PROCEEDING BOOK

(Abstracts and Full-Text Papers)

6th INTERNATIONAL EURASIAN CONFERENCE ON SCIENCE, ENGINEERING and TECHNOLOGY

(EurasianSciEnTech 2025)

25 – 27 June 2025
Ankara / Türkiye

ISBN: 978-605-72134-5-7

EurasianSciEnTech 2025

www.eurasianscientech.org

6th International Eurasian Conference on Science, Engineering and Technology (EurasianSciEnTech 2025)

June 25-27, 2025 / Ankara, Turkey
www.EurasianSciEnTech.org

PROCEEDING BOOK

(Abstracts and Full-Text Papers)

Editor

Prof. Dr. Muhittin DOĞAN

Copyright © 2025

ISBN: 978-605-72134-5-7

Publication Date: July 2025

Organized by

Avrasya Araştırma Geliştirme Bilim ve Teknoloji Merkezi

All rights reserved. The right to publish this book belongs to EurasianSciEnTech 2025. No part of this publication may be reproduced, stored in a retrieval system, or transmitted in any form or by any means, electronic, mechanical, photocopying, recording or otherwise, without permission. This Proceeding Book has been published as an electronic publication (e-book). Citation can not be shown without the source, reproduced in any way without permission.

Authors are responsible for the contents of their abstracts and full-text papers.

Congress Web Page: www.eurasianscientech.org
E-mail: info@eurasianscientech.org

CHAIRMAN OF CONFERENCE

Prof. Dr. Muhittin DOĞAN	**Gaziantep University, Turkey**

ORGANIZING COMMITTEE

Prof. Dr. Ahmet EKİCİBİL	**Çukurova University, Türkiye**
Prof. Dr. Ahmet DEMİRBAŞ	**Sivas Cumhuriyet University, Türkiye**
Prof. Dr. Ali BİLGİLİ	**Ankara University, Türkiye**
Prof. Dr. Ayla BALABAN GÜNDÜZALP	**Gazi University, Türkiye**
Prof. Dr. Ergül YAŞAR	**İskenderun Technical University, Türkiye**
Prof. Dr. Faruk KARADAĞ	**Çukurova University, Türkiye**
Prof. Dr. Mehmet Cengiz TAPLAMACIOĞLU	**Gazi University, Türkiye**
Prof. Dr. Mohammed A. IBRAHIM SHARAF	**İstanbul University-Cerrahpaşa, Türkiye**
Prof. Dr. Murat ARI	**Çankırı Karatekin University, Türkiye**
Prof. Dr. Nabeel Ahmad	**Dev Bhoomi Uttarakhand University, India**
Prof. Dr. Ümmühan ÖZDEMİR ÖZMEN	**Gazi University, Türkiye**
Assoc. Prof. Dr. Alevcan KAPLAN	**Batman University, Türkiye**
Assoc. Prof. Dr. Barkat ULLAH	**Islamia College University, Pakistan**
Assoc. Prof. Dr. Demet DOĞAN	**Gaziantep University, Türkiye**
Assoc. Prof. Dr. Ebru SARALOĞLU GÜLER	**Başkent University, Türkiye**
Assoc. Prof. Dr. Haluk GÖZDE	**Turkish Aerospace (TUSAŞ), Türkiye**
Assist. Prof. Dr. Ahmad Ali	**University of Mumbai, India**
Dr. Abdul Bari Shah	**Seoul National University, South Korea**
Dr. Abdul RAZZAQ	**Quarshi University, Pakistan**
Dr. Majid Iqbal	**University of Chinese Academy of Sciences, China**
Dr. Muhammad Nauman Khan	**Islamia College University, Pakistan**
Dr. Sana Wahab	**Quaid-i-Azam University, Pakistan**
Dr. Victorinne Lorette Yimgang	**University of Yaoundé I, Cameroon**

INTERNATIONAL SCIENTIFIC COMMITTEE*

Prof. Dr. Abd. Rahim Abu TALİB	**Universiti Putra Malaysia, Malaysia**
Prof. Dr. Adnan BOZDOĞAN	**Osmaniye Korkut Ata University, Türkiye**
Prof. Dr. Adnan QADIR	**NED University of Engineering & Technology, Pakistan**
Prof. Dr. Ahmet EKİCİBİL	**Çukurova University, Türkiye**
Prof. Dr. Ahmet ŞEKEROĞLU	**Niğde Ömer Halisdemir University, Türkiye**
Prof. Dr. Ali BİLGİLİ	**Ankara University, Türkiye**
Prof. Dr. Ali Osman AYAŞ	**Adıyaman University, Türkiye**
Prof. Dr. Ali Tuncay ÖZYILMAZ	**Hatay Mustafa Kemal University, Türkiye**
Prof. Dr. Alpaslan DAYANGAÇ	**Osmaniye Korkut Ata University, Türkiye**
Prof. Dr. Aslıhan DEMİRDÖVEN	**Tokat Gaziosmanpasa University, Türkiye**
Prof. Dr. Aycan TOSUNOĞLU	**Uludağ University, Türkiye**
Prof. Dr. Ayla UYSAL	**Süleyman Demirel University, Türkiye**

Prof. Dr. Aysel GÜVEN	**Baskent University, Türkiye**
Prof. Dr. Ayşe AVCI	**Sakarya University, Türkiye**
Prof. Dr. Ayşe AYDOĞDU	**Gazi University, Türkiye**
Prof. Dr. Ayşe BEDELOĞLU	**Bursa Technical University, Türkiye**
Prof. Dr. Azize AYOL	**Dokuz Eylül University, Türkiye**
Prof. Dr. Başak HANEDAN	**Atatürk University, Türkiye**
Prof. Dr. Bengi USLU	**Ankara University, Türkiye**
Prof. Dr. Berna DENGİZ	**Baskent University, Türkiye**
Prof. Dr. Bushra MIRZA	**Quaid-i-Azam University, Pakistan**
Prof. Dr. Bülent AKAY	**Ankara University, Türkiye**
Prof. Dr. Bülent KABAK	**Hitit University, Türkiye**
Prof. Dr. Bülent YEŞİLATA	**Ankara Yildirim Bayazit University, Türkiye**
Prof. Dr. Cihangir DURAN	**Ankara Yıldırım Beyazıt University, Türkiye**
Prof. Dr. Deniz Sunar ÇERÇİ	**Adıyaman University, Türkiye**
Prof. Dr. Deniz UZUNSOY	**Bursa Technical University, Türkiye**
Prof. Dr. Didem ÖZÇİMEN	**Yildiz Technical University, Türkiye**
Prof. Dr. Dilek ERDİRENÇELEBİ	**Konya Technical University, Türkiye**
Prof. Dr. Ebru ŞENADIM TÜZEMEN	**Cumhuriyet University, Türkiye**
Prof. Dr. Ebru ŞENEL	**Ankara University, Türkiye**
Prof. Dr. Emine GÜNERİ	**Erciyes University, Türkiye**
Prof. Dr. Erol ATAY	**Hatay Mustafa Kemal University, Türkiye**
Prof. Dr. Fakhru'l Razi bin Ahmadun	**National Defence University Malaysia, Malaysia**
Prof. Dr. Farhat JABEEN	**Government College University, Pakistan**
Prof. Dr. Faruk KARADAĞ	**Çukurova University, Türkiye**
Prof. Dr. Fatma MEYDANERİ TEZEL	**Karabuk University, Türkiye**
Prof. Dr. Fatma Suna BALCI	**Gazi University, Türkiye**
Prof. Dr. Ferruh ERDOĞDU	**Ankara University, Türkiye**
Prof. Dr. Gamal BADR	**Assiut University, Egypt**
Prof. Dr. Gıyasettin KAŞIK	**Selçuk University, Türkiye**
Prof. Dr. Gul Majid Khan	**Quaid-i-Azam University, Pakistan**
Prof. Dr. Gülay ZENGİN	**Gaziantep University, Türkiye**
Prof. Dr. Hakan GÜNEYLİ	**Cukurova University, Türkiye**
Prof. Dr. Handan UYSAL	**Atatürk University, Türkiye**
Prof. Dr. Hülya METİN GÜBÜR	**Mersin University, Türkiye**
Prof. Dr. Hüseyin CANBOLAT	**Ankara Yıldırım Beyazıt University, Türkiye**
Prof. Dr. Ioan SEBEŞAN	**Politehnica University of Bucharest, Romania**
Prof. Dr. Kerim KÜÇÜK	**Dokuz Eylül University, Türkiye**
Prof. Dr. Maria DAGLIA	**University of Naples Federico II, Italy**
Prof. Dr. Mehmet Bertan YILMAZ	**Çukurova University, Türkiye**

Prof. Dr. Mehmet SARI	**Aksaray University, Türkiye**
Prof. Dr. Medeni MASKAN	**Gaziantep University, Türkiye**
Prof. Dr. Meltem SARIOĞLU CEBECİ	**Cumhuriyet University, Türkiye**
Prof. Dr. Muhammad ANSAR	**Quaid-i-Azam University, Pakistan**
Prof. Dr. Mustafa AKYOL	**Adana Alparslan Türkeş Science and Technology University, Türkiye**
Prof. Dr. Mustafa DJAMGOZ	**Imperial College London, United Kingdom**
Prof. Dr. Murat Hüsnü SAZLI	**Ankara University, Türkiye**
Prof. Dr. Mustafa ÇİĞDEM	**Yıldız Technical University, Türkiye**
Prof. Dr. Nabeel Ahmad	**Dev Bhoomi Uttarakhand University, India**
Prof. Dr. Necati OLGUN	**Gaziantep, University, Türkiye**
Prof. Dr. Neriman BAĞDATLIOĞLU	**Celal Bayar University, Türkiye**
Prof. Dr. Nil TOPLAN	**Sakarya University, Türkiye**
Prof. Dr. Niyazi ŞAHİN	**Ankara Yıldırım Beyazıt University, Türkiye**
Prof. Dr. Nuri ÖZALP	**Ankara University, Türkiye**
Prof. Dr. Olcayto KESKİNKAN	**Çukurova University, Türkiye**
Prof. Dr. Oya BOZDAĞ DÜNDAR	**Ankara University, Türkiye**
Prof. Dr. Rani Faryal Faheem TAHIR	**Quaid-i-Azam University, Pakistan**
Prof. Dr. Ozan TEKİNALP	**Middle East Technical University, Türkiye**
Prof. Dr. Sadaf Zaidi	**Aligarh Muslim University, India**
Prof. Dr. Salim ÇERÇİ	**Adıyaman University, Türkiye**
Prof. Dr. Sarwat JAHAN	**Quaid-i-Azam University, Pakistan**
Prof. Dr. Selma DÜZYOL	**Konya Technical University, Türkiye**
Prof. Dr. Sezgin AYDIN	**Gazi University, Türkiye**
Prof. Dr. Sibel YILDIZ	**Karadeniz Technical University, Türkiye**
Prof. Dr. Siti Khairunniza bt. Bejo	**Universiti Putra Malaysia, Malaysia**
Prof. Dr. Şule UĞUR	**Gazi University, Türkiye**
Prof. Dr. Tayfun DEDE	**Karadeniz Technical University, Türkiye**
Prof. Dr. Tevfik AĞAÇAYAK	**Konya Technical University, Türkiye**
Prof. Dr. Ümmühan ÖZDEMİR ÖZMEN	**Gazi University, Türkiye**
Prof. Dr. William A. COETZEE	**New York University, USA**
Assoc. Prof. Dr. Aslı GİRAY	**Alanya Alaaddin Keykubat University, Türkiye**
Assoc. Prof. Dr. Bahar MERYEMOĞLU	**Cukurova University, Türkiye**
Assoc. Prof. Dr. Burhan TİRYAKİOĞLU	**Marmara University, Türkiye**
Assoc. Prof. Dr. Demet DOĞAN	**Gaziantep University, Türkiye**
Assoc. Prof. Dr. Dian Darina Indah Binti Daruis	**Universiti Putra Malaysia, Malaysia**
Assoc. Prof. Dr. Doğan KAYA	**Cukurova University, Türkiye**
Assoc. Prof. Dr. Ebru SARALOĞLU GÜLER	**Başkent University, Türkiye**
Assoc. Prof. Dr. Mahmoud HAFEZİEH	**Iranian Fisheries Sciences Research Institute, Iran**
Assoc. Prof. Dr. Mohammad SUDAGAR	**Gorgan University, Iran**

Assoc. Prof. Dr. Muhammad Mohsin Amman	**NED University of Engineering & Technology, Pakistan**
Assoc. Prof. Dr. Muhsine Bilge İMER	**Middle East Technical University, Türkiye**
Assoc. Prof. Dr. Mehmet YALÇIN	**Hatay Mustafa Kemal University, Türkiye**
Assoc. Prof. Dr. Nemanja Kašiković	**University of Novi Sad, Serbia**
Assoc. Prof. Dr. Özge TUFAN ÇETİN	**Akdeniz University, Türkiye**
Assoc. Prof. Dr. Roselina Arelhi	**University of Nottingham, Malaysia**
Assoc. Prof. Dr. Samra MEDEDOVIC	**Dzemal Bijedic University of Mostar, Bosnia and Herzegovina**
Assoc. Prof. Dr. S.D. SARASWATHY	**Bharathidasan University, India**
Assoc. Prof. Dr. Selda KILIÇ ÇETİN	**Cukurova University, Türkiye**
Assoc. Prof. Dr. Semra ÇİÇEK	**Atatürk University, Türkiye**
Assoc. Prof. Dr. Sezen Canım ATEŞ	**Istanbul Yeni Yüzyıl University, Türkiye**
Assoc. Prof. Dr. Shahram DADGAR	**Iranian Fisheries Sciences Research Institute, Iran**
Assoc. Prof. Dr. Süleyman Sungur TEZCAN	**Gazi University, Türkiye**
Assoc. Prof. Dr. Ümit AYATA	**Bayburt University, Türkiye**
Assist. Prof. Dr. Ahmad Ali	**University of Mumbai, India**
Assist. Prof. Dr. Emine ÇELİKOĞLU	**Amasya University, Türkiye**
Assist. Prof. Dr. Halil İbrahim DEMİR	**Sakarya University, Türkiye**
Assist. Prof. Dr. Hıdır DÜZKAYA	**Gazi University, Türkiye**
Assist. Prof. Dr. Mahmut DURGUN	**Tokat Gaziosmanpasa University, Türkiye**
Assist. Prof. Dr. Levent ÇOLAK	**Baskent University, Türkiye**
Assist. Prof. Dr. Poonam Agarwal	**Jawaharlal Nehru University, India**
Assist. Prof. Dr. Tuba PEHLİVAN	**Gaziantep University, Türkiye**
Assist. Prof. Dr. Umut ÇELİKOĞLU	**Amasya University, Türkiye**
Assist. Prof. Dr. Yıldıray PALABIYIK	**Istanbul Technical University, Türkiye**
Dr. Aainaa Izyan Nafsun	**Universiti Putra Malaysia, Malaysia**
Dr. Abdul Bari Shah	**Seoul National University, South Korea**
Dr. Antonio SUREDA GOMILA	**University of the Balearic Islands, Spain**
Dr. Atanas G. ATANASOV	**University of Vienna, Austria**
Dr. Francesca CIGNARELLA	**Washington University, USA**
Dr. Hüsna TOPKAYA	**Batman University, Türkiye**
Dr. Lim Kar Sing	**Universiti Malaysia Pahang, Malaysia**
Dr. Ramin Ekhteiari SALMAS	**King's College London, United Kingdom**
Dr. Ravichandran RAMASAMY	**New York University, USA**
Dr. Sachiyo ABURATANI	**National Institute of Advanced Industrial Science and Technology, Japan**
Dr. Sergey SHITYAKOV	**University Hospital Würzburg, Germany**

***This list is arranged in alphabetical order.**

FOREWORD

6th International Eurasian Conference on Science, Engineering and Technology (EurasianSciEnTech 2025) was successfully held on June 25-27, 2025 with a great participation from many countries

The objective of *EurasianSciEnTech 2025* was to bring leading academicians, researchers, scholars as well as industrial professionals together from all over the world to exchange and share their experiences and research results to discuss the practical challenges encountered and the solutions adopted. In this context, we welcomed precious scientists and the greatest appreciation goes to all participants whose contributions have made this conference a success. I would like to thank the organizing committee and the scientific committee for providing this intense and high quality scientific environment.

I believe that the *EurasianSciEnTech 2025* has made important contributions to you at large and hope to see you at the *7th International Eurasian Conference on Science, Engineering and Technology* (*EurasianSciEnTech 2026*).

Prof. Dr. Muhittin DOĞAN

Chairman of *EurasianSciEnTech 2025*

Contents

1. ORAL PRESENTATIONS **2**

1.1. ABSTRACTS **3**

Synthesis of sulfamethoxazole surface imprinted core-shell magnetic nanoparticles for selective detection of sulfamethoxazole in poultry by an electrochemical biosensor 5

Herbal cold cream formulation from *Lavandula stoechas* essential oil 6

Optimization of U-Bending Process Parameters for 304L Austenitic Stainless Steel 7

Data-Driven Optimization of Martensitic Phase Transformation Models in 304L Steel 8

İndiyum monotellüride dayalı ileri malzemelerin elde edilmesi ve bazı termofiziksel özellikleri 9

Positive solutions to a system of fractional q-difference equations with multi-point boundary conditions 11

Exploring Alcohol-Related Metabolites in Bone: A Pilot Study Using NMR Spectroscopy 12

Antileishmanial activity and chemical composition of fractions from an endophytic fungus, AMrb9 inhabiting Cameroonian *Annona muricata* L. (Annonaceae) 13

To Compare maternal outcomes aming pregnant woman with COVID-19 infection, stratified by body mass index : normal weight, overweight and obesity. 14

Metabolomic Characterization of Human Vitreous Fluid Using ^{1}H-NMR Spectroscopy 15

Bridging Traditional and Scientific Knowledge: Quantitative Ethnopharmacological Investigation in Marghazar Valley, Swat, Pakistan 16

Influence of Edaphic Factors on Vegetation and Plant Community Dynamics in the Dry Temperate Region, Ojhor Valley, Eastern Hindu Kush, Pakistan 17

Investigation of the Material Effect on Rotor Mechanical Stress 18

A novel binary mixture of lauric acid/caprylic acid as phase change material for refrigerated trucks 19

Investigation of Potential Antiviral Activity of *Hypericum perforatum* Extract Against SARS-CoV-2 20

Silver Loaded Photocrosslinked Silk Sericine-Keratin-F127 Hydrogels for Wound Healing Applications 21

Synthesis and Characterization of a Novel Chromenylium-Cyanine Type Compound 22

A New Smartphone-Assisted Near-Infrared Fluorescent Probe for Visual Detection of Mercury(II) in Food and Water Samples 23

The Investigation of the Latest Developments in Green Energy Technologies to Reduce Carbon Emissions 24

Biosynthesis of *Helichrysum arenarium* L.-Cu(II) hybrid nanoflowers and evaluation of their cytotoxic activities 25

Electrochemical Surface Modification of Screen-Printed Gold Electrodes for Enhanced Performance and Kinetics 26

Deniz Dibi Tarama Faaliyetlerinden Elde Edilen Dip Çamurlarının Alternatif Bertaraf Yöntemlerinin Araştırılması 27

Comparative analysis of transport-oriented urban approaches 28

Hatay ili Arsuz Bölgesi Topraklarının Molibden İçeriği ve Topraktaki Bazı Ağır Metaller ile İlişkilerinin Belirlenmesi 29

Investigation of the effect of layer thickness on the wear properties of PEEK materials 30

Powder metallurgical synthesis and characterization of Al-10 wt.% Si-x($Hf_{0.2}Ti_{0.2}Zr_{0.2}V_{0.2}Ta_{0.2}$)$B_2$ 31

Kolon kanseri ve bağırsak mikrobiyotası: ön çalışma 32

Damping–mixing enthalpy relationship in Mg-Ca and Mg-Ni alloys: Influence of short-range order 33

Kiraz domatesin raf ömrünü uzatmak için PBAT esaslı nanokompozit filmlerin geliştirilmesi ve karakterizasyonu 34

A New Role for Cyclobenzaprine: Cytotoxic Effects in Lung Cancer Cells 35

Improvement of Functional Properties in Bread Enriched with Aronia (*Aronia melanocarpa*) Juice 36

Impact of *Aronia melanocarpa* juice substitution on the rheological properties of wheat flour 37

Revolutionizing Skincare: The Rise of Probiotics in the Cosmetic Market 38

Ev tekstili kumaşların ıslanma davranışı analizi için yöntem geliştirilmesi 39

Health impact of particulate matter (PM): case study for Artvin 40

The Effect of Nano-Hydroxyapatite Forms on the Growth of Barley Plants Grown in Hydroponic Conditions Under Combined Boron and Salinity Stress 41

Assessment of Fishing Zones (FZ) and No-Fishing Zones (NFZs) in the Gökova and Datça–Bozburun Special Environmental Protection Areas (SEPAs) in Terms of Alien Species 42

Kedi ve Köpeklerde Göz Ultrasonografisi ile Normal Göz Yapılarının Değerlendirilmesi 43

Kedi ve Köpeklerde Göz Ultrasonografisi ile Patolojik Bulguların Değerlendirilmesi 44

Electrocatalysis of Carbon Dioxide into Green Energy Resources Using Metal Nanoparticles Coupled with Metal Oxide Nanocomposite 45

Interfacial film flows on multi-layer thin films 46

Çok Ölçütlü Grup Öneri Sistemlerinde Popülerlik Yanlılığı 47

Diabetes Classification Using MLP, SVM and Random Forest 48

The Biotechnological Importance of Keratin and its Isolation Process from Waste Hair Samples 49

Adsorptive Stripping Voltammetric Determination of Apigenine on a Glassy Carbon Electrode Improved by The Use of Surfactant 50

Green *Papaver somniferum* L. seed and shell extract in a 1 M HCl solution for mild steel corrosion prevention 51

Comparative Study: Global Aquaculture Production Statistics of Common Carp (*Cyprinus carpio*, Linnaeus, 1758) 52

Comparison of Classical and Ultrasound-Assisted Extraction of Phytochemicals and Antioxidant Activity of *Salvia officinalis* L. 53

An overview of the challenges of a collaborative filtering recommender system 54

EMI Shielding and Life Cycle Assessment 55
Hydrochar production from oil-extracted spent coffee grounds by hydrothermal carbonization 56
Biocompatibility investigation of TiTaHfNbZr alloys with femtosecond laser surface modification 57
A Study on Awareness and Cryptographical Solutions Against Sim Swapping Attack 58
The Composition and Characterization of Octopamine-Derived Cyclomatrix Tetrameric Polyphosphazenes 59
Evaluation of cutting parameter effects on surface roughness and temperature in face milling of a tractor part 60
Environmental interactions of early life stages of European Sprat (*Sprattus sprattus*) along the vertical water column in Sinop Bay, 2023-2024 61
Effect of nano calcium on broad bean plant growth and calcium uptake in soil and soilless conditions . 62
Biological Control Potential of EPNs Against the Citrus Mealybug 63
Differential effects of lipopolysaccharide and SARS-CoV-2 spike protein on RAS-related gene expression in normal and colon cancer epithelial cells 64
Synthesis and Characterization of Curcumin and Lysine Derived Carbon Dots 65
The Effect of Different Cobalt Contents on the Properties of Tungsten Carbide Materials Sintered at Low Temperature 66
Conventional and Microwave-Assisted Synthesis and Characterization of PEG-Based Esters 67
Effect Of Cooling 16MnCr5 Steel Under Different Pressure On Hardness And Microstructure Properties 68
L-Alanin, L-İzolösin, ve L-Valin Amino Asit Metil Esterlerinin *Candida albicans* ile Bazı Gram pozitif ve Gram negatif Bakteri Suşlarına Karşı Antimikrobiyal Etkilerinin Araştırılması 69
UV-Curable Emulsion Hydrogel System Based on Modified PVA as a Wound Dressing Material 70
Monitoring of endangered dusky grouper (*Epinephelus marginatus*) in The Karaburun-Ildır Gulf Special Environmental Protection Area with different methods 71
Microwave-assisted preparation and characterization of derivatives starting from flurbiprofen 72
Elastic and Mechanical Property Enhancement of NASICON-Type LATP via Indium Doping: Implications for Solid-State Li-Ion Battery Applications 73
Production and quality monitoring of marinade from mussels smoked with different wood chips 74
Thermal Analysis-Based Investigation of the Pyrolysis Kinetics of *Spirulina platensis* 75
Quantitative Analysis Of CoQ10 Content Of Nutraceuticals From Turkish Market 76
Time – space tradeoff in array merging problem 77
The infinite sum of reciprocal Fibonacci numbers 78
On the relations between three reduced series of numbers 79
Integrated Microfluidic Chip Platform for Cyclotide Isolation from Plant Extract 80
Rapid detection of expired tablets using Second Derivative FTIR: An iron supplement tablet example.. 82

Magnetic Characterization of $Pt_{17}Cu_{14}Ni_{69}$ Nanoparticles with Enhanced Low-Temperature Magnetic Stability 83

Investigation of photocatalytic properties of $ZnFe_2O_4$ spinel nanoparticles 84

Biomass, distribution and some population parameters of Big-Scale Sand Smelt, *Atherina boyeri* (Risso, 1810) in the Sea of Marmara 85

Menfez kesitlerinde karayolu göçme nedenlerinin araştırılması 86

A Multi-Criteria Decision-Making Approach for Green Hydrogen Production via Renewable Energy Sources 87

Otomotiv Şartlarına Uygun Uv Dayanımı Sağlayan PBT/PET Harmanlarının Geliştirilmesi 88

A genome-wide *in silico* analysis of *PR1* (pathogenesis-related 1) genes in the watermelon (*Citrullus lanatus*) 89

Assessment of the UV-B Protective Potential of Pollenkitt in *Narcissus tazetta* 90

Antioxidant Responses in *Camellia sinensis* Pollen Exposed to Low Temperatures 91

Functional Analysis of Missense SNPs in the CYP2D6 Gene Using *In Silico* Methods 92

European Ionospheric Response to the May 2024 Gannon Geomagnetic Superstorm 93

Numerical simulations of 3D Magnetotellurics for Hydrocarbon exploration: Focus on overthrust structures 94

Endüstriyel Meyve Posalarının Antidiyabetik Potansiyeli: a-Amilaz İnhibisyonu 95

Gemi Emisyonlarını Azaltmaya Yönelik Yakıt Alternatiflerinin Seçiminde Etkili Faktörlerin Belirlenmesi 96

Effect of Fat Content and Fermentation Time on Kefir Quality 97

Sustainable Production from Waste Rooster Combs: High-Purity Hyaluronic Acid Isolation and Structural Analysis 98

Genetic identification of *Myomimus roachi* (Rodentia: Gliridae) from Türkiye using DNA barcoding 99

A faunistic survey on wild bees of the Aegean region, Turkiye 100

Determination of the role of fullerenol and green-synthesized iron nanoparticles in enhancing drought tolerance in safflower plants through photochemical mechanisms 101

Removal of 2-(4-isobutylphenyl)propanoate (ibuprofen) from aqueous solutions by adsorption onto carbon fiber 102

Thermodynamic analysis of internal heat recovery between the condenser and evaporator outlets in an air-source heat pump 103

Size Effect on WS_2 Structures in Electrochemical Ammonia Synthesis via Nitrogen Reduction Reaction 104

Electrochemical NH_3 production by different size Molybdenum Sulfide 105

Karpal tünel sendromu olan bireylerde boyun pozisyon hissi ve eklem hareketi arasındaki ilişki 106

İletken Nanokompozit Polimerlerin Eldesi Ve Özelliklerinin Araştırılması 107

Omega-3 Rich Edible Oil Alternative: Functional Potential and Limitations of *Camelina sativa* Oil 108

In vitro evaluation of a dual drug-loaded delivery system for the treatment of hepatocellular carcinoma 109

Influence of Mg^{2+} Ions on the Crystallization and Filtration Characteristics of Lithium Carbonate 110

Impact of Methyl Substitution on Photocatalytic Activity of BODIPY-Thiophene-Integrated COP-TiO_2 Systems 111

Potential effects of *Moluccella leavis*-silver nanoparticles on lung cancer cell viability and apoptotic cell death 112

Hotair Tutkalı ile PP Kenar Bandı Üretim Sürecinde Yapışma Performansının Artırılması 113

PVC Kenar Bandı Üretim Kalitesinin İyileştirilmesi İçin Plastifiyan Miktarının Artırılması 114

Repositioning Existing Drugs to Target DNMT3A in Liver Cancer: A Site-Focused Structural Approach 115

Türkiye'deki Yeşil Limanların Sürdürülebilirlik Üzerine Etkileri 116

Aronia melanocarpa Meyve Ekstresinin İnsan Meme Kanseri Hücreleri Üzerine Etkisi 117

Enhancing ammonium perchlorate decomposition via samarium-doped ceria catalysts for solid rocket propellants 118

Novel tomato-based interventions: Impact on survival rates in common cancers 119

Antimicrobial target identification in *Vibrio cholerae* via reporter metabolite analysis 120

Effect Of Feder Produced By Plastic Injection On Material Behavior 121

Design of inner-outer layered garments with enhanced comfort effect for men's upper clothing 122

A computer simulation study on coalescence of metal nanoparticles 123

Production and Characterization of Biochar from Cabbage Waste Using Hydrothermal Carbonization 124

Finite Element Analysis of Natural Rubber-Based Damping Components 125

Resolved GMCs in Lenticular Galaxy NGC383 126

A comparative investigation on short-beam strength of 3D-printed hybrid curved composites 127

Effect of organic alizarin sensitizer on the efficiency of TiO_2-based dye-sensitized solar cells under different light intensities 128

Synthesis and characterization of graphene-derived materials as a composite additive 129

Preservation of Quality in Seafood Products with Smart Packaging Technologies 130

Protective Effect of *Cotinus coggygria* Scop. Extract on Ethanol-Induced Kidney Damage 131

Magnetic properties of spin-3/2 antiferromagnetic Blume-Capel model in triangular lattice 132

Protective Effects of *Cotinus coggygria* Scop. Extract Against Ethanol-Induced Glycosylation Anomalies in Small Intestinal Tissue 133

Artificial Intelligence and Ethics in Education 134

Responsive Polymer Brush Architectures Explored via Dissipative Particle Dynamics 135

Arıtma çamurunun sorgum yetiştiriciliğinde kullanım potansiyeli 136

Determination of antibacterial, antifungal, and insecticidal effects of secondary metabolites from entomopathogenic fungi 137

Production of Al-doped ZnO materials and investigation of their properties 138

Some bounds on distance based energy of graph products 139

Çilek (*Fragaria ananassa)* Yaprağı Ekstresi Kullanılarak Altın Nanoparçacıkların Yeşil Sentezi ve Karakterizasyonu 140

Histological Evaluation of the Effect of Baicalin on Cisplatin-Induced Parotid Gland Injury 141

Effect of *Alcea rosea* var. *nigra* flower extract on cancerous and non-cancerous pleural mesothelial cells 142

Protective Effects of Alpha Lipoic Acid Against Valproic Acid-Induced Small Intestinal Damage 143

Tarım İşletmeleri ve Sürdürülebilirlik Perspektifinden IV. Tarım Orman Şûrası Kararları 144

Techno-economic assessment of off-grid hybrid renewable energy systems for urban electricity demand 145

Plastivore insects: an overview 146

Effect of Glaucocalyxin A on Cell Migration Capacity in Lung Cell Line 147

Contribution of using a tuned mass damper (TMD) as a passive control device in building performance 148

Eskişehir Sazova Bilim Kültür ve Sanat Parkı Floristik Yapısı İle İlgili Ön Çalışmalar 149

The role of microbiome research in improving gut health of farmed species for sustainable disease resistance in aquaculture. 150

Effects of sustainable diets such as insect-based, essential oil-supplemented and single-cell protein on disease resistance in aquaculture 151

İkincil A356 Alüminyum Alaşımının Korozyon Davranışına Minör Skandiyum (Sc) ve Lantan (La) Eklentisinin Etkisi 152

Design and Evaluation of Chitosan/PVP-Based Films for Advanced Wound Dressings in Biomedical Applications 153

Evaluation of volatile oil composition and structural discrepancies in different parts of *Chenopodium botrys* L. 154

Kinetic and Equilibrium Studies on the Adsorption of Remazol Red by Natural Zeolite 155

The Role of Food Choice Motivations and Food Neophobia in Organic Food Consumption 156

Adsorptive Removal of Polystyrene Nanoplastics from Water: Role of Activated Carbon and Ion Exchange Resin 157

The role of swimming exercise in preserving uterine and ovarian reserves in a DSS-induced chronic ulcerative colitis mouse model 158

Bi-objective optimization of time and cost in project scheduling: an application in a construction project 159

Arıtılmış atıksuların tarımsal sulamada kullanımı 160

Protective effect of white cabbage extract against amiodarone-induced small intestinal damage in rats. 161

Transcript levels of genes encoding pyroptotic effector proteins in triple-negative breast cancer (TNBC) and non-TNBC, and based on hormone receptor (HR) and HER2 status 162

In vitro Antioxidant and Anticancer Activities of Methanolic Extract of *Onobrychis oxyodonta* 163

Determination of pathotype, serogroup, and antibiotic susceptibility of *Escherichia coli* recovered from a cat with cystitis 164

Cadmium (II) Adsorption from Aqueous Media using Mercapto-Functionalized Silica Xerogels 165

Millimeter-Wave Radar for Short-Range Mobility Detection 166

The characterization of *Acinetobacter lwoffii* isolates from sheep necropsy materials 167

Animal Welfare Standards in Calf Management 168

The effect of direct kisspeptin-54 application on gonadotropin receptor expressions in granulosa cells of PCOS patients 169

The Effect of Different LED Light Conditions on the Total Phenolic and Flavonoid Contents of Fenugreek (*Trigonella foenum-graecum* L.) Microgreens 170

Evaluation of Antioxidant Activities of Leaf and Fruit Extracts of *Cotoneaster coriaceus* Franch. by DPPH Assay 171

Measuring Perceived Accessibility: The Role of Subjective Experiences in Transportation Planning 172

Biotypes of *Bemisia tabaci* populations in Southwestern Türkiye 173

Mikroalglerin sürdürülebilir bir üretim için uygulama alanları üzerine güncel bir inceleme 174

Granulocyte: the key hemocyte of humoral and cell-mediated immunity 175

Istilacı *Cirsium arvense* (L.) SCOP.'in Grime'in CSR Stratejilerine Göre Sınıflandırılması 176

Elektrosprey ve 3B Biyoyazıcı Yöntemleri ile *Cinchona* Ekstresi ve Arap Zamkı İçeren Fonksiyonel Yara Örtülerinin Geliştirilmesi 177

Development of a surrogate model for dual optical element concentrated photovoltaic system using machine learning 178

Seramik Karo Üretiminde Sürdürülebilir Teknolojilerin Geliştirilmesi 179

Linking Forest Management to Water Treatability: Improved Coagulation Performance Following Silvicultural Activities in Forested Watershed 180

Aspergillus fumigatus ERG6 Protein Modelinin Antifungal Ajanlarla Moleküler Etkileşim Analizi 181

Hypericum perforatum Modulates Innate Immune Responses in *Galleria mellonella*: A Dose-Dependent Analysis 182

Cytotoxic and Antimicrobial Properties of Brown Algae Extracts: A Study on *Cystoseira foeniculacea* and *Sargassum vulgare* 183

Evolution of the Dmrt1 Sex Gene in the Anatolian Water Frog Complex (Genus: *Pelophylax*) in Türkiye 184

Development of Composite Anode Electrodes Containing Metal Oxide-N Doped Reduced Graphene Oxide for Lithium Ion Batteries 185

Structural and Antibacterial Activity Properties of Lignite-Derived Carbon Coating on Ceramic Tiles. 186

Mucormycosis Cases Under the Microscope: A 19 Year Retrospective Pathology-Based Surveillance Study 187

Environmental and mechanical impacts of incorporating synthetic C-S-H in cement systems 188

Evaluation and integration of YOLOv8 and SAM deep learning models for brain tumor detection and segmentation in MRI 189

From Waste to Worth: Sustainable Nanofibers from *Aloe vera* and Recycled Polystyrene 190

Investigation of the Cadmium (Cd) removal potential of two aquatic macrophytes (*Limnobium laevigatum*, *Egeria densa*) in two different media with a microcosm approach 191

Green Synthesis of Copper Oxide Nanoparticle via *Rubus Idaeus* 192

Cyclic amine linked *p*-benzoquinones and their antimicrobial analyses 193

Potentiometric determination of skin antiseptic rivanol and its greenness assessment 194

Thermal and Chemical Assessment of Rolled Tobacco from Two Turkish Regions: Aegean and Southeast 195

Alterations in Oxidative Stress and Antioxidant Enzyme Activities Due to Phosmet Exposure in *Eisenia fetida* 196

Comparative evaluation of CKAN and CNN deep learning models for classifying tumor-infiltrating lymphocytes in cancer histopathology images 197

Multi-Criteria Assessment of Turkish Cities for Biogas Plant Siting 198

Optimization of Bioethanol Production from Tobacco and Tobacco Product Wastes 199

Efficient Dye Removal Using NH_2 functional polymer gel 200

Effects of Olive Leaf Extract on Enzyme Activities of Actinobacteria Isolates and Molecular Identification of Isolates 201

Evaluation of Solvent Type and Concentration on the Extraction Efficiency of Phenolic Compounds from *Urtica dioica* 202

Lignoselülozik Kaynaklı Karbon Kuantum Noktalarının Asidik Ortamda Korozyon İnhibitörü Olarak Geliştirilmesi 203

Genetic Identification of Some Medicinal and Aromatic Hawthorn (*Crataegus* spp.) Species Naturally Distributed in Artvin 204

Ethnobotanical Uses and the Medicinal - Economic Significance of *Valeriana* Species 205

Performance Analysis of Metaheuristic Algorithms in the Parameter Tuning of BLDC Motor PID Controllers 206

Traditional Plants Used For Medicinal-Aromatic Purposes in South Villages of Ardanuc, Artvin (Türkiye) 207

The Modification of Partial Oxidation Based Magnetic Nanoparticles with Cyclodextrin and Application in Magnetic Hyperthermia 208

Synthesis and characterization of the poly(ε-caprolactone-g-styrene) three arm block-brush copolymer via RAFT bulk polymerization 209

Uçak Bakım Ve Onarım Verileri İle İstatistiksel Uygulama 210

Traditional plant uses in the villages surroundings of Karagöl-Sahara National Park 211

Sürdürülebilir Enerji Yönetimi için IoT Çözümü: Raspberry Pi, Docker ve Bulut Tabanlı İzleme Mimarisi 212

An Important Step Towards Rural Development: Medicinal-Aromatic Plant Cultivation Studies in Artvin 214

Immobilization of Urease on Cellulose Nanocrystals via Different Modifications 215

Contribution of Artvin Coruh University to Regional Development: Establishment of a Facility for Processing and Storing Aromatic Plants in Artvin 216

The role of hormesis in nutrition and health 217

BIX-induced Somatic Embryogenesis through Epigenetic Reprogramming in *Arabidopsis thaliana* 218

Dünya'da ve Türkiye'de Su Ürünleri Mutfağı 219

A fuzzy c-means ensemble approach for robust price dynamics forecasting in Turkey 220

Radiation Shielding Properties of Gd_2O_3 Reinforcement Paraffin Materials: MCNP6.2 Simulation Analysis 221

Current research on anti-Alzheimer's drugs: Secretase Inhibitors 222

Seasonal effects of air pollution on childhood allergic rhinitis: A case study from Northwestern Türkiye 223

Analyzing the impact of air pollution on asthma with machine learning in Edirne, Türkiye 224

Effect of Pesticide Exposure on ACTH and Cortisol Levels in Fish 225

Medicinal Mushrooms as Natural Antioxidant Sources: Their Potential in Combating Oxidative Stress 226

Phytoremediation potential of some aquatic medicinal plants for heavy metals 227

Impact of climate change on sustainability of agricultural food security 228

Effect of nanotechnological applications used in agricultural production on food safety 229

Scalability analysis and performance evaluation of massive MIMO network 230

Effects of The Diatomaceous Earth and Entomopathogenic Fungi Against The Tomato Leafminer Moth, *Tuta absoluta* (Meyrick) [Lepidoptera: Gelechiidae] in Field Condition 231

Design and optimization of a solar-wind hybrid system with enhanced efficiency measures for Türkiye 232

A Preliminary Evaluation of Bioactive Compounds in *Galium divaricatum* 233

Simulation of Charging and Sustainability of Electric Motors in Aviation from a Hybrid Renewable Energy System 234

Pharmacological Potential of Essential Oils: Current Approaches to Naturally Sourced Therapeutic Agents 235

1.2. FULL-TEXT PAPERS 236

Hormone-related risk factors for breast cancer based on estrogen and progesterone receptor status- a retrospective study from Albania. 238

Active Control of Air Suspension Systems in Commercial Vehicles 243

A Hybrid Approach Using AHP-TOPSIS for the Patent Process in the R&D Company 250

HER-2/neu receptor expression in breast cancer among Albanian females. 264

Elektrikli Otobüsler için Şarj Altyapısının Dağıtım Optimizasyonu 268

How classroom participation and course projects affect final grades in biology courses in online teaching? 279

Antibiotics use in pediatric age groups 282

PVD Yöntemi ile Kaplanmış Isıl İşlemli AISI 4140 Çeliklerin Islanabilirlik Özelliğinin İncelenmesi 286

Determination of Chemical Content, Cholinesterase Enzyme and Tyrosinase Enzyme Activities of *Citrus hystrix* Extracts 291

Optimizing Renewable Energy Integration in the Kurdistan Province Microgrid: A Comparative Analysis of Feed-in Tariff and Net Metering Policies 300

Localizing fetal skulls by fitting 309

Toz Gıdalar ve Raf Ömrü Sırasındaki Adezyona Bağlı Değişimler 318

Clays as supplementary cementitious materials, a FTIR investigation on structural modification 324

Sazan balığının (*Cyprinus carpio*) COI gen dizilerine dayalı filogenetik karşılaştırmaları 330

Fast Food Consumption Trends: A Comparative International Analysis and Standardisation of Measurement Methods 338

The Role of Radiation Technologies in Sustainable Textile Finishing Applications 344

MOSH/MOAH Kontaminasyonu: Kaynakları, Analitik Tespiti ve Sağlık Üzerindeki Etkileri 349

Çevresel kirleticilerin sağlık riski değerlendirmesi-literatür taraması 358

Sürdürülebilir Grafik Tasarım: Çevre Dostu Tasarım İlkeleri 368

Effect of different solvents on the solubility of pea protein isolate and optimization using artificial neural network-genetic algorithm (ANN-GA) 377

How does the concept of sustainable development affect the acquisition of knowledge by students in the pre-university and university systems? 386

AlNi-Graphene Modified Natural Wool Materials for Solar Steam Generator Applications 391

Design Optimization of Corona Rings for Electric Field Control Using Finite Element Analysis 400

Half-Metallic Properties of $CsIrI_3$ Perovskite: A First-Principles Study 407

Yolov8 ile Yolov11 Algoritmalarinin Gerçek Zamanli Araç Nesne Tespiti Ve Trafik Yoğunluğu Analizinde Karşılaştırılması 414

In vitro and *in silico* evaluation of schiff base and bis-α-aminophosphonate derivatives as potent α-glucosidase ve tyrosinaze inhibitors 423

Stabilization of Marl Soil Using Sewage Sludge and Polypropylene Fibers under Freeze-Thaw Conditions 429

Sustainable Pasture Management Through Community Engagement: Preserving Ecosystem Services in Korab-Koritnik Nature Park, Albania 436

Değişken zemin koşulları altında TBDY 2018'e göre farklı döşeme tiplerinin yapı maliyetine etkisinin incelenmesi 445

DBYBHY-2007 ve TBDY-2018 yönetmeliklerine göre konut tipi betonarme binaların performansı ve kaba inşaat maliyeti açısından değerlendirilmesi 453

Raspberry Pi Kullanarak Etkili ve Ekonomik Elektronik Ücret Toplama Sistem Tasarımı 462

Carbonized Turkish Tea Waste for Interfacial Solar Steam Generation 468

Sustainable Water Evaporation System Based on Carbonized Turkish Coffee Waste and Cellulosic Sponge 474

Fuzzy backstepping control of quarter car suspension system 480

Synthesis and characterization of new generation nucleating agents for use in recycled PET masterbatches 490

Mancozeb Toksisitesinin Nil Tilapiası *Oreochromis niloticus'un* Solungaçlarında SOD enzim aktivitesine etkisi 496

İmidacloprid Toksisitesinin *Oreochromis niloticus* Beyin dokusunda Asetilkolinesteraz Aktivitelerinde Oluşan Yanıtlar 500

The use of perlite and vermiculite aggregates in the production of lightweight mortars 504

Pedestrian Detection and Target Classification in Urban Forestry Environment with FMCW Automotive Radar and CNN 511

Comparative Analysis of the Health Systems in Turkey and Mauritania 521

Leadership Studies in Healthcare Institutions: A Bibliometric and Content Analysis 528

Machine Strength Grading of Fir Structural Boards According to TS EN 14081-2 Standards 536

Comparison of Dimensional Accuracy Performance of PLA and ABS Filament in 3D FDM Printing 543

A case study on the effects of high horizontal and vertical accelerations on structural damage in Antakya during the 2023 Türkiye earthquakes 549

The Oral Microbiota and Its Relation to Oral Health and Systemic Diseases: A comprehensive Review 559

Antifungal activity and biocompatibility on fibroblast cells of Sea Urchin (*Diadema setosum*) gonad lipid extract based PVA (polyvinyl alcohol) hydrogel 567

The Effect of Ultrasonic-Assisted Cellulose Nanocrystalline Dispersion on the Epoxy Coating for Anti-Corrosion Resistance 574

Neural network-driven perturbation and observation method for global maximum power point tracking in PV systems 583

Electrochemical determination of phosphate by measuring the phosphomolybdate complex using a reduced graphene oxide-doped with copper ions carbon paste electrode (rGO@Cu/CPE) sensor 593

Random metric lattices and some betweenness relations in random metric spaces 602

Assessment of eating habits, physical activity, and lifestyle among medical students at the University of Medicine, Tirana (2025) 607

Literature review of orofacial praxis skills in children with autism spectrum disorder 616

Restriksiyon enzimleri kullanılarak farklı türlerde cinsiyetin belirlenebilmesinin PZR-RFLP yöntemiyle araştırılması 620

Manual or Automated? A UI Testing Comparison 625

The Comparison of Body Performance of Some Invasive Species Distributed in Kemer, Antalya 634

Identification and Classification of Entity Names in Turkish Celebrity News Contents 639

Demand forecasting performance using multi-channel sales data: a comparative analysis of e-commerce and traditional channels 648

Bottled Drinking Water And Microbiological Quality 658

Study of Health Behaviors among Adolescents in Tirana (2024): Smoking, Alcohol, Drugs, and Physical Activity 664

Ulaşım odaklı kentsel yaklaşımların karşılaştırmalı analizi 672

Şehir içi taşımacılık yapan araçların hidrojen yakıt ikmal istasyonu için mikro şebeke tasarımı; Muş ili örneği 681

Farklı kalınlıklarda akrilik ve Silika (SiO_2) ile güçlendirilmiş akrilik bazlı basınca duyarlı yapıştırıcı bantların PVC yüzeyler üzerinde mekanik özelliklerinin karşılaştırılmalı analizi 686

Effect of lugol's solution on antibacterial activity and scoby growth in kombucha tea 693

Erbiyum Katkılı Fiber Yükselteç ile Farklı Senaryolarda Oluşturulan Düzeneklerde Çıkış Kazancı ve Gürültü Analizi 698

Uzay Yoluyla Haberleşme Ağını Genişletmek: Karasal Olmayan Ağ (NTN) Teknolojileri ve Kullanım Alanlarının Genel Bir Değerlendirmesi 708

Sodyum lignosülfonatın beton katkı maddesi olarak etkisinin incelenmesi 718

Enhanced Impact-Sliding Wear Performance of AISI H13 Extruding Die Steel Through Quenching & Tempering Heat Treatment Process 723

Effect of Cathode Shape and Anodization Time on The Formation of TiO_2 Nanotubes on Ti6Al4V ELI Alloy 730

Photocatalytic Hydrogen Generation by a Novel Push-Pull Donor-π-Acceptor Dye Sensitized TiO_2 737

Score plot distribution of thermal reduced graphene oxide considering the process operating parameters: A tutorial 749

Pardosa roscai (Roewer, 1951) türünün mayoz bölünme özelliklerinin belirlenmesi 753

Abiyotik stres koşullarındaki bahçe bitkilerine hümik asit uygulanması 757

Abiyotik stres koşullarındaki bahçe bitkilerine mikoriza uygulaması 763

Design and prototyping process of the gas shutoff system developed for safe natural gas supply 771

Synergistic modulation of epithelial-mesenchymal transition-related proteins by oxaliplatin and thymoquinone in HCT116 colorectal cancer cells 780

Development Of Decision Support Systems In Agriculture With Open Source Linear Programming Libraries 787

Non-stationary analysis of extreme temperatures in Erzurum using physical covariates 796

Detection and assessment of pedestrian crossings physical conditions using YOLOv12 model 801

Microstructural analysis of polyvinyl alcohol hydrogels modified with GNPs/AgNPs/GO/NAC 806

Mikroalglerden fikosiyanin: üretim, stabilite ve ticari potansiyel üzerine inceleme 811

Taşınabilir Cihazlarda Faz Değiştiren Madde (FDM) İle Isıl Yönetim ve Termal Kılıf Tasarımı: Akıllı Telefon Uygulaması 817

Ortaöğretim Kurumları İçin Çok Kriterli Karar Verme Tabanlı Sürdürülebilirlik Skorlama Algoritması Geliştirilmesi 826

Perlit agregalı polimer betonların kılcal su emme özelliklerinin deneysel olarak incelenmesi 839

Reinforcement Learning for Aerial Robots: Real-World Evaluation of Infeasible Trajectory Tracking. 845

Araçtan şebekeye (V2G) şarj teknolojisinin enerji yönetimi açısından değerlendirilmesi 850

Park ve Bahçelerde Bulunan Zehirli Bitkiler ve Bunların Tıbbi Kullanımları Üzerine Bir İnceleme 858

Improving PPO-Based Reinforcement Learning for Energy Forecasting with Chaotic Initialization and American Zebra Optimization 865

Understanding The Rationale and Advantages Of Embedded Systems Modelling with Emphasis on Electronic Differantial Using Ackermann Steering 874

Feature Selection in Industry 5.0: Adapting to The Dynamic Evolution of Data 883

Resource Dependent Assembly Line Balancing Under Grey Uncertainty 893

Effects of *Craterellus lutescens* (chick) fungus on peroxidation of olive oil 899

TRP Channels in Colorectal Cancer 904

Voltage Regulation Analysis with PV System Integration: A Campus Distribution Network Case Study 914

Design of an innovative reel transfer mechanism for automatic winding machines 923

Language application “Hey!” — development, possibilities and future 929

Investigation of Molecular Responses in Cervical Cancer Cells Treated with Abraxane via RNA Sequencing 936

Antiquorum Sensing and Antibiofilm Potentials of *Origanum vulgare* L. 951

Synthesis of Silver Nanoparticles by Green Chemistry Using St. John's Wort Extract and Investigation of Their Antimicrobial Properties 955

Uplink-NOMA Transmission over Málaga Channels 963

Yenilenebilir enerji kaynağı olarak güneş enerjisinin önemi ve Türkiye'deki gelecek perspektifi 969

Geleneksel ve Hazır Köfte Harcı Kullanılarak Hazırlanan Maydanoz Tohumu ve Çörek Otu Yağı İlave Edilen Kolyoz Balığı Köftelerinin Besin Değeri ve Duyusal Kalite Özelliklerinin Belirlenmesi 979

Akıllı Telefon Tabanlı Glukoz/Laktat Çoklu Analiz Sisteminin Geliştirilmesi ve Validasyonu 988

Hibrit tahrikli bir şehir içi otobüs şanzımanın termal optimizasyonu 998

Kripto Para Türlerinin Teknik Özelliklerinin Karşılaştırmalı Analizi ve Balon Fiyat Tespiti 1008

Endüstri 5.0 uyumlu teknoloji seçimi için çok kriterli karar verme yaklaşımı uygulamaları 1017

Bitkilerden elde edilen doğal bileşikler ve pulmuner fibrozisin baskılanmasındaki etki mekanizmaları – Bir derleme çalışması 1024

Inconel 625 süper alaşımının tornalanmasında kesme hızının işleme performansına etkisi 1031

İnce kesitli küresel dökme demirlerde döküm sıcaklığı, kesit kalınlığı ve ısıl işlem parametrelerinin mikro yapı ve sertliğe etkisi 1038

Model Organizma Olarak *Drosophila melanogaster*'de Levetirasetamın Toksisitesi ve Roselle'nin Olası Koruyucu Etkisi 1045

Bakır Tabanlı Bazı Alaşımların Gama Radyasyonu ile Etkileşimlerinin İncelenmesi 1052

Seçilen Kauçukların Gama Radyasyonu Zırhlama Parametrelerinin Değerlendirilmesi 1059

High-Performance X-Band microwave absorbers: Synergistic effects of MoS_2, $CoFe_2O_4$, and conducting polymer coating 1065

EpiXS tabanlı hesaplamalarla gelişmiş seramik numunelerin gama radyasyonu azaltma kapasitelerinin değerlendirilmesi 1074

Bazı Cam Türlerinin Birincil ve İkincil Radyasyon Etkileşimlerinin İncelenmesi 1081

Biyobozunur Doğal İçerikli Yara Kremi Geliştirilmesi ve *İn Vitro* Biyouyumluluk Değerlendirmesi 1090

The single crystal x-ray crystallographic elucidation of thiazole-based heterocycles with supramolecular interactions 1102

Secure and efficient energy billing using blockchain and smart contracts 1110

Kil Minerallerinin Gama Işınları ile Etkileşiminin Araştırılması 1116

Elektroensefolografi ve Elektrokardiyografi Sinyalleri Kullanılarak Epilepsi Nöbetlerinin Yapay Zeka ile Tahmin Edilmesi 1125

DFT Calculations for MEP, HOMO-LUMO, NLO, SAR studies of 3-Methyl-4-(3-methoxy-4-isobutyryloxy benzylidene amino)-4,5-dihydro-1*H*-1,2,4-triazol-5-one 1131

Bazı B Vitaminlerin Gama Radyasyonları ile Etkileşimlerinin Araştırılması 1138

İnsansız Araç Mühendisliğinin Geleceği: Teknolojik Gelişmeler ve Uygulama Alanları 1146

Fotovoltaik/termoelektrik (PV/TEG) hibrit sistemlerdeki son gelişmeler ve gelecek perspektifleri 1153

Use of Cyclomatic Complexity and Maintainability Index Metrics in Agile Development: Trends, Challenges, and Research Directions 1160

Evaluation on passive cooling of photovoltaic panels with phase change material 1169

The Place and Importance of Nanomaterial Additives in Passive Cooling of Photovoltaic Panels with Phase Change Materials 1185

Evaluation Of Doppler Indices In Dogs With Mammary Tumors Treated With Homeopathic Medicine 1197

Hareketli Hedefleri İzlemek İçin Yer Tabanlı Platformda Kullanılan İzleme Algoritmalarının Karşılaştırmalı Analizi 1207

Advanced oxidation of acid violet (AV-19) from aquatic environments by homogeneous and heterogeneous Fenton and photo-Fenton processes 1223

Rhabdomyosarcoma in a Malaklı Mixed-Breed Bitch 1231

Degradation and mineralization of acid fuchsin dye from aqueous media by means of electrochemical water treatment methods 1237

Bazı ikili alüminat seramiklerin gama radyasyon zırhlama özelliklerinin teorik hesaplanması 1245

Bazı Silikat Cam Elyaflarının Gama Radyasyon Kalkanı Özellikleri Üzerine Bir Çalışma 1253

A Machine-Learning Approach to Precision Agriculture for Seasonal-aware Clustering of Agricultural Crops 1260

Erp Uygulamalarında İş Süreçlerinin Analizi: Bir Elektrik Dağıtım Şirketi Örneği 1269

Comparison of Anomaly Detection in Logged Data Analysis 1272

Thermo-Responsive Structural Transitions of Graphene-Grafted PNIPAM–PLGA Polymer Brushes Explored by DPD 1281

Injectable Ca^{2+}-Bridged CMC/PVA Supramolecular Hydrogel with Self-Healing, Hemocompatibility, and Controlled Procaine Release for Advanced Wound Care 1289

Application of a New Numerical Approach for Neural Ordinary Differential Equations 1299

Temperature dependent electrical behavior of nickel silicide Schottky diodes on *p*-type silicon 1306

In vivo phage display in targeted drug delivery applications 1313

Ergonomic Analysis of Working Postures in Crankshaft Packaging Processes and Recommendations for Improvement 1318

Transfer learning-based pneumonia detection on pediatric chest x-rays using a CNN model 1324

Nanoplastic Toxicity in Fish: The Trojan Horse Effect 1331

Understanding Pesticide Toxicity in Fish: Detoxification versus Bioactivation 1335

Toprakta mikroplastik (MP) kirliliğinin mikrobiyal ekoloji üzerindeki etkileri 1339

Determination of geocell-soil interfacial behavior of sandy soils by large-scale shear box tests 1344

Effects of polyvinyl alcohol applications on morphological and physiological parameters of different wheat (*T. aestivum* L.) varieties grown in hydroponic environment under lead stress 1352

Effects of polyvinyl alcohol applications on biochemical parameters of different wheat 1359

(*T. aestivum* L.) cultivars grown under lead stress 1359

Photoremoval of Dissolved Organic Waste and Dielectric-Energy Storage with SmCuO/ZnO/$CuMn_2O_4$ Tri-Composite 1366

Influence of Shot Peening on Surface Residual Stress and Microstructure Evolutions of R260 Rail Steel 1378

Influence of Shot Peening on Impact-Sliding Wear Behaviour of R260 Rail Steel 1383

API ZYM enzymatic characterization of lactic acid bacteria isolated from boza 1390

Development of a Renewable Energy-Powered Autonomous Irrigation zystem for Sustainable Landscape Management 1396

Synthesis and optical properties of erbium-doped lithium calcium borate ($Li_6CaB_3O_{8.5}:Er^{3+}$) 1402

Potasyumun Alımı, Taşınması ve kullanım etkinliği: Moleküler ve Biyoteknolojik Yaklaşımlar 1406

DBYBHY-2007 ve TBDY-2018 yönetmeliklerine göre konut tipi betonarme binaların performansı ve kaba inşaat maliyeti açısından değerlendirilmesi 1417

Evaluation of Blueberry Pruning Waste as Antimicrobial Agent in Edible Film Content Containing Probiotic 1426

Development of Edible Composite Film with Clove Extract and Probiotic to Improve Strawberry Shelf Life 1432

Toxic Traces of Some Heavy Metals 1437

Yeni bir Schiff bazı temelli rutenyum(II) aren kompleksinin sentezi ve meme kanseri hücrelerine karşı sitotoksik aktivitesi 1443

2. POSTER PRESENTATIONS 1453

2.1. ABSTRACTS 1453

Effect of pre-treatment on mechanical properties of quenched and tempered medium carbon steels 1456

Investigation of the effects of some plant lectin proteins on the digestive enzymes of the agricultural pest *Halyomorpha halys* (stal) beetles 1457

Development of Novolac Resin Using Biobased Raw Materials 1458

Development of Room Temperature Curable Phenolic Foam Suitable for Mining and Construction Sectors 1459

Effect of Chain Transfer Agent/ Crosslinking Agent ratio on Thermoplastic Properties of Acrylic Materials 1460

Development and Pilot Scale Production of High Solid Melamine-Formaldehyde Resin for Use in Textiles 1461

Development of A Cold-Box Resin to Be Used as A Binder in Core Manufacturing for Foundry Industry 1462

Biomaterials from the aquatic organisms: resources, extraction and applications 1463

The impact of external magnetic field on chlorophyll content, leaf morphology, and gene expression in the Fragaria × ananassa 1464

Silver nanoparticle synthesis with grey juniper (*Juniperus excelsa*) extract 1465

Mathematical Modelling Study Of Infrared Dried Prickly Pear 1466

Cellulose Extraction and Optimization from Pine Needles 1467

The Protective Effects of Chard on Kidney Damage Induced by Valproic Acid Toxicity in Rats 1468

Gıdaların Kurutulmasında Yeni Yaklaşımlar: Mikrodalga ve Mikrodalga-Vakum Teknolojileri 1469

Yeni Nesil Mikrobiyal Terapötikler: Postbiyotikler ve Paraprobiyotikler 1470

Effects of Some Plant Extracts and Metal Salts on Aldose Reductase Activity 1471

In vitro antioxidant activities *of Helianthus tuberosus* L. extracts 1472

Multi 7: A food supplement with antioxidant activity 1473

Multi 7: A food supplement with inhibitory activity of diabetes-related enzymes 1474

Bridging the Knowledge Gap: Investigating Short-Chain PFAS Effects on Lipid Metabolism and Immune System 1475

Effects of sustainable diets such as insect-based, essential oil-supplemented and single-cell protein on disease resistance in aquaculture 1476

Effects of *Helianthus tuberosus* L. extracts on enzyme activities in diabetes mellitus 1477

Microwave drying of beef and lamb liver: Investigation of drying kinetics and color change 1478

Effect of heat treatment on antioxidant capacity of Karayaka sheep milk 1479

Monitoring Organophosphate Resistance in *Bemisia tabaci* Populations from the Mediterranean and Aegean Regions of Türkiye 1480

Antioxidant activities of polycaprolactone/sodium alginate/chestnut honey nanofibers 1481

Fabrication and characterization of polycaprolactone/cellulose acetate/polselenophene nanofibers 1482

Simultaneous Quantitative Analysis of the Active Pharmaceutical Ingredients in Oral Antiseptic Solution By HPLC 1483

Phytoremediation potential of *Limnobium laevigatum* enhanced by ZnO nanoparticles in arsenic-contaminated waters 1484

2.2. FULL-TEXT PAPER 1486

The Anti-cancer impact of Metformin In the Prostate Cancer 1488

Densities Of 1,2-Dichloroalkane With Tertio Butyl Methyl Ether At Different Temperatures. 1502

1. ORAL PRESENTATIONS

1.1. ABSTRACTS

➢ *ORAL PRESENTATION*

Synthesis of sulfamethoxazole surface imprinted core-shell magnetic nanoparticles for selective detection of sulfamethoxazole in poultry by an electrochemical biosensor

Pwadubashiyi Coston Pwavodi [1*] (*https://orcid.org/0000-0002-4486-4703)*

[*1]Cyprus International University, Faculty of Engineering, Department of Biomedical/Medical Engineering/Bioengineering. Haspolat, 99258, Nicosia, North Cyprus.

Abstract

Foodborne illness poses a threat to both human and animal health. Campylobacter and Salmonella spp. are the most frequent causes of human foodborne bacterial diseases connected to poultry in recent years. Sulfamethoxazole (SMX) is administered into poultry products' diets as a preventive treatment technique for future illnesses to ensure the long-lasting availability of poultry products. Unfortunately, they have been abusively used, and due to the extensive, abusive use of antibiotics over many years, the dissemination of antibiotic-resistant strains of different bacterial organisms, such as Carbapenem-Resistant Acinetobacter, have been introduced to the environment. Sulfamethoxazole was determined using a unique sensitive voltammetric sensor presented in this study. The developed sensor uses a carbon paste electrode modified with Sulfamethoxazole surface imprinted core-shell magnetic nanoparticles as a recognition element. For the electrosensitive determination of SMX, a carbon paste electrode with a non-imprinted polymer (NIP) modification was also created. Electrochemical techniques such as Cyclic Voltammetry (CV), Differential Pulse Voltammetry (DPV), and Electrochemical Impedance Spectroscopy (EIS) were used to evaluate the electrochemical behaviour of Sulfamethoxazole at a modified carbon paste electrode. Integrating Fe_3O_4 nanoparticles into the CPE sensor resulted in a sensor with exceptional sensitivity, repeatability, selectivity, reproducibility, stability, and low preparation cost. The Limit of detection LOD and the Limit of quantification LOQ are 6.45788 $x10^{-8}$ M and 2.1311 $x10^{-8}$ M, respectively. The concentration of SMX in actual tap water samples was determined using the modified electrochemical sensor.

Keywords: Sulfamethoxazole, Molecularly Imprinted Polymer, Nanotechnology, Carbon Paste Electrode, Electrochemical Biosensor, Fe_3O_4 Nanoparticles

➢ *ORAL PRESENTATION*

Herbal cold cream formulation from *Lavandula stoechas* essential oil

Sondos Mahmoud[1] (*https://orcid.org/0009-0004-6752-5378*)
Najat Agiel[2*](*https://orcid.org/0000-0003-4620-0019*)

[1,2]European University of Lefke, Faculty of Pharmacy, Pharmacognosy, TRNC.

Abstract

Cold creams can be used in cosmotics as moisturizer and pharmaceutically for many purposes as;, antiacne, antimicrobial and to treat skin injuries. The aim of this study was to design a moisturizing cold cream containing essential oils extracted from herbal plants to be used as a way to moisturize and nourish the skin. Using clevanger appartus the essential oil was obtained by hydrodistillation of *Lavandula stoechas* growing in Northern Cyprus. The cream material included liquid vaseline, borax powder, distilled water, white bees wax, and citric acid. Tests for physical characteristics, stability, pH balance, washability, ease of application, and irritant potential were all part of the evaluation procedure. The cream's smooth texture, light creamy color, and non-greasy application were all according to the standard conditions. Under normal storage settings, stability tests verified that the cream's chemical and physical characteristics were preserved for two months. Microbial analyses verified the product's safety and resistance to contamination, while irritation testing revealed no adverse effects either. The results show the possibility of using herbal skin care products with essential oils are safe and efficient. The cold cream with a lavender oil basis effectively mixes the advantages of natural skincare with visual appearance. It is a good candidate for consumer usage due to its formulation, physical characteristics, and stability. To improve its competitiveness in the market, future research should concentrate on scalability and increasing its functional purpose.

Keywords: Cold cream, Herbal formulations, Skin protection, lavender oil, Hydrodistillation.

➢ *ORAL PRESENTATION*

Optimization of U-Bending Process Parameters for 304L Austenitic Stainless Steel

BOUDEDJA Amar[1*] (https://orcid.org/0000-0002-3867-927X), BENCHERIF Mokhtar[1] (https://orcid.org/0000-0002-1229-8874), ALMANSBA Madjid[1] (https://orcid.org/0000-0001-6551-5230) , FERHOUM Rabah[1] (https://orcid.org/0000-0001-8151-916X), HABAK Malek[2] (https://orcid.org/0000-0003-1498-4680), BELMIHOUB Khellaf[3] (https://orcid.org/0009-0000-5759-2340)

[1] Laboratory of Elaboration, Characterization of Materials and Modeling, University Mouloud Mammerie of Tizi Ouzou, Faculty of Construction, Tizi Ouzou, Algeria.
[2] Roberval Laboratory Department of Mechanical Engineering Royallieu Research Center CS 60319 - 60203 Compiègne Cedex, France
[3] University Mouloud Mammerie of Tizi Ouzou, Faculty of construction, Department of mechanical engineering, Tizi Ouzou, Algeria.

Abstract

This comprehensive study investigates the optimization of U-bending process parameters for 1.5 mm thick AISI 304L austenitic stainless-steel sheets through an integrated experimental and computational approach. The research methodology was conducted in three primary phases: material characterization, experimental forming trials, and data-driven optimization. In the initial phase, quasi-static uniaxial tensile tests were performed at room temperature (23°C) following ASTM E8 standards to determine the fundamental mechanical properties of the material, including yield strength, ultimate tensile strength, and elongation at fracture. These properties served as critical inputs for subsequent numerical analysis and process optimization. The experimental phase involved systematic U-bending trials conducted under displacement-controlled conditions (5 mm/min) using a universal tensile testing machine. A full factorial experimental design was implemented, varying three key process parameters: die radius (ranging from 2, 4, 6, 8), punch radius (4, 6, 8, 13.2), and punch-die clearance (2 to 5.6). Post-forming metrology included precise measurements of springback angles using optical coordinate measurement and thickness reduction analysis through micrometer gauging at predetermined locations. Statistical analysis of variance (ANOVA) was performed to quantify parameter significance and interaction effects. For the optimization framework, the experimental dataset was enhanced through Gaussian noise injection ($\sigma = 0.05$ mm) during interpolation to account for process variability and improve model robustness. The augmented dataset was processed using a customized Python workflow incorporating NumPy and Pandas for data manipulation, followed by implementation of a multi-layer perceptron (MLP) neural network with Bayesian hyperparameter optimization. The neural network architecture featured three hidden layers with ReLU activation functions and was trained to predict springback and thinning responses based on input parameter combinations. Preliminary validation results demonstrate the neural network's capability to accurately capture the complex nonlinear relationships between process parameters and forming outcomes. The Gaussian noise interpolation proved particularly effective in preventing model overfitting while maintaining prediction accuracy within experimental error bounds. This research establishes a methodological framework that effectively combines traditional metal forming analysis with modern data science techniques, providing valuable insights for industrial process optimization.

Keywords: U-bending, 304L stainless steel, springback prediction, Gaussian process interpolation, neural network optimization, metal forming process control.

➢ *ORAL PRESENTATION*

Data-Driven Optimization of Martensitic Phase Transformation Models in 304L Steel

BENCHERIF Mokhtar[1*] (https://orcid.org/0000-0002-1229-8874), BOUDEDJA Amar[1] (https://orcid.org/0000-0002-3867-927X), ALMANSBA Madjid[1] (https://orcid.org/0000-0001-6551-5230) , FERHOUM Rabah[1] (https://orcid.org/0000-0001-8151-916X), HABAK Malek[2] (https://orcid.org/0000-0003-1498-4680), BELMIHOUB Khellaf[3]

[*1] Laboratory of Elaboration, Characterization of Materials and Modeling, University Mouloud Mammerie of Tizi Ouzou, Faculty of Construction, Tizi Ouzou, Algeria.
[2]2Laboratoire Roberval, Département d'Ingénierie Mécanique, Centre de Recherches de Royallieu, CS 60319 - 60203 Compiègne Cedex, France
[3] University Mouloud Mammerie of Tizi Ouzou, Faculty of construction, Department of mechanical engineering, Tizi Ouzou, Algeria.

Abstract

The accurate modeling of deformation-induced martensitic transformation in metastable austenitic steels is crucial for predicting and optimizing mechanical performance in engineering applications. This study presents a comparative evaluation of several nonlinear predictive models designed to estimate the martensite volume fraction as a function of magnetic flux density in 304L stainless steel. Motivated by the limitations of classical phase quantification techniques such as X-ray diffraction (XRD) and Electron Backscatter Diffraction (EBSD), we developed a data-driven methodology combining physical modeling with advanced optimization algorithms inspired by artificial intelligence. Six mathematical models, including the Olson-Cohen, Koistinen-Marburger, Modified Avrami, Saturation-type, Gompertz, and a custom hybrid exponential model, were investigated. Each model was calibrated using six optimization strategies: Levenberg–Marquardt, Genetic Algorithm, Particle Swarm Optimization, Differential Evolution, Simulated Annealing, and Grey Wolf Optimizer. The evaluation criteria included mean squared error (MSE), coefficient of determination (R^2), residual distribution, parameter sensitivity, and computation time. Results indicate that the choice of optimization algorithm significantly affects model accuracy and stability. The best-performing models were characterized by low residuals, narrow confidence intervals, and high predictive correlation with experimental data derived from XRD and magnetic measurements. This work demonstrates the effectiveness of AI-based optimization in refining physically meaningful models for phase transformation and provides a robust framework for future integration of machine learning techniques in smart materials characterization.

Keywords: Martensitic Transformation, TRIP Steels, Optimization Algorithms, Phase Quantification, Data-Driven Modeling, Predictive Materials Science

➢ *ORAL PRESENTATION*

İndiyum monotellüride dayalı ileri malzemelerin elde edilmesi ve bazı termofiziksel özellikleri

Çingiz Abilov* (*ORCID: https://orcid.org/0000-0001-7617-5737*), Mehriban Hasanova (*ORCID: https://orcid.org/0000-0002-2532-2597*), Elmira Gasimova (*ORCID: https://orcid.org/0000-0002-9497-9066*),
Nigar Huseynova (*ORCID: https://orcid.org/0009-0009-0180-0214*)

Azerbaycan Teknik Üniversitesi, Enerji ve Otomasyon Fakültesi,
Mühendis Fiziği ve Elektronik Bölümü, Bakü, Azerbaycan.

Özet

$InTe$-Cr_2Te_3 ($CoTe_2$, $TlGaTe_2$, $TlInSe_2$, $CuGaTe_2$, $Bi_{1.3}Sb_{0.7}Te_3$, $CuCr_2Te_4$, Cu_2ZnSnS_4) sisteminin sekiz faz diyagramı incelendi ve oluşturuldu. Başlangıç bileşenleri arasındaki fizikokimyasal etkileşimin karmaşık bir doğası, InTe'ye dayalı sınırlı katı çözeltilerin oluşumu ile ortaya çıktı. İncelenen sistemlerdeki etkileşimin doğasının karmaşıklığı, bir yandan yapının kusurlu olmasıyla, diğer yandan çok bileşenli kompozisyon ve sentezlenen yarı iletken malzemelere dahil edilen elementlerin farklı konfigürasyonlarıyla ilişkilidir.
Fonon termal iletkenliğinin mikro sertliğe bağımlılığından, indiyum monotellürid temelinde elde edilen katı çözelti alaşımlarında kimyasal bağ mukavemetinin zayıflaması belirlendi. İkinci etkileşimli bileşenlerde, krom içeren bileşenlerden kobalt içeren bileşenlere doğru hareket edildiğinde, InTe'ye dayalı katı çözeltiler bölgesinin genişliğinin arttığı, bunun da görünüşe göre kromun elektron konfigürasyonunun diğer 3d elementlere kıyasla kararlılığıyla ilişkili olduğu bulundu. Ana termodinamik parametrelerin hesaplanması, InTe'ye dayalı elde edilen alaşımların kararlı düzenli katı çözeltiler olduğunu gösterdi.

Anahtar Kelimeler: Faz diyagramı, Katı çözelti, Mikrosertlik

➢ *ORAL PRESENTATION*

Existence of positive solutions for a system of Hadamard fractional boundary value problems

Alexandru Tudorache[1] (*ORCID: https://orcid.org/0000-0003-0151-505X*), Rodica Luca Tudorache[2*] (*ORCID: https://orcid.org/0000-0003-3901-5747*)

[1] "Gheorghe Asachi" Technical University, Department of Computer Science and Engineering, Iasi, Romania.
[2*] "Gheorghe Asachi" Technical University, Department of Mathematics, Iasi, Romania

Abstract

We study the existence, uniqueness, and multiplicity of positive solutions for a system of Hadamard fractional differential equations which contain fractional integral terms, and it is defined on a finite interval. This system is supplemented with general coupled nonlocal boundary conditions encompassing Hadamard fractional derivatives and Riemann-Stieltjes integrals. To establish the main results, we apply several fixed point theorems, including the Banach contraction mapping principle, the Schauder fixed point theorem, the Guo-Krasnosel'skii fixed point theorem, and the Leggett-Williams fixed point theorem.

Keywords: Hadamard fractional differential equations, nonlocal coupled boundary conditions, existence, uniqueness, multiplicity, positive solutions.

➢ *ORAL PRESENTATION*

Positive solutions to a system of fractional q-difference equations with multi-point boundary conditions

Rodica Luca Tudorache [1*] (*ORCID: https://orcid.org/0000-0003-3901-5747*),
Alexandru Tudorache [2] (*ORCID: https://orcid.org/0000-0003-0151-505X*)

[1*] "Gheorghe Asachi" Technical University, Department of Mathematics, Iasi, Romania,
[2] "Gheorghe Asachi" Technical University, Department of Computer Science and Engineering, Iasi, Romania.

Abstract

We explore the existence, uniqueness, and multiplicity of positive solutions to a system of fractional q-difference equations that includes fractional q-integrals. This investigation is carried out under coupled multi-point boundary conditions featuring q-derivatives and fractional q-derivatives of various orders. The proofs of our principal findings employ a range of fixed point theorems, including the Guo-Krasnosel'skii fixed point theorem, the Leggett-Williams fixed point theorem, the Schauder fixed point theorem, and the Banach contraction mapping principle.

Keywords: fractional q-difference equations, fractional q-integrals, coupled multi-point boundary conditions, positive solutions, existence, uniqueness, multiplicity.

➢ *ORAL PRESENTATION*

Exploring Alcohol-Related Metabolites in Bone: A Pilot Study Using NMR Spectroscopy

Pong Pornjarernpong (*ORCID: https://orcid.org/0009-0004-7301-6350*), Churdsak Jaikang (*ORCID: https://orcid.org/0000-0002-9262-0404*), Somlada Watcharakhom (*ORCID: https://orcid.org/0009-0006-9353-7668*), Yutti Amornlertwatana (*ORCID: https://orcid.org/0000-0002-0619-1333*)
Department of Forensic Medicine, Faculty of Medicine, Chiang Mai University, Chiang Mai 50200 Thailand

Abstract

Ethanol is one of the most commonly consumed psychoactive substance worldwide. In forensic investigations, ethanol levels are typically assessed using blood or vitreous fluid samples. However, in decomposed bodies, alternative specimens must be considered. This study aimed to investigate ethanol metabolites in decreased individual's bone and their correlation with blood alcohol concentration (BAC). Bone and blood samples (n = 79) were collected, samples were categorized into two groups—BAC-positive and BAC-negative—based on blood alcohol concentration and ethanol metabolites were analyzed using proton nuclear magnetic resonance (^1H-NMR) spectroscopy. All samples showed the presence of ethanol-related metabolites, including ethanol, ethyl oleate, ethyl cis-9-octadecenoate, ethyl glucuronide, ethyl sulfate, N-acetyl taurine, acetic acid, acetaldehyde, acetone, 5-hydroxyindoleacetic acid (5-HIAA), and 5-hydroxytryptophol (5-HTOL). No significant differences in metabolite levels were observed between the two groups, and no correlations were found between level of bones' metabolite and BAC. These results suggest that the detected ethanol's metabolites may reflect chronic ethanol consumption rather than acute intake. These preliminary findings highlight the potential of bone metabolomics as a tool for retrospective assessment of ethanol use, particularly in cases where conventional specimens are unavailable. Further research with larger sample sizes is needed to validate and refine this approach.

Keywords: Ethanol, Metabolomic, Bone, Metabolite, Bone metabolomic, Postmortem metabolomic

➢ *ORAL PRESENTATION*

Antileishmanial activity and chemical composition of fractions from an endophytic fungus, AMrb9 inhabiting Cameroonian *Annona muricata* L. (Annonaceae)

Victorine Lorette Yimgang[1*], Eric Coffie[2], Barbara Zenabu Anibea[2], Christine Achiaa Antwi[3], Theresa Manful Gwira[3], Rufin Marie Toghueo Kouipou[1], Alevcan Kaplan[4], Dorcas Osei Safo[2], Fabrice Fekam Boyom[1]

[1]Antimicrobial & Biocontrol Agents Unit (AmBcAU), Laboratory for Phytobiochemistry and Medicinal Plants Studies, Department of Biochemistry, Faculty of Science, University of Yaoundé I, Cameroon, P.O. Box 812, Messa, Yaoundé, Cameroon
[2]Department of Chemistry, University of Ghana, Accra, Ghana
[3]Department of Biochemistry, Cell and Molecular Biology, University of Ghana, Accra, Ghana
[4]Department of Crop and Animal Production, Sason Vocational School, Batman University, Turkiye

Abstract

Leishmaniasis is one of the most neglected tropical diseases caused by intracellular parasite belongs to genus Leishmania affecting both humans and animals. Approximately, it affected 350 million people worldwide every year precisely in the undeveloped and developing countries. In animals, dogs are considered to be the main reservoir of zoonotic leishmaniosis and the seroprevalence reported in the Mediterranean Basin ranges from 5 % to 30 % depending on the region. Various chemical drugs are used to treat and control this disease including pentavalent antimonial and antimicrobial. However, this chemotherapy has several limitations such as toxic side effects, high costs, frequent relapses, the development of resistance, and the requirement for long-term treatment. Therefore, there is a pressing need for drug discovery to treat this particular disease. In this scenario, microbial natural products are emerging as an interesting source for new antileishmanial drugs. This study aims to evaluate the antileishmanial potency of fractions of an endophytic fungi extract sheltered by a Cameroonian medicinal plant. Five fractions isolated from AMrb9 extract were screened against promastigotes stage of *Leishmania donovani* MHOM/SD/62/1S strain in a terminally differentiated THP1 (Human Acute Monocytic Leukemia) cell line and their cytotoxicity was also evaluated on the same cell line. Thereafter, the chemical composition of active fractions was determined using GC-MS analysis. Graphpad prism 8.0 was used to determine Inhibitory Concentration 50 (IC_{50}) and Cytotoxic Concentration 50 (CC_{50}) and Microsoft excel 2016 to calculate Selectivity Indexes (SI).Three fractions exhibited antileishmanial activity with IC_{50} values ranging from 3.40 -6.54 µg/mL. Globally, no active fraction showed cytotoxicity with significant SI greater than 40. GC-MS analysis of the three selective fractions revealed broad-spectrum antileishmanial compounds such as Endo-Borneol, Alpha terpineol, 1- oxo- forskolin, 3,5-octadione 2,2,7 trimethyl and alloaromadendrene being the most abundant. These findings suggest that three of the five fractions used in this study have the potential to produce antileishmanial molecules and can be used as starting point of new drugs to cure this disease and therefore improve treatment outcomes for patients and animals with leishmaniasis, reducing morbidity and mortality rates associated with the disease.

Keywords: Antileishmanial, cytotoxicity, fractions, resistance

➢ *ORAL PRESENTATION*

To Compare maternal outcomes aming pregnant woman with COVID-19 infection, stratified by body mass index : normal weight, overweight and obesity.

Vera Beca* ; Mirela Rista; Daniela Nakuci; Eliona Demaliaj

University Hospital of Obstetrics and Gynecology 'Queen Geraldine', Tirana, Albania
*Corresponding author: Vera Beca PhDc , University Hospital of Obstetrics and Gynecology 'Queen Geraldine', Tirana

Abstract

Background and Objectives :Obesity in the female population represents a significant public health concern. It is particularly associated with adverse outcomes during pregnancy, increasing the risk of various maternal and fetal complications. During the COVID-19 pandemic, a notable association was observed between elevated body mass index (BMI) and SARS-CoV-2 infection, contributing to an increased incidence of unfavorable maternal and perinatal outcomes. The aim of this study is to examine the association between obesity, elevated body mass index (BMI), and COVID-19 severity, including the risk of developing severe complications requiring intensive care among pregnant women. Material and Methods: A retrospective study was conducted at a leading women's health hospital, including pregnant women with confirmed positive cases of SARS-CoV-2. Participants were classified into three groups based on their pre-pregnancy body mass index (BMI): obesity (BMI ≥ 30), overweight (BMI 25–29.9), and normal weight (BMI 18.5–24.9). An association was observed between elevated BMI and the presence of symptoms, obstetric characteristics, and the occurrence of complications such as sepsis, antimicrobial resistance, and other adverse outcomes in pregnant women Results: A total of 83 pregnant women with confirmed SARS-CoV-2 infection and documented pre-pregnancy BMI were included in the analysis. Obesity was significantly associated ($P < 0.01$), with an increased risk of severe maternal complications, including sepsis ,acute respiratory distress syndrome and the need for mechanical ventilation . Multivariate regression analysis confirmed obesity as an independent predictor of adverse perinatal outcomes. Conclusion:Overweight and obesity were associated with more severe clinical courses of COVID-19 during pregnancy, as well as with higher rates of maternal and perinatal complications. These findings underscore the importance of targeted monitoring and management of pregnant women with elevated BMI during infectious disease outbreaks

Keywords: Obesity, COVID-19 , sever pathology

➢ *ORAL PRESENTATION*

Metabolomic Characterization of Human Vitreous Fluid Using ^{1}H-NMR Spectroscopy

Thanakrit Trichag* (*ORCID: https://orcid.org/0009-0002-5513-1182*),
Churdsak Jaikang (*ORCID: https://orcid.org/0000-0002-9262-0404*),
Kanicnan Intui (*ORCID: https://orcid.org/0009-0009-0171-9790*)

Chiang Mai University, Faculty of Medicine, Department of Forensic Medicine, Chiang Mai, Thailand.

Abstract

Vitreous humor serves as a critical biological matrix in forensic investigations due to its biochemical stability and resistance to postmortem changes. It facilitates the reconstruction of circumstances surrounding death by allowing accurate analysis of substances such as drugs, alcohol, glucose, and electrolytes. This makes it a valuable alternative specimen in cases where traditional samples like blood are decomposed or contaminated. Despite its recognized forensic value, the comprehensive chemical profiling of compounds contained in vitreous humor remains limited. This study aims to advanced analytical studies to explore the full spectrum of endogenous and exogenous compounds in vitreous humor, which may enhance its utility in forensic diagnostics. Vitreous humor samples (n=76) were typically collected postmortem from the eye and lyophilized. The samples were analyzed using ^{1}H-NMR spectroscopy. A total of 217 biochemical compounds were identified in vitreous fluid. The most organic compounds contained in vitreous humor are organic acids and their derivatives (46%), organoheterocyclic compounds (16%), and organic oxygen compounds (15%), respectively. These compounds and the ^{1}H-NMR technique highlight the potential for further application in forensic investigations.

Keywords: vitreous fluid, biochemical compounds, ^{1}H-NMR, forensic investigations

➢ *ORAL PRESENTATION*

Bridging Traditional and Scientific Knowledge: Quantitative Ethnopharmacological Investigation in Marghazar Valley, Swat, Pakistan

Muhammad Nauman Khan[1,2*], Sajjad Ali[3], Tabassum Yaseen[3], Barkat Ullah[1], Abdul Razzaq[4,5], Alevcan Kaplan[6], Fethi Ahmet Ozdemir[7]

1. Department of Botany, Islamia College University, Peshawar, 25120, Pakistan
2. Biology Laboratory, University Public School, University of Peshawar, 25120 Peshawar, Pakistan
3. Department of Botany, Bacha Khan University, Charsadda, Khyber Pakhtunkhwa, Pakistan
4. Qarshi Herb Research Center, Qarshi Industries (Pvt.) Ltd. Hattar, Haripur, Pakistan
5. Qarshi University, Lahore, Punjab, Pakistan
6. Department of Crop and Animal Production, Sason Vocational School, Batman University, Batman 72060, Turkiye
7. Department of Molecular Biology and Genetics, Faculty of Science and Art, Bingol University, 12000, Bingol, Turkiye

Corresponding author e-mail: nomiflora@uop.edu.pk

Abstract

This study presents the first ethnobotanical exploration aimed at documenting the traditional medicinal use of plants with therapeutic potential in the Marghazar Valley, located in the Hindukush Range, Pakistan. A total of 25 respondents, including local residents of both genders and traditional healers, were interviewed using semi-structured and open-ended questionnaires. The collected data were analyzed using quantitative ethnobotanical indices such as Use Value (UV), Frequency of Citation (FC), Relative Frequency of Citation (RFC), and Family Use Value (FUV). In total, 108 medicinal plant species from 56 families were recorded as being used to treat various human ailments. The most represented family was Asteraceae (9 species), followed by Lamiaceae (7 species). Herbs comprised the most common life form (56%), and leaves were the most frequently used plant part. Decoctions were the most commonly used method of remedy preparation, with several different modes of administration reported. The RFC values ranged from 0.08 to 0.76, with *Justicia adhatoda* having the highest RFC (0.76). Other notable plants with high RFC values included *Ficus palmata*, *Geranium collinum*, *Acacia nilotica*, and *Hyoscyamus niger*. *Justicia adhatoda* was the most frequently cited plant, commonly used for treating cough, swelling, rheumatism, snake bites, and eye infections. Plants with the highest UVs were *Justicia adhatoda* (1.36) and *Cichorium intybus* (1.24). Among families, Acanthaceae showed the highest FUV (1.36), followed by Zygophyllaceae (1.08), while Aspleniaceae and Polygalaceae had the lowest FUV*s* (0.16). Notably, families with fewer species but high UVs often had relatively high FUV*s*. For example, a decoction prepared from the whole plant of *Asplenium dalhousiae* is traditionally used to treat gonorrhea, tuberculosis, and hepatitis. The high UVs of certain plants identified in this study suggest the potential presence of valuable phytochemicals, highlighting the need for further pharmacological investigations to discover new therapeutic agents.

Keywords: Quantitative ethnobotanical indices, medicinal plants, local community, decoction, herbal remedies

➢ *ORAL PRESENTATION*

Influence of Edaphic Factors on Vegetation and Plant Community Dynamics in the Dry Temperate Region, Ojhor Valley, Eastern Hindu Kush, Pakistan

Muhammad Nauman Khan[1,2*], Barkat Ullah[1], Abdul Razzaq[3,4], Fazal Manan[5], Zeeshan Ahmad[6], Majid Iqbal[7,8], Alevcan Kaplan[9]

1. Department of Botany, Islamia College University, Peshawar, 25120, Pakistan
2. Biology Laboratory, University Public School, University of Peshawar, 25120 Peshawar, Pakistan
3. Qarshi Herb Research Center, Qarshi Industries (Pvt.) Ltd. Hattar, Haripur, Pakistan
4. Qarshi University, Lahore, Punjab, Pakistan
5. Department of Plant Sciences, Quaid-i-Azam University, Islamabad, 45320, Pakistan
6. CAS Key Laboratory of Tropical Forest Ecology, Xishuangbanna Tropical Botanical Garden, Chinese Academy of Sciences, Mengl, 666303, China
7. Key Laboratory of Ecosystem Network Observation and Modeling, Institute of Geographic Sciences and Natural Resources Research, Chinese Academy of Sciences, 11A, Datun Road, Chaoyang District, Beijing, 100101, China
8. University of Chinese Academy of Sciences, (UCAS), Beijing 100049, China
9. Department of Crop and Animal Production, Sason Vocational School, Batman University, Batman 72060, Turkiye

Corresponding author e-mail:nomiflora@uop.edu.pk

Abstract

Vegetation patterns in a region are shaped by a complex interplay of environmental factors, including climate, soil characteristics, and anthropogenic influences. This study investigates the influence of edaphic (soil-related) factors on vegetation structure and plant community dynamics in the dry temperate region of the Ojhor Valley, Eastern Hindu Kush, Pakistan. The study area was stratified into four ecological zones based on altitudinal gradients, climatic conditions, species composition, and vegetation physiognomy. Vegetation sampling was conducted using the transect and quadrat method, with quadrat sizes of 20 × 20 m for trees, 10 × 10 m for shrubs, and 2 × 2 m for herbs. Data were compiled in Microsoft Excel and analyzed using multivariate statistical techniques. PCORD version 5 was employed to classify plant species into four distinct communities, named after their most dominant species. These included: *Salix tetrasperma–Crataegus songarica–Rheum tibeticum* community (elevation: 6,500–7,800 ft; Galeh-Hinjil-Dronil), *Populus alba–Hippophae rhamnoides–Arenaria griffithii* community (8,000–9,000 ft; Breshgram), *Onobrychis cornuta–Cousinia pineticola* community (9,000–10,500 ft; Susoom), and *Berberis calliobotrys–Ranunculus hirtellus* community (11,000–14,000 ft; Susoom). To examine species-environment relationships, Detrended Correspondence Analysis (DCA) and Canonical Correspondence Analysis (CCA) were performed using CANOCO version 4.5. The results highlighted that key edaphic factors—electrical conductivity (EC), calcium carbonate ($CaCO_3$), organic matter (OM), pH, phosphorus (P), and potassium (K)—played significant roles in shaping the distribution and composition of plant communities. This study underscores the importance of soil properties in determining vegetation patterns and provides a scientific basis for ecological conservation and land-use planning in the dry temperate zones of the Eastern Hindu Kush.

Keywords: Vegetation dynamics, Plant communities, Edaphic factors, Altitudinal variations, Dry temperate region, Chitral

➢ *ORAL PRESENTATION*

Investigation of the Material Effect on Rotor Mechanical Stress

Yusuf Bello Saleh[1*] (https://orcid.org/0000-0002-9746-0497), Abdullahi Abba Abdullahi[2]

[*1]Ahmadu Bello University, DAC, ABET, Kaduna, Nigeria.
[2]Firat University, Technology, Software, Elazig, Turkey.

*Corresponding author e-mail: yusufbellosaleh@gmail.com

Abstract

This study investigates the effect of different materials on mechanical stress in rotors, with an emphasis on materials that are commonly used in rotor design while keeping consistent density. The objective is to determine how material properties affect stress distribution and identify optimal materials for mechanical stress. Several materials were analysed under equal operating conditions, and the results demonstrating that M19-24 has the lowest mechanical stress when compared to its equivalents. Specifically, the M19-24 material reduces mechanical stress by approximately 34.2% when compared to other evaluated materials. These findings highlight the importance of material selection in rotor design, suggesting that M19-24 could improve rotor durability and performance by reducing stress-induced failures. The study offers significant data for engineers when choosing materials to improve rotor mechanical integrity.

Keywords: Rotor mechanical stress, rotor disposition, material properties.

➢ *ORAL PRESENTATION*

A novel binary mixture of lauric acid/caprylic acid as phase change material for refrigerated trucks

Bercem Kiran-Yildirim[1*] (*ORCID: https://orcid.org/0000-0002-7504-0176*), Zeynep Lara Pazar[1] (*ORCID: https://orcid.org/0009-0001-2645-1462*), Ozlem Turhan[1] (*ORCID: https://orcid.org/ 0009-0009-6151-8085*)

[*1] Marmara University, Faculty of Engineering, Department of Chemical Engineering, Istanbul, Turkey.

*Corresponding author e-mail: bercem.kiran@marmara.edu.tr

Abstract

The cold chain is critical for ensuring food security and preservation and comprises multiple stages, including pre-cooling, freezing, cold storage, refrigerated transportation, distribution, and domestic refrigeration. The refrigerated truck is one of the essential components of refrigerated transportation. Refrigerated trucks can be classified into four groups based on refrigeration technology: mechanical refrigerated trucks, cold plate refrigerated trucks, liquid nitrogen/dry ice refrigerated trucks, and liquefied natural gas (LNG) refrigerated trucks[1]. Phase change materials (PCMs) are used in cold plate refrigerated trucks, enabling heat preservation, temperature control, and refrigeration with improved energy efficiency. PCMs are able to store or release heat during phase change in response to temperature variations, thereby reducing temperature fluctuations and enhancing system performance. Thus, there are lots of studies focused on incorporating PCMs into cooling systems. In this study, the efficiency of the cooling system operating between 4 ºC and 12 ºC [2] was evaluated with novel mixtures of lauric acid and caprylic acid as PCMs to identify a suitable option for mechanical refrigerated trucks. The results demonstrated that the total energy consumption of the system over a 24-hour running period could be reduced by up to 27.8% using a solution composed of 86.6 wt.% caprylic acid and 13.4 wt.% lauric acid. This reduction further increased with the addition of acetone. The energy savings reached 32.2% with a solution containing 90.0 wt.% caprylic acid, 9.0 wt.% lauric acid, and 1.0 wt.% acetone, and were maximized at 38.6% using a solution of 90.0 wt.% caprylic acid and 10.0 wt.% acetone. Furthermore, the electricity cut-off was simulated following the running period in the cases with and without PCMs. The time required for the air inside the cabinet to reach the ambient temperature was approximately 1.6 times longer with solutions containing aceton, compared to the case without PCM. In contrast, this value was 1.4 times longer with the solution composed of 86.6 wt.% caprylic acid and 13.4 wt.% lauric acid. In conclusion, while acetone-containing solutions showed better performance in reducing energy consumption and maintaining product temperature for a longer duration during power failures in mechanical refrigerated trucks, the 86.6 wt.% caprylic acid–13.4 wt.% lauric acid solution can be recommended as a non-toxic alternative PCM, offering a practical balance between effectiveness and safety.

Keywords: Cold chain, refrigerated trucks, phase change materials, fatty acids

References:

[1] Chen, Y., Zhang, X., Ji, J., and Zhang, C. 2024. Cold chain transportation energy conservation and emission reduction based on phase change materials under dual-carbon background: A review. *Journal of Energy Storage*, 86, 111258.

[2] Tong, S., Nie, B., Li, Z., Li, C., Zou, B., Jiang, L., Jin, Y., and Ding, Y. 2021. A phase change material (PCM) based passively cooled container for integrated road-rail cold chain transportation–an experimental study. *Applied Thermal Engineering*, 195, 117204.

Acknowledgements

This research was supported financially by the Scientific and Technological Research Council of Turkey (TUBITAK), 2209-A - University Student Research Project Support Program (Project no: 1919B012413745).

➢ *ORAL PRESENTATION*

Investigation of Potential Antiviral Activity of *Hypericum perforatum* Extract Against SARS-CoV-2

Gülşah Akbaş[1,2] (ORCID: https://orcid.org/0000-0001-5378-7829) Jenya Dursun[1], (ORCID: https://orcid.org/0009-0006-9732-9217), Şeyma Aydınlık[1] (ORCID: https://orcid.org/0000-0001-5238-2432), Yüksel Çetin[1]* (ORCID: https://orcid.org/0000-0001-5101-3870)

*[1]TUBITAK Marmara Research Center, Life Sciences, Biotechnology R&D, Kocaeli, Turkiye
[2]Yildiz Technical University, Faculty of Arts and Sciences, Department of Molecular Biology and Genetics, Istanbul, Turkiye

*Corresponding author e-mail: yuksel.cetin@tubitak.gov.tr

Abstract

In the context of a pandemic, a principal challenge in antiviral drug development lies in identifying novel virus-host interactions and concerning drug efficacy and safety. These critical needs have highlighted the potential utility of phytochemicals derived from commonly used herbs and spices as antiviral agents and immunomodulatory compounds. The aim of this study was to investigate the potential antiviral activity and immunomodulatory effects of *Hypericum perforatum* against SARS-COVCoV-2 using in vitro systems, with the goal of supporting its potential application as a therapeutic agent. To comprehensively evaluate the effects of *H. perforatum* extract on cellular functions, a series of in vitro assays were performed using HEK293T, Vero E6, Caco-2, and Calu-3 cell lines. These included the MTT assay for assessing cell viability, Hematoxylin and Eosin (H&E) staining for morphological analysis, Annexin V/PI/Hoechst staining for the detection of apoptosis, and the DCFDA assay for quantifying intracellular oxidative stress. To investigate the antiviral potential of *H. perforatum* extract, high-throughput screening was conducted to evaluate its ability to inhibit the binding of the SARS-CoV-2 receptor-binding domain (RBD) to the ACE2 receptor using an ELISA, and pseudovirus S1 neutralization assay as well as its inhibitory activity against the viral main protease (Mpro) via a Fluorescence Resonance Energy Transfer (FRET) assay. The results indicated that *H. perforatum* extract exhibited notable antioxidant capacity and demonstrated substantial antiviral activity, achieving up to 34% neutralization of SARS-CoV-2 infection at a concentration of 100 µg/mL. Additionally, it inhibited SARS-CoV-2 main protease (Mpro) activity by 75% to 81% at 5 - 500 µg/mL. Furthermore, the extract displayed significant immunomodulatory effects by downregulating key proinflammatory cytokines, including TNF-α, IL-1β, IL-6, and IL-8. These findings highlight *H. perforatum* as a promising therapeutic candidate, either used alone or in combination with antiviral drugs, for the management of viral infections.

Keywords: SARS-CoV-2, *Hypericum perforatum*, Antiviral activity, Antioxidant effect, MTT assay, DCFDA assay

➢ *ORAL PRESENTATION*

Silver Loaded Photocrosslinked Silk Sericine-Keratin-F127 Hydrogels for Wound Healing Applications

İrem YAKAR[1*] (*ORCID: https://orcid.org/0009-0008-5083-4691*), Ayben TOP[1] (*ORCID: https://orcid.org/0000-0003-0554-2506*)

[1]Izmir Institute of Technology, Faculty of Engineering, Chemical Engineering, İzmir, Türkiye.

*Corresponding author e-mail: iremyakar@iyte.edu.tr

Abstract

Hydrogels offer many advantages in wound dressing applications. The moist environment of the hydrogels accelerates the cellular wound healing process and makes them suitable for treating dry and necrotic wounds. Additionally, hydrogel matrices can transport therapeutic materials such as drugs, antibiotics, antioxidants, and growth factors into the wound site [1-2]. In this study, we prepared antibacterial and antioxidant hydrogels using sustainable natural polymers, silk sericin, keratin, and a synthetic polymer, Pluronic F127. Silk sericin was extracted by autoclaving silk cocoons in deionized water at 120°C for 30 minutes. Keratin was obtained from wool by peracetic acid oxidation. The methacrylated forms of keratin and F127 were synthesized using methacrylic anhydride (MA). Hydrogel formulations containing silver at different concentrations, sericin, keratin-MA, and Pluronic F127-MA were prepared. These formulations were crosslinked under UV light using Irgacure as a photoinitiator to form self-supporting hydrogels. The swelling ratios of the hydrogels were similar and approximately 15 ± 3. All hydrogels maintained their structural integrity for more than 5 days in PBS. The addition of silver accelerated hydrogel degradation. Antibacterial tests using the disc diffusion method indicated that all silver-containing hydrogels exhibited antibacterial activity against *E. coli* and *S. aureus*. Antioxidant activities of hydrogels were determined using DPPH assay and attributed to sericin in the hydrogel composition. Cytotoxicity analysis with L929 cells confirmed that all hydrogels have acceptable cytotoxicity (above 75 %). The *in vitro* wound healing potential of the hydrogels was evaluated using the scratch test. The hydrogel extracts exhibited wound closures between 35 % and 82 %, depending on the composition. Thus, our results suggest that these antioxidant and antibacterial hydrogel formulations have potential in wound healing applications.

Keywords: Hydrogels, Wound Healing, Photocrosslinking, Silk Sericin, Wool Keratin

References:

1. Brumberg, V., Astrelina, T., Malivanova, T., Samoilov, A. 2021. "Modern Wound Dressings: Hydrogel Dressings", Biomedicines, 9(9), 1235.
2. Koehler, J., Brandl, F. P., Goepferich, A. M. 2018. "Hydrogel Wound Dressings for Bioactive Treatment of Acute and Chronic Wounds", European Polymer Journal, 100, 1-11.

Acknowledgments: This study was supported by the Scientific and Technological Research Council of Turkey (TUBITAK) with Grant Number 223M522.

➢ *ORAL PRESENTATION*

Synthesis and Characterization of a Novel Chromenylium-Cyanine Type Compound

Yusuf Alcay[1] (*ORCID: https://orcid.org/0000-0003-4948-7609*),
Ismail Yilmaz[1]*(*ORCID: https://orcid.org/0000-0002-5046-7456*)

[1] Istanbul Technical University, Faculty of Science and Letters, Department of Chemistry, Istanbul, Türkiye.

*Corresponding author e-mail: iyilmaz@itu.edu.tr

Abstract

Fluorescent probes play a pivotal role in biological imaging due to their ability to visualize and track biomolecules in real time. However, a significant limitation of conventional fluorophores lies in their absorption and emission within the visible spectrum, which often leads to inadequate tissue penetration, high levels of background autofluorescence, and light scattering issues. These drawbacks hinder the efficacy of imaging in complex biological environments. Near-infrared (NIR) fluorophores exhibit minimal interference from endogenous autofluorescence, resulting in clearer and more accurate imaging outcomes [1]. Among NIR fluorophores, chromenylium-cyanine dyes have gained considerable attention due to their high fluorescence quantum yields, large molar absorption coefficients, and tunable optical properties. These characteristics make them highly suitable for a range of biological and environmental sensing applications. These dyes exhibit dynamic spirolactam ring-opening and -closing behavior in response to environmental factors such as pH or target analytes, thereby offering potential as responsive chemosensors. The inclusion of the indolinium ring enhances their resonance stabilization, promoting efficient NIR absorption and emission. With their unique combination of high sensitivity, environmental responsiveness, and favorable photophysical characteristics, chromenylium-cyanine fluorophores are poised to become powerful tools in the fields of bioimaging and chemosensor development [2]. For this purpose, a novel chromenylium-cyanine-based compound containing an indole ring (**INIR10**) was synthesized and characterized using conventional techniques such as ^{1}H NMR, ^{13}C NMR, FTIR, and HRMS.

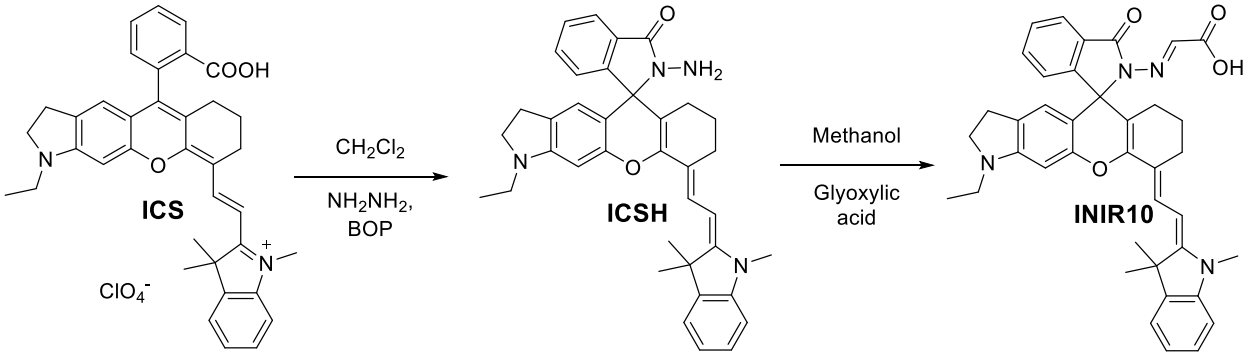

Figure 1. Synthesis of novel chromenylium-cyanine fluorophore, **INIR10**.

Keywords: chromenylium, cyanine, NIR, synthesis.

References:

[1] E. Ozdemir, Y. Alcay, O. Yavuz, M.S. Yildirim, H. Aribuga, U. Ertugral, K. Kaya, I. Yilmaz, Colorimetric and near-infrared spectrophotometric monitoring of bisulfite using glyoxal modified chromenylium-cyanine chemosensor: Smartphone and paper strip applications for on-site food and beverages control, Talanta 261 (2023) 124660. https://doi.org/10.1016/j.talanta.2023.124660.

[2] M.S. Yildirim, Y. Alcay, E. Ozdemir, U. Ertugral, O. Yavuz, H. Aribuga, K. Kaya, Y. Ozkilic, N.Ş. Tuzun, A.B.O. Sert, I. Yilmaz, Molecular architecture of a novel indoline-fused chromenylium-cyanine probe carrying methionine biomolecule for ultrasensitive analyzing Hg2+ ion in real samples, Journal of Environmental Chemical Engineering 12 (2024). https://doi.org/10.1016/j.jece.2024.114388.

This study was supported by Scientific and Technological Research Council of Turkey (TUBITAK) under the Grant Number 123Z402. The authors thank to TUBITAK for their supports.

➢ *ORAL PRESENTATION*

A New Smartphone-Assisted Near-Infrared Fluorescent Probe for Visual Detection of Mercury(II) in Food and Water Samples

Emre Ozdemir[1] (ORCID : *https://orcid.org/0000-0001-6921-7871*), Yusuf Alcay[1] (*ORCID: https://orcid.org/0000-0003-4948-7609*), Ozgur Yavuz[1] (*ORCID:* https://orcid.org/0000-0002-0660-7474), Muhammed Ikbal Gunduz[1] (*ORCID: https://orcid.org/0000-0002-6683-9875*), Ismail Yilmaz[1*] (*ORCID: https://orcid.org/0000-0002-5046-7456*)

*[1]Istanbul Technical University, Faculty of Science and Letters, Department of Chemistry, Istanbul, Turkiye

*Corresponding author e-mail: iyilmaz@itu.edu.tr

Abstract

Mercury (Hg^{2+}) pollution poses a serious threat to environmental and human health due to its bioaccumulative and toxic nature, necessitating the development of rapid, selective, and cost-effective detection methods. In this study, a novel phenylthiourea-based indoline-fused chromenylium-cyanine dye (**INIR2**) was synthesized and employed as a chemodosimetric probe for the selective detection of Hg^{2+} ions through colorimetric, fluorometric, and smartphone-based approaches. The **INIR2** probe was synthesized by reacting **ICSH** with phenyl isothiocyanate in DMF at room temperature, followed by extraction and purification via column chromatography (yield: 69%). Structural characterization was confirmed by FT-IR, ^{1}H-NMR, ^{13}C-NMR, and HRMS. For the sensing study, **INIR2** was reacted with $HgCl_2$ to form **INIR2H**, a green-colored product isolated after purification. HRMS data confirmed the formation of **INIR2H** with a mass peak at m/z 672.33276, consistent with the expected loss of HgS. Spectral shifts and NMR data supported the proposed spirolactam ring-opening and imidazole formation mechanism upon Hg^{2+} interaction. **INIR2** exhibited a fast response (10 s), broad working pH range (3–9), and high selectivity towards Hg^{2+} over other competing species. Spectral studies revealed exceptionally low limits of detection (LOD) at 0.11 nM (UV-Vis), 0.18 nM (fluorescence), and 33.3 nM (smartphone method), with the latter achieving the highest sensitivity reported to date for mobile-based Hg^{2+} sensing. The probe's applicability was validated in real samples including drinking, tap, and lake water, as well as corn and rice matrices, with recovery rates close to 100%. The findings highlight **INIR2** as a powerful, versatile platform for Hg^{2+} monitoring in environmental systems.

Keywords: 3-6 words. (chromenylium-cyanine, smartphone, food, mercury, UV-Vis, fluorescence)

This study was supported by Scientific and Technological Research Council of Turkey (TUBITAK) under the Grant Number 123Z402. The authors thank to TUBITAK for their supports.

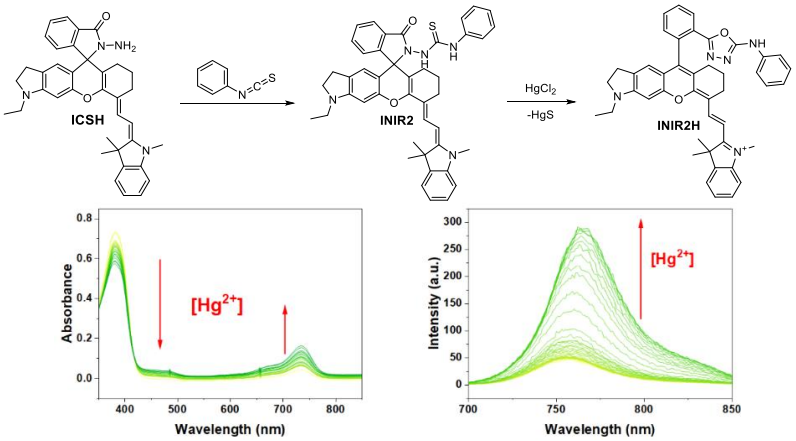

Figure 1. Synthetis route of **INIR2** and its proposed molecular rearrangement with Hg^{2+}, UV-Vis and fluorescence spectra changes of **INIR2**.

References:
[1] A methionine biomolecule-modified chromenylium-cyanine fluorescent probe for the analysis of Hg2+ in the environment and living cells, Talanta, Volume 259, 2023, 124471, ISSN 0039-9140, https://doi.org/10.1016/j.talanta.2023.124471.

➢ *ORAL PRESENTATION*

The Investigation of the Latest Developments in Green Energy Technologies to Reduce Carbon Emissions

Kasım ATMACA[1*] (*ORCID: https://orcid.org/0000-0002-6570-4127*)

[*1]Sinop University, Faculty of Engineering and Architecture, Department of Environmental Engineering, Sinop, Türkiye.

*Corresponding author e-mail: katmaca@sinop.edu.tr

Abstract

Today, climate change and increasing carbon emissions are among the most important problems faced by humanity. In the context of reducing carbon emissions, green energy transition is of vital importance. Since green energy is obtained from natural resources, it has less harmful effects on the environment compared to fossil fuels and has the capacity to reduce carbon emissions. Green energy technologies include advanced solar panels, energy storage systems, smart grids, carbon capture and storage systems, and hydrogen energy. These innovations in green energy technologies offer great promise for the future of sustainable energy. Future urban planning needs to be considered together with this transformation. In this study, recent and new developments in sustainable buildings and environment, transportation systems, waste management and reduction of pollutant emissions in cities in the context of green energy were examined. Additionally, the difficulties encountered in the development and implementation of green energy in cities and solution proposals were compared.

Keywords: Climate change, carbon emissions, green energy, sustainable systems

➢ *ORAL PRESENTATION*

Biosynthesis of *Helichrysum arenarium* L.-Cu(II) hybrid nanoflowers and evaluation of their cytotoxic activities

Burcu SOMTÜRK YILMAZ[1]*(ORCID: https://orcid.org/0000-0002-2775-3083)

[1]Drug Application and Research Center, Erciyes University, 38280 Kayseri, Türkiye

*Corresponding author e-mail: burcu_smtrk@hotmail.com

Abstract

Golden grass, named after its golden yellow color "*Helichrysum arenarium*" in Latin, is a herbaceous plant that blooms yellow flowers that are 50-60 centimeters long. It is also known by different names among the public: Golden flower, immortelle flower, sun flower, bee flower, etc. and its homeland is Europe. It grows in Eastern Anatolia in our country. The flower of *Helichrysum arenarium* has many biological activities, especially antibacterial, antiviral, antifungal, anti-inflammatory, antiproliferative, antimicrobial, antiallergic, antioxidant, antiradical, cholinergic, hepatoprotective and detoxification activities. In this study, hybrid nanoflower synthesis was carried out using *Helichrysum arenarium* L. plant and Cu(II) metal ion. Then, characterization process was carried out with SEM, EDX, XRD, FTIR, Mapping and NTA. Anticancer activities of synthesized hybrid nanoflowers were carried out on MCF7 cell line. As a result, it was observed that anticancer activity increased when the plant extract was converted into hybrid nanoflower form.

Keywords: Nanoflower, Cytotoxic, *Helichrysum arenarium L.*

➢ *ORAL PRESENTATION*

Electrochemical Surface Modification of Screen-Printed Gold Electrodes for Enhanced Performance and Kinetics

Turgut Sönmez (https://orcid.org/0000-0002-3927-2551)

Karabük University, Faculty of Science, Department of Chemistry, Karabük, Türkiye

*Corresponding author e-mail: turgutsonmez@karabuk.edu.tr

Abstract

Screen-printed electrodes (SPEs) as a sensing platform have gained popularity as an alternative to the classical three-electrode electrochemical setup (which typically consists of a carbon working electrode (WE), a platinum counter electrode (CE), and an Ag/AgCl reference electrode (RE) in a glass cell).[1, 2] This shift is driven by several advantages, including low cost, ease of fabrication, mass production capability, and disposability.[1-3] As shown in the left figure, the three electrodes are integrated onto the same flat substrate through the combination of various layers, forming a compact chip of just a few cm^2.[1] SPEs can be used for the detection and quantification of analytes in a wide range of applications, including environmental analysis, heavy metal detection, pesticides, oxygen concentration, glucose monitoring, and DNA analysis.[3, 4] To optimize surface performance, sensitivity, and stability, a surface activation process is essential. Therefore, electrochemical surface modification in an acidic environment is of great interest.

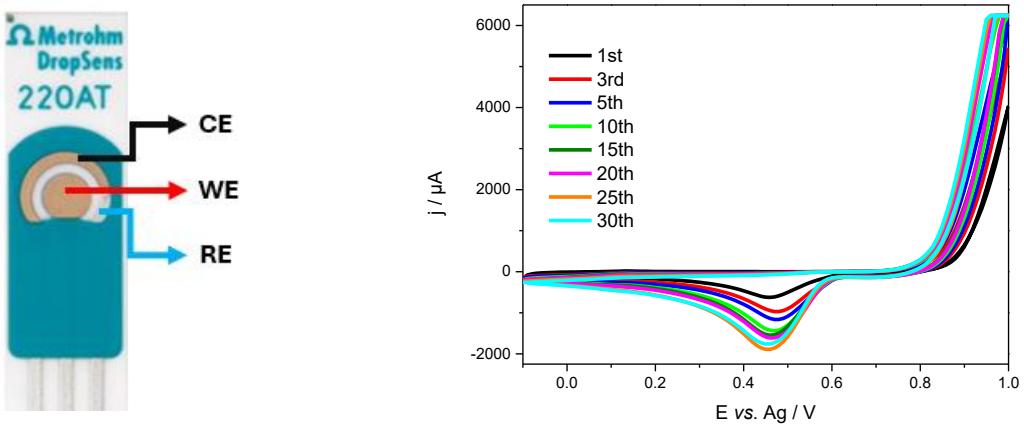

Figure. *Image of the screen-printed gold electrode (SPGE) (left) and cyclic voltammograms of SPGE (right) recorded in 0.5 M HCl at 25 °C. 1st - 30th scan. 100 mV/s.*

In this study, we performed electrochemical surface modification of a screen-printed gold electrode (SPGE) in 0.5 M HCl using cyclic voltammetry (CV). As shown in Figure (right), the reduction peak current at approximately 0.45 V *vs.* Ag increases steadily until the 25th scan, after which the activity stabilizes. The current exhibits more than a three-fold increase between the 1st and 25th scans. Our results demonstrate that the sensing activity of the SPGE in HCl has been enhanced nearly 100 times compared to our recent report[3] of SPGE performance in H_2SO_4. Surface-modified and unmodified SPGEs were subsequently used for O_2 detection, with their performance and kinetics compared. The underlying mechanisms responsible for the enhanced surface activity were also investigated.

Keywords: Screen Printed Electrodes, Biosensors, Surface Modification, Cyclic Voltammetry

References:

[1] R.D. Crapnell, A.G.-M. Ferrari, N.C. Dempsey, C.E. Banks, Sensors & Diagnostics, 1 (2022) 405-428.
[2] R.D. Crapnell, C.E. Banks, ChemElectroChem, (2024) e202400370.
[3] N.D. Zakaria, I.L. Salih, H.H. Hamzah, T. Sönmez, M.H. Omar, N.M. Nor, K.A. Razak, V. Balakrishnan, Analyst, 149 (2024) 5401-5410.
[4] M. Li, Y.-T. Li, D.-W. Li, Y.-T. Long, Analytica chimica acta, 734 (2012) 31-44.

➢ *ORAL PRESENTATION*

Deniz Dibi Tarama Faaliyetlerinden Elde Edilen Dip Çamurlarının Alternatif Bertaraf Yöntemlerinin Araştırılması

Elif Erdeve Özvan[1*] (*ORCID: https://orcid.org/0000-0002-3355-3432*), Ayşe Özgüven[2] (*ORCID: https://orcid.org/ 0000-0003-1071-2813*), Dilara Öztürk[2] (*ORCID: https://orcid.org/0000-0003-2689-560X*), Mehmet Türkmenoğlu[3] (*ORCID: https://orcid.org/0000-0001-6088-4416)*

[*1]Van Yüzüncü Yıl Üniversitesi, Van Meslek Yüksekokulu, İnşaat Teknolojisi Programı, Van, Türkiye.
[2] Van Yüzüncü Yıl Üniversitesi, Mühendislik Fakültesi, Çevre Mühendisliği Bölümü, Van, Türkiye.
[3] Van Yüzüncü Yıl Üniversitesi, Mühendislik Fakültesi, Maden Mühendisliği Bölümü, Van, Türkiye.

*Sorumlu yazar e-posta : eliferdeveozvan@yyu.edu.tr

Özet

Sanayi ve kentleşme faaliyetlerinin artmasıyla beraber atıksu arıtma tesislerinin artması ve buna bağlı olarak yüzeysel sulara atıksu deşarjlarının artması sonucunda nehir, göl ve denizlerde dip çamurları oluşmaktadır. Kanalizasyon deşarjları, tarımsal uygulamalar, inşaat ve hafriyat atıkları gibi birçok insan faaliyetleri sonucunda da organik ve inorganik maddeler (patojenler, ağır metaller, organik kirleticiler ve diğer toksik maddeler) dip çamurunda birikmektedir. Bu durum insan ve suda yaşayan organizmaların sağlıklarını tehdit etmektedir. Dip çamurunun susuzlaştırıldıktan sonra tasfiye edilmesi veya tekrar kullanılması hem ekonomi hem de çevre sağlığı için oldukça önemlidir. Çamurların susuzlaştırılmasında genellikle mekanik yöntemler kullanılmaktadır. Fakat mekanik yöntemlerin etkinliğini geliştirmek için çamura polielektrolit eklenerek çamurun susuzlaştırılma kapasitesinin daha iyi hale getirilmesi gereklidir. Dip çamurunun susuzlaştırılması üzerine yapılan araştırmalar genellikle geo-tekstil ve poliakrilamid ilaveli susuzlaştırma metodlarını içermektedir. Bu çalışmada, Türkiye'de gerçekleştirilen deniz dibi tarama faaliyetlerinden elde edilen çamurların alternatif bertaraf yöntemleri sunulmuş ve bu faaliyetlerin çevresel potansiyel etkileri vurgulanmıştır. Deniz tarama faaliyetleri sonucu elde edilen dip çamurlarının ağır metal içeriği göz önünde bulundurularak susuzlaştırıldıktan sonra bertaraf alternatifleri için mevcut olan yöntemler incelenmiştir. Türkiye'de dip çamurlarının ham madde olarak kullanımı veya geri kazanımıyla ilgili olarak az sayıda çalışma yapılmıştır. Bazı çalışmalarda dip çamurlarının bağlayıcılık özelliği iyi olan çeşitli malzemelerle karıştırılıp, inşaat malzemesi olarak hafif agrega yapımında veya yol yapımında dolgu malzemesi olarak kullanılabilirliği araştırılmıştır. Dip çamurlarının dolgu malzemesi olarak kullanılabilmesi için karayolları teknik şartnamesinde verilen limit değerler göz önünde bulundurulmalıdır. Dip çamurunun çevresel etkilerinin değerlendirildiği çalışmalarda ''Atık Yönetimi Yönetmeliği (AYY) (02.04.2015-R.G.29314)''ye göre ''tehlikesiz atık (atık kodu 17 05 06)'' sınıfında olup olmadığı belirtilmelidir. Yapılan araştırmalar sonucunda dip çamurlarının susuzlaştırılması için hangi yöntemlerin kullanılabileceği, dip çamurunun bertaraf edilmesinden kaynaklanan çevresel risklerin azaltılması için uygun teknolojilerin nasıl seçileceği vurgulanmıştır.

Anahtar Kelimeler: Bertaraf yöntemleri, dip çamuru tarama, çevresel etkiler.

➢ *ORAL PRESENTATION*

Comparative analysis of transport-oriented urban approaches

Rukiye Gizem Öztaş Karlı[1*] (*ORCID: https://orcid.org/0000-0003-0999-418X)*

[*1]Bartın University, Engineering, Faculty of Engineering, Architecture and Design, Department of Landscape Architecture, Bartın, Türkiye.

*Corresponding author e-mail: roztas@bartin.edu.tr

Abstract

In contemporary cities, transportation systems are no longer limited to facilitating mobility alone; they are increasingly re-evaluated in line with multidimensional goals such as sustainability, accessibility, and quality of urban life. In this context, transport-oriented urban models have emerged as frameworks with the potential to reshape urban space across varying scales and planning paradigms. Although models such as the 15-Minute City, Net Zero Carbon City, and Transit-Oriented Development (TOD) have been implemented in various urban contexts, studies that comparatively analyze these approaches remain limited. In particular, there appears to be a lack of systematic evaluation in the literature concerning their planning principles, sustainability dimensions, and contextual adaptability. This study aims to address this gap by providing a comparative conceptual analysis of the aforementioned three approaches. Within a conceptual framework, the research will examine the fundamental principles, transportation visions, and implementation challenges of each model based on academic literature, international policy documents, urban strategy reports, and exemplary cases. Through a qualitative comparative method, the study will identify and interpret the advantages, limitations, and contextual adaptability of each approach. Ultimately, the study seeks to contribute to the academic discourse by offering an integrated understanding of transport-oriented urban approaches and to provide a conceptual foundation for strategic syntheses that may be applicable in developing countries such as Türkiye.

Keywords: Sustainable urban mobility, Urban planning models, Comparative analysis

➢ *ORAL PRESENTATION*

Hatay ili Arsuz Bölgesi Topraklarının Molibden İçeriği ve Topraktaki Bazı Ağır Metaller ile İlişkilerinin Belirlenmesi

Mehmet YALÇIN (ORCID: 0000-0002-1690-7681)

Hatay Mustafa Kemal Üniversitesi, Toprak Bilimi ve Bitki Besleme Bölümü, Hatay/Türkiye

*Sorumlu yazar e-posta: myalcin@mku.edu.tr

Özet

Bu çalışmada Hatay ili Arsuz bölgesi topraklarının molibden içeriğinin belirlenmesi ve toprak içerisindeki bazı ağır metaller ile ilişkilerinin saptanması amaçlanmıştır. Bu amaç için Arsuz ilçesi topraklarını temsil edecek şekilde 0-30 cm derinlikten ve 70 noktadan olmak üzere toplamda 70 toprak örneği alınmıştır. Alınan toprak örneklerinde; Kadmiyum (Cd), Cobalt (Co), Krom (Cr), Nikel (Ni), Demir (Fe) ve Molibden (Mo) içerikleri belirlenmiştir. Araştırma sonuçlarına göre; toprakların Cd içerikleri 0.01-0.03 µg/kg; Co içeriği 0.02-2.96 µg/kg; Cr 0.01-0.85 µg/kg, Ni içerikleri 0.35-17.60 mg/kg; Fe içerikleri 1.65-18.72 mg/kg ve Mo içerikleri 0.01-0.18 µg/kg arasında bulunmuştur. Toprakların Mo ile Cd, Co ve Fe içerikleri arasında pozitif önemli ilişkiler belirlenmiştir. Aynı zamanda Cd ile Co, Ni, Fe ve Co ile Ni ve Fe aralarında ise pozitif önemli ilişkiler belirlenmiştir. Bölge topraklarının ağır metal içerikleri sınır değerler ile karşılaştırıldığında herhangi bir ağır metal kirliliğine rastlanmamıştır.

Anahtar kelimeler: molibden içeriği, Arsuz ilçesi, ağır metaller

➢ *ORAL PRESENTATION*

Investigation of the effect of layer thickness on the wear properties of PEEK materials

Şakir Altınsoy (*ORCID: https://orcid.org/0000-0002-1893-2266*)

İstanbul Yeni Yüzyıl University, Faculty of Engineering and Architecture, Department of Biomedical Engineering, Istanbul / Türkiye

*Corresponding author e-mail: sakir.altinsoy@yeniyuzyil.edu.tr

Abstract

In recent years, the Additive Manufacturing method has gained an important place in the industry by facilitating the production of complex geometry parts that are difficult to manufacture with traditional production methods. This method offers various advantages in today's production sectors where lightweight structures and raw material savings are essential. Polyetheretherketone (PEEK), an advanced engineering material with high melting temperature, and chemical and wear resistance, provides both functional and economical solutions when combined with Additive Manufacturing technologies. In this study, test specimens with Ø10x25 mm dimensions were produced with the Additive Manufacturing method using PEEK material in different layer thicknesses (50, 75, and 100 µm). In order to examine the wear behavior of the samples, three different loads (20, 40, and 60 N) and two different sliding speeds (0.5 and 1.0 m/s) were used in a dry environment disk-on-pin wear test setup. The test samples were produced at an 80% fill rate. The results obtained show that the layer thickness in samples produced from PEEK material does not have a significant effect on both volume loss and average friction coefficient, but the wear resistance decreases with the increase in applied load and sliding speed. It was also determined that the increase in sliding speed affects the average friction coefficient.

Keywords: PEEK, additive manufacturing, layer thickness, wear.

➢ *ORAL PRESENTATION*

Powder metallurgical synthesis and characterization of Al-10 wt.% Si-x($Hf_{0.2}Ti_{0.2}Zr_{0.2}V_{0.2}Ta_{0.2}$)$B_2$

İlayda Süzer[1*] (*ORCID: 0000-0003-1825-7253*), Duygu Ağaoğulları[2] (*ORCID: 0000-0002-0623-5586*)

[*1]Istanbul Technical University, Faculty of Chemical and Metallurgical Engineering, Department of Metallurgical and Materials Engineering, Particulate Materials Laboratories (PML), Graphene & 2D Materials Laboratory, Maslak, Istanbul, 34469, Türkiye

*Corresponding author e-mail: suzeri@itu.edu.tr

Abstract

This study reports on the sintering of Al-10 wt.% Si-x($Hf_{0.2}Ti_{0.2}Zr_{0.2}V_{0.2}Ta_{0.2}$)$B_2$ (x= 1, 2, 5, 10, 15 wt.%) composites by traditional powder metallurgy methods. Firstly, high entropy ($Hf_{0.2}Ti_{0.2}Zr_{0.2}V_{0.2}Ta_{0.2}$)$B_2$ diboride (HEB) ceramics were synthesized via planetary ball milling (6 h) assisted spark plasma sintering (2000 ^oC, 30 MPa). After the prealloying of Al-10 wt.% Si (Al10Si) matrix during 4 h, HEB ceramics were milled down to particles and then incorporated into the matrix at five different weight ratios with in the presence of stearic acid. Next, prepared powder mixtures were mechanically alloyed for 6 h. The powders were cold pressed and debinded at 420 ^oC during 2 h and then pressureless sintered at 630 ^oC during 2 h. X-ray diffractometer (XRD), scanning electron microscope/energy dispersive spectrometer (SEM/EDS), Archimedes' density, hardness (50 g, 10 sec) and dry sliding wear tests were conducted as characterization studies. In addition to Al, Si and HEB phases, Fe contamination originating from the milling media was also detected. The composite containing 15 wt.% HEB reinforcement had the highest Archimedes' density of 2.84 g/cm^3 had the highest hardness value of nearly 3.87 GPa and the 10 wt.% HEB reinforcement composites had the lowest wear rate of approximately $2.14x10^{-4}$ mm^3/Nm.

Keywords: High entropy diborides, microstructure, mechanical alloying, hardness, phase analysis, Al-matrix composites.

Acknowledgement: This study was supported by Scientific Research Projects Department of Istanbul Technical University with the project number of MGA-2023-44054 (ITU BAP/YAP Project).

➢ *ORAL PRESENTATION*

Kolon kanseri ve bağırsak mikrobiyotası: ön çalışma

Samet Uçak[1*] (*ORCID: https://orcid.org/0000-0002-3461-2481*),
Seval Kaya[2] (*https://orcid.org/0000-0001-6251-6529*)

[*1]İstanbul Aydın Üniversitesi, Tıp Fakültesi, Tıbbi Biyoloji ve Genetik Anabilim Dalı, İstanbul, Türkiye.
[2]İstanbul Aydın Üniversitesi, Tıp Fakültesi, Histoloji ve Embriyoloji Anabilim Dalı, İstanbul, Türkiye.

*Sorumlu yazar e-posta: sametucak@aydin.edu.tr

Özet

Kolon kanseri, dünya çapında önemli bir morbidite ve mortalite nedenidir. Son yıllarda, bağırsak mikrobiyotasının kolon kanseri patogenezindeki rolü giderek daha fazla araştırılmaktadır. Mikrobiyota bileşimindeki değişiklikler (disbiyozis), kronik inflamasyon, genotoksik metabolit üretimi ve immün modülasyon yoluyla kolon karsinogenezini tetikleyebilmektedir. Bu çalışma ön çalışma olup, kolon kanseri mikrobiyotasının yeni nesil dizileme (NGS) yöntemi ve metagenomik analiz kullanılarak belirlenmesi amaçlanmıştır. Kolon CA (+) klinik tanısı almış 10 hastadan alınan doku örneklerinden QIAamp DNA Micro Kiti kullanılarak DNA izolasyonu gerçekleştirilmiştir. Toplam DNA örneklerinden, bakteriyel 16S rRNA gen bölgesi polimeraz zincir reaksiyonu (PZR) kullanılarak amplifiye edilmiş ve oluşturulan kütüphanelerin sekans analizleri Illumina platformunda yeni nesil dizileme (NGS) yöntemiyle yapılmıştır. Metagenomik analizlerde incelenen 10 kolon kanseri mikrobiyota örneğinde, cins seviyesinde baskın türün *Enterococcus* olduğu gözlemlenmiş; bunu sırasıyla *Escherichia/Shigella* ve *Staphylococcus* izlemiştir. Literatürde *Enterococcus*'un (özellikle *E. faecalis*), kolon kanserinde artış gösterdiği, ROS üretimi, DNA hasarı ve kronik inflamasyon yoluyla tümör oluşumunu tetikleyebildiği, *Escherichia/Shigella*'nın (özellikle pks+ *E. coli*), kolon kanserinde artış gösterdiği, kolibaktin toksini ile DNA hasarı yaparak ve kronik inflamasyonu tetikleyerek tümör oluşumunu desteklediği, *Staphylococcus*'un kolon kanserinde artış gösteren bakterilerden olduğu, biyofilm oluşturarak kronik inflamasyona ve immün modülasyona yol açtığı, toksinleriyle epitel bariyeri bozabildiği, ancak direkt kanserojen etkisinin tartışmalı olduğu bildirilmiştir. Bu bakterilerin artışı, sağlıklı mikrobiyota dengesinin (örn. *Faecalibacterium prausnitzii* gibi anti-inflamatuvar türlerin) bozulmasıyla ilişkilendirilmektedir. Mikrobiyota modülasyonu (pro/prebiyotik uygulamaları, fekal transplantasyon ve spesifik antibiyotik tedavileri) kolon kanseri tedavisinde yeni terapötik seçenekler sunmaktadır. Mikrobiyota profilleme teknikleri ise hastalığın erken evre tanısında potansiyel biyobelirteçler olarak umut vaat etmektedir.

Anahtar Kelimeler: Bağırsak mikrobiyotası, Disbiyozis, Kolon kanseri.

➢ *ORAL PRESENTATION*

Damping–mixing enthalpy relationship in Mg-Ca and Mg-Ni alloys: Influence of short-range order

Yiğit Türe[1*] (*https://orcid.org/0000-0002-5238-2624*)

[*1]Eskisehir Technical University, Information Technologies Vocational School, Electronics and Automation Department, Eskisehir, Turkey.

*Corresponding author e-mail: yture@eskisehir.edu.tr

Abstract

In addition to their high specific strength, magnesium (Mg) and its alloys exhibit notable damping capacity. However, the type and concentration of alloying elements must be carefully considered. In Mg-based alloys, the relationship between damping behavior and mixing enthalpy can offer valuable insights into the fundamental mechanisms that govern material properties. This study investigates this relationship using two alloy systems: one containing calcium (Ca), which is soluble in Mg, and the other containing nickel (Ni), which is insoluble in Mg. Damping test data at low strain amplitude levels (relevant to ride comfort) were utilized to establish the correlations. These data were obtained from previously published studies in the literature. Given the importance of solubility, the effect of short-range order (SRO) was also examined within the main framework of the study. The results revealed that the correlation between damping capacity and mixing enthalpy exhibited a similar decreasing trend in both alloy systems as the concentration of the alloying element increased. The pronounced reduction in damping observed in Ca-containing alloys was attributed to the formation of SRO structures.

Keywords: Magnesium alloy, damping, enthalpy of mixing, short range order

➢ *ORAL PRESENTATION*

Kiraz domatesin raf ömrünü uzatmak için PBAT esaslı nanokompozit filmlerin geliştirilmesi ve karakterizasyonu

Seden Aksu[1] (*https://orcid.org/ 0009-0006-1476-8418*),
Şükran Melda Eskitoros Toğay[1*] (*https://orcid.org/ 0000-0002-7473-8417*)

[*1]Sağlık Bilimleri Üniversitesi, Gülhane Sağlık Meslek Yüksekokulu, Eczane Hizmetleri Programı, Ankara, Türkiye

*Sorumlu yazar e-posta: melda.togay@sbu.edu.tr, meskitoros@gmail.com

Özet

Plastik atıkların çevresel etkilerini azaltmak amacıyla biyobozunur ambalaj malzemelerine olan ilgi giderek artmaktadır. Bu doğrultuda, gıda ürünlerinin raf ömrünü uzatmada kullanılabilecek, çevre dostu ve antimikrobiyel özelliklere sahip polimer esaslı yeni nesil ambalaj çözümleri geliştirilmektedir. Bu çalışmada, biyolojik olarak parçalanabilir poli(bütilen adipat-ko-tereftalat) (PBAT) esaslı nanokompozit filmler, titanyum dioksit (TiO_2) ve indirgenmiş grafen oksit (rGO) nano dolgu maddeleriyle katkılandırılarak hazırlanmıştır. Filmler, çözelti döküm yöntemiyle üretilmiş ve saf PBAT ile birlikte PBAT/TiO_2, PBAT/rGO ve PBAT/TiO_2-rGO kompozitleri elde edilmiştir. Hazırlanan filmlerin karakterizasyonu; yüzey morfolojisini incelemek için atomik kuvvet mikroskobu (AFM), kimyasal yapı analizleri için Fourier dönüşümlü kızılötesi spektroskopisi (FTIR), yüzeyin hidrofilik/hidrofobik doğasını değerlendirmek için temas açısı ölçümleri ve nem ile etkileşimini belirlemek üzere su absorplama testleri ile gerçekleştirilmiştir. Özellikle rGO ve TiO_2 nano dolgu maddelerini birlikte içeren filmler, daha düşük su absorplama oranları ve daha homojen yüzey yapılarıyla dikkat çekmiştir. Filmlerin gıda ambalajı olarak uygulanabilirliğini değerlendirmek üzere, 28 gün süren kiraz domates raf ömrü testi gerçekleştirilmiştir. Domatesler düzenli aralıklarla izlenmiş, ağırlık kaybı oranları hesaplanmış ve yüzey bozulmaları değerlendirilmiştir. PBAT/TiO_2-rGO kompozit film ile sarılan domateslerin 28. güne kadar görünür mikrobiyal bozulma göstermediği ve ağırlık kaybının %15'in altında kaldığı gözlemlenmiştir. Bu bulgular, geliştirilen PBAT/TiO_2-rGO kompozit filmin çevre dostu ambalaj uygulamaları için potansiyel taşıdığını göstermektedir.

Anahtar kelimeler: Poli(bütilen adipat-ko-teraftalat), İndirgenmiş grafen oksit, Titanyum dioksit, Kiraz domates, Nanokompozit film

Teşekkür
Bu çalışma, TÜBİTAK 2209-A Üniversite Öğrencileri Araştırma Projeleri Destekleme Programı tarafından 1919B012406919 numaralı proje kapsamında desteklenmiştir.

➢ *ORAL PRESENTATION*

A New Role for Cyclobenzaprine: Cytotoxic Effects in Lung Cancer Cells

Asli ELDEM[1] (https://orcid.org/0000-0003-3510-6748)

Department of Analytical Chemistry, Faculty of Pharmacy, İzmir Kâtip Çelebi University, İzmir, Turkiye

*Corresponding author e-mail: aslierdem45@gmail.com

Abstract

Cyclobenzaprine is a tricyclic compound commonly used as a muscle relaxant, but its anticancer potential has not been sufficiently explored. In this study, the cytotoxic and antiproliferative effects of cyclobenzaprine on the human lung adenocarcinoma cell line A549 were investigated following 24 hours of treatment. Cell viability was evaluated using the MTT assay, while long-term proliferative capacity was assessed via the colony formation assay. Cyclobenzaprine was applied at various concentrations (1, 5, 10, 12.5, 15, 20, 50 µM), and based on dose–response analysis, the IC_{50} value was determined to be 22.3 µM. At this concentration, a significant reduction in cell viability was observed. Furthermore, colony formation ability was notably inhibited. Both the number and size of colonies were found to be significantly lower in the treated groups compared to the control group ($p < 0.05$). These results indicate that cyclobenzaprine effectively suppresses the viability and clonogenic potential of A549 cells. The findings suggest that cyclobenzaprine may directly affect cell proliferation and could be considered a potential anticancer agent. This study also presents a novel perspective on the repurposing of cyclobenzaprine for oncological applications beyond its conventional therapeutic roles. In conclusion, further research is proposed to elucidate the underlying mechanisms of its antiproliferative effects, particularly focusing on apoptosis, cell cycle regulation, and related signaling pathways. These future studies may provide deeper insights into cyclobenzaprine's mechanism of action and strengthen the rationale for its potential use in cancer therapy. Overall, these findings highlight the promise of cyclobenzaprine as an anticancer compound and provide a foundation for more extensive preclinical investigations.

Keywords: A549, Cyclobenzaprine,Cell viability

➢ *ORAL PRESENTATION*

Improvement of Functional Properties in Bread Enriched with Aronia (*Aronia melanocarpa*) Juice

Sultan ACUN[1*] (https://orcid.org/0000-0003-1954-6102), Şeyma ULUTÜRK[2] (https://orcid.org/0000-0001-7060-5337), Kerem MERTOĞLU[3] (https://orcid.org/0000-0002-0490-9073), İlknur ESKİMEZ[4] (https://orcid.org/0000-0003-4453-505X), Hülya GÜL[5] (https://orcid.org/0000-0002-6791-817X)

[1*] Amasya University, Suluova Vocational School, Department of Food Processing, Amasya, Türkiye
[2] Süleyman Demirel University, Graduate School of Natural and Applied Sciences, Department of Food Engineering, Isparta, Türkiye
[3] Usak University, Faculty of Agriculture, Department of Horticulture, Usak, Türkiye
[4] Isparta University of Applied Sciences, Faculty of Agriculture, Department of Horticulture, Isparta, Türkiye
[5] Süleyman Demirel University, Faculty of Engineering and Natural Sciences, Department of Food Engineering, Isparta, Türkiye

*Corresponding author e-mail: sultan.acun@amasya.edu.tr

Abstract

Bread is one of the most widely consumed food products worldwide and constitutes an essential part of the daily diet. Due to its frequent consumption, improving the nutritional and functional value of bread offers a practical approach to supporting public health. In this context, the use of natural ingredients rich in bioactive compounds has gained increasing attention. Aronia (*Aronia melanocarpa*) is a fruit known for its high content of phenolic compounds such as anthocyanins and flavonoids, and for its strong antioxidant capacity. In this study, the effect of incorporating aronia juice at levels of 50% and 100% in bread formulations was investigated in terms of its contribution to the product's bioactive profile. The enrichment of bread with aronia juice led to a remarkable increase in both phenolic content and antioxidant potential compared to the control. Specifically, phenolic content increased by approximately 176% and 393%, while antioxidant activity improved by 89% and 228% in the 50% and 100% juice formulations, respectively. The results demonstrate that aronia juice can serve as a natural source of phenolics and antioxidants in cereal-based products. Its inclusion in bread formulations significantly enhances both nutritional and functional properties. These findings suggest that the utilization of fruit-derived bioactive components may contribute to the development of novel functional bakery products with potential health-promoting effects.

Keywords: *Aronia melanocarpa*, functional products, phenolic compounds, antioxidant activity, bread

➢ *ORAL PRESENTATION*

Impact of *Aronia melanocarpa* juice substitution on the rheological properties of wheat flour

Şeyma ULUTÜRK[1] (https://orcid.org/0000-0001-7060-5337), Hülya GÜL[2*] (https://orcid.org/0000-0002-6791-817X), İlknur ESKİMEZ[3] (https://orcid.org/0000-0003-4453-505X), Kerem MERTOĞLU[4] (https://orcid.org/0000-0002-0490-9073), Sultan ACUN[5] (https://orcid.org/0000-0003-1954-6102)

[1] Süleyman Demirel University, Graduate School of Natural and Applied Sciences, Department of Food Engineering, Isparta, Türkiye
[2*]Süleyman Demirel University, Faculty of Engineering and Natural Sciences, Department of Food Engineering, Isparta, Türkiye
[3] Isparta University of Applied Sciences, Faculty of Agriculture, Department of Horticulture, Isparta, Türkiye
[4] Usak University, Faculty of Agriculture, Department of Horticulture, Usak, Türkiye
[5] Amasya University, Suluova Vocational School, Department of Food Processing, Amasya, Türkiye

*Corresponding author e-mail: hulyagul@sdu.edu.tr

Abstract

Aronia melanocarpa is a rich source of polyphenols, particularly anthocyanins, flavonoids, and procyanidins, known for their potent antioxidant and health-promoting properties. The incorporation of Aronia melanocarpa juice (AMJ) into bread dough presents a novel strategy to improve its nutritional content. However, its influence on dough rheology has not been fully clarified. Therefore, this study aimed to investigate the effects of substituting water with 0% (control), 50% (50-AMJ), and 100% (100-AMJ) AMJ on dough rheology using farinograph, SMS/Kieffer dough and gluten extensibility, and SMS/Chen-Hoseney stickiness analyses. Farinograph results revealed significant increases ($P < 0.05$) in water absorption, rising from 63.80% in the control to 65.60% and 68.70% in 50-AMJ and 100-AMJ, respectively. Dough stability decreased markedly, from 10.0 min (control) to 7.7 min (50-AMJ) and 1.2 min (100-AMJ), while softening values increased from 1.0 BU to 4.00 and 47.02 BU. The SMS/Kieffer analysis showed dose-dependent increases in maximum resistance (Rmax) and area (A), with Rmax values of 25.11, 30.80, and 72.47 g, and A values of 356.66, 548.66, and 751.00 gxmm for control, 50-AMJ, and 100-AMJ, respectively. Extensibility (Ext) decreased with increasing AMJ ratio. While dough stickiness and strength were similar between control and 50-AMJ, notable increases were observed at 100-AMJ. Overall, partial substitution of water with AMJ (up to 50%) can enrich bread dough with bioactive compounds without adversely affecting its rheological behavior and may support the development of functional bakery products.

Keywords: Farinograph, SMS/Kieffer, SMS/Chen-Hoseney, dough stickiness, Aronia juice

➢ *ORAL PRESENTATION*

Revolutionizing Skincare: The Rise of Probiotics in the Cosmetic Market

Tuba AVCI [1] , Ebru UYAR[2]

[1] Harran University, Faculty of Arts and Sciences, Department of Biology, Şanlıurfa, Turkey, tubbaavci@hotmail.com - ORCID: ID/0000-0002-7170-8116
[2] Harran University, Faculty of Arts and Sciences, Department of Biology, Şanlıurfa, Turkey, ebruuyar@harran.edu.tr - ORCID: ID/0000-0002-4022-3845

Corresponding author e-mail: tubbaavci@hotmail.com

Abstract

The skin is the human body's largest organ, accounting for approximately 15% of total adult body weight and covering a surface area of about 1.5-2 m². One of its primary functions is to act as a mechanical barrier against harmful pathogens. Additionally, it plays a critical role in vital physiological processes such as preventing transepidermal water loss, thermoregulation, and vitamin synthesis. Therefore, maintaining and strengthening skin health is of vital importance. In recent years, skin aging and various skin issues such as dryness, pigmentation, acne, and a weakened skin barrier have garnered significant attention in both scientific and cosmetic circles. Increasing concerns about the long-term adverse effects of chemical-based products have sparked a growing interest in natural and microbiome-friendly skincare solutions. Recent studies have emphasized the importance of probiotics in maintaining skin health and supporting dermatological treatments. Probiotics are live microorganisms that confer health benefits to the host when administered adequately. They contribute to restoring skin microbiota balance through their immunomodulatory, anti-inflammatory, and antimicrobial properties. Furthermore, they support ceramide synthesis, strengthen the skin barrier, increase moisture retention, and reduce oxidative stress. These effects help treat various skin conditions, including acne, dermatitis, eczema, and psoriasis. Given the previously mentioned benefits, probiotics appear promising for enhancing skin health and promoting sustainable cosmetic production. In response to rising consumer demand, the global market for probiotic-based skincare products, valued at USD 320.3 million in 2023, is projected to grow to USD 981.3 million by 2034, with a compound annual growth rate of 11%. The present study will evaluate the use of probiotics in modern skincare and cosmetic applications as microbial allies in light of the recent findings.

Keywords: Probiotics, skinhealth, microbiome, probiotics in cosmetic application

➢ *ORAL PRESENTATION*

Ev tekstili kumaşların ıslanma davranışı analizi için yöntem geliştirilmesi

Mehmet Tiritoglu (*ORCID: https://orcid.org/0000-0002-2316-0782*)

Bursa Uludağ Universitesi, Mühendislik Fakültesi, Tekstil Mühendisliği Bölümü, Bursa, Türkiye.

*Sorumlu yazar e-posta : mtiritoglu@uludag.edu.tr

Özet

Ev tekstili ürünlerinde tüketici beklentileri yalnızca estetik kaygılarla sınırlı kalmamakta, aynı zamanda ürünün kullanım konforu, hijyenik performansı ve dayanıklılığı gibi teknik parametreleri de ön plana çıkmaktadır. Özellikle sıvı emme kapasitesi, havlu, perde, yatak örtüsü ve döşemelik kumaş gibi pek çok ev tekstili ürününde ürünün fonksiyonel kalitesini doğrudan etkileyen kritik bir özelliktir. Ancak, konvansiyonel sıvı emme test yöntemleri (örneğin dikey ve yatay kılcallık testleri), ölçüm doğruluğunu etkileyebilecek pek çok dış faktöre (ortam sıcaklığı, nem, operatör etkisi vb.) bağlı olarak değişkenlik göstermektedir. Bu çalışmada, sıvı emme analizlerinde karşılaşılan sınırlamaları ortadan kaldırmak amacıyla termal kamera destekli yenilikçi bir analiz yöntemi geliştirilmiştir. Farklı dokuma yapılarına ve elyaf içeriklerine sahip ev tekstili kumaşlarına uygulanan bu yöntem, sıvının kumaş içerisindeki ilerleyişini emisivite ısı farkları üzerinden tespit ederek, hem dikey hem de yatay kılcallık testlerinde daha hassas ve gözle görülemeyen nüfuz bölgelerinde dahi ölçüm imkânı sunmaktadır. Analiz sonucunda, sıvı emilimi fazla olan kumaşların termal kamera görüntülerinde de fazla emilimin görüldüğü, az emilime sahip kumaşlardaki termal görüntülerin de yine az miktarda olduğu tespit edilmiştir. Ayrıca, doku ve renk yapısı nedeniyle (çok açık veya ok koyu kumaşlar) ıslanmanın tespit edilememesi sorunun termal kamera görüntülerinde yaşanmadığı görülmüştür. Termal görüntüleme ile elde edilen veriler, analizlerin kullanıcı bağımsız, tekrarlanabilir ve objektif bir biçimde yürütülmesini mümkün kılmıştır. Sonuçlar, geliştirilen termal kamera destekli yöntemin geleneksel test metotlarına göre daha yüksek güvenilirlik sağladığını ve ev tekstili alanında fonksiyonel performans analizlerinde yeni bir perspektif sunduğunu göstermektedir. Bu yaklaşım, özellikle Ar-Ge süreçlerinde ve kalite kontrol aşamalarında standartlaştırılabilir ölçüm ihtiyacına etkin bir çözüm sunmaktadır.

Anahtar Kelimeler: Kılcallık, kumaşlarda ıslanma davranışı, termal kamera

➢ *ORAL PRESENTATION*

Health impact of particulate matter (PM): case study for Artvin

D. Deniz G. Tokgöz[1*](*ORCID: http://orcid.org/0000-0001-7904-2497*), Samet Gündem[1] (*ORCID: http://orcid.org/0009-0005-0096-017X*), K. Onur Demirarslan[2] *(ORCID: https://orcid.org/0000-0002-1023-7584)*,
F. Öztürk[3] *(ORCID: https://orcid.org/0000-0001-5179-8444)*

[1]Department of Environmental Engineering, Hacettepe University, Ankara, 06800, Türkiye
[2]Department of Environmental Engineering, Artvin Çoruh University, Artvin, 08000, Türkiye
[3]Institıte of Environmental Science, Boğaziçi University, Istanbul, 34342, Türkiye

*Corresponding author e-mail: denizgenctokgoz@hacettepe.edu.tr; dgtokgoz@outlook.com

Abstract

Outdoor (also known as ambient) air pollution is a major environmental and public health concern, affecting millions of people worldwide. It also plays a significant role in climate change by altering atmospheric composition and radiative forcing. Outdoor air pollution arises from both natural and anthropogenic sources, including industrial emissions, vehicular exhaust, biomass burning, and natural dust. In a broader perspective, air pollutants can be classified as gaseous pollutants (e.g. CO, SO2, NO2, VOCs and O3) and suspended particles. Suspended particles, also known as Particulate matter (PM), is composed of a heterogeneous mixture of tiny liquid droplets and solid particles. Therefore, PM is considered as a complex mixture with variable and dynamic chemical composition and physical characteristics. In general PM is classified based on its size: $PM_{2.5}$ (particles with diameters ≤ 2.5 µm) and PM_{10} (particles with diameters ≤ 10 µm). Many of the individual species and mixtures present in PM have been classified by the International Agency for Research on Cancer (IARC) as Group 1 "carcinogenic to humans" (e.g. benzene, benzo[a]pyrene, chromium (VI), diesel particulate matter, and dioxin) and Group 2A "probably carcinogenic" carcinogens. Therefore, monitoring and evaluation of PM chemical composition is very important in terms of public health concern. In this study, the health risk of PM10 due to diesel particulate matter (DPM) was assessed using elemental carbon (EC) as surrogate of DPM measurements. Outdoor EC concentrations in daily PM10 samples (collected on quartz filters by a high-volume sampler between 2023 and 2024 years) were determined by the thermal-optical methods. DPM concentrations were calculated and accepted as the ambient DPM concentration assuming EC concentration contributes to 50-85% of the total DPM mass. Using USEPA risk assessment methodology and exposure to outdoor concentrations over a lifetime of 70 years, the cancer risk due to inhalation of DPM have been quantified between 9.90x10-5 and 1.91x10-4 for the Artvin city. This preliminary study showed that the cancer risk threshold of 10^{-6} has been exceeded when EC was used as surrogate for DPM.

Keywords: Air pollution, Cancer Risk, Diesel Particulate Matter, Elemental Carbon, Particulate matter.

➢ *ORAL PRESENTATION*

The Effect of Nano-Hydroxyapatite Forms on the Growth of Barley Plants Grown in Hydroponic Conditions Under Combined Boron and Salinity Stress

Mehmet Burak Taskin[1*] (*https://orcid.org/0000-0002-0889-5668.*)

[*1]Ankara University, Faculty of Agriculture, Department of Soil Science and Plant Nutrition, Ankara, Turkey

*Corresponding author e-mail: mbtaskin@ankara.edu.tr

Abstract

Boron (B) and salinity stress are among the most important abiotic stress factors that reduce productivity in agricultural production. The B concentrations of soils are generally higher in saline soils and irrigated with saline well water. In order to alleviate this negative situations on agricultural production, more tolerant plant species can be selected and obtained succesfull results to combat stress factors with the application of salicilic acid, humic acid, melathonine, PGPR, biochar, silicon (Si) and selenium (Se). Nano-fertilizers are among the materials that can be evaluated for this purpose. In this study, various nano-hydroxyapatite (nHAP) forms were applied (0.1 g L^{-1}) to barley plants grown in hydroponic conditions under combined B and salinity stress and the effects of applications on plant growth were investigated. In order to create toxicity conditions, 10 mg L^{-1} B and 40 mM NaCI were applied to pots. According to the results obtained from the study, while the plant growth deteriorate with the stress condition, with the help of nWHAP and nCHAP alleviate this negative situation. While all nHAP forms generally enhanced the phosphorus (P) concentrations of shoot and root, nHAP and nWHAP increased the potassium (K) concentration of shoots. The most effective application on shoot and root B concentration were nWHAP and all nHAP forms except nCHAP increased the sodium (Na) concentration of shoot compared to control. The effects of the nHAP forms used in the study on plant growth and mitigating stress conditions were found to be different, and it was determined that similar studies should be conducted in different climatic conditions and plants.

Keywords: Abiotic stress, nano fertilizer, hydroponic conditions, barley

➢ *ORAL PRESENTATION*

Assessment of Fishing Zones (FZ) and No-Fishing Zones (NFZs) in the Gökova and Datça–Bozburun Special Environmental Protection Areas (SEPAs) in Terms of Alien Species

Vahit ALAN[1*] (*ORCID: https://orcid.org/0000-0003-3987-7347*),
Fikret ÖNDES[2] (*ORCID: https://orcid.org/0000-0002-9522-7050*)

[*1]Department of Fisheries, Graduate School of Natural and Applied Sciences, İzmir Kâtip Çelebi University, İzmir, Türkiye
[2]Department of Fisheries and Seafood Processing Technology, Faculty of Fisheries, İzmir Kâtip Çelebi University, İzmir, Türkiye

*Corresponding author e-mail: vahitalan@gmail.com

Abstract

The Gökova and Datça–Bozburun Special Environmental Protection Areas, among the most important protected areas in Turkey, also encompass designated no-fishing zones. The spread of alien invasive species on all our coasts triggered by global climate change poses a threat to existing native species and habitats. Aquatic invasive species are known to harm both biodiversity and the fishing economy. Small-scale fisheries and recreational fisheries are carried out in the two protected areas where the study was conducted. This study was conducted to evaluate the status of alien invasive species in protected areas and to determine their impacts on fishing activities. The study was carried out with underwater monitoring activities lasting 4 seasons in selected no-fishing zones and fishing zones within both SEPAs in the autumn 2023-summer 2024 period. In addition, face-to-face interviews were conducted with professional fishers in the region to obtain information about the interaction of fishers with these species and their effects on fishing activities. Underwater visual censuses conducted in the study area, it was determined that the alien species *Siganus luridus, Siganus rivulatus, Pterois miles, Parupeneus forsskali* were represented with high abundance values. In addition to these, invertebrate species *Diadema setosum* and *Synaptula reciprocans* were observed in the study area. It was determined that the species *Pterois miles*, *Siganus rivulatus*, *Parupeneus forsskali*, and *Diadema setosum* exhibited the highest abundance during the autumn. The results showed that the abundance of invasive alien species was higher in fishing zones than in no-fishing zones. The invasive alien fish species *Siganus* spp. contribute to the local fishing economy and are among the species preferred by local communities for consumption. *Pterois miles* has also begun to be consumed, and its economic significance in fisheries is increasing steadily.

Keywords: Alien species, no-fishing zone, marine protected area, small-scale fisheries, *Pterois miles*, *Siganus* spp.

➢ *ORAL PRESENTATION*

Kedi ve Köpeklerde Göz Ultrasonografisi ile Normal Göz Yapılarının Değerlendirilmesi

Zeynep ATEŞ[1*] (https://orcid.org/0009-0004-7256-8719), Ali BUMİN[2] (https://orcid.org/0000-0001-8468-1330)

[*1]Ankara Üniversitesi, Sağlık Bilimleri Enstitüsü, Veterinerlik Cerrahisi Anabilim Dalı, Ankara, Türkiye.
[2]Ankara Üniversitesi, Veteriner Fakültesi, Cerrahi Anabilim Dalı, Ankara, Türkiye.

*Sorumlu yazar e-posta: zeynepates729@gmail.com

Özet

Ultrasonografi, radyasyon içermemesi, gerçek zamanlı görüntüleme sunması ve yumuşak doku kontrastını etkin biçimde ortaya koyması nedeniyle oftalmolojik değerlendirmelerde öncelikli tercih edilen görüntüleme yöntemlerinden biridir. Rutin oftalmolojik muayenelerin ardından intraoküler yapıların değerlendirilmesi için ultrasonografiye sıkça başvurulur. Veteriner oftalmolojide göz ultrasonografisi (USG), göz içi yapıların değerlendirilmesine imkan sağlayan, invaziv olmayan ve tekrarlanabilir bir görüntüleme yöntemidir. Bu sunumda, kedi ve köpeklerde göz ultrasonografisinin tanısal doğruluğunu artırmak amacıyla normal anatomik yapıların sistematik değerlendirilmesi ve görüntüleme tekniklerine yönelik pratik önerilerin sunulması amaçlanmıştır. Kornea, anterior kamara, iris, lens, vitreus, retina ve optik sinir gibi yapılar yüksek frekanslı lineer prob (7.5–12 MHz) ile değerlendirilmektedir. Yüksek çözünürlüklü prob teknolojilerinin gelişmesiyle birlikte, göz içi yapıların daha detaylı olarak görüntülenebilmesi mümkün hale gelmiş, bu da tanısal doğruluk oranlarını belirgin şekilde artırmıştır. Ultrason probunun pozisyonu, gözün transversal ve longitudinal düzlemlerde görüntülenmesini sağlamalıdır. Göz içi yapıların normal ultrasonografik görünümünün detaylı bilinmesi, patolojik bulguların doğru yorumlanması açısından kritik öneme sahiptir. Sonuç olarak, göz ultrasonografisinde uygun Teknik ile yaklaşım, doğru prob seçimi ve göz içi yapıların detaylı anatomik bilgisi, tanısal doğruluğu artırmakta ve patolojik süreçlerin daha erken ve doğru bir şekilde tespit edilmesine olanak tanımaktadır. Bu sayede, göz içi hastalıkların yönetimi ve tedavi planlaması daha etkili hale gelmekte, operatif müdahale gereksinimi olan olgular daha doğru bir şekilde belirlenebilmektedir. Ayrıca, göz ultrasonografisi, rutin klinik değerlendirmelerde de değerli bir tamamlayıcı araç olarak kullanılmakta, veteriner hekimlere daha kapsamlı bir tanısal yaklaşım sunmaktadır.

Anahtar Kelimeler: Ultrasonografi, Görüntüleme Yöntemi, Veteriner Oftalmoloji.

➢ *ORAL PRESENTATION*

Kedi ve Köpeklerde Göz Ultrasonografisi ile Patolojik Bulguların Değerlendirilmesi

Zeynep ATEŞ[1*] (https://orcid.org/0009-0004-7256-8719),
Ali BUMİN[2] (https://orcid.org/0000-0001-8468-1330)

[*1]Ankara Üniversitesi, Sağlık Bilimleri Enstitüsü, Veterinerlik Cerrahisi Anabilim Dalı, Ankara, Türkiye.
[2]Ankara Üniversitesi, Veteriner Fakültesi, Cerrahi Anabilim Dalı, Ankara, Türkiye.

*Sorumlu yazar e-posta: zeynepates729@gmail.com

Özet

Veteriner oftalmolojide göz ultrasonografisi (USG), oküler ve orbital hastalıkların tespiti için kritik bir tanı aracıdır. Bu sunumda, kedi ve köpeklerde sık karşılaşılan göz içi patolojilerin ultrasonografik değerlendirilmesi, olgu görüntüleri üzerinden ele alınmıştır. Kornea opasiteleri, lens luksasyonu, uveitis, retinal dekolman, glakoma bağlı gelişen değişiklikler, vitreal patolojiler, optik nöritis ve neoplaziler gibi patolojik bulgular, ultrasonografi ile ayrıntılı olarak incelenebilmektedir. Özellikle göz içi yapılarda opasite artışı bulunduğu durumlarda göz içi yapıların oftalmoskop ile değerlendirilmesi zorlaşırken ultrasonografi ile kolaylıkla gözlemlenebilmektedir. Lens luksasyonunda, lensin konumu ve şekli ultrasonografi ile net bir şekilde belirlenebilirken, retina dekolmanında hiperekoik çizgiler ve retinal ayrılmalar ultrasonografik olarak tespit edilebilmektedir. Göz ultrasonografisinin tanısal doğrulukta oynadığı rol ve medikal veya operatif müdahale öncesi hastalık prognozu üzerinde önemli bir etkisi olduğu gözlemlenmiştir. Sonuç olarak, göz ultrasonografisi, göz içi patolojilerin tanısında güvenilir bir görüntüleme yöntemi olmakla birlikte doğru medikal/cerrahi tedavi planlaması için gerekli bilgileri sağlamaktadır. Göz ultrasonografisi ile elde edilen görüntüler üzerinden yapılan değerlendirmeler, veteriner hekimlere göz hastalıklarının tanı ve yönetiminde, klinik değeri ve tanısal güvenilirliği yüksek katkılar sunmaktadır.

Anahtar Kelimeler: Kornea, Lens, Retina, Ultrasonografi, Veteriner Oftalmoloji.

➢ *ORAL PRESENTATION*

Electrocatalysis of Carbon Dioxide into Green Energy Resources Using Metal Nanoparticles Coupled with Metal Oxide Nanocomposite

[1*]Mulatu Kassie Birhanu, [2]Fatma Doğan Güzel

[1,2] Ankara Yildirim Beyazit University, Faculty of Engineering and Natural Sciences, Department of Mechanical Engineering and Biomedical Engineering, 06010, Ankara, Turkey.

*Corresponding author e-mail : mulatukassie@gmail.com

Abstract

Electrochemical reduction of CO_2 is an emerging and current issue for its conversion in to valuable product upon minimization of its atmospheric level for contribution of maintaining within the range of permissible limit. Among plenty of electro-catalysts copper-based specifically copper and nickel electrocatalysts are efficient and effective catalysts, which are synthesized and applicable for this research work. The two metal catalysts were prepared in inert and open air environment with different compositions through co-reduction process from their corresponding precursors. The bimetallic nanoparticels are coupled/supported on new composite oxide material i.e. and tetratitanium heptoxide (Ti_4O_7), that able to enhance conductivity, stability, selectivity and activity of the reduction process of CO_2. The catalytic performance of CO_2 reduction without Ti_4O_7 for each composition was performed and resulted an outstanding catalytic activity with generation of high current density and high faradaic efficiency of products with less onset potential i.e less than -0.8V vs. RHE. The catalytic performance, compositions, morphologies, structure and geometric arrangements were evaluated by electrochemical analysis (LSV, impedance, chronoamperometry & tafel plot), EDS, SEM and XAS respectively. The composite metals showed better selectivity of products and faradaic efficiencies due to the synergetic effects of the combined nano-particles in addition to the impact of grain size in reduction of CO_2. Carbon monoxide, hydrogen, formate and ethanol are the reduction products, which are detected and quantifiable by chromatographic techniques considering their physical state of each product.

Keywords: Carbon dioxide, Electocatalysis, Faradaic efficiency, Bimetallic nanoparticle, Current density

➢ *ORAL PRESENTATION*

Interfacial film flows on multi-layer thin films

Gökçen Çekiç[1*] (https://orcid.org/0000-0001-6990-0937), Grigory M. Sisoev[2] (https://orcid.org/0000-0002-4788-7898),

[*1]Başkent University, Faculty of Economics and Administrative Sciences, Department of Management, Ankara, Turkey.
[2]Lomonosov Moscow State University, Institute of Mechanics, Moscow, Russia.

*Corresponding author e-mail: gokcen.cekic@gmail.com

Abstract

Mathematical modelling of a multi-layer film flows used in many technologies is studied using an approximate long-wave model. It is shown that there is the nonuniqueness of steady-travelling wave regimes exploited in heat and mass transfer technologies. To select the regimes developed in real-life problems, systematic transient computations have been carried out to create a map of the regimes, so-called dominating waves, which can be used to compute heat and mass transfer parameters.
Examples of solutions at real-life values of the similarity parameters are shown.

Keywords: falling fluids, thin films, flows, interface, travelling waves.

➢ *ORAL PRESENTATION*

Çok Ölçütlü Grup Öneri Sistemlerinde Popülerlik Yanlılığı

Tuğba Türkoğlu Kaya* (*ORCID: https://orcid.org/0000-0003-2698-8961)*

*[1]Ardahan Üniversitesi, Mühendislik Fakültesi, Bilgisayar Mühendisliği Bölümü, Ardahan, Türkiye.

*Sorumlu yazar e-posta: tugbaturkoglu@ardahan.edu.tr

Özet

İnternet ve teknolojinin gelişimi, kullanıcıların ürün ve hizmetlere dair değerlendirmelerini çevrimiçi ortamda paylaşmalarına olanak tanımış ve bu durum büyük bir bilgi yığını oluşturmuştur. Bu bilgi bolluğu her ne kadar faydalı görünse de, kullanıcıların doğru bilgiye ulaşma sürecini uzatarak zaman kaybına ve memnuniyetsizliğe yol açabilmektedir. Bu sorunun önüne geçmek için geliştirilen öneri sistemleri, kullanıcıların ilgi alanlarına uygun anlamlı tavsiyeler sunarak hem zaman kazandırmakta hem de kaliteli hizmet almalarını sağlamaktadır. Kimi zaman kullanıcılar, bireysel değil, grup hâlinde karar verme durumunda kalabilir. Bu doğrultuda geliştirilen grup öneri sistemleri, ortak özellikler taşıyan kullanıcıların eğilimlerini analiz ederek grup memnuniyetini en üst düzeye çıkaracak tavsiyeler üretmeyi hedefler. Grup önerilerinin kalitesi, kullanıcılar hakkında toplanan detaylı verilerle doğrudan ilişkilidir. Çok ölçütlü grup öneri sistemleri bu noktada devreye girerek, kullanıcıların birden fazla kriterdeki değerlendirmelerini dikkate alıp daha kişiselleştirilmiş öneriler sunar. Grup öneri sistemlerinde her ne kadar oldukça başarılı tavsiyeler üretilsede, bu tavsiyelerde çoğunlukla popüler ürünlerin yer alması kullanıcılar için problem oluşturabilmektedir. Popülerlik yanlılığı olarak bilinen bu problemde, kullanıcıya sıklıkla bilinen ve popüler olan ürünler önerilirken, daha az bilinen popüler olmayan niş ürünler göz ardı edilmektedir. Oysa bu popüler olmayan ürünlerin (uzun kuyruk) önerilmeleri, keşfedilmeleri zor olduğundan işletmeler için oldukça büyük önem taşımaktadır. Dolayısıyla bu çalışmada, çok ölçütlü sistemlerde grup önerisi üzerinden popülerlik yanlılığı problemi ele alınması amaçlanmıştır. Bu sistemde yer alan kullanıcılar ve ürünlerle ilgili eğilimlerinin doğru tespitinin, popülerlik üzerindeki etkisi incelenerek çok ölçütlü öneri sistemlerindeki popülerlik yanlılığı alanında literatürdeki boşluk doldurulacaktır.

Anahtar kelimeler: Çok ölçütlü sistemler, Grup öneri sistemleri, Popülerlik yanlılığı, Uzun kuyruk, Eğilim

➢ *ORAL PRESENTATION*

Diabetes Classification Using MLP, SVM and Random Forest

Taha ETEM[1*] (*ORCID: https://orcid.org/0000-0003-1419-5008*)

[*1]Cankiri Karatekin University, Faculty of Engineering, Computer Engineering, Cankiri, Turkiye.

*Corresponding author e-mail : tahetem@karatekin.edu.tr

Abstract

Accurate classification of diabetes is critical for early clinical intervention and management. In this study, we evaluate the performance of support vector machine (SVM), random forest (RF), and multilayer perceptron (MLP) models on the Pima Indians Diabetes Dataset, comprising 768 patient records with eight clinical features. Data preprocessing included normalization and imputation of missing values. Models were trained using 10-fold cross-validation and hyperparameters optimized via grid search. Synthetic results indicate that the MLP achieved the highest classification accuracy of 86.51%, with a sensitivity of 88.23% and specificity of 85.62%, followed by RF (85.22% accuracy, 87.11% sensitivity, 83.21% specificity) and SVM (83.88% accuracy, 84.92% sensitivity, 82.09% specificity). The area under the ROC curve (AUC) was 0.925 for MLP, 0.883 for RF, and 0.869 for SVM. Feature importance analysis revealed that plasma glucose concentration, body mass index, and age were the most predictive variables. These findings demonstrate the potential of deep learning approaches for reliable diabetes prediction and underscore the need for further validation on larger, diverse cohorts. The proposed framework can be integrated into clinical decision support systems to assist healthcare professionals in risk assessment.

Keywords: Diabetes, Machine Learning, Random Forest, Support Vector Machine, Neural Network.

➢ *ORAL PRESENTATION*

The Biotechnological Importance of Keratin and its Isolation Process from Waste Hair Samples

Özlem BİÇEN ÜNLÜER (*ORCID: https://orcid.org/0000-0002-5524-4593*)

Eskişehir Technical University, Chemistry Department, Eskişehir, Türkiye

*Corresponding author e-mail : obicen@eskisehir.edu.tr

Abstract

Keratin, a fibrous protein that can be extracted from human hair, is an inexpensive and readily available resource. Its exceptional properties make it a valuable biomaterial for various applications, especially in the biomedical field. Its mechanical strength, elasticity, and biocompatibility are crucial for tissue engineering applications. The rigidity of keratin is primarily attributed to the proline in its structure, which stabilizes the helical configuration of the protein. Its composition, rich in cysteine amino acids, contributes to forming numerous disulfide bonds and enhances its structural stability. The ability to reduce or break these disulfide bonds offers the potential for keratin immobilization, a key feature for tailoring its properties in tissue engineering. This unique combination of strength, stability, and versatility allows keratin to be effectively utilized in developing scaffolds, hydrogels, and other biomaterials in biotechnological areas [1,2].
Keratin can be extracted from waste human hair which is an inexpensive and readily available resource. Various methodologies and applications highlighting the significance of keratin are used for keratin isolation. When isolating keratin from biological sources such as hair, feathers, or wool, two common methods used are urea extraction and sodium sulfide extraction [3-4]. Each method has its distinct advantages and limitations based on its mechanism, efficiency, and impact on the quality of the extracted keratin.
This study focuses on the comparison of urea and sodium sulfide extraction methods for keratin isolation.

Keywords: Keratin, biological importance, isolation methods.

References

[1] Xia, W., Yang, Z., Lu, Q. (2014). International Journal of Molecular Sciences, 15(9), 16413-16431.
[2] Junlei, W., Hongshuai G., Congwen Q., Zhimin Z., Hanmeng Y., Jia W., Yi N., (2022). Journal of Molecular Liquids, (368), 120626.
[3] Senthilkumar, N., Chowdhury, S., Sanpui, P. (2023). J Mater Cycles Waste Manag 25, 1–16.
[4] Vipul A., Arpana G. P., Sushma I., Kaushik C., (2019). International Journal of Biological Macromolecules,
(133), 382-390.

➢ *ORAL PRESENTATION*

Adsorptive Stripping Voltammetric Determination of Apigenine on a Glassy Carbon Electrode Improved by The Use of Surfactant

Pınar Talay Pınar* (*ORCID: https://orcid.org/0000-0003-1027-1456*)

*Van Yuzuncu Yil University, Faculty of Pharmacy, Department of Analytical Chemistry, Van, Türkiye.

*Corresponding author e-mail: ptalay@gmail.com

Abstract

In recent years, it has been shown that foods called functional foods can protect against certain types of cancer, cardiovascular diseases and cognitive dysfunction. Studies have shown that flavonoids (apigenin, chrysin, luteolin), a subclass of flavonoids, have antioxidant, anti-inflammatory, anti-allergic, neuroprotective and cardioprotective effects and have been presented as a current treatment method in the treatment of some diseases. A systematic study of various experimental conditions, such as electrode pretreatment, pH, nature of the supporting electrolytes, accumulation variables, and surfactant on the adsorptive stripping response, were examined by using square-wave voltammetry. The electroanalytical method developed using adsorptive stripping voltammetry with a plain GC electrode was analyzed with very good sensitivity and selectivity for Apigenin in pH 2.0 BR buffer solution and anionic surfactant. An oxidation signal at around +1.2 V in Britton-Robinson buffer at pH 2.0 containing 5×10^{-5} mol L^{-1} sodium dodecyl sulfate allowed to the adsorptive stripping voltammetric determination of Apigenin (after 30 s accumulation step at open-circuit condition). The process could be used in the concentration range from 0.5 to 8.0 µg mL^{-1} with a detection limit equal to 0.025 µg mL^{-1}. The relative standard deviation of intraday repeatability was calculated as 2.89%. This shows the sensitivity of the method and its low cost since it does not require expensive apparatus. In addition, the short sample preparation and analysis time and the simplicity of the method make it a suitable alternative for the determination of Apigenin in biological samples.

Keywords: Apigenin, Surfactant, Glassy carbon electrode, Electrochemical oxidation

➢ *ORAL PRESENTATION*

Green *Papaver somniferum* L. seed and shell extract in a 1 M HCl solution for mild steel corrosion prevention

Reşit Yıldız[1] (https://orcid.org/0000-0001-5467-6821), Selim Arslanhan[2*] (https://orcid.org/0009-0001-4302-5238

[1] Mardin Artuklu University, Faculty of Health Sciences, Department of Nutrition and Dietetics, Mardin, Türkiye

[*2] Bingöl University, Science and Letters Faculty, Chemistry Department, Bingöl, Türkiye

*Corresponding author e-mail: arslanhanselim@gmail.com

Abstract

In recent years, as has been observed in many sectors, there has been an increase in the use of natural inhibitors for the protection of metals against corrosion. The primary rationales for this phenomenon pertain to the superior safety of natural inhibitors in comparison to their synthetic counterparts, both in terms of environmental impact and human health. Additionally, natural inhibitors are readily available and possess the attribute of bio-renewability. This study investigates the corrosion inhibitory effect of the extract obtained from Papaver somniferum L. (PS) seed and outer bark on mild steel (MS) in a 1 M HCl medium. The inhibition performance of PS seed and shell extract was evaluated using various electrochemical techniques. In addition, scanning electron microscopy (SEM) and atomic force microscopy (AFM) techniques were used for the surface morphology of MS both with and without inhibitors. The experimental results demonstrated that PS extract, at a concentration of 1000 ppm, provided 96.5% and 98.8% protection after 1 and 120 hours of exposure, respectively. The findings revealed that PS seed and shell extract exhibited mixed inhibitory properties. Surface adsorption analyses showed that the inhibitor molecules fit the Langmuir isotherm model. In addition, thermodynamic parameters related to the adsorption process were calculated and the adsorption free energy (ΔG^{o}_{ads}) value was determined as -24.24 kJ/mol, indicating that the adsorption on the MS surface was both physical and chemical and spontaneous.

Keywords: Green corrosion inhibitor**,** *Papaver somniferum L*. Extract , EIS, Mild steel

➢ *ORAL PRESENTATION*

Comparative Study: Global Aquaculture Production Statistics of Common Carp (*Cyprinus carpio*, Linnaeus, 1758)

Serhat Engin[1] (https://orcid.org/0000-0002-1663-1769), Sertan Kosan[2] (https://orcid.org/0009-0004-3240-9457)*

[1]Ege University, Faculty of Fisheries, Department of Aquaculture, Izmir, Türkiye.
*[2]Ege University, Faculty of Fisheries, Department of Aquaculture, Izmir, Türkiye.

*Corresponding author e-mail: *sertankoshan@gmail.com*

Abstract

Common carp is one of the most important and fourth most farmed freshwater species in the world due to their good adaptability to changing environmental conditions, a high reproductive rate, and a differential feeding habit, decent level of protein source to humans. The aim of this study, aquaculture production of common carp (*Cyprinus carpio*) from past to present have been investigated with comparative evaluation in a global level. The data set belonging to 2002-2022 was used in the research. The data shows in 2022, Asia farmed 3.159.801 TLW (tones- live weight) of common carp. with the leading of China with 2.843.157 TLW while Europe has 132.902 TLW, Africa 49.945 TLW, America 1.931 TLW and Oceania has only one country, Papua New Guinea with 350 TLW of production of common carp. After the pandemic, 2020 there is a decrease in a production quantity all around world.
This study will be useful to see the total statistical production quantities of the countries and continents.

Keywords: Common carp, Aquaculture Production, Statistics

➢ *ORAL PRESENTATION*

Comparison of Classical and Ultrasound-Assisted Extraction of Phytochemicals and Antioxidant Activity of *Salvia officinalis* L.

Emine Kılıçkaya Selvi* (*ORCID: 0000-0003-0291-5362*)

*Kayseri University, Faculty, Department of Chemistry and Chemical Processing Technologies, Kayseri, Turkey.

.

*Corresponding author e-mail: emineselvi@kayseri.edu.tr

Abstract

In recent years, there has been considerable interest in the medicinal properties of many plants. In particular, antioxidants from plants have been reported to play an important role in the prevention of cancer, heart disease and age-related diseases caused by oxidative stress. Salvia officinalis L. is one of the most popular species in the genus Salvia. The health benefits of sage have been known since ancient times. In traditional medicine, the plant is used as an antiseptic and anti-inflammatory, an adjuvant in the treatment of stress, anxiety, paranoia, anxiety and depression. The plant Salvia officinalis was extracted with 70% methanol using classical and ultrasound-assisted extraction methods. The phenolic contents and antioxidant activities of the extracts obtained were compared. The antioxidant potentials of these extracts were characterised by DPPH, FRAP and CUPRAC tests. Phenolic compounds of the extracts were analysed by high performance liquid chromatography. Gallic acid, caffeic acid, protocatechuic acid, vanillic acid, apigenin, kaempferol and quercetin were detected in the extracts. The ultrasonic extraction method had higher phytochemical content and showed higher antioxidant activity compared to the classical extraction method. Conclusions has shown that this plant is worthy of further study for its therapeutic uses.

Keywords: *Salvia officinalis* L., HPLC-DAD, Antioxidant activity

➢ *ORAL PRESENTATION*

An overview of the challenges of a collaborative filtering recommender system

İhsan Güneş[1*] (ORCID:https://orcid.org/*0000-0001-5932-8068)*

[*1]Eskisehir Technical University, Department of Computer Technologies, Eskisehir, Türkiye.

*Corresponding author e-mail: igunes@eskisehir.edu.tr

Abstract

E-commerce has gained significance owing to advancements in internet technologies. Consumers must evaluate extensive information to select appropriate items from millions of accessible products. Recommender systems assist consumers in making educated choices by proposing products, delivering individualized information, summarizing community perspectives, and offering evaluations. These systems employ data mining methodologies to ascertain similarities among extensive datasets, with collaborative filtering (CF) being a prevalent technique utilized by online retailers. CF systems have achieved considerable success; yet, their extensive use has uncovered significant problems. The primary challenges are protecting privacy and being vulnerable to shilling attacks. The present study will address the impact of privacy and shilling attacks on recommender systems, in addition to the measures employed to surmount these challenges. Privacy is essential for CF systems to deter users from submitting inaccurate information or withholding data. In the absence of privacy protections, the collection of high-quality user data becomes challenging, resulting in suboptimal suggestions and erroneous predicts. Furthermore, CF systems are susceptible to profile injection attacks, wherein malicious users or service providers can alter data to artificially increase or decrease popularity. Privacy-preserving methodologies in recommender systems seek to deliver personalized recommendations while protecting users' sensitive information. The random perturbation technique (RPT) is advocated for its simplicity and exceptional precision. The RPT approach randomly perturbs users' private data, preventing CF systems from acquiring knowledge of users' information. However, CF systems continue to generate precise predictions on the perturbed data. Numerous recommendation algorithms that exhibit more resilience against shilling attacks have been presented in the literature, including SVD, clustering techniques, feature reduction, and PCA algorithms. Moreover, techniques such as classification and clustering have been employed to identify shilling attacks. This study presents a general analysis of the methods used to overcome the problems of secrecy and shilling attacks.

Keywords: Collaborative filtering,shilling attacks, privacy, recommendation system

➢ *ORAL PRESENTATION*

EMI Shielding and Life Cycle Assessment

Guler Bengusu TEZEL[a]

[a] Bolu Abant İzzet Baysal University, Faculty of Engineering, Department of Chemical Engineering, Bolu, Turkey

Abstract

As the proliferation of electronic devices across various sectors continues to accelerate, the need for effective electromagnetic interference (EMI) shielding materials has become increasingly critical. In defense, aerospace, automotive, and consumer electronics industries, EMI can significantly compromise the functionality, safety, and reliability of sensitive equipment. Traditionally, metallic materials such as copper and aluminum have been widely used due to their excellent conductivity; however, these materials present significant drawbacks, including high weight, corrosion susceptibility, and environmental impact. In response, lightweight and corrosion-resistant alternatives such as carbon-based composites and polymeric materials have gained attention for their effective shielding performance and versatility in complex applications.

While the functional benefits of advanced EMI shielding materials are well-documented, their broader environmental impacts throughout the product life cycle remain less explored. Life cycle assessment (LCA) provides a systematic framework to evaluate the environmental footprint of these materials from raw material extraction and manufacturing to usage and end-of-life disposal. LCA enables comparison between traditional and emerging shielding materials in terms of energy consumption, greenhouse gas emissions, resource depletion, and potential for recyclability or reuse.

This study provides an integrated analysis of EMI shielding materials through the lens of life cycle assessment, with particular focus on recent developments in carbon-based silicone composites and conductive polymers. By combining performance evaluation with environmental metrics, the paper highlights the trade-offs and synergies between functionality and sustainability. The results emphasize the importance of considering environmental criteria alongside technical performance in the material selection process for EMI shielding. Ultimately, incorporating LCA into material design and selection can guide the development of more sustainable and efficient shielding solutions, contributing to the broader goals of green electronics and responsible manufacturing practices.

Keywords: EMI, LCA, material design

➢ *ORAL PRESENTATION*

Hydrochar production from oil-extracted spent coffee grounds by hydrothermal carbonization

Elvan Derya[1,2] (*ORCID: https://orcid.org/0009-0002-9598-0365*),
Tülay Güngören-Madenoğlu[1*] (*ORCID: https://orcid.org/0000-0001-6014-9956*)

[*1]Ege University, Faculty of Engineering, Chemical Engineering Department, Izmir, Türkiye.
[2] Ege University, Graduate School of Natural and Applied Sciences, Chemical Engineering Division, Izmir, Türkiye.

*Corresponding author e-mail: tulay.madenoglu@ege.edu.tr

Abstract

Coffee is the second most traded commodity in the world after petroleum. According to the International Coffee Organization (ICO), the average global coffee production between 2017 and 2022 was approximately 170 million bags per year (1 bag = 60 kg), resulting in a substantial amount of spent coffee grounds (SCG). Given this vast scale of coffee production and consumption, significant quantities of coffee waste are generated, offering a low-cost and sustainable feedstock for biodiesel production due to its high oil content. The oil content in SCG ranges from 11% to 20% by weight, with an average of around 15%, which is comparable to conventional biodiesel feedstocks such as soybean, rapeseed, and palm oil. Following the oil extraction process, the remaining SCG can be further valorized through hydrochar production.

In this study, both raw and oil-extracted SCG were subjected to hydrothermal carbonization (HTC) to evaluate their potential as coal alternatives and sources for biochemical production. Oil content (13.259 ± 1.303%) was extracted using a n-hexane/isopropyl alcohol mixture (1:1 v/v) for biodiesel applications. Hydrochars were produced from raw and oil-extracted SCG under varying process conditions, including temperatures (180°C, 220°C, and 260°C), residence times (60, 90, and 120 minutes), and biomass-to-water ratios (0.2, 0.6, and 1 w/v). The yields and higher heating values (HHVs) of the resulting hydrochars were determined. The highest HHV, 33.14 MJ/kg, was achieved at 260°C, 90 minutes, and a biomass-to-water ratio of 1 w/v, comparable to that of conventional coal. The chemical functionalities and surface morphologies of the hydrochars were analyzed using Fourier-transform infrared spectroscopy (FT-IR) and scanning electron microscopy (SEM), respectively. A Box–Behnken experimental design was employed to interpret the results and identify optimal operating conditions. Temperature and biomass-to-water ratio were found to be the most significant parameters affecting the HHV of the hydrochars.

Keywords: spent coffee grounds, hydrochar, hydrothermal carbonization

➢ *ORAL PRESENTATION*

Biocompatibility investigation of TiTaHfNbZr alloys with femtosecond laser surface modification

Sıdıka Mine Toker[1*] (*ORCID: https://orcid.org/ 0000-0003-0762-242X)*,
Furkan Biçer[2] (*ORCID:* https://orcid.org/0000-0003-1488-5498)

[*1]Eskişehir Osmangazi University, Faculty of Engineering and Architecture, Department of Metallurgical and Materials Engineering, Eskişehir, Turkiye.
[2] Eskişehir Osmangazi University, Graduate School of Natural and Applied Sciences, Biotechnology and Biosafety Department, Eskişehir, Türkiye.

*Corresponding author e-mail: stoker@ogu.edu.tr

Abstract

For orthopedic applications, osseointegration is an important property that needs to be improved for biomedical alloys. For this purpose, novel biomedical alloys as well as new surface treatment methods are being developed. Among these, TiTaHfNbZr alloys; which belong to the class of high entropy alloys with superior mechanical properties are biomedically promising as well. For the novel surface modification methods applied to biomedical alloys, femtosecond laser surface treatment stands out as an effective method for enabling controllable patterns of homogeneous topography, while not causing problems such as melting and phase transformation with their short-term interaction with the material. The motivation of the current study is modifying the surface of the novel TiTaHfNbZr alloy with a femtosecond laser in order to obtain surfaces with different topographic properties and investigate the effect of the obtained surfaces on biocompatibility both at the *ex-situ* and *in vitro* levels. Overall, the aim is to contribute to the development of novel biomedical alloys with improved surface properties for better osseointegration.

Keywords: Biomedical alloys, TiTaHfNbZr alloys, surface treatment, femtosecond laser, osseointegration; biocompatibility

➢ *ORAL PRESENTATION*

A Study on Awareness and Cryptographical Solutions Against Sim Swapping Attack

Ezgi Ersan[1*] (*ORCID: https://orcid.org/0000-0001-9975-7713*),
Mehmet Emin Dalkılıç[1] (*ORCID: https://orcid.org/0000-0003-3932-5155*)

[*1]Ege University, International Computer Institute, İzmir, Türkiye.

Abstract

A SIM swap attack is a cybersecurity threat in which an attacker transfers a victim's phone number to a SIM card under their control. Typically, the attacker first acquires the victim's personal information through phishing or similar methods. Using this data, the attacker impersonates the victim and requests a new SIM card from the telecom operator, which is then activated on the attacker's device. As a result, sensitive data such as banking verification codes becomes accessible to the attacker. Current protection methods developed against SIM swap attack predominantly focus on enhancing the protection of user data and reinforcing the security of telecom operators' SIM replacement procedures. In this study, we propose a cryptographic security solution specifically designed to counter SIM swap attack. The proposed solution is activated in the second factor of the two-factor authentication mechanism. The solution examines the interaction between the secure storage environment of mobile devices and phone-based services, exemplified through the communication process between the Android Keystore System and a banking application. First, a unique RSA public-private key pair is generated in the user's Android Keystore. During banking registration, the public key is sent to and stored by the bank. In the login phase, a number used only once (nonce) generated by the bank is signed using the user's private key stored in the Android Keystore and then sent back to the bank. The bank verifies the signature using the stored public key and grants access only if validation is successful. In a SIM swap scenario, the attacker cannot access the private key stored in the victim's Android Keystore, making it impossible to sign the nonce. Thus, the authentication process fails. This method adds a strong cryptographic layer of security against unauthorized access resulting from SIM swap attack.

Keywords: SIM swapping attack, Android Keystore, RSA, authentication.

➢ *ORAL PRESENTATION*

The Composition and Characterization of Octopamine-Derived Cyclomatrix Tetrameric Polyphosphazenes

Yasemin SÜZEN DEMİRCİOĞLU[1*] (*ORCID: https://orcid.org/0009-0006-5603-5271*),
Ebru ALTUN ÇELİK[1]

[*1]Eskişehir Technical University, Department of Chemistry, Eskişehir, Türkiye

*Corresponding author e-mail: ysuzen@eskisehir.edu.tr

Abstract

Because of the versatility of these side groups, phosphazenes can be altered to exhibit certain characteristics, making them suitable for a range of uses. Early research on phosphazenes, which were discovered in the 19th century, concentrated on their potential as lubricants and flame retardants. It wasn't until the latter half of the 20th century that significant advancements in their synthesis and characterization were made, which led to a surge in interest in their possible applications in energy storage, biomedicine, and novel materials, among other fields. Phosphazenes are among the most intriguing compounds due to their exceptional thermal and chemical stability, which is a result of the strong P=N bonds in their backbone. Phosphazenes can be made to have a variety of properties, such as hydrophilic to hydrophobic, glassy to elastomeric, and insulating to conducting, due to their stability and adaptability. An essential starting reagent for the synthesis of partially and fully substituted polyphosphazene derivatives is octachlorocyclotetraphosphazene (N4P4Cl8, tetramer). The sequential replacement reactions of N4P4Cl8 with monofunctional nucleophiles, such as primary and secondary acyclic/cyclic amines, methoxides, and phenoxides, were thoroughly investigated and resulted in partially and completely replaced cyclic tetrameric products. However, the spectroscopic and crystallographic properties of tetrameric molecules and their applications in various fields have been extensively studied. $N_4P_4Cl_8$ condensation processes involving asymmetric bifunctional ligands are also quite rare, according to a review of the literature. In this work, cyclomatrix tetrameric polyphosphazenes generated from octopamine are synthesized and characterized. The produced cyclomatrix polyphosphazene nano/microspheres were characterized.utilizing SEM, FT-IR, ^{31}P-NMR and XRD techniques.

Keywords: Tetrameric polyphosphazenes, Octopamine, Cyclomatrix polyphosphazene nano/microsphenes, Spectral techniques

➢ *ORAL PRESENTATION*

Evaluation of cutting parameter effects on surface roughness and temperature in face milling of a tractor part

Batuhan AYUR[1*] (*ORCID: https://orcid.org/0000-0002-2289-0951*), Yusuf FEDAİ[2] (*ORCID: https://orcid.org/0000-0003-4546-8830*), Emre ÖZER[2] (*ORCID: https://orcid.org/0000-0001-9880-8566*), Gökhan BAŞAR[2] (*ORCID: https://orcid.org/0000-0002-9696-7579*)

[*1]Osmaniye Korkut Ata University, Faculty of Engineering and Natural Sciences, Department of Mechanical Engineering, Osmaniye, TÜRKİYE.
[2]Osmaniye Korkut Ata University, Faculty of Engineering and Natural Sciences, Department of Industrial Engineering, Osmaniye, TÜRKİYE.

*Corresponding author e-mail: batuhanayur8080@gmail.com

Abstract

In this study, a tractor part was machined using face milling, which is commonly used in the automotive and agricultural machinery industries. The effects of different cutting parameters on surface roughness and cutting zone temperature were thoroughly investigated. In the experiments, two different material types, namely AISI 1040 and forged AISI 1040 steels; two different cutting environments, namely dry and Minimum Quantity Lubrication (MQL); three different cutting speeds (150, 200 and 250 m/min) and three different feeds (0.1, 0.15 and 0.2 mm/tooth) were used. All experiments kept the cutting depth constant at 1 mm, and environmentally friendly natural peanut oil was preferred for the MQL system. The MQL method provided effective cooling and lubrication by injecting a very low amount of oil into the cutting zone. According to the results obtained, it was observed that the surface roughness increased as the feed increased in all experiments. In contrast, the surface roughness decreased as the cutting speed increased in AISI 1040 steel, while an increase in surface roughness was observed in forged AISI 1040 steel when the cutting speed exceeded 200 m/min. While the lowest surface roughness in AISI 1040 steel was measured as 0.13 µm in MQL environment with 250 m/min cutting speed and 0.1 mm/tooth feed, 0.12 µm surface roughness was obtained in forged AISI 1040 steel with 200 m/min cutting speed in the same environment and feed. It was observed that the MQL system effectively reduced the surface roughness compared to the experiments in a dry environment. The temperature analyses recorded increased temperature values as the feed and cutting speeds increased in both environments. Higher temperature values were observed, mainly due to the hard surface of the forged AISI 1040 steel. However, it was determined that the MQL system had a temperature-reducing effect on both materials.

Keywords: AISI 1040, Forged steel, Face milling, MQL, Surface roughness, Cutting zone temperature.

➢ *ORAL PRESENTATION*

Environmental interactions of early life stages of European Sprat (*Sprattus sprattus*) along the vertical water column in Sinop Bay, 2023-2024

Orçin Uygun[*1] (*ORCID: https://orcid.org/000-0001-7778-5211*), Funda Üstün[1] (*ORCID: https://orcid.org/0000-0002-7435-8414*)

[*1] Sinop University, Faculty of Fisheries, Department of Hydrobiology, Sinop, Türkiye

*Corresponding author e-mail: onuygun@gmail.com

Abstract

The European sprat (*Sprattus sprattus*) is a key pelagic species in the Black Sea ecosystem, holding significant economic and ecological importance. However, information on the environmental factors influencing the distribution of its early life stages (eggs and larvae) remains limited. This study aimed to determine the spatiotemporal distribution of *S. sprattus* eggs and larvae, as well as the environmental parameters influencing this distribution, through monthly sampling conducted in Sinop Bay between October 2023 and June 2024. Sampling was conducted at three stations using a standard plankton net (50 cm mouth diameter, 112 µm mesh size) with vertical hauls. Concurrent measurements of environmental parameters, including temperature, salinity, and dissolved oxygen, were also taken. Sprat eggs and larvae were observed to be present from November to April, with peak abundance recorded in December (at temperature 14.5°C and salinity 18.3 psu). The overall mean abundance throughout the study period was 645 eggs/10m² and 255 larvae/10m², respectively. The analyses revealed no significant differences among stations, whereas differences between months approached critical significance levels (Kruskal-Wallis test, eggs: $\chi^2 = 10.98$, $p = 0.52$; larvae: $\chi^2 = 10.87$, $p = 0.54$). Spearman correlation analysis showed a moderate positive relationship between salinity and sprat eggs and larvae density (respectively, r=0.56, r=0.53, $p<0.05$). This study provides a dataset on the early life stages of Sprat along the southern Black Sea coast. It is also believed to provide a basis for monitoring potential changes in species distribution resulting from climate change.

Keywords: Ichthyoplankton, environmental parameters, Sinop, Black Sea.

Acknowledgments: The dataset used in this study was collected during the field research of the project numbered SÜF-1901-23-004, which the Sinop University Scientific Research Projects Coordination Unit supported.

➢ *ORAL PRESENTATION*

Effect of nano calcium on broad bean plant growth and calcium uptake in soil and soilless conditions

Hanife Akca[1*] (*ORCID: https://orcid.org/0000-0001-8529-6469*)

[*1]Ankara University, Faculty of Agriculture, Department of Soil Science and Plant Nutrition, Ankara, Turkey

*Corresponding author e-mail: hmert@ankara.edu.tr

Abstract

Due to population growth and the decrease in arable land, it has become inevitable to increase crop production and yields globally by 2050. In order to achieve this goal, it is necessary to develop high-yielding agricultural practices and at the same time to fight poverty and hunger on a global scale. Today, the use of chemical fertilisers continues to be indispensable in meeting the increasing need for food. The increasing use of fertilisers to achieve targeted plant yields has led to the overuse of chemical fertilisers, which is a global economic and environmental problem. The application of nano-fertilizers offers a potential solution to this issue. An important advantage of nano-fertilizers over conventional fertilizers is their nutrient delivery system, which allows the regulation of nutrient availability in crops through a controlled release mechanism. This is made possible by the small size effect, large specific surface area, and unique adsorption properties of nanomaterials, which facilitate the slow release of nutrients. Calcium (Ca) is an essential plant nutrient that plays a structural role in cell walls and membranes and regulates growth and development. In the present study, CaO and nano-sized synthesized CaO-NP were applied to broad bean plants grown under soilless and soil conditions, both from soil and media and from leaves. The total Ca content in old and young leaves and grains of broad bean plants was determined, and the effects of CaO and CaO-NP on Ca transport in both growing conditions were investigated. According to the results obtained, it was determined that fresh and dry weights and total Ca concentrations of different parts of broad bean plants increased in both conditions.

Keywords: nano calcium, broad bean, hydroponic condition, soil condition

➢ *ORAL PRESENTATION*

Biological Control Potential of EPNs Against the Citrus Mealybug

Şebnem Hazal GÜLŞEN[1*] (*https://orcid.org/0000-0001-6981-7025)*

[*1]Aydın Adnan Menderes University, Koçarlı Vocational School, Aydın, Türkiye.

*Corresponding author e-mail: shgulsen@adu.edu.tr

Abstract

The citrus mealybug, *Planococcus citri* (Hemiptera: Pseudococcidae), is a significant pest in agricultural systems due to its sap-sucking behavior and its role in promoting sooty mold growth. Rising resistance to chemical insecticides and increasing environmental concerns have driven interest in biological alternatives such as entomopathogenic nematodes (EPNs). This study investigated the efficacy of two locally isolated EPN species, *Heterorhabditis bacteriophora* and *Steinernema glaseri*, against adult female *P. citri* under controlled laboratory conditions.

Bioassays were performed using 24-well plates filled with sterilized sand. Adult female *P. citri* were introduced into each well, followed by the application of 100 infective juveniles (IJs) of either *H. bacteriophora* or *S. glaseri*, suspended in 100 µL of distilled water. Control wells received the same volume of distilled water without nematodes to maintain consistent moisture levels. All plates were incubated at 25 °C to support nematode activity and host susceptibility.

The results showed that *H. bacteriophora* caused 75% mortality of the mealybugs, while *S. glaseri* achieved 67% mortality. No mortality was recorded in the control wells, confirming the nematodes' pathogenicity. These findings highlight the potential of locally isolated EPNs as effective biocontrol agents against female *P. citri*.

This study supports the use of indigenous EPN isolates as part of integrated pest management (IPM) strategies targeting *P. citri*. Further investigations in field conditions are recommended to evaluate their practical application and long-term effectiveness in agricultural settings.

Keywords: *Planococcus citri*, Entomopathogenic nematodes, Biologic control

➢ *ORAL PRESENTATION*

Differential effects of lipopolysaccharide and SARS-CoV-2 spike protein on RAS-related gene expression in normal and colon cancer epithelial cells

Aysegul Yilmaz[1*] *(https://orcid.org/0000-0002-9541-9853)* Safiye Gocer[1] (*https://orcid.org/0000-0003-1787-9755)*

[*1]Lokman Hekim University, Faculty of Medicine, Department of Medical Microbiology, Ankara, Turkiye.

*Corresponding author e-mail: aysegul.yilmaz@lokmanhekim.edu.tr

Abstract

Colorectal cancer remains one of the leading causes of cancer-related morbidity and mortality worldwide, and a better understanding of the molecular responses to pathogen-associated stimuli may contribute to improved therapeutic approaches. This study aims to evaluate the effects of lipopolysaccharide (LPS) and SARS-CoV-2 spike protein on the expression of key RAS-related genes (ACE2, EGFR and IGF2R) in colon cancer cells (COLO205) and healthy colon epithelial cells (CRL-1831). Both cell lines were treated with LPS and spike protein for 12, 48, and 72 hours. Gene expression levels were evaluated using qPCR method and significant time and cell type–dependent differences were observed. Results showed that ACE2 expression decreased in the cancer cell group at 12 hours following both treatments, whereas an increase was observed in the healthy cell group under the same conditions. EGFR expression was reduced in the healthy cells at 72 hours after both LPS and spike treatments, while a significant increase was detected in the cancer cells at the same time point. IGF2R expression was upregulated in the cancer group at 12 hours for both treatments compared to the control. At 48 hours, spike protein treatment led to increased IGF2R expression in healthy cells, while causing a significant decrease in the cancer cells. These findings suggest that LPS and spike protein elicit differential gene expression responses depending on the cell type and duration of exposure. The results emphasize the importance of cellular context in understanding pathogen-related signaling alterations and highlight the need for tailored therapeutic approaches in infection-associated conditions, particularly in cancer biology.

Keywords: Epithelial cells, Spike protein, Lipopolysaccharide, RAS-related genes, Pathogen-host interaction

➢ *ORAL PRESENTATION*

Synthesis and Characterization of Curcumin and Lysine Derived Carbon Dots

İrem YAKAR[1*] (*ORCID: https://orcid.org/0009-0008-5083-4691*), Ayben TOP[1] (*ORCID: https://orcid.org/0000-0003-0554-2506*)

[1]Izmir Institute of Technology, Faculty of Engineering, Chemical Engineering, İzmir, Türkiye.

*Corresponding author e-mail: iremyakar@iyte.edu.tr

Abstract

Antibacterial materials are designed to inhibit or kill bacterial growth, making them essential in various applications where hygiene and infection control are crucial such as wound care and medical devices. Carbon dots (CD) are nano-scale materials with unique optical properties, chemical stability, biocompatibility, with ease of synthesis and functionalization. The properties of the carbon dots are dictated by the precursors used in the synthesis. In this study carbon dots were synthesized using antibacterial precursors, curcumin and lysine, via the furnace method. Structural and optical properties of the CDs were determined. The synthesized CDs exhibit mild antibacterial activity against common wound pathogens, including Staphylococcus aureus and Escherichia coli. The promising results highlight the potential of antibacterial carbon dots as an effective, safe, and multifunctional therapeutic agent for wound healing. Future work will focus on optimizing the synthesis process and evaluating the biocompatibility and antioxidant activity of these CDs.

Keywords: Carbon Dots, Curcumin, Lysine, Antibacterial.

Acknowledgements:
We thank İzmir Institute of Technology Integrated Research Center for making XRD, ATR, UV, DLS and antimicrobial analyses possible. We extend our sincere gratitude to Yekta Günay for DLS, UV, and ATR and Evrim Paşık for antibacterial analysis.

➢ *ORAL PRESENTATION*

The Effect of Different Cobalt Contents on the Properties of Tungsten Carbide Materials Sintered at Low Temperature

Kubat Mete KUTLU[1*] (*ORCID: 0009-0007-9958-2328*), Bilge YAMAN ISLAK[2] (*ORCID: 0000-0003-0766-8014)*

[*1,2] Eskisehir Osmangazi University, Faculty of Engineering and Architecture, Department of Metallurgical & Materials Engineering, Eskisehir, Turkey

*Corresponding author e-mail: byaman@ogu.edu.tr

Abstract

In this study, the Spark Plasma Sintering (SPS) technique was utilized for the production of tungsten carbide (WC) composites, offering significant advantages over conventional sintering methods, such as shorter processing times, lower sintering temperatures, and improved control over microstructural evolution. The research focused on evaluating the influence of varying cobalt binder contents on the mechanical and tribological properties of WC-based composites sintered at a relatively low temperature. Within the scope of this research, tungsten carbide (WC) samples containing 3 wt.% and 6 wt.% cobalt binder were sintered at a relatively low temperature of 1100 °C using the SPS technique. The mechanical and tribological behaviors of the resulting materials were systematically evaluated. The tribological tests conducted under dry conditions revealed surface morphologies through profilometer profiles, and both the coefficient of friction and wear rates were determined. The study showed that samples with a higher cobalt content exhibited a lower coefficient of friction and more stable wear behavior. This improvement in tribological behavior is attributed to the enhanced toughness and plasticity provided by the increased metallic binder phase, which helps to better accommodate stress and reduce crack propagation during sliding.

Keywords: Tungsten carbide-cobalt; cemented carbide; powder processing; spark plasma sintering; wear.

➢ *ORAL PRESENTATION*

Conventional and Microwave-Assisted Synthesis and Characterization of PEG-Based Esters

Gulsen Karaca[1,4] (*ORCID: https://orcid.org/0000-0002-2231-1454)*
Omur ARAS[2,3*] (*ORCID: https://orcid.org/0000-0003-4577-028X)*

[1] Bursa Technical University, Institute of Graduate Education, Department of Chemical Engineering, Bursa, Türkiye.
[*2] Bursa Technical University, Faculty of Engineering and Natural Sciences, Department of Chemical Engineering, Bursa, Türkiye
[*3] Department of Chemical Engineering, Faculty of Engineering, Kyrgyz-Turkish Manas University, Bishkek, Kyrgyzstan.
[4] Sözal Chemical Industry and Trade Inc., Research and Development Center, Bursa, Türkiye.

*Corresponding author e-mail: omur.aras@btu.edu.tr

Abstract

The process of esterification generally refers to the chemical reaction between a carboxylic acid and an alcohol, resulting in the formation of esters along with water as a by-product. Esters are chemical compounds characterized by their distinctive sweet odor. In the chemical structure of esters, represented as R–COOR', R and R' denote organic groups (alkyl and/or aryl groups), while -COO represents the carboxyl group. Esterification reactions proceed very slowly in the absence of a catalyst; therefore, a catalyst is required to accelerate the reaction and shift the equilibrium toward the product side. Esterification reactions play a crucial role in both industrial and biological systems, serving as fundamental processes in the production of pharmaceuticals, polymers, and specialty chemicals. The esterification of polyethylene glycols (PEGs) with chloroacetic acid (CAA) is particularly important due to its applications in biocompatible materials, surfactants, and controlled drug delivery systems. In this study, the esterification reaction of PEGs with different molecular weights (PEG200, PEG300, and PEG400) and chloroacetic acid was investigated using both conventional and microwave (MW) methods. In the conventional method, p-toluenesulfonic acid (p-TSA) was used as a catalyst. To observe the temperature dependence of the esterification reaction between PEGs and CAA, the reactions were conducted at different temperatures. For each temperature, the progress of the reaction was monitored and the conversion was calculated. Structural confirmation of the synthesized products was carried out using Fourier Transform Infrared Spectroscopy (FTIR) and Nuclear Magnetic Resonance (NMR) spectroscopy. The FTIR spectra confirmed that the targeted structural transformations had occurred and that characteristic functional groups (C–Cl, C=O, C–O) had formed. Signals specific to the ester structure were also detected in the ^{1}H-NMR spectra. These findings indicate that the compound was successfully synthesized in the desired structure.

Keywords: Esterification, Microwave, Characterization

➢ *ORAL PRESENTATION*

Effect Of Cooling 16MnCr5 Steel Under Different Pressure On Hardness And Microstructure Properties

Mehmet EKICI[1*] (*ORCID: https://orcid.org/0000-0001-6259-3524*)

[*1]Yalova University, Vocational School of Yalova, Yalova, Turkey.

*Corresponding author e-mail: mekici@yalova.edu.tr

Abstract

In this study, the microstructure and hardness properties of hot rolled commercial 16MnCr5 steel were investigated after normalization and austenitization processes and subsequent hot forming processes. First, the steel was subjected to normalization process at 1000°C for 40 minutes to ensure homogeneous distribution of ferritic-pearlitic microstructure along the rolling direction. Then, austenitization was performed at 950°C for 10 minutes in accordance with the TTT diagram and the material was shaped under varying die pressures (25 kN, 50 kN, 75 kN, 100 kN) and then controlled cooling was performed. The cooling rate was aimed to be sufficient to promote martensitic transformation. Hardness measurements were performed using the Zwick/Roell ZHV 10 device by taking five measurements for 15 seconds under a load of 5 kgf for each sample and the average values were calculated. Although an increase in the cooling rate was observed, the expected linear increase in hardness values was not obtained. This was attributed to the fact that the austenitizing temperature of 950°C was insufficient for complete austenite formation, as evidenced by the presence of a small amount of ferrite phase in the microstructure. Microstructure analyses revealed similarities with dual phase (DP) steels with high martensite content. It was concluded that the austenitizing temperature should be increased to 1000°C or higher to obtain a fully martensitic structure and higher hardness values.

Keywords: Hot stamping, 16MnCr5 alloy, contact pressure, microstructure

➢ *ORAL PRESENTATION*

L-Alanin, L-İzolösin, ve L-Valin Amino Asit Metil Esterlerinin *Candida albicans* ile Bazı Gram pozitif ve Gram negatif Bakteri Suşlarına Karşı Antimikrobiyal Etkilerinin Araştırılması

Tuğçe Deniz Karaca[1*] (*ORCID: https://orcid.org/0000-0002-7471-1759*), Gülcan Şahal[2] (*ORCID: https://orcid.org/0000-0001-5994-1727*), Handan Sevim Akan[3] (*ORCID: https://orcid.org/0000-0002-8511-5258*)

[*1] Gazi Üniversitesi, Sağlık Hizmetleri Meslek Yüksekokulu, İlk ve Acil Yardım Programı, Ankara, Türkiye.
[2] Hacettepe Üniversitesi, Fen Fakültesi, Biyoloji Bölümü, Ankara, Türkiye.
[3]Hacettepe Üniversitesi, Fen Fakültesi, Biyoloji Bölümü, Ankara, Türkiye.

*Corresponding author e-mail: tdenizkaraca@gazi.edu.tr

Özet

Antimikrobiyal direnç, özellikle çoklu ilaç direnci, antimikrobiyallerin aşırı kullanımı ve dirençli mikroorganizmaların artışı nedeniyle giderek daha ciddi bir halk sağlığı sorunu haline gelmiştir ve mevcut antibiyotiklere alternatif olarak yeni kemoterapötik ajanlara duyulan ihtiyaç da her geçen gün artmaktadır. Son yıllarda bu alanda amino asit türevleri ile ilgili yapılan çalışmalar dikkat çekicidir. Bu nedenle bu çalışmada, L-Alanin, L-İzolösin, ve L-Valin Metil Esterlerinin *Bacillus subtilis* ATCC 6633, *Candida albicans* ATCC 10231, *Escherichia coli* ATCC 35218, *Klebsiella pneumoniae* MTCC 109, *Pseudomonas aeruginosa* ATCC 27853 ve *Staphylococcus aureus* ATCC 25923 suşlarına karşı antimikrobiyal etkilerinin araştırılması amaçlanmıştır. Test edilen esterlerin Minimum İnhibisyon Konsantrasyonu (MİK) ve Minimum Mikrobisidal Konsantrasyonu (MMK) değerleri Sıvı Dilüsyon Yöntemi ile, inhibisyon zon çapları (ZOI) ise Disk Difüzyon (DD) Yöntemi ile belirlendi. Çalışmamızın sonuçlarına göre, L-Alanin Metil Ester, *B. subtilis* ATCC 6633 (MİK: 50 mg/mL), *S. aureus* ATCC 25923 (MİK: 100 mg/mL) ve *K. pneumoniae* MTCC 109 (MİK: 100 mg/mL) suşlarına karşı en etkili antimikrobiyal madde olarak belirlendi. Ayrıca, L-İzolösin Metil Ester'in *E. coli* ATCC 35218 (MİK: 100 mg/mL; ZOI: 9.3 ± 0.6 mm) ve *K. pneumoniae* MTCC 109 (MİK: 200 mg/mL; ZOI: 7.7 ± 0.6 mm) suşlarına karşı da antimikrobiyal aktivite gösterdiği tespit edildi. Bunun yanı sıra, L-Alanin Metil Ester ve L-İzolösin Metil Esterin düşük düzeyde de olsa *C. albicans* ATCC 10231 suşuna karşı antifungal aktivite sergilediği gözlenirken, *P. aeruginosa* ATCC 27853 suşuna karşı test edilen tüm metil esterlerin benzer antimikrobiyal etki gösterdikleri saptandı (MİK: 200 mg/mL). Elde edilen bulgular, L-Alanin Metil Ester ve L-İzolösin Metil Ester'in, çalışmamızda test edilen tüm mikroorganizmalara karşı antimikrobiyal potansiyele sahip olduğunu göstermektedir.

Anahtar Kelimeler: Antimikrobiyal Direnç, Antimikrobiyal Etki, Amino Asit Alkil Ester, Minimum İnhibisyon Konsantrasyonu (MİK), İnhibisyon Zonu Çapı (ZOI)

Bu çalışma 9467 ID kodlu Gazi Üniversitesi BAP Projesi tarafından desteklenmektedir.

➢ *ORAL PRESENTATION*

UV-Curable Emulsion Hydrogel System Based on Modified PVA as a Wound Dressing Material

Bora Gümüş[1] (0009-0009-9015-2086), Fatma Nur Parın[2*] (0000-0003-2048-2951)

[1]Bursa Technical University, Institute of Graduate Education, Polymer Materials Engineering Department, Bursa, Türkiye
[2*]Bursa Technical University, Faculty of Engineering and Natural Sciences, Polymer Materials Engineering, Bursa, Türkiye

*Corresponding author e-mail: nur.parin@btu.edu.tr

Abstract

Wound dressing materials are of critical importance for accelerating the wound healing process, reducing infection risks, and improving the quality of recovery. In this study, a UV-curable emulsion hydrogel system was developed, modified with polyvinyl alcohol (PVA) and maleic anhydride (MAH), combined with gelatin, and emulsified with lavender oil. Lavender oil was utilized in this system due to its natural antibacterial properties, aimed at preventing infection and accelerating the healing process. The chemical structure of the resulting hydrogel was analyzed using Fourier Transform Infrared Spectroscopy (FTIR) to investigate the interactions of functional groups. The surface morphology and porosity were examined using Scanning Electron Microscopy (SEM) to assess the structural integrity and biological activity of the system. Antibacterial activity was tested against common wound infection pathogens such as *Staphylococcus aureus* and *Escherichia coli*. FTIR analyses confirmed the successful modification of PVA–MAH and the interaction with gelatin, as well as the effective encapsulation of lavender oil into the system. SEM images revealed that the UV-cured hydrogel possessed a smooth surface structure and adequate porosity. These features suggest that the hydrogel was designed to improve water absorption capacity. Antibacterial tests demonstrated that lavender oil exhibited high activity against both bacterial strains, confirming that the system could significantly reduce infection risk when used as a wound dressing.

Keywords: Lavender essential oil, modified polyvinyl alcohol (PVA), UV-curable hydrogel, wound dressing, antibacterial activity

➢ *ORAL PRESENTATION*

Monitoring of endangered dusky grouper (*Epinephelus marginatus*) in The Karaburun-Ildır Gulf Special Environmental Protection Area with different methods

Kaan KIRŞAN[*1] (*ORCID: https://orcid.org/0009-0001-7640-7515*),
Tuğçe ŞENSURAT GENÇ[2] (*ORCID: https://orcid.org/0000-0002-5528-3322*)

[*1]Cukurova University, Faculty of Fisheries, Department of Basic Science, Adana, Türkiye
[2]İzmir Katip Çelebi University, Faculty of Fisheries, Department Of Fisheries and Fish Processing Technology, İzmir, Türkiye

*Corresponding author e-mail: kaan.kirsan@gmail.com

Abstract

Over the past fifty years, marine biodiversity has significantly declined due to overfishing, pollution, climate change, and other anthropogenic pressures. In response to these threats, the number of marine protected areas has rapidly increased globally over the past two decades, and these protected areas are now considered effective tools for conserving biodiversity and mitigating human impacts. The IUCN Red List of Threatened Species assesses the conservation status of species based on their population trends, distribution, ecological characteristics, and the threats they face. *Epinephelus marginatus* (dusky grouper) was listed as an endangered species on the IUCN Red List in 1996. However, its fishing has been completely banned along the Turkish coasts since 2016. In our study, we aimed to monitor the endangered *Epinephelus marginatus* in the Karaburun-Ildır Special Environmental Protection Area in the Aegean Sea using various non-destructive methods. The presence, abundance, and size structure of the species were recorded for the first time using baited remote underwater video systems (BRUVs), while underwater visual census (UVC) methods were applied in darker and more complex habitats where BRUVs were less effective. A total of 50 successful BRUV deployments were conducted during the study. In addition, 15 UVC surveys, each lasting 15 minutes at depths between 25 and 35 meters, were performed. Furthermore, to assess the status of the species before and after the 2016 fishing ban, face-to-face interviews were conducted with local stakeholders, including recreational and industrial fishers, spear fishers, and divers. Based on the collected data, it was concluded that the grouper population in the region has increased following the 2016 fishing ban. However, follow-up conversations after the spear fisher surveys suggested that some individuals may still be illegally targeting the species. These findings indicate that human pressure on the species continues within the protected area.

Keywords: Dusky grouper, Baited Remote Underwater Video Systems, Threatened Species, Underwater Visual Census, Local Ecological Knowledge

➢ *ORAL PRESENTATION*

Microwave-assisted preparation and characterization of derivatives starting from flurbiprofen

Ecem Gökoğlan[1*] (*https://orcid.org/0000-0002-2488-9698*),
Ş. Güniz Küçükgüzel[1] (*https://orcid.org/0000-0001-9405-8905)*

[*1]Fenerbahçe University, Faculty of Pharmacy, Department of Pharmaceutical Chemistry, Istanbul, Türkiye.

*Corresponding author e-mail: ecem.gokoglan@fbu.edu.tr

Abstract

The microwave-assisted synthesis method is one of the green chemistry methods, and its importance is increasing daily. It is an environmentally friendly method compared to conventional synthesis methods, where microwave radiation is used as a heat source. It has become a preferred method compared to other methods in terms of using less solvent, significantly shortening the reaction time (from days to minutes), saving energy, increasing the reaction efficiency, and obtaining pure product. It reduces the carbon footprint since it reduces the amount of waste formed at the end of the reaction and creates less toxic products. In this study, to compare conventional and microwave synthesis methods, derivatives previously synthesized by the conventional method were synthesized using the microwave-assisted approach. Based on the active substance flurbiprofen ((±)-2-fluoro-α-methyl-(1,1'-biphenyl)-4-acetic acid), a non-steroidal anti-inflammatory drug, various thioether derivatives previously synthesized by a conventional method were synthesized by the microwave method (Gökoğlan et al., 2023). The impurity controls of the synthesized derivatives were carried out using TLC and melting point analysis, while their structures were confirmed by the FT-IR spectroscopic method. Conventional and microwave-assisted synthesis methods were compared in terms of reaction time and reaction percentage yields. As a result of the study, it was observed that the product was obtained in a much shorter time and with a higher yield using the microwave-assisted synthesis method.

Keywords: Flurbiprofen, conventional synthesis, microwave-assisted synthesis, green chemistry

Gökoğlan, E., Dere, D., Bedir, İ., Yelekçi, K., Telci, D., & Küçükgüzel, Ş. G. (2023). Synthesis and investigation of cytotoxic effects of compounds derived from flurbiprofen. Journal of Molecular Structure, 1289, 135876.

➢ *ORAL PRESENTATION*

Elastic and Mechanical Property Enhancement of NASICON-Type LATP via Indium Doping: Implications for Solid-State Li-Ion Battery Applications

Savaş Şehirli[*1] (*ORCID: https://orcid.org/0000-0002-2049-5464*), Yasemin Çiftçi[2] (*ORCID: https://orcid.org/0000-0003-1796-0270*), Gültekin Çelik[3] (*ORCID: https://orcid.org/0000-0001-8587-322X*), Fatih Öksüzoğlu[4] (*ORCID: https://orcid.org/0000-0003-0869-2606*)

[*1]Selcuk University Institute of Science Campus Konya
[2]Gazi University Faculty of Science Department of Physics Ankara
[3]Selcuk University Faculty of Science Department of Physics Campus Konya
[4]Tarsus University Graduate Education Institute Tarsus / Mersin

*Corresponding author e-mail : savassehirli@hotmail.com

Abstract

The mechanical properties of NASICON-type solid electrolytes, $Li_{1.3}Al_{0.3}Ti_{1.7}(PO_4)_3$ (LATP) and its indium-doped derivative $Li_{1.3}Al_{0.3}In_{0.1}Ti_{1.6}(PO_4)_3$ (LATIP), were systematically investigated via first-principles density functional theory (DFT). Elastic stiffness tensors (C_{ij}) reveal that indium incorporation significantly enhances lattice rigidity. LATP exhibits calculated bulk, shear, and Young's moduli of 95.1 GPa, 68.23 GPa, and 155.43 GPa, respectively, whereas LATIP shows higher values of 127.32 GPa, 83.64 GPa, and 172.83 GPa. The Poisson's ratio increases from 0.26 (LATP) to 0.274 (LATIP), indicating improved ductility. Moreover, Pugh's ratio (B/G) rises from 1.79 to 1.88, surpassing the brittle–ductile threshold (1.75) and confirming enhanced mechanical plasticity. These improvements are critical for resisting lithium dendrite penetration and ensuring stable electrode–electrolyte interfaces. The superior combination of rigidity, ductility, and mechanical robustness makes LATIP a promising candidate for high-performance solid-state lithium batteries.

Keywords: LATP, LATIP, Mechanical properties, DFT, Pugh's ratio, Dendrite resistance

➢ *ORAL PRESENTATION*

Production and quality monitoring of marinade from mussels smoked with different wood chips

Emre Uluturhan[1*] (*ORCID: https://orcid.org/0009-0005-6864-8852*), Aslı Cadun Yünlü[1] (*ORCID: https://orcid.org/0000-0002-6139-7983*), Fevziye Nihan Bulat[1] (*ORCID: https://orcid.org/0000-0001-5165-3632*), Ömer Alper Erdem[1] (*ORCID: https://orcid.org/0000-0002-1745-1751)*

[*1] Ege University, Faculty of Fisheries, Department of Fishing Technology and Seafood Processing Technology, İzmir, Türkiye.

*Corresponding author e-mail: emreuluturhan1@gmail.com

Abstract

In Turkey, it is commonly prepared and consumed as stuffed mussels or fried dishes mussels. As an alternative to the aforementioned processing methods, a third method was considered, which involved the application of two traditional methods. In the study, it was aimed to use the incense gun, which has recently been adopted by many food groups in the food industry. The marinade was prepared by smoking mussels using cherry and oak wood shavings with an incense gun. A comprehensive examination encompassing sensory, chemical (pH, aromatic compounds), physical (colour, cooking loss, water holding capacity (WHC) and microbiological qualities (total viable count and yeast-mould)) attributes was conducted during the storage period. The mussels as frozen obtained from a local supplier in İzmir, Türkiye, were meticulously thawed, and then divided into three groups. The experimental design entailed the allocation of mussels to one of three groups: a control group, and two groups that were exposed to fumigants, with cherry shavings or oak shavings serving as the fumigants. Subsequent to the smoking process, three groups were subjected to marinating with 14% apple cider vinegar and 14% salt at the previously determined ratios. Subsequent to the maturation process of the mussels being completed, they were placed in sunflower oil with rosemary in jars and stored at 0-4°C.

Keywords: Mussel, marinade, smoking gun, quality monitoring

This study was supported by 2209-A University Students Research Projects Support Program of TÜBİTAK.

➢ *ORAL PRESENTATION*

Thermal Analysis-Based Investigation of the Pyrolysis Kinetics of *Spirulina platensis*

Sevgi Polat[1*] (*ORCID: https://orcid.org/0000-0002-0934-2125),* Ömer Faruk Kılıç[1]

[1]Marmara University, Engineering Faculty, Chemical Engineering Department, 34854 Istanbul, Turkey

*Corresponding author e-mail: sevgi.polat@marmara.edu.tr

Abstract

Bio-oil derived from microalgae pyrolysis holds significant potential as a renewable, sustainable, and environmentally friendly energy source. Utilizing pyrolysis technology to convert Spirulina platensis microalgae into energy offers a promising solution to future energy demands. This study investigates the thermodynamics and non-isothermal kinetics of Spirulina platensis within a temperature range of 30 to 600 °C. Thermogravimetric analysis (TGA) was conducted at heating rates of 5, 10, and 20 °C/min to examine the thermal decomposition behavior. The kinetic parameters were evaluated using the model-fitting Coats-Redfern method. The thermal degradation process revealed three main stages: dehydration, active pyrolysis, and passive pyrolysis. The activation energy (Ea) calculated using the Coats-Redfern method was approximately 55.0 kJ/mol.

Keywords: Microalgae, pyrolysis, TGA kinetics, Coats-Redfern method.

Acknowledgements: This work is funded by the Scientific and Technological Research Council of Turkey (TUBİTAK) with project number 224M617 and the Scientific Research Projects Coordination Unit of Marmara University under the project code FYL-2024-11408.

➢ *ORAL PRESENTATION*

Quantitative Analysis Of CoQ10 Content Of Nutraceuticals From Turkish Market

Tuğba Buse Şentürk[1](*ORCID: https://orcid.org/0000-0002-0138-2480*), Ayşe Sueda Müftüoğlu[2*](*ORCID: https://orcid.org/0009-0001-8156-7839*), Timur Hakan Barak[1](*ORCID: https://orcid.org/0000-0002-7434-3175)*, Engin Celep[1](*ORCID: https://orcid.org/0000-0002-9748-4325*)

[*1] Department of Pharmacognosy, Faculty of Pharmacy, Acıbadem Mehmet Ali Aydınlar University, 34752, Istanbul, Türkiye.
[2] Faculty of Pharmacy, Acıbadem Mehmet Ali Aydınlar University, 34752, Istanbul, Türkiye.

*Corresponding author e-mail: Ayse.Muftuoglu@live.acibadem.edu.tr

Abstract

Coenzyme Q10 (CoQ10) is a fat-soluble, vitamin-like benzoquinone compound synthesized endogenously from tyrosine. Its potential health benefits have led to a growing consumer demand, making it the third most popular dietary supplement after multivitamins and fish oil [1]. However, the lack of standardized regulations in the production and labelling of dietary supplements raises concerns regarding product quality [2]. Since official market controls are infrequent, particularly for non-vitamin supplements, consumers are unable to verify the actual CoQ10 content, thereby increasing the risk of misleading practices. This study aimed to assess the accuracy of CoQ10 content labelling in dietary supplements available in the Turkish market. Ten CoQ10-containing supplements, in the form of soft gels, tablets, or sachets, were purchased from various sales channels, including pharmacies and non-pharmacy markets. The CoQ10 content was analysed using High-Performance Thin-Layer Chromatography (HPTLC) to determine compliance with the declared amounts. Results showed that within the generally accepted 90%-110% label compliance range, only 50% (5/10) of the samples met the label claims. One sample (10%) contained less CoQ10 than declared, while four (40%) exceeded the stated content. These findings indicate significant deviations in half of the analysed supplements, which could impact efficacy and safety. Given that CoQ10's bioavailability depends on formulation and individual metabolism, deviations from the recommended dose may result in pharmacokinetic inconsistency and unexpected physiological effects. In conclusion, stricter quality control measures as well as regulatory oversight are necessary to ensure dietary supplements meet label claims. Regular inspections and standardized international guidelines should be implemented to enhance consumer safety and minimize inconsistencies in supplement content.

Keywords: Coenzyme Q10, Dietary supplements, Label compliance, HPTLC analysis, Quality control.

References:

[1] Arenas-Jal, M., Suñé-Negre, J. M., & García-Montoya, E. (2020). Coenzyme Q10 supplementation: Efficacy, safety, and formulation challenges. Comprehensive reviews in food science and food safety, 19(2), 574-594.
[2] Pravst, I., & Žmitek, K. (2011). The coenzyme Q10 content of food supplements. Journal für Verbraucherschutz und Lebensmittelsicherheit, 6, 457-463.

➢ *ORAL PRESENTATION*

Time – space tradeoff in array merging problem

Subhan Guliyev[1*] (*ORCID: https://orcid.org/0009-0004-1971-3622*),
Mehmet Emin Dalkilic[2] (*ORCID: https://orcid.org/0000-0003-3932-5155*)

[*1]Ege University, International Computer Institute, Turkey.
[2] Ege University, International Computer Institute, Turkey

*Corresponding author e-mail: subhan.quliyev02@gmail.com

Abstract

Merge algorithms are so widely used today that they are incorporated even into standard programming libraries. The problem of merging two distinct sorted arrays, comprising a total of N elements, is conventionally addressed by allocating an auxiliary buffer of size N – an approach employed in the Merge Sort algorithm. However, this additional memory requirement constitutes a significant drawback compared to in-place merging algorithms that perform the merge without extra storage.
Since Kronrod's seminal work in 1969 (Kronrod, 1969), computer scientists have devoted over fifty years to devising an efficient merge method that obviates auxiliary space (Pardo, 1977; Dvorak & Durian, 1987; Huang & Langston, 1988; Symvonis, 1995; Ellis & Markov, 2000; Kim & Kutzner, 2004; Dalkilic et al., 2011; Mergen & Moreira, 2017; Salah et al., 2020), yet a fully satisfactory solution remains elusive.
In this study, an alternative perspective on the array-merging problem is proposed. By leveraging the inherent time–memory trade-off—sacrificing a modest amount of extra memory to reduce execution time—a new merging algorithm was designed and implemented. This merge algorithm based on time-space trade-off has been implemented in the C++ programming language and the performance of the algorithm has been tested for different problem lengths (N) created with the rand() function and different additional memory lengths (k). Experimental results demonstrate that as the buffer size increases (constant, log N, $(\log N)^2$, …, N), the algorithm's time complexity correspondingly decreases.
It is concluded that this time–memory trade-off-based merging algorithm is highly practical: allocating a small additional buffer accelerates the merge process, and the algorithm's straightforward implementation ensures its suitability for real-world applications.

Keywords: array merging problem, optimal memory usage, time – memory tradeoff.

➢ *ORAL PRESENTATION*

The infinite sum of reciprocal Fibonacci numbers

Abdullah Açıkel *(ORCID: https://orcid.org/0000-0002-4819-9384)*

Hatay Mustafa Kemal University, The faculty of arts and sciences, Department of Mathematics, Hatay, Turkey.

Corresponding author e-mail: aacikel@mku.edu.tr, abdullahacikel3107@gmail.com

Abstract

In this paper, we consider infinite sums from the reciprocals of the Fibonacci numbers. Then applying the floor function to the reciprocals of this sums, we obtain a new identity involving the Fibonacci numbers.

Keywords: Fibonacci numbers, Floor function, Reciprocal.

➢ *ORAL PRESENTATION*

On the relations between three reduced series of numbers

Abdullah Açıkel *(ORCID: https://orcid.org/0000-0002-4819-9384)*

Hatay Mustafa Kemal University, The Faculty of Arts and Sciences, Department of Mathematics, Hatay, Turkey.

Corresponding author e-mail: aacikel@mku.edu.tr, abdullahacikel3107@gmail.com

Abstract

Reduction number sequences have an important role among number sequences. In this paper, three different reduction number series were considered and some relationships were determined between them.

Keywords: Tribonacci, Perrin, Padovan.

➢ *ORAL PRESENTATION*

Integrated Microfluidic Chip Platform for Cyclotide Isolation from Plant Extract

Beyza Dağhan[*1] (*ORCID: https://orcid.org/0009-0009-5482-5087*), Mesut Bora Akdoğan[1] (*ORCID: https://orcid.org/0009-0006-8584-0309*), Aliakbar Ebrahimi[2] (*ORCID: https://orcid.org/0000-0001-6437-7796*) , Reza Didarian[2] (*ORCID: https://orcid.org/0000-0001-9329-878X*), Mulatu Kassie Birhanu[2] (*ORCID: https://orcid.org/0000-0001-5287-6862*), Hossein Hashempour[3] (*ORCID: https://orcid.org/0000-0001-8518-6411*), Zahra Zendeh[2] (*ORCID: https://orcid.org/0000-0003-2668-3869*), Fatma Dogan Guzel[1] (*ORCID: https://orcid.org/0000-0001-7200-4615*),

[*1]Ankara Yıldırım Beyazıt Üniversitesi, Mühendislik ve Doğa Bilimleri Fakültesi, Makine Mühendisliği, Ankara, Türkiye.
[2]Ankara Yıldırım Beyazıt Üniversitesi, Mühendislik ve Doğa Bilimleri Fakültei, Biyomedikal Mühendisliği, Ankara, Türkiye.
[3] Azarbaijan Shahid Madani University, Faculty of Basic Sciences, Department of Chemistry, Tabriz, Iran

*Corresponding author e-mail : fdogan@aybu.edu.tr

Abstract

Microfluidic chips are coin biotechnology research[1]. Microfluidic chip technology offers a promising, low-cost, and easy-to-implement platform for developing efficient seperation methodologies[2]. This study presents a separation method based on two different microfluidic chip designs. As compact microfluidic designs offer advantages in speed, efficiency and cost[3] . Implementation of three inlets with usage of an applied electric current enables a separation based on molecular charge or mobility, allowing for precise and active control during the process. On this current based chip middle inlet introduces plant extract, with other inlets adding reagents. To achive the optimum conditions for seperation different voltages are utilized. The other chip features two inlets and contains a PET membrane placed between two separate channels, enabling passive separation through selective diffusion without the need for external forces. The membrane-based design offers a simple and cost-effective alternative, suited for small-scale laboratory applications. In membrane-based design dilute acid solution—either HCl or phosphoric acid—was introduced into the second inlet. Flow rates of 0.5 µL/min, 1 µL/min, and 2 µL/min were used during testing. To evaluate the method's effectiveness, a plant extract from Viola ignobilis, collected in Iran's West Azerbaijan province used in both design applications. Cyclotides are the target compounds in the plant extract. They are small, highly stable cyclic peptides of interest for their potential biomedical applications[4].

Keywords: microfluid. microfluidic chip. seperation. cyclotide.

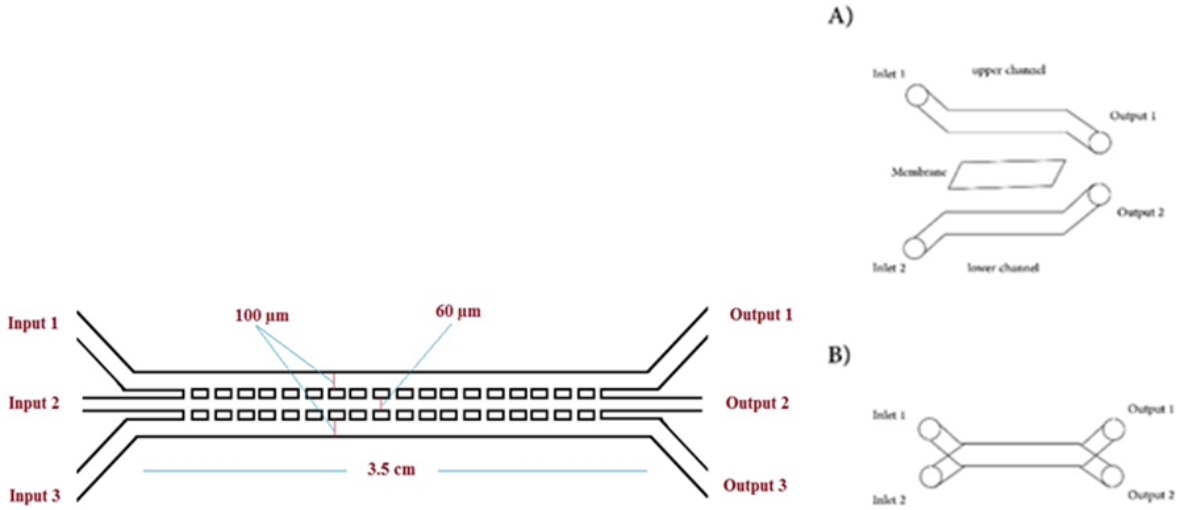

Referances

1 A. N. Dizaji et al., "Investigation of the Effect of Channel Structure and Flow Rate on On-Chip Bacterial Lysis," in IEEE Transactions on NanoBioscience, vol. 20, no. 1, pp. 86-91, Jan. 2021, doi: 10.1109/TNB.2020.3031346

2 Kaur, J., Ghorbanpoor, H., Öztürk, Y., Kaygusuz, Ö., Avcı, H., Darcan, C., Trabzon, L. and Güzel, F.D. (2021), On-chip label-free impedance-based detection of antibiotic permeation. IET Nanobiotechnol, 15: 100-106. https://doi.org/10.1049/nbt2.12019

3 DIDARIAN, REZA; EBRAHIMI, ALIAKBAR; GHORBANPOOR, HAMED; BAGHEROGHLI, HESAM; GÜZEL, FATMA DOĞAN; FARHADPOUR, MOHSEN; LOTFIBAKHSHAYESH, NASRIN; HASHEMPOUR, HOSSEIN; and AVCI, HÜSEYİN (2023) "On chip microfluidic separation of cyclotides," Turkish Journal of Chemistry: Vol. 47: No. 1, Article 25. https://doi.org/10.55730/1300-0527.3534

4 Ebrahimi, A., Didarian, R., Ghorbanpoor, H. et al. High-throughput microfluidic chip with silica gel-C18 channels for cyclotide separation. Anal Bioanal Chem 415, 6873–6883 (2023). https://doi.org/10.1007/s00216-023-04966-3

Acknowledgement

Auhtors would like to thank Ankara Yıldırım Beyazıt University BAP with a project number of 2658.

➢ *ORAL PRESENTATION*

Rapid detection of expired tablets using Second Derivative FTIR: An iron supplement tablet example

Sinem Çolak[1*] *(https://orcid.org/0000-0001-6731-327X)*

[*1] Zonguldak Bülent Ecevit University, Çaycuma Food and Agriculture Vocational School, Department of Chemistry and Chemical Processing Technologies, Zonguldak, Turkey

*Corresponding author e-mail:sinem.colak@beun.edu.tr

Abstract

Iron supplements are important supports used to complete the deficient iron levels in the body and to eliminate problems such as anemia. Iron tablets are one of the most effective solutions for iron lack anemia. Nowadays, it is common to repackage medicines used for both supplementation and medication, which can cause serious problems. Therefore, fast and reliable analytical methods for the detection of these situations are very important. In this study, expired (in 2023) and non-expired (in 2028) commonly used iron tablets obtained from local pharmacies were used. Each capsule contains 567.7 mg of iron (II)-glycinesulfate-complex equivalent to 100 mg Fe^{+2}. The powder samples in the capsule were analyzed using a FTIR-ATR spectrometer. Spectra were obtained in the mid-infrared region (4000-550 cm^{-1}) with 16 scans and a resolution of 4 cm-1. Peak analysis was performed on the raw peak data with Origin Pro 2018 software. After Savitzky-Golay correction, the 2nd order derivative of the data point was calculated. All peaks of the 2nd order derivative curve were found using the Local Maximum method. The Savitzky-Golay technique was used to remove noise and background effects from the spectra. Using the 2nd derivative of the FTIR spectrum, overlapping peaks in the raw spectrum were distinguished. Furthermore, baseline errors were eliminated and peak visibility was improved. In the spectrum, O-H stretching at 3239 cm^{-1}, O=S=O stretching at 1140 cm^{-1}, C=S at 1096 cm^{-1}, C-S at 585 cm^{-1} and S-O stretching peaks at 600-700 cm^{-1}. The band range of 1020-628 cm^{-1} belongs to the Fe-O peak. C-N bending peak at 1300 cm^{-1}, C-H stretching peak at 1490 cm^{-1} and C-H bending peak at 1387 cm^{-1} were also observed. This study showed that derivatized FTIR spectra of expired drugs improved the peaks and can be used in chemometric methods for better discrimination.

Keywords: FTIR-ATR, Savitzky-Golay technique, tablet

➢ *ORAL PRESENTATION*

Magnetic Characterization of $Pt_{17}Cu_{14}Ni_{69}$ Nanoparticles with Enhanced Low-Temperature Magnetic Stability

Ilknur Baldan Isik[1*] (*ORCID: 0000-0002-8786-7672*), Dogan Kaya[1,2] (*ORCID: 0000-0002-6313-7501*), Hasan Huseyin Isik[1] (*ORCID:* 0000-0001-5172-8200), Faruk Karadağ[1] (ORCID: 0000-0001-7862-9085), Ahmet Ekicibil[1] (ORCID: 0000-0003-3071-0444)

[*1]Cukurova University, Faculty of Art and Sciences, Department of Physics, Adana, Türkiye
[2]Cukurova University, Institute of Natural and Applied Sciences, Department of Advance Materials and Nanotechnology, Adana, Türkiye

*Corresponding author e-mail: ibaldan@cu.edu.tr

Abstract

Ternary PtCuNi alloys have attracted significant attention recently due to their magnetic properties and catalytic performance. The superparamagnetic behaviour of these alloys arises from the random orientation of magnetic moments induced by thermal energy due to the nanosize, which provides notable advantages in magnetic sensitivity and various applications [1]. In particular, PtCuNi nanostructures have been reported to exhibit unique magnetic properties and stability, demonstrating superparamagnetic characteristics that make them promising candidates for a wide range of applications, from magnetic sensors to biomedical uses [2, 3]. In this study, the PtCuNi material was synthesized using the polyol method. The structural and morphological properties were investigated using X-ray diffraction, scanning electron microscopy, and energy dispersive X-ray spectroscopy analyses. The structural and morphological analyses revealed that the PtCuNi material possesses a face-centered cubic crystal structure with spherical morphology, with an 8.89 nm in particle size. We measured the magnetization of $Pt_{17}Cu_{14}Ni_{69}$ nanoparticles (NPs) as a function of temperature and magnetic field. Under a 500 Oe applied magnetic field, the ZFC magnetization of $Pt_{17}Cu_{14}Ni_{69}$ NPs rises with increasing temperature and attains its maximum around 6.4 K. The maximum saturation magnetization of $Pt_{17}Cu_{14}Ni_{69}$ NPs was measured to be 13.21 and 0.48 emu/g at 5 K and 320 K, respectively. The coercivity value was determined as 145.5 Oe, indicating that the magnetic moments exhibit considerable stability at low temperatures. Moreover, since the hysteresis loop did not reach full saturation, it suggests that superparamagnetic behaviour is predominant and the magnetic moments are not fully aligned under the applied magnetic field. These results demonstrate that PtCuNi NPs exhibit pronounced magnetic properties at low temperatures; however, full magnetic saturation could not be achieved, further confirming the dominance of superparamagnetic behaviour in these nanostructures.

Keywords: PtCuNi NPs, XRD, SEM, Magnetic properties.

References:

[1] J.-J. Du, et al, Materials Chemistry and Physics, 155, 47-51, 2015.
[2] I. Baldan Isik et al, Electrochimica Acta, 477, 143794, 2024.
[3] I. Ban et al, Nanotechnology Reviews, 7 (2), 187-207, 2018.

Acknowledgements: This study was mainly funded by Cukurova University, Adana, Turkey, through the Scientific Research Funding Grant No: FBA-2021-14176.

➢ *ORAL PRESENTATION*

Investigation of photocatalytic properties of $ZnFe_2O_4$ spinel nanoparticles

Hasan Huseyin Isik[1,*] (*ORCID: https://orcid.org/0000-0001-5172-8200*), Dogan Kaya[2] (*ORCID: https://orcid.org/0000-0002-6313-7501*), Ilknur Baldan Isik[1] (*ORCID: https://orcid.org/0000-0002-8786-7672*), Ahmet Ekicibil[1] (*ORCID: https://orcid.org/0000-0003-3071-0444*), Faruk Karadag[1] (*ORCID: https://orcid.org/0000-0001-7862-9085*)

[1]Çukurova University, Faculty of Art and Sciences, Department of Physics, Adana, Turkey
[2]Çukurova University, Institute of Natural and Applied Sciences, Department of Advanced Materials and Nanotechnology, Adana, Turkey

*Corresponding author e-mail: hhisik@student.cu.edu.tr

Abstract

Zinc ferrite ($ZnFe_2O_4$) is a spinel-structured mixed metal oxide known for its diverse physical and chemical properties, making it a promising material for applications in catalysis, magnetic devices, and energy storage. In this study, $ZnFe_2O_4$ nanoparticles (NPs) were synthesized mixing precursors with citric acid and annealing at 800 °C for 12 h by sol-gel method. The structural properties of the NPs were determined by X-ray diffraction analysis which confirmed the formation of a well-crystallized cubic spinel structure with space group of Fd-3m and lattice parameters of $a=b=c=$ 8.46 Å. Scanning electron microscopy images revealed that the NPs had a relatively uniform morphology with an average particle size of approximately 220 nm. The photocatalytic performance of $ZnFe_2O_4$ NPs was tested through the degradation of methylene blue (MB) under UV light irradiation. The results demonstrated that $ZnFe_2O_4$ NPs was able to degrade nearly 80% of MB within 60 min of UV exposure. This high photocatalytic efficiency is attributed to the material's stable crystal structure, suitable particle size, and effective absorption of UV light, which together enhance the generation and separation of photogenerated charge carriers. These findings suggest that $ZnFe_2O_4$ is a promising photocatalyst for environmental applications, particularly in the degradation of organic dye pollutants in wastewater treatment.

Keywords: $ZnFe_2O_4$, XRD, SEM, photocatalytic

Acknowledgements: We thank the Çukurova University Research Fund (FDK-2023-15837) for financially supporting this research

➢ *ORAL PRESENTATION*

Biomass, distribution and some population parameters of Big-Scale Sand Smelt, *Atherina boyeri* (Risso, 1810) in the Sea of Marmara

Oğuz Yılmaz[1*] (*ORCID: https://orcid.org/0009-0009-6729-5302*), Ali İşmen[2] (*ORCID: https://orcid.org/0000-0003-2456-0232*)

[*1]Çanakkale Onsekiz Mart University, School of Graduate Studies, Fisheries and Fish Processing Department, Çanakkale, Türkiye.
[2] Çanakkale Onsekiz Mart University, Marine Science and Technology Faculty, Fisheries and Fish Processing Çanakkale, Türkiye.

*Corresponding author e-mail: yilmazoguztr@gmail.com

Abstract

Big-scale Sand Smelt, *Atherina boyeri*, is an estuarine resident species, which usually lives lower parts of the rivers, lagoons, and the coastal areas of the seas. The aim of the present study is to reveal the mean abundance, spatial and temporal variation of abundance and reveal some biological parameters (length-frequency distribution, length-weight relationship, otolith-fish size relationship, otolith shape analyses etc.) of the *A.boyeri*, distributed in the coastal waters of the Sea of Marmara. Individuals were obtained with beach seine sampling at 12 various stations from the coastal areas of the Marmara Sea between December 2021 and March 2022. A total of 1728 individual were obtained, and ranged in length between 3.07 and 15.30 cm TL and weighted from 0.05 to 21.15 g. The lowest and the highest mean lengths were calculated in March (6.24 cm TL) and January (7.30 cm TL), respectively. The mean CPUE (Catch per Unit Effort) and CPUA (Catch per Unit Area) were detected as 18 ind./haul and 0.48 ind./300 m^2, respectively. The lowest and the highest CPUE were found in March (11.58 ind./haul) and January (23.75 ind./haul), respectively. The highest abundance was found in Erdek station, with a 28.4% of the total catch and 61.4 ind./haul mean abundance. The lowest and the highest mean lengths were found in Erdek (6.00 cm) and Ayazma (10.89 cm), respectively. The total length-fork length relationship and the length-weight relationship were calculated as FL:0.927*TL+0.0811 (r^2: 0.992) and W=0.005*$TL^{3.054}$ (r^2=0.932), respectively. Otolith length was ranged between 1.010 and 4.198 mm (2.284±0.051 mm) in length. A strong linear relationship was detected between the total length-otolith length, with a given formula: OL=0.0377*TL-0.397 (r^2=0.92). Due to the restricted scientific information related the fish biology of the *A.boyeri* stocks distributed in the Sea of Marmara, the results of the present study may be useful for the researchers and the fisheries management authority of Türkiye.

Keywords: Abundance, spatial variation, temporal variation, otolith, size, relationship

"Bu Abstract (Özet) bölümü Çanakkale Onsekiz Mart Üniversitesi Lisansüstü Eğitim Enstitüsü Su Ürünleri Av. Ve İşleme Tek. Marmara Denizi'nde Gümüş Balığı'nın (Atherina boyeri Risso, 1810) Bolluğu, Dağılımı ve Bazı Biyolojik Özellikleri konulu Yüksek Lisans Tezimin bazı bölümlerinden oluşturulmuştur."

➢ *ORAL PRESENTATION*

Menfez kesitlerinde karayolu göçme nedenlerinin araştırılması

Abdulmuttalip YOLUR (*ORCID: https://orcid.org/0009-0009-5648-5995*),
Necati KAYAALP (*ORCID: https://orcid.org/0000-0002-6136-5025*)

Dicle Ünüversitesi. Mühendislik Fakültesi, İnşaat Mühendisliği, Diyarbakır, Türkiye

*Sorumlu yazar e-posta: abdulmuttalipyolur@gmail.com

Özet

Son yıllarda Türkiye'de meydana gelen sel ve taşkın olayları, birçok il ve devlet karayolunda menfez ve köprü yaklaşımlarında çökmelere neden olmuştur. Bu çalışma, karayollarında kullanılan menfezlerin, yağış dönemlerinde gerçekleşen taşkın ve sellerde menfez kesitlerinde karayolu göçme mekanizmalarının araştırılmasını amaçlamaktadır. Karayollarını dış kaynaklı yağış ve toprak kayması gibi doğal afetlerden korumak amacıyla inşa edilen yapılar, 'sanat yapıları' olarak adlandırılmaktadır. Bu yapıların temel amacı, karayolunun işlevselliğine katkıda bulunmak, ekonomik ömrünü uzatmak ve güvenli trafik akışını sağlamaktır. Özellikle, karayolu altyapısında en büyük hasara yol açabilecek zemin suyunun güvenli bir şekilde uzaklaştırılması için sanat yapılarına başvurulmaktadır. Drenaj yapılarının etkin bir şekilde işlevlerini yerine getirebilmesi için, işlevine uygun tipte seçilmeli, teknik açıdan uygun konumda ve yeterli boyutlarda inşa edilmeli ve düzenli aralıklarla bakım işlemleri gerçekleştirilmelidir. Menfezler, karayolu veya demiryolu altyapısında, yağışlarla birlikte oluşan su akışının karayoluna zarar vermeden tahliyesini sağlamak, yol altından kablo, boru vb. malzemelerin geçişini kolaylaştırmak gibi amaçlarla inşa edilen mühendislik yapılarıdır. Kullanım amacına veya bulunduğu yere göre farklı türleri bulunan menfezlerin temel görevi, karayolunun bir tarafından diğer tarafına enine geçişler sağlamaktır. Menfez çeşitleri arasında köprü menfezler, kutu menfezler, kemerli menfezler, tabliyeli menfezler (standart köprüler) ve boru (büz) menfezler yer almaktadır.

Anahtar Kelimeler: Menfez, Drenaj, Taşkın

➢ *ORAL PRESENTATION*

A Multi-Criteria Decision-Making Approach for Green Hydrogen Production via Renewable Energy Sources

Medine Türkmen (https://orcid.org/0009-0007-6842-2049)
Serap Ulusam Seçkiner (https://orcid.org/0000-0002-1612-6033)

Gaziantep University, Engineering Faculty, Industrial Engineering Department, Gaziantep, Türkiye.

*Corresponding author e-mail: mt9006@mail2.gantep.edu.tr

Abstract

The global transition toward cleaner energy systems has intensified interest in green hydrogen as a sustainable and low-emission alternative to fossil-based fuels. However, selecting the most appropriate hydrogen production method remains a complex decision-making challenge due to the interplay of technical, economic, environmental, and social factors. This study applies the Analytic Hierarchy Process (AHP), a widely recognized multi-criteria decision-making (MCDM) approach, to systematically evaluate and rank various green hydrogen production technologies. A hierarchical framework was developed incorporating critical criteria such as investment cost, operational efficiency, environmental sustainability, and technological maturity. Expert judgments were used to assign relative weights to each criterion, and competing alternatives were assessed accordingly. The AHP analysis identified RW-Biomass: Bio Photolysis as the most favourable hydrogen production method, achieving the highest overall priority score (0.102), indicating its strong performance across the selected evaluation criteria. These results highlight the method's potential in aligning sustainability goals with practical energy planning and provide valuable insights for decision-makers in shaping future hydrogen strategies. The study confirms the effectiveness of AHP in delivering structured, transparent, and evidence-based assessments in the context of sustainable energy development.

Keywords: Green Hydrogen, Multi-Criteria Decision Making (MCDM), Analytic Hierarchy Process (AHP), Sustainability, Hydrogen Production Technologies

➢ *ORAL PRESENTATION*

Otomotiv Şartlarına Uygun Uv Dayanımı Sağlayan PBT/PET Harmanlarının Geliştirilmesi

Dilara SÜZER (ORCID NO: 0009-0007-2687-9294)

Technology&Innovation Product Specialist, Epsan Plastik

*Sorumlu yazar e-posta: dilara.s@epsan.com

Özet

Polyester reçineleri, diasit ve dialkolün reaksiyonu sonucu suyun uzaklaştırılmasıyla üretilirler. Polyester reçineler, farklı takviyeler ile mekanik özellikleri iyileştirilerek sert, esnek veya dayanıklı hale getirilebilir. Polibutilen tereftalat (PBT) ve Polietilen Tereftalat (PET), polyester ailesinin en yaygın kullanılan üyeleridir. Termoplastik polyesterler, Naylon 6 ve Naylon 66'ya benzer özellikler sergilemekle birlikte, daha düşük su emme kapasitesine ve daha yüksek boyutsal kararlılığa sahiptir. Ancak, ultraviyole (UV) radyasyonun etkisiyle polimer zincirinde parçalanmalar meydana gelebilir. PBT ve PET, geniş fiziksel ve termal özellikleriyle mühendislik plastikleri arasında önemli bir yere sahiptir. Bu polimerlerin UV dayanımlarının artırılması için uygun katkılar ile takviye edilmesi gerekmektedir. Bu çalışma ile PBT/PET kompozitleri için UV dayanımı artırılmış, dış hava koşullarına ve mekanik yüklere karşı daha dirençli yeni bir malzeme geliştirilmesi hedeflenmiştir. Uluslararası standartlara uygun test edilen ve onaylanan ürünler, otomotiv sektöründe rekabet avantajı sağlayacaktır. Özellikle UV dayanımı yüksek ve mekanik özellikleri iyileştirilmiş yeni bir mühendislik plastiği sunularak sektörde önemli bir yenilik sağlaması beklenmektedir. Çalışma kapsamında, %30 cam elyaf ile güçlendirilmiş PBT/PET kompozitlerine iki farklı UV katkısı eklenerek üretilmiş ve performansları karşılaştırılmıştır. Ayrıca, Akrilonitril-Stiren-Akrilat (ASA) katkısı farklı oranlarda kullanılarak malzemenin UV dayanımı ve mekanik özellikler üzerindeki etkisi değerlendirilmiştir. Literatür taramaları tamamlandıktan sonra belirlenen, kontrol numunesi haricinde altı farklı formülasyon, tek yönlü çift vidalı ekstrüder kullanılarak üretilmiştir. Elde edilen granüller enjeksiyon kalıplama makinesinde test plakaları haline getirilerek yoğunluk, mekanik ve UV dayanım testleri için örnekler elde edilmiştir. UV testi hizmet alımı yolu ile yapılmıştır. Karakterizasyon testleri sonucunda, ASA katkısının karışımın mekanik özelliklerine olumlu katkı sağladığı tespit edilmiştir. %15 oranda ASA kullanılan ürünün mekanik değerlerinin; %10 kullanım oranına göre yaklaşık %7,5 artığı gözlemlenmiştir. Ayrıca bu ürün UV testlerinden de başarıyla geçmiştir. Hem mekanik özellikler hem de UV dayanım açısından hedeflenen kriterler sağlanmıştır.

Anahtar kelimeler: PBT, PET, ASA, UV, Otomotiv

➢ *ORAL PRESENTATION*

A genome-wide *in silico* analysis of *PR1* (pathogenesis-related 1) genes in the watermelon (*Citrullus lanatus*)

Tamella Suleymanova[1], Mehmet Emin Uras[2*] (*ORCID: https://orcid.org/0000-0002-0444-9994*), Mustafa Zafer Karagözlü[2] (*ORCID: https://orcid.org/0000-0002-6749-8654*)

[*1]Haliç University, Institute of Graduate Studies, İstanbul, Türkiye.
[2]Haliç University, Faculty of Arts and Sciences, Department of Molecular Biology and Genetics, İstanbul, Türkiye.

*Corresponding author e-mail: meminuras@halic.edu.tr

Abstract

The watermelon (*Citrullus lanatus* (Thunb.) Matsum. & Nakai), a member of the gourd family (Cucurbitaceae), is a widely consumed fruit around the world. It is known for its high-water content and is a prominent food source and notable horticultural crop that is also associated with numerous health benefits. Watermelon cultivation presents significant challenges arising from the presence of both biotic and abiotic stressor factors. In this study, a genome-wide in silico analysis of pathogen-associated 1 (PR1) genes, an important part of the molecular response system activated by biotic stress factors, was performed in the *C. lanatus* genome. The analyses have identified 19 distinct PR1 genes/proteins in the *C. lanatus* genome. The genes in question range in length from 384 to 690 base pairs (bp) and are primarily composed of a single exon. They are located on chromosomes 3, 4, 6, 10, and primarily on chromosome 2, and they regulate the synthesis of ClPR1 proteins, which have a molecular weight ranging from 16 to 215 kilodaltons. These proteins are typically localized in the extracellular space and possess a CAP_PR-1 (IPR001283/IPR034113) domain that confers antibacterial, antifungal, and antiviral properties. ClPR1 proteins are predominantly hydrophilic and comprise a total of 10 conserved motifs, of which 4 are shared among all. The proteins contain a series of special motifs, including CAP1 to CAP4 and CBM, which have been associated with pathogen tolerance. The 3D structures of the proteins were generated based on the homology of the previously characterized *Solanum lycopersicum* 1CFE PR14A protein, and secondary structure analysis was performed. The information obtained on PR1 genes and proteins identified in the watermelon genome has been presented to scientific literature to contribute to the development of disease-resistant varieties.

Keywords: Biotic factors, plant pathogens, tolerance, molecular response.

➢ *ORAL PRESENTATION*

Assessment of the UV-B Protective Potential of Pollenkitt in *Narcissus tazetta*

Melse Su Bilgili[1*] (*ORCID: https://orcid.org/0000-0002-2062-7295*),
Aslıhan Çetinbaş-Genç[2] (*ORCID: https://orcid.org/0000-0001-5125-9395*)

[*1]Marmara University, Institute of Pure and Applied Sciences, Istanbul, Türkiye
[2] Marmara University, Faculty of Science, Department of Biology, Istanbul, Türkiye

*Corresponding author e-mail: melsesubilgili@gmail.com

Abstract

This study aimed to assess the UV-B protective potential of the pollenkitt in pollen grains of *Narcissus tazetta*. For this purpose, pollenkitt isolates were obtained from pollen grains using dH_2O (dH_2O group, control) and ethanol (ethanol group). Additionally, pollen grains were first exposed to UV-B radiation, followed by isolation of pollenkitt using dH_2O (UV-B+dH_2O group) and ethanol (UV-B+ethanol group). Furthermore, pollenkitt isolates obtained through dH_2O and ethanol isolation were subsequently exposed to UV-B radiation (dH_2O+UV-B group and ethanol+UV-B group). DPPH% activity, total phenolic and flavonoid content, and UV-B absorption capacity of all pollenkitt isolates were analyzed. The findings were evaluated using heat-maps, correlation analysis, and PCA biplots. According to our findings, ethanol was more effective than dH_2O in pollenkitt isolation. DPPH% activity decreased, while phenolic and flavonoid contents increased in the ethanol, UV-B+ethanol, and ethanol+UV-B groups compared to the control. However, the UV-B absorption capacity of the isolates decreased in all treatment groups compared to the control. The heat-map ranking of UV-B protective potential from highest to lowest was: UV-B+ethanol, ethanol+UV-B, ethanol, dH_2O, dH_2O+UV-B, UV-B+dH_2O. Correlation analysis showed a positive link between phenolic and flavonoid contents and a negative link with DPPH activity. According to the PCA biplot analysis, UV-B absorbance values contributed the most to the overall variance, whereas total flavonoid and phenolic contents contributed the least. The UV-B+ethanol, ethanol, and ethanol+UV-B groups were linked to phenolic and flavonoid contents, while the UV-B+dH_2O and dH_2O+UV-B groups aligned with DPPH activity, and the dH_2O group with UV-B absorbance. The findings suggest that ethanol-isolated samples exposed to UV-B may indicate a protective role of pollenkitt against UV-B radiation. This work was financially supported by the Marmara University Scientific Research Projects Commission (Project no: FYL-2025-11606).

Keywords: DPPH activity, flavonoids, phenolic compounds, pollen, pollenkitt, UV-B

➢ *ORAL PRESENTATION*

Antioxidant Responses in *Camellia sinensis* Pollen Exposed to Low Temperatures

Sena Acar* (*ORCID: https://orcid.org/0009-0003-5912-5852*), Aslıhan Çetinbaş-Genç[2] (*ORCID: https://orcid.org/0000-0001-5125-9395*)

*[1]Marmara University, Institute of Pure and Applied Sciences, Istanbul, Türkiye
[2] Marmara University, Faculty of Science, Department of Biology, Istanbul, Türkiye

*Corresponding author e-mail: senaacar.mu@gmail.com

Abstract

The aim of this study was to investigate the antioxidant responses of pollen grains of *Camellia sinensis* under low-temperature stress. For this purpose, pollen grains from the low-temperature stress treatment groups were germinated at 5, 10, and 15 °C, while control group pollen grains were germinated at room temperature in a germination medium containing 8% sucrose for 4 hours. According to the findings, pollen germination rates and pollen tube lengths decreased significantly in response to temperature reduction compared to the control group. The antioxidant response of pollen grains to low-temperature stress was assessed by analysing the total antioxidant activity as well as the activity or levels of enzymatic and non-enzymatic antioxidants. DPPH% activity significantly decreased only after the 5 °C treatment. Conversely, total phenolic and flavonoid contents significantly decreased at all treatment temperatures compared to the control group. Superoxide dismutase activity increased significantly only after the 5 °C treatment, while no significant changes were observed in catalase activity at any temperature. However, ascorbate peroxidase activity showed a significant increase after 5 and 10 °C treatments. Overall, the results indicate that low temperatures disrupt the oxidative stress balance in *Camellia sinensis* pollen grains, exerting a notable inhibitory effect on pollen performance. This work was financially supported by the Marmara University Scientific Research Projects Commission (Project no: FYL-2025-11603).

Keywords: antioxidant response, *Camellia sinensis*, low-temperature stress, pollen

➢ *ORAL PRESENTATION*

Functional Analysis of Missense SNPs in the CYP2D6 Gene Using *In Silico* Methods

[*1]Hacer Menekşe Polat, [2]Esma Eryılmaz Doğan
[*1](ORCID: https://orcid.org/0000-0003-3216-4731), [2](ORCID: https://orcid.org/0000-0001-6809-7513)

Selçuk University, Faculty of Technology, Department of Biomedical Engineering, Konya, Türkiye

*Corresponding author e-mail: eeryilmaz@selcuk.edu.tr

Abstract

The CYP2D6 gene is a key member of the cytochrome P450 enzyme family involved in drug metabolism. Missense single nucleotide polymorphisms (SNPs) in this gene can alter protein function and contribute to interindividual variability in drug response. In this study, selected missense SNPs in the human CYP2D6 gene were analyzed using various in silico prediction tools, including SIFT, PolyPhen-2, PANTHER, FATHMM, and MutPred2. The functional effects of these variants were evaluated and their potential deleterious impact was classified. According to the results, the R296C variant was predicted to be deleterious by all five tools, highlighting it as the most critical variant in this study. Additionally, R245S, R296S, and R245G were identified as potentially harmful by at least three of the prediction tools. These findings indicate that these variants may significantly impair the function of the CYP2D6 protein. In future phases of this study, these variants will be further investigated through protein-protein and gene-gene interaction analyses, as well as three-dimensional structural evaluations using tools such as I-TASSER and HOPE. The results are expected to contribute to a better understanding of genetic variations in drug metabolism and to support the advancement of personalized medicine.

Keywords: CYP2D6, missense SNP, *in silico* analysis, protein interactions, pharmacogenetics

➢ *ORAL PRESENTATION*

European Ionospheric Response to the May 2024 Gannon Geomagnetic Superstorm

Elif Çiftçi[1*] (*ORCID: https://orcid.org/0009-0002-4391-0058*), Özlem Hacıoğlu[2] (*ORCID: https://orcid.org/0000-0002-0747-6752*), Burak Kotan[3] (*https://orcid.org/0000-0003-2105-7498)*

[*1]Bogazici University, Kandilli Observatory and Earthquake Research Institute, Department of Geophysics, İstanbul, Türkiye
[2]Karadeniz Technical University, Department of Geophysical Engineering, Trabzon, Türkiye
[3]Bogazici University, Kandilli Observatory and Earthquake Research Institute, Department of Geodesy, İstanbul, Türkiye

*Corresponding author e-mail: elif.tolak@bogazici.edu.tr

Abstract

The Gannon Geomagnetic Superstorm of May 2024, classified as a G5-level extreme space weather event, caused profound disturbances in Earth's magnetosphere and ionosphere, particularly over the European sector. This study investigates the ionospheric response to the storm by integrating Global Navigation Satellite System (GNSS)-based Total Electron Content (TEC) data from the Centre for Orbit Determination in Europe (CODE), ground-based geomagnetic observations from the IZN observatory in Türkiye, and key interplanetary parameters. The results reveal a clear storm-time evolution: a significant TEC enhancement during the main phase, followed by widespread and persistent TEC depletions during the early recovery phase, reaching up to –35 TECU across mid-latitudes. Geomagnetic field perturbations at IZN, including marked negative deviations in the horizontal component (ΔH), fluctuations in declination (ΔD), and enhancements in the vertical component (ΔZ), coincide temporally with TEC depressions, indicating strong magnetosphere–ionosphere coupling. The simultaneous occurrence of intense interplanetary electric field (IEFy) penetration, southward turning of the interplanetary magnetic field (IMF), and ring current intensification supports the interpretation of enhanced high-latitude energy input as a key driver of mid-latitude ionospheric disturbances. This study highlights the necessity of continuous space weather monitoring to better understand and mitigate extreme ionospheric variability during future storm scenarios.

Keywords: Gannon superstorm, space weather, geomagnetic storm, GNSS, Total Electron Content, Europe

➢ *ORAL PRESENTATION*

Numerical simulations of 3D Magnetotellurics for Hydrocarbon exploration: Focus on overthrust structures

Özlem Hacıoğlu[1*] (*ORCID: https://orcid.org/0000-0002-0747-6752*)

[*1]Karadeniz Technical University, Department of Geophysical Engineering, Trabzon, Türkiye

*Corresponding author e-mail: ozlem.hacioglu@ktu.edu.tr

Abstract

The seismic reflection method has been widely utilized in oil and gas exploration to detect potential hydrocarbon zones due to its capability to provide detailed insights into sedimentary layers. However, in regions where high-velocity rocks overlie low-velocity sediments such as resistive volcanic cover above more conductive zones in overthrust terrains seismic methods face challenges in distinguishing hydrocarbon-bearing areas from other sedimentary units. This difficulty arises from the decrease in seismic velocity at the base of the volcanic layers and the dispersive nature of volcanic rocks. In such cases, the magnetotelluric method can be employed to achieve sufficient investigation depths and to image subsurface structures effectively.

In this study, a synthetic dataset from a station network was used to demonstrate the significance of three-dimensional magnetotellurics in areas covered by high-resistivity rocks, aiming to identify hydrocarbon-bearing zones and typical thrust-related structures. Various representative reservoir models characterized by high-resistivity cover layers overlying lower-resistivity units and incorporating folded and overthrust geometries were constructed to compute synthetic magnetotelluric responses and assess the effectiveness of the method.

The results indicate that the subsurface models derived from inversion accurately reconstructed the initial hydrocarbon trap scenarios, emphasizing that 3D magnetotellurics should be considered prior to seismic surveys in contractional tectonic regimes, particularly in fold-and-thrust belts. However, it is important to acknowledge the limitations of the method in hydrocarbon exploration.

Keywords: Hydrocarbons, Fold-and-thrust Belts, Trap, Synthetic Modeling

➢ *ORAL PRESENTATION*

Endüstriyel Meyve Posalarının Antidiyabetik Potansiyeli: a-Amilaz İnhibisyonu

Esma Aslan[1*] (*https://orcid.org/0009-0002-3266-0882*),
Nurullah Zekeriya Akar[1] (*https://orcid.org/0000-0003-2485-2382)*

[*1]İstanbul Gelişim Üniversitesi, İstanbul Gelişim Meslek Yüksekokulu, Gıda Teknolojisi, İstanbul, Türkiye.

*Sorumlu yazar e-posta: 4esmaaslan@gmail.com

Özet

Diyabetin küresel prevalansının önümüzdeki yıllarda önemli ölçüde artacağı ve bu artışın özellikle ilaç erişiminin kısıtlı olduğu gelişmekte olan ülkelerde önemli bir sosyoekonomik yük oluşturacağı öngörülmektedir. Postprandiyal hiperglisemi, tip 2 diyabet gelişiminde başlıca risk faktörlerinden biridir. Bu nedenle, tip 2 diyabetin yönetiminde en etkili yaklaşımlardan biri, yemek sonrası karbonhidrat emilimini düzenlemek ve glukozun kana geçişini geciktirmektir. Nişasta, diyetle alınan başlıca karbonhidrat kaynağı olduğundan nişasta sindiriminin yavaşlatılması diyabetik bireylerde glisemik kontrolü sağlamada etkili yöntemlerden biridir. Bu bağlamda karbonhidrat sindiriminde görevli olan α-amilaz enziminin inhibisyonu, postprandiyal glukoz düzeylerini azaltarak antidiyabetik diyetlerin geliştirilmesine olanak sağlayabilir. Meyve ve sebzeler ile bunların işlenmesi sonucu oluşan yan ürünler, α-amilaz inhibitör aktivitesi gösteren flavonoidler, fenolik asitler gibi sekonder metabolitler açısından zengindir. Bu çalışmada, Türkiye meyve suyu endüstrisinde yaygın olarak işlenen elma, kayısı ve şeftali posalarının α-amilaz inhibitör aktiviteleri araştırılmıştır. Endüstriyel yan ürünü olan meyve posaları kontrollü koşullarda kurutulup öğütülerek sulu ekstraktları hazırlanmıştır. Ekstraktların a-amilaz inhibitör aktiviteleri nişasta-iyot renk esaslı spektrofotometrik yöntemle belirlenmiştir. A-amilaz inhibisyon oranları sırasıyla elma için %13.52, kayısı için %54.76 ve şeftali için %5.14 olarak tespit edilmiştir. Elde edilen sonuçlar özellikle kayısı posasının a-amilaz enzimi üzerine anlamlı bir inhibitör etkiye sahip olduğu ve antidiyabetik beslenme için iyi bir kaynak olabileceğini gösterdi.

Anahtar Kelimeler: Meyve Posası, Antidiyabetik, a-Amilaz, İnhibisyon

➢ *ORAL PRESENTATION*

Gemi Emisyonlarını Azaltmaya Yönelik Yakıt Alternatiflerinin Seçiminde Etkili Faktörlerin Belirlenmesi

Bağcan Çatı[1*] *(ORCID: https://orcid.org/0009-0007-6095-6644)*, Mehmet Ali Vahdet Yılmaz[2] *(ORCID: https://orcid.org/0009-0004-8985-2994),* Remzi Fışkın[3,4] *(ORCID: https://orcid.org/0000-0002-5949-0193)*

[*1]Ordu Üniversitesi, Fen Bilimleri Enstitüsü, Deniz Ulaştırma İşletme Mühendisliği Ana Bilim Dalı, Ordu, Türkiye.
[2]Karadeniz Teknik Üniversitesi, Deniz Bilimleri Fakültesi, Deniz Ulaştırma İşletme Mühendisliği Bölümü, Trabzon, Türkiye.
[3]Ordu Üniversitesi, Deniz Bilimleri Fakültesi, Deniz Ulaştırma İşletme Mühendisliği Bölümü, Ordu, Türkiye.
[4]Danimarka Teknik Üniversitesi, İşbirlikçi Otonom Sistemler Merkezi, Kopenhag, Danimarka.

*Sorumlu yazar e-posta: bagcan5960@gmail.com

Özet

Enerji üretiminde kullanılan yakıtlardan kaynaklanan karbon, azot ve sülfür emisyonları, çevresel sürdürülebilirlik ve insan sağlığı açısından önemli tehditler oluşturmaktadır. Artan dünya nüfusuna bağlı olarak deniz taşımacılığı da belirgin şekilde artmış; bu durum, gemi kaynaklı emisyonlarda kayda değer bir yükselişe yol açmıştır. Bu bağlamda, Uluslararası Denizcilik Örgütü (IMO) tarafından 2020 yılında yürürlüğe giren düzenlemeler ile Emisyon Kontrol Alanları'nda (ECA) deniz yakıtlarındaki sülfür içeriği %0,1; diğer bölgelerde ise %0,5 ile sınırlandırılmıştır. Ayrıca IMO, 2050 yılına kadar karbon nötr olma hedefi doğrultusunda çevre dostu yakıtların kullanımını teşvik etmektedir. Bu çalışmada, günümüzde yeni inşa edilen gemilerde öne çıkan dört farklı yakıt alternatifinin (sıvılaştırılmış doğal gaz (LNG), metanol, geleneksel yakıt ve scrubber ile donatılmış geleneksel yakıt) tercih edilirliğini etkileyen faktörler belirlenmiştir. Söz konusu alternatifler teknik, maliyet ve sosyal ana başlıkları altında sınıflandırılmış ve bu başlıklar altında yer alan alt kriterler, uzman görüşleri doğrultusunda literatür desteğiyle ortaya konmuştur. Çalışma, henüz değerlendirme aşamasına geçilmemiş bir ön araştırma niteliğindedir. Devam eden süreçte, belirlenen bu kriterler doğrultusunda çok kriterli karar verme (ÇKKV) yöntemleri olan Analitik Hiyerarşi Süreci (AHP), Ağırlıklı Toplam Ürün Değerlendirmesi (WASPAS) ve Gri İlişkisel Analiz (GRA) gibi yöntemler ile alternatiflerin karşılaştırmalı analizlerinin gerçekleştirilmesi planlanmaktadır. Bu kapsamda elde edilecek bulguların, denizcilik sektöründe sürdürülebilir ve dengeli yakıt tercihi yapmak isteyen karar vericilere yol göstermesi hedeflenmektedir.

Anahtar Kelimeler: Emisyon, Yeni İnşa Gemiler, Sürdürülebilirlik, Deniz Taşımacılığı

➢ *ORAL PRESENTATION*

Effect of Fat Content and Fermentation Time on Kefir Quality

Hatice Sıçramaz[1*] (*ORCID: https://orcid.org/0000-0002-5943-9566*),
Buse Güven[1] (*ORCID: https://orcid.org/0009-0000-1342-5823*)

[*1]Sakarya University, Faculty of Engineering, Department of Food Engineering, Sakarya, Turkey.

*Corresponding author e-mail: haticesicramaz@sakarya.edu.tr

Abstract

Kefir has been gaining increasing global attention both as a traditional food and a functional food due to its probiotic nature. In response to growing consumer demand, optimizing both the nutritional value and sensory quality of kefir has become a significant area of research. This study aimed to evaluate the effects of fat content and fermentation time on the quality of kefir. For this purpose, kefir was produced using low-fat (0.1%) and full-fat (3.1%) UHT milk, and subjected to two different incubation times: 20 and 26 hours. The resulting kefir samples were analyzed in terms of pH, water-holding capacity (WHC), viscosity, and sensory attributes. According to the results, after 20 hours of fermentation, both full-fat and low-fat kefir exhibited similar pH values. However, at 26 hours, pH levels decreased in both, with a more pronounced drop in the low-fat sample. WHC followed the descending order: full-fat (26 h), full-fat (20 h), low-fat (26 h), and low-fat (20 h) kefir, with respective values of 58%, 50%, 32%, and 28%. Viscosity was notably higher in full-fat samples, whereas the lowest viscosity was recorded in the low-fat kefir fermented for 20 hours. Sensory evaluation revealed that full-fat kefirs were perceived as less sour, and the sourest sample was identified as the low-fat kefir fermented for 26 hours. The most preferred sample in terms of taste and overall acceptability was the full-fat kefir fermented for 26 hours, while the least favored was the low-fat kefir with the same fermentation time. These findings indicated that both fat content and fermentation time are critical parameters affecting the physicochemical properties and consumer acceptance of kefir.

Keywords: kefir, fermentation time, fat content, physicochemical properties, sensory evaluation.

➢ *ORAL PRESENTATION*

Sustainable Production from Waste Rooster Combs: High-Purity Hyaluronic Acid Isolation and Structural Analysis

Banuay Coşkun[1] (*ORCID: https://orcid.org/0000-0003-2645-8565*

[1] Eskişehir Technical University, Chemistry Department, Eskişehir, Türkiye

*Corresponding author e-mail: banuaycoskun@ogr.eskisehir.edu.tr

Abstract

Hyaluronic acid (HA) is a natural polysaccharide widely used in medicine, cosmetics, and tissue engineering due to its biocompatibility and biodegradability. However, it faces performance and industrial applicability limitations when isolated from biological sources due to impurities such as proteins, lipids, and nucleic acids. This study aims to achieve high-purity HA production from a low-cost animal waste source, rooster combs, while analyzing the process's sustainability of the process and structural properties of polymer [1,2]. Rooster comb tissues were processed using an optimized protocol that involved mechanical separation, sequential alcohol precipitation, ultracentrifugation, and dialysis, leading to the isolation of pure HA. UV-VIS spectroscopy confirmed the effective removal of impurities, as shown by a notable increase characteristic absorption peaks of HA at 200-220 nm after purification. Gel Permeation Chromatography (GPC) analysis revealed a homogeneous molecular weight distribution and a high molar mass for HA, while FTIR spectroscopy confirmed the preservation of its core functional groups (carboxylate, acetamide). This study demonstrates that rooster comb waste can be a sustainable resource for industrial-scale HA production, offering a 35% cost advantage compared to conventional methods. The obtained high-purity HA can be accepted as suitable for critical applications such as cosmetic formulations, viscosupplementation eye drops, and intra-articular injections [3-5]. These findings suggest the biotechnological valorization of animal waste, which would contribute to a circular economy for a green world and a viable economic model.

Keywords: Hyaluronic acid, rooster comb waste, sustainable production.

References:

[1] Snetkov, P., Zakharova, K., Морозкина, C. H., Olekhnovich, R. O., & Uspenskaya, M. V. (2020). Hyaluronic acid: the influence of molecular weight on structural, physical, physico-chemical, and degradable properties of biopolymer. Polymers, 12(8), 1800.

[2] Schulz, A., Germann, A., Heinz, W. R., Engelhard, M., Menz, H., Rickmann, A., … & Szurman, P. (2022). Translation of hyaluronic acid–based vitreous substitutes towards current regulations for medical devices. Acta Ophthalmologica, 101(4), 422-432.

[3] Shen, D., Chen, M., Chen, K., Wang, T., Lu, L., & Yang, X. (2018). Efficacy of hyaluronic acid after knee arthroscopy: a systematic review and meta-analysis. Journal of Rehabilitation Medicine, 50(10), 860-865.

[4] Qiao, J., Jia, Q., Jin, H., Li, F., He, C., Yang, J. & Fu, L. (2019). Long-term follow-up of longevity and diffusion pattern of hyaluronic acid in nasolabial fold correction through high-frequency ultrasound. Plastic &Amp; Reconstructive Surgery, 144(2), 189e-196e.

[5] Zheng, F., Xin, X., He, F., Liu, J., & Cui, Y. (2020). Meta-analysis on the use of hyaluronic acid gel to prevent intrauterine adhesion after intrauterine operations. Experimental and Therapeutic Medicine.

➢ *ORAL PRESENTATION*

Genetic identification of *Myomimus roachi* (Rodentia: Gliridae) from Türkiye using DNA barcoding

Ercüment Çolak[1] (*ORCID: https://orcid.org/0000-0001-5826-1615*), Engin Selvi[1*] (*ORCID: https://orcid.org/0000-0001-5370-3023*) , Teoman Kankılıç[2] (*ORCID: https://orcid.org/0000-0002-9576-5887*), Perinçek Seçkinozan ŞEKER[3*] (*ORCID: https://orcid.org/0000-0002-6103-4840*), Reyhan Çolak[1](*ORCID: https://orcid.org/0000-0003-1031*), Nuri Yiğit[1] (*ORCID: https://orcid.org/0000-0001-8426-2144*)

[*1]Ankara University, Faculty of Science, Department of Biology, Ankara, Türkiye.
[2]Ömer Halisdemir University, Faculty of Science and Letter, Department of Biotechnology, Niğde, Türkiye.
[*3]Artvin Çoruh University, Artvin Vocational School, Department of Forestry, Artvin, Türkiye.

*Corresponding author e-mail: eselvi@ankara.edu.tr, seckinperincek@artvin.edu.tr

Abstract

Myomimus roachi, or Roach's mouse-tailed dormouse, is a small rodent in the family Gliridae, found only in Bulgaria, Greece, and Türkiye. It inhabits scrubland and semi-open environments such as orchards and riverbanks. Due to its limited range and habitat degradation, it is classified as Vulnerable (VU) by the IUCN. Genetic characterization is vital for understanding evolutionary history of the species and supporting conservation efforts. The Cytochrome c Oxidase Subunit I gene (*COI*), known as the DNA barcode, is widely used for reliable species identification in such studies. In this context, the current study analyzed the *COI* gene sequences of eight *M. roachi* samples from Edirne and Çanakkale in Türkiye to assess genetic variation and support conservation strategies for the first time. Multiple sequence alignment of the 563 bp long partial sequence of the *COI* gene revealed 508 monomorphic and 55 polymorphic sites, including 3 parsimony-informative sites. The estimated average transition/transversion ratio was 1.40. Nucleotide frequencies were as follows: A = 25.22%, T/U = 31.82%, C = 26.98%, and G = 15.99%. Analysis of partial gene sequences from the eight samples revealed a total of five haplotypes, which clustered into two distinct genetic groups: three from Edirne and two from Çanakkale. The haplotype diversity (Hd) observed in all samples of *M. roachi* was 0.857 ± 0.108, while the nucleotide diversity (π) was 0.02582 ± 0.01608. In the Edirne population of *M. roachi*, Hd was 0.700 ± 0.218 and π was 0.03837 ± 0.02177. On the other hand, in the Çanakkale population, Hd was 0.667 ± 0.314, and π was 0.00118 ± 0.00056. Both populations exhibited moderate haplotype diversity may indicate that the populations have retained genetic diversity from the past or are recovering from a historical reduction in size. The higher standard error observed in the Çanakkale population may be due to the small sample size or an uneven distribution of haplotypes. Based on nucleotide diversity, the greater genetic variation observed in the Edirne population may suggest a larger effective population size, an older evolutionary history, or a less recent bottleneck. On the other hand, the Çanakkale population, with low nucleotide diversity, may have experienced a recent founder effect, bottleneck, or lower mutation rate, and could be more genetically homogenous. The multimodal mismatch distribution observed in *M. roachi* suggested the presence of population structure or long-term demographic stability, rather than a recent population expansion. The relatively low Raggedness statistic (r = 0.1735) indicated a moderately smooth mismatch distribution, which may also reflect moderate genetic structuring or a recovery following a historical bottleneck. Based on the Kimura 2-parameter model, the genetic distance between the Edirne and Çanakkale was approximately 2.36%. The fixation index (FST: 0.11640), a measure of population differentiation due to genetic structure, revealed also moderate genetic differentiation ($0.05 < FST < 0.15$) between the Edirne and Çanakkale populations. These findings highlighted the presence of genetic structure between two populations of *M. roachi* and emphasized the importance of regional conservation strategies to preserve the species' genetic diversity and evolutionary potential. Overall, the genetic differentiation and diversity observed between the Edirne and Çanakkale populations provided valuable insights into the evolutionary dynamics of *M. roachi* and underscored the need for further studies with larger sample sizes to better inform conservation efforts. Also, this study represented a pioneering effort in evaluating the genetic structure of *M. roachi* populations in Türkiye at the molecular level for the first time.

Keywords: *Myomimus roachi*, DNA barcoding, genetic structure, Türkiye

➢ *ORAL PRESENTATION*

A faunistic survey on wild bees of the Aegean region, Turkiye

Serap SENOL TUNCAY[1*] (*ORCID ID: 0009-0002-2523-6768*), Baris GULCU[2] (*ORCID ID: 0000-0002-4808-1538*), Canan HAZIR[3] **(***ORCID ID: 0000-0003-4471-5115***),** Harun CIMEN[4] (*ORCID ID: 0000-0002-0106-4183*), Mustapha TOURAY[5] (*ORCID ID: 0000-0002-9550-0782*), Sebnem Hazal GULSEN[6] (*ORCHOD ID: 0000-0001-6981-7025*), Selcuk HAZIR[7] (*ORCID ID: 0000-0001-9298-1472*)

[1]Mimar Sinan District, Sair Omer Boulevard, Huzurkent site, Block C, Efeler, Aydin, TURKIYE.
[2]Department of Biology, Faculty of Arts and Science, Duzce University, Duzce, TURKIYE.
[3]Environmental Health Programme, Aydin Health Services Vocational School, Aydin Adnan Menderes University, Aydin, TURKIYE.
[4]Recombinant DNA and Recombinant Protein Application and Research Center, Aydin Adnan Menderes University, Aydin, TURKIYE.
[5]Department of Biosciences, Faculty of Science and Engineering, Swansea University, Swansea, UK.
[6]Department of Plant and Animal Production, Kocarli Vocational School, Aydin Adnan Menderes University, Aydin, TURKIYE.
[7]Department of Biology, Faculty of Science, Aydın Adnan Menderes University, Aydin, TURKIYE.

*Corresponding author e-mail: srpsenol@gmail.com

Abstract

Bees are the most important pollinators of native and cultivated plants. An estimated one-third of the human diet consists of fruits, vegetables, and nuts that depend primarily on bee pollination. Approximately 73% of cultivated plants in the world are pollinated by bees. Bees pollinate not only cultivated plants but also wild plants in nature, enabling these plants to multiply and spread, wildlife to develop, and diversity in plants and animals to increase. There are approximately 20,000 identified species of bees in the world. While some groups, such as honey bees and bumblebees, have been well studied, studies on the remaining wild bee species, which constitute the vast majority, are insufficient. Although the number of bee species recorded in Turkiye is 1495, this number is estimated to be around 2000.
In spite of the fact that Turkiye is a country with a rich diversity of plants and pollinators, there are limited studies on wild bee diversity. The aim of this study is to determine the diversity of wild bees in the Aegean Region of Turkiye. Within the scope of the research, a total of 444 wild bee specimens were collected from Afyonkarahisar, Aydin, Balikesir, Izmir, Kutahya and Manisa provinces in 2023 and 2024, when climatic conditions were suitable. The collected specimens are kept in the Turkish Wild Bee Museum established within Aydin Adnan Menderes University. According to morphological diagnosis, wild bee samples belonging to the families Andrenidae, Apidae, Colletidae, Halictidae and Megachilidae were identified. After morphological identification, one to two legs of the pinned bee specimens were preserved in absolute ethanol for future molecular identification. Mitochondrial DNA cytochrome oxidase I (COXI) gene will be used for molecular identification of the species.

Keywords: Wild bees-Turkiye-Pollination-Biodiversity.

➢ *ORAL PRESENTATION*

Determination of the role of fullerenol and green-synthesized iron nanoparticles in enhancing drought tolerance in safflower plants through photochemical mechanisms

Şeküre ÇULHA ERDAL

Hacettepe University, Faculty of Science, Department of Biology, 06800, Ankara, Turkey

*Corresponding author e-mail: sekureculha85@hacettepe.edu.tr

Abstract

In recent years, nanoparticle applications in sustainable agriculture have been explored as a strategy to mitigate the impact of drought on the yield and growth of agricultural plants. This study aims to evaluate the potential of organic-based iron nanoparticles (FeNP) and/or fullerenol in mitigating the effects of drought on safflower plants by analyzing their impact on the photosynthetic pathway, a key determinant of plant productivity. Safflower cultivar (*Carthamus tinctorius* L., Olas) was grown in controlled growth room for 18 days and then plants were initially treated with fullerenol via foliar application (10 mg/L) and FeNP via soil application (60 mg/L), and were subsequently exposed to drought induced by PEG for 7 days (Application groups: Control, Drought, Fullenerol, FeNP, Fullenerol+FeNP, Fullenerol+Drought, FeNP+Drought; Fullenerol+FeNP+Drought). Analysis of the fluorescence transient (OJIP) curve (Kautsky curve) in safflower leaves revealed that, while a typical OJIP polyphasic rise was observed, there were variations compared to the control in drought and nanoparticle treatments. There was a significant reduction in the J-I-P phases, which indicates the electron transfer from Q_A to PSI, under the drought treatment, but nanoparticle applications attenuated this effect. Besides, drought caused significant decrease in the photosynthetic performance indexes (PIs—PI_{ABS} and PI_{TOT}) and their partial components [RC/ABS, $\varphi P_0/(1-\varphi P_0)$, $\psi_0/(1-\psi_0)$ and $\delta R_0/(1-\delta R_0)$] of safflower cultivar. However, the applications of FeNP and fullerenol anf their combination maintained the performance indexes at significantly higher levels in drought-stressed plants. Comparable results were also observed in quantum yields and energy flux per reaction center. The findings indicate that the adverse effects of drought on photosynthesis can be effectively mitigated through the combined application of fullerenol and Fe nanoparticles.

Keywords: Safflower, carbon-based fullerenol nanoparticle, green-synthesized iron nanoparticles, photosynthetic pathway

➢ *ORAL PRESENTATION*

Removal of 2-(4-isobutylphenyl)propanoate (ibuprofen) from aqueous solutions by adsorption onto carbon fiber

Timur TONGUR[1*] (https://orcid.org/0000-0003-3030-8930)

[1]*Akdeniz University, Faculty of Science, Department of Chemistry, Antalya, Turkey*

*Corresponding author e-mail :timurtongur@akdeniz.edu.tr

Abstract

Underground and surface water resources are increasingly threatened by various chemical pollutants, including salts, dyes, production wastes, pesticides, heavy metals, and pharmaceuticals originating from industrial and commercial usage. It has become inevitable to deal with water contamination at the source of the problem or before use. Accordingly, effective decontamination methods are essential to ensure the safety of consumable water. Among the available techniques, adsorption is the most preferred technique due to its cost-effectiveness, low energy requirement, high removal efficiency, and operational simplicity. In the present study, the adsorption-based removal of 2-(4-isobutylphenyl)propanoate (ibuprofen), which is an active pharmaceutical ingredient, from aqueous solution was examined by using activated carbon fiber (ACF) as the adsorbent. Excellent adsorption efficiency (95%) was achieved for ibuprofen. Adsorption kinetic was evaluated by applying experimental data to pseudo-first order and pseudo-second order kinetic models and the experimental data were fitted to pseudo-second-order kinetic model. Furthermore, adsorption isotherms were obtained at 25 °C through batch experiments and evaluated using both Langmuir and Freundlich isotherm models. The experimental data was well-fitted to Langmuir isotherm model that means homogenous and monolayer coverage was occurred. Gibbs free energy was found to be negative (–13.68 kJ mol^{-1}) that indicated a spontaneous and thermodynamically favorable adsorption process.

Keywords: adsorption kinetics, adsorption isotherms, ibuprofen, UV-vis spectrophotometer

➢ *ORAL PRESENTATION*

Thermodynamic analysis of internal heat recovery between the condenser and evaporator outlets in an air-source heat pump

Kutbay Sezen[1*] (*ORCID: https://orcid.org/0000-0003-1018-5793*)

[*1]Alanya Alaaddin Keykubat University, ALTSO Vocational School of Higher Education, Air Conditioning and Refrigeration Technology, Antalya, Türkiye.

*Corresponding author e-mail: kutbay.sezen@alanya.edu.tr

Abstract

Enhancing the efficiency and reliability of vapor compression refrigeration systems remains a key goal in the development of sustainable HVAC technologies. One method being explored is internal heat recovery, which modifies the refrigerant's thermal conditions and may impact the system's overall performance. This study investigates the impact of internal heat recovery between the condenser outlet and evaporator outlet in an air-source heat pump system using R32 refrigerant. A numerical model was developed to evaluate the effect of varying levels of internal heat exchange on thermodynamic performance, assuming constant isentropic and adiabatic efficiencies for the compressor. Simulations were conducted in both cooling and heating modes, and variations in subcooling, superheating, compressor work, and coefficient of performance (COP) were analysed. The results indicate that as the amount of internal heat recovery increases, superheating rises more significantly than subcooling—nearly twice as much. In heating mode, subcooling increases from 5 °C to 11.4 °C and superheat from 5 °C to 17.1 °C, while COP decreases from 3.19 to 3.09 as the recovered heat increases from 0 to 300 W. In cooling mode, with 300 W of internal heat recovery, subcooling rises from 5 °C to 9.5 °C and superheat from 5 °C to 13.2 °C, while COP drops from 2.64 to 2.52. These findings show that internal heat recovery does not enhance thermodynamic performance; rather, it leads to a slight performance drop under constant-efficiency assumptions. The model does not account for potential improvements in isentropic or adiabatic efficiency that may result from increased superheat. Despite the minor decrease in calculated performance, internal heat recovery may offer practical benefits such as improving vapor quality at the compressor inlet, increasing system reliability, and potentially enhancing isentropic efficiency under real-world operating conditions. Future work may extend this analysis by incorporating experimental measurements of how isentropic and adiabatic efficiencies vary with refrigerant superheat, potentially revealing performance benefits not captured under the current assumptions.

Keywords: Internal heat recovery, air-source heat pump, thermodynamic performance, superheating, subcooling

➢ *ORAL PRESENTATION*

Size Effect on WS_2 Structures in Electrochemical Ammonia Synthesis via Nitrogen Reduction Reaction

Talha Kuru[1, 2*] (*ORCID: https://orcid.org/0000-0001-9662-8211*), Yigit Osman Akyıldız[2,3] (*ORCID: https://orcid.org/0000-0001-7057-7268*), Ali Keleş[2], Barış Arıcı[2], Emre Aslan[3] (*ORCID: https://orcid.org/0000-0002-7672-2873*), İmren Hatay Patır[1] (*ORCID: https://orcid.org/0000-0003-2937-6557*)

[1]Selcuk University, Department of Biotechnology, 42030, Konya, Türkiye, e-mail: talha59510@gmail.com
[2]YEO Technology R&D Center, 34870, İstanbul, Türkiye
[3]Selcuk University, Department of Biochemistry, 42030, Konya, Türkiye

*Corresponding author e-mail: talha59510@gmail.com

Abstract

Ammonia is gaining attention as a renewable energy carrier due to its high hydrogen content, ease of storage, and carbon-free combustion. However, the vast majority of global ammonia production still relies on the Haber–Bosch process, an energy-intensive method that operates under high temperature and pressure and is responsible for significant carbon dioxide emissions, thereby raising environmental and sustainability concerns. Electrochemical ammonia synthesis has emerged as a sustainable alternative to the energy-intensive Haber–Bosch process, offering potential for ammonia production under ambient conditions. However, the low Faradaic efficiencies of current electrochemical methods remain a major challenge. Transition metal dichalcogenides (TMDs) are a class of layered materials known for their unique electronic, optical, and mechanical properties, which can be finely tuned by changing their composition or structure. Among TMDs, tungsten disulfide (WS_2) stands out due to its excellent chemical stability, layered crystal structure, and favorable electronic properties. Its exposed edge sites and strong adsorption capability for nitrogen-containing species make it a particularly attractive electrocatalyst for ammonia synthesis. Nanostructured materials often exhibit enhanced electrocatalytic performance compared to their bulk or microscale counterparts due to their higher surface area, increased density of active sites, and shortened ion/electron diffusion paths. In contrast, microscale structures may suffer from limited surface reactivity and slower charge transport, which can reduce their overall catalytic efficiency in electrochemical reactions. In this study, bulk (micro) and nanoscale WS_2 structures were investigated as electrocatalysts for electrochemical ammonia synthesis. The structural and morphological properties of the commercial WS_2 samples were characterized by EDX and TEM, respectively. Electrochemical tests and Indophenol blue method revealed that the nanoscale WS_2 achieved an ammonia production amount of 0.101 $\mu g\ h^{-1}\ mg^{-1}$, outperforming its microscale WS_2 (0.089 $\mu g\ h^{-1}\ mg^{-1}$), highlighting the significant impact of morphology and particle size on catalytic performance.

Keywords: Ammonia, Electrocatalyst, TMD, WS_2

➢ *ORAL PRESENTATION*

Electrochemical NH_3 production by different size Molybdenum Sulfide

Yigit Osman Akyıldız[1, 2*] (*ORCID: https://orcid.org/0000-0001-7057-7268*), Talha Kuru[2, 3] (*ORCID: https://orcid.org/0000-0001-9662-8211*), Ali Keleş[2], Barış Arıcı[2], Emre Aslan[1] (*ORCID: https://orcid.org/0000-0002-7672-2873*), İmren Hatay Patır[3] (*ORCID: https://orcid.org/0000-0003-2937-6557*)

[*1]YEO Technology R&D Center, 34870, İstanbul, Türkiye, e-mail: yigitakyy@gmail.com
[2]Selcuk University, Department of Biochemistry, 42030, Konya, Türkiye
[3]Selcuk University, Department of Biotechnology, 42030, Konya, Türkiye

*Corresponding author e-mail: yigitakyy@gmail.com

Abstract

Nowadays, energy consumption is steadily increasing, and most of the demand is met through fossil fuels. However, their limited availability and high carbon emissions make them environmentally and economically unsustainable. Therefore, the use of renewable energy sources is becoming increasingly important. Ammonia (NH_3) is a key chemical with high energy density. Currently, a large portion of global NH_3 production depends on energy-intensive and costly processes such as the Haber-Bosch method. Producing NH_3 *via* electrochemical nitrogen reduction using hydrogen from water electrolysis powered by renewable electricity is considered a greener alternative. A major challenge in electrochemical nitrogen reduction (NRR) is the high dissociation energy (911 kJ mol^{-1}) of the nitrogen triple bond, along with the competing hydrogen evolution reaction (HER). Thus, the efficiency of NRR strongly depends on the selectivity, structure, composition, and surface morphology of the electrocatalyst. The reliance on Pt like expensive and noble metals in conventional catalysts limits widespread application, driving the search for cost-effective and efficient alternatives. Recently, molybdenum disulfide (MoS_2) has received attention for its catalytic activity in hydrodesulfurization, HER, and CO_2 reduction. Moreover, considering the critical roles of Mo and S elements in nitrogenase enzymes involved in biological nitrogen fixation, MoS_2 has been proposed as a potential NRR-active material. However, the limited active surface area of microscale MoS_2 restricts its practical use in energy applications. In this study, the effect of different particle sizes (micro and nano) of MoS_2, a member of the transition metal dichalcogenides, on electrochemical NRR performance was investigated. Ammonia production by the catalysts was evaluated electrochemically via linear sweep voltammetry (LSV) under nitrogen and argon atmospheres. Additionally, the amount of NH_3 formed was quantified spectroscopically using indophenol blue assays based on a standard calibration curve.

Keywords: Electrocatalysts, Electrochemical NRR, Molybdenum Sulfide

➢ *ORAL PRESENTATION*

Karpal tünel sendromu olan bireylerde boyun pozisyon hissi ve eklem hareketi arasındaki ilişki

Rabia ALACA[1*] (ORCİD: https://orcid.org/0009-0008-9588-9426)
Özge AL[1] (ORCİD: 0000-0001-5292-3593)

[1*]Erciyes Üniversitesi, Tıp Fakültesi, Anatomi Anabilim Dalı, Kayseri, Türkiye

*Sorumlu yazar e-posta: rabiaaalaca38@gmail.com

Özet

Karpal tünel sendromu, nervus medianus'un ligamentum transversum carpale'nin baskısıyla osteofibröz kanalda sıkışması sonucu gelişen bir tuzak nöropatidir. Bu sendrom, sinirin dağılım gösterdiği bölgelerde el ve el bileğinde uyuşma, karıncalanma ve ağrı ile karakterizedir. İlerlemiş vakalarda güçsüzlük ve elin thenar bölgesinde atrofiye yol açmaktadır. Karpal tünel sendromu olan bireyler günlük yaşam aktivitelerinde kısıtlanırken, el ve el bileğine ek olarak omuz ve boyun ağrısından da şikâyet etmektedir. Karpal tünel sendromuna sahip bireylerin birçoğunda servikal lordoz, disk hernisi gibi boyun problemleri beraber seyretmektedir. Çalışmamızda boyun eklem hareketleri ve boyun pozisyon hissi ayrı ayrı değerlendirilmiş ve sağlıklı bireylerle karşılaştırılmıştır. Değerlendirme sonucunda, sağ tarafı etkilenmiş bireylerde sağ boyun rotasyonunda, sol tarafı etkilenmiş bireylerde ise sol boyun rotasyonunda anlamlı farklılıklar gözlemlenmiştir. Boyun pozisyon hissi değerlendirilmesi sonucunda, boyun ekstansiyon hareketi sırasında anlamlı düzeyde fark tespit edilmiştir. Elde edilen bulgular, karpal tünel sendromu olan bireylerin tedavisinde boyun bölgesinin de değerlendirilmesinin yararlı olabileceğini göstermektedir.

Anahtar Kelimeler: Boyun Pozisyonu, Eklem Hareketi, Gonyometre, Karpal Tünel Sendromu.

Bu bildiri özeti Erciyes Üniversitesinde, Özge AL danışmanlığında Rabia ALACA tarafından hazırlanan "Karpal tünel sendromu olan bireylerde boyun pozisyon hissi ve eklem hareketi arasındaki ilişki" adlı yüksek lisans tezinin bir kısmından üretilmiştir.

➢ *ORAL PRESENTATION*

İletken Nanokompozit Polimerlerin Eldesi Ve Özelliklerinin Araştırılması

Ilke Demirkaya[1*] (*https://orcid.org/0000-0002-9402-6724*), İbrahim Kurtay[1] (*https://orcid.org/0009-0005-0589-6787*), Ilknur Babahan-Bircan[1] (*https://orcid.org/0000-0002-1336-671X*)

[1] Aydın Adnan Menderes Üniversitesi, Fen Fakültesi, Kimya Bölümü, 09010 Efeler, Aydın, Türkiye

*Sorumlu yazar e-posta : ilkedemirkaya@yahoo.com

Özet

Metallerin elektriksel özelliklerini, polimerlerin özellikleriyle birleştirerek tek bir malzemede toplayabilmek her zaman ilgi çeken bir araştırma konusu olmuştur. İletken polimerler çeşitli elektrokimyasal özelliklerinden dolayı çok değişik alanlarda kullanılabilmektedirler. Özellikle, sensörler, şarj olabilen piller, fotokimyasal hücreler, elektrokromik aletler ve iyon seçici elektrotların yapımında kullanım potansiyeline sahip oldukları bilinmektedir. Bir polimerin iletken özellik gösterebilmesi için yapısında konjuge çift bağ içeren zincir bulundurması gerektiği Glarum et al. 1963, tarafından belirtilmiştir. Konjuge polimerlerde elektriksel iletkenliğin yapıda yer alan konjuge π bağları ile sağlandığı ise Berets et al. 1968, tarafından ileri sürülmüştür. Bu sebepten dolayı çıkış maddesi olarak kullanılacak polimer zincirinde korunabilen aromatik veya konjuge karbon- karbon çift bağları bulunduracak yapıda olması gerekmektedir. Bu çalışmada, epoksi türevlerinin nanopartiküller varlığında amin türevleri ile reaksiyonundan iletken polimerler ve bunlardan nanokompozit kaplamalar elde edilerek karakterizasyonları yapılarak çeşitli özelliklerinin incelenmiştir. Baslangıç maddesi olarak seçilen ticari epoksi silan türevleri, N(Azot) içeren çeşitli aromatik bileşiklerle (azol ve tiyazol türevleri) reaksiyona girerek iletken polimerler eldesi gerçekleştirilmiştir. Bu reaksiyonlarda iletkenliği artırmak amaçlı karbon ve Fe nanopartiküller kullanılmıştır. Glisidil epoksi silan türevleri, nanopartikül varlığında aromatik amin türevleri halka açılması reaksiyonunu gerçekleştirerek çapraz bağlı iletken polimerler ve bunlardan elde edilen nanokompozit kaplamalar elde edilmiştir. Elde edilen iletken polimerler alüminyum, yüzeylere uygulanarak bu yüzeyler için kullanılabilirliği test edilerek iletken nanokompozit kaplamalar elde edilmiştir. Elde edilen yeni iletken polimerlerin karakter analizi IR, NMR, diferansiyel taramalı kalorimetre (DSC), termogravimetrik analiz (TGA) ve jel içeriği testleri ile yapılmıştır. Ayrıca bu çalışmada elde edilen yeni iletken epoksi-nanokompozit kaplamaların mekanik özellikleri de ayrıca incelenmiştir.

Anahtar Kelimeler: İletken Polimerler, Nanokompozit Kaplamalar, Epoksi Polimerler

➢ *ORAL PRESENTATION*

Omega-3 Rich Edible Oil Alternative: Functional Potential and Limitations of *Camelina sativa* Oil

Necattin Cihat ICYER (*ORCID: https://orcid.org/0000-0002-3190-9669*)

Mus Alparslan University, Faculty of Engineering and Architecture, Department of Food Engineering, Mus, Türkiye.

*Corresponding author e-mail: n.icyer@alparslan.edu.tr, n.icyer@gmail.com

Abstract

One of the ancient oilseeds with a highly valuable fatty acid profile as an omega-3 source is *Camelina sativa*, also known as camelina seed. The fatty acid composition of camelina seed oil was determined by gas chromatography with the Soxhlet oil extraction system and the presence of significant amounts of polyunsaturated fatty acids (PUFA) was detected. In the fatty acid profile of camelina seed oil, 55.18% of the total fatty acids are α-linolenic acid (C18:3 n-3), which demonstrates its strong potential as an alternative to marine-based omega-3 sources. The oil also contained moderate levels of palmitic acid (C16:0, 13.43%), stearic acid (C18:0, 6.21%), linoleic acid (C18:2, 7.27%) and oleic acid (cis-C18:1, 3.04%). Minor fatty acids included arachidic acid (C20:0, 4.11%), homo-γ-linolenic acid (C20:3, 3.22%), erucic acid (C22:1, 6.18%) and eicosadienoic acid (C20:2, 0.92%). The presence of trans-oleic acid was detected as (0.24%). The total PUFA content of this oil was 66.59%. The free fatty acid value of the oil obtained from camelina seed was found as 0.66±0.37% and peroxide value as 3.21±1.01 (meq g O2/kg).
Although the high α-linolenic acid (C18:3 n-3) content positions camelina seed oil as a valuable ingredient for functional food formulations and nutraceutical development, the high erucic acid (C22:1, 6.18%) content in its fatty acid profile constitutes a significant obstacle to human consumption. Because high erucic acid intake has been associated with potential cardiovascular risks. In conclusion, camelina seed oil exhibits a highly valuable fatty acid profile with potential applications in the development of functional food ingredients. However, to ensure compliance with food safety standards, erucic acid content requires a process similar to the historical development of canola oil.

Keywords: Camelina sativa, omega-3, edible oil, gas chromatography

➢ *ORAL PRESENTATION*

In vitro evaluation of a dual drug-loaded delivery system for the treatment of hepatocellular carcinoma

Ümmühan Fulden Aydın[1*](*ORCID: https://orcid.org/0000-0003-2603-739x.*), Şenay Şanlıer[2](*ORCID: https://orcid.org/0000-0001-6532-7221*), Abdullah Tuli[1] (*ORCID: https://orcid.org/0000-0002-6475-1087*)

[*1] Çukurova University, Faculty of Medicine, Department of Medical Biochemistry, Adana, Türkiye.
[2] Ege University, Faculty of Science, Department of Biochemistry, İzmir, Türkiye

*Corresponding author e-mail: bozkayafulden@gmail.com

Abstract

Liver cancer is the sixth most diagnosed cancer and the third leading cause of cancer-related deaths. Hepatocellular carcinoma comprises 75-85% of liver cancer cases in adults, 60% of which are advanced cases that are not amenable to local treatment. In advanced hepatocellular carcinoma cases, systemic drug therapy is used, which is associated with many side effects. Nowadays, drug delivery systems developed with nanotechnological approaches can be used to reduce the side effects of drugs and increase the effectiveness of treatment. The aim of this study was to load sorafenib, which is used in the treatment of hepatocellular carcinoma, and vismodegib, an inhibitor of the hedgehog pathway that has been found to be activated in hepatocellular carcinoma, into a liposomal drug carrier system, to examine their synergistic effects and to investigate their in vitro therapeutic efficacy on liver cancer. Liposomes prepared by thin lipid film hydration method and loaded with sorafenib and vismodegib drugs were characterized. In vitro drug release, stability and hemolysis assays were performed. In vitro cytotoxicity and apoptotic effect of the carrier were investigated. According to the data obtained, it was determined that the drug carrier system has appropriate properties, releases drugs in a controlled manner, does not cause hemolysis and has cytotoxic and apoptotic effects on hepatocellular carcinoma cells. In conclusion, it can be said that the obtained dual drug-loaded carrier system has the potential to reduce side effects and increase therapeutic efficacy in the treatment of hepatocellular carcinoma.

Keywords: hepatocellular carcinoma, dual drug delivery, sorafenib, vismodegib, HepG2 cells, apoptosis

Acknowledgement: This study is supported by Çukurova University, Department of Scientific Research Projects (Project ID: 14316).

➢ *ORAL PRESENTATION*

Influence of Mg^{2+} Ions on the Crystallization and Filtration Characteristics of Lithium Carbonate

Sevgi Polat[1*] (*ORCID: https://orcid.org/0000-0002-0934-2125)*

[1]Marmara University, Engineering Faculty, Chemical Engineering Department, 34854 Istanbul, Turkey

*Corresponding author e-mail: sevgi.polat@marmara.edu.tr

Abstract

With the rapid advancement of technology, global energy demand has increased significantly. Lithium-ion batteries—offering high energy density, safety, long cycle life, rapid charging capability, and environmental friendliness—are widely used across various sectors, including electric vehicles, consumer electronics, and photovoltaic systems. As non-renewable energy sources continue to deplete and energy storage needs grow, the use of lithium-ion batteries is expected to expand further. This trend underscores the critical importance of recovering lithium carbonate, the primary raw material in lithium-ion batteries, for both environmental sustainability and resource conservation. Hydrometallurgical processes are commonly utilized for lithium recovery from spent batteries, wherein lithium ions are precipitated as lithium carbonate via reaction with sodium carbonate. However, the presence of impurity metal ions during recovery can significantly affect the structural, morphological, and functional properties of the resulting lithium carbonate, ultimately influencing the electrochemical performance of new batteries.
This study investigates the effect of Mg^{2+} ions on the crystallization of lithium carbonate. Lithium carbonate crystals were synthesized through reactive crystallization in both the absence and presence of varying Mg^{2+} ion concentrations. The structural characterization was performed using X-ray diffraction (XRD) and Fourier-transform infrared spectroscopy (FTIR). The variations in crystal morphology and particle size were characterized using scanning electron microscopy (SEM) and particle size analysis. Zeta potential measurements confirmed a reduction in crystal agglomeration in the presence of Mg^{2+} ions. Additionally, the influence of Mg^{2+} concentration on the filtration behavior of the crystals was assessed and the changes in specific cake resistance and porosity were quantitatively determined based on Darcy's law.

Keywords: Crystallization, lithium carbonate, characterization, metal ion effect.

➢ *ORAL PRESENTATION*

Impact of Methyl Substitution on Photocatalytic Activity of BODIPY-Thiophene-Integrated COP-TiO_2 Systems

Kübra Turgut[a] (*ORCID: https://orcid.org/0009-0009-9466-4185)*, Mücahit Özdemir[b] *(ORCID: https://orcid.org/0000-0002-0840-4953)*, Gizem Yıldız[c] (*ORCID: https://orcid.org/0000-0001-9845-8076)*, Bahattin Yalçın[b] *(ORCID: https://orcid.org/0000-0003-4448-1101)*, Sermet Koyuncu[d] (*ORCID: https://orcid.org/0000-0001-8352-8326)*, Baybars Köksoye* *(ORCİD: https://orcid.org/0000-0001-7939-5380)*, İmren Hatay Patır[a]*(*ORCID: https://orcid.org/0000-0003-2937-6557)*

[a] Selçuk University, Department of Biotechnology, 42130 Konya, Türkiye
[b] Marmara University, Department of Chemistry, 34722 İstanbul, Türkiye
[c] Selçuk University, Department of Biochemistry, 42130 Konya, Türkiye
[d] Çanakkale Onsekiz Mart University, Department of Chemical Engineering, 17020 Çanakkale, Türkiye
[e] Bursa Technical University, Department of Chemistry, 16310 Bursa, Türkiye

*Corresponding author e-mail: kubratrgt1809@gmail.com

Abstract

The adverse effects of environmental pollution and climate change have significantly increased interest in environmentally friendly, sustainable, and renewable energy sources. In this context, extensive research has been conducted on renewable energy systems to reduce dependence on fossil fuels. Photocatalytic hydrogen production, which enables the generation of hydrogen gas through the decomposition of water under solar irradiation, is considered a promising approach for clean energy production. In this study, a boron-dipyrromethene (BODIPY)-thiophene-based covalent organic polymer (COP) structure was designed by utilizing the advantageous properties of BODIPY dyes, such as high molar absorptivity, tunable optoelectronic features, and high fluorescence quantum yields. The effect of a methyl group on the photocatalytic performance of the COP structure was systematically investigated. Integration of the BODIPY dye into the COP framework was employed to enhance light-harvesting capability, and the resulting structure was evaluated as a photocatalyst under simple experimental conditions. Surface, thermal, and structural characterizations of the synthesized polymers were carried out using scanning electron microscopy coupled with energy-dispersive X-ray spectroscopy (SEM-EDX), transmission electron microscopy (TEM), and Fourier-transform infrared spectroscopy (FT-IR). The prepared BODIPY-Th-COP-CH_3_TiO_2 photocatalyst demonstrated a hydrogen evolution rate of 0.132 mmol g^{-1} h^{-1} under 8 hours of visible light irradiation in the presence of methanol as a sacrificial electron donor, without the need for any additional co-catalyst. These results indicate that BODIPY-thiophene-based COP systems containing methyl groups hold significant potential as effective photocatalyst candidates for sustainable hydrogen production.

Keywords: Photocatalytic Hydrogen Evaluation, BODIPY, Covalent Organic Polymers

➢ *ORAL PRESENTATION*

Potential effects of *Moluccella leavis*-silver nanoparticles on lung cancer cell viability and apoptotic cell death

Pınar Yumrutaş, Mustafa Pehlivan, Demet Taşdemir, Pınar Aksoy, Yağmur Töremişoğlu, Önder Yumrutaş

[1*]Department of Respiratory Disease and Cancer Biology, Faculty of Medicine, Gaziantep University, 27410, Gaziantep, Turkey
[2]Department of Biology, Faculty of Science, Gaziantep University, 27410, Gaziantep, Turkey
[3]Department of Medical Biochemistry, Faculty of Medicine, Gaziantep University, 27410, Gaziantep, Turkey
[4]Department of Medical Biology, Faculty of Medicine, Adiyaman University, 02200 Adiyaman, Turkey

*Corresponding author e-mail: pinargokcekk@gmail.com

Abstract

Lung cancer is the leading cause of cancer death worldwide. Nanotechnology is currently used in many fields including medicine. methods such as surgery, radiotherapy, chemotherapy, immunotherapy are used in cancer treatment. however, existing methods have limited effect and it is important to identify new agents. Medicinal plants contain important anticancer agents and these agents can be organized in nanoparticle form to enter cells faster and show stronger activity. In this context, the aim of this study was to determine the anticancer activity of Moluccella laevis-silver nanoparticles from the Lamiaceae family on lung cancer cells. The cytotoxic activity of ML-AgNP on lung cancer cells was determined by MTT method. The morphological characteristics of ML-AgNP-treated A549 cells were determined by Inverted phase-contrast microscopy. Percentages of early apoptotic, late apoptotic and necrotic cells after ML-AgNP treatment were determined by flow cytometry after Annexin-V/propodium iodide staining. Chemical characterization of ML-AgNP was determined by XRD, FTIR and SEM-electron microscopy. ML-AgNP treatment of A549 cells resulted in decreased proliferation and altered cell morphology. However, 200 and 500 mg/ml ML-AgNP weakly increased the percentage of early and late apoptotic cells. However, no change was observed in the percentage of necrotic cells. In this study, ML-AgNP showed cytotoxic effect on lung cancer cells and induced apoptotic cell death.

Keywords: Moluccella laevis, Nanoparticles, Apoptosis, Antiproliferation

➢ *ORAL PRESENTATION*

Hotair Tutkalı ile PP Kenar Bandı Üretim Sürecinde Yapışma Performansının Artırılması

Ertuğ YILDIRIM[1*] (*ORCID: https://orcid.org/0000-0002-4285-6929*), İsmail Bilgin DEMİRCİ[2] (*ORCID: https://orcid.org/0000-0002-8353-802X)*

[*1]Sakarya Üniversitesi, Fen Edebiyat Fakültesi, Kimya Bölümü, Sakarya, Türkiye.
[2]Yalova Üniversitesi, Mühendislik Fakültesi, Polimer Malzeme Mühendisliği Bölümü, Yalova, Türkiye.

*Sorumlu yazar e-posta: ertug.yildirim@tece.com.tr

Özet

Mobilya üretiminde kullanılan kenar bantları, mobilya tasarımında hem estetik hem de işlevsel açıdan kritik bir öneme sahiptir. Bu bantlar, mobilyaların dış kenarlarını kapatarak daha şık bir görünüm sağlar ve aynı zamanda bu yüzeyleri dış etkenlere karşı korur. Mobilya üretiminde kullanılan malzemeler genellikle darbelere, suya, kimyasallara ve aşınmaya maruz kaldığı için kenar bantlarının dayanıklılığı, ürünün genel ömrünü doğrudan etkiler. Kenar bantları, aynı zamanda montaj ve kullanım sırasında karşılaşılan mekanik zorlamalara karşı direnç göstererek ürünlerin uzun ömürlü olmasını sağlar.

Polipropilen (PP) bazlı kenar bantları, hafiflik, dayanıklılık ve düşük maliyet gibi avantajlarıyla mobilya sektöründe yaygın olarak kullanılmaktadır. Ancak, PP'nin düşük yüzey enerjisi nedeniyle yüzeylere yeterli düzeyde yapışamaması, üretim kalitesini ve ürün ömrünü olumsuz etkileyebilmektedir. Bu bağlamda, söz konusu yapışma sorununu çözmeye yönelik olarak, PP kenar bantlarının MDF ve sunta gibi yüzeylere daha güçlü bir şekilde yapışmasını sağlayacak bir Hotair tutkal formülasyonu geliştirilmesi hedeflenmiştir.

Hotair teknolojisi, yüksek sıcaklıkla PP'nin yüzey enerjisini artırarak yapışma kuvvetini artırma potansiyeline sahiptir. Bu çalışmada, farklı bağlayıcılar içeren çeşitli tutkal formülasyonları hazırlanmıştır. Her bir formülasyonun soyulma dayanımı, yapışma kuvveti ve genel mekanik özellikleri detaylı olarak incelenmiş, farklı uygulama sıcaklıkları (350°C ve 400°C) ile uygulama hızlarında (14 m/dak ve 20 m/dak) gerçekleştirilen denemelerle, sıcaklık ve hız gibi uygulama parametrelerinin etkileri karşılaştırmalı olarak değerlendirilmiştir.

Çalışmanın amacı, daha düşük maliyetli, yüksek performanslı ve uzun ömürlü kenar bantları üretimini mümkün kılacak optimize edilmiş bir tutkal çözümü sunmaktır. Mobilya sektöründe maliyet etkinliği sağlayacağı ve ürün kalitesini artıracağı öngörülmektedir. Ayrıca, geliştirilen bu yenilikçi tutkal formülasyonlarının sürdürülebilirlik açısından da avantaj sunarak sektörde rekabet gücünü yükselteceği düşünülmektedir.

Bu çalışma ile PP bazlı kenar bantlarının yapışma zayıflığını ortadan kaldıracak, yüksek sıcaklıklarda dahi güçlü tutunma sağlayan ve üretim verimliliğini artıran bir Hotair tutkal teknolojisinin geliştirilmesi amaçlanmaktadır. En iyi performansı gösteren formülasyonlar, hem ekonomik hem de teknik açıdan avantaj sağlayacak şekilde sektöre kazandırılacaktır.

Anahtar Kelimeler: Polipropilen (PP), kenar bandı, Hotair tutkal teknolojisi, yapışma performansı.

➢ *ORAL PRESENTATION*

PVC Kenar Bandı Üretim Kalitesinin İyileştirilmesi İçin Plastifiyan Miktarının Artırılması

Samet FİLİZ[1*] (*ORCID: https://orcid.org/0009-0000-9793-9556*), Ertuğ YILDIRIM[2] (ORCID: https://orcid.org/0000-0002-4285-6929), İsmail Bilgin DEMİRCİ[3] (ORCID: https://orcid.org/0000-0002-8353-802X)

[*1]Bursa Teknik Üniversitesi, Mühendislik Fakültesi, Kimya Mühendisliği Bölümü, Bursa, Türkiye.
[2]Sakarya Üniversitesi, Fen Edebiyat Fakültesi, Kimya Bölümü, Sakarya, Türkiye.
[3]Yalova Üniversitesi, Mühendislik Fakültesi, Polimer Malzeme Mühendisliği Bölümü, Yalova, Türkiye.

*Sorumlu yazar e-posta: samet.filiz@tece.com.tr

Özet

PVC (Polivinil Klorür), dayanıklılığı, işlenebilirliği ve uygun maliyeti sayesinde mobilya sektöründe kenar bandı üretiminde yaygın olarak kullanılan bir polimerdir. Kenar bantları, mobilyaların estetik görünümünü tamamlamanın yanı sıra dış etkilere karşı koruma sağlar. Ancak PVC'nin doğal olarak sert ve kırılgan yapısı, kullanım sırasında performans düşüklüğüne yol açabilir. PVC'nin performansını artırmak amacıyla plastifiyanlar kullanılır. Bu katkı maddeleri, PVC'nin moleküler yapısını değiştirerek daha esnek, işlenebilir ve dayanıklı hale gelmesini sağlar. Ayrıca termal ve kimyasal stabiliteyi artırarak malzemenin kullanım alanını genişletir. Plastifiyan türü ve kullanım oranı, üretim sürecinde ve ürünün son özelliklerinde kritik rol oynamaktadır.

Endüstride yaygın olarak kullanılan plastifiyanlar arasında DOP, DOTP, DINP ve TOTM gibi ftalat ve tereftalat bazlı türler yer alırken, çevre dostu seçeneklerden biri olan ESBO (Epoksidize Soya Yağı) da önem kazanmaktadır. Plastifiyan oranının artması genellikle esnekliği artırırken, fazla kullanımı malzemenin mekanik dayanımını olumsuz etkileyebilir. Bu nedenle doğru plastifiyan seçimi ve dozajı büyük önem taşır.

Bu çalışma kapsamında, farklı oranlarda (%2,8, %4,3, %5,8, %7,3) plastifiyan içeren PVC kenar bantları üretilmiş ve bu bantların tokluk, esneklik ve dayanıklılık gibi fiziksel özellikleri detaylı şekilde karşılaştırılmıştır. Amaç, plastifiyan miktarının artırılmasının ürün performansına etkisini ortaya koymak ve en uygun plastifiyan oranını belirlemektir.

Elde edilen veriler, PVC kenar bandı üretiminde plastifiyan miktarının dikkatli şekilde optimize edilmesinin ürün kalitesini artırabileceğini göstermektedir. Epoksitlenmiş soya yağının (ESBO) PVC formülasyonlarında plastikleştirici ve yüzey modifiye edici olarak etkili bir rol oynadığı net bir şekilde ortaya konmuştur. Farklı ESBO oranlarının (%2,8, %4,3, %5,8 ve %7,3) ürünün mekanik ve fiziksel özelliklerini önemli ölçüde etkilediği, özellikle %7,3 oranının en yüksek parlaklık, elastik modül ve kopma dayanımı gibi değerlerle en iyi performansı sağladığı tespit edilmiştir. Bununla birlikte, daha düşük ESBO oranları da belirli uygulamalar için esneklik ve darbe dayanımı açısından avantajlar sunabilmektedir.

Anahtar Kelimeler: Plastifiyan, PVC, Kenar bandı, ESBO (Epoksidize Soya Yağı)

➢ *ORAL PRESENTATION*

Repositioning Existing Drugs to Target DNMT3A in Liver Cancer: A Site-Focused Structural Approach

Shatha Khadra[1] (ORCID: 0009-0006-6331-1369) , Nasma Anjrini[1] (ORCID: 0009-0005-7498-1133), Tugba Bal[1-2,*] (ORCID: 0000-0003-2100-285X)

[1]Department of Bioengineering, Graduate School of Sciences, Üsküdar University, 34662, Istanbul, Turkiye
[2]Department of Bioengineering, Faculty of Engineering and Life Sciences, Üsküdar University, 34662, Istanbul, Turkiye

*Corresponding author e-mail: tugba.bal@uskudar.edu.tr

Abstract

Liver cancer, particularly hepatocellular carcinoma (HCC), is one of the most aggressive and difficult-to-treat cancers globally. One of the underlying drivers of this disease is abnormal DNA methylation and epigenetic change that can silence critical tumor-suppressor genes. A key enzyme involved in this process is DNMT3A which has emerged as a promising therapeutic target. In this study, we explored two distinct binding regions within the catalytic domain of DNMT3A with the goal of identifying existing FDA-approved drugs that can potentially bind and inhibit its activity.

The present study initially evaluates the potential of numerous drugs by molecular docking and molecular dynamics simulations to understand how well various compounds interact with each site. In silico approach demonstrated that second site has stronger interactions, especially with several peptide-based drugs such as Lanreotide (–10.025 kcal/mol) and Desmopressin (–9.974 kcal/mol), suggesting this site may be more structurally favorable for larger, flexible ligands. While the binding scores were encouraging, medicinal chemistry properties and ADMET were also investigated, and several violations were noted suggesting that may still be effective as injectables or targeted treatments. This comparison emphasizes the need to consider both binding performance and practical drug characteristics when identifying repositioning candidates.

In summary, our findings suggest that second site identified in DNMT3A is a particularly promising target for strong, stable binding especially by peptide-based drugs while the other site remains a valuable option for small molecules. This dual-site approach enhances our understanding of DNMT3A's structural behavior and opens the door for repositioning safe, existing drugs in the treatment of liver cancer.

Keywords: DNMT3A, hepatocellular carcinoma, drug repositioning, molecular dynamics, ADMET, medicinal chemistry rules

➢ *ORAL PRESENTATION*

Türkiye'deki Yeşil Limanların Sürdürülebilirlik Üzerine Etkileri

Bağcan Çatı[1*] *(ORCID: https://orcid.org/0009-0007-6095-6644)*, Remzi Fışkın[2, 3] *(ORCID: https://orcid.org/0000-0002-5949-0193)*

[*1]Ordu Üniversitesi, Fen Bilimleri Enstitüsü, Deniz Ulaştırma İşletme Mühendisliği Ana Bilim Dalı, Ordu, Türkiye.
[2]Ordu Üniversitesi, Deniz Bilimleri Fakültesi, Deniz Ulaştırma İşletme Mühendisliği Bölümü, Ordu, Türkiye.
[3]Danimarka Teknik Üniversitesi, İşbirlikçi Otonom Sistemler Merkezi, Kopenhag, Danimarka.

*Sorumlu yazar e-posta: bagcan5960@gmail.com

Özet

Küresel deniz taşımacılığının artmasıyla birlikte, limanların çevresel etkilerini azaltmak kaçınılmaz bir gereklilik hâline gelmiştir. Uluslararası Denizcilik Örgütü'nün (IMO) 2050 yılına kadar sera gazı emisyonlarını net sıfıra indirme hedefi doğrultusunda, limanların enerji verimliliği, atık yönetimi, hava ve su kalitesi yönetimi, dijitalleşme gibi alanlarda yenilikçi çözümler üretmesi kritik öneme sahiptir. Türkiye, stratejik coğrafi konumu ve artan deniz ticareti hacmi ile limanlarının sürdürülebilirliğini sağlama konusunda önemli bir potansiyele sahiptir. Limanların çevresel etkilerini en aza indirecek uygulamaların geliştirilmesi, sadece yerel düzeyde değil, aynı zamanda küresel çevre politikaları açısından da önem arz etmektedir. Bu bağlamda yeşil (ekolojik) limanlar; faaliyetlerinin çevresel, sosyal ve ekonomik boyutlarda sürdürülebilirliğini dengelemeyi amaçlayan limanlardır. Türkiye'de Ulaştırma ve Altyapı Bakanlığı tarafından geliştirilen "Yeşil Liman Sertifikası", limanların çevre dostu teknolojilere uyumunu teşvik etmekte ve uluslararası standartlara uyum sağlamaktadır. Çalışma, literatür taraması ve ulusal raporların incelenmesi yöntemi ile Türkiye'deki gönüllülük esasına dayalı yeşil limanların sürdürülebilirlik boyutlarını ele almaktadır. Bulgular, yeşil limanların sadece çevresel sürdürülebilirliğe değil, aynı zamanda ekonomik sürdürülebilirliğe ve saygınlık kazandırıcı etkilere de katkı sağladığını göstermektedir. Türkiye'nin yeşil liman dönüşümünün hızlandırılması, hem çevresel koruma hem de uluslararası rekabet gücü açısından kritik öneme sahiptir. Bu çalışma, yeşil liman uygulamalarının yaygınlaştırılmasının sürdürülebilir kalkınma hedeflerine önemli ölçüde katkı sağlayabileceğini ortaya koymaktadır.

Anahtar Kelimeler: Yeşil Liman, Sürdürülebilirlik, Türkiye

➢ *ORAL PRESENTATION*

Aronia melanocarpa Meyve Ekstresinin İnsan Meme Kanseri Hücreleri Üzerine Etkisi

Betül YÜKSEL[1*] (*ORCID: https://orcid.org/0009-0005-3512-3152)* ,Özge AL[1] (*ORCID: https://orcid.org/0000-0001-5292-3593*), Neriman LÖKER[2] (*ORCID:* https://orcid.org/0009-0002-2073-6317), Hazal ÇOBUR[2] (*ORCID:* https://orcid.org/0000-0002-6464-6893), Melike VURMAZ[3] (*ORCID:*https://orcid.org/0000-0001-5162-7514) Zeynep SARIMERMER YÜCEL[1] (*ORCID: https://orcid.org/0009-0008-4662-0957),* Serhat AL[2] (*ORCID: https://orcid.org/0000-0003-2721-9275),* Mehtap NİSARİ[1] (*ORCID: https://orcid.org/0000-0002-1126-7478),* Ali Adnan HAYALOĞLU[3] (*ORCID: https://orcid.org/0000-0002-4274-2729)*

[*1] Erciyes Üniversitesi, Tıp Fakültesi, Anatomi Anabilim Dalı, Kayseri, Türkiye.
[2]Erciyes Üniversitesi, Veterinerlik Fakültesi, Veteriner Halk Sağlığı Anabilim Dalı, Kayseri, Türkiye.
[3]İnönü Üniversitesi, Mühendislik Fakültesi, Gıda Mühendisliği, Malatya, Türkiye.

*Sorumlu yazar e-posta: sbetulyuksl@gmail.com

Özet

Meme kanseri dünya çapında kadınlar arasında en sık görülen ve yüksek mortalite oranına sahip kanser türüdür. Meme kanseri tedavi seçeneklerine yönelik çalışmalar günümüzde artarak devam etmektedir. Doğal ürünlerin kanser karşıtı ajanlar olarak kullanılmasının, ulaşılabilir ve uygulanabilirlikleri ve sitotoksisiteyi azaltıcı etkileri sayesinde tedavi etkinliğini arttırıcı bir yaklaşım olduğu kabul edilmektedir. Doğal ürün olan bitkiler, geçmişten günümüze çeşitli hastalıkların önlenmesi ve tedavisinde kullanılmaktadır. Yüksek antosiyanin ve antioksidan içeriğine sahip olduğu bilinen *Aronia melanocarpa* meyvesinin çeşitli patolojik durumlara karşı koruyucu etkileri kanıtlanmış olup günümüzde bitkisel ilaç ve fonksiyonel bir besin olarak kullanılmaktadır. Gerçekleştirilen bu çalışmada *Aronia melanocarpa* meyve ekstresinin insan umblikal ven endotel hücreleri (HUVEC) ve insan meme kanseri hücre hatlarından MCF-7 ile MDA-MB-231 üzerine olan etkisinin in vitro yöntemlerle araştırılması amaçlanmıştır. *Aronia melanocarpa* meyvesinden elde edilen ekstre ile oluşturulan 12 farklı konsantrasyonun her üç hücre hattında hücre canlılığına olan etkisi MTT tahlili ile değerlendirildi. *A.melanocarpa* meyve ekstresinin her üç hücre hattı için IC50 değerleri GraphPad Prism 10.4.2 yazılımı kullanılarak hesaplandı. MTT tahlili sonucunda *Aronia melanocarpa* meyve ekstresinin 24 saatlik uygulama sonrası HUVEC hücre hattı için IC50 değeri 19.89 mg/mL; MCF-7 meme kanseri hücre hattı için 10,76 mg/mL; MDA-MB-231 meme kanseri hücre hattı için ise IC50 değeri 15,39 mg/mL olarak hesaplandı.

Anahtar Kelimeler: Aronia Melanocarpa, Kanser, HUVEC, MCF-7, MDA-MB-231.

*Bu çalışma Erciyes Üniversitesi Bilimsel Araştırma Projeleri Birimi tarafından TYL-2024-13903 proje kodu ile desteklenmektedir ve yüksek lisans tezinden üretilmiştir.

➢ *ORAL PRESENTATION*

Enhancing ammonium perchlorate decomposition via samarium-doped ceria catalysts for solid rocket propellants

Dilara GÜÇTAŞ GÜREL[1*] (*ORCID: https://orcid.org/0000-0002-0810-3923*),
M.A. Faruk ÖKSÜZÖMER[1] (*ORCID: https://orcid.org/0000-0003-0827-8667*)

[*1]İstanbul University - Cerrahpaşa, Faculty of Engineering, Chemical Engineering Department, İstanbul, Türkiye

*Corresponding author e-mail: dilara.guctas@iuc.edu.tr

Abstract

This study focuses on enhancing the performance of conventional aluminum fuel used in solid rocket propellants by incorporating a suitable catalyst into the propellant composition. In solid propellants, the combustion of metallic fuel occurs through the presence of an oxidizer, most commonly ammonium perchlorate (AP). The decomposition of AP releases oxygen, which facilitates the combustion of the metallic fuel. Therefore, accelerating the decomposition of the oxidizer is crucial for improving the overall combustion efficiency of the propellant system. To achieve this, a catalyst with an oxide structure containing oxygen vacancies, specifically samarium-doped ceria (SDC20), was selected due to its potential to promote AP decomposition. Since the preparation method of the catalyst significantly influences its catalytic activity, SDC20 was synthesized using various techniques. The synthesized catalysts were then incorporated into model propellant formulations to evaluate their effectiveness in enhancing AP decomposition. The catalytic effect was assessed via thermogravimetric and differential thermal analysis (TG-DTA), focusing on the change in the activation energy of AP decomposition. Typically, the high temperature decomposition activation energy of pure ammonium perchlorate ranges between 200–250 kJ/mole. With the incorporation of SDC20 catalysts, this value was successfully reduced to approximately 130-150 kJ/mole, indicating a notable improvement in thermal decomposition behavior. The findings of this study highlight the critical role of catalyst synthesis methods in tailoring the thermal characteristics of oxidizers in solid rocket propellants. The optimized catalyst not only improves the decomposition kinetics of AP but also contributes to the development of more efficient and responsive propulsion systems. This research offers a promising approach to advancing solid propellant technology through rational catalyst design.

Keywords: Solid Rocket Propellant, Catalyst, SDC20, Ammonium perchlorate decomposition

➢ *ORAL PRESENTATION*

Novel tomato-based interventions: Impact on survival rates in common cancers

Gokhan Gorgisen[1*](ORCID: https://orcid.org/0000-0001-6040-7863), Salih Yabalak[2] (ORCID: https://orcid.org/0009-0000-5024-9128), Ozan Tas[3] (ORCID: https://orcid.org/0000-0001-6421-5092), Neriman Ezgi Cifte[3] (ORCID: https://orcid.org/0000-0001-9664-0325), Mecit Halil Oztop[3] (ORCID: https://orcid.org/0000-0001-6414-8942)

[*1] University of Health Sciences, Gülhane Medical School, Department of Medical Biology, Ankara, Türkiye.
[2] Van Yuzuncu Yıl University, Institute of Health Sciences, Department of Molecular Medicine, Van, Türkiye.
[3]Middle East Technical University, Faculty of Food Engineering, Ankara, Türkiye

*Corresponding author e-mail: gokhangorgisen@gmail.com

Abstract

Tomato-based products are recognized for their inherent anticancer and anti-inflammatory properties, primarily attributed to their rich content of bioactive compounds, including lycopene, β-carotene, vitamin C, and polyphenols. In this study, functionalized tomato products—specifically juice and sauce—were formulated by incorporating plant proteins (pea protein and RuBisCO) and lyophilized olive powder to investigate the effects of compositional variations on their health-related potential. While all products were enriched with lyophilized olive powder, pea protein and RuBisCO were individually incorporated into the formulations to assess their distinct contributions. The engineered products were designed to systematically evaluate the influence of these ingredients on anticancer properties. Additionally, the impact of processing methods, namely conventional water bath and microwave pasteurization, was examined for both juice and sauce formulations. The MTT assay was performed to determine the survival rates of various cancer cell lines, including breast cancer, glioblastoma, colorectal cancer, and melanoma. Our findings revealed that the newly developed tomato products reduced cancer cell viability in a concentration- and cancer type-dependent manner. These results demonstrate that the engineered tomato products exhibit significant anticancer effects, though their precise mechanisms of action and broader implications for cell survival warrant further investigation.

Keywords: FunTomP, tomato products, anticancer

Acknowledgement: To the project, the Partnership for Research and Innovation in the Mediterranean Area PRIMA H2020 GA2032: “FunTomP—Functionalized Tomato Products”.

➢ *ORAL PRESENTATION*

Antimicrobial target identification in *Vibrio cholerae* via reporter metabolite analysis

Fatma Gizem Avci[1,2*] (*ORCID: https://orcid.org/0000-0001-6618-0487*)

[1] Üsküdar University, Faculty of Engineering and Natural Sciences, Department of Bioengineering, Istanbul, Türkiye.
[2] Bielefeld University, Faculty of Biology and Center for Biotechnology (CeBiTec), Genetics of Prokaryotes, Bielefeld, Germany.

*Corresponding author e-mail: fatmagizem.avci@uskudar.edu.tr

Abstract

Vibrio cholerae, the causative agent of cholera, continues to pose a global health threat, with an estimated 1.3 to 4 million cases and up to 143,000 deaths annually. The disease is primarily transmitted through contaminated water or food. While mild cases are manageable with oral rehydration therapy, severe infections require a combination of intravenous fluids and antimicrobial treatment. Although antibiotics such as tetracycline, fluoroquinolones, and azithromycin have been successfully used to treat cholera patients, treatment failures have become increasingly common recently due to the emergence and spread of antimicrobial-resistant *V. cholerae* strains. This highlights a critical need to identify novel drug targets and develop alternative therapeutic strategies.

In this study, a systems biology approach was employed to uncover potential antimicrobial targets. Transcriptomic data of *V. cholerae* O1 El Tor N16961 exposed to eleven different stress conditions mimicking the human host environments were integrated with its genome-scale metabolic model to identify reporter metabolites, the key metabolites around which significant transcriptional changes occur. The analysis revealed significant enrichment in metabolic pathways, including amino acid biosynthesis, fatty acid metabolism, and carbohydrate metabolism. Further investigation of common reporter metabolites highlighted FabV, ArgE, and MenE as promising antimicrobial target candidates. These findings offer valuable insights into the metabolic adaptability of *V. cholerae* and potential antimicrobial targets for developing new antimicrobial therapies.

Keywords: *Vibrio chlorea*, antimicrobial resistance, reporter metabolite, enrichment analysis, drug target.

➢ *ORAL PRESENTATION*

Effect Of Feder Produced By Plastic Injection On Material Behavior

Yunus Çivici[1*](ORCID ID: https://orcid.org/0000-0003-3047-5034),
Onuralp Uluer[2] (ORCID ID: https://orcid.org/0000-0001-7488-3166

[1]Gazi University, Graduate School of Natural and Applied Sciences, Department of Manufacturing Engineering, Ankara, Turkey
[2]Gazi University, Faculty of Technology, Department of Manufacturing Engineering, Ankara, Turkey

*Corresponding author e-mail :yunus.civici@outloook.com , uluer@gazi.edu.tr

Abstract

Plastic injection molding is one of the most commonly used manufacturing methods due to its ability to produce complex geometries with high precision and cost efficiency. In injection-molded parts, various structural features are utilized to enhance mechanical strength and minimize manufacturing defects. Among these features, rib structures (also known as “feder” structures) play a critical role in reducing stress concentrations, improving shape stability, and preventing crack initiation. The purpose of this study is to review the current literature on the influence of rib structures on the material behavior of plastic injection molded parts and to provide a comprehensive overview of the research conducted in this field. This research is based on a systematic review of national and international studies focusing on rib design and its impact on the mechanical behavior of plastic components. Key parameters such as rib geometry, placement, rib-to-wall thickness ratio, and transition radii have been examined in the context of their effects on stress distribution and overall mechanical performance. Additionally, studies involving different types of thermoplastics (e.g., PP, ABS, PC, PA6) have been analyzed to understand material-specific behaviors. The literature reveals that well-designed rib structures significantly improve part strength, crack resistance, and molding quality. Specifically, rounded transitions at the rib base reduce stress concentrations, while maintaining an optimal rib-to-wall thickness ratio enhances structural integrity without causing molding defects such as sink marks. The findings underscore the importance of rib design in optimizing the performance of plastic parts and highlight the need for continued research in this area to support more efficient and reliable product development.

Keywords: Plastic Injection Molding; Rib Structures; Material Behavior; Stress Distribution; Mechanical Performance

➢ *ORAL PRESENTATION*

Design of inner-outer layered garments with enhanced comfort effect for men's upper clothing

Tuğçe Eren[1] (*ORCID: https://orcid.org/0009-0005-9116-1065*),
Seda Kızıl[1] (*ORCID: https://orcid.org/0009-0002-1920-230X*)

[*1] ÇGS-Çetinkaya Giyim Sanayi Tasarım Departmanı, İstanbul/Türkiye.

*Corresponding author e-mail: teren@cetinkaya.com.tr

Abstract

Nowadays, comfort has become an increasingly important factor in individuals' clothing preferences. To meet this demand, dual-layer fabrics incorporating different yarns on the inner and outer surfaces are being utilized, and multi-layered garment designs are also being adopted. When a garment consists of multiple layers, the air trapped between these layers, especially the outermost layer, plays a crucial role. Garments that fit closely to the body contain less air compared to those that hang loosely. In multi-layered garments, the total thermal insulation is greater than the insulation provided by a single layer alone (Marmaralı, A., Kretzschmar, D. S., Özdil, N., & Oğlakcıoğlu, G. N. (2006). Parameters affecting thermal comfort in clothing. Tekstil ve Konfeksiyon, 16(4), 241-246). Based on this, the present study was designed to enhance moisture management comfort in terms of water vapour permeability and wear comfort in men's upper garments by using combinations of knitted and woven fabrics with different fiber contents. By designing and testing inner-outer fabric combinations focused on fiber and fabric types, this study aims to help designers better understand fabric and garment properties, as well as their interactions, enabling them to develop garments with improved wear and moisture comfort. As a result, fabric and design combinations that promote comfort have been proposed based on the findings and evaluations.

Keywords: Comfort, inner-outer combination, men's clothing, water vapor permeability

➢ *ORAL PRESENTATION*

A computer simulation study on coalescence of metal nanoparticles

Songül Taran[1*] (*ORCID: https://orcid.org/0000-0001-8115-2169)*

[*1]Düzce University, Faculty of Arts and Sciences, Department of Physics, Düzce, Türkiye.

*Corresponding author e-mail: songultaran@duzce.edu.tr

Abstract

Bimetallic nanoparticles are of great interest in a broad variety of applications due to their high degree of tunability of the physical and chemical properties [1]. The coalescence process of two metal nanoparticles is widely accepted as one of the growth mechanisms of nanoparticles [2]. In coalescence, independent nanoparticles collide and merge to form a larger aggregate [3]. In order to understand nanoparticle coalescence, a considerable progress has been made by using computational methods [4] and Molecular dynamics (MD) simulations are particularly well suited to this phenomenon [5]. In this study, the coalescence of two different metal nanoparticles were performed by using MD simulations. Visualizations and analysis of MD trajectories were carried out by using OVITO [6]. The coalescence process was analyzed by dependence on temperature, geometric structure, nanoparticle size and composition. It was obtained that it can be possible to tune the structural and chemical ordering properties of the resultant configurations obtained at the end of the coalescence process by changing temperature, geometric structure, nanoparticle size and composition.

Keywords: Metal nanoparticles, coalescence, molecular dynamics simulations.

References:

[1] Ferrando R. Structure and Properties of Nanoalloys. In: Palmer RE, editor. Front. Nanosci. Elsevier; 2016.
[2] Zinzani S, Baletto F. Coalescence of AuPd nanoalloys in implicit environments. Phys. Chem. Chem. Phys. 2024;26:21965–21973.
[3] Nelli D, Cerbelaud M, Ferrando R, et al. Tuning the coalescence degree in the growth of Pt-Pd nanoalloys. Nanoscale Adv. 2021;3:836–846.
[4] Jiang L, Guo Y, Liu Z, et al. Computational understanding of the coalescence of metallic nanoparticles: a mini review. Nanoscale. 2024.
[5] Nelli D, Dighero E, Ferrando R. Coalescence-induced shape transformations in Pd and AuPd clusters. 2024;16.
[6] Stukowski A. Visualization and analysis of atomistic simulation data with OVITO-the Open Visualization Tool.
Model. Simul. Mater. Sci. Eng. 2010;18:015012.

➢ *ORAL PRESENTATION*

Production and Characterization of Biochar from Cabbage Waste Using Hydrothermal Carbonization

Koray ALPER[1*] *(https://orcid.org/0000-0001-6845-2087)*

[*1] Zonguldak Bülent Ecevit University, Devrek Vocational School, Department of Environmental Protection Technologies, Zonguldak, Turkey

*Corresponding author e-mail: korayalper@beun.edu.tr

Abstract

As the environmental impact of organic waste from the food and agricultural sectors grows, transforming such waste into value-added products has become critical for sustainability. In this study, low-value cabbage waste was converted into functional biochar via hydrothermal carbonization (HTC) at 200°C, 225°C, 250°C, and 275°C for 3 and 6 hours in deionized water. The goal was to produce biochar suitable for environmental applications, particularly adsorption. Yield analysis indicated a clear influence of both temperature and time. At 200°C for 3 hours, the yield was 29.18%, increasing to 31.85% after 6 hours. The highest yield (33.89%) occurred at 225°C for 6 hours, highlighting the effect of extended reaction conditions on biochar formation and process optimization. FT-IR analysis revealed temperature- and time-dependent changes in functional groups. A decrease in –OH bands (3300–3400 cm^{-1}) and C–O bands (1000–1100 cm^{-1}) indicated the breakdown of oxygenated groups, while the increased intensity of C=C bands (~1600 cm^{-1}) reflected enhanced aromaticity. SEM images confirmed morphological changes such as increased porosity and surface roughness, especially at higher temperatures. TGA results showed improved thermal stability with increased carbonization. XRD analysis revealed a reduction in crystallinity and a transition toward amorphous carbon structures, confirming advanced carbon development. TOC and COD analyses of the liquid phase demonstrated a decrease in organic content at higher temperatures and durations, suggesting more environmentally benign effluents. This study offers a promising approach to organic waste valorization by producing eco-friendly, structurally stable, and adsorptive biochars. Hydrothermal carbonization of cabbage waste supports sustainable waste management and environmental remediation goals through efficient resource recovery.

Keywords: Cabbage waste, Hydrothermal carbonization, Biochar, Waste valorization.

➢ *ORAL PRESENTATION*

Finite Element Analysis of Natural Rubber-Based Damping Components

Nedimcan ÖNDER[1*] (*ORCID: https://orcid.org/0000-0001-7644-8694*),
Hasan KASIM[2] (*ORCID: https://orcid.org/0000-0002-3024-5207*)

[*1]Pe-Ga Otomotiv Süspansiyon San. ve Tic. A.Ş, Bursa, Türkiye
[2] Pe-Ga Otomotiv Süspansiyon San. ve Tic. A.Ş, Bursa, Türkiye

*Corresponding author e-mail: nedimcan@pegaairsprings.com

Abstract

Rubber bumpers are widely used in various industrial applications, particularly in the automotive sector, due to their ability to carry loads, absorb vibrations, and dampen impacts. Natural rubber-based materials are preferred in such applications because of their high elasticity and favorable mechanical performance. However, the performance of these materials may vary depending on parameters such as hardness, filler content, and deformation conditions. Therefore, conducting both experimental and numerical analyses is essential for reliable design and material optimization.In this study, mechanical tests were conducted at room temperature on three equivalent natural rubber bumpers. The tests included hardness measurements using the Shore A scale, ash testing to determine inorganic filler content, and load-bearing tests under 25 mm deformation. The measured hardness values were 76.7, 76.9, and 78.0 Shore A, while the corresponding load capacities were 11,920 N, 13,155 N, and 14,252 N. According to the ash test results, the filler contents were 9.7%, 7.5%, and 6.5%, indicating that a lower filler ratio correlates with increased load-bearing capacity.Based on the average experimental values, a finite element analysis was performed using ANSYS software and a hyperelastic Mooney-Rivlin material model. The numerical model was constructed using a representative rubber mount with 77.2 Shore A hardness, a load capacity of 13,109 N, and 7.9% ash content. The simulation yielded a load value of 14,058 N, resulting in a 7.2% deviation from the experimental result—well within acceptable engineering limits for such materials. The developed model offers a reliable numerical analysis approach that can be used in the design of new rubber mount applications.

Keywords: Rubber Bumpers , Finite Element Analysis , Hyperelastic Material Modeling

➢ *ORAL PRESENTATION*

Resolved GMCs in Lenticular Galaxy NGC383

Selçuk Topal[1,2*] (*ORCID: https://orcid.org/0000-0003-2132-5632*), Martin Bureau[2], Anan Lu[3] (*ORCID: https://orcid.org/0000-0003-2877-5935)*, Pandora Dominiak[2] (*ORCID: https://orcid.org/0009-0002-6380-3428),* Woorak Choi[4], Timothy A. Davis[5] (*ORCID: https://orcid.org/0000-0003-4932-9379),* Fu-Heng Liang[6] (*ORCID: https://orcid.org/0000-0003-2496-1247*), Ilaria Ruffa[7] (ORCID: https://orcid.org/0000-0002-4578-1205), Lijie Liu[8] *(ORCID: https://orcid.org/0000-0003-4956-706X)*, Hengyue Zhang[2] *(ORCID: https://orcid.org/0000-0003-4079-2447)*

[1]Van YuzuncuYil University, Faculty of Science, Department of Physics, Van, Turkey
[2]University of Oxford, Sub-department of Astrophysics, Department of Physics, Oxford, UK
[3]McGill University, Trottier Space Institute and Department of Physics, Montreal, Canada
[4]Yonsei University, Department of Astronomy, Seoul, Republic of Korea
[5]Cardiff University, Cardiff Hub for Astrophysics Research & Technology, School of Physics & Astronomy, Cardiff, UK
[6]Zentrum für Astronomie der Universität Heidelberg, Astronomisches Rechen-Institut, Heidelberg, Germany
[7]Arcetri Astrophysical Observatory, INAF,Largo Enrico Fermi 5, I-50125 Florence, Italy
[8]University of Copenhagen, Niels Bohr Institute, Copenhagen, Denmark

*Corresponding author e-mail: selcuktopal@yyu.edu.tr

Abstract

Spiral galaxies are known for their high levels of star formation activity. However, the process by which late-type galaxies evolve into early-type ones is not well understood. Lenticular galaxies are key to investigating such transitions. Giant molecular clouds (GMCs) are the birthplaces and deathbeds of stars in galaxies. High-angular-resolution observations are essential to probe the physical properties and kinematics of GMCs, and to improve our understanding of star formation processes in galaxies. In this study, we present high-resolution, high-sensitivity observations of carbon monoxide (CO) in the nearby lenticular galaxy NGC 383. Data were obtained using the Atacama Large Millimetre Array, achieving an angular resolution of 0.085 arcsec x 0.052 arcsec (approximately 22 parsecs) and a velocity resolution of 2 km/s. This excellent resolution enables us to resolve the GMCs both spatially and spectrally. Here, we present the initial results of our analysis, based on a modified GMC identification algorithm. This algorithm enables us to determine various physical parameters, such as the boundaries and dimensions of GMC structures, as well as star formation at the GMC scale. Our results suggest that the GMCs are gravitationally unbound and likely to undergo gravitational collapse. We will also discuss results based on Larson relations (i.e. relations between the size, velocity dispersion, and luminosity of GMCs) and their physical interpretation for hundreds of GMCs identified across the disc of the galaxy.

Keywords: *galaxies, lenticular galaxies, ISM, molecular gas*

A comparative investigation on short-beam strength of 3D-printed hybrid curved composites

Sedat Süsler[1*] (*ORCID: https://orcid.org/0000-0002-5947-8231*)

[*1]Kocaeli University, Faculty of Aeronautics and Astronautics, Department of Aerospace Engineering, Kocaeli, Turkiye.

*Corresponding author e-mail: sedat.susler@kocaeli.edu.tr

Abstract

Assessing the mechanical behaviors of composites reinforced with continuous and long fibers via additive manufacturing under different loading scenarios is essential for understanding their capabilities and limitations in real-world industrial use, as well as for enhancing 3D printing technologies and materials. A crucial factor defined by ASTM D2344/2344M-22 standard is the short beam strength (SBS), which indicates the interlaminar shear strength (ILSS) of a composite. This research conducts a comparative investigation into the short-beam strength of both flat and curved additively manufactured fiber polymer laminates. The study focuses on the performance of a laminated hybrid composite material form with the lay-up configuration 3/2 that contains three layers of short-fiber carbon-reinforced nylon (Onyx®) and two layers of unidirectional continuous carbon fiber-reinforced nylon. The short-beam specimens were subjected to three-point bending tests with a crosshead movement of 1 mm/min after they had been printed with the build configuration of on-edge orientation by a Markforged Mark Two™ 3D printer. Load and crosshead displacement were recorded throughout each test. Load-displacement and short-beam stress-displacement histories, damage modes, and mean values of maximum loads, SBSs, and specific SBSs were compared with each other and their non-hybrid configurations (three layers of Nylon White® and two layers of unidirectional continuous carbon fiber reinforced nylon). There was progress on energy storage capacity before the complete failure of the composite; however, the existence of the curve created a significant decrease of 19.6% in SBS and an increase in standard deviation, which is a sign of a decrease in foreseeability of material behavior, unlike non-hybrid design. This study aims to enhance the understanding of the mechanical behavior of 3D-printed hybrid composites manufactured using the continuous filament fabrication (CFF) technique—a method derived from fused deposition modeling (FDM)—and to support future engineering applications through deeper insights into their structural performance.

Keywords: Fused deposition modeling, continuous filament fabrication, short-beam strength, interlaminar shear strength, curved structures, hybrid composites

➢ *ORAL PRESENTATION*

Effect of organic alizarin sensitizer on the efficiency of TiO_2-based dye-sensitized solar cells under different light intensities

Fatih Akpınar[1*] *ORCID: (https://orcid.org/0009-0005-0102-3823)*, Sümeyra Tuna Yıldırım[2] (*https://orcid.org/0000-0001-5564-9630*), Sefa Gözcü[3] (*https://orcid.org/0000-0002-0735-4229*), Aykut Astam[4] (https://orcid.org/0000-0002-4321-3626), Memet Ali Yıldırım[5] (https://orcid.org/0000-0002-6175-1807)

[*1]Erzincan Binali Yıldırım University, Institute of Science and Technology, Department of Electrical and Electronics Engineering, Erzincan, TURKEY.
[2]Erzincan Binali Yıldırım University, Pharmacy Faculty, Department of Analytical Chemistry, Erzincan, TURKEY.
[3]Erzincan Binali Yıldırım University, Pharmacy Faculty, Department of Pharmacognosy, Erzincan, TURKEY.
[4]Erzincan Binali Yıldırım University, Science and Art Faculty, Department of Physics, Erzincan, TURKEY.
[5]Erzincan Binali Yıldırım University, Engineering- Architecture Faculty, Department of Electrical and Electronics Engineering, Erzincan, TURKEY.

*Corresponding author e-mail: fatihakpnrr24@gmail.com

Abstract

Dye-sensitized solar cells (DSSC) are one of the most promising alternatives to silicon solar cells in terms of efficiency and easy production. In this study, the effect of organic alizarin ($C_{14}H_8O_4$) dye sensitizer on the efficiency of TiO_2-based DSSC under different light intensities was investigated. TiO_2 nanoparticles to be used as photoanodes in DSSC were synthesized using a low-cost and environmentally friendly hydrothermal method at 120 °C for a 12-hour deposition time. The synthesized TiO_2 nanoparticles were calcined in a muffle furnace at 450 °C. The calcined TiO_2 nanoparticles were made into paste and coated on a 0.49 cm^2 area on the fluorine-doped tin oxide (FTO) coated glass surface using the doctor-blade method. The structural and optical properties of the coated TiO_2 photoanode film were characterized by XRD and optical absorption measurements. XRD measurements revealed that the TiO_2 film was in the anatase phase, while optical analysis showed that the film had a maximum transmittance of 80% in the visible wavelength range and a direct bandgap energy of 3.28 eV. For DSSC fabrication, TiO_2 photoanode film coated on FTO was sensitized by soaking in an alizarin dye solution for 6 hours. Then, fabrication was completed by using iodide/triiodide (I^-/I_3^-) redox electrolyte solution and a Pt counter electrode. J-V measurements were performed under different light intensities (20, 60, 100 mW/cm^2) to determine the photovoltaic parameters of the fabricated DSSC. From these measurements, it was determined that the DSSC's J_{sc}, V_{oc}, and η parameters varied in the ranges of 5.70-9.59 mA/cm^2, 0.66-0.76 V, and 4.01-9.27%, respectively, depending on the light intensity. Based on these findings, it was concluded that organic alizarin dye has the potential to be used in DSSCs.

Keywords: DSSC, TiO_2, Alizarin, Light Intensity.

➢ *ORAL PRESENTATION*

Synthesis and characterization of graphene-derived materials as a composite additive

Elif Aydın[1*] (*ORCID: https://orcid.org/0009-0003-2016-0394*), Emine Ekinci[2] (*ORCID: https://orcid.org/0000-0002-0958-1513*), Birce Pekmezci Karaman[3] (*ORCID: https://orcid.org/0000-0002-9051-2354)*

[*1]Gazi University, Graduate School of Natural and Applied Sciences, Chemical Engineering, Ankara, Turkey.
[2,3]Gazi University, Faculty of Engineering, Chemical Engineering Department, Maltepe, Ankara, Turkey.

*Corresponding author e-mail: [*1]23830901001@gazi.edu.tr, [2]eminekaya@gazi.edu.tr, [3]bircepekmezci@gazi.edu.tr

Abstract

Graphene and its derivatives, graphene oxide (GO) and reduced graphene oxide (rGO), are considered promising nanomaterials due to their exceptional mechanical, thermal, and electrical properties. This study aims to synthesize graphene nanoplatelets (GNP), graphene oxide (GO), and reduced graphene oxide (rGO) through green synthesis routes by employing the modified Hummers method. The process designed in accordance with sustainable chemistry principles, minimizing the use of toxic reagents and optimizing energy efficiency. GO will be produced through the chemical oxidation of graphite using a modified version of the classical Hummers method, which enhances safety and environmental compatibility. In the subsequent step, GO will be reduced to rGO using environmentally reducing agents such as ascorbic acid, replacing conventional hazardous chemicals like hydrazine. The synthesized nanomaterials thoroughly characterized using a range of techniques including X-ray diffraction (XRD), Raman spectroscopy, scanning electron microscopy (SEM), and transmission electron microscopy (TEM) etc. These analyses aim to investigate the structural, chemical, and morphological features of the materials and to determine the effectiveness of the modified method in producing high-quality graphene derivatives. Process parameters such as oxidant ratio, reaction time, and temperature systematically varied to optimize yield and product performance. This research intends to contribute to the development of scalable, eco-friendly production strategies for graphene-based materials. The synthesized graphene derivatives further applied as reinforcing agents in ceramic matrix composite systems.

Keywords: Graphene, graphene oxide, reduced graphene oxide, graphene-derived materials, composite

Acknowledgements: We gratefully acknowledge financial support from University Research Funds through Gazi University (ADEP Project Number: FGA-2024-9139), Prof. Dr. Nuray Oktar for invaluable guidance and support, and Nanografi Inc. for providing materials/facilities.

➢ *ORAL PRESENTATION*

Preservation of Quality in Seafood Products with Smart Packaging Technologies

Hatice Gündüz[1*] (ORCID: https://orcid.org/0000-0002-9899-8635)
Fatma Öztürk[1] (ORCID: https://orcid.org/0000-0003-4763-3801)

*[1]Izmir Katip Celebi University, Faculty of Fisheries,
Department of Fisheries and Fish Processing Technology,
Izmir, Turkey.

*Corresponding author e-mail: hatice.gunduz1@ikcu.edu.tr

Abstract

Food packaging is a fundamental process for preserving products, facilitating transportation, and extending shelf life. Environmental concerns and health risks associated with conventional packaging have increased interest in sustainable, biodegradable alternatives. These alternatives contribute to waste reduction and support the circular economy while promoting resource efficiency. In this context, emerging smart packaging systems offer innovative solutions capable of performing functions such as detection, monitoring, recording, and communication.
Freshness is a key indicator of product quality in seafood, which is known for its high nutritional value and sensitive sensory properties. Smart packaging technologies play a critical role in maintaining quality during the transportation and storage of these products, while also enhancing consumer safety.
Applications of smart packaging in seafood include a variety of systems such as biosensors for monitoring freshness and spoilage, color-changing indicators, time–temperature indicators, gas sensors, and RFID tags. This study aims to evaluate smart packaging techniques used for monitoring the freshness of seafood products and to discuss existing limitations as well as future development opportunities.

Keywords: Smart packaging, Seafood, Freshness monitoring, Sustainable packaging, Bio-based materials, Food safety, Packaging technologies

➢ *ORAL PRESENTATION*

Protective Effect of *Cotinus coggygria* Scop. Extract on Ethanol-Induced Kidney Damage

Fatma Gulnaz Karakus [1,2*](ORCID: http://orcid.org/0000-0003-2086-2444), Sevim Tunali [2] (ORCID: http://orcid.org/0000-0003-3363-1290), Refiye Yanardag [2] (ORCID: https://orcid.org/0000-0003-4185-4363)

[1] Istanbul University-Cerrahpaşa, Institute of Graduate Studies, Avcilar, Istanbul, Türkiye
[2] Istanbul University-Cerrahpaşa, Faculty of Engineering, Department of Chemistry, Avcilar, Istanbul, Türkiye

*Corresponding author e-mail: f.g.guler@hotmail.com

Abstract

Plants are considered as an important resource in new phytomedicinal product development studies due to their wide clinical benefits, high efficiency, low costs and fewer side effects. *Cotinus coggygria* Scop. (*C. coggygria*) plant stands out among these natural resources with its strong antioxidant effect due to its flavonoids and phenolic compounds. Ethanol consumption can cause serious damage to tissues and organs as a result of oxidative stress and inflammation. In this study, the protective effect of *C. coggygria* aqueous extract was investigated to prevent ethanol-induced kidney damage. In the study, 5-6 months old male Sprague Dawley rats were divided into four groups: Group I (control group), Group II (group administered 50 mg/kg *C. coggygria* aqueous extract), Group III (group administered 1 mL absolute ethanol) and Group IV (group administered *C. coggygria* aqueous extract and 1 mL absolute ethanol one hour later). *C. coggygria* aqueous extract and ethanol were administered to rats by gavage method. One hour after ethanol administration, blood and tissue samples of rats were collected under anaesthesia and various biochemical analyses were performed. When the results were evaluated, it was found that there was an increase in urea and uric acid amounts in serum samples; lactate dehydrogenase, xanthine oxidase and arginase enzyme activities, as well as reactive oxygen species, total oxidant content and oxidative stress index increased in kidney tissues of ethanol-treated rats. On the other hand, a decrease in sodium-potassium ATPase enzyme activity and total antioxidant content was observed. It can be suggested that these biochemical parameters were reversed by the application of *C. coggygria* extract and this plant extract showed a protective effect.

Keywords: *Cotinus coggygria* Scop., Kidney, Ethanol.

➢ *ORAL PRESENTATION*

Magnetic properties of spin-3/2 antiferromagnetic Blume-Capel model in triangular lattice

Ahmed Tawfik Hasan Al-Askari[1] (*https://orcid.org/0009-0003-2357-8470*),
Ulvi Kanbur[1*] (*https://orcid.org/0000-0002-9290-8045*)

[1]University of Karabuk, Faculty of Science, Department of Physics, Karabuk, Türkiye.

*Corresponding author e-mail: ulvikanbur@karabuk.edu.tr

Abstract

We study the magnetic properties of the antiferromagnetic Blume-Capel model on a triangular lattice by means of Monte Carlo simulations. We investigate staggered magnetization, staggered susceptibility, specific heat, and Binder parameters of the model. Those quantities of the spin system are computed for different sizes and anisotropy parameters over a range of temperatures. The ground state and finite temperature results suggest different phases of the model, importantly, a Berezinskii-Kosterlitz-Thouless type phase at higher temperatures. The low-temperature phase is expected to be the antiferromagnetic long-range ordering on two sublattices, while the remaining one remains in a nonmagnetic state.

Keywords: Blume-Capel model, Monte Carlo simulation, antiferromagnetism.

➢ *ORAL PRESENTATION*

Protective Effects of *Cotinus coggygria* Scop. Extract Against Ethanol-Induced Glycosylation Anomalies in Small Intestinal Tissue

Fatma Gulnaz Karakus [1,2*](ORCID: http://orcid.org/0000-0003-2086-2444), Sevim Tunali [2] (ORCID: http://orcid.org/0000-0003-3363-1290), Refiye Yanardag [2] (ORCID: https://orcid.org/0000-0003-4185-4363)

[1] Istanbul University-Cerrahpaşa, Institute of Graduate Studies, Avcilar, Istanbul, Türkiye
[2] Istanbul University-Cerrahpaşa, Faculty of Engineering, Department of Chemistry, Avcilar, Istanbul, Türkiye

*Corresponding author e-mail: f.g.guler@hotmail.com

Abstract

Alcohol use disorder and ethanol dependence is a common condition that causes serious health problems on a global scale. As a result of ethanol metabolism, acetaldehyde accumulates in the organism and causes oxidative stress. The free radicals, generated in this process, affect the glycosylation of proteins and lipids and cause cellular damage. *Cotinus coggygria* Scop. (*C. coggygria*) plant has been used in various treatment processes for many years due to its strong antioxidant and anti-inflammatory components. In our study, the protective effect of *C. coggygria* aqueous extract against ethanol-induced small intestinal damage in rats was investigated. In our study, 5-6 months old male Sprague Dawley rats were divided into four groups: Group I (control group), Group II (group administered 50 mg/kg *C. coggygria* aqueous extract), Group III (group administered 1 mL absolute ethanol) and Group IV (group administered *C. coggygria* aqueous extract and 1 mL absolute ethanol one hour later). *C. coggygria* aqueous extract and ethanol were administered to rats by gavage method. One hour after ethanol administration, blood and tissue samples were obtained from anaesthetised rats and various biochemical analyses were performed. The results showed that ethanol-induced small intestinal tissue damage caused an increase in hexose, hexosamine and sialic acid levels. Administration of *C. coggygria* aqueous extract may play a protective role against ethanol-induced tissue damage by reducing these negative effects.

Keywords: *Cotinus coggygria* Scop, Small Intestine, Ethanol.

➢ *ORAL PRESENTATION*

Artificial Intelligence and Ethics in Education

Gülden Bozok[1*] (*ORCID: https://orcid.org/0009-0008-4104-417X*),
Murat Osman Ünalır[2] (*ORCID: https://orcid.org/0000-0003-4531-0566)*

[*1]Ege University, Graduate School of Natural and Applied Sciences, Department of Computer Engineering, İzmir, Türkiye.
[2]Ege University, Graduate School of Natural and Applied Sciences, Department of Computer Engineering, İzmir, Türkiye.

*Corresponding author e-mail :guldenbozok@gmail.com

Abstract

The integration of artificial intelligence (AI) into education brings not only technological and pedagogical advancements but also raises significant ethical and legal concerns (1). Key issues such as data privacy, algorithmic transparency, accountability, and fairness are increasingly emphasized in educational AI research (2). This study aims to examine how ethical dimensions of AI are addressed in the educational context by analyzing the relevant academic literature. The research is designed as a qualitative study based on the descriptive survey model and utilizes the systematic mapping method. Data were collected from three major academic databases: Scopus, Web of Science, and ERIC. A total of 611 articles published between 2020 and 2024 were selected for full-text analysis based on predetermined inclusion and exclusion criteria. Findings show that the most frequently addressed ethical theme is data privacy and security (30.48%), followed by transparency and explainability of algorithmic decisions (19.70%), responsibility and accountability (10.78%), and discrimination and bias (9.88%). Other prominent themes include legal insufficiencies (6.41%), ethical design principles (6.35%), digital ethics education (3.29%) and challenges in developing ethical frameworks (4.79%). The results suggest that ethical concerns in AI-supported education are multifaceted and require comprehensive policy and design approaches. Particularly, the dominance of themes such as privacy and algorithmic fairness highlights the need for transparent, accountable, and human-centered AI systems in education. The study concludes that the ethical integration of AI in education is not merely a support mechanism but a transformative process that demands ethical sensitivity and regulatory foresight.

Keywords: Artificial intelligence, ethics in education, educational technology, digital ethics

References

1. İşler, B., & Kılıç, M. Y. (2021). The use and development of artificial intelligence in education. *e-Journal of New Media / Yeni Medya Elektronik Dergi – eJNM*, *5*(1),1 11. https://doi.org/10.17932/IAU.EJNM.25480200.2021/ejnm_v5i1001
2. Bushuyev, S., Bushuyeva, N., Murzabekova, S., Khusainova, M., & Saidullayev, R. (2024). Transformation of the education landscape in an AI environment. In *Proceedings of the International Scientific Conference* (pp. 57–64). https://doi.org/10.56889/strd5315

➢ *ORAL PRESENTATION*

Responsive Polymer Brush Architectures Explored via Dissipative Particle Dynamics

Agnė Kilnaitė[1]* (ORCID: https://orcid.org/0009-0003-4422-5367),
Atakan Meran[1] (ORCID: https://orcid.org/0000-0001-8804-1365)

[1]Üsküdar University, Graduate School of Science, Department of Bioengineering, Istanbul, Türkiye

*Corresponding author e-mail: agne.kilnaite@st.uskudar.edu.tr

Abstract

Molecular brushes are polymer architectures consisting of a linear backbone that is densely grafted with side chains. Molecular brushes with core-shell side chains show promising structural and responsive behavior, making them suitable for applications such as drug delivery systems and advanced functional materials. In this study, the behavior of brushes with core-shell copolymer side chains was investigated using dissipative particle dynamics (DPD) simulations performed in LAMMPS. The polymer segments and solvent molecules were modeled as coarse-grained beads that interacted via conservative, dissipative, random and harmonic bond forces. PEG, PCL, and PLLA were selected as representative polymers with distinct hydrophilic, semi-crystalline, and biodegradable properties, respectively. To investigate phase behavior, the interaction parameters were systematically varied to adjust their compatibility.
Preliminary simulation results demonstrated the sensitivity of brush morphology to variations in grafting density and backbone configuration. The responsiveness of the polymer brush system to these molecular design factors highlights the value of coarse-grained modeling in capturing mesoscale behavior that is often challenging to observe experimentally. These results confirm the practicality of DPD as a predictive tool for investigating soft matter and reveal possibilities for adjusting polymer brush configurations to achieve specific functions.

Keywords: Molecular brush, dissipative particle dynamics, core-shell, polymer modeling.

➢ *ORAL PRESENTATION*

Arıtma çamurunun sorgum yetiştiriciliğinde kullanım potansiyeli

Mustafa Kutay Karadayı[1*] (*ORCID: https://orcid.org/ 0009-0004-3441-5658)*, Osman Sönmez[1](*ORCID: https://orcid.org/0000-0002-9134-6466*), Fatma Nur Kılıç[1] (*ORCID: https://orcid.org/0000-0003-3498-2455*)

[1]Erciyes Üniversitesi, Ziraat Fakültesi, Toprak Bilimi ve Bitki Besleme, Kayseri, Türkiye

*Sorumlu yazar e-posta: fatmanur@erciyes.edu.tr

Özet

Arıtma çamurlarının artan hacmi ve bertaraf edilmesi günümüzde ciddi bir problem haline gelmiştir. Belediye tesislerinde arıtma çamurlarının işlenmesi veya bertaraf edilmesi işletme maliyetlerinin temel bölümünü oluşturmakta, bundan dolayı ekonomik ve çevresel açıdan sürdürülebilir yöntemlerin kullanılması gerekmektedir. Sürdürülebilirliğin sağlanması ve maliyetin düşürülmesi amacıyla arıtma çamurlarının tarımda arazi tabanlı uygulanması alternatif yöntemler arasında yer almıştır. Bu çalışmada; analizleri belirlenen atık çamurun (%7,5, %15, %20, %25, %50, %75) toprakla seyreltilerek farklı gübre dozlarında (%25, %50, %100) sorgum bitkisinin gelişimi üzerine etkileri incelenmiş ve kullanılabilirliği değerlendirilmiştir. Bulgular, arıtma çamurunun ilave edilen miktarının artmasının sorgum bitkisinin gelişimine engel olduğu ancak miktarı seyreltildiğinde sorgum gelişimini teşvik ettiği, özellikle arıtma çamurunun dozunun azaltılmasının ve gübre ilavesinin birlikte etkisinin bitki-kök boyu, sap çapı, bitki-kök yaş ağırlığı, bitki-kök kuru ağırlığı gibi fizyolojik parametreleri kontrol grubuna kıyasla önemli düzeyde etkilediği belirlenmiştir ($p<0,001$). En yüksek değerler bitki boyunda A7,5-G50 grubunda 76,16 cm, kök derinliğinde A7,5-G25 grubunda 35 cm, bitki ve kök yaş ağırlığı A7,5-G100 grubunda sırasıyla 66,79 g ve 41,07 g ölçülmüştür. Ayrıca uygulanan atık çamur miktarının artması kontrol grubuna kıyasla toprak pH değerlerinde azalmaya, EC ve organik madde değerlerinde artışa neden olmuştur. Bulgular değerlendirildiğinde, arıtma çamurunun yüksek oranlarda toprağa ilavesinin bitkisel üretimi olumsuz yönde etkileyebileceği; ancak uygun dozlarda uygulandığında bitki gelişimini destekleyici yönde anlamlı sonuçlar elde edilebileceği düşünülmektedir.

Anahtar Kelimeler: Arıtma çamuru, sorgum, tarımsal sürdürülebilirlik

➢ *ORAL PRESENTATION*

Determination of antibacterial, antifungal, and insecticidal effects of secondary metabolites from entomopathogenic fungi

Seda BİRYOL[1*] (ORCID: https://orcid.org/0000-0003-0881-5004), Ali SOYDİNÇ[2] (ORCID: https://orcid.org/0000-0003-4208-2000) , Mehtap USTA[3](ORCID: https://orcid.org/0000-0001-7656-5655), Sevda İŞIK[2] (ORCID:https://orcid.org/0000-0002-1032-1807)

[1]Trabzon University, Tonya Vocational School, Department of Medical Services and Techniques, Trabzon/TÜRKİYE
[2]Trabzon Regional Directorate of Forestry, Trabzon/TÜRKİYE
[3]Trabzon University, Tonya Vocational School, Health Care Services Department, Trabzon/TÜRKİYE

*Corresponding author e-mail: sedabiryol@trabzon.edu.tr

Abstract

Entomopathogenic fungi (EPF) are known to produce a range of secondary metabolites, which have been observed to possess a variety of biological activities, including antibacterial, antifungal and insecticidal properties. This study aimed to obtain the total secondary metabolites of four *Metarhizium* sp. (Metch) (OZM-4, OZM-8, OZM-22b, OZM-14) isolated from *Dendroctonus micans* (Kugelann) (Coleoptera: Curculionidae, Scolytinae) and to elucidate the antibacterial and antifungal properties of these metabolites. Following the experimental design, two different solvents, ethyl acetate and chloroform, were employed in the synthesis of the secondary metabolites. Among the metabolites obtained using chloroform, OZM-4(K) was found to have the most effective antibacterial effect, as evidenced by the formation of an inhibition zone of 19.17 mm on *Staphylococcus aureus* ATCC 25923 and 17.62 mm on *Escherichia coli* ATCC 2471. OZM22b (E), one of the metabolites obtained by using ethyl acetate, demonstrated the most effective antibacterial effect, with an inhibition zone of 26.03 mm on *Bacillus subtilis* ATCC TCC6051U and 16.91 mm on *S. aureus*. It was established that OZM22b (K) exhibited the most pronounced antifungal activity against *Candida albicans*, manifesting as an inhibition zone of 12.33 mm. It was established that the metabolite derived from OZM14 (E) exhibited a pronounced antifungal effect on *C. albicans*, manifesting as an inhibition zone of 18.26 mm. The insecticidal effects on *D. micans* pest metabolites obtained using ethyl acetate showed mortality rates between 13% and 80% in larvae. Total metabolites obtained using chloroform showed mortality in larvae at a rate of 13% to 93%. In this context, the results obtained showed that the determination of the insecticidal effects of secondary metabolites obtained from EPFs on both human pathogenic bacteria and fungi, as well as the spruce pest *D. micans*, demonstrated that these compounds, derived from natural sources, have potential applications in agriculture and health.

Keywords: Antimicrobial, Entomopathogenic fungus, Insecticidal, *Metarhizium*, Microbiology, Secondary metabolite

Acknowledgement: This research was supported by the Trabzon University Scientific Research Projects Coordination Unit (BAP, Project Number: 23TAP00246).

➢ *ORAL PRESENTATION*

Production of Al-doped ZnO materials and investigation of their properties

Mariam Chari[1*] (ORCID: https://orcid.org/0009-0003-9035-5277), Zafer Gültekin[2] (ORCID: https://orcid.org/ 0000-0001-8026-0379), Handan Engin Kırımlı[3] (ORCID: https://orcid.org/ 0000-0003-0300-3381)

[*1] Bursa Uludag University, Faculty of Science, Department of Physics, Bursa, Türkiye.
[2] Bursa Uludag University, Faculty of Science, Department of Physics, Bursa, Türkiye.
[3] Bursa Uludag University, Faculty of Science, Department of Physics, Bursa, Türkiye.

*Corresponding author e-mail: Uumariam9@gmail.com

Abstract

In this study, undoped ZnO and different amounts of Al doped ZnO (AZO) thin films were prepared on glass substrates by sol-gel spin-coating method. In order to see the effects on the structural properties, morphology and optical properties of the films, the initial precursor concentration was changed by adding Al at 1%, 3%, 5% and 7%. The films were characterized by UV-vis transmittance measurements, X-ray diffraction (XRD) and scanning electron microscopy (SEM-EDS). In addition, ZnO and AZO thin films produced by sol-gel spin-coating technique were analyzed with the contact angle device. XRD measurements revealed that all the obtained films were polycrystalline with hexagonal structure. Absorption and transmittance measurements were taken to determine the forbidden energy band gap of the prepared undoped and doped ZnO thin films. The absorption spectrum of ZnO and AZO thin films varies significantly with Al content, especially in the 300-400 nm UV region. All films have high transmittance in the visible range (400-800 nm) at 85-95%. The optical band gap of all films was investigated by measuring the optical absorbance depending on the wavelength and was found to be between 3.2-3.3 eV. In addition, SEM analysis was performed to obtain a detailed understanding of the surface morphology of the thin films. The elemental composition was examined by EDX. The SEM image of Al-doped ZnO reveals a more homogeneous and smoother structure compared to undoped ZnO. Surface contact measurements were determined to support the SEM analysis for surface morphology (roughness). The change in contact angle indicates the increase or decrease in the surface roughness of the film. The results are consistent with the SEM images.

Keywords: Aluminum-doped zinc oxide (AZO), Sol-gel spin coating method, Transparent conductive oxide (TCO), Contact angle.

➢ *ORAL PRESENTATION*

Some bounds on distance based energy of graph products

Kübra Nur Koral[1] (*ORCID: https://orcid.org/0009-0006-8908-378X*),
Ezgi Aydemir[1*] (*ORCID: https://orcid.org/0000-0001-8557-1301*)

[1]University of Igdir, Faculty of Arts and Sciences, Department of Mathematics, Igdir, Türkiye.

*Corresponding author e-mail: ezgi.kaya@igdir.edu.tr

Abstract

Let G be a simple connected and undirected graph with n vertices. The energy of a graph is defined as the sum of the absolute values of all eigenvalues of the adjacency matrix of graph. For vertices u,v in $V(G)$, the distance $d(u,v)$ is the length of the shortest path between u and v in G. A topological index is a number related to graph which is invariant under graph isomorphism. Distance based topological indices TI and to each topological index associated a general extended adjacency matrix A_{TI} can be represented in the form $TI=TI(G)=\sum_{u\sim v} f(n_u(e)n_v(e))$ where for a given edge $e=uv$, the quantity $n_u(e)$ denotes the number of vertices closer to u than v, the quantity $n_v(e)$ denotes the number of vertices closer to v than u, and $A_{TI} = (f_{uv})$, here $f_{uv} = f(n_u(e)n_v(e)$ if $u\sim v$, $f_{uv} = 0$ otherwise, respectively. Let G_1 and G_2 be two graphs. Their product (Cartesian product, corona product, strong product, lexicographic product) also is a graph. In this study, we obtain the distance based eigenvalues and energy of product of two graphs from the eigenvalues of the given graphs.

Keywords: Distance, Co-PI energy, Corona Product, Graph products, Graph Theory.

➢ *ORAL PRESENTATION*

Çilek (*Fragaria ananassa)* Yaprağı Ekstresi Kullanılarak Altın Nanoparçacıkların Yeşil Sentezi ve Karakterizasyonu

Sümeyye YILMAZ KARAOĞLU[1,2*] (*ORCID: https://orcid.org/0000-0001-5529-7380*),
Tuğba TUNALI AKBAY[2] (*ORCID: https://orcid.org/0000-0002-2091-9298*)

[*1]Fenerbahçe Üniversitesi, Sağlık Hizmetleri Meslek Yüksekokulu, İstanbul, Türkiye.
[2] Marmara Üniversitesi, Diş Hekimliği Fakültesi, Temel Tıp Bilimleri, İstanbul, Türkiye.

*Sorumlu yazar e-posta: smylmz@icloud.com

Özet

Bu çalışma, çilek (Fragaria × ananassa) yaprağı ekstresi kullanılarak çevre dostu bir altın nanoparçacık (AuNP) sentez yönteminin geliştirilmesini ve bu nanoparçacıkların potansiyel biyomedikal uygulamalar açısından karakterizasyonunu amaçlamıştır.
Yeşil sentez yöntemi, fenolik bileşikler ve flavonoidler açısından zengin olan çilek yapraklarının sıcak su ekstraktı kullanılarak gerçekleştirilmiştir. Bu fitokimyasallar, güçlü antioksidan ve metal indirgeme özellikleri sayesinde 0.1 mM'lik kloroaurik asitten ($HAuCl_4$) Au^{3+} iyonlarının indirgenmesini sağlamış ve oluşan altın nanoparçacıklarının stabilizasyonuna katkıda bulunmuştur. Nanoparçacık oluşumu, karakteristik kırmızı rengin ortaya çıkmasıyla görsel olarak doğrulanmıştır.
Sentez sonrası, altın nanoparçacıklar, santrifüjleme ve etanol ile yıkama işlemleri (örnek:etanol = 1:5 oranında) ile saflaştırılmıştır. Karakterizasyon çalışmaları, transmisyon elektron mikroskobu (TEM), UV–vis spektrofotometresi ve dinamik ışık saçılımı (DLS) teknikleri kullanılarak gerçekleştirilmiştir. TEM görüntüleri, çapları 40–80 nm arasında değişen, çoğunlukla küresel şekilli nanoparçacıklar göstermiştir. UV–vis spektrumunda, AuNP'lerin yüzey plazmon rezonansına karşılık gelen 420 nm'de bir tepe gözlemlenmiştir. DLS analizi ise parçacık boyutu dağılımını doğrulamıştır.
Sonuç olarak, çilek yaprağı ekstresinin, altın nanoparçacıklarının yeşil sentezinde etkili ve sürdürülebilir bir ajan olduğu gösterilmiştir. Elde edilen nanoparçacıkların kolloidal stabilitesi ve boyut aralığı, onları lateral akış testleri ve diğer biyosensör sistemlerinde kullanım için uygun hale getirmektedir. Tanı uygulamalarının ötesinde, farklı uygulama gereksinimlerine göre boyutları ayarlanabilen altın nanoparçacıklar; ilaç taşıma, fototermal terapi, biyo-görüntüleme ve antimikrobiyal uygulamalar gibi alanlarda da benzersiz optik ve yüzey özellikleri sayesinde umut vadeden adaylardır.

Anahtar kelimeler: nano partiküller, nano altın, yeşil sentez

➢ *ORAL PRESENTATION*

Histological Evaluation of the Effect of Baicalin on Cisplatin-Induced Parotid Gland Injury

Duha İbrahimoğlu[1*] (*ORCID: https://orcid.org/0009-0005-1243-3334*),
Esin Ak[2] (*ORCID: https://orcid.org/0000-0002-3467-7808)*

[*1] Marmara University, Institute of Health Sciences, Department of Basic Medical Sciences, Istanbul, Turkey
[2] Marmara University, Faculty of Dentistry, Department of Basic Medical Sciences, Istanbul, Turkey

*Corresponding author e-mail: duhaibrahimoglu@gmail.com

Abstract

Cisplatin is an effective chemotherapeutic agent frequently used in the treatment of various cancers. However, it has adverse effects on non-target tissues, including the salivary glands. Baicalin, a flavonoid compound derived from Scutellaria baicalensis, possesses various pharmacological properties, including antioxidant, anti-inflammatory, and cytoprotective effects The aims of this study is to investigate the effects of baicalin on cisplatin-induced parotid gland damage. In this study, twenty-eight adult female rats were divided into four groups as Control (n=6), Baicalin (n=6), Cisplatin (n=8), and Cisplatin + Baicalin (n=8) groups. In the Control group, rats were given vehicle solution (Dimethyl sulfoxide (DMSO)) intraperitoneally (i.p.) for five days. In the Baicalin group, rats were given baicalin (100 mg/kg, dissolved in DMSO) i.p. for five days. In the Cisplatin group, rats were given a single dose of 7 mg/kg cisplatin on day the first day of the experiment and the vehicle solution (DMSO) i.p. daily for five days. In the Cisplatin + Baicalin group, rats were given a single dose of cisplatin (7 mg/kg) on day first day of the experiment, followed by baicalin (100 mg/kg, dissolved in DMSO) i.p. daily for five days. On the sixth day of the experiment, all rats were sacrificed and parotid glands were taken for histological analysis. Cisplatin administration caused a damage in acinar and ductal structures, as well as vascular congestion. However, baicalin treatment notably ameliorated the morphological alterations in the parotid gland induced by cisplatin administration. According to our histological results, baicalin treatment appears to have a protective role on cisplatin-induced parotid gland damage.

Keywords: Cisplatin, Baicalin, Parotid gland, Oxidative stress, Histopathology

➢ *ORAL PRESENTATION*

Effect of *Alcea rosea* var. *nigra* flower extract on cancerous and non-cancerous pleural mesothelial cells

Israt JAHAN[1*] (*ORCID: https://orcid.org/0000-0003-4166-1617*)

[1*]Mardin Artuklu University, Vocational School of Health Services, Department of Health Care Services, Mardin, Türkiye

*Corresponding author e-mail: ijahan@artuklu.edu.tr (I. Jahan)

Abstract

Black hollyhock (*Alcea rosea* var. *nigra*), a member of the Malvaceae (mallow) family, is native to Asia and has been extensively cultivated across Europe since medieval times. The flowers range in color from deep maroon to almost black and may appear as single or double blooms, typically measuring 3 to 4 inches in diameter. The flower, along with other parts of the plant, has been used in traditional medicine to treat pain, ulcers, wounds, diabetes, and more, largely due to its rich content of anthocyanins, mucilage, flavonoids, and tannins. In this study, fresh flowers were collected from the Tigris River shoreline in Diyarbakır during mid-June, and dried under ambient conditions, and extracted with a methanol-to-water mixture (5:1, v/v). Different concentrations of the flower extract were used to evaluate the *in vitro* cytotoxic effects on healthy lung epithelial (MeT-5A) and two malignant pleural mesothelioma, i.e, biphasic mesothelioma (NCI-H2452) and sarcomatoid mesothelioma (NCI-H2052) cell lines. Cell proliferation in healthy epithelial cells (MeT-5A) was observed at concentrations of 15.625, 31.25, and 62.5 µg/mL, with corresponding cell viability values of 112.05%, 118.01%, and 109.95%, respectively. The strongest anti-proliferative effects were observed in NCI-H2052 and NCI-H2452 cell lines at a concentration of 500 µg/mL, with cell viability reduced to 58.63% and 72.13%, respectively. Remarkably, healthy epithelial cells exhibited no significant signs of cytotoxicity at the given treatments.

Keywords: *Alcea rosea* var. *nigra*, MTT assay, Human Mesothelioma, Proliferation, Cytotoxicity

➢ *ORAL PRESENTATION*

Protective Effects of Alpha Lipoic Acid Against Valproic Acid-Induced Small Intestinal Damage

Jahan Babazade[1] * (*ORCID: https://orcid.org/0009-0001-1954-1750*), Ismet Burcu Turkyilmaz Mutlu[2] (*ORCID: https://orcid.org/0000-0003-2789-5943*), Refiye Yanardag[2] (*ORCID: https://orcid.org/0000-0003 4185-4363*)

[1]Istanbul University-Cerrahpaşa, Institute of Graduate Studies, Istanbul, Türkiye.
[2]Istanbul University-Cerrahpaşa, Faculty of Engineering, Department of Chemistry, Istanbul, Türkiye

*Corresponding author e-mail: jahan.babazade@gmail.com

Abstract

Valproic acid (VPA), also known as 2-propylpentanoic acid, is a broad-spectrum antiepileptic drug used in the treatment of generalized and focal seizures. Alpha lipoic acid (ALA), due to the functional dithiolane ring in its structure, possesses antioxidant properties. The small intestine is the part of the digestive tract and digestive processes are completed in this tissue.
In this study, we aimed to investigate the effects of ALA against VPA-induced small intestinal damage. The experimental groups were divided into four groups as follows: Control group, VPA given group, ALA given group and VPA+ALA given group. VPA and ALA were given at doses of 500 mg/kg (i.p) and 50 mg/kg (orally) for 15 days, respectively. At the end of the experiment, the tissues were taken, homogenized in cold physiological saline and centrifuged. In supernatants, GSH and TAC levels were found to be decreased whereas LPO, TOS and OSI levels were increased at VPA given group. Administration of ALA reversed these effects in VPA group. We can conclude that ALA ameliorated small intestine damage caused by VPA.

Keywords: Valproic Acid, Alpha Lipoic Acid, Small Intestine, Oxidative Stress

➢ *ORAL PRESENTATION*

Tarım İşletmeleri ve Sürdürülebilirlik Perspektifinden IV. Tarım Orman Şûrası Kararları

Hüseyin Tayyar Güldal[1*] (*ORCID: https://orcid.org/0000-0003-4477-3980)*

[1] Ankara Üniversitesi, Ziraat Fakültesi, Tarım Ekonomisi Bölümü, Ankara, Türkiye

*Sorumlu yazar e-posta: htguldal@ankara.edu.tr

Özet

Tarım ve Orman Şûrası, Türkiye'de tarım ve kırsal kalkınma politikalarının şekillendirilmesine katkı sunmak amacıyla düzenlenen yüksek düzeyli bir istişare platformudur. İlk olarak 1997 yılında yapılan şûranın dördüncüsü 30 Ocak 2025 tarihinde, 16 farklı çalışma grubunun katılımıyla gerçekleştirilmiştir. Bu çalışma amaç, IV. Tarım Orman Şûrası sonuç bildirgesinde yer alan kararların, tarım işletmelerine yönelik sürdürülebilirlik eğilimleri açısından nasıl bir çerçeve sunduğunu değerlendirmektir. Çalışmada, şûra sonucu alınan kararlar tematik olarak gruplandırılmış, bu kararların Birleşmiş Milletler Sürdürülebilir Kalkınma Amaçları (SKA) ile olası ilişkileri incelenmiştir. Çalışma sonucunda özellikle SKA 2 (Açlığa Son) ve SKA 13 (İklim Eylemi) ile bağlantılı başlıklar ön plana çıkmaktadır. Üretim planlaması, su kullanımı, dijitalleşme, iklim uyumu ve kırsal altyapı gibi alanlara yönelik kararların, tarım işletmelerinin sürdürülebilirlik kapasitesine katkı sunabilecek potansiyeller barındırdığı görülmektedir. Bununla birlikte, bazı kararların önceki şûralarda da yer aldığı ve benzer önerilerin tekrarlandığı dikkat çekmektedir. Bu durum, politika belgelerinin uygulanabilirliğinin işletme düzeyinde nasıl yansıdığına dair daha fazla değerlendirme ihtiyacını gündeme getirmektedir. Çalışmada, şûra kararlarının tarım işletmeleriyle ilişkili yönleri öne çıkarılmış ve sürdürülebilirlik hedefleriyle kurulan bağlar üzerine genel bir değerlendirme sunulmuştur.

Anahtar Kelimeler: Üretim planlaması, şûra kararları, sürdürülebilir kalkınma amaçları

➢ *ORAL PRESENTATION*

Techno-economic assessment of off-grid hybrid renewable energy systems for urban electricity demand

Hacımurat Demir[1*] (*ORCID: https://orcid.org/0000-0002-4819-2633*)

[*1]Aksaray University, Engineering Faculty, Department of Mechanical Engineering, Aksaray, Türkiye.

*Corresponding author e-mail: hmdemir@aksaray.edu.tr

Abstract

The growing environmental concerns associated with fossil fuel consumption and the critical demand to decrease carbon emissions have intensified global efforts toward the deployment of clean and sustainable energy systems. In this context, hybrid renewable energy systems (HRES) offer a promising solution for meeting urban electricity demands without relying on conventional, carbon-intensive power generation. This study presents a comparative techno-economic analysis of six different grid-independent HRES configurations designed to meet the annual electricity demand of a city. All configurations were modelled and optimized using HOMER software and include various combinations of generators, PV panels, wind turbines, lithium-ion batteries, and converters. The estimation of key performance indicators, including Net Present Cost (NPC), Levelized Energy Cost (LCOE), Renewable Fraction (RF), and Excess Electricity (EE), was made for each configuration during a 20-year project lifespan under consistent economic and resource assumptions. The third configuration, comprising one generator, 154 wind turbines, 118 MW PV panels, and 11,923 battery arrays, achieved a renewable energy ratio of 71.6%, the lowest LCOE of $0.259/kWh, and an NPC of $2.26 billion. In fully renewable scenarios (fourth and sixth configurations), higher costs (LCOE ranging from $0.375 to $0.611/kWh) and significantly excess production (55.7-69%) were generated. The second configuration minimized excess electricity (10.7%) but relied heavily on PV and generator backup, resulting in a moderate LCOE of 0.319 $/kWh. The results stated that both technical and economic parameters must be comprehensively evaluated in off-grid energy systems. The effective integration of renewable energy resources with adequate storage and backup production units that can be enabled, when necessary, offers a more feasible and sustainable approach than fully renewable but high-cost solutions. Moreover, the findings provide important insights for researchers, investors, and decision-makers involved in the design and implementation of renewable energy systems, particularly at the urban scale or in isolated settlements.

Keywords: Hybrid renewable energy system, Energy generation, Renewable energy, Wind energy, Solar energy.

➢ *ORAL PRESENTATION*

Plastivore insects: an overview

Elif Fatma Topkara[1*] (*ORCID: https://orcid.org/0000-0002-4743-2914*)

[1*]Ondokuz Mayıs University, Faculty of Sciences, Department of Biology, Samsun, Turkey

[*]Corresponding author e-mail: topkaraelif@hotmail.com

Abstract

The increasing global production of plastics, which are frequently used today, causes plastic pollution. Traditional methods used for the disposal of plastics are inadequate in dealing with plastic pollution. The idea of biodegradation of plastics has been put forward as a new alternative to develop a sustainable approach to this problem, which continues to increase every year. Biodegradation of plastics by insects offers a different alternative to traditional plastic waste management. Insect larvae that can consume plastic materials are called “plastivores”. The ability of plastivore insects to digest plastic is mediated by gut microorganisms. Microorganisms in the insect gut initiate enzyme activity, along with metabolic processes such as oxidation and depolymerization. In this way, polymer plastic slowly degrades into smaller monomers, which are then converted into biomass, carbon dioxide, and water that are then excreted as waste by insect larvae. One of the important benefits of this approach is that insects complete the degradation of plastics in a much shorter time, whereas in natural environments they occur very slowly. In addition, environmental friendliness, minimum cost, and the absence of secondary contamination are also advantages. In addition, plastivore larvae have good utilization and financial value as a source of animal feed. In addition, small plastic particles such as microplastics can be completely degraded into water and carbon dioxide, thus minimizing the adverse effect on the environment. Various studies have investigated the ability of insects from different orders to degrade plastics. Identifying new candidate insects from different species that can degrade plastics will undoubtedly be important in helping solve this problem. In addition, the ability of microorganisms/enzymes isolated from these insects to degrade different types of plastics should be investigated in detail.

Keywords: Plastic waste, Plastivore insects, Pollution.

➢ *ORAL PRESENTATION*

Effect of Glaucocalyxin A on Cell Migration Capacity in Lung Cell Line

Merve BOZKURT[1*] (*ORCID: https://orcid.org/0009-0005-3513-6412*), Nuray BOSTANCIERİ[2] (*ORCID: https://orcid.org/0000-0002-3765-8274*), Çiğdem KARACA[3] (*ORCID: https://orcid.org/0000-0003-2106-2422*)

*[1]Gaziantep University, Faculty of Medicine, Department of Histology and Embryology, Gaziantep, Türkiye.
[2]Gaziantep University, Faculty of Medicine, Department of Histology and Embryology, Gaziantep, Türkiye.
[3]Gaziantep Islamic Science and Technology University, Faculty of Medicine, Department of Histology and Embryology, Gaziantep, Türkiye.

*Corresponding author e-mail: mervehistoloji@gmail.com

Abstract

The aim of the study was to investigate the effect of Glaucocalyxin A on cell migration in A549 cell line in which cell migration capacity was induced by TGF- β.
Three replicate MTT assays were performed to determine the IC50 dose of Glaucocalyxin A on A549 cell line. Increasing doses of Glaucocalyxin A were added to 85% confluent cells seeded in 96-well plate. As a result of the analysis, the IC50 dose was measured as 10 µM at 24th and 48th hours of the experiment. After determination of the doses, four experimental groups were formed in 6-well cell culture plates. Our groups were; control group without treatment, T group with 5 ng/mL TGF- β, G group with 10 µM Glaucocalyxin A, T+G group with both 5 ng/mL TGF- β and 10 µM Glaucocalyxin A. In order to evaluate the migration level of the cells, a line was drawn in the wells with a 1000 µl micropipette tip and a wound site model was created. After the cells were checked under an inverted microscope, they were incubated at 37°C and 5% CO2. The experimental groups were examined at 24 hours and 48 hours under an inverted microscope and the images were recorded. Images were evaluated with the help of Image J program.
The wound closure rate of the TGF- β group was significantly higher than that of the control group at 24 and 48 hours ($p<0.001$). The wound closure rate in the G and T+G groups was significantly lower at 24 and 48 hours of the study compared to the control and TGF- β groups ($p<0.001$). Wound site patency in the G group was significantly higher compared to all groups at 24 and 48 hours of the study.
Based on the results we obtained in our study, we concluded that Glaucocalyxin A has an inhibitory effect on cell migration at increasing concentrations and that it can also show this effect in the presence of TGF-β. We believe that further studies are needed to determine the other effects of Glaucocalyxin A on A549 cells.

Keywords: Glaucocalyxin A, Cell migration, A549

This study was supported by Gaziantep University Scientific Research Projects Management Unit with project number TF.UT.23.38.

➢ *ORAL PRESENTATION*

Contribution of using a tuned mass damper (TMD) as a passive control device in building performance

Osman Akyürek[1*] (*ORCID: https://orcid.org/0000-0001-8161-1775*)

[*1]Nevsehir Haci Bektas Veli University, Faculty of Architecture and Engineering, Department of Civil Engineering, Nevsehir, Türkiye.

*Corresponding author e-mail: oakyurek@nevsehir.edu.tr

Abstract

A tuned mass damper (TMD) is a well-known passive control device widely used in structures located in regions prone to high seismic activity. Its effectiveness in enhancing the seismic energy absorption capabilities of buildings and systems is well recognized across various engineering industries, from automobiles to shipping. However, the impact of TMDs on overall building performance has not been extensively studied. In this research, a TMD device with a 5% mass ratio is integrated into a 7-story reinforced concrete (RC) building. The analysis is conducted using structural finite element software, SAP 2000. The results are compared to those of the building without a TMD. While the TMD does not significantly change the capacity curve of the building, it enhances the performance point by reducing it by 26% compared to the uncontrolled structure. This indicates that TMD systems can be a promising alternative to conventional retrofitting methods.

Keywords: Capacity curve, Pushover nonlinear analysis, Tuned mass damper.

➢ *ORAL PRESENTATION*

Eskişehir Sazova Bilim Kültür ve Sanat Parkı Floristik Yapısı İle İlgili Ön Çalışmalar

Erhan DURGUT[1*] (0009-0004-7349-6294), Ebru ATAŞLAR[2] (0000-0001-5755-4256)

[*1]Eskişehir Osmangazi Üniversitesi, Fen Bilimleri Enstitüsü, Biyoloji Anabilim Dalı, 26040, Eskişehir, Türkiye
[2]Eskişehir Osmangazi Üniversitesi, Fen Fakültesi, Biyoloji Bölümü, 26040, Eskişehir, Türkiye

* Sorumlu yazar e-posta: edurgut26@gmail.com

Özet

İç Anadolu Bölgesi floristik yapısının bitki çeşitliliğini içerisinde barındıran Eskişehir, Türkiye bitki çeşitliliği için önemli bir görev üstlenmektedir. Eskişehir, İran-Turan fitocoğrafik bölgesinde yer almasına rağmen yeryüzü şekillerinin çeşitliliği ve jeomorfolojik farklılıklar sebebiyle mikroklimal iklim bölgelerine de sahiptir. Bu nedenle Eskişehir'deki bazı bölgelerde Akdeniz iklimi de gözlemlenmekte, Akdeniz fitocoğrafik bölgesinde doğal olarak yetişmekte olan bitki türleri de gözlenmektedir. Ayrıca, Eskişehir'in bitki çeşitliliği peyzaj çalışmalarına da katkı sağlamaktadır.
Bu çalışma, Eskişehir Sazova Bilim Kültür ve Sanat Parkı'nın floristik yapısı ile ilgili ön bilgileri kapsamaktadır. Araştırma, Ocak 2024 - Ekim 2024 tarihleri arasında on beş günlük periyotlar şeklinde gerçekleştirilmiş olup bitkilerin yapraklı, çiçekli ve meyve/tohum durumları fotoğraflanmış ve toplanmıştır. Daha sonra tür teşhisleri yapılarak floristik yapısı ile ilgili ön bilgilere ulaşılmıştır. İncelemeler sonucunda, Eskişehir Sazova Bilim Kültür ve Sanat Parkı'nın genel floristik yapısına ait tür sayısı bakımından zengin olan bazı familyalar şu şekilde sıralanmaktadır; *Asteraceae, Betulaceae, Brassicaceae, Cupressaceae, Fabaceae, Liliaceae, Pinaceae, Rosaceae, Sapindaceae*

Anahtar Kelimeler: Taksonomi, Park Florası, Kent Ekolojisi, Sazova

➢ *ORAL PRESENTATION*

The role of microbiome research in improving gut health of farmed species for sustainable disease resistance in aquaculture.

Ulviye Karacalar (https://orcid.org/0000-0002-9093-2324)

Ege University, Fisheries Faculty, Aquaculture Department, Fish Disease Unit, Izmir, Türkiye.

*Corresponding author e-mail: ukaracalar@yahoo.com

Abstract

More than 50% of seafood produced worldwide comes from aquaculture, the fastest growing sector in food production (FAO, 2022). However, disease outbreaks and antibiotic use pose serious challenges to sustainability, particularly given the potential for antibiotic resistance genes to spread to other pathogenic systems. According to recent research focused on identifying microbiome species found in the gastrointestinal tracts of fish and shellfish, a large number of bacterial and viral diseases that continuously affect aquaculture and cause major financial losses can be successfully controlled. Aquaculture has recently seen significant advances with the emergence of new insights into the applications of high-throughput sequencing, metagenomics, and probiotics as well as pro- and prebiotics. This research aims to focus on the current state of research on the impact of the gut microbiome in farmed fish and shellfish on nutrient metabolism, immune regulation and disease prevention, while summarizing genetic and technological innovations introduced for microbiome manipulation (probiotics, prebiotics, synbiotics and sustainable feeds) and early pathogen detection, particularly on the basis of sustainability.

Keywords: Aquaculture microbiome , gut health, disease resistance, sustainable aquaculture

➢ *ORAL PRESENTATION*

Effects of sustainable diets such as insect-based, essential oil-supplemented and single-cell protein on disease resistance in aquaculture

Ulviye Karacalar (https://orcid.org/0000-0002-9093-2324)

Ege University, Fisheries Faculty, Aquaculture Department, Fish Disease Unit, Izmir, Türkiye.

*Corresponding author e-mail : ukaracalar@yahoo.com

Abstract

Aquaculture is one of the fastest growing sectors and has the potential to contribute to sustainable food production in the future. However, with the intensification of production, the sector has been faced with disease outbreaks that cause global losses exceeding US$ 6 billion per year, and serious problems such as antimicrobial resistance (AMR) and environmental pollution due to antibiotics and chemical treatments have also faced significant limitations in sustainable production. In response to these problems, many researchers have succeeded in developing sustainable feed alternatives that not only meet nutritional demands but also provide health benefits to farmed aquatic animals. Studies have shown that the use of alternative ingredients in feed ingredients (especially insect-based proteins, essential oil (EO) supplements and single-cell proteins (SCPs)) contributes to both environmental sustainability and a significant increase in the potential to increase host disease resistance. Key findings show that insect feeds increase survival rates against bacterial infections through their immune-stimulating effect, essential oils exhibit broad antimicrobial activity and single-cell proteins significantly increase antiviral resistance. The aim of this research is to evaluate the immunomodulatory and antimicrobial effects of sustainable feeds in aquaculture species and to present current studies on promising feed ingredients that could be alternatives to fishmeal-based diets.

Keywords: Aquatic animals, insect-based feed, essential oil-supplemented, antimicrobial effects, immunomodulatory

➢ *ORAL PRESENTATION*

İkincil A356 Alüminyum Alaşımının Korozyon Davranışına Minör Skandiyum (Sc) ve Lantan (La) Eklentisinin Etkisi

Hayat Oyman[1,*] (https://orcid.org/0009-0006-9634-0158)
Simge İrizalp[1] (https://orcid.org/0000-0002-0339-5699)
Burçak Kardelen Köroğlu[2] (https://orcid.org/0000-0003-0200-8252)
Batuhan Doğdu[2] (https://orcid.org/0000-0003-4110-7341)
Caner Kalender[2] (https://orcid.org/0000-0003-3398-3181)

*[1]Manisa Celal Bayar Üniversitesi, Mühendislik ve Doğa Bilimleri Fakültesi, Manisa, Türkiye
[2]CMS Jant ve Makina Sanayii A.Ş. ,Çiğli/İzmir

*Sorumlu yazar e-posta: hayatoyman@hotmail.com

Özet

Birincil alüminyum üretiminin yüksek enerji tüketimi ve çevresel etkileri, geri dönüştürülmüş (ikincil) alüminyum alaşımlarının kullanımını teşvik etmektedir. Ancak, bu tür alaşımların yapısal ve kimyasal safsızlıkları, malzeme özelliklerini olumsuz etkileyebilmektedir. Literatürde nadir toprak elementlerinin (Rare Earth Elements, REE) A356 tipi alüminyum alaşımı üzerindeki mikro yapı ve mekanik özelliklere etkisi araştırılmış olsa da, korozyon davranışına etkileri sınırlı sayıda çalışmayla ele alınmıştır. Üstelik mevcut çalışmalarda elde edilen bulgular arasında belirgin bir tutarsızlık bulunmakta olup, farklı REE ilavelerinin oranlarına bağlı etkilerin sistematik ve detaylı bir şekilde incelenmesine duyulan ihtiyaç devam etmektedir. Bu doğrultuda yürütülecek kapsamlı araştırmalar, hem akademik literatüre hem de alaşım geliştirme süreçlerinde uygulamaya yönelik sanayiye önemli katkılar sağlayacaktır. Bu çalışma, geri dönüştürülmüş A356 alaşımına farklı oranlarda La, Sc, Ti ve Zr eklenmesiyle elde edilen mikroyapısal değişimlerin, alaşımın korozyon performansı üzerindeki etkilerini sistematik olarak ortaya koymayı amaçlamaktadır.

Çalışmada, çeşitli mikroalaşım kombinasyonları hazırlanarak, numuneler %3,5 NaCl içeren asidik ortamda ASTM G31 standardına uygun olarak daldırma tipi korozyon testine tabi tutulmuştur. Bulgular, La ilavesinin belirli oranların üzerinde intermetalik faz oluşumunu teşvik ettiğini, bu fazların mikroyapıda heterojen dağılımı nedeniyle galvanik hücre oluşumunu artırarak korozyon direncini azalttığını göstermiştir. Öte yandan, Sc elementinin özellikle Zr ile birlikte kullanıldığında tane yapısını rafine ettiği ve korozyon hızını önemli ölçüde düşürdüğü tespit edilmiştir. %0,1 Sc + %0,2 Zr içeren numunede ölçülen 0,07177 mm/yıl korozyon hızı, tüm kombinasyonlar arasında en iyi performansa işaret etmektedir. Kıyas olması bakımından SAA-A356 alaşımı 0,76264 mm/yıl korozyon hızına sahiptir. %0,1 Sc + %0,2 Zr içeren numunede, korozyon hızında yaklaşık %90,6 oranında iyileşme sağlanmıştır.

Bu çalışma, literatürde eksikliği hissedilen bir alana katkı sunarak, geri dönüştürülmüş alüminyum alaşımlarının sürdürülebilirliğini artıracak yeni mikroalaşımlama stratejilerinin geliştirilmesine bilimsel zemin hazırlamaktadır. Ayrıca, mikroalaşımlama işleminin ilave tezgah yatırımı gerektirmemesi, özellikle ikincil alüminyum alaşımları (SAA) gibi düşük maliyetli hammadde grupları açısından bu yöntemi endüstriyel uygulamalar için tercih edilebilir ve uygulanabilir bir çözüm haline getirmektedir.

Anahtar Kelimeler: Al-Si döküm alaşımı, İkincil alüminyum alaşımı, Korozyon davranışı, Nadir toprak elementleri

➢ *ORAL PRESENTATION*

Design and Evaluation of Chitosan/PVP-Based Films for Advanced Wound Dressings in Biomedical Applications

Özlem Ayşe Tosyalı[1*] (*ORCID: https://orcid.org/0000-0002-8878-5863*), Okşan Karal-Yılmaz[2] *(ORCID https://orcid.org/0000-0001-6780-9814)*

[*1] İstanbul Beykent University, Faculty of Engineering&Architecture, Department of Biomedical Engineering, Istanbul, Türkiye

[2]İstanbul Beykent University, Faculty of Engineering&Architecture, Department of Chemical Engineering, Istanbul, Türkiye

*Corresponding author e-mail: aysetosyali@beykent.edu.tr

Abstract

Wound dressings play a vital role in shielding wounds from external contaminants, preserving a moist environment that promotes healing, and supporting a faster recovery process. Among advanced wound dressings, hydrogel films have gained attention due to their tunable properties and ability to act as platforms for the co-delivery of various therapeutic agents. In our study, we developed chitosan (CH) and polyvinylpyrrolidone (PVP)-based hydrogel films loaded with silver nanoparticles (AgNPs) and vancomycin hydrochloride (VH) as a co-delivery platform for wound dressing applications, prepared via the solvent casting method. CH, a naturally derived biopolymer, has been extensively studied for such applications owing to its biodegradability, biocompatibility, hemostatic effect, and antimicrobial activity. AgNPs possess excellent physical and chemical stability, along with strong bactericidal properties. In this study, AgNPs were synthesized *in situ* via a green method using CH as a natural reducing and stabilizing agent, avoiding toxic-reducing reagents. To enhance mechanical strength, the synthesized AgNPs-CH nanocomposite was blended with PVP, a synthetic, water-soluble polymer widely used in wound dressings for its excellent biocompatibility and film-forming ability. VH is a glycopeptide antibiotic was incorporated to target gram-positive bacteria.

The successful synthesis of AgNPs-CH was confirmed by a visible color change from light yellow to dark yellow, and UV-Vis spectroscopy revealed a characteristic surface plasmon resonance absorption band at ~425 nm, indicative of spherical AgNPs. The chemical structure of the resulting hydrogel films was confirmed by FTIR analysis. All films demonstrated favorable swelling behavior at pH 7.4 and 37 °C. *In vitro* release studies demonstrated a sustained release profile of VH from the composite films.

In summary, our findings demonstrate that the AgNPs-CH/PVP-VH film is a suitable candidate for development as a multifunctional wound dressing platform.

Keywords: wound dressing, chitosan, polyvinylpyrrolidone, silver nanoparticles, drug release

➢ *ORAL PRESENTATION*

Evaluation of volatile oil composition and structural discrepancies in different parts of *Chenopodium botrys* L.

Pelin Yılmaz Sancar[1*] (*ORCID: https://orcid.org/0000-0002-6134-622X*),
Azize Demirpolat[2] (*ORCID: https://orcid.org/0000-0001-7192-185X*)

[*1] Fırat University, Faculty of Science, Department of Biology, Elazığ, Türkiye.
[2] Bingöl University, Vocational School of Food, Agriculture and Livestock, Bingöl, Türkiye.

*Corresponding author e-mail: peyilmaz@firat.edu.tr

Abstract

In this study, the essential oil composition of *Chenopodium botrys* L. was analyzed separately from its aerial parts and seeds using Gas Chromatography-Mass Spectrometry (GC-MS). The components of the essential oils obtained from both parts were identified based on peak area percentages, and the major constituents were determined. *C. botrys* is an aromatic plant reported to possess various biological activities such as antimicrobial, anti-inflammatory, and anticancer potential. The composition of essential oils derived from the aerial parts and seeds is significant for understanding the variation in these biological effects and the plant's potential applications. Findings revealed both similarities and notable differences between the essential oil profiles of different plant parts.

According to the GC-MS results, the seed essential oil contained 22 components, with the major ones being 2,3-Dimethylpentane (43.5%), Cyclopentane, methyl- (8.32%), Elemol (11.16%), and β-Eudesmol (4.93%). In contrast, the aerial part oil yielded 19 components, with Cyclopentane, methyl- (52.56%), Elemol (16.10%), and 4,4-Dimethyladamantan-2-ol (6.02%) identified as the main constituents. Cyclopentane, methyl- was found in both parts in significant amounts, being particularly dominant in the aerial oil. Notably, 2,3-Dimethylpentane was only detected as a major compound in the seed oil. Additionally, sesquiterpene alcohols such as Elemol and Selina-6-en-4-ol were major components in both oils, indicating their potential therapeutic relevance.

These compositional differences suggest that the biosynthetic pathways of *C. botrys* may vary between aerial and seed tissues, potentially affecting the pharmacological properties of their essential oils. Both oils exhibit rich chemical profiles with key constituents such as Cyclopentane, methyl-, Elemol, Selina-6-en-4-ol, and β-Eudesmol, which highlight the pharmaceutical and industrial potential of the plant. The data obtained provide a valuable basis for further studies on the bioactive properties and possible therapeutic uses of *Chenopodium botrys* essential oils.

Keywords: *Chenopodium botrys*, essential oils, GC-MS, aerial parts, seeds, chemical composition

➢ *ORAL PRESENTATION*

Kinetic and Equilibrium Studies on the Adsorption of Remazol Red by Natural Zeolite

Buse Nur DÜKANLI (ORCID: https://orcid.org/0009-0004-2488-7344),
Elçin DEMİRHAN (ORCID: https://orcid.org/0000-0002-4885-2902)

Yildiz Technical University, Faculty of Chemical and Metallurgical Engineering, Department of Chemical Engineering, Istanbul, Turkey

*Corresponding author e-mail: nur.dukanli@std.yildiz.edu.tr, demirhan@yildiz.edu.tr

Abstract

Water pollution has become an increasingly serious global challenge that threatens both human health and the environment [1]. Among pollutants, dyes released from textile industries are particularly concerning due to their complex chemical structures and resistance to degradation [2]. Remazol Red, a reactive dye extensively used for dyeing cellulose-based fibers, is characterized by its high solubility and bright color, which can cause severe environmental pollution if discharged untreated into water bodies [3]. Adsorption has been widely recognized as an effective and cost-efficient method for removing dyes from aqueous solutions, offering operational simplicity and high removal efficiency [4].
In this study, natural zeolite was utilized as an adsorbent to investigate the removal of Remazol Red dye from aqueous solutions under varying experimental conditions, including temperature (25°C, 35°C, and 45°C), pH (2, 3, and 4), and adsorbent dosage (0.1, 0.3, and 0.5 g/100 mL). The adsorption kinetics were analyzed using pseudo-first-order and pseudo-second-order models, while Langmuir and Freundlich isotherm models were applied to describe the equilibrium behavior of dye adsorption on zeolite. The results obtained in this study indicate that natural zeolite can be considered an environmentally friendly, reusable, and cost-effective adsorbent for the removal of Remazol Red dye from aqueous solutions, showing promising performance in terms of adsorption efficiency, kinetic behavior, and equilibrium modeling.

Keywords: Remazol Red, Zeolite, Adsorption Kinetics, Isotherm Models, Dye Removal.

References:

[1] Yakartepe M. ve Yakartepe Z., "Tekstil Terbiye Teknolojisi" T.K.A.M., İstanbul, 1995.
[2] Wang J. and Guo X., "Adsorption kinetic models: Physical meanings, applications, and solving methods," Journal of Hazardous Materials, vol. 390, p. 122156, May 2020.
[3] Bozic, M., & Kokol, V. (2008). "Ecological alternatives to the reduction and oxidation processes in dyeing with reactive dyes." Dyes and Pigments, 76(2), 299–309.
[4] Ghaly, A. E., Ananthashankar, R., Alhattab, M., & Ramakrishnan, V. V. (2014). "Production, Characterization and Treatment of Textile Effluents: A Critical Review." Journal of Chemical Engineering & Process Technology, 5(1).

➢ *ORAL PRESENTATION*

The Role of Food Choice Motivations and Food Neophobia in Organic Food Consumption

Muhammet Ali ÇAKIR[1*] (*https://orcid.org/0000-0001-5066-1956),* Merve PEHLİVAN[2] (*https://orcid.org/0000-0003-1640-8724),* Neslişah Denkçi[2] (https://orcid.org/0009-0004-4690-0378)

[*1] Kırklareli University Faculty of Health Sciences, Kırklareli, Turkey,
[2] Trakya University Faculty of Health Sciences, Edirne, Turkey,

*Corresponding author e-mail: m.ali.cakir@klu.edu.tr

Abstract

The consumption of organic foods has gained increasing attention due to rising concerns about health, food safety, and environmental sustainability. This study aimed to explore the relationships between organic food consumption, food choice motivations, and food neophobia among adults living in Kırklareli, Türkiye. A total of 506 individuals aged 18–64 years participated in the study. Data were collected through a structured questionnaire including sociodemographic characteristics, the Food Choice Questionnaire (FCQ), the Turkish version of the Food Neophobia Scale (T-FNS), and the Organic Food Consumption Scale (OGTÖ). Descriptive findings showed that the majority of participants had a moderate level of organic food consumption and expressed motivations related to health, natural content, and ethical concerns. Correlation analyses revealed positive associations between organic food consumption and motivations such as health, natural content, ethical concerns, weight control, and personal identity. Additionally, a positive relationship was found between organic food consumption and trust in new foods, whereas willingness to try new foods was negatively associated. These findings suggest that although individuals may view organic products as beneficial and trustworthy, unfamiliarity or food neophobia may limit their openness to novel food products. In conclusion, organic food consumption appears to be influenced by a combination of health-driven, value-based, and psychological factors. Understanding these motivations may support the development of targeted nutrition education strategies that promote sustainable and informed dietary choices.

Keywords: Organic food, food neophobia, food choice, health motivation, consumer behavior

➢ *ORAL PRESENTATION*

Adsorptive Removal of Polystyrene Nanoplastics from Water: Role of Activated Carbon and Ion Exchange Resin

Soner GÖKÇEDAĞ[1*](https://orcid.org/my-orcid?orcid=0009-0002-2896-3645), Dilara Leyla KAPLAN[1] (https://orcid.org/0009-0001-2958-2193), Sıla MERT[1](https://orcid.org/my-orcid?orcid=0009-0005-1783-8066), Emine EKİNCİ[1] (ORCID: https://orcid.org/0000-0002-0958-1513), Birce PEKMEZCI KARAMAN[1] (ORCID: https://orcid.org/0000-0002-9051-2354)

[*1]Gazi University, Faculty of Engineering, Department of Chemical Engineering, Ankara, Türkiye.

*Corresponding author e-mail : sonergkcdg@gmail.com, bircepekmezci@gazi.edu.tr

Abstract

Plastic waste has begun to pose serious threats to aquatic environments and human health with the increasing use of plastics. Most plastic materials can persist in the environment for hundreds of years under suitable conditions, leading to long-term pollution. As plastics degrade, microplastics (particles smaller than 5 mm) and even smaller nanoplastics (less than 1 µm) are released into ecosystems, raising growing environmental concerns. This project aims to remove nanoplastics from water through adsorption using two different adsorbents: powdered activated carbon (PAC) and Sepabeads SP-207, a commercial ion exchange resin. Activated carbon was chosen for its high surface area and porous structure, which enhances its adsorption potential. Sepabeads SP-207, composed of a hydrophobic aromatic polymer structure, was selected for its strong affinity toward organic pollutants. Batch adsorption experiments were performed with 1 µm polystyrene nanoplastics under controlled laboratory conditions. The equilibrium data fitted best to the Freundlich isotherm model for both adsorbents, indicating heterogeneous multilayer adsorption. Kinetic analyses revealed that the adsorption behavior of SP-207 followed a pseudo-second-order model, suggesting chemisorption, while PAC followed a pseudo-first-order model, suggesting physical adsorption. According to equilibrium results, SP-207 exhibited a removal efficiency of 73.46%, while PAC achieved 69.07%. These results demonstrate that both materials are effective, though they operate via different adsorption mechanisms. The results of this study emphasize the effectiveness of adsorbent technologies in combating water pollution and provide forward-looking solutions in the field of environmental protection and sustainability. This important research is a significant step toward leaving a cleaner and healthier environment for future generations.

Keywords: Microplastics, Nanoplastics, Adsorption, Adsorbent.

Acknowledgements: We gratefully acknowledge financial support from Gazi University Scientific Research Projects (BAP) Coordination Unit (Project No: FLO-2024-9570).

➢ *ORAL PRESENTATION*

The role of swimming exercise in preserving uterine and ovarian reserves in a DSS-induced chronic ulcerative colitis mouse model

İshak Gökçek[1*] (*ORCID: https://orcid.org/0000-0002-0590-6405*)

[*1] University of Hatay Mustafa Kemal, Faculty of Veterinary, Department of Veterinary Physiology, Hatay, Türkiye.

*Corresponding author e-mail: ishakgokcek@hotmail.com; igokcek@mku.edu.tr

Abstract

In this study, the effects of exercise on ovarian reserves and uterine lipid peroxidation were investigated in mice with chronic colitis. Fifty female Balb-c mice were randomly divided into five groups of ten animals each: Control (C), Colitis (CLT), Exercise (EX), Colitis+Exercise (CLT+EX), and Colitis+Sulfasalazine (CLT+SSZ). The experimental period lasted for thirty-five days. Chronic colitis was induced in the mice by adding 1.5% Dextran sulphate sodium (DSS) to their drinking water, following three cycles of 5 days of DSS administration followed by 5 days of regular drinking water. Also, in the CLT+SSZ group, sulfasalazine (10 mg/kg) was administered regularly for thirty-five days to the animals in which colitis was induced. The swimming exercise protocol was applied to the animals for thirty-five days, one hour per day, five days a week. At study completion, blood samples were collected to assess AMH levels, and uterine tissues were analyzed for malondialdehyde (MDA) concentrations. The findings revealed a statistically significant reduction in AMH levels in the CLT group ($p=0.007$). Moreover, uterine MDA concentrations were markedly elevated in the CLT group, whereas MDA levels in the CLT+EX group were comparable to those observed in the control group, with no significant difference noted ($p=0.001$). In conclusion, moderate-intensity swimming exercise has the potential to reduce ovarian lipid peroxidation and to exert protective effects on ovarian reserves. Nevertheless, further comprehensive analyses are warranted to elucidate the underlying molecular mechanisms.

Keywords: Swimming exercise, Chronic ulcerative colitis, Ovarian reserves, Uterine, DSS

➢ *ORAL PRESENTATION*

Bi-objective optimization of time and cost in project scheduling: an application in a construction project

Fatma Yavuz[1*] (*ORCID: https://orcid.org/009-0009-5865-2208*),
Fatih Kasımoğlu[2] (*https://orcid.org/0000-0001-5818-9342*)

[*1,2]University of Turkish Aeronautical Association, Faculty of Engineering, Industrial Engineering Department, Ankara, Turkey.

*Corresponding author e-mail: fatmayvuzz99@gmail.com

Abstract

Completing projects in the most efficient way with limited resources is of great importance, especially in dynamic and time-pressured areas such as the construction sector. In this study, optimization was performed by considering time and cost criteria for a construction project within the scope of multi-objective project scheduling. In the study, instead of classical heuristic algorithms, a mathematical programming-based approach was adopted; project planning was modeled within the framework of Crashing, Deadline and Budget techniques. The developed model was solved in the GAMS (General Algebraic Modeling System) program and alternative scenarios that provide time-cost balance were evaluated. The most appropriate solution was determined, especially in terms of shortening activity periods (crashing), project delivery time (deadline) and budget limitations. The model aimed to minimize both the total project duration and cost under the specified constraints, and realistic and applicable results were obtained in this direction. When we crashed, the minimum duration was found to be 202 days, and the cost for this day is 106,293,100,000 TL. When we increase the duration to 230 days, our cost becomes 78,293,100,000 TL. When we make the duration 260 days, our minimum cost becomes 48,293,100,000 TL. The results of the study were supported by the optimization results obtained through the GAMS software and a solution proposal with sectoral applicability in terms of project management was presented. This approach provides an effective reference model for decision makers who want to evaluate time and cost constraints simultaneously in engineering projects.

Keywords: Project Scheduling, Multiobjective Optimization, Critical Path Method, Project Crashing

➢ *ORAL PRESENTATION*

Arıtılmış atıksuların tarımsal sulamada kullanımı

Zeynep Nur Savaştaer[1] (*ORCID: https://orcid.org/0000-0003-1201-1092*),
Özlem Demir[1] (*ORCID: https://orcid.org/0000-0002-0727-1845*)

[1] Harran Üniversitesi, Mühendislik Fakültesi, Çevre Mühendisliği Bölümü, Şanlıurfa, Türkiye

*Sorumlu yazar e-posta: savastaerzeynep@gmail.com:

Özet

Su, yaşam ve endüstriyel süreçler için hayati önem taşıyan temel bir doğal kaynaktır; bu nedenle ulusal kalkınmada temel bir rol oynamaktadır. Önümüzdeki yıllarda, küresel nüfusun %40'ının su kıtlığı stresiyle karşı karşıya kalacağı tahmin edilmektedir. Su kıtlığı, küresel ekonomiyi ve insanlığın geçim kaynaklarını etkileyen en önemli endişe kaynağıdır. İklim değişikliği, hızlı nüfus artışı, tatlı su kirliliği ve tükenmesi durumu daha da kötüleştiren faktörler arasındadır. Henüz kapsamlı bir şekilde kullanılmamış olsa da atıksuyun ıslahı ve yeniden kullanımı, bu sorunu hafifletmek için potansiyel mekanizmalar olarak kabul edilmektedir.

Suyun güvenli bir şekilde yeniden kullanılabilmesi için, atıksuyun farklı alanlarda yeniden kullanım amaçlarına uygun, iyi kalitede atıksu elde edilmesi için yeterince arıtılması gerekir. Geri kazanılan atıksu, alternatif bir su kaynağı görevi görerek doğal su kaynakları üzerindeki baskıyı azaltmaktadır.

Tarım, ortalama su tüketiminin %80'ini oluşturan en yoğun su sektörüdür. Sonuç olarak, su kaynaklarının tarım ve diğer sektörler için etkin ve sürdürülebilir bir şekilde yönetilmesi için entegre su kaynakları yönetimi gerekmektedir. Özellikle, alternatif su kaynakları arasında yer alan arıtılmış atıksuyun yeniden kullanımı, sürdürülebilir, iklim açısından akıllı ve dayanıklı bir tarım sisteminin elde edilmesine katkıda bulunmaktadır.

Arıtılmış atıksuyun tarımsal sulamada kullanılması, su kıtlığıyla başa çıkmada etkili bir strateji olarak yaygın olarak kabul edilmekte ve dünya çapında ilgi görmektedir. Tatlı su kaynaklarını korumanın yanı sıra, bu uygulamanın kimyasal gübrelerin yerini alabilecek besinlerin sağlanması ve böylece politantların hassas su kaynaklarına deşarjını azaltmak da dahil olmak üzere çeşitli avantajları vardır. Bu iki yönlü fayda için, arıtılmış atıksuların tarımda kullanılması, yoğun tarım alanlarında yeraltı sularını korumak için iyi bir strateji olarak kabul edilebilir.

Bu çalışma kapsamında, alternatif kaynak olarak değerlendirilebilecek olan arıtılmış atıksuların uygun kaliteye getirildikten sonra yeniden kullanımı konusu çalışılmıştır. Birçok alanda kullanım imkânı olan arıtılmış atıksuların sulama ihtiyacının fazla olması nedeniyle özellikle tarım sektöründe yeniden kullanılması değerlendirilmiştir.

Anahtar kelimeler: Atıksu, geri kazanım, yeniden kullanım, tarımsal sulama.

➢ *ORAL PRESENTATION*

Protective effect of white cabbage extract against amiodarone-induced small intestinal damage in rats.

Orkhan Mammadli[1] * *(ORCID: https://orcid.org/0009-0006-4326-7081)*, Ismet Burcu Turkyilmaz Mutlu[2] (*ORCID: https://orcid.org/0000-0003-2789-5943*), Refiye Yanardag[2] (*ORCID: https://orcid.org/0000-0003 4185-4363*)

[1]Istanbul University-Cerrahpaşa, Institute of Graduate Studies, Istanbul, Türkiye.
[2]Istanbul University-Cerrahpaşa, Faculty of Engineering, Department of Chemistry, Istanbul, Türkiye

*Corresponding author e-mail: orxanmemmedli2023@gmail.com

Abstract

Amiodarone (AMD) is a class III antiarrhythmic drug and due to its iodine containing structure, AMD tends to accumulate in many organs. AMD can generate oxidative stress by forming reactive oxygen products. White cabbage (*Brassica oleracea* L. var. capitata) is one of the most consumed vegetables in the world and has important antioxidant potential due to its rich phytochemical content. The small intestine is a part of the digestive system and digestive processes are completed in this tissue.
In this study, we aimed to investigate the effects of white cabbage aqueous extract against AMD-induced small intestinal damage. The experimental groups were divided into four groups as follows: Control group, white cabbage aqueous extract given group, AMD given group and AMD+white cabbage extract given group. AMD and white cabbage aqueous extract were given at doses of 50 mg/kg (orally) and 500 mg/kg (orally) for 7 days, respectively. At the end of the experiment, the small intestine tissues were taken, homogenized in cold physiological saline and centrifuged. In supernatants, glutathione levels were found to be decreased whereas lipid peroxidation levels, catalase and xanthine oxidase activities were increased at AMD given group. Administration of white cabbage aqueous extract reversed these effects in AMD group. We can conclude that white cabbage ameliorated small intestine damage induced by AMD.

Keywords: Amiodarone, White Cabbage, Small Intestine, Oxidative Stress

➢ *ORAL PRESENTATION*

Transcript levels of genes encoding pyroptotic effector proteins in triple-negative breast cancer (TNBC) and non-TNBC, and based on hormone receptor (HR) and HER2 status

Caglar BERKEL[1*] (*https://orcid.org/0000-0003-4787-5157*)

[*1] Tokat Gaziosmanpasa University, Faculty of Science and Arts, Department of Molecular Biology and Genetics, Tokat, Türkiye.

*Corresponding author e-mail: caglar.berkel@gop.edu.tr

Abstract

Breast cancer is classified into multiple molecular subtypes based on the status of hormone receptors (estrogen receptor (ER) and progesterone receptor (PR)) and HER2 (ERBB2), with large differences in response to therapy and prognosis. TNBC (triple-negative breast cancer) is the subtype with the highest mortality rates. Pyroptosis is a regulated pro-inflammatory cell death mechanism resulting in the formation of membrane pores mediated by gasdermin (GSDM) proteins. Certain pro-inflammatory molecules such as IL-18 can be released from these gasdermin pores to the extracellular space. Here, I studied how the transcript levels of gasdermin family of genes (6 members present in humans: GSDMA-F) differ between TNBC and non-TNBC, using publicly available TCGA-BRCA transcriptomics dataset. I found that the expression of GSDMC and GSDME was increased; in contrast, the expression of GSDMD was decreased in TNBC compared with non-TNBC. I further investigated ER-, PR-, and HER2-dependent changes in the mRNA expression of GSDMC, GSDMD and GSMDE in breast tumors from patients. I observed decreased GSDMC mRNA expression in breast tumors with ER-positive and PR-positive status than in those with ER-negative and PR-negative status, respectively. In contrast, HER2-positive breast tumors had higher expression of GSDMC compared to HER2-negative breast tumors, at the transcript level. Unlike GSDMC, the mRNA expression of GSDMD was higher in ER-positive and PR-positive breast cancer samples than in ER-negative and PR-negative samples, respectively. I found that GSDME transcript levels were lower in ER-positive breast tumors compared to ER-negative breast tumors. Finally, I showed that breast tumors from premenopausal women had slightly higher transcript levels of GSDME than breast tumors from postmenopausal women. Combined, this study points to the possible differences in pyroptotic cell death between TNBC and non-TNBC, and also between different breast cancer subgroups defined based on hormone receptor (ER, PR) and HER2 status.

Keywords: Breast cancer, pyroptosis, triple-negative breast cancer, estrogen receptor, progesterone receptor, HER2

➢ *ORAL PRESENTATION*

In vitro Antioxidant and Anticancer Activities of Methanolic Extract of *Onobrychis oxyodonta*

Samed Şimşek[1*] (*ORCID: https://orcid.org/0000-0001-8451-3425*), Tuğçe Varol[2] (*ORCID: https://orcid.org/0000-0001-7027-462X*)

[*1]Erzincan Binali Yildirim University, Cayirli Vocational School, Department of Medical Services and Techniques, Erzincan, Turkey.
[2]Erzincan Binali Yildirim University, Institute of science, Biology, Erzincan, Turkey.

*Corresponding author e-mail: samed.simsek@erzincan.edu.tr

Abstract

Onobrychis species are widely recognized among medicinal and aromatic plants for their high phenolic content and significant antioxidant potential. Onobrychis oxyodonta, one of these species growing naturally in various regions of Turkey, was evaluated in this study in terms of its biological activity. This study aimed to evaluate the total phenolic and flavonoid contents, as well as the antioxidant and anticancer potential of the methanolic extract obtained from this plant. The total phenolic and flavonoid contents of the extract were determined as 70.24 ± 0.58 mg GAE/g and 26.43 ± 0.36 mg QE/g, respectively. Antioxidant capacity was calculated using the FRAP method as 98.75 ± 0.21 µg TE/g, and DPPH radical scavenging activity was IC_{50}: 27.39 ± 1.34 µg/mL. Anticancer activity was evaluated on A549, Calu1, and H1650 lung cancer cell lines and the Beas2B normal lung epithelial cell line. GI_{50} values below 10 µg/mL in all cancer lines indicate strong growth inhibitory activity. TGI values were 179.88 µg/mL (5FU: 105.40) in A549, 78.70 (5FU: 98.51) in Calu1, and 4.86 (5FU: 97.74) in H1650. Calu1 and H1650 cells showed superior inhibition compared to 5FU. LC_{50} values above 500 µg/mL in all cell lines indicate low general cytotoxicity. In Beas2B cells, the extract's TGI was 454.67 µg/mL, compared to 112.19 µg/mL for 5FU, suggesting lower toxicity in normal cells. The Tumor Selectivity Index (TSI) was >2, confirming selective toxicity toward tumor cells. Membrane integrity and cytotoxicity assays showed that the extract induced higher toxicity (10.9–29.6%) than 5FU in all lines except A549, with 5FU showing 6.7–10.9% toxicity. These results suggest that Onobrychis oxyodonta extract has strong anticancer potential and may provide selective cytotoxic effects with lower toxicity in normal cells.

Keywords: Anticancer potential, Antioxidant activity, *Onobrychis oxyodonta*, Tumor selectivity ındex (TSI).

➢ *ORAL PRESENTATION*

Determination of pathotype, serogroup, and antibiotic susceptibility of *Escherichia coli* recovered from a cat with cystitis

Özgür GÜRAN*[1] (*https://orcid.org/0009-0009-7520-4503*), Emre KARAKAYA[1] (https://orcid.org/0000-0003-2390-6190), Celil BENDEŞ[2], (*ORCID: https://orcid.org/0009-0008-5777-1443),* Gencay EKİNCİ[3] *https://orcid.org/0000-0002-4551-8749*

*[1]Erciyes University, Faculty of Veterinary Medicine, Department of Microbiology, Kayseri, Türkiye.
[2]Erciyes University, Institute of Health Sciences, Department of Veterinary Internal Medicine, Kayseri, Türkiye
*[3]Erciyes University, Faculty of Veterinary Medicine, Department of Internal Medicine, Kayseri, Türkiye

*Corresponding author e-mail: ozgurguran@erciyes.edu.tr

Abstract

This study aimed to identify, patotype, serotype, and determine the antibiotic susceptibility of an *Escherichia coli* isolate recovered from a cat urine sample. For the purpose, a 16-year-old male cat presented to Erciyes University Faculty of Veterinary Medicine, Department of Internal Medicine, with the complaint of dysuria. Clinical examinations and hemogram analysis revealed elevated WBC levels, and a diagnosis of cystitis was made. Urine sample was collected via cystocentesis and subjected to bacteriological analysis at the Department of Microbiology. The sample was inoculated on 7% sheep blood agar and MacConkey agar, and the media incubated aerobically, microaerophilically, and anaerobically at 37°C for 24-72h. Following incubation, colonies were evaluated, and pure culture was obtained. In the phenotypic identification of the isolate, Gram staining, motility, oxidase, catalase, and carbohydrate-fermentation tests were performed. *E. coli* species-specific PCR was used for molecular identification. Multiplex PCR was used to detect Uropathogenic *E. coli* (UPEC) pathotypes and serogroups. The disk diffusion method was used to determine antibiotic susceptibility. As a result of phenotypic tests and molecular analyses, the isolate was identified as *E. coli*. In UPEC analysis, it was revealed that the isolate was not UPEC. As a result of UPEC analysis, it was revealed that the *E. coli* isolate was not UPEC. In serogrouping, it was determined that the isolate was not included in the 4 serogroups tested. In the antibiotic susceptibility, the isolate was determined to be resistant to 9 out of 14 antibiotics. Treatment commenced with meropenem at 12mg/kg q12h/14. Complete blood counts monitored on days 1 and 7 showed WBC levels of 23.5×10^9/L and 18.9×10^9/L, respectively, indicating clinical improvement. In conclusion, performing antimicrobial susceptibility testing for *E. coli*, an important etiological agent in urinary tract infections, determining pathotypes/serogroups, and then selecting appropriate antibiotics to start treatment are beneficial for successful therapeutic outcomes.

Keywords: Antibiotic Susceptibility, Cystitis, *Escherichia coli*, Hemogram, UPEC.

➢ *ORAL PRESENTATION*

Cadmium (II) Adsorption from Aqueous Media using Mercapto-Functionalized Silica Xerogels

Selay Sert Çok[1*] (*ORCID: https://orcid.org/0000-0001-7595-2151*),
Zoltán Dudás[2] (*ORCID: https://orcid.org/0000-0001-7839-8934)*

[*1]Ege University, Faculty of Engineering, Chemical Engineering Department, İzmir, Turkey.
[2]HUN-REN Centre for Energy Reseach, Budapest Neutron Centre, Budapest, Hungary.

*Corresponding author e-mail: selay.sert@ege.edu.tr

Abstract

The effective removal of cadmium ions from water is a growing environmental concern due to the toxic and bioaccumulative nature of Cd(II). In this study, a series of mercapto-functionalized silica xerogels were synthesized via a facile, ambient-pressure sol-gel method using tetraethyl orthosilicate (TEOS) and 3-mercaptopropyltrimethoxysilane (MPTMS) as a sulphur-containing organosilane. The incorporation of MPTMS into the silica matrix was confirmed by FTIR spectroscopy, and SEM imaging revealed a uniform, interconnected porous structure. Nitrogen sorption analysis showed mesoporous characteristics with surface areas exceeding 300 m^2/g and porosity greater than 85%. Batch adsorption experiments were conducted to evaluate the materials' performance in Cd(II) removal from aqueous solutions. The results indicated rapid adsorption kinetics and high removal efficiency (>95%), especially for samples with higher thiol content. The strong affinity between Cd(II) ions and thiol (-SH) groups suggests that chemisorption is the dominant mechanism. These findings demonstrate the potential of mercapto-modified silica xerogels as highly efficient and regenerable adsorbents for cadmium remediation in water treatment applications, offering a sustainable strategy for mitigating heavy metal pollution.

Keywords: silica xerogels, mercapto functionalization, heavy metal adsorption, cadmium (II) removal

➢ *ORAL PRESENTATION*

Millimeter-Wave Radar for Short-Range Mobility Detection

Mehmet Ziya Keskin[1*] (*ORCID: https://orcid.org/0000-0001-5278-5602*)
Abdulkadir Yentür[1] *(ORCID: https://orcid.org/0000-0002-9828-929X)*
İbrahim Tuna Özdür[1] *(ORCID: https://orcid.org/0000-0001-6452-0804)*
Veli Tayfun Kılıç[2] (*ORCID: https://orcid.org/0000-0001-6806-9053)*

[*1]TOBB University of Economics and Technology, Department of Electrical and Electronics Engineering, Ankara, Türkiye.
[2]Abdullah Gül University, Department of Electrical and Electronics Engineering, Ankara, Türkiye, Kayseri, Türkiye.

*Corresponding author e-mail: mehmetziya.keskin@etu.edu.tr

Abstract

The adoption of millimeter-wave (mmWave) sensors is rapidly growing in diverse sectors, driven by their low power requirements, small footprint, and effectiveness in applications like object detection and tracking. In this study, we present the development of a short-range mobility detection system based on W-band mmWave radar technology, specifically operating in the 76–81 GHz frequency range, where commercial single-chip integrated circuits are available. The proposed system is capable of detecting multiple moving targets—such as humans, animals, and vehicles—in real time and at varying distances. Designed for use in environments with high mobility, it features simultaneous multi-object tracking and reliable positional data output to a central computing unit. The system maintains low power consumption and offers a flexible, integrated architecture that can be adapted to both portable and fixed installations. To enhance the system's performance, we investigate gain optimization in a patch antenna array configuration. We analyse the S-parameters and radiation patterns of a reference antenna through both simulation and experimental measurements, ensuring design accuracy and validating the radar's effective coverage. A wide operational bandwidth underpins high-resolution detection, and an intuitive interface allows users to set detection thresholds, range limits, and speed windows. The resulting platform offers a compact, energy-efficient, and high-precision solution for mobility sensing, with clear potential in smart-city infrastructure, security, and real-time monitoring applications.

Keywords: Antenna array, mmWave, microstrip patch, series fed.

➢ *ORAL PRESENTATION*

The characterization of *Acinetobacter lwoffii* isolates from sheep necropsy materials

Özgür GÜRAN[*1] (*https://orcid.org/0009-0009-7520-4503*), Cansu GÜRAN[2] (https://orcid.org/0009-0004-2573-8519), Emre KARAKAYA[1] (https://orcid.org/0000-0003-2390-6190), Fuat AYDIN[1], (*ORCID:* https://orcid.org/0000-0002-5467-011X*)*.

[*1]Erciyes University, Faculty of Veterinary Medicine, Department of Microbiology, Kayseri, Türkiye.
[2]Erciyes University, Institute of Health Sciences, Department of Veterinary Microbiology Kayseri, Türkiye.

*Corresponding author e-mail: ozgurguran@erciyes.edu.tr

Abstract

Acinetobacter lwoffii (*A. lwoffii*) is an opportunistic pathogen that causes infections in humans and animals. In this study, it was aimed to characterize A. lwoffii isolates from necropsy materials (lungs, liver, spleen, and abscessed lymph nodes) of 4 different sheep. The necropsy materials brought to Erciyes University, Faculty of Veterinary Medicine, Department of Microbiology Laboratory were subjected to bacteriological analysis and for this purpose, 7% defibrinated sheep blood agars were inoculated from necropsy materials. The inoculated media were incubated in aerobic, microaerobic, and anaerobic environments at 37°C for 24-48 hours. After incubation, convex, gray-white, and S-type colonies were evaluated. It was obtained the pure cultures of colonies on blood agar. Phenotypic identification of isolates was performed by Gram staining, motility test, and biochemical tests. In molecular identification, 16S rRNA gene sequence analysis using 27F and 1492R primers was used. Enterobacterial Repetitive Intergenic Consensus Sequence-Based Polymerase Chain Reaction (ERIC-PCR) was performed to genotype the recovered *A. lwoffii* isolates. The Kirby-Bauer disk diffusion method determined the susceptibility to amoxicillin+clavulanic acid, ampicillin, ciprofloxacin, erythromycin, gentamicin, and tetracycline of the isolates. As a result of the cultural examination, four isolates from sheep necropsy samples were identified as *A. lwoffii* by phenotypic/molecular analysis. In the result of ERIC-PCR used for genotyping, it was determined that all 4 A. lwoffii isolates exhibited different ERIC profiles. In the antibiotic susceptibility test, 2 (50%), 2 (50%), and 1 (25%) of 4 *A. lwoffii* isolates were found to be resistant to erythromycin, gentamicin, and ampicillin, respectively. In conclusion, considering the different ERIC profiles and antibiotic resistance, *A. lwoffii* may be thought the etiological agent of various infections in sheep.

Keywords: *Acinetobacter lwoffii*, antibiotic susceptibility, ERIC-PCR, identification, sheep necropsy material.

➢ *ORAL PRESENTATION*

Animal Welfare Standards in Calf Management

Mohamad Salem NAJAR[1*] (*ORCID: https://orcid.org/0009-0001-7568-4123*), Filiz AKDAĞ[2] (*ORCID: https://orcid.org/*0000-0001-9142-9731)

[*1]Ondokuz Mayis University, Postgraduate Institute, Department of Animal Breeding and Husbandry, Samsun,Türkiye
[2] Ondokuz Mayis University, Faculty of Veterinary Medicine, Department of Animal Breeding and Husbandry, Samsun,Türkiye

*Corresponding author e-mail: salemhn.22@gmail.com

Abstract

Cattle farming play a vital role in meeting the human demand for animal-based food products. In cattle farming, the primary objectives include maintaining an optimal herd size, applying effective culling and selection strategies, and ensuring productivity by achieving a minimum of one calf per cow per year and raising healthy offspring. The achievement of these objectives is closely associated with improvements in animal welfare, supported by evidence-based husbandry practices that promote healthy physiological development, high standards of well-being, productivity, and long-term sustainability. According to various international frameworks, animal welfare is assessed based on four core principles: appropriate housing, sufficient nutrition, good health, and the ability to express natural behaviours-each supported by specific evaluation criteria. In assessing calf welfare, key indicators include the absence of prolonged hunger and thirst; access to a comfortable and thermally appropriate resting environment; freedom of movement; absence of injury and disease; minimization of pain resulting from management procedures; the ability to express social and species-specific behaviours; the capacity to experience positive emotional states; and the presence of positive human-animal interactions. This study aims to explore the specific welfare criteria used in evaluating the well-being of calves.

Keywords: Behaviour, calf, health, nutrition, housing.

➢ *ORAL PRESENTATION*

The effect of direct kisspeptin-54 application on gonadotropin receptor expressions in granulosa cells of PCOS patients

Erkan ERENER[1] * (ORCID: https://orcid.org/0000-0003-2550-8524), Adem KOCAMAN[2] (ORCID:https://orcid.org/0000-0002-4457-9144), Bülent AYAS[2] (ORCID: https://orcid.org/0000-0003-4411-2496)

[1]Department of Histology and Embryology, Faculty of Medicine, Istanbul Medeniyet University, Istanbul, Turkey.
[2]Department of Histology and Embryology, Faculty of Medicine, Ondokuz Mayis University, Samsun, Turkey

Corresponding Author e-mail: erkan.erener@medeniyet.edu.tr

Abstract

Polycystic ovary syndrome (PCOS) is one of the leading causes of female infertility. In this study, the effects of PCOS and the direct in vitro kisspeptin application on the expression of genes concerning steroidogenesis, estrogen receptors and inhibin in the granulosa cells were investigated via qRT-PCR method. . This study was approved by The Clinical Studies Ethical Committee of Ondokuz Mayis University via decision numbered 2019/724 with the date of 19/01/2019. The samples were obtained from 32 patients,16 of which are PCOS and 16 are non-PCOS patients. Half of the granulosa cells collected from the patients were applied with in vitro Kisspeptin-54. The groups were formed as 16 patients in the Control and Control-Kiss groups and 16 patients in the Pcos and Pcos-Kiss groups. It was found that serum and follicular fluid KISS1 level are significantly higher in PCOS group in comparison to the Control group ($p=0,017$; $p<0,05$; $p=0,0004$; $p<0,001$). The ESR1nad ESR2 gene expressions were significantly higher in the PCOS group in comparison to the Control group ($p<0,05$). Between the Kisspeptin applied groups, the ESR1 and 2 gene expression were significantly higher in PCOS-Kiss group in comparison to Control-Kiss group ($p<0,05$). Regarding FSHR gene expression change, the PCOS group was significantly lower in comparison to the Control group ($p<0,05$). Between the Kisspeptin-54 appplied groups, in terms of FSHR gene expression, PCOS-Kiss group was significantly lower in comparison to the Control-Kiss group ($p<0,05$). In terms of LHCGR gene expression change, PCOS group and PCOS-Kiss were significantly higher in comparison to Control group and Control-Kiss group ($p<0,05$). The results of this study indicates that direct in vitro kisspeptin application affects the expression of steroidogenic and gonadotropin receptor gene expressions in non-PCOS and PCOS granulosa cells and thus its intraovarian application can alleviate the follicular atresia encountered in these patients.

Keywords: Kisspeptin, PCOS, Granulosa Cells, Gonadotropins

➢ *ORAL PRESENTATION*

The Effect of Different LED Light Conditions on the Total Phenolic and Flavonoid Contents of Fenugreek (*Trigonella foenum-graecum* L.) Microgreens

Zehra Demirci[1]* (https://orcid.org/0009-0007-9307-7400),
Muhammet Dogan[2] (https://orcid.org/0000-0003-3138-5903),
Bugrahan Emsen[3] (https://orcid.org/0000-0002-9636-2596)

*[1]Department of Biology, Graduate School of Natural and Applied Sciences, Karamanoglu Mehmetbey University, Karaman, Türkiye.
[2]Department of Nutrition and Dietetics, Faculty of Health Sciences, Karamanoglu Mehmetbey University, Karaman, Türkiye
[3]Department of Biology, Kamil Ozdag Faculty of Science, Karamanoglu Mehmetbey University, Karaman, Türkiye

*Corresponding author e-mail: zehra.demirci502@gmail.com

Abstract

This study aimed to investigate the effects of different LED light spectra (white, red, and blue) on the total phenolic and flavonoid contents of fenugreek (*Trigonella foenum-graecum* L.) microgreens grown under controlled environmental conditions. By keeping variables such as temperature and substrate constant, the role of light quality on the biochemical properties of microgreens was isolated and evaluated. Seeds were first germinated in darkness, and upon sprouting, containers were exposed to white, red, or blue LED lights under a 16-hour light / 8-hour dark photoperiod. Standard light intensity was maintained across all treatments. Harvested plant samples (10 g) were pulverized using an ultra-centrifugal mill and subjected to Soxhlet extraction with acetone or water as solvents. Extracts were filtered, concentrated with a rotary evaporator, and freeze-dried to obtain high-yield crude extracts. The total phenolic content, expressed as gallic acid equivalents (GAE), varied significantly among treatments. The highest phenolic content was observed in the acetone extract of fenugreek microgreens grown under blue LED light (231.41 ± 5.69 µg GAE/ mg extract), followed by the acetone extract of those grown under red LED light (210.85 ± 5.00 µg GAE/ mg extract), and the acetone extract of those grown under white LED light (204.71 ± 1.90 µg GAE/ mg extract). Water extracts showed lower phenolic levels, with the water extract of microgreens grown under blue LED light (147.71 ± 4.18 µg GAE/ mg extract) being the highest among them. Regarding total flavonoid content (quercetin equivalents (QE)), the acetone extract of microgreens grown under red LED light (631.80 ± 11.60 µg QE/mg extract) demonstrated the highest concentration, followed by the acetone extract of those grown under white LED light (509.35 ± 8.52 µg QE/mg extract) and the acetone extract of those grown under blue LED light (398.42 ± 5.14), indicating that red light in combination with acetone extraction was most effective in accumulating flavonoids. Again, water extracts contained markedly lower flavonoid content, with the water extract of microgreens grown under red LED light (73.84 ± 2.56 µg QE/mg extract) showing the lowest. These findings suggest that LED light quality significantly influences the accumulation of phenolic and flavonoid compounds in fenugreek microgreens. Red and white LED lights, particularly when paired with acetone extraction, enhanced the phytochemical richness of the microgreens, indicating potential strategies for improving their functional food value.

Keywords: Antioxidant activity, Fenugreek microgreens, LED light spectra, Soxhlet extraction

Acknowledgements
This research was supported by the Scientific Research Projects Commission of Karamanoğlu Mehmetbey University under Project Number 19-YL-24. The authors gratefully acknowledge the financial support provided by the Commission. This study is also derived from the master's thesis of Zehra Demirci, conducted under the supervision of Muhammet Doğan and the co-supervision of Bugrahan Emsen.

➢ *ORAL PRESENTATION*

Evaluation of Antioxidant Activities of Leaf and Fruit Extracts of *Cotoneaster coriaceus* Franch. by DPPH Assay

Yazgı Doga Atıcı[1]*(https://orcid.org/0009-0001-0239-1063),
Muhammet Dogan[2] (https://orcid.org/0000-0003-3138-5903),
Bugrahan Emsen[3] (https://orcid.org/0000-0002-9636-2596)

*[1]Department of Biology, Graduate School of Natural and Applied Sciences, Karamanoglu Mehmetbey University, Karaman, Türkiye.
[2]Department of Nutrition and Dietetics, Faculty of Health Sciences, Karamanoglu Mehmetbey University, Karaman, Türkiye
[3]Department of Biology, Kamil Ozdag Faculty of Science, Karamanoglu Mehmetbey University, Karaman, Türkiye

*Corresponding author e-mail: dogatici@gmail.com

Abstract

This study aimed to evaluate the antioxidant activities of leaf and fruit extracts of *Cotoneaster coriaceus* Franch. using the DPPH (2,2-diphenyl-1-picrylhydrazyl) radical scavenging assay. Plant materials were collected, dried, and powdered. Extraction was performed using Soxhlet apparatus with three solvents of differing polarities: acetone, ethyl acetate, and water. The antioxidant activities of the obtained extracts were analyzed spectrophotometrically based on their ability to scavenge DPPH free radicals at various concentrations. The results demonstrated that the antioxidant capacities of the extracts varied significantly depending on both the plant part and the solvent used. Among all samples, the acetone extract of the leaves exhibited the strongest activity, with the lowest IC_{50} value of 10.55 µg/mL. This extract showed a rapid increase in activity between 12.5 µg/mL and 50 µg/mL, reaching over 92% inhibition and maintaining this level at higher concentrations, indicating an early saturation point. The acetone extract of the fruit also exhibited strong activity (IC_{50} = 31.15 µg/mL), with inhibition values sharply rising from 22.99% at 12.5 µg/mL to 91.70% at 100 µg/mL, followed by a plateau. In contrast, ethyl acetate extracts from both parts demonstrated weaker antioxidant activity at low concentrations but improved significantly at higher doses, reaching around 89% inhibition at 400 µg/mL. Water extracts showed moderate activity. Leaf water extract rose from 26.10% inhibition at 12.5 µg/mL to 89.85% at 400 µg/mL, showing a marked increase after 100 µg/mL. Similarly, fruit water extract exhibited a gradual rise, peaking at 89.61% at the highest tested concentration. In conclusion, *C. coriaceus*, particularly its leaf acetone extract, possesses significant antioxidant potential. These findings suggest that this species could serve as a promising natural source of antioxidants for pharmaceutical or nutraceutical applications.

Keywords: Antioxidant activity, DPPH assay, IC_{50} value, Leaf extract

➢ *ORAL PRESENTATION*

Measuring Perceived Accessibility: The Role of Subjective Experiences in Transportation Planning

Zehra Özçelik (*ORCID: https://orcid.org/0009-0009-0108-1635)*

Yıldız Technical University, Faculty of Architecture, Department of City and Regional Planning, İstanbul, Türkiye.

*Corresponding author e-mail : zehra.ozcelik@yildiz.edu.tr

Abstract

Objective accessibility criteria based solely on spatial data are insufficient for understanding the impact of transportation systems on the daily life experiences of city dwellers. This study focuses on the concept of perceptual accessibility, which goes beyond the limitations of traditional measurements to examine individuals' perceptions of their ability to lead a satisfying life using transportation systems. Perceived accessibility encompasses individual assessments such as access to desired activities via a specific mode of transportation, the ease of performing these activities, and the ability to maintain overall quality of life (Lättman et al., 2016; Pot et al., 2024).

Within the scope of the research, survey data collected from 183 participants was used to evaluate individuals' patterns of transportation system use, their access to daily life activities, and the impact of this access on their quality of life. The study aimed to measure individuals' perceptions of their experiences in scenarios they imagined using different modes of transportation, based on personal statements.

The collected data were analyzed in SPSS. Descriptive statistics, Pearson correlation analysis, reliability testing (Cronbach's Alpha = 0.70), and exploratory factor analysis (EFA) were performed, demonstrating that perceived accessibility represents a multi-layered user experience.

The results demonstrate how dimensions that cannot be measured objectively can emerge from the user perspective, highlighting the need for transportation policies to be shaped with a more holistic approach aimed at reducing social exclusion, enhancing subjective well-being, and promoting the adoption of sustainable transportation modes. The usability of perceptual accessibility criteria in policy monitoring and evaluation processes is particularly high when assessing goals aimed at reducing car dependency and visions such as “the ease of living without a car.”

This study aims to contribute to the development of user-centered and more equitable urban transportation solutions by providing insights into how individuals perceive their environment, rather than focusing solely on physical accessibility, within the field of urban planning.

Keywords: Perceived accessibility, transportation modes, daily life activities, survey, SPSS

References

Lättman, K., Olsson, L. E., & Friman, M. (2016). Development and test of the Perceived Accessibility Scale (PAC) in public transport. *Journal of Transport Geography*, *54*, 257–263.

Pot, F. J., Heinen, E., & Tillema, T. (2024). Sufficient access? Activity participation, perceived accessibility and transport-related social exclusion across spatial contexts. *Transportation*, *52*(4), 1679–1707.

➢ *ORAL PRESENTATION*

Biotypes of *Bemisia tabaci* populations in Southwestern Türkiye

Ömer YÜZER[1*] (*ORCID: https://orcid.org/0000-0003-0209-324X*), Alper TONGUÇ[2] (*ORCID: https://orcid.org/ 0000-0002-2613-3114*), Ersin DOĞAÇ[2] (*ORCID: https://orcid.org/0000-0003-4426-2187*)

[*1]Doğuş University, Vocational School, Department of Medical Laboratory Techniques, Istanbul, Türkiye.
[*1]Mugla Sıtkı Kocman University, Institute of Science, Department of Molecular Biology and Genetics, Muğla, Türkiye.
[2]Muğla Sıtkı Koçman University, Faculty of Science, Department of Molecular Biology and Genetics, Mugla, Türkiye.

*Corresponding author e-mail: oyuzer@dogus.edu.tr

Abstract

Bemisia tabaci, belonging to the Aleyrodidae family, is commonly known as the tobacco whitefly or sweet potato whitefly. First described by Gennadius (1889) in Greece, this species is one of the leading agricultural pests worldwide. Currently, at least 24 distinct biotypes are recognized. MEAM 1 and MED biotypes are the most notable due to the significant agricultural damage they cause globally. This study aimed to identify the biotypes of *B. tabaci* populations distributed in the southwestern provinces of Türkiye. To this end, a total of 360 individuals were collected, with 60 individuals sampled from each of six different provinces. DNA samples extracted from these individuals were subjected to partial amplification of the mitochondrial cytochrome oxidase I gene, followed by sequencing of the amplified region. The obtained sequences were analysed using the NCBI Nucleotide BLAST tool for biotype identification. Three biotypes (MEAM 1, MED Q1, and MED Q2) were identified across the six studied provinces. According to the results, the population in İzmir consisted entirely of MED Q1 (100%). In Aydın, 88% were MEAM 1 and 12% were MED Q1. In Muğla, 75% were MED Q2 and 25% were MEAM 1. Based on these findings, among the 180 individuals from the Aegean region, 38% were MEAM 1, 37% MED Q1, and 25% MED Q2. In the Mediterranean region, the population in Antalya was composed of 50% MED Q2 and 50% MEAM 1; in Mersin, all individuals were MEAM 1; and in Adana, 80% were MEAM 1, 12% MED Q1, and 8% MED Q2. Accordingly, among the 180 individuals from the Mediterranean region, 77% were MEAM 1, 19% MED Q2, and 4% MED Q1. Based on all results, it was determined that the MEAM 1 biotype is the dominant biotype in both the Aegean and Mediterranean regions of southwestern Türkiye.

Keywords: *Bemisia* tabaci, biotype, mitochondrial cytochrome oxidase I, MEAM 1, MED, Türkiye.

Acknowledgement: This research was supported by Mugla Sıtkı Koçman University, Scientific Research Projects Coordination Unit (Research Project Number: 23/161/01/1/5).

➢ *ORAL PRESENTATION*

Mikroalglerin sürdürülebilir bir üretim için uygulama alanları üzerine güncel bir inceleme

Melike Yalçınkaya[1*](*ORCID:* 0009-0001-6910-7450) , Seda Balkan[2](*ORCID:* 0000-0001-7148-4792)

[*1]Kırklareli Üniversitesi, Fen Bilimleri Enstitüsü, Moleküler Biyoloji ve Genetik ABD, Kırklareli, Türkiye.
[2]KırklareliÜniversitesi,Fen Edebiyat Fakültesi, Moleküler Biyoloji ve Genetik Bölümü, Kırklareli, Türkiye.

*Sorumlu yazar e-posta: melikeshen.mbg@gmail.com

Özet

Fotosentetik bir mikroorganizma olan mikroalgler, kök, gövde ve yapraktan yoksun olan en ilkel bitki türleridir.Sucul sistemlerde birincil besin zincirinin büyük bir bölümünü oluşturan mikroalgler hem tatlı sularda hem de deniz sistemlerinde yaygın olarak bulunurlar. Chlorella, Spirulina ve Scenedesmus genellikle tatlı su mikroalgleri, Dunaliella, Nannochloropsis ve Isochrysis ise bazı deniz mikroalg türleridir. Bu derlemede, sürdürülebilir bir üretim için mikroalglerin biyolojik rolleri ve biyoteknolojik potansiyelleri hakkında güncel bir genel bakış sağlanması amaçlanmıştır. Mikroalgler tarafından sentezlenen çoklu doymamış yağ asitleri, karotenoidler, fikobiliproteinler, peptitler, steroller, polisakkaritler, fenolik bileşikler, vitaminler, mikosporin benzeri amino asitler ve alkaloidlerin sağlık, kozmetik ve fonksiyonel gıdalardaki uygulamaları, biyoyakıt üretimi ve depolama kararlılığını artırmayı amaçlayan gelişmiş teknolojiler, endüstriyel atıklar, boyalar, pestisitler ve ilaçlar gibi kalıcı dirençli kirleticilerin yeni teknolojik ilerlemeler (örneğin, nanoteknoloji) ile biyoremediasyon sürecinin sürdürülebilirliği ve uygulanabilirliği, oksijen eksikliğiyle artan hastalıkların tedavisinde mikroalg bazlı biyomalzemelerin geliştirilmesi, fosil yakıtlara bağımlılığın azaltılmasında temiz enerji üretimi için sürdürülebilir bir kaynak olarak mikroalglerin kullanılmasının uygulanabilirliği, küresel karbon azaltma stratejilerinin temel bir bileşeni olarak mikroalg temelli tekniklerin potansiyeli ve mikroalglerin antioksidan aktiviteleri konularına odaklanılmıştır.

Anahtar kelimeler: Mikroalg, biyoteknolojik potansiyel, sürdürülebilirlik.

➢ *ORAL PRESENTATION*

Granulocyte: the key hemocyte of humoral and cell-mediated immunity

Serhat KAYA*
(*ORCID: https://orcid.org/ 0000-0002-0984-2824*)

*Çanakkale Onsekiz Mart University, Faculty of Science, Department of Biology, Çanakkale, TÜRKİYE.

*Corresponding author e-mail: serhatkaya@comu.edu.tr

Abstract

Insect haemocytes are multifunctional cellular components that play essential roles not only in classical immune responses – such as phagocytosis, encapsulation, nodule formation, and melanisation- but also in non-immune physiological processes including tissue repair, hypoxia adaptation, vitellogenin and ferritin transport, apoptotic cell clearance, and haematopoietic niche formation. The number and types of haemocytes vary depending on insect species, developmental stage, and physiological conditions. Major haemocyte types are prohemocytes, plasmatocytes, granulocytes, spherule cells, and oenocytoids. These haemocytes collectively regulate both humoral and cellular immune pathways through the coordination of antimicrobial peptide synthesis, coagulation, reactive oxygen species production, and immune signalling. Among these, granulocytes have received increasing attention for their versatile roles in immunity. As spherical, granule-rich cells, granulocytes are typically the first to encounter pathogens and initiate immune responses by exocytosing granules that activate other haemocytes, particularly plasmatocytes, and facilitate capsule or nodule formation via opsonin-like factors. Resembling vertebrate macrophages, granulocytes exhibit high phagocytic capacity, elevated lysosomal activity, and strong expression of immune-related genes. Recent findings also suggest that granulocytes may contribute to long-term immune protection in insects, mimicking adaptive-like memory responses. The aim of this review is to give an in-depth primer on insect haemocyte functions, with a special focus on the emerging immunological significance of granulocytes. Taken together, this review highlights the immunological versatility of insect haemocytes and proposes new perspectives for investigating innate immune memory in invertebrates.

Keywords: Insects, haemocyte, granulocytes, immune responses

➢ *ORAL PRESENTATION*

Istilacı *Cirsium arvense* (L.) SCOP.'in Grime'in CSR Stratejilerine Göre Sınıflandırılması

Elif KOCAMAN(ORCID:https://orcid.org/0009-0001-8651-6096)

Ondokuz Mayıs Üniversitesi Lisansüstü Eğitim Enstitüsü Biyoloji Ana Bilim Dalı Yüksek Lisans, Haziran/2025 Samsun / Türkiye

*Sorumlu yazar e-posta: eliftunckocaman@gmail.com

Özet

Ekosistemde bulunan canlı türlerinin çeşitliliği ne kadar fazla ise o ekosistemin direnci de dolaylı olarak o kadar fazladır ancak son yıllarda Türkiye'de de biyoçeşitlilik ve endemizm ciddi tehlike altındadır. Biyosferdeki antropojenik bozulmalar, sanayileşme hızı, tarım, artan nüfus, hızlı ve çarpık kentleşme ve madencilik stres ve tahribat faktörleri oluşturarak ekolojik ve çevresel sorunlara sebep olmaktadır. İklim, tahribatın sıklığının ve yoğunluğunun artması ve yerli türlerin rekabet özellikleri sonucunda, birçok farklı yollarla ortama yerleşen yabancı türler yerli türlerle rekabete girip alana yerleşerek, zamanla biyolojik istilalara sebep olmakta, İstilacı türlerin rekabette üstün gelmesi ve yayılmacı yapısıyla zamanla biyoçeşitlilik ve endemizm yok olmaktadır. Çalışmamızın amacı Samsun ili sınırları içinde yayılım gösteren istilacı yabancı tür *Cirsium arvense* L. in Grime'in CSR (Rekabetçi, strese- dirençli, ruderal) metodu kullanılarak ana ve ara stratejiler halinde sınıflandırılmasıdır. Grime (1977), bitkileri ekolojik faktörleri dikkate alarak sınıflandırmaya çalışmıştır. Bunu yaparken de başlıca stres ve tahribat faktörlerine karşı bitkilerin geliştirdikleri cevapları, dikkate almıştır. Buna göre bitkileri Rekabetçi (C), Strese- toleranslı (S) ve Ruderal (R) olmak üzere üç gruba ayırmıştır. Ancak bitki türleri sadece bu üç grup halinde sınıflandırılmamakta, çok sayıda ara stratejiler de göstermektedirler. Bu sınıflandırmaya dayanarak türlerin Grime stratejilerinin hangilerini benimsedikleri belirlenmiştir. Bu çalışma kapsamında öncelikle Samsun ilinde bulunan yedi adet farklı habitat Nebiyan Dağı, Kocadağ, Balaç köyü, Deniz kenarı, OMÜ Gölet, OMÜ Prof. Dr.Tahsin Tuncalı Parkı ve Bafra Kuş Cenneti'ne gidilmiştir. Bu bölgelerde bitki bireylerinin ayrı ayrı kanopi boyu, lateral yayılma durumu, çiçeklenme başlangıcı, çiçeklenme periyodu, kuru yaprak ağırlığı, yaş yaprak ağırlığı, spesifik yaprak alanı, yapraktaki kuru madde içeriği belirlenmiştir. Çalışma sonucunda; Deniz kenarı,,OMÜ Gölet, Kocadağ, Nebiyan Dağı ve OMÜ Prof. Dr. Tahsin Tuncalı Parkı'nda Rekabetçi (R)strateji ve Strese- toleranslı/ Rekabetçi Strateji (SC), Bafra Kuş Cenneti ve Balaç Köyü'nde ise Rekabetçi Strateji (R) ve Rekabetçi/ Ruderal Strateji göstermektedir. StrateFy yöntemine göre ise Strese- toleranslı strateji göstermiştir. İstilacı yabancı bitkilerle mücadelede, bitkinin stratejisini bilmek mücadelenin birinci adımıdır.

Anahtar Kelimeler: CSR stratejileri, Stres, Tahribat, *cirsium arvense*

➢ *ORAL PRESENTATION*

Elektrosprey ve 3B Biyoyazıcı Yöntemleri ile *Cinchona* Ekstresi ve Arap Zamkı İçeren Fonksiyonel Yara Örtülerinin Geliştirilmesi

Ceylan Büyüktaş[1*] (*ORCID: https://orcid.org/ 0009-0001-8317-1248*), Sinem Koçer[2] (*ORCID:https://orcid.org/0000-0003-0517-7422*), Azime Erarslan[3] (*ORCID: https://orcid.org/0000-0002-9470-4310*), Anıl Tevfik Koçer[4] (*ORCID: https://orcid.org/0000-0003-1519-1711*)

[*1]Yıldız Teknik Üniversitesi, Fen Bilimleri Enstitüsü, Biyoteknoloji Anabilim Dalı, İstanbul, Türkiye.
[2]İstanbul Yeni Yüzyıl Üniversitesi, Eczacılık Fakültesi, Eczacılık Teknolojisi Bölümü, İstanbul, Türkiye.
[3]Yıldız Teknik Üniversitesi, Kimya-Metalurji Fakültesi, Biyomühendislik Bölümü, İstanbul, Türkiye.
[4]Sağlık Biyoteknolojisi Mükemmeliyet Ortak Uygulama ve Araştırma Merkezi, İstanbul, Türkiye

*Sorumlu yazar e-posta: ceylan.2390@gmail.com

Özet

Yara iyileşmesi sürecinin karmaşıklığı ve yüksek enfeksiyon riski nedeniyle enfeksiyonu önleyebilecek, hücre canlılığını destekleyebilecek ve iyileşme sürecini hızlandırabilecek özellikte yara örtülerine duyulan ihtiyaç giderek artmaktadır. Bu açıdan bakıldığında doğadan elde edilen biyopolimerler ve bitkisel ekstreler, sahip oldukları antimikrobiyal ve biyolojik özellikler sayesinde yara iyileştirme uygulamalarında dikkat çekmektedir. Bu çalışmada, doğadan elde edilen *Cinchona* (Kınakına) ekstresi ve Arap zamkının biyolojik ve antimikrobiyal potansiyelleri, yeni nesil bir yara örtüsü tasarımında değerlendirilmiştir. Bu kapsamda ilk olarak PVA/kitosan/Arap zamkı içeren çözeltilerin 3B biyoyazıcı ile basılabilirlikleri değerlendirilmiştir. Optimum formülasyon belirlendikten sonra basılan yara örtülerinin üzerine ikinci katman olarak PCL/*Cinchona* ekstresi elektrosprey yöntemiyle püskürtülmüş ve elde edilen çift katmanlı yapının karakterizasyonları gerçekleştirilmiştir. Bitki ekstraksiyonu maserasyon yöntemi ile gerçekleştirilmiş ve ekstrenin antioksidan kapasitesi DPPH analizi ile maksimum %94.04 radikal giderme oranı olarak tespit edilmiştir. Karakterizasyon çalışmaları kapsamında FTIR analizi, her iki tabakada da karakteristik fonksiyonel grupların başarılı bir şekilde entegre edildiğini; SEM analizi ise yara örtüsü yüzeylerinin düzgün bir yapıya sahip olduğunu göstermiştir. Yara örtüsünün antimikrobiyal etkinliği *Staphylococcus aureus* ve *Escherichia coli* suşlarına karşı disk difüzyon yöntemi ile değerlendirilmiş; inhibitör zon çapları sırasıyla 14.2 mm ve 12.8 mm olarak ölçülmüştür. Elde edilen bulgular, doğadan elde edilen malzemelerle geliştirilen bu çift katmanlı yapının, fonksiyonel ve antimikrobiyal özellikleri sayesinde yara örtüsü uygulamalarında etkin bir alternatif olabileceğini göstermektedir.

Anahtar Kelimeler: 3B yazıcı, Elektrosprey, Biyopolimer, *Cinchona,* Arap zamkı, Yara Örtüsü

➢ *ORAL PRESENTATION*

Development of a surrogate model for dual optical element concentrated photovoltaic system using machine learning

Mahir Jafarov[1*] (*ORCID: 0009-0006-0934-8638*), Osman Turan[2] (*ORCID: 0000-0003-3421-2020*)

[*1]Bursa Technical University, Faculty of engineering and Natural Science, Department of Mechanical Engineering, Bursa, Turkey.

*Corresponding author e-mail: mahir.cafarov2022@gmail.com

Abstract

In this study, a machine learning-based approximate model was developed to accurately predict the electrical performance of dual optical element concentrated photovoltaic (CPV) systems. The model was built based on a total of 25 different CPV configurations composed of various combinations of primary and secondary Fresnel lenses. For each configuration, the inter-lens distance (L_d) was systematically varied, and approximately 220 experimental data points were collected under two different solar irradiance levels (G = 500 and 1000 W/m²). Key optical and geometrical parameters, including concentration ratios (C_1, C_2), f-numbers (f_1, f_2), and inter-lens distance, were used as input features for the model. The extensive dataset was processed using the XGBoost regression algorithm combined with the MultiOutputRegressor approach to simultaneously predict short-circuit current (I_{sc}) and open-circuit voltage (V_{oc}). Additionally, Optuna was employed for hyperparameter optimization to enhance model accuracy.The developed model successfully captured the complex nonlinear relationships between optical design parameters and the electrical outputs of the CPV system, achieving high prediction accuracy. This capability enables rapid and reliable evaluation of system performance without the need for extensive physical prototyping and long-duration experiments. Through virtual experiments and parametric studies, the proposed approach facilitates design optimization and provides valuable insights for the development of high-performance dual optical element CPV systems.

Keywords: CPV System, Fresnel Lens, Optical Parameter, XGBoost, Machine Learning.

➢ *ORAL PRESENTATION*

Seramik Karo Üretiminde Sürdürülebilir Teknolojilerin Geliştirilmesi

Buse Erdoğan[1*] (*https://orcid.org/0009-0003-2613-2271),*
Demet Topaloğlu Yazıcı[2](*https://orcid.org/0000-0002-9409-7397*)

[*1]Eskişehir Osmangazi Üniversitesi, Kimya Mühendisliği, Eskişehir, Türkiye.
[2] Eskişehir Osmangazi Üniversitesi, Kimya Mühendisliği, Eskişehir, Türkiye.

*Sorumlu yazar e-posta: 1buseerdogan@gmail.com

Özet

Endüstriyel seramik üretimde hammadde maliyetlerinde hedeflenen iyileşme ve artan çevre bilinciyle uyumlu üretim süreçlerin geliştirilmesi amacıyla bu çalışma planlanmıştır. Seramik endüstrisi gibi kaynak tüketimi yoğun olan sektörlerde, üretim sırasında ortaya çıkan atıkların yeniden değerlendirilmesi hem doğal kaynakların korunması hem de işletme maliyetlerinin düşürülmesi açısından büyük önem taşımaktadır. Seramik karolar, sahip oldukları üstün mekanik dayanım, kimyasal etkilere karşı gösterdikleri direnç ve düşük su emme oranları gibi özellikleri sayesinde inşaat sektöründe vazgeçilmez yapı malzemeleri arasında yer almaktadır. Ancak bu ürünlerin üretim süreçlerinde ortaya çıkan atıkların değerlendirilmemesi, hem çevresel anlamda kirliliğe yol açmakta hem de işletmeler için önemli bir ekonomik yük oluşturmaktadır. Bu nedenle, seramik endüstrisinde atık yönetimi ve geri dönüşüm uygulamaları giderek daha fazla önem kazanmaktadır. Bu çalışmada, seramik karo üretiminde kullanılan ve zamanla atık haline gelen fırın rulolarının yeniden değerlendirmesi için karolarda kullanımı denenmiş ve standart karolar ile karşılaştırılmıştır. Fırın rulo atıklarının, yüksek sıcaklığa dayanıklı yapıları sayesinde seramik karolarda alternatif hammadde olarak kullanılabilme potansiyeli incelenmiştir. Elde edilen verimli bulgular sonucunda karo yüzeylerinde kaplama uygulamaları ile bazı özelliklerin geliştirilebileceği tespit edilmiştir. Çalışma kapsamında, standart seramik karo reçetesine belirli oranlarda fırın rulo atığı eklenerek örnekler hazırlanmıştır. Üretilen karolar üzerinde temas açısı ölçümleri, renk analizleri, su emme testleri, mekanik dayanım testleri ve taramalı elektron mikroskobu (SEM) analizleri gerçekleştirilmiştir. Sonuçlar, uygun miktarda fırın rulo atığı ilavesinin karoların mekanik özelliklerini iyileştirdiğini göstermiştir. Bu bulgular, atık malzemelerin geri kazanımının hem ekonomik hem de çevresel açıdan avantaj sağladığını ortaya koymaktadır. Sonuç olarak, bu araştırma, seramik endüstrisinde sürdürülebilir üretim için yenilikçi ve uygulanabilir bir yaklaşım sunmaktadır.

Anahtar Kelimeler: Seramik hammaddeleri, Karo, Sürdürülebilir üretim, Karakterizasyon.

➢ *ORAL PRESENTATION*

Linking Forest Management to Water Treatability: Improved Coagulation Performance Following Silvicultural Activities in Forested Watershed

Habibullah Uzun (*https://orcid.org/0000-0001-7675-0885)*

Department of Environmental Engineering, Istanbul Technical University, Istanbul, Türkiye

*Corresponding author e-mail: uzunh@itu.edu.tr

Abstract

This study examines the impact of silvicultural forest treatments, including thinning, regeneration, and controlled burns (Prescribed [Rx] burnings), on the treatability (i.e., enhanced alum coagulation) of dissolved organic carbon (DOC) and related water quality parameters within a 155-hectare experimental forest (WS 77) located in the Santee Experimental Forest, South Carolina (SC). Watershed 80 (WS 80), which remained untreated by fire or other interventions, served as a control. Raw water samples were collected from two distinct periods: before treatment in 2016, when only prescribed burning was conducted, and post-treatment in 2024, following four different treatment methods. The study examined various parameters related to water quality (WQ) and treatability, including DOC, dissolved organic nitrogen (DON), specific ultraviolet absorbance (SUVA), turbidity, and ultraviolet absorbance at 254 nm (UV_{254}). Following the implementation of silvicultural treatment (2019-2022), the efficiency of removal in WS 77 exhibited a marked improvement, rising from an average of 45% in 2016 to 65% in 2024. However, an increase in $SUVA_{254}$ in the raw water was observed, indicating a shift towards more aromatic DOC species, which are more effectively removed through alum-coagulation. Raw water turbidity decreased by over 50%, likely due to reduced surface erosion and organic matter mobilization in WS 77. Overall, WS 80 exhibited only modest changes during the same period, highlighting the role of Forest management in modifying DOC characteristics conducive to alum-coagulation. These findings align with recent literature indicating that low-intensity fire regimes promote the formation of aromatic, humic-like dissolved organic matter (DOM) and decrease hydrophilic DOC fractions that resist coagulation. This study offers field-based evidence that silvicultural activities, including prescribed burning (Rx), can effectively source water protection strategies, enhancing coagulation performance and reducing the demand for treatment chemicals. Continued molecular characterization of dissolved organic matter is recommended to elucidate further fire-induced shifts in natural organic matter (NOM) composition and optimize treatment processes.

Keywords: Forest Management, Water Treatment, Enhanced Coagulation, DOC

➢ *ORAL PRESENTATION*

Aspergillus fumigatus ERG6 Protein Modelinin Antifungal Ajanlarla Moleküler Etkileşim Analizi

Sinem Koçer[*1] (ORCID:https://orcid.org/0000-0003-0517-7422)

[*1] İstanbul Yeni Yüzyıl Üniversitesi, Eczacılık Fakültesi, Eczacılık Teknolojisi Ana Bilim Dalı, İstanbul

*Sorumlu yazar e-posta: sinem.kocer@yeniyuzyil.edu.tr

Özet

Aspergillus fumigatus, bağışıklık sistemi baskılanmış bireylerde alerjik ve kronik akciğer patolojilerine neden olan en yaygın ve fırsatçı hava mantarı patojenidir. Mantar zarında bulunan ergosterol, zar akışkanlığı düzenlemesi, integral proteinlerin aktivitesi, hücre döngüsünün kontrolü gibi çok sayıda biyolojik işlevde görev alır. Bu nedenle, ergosterol biyosentezi, bu organizmanın hayatta kalması için kritik olduğundan bu yolaktaki enzimler antifungal tedavilerde önemli hedeflerdendir. Bu çalışmada, ergosterol biyosentezinde görev alan sterol 24-C-metiltransferaz (AfERG6, UniProt ID: Q4W9V1, NCBI Protein ID: XP_746550) proteini hedeflenmiştir. ERG6'nın üç boyutlu yapısı AlphaFold üzerinden modellenmiştir. Chimera 1.13.1 programı ile 1000 adımda (steepest descent) minimizasyonu yapılmış ve yapısal doğrulama analizleri (ERRAT, Verify3D, Ramachandran plot grafiği ve ProSA-web) ile modelin güvenilirliği değerlendirilmiştir. ERRAT genel kalite faktörü 94,5652 olup yüksek yapısal güvenilirlik göstermiştir. Verify3D analizine göre rezidülerin %88,06'sı kabul edilebilir 3D-1D skoru sağlamıştır. Ramachandran plot sonuçları, rezidülerin %92,3'ünün en uygun bölgede yer aldığını göstermiştir. ProSA-web analizi ise −8,18 Z-skoru ile modelin deneysel protein yapılarıyla uyumlu olduğunu ortaya koymuştur. Tüm validasyon sonuçları değerlendirildiğinde oluşturulan AfERG6 modelinin moleküler yanaştırma analizleri için uygun olduğu tespit edilmiştir. Potansiyel bağlanma cepleri DogSiteScorer ile belirlenmiş ve en yüksek ilaçlanabilirlik skoruna sahip bölge (Drug Score: 0,81) seçilmiştir. Bu hedef bölgeye yönelik olarak, üç antifungal ajan— Posakonazol, Terbinafin, Flusitozin — ile moleküler yanaştırma çalışmaları SwissDock üzerinden AutoDock Vina metodu kullanılarak gerçekleştirilmiştir. Moleküler yanaştırma analizleri, en güçlü bağlanmanın −8.152 kcal/mol ile Terbinafin tarafından gerçekleştirildiğini ortaya koymuştur. Flusitozin, −5,258 kcal/mol bağlanma enerjisi ile göreceli olarak daha zayıf bir etkileşim sergilemiştir. Öte yandan, Posakonazol için hesaplanan pozitif bağlanma enerjisi (3,746 kcal/mol), hedef proteinle düşük affiniteli veya uygun olmayan bir etkileşimi işaret etmektedir. Elde edilen bu veriler, özellikle Terbinafin'in AfERG6 proteini ile etkileşim potansiyeli açısından umut verici bir aday olabileceğini göstermektedir. Ancak, bu sonuçlar ön tahmin niteliğinde olup, farklı bağlanma ceplerinde yapılacak ileri düzey moleküler yanaştırma analizleriyle desteklenmesi gerekmektedir.

Anahtar Kelimeler: *Aspergillus fumigatus,* ergosterol biyosentezi, antifungal ajan, moleküler yanaştırma

➢ *ORAL PRESENTATION*

Hypericum perforatum Modulates Innate Immune Responses in *Galleria mellonella*: A Dose-Dependent Analysis

Serhat KAYA*
(*ORCID: https://orcid.org/ 0000-0002-0984-2824*)

*Çanakkale Onsekiz Mart University, Faculty of Science, Department of Biology, Çanakkale, TÜRKİYE.

*Corresponding author e-mail: serhatkaya@comu.edu.tr

Abstract

Hypericum perforatum is a widely recognized medicinal plant known for its antimicrobial, anti-inflammatory, and antioxidant properties. Recently, its potential immunomodulatory effects have garnered attention, particularly in experimental models such as *Galleria mellonella*, an invertebrate increasingly used to investigate innate immune responses. The choice of *G. mellonella* in such research is especially valuable, as its immune system shares notable similarities with that of vertebrates and supports the 3R principles by offering an ethical, cost-effective alternative to vertebrate models. The study using this model have shown that *H. perforatum* extract can influence phenoloxidase activity and the expression of antimicrobial peptides like hemolin and gallerimycin, suggesting its ability to modulate immune signaling and effector mechanisms. Larvae reared under controlled conditions were injected with four doses of *H. perforatum* extract, and immune responses were evaluated 24 hours post-injection. Hemolymph samples were collected to assess total hemocyte counts, phenoloxidase and antioxidant enzyme activities, as well as encapsulation and melanization responses using standard light microscopy-based and spectroscopic techniques. *Hypericum perforatum* administration modulated immune responses in *G. mellonella* in a dose-dependent manner, with higher doses significantly enhancing strong encapsulation and lower doses promoting strong melanization responses. The results indicate that *H. perforatum* modulates hemocyte count in a dose-dependent manner, with moderate concentrations significantly increasing total hemocyte numbers, while the highest concentration showed no immunostimulatory effect, suggesting a potential shift toward immunosuppression or tolerance at elevated levels. However, despite these cellular immune modulations, *Hypericum* extract did not exhibit a measurable effect on DPPH radical scavenging activity in *G. mellonella* hemolymph, indicating limited systemic antioxidant impact under the tested conditions. These findings suggest that *H. perforatum* may act as a dose-dependent immunomodulator in *G. mellonella*, enhancing cellular immune responses at moderate concentrations while showing potential immunosuppressive effects at higher doses.

Keywords: *Hypericum perforatum*, *Galleria mellonella*, DPPH, immune responses

Acknowledgement: This study was supported by the Scientific Research Projects Commission of Çanakkale Onsekiz Mart University under project number FBA-2023-4319.

➢ *ORAL PRESENTATION*

Cytotoxic and Antimicrobial Properties of Brown Algae Extracts: A Study on *Cystoseira foeniculacea* and *Sargassum vulgare*

Damla Kirci[1*] (*ORCID: https://orcid.org/0000-0002-3479-3999)*

[*1]izmir Katip Çelebi University, Faculty of Pharmacy, Department of Pharmacognosy, Izmir, Türkiye.

*Corresponding author e-mail: damla.kirci@ikc.edu.tr

Abstract

This study investigates the cytotoxic and antimicrobial activities of methanolic extracts derived from *Cystoseira foeniculacea* and *Sargassum vulgare*, two edible brown algae collected from the Mediterranean Sea. Cytotoxic effects were assessed on HepG2, MCF-7, and MDA-MB-231 cell lines, while antimicrobial activity was evaluated against clinically relevant bacteria and yeast strains. *Cystoseira foeniculacea* exhibited potent antiproliferative effects, particularly on HepG2 (IC_{50}: 35.25 µg/mL) and MCF-7 (IC_{50}: 105.5 µg/mL) cells. In contrast, *Sargassum vulgare* displayed limited cytotoxicity but demonstrated selective antimicrobial activity against *Enterococcus faecalis* and *Candida albicans*, with MIC values of 128 µg/mL and 512 µg/mL, respectively. Both extracts were ineffective against Gram-negative bacteria. The findings highlight species-specific therapeutic potential and support further investigation of these macroalgae as sources of multi-target natural products. Future work should focus on bioactivity-guided fractionation and *in vivo* validation.

Keywords: *Cystoseira foeniculacea, Sargassum vulgare*, cytotoxicity, antimicrobial activity, methanolic extract, macroalgae

➢ *ORAL PRESENTATION*

Evolution of the Dmrt1 Sex Gene in the Anatolian Water Frog Complex (Genus: *Pelophylax*) in Türkiye

Doğa Koçyiğit[1] (*ORCID: https://orcid.org/0009-0009-1094-0892),* Buse Ceyda Öncel[1] (*ORCID: https://orcid.org/0009-0009-8422-0994*), Çiğdem Akın Pekşen[1,2*] *(ORCID: https://orcid.org/0000-0001-5736-3062*), Albert J. Poutska[3], Jose H. Grau[4] *(ORCID: https://orcid.org/0000-0002-5328-3652),* Jörg Plötner[4] *(ORCID: https://orcid.org/0000-0001-8224-6378)*

[*1]Başkent University, Faculty of Science and Letter, Department of Molecular Biology and Genetics, Ankara, Turkey.
[2] Başkent University, Institute of Transplantation and Gene Sciences, Ankara, Turkey.
[3]Max Planck Institute for Molecular Genetics, Evolution and Development Group, Ihnestrasse 73, 14195 Berlin, Germany.
[4]Museum für Naturkunde Berlin, Leibniz-Institut für Evolutions- und Biodiversitätsforschung, Invalidenstraße 43, 10115 Berlin, Germany.

*Corresponding author e-mail: cerigensis@gmail.com

Abstract

The sexual development is an important mechanism in life which, is subject to the spatial and temporal expression of numerous genes. One of these genes, designated as DMRT1 (Doublesex and Mab-3 Related Transcription factor 1), is homologous to the DSX gene of *Drosophila melanogaster* and the MAB-3 gene of Caenorhabditis elegans. The DMRT1 gene encodes a transcription factor containing a conserved zinc finger domain, which is involved in sex determination and differentiation. Despite its vital function, the studies related to the evolution of this gene are limited. In this study we investigated evolution of the dmrt1 gene across various lineages of the Anatolian water frogs complex (*Pelophylax*). This group consists of recently diverged lineages (*Caralitanus, Cerigensis*, Cf. *bedriagae* and *Euphrates*) and olderly diverged lineages (*Cilician* and *Ridibundus*). This high genetic and phylogenetic diversity make them a valuable model for studying molecular evolution of genes. In the present study, we amplified and sequenced the coding sequence of the Dmrt1 sex gene. This analysis involved the analysis of five exons, with a total length of 1005 base pairs, from six lineages of the Anatolian water frog complex, including both male and female individuals. The analysis of the DNA sequences of the Dmrt1 was performed at both nucleotide and amino acid levels. Sequencing results revealed that the coding sequences of the Dmrt1 gene obtained from both female and male individuals from each lineage were found to be identical. Furthermore, the position of conserved motifs, including the DM domain, the male-specific motif and the P/S-rich element, was identified throughout the coding sequence of the gene. The resulting phylogenetic trees demonstrated that the Dmrt1 gene is highly conserved between closely and distantly related *Pelophylax* lineages, including one or two SNPs. These findings contribute to a deeper understanding of the evolution of sex-determination genes in amphibians and lay the groundwork for future research on other sex-determining genes.

Keywords: Dmrt1 gene, sex gene, *Pelophylax*, water frog, Anatolia

➢ *ORAL PRESENTATION*

Development of Composite Anode Electrodes Containing Metal Oxide-N Doped Reduced Graphene Oxide for Lithium Ion Batteries

Alican Çördük[1*] *0009-0001-0687-6471* Zekerya Dursun[2*] 0000-0001-8887-3356

[*1] Ege University, Faculty of Science, Chemistry Department, İzmir, Türkiye.
[*2] Ege University, Faculty of Science, Chemistry Department, İzmir, Türkiye

**Corresponding author e-mail : 91220001360@ogrenci.ege.edu.tr

Abstract

Clean and renewable alternative energy sources are needed because fossil-based energy sources have limited reserves and cause environmental problems. The growing demand for energy with the rise of renewable sources, requires more efficient energy storage devices. Lithium-ion batteries (LIBs) have become essential due to their high energy density and long cycle life. The choice of electrode materials is crucial, as it directly affects LIB performance. While graphite is widely used, its relatively low theoretical capacity limits battery performance. Metal oxides offer higher capacities but suffer from volume expansion and poor cycling stability. Two-dimensional materials like graphene oxide (GO) can enhance the electrical performance of metal oxides in composites. In this study, graphite was first converted to GO using a modified Hummers method and then nitrogen-doped by hydrothermal treatment with urea. Binary and ternary N-doped GO (N-GO) based metal oxide composites (MnO_2, NiO, V_2O_5) were synthesized with hydrothermal method, ensuring homogeneous distribution of metal oxides in the N-GO matrix. The composites were characterized by SEM, Raman spectroscopy, XRD, and XPS, confirming uniform nanometer-scale distribution, crystalline phases, and successful nitrogen doping. Electrochemical performance was evaluated by cyclic voltammetry and galvanostatic charge-discharge tests in button cells.The N-GO/NiO binary hybrid anode showed a high initial discharge capacity of 520 mAh/g at 100 mA/g, retaining 480 mAh/g after 50 cycles, reflecting NiO's high theoretical capacity. In contrast, the N-GO/V_2O_5 binary hybrid anode exhibited a lower initial capacity of 250 mAh/g and 220 mAh/g after 50 cycles, consistent with V_2O_5's lower theoretical capacity. The N-GO/NiO/V_2O_5 hybrid composite anode (20 wt% N-GO, 40 wt% NiO, 40 wt% V_2O_5) achieved 410 mAh/g initially and 370 mAh/g after 50 cycles, surpassing graphite. These results demonstrate the promise of N-GO-based hybrid metal oxide composites as robust anodes for next-generation LIBs, especially where stability and high-rate performance are required.

Keywords: Graphene oxide, Metal oxide, Anode material, Cyclic voltammetry, Cycling stability, Current density

➢ *ORAL PRESENTATION*

Structural and Antibacterial Activity Properties of Lignite-Derived Carbon Coating on Ceramic Tiles

Emre Dal[1*] (*ORCID: https://orcid.org/ 0009-0006-3777-3180.*), Fatma Sarf[2] (*ORCID: https://orcid.org/000-0002-4445-48000*), Emin Yakar[3] (*ORCID: https://orcid.org/*0000-0002-7775-0251)

[*1,2]Çanakkale Onsekiz Mart University, Çan Vocational School, Çanakkale, Turkey.
[3]Çanakkale Onsekiz Mart University, Engineering Faculty, Materials Science and Engineering, Çanakkale, Turkey.

*Corresponding author e-mail: emredal1973@gmail.com

Abstract

In this study, lignite-derived carbons coated on ceramic tiles by spin coating. Their structural, morphological, surface wettability and antibacterial activity properties were investigated by XRD, SEM, surface contact angle measurement system and acredite ISO 22196 measurement, respectively. Graphitic carbon structure with typical (002) and (100) peaks were observed with relative homogenous carbon coating on ceramic tiles. Enhanced *E.coli* antibacterial activity is integrated into the hydrophilic surface. According to these results, this coating can be preferred in areas with high pollution levels such as toilets, bathrooms.

Keywords: antibacterial coating, ceramic surface, *E.coli*

➢ *ORAL PRESENTATION*

Mucormycosis Cases Under the Microscope: A 19 Year Retrospective Pathology-Based Surveillance Study

Bilal Tunçtürk[1*] (ORCID ID: https://orcid.org/0000-0003-1738-1025),
Ulaş Alabalık[2] (ORCID ID: https://orcid.org/0000-0003-4551-8439)

[*1] Diyarbakır Selahaddin Eyyubi State Hospital, Department of Medical Pathology, Diyarbakır, Turkey
[2]Dicle University, Faculty of Medicine, Department of Medical Pathology, Diyarbakır, Turkey

*Corresponding author e-mail : dr.bilaltuncturk@gmail.com

Abstract

Mucormycosis is a rare but fatal fungal infection caused by fungi belonging to the order Mucorales. It poses a serious threat especially in immunosuppressed individuals. Conditions such as diabetes mellitus, hematologic malignancies, organ transplantation, long-term corticosteroid use are among the main risk factors for mucormycosis. With the COVID-19 pandemic, the diagnosis of COVID-19 Associated Mucormycosis (CAM) entered the literature. Histopathologically, the presence of thick hyphae branching 90 degrees is important in the diagnosis. In this single center study, we aimed to retrospectively evaluate the epidemiological data and clinical features of the patients.

Thirty-nine cases diagnosed with mucormycosis between 2006 and 2025 in the Department of Pathology, Dicle University Faculty of Medicine were retrospectively reviewed and included in our study. Demographic and clinical findings obtained from the hospital information management system were included in the evaluation.

Twenty (51%) of our patients were male and 19 (49%) were female. The age range varies between 6 and 80 years, with an average age at diagnosis of 53.5 years. We have 13 patients (33%) in 13 years before 2019 and 26 patients (66%) in 7 years after 2019. Among our patients, 15 (38%) had hematologic malignancy, 11 (28%) had diabetes mellitus, 2 (5%) had non-hematologic malignancy, 2 (5%) had chronic steroid use, and 1 (2.5%) had coexistence of diabetes and malignancy. Seventeen (43%) cases were localized in the nasal passage, 14 (35%) in the paranasal sinus, 6 (15%) in the hard or soft palate of the mouth, and 2 (5%) in the nasal wing.

There was no significant difference in the number of cases between men and women. Rhinocerebral mucormycosis typically starts in the paranasal sinuses by inhalation of spores and rapidly spreads to the orbit and brain. In our study, 31 of our cases (80%) were sampled from the nasal cavity and sinuses. When the number of cases between 2019 and 2025 is compared with the number of cases between 2006 and 2019, it is noteworthy that twice as many cases were seen in half the time. The emergence of this significant difference highlights the impact of the Covid-19 pandemic. Mucormycosis is an opportunistic infection and 31 of our cases (80%) had underlying diabetes, malignancy or steroid use.

Mucormycosis has a remarkable clinical significance due to its high mortality rates and aggressive nature. Untreated, the mortality rate approaches 100%, while with treatment the rate drops significantly but is still high. Current data suggest that overall mortality rates range from 32% to 71%, depending on clinical form, underlying conditions and treatment efficacy. The high mortality rate of the disease reaffirms the importance of early diagnosis and aggressive treatment strategies. Diabetes control, avoidance of unnecessary steroid use and evaluation of immunosuppression status are important to reduce the prevalence. In patients in the risk group, mucormycosis should be considered in the differential diagnosis in case of antibiotic resistance.

Keywords: Mucormycosis, Opportunistic infection, Mortal, Immunosuppressive

➢ *ORAL PRESENTATION*

Environmental and mechanical impacts of incorporating synthetic C-S-H in cement systems

Nevin Karamahmut Mermer[1*] (*ORCID:0000-0001-6645-4724*),
Melis Ünal[2] (*ORCID: 0000-0001-9423-2184*)

[*1]Kalekim Construction Chemicals Co., R&D Department, Istanbul, Türkiye.
[2] Istanbul Technical University, Chemistry Department, Istanbul, Türkiye.

*Corresponding author e-mail: nevinmermer@kale.com.tr

Abstract

In considering the carbon emissions and environmental impacts of the cement industry, the utilization of cement with decreased clinker content has been established and executed both academically and commercially in numerous countries with regulatory frameworks. The temperature throughout the cement production process is the stage with the greatest environmental impact across the whole production cycle. Given its status as one of the most utilized materials, the environmental impact of sustainability research in this domain will be significant. Upon the reaction of the primary constituents of cement, C_3S (tricalcium silicate) and C_2S (dicalcium silicate), with water, calcium silicate hydrate (C-S-H) and calcium hydroxide (CH) are produced. C-S-H is the primary product of cement hydration. C-S-H gel constitutes the fundamental binding phase that imparts mechanical strength and durability to concrete. C-S-H, the substance formed during the hydration reaction of cement, can also be synthesized artificially. The maximal manufacturing temperature of C-S-H is 220°C. It can be utilized directly as an additive for cement or for surface coating/composite products. In the study, 1%, 2%, 3%, 4%, and 5% synthetic C-S-H was incorporated into the cement paste. Strength tests were performed based on EN 196-1 "Methods of testing cement — Part 1: Determination of strength" standard. Bending and compression tests were conducted after 2, 7, and 28 days of curing to assess performance. Material was taken from cement pastes and cured in compliance with the standards. Upon completion of the curing period for the samples, the reaction was stopped by a solvent exchange method, followed by XRD and FTIR studies to monitor the reaction process. The results were assessed by analyzing the microstructure and performance, revealing that the optimal C-S-H content is 2%.

Keywords: Synthetic C-S-H, environmental impact, reaction monitoring, microstructure.

➢ *ORAL PRESENTATION*

Evaluation and integration of YOLOv8 and SAM deep learning models for brain tumor detection and segmentation in MRI

Salajdin Maloku[1*] (*0009-0007-8128-3741*), Savaş İzzetoğlu[1] (*0000-0002-1546-1083*)

*[1]Ege University, Faculty of Science, Department of Biology, Molecular Biology Section, İzmir, Türkiye.

*Corresponding author e-mail : salajdinmaloku@gmail.com

Abstract

Brain tumors pose significant diagnostic challenges due to their variability in size, location, and morphology. Accurate detection and segmentation are critical for treatment, yet manual annotation is time-consuming and prone to variability. This study investigates the application and comparative performance of various You Only Look Once (YOLOv8) models and integrates the Segment Anything Model (SAM) algorithm to build a deep learning-based, automated pipeline for zero-shot segmentation of brain MRI scans. The dataset comprises annotated MRI images, well balanced among four classes: pituitary tumor, meningioma, glioma, and no tumor. Five YOLOv8 architectures (x-large, large, medium, small, nano) were evaluated under identical conditions on unseen test data using mAP50-95, mAP50 and F1-score metrics. Cost-efficiency was assessed based on performance, training time, inference time and memory consumption. Among the tested models, smaller architectures demonstrated superior cost-effectiveness, with the small variant achieving the highest mAP50-95 score of 0.549 and offering the best trade-off between performance and practicality. In contrast, the x-large model offered no marginal performance gain with a mAP50-95 score of 0.535 at over double the training time and memory cost. None of the models performed notably well in detecting gliomas with the highest score AP50-95 of 0.353 attained by the small model. The 'no tumor' class was consistently the easiest to detect with the highest score of 0.712 AP50-95 attained by the x-large model. Finally, the model with the best raw detection performance was used to generate bounding-box prompts for SAM, facilitating the construction of the emerging YOLOv8-SAM pipeline for zero-shot segmentation on brain MRI scans for a visual presentation of the tumor boundaries. This study highlights the ease of integrating SAM into the YOLOv8 pipeline, particularly for medical imaging tasks requiring precise tumor boundary detection.

Keywords: brain tumor, MRI, YOLOv8, SAM, object detection, segmentation

➢ *ORAL PRESENTATION*

From Waste to Worth: Sustainable Nanofibers from *Aloe vera* and Recycled Polystyrene

Fatma Rabia Karaduman* (*ORCID: https://orcid.org/0000-0001-7317-3445*)

* Kırıkkale University, Faculty of Engineering and Natural Sciences, Department of Chemistry, Kırıkkale, Türkiye.

*Corresponding author e-mail: fatmarabiakaraduman@gmail.com

Abstract

Polystyrene waste poses a significant environmental concern due to its non-biodegradable nature and widespread accumulation in natural ecosystems. As such, developing effective recycling and upcycling strategies is critical for mitigating its ecological impact and promoting sustainable material use. *Aloe vera* is a natural bioactive compound with well-documented antimicrobial, anti-inflammatory, and healing properties, making it an ideal additive for biomedical applications such as wound dressings and tissue engineering. Its inherent biocompatibility and hydrophilicity also enhance filtration performance and environmental remediation potential when incorporated into polymeric nanofibers. This study investigates the fabrication of nanofibers from recycled polystyrene and *Aloe vera*, highlighting their potential applications in various areas.

Post-consumer polystyrene from food containers and coffee cups was dissolved in a natural solvent (DL-limonene), blended with different concentrations of *Aloe vera*, and processed via electrospinning to fabricate nanofibers. Before blending, *Aloe vera* leaves were washed with distilled water, sliced, freeze-dried, ground, and sieved to obtain particles smaller than 100 µm. The morphology and structure of the resulting fibers were characterized using scanning electron microscopy (SEM), Fourier-transform infrared spectroscopy (FTIR), and contact angle (CA) measurements. The fabricated nanofibers exhibit strong potential for applications in biomedical, filtration, wound healing, and environmental fields. Future research should focus on functional evaluations such as antibacterial activity, biodegradability, and mechanical performance to further assess their practical applicability.

Keywords: *Aloe vera*, electrospinning, recycled polystyrene, sustainable nanofibers

➢ *ORAL PRESENTATION*

Investigation of the Cadmium (Cd) removal potential of two aquatic macrophytes (*Limnobium laevigatum*, *Egeria densa*) in two different media with a microcosm approach

Danial NASSOUHI[*1] (*https://orcid.org/0000-0003-3693-6313*), Mehmet Borga ERGÖNÜL[1] (https://orcid.org/0000-0002-0263-9129)

[*1]Department of Biology, Faculty of Science, Ankara University, 06100 Ankara, Turkey

*Corresponding author e-mail: dnassouhi@ankara.edu.tr

Abstract

Contamination of aquatic habitats by heavy metals is regarded as one of the most critical environmental concerns, posing severe risks to both aquatic life and human health. Owing to their persistence, heavy metals tend to accumulate in aquatic environments, leading to long-term ecological and toxicological consequences. In recent years, biological methods for heavy metal removal, have gained increasing attention due to their affordability, reduced energy demand, and environmentally friendly nature. As a branch of bioremediation, phytoremediation, utilizes plants with high biomass productivity and pollutant uptake capacity to absorb, accumulate, transform, or stabilize heavy metals in water and sediments, offering an effective and eco-friendly remediation strategy. However, current research often overlooks the synergistic or antagonistic effects of multiple plant species and the crucial influence of biological, and physicochemical properties of water on phytoremediation efficacy.

This study aimed to investigate the Cd removal performance of *Limnobium laevigatum* (Humb. & Bonpl. ex Willd.) Heine and *Egeria densa* Planch. by exposing them to 1, 2.5, and 5 ppm concentrations of cadmium for 1, 4, and 7 days in two different mediums (25% Hoagland and pond water) individually and together. Cadmium concentrations were determined by ICP-OES, and the percentage removal, Cd concentration accumulated in plants, and bioconcentration factors (BCF) were calculated to investigate the removal performance of the macrophytes.

The results showed that the macrophytes exhibited a higher percentage removal when exposed to Cd individually in both mediums. Additionally, the Cd concentration accumulated in the macrophytes was higher when the macrophytes were exposed to Cd individually than in the co-cultured groups. Similar findings were seen in the BCF values. Overall, the data obtained from the study showed that both plants exhibited a more successful removal when individually exposed to Cd in both mediums.

Keywords: *Limnobium laevigatum*, *Egeria densa*, cadmium, phytoremediation

➢ *ORAL PRESENTATION*

Green Synthesis of Copper Oxide Nanoparticle via *Rubus Idaeus*

Ines Nour-Eddine[1] (*ORCID: https://orcid.org/0009-0006-1267-2965*), Tuğba Erkoç[1*] (*ORCID: https://orcid.org/0000-0002-3416-7074*)

[*1]Üsküdar University, Faculty of Engineering and Natural Sciences, Department of Chemical Engineering (English), Istanbul, Türkiye.

*Corresponding author e-mail: tugba.erkoc@uskudar.edu.tr

Abstract

The aim of the present study is to prepare copper oxide nanoparticle by green synthesis method at temperature T=60°C using *Rubus Idaeus*. The aqueous extract of *Rubus Idaeus* was found to act as both a natural reducing agent and a capping agent, contributing to the eco-friendly synthesis of nanoparticles. The synthesized copper oxide nanoparticle was allowed to dry at 50 °C in a vacuum oven. Fourier transform infrared spectroscopy (FT-IR), X-ray diffraction (XRD) and scanning electron microscope (SEM) techniques were used for the characterization of the synthesized copper oxide nanoparticle. XRD and FT-IR analyses confirmed the successful synthesis of a copper oxide nanoparticle through characteristic structural and spectral features. SEM analysis demonstrated that the copper oxide nanoparticle had a size below 100 nm, highlighting its nanoscale nature.

Keywords: Copper oxide, Nanoparticle, Green synthesis, Nanotechnology.

➢ *ORAL PRESENTATION*

Cyclic amine linked *p*-benzoquinones and their antimicrobial analyses

Mahmut Yıldız[1*] (*https://orcid.org/0000-0001-6317-5738*), Hatice Yıldırım[2] (*https://orcid.org/0000-0003-3988-6120*), Nilüfer Bayrak[3] (*https://orcid.org/0000-0002-0777-4012*), Selin Melis Çakmak[4] (*https://orcid.org/0000-0002-1213-4626*), Emel Mataracı-Kara[4] (*https://orcid.org/0000-0002-4428-5066*), Berna Özbek-Çelik[4] (*https://orcid.org/0000-0001-8909-8398*), Amaç Fatih Tuyun[3] (*https://orcid.org/0000-0001-5698-1109*)

[*1]Gebze Technical University, Faculty of Science, Department of Chemistry, Kocaeli, Türkiye
[2]Istanbul University-Cerrahpasa, Faculty of Engineering, Department of Chemistry, Istanbul, Türkiye
[3]Istanbul University, Faculty of Science, Department of Chemistry, Istanbul, Türkiye
[4]Istanbul University, Faculty of Pharmacy, Department of Pharmaceutical Microbiology, Istanbul, Türkiye

*Corresponding author e-mail: yildizm@gtu.edu.tr

Abstract

Due to the adaptation of microorganisms to the antibiotics, their excessive use and/or abuse and mutations, the bacteria causing the infections are becoming more resistant, known also as antimicrobial resistance (AMR) [1]. Therefore, improving or developing new antimicrobial drugs with good inhibitory properties against the resistant pathogens remains still a substantial demand. Owing to the biological and pharmacological features of quinone compounds, they are of great importance in drug development researches as lead and key molecules. Since quinone molecules exhibit biological activity, for many years they have been investigated for their different activities such as antiviral, antioxidant, antifungal, antibacterial, anticancer, etc. [2-3]. The introduction of amine molecules into the *p*-quinone structures gives aminoquinone derivatives and improves biological activity substantially [4]. Aminoquinones have received remarkable attention because of their various applications and increasing efficacy in medicinal chemistry [5]. Accordingly, in the search of new potential lead molecule, cyclic amine bonded novel amino-*p*-benzoquinone compounds designed, synthesized and characterized in the present work. Their antimicrobial activity was evaluated against a panel of the Gram-positive and Gram-negative pathogenic bacterial strains in addition to three different fungal strains. In order to understand deeply the chemical properties enhancing the antimicrobial activity, substitued cyclic secondary amine moieties were introduced bearing various group(s) and/or atom(s) in different positions and their influences on the biological activity were analyzed.

Keywords: Quinone, *p*-Benzoquinone, Cyclic amine, Antibacterial activity, Antifungal activity.

References:

[1] M.M. Masadeh, N.M. Mhaidat, K.H. Alzoubi, E.I. Hussein, E.I. Al-Trad, Infect. Drug Resist., 6, 27-32, 2013.
[2] P. M. S. Sahoo, S. Behera, R. Behura, A. Acharya, D. Biswal, S. K. Suna, R. Sahoo, R. C. Soren, B. R. Jali, Biointerface Res. Appl. Chem., 12(3), 3247-3258, 2021.
[3] E. S. Ahmadi, A. Tajbakhsh, M. Iranshahy, J. Asili, N. Kretschmer, A. Shakeri, A. Sahebkar, Mini Rev. Med. Chem., 20(19), 2019-2035, 2020.
[4] R. Pingaew, V. Prachayasittikul, A. Worachartcheewan, C. Nantasenamat, S. Prachayasittikul, S. Ruchirawat, V. Prachayasittikul, Eur. J. Med. Chem., 103, 446-459, 2015.
[5] D. Aminin, S. Polonik, Chem.Pharm.Bull., 68, 46-57, 2020.

➢ *ORAL PRESENTATION*

Potentiometric determination of skin antiseptic rivanol and its greenness assessment

Onur Cem Altunoluk[1,*] (*ORCID: https://orcid.org/0000-0003-3558-3499)*, Oguz Özbek[2] (*ORCID: https://orcid.org/0000-0001-5185-9681*), Caglar Berkel[2] (*ORCID: https://orcid.org/0000-0003-4787-5157)*

[*1]Tokat Gaziosmanpaşa University, Faculty of Science and Arts, Department of Chemistry, Tokat, Türkiye
[2]Tokat Gaziosmanpaşa University, Faculty of Science and Arts, Department of Molecular Biology and Genetics, Tokat, Türkiye

*Corresponding author e-mail: altunolukonurcem@gmail.com

Abstract

The skin antiseptic rivanol, also known as ethacridine lactate, is 6,9-diamino-2-ethoxyacridine lactate [1]. Different analytical methods have been reported to determine rivanol concentration in different samples, such as HPLC–UV, SPE–HPLC and Laser Induced Fluorescence [2]. However, these methods lack certain advantages provided by potentiometric techniques. Potentiometric devices offer versatile advantages over their alternatives, including wide concentration range, ease of preparation and use, low cost, fast response time, low detection limit, long lifetime, high selectivity and good reproducibility [3, 4]. In this study, polymer membrane potentiometric sensor was developed for the determination of rivanol. Potentiometric performance properties of the prepared sensors were tested under laboratory conditions using rivanol solutions. Polymer membrane rivanol sensors had a low detection limit and good reproducibility in a wide linear concentration range. At the same time, greenness evaluation of the prepared sensor was performed using complex–GAPI and AGREE tools. Finally, the fabricated sensor was applied to bovine serum albumin (BSA) protein solutions containing different amounts of rivanol and the obtained results were compared with the spectrophotometric method. As a result, the prepared sensors can determine rivanol with high recoveries and can be considered as green sensors.

Keywords: Rivanol, sensor, potentiometry, skin antiseptic

References

[1] W.Y. Li, J.G. Xu, X.W. He, Anal. Lett 33 (2000) 3183-3194.
[2] I. Palarie, M. C. Varut, L. M. E. Chirigiu, Rev. Chim, 70 (2019) 140-142.
[3] O. Özbek, O. C. Altunoluk, Anal. Biochem, (2024) 115657.
[4] O. C. Altunoluk, O. Özbek, E. Kalay, F. S. Tokalı, O. N. Aslan, Electroanalysis, 36 (2024) e202300407.

➢ *ORAL PRESENTATION*

Thermal and Chemical Assessment of Rolled Tobacco from Two Turkish Regions: Aegean and Southeast

Pelin Güzel[1] *(ORCID: https://orcid.org/0000-0001-9704-4250),* Doğa Topcu[2], Deniz Uykun Mangaloğlu[1,3*] *(ORCID: https://orcid.org/0000-0002-5295-3976),* Işık Çoban[1,2] *(ORCID: https://orcid.org/0000-0002-8736-8101*)

[*1]Research and Development Laboratory of Tobacco and Tobacco Products Analysis, Istanbul Medeniyet University, 34700 Istanbul, Türkiye
[2]Istanbul Medeniyet University, Faculty of Engineering and Natural Sciences, Bioengineering Dept., Istanbul, Türkiye
[3] Department of Chemical Engineering, Istanbul Technical University, 34469 Istanbul, Türkiye

*Corresponding author e-mail: deniz.mangaloglu@medeniyet.edu.tr

Abstract

Tobacco is recognized as one of the most commonly consumed and highly addictive substances both worldwide and within Türkiye. The leaves of the tobacco plant are particularly significant, as nicotine is predominantly synthesized in the roots and subsequently accumulates in the leaf tissues. Before reaching a consumable state, tobacco undergoes several technological processing steps.
In this study, a total of 35 rolled tobacco samples originating from the Southeastern and Aegean regions of Türkiye were analyzed. The nicotine and reducing sugar contents were quantified using an Autoanalyzer system, and the moisture content of the samples was also measured. To investigate the thermal behavior of the tobaccos, Thermogravimetric Analysis (TGA) and Differential Thermogravimetric Analysis (DTG) were performed on three representative samples from each region. The experiments were conducted in a temperature range of 105°C to 800°C, with a constant heating rate of 10°C per minute. The decomposition stages corresponding to hemicellulose and cellulose breakdown were identified, and reaction kinetics were evaluated based on the thermal degradation profiles.
Kinetic modeling was carried out using the Coats-Redfern method, focusing on the 200°C to 350°C temperature interval. The most suitable reaction models for different stages of pyrolysis were identified based on correlation coefficients, and activation energies were calculated accordingly. According to the kinetic analysis of the pyrolysis process, different reaction mechanisms were observed for the Southeastern and Aegean tobacco samples across specific temperature ranges. In the first temperature interval (473 K – 553 K), the one-dimensional diffusion model was found to be appropriate for all samples. In the second temperature interval (553 K – 623 K), one sample followed a unique reaction model, while the other two samples were best described by the bi-directional diffusion model for the Southeastern region, and for the Aegean region, all three samples conformed to a second-order reaction model.

Keywords: Tobacco, Thermogravimetric Analysis (TGA), Derivative thermogravimetric analysis (DTG), Autoanalyzer, Reducing Sugar, Total Alkaloids.

➢ *ORAL PRESENTATION*

Alterations in Oxidative Stress and Antioxidant Enzyme Activities Due to Phosmet Exposure in *Eisenia fetida*

Muhterem Elif Demirağ[1*] (*ORCID: https://orcid.org/0009-0007-6343-1309*),
Esra Akat Çömden[1] (*ORCID: https://orcid.org/0000-0001-7080-3106*)

[*1]Ege University, Faculty of Science, Department of Biology, Izmir, Turkey.

*Corresponding author e-mail: muhterem.elif.demirag@ege.edu.tr

Abstract

In recent years, the use of pesticides has increased significantly due to population growth and the rising demand for food. This increase has raised concerns about soil health and biodiversity, as pesticides affect not only pests but also non-target organisms. Studies have demonstrated that pesticides have various toxic effects on non-target organisms, including oxidative stress, genetic damage, endocrine disruption and histopathological alterations. Furthermore, pesticide residues can circulate through ecosystems, impacting organisms in distant habitats. Therefore, understanding the damage caused by pesticides is essential for developing sustainable agricultural strategies to mitigate their adverse effects. In this study, the effects of Phosmet, an organophosphate pesticide widely used in fruit and vegetable cultivation against harmful insects, were investigated on *Eisenia fetida.* The earthworms were assigned to five groups, including a negative control (0 mg/kg), a solvent control (0 mg/kg) and three groups exposed to different concentrations of Phosmet (5 mg/kg, 10 mg/kg, 20 mg/kg). Samples were collected on days 7, 14, 21, and 28 of the exposure periods. The study evaluated changes in the activities of antioxidant enzymes (superoxide dismutase, catalase, and glutathione S-transferase), total energy reserves (carbohydrates, proteins, lipids) and histopathological alterations in relation to concentration and exposure duration. As earthworms play a crucial role in maintaining soil health, their responses to pesticide exposure provide critical insights into ecological risk. Accordingly, comprehensive pesticide risk assessment is essential, and this study provides valuable data relevant to environmental toxicology.

Keywords: Phosmet, histopathology, earthworm, oxidative stress, ecotoxicology.

Acknowledgement: The study was financially supported by Ege University Office of Scientific Research Projects (Project number: FM-YLT-2023-31935)

➢ *ORAL PRESENTATION*

Comparative evaluation of CKAN and CNN deep learning models for classifying tumor-infiltrating lymphocytes in cancer histopathology images

Seyit Metin Köroğlu[1*] (*0009-0003-5731-1504*), Savaş İzzetoğlu[1] (*0000-0002-1546-1083*)

[*1]Ege University, Faculty of Science, Department of Biology, Molecular Biology Section, İzmir, Türkiye.

*seyit.metin.koroglu@ege.edu.tr

Abstract

Histopathology is still the gold standard for diagnosis of many cancers, including Prostate Adenocarcinoma (PRAD). While tumor cell morphology is primarily focused, the tumor microenvironment, particularly the presence and distribution of tumor-infiltrating lymphocytes (TILs), have gained importance as a biomarker in cancer research for predicting clinical outcomes and guiding treatment since they play a crucial role in cancer prognosis and response to immunotherapy. Machine learning (ML), especially deep learning (DL), models are being developed and used more and more every day in histopathological image classification problems. Kolmogorov-Arnold Network (KAN) is a new promising ML method that is based on Kolmogorov-Arnold representation theorem and Convolutional KAN (CKAN) is a recently differentiated model which came along by integrating KANs into convolution layers that leads to changing the classic linear transformation of the convolution to learnable nonlinear activations in each pixel. The purpose of this study is to test CKAN models, which have not been previously applied or evaluated on histopathological images, and to compare them with standard methods for classification tasks. For this aim, TCGA-TIL-PRAD dataset, which has 4865 TIL-negative and 730 TIL-positive patches obtained from Whole Slide Images taken from The Cancer Genome Atlas (TCGA), is used. Data preprocessing, augmentation and weighted random sampling were employed to handle class imbalance. CKAN and CNN models were built with the same number of layers and trained with the same parameters to classify these patches. Model performance was evaluated using accuracy, precision, recall, F1-score, and Area Under the Curve (AUC). CNN performed 71% accuracy, AUC of 0.5778, with an F1-score of 0.26 for TIL-positives. However, CKAN model had 79% accuracy, AUC to 0.6495, with an F1-score of 0.32 for TIL-positives. According to metrics, CKAN outperforms CNN and shows a promising preliminary result for effectively identifying TILs while offering valuable insights for personalized immunotherapy.

Keywords: Histopathology, PRAD, TILs, Deep Learning, Convolutional Kolmogorov-Arnold Networks

➢ *ORAL PRESENTATION*

Multi-Criteria Assessment of Turkish Cities for Biogas Plant Siting

Cheikha Hacena Ahmed El alem[1] (*ORCID: https://orcid.org/0009-0004-1521-1959*),
Seza Özge Gönen[1*] (*ORCID: https://orcid.org/0000-0002-5870-6319*)

[*1]Üsküdar University, Faculty of Engineering and Natural Sciences,
Department of Chemical Engineering, Istanbul, Türkiye.

*Corresponding author e-mail: sezaozge.gonen@uskudar.edu.tr

Abstract

This study evaluates the suitability of various cities in Turkey for the establishment of biogas plants, with a specific focus on the use of small cattle manure as the sole feedstock. To identify the most appropriate locations, a multi-criteria decision-making approach was applied. Three criteria were taken into account in the evaluation process. The comparative analysis of cities based on these factors resulted in a prioritized ranking of potential sites. According to the analysis, Van, Diyarbakır, and Mersin emerged as the most favorable cities for biogas plant siting. The findings of this study are expected to guide policymakers and investors in strategic planning and resource allocation for sustainable energy projects in Turkey.

Keywords: Biogas, Multi-criteria decision-making, Renewable energy, Sustainability

➢ *ORAL PRESENTATION*

Optimization of Bioethanol Production from Tobacco and Tobacco Product Wastes

Ayşenur Uzunbay[1] (*ORCID: https://orcid.org/0009-0001-9192-2160*), Emrullah Yılmaz[1] , Betül Taşbakır[1], Pelin Güzel[2]* *(ORCID: https://orcid.org/0000-0001-9704-4250)*, Deniz Uykun Mangaloğlu[2] *(ORCID: https://orcid.org/0000-0002-5295-3976)*, Işık Çoban[1,2] (*ORCID*: https://orcid.org/0000-0002-8736-8101)

*[1]Istanbul Medeniyet University, Engineering and Life Sciences Faculty, Department of Bioengineering, 34700, Istanbul, Türkiye.
[2]Research and Development Laboratory of Tobacco and Tobacco Products Analysis, Istanbul Medeniyet University, 34700, Istanbul, Türkiye.

*Corresponding author e-mail: pelin.guzel@medeniyet.edu.tr

Abstract

The supply of energy resources is one of the cornerstones of economic growth and social development. In this context, the exploration and development of alternative energy sources beyond fossil fuels is of great importance. As the demand for sustainable energy and raw materials in industrial sectors increases, interest in biomass continues to grow, intensifying competition over biogenic carbon sources. Among renewable energy sources, cellulose—and especially hemicellulose—are considered high-potential raw materials. Cellulose-based ethanol production stands out as an effective alternative to the adverse impacts of fossil-derived fuels. Agricultural and industrial residues such as grass clippings, bamboo, rice straw, empty palm fruit bunches, and sugarcane bagasse are commonly utilized in bioethanol production from cellulosic sources. This study investigates the optimization of bioethanol production using waste from tobacco and tobacco products. Bioethanol production consists of four main stages: pretreatment, hydrolysis, fermentation, and distillation. For the processing of complex raw materials like lignocellulosic biomass, it is necessary to optimize various parameters in each of these stages. Acidic, basic, and enzymatic methods were compared for the hydrolysis of lignocellulosic waste, and enzymatic hydrolysis was found to yield the highest sugar content. Specifically, an enzyme combination of 60% cellulase and 40% hemicellulase produced the most effective results in terms of both total and reducing sugar yields. During the fermentation phase, parameters such as duration, initial sugar concentration, and inoculum amount were optimized using the Response Surface Methodology (RSM). Theoretical and experimental data were compared for product yield calculations, and the highest yield obtained at the end of fermentation was approximately 13.73%.
The results of this study emphasize the importance of converting waste into value-added products in terms of sustainability and suggest that this research may serve as a scientific basis for future large-scale bioethanol production projects.

Keywords: Bioethanol, tobacco waste, enzymatic hydrolysis, fermentation optimization, response surface methodology

➢ *ORAL PRESENTATION*

Efficient Dye Removal Using NH_2 functional polymer gel

Şeyda GETİR[1*] *(https://orcid.org/0000-0003-1194-0308),* Atakan TOPRAK[2] *(https://orcid.org/0000-0003-0080-1456)*

[*1]Zonguldak Bülent Ecevit University, Çaycuma Food and Agriculture Vocational School, Department of Chemistry and Chemical Processing Technologies, Zonguldak, Turkey
[2]Zonguldak Bülent Ecevit University, Çaycuma Food and Agriculture Vocational School, Department of Chemistry and Chemical Processing Technologies, Zonguldak, Turkey

*Corresponding author e-mail:seyda.getir@beun.edu.tr

Abstract

Nowadays, it is necessary to prevent the increasing water pollution caused by dye residues in industrial and agricultural waste, which poses a potential threat to both the environment and human health. As it is known, the separation of dyes is quite tricky due to their complex and stable chemical structures. Removal of these dyes from wastewater is carried out using various physical and chemical methods, including membrane separation, ion exchange, chemical precipitation, and adsorption. Among these, adsorption is widely accepted as a globally appreciated water treatment process due to its versatility, economic feasibility, and broad applicability. In the study, the copolymer of widely found Polymethyl methacrylate (PMMA) with NH_2 functional groups was synthesized. Synthesized PMMA-NH_2 was reacted with $FeCl_3$ by Fridel Krafts to produce Fe-PPMA-NH_2 with increased crosslink formation. Fe-PPMA-NH_2 anionic Congo red (CR) and Methyl orange (MO) dye adsorption and kinetic studies were carried out. The CR and MO adsorption capacities of Fe-PPMA-NH_2 were calculated to be 3984 and 1046 mg/g, respectively. The obtained results showed that Fe-PPMA-NH_2 is a highly effective and promising adsorbent for the adsorption of Congo red (CR) and Methyl orange (MO) from aqueous solutions, thanks to its NH_2 functional groups.

Keywords: Polimer Adsorbent, Dye Adsorption

➢ *ORAL PRESENTATION*

Effects of Olive Leaf Extract on Enzyme Activities of Actinobacteria Isolates and Molecular Identification of Isolates

Fadime Özdemir[1*] (*ORCID: https://orcid.org/0000-0002-8557-5166*), Öznur Bilgin[1] (*ORCID: https://orcid.org/0009-0007-0421-9607*), Fatih Tozoğlu[2] (*ORCID:https://orcid.org/0000-0002-8882-9264*)

[*1] Bilecik Şeyh Edebali University, Faculty of Science, Department of Molecular Biology and Genetics, Bilecik, Turkey.
[2] Bilecik Şeyh Edebali University, Central Research Laboratory, Bilecik, Turkey.

*Corresponding author e-mail: fadime.ozdemir@bilecik.edu.tr

Abstract

The main components of the extract obtained from Olive Leaf are oleuropein and hydroxytyrosol. In particular, oleuropein has been found to possess hypotensive, coronary vasodilatory, and antiarrhythmic activity in animal experiments. Actinobacteria have a wide range of applications in fields such as medicine, agriculture, industry, food, and the detergent industry. In this study, the production capacities of industrially important cellulase, protease and amylase enzymes synthesized by Actinobacteria isolates were determined and the effects of olive leaf extract on these enzyme activities were investigated.
It was found that the addition of olive leaf extract increased cellulase enzyme activity in isolate GBT32, and protease enzyme activity was also increased in the same isolate. Additionally, amylase activity was enhanced in isolates VYN25, and GBT17.
Based on 16S rRNA sequencing studies, isolate GBT17 was found to be related to *Micromonospora cremea*, while isolate VYN25 was related to *Micromonospora hortensis*. Isolates GBTUV4 and GBT32 were found to be related to the genus *Streptomyces*. Isolate GBTUV4 showed close relation to *Streptomyces durocortorensis*, and isolate GBT32 to *Streptomyces badius*.
In conclusion, the results indicate that the studied Actinobacteria isolates possess high biological activity and have potential applications in medicine, agriculture, and various industries such as food, detergent, and paper.

Keywords: Actinobacteria, biologically active substance, 16S rRNA sequence analysis

➢ *ORAL PRESENTATION*

Evaluation of Solvent Type and Concentration on the Extraction Efficiency of Phenolic Compounds from *Urtica dioica*

Hussein Abbas Lazim Maliki[1*] *ORCID: https://orcid.org/ 0000-0002-7378-6468*),
Esra Gökçe Gündüzer[2] *(ORCID: https://orcid.org/0000-0002-4474-7523*)

[*1]Gazi University, Graduate School of Natural and Applied Sciences, Biology Department, Ankara, Türkiye.
[2]Gazi University, Faculty of Science, Biology Department, Ankara, Türkiye.

*Corresponding author e-mail: esragokce@gazi.edu.tr

Abstract

Urtica dioica, commonly known as stinging nettle, is a plant that has been used in traditional medicine for centuries. Its medicinal importance arises from its content of biologically active compounds exhibiting various pharmacological properties. This plant contains a wide range of phytochemicals such as flavonoids, phenolic compounds, terpenoids, and sterols, which are known for their antioxidant, anti-inflammatory, and antimicrobial activities. These properties suggest that *Urtica dioica* could serve as a potential natural source for the prevention and treatment of various diseases. The type and concentration of the solvent used are critical for the efficient extraction of bioactive compounds from plant material. These factors directly influence both the extraction yield and the bioavailability of the extracted compounds. This study aimed to evaluate the effects of different solvent types (water, ethanol, methanol, dichloromethane) and their concentrations (20%, 50%, 70%, and 100%) on the total phenolic content extracted from *Urtica dioica*. Following the extraction process performed using the ultrasonication method, total phenolic contents were quantitatively determined using the Folin–Ciocalteu reagent, and absorbance values were measured with a UV-Visible spectrophotometer. According to the findings, among all tested solvents and concentrations, water (132.97 mg GAE/g) and 20% dichloromethane (136.98 mg GAE/g) extracts yielded the highest total phenolic contents. It was observed that both the solvent type and its concentration significantly affected the total phenolic content. Although optimal extraction yield varied depending on the solvent, in general, solvents with higher polarity were more effective. Moreover, an inverse relationship was noted between solvent concentration and phenolic content; the lowest total phenolic content values were obtained from pure (100%) solvents. These results indicate that water, due to its high polarity and non-toxic nature, is an effective and safe solvent for the extraction of phenolic compounds from *Urtica dioica*, and may be considered suitable for future pharmaceutical applications.

Keywords: *Urtica dioica*, nettle, total phenolic compound, ultrasonic extraction

➢ *ORAL PRESENTATION*

Lignoselülozik Kaynaklı Karbon Kuantum Noktalarının Asidik Ortamda Korozyon İnhibitörü Olarak Geliştirilmesi

Damla Zorcu[1*] , Seden Beyhan[1] (*https://orcid.org/0000-0002-0504-8607)*

[1]İstanbul Teknik Üniversitesi, Fen-Edebiyat Fakültesi, Kimya Bölümü, İstanbul, Türkiye

*Sorumlu yazar e-posta: zorcu18@itu.edu.tr

Özet

Bu çalışmada, defne yapraklarından hidrotermal yöntemle sentezlenen karbon kuantum noktalarının (CQD), 1 M HCl çözeltisinde karbon çeliğinin korozyon davranışı üzerindeki etkisi incelenmiştir. CQD'ler, defne yapraklarının 225 °C'de 24 saat hidrotermal işleme tabi tutulmasıyla elde edilmiştir. Korozyon hızı ve inhibisyon verimliliği, 24 saatlik ağırlık kaybı testleriyle değerlendirilmiştir. CQD içermeyen çözeltide çeliğin ağırlık kaybı 0,4717 g ve korozyon hızı 49,14 $g \cdot m^{-2} \cdot h^{-1}$ olarak ölçülmüştür. CQD konsantrasyonu arttıkça, bu değerlerde belirgin bir azalma gözlemlenmiştir. 1000 mg/L CQD konsantrasyonunda ağırlık kaybı 0,0175 g'a, korozyon hızı ise 1,82 $g \cdot m^{-2} \cdot h^{-1}$'e düşmüş ve %96,29 inhibisyon verimliliği elde edilmiştir. Elektrokimyasal analizler, bu sonuçları desteklemiştir. 500 mg/L CQD içeren, 1 M HCl ortamında açık devre potansiyeli −423,5 mV'den −404,2 mV'ye kaymış, polarizasyon direnci ise 3,11'den 4,68 $\Omega \cdot cm^2$'ye yükselmiştir. Bu durum, CQD'lerin metal yüzeyini daha pasif hâle getirerek korozyon hızını azalttığını göstermektedir. Elde edilen bulgular, defne yaprağı kaynaklı karbon kuantum noktalarının asidik ortamlarda karbon çeliği için etkili bir korozyon inhibitörü olduğunu ortaya koymuştur. Bu çevre dostu yaklaşım, metal yüzeylerin korunmasında sürdürülebilir bir alternatif olarak değerlendirilebilir.

Anahtar Kelimeler: Korozyon, karbon kuantum noktaları, defne yaprağı, hidrotermal sentez, karbon çeliği

➢ *ORAL PRESENTATION*

Genetic Identification of Some Medicinal and Aromatic Hawthorn (*Crataegus* spp.) Species Naturally Distributed in Artvin

Hayal AKYILDIRIM BEĞEN[1] *(https://orcid.org/0000-0003-2028-5827)*, Özgür EMİNAĞAOĞLU[2] *(https://orcid.org/0000-0003-0064-0318)*, Perinçek Seçkinozan ŞEKER[3] *(https://orcid.org/0000-0002-6103-4840)*, Ahmet Yesari SELÇUK[3] *(https://orcid.org/ 0000-0002-2785-2823)*, Batuhan Yaman YAKIN[4] *(https://orcid.org/0000-0003-4570-5111)*, Nasibe Tekiner AYDIN[4] *(https://orcid.org/0000-0003-2396-7786)*, Ayşegül SARAL SARIYER[5] *(https://orcid.org/ 0000-0002-7757-6812)*, Emrah SARIYER[1] *(https://orcid.org/ 0000-0003-1721-0314)*, Damla İpek TOK [6] *(https://orcid.org/0009-0008-8837-6059)*

[1]Health Services, Vocational School, Artvin Çoruh University, Artvin, Türkiye.
[2]Department of Forestry, Artvin Çoruh University, Artvin, Türkiye.
[3]Department of Forestry, Artvin Vocational School, Artvin Çoruh University, 08000 Artvin, Türkiye.
[4]Ali Nihat Gökyiğit Botanical Garden, Artvin Çoruh University, Artvin, Türkiye.
[5]Faculty of Health Sciences, Department of Nutrition and Dietetics, Artvin Çoruh University, Artvin, Türkiye.
*[6] Graduate Education Institute, Artvin Çoruh University, Artvin, Türkiye

*Corresponding author e-mail: ipekdamla98@gmail.com

Abstract

Hawthorn (*Crataegus*) species, which are of high importance in terms of medicinal and aromatic properties, are widely used as food, dietary supplements, and phytopharmaceutical products, and also hold significant economic value. Particularly in Europe and China, the leaves, flowers, and fruits of *Crataegus* species are offered for over-the-counter sale in the form of herbal drugs, tinctures, tablets, teas, and extracts. Species with large fruits, such as *C. azarolus* subsp. *pontica,* are especially important in the Caucasus and Mediterranean countries for both traditional local consumption and small-scale commercial production. In Türkiye, the genus is represented by approximately 29 species. The presence of rich ecosystems in the province of Artvin provides a favorable environment for the natural distribution of hawthorn species. The natural occurrence of these species in the region constitutes an important local genetic resource in terms of species diversity and ecosystem sustainability. The DNA barcoding technique, one of the modern molecular biology methods, has proven successful not only in identifying living species and discovering unknown ones, but also in verifying the authenticity of processed or unprocessed food products of commercial importance, and in detecting food fraud in already produced and marketed items. In this study, the goal is to genetically identify four different hawthorn species (*Crataegus* spp.) naturally distributed in and around Artvin by generating sequence data from three different gene regions (ITS, matK, rbcL), and to create a reference dataset for these species. The DNA sequences obtained from these gene regions have been uploaded to reference databases such as NCBI and BOLD Systems. Additionally, the study aims to contribute to the establishment of a National DNA Barcode Database by completing the DNA barcoding processes for four plant species prioritized for the project that naturally occur in Artvin, and registering them on behalf of Türkiye.

Keywords: Artvin, *Crataegus*, DNA Barkoding, Medicinal-Aromatic, Türkiye

➢ *ORAL PRESENTATION*

Ethnobotanical Uses and the Medicinal - Economic Significance of *Valeriana* Species

Hayal AKYILDIRIM BEĞEN[1] (*https://orcid.org/0000-0003-2028-5827)* Özgür EMİNAĞAOĞLU[1] (*https://orcid.org/0000-0003-0064-0318)* Damla İpek TOK *[2] (*https://orcid.org/0009-0008-8837-6059)*

[1] Ali Nihat Gökyiğit Botanical Garden Application and Research Center, Artvin Coruh University, Artvin, Türkiye
*[2] Graduate Education Institute, Artvin Çoruh University, Artvin, Türkiye

*Corresponding author e-mail: ipekdamla98@gmail.com

Abstract

The genus *Valeriana* (Caprifoliaceae) represents a significant group of plants, comprising 441 species worldwide. The genus name is believed to derive from the medieval term rooted in the Latin word valere, meaning "to be healthy," likely referring to the plant's traditional medicinal uses for conditions such as nervousness and hysteria. Among them, species like *Valeriana officinalis* (commonly known as medicinal valerian) are frequently investigated in pharmacological studies due to their sedative, anxiolytic, and antispasmodic effects. Clinical studies have demonstrated that root extracts of *V. officinalis* reduce anxiety and sleep disorders. In aromatherapy, valerian essential oil is used in diffusers and massage oils for its calming effects. From an economic standpoint, *Valeriana* products represent a market valued at over $100 million annually in the global herbal medicine sector. Türkiye is an important center of diversity for the genus *Valeriana,* hosting 15 species. Of these, 12 are endemic and are primarily distributed across the microhabitats of Anatolia. Common species in Türkiye, such as *V. dioscoridis* (in the Mediterranean region) and *V. alliariifolia* (in rocky habitats), have been frequently studied in ecological, medicinal and taxonomic research. These are perennial herbaceous plants characterized by their fragrant leaves, stems, flowers, and roots. According to inventory studies on medicinal and aromatic plants in Türkiye, valerian species are predominantly used as sedatives, and in the treatment of digestive disorders, nausea, and menstrual cramps. *Valeriana officinalis*, in particular, is commonly used as a sleep aid. In the context of medicinal plant trade in Türkiye, species such as *Valeriana dioscoridis* and *V. officinalis* are utilized in the natural products and dietary supplements industries. However, due to overharvesting and habitat loss, wild populations of some species are under threat, highlighting the growing importance of sustainable agricultural practices.

Key Words: Artvin, herbal usage, Medicinal-Aromatic, Türkiye, *Valeriana*

➢ *ORAL PRESENTATION*

Performance Analysis of Metaheuristic Algorithms in the Parameter Tuning of BLDC Motor PID Controllers

Abdulkadir YILMAZ[1] (0009-0000-4449-8435), Murat DEMİR[2] (ORCID:0000-0003-4407-9673)

[1] National Defence University, Air Non-Commissioned Officer Vocational School, Aviation Sciences, İzmir, Türkiye
[2] İzmir Bakırçay University, Faculty of Engineering and Architecture, Electrical-Electronics Engineering, İzmir, Türkiye

Corresponding author e-mail: abdulkadir.yilmaz2@msu.edu.tr

Abstract

Brushless DC (BLDC) motors are widely preferred in industrial applications due to their high efficiency, long service life, and low maintenance requirements [1]. Proportional–Integral–Derivative (PID) controllers are frequently employed for precise speed control in such systems. However, manual tuning of PID parameters often results in time-consuming and suboptimal outcomes, particularly in nonlinear systems [2]. In this study, four different metaheuristic algorithms were investigated for the optimal tuning of PID controller parameters: Genetic Algorithm (GA) [3], Particle Swarm Optimization (PSO) [4], Grey Wolf Optimizer (GWO) [5], and Red Panda Optimization (RPA) [6].
The simulations were carried out in MATLAB/Simulink, and performance was evaluated based on settling time, overshoot, and mean squared error (MSE) criteria [7]. A comparative analysis was conducted by assessing the convergence speed and accuracy of each algorithm. The results indicate that GWO and RPA demonstrated superior performance in terms of faster convergence and lower MSE values. Notably, the application of RPA in this domain remains limited in the literature, making the findings of this study a novel contribution [6].
This work highlights the effectiveness of metaheuristic algorithms in PID controller design for BLDC motor applications. Moreover, it provides a comparative framework that aids in selecting appropriate optimization strategies by balancing classical and next-generation approaches.

Keywords: Brushless DC motor, optimization, PID controller, metaheuristic algorithms, speed control

References:
[1] Krishnan R. (2010). Permanent Magnet Synchronous and Brushless DC Motor Drives. CRC Press. DOI:10.1201/9781420014235
[2] Åström KJ, Hägglund T. (2006). Advanced PID Control. ISA.
[3] Holland JH. (1992). Adaptation in Natural and Artificial Systems. MIT Press.
[4] Kennedy J, Eberhart R. (1995). Particle Swarm Optimization. In: Proc. IEEE ICNN.
[5] Mirjalili S, Mirjalili SM, Lewis A. (2014). Grey wolf optimizer. Advances in Engineering Software, 69:46–61. DOI:10.1016/j.advengsoft.2013.12.007
[6] Gautam S, Pradhan AK. (2022). Red Panda Optimization (RPO): A novel nature-inspired metaheuristic algorithm. Expert Systems with Applications, 200:117004.
[7] Ogata K. (2010). Modern Control Engineering (5 ed.). Prentice Hall.

➢ *ORAL PRESENTATION*

Traditional Plants Used For Medicinal-Aromatic Purposes in South Villages of Ardanuc, Artvin (Türkiye)

Özgür EMINAGAOGLU[1*] *(https://orcid.org/0000-0003-0064-0318)*, Hayal AKYILDIRIM BEGEN[1] *(https://orcid.org/0000-0003-2028-5827)*, Funda ERSEN BAK[2] *(https://orcid.org/0000-0003-2659-3310)*, Melahat OZCAN[2] *(https://orcid.org/0000-0002-2638-3914)* Nasibe TEKINER AYDIN[1] *(https://orcid.org/0000-0003-2396-7786)* Sevval SALIOGLU[2] *(https://orcid.org/0000-0002-7601-5140)*, Canan ACIKGOZ HARSIT[2] *(https://orcid.org/0000-0002-7174-1936)*, Emine YAZICIOGLU[1] *(https://orcid.org/0000-0001-9856-9374),* Bahar ASLAN[1] *(https://orcid.org/0000-0002-7454-3943)*

[1] Artvin Coruh University, Ali Nihat Gökyigit Botanical Garden Application and Research Center, Artvin, Türkiye
[2] Artvin Coruh University, Faculty of Forestry, Department of Forest Engineering, Artvin, Türkiye

*Corresponding author e-mail: oeminagaoglu@artvin.edu.tr

Abstract

A variety of traditional medicinal plants has been widely used by different indigenous people in Türkiye. This study, which was conducted between 2021 and 2023 to record the traditional medicinal plant usage culture of the inhabitants of South Villages of Ardanuç (Aydınköy, Ballı, Bereket, Ekşinar, Ferhatlı, Gümüşhane, Meşeköy, Ovacık, Örtülü, Peynirli, Sakarya, Tepedüzü, Torbalı, Tosunlu, Zekeriyaköy) was the first to be conducted in the district. face-to-face interviews with individuals with advanced ethnobotanical knowledge were conducted in the villages (15) of the district, and the medicinal plants which were used were gathered and identified. Besides descriptive statistics, the data were analyzed using some ethnobotanical analysis tools like preference ranking, paired comparison, direct matrix ranking, informant consensus factor, and fidelity level index. The information gathered as a result of the interviews with participants was recorded for this purpose. A total of 105 species of medicinal plants were identified and collected with 90 genera and 46 families were used to treat 44 different diseases. The most used medicinal plants were from the family Rosaceae followed by Urticaceae, and Asteraceae. The usage value (UV) was calculated for each species. Out of these, 70 species (66.67%) were used against human ailments. The most frequently used plant part was fruit (26.69%), followed by leaves (20.61%), and herba (15,71%). The most widely used method of preparation was uncooked (30.51%) followed by decoction (17.63%). The most common route of administration was oral (71,64%) followed by dermal (28.36%). The disease category with FIC value (0.76) was the skin diseases. *Berberis vulgaris* was the most preferred species. Anthropogenic factors are the major threats to medicinal plants. In general, the study area is rich in medicinal plants that have a significant role in the management of various human and livestock diseases.

Keywords: Artvin, Ardanuç, Medicinal-Aromatic Plants, Traditional

Acknowledgement: This study was carried out within the scope of the Project titled ‘Artvin’de Tıbbi Aromatik Bitki Potansiyel Alanlarının Belirlenmesi (Envanteri), Halkın Bilgi Düzeyinin Ölçülmesi, Canlı Materyal ve Tohum Temini (Determination (Inventory) of Potential Areas for Medicinal and Aromatic Plants in Artvin, Measurement of Public Awareness Level, Provision of Living Materials and Seeds)’, numbered 2021-TAB-01, carried out at Artvin Çoruh University.

References:

Eminağaoğlu Ö (ed) (2015). *Artvin'in Doğal Bitkileri*. İstanbul: Promat.
Eminağaoğlu, Ö. (Ed) (2023). *Artvin’in Tıbbi-Aromatik Bitkileri.* Artvin: Zafer Medya.
Eminağaoğlu, Ö. (Ed) (2012). *Artvin'de Doğa Mirası, Camili'nin Doğal Bitkileri*

➢ *ORAL PRESENTATION*

The Modification of Partial Oxidation Based Magnetic Nanoparticles with Cyclodextrin and Application in Magnetic Hyperthermia

Miray Senkal[1*] (*https://orcid.org/0009-0000-5725-4157)* Cem L. Altan[1] (*https://orcid.org/0000-0002-1347-5772)*

[1]Yeditepe University, Faculty of Engineering, Chemical Engineering Department, Istanbul, Turkey.

*Corresponding author e-mail: miray.senkal@yeditepe.edu.tr

Abstract

Magnetic iron oxide nanoparticles are one of the most preferred materials for nanotechnology-based applications due to their excellent magnetic properties along with extremely adequate biocompatibility. The efficient incorporation of magnetic nanoparticles to relevant applications relies on utilization of specific surface functionalization. The surface modification allows both the binding of niche molecules to the surface and enhance the colloidal stability. β-Cyclodextrin (β-CD) is a cyclic oligosaccharide consisting of both a hydrophilic outer surface and a hydrophobic cavity. The structural characteristics of this system facilitate the formation of complexes with a range of hydrophobic guest molecules, including drugs. These guest molecules can be encapsulated within the non-polar cavity of β-CD, thereby rendering β-CD a highly versatile platform for applications in the controlled release of drugs. Although, magnetic nanoparticles are shown to be modified with several molecules for biomedical applications, the surface functionalization of relatively larger and unconventional partial oxidation based magnetic nanoparticles with β-CD has not been studied extensively. Consequently, the objective of this study was to synthesize magnetic nanoparticles in the presence of β-CD possessing adequate colloidal stability in aqueous medium and subsequently analyze its potential in hyperthermia applications via studying the local temperature enhancements at varying concentrations, magnetic field strengths and frequencies. The results demonstrated that the magnetic nanoparticles synthesized using the partial oxidation method exhibited an average size of 27 nm and a saturation magnetization of 48.4 emu/g. Furthermore, the obtained nanoparticles exhibited sufficient colloidal stability and morphological changes after modification with β-CD. In addition, hyperthermia analyses conducted in the presence of an alternating magnetic field have indicated that local temperatures increased in conjunction with concentration, magnetic field strength, and frequency. The findings demonstrate the preliminary possibility of magnetic nanoparticles modified with β-CD and synthesized using the partial oxidation method for utilization in both drug delivery and hyperthermia applications.

Keywords: Magnetic nanoparticles, Cyclodextrin, Hyperthermia

➢ *ORAL PRESENTATION*

Synthesis and characterization of the poly(ε-caprolactone-g-styrene) three arm block-brush copolymer via RAFT bulk polymerization

Melahat Göktaş*[1], Ümran Aslan[2], Cengiz Aykaç[3]

[1]Van Yüzüncü Yıl University, Faculty of Education, Department of Chemistry, Van, 65080 Turkey
[2,3]Van Yüzüncü Yıl University, Institute of Science, Van, 65080 Turkey

*Corresponding author: E-mail: melahat_36@hotmail.com

Abstract

The graft copolymers can be designed by grafting another polymer chain or monomer to the active center of the polymer chain and are a important class of the macromolecular structure [1,2]. Reversible addition/fragmentation chain transfer (RAFT) polymerization is one of the CRP techniques which introduced by the Rizzardo and co-worker [3]. This polymerization technique based on the radical closing mechanism and the molecular control of the copolymers which prepared via RAFT is achieved by chain transfer agent (RAFT-agent). In this study, three arm block-brush copolymer was prepared by a combination of ring- opening polymerization (ROP) and RAFT bulk polymerization in two-step procedure. For this purpose, macropolymeric ester based RAFT agent (multifunctional macro-RAFT agent) was obtained from reaction of the brominated/chlorine-terminated poly(ε-caprolactone) (PCL-Br/Cl) which synthesized by ROP of the ε-caprolactone and ethylxanthic acid potassium salt. Then, the poly(ε-caprolactone-*g*-styrene) [(PCL-*g*-PSt)] three arm block-brush copolymer was synthesized via RAFT bulk polymerization using multifunctional macro-RAFT agent based on PCL. This polymerization was carried out at 80 °C by changing the polymerization time and investigation of the polymerization time and polymerization temperature on the molecular weight, monomer conversion and dispersity. As a result of this polymerization, very high molecular weight polymers with low dispersity were obtained. The products were characterized by using multi-instruments such as proton nuclear magnetic resonance spectroscopy, Infrared spectroscopy, gel permeation chromatography, thermo gravimetric analysis, differential scanning calorimetry.

References

1. Göktaş M, Aykaç C, Hazer B and A Richard D (2024), *J. Polym. Environ*. 32:2629–2643
2. Göktaş M, Aslan Ü (2024), *Polym. Bull.* 81:11127–11143.
3. Chiefari J, Chong Y K, Ercole F, Krstina J, Jeffery J, Le TPT, Mayadunne RTA, Meijs GF, Moad CL, Moad G, Rizzardo E, Thang SH (1998), Macromolecules 31:5559-5562.

➢ *ORAL PRESENTATION*

Uçak Bakım Ve Onarım Verileri İle İstatistiksel Uygulama

ONUR BATIN DOĞAN[1]* (ORCID: https://orcid.org/0000-0003-4632-2884),
FATMA SEVİNÇ KURNAZ[1] (ORCID: https://orcid.org/0000-0002-5958-7366)

*[1]Yıldız Teknik Üniveristesi, Fen Edebiyat Fakültesi, İstatistik, İstanbul, Türkiye.

*Sorumlu yazar e-posta: onurbatindogan@gmail.com

Özet

Uçak Bakım, Onarım ve Yenileme (Maintenance, Repair, and Overhaul- MRO), sektörü havacılık açısından operasyonel süreklilik ve maliyet etkinliği açısından kritik öneme sahiptir. Uçak komponentlerinin alış fiyatlarının doğru bir şekilde öngörülmesi, pazar dinamikleri, parça özellikleri, tedarikçi çeşitliliği ve talep değişkenliği gibi çok sayıda faktörden etkilenmesi nedeniyle karmaşık bir problem teşkil etmektedir. Geleneksel fiyat tahmin yöntemleri bu faktörler arasındaki doğrusal olmayan ve dinamik ilişkileri yakalamada sıklıkla yetersiz kalmaktadır.
Çalışmanın temel amacı MRO sektöründe uçak komponentlerinin alış fiyatlarını yüksek doğrulukla tahmin etmek üzere bir derin öğrenme modeli geliştirmek ve performansını değerlendirmektir. Bu amaç doğrultusunda geçmiş satınalma kayıtları komponent teknik detayları tedarikçi verileri ve ilgili pazar göstergelerini içeren kapsamlı bir veri seti derlenmiştir. Çalışmada farklı derin öğrenme mimarileri incelenmiş ve en uygun yapı belirlenmiştir.
Derin öğrenme yaklaşımının çok boyutlu ve karmaşık veri setlerindeki gizli örüntüleri ve faktörler arası etkileşimleri etkin bir şekilde modelleyebilme kabiliyeti sayesinde geleneksel yöntemlere kıyasla fiyat tahmin doğruluğunu önemli ölçüde artırması beklenmektedir. Bu araştırma MRO şirketlerine komponent tedarik ve tamir süreçlerinde daha bilinçli kararlar alma, bütçeleme süreçlerini iyileştirme ve maliyet optimizasyonu sağlama potansiyeli taşıyan veri odaklı bir yaklaşım sunmaktadır. Çalışma derin öğrenme tekniklerinin MRO tedarik zinciri yönetimindeki pratik uygulamalarına ve potansiyel faydalarına ışık tutmayı hedeflemektedir.

Anahtar Kelimeler: Uçak Bakım Onarım ve Yenileme, havacılık, derin öğrenme, fiyat tahmini

➢ *ORAL PRESENTATION*

Traditional plant uses in the villages surroundings of Karagöl-Sahara National Park

Özgür EMINAGAOGLU*,2 *(https://orcid.org/0000-0003-0064-0318)*, Melahat OZCAN[1] *(https://orcid.org/0000-0002-2638-3914)* Funda ERSEN BAK[1] *(https://orcid.org/0000-0003-2659-3310)*, Hayal AKYILDIRIM BEGEN[2] *(https://orcid.org/0000-0003-2028-5827)*, Sevval SALIOGLU*[1] *(https://orcid.org/0000-0002-7601-5140)*, Nasibe TEKINER AYDIN[2] *(https://orcid.org/0000-0003-2396-7786)* Canan ACIKGOZ HARSIT[1] *(https://orcid.org/0000-0002-7174-1936)*, Emine YAZICIOGLU[2] *(https://orcid.org/0000-0001-9856-9374),* Bahar ASLAN[2] *(https://orcid.org/0000-0002-7454-3943)*

[1] Artvin Coruh University, Faculty of Forestry, Department of Forest Engineering, Artvin, Türkiye

[2] Artvin Coruh University, Ali Nihat Gökyigit Botanical Garden Application and Research Center, Artvin, Türkiye

*Corresponding author e-mail: oeminagaoglu@artvin.edu.tr

Abstract

Most indigenous people in the world, as well as in Türkiye have used medicinal and aromatic plants to treat many diseases. Plant diversity is very rich in Şavşat district of Artvin Province and it is understood from the reports that Şavşat people used and rely on them different purposes, including health issues. In this study, we investigated the traditional uses of medicinal and aromatic plants, including their uses herbal mixtures¸ modes of preparation, commonly used plant parts and disease categories treated with documented plant species. In this investigation, we aimed to examine the traditional uses of medicinal-aromatic plants in the villages surroundings of Karagöl-Sahara National Park of Şavşat District. This study carried out to record the traditional medicinal plant usage culture of the inhabitants with face-to-face interviews local inhabitants from 10 villages of the district having advanced ethnobotanical knowledge. The information gathered as a result of the interviews with 63 participants was recorded. Disease categories treated with documented plant species, using ethnobotanical indices such as Fledity Level (FL), relative frequency citation (RFC), and informant consensus factor (ICF). In total, 106 medicinal-aromatic plant taxa belonging to 83 genera and 43 families using in different ethnobotanical purposes were identified and collected. Out of these, 73 species (68.87%) were used against human ailments. The most frequently used plant part was fruit (52) (49.06%), followed by leaves (50) (47,16%), and the whole plant material was (28) (24.42%). The human ailment category with the highest Informant Consensus Factor (ICF) value was the skine disorders (0.85) and Musculoskeletal disease (0,79) respectively. Most cited medicinal and aromatic plants were determined as *Urtica dioica* L. The highest ICF value was detected for skin disorders (0.85), We determined that *Urtica dioica* L., *Plantago major* L. and *Malus sylvestris* L. have widely traditional uses, with high using reports.

Keywords: Artvin, Şavşat, Medicinal and Aromatic Plants, Traditional uses, Türkiye.

Acknowledgement: The study was funded by the project etitled “Identification of Potential Areas for Medicinal and Aromatic Plants in Artvin (Inventory), Measurement of Public Awareness, Procurement of Live Material and Seeds” (Project number: 2021-TAB-01) and supported within the scope of the project themed “Regional Development Oriented Mission Differentiation and Specialization of Universities”. We would like to thank the Presidency of Strategy and Budget of the Republic of Turkiye for their support.

➢ *ORAL PRESENTATION*

Sürdürülebilir Enerji Yönetimi için IoT Çözümü: Raspberry Pi, Docker ve Bulut Tabanlı İzleme Mimarisi

Hüseyin Parmaksız[1*](*ORCID:* https://orcid.org/0000-0001-8455-5625), Emine Nur Çalı[1] (*ORCID: https://orcid.org/0009-0000-9626-0496*), Zeynep Özer[1] (*ORCID:* https://orcid.org/0009-0001-9383-229X)

[*1]Bilecik Şeyh Edebali Üniversitesi, İktisadi ve İdari Bilimler Fakültesi, Yönetim Bilişim Sistemleri Bölümü, Bilecik, Türkiye.

[*]Sorumlu yazar e-posta: huseyin.parmaksiz@bilecik.edu.tr

Özet

EIA [1], IRENA [2], TotalEnergies [3], McKinsey [4] ve ExxonMobil [5,6] tarafından yayınlanan raporlar, enerji tüketiminin önümüzdeki yıllarda önemli ölçüde artacağını ve bu artışın sürdürülebilirlik için ciddi riskler oluşturabileceğini ortaya koymaktadır. Artan küresel enerji talebi, sürdürülebilirlik hedefleri ve uzaktan erişilebilir izleme çözümlerine duyulan ihtiyaç, enerji yönetim sistemlerinde yeni nesil yaklaşımları gerekli kılmaktadır. Bu gereksinimlere yanıt olarak, bu çalışma düşük maliyetli, modüler, yerel ve bulut tabanlı bir enerji izleme sistemi önermektedir. Kenar hesaplama sistemi, Raspberry Pi üzerinde çalışan Raspbian OS Lite (bookworm) ve Docker konteyner mimarisi üzerine inşa edilmiştir. DHT11 ortam sıcaklığı ve nem verilerini toplarken, PZEM-004T (v3.0) [7] modülü akım, voltaj ve enerji tüketimi verilerini toplamaktadır. Toplanan veriler, MQTT [8] protokolü aracılığıyla güvenli bir şekilde (TLS/SSL ile şifrelenmiş biçimde) Amazon Web Services (AWS) bulut altyapısına iletilmekte; kenar hesaplama (edge computing) ise Docker konteynerleri içerisinde çalışan InfluxDB veri tabanında zaman serisi formatında depolanmaktadır. Bu veriler, yine Docker üzerinde barındırılan Grafana arayüzü kullanılarak gerçek zamanlı analiz edilmekte ve görselleştirilmektedir. Olağandışı durumlar, AWS Simple Email Service (SES) tabanlı e-posta bildirim sistemi aracılığıyla ilgililere anlık olarak iletilmekte; bu sayede hızlı müdahale süreçlerini başlatan yanıt mekanizmaları etkin bir şekilde devreye alınmaktadır. Telegram Bot API ile bildirim mekanizması yedeklenmektedir. Çalışmanın genel mimari yapısı Şekil 1'de sunulmuştur. Çalışma, bireysel kullanıcılar ve KOBİ'ler için uygulanabilir bir çözüm sunarak enerji verimliliği, çevresel sürdürülebilirlik ve siber güvenlik risklerine katkıda bulunmaktadır. Ayrıca çalışmanın modüler yapısı ve genişletilebilir mimarisi; akıllı ev otomasyonu, elektrikli araçlar, OCPP destekli şarj istasyonları, yenilenebilir enerji sistemleri, endüstriyel IoT uygulamaları, mikro şebeke entegrasyonları gibi çeşitli enerji yönetimi senaryolarında kullanılma potansiyeli sunmakta olup, bu alanlarda geliştirilecek yeni nesil enerji yönetim sistemlerine rehberlik edebilir yapıdadır. Özellikle mimarinin esnek tasarımı, sadece enerji yönetimiyle sınırlı kalmayıp, donanımsal anomali tespiti gibi siber güvenlik uygulamalarında da değerlendirilebilecek bir altyapı sunmaktadır. Bu sayede IoT cihazlarından kaynaklı olağandışı veri davranışları erkenden tespit edilerek, sistem güvenliği proaktif şekilde sağlanabilmektedir.

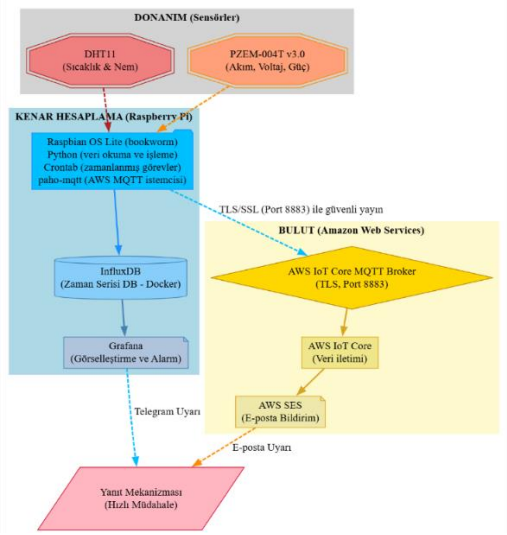

Şekil 1. IoT, Docker, MQTT ve bulut tabanlı izleme ve uyarı sistemi.

Anahtar Kelimeler: Kenar hesaplama, IoT, Docker, Bulut bilişim, Siber güvenlik.

Referanslar

[1] U.S. Energy Information Administration. (2023). *International energy outlook 2023*. https://www.eia.gov/outlooks/ieo/pdf/IEO2023_Narrative.pdf

[2] International Renewable Energy Agency. (2023). *World energy transitions outlook 2023: 1.5 °C pathway* (Vol. 1). International Renewable Energy Agency. https://solarquarter.com/wp-content/uploads/2023/07/1688542036127.pdf

[3] TotalEnergies. (2023). Energy outlook 2023.https://totalenergies.com/system/files/documents/2023-11/EN_CP_TEO_2023.pdf

[4] McKinsey & Company. (2024). *Global energy perspective 2024*. https://www.mckinsey.com/industries/energy-and-materials/our-insights/global-energy-perspective

[5] ExxonMobil. (2023). *2023 global outlook: Executive summary*. https://corporate.exxonmobilresources.com/-/media/global/files/global-outlook/2023/2023-global-outlook-executive-summary.pdf

[6] ExxonMobil. (2024). *Global outlook: Our view to 2050*. https://corporate.exxonmobil.com/sustainability-and-reports/global-outlook#Projectionsandkeytakeaways

[7] Yasa, K. A., Purbhawa, I. M., Yasa, I. M. S., Teresna, I. W., Nugroho, A., & Winardi, S. (2023). IoT-based electrical power recording using ESP32 and PZEM-004T microcontrollers. *Journal of Computer Science and Technology Studies, 5*(4), 62–68. https://doi.org/10.32996/jcsts.2023.5.4.7

[8] Chen, Y., Sumiyoshi, D., Sakai, R., Yamamoto, T., Ueno, T., & Oh, J. (2024). *Development of low-cost IoT units for thermal comfort measurement and AC energy consumption prediction system (arXiv preprint arXiv:2411.19536)*. arXiv. https://doi.org/10.48550/arXiv.2411.19536

➢ *ORAL PRESENTATION*

An Important Step Towards Rural Development: Medicinal-Aromatic Plant Cultivation Studies in Artvin

Özgür EMİNAĞAOĞLU[1*] (*ORCID: https://orcid.org/0000-0003-0064-0318*), Hayal AKYILDIRIM BEĞEN[2] (*ORCID: https://orcid.org/0000-0003-2028-5827*), Melahat ÖZCAN[1] (*ORCID: https://orcid.org/0000-0002-2638-3914*), Emine YAZICIOĞLU[3] (*ORCID: https://orcid.org/0000-0001-9856-9374*), Nasibe TEKİNER AYDIN[3] (*ORCID: https://orcid.org/0000-0003-2396-7786*), Şevval SALİOĞLU[1] (*ORCID: https://orcid.org/0000-0002-7601-5140*), Canan AÇIKGÖZ HARŞIT[1] (*ORCID: https://orcid.org/0000-0002-7174-1936*), Bahar ASLAN[3] (*ORCID: https://orcid.org/0000-0002-7454-3943*)

[*1]Artvin Çoruh University, Faculty of Forestry, Department of Forest Engineering, Artvin, Türkiye.
[2]Artvin Çoruh University, Health Vocation School, Programme of Medical Laboratory Techniques, Artvin, Türkiye.
[3]Artvin Çoruh University, Ali Nihat Gökyiğit Botanical Garden Aplication and Research Center, Artvin, Türkiye.

*Corresponding author e-mail: oeminagaoglu@artvin.edu.tr

Abstract

Artvin is rich in terms of medicinal-aromatic plant biodiversity. Uncontrolled collection of medicinal plants from nature may pose a danger of extinction for these species. The need to cultivate these plants comes to the fore as a way to meet the demand for medicinal plants. The study aims to determine their ecological requirements, create suitable cultivation areas, collect live plant materials and seeds of the target species, conduct soil analyses, establish a production greenhouse, distribute seedlings to the local community free of charge, provide training on cultivation, and set up Model Gardens in suitable areas identified in eight different districts of Artvin for the cultivation of these species. In the project aimed at developing medicinal-aromatic plant cultivation, cultivation continues using seeds, cuttings, and live plant specimens collected during field studies. Of the 54 species, 43 herbaceous species have been planted in the raised beds, while the remaining 11 woody species have been planted in suitable areas within the TAB plots. Soil texture, soil reaction (pH) and salinity (EC), organic matter content, analyses were conducted on 162 samples from 11 different areas. Model garden projects have been created for trees, shrubs, climbers, and herbaceous medicinal-aromatic species. Detailed photographs of the collected seeds have been taken with the imaging system set up in the Artvin Çoruh University Herbarium (ARTH) and uploaded into the system. Studies on creating a virtual seed bank are ongoing. For the germination of the seeds, direct sowing and soaking in distyle water for 24 hours in 500 and 1000 ppm Gibberellic acid solutions were applied. Peat, Peat + Perlite was used as seed growth media. While the emergence rate varied between 5-10% in control and distyle water soaking treatment, over 90% was obtained in *Helichrysum orientale* and *Inula orientalis* seeds with 1000 ppm GA_3 treatment and peat media.

Keywords: Artvin, model garden, cultivation, medicinal-aromatic plant, natural plants, Türkiye

Acknowledgement: This study was produced from the project numbered 2021-TAB-05 titled “Development of Medicinal and Aromatic Plant Cultivation” supported by the Presidency of the Republic of Türkiye Strategy and Budget Directorate within the scope of the project themed “Regional Development Oriented Mission Differentiation and Specialization of Universities”. We would like to thank the Presidency of Strategy and Budget of the Republic of Türkiye for their support.

➢ *ORAL PRESENTATION*

Immobilization of Urease on Cellulose Nanocrystals via Different Modifications

Elif TOKU[1,2,3*] (*ORCID: https://orcid.org/0009-0006-4836-9888*), Özlem ALPTEKİN[2] (*ORCID: https://orcid.org/0000-0002-0458-7609*), Serap YALIN[3] (*ORCID: https://orcid.org/0000-0002-1286-2172)*

[*1] Mersin University, Institute of Health Sciences, Department of Biochemistry, Mersin, Türkiye
[2] Çukurova University, Faculty of Pharmacy, Department of Biochemistry, Adana, Türkiye
[3] Mersin University, Faculty of Pharmacy, Department of Biochemistry, Mersin, Türkiye

*Corresponding author e-mail: eliftoku01@gmail.com

Abstract

Immobilization of enzymes is an effective method for improving the properties and applications of enzymes. Various support materials are used for enzyme immobilization, and cellulose nanocrystals (CNC), with their eco-friendly structure and biocompatible nature, are among the notable cellulose nanomaterials for this purpose. Urease (urea amidohydrolase, EC 3.5.1.5) is an enzyme that catalyzes the hydrolysis of urea into ammonia and carbon dioxide. In this study, Jack bean urease was immobilized onto CNC by different immobilization methods. CNC was activated with 3-aminopropyltriethoxysilane (3-APTES) then modified with glutaraldehyde (GA). Urease was immobilized onto this modified support by covalent immobilization ($IU_{CNC\text{-}GA}$). CNC modified with GA was further functionalized separately with polyethyleneimine (PEI) and 1,2-bis(3-aminopropylamino)ethane (1,2BIS). These modified supports were used for ionic adsorption of urease ($IU_{CNC\text{-}PEI}$ and $IU_{CNC\text{-}1,2BIS}$). The urease immobilization was carried out in 50 mM phosphate buffer at pH 7.0 and 25 °C for 2 hours. The amount of immobilized urease was determined as 1.5 mg/g support, 1.9 mg/g support and 2.5 mg/g support for $IU_{CNC\text{-}GA}$, $IU_{CNC\text{-}PEI}$, and $IU_{CNC\text{-}1,2BIS}$, respectively. The amount of immobilized urease affected the modification methods of CNC. The characterization of immobilized urease will be carried out.

Keywords: Cellulose nanocrystals, CNC, urease, immobilization

Acknowledgments

*This paper is derived from a master's thesis.

- This study was supported by the Scientific Research Projects Unit of Mersin University. Project Number: 2024-TP2-5043
- This study was supported by the Scientific and Technological Research Council of Turkey (TÜBİTAK).
  Project Number: 124Z971

References:

1. Aggarwal, S., & Ikram, S. (2025). Aluminum oxide nanoparticles-impregnated aminated silica surfaces for covalent immobilization of urease via glutaraldehyde activation: Stability and kinetic studies. *ChemistrySelect, 10*, e202405033.
2. Al-Garawi, Z. S., Taha, A. A., Abd, A. N., & Tahir, N. T. (2022). Immobilization of urease onto nanochitosan enhanced the enzyme efficiency: Biophysical studies and in vitro clinical application on nephropathy diabetic Iraqi patients. *Journal of Nanotechnology,* 8288585.
3. Alptekin, Ö. (2022). Characteristics of immobilized urease onto modified zirconium (IV) oxide via glutaraldehyde: Kinetic, stability, and operational stabilities in bioreactors. *Chemical Papers, 76*, 749–761.
4. Khalid, W., Heng, L., & Arip, M. (2018). Surface modification of cellulose nanomaterial for urea biosensor application. *Sains Malaysiana, 47*(5), 941–949.
5. Tükel, S. S., & Alptekin, Ö. (2004). Immobilization and kinetics of catalase onto magnesium silicate. *Process Biochemistry, 39*(12), 2149–2155.

➢ *ORAL PRESENTATION*

Contribution of Artvin Coruh University to Regional Development: Establishment of a Facility for Processing and Storing Aromatic Plants in Artvin

Özgür Eminağaoğlu[1] (https://orcid.org/0000-0003-0064-0318), Hayal Akyıldırım Beğen[1] (https://orcid.org/0000-0003-2028-5827), Alper Durmaz[1] (https://orcid.org/0000-0001-6927-3283), Kamil Öztürk[2] (https://orcid.org/0000-0003-2036-9780), Zehra Eminağaoğlu[3] (https://orcid.org/0000-0003-4337-6860), Abdüssamed Kabakuş[4] *(https://orcid.org/0000-0002-3049-9493),* Şevval Salioğlu[5] (https://orcid.org/0000-0002-7601-5140), Canan Açikgöz Harşit[5] (https://orcid.org/0000-0002-7174-1936), Hayrettin İlker Özdemir[6] (https://orcid.org/0000-0002-5480-7227), Bahar Aslan[1] (https://orcid.org/0000-0002-7454-3943), Çağlar Yazici[7]

*[1]Artvin Çoruh University, Ali Nihat Gökyiğit Botanical Garden Application and Research Center, Artvin, Türkiye
[2]Artvin Çoruh University, Medicinal and Aromatic Plants Application and Research Center, Artvin, Türkiye
[3]Artvin Çoruh University, Department of Architecture, Faculty of Art and Design, Artvin, Türkiye
[4] Artvin Çoruh University, Artvin Vacational School, Artvin, Türkiye
[5]Artvin Çoruh University, Department of Forest Engineering, Faculty of Forestry, Artvin, Türkiye
[6]Aydın Adnan Menderes University, Koçarlı Vocational School, Department of Plant and Animal Production, Aydın, Türkiye
[7]Artvin Çoruh University, Department of Construction and Technical Affairs, Artvin, Türkiye

*Corresponding author e-mail: cananacikgozharsit@artvin.edu.tr

Abstract

This study summarizes the work carried out between 2021 and 2025 under the project titled *"Establishment of a Facility for Processing and Storing Aromatic Plants in Artvin"* (Project No: 2021-TAB-02), supported by the Presidency of Strategy and Budget of the Republic of Turkey and coordinated by Artvin Çoruh University. The main goal was to convert local plant resources into high-value-added products using modern extraction and drying technologies. A Plant Processing and Product Development Center is established with units for distillation, extraction, evaporation, and spray drying. The facility includes support systems such as a purified water treatment unit and environmental control equipment. Each main vessel has a capacity of 500 liters, allowing efficient processing of plant materials into essential oils, extracts, and powders. Field studies targeted species such as *Malus sylvestris, Pyrus communis, Cornus mas, Diospyros lotus, Rubus idaeus, Rosa canina, Cydonia oblonga, Ficus carica, Vitis vinifera*, and *Vaccinium arctostaphyllos*. Collected plant materials were propagated and conserved in the university's botanical garden. Extraction and spray drying trials were conducted on species including *Olea europaea, Valeriana erotica, Amaranthus retroflexus, Xanthium strumarium, Erigeron canadensis, Teucrium hyrcanum, Origanum rotundifolium, Salvia sclarea, Ferula orientalis, Epimedium pinnatum*, and *Tribulus terrestris*. These species, among nearly 60 plant types processed during the project, were successfully extracted and spray-dried. The resulting extracts were formulated into value-added products intended for commercial sale. Stable powder products with long shelf life were obtained through optimized procedures. Freeze-drying trials were successfully performed on *Malus domestica* (apple), *Pyrus communis* (pear), *Cydonia oblonga* (quince), *Aronia melanocarpa* (aronia), and *Vaccinium* sp. (blueberry). From fresh weight to dried product, the approximate yields were as follows: *Malus domestica* ~12%, *Pyrus communis* ~11%, *Cydonia oblonga* ~9.3%, *Aronia melanocarpa* ~7.2%, and *Vaccinium* sp. ~6.8%. The drying efficiency ranked from highest to lowest was: apple, pear, quince, aronia, and vaccinium. Additional demand for freeze drying of various fruits has also been received from local producers. Future freeze-drying operations will be planned in line with incoming demands.
In the next phase, a new 1,000 m² facility will be built with expanded lines for fruit processing, jam production, pasteurization, and packaging, supporting sustainable botanical product development in the region.

Keywords: Medicinal and Aromatic Plants, Plant Extraction Technologies, Spray Drying and Freeze Drying, High-Value-Added Plant Products, Sustainable Botanical Processing.

➢ *ORAL PRESENTATION*

The role of hormesis in nutrition and health

Merve Başak Sarraç[1*], Gamze Toydemir[1] (*ORCID: https://orcid.org/0000-0003-3738-0986)*

[1] Alanya Alaaddin Keykubat University, Faculty of Engineering, Department of Food Engineering, Antalya, Türkiye.

*Corresponding author e-mail : basaksarrac01@gmail.com

Abstract

Hormesis is a two-phase phenomenon characterized by inverted U, U, or J-shaped dose-response curves that cannot be explained by classical threshold or linear-no-threshold toxicology models. At low doses, hormetic agents are well-reported to generate mild stress conditions that trigger cellular adaptive responses, such as enhanced antioxidant defense, improved levels of heat shock proteins, etc.; whereas these agents cause toxic effects at high doses. The molecular basis of hormetic response is supported by receptor theory, which explains that a small number of high-affinity receptors are activated at low doses; while a large number of low-affinity receptors are activated at high doses. Components of food, especially the ones that are not abundant in the diet (e.g., plant bioactives, micronutrients) are gaining an increasing interest as promising nutritional agents that exert their potential health benefits by hormesis. Several phytochemicals and micronutrients, including polyphenols, organosulfur compounds, vitamins, etc., have been related with reduced inflammation and lower risk of degenerative diseases when consumed at low doses; however, in contrast, their excessive intake have been documented to produce detrimental effects. Distinctively, some food contaminants (e.g., heavy metals, mycotoxins) have also been reported to induce hormetic responses through exhibiting dose-dependent biphasic effects which is characterized by low-dose stimulation and high-dose inhibition depending on the level and duration of exposure. Depending on this background, it is essential to gain a deep knowledge on nutritional hormesis and its mechanisms in order to provide a critical framework for precise regulation of the optimal intake of diet-derived hormetic agents. Therefore, this presentation aimed to discuss how nutrition and hormetins within the diet could reduce the risk of disease and promote health through modifying the key biochemical targets and their importance in developing promising therapeutic strategies.

Keywords: nutritional hormesis, dose-response, phytochemicals, contaminants

➢ *ORAL PRESENTATION*

BIX-induced Somatic Embryogenesis through Epigenetic Reprogramming in *Arabidopsis thaliana*

Burcu Gündüz [1*] *(ORCID: https://orcid.org/0009-0005-9683-9971)*, Sinan Meriç [1] *(ORCID: https://orcid.org/0000-0003-0336-0004)*

[*] Istanbul Kültür University, Faculty of Science and Letters, Department of Molecular Biology and Genetics, 34156 Ataköy, Istanbul, Turkey

[*] Corresponding author e-mail: s.meric@iku.edu.tr

Abstract

Somatic embryogenesis (SE) can be induced in vitro through various approaches, including stress treatments, tissue culture techniques, and genetic engineering. The most commonly used method involves incorporating high levels of plant hormones into the culture medium. Other methods utileze wounding, extreme pH, osmotic or heat shock, and exposure to certain chemicals. The growth regulator 2,4-dichlorophenoxyacetic (2,4-D) is widely used in both direct and indirect SE, playing critical role in cell dedifferentiation and SE recovery. BIX-01294 is a diazepine-quinazoline-amine derivative histone lysine methyltransferase inhibitor (HKMT) that was identified as a specific G9a HKMT and reduced global H3K9me2 levels in several mammalian cell lines. Short-term application of the HKMT inhibitor BIX-01294 increase cell reprogramming, totipotency and embryogenesis initiation efficiency by decreasing H3K9 methylation. In this study, the effects of BIX-01294 on SE in Arabidopsis thaliana Col-0 ecotype were investigated with different concentrations. It was determined that the HKMT inhibitor in the medium at different concentrations was sufficient to induced embryogenesis with 0.1 µM. The SE number formed from immature zygotic embryos (IZEs) in the presence of 2.5 µM BIX-01294 and 2,4-D at the end of the 21st day was determined to be 35.41% and 31.25%, respectively. BIX-01294 increased SE formation by 1.13-fold in bent cotyledon stage immature zygotic embryos compared to 2,4-D. Moreover, the average number of somatic embryos produced per explant was also determined to be dramatically higher in 2.5 µM BIX-01294 than in the presence of 2,4-D.

Keywords: *Arabidopsis thaliana*, BIX-01294, Reprogramming, Somatic Embryogenes, RNA-seq.

➢ *ORAL PRESENTATION*

Dünya'da ve Türkiye'de Su Ürünleri Mutfağı

Buminhan Burkay SELÇUK[1*] https://orcid.org/0000-0003-4650-5592, Fikret ÇAKIR[2] https://orcid.org/0000-0001-5261-2365

[*1]Çanakkale Onsekiz Mart Üniversitesi, Deniz Bilimleri ve Teknolojisi Fakültesi, Lisansüstü Eğitim Enstitüsü, Çanakkale, TÜRKİYE.
[2] Çanakkale Onsekiz Mart Üniversitesi, Deniz Bilimleri ve Teknolojisi Fakültesi, Avlama ve İşleme Teknolojisi Anabilim dalı, Çanakkale, TÜRKİYE.

*Sorumlu yazar e-posta: buminhanselcuk@gmail.com

Özet

Nüfus artışıyla birlikte dünya genelinde nitelikli gıdaya ulaşmanın zorlaştığı, özellikle proteince zengin gıda arzını karşılamanın zorlaştığı bir durum ile dünya karşı karşıyadır. Sucul canlı kaynakları hem proteince zengin hem de diğer hayvansal proteinlere göre daha ucuz ve daha kolay sindirilebilir ürünlerdir. Bu yüzden her geçen gün sucul canlı kaynakların tüketimine olan ilgi artmakta ve su ürünleri üretim miktarları da hem Dünya'da hem de Türkiye'de buna paralel olarak yükselmektedir. Dünya balıkçılık ve tarım organizasyonuna göre 2022 yılı itibarıyla Dünya'da toplam su ürünleri üretim miktarı 186 milyon ton, kişi başına düşen ortalama su ürünleri tüketimi 22 kg iken, ülkemizde üretim miktarı 1 milyon ton ve su ürünleri tüketimi yıllık 7.2 kg'dır. Bu durum ülkemizde halen su ürünlerinin öncelikli protein kaynağı olarak tercih edilmediğinin bir göstergesidir. Besin olarak insanlar tarafından tüketilen su ürünleri kaynaklarının başlıca deniz ve tatlı su balıkları, kabuklu su ürünleri (Karides, istiridye, midye vb.) ve kafadanbacaklılar (ahtapot, kalamar, sübye vb.) gibi sucul canlılardan oluşmakta ve bu canlı kaynaklar bir çok kültürde önemli yere sahip olmaktadır. Sucul canlı kaynaklar hiç işlem görmeden çiğ olarak, farklı pişirme teknikleri ile (tuza gömme, kurutma, kızartma, marinasyon, konserve vb.) ve ileri işleme teknikleri ile (kroket, surumi, köfte, pastırma, cips vb.) dünya su ürünleri mutfağında sokak lezzetlerinden en lüks restorantlara kadar yer bulmaktadır. Dünya üzerinde en fazla gelişmiş su ürünleri mutfağı ve su ürünleri yemek çeşitliliği uzakdoğu ülkelerinde görülmekte ve en öne çıkan yemekler suşi, kamaboko, katsuobushi, shrimp paste (karides ezmesi) olduğu bilinmektedir. Avrupa ülkelerinde havyar ve botarga, Avustralya'da gravlax, Güney Amerika'da Ceviche, Kuzey Amerika'da ise Tuna Tartar yemekleri öne çıkmaktadır. Ülkemizde çoğunlukla su ürünleri kızartma ve ızgara olarak işlem görmeksizin pişirilmekte ve su ürünleri mutfağının Dünya geneline göre gelişmemiş olduğu görülmektedir. Dünya su ürünleri mutfağının gelişiminde yaşanılan coğrafya ve kültürün en etkili faktörler olduğu anlaşılmaktadır.

Anahtar Kelimeler: Yemek, sucul canlı kaynaklar, tüketim, alışkanlık, besin

➢ *ORAL PRESENTATION*

A fuzzy c-means ensemble approach for robust price dynamics forecasting in Turkey

Erdinç Karakullukçu[1*] (*ORCID: https://orcid.org/0000-0001-8805-1694*)

[*1]Karadeniz Technical University, Faculty of Science, Department of Computer Sciences, Trabzon, Turkey.

*Corresponding author e-mail: erdinc.karakullukcu@ktu.edu.tr

Abstract

In Turkey's dynamic and inflation-sensitive economic landscape, accurately forecasting the Domestic Producer Price Index (PPI (YI-UFE)) and the Consumer Price Index (CPI (TUFE)) is paramount. These indices are critical for guiding monetary policy, informing investment choices, and ensuring economic stability. PPI offers an early indication of future consumer price movements, while CPI directly reflects household cost changes. Both indices in Turkey exhibit a consistent upward trend, necessitating robust prediction models. This study explores various individual forecasting techniques, including Holt's Exponential Smoothing, Auto ARIMA, Theta Method, Piecewise Linear Trend, Prophet Method, LOESS, and Support Vector Regression, acknowledging their inconsistent performance across different conditions. To address this limitation, an innovative ensemble methodology is introduced. This approach utilizes the Fuzzy C-Means clustering algorithm to strategically group and combine the forecasts from these diverse individual models. By leveraging the collective intelligence of clustered predictions, the ensemble method aims to deliver more reliable and stable forecasts. Rigorous evaluation of this ensemble approach demonstrated its superior performance. The proposed method consistently achieved lower Mean Absolute Percentage Error (MAPE) and Root Mean Squared Error (RMSE) compared to individual models when predicting PPI and CPI. This highlights the significant potential of the ensemble strategy in enhancing the accuracy and stability of key economic indicator forecasts within complex and volatile economic environments.

Keywords: Forecasting, meta fuzzy functions, Turkish economy, ensemble methods, fuzzy c-means

➢ *ORAL PRESENTATION*

Radiation Shielding Properties of Gd_2O_3 Reinforcement Paraffin Materials: MCNP6.2 Simulation Analysis

Seyit Çağlar* (*ORCID: https://orcid.org/0000-0002-0701-3029*)

*Department of Metallurgical and Materials Engineering, Zonguldak Bülent Ecevit University, Zonguldak 67100, Türkiye

*Corresponding author e-mail: s.caglar@beun.edu.tr

Abstract

This study investigates the effects of Gd_2O_3 (gadolium oxide) doping on the radiation shielding performance of paraffin-based polymer matrix materials. The study analyzed the radiation interaction properties of paraffin materials doped with 3%, 6%, 9%, 12%, and 15% Gd_2O_3 using a Monte Carlo-based MCNP6.2 simulation program. According to the simulation results, a significant increase was observed in the attenuation capacity of the material against both thermal and fast neutrons with increasing Gd_2O_3 doping ratio. In addition, it has been determined that the radiation absorption ability has improved regarding photon interactions. In this context, a significant improvement in the linear attenuation coefficient (LAC) was achieved; the LAC value of 6.582 in the undoped material increased to 7.554 with 15% Gd_2O_3 doping, which corresponds to an increase of approximately 14.77%. The obtained findings reveal that Gd_2O_3-doped paraffin-based composites improve not only neutron but overall radiation shielding properties and therefore have the potential for use in a wide variety of fields such as radioactive material transportation and storage, nuclear medicine applications, nuclear power plants, and space technologies.

Keywords: Gd_2O_3-reinforcement paraffin, radiation shielding, MCNP6.2

➢ *ORAL PRESENTATION*

Current research on anti-Alzheimer's drugs: Secretase Inhibitors

Ayşe Nur ER[1] (*ORCID:* https://orcid.org/0009-0002-1566-1306) ,
Cem YAMALI[1*] (*ORCID: https://orcid.org/0000-0002-4833-7900*)

[1]Çukurova University, Faculty of Pharmacy, Adana, Türkiye

*Corresponding authors e-mail: c.yamali@yahoo.com; aysenurer.2000@gmail.com

Abstract

Alzheimer's disease (AD) is a progressive neurodegenerative disorder that increasingly affects the aging global population, leading to gradual loss of memory, cognition, and behavioral functions. The clinical manifestations of the disease are associated with the accumulation of amyloid beta (Aβ) plaques and tau protein-related neurofibrillary tangles in the brain. One of the key pathological mechanisms of AD involves the proteolytic cleavage of amyloid precursor protein (APP) by secretase enzymes, resulting in the generation of Aβ peptides. Therefore, secretase inhibitors, which aim to reduce Aβ production, have emerged as important pharmacological agents in the therapeutic landscape of AD.

This study focuses on the biological functions of α-, β-, and γ-secretase enzymes and evaluates the pharmacological properties of their inhibitors. The efficacy, safety, and therapeutic potential of secretase inhibitors under clinical and preclinical investigation has been conducted. Although β-secretase (BACE1) inhibitors significantly reduce Aβ levels, they have failed to provide cognitive benefits in clinical trials. On the other hand, γ-secretase inhibitors have been associated with severe adverse effects due to their interaction with multiple physiological substrates, indicating the limitations of single-target treatment strategies. Meanwhile, new-generation agents such as γ-secretase modulators (GSMs), which offer higher selectivity and fewer side effects, represent a promising direction for future AD therapies.

The findings of this study highlight the significance of secretase-targeted therapies in the development of AD drugs, while also emphasizing the need for multi-targeted and combinational therapeutic strategies.

Keywords: Alzheimer's disease, secretase inhibitors, amyloid beta, β-secretase, γ-secretase

➢ *ORAL PRESENTATION*

Seasonal effects of air pollution on childhood allergic rhinitis: A case study from Northwestern Türkiye

Hilal Arslan[1*] *(ORCID: https://orcid.org/0009-0006-6018-2784)*

[*1] University of Health Sciences, Hamidiye Faculty of Health Sciences, Department of Occupational Health and Safety, Istanbul, Türkiye.

*Corresponding author e-mail: hilal.arslan@sbu.edu.tr

Abstract

Allergic rhinitis is recognized as a common inflammatory disease of the upper respiratory tract, with its prevalence increasing, particularly among children. This increase has been attributed to environmental risk factors, particularly air pollution. In this study, short-term seasonal exposure to $PM_{2.5}$, SO_2 and NO_2, and its impact on allergic rhinitis prevalence among children in Edirne, Türkiye, were analyzed using Generalized Additive Model based on data collected between 2013 and 2018. Edirne was selected as study area due to its high vehicle emissions resulting from transportation and border trade, as well as intensive agricultural activities. A significant association was identified between $PM_{2.5}$ exposure and allergic rhinitis cases in adolescents aged 13-17 years, particularly at lag2 (RR: 1.0101; 95% CI: 1.0010-1.0192) and lag3 (RR: 1.0082; 95% CI: 1.0013-1.0151). Similarly, NO_2 exposure was found to be significantly associated with allergic rhinitis cases in the same age group between lag0-lag5, with the highest risk observed at lag0 (RR: 1.0516; 95% CI: 1.0177-1.0867). However, no statistically significant association was observed between SO_2 exposure and allergic rhinitis in any age group (0-5, 6-12, 13-17). When seasonal variations in air pollution exposure were examined, significant associations were found in 13-17 years age group during autumn, with $PM_{2.5}$ between lag0-lag3, with SO_2 between lag0-lag3, and with NO_2 between lag0-lag2. In the 6-12 years age group, NO_2 exposure was significantly associated with allergic rhinitis between lag3-lag7. In particular, increased NO_2 concentrations were recorded during morning and evening hours, likely due to traffic emissions near school routes. The findings of this study indicate that fossil fuel consumption, increased traffic density, atmospheric inversion events, and seasonal allergen exposure have contributed to the increase in allergic rhinitis cases, particularly in autumn. These results highlight the necessity of implementing targeted interventions to minimize air pollution exposure and its adverse health effects on children.

Keywords: Allergic Rhinitis, air pollution, childhood health, Distributed Lag Non-Linear Model, Northwestern Türkiye

➢ *ORAL PRESENTATION*

Analyzing the impact of air pollution on asthma with machine learning in Edirne, Türkiye

Hilal Arslan[1*] *(ORCID: https://orcid.org/0009-0006-6018-2784)*

[*1] University of Health Sciences, Hamidiye Faculty of Health Sciences, Department of Occupational Health and Safety, Istanbul, Türkiye.

*Corresponding author e-mail: hilal.arslan@sbu.edu.tr

Abstract

Air pollution, exacerbated by increasing industrialization and urbanization, poses a significant threat to public health, particularly in relation to respiratory diseases such as asthma. Epidemiological studies have shown a positive association between air pollutant exposure and higher asthma incidence. This study examined the impact of air pollution on asthma diagnoses in Edirne, a city in northwestern Türkiye, using machine learning models. The dataset includes air quality and meteorological parameters obtained between 2013 and 2018, specifically focusing on four criteria air pollutants: $PM_{2.5}$, SO_2, NO_2, and O_3. Prior to modelling, all variables were standardized using Z-score normalization to ensure a mean of 0 and a standard deviation of 1. The data were divided into training (80%) and testing (20%) subsets, and model validation was conducted using 10-fold cross-validation. The Spearman correlation analysis indicated that $PM_{2.5}$ had the strongest association with asthma diagnoses. Three classification algorithms- Support Vector Machine (SVM), K-Nearest Neighbors (KNN), and Kernel Naive Bayes (KNB) were employed to model the predictive relationship between air pollution exposure and asthma incidence. Model performance was assessed using receiver operating characteristic (ROC) curves and the area under the curve (AUC) metric. The highest AUC value was achieved with SVM (0.802), followed by KNN (0.789), and KNB (0.777), indicating moderate to strong predictive performance. These findings highlight the significant role of air pollutants and meteorological factors in asthma prevalence and emphasize the potential of machine learning approaches in environmental health research.

Keywords: Asthma, air pollution, machine learning, support vector machine, Edirne, Türkiye

➢ *ORAL PRESENTATION*

Effect of Pesticide Exposure on ACTH and Cortisol Levels in Fish

Nuh Korkmaz[1*] (*ORCID: https://orcid.org/ 0000-0001-8299-910X*)

[*1]Osmaniye Korkut Ata University, Faculty of Engineering and Natural Sciences, Department of Biology, Osmaniye, Türkiye.

*Corresponding author e-mail: korkmazhun@gmail.com

Abstract

Pesticide pollution poses an increasing threat to aquatic ecosystems. Fish are among the organisms that are constantly exposed to these chemical agents, and pesticides can trigger various physiological stress responses. In particular, activation of the hypothalamic-pituitary-interrenal (HPI) axis increases the release of stress hormones in fish. In this context, changes in the levels of hormones such as adrenocorticotropic hormone (ACTH) and cortisol are considered important indicators of the endocrine disrupting effects of pesticides.

Studies in the literature show that different types of pesticides (insecticides, herbicides, fungicides) can significantly affect ACTH and cortisol levels in fish. Pesticide exposure generally results in excessive activation of the HPI axis, which leads to a significant increase in plasma cortisol levels. Some studies have shown that even low-dose exposure increases ACTH release and triggers cortisol secretion. However, depending on the type, dose, duration of exposure and fish species, differences in the severity of stress responses are observed. It has also been reported that long-term or high-dose pesticide exposure can cause chronic effects such as depletion in the HPI axis and a decrease in cortisol response.

The effects of pesticides on ACTH and cortisol levels in fish are critical for the health status and ecosystem balance of aquatic organisms. Changes in these hormones can be used as a biomarker of physiological stress caused by pesticides. Controlling pesticide use and reducing pesticide contamination in aquatic environments are of great importance for the sustainability of fish populations

Keywords: Fish, Pesticide, ACTH, Cortisol, Stress Response

➢ *ORAL PRESENTATION*

Medicinal Mushrooms as Natural Antioxidant Sources: Their Potential in Combating Oxidative Stress

Celal Bal[1*] (*ORCID: https://orcid.org/0000-0001-6856-3254*)

[*1] Oguzeli Vocational School, University of Gaziantep, Gaziantep, Türkiye.

*Corresponding author e-mail: bal@gantep.edu.tr

Abstract

Oxidative stress is an important biochemical condition that occurs when the balance in the detoxification of reactive oxygen species (ROS) formed as a result of cellular metabolism is disrupted and plays a role in the pathogenesis of many chronic diseases. Antioxidants are molecules that protect cells from oxidative damage by neutralizing these harmful free radicals. In recent years, interest in natural antioxidant sources has increased and especially medicinal mushrooms have attracted attention with their rich phenolic compounds, polysaccharides and compounds such as ergothioneine. In this study, the antioxidant capacities of various medicinal mushroom species were examined and the potential therapeutic uses of these effects were evaluated. It has been documented in many studies that extracts of mushrooms such as Ganoderma lucidum, Pleurotus ostreatus, Lentinula edodes and Hericium erinaceus exhibit high activity in in vitro antioxidant tests such as DPPH, FRAP, ABTS and CUPRAC. These activities show that mushroom extracts can be used not only as preventive health components but also as natural antioxidant additives in the pharmaceutical and food industries. In addition, it has been shown that the antioxidant effects of some mushroom species are not limited to free radical scavenging activity but also activate endogenous antioxidant defense systems (SOD, CAT, GPx). In this respect, medicinal mushrooms are promising natural agents in the prevention and supportive treatment of diseases associated with oxidative stress. In this presentation, the antioxidant properties of selected mushroom species, the mechanisms of these effects and potential avenues for future clinical applications will be discussed in detail.

Keywords: Medicinal mushrooms, Antioxidant activity, Oxidative stress, Natural antioxidants

➢ *ORAL PRESENTATION*

Phytoremediation potential of some aquatic medicinal plants for heavy metals

Beyza Yıldırım*, Muhittin Doğan

University of Gaziantep, Faculty of Arts and Sciences, Department of Biology, Gaziantep, Türkiye

*Corresponding author e-mail: yildirimbeyza2002@gmail.com

Abstract

Accumulation of heavy metals in the environment poses serious threats to both ecosystem health and human health. Therefore, phytoremediation, an environmentally friendly and sustainable method, stands out as an important solution in the remediation of contaminated areas. In this study, the heavy metal removal potential of some aquatic macrophytes with medical importance was evaluated. The capacity of plants to absorb and accumulate heavy metals and phytoremediation mechanisms were examined. Additionally, medical aspects of the macrohytes, such as their use in the public or pharmaceutical field, were also discussed.

Key words: Phytoremediation, medicinal aquatic plants, heavy metal

➢ *ORAL PRESENTATION*

Impact of climate change on sustainability of agricultural food security

Gülcan Çınar* *(https://orcid.org/0000-0001-6167-3362)*, Muhittin Doğan

University of Gaziantep, Faculty of Arts and Sciences, Department of Biology, Gaziantep, Türkiye

* Corresponding author e-mail: gulcancnar03@gmail.com

Abstract

Global warming causes climate change by releasing greenhouse gases into the atmosphere and increasing the temperature of the world. It is a known fact that this warming will accelerate hydrological disasters, cause extreme weather events such as droughts and floods, and increase climate change. Global climate change poses a threat to the global climate due to increasing carbon emissions and the effects of other greenhouse gases. Global climate variability causes increases in evaporation, temperature, and precipitation, which are very important factors for the life of living things. This situation causes a continuous decrease in water resources, endangers natural life, and has negative effects on agricultural production. Plants are significantly affected by climate variability, which causes a decrease in agricultural production. Food production is a serious component that can be affected by changes in climate. Climate change also threatens global food systems, which feed all living things on the planet. Climate change and variability can be effective in the emergence of dangers at various stages of the food chain, from primary production to consumption. There are multiple ways in which climate-related factors can affect food security. In this study, the risks of global warming and climate change on food security and food safety in agricultural production were examined.

Key words: Global warming, climate change, food security, sustainability

➢ *ORAL PRESENTATION*

Effect of nanotechnological applications used in agricultural production on food safety

Gülcan Çınar* *(https://orcid.org/0000-0001-6167-3362)*, Muhittin Doğan

University of Gaziantep, Faculty of Arts and Sciences, Department of Biology, Gaziantep, Türkiye

* Corresponding author e-mail: gulcancnar03@gmail.com

Abstract

Nanotechnology is considered the most important technological development of recent years and is used in many areas due to its potential applications. Today, their use in agricultural production to maintain an environmentally friendly agriculture offers a great opportunity. Globally, food safety and security are currently receiving great attention with the aim of ensuring the sustainable supply of nutrient-rich and safe foods. Nanotechnology has become a promising solution to many problems faced by some applications used globally, and has also made great contributions to applications in the agricultural, environmental and food sectors. Nanotechnology in agriculture has significant effects at every stage of agricultural production, including seed germination, growth, harvesting, processing, storage and transportation of agricultural products. Nanofertilizers, nanoherbicides, nanofungicides, nanobiosensors, nanoscale genetic carriers, nanobioremediation agents and nanocomposites for packaging are new applications of nanotechnology in the field of product development. Nanotechnology minimizes loss and increases efficiency by ensuring the delivery of nutrients to the target area of the plant. Nanoscale materials are used to increase agricultural yields, improve food quality and safety, improve water and nutrient efficiency, and reduce environmental pollution. Nanotechnology has emerged as a promising avenue that offers significant opportunities to revolutionize food safety practices and increase agricultural productivity in a sustainable manner. This study aims to provide information on nanotechnological applications used in agricultural production, taking into account current developments.

Key words: Nanotechnology, agricultural production, food safety, food security

➢ *ORAL PRESENTATION*

Scalability analysis and performance evaluation of massive MIMO network

Onem Yildiz[1*] (*ORCID: https://orcid.org/0000-0003-0675-6637*)

[*1]Aydin Adnan Menderes University, Faculty of Engineering, Department of Electrical and Electronics Engineering, Aydin, Türkiye.

*Corresponding author e-mail: onem.yildiz@adu.edu.tr

Abstract

The exponential growth in mobile data traffic and the emergence of ultra-reliable low-latency applications are driving the need for revolutionary wireless architectures that go beyond conventional cellular systems. Cellular massive MIMO networks, in which numerous access points (APs) equipped with multiple antennas cooperatively serve users, offer the potential for enhanced coverage, increased throughput, and improved spectral efficiency. However, despite their promise, optimal deployment strategies for such networks remain insufficiently explored—particularly regarding the trade-offs between AP density, antenna configurations, and overall system efficiency in densely populated user environments. This study presents a comprehensive analysis of these trade-offs using high-resolution simulation data, examining the joint impact of antenna diversity, AP scaling, and user load on system performance. Results show over 160% improvement in user throughput when increasing AP density under moderate antenna configurations, while antenna diversity contributes additional throughput gains ranging from 20% to over 70%, depending on AP density. Conversely, a tenfold increase in user count leads to more than 98% degradation in per-user throughput, underlining the limits of scalability. Efficiency analysis further reveals that maximum throughput per AP is reached at moderate AP densities, beyond which performance per AP declines due to resource contention and coordination overhead. These findings highlight deployment sweet spots where system throughput and spectral efficiency are balanced, offering practical guidelines for scalable wireless infrastructure design in next-generation networks.

Keywords: 5G, massive MIMO, antenna diversity, system efficiency.

➢ *ORAL PRESENTATION*

Effects of The Diatomaceous Earth and Entomopathogenic Fungi Against The Tomato Leafminer Moth, *Tuta absoluta* (Meyrick) [Lepidoptera: Gelechiidae] in Field Condition.

Zainelabdin Adam Mohmmed Ali, Orkun Barış Kovancı*

Bursa Uludağ University, Faculty of Agriculture, Department of Plant Protection
Campus of Görükle, 16059 Bursa/TÜRKİYE

*Corresponding author e-mail: baris@uludag.edu.tr

Abstract

Field tests were done by the Department of Plant Protection at the Faculty of Agriculture, Bursa Uludağ University. The tomato varieties Albeni and UG 12406 740 are provided by United Genetics Turkey Seedling Company. This study sought to evaluate the impact of diatomaceous earth and entomopathogenic fungi on the mortality of the tomato leafminer moth, *Tuta absoluta*, as an alternative to insecticides. Diatomaceous Earth (DE) was combined with *Paecilomyces fumosoroseus* strain PFs-1 (Priority) and *Verticillium lecanii* strain Bb-1 (Nibortem) to manage *T. absoluta* larvae, alongside a positive control of Azadirachtin (Nimbecidine) and an untreated control group. In field studies with the Albeni variety, optimal toxic effects (elevated mortality, minimal infestation) were seen with Nibortem + DE: mortality increased steadily over time (40% to 93.3% on day 7). Infested fruit: 44.6%. Mortality demonstrated a gradual escalation (46.1% → 92.3%). Infested fruit: 52.4%, demonstrating a considerable protective effect. Nembecidine, utilized as a positive control, demonstrated the highest death rate by day 7 (100%). Infested fruit: 37.9% – the lowest infestation rate, signifying strong field efficacy. In the UG 12406 740 variety optimal Toxic Effects (Elevated Mortality, Minimal Infestation) Nibortem + DE: Mortality progressively escalated over time (55.5% → 88.8% by day 7). Infested fruit: 37.4% — significantly lower than individual treatments. Proposes a synergistic interaction between Nibortem and Diatomaceous Earth. Priority + DE: Mortality exhibited a progressive increase (44.4 → 77.7). Infested fruit: 47.6%, indicating a significant protective effect. Demonstrates that the combination of Priority and DE yields superior performance compared to each independently. Nembecidine, utilized as a positive control, exhibited the highest death rate by day 7 (92.3%). Infested fruit: 29.6% — the minimal infestation, indicating robust field performance. Thus, Nibortem+ DE and Priority+ DE can be considered a viable alternative to chemical control for the management of *T. absoluta* larvae.

Keywords: *Verticillium lecanii*, *Tuta absoluta*, Synergistic interaction, Biological control

➢ *ORAL PRESENTATION*

Design and optimization of a solar-wind hybrid system with enhanced efficiency measures for Türkiye

Nazif Erdem Gülçin[1*] (*ORCID: https://orcid.org/0009-0006-7153-2727)*, Betül Çetin[2] (*ORCID: https://orcid.org/0009-0004-0937-0427*) , Zuhal Er[3] (*ORCID: https://orcid.org/0000-0002-9737-1435),* Osman Giray Oğuzman[4] (*ORCID: https://orcid.org/0000-0001-6046-7030)*

[*1]Istanbul Technical University, Science and Letters, Physics Engineering, İstanbul, Türkiye.
[2]Istanbul Technical University, Science and Letters, Physics Engineering, İstanbul, Türkiye.
[3]Istanbul Technical University, Science and Letters, Physics Engineering, İstanbul, Türkiye.
[4]Gebze Technical University, Aerospace, Aeronautical Engineering, Kocaeli, Türkiye.

*Corresponding author e-mail: gulcin18@itu.edu.tr

Abstract

Energy is one of the most pressing global issues of the 21st century, with energy independence being essential to national sovereignty. In line with global carbon neutrality goals and Türkiye's 2035 and 2050 energy targets, this project proposes an optimized hybrid renewable energy system combining solar tracking-enabled photovoltaic panels and wind turbines.

The study focuses on enhancing system performance through multiple optimization strategies, including wind farm orientation, wind turbine blade design, and anti-soiling coatings for solar panels. Using Python-based computational modeling and simulation tools, the project evaluates annual solar irradiance and wind speed data to identify the most suitable geographic locations across Türkiye. It also includes optimal PV panel sizing and tilt angle selection, dynamic solar tracking integration, and region-specific turbine selection based on wind profiles.

A key component involves the positional optimization of wind farms to increase capacity factor and reduce wake effects. In parallel, innovative blade design improvements are considered to enhance aerodynamic efficiency. For the solar component, the implementation of dust-repellent coatings is investigated to reduce performance loss due to soiling. The integration of these elements aims to improve operational efficiency and extend system lifespan.

By synthesizing solar and wind technologies into a unified energy solution, this project not only targets higher energy yield and CO_2 emission reduction but also reduces Türkiye's dependency on imported fossil fuels. Furthermore, the model developed will be evaluated for its scalability and adaptability to other regions and renewable infrastructure projects.

Keywords: Renewable energy, wind farm orientation optimization, solar panel coating, blade design optimization, solar tracking systems, energy efficiency

➢ *ORAL PRESENTATION*

A Preliminary Evaluation of Bioactive Compounds in *Galium divaricatum*

Nurdan Yazici[1*] (*ORCID: https://orcid.org/0000-0001-7617-1701*), Ayşenur Koçan[2] (*ORCID: https://orcid.org/0009-0006-4714-2446*), Hava Dudu Cavlak[2] (*ORCID: https://orcid.org/0009-0000-0535-579X*)

[*1] Karadeniz Technical University, Faculty of Pharmacy, Department of Pharmacognosy, Trabzon, Türkiye
[2]Karadeniz Technical University, Faculty of Pharmacy, Trabzon, Türkiye

*Corresponding author e-mail: nurdanyazici@ktu.edu.tr

Abstract

The genus *Galium* L., a member of the Rubiaceae family comprising nearly 600 species, is known as "yoğurt otu" (yoghurt herb) in traditional Anatolian medicine. Various *Galium* species have long been utilized for their diuretic, antidiarrheal, antispasmodic, and sedative properties, and in certain regions of Türkiye, notably Elazığ and Tunceli, they are also used to help regulate blood glucose levels. Phytochemical investigations have identified the presence of a wide range of bioactive constituents in *Galium* species, including flavonoids, tannins, iridoids, and saponins.

In the present study, methanol extract was prepared from the aerial parts of *Galium divaricatum*. Enzyme inhibition assays demonstrated that while the extract showed no inhibitory effect on α-amylase, it effectively inhibited the α-glucosidase enzyme, with an IC_{50} value of 20.66 ± 2.43 µg/mL, and the reference drug acarbose inhibited the α-glucosidase enzyme, with an IC_{50} value of IC_{50} 62.37 ± 3.58 µg/mL. LC-MS/MS analysis of the methanol extract confirmed the presence of several phenolic and flavonoid constituents, including quinic acid (36.467 µg/g), chlorogenic acid (35.624 µg/g), cynaroside (25.963 µg/g), and isoquercitrin (11.313 µg/g). Each of these compounds is known for specific biological activities: cynaroside exhibits anti-inflammatory effects, chlorogenic acid is a potent antioxidant, quinic acid functions as an α-glucosidase inhibitor, and isoquercitrin contributes to blood glucose regulation.

Collectively, these findings suggest that *Galium divaricatum* is not only rich in compounds with strong antioxidant, antiinflammatory, and antidiabetic properties, but may also hold therapeutic potential in the management of diabetes mellitus—a chronic and progressively prevalent disease with systemic consequences. This study adds to the growing body of evidence supporting the medicinal value of traditionally used plants in modern therapeutic contexts.

This work was supported by Office of Scientific Research Projects of Karadeniz Technical University under Grant [number TLÖ-2024-16264].

Keywords: Alpha-glucosidase, Diabetes, *Galium divaricatum*, LC-MS/MS

➢ *ORAL PRESENTATION*

Simulation of Charging and Sustainability of Electric Motors in Aviation from a Hybrid Renewable Energy System

Betül Çetin[1*] (*ORCID: https://orcid.org/0009-0004-0937-0427*), Nazif Erdem Gülçin[1] (*ORCID: https://orcid.org/0009-0006-7153-2727*), Osman Giray Oğuzman [1 2] (*ORCID: https://orcid.org/0000-0001-6046-7030*), Zuhal Er[1] (ORCID: *https://orcid.org/0000-0002-9737-1435*)

[*1]Istanbul Technical University, Faculty of Science and Letters, Physics Engineering, Istanbul, Türkiye.
[2]Gebze Technical University, Aerospace Faculty, Aeronautical Engineering, Kocaeli, Türkiye.

*Corresponding author e-mail: cetinb19@itu.edu.tr

Abstract

Fossil fuels are known to constitute approximately half of the world's energy production, yet international organizations like the European Union have begun investing in renewables for carbon neutrality. In line with COP28 decisions, Türkiye aims to increase its renewable energy usage between 2035 and 2050. Meanwhile, the International Air Transport Association (IATA) targets carbon neutrality in air transportation by 2050. Given the high energy consumption and carbon emissions in the aviation industry, progress in reducing environmental impacts is accelerating faster than in other sectors. This study seeks to generate tangible results for reducing Türkiye's energy dependence and carbon emissions. Its primary objective is to develop a simulation-based Python system to enhance energy efficiency and reduce carbon emissions within the sector.

The project will employ data analysis to identify optimal locations based on solar radiation, annual average wind speeds, and energy production potential. Performance of photovoltaic panels and wind turbines in selected regions will be assessed. Parameters such as solar panel size, tilt angles, and suitable turbine choices for wind speeds will be optimized. Python-based optimization techniques will evaluate the hybrid system's performance and analyse ways to increase the efficiency of energy production processes for electric motors in airports and ports.

Solar-wind hybrid systems hold significant promise for countries like Türkiye, potentially meeting 70-100% of an airport's daily energy needs. Integrating these systems could reduce fossil fuel-based carbon emissions by 50-80%. To achieve zero-carbon targets, specialized software will simulate and compare various propulsion systems, bolstering environmental sustainability. Ultimately, this approach simplifies incorporating renewable energy solutions into design, empowering companies to optimize long-term energy and cost planning effectively.

Keywords: Hybrid Energy, Renewable-Powered Airports, Solar Panels, Wind Turbines

➢ *ORAL PRESENTATION*

Pharmacological Potential of Essential Oils: Current Approaches to Naturally Sourced Therapeutic Agents

Oguzhan Koçer[1*] (*ORCID: https://orcid.org/0000-0002-0104-7586*)

[*1] Osmaniye Korkut Ata University, Vocational School of Health Services, Department of Pharmacy Services, Osmaniye, Türkiye

*Corresponding author e-mail: oguzhankocer@hotmail.com

Abstract

Essential oils consist of a mixture of low molecular weight, volatile compounds obtained from different parts of aromatic plants such as flowers, leaves, fruits, stems, roots and barks by steam distillation or cold pressing methods. These natural oils, which generally include compound classes such as monoterpenes, sesquiterpenes, aldehydes, alcohols, phenols and esters, fulfill important physiological functions in plants such as antimicrobial defense, environmental stress tolerance and insect defense. In recent years, scientific and commercial interest in essential oils has increased significantly due to increasing antibiotic resistance, side effects of synthetic drugs and the tendency towards natural. The broad-spectrum biological activities of essential oils such as antimicrobial, antifungal, antiviral, antioxidant, anti-inflammatory, cytotoxic, neuroprotective and insecticidal have been demonstrated in various in vitro and in vivo studies. In particular, essential oils obtained from some species have been found to be effective against pathogenic bacteria at a level similar to antibiotics; they also showed significant potential in preventing oxidative stress by fighting free radicals. It has also been reported that essential oil components can have anxiolytic, sedative and antidepressant effects on the central nervous system. However, in order to use the therapeutic potential of essential oils safely and effectively, standardization, toxicity assessments and pharmacokinetic profiles need to be clearly demonstrated. In this review presentation, the chemical compositions, biological effects and potential areas of use of essential oils are discussed in the light of current literature data.

Keywords: Essential oils, antimicrobial effect, antioxidant, phytotherapy, natural products, pharmacological activity

1.2. FULL-TEXT PAPERS

➢ *ORAL PRESENTATION*

Hormone-related risk factors for breast cancer based on estrogen and progesterone receptor status- a retrospective study from Albania.

[1]Albina Hasa, [2,3]Merita Xhetani, [4]Floriana Marku

[1]Aldent University, Faculty of Technical Medical Sciences, Department of Medical Laboratory Technician and Imaging, Tirana, Albania
[2]University of Tirana, Faculty of Natural Sciences, Department of Biology, Tirana, Albania
[3]Center of Molecular Diagnostics and Genetic Research, Tirana, Albania
[4]University of Medicine, Faculty of Medicine, Department of Public Health, Tirana, Albania.

Abstract
Breast cancer is a heterogeneous, hormone-dependent malignancy that represents the primary cause of cancer among women and is one of the most prevalent contributors to cancer-related mortality nowadays. Our research aims to assess the expression of ER and PR status in women diagnosed with breast cancer, as well as to assess the correlations between these receptors and prognostic parameters of the disease. A retrospective study of 252 women with breast cancer was conducted at the oncology department of Mother Teresa University Hospital in Albania between 2021 and 2024. Statistical analysis was performed utilizing SPSS. The over-45 age group has the highest diagnostic rate (92.5%) compared to the under-45 age group (7.5%). The most common morphological type observed was ductal carcinoma, accounting for 81.3% of the cases. A significant association was observed between the disease stage and the receptors assessed in the study ($p<0.001$). Our analysis of the association between receptor status and age group revealed a statistically significant association between the two variables ($p=0.02$). A strong association was observed between ER and PR expression receptors ($p=0.00$)
Keywords: breast cancer, Albanian population, ER receptor, PR receptor.

INTRODUCTION

Globally, breast cancer is the most common type of cancer and the leading cause of cancer-related deaths among those under 70 (Esmat E, 2024).
Receptor status has been consistently demonstrated to be one of the most significant predictive factors that affect five-year survival rates, mortality, and disease-free survival rates. (Davey MG, 2021), (Falck AK, 2013). Estrogen receptors (ER) and progesterone receptors (PR) are highly expressed in breast cancer cells and are regarded as diagnostic and prognostic biomarkers for the disease. The overall survival and time to recurrence are positively correlated with increased ER/PR expression, whereas a more aggressive course of the disease, as well as a worse prognosis and recurrence, are typically associated with low ER and PR levels (Łukasiewicz S, 2021).

MATERIALS AND METHODS

The research comprised 252 Albanian women. The data of our study were acquired from patients diagnosed with breast cancer at the oncology service of Mother Teresa University Hospital throughout the years 2021-2024. In the medical records of each patient, all the data directly associated with breast cancer were evaluated.
Statistical analysis was conducted utilizing SPSS. Descriptive and analytic data were evaluated. A p-value of less than or equal to 0.05 was deemed statistically significant. Tables and graphs illustrate the results.

RESULTS

The study included 252 female participants. The over-45 age group had the highest diagnostic rate (92.5%) compared to the under-45 age group (7.5%). The subjects' average age was 62.2 years, with a standard deviation of 11.73. Ductal carcinoma was the most prevalent form at 81.3%. The left breast had the highest prevalence of the disease (57.1%). According to the receptor measurements in the study, ER+ had the highest percentage of positive receptors (85.3%), followed by PR+ (80.6%). Of the subjects, 88.9% were non-TN, and 11.1% were TN. The mean age of subjects with ER and PR overexpression was 63, 63 compared with those lacking ER and PR expression (59; 60).

The analysis of the association between receptor status (TN and non-TN) and age group using the non-parametric Chi-square test revealed a statistically significant association between the two variables ($p=0.02$). A statistically significant correlation ($p<0.001$) existed between the receptors' status and the disease's stage. ER had a strong, positive, and significant association with PR ($r = .589$, $p < 0.01$).

Table 1: Distribution of receptors according to disease grade.

<<		Stage				r, p
		Stage I	Stage II	Stage III	Stage IV	
		Count	Count	Count	Count	
ER	0%/ negative	0	20	13	2	
	1-9%/ low positive	1	2	3	0	r=-0.228;
	10-100%/ positive	15	154	39	0	p=<0.001
	Total	16	176	55	2	
PR	0%/ negative	2	27	15	1	
	1-9%/ low positive	0	4	0	0	r=-0.129;
	10-100%/ positive	14	144	40	0	p= 0.042
	Total	16	175	55	1	
Receptor Status	TN	0	15	11	2	r=-0.218;
	Non-TN	16	161	44	0	p=<0.001
	Missing	0	0	0	0	
	Total	16	176	55	2	

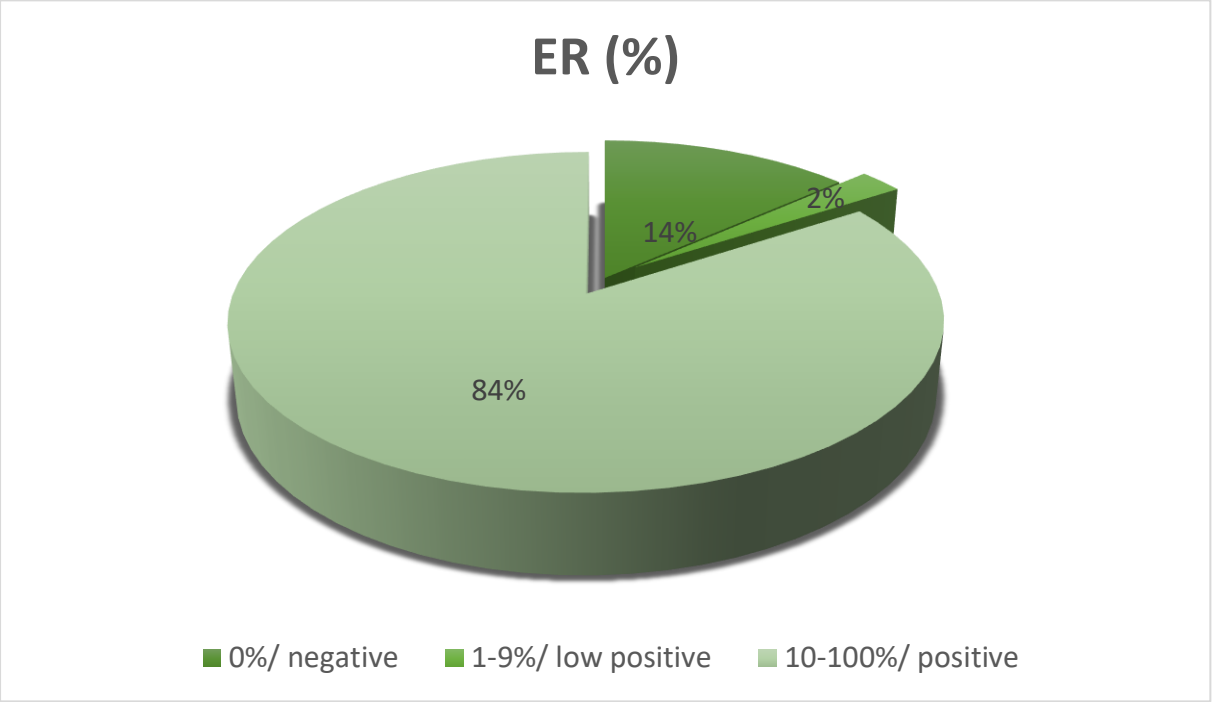

Chart 1: ER receptor distribution

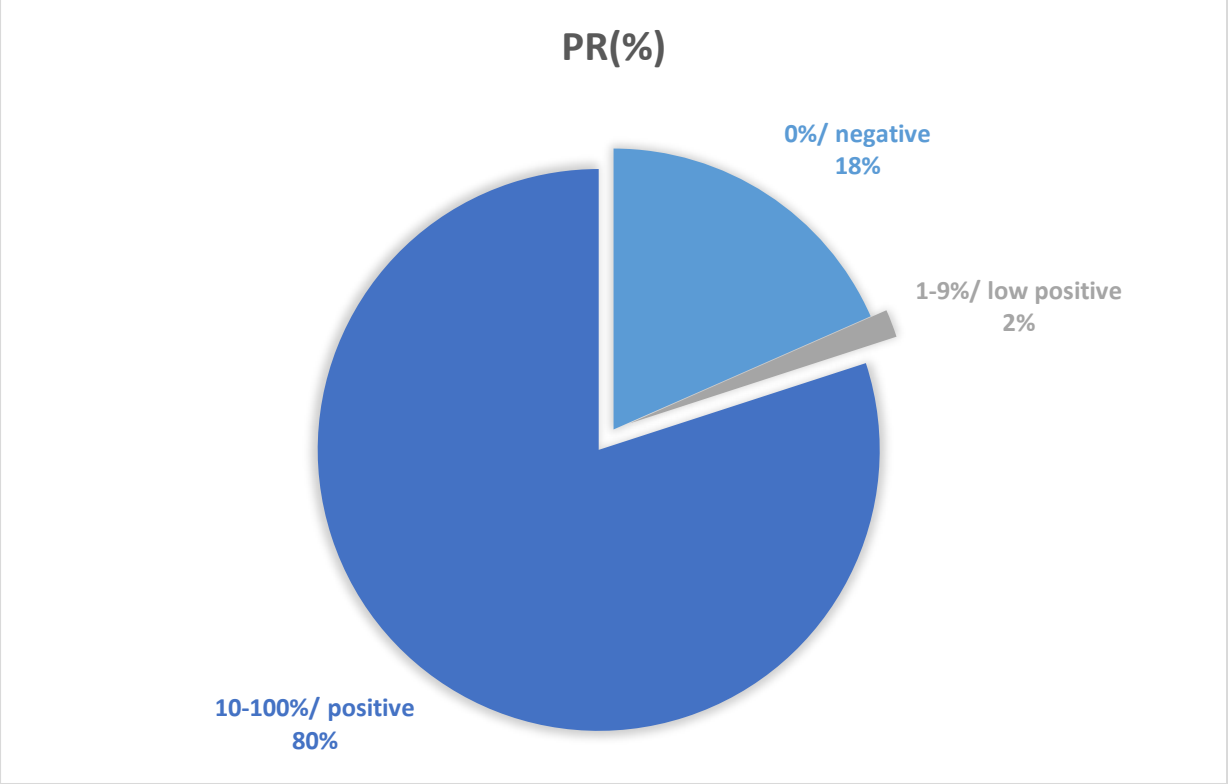

Chart 2: PR receptor distribution

DISCUSSIONS

Approximately 80% of individuals diagnosed with breast cancer are over the age of 50, and over 40% are aged above 65 (McGuire A, 2015) (Łukasiewicz S, 2021). In our study, the mean age of the subjects was 62.6 years. The over-45 age group has the highest diagnostic rate (92.5%) compared to the under-45 age group (7.5%).

Ductal carcinoma was the most common histological type (81.3%) of breast cancer, comparable to other studies. (Azizun-Nisa, 2008), (Sharif MA, 2009), (Anupama Dayal, 2016), (Pathak TB, 2011), (Ellis IO, 1992), (Hiral Samir Shah, 2020).

Measurable amounts of ER and PR receptors were found in about 50–85% and 60-70% of patients with breast cancer (Senel, 2021). In our study, the ER receptor was positive in 85.3% of the subjects and the PR receptor in 80.6%. Other studies have found varying expressions of estrogen and progesterone receptors in breast cancer (Yip CH, 2014) (Łukasiewicz S, 2021) (MN., 2014).
The HER2 gene is 15-25% positive in breast cancer (Senel, 2021) (Kohler BA, 2015). In our study, HER2/neu was 14.277%.

Clinical observations and biomarker studies indicate that late-onset breast cancers grow more slowly. They are biologically less aggressive than early-onset breast cancers, even when controlled for hormone receptor (for example, estrogen receptor, ER) and growth factor receptor (for example, HER2) expression, supporting the conclusion that the biology of breast cancer is age-dependent (CC., 2008).

In our study, a significant association was observed between the disease stage and the receptors assessed in the study ($p<0.001$). Advanced stages were likelier to exhibit low positivity for ER and PR ($p\leq0.001$; $p = 0.04$). ER and PR expression increased with rising age. Our results are consistent with the literature (Azizun-Nisa, 2008) (Tero A. H. Jarvinen, 2000).

Given our current findings on breast cancer and the role of hormonal status in this disease, as well as the role of BRCA genes in the development of inherited breast cancer in our most recent article (Xhetani, 2024) (Hasa, 2024), we intend to conduct additional research on BRCA genes in women with a family history of breast cancer.

CONCLUSION

ER and PR receptor expression is higher in differentiated low-grade tumors compared to high-grade tumors. Their expression rises with age. ER and PR receptors are essential for prognostic evaluation, risk assessment of disease recurrence, and therapeutic decision-making.

ACKNOWLEDGEMENTS

I wish to express deep regards to the oncology department of Mother Teresa University Hospital in Albania for their cooperation in this study.

Reference

Ambroise M, G. M. (2011). Immunohistochemical profile of breast cancer patients at a tertiary care hospital in South India. *Asian Pac J Cancer Prev., 12*(3), 625-9.

Anupama Dayal, R. J. (2016, November 8). Correlation of Her-2/neu Status With Estrogen, Progesterone Receptors and Histologic Features in Breast Carcinoma. *Annals of Pathology and Laboratory Medicine, 3*.

Azizun-Nisa, B. Y. (2008 , Oct-Dec). Comparison of ER, PR, and HER-2/neu (C-erb B 2) reactivity pattern with histologic grade, tumor size, and lymph node status in breast cancer. *Asian Pacific Journal of Cancer Prevention, 9*(4), 553-6.

Bhagat, V. (2012). CORRELATION OF HORMONAL RECEPTOR AND Her-2/neu EXPRESSION IN BREAST CANCER: A STUDY AT TERTIARY CARE HOSPITAL IN SOUTH GUJARAT. *National Journal of Medical Research, 2*(03), 295–298.

CC., B. (2008, Apr). Impact of aging on the biology of breast cancer. *Crit Rev Oncol Hematol., 66*((1)), 65-74.

Davey MG, H. S. (2021, Sep 3). Ki-67 as a Prognostic Biomarker in Invasive Breast Cancer. *Cancers (Basel), 13*(17), 4455.

Ellis IO, G. M. (1992, Jun). Pathological prognostic factors in breast cancer. II. Histological type. Relationship with survival in a large study with long-term follow-up. *Histopathology, 20* (6), 479-89.

Esmat E, H. A.-G. (2024, Mar 27). Association of hormone receptors and human epidermal growth factor receptor-2/neu expressions with clinicopathologic factors of breast carcinoma: a cross-sectional study in a tertiary care hospital, Kabul, Afghanistan. *BMC Cancer, 24*((1), 388.

Falck AK, F. M. (2013, Nov). St Gallen molecular subtypes in primary breast cancer and lymph node metastases--aspects on distribution and prognosis for patients with luminal A tumours: results from a prospective randomised trial. *BMC Cancer., 25*(13), 558.

Hasa, A. X. (2024, December). BRCA1 and BRCA2 genes: Key genetic drivers in breast cancer risk and management. *Journal of Natural Sciences, 36*.

Hiral Samir Shah, N. A. (2020). CORRELATION OF ESTROGEN RECEPTOR(ER), PROGESTERONE RECEPTOR(PR) AND HER2/NEU EXPRESSION WITH CLINICOPATHOLOGICAL PARAMETERS IN PRIMARY BREAST CARCINOMA -A STUDY OF 175 CASES. *National Journal of Medical Research, 10* (02), 70–75.

Kohler BA, S. R. (2015, Mar 30). Annual Report to the Nation on the Status of Cancer, 1975-2011, Featuring Incidence of Breast Cancer Subtypes by Race/Ethnicity, Poverty, and State. *J Natl Cancer Inst., 107* (6).

Łukasiewicz S, C. M. (2021, Aug 25). Breast Cancer-Epidemiology, Risk Factors, Classification, Prognostic Markers, and Current Treatment Strategies-An Updated Review. *Cancers (Basel), 13* (17), 4287.

M., A. (2012). Correlation of hormone receptors with HER-2 Neu protein expression and the histological grade in invasive breast cancers in a cohort of Saudi Arabia. *Turk Patoloji Derg., 28*((1)), 38-43.

McGuire, A. B. J. (2015, May 22). Effects of age on the detection and management of breast cancer. *Cancers (Basel), 7*(2), 908-29.

MN., K. (2014). Immunohistochemistry subtypes (ER/PR/HER) of breast cancer: where do we stand in the West of Saudi Arabia? *Asian Pac J Cancer Prev., 15*(19), 8395-400.

MS., A.-A. (2006, Feb). HER-2 positivity and correlations with other histopathologic features in breast cancer patients—hospital-based study. *J Pak Med Assoc., 56*(2), 65-8.

Pathak TB, B. R. (2011). Estrogen and progesterone receptor expression in breast carcinoma. *Journal of Pathology of Nepal*, 100-103.

Senel, F. (2021, Oct–Dec). The hormone receptor status in breast cancer and the relationship of subtypes with clinicopathological features. *Indian Journal of Pathology and Microbiology, 64* (4), 671-676.

Sharif MA, M. N. (2009, February). Morphological profile and association of HER-2/neu with prognostic markers in breast carcinoma in Northern Pakistan. *Coll Physicians Surg Pak, 19*(2), 99-103.

Tero A. H. Jarvinen, M. P.-H. (2000, January). Estrogen Receptor Is Coexpressed with ER and PR and Associated with Nodal Status, Grade, and Proliferation Rate in Breast Cancer. *American Journal of Pathology, 156*(1).

Xhetani, M. H. (2024, Dec 1). BRCA1 mutations in family members with a breast cancer history. *EUROPEAN JOURNAL OF HUMAN GENETICS, 32*, 913-913.

Yip CH, R. A. (2014, Nov). Estrogen and progesterone receptors in breast cancer. *Future Oncol., 10*(14), 2293-301.

➢ *ORAL PRESENTATION*

Active Control of Air Suspension Systems in Commercial Vehicles

İ. Sina Kuseyri
Marmara University Department of Mechanical Engineering, Maltepe-İstanbul, Turkey

Corresponding author e-mail : sina.kuseyri@marmara.edu.tr

Abstract

Commercial vehicles such as public transportation busses can benefit from the height control of the chassis that an air suspension provides. Main benefits of height control are retaining a pitch angle parallel to the road for passenger comfort regardless of the load and road disturbance, and easy accessibility to vehicle for especially old or disabled people. Electronically controlled air suspension systems are commonly used in commercial vehicles to enhance ride comfort and improve handling stability. This paper focuses on the vehicle height adjustment process in actively controlled air suspension systems. A non-linear mathematical model for adjusting vehicle height is developed by integrating vehicle dynamics, suspension pneumatics, and the thermodynamic effects of compressible flow. A PID controller is proposed for accurate control of vehicle height. Effectiveness and performance of the proposed controller are verified by simulations.

Keywords: Modeling and simulation, air suspension, active control

1 Introduction

The background of ECAS is closely linked to advancements in both air suspension and electronic control technologies, bringing together the best of both worlds to create a highly adaptable and customizable suspension system. Initially adopted in high-end luxury vehicles, ECAS systems have gradually expanded their presence to other automotive segments, including commercial trucks and buses, further emphasizing their effectiveness and versatility in addressing the challenges of diverse driving scenarios. The advantages of ECAS in public transportation buses are notable for their contribution to both passenger comfort and overall vehicle performance. ECAS allows public buses to adjust their ride height based on the number of passengers, cargo load, or road conditions. Customizable ride height contributes to improved accessibility, making boarding and disembarking easier for passengers. The precise control over air pressure in ECAS results in a smoother and more comfortable ride for passengers.

In conventional passive air suspension systems vehicle height is continuously regulated by the direct connection between the air reservoir and air suspensions [1]. To keep the vehicle height constant in rough terrain, high pressure air is continuously supplied to the air springs. In ECAS, on the other hand, control is taken over by an electronic control device (ECU). Hence, air supply to the suspensions can be provided only if the vehicle height exceeds the predefined tolerance [2]. Therefore, actively controlled air suspension systems consume less pressurized air leading to energy savings during the ride.

In [3] the evolution of vehicle pneumatic suspension systems is reviewed. An adaptive LQR controller is designed in [4], and its performance is validated by experiments. Robust controllers for air suspension systems are designed in [5] using finite-time approach and in [6] considering unmodeled dynamics and parametric uncertainties. In [7] and [8] authors design model predictive controllers with a cooperative control method and with multi-mode switching damping respectively. In [9] authors proposed a fuzzy PID controller with nonlinear delay factors to control an ER damper. In [10] authors designed a fuzzy PID controller for damping control of the shock absorber by combining a PID control algorithm with the fuzzy control concept that involves a genetic algorithm-optimized fuzzy PID air suspension control approach.

In this paper we propose a basic PID controller for hight adjustment and road disturbance rejection of ECAS. It is shown that this basic controller is effective with acceptable performance. Modeling of electrical and mechanical parts of the drive system is presented in Section 2. Model based numerical simulation results are in Section 3. Finally we summarize the conclusions of our study in Section 4, and provide suggestions for further research.

2. System Dynamics

The height adjustment function of the ECAS system is achieved by inflating and deflating the air springs. The circuit diagram for this process is shown in Figure 1. It includes four air springs, one at each corner of the vehicle, a solenoid valve that regulates the airflow into the air springs, a compressor that provides compressed air when the gas pressure in the reservoir falls below a certain threshold, a reservoir that stores the compressed air, an air filter that removes impurities from the system, and an air dryer that removes moisture from the intake air to prevent damage caused by excess moisture.

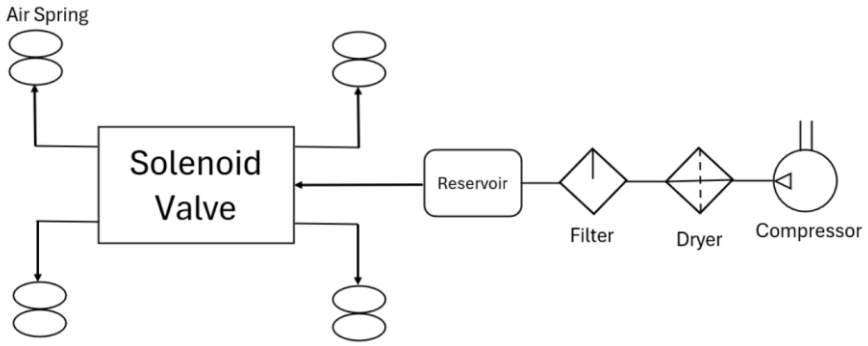

Figure 1: Pneumatics of the ECAS system

The displacement of the sprung mass (vehicle) is adjusted by inflating and deflating the air springs, which modifies the vehicle's height to achieve the desired driving performance.

During inflation, compressed air from the reservoir is directed into the air springs through the pipeline, raising the vehicle's height. In the deflation process, air is released from the air springs into the atmosphere via the pipeline, lowering the vehicle's height.

Based on the described height adjustment processes, a mathematical model for vehicle height adjustment can be derived by integrating vehicle dynamics, the compressible flow equations through the solenoid valve, and the thermodynamic behavior of the air in the air springs. The following assumptions/simplifications are made during this derivation:
i) Air is treated as an ideal gas, and its kinetic energy is considered negligible in all air springs.
ii) The pressure within the air reservoir remains constant, and there is no gas leakage from the system.
iii) The solenoid valve is modeled as a throttle (orifice).
iv) The pressure and temperature of the gas in the air springs are assumed to be uniformly distributed.
v) Rate of change of the volume and the effective area of air springs are constant.

2.1 Thermofluid models for the valve and air springs

As the solenoid valve in the gas circuit is simplified as an orifice, when the solenoid valve is open, area-normalized mass flow rate through the valve is

$$q_m = S_e P_u \phi \tag{1}$$

where the definition of parameter ϕ changes upon the choked and unchoked flow conditions.

$$\phi = \begin{cases} \sqrt{\dfrac{k}{RT}\left(\dfrac{2}{k+1}\right)^{\frac{k+1}{k-1}}} & \dfrac{P_d}{P_u} \le C_r \\ \sqrt{\dfrac{2k}{(k-1)RT}\left[\left(\dfrac{P_d}{P_u}\right)^{\frac{2}{k}} - \left(\dfrac{P_d}{P_u}\right)^{\frac{k+1}{k}}\right]} & \dfrac{P_d}{P_u} > C_r \end{cases} \tag{2}$$

In Equations (1) & (2) q_m is area-normalized mass flow rate, S_e is effective area of the valve, P_u is the upstream pressure, P_d is downstream pressure, R is the gas constant, k is polytropic index, T is the temperature, and C_r is the critical pressure ratio. The upper and lower parts in Equation (2) are for the choked and unchoked flow conditions respectively.

During the elevation of the vehicle, the upstream pressure is the pressure of the air in the reservoir, i.e., $P_u = P_r$, and the downstream pressure is the pressure of the air in the air spring, i.e., $P_d = P_s$. While lowering the vehicle, the upstream pressure is the pressure of the air in the air spring, i.e., $P_u = P_s$, and the downstream pressure is the atmospheric pressure, i.e., $P_d = P_{atm}$.

The variable mass thermodynamic model of air spring is derived to obtain a relationship of air pressure and the area-normalized mass flow rate of the pipeline. The charging and discharging process of the air spring is independent of each other and they are relatively fast, so they can be regarded as adiabatic processes. Assuming ideal gas conditions, the nonlinear dynamic model of the simplified air spring is

$$\dot{P_s} = \frac{kRT}{V} q_m - \frac{kP_s}{V}\dot{V}, \tag{3}$$

where rate of change of the volume of the air spring is

$$\dot{V} = \frac{dV}{dx}\dot{x} = V_x\dot{h}. \tag{4}$$

2.2 Mechanical model of the air suspension

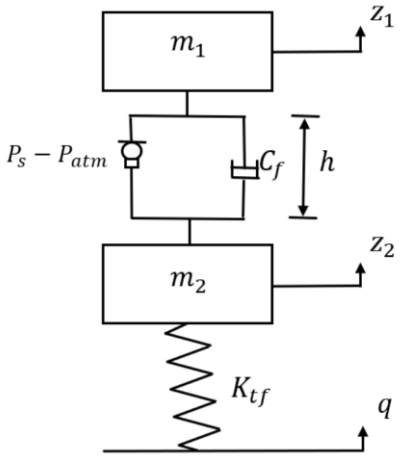

Figure 2: Quarter-vehicle mechanical model of the air suspension

Equations of motion for the quarter-vehicle mechanical model of the suspension system shown in Figure 2 are

$$m_1\ddot{z}_1 = (P_s - P_{atm})A_e + C_f\dot{h} - m_1 g \tag{5a}$$
$$m_2\ddot{z}_2 = K_{tf}(q - z_2) - (P_s - P_{atm})A_e - C_f\dot{h} \tag{5b}$$
$$\dot{h} = \dot{z}_2 - \dot{z}_1 \tag{5c}$$

In this model mass of the quarter-vehicle, m_1, can vary depending on the load on the vehicle.

3 Numerical Simulations and Results

Numerical simulations reflecting the active air suspension system performance during the cruise on a relatively rough road, and during the passage through a bump in this section. We also verify the performance of active control during the ascent and descent of the vehicle. Mathematical model of the air suspension system combined with the PID controller is composed in MATLAB/Simulink.

Rough road condition is modeled by a first order filter that takes white noise as its input [11]

$$q = n - \frac{1}{\omega_c v}\dot{q}, \tag{6}$$

where q is the vertical displacement of the road, n is the white noise signal, ω_c= 0.8 rad/s is the cut-off frequency, v= 7.5 m/s is the vehicle's speed. Bump on the road is modeled by

$$q = 0.15 \sin(9\pi t). \tag{7}$$

Hence bump has a height of 15cm, and a width of 83cm during the cruise with a speed of 7.5 m/s. We take only the half period of the sine signal to represent the bump.

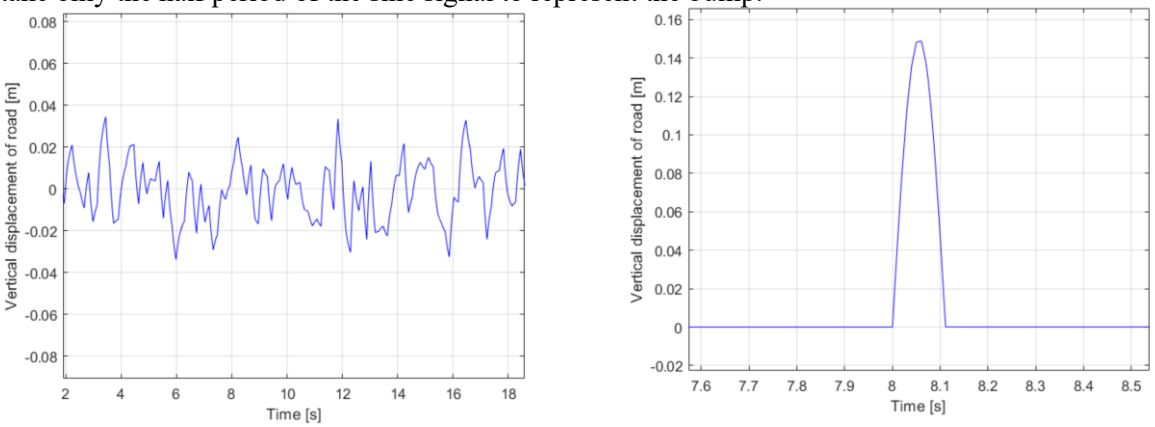

Figure 3: Rough road and bump models

Parameters of the suspension system used in the simulations is given in Table 1 [2]. PID controller gains, optimized by trial and error, are 3,5, 0.06, and 1.5 respectively with the filter coefficient 100.

Table 1: Air suspension parameters

Parameter	Symbol	Value
Sprung mass (kg)	m_1	1550
Unsprung mass (kg)	m_2	200
Nominal bus height (m)	h	0.5
Damping coefficient (kN.s/m)	C_f	8.3
Tire vertical stiffness (kN/m)	K_{tf}	750
Effective air spring area (m^2)	A_e	0.042
Unit change in volume (m^3/m)	dV/dx	0.045
Reservoir pressure (MPa)	P_r	0.8
Effective valve area (m^2)	S_e	$7.34x10^{-6}$
Polytropic index	k	1.38
Critical pressure ratio (kg)	C_r	0.528
Temperatue (K)	T	300

Response of the active air suspension system to a bump and to rough road disturbance is shown in Figure 4. When the vehicle passes over an 15 cm height bump, its height rises 5 cm during the transient response. Hence ECAS system bump suppression performance is 67%. Bus reaches the steady-state in 3 seconds.

The road disturbance model is a pseudorandom signal taking values in the range of $\pm$ 0.03 m The ECAS system is so adjusted that it does not take any action if the disturbance is within $\pm$ 0.02 m margin. If the road disturbance exceeds this margin controller activates air valves and bus height is adjusted. This mode is the main benefit of the active air suspension over the passive air suspension systems in disturbance rejection. Frequent switching of the air valve can cause premature wear of the components. Moreover, high energy consumption of the vehicle to generate compressed air is mitigated.

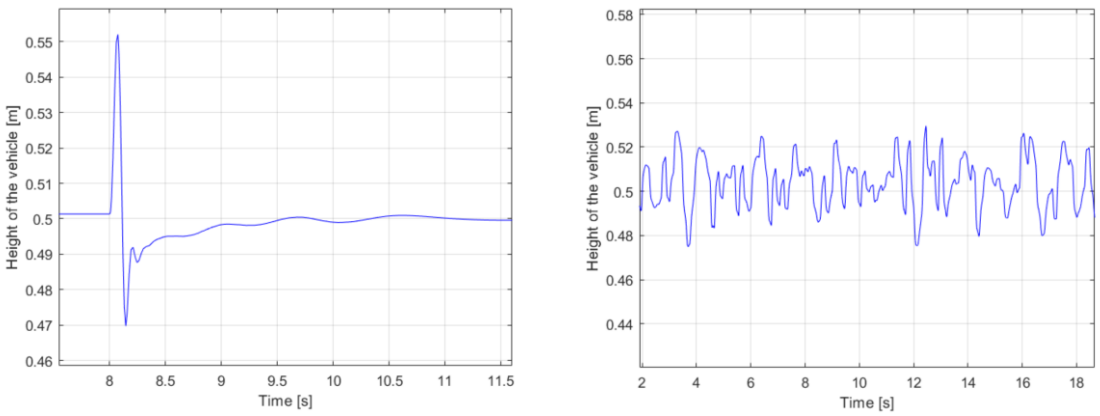

Figure 4: Bump and rough road responses

The ECAS system also enables the driver to adjust the height of the bus. In Figure 5 height adjustment processes are simulated.

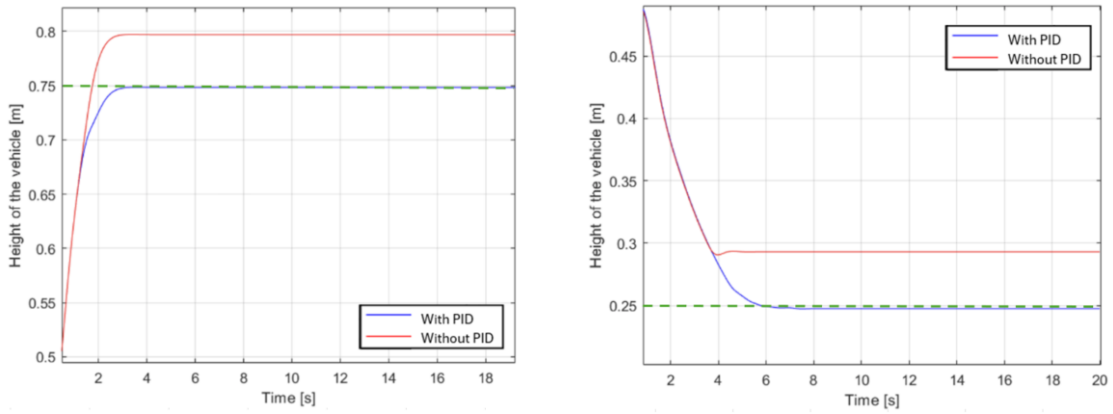

Figure 5: Height adjustment processes

Dashed green line is the target height in the simulations which is 0.75 m during the ascent of the vehicle body, and 0.25 m during the descent. Without feedback control system height is elevated to 0.8 m during descent which is 5 cm above the reference command. Feedback PID control achieves almost zero steady-state error. Similarly, during the descent of the vehicle feedback PID control achieves zero steady-state error as opposed to 4 cm error in the case without feedback. Moreover, it is clear from the figures that settling time during the vehicle ascent process (3 seconds) is approximately half of the settling time of vehicle descent process (6 seconds) hence, ascending the bus is faster than descending it. The difference stems from the fact that, during the ascent process, upstream pressure is reservoir pressure which is 0.8 MPa, whereas during the descent upstream pressure is the internal pressure of the air spring which is around 0.58 MPa.

4 Conclusion and Recommendations for Future Work

In this paper we have studied electronically controlled air suspension systems which represent a significant advancement in the field of public transportation, offering enhanced ride quality, improved safety, and enabling height adjustment. The implementation of ECAS in public buses addresses the critical need for adaptive suspension solutions that can respond dynamically to varying load conditions and road surfaces, thereby optimizing passenger comfort and vehicle stability and passengers' accessibility by height adjustment. The ECAS system used with the system specified in our work had a suppression performance for the bump on the road up to 67%. We have shown that Feedback PID control leads to zero steady state error during the height adjustment processes. Moreover, it is possible to deactivate the air valves if the road disturbance is less than a margin that can easily be tolerated by the passengers. Frequent switching of the air valve can cause premature wear of the mechanical components. Moreover, high energy consumption of the vehicle to generate compressed air can be mitigated. We recommend further studies to be made on the quantification of possible energy savings of active air suspension systems over their passive counterparts.

References

[1] Huang T., Chen G., Zong C., Zhou T., 2015, "Research on Vehicle Height Adjustment Control of Electronically Controlled Air Suspension", SAE Technical Paper, 2015-01-2750, doi:10.4271/2015-01-2750.

[2] Dou H., Chen L., Wang S., 2014, "Research on vehicle height adjustment control of electronically controlled closed loop air suspension", Journal of Mechanical Design and Manufacture, vol. 9, pp. 171-174.

[3] Atindana V.A., Xu X., Nyedeb A.N., Quaisie J.K., Nkrumah J.K., and Assam S.P., 2023 "The Evolution of Vehicle Pneumatic Vibration Isolation: A Systematic Review", Shock and Vibration, vol.2023, pp.1-23.

[4] Gokul P.S., Malar M.K., 2019, "A contemporary adaptive air suspension using LQR control for passenger vehicles", IPA Transactions, vol. 93, pp. 244-254.

[5] Yin C., Zhao D., Zhang J., Wang S., Xu X., Sun X., and Shi D., 2020, "Body height robust control of automotive air suspension system using finite-time approach", Asian Journal of Control, vol. 2021, pp. 1-13.

[6] Sun X., Yuan C., Wong P.K., Cabecinhas D., and Silvestre C., 2019, "Robust Ride Height Control for Active Air Suspension Systems With Multiple Unmodeled Dynamics and Parametric Uncertainties", IEEE Access, vol. 7, pp. 59185-59199.

[7] Geng G., Zeng S., Sun L., Li Z., and Yu W., 2022, "Cooperative Control of Inter-connected Air Suspension Based on Energy Consumption Optimization", Shock and Vibration, vol. 2022, pp. 1-13.

[8] Sun X., Yuan C., Cai Y., Wang S., and Chen L., 2017, "Model predictive control of an air suspension system with damping multi-mode switching damper based on hybrid model", Mechanical Systems and Signal Processing, vol. 94, pp. 94-110.

[9] Zhang P., Chen W., Wang H., Wang J., Lu H., and Cheng Z., 2022, "Fuzzy PID control method for damping of electronically controlled air suspension shock absorbers for vehicles", Eng. Res. Express, Vol. 4, 045020.

[10] Zhang S., Li M., Li J., Xu J., Wang Z., and Liu S., 2024, "Research on Ride Comfort Control of Air Suspension Based on Genetic Algorithm Optimized Fuzzy PID", Applied Sciences, vol. 14, no. 17, 7787.

[11] Liu H., Gao H., and Li P., 2013, "Handbook of Vehicle Suspension Control Systems", Institution of Engineering and Technology.

➢ *ORAL PRESENTATION*

A Hybrid Approach Using AHP-TOPSIS for the Patent Process in the R&D Company

Dilek Çelik[1*](*ORCID: https://orcid.org/0009-0002-8107-0547*),
Burçak Könen[1*](*ORCID: https://orcid.org/0009-0001-7025-7747*),
Nida Nur Uzel[1*](*ORCID: https://orcid.org/0009-0001-6690-2299*),
Gülçin Dinç Yalçın[1*](*ORCID: https://orcid.org/0000-0001-7696-7507*)

[1] Eskişehir Teknik Üniversitesi, İki Eylül Kampüsü, Mühendislik Fakültesi, Endüstri Mühendisliği Bölümü, 26555, Eskişehir, Türkiye

*Corresponding author e-mail: gdinc@eskisehir.edu.tr

Abstract
The objective of this study is to propose a methodology for the decision-making process concerning the patenting of innovations within an R&D company. The patenting process is to be integrated into the company's workflow at an opportune stage, in order to avoid loss of time and disruption to the process. Multi-criteria decision-making techniques are to be used to this end. Literature research was conducted to identify possible selection criteria, and these criteria were finalized through a survey. The AHP method was used to weight the criteria, and the TOPSIS method was used to evaluate and rank the existing projects that met the company's objectives and strategies. The development of a decision support system was undertaken to prioritize the patenting of projects and to allow it to be used by different companies.
Keywords: Multi Criteria Decision Making, AHP, TOPSIS, Patent, R&D Project, Decision Support System.

INTRODUCTION

Companies do not only create value but also compete with each other. To benefit from the advantages arising from the innovation process, companies must protect their innovations from being imitated by others. One of the mechanisms that enables companies to safeguard themselves in this regard is the patent system. A patent is a legal document that grants its holder exclusive rights to prevent others from making, using, or selling the invention without their consent for a specific time and place (Turkish Patent Institute, 2017). Patents play a crucial role in promoting innovation and economic growth. In addition to protecting an invention, patents also serve as a motivational factor for future ideas that have yet to be developed (Bennett, 2020). Obtaining a patent can provide a significant advantage for a company, especially for a research and development (R&D) company. However, the process of obtaining a patent is lengthy and challenging. Companies may find it daunting to determine which product or project to patent from the developed ones.

In their studies, Mehrez and Sinuany-Stern (1983) used Multi-Criteria Decision Making (MCDM) methods to address the project selection problem. MCDM methods, such as Analytic Hierarchy Process (AHP), Technique for Order of Preference by Similarity to Ideal Solution (TOPSIS), and Elimination and Choice Expressing the Reality (ELECTRE), are commonly used for solving decision-making problems. AHP, a MCDM method, is useful for solving complex problems with a small number of alternatives (Mahmoodzadeh et al., 2007). Developed by Saaty (1977), this mathematical theory is based on pairwise comparisons. AHP is structurally simple and popular for weighting criteria in decision-making.

In addition, the TOPSIS method was developed by Hwang and Yoon (1981) and has been applied in various fields by ranking a large number of alternatives and quickly identify the best option. The combination of AHP and TOPSIS has been frequently used in research due to the superiority of AHP in determining criteria weights compared to other methods and the ability of TOPSIS to identify the best alternative (Tavana and Hatami-Marbini, 2011). This combination has yielded positive results when used together.

The objective of this study is to create a systematic decision-making process for prioritising finished products or ongoing R&D projects of an R&D company in Eskişehir for patenting. The projects are ranked based on their importance, and a systematic decision-making process is used to identify the most suitable project for patenting. During the study, criteria for evaluating the projects were identified through a literature review. The specific criteria to be included in the project were then decided through an internal

survey within the company and surveys conducted with other companies. A decision support system for the Analytic Hierarchy Process (AHP) was created in Excel VBA to calculate the weights of the criteria based on the evaluations. The projects were ranked in order of importance using the Technique for Order of Preference by Similarity to Ideal Solution (TOPSIS) method, based on the assigned weights.

This study is unique in its focus on prioritising which product's patent process the company should initiate, among existing products and projects. This prioritisation is achieved through the use of multi-criteria decision-making techniques. The project's innovation lies in using multi-criteria decision-making techniques to determine which product or project the company should prioritize for initiating the patent process. This is done by considering the crucial criteria for the company before starting the patenting process. Moreover, the project's innovative and technological aspects are emphasised by the decision support system developed in the study. This system is intended for use not only by the company but also by other R&D firms in the future.

When reviewing the literature, it is evident that research tends to focus more on post-patenting processes, such as patent valuation, rather than determining which product should be patented. There is a noticeable gap in the literature regarding sufficient studies on the specific question of which product/project should be prioritised for patenting. Consequently, efforts have been made to explore studies that might be relevant to this topic.

Literature Review

In a study on the patenting process, patent-holding academics were surveyed to identify the difficulties they encountered. Qualitative research methods, specifically phenomenology and the trial model of content analysis, were employed to analyze the data (Tacgın, 2020). The study gathered information from academics and conducted literature reviews to identify codes within the scope of these studies. The identified difficulties include time constraints, financial limitations, the patronage system, and bureaucratic obstacles. To address these issues, it was concluded that administrations should engage in incentivizing activities and pursue process improvements in patenting.

Deger (2011) examined patent valuation and discussed four commonly used approaches: the market-based, income-based, cost-based, and option-based approaches. The study evaluated these methods and others to determine the most appropriate approach for patent valuation. The conclusion was that the option-based approach is the most suitable method.

A study on patent valuation was conducted, evaluating a company's ten patents using multi-criteria decision-making techniques, namely TOPSIS and VIKOR, with twelve criteria. The patents were then ranked using MOORA and ARAS. The criterion weights were determined using the entropy method. Although the obtained results had the same criterion weights, differences in rankings were observed due to the use of different methods. To address this issue, it is recommended that future studies conduct a sensitivity analysis to examine the impact of different weights on the results (Deniz, 2020).

A study (Yildirim and Yildirim, 2022)on R&D project selection using an Integrated Fuzzy Intuitive Group Decision-Making approach aimed to choose the most suitable R&D project among four alternatives for the year 2021. Linguistic evaluation expressions were used for this selection, and they were evaluated using fuzzy intuitive numbers. A decision matrix was used to identify the most ideal project, applying the Intuitive Fuzzy Grey Relational Analysis method. The study is based on Grey System Theory, which involves the mathematical modeling and analysis of grey systems to address uncertainties. Grey System Theory aims to enhance data analysis, predictions, and decision-making in situations involving a lack of information or uncertainty. The study determined the ideal project based on analysis scores.

Binici and Aksakal (2020) addressed the selection of R&D projects in their study. An expert group determined five criteria, including four benefit criteria and one budget criterion, for project evaluation. The Utilitee Additive (UTA) method was applied based on the identified criteria, and a mathematical model was formulated. The UTA method is used to evaluate various criteria and rank alternatives. It employs a mathematical model based on a specific decision matrix and criterion weights. The decision-maker's preferences are expressed through this matrix, which includes the performance of each alternative for each criterion. Criterion weights are factors that determine the importance and impact of each criterion. The mathematical model was solved using the General Algebraic Modeling System (GAMS), which resulted in the ranking of projects.

Bal and Taşçı (2021) conducted a study on patent evaluation, focusing on measuring patent value and identifying the key factors that determine it. They then scored the patent values of a climate control company. Ten patents were selected through literature reviews and scored using a rating table for indirect indicators, while direct indicators were evaluated using a Likert scale ranging from 1 to 5. The results showed that the 8 direct and indirect indicators used in the patent evaluation process significantly influenced the patent score.

The study by Demir and Soydoğan (2017) analysed the impact of patents on company performance in Turkey. The study aimed to determine whether patents had an effect on the economic performance of the firms. The study analysed the impact of patents on company performance using various methods, including Return on Assets (ROA), Return on Equity (ROE), number of employees, and export values. Statistical and trend analysis approaches were employed. The results showed a strong positive correlation between the number of patents and the number of employees, as well as between the number of patents and export values. However, no significant correlation was found between the number of patents and ROA or ROE values.

Göktaş and Gömleksiz (2011) conducted an analysis of the relationships between R&D expenditures, patents granted as an innovation indicator, researchers, and entrepreneurs. The study tested the relationships between innovation and entrepreneurship rates, R&D expenditures in sectoral classification, and the number of researchers for 25 countries, using the number of patent grants as an innovation indicator. The analysis was carried out through panel data analysis. The study indicates a significant correlation between innovation and R&D based on the coefficients linking patent grants, R&D activities, and the number of researchers.

Arıbaş and Özcan (2016) introduced a new methodology for evaluating academic research projects by combining AHP and TOPSIS methods. The study began by establishing criteria for comparing academic research projects. These criteria were then weighted using the AHP method and applied to TOPSIS to determine the importance of each project and rank them based on a sample. These criteria were then weighted using the AHP method and applied to TOPSIS to determine the importance of each project and rank them based on a sample. The results were then compared for a comprehensive evaluation.

Ömürbek et al. (2015) conducted a study on project selection in which they employed the AHP and TOPSIS methods to select a program for Enterprise Project Management Software from among alternative programs. The criteria identified in the literature were initially weighted using the AHP method through Excel. The study employed the TOPSIS approach to analyse various EPM algorithms and select the most suitable tool for the organization from the available options.

Durgun and Turan (2016) discuss the importance, advantages, eligibility conditions, and process workflows of obtaining patents in relation to protecting intellectual property rights arising from R&D activities and innovative ideas in companies. The study focuses on the management of the patent process within companies and includes a schematic of the patent application decision process. Assessments are conducted to evaluate the commercial potential of patents based on specific parameters. It is concluded that protecting innovative ideas is possible through obtaining patents, which is a result of innovation.

Yavuz and Baki (2019) conducted a study in which they ranked patents owned by an automotive company based on their values. They used multi-criteria decision-making methods due to the limited number of studies on this subject. The entropy method was chosen to determine criteria weights because of its realistic and objective weighting capabilities. The TOPSIS and VIKOR methods were used to rank the alternatives due to the benefit and cost-oriented nature of the criteria. A Spearman correlation analysis was applied to determine if there was a correlation between the results generated by the two methodologies. The comparison of the results demonstrated the applicability of the model.

Güryeli (2016) conducted a literature review on the selection of R&D projects and then used the AHP to model this subject and determine the relative weights of project evaluation criteria. Expert opinions were used to explore the prioritization levels of project evaluation criteria and the factors that referees gave more value to when evaluating projects in the AHP model. Furthermore, future research could expand the evaluation criteria within the scope of this study or develop a new network by modifying the existing structure. A new model could be created by examining the interactions between primary and sub-criteria in this new network.

Ceylan and Gürsev (2020) identified the general characteristics of software development projects and analysed the success criteria of these projects. The projects operate using different project management methodologies, such as Scrum, Kanban, and Waterfall. To determine the solution method for making selections based on importance ranking within certain criteria, the authors conducted a literature review. The research determined that the most appropriate methods for solving the MCDM problem are the AHP and the TOPSIS. Then AHP was chosen for its simplicity, ease of use, and effectiveness, while TOPSIS was selected for its ability to evaluate criteria based on their weights. The methods were explained in detail, and their applications were demonstrated. The study concluded that the Waterfall model did not improve company efficiency. Instead, project management techniques such as Scrum and Kanban were found to be more beneficial.

In a study on personnel selection in hospitality establishments, the AHP and TOPSIS methods were used to select personnel. To achieve the goal of personnel selection in human resource management, this text first details the definition and scope of the process and identifies the criteria. The identified criteria are then weighted using the AHP method, and the TOPSIS method is employed to select from 10 applicants. A resource has emerged that could be beneficial for other hospitality establishments. It provides a detailed analysis of different criteria and serves as a reference for developing applications related to personnel selection (Icigen and Cetin, 2017).

As indicated by the literature, MCDM methods are used to select projects prior to initiating them as R&D projects. However, this study employed MCDM methods for the completed R&D projects. R&D companies may focus on developing new projects and may not have time to patent them. They may have several completed projects that require patents. Due to time constraints, they may not be able to patent all of them simultaneously. Therefore, it is important to prioritize which projects to patent first. This study aims to assist R&D companies in prioritising their finished projects for patenting by using MSDM methods.

MATERIALS AND METHODS

The literature review has led to the conclusion that the most suitable multicriteria decision-making method for the project is TOPSIS. This decision is based on TOPSIS's ability to provide simple outputs, yield easily understandable results, measure distances to both positive and negative ideal solutions, and efficiently rank numerous alternatives. The TOPSIS method was applied, and the AHP was chosen to weight the criteria due to its ability to address both abstract and concrete criteria simultaneously in the decision-making process. AHP also allows for consistency checking, has broad application potential, and facilitates group decision-making by assigning weights to the criteria.

AHP Method

AHP, which was developed by Thomas L. Saaty in the 1970s, is a decision-making technique used to solve complex situations involving a large number of criteria. It allows for modelling in a hierarchical structure that shows the connections between criteria, sub-criteria, and alternatives. The most significant aspect of AHP is its ability to incorporate both objective and subjective evaluations of the decision-maker into the decision process. In essence, AHP is a method that combines an individual's knowledge, experience, thoughts, and intuitions in a logical manner. It has a broad range of applications and can be effectively used to solve various decision-making problems.

1. Determination of Selection Criteria
2. Weighting Using the AHP Method (Durak et al., 2021)

Step 1: In this stage, the decision-making problem is decomposed into fundamental building blocks, forming a hierarchical structure.

Step 2: After creating the hierarchical model, pairwise comparison matrices are established to determine the relative importance of all elements over each other.

Step 3:

The equation below is used to calculate the eigenvector value of the criteria in pairwise comparisons.

$$W_i = \frac{1}{n} \sum_{j=1}^{n} \frac{a_{ij}}{\sum_{j=1}^{n} a_{ij}}$$

- The maximum eigenvalue (λmax) is determined using the following equation to calculate the consistency indicator value.

$$\lambda_{max} = \frac{1}{n} \sum_{i=1}^{n} \frac{(a_w)_i}{w}$$

- The consistency index (CI) is calculated using the following equation.

$$CI = \frac{\lambda_{max} - n}{n - 1}$$

- The consistency ratio (CR) indicates whether the values given during pairwise comparisons are consistent with each other. The consistency ratio should be less than 0.10. In cases where it is high, the decision matrix needs to be revised and corrected.

$$CR = \frac{CI}{RI}$$

TOPSIS Method

The TOPSIS is a multiple criteria decision-making technique developed by Hwang and Yoon in 1981. It assumes that the alternative solution point is closest to the positive-ideal solution and farthest from the negative-ideal solution. The TOPSIS approach can be applied directly to the data without qualitative transformation (Omurberk et al., 2015).

1. Creation of the Decision Matrix

2. Normalization of the Decision Matrix

$$y_{ij} = x_{ij} \div \sqrt{\sum_{i=1}^{I} x_{ij}^2}$$

3. Weighting of the Normalized Decision Matrix

$$v_{ij} = W_j * y_{ij}; (i = 1,2, \dots, I; j = 1,2, \dots, J)$$

$$V = \begin{bmatrix} v_{11} & v_{12} & \cdots & v_{1J} \\ v_{21} & v_{22} & \cdots & v_{2J} \\ \cdots & \cdots & \cdots & \cdots \\ v_{I1} & v_{I2} & \cdots & v_{IJ} \end{bmatrix}$$

4. Determination of Ideal and Negative-Ideal Solutions

$$A^* = [\, v_1^*, v_2^*, \dots, v_J^*]$$

$$A^- = [\, v_1^-, v_2^-, \dots, v_J^-$$

$$v_j^* = \begin{cases} \max v_{ij}, if\ criteria\ j\ are\ beneficial \\ \min v_{ij}, if\ criteria\ j\ are\ cost \end{cases}$$

$$v_j^- = \begin{cases} \min v_{ij}, if\ criteria\ j\ are\ beneficial \\ \max v_{ij},\ if\ criteria\ j\ are\ cost \end{cases}$$

5. Calculation of Separation Measure

$$S_i^* = \sqrt{\sum_{j=1}^{J}(v_{ij} - v_j^*)^2} \qquad S_i^- = \sqrt{\sum_{j=1}^{J}(v_{ij} - v_j^-)^2}$$

6. Calculation of Proximity to the Ideal Solution

$$V_i = \frac{S_i^-}{S_i^- + S_i^*}$$

7. Ranking of Alternatives

Application of AHP and TOPSIS Methods for Product Selection

Priliminary Search for Products to be Patented:

The company has identified 20 products for patenting purposes. Literature reviews were conducted using Turkish Patent Institute (Türkpatent) (2023) for patents obtained only in Turkey, and Espacenet (2023), Google Patents (2023), and Patentscope (2023) for patents obtained both in Turkey and worldwide. After researching these 20 products and consulting with the company, it was decided to proceed with patent applications for six of them. These six products were chosen because they are less commonly discussed in the literature and have a higher priority for the company.

Determination of Criteria:

After conducting a literature review and consulting with the company, we identified potential criteria that are crucial for obtaining a patent. We then conducted an open-ended questionnaire survey among the company employees based on these criteria to determine if there are any other important factors. It is important to note that these criteria should be capable of obtaining numerical values. Accordingly, the survey employs the most suitable method for criteria that can take numerical values. Table 1 lists the potential criteria included in the survey.

Table 1. Possible Criteria

Criteria Code	**Possible Criterias Criteria**
PC1	The Annual Sales Amount of Product
PC2	The Variety of Sectoral Use of Product
PC3	Product Time to Market
PC4	Return of Profit of Product
PC5	Adaptability of the Product to Technology
PC6	The Cost of Product

The survey was participated in by seven employees. The following are additional criteria suggested by the employees, along with a percentage graph of the criteria that are considered a priority based on the survey results (See Figure 1 below).

Criterion Suggestions:

- Innovation, sustainability
- Feasibility of the product
- Number of personnel working on the Project

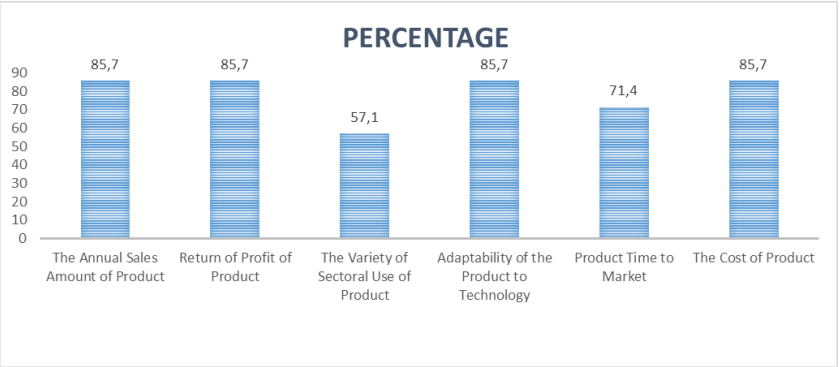

Figure 1. Percentages of Criteria

After reviewing the survey results and discussing with the company, we concluded that the criterion 'Adaptability of the Product to Technology' was not applicable since all of the company's products already have up-to-date technological features. During discussions with the company management regarding employee suggestions, it was emphasized that these criteria do not hold significant importance in the context of patent acquisition. Thus, we reached an agreement on the remaining five criteria to be used in our study. The finalised criteria are listed in Table 2.

Table 2. Finalised Criteria

Criteria Code	Criteria
C1	The Annual Sales Amount of Product
C2	The Variety of Sectoral Use of Product
C3	Return of Profit of Product
C4	The Cost of Product
C5	Product Time to Market

Application of AHP Method :

A study was conducted to determine the criteria and assess their importance among employees of the company through a company-wide survey. The employees ranked the criteria by assigning numbers from 1 to 9, including even numbers, to each criterion. To improve the study and obtain better results, it was decided to conduct a broader survey involving individuals with expertise in the field. The survey had 39 participants, 33 of whom provided rankings and the remaining 6 provided a single numerical score without ranking. The priority rankings of the 33 individuals and 4 company employees are presented in Figure 2 ant the meaning of rankings are listed in Table 3.

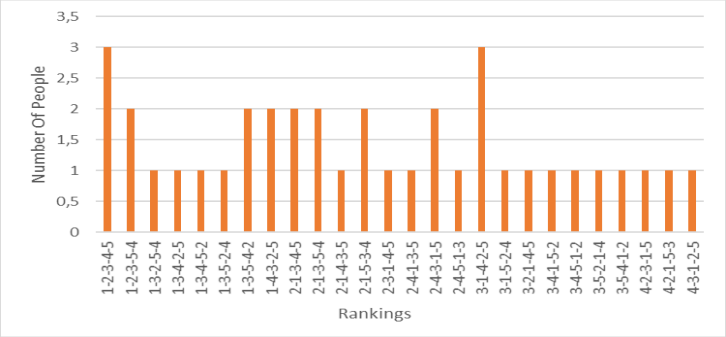

Figure 2. The Rankings Obtained as a Result of the Survey

Table 3. 1-9 Scale Used in Pairwise Comparison Method

DEGREES		DEFINITION
1	[redacted]	Equally important
3	[redacted]	A little more important
5	[redacted]	Strongly important
7	[redacted]	Very strongly important
9	[redacted]	Extremely important
2-4-6-8		Intermediate (Average) Values

The Analytic Hierarchy Process (AHP) steps were analysed to develop a decision support system using Excel VBA (See Figure 3). The system comprises of five buttons, namely: Pairwise Comparison Button, Criteria Weight Button, Normalisation Button, Consistency Ratio Button, and Result Button.

The Pairwise Comparison Button is used to establish the importance degrees of each criterion relative to other criteria on a scale of 1-9 in the first step of the pairwise comparison matrix. The matrix used for pairwise comparison is constructed by filling the upper triangular matrix with user-inputted superiority values (x_{ij}), while the values in the lower triangular matrix are determined by taking the reciprocal of the corresponding upper triangular values ($x_{ji} = \frac{1}{x_{ij}}$). The sum of values in each column is then calculated to construct the pairwise comparison matrix. A copy of this matrix is stored in a separate table. To normalize the values in the pairwise comparison matrix, use *the normalization button*. Normalization is accomplished by dividing each value in a column by the sum of that column. *The criterion weighting button* calculates the arithmetic mean of each row for the normalized values, which form the criterion weights. At *Consistency Test Button- 2* , to perform the consistency test, divide the values in each column of the pairwise comparison matrix by the criterion weights calculated for each row and then sum the resulting values row-wise.

At *Consistency Test Button- 2* , the values for each row are summed and then divided by the criterion weights. The resulting values are then averaged to obtain the maximum lambda (lambda max) value. Depending on the number of criteria (n), the Random Index (RI) is determined (1.115 for n=5). The table below shows the Random Consistency Index values. The Consistency Index (CI) can then be calculated. To determine consistency, divide the Consistency Index by the Random Consistency Index to obtain the

Consistency Ratio (CR). If the CR is less than 0.1, the criterion weights are consistent. If the CR is greater than 0.1, the user is prompted to re-enter the superiority values.

The geometric mean of the criterion weights obtained from 37 people is taken, and the final criterion weights for each criterion are shown in Table 4.

Figure 3. AHP Excel Interface



Table 4. Final Criteria Weights

Criteria	**Weights**
C1	0.138606
C2	0.246019
C3	0.101705
C4	0.232352
C5	0.281319

Application of TOPSIS :

The TOPSIS method has been applied with the final criterion weights obtained from the AHP method. The steps of the TOPSIS method have been coded in Excel VBA, and a user interface has been created. The Excel interface is shown in Figure 4.

Weight	0.138606	0.246019	0.101705	0.232352	0.281319	
	C1- Annual Sales Amaount of Product	C2- The Variety of Sectoral Use of Product	C3- Return of Profit of Product	C4- The cost of Product	C5- Product Time to Market	Topsis
1. Ürün	480	17	0.2	17508.03	18	
2. Ürün	5	17	0.4	23938.56	36	
3. Ürün	40	17	0.3	32829.29	24	
4. Ürün	5	17	0.5	34216.07	18	
5. Ürün	100	17	0.5	30493.11	24	
6. Ürün	30	17	0.3	23582.97	18	
	492.8995841	41.641326	0.9380832	67926.974	58.480766	
1. Ürün	0.973829184	0.4082483	0.2132007	0.2577478	0.3077935	*Normalization matrix
2. Ürün	0.010144054	0.4082483	0.4264014	0.3524161	0.615587	
3. Ürün	0.081152432	0.4082483	0.3198011	0.4833027	0.4103913	
4. Ürün	0.010144054	0.4082483	0.5330018	0.5037185	0.3077935	
5. Ürün	0.20288108	0.4082483	0.5330018	0.4489102	0.4103913	
6. Ürün	0.060864324	0.4082483	0.3198011	0.3471812	0.3077935	
1. Ürün	0.134978568	0.1004368	0.0216836	0.0598882	0.0865882	*weighted normalization matrix
2. Ürün	0.001406027	0.1004368	0.0433672	0.0818846	0.1731763	
3. Ürün	0.011248214	0.1004368	0.0325254	0.1122963	0.1154509	
4. Ürün	0.001406027	0.1004368	0.0542089	0.11704	0.0865882	
5. Ürün	0.028120535	0.1004368	0.0542089	0.1043052	0.1154509	
6. Ürün	0.00843616	0.1004368	0.0325254	0.0806683	0.0865882	
Vj*	0.134978568	0.1004368	0.0542089	0.0598882	0.0865882	
Vj-	0.001406027	0.1004368	0.0216836	0.11704	0.1731763	
						Si*
1. Ürün	0	0	0.0010579	0	0	0.0325254
2. Ürün	0.017841624	0	0.0001175	0.0004838	0.0074975	0.1610606
3. Ürün	0.0153092	0	0.0004702	0.0027466	0.0008331	0.1391368
4. Ürün	0.017841624	0	0	0.0032663	0	0.1452857
5. Ürün	0.011418639	0	0	0.0019729	0.0008331	0.1192668
6. Ürün	0.016012981	0	0.0004702	0.0004318	0	0.1300576
						Si-
1. Ürün	0.017841624	0	0	0.0032663	0.0074975	0.1691315
2. Ürün	0	0	0.0004702	0.0012359	0	0.0413047
3. Ürün	9.68686E-05	0	0.0001175	2.25E-05	0.0033322	0.0597423
4. Ürün	0	0	0.0010579	0	0.0074975	0.0924955
5. Ürün	0.000713665	0	0.0010579	0.0001622	0.0033322	0.072567
6. Ürün	4.94228E-05	0	0.0001175	0.0013229	0.0074975	0.0948018
	Vi	Ranking				
1. Ürün	0.83870933	1				
2. Ürün	0.20410967	6				
3. Ürün	0.300395057	5				
4. Ürün	0.388993977	3				
5. Ürün	0.378280572	4				
6. Ürün	0.421604855	2				

Figure 4. TOPSIS Excel Interface

The values corresponding to each criterion for the product/system to be patented were obtained from the company, and the relevant data is provided in Table 5.

Table 5. Criteria Values

Product	The Annual Sales Amount of Product	The Variety of Sectoral Use of Product	Return of Profit of Product	The Cost of Product	Product Time to Market
1st. Product	480 Product	17	20 %	17508.03 €	18 months
2nd. Product	5 Product	17	40 %	23938.56 €	36 months
3rd. Product	40 Product	17	30 %	32829.29 €	24 months
4th. Product	5 Product	17	50 %	34216.07 €	18 months
5th. Product	100 Product	17	50 %	30493.11 €	24 months
6th. Product	30 Product	17	30 %	23582.97 €	18 months

The interface of the method includes a "TOPSIS" button. All steps are executed by clicking the "TOPSIS" button. The ranging values are given in Table 6.

Table 6. Vi Values

Product	Vi
1st. Product	0.83870933
2nd. Product	0.20410967
3rd. Product	0.300395057
4th. Product	0.388993977
5th. Product	0.378280572
6th. Product	0.421604855

RESULTS AND DISCUSSION

According to the results of the TOPSIS method based on the values obtained from the company for the products and their criterion values, the maximum value of Vi is 0.83870933. As a result, it is observed that the first product should be patented, which aligns with the goal of our study. Additionally, the prioritization of products to be patented is clarified. The recommended ranking for patent acquisition based on the identified criteria and their values for six products in our study is provided in Table 7.

Table 7. Prioritisation of Products to be Patented

Ranking	Product No
1.	1st. Product
2.	6th. Product
3.	4th. Product
4.	5th. Product
5.	3rd. Product
6.	2th. Product

Electre Method:

The Electre method was used in our study as an alternative to the TOPSIS method for comparison and control. The products obtained equal scores and were ranked 1-6-4-5-2-3 (Ranking-1), 1-6-4-5-3-2 (Ranking-2), 1-6-5-4-2-3 (Ranking-3), and 1-6-5-4-3-2 (Ranking-4) respectively in terms of priority for patent acquisition among the six products. Based on the results, it is recommended to prioritize patent acquisition for the first product, similar to the TOPSIS method.

Spearman Correlation :

The consistency of MCDM methods are compared with Spearman Correlation coefficient values whic is computed as $r_s = 1 - \frac{6\sum_i d_i^2}{I(I^2-1)}$ where r_s and d_i are the Spearman Correlation coeffient and difference between rankings, respectively. The Spearman Correlation coeffient values of rankings from both TOPSIS and Electre are given in Table 8 and as shown from Table 8, the rankings are consistency.

Table 8. Spearman Correlation coefficient values between rankings

Methods	TOPSIS	Electre (Ranking-1)	Electre (Ranking-2)	Electre (Ranking-3)	Electre (Ranking-4)
TOPSIS	1	0.9428	1	0.8857	0.9428
Electre (Ranking-1)	0.9428	1	0.9428	0.9428	0.8857
Electre (Ranking-2)	1	0.9428	1	0.8857	0.9428
Electre (Ranking-3)	0.8857	0.9428	0.8857	1	0.9428
Electre (Ranking-4)	0.9428	0.8857	0.9428	0.9428	1

CONCLUSION

Companies aim to distinguish their products and projects from others by obtaining patents. However, some companies tend to overlook this process due to its time-consuming nature. Therefore, it is important for companies to effectively use the patent acquisition process and ensure that the right product/project receives a patent.

The study analysed the relationships between projects at an R&D company in Eskisehir, Türkiye and the importance levels of identified criteria using the AHP and TOPSIS methods. Each project was evaluated based on five criteria: Annual Sales Volume of the Product, Sectoral Usage Diversity of the Product, Profitability of the Product, Cost of the Product, and Time to Market for the Product.

An assessment was conducted to determine the consistency of the identified criteria. The assessment was

carried out using a decision support system created in Excel VBA. A total of 39 participants took part in the assessment, including 4 employees from the company and 35 individuals working on R&D from different companies. Upon examining the results of the assessment, the consistency of the criteria weights was confirmed for 37 responses. To ensure consistency ratios were uniform, we calculated the geometric averages of each individual's consistency ratios to determine the final criteria weights. Prior to applying the TOPSIS method, we conducted a literature review on patent acquisition for 20 R&D projects identified and communicated by the company. After screening, we narrowed the scope of the study to 6 projects. Using the TOPSIS method, a priority order was established among the six projects for patent acquisition. Based on the results, it was recommended that the company pursue a patent acquisition study for the first product. This recommendation was validated using the alternative method, Electre.

ACKNOWLEDGEMENTS

This study was conducted within the scope of Project No. 22LÖP395 by the Scientific Research Projects Coordination Unit of Eskişehir Technical University and supported by TÜBİTAK (The Scientific and Technological Research Council of Turkey) within the framework of the 2209B University Students Research Projects Support Program.

REFERENCES

Aribaş M & Özcan U. (2016). Evaluation of academic research projects using AHP and TOPSIS methods. Journal of Polytechnic, 19(2):163-173. (article in turkish with an abstract in English)

Bal S & Taşçı T. (2021). Determination of direct and indirect indicators in the patent evaluation process and their application in an air conditioning company. European Journal of Science and Technology, 23:868-874. (article in Turkish with an abstract in English)

Bennett DE. The power of patents and their strategic use. Accessed 13 March 2023. https://coatsandbennett.com/wp-content/uploads/2020/06/power-of-patents.pdf

Binici E & Aksakal E. (2020). A new approach to R&D Project selection problem and a solution proposal: UTA method. Pamukkale University Journal of Engineering Sciences, 26(1):211-226.

Ceylan Z, Gürsev S. (2020). Coomparison of Scrum-Kanban-Waterfall applications in information technology projects using AHP and TOPSIS methods. Journal of Information Technologies, 13(3):329-339.

Değer A. (2011). Patent valuation and reel options. Business and Economics Research Journal, 2(1):153-172.

Demir AZ & Soydoğan D. (2017). Patent innovation relationship and patent's effects on company performance. Journal Of International Social Research, 10(49):589-595. (article in Turkish with an abstract in English)

Deniz N. (2020). Patent evaluation with MOORA and ARAS multi criteria decision making techniques in technology management. Dumlupınar University Journal of Social Bilimler Sciences, 64:191-207.

Durgun I & Turan S. Patent Process Management in Companies. In 4th International Symposium on Innovative Technologies in Engineering and Science; 3-5 November 2016; Alanya, Antalya, Turkey, pp. 1083-1091. (article in turkish with an abstract in English)

Durak I, Arslan HM & Ozdemir Y. (2021). Application of AHP-TOPSIS methods in technopark selection of technology companies: Turkish case. Technology Analysis & Strategic Management 2021, 34(10):1109-1123.

Espacenet. Otomatik Yönlendirmeli Araç. Accessed 13 March 2023. https://worldwide.espacenet.com

Hwang CL & Yoon K. Multiple Attribute Decision Making: Methods and Applications. A State-of-The-Art Survey Lecture Notes in Economics and Mathematics Systems, No. 186, New York: Springer-Verlag, 1981.

İçigen ET & Çetin Eİ. (2017). AHP temelli TOPSIS yöntemi ile konaklama işletmelerinde personel seçimi. Balkan Journal Of Social Sciences 2017, 7(13):79-187. (article in turkish with an abstract in English)

Google Patents. Otomatik Yönlendirmeli Araç. Accessed 13 March 2023. https://patents.google.com

Göktaş AGD & Gömleksiz YLÖM. (2011). Effects of R&D activities and entrepreneurs on innovation: evidence from patent data. PARADOKS Echonomy, Sociology and Policy Journal, 7(2):27-44. (article in turkish with an abstract in English)

Güryeli M. (2016). An investigation to R&D Project selection problem with AHP method: An application to public sponsored technological product investment program. M.sc, Adnan Menderes University, Aydın, Turkey. (thesis in turkish with an abstract in English)

Mahmoodzadeh S, Shahrabi J, Pariazar M & Zaeri M.S. (2007). Project selection by using fuzzy AHP and TOPSIS technique. World Academy of Science Engineering and Technology, 30:333-338.

Mehrez A & Sinuany-Stern Z. (183). An interactive approach for project selection. Journal of the Operational Research Society, 34(7):621-626.

Ömürbek N, Makas Y & Ömürbek V. (2015). Selecting software programs for enterprise project management with AHP and TOPSIS. Journal of Süleyman Demirel University Institute of Social Sciences, 21:59-83. (article in turkish with an abstract in English)

Patentscope. Otomatik Yönlendirmeli Araç. Accessed 13 March 2023. https://www.wipo.int/patentscope/en

Saaty TL. (1977). A scaling method for priorities in hierarchical structures. Journal of Mathematical Psychology, 15(3): 234-281.

Taçgın Z. (2020). A Qualitative study reflecting the patents opinions on the patenting process. Journal of Balkan and Near Eastern Studies 2020, 6(1):75-88. (article in Turkish with an abstract in English)

Tavana M & Hatami-Marbini A. (2011). A group AHP-TOPSIS frame work for human space flight mission planning at NASA. Expert Systems with Applications 2011, 38(11):13588-13603.

Turkish Patent Institute. Utility Model/Patent 2017. Accessed 13 March 2023. https://www.turkpatent.gov.tr/en

Türkpatent. Otomatik Yönlendirmeli Araç. Accessed 13 March 2023. https://www.turkpatent.gov.tr

Yıldırım BF & Yıldırım SK. (2022). A new integrated intuitonstic fuzzy group decision making approach for R&D project selection process. Journal of Engineering Sciences and Designs 2022, 10(2):643 – 653. (article in Turkish with an abstract in English)

Yavuz N & Baki B. (2019). The ranking of the patent values with multi criteria decision-making methods: an application in automotive sector. Karadeniz Teknik Üniversitesi Sosyal Bilimler Enstitüsü Sosyal Bilimler Dergisi, 9(17):27-52. (article in turkish with an abstract in English)

➢ *ORAL PRESENTATION*

HER-2/neu receptor expression in breast cancer among Albanian females.

[1]Albina Hasa, [2,3]Merita Xhetani,

[1]Aldent University, Faculty of Technical Medical Sciences, Department of Medical Laboratory Technician and Imaging, Tirana, Albania
[2]University of Tirana, Faculty of Natural Sciences, Department of Biology, Tirana, Albania
[3]Center of Molecular Diagnostics and Genetic Research, Tirana, Albania

Abstract
Globally, breast cancer is the most common type of cancer and the second leading cause of cancer mortality. Our research aims to evaluate the expression of the HER-2/neu receptor in women diagnosed with breast cancer and to examine its correlation with other prognostic indicators of the disease. A retrospective study of 252 women with breast cancer was conducted at the oncology department of Mother Teresa University Hospital in Albania between 2021 and 2024. Statistical analysis was performed utilizing SPSS. The age group over 45 years old has the highest rate (92.5%), compared to the age group under 45 years old (7.5%). A significant association between HER-2/neu and the variables, disease stage, and age was observed (p=0.033; p=0.035). An inverse association was observed between Her-2/neu expression and receptor status.
Keywords: Breast cancer, Albanian population, HER-2/neu receptor.

INTRODUCTION

Globally, breast cancer is the most common type of cancer and the second leading cause of cancer mortality (Pathak TB B. R., 2011).
Her-2/neu, known as c-erbB-2, is a protooncogene located on chromosome 17. It is amplified and/or overexpressed in 15% to 25% of invasive breast carcinomas, leading to a worse clinical outcome (Kaptain, 2001). HER2-positive Breast cancer is defined as breast cancer that tests positive for the protein human epidermal growth factor receptor 2 (HER2). This protein promotes the proliferation of cancer cells.
The interaction of ER, PR, and Her-2/neu has become crucial in the treatment of breast cancer (Allred, 2010).

MATERIALS AND METHODS

The research comprised 252 Albanian women. The data of our study were acquired from patients diagnosed with breast cancer in the oncology service of the Mother Teresa University Hospital throughout the years 2021-2024. We have analysed all the data related to breast cancer in the medical records of all the subjects included in the study (personal data, clinical manifestation, histopathological classification, stage, and receptor status.
Statistical analysis was conducted utilizing SPSS. Descriptive and analytic data were evaluated. A p-value of less than or equal to 0.05 was deemed statistically significant. Tables and graphs illustrate the results.

RESULTS

7% of participants were under 45, while 93% were above 45, with an average age of 62.2 years. The majority of breast cancer patients were grade II (69.8%), and ductal carcinoma was the most prevalent form at 81.3%. The left breast was mostly affected (57.1%). According to the receptor measurements in the study, 14.27% of the subjects were HER-2/neu positive. The mean age of subjects with Her-2/neu overexpression was 58, compared with those lacking Her-2/neu, ER, and PR expression, 63. Of the subjects, 88.9% were

non-TN, and 11.1% were TN. The analysis of the association between receptor status (TN and non-TN) and age group revealed a statistically significant association (p = 0.02). There was also a significant association between HER-2/neu and the age variable (p = 0.035).

A statistically significant correlation (p =0.035) existed between HER-2/neu and age. There was a significant association between the HER-2/neu receptor and disease stage (p = 0.033). HER-2/neu had a weak, negative, but significant correlation with ER (r = -0.174, p = 0.006) and PR (r = -0.171, p = 0.008).

Table 1: Distribution of receptors according to each other.

			Er	Pr	Her2	Receptor Status
Spearman's rho	Er	Correlation Coefficient	1.000	.589**	-.174**	.678**
		Sig. (2-tailed)	.	.000	.006	.000
		N	252	250	245	252
	Pr	Correlation Coefficient	.589**	1.000	-.171**	.578**
		Sig. (2-tailed)	.000	.	.008	.000
		N	250	250	243	250
	Her2	Correlation Coefficient	-.174**	-.171**	1.000	-.084
		Sig. (2-tailed)	.006	.008	.	.191
		N	245	243	245	245
	Receptor status	Correlation Coefficient	.678**	.578**	-.084	1.000
		Sig. (2-tailed)	.000	.000	.191	.
		N	252	250	245	252

Table 2: The association of HER-2/neu with ER & PR.

HER-2	ER			PR		
	0%	1-9%	10-100%	0%	1-9%	10-100%
0-1+ /negative	27	2	181	33	4	172
2+/ equivocal	0	0	12	1	0	11
3+ / positive	8	3	12	11	0	11

DISCUSSIONS

The HER2 gene is 15-25% positive in breast cancer (Senel, 2021) (Kohler BA, 2015). HER2/neu in our study was 14.277%.

Measurable amounts of ER and PR receptors are found in about 50–85% and 60-70% of patients with breast cancer (Senel, 2021). In our study, the ER receptor was positive in 85.3% of the subjects & the PR receptor was 80.6%. Other studies have found varying expressions of estrogen and progesterone receptors in breast cancer, (Yip CH, 2014) (Łukasiewicz S, 2021), (Ambroise M, 2011), (MN., 2014).

A significant inverse relation between Her-2/neu overexpression and ER and PR expression was found in different studies. (Anupama Dayal, 2016), (Azizun-Nisa, 2008), (M., 2012), (MS., 2006), (Bhagat, 2012).

Our study resulted in an inverse association between Her-2/neu and ER, PR receptor status. Her2/neu has a weak, negative, but significant correlation with ER (r=-.174, p=0.006) and PR (r=-.171, p=0.008). ER has a strong, positive, and significant association with PR (r=.589, p<0.01).

In a study, HER-2/neu positivity decreased with rising age. ER and PR expression were significantly lower in HER-2/neu positive as compared with HER-2/neu negative tumors (ER 83.8% vs 69.8%; PR 91.9% vs 77.8%). In the HER-2/neu positive tumors, ER and PR expression in high-grade tumors was significantly decreased compared with intermediate-grade tumors (ER 5.6% vs. 10.5%; PR 0% vs. 5.3%) (Azizun-Nisa, 2008). In another study, there is a strong association between ER receptor and histological grade(p=0.0003) (Tero A. H. Jarvinen, 2000).

In our study, a significant association was observed between the disease stage and HER-2/neu assessed in the study (p=0.003). Advanced stages were more likely to exhibit increased positivity for HER2/neu.

Ductal carcinoma is the most common histological type (81.3%) of breast cancer, comparable to other studies. (Azizun-Nisa, 2008), (Sharif MA, 2009), (Anupama Dayal, 2016), (Pathak TB B. R., 2011), (Ellis IO, 1992), (Hiral Samir Shah, 2020).

13.9% (35/252) of the subjects were identified with a family history of cancer. In our most recent article, which is a review of the significance of the BRCA1 and BRCA2 genes, we underscore the significance of these genes in the diagnosis of hereditary breast cancer (Xhetani, 2024) (Hasa, 2024).
Based on our current findings on breast cancer, we intend to conduct additional research on BRCA genes in women with a family history of breast cancer.

CONCLUSION

A significant association was found between different histological grades and HER-2/neu immunoreactivity. The overexpression of HER-2/neu leads to a worse prognosis. There is an inverse association between HER-2/neu and ER/PR receptors. ER/PR receptors show an inverse association with histological grades of tumor; the higher the overexpression of ER/PR receptors, the better the diagnosis. The combined assessment of HER-2/neu and ER/PR may provide significant prognostic insights for the clinical management of breast cancer patients.

ACKNOWLEDGEMENTS

I wish to express deep regards to the oncology department of Mother Teresa University Hospital in Albania for their cooperation in this study.

References

Allred, D. (2010). Issues and Updates: Evaluating Estrogen Receptor-α, Progesterone Receptor, and HER2 in Breast Cancer. *Modern Pathology, 23*, S52-S59.

Ambroise M, G. M. (2011). Immunohistochemical profile of breast cancer patients at a tertiary care hospital in South India. *Asian Pac J Cancer Prev., 12*(3), 625-9.

Anupama Dayal, R. J. (2016, November 8). Correlation of Her-2/neu Status With Estrogen, Progesterone Receptors and Histologic Features in Breast Carcinoma. *Annals of Pathology and Laboratory Medicine., 3*.

Azizun-Nisa, B. Y. (2008 , Oct-Dec). Comparison of ER, PR and HER-2/neu (C-erb B 2) reactivity pattern with histologic grade, tumor size and lymph node status in breast cancer. *Asian Pacific Journal of Cancer Prevention., 9*(4), 553-6.

Bhagat, .. V. (2012). CORRELATION OF HORMONAL RECEPTOR AND Her-2/neu EXPRESSION IN BREAST CANCER: A STUDY AT TERTIARY CARE HOSPITAL IN SOUTH GUJARAT. *National Journal of Medical Research,, 2*(03), 295–298.

CC., B. (2008, Apr). Impact of aging on the biology of breast cancer. *Crit Rev Oncol Hematol., 66*((1)), 65-74.

Davey MG, H. S. (2021, Sep 3). Ki-67 as a Prognostic Biomarker in Invasive Breast Cancer. *Cancers (Basel), 13*(17), 4455.

Ellis IO, G. M. (1992, Jun). Pathological prognostic factors in breast cancer. II. Histological type. Relationship with survival in a large study with long-term follow-up. *Histopathology., 20*(6), 479-89.

Esmat E, H. A.-G. (2024, Mar 27). Association of hormone receptors and human epidermal growth factor receptor-2/neu expressions with clinicopathologic factors of breast carcinoma: a cross-sectional study in a tertiary care hospital, Kabul, Afghanistan. *BMC Cancer., 24*(1), 388.

Falck AK, F. M. (2013, Nov). St Gallen molecular subtypes in primary breast cancer and matched lymph node metastases--aspects on distribution and prognosis for patients with luminal A tumours: results from a prospective randomised trial. *BMC Cancer., 25*(13), 558.

Hasa, A. X. (2024, December). BRCA1 and BRCA2 genes: Key genetic drivers in breast cancer risk and management. *Journal of Natural Sciences, 36*.

Hiral Samir Shah, N. A. (2020). CORRELATION OF ESTROGEN RECEPTOR(ER), PROGESTERONE RECEPTOR(PR) AND HER2/NEU EXPRESSION WITH CLINICOPATHOLOGICAL PARAMETERS IN PRIMARY BREAST CARCINOMA -A STUDY OF 175 CASES. *National Journal of Medical Research, 10*(02), 70–75.

Kaptain, S. T. (2001). Her-2/neu and breast cancer. *Diagnostic Molecular Pathology, 10*(3), 39-152.

Kohler BA, S. R. (2015, Mar 30). Annual Report to the Nation on the Status of Cancer, 1975-2011, Featuring Incidence of Breast Cancer Subtypes by Race/Ethnicity, Poverty, and State. *J Natl Cancer Inst., 107*(6).

Łukasiewicz S, C. M. (2021, Aug 25). Breast Cancer-Epidemiology, Risk Factors, Classification, Prognostic Markers, and Current Treatment Strategies-An Updated Review. *Cancers (Basel), 13*(17), 4287.

M., A. (2012). Correlation of hormone receptors with Her-2 Neu protein expression and the histological grade in invasive breast cancers in a cohort of Saudi Arabia. *Turk Patoloji Derg., 28*(1), 38-43.

McGuire A, B. J. (2015, May 22). Effects of age on the detection and management of breast cancer. *Cancers (Basel), 7*(2), 908-29.

MN., K. (2014). Immunohistochemistry subtypes (ER/PR/HER) of breast cancer: where do we stand in the West of Saudi Arabia? *Asian Pac J Cancer Prev., 15*(19), 8395-400.

MS., A.-A. (2006 , Feb). HER-2 positivity and correlations with other histopathologic features in breast cancer patients--hospital based study. *J Pak Med Assoc., 56*(2), 65-8.

Pathak TB, B. R. (2011). Estrogen and progesterone receptor expression in breast carcinoma. *Journal of Pathology of Nepal*, 100-103.

Pathak TB, B. R. (2011). Estrogen and progesterone receptor expression in breast carcinoma. *Journal of Pathology of Nepal, Vol. 1*, 100 - 103.

Senel, F. (2021, Oct–Dec). The hormone receptor status in breast cancer and the relationship of subtypes with clinicopathological features. *Indian Journal of Pathology and Microbiology, 64*(4), 671-676.

Sharif MA, M. N. (2009, February). Morphological profile and association of HER-2/neu with prognostic markers in breast carcinoma in Northern Pakistan. *Coll Physicians Surg Pak, 19*(2), 99-103.

Tero A. H. Jarvinen, M. P.-H. (2000, January). Estrogen Receptor Is Coexpressed with ER and PR and Associated with Nodal Status, Grade, and Proliferation Rate in Breast Cancer. *American Journal of Pathology, 156*(1).

Xhetani, M. H. (2024, Dec 1). BRCA1 mutations in family members with breast cancer history. *EUROPEAN JOURNAL OF HUMAN GENETICS, 32*, 913-913.

Yip CH, R. A. (2014, Nov). Estrogen and progesterone receptors in breast cancer. *Future Oncol., 10*(14), 2293-301.

➢ *ORAL PRESENTATION*

Elektrikli Otobüsler için Şarj Altyapısının Dağıtım Optimizasyonu

Yaren Altuğlu[1], Sevide Nur Kar[1], Gülçin Dinç Yalçın[1] *(*ORCID: https://orcid.org/0000-0001-7696-7507*)

[1]Eskişehir Teknik Üniversitesi, İki Eylül Kampüsü, Mühendislik Fakültesi, Endüstri Mühendisliği Bölümü, 26555, Eskişehir, Türkiye

*Sorumlu yazar e-posta: gdinc@eskisehir.edu.tr

Özet

Sürdürülebilir olması sebebiyle toplu taşıma sistemlerinde elektrikli otobüslerin kullanılması büyük önem kazanmaktadır. Avantajlarının olmasının yanında kesintisiz hizmet veren elektrikli otobüslerin nasıl şarj edileceği ve şarj istasyonlarının konumlandırılması büyük bir sorun olarak görülmektedir. Günümüzde sürdürülebilir ulaşım sistemlerine yönelik artan talep, şehirlerde toplu taşıma araçlarının elektrifikasyonu çalışmalarını hızlandırmaktadır. Bu yönde artan talep sebebiyle, Eskişehir gibi büyük şehirlerde, otobüs filosunun elektrikli otobüslere dönüştürülmesi aşamasında, etkili bir şarj altyapısı planlaması yapılması sürecin hızlanması için oldukça önemlidir. Elektrikli araçlara olan ilgi arttıkça, şarj altyapısının kullanılabilirliğini ve verimliliğini bulma konusu, incelenmesi gereken karmaşık bir soru haline gelmektedir. Bu çalışmanın amacı, kentlerdeki elektrikli otobüsler için şarj altyapısının dağıtımını optimize etmek için geliştirilen bir matematiksel model önerisi ve uygulamasını sunmaktadır. Model Eskişehir otobüs ağı için test edilmiştir. Geliştirilecek model, sürdürülebilirlik ve emisyonun azaltılmasında katkı sağlayan yakıt alternatiflerini dikkate alarak şehirdeki elektrikli otobüsler için şarj altyapısının dağıtımını optimizasyonunu da içermektedir. Kullanılan modellemede, endeks olarak şehirdeki otobüs rotaları, durakları ve tercih edilen yakıt türü belirlenmiştir. Modelleme, duraklarının stratejik konumlandırılması, şarj istasyonlarının kapasitesi ve yerleşimi gibi faktörleri içermektedir. Modelde amaç fonksiyonları sistemdeki toplam yıllık maliyetler ve toplam emisyon olarak planlanmıştır. Modellemenin sonunda elektrikli otobüsler için şarj altyapısının uygulanabilirliği ve verimliliğiyle ilgili sonuçlar elde edilmiş ve yorumlanmıştır.

Anahtar Kelimeler: Elektrikli otobüs, optimizasyon, çok amaçlı optimizasyon, şarj istasyonu, şarj altyapısı, sürdürülebilirlik

Distribution Optimisation of Charging Infrastructure for Electric Buses

Abstract

The utilisation of electric buses within public transport systems is gaining significant importance due to their sustainability. In addition to their inherent advantages, the challenges of charging these vehicles in a manner that ensures uninterrupted service, as well as the strategic positioning of charging stations, are of paramount importance.The increasing demand for sustainable transport systems is a key factor in the accelerated electrification of public transport vehicles in urban areas. In this context, it is imperative to plan an effective charging infrastructure during the conversion of the bus fleet to electric buses in order to accelerate the process, as interest in electric vehicles continues to grow. The availability and efficiency of charging infrastructure is a complex question that needs to be examined.The aim of this paper is to propose and implement a mathematical model to optimise the deployment of charging infrastructure for electric buses in cities. The model has been tested on the Eskisehir bus network, and the results obtained have been interpreted.The model being developed includes the optimisation of the deployment of charging infrastructure for electric buses in the city, taking into account fuel alternatives that contribute to sustainability and emission reduction.In the modelling used, bus routes, stops and preferred fuel type in the city are determined as an index.The modelling includes factors such as strategic positioning of bus stops, capacity and placement of charging stations. The model's objective functions are defined as total annual costs and total emissions in the system. The results of the modelling process yield insights into the feasibility and efficiency of charging infrastructure for electric buses.

GİRİŞ

Bu çalışmanın motivasyonu "Bir ilde elektrikli otobüslerin kentsel bağlamda elektrikli otobüsler için şarj altyapısının dağıtımını optimize etmek için matematiksel model geliştirilebilir mi?" sorusunu temel almaktadır. Enerji sektöründeki yaşanan hızlı değişimler ve sıfır emisyon hedefi sürdürülebilir ulaşım sistemlerine olan ilgiyi arttırmıştır. Sıfır emisyon hedefinin gerçekleşmesi ve sürdürülebilirliğin artması için ulaşım sektöründeki değişimler önem arz etmektedir. Dünya genelinde ve Eskişehir gibi büyük şehirlerde elektrikli otobüs filolarının kullanılması, çevre dostu ulaşım sistemlerinin oluşturulması hedeflemektedir. Bu bağlamda, Eskişehir'de elektrikli otobüslerin şarj altyapısının optimize edilmesi, enerji verimliliğini artırabilir ve çevresel etkileri minimize edebilir. Eskişehir için daha önce böyle bir çalışmanın yapılmaması sebebiyle gelecekte elektrikli otobüslerin yaygınlaşması durumunda yapılacak modelleme bir örnek teşkil edecektir. Bu araştırma, Eskişehir'de elektrikli otobüslerin şarj altyapısının etkin bir şekilde dağıtılmasını amaçlayan kapsamlı bir optimizasyon modelini içerir. Model, otobüs hatları, duraklar, enerji talepleri, mevcut altyapı ve otobüs rotaları gibi çeşitli unsurları dikkate alarak geniş bir çerçeve sunar. Bu konuda yapılan çalışmalarla ilgili literatür araştırması yapıldığında başta Avrupa ülkeleri olmak üzere Amerika gibi ülkelerde bu alanda önemli araştırmalar yapılmıştır.

Wirges vd. (2012), Almanya'nın Stuttgart şehri için elektrikli araçların yaygınlaşmasına yönelik mekansal-zamansal modeli şarj altyapısı yatırımlarının finansmanına yönelik ekonomik modelle birleştirmiştir. Usman vd. (2016), Belçika'nın Flanders kentindeki bir çalışma bölgesinde faaliyet tabanlı FEATHERS modelini kullanarak elektrikli araçlara yönelik şarj optimizasyon süreci için bir çerçeve sunmuştur. Bu çalışmada kullanılan metodolojiye daha çok benzeyen Baouche vd. (2014) ve Cavadas vd (2015), Fransa'nın Lyon ve Portekiz'in Coimbra şehirlerindeki yolcu elektrikli araçları için şarj istasyonlarının konumunu belirlemek amacıyla tamsayılı optimizasyon tekniklerini kullanmıştır. Ancak bu çalışmalar, otobüs gibi Ağır Hizmet Araçlarını değil, elektrikli Hafif Hizmet Araçlarını ele aldıkları için mevcut çalışmadan farklılık göstermektedir. Ribau vd. (2014) tarafından yapılan çalışmada, Portekiz'in Lizbon ve Porto şehirlerinde temsili sürüş çevrimlerini kullanarak, hidrojenle çalışan yakıt hücreli hibrit bir otobüs için enerji yönetimi stratejisi olarak gerçek kodlu bir genetik algoritma (GA) kullanılmıştır. Kunith vd. (2017) tarafından yapılan çalışma, Berlin, Almanya'daki 17 otobüs güzergahı için şarj istasyonu konumunu ve pil kapasitesini belirlemek amacıyla karma tamsayılı doğrusal maliyet optimizasyon modeli geliştirmiştir. Her bir rota için enerji tüketim profilleri oluşturularak, farklı şarj gücü ve çalışma koşulları senaryoları analiz edilmiştir.

Literatürde dizel otobüslerin kademeli olarak elektrikli otobüslere değiştirilmesini ve kademeli olarak şarj altyapısının sağlanmasını ele alan çalışmalar da bulunmaktadır. Örneğin Lin vd. (2019) elektrikli otobüslerin hızlı şarj istasyonları için çok aşamalı bir planlama stratejisi önermişlerdir. Sebastiani vd. (2016), tam elektrikli bir otobüs ağı için şarj cihazlarını en iyi şekilde tahsis etmek amacıyla hem şarj istasyonlarının sayısını hem de şarj olayları sırasında istasyonlarda harcanan ekstra süreyi en aza indirmeyi amaçlayan ayrık bir olay simülasyon yöntemi geliştirmişlerdir. An (2020) tarafından yapılan çalışma, talep belirsizliği altında elektrikli otobüs şarj tesisi konum optimizasyon problemini ele almış ve stokastik bir tamsayı programı önermiştir. Lotfi vd. (2020) farklı elektrikli otobüs tipleri, şarj altyapıları ve otobüs güzergahları için en uygun şarj altyapılarını ve pil kapasitelerini belirlemiştir. Bagherinezhad vd. (2020) elektrikli otobüslerin mekansal-zamansal şarj olaylarını, otobüsün operasyonel kısıtlamalarını ve şarj istasyonu güç dağıtım kısıtlamalarını karşılarken elektrik şebekesinin işletme maliyetini en aza indirme perspektifinden planlamıştır. Brezilya'da yapılan bir araştırmada (Zaneti vd., 2022) Campinas Üniversitesi'nde bir sürdürülebilir şarj istasyonundaki elektrikli otobüsün farklı şarj tipleri altındaki operasyonel maliyetlerini minimize etmeyi amaçlayan bir optimizasyon modeli incelenmiştir. Optimizasyon modeli, gerçek verilerle desteklenmiş olup, fotovoltaik panellerden elde edilen ve Unicamp tesislerinde dolaşan bir elektrikli otobüsün işletmesine dair verilerle çözümlenmiştir. Başka bir çalışma (Sang vd., 2022) Nanjing şehrindeki bir örnek üzerinden gösterilmiştir. Bu çalışma elektrikli otobüslerin (EO'lar) hava kirliliği ve sera gazı emisyonlarını azaltmada etkili bir ulaşım modu olduğunu vurgulayarak, EO şarj istasyonu (EO Şİ) yer seçiminin kritik öneme sahip olduğunu belirtmiştir. Ele alınan belirsizlik ve karmaşık ilişkiler için bulanık karar verme ve DEMATEL yöntemi, tercih sıralama organizasyon yöntemi (PROMETHEE) ve gelecek teorisi (PT) yöntemlerini birleştirerek farklı sonuçlar alınmıştır. Dinç Yalçın vd. (2023) Türkiye için de bu konuda araştırmalar yapılmıştır, bu çalışmalardan birinde Türkiye'deki bir şehirlerarası otobüs şirketinin verileriyle gerçekleştirilen bir vaka çalışması üzerinden, elektrikli otobüs şarj istasyonlarının konumlandırılması konusunda bir çok amaçlı matematiksel model önerilmiştir. Bu model bütçe kısıtlamalarını dikkate alarak, tüm şehirlerarası otobüslerin elektrikli olamayabileceği gerçeğini

içermektedir. Bu, literatürde genellikle göz ardı edilen bir faktördür. Elektrikli otobüs sayısını maksimize etmeyi ve şarj istasyonu sayısını minimize etmeyi amaçlayan çok amaçlı bir matematiksel model önermiş ve bu model, ağırlıklı toplam yöntemi kullanılarak çözülmüştür. Sıfır emisyonlu bir toplu taşıma çözümü sunma potansiyeline sahip olan yakıt hücreli hibrit otobüsleri içeren çalışmalar da incelendi (Wu ve Bucknall, 2013). Bu otobüsler bataryalar, yakıt hücreleri veya her ikisini kullanarak elektrikle çalışan otobüsleri içerir. İncelenen bir makalede bahsedilen yakıt hücreli hibrit otobüsler, bir dizi polimer elektrolit zarlı (PEM) yakıt hücresi ve bir nano-fosfat lityum-iyon bataryadan güç alırlar. Bu tasarım, otobüsün elektrikle çalışan bir motoru tahrik etmesini sağlar. Bu nedenle, yakıt hücreli hibrit otobüsler, elektrikli otobüs kategorisine dahil edilebilir. Elektrikli ve hibrit araçlar, karayolu taşıma ağlarında giderek artan bir rol oynamaktadır (Gagarin ve Corcoran, 2018). Avantajlarına rağmen, geleneksel dizel/benzinli araçlara kıyasla sınırlı bir menzile sahiptirler ve önemli bir pil şarj süresine ihtiyaç duyarlar

MATERYAL VE METOD

Veriler:

Projede kullanılacak parametre ve küme değerleri için araştırmalar yapılmıştır. Araştırma için ana veri kaynağı olarak Eskişehir Belediyesi internet sitesi alınmıştır (Eskişehir Belediyesi, 2024). Buna ek olarak çeşitli kaynaklarda diğer verilere ulaşılmıştır. Eskişehir için toplamda merkezi ve ilçeleri kapsayacak şekilde 115 otobüs hattı bulunmaktadır. Yapılan analizler sonucunda güncel olarak kullanılan toplam hat sayısı 111 olarak belirlenmiştir. Elektrikli araçlar için elde edilen veriler aşağıdaki Tablo 1'de gösterilmiştir. Değerlere ulaşılan siteler kaynakça kısmında belirtilmiştir.

Tablo 1. Elektrikli Araçlar için Parametreler

Teknoloji 1 (Elektrikli)	Değerler	Birimler	Kaynaklar
Bakım maliyeti	3.000,00	₺	(Hedef Filo, 2024)
Altyapı maliyeti	1.023.870,00	₺	(T.C. Sanayi ve Teknoloji Bakanlığı,2021)
Araçlar için maliyetler	1.456.666,00	₺	(T.C. Sanayi ve Teknoloji Bakanlığı,2021)
Km başına yakıt maliyeti	3,30	₺	(Sigortam.net, 2024)
Enerji Tüketimi	1,50	kWh / km	(Dolu Batarya, 2024; Karsan, 2024a)
Maksimum pil kapasitesi	599	kWh	(Karsan, 2024b)
Yakıt başına emisyon faktörü	0	gr/CO2	(Karsan, 2024c)

Dizel araçlar için elde edilen veriler aşağıdaki Tablo 2'de gösterilmiştir. Dizel araçlarda yeni bir şarj istasyonu kurulumu ve araç satın alması yapılmayacağı için bu değerle 0 olarak alınmıştır.

Tablo 2. Dizel Araçlar için Parametreler

Teknoloji 2 (Dizel)	Değerler	Birimler	Kaynaklar
Bakım maliyeti	₺9.000,00	Tl	(TRT Haber, 2023)
Altyapı maliyeti	0	Tl	-
Araçlar için maliyetler	0	Tl	-
Km başına yakıt maliyeti	₺13,20	Tl	(Buskirala, 2024)
Enerji Tüketimi	0,3	kWh / km	(Graurs ve Bērziņš, 2015)
Maksimum pil kapasitesi	480	L	(Buskirala, 2024)
Yakıt başına emisyon faktörü	63	gr/CO2	(International Energy Agency, 2024)

Güzergâh uzunluğu hesaplanırken belediyedeki konumlar girilerek Google Maps yardımı ile hesaplanmıştır. Yıllık toplam yolculuk sayıları ise Eskişehir Büyükşehir Belediyesi sitesinden her hat için günlük yolculuk sayılarının tek tek elde edilip yıllık bazda hesaplanmasıyla oluşturulmuştur. Araç için yıllık maliyetler (araç bedeli) / (araç ömrü) ne oranlanarak hesaplanmıştır. Bir araç ömrü için kesin bir bilgi bulunmadığı için ortalama bir değer alınarak hesaplamalar yapılmıştır. Otobüsün çalıştırılması durumundaki ilk güç maksimum kapasite ile aynı olarak kabul edilecek ve bu şekilde modelde kullanılacaktır.

Matematiksel Model:

Bu kısımda Xylia vd. (2017) çalışmasından ele alınarak hazırlanan matematiksel model açıklanacaktır.

Kümeler	
l	Otobüs Rotası
s	Otobüs Durağı
tech	Otobüs Teknolojisi (yakıt türü)
L	Rota sayısı
$\tilde{L}$	Tüm otobüs güzergahlarının seti
S	Otobüs durağı sayısı
$\tilde{S}$	Tüm otobüs duraklarının seti
$S^{başlangıç}$	Başlatma duraklarının sayısı
$\widetilde{S^{başlangıç}}$	Rotaların başlangıcındaki durakların alt kümesi
$S^{bitiş}$	Son durak sayısı
$\widetilde{S^{bitiş}}$	Rotaların sonundaki durakların alt kümesi
S^{orta}	Orta durak sayısı
$\widetilde{S^{orta}}$	Rotaların ortasındaki durakların alt kümesi
$\widetilde{TECH}$	Tüm veri yolu teknolojilerinden oluşan set

İkili değişkenler	
$US_{l,s,tech}$	Otobüs durağında şarj istasyonunun kurulu olup olmadığını gösteren ikili değişken {0,1}
$TUS_{l,tech}$	Otobüs güzergahlarını belirli teknolojiyle ilişkilendiren ikili değişken {0,1}

Pozitif değişkenler	
C_{total}	Toplam maliyetler
E_{total}	Toplam enerji tüketimi
U_{total}	Toplam emisyonlar
$P^{in}_{l,s,tech}$	Otobüsün istasyona geldiğinde kalan gücü
$P^{out}_{l,s,tech}$	Otobüsün istasyondan ayrılırken olan gücü
$P^{şarj}_{l,s,tech}$	Otobüsün istasyonda şarjı için gereken güç

Parametreler	
$C_{l,tech}^{bakım}$	İşletme ve bakım maliyetleri
$C_{l,tech}^{yakıt}$	Yıllık yakıt maliyetleri
$C_{l,tech}^{altyapı}$	Altyapının yıllık maliyetleri
$C_{l,tech}^{araç}$	Araçlar için yıllık maliyetler
Cap_{tech}	Otobüste depolanan maksimum güç
$Cons_{tech}$	Her otobüs yakıt türü için enerji tüketimi
$D_{l,s-s,l}$	Durak s−1 ile s arasındaki mesafe
EF_{tech}	Her teknoloji için yakıt başına emisyon faktörü
P_{tech}^{ilk}	Çalıştırma durdurmadaki güç
SOC^{min}	Pilin minimum şarj durumu
TC_l	Otobüs güzergahı gezileri (yıllık toplam yolculuk sayısı)
L_l	Tüm otobüs güzergahlarının sayısı

$$C_{total} = \begin{cases} \sum_{l=1}^{L}\sum_{s=1}^{S}\sum_{tech=1}^{Tech} C_{l,tech}^{altyapı} * US_{l,s,tech} \\ + \sum_{l=1}^{L}\sum_{tech=1}^{TECH}[(C_{l,tech}^{bakım} + C_{l,tech}^{yakıt}) * L_l * TC_l + C_{l,tech}^{araç} * TUS_{l,tech} \end{cases} \quad (1)$$

$$U_{total} = \sum_{l=1}^{L}\sum_{tech=1}^{TECH}(EF_{tech} * L_l * TC_l * TUS_{l,tech}) \quad (2)$$

C_{total} içerisinde iki ayrı toplam içermektedir. Birincisi altyapı maliyetleri ($C_{l,tech}^{altyapı}$) ile durakta şarj istasyonu olup olmamasının ($US_{l,s,tech}$) ikili değişkeninin çarpılması ve indeksler ile toplanması ile elde edilir. Bu şarj istasyonu açılması durumunda oluşacak alt yapı maliyetini verecektir. U_{total} tercih edilen teknolojinin emisyon faktörü (EF_{tech}), otobüs güzergâh sayısı (L_l), yıllık toplam yolculuk sayısı (TC_l), Otobüs güzergahlarını belirli teknolojiyle ilişkilendiren ikili değişken ($TUS_{l,tech}$) çarpılması ile elde edilir.

$$P_{l,s,tech}^{in} = P_{ltech}^{ilk} * TUS_{l,tech}, \quad l \in \tilde{L}, \quad tech \in \widetilde{TECH}, \quad s \in \tilde{S} \quad (3)$$

Kısıt 3, güzergahların başlangıç duraklarında tam şarj olduğu durumlar için geçerlidir. P_{tech}^{ilk} Otobüsün maksimum şarjını vermektedir.

$$P_{l,s,tech}^{in} = P_{l,s,tech}^{out}, l \in \tilde{L}, s \in \widetilde{S^{end}}, tech \in \widetilde{TECH} \quad (4)$$

Kısıt 4 rotaların son durak için şarja gerek olmadığını ve gidilecek mesafenin olmadığını varsaymaktadır.

$$P_{l,s,tech}^{out} \geq \begin{cases} Cons_{tech} * L_l * (1 + SOC^{min}) * TUS_{l,tech}, \\ l \in \tilde{L}, s \in \widetilde{S^{start}} \text{ or } s \in S, \ tech \in \widetilde{TECH} \end{cases} \quad (5)$$

Kısıt 5 bir sonraki durağa gidilmesi için yeterli enerjinin olmasını garanti altına almak için kullanılmıştır. Otobüsün yakıt türü için harcanan enerji miktarı, iki durak arası mesafe, (1+ Pilin minimum şarj durumu (SOC^{min})) ve $TUS_{l,tech}$ çarpılır ve sonucunun otobüs duraktan ayrılırken enerji miktarından küçük olması kısıtı oluşturulur.

$$\sum_{tech=1}^{TECH} TUS_{l,tech} = 1 \quad l \in L \tag{6}$$

Kısıt 6 her hattın bir teknolojiye kesinlikle atanmasını sağlamak için eklenmiştir.

$$US_{l,s,t} = TUS_{l,t} \quad \forall t = 1, l \in L, s \in S \tag{7}$$

Kısıt 7 eğer bir hat elektrikli oluyorsa başlangıç ve bitiş noktasına şarj istasyonu kurulması için eklenmiştir. (5)

BULGULAR VE TARTIŞMA

Model çözdürüldükten sonra elde edilen sonuçlar Tablo 3'te gösterilmiştir.

Tablo 3. Matematiksel Model Amaç fonksiyonu Değerleri

Amaç Fonksiyonu	**Değeri**
Toplam Maliyet (C_{total})	₺684.968.395,60
Toplam Emisyon (U_{total})	183.513.657,60 gr/ CO2

Optimizasyon öncesi ve sonrası emisyon değerleri hesaplatılmıştır. Sonucunda %92.63 emisyonda azalma olacağı sonucuna varılmıştır. Emisyon değerleri aşağıdaki Tablo 4' te gösterilmiştir.

Tablo 4. Emisyon Değerleri Karşılaştırılması

Toplam Emisyon	**Değeri**
Optimizasyon Öncesi Toplam Emisyon	2,477,558,538 gr/ CO2
Optimizasyon Sonrası Toplam Emisyon	183.513.657,60 gr/ CO2

Modeli çalıştırmadan önce 111 hat dizelken optimizasyon sonrası 71 hat elektrikli 40 hat dizel olacak şekilde sonuç elde edilmiştir. Şekil 1'de sonuçlar gösterilmiştir.

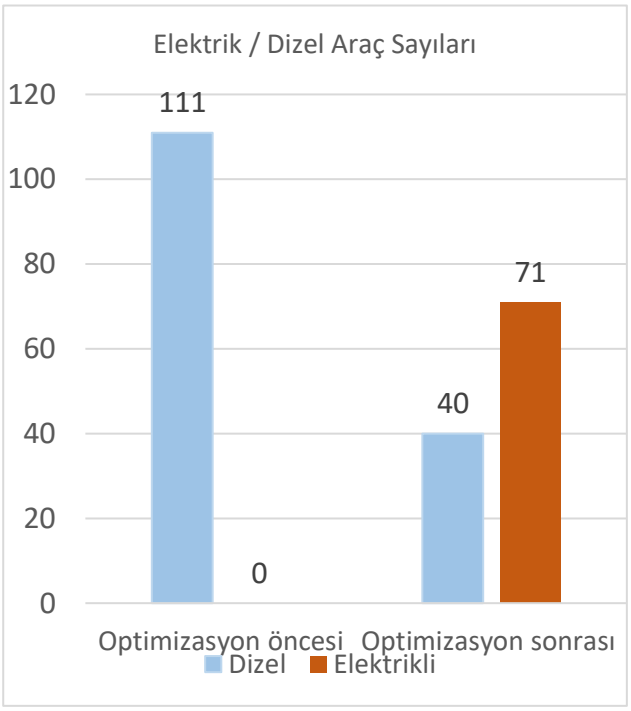

Şekil 1. Elektrik / Dizel Araç Sayıları

ANALİZLER

Analiz 1

Elde edilen sonuçlarında hatlar tek tek incelenmiştir Elektrikli hatlar için günlük gidilen toplam yol(km) tam dolum kapasitesine bölünerek hesaplamalar gerçekleşmiştir ve hatlar için gerekli tam dolum sayıları Şekil 2'de verilmiştir.

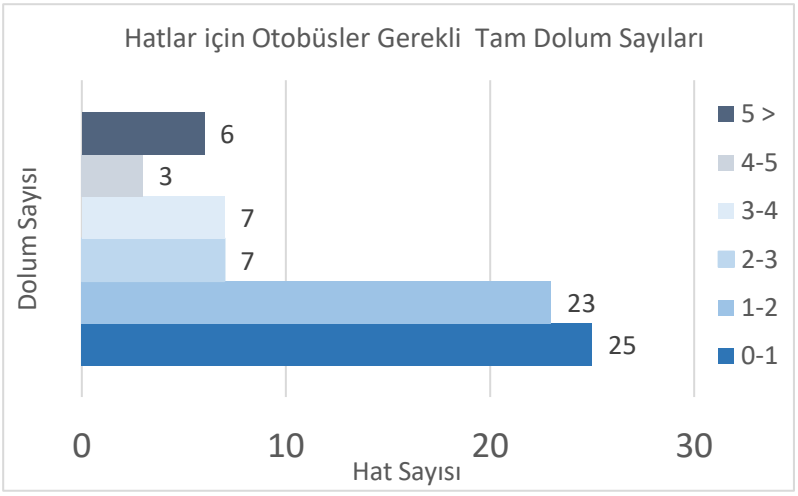

Şekil 2. Hatlar için Otobüsler Gerekli Tam Dolum Sayıları

Yapılan hesaplamalar sonucunda günde 0-1 ve 1-2 dolum arasında tam dolum gerektiren hatların tek bir noktaya şarj istasyonu konumlandırılmasının yeterli olduğu kararına varıldı. Bunla ilgili hat durakların konumları da önemsenerek şarj istasyonu sayısında ve şarj istasyonu konumunda azalma sağlanmaktadır. Model sonucu oluşan konum 76 iken analiz 1 sonucu 34 konuma düşmüştür. 152 şarj istasyon sayısı 94 şarj istasyonuna düşürülmüştür.

Analiz 2

Analiz iki ortak lokasyonlar üzerine bir inceleme gerçekleştirmek adına yapılmıştır. Modeldeki şarj istasyonları konumları incelendiğinde pek çok otobüsün aynı konumlarda başlangıç veya bitiş noktası olduğu fark edilmiştir. Ortak duraklar için incelemeler yapılmış ve sonucunda kurulum yapılacak istasyonlar aşağıda Tablo 5'te gösterilmiştir.

Tablo 5. Şarj İstasyonu Kurulumu Yapılacak Yerler

Şarj İstasyonu Kurulum Yerleri	**İstasyon Sayısı**	**Şarj İstasyonu Kurulum Yerleri**	**İstasyon Sayısı**
Çankaya Mh.	1 ADET / 2 SOKET	Muttalip Mahallesi	1 ADET / 2 SOKET
Yeşiltepe Mh.	2 ADET / 4 SOKET	Organize San.	1 ADET / 2 SOKET
Sakarya 1 Cd.	1 ADET / 2 SOKET	Otogar	5 ADET / 10 SOKET
Eskişehir Osmangazi Üniversitesi	1 ADET / 2 SOKET	Diş Hastanesi	1 ADET / 2 SOKET
Yaşamkent	1ADET / 2 SOKET	Bademlik	1 ADET / 2 SOKET
Odunpazarı	27ADET / 54 SOKET	Şehir Hastanesi	4 ADET / 8 SOKET
İki Eylül Kampüsü	3 ADET / 6 SOKET	Şirintepe Mh.	1 ADET / 2 SOKET
Osmangazi Mh.	1 ADET / 2 SOKET	Karapınar Toki	1 ADET / 2 SOKET
Vadişehir Mh.	3 ADET / 6 SOKET	Batıkent Mh.	2 ADET / 4 SOKET
Askeri Birlik	1 ADET / 2 SOKET	Sarısungur Mh.	1 ADET / 2 SOKET
Orhangazi Fidanlık Mevki	1 ADET / 2 SOKET	Turgutlar Mh.	1 ADET / 2 SOKET
Yenikent Mh.	3 ADET /6 SOKET	Ihlamurkent Mh.	1 ADET / 2 SOKET
Tepebaşı Belediyesi	2 ADET / 4 SOKET	Yıldız	1 ADET / 2 SOKET
Anadolu Ünv. Yunusemre Kamp.	1 ADET / 2 SOKET	Çukurhisar Mh.	1 ADET / 2 SOKET
75.Yıl Mah.	2 ADET / 4 SOKET	Prof. Dr. Nabi Avcı Blv	1 ADET / 2 SOKET
Yunusemre Devlet Hastanesi	5 ADET / 10 SOKET	Eski Otogar	1 ADET / 2 SOKET
Kıymetli Sk.	1 ADET / 2 SOKET	Sümer Mh	1 ADET / 2 SOKET

Şekil 3'te şarj istasyonlarının konumları harita üzerinde gösterilmiştir.

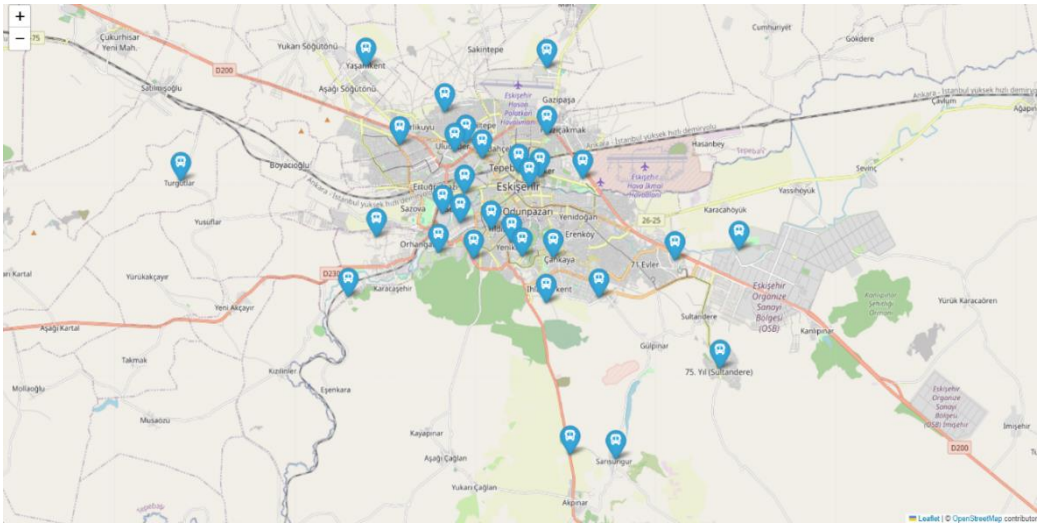

Şekil 3. ***Şarj İstasyonu Konumları***

Analiz 1 sonucu ₺59.384.460,00 ve analiz 2 sonucu ₺72.694.770,00 kazanç elde edilmiştir.

Tablo 6. Analiz Sonuçları

Model veya Analiz	Toplam Maliyet (Ctotal)	Kazanç
Model	Ł684.968.395,60	-
Analiz 1	Ł625.583.935,60	Ł59.384.460,00
Analiz 2	Ł612.273.625,60	Ł72.694.770,00

SONUÇ

Bu çalışmada Eskişehir şehir içi otobüs hatlarının hangilerinin elektrikli olabileceği ve Optimizasyon çalışmasının başlangıcında, Eskişehir'deki toplu taşıma sisteminin toplam emisyon değeri 2,477,558,538 gram (iki milyar dört yüz yetmiş yedi milyon beş yüz elli sekiz bin beş yüz otuz sekiz) olarak hesaplanmıştı. Optimizasyon sonrasında ise bu değer 31,084,326.00 gram (otuz bir milyon seksen dört bin üç yüz yirmi altı) seviyesine düşürülmüştür. Bu, %92.63 gibi çok büyük bir azalmaya işaret ediyor. Bu, sürdürülebilirlik adına atılan büyük bir adım olacaktır.

TEŞEKKÜR

Bu çalışma Eskişehir Teknik Üniversitesi Bilimsel Araştırma Projeleri Koordinasyon Birimi tarafından 24LÖP017 nolu proje kapsamında desteklenmiştir.

KAYNAKLAR

Xylia, M., Leduc, S., Patrizio, P., Kraxner, F., & Silveira, S. (2017). Locating charging infrastructure for electric buses in Stockholm. Transportation Research Part C: Emerging Technologies, 78, 183-200.

Wirges, J., Linder, S., & Kessler, A. (2012). Modelling the development of a regional charging infrastructure for electric vehicles in time and space. European Journal of Transport and Infrastructure Research, 12(4).

Usman, M., Knapen, L., Vanrompay, Y., Bellemans, T., Janssens, D., & Wets, G. (2016). A coordinated framework for optimized charging of EV fleet in smart grid. Procedia Computer Science, 94, 332-339.

Baouche, F., Billot, R., Trigui, R., & El Faouzi, N. E. (2014). Efficient allocation of electric vehicles charging stations: Optimization model and application to a dense urban network. IEEE Intelligent transportation systems magazine, 6(3), 33-43.

Cavadas, J., de Almeida Correia, G. H., & Gouveia, J. (2015). A MIP model for locating slow-charging stations for electric vehicles in urban areas accounting for driver tours. Transportation Research Part E: Logistics and Transportation Review, 75, 188-201.

Ribau, J., Viegas, R., Angelino, A., Moutinho, A., & Silva, C. (2014). A new offline optimization approach for designing a fuel cell hybrid bus. Transportation Research Part C: Emerging Technologies, 42, 14-27.

Kunith, A., Mendelevitch, R., & Goehlich, D. (2017). Electrification of a city bus network—An optimization model for cost-effective placing of charging infrastructure and battery sizing of fast-charging electric bus systems. International Journal of Sustainable Transportation, 11(10), 707-720.

Lin, Y., Zhang, K., Shen, Z. J. M., Ye, B., & Miao, L. (2019). Multistage large-scale charging station planning for electric buses considering transportation network and power grid. Transportation Research Part C: Emerging Technologies, 107, 423-443.

Sebastiani, M. T., Lüders, R., & Fonseca, K. V. O. (2016). Evaluating electric bus operation for a real-world BRT public transportation using simulation optimization. IEEE Transactions on Intelligent Transportation Systems, 17(10), 2777-2786.

An, K. (2020). Battery electric bus infrastructure planning under demand uncertainty. Transportation Research Part C: Emerging Technologies, 111, 572-587.

Lotfi, M., Pereira, P., Paterakis, N., Gabbar, H. A., & Catalão, J. P. (2020, June). Optimizing charging infrastructures of electric bus routes to minimize total ownership cost. In 2020 IEEE International Conference on Environment and Electrical Engineering and 2020 IEEE Industrial and Commercial Power Systems Europe (EEEIC/I&CPS Europe) (pp. 1-6). IEEE.

Bagherinezhad, A., Palomino, A. D., Li, B., & Parvania, M. (2020). Spatio-temporal electric bus charging optimization with transit network constraints. IEEE Transactions on Industry Applications, 56(5), 5741-5749.

Zaneti, L. A., Arias, N. B., de Almeida, M. C., & Rider, M. J. (2022). Sustainable charging schedule of electric buses in a University Campus: A rolling horizon approach. Renewable and Sustainable Energy Reviews, 161, 112276.

Sang, X., Yu, X., Chang, C. T., & Liu, X. (2022). Electric bus charging station site selection based on the combined DEMATEL and PROMETHEE-PT framework. Computers & Industrial Engineering, 168, 108116.

Yalçın, G. D., Doğan, E., Kaya, A. Y., & Oğuz, E. C. (2023). A Mathematical Model for the Location of Charging Station for Electric Buses. Journal of Industrial Engineering (Turkish Chamber of Mechanical Engineers), 34(2).

Wu, W., & Bucknall, R. W. (2013, September). Conceptual evaluation of a fuel-cell-hybrid powered bus. In 2013 48th International Universities' Power Engineering Conference (UPEC) (pp. 1-5). IEEE.

Gagarin, A., & Corcoran, P. (2018). Multiple domination models for placement of electric vehicle charging stations in road networks. Computers & Operations Research, 96, 69-79.

Eskişehir Belediyesi. (20 Nisan 2024). Otobüs saatleri. Eskişehir Belediyesi. https://www.eskisehir.bel.tr/otobus-saatleri

Hedef Filo. (20 Nisan 2024). Elektrikli araç bakımı nedir? Bakımı önemli parçalar nelerdir?. Hedef Filo. https://ev.hedeffilo.com/ev-gundem/blog/elektrikli-arac-bakimi-nedir-bakimi-onemli-parcalar-nelerdir

T.C. Sanayi ve Teknoloji Bakanlığı. (2021). İstanbul ili elektrikli araçlar şarj istasyonu ön fizibilite raporu. https://www.yatirimadestek.gov.tr/pdf/assets/upload/fizibiliteler/stanbul-ili-elektrikli-araclar-sarj-istasyonu-on-fizibilite-raporu2021.pdf

Sigortam.net. (20 Nisan 2024). Elektrikli araba şarj maliyeti ne kadar?. Sigortam.net. https://www.sigortam.net/elektrikli-araba-sarj-maliyeti-ne-kadar

Dolubatarya. (20 Nisan 2024). Yerli elektrikli otobüs modelleri teknik özellikleri (Menzil ve güç). Dolubatarya. https://dolubatarya.com/haber/yerli-elektrikli-otobus-modelleri-teknik-ozellikleri#ata

Karsan. (20 Nisan 2024a). Genel bakış - e-ATA 18. Karsan. https://www.karsan.com/tr/genel-bakis-e-ata-18

Karsan. (20 Nisan 2024b). Teknik özellikler - e-ATA 18. Karsan. https://www.karsan.com/tr/teknik-ozellikler-e-ata-18

Karsan. (20 Nisan 2024c). Genel bakış - e-ATAK. Karsan. https://www.karsan.com/tr/genel-bakis-e-atak

TRT Haber. (2023, Mart 18). Elektrikli otomobiller bakım ve satın alma maliyeti konusunda da rekabet ediyor. TRT Haber. https://www.trthaber.com/haber/ekonomi/elektrikli-otomobiller-bakim-ve-satin-alma-maliyeti-konusunda-da-rekabet-ediyor-

858115.html#:~:text=S%C3%B6z%20konusu%20aksamlar%C4%B1n%C4%B1n%202%20y%C4%B1l,30%20bin%20liraya%20kadar%20y%C3%BCkselebiliyor

Buskirala. (20 Nisan 2024). Otobüsün yakıt deposu kaç litredir?. Buskirala. https://blog.buskirala.com/otobusun-yakit-deposu-kac-litredir#:~:text=Otob%C3%BCslerin%20yak%C4%B1t%20deposu%20hacimleri%20ile,ara%C3%A7larda%2034%20litreye%20kadar%20%C3%A7%C4%B1kabilir

Graurs, A., & Bērziņš, J. (2015). Electric vehicle charging station optimization. Proceedings of the 2015 International Conference on Transport, 060, 1-8.

International Energy Agency (IEA). (20 Nisan 2024). Well-to-wheel wake-wing GHG intensity of motorised passenger transport modes. International Energy Agency. https://www.iea.org/data-and-statistics/charts/well-to-wheel-wake-wing-ghg-intensity-of-motorised-passenger-transport-modes-2

➢ *ORAL PRESENTATION*

How classroom participation and course projects affect final grades in biology courses in online teaching?

Sara Pupe[1] https://orcid.org/0009-0009-6698-283X

[1]Department of Biology, Aldent University, Albania

Abstract
The development of technology has had a great development and impact on teaching methods. Along with the evolution of technology, the variety of teaching methods have also evolved, influencing an increase in student learning outcomes. In the framework of the variety of teaching, online teaching has an important place. The research was carried out in UT (University of Tirana) mainly in the faculty of natural sciences, in the biology department mainly in the bachelor cycle (I-III) and in the master cycle (I, II) where the aim is to focus on participation during the lesson, course projects, and the calculation of the final grade in the context of teaching.A correlational research design was used in this study. Random samples of respondent groups (N=150) and master groups (N=60) were used in the research. In order to reach the most accurate conclusion, a defined list of student participation in lectures and the degree of academic progress was used, leaving secondary data. From the research study results a high and positive correlation between the participation in the auditorium and that of online teaching and the variables of the final grade of the course. The studies show that the amount of variance of the final grade levels explained by the participation in the auditorium is 54.2% while with the points of the subject project is 67.5%, other variance can be described by other variables, the points help a lot in the final grade of the student's academic performance.
Keywords: Online learning, design, correlation, final grades, course projects, classroom participation

INTRODUCTION

The teaching of natural sciences must necessarily include a variety of teaching methodologies in order to increase the level of student learning. In the multitude of teaching varieties, an important place is voice and online teaching. Scientific competences and methodology are two main teaching competences. Teachers and lecturers who demonstrate a high level of scientific competences also show a high level of methodological competence. The use of digital tools in the teaching process plays an important role in the transformation of traditional teaching practices, leading to an increase in the level of students and studies and an increase in the level of acquisition of biological knowledge.This study aims to find out the relationship between participation in lectures, course projects and the final grade in the online learning environment. Studies and research have shown that the academic performance of students and learning is affected by many variables including age, gender, education, social background, access to school instructions, schooling trends, etc. Students should develop a variety of biological activities before and after learning. in the auditorium with the sole purpose of making the most of a blended teaching and learning. The study was conducted at the university in the Department of Biology of the bachelor and master cycle using a research design as well as being supported by two research questions that were used during the study as :

1. Is there variance in final grade explained by lecture attendance in an online learning context?
2. Is there a variance in the final grade described by the course projects in the online learning environment?

The research study is based on a review of existing works about online learning through ERIC and EBSCO using the terms "lecture participation", "course project", and "final grade". The conclusion of the study should result in a relationship between the three variables of leadership, participation in lectures, course projects, and the final grade in the student profile. Project work performance of students is positively related to their involvement in online teaching activities (Brechler,Teah&Robe,2011:Graff,2006) which links curriculum modules where they are more accessible in the ompjuter-based approach than in conventional lecture teaching. Mathneës&Pulcim(2017) found that performance-based rewards helped boost students Ward,Jacobs&Thompson(2016) show that in a traditionally at-risk population suffered from lower university results as well as lower retention and lower completion rates.Online students had lower academic results while being more likely to attend a formal setting. rather than just in the auditorium. Meanwhile, the leadership style through isolation and the lack of aspiration for the future significantly affect the teacher-

student interaction and the academic performance of students in a complex way (Xhomara, 2018: Bek, 2017).Academic progress is directly related in a positive and significant way to students' prior course content, course record, previous academic achievements and application of learned material in practice. Academic and social engagement of students in universities is important for study engagement, progress and dropout prevention {(Dama, Gadis & Marodze (2020)}. Academic self-efficacy, the level of student participation, internal and external motivation variables as well as individual study work and the support of lecturers predict students' performance in the exam (Sezer, Inel, Seckin, Ulucinar, 2017).There is a significant relationship between academic progress and the time students participate in online as well as prior knowledge, problem-based instruction, comprehensive learning, and work assessments (Nieuwoudt, 2020: Fematt, et, al, 2021).

MATERIALS AND METHODS

For the realization of this study, research methods were applied, where contemporary literature was browsed and reviewed. At the same time, quantitative and qualitative methods were used, and a correlative research design was chosen. Two groups of students were selected in the bachelor's and master's cycle and they were subjected to a survey for the final grade in online learning. These two groups of students were subjected to a systematic study of their participation in lectures as well as the degree of their academic reinforcement to collect secondary data. Also in the research, random samples of the groups of respondents (N=150) were used for the bachelor's cycle and (N=60) for the master cycle. The composition of the two groups is 110 women and 40 men for the bachelor group, while for the master group 45 women and 15 men.

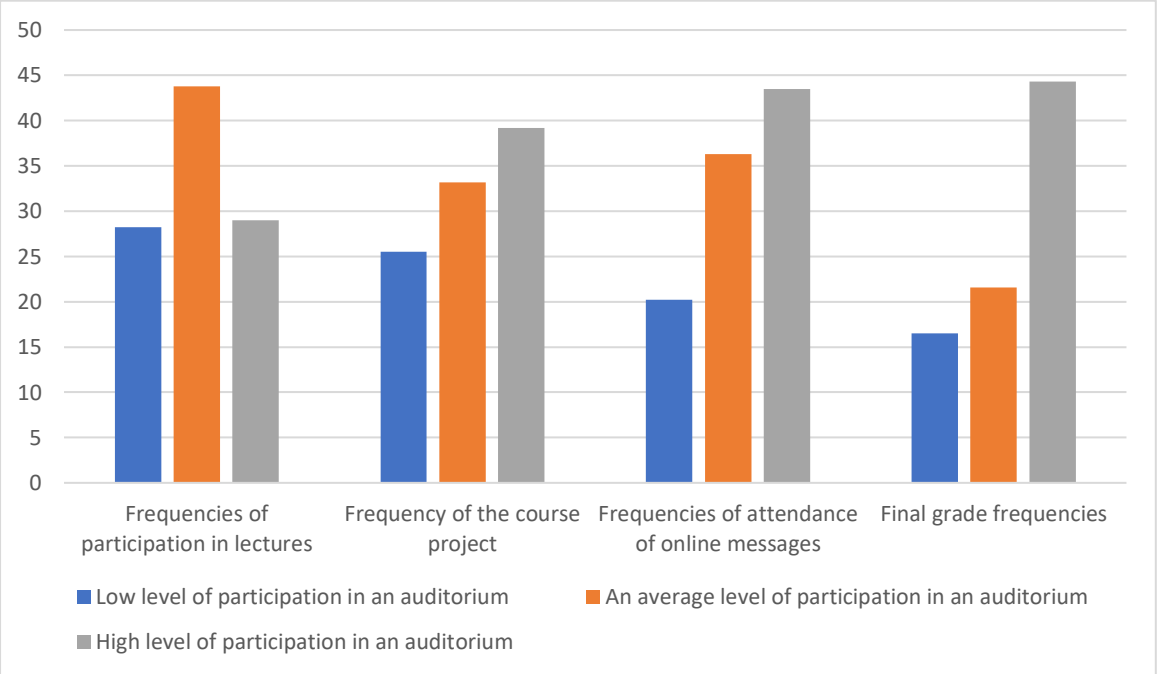

Figure 1. Percentage of participation in lectures, course project, online teaching, final grade

RESULTS and DISCUSSION

The statistical results of the correlation were used to understand the relationship between the participation in lectures and the final grade as well as between the course projects and the final grade. The results are based on descriptive analyzes based on the frequencies of participation in the auditorium, online learning and course projects, final grades. the final results were based on surveys conducted for each frequency.

- **Frequencies of participation in lectures**

From the survey of respondents, it results that 28.2% state that they have a low level of participation in an auditorium, 43.8% often have an average level of participation in an auditorium, and 29% of respondents have a high level of participation in an auditorium. So the result is that the majority of students (72.8%) have an average and high participation in an auditorium.

● **Frequency of the course project**

The survey results show that 25.5% of the respondents have a low level of the results of their project, 33.2% have an average level and 39.2% have a high level of the results of their project. Thus, the majority of students (72.5%) have an average and high level of the results of their projects

● **Frequencies of attendance of online messages**

The survey results show that 20.2% of students have a low participation in online education, 36.3% have an average level, 43.5% have a high level of participation in online education. The results show that the majority of students (79.8%) have an average and high level of participation. attendance in online education

●**Final grade frequencies**

The survey results show that 16.5% of the respondents say they have failed, where 21.6% say they have a low level of the final grade, 44.3% say they have an average level of the final grade, 17.6% say they have a high level of the final grade. The majority of students (61.9%) have a medium or high final grade.

CONCLUSION

The research carried out clearly shows the relationship between participation in lectures, course projects, and the final grade in the context of online teaching. In the beginning, before starting the research, it was assumed that participation in lectures and course projects affect the final grade of students. The research study shows that the majority of students (72.8%) have an average and high level of attendance of students in online teaching, 61.9% of students have a medium or high final grade. Studies reveal a high positive correlation between lecture participation and the final grade as the increase in the results of participation in the classrooms was accompanied by an increase in the final grade. Also the study shows that the increase in course project points accompanied with an increase in the final grades. The results of this study have practical importance because it creates an opportunity to reason and support students by letting you know that participation in auditor and in course projects help in the final grade.

REFERENCES

Cui, T. G., & Coleman, A. (2020). Investigating Student`s Attitudes,Motives,Partepation,and Performance.Regarding out-of-class Commumcation(occ).In a Flipped Classroom.Eletronic Journal of e-learning,18(6), 550-556.

Graff, M. (2006). The Importance of online Community in Student Academic Performance.Electronic Journal of e-learning,4(2), 127-132.

Delfino, A. P., (2019). Student Engogment and Academic Performance of Students of Partido State University.Asian Journal of University Education. 15(1)

Bekg, H. I. (2017). Understanding the Effect of Louneliness on Akademic Participation and Succes among International University Students.Journal Education and Practice, 8(14), 46-50.

Perez-Lopez, M. C., & Iborrondo-Davila, M. P. (2020). Key Variables for Academic Performance in University Accounting Studies.A Mediation Model.Iunovations in Education and Teaching International, 53(3), 374-385.

Ward, T. Q., Jacobs, J.Q., & Thompson, R. T. (2016). International Freshman Performance :GPA,Retention,Graduation,Collage and University, 91(1), 2-10.

Xhomara, N. (2016). Kompetenca shkencore dhe metodologjia mesimedhines. Monografi.

Xhomara, N.Q., & Hasan N. (2018). Amound of students study time as an important preditor of academic achievement of students.

Sothan, S. P., (2019). The determinants of Acamedic Performance:Evidence from a Cambodian University.Studies in Higer Education, 44(11), 2096-2111.

Mathnews, K. & Kurap 152,A. (2015). Impact of Writing Proficiency and Writing Center Partecipation an Academic Performance International Journal of Educational Management,20(4), 385-394.

➢ *ORAL PRESENTATION*

Antibiotics use in pediatric age groups

Klodiola Dhamo* (ORCID: *https://orcid.org/0009-0004-6422-7471)*

[*1] Aldent University, Faculty of Medical Sciences, Department of Pharmacy, Tirana, Albania.

Abstract

The pediatric use of antibiotics is essential for managing infections in children. However, inappropriate prescribing can lead to negative effects and antibiotic resistance. This study aims to analyze antibiotic prescription patterns, dosages, and potential drug interactions in pediatric patients in Tirana. The objective of this study is to evaluate prescription patterns, dosage forms, and possible drug interactions of antibiotics used in pediatric patients in Tirana during the period of January-February 2024. This study analyzed 115 antibiotic prescriptions collected from pharmaceutical institutions in Tirana. The collected data included gender, age group, the name of the prescribed antibiotic, pharmacological class, dose, dosing regimen, route of administration, and the specialty of the prescribing doctor. The data were statistically analyzed using SPSS 21 to identify patterns and correlations. The results revealed a balanced gender distribution among pediatric patients, with the highest number of prescriptions in the 1-5 years old age group. Second- and third-generation cephalosporins were the most prescribed antibiotics, followed by amoxicillin and amoxicillin-clavulanate. Suspensions were the most prescribed form. It is recommended to implement guidelines for the prescription of pediatric antibiotics to prevent overuse and resistance. Careful monitoring of possible drug interactions is essential.
Keywords: *Antibiotics, prescription, pediatric patients, prescriptions*

INTRODUCTION

Antibiotic prescribing guidelines set care standards, focus efforts on improving quality, and enhance patient outcomes. There are many factors that influence antibiotic prescribing in pediatric populations, ranging from clinical decision-making by physicians, parents' expectations, to social or cultural factors. Specific diagnoses, maternal education levels, and parents' perceptions of antibiotic use also play a crucial role in shaping prescription patterns. Furthermore, the qualifications of doctors, experience, knowledge sources, and the hospital practice environment contribute to variations in antibiotic prescribing practices. Approximately 60% of hospitalized children receive antibiotics, with one-quarter of antibiotic use considered inappropriate. Although antibiotics are critical for improving clinical outcomes in children with infections, their use in pediatric populations, although widespread, has raised concerns due to potential long-term health consequences, extending beyond antibiotic resistance. Bacterial antimicrobial resistance is a phenomenon caused by changes occurring in bacteria that make the drugs used to treat infections less effective. Infectious pathogens are capable of evolving, and over time, many have developed resistance to previously known or newly developed antibiotics.

MATERIALS AND METHODS

This study used a cross-sectional methodology to analyze antibiotic prescription patterns in pediatric patients in Tirana. Data collection was carried out through a review of 115 pediatric antibiotic prescriptions obtained from pharmaceutical institutions in Tirana during January and February 2024. The collected data included patient demographics (age and gender), details of the prescribed antibiotic (name, pharmacological class, dose, form, and dosing regimen), method of administration, and the specialty of the prescribing doctor. Information on any concurrent medications and potential drug interactions was also analyzed. The data were systematically organized and analyzed to identify trends and adherence to pediatric prescription guidelines.

Statistical analysis through basic frequencies and percentages, as well as advanced SPSS analysis, was used to assess correlations and patterns in the data.

RESULTS

Table 1. 1 Distribution of patients by age and gender

Age	Gender	Frequency	Percentage (%)
0-6 months	Male	7	5,6
	Female	5	4,4
6 months – 1 year	Male	9	7,8
	Female	8	7
1 – 5 years	Male	22	19,1
	Female	18	15,9
5 – 10 years	Male 1	16	13,9
	Female	13	11,1
10 – 17 years	Male	9	7,8
	Female	8	7

55% of the patients (n=63) considered in the study are male, 35% of the patients (n=40) belong to the 1-5 years age group, followed by 25% of the patients (n=29) who belong to the 5-10 years age group.

Table 2. Type of prescribed antibiotic

Antibiotics name	Pharmacological class	Frequency	Percentage (%)
Amoxicillin	Penicillin	12	10,4
Amoxicillin-Clavulanate	Penicillin, Beta-lactamase inhibitors	12	10,4
Cefalexine	Cephalosporins I generation	6	5,2
Cefuroxime	Cephalosporins II generation	6	5,2
Cefaclor		14	12,2
Cefixime	Cephalosporins III generation	17	14,8
Ceftazidime		6	5,2
Ceftriaxone		17	14,8
Azythromycin	Macrolides	12	10,4
Metronidazole	Nitroimidazoles	6	5,2
Sulfamethoxazole-trimethoprim	Sulfphonamides	9	7,8

Regarding the type of antibiotic, cefixime and ceftriaxone are the most commonly used antibiotics, accounting for 14.8% of cases (n=17) each, followed by cefaclor with 12.2% of cases (n=14).
Regarding the pharmacological class, third-generation cephalosporins make up the most prescribed pharmacological class, accounting for 34.8% of cases.

Table.3 Description of the antibiotics by dosage form

Antibiotic	Dosage Form	Description	Frequency	Percentage (%)
Amoxicillin	125 mg/5 ml, 250 mg/5 ml	Suspension	9	7,8
	250 mg, 500 mg	Tablet	3	2,6
Amoxicil lin-clavulana te	200 mg/28.5 mg/5 mL, 400 mg/57mg/5 mL	Suspension	9	7,8
	250 mg/125 mg, 500 mg/125 mg	Tablet	3	2,6
Cephalexine	125 mg/5 mL, 250 mg/5 mL	Suspension	5	4,3
	250 mg, 500 mg	Capsule	1	0,9
Cephuroxime	125 mg/5 mL, 250 mg/5 mL	Suspension	5	4,3
	250 mg, 500 mg	Tablet	2	1,7
Cephaclor	125 mg/5 mL, 250 mg/5 mL	Suspension	12	10,4
	250 mg, 500 mg	Capsule	2	1,7
Cephixime	100 mg/5 mL	Suspension	14	12,2
Cephtazidime	50 mg/kg, 100mg/kg	Injection	6	5,2
Cephtriaxone	50 mg/kg, 75mg/kg	Injection	17	14,8
Azythromycin	200 mg/5 mL	Suspension	12	10,4
Metronidazole	200 mg/5 mL	Suspension	6	5,2
Sulfamethoxazole-trimethoprim	200 mg/40 mg/5 mL	Suspension	9	7,8

65.2% of the dosage forms (n=75) are suspensions. 22.6% of the dosage forms (n=26) are injection suspensions**.**

Tabela.4 Distribution of patients by method of administration

Method of administration	Frequency	Percentage (%)
Oral	89	77,4
Intramuscular	16	13,9
Intravenous	10	8,7

In 77.4% of cases (n=89), the method of antibiotic administration is oral

Tabela.5: Distribution of patients by antibiotic administration regimen

Therapy regimen	Frequency	Percentage (%)
Once a day for 5 days	29	25,2
Twice a day for 7 days	43	37,4
Twice a day for 10 days	6	5,2
Three times a day for 7 days	18	15,7
Three times a day for 10 days	19	16,5

Tabela.6 Distribution by doctor's specialty

Doctor's specialty	Frequency	Percentage (%)
General practitioner	29	25,2
Pediatrician	45	39,1
Emergency physician	41	35,7

35.7% of antibiotic prescriptions were given by a pediatrician, followed by 35.7% given by an emergency physician.

CONCLUSION

The study on pediatric antibiotic prescriptions in Tirana revealed a balanced gender distribution among pediatric patients. The youngest age groups, particularly those aged 1-5 years, accounted for the largest number of prescriptions. Second- and third-generation cephalosporins were the most commonly prescribed antibiotics. Amoxicillin and amoxicillin-clavulanate were also frequently prescribed, reflecting their role in treating common pediatric infections. Suspensions were the most recommended form, especially for younger children.

RECOMMENDATIONS

It is recommended to implement guidelines for pediatric antibiotic prescribing to prevent overuse and resistance. Healthcare providers should be educated on the importance of proper antibiotic use and potential side effects. It is recommended to ensure that liquid formulations are available and used for younger children for ease of administration. Regular training sessions on pediatric antibiotic prescribing practices should be developed for healthcare professionals. The use of probiotics alongside antibiotics should be encouraged to maintain intestinal health.

REFERENCES

Alter, S. J., Vidwan, N. K., Sobande, P. O., Omoloja, A., & Bennett, J. S. 2011. Common childhood bacterial infections. Current problems in pediatric and adolescent health care, 41(10), 256–283. https://doi.org/10.1016/*j.cppeds*.2011.06.001

D.G. Wolf et al.2010 Association of human metapneumovirus with radiologically diagnosed community-acquired alveolar pneumonia in young children. *J Pediatr*

Ku, L.C.; Brian Smith, P.2015 Dosing in neonates: Special considerations in physiology and trial design. *Pediatr. Res*, 77, 2–9.

L.; Gasthuys, E.; Vermeulen, A. 2023 Predicting Volume of Distribution in Neonates: Performance of Physiologically Based Pharmacokinetic Modelling. *Pharmaceutics* 2023, 15, 2348

Lutsar, I.; Metsvaht, T. 2010 Understanding pharmacokinetics/pharmacodynamics in managing neonatal sepsis. Curr. Opin. *Infect. Dis*, 23, 201–207

Men, P.; Li, H.-B.; Zhai, S.-D.; Zhao, R.-S.2016 Association between the AUC0-24/MIC ratio of vancomycin and its clinical effectiveness: A systematic review and meta-analysis. *PLoS ONE*, 11, e0146224.

Rodríguez-Gascón, A.; Solinís, M.Á.; Isla, A. 2021 The role of PK/PD analysis in the development and evaluation of antimicrobials. *Pharmaceutics*, 13, 833.

Smits, A.; Annaert, P.; Van Cruchten, S.; Allegaert, K. A 2020 Physiology-Based Pharmacokinetic Framework to Support Drug Development and Dose Precision During Therapeutic Hypothermia in Neonates. *Front. Pharmacol*, 11, 587.

Van Donge, T.; Van den Anker, J.; Pfister, M. Key 2018 Components for Antibiotic Dose Optimization of Sepsis in Neonates and Infants. *Front. Pediatr*, 29, 325.

➢ *ORAL PRESENTATION*

PVD Yöntemi ile Kaplanmış Isıl İşlemli AISI 4140 Çeliklerin Islanabilirlik Özelliğinin İncelenmesi

Emre Deniz Yalçın* (*ORCID: https://orcid.org/0000-0001-9691-1017*)

*Karadeniz Teknik Üniversitesi, Abdullah Kanca Meslek Yüksekokulu, Makine Programı, Trabzon, Türkiye

*Sorumlu yazar e-posta: emredenizyalcin@ktu.edu.tr

Özet

Bu çalışma kapsamında imalat endüstrisinde özellikle savunma ve havacılık başta olmak üzere birçok üretim alanında önemli ve etkin bir yere sahip olan AISI 4140 çeliklere daha iyi mekanik, fiziksel ve kimyasal yetenekler kazandırmak için çeşitli ısıl işlemler yapılmıştır. Isıl işlem prosesi tamamlanan numuneler çeşitli metalografik işlemleri ve yüzey pürüzlülük ölçümlerinden sonra numunelerin yüzeylerine son yıllarda endüstride yaygın bir kaplama yöntemi olarak kullanılan PVD (Physical Vapor Deposition) kaplama yöntemi ile Argon ve Nitrojen atmosferi altında kaplanma uygulanmıştır. PVD kaplama yöntemi, özellikle alt tabakadaki yüzeyi aşınma ve korozyon gibi etkenlerden koruması ile bilinmektedir. Bununla birlikte PVD kaplama çeşidi olarak iyi mekanik ve fiziksel özellikler ile yüksek kimyasal kararlılıkta olan sert ve yüksek darbe tokluğuna sahip bir kaplama olan TiCN (Titanyum Karbon Nitrür) kaplama çeşidi uygulanmıştır. Oluşturulan PVD kaplamalı 4140 çeliklerdeki kaplama tabakasındaki ıslanabilirlik özellikleri incelenmiş olup üç farklı kontak açısı tespit edilmesi ve elde edilen verilerin PVD kaplamalı 4140 çeliklerin ıslanabilirlik özellikleri hakkındaki bazı bilimsel değerleri ortaya çıkarmıştır.
Anahtar Kelimeler: AISI 4140, Isıl işlem, PVD kaplama, Isnalabilirlik

Investigation of the Wetting Properties of Heat Treated AISI 4140 Steels Coated with PVD Method

Abstract

Within the scope of this study, various heat treatments were carried out to give better mechanical, physical and chemical properties to AISI 4140 steels, which have an important and effective place in many production areas, especially in defence and aerospace in the manufacturing industry. After various metallographic processes and surface roughness measurements, PVD (Physical Vapour Deposition) coating method, which has been widely used as a coating method in the industry in recent years, was applied to the surfaces of the samples under Argon and Nitrogen atmosphere. PVD coating method is especially known for protecting the surface of the substrate from factors such as wear and corrosion. In addition, TiCN (Titanium Carbon Nitride), a hard and high-impact toughness coating with good mechanical and physical properties and high chemical stability, was applied as PVD coating type. The wettability properties of the coating layer on the PVD-coated 4140 steels were investigated and three different contact angles were determined and the data obtained revealed some scientific values about the wettability properties of PVD-coated 4140 steels.

Keywords: AISI 4140, Heat treatment, PVD coating, Wettability

GİRİŞ

Gelişen teknolojiler dengesinde çelik endüstrisinde her geçen gün yeni yöntemler ve gelişmeler kaydedilmektedir. Stratejik bir değere sahip olan AISI 4140 çelikler demir-çelik endüstrisinde çok fazla rağbet gören ve sürekli innovasyon içeren çalışmalara tabi tutulan bir çelik türüdür. Başlıca kullanım alanları olarak; savunma ve havacılık sanayi, otomotiv, makine imalat ve inşaat olmak üzere pek çok alanda 4140 çeliklere ihtiyaç duyulmaktadır. Bunda 4140 çeliklerin mukavemet dayanımı, aşınma ve korozyona karşı gösterdiği karşı direnç önemli bir rol oynamaktadır (Meysami ve ark 2010). 4140 çeliklerin mekanik, fiziksel ve kimyasal özelliklerini geliştirmek için çeşitli ısıl işlemler ve kaplama yöntemleri geliştirilmektedir. Bunlar ısıl işlem olarak, su verme sertleşmesi, yağda soğutma, havada soğutma ve fırında tavlama gibi sıralanabilir. Kaplama yöntemi olarak da kısaca PVD olarak bilinen fiziksel buhar biriktirme

yöntemi ve CVD olarak bilinen kimyasal buhar biriktirme yöntemleri gelmektedir (Knapp ve ark. 2017). Özellikle çelik malzemelerin aşırı stres altında çalıştıkları durumlarda mekanik özelliklerini geliştirmek amacı ile PVD kaplama yöntemleri son yıllarda yaygın olarak kullanılmaktadır (Şimşir ve ark 2021). Yapışma, iyi bir ara yüzey oluşturma, istenilen kalınlık ve esneklik PVD kaplamalarda istenilen temel özellikler arasında yer almaktadır (Warcholinski ve Gilewicz 2011).
Islanabilirlik tanım olarak katı bir ortam ile sıvı ortamın birleştiğinde moleküler etkileşim ile temas sürdürme kabiliyeti olarak ifade edilir. Katı yüzeyler için ıslanabilirlik, yüzeyin sıvı ile ıslanabileceği ıslatma derecesi olarak tanımlanır (Samanta ve ark.2020). Katı yüzeylerin hidrofobikliğini veya hidrofilikliğini değerlendirmek için CA denilen statik temas açısı parametresi kullanılmaktadır. $0° < \theta < 90°$ ise yüzey hidrofiliktir, $90° < \theta < 180°$ ise yüzey hidrofobik, $\theta > 150°$ ise yüzey süperhidrofobik, $\theta = 180°$ ise yüzey bütünüyle hidrofobiktir ve sıvı damlacık katı yüzeyde küresel bir yapıdadır (Ma ve ark. 2019). Gelişen teknolojilerle birlikte yakın zaman içinde çelik, alüminyum ve titanyum gibi bazı mühendislik alaşımlarının yüzey ıslanabilirlik (wettability) özellikleri iyileştirilerek biyomedikal, havacılık ve çeşitli stratejik malzemelerin üretilmesi tasarımcı mühendisler ve dizaynırlar tarafından ilgi görmüştür.
Bu çalışma kapsamında özellikle savunma ve havacılık sanayinde önemli bir yere sahip olan 4140 çeliklerin ısıl işlemleri yapılarak yüzeylerine PVD yöntemi ile TiCN kaplaması uygulanarak oluşan kaplama tabakasındaki ıslanabilirlik özellikleri incelenmiş ve ortaya koyulan veriler irdelenmiştir.

MATERYAL VE METOD

Has çelik firmasından temin edilen AISI 4140 çelik malzeme, 30 mm çapında ve 5 mm kalınlıkta silindirik şekilde hazırlanmış olup ısıl işlem fırınında 700-820-840° C de ısıtıldıktan sonra sırasıyla havada, suda ve yağ ortamında soğutularak ısıl işleme tabi tutulmuştur. Kaplama öncesinde numunelere gerekli metalografik yüzey işlemleri (zımparalama ve parlatma) yapılarak kaplamaya hazır hale getirilmiştir. TiCN PVD kaplamalar- Ar (%99,99), N2 (%99,99) ve C2H2 (%99,99) karışım atmosferinde InterAtom PVD-32 model kaplayıcı kullanılarak üretilmiştir. Kaplama işlemi tamamlanan numuneler ıslanabilirlik deneyleri için uygun hale getirilmiştir. Numunelerin yüzey pürüzlülük ölçümleri MarSurf PS1 marka cihaz ile gerçekleştirilmiştir. TiCN ile kaplanmış 4140 çelik numunelerin yüzeylerinde meydana gelen ıslanma davranışlarının değişimini araştırmak için kontak açısı değerleri incelenmiştir. Deneylerde temas açısı ölçümleri, 3 µL damıtılmış su damlacıkları kullanılarak elektrot yüzeylerinde beş kez farklı farklı pozisyonda uygulanarak gerçekleştirilmiştir. Ölçüm süreci, Leica optik lens sistemi aracılığıyla görüntülerin yakalanmasını, mobil bir cihaza aktarılmasını ve temas açılarını nicel olarak belirlemek için ImageJ yazılımı ile analiz edilmiştir.

BULGULAR ve TARTIŞMA

Isıl işlemli TiCN kaplamalı numunelerin ısıl işlem türüne göre kodlandırılması Tablo 1 de verilmiştir. Bununla birlikte Tablo 2'de ve Şekil 1'de gösterilen değerler numunelerin yüzey pürüzlülük değerlerini belirtmektedir. Ra değeri (ortalama pürüzlük) ve Rz değeri(ortalama derinlik) olarak en iyi değer P3 numunesinde görülmektedir. Düşük ve yüksek Ra ve Rz seviyelerinin olmaması ve bu seviyelerin birbirine çok yakın olması sıcaklık, basınç, ısıl işlem ve kaplama parametrelerinin optimal düzeyde belirlendiği anlamına gelmektedir.

Tablo 1. Numunelerin kodları

Isıl İşlem Türü	Kod
700° Fırında soğutma	P1
820° havada Soğutma	P2
840° Yağda Soğutma	P3

Tablo 2. Numunelerin yüzey pürüzlülük değerleri

Kod	Ra (µm)	Rz (µm)
P1	0,343	2,554
P2	0,252	2,396
P3	0,209	2,252

Şekil 2' de numunelerin kontak açısı değerleri numunelerin damlacık görüntüleri verilmiştir. Kontak açısı en yüksek P1 numunesinde 102° olarak, P2 numunesinde ise 95° olarak ölçülmüştür. Burada P1 numunesinin ve P2 numunesinin yüzeyleri hidrofobik olarak nitelendirilmiştir. P1 numunesinin kontak açı değeri daha büyük olduğu için P1 numunesi, P2 numunesine göre daha hidrofobiktir. P2 numunesi yüzeyindeki ıslanabilirlik P1 numunesine göre daha fazladır. En düşük kontak açısı 88° ile P3 numunesinde ölçülmüş ve P3 numunesi yüzeyi hidrofilik olarak belirlenmiştir. Şekil 2'de bulunan damlacık görüntülerinde P3 numunesinde damlacığın yüzeye yayılması daha belirgin bir şekilde görülmektedir. Bir malzemede yüzey pürüzlülük değerinin artması, katı-sıvı temas bölgesinde büyümeye neden olacağı için kontak açısı da artış göstermesi Cassie Baxter modeli ile açıklanmaktadır. Deney numunelerinin yüzeyindeki mikro yükseklikler ve bu yüksekliklerin aralıkları büyük olduğunda damlacığın temas ettiği yüzeyin alt kısmında oluşan hava boşlukları damlacığın yüzeyi ıslatmasını önlemektedir. Şekil 3 incelendiğinde, numunelerde Ra değeri azaldıkça temas açısının da azaldığı görülmüştür. Bu durum yüzey morfolojisi ve yüzey enerjisi ile açıklanabilir.

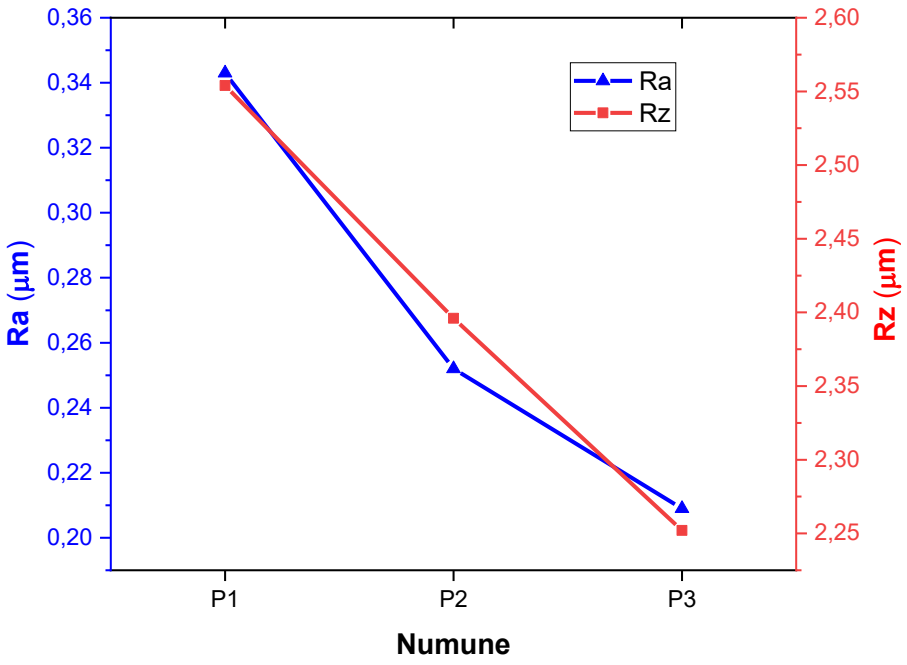

Şekil 1. Numunelerin yüzey pürüzlülük Ra ve Rz değerleri grafiği

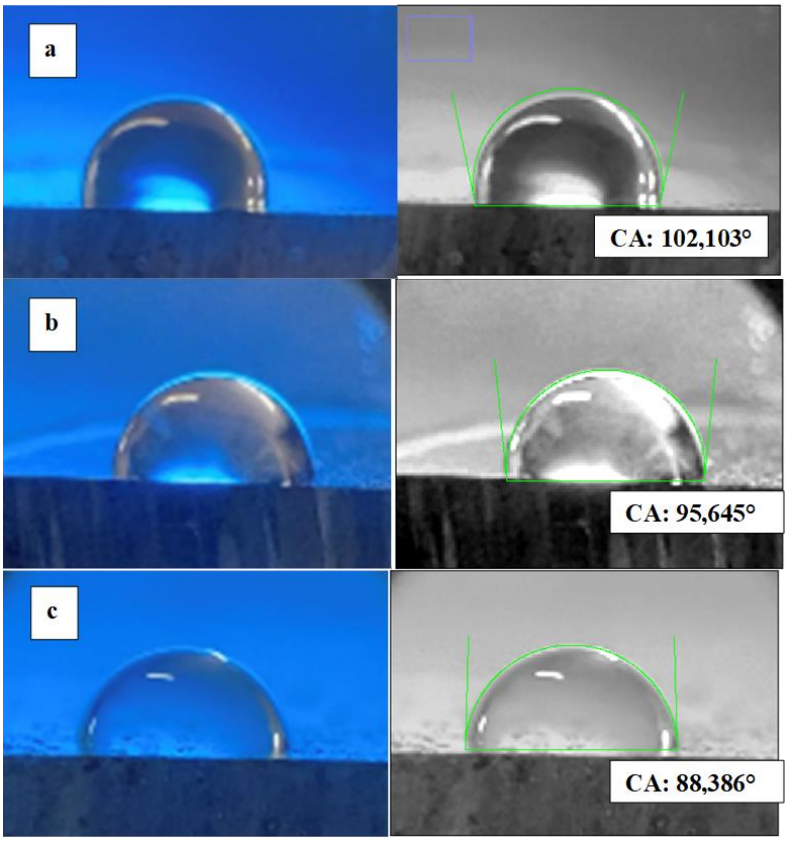

Şekil 2. Numunelerin damlacık görüntüleri, a) P1, b) P2, c) P3

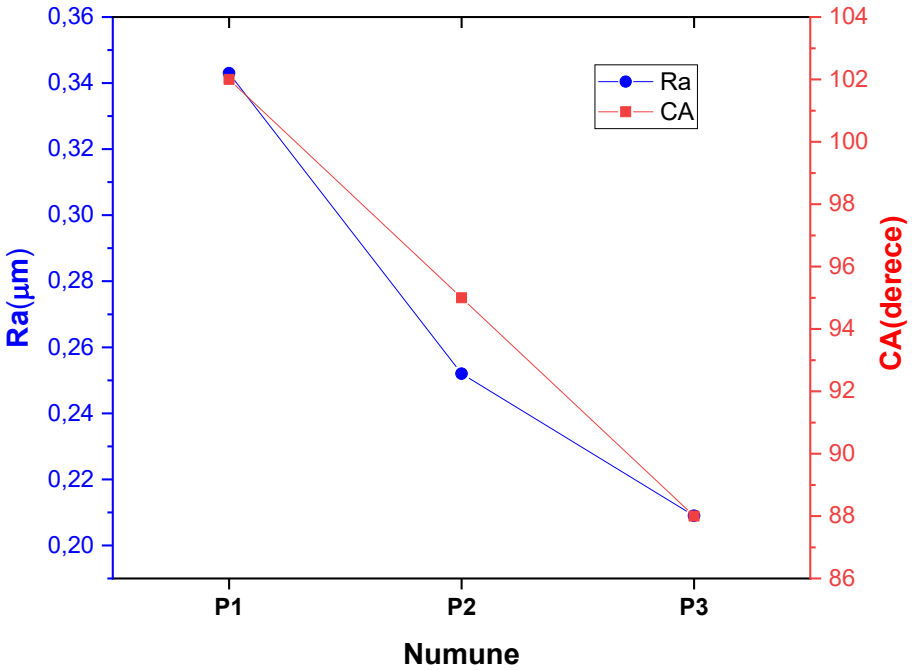

Şekil 3. Numunelerin kontak açısı ve yüzey pürüzlülük grafiği

SONUÇ

TiCN kaplamalı numunelerin fiziksel ve Islanabilirlik özellikleri incelenmiştir. Kaplama işlemi yapılmadan önce uygulanan ısıl işlemler numunelerin ıslanabilirlik özelliklerini etkilemiştir. Bununla birlikte her bir numune farklı kontak açısı ile damlacıkların numene yüzeyinde yayılmasında farklılıklar göstermiştir. P3 numunesine uygulanan yağda soğutma işlemi ve sonrasında TiCN kaplaması yüzey kimyasını etkilemesi ve ayrıyeten yüzeyi daha hidrofilik hale getirmiştir. Özellikle yağda soğutma işleme diğer havada ve fırın

içerisinde yapılan soğutma işlemine göre daha hızlı bir soğutma yöntemi olduğu için numune yüzeyinde mikro boyutta çatlaklar ve nano gözenekler malzeme yüzeyindeki tane sınırlarını değiştirmiş olduğu kanısına varılmıştır. Bu yapısal değişim suyun yayılmasını hidrofilik bir yapıya doğru yönlendirmiştir. Bu durum Wenzel ıslatma modeli ile açıklanabilir. P1 numunesindeki en yüksek temas açısı ile ıslanabilirliğin en az olduğu görülmüştür. Bununla birlikte ıslanabilirliğin az olması ile korozyona maruz kalma ve korozyondan etkilenen yüzey alanlarında azalmalar meydana gelecektir.

KAYNAKLAR

Knapp, M., Hoffmann, R., Cimalla, V., & Ambacher, O., Wettability Investigations and Wet Transfer Enhancement of Large-Area CVD-Graphene on Aluminum Nitride. Nanomaterials, 7(2017), 226. https://doi.org/10.3390/nano7080226.

Ma C., Kang M., Wang X., et al. (2019). Fabrication of Regular Hierarchical Structures with Superhydrophobic and High Adhesion Performances on a 304 Stainless Steel Surface via Picosecond Laser. J Bionic Eng, 16, 806-813.

Meysami A.H., Ghasemzadeh R., Seyedein S.H., Aboutalebi M.R., (2010). An investigation on the microstructure and mechanical properties of direct-quenched and tempered AISI 4140 steel, Mater Des 31, 1570–1575.

Samanta A., Wang Q., Shaw S. K. (2020). Roles of Chemistry Modification for Laser Textured Metal Alloys to Achieve Extreme Surface Wetting Behaviors. Materials and Design, 192, 108744.

Simsir M., Palaci Y., Özer A., (2021). A comparative study of hardness/scratch/wear properties of TiCN and TiAlN coatings on DIN 1.2842 steel by CA-PVD method, Journal of the Australian Ceramic Society 57, 1027–1037.

Warcholinski B., Gilewicz A., (2011). Multilayer coatings on tools for woodworking, Wear 271 2812–2820.

➢ *ORAL PRESENTATION*

Determination of Chemical Content, Cholinesterase Enzyme and Tyrosinase Enzyme Activities of *Citrus hystrix* Extracts

Bihter Şahin[1*] (*ORCID: https://orcid.org/ 0000-0001-8657-052X*),
Beyda Toğluk[1] (*ORCID: https://orcid.org/0009-0004-5830-9972*)

[*1]Bandırma Onyedi Eylül University, Susurluk Agriculture and Forest Vocational School, Department of Chemistry and Chemical Processing Technologies, Balıkesir, Türkiye

*Corresponding author e-mail: bsahin@bandirma.edu.tr

Abstract
Kaffir lime (*Citrus hystrix*) is an herbal plant from the *Rutaceae* family, grown and widely distributed in many countries, especially in Southeast Asia. It is frequently used as aromatic oil and spice due to its strong odor. As a result of the studies carried out in this study, the phenolic and organic acid content concentrations of ethyl acetate, methanol, ethanol and water extracts obtained from the shells of *C. hystrix*, which is a value of our country, were calculated qualitatively and quantitatively with the help of HPLC-DAD device. Anticholinesterase activity, tyrosinase enzyme inhibition activity and bioactivities were determined spectroscopically and in vitro. CH1 extract obtained from *Citrus hystrix* peels was found to be the extract with the highest phenolic content. It was also determined that CH1 extract showed the best enzyme inhibition activity. As a result of this, the expectation of finding natural and new enzyme inhibitors because of the isolation of the active substance by chromatographic methods from the extracts of different polarities of Kaffir lime collected from Köyceğiz district of Muğla has increased.
Keywords: *Citrus hystrix*, Enzyme inhibitory activity, HPLC-DAD, Phenolic composition

INTRODUCTION

Citrus hystrix or Kaffir lime, commonly known as "magrood", is a plant belonging to the family *Rutaceae*. The leaves and fruits of *C. hystrix* have a pleasant lemon scent and are called medicinal lime. Kaffir lime is one of the indispensable ingredients especially in Far Eastern cuisine. Kaffir lime has a bitter-sour taste, and its aroma is quite intense compared to other lemon varieties.

C. hystrix leaves are used as a flavoring in dishes in Thailand at that time. The fruit is not eaten fresh, but canned or used as a spice in meals. It is also used as a hair shampoo or medicine (Allen, 1967). Various parts of *C. hystrix*, such as its leaves, branches, fruit peels and juice, are rich in essential oils. (Akiyoshi et al., 1990). Since it is rich in essential oils, it has also been used as an insect repellent and for the treatment of insect bites.

Kaffir lime peel and leaves are known to be a source of phenolic compounds and antioxidant compounds (Tachakittirungrod et al., 2007; Jantarach and Thanaboripat, 2010; Anuchapreeda et al., 2020). It is known that many bioactive compounds obtained from various citrus fruits inhibit cancer cell proliferation (Patil et al., 2009). In addition to the positive effect of citrus fruits on cancer treatment, it can also be described as the plague of the age, irreversible nerve cell loss, the cause of which is not yet fully known; difficulties in cholinergic neurotransmission, memory and mental functions, thinking and interpretation; It has become a matter of curiosity to investigate the effect of neurodegenerative Alzheimer's disease (Tayeb et al., 2012), which is known for its personality and behavioral disorders.

In the physiology of this disease, which is quite complex to understand, neuron and axon loss occurs. As a result, there is a decrease in the acetylcholine level. Therefore, increasing acetylcholine levels is an important way to treat Alzheimer's disease. Another method to increase acetylcholine levels is to suppress cholinesterase enzymes that break down acetylcholine. Acetylcholinesterase (AChE; acetylcholinesterase) and butyrylcholinesterase (BChE, butyrylcholinesterase) are enzymes that are encoded by different genes but differ from each other due to their differences in their substrate selectivity and some catalytic mechanisms. As a result of the data obtained in the research, it is necessary to increase the concentration of melanin pigment in the body, which, unlike Alzheimer's disease, provides defense against skin photocarcinoma (Liesener et al., 2007).

Tyrosinase enzyme increases the concentration of melanin pigment by specifically acting on the tyrosine substrate. Melanin is one of the factors that affect skin and hair color in humans. Melanin is necessary to protect human skin against radiation (Parvez et al., 2007).

Melanin plays a protective role against skin photocarcinoma and protects the skin against UV damage and reactive oxygen species (ROS) by absorbing ultraviolet (UV) rays. It purifies toxic substances and drug residues from the organism. In recent years, it has been known that a large number of potent tyrosinase inhibitors have become available from natural and synthetic sources (Khan, 2012). Tyrosinase inhibitors such as arbutin, kojic acid and hydroquinones are used as whitening and antihyperpigment agents because they prevent melanin production in the skin.

Since *Citrus* species have many medicinal activities, the expectation of finding natural and new enzyme inhibitors from *C. hystrix* is increasing. The phenolic contents of 4 different extracts, namely ethyl acetate, ethanol, methanol and water, from the shells of *C. hystrix* collected from Muğla, which was the subject of the study, were determined by HPLC-DAD and their concentrations were determined spectroscopically and in vitro. In addition, acetylcholinesterase, butyrylcholinesterase and tyrosinase enzyme inhibition activity experiments were performed on the extracts of different qualities. Bioactivity results of ethanol, ethyl acetate, methanol and water extracts with qualitatively different polarities were calculated with the results obtained from chemical content and enzyme activity tests with 3 different methods.

MATERIALS AND METHODS

Preparation and extraction procedures of *C. hystrix*

Kaffir lime (*C. hystrix*) was collected from Köyceğiz district of Muğla, the peels were separated from the fruit, dried in the shade and at room temperature. It was cut into small pieces and ready for extraction. After removing the oily parts with hexane, the peels of *C. hystrix* were extracted with ethyl acetate (CH1), methanol (CH2), ethanol (CH3), and water (CH4) extracts by applying the sequential extraction method until their colors lightened (x3 times). Thus, extracts were obtained.

Preparation of samples for HPLC-DAD analysis

Ethyl acetate, ethanol, methanol and water extracts of *C. hystrix* peels were weighed as 8 mg, then dissolved in 1 mL of methanol, homogenized and filtered through 0.45 µm PTFE filters, and then made ready for HPLC-DAD injection.

HPLC-DAD analysis parameters

Phenolic component analysis of ethyl acetate, ethanol, methanol and water extracts of *C. hystrix* peels, Tokul-Ölmez et al. The 2020 method gradient solvent system was applied. In this study, comparison was made with 42 phenolic standard substances (fumaric acid, gallic acid, protocatechin acid, thiobromine, thiophylline, catechin, 4-hydroxybenzoic acid, 6,7-dihydroxycoumarin, methyl-1,4-benzoquinone, vanillic acid, caffeic acid, vanillin, chlorogenic acid, *p*-coumaric acid, ferrulic acid, cynarin, coumarin, propylgallate, routine, *trans*-2-hydroxy cinnamic acid, ellagic acid, myricetin, fisetin, quercetin, *trans* cinnamic acid, luteolin, rosmarinic acid, campferol, apigenin, chrysin, 4-hydroxyresorquinol, 1,4-dichlorobenzene, pyrocatechol, 4-hydroxy benzaldehyde, epicatechin, 2,4-dihydroxybenzaldehyde, hesperedin, oleuropein, naringenin, hesperetin, genistein, curcumin). The column temperature was set at 35ºC. The solvent system was methanol and 0.1% acidified water. Chromatographic separation will be performed on a C_{18} (5 µm, 4.6 mm x 250 mm) reverse phase column and Inertsil C_{18} guard column. A diode array detector (DAD) was used with absorbance using a wavelength of 254 nm. The solvent system was applied as stated in the literature (Tokul-Ölmez et al., 2020).

Anticholinesterase enzyme inhibition activity

Acetylcholinesterase and butyrylcholinesterase inhibition activities of ethyl acetate, ethanol, methanol and water extracts of *C. hystrix* peels were measured by a spectrophotometric method known as the Ellman method (Ellman et al., 1961), and acetylcholinesterase obtained from electric fish and butyrylcholinesterase obtained from horse serum were used as enzymes. Substrates were used as acetylcholine iodide and butyrylcholinen iodide, yellow colored 5,5'-dithiobis-(2-nitrobenzoic acid) (DTNB) was used to measure the activity. 160 µL of 0.1M pH=8 phosphate buffer, 10 µL of extracts containing 2 mL sample solution at

2000 ppm concentration, and 10 µL of AChE and/or BChE solution were added to each well of the 96-well microplates. 10 µL of methanol was used as a control. It was incubated for 15 minutes at 25 °C. Then, 10 µL of DTNB solution and 10 µL of AcI or BuI were added and the kinetic absorbances were measured for 10 minutes at a wavelength of 412 nm. The results are given in Table 5.

Tyrosinase enzyme inhibition activity

Tyrosinase inhibition activity of *C. hystrix* peel extracts was determined using the spectrophotometric method (Hearing, 1987). Tyrosinase fungus was used as an enzyme and L-DOPA was used as the substrate. After adding 150 µL of 0.005 M pH=6.8 phosphate buffer to the microplates and 20 µL of tyrosinase enzyme prepared from tyrosinase fungus onto 10 µL stock solutions of *C. hystrix* peel extracts at different concentrations, the samples were mixed for 3 minutes and incubated for 10 minutes at 37°C. At the end of the incubation, as soon as 20 µL L-DOPA solution was added to the microplate, the kinetic absorbance of the samples was measured at 475 nm wavelength for 10 min at 37°C. The results are given as IC_{50} concentrations in Table 5. With this study, Kaffir lime peels collected from Muğla Köyceğiz were evaluated in this context for the first time.

RESULTS and DISCUSSION

HPLC-DAD analysis

Ethyl acetate, methanol, ethanol and water extracts obtained from *C. hystrix* were prepared at concentrations in accordance with the specified procedure and HPLC-DAD analysis were performed. According to HPLC-DAD results of ethyl acetate extract (CH1) obtained from *C. hystrix*; pyrocatechol (2.18 mg/g), catechin (0.11 mg/g), vanilic acid (0.45 mg/g), *trans*-2-hydroxycinnamic acid (1.08 mg/g), ellagic acid (5.74 mg/g), kaempferol (4.89 mg/g), and curcumin (11.98 mg/g) phenolic acids were detected. Chlorogenic acid, ferulic acid, cynarin, hesperedin, myricetin, quercetin, naringenin, hesperetin, oleuropein, chrysin, and 4-hydroxyresorcinol were detected in trace amounts.

Table 1. Phenolic component contents of CH1 extract (mg/g)

No	Compounds name	Retention time	Calibration Equation	Area	Concentration
1	Pyrocatechol	23.844	y = 3772.8x + 23692	68144	2.18
2	Catechin	30.100	y = 2611.2x + 74392	10074	0.11
3	Vanilic acid	34.990	y = 66764x + 46508	60998	0.45
4	Chlorogenic acid	40.157	y = 46920x - 36953	124	*tr**
5	Ferrulic acid	42.706	y = 42245x + 110701	97536	*tr**
6	Cynarin	43.805	y = 42559x - 2E+06	295	*tr**
7	Hesperedin	47.127	y = 2949.5x + 9083.5	27	*tr**
8	*Trans*-2-hydroxycinnamic acid	48.124	y = 53442x + 104662	162379	1.08
9	Ellagic acid	49.731	y = 235073x - 7E+06	120116	5.74
10	Myricetin	50.842	y = 119666x + 161404	18	*tr**
11	Oleuropein	51.226	y = 6962.8x + 4273.4	0	*tr**
12	Naringenin	54.970	y = 5906.1x + 8703	160	*tr**
13	Quercetin	55.296	y = 89397x - 80467	0	*tr**
14	Hesperetin	56.770	y = 4524.4x + 10178	0	*tr**
15	Kaemferol	62.210	y = 92669x + 58328	511479	4.89
16	Chyrsin	72.645	y = 26957x + 286396	0	*tr**
17	Curcumin	72.798	y = 15850x + 140009	329892	11.98
18	4-hydroxyresorcinol	72.932	y = 2389.3x + 109133	1765	*tr**

**tr*: trace amount of compound.

Phenolic component contents of CH1 (mg/g) were listed Table 1 and the detected compounds were given in the chromatogram in Figure 1.

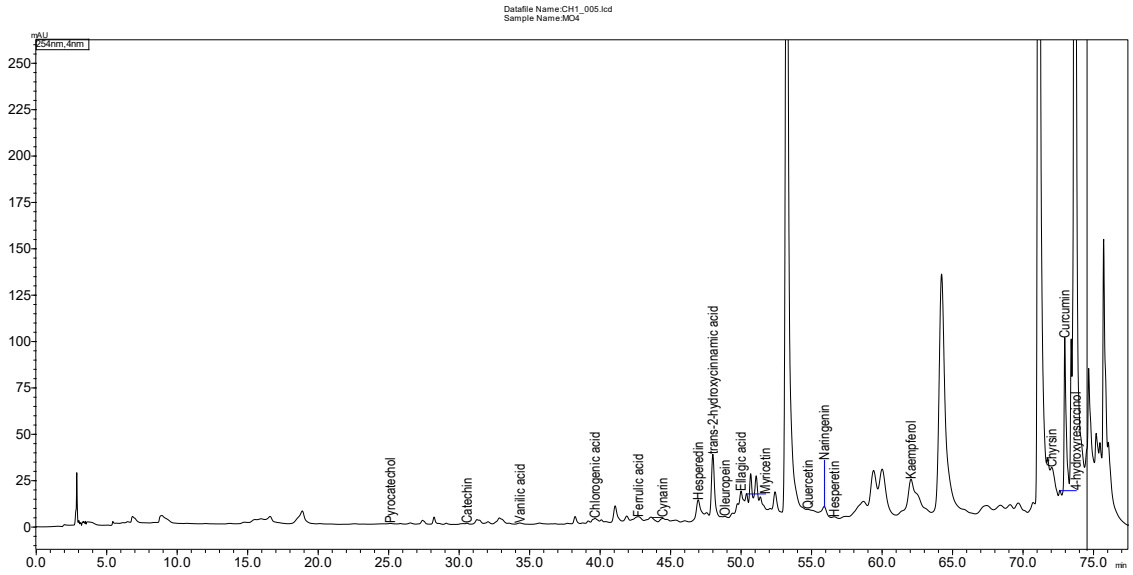

Figure 1. HPLC-DAD chromatogram of CH1 extract at 254 nm wavelength

HPLC-DAD results CH2 of extract (methanol) obtained from *C. hystrix*; chlorogenic acid (0.25 mg/g), hesperedin (2.06 mg/g), fisetin (0.28 mg/g), and 4-hydroxyresorcinol (17.65 mg/g) phenolic acids were detected. Vanilic acid, oleuropein, ellagic acid, myricetin, naringenin, genistein, curcumin, and 1,4-dichlorobenzene were detected in trace amounts. Phenolic component contents of CH2 (mg/g) were listed Table 2.

Table 2. Phenolic component contents of CH2 extract (mg/g)

No	Compounds name	Retention time	Calibration Equation	Area	Concentration
1	Vanilic acid	34.960	y = 66764x + 46508	10500	*tr*
2	Chlorogenic acid	38.266	y = 46920x - 36953	71620	0.25
3	Hesperedin	47.604	y = 2949.5x + 9083.5	56488	2.06
4	Oleuropein	51.226	y = 6962.8x + 4273.4	0	*tr*
5	Ellagic acid	49.731	y = 235073x - 7E+06	2321	*tr*
6	Myricetin	50.842	y = 119666x + 161404	102	*tr*
7	Fisetin	52.513	y = 100784x + 16688	237998	0.28
8	Naringenin	54.970	y = 5906.1x + 8703	22	*tr*
9	Genistein	58.875	y = 69160x + 5753.8	700120	*tr*
10	Curcumin	72.798	y = 15850x + 140009	0	*tr*
11	4-hydroxyresorcinol	72.932	y = 2389.3x + 109133	440123	17.65
12	1,4-dichlorobenzene	74.590	y = 7482.7x + 100774	20	*tr*

**tr*: trace amount of compound.

The detected compounds are given in the chromatogram in Figure 2.

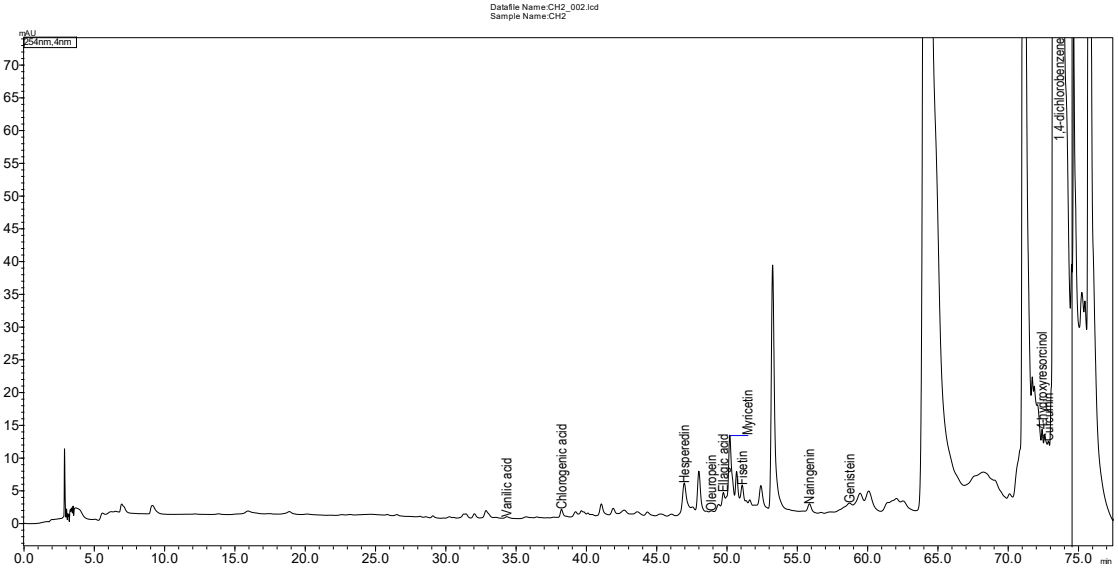

Figure 2. HPLC-DAD chromatogram of CH2 extract at 254 nm wavelength

The results in Table 3; 4-hydroxyresorcinol (18.73 mg/g) were detected as the major factor in *C. hystrix*; CH3 extract. It was calculated as cynarin (5.90 mg/g), hesperedin (2.38 mg/g), protocatechuic acid (1.71 mg/g), rosmarinic acid (0.54 mg/g), chlorogenic acid (0.42 mg/g), fisetin (0.40 mg/g) and genistein (0.13 mg/g), respectively. Catechin, vanilic acid, epicatechin, *trans*-2-hydroxycinnamic acid, and chyrsin were detected in trace amounts.

Table 3. Phenolic component contents of CH3 extract (mg/g)

No	Compounds name	Retention time	Calibration Equation	Area	Concentration
1	Protocatechuic acid	25.499	y = 65753x - 6932.1	44633	1.71
2	Catechin	30.628	y = 2611.2x + 74392	7541	*tr**
3	Vanilic acid	34.960	y = 66764x + 46508	30201	*tr**
4	Epicatechin	35.784	y = 2097.6x + 7998.2	3959	*tr**
5	Chlorogenic acid	38.266	y = 46920x - 36953	120324	0.42
6	Cynarin	43.799	y = 42559x - 2E+06	9541	5.90
7	Hesperedin	47.604	y = 2949.5x + 9083.5	65263	2.38
8	*Trans*-2-hydroxycinnamic acid	48.157	y = 53442x + 104662	260771	*tr**
9	Fisetin	52.513	y = 100784x + 16688	339998	0.40
10	Genistein	58.875	y = 69160x + 5753.8	77468	0.13
11	Rosmarinic acid	60.267	y = 100183x + 58325	489238	0.54
12	Chyrsin	72.645	y = 26957x + 286396	237669	*tr**
13	4-hydroxyresorcinol	72.932	y = 2389.3x + 109133	467055	18.73

**tr*: trace amount of compound.

The HPLC-DAD chromatogram of the CH3 extract at 254 nm wavelength is given in Figure 3.

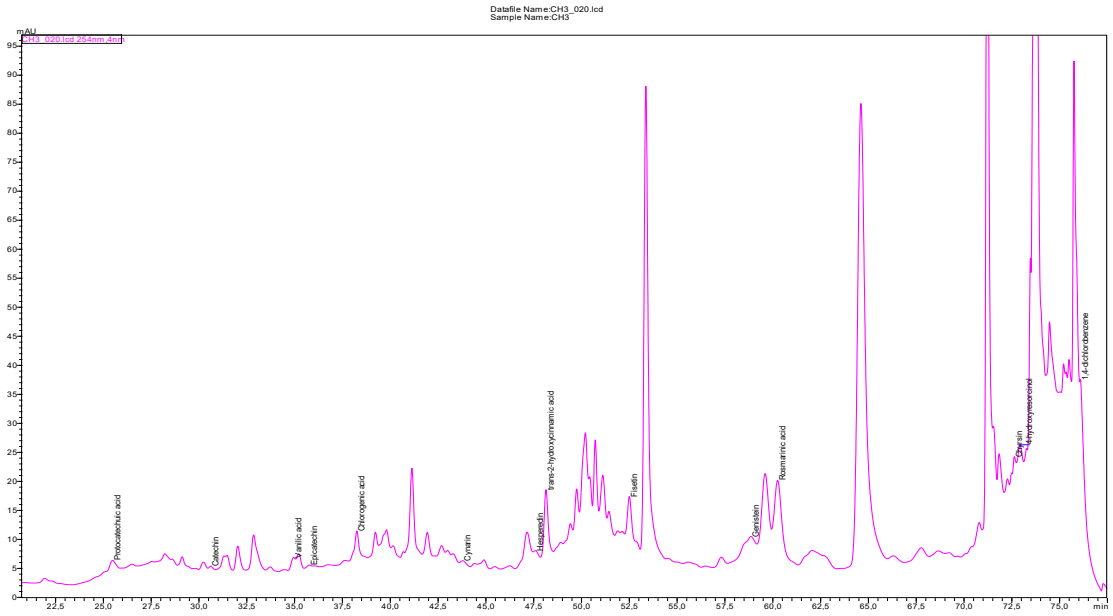

Figure 3. HPLC-DAD chromatogram of CH3 extract at 254 nm wavelength

According to the results, in Table 4; Ellagic acid (37.35 mg/g) were detected as the major compound in *C. hystrix* CH4 extract and respectively pyrocatechol (22.02 mg/g), hesperedin (10.06 mg/g), cynarin (6.00 mg/g), fumaric acid (2.72 mg/g), gallic acid (2.28 mg/g), rosmarinic acid (0.96 mg/g), 4-hydroxy benzaldehyde (0.56 mg/g), *p*-coumaric acid (0.50 mg/g), *trans*-2-hydroxycinnamic acid (0.39 mg/g), and chlorogenic acid (0.21 mg/g). 6,7-dihydroxycoumarin, vanilic acid, caffeic acid, vanillin, ferrulic acid and *trans* cinnamic acid were detected as a trace amounts.

Table 4. Phenolic component contents of CH4 extract (mg/g)

No	Compounds name	Retention time	Calibration Equation	Area	Concentration
1	Fumaric acid	14.304	y = 1988.9x - 4655.8	38621	2.72
2	Gallic acid	15.248	y = 45540x - 84708	745745	2.28
3	Pyrocatechol	23.844	y = 3772.8x + 23692	688317	22.02
4	4-hydroxy benzaldehid	32.867	y = 34376x + 4239.6	157998	0.56
5	6,7-dihydroxycoumarin	33.663	y = 27607x + 208788	1978	*tr**
6	Vanilic acid	34.99	y = 66764x + 46508	0	*tr**
7	Caffeic acid	35.072	y = 49533x + 213471	2053	*tr**
8	Vanillin	37.620	y = 21426x + 195103	10956	*tr**
9	Chlorogenic acid	40.157	y = 46920x - 36953	42197	0.21
10	*p*-Coumaric acid	41.138	y = 17265x + 343183	412654	0.50
11	Ferrulic acid	42.706	y = 42245x + 110701	105745	*tr**
12	Cynarin	43.805	y = 42559x - 2E+06	43529	6.00
13	Hesperedin	47.127	y = 2949.5x + 9083.5	246427	10.06
14	*Trans*-2-hydroxycinnamic acid	48.124	y = 53442x + 104662	271572	0.39
15	Ellagic acid	49.731	y = 235073x - 7E+06	240325	37.35
16	*Trans* cinnamic acid	56.446	y = 88190x + 158733	1270	*tr**
17	Rosmarinic acid	60.249	y = 100183x + 58325	826602	0.96

**tr*: trace amount of compound.

The HPLC-DAD chromatogram of the CH4 extract at 254 nm wavelength is given in Figure 4.

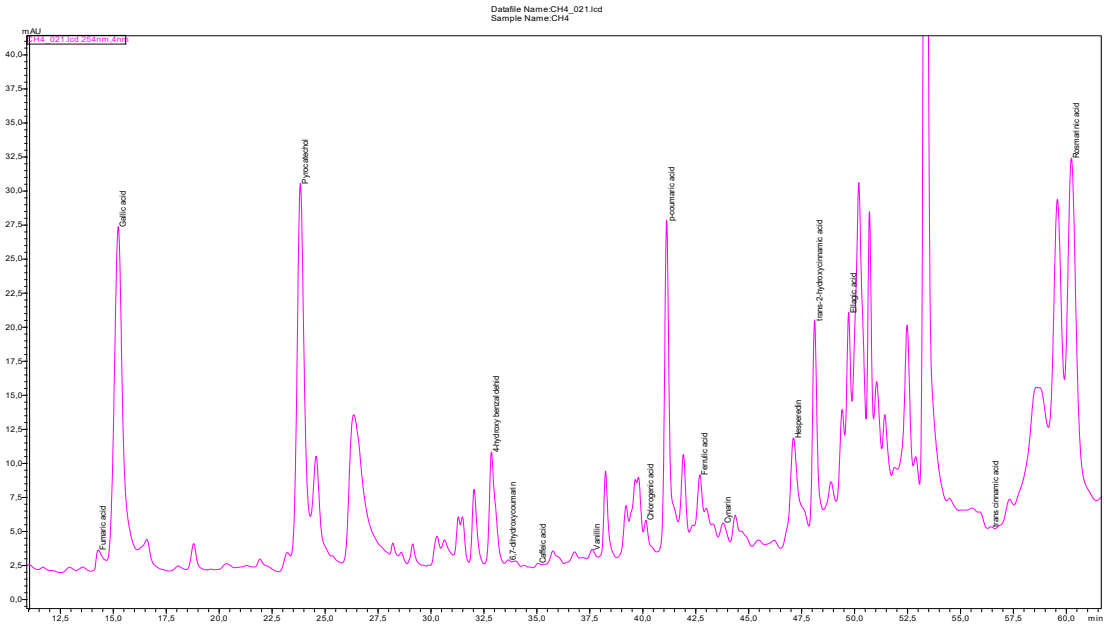

Figure 4. HPLC-DAD chromatogram of CH4 extract at 254 nm wavelength

Enzyme inhibition activity

According to the enzyme activity results given in Table 5; It was found that CH3 (ethanol) (IC_{50}: 117.68±0.60 µg/mL) extract showed better acetylcholinesterase enzyme activity than other extracts.

In the results of butyrylcholinesterase enzyme inhibition activity, it was determined that CH1 (ethyl acetate) (IC_{50}: 11.08±2.89 µg/mL) extract showed better enzyme activity compared to the standard reference substance studied, galantamine (IC_{50}: 34.58±0.60 µg/mL). CH1 extract was followed by CH2, and activity was observed in the CH4 extract at a concentration of IC_{50}: > 200 µg/mL.

Kojic acid was used as the standard reference substance in tyrosinase enzyme inhibition. According to the results of the 4 extracts obtained; CH2 (methanol) and CH3 (ethanol) tyrosinase enzyme inhibitions were calculated as IC_{50}: > 200 µg/mL. CH1 (IC_{50}: 111.96±1.45 µg/mL) extract, which showed the best activity, was followed by CH3 (IC_{50}: 141.51±2.65 µg/mL) extract.

Table 5. Anticholinesterase and tyrosinase enzyme inhibition results of *Citrus hystrix* extracts (25-200 µg/mL)

Codes	Acetylcholinesterase enzyme inhibition (AcHE)	Butyrylcholinesterase enzyme inhibition (BcHE)	Tyrosinase inhibition
CH1 (*ethyl acetate*)	*NA**	11.08±2.89	111.96±1.45
CH2 (*methanol*)	*NA**	56.15±0.27	> 200
CH3 (*ethanol*)	117.68±0.60	*NA**	141.51±2.65
CH4 (*water*)	> 200	> 200	> 200
Galantamine	16.39±0.81	34.58±0.60	*NT***
Kojic acid	*NT***	*NT***	24.99±0.13

**NA:* not active.
***NT:* not tested.

CONCLUSION

In our study, four extracts with different properties (ethyl acetate, ethanol, methanol, water) of *Citrus hystrix* were obtained fruit peels which collected from Muğla in 2022. After the extracts were prepared, their phenolic contents were determined with the help of HPLC-DAD. The HPLC-DAD analysis gave insight into the phenolic and organic acid composition of *C. hystrix* four extracts. In this way, phenolic content was determined both qualitatively and quantitatively. The results were presented in Table 1-4. As a result of our comparisons with the 42 phenolic compounds included in the phenolic method we applied, the highest number of phenolic compounds were detected in the CH1 extract. In addition, vanillic acid, chlorogenic acid and hesperidin compounds were found in common in the scanned extracts.

A certain substance is known to help treat skin conditions like hyperpigmentation and melanoma. It works by inhibiting the tyrosinase enzyme, which is crucial in the process of producing melanin, the pigment responsible for skin color (Parvez et al., 2007). Additionally, the substance contains compounds that inhibit acetylcholinesterase and butyrylcholinesterase enzymes, which are believed to help prevent nerve damage in Alzheimer's disease. So, for this reason, considering the studies in the literature on *Citrus* species with biological activity, we investigated the anticholinesterase and tyrosinase inhibition activities of 4 different extracts obtained from kaffir lime peels. IC_{50} values were calculated by screening the anticholinesterase and tyrosinase enzyme inhibition activities of the 4 extracts we obtained.

According to these results, it is seen that the ethyl acetate extract, which we code as CH1, gives more interesting results compared to other extracts, both in terms of its phenolic content and the anticholinesterase and tyrosinase enzyme inhibition results. We see in many literature studies that phenolic content and antioxidant properties support each other (Jantarach and Thanaboripat, 2010; Anuchapreeda et al., 2020). While CH1 (11.08±2.89 µg/mL) showed better butyrylcholinesterase activity than galantamine (34.58±0.60 µg/mL), which was used as the standard reference compound, CH2 (56.15±0.27 µg/mL) extract was closer to galantamine (34.58±0.60 µg/mL). It was found to show butyrylcholinesterase activity. As a result of tyrosinase enzyme inhibition activity; It was found that CH1 extract showed the best activity. On the other hand, it was determined that CH4 extract (>200 µg/mL) showed low activity against all enzyme types.

In the light of all the data obtained as a result of this study, it is recommended to conduct in vivo and in vitro studies of the rich contents of *C. hystrix* fruits with different extract types, based on our aim, phenolic content determinations. With future studies, beneficial compounds originating from natural products will be introduced to the food and health sector.

ACKNOWLEDGEMENTS

This study was financially supported by TUBITAK with the number 2209-A with the project numbered 1919B012220664 within the scope of the University Students Research Projects Support Program in the 2022/2. I would like to thank Prof. Dr. Mehmet ÖZTÜRK from Muğla Sıtkı Koçman University for support in the completion of my experimental studies. The editor and referees should be thanked for their contributions during the review and evaluation of the manuscript.

REFERENCES

Akiyoshi, A., Kenichi, A., & Toshiya S. (1990). The chemical composition of *Citrus hystrix* DC. (Swingi) Journal of Essential Oil Research, 2, 179-183. https://doi.org/10.1080/10412905.1990.9697857.

Allen, B.M. (1967). *Malayan fruits an introduction to the cultivated species*. Donald Moore Press Ltd., Singapore, 154–155.

Anuchapreeda, S., Anzawa, R., Viriyaadhammaa, N., Niumkam, W., Chaiyana, W., Okonogi, S., & Usuki, T. (2020). Isolation and biological activity of agrostophillinol from kaffir lime (Citrus hystrix) leaves. *Bioorganic & Medicinal Chemistry Letters*, 127256. https://doi:10.1016/j.bmcl.2020.127256.

Ellman, G. L., Courtney, K. D., Andres, V., & Featherston, R. M. (1961). A new and rapid colorimetric determination of acetylcholinesterase activity. *Biochemical Pharmacology*, *7*, 88–95. https://doi.org/10.1016/0006-2952(61)90145-9.

Jantarach, J., & Thanaboripat, D. (2010). The efficacy of ethyl acetate extract of Trichoderma culture broth on growth inhibition and aflatoxin production by *Aspergillus flavus* IMI242684. *KMITL Science and Technology Journal*, *10*(1), 19-29.

Khan, M.T.H. (2012). Novel tyrosinase inhibitors from natural resources-their computational studies. *Current Medicinal Chemistry*, *19*, 2262-2272. https://doi.org/10.2174/092986712800229041.

Liesener, A., Perchuc, A.-M., Schöni, R., Schebb, N.H., Wilmer, M., & Karst U. (2007). Screening of acetylcholinesterase inhibitors in snake venom by electrospray mass spectrometry. *Pure and Applied Chemistry*, *79*(12), 2339-2349. https://doi.org/10.1351/pac200779122339.

Parvez, S., Kang, M., Chung, H., & Bae, H. (2007). Naturally occurring tyrosinase inhibitors: Mechanism and applications in skin health, cosmetics and agriculture industries. *Phytotherapy Research*, *21*(9), pp. 805-816. https://doi.org/10.1002/ptr.2184.

Patil, J.R., Jayaprakasha, G., Murthy, K.C., Tichy, S.E., Chetti, M.B., & Patil, B.S. (2009). Apoptosis-mediated proliferation inhibition of human colon cancer cells by volatile principles of *Citrus aurantifolia*. *Food Chemistry*, *114*, 1351-1358. https://doi.org/10.1016/j.foodchem.2008.11.033.

Tachakittirungrod, S., Okonogi, S., & Chowwanapoonpohn, S. (2007). Study on antioxidant activity of certain plants in Thailand: mechanism of antioxidant action of guava leaf extract. *Food Chemistry*, *103*, 381-388. https://doi.org/10.1016/j.foodchem.2006.07.034.

Tayeb, H.O., Yang, H.D., Price, B.H., & Tarazi, F.I. (2012). Pharmacotherapies for Alzheimer's disease: beyond cholinesterase inhibitors, *Pharmacology & Therapeutics*, *134*(1), 8-25. https://doi.org/10.1016/j.pharmthera.2011.12.002.

Tokul Ölmez, Ö., Şahin, B., Çakır, C., & Öztürk, M. (2020). Rapid and easy method for simultaneous measurement of widespread 27 compounds in natural products and foods. *Journal of Chemical Metrology*, *14*(1), 1-11. https://doi.org/10.25135/jcm.38.20.03.1589.

➢ *ORAL PRESENTATION*

Optimizing Renewable Energy Integration in the Kurdistan Province Microgrid: A Comparative Analysis of Feed-in Tariff and Net Metering Policies

Fooad Karimi Ghaleh Jough[1*] (*https://orcid.org/0000-0003-0697-516X)*
Mohammadreza Gholami[2](*https://orcid.org/0000-0002-9136-5026*)

[*1]Department of Civil Engineering, Faculty of Engineering Final International University, Via Mersin 10, Kyrenia, Turkey.
[2]Department of Electrical and Electronic, Faculty of Engineering Final International University, Via Mersin 10, Kyrenia, Turkey.

Abstract

This study explores the optimization of renewable energy integration within the microgrid (MG) framework of Kurdistan province, Iran, through a comparative analysis of Feed-in Tariff (FiT) and Net Metering (NM) policies. Building upon existing research on MG operation, renewable energy technologies, and energy policy frameworks, our investigation aims to assess the effectiveness of FiT and NM in promoting renewable energy adoption, enhancing grid stability, and optimizing economic outcomes within the Kurdistan MG context. Methodologically, we extend a previously developed optimization model to incorporate the simulation of FiT and NM policies, considering their respective regulatory frameworks, incentive structures, and operational implications. The study evaluates the impacts of these policies on key performance metrics such as energy generation, grid stability, and economic costs. Our findings highlight the nuanced effects of FiT and NM on MG operation, reducing the total cost and more exporting power to the main grid. Ultimately, this research contributes valuable insights to the discourse on renewable energy policy and MG management, offering guidance for policymakers, utilities, and stakeholders involved in energy transition efforts.

Keywords: Renewable energy integration; Feed-in Tariff (FiT); Net Metering (NM); Energy policy; Grid stability; Economic analysis

INTRODUCTION

Utilizing renewable energy sources (RES) holds paramount importance in the pursuit of sustainable energy systems globally. By harnessing RES such as solar, wind, hydro, and biomass, societies can mitigate greenhouse gas emissions, reduce dependence on fossil fuels, and enhance energy security (Alam et al., 2020). Moreover, RES offer immense potential for decentralized energy generation, enabling communities to achieve greater energy independence and resilience against external disruptions. Embracing RES not only contributes to mitigating climate change but also fosters economic development through job creation, technological innovation, and the establishment of green industries (Impram et al., 2020). In the context of Kurdistan province in Iran, where abundant renewable resources exist, leveraging RES presents a strategic opportunity to meet growing energy demands while minimizing environmental impacts and promoting regional development.

Microgrids (MG) represent a transformative paradigm in the modern energy landscape, offering localized, resilient, and sustainable solutions to energy distribution and management challenges. These self-contained energy systems integrate various distributed energy resources (DERs), including renewable energy sources (RES), energy storage systems (ESS), and demand response technologies, to efficiently supply electricity to local communities or specific facilities (D'Silva et al., 2020). MGs can operate either autonomously or in conjunction with the main grid, providing flexibility, reliability, and stability to energy networks. They empower end-users with greater control over their energy consumption, enhance grid resilience against disruptions, and facilitate the integration of intermittent renewable generation (Sharmila et al., 2019). Additionally, MGs hold significant promise for electrifying remote or underserved areas, improving energy access, and fostering economic development.

While RES offer tremendous potential for sustainable electricity generation, they also pose several challenges, including intermittency, variability, and limited predictability. The inherent fluctuations in RES output can lead to grid instability and mismatches between supply and demand, particularly during periods of low generation or high demand. Energy storage systems (ESS), such as battery energy storage, emerge as a viable solution to mitigate these challenges by enabling the capture and storage of excess renewable energy during periods of surplus generation for later use when demand exceeds supply (Bahramirad et al., 2012; Buchana and Ustun, 2015; IRENA, 2015). By smoothing out fluctuations, enhancing grid reliability, and providing ancillary services like frequency regulation, ESS complement RES integration efforts, unlocking their full potential while facilitating the transition towards a more sustainable and resilient energy future (Das et al., 2018; Nazaripouya et al., 2019).

Despite the promising benefits of RES and BESS, their widespread adoption faces significant economic barriers, with high upfront costs being a primary concern. The initial investment required for deploying RES infrastructure, such as solar panels, wind turbines, and associated grid integration equipment, can be substantial, deterring some stakeholders from pursuing renewable energy projects. Similarly, BESS technologies involve considerable capital expenditure for procurement, installation, and maintenance, further exacerbating the financial burden of transitioning to renewable energy-based systems. Additionally, the economic viability of RES and BESS solutions is contingent upon various factors, including local resource availability, regulatory frameworks, and market conditions, which can introduce uncertainty and risk for investors and project developers (Chen et al., 2012; Bahramirad and Camm, 2012; Gupta et al., 2017).

The necessity of robust energy policies to address the economic challenges associated with renewable energy adoption, particularly in regions like Kurdistan province in Iran, cannot be overstated. Well-designed energy policies play a pivotal role in creating a conducive environment for investment, innovation, and market development in the renewable energy sector. By providing financial incentives, energy policies can help offset the high upfront costs of renewable energy infrastructure and incentivize private sector participation. Moreover, clear and consistent regulatory frameworks, including renewable energy targets, grid access regulations, and permitting procedures, can reduce uncertainty and perceived risk for investors, facilitating greater capital flows into renewable energy projects.

Net Metering (NM) and Feed-in Tariffs (FiT) stand out as two well-known policies that have been widely implemented to incentivize renewable energy adoption and address economic barriers. Net Metering allows energy consumers who generate electricity from renewable sources, such as solar panels or wind turbines, to offset their electricity bills by exporting excess energy back to the grid. Under NM, the electricity meter runs backward when the renewable energy system generates more electricity than the consumer's immediate needs, effectively allowing them to "bank" excess energy credits for future use. This policy not only encourages the deployment of distributed renewable energy systems but also promotes self-consumption and grid stability by aligning generation with demand patterns (Marcelino et al., 2023; Poullikkas and Kourtis, 2013; Zhao, 2018). On the other hand, Feed-in Tariffs (FiT) offer renewable energy producers a guaranteed price for the electricity they generate and feed into the grid. FiT schemes typically involve long-term contracts between renewable energy producers and utilities or government entities, wherein producers receive a fixed tariff for each unit of electricity generated, often above market rates. FiTs provide revenue certainty and financial incentives for renewable energy investments, thereby stimulating market growth, attracting private sector investments, and accelerating the deployment of renewable energy technologies (Pyrgou et al., 2016; Bayod-Rújula et al., 2017; Meena et al., 2019).

Our contribution to the field lies in the formulation and application of NM and FiT policies within the context of Kurdistan province in Iran. Through a detailed case study, we have implemented these two policies and conducted a comprehensive comparison of their economic impacts relative to a scenario without any policy intervention. By integrating economic analysis with real-world data and simulation results, we have quantified the economic benefits and trade-offs associated with NM, FiT, and the absence of policy support. By elucidating the comparative economics of NM, FiT, and no policy scenarios, our research offers valuable guidance to policymakers, utilities, and stakeholders seeking to design and implement effective renewable energy policies tailored to local conditions and objectives.

The study is structured into several key sections. In Section 2, the methodology employed in the investigation is elaborated, outlining the approach taken to model and simulate the implementation of energy policies. Section 3 delves into the mathematical formulation of the model used to assess the economic implications of NM, FiT, and no policy scenarios. This section elucidates the key variables, constraints, and objective functions incorporated into the model to facilitate a rigorous analysis of the economic impacts of different policy regimes. In Section 4, the findings of the study are presented and discussed. Section 5 encapsulates the conclusions drawn from the analysis, synthesizing the key insights gleaned from the research and offering recommendations for policymakers and stakeholders.

METHODOLOGY

This section outlines the methodology employed to assess the economic implications of implementing NM and FiT policies within the MG framework of Kurdistan province. The methodology comprises several steps, including data collection, model formulation, and economic analysis.

- Step 1: Data Collection: The first step involves gathering relevant data to characterize the MG system and its operational parameters. This includes 24-hourly load demand profiles, solar and wind turbine output data, BESS size, and electricity prices based on time of use.
- Step 2: Model Formulation: Once the data is collected, an optimization model is formulated to simulate the operation of the MG under different policy scenarios. The model incorporates variables representing energy generation, storage, and consumption, as well as constraints related to grid stability, energy balance, and policy compliance.
- Step 3: Economic Analysis: The economic analysis begins by calculating the total cost of MG operation without any energy policy in place. This baseline cost serves as a reference point for comparing the economic impacts of NM and FiT policies. Subsequently, the selected policy (NM or FiT) is integrated into the optimization model, and the total cost of MG operation is recalculated. This process is repeated iteratively until the economic implications of both NM and FiT policies are fully considered.
- Step 4: Analysis of Results: Finally, the results of the economic analysis are analyzed to evaluate the comparative economic performance of NM and FiT policies relative to the baseline scenario without any policy intervention. Key metrics such as energy costs, revenue generation, and return on investment are examined to assess the effectiveness of each policy in promoting renewable energy adoption, enhancing grid stability, and optimizing economic outcomes within the Kurdistan province MG context.

6 the calculation of the total cost of MG operation and the modeling of regulatory frameworks governing NM and FiT policies.

Total cost of MG

The total cost of the MG, which is the objective of our problem, is defined by Eq. 1.

$$\min TC = CR + C_{BESS} + C_{exchanged} + CRI - CRE \tag{1}$$

In this context, TC symbolizes the overall expenditure of the MG, determined by the expenses linked with RES (CR), the BESS (C_{BESS}), and the energy transactions with the primary grid. Moreover, CRE and CRI denote the income obtained from selling surplus energy to the grid and procuring energy from the main grid, respectively. The determination of C_{BESS} and $C_{exchanged}$ is delineated in Equation 2 and Equation 3, correspondingly.

$$C_{BESS} = PC_{BESS} \times P_rated_{BESS} + EC_{BESS} \times E_rated_{BESS} \tag{2}$$

$$C_{exchanged} = \sum_{t=1}^{NT} \rho_{i,t} \times EP_t \tag{3}$$

Here,

The power and energy expenditures related to the BESS are symbolized by PC_{BESS} and EC_{BESS}, respectively. Furthermore, P_rated_{BESS} and E_rated_{BESS} denote the rated power and energy capacity of the BESS. Within Equation 3, EP_t represents the power transacted with the primary grid at time t, while $\rho_{i,t}$ signifies the cost per kilowatt-hour (KWh) of energy exchanged with the primary grid during time t of the day. We designate the energy exported and imported during time period t as $E_{export,t}$ and $E_{import,t}$ respectively.

$$CRE = \sum_{t=1}^{NT} E_{export,t} \times R_{export} \tag{4}$$

$$CRI = \sum_{t=1}^{NT} E_{import,t} \times R_{import} \tag{5}$$

The modeling of the BESS relies on its inherent constraints. The quantity of energy stored in the BESS at time t is determined by Equation 6, where the charging and discharging power of the BESS are denoted by P^c_{BESS} and P^d_{BESS}, respectively.

$$E_{BESS,T} = E_{BESS,T-1} + (P^c_{BESS} \times \eta_c - \frac{P^d_{BESS}}{\eta_d}) \times \Delta t \quad \forall t \in NT \tag{6}$$

Here, the efficiency of charging and discharging of the BESS is represented by η_c and η_d, respectively. The upper and lower bounds of the BESS's rated values are outlined as constraints in Equation 7 and Equation 8, respectively.

$$-P^R_{BESS} \le P_{BESS,t} \le P^R_{BESS} \quad \forall t \in NT \tag{7}$$

$$0 \le E_{BESS,t} \le E^R_{BESS} \quad \forall t \in NT \tag{8}$$

Additionally, Equation 9 illustrates the constraint imposed on the power interchange between the main grid and the microgrid, which is restricted by the maximum capacity of the transmission lines linking them ($P^{max}_{exchanged}$)

$$0 \le P_t \le P^{max}_{exchanged} \quad \forall t \in NT \tag{9}$$

Energy Policies Formulation

The regulatory frameworks are integrated into the problem formulation through their respective constraints. In the case of the NM policy, the revenue generated from exporting energy is calculated based on the net energy exported to the grid (as depicted in Equation 10). Similarly, the revenue derived from importing energy is determined by the net energy imported from the grid (as illustrated in Equation 11). The net energy exported or imported is computed as the disparity between the total energy exported to the grid and the total energy imported from the grid (as outlined in Equations 12 and 13).

The constraints associated with the regulatory frameworks are embedded within the problem formulation. Specifically, for the NM policy, the revenue generated from exporting and importing energy is determined by Equation 19 and Equation 20, respectively. Furthermore, the net energy exported ($N_E_{export,t}$) or imported ($N_E_{import,t}$) is calculated as the difference between the total energy exported to the grid and the total energy imported from the grid, as outlined in Equation 21 and Equation 22, respectively (Gholami et al., 2024).

$$CRE_{Net-metering} = \sum_{t=1}^{NT} N_E_{export,t} \times R_{export} \quad (10)$$

$$CRI_{Net-metering} = \sum_{t=1}^{NT} N_E_{import,t} \times R_{import} \quad (11)$$

$$N_E_{import} = \sum_{t=1}^{NT} E_{import,t} - E_{export,t} \quad (12)$$

$$N_E_{export,t} = \sum_{t=1}^{NT} E_{export,t} - E_{import,t} \quad (13)$$

Finally, under the FiT framework, the main grid procures the electricity generated by the MG at a pre-established fixed rate, typically exceeding the retail rate of electricity. The revenue generated from exporting energy within the FiT framework is computed by modifying the parameter FiT_{rate} in Equation 14 to reflect this fixed rate.

$$CRE_{FiT} = \sum_{t=1}^{NT} E_{export,t} \times R_{export} \times FiT_{rate} \quad (14)$$

RESULTS

The MG under investigation represents a real rural village situated at coordinates 35°59'N, 47°30'E in Kurdistan province, Iran [20]. This rural village consists of approximately 200 houses, with an average of 5 occupants per house, along with facilities such as a boarding clinic, mosque, double-shifted school, and agricultural electricity consumption, primarily for electric water pumps. The hourly electrical load profile for the month of July, depicted in Figure 1, exhibits the highest energy consumption and peak demand among all months, with highest peak demand reaching 580 kW. Figures 1 illustrate the 24-hour variations in wind turbine (WT) and photovoltaic (PV) array output powers as well, obtained from (Ataee et al., 2016). The MG infrastructure comprises wind turbines, PV arrays, A 100 KW battery system, and local loads, all interconnected with the external grid.

Also, this section outlines the input data related to RES and electricity prices based on time of use (ToU) tarrif from the main grid for the MG. The data includes the following costs: The cost of energy generated by PV and WT arrays are considered $0.048 and $0.033 per kilowatt-hour (kWh). Also, the cost of energy exchanged with the main grid varies based on the demand period: During peak demand periods, the cost is 0.024 ($/ kWh). During intermediate demand periods, the cost is 0.012 ($/ kWh), and during off-peak demand periods, the cost is 0.006($/ kWh). These cost parameters are crucial for assessing the economic viability of different energy generation and consumption scenarios within the MG framework.

The Fig.2 show the imported power from the grid with and without battery in case of using no energy policy. The analysis of imported power from the main grid for the MG reveals differences when comparing scenarios with and without the BESS. In the scenario without BESS, the imported power values fluctuate, with notable peaks at 450 kW and 480 kW. The overall trend shows considerable reliance on the main grid during high demand periods. In contrast, the scenario with BESS demonstrates a reduction in the imported power during certain peak times, particularly in the afternoon and evening hours. For example, the imported power is reduced to 400 kW. Additionally, the presence of BESS seems to smooth out some of the fluctuations observed in the no-BESS scenario, indicating better load balancing and energy management.

Figures 3 and 4 illustrate the power imported, exported, and battery usage under the NM and FiT policies (with a rate of 1.5), respectively. As shown in the FiT scenario, there are more opportunities for exporting energy to the grid compared to the NM policy. This is due to the fixed rate provided by FiT, which incentivizes higher energy exports by ensuring a guaranteed return for the electricity generated. Additionally, the FiT policy supports a larger BESS size, which can be installed to maximize energy storage and export potential. The increased BESS capacity under FiT allows for greater energy management

flexibility, enabling the MG to store excess renewable energy and export it when grid prices are favorable, further enhancing economic benefits.

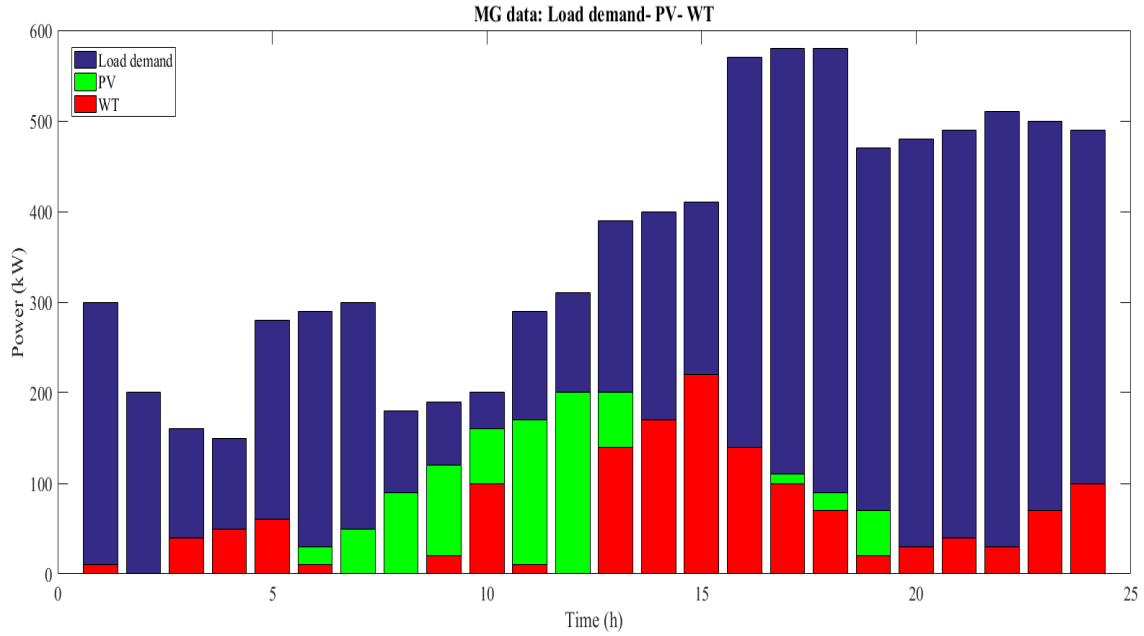

Figure 1. Data for MG under study: a rural village in Kurdistan province, Iran [Main]

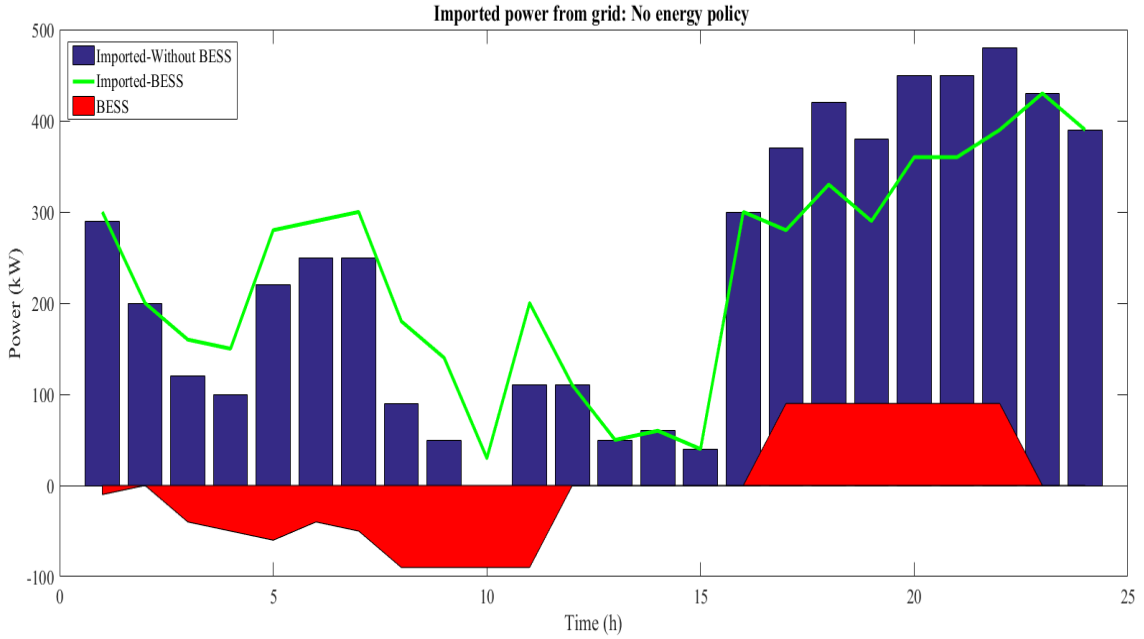

Figure 2. Imported power from the main grid: No policy is applied

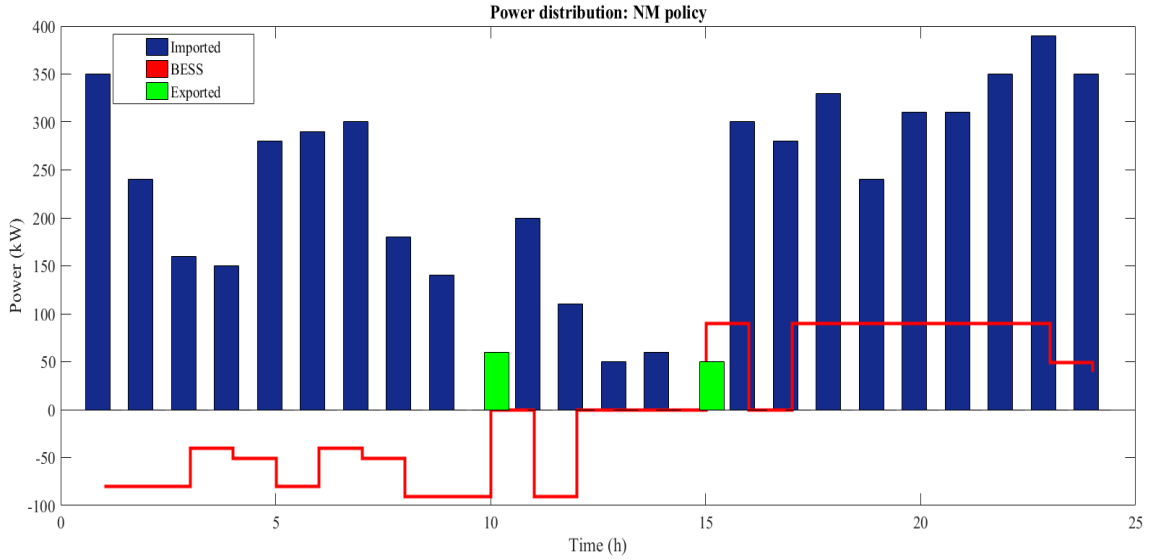

Figure 3. Imported and exported power: NM framework is applied

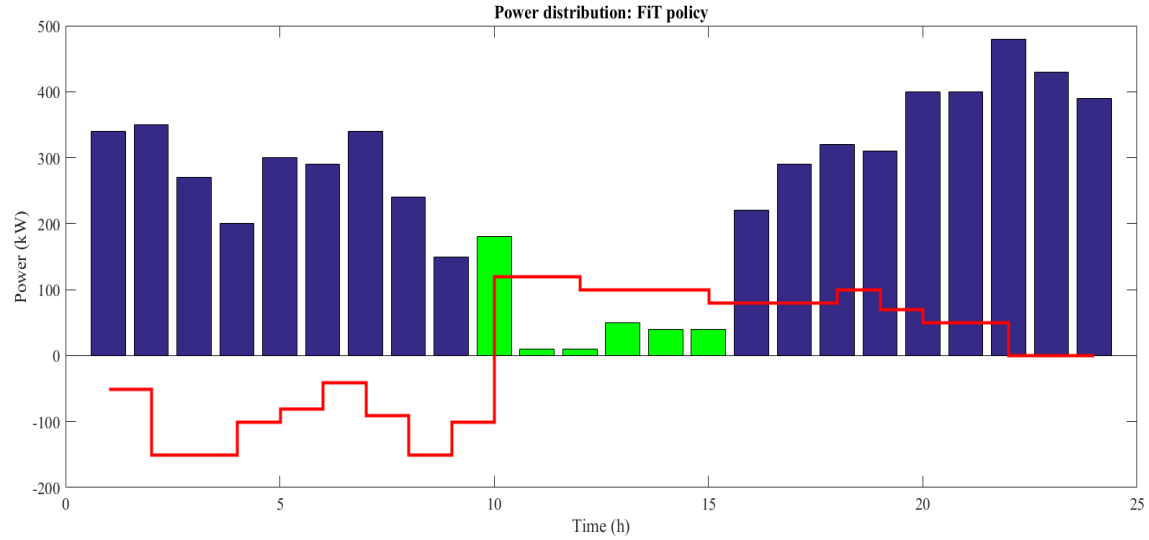

Figure 4. Imported and exported power: FiT framework is applied

Furthermore, Table 1 provides a comparative analysis of different case studies, focusing on total cost, total imported energy, and total exported energy. The scenarios include a MG without BESS and no policy, with BESS and no policy, under the NM policy, and under the FiT policy.

Table 1. Comparative Analysis of Different Case Studies

Case study	Total Cost ($)	Total Imported (kWh)	Total Exported (kWh)
MG –NO BESS- No Policy	307.59	5550	0
MG–BESS- No Policy	290.95	5620	0
MG –NO BESS- NM Policy	285.39	5370	110
MG –NO BESS- FiT Policy	273.51	5730	330

The analysis reveals that the total cost is highest for the scenario without BESS and no policy ($307.59), while the FiT policy scenario without BESS results in the lowest total cost ($273.51). The total imported energy is relatively consistent across scenarios, ranging from 5370 kWh to 5730 kWh. However, significant

differences are observed in exported energy. Under the NM policy, 110 kWh is exported, whereas the FiT policy facilitates a much higher export of 330 kWh. This indicates that the FiT policy provides better economic incentives for exporting surplus energy, thereby reducing overall costs and increasing energy export opportunities.

CONCLUSION

The integration of RES and BESS in MGs represents a critical step towards sustainable and reliable energy systems. This study focuses on evaluating the economic implications of different energy policies—NM and FiT—applied to a real-world MG in a rural village in Kurdistan province. The MG in question includes a combination of WT, PV arrays, batteries, and local loads. In this research, we developed a comprehensive methodology that involves collecting detailed hourly data on load demand, solar output, wind turbine output, and BESS size, as well as electricity prices based on time of use. Using this data, we formulated an model to calculate the total cost of MG operation under different policy scenarios. We then integrated the regulatory frameworks for NM and FiT into the model to evaluate their economic impacts. The analysis revealed significant findings. The FiT policy, with a higher fixed rate, provided greater incentives for energy export, resulting in a higher total exported energy and the lowest total operational cost among the scenarios studied. The NM policy also facilitated energy export but to a lesser extent. The inclusion of BESS in the microgrid demonstrated potential for cost savings and enhanced energy management, albeit with limited impact during off-peak periods. Highlighting the achievements, we demonstrated that the FiT policy leads to substantial economic benefits by maximizing energy export opportunities and reducing overall costs. Future work will focus on further refining the optimization model by incorporating more detailed data and exploring additional policy scenarios.

REFERENCES

Alam, M. S., Al-Ismail, F. S., Salem, A., & Abido, M. A. (2020). High-level penetration of renewable energy sources into grid utility: Challenges and solutions. *IEEE Access, 8*, 190277–190299. https://doi.org/10.1109/ACCESS.2020.3031481

Ataee, S., Feizi, M. R., & Bevrani, H. (2016). Optimal operation of renewable energy based grid connected microgrid. *2nd National Conference of Technology, Energy and Data on Electrical & Computer Engineering.*

Bahramirad, S., & Camm, E. (2012). Practical modeling of Smart Grid SMSTM storage management system in a microgrid. *Proceedings of the IEEE Power Engineering Society Transmission and Distribution Conference*, 1–7. https://doi.org/10.1109/TDC.2012.6281697

Bahramirad, S., Reder, W., & Khodaei, A. (2012). Reliability-constrained optimal sizing of energy storage system in a microgrid. *IEEE Transactions on Smart Grid, 3*(4), 2056–2062. https://doi.org/10.1109/TSG.2012.2217991

Buchana, P., & Ustun, T. S. (2015). The role of microgrids & renewable energy in addressing Sub-Saharan Africa's current and future energy needs. *2015 6th International Renewable Energy Congress (IREC 2015).* https://doi.org/10.1109/IREC.2015.7110977

Chen, S. X., Gooi, H. B., & Wang, M. Q. (2012). Sizing of energy storage for microgrids. *IEEE Transactions on Smart Grid, 3*(1), 142–151. https://doi.org/10.1109/TSG.2011.2160745

Das, C. K., Bass, O., Kothapalli, G., Mahmoud, T. S., & Habibi, D. (2018). Overview of energy storage systems in distribution networks: Placement, sizing, operation, and power quality. *Renewable and Sustainable Energy Reviews, 91*, 1205–1230. https://doi.org/10.1016/j.rser.2018.03.068

D'Silva, S., Shadmand, M., Bayhan, S., & Abu-Rub, H. (2020). Towards grid of microgrids: Seamless transition between grid-connected and islanded modes of operation. *IEEE Open Journal of the Industrial Electronics Society, 1*, 66–81. https://doi.org/10.1109/OJIES.2020.2988618

Gholami, M., Muyeen, S. M., & Mousavi, S. A. (2024). Optimal sizing of battery energy storage systems and reliability analysis under diverse regulatory frameworks in microgrids. *Energy Strategy Reviews, 51*, 101255. https://doi.org/10.1016/j.esr.2023.101255

Gupta, P. P., Jain, P., Sharma, S., & Bhakar, R. (2017). Reliability-security constrained unit commitment based on benders decomposition and mixed integer non-linear programming. *2017 International*

Conference on Computing, Communication and Automation (COMPTELIX), 328–333. https://doi.org/10.1109/COMPTELIX.2017.8003988

Impram, S., Varbak Nese, S., & Oral, B. (2020). Challenges of renewable energy penetration on power system flexibility: A survey. *Energy Strategy Reviews, 31*, 100539. https://doi.org/10.1016/j.esr.2020.100539

IRENA. (2015). *From baseload to peak: Renewables provide a reliable solution.* https://www.irena.org/DocumentDownloads/Publications/IRENA_Baseload_to_Peak_2015.pdf

Marcelino, C. G., Leite, G. M. C., Wanner, E. F., Jiménez-Fernández, S., & Salcedo-Sanz, S. (2023). Evaluating the use of a net-metering mechanism in microgrids to reduce power generation costs with a swarm-intelligent algorithm. *Energy, 266*, 126317. https://doi.org/10.1016/j.energy.2022.126317

Meena, N. K., Yang, J., & Zacharis, E. (2019). Optimal planning and operational management of open-market community microgrids. *Energy Procedia, 159*, 533–538. https://doi.org/10.1016/j.egypro.2018.12.002

Nazaripouya, H., Chung, Y.-W., & Akhil, A. (2019). Energy storage in microgrids: Challenges, applications and research need. *International Journal of Energy Smart Grid, 3*(2), 60–70. https://doi.org/10.23884/ijesg.2018.3.2.02

Poullikkas, I. H., Kourtis, G., & Andreas, G. (2013). A review of net metering mechanism for electricity renewable energy sources. *International Journal of Energy and Environment, 4*(6), 975–1002. https://www.osti.gov/etdeweb/biblio/22188315

Pyrgou, A., Kylili, A., & Fokaides, P. A. (2016). The future of the Feed-in Tariff (FiT) scheme in Europe: The case of photovoltaics. *Energy Policy, 95*, 94–102. https://doi.org/10.1016/j.enpol.2016.04.048

Sharmila, N., Nataraj, K. R., & Rekha, K. (2019). An overview on design and control schemes of microgrid. *2019 Global Conference for Advancement in Technology (GCAT)*, 20–23. https://doi.org/10.1109/GCAT47503.2019.8978407

Zhao, Y. (2018). Solar energy sharing in net metered community microgrids: Can the social goals be achieved? *2018 52nd Annual Conference on Information Sciences and Systems (CISS)*, 1–6. https://doi.org/10.1109/CISS.2018.8362287

➢ *ORAL PRESENTATION*

Localizing fetal skulls by fitting

Umut Konur[1*] (*ORCID: https://orcid.org/0000-0003-1322-6669*)

[*1]Zonguldak Bülent Ecevit University, Faculty of Engineering, Department of Computer Engineering, Zonguldak, Türkiye

*Corresponding author e-mail : konur@beun.edu.tr

Abstract

A promising idea to segment fetal skull images is to first localize the sought structures and then refine the regions to arrive at more precise outcomes. In this work, we propose a methodology to achieve satisfactory localization of transcerebellar fetal skulls visible in gray-scale ultrasound (US) images. The approach depends on scale reduction of images to decrease the search space, extract feature points and do model fitting. Knowing that the structures resemble ellipses to a manageable extent, the selected model for fitting is an ellipse. Measuring how good a certain fit is, usually depends on meta information describing how a skull is likely to look like, such as intensities of border pixels, shape descriptors, etc. The method actually selects the best among many fits. The experiments on sample images provide good results.

Keywords: localization, scale, feature, fitting, transcerebellar.

INTRODUCTION

Segmentation of fetal skulls is required to provide input to computerized diagnosis systems (Konur et al., 2015; Konur, 2018). The process must be automated to minimize human intervention and effort. It can be argued that a segmenter could be built benefiting a training set of images whose desired segmentations are available, however, the rarity of medical data sets usually prevents the possibility of training sound models. For example, a deep learning method (Minaee et al., 2022) would need a very large training set of images to produce successful outputs and generalize well enough for all possible inputs. Lack of training data arises the need for other approaches where no training is required except the availability of some meta information (or expert knowledge) defining how a transcerebellar fetal skull looks like.

In the scope of this work, each input US image contains one and only one fetal skull structure in transcerebellar view mode excluding the possibilities of partial existence (i.e. the entire skull is located within image borders) and occlusion (this is rarely the case such as in twin pregnancies). Clearly, successful segmentation would depend on a good initial guess of skull position. This guess is definitely not all that must be done to arrive at satisfactory segmentation, however, it is probably the most important stage since starting wrong cannot lead to the right. Assuming that a skull is well-localized, the region can hopefully be refined for detailed and precise structure. In fact, this work deals with localizing fetal skulls in underscaled (Burt and Adelson, 1983) versions of images and identify skull regions. Thus, refinements for ultimate segmentation must be done at the lowest scale and, if desired, carried on to higher scales.

Model fitting (Forsyth and Ponce, 2012) is the main approach for localizing skulls. It is known that boundaries of fetal skulls (in transcerebellar view) have considerably large intensities and resemble ellipses. Hence, the natural choice is to fit an ellipse to any input image and report the result as the skull position (i.e. localize the fetal skull). Geometric models are fit using points, so feature points extracted from images are used to obtain ellipses. There exist many feature points and thus many ellipses can be fit. Selecting the best ellipse is yet another issue. The methodology in this work is to fit an ellipse using a set of 3 feature points, do this many times similar to the RANSAC (Fischler and Bolles, 1981; Forsyth and Ponce, 2012)

procedure with randomly selected sets of 3 points and identify the best ellipse. Obviously, a score of goodness of any fit is necessary to compare and select among fits.

The following sections describe how undersampling and feature points extraction are performed, the 3-point ellipse fitting procedure, goodness of fit measures usually derived from meta information and their utilization. Visual results on sample images are presented along with a discussion and conclusion. The algorithmic details, assumptions, design decisions and followed paths of the methodology are mentioned in the flow to some extent as the need arises to ensure complete comprehension.

METHODOLOGY

Undersampling

Input images (I) are of size 400 x 520. Since speckle noise is a characteristic of US imaging, each image is first filtered to eliminate speckle noise (Yu and Acton, 2002). Although this step does not crucially affect the performance of the overall scheme, it should not be skipped regardless of its minor gains. Next, a Gaussian image pyramid (Burt and Adelson, 1983) of 4 levels is generated out of the noise-free image (NF). The output is an underscaled (reduced) version (R) of NF and of size 50 x 65. R is to serve as the input to the next step where feature points are extracted to fit an appropriate ellipse. Figure 1 shows an example of an input and its underscaled version.

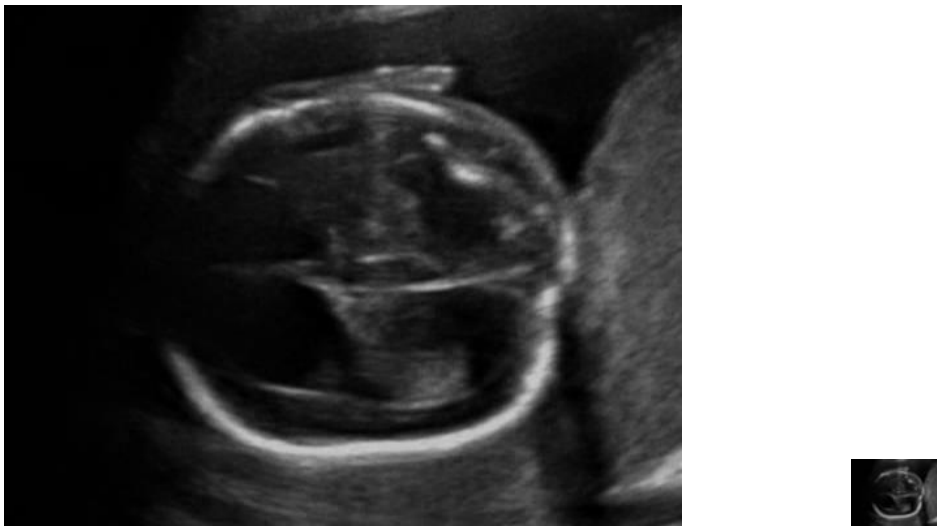

Figure 1. Sample input I (left) and its underscaled version R (right)

Feature Points Extraction

Retrieving feature points is primarily based on edge detection from R. The Sobel mask (Sobel and Feldman, 1968) is first run on R to determine the threshold value (thr) used in detection. In order not to overlook and exclude potentially important feature points, the same mask is run again on R with a new threshold value of $0.8\ x\ thr$. These parameter adjustments are arbitrary and values are selected empirically. In fact, retrieving few edge points could lead to degrading the ellipse fitting process whereas having too many of them could lead to an explosion in the number of detectable ellipses and complicate the search to select the best among them, many of which are unrelated at all in the context of the problem. The output of edge detection is the binary feature points image (F). R is also treated with Harris corner detection (Harris and Stephens, 1988) to retrieve a binary corner points image (H). H is later to be used for breaking connections between segments potentially belonging to different structures in R. This action is important because one of the goodness of fit measures used in this work depends on broken curves out of which ellipses are fit. A Harris corner detector may use different threshold values to detect each corner point and probably many are detected. In order to get rid of some detected corner points which are insignificant and thus must not be

removed, the average of minimum and maximum threshold values is considered and only those corner points exceeding that value are included in H. F and H are then used to obtain the binary broken curves image (B) just mentioned. This stage of the procedure benefits from basic image processing operations (Gonzalez and Woods, 2018). The holes in F are filled to get G whose binary skeleton image is found to get B further to be refined. First, those points both marked in B and H are turned to unmarked (i.e. corner points are removed) in B. Next, the points where branches may have formed during skeletonization and their immediate neighbors are also turned to unmarked in B. The final B goes through a process of connected components labeling. It may be the case that some connected components arose from tiny skeletons or spurs in B and thus contain only a single point. Such points (components including a single point) are also removed. At the end; B, where labels of all included points is also available as a label image L and indicate to which connected component points in B belong, is the desired disconnected curves image to be used in one specific goodness of fit measurement grading how well a particular ellipse is fit. It is worth to mention here that measuring the quality of a fit does not depend entirely on this single measure and many measures are employed, all to be detailed in the flow. As the outputs of the feature points extraction stage, Figure 2 shows the feature points image and the disconnected curves image, both derived from the input of Figure 1.



Figure 2. Feature points image F (left) and disconnected curves image B (right)

3-Points Ellipse Fitting

The usual way to fit an ellipse requires 5 points known to be on it. The current work cannot a priori assume that a correct selection of 5 points from the set of feature points can be performed and a correct (i.e. perfect) ellipse determined. Indeed, what is being done is to determine the location of a fetal skull with an ellipse fit as correctly as possible. Therefore, a more traceable approach using only 3 feature points in the fitting procedure is used to determine the "best" ellipse that localizes the fetal skull in the image. Doing this with a sufficiently large number of randomly selected sets of 3 points, similar to the RANSAC procedure (Fischler and Bolles, 1981), where the points are assured to be non-collinear and selecting the best fit is expected to give a satisfactory result. The 3-points fitting method, outlined in (Song and Wang, 2007), assumes that these points P_0, P_1, P_2 are on the ellipse and estimates the tangent lines to the ellipse at these points. The 3 points and their tangents determine the center C of the ellipse at coordinates (c_x, c_y) as shown in Figure 3.

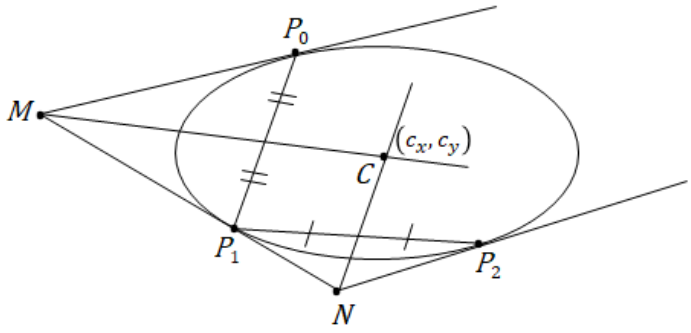

Figure 3. Determining ellipse çenter with 3 points and tangent lines

Knowing the center coordinates allows to move the center to the origin of the XY-plane and work in a new reference frame. The transformed coordinates x' and y' are as shown in Eq. (1):

$$x' = x - c_x\,,\quad y' = y - c_y \qquad (1)$$

The ellipse can then be written with three parameters as Eq. (2) shows:

$$a_0 x'^2 + 2a_1 x' y' + a_2 y'^2 = 1 \qquad (2)$$

Transforming the 3 points with coordinates $(x_0,y_0),(x_1,y_1),(x_2,y_2)$ to the new frame and naming them (x'_0,y'_0), (x'_1,y'_1), (x'_2,y'_2); the three parameters $A = [a_0 \quad a_1 \quad a_2]^T$ can be written as in Eq. (3)

$$A = Q^{-1}K \qquad (3)$$

where K and Q are stated in Eqs. (4) - (5):

$$K = [1 \quad 1 \quad 1]^T \qquad (4)$$

$$Q = \begin{bmatrix} x_0'^2 & 2x'_0y'_0 & y_0'^2 \\ x_1'^2 & 2x'_1y'_1 & y_1'^2 \\ x_2'^2 & 2x'_2y'_2 & y_2'^2 \end{bmatrix} \qquad (5)$$

Estimating the tangent lines at the 3 ellipse points is with the least squares method. At a particular point, a 5 x 5 window around the point such that it is located at the center of the window is used and line parameters are computed with the feature points inside the window. Figure 4 shows such an example with feature pixels in white color and others in gray. The result of fitting is both the ellipse parameters and the best approximation of a binary ellipse image E whose 1-valued pixels locate the ellipse boundary.

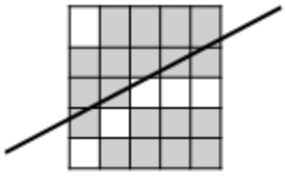

Figure 4. Estimating tangent lines at ellipse points

Goodness of Fit Measures

The primary metrics used to produce a score in [0, 1] and evaluate the goodness of a fit is two-fold. The first is computed using the normalized average distance between the particular ellipse and those points of the broken curves image B belonging to the connected curves that the ellipse shares a point with. The second is the normalized average intensity of ellipse boundary pixels retrievable from R.

Distance Score:

For an ellipse obtained as the output of a particular fit, some connected curves in B have a point in common with it and others do not. Only the points of those curves that have a common point with the ellipse are considered and the average Euclidian distance between curve points and the ellipse boundary is computed. We note that the curves image B and the ellipse image E are discrete but distance computation involves points in B with integer coordinates and the idealized ellipse points (with non-integer coordinates in

general) computable using ellipse parameters. With d_i denoting the Euclidian distance between the ith point of involved connected curves in B with n_c points in total and the ellipse (the shortest distance between the ith point and an ellipse point), the average distance is $\bar{d}$ as shown in Eq. (6):

$$\bar{d} = \frac{\sum_{i=1}^{n_c} d_i}{n_c} \quad (6)$$

Assuming all ellipses are somehow normalized to a certain frame, smaller values of this metric would indicate better fits. Since ellipses cannot directly be viewed in a normalized frame, another action must be followed to achieve normalization. This can be performed by considering the combined geometry of the ellipse and involved connected curves. Let x_m and x_M be the minimum and maximum x-coordinates of all the points of the combined geometry including all ellipse points and points of involved connected curves. Let y_m and y_M be that for y-coordinates. Then, the diagonal of the bounding box of the combined geometry has length l expressed in Eq. (7):

$$l = \sqrt{(x_M - x_m)^2 + (y_M - y_m)^2} \quad (7)$$

The distance normalization can be achieved by using $\bar{d}/l$. For the metric to be a score that favors small normalized distances, the distance score s_d can be defined as in Eq. (8):

$$s_d = 1 - \bar{d}/l \quad \textbf{(8)}$$

Intensity Score:

Boundaries (i.e. outlines) of transcerebellar skulls, in general, are known to have higher intensities than the rest of the image. Feature points used to fit ellipses are also derived from edge segments that separate pixels with higher intensity from those with lower intensity. This suggests that ellipses whose points occupy pixels with a high average intensity are more likely to be good fits. n_e being the number of pixels of an ellipse in E and t_i being the intensity of the pixel in R corresponding to the ith ellipse pixel, the average ellipse intensity $\bar{t}$ can be computed using Eq. (9):

$$\bar{t} = \frac{\sum_{i=1}^{n_e} t_i}{n_e} \quad (9)$$

Since lighting conditions may be different for input images, this value must also be normalized. This can be done by using the maximum intensity t_M in the input R and compute an intensity score s_t by Eq. (10):

$$s_t = \bar{t}/t_M \quad (10)$$

Combined Score:

With a hypothetic view that distance score and intensity score are equally important, a combined fit score s_f can be formulated as the average of both scores as Eq. (11) shows:

$$s_f = (s_d + s_t)/2 \quad (11)$$

Valid and Invalid Fits:

It should be stated that some fit attempts or actual fits are skipped over and not counted as valid due to several reasons. Some reasons are related to issues arising during or at the end of ellipse fitting stage and thus before score computation. Some others become evident with observations encountered during score computation. Deeming an actual fit as invalid is always based on meta information specific to the problem context such as the trustworthiness of a fit depending on the ratio of points of connected curves intersecting the fit ellipse to the number of ellipse points (i.e. circumference of the ellipse), how transcerebellar fetal skulls are supposed to look like, the intensity distribution of their neighborhoods, etc.

First, if linear algebraic issues arise while computing Q^{-1} such as singularity or numerical inconvenience (e.g. very small or large values), the attempt to fit an ellipse for the particular set of 3 points is ignored and a new attempt is initiated. Such attempts are repeated until a sufficient number of "valid" ellipses are fit using feature points (pixels) in F. Some of the fits may result with identical valid ellipses. Nevertheless, each such fit (either unique or repeating) is OK and counted. Provided that a fit attempt is successful, cases that make the fit "invalid" and further cause the initiation of a new attempt are the following:

- The assumption on ellipses modelling transcerebellar fetal skulls is that they entirely lie within image boundaries. Therefore, if an ellipse has a point with either x or y coordinate outside the image, such a fit is rejected.
- An ellipse is expected to have major and minor radii lengths with a ratio of around 1,2. The implementation analytically computes this ratio for each ellipse and rejects the fit if it is not in the (1,1 1,3) interval.
- If the area of an ellipse is too small, it is foreseen that the fit is useless. The implementation assumes that if the area of the ellipse, as measured by the number of pixels its region covers, is less than one sixty-fourth of the total number of pixels of the input image (its underscaled version R) the ellipse must be rejected. The number of pixels the elliptical region spans is analytically measured using its major and minor radii lengths and usually is not an integer value. The number of pixels of an input image is 50 x 65 = 3250. Thus, the implementation rejects ellipses with areas less than 3250/64 = 50,78125 pixels.
- If the ratio of the total number of points of broken curves involved in distance computation (these are broken curves in B that the one-pixel thick ellipse boundary image E intersects with) to an accurate enough approximation of the circumference of the ellipse is less than 0.4, the fit is rejected. This is because a small ratio would indicate a rather non-representative set of points that should ideally be definitive for E.
- If the average intensity of pixels in R whose coordinates coincide with those of E (t_{Eavg}) is not more than the average intensity of pixels in R, whose coordinates coincide with those of the internal region of E (t_{IEavg}), the fit is rejected because boundary pixels, on average, must have higher intensities.
- t_{Eavg} and t_{IEavg} must not be very close because skull boundaries and interiors differ in intensity values at least to some extent. Knowing that t_{Eavg} is more than t_{IEavg}, a fit is rejected if $(t_{Eavg} - t_{IEavg})/t_{Eavg}$ is not more than 0.15.
- Going deeper in the internal region of E and excluding another one-pixel thick boundary of the internal region produces a so-called "deeper" region of E (i.e. there is a one-pixel thick borderline between E and the deeper region of E). What is desired for a valid fit is that this deeper region D must not contain too many points from the broken curves image B. This is because, skull interiors which coincide with D do not contain too many points that are extracted from the edge image which

could potentially cause fitting other useless ellipses. In fact, the actual meta information indicates that skull interiors do not contain too many pixels that an edge detector outputs. If the ratio of pixels that are both in B and D to pixels in D is not less than 0.25, the fit is rejected.

Number of Valid Fits:

In order to select the best fit among many ellipses, a decision on how many valid ellipses should be fit before the selection must be made. These ellipses could be either unique in the set of all fits or they may be repeating. Since the followed procedure is RANSAC-like, the classical methodology to determine the number of iterations N with RANSAC (Fischler and Bolles, 1981) is adopted and the estimated N is used as the number of valid ellipses from which the best is selected. This estimation uses the number of model points n, desired probability of a successful fit p and an estimate of outlier ratio ε shown in Eq. (12):

$$N = \frac{\log(1-p)}{\log(1-(1-\varepsilon)^n)} \qquad (12)$$

Experiments on the available data set of this work show that a much smaller N is sufficient to produce satisfactory results and the estimation in Eq. (13) is used:

$$N = \left\lceil \left(\frac{\log(1-p)}{\log(1-(1-\varepsilon)^n)} \right) / 4 \right\rceil \qquad (13)$$

Selection of the Best Fit:

The "best" fit is to be selected from the members of a subset W of all valid fits. Heuristically, W contains those fits with highest distance scores s_d and should not exclude those fits among which potentially the best fit can be selected. This further requires that a minimum number of elements n_N must be present in W. After determining the elements of W, the member with the highest combined score s_f is selected as the best fit. Although unlikely for disparate fits, ties are broken arbitrarily. The selection procedure requires parameters some of which could be updated in the flow and is as follows:

1. Retrieve maximum distance score value max_s_d of all $N = 511$ fits.
2. Set minimum number of subset elements $n_N = \lceil N \; x \; 0.02 \rceil = \lceil 511 \; x \; 0.02 \rceil = 11$.
3. Set minimum distance score threshold value $min_thr_s_d = 0.990 \; x \; max_s_d$.
4. Set current distance score threshold value $thr_s_d = 0.996 \; x \; max_s_d$.
5. Set step size for distance score values $step_s_d = 0.002 \; x \; max_s_d$.
6. Retrieve the set of those fits W with distance scores $s_d > thr_s_d$.
7. If the number of elements of W is at least n_N ($|W| \geq n_N$), goto 12.
8. Update $thr_s_d = thr_s_d - step_s_d$.
9. If thr_s_d equals $min_thr_s_d$ goto 10, else goto 6.
10. If $|W| \geq 1$ goto 12 (If the minimum distance score threshold value is reached, nonempty W is sufficient and no more members are forced.), else goto 11.
11. Update $min_thr_s_d = min_thr_s_d - step_s_d$ and $n_N = 1$. (If the minimum distance score threshold value has undergone an update, nonempty W is sufficient from then on.). Goto 6.
12. Retrieve, from W, the fit with highest combined fit score s_f. Break ties arbitrarily.

RESULTS AND DISCUSSION

The available data set contains 357 US images each of which allows viewing one and exactly one transcerebellar fetal skull in its entirety. No partial existence or occlusion takes place. Figure 5 shows the discussed scheme on six inputs and associated outputs.

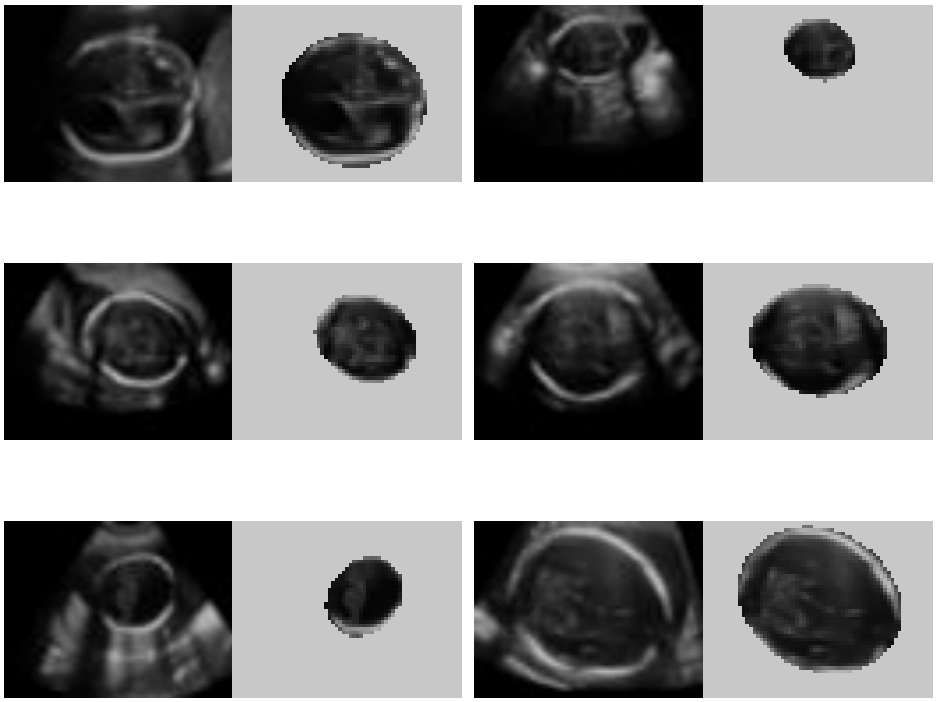

Figure 5. Undersampled inputs and associated outputs

It can be observed that visually satisfactory results are obtained for the majority of the inputs in the data set. In fact, the majority of all available inputs of transcerebellar skulls have been well-localized and accurate segmentations are very likely to be obtained after further refinements on localization outputs. In this work, rather heuristic ways are proposed for evaluating how good fit ellipses are and selecting the best one from among them. These are based on many factors, arguable and perhaps can be improved with better capture and exploitation of meta information. The demonstrations are not based on numerical indicators since the quality of segmentation can generally (if not always) be visually assessed by human experts and localization outputs cannot be considered ultimate segmentation.

CONCLUSION

The proposed scheme to localize fetal skulls is not a full segmenter but only a start that would lead for more proper segmentation after other processing. Hence, expectations for perfect localization may also be redundant and roughness (i.e. imprecision) can be acceptable to some extent assuming that proper post-processing will refine localization outputs and arrive at good enough segmentation outputs. Since the potential applications that can benefit from localizing skulls are not supposed to be real-time and the time it takes to produce an output is not critical, arguments on how fast (or slow) localizations are obtained is out of discussion. Indeed, for most inputs execution lasts in the order of a couple of minutes. One can assess that spending minutes or hours or even a day before reaching an output is actually worthy. Finally, a clear advantage is to perform with no training at all and it is evident that there is room for future work.

ACKNOWLEDGEMENTS

The author expresses his gratitudes to İbrahim Kalelioğlu and Füsun Varol from Obstetrics and Gynecology Departments of the Medical Faculties of Istanbul University and Trakya University, respectively, for providing ultrasound data whose research-aimed use has been ethically approved.

REFERENCES

Burt, P., & Adelson, E. (1983). The Laplacian pyramid as a compact image code. IEEE Transactions on Communications, 31(4), 532-540.

Fischler, M.A., & Bolles, R. C. (1981). Random sample consensus: a paradigm for model fitting with applications to image analysis and automated cartography., Communications of the ACM, 24(6), 381-395.

Forsyth, D. A., & Ponce, J. (2012). Computer vision: a modern approach (2nd ed.). Pearson.

Gonzalez, R. C., & Woods, R.E. (2018). Digital image processing (4th ed.). Pearson.

Harris, C., & Stephens, M. (1988). A combined corner and edge detector", Proc. 4th Alvey Vision Conference, 147-152.

Konur, U., Gürgen, F. S., Varol, F., & Akarun, L. (2015). Computer aided detection of spina bifida using nearest neighbor classification with curvature scale space features of fetal skulls extracted from ultrasound images. Knowledge Based Systems, 85, 80-95.

Konur, U. (2018). Computerized detection of spina bifida using SVM with Zernike moments of fetal skulls in ultrasound screening. Biomedical Signal Processing and Control, 43, 18-30.

Minaee, S., Boykov, Y., Porikli, F., Plaza, A., Kehtarnavaz, N., & and Terzopoulos, D. (2022). Image segmentation using deep learning: a survey. IEEE Transactions on Pattern Analysis and Machine Intelligence, 44(7), 3523-3542.

Sobel, I., & Feldman, G. (1968). A 3x3 isotropic gradient operator for image processing. Stanford Artificial Intelligence Project.

Song, G., & Wang, H. (2007) A fast and robust ellipse detection method based on pseudo-random sample consensus. Proc. Computer Analysis of Images and Patterns, 669-676.

Yu, Y., & Acton, S. T. (2002). Speckle reducing anisotropic diffusion. IEEE Transactions on Image Processing, 11(11), 1260–1270.

➢ *ORAL PRESENTATION*

Toz Gıdalar ve Raf Ömrü Sırasındaki Adezyona Bağlı Değişimler

Fatih Kırbayır*(0000-0002-7959-8927), Didar Ucuncuoglu*(0000-0002-2640-5976)

*Çankırı Karatekin Üniversitesi, Mühendislik Fakültesi, Gıda Mühendisliği Bölümü, Çankırı, Türkiye

*Sorumlu yazar e-posta:krbyr.f@gmail.com , a.emir.57@gmail.com, didaru@karatekin.edu.tr

Özet

Adezyon, farklı yüzeyler arasında moleküller ya da kristallerin çekim kuvvetleriyle birbirine yapışması olarak tanımlanmakta olup; kristal köprü oluşumu, elektrostatik adezyon ve mekanik kilitlenme gibi mekanizmalarla gerçekleşmektedir. Toz gıdalarda adezyon kapasitesi; nem ve su aktivitesi, elektrostatik yüklenme, yüzey pürüzlülüğü, parçacık boyutu ve şekli gibi birçok faktörden etkilenmektedir. Adezyon, özellikle gıda işleme ve paketleme süreçlerinde kalite ve raf ömrü açısından önemli bir parametre olup; üretim hattında yapışma, paketleme sorunları ve üründe topaklanma gibi problemlere neden olabilmektedir. Bu nedenle, gıdalarda adezyonun özellikle depolama ve işleme süreçlerinde kalite kontrolü açısından izlenmesi gerekmektedir. Bu derleme çalışmasında; toz gıdalar, bu ürünlerde adezyon kapasitesini etkileyen faktörler, raf ömrü süresince meydana gelen fiziksel, kimyasal ve morfolojik değişiklikler ile bunların önlenmesine yönelik yaklaşımlar ele alınmaktadır.

Anahtar Kelimeler: Adezyon, Toz Gıdalar, Raf ömrü, Kalite Kontrol

Powdered foods and adhesion-related quality changes during shelf life

Abstract

Adhesion refers to the phenomenon of molecules or crystals sticking together due to attractive forces between different surfaces, which may occur through mechanisms such as crystal bridge formation, electrostatic attraction, and mechanical interlocking. In powdered foods, adhesion capacity is influenced by various factors including moisture content and water activity, electrostatic charging, surface roughness, and particle size and shape. Adhesion is a critical factor in food processing and packaging, as it can significantly affect product quality and shelf life. It often leads to issues such as sticking on production lines, packaging difficulties, and caking in the final product. Therefore, monitoring and controlling adhesion in powdered food products during processing and storage is essential for maintaining quality standards. This review discusses powdered foods, factors affecting their adhesion capacity, the physical, chemical, and morphological changes that occur during shelf life, and strategies to prevent adhesion-related problems.

Keywords: Adhesion, Powdered Foods, Shelf Life, Quality Control

1. GİRİŞ

Adhezyon, farklı cins moleküller veya yüzeyler arasındaki çekim kuvveti nedeniyle meydana gelen yapışma olayını ifade eden bir fizikokimyasal kavramdır (Mittal, 2011) ve intermoleküler etkileşimlere dayanmaktadır (Israelachvili, 2011). Adhezyon gerçekleşirken iki yüzey arasında belirli fiziksel veya kimyasal bağlar oluşmakta ve böylece mekanik, kimyasal ve elektrostatik yapışma ile dispersiyon kuvvetleri oluşmaktadır. Mekanik adezyon, bir molekülün diğer bir molekül üzerine fiziksel olarak tutunması ile gerçekleşmektedir (Kinloch, 1987). Farklı yüzeyler arasında kovalent, iyonik veya hidrojen bağları gibi bağların oluşumu ile kimyasal adezyon gerçekleşmektedir (Pocius, 2002). Farklı malzemelerin yüzeyleri arasında elektrik yükü farkı nedeniyle elektrostatik adezyon meydana gelmektedir (Derjaguinve ark., 1987). Moleküller arasında geçici dipol etkileşimleri sonucu ortaya çıkan zayıf çekim kuvvetlere van der Waals Kuvvetleri adı verilmekte olup daha çok sıvı damlacıkların katı yüzeylere tutunmasına neden olmaktadır. Sıvı yağların ambalajlandığı paket materyaline yapışarak akması bu mekanizmaya örnek

gösterilmiştir.Toz gıdalarda ise nem ve su aktivitesi artışına bağlı olarak higroskopik adezyon gerçekleşmektedir (Israelachvili, 2011).

Adhezyon, doğada ve endüstride birçok önemli süreçte gerçekleşmekte ya da zaman içinde ortaya çıkabilmektedir. Moleküllerin veya hücrelerin birbirlerine ve bulundukları ortama tutunmasında önemli rol oynamaktadır (Alberts et al., 2014). Kompozit malzeme, kaplama ve yapıştırıcı ürünlerinin geliştirilmesinde de adezyon kritik bir faktördür (Kinloch, 1987). Benzer şekilde biyosensör, protez, yara bandı, mikroelektromekanik sistemlerin üretilmesi ve nano ölçekli kaplama materyallerinin geliştirilmesinde yine moleküllerin adezyon kapasitesi önemli bir parametredir (Peppas ve ark., 2004). Diğer taraftan, toz gıda üretiminde adhezyon kapasitesine bağlı kalite kusurları da gelişebilmektedir.Bunlardan en önemlisi, higroskopik adhezyona bağlı topaklanma fiziksel kusuru (Ueda ve ark., 2023), kimyasal reaksiyonlar (Hedegaard & Skibsted, 2024) veya morfolojik bozunmalardır (Ueda ve ark., 2023). Sunulan derlemede bu kusurlar tartışılmıştır.

2. TOZ GIDALAR

Genellikle amorf ya da kristal yapıya sahip toz gıdalar katı formda olup partikül boyutları küçültülerek bu forma getirilmiş endüstriyel ürünlerdir (Ermiş, 2015). Endüstriyel öneme sahip toz gıdalara başlıca baharatlar, süt tozu, toz çorba karışımları, tuz, un, şeker, yumurta tozu, bebek mamaları, kahve çeşitleri, kakao ve katkı maddeleri ile katkı maddeleri karışımları örnek olarak verilebilir (Ueda ve ark., 2023). Gıda hammaddelerinin çeşitli mühendislik uygulamalarıyla toz forma getirilmesi, üretim, taşıma, depolamada pek çok avantaj sağlamaktadır (Forny ve ark., 2011). Buna en güzel örneklerden biri, raf ömrü çok kısa olan süt yerine süt tozu kullanımıdır. Son yıllarda verimli ve sürdürülebilir gıda üretimi konusunda yapılan çalışmalar büyük önem kazanmıştır. Bu çalışmalar, ürüne ait proses tasarımı, maliyetlerin azaltılması, paketleme ve depolama kusurları ile nihai tüketiciye ulaşıncaya kadar meydana gelecek kalite kusurlarını önlemeye yöneliktir. Sunulan derlemede, başlıca toz gıdalar, bunların önemi, üretimden tüketilinceye kadarki süreçte meydana gelebilecek adezyona bağlı kalite kusurları tanımlanmış olup muhtemel önleme yöntemleri tartışılmıştır.

Baharatlar, toz formunda satışı yapılabilen ve adhezyon kusurları gözlemlenebilen gıda ürünlerindendir. Bu bağlamda, baharatların üretiminde yüksek nemlilik, higroskopik özelliklerinden dolayı partiküllerinin birbirine yapışarak aglomere olmasına sebep olabilmektedir. Baharatların toz formunda taşınması ve depolanması sırasında, yüzey etkileşimlerinin kontrol edilmesi, tozun akışkanlık özelliklerini ve ürün kalitesini doğrudanetkilemektedir.Kalite kaybını önlemek için baharatların düşük nemli ortamlarda depolanması ve uygun paketleme tekniklerinin kullanılması gereklidir (Fitzpatrick, 2017).

Süt tozu, adhezyonun çok belirgin olduğu gıda ürünlerinden biridir. Üretim sürecinde süt, suyun uzaklaştırılmasıyla toz hale gelir ve bu noktada partikül boyutunun küçültülmesi işlemi gerçekleştirilir. Bu işlemler sırasında adhezyon, özellikle higroskopik özelliklerden kaynaklanan topaklanma ve akışkanlık sorunları yarattığı bildirilmiştir(Fitzpatrick ve ark., 2007). Ayrıca, depolama koşullarının uygunsuzluğu süt tozu partiküllerinin birbirine yapışarak işlenebilirliklerini ve çözünürlüğünü de etkilemektedir. Süttozu su ile karıştırıldığında homojen bir çözeltinin oluşmamasına ve nihayetinde besleyici değerde önemli kayıplara yol açmaktadır. Ayrıca, sütün içerdiği protein ve yağlar, partiküllerin birbirine yapışma kapasitesini artırarak, uzun süreli depolama sırasında ürünün kalitesinin hızla düşmesine neden olmaktadır. Bu nedenle süt tozunun üretiminde, adhezyon gücünün minimize edilmesi için uygun koruyucu tedbirler alınması gerekli görülmüştür(Huppertz ve ark., 2016).

Toz çorba karışımları, pratik kullanımı açısından önemli bir ürün kategorisidir. Bu tür tozlar, genellikle yüksek oranda tuz ve baharat içermekte bu da partiküller arasındaki adhezyonun artmasına yol açmaktadır. Üretim sırasında, tozun nem içeriği, partiküllerin birbirine yapışma kapasitesini doğrudan etkiler. Fiziksel ve kimyasal özellikleri farklı katkı maddelerini de içeren çok bileşenli karışımlar olan hazır çorba tozlarında, her bir bileşenin adhezyon kapasitesi birbirinden farklı olabileceğinden homojen bir karışım elde edilmesi daha zordur. Ayrıca,her bileşenin adhezyon özelliklerinin dikkate alınarak doğru oranda karıştırılması ve nemin minimize edilmesi gereklidir. Bu nedenle, adhezyonun kontrol edilmesi hem üretim verimliliği hem de son ürünün kalitesi için önemlidir(Fitzpatrick ve ark., 2007).

Tuz, genellikle kristal yapıya sahip bir bileşik olup rafine edilerek ya da edilmeden farklı formlarda işlenen bir endüstriyel üründür. Yüksek nemli ortamlar, tuz kristallerinin birbirine yapışarak topaklanmasına yol açmakta bu da ürünün taşınmasını ve depolanmasını zorlaştırmaktadır. Tuzun adhezyon özellikleri, özellikle gıda endüstrisinde büyük önem taşır çünkü tuzun etkinliği ve kullanım kolaylığı, doğru bir şekilde paketlenmesi ve depolanması ile doğrudan ilişkili olduğu tespit edilmiştir. Tuzun ideal koşullarda saklanması, nemden korunması ve gerektiğinde topaklanma önleyici ajanlarının kullanılması kalite kusurlarını önlemeye yardımcı olmaktadır. Depolama sırasında tuzların topaklaşması ve topakların sertleşmesi özellikle tuzun toz formda kullanıldığı ürünlerde tüketici memnuniyetini de düşürmektedir(Li ve ark., 2019).

Un, çok yaygın kullanılan bir toz gıda maddesidir ve endüstriyel gıda üretiminin temel bileşenlerinden biridir. Un partikülleri arasında adhezyon, genellikle nem oranı ve sıcaklık gibi çevresel faktörlere bağlı olarak değişir. Özellikle yüksek nem, un partiküllerinin birbirine yapışmasına neden olmaktadır. Unun ambalajlanması, taşınması ve depolanması sırasındaüreticiler adhezyonun minimuma indirilmesi için kontrollü ortamlar sağlamayı hedeflemektedirler. Un üretiminde uygun nem seviyelerinin korunması ve paketleme sırasında hava geçirmez malzemelerin kullanılması pek çok kalite problemlerinin önlenmesine yardımcı olmaktadır(Hasmadi, 2020).

Şeker, özellikle toz formunda, higroskopik özelliklerinden dolayı adhezyon sorunlarının yaygın yaşandığı gıdalardan biridir. Şeker kristallerinin etkileşimleri, çevresel koşullar altında birbirine yapışmalarına sebep olmaktadır. Bu özellik, şekerin taşınması, depolanması ve işlenmesi sırasında çeşitli zorluklara neden olmaktadır. Özellikle nemli ortamlarda, şeker kristallerinin birbirine yapışarak topaklanması, ürünün istenilen akışkanlık özelliklerini kaybetmesine yol açar. Bu da şekerin kullanımını ve paketlenmesini zorlaştıran faktörlerin başında gelmektedir(Li ve ark., 2017).

Yumurta tozu, özellikle yüksek protein içeriği ve yağ oranı ile bilinmektedir.Nem içeriğinin yükselmesi ile birliktepartiküller arasındaki adhezyon kapasitesini artarak topaklanmaya neden olmaktadır. Bu nedenle yumurta tozu üretiminde topaklanma önleyici kimyasalların kullanılması gerekmektedir(Mazalli ve ark., 2007)

Bebek mamaları, genellikle kolloidal sıvı formdaki karışımlarda hacim azaltma amacıyla kurutularak toz formunda üretilmekte olup yüksek besin değerine sahiptir. Bebek mamalarının üretim aşamaları sırasında adhezyonun önlenmesi, ürünün besin değerini ve kullanım kolaylığını etkilemektedir. Bebek mamaları üretiminde ve depolanmasında, adhezyonla ilişkili sorunların minimize edilmesi için, genellikle modifiye atmosfer uygulamaları tercih edilmektedir(De ve ark., 2016).

Kahve, dünya genelinde çok tüketilen bir gıda maddesidir ve genellikle toz formunda veya öğütülmüş olarak satılır. Kahve tozlarının adhezyon kapasitesi, partiküllerin boyutu ve şekliyle doğrudan ilişkilidir. Kahve partiküllerinin nemli ortamlarda birbirine yapışma eğilimi, kahve kalitesini azaltmaktadır. Bu nedenle kahve üreticileri, kahvenin öğütülmesi ve paketlenmesi sırasında, partiküllerin akışkanlık özelliklerini korumak için kontrollü atmosferde işleme, paketleme ve depolama yapılmaktadır (Dogan ve ark., 2019).

Kakao, zengin aroması ve besin içeriği ile bilinen bir toz gıda maddesidir. Kakao tozunda yağ içeriği yüksek olup toz partiküllerinin birbirine yapışmasını hızlandırmaktadır. Paketleme ve depolamada nem kontrolü son ürünün kalitesi açısından oldukça önemlidir(Guehi ve ark., 2010).

Son olarak, toz formdaki gıda katkı maddeleri, yüksek higroskopik özelliklere sahip olduğundan bu ürünlerin ambalajlanması, depolanması ve satışı sırasında topaklanma en önemli sorun olarak görülmektedir. Katkı maddelerinin homojen bir şekilde dağılması ve etkileşiminin kontrol edilmesi, ürünün son kalitesini ve raf ömrünü etkileyen önemli bir faktördür.

3. TOZ GIDALARDA KALİTE KUSURLARI VE ÖNLENMESİ

Toz gıdalarda, gıda hammaddelerinde veya gıda katkı maddelerinde adezyona bağlı en sık karşılaşılan sorun topaklanma sorunudur (Zafar ve ark., 2017). Ancak, yukarıda açıklanan herhangi bir nedenle topaklanma başladığı andan itibaren besin değeri kaybı, aroma kaybı ya da değişikliği, kötü koku oluşumu, renk ve tekstür bozulmaları, reolojik değişimler, yüzde çözünür madde miktarında değişim, besin yapısındaki homojen matrisin bozulması gibi fiziksel, tekstürel veya kimyasal birincil kalite kusurları meydana gelmektedir (Afrassiabian ve ark., 2016).

Toz gıda üretiminde adhezyona bağlı sorunların önlenmesi için sanayide ürünlerin fiziksel ve kimyasal kalitesini korumaya yönelik çeşitli yöntemler uygulanmaktadır.Bunlardan ilki proses koşulların ayarlanması ve prosese uygun makine kullanılmasıdır. İkincisi topaklanma önleyici katkı maddelerinin kullanılmasıdır. Yaygın kullanılan diğer bir yöntem ise ürün paketlemede hava ve nem geçirmeyen bariyer içeren ambalaj materyallerinin kullanılmasıdır (Chen ve ark., 2015).

Toz gıda üretiminde, özellikle mikserler ve öğütücüler, partiküllerin daha homojen bir şekilde karışmasını sağlamak için kullanılmaktadırlar. Bu makineler, adhezyonun önlenmesine yardımcı olmak amacıyla düşük hızda ve kontrollü ortamda çalıştırılmaktadır. Ayrıca, sıkıştırma ve topaklanma eğilimlerini azaltacak şekilde tasarlanmış olan yüksek kaliteli mikserler ve vibrasyonlu öğütücüler kullanılarak, partikül boyutu ve dağılımı üzerinde kontrol sağlanabilmektedir. Bu yöntem, özellikle çorba karışımları ve süt tozu gibi ürünlerde, adhezyonun önlenmesi açısından önemli rol oynamaktadır(Chen ve ark., 2018).

Toz gıdalarda, adhezyona bağlı kusurları engellemek için sıklıklatopaklanma önleyici katkı maddeleri kullanılmaktadır. Türk Gıda Kodeksi Gıda Katkı Maddeleri Yönetmeliği'ne göre, topaklanmayı önleyici katkı maddeleri, E 500 ile E 599 arasında sınıflandırılan ve "topaklanmayı önleyici" fonksiyonel sınıfına dahil edilen maddelerdir.Bu maddeler arasında E500 (sodyum karbonat), E504 (magnezyum karbonat), E552 (kalsiyum silikat), E553 (magnezyum silikat), E559 (alüminyum silikat) ve E551 (silikon dioksit) yer alır. Örneğin, E551 ve E553 maddelerinin kullanımı, yalnızca kurutulmuş toz formdaki gıdalarda ve belirli gıda kategorilerinde sınırlıdır. E500 (Sodyum Karbonat), unlu mamuller, kabartma tozu ve bazı içeceklerde kullanılır. E504 (Magnezyum Karbonat), şeker, tuz, çikolata, reçel, marmelat ve süt tozu gibi gıdalarda topaklanmayı önlemek amacıyla kullanılır. E552 (Kalsiyum Silikat), tuz, baharatlar, süt tozu, şeker, kabartma tozu, pudra şekeri, hazır çorbalar ve hububat ürünleri gibi toz gıdalarda yaygın olarak kullanılır. E553 (Magnezyum Silikat), unlu mamuller, tuz ve baharatlar gibi toz gıdalarda kullanılır.E559 (Alüminyum Silikat), hazır kahve, süt tozu ve aromalar gibi ürünlerde kullanılır. E551 (Silikon Dioksit), tuz, un, toz çorbalar, kahve, vanilya tozu, kabartma tozu, kurutulmuş yumurta sarısı ve tortilla cipsleri gibi çok çeşitli ürünlerde kullanılır (TGK., 2013). Bu katkı maddeleri, tozların daha akışkan olmasını sağlayarak, ürünlerin taşınmasını, depolanmasını ve kullanılmasını kolaylaştırmaktadır. Ayrıca, bu maddeler, ürünlerin raf ömrünü uzatmaya ve nemle olan etkileşimini azaltmaya da yardımcı olmaktadır. Bu nedenle birçok toz formda paketlenmiş gıdada topaklanmayı önleyici katkı maddesi kullanılmaktadır.

Toz gıda ürünlerinin nem oranı, adhezyonun en büyük tetikleyicisi olduğundan üretim, depolama ve taşıma süreçlerinde nem kontrolü büyük önem taşımaktadır. Bu nedenle, ürünlerin paketleneceği ve depolanacağı ortamda nem oranı sürekli olarak izlenmekte, nem alıcılar veya su tutucular kullanılmakta ve iklimlendirme kontrol sistemleri kullanılmaktadır. Ayrıca, nem ve hava geçirmez özellikli uygun ambalaj materyali kullanılarak toz gıdaların nem alması engellenmektedir.Bu bağlamda, toz gıda ürünlerinde yaygın olarak kullanılan ambalaj materyalleri; Alüminyum Folyo (Alüminyum Laminantlar), Alüminyumun geçirimsizlik özelliği, ürünün dış ortamla etkileşimini minimize ederek topaklanma riskini önemli ölçüde azaltmaktadır. Yüksek nem, oksijen, ışık ve koku bariyeri sağlayan bu materyal, kurutulmuş çorba, baharat ve toz içecek gibi ürünlerde sıkça tercih edilmektedir. Metalize filmler, ince bir alüminyum tabakası ile kaplanmış plastik filmlerden oluşan bu yapı hem ışığa hem de neme karşı etkili bir bariyer sağlar. Baharat ve otlarda aroma kaybı ve topaklanmayı önlemek için kullanılır. BOPA (Çift Yönlü Gerdirilmiş Poliamid) Filmleri, Yüksek oksijen ve nem bariyeri özellikleri sayesinde, vakumlu ambalajlamada tercih edilen BOPA filmleri de etkili bir seçenektir. BOPP/BOPET Filmleri, Akrilik veya PVC (polivinilden klorür) kaplamalarla güçlendirilen bu filmler, oksijen ve nem geçişine karşı direnç göstererek, toz gıdaların uzun süre tazeliğini korumasına yardımcı olur. Süt tozu ve şeker gibi ürünlerde kullanmaktadır. PET/EVOH/PE Laminantlar, EVOH (etilen-vinil alkol) katmanı oksijen bariyeri sağlarken, PE (polietilen) katmanı nem geçişini önlemektedir. Bu çok katmanlı yapı, özellikle şarküteri ürünleri ve toz içeriğe sahip ürünlerde

kullanılmakta, topaklanmanın engellenmesinde önemli bir rol oynamaktadır. Uygun ambalaj materyallerinin kullanımı, toz gıdalarda karşılaşılan topaklanma gibi kalite problemlerinin önlenmesinde kritik bir rol oynamaktadır. Bu materyaller, hem fiziksel bariyer etkisi sağlayarak dış etkenlere karşı koruma sunmakta hem de tüketiciye güvenli, taze ve kaliteli ürün ulaştırılmasını mümkün kılmaktadır(Muller, 2017).

4. SONUÇ

Toz gıdalarda adezyon olgusu, ürünün kalitesi ve raf ömrü stabilitesi açısından kritik bir rol oynamaktadır. Özellikle depolama ve işleme süreçlerinde gözlenen topaklanma gibi fiziksel bozulmalar, yalnızca ürünün görünümünü ve akışkanlığını değil, aynı zamanda tüketici memnuniyetini ve endüstriyel uygulamalardaki verimliliği de olumsuz yönde etkileyebilmektedir. Bu durum, üretim hattında zaman kaybı, ambalajlama sorunları ve hatta ürün geri çağırmaları gibi ciddi sonuçlara yol açabilmektedir.

Toz gıdaların endüstriyel ve tüketici düzeyindeki kullanılabilirliği, yalnızca besinsel içeriğine değil; aynı zamanda fiziksel stabilitesine, serbest akış özelliklerine ve ambalaj içerisindeki davranışına da bağlıdır. Bu bağlamda, adezyonun kontrol altına alınması, ürünün hem işlenebilirliğini hem de raf ömrü boyunca kalitesini koruyabilmesi açısından stratejik öneme sahiptir.

Adezyonun, kristal köprü oluşumu, elektrostatik çekim ve mekanik kilitlenme gibi farklı mekanizmalarla ortaya çıkması; sürecin kontrolünü karmaşık hale getirse de nem kontrolü, uygun ambalajlama stratejileri, partikül mühendisliği ve yüzey modifikasyonları gibi çeşitli önleyici yöntemlerle bu etki azaltılabilmektedir. Bu nedenle, toz gıdaların üretim ve depolama aşamalarında; nem düzeyi, parçacık morfolojisi ve yüzey özelliklerinin dikkatle izlenmesi ve optimize edilmesi büyük önem taşımaktadır.

Mikroskobik ölçekteki yüzey etkileşimlerinin topaklanma, yapışma, dağılmama gibi makroskobik kalite kusurlarına dönüşmesi, gıda biliminde çok boyutlu bir değerlendirme gerektirmektedir. Bu nedenle, sorunun yalnızca fiziksel değil, aynı zamanda mühendislik ve malzeme bilimi perspektifinden de ele alınması gerekmektedir.

Modern üretim ortamlarında bu tür kalite kusurlarının öngörülmesi ve önlenmesi; yüzey kaplama teknolojileri, kontrollü ortam koşulları, formülasyon optimizasyonları ve süreç modellemeleri gibi disiplinler arası çözümlerle mümkün hale gelmektedir. Dolayısıyla, adezyon sadece bir zorluk değil, aynı zamanda daha rafine ve dayanıklı ürünler geliştirmek için bir fırsat alanı olarak da değerlendirilmelidir.

Gelecekte, nano-ölçekli yüzey analizleri, gelişmiş modelleme teknikleri ve yapay zekâ destekli kalite kontrol sistemlerinin kullanımıyla adezyon kaynaklı problemlerin daha etkin şekilde yönetilmesi mümkün hale gelecektir. Böylece hem üretim süreçlerinin sürdürülebilirliği artırılacak hem de nihai ürün kalitesinde istikrar sağlanabilecektir. Tüm bu bilgiler ışığında, toz gıdalarda gözlemlenen adezyona bağlı kalite kusurlarının bütüncül kalite yönetimi stratejilerinde temel bir kriter olarak değerlendirilmesi gerektiği çıkarımı yapılmıştır.

TEŞEKKÜR
Bu çalışma Çankırı Karatekin Üniversitesi Bilimsel Araştirma Projeleri kapsamında desteklenmiştir (2025).

KAYNAKÇA

Afrassiabian, Z., Leturia, M., Benali, M., Guessasmac, M., & Saleh, K. (2016). An overview of the role of capillary condensation in wet caking of powders. Chemical Engineering Research and Design, 110, 245–254.

Chen, X. D., & Özkan, N. (2007). Stickiness, functionality, and microstructure of food powders. Drying Technology, https://doi.org/10.1080/07373930701397400 [17.04.25]

Chen, M., Wu, S., Tang, W., & Gong, J. (2015). Caking and adhesion free energy of maltitol: Studying of mechanism in adhesion process. Powder Technology, 272, 235–240. https://doi.org/10.1016/j.powtec.2014.12.012 0032-5910/©. [08.04.25]

Chen, M., Wu, S., Xu, S., Yu, B., Shilbayeh, M., Liu, Y., Zhu, X., Wang, J., & Gong, J. (2018). Caking of crystals: Characterization, mechanisms and prevention. Powder Technology, 337, 51–67. https://doi.org/10.1016/j.powtec.2017.04.052. [10.04.25)

De Maria, F., Drogue, S., "EU Trade Regulation for Baby Food: Protecting Health or Trade?", The World Economy, 40 (7), 1430-1453, Aug 2016.

Dogan, ˘ M., Aslan, D., Gürmeriç, V., Ozgür, ¨ A., Goksel ¨ Saraç, M., 2019. Powder caking and cohesion behaviours of coffee powders as affected by roasting and particle sizes: principal component analyses (PCA) for flow and bioactive properties. Powder T.

Ermiş E. 2015. Food Powders: Properties and Characterization. Gida / J. Food 40, 287–294. doi:10.15237/gida.GD14072 [03.03.25]

Fitzpatrick, J. J., O'Connor, J., Cudmore, M., & Dos Santos, D. (2017). Caking behaviour of food powder binary mixes containing sticky and non-sticky powders. Journal of Food Engineering, https://doi.org/10.1016/j.jfoodeng.2017.02.021 204, 73–79.[13.04.25]

Fitzpatrick, J. J., Hodnett, M., Twomey, M., Cerqueira, P. S. M., O'Flynn, J., & Roos, Y. H. (2007). Glass transition and the flowability and caking of powders containing amorphous lactose. Powder Technology, 178(2), 119–128. 92 https://doi.org/10.1016/j.[13.04.25]

Fitzpatrick, J. J. (2007). Particle properties and the design of solid food particle processing operations. Food and Bioproducts Processing, 85(4 C), 308–314. https://doi.org/10.1205/fbp07056. [13.04.25]

Forny L, Marabi A, Palzer S. 2011. Wetting, disintegration and dissolution of agglomerated water soluble powders. Powder Technol. 206, 72–78.

Guehi, TS , Zahouli, IB , Ban-Koffi, L. , Fae, MA & Nemlin, JG (2010). Performance of different drying methods and their effects on chemical quality attributes of raw cocoa material. International Journal of Food Science and Technology , 45 , 1564–1571.

Gupta, S., Singh, R., & Verma, P. (2022). Impact of Moisture on the Quality of Milk Powder: An Adhesion and Clumping Study. Dairy Science & Technology, 99(3), 287-297.

Hasmadi, M., Noorfarahzilah, M., Noraidah, H., Zainol, M.K. and Jahurul, M.H.A. (2020). Functional properties of composite flour: a review. Food Research, 4(6), 1820–1831. https://doi.org/10.26656/fr.2017.4(6).419. [21.04.25]

Hill, A., & Tully, M. (2018). Preparation and feeding of infant formula: Best practices and recommendations. Pediatric Nutrition Reviews, 6(3), 98-106.

Huppertz et al. (2016). Huppertz, T., & Gazi, I. (2016). Lactose in dairy ingredients: Effect on processing and storage stability. Journal of Dairy Science, 99(8), 6842–6851. https://doi.org/10.3168/jds.2015-10033.[21.04.25]

Israelachvili, J. (2011). Intermolecular and Surface Forces. Academic Press.

Lestari, P., & Subagio, A. (2020). Coffee production process and its impact on quality: A review. Journal of Food Science and Technology, 57(3), 835-843.

Li, A., Cai, L., Chen, Z., Wang, M., Wang, N., Nakanishi, H., Gao, X. D., & Li, Z. (2017). Recent advances in the synthesis of rare sugars using DHAP-dependent aldolases. Carbohydrate Research, https://doi.org/10.1016/j.carres.2017.10.009. [21.04.25]

Li, F., Wang, X., Guo, Q., Zhang, B., Pei, Q., & Yang, S. (2019). Moisture Adsorption Mechanism of Earthen Plaster Containing Soluble Salts in the Mogao Grottoes of China. Studies in Conservation, 64(3), 159–173. https://doi.org/10.1080/00393630.2018.1537. [21.04.25]

Mazalli, M.R., Bragagnola, N., 2007, Effect of storage on cholesterol oxide formation and fatty acid alterations in egg powder, J. Agric. Food Chem., 55: 2743-2748.

Muller, C. R. (2017). Caking considerations: causes, mechanisms, quantification. https://www.foodprocessing.com.au/content/materials-handling-storage-and supply-chain/article/caking-considerations-causes-mechanisms-quantification 42795435.

Türk Gıda Kodeksi Gıda Katkı Maddeleri Yönetmeliği, Resmi Gazete, 2013.

Zafar, U., Vivacqua, V., Calvert, G., Ghadiri, M., & Cleaver, J. A. S. (2017). A review of bulk powder caking. Powder Technology, 313, 389–401. https://doi.org/10.1016/j.powtec.2017.02.024.

➢ *ORAL PRESENTATION*

Clays as supplementary cementitious materials, a FTIR investigation on structural modification

Sidorela Vishkulli[1*](*ORCID: https://orcid.org/0009-0003-5671-6075.*), Sonila Vito[1](*ORCID: https://orcid.org/0009-0008-3577-2429*), Ilirjana Boci[1](*ORCID: https://orcid.org/0009-0005-1019-056X)*

[*1]University of Tirana, Faculty of Natural Sciences, Department of Industrial Chemistry, Tirana, Albania.

Abstract

Due to diminishing fly ash and slag supplies as a result of global decarbonization attempts, alternative supplementary cementitious materials are needed to ensure the long sustainability of cement industry. Clays offer an attractive opportunity as an abundant, low-cost and environmentally friendly material. Their use as supplementary cementitious materials is becoming increasingly interesting for cement industry. The suitability of clays to be used as SCMs varies according to their origin and composition as well as their treatment processes. This study aims at investigating the potential of natural and thermally treated selected clays from south-east part of Albania as SCM. After grinding and sieving, the clays are treated thermally for one hour in three different temperature values, 550, 650 and 750°C respectively. The raw and treated clays are analyzed with FTIR spectrometer in order to identify the structural changes induced by thermal treatment. The optimal value of the treating temperature that ensures the complete modification of clays has been identified.

Keywords: natural clays, thermal treatment, reactivity, FTIR spectra, binder, cement-based materials

INTRODUCTION

Sustainable development, understood as progress that meet the needs of the present without compromising the ability of future generations to meet their needs, is now the basic idea behind the current paradigm of technological progress. The greatest threat to the achievement of the objectives of sustainable development is the excessive emission of greenhouse gases including, above all, carbon dioxide, which results in global warming with many serious negative consequences for future development and its prospects. The building industry makes a significant contribution to increasing carbon dioxide content in the atmosphere (Jaskulsi et. al., 2020). Concrete is the most used material in the world. Ordinary Portland cement is the main cementitious material in concrete recipes, which acts as binder for coarse and fine aggregates (Cao et. al., 2021). The production process of cement is energy intensive and produces large quantities of CO_2 which are released into the atmosphere (Tironi et. al., 2012). The global production of cement is expected to grow with the development and urbanization of nations. The possibilities of reducing the energy intensity of cement production are limited, although it is already possible to reduce heat consumption to 2.9GJ/t of clinker. The use of alternative fuels further reduces carbon dioxide emissions from fossil fuels. However, the use of limestone in clinker production cannot be eleminated or reduced (Jaskulsi et. al., 2020). Scientists are looking for effective strategies to reduce carbon dioxide emissions. Currently, the most promising strategy is the use of supplementary cementitious materials, which are aluminosilicate materials with hydraulic and/or pozzolanic activity (Vallina et. al., 2024). According to ASTM C125, a pozzolan is a siliceous or siliceous – aluminous material that, on its own, has little or no cementitious value. However, when finely divided and in the presence of moisture, it chemically reacts with calcium hydroxide at normal temperatures to form compounds exhibiting cementitious properties (Drissi et. al., 2024). The most commonly used SCM so far is fly ash from coal power plants (Vallina et. al., 2024; Poussardin et. al., 2024). However this additive which is used in production of both cement and concrete, is slowly losing its primary importance due to the progressive decommisioning of coal and lignite power plants. As a result, the supply of fly ash will be significantly reduced in the near future. Another cement additive used to reduce clinker content is a granulated blast furnace slag (Vallina et. al., 2024). However, it has no potential to replace fly ash, not at least because its global supply is far below potential demand. Additionally, it is only available in countries where the steel industry exists (Jaskulsi et. al., 2020). The decreasing supply of fly ash from the power industry is encouraging the search for new sources of pozzolan additives for cement and concrete production. Ashes from biomass combustion, volcanic tuffs, clays are potential alternatives to be used as SCM. Among these SCMs, calcined clays are attracting interest due to their abundance and high

availability, and ease of activation (Vallina et. al., 2024, Hanein et. al., 2022). The advantage of using calcined clay as a SCM is related to both energy and CO_2 emissions. Compared to the calcination of limestone for the production of Portland cement, which releases large quantities of CO_2 due to the decomposition of limestone ($CaCO_3$) at temperatures of around 1450°C, clay calcination takes place at lower temperatures (between 600 and 800°C) and emits much less CO_2, resulting in lower energy consumption and lower greenhouse gas emissions (Pinheiro et. al., 2024). The quality and suitability of clays for use as supplementary cementitious materials is highly dependend on the specific mineral composition, particle morphology, and particle size (Stefanini et. al., 2024; Saikia & Parthasarathy, 2010; Djomgoue & Njopwouo, 2013). Natural clays have different ability to react in cementitious reactions. Usually they have moderate or low pozzolanic activity. In order to make them more reactive, they need to be activated. As a result of activation, clay minerals undergo processes of dehydroxylation and amorphisation and the accompanying change in coordination of Al ions (Hazarika et. al., 2024). The resulting Al and Si – containing amorphous phase can undergo a series of reactions with calcium hydroxide (from cement hydration) and other binder constituents, such as sulfates or carbonates, to form a variety of calcium silicate/aluminate hydrates (C-S(A)-H, hemi/mono-carboaluminates, monosulfoaluminates, ettringite, iron – silicon hydrogarnet, etc.). These hydrated compounds are responsible for the improved mechanical properties of cements containing SCMs (Vallina et. al., 2024). Among different methods of activation, thermal activation is more common. The optimum calcination temperature to reach the maximum pozzolanic activity depends on the mineralogy of the clays. A complete removal of hydroxyl groups upon calcinations results in collapsed and disarranged metastable structure with low crystallinity. Raw clays are often polymineral materials making it difficult to find the optimum calcinations temperature. If raw clays are heated at too high temperatures (>900°C), recrystallization can take place, resulting in a decreased reactivity (Jaskulsi et. a.l, 2020; Hanein et. al., 2022; Hazarika et. al., 2024; Danner et. al., 2018).

The aim of this experimental work is to explore the feasibility of using some selected clays from south-east part of Albania as SCM. Thermally activation is used to activate the clays. The effect of different calcination temperatures on the structure and morphology of clays has been studied. The optimal treating temperature has been predefined. Further analysis and tests will be used to further characterize their properties and efficiency as supplementary cementitious materials.

MATERIALS AND METHODS

Materials

The clay samples were obtained from different locations in south-east part of Albania. They were crushed, grinded and homogenized in order to remove any organic waste and to transform them in a powder form. They were stored in plastic containers for further experiments.

Methods

Calcination of clays

The thermal treatment of raw clays was performed at a laboratory muffle furnace. Three different temperatures (550, 650 and 750°C) were used as calcination parameters. The calcination was done for one hour for each clay and calcination temperature. The samples were left to cool down until room temperature. They were stored in plastic containers and further tested with FTIR spectrometer and pozzolanic test.

Fourier transform infrared spectroscopy (FTIR)

The raw and calcined clays were characterized for their vibrational spectra with Fourier transform infrared spectroscopy using Shimadzu model instrument in the range 400-4000cm^{-1} with ATR method. For each sample 20 scans in the 400 – 4000cm^{-1} spectral range were recorded with a resolution of 2cm^{-1}. A spectrum of the atmosphere was recorded for background correction of the samples.

Pozzolanic activity test

The pozzolanic activity of calcined clays was measured by Frattini test according to EN 196-5. The pozzolanic activities of untreated clays and thermally treated clays were compared. Three samples were prepared for each composition. 20g of blended cement (70% PC and 30% by mass of ground calcined clay) and mixed with 100ml of boiled distilled water. After preparation the samples were left for 8 days in a sealed plastic container in an oven at 40°C. The suspension was filtered in vacuum through a 8µm nominal pore size filter paper and allowed to cool down at room temperature. The filtrated solution was analyzed for [OH^-] by titration against HCl 0.1M with methyl orange indicator and for [Ca^{2+}] by pH adjustment to 13, followed by titration with 0.03M EDTA solution using Murexide indicator. The concentrations of hydroxyl and [Ca^{2+}] ions are plotted and show a concentration of CaO as a function of [OH^-] ions at 40°C.

RESULTS AND DISCUSSIONS

FTIR results of raw and thermally treated clays

The FTIR spectra of the raw and calcined clays at different temperatures are shown in figures 1-3.
In general, the constituent units of clay minerals include the hydroxyl groups, tetrahedral silicate/aluminate anions, octahedral metal cations, and interlayer cations.

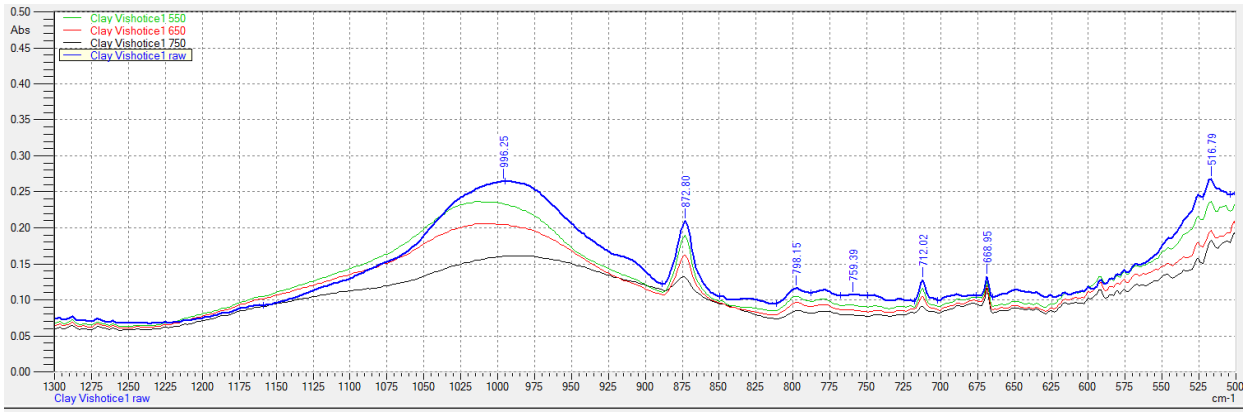

Figure 1. FTIR spectra of Vishotice1 clay, natural and thermally treated

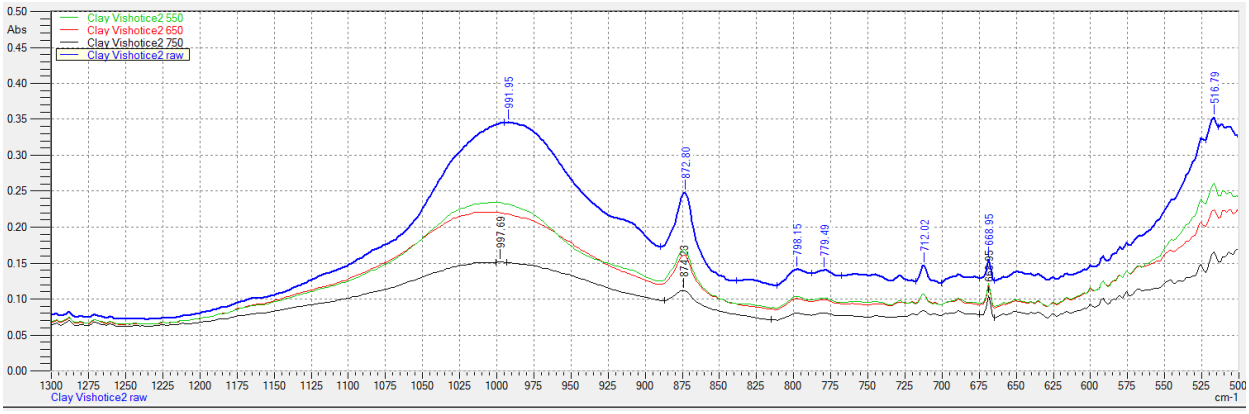

Figure 2. FTIR spectra of Vishotice2 clay, natural and thermally treated

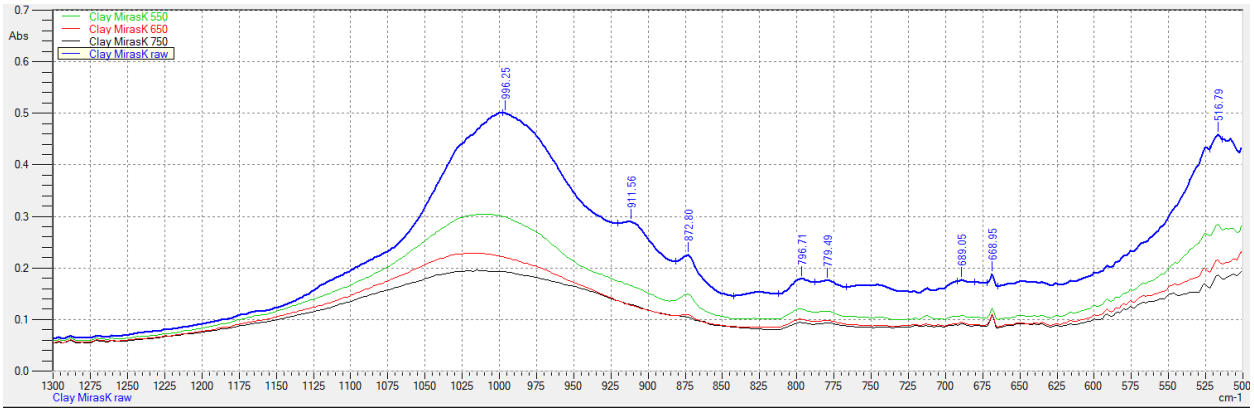

Figure 3. FTIR spectra of MirasK clay, natural and thermally treated

For all the raw clays, the band around 996cm^{-1} is attributed to Si-O stretching band in the kaolinite. The band located around 873cm^{-1} is attributed to calcite and is found in all the studied clays. The bands located around 770-795 cm^{-1}are attributed to the deformation vibrations of Si-O stretching (indicating the presence of quartz) and bands around 750cm^{-1} are from the deformation of Si–O vibrations (characteristic for kaolinite). The adsorption bands observed around 669cm^{-1} are attributed to Si-O-Al (octahedral Al) bending vibrations, characteristic for quartz. For all the clays, the bands located around 500-520cm^{-1} are attributed to Al-O-Si bending vibrations. For MirasK raw clay is observed a characteristic band around 900cm^{-1} which corresponds to the Al–OH deformation.

The FTIR spectrums of all calcined clays taken into the study present the absence of detectable –OH and Al-OH bands, the disappearance of the Si-O characteristic bands of kaolinite present in the raw clays, the disappearance of the Si-O-Al and Al-O-Si bands. All the obtained results from the FTIR analysis confirm the transformation and modification of raw clays through thermal treatment. These changes are more evident in higher temperatures of calcinations implying that 750°C is the optimal temperature for heat treatment of these selected clays from Albania.

The calcination of these clays at different temperatures causes decomposition of several minerals and the formation of new phases. The FTIR spectra of the raw clays indicates that these clays have high content of kaolinite which during thermal treatment forms meta-kaolinite. This is more evident in MirasK clay which has also a characteristic peak of kaolinite compared to the two other clays. This peak is completely disappeared after thermal treatment indicating the completely modification of the clay structure. This new phase has its influence in the reactivity of the clay since it is more reactive in the cementitious reactions. These results indicate that heat treatment is a good method of activation for kaolinitic clays. The same results are reported in literature.

Pozzolanic activity of clays

The Frattini test reults are plotted together with the lime solubility curve, which represents the concentration of Ca^{2+} in an alkaline solution at 40°C. The solubility curve was evaluated for [OH^{-}] in the range between 35mmol/l and 100mmol/l and a theoretical concentration of [CaO] was calculated by equation 1:

$$[CaO] = \frac{350}{([OH^{-}]-15)} \qquad (1)$$

Materials with an evident pozzolanic reactivity are located below the lime solubility curve while non-pozzolanic materials are above this curve. The experimental results obtained for our clays are shown in figure 4.

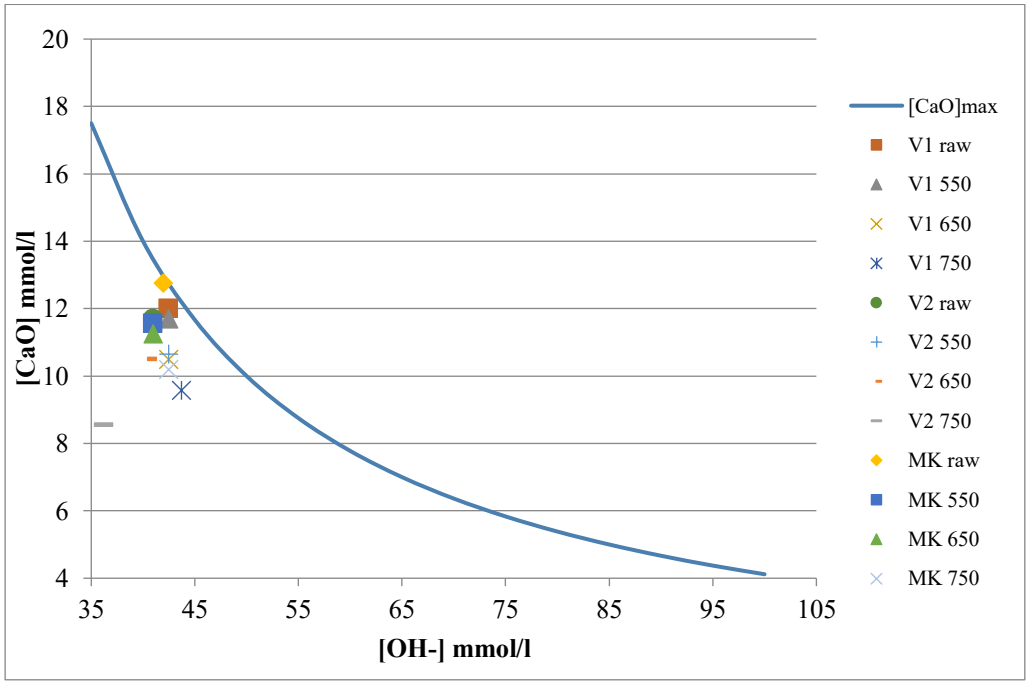

Figure 4. Frattini test results for cement paste containing 30wt% of different natural and treated clays after 8 days

All natural clays were under the solubility line thus indicating good pozzolanic reactivity. After 8 days, mixes containing activated clays showed an increased pozzolanic reactivity. Their points are located below the solubility line and below the points that represent the natural clays. According to the standard, below the solubility line indicates that the analysed material is a pozzolan and that a significant amount of Ca^{2+} ions produced by the cement hydration, was consumed in the pozzolanic reaction. Hence, all studied thermally treated clays were classified as pozzolanic materials and their pozzolanicity was increased proportionally with temperature.

CONCLUSIONS

Thermally treated clays are a valuable resource of supplementary cementitious materials. Enhancement of the pozzolanic reactivity of selected natural clays from south-east part of Albania after thermal treatment was investigated through FTIR and Frattini test. From the obtained results it is evident that thermal treatment of clays increases their reactivity. All the clays contained kaolinite in several amounts. Clays with higher kaolinite content were more reactive due to transformation of kaolinite to metakaolinite. The optimal treating temperature for all the clays was found to be 750°C. In this temperature most of the peaks were diminished and disappeared suggesting that the clays were modified structurally (got amorphised) and increased their reactivity as cementitious material. These results were confirmed by pozzolanic activity tests. Clays showed increased pozzolanic activity at higher treatment temperatures.

ACKNOWLEDGEMENTS

This work was financially supported to by the Research Expertise from the Academic Diaspora (READ) Program, developed by the Albanian-American Development Foundation (AADF) in coordination with the Institute of International Education (IIE).

REFERENCES

Cao Y., Wang Y., Zhang Z., Ma Y., Wang H. (2021). Turning sandstone clay into supplementary cementitious material: activation and pozzolanic activity evaluation. Composites Part B: Engineering, vol. 223, https://doi.org/10.1016/j.compositesb.2021.109137

Danner T., Norden G., Justnes H. (2018). Characterization of calcined raw clays suitable as supplementary cementitious materials. Applied Clay Science, vol. 162, https://doi.org/10.1016/j.clay.2018.06.030

Stefanini L., Ansari D., Walkley B., Provis J.L. (2024). Characterisation of calcined waste clays from kaolinite extraction in alkali-activated GGBFS blends. Materials today communications, vol. 38, https://doi.org/10.1016/j.mtcomm.2023.107777

Djomgoue P. & Njopwouo D. (2013). FT-IR spectroscopy applied for surface clays characterization. Journal of Surface Engineered Materials and Advanced Technology, vol. 3, https://doi.org/10.4236/j.semat.2013.34037

Drissi M., Horma O., Mezrhab A., Karkri M. (2024). Exploring raw red clay as a supplementary cementitious material: Composition, thermo-mechanical performance, cost and environmental impact. Buildings, 14(12), https://doi.org/10.3390/buildings14123906

EN 196-5 Methods of testing cement – Part 5: Pozzolanicity test for pozzolanic cements 2011

Hanein Th., Thienel K.C., Zunino F., Marsh A.T.M., Maier M., Wang B., Canut M., Juenger M.C.G., Haha M.B., Avet F., Parashar A., Al-Jaberi L.A., Almenares-Reyes R.S., Alujas-Diaz A., Scrivener K.L., Bernal S.A., Provis J.L., Sui T., Bishnoi S., Martirena-Hernández F. (2022). Clay calcination technology: state-of-the-art review by the RILEM TC 282-CCL. Materials and Structures, 55:3, https://doi.org/10.1617/s11527-021-01807-6

Hazarika A., Huang L., Babaahmadi A. (2024). Characterization, activation, and reactivity of heterogeneous natural clays. Materials and Structures, vol. 57, 68, https://doi.org/10.1617/s11527-024-02335-9

Jaskulski R., Jozwiak-Niedzwiedzka D., Yakymechko Y. (2020). Calcined clay as supplementary cementitious material.materials, (13)21, https://doi.org/10.3390/ma13214734

Pinheiro V. D., Fernandes de Abreu R., Alexandre J., de Castro Xavier G., Marvila M. T., Garcez deAzevedo A. R. (2024). Pozzolanic potential of calcined clays at medium temperature as supplementary cementitious material. Sustainability, 16(17), https://doi.org/10.3390/su16177508

Poussardin V., Wilson W., Paris M., Hamou A. T., Deneele D. (2024). Calcined clays as supplementary cementitious materials: A comparison between palygorskite and kaolinite, Construction and Building Materials, vol.416, https://doi.org/10.1016/j.conbuildmat.2024.135180

Saikia B. J. & Parthasarathy G. (2010). Fourier transform infrared spectroscopic characterization of kaolinite from Assam and Meghalaya, Northeastern India. Journal of Modern Physics, vol. 1, no. 4, https://doi.org/10.4236/jmp.2010.14031

Tironi A., Trezza M. A., Scian A. N., Irassar E. F. (2012). Kaolinitic calcined clays: Factors affecting its performance as pozzolans. Construction and Building Materials, vol. 28, https://doi.org/10.1016/j.conbuildmat.2021.08.064

Vallina D., Rodriguez-Ruiz M. D., Santacruz I., Cuesta A., Aranda M. A. G., De la Torre A. G. (2024). Supplementary cementitious material based on calcined montmorillonite standards. Construction and Building Materials, vol. 426, https://doi.org/10.1016/j.conbuildmat.2024.136193

➢ *ORAL PRESENTATION*

Sazan balığının (*Cyprinus carpio*) COI gen dizilerine dayalı filogenetik karşılaştırmaları

Serdar YEDİER[1] (*ORCID:* https://orcid.org/0000-0003-0017-3502)
Zeynep AKBAŞ[1*] (*ORCID:* https://orcid.org/0009-0001-0738-9288)
Seda KONTAŞ YALÇINKAYA[2] (*ORCID:* https://orcid.org/0000-0002-6582-6722)
Derya BOSTANCI[1] (*ORCID:* https://orcid.org/0000-0003-3052-9805)

[1]Ordu University, Faculty of Arts and Sciences, Department of Molecular Biology and Genetics, Ordu, Türkiye
[2]Ordu University, Fatsa Faculty of Marine Sciences, Department of Fisheries Technology Engineering, Ordu 52400 Türkiye

*Sorumlu yazar e-posta: akbaszeynep133@gmail.com

Özet
Bu çalışma, Amasya'daki Yedikır Baraj Gölü'nden örneklenen sazan balıklarının (*Cyprinus carpio*), diğer sazan popülasyonlarıyla filogenetik düzeyde karşılaştırılmasını amaçlamaktadır. Laboratuvar ortamında, örneklenen balıkların temel morfometrik ölçümleri yapılmış ve ardından genomik DNA izolasyonu gerçekleştirilmiştir. Türler arası filogenetik farklılıkların belirlenmesinde yaygın olarak kullanılan COI (Sitokrom Oksidaz I) gen bölgesi üzerinden filogenetik değerlendirmeler yapılmıştır. İzole edilen DNA örnekleri, evrensel primerler kullanılarak polimeraz zincir reaksiyonuna (PCR) tabi tutulmuştur. PCR ile elde edilen DNA dizileri dizileme yöntemiyle analiz edilmiş ve biyoinformatik yazılımlar aracılığıyla işlenmiştir. COI gen bölgesine ait filogenetik analiz için, GenBank ve BOLD (Barcode of Life Data System) veri tabanlarından *Cyprinus carpio* türüne ait dizi verileri toplanmıştır. 650 baz çiftinden kısa olan ya da doğrulanmamış olarak etiketlenen diziler analiz dışında bırakılmıştır. Elde edilen veriler öncelikle ülkelere göre gruplandırılmış; ardından Yedikır Baraj Gölü'nden elde edilen örnekler bu gruplara entegre edilerek filogenetik ağaçlar oluşturulmuştur. Veriler, nükleotid dizilerinin hizalanması ve filogenetik ilişkilerin belirlenmesi için MEGA yazılımı ile analiz edilmiştir. Sazan popülasyonlarının taksonomik durumlarını değerlendirmek amacıyla Neighbor-Joining (NJ) ve Maximum Likelihood (ML) yöntemleri kullanılmıştır. Analiz sonuçları, Yedikır Baraj Gölü'nden elde edilen sazanların belirgin grupları oluşturduğunu göstermiştir. Ayrıca, küresel popülasyonların genel olarak ülke temelli gruplandığı; ancak bazı haplotiplerin birden fazla ülkede yayılım gösterdiği de tespit edilmiştir.

Anahtar Kelimeler: *Cyprinus carpio*, COI, filogenetik analiz, biyoinformatik

Phylogenetic comparisons of common carp (*Cyprinus carpio*) using COI gene sequences

Abstract
This study aims to compare the common carp (*Cyprinus carpio*) sampled from Yedikır Dam Lake in Amasya with other carp populations at the phylogenetic level. In the laboratory, the basic morphometric measurements of the sampled fish were conducted, followed by genomic DNA isolation. Phylogenetic evaluations were performed using the COI (mitochondrial Cytochrome Oxidase I) gene region, which is widely used for interspecies phylogenetic differentiation. The isolated DNA samples were subjected to polymerase chain reaction (PCR) using universal primers. The DNA sequences obtained from PCR were analysed through sequencing and processed using bioinformatics software. For the phylogenetic analysis of the COI gene region, sequence data related to common carp were collected from the GenBank and BOLD (Barcode of Life Data System) databases, excluding sequences under 650 bp and those labelled as unverified. The collected data were initially grouped by country. Subsequently, the Yedikır Dam Lake samples were integrated into these groups, and phylogenetic trees were constructed. The data were analysed using MEGA software, which allowed for the alignment of nucleotide sequences and the detection of phylogenetic relationships. Neighbor-Joining and Maximum Likelihood methods were employed to evaluate the taxonomic status of carp populations. The analysis results indicated that the carp sampled from

Yedikır Dam Lake formed distinct haplotype groups. Additionally, it was found that global populations were generally grouped by country, although some haplotypes were distributed across multiple countries.

Keywords: *Cyprinus carpio*, COI, phylogenetic analysis, bioinformatics

GİRİŞ

Geleneksel balık sistematiği uzun yıllar boyunca morfolojik karakterlere dayanarak yürütülmüş olsa da, son yıllarda moleküler teknikler bu alanda devrim yaratmıştır (Nelson, 2006). Morfolojik benzerlikler bazen farklı türlerin ayırt edilmesini güçleştirdiğinden, genetik veriler türlerin daha doğru sınıflandırılmasını sağlamaktadır (Hebert ve Gregory, 2005). Moleküler sistematik, türler arasındaki evrimsel ilişkileri ortaya koymakta güçlü bir araç haline gelmiştir (Avise, 2000).

Moleküler analizler, yalnızca tür tanımlamada değil, aynı zamanda popülasyon yapısının ortaya konmasında, genetik çeşitliliğin ölçülmesinde ve göç yollarının belirlenmesinde de yaygın olarak kullanılmaktadır (Ward ve ark., 2005). Mitokondriyal DNA'ya dayanan analizler, özellikle de COI (*Cytochrome Oxidase I*) gen bölgesi, hayvanlar arasında yaygın olarak kullanılan bir moleküler barkodlama aracı haline gelmiştir (Hebert ve ark., 2003; Thai ve ark., 2004). COI dizileri üzerinden yapılan filogenetik çalışmalar, popülasyonlar arası ilişkileri anlamada yüksek çözünürlük sunmakta, bu sayede türler arası farklılıklar kadar tür içi varyasyonlar da detaylı biçimde incelenebilmektedir (Zhang ve Hanner, 2012).

Bu yöntemler, özellikle ekonomik ve ekolojik açıdan önemli türler için vazgeçilmez hale gelmiştir. Bunlardan biri de, hem doğal popülasyonları hem de yetiştiriciliği yaygın olan sazan balığıdır (*Cyprinus carpio*) (David ve ark., 2007). Sazan balığı, Asya ve Avrupa kökenli iki ana evrimsel hattı temsil eden geniş bir yayılım gösterir ve uzun süredir kültüre alınmış bir tür olması nedeniyle oldukça karmaşık bir genetik yapıya sahiptir (Xu ve ark., 2014). Yapılan çalışmalar, sazanın evcilleştirilme süreci boyunca çok sayıda stok transferi ve melezleme gerçekleştiğini ve bunun sonucunda farklı bölgelerde yaşayan popülasyonlar arasında genetik benzerliklerin oluştuğunu göstermektedir (Balon, 2004; Kalous ve ark., 2012). Avrupa'daki popülasyonların Asya kökenli bireylerle yüksek düzeyde genetik örtüşme gösterdiğini, bunun da kültürel taşınımın bir sonucu olabileceğini belirtmiştir. Aynı şekilde, coğrafi olarak uzak bölgelerdeki sazan popülasyonlarının benzer genotiplere sahip olması, bu türün doğal yayılımının çok ötesinde, insan eliyle gerçekleşen taşınım ve adaptasyon süreçlerinin etkili olduğunu düşündürmektedir (Kohlmann ve ark., 2005). Bu tür genetik karışımlar, yalnızca filogenetik analizlerde değil, aynı zamanda tür koruma, stok yönetimi ve biyoçeşitlilik politikaları açısından da dikkate alınması gereken önemli dinamiklerdir (Cawthorn ve ark., 2012).

Sazan balığı gibi geniş dağılıma sahip ve genetik olarak zengin türlerde, düzenli genetik izleme çalışmaları yapmak, mevcut genetik çeşitliliğin korunması ve potansiyel tehlikelere karşı önlem alınması açısından son derece önemlidir (Hänfling ve ark., 2005). Özellikle iç su ekosistemlerinde türlerin karşılaştığı çevresel baskılar, habitat değişiklikleri ve melezleşme gibi etkenler, genetik yapıyı hızla değiştirebilmekte; bu da türlerin uzun vadeli sürdürülebilirliğini tehdit edebilmektedir (Allendorf ve ark., 2012).

Bu çerçevede, Türkiye'nin farklı sucul ekosistemlerinde yayılım gösteren sazan balığı popülasyonlarının genetik yapısının ortaya konması, hem yerel hem de küresel düzeyde yapılan araştırmalara önemli katkılar sağlayacaktır. Bu çalışmada, Karadeniz Bölgesi'nde yer alan Amasya Yedikır Baraj Gölü'nden elde edilen *Cyprinus carpio* bireylerinin mitokondriyal COI gen bölgesi üzerinden genetik yapısı analiz edilerek, dünya genelindeki diğer popülasyonlarla filogenetik açıdan karşılaştırılması amaçlanmıştır. Bu sayede, hem türün evrimsel geçmişine dair yeni bilgiler edinilmesi hem de gelecekte yapılacak koruma ve yönetim stratejilerine genetik açıdan temel oluşturulması hedeflenmektedir.

MATERYAL VE METOD

Cyprinus carpio bireyleri Amasya Yedikır Baraj gölünden örneklenmiş ve bu balık örnekleri Ordu Üniversitesi Moleküler Biyoloji ve Genetik Bölümü Hidrobiyoloji Laboratuvarına getirilerek öncelikle balıkların ağırlık ve total boy verileri ölçülmüştür (Şekil 1). Morfometrik ölçümlerden sonra elde edilen balıklardan genetik çalışmalarda kullanılmak üzere bir miktar kuyruk yüzgeci dokusu makas yardımı ile kesilmiş ve 1.5 ml'lik mikrosantrifüj tüplerde %98'lik etanol ilave edilerek moleküler analizlerde kullanılmak üzere derin dondurucuda saklanmıştır.

Bu çalışmada *Cyprinus carpio* türünün moleküler analizleri ayrım gücünün yüksek olması sebebiyle DNA'nın COI gen bölgesi üzerinden gerçekleştirilmiştir.



Şekil 1. Sazan Balığının (*Cyprinus carpio*) genel görünüşü

DNA'nın eldesi derin dondurucuda saklanan kuyruk yüzgeci dokularından DNA izolasyonu yoluyla gerçekleştirilmiştir. Toplam DNA'nın ekstraksiyonunda Hibrigen DNA ekstraksiyon kiti kullanılmıştır. Total DNA izolasyonu için her bireyin kuyruk dokusundan parça alınmış ve alınan bu parçalardan DNA izole edilmiştir.

DNA'nın agaroz jel elektroforeziyle kontrolü aşamasında, 0.8 g agaroz 1xTBE buffer ile 100 ml'lik agaroz jel hazırlanmıştır. Isıtıcıda agarozu erittikten sonra, üzerine 4µl ethidium bromide ilave edilerek karışması sağlanacak ve hazırlanan jel elektroforez küvetine dökülmüştür. Küvet elektroforez tankının içine yerleştirilip tank 1xTBE buffer ile doldurulmuştur. Bundan sonraki aşamada her bir örnek için 3µl genomik DNA, 2 µl Nuclease Free Water ve 1 µl de 6xLoading Dye pipetajlanmış ve kuyucuklara sırasıyla yüklenmiştir (Şekil 2).

Yükleme işlemi bittikten sonra örnekler elektroforezde yürütülmüştür. Yürütme işlemi tamamlandıktan sonra jel UV görüntüleyici yardımıyla incelenmiş ve oluşan bantlar gözlemlenerek DNA kalitesi belirlenmiştir. Çalışma sonucunda istenilen kalitede bant veren örnekler PCR için ayrılmıştır.

COI Gen Bölgesinin PZR ile amplifikasyonu için uygun PZR koşulları belirlenmiştir (Şekil 3). Mitokondriyal gen bölgelerinin çoğaltılmasında kuyruk yüzgeci dokusundan elde edilmiş total DNA kullanılmıştır. DNA'nın COI bölgesi PZR ile çoğaltılmıştır. Çalışmamız kapsamında PZR ile çoğaltımda reaksiyon başına kullanılacak olan dNTP, $MgCl_2$, kalıp DNA ve primer miktarları ve konsantrasyonları optimize edilmiştir.



Şekil 2. DNA'nın Agaroz Jel Elektroforeziyle Kontrolü



Şekil 3. Çalışmada kullanılan PZR koşulları

Sazan balığı türü için literatür doğrultusunda belirlenmiş olan aşağıdaki primer dizileri kullanılmıştır (Ward vd., 2005).

FishF1 TCAACCAACCACAAAGACATTGGCAC

FishR1 TAGACTTCTGGGTGGCCAAAGAATCA

Çoğaltılan COI gen bölgesinin agaroz jel elektroforeziyle kontrolünde PZR ürünlerinin istenilen görüntüyü verebilmesi için çalışmada agaroz jel konsantrasyonu %1 olarak ayarlanmıştır. Daha önceden de belirtilen elektroforez aşamaları uygulanmış ve her bir örnek için 3 µl PZR ürünü, 2 µl NFW ve 1 µl 6x Loading Dye pipetajlanarak kuyucuklara sırasıyla yüklenmiş ve 100V'da 45dk yürütme işlemi yapılmıştır. Yürütme işlemi tamamlandıktan sonra jel UV görüntüleyici yardımıyla oluşan bantlar gözlemlenerek ilgili bölgenin varlığı ve kalitesi belirlenmiştir. Çalışma sonucunda istenilen kalitede bant veren örnekler sekans için ayrılarak -20°C'de muhafaza edilmiştir.

PZR ürünlerinin saflaştırması ve dizilerin elde edilmesi aşamasında DNA izolasyon kitleri kullanılmıştır. Saflaştırılan PZR ürünlerinin nükleotid dizileri Macrogen firmasından hizmet alımı yapılarak gerçekleştirilmiştir. Hizmet alımı sonrasında elde edilen ham sekans verileri biyoinformatik programlarla işlenmiş ve tür için filogenetik ağaçlar oluşturulmuştur.

Yedikır Baraj Gölü'nden elde edilen *Cyprinus carpio* bireylerine ait COI (mitokondriyal Cytochrome c Oxidase I) gen bölgesi dizileri, filogenetik analiz amacıyla dünyanın farklı bölgelerinden GenBank ve BOLD (Barcode of Life Data System) veritabanlarından temin edilen COI sekansları ile karşılaştırılmıştır. Analize dahil edilecek diziler seçilirken, 650 baz çifti altında kalan ya da "unverified" (doğrulanmamış) olarak işaretlenen kayıtlar çalışma dışı bırakılmıştır. Seçilen sekanslar FASTA formatında toplanmış ve

analiz öncesi ChromasPro 2.2.0 yazılımı ile manuel olarak temizlenip hizalanmıştır. Ardından, filogenetik ilişkileri ortaya koymak amacıyla MEGA (Molecular Evolutionary Genetics Analysis) programı kullanılmıştır. Diziler, MEGA yazılımı içerisinde ClustalW algoritması ile çoklu hizalamaya tabi tutulmuştur. Filogenetik ağaçlar, Neighbor-Joining (NJ) ve Maximum Likelihood (ML) yöntemleri kullanılarak ayrı ayrı oluşturulmuştur. NJ yöntemi için Kimura 2-parameter modeli, ML yöntemi içinse en uygun model otomatik olarak belirlendikten sonra uygulanmıştır. Her iki analizde de bootstrap analizi yapılarak ağaçların istatistiksel güvenilirliği değerlendirilmiştir. Analiz sonucunda, Yedikır Baraj Gölü'nden elde edilen örneklerin genetik olarak diğer ülke popülasyonlarına olan uzaklıkları ve filogenetik ilişkileri görselleştirilmiştir.

SONUÇLAR VE TARTIŞMA

Çalışmada elde edilen sazan bireylerinin ortalama total boyları 19,5±1,5 cm, ortalama ağırlıkları ise 114,5±5,2 g olarak hesaplanmıştır. Sazan bireylerinin çoğaltılan COI gen bölgesine ait PZR ürünleri, %1 agaroz jel kullanılarak elektroforez yöntemiyle incelenmiştir. Jel üzerinde gözlemlenen bantlar net, tekil ve yaklaşık 650 bp civarında olup istenilen amplifikasyonun başarıyla gerçekleştiğini göstermektedir. Bantların konumu DNA ladder ile karşılaştırıldığında hedef gen bölgesiyle uyumlu olduğu gözlemlenmiştir (Şekil 4). Ayrıca, jel görüntüsünde non-spesifik bantlara ya da primer-dimer oluşumlarına rastlanmamıştır. Bu durum hem kullanılan primer çiftinin uygunluğunu hem de PCR koşullarının başarılı şekilde optimize edildiğini göstermektedir (Şekil 4).



Şekil 4. Çalışmada çoğaltılan COI gen bölgesine ait verilerin jel görüntüsü

Yedikır Baraj Gölü'nden elde edilen *Cyprinus carpio* bireylerine ait COI gen bölgesine ait ham dizi verileri ChromasPro 2.2.0 programıyla analiz edilmiştir (Technelysium Pty. Ltd., Tewantin, Australia). Bu analizde forward ve reverse okumalara ait diziler karşılaştırılarak ve her bir örnek için consensus dizileri oluşturmuştur. Oluşturulan bu diziler ile GenBank ve BOLD veritabanlarından temin edilen farklı ülkelerde yayılış gösteren *Cyprinus carpio* tütüne ait diziler karşılaştırılmıştır.

MEGA yazılımı kullanılarak gerçekleştirilen filogenetik analizlerde, hem Neighbor-Joining (NJ) hem de Maximum Likelihood (ML) yöntemleri kullanılmış ve dış grup olarak da *Barbus barbus* türü tercih edilmiştir. MEGA yazılımı ile sazan bireylerinin COI bölgelerine ait veriler ve Kimura 2-parameter modeli kullanılarak oluşturulan Neighbor-Joining (NJ) ağacı Şekil 5'te sunulmuştur. MEGA yazılımı ile sazan bireylerinin COI bölgelerine ait veriler ve HKY (Hasegawa-Kishino-Yano) modeli kullanılarak oluşturulan Maximum Likelihood (ML) ağacı Şekil 6'te sunulmuştur.

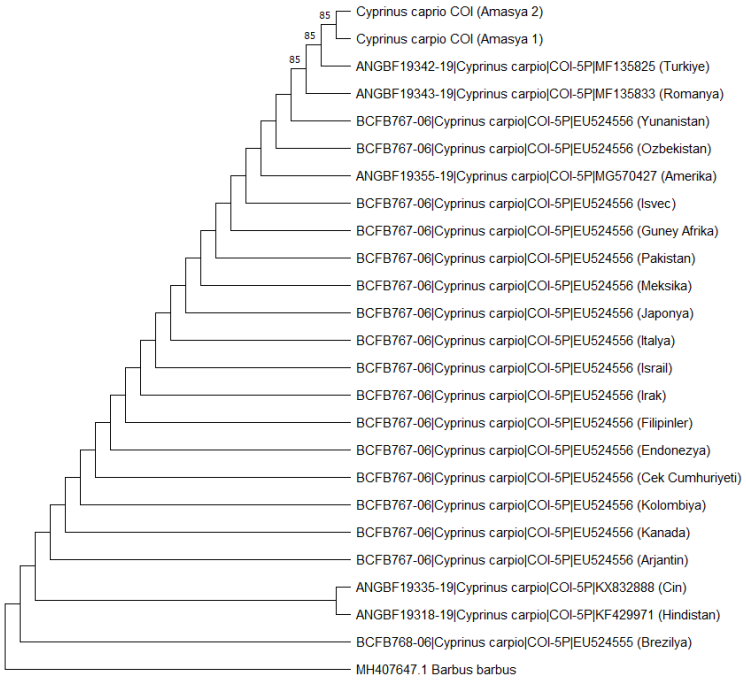

Şekil 5. *Cyprinus carpio* bireylerinin COI gen bölgesine ait Neighbor-Joining ağacı

Elde edilen sonuçlar, Amasya örneklerinin kendi içerisinde tutarlı olduğunu göstermiş olup bu örnekler öncelikle yine Türkiye örnekleriyle aynı filogenetik dalda yer almıştır. Ayrıca, Amasya örneklerinin özellikle Romanya örnekleriyle de benzerlik gösterdiğini ve bu iki grubun aynı klad içerisinde gruplanabildiğini ortaya koymuştur. Bu durum, coğrafi yakınlık veya tarihsel stok alışverişi gibi etkenlerin genetik benzerlik üzerinde etkili olabileceğini düşündürmektedir.

Buna karşılık, diğer ülkelerden elde edilen örneklerin kümelenmesinde ise belirgin bir coğrafi desenler görülmemiştir. Örneğin, Amerika Birleşik Devletleri ve Japonya, Filipinler ve Meksika örneklerinin aynı klad içinde yer alması, sazan balığının kültürel taşınımı ve insan eliyle yayılımı sonucunda dünya genelinde genetik olarak karışık yapılar oluşturduğunu göstermektedir. Aynı genotiplerin farklı kıtalarda bulunması, türün doğal yayılımı dışında geniş çaplı yetiştiricilik ve adaptasyon süreçlerinin bir sonucu olabilir. Ancak bazı dalların düşük bootstrap değerlerine sahip olması, COI gen bölgesinin tüm popülasyonları ayırt etmede sınırlı kalabildiğini ve genetik farklılıkların kesin bir şekilde yorumlanabilmesi için daha fazla gen bölgesi ile desteklenmesi gerektiğini göstermektedir.

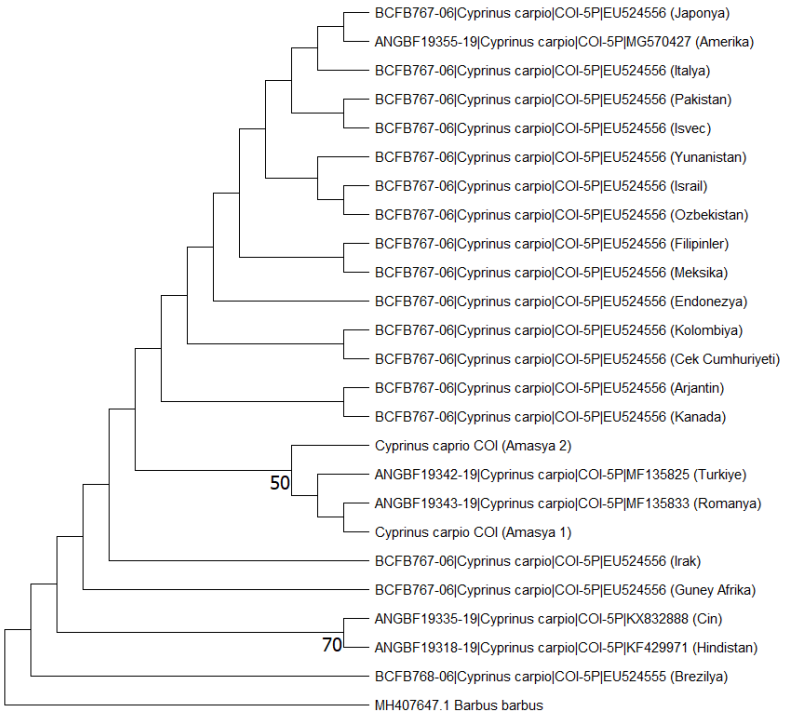

Şekil 6. *Cyprinus carpio* bireylerinin COI gen bölgesine ait Maximum Likelihood ağacı

Bu çalışmada, Yedikır Baraj Gölü'nden elde edilen *Cyprinus carpio* örnekleriyle gerçekleştirilen filogenetik analizler, türün genetik yapısına dair bazı önemli ipuçları sunmuştur. Ancak analizlerin sınırlı sayıda gen bölgesine ve örneklem alanına dayanması, elde edilen verilerin geniş çaplı genetik yapı hakkında kesin yargılar vermesi açısından bazı kısıtlamalar doğurmaktadır. Yapılan analizlerde bazı uzak coğrafyalardaki örneklerin aynı klad içerisinde yer alması, insan eliyle gerçekleştirilen kültürel taşınımın sazan balığı popülasyonlarında genetik karışıklığa yol açtığını düşündürmektedir. Bu durum, doğal yayılımdan ziyade, türün yetiştiricilik, stok aktarımı ya da ticari transferler gibi süreçlerle global ölçekte yayılmış olabileceğine işaret etmektedir. Literatürde de benzer bulgular mevcuttur; örneğin Kalous ve ark. (2012) farklı kıtalardan yayılış gösteren balık örneklerinin benzer genetik özellikler taşıyabildiğini belirtmiştir. Bu tip genetik benzerliklerin belirlenmesi, türün kökenini anlamakla birlikte, mevcut stokların geçmişte ne tür müdahalelere maruz kaldığını da ortaya koyabilmektedir.

Özellikle bu çalışmada Türkiye örneklerinin Romanya örnekleriyle yüksek genetik benzerlik göstermesi, tarihsel stok alışverişlerinin veya coğrafi yakınlığın etkili olduğunu düşündürmektedir. Xu ve ark. (2014) ve Balon (2004) sazan balığının uzun süredir kültüre alınması, sık sık popülasyonlar arasında taşınım yapılması ve kontrollü melezlemelerin genetik çeşitliliği etkilediği belirtilmiştir. Bu yönüyle elde edilen bulgular, daha önceki çalışmalarla da örtüşmektedir. Öte yandan, bazı örneklerin düşük bootstrap değerleriyle ayrılması, yalnızca COI gen bölgesinin tüm popülasyonları ayırt etmede yeterli olmadığını göstermektedir. Thai ve ark. (2004) ile Zhang ve Hanner (2012) gibi araştırmalar da, tür içi varyasyonları ve daha hassas filogenetik ayrımları tespit edebilmek için çoklu gen bölgelerinin birlikte analiz edilmesi gerektiğini vurgulamaktadır. Bu bağlamda, ileriki çalışmalarda nükleer DNA işaretleyicileri veya mikrosatellit analizleriyle desteklenen daha kapsamlı bir yaklaşım, genetik yapının daha net anlaşılmasını sağlayacaktır. Ayrıca, bu tür çalışmalar yalnızca akademik düzeyde değil, aynı zamanda su ürünleri yetiştiriciliği, doğal popülasyonların korunması ve stok yönetimi açısından da kritik öneme sahiptir. Özellikle insan etkisiyle hızla değişen iç su ekosistemlerinde, türlerin karşı karşıya kaldığı genetik baskılar zamanla adaptasyon kapasitesini azaltabilir (Hänfling ve ark., 2005). Bu nedenle, yerel düzeyde yapılan bu tür çalışmalar, küresel biyoçeşitlilik politikaları açısından da değer taşımaktadır. Sonuç olarak, bu çalışma bölgesel düzeyde sazan balığının genetik yapısı hakkında temel bilgiler sağlamış; ancak türün evrimsel ilişkilerinin ve küresel dağılımının tam olarak anlaşılabilmesi için daha kapsamlı, çoklu genetik belirteçlerin ve geniş alanlı örneklemelerin kullanıldığı ileri analizlere ihtiyaç duyulduğunu ortaya koymuştur.

REFERANSLAR

Allendorf, F. W., Luikart, G., & Aitken, S. N. (2012). *Conservation and the genetics of populations*. Wiley-Blackwell, 624 p.

Avise, J. C. (2000). *Phylogeography: The history and formation of species*. Harvard University Press, Cambridge. https://doi.org/10.2307/j.ctv1nzfgj7

Balon, E. K. (2004). About the oldest domesticates among fishes. *Journal of Fish Biology,* 65 (Suppl. A), 1–27.

Cawthorn, D.-M., Steinman, H. A., & Witthuhn, R. C. (2012). DNA barcoding reveals a high incidence of fish species misrepresentation and substitution on the South African market. *Food Research International*, 46(1), 30–40.

David, L., Rosenberg, N. A., Lavi, U., Feldman, M. W., & Hillel, J. (2007). Genetic diversity and population structure inferred from the partially duplicated genome of domesticated carp, *Cyprinus carpio* L. *Genetics Selection Evolution*, 39(3), 319–340.

Hänfling, B., Bolton, P., Harley, M., & Carvalho, G. R. (2005). A molecular approach to detect hybridisation between crucian carp (*Carassius carassius*) and non-indigenous carp species (*Carassius auratus* and *Cyprinus carpio*). *Freshwater Biology*, 50(3), 403–417.

Hebert, P. D. N., & Gregory, T. R. (2005). The promise of DNA barcoding for taxonomy. *Systematic Biology*, 54(5), 852–859.

Hebert, P. D. N., Cywinska, A, Ball, S. L, deWaard, J. R. (2003). Biological identifications through DNA barcodes. *Proceedings of the Royal Society of London. Series B*. 270: 313-321.

Kalous, L., Bohlen, J., Ráb, P., & Petrtýl, M. (2012). Hidden diversity within the Prussian carp and designation of a neotype for *Carassius gibelio* (Teleostei: Cyprinidae). Ichthyological Exploration of Freshwaters. 23:11-18.

Kohlmann, K., Kersten, P., & Flajšhans, M. (2005). Genetic variability and structure of common carp (*Cyprinus carpio* L.) populations throughout Europe. *Aquaculture International*, 13(4), 365–373.

Nelson, J. S. (2006). *Fishes of the world* (4th ed.). Hoboken (New Jersey, USA): John Wiley & Sons, 601 p.

Thai, B. T., Burridge, C. P., Pham, T. A., & Austin, C. M. (2005). Using mitochondrial nucleotide sequences to investigate diversity and genealogical relationships within common carp (*Cyprinus carpio* L.). *Animal genetics*, 36(1), 23–28.

Ward, R. D., Zemlak, T. S., Innes, B. H., Last, P. R., & Hebert, P. D. N. (2005). DNA barcoding Australia's fish species. *Philosophical Transactions of the Royal Society B: Biological Sciences*, 360(1462), 1847–1857.

Xu, P., Zhang, X., Wang, X., Li, J., Liu, G., Kuang, Y., et. al. (2014). Genome sequence and genetic diversity of the common carp, *Cyprinus carpio*. *Nature Genetics*, 46(11), 1212–1219.

Zhang, J., & Hanner, R. (2012). Molecular approach to the identification of fish in the South China Sea. *Plos* One, 7: e30621.

➢ *ORAL PRESENTATION*

Fast Food Consumption Trends: A Comparative International Analysis and Standardisation of Measurement Methods

Mirva Hoxha[1] (ORCID: https://orcid.org/0009-0004-2757-3340)
Admir Nake[2] (ORCID: https://orcid.org/0000-0001-6621-4034)

[*1] Aldent University, Faculty of Medical Tecnical Sciences, Department of Nursing, Tirana, Albania.
[2]Medical University of Tirana, Faculty of Technical Medical Sciences,Tirane/Albania

Abstract

Fast food consumption has become a global trend. The process of globalisation has significantly increased the number of outlets offering this service almost worldwide. This article aims to analyse trends in fast-food consumption across different countries, based on a cross-sectional study conducted to standardise the questionnaire. Within this framework, factors influencing dietary choices, including socio-economic and cultural aspects and their impact on health, will be examined.

Numerous studies in various countries focusing on the assessment of fast-food consumption have explored consumption patterns among young people in those countries. These studies highlight a shift from traditional home-cooked meals—which include healthy, nutrient-rich, locally available foods—towards fast and processed foods. This paper provides an extensive review of materials from several countries to analyse fast-food consumption patterns among young people, alongside data related to age and education levels from a cross-sectional study of 140 randomly selected cases.

Education is also a factor contributing to increased fast-food consumption, linked to a lack of information regarding the health effects of fast food compared to nutritious meals.

Keywords: fast food, consumption, globalisation, healthy foods

INTRODUCTION

Globally, traditional dietary patterns are being replaced by fast food. Local nutrient-rich recipes and dietary practices are now substituted with fast food. Despite its negative health impacts, fast food remains popular among young people.

Nutrients are essential for human growth and development. Daily choices of nutrient-rich foods are a fundamental part of a healthy lifestyle (1). However, fast-food consumption is steadily rising among youth and children. Fast food is defined as food that can be quickly prepared and served within a short timeframe (6). The term was first introduced in 1950 by Merriam-Webster in the UK. According to the National Institutes of Health (NIH), fast food is defined as easily accessible, quickly served, and an affordable alternative to home-cooked meals (8). This includes restaurants, street vendors, home-delivery services, online platforms, and more. Fast food is commonly available in public spaces such as colleges, schools, shopping centres, cinemas, parks, street corners, airports, petrol stations, and even hospitals (5). Fast food has some advantages include fast service, availability, affordability and convenience. The fast-food industry operates swiftly to fulfil orders and cater to customers. Fast food originated as a commercial strategy to meet the needs of time-constrained workers (7).

In recent years, there has been identified a significant rise in fast-food consumption, particularly among employees and among other people who provide services at institutions and several working places. Many workers even take fast food home for consumption as snacks or full meals. Fast food is typically pre-portioned, leaving consumers with no control over serving sizes or nutritional content (11). Studies indicate that individuals with higher-than-average monthly incomes, as defined by INSTAT (https://www.instat.gov.al/al/statistika/t%C3%AB-dh%C3%ABna-ky%C3%A7e/), consume more fast food. Fast food is calorie-dense but nutrient-poor, often containing refined flour, sugars, low-quality oils, trans fats, and harmful additives (15). The increasing fast-food consumption trends among adolescents and youth adults are concerning dietary issues, as they are loaded with calories and fat and are strongly linked to obesity and obesity-related chronic diseases (12).

Electronic media plays a significant role in advertising fast food. Other promotional methods, such as posters, magazines, billboards, radio, and cinema, are also used to encourage and promote fast food consumption (6). The existence of a wide variety of fast foods, affordable price, convenience and readily available fast-food options are also reasons for consuming fast foods and drives its popularity.

Regular fast-food consumption without physical activity leads to obesity. Fast food consumption among youth contributes to rising obesity rates, which is a global health concern (14).

MATERIALS AND METHODS

A standardised questionnaire was used to compare consumer behaviours internationally. International Comparison of Fast-Food Consumption, key consumption trends in developed vs. developing countries and cultural factors, the impact and the influence of globalization on food dietary choices.

This study was focused on and analyses fast-food consumption trends among 141 randomly selected participants (simple random sampling) with the aim of validating the questionnaire that will be used further in many other people and that will be accompanied by data on physical and laboratory parameters (glycemia, lipidogram). The analysis was conducted using IBM SPSS Statistics 21, incorporating physical and laboratory parameters (blood glucose, lipid profiles).

RESULTS

Table 2: Descriptive Statistics of Participants

	N	Minimum	Maximum	Mean	Std. Deviation
Age of Participant	141	1	5	1.43	.920
Gender of Participant	141	1	2	1.14	.350
Family Economic Status (Reference INSTAT 2023)|	141	1	3	1.76	.559
Fast-Food Consumption	141	1	3	2.04	.985
Education Level of Participant	141	1	2	1.04	.186
Valid N (listwise)	141	1			

The table above presents descriptive statistics of the questionnaire results depending on the alternatives presented for each question.

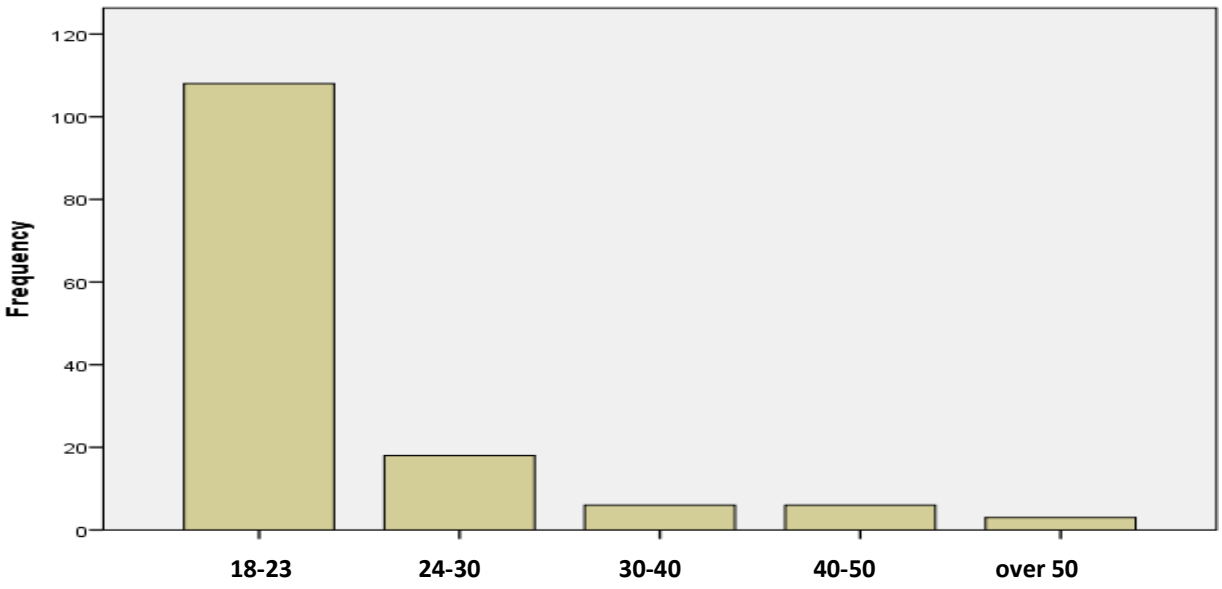

Graph 1: Distribution of participants by age group

The graph above shows higher participation among 18–23-year-olds.

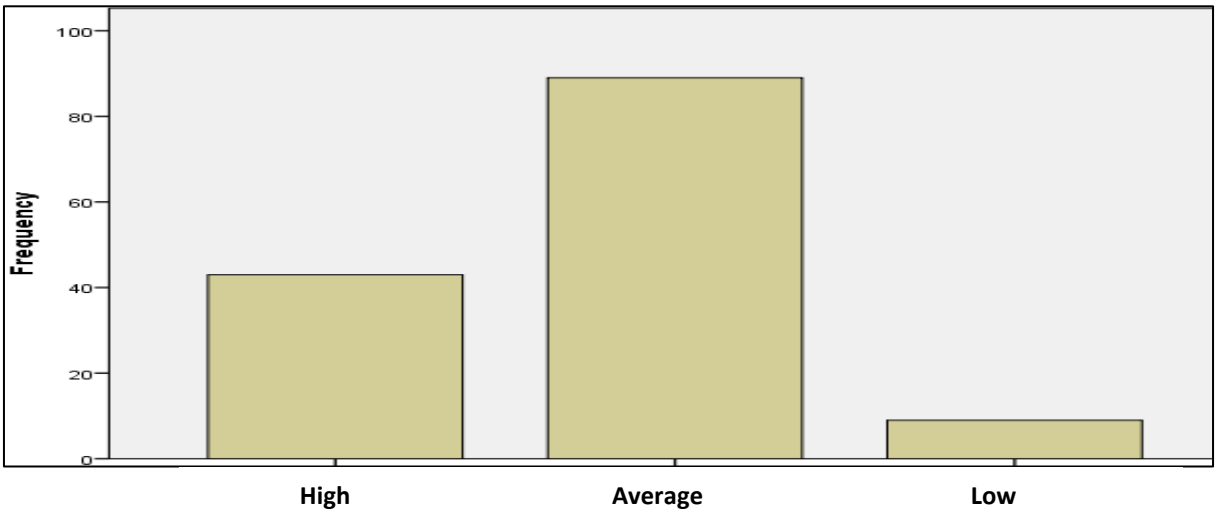

Family Economic Status (Referred to INSTAT 2023)

Graph 2: Family Economic Status

The graph above presents the economic status of the participants based on the average monthly income (400 euros per month per capita).

Table 3: Do you eat fast-food?

		Frequency	Percent %	Valid Percent %	Cumulative Percent
Valid	Yes	65	46.1	46.1	46.1
	No	5	3.5	3.5	49.6
	Rare	71	50.4	50.4	100.0
	Total	**141**	**100.0**	**100.0**	

Table 3 describes the frequency of fast food consumption among respondents, where it is noted that 96.5% of the participants consume fast food. And only 3.5% do not consume it at all.

Table 4: Correlation between age and fast-food consumption

Correlations[b]				
			Age of respondent	Do you consume fast-food?
Spearman's rho	Age of respondent	Correlation Coefficient	1.000	.291**
		Sig. (2-tailed)	.	.000
	Do you consume fast-food?	Correlation Coefficient	.291**	1.000
		Sig. (2-tailed)	.000	.
. Correlation is significant at the 0.01 level (2-tailed). b. Listwise **N = 141				

The table above shows a significant positive relationship between age and fast-food consumption in our respondents, which confirms the same results as those of the various countries considered during the study.

Table 5: Correlation between fast-food consumption and education level

Correlations[b]				
			Do you consume fast-food?	Education level of the respondent
Spearman's rho	Do you consume fast-food?	Correlation Coefficient	1.000	-.203*
		Sig. (2-tailed)	.	.016
	Education level of the respondent	Correlation Coefficient	-.203*	1.000
		Sig. (2-tailed)	.016	.
*. Correlation is significant at the 0.05 level (2-tailed).				
b. Listwise N = 141				

So, based on the above table, a significant correlation exists between education and fast-food consumption, and there was also no correlation between consumption and the economic status of the respondents.

DISCUSSION

Eating out of home and fast food consumption is a global concern; fast food consumption is highest in countries such as Australia, the United States, and the United Kingdom. According to a report from the National Health and Nutrition Examination Survey (NHANES, 2018) in the United States, between 2013 and 2016, 36.6% of American adults consumed fast food daily. A study of Australian youth on the consumption of fast food prepared for delivery showed that Australian males consumed more fast food for delivery than females (16).

Various European studies have shown that fast food consumption and the takeaway culture are growing every day. A government report in the UK found that 22% of residents bought takeaway food at least once a week and 58% bought it several times a month (9).

In a study in Romania among young people, it was found that the 18-24 age group consumed the most fast food products. The price of fast food and convenience were factors that influenced their decision to consume fast food (4)

A study in Germany reported that pizza was the most consumed fast food product among adolescents. In the same study, it was reported that girls received 6.5% of their daily energy from fast food, while boys received 7.8% of their daily energy from fast food (13)

The presence of excessive calories, saturated and trans fats, and a lack of many important nutrients, such as vitamins, minerals, dietary fibres, essential amino acids, phytochemicals, and antioxidants, is harmful to our body and health (2)

Frequent consumption of this type of food can lead to the development of deficiencies in many important nutrients. Fast food vendors mainly use hydrogenated oil to prepare fast food products and thus this type of food is rich in trans fats.

Regular consumption of fast food products leads to an increase in energy intake in adults and children which is linked to obesity and chronic diseases (10).

Studies have shown that fast food provides 158 to 163 calories per 100 grams and is also very poor in vitamin A, carotenoids and vitamin C, which are good for health and play a role in cancer prevention (3)

CONCLUSIONS

The dominant group in the study consists of young people aged 18-23, who represent 76.6% of the respondents, which indicates a high interest of this age group in the issue of fast food consumption. Participation by gender was uneven, with 85.8% of respondents being female and 14.2% male. The vast majority of participants (96.5%) have a high level of education, indicating that even individuals with advanced education tend to consume fast food. Despite higher education, 96.5% of respondents consume fast food, although with different frequencies. There is a statistically significant relationship between age, level of education and fast food consumption. The fast food industry is growing rapidly and is actively targeting youth through aggressive and intensive marketing and advertising strategies. Young adults report high rates of fast food consumption, which is a major public health concern due to associated risks. High consumption of fast food among young adults is associated with a number of serious health problems, while young people often lack the necessary information about these risks.

RECOMMENDATIONS

- Develop and implement awareness programs that inform young adults about the health risks associated with the consumption of fast food.
- Promote educational activities aimed at increasing knowledge about the negative consequences of unhealthy diets and the importance of a balanced diet.
- Provide support through individual or group nutritional counselling to help young people make informed decisions about their eating habits and dietary choices.
- Encourage the consumption of healthy foods in schools, universities and workplaces as a way to positively influence young people's behaviours, as well as undertake campaigns that promote lifestyle changes through inspiring stories, modelling healthy behaviours and rewards or incentives for active involvement.

REFERENCES

1. Arya C, Dubey N. A critical review on fast-food consumption pattern among South Asian and Southeast Asian young adults. *Int J Community Med Public Health* 2023.
2. Ashakiran, Deepti R. Fast Foods and Their Impact on Health. *JKIMSU*. 2012.
3. Brown DJ, Goodman J. Vitamins A, C, E and Cardiovascular Disease.
4. Chitnis SP. Fast-Food Industry in India. *Int J Trend Sci Res Dev*. 2019.
5. Choudhury SR. Fact Finding on Fast Food: A Review. 2022.
6. Das JC. Fast food Consumption in Children: A Review. *Med Clin Rev*. 2015.
7. French SA. Pricing Effect on Food Choices. *J Nutr*. 2003.
8. Hellesvig-Gaskell K. Definition of Fast Food. *Livestrong*. 2016.
9. Jahan I et al. Fast Food and Health. *EMCJ*. 2020.
10. Jahan I et al. Fast Food Consumption and Its Impact on Health. *EMCJ*. 2020.
11. Mandoura N et al. Factors Associated with Consuming Junk Food among Saudi Adults. *Cureus*. 2017.
12. Mohiuddin AK, Nasirullah M. Fast Food Addiction: A Major Public Health Issues. Indian J Nutrition. 2019
13. Moosburger R et al. Fast Food Consumption Among German Adolescents. *J Heal Monitoring*. 2020.
14. Sachithananthan V. Effect of Fast-Food on Adolescent Girls' BMI. *Int J Adv Res Biological Sci*. 2015.
15. Sason R, Sharma M. A Review Article on Effects of Incompatible Food W.S.R. to Junk Food on Health and Its Ayurvedic Aspects. Int J Heal Sci Res. 2019
16. Smith KJ et al. Fast Food Consumption in Australian Youth. *Int J Behav Nutr Phys Act*. 2009.

➢ *ORAL PRESENTATION*

The Role of Radiation Technologies in Sustainable Textile Finishing Applications

Mehtap Sahin[1*] (*ORCID: https://orcid.org/0000-0001-8262-6813*),
Buket Arik[2] (*ORCID: https://orcid.org/0000-0003-0647-5851*)

[*1] ZGK Goksin Kimya, Marketing Department, Denizli, Turkiye.
[2] Pamukkale University, Faculty of Engineering, Textile Engineering Department, Denizli, Turkiye

Corresponding author e-mail : mehtapsahin96@gmail.com

Abstract

In recent years, the need for new technologies as sustainable alternatives to conventional methods has increased in line with goals such as sustainability, low energy, water, and chemical consumption, and reduction of environmental impact and processing times in the textile industry. In this context, radiation technologies offer the potential to increase the efficiency of production processes while improving the ecological sustainability of the textile industry. Radiation technologies such as plasma, microwave, and ultraviolet (UV) irradiation have provided many important benefits and improvements in surface modification and functional finishing of textile materials. These technologies can be used in textile applications like pre-treatment, dyeing, printing, and functional finishing. In this review, the operation mechanisms, important parameters and properties; the contributions to sustainable production; the present textile finishing applications, and the future perspectives of radiation technologies have been evaluated and discussed.

Keywords: Textile Finishing, Sustainability, Radiation, Plasma, Microwave, Ultraviolet

Introduction

The textile industry has searched for sustainable and innovative solutions as alternatives to conventional methods, due to fast-changing consumer demands and growing environmental awareness. Conventional dyeing, printing, and finishing processes involve using large amounts of water and chemicals, which cause serious environmental problems. Especially the wastewater generated from dyes, salts, and various auxiliary chemicals pollutes freshwater sources and poses significant risks to ecosystems (Diaz-Garcia et al., 2024). Additionally, since textile production is responsible for about 20% of global clean water pollution, the transition to sustainable practices in the textile industry is quite essential (European Parliament, 2023).

In response to these growing concerns, many research projects and programs have been developed to reduce the environmental impact of wet textile processes. These efforts mainly focus on lowering energy use, reducing wastewater discharge, and limiting chemical consumption (H. Catarino et al., 2024). While some of these technologies are already used in industry, others are still under development and require more studies to improve their performance, cost-effectiveness, and scalability.

One innovative approach that supports this transformation in textile finishing is the use of radiation-based technologies. Applications such as plasma, microwave, and ultraviolet (UV) offer promising alternatives for sustainable textile production due to their potential to reduce environmental impact and improve processing efficiency.

Radiation technologies in textile finishing are processes that use ionizing or non-ionizing radiation energy to improve the physical and chemical properties of fabrics. Compared to conventional methods, these technologies offer more efficient, eco-friendly, and sustainable solutions (Teker et al., 2024).

In this study, the prominent applications of common radiation technologies like plasma, microwave, and ultraviolet, benefits to sustainability, future perspectives, and limitations in textile finishing have been reviewed.

Plasma Technology and Its Applications in Textiles

Plasma technology is an innovative method that allows textile surfaces to be modified in an eco-friendly and energy-efficient way. Plasma is a partially ionized gas made up of ions, free electrons, and excited molecules. Thanks to this structure, it can cause physical and chemical changes on the textile surface and improve the functional properties of the material (Haji & Kan, 2021).

Plasma treatments are 'dry' processes that do not require water or chemicals. Compared to conventional wet treatments, they reduce environmental impact and save energy. Low-pressure (vacuum) and atmospheric plasma systems are used to improve adhesion, enhance color fastness, increase hydrophilicity, and apply functional finishes to textile surfaces. (Donkor et al, 2024).

Textiles treated with plasma show improved dyeability, print quality, lamination compatibility, and response to functional coatings. Moreover, low operating temperatures enable the synthetic and delicate fibers to be treated without damage. This makes plasma especially useful for difficult-to-dye fibers such as polyester, polypropylene, and PTFE (Primc & Mozetič, 2024).

Plasma technology imparts hydrophilic and adhesive characteristics to textile fiber surfaces by polymerization, cleaning, etching, grafting, and activation reactions with the help of excited and energetic species like ions, free radicals, electrons, and metastables (Zhang et al 2022). In this way, plasma treatment improves the wetting, dyeing affinity, and reactivity of textile fibers in an environmentally benign approach (Hamida et al 2024). The important parameters that affect the efficiency of the plasma treatments are the nature of the gas, pressure, flow rate, power, frequency, and duration (Haji and Naebe 2020) (Zhang et al 2022).

However, there are some limitations to the widespread use of plasma technology. High initial investment costs, the temporary effect of some plasma treatments, and challenges in achieving uniform surface treatment can restrict its industrial use.

In the study by Serrano-Martínez et al. (2023), the effects of low-pressure oxygen plasma treatment on the surface properties and printing performance of cotton fabrics were investigated. The plasma treatment introduced hydrophilic functional groups on the fabric surface, increasing the surface energy. This modification led to improved pigment adhesion and enhanced print quality, especially in metallic pigment-based printing processes. Additionally, improvements in color fastness values were observed, highlighting the potential of plasma treatment as an eco-friendly and effective method for textile surface modification.

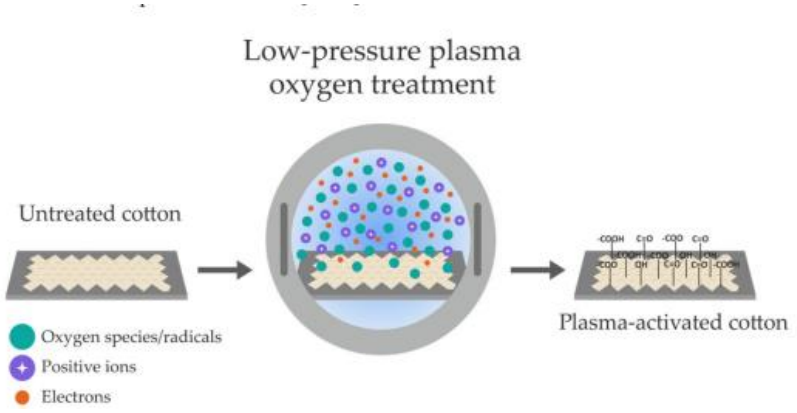

Figure1. Stretch of the low-pressure oxygen plasma activation treatment of cotton textiles. (Serrano-Martínez et al., 2023).

Ghasemian et al. (2025) applied atmospheric pressure plasma to wool fibers, followed by treatment with protease and glutaminase enzymes. This combined treatment changed the surface morphology of the wool and improved the color depth and wash fastness properties of the natural dyed fabrics. The synergistic effect of plasma and enzymatic treatment increased dye affinity and made the dyeing process more environmentally friendly.

Microwave Technology and Its Applications in Textiles

Microwave technology is gaining more and more attention as an innovative and sustainable approach to textile finishing. This technology covers the frequencies of the electromagnetic spectrum between 300 MHz and 300 GHz, with the frequency of 2.45 GHz generally preferred in industrial applications. Microwaves

provide direct heat generation by vibrating polar molecules in the textile material under a high-frequency electric field. This significantly shortens the process time, increases energy efficiency, and reduces environmental impacts (Adeel et al., 2023).

Microwave-assisted dyeing processes are carried out at lower temperatures compared to conventional methods, reducing energy consumption and providing more homogeneous dye uptake. In addition, the dyestuff uptake increases due to physical changes in the surface properties of the fabrics subjected to microwave pretreatment, resulting in stronger color depth and high fastness values (Rehman et al., 2022).

Recent studies have shown that microwave-treated natural and synthetic dyes give effective results, especially in protein-based fibers such as silk, wool, and nylon. Microwave radiation physically modifies the surface of such fibers, increasing the diffusion of dye molecules and thus improving the dyeing quality (Adeel et al., 2023; Rehman et al., 2022). In addition, the color fastness of fabrics treated with this method was evaluated as good to very good according to ISO standards, and less waste generation was observed from an environmental point of view (Adeel et al., 2023).

Rehman et al. (2022) showed that microwave radiation can be successfully used for dyeing polyamide (nylon) fabrics with natural dyes such as saffron and safflower. The dyes extracted with microwave support were obtained in a shorter time and demonstrated high performance in terms of color fastness and intensity.

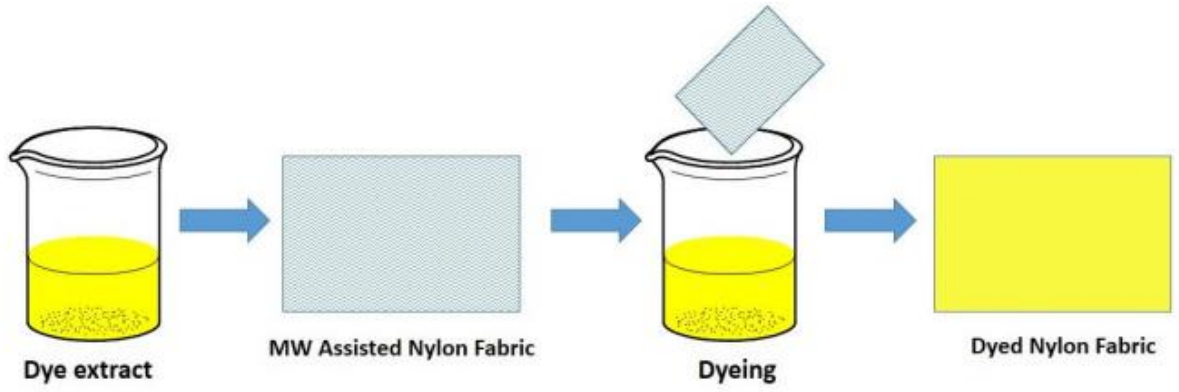

Figure2. A schematic representation of the nylon fabric dyeing process. (Rehman et al. 2022)

Adeel et al. (2023) found that microwave treatment caused physical changes on the fabric surface, which enhanced the penetration of dye molecules, resulting in darker and more vibrant shades. Additionally, fabrics dyed with microwaves showed better results in washing, light, and rubbing fastness tests.

Ultraviolet (UV) Technology and Its Applications in Textiles

Ultraviolet (UV) technology is a sustainable method used in many textile applications, including surface modification, color fastness improvement, and curing of functional coatings. UV treatment improves the coloring process of textiles due to surface modification of the textile substrate. UV technology can be used for bleaching and surface modification processes before coloring processes such as dyeing and printing. This technology works only on the surface without changing the volume properties of the fabrics. It is used to improve dye absorption, increase color fastness, and reduce the pilling problem (Lara et al. 2022).

In conventional bleaching, chemicals like hydrogen peroxide (H_2O_2) are widely used. When combined with UV, the same or better whiteness levels can be achieved with less chemical usage. This UV-assisted bleaching process reduces environmental impact and lowers energy and water consumption (Wang et al, 2020). Similarly, pretreating fibers like polyester and cotton with UV rays improves dye bonding, color depth, and wash fastness.

UV curing technology has emerged as a sustainable method in textile finishing to impart functional properties such as conductivity, antibacterial activity, flame retardancy, and smart responsiveness. For instance, graphene oxide has been reduced to graphene under UV light to render cotton and wool fabrics conductive. UV irradiation has also been applied to modify cotton fiber surfaces, resulting in light-activated antibacterial properties. Furthermore, low-toxicity flame retardants have been successfully grafted onto polyester/cotton fabrics using UV curing, enhancing fire resistance. Additionally, UV-curable photochromic inks have enabled the development of UV-sensing smart textiles capable of reversible color

change under sunlight. These examples highlight the versatile and eco-friendly potential of UV technology in modern textile treatment processes (Catarino et al. 2025)

However, industrial-scale use of UV technology is still limited. There are challenges such as operational costs, safety for workers, and its effectiveness being limited to fabric surfaces. Still, pilot applications and UV-curing solutions developed by companies like Rudolf GmbH and Trelleborg show promising potential for wider use (Rudolf GmbH & Trelleborg, 2023).

Wang et al. (2020) developed a UV/H_2O_2 system as an alternative to conventional bleaching for cotton fabrics. This system produced perhydroxyl radicals (HOO^-) under UV light, enabling effective bleaching and reducing chemical use and environmental impact. The treated fabrics reached similar whiteness levels by using lower NaOH concentrations.

Čuk et al. (2021) found that UV treatment on cotton fabric surfaces increased dye uptake. Both the fabric and the reactive dye were exposed to UV light, activating reactive groups and forming reactive carbon on the fiber surface. As a result, high color depth and wash fastness were achieved with low chemical and energy consumption. This method was proposed as a sustainable alternative to conventional pretreatments.

Conclusion

Radiation technologies used in textile finishing make significant contributions to the industry in line with sustainability goals. Methods such as plasma, UV, and microwave help to create eco-friendly production processes by reducing energy and water consumption. At the same time, they shorten processing times and improve the physical and chemical properties of textile materials.

Plasma technology offers an effective solution for surface modification and functionalization, while microwave energy ensures energy efficiency with uniform heat distribution. UV radiation is used in many areas such as adding antimicrobial properties, surface modification, improving color fastness, and surface disinfection.

However, some disadvantages limit the widespread use of these technologies, such as high initial investment costs, limited material compatibility, and potential health risks. In the future, overcoming these obstacles will require proper infrastructure investments and innovative studies to make these technologies more widely available.

In conclusion, the broader application of radiation technologies in textile finishing will play a critical role in achieving environmental and economic sustainability goals. New research in this field will increase the effectiveness of these technologies and lead to the transformation of the textile industry.

References

Adeel, S., Akram, H., Usman, M., Bokhari, T. H., Aftab, M., & Ozomay, M. (2023). Eco-friendly microwave assisted sustainable coloration of silk and wool fabric with Acid Blue 07 dye. Environmental Science and Pollution Research, 30, 74939–74951. https://doi.org/10.1007/s11356-023-27471-7

Catarino, M. L., Sampaio, F., & Gonçalves, A. L. (2025). Sustainable wet processing technologies for the textile industry: A comprehensive review. Sustainability, 17(7), 3041. https://doi.org/10.3390/su17073041

Čuk, N., Šala, M., & Gorjanc, M. (2021). Development of antibacterial and UV protective cotton fabrics using plant food waste and alien invasive plant extracts as reducing agents for the in-situ synthesis of silver nanoparticles. Cellulose, 28(5), 3215–3233. https://doi.org/10.1007/s10570-021-03715-y:contentReference[oaicite:0]{index=0}

Diaz-Garcia, P., et al. (2024). Understanding and addressing the water footprint in the textile sector: A review. Sustainability Transformation, 1(1), Article e0000072. https://doi.org/10.1371/journal.pstr.0000072

Donkor, S. O., Sun, D., Bucknall, D., & Buckman, J. (2024). Surface activation of cotton fabric with low-temperature air plasma treatment for metallic printing. Fibers and Polymers, 25, 4321–4332. https://doi.org/10.1007/s12221-024-00738-7

European Parliament. (2023). The impact of textile production and waste on the environment. https://www.europarl.europa.eu/topics/en/article/20201208STO93327/the-impact-of-textile-production-and-waste-on-the-environment-infographics

Ghasemian, R., Barani, H. & Khazaei, F. Surface modification and performance of wool fibers after combined plasma and enzyme treatments. Sci Rep 15, 9079 (2025). https://doi.org/10.1038/s41598-025-93665-3

H Catarino, M. L., Sampaio, F., & Gonçalves, A. L. (2024). Sustainable wet processing technologies for the textile industry: A comprehensive review. Sustainability, 17(7), 3041. https://doi.org/10.3390/su17073041

Haji, A., & Kan, C.-W. (2021). Plasma treatment for sustainable functionalization of textiles. In M. A. Khan & A. Shahid (Eds.), Green chemistry for sustainable textiles (pp. 265–277). Elsevier. https://doi.org/10.1016/B978-0-323-85204-3.00034-8

Haji, A., & Naebe, M. (2020). Cleaner dyeing of textiles using plasma treatment and natural dyes: A review. Journal of Cleaner Production, 265, 121866. https://doi.org/10.1016/j.jclepro.2020.121866

Hamida, S. B., Štěpánová, V., Zahedi, L., Kováčová, M., Nasadil, P., Valášková, K., Humpolíček., P., & Kováčik, D. (2024). Enhancement of the dyeability and antibacterial properties of cotton fabric by plasma assisted cationization using chitosan and quaternized poly[bis (2-chloroethyl) ether-alt-1, 3-bis [3-(dimethylamino) propyl] urea. Cellulose, 31, 7119–7136. https://doi.org/10.1007/s10570-024-06027-z

Lara, L., Cabral, I., & Cunha, J. (2022). Ecological approaches to textile dyeing: A review. Sustainability, 14(14), 8353. https://doi.org/10.3390/su14148353

Primc, G., & Mozetič, M. (2024). Surface modification of polymers by plasma treatment for appropriate adhesion of coatings. Materials, 17(7), 1494. https://doi.org/10.3390/ma17071494

Rehman, F. U., Adeel, S., Haddar, W., Bibi, R., Azeem, M., Mia, R., & Ahmed, B. (2022). Microwave-assisted exploration of yellow natural dyes for nylon fabric. Sustainability, 14(9), 5599. https://doi.org/10.3390/su14095599

Rudolf GmbH & Trelleborg Engineered Coated Fabrics. (2023). UV-curable textile coatings and scalability studies. Companywhitepaper/internalpilotreports.

Serrano-Martínez, V. M., Ruzafa-Silvestre, C., Hernández-Fernández, C., Bañón-Gil, E., Arán-Ais, F., & Orgilés-Calpena, E. (2024). Improving cotton fabric dyeability by oxygen plasma surface activation. Surfaces, 7(4), 1079–1095. https://doi.org/10.3390/surfaces7040071

Teker, M., Usluoğlu, A., & Alşan, H. G. (2023). Microwave-assisted textile processes: A review. International Journal of Science, Technology and Design, 4(2), 56-65.

Wang, N., Tang, P., Zhao, C., Zhang, Z., & Sun, G. (2020). An environmentally friendly bleaching process for cotton fabrics: Mechanism and application of UV/H_2O_2 system. Cellulose, 27(2), 1071–1083. https://doi.org/10.1007/s10570-019-02812-3

Zhang, Y., Rather, L. J., & Li, Q. (2022). Recent advances in the surface modification strategies to improve functional finishing of cotton with natural colourants-A review. Journal of Cleaner Production, 335, 130313. https://doi.org/10.1016/j.jclepro.2021.130313

➢ *ORAL PRESENTATION*

MOSH/MOAH Kontaminasyonu: Kaynakları, Analitik Tespiti ve Sağlık Üzerindeki Etkileri

Kıvılcım Yıldız[1*], Burcu Durmuş[2]

[*1]Manisa Celal Bayar Üniversitesi, Mühendislik ve Doğa Bilimleri Fakültesi, Gıda Mühendisliği, Manisa, Türkiye.
[2] Manisa Celal Bayar Üniversitesi, Mühendislik ve Doğa Bilimleri Fakültesi, Gıda Mühendisliği, Manisa, Türkiye.

*Sorumlu yazar e-posta: kivilcim.celik@cbu.edu.tr

Özet

Katı ve sıvı yağlar, insan beslenmesinin temel bileşenleri arasında yer almakta olup, günümüzde dünya genelinde üretilen yağların yaklaşık %80'ini sıvı yağlar oluşturmaktadır. Ancak bu yağların kalitesi ve stabilitesi, içerdiği bileşikler nedeniyle olumsuz etkilenebilmektedir. Aynı zamanda bu yağlar üretim süreçlerinde çeşitli kontaminantlara maruz kalabilmektedir. Bu kontaminantlardan mineral yağlar, gıda güvenliği açısından önemli risk faktörü olup sağlık üzerinde olumsuz etkiler oluşturabilmektedir. Mineral yağlar birçok gıda ürününde ve özellikle işlenmiş yağlarda bulunmakla birlikte üretim sürecinin herhangi bir aşamasında ve tedarik zinciri boyunca bulaşma riski taşımaktadır. Başlıca kontaminasyon kaynakları; yakıt kalıntıları, egzoz gazları, toz önleyici ve yüzey temizleme ürünleri, ambalaj malzemeleri, proses kaynaklı bulaşılar olarak sıralanmaktadır. Yapılan çalışmalarda mineral yağların en fazla yemeklik yağlarda olduğu tespit edilmiştir. Mineral yağ bileşenleri, MOSH (Mineral Yağ Doymuş Hidrokarbonlar) ve MOAH (Mineral Yağ Aromatik Hidrokarbonlar) olmak üzere iki ana gruba ayrılmaktadır. Mineral yağ olan MOSH/MOAH, fosil kökenli karmaşık hidrokarbonların karışımından oluşmaktadır. Bulaşı kaynakları; paketleme kaynaklı, proses kaynaklı, plantasyon kaynaklı, çevresel etmenler kaynaklı ve sevkiyat kaynaklı olarak gruplandırılmaktadır. MOSH bileşikleri insan vücudunda birikerek özellikle karaciğer fonksiyonları üzerinde olumsuz etkilere yol açarken, MOAH bileşiklerinin genotoksik özellikler gösterebildiği ve hücrelerde DNA hasarına neden olarak kanserojen potansiyel taşıdığı belirlenmiştir. Bu nedenle, MOSH/MOAH bileşiklerinin gıdalardaki varlığı ve seviyelerinin yakından takip edilmesi gerekmektedir. MOSH/MOAH tespiti için en yaygın kullanılan yöntemler arasında gaz kromatografisi ile birleştirilmiş sıvı kromatografisi (LC-GC) ve kapsamlı çok boyutlu gaz kromatografisi (GC-GC) teknikleri yer almaktadır. Ancak bu bileşiklerin doğada yaygın bulunması ve çapraz kontaminasyona açık olması nedeniyle analizin doğruluğu zorlaşmaktadır. Mineral yağların insan sağlığı üzerindeki potansiyel riskleri göz önüne alındığında, MOSH/MOAH bulaşının azaltılması için kontaminasyon kaynaklarının belirlenmesi ve önleyici tedbirlerin geliştirilmesi büyük önem taşımaktadır. Bu doğrultuda, gıda endüstrisinde üretim süreçlerinin gözden geçirilmesi, ambalaj malzemelerinin güvenliğinin sağlanması ve ileri analiz tekniklerinin kullanılması gerekmektedir. Bu çalışmada, mineral yağların sağlık üzerine etkileri, kontaminasyon kaynakları, tespit yöntemleri ve MOSH/MOAH seviyelerinin azaltılmasına yönelik stratejiler ele alınacaktır.

Anahtar Kelimeler: MOSH, MOAH, mineral yağlar, kontaminant

MOSH/MOAH Contamination: Sources, Analytical Detection, and Health Effects

Abstract

Fats and oils are fundamental components of human nutrition, with liquid oils currently accounting for approximately 80% of the total fat production worldwide. However, the quality and stability of these oils can be adversely affected by their chemical composition. Additionally, these oils may be exposed to various contaminants during production processes. Among these contaminants, mineral oils pose significant risk factors in terms of food safety and can have negative impacts on human health. While mineral oils are found in many food products, especially processed oils, there is a risk of contamination at any stage of the production process and throughout the supply chain. The main sources of contamination include fuel residues, exhaust gases, anti-dust and surface cleaning agents, packaging materials, and process-related

contaminations. Studies have identified that mineral oils are most commonly found in edible oils. Mineral oil components are classified into two main groups: MOSH (Mineral Oil Saturated Hydrocarbons) and MOAH (Mineral Oil Aromatic Hydrocarbons). These compounds are mixtures of complex fossil-derived hydrocarbons. Sources of contamination are categorized as packaging-related, process-related, plantation-related, environmental, and transport-related. MOSH compounds can accumulate in the human body, particularly affecting liver functions, while MOAH compounds have been shown to exhibit genotoxic properties and may cause DNA damage in cells, indicating their potential carcinogenicity. Therefore, the presence and levels of MOSH/MOAH compounds in foods must be closely monitored. The most commonly used methods for the detection of MOSH/MOAH include liquid chromatography coupled with gas chromatography (LC-GC) and comprehensive two-dimensional gas chromatography (GC-GC) techniques. However, due to the widespread occurrence of these compounds in the environment and the possibility of cross-contamination, achieving analytical accuracy is challenging. Considering the potential health risks of mineral oils, it is crucial to identify the sources of MOSH/MOAH contamination and develop preventive measures. In this context, it is necessary to review production processes in the food industry, ensure the safety of packaging materials, and utilize advanced analytical techniques. This study will address the health impacts of mineral oils, sources of contamination, detection methods, and strategies for reducing MOSH/MOAH levels.

Keywords: MOSH, MOAH, mineral oils, contaminant

GİRİŞ

Tüketiciler, gıda zincirinde bulunan çeşitli mineral yağ hidrokarbonlarına (MOH) maruz kalabilmektedir (Bratinova ve ark., 2023). Mineral yağ hidrokarbonları (MOH), çevresel ve proses kaynaklı kontaminantlardır. Genellikle petrol türevli olup 10 ile 50 arasında karbon atomu içeren lipofilik (yağda çözünebilen) bileşiklerin kompleks bir karışımını temsil etmektedir (Bratinova ve ark., 2023; Xue ve ark., 2024). Gıdalardaki mineral yağ hidrokarbonlarının (MOH) başlıca kaynakları; gıda ile temas eden malzemelerden (FCM) migrasyon, gıda sınıfına uygun olmayan yağlayıcıların neden olduğu istem dışı kontaminasyon, çevresel kaynaklar veya katkı maddesi ve proses yardımcı maddesi olarak rafine mineral yağların kullanımıdır (Bratinova ve ark., 2023). Bu kontaminantlar, kimyasal yapılarına göre mineral yağ doymuş hidrokarbonlar (MOSH) ve mineral yağ aromatik hidrokarbonlar (MOAH) olmak üzere iki ana kategoriye ayrılmıştır. Her iki kategori, kendi içerisinde çeşitli alt sınıflara ayrılabilmektedir (Albendea ve Purcaro, 2025). MOSH ve MOAH'ın toksikolojik etkileri ve analitik zorlukları farklıdır (Bauwens ve Purcaro, 2024). MOAH fraksiyonunda sınıflandırma, bileşiklerin içerdiği aromatik halka sayısına göre yapılmakta olup, özellikle 3 ila 7 aromatik halka içeren bileşiklerin kanserojen, genotoksik ve mutajenik etkilerle ilişkili olduğu belirtilmiştir (Albendea ve Purcaro, 2025). Bu durum göz önüne alınarak Avrupa Gıda Güvenliği Otoritesi (EFSA), gıdaların MOAH içermemesi gerektiğini önermiştir ve Avrupa Komisyonu, gıdalarda ve gıda ile temas eden malzemelerde mineral yağ hidrokarbonlarının (MOH) varlığının izlenmesi gerekliliğini belirten (AB) 2017/84 sayılı tavsiye kararı yayımlamıştır (EFSA, 2012; Commission, 2017; Jaen ve ark., 2022a). MOSH bileşikleri açısından ise parafinler (doğrusal ve dallanmış alkanlar) ile naftenler arasında bir sınıflandırma yapılmaktadır. Mevcut toksikolojik veriler, MOSH bileşiklerinin hem hayvan hem de insan organ ve dokularında birikebildiğini ortaya koymakta olup bu birikimin ise karbon zincir uzunluğuna (genellikle C16–C35) ve hidrokarbonların yapısal özelliklerine bağlı olarak değişkenlik gösterdiğini belirtmektedir (Albendea ve Purcaro, 2025).

Geçmişte belirli ürünler için geçici limitler getirilmiştir; örneğin, 2008–2014 yılları arasında, mineral yağla kontamine olmuş Ukrayna ayçiçek yağı tedariki sonrasında Avrupa Komisyonu tarafından bu ürün için 50 mg/kg'lık geçici bir limit uygulanmıştır (Purcaro ve ark., 2016). 2022 yılında Avrupa Birliği Üye Devletleri ile Avrupa Komisyonu, yağlar ve katı yağlardaki toplam MOAH için 2 mg/kg'lık bir limit belirleme konusunda anlaşmaya varmışlardır (EC, 2022). Bu limit, Avrupa Komisyonu Ortak Araştırma Merkezi'nin (JRC) güncellenmiş kılavuzunda belirtilen en yüksek kabul edilebilir kantifikasyon sınırına karşılık gelmektedir (Bratinova ve ark., 2023). 2023 yılı sonunda Avrupa Komisyonu Sağlık ve Gıda Güvenliği Genel Müdürlüğü, bu sınır değerinin zeytinyağları da dâhil olmak üzere çoğu bitkisel yağ için geçerli olmasını öngören ve (AB) 2023/915 sayılı Yönetmelik'te değişiklik yapılmasına ilişkin bir taslak düzenlemeyi paydaşlara sunmuştur. Bu düzenlemenin 1 Ocak 2026 tarihinde yürürlüğe girmesi beklenmektedir. Bununla birlikte, zeytin küspe yağı için başlangıçta daha yüksek bir limit olan 10 mg/kg kabul edilmiştir; bu değerin 2030 yılına kadar kademeli olarak 2 mg/kg'a düşürülmesi planlanmaktadır (Craig, 2024).

Diğer yandan, mineral yağ doymuş hidrokarbon (MOSH) içeriğine ilişkin olarak, bitkisel yağlar ve katı yağlar için 15 mg/kg düzeyinde bir gösterge değer belirlenmesine yönelik bir öneri gündemdedir. Bu değerin aşılması halinde, gıda işletmecilerinin kontaminasyon kaynağını belirlemeye yönelik araştırmalar yürütmeleri ve gerekli risk azaltıcı önlemleri uygulamaları beklenmektedir (Ursol ve ark., 2025).

MOSH&MOAH'ın Gıdalarda Bulunma Kaynakları

Gıda tedarik zinciri, birbirine bağlı birçok adımdan oluşmakta olup hem doğal olarak bulunan hem de kontaminant niteliğindeki hidrokarbonlar bu zincirin herhangi bir aşamasında gıdaya bulaşabilmektedir. Mineral hidrokarbonların gıda hammaddelerinde ve işlenmiş ürünlerde tespit edilmesi; çevresel hava ve su kaynakları, tarımsal faaliyetler, işleme aşamaları ile gıda ile temas eden materyallerden kaynaklanan kontaminasyonlardan ileri gelebilmektedir (Bevan ve ark., 2020).

Gıda ürünlerinin korunması, taşınması ve depolanması amacıyla birincil, ikincil ve üçüncül ambalaj malzemesi olarak yaygın biçimde kullanılan kağıt ve karton, çeşitli kaynaklardan kaynaklanan mineral yağ hidrokarbonları (MOH) ile kontaminasyona açık hale gelebilmekte ve bu bileşikler ambalajdan gıdaya geçebilmektedir. Gıdalar, bu tür kimyasal bulaşanların yanı sıra dağıtım ve depolama sırasında mikrobiyal kontaminasyona karşıda hassastır. Bu durum, hem gıda güvenliğini tehdit etmekte hem de ekonomik kayıplara yol açmaktadır (Jaen ve ark., 2022b; Zhang ve ark., 2025).

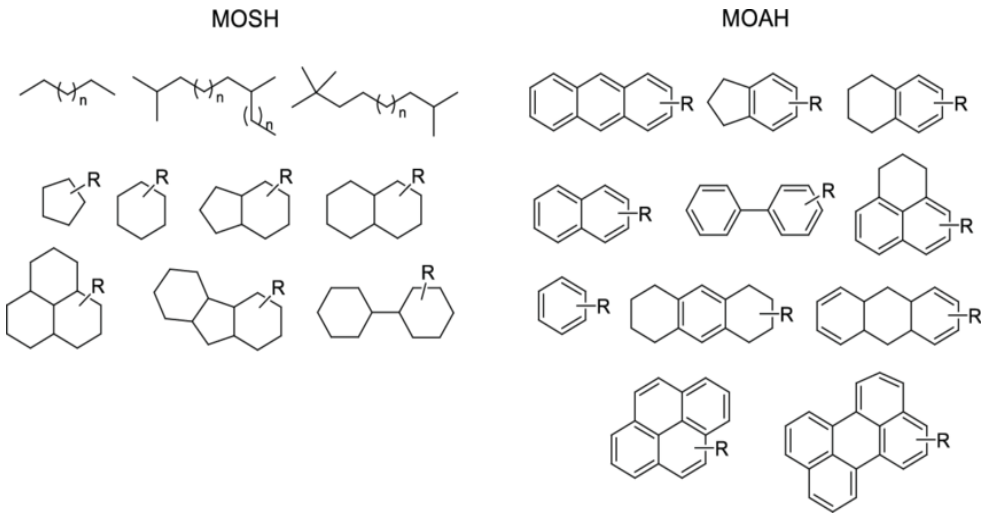

Şekil 1. Mineral yağ doymuş hidrokarbonlarda (MOSH) ve mineral yağ aromatik hidrokarbonlarda (MOAH) bulunan temsili bileşiklerin kimyasal yapıları (Weber ve ark., 2018).

MOSH bileşikleri; lineer, dallanmış ve siklik yapıda doymuş hidrokarbonlardan oluşurken, MOAH fraksiyonu ise farklı sayıda yoğunlaştırılmış benzen halkası içeren ve büyük oranda (%98'in üzerinde) alkillenmiş aromatik hidrokarbonları kapsamaktadır. Bu yapısal farklılıklar Şekil 1'de detaylı olarak gösterilmektedir (Ursol ve ark., 2025; EFSA, 2012).

MOSH&MOAH'ın kimyasal yapılarından kaynaklanan apolar özellikleri, bu bileşiklerin yağlı matrislerle yüksek düzeyde etkileşim göstermesine neden olmakta ve bu durum, özellikle bitkisel yağlarda yaygın olarak bulunmalarını beraberinde getirmektedir. Yapılan analizlerde, MOSH'ın çevresel kontaminasyona bağlı seviyeleri, elle toplanmış hammaddeden laboratuvar ortamında doğrudan ekstrakte edilen örnekler de dahil olmak üzere neredeyse tüm bitkisel yağlarda tespit edilmiştir. Ancak mevcut miktarların düşük olması ve oksidasyona uğrama olasılığı nedeniyle çevresel kirlenmeye maruz kalmış örneklerde MOAH varlığına dair güçlü bir kanıt bulunmamaktadır (Menegoz Ursol ve ark., 2022).

Gıdalarda mineral yağ hidrokarbonları (MOH) kontaminasyonu çeşitli kaynaklardan kaynaklanabilmekte olup, özellikle geri dönüştürülmüş karton materyallerin ambalaj malzemesi olarak kullanımı önemli bir risk faktörü olarak değerlendirilmektedir. Gazete kâğıdı gibi geri dönüştürülmüş kağıtlara mineral yağ bazlı mürekkeplerle baskı yapılması, MOH kontaminasyonunun başlıca nedenlerinden biri olarak öne çıkmaktadır (Nestola ve Schmidt, 2017). Bu kontaminasyon, özellikle oda sıcaklığında buharlaşabilen

<C25 zincir uzunluğuna sahip hidrokarbonların gıdaya göç etmesiyle meydana gelmektedir. Her ne kadar mineral yağ içermeyen mürekkeplerle basılmış saf (virgin) kartonların kullanımıyla bu sorun büyük ölçüde giderilmiş olsa da, ambalaj üretiminde kullanılan tutkallar hâlâ potansiyel bir MOH kaynağı olmaya devam etmektedir. Ayrıca tarımsal üretim sürecinde kullanılan hasat makinelerine ait yağlayıcılar ve dizel yağları da mineral yağ hidrokarbonları (MOH) açısından önemli bir kontaminasyon kaynağı oluşturmaktadır. Bu duruma örnek olarak, ayçiçeği tohumlarında yağlayıcılardan kaynaklı yaklaşık 5 mg/kg ve dizel yağlarından kaynaklı yaklaşık 3 mg/kg düzeylerinde MOH tespit edilmiştir (Bevan ve ark., 2020).

Gıda ile temas eden malzemelerde sıcak eriyen yapıştırıcılar en çok kağıt, karton, belirli plastik filmler, metal ve cam gibi substratlarda kullanılır. Yapıştırıcılar çoğunlukla doğrudan gıdayla temas etmese de, yapılan bilimsel araştırmalar, üretimde kullanılan katkı maddeleri ile bileşenlerin bozunması ya da safsızlıklardan kaynaklanan istem dışı eklenen maddeler nedeniyle yapıştırıcılardan gıdaya çeşitli bileşiklerin geçiş yaptığını ortaya koymuştur. MOAH ise geri dönüştürülmüş kağıt ve karton ile bu yüzeylere uygulanan baskı mürekkeplerinden gıdaya geçebilmektedir. Çünkü mineral yağ hidrokarbonları (MOH), plastik ürünler, mumlar, yağlayıcılar ve yapıştırıcıların üretiminde kullanılmaktadır (Jaen ve ark., 2022c).

Albendea ve Purcaro (2025) tarafından yürütülen çalışmada, farklı et örneklerinde tespit edilen MOH kontaminasyon düzeylerinin önemli derecede değişkenlik gösterdiği rapor edilmiştir. Bu durum, nihai kontaminasyon seviyesinin; hayvanın mineral yağ hidrokarbonlarına (MOH) maruziyet derecesi, MOH'un farklı türlerdeki sergilediği toksikokinetik özellikler ile etin ticarileştirilmeden önce maruz kaldığı potansiyel dış kontaminasyon kaynakları gibi çok sayıda faktöre bağlı olarak değişebileceğini ortaya koymaktadır.

Mineral yağ bileşikleri, kozmetik ürünlerde içerik olarak bulunabileceği gibi, gıdalarda katkı maddesi veya istenmeyen kirletici olarak da bulunabilmektedir. Paketleme malzemeleri gibi gıda ile temas eden malzemeler de dahil olmak üzere teknik ürünlerde geniş uygulama alanı olması nedeniyle bu bileşiklerin özellikle yağ içeriği yüksek olan çikolata ve benzeri yağ bazlı gıdalara geçişi daha kolay gerçekleşmektedir (Weber ve ark., 2018). Hot melt (sıcak eriyen) yapıştırıcılar, katlanabilir kutuların yapıştırılması gibi gıda ambalajlarında yaygın olarak kullanılmaktadır. Düşük moleküler ağırlıklı hidrokarbonların bir kısmı, hot melt yapıştırıcılar doğrudan gıda ile temas edecek şekilde uygulanmadığından gaz fazı yoluyla gıdaya göç edebilmektedir. Yapılan bir çalışmada geri dönüştürülmüş ve saf lifli karton malzemeden üretilen katlanabilir kutulardan makarnaya hot melt yapıştırıcılardan doymuş hidrokarbonların göç ettiği bildirilmiştir (Lommatzsch ve ark., 2016). Mineral yağların diğer uygulama alanları arasında baskı mürekkepleri, kozmetik ürünler, ayırıcı maddeler (örneğin fırıncılık ve şekerleme endüstrileri için), gıda ambalaj malzemeleri (örneğin mumlu kağıt ve mumlu karton) ile teknik ürünler (örneğin yağlama yağları) gibi çeşitli kullanım alanları yer almaktadır (Weber ve ark., 2018). EFSA raporlarına göre, makinelerde kullanılan mineral yağlar nedeniyle çikolata ve fırıncılık ürünlerinde mineral yağ hidrokarbonlarına (MOH) rastlanmıştır (EFSA, 2012). Özellikle fırın ve çikolata sektörlerinde, ürünlerin kalıptan kolay ayrılmasını sağlamak ve yüzeylerin yağlanmasını kolaylaştırmak amacıyla parafin bazlı yağlar yaygın olarak kullanılmaktadır. Bu uygulamalar sonucunda ürünlerde 500–3000 mg/kg arasında MOH seviyeleri tespit edilmiş; bazı bisküvi örneklerinde ise 11 000 mg/kg'a kadar ulaşan yüksek düzeyler rapor edilmiştir (Bevan ve ark., 2020).

MOSH&MOAH'ın Analitik Tespiti

Mineral yağlar üzerine yapılan çok sayıda çalışmaya rağmen, bu maddelerin kimyasal analizleri hâlâ önemli bir analitik zorluk oluşturmaktadır. Bu zorluğun başlıca nedeni, mineral yağların kimyasal yapılarının son derece karmaşık olması ve bileşenlerin kromatografik olarak etkin bir şekilde ayrılmasının güçlüğüdür. Özellikle MOSH ve MOAH fraksiyonları, çözünmemiş çok sayıda bileşeni içeren geniş ve belirsiz tepe (hump) yapıları sergilemekte, bu da farklı yapıdaki bileşenlerin tespit edilmesini zorlaştırmaktadır (Biedermann & Grob, 2015; Gharbi ve ark., 2017). Bu durum, analiz edilen bileşenlerin doğru bir şekilde ayırt edilememesine ve dolayısıyla hatalı kantitatif sonuçlara yol açabilmektedir. Yapılan bir çalışmada, mineral yağ hidrokarbon (MOH) kontaminasyonunun düşük seviyelerde olduğu durumlarda mevcut analitik yöntemlerin kontaminasyonun varlığına ilişkin güvenilir sonuçlar sağlayamadığı belirtilmiştir. Bu nedenle, analizlerin doğruluğunu artırmak amacıyla iki boyutlu gaz kromatografisi (GC×GC), kütle spektrometresi (MS) ve kimyasal belirteçlerin kullanımı gibi tamamlayıcı tekniklerin uygulanması önerilmektedir. MOH kontaminasyonunun kaynağını belirlemede kimyasal belirteçlerin kullanımı oldukça

önemlidir. Örneğin, geri dönüştürülmüş kâğıt veya karton kaynaklı kontaminasyonu tespit etmek amacıyla diizopropilnaftalin yaygın bir gösterge bileşik olarak kullanılmaktadır. Kontaminasyonun karmaşık yapıda olduğu durumlarda, MOSH ve MOAH bileşiklerinin karakterizasyonu için kütle spektrometresi ve gösterge bileşiklerin kullanımı önerilmektedir. Ayrıca, kütle spektrometresinin tanımlayabildiği belirteç madde sayısının artmasıyla birlikte bu tekniğin ayırt edici gücünün de artacağı sonucuna varılmıştır (Jaen ve ark., 2022a).

Avrupa Komisyonu Ortak Araştırma Merkezi'nin (JRC) MOH'ların gıdalar ve gıda ile temas eden malzemelerdeki örnekleme ve analizine ilişkin rehberine göre alev iyonizasyon detektörü (FID) ile eşleştirilmiş çevrim içi yüksek performanslı sıvı kromatografi (LC)-gaz kromatografi (GC) yöntemi, MOH analizinde referans yöntem olarak kabul edilmektedir (Bratinova ve Hoekstra, 2019; Menegoz Ursol ve ark., 2022).

Kimyasal açıdan bakıldığında, MOAH çoğunlukla dallanmış aromatik halkalar içeren bileşiklerden oluşur ve genellikle doymuş hidrokarbonlar (MOSH) ile birlikte bulunurlar. Bu nedenle, MOAH'ın analiz edilebilmesi için MOSH'tan ayrılması gerekmektedir. MOAH analizinde tavsiye edilen yöntem, alev iyonizasyon detektörlü çevrimiçi sıvı kromatografi-gaz kromatografi (HPLC-GC-FID) tekniğidir (Jaen ve ark., 2022a). Gıdalar, gıda ile temas eden materyaller, dokular ve kozmetik ürünler gibi matrislerde mineral yağ doymuş hidrokarbonları (MOSH) ve aromatik hidrokarbonların (MOAH) analizi, çoğunlukla normal faz yüksek performanslı sıvı kromatografisinin (HPLC) gaz kromatografisi (GC) ve alev iyonizasyon dedektörü (FID) ile çevrimiçi bağlantılı kullanıldığı HPLC-GC-FID yöntemiyle gerçekleştirilmektedir (Biedermann ve ark., 2017).

Yapılan bir çalışmada, LC-GC × GC-FID/MS tekniğinin kullanımı, mineral yağ hidrokarbonlarının (MOH) rutin tayininde yaygın olarak kullanılan LC-GC-FID tekniğiyle karşılaştırılmıştır. Çalışma sonucunda, her iki yöntemin benzer sonuçlar sağladığı belirlenmiştir. Bununla birlikte, LC-GC × GC-FID/MS tekniği, özellikle işlenmemiş et numunelerinde tespit edilen MOSH ve MOAH kontaminasyon profiline ilişkin daha ayrıntılı ve kapsamlı bilgiler sunma açısından avantaj sağlamıştır (Albendea ve Purcaro, 2025). LC-GC-FID yöntemi, mineral yağ hidrokarbonlarının kantitatif analizinde güçlü ve güvenilir bir teknik olup, günümüzde rutin analizlerde yaygın olarak tercih edilmektedir. Ancak, bazı durumlarda hidrokarbonların türlerine ilişkin daha ayrıntılı bilgiye ihtiyaç duyulabilmektedir. Bu gibi durumlarda, kapsamlı iki boyutlu gaz kromatografisi (GC×GC) yöntemi, daha gelişmiş ayırım gücü sayesinde tercih edilen bir teknik olarak öne çıkmaktadır (Weber ve ark., 2018).

Günümüzde geliştirilen ileri düzey kromatografik yaklaşımlarda, LC-GC-FID ile elde edilen pozitif sonuçlar, doğrulama amacıyla GC×GC-MS analizleriyle desteklenmektedir. Weber ve ark. (2018), MOSH fraksiyonlarının bir kısmının MOAH olarak yanlış sınıflandırılması durumunda anlamlı düzeyde aşırı kantifikasyonun meydana gelebileceğini belirtmişlerdir. Bu nedenle, analitik özgüllüğün artırılması amacıyla, şüpheli numunelerin karakterizasyonunun LC-GC-FID, LC-MS, GC-MS veya GC×GC-MS gibi gelişmiş kromatografik tekniklerden biri kullanılarak gerçekleştirilmesi gerektiği sonucuna varılmıştır (Weber ve ark., 2018). Hot-melt yapıştırıcılardan kaynaklanan, düşük moleküler ağırlığa sahip hidrokarbonlar (en az C50 karbon numarasına kadar), MOSH ve MOAH analizlerinde yaygın olarak kullanılan çevrimiçi HPLC-GC-FID yöntemi ile analiz edilebilmektedir (Lommatzsch ve ark., 2016).

MOSH&MOAH'ın Sağlık Üzerindeki Etkileri

Mineral yağlar, günümüzde birçok gıda ürününde ve işlenmiş yağda tespit edilmekte olup, üretim sürecinin herhangi bir aşamasında ve tedarik zinciri süresince kalabilmektedirler (Grob, 2018). Bu kontaminasyonun potansiyel kaynakları arasında yakıtlar, egzoz gazları, toz önleyici ve yüzey temizleyici ürünler, yağlar ve ambalaj malzemeleri yer almaktadır (Polyakova ve ark., 2022). İnsanlarda MOH emilimini değerlendiren kontrollü çalışmalar sınırlı olsa da, MOSH'un karaciğer, dalak, yağ dokusu, mezenterik lenf nodları, akciğer ve anne sütü gibi farklı insan dokularında tespit edilmesi; bu bileşiklerin emildiğini, vücutta dağıldığını ve bazı dokularda biriktiğini ortaya koymaktadır (Bevan ve ark., 2020).

Yapılan çalışmalarda fare denekleri üzerine mineral yağ uygulandığında deri tümörlerine rastlandığı gözlenmiştir (Carrillo ve ark., 2022). Yapılan bir başka çalışmada, farklı MOSH fraksiyonları içeren diyetlerle beslenen farelerde karaciğer granülomlarının oluştuğu tespit edilmiştir. Ancak araştırmacılar, granülom oluşumunun artan MOSH maruziyetinden ziyade, MOSH bileşiklerinin karbon zinciri

uzunluğuna bağlı olarak arttığını belirtmişlerdir. Özellikle karbon sayısı >C25 olan MOSH'lara maruz kalımın, granülom oluşumunu daha fazla teşvik ettiği saptanmıştır (Nygaard ve ark., 2019).

İnsanlar üzerinde yapılan çalışmalar sınırlı olmakla birlikte, mevcut karaciğer biyopsi/otopsi örneklerinde MOH içeriğinin analizi yapıldığında kaynağın tıbbi kullanım veya ambalajdan kaynaklandığı şeklinde yorumlanmıştır. Ayrıca, insan dokularında biriken MOSH bileşiminin dokular arasında C uzunluklarına göre farklılık gösterdikleri gözlemlenmiştir. Örneğin, C25–C30 aralığındaki MOSH bileşikleri karaciğer ve dalakta birikirken, C16–C36 aralığındaki bileşiklerin ise karın dokusunda birikme eğiliminde olduğu bildirilmiştir. Bu aralıkların dışında kalan karbon zinciri uzunluğuna sahip MOSH bileşiklerinin doku birikimi ise net olarak belirlenememiştir (Bevan ve ark., 2019).

Hayvan deneylerine ilişkin mevcut verilerin büyük bir kısmı, çeşitli mineral yağ ve mumların yüksek diyet konsantrasyonlarında (%2'ye kadar) sıçanlara uygulanmasına dayanmaktadır ve bu çalışmaların odak noktası çoğunlukla karaciğer, dalak ve mezenterik lenf düğümlerinde (MLN) granülom oluşumunun değerlendirilmesidir (Barp ve ark., 2017).

Sezaryen sırasında alınan karın yağ dokusu örneklerinde, kadın gönüllülerde MOSH seviyeleri 15–360 mg/kg arasında değişmiş; ortalama 60.7 mg/kg, medyan ise 52.5 mg/kg olarak raporlanmıştır. Bu örneklerin %80'inin 30–200 mg/kg arasında olduğu bildirilmiştir (Bevan ve ark., 2020). Barp ve ark. (2014) tarafından yapılan bir diğer çalışmada ise, 25–91 yaş aralığında (ortalama 67) bulunan 37 bireyin çeşitli dokularında MOSH düzeyleri incelenmiş ve bireylerin %25'inde toplam MOSH birikiminin 5 gramı aştığı belirlenmiştir. Bu birikimin zamanla oluştuğu düşünülürken, örneklerde MOAH varlığına rastlanmamıştır. En yüksek MOSH düzeyleri mezenterik lenf nodlarında saptanmış; bunu sırasıyla karaciğer, yağ dokusu, dalak ve akciğer takip etmiştir. Böbrek, kalp ve beyin dokularında ise oldukça düşük düzeylerde bulunmuştur.

SONUÇ

Mineral yağlar, petrol kökenli maddeler olup doymuş ve aromatik hidrokarbonlardan oluşan karmaşık ve değişken bir bileşime sahiptir. Avrupa Gıda Güvenliği Otoritesi (EFSA), 2012 yılında yayımladığı "Gıdalarda Mineral Yağ Hidrokarbonları" konulu bilimsel görüşünde, bazı MOSH'ların (özellikle dallanmış ve siklo-alkanlar) insan dokularında birikim gösterebileceğine dikkat çekmiştir. Bununla birlikte, mevcut birikim verilerinin sınırlı olması nedeniyle, gıdayla maruziyete ilişkin güvenli alım düzeylerinin türetilemediği ifade edilmiştir (Isola ve ark., 2023). Karbon sayısı C20'nin altında olan alkanlar vücutta etkin bir şekilde emilmekte ve hızla metabolize edilerek birikmeleri engellenmektedir. Buna karşılık, C35'in üzerindeki alkanlar hücre zarlarını geçebilecek özellikte olmadıkları için biyoyararlanımları oldukça düşüktür ve bu nedenle dokularda anlamlı düzeyde birikim göstermemektedir. Karbon zincir uzunluğu C20–C35 aralığında olan alkanlar ise bazı dokularda birikme potansiyeline sahiptir. Güncel literatür verileri, aromatik hidrokarbonların insan dokularında tespit edilmediğini ortaya koymaktadır. Bu durum söz konusu bileşiklerin biyolojik olarak tutulma potansiyelinin bulunmamasına veya gıda ile temas eden materyaller üzerindeki düzenleyici kontrollerin etkili olması nedeniyle maruziyetin gerçekleşmemesine bağlanmaktadır (Barp ve ark., 2014). İnsan dokularında birikim gösteren MOSH fraksiyonları (özellikle C20–C35 aralığında yer alan yüksek derecede dallanmış alkanlar ve yoğunlaşmış sikloalkanlar) hayvan dokularında da bulunmakta ve karaciğer örneklerinde gerçekleştirilen GCxGC-FID kromatogramlarında "gri bulut" şeklinde görselleştirilebilmektedir (Isola ve ark., 2023).

MOSH bileşenlerinin karaciğer ve lenf düğümlerinde birikme eğiliminde olduğu bilinmekte olup, bu durum inflamasyon ve doku hasarına yol açabilmektedir. Öte yandan, MOAH fraksiyonu içerisinde yer alan polisiklik aromatik hidrokarbonlar (PAH'lar) potansiyel kanserojen özellikleriyle öne çıkmaktadır. Bu bileşikler metabolik aktivasyon sonucu DNA adükleri oluşturabilmekte, gen ekspresyonunu bozarak mutasyonlara neden olabilmekte ve dolayısıyla kanser riskini artırabilmektedir. Ayrıca, mineral yağların gıdalarda uzun süreli birikimi karaciğer fonksiyonlarını olumsuz etkileyerek bağışıklık sisteminin zayıflamasına neden olabilmekte ve kronik toksik etkiler ortaya çıkarabilmektedir (Deng ve ark., 2025).

Mineral yağ hidrokarbonları; çevresel yaygınlıkları, çapraz kontaminasyona açıklıkları ve doğal olarak bulunan birçok bileşenle birlikte ekstrakte edilmeleri nedeniyle analizi güç, yüksek belirsizlik içeren bileşiklerdir. Bu nedenle, bu kontaminantların güvenilir biçimde tespiti ve nicelendirilmesine yönelik analitik yöntemlerin geliştirilmesi, günümüzde hâlâ devam eden önemli bir araştırma konusudur. Sonuç olarak mineral yağ hidrokarbonları, doğrudan gıda bileşenlerinden ziyade, genellikle dış kaynaklı

kontaminasyon yoluyla gıdalara bulaşmakta ve bu durum gıda güvenliği açısından ciddi bir risk oluşturmaktadır. MOSH&MOAH kontaminasyonunun temel nedenleri arasında; gıda ile temas eden malzemelerden migrasyon, çevresel bulaşılar, proses ekipmanlarının yetersiz hijyeni veya aşınması sonucu yağlayıcı kullanılması ve ambalaj malzemelerinden kaynaklanan bulaşılar gibi endüstriyel ve çevresel faktörler yer almaktadır. Bu faktörlerden kaynaklı kontaminasyonlar gıdada istenmeyen MOH varlığına yol açmaktadır. Bu bağlamda, Avrupa Birliği'nin 2030 yılına kadar zeytin küspe yağı için MOAH sınırını kademeli olarak 2 mg/kg düzeyine indirme hedefi bu kontaminantların yönetiminde daha sıkı bir yaklaşımın benimsenmesini zorunlu kılmaktadır. Benzer şekilde, MOSH için önerilen 15 mg/kg'lık gösterge değer, üretici firmaların kontaminasyon kaynaklarını daha dikkatli izlemelerini ve düzeltici önlemler geliştirmelerini gerektirmektedir.

KAYNAKLAR

Albendea, P., Purcaro, G. (2025). Study on the content and profile of MOSH and MOAH in unprocessed meat by LC/GC × GC-FID/MS. *Food Chemistry*, 480, 143880. https://doi.org/10.1016/j.foodchem.2025.143880

Barp, L., Biedermann, M., Grob, K., Blas-Y-Estrada, F., C Nygaard, U., Alexander, J., Cravedi, J.P. (2017). Mineral oil saturated hydrocarbons (MOSH) in female Fischer 344 rats; accumulation of wax components; implications for risk assessment. Science of the Total Environment, 583, 319–333. https://doi.org/10.1016/j.scitotenv.2017.01.071

Barp, L., Kornauth, C., Wuerger, T., Rudas, M., Biedermann, M., Reiner, A., Concin, N., Grob, K. (2014). Mineral oil in human tissues, Part I: Concentrations and molecular mass distributions. Food and Chemical Toxicology, 72, 312–321. https://doi.org/10.1016/j.fct.2014.04.029

Bauwens, G., Purcaro, G. (2024). Improved microwave-assisted saponification to reduce the variability of MOAH determination in edible oils. Analytica Chimica Acta, 1312, 342788. https://doi.org/10.1016/j.aca.2024.342788

Bevan, R., Harrison, P.T.C., Jeffery, B., Mitchell, D. (2019). Evaluating the risk to humans from mineral oils in foods: Current state of the evidence. *Food and chemical toxicology*, 110966.

Bevan, R., Harrison, P.T.C., Jeffery, B., Mitchell, D. (2020). Evaluating the risk to humans from mineral oils in foods: Current state of the evidence. *Food and Chemical Toxicology,* 136. https://doi.org/10.1016/j.fct.2019.110966

Biedermann, M., & Grob, K. (2015). Comprehensive two-dimensional gas chromatography for characterizing mineral oils in foods and distinguishing them from synthetic hydrocarbons. Journal of Chromatography A, 1375, 146–153. https://doi.org/10.1016/j.chroma.2014.11.064

Biedermann, M., Munoz, C., Grob, K. (2017). Update of on-line coupled liquid chromatography – gas chromatography for the analysis of mineral oil hydrocarbons in foods and cosmetics. Journal of Chromatography A, 1521, 140–149. https://doi.org/10.1016/j.chroma.2017.09.028

Bratinova, S., Hoekstra, E. (2019). Guidance on sampling, analysis and data reporting for the monitoring of mineral oil hydrocarbons in food and food contact materials, EUR 29666 EN. Publications Office of the European Union, Luxembourg. https://op.europa.eu/s/z5VS

Bratinova, S., Roubouch, E., & Hoekstra, E. (2023). Guidance on sampling, analysis and data reporting for the monitoring of mineral oil hydrocarbons in food and food contact materials. In EUR 31473 EN (2nd ed.). Luxembourg: Publications Office of the European Union. https://doi.org/10.2760/963728

Carrillo, J.C., Kamelia, L., Romanuka, J., Kral, O., Isola, A., Niemela, H., Steneholm, A., (2022). Comparison of PAC and MOAH for understanding the carcinogenic and developmental toxicity potential of mineral oils. *Regulatory Toxicology and Pharmacology*, 132, 105193.

Commission, E. (2017). Commission Recommendation (EU) 2017/84 of 16 January 2017 on the monitoring of mineral oil hydrocarbons in food and in materials and articles intended to come into contact with food. Official Journal of the European Union, L12 (84), 95–96. https://doi.org/10.2903/j.efsa.2012.2704.L

Craig, S. (2024). Trying to run before you can walk: Control and enforcement of mineral oil aromatic hydrocarbon contamination of food in the European Union. European Food and Feed Law Review, 19(1), 11–18. https://www.khlaw.com/sites/default/files/2024-03/EU-Control-and-Enforcement-of-Mineral-Oil-Aromatic-Hydrocarbons.pdf

Deng, J., Jiang, H., Chen, Q. (2025). Qualitative and quantitative analysis of mineral oil pollution in peanut oil by Fourier transform near-infrared spectroscopy. Food Chemistry, 469, 142590. https://doi.org/10.1016/j.foodchem.2024.142590

Efsa. (2012). Scientific Opinion on Mineral Oil Hydrocarbons in Food. In EFSA Journal 10(6) https://doi.org/10.2903/j.efsa.2012.2704

European Commission. (2022). Summary Report. Standing committee on Plants, Animals, Food and Feed. Section Novel Food and Toxicological Safety of the Food Chain, 21 April 2022. https://food.ec.europa.eu/system/files/2022-07/reg-com_toxic_20220421_sum.pdf

Gharbi, I., Moret, S., Chaari, O., Issaoui, M., Conte, L. S., Lucci, P., & Hammami, M. (2017). Evaluation of hydrocarbon contaminants in olives and virgin olive oils from Tunisia. Food Control, 75, 160–166. https://doi.org/10.1016/j. foodcont.2016.12.003

Grob, K. (2018). Mineral oil hydrocarbons in food: a review. *Food Additives & Contaminants. Part a, chemistry, analysis, control, exposure, risk, assessment*.35(9),1845-1860. https://doi.org/10.1080/19440049.2018.1488185

Isola, A.L., Carrillo, J.C., Lemaire, P., Niemela, H., Steneholm, A. (2023). Lack of human-relevant adversity of MOSH retained in tissues: Analysis of adversity and implications for regulatory assessment. *Regulatory Toxicology and Pharmacology*, 137, 105284. https://doi.org/10.1016/j.yrtph.2022.105284

Jaen, J., Domeno, C., Nerín, C. (2022a). Development of an analytical method for the determination of mineral oil aromatic hydrocarbons (MOAH) from printing inks in food packaging. Food Chemistry, 397, 133745. https://doi.org/10.1016/j.foodchem.2022.133745

Jaen, J., Domeno, C., Ubeda, S., Aznar, M., Nerin, C., (2022b). Migration of mineral oil aromatic hydrocarbons (MOAH) from cardboard containers to dry food and prediction tool. Food Control, 138, 109016. https://doi.org/10.1016/j.foodcont.2022.109016

Jaen, J., Domeno, C., Vera, P., Nerín, C. (2022c). Migration of mineral oil aromatic hydrocarbon (MOAH) from hot melt adhesives used in food packaging materials. Food Packaging and Shelf Life, 33, 100885. https://doi.org/10.1016/j.fpsl.2022.100885

Lommatzsch, M., Biedermann, M., Grob, K., Simat, T.J. (2016). Analysis of saturated and aromatic hydrocarbons migrating from apolyolefin-based hot-melt adhesive into food. *Food Additives & Contaminants: Part A*, *33*(3), 473–488. https://doi.org/10.1080/19440049.2015.1130863

Menegoz Ursol, L., Conchione, C., Srbinovska, A., Moret, S. (2022). Optimization and validation of microwave assisted saponification (MAS) followed by epoxidation for high-sensitivity determination of mineral oil aromatic hydrocarbons (MOAH) in extra virgin olive oil. *Food Chemistry*, 370, 130966. https://doi.org/10.1016/j.foodchem.2021.130966

Nestola, M., Schmidt, T.C. (2017). Determination of mineral oil aromatic hydrocarbons in edible oils and fats by online liquid chromatography–gas chromatography–flame ionization detection – Evaluation of automated removal strategies for biogenic olefins. Journal of Chromatography A, 1505, 69–76. https://doi.org/10.1016/j.chroma.2017.05.035

Nygaard, U.C., Vege, A., Rognum, T., Grob, K., Cartier, C., Cravedi, J.P., Alexander, J. (2019). Toxic effects of mineral oil saturated hydrocarbons (MOSH) and relation to accumulation in rat liver. *Food and chemical toxicology*, 123, 431-442.

Polyakova, A., Van Leeuwen, S., Peters, R. (2022). Review on chromotographic and specific detection methodologies for unravelling the complexity of MOAH in foods. *Analytica Chimica Acta,* 1234, 1-15. https://doi.org/10.1016/j.aca.2022.340098

Purcaro, G., Barp, L., Moret, S., 2016. Determination of hydrocarbon contamination in foods. A review. Anal Methods 8, 5755–5772.

Ursol, L.M., Conchione, C., Peroni, D., Moret, S. (2025). A study on the impact of industrial-scale refining on olive oil and olive pomace oil contamination with mineral oils. Food Chemistry, 466, 142207. https://doi.org/10.1016/j.foodchem.2024.142207

Weber, S., Schrag, K., Mildau G., Kuballa, T., Walch, G.S., Lachenmeier, W.D. (2018). Analytical methods for the determination of mineral oil saturated hydrocarbons (MOSH) and mineral oil aromatic hydrocarbons (MOAH)- a short review. *Analytical Chemistry Insights,* 4(13). https://doi.org/10.1177/1177390118777757

Xue, M., Huang, R., Wen, Z., Li, W., Chai, X., Huang, L. (2024). Adsorption and barrier properties of bio-based coating on paper against MOSH for improving food packaging safety. *Progress in Organic Coatings,* 194, 108590. https://doi.org/10.1016/j.porgcoat.2024.108590

Zhang, Q., Huo, Y., Yang, Q., Zhao, F., Li, M., Ju, J. (2025). Migration of chemical substances from packaging materials to food. *Food Chemistry,* 485, 144544. https://doi.org/10.1016/j.foodchem.2025.144544

➢ *ORAL PRESENTATION*

Çevresel kirleticilerin sağlık riski değerlendirmesi-literatür taraması

Samet Gündem[1*] (*ORCID: https://orcid.org/0009-0005-0096-017X*),
D. Deniz G. Tokgöz [1] (*ORCID: https://orcid.org/0000-0001-7904-2497.*)

[*1]Hacettepe Üniversitesi, Mühendislik Fakültesi, Çevre Mühendisliği Bölümü, Ankara, Türkiye

*Sorumlu yazar e-posta: sametgundem@hacettepe.edu.tr

Özet
Sağlık Riski Değerlendirmesi (SRD), çevresel kirleticilerin insan sağlığı üzerindeki olası etkilerini belirlemek ve bu riskleri yönetmek için kullanılan bilimsel bir yaklaşımdır. Bu çalışmada, sağlık riski analizi: tehlike tanımlama, doz-tepki değerlendirmesi, maruziyet değerlendirmesi ve risk karakterizasyonu olmak üzere dört aşamada açıklanmıştır. Tehlike tanımlama aşamasında, belirli bir kimyasal maddenin insan sağlığına zarar verip vermediği belirlenmektedir. Doz-tepki değerlendirmesi, belirli bir maruziyet seviyesinin insan sağlığı üzerindeki etkilerini belirlemek için yapılmaktadır. Maruziyet değerlendirmesinde, insanların çevresel kirleticilere ne kadar ve hangi yollarla maruz kaldığı incelenmektedir. Son aşama olan risk karakterizasyonunda ise elde edilen veriler birleştirilerek sağlık riskleri niceliksel olarak belirlenmektedir. Bu çalışmada kriter hava kirleticilerinden olan partikül maddenin (PM) sağlık riski değerlendirmesi için lireratür taraması yapılmış ve yukarıda bahsedilen aşamaların açıklanmasında literatürde PM ile ilgili çalışmalara vurgu yapılmıştır. Çalışmada ayrıca risk değerlendirme sürecinde karşılaşılan belirsizlikler, kullanılan modeller ve veri eksiklikleri gibi faktörler de ele alınmıştır. Literatür taraması sonucunda, SRD'nin çevresel politikaların oluşturulmasında ve halk sağlığının korunmasında önemli bir araç olduğu, doğru ve kapsamlı analizlerin yapılabilmesi için güncel veri kaynakları ve gelişmiş modelleme tekniklerinin kullanılması gerektiği sonucuna varılmıştır.

Anahtar Kelimeler: Sağlık Riski, Hava Kirliliği, Partikül Madde, Kanser, Kanser Dışı, Soluma, Yutma, Deri Yolu.

Health risk assessment of environmental pollutants-literature review

Abstract
Health Risk Assessment (HRA) is a scientific approach used to determine and manage the potential effects of environmental pollutants on human health. This study explains health risk analysis in four stages: hazard identification, dose-response assessment, exposure assessment, and risk characterization. In the hazard identification stage, it's determined whether a specific chemical substance harms human health. Dose-response assessment aims to establish the effects of a particular exposure level on human health. Exposure assessment investigates how much and by what means people are exposed to environmental pollutants. Finally, in the risk characterization stage, the gathered data are combined to quantitatively determine health risks. In this study, a literature review was conducted for the health risk assessment of particulate matter (PM), a criterion air pollutant, emphasizing PM-related studies in the explanation of the aforementioned stages. The study also addressed factors such as uncertainties encountered in the risk assessment process, the models used, and data deficiencies. The literature review concluded that HRA is a crucial tool in shaping environmental policies and protecting public health, and that accurate and comprehensive analyses require the use of up-to-date data sources and advanced modeling techniques.

Keywords: Health Risk, Air Pollution, Particulate Matter, Cancer, Non-Cancer, Inhalation, Ingestion, Dermal Route.

GİRİŞ

Hızlı sanayileşme nedeniyle hava kirliliği küresel bir sorun haline gelmiş, hava kalitesini düşürerek çevresel dengesizliklere ve yılda 7 milyondan fazla erken ölüme yol açmaktadır (Fowler et al., 2020; Fadel et al., 2022; WHO 2016). Hava kirliliğinin sağlık etkileri tek bir maddeye bağlanamaz; atmosferdeki farklı gaz, partikül ve sıvıların birleşik etkileri söz konusudur (Elkama et al., 2021). Özellikle partikül madde (PM), ciddi bir tehdit olup Uluslararası Kanser Araştırma Ajansı (IARC, 2016) tarafından Grup 1 kanserojen olarak sınıflandırılmıştır. Gelişmekte olan bölgelerde PM maruziyeti, miyokard enfarktüsü, vasküler disfonksiyon, pulmoner yetersizlik, akciğer kanseri, KOAH ve astım gibi kardiyovasküler ve solunum yolu hastalıklarıyla ilişkilendirilmiştir (Du et al., 2016; Manisalidis et al., 2020; Fadel et al., 2022).

Hava kirleticileri organik ve inorganik olarak iki ana kategoriye ayrılır. Organik kirleticiler arasında polisiklik aromatik hidrokarbonlar (PAH'lar) ve benzen, toluen, etilbenzen, ksilen (BTEX) gibi bileşikler bulunur. BTEX, kentsel alanlarda en yaygın uçucu organik bileşikler (VOC'ler) olup sağlık riski taşırken (Kermani et al., 2020; Fadel et al., 2022), PAH'lar mutajenik ve kanserojenik etkileri nedeniyle tehdit oluşturur (Niu et al., 2017; Kermani et al., 2020). İnorganik kirleticiler arasında kurşun, kadmiyum, cıva, krom gibi ağır metaller ve asbest lifleri yer alır. Bu metaller çevrede kalıcı olup insan sağlığına ve ekosistemlere zarar verir (Wang et al., 2019; Kermani et al., 2020), asbest ise mezotelyoma ve akciğer kanserine yol açabilir (Taghizadeh et al., 2019; Kermani et al., 2020).

Atmosferik PM'nin bileşimi emisyon kaynakları, kimyasal olaylar ve kirletici taşınımı gibi faktörlere bağlıdır (Yu & Park, 2021; Fadel et al., 2022). Kentsel bölgelerde, toplam PM kütlesinin %20-70'ini oluşturan karbon bazlı aerosoller (organik karbon (OK) ve elementel karbon (EK)), hava kalitesini ve iklim değişikliğini olumsuz etkiler (Sharma et al., 2020). OK ve EK, organik materyallerin eksik yanması sonucu oluşur (Valle-Hernández et al., 2024). PM'deki OK, EK ve PAH'lar, reaktif oksijen türleri (ROT) üreterek oksidatif stres, iltihaplanma, astım ve diğer solunum hastalıklarını tetikleyebilir (Morgenstern et al., 2008; Yadav et al., 2021). Özellikle PM2.5 içindeki EK konsantrasyonları ile akciğer kanseri arasında güçlü bir ilişki bulunmuştur (Gauderman et al., 2004; Yadav et al., 2021).

İnsanların hava kirleticilerine maruz kalması başlıca soluma, yutma ve deri yoluyla emilim ile gerçekleşir. Solunan partiküller, boyut, şekil ve bileşime bağlı olarak solunum sistemi içinde farklı bölgelerde tutulur (Bell et al., 2009; Cochard et al., 2020). Özellikle PM2.5, alveollere ulaşarak kana karışabilir ve erken ölümlere neden olabilir (WHO, 2021; Fadel et al., 2022). Solunamayan partiküller yutma yoluyla vücuda girip ince bağırsakta emilebilir (Fadel et al., 2022). Deri yoluyla maruziyet ise kimyasalların deriden kana karışmasıyla olur, ancak diğer yollara göre daha sınırlıdır (Tuncel & Atimtay, 2023).

Sağlık risk değerlendirmesi çalışmaları, kimyasallara maruziyetin potansiyel olumsuz etkilerini tahmin etmek için önemlidir (USEPA, 2022; Fadel et al., 2022). Bu değerlendirmeler kanser ve kanser dışı sağlık risklerini inceler (OEHHA, 2001; Fadel et al., 2022). Değerlendirme araçları arasında BenMap-CE, COBRA, Air Q+ ve HAPIT bulunur (Gao et al., 2015; Farzaneh, 2019; Fadel et al., 2022). Ancak bu araçlar genellikle kükürt oksitler, azot oksitler, ozon ve partikül madde gibi temel kirleticilerin risklerini değerlendirmekle sınırlıdır (Fadel et al., 2022).

BULGULAR ve TARTIŞMA

1. Risk Değerlendirme Süreci

Sağlık riski değerlendirmesi (SRD), kimyasal maruziyetin insan sağlığı üzerindeki olası etkilerini belirlemeye yönelik dört aşamalı, yapılandırılmış bir yaklaşımdır (Tuncel & Atimtay, 2023). İlk iki aşama kimyasalın özelliklerini ve toksikolojik etkilerini incelerken, son iki aşama belirli maruziyet senaryolarına odaklanır (Tuncel & Atimtay, 2023).

1) Tehlike Tanımlama: Bu aşama, maruz kalınan kimyasalların olumsuz sağlık etkilerine yol açma potansiyelini belirleme sürecidir (Masters, 1991; OEHHA, 2001; Fadel et al., 2022). Dünya Sağlık Örgütü (WHO, 2021) gibi küresel sağlık kuruluşlarının toksisite sınıflandırmaları da değerlendirilir (Fadel et al., 2022). Bir kimyasalın kanserojen olup olmadığı, insanlardaki kanser insidansı, hayvan deneyleri, genotoksisite testleri, metabolik ve farmakokinetik özellikler ile fiziksel ve kimyasal özellikler dikkate alınarak belirlenir (Tuncel & Atimtay, 2023). Toksik kimyasalların kanserojen etkisi, "Weight of Evidence" (WoE) yaklaşımıyla vaka çalışmaları, epidemiyolojik araştırmalar ve hayvan deneyleri üzerinden değerlendirilir (Tuncel & Atimtay, 2023).

2) Doz-Tepki Değerlendirmesi: Bu aşamada, bir kirleticiye maruz kalınan doz ile canlının bu doza karşı gösterdiği sağlık tepkisi arasındaki ilişki incelenir (Patterson vd, 2002; Tuncel & Atimtay, 2023). Sağlık tepkisi, gözlemlenen olay sayısı veya bir popülasyonda tepkinin meydana gelme olasılığı olarak tanımlanabilir (USEPA, 1997; Tuncel & Atimtay, 2023). Bu ilişkinin doğası, kimyasalın özelliklerine ve kanserle ilişkili olup olmadığına göre değişir (OEHHA, 2001). Kanserojen kimyasallara çok düşük dozlarda bile maruz kalmak kanser riskini artırabilirken, kanser dışı tepkiler için bir eşik doz kabul edilir (Tuncel & Atimtay, 2023). Bazı kimyasallar her iki tür tepkiye de neden olabilir (Masters, 1991).

Kanser Risk Değerlendirmesi

USEPA'ya göre (1991), hiçbir maruziyet seviyesi tamamen kansersiz kabul edilemez; en düşük seviyelerde bile kanser riski bulunur. Moleküler olaylar mutasyonları tetikleyerek hücre hasarına ve kansere yol açabilir (Haber et al., 2012; Fadel et al., 2022). Bu etkiler, eşik değeri olmayan etkiler olarak sınıflandırılır ve herhangi bir maruziyet düzeyinde olumsuz sonuçlar doğurabilir (Fadel et al., 2022). Bu nedenle, kanserojen kirleticilere maruz kalmanın, doğrusal doz-tepki ilişkisi varsayımıyla, en düşük seviyelerde bile kanser riskini artırdığı kabul edilir (Fadel et al., 2022).

Kanser risk değerlendirmesi, kanserojen kimyasallara maruz kalma sonucu bireyin yaşamı boyunca kansere yakalanma olasılığını tahmin etmeyi amaçlar (OEHHA, 2001; Fadel et al., 2022). Bu risk, genellikle 70 yıllık bir yaşam süresi boyunca her bir milyon kişi başına tahmin edilen kanser vakası sayısı olarak ifade edilir (OEHHA, 2001; Fadel et al., 2022). Doz-tepki eğrisinin eğimi, potansiyel faktör (PF) veya eğim faktörü (EF) olarak adlandırılır ve birim doz başına kanser riskini tanımlar (USEPA, 1997; Tuncel & Atimtay, 2023). Belirli bir maruziyet yoluna ilişkin kanser riski, yaşam boyu ortalama günlük dozun, kanserojen eğim faktörüyle çarpılmasıyla hesaplanır (USEPA, 1989; Fadel et al., 2022).

Kanser Dışı Risk Değerlendirmesi

Kanser dışı sağlık riskleri, kanser risklerinin aksine, belirli bir eşik değerinin altında zararlı etki oluşturmadığı varsayılan sağlık sorunlarını içerir. Bu durum, vücudun adaptif koruyucu mekanizmalarına dayanır (Haber et al., 2012). Astım, nörolojik bozukluklar, doğum kusurları ve kardiyovasküler hastalıklar gibi sorunlar, kimyasal maruziyet arttıkça kötüleşebilir (OEHHA, 2001; Fadel et al., 2022).

Eşik değeri belirlemek için hayvan deneylerinde kirleticilere farklı dozlarda maruziyet uygulanır. Toksisite testleri, eşik altındaki dozların tepki oluşturmadığını, eşik üzerindeki dozların ise tepki vereceğini gösterir (Robson ve Toscana, 2007; Tuncel & Atimtay, 2023). Toksik etkilerin sınırları, Gözlemlenebilir Tepki Olmayan En Yüksek Doz ve En Düşük Dozda Gözlemlenen Tepki Düzeyi terimleriyle tanımlanır (Robson ve Toscana, 2007). Gerçek eşik, bu iki değer arasında bir noktadadır.

Farklı sağlık kuruluşları güvenli maruziyet sınırlarını farklı şekillerde tanımlar. USEPA Referans Doz (RfD) ve Referans Konsantrasyon (RfK) kavramlarını kullanırken, Dünya Sağlık Örgütü (WHO) Kabul Edilebilir Günlük Alım (KEGA) terimini tercih eder (Fadel et al., 2022). RfK, ömür boyu zararlı etki riski taşımayan tahmini soluma konsantrasyonunu, RfD ise günlük kabul edilebilir oral maruziyet değerini belirtir (USEPA IRIS, 2021; Tuncel & Atimtay, 2023). Uluslararası Kimyasal Güvenlik Programı ve Toksik Maddeler ve Hastalıklar Kaydı Ajansı (ATSDR) ise sırasıyla Tolere Edilebilir Alım (TEA) ve Minimum Risk Seviyesi (MRS) kavramlarını benimsemiştir (Pohl & Abadin, 1995; Fadel et al., 2022).

USEPA'ya (1989) göre, kanser dışı sağlık riski Tehlike Katsayısı (TK) ile ölçülür. TK, bireyin maruziyet düzeyinin (Ortalama Günlük Doz, OGD) RfD veya RfK gibi bir referans değere oranlanmasıyla hesaplanır (Fadel et al., 2022). Birden fazla kimyasal veya maruziyet yolundan kaynaklanan riskleri değerlendirmek için ise birden fazla tehlike katsayısının toplamı olan Tehlike İndeksi (Tİ) kullanılır (USEPA, 1991; Fadel et al., 2022). Belirsizlik faktörleri, genellikle on kat olarak belirlenir ve hamileler, bebekler, yaşlılar gibi hassas gruplar ile sağlıklı bireyler arasındaki farkları hesaba katmak için kullanılır. İnsan veya hayvan verileri yetersiz olduğunda da 10 katlık bir faktör geçerli olabilir. Her kimyasal için eğim faktörü, referans doz ve referans konsantrasyon farklıdır. Bu parametreler, EPA'nın IRIS Programı veri tabanında listelenmektedir (USEPA IRIS, 2021; Tuncel & Atimtay, 2023).

3) Maruziyet Değerlendirmesi: Bu aşama, insanların bir kimyasala ne kadar ne sıklıkla ve ne süreyle maruz kaldığını ölçme veya tahmin etme sürecidir (USEPA 1992; Tuncel & Atimtay, 2023). Özellikle hava yoluyla ya da diğer maruziyet yolları incelenir (USEPA, 1991; Fadel et al., 2022). Kimyasal alımını tahmin etmek için yaş, cinsiyet, vücut ağırlığı, solunum oranları ve günlük aktiviteler gibi faktörler dikkate alınır. Bu parametrelerle ilgili çalışmalar belirli bir popülasyon üzerinde gerçekleştirilmiş veya modelleme

yoluyla elde edilmiş olup literatürde yer almaktadır. Ancak, bu verilere ulaşılamadığında, maruziyet tahmini küresel referans değerler kullanılarak yapılır (USEPA, 1997; Tuncel & Atimtay, 2023).

4) Risk Kategorizasyonu: Bu son aşamada, önceki adımlardan elde edilen tüm veriler birleştirilerek maruz kalan nüfus için genel sağlık riski tahmini yapılır (Fadel et al., 2022). Doz-tepki değerlendirmesi sırasında elde edilen veriler, belirli bir popülasyonda kanserojen ve kanserojen olmayan etkileri içeren sayısal risk tahmini yapmak amacıyla maruziyet değerlendirmesinden sağlanan verilerle birleştirilir (USEPA, 1992; Tuncel & Atimtay, 2023). Kanser risk hesaplamaları, USEPA, IRIS (2021) tarafından sağlanan birim risk veya eğim faktörü değerleri temel alınarak gerçekleştirilir.

2. Risk Değerlendirme Metodolojisi

Sağlık risk değerlendirmesi, maruziyetin şiddetini belirlemek için kirletici madde konsantrasyonu, alım oranı ve maddenin toksik özellikleri gibi birden fazla faktörü göz önünde bulundurur (Fadel et al., 2022). Ayrıca vücut ağırlığı, maruziyet süresi ve sıklığı gibi bireysel özellikler de önemlidir. Bu parametreler, zararlı bileşiklerin insan sağlığı üzerindeki potansiyel etkilerini değerlendirmeye yardımcı olur.

İnsanların kirleticilere maruz kalma düzeylerine bağlı olarak sağlık risklerini değerlendirme yöntemi ilk kez 1970'lerde uygulanmaya başlanmış, ardından farklı risk türleri ve değerlendirme kriterleri için çeşitli yöntemler geliştirilmiştir (Tuncel & Atimtay, 2023). Birleşik Devletler Çevre Koruma Ajansı (USEPA), sağlık risk değerlendirme çerçevesini ilk olarak 1989 ve 1991 yıllarında tanıtmıştır (USEPA, 1989; 1991; Fadel et al., 2022). O zamandan bu yana, bu yaklaşım, çeşitli partikül madde bileşenlerine geniş bir şekilde uygulanmıştır (Fadel et al., 2022). Hem kanser hem de kanser dışı risk değerlendirmeleri, günlük maruziyet düzeylerinin değerlendirilmesini gerektirir. Bu değerler, mg/kg-gün cinsinden doz veya mg/m^3 cinsinden konsantrasyon olarak ifade edilebilir. Kanser dışı risk için günlük maruziyet dozu, ortalama günlük doz (OGD_i) olarak adlandırılırken, soluma maruziyet konsantrasyonu, havadaki maruziyet konsantrasyonu (MK_i) olarak belirtilir (Fadel et al., 2022). Bu değerler, birden fazla maruziyet yolunu dikkate alan ve solunum riskini hesaplamaya yönelik denklemler (Eşitlik 1, 2, 3 ve 4) kullanılarak belirlenir.

$$OGD_{i-soluma} = \frac{C_i \times MO_{soluma} \times TMSü \times MSı \times 10^{-6}}{VA \times OZ} \quad (1)$$

$$OGD_{i-yutma} = \frac{C_i \times MO_{yutma} \times TMSü \times MSı \times 10^{-6}}{VA \times OZ} \quad (2)$$

$$OGD_{i-deri} = \frac{C_i \times YA \times DYF \times DAF \times TMSü \times MSı \times 10^{-6}}{VA \times OZ} \quad (3)$$

$$MK_i = \frac{C_i \times MSü \times TMSü \times MSı \times 10^{-6}}{OZ} \quad (4)$$

Havadaki konsantrasyon (C_i), kirleticinin havadaki ortalama seviyesini (ng/m^3) ifade eder (USEPA, 2011; Fadel et al., 2022). Solunum yoluyla maruziyet oranı (MO_{soluma}), yetişkinler için 20 m^3/gün, çocuklar için ise 10 m^3/gün olarak belirlenmiştir (USEPA, 2011; Fadel et al., 2022). Yutma oranı (MO_{yutma}) ise çocuklar için 100 mg/gün, yetişkinler için 50 mg/gün raporlanmıştır (USEPA, 2011; Fadel et al., 2022). Solunum ve yutma oranları gibi bazı parametreler vücut ağırlığı (VA) gibi bireysel özelliklerle ilişkilidir. Maruziyet sıklığı (MSı) ve süresi (MSü) ise kirletici maddeyle temasa dair verileri yansıtır (Fadel et al., 2022).

Kanser riski değerlendirmesi için maruziyet süresi genellikle 70 yıl (25.500 gün) olarak kabul edilir ve yaşam boyu ortalama günlük doz (YB-OGD_i) Denklemler 1–4 kullanılarak hesaplanır (USEPA, 1989; 2011; Fadel et al., 2022). Maruziyet parametreleri yaş grubu (yenidoğan, çocuk, ergen, yetişkin), cinsiyet, meslek ve bölgesel demografik özelliklere göre değişir. Veri eksikliğinde USEPA tarafından belirlenen standart değerler kullanılır; örneğin, standart vücut ağırlığı değerleri yenidoğanlar için 7.8 kg, çocuklar için 25 kg, ergenler için 61 kg ve yetişkinler için 70 kg'dır (USEPA, 1991, 1997, 2011; Fadel et al., 2022). USEPA, maruziyet değerlendirmelerini desteklemek amacıyla 2011 yılında güncellenmiş bir Maruziyet Faktörleri El Kitabı geliştirmiştir (USEPA, 2011; Fadel et al., 2022). Benzer şekilde, Çin Çevre Bilimleri Araştırma Akademisi (CRAES) de kendi nüfusuna yönelik bir el kitabı yayınlamıştır (Duan, 2016; Fadel et al., 2022). Bu veri setleri, araştırmacıların nüfusa özgü maruziyet risklerini değerlendirmesine yardımcı olur.

Maruziyet sıklığı (MSı) mesleğe ve yaşam biçimine göre değişir; saha çalışanları ve kapalı alan çalışanları için 250 gün/yıl, sakinler için 350 gün/yıl belirlenmiştir (USEPA, 2002, 2004; Fadel et al., 2022). Maruziyet süresi (MSü) çocuklar için 6 saat/gün, yetişkinler için 8 saat/gün olarak tanımlanmıştır (Liu et al., 2018; Fadel et al., 2022). Toplam maruziyet süresi (TMSü) USEPA rehberine göre yenidoğanlar için 1 yıl,

çocuklar için 11 yıl, ergenler için 6 yıl ve yetişkinler için 52 yıldır (USEPA, 2011; Fadel et al., 2022). Ortalama zaman (OZ) ise kanserojen olmayan maddeler için OZ = TMSü × 365 gün, kanserojenler için ise OZ = 70 yıl × 365 gün olarak kabul edilmiştir (USEPA, 1989; Fadel et al., 2022).

Cilde maruz kalan yüzey alanı (YA) çocuklar için 2800 cm^2, yetişkinler için 5700 cm^2, açık alan çalışanları ve inşaat işçileri için 3300 cm^2'dir (USEPA, 2002, 2011; Fadel et al., 2022). Dermal yapışma faktörü (DYF) çocuklar için 0.2 mg/cm^2, yetişkinler için 0.07 mg/cm^2, açık alan çalışanları için 0.2 mg/cm^2 olarak verilmiştir (USEPA, 2002; Fadel et al., 2022). Dermal adsorpsiyon faktörü (DAF) bileşiğin türüne bağlıdır: poliaromatik hidrokarbonlar için 0.13, arsenik için 0.03, kadmiyum için 0.001 ve diğer elementler için 0.01 (USEPA, 2002, 2011; Fadel et al., 2022). Bu parametreler, çeşitli çevresel etkenlerin sağlık üzerindeki potansiyel etkilerini anlamada kritik bir rol oynar.

Kanser Dışı Risk Değerlendirmesi

Kanser dışı risk değerlendirmesi, tahmin edilen maruziyetin belirlenmiş referans değerlerle karşılaştırılmasını içerir. Ortalama günlük doz (OGD_i), referans doz (RfD_i) ile karşılaştırılırken, hava içindeki maruziyet konsantrasyonu (MK_i), solunum için referans konsantrasyon (RfK_i) ile karşılaştırılır. Referans doz (RfD_i), mg/kg/gün cinsinden ölçülen, insanlarda, özellikle hassas popülasyonlar arasında, yaşam boyu olumsuz sağlık etkilerine yol açma olasılığı düşük olan tahmin edilen günlük maruziyet seviyesini temsil eder (USEPA, 2022; Fadel et al. 2022). Benzer şekilde, referans konsantrasyon (RfK_i), mg/m^3 cinsinden ifade edilerek solunum risklerini değerlendirmek için kullanılır (Fadel et al. 2022). OGD_i ile RfD_i veya MK_i ile RfK_i arasındaki oran, kanser dışı risk değerlendirmesinde önemli bir gösterge olan tehlike katsayısını (TK_i) belirler. Bu oran, USEPA (1989, 1991, 2011) tarafından belirlenen Denklem 5 kullanılarak hesaplanır.

$$TK_i = \frac{OGD_i}{RfD_i} = \frac{MK_i}{RfK_i} \quad (5)$$

Fadel et al. (2022) tarafından derlenen referans doz (RfD_i) ve referans konsantrasyon (RfK_i) değerleri, polisiklik aromatik hidrokarbonlar (PAH'lar), ağır metaller, ftalatlar, dioksinler, furanlar ve dioksin benzeri poliklorlu bifeniller (PCB'ler) gibi çeşitli kimyasal sınıflar için kapsamlı bir kaynak sunmaktadır. Bu değerler, farklı maruziyet yolları ve türler için özel olup, kanser dışı risk değerlendirmesinde yardımcı olur. USEPA (2011) tarafından belirtilenlere göre, standart olmayan popülasyonlar için vücut ağırlığı düzeltmesi gerekmemektedir, çünkü Entegre Risk Bilgisi Sistemi (IRIS), RfD_i ve RfK_i değerlerini belirlerken varsayılan 70 kg vücut ağırlığını kabul etmemektedir (Fadel et al. 2022). Ayrıca, deri yoluyla maruziyet değerlendirilirken, dermal referans doz (RfD_{dermal}) ağız yoluyla alınan referans doz (RfD_{oral}) ile gastrointestinal emilim faktörü (GEF) kullanılarak Eşitlik 6'da açıklandığı şekilde türetilebilir (Fadel et al. 2022).

$$RfD_{dermal} = RfD_{oral} \times GEF \quad (6)$$

Risk değerlendirmesinde, gastrointestinal emilim faktörü (GEF) genellikle 1 olarak kabul edilir (USEPA 2004). Ancak antimon, baryum, berilyum, kadmiyum, krom (VI), manganez, nikel, gümüş ve vanadyum gibi bazı inorganik bileşikler için spesifik değerler (sırasıyla 0.15, 0.07, 0.007, 0.025, 0.025, 0.04, 0.04, 0.04 ve 0.026) kullanılır (USEPA 2004).

Kanser dışı risk değerlendirmesi, birden fazla kimyasal maddeye maruziyeti de kapsar (Fadel et al., 2022). Bu riskler; birden fazla maruziyet yoluyla bireysel tür bazında, belirli bir maruziyet yolu için tüm türlerin risklerini toplayarak veya tüm yollar boyunca tüm türlerin risklerini birleştirerek değerlendirilebilir (USEPA 1989, 1991, 2011). Toplam tehlike katsayısı (TTK_i), bir kimyasalın birden fazla maruziyet yolu boyunca kümülatif kanser dışı riskini temsil eder ve Denklem 7 kullanılarak hesaplanır. Bir kimyasal ailesinin belirli bir maruziyet yolu için toplu kanser dışı riskini değerlendirirken tehlike indeksi (Tİ) Denklem 8 ile hesaplanır. Son olarak, bir kimyasal ailesi için birden fazla maruziyet yolundan kaynaklanan toplam kanser dışı riski tahmin etmek için toplam tehlike indeksi (TTİ) Denklem 9'da gösterilmiştir. USEPA'ya (1997; 2011) göre, TK_i, TTK_i, Tİ ve TTİ değerlerinin 1'i aşması, kanser dışı sağlık etkilerinin daha yüksek olasılığını ve artan bir endişe seviyesini gösterir.

$$TTK_i = TK_{i-soluma} + TK_{i-yutma} + TK_{i-deri} \quad (7)$$

$$T\dot{I}_{soluma/yutma/deri} = \sum_i TK_{i-soluma/yutma/deri} \quad (8)$$

$$TT\dot{I} = T\dot{I}_{soluma} + T\dot{I}_{yutma} + T\dot{I}_{deri} \quad (9)$$

Kanser Riski Değerlendirmesi

Bir kimyasalın belirli bir maruz kalma yoluyla kanser riski (KR_i), maruziyet konsantrasyonu (MK_i) veya yaşam boyu ortalama günlük doz ($YB\text{-}OGD_i$) kullanılarak Denklem 10 ve Denklem 11 ile belirlenir (Fadel et al. 2022). Soluma yoluyla kanser riskini tahmin etmek için Soluma Birimi Riski (SBR_i) (m^3/mg cinsinden) kullanılır (USEPA 1997; Fadel et al. 2022). Benzer şekilde, kanser eğim faktörü (KEF_i) (kg gün/mg cinsinden), belirli bir maruziyet yolu için birim doz başına kanser riskini nitelendirir. Partikül madde içinde bulunan farklı bileşikler için KEF ve SBR değerleri Fadel et al. (2022) çalışmasında özetlenmiştir. Bu değerler, standart dışı vücut ağırlığına sahip bireyler için $(VA/70)^{1/3}$ düzeltme faktörü kullanılarak ayarlanır (USEPA 1997; Fadel et al. 2022). Ayrıca, deri kanser eğim faktörü, gastrointestinal emilim faktörü (GEF) mevcutsa, oral KEF değerlerinden Denklem 12 ile türetilebilir (Fadel et al. 2022).

$$KR_{i-soluma} = MK_i \times SBR_i \quad (10)$$

$$KR_{i-soluma/yutma/deri} = YB - OGD_i \times KEF_i \quad (11)$$

$$KEF_{deri} = KEF_{oral}/GEF \quad (12)$$

Belirli bir kimyasalın toplam kanser riski, birden fazla maruz kalma yolu boyunca risklerin toplamı olarak hesaplanır, bu Denklem 13'de gösterilmektedir (Fadel et al. 2022). Bir maruz kalma yolu içinde bir kimyasal grubu için, bir kimyasal ailesinin kanser riski Denklem 14 kullanılarak belirlenir (Fadel et al. 2022). Ayrıca, tüm yollar boyunca kümülatif maruz kalmayı göz önünde bulundururken, kümülatif kanser riski (KKR) Denklem 15 kullanılarak hesaplanır (Fadel et al. 2022).

$$Toplam\ KR_i = KR_{i-soluma} + KR_{i-yutma} + KR_{i-deri} \quad (13)$$

$$KR_{soluma/yutma/deri} = \sum_i KR_{i-soluma/yutma/deri} \quad (14)$$

$$Kümülatif\ KR\ (KKR) = KR_{soluma} + KR_{yutma} + KR_{deri} \quad (15)$$

USEPA'ya (1991; 1997) göre, 10^{-6}'lık bir kanser riski eşiği (bir milyon kişi başına bir ek kanser vakası) kabul edilebilir risk seviyelerini tanımlamak için kullanılır. 10^{-6} ile 10^{-4} arasındaki riskler, potansiyel endişe yaratırken, 10^{-4}'ün üzerindeki değerler yüksek kanser riski anlamına gelir (Chiang et al. 2009; Fadel et al. 2022). Ayrıca, kanser riski değerlendirmeleri yaş gruplarına göre sınıflandırılabilir ve ömür boyu kanser riski (ÖBKR) veya artan ömür boyu kanser riski (ÖBKR) tahmin etmek için Denklem 16 kullanılarak hesaplanabilir (Fadel et al. 2022).

$$\ddot{O}BKR = (KKR_{bebek} \times \frac{Esü_{bebek}}{70}) + (KKR_{çocuk} \times \frac{Esü_{çocuk}}{70}) + (KKR_{genç} \times \frac{Esü_{genç}}{70}) + (KKR_{yetişkin} \times \frac{Esü_{yetişkin}}{70}) \quad (16)$$

3. Risk Değerlendirmesinde Türlerin Konsantrasyonu

Hava kirleticilerinin risk değerlendirmesi hem gaz hem de partikül fazındaki bileşenlere maruz kalmayı inceler (Fadel et al. 2022). Değerlendirilen kimyasal sınıflar arasında elementler, polisiklik aromatik hidrokarbonlar (PAH'lar), ftalatlar, dioksinler, furanlar ve dioksin benzeri poliklorobifeniller bulunur. PAH'lar, çevrede uzun süre kalan ve toksisite açısından farklılık gösteren hidrofobik bileşiklerdir (Abdel-Shafy & Mansour 2016; Fadel et al. 2022). Ftalatlar, plastiklerde yaygın kullanılan sentetik kimyasallardır (USEPA 2012). Dioksinler, furanlar ve dioksin benzeri poliklorobifeniller ise uzun mesafeli atmosferik taşınıma izin veren yarı uçucu organik kirleticilerdir (Srogi 2008; Koukoulakis et al. 2020). Bu organik ve inorganik kirleticiler, partikül maddede az miktarda bulunsa da toksisiteye önemli katkı sağlarlar (Akhtar et al. 2010; Fortoul et al. 2015). Amonyum, sülfatlar, deniz tuzları ve kabuk elementleri gibi partikül madde kütlesinin büyük kısmını oluşturan bileşenlerin toksisitesi ise minimaldir (Borm et al. 2007; Fadel et al. 2022).

Elementler ve ftalatlar için risk değerlendirmesi genellikle bireysel yapılır. Örneğin, diethylftalat ve dibutylftalat sadece kanser dışı etkiler için değerlendirilirken, bis(2-ethylhexyl) ftalat ve butil benzilftalat hem kanser hem de kanser dışı riskler için değerlendirilir (Fadel et al. 2022). PAH'lar ve dioksinler arasında, benzo[a]piren (B[a]P) ve 2,3,7,8-tetrahlorodibenzop-diyoksin (2,3,7,8-TCDD) insan kanserojenleri olarak bilinir (IARC 2021; Fadel et al. 2022). Toksisitelerini nicelendirirken, toksik eşdeğer faktörü (TEF) uygulanır ve B[a]P ile 2,3,7,8-TCDD'ye referans toksisite değeri olarak 1 atanır (Berg et al. 2006; Fadel et al. 2022). PAH'lar, dioksinler ve furanlar için sağlık riski değerlendirmesi, benzo[a]piren eşdeğer konsantrasyonu (B[a]P_{eq}) ve 2,3,7,8-TCDD'nin toksik eşdeğer konsantrasyonu (WHO-TEK) kullanılarak yapılır. Bu değerler, Denklem 17 ve Denklem 18 kullanılarak belirlenir.

$$WHO - TEK = \sum_{i=1}^{n} C_i \times TEF_i \quad (17)$$

$$B[a]P_{eq} = \sum_{j=1}^{n} C_j \times TEF_j \quad (18)$$

C_i ve C_j (ng/m^3), dioksin, furan, dioksin benzeri PCB'ler, PAH'lar ve bunların türevlerinin konsantrasyonlarını temsil eder. TEF_i ve TEF_j, 2,3,7,8-TCDD ve B[a]P'ye göre toksik eşdeğer faktörleri belirtir (Collins ve diğerleri, 1998; Berg ve diğerleri, 2006; Fadel et al. 2022). İlgili TEF_i ve TEF_j değerleri, her konjenörün 2,3,7,8-TCDD ve B[a]P'ye kıyasla göreli toksisitesini belirten değerler Fadel et al. (2022)'in çalışmasında detaylandırılmıştır. Hesaplanan B[a]P_{eq} veya WHO-TEK değerleri, günlük doz veya maruz kalma konsantrasyonunu belirlemek için daha sonra Denklemler 1-4'e dahil edilir, ardından kanser ve kanser dışı risklerin tahmin edilmesinde kullanılır.

4. Risk Değerlendirmede Belirsizlikler

Hava kirliliğinin insan sağlığına etkilerini niceliksel olarak değerlendiren çalışmalar, somut veriler sunsa da hava kirliliğinin karmaşık yapısı nedeniyle belirli gruplar ve genel popülasyon için kullanılan parametreler farklılık gösterebilir (Tuncel & Atimtay, 2023). Özellikle hayvan deneylerinden elde edilen verilerin insanlara uyarlanması gibi faktörler, sağlık riski modellerinde belirsizliklere yol açar. Bu belirsizliklerin derecesi; seçilen modeller, kullanılan parametreler ve veri eksikliği gibi etkenlere bağlı olarak değişir (IPCS, 2014; Tuncel & Atimtay, 2023) ve yalnızca analiz yapan uzmanlara değerlendirme aralıklarını ve olasılıkları göstermekle kalmaz, aynı zamanda karar vericiler ve toplum için sağlık risklerinin yorumlanmasını da etkileyebilir (ENHEALTH, 2012; Tuncel & Atimtay, 2023). Sağlık riski tahmininde bu belirsizlikler dört temel aşamada karşılaşılabilmektedir: maruziyet değerlendirmesinde; betimsel ve toplulaştırma hataları, model yapısı, doğrulama süreçleri ve parametre seçimleri belirsizliğe neden olur. Doz-tepki ilişkisi aşamasında ise veri kalitesi, çalışmalar arasındaki tutarsızlıklar ve farklı türler arası ekstrapolasyon gibi unsurlar belirsizlik kaynaklarıdır. Ayrıca, maruziyet süresi, dozu tahmin etme ve model seçimi gibi faktörler de sonuçları etkileyebilir. Son olarak, risk karakterizasyonunda; toksisite kriterleri ve senaryo değerlendirme süreçleri karar verme aşamasında belirsizliğe yol açmaktadır (Dong vd., 2015).

SONUÇ

Bu çalışma, hava kirleticilerine maruziyetin insan sağlığı üzerindeki etkilerini değerlendirmek için kullanılan Sağlık Riski Değerlendirmesi (SRD) sürecinin önemini vurgulamaktadır. PM2.5 ve PM10 gibi ince partiküller, solunum ve dolaşım sistemi hastalıkları açısından önemli bir risk faktörü oluşturmakta ve özellikle hassas gruplar (çocuklar, yaşlılar ve kronik hastalar) için ciddi sağlık sorunlarına yol açabilmektedir. Çalışmada ele alınan maruziyet değerlendirmesi, doz-tepki analizi ve risk karakterizasyonu, hava kirliliğine bağlı sağlık risklerini anlamada kritik bileşenlerdir. Ancak, bu süreçler belirsizlikler ve veri eksiklikleri nedeniyle kesin tahminler sunmakta zorlanmaktadır. Daha doğru risk değerlendirmeleri yapmak için maruziyet ölçümlerinin geliştirilmesi, modelleme tekniklerinin iyileştirilmesi ve uzun vadeli sağlık etkilerini içeren epidemiyolojik çalışmaların artırılması gerekmektedir. Gelecekteki araştırmalar, risk tahminlerindeki belirsizlikleri azaltmaya odaklanmalı ve politik karar alıcılara hava kirliliğinin sağlık üzerindeki etkilerini minimize etmeye yönelik daha sağlam kanıtlar sunmalıdır. Sağlık riski değerlendirme süreçlerinin iyileştirilmesi, çevre politikalarının geliştirilmesine ve halk sağlığının korunmasına önemli katkılar sağlayacaktır.

KAYNAKLAR

Abdel-Shafy HI, Mansour MSM (2016) A review on polycyclic aromatic hydrocarbons: source, environmental impact, effect on human health and remediation. Egypt J Pet 25(1):107–123.

Akhtar U, McWhinney R, Rastogi N, Abbatt J, Evans G, Scott J (2010) Cytotoxic and proinflammatory effects of ambient and sourcerelated particulate matter (PM) in relation to the production of reactive oxygen species (ROS) and cytokine adsorption by particles. Inhal Toxicol 22(Suppl 2):37–47.

Bell ML, Ebisu K, Peng RD, Samet JM, Dominici F (2009) Hospital admissions and chemical composition of fine particle air pollution. Am J Respir Crit Care Med.

Borm PJA, Kelly F, Künzli N, Schins RPF, Donaldson K (2007) Oxidant generation by particulate matter: from biologically effective dose to a promising, novel metric. Occup Environ Med 64(2):73–74.

Chiang KC, Chio CP, Chiang YH, Liao CM (2009) Assessing hazardous risks of human exposure to temple airborne polycyclic aromatic hydrocarbons. J Hazard Mater 166(2–3):676–85.

Cochard M, Ledoux F, Landkocz Y (2020) Atmospheric fine particulate matter and epithelial mesenchymal transition in pulmonary cells: state of the art and critical review of the in vitro studies. J Toxicol Environ Health B Crit Rev 23(7):293–318.

Collins JF, Brown JP, Alexeeff GV, Salmon AG (1998) Potency equivalency factors for some polycyclic aromatic hydrocarbons and polycyclic aromatic hydrocarbon derivatives. Regul Toxicol Pharmacol 28(1):45–54.

Dong, Z., Liu, Y., Duan, L., Bekele, D., Naidu, R., 2015. Uncertainties in human health risk assessment of environmental contaminants: a review and perspective, Environ. Int. 85, 120-132.

Du Y, Xu X, Chu M, Guo Y, Wang J (2016) Air particulate matter and cardiovascular disease: the epidemiological, biomedical and clinical evidence. J Thorac Dis 8(1):E8–E19.

Duan X (2016) Highlights of the Chinese exposure factors handbook (children)-Chinese version. China Environmental Science Press, Beijing

Elkama, A., Şüküroğlu, A. A., & Çakmak, G. (2021). Exposure to particulate matter: a brief review with a focus on cardiovascular effects, children, and research conducted in Turkey. Arhiv za higijenu rada i toksikologiju, 72(4), 244-252.

ENHEALTH, 2012. Environmental Health Risk Assessment, Guidelines for Assessing Human Health Risks From Environmental Hazards. Environmental Health Standing Committee, Canberra, Australia.

Fadel, M., Courcot, D., Afif, C., & Ledoux, F. (2022). Methods for the assessment of health risk induced by contaminants in atmospheric particulate matter: a review. Environmental Chemistry Letters, 20(5), 3289-3311.

Farzaneh H (2019) Climate change multiple impact assessment models. Energy systems modeling. Springer, Singapore, pp 107–129

Fortoul TI, Rodriguez-Lara V, Gonzalez-Villalva A, Rojas-Lemus M, Colin-Barenque L, Bizarro-Nevares P, García-Peláez I, Cano MU-, López-Zepeda S, Cervantes-Yépez S, López-Valdez N, Meléndez-García N, Espinosa-Zurutuza M, Cano-Gutierrez G, Cano-Rodríguez MC (2015) Health Effects of Metals in Particulate Matter

Fowler D, Brimblecombe P, Burrows J, Heal MR, Grennfelt P, Stevenson DS, Jowett A, Nemitz E, Coyle M, Liu X, Chang Y, Fuller GW, Sutton MA, Klimont Z, Unsworth MH, Vieno M (2020) A chronology of global air quality. Philos Trans Royal Soc A 378(2183):20190314.

Gao T, Wang XC, Chen R, Ngo HH, Guo W (2015) Disability adjusted life year (DALY): a useful tool for quantitative assessment of environmental pollution. Sci Total Environ 511:268–287.

Gauderman WJ, Avol E, Gilliland F, Vora H, Thomas D, Berhane K, McConnell R, Kuenzli N, Lurmann F, Rappaport E, Margolis H, Bates D, Peters J (2004) The effect of air pollution on lung development from 10 to 18 years of age. N Engl J Med.

Haber LT, Strawson JE, Maier A, Baskerville-Abraham IM, Parker A, Dourson ML (2012) Noncancer risk assessment: principles and practice in environmental and occupational settings. In: Patty's Toxicology. pp. 89–132

Hava Kirliliği, Tuncel Süleyman Gürdal, Atimtay Aysel, Editör, Nobel Akademik Yayıncılık, Ankara, 2023

IARC (2021) IARC monographs on the identifcation of carcinogenic hazards to Humans.

International Agency for Research on Cancer. Outdoor air pollution. IARC monographs on the evaluation of carcinogenic risks to humans. Volume 109. Lyon: IARC; 2016

International Programme on Chemical Safety (IPCS), 2014; U.K. IGHRC, 2003

Kermani, M., Asadgol, Z., Gholami, M., Jafari, A. J., Shahsavani, A., Goodarzi, B., & Arfaeinia, H. (2021). Occurrence, spatial distribution, seasonal variations, potential sources, and inhalation-based health risk

assessment of organic/inorganic pollutants in ambient air of Tehran. Environmental geochemistry and health, 43, 1983-2006.

Koukoulakis KG, Kanellopoulos PG, Chrysochou E, Costopoulou D, Vassiliadou I, Leondiadis L, Bakeas E (2020) Atmospheric concentrations and health implications of PAHs, PCBs and PCDD/Fs in the vicinity of a heavily industrialized site in Greece. Appl Sci 10(24):9023.

Liu J, Chen Y, Chao S, Cao H, Zhang A, Yang Y (2018) Emission control priority of PM2.5 bound heavy metals in different seasons: a comprehensive analysis from health risk perspective. SciTotal Environ 644:20–30.

Masters, G. M., 1991. Introduction to environmental engineering and science. Prentice Hall International Publication. 291-292.

Morgenstern V, Zutavern A, Cyrys J, Brockow I, Koletzko S, Krämer U, Behrendt H, Herbarth O, Von Berg A, Bauer CP, Wichmann HE, Heinrich J, Wichmann HE, Bolte G, Belcredi P, Jacob B, Schoetzau A, Mosetter M, Schindler J, Schäfer T et al (2008) Atopic diseases, allergic sensitization, and exposure to trafficrelated air pollution in children. Am J Respir Crit Care Med.

Niu, X., Ho, S. S. H., Ho, K. F., Huang, Y., Sun, J., Wang, Q., et al. (2017). Atmospheric levels and cytotoxicity of polycyclic aromatic hydrocarbons and oxygenated-PAHs in PM2. 5 in the Beijing-Tianjin-Hebei region. Environmental Pollution, 231, 1075–1084.

OEHHA (2001) A guide to health risk assessment. California environmental protection agency, office of environmental health hazard assessment.

Patterson, J., Hakkinen, P.J., Wullenweber, A.E., 2002. Human health risk assessment: selected internet and world wide web resources, Toxicology.173, 23-143.

Pohl HR, Abadin HG (1995) Utilizing uncertainty factors in minimal risk levels derivation. Regul Toxicol Pharmacol 22(2):180–188.

Robson, M. and Toscana, W., 2007. “Risk assessment for environmental health.” John Wiley&Sons

S.K. Sharma, N. Choudhary, P. Srivastava, M. Naja, N. Vijayan, G. Kotnala, T.K. Mandal, Variation of carbonaceous species and trace elements in PM10 at a mountain site in the central Himalayan region of India, J. Atmos. Chem., 77, 2020, 1–14.

Taghizadeh, F., Jafari, A. J., Gholami, M., Kermani, M., Arfaeinia, H., Mohammadi, S., et al. (2019). Monitoring of airborne asbestos fibers in an urban ambient air of Shahryar City, Iran: levels, spatial distribution, seasonal variations, and health risk assessment. Environmental Science and Pollution Research, 26, 6450–6459.

USEPA (1989) General quantitative risk assessment guidelines for noncancer health effects. External review draft. Risk assessment forum technical panel on risk assessment guidelines for noncancer health effects

USEPA (1991) Risk assessment guidance for superfund: Volume I-human health evaluation manual (Part B, development of riskbased preliminary remediation goals) Publication 9285.7-01B. Office of emergency and remedial response, Washington, DC. NTIS PB92-963333

USEPA (1994) Methods for derivation of inhalation reference concentrations and application of inhalation dosimetry. Environmental criteria and assessment office, office of health and environmental assessment, office of research and development, U.S. environmental protection agency, Research Triangle Park, NC

USEPA (2002) Supplemental guidance for developing soil screening levels for superfund sites.U.S. Environmental protection agency, Washington, DC

USEPA (2004) Risk assessment guidance for superfund volume I. Human health evaluation manual (Part E, supplemental guidance for dermal risk assessment), Final. EPA/540/R/99/005. Office of solid waste and emergency response, Washington, DC. PB99-963312

USEPA (2012) Phthalates action plan. Washington, DC: U.S. EPA.

USEPA (2022) Human health risk assessment.

USEPA IRIS, 2021, Chemical Assessment Summary, Environmental Protection Agency Integrated Risk Information System, Washington, D.C

USEPA, 1992. Dermal exposure assessment:principles and applications.Office of ResearchandDevelopment, Office of Health and Environmental Assessment/ OHEA, U.S. Environmental Protection Agency, Washington, D.C

USEPA, 1997. Exposure Factors Handbook Vol. I-III. EPA/600/P-95/002Fa, U.S. Environmental Protection Agency, Washington, D.C.

Valle-Hernández, B. L., Figueroa-Lara, J. D. J., Torres-Rodríguez, M., Ginéz-Hernández, N., Álvarez-Lupercio, T., & Mugica-Álvarez, V. (2024). Levels, Sources and Risk Assessment of Carbonaceous

and Organic Species Associated with PM2. 5 in Two Small Cities of Morelos, Mexico. Atmosphere, 15(12), 1496.

Wang, F., Wang, J., Han, M., Jia, C., & Zhou, Y. (2019). Heavy metal characteristics and health risk assessment of PM2. 5 in students' dormitories in a university in Nanjing, China. Building and Environment.

WHO (2016) Ambient air pollution : a global assessment of exposure and burden of disease. Switzerland, Geneva.

WHO (2021) WHO human health risk assessment toolkit: chemical hazards, second edition. Geneva: World Health Organization; 2021 (IPCS harmonization project document, no. 8). Licence: CC BY-NC-SA 3.0 IGO

Yadav, A. K., Sarkar, S., Jyethi, D. S., Rawat, P., Aithani, D., Siddiqui, Z., & Khillare, P. S. (2021). Fine particulate matter bound polycyclic aromatic hydrocarbons and carbonaceous species in Delhi's atmosphere: seasonal variation, sources, and health risk assessment. Aerosol Science and Engineering, 5, 193-213.

Yu GH, Park S (2021) Chemical characterization and source apportionment of PM2.5 at an urban site in Gwangju, Korea. Atmos Pollut Res 12(6):101092–90.

Manisalidis I, Stavropoulou E, Stavropoulos A, Bezirtzoglou E (2020) Environmental and health impacts of air pollution: a review. Front Public Health 8:14.

➢ *ORAL PRESENTATION*

Sürdürülebilir Grafik Tasarım: Çevre Dostu Tasarım İlkeleri

Ali Aşur DELEN (ORCID:0000 0003 3767 8336)

Beykoz Üniversitesi, Sanat ve Tasarım Fakültesi, Grafik Tasarım Bölümü, İstanbul, Türkiye

*Sorumlu yazar e-posta: aliasurdelen@beykoz.edu.tr

Özet

Bu çalışma, grafik tasarım alanında sürdürülebilirlik ilkesinin teorik temelleri ile uygulama alanlarını kapsamlı biçimde incelemektedir. Artan çevresel sorunlar karşısında tasarımcıların sorumluluk üstlenmesi gerektiği vurgulanarak, çevre dostu tasarım anlayışının tarihsel gelişimi, temel ilkeleri ve güncel uygulamaları ele alınmıştır. Geri dönüştürülmüş malzemelerin kullanımı, çevreye duyarlı baskı teknikleri, düşük enerji tüketimli dijital araçlar ve minimalist tasarım yaklaşımı gibi başlıklarda somut önerilere yer verilmiştir. Ayrıca grafik tasarım yoluyla çevresel farkındalık oluşturma gücü örnek kampanyalar üzerinden değerlendirilmiş; bireysel tasarımcılar ve kurumsal yapıların bu süreçte üstlenebileceği sorumluluklar tartışılmıştır. Kavramsal bir çerçevede ilerleyen çalışma, sürdürülebilir grafik tasarımın sadece çevreyi korumakla kalmayıp, aynı zamanda toplumsal bilinç oluşturma ve davranış değişikliği yaratma potansiyeline sahip olduğunu ortaya koymaktadır. Sonuç olarak, sürdürülebilirlik yaklaşımı, tasarım sürecine yeni olanaklar kazandıran bir etik çerçeve olarak ele alınmakta ve tasarımcıların bu dönüşümde aktif rol üstlenmesi gerektiği vurgulanmaktadır.

Anahtar Kelimeler: Sürdürülebilirlik, Grafik Tasarım, Ekolojik İletişim, Görsel Kültür, Dijital Üretim

Sustainable Graphic Design: Eco-Friendly Design Principles

Abstract

This study comprehensively examines the theoretical foundations and application areas of the principle of sustainability in the field of graphic design. Against the backdrop of mounting environmental challenges, the text emphasises the responsibility of designers to embrace environmentally friendly design principles, tracing their historical evolution, fundamental principles, and contemporary applications. The text provides concrete recommendations on topics such as the use of recycled materials, environmentally friendly printing techniques, low-energy digital tools and minimalist design approaches. Additionally, the power of graphic design to raise environmental awareness is evaluated through exemplary campaigns, and the responsibilities that individual designers and corporate entities can take on in this process are discussed. The conceptual framework of the study reveals that sustainable graphic design not only protects the environment, but also has the potential to create societal awareness and behavioural change. In conclusion, the sustainability approach is considered to be an ethical framework that can open up new possibilities in the design process, and it is emphasised that designers must play an active role in this transformation

Keywords: Graphic Design, Sustainability, Eco-Friendly Design, Design Principles, Minimalist Approach.

GİRİŞ

Günümüzde iklim değişikliği, doğal kaynakların tükenmesi, çevre kirliliği ve ekosistem tahribatı gibi küresel çevre sorunları, yalnızca çevre bilimleri alanında değil, yaratıcı endüstrilerde de sorumluluk bilincini tetikleyen temel dinamiklerden biri haline gelmiştir. Bu bağlamda, grafik tasarım gibi görsel iletişimi merkezine alan disiplinlerin, sürdürülebilirlik ilkeleriyle uyumlu bir yaklaşım geliştirmesi kaçınılmazdır. Grafik tasarımın yalnızca estetik ve işlevsel bir iletişim aracı olmanın ötesine geçerek, çevresel etkileri göz önünde bulunduran bir üretim süreci haline gelmesi, tasarım pratiğinin yeniden tanımlanmasını gerektirmektedir (Papanek, 1971; Jedlicka, 2010).

Sürdürülebilir grafik tasarım, sadece geri dönüştürülebilir malzemelerin tercih edilmesiyle sınırlı kalmayıp; baskı tekniklerinden dijital üretim araçlarına, kullanıcı arayüzlerinden görsel dil tercihlerine kadar tüm süreçlerde doğaya duyarlı stratejiler geliştirilmesini kapsayan bütüncül bir yaklaşımdır (Allameh ve Jozam, 2020; Mirković ve ark., 2019). Bu kapsamda, kaynak kullanımını azaltan, karbon ayak izini düşüren ve

üretim döngüsünde ekolojik dengeyi gözeten tasarım çözümleri ön plana çıkmaktadır. Grafik tasarımcılar bu süreçte, geleneksel yöntemleri sorgulayan ve sürdürülebilir alternatifleri benimseyen karar vericiler olarak konumlanmaktadır (Regions, 2014). Aynı zamanda grafik tasarım, çevresel sorunlara ilişkin farkındalık yaratma ve toplumsal davranışları etkileme potansiyeline sahip güçlü bir iletişim aracıdır. Etkileyici görseller aracılığıyla geniş kitlelere ulaşabilen tasarımlar, çevre duyarlılığını artırmak ve sürdürülebilir yaşam alışkanlıklarını teşvik etmek açısından kritik bir rol üstlenmektedir (Strawzell, 2013; Utoyo ev ark., 2021). Bu bağlamda, grafik tasarım yalnızca mesaj taşıyan bir araç değil, aynı zamanda çevresel bilinç üretme sürecinin aktif bir bileşenidir. Örneğin, Şekil 1'de yer alan ve çevre ikonlarıyla dijital olarak bütünleştirilmiş bir deniz kaplumbağası görseli, tasarım ile doğa arasındaki ilişkinin sembolik temsillerinden biridir. Bu tür görseller, grafik tasarımın sürdürülebilirlik kavramını estetik düzlemde nasıl görünür kılabileceğine dair güçlü bir örnek sunar.



Şekil 1. Sürdürülebilir grafik tasarım kavramını sembolik olarak ifade eden bir görsel. Çevre ikonları ve bir deniz kaplumbağası, tasarım ile ekoloji arasındaki bağı vurgulamaktadır.

Dijitalleşmenin tasarım üretiminde merkezi bir konuma gelmesiyle birlikte, enerji verimliliği sağlayan dijital içerikler, çevre dostu kullanıcı arayüzleri ve minimalist tasarım anlayışları da sürdürülebilirlik ekseninde yeniden değerlendirilmelidir (VanEenoo, 2011; Palafox, 2019). Böylece grafik tasarım, yalnızca fiziksel üretim değil, aynı zamanda dijital ortamda da ekolojik sorumluluk taşıyan bir faaliyet alanı haline gelmektedir.

Bu çalışma, sürdürülebilir grafik tasarım kavramını kuramsal, tarihsel ve uygulamalı yönleriyle ele almakta; çevre dostu tasarım ilkelerinin tasarım sürecine entegrasyonunu örneklerle destekleyerek ortaya koymayı amaçlamaktadır. Malzeme seçimi, üretim teknikleri, dijital araç kullanımı ve toplumsal farkındalık kampanyaları bağlamında sürdürülebilirlik ilkesinin grafik tasarıma nasıl yansıtılabileceği analiz edilmekte; bireysel tasarımcılar ve kurumlar düzeyinde üstlenilebilecek roller kapsamlı biçimde değerlendirilmektedir. Sonuç olarak bu çalışma, grafik tasarımı yalnızca estetik bir ifade aracı olarak değil, aynı zamanda çevresel dönüşümün destekleyicisi olan stratejik bir iletişim pratiği olarak konumlandırmaktadır.

SÜRDÜRÜLEBİLİR GRAFİK TASARIM: TANIM VE KAVRAMSAL ÇERÇEVE

Grafik tasarımda sürdürülebilirlik, tasarım ürünlerinin yaşam döngüsü boyunca çevreye en az zarar verecek şekilde planlanması anlamına gelir. Bu yaklaşım, sadece geri dönüştürülebilir malzemeler kullanmak veya "yeşil" temalı görseller oluşturmakla sınırlı kalmayıp, tasarım sürecinin her aşamasında çevresel sorumluluk bilinciyle hareket etmeyi gerektirir. Fikir geliştirme, üretim, dağıtım ve kullanım aşamalarında çevresel etkileri minimize etmek sürdürülebilir grafik tasarımın temelini oluşturur. Sürdürülebilir grafik tasarım, "tüm yaşamın iyiliğini gözeten tasarım" olarak da tanımlanabilir ve bugünün ihtiyaçlarını karşılarken gelecek nesillerin kaynaklarını tehlikeye atmayan tasarımlar ortaya koymayı hedefler. Geleneksel grafik tasarım uygulamalarının önemli bir çevresel ayak izi olabilir. Kağıt kullanımı ormansızlaşmaya ve atık oluşumuna sebep olurken, kullanılan mürekkepler ve baskı kimyasalları üretim ve bertaraf süreçlerinde zararlı organik bileşikler yayarak hava ve su kirliliğine neden olabilir (Regions, 2014). Baskı süreçleri, enerji tüketimi ve nakliye de düşünüldüğünde karbon salınımına yol açabilir. Dijital grafik tasarım da enerji tüketimi açısından tamamen zararsız değildir; bilgisayarlar, sunucular ve veri merkezlerinin çalışması elektrik tüketimine neden olur ve bu enerjinin fosil yakıtlardan sağlanması karbon emisyonlarına yol açar. Sürdürülebilir grafik tasarımın önemi, hem tasarım sektöründe hem de toplumda giderek daha fazla anlaşılmaktadır. Tasarımcılar, mesajlarını görselleştirirken doğal kaynakları sorumlu bir şekilde kullanma yükümlülüğünü taşırlar. Bu yaklaşımın benimsenmesi, çevreye doğrudan fayda sağlamanın yanı sıra topluma da örnek olur. Tüketiciler, üzerinde "FSC sertifikalı kağıda basılmıştır" ibaresi bulunan bir broşür veya geri dönüştürülmüş malzemelerle üretilmiş bir ambalajla karşılaştıklarında, markaların ve tasarımcıların çevreye duyarlılığı hakkında olumlu bir algı geliştirirler. Sürdürülebilir

tasarım, doğru olanı yapmanın ötesinde, iletişim kurduğu kitleyi eğiten ve farkındalık kazandıran bir araç haline gelir (Allameh ve Jozam, 2020).

ÇEVRE VE TASARIM İLİŞKİSİNİN TARİHİ GELİŞİMİ

Grafik tasarım ile çevre bilincinin kesişimi yeni bir olgu değildir. 20. yüzyılın ikinci yarısından itibaren tasarımcılar, toplumsal ve çevresel meselelere görsel iletişimle dikkat çekmeye başlamıştır. Özellikle 1960'lar ve 1970'lerde yükselen çevre hareketi, grafik tasarımcılar için de ilham kaynağı olmuştur. 22 Nisan 1970'de kutlanan ilk Dünya Günü, çevresel farkındalık adına dönüm noktasıydı. Bu etkinlik kapsamında ünlü sanatçılar ve tasarımcılar çevre temalı posterler tasarladılar. Örneğin, Amerikalı sanatçı Robert Rauschenberg, ilk Dünya Günü için bir poster tasarlayarak çevre kirliliğine dikkat çekti. (Şekil 2)



Şekil 2. Robert Rauschenberg, ilk Dünya Günü için yaptığı poster (Rauschenberg, 1970)

Benzer şekilde karikatürist Walt Kelly, "Pogo" karakterini kullanarak "We have met the enemy and he is us" sloganıyla çevre sorunlarına insanın kendi etkisini vurgulayan bir poster hazırladı. Bu dönemden bir başka çarpıcı çalışma da grafik tasarımcı Seymour Chwast'ın 1968 tarihli "End Bad Breath" posteri idi. Her ne kadar Chwast'ın posteri doğrudan çevre kirliliğinden ziyade Vietnam Savaşı'na atıf yapsa da, kullanılan metafor (Uncle Sam'in ağzından dumanlar çıkması) hava kirliliği ve zehirli propagandayla özdeşleştirilerek dönemin protest ruhunu yansıtıyordu. Tasarımcılar, güçlü mesajlar içeren görsellerle kamusal tartışmalara katılmış ve değişim çağrılarını desteklemişlerdir (Strawzell, 2013).

1970 yılındaki ilk Dünya Günü'nde bir tasarım öğrencisi olan Gary Anderson, bugün tüm dünyada tanınan geri dönüşüm sembolünü yarattı (Şekil 3). Üç kıvrımlı oktan oluşan bu simge, kağıt geri dönüşümünü teşvik etmek amacıyla bir yarışma kapsamında geliştirilmiş ve hızla evrensel bir işaret haline gelmiştir. Sembolün üç okla çizdiği döngü, azalt-yeniden kullan-geri dönüştür (3R: reduce, reuse, recycle) prensiplerini temsil eder. Bu logo, belki de sürdürülebilir tasarımın grafik alandaki ilk ikonik örneğidir ve kamu malı (public domain) olarak serbestçe kullanıma açık olduğundan, çevre dostu uygulamaların yaygınlaşmasında büyük payı olmuştur. Geri dönüşüm sembolü, baskı tasarımında önemli bir yere sahiptir (Strawzell, 2013).



Şekil 3. Evrensel geri dönüşüm sembolü. (Container Corporation of America, 1970)

1980'ler ve 1990'lar, sürdürülebilir tasarım kavramının farklı tasarım disiplinlerinde kuramsal olarak ele alınmaya başlandığı dönemlerdir. 1987'de yayınlanan Brundtland Raporu ile sürdürülebilir kalkınma kavramı uluslararası ölçekte dikkat çekmiş; bu durum tasarım dünyasında da yankı bulmuştur. 1990'larda özellikle mimarlık ve endüstriyel tasarım alanlarında "yeşil tasarım" hareketi ivme kazanırken, grafik tasarım topluluğu da matbaa endüstrisindeki çevre sorunlarına eğilmeye başlamıştır. Bu dönemde Amerikan Grafik Tasarımcılar Birliği gibi mesleki kuruluşlar, tasarım ve baskı süreçlerinde çevresel sorumluluğu teşvik eden kılavuzlar yayımlamışlardır. Örneğin, AIGA'nın "Design and Environment" girişimleri, tasarımcılar ile kağıt/başım tedarikçileri arasındaki diyaloğu geliştirmeyi ve daha sürdürülebilir seçimleri özendirmeyi amaçlamıştır. 2000'lere gelindiğinde, dijital devrim ile birlikte grafik tasarımın

üretim ve dağıtım yöntemleri değişirken, sürdürülebilirlik boyutu yeni sorular ve fırsatlarla gündeme gelmiştir (örneğin çevrimiçi tasarımın enerji maliyeti, elektronik atıklar, vb.). Son yıllarda ise sürdürülebilir grafik tasarım, tasarım eğitiminin ve profesyonel pratiklerin ayrılmaz bir parçası haline gelmeye başlamıştır. Tasarım konferanslarında, akademik yayınlarda ve endüstri bloglarında sürdürülebilirlik sıkça tartışılan bir konu olmuş; genç tasarımcılar arasında eko-inovasyon, döngüsel tasarım ve sosyal sorumluluk kavramları önem kazanmıştır (Alahira ve ark., 2024). Özetle, grafik tasarımcılar tarih boyunca toplumsal meselelere duyarlı olmuş ve çevre hareketine de yaratıcı katkılar sunmuştur. Geçmişteki bu birikim, günümüz tasarımcılarına ilham vermekte ve sürdürülebilirlik odaklı bir tasarım kültürünün temellerini oluşturmaktadır.

SÜRDÜRÜLEBİLİR GRAFİK TASARIM İLKELERİ

Grafik tasarımda sürdürülebilirlik, teori kadar pratikte de kendini göstermelidir. Bir tasarımın sürdürülebilir olması, onu hayata geçirme sürecindeki tercihlerin çevre dostu olmasıyla mümkündür. Bu bölümde, sürdürülebilir tasarım anlayışının somut uygulama alanları ele alınacaktır: Geri dönüştürülmüş malzeme kullanımı, çevre dostu baskı teknikleri ve düşük enerji tüketimli dijital araçlar. Bu uygulamalar, grafik tasarımcının karar verebileceği farklı aşamalara karşılık gelir ve birlikte ele alındığında tasarım sürecinin bütününde bir dönüşümü ifade eder.

GERİ DÖNÜŞTÜRÜLMÜŞ MALZEMELERİN KULLANIMI

Basılı tasarım ürünlerinde en temel malzeme kağıttır ve kağıdın sürdürülebilir kaynaklardan gelmesi, çevresel etkinin azaltılmasında kritik bir rol oynar. Sürdürülebilir grafik tasarımın en önemli uygulamalarından biri geri dönüştürülmüş kağıt kullanımıdır. Geri dönüşüm kağıdı, atık kağıtların toplanıp yeniden hamur haline getirilmesiyle üretilir ve bu sayede yeni odun hamuruna duyulan ihtiyacı azaltır. Bu süreç, hem ağaç kesimini azaltır hem de kağıt atıklarının çöp sahalarında birikmesini önler. Geri dönüştürülmüş kağıt kullanımının karbon ayak izini küçülttüğü ve atık miktarını düşürdüğü belirtilmektedir. Günümüzde geri dönüşüm kağıtları, geçmişe kıyasla çok daha yüksek kalitede üretilebilmektedir. Farklı dokulara ve dayanıklılıklara sahip geri dönüştürülmüş kağıtlar, kartvizitlerden parlak dergilere kadar çeşitli ihtiyaçlara cevap verebilmektedir. Bu gelişmeler, tasarımcıların estetik veya kalite kaygısı duymadan geri dönüşümlü kağıda yönelebilmelerini sağlamaktadır. Kağıt seçiminde bir diğer sürdürülebilir yaklaşım, alternatif liflerden üretilmiş kağıtlar kullanmaktır. Örneğin, ağaç dışı kaynaklardan (keten, kenevir, buğday sapı gibi tarımsal atıklardan) yapılan kağıtlar son yıllarda dikkat çekmektedir (Plazonić ve ark, 2016). Bu tip kağıtlar, odun lifi yerine hızlı yenilenebilir veya atık lifleri kullandığı için ormanlar üzerindeki baskıyı azaltır. Tasarımcıların mümkün olduğunca odun dışı kağıtları veya %100 post-tüketici atıklardan üretilmiş kağıtları tercih etmesi önerilmektedir. PCW ibaresi, kağıdın tamamının tüketici sonrası atıklardan geri dönüştürüldüğünü, yani çöpe gidecek malzemelerin yeniden değerlendirildiğini gösterir. Bu tür kağıtlar, aksi halde çöplüklerde çürüyecek ve metan gazı salacak atıkları değerli bir kaynağa dönüştürür. Kağıt üretimi sırasında uygulanan işlemler de sürdürülebilirlik açısından önemlidir. Örneğin, beyazlatma (ağartma) işlemlerinde geleneksel olarak kullanılan klor, zararlı yan ürünler oluşturur. Bu nedenle, klor içermeyen (TCF – Totally Chlorine Free) veya elemental klor içermeyen kağıtlar tercih edilmelidir. Geri dönüştürülmüş kağıtlarda ise mümkünse PCF yöntemle, yani geri dönüştürme sürecinde klor kullanılmadan beyazlatma yapılmış kağıtlar kullanılabilir. Bu sayede klor kaynaklı dioksin gibi toksik maddelerin su sistemlerine karışmasının önüne geçilir. Kağıt tedarikinin sürdürülebilir olması sadece geri dönüşümle değil, aynı zamanda sorumlu ormancılık uygulamalarıyla da ilgilidir. Eğer bakir (geri dönüştürülmemiş) kağıt kullanılıyorsa, bunun FSC sertifikalı olmasına dikkat edilmelidir (FSC Paper, 2024). Forest Stewardship Council sertifikası, ilgili kağıdın veya ahşap ürünün sürdürülebilir orman yönetimi kriterlerine uygun kaynaklardan geldiğini garanti eder. FSC sertifikalı ormanlar, ağaç kesiminin kontrollü yapıldığı, biyoçeşitliliğin korunduğu, orman işçilerinin ve yerel halkın haklarının gözetildiği işletmelerdir. FSC'nin "Recycled", "FSC 100%" ve "FSC Mix" gibi etiketleri bulunmaktadır; örneğin "FSC Recycled" etiketi taşıyan bir kağıdın tamamen geri dönüştürülmüş içerikten yapıldığı anlamına gelir. Benzer şekilde PEFC sertifikası da dünya genelinde kabul gören bir diğer orman sertifikasyon sistemidir ve sürdürülebilir orman yönetimini teşvik eden standartları vardır

Sonuç olarak, bir grafik tasarım projesinde kağıt seçimi yapılırken sürdürülebilirlik adına sorulacak temel sorular şunlardır: Bu kağıt geri dönüştürülmüş mü? Değilse, sertifikalı sürdürülebilir bir kaynaktan mı geliyor? Üretiminde klor gibi zararlı kimyasallar kullanılmış mı? Bu sorulara verilen yanıtlar, tasarım

ürününün çevresel profilini belirler. Sürdürülebilir malzeme kullanımı, tasarımcıların kontrol edebileceği somut bir alandır ve nispeten küçük bir tercih değişikliğinin (örneğin kuşe kağıt yerine geri dönüştürülmüş kâğıt seçmek) bile ölçek etkisiyle ciddi kazanımlar sağlayabileceği unutulmamalıdır.

ÇEVRE DOSTU BASKI TEKNİKLERİ

Baskı süreçlerinde çevresel etkilerin azaltılması, sürdürülebilir grafik tasarım uygulamalarının temel hedeflerinden biridir. Özellikle kullanılan mürekkep türleri ve baskı sonrası işlemler, çevreye olan etkinin belirleyicileri arasında yer alır. Geleneksel ofset baskılarda kullanılan petrol türevi mürekkepler, üretim ve uygulama sırasında yüksek oranda uçucu organik bileşikler (VOC) salımı yapar. Bu bileşikler hem insan sağlığına zararlıdır hem de hava kalitesini olumsuz etkiler. Buna karşılık, soya ve diğer bitkisel yağ bazlı mürekkepler, VOC oranı düşük, yenilenebilir kaynaklara dayalı çevre dostu alternatiflerdir. Ayrıca bu tür mürekkepler, geri dönüşüm sırasında kâğıttan daha kolay ayrışarak geri kazanımı kolaylaştırır (Mirković ve ark., 2019). Renk ve efekt katkı maddeleri de sürdürülebilirlik açısından dikkatle seçilmelidir. Fosforlu veya metalik mürekkepler genellikle ağır metaller içerdiğinden, çevre dostu baskı prensipleri bu tür katkıların kullanımını sınırlandırır. Aynı şekilde, parlak selefon kaplamalar ve UV lak gibi uygulamalar da geri dönüşüm sürecini zorlaştırır. WWF, biyolojik olarak parçalanabilir laminatların dahi yapıştırıcıları nedeniyle geri dönüşüme engel oluşturabileceğini belirtmektedir (Sürdürülebilir Grafik Tasarım: Çevre Dostu Tasarım İlkeleri, n.d.). Bu nedenle, su bazlı vernikler veya kabartma gibi geri dönüşüm dostu tekniklerin tercih edilmesi önerilir.

Teknolojideki gelişmeler, baskı sektöründe daha çevreci uygulamaların yaygınlaşmasını sağlamaktadır. Eko-solvent yazıcılar, geleneksel solventlere göre daha az toksik çözücüler kullanarak dış mekân baskılarında güvenli seçenekler sunar. UV-LED baskı teknolojisi ise solvent içermez; UV ışığı ile anında kürlenen mürekkepler sayesinde VOC salınımı engellenir ve enerji verimli LED sistemleri kullanılır (Hall, A., 2024). Bunun yanı sıra, su kullanmayan ofset sistemleri ve kimyasalsız baskı kalıpları sayesinde hem su tüketimi azalır hem de atık suya karışan kirleticiler engellenir. Baskı sürecinde atık yönetimi de sürdürülebilirlik açısından kritik bir başlıktır. Sayfa yerleşimlerinin, kâğıt ölçüleri ve baskı tekniklerine uygun planlanması; kesim sonrası oluşabilecek fire miktarını en aza indirir. Ayrıca, sayfa üzerindeki mürekkep kaplama oranının azaltılması (yoğun renkli zeminler yerine açık tonlu arka planlar gibi) hem malzeme hem de enerji tasarrufu sağlar. Baskı sonrası ciltleme aşamasında kullanılan malzemelerin de çevreye etkisi göz önünde bulundurulmalıdır. Termal tutkallı veya plastik spiralli ciltleme yöntemleri geri dönüşüm açısından zorluk yaratırken; tel veya iplik dikişli ciltleme yöntemleri, kolay ayrıştırılabilir olmaları sayesinde çevre dostu seçenekler olarak öne çıkar (Abed El Salam, S. H.).

Sonuç olarak, tasarımcıların baskı öncesi süreçleri dikkatle planlaması ve matbaalarla etkin iletişim kurması sürdürülebilir uygulamaların başarısı açısından büyük önem taşır. Tasarım kararları, yalnızca estetik değil; aynı zamanda malzeme seçimi, baskı yöntemi ve geri dönüşüm uygunluğu gibi çevresel faktörleri de gözetmelidir. Bu yaklaşımla, baskı süreçleri boyunca çevre üzerindeki etki en aza indirilebilir.

DÜŞÜK ENERJİ TÜKETİMLİ DİJİTAL ARAÇLAR

Dijital ekranlar karşısında geçirilen sürenin artmasıyla birlikte, dijital grafik tasarım giderek daha merkezi bir rol oynamaktadır. Ancak dijital tasarım süreçlerinin fiziksel kaynak kullanmaması her zaman çevre dostu olduğu anlamına gelmez. İnternetin altyapısını oluşturan veri merkezleri ve kullanılan cihazlar, yüksek enerji tüketimi ve elektronik atık gibi çevresel sorunlara yol açabilir. Bu nedenle, dijital sürdürülebilirlik; yalnızca ürün değil, üretim araçları ve barındırma altyapısıyla birlikte düşünülmelidir. Tasarımcılar, kullandıkları donanımın enerji verimliliğine dikkat ederek sürece katkı sağlayabilirler. Energy Star gibi sertifikalı düşük tüketimli cihazların kullanımı, uyku modlarının etkinleştirilmesi ve gereksiz durumlarda cihazların kapatılması, toplam enerji tüketimini azaltan basit ama etkili adımlardır (Pimentel ve ark., 2008). Dijital ürünlerin enerji verimliliği ise özellikle web ve mobil arayüz tasarımında belirginleşir. Bu alanda gelişen “yeşil UX/UI” yaklaşımı, görsel ve işlevsel unsurların veri transferini minimumda tutacak şekilde optimize edilmesini önerir. Gereksiz animasyonlar, yüksek çözünürlüklü medya dosyaları ve karmaşık sayfa yapıları, cihazlarda ve sunucularda fazladan enerji tüketimine neden olabilir. Buna karşılık, sadeleştirilmiş tasarım, sıkıştırılmış görseller ve temiz kod yapısı, hem performansı artırır hem de çevresel etkiyi azaltır. Koyu arka plan tasarımları da özellikle OLED ve AMOLED ekranlı cihazlarda enerji tasarrufu sağlamaktadır. Bu nedenle birçok uygulama, kullanıcıya karanlık mod seçeneği

sunmaktadır. Ancak bu stratejinin her ekran türü için geçerli olmadığını ve erişilebilirlik açısından dikkatle uygulanması gerektiğini unutmamak gerekir. Barındırma altyapıları da dijital tasarımın sürdürülebilirliğinde kritik bir rol oynar. Web sitelerini destekleyen sunucular sürekli çalıştığından, bu sistemlerin yenilenebilir enerjiyle çalışıp çalışmadığı çevresel etkiyi doğrudan etkiler. Yeşil enerjiyle çalışan veri merkezlerini tercih eden hosting firmaları, daha sorumlu bir dijital tasarım yaklaşımının parçası olabilir (Website Sustainability, 2024). Tasarımcılar bu konuda farkındalık oluşturarak, müşterilerini de bilinçli tercihlere yönlendirebilir. Ayrıca, dijital içeriklerin dosya formatı ve boyutu da enerji tüketimini etkileyen önemli bir unsurdur. Statik görsellerin tercih edilmesi, animasyonların sınırlı kullanımı ve gereksiz medya öğelerinin kaldırılması; sunucu yükünü ve veri aktarım ihtiyacını azaltarak sürdürülebilirliği destekler. Örneğin, LED ekranlar için hazırlanan koyu zeminli dijital posterler, daha az enerji tüketir.

Sonuç olarak, dijital grafik tasarım sürecinde sürdürülebilirlik yalnızca estetik kararlarla sınırlı kalmamalı; kullanılan araçlardan, tasarım stratejilerine ve barındırma altyapısına kadar bütüncül bir yaklaşım benimsenmelidir. Enerji verimliliği, temiz enerji kullanımı ve veri yönetimi gibi faktörler dikkate alındığında, dijital tasarım çevresel sorumlulukla uyumlu bir üretim alanı haline gelebilir.

MİNİMALİST TASARIM İLE ENERJİ VE KAYNAK TASARRUFU

Minimalizm, tasarımda yalnızca estetik bir tercih değil, aynı zamanda sürdürülebilirlik açısından da önemli bir yaklaşımdır (vanEenoo, 2011). “Az çoktur” anlayışıyla hareket eden minimalist tasarım, gereksiz unsurları ortadan kaldırarak yalnızca temel öğelere odaklanır. Bu sadeleştirme, hem üretim hem de kullanım aşamalarında kaynakların daha verimli kullanılmasına katkı sağlar. Basılı materyallerde minimalizm; daha az mürekkep kullanımı, sınırlı sayfa sayısı ve kompakt boyutlar gibi avantajlar sunar. Örneğin, geniş beyaz alanlar içeren sade bir poster tasarımı, malzeme ve enerji tasarrufu sağlar. Ambalaj tasarımlarında ise gereksiz katmanlardan kaçınmak bu yaklaşımı destekler. Dijital mecralarda da minimalist tasarım enerji tüketiminin azaltılmasına katkı sunar. Basit arayüzler, cihazların işlem gücünü daha az kullanarak web sitelerinin daha hızlı yüklenmesini ve mobil cihazların pil ömrünün uzamasını sağlar (Selcová, 2014). Küçük dosya boyutları ve statik içerikler veri transferini ve enerji kullanımını düşürür (Palafox, 2019). Bu yönüyle minimalizm, tasarımcının kaynak kullanımına dair bilinçli kararlar almasını gerektirir. Tasarım sürecinin başında "Bu kadar sayfaya ihtiyaç var mı?" veya "Bu grafik mesajı gerçekten güçlendiriyor mu?" gibi sorgulamalar yapılmalıdır. Renk sayısını azaltmak ise doğrudan mürekkep tüketimini azaltarak çevresel etkiyi sınırlar. Minimalist tasarımlar aynı zamanda uzun ömürlüdür; geçici trendlere bağlı kalmaz ve zamansız nitelikleri sayesinde yıllarca kullanılabilir (Gumber, 2023). Sade bir logo, güçlü bir görsel kimlik sunarken sürekli yenileme ihtiyacını da azaltır. Her ne kadar her proje için uygun olmasa da minimalizmin temel ilkesi, yalnızca gerekli olanı korumak ve fazlalıkları elemektir. “Bu öğe olmazsa ne kaybederim?” sorusu, tasarımın işlevselliğini ve sürdürülebilirliğini değerlendirmek açısından önemli bir yol göstericidir.

Özetle, minimalizm sürdürülebilir grafik tasarımın görünmeyen ancak etkili bir dayanağıdır. Gösterişten uzak, amacı merkeze alan her tasarım; daha az kaynakla üretim yapılmasını, kullanım sırasında daha az enerji tüketilmesini ve dolayısıyla çevresel etkilerin azaltılmasını sağlar. Minimalist yaklaşım, tasarımcılara hem estetik hem de etik bir çerçeve sunar. Nihayetinde, en sürdürülebilir malzeme hiç tüketilmeyen malzemedir — minimalizm ise bunu baştan hedefler: Gereksiz tüketimi önlemek.

GRAFİK TASARIM YOLUYLA ÇEVRESEL FARKINDALIK

Grafik tasarım, çevresel sorunlara dikkat çekmek ve toplumsal farkındalık oluşturmak açısından güçlü bir iletişim aracıdır. Görsel tasarımlar; karmaşık çevre meselelerini sadeleştirerek geniş kitlelere etkili biçimde aktarabilir. Özellikle afişler, sosyal kampanya görselleri ve infografikler, çevresel farkındalık oluşturma süreçlerinde önemli rol oynar (Utoyo et al., 2021). 1970'lerden bu yana grafik tasarım, çevre hareketlerinin görsel yüzü haline gelmiş; bu dönemde tasarımcılar ormansızlaşma, kirlilik ve iklim değişikliği gibi sorunlara dikkat çekmek amacıyla çarpıcı görsel metaforlar geliştirmiştir.



Şekil 4. Basit ve etkili bir çevre farkındalığı posteri örneği.

Benzer şekilde, küresel ölçekte düzenlenen kampanyalar için geliştirilen grafik tasarımlar da çevresel iletişimde kritik rol oynar. Dünya Saati etkinliği kapsamında tasarlanan "60+" logosu, karanlık zemin üzerinde dünya sembolüyle enerji tasarrufu çağrısında bulunur. Bu logo, yalnızca bir saatlik eylemle sınırlı kalmayıp, sürdürülebilir yaşam alışkanlıklarına dikkat çekmeyi amaçlamaktadır. Kampanya sürecinde şehir silüetlerinin karartılması gibi sembolik görseller, bu mesajı daha da pekiştirmiştir. Grafik tasarım ayrıca, infografikler aracılığıyla çevresel verileri sadeleştirip anlaşılır hale getirmekte de etkilidir. Örneğin, plastik atıkların okyanuslara etkisini gösteren infografikler; konunun hem bilimsel hem de duygusal boyutuna hitap ederek izleyicide farkındalık yaratır. Ayrıca grafik tasarım, çevre odaklı protesto ve aktivizmin de görsel dilini oluşturur. İklim grevlerinde kullanılan dövizler, yaratıcı tipografiler ve "There is no Planet B" gibi küresel sloganlar, genç kuşağın çevresel kaygılarını görünür kılar. Bu süreçte Do The Green Thing, Poster for Tomorrow gibi platformlar, tasarımcıların çevreci mesajlarını paylaşabilecekleri ortamlar sunar ve katılımcı farkındalığı teşvik eder.

Sonuç olarak, grafik tasarım; bilgi aktarımı, toplumsal etki ve duygusal bağ kurma potansiyeli sayesinde çevresel iletişimde vazgeçilmez bir araçtır. Etkili bir görsel, karmaşık bir rapordan daha hızlı ve kalıcı biçimde etki yaratabilir. Tasarımcılar bu potansiyelin farkında olarak, çevre temelli projelerde yalnızca estetik değil, etik sorumluluk da üstlenmelidir. Bu bağlamda grafik tasarım, yalnızca bir iletişim biçimi değil, aynı zamanda sürdürülebilir bir gelecek için dönüşüm aracı olarak değerlendirilmelidir.

SÜRDÜRÜLEBİLİR GRAFİK TASARIM UYGULAMALARINA YÖNELİK ÖNERİLER

Sürdürülebilir grafik tasarım ilkelerini hayata geçirmek, hem bireysel tasarımcıların hem de kurumların bilinçli çabalarını gerektirir. Yalnızca tasarımcıların kendi pratiklerini değiştirmesi yetmez; müşterilerin, baskı tedarikçilerinin ve genel iş kültürünün de bu değişime uyum sağlaması önemlidir. Bu bölümde, bireysel düzeyde tasarımcıların neler yapabileceği ve kurumsal düzeyde hangi politikaların uygulanabileceği ele alınacaktır.

Bireysel Tasarımcılar Olarak: Grafik tasarımcılar, projelerin her aşamasında sürdürülebilirlik için adımlar atabilirler. Tasarımcılar, her projede "Bu işi daha çevre dostu nasıl yapabilirim?" sorusunu sormalıdır. Örneğin, kağıt seçiminde müşteriyi geri dönüşümlü kağıda yönlendirebilir veya tek renkli tasarımlar önerebilirler. Sürdürülebilirlik konusunda güncel kalmak ve yeni çıkan çevre dostu malzemeler hakkında bilgi edinmek önemlidir. Re-nourish gibi kaynaklar ve karbon ayak izi hesaplama araçları tasarımcılara yardımcı olabilir. Müşteri iletişiminde sürdürülebilirlik elçisi olarak, önerilen çözümlerin çevresel faydalarını vurgulamak önemlidir. Ofis içinde kağıt israfını önlemek ve elektronik cihazları verimli kullanmak da bireysel düzeyde atılabilecek adımlardır. Uzaktan çalışma ve dijital onay süreçleri yaygınlaştırılarak karbon ayak izi düşürülebilir. Sürdürülebilir tasarım, çevresel, sosyal ve ekonomik faktörleri ön planda tutarak kaynakların verimli kullanılmasını ve gelecek nesillerin ihtiyaçlarının karşılanmasını sağlar.

Kurumsal Düzeyde (Ajanslar ve Şirketler): Kurumsal düzeyde, grafik tasarım hizmeti veren ajanslar, matbaalar veya tasarıma ihtiyaç duyan şirketler, sürdürülebilirliği iç politikalarıyla teşvik edebilirler. Kurumlar, üst yönetim desteğiyle kapsamlı bir sürdürülebilirlik politikası oluşturup uygulayabilirler. Örneğin, bir reklam ajansı, tedarikçi seçiminde yeşil kriterler belirleyebilir ve sadece FSC sertifikalı kağıt kullanan matbaalarla çalışabilir. Şirketler, tasarım çalışmalarının etkisini azaltmak için basit önlemler alabilirler (Alahira ve ark., 2024). Örneğin, katalog boyutlarını küçültebilir, geri dönüştürülmüş kağıt seçebilir ve baskı adedini optimize edebilirler. Kurumlar, basılı iletişimi dijital ortama kaydırarak kağıt

tüketimini azaltabilirler. Kurum içi tasarım ekipleri veya ajanslar, çalışanlarına yönelik eğitimlerle sürdürülebilir tasarım farkındalığı yaratmalıdır. Şeffaflık ve hesap verebilirlik mekanizmaları kurmak da önemlidir; şirketler, yıllık sürdürülebilirlik raporlarında iletişim faaliyetlerinin çevresel etkisini raporlayabilirler. Tedarik zinciri iş birlikleri de kurumsal düzeyde kritik bir faktördür. Tasarım ajansları, birlikte çalıştığı matbaaları yeşil uygulamalar konusunda teşvik edebilir (Studio Carbon Negative, 2013). Kurumlar arası iyi uygulama paylaşımları da önemlidir (MaCher: Sustainable Promotional & Packaging Design, 2025). Sektör dernekleri veya mesleki konferanslar yoluyla, firmalar sürdürülebilir tasarım yolculuklarını ve öğrendiklerini birbirine aktarmalıdır (Harris, 2021).

Son olarak, hem bireysel hem de kurumsal düzeyde belki de en kritik unsur, tutarlılık ve samimiyettir. "Yeşil yıkama" (greenwashing) olarak bilinen, sadece çevreci görünmek için yüzeysel adımlar atıp bunu abartılı biçimde pazarlama hatasına düşmemek gerekir. Tasarımcılar, eğer bir proje gerçekten çevreci değilse onu öyleymiş gibi göstermemeli; kurumlar da sürdürülebilirlik ilkelerini reklam sloganı yapıp iç uygulamalarında bunu boşlamamalıdır. Bu denge kurulduğunda, yapılan işler hem etik hem de iletişim açısından güçlü olacaktır.

SONUÇ

Sürdürülebilir grafik tasarım, gezegenimizin geleceği için tasarım disiplininin üstlendiği kritik bir sorumluluktur. Bu yaklaşım, grafik tasarım süreçlerinde ekoloji, ekonomi ve estetiğin dengeli bir biçimde bir araya getirilmesini gerektirir. İncelediğimiz üzere, sürdürülebilirlik kavramı basılı malzeme seçiminden baskı tekniklerine, dijital tasarım uygulamalarından minimalist anlayışa kadar geniş bir yelpazede somut adımlara dönüşebilmektedir. Her bir adım, tek başına küçük görünse de birleştiğinde anlamlı bir fark yaratır. Elbette sürdürülebilir tasarım, bir gecede tamamlanacak bir hedef değildir; bu daha çok süreklilik arz eden bir yolculuktur. Tasarımcılar ve kurumlar, teknolojinin ve bilginin gelişimiyle birlikte sürekli öğrenmeli, uygulamalarını güncellemelidir. Örneğin, bugün ideal gördüğümüz bir malzeme veya teknik, yarın daha iyisi bulunduğunda değişebilir. Bu yüzden esneklik ve yeniliğe açıklık önemlidir. Sürdürülebilirlik, tasarım pratiğine yerleştiğinde, aslında inovasyonu da beraberinde getirir – çünkü daha iyiyi, daha verimliyi arama çabası, yaratıcılıkla beslenecektir. Bu makalede vurguladığımız gibi, grafik tasarım yoluyla sadece ürünlerin çevresel ayak izi azaltılmakla kalmaz, aynı zamanda toplumun çevre konusundaki algısı da şekillendirilebilir. Tasarım, bir sorun karşısında umutsuzluğu değil, aksine çözümün parçası olma motivasyonunu tetiklemelidir. Çarpıcı bir poster, ilham verici bir logo, bilgi dolu bir infografik – bunların her biri insanları düşünmeye ve eyleme geçmeye davet edebilir. Sürdürülebilir grafik tasarım, "gelecek nesillerin ihtiyaçlarını tehlikeye atmadan bugünün ihtiyaçlarını karşılamak" şeklindeki genel sürdürülebilirlik prensibinin tasarım alanındaki yansımasıdır. Grafik tasarımcılar, bu prensibi rehber edinerek işlerini yürüttüklerinde, mesleklerini gezegenimiz için bir fayda unsuruna dönüştürürler. Sonuçta, gezegenimizin kaynakları sınırlıdır ve yaratıcı endüstriler olarak bizler de üzerimize düşeni yapmalıyız. Küçük başlayıp büyük düşünerek, her tasarım projesini sürdürülebilirlik ekseninde değerlendirmek, uzun vadede kültürel bir değişimi tetikleyecektir.

Özetle, sürdürülebilirlik tasarımın kısıtlayıcı bir unsuru değil, aksine yeni imkanlar açan bir çerçevedir. Bu çerçeve içinde üretilen işler, hem tasarımcısına etik bir tatmin sağlar, hem kullanıcılarına değer katar, hem de dünyamızın sürdürülebilir geleceğine katkıda bulunur. Grafik tasarımın yaratıcılığı ile sürdürülebilirliğin gereklilikleri buluştuğunda, ortaya çıkan sonuç, bugünün ve yarının dünyası için umut vadeden bir iletişim olacaktır. Tasarımcılar olarak unutmamalıyız ki "doğayı tasarlayamayız, ama tasarımla doğayı koruyabiliriz".

KAYNAKLAR

- Abed El Salam, S. H. (n.d.). The impact of the sustainability development on graphic design. Journal of Heritage and Design, 3, 429–442.
- Alahira, J., Ninduwezuor-Ehiobu, N., Olu-lawal, K. A., et al. (2024). Eco-innovative graphic design practices: Leveraging fine arts to enhance sustainability in industrial design.
- Allameh, E., & Heidari Jozam, M. (2020). Sustainable street furniture. Periodica Polytechnica Architecture, 51(1), 65–74. https://doi.org/10.3311/PPar.15212
- Dawson, A. (2023). The carbon impact of web standards [PDF]. Website Sustainability. https://websitesustainability.com/cache/files/research23.pdf.

- Earth Hour. (2025). Earth Hour campaign overview. Earth Hour. Erişim: https://www.earthhour.org/
- EDDY. (2024, October 17). Sustainable graphic design: Eco-friendly practices and material. Rocky Mountain College of Art + Design. https://www.rmcad.edu/blog/sustainable-graphic-design-eco-friendly-practices-and-material/
- FSC Paper. (2024). *Sustainable paper certifications*. Forest Stewardship Council. Erişim: https://fsc.org/en/businesses/paper-packaging
- Gumber, S. (2023). Minimalism in design: A trend of simplicity in complexity. ShodhKosh: Journal of Visual and Performing Arts, 4(2), 357–365. https://doi.org/10.29121/shodhkosh.v4.i2.2023.539
- Hamlett, P. (2003). Sustainability and graphic design. Communication Arts.
- Harris & Associates. (2020, January 08). Corporate sustainability program. Harris & Associates. https://www.weareharris.com/about/corporate-sustainability/
- Jedlicka, W. (2010). Sustainable graphic design: Tools, systems and strategies for innovative print design. John Wiley & Sons.
- Lopez Palafox, C. (2019). When less is more: Minimalism and the environment. Environmental and Earth Law Journal, 9(1), Article 5.
- MaCher. (2025). Sustainable promotional & packaging design. MaCher. Erişim: https://macher.com/sustainability/
- Mirković, D., Ševo, M., Kostić, M., & Dragićević, M. (2019). Ecologically sustainable printing: Aspects of printing materials. Journal of Graphic Engineering and Design, 10(1), 13–20.
- Palafox, C. L. (2020). When less is more: Minimalism and the environment. *Earth Jurisprudence & Envtl. Just. J.*, *10*, 64.
- Papanek, V. (1971). Design for the real world: Human ecology and social change. New York, NY: Pantheon Books.
- Pimentel, D., Gardner, J., & Bonnifield, A. (2009). Energy efficiency and conservation for individual Americans. Environment, Development and Sustainability, 11(3), 547–552.
- Plazonić, I., Bates, I., & Barbarić-Mikočević, Ž. (2016). The effect of straw fibers in printing papers on dot reproduction attributes, as realized by UV inkjet technology. Nordic Pulp & Paper Research Journal, 31(3), 398–405.
- Posters Against Plastic Pollution. (2021). Visual campaign archive. https://www.postersagainstplastic.org
- Rawpixel. (2024). Sustainable graphic design: Tips to create eco-friendly designs. Rocky Mountain College of Art + Design. (2024, October 17). *Sustainable graphic design: Eco-friendly practices and material*. RMCAD.
- Selcová, Ľ. (2014). The concept of minimalism in sustainable residential buildings. Advanced Materials Research, 899, 611–614.
- Sison, M. D. (2013). Creative Strategic Communications: A Case Study of Earth Hour. International Journal of Strategic Communication, 7(4), 273–291.
- Strawzell, K. B. (2013). Psychology of poster design: The power of color and other design elements (Bachelor's honors thesis, Eastern Kentucky University). Eastern Kentucky University.
- Studio Carbon Negative. (2013). Eco-friendly printing and communication services. Studio Carbon Negative.
- Utoyo, A. W., Aprilia, H. D., Kuntjoro-Jakti, R. A. D. R. I., & Kurniawan, A. (2021, April). Visual communication design: Poster as an important way to encourage social distance in Jakarta when the epidemic 19. In IOP conference series: earth and environmental science (Vol. 729, No. 1, p. 012140). IOP Publishing.
- VanEenoo, C. (2011). Minimalism in Art and Design: Concept, influences, implications and perspectives. Journal of Fine and Studio Art, 2(1), 7-12.

➢ *ORAL PRESENTATION*

Effect of different solvents on the solubility of pea protein isolate and optimization using artificial neural network-genetic algorithm (ANN-GA)

Mustafa Onur Yuzer (https://orcid.org/0000-0002-8192-2298)

Bayburt University, Department of Food Processing, Bayburt, Türkiye

*Corresponding author e-mail: mustafaonuryuzer@gmail.com

Abstract
The limited solubility of plant proteins is a significant factor in determining the range of applications for these proteins. This results in the prevention of interactions with other proteins and limits their application in food products, as well as offering reduced solubility. One potential solution to this issue may be to optimise the factors that can influence solubility, as opposed to modifying the protein structure to enhance low solubility. Current research is focusing on the functionality and applications of pea protein, and various processes are under investigation with a view to improving the technofunctional properties and processing qualities of pea proteins. ANN-GA was utilised to optimise and study the effects of solvents, including distilled water, sodium chloride (NaCl) and potassium phosphate buffer (PPB), as well as different centrifugation speeds and times on pea protein isolate (PPI) solubility with maximum solubility. The response parameter that demonstrated optimal performance was the solubility value. The optimal states for the ANN-GA model were as follows: distilled water as the solvent, a centrifugation speed of 10407 g and a duration of 17 min, which resulted in a maximum protein solubility of 9.35%. The generated artificial neural network (ANN) model demonstrates a high degree of predictive capability. Consequently, solubility values were enhanced by optimising solely the conditions of the solubility analysis, without modifying the structure of PPI. In subsequent studies, the solubility values of proteins may be enhanced by modifying the conditions of the solubility analysis, in addition to the application of diverse treatments.
Keywords: Pea protein isolate, Solubility, ANN-GA, Optimization

INTRODUCTION

The demand for plant protein is increasing on a daily basis. The reasons for this increasing trend include changes in consumers' diets and lifestyles, strong factors associated with plant protein production compared to animal proteins, and less environmental impact (Akharume et al., 2021; Yüzer, 2023). Pea (*Pisum sativum*) is a pulse that can be widely cultivated across the globe, and its shell can be readily removed. Its primary application is as a commercial source of starch, protein and fibre when compared to other pulses (Arntfield and Maskus, 2011). It has been reported that peas can contain up to 30% protein (Chen et al., 2019; Aluko et al., 2009). Pea seeds are processed to obtain pea proteins commercially (Chen et al., 2019). There is a significant amount of research demonstrating the antioxidant potential of pea proteins (Ndiaye et al., 2012; Sun & Xiong, 2012; Sun & Xiong et al., 2012). In addition, these proteins have been demonstrated to possess antioxidant properties (Ge et al., 2020), with some studies even attributing a role in lowering cholesterol (Sirtori et al., As demonstrated in the studies conducted by Swiatecka et al. (2011, 2012), Sun and Xiong (2015), Aluko et al. (2015) and Liao et al. (2019), the properties of the substance in question include the regulation of intestinal bacteria, the provision of antihypertensive effects and the attenuation of inflammation. Collectively, these characteristics are associated with a range of health benefits. Pea protein isolate (PPI) is a prominent ingredient in the realm of plant protein, characterised by its high nutritional value, minimal allergenicity, and cost-effectiveness. However, its wide range of applications in various food systems is greatly limited due to its low solubility (Gao et al., 2024).

Determining the functional properties of proteins, it is possible to have information about how that protein isolate will be used in which food system. One of the most important of these functional properties is the solubility of protein. Changing the chemistry of protein or the test system in order to eliminate or improve these deficiencies of proteins that do not function at the desired level can change the functional properties of the isolates (Arntfield and Maskus, 2011). Plant based proteins characteristically possess a globular and rigid structural configuration, which hinders their interaction with other proteins and limits their application in food products as well as offering lower solubility (McClements & Grossmann, 2021; Higa et al., 2024). The utilisation of a multitude of plant proteins is constrained by their suboptimal solubility characteristics.

Furthermore, solubility is contingent upon the state of protein denaturation or aggregation. Consequently, one should aim to minimise protein denaturation and ensure that proteins are in a suitable aggregation state. The development of protein isolation and purification procedures is of potential significance for this purpose. This involves controlling factors such as solvent conditions, temperature, time, pH and ionic strength (McClements & Grossmann, 2021). To overcome the lack of technofunctional functionality of proteins, plant proteins can be subjected to different treatments to modify their structure, which can lead to an improvement in their functional properties. One solution may be to optimise the factors that can influence solubility rather than changing the structure of the protein with modifications to improve low solubility. With current research focusing on the functionality and applications of pea protein, various processes are being investigated to improve the technofunctional properties and processing qualities of pea proteins. These treatments include ultrasound, glycation, hydrolysis, acetylation, heat-assisted pH shift and treatment with enzymes. However, there is no research on optimising the conditions of solubility analysis without changing the PPI structure.

There are many different solubility measurements for measuring protein solubility. Although the principles of the methods are similar, the solvent used and the centrifugation conditions preferred during the analysis affect the solubility. In different studies in which the solubility of PPIs was determined, water (Gao et al., 2022; Gao et al., 2024; Othmeni et al., 2025; Schumacher et al., 2025), phosphate buffers (Mozafarpour et al., 2022; Vatansever et al., 2022; Zhang et al., 2022), citrate buffers (Kravchenko et al., 2024) and solutions containing NaCl (Xu et al., 2023) were used as solvents. Similarly, different centrifugation conditions were preferred in these studies. Therefore, a comparative study of these factors that may affect solubility will provide information about the most effective conditions.

In recent decades, there has been a notable shift in preference towards the utilisation of artificial neural networks (ANNs) for the purpose of nonlinear multivariate modelling. ANN is a technique that is trained on data in the experimental range and thus can predict responses and develop generalization and predictive modeling. Thus, a computational and mathematical modeling will be developed that examines the effect of input variables on the investigated outputs (Raj and Dash, 2020). The application of this technique has been extensively and successfully implemented across multiple disciplines. Furthermore, genetic algorithm (GA) is an AI-based optimization algorithm that optimizes the independent variables in ANN models. The hybrid methodology of artificial neural network and genetic algorithm (ANN-GA) has become increasingly common in the field of AI-based approaches (Desai et al., 2008; Patra et al., 2022).

The present study has two objectives; (i) to determine the effect of different solvents and differences in experimental conditions on solubility of PPI, and (ii) to determine the performance of artificial intelligence-based optimisation techniques to be used in the optimisation of these effects. ANN-GA was used to optimise and study the effects of solvents such as distilled water, sodium chloride (NaCl) and potassium phosphate buffer (PPB) and different centrifugation speeds and times on PPI solubility with maximum resolution. The optimum conditions given by this approach were experimentally verified. To our knowledge, this is the first study on the use of ANN-GA for the optimization of PPI solubility. Thus, it is expected to improve the solubility analysis without changing the structure of the PPI, only by optimising its conditions.

MATERIALS AND METHODS

Materials

Pea protein isolate (81.7%) used in the study was purchased directly from a local market. All chemicals were purchased from Sigma Aldrich for analytical purity. Ultrapure water was obtained by passing distilled pure water through an additional activated carbon purification system (Millipore, Bedford, USA).

Experimental Design

A Box-Behnken experimental design was used to evaluate the solubility property of PPI. Different solvents (10 mM PPB with pH 7, 0.5 M NaCl solution and ultrapure water), different centrifugation speeds (8000, 10000 and 12000 g) and times (10, 15 and 20 min) were selected as independent variables. Box-Behnken experimental design from Design-Expert software (V13, Stat-Ease Inc., Minneapolis, USA) helped to obtain combinations of process parameters and total experimental runs. Table 1 shows the experimental design and results.

Determination of Solubility

Percent solubility of the samples was determined at pH 7 by modifying Yüzer (2023). Protein isolate at 10 mg/mL concentration was prepared with the indicated solvents. 1 N HCl or 1 N NaOH was used to adjust the pH of the dispersions. The dispersions were stirred with a magnetic stirrer for 30 min at room temperature, then centrifuged (Hermle Z216, Hermle Labortechnik GmbH, Wehingen, Germany) at different centrifugation speeds and for different times given in the experimental design. After centrifugation, the supernatant was analysed for protein using the method of Bradford (1976). For this purpose, 50 µL of the supernatant was taken and 1.5 mL of Bradford reagent was added and the absorbance of the mixture was read at 595 nm wavelength in a spectrophotometer (Shimadzu, UV-1201V, Japan) after 10 min. Bovine serum albumin standard curve was used to calculate the protein content. The solubility was calculated by the following equation:

$$\text{Solubility (\%)} = \frac{\text{Protein content of the supernatant}}{\text{Total protein content of the sample}} \text{x} 100 \quad (1)$$

ANN Modeling and GA Optimization

The implementation of neural network fitting in MATLAB (R2021a, The Math Works, Inc., Natick, MA, USA) was facilitated by the utilisation of an ANN modelling tool. The artificial neural network (ANN) model comprised three layers: an input layer, a hidden layer, and an output layer. The input layer consists of three independent variables: solvent, centrifuge speed and time. In the output layer, the dependent variable is expressed as a percentage of resolution (Figure 1). A trial-and-error approach was adopted, with the number of neurons varying between 10 and 20. Following this, the number of hidden neurons was finalised at 16, in order to achieve the optimum model performance. The protein resolution results were represented by a neuron that formed the output layer. The ANN model was created by encoding the input and output data points. The tansig function was utilised as the transfer function for the hidden layer, while purelin represented the transfer function of the output layer. The Levenberg-Marquardt (LM) back propagation (trainlm) method was utilised in the training of the data. Of the total data, 70% was allocated to training, 15% to testing and 15% to validation. The network was trained until it reached the lowest mean squared error (MSE) and maximum R^2. Subsequent to the training of the ANN, the weights and bias values were determined by means of the following equation. These values were then utilised to determine the predicted outputs.

$$y_i = purelin\{W_{OH} \times tansig\,(U_{IH} \times x_i + TH) + TO\} \quad (2)$$

Where x_i and y_i are the input and estimated coded output parameters. W_{OH} are the weights between the hidden and output layers, while U_{IH} are the weights between the input and hidden layers. TO and TH are the bias values of the output and hidden layer neurons, respectively (Patra et al., 2022).

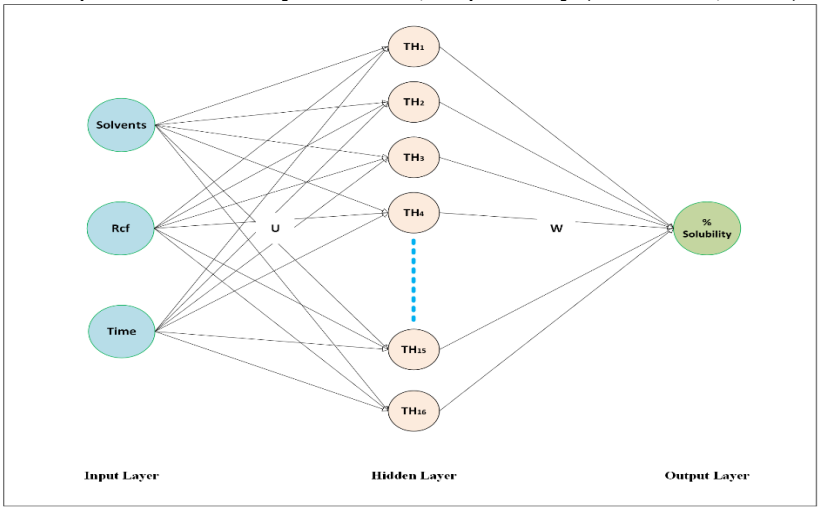

Figure 1. The architecture of artificial neural network model

The GA optimisation procedure was performed using MATLAB's GA package. GA optimisation mimics natural selection, using biologically inspired operators such as selection, mutation and crossover to improve solutions (Patra et al., 2022). The three basic parameters chosen for GA optimisation were population type (double vector), size (50) and crossover rate (0.8). The fitness function (f), shown below, was created to maximise the output responses.

$$f = -(y_i) \tag{3}$$

Where y_i is the actual values of the protein solubility (%) response predicted by the ANN and the maximisation of the specified function (f) in the GA has a negative sign.

Statistical Analysis

In order to verify the performance of the developed ANN model, the average absolute deviation (AAD), mean squared error (MSE), normal mean squared error (NMSE), mean percentage error (MPE), root mean squared error (RMSE), normal root mean squared error (NRMSE) and coefficient of determination (R^2) between the predicted and experimental responses were calculated using the formulae given below. The model that shows the lowest values for AAD, MSE, RMSE, NMSE, NRMSE and MPE and the highest R^2 value is considered to be the most effective model in accurately representing the responses.

$$AAD\ (\%) = \left[\frac{\sum_{i=1}^{n}(|Y_{pre} - Y_{exp}|/Y_{exp})}{n}\right] x100 \tag{4}$$

$$MSE = \frac{\sum_{i=1}^{n}(Y_{pre} - Y_{exp})^2}{n} \tag{5}$$

$$NMSE = \frac{MSE}{Y_m} \tag{6}$$

$$RMSE = \sqrt{\frac{\sum_{i=1}^{n}(Y_{pre} - Y_{exp})^2}{n}} \tag{7}$$

$$NRMSE = \frac{RMSE}{Y_m} \tag{8}$$

$$MPE = \frac{100}{n}\sum\left|\frac{(Y_{pre} - Y_{exp})}{Y_{pre}}\right| \tag{9}$$

$$R^2 = 1 - \frac{\sum_{i=1}^{n}(Y_{pre} - Y_{exp})^2}{\sum_{i=1}^{n}(Y_m - Y_{exp})^2} \tag{10}$$

Where Y_{exp} is the observed value, Y_{pre} is the predicted value obtained from ANN, Y_m is the mean value of experimental data and n is the number of experiments (n=34).

RESULTS and DISCUSSION

The solubility of a protein is not only considered as a primary functional property, but is often a prerequisite for other functional properties (Wang et al., 2016). Table 1 shows the solubility values of PPI obtained in different solvents and solubility test conditions. It is seen that the solvent with the lowest solubility is NaCl solution. The highest solubility values were determined in the samples in which ultrapure water was used as solvent.

Table 1. Experimental design, predicted and actual values of responses of solubility (%)

Run	Solvents	Rcf (g)	Time (min)	Exp. value	ANN Predict
1	NaCl	10000	20	5,14	5,14
2	Water	10000	15	9,33	9,25
3	PPB	10000	20	6,96	6,96
4	Water	12000	20	8,08	8,08
5	Water	10000	15	8,98	9,25
6	NaCl	8000	15	4,20	4,16
7	NaCl	12000	15	4,47	4,41
8	Water	8000	10	6,59	6,41
9	PPB	12000	15	6,04	5,96
10	PPB	10000	10	6,08	6,08
11	Water	12000	10	7,67	7,67
12	PPB	8000	15	5,67	5,67
13	Water	10000	15	9,20	9,25
14	NaCl	10000	10	4,41	4,37
15	Water	10000	15	9,53	9,25
16	Water	10000	15	9,18	9,25
17	Water	8000	20	7,81	7,71

Detection of hidden layers, determination of connection weights and generation of bias values were performed as explained in the methods section. The connection weight and bias values for response resolution are given in the following matrices.

$$U = \begin{bmatrix} -3.5581 & 1.0355 & 0.6507 \\ -2.6580 & 0.2116 & 2.2747 \\ 2.0650 & 1.1006 & 2.4704 \\ 2.9846 & 1.7670 & 0.3342 \\ -3.0099 & -1.1022 & 1.5320 \\ -2.5538 & -2.3024 & -0.7012 \\ -2.5296 & 0.4843 & -2.4495 \\ -1.0877 & 1.9962 & -2.7485 \\ -0.9075 & 2.7998 & -1.9465 \\ 2.6607 & -2.2209 & 0.7548 \\ -0.4263 & -1.7149 & -2.9614 \\ 2.3373 & -2.5313 & -0.5142 \\ -3.0692 & -1.4684 & 0.7243 \\ -2.0183 & -2.5300 & 1.6212 \\ -2.5242 & -1.7430 & 1.6468 \\ 0.9360 & -2.6839 & 2.3272 \end{bmatrix} \quad TH = \begin{bmatrix} 3.2971 \\ 3.0866 \\ -2.7152 \\ -2.1735 \\ 1.6334 \\ 1.3163 \\ 0.2684 \\ 0.0605 \\ -0.2911 \\ 0.4981 \\ -1.3316 \\ 1.8278 \\ -2.2610 \\ -2.4624 \\ -3.0588 \\ 3.3882 \end{bmatrix} \quad TO = -0.0874$$

$$W = \begin{bmatrix} -0.6721 & 0.4405 & -0.0593 & 0.4046 & -0.4249 & 0.3158 & 0.2061 & -0.8895 & 0.0787 \\ -0.7427 & -0.2999 & 0.4908 & 0.4607 & -0.4323 & -0.2324 & -0.4855 \end{bmatrix}$$

U is the link weights between the input and hidden layers and W is the link weights between the hidden and output layers. TH and TO are the bias values of the hidden and output layer, respectively.

The best ANN model for the resolution value was reached in the 4th period. At this point, the experimental studies used during the training of the models were categorised as training (1, 2, 3, 4, 7, 8, 11, 12, 13, 15, 17), validation (5, 6, 10) and testing (9, 14, 16), respectively. Similarly, the R^2 values were 0.996, 0.996 and 0.996 for training, validation and testing, respectively (Figure 3a), while the R^2 value of the solubility was 0.9951 according to the developed model. The error histogram and the performance graph of each response are shown in Figure 3 (b and c). The error values are calculated between the experimental responses and the output responses predicted from the ANN model.

The optimization process was executed using the genetic algorithm (GA), with the objective of attaining the maximum resolution value. As demonstrated in Figure 2, the optimisation was concluded following the 10th generation, with an average fitness value of -9.4389 being attained. At this best-fit point, centrifugation speed of 10407 g, processing time of 17 min and ultrapure water as solvent were determined as optimum conditions. The solubility value during these optimum conditions was estimated to be 9.44%. As a result of the experiment performed using the optimum conditions to verify the GA optimisation, the solubility was determined as 9.35%.

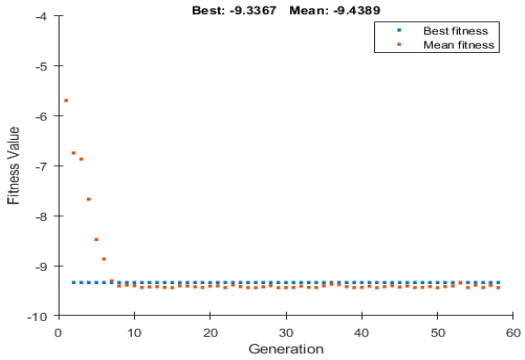

Figure 2. The variation of fitness value with respect to generations during genetic algorithm optimization of solubility

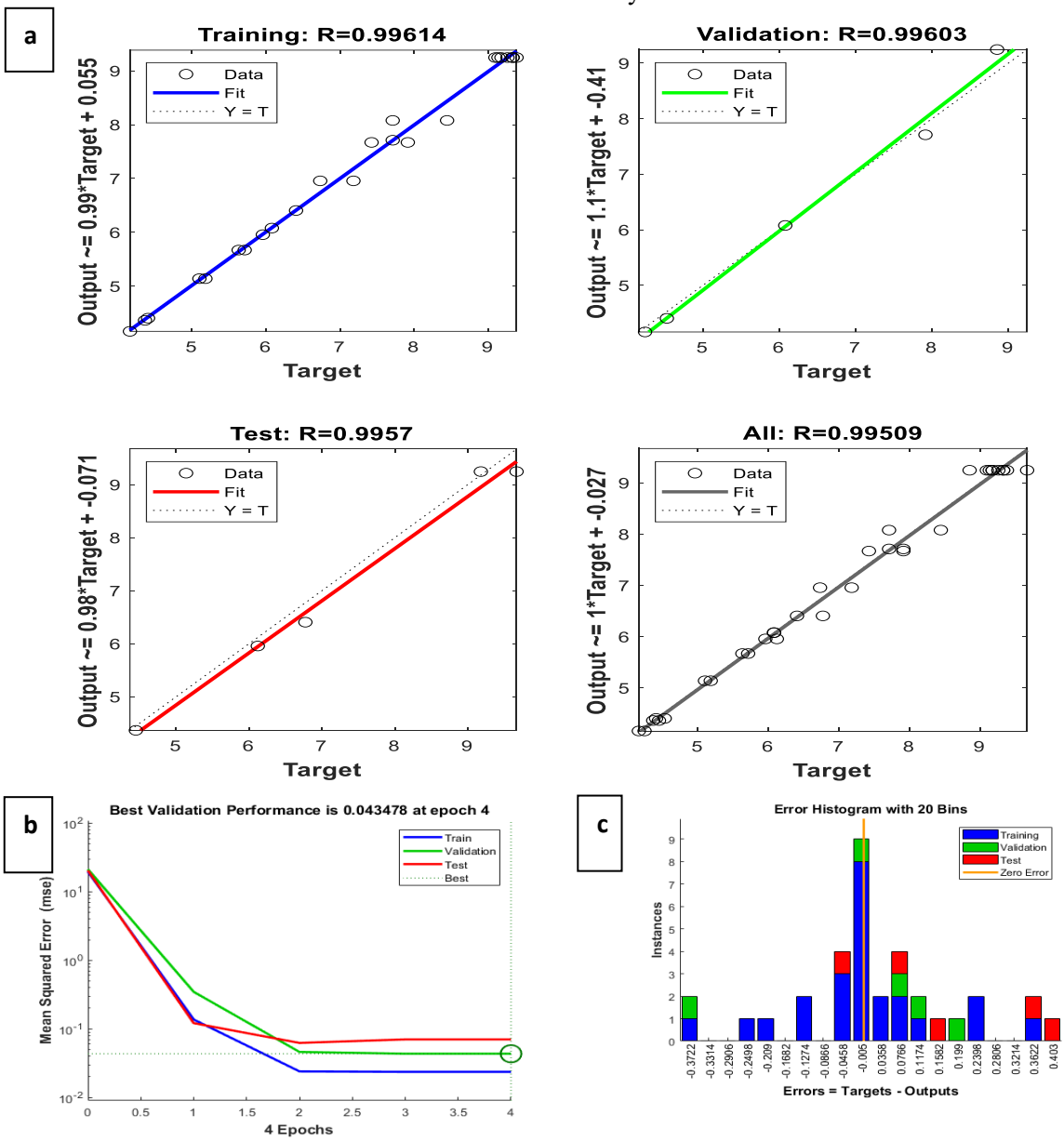

Figure 3. Post-training performance (a), best validation performance (b) and error histogram of solubility (c) of generated artificial neural network model

Using MATLAB (version R2021a), the prediction performance of the ANN model was evaluated using various metrics including R^2, MPE, MSE, NRMSE, AAD, RMSE and NMSE (Table 2). The ANN model demonstrated robust performance metrics in predicting protein solubility. The model demonstrated a high R^2 value of 0.9899. With regard to precision, the ANN model displays a low RMSE value of 0.1825 for solubility. Furthermore, the mean absolute deviation (AAD) value was found to be 1.73% for the artificial

neural network (ANN) model. In a similar manner, the ANN model demonstrated a reduced MSE value of 0.033 for resolution. The obtained results highlight that the ANN model, which performs well in the calculated evaluation criteria, is superior in optimizing protein solubility. The superiority of the ANN model over the RSM model is attributable to the former's utilisation of nonlinear polynomials, which ensure a higher level of prediction accuracy (Ware et al., 2025). In contrast, the RSM model is constrained to the use of quadratic equations for the generalisation of data. As evidenced by numerous scientific papers, the ANN model has been shown to outperform RSM modelling (see Shende et al., 2024; Ware et al., 2025).

Table 2. Summary of all statistical parameters of protein solubility

Coefficient	Value
AAD (%)	1,73
MSE	0,033
NMSE	0,0098
RMSE	0,1825
NRMSE	0,0260
MPE	0,4235
R^2	0,9899

CONCLUSION

Optimization of protein solubility was successfully performed using ANN-GA with different solvents, centrifugation speeds and times. The optimised response parameter was the solubility value. The optimum conditions for the ANN-GA model were pure water as solvent, centrifugation speed of 10407 xg and time of 17 min, which gave a maximum protein solubility of 9.35%. The generated ANN model is highly predictive. It can thus be concluded that the ANN-GA model is a quantitatively effective tool for the optimisation of process parameters with regard to the solubility of pea protein isolate. Studies to improve protein solubility usually focus on improving solubility by including a different treatment. In this study, only the analysis conditions were optimised. In future studies, the solubility property of proteins developed with different modifications can be further increased by changing the conditions of solubility analysis in addition to these treatments.

REFERENCES

Aluko, R. E., Girgih, A. T., He, R., Malomo, S., Li, H., Offengenden, M., & Wu, J. (2015). Structural and functional characterization of yellow field pea seed (*Pisum sativum* L.) protein-derived antihypertensive peptides. Food Research International, 77, 10-16. https://doi.org/https://doi.org/10.1016/j.foodres.2015.03.029

Aluko, R. E., Mofolasayo, O. A., & Watts, B. M. (2009). Emulsifying and Foaming Properties of Commercial Yellow Pea (*Pisum sativum* L.) Seed Flours. Journal of Agricultural and Food Chemistry, 57(20), 9793-9800. https://doi.org/10.1021/jf902199x

Arntfield, S. D., & Maskus, H. D. (2011). 9 - Peas and other legume proteins. In G. O. Phillips & P. A. Williams (Eds.), Handbook of Food Proteins (pp. 233-266). Woodhead Publishing. https://doi.org/https://doi.org/10.1533/9780857093639.233

Bhagya Raj, G. V. S., & Dash, K. K. (2020). Ultrasound-assisted extraction of phytocompounds from dragon fruit peel: Optimization, kinetics and thermodynamic studies. Ultrasonics Sonochemistry, 68, 105180. https://doi.org/https://doi.org/10.1016/j.ultsonch.2020.105180

Chen, M., Lu, J., Liu, F., Nsor-Atindana, J., Xu, F., Goff, H. D., Ma, J., & Zhong, F. (2019). Study on the emulsifying stability and interfacial adsorption of pea proteins. Food Hydrocolloids, 88, 247-255. https://doi.org/https://doi.org/10.1016/j.foodhyd.2018.09.003

Choi, H.-J., Naznin, M., Alam, M. B., Javed, A., Alshammari, F. H., Kim, S., & Lee, S.-H. (2022). Optimization of the extraction conditions of Nypa fruticans Wurmb. using response surface methodology and artificial neural network. Food Chemistry, 381, 132086. https://doi.org/https://doi.org/10.1016/j.foodchem.2022.132086

Desai, K. M., Survase, S. A., Saudagar, P. S., Lele, S. S., & Singhal, R. S. (2008). Comparison of artificial neural network (ANN) and response surface methodology (RSM) in fermentation media optimization:

Case study of fermentative production of scleroglucan. Biochemical Engineering Journal, 41(3), 266-273. https://doi.org/https://doi.org/10.1016/j.bej.2008.05.009

Dominika, Ś., Arjan, N., Karyn, R. P., & Henryk, K. (2011). The study on the impact of glycated pea proteins on human intestinal bacteria. International Journal of Food Microbiology, 145(1), 267-272. https://doi.org/https://doi.org/10.1016/j.ijfoodmicro.2011.01.002

Gao, K., Xu, Y., Rao, J., & Chen, B. (2024). Maillard reaction between high-intensity ultrasound pre-treated pea protein isolate and glucose: Impact of reaction time and pH on the conjugation process and the properties of conjugates. Food Chemistry, 434, 137486. https://doi.org/https://doi.org/10.1016/j.foodchem.2023.137486

Gao, K., Zha, F., Yang, Z., Rao, J., & Chen, B. (2022). Structure characteristics and functionality of water-soluble fraction from high-intensity ultrasound treated pea protein isolate. Food Hydrocolloids, 125, 107409. https://doi.org/https://doi.org/10.1016/j.foodhyd.2021.107409

Ge, J., Sun, C.-X., Corke, H., Gul, K., Gan, R.-Y., & Fang, Y. (2020). The health benefits, functional properties, modifications, and applications of pea (Pisum sativum L.) protein: Current status, challenges, and perspectives. Comprehensive Reviews in Food Science and Food Safety, 19(4), 1835-1876. https://doi.org/https://doi.org/10.1111/1541-4337.12573

Higa, F., Nickerson, C., & Nickerson, M. T. (2025). Effect of pH shifting and temperature on the functional properties of a commercial pea protein isolate. Cereal Chemistry, 102(1), 89-101. https://doi.org/https://doi.org/10.1002/cche.10847

Huang, S.-M., Kuo, C.-H., Chen, C.-A., Liu, Y.-C., & Shieh, C.-J. (2017). RSM and ANN modeling-based optimization approach for the development of ultrasound-assisted liposome encapsulation of piceid. Ultrasonics Sonochemistry, 36, 112-122. https://doi.org/https://doi.org/10.1016/j.ultsonch.2016.11.016

Jaddu, S., Abdullah, S., Dwivedi, M., & Pradhan, R. C. (2023). Optimization of functional properties of plasma treated kodo millet (open air multipin) using response surface methodology (RSM) and artificial neural network with genetic algorithm (ANN-GA). Journal of Food Process Engineering, 46(10), e14207. https://doi.org/https://doi.org/10.1111/jfpe.14207

Kravchenko, I. V., Furalyov, V. A., Kostyleva, E. V., Sereda, A. S., Kurbatova, E. I., Tsurikova, N. V., Pshennikova, E. S., Boyarintseva, T. V., Popov, V. O., & Fedorov, A. N. (2024). Effect of Different Classes of Proteases on the Techno-Functional Properties of Pea Protein Isolates. Applied Biochemistry and Microbiology, 60(1), 106-117. https://doi.org/10.1134/S0003683824010083

Liao, W., Fan, H., Liu, P., & Wu, J. (2019). Identification of angiotensin converting enzyme 2 (ACE2) up-regulating peptides from pea protein hydrolysate. Journal of Functional Foods, 60, 103395. https://doi.org/https://doi.org/10.1016/j.jff.2019.05.051

McClements, D. J., & Grossmann, L. (2021). The science of plant-based foods: Constructing next-generation meat, fish, milk, and egg analogs. Comprehensive Reviews in Food Science and Food Safety, 20(4), 4049-4100. https://doi.org/https://doi.org/10.1111/1541-4337.12771

Mozafarpour, R., Koocheki, A., & Nicolai, T. (2022). Modification of grass pea protein isolate (Lathyrus sativus L.) using high intensity ultrasound treatment: Structure and functional properties. Food Research International, 158, 111520. https://doi.org/https://doi.org/10.1016/j.foodres.2022.111520

Ndiaye, F., Vuong, T., Duarte, J., Aluko, R. E., & Matar, C. (2012). Anti-oxidant, anti-inflammatory and immunomodulating properties of an enzymatic protein hydrolysate from yellow field pea seeds. European Journal of Nutrition, 51(1), 29-37. https://doi.org/10.1007/s00394-011-0186-3

Othmeni, I., Blecker, C., & Karoui, R. (2025). pH-dependent emulsifying properties of pea protein isolate: Investigation of the structure – Function relationship. International Journal of Biological Macromolecules, 290, 139105. https://doi.org/https://doi.org/10.1016/j.ijbiomac.2024.139105

Patra, A., Abdullah, S. & Pradhan, R.C. (2022). Optimization of ultrasound-assisted extraction of ascorbic acid, protein and total antioxidants from cashew apple bagasse using artificial neural network-genetic algorithm and response surface methodology. Journal of Food Processing and Preservation, 46(3), e16317.

Pavani, M., Singha, P., Rajamanickam, D. T., & Singh, S. K. (2024). Impact of extrusion processing on bioactive compound enriched plant-based extrudates: A comprehensive study and optimization using

RSM and ANN-GA. Future Foods, 9, 100286. https://doi.org/https://doi.org/10.1016/j.fufo.2023.100286

Schumacher, T., Steinmacher, T., Köster, E., Wagemans, A., Weiss, J., & Gibis, M. (2025). Physico-chemical characterization of ten commercial pea protein isolates. Food Hydrocolloids, 162, 110996. https://doi.org/https://doi.org/10.1016/j.foodhyd.2024.110996

Shende, A. S., Jayasree Joshi, T., & Srinivasa Rao, P. (2024). Microwave-assisted aqueous extraction of bioactive components from Malabar spinach (Basella alba) leaves and its optimization using ANN-GA and RSM methodology. Journal of Food Measurement and Characterization, 18(1), 287-298. https://doi.org/10.1007/s11694-023-02182-2

Sirtori, C. R., Triolo, M., Bosisio, R., Bondioli, A., Calabresi, L., De Vergori, V., Gomaraschi, M., Mombelli, G., Pazzucconi, F., Zacherl, C., & Arnoldi, A. (2012). Hypocholesterolaemic effects of lupin protein and pea protein/fibre combinations in moderately hypercholesterolaemic individuals. British Journal of Nutrition, 107(8), 1176-1183. https://doi.org/10.1017/S0007114511004120

Sun, W., & Xiong, Y. L. (2015). Stabilization of cooked cured beef color by radical-scavenging pea protein and its hydrolysate. LWT - Food Science and Technology, 61(2), 352-358. https://doi.org/https://doi.org/10.1016/j.lwt.2014.12.048

Świątecka, D., Markiewicz, L. H., & Wróblewska, B. (2012). Experimental immunologyPea protein hydrolysate as a factor modulating the adhesion of bacteria to enterocytes, epithelial proliferation and cytokine secretion – an in vitro study. Central European Journal of Immunology, 37(3), 227-231. https://doi.org/10.5114/ceji.2012.30798

Vatansever, S., Ohm, J.-B., Simsek, S., & Hall, C. (2022). A novel approach: Supercritical carbon dioxide + ethanol extraction to improve techno-functionalities of pea protein isolate. Cereal Chemistry, 99(1), 130-143. https://doi.org/https://doi.org/10.1002/cche.10489

Ware, K., Kashyap, P., Gorde, P. M., Yadav, R., & Sharma, V. (2025). Comparative analysis of RSM and ANN-GA based modeling for protein extraction from cotton seed meal: Effect of extraction parameters on amino acid profile and nutritional characteristics. Food and Bioproducts Processing, 150, 63-77. https://doi.org/https://doi.org/10.1016/j.fbp.2024.12.016

Xu, G., Kang, J., You, W., Li, R., Zheng, H., Lv, L., & Zhang, Q. (2023). Pea protein isolates affected by ultrasound and NaCl used for dysphagia's texture-modified food: Rheological, gel, and structural properties. Food Hydrocolloids, 139, 108566. https://doi.org/https://doi.org/10.1016/j.foodhyd.2023.108566

Yüzer, M.O. (2023). Soya proteini izolati-fruktoz glikasyon konjugatlarinin yapisi ve bazi teknofonksiyonel özellikleri üzerine ultrason işleminin etkisi. Gıda, 48(6), 1351-1365. https://doi.org/10.15237/gida.GD23079

Zhang, B., Kang, X., Cheng, Y., Cui, B., & Abd El-Aty, A. M. (2022). Impact of high moisture contents on the structure and functional properties of pea protein isolate during extrusion. Food Hydrocolloids, 127, 107508. https://doi.org/https://doi.org/10.1016/j.foodhyd.2022.107508

➢ *ORAL PRESENTATION*

How does the concept of sustainable development affect the acquisition of knowledge by students in the pre-university and university systems?

Sara Pupe[1] ORCID https://orcid.org/0009-0009-6698-283X

[1]Department of Biology, Aldent University, Albania

Abstract

The concept of sustainable development has taken an important place in school curricula by giving students and teachers a wider access to each of their fields, while also learning to make informed decisions and people, both individually and collectively, for other society and to protect the planet. The treatment and importance of the concept of sustainable schools is to equip students and teachers with knowledge, values, values to address issues such as development, university skills, economic biodiversity, global warming. The research used random samples of respondent groups (N=150) including Aldent University, the Faculty of Natural Sciences, the University of Vlora, and the Andon Zako Cajupi, Petro Nini Luarasi, and Sinan Tafaj High Schools. Most of them agreed that many factors such as energy conservation practices and solid waste recycling influence the development of the sustainable concept.

Keywords: Concept of sustainable development, teaching, biological knowledge, curriculum, correlation, education

INTRODUCTION

The concept of sustainable development is gaining particular importance in today's society, to address the pressure that the challenges of environmental degradation, social inequality and economic instability impose. Education plays an important role in shaping pupils and students with knowledge and concepts on sustainable development, skills and values to give voice and solutions to complex issues (Borg et al., 2014). The concept of sustainable development is complex and includes many disciplines of knowledge. Sustainable development as an approach has three dimensions: that of the environment, society and economy, and to achieve its realization, education in schools constitutes a key element. On the other hand, traditional methods of scientific education in our schools are not sufficient to achieve the cultivation of an advanced mindset of sustainable development, therefore this constitutes the challenge of today's educational system in our country and around the globe (Freeman & Morgan, 2009). Determining the knowledge and competencies that need to be given to students regarding the formation of appropriate concepts for sustainable development is and remains an issue under discussion (Aarnio-Linnanvuori, 2019). In this context, it is of great importance how students perceive and interact with the concept of sustainable development within the framework of science education at school. The purpose of this study focuses on assessing the perception that students have about sustainable development. By analyzing the level of their knowledge, attitudes and awareness of the principles of sustainable development, this study aims to create an efficient model for effective sustainable development education in pre-university and university education.

The study was conducted using a research design and supported by two research questions that were used during the study:

1. Is economic development, nature conservation, biodiversity, global warming important for understanding the concept of sustainable development and do these situations affect school curricula?
2. Do energy conservation practices, construction and renovation of buildings based on green design principles, solid waste recycling, poverty eradication, political instability on the concept of sustainable development matter?

The research study was conducted in Google Forms where the data were processed using descriptive methods. The conclusion of the study should result in 3 main variables: the importance that external factors offer on the understanding of sustainable development among students of the pre-university and university systems, the institutions and the importance that they offer and treat these on the understanding of sustainable development for student learning, as well as the curriculum of which subject has the concept of sustainable development more in focus. In an effort to move beyond the rhetoric of sustainability and pursue

a more meaningful agenda for sustainable development in education, a clear definition of this concept and an explanation of its main dimensions are needed (Gray, Citation2010; Mensah & Enu-Kwesi, Citation2018). This need, according to Gray (Citation2010), as cited in Giovannoni and Fabietti (Citation2014), has been supported by both academics and practitioners with the aim of promoting sustainable development to make teaching and learning as successful as possible so that students learn as quickly as possible. The development of the concept of sustainability in education is defined as an evolutionary process in which human capacity increases in terms of initiating new structures, confronting problems, adapting to continuous change, and striving purposefully and creatively to achieve new goals and high results in different subjects (Peet, Citation 1999 cited in Du Pisani, Citation2006). Todaro and Smith (Citation2006) also define development as a multidimensional process that includes major changes in social structures, attitudes, and institutions, as well as economic growth, reducing inequality, and eradicating absolute poverty. Several theories have been presented to explain the concept of development. They include theories of modernization, dependency, world systems, and globalization, which also influence the approach to school curricula. In the development literature, most academics, researchers and practitioners (Gray & Milne, Citation2013: Tjarve, & Zemīte, Citation2016; Mensah & Enu-Kwesi, Citation2018; Thomas, Citation2015) apply the concept to provide a mechanism through which students can interact with the environment without risking damaging the resource for the future. The concept of sustainable development constitutes a lifelong learning effort, providing students with the cognitive, socio-emotional and behavioral dimensions essential for addressing interconnected global challenges such as climate change, biodiversity loss, unsustainable resource use and social inequality (UNESCO, 2023a). The preceding factors highlighted the reinforcing calls for strengthening systems thinking, interdisciplinary collaboration, and sustainability-focused educational leadership as imperatives to drive sustainability advances in biology and nursing education (Osingada and Porta 2020; Lopez-Medina et al. 2019). The concept attributes and defining components similarly provide a strategic framework to guide curriculum development, the design of sustainability learning objectives, and content delivery models.

MATERIALS AND METHODS

Preparation of the questionnaire with multiple choice questions, Likert scale and discussion questions. The sample selection will be done by randomly selecting students and pupils while maintaining a balance between gender representation, academic programs and profile of high schools and years of study. Pre-pilot testing will be carried out with a small group to test the clarity of the questionnaire, understandability and on this basis the necessary adjustments will be made. Data collection will be done according to an appropriate method such as conducting online or in-person questionnaires, or combined. Before data collection, each participant in the study will sign a consent statement, to guarantee voluntariness and anonymity. Data analysis will be done quantitatively, using statistical programs, such as descriptive analysis, frequencies, means and standard deviations, and qualitatively by analyzing the developmental questions. Care will be taken to maintain ethics in the study, that is, to respect anonymity and confidentiality. In this research, respondents (N= 150) were used, 120 females and 30 males, where the schools and universities that participated were: Aldent University, Faculty of Natural Sciences, University of Vlora, and Andon Zako Cajupi High School, Petro Nini Luarasi, Sinan Tafaj

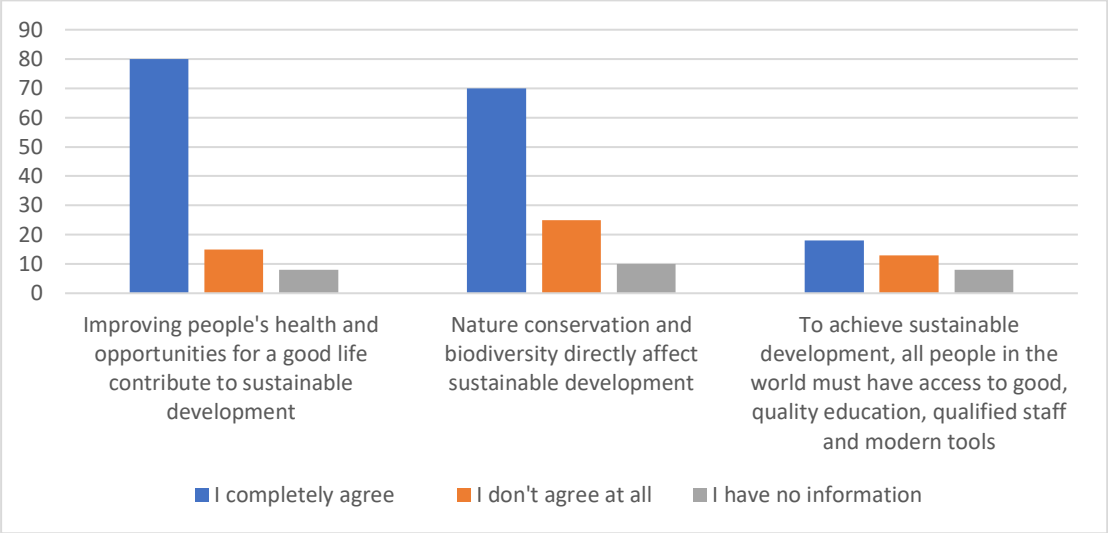

Figure 1. The importance of environmental and health factors in understanding the concept of sustainable development

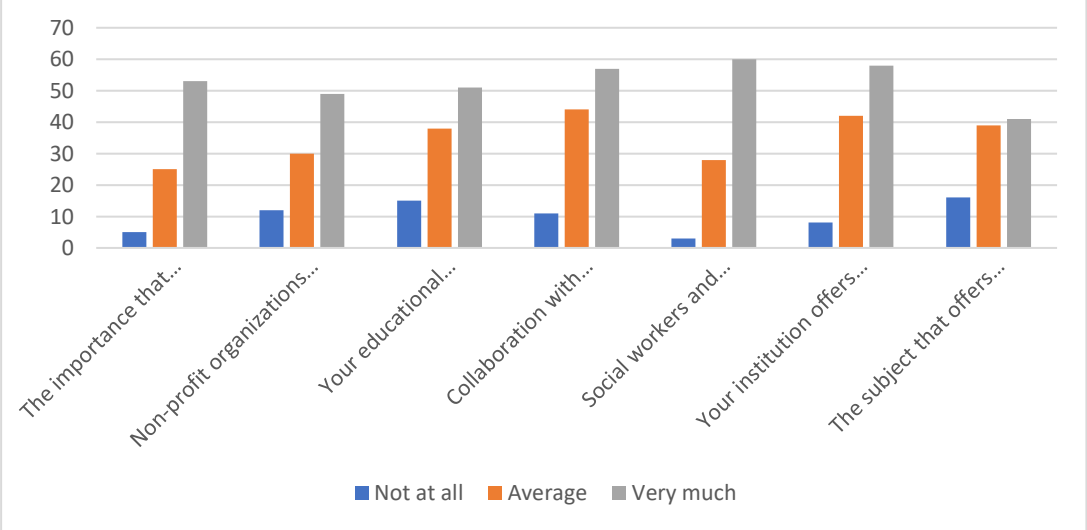

Figure 2. The importance that the educational institution offers to various organizations for the concept of sustainable development

RESULTS and DISCUSSION

The statistical results of the correlation were used to understand the relationship between the importance that external factors provide on the understanding of sustainable development among students of the pre-university and university systems, the institutions and the importance that they provide and treat on the understanding of sustainable development for student learning, as well as the curriculum of which subject has the concept of sustainable development more in focus

●To achieve sustainable development, all people in the world must have access to good, quality education, qualified staff and modern tools

The survey of respondents shows that 18% completely agree with this, 13% do not agree at all and 8% have no information on this

●The importance that your school or university offers for extracurricular courses or training to expand the concept of sustainable development

The survey of respondents shows that about 5% of these institutions do not offer any training and courses at all, and about 25% offer average courses and training, and about 53% offer a lot of extracurricular courses and training to understand the concept of sustainable development.

● Non-profit organizations offer financial assistance for material bases that help you in the process of understanding the concepts
The survey of respondents shows that about 12% of these institutions do not provide financial assistance and material support at all, and about 30% provide average and about 49% of them provide a lot of financial assistance and material support.

● Your educational institution offers a variety of scientific literature, also giving you access to examples or good practices of implementing the principle of sustainable development
.The survey of respondents shows that about 15% offer a variety of scientific literature, also giving access to examples or good practices of implementing the concept of sustainable development, and about 38% provide an average of this variety of literature and about 51% of them offer a lot of literature to help understand the concept of sustainable development.

● Collaboration with environmental organizations to practice various activities to understand how development concepts are related to each other in the way they function and their use
The survey of respondents shows that about 11% offer collaborations with environmental organizations to practice various activities to understand how development concepts are related to each other in the way they function and their use, and about 44% offer average collaborations and about 57% of them offer collaborations with these organizations.

● Social workers and psychologists at your institution offer you meetings with people with disabilities so that you can explain to them the basic concepts of sustainable development
The survey of respondents shows that about 3% offer meetings with social workers and psychologists with people with disabilities in order to explain to them the basic concepts of sustainable development, and about 28% offer an average of meetings, and about 60% of them offer many meetings with psychologists and social workers to increase the effectiveness of the concept of sustainable development.

● Your institution offers meetings with electrical engineers or renewable energy businesses (wind, solar, water) to understand the importance of implementing the principle of sustainable development in the renewable energy sector
The survey of respondents shows that about 8% of educational institutions offer meetings with electrical engineers or renewable energy businesses (wind, solar, water) to understand the importance of implementing the principle of sustainable development in the renewable energy sector, and about 42% offer an average of meetings with electrical engineers and about 58% of them offer many of these meetings to learn as much as possible about the concept of sustainable development.

● Improving people's health and opportunities for a good life contribute to sustainable development
The survey of respondents shows that about 80% completely agree that improving people's health contributes to a better life, 15% do not agree at all about this aspect, and about 6% have no information about it.
● Nature conservation and biodiversity directly affect sustainable development
The survey of respondents shows that 70% agree with it, about 25% do not agree at all that it affects sustainable development, and about 10% do not have any information.

CONCLUSION

The majority of pupils and students are well acquainted with the concept of sustainable development, whether from school curricula or under the influence of social networks or the media. Most of them agreed that many factors such as: economy, nature conservation, biodiversity or global warming influence the development of the sustainable concept. On the other hand, they indicate that the educational institutions where they study offer, on average, extracurricular training or meetings with non-profit organizations or conversations with social workers to exchange experiences or to better understand the functionality and practice of the sustainable concept. The vast majority of them think that energy conservation practices, solid waste recycling, political instability, effective management of natural resources also have great importance and great impact, causing sustainable concepts to evolve over time and this brings a major benefit to increase the quality of education in the process of effective teaching and learning. The majority of them believe that energy conservation practices, solid waste recycling, political instability, and effective management of natural resources are also of great importance and impact, causing the concepts of

sustainable development to evolve over time and this brings a major benefit to increasing the quality of education in the process of effective teaching and learning. The results of this study are very important for understanding the importance of all the above-mentioned factors for the concept of sustainable development and for understanding how they influence these concepts for the most effective teaching and learning for students in the pre-university and university systems.

REFERENCES

Benaim, C. A., & Raftis, L. (2008). The Social Dimension of Sustainable Development: Guidance and Application: Thesis submitted for completion of Master of Strategic Leadership towards Sustainability, Blekinge Institute of Technology, Karlskrona, Sweden, 47(6)

Brodhag, C., & Taliere, S. (2006). Sustainable development strategies: Tools for policy coherence. Natural Resources Forum, 30, 136–145.

Osingada, C. P., and C. M. Porta. 2020. "Nursing and SustainableDevelopment Goals (SDGs) in a COVID-19 World: The State of theScience and a Call for Nursing to Lead." Public Health Nursing 37, no.5: 799–805.

Lopez-Medina, I. M., C. Álvarez-Nieto, J. Grose, et al. 2019."Competencies on Environmental Health and Pedagogical Approachesin the Nursing Curriculum: A Systematic Review of the Literature."Nurse Education in Practice 37: 1–8.

Aarnio-Linnanvuori, E. (2019). How do teachers perceive environmental responsibility? Environmental Education Research, 25(1), 46-61.

Borg, C., Gericke, N., Howglund, H. –O., & Bergman, E. (2014). Subject and experience-bound differences in teachers' conceptual understanding of sustainable development. Environmental Education Research, 20(4), 526-551.

C.M. Chou, C.H. Shen, H.C. Hsiao, and T.C. Shen. (2019). Factors influencing teachers' innovative teaching behavior with information and communication technology (ICT): The mediator role of organisational innovation climate. Educational Psychology. 39(1): 65-85

R. Stankić, G.B. Jovanović, and A.J.Soldić. (2018). Information and communication technologies in education as a stimulus to economic development. Economic Horizons. 20(1): 61-73.

J. L. Arvai, V. E. Campbell, A. Baird, and L. Rivers, "Teaching students to make better decisions about the environment: Lessons from the decision sciences," The Journal of Environmental Education,vol. 36, 1, pp. 33-44.

P. Kwangmuang, S. Jarutkamolpong, W. Sangboonraung, and S. Daungtod, "The development oflearning innovation to enhance higher order thinking skills for students junior high schools,pp.678-895,August 2020

➢ *ORAL PRESENTATION*

AlNi-Graphene Modified Natural Wool Materials for Solar Steam Generator Applications

Kader Dağcı Kıranşan[1*] (*ORCID: https://orcid.org/0000-0002-0764-9393*), Ezgi Salper[1] (*ORCID: https://orcid.org/0009-0009-2252-807X)*, Ezgi Topçu[1] (*ORCID: https://orcid.org/0000-0003-1506-9089*), Elif Erçarıkcı[1] (*ORCID: https://orcid.org/0000-0002-8490-1644*), Zeynep Karcıoğlu Karakaş[2](*ORCID: https://orcid.org/*0000-0001-9778-5956

[*1] Atatürk University, Faculty of Science, Department of Chemistry, Erzurum, Turkey.
[2] Atatürk University, Faculty of Engineering, Department of Environmental Engineering, Erzurum, Turkey.

*Corresponding author e-mail:kdagci@atauni.edu.tr

Abstract
In this study, an AlNi-Gr composite was obtained by interacting AlNi, which was prepared using a simple hydrothermal method and low-cost, readily available metals, with graphene. Using the AlNi-Gr composite, a photothermal paste was prepared and immobilized onto the surface of natural wool (NW) material to produce AlNi-Gr/NW. The AlNi-Gr/NW photothermal material demonstrated a high evaporation rate (3.4 $kg \cdot m^{-2} \cdot h^{-1}$) due to the combined photothermal activity of both AlNi and graphene structures, and exhibited high thermal efficiency (88%) owing to the thermal insulation property of the NW material. It was also determined that AlNi-Gr/NW maintained a steam generation performance close to that in pure water, even in systems containing saline, acidic, basic, heavy metal-contaminated, or dye-polluted water. Consequently, AlNi-Gr/NW, with its high steam generation performance, was employed as a photothermal material in a solar steam generator system for obtaining potable water from wastewater and seawater, achieving a salt and metal ion removal efficiency of 93%.
Keywords: AlNi, Graphene, Photothermal material, Solar steam generator.

INTRODUCTION

The rapid urbanization and population growth, along with the swift advancements observed in modern industry, have significantly increased the demand for both energy and potable water. In response to this growing need, traditional technologies such as multi-stage flash evaporation, thermal distillation, ion exchange, and reverse osmosis are widely used for seawater desalination (Ghaffour at al.,2013; Fan et al., 2027; Li et al., 2011, Qasim et al., 2019). The solar steam generation method has garnered attention due to its use of natural and sustainable solar energy as the input, low cost, and low carbon footprint (Liu et al., 2020; Geng et al., 2029; Xiao et al., 2021). A solar steam generation system typically consists of a region with high water adsorption capacity for continuous water supply and a photothermal absorber region that converts solar energy into thermal energy to produce steam (Ginting et al., 2022; Ginting et al., 2022; Lau et al. 2029).
There are five essential features of an ideal photothermal evaporator:

(i) the ability to absorb solar energy across a broad spectral range,

(ii) uniform heat distribution on the surface,

(iii) good wettability of the porous material,

(iv) excellent chemical and mechanical stability, and

(v) salt resistance to prevent salt accumulation (Ni et al., 2026; Shi et al., 2020).

Extensive research has been conducted to minimize heat losses in photothermal materials and improve solar steam generation efficiency. In this context, natural wool (NW), which is low-cost, readily available, and has a high water transport capacity, is considered highly effective as a 3D base material in solar steam

generator systems. NW is commonly used in yarn production and household textile products. However, in recent years, the usage of wool has declined due to the emergence of alternative materials in home textiles.

Thanks to its excellent thermal and sound insulation properties, natural wool is being reconsidered—especially in solar steam generator applications due to its natural structure, ease of access, low cost, and biodegradability. In recent years, modifying inexpensive and easily accessible natural materials like NW with new materials possessing different chemical structures for various applications has become a popular topic. There is growing interest in the design of inorganic materials with hierarchical and complex morphologies. Accordingly, parameters such as synthesis environment, type of surfactant, and polymer templates have been altered to synthesize inorganic materials with different crystal structures, particle sizes, and morphologies (Zhang et al., 2023; Li et al., 2016; Zhang et al., 2026).

In this regard, layered double hydroxides (LDHs) have gained increasing attention due to their anion exchange properties and potential applications in catalysis, environmental remediation, bionanocomposites, and biosensors. Recently, various synthetic techniques such as sonochemistry, microwave, hydrothermal, and sol-gel methods have been employed for LDH synthesis to control crystal growth. New LDH morphologies have also been reported through the use of organic solvents, surfactants, macromolecules, and biomolecules (Zhang et al., 2012; Cheng et al., 2013).

Graphene, with its planar structure and highly negative charge centers due to oxygen-containing functional groups, has been reported to interact effectively with positively charged LDHs (Li et al., 2017). The resulting composite material retains both the physical and chemical properties of graphene and LDHs.

To date, numerous photothermal materials have been developed through immobilizing various chemical materials including carbon-based, metallic, and semiconducting materials onto 3D base substrates. At this point, a composite material was prepared by doping AlNi LDH, synthesized via a simple hydrothermal method, with graphene. The AlNi-LDH-Gr-based photothermal paste was immobilized onto NW, and the resulting composite material was used as a photothermal agent in a solar steam generation system. Composites containing different ratios of AlNi-LDH and graphene were prepared, and their steam generation performances were compared. It was found that the optimally composed AlNi-LDH-Gr/NW material had a steam generation rate of 3.41 $kg \cdot m^{-2} \cdot h^{-1}$, while AlNi-LDH/NW and Gr/NW exhibited lower rates of 1.8 and 1.6 $kg \cdot m^{-2} \cdot h^{-1}$, respectively. Moreover, the AlNi-LDH-Gr/NW material demonstrated over 90% removal efficiency of salts and heavy metals from wastewater, indicating its effectiveness and practicality in clean water production from polluted sources.

MATERIALS AND METHODS

Hydrothermal Synthesis of NiAl-LDH

A 75 mL solution containing 0.2 M $Ni(NO_3)_2 \cdot 6H_2O$ and 0.1 M $Al(NO_3)_3 \cdot 9H_2O$ was prepared and stirred for 15 minutes to obtain Solution A. Then, 15 mmol of urea solution was slowly added to Solution A to form Solution B. After stirring for another 15 minutes, Solution B was transferred into a Teflon-lined autoclave and subjected to hydrothermal treatment at 180 °C for 12 hours. After the autoclave was cooled down, the resulting AlNi-LDH was filtered, washed several times with ethanol and water, and dried at 60 °C for 12 hours to obtain solid NiAl-LDH (Li et al., 2017).

Synthesis of the NiAl-Gr Composite

During the NiAl-LDH preparation procedure, various volumes (2, 4, 6 mL) of a GO dispersion at a concentration of 7 mg/mL were added into the previously described Solution B. The resulting composite solution was first subjected to ultrasonic treatment for 30 minutes. It was then transferred into a 50 mL Teflon-lined autoclave and treated hydrothermally at 180 °C for 12 hours. After cooling, the resulting AlNi-Gr composites with varying compositions were filtered, washed with ethanol and water several times, and dried at 60 °C for 12 hours, yielding AlNi-Gr composites with different AlNi/Gr ratios.

Preparation of NiAl-LDH, NiAl-Gr, and Gr Gels and Their Immobilization on NW Material
Different mixtures were prepared by adding NiAl-LDH, AlNi-Gr composites, or graphene (Gr) individually at a concentration of 5 mg/mL into a solution containing 5 wt% polyvinyl alcohol (PVA). The mixtures were heated at 85 °C for 2 hours to ensure complete dissolution of the PVA (33). Figure 1.b shows the gel preparation procedures along with digital photographs of the gels. The prepared NiAl-LDH gel, Gr gel, and composite gels (AlNi-Gr-1, AlNi-Gr-2, and AlNi-Gr-3) were applied onto NW substrates (natural wool) with a diameter of 2 cm and a height of 0.5 cm using a brush. The coated materials were then dried in an oven at 80 °C for 12 hours and made ready for use in the solar steam generation system.

Steam Generation Experiments
Solar steam generation experiments were carried out using the setup shown in Figure 5.a. The prepared AlNi/NW, Gr/NW, and AlNi-Gr/NW materials were directly used as photothermal materials. During the process, surface temperatures were monitored using an IR camera (FLIR), and water weight loss was measured using an electronic balance (Shimadzu). A solar simulator (Optosence) with an intensity ranging from 1 sun (1 kW/m²) to 10 suns (10 kW/m²) was used as the light source. All purification experiments were conducted under 10 suns. All experiments were performed at room temperature.

RESULTS AND DISCUSSION

Photothermal Performance and Solar Steam Generation Efficiency

The photothermal performance of the fabricated Gr/NW, AlNi/NW, and AlNi-Gr/NW materials was comprehensively investigated for solar steam generation applications.

The evaporation rates of these materials after 1 hour of irradiation under 1 sun (1 kW m^{-2}) were found to be 1.68, 1.82, 2.2, 3.4, and 2.9 kg m^{-2} h^{-1} for Gr/NW, AlNi/NW, AlNi-Gr1/NW, AlNi-Gr2/NW, and AlNi-Gr3/NW, respectively. Among these, the AlNi-Gr2/NW composite exhibited the highest evaporation rate, highlighting the synergistic effect of the layered double hydroxide (LDH) and graphene components.

To further optimize the system, the diameter of the photothermal material and the mass of the immobilized AlNi-Gr2 composite were systematically varied. When the composite mass was kept constant at 1.5 g, the effect of varying diameters (3.0–5.0 cm) on the evaporation rate was studied. It was found that a 4.0 cm diameter yielded the maximum evaporation rate, whereas further increases led to slight reductions, likely due to decreased photothermal conversion efficiency per unit area. However, the diameter showed no statistically significant influence on overall evaporation performance.

Subsequently, the effect of the immobilized composite mass (0.5–2.5 g) was investigated with a constant material diameter of 4.0 cm. The evaporation rate increased with composite loading up to 1.5 g but declined beyond this point. This decline was attributed to partial blockage of the NW scaffold's pores, leading to reduced water transport capacity and consequently lower evaporation efficiency, consistent with previous findings. Hence, 1.5 g was determined to be the optimal composite loading.

Surface Temperature Profiles and Photothermal Conversion Efficiency

Surface temperature changes of Gr/NW, AlNi/NW, and AlNi-Gr2/NW were monitored under 1 sun irradiation for 120 seconds using infrared thermography (Figure 1a). Compared to the bare water surface, which showed a modest temperature increase from 20 °C to 23 °C, the photothermal materials exhibited significantly higher surface temperatures: Gr/NW reached 44 °C, AlNi/NW reached 46 °C, and AlNi-Gr2/NW exceeded 64 °C within 45 seconds. The exceptional thermal response of AlNi-Gr2/NW was attributed to efficient electron delocalization within the conjugated graphene layers and the presence of Ni and Al atoms, which facilitated rapid conversion of absorbed light into thermal energy.

Thermal camera images taken after 60 seconds of irradiation further confirmed the superior photothermal activity of AlNi-Gr2/NW compared to AlNi/NW and Gr/NW (Figure 1.b). Based on the calculated evaporation enthalpies, the solar steam generation efficiencies were determined as 50% for Gr/NW, 53% for AlNi/NW, and 88% for AlNi-Gr2/NW, as presented in Figure 5f. Moreover, the AlNi-Gr2 composite

layer served as an insulating barrier that minimized heat loss, further enhancing its photothermal conversion capability.

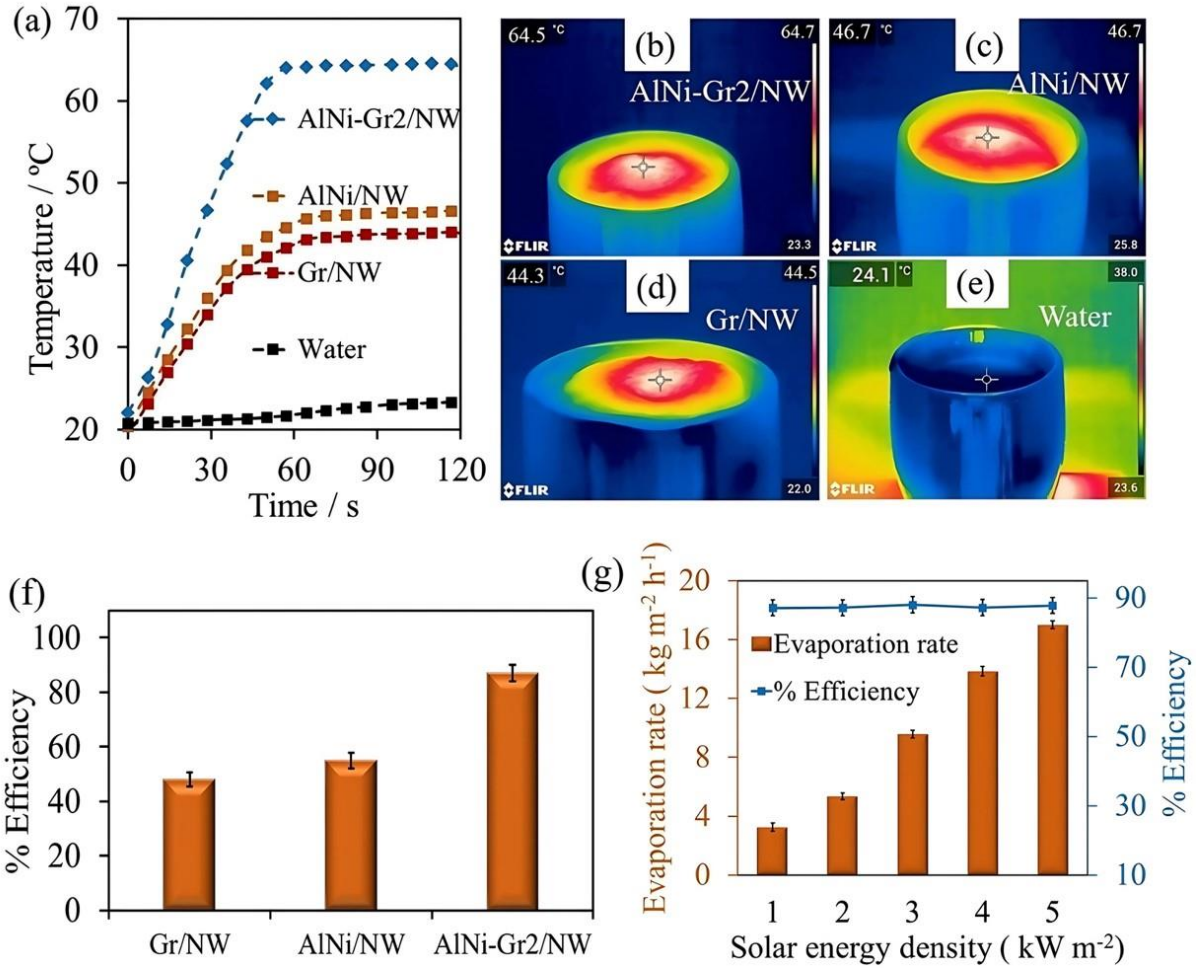

Figure1. (a) Graph showing the surface temperature changes of Gr/NW, AlNi/NW, AlNi-Gr2/NW, and bare water surface over a 120-second irradiation period. (b) Thermal camera images displaying the surface temperatures of AlNi-Gr2/NW, AlNi/NW, Gr/NW, and the bare water surface after 60 seconds of irradiation under 1 sun (1 kW/m²). (f) Graph showing the photothermal conversion efficiencies (%) of Gr/NW, AlNi/NW, and AlNi-Gr2/NW materials. (g) Graph illustrating the changes in evaporation rate and photothermal efficiency (%) of the AlNi-Gr2/NW material with increasing solar irradiance intensity.

Evaluation in Various Water Matrices

To assess the practical applicability of AlNi-Gr2/NW, solar evaporation performance was evaluated in various water matrices, including pure water, acidic (pH 2), basic (pH 12), saline (3.5% NaCl), heavy metal-containing (100 mg/L Cu^{2+}), and dye-containing (1.0 g/L methyl blue) solutions under optimized conditions. The results are depicted in Figure 2.a. Remarkably, the material exhibited consistent evaporation performance across all tested conditions, with an average standard deviation of 4.27% in steam generation efficiency and 0.68 in evaporation yield, indicating strong tolerance to varying water chemistries.

Corresponding surface temperature changes during irradiation were monitored (Figure 2.b), and thermal images after 60 seconds are shown in Figure 2.c. The surface temperature variations remained within a 3.2% standard deviation, further confirming the stability and robustness of AlNi-Gr2/NW under diverse water compositions.

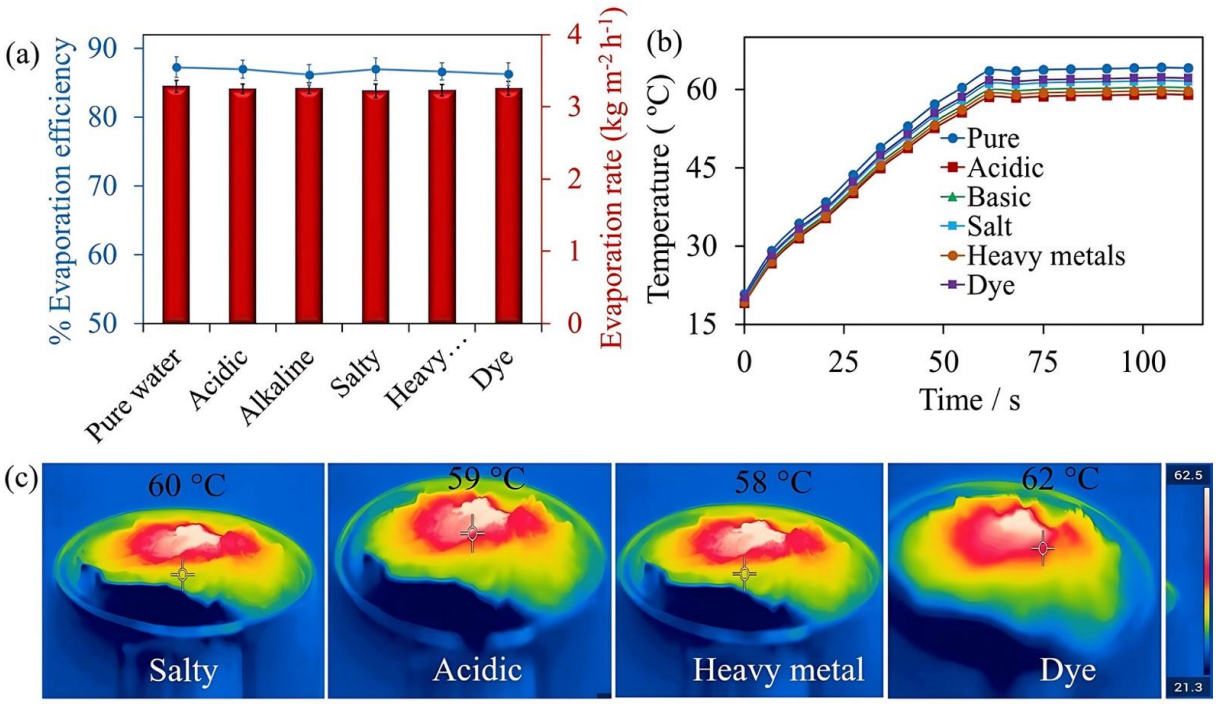

Figure 2. (a) Evaporation efficiency and evaporation yield of AlNi-Gr2/NW material after 1 hour of irradiation under 1 sun intensity (1 kW m^{-2}) in various water samples: pure water, acidic (pH 2), basic (pH 12), saline (3.5% NaCl), heavy metal-contaminated (100 mg/L Cu^{2+}), and dye-contaminated (1.0 g/L methyl orange) solutions. (b) Surface temperature changes of AlNi-Gr2/NW recorded as a function of irradiation time for different water matrices. (c) Thermal camera images showing the surface temperatures of AlNi-Gr2/NW after 60 seconds of irradiation under 1 sun for each water type.

Desalination Performance of AlNi-Gr2/NW Material

The applicability of the synthesized AlNi-Gr2/NW material for potable water production from saline water was investigated. A synthetic salt solution containing 0.1% Na^+, K^+, Mg^{2+}, and Ca^{2+} ions was prepared, and the desalination process was carried out under 10 sun irradiation using a closed experimental setup until approximately 10 mL of distilled water was collected from an initial 20 mL of saline feed solution. The experimental system used for the desalination studies is depicted in Figure 3.a. Ion concentrations before and after distillation were analyzed, and the results presented in Figure 3.a and Table 1 demonstrate that the AlNi-Gr2/NW photothermal material achieved a salt removal efficiency of 91%.

Table 1. The ion contents after solar desalination of solution containing 0.1% Na^+, K^+, Mg^{+2} ve Ca^{+2} with AlNi/NW, Gr/NW, and AlNi-Gr/NW.

Material	Na^+ (ppm)	K^+ (ppm)	Mg^{+2} (ppm)	Ca^{+2} (ppm)
AlNi-Gr/NW	0.9	1.1	2.2	3.0
AlNi/NW	0.8	0.9	2.5	3.0
Gr/NW	1.1	1.2	1.9	3.0
Initially, 900 ppm Na+, 935 ppm K^+, 550 ppm Mg^{+2}, and 905 ppm Ca^{+2} were detected in 0.1% ion solution.				

Heavy Metal, Acid-Base, and Dye Removal Performance of AlNi-Gr2/NW Photothermal Material

In a similar manner to the salt removal experiments, aqueous solutions containing 225 mg/mL Pb^{2+}, 100 mg/mL Cu^{2+}, 90 mg/mL Ni^{2+}, 75 ppm Cr^{3+}, and 150 mg/mL Zn^{2+} were prepared. Following the distillation process, the ion concentrations in the distilled water collected from the bottom chamber were analyzed using ICP-MS. The pre- and post-distillation ion concentrations are presented in Figure 3.b and Table 2. According to the data, the heavy metal removal efficiency of the AlNi-Gr2/NW photothermal material was calculated as 97.5%.

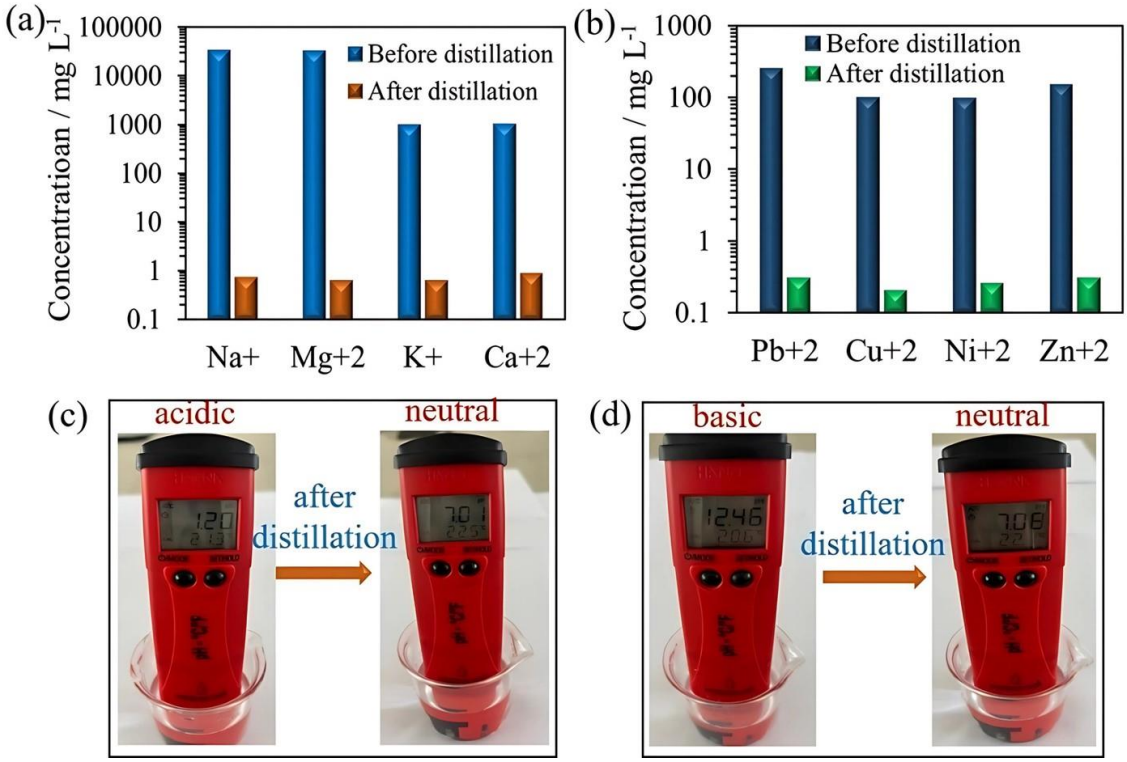

Figure 3. (a) Graph showing the changes in ion concentrations after distillation using the AlNi-Gr2/NW photothermal material on a solution containing 0.1% Na^{+}, K^{+}, Mg^{2+}, and Ca^{2+} ions; (b) Graph illustrating the changes in ion concentrations after distillation using a solution containing 225 mg/mL Pb^{2+}, 100 mg/mL Cu^{2+}, 90 mg/mL Ni^{2+}, 75 ppm Cr^{3+}, and 150 mg/mL Zn^{2+} ions; (c) Photographs displaying the pH values of an acidic solution before and after treatment; and (d) Photographs displaying the pH values of a basic solution before and after treatment, all obtained using the AlNi-Gr2/NW photothermal material.

Table 2. The ion contents after solar purification of heavy metal solution with AlNi-Gr/NW, AlNi/NW, and Gr/NW.

Material	Pb^{+2} (ppm)	Cu^{+} (ppm)	Ni^{+2} (ppm)	Cr^{+2} (ppm)	Zn^{+2} (ppm)
AlNi-Gr/NW	0.15	0.23	0.12	0.11	0.14
AlNi/NW	0.16	0.26	0.13	0.11	0.15
Gr/NW	0.17	0.27	0.13	0.12	0.15
Initially, 900 ppm Na+, 935 ppm K^{+}, 550 ppm Mg^{+2}, and 905 ppm Ca^{+2} were detected in heavy metal solution.					

In addition to desalination and heavy metal removal, the AlNi-Gr2/NW material was evaluated for its performance in treating acidic (pH 2) and basic (pH 12) solutions. The pH values of the distilled water were measured using a pH meter. As illustrated in Figure 3.c, after the distillation of the acidic solution using

AlNi-Gr2/NW, the pH of the distillate approached neutrality. Similarly, Figure 3.d shows that the initially basic solution also yielded a neutral pH after distillation, indicating the material's suitability for purifying solutions with extreme pH values.

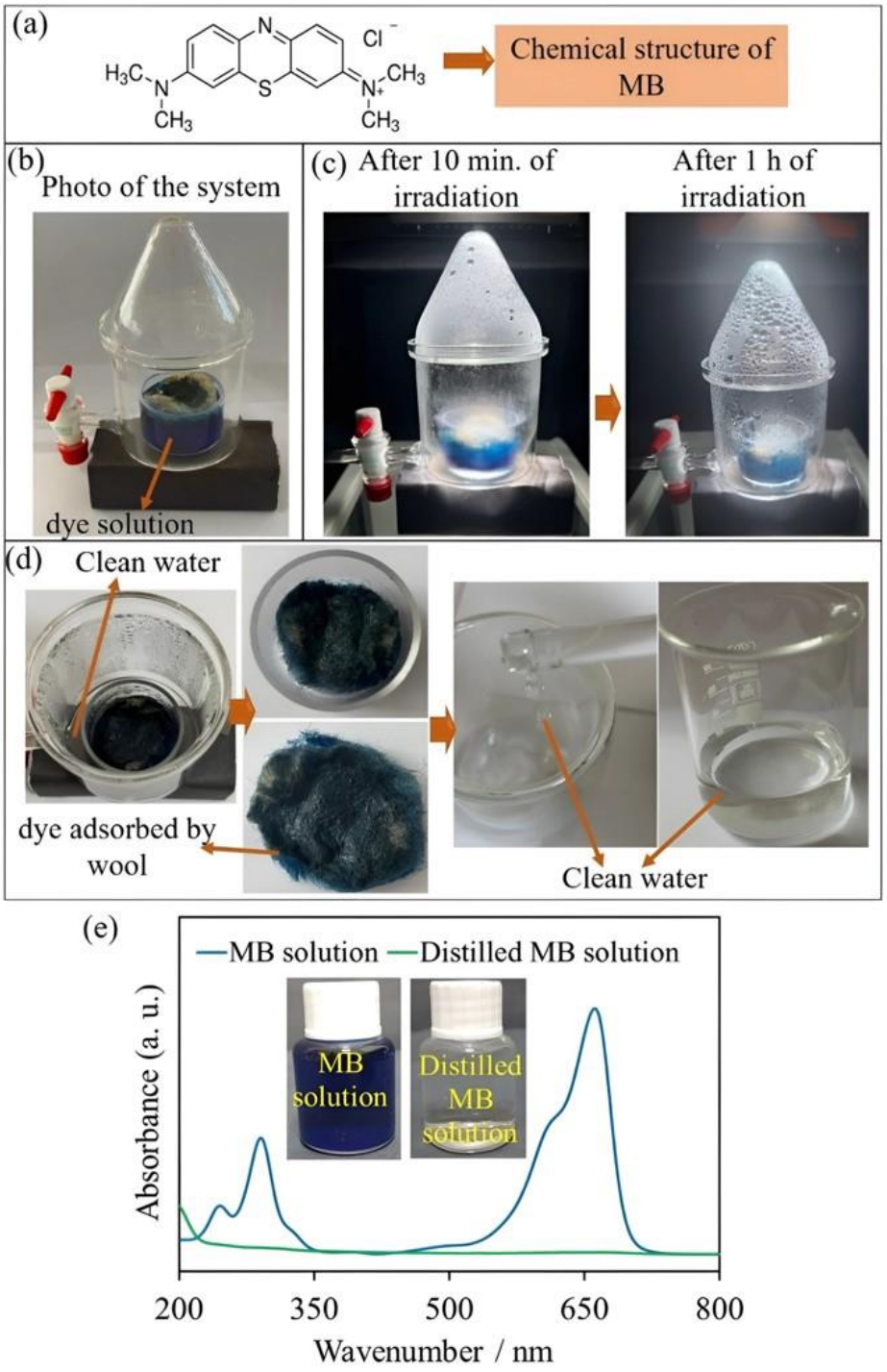

Figure 4. (a) Chemical structure of methylene blue (MB). (b) Schematic of the experimental setup used for dye removal via solar-driven distillation. (c) Photographs of the distillation system at various irradiation times. (d) Images of the AlNi-Gr2/NW photothermal material after MB adsorption and the collected distillate. (e) UV-Vis absorption spectra of the initial MB solution and the collected distillate, along with corresponding visual images, demonstrating complete dye removal.

The AlNi-Gr2/NW material was further tested for its capacity to treat dye-contaminated water. A 1.0 g/L methylene blue (MB) solution was subjected to solar distillation under 10 sun illumination. The distillation process is illustrated in Figure 4.a–d. Initial and intermediate stages of distillation were documented

photographically (Figure 4.b–c), and the final distillate collected in the receiving container was observed to be colorless and clear (Figure 4.d). Furthermore, the AlNi-Gr2/NW material exhibited visible adsorption of MB dye, as indicated by a blue coloration after distillation (Figure 4.c).

UV-visible absorption spectroscopy of the collected distillate revealed the absence of any MB characteristic absorption peaks, confirming effective dye removal (Figure 4.d, inset). These results demonstrate the potential of the AlNi-Gr2/NW photothermal material in the treatment of dye-contaminated wastewater.

CONCLUSION

In summary, a 3D AlNi-Gr/NW photothermal material with a highly porous structure and excellent light absorption capacity was successfully fabricated for clean water generation from wastewater using solar energy a natural and sustainable energy source. NW substrate, selected for its high water transport capacity, low cost, easy availability, and exceptional thermal insulation, significantly minimized heat loss during operation. Moreover, due to the unique morphology of the NW, incident light undergoes multiple reflections, thereby enhancing the overall light absorbance of the system.

The surface-deposited AlNi and Gr structures demonstrated broad-spectrum solar absorption and superior photothermal activity, resulting in a high steam generation rate of 3.4 kg m^{-2} h^{-1} and rapid surface temperature elevation to above 65 °C within just 1 minute under solar irradiation. The synergistic integration of AlNi-Gr's high photothermal efficiency and NW's excellent transport properties yielded an impressive thermal conversion efficiency of approximately 88%.

Thanks to the NW's 3D penetration channels and anisotropic macroporous architecture, the AlNi-Gr/NW system showed outstanding performance in extracting clean water from saline and wastewater, along with excellent fluid circulation and self-cleaning stability. Designed using cost-effective and readily available materials, the AlNi-Gr/NW photothermal material demonstrates strong potential for widespread application in solar driven water purification systems, particularly in addressing the global challenges of clean water supply from seawater and wastewater.

ACKNOWLEDGEMENTS

The work is supported by the Ataturk University through a Scientific Project: FCD-2025-15134.

REFERENCES

Alam, M. S., Kaur, G., Jabbar, Z., Javed, K., & Athar, M. (2007). Eruca sativa seeds possess antioxidant activity and exert a protective effect on mercuric chloride induced renal toxicity. Food and chemical toxicology, 45(6), 910-920.

Liu, C., K. Hong, X. Sun, A. Natan, P. Luan, Y. Yang and H. Zhu, (2020), An 'antifouling'porous loofah sponge with internal microchannels as solar absorbers and water pumpers for thermal desalination, J. Mater. Chem. A, 8, 12323–12333.

Ni, G., G. Li, S. V. Boriskina, H. Li, W. Yang, T. Zhang and G. Chen, (2016), Steam generation under one sun enabled by a foating structure with thermal concentration, Nat. Energy, 1, 1–7.

Geng, H., Q. Xu, M. Wu, H. Ma, P. Zhang, T. Gao, L. Qu, T. Ma and C. Li, (2019), Plant leaves inspired sunlight-driven purifer for high-efficiency clean water production, Nat. Commun., 10, 1–10.

Li, H., L. Zou, (2011), Ion-exchange membrane capacitive deionization: a new strategy for brackish water desalination, Desalination, 275, 62–66.

Xiao, J., Y. Guo, W. Luo, D. Wang, S. Zhong, Y. Yue, C. Han,R. Lv, J. Feng and J. Wang, (2021), A scalable, cost-effective and salt-rejecting MoS_2/SA@melamine foam for continuous solar steam generation, Nano Energy, 87, 106213.

Cheng, J.P., J.H. Fang, M. Li, W.F. Zhang, F. Liu, X.B. Zhang, (2013) Enhanced electrochemical performance of CoAl-layered double hydroxide nanosheet arrays coated by platinum film, Electrochim. Acta 114, 68-75.

Lau, K. S., R. T. Ginting, S. T. Tan, S. X. Chin, S. Zakaria and C. H. Chia, (2019), Sodium cholate as efficient green reducing agent for graphene oxide via fow reaction for fexible supercapacitor electrodes, J. Mater. Sci.: Mater. Electron., 30, 19182–19188.

Li, L., K. S. Hui , K. N. Hui, Q. Xia, J. Fu, Y. Rç Cho, (2017), Facile synthesis of NiAl layered double hydroxide nanoplates for high-performance asymmetric supercapacitor, Journal of Alloys and Compounds, 721, 803-812

Shi, L., X. Wang, Y. Hu, Y. He and Y. Yan, (2020), Solar-thermal conversion and steam generation: a review, Appl. Therm. Eng., 179, 115691.

Zhang, L.J., J. Wang, J.J. Zhu, X.G. Zhang, K.S. Hui, K.N. Hui, (2013), 3D porous layered double hydroxides grown on graphene as advanced electrochemical pseudocapacitor materials, J. Mater. Chem. A 1, 9046-9053.

Zhang, L.J., X.G. Zhang, L.F. Shen, B. Gao, L. Hao, X.J. Lu, F. Zhang, B. Ding, C.Z. Yuan, (2012), Enhanced high-current capacitive behavior of graphene/CoAl-layered double hydroxide composites as electrode material for supercapacitors, J. Power Sources 199, 395-401.

Qasim, M., M. Badrelzaman, N. N. Darwish, N. A. Darwish and N. Hilal, (2019), Reverse osmosis desalination: a state-of-theart review, Desalination, 459, 59–104.

Ghaffour, N., T. M. Missimer and G. L. Amy, (2013), Technical review and evaluation of the economics of water desalination: current and future challenges for better water supply sustainability, Desalination, 309, 197–207.

Zhang, Q.B., B.T. Zhao, J.X. Wang, C. Qu, H.B. Sun, K.L. Zhang, M.L. Liu, (2016), High-performance hybrid supercapacitors based on self-supported 3D ultrathin porous quaternary Zn-Ni-Al-Co oxide nanosheets, Nano Energy, 28, 475-485.

Ginting, R. T., H. Abdullah and V. Fauzia, (2022), Facile preparation of MXene and protonated-g-C_3N_4 on natural latex foam for highly efficient solar steam generation, Mater. Lett., 313, 131779.

Ginting, R. T., H. Abdullah, E. Taer, O. Purba and D. Perangin-angin, (2022), Novel strategy of highly efficient solardriven water evaporation using MWCNTs-ZrO2-Ni@CQDs composites as photothermal materials, Colloids Surf., A, 642, 128653.

Li, X. J., Y. Zhang, W. Xing, L. Li, Q.Z. Xue, Z.F. Yan,(2016), Sandwich-like graphene/polypyrrole/layered double hydroxide nanowires for high-performance supercapacitors, J. Power Sources 331, 67-75.

Fan, Y., S. Chen, H. Zhao and Y. Liu, (2017), Distillation membrane constructed by TiO_2 nanofber followed by fuorination for excellent water desalination performance, Desalination, 405, 51–58.

➢ *ORAL PRESENTATION*

Design Optimization of Corona Rings for Electric Field Control Using Finite Element Analysis

Burak Esenboğa[1*] (*ORCID: https://orcid.org/0000-0002-7777-259X)*

[*1]Adana Alparslan Türkeş Science and Technology University, Engineering Faculty, Department of Electrical and Electronics Engineering, Adana, Türkiye.

*Corresponding author e-mail: besenboga@atu.edu.tr

Abstract
In high-voltage power transmission systems, corona rings are essential components designed to mitigate electric field concentrations at critical points of insulator assemblies, thereby enhancing system reliability and longevity. This study presents a comprehensive design optimization of corona rings aimed at controlling electric field distributions using the Finite Element Method (FEM). To reduce the electric field intensity on the surface of composite insulators, particularly near the end fittings, three primary corona ring design parameters are considered for optimization. These parameters are the ring's outer radius, the tube radius, and its vertical positioning relative to the insulator. This geometric optimization is achieved through a parametric sensitivity analysis, systematically varying each parameter to assess its impact on the electric field distribution. The optimized configuration is analyzed using the ANSYS Maxwell electromagnetic solver. Simulation results indicated that the maximum electric field strength is reduced to 228 kV/m, significantly below the target threshold of 450 kV/m. This substantial reduction confirms the effectiveness of the optimization process in enhancing the electric field distribution along the insulator surface. The findings underscore the importance of precise corona ring design in improving the performance and durability of composite insulators in high-voltage applications.

Keywords: Corona Ring, Design Optimization, Electric Field Distribution, Composite Insulator, Finite Element Method.

INTRODUCTION

In high-voltage (HV) power transmission systems, composite insulators have become increasingly popular due to their superior mechanical strength, lighter weight, and enhanced resistance to pollution compared to traditional porcelain or glass insulators. Despite these advantages, composite insulators are still vulnerable to electric field intensification, particularly near metallic end fittings where abrupt geometric transitions lead to localized field enhancements. These intensified electric fields can initiate partial discharges, surface tracking, and corona effects, ultimately compromising the insulator's long-term performance and reliability (Doshi et al., 2011; Saleem and Akbar, 2022).

Khajavi et al. (2023) optimized corona ring design for a 230 kV composite insulator by considering the effects of the tower structure, conductor, hardware, and mutual phases, which were previously overlooked. Using 3D FEM simulations in COMSOL, the Nelder-Mead (NM) and BOBYQA algorithms were applied to minimize electric field intensity (EFI) along the creepage distance. The NM method achieved a 76.5% reduction in EFI at the triple point and increased the insulator's voltage withstand length. The results emphasized the importance of including environmental factors in EFI modeling for more effective high-voltage insulator design. Jthear et al. (2023) focused on the use of corona rings at the ends of 765 kV and 500 kV polymer insulators to minimize electric field strength and improve voltage distribution. By applying a two-dimensional Finite Element Method and optimizing corona ring parameters with the Nelder-Mead algorithm, the research successfully reduced electric field strength by 69% for the 765 kV insulator and 32% for the 500 kV insulator. This approach demonstrated high performance and speed, providing an efficient methodology that can be applied to insulators of various voltage levels, ensuring better insulation reliability in power transmission systems. Li et al. (2012) used FEM to optimize grading ring configurations for ceramic insulators in 1000 kV UHV substations, improving potential distribution and reducing corona effects. By adjusting parameters like mounting height and diameter, the research finds that double rings at terminal insulators and proper jumper configurations can enhance electric field uniformity. The optimized design, validated through testing and applied in a pilot project in China, successfully prevented corona in the field. Ahsan et al. (2024) presented a grading device design for insulated cross-arms (ICA) on a 132 kV

lattice tower, using FEA to optimize electric field stress. The grading devices, including a ring for the LV end and a single-piece device for the HV end, reduced electric field stress by 70% and 80%, respectively. The study demonstrates the value of FEA in accelerating the design process and improving the reliability of ICA in power transmission systems.

To mitigate these adverse effects, corona rings are installed to redistribute electric field lines more uniformly along the insulator surface. Properly designed corona rings reduce the electric field magnitude near critical points, thereby preventing corona inception and minimizing the risk of dielectric degradation (Aramugam et al., 2023). However, the effectiveness of corona rings is highly sensitive to their geometric configuration, including factors such as the outer diameter of the ring, the tube radius, and the axial position relative to the insulator. Suboptimal designs may fail to sufficiently suppress field intensity, especially under high-voltage operation or polluted environments (Illias et al., 2021).

The optimization of corona ring geometry has gained significant attention in recent years, driven by both empirical testing and numerical simulation approaches. Among these, the Finite Element Method (FEM) has emerged as a powerful computational tool for modeling complex electromagnetic phenomena and predicting electric field distributions around HV components (Aziz et al., 2023). FEM-based tools such as ANSYS Maxwell enable parametric studies and design iterations, offering insights into how geometric changes influence local electric fields.

This study aims to optimize the design of corona rings used with composite insulators in high-voltage applications by systematically evaluating three primary parameters: the ring's outer radius, the tube radius, and its vertical positioning with respect to the insulator. A parametric sensitivity analysis is conducted to assess the impact of each factor on the electric field distribution, with the goal of minimizing the peak field strength near the end fittings. The optimized configurations are validated using FEM simulations in ANSYS Maxwell. The study presents that geometric optimization of corona rings can substantially improve the electrical performance and reliability of composite insulators, supporting safer and more durable HV transmission systems.

MATERIALS AND METHODS

A 3D composite insulator is designed using the FEM and ANSYS Maxwell software to analyse the electric field (EF) distribution and voltage profile along the insulator surface under clean and dry conditions. By incorporating corona rings (CRs) at both ends of the insulator, the electric field intensity is both enhanced and regulated to remain below the critical threshold.

Finite Element Method

FEM is a widely adopted numerical technique used for solving complex boundary value problems that arise in electromagnetics, structural analysis, and other physical systems governed by partial differential equations. In this study, FEM is employed within the ANSYS Maxwell simulation environment to analyse the electric field distribution around high-voltage composite insulators under specified boundary conditions. The electrostatic field behaviour in dielectric materials is governed by Poisson's equation, derived from Maxwell's equations under static conditions. The general relationship between electric field E and electric potential V is given by Equation 1.

$$E = -\nabla V \tag{1}$$

Equation 2 is obtained by substituting Equation 1 into Gauss's law for electric fields.

$$\nabla \cdot (\varepsilon \nabla V) = -\rho \tag{2}$$

In Equation 2, ρ represents the volume charge density within the dielectric medium, measured in coulombs per cubic meter (C/m³). The term ε denotes the absolute permittivity of the material, defined as the product of the vacuum permittivity ε_0 and the relative permittivity ε_r. The vacuum permittivity ε_0 is a physical

constant with a value of 8.854×10^{-12} 8farads per meter (F/m), while ε_r is a dimensionless quantity that characterizes the material's ability to permit electric field lines relative to a vacuum.

These equations are solved numerically in ANSYS Maxwell through its electrostatic solver, which computes the electric field distribution and potential profile throughout the simulation domain. Boundary conditions such as voltage sources, grounded surfaces, and material interfaces are defined explicitly to reflect the operational scenario under analysis.

Parametric Sensitivity Analysis

Parametric Sensitivity Analysis (PSA) in ANSYS Maxwell is a method used to evaluate how variations in design parameters influence the performance of an electromagnetic system. By identifying which parameters are most influential, PSA helps guide subsequent optimization efforts and reduces computational complexity by narrowing the focus to only those variables that significantly impact system performance.

To optimize the electric field distribution around high-voltage composite insulators, a parametric sensitivity analysis was performed using ANSYS Maxwell. This analysis focuses on evaluating how variations in key geometric parameters of the corona ring namely, the outer radius of the ring, the tube radius, and the vertical distance from the insulator affect the local electric field intensity. These parameters are selected due to their critical role in shaping the electric field distribution, particularly near the high-stress regions at the insulator terminals. The 400 kV composite insulator, illustrated in Figure 1, consists of high-voltage and ground-side end fittings, a silicone rubber housing, and a fiberglass-reinforced plastic (FRP) core that provides enhanced mechanical strength. For simulation purposes, external elements such as towers, conductors, and associated accessories are excluded. The insulator features 22 sheds, with alternating diameters of 160 mm and 98 mm, and a uniform spacing of 40 mm between them. The total length of the insulator structure is 2400 mm.

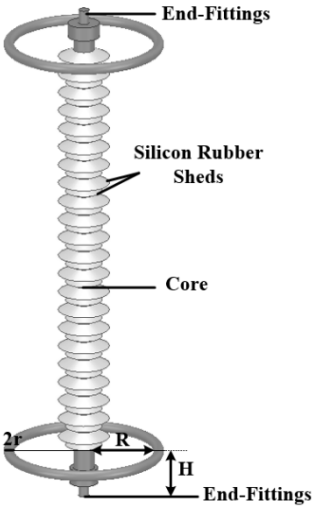

Figure 1. 3D model of a designed composite insulator in ANSYS/Maxwell

The parametric sensitivity analysis is conducted within a parametric simulation framework, allowing for systematic variation of each parameter while monitoring the corresponding changes in maximum electric field values along the insulator surface. By analyzing the trends, the most influential parameters are identified, forming the basis for targeted geometric optimization. The design parameters of the composite insulator and the corona ring are given in Table 1.

Table 1. The parameters of designed composite insulator and corona ring

Material	Parameter	Value
Composite Insulator	Rated Voltage	400 kV
	Number of Sheds	22
	Shed Spacing	40 mm
	Shed Diameters	160/98 mm
Corona Ring	Radius (R)	215 mm
	Ring Tube Thickness (r)	30 mm
	Vertical Ring Position (H)	200 mm

Material properties must vary throughout the model rather than being uniform. The model is discretized into smaller elements such as squares, triangles, or lines to accurately analyze complex geometries. This process applies to 3D models and follows key steps, including completing the geometry, assigning appropriate material properties, and defining boundary conditions. Accordingly, Table 2 presents the permittivity values assigned to various parts of the insulator and its surrounding environment.

Table 2. The permittivity values of the designed system component

Material	Relative Permeability
Air (Region)	1
Sheds (Silicon Rubber)	3.5
Aluminum (Corona Ring)	1
FRP (Core)	6
Aluminum (End Fittings)	1

In this study, completing the FEM analysis requires defining two essential boundary conditions. These are one at the grounded end and one at the high-voltage (active) end. Under steady-state conditions, the grounded end or connected to the transmission tower is assigned to a zero-voltage boundary condition. Meanwhile, the active end is set to the appropriate applied voltage specific to each insulator. In ANSYS Maxwell, these conditions are implemented by assigning voltage values and excitation forces to the active terminals.

RESULTS and DISCUSSION

Based on industry standards and manufacturer guidelines, corona rings are typically mounted at the high-voltage end of the insulator. For systems operating at voltages of 230 kV or below, a single CR is generally sufficient. However, for higher voltage levels, such as 345 kV and above, it is recommended to install CRs at both ends of the insulator (M'Hamdi et al., 2022). When determining the design parameters of CRs, a range of values is selected for each variable. For instance, the outer radius of the ring is typically varied between 150 mm and 250 mm. Importantly, the minimum ring radius must exceed the diameter of the largest insulator shed to avoid physical contact between the two components. The initial dimensions of designed corona ring and the range variations used for optimization are presented in Table 3.

Table 3. The initial dimensions of designed corona ring and the range variations

Parameter	Original Value	Lower Value	Upper Value
Radius (R)	215 mm	150 mm	250 mm
Ring Tube Thickness (r)	30 mm	20 mm	40 mm
Vertical Ring Position (H)	200 mm	0 mm	600 mm

This section presents the simulation results for all insulator configurations, highlighting the impact of incorporating corona rings and optimizing their positioning and dimensions. The analysis clearly demonstrates that the presence and proper adjustment of corona rings significantly reduce the electric field intensity along the insulator surface, particularly at critical stress points near the energized end. As shown in Figure 2, a significant concentration of electric field occurs at the critical junction where the core rod, polymer sheath, and metallic end fitting converge. This interface is widely recognized as the most vulnerable point of the composite insulator structure due to its susceptibility to intensified electric field stress.

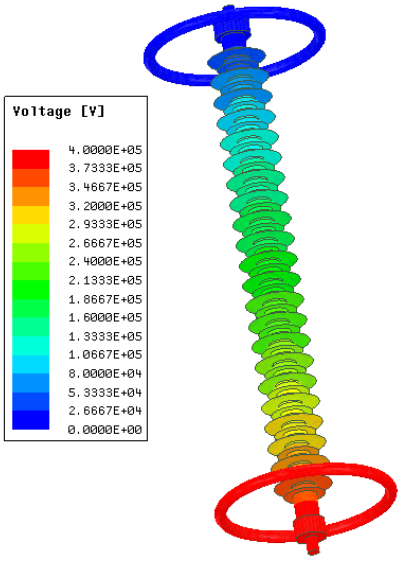

Figure 2. Voltage distribution of composite insulator

To mitigate these stresses particularly in high-voltage applications, it becomes essential to implement corona rings. These devices play a crucial role in redistributing the electric field, effectively diverting high-intensity fields away from the interface region and reducing the risk of partial discharge or long-term degradation. The impact of corona rings on electric field distribution is further analyzed and presented through simulation results in Figures 3, which demonstrate the effectiveness of this approach in enhancing the electrical performance and reliability of the insulator.

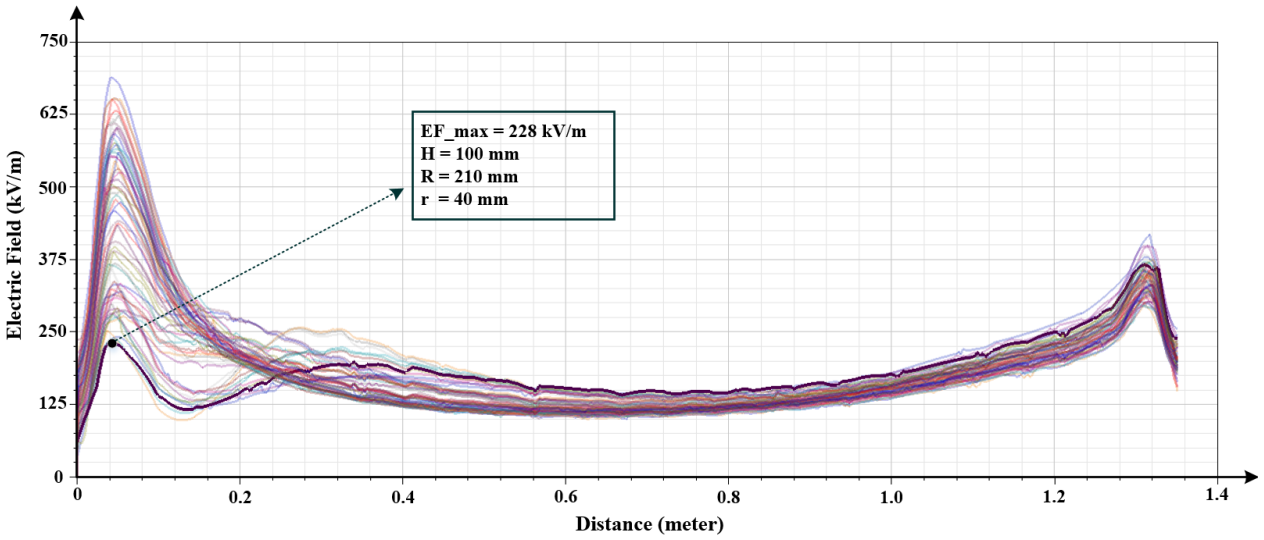

Figure 3. EF distribution of composite insulator after the parametric optimization of the corona ring

Figure 4 illustrates the potential distribution curves along the surface of the composite insulator for both the nominal and optimized designs. The comparison reveals how the optimized corona ring parameters contribute to a more uniform voltage distribution, effectively reducing the electric field concentration at critical points such as the high-voltage end. This improvement enhances the dielectric performance and reliability of the insulator under high-voltage stress.

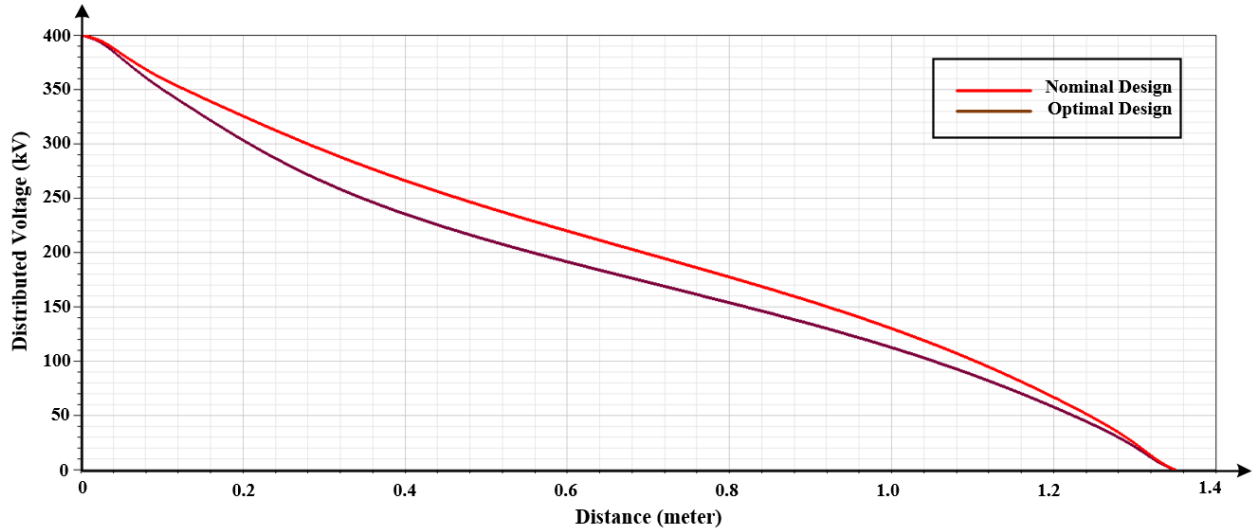

Figure 4. Potential distribution curves of composite insulators

CONCLUSION

The study demonstrates the effectiveness of optimizing corona ring geometry to improve the EF distribution along composite insulators used in high-voltage transmission systems. By employing Finite Element Method simulations and a parametric sensitivity analysis, key design parameters including the ring's outer radius, tube radius, and vertical position are systematically evaluated. The optimal configuration, identified as 210 mm outer radius, 40 mm tube radius, and 100 mm vertical distance from the insulator, significantly reduced the peak electric field intensity to 228 kV/m well below the 450 kV/m threshold. These results confirm that precise design and placement of corona rings play a critical role in enhancing insulator performance, reducing the risk of localized electrical stress, and increasing long-term reliability in high-voltage environments.

REFERENCES

Ahsan, M., Baharom, M. N. R., Zainal, Z., Khalil, I. U., Sahari, N., Ali, E., & Ghaly, R. N. (2024). Improving electric field stress using grading ring devices for insulated cross-arm. Results in Engineering, 23, 102550.

Aramugam, K., Illias, H. A., Ching, Y. C., Ali, M. S., & Makmud, M. Z. H. (2023). Optimal design of corona ring for 132 kV insulator at high voltage transmission lines based on optimisation techniques. Energies, 16(2), 778.

Aziz, E., Aouabed, F., Abdellah, H., & Dineva, A. (2023). Case study: optimizing grading ring design for high voltage polymeric insulators in power transmission systems for enhanced electric field and voltage distribution by using a finite element method. Energies, 16(13), 5235.

Doshi, T., Gorur, R. S., & Hunt, J. (2011). Electric field computation of composite line insulators up to 1200 kV AC. IEEE Transactions on Dielectrics and Electrical Insulation, 18(3), 861-867.

Illias, H. A., Chean, Y. S., Ling, L. Y., Mokhlis, H., Ariffin, A. M., & Yousof, M. F. M. (2021). Corona Ring Design Impact on the Electric Field Distribution Surrounding an Insulator String. In 2021 IEEE International Conference on the Properties and Applications of Dielectric Materials (ICPADM) (pp. 402-405). IEEE.

Jthear, Y. K., Sultan, A. J., & Bonneya, M. F. (2023). Optimization of Corona Rings Parameters for 765kV and 500kV Polymer Insulators. In 2023 6th International Conference on Engineering Technology and its Applications (IICETA) (pp. 696-700). IEEE.

Khajavi, M., Bagheri, S., & Shemshadi, A. (2023). Optimal design of corona ring in composite insulator considering the effects of tower structure, conductor, hardware and mutual phases. Electric Power Systems Research, 223, 109686.

Li, J., Peng, Z., & Yang, X. (2012). Potential calculation and grading ring design for ceramic insulators in 1000 kV UHV substations. IEEE Transactions on Dielectrics and Electrical Insulation, 19(2), 723-732.

M'Hamdi, B., Benmahamed, Y., Teguar, M., Taha, I. B., & Ghoneim, S. S. (2022). Multi-objective optimization of 400 kV composite insulator corona ring design. IEEE Access, 10, 27579-27590.

Saleem, M. Z., & Akbar, M. (2022). Review of the performance of high-voltage composite insulators. Polymers, 14(3), 431.

➢ *ORAL PRESENTATION*

Half-Metallic Properties of $CsIrI_3$ Perovskite: A First-Principles Study

Doğukan Alkan (*ORCID: https://orcid.org/0009-0009-8561-5269*), İlknur Kars Durukan (*ORCID: https://orcid.org/0000-0001-5697-0530*), Yasemin Öztekin Çiftçi (*ORCID: https://orcid.org/ 0000-0003-1796-0270*)s

Gazi University. Faculty of Sciences, Physics, Ankara, Turkey

Corresponding author e-mail: dogukan.alkan@gazi.edu.tr

Abstract

Thanks to their unique combination of high spin polarization and structural tunability, half-metallic perovskites play a key role in the development of spintronic devices. Thus, we aim to study the structural, elastic, electronic, and optical properties of $CsIrI_3$ using density functional theory (DFT) to identify potential half-metallic behavior. The calculations are performed using generalized gradient approximation (GGA) with Perdew-Burke-Ernzerhof (PBE) functional. The results of the elastic calculations indicate that the material satisfies the Born stability conditions. Being a semiconductor in spin down state and a metal in spin up state demonstrates that the material is half-metallic and exhibits ferromagnetic or ferrimagnetic properties. We also found that total magnetic moment is an integer value of $1\mu_B$. In addition, the material exhibits strong optical activity in the ultraviolet region, highlighting its potential for applications in ultraviolet optoelectronics. These findings suggest that $CsIrI_3$ perovskite is a strong candidate for spintronic and ultraviolet optoelectronic devices, encouraging future experimental validation and exploration of its potential in technological and scientific domains.

Keywords: First-principles calculations, Half-Metallicity, $CsIrI_3$, Electronic Structure, Magnetic Properties, Elastic Properties

INTRODUCTION

Half-Metallic materials are indispensable for spintronics applications due to their excellent spin transport properties and complete spin polarisation at the fermi level. The growing need for spintronics technology arises from limitations of Moore's law, as well as the increasing complexity and inefficiencies encountered when scaling down transistor sizes. Major challenges such as excessive heat generation, increased power consumption, and the need for larger chip areas emerge as we attempt to enhance computer power and data storage capacities. Spintronics offers a promising solution to these challenges by utilizing electron's spin degree of freedom, rather than relying on solely on charge transport. Moreover, spin-dependent transport does not require excessive current resulting in reduced heat generation and, consequently, a lower demand for complex cooling systems, as well as the power required to operate them. In addition, the non-volatile nature of spin significantly reduces power consumption for data storage devices. Spintronic circuits also occupy less space compared to traditional charge-based circuits, enabling increased computing density and helping to overcome the scaling limitations of current technologies. Therefore, the development of spintronics is crucial, resulting the need for new half-metallic materials to support the advancement of these technologies.

As its name suggests, uniqueness of half-metals lies in their ability to act as metals for spin-up states, while behaving as semiconductor or insulator for spin-down states. When unpolarised current applied to a half-metal, only spin-up electrons contribute to current while spin-down electrons are either reflected, filtered out or do not participate at all, effectively behaving as perfect spin filter. This effect is one of the key reasons for the use of half-metals in spintronics and has also been studied experimentally. For instance, a study by (Zhou et al., 2008) investigated one-dimensional half-metallic iron-cyclopentadienyl sandwich molecular wires (SMWs) to assess their spin-filter efficiency, showing that SMWs exhibit perfect spin-filtering properties. Similarly, another study (Yang et al., 2019) shows that half-metallic Cr2NO2 exhibit excellent spin-filter performance. Despite this, many half-metals exhibit high Curie temperatures, which are essential for both thermal stability and compatibility with manufacturing processes that involve elevated

temperatures. For example, a study by (Zhehong et al., 2022) reported that half metallic compound $LaCu_3Fe_2ReO_{12}$ exhibits curie temperature of 710K. As a result, half-metallic materials remain among the most promising candidates for spintronics due to their remarkable electronic and magnetic properties.

Although Heusler alloys currently dominate materials used in spintronic devices, they often lack the structural and electronic tunability required for next-generation applications. In contrast, perovskite oxide materials have governed significant attention due to their wide compositional diversity, structural flexibility, and tuneable electronic applications. Among them, perovskite oxides such as $SrRuO_3$ (Gu et al., 2022) and $La_{1-x}Sr_xMnO_3$ (Chanu and Phanjoubam, 2023) have demonstrated promising spintronic behaviour and are extensively studied for their magnetic ordering and high Curie temperatures. However, the exceptional tunability of halide perovskites has led some researchers to explore their potential for half-metallic behaviour, making them intriguing candidates for spintronic applications (Khan et al., 2024). Despite this growing interest, the lack of experimental studies on single halide perovskites and the scarcity of theoretical work have created a gap for this material in spintronic research. In this context, the present study aims to explore the half-metallic characteristics of $CsIrI_3$ perovskite using first-principles calculations, to assess its suitability for spintronic applications.

MATERIALS AND METHODS

This calculations are performed with Density Functional Theory(DFT) with CASTEP. Ultrasoft psuedopotential and GGA_PBE functional are employed, with 20x20x20 k-point mesh. A cut-off energy of 550 eV is used in the calculations. The material under this study is cubic perovskite that belongs to the Pm3m space group. The atomic coordinates are as follows: Cs at (0, 0, 0), Ir at (0.5, 0.5, 0.5), and I at (0.5, 0.5, 0.0). In geometrical optimisation, the lattice parameter allowed to change while the shape remains fixed. Throughout the calculations, convergence criteria and SCF tolerance are set to ultra-fine quality, and spin polarisation is enabled to account for magnetism.

RESULTS and DISCUSSION

Geometrical optimisation calculations converged successfully at lattice parameter 5.68 Å, with total energy of -2050.029 eV. Additional structure parameters, including the cell volume and density, are presented in Table 1. It is important to note that the structure retained its cubic symmetry throughout the optimisation process, confirming the stability of cubic phase. Hirshfeld and Mulliken population analysis indicate that the magnetic moment is primarily contributed by the Iridium atom, while other atoms exhibit negligible contributions. This, combined with the observation of an integer magnetic moment of 1uB, rules out the possibility of antiferromagnetic ordering and suggests that the material is either ferromagnetic or ferrimagnetic nature.

Table 1. Structural Parameters of CsIrI3

Material	Lattice Parameter	Cell Volume	Density	Energy	Enthalpy
$CsIrI_3$	5.68 Å	184.01 $Å^3$	6.37 g / cm^3	-2050.029eV	-2050.032 eV

The elastic constants, as presented in Table 2, satisfy the Born stability criteria, thereby confirming the elasticity of the material. This indicates that CsIrI3 can maintain its structural integrity under small deformations, which is a critical requirement for practical device applications.

Table 2. Elastic Constants of CsIrI3

Index	11	12	44
Cij (GPa)	64.98	13.86	11.77

Some of the elastic properties are summarized in Table 3. The calculated bulk modulus indicates that the material exhibits low resistance to volume change in under applied pressure, which is characteristic of mechanically soft materials. Furthermore, the Pugh's ratio (B/G) exceeds 1.75, suggesting that the material is ductile. These mechanical characteristics imply that CsIrI3 is suitable for strain-sensitive spintronic applications. Additionally, the material is elastically anisotropic, as indicated by the elastic anisotropy index deviating from unity.

Table 3. Elastic Properties of CsIrI3

Property	Symbol	Value
Bulk Modulus	B	30.90 GPa
Sheer Modulus	G	17.28 GPa
Pugh's Ratio	B/G	1.79
Poisson Ratio	V	0.26
Young Modulus	E	43.71 GPa
Elastic Anisotropy Index	A	0.46

To confirm half-metallic nature of the material, band structure calculations are essential. By enabling spin polarization in calculations, both the band structure and density of states (DOS) outputs provide separate results for spin-up and spin-down channels. This allows for a detailed analysis of the electronic states associated with each spin orientation, where a metallic behavior in one spin channel and semiconducting or insulating behavior in the other indicates half-metallicity. The results of the band structure calculations for spin-up channel are presented in **Figure 1(a),** while those for spin-down channel are shown in **Figure 1(b)**. Absence of a band gap near the Fermi level in **Figure 1(a)**, indicates that the spin-up channel exhibits metallic behavior, while the presence of clear band gap in **Figure 1(b)** demonstrates that spin-down channel behaves as semiconductor. This contrasting electronic behavior between the two spin channels is characteristics of half-metallicity.

The partial density of states (PDOS) calculations allows us to identify which atoms and orbitals contribute to the half-metallic behavior of CsIrI3. Through PDOS analysis, it is possible to distinguish the dominant atomic orbitals responsible for the metallic spin-up states and the semiconducting nature of the spin-down channel. The PDOS results for the spin-up and spin-down channels are presented in **Figure 2(a)** and **Figure 2(b)**, respectively. The PDOS analysis, as shown in **Figure 2(a)**, reveals both Ir and I atoms contribute significantly to the states at fermi level, primarily through hybridization between Ir d-orbitals and I p-orbitals. These orbitals are the main contributors to the metallic behavior observed in spin-up channel, while the Cs atom shows negligible participation near the Fermi level. In contrast to spin-up channel, a band gap is observed in the spin-down channel, as shown in the **Figure 2(b)**. This band gap is primarily associated with electronic states of Ir and I atoms, with Ir atoms contributing more significantly to the gap formation. Therefore, these results confirm the half-metallic nature of $CsIrI_3$, characterized by metallic behavior in the spin-up channel and semiconducting behavior in the spin-down channel.

To determine whether the material exhibits optical activity in specific energy regions, optical property calculations performed, and the absorption spectrum analyzed, as shown in **Figure 3**. This analysis helps to identify the energy ranges where $CsIrI_3$ strongly absorbs light, providing insight into its potential for optoelectronic or spintronic applications.

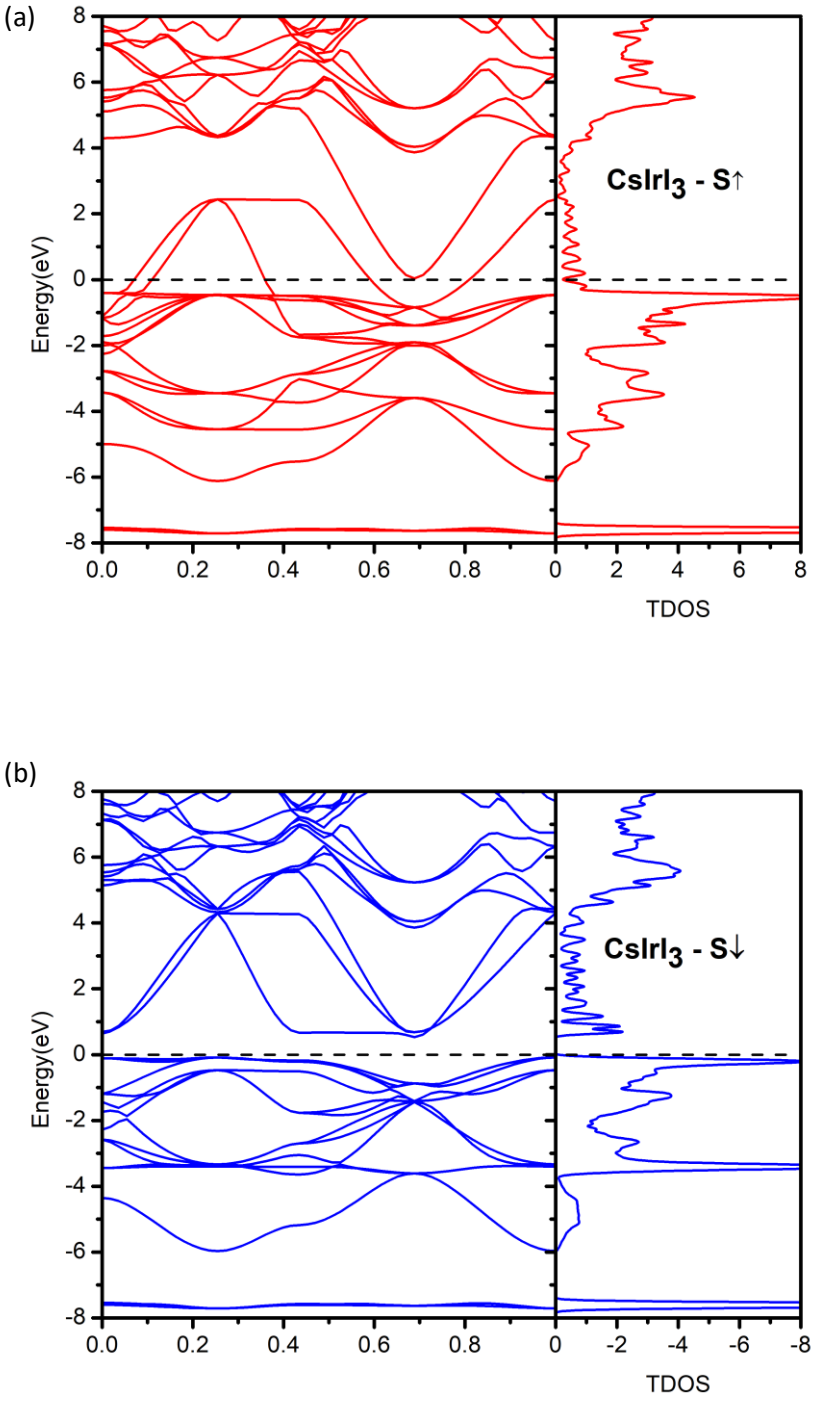

Figure 1. (a) Spin-polarized band structure of $CsIrI_3$ for the spin-up channel, showing metallic behavior with no band gap at the Fermi level. (b) Calculated band structure of $CsIrI_3$ for the spin-down channel. The presence of a band gap at the Fermi level indicates semiconducting behavior for this spin orientation.

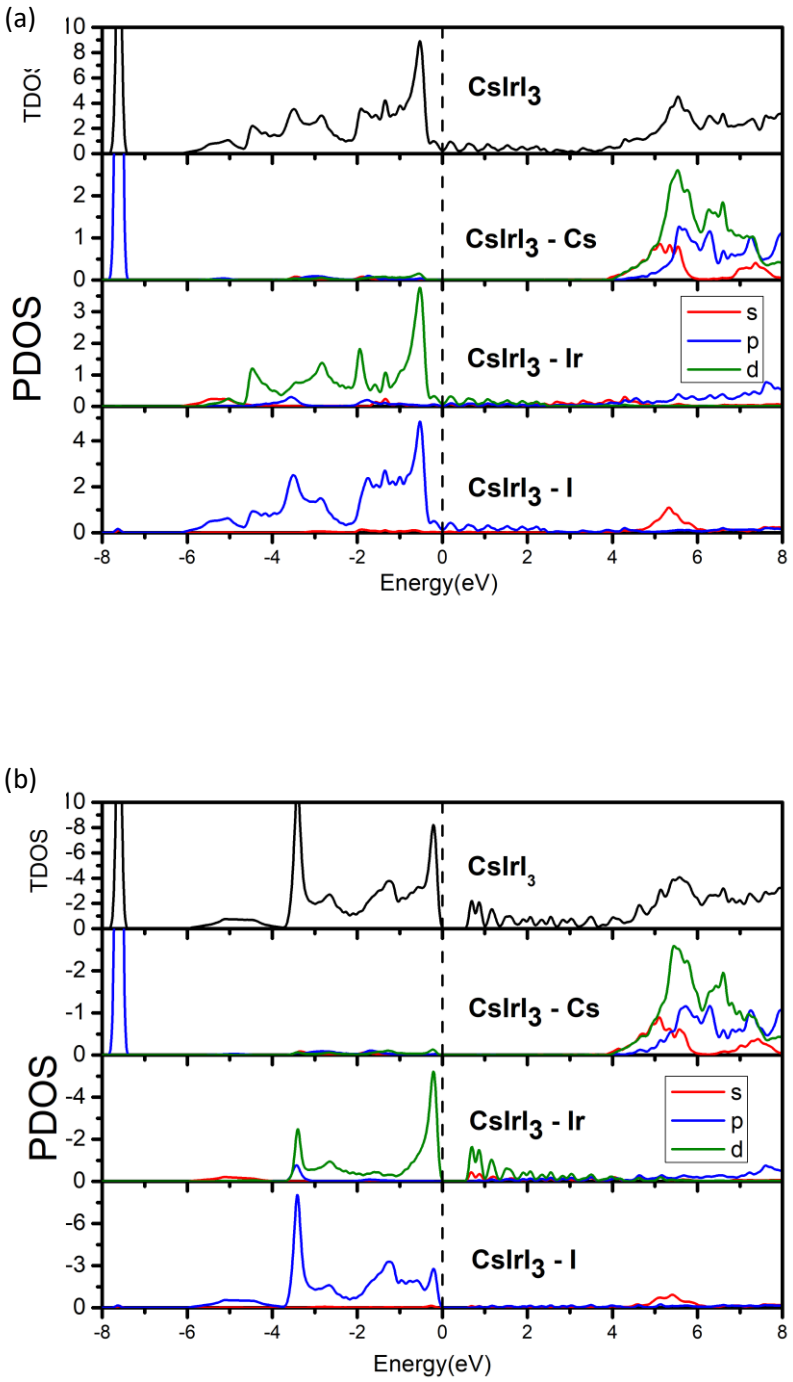

Figure 2. (a) Partial density of states (PDOS) of $CsIrI_3$ for the spin-up channel, showing metallic behavior mainly due to Ir d and I p orbital contributions. (b) Partial density of states (PDOS) of $CsIrI_3$ for the spin-down channel, showing a band gap at the Fermi level with dominant Ir d and I p orbital contributions.

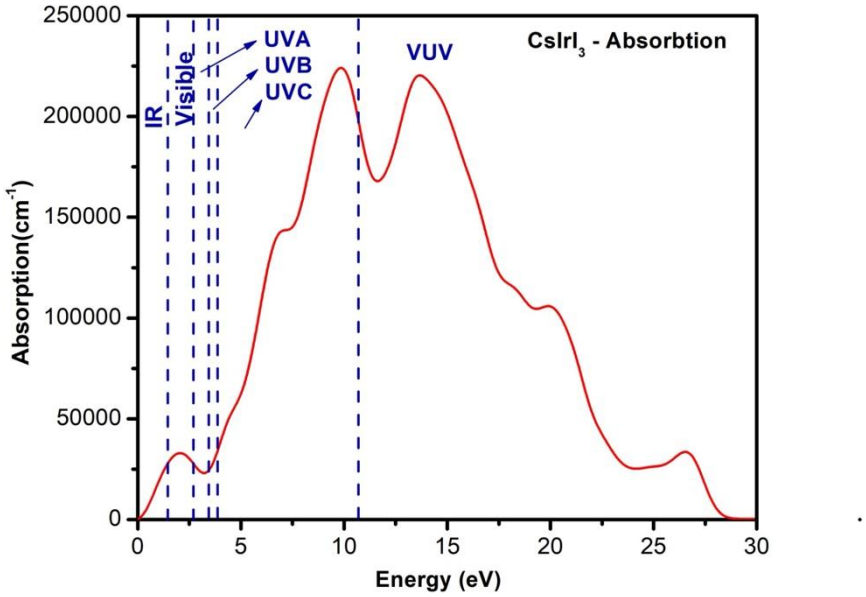

Figure 3. Optical absorption spectrum of $CsIrI_3$, showing strong absorption in the ultraviolet (UV) region, with negligible absorption in the infrared (IR) and weak absorption in the visible region.

As shown in **Figure 3,** the material exhibits negligible absorption in the infrared (IR) region and only weak absorption in the visible region, while demonstrating significantly stronger absorption in the ultraviolet (UV) region. Notably, two distinct absorption peaks are observed within the UV region. One peak lies in the far-ultraviolet(UVC) region, near the boundary of the vacuum ultraviolet(VUV), while the other is located within the vacuum ultraviolet region, close to the far-ultraviolet range. These peaks highlight strong UV absorption, supporting the potential use of $CsIrI_3$ in UV-sensitive spintronic applications.

CONCLUSION

These results, obtained through first-principles calculations, confirm that this material elastically stable and exhibits half-metallic behaviour. Half-metallicity is confirmed by metallic behaviour in spin-up channel, and semiconductor behaviour in spin-down channel, as revealed by band structure calculations. The behaviour is primarily influenced by the hybridisation between Ir d-orbitals and I p-orbitals, which are the main contributors to the electric states near Fermi level. The difference in spin channels also indicates the presence of magnetic behaviour, and with Hirshfeld and Mulliken population analysis the magnetic moment is 1uB. Additionally, elastic calculations show that the material is ductile and elastically anisotropic. The absorption spectrum indicates that the material exhibits strong optical activity in the ultraviolet (UV) region, while showing weak absorption in the visible region and negligible absorption in the infrared (IR) region. As a result, $CsIrI_3$ shows potential for use in spintronic applications that require strain sensitivity or optical activity in the ultraviolet (UV) region. Therefore, experimental validation and integration into device structures are essential to fully explore and realize the potential of $CsIrI_3$ for practical spintronic applications.

REFERENCES

Gu, Y., Wang, Q., Hu, W., Liu, W., Zhang, Z., Pan, F., & Song, C. (2022). An overview of srruo3-based heterostructures for spintronic and topological phenomena. *Journal of Physics D: Applied Physics*, *55*(23), 233001. https://doi.org/10.1088/1361-6463/ac4fd3

Khan, M. U., Rahman, A. U., Ahmad, M., Yaseen, M., & Ahmed, M. A. (2024). Exploring room-

temperature ferromagnetism and half-metallicity in new Halide Perovskites RbCrX$$_3$$ (X: F, cl, br, I) using first-principles and Monte Carlo Simulations. *The European Physical Journal Plus*, *139*(2). https://doi.org/10.1140/epjp/s13360-024-04898-6

Liu, Z., Zhang, S., Wang, X., Ye, X., Qin, S., Shen, X., Lu, D., Dai, J., Cao, Y., Chen, K., Radu, F., Wu, W., Chen, C., Francoual, S., Mardegan, J. R., Leupold, O., Tjeng, L. H., Hu, Z., Yang, Y., & Long, Y. (2022). Realization of a half metal with a record-high curie temperature in perovskite oxides. *Advanced Materials*, *34*(17). https://doi.org/10.1002/adma.202200626

Paris Chanu, L., & Phanjoubam, S. (2023). On the structural and magnetic properties of SR-substituted LaMnO3 nanoparticles (La1-xsrxmno3). *Materials Today: Proceedings*. https://doi.org/10.1016/j.matpr.2023.04.621

Yang, J., Zhang, S., Li, L., Wang, A., Zhong, Z., & Chen, L. (2019). Rationally designed high-performance spin filter based on two-dimensional half-metal CR2NO2. *Matter*, *1*(5), 1304–1315. https://doi.org/10.1016/j.matt.2019.07.022

Zhou, L., Yang, S.-W., Ng, M.-F., Sullivan, M. B., Tan, & Shen, L. (2008). One-dimensional iron−cyclopentadienyl sandwich molecular wire with half metallic, negative differential resistance and high-spin filter efficiency properties. *Journal of the American Chemical Society*, *130*(12), 4023–4027. https://doi.org/10.1021/ja7100246

➢ *ORAL PRESENTATION*

Yolov8 ile Yolov11 Algoritmalarinin Gerçek Zamanli Araç Nesne Tespiti Ve Trafik Yoğunluğu Analizinde Karşılaştırılması

Mert DURUKAN[1*] (ORCID: *https://orcid.org/0009-0006-9583-0163*),
Jale BEKTAŞ[2] (*https://orcid.org/0000-0002-8793-1486*)

[*1]Mersin University, Faculty of Engineering, Computer Engineering, Mersin, Turkey.
[2] Mersin University, Faculty of Engineering, Computer Engineering, Mersin, Turkey.

*Corresponding author e-mail: 1mertdurukan@gmail.com

Abstract

This study aims to compare the performance of the advanced object detection architectures YOLOv8 and YOLOv11 in real-time vehicle detection and traffic density analysis. Traffic density assessment plays a critical role in smart city applications, traffic management systems, and enhancing driver safety. The study utilizes the 'Real-Time Traffic Density Estimation' dataset from Kaggle, previously trained on YOLOv8. Both models will be trained and tested on this dataset to evaluate and compare their effectiveness in detecting vehicles and analyzing traffic density. The results will highlight the improvements and evolutionary developments from YOLOv8 to YOLOv11, emphasizing their impact on solving real-time traffic monitoring challenges.
Keywords: YOLOv11, Nesne Tespiti, Trafik Yoğunluğu, Derin Öğrenme, Bilgisayarla Görü

INTRODUCTION

Günümüzde artan araç sayısı, şehir içi ulaşımı daha karmaşık hale getirmekte ve trafik yönetim sistemlerinin önemini her geçen gün artırmaktadır. Özellikle büyük şehirlerde, trafik yoğunluğunun etkin bir şekilde izlenmesi ve yönetilmesi, ulaşım planlaması, çevresel etki analizi ve sürücü güvenliği açısından kritik bir rol oynamaktadır. Bu bağlamda, gerçek zamanlı trafik yoğunluğu tespiti; akıllı şehir uygulamalarının temel bileşenlerinden biri haline gelmiştir.

Trafik yoğunluğunun belirlenmesinde geleneksel yöntemler, genellikle manyetik sensörler, döngü dedektörleri veya insan gücüne dayalı gözlemler gibi fiziksel altyapı gerektiren sistemleri içermektedir. Ancak bu yöntemler; kurulum maliyetlerinin yüksek olması, bakım zorlukları ve esnekliğin düşük olması gibi dezavantajlara sahiptir. Son yıllarda, bilgisayarla görme ve yapay zeka tekniklerindeki gelişmeler sayesinde, trafik izleme sistemlerinde kamera görüntüleri üzerinden otomatik analiz yapılması daha yaygın hale gelmiştir. Bu tür görüntü tabanlı çözümler, daha düşük maliyetli, kolay ölçeklenebilir ve gerçek zamanlı sonuçlar üretmeye uygun yapılar sunmaktadır.

Nesne tespiti (object detection), görüntülerdeki nesnelerin konumlarını ve türlerini belirlemeyi amaçlayan bilgisayarla görme problemlerinden biridir. Özellikle trafik yoğunluğu analizi gibi dinamik ortamlarda, doğru ve hızlı nesne tespiti yapan algoritmaların kullanılması, sistemin başarımını doğrudan etkilemektedir. Bu alanda en çok dikkat çeken ve yaygın kullanılan modellerden biri, "You Only Look Once (YOLO)" mimarisidir(Redmon & Farhadi, 2018). YOLO, gerçek zamanlı nesne tespiti konusunda yüksek hız ve doğruluk oranlarıyla öne çıkan bir algoritmadır. YOLO mimarisi, gelişen donanım ve yazılım olanaklarıyla birlikte sürekli evrim geçirmekte ve yeni sürümleriyle daha karmaşık senaryolara çözüm sunmaktadır.

Bu çalışma kapsamında, en güncel YOLO sürümlerinden biri olan YOLOv11 mimarisi kullanılarak gerçek zamanlı trafik yoğunluğunun tespiti amaçlanmaktadır. Çalışmada, Kaggle platformunda yer alan ve daha önce YOLOv8 ile eğitilmiş olan "Real-Time Traffic Density Estimation" veri seti kullanılacaktır . Bu veri seti; farklı hava koşulları, günün farklı zamanları ve çeşitli trafik senaryolarını içeren, etiketlenmiş görüntülerden oluşmaktadır. YOLOv11 ile bu veri seti üzerinde gerçekleştirilecek model eğitimi ve test süreci sonucunda elde edilen performans metrikleri, önceki nesil YOLOv8 mimarisi ile karşılaştırılarak analiz edilecektir.

Bu karşılaştırmalı analiz sayesinde, YOLO mimarisinin evrimsel gelişiminin, özellikle trafik yoğunluğu gibi gerçek zamanlı ve kritik öneme sahip problemlere olan katkısı değerlendirilecektir. Elde edilen

sonuçlar; yalnızca akademik düzeyde bir model başarımı değil, aynı zamanda akıllı şehirlerde uygulanabilirlik açısından da yol gösterici olacaktır.

YOLO mimarisi ilk olarak 2016 yılında Redmon ve arkadaşları tarafından tanıtılmıştır (Redmon et al., 2016). YOLOv1, gerçek zamanlı nesne tespitine olanak sağlayan ilk mimaridir ancak doğruluk konusunda bazı sınırlamaları bulunmaktaydı. Bu sorunlar, sırasıyla YOLOv2 ve YOLOv3 sürümlerinde çözülmeye çalışılmış; özellikle YOLOv3 ile daha derin mimariler, daha küçük nesne tespiti ve residual bağlantılar gibi iyileştirmeler yapılmıştır (Redmon & Farhadi, 2018).

Daha sonra tanıtılan YOLOv4, verimlilik odaklı bazı teknikleri (CSPDarknet53, PANet, Mish aktivasyon fonksiyonu) kullanarak hem hız hem de doğruluk açısından önemli iyileştirmeler sunmuştur (Bochkovskiy et al., 2020). YOLOv5 ve YOLOv6 ise açık kaynak topluluklarının katkısıyla geliştirilmiş, modülerlik ve kullanım kolaylığı açısından öne çıkmıştır. YOLOv7 ile hız ve doğruluk optimizasyonu daha ileriye taşınmış; YOLOv8 ise anchor-free yaklaşım, yeni veri artırma teknikleri ve otomatik öğrenme oranı gibi modern özelliklerle donatılmıştır (Jocher et al., 2023).

Son olarak geliştirilmiş olan YOLOv11, hem donanımsal kaynaklara uygunluğu hem de karmaşık sahnelerdeki doğruluk oranları açısından önemli iyileştirmeler sunmaktadır. Bu sürümde, yeni nesil transformer tabanlı katmanların entegre edildiği ve sinir ağı içerisindeki bilgi akışının daha etkili hale getirildiği görülmektedir. Ayrıca, YOLOv11'de kullanılan gelişmiş veri artırma yöntemleri (mosaic, mixup, cutmix vb.) sayesinde modelin genelleme yeteneği artmıştır. Backbone yapısında yapılan iyileştirmeler sayesinde hem küçük hem büyük nesne tespitlerinde daha başarılı sonuçlar alınmaktadır (Zhang et al., 2024).

Özetle, YOLO mimarisinin evrimsel gelişimi, trafik yoğunluğu gibi zaman duyarlı ve dinamik problemlerin çözümünde onu en uygun modellerden biri haline getirmiştir. YOLOv11, özellikle yüksek çözünürlüklü görüntülerde çoklu nesne tespiti yaparken dahi gerçek zamanlı çalışabilme kapasitesi ile bu alandaki ihtiyaçlara etkili bir çözüm sunmaktadır .

Ultralytics'in en son yinelemesi olan UltralyticsYOLO11, nesne algılama görevleri için hız ve doğruluk açısından mükemmel olacak şekilde tasarlanmıştır. gibi önceki YOLO modelleri üzerine inşa edilmiştir. YOLOv8 YOLO11 , uç cihazlardan bulut sunucularına kadar farklı donanım platformlarında performansı optimize etmek için mimari geliştirmeler içermektedir. Nesne algılama, örnek segmentasyonu, görüntü sınıflandırma ve poz tahmini dahil olmak üzere bir dizi bilgisayarla görme görevini destekleyen çok yönlülüğü ile öne çıkmaktadır.

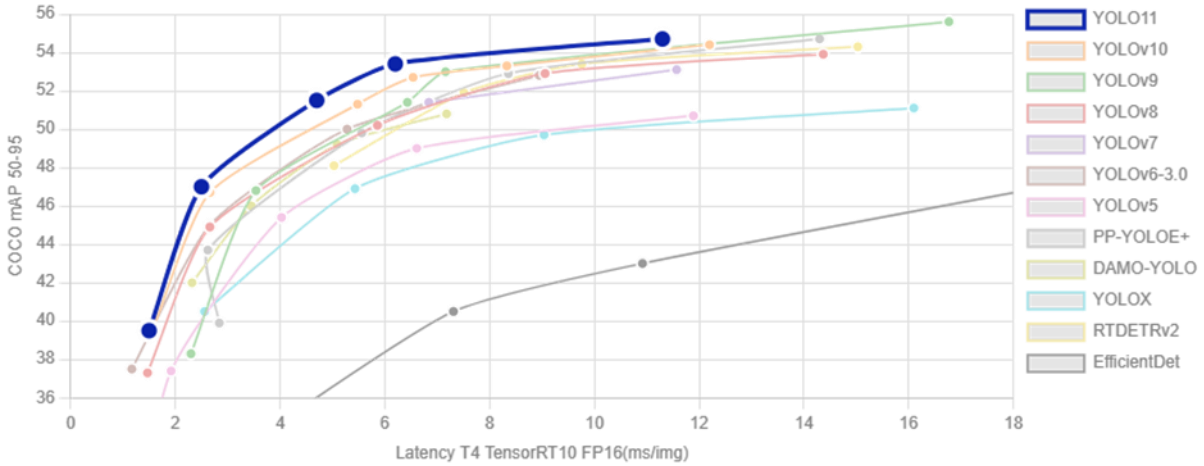

Figure 1. YOLOV11 mimarisi ve diğer mimarilerin karşılaştırılması.

YOLO11, farklı performans ihtiyaçlarına uygun bir dizi model (YOLO11n, YOLO11s, YOLO11m, YOLO11l, YOLO11x) sunmaktadır. Nano versiyon olan YOLO11n, sadece 2,6M parametre ve 56,1 ms CPU ONNX hızı ile 39,5 mAPval 50-95 değerine ulaşır. Daha büyük olan YOLO11x, doğruluğa öncelik

vererek 54,7'lik bir mAPval 50-95'e ulaşır. YOLO11 , çıkarım hızını daha da artırmak için karma hassasiyetli eğitim gibi teknikler kullanır.

Trafik yoğunluğu tahmini gibi gerçek zamanlı uygulamalarda, modelin hem hızlı hem de doğru sonuç üretmesi kritik öneme sahiptir. YOLO mimarisi bu gereksinimleri karşılamada öne çıkmaktadır. YOLOv3 ile birlikte küçük nesne tespiti gibi problemler üzerine yoğunlaşılmış, ardından gelen YOLOv4 ve YOLOv5 sürümleriyle doğruluk-hız dengesinde önemli gelişmeler kaydedilmiştir(Bochkovskiy & Wang & Liao, 2020). Daha sonra açık kaynaklı Ultralytics tarafından geliştirilen YOLOv8, modüler yapısı ve yüksek doğruluk oranıyla dikkat çekmiştir . Son olarak geliştirilen YOLOv11, farklı boyutlardaki modelleriyle (n, s, m, l, x) kullanıcıya esneklik sunmakta ve hem CPU hem de GPU ortamları için optimize edilmiş yüksek performanslı bir çözüm sunmaktadır.

Trafik yoğunluğu tahmini özelinde, YOLO algoritması görüntülerdeki araçların hızlı ve doğru şekilde tespit edilmesini sağlar. Bu sayede belirli bir zaman aralığında geçen araç sayısı belirlenerek yoğunluk tahmini yapılabilir. Bu yöntem, özellikle sabit kameralar veya dronlar gibi düşük maliyetli görüntü kaynaklarıyla entegre edildiğinde geleneksel sensör tabanlı sistemlere kıyasla daha esnek ve ekonomik çözümler sunar (Ma & Zhu & Li, 2021).

YOLO mimarisi, trafik sahnelerinin değişken yapısı (gün ışığı değişimleri, hava koşulları, araç çeşitliliği) karşısında da sağlam bir performans sergilemektedir. Özellikle YOLO'nun transfer öğrenme desteği sayesinde, önceden eğitilmiş modeller küçük veri setleriyle dahi etkin sonuçlar verebilmektedir (Tan & Le, 2019). Bu özellik, etiketleme maliyetlerinin yüksek olduğu trafik verisi gibi durumlarda büyük avantaj sağlamaktadır.

Bu çalışmada, YOLOv11 mimarisi kullanılarak Kaggle platformunda yer alan "Real-Time Traffic Density Estimation" veri seti üzerinde model eğitimi yapılmakta ve elde edilen sonuçlar, YOLOv8 ile kıyaslanarak analiz edilmektedir. Bu karşılaştırma ile YOLO mimarisinin sürümler arası gelişiminin trafik yoğunluğu tahminindeki başarım üzerindeki etkisi değerlendirilecektir.

MATERIALS AND METHODS

Bu çalışmada, gerçek zamanlı trafik yoğunluğu tespiti amacıyla, en güncel nesne tespiti algoritmalarından biri olan YOLOv11 mimarisi tercih edilmiştir. YOLO ailesinin en son sürümü olan YOLOv11, seleflerine kıyasla daha yüksek doğruluk oranı, iyileştirilmiş hız-performans dengesi ve gelişmiş model genel performansı ile öne çıkmaktadır. Bu bölümde, uygulanan yöntem, model eğitimi süreci ve kullanılan veri kümesine ilişkin detaylar açıklanacaktır.

YOLOv11, Ultralytics tarafından geliştirilen önceki YOLO sürümlerinin üzerine inşa edilmiş, optimize edilmiş bir nesne tespiti mimarisidir. YOLOv11'de Efficient Layer Aggregation Networks (ELAN++), Bidirectional Feature Pyramid Network (BiFPN) ve Dynamic Head (DyHead) gibi yeni nesil mimari bileşenler entegre edilmiştir. Bu sayede, hem düşük hem de yüksek çözünürlüklü özellik haritalarının etkin bir şekilde birleştirilmesi sağlanarak çok ölçekli nesne tespitinde doğruluk artırılmıştır.

Ayrıca YOLOv11, transformer tabanlı dikkat mekanizmalarını da desteklemektedir. Bu yapı, özellikle yoğun trafik gibi karmaşık senaryolarda araçların birbiriyle çakıştığı durumlarda, ayrım gücünü artırmakta ve nesne sınırlarının daha net belirlenmesini sağlamaktadır. Modelin temel yapı taşları aşağıdaki gibidir:

Backbone (Omurga): ELAN++ ile güçlendirilmiş CSP yapısı sayesinde özellik çıkarımı daha verimli hale gelmiştir.

Neck (Boyun Yapısı): BiFPN kullanılarak farklı katmanlardan gelen özellik haritaları optimize bir şekilde harmanlanmaktadır.

Head (Başlık Yapısı): Dynamic Head modülü ile farklı görevler (sınıflandırma, regresyon, nesne skoru) arasında görev odaklı dikkat mekanizmaları uygulanarak daha esnek öğrenme sağlanmaktadır.

Model eğitimi için Kaggle platformunda yayımlanan Real-Time Traffic Density Estimation veri seti kullanılmıştır. Bu veri seti; farklı trafik koşullarını temsil eden binlerce etiketlenmiş görüntüden oluşmakta olup, farklı hava koşulları, günün saatleri ve yol tiplerini içermektedir. Görüntüler, "car", "truck", "bus", "motorbike" gibi sınıflara ayrılmıştır. Veri seti eğitim (%70), doğrulama (%20) ve test (%10) olmak üzere üç alt kümeye bölünmüştür. Etiketleme formatı, YOLO'nun kullandığı bounding box (sınırlayıcı kutu) biçimine uygun olarak hazırlanmıştır.

Veri seti, her bir görüntünün 640x640 piksellik tekdüze bir çözünürlüğe yeniden boyutlandırıldığı bir standartlaştırma sürecinden geçer. Modelin genelleme yeteneğini güçlendirmek için, 536 görüntüden oluşan eğitim verilerine artırmalar uygulandı. Doğrulama seti 90 görüntü içerir ve performans değerlendirmesinin bütünlüğünü korumak için artırılmamış halde kalır.

Model eğitimi sürecinde YOLOv11-custom konfigürasyonu tercih edilmiştir. Eğitim işlemi için aşağıdaki hiperparametreler kullanılmıştır:

Table 1. YOLOv11 ve YOLOv8 Model Eğitiminde Kullanılan Hiper Parametreler

Parametre	**Değer**
Batch Size	32
Initial Learning Rate	0.0001
Learning Rate	0.1
Epoch Sayısı	100
Dropout	0.1
Optimizer	SGD (Momentum: 0.937)
Loss Function	CIoU Loss (box loss), Binary Cross Entropy (class loss)

Bu hiperparametreler literatürde var olan YoloV8 modeli ile tam bir karşılaştırma yapılabilmesi adına, YoloV8'de kullanılan parametreler ile birebir seçilmiştir.

Model eğitimi, Google Colab ortamında T4 GPU kullanılarak gerçekleştirilmiştir. Eğitim süreci boyunca her epoch sonunda doğrulama metrikleri izlenmiş, modelin overfitting eğilimleri kontrol edilmiştir. En iyi doğrulama başarımı gösteren model, test veri seti üzerinde değerlendirilerek YOLOv8 ile karşılaştırılmıştır.

YOLOv11'in Yolov8'den daha iyi performans göstermediği görülmüştür.

YOLOv8 ve YOLOv11 mimarileri kullanılarak elde edilen trafik yoğunluğu tahmin sonuçları karşılaştırılmıştır. Karşılaştırma; Box Loss Learning Curve, Classification Loss Learning Curve, Distribution Focal Loss Learning Curve metrikleri üzerinden yapılmıştır.

Öğrenme Eğrileri Analizi (Learning Curves Analysis) karşılaştırıldığında,

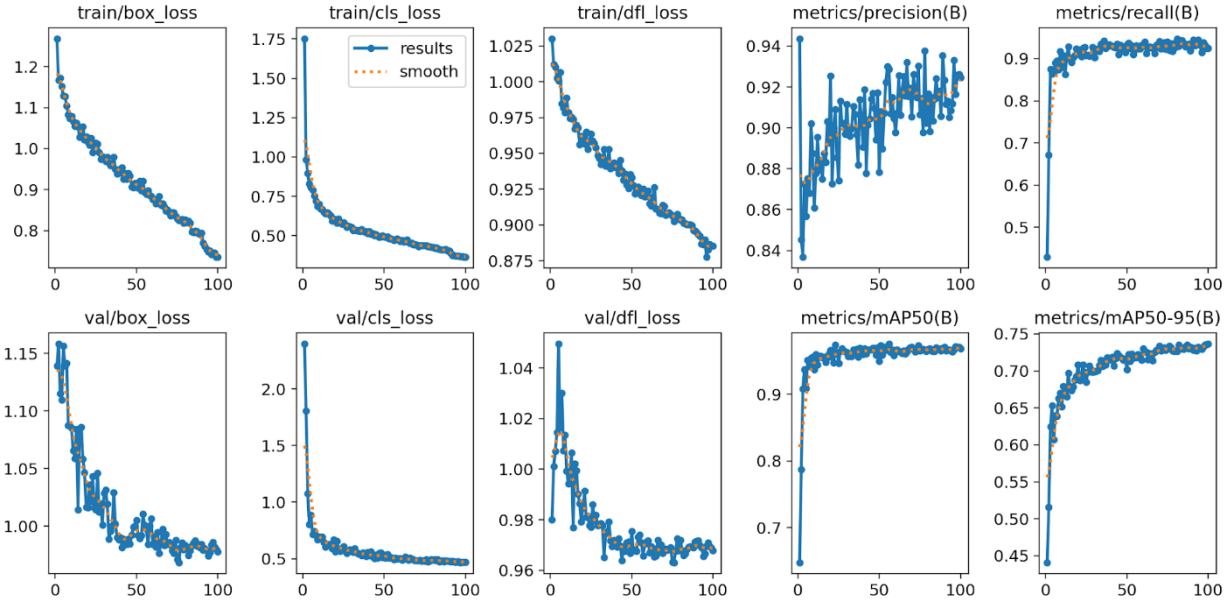

Figure 2. YOLOv8 performans metrikleri grafiği

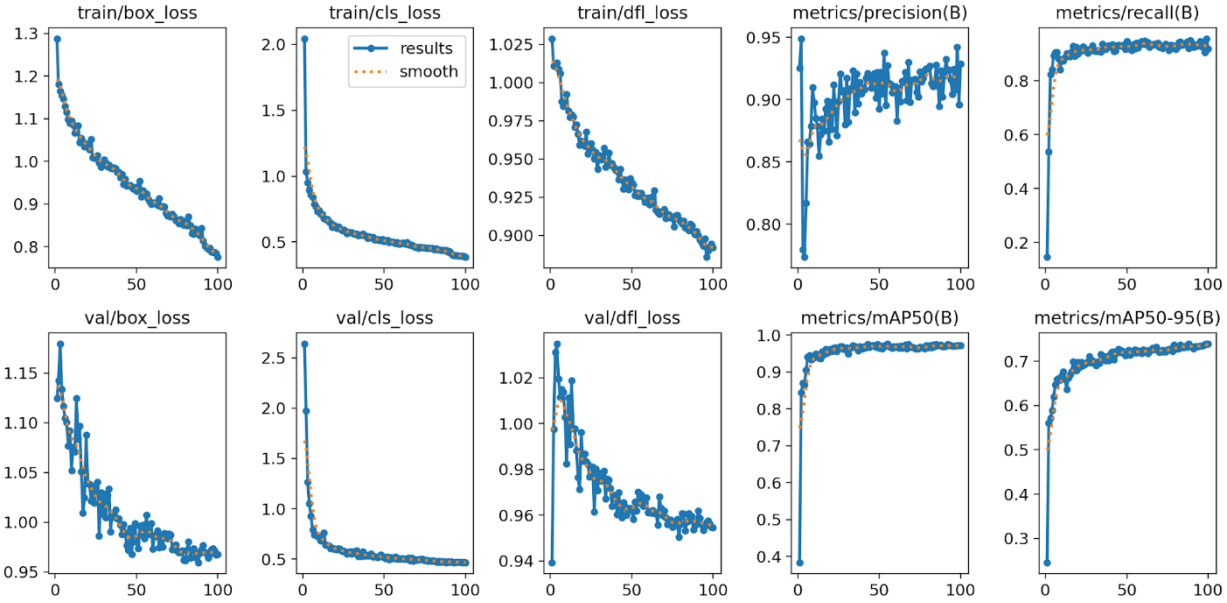

Figure 3. YOLOv11 performans metrikleri grafiği

Performance Metrics Comparison (Last Epoch Only):

	Metric	YOLO11 (Last Epoch)	YOLOv8 (Last Epoch)
0	epoch	100.00000	100.00000
1	time	1094.63000	1026.70000
2	train/box_loss	0.77526	0.73564
3	train/cls_loss	0.38572	0.36463
4	train/dfl_loss	0.89195	0.88532
5	metrics/precision(B)	0.92881	0.92458
6	metrics/recall(B)	0.91895	0.92423
7	metrics/mAP50(B)	0.97131	0.96841
8	metrics/mAP50-95(B)	0.73870	0.73649
9	val/box_loss	0.96777	0.97778
10	val/cls_loss	0.46664	0.47013
11	val/dfl_loss	0.95449	0.96772
12	lr/pg0	0.00004	0.00004
13	lr/pg1	0.00004	0.00004
14	lr/pg2	0.00004	0.00004

Figure 4. YOLOv8 ve YOLOv11 performans metrikleri karşılaştırma grafiği.

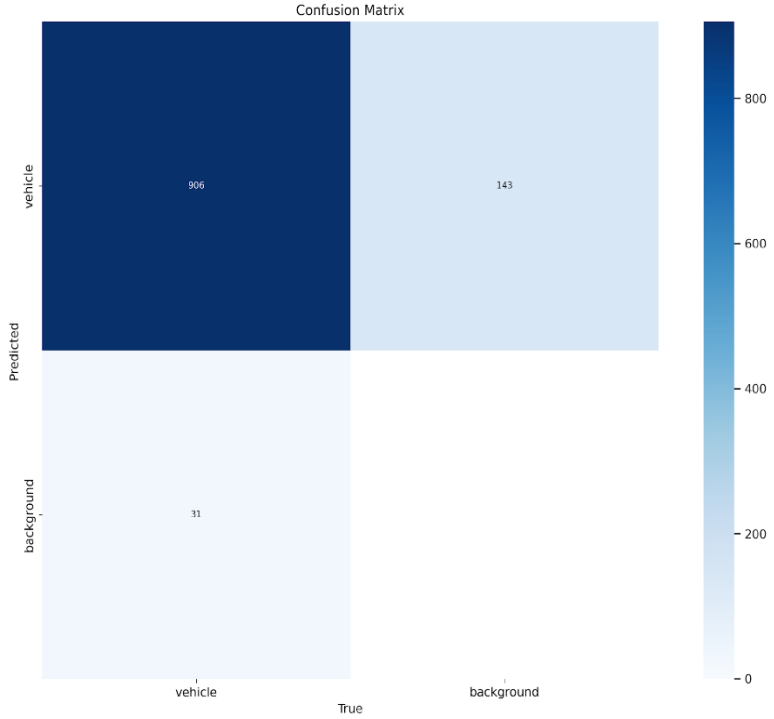

Figure 5. YOLOv8 confusion matrix.

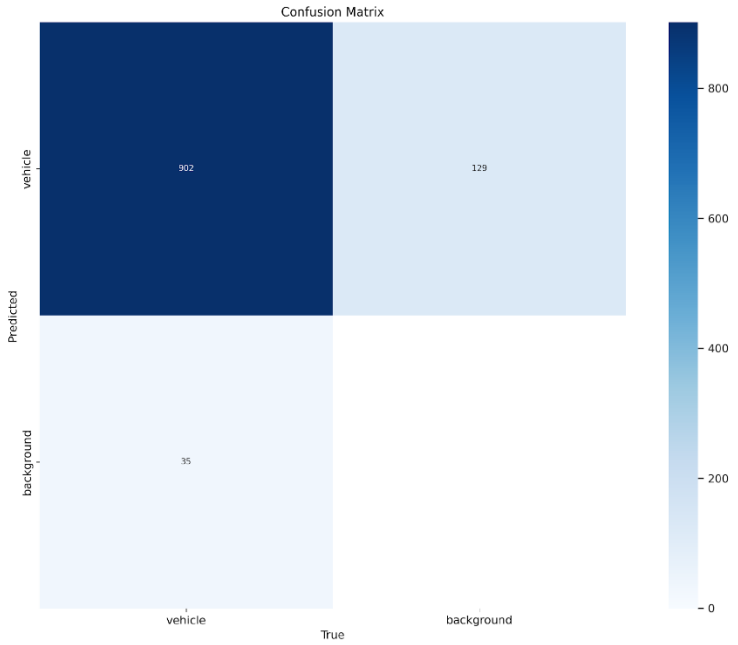

Figure 6. YOLOv11 confusion matrix.

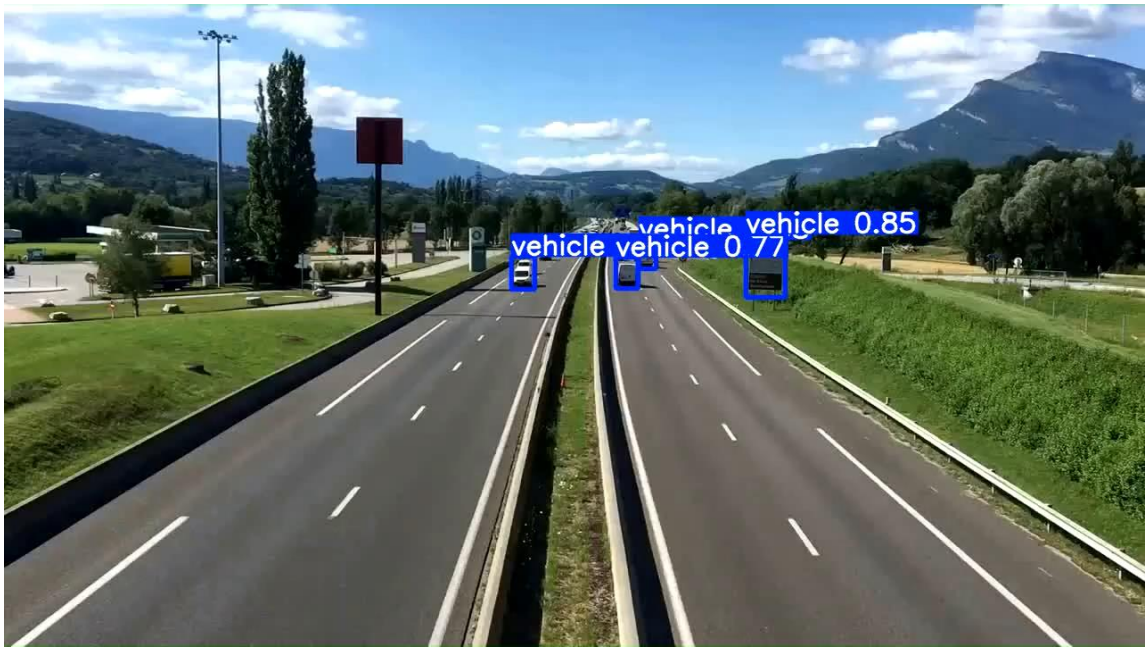

Figure 7. Eğitilen YOLOv8 modellinin test verileri üzerinde test edilmesi



Figure 8. Eğitilen YOLOv11 modellinin test verileri üzerinde test edilmesi

RESULTS

YOLOv8 ve YOLOv11 modelleri, trafik görüntüleri üzerinde eğitilerek nesne tespiti performansları karşılaştırmalı olarak analiz edilmiştir. Her iki model de aynı veri kümesi üzerinde, benzer eğitim koşulları altında eğitilmiş ve test edilmiştir. Elde edilen sonuçlara göre, YOLOv11 modelinin mimarisinde yapılan güncellemeler doğruluk, kararlılık ve hassasiyet açısından avantajlar sunsa da, incelenen trafik veri seti özelinde bu avantajlar sınırlı kalmış ve YOLOv8, özellikle trafik yoğunluğu ölçümü gibi gerçek zamanlı analizlerde daha verimli bir performans sergilemiştir.

YOLOv8'in başarısı, optimize edilmiş katman yapısı, daha kısa eğitim süresi ve yüksek işlem hızı ile dengeli bir doğruluk sağlamasından kaynaklanmaktadır. Bu yönleriyle gerçek zamanlı uygulamalarda öne çıkmaktadır. Öte yandan, YOLOv11 modeli, daha karmaşık yapısıyla bazı durumlarda daha doğru ve hassas tespitler yapabilse de, genel doğruluk artışı sınırlı kalmış ve işlem süresi açısından dezavantaj oluşturmuştur.

Sonuç olarak, trafik yoğunluğunu ölçme gibi hız ve verimlilik gerektiren senaryolarda YOLOv8 modeli daha uygun bir tercih olacaktır. Ancak, doğruluk ve hassasiyetin ön planda olduğu uygulamalarda YOLOv11 değerlendirilebilir. Gelecekte farklı veri setleri ve uygulama senaryoları ile yapılacak analizler, bu modellerin seçiminde daha isabetli kararlar verilmesine katkı sağlayacaktır.

DISCUSSION

Elde edilen sonuçlar, model seçiminin yalnızca doğruluk metriklerine değil, uygulama bağlamındaki ihtiyaçlara göre yapılması gerektiğini göstermektedir. YOLOv8'in daha kısa eğitim süresi ve dengeli performansı, gerçek zamanlı trafik yoğunluğu analizleri için daha uygun bir çözüm sunduğunu ortaya koymuştur. Buna karşılık, YOLOv11'in bazı metriklerde sağladığı sınırlı iyileştirmeler, doğruluk açısından potansiyel taşısa da işlem süresi ve kaynak kullanımı açısından dezavantaj oluşturabilir. Bu durum, model tercihlerinde doğruluk-hız dengesinin kritik bir rol oynadığını ve bağlama özgü değerlendirmelerin gerekliliğini vurgulamaktadır. Ayrıca, çalışmanın tek bir veri seti ile sınırlı olması, farklı koşullarda yapılacak deneylerle desteklenmesi gerektiğini göstermektedir.

CONCLUSION

Bu çalışma, YOLOv8 ve YOLOv11 modellerinin trafik yoğunluğu tespiti özelindeki performanslarını karşılaştırmalı olarak değerlendirmiştir. Elde edilen bulgular, YOLOv8'in daha kısa eğitim süresi ve dengeli doğruluk-hız performansı ile gerçek zamanlı uygulamalarda daha uygun bir seçenek olduğunu göstermiştir. Öte yandan, YOLOv11 belirli metriklerde sınırlı iyileştirmeler sunmakla birlikte, işlem süresi açısından daha maliyetlidir. Bu doğrultuda, model seçiminin kullanım senaryosuna göre yapılması gerektiği ve sadece doğruluk değil, sistem gereksinimleri ve hız gibi kriterlerin de dikkate alınmasının önemli olduğu sonucuna varılmıştır. Gelecek çalışmalarda farklı veri setleri ve uygulama alanlarında bu modellerin kapsamlı analizlerinin yapılması önerilmektedir.

REFERENCES

Bochkovskiy, A., Wang, C. Y., & Liao, H. Y. M. (2020). YOLOv4: Optimal speed and accuracy of object detection. *arXiv*, article 2004.10934.

Juliansyah, A., Wibowo, S. H., & Heryanto, D. (2024). Development of a real-time traffic density detection website using YOLOv8-based digital image processing with OpenCV. *Journal of Information Systems and Informatics*, 6, 38–49.

Real-time traffic density estimation dataset. (2025, April 20). In *Kaggle*. https://www.kaggle.com/code/farzadnekouei/real-time-traffic-density-estimation-with-yolov8/

Redmon, J., Divvala, S., Girshick, R., & Farhadi, A. (2016). You only look once: Unified, real-time object detection. In *Proceedings of the IEEE Conference on Computer Vision and Pattern Recognition* (pp. 779–788). Las Vegas, Nevada, USA.

Redmon, J., & Farhadi, A. (2018). YOLOv3: An incremental improvement. *arXiv*, article 1804.02767.

Shaqib, M., Islam, M. N., Rahman, M. A., & Hossain, M. S. (2024). Vehicle speed detection system utilizing YOLOv8: Enhancing road safety and traffic management for metropolitan areas. *arXiv*, article 2401.07413.

YOLOv8 documentation & codebase. (2025, April 19). In *GitHub*. https://github.com/ultralytics/ultralytics

➢ *ORAL PRESENTATION*

In vitro and *in silico* evaluation of schiff base and bis-α-aminophosphonate derivatives as potent α-glucosidase ve tyrosinaze inhibitors

Emel Ekinci*[1] (*ORCID: 0000-0003-2323-2747*), Harun Çiftçi[2] (*ORCID: 0000-0002-3210-5566*), Şevki Adem[3] (*ORCID: 0000-0003-2146-5870*), Özlem Gündoğdu Aytaç[4] (*ORCID: 0000-0002-6943-9674*)

*[1]Çankırı Karatekin University, Central Research Laboratory Application and Research Center, Çankırı, Türkiye.
[2]Çankırı Karatekin University, Institute of Science, Department of Chemistry, Çankırı, Türkiye.
[3]Çankırı Karatekin University, Faculty of Science, Department of Chemistry, Çankırı, Türkiye.
[4]Ahi Evran University, Vocational School of Kaman, Department of Food Processıng, Kırşehir, Türkiye.

*Corresponding author e-mail: emelekinci@karatekin.edu.tr

Abstract

In this study, the inhibitory effects of synthesized Schiff bases (7-11) and bis-α-aminophosphonate (13-16) derivatives on α-glucosidase and tyrosinase enzymes and the molecular level mechanisms of these effects were investigated. As a result of *in vitro* studies, it was determined that bis-α-aminophosphonate derivatives were more potent inhibitors than Schiff bases. Among the tested compounds, compound 16 exhibited the strongest inhibition against α-glucosidase with an IC_{50} value of 32.54 ± 0.6 µg/mL, outperforming the reference compound acarbose (IC_{50} = 80.60 ± 2.1 µg/mL). In tyrosinase inhibition assays, compound 9 showed the highest activity among the synthesized molecules (IC_{50} = 187.34 ± 3.7 µg/mL), though still significantly less potent than the standard inhibitor tropolone (IC_{50} = 1.06 ± 0.4 µg/mL). Molecular docking studies, which are consistent with the experimental results, showed that these substances bind to the active sites of the target enzymes with high affinity. These findings indicate that compound 16 in particular can be evaluated among potential inhibitor candidates targeting the α-glucosidase enzyme.

Keywords: Schiff bazları, α-Aminofosfonatlar, α-Glikozidaz, Tirozinaz, Moleküler docking.

INTRODUCTION

Hyperglycemia, a defining characteristic of diabetes mellitus (DM), results from insufficient insulin production or action (Ke *et. al* 2024, Feitosa *et. al* 2024). As a major global health issue, DM is among the most prevalent chronic metabolic disorders. In 2021, approximately 10.5% of the global population aged 20–79—about 536.6 million individuals—were living with diabetes. This number is projected to rise to 12.2% (783.2 million people) by 2045 (Sun *et. al* 2022, Fayed *et. al* 2024). According to WHO estimates, diabetes may rank as the sixth leading cause of mortality worldwide by 2030 (Wahidin *et al*. 2024). A key target in diabetes management is the α-glucosidase enzyme, which facilitates the final step of carbohydrate digestion in the small intestine by converting complex carbohydrates into glucose (Peytam *et. al* 2025). Inhibiting this enzyme slows glucose absorption and helps regulate postprandial blood sugar levels (Peytam *et. al* 2025). α-Glucosidase inhibitors such as acarbose and miglitol are already approved for managing type 2 diabetes mellitus (T2DM), though their use is often limited by gastrointestinal side effects like bloating, diarrhea, and abdominal pain (Van de Laar *et al.* 2005). Despite advances in treatment, the global burden of diabetes persists (Bouchi *et al.* 2024, DiNicolantonio *et al.* 2015), prompting the search for safer and more effective α-glucosidase inhibitors. In recent years, many promising candidates have been identified with the potential to improve efficacy and minimize adverse effects (Adip *et al.* 2019, Peytam *et al.* 2020, Peytam *et al.* 2021, Singh *et al.* 2023, Mushtaq *et al.* 2023, Pan *et al.* 2024).

Hyperpigmentation, a condition characterized by localized skin darkening, results from excessive melanin accumulation and can arise due to UV exposure, hormonal imbalances, inflammation, or aging (Thawabteh *et al.* 2023, Kang *et al.* 2021). Tyrosinase (EC 1.14.18.1), a copper-containing oxidoreductase enzyme, catalyzes key reactions in melanogenesis, including the hydroxylation of L-tyrosine and its subsequent oxidation to dopaquinone (Pillaiyar *et al.* 2017). Inhibiting this enzyme reduces melanin synthesis, making tyrosinase a critical target for treating pigmentation disorders. Beyond dermatology, tyrosinase also plays

roles in food spoilage, antibiotic resistance, and neurodegenerative processes (Min *et al.* 2019, Peng *et al.* 2022). Given its broad relevance in cosmetics, agriculture, and pharmaceuticals, extensive efforts have focused on discovering effective tyrosinase inhibitors (Moghadam *et al.* 2025).

Schiff bases represent an important class of nitrogen-containing heterocyclic compounds and exhibit a wide range of biological activities. These compounds are known for their anticonvulsant, antidepressant, anti-inflammatory, analgesic, antimicrobial, antimalarial, anticancer, and antioxidant properties (Gopalakrishnan *et al.* 2007, Das *et al.* 2012). First synthesized by the German chemist Hugo Schiff in 1864, Schiff bases are typically formed via the condensation of amines with aldehydes or ketones (Aytac *et al.* 2023). They are generally represented by the formula R-CH=N-Ar, where the imine (azomethine) bond is classified as an aldimine if derived from an aldehyde and as a ketimine if derived from a ketone (Karaca 2018). Acting as key intermediates in the synthesis of nitrogen-based heterocycles, Schiff bases have recently garnered attention for their enhanced biological activities and enzyme inhibitory potential (Shukla *et al.* 2016, More *et al.* 2019, Shokrollahi *et al.* 2020, Tunç and Alım, 2021). Similarly, organophosphorus compounds have become prominent in medicinal chemistry due to their chemical diversity and pharmacological significance (Gundluru *et al.* 2016). Among them, α-aminophosphonates stand out as structural analogs of amino acids, in which a phosphonic acid moiety replaces the carboxyl group (Amira *et al.* 2021, Baren *et al.* 2023, Mandour *et al*. 2023). These compounds exhibit broad biological effects, including enzyme inhibition and anticancer activity. Their structural versatility has led to increasing interest in developing multifunctional molecules, particularly through the combination of Schiff base and α-aminophosphonate frameworks, for potential therapeutic applications ranging from neurodegenerative diseases to cancer.

In this study, Schiff bases (**7–11**) and bis-α-aminophosphonate derivatives (**13–16**), previously synthesized by our research group (Ekinci *et al.* 2025), were assessed for their inhibitory potential against α-glucosidase and tyrosinase enzymes. Alongside in vitro enzyme inhibition assays, molecular docking simulations were carried out to investigate their binding interactions at the molecular level. By combining experimental techniques with computational modeling, this integrative strategy offers meaningful insights into the possible therapeutic relevance of these compounds.

MATERIALS AND METHODS

1. Enzyme Activity Studies

The α-glucosidase inhibitory activity was evaluated using p-nitrophenyl-α-D-glucopyranoside (PNP-G) as the substrate, following the method of Tao *et al.* (2013). In a 96-well plate, test compounds were incubated with α-glucosidase (0.5 U/mL) in phosphate buffer (100 mM, pH 6.8) at 37 °C for 15 minutes. The reaction was initiated by adding PNP-G (5 mM), and absorbance was recorded over 5 minutes. Tyrosinase inhibition was evaluated spectrophotometrically at 492 nm using mushroom tyrosinase and L-DOPA as substrate, following the method of Yırtıcı *et al.* (2022). The assay mixture contained phosphate buffer (100 mM, pH 6.8), deionized water, L-DOPA (2.5 mM), and enzyme solution. Each compound was tested at five concentrations, and IC_{50} values were determined from activity versus concentration plots.

Molecular Docking Analysis

Molecular docking studies were carried out to predict the binding conformations and non-covalent interactions between the molecules and the target enzymes. Docking calculations were performed using the Molegro Virtual Docker software. Additionally, two-dimensional and three-dimensional interaction diagrams were visualized using BIOVIA Discovery Studio. The crystal structures of the target proteins (α-glucosidase and tyrosinase, with PDB IDs 3A4A and 2Y9X, respectively) were obtained from the RCSB database (www.pdb.org). The active sites of α-glucosidase and tyrosinase were identified based on the experimentally determined structures (PDB codes 3A4A and 2Y9X), and the docking procedure was applied to analyze the interactions of compounds **7**–**11** and **13**–**16** within these active regions (Cheung *et al.* 2012, Nachon *et al.* 2013).

RESULTS and DISCUSSION

Enzyme Activity

In this study, the inhibitory effect of all compounds on α-glucosidase and tyrosinase was investigated at five different concentrations. Activity (%)-Concentration graphs were drawn for each compound and IC_{50} values were calculated. Enzyme activity results are given in **Table 1**.

Table 1. IC_{50} values of compounds against α-glucosidase and tyrosinase.

α-Glycosidase		Tyrosinase	
Compounds	**IC_{50} (µg/mL)**	**Compounds**	**IC_{50} (µg/mL)**
7	173,29±3,4	**7**	-
8	115,52±2,3	**8**	-
9	-	**9**	187,34±3,7
10	-	**10**	-
11	-	**11**	693,15±6,8
13	99,02±0,9	**13**	-
14	-	**14**	231,05±2,5
15	-	**15**	346,57±3,2
16	32,54±0,6	**16**	330,07±3,0

As a result of the activity studies performed, compounds **9**-**11** of Schiff bases and **14** and **15** of bis-α-aminophosphonates did not show inhibition against α-glucosidase. On the other hand, compounds **7** and **8** of Schiff bases showed inhibition with IC_{50} values of 173.29 and 115.52 µM, respectively. Among bis-α-aminophosphonates, compounds **13** and **16** showed inhibition with IC_{50} values of 99.02 and 32.54 µM, respectively. Therefore, it is clear that bis-α-aminophosphonates, when compared to Schiff bases, show stronger inhibition against α-glucosidase. In addition, according to the obtained IC_{50} values, compound **16** is the strongest inhibitor among the molecules. According to the tyrosinase activity study, compounds **7**, **8**, **10** and **13** did not show any inhibitory effect against tyrosinase. The IC_{50} values of compounds **9** and **11** from Schiff bases were calculated as 187.34 and 693.15 µM, respectively. On the other hand, the IC_{50} values of molecules **14**, **15** and **16** from bis-α-aminophosphonates were calculated as 231.05, 346.57 and 330.07 µM, respectively. According to the calculated IC_{50} values, compound **9** showed the best inhibitory properties among the compounds.

Molecular Docking

Molecular docking studies were performed to predict the binding conformations between Schiff bases, bis-α-aminophosphonates and the relevant enzymes. The compatibility of the results of the docking studies with in vitro studies was evaluated. The molecular docking results of the complexes formed between Schiff bases and bis-α-aminophosphonate molecules and the relevant enzymes are given in **Table 2**. Both Schiff bases and bis-α-aminophosphonates exhibited stronger interactions with α-glucosidase compared to the reference compound acarbose. Similarly, the compounds exhibited stronger interactions with tyrosinase compared to the reference molecule tropolene.

Table 2. Molecular docking results of compounds with α-glycosidase and tyrosinase enzymes.

α-Glycosidase		Tyrosinase	
Compound	**MolDock Score**	**Compound**	**MolDock Score**
7	-123,71	**9**	-96,10
8	-112,07	**11**	-93,19
13	-191,14	**14**	-142,93
16	-189,47	**15**	-171,32
Acarbose	-71,77	**16**	-123,63
		Tropolone	-64,36

Compound **16** formed a hydrogen bond with Arg442 and a π-donor hydrogen bond with Arg315 in the binding site of α-glucosidase. Additionally, π-anion interactions were observed with Asp242, Asp307, and Asp352, and a π-cation interaction with Arg315. Alky interactions were detected between compound 16 and Val216, Phe303, Phe178, Phe314, and Lys156, while π-alkyl interactions were observed with Val216 and Arg442. Moreover, π-sigma interactions were found with Tyr72 and Pro312. The benzene ring attached to the phosphonate group of compound **16** exhibited a π–π interaction with Phe303 (**Figure 1**). Compound **9** formed a hydrogen bond with Asn260 located in the binding site of tyrosinase. Additionally, π-sigma interaction was observed with His85. π-alkyl interactions were detected between compound **9** and Met257,

Phe264, and Val248. The benzene rings of compound **9** exhibited π–π interactions with Phe264 and His244 (**Figure 1**).

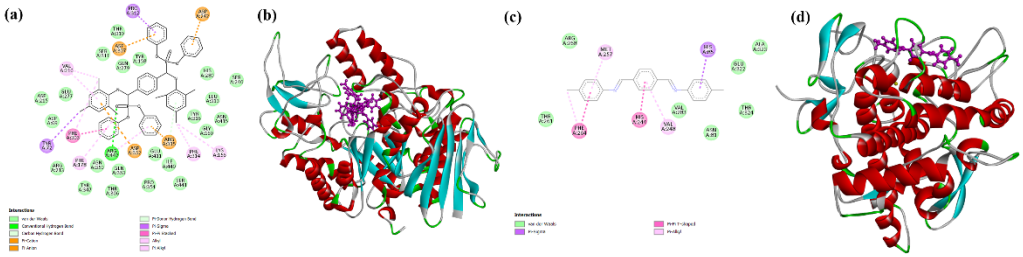

Figure 1. (a) 3D and (b) 2D docking poses of compound **16** with α-glucosidase, (a) 3D and (b) 2D docking poses of compound **9** with tyrosinase**.**

CONCLUSION

In conclusion, Schiff base and bis-α-aminophosphonate derivatives synthesized in our previous study were evaluated for their inhibitory activities against α-glucosidase and tyrosinase enzymes by both in vitro experiments and molecular docking studies. The results showed that bis-α-aminophosphonates, especially compound **16**, exhibited superior inhibitory potential against α-glucosidase. Compound **9** showed the most promising tyrosinase inhibition among the tested molecules. Molecular docking analyses supported the experimental findings, confirming the favorable binding interactions between the active compounds and the catalytic sites of the enzymes. Overall, compound **16** emerges as a promising lead for further development as an α-glucosidase inhibitor, potentially contributing to therapeutic strategies for diabetes management.

ACKNOWLEDGEMENTS

This work was financially supported by The Scientific Research Projects Coordination Office of Çankırı Karatekin University (BAP, Project No: FF081123D05). The computations reported in this study were partially performed at TUBITAK ULAKBIM High Performance and Grid Computing Center (TRUBA resources).

REFERENCES

Adib, M., Ansari, A., Asadipour, A., Mahdavi, M., Shafiee, A. and Foroumadi, A. (2019). Design and synthesis of new fused carbazole-imidazole derivatives as anti-diabetic agents: in vitro α-glucosidase inhibition, kinetic, and in silico studies. Bioorganic & Medicinal Chemistry Letters, (29), 713–718.

Amira, A., Aouf, Z., K'tir, H., Chemam, Y., Ghodbane, R., Zerrouki, R. and Aouf, N.-E. (2021). Recent advances in the synthesis of α-aminophosphonates: a review. ChemistrySelect, (6), 6137–6149. https://doi.org/10.1002/slct.202101360.

Aytac, S., Gundogdu, O., Bingol, Z. and Gulcin, I. (2023). Synthesis of schiff bases containing phenol rings and investigation of their antioxidant capacity, anticholinesterase, butyrylcholinesterase, and carbonic anhydrase inhibition properties. Pharmaceutics, (15), 779.

Baren, M. H., Ibrahim, S. A., Al-Rooqi, M. M., Ahmed, S. A., El-Gamil, M. M. and Hekal, H. A. (2023). A new class of anticancer activity with computational studies for a novel bioactive aminophosphonates based on pyrazole moiety. Scientific Reports, (13), 14680.

Bouchi, R., Fukuda, T., Takeuchi, T., Sugawara, A., Ohsugi, M. and Yoshimoto, T. (2024). A consensus statement from the Japan diabetes society (JDS): a proposed algorithm for pharmacotherapy in people with type 2 diabetes—2nd edition (English version). Diabetology International, (15), 327–345.

Cheung, J., Rudolph, M. J., Burshteyn, F., Cassidy, M. S., Gary, E. N., Love, J., Franklin, M. C. and Height, J. J. (2012). Structures of human acetylcholinesterase in complex with pharmacologically important ligands. Journal of Medicinal Chemistry, (55), 10282–10286.

Das, S., Das, V. K., Saikia, L. and Thakur, A. J. (2012). Environment-friendly and solvent-free synthesis of symmetrical bis-imines under microwave irradiation. Green Chemistry Letters and Reviews, (5), 457–474.

DiNicolantonio, J. J., Bhutani, J. and O'Keefe, J. H. (2015). Acarbose: safe and effective for lowering postprandial hyperglycaemia and improving cardiovascular outcomes. Open Heart, (2), e000327.

Ekinci, E., Çiftçi, H., Adem, Ş., Gündoğdu Aytaç, Ö. and Eyüpoğlu, V. (2025). A comprehensive investigation of Schiff bases and bis-α-aminophosphonates as potent agents against Alzheimer's disease by computer-aided drug discovery techniques and in vitro examinations. Journal of Molecular Structure, (1333), 141734.

Fayed, E. A., Thabet, A., Abd El-Gilil, S. M., Elsanhory, H. M. and Ammar, Y. A. (2024). Fluorinated thiazole–thiosemicarbazones hybrids as potential PPAR-γ agonist and α-amylase, α-glucosidase antagonists: Design, synthesis, in silico ADMET and docking studies and hypoglycemic evaluation. Journal of Molecular Structure, (1301), 137374.

Fayed, E. A., Thabet, A., Abd El-Gilil, S. M., Elsanhory, H. M. and Ammar, Y. A. (2024). Fluorinated thiazole–thiosemicarbazones hybrids as potential PPAR-γ agonist and α-amylase, α-glucosidase antagonists: Design, synthesis, in silico ADMET and docking studies and hypoglycemic evaluation. Journal of Molecular Structure, (1301), 137374.

Feitosa, S. G. D., Lins, I. M. S., dos Maciel, L. G. and Anjos, J. V. (2024). Discovery of novel heterocyclic derivatives containing oxadiazolone or pyrimidinone cores as DPP-4 inhibitors. Journal of Heterocyclic Chemistry.

Gopalakrishnan, M., Sureshkumar, P., Kanagarajan, V. and Thanusu, J. (2007). New environmentally-friendly solvent-free synthesis of imines using calcium oxide under microwave irradiation. Research on Chemical Intermediates, (33), 541–548.

Gundluru, M., Sarva, S., Kandula, M. K. R., Netala, V. R., Tartte, V. and Cirandur, S. R. (2016). Phosphosulfonic acid-catalyzed green synthesis and bioassay of α-aryl-α′-1,3,4-thiadiazolyl aminophosphonates. Heteroatom Chemistry, (27), 269–278.

Kang, H. Y., Bahadoran, P., Park, K. and Yaar, M. (2021). Alterations of the pigmentation system in the aging process. Pigment Cell & Melanoma Research, (34), 800–813.

Karaca, E. Ö. (2018). Politeknik Dergisi. (n.d.). Yeni Schiff bazı bileşiklerinin sentezi ve yapılarının aydınlatılması. 245 – 249.

Ke, Y., Jin, W., Zhang, X., Zhang, S., Zhang, L. and Liu, L. (2024). Xanthones with multiple roles against diabetes: their synthesis, structure-activity relationship, and mechanism studies. Drug Development Research, (85), e22170.

Mandour, H. S. A., Hamed, M. A., Saad-Allah, K. M., Abd Elnabi, M. K., Abosharaf, H. A. and El-Gharably, A. A. (2023). Antimicrobial and molecular docking studies of novel synthesized α-aminophosphonates based on pyrozol moiety as anticancer agents via α-topoisomerase II inhibition. ChemistrySelect, (8), e202300254.

Min, K., Kim, M., Yun, J., Park, S. and Lee, Y. (2019). A perspective on the biotechnological applications of the versatile tyrosinase. Bioresource Technology, (289), 121730.

Moghadam Farid, S., Moradi Dehaghi, S., Iraji, A., Shahraki, S., Ghanei, M. and Zolfaghari, E. (2025). Synthesis, biological evaluations, and in silico assessments of phenylamino quinazolinones as tyrosinase inhibitors. Scientific Reports, (15), 846.

More, M. S., Joshi, P. G., Mishra, Y. K. and Khanna, P. K. (2019). Metal complexes derived from Schiff bases and semicarbazones for biomedical and allied applications: a review. Materials Today Chemistry, (14), Article 100195.

Mushtaq, A., Azam, U., Mehreen, S. and Naseer, M. M. (2023). Synthetic α-glucosidase inhibitors as promising anti-diabetic agents: recent developments and future challenges. European Journal of Medicinal Chemistry, (249), 115119.

Nachon, F., Carletti, E., Ronco, C., Trovaslet, M., Nicolet, Y., Jean, L. and Renard, P.-Y. (2013). Crystal structures of human cholinesterases in complex with huprine W and tacrine: elements of specificity for anti-Alzheimer's drugs targeting acetyl- and butyryl-cholinesterase. Biochemical Journal, (453), 393–399.

Pan, G., He, Y., Hu, L., Zhou, Y., Zhang, Y. and Liu, Y. (2024). A review on the in vitro and in vivo screening of α-glucosidase inhibitors. Heliyon, (2024).

Peng, Z., Jin, G., Li, X., Zhang, W., Zheng, J. and Liu, W. (2022). A systematic review of synthetic tyrosinase inhibitors and their structure–activity relationship. Critical Reviews in Food Science and Nutrition, (62), 4053–4094.

Peytam, F., Foroumadi, P., Gulcan, H. O., Edraki, N., Abdolmaleki, A. and Emami, S. (2025). Design, synthesis, and evaluation of triazolo[1,5-a]pyridines as novel and potent α-glucosidase inhibitors. Scientific Reports, (15), 17813.

Peytam, F., Foroumadi, P., Abdolmaleki, A., Edraki, N., Emami, S. and Amanlou, M. (2020). Design and synthesis of new imidazo[1,2-b]pyrazole derivatives, in vitro α-glucosidase inhibition, kinetic and docking studies. Molecular Diversity, (24), 69–80.

Peytam, F., Foroumadi, P., Emami, S., Abdolmaleki, A., Amanlou, M. and Edraki, N. (2021). Synthesis and biological evaluation of new dihydroindolizino[8,7-b]indole derivatives as novel α-glucosidase inhibitors. Journal of Molecular Structure, (1224), 129290.

Pillaiyar, T., Manickam, M. and Namasivayam, V. (2017). Skin whitening agents: medicinal chemistry perspective of tyrosinase inhibitors. Journal of Enzyme Inhibition and Medicinal Chemistry, (32), 403–425.

Shokrollahi, S., Amiri, A., Fadaei-Tirani, F. and Schenk-Joß, K. (2020). Promising anti-cancer potency of 4,5,6,7-tetrahydrobenzo[d]thiazole-based Schiff-bases. Journal of Molecular Liquids, (300), Article 112262.

Shukla, R., Singh, A. P., Sonar, P. K., Mishra, M. and Saraf, S. K. (2016). Schiff bases of benzothiazol-2-ylamine and thiazolo[5,4-b]pyridin-2-ylamine as anticonvulsants: synthesis, characterization and toxicity profiling. Central Nervous System Agents in Medicinal Chemistry, (16), 240–248.

Singh, A., Malik, R., Sharma, S., Kumar, M. and Kumar, P. (2023). Recent developments in synthetic α-glucosidase inhibitors: a comprehensive review with structural and molecular insight. Journal of Molecular Structure, (1281), 135115.

Sun, H., Saeedi, P., Karuranga, S., Pinkepank, M., Ogurtsova, K., Duncan, B. B., Stein, C. and Basit, A. (2022).
IDF Diabetes Atlas: Global, regional and country-level diabetes prevalence estimates for 2021 and projections for 2045. Diabetes Research and Clinical Practice, (183), 109119.

Tao, Y., Zhang, Y., Cheng, Y. and Wang, Y. (2013). Rapid screening and identification of α-glucosidase inhibitors from mulberry leaves using enzyme-immobilized magnetic beads coupled with HPLC/MS and NMR. Biomedical Chromatography, (27), 148–155.

Thawabteh, A. M., Juma, S., Bader, M., Sawafta, M. and Alkhatib, R. (2023). Skin pigmentation types, causes and treatment—A review. Molecules, (28), 4839.

Tunç, T. and Alım, Z. (2021). Synthesis of new schiff bases and assessment of their in vitro biological effects on acetylcholinesterase and carbonic anhydrase isoenzymes activities. Russian Journal of Organic Chemistry, (57), 247–254.

Van de Laar, F. A., Lucassen, P. L., Akkermans, R. P., van de Lisdonk, E. H., Rutten, G. E. and van Weel, C. (2005).
Alpha-glucosidase inhibitors for type 2 diabetes mellitus. Cochrane Database of Systematic Reviews, (2005).

Wahidin, M., Lazuardi, L., Hidayat, R., Kristina, S. A. and Wibowo, L. (2024). Projection of diabetes morbidity and mortality till 2045 in Indonesia based on risk factors and NCD prevention and control programs. Scientific Reports, (14), 5424.

Yırtıcı, U., Ergene, A., Atalar, M. N. and Adem, S. (2022). Phytochemical composition, antioxidant, enzyme inhibition, antimicrobial effects, and molecular docking studies of Centaurea sivasica. South African Journal of Botany, (144), 58.

➢ *ORAL PRESENTATION*

Stabilization of Marl Soil Using Sewage Sludge and Polypropylene Fibers under Freeze-Thaw Conditions

[1] Mohamed Bashir Said RADDAD, [2] İnan KESKİN, [3]AmirHossein VAKİLİ

[1] Department of Civil Engineering, Karabük University, 78050, Karabük, TÜRKİYE
[2] Department of Civil Engineering, Karabük University, 78050, Karabük, TÜRKİYE
[3] Department of Civil Engineering, Faculty of Engineering, Zand Institute of Higher Education, Shiraz, IRAN

*Corresponding author e-mail : inankeskin@karabuk.edu.tr

Abstract
In this study, the stabilisation of marl soil using Iron and steel cooling water sludge (SS) and polypropylene fibres (PPF) was investigated. Marl soil is a type of soil characterised by high clay and calcium carbonate content and is a poor subgrade for construction purposes due to its low strength and sensitivity to environmental stressors. SS is proposed as a soil modifier that can increase soil strength and provide environmental sustainability. PPF also help to improve soil cohesion, reduce cracking and improve overall mechanical properties. In this study, the strength and durability of marl soil stabilised withSS and PPF under freeze-thaw cycles were investigated. Freeze-thaw cycles can cause mechanical and structural changes in the soil, jeopardising the stability of the infrastructure. Therefore, it is important to develop soil stabilisation techniques, especially under such environmental conditions. In this research, the performance of different stabilisation materials under freeze-thaw conditions, optimisation of curing periods and development of predictive models to evaluate soil performance are discussed. The study showed that SS and PPF are potentially effective materials for stabilizing marl soil and can improve soil behaviour under freeze-thaw conditions.
Keywords: Freeze-Thaw Cycles, Soil Stabilisation, Marl Soil, Sewage Sludge (SS), Polypropylene Fibres (PPF).

INTRODUCTION

Soil stabilization is an important geotechnical technique that improves the mechanical and structural properties of weak soils, especially for construction purposes. Marl soil is a type of soil characterized by high clay and calcium carbonate content. They are difficult to work with due to their low strength, periodic swelling, and shrinkage[1]. Soil stability is crucial for infrastructure, but freeze-thaw cycles pose challenges by weakening soil structure, reducing strength, and increasing permeability. Conventional stabilization methods have limited success in addressing these effects [2]. To reduce these problems, SS, a by-product of wastewater treatment processes, is proposed as a potential solution. SS contains organic and inorganic components that increase soil strength by binding particles together and densifying the soil matrix, thus increasing the load-carrying capacity and resistance to soil deformation. In addition, SS reduces soil retention under freeze-thaw conditions, prevents the formation of ice lenses, and provides the capacity to maintain structural integrity for many cycles under freeze-thaw conditions [3]. Therefore, such materials offer the dual benefits of improved mechanical strength and freeze-thaw resistance.An innovative approach is using wastewater sludge (SS) as a soil modifier, offering both environmental and stability benefits by reducing waste and promoting resource recycling [4]. Additionally, polypropylene fibers (PPF) enhance soil strength and durability under freeze-thaw conditions [5]. When combined with SS, PPFs create a synergistic effect, improving soil cohesion and overall stability. Soıl stabılızatıon technıques lose theır effectıveness under freeze-thaw condıtıons, sıgnıficantly ımpactıng the long-term stabılıty and ıntegrıty of ınfrastructure. The problem becomes crıtıcal ın regıons wıth contrastıng clımates, where freeze-thaw cycles cause the soıl to expand and contract, leadıng to damage to structures. Therefore, there ıs an urgent need to ıdentıfy and develop ınnovatıve technıques and materıals that can enhance soıl resılıence agaınst the effects of freeze-thaw cycles [6].

Soil stabilization techniques lose their effectiveness under freeze-thaw conditions, significantly impacting the long-term stability and integrity of infrastructure. The problem becomes critical in regions with contrasting climates, where freeze-thaw cycles cause the soil to expand and contract, leading to damage to structures. Therefore, there is an urgent need to identify and develop innovative techniques and materials that can enhance soil resilience against the effects of freeze-thaw cycles

The limited comprehensive analysis of the performance of various stabilization materials under freeze-thaw conditions makes it difficult to develop effective soil improvement strategies in complex environmental conditions. Current deficiencies in optimization of curing time and additive ratios prevent consistent and predictable results from soil stabilization. Furthermore, the lack of reliable models to evaluate soil behavior under environmental stress conditions makes long-term performance analyses uncertain. This study aims to provide comprehensive and comparative data on the stabilization performance under different curing times and freeze-thaw cycles by investigating the effects of wastewater sludge (SS) and polypropylene fibers (PPF) on marl soil.

MARL SOIL AND SITE DESCRIPTION

Soil samples of marl were collected from the Karabük region, which is considered a complex geological area with significant seismic activity. This region is part of the highly active Alpine-Himalayan seismic belt and lies north of the North Anatolian Fault Zone, a high seismic hazard area. Marl soil is a fine-grained sedimentary material with a high calcium carbonate content, which increases its bearing capacity. However, it remains relatively weak under severe environmental stresses, such as freeze-thaw cycles and earthquakes.

The harsh climate and elevated seismic risks in the region make Karabük an ideal location for studying innovative techniques for marl soil stabilization. A picture of the sampling area around Karabük city is shown in Figure 1.

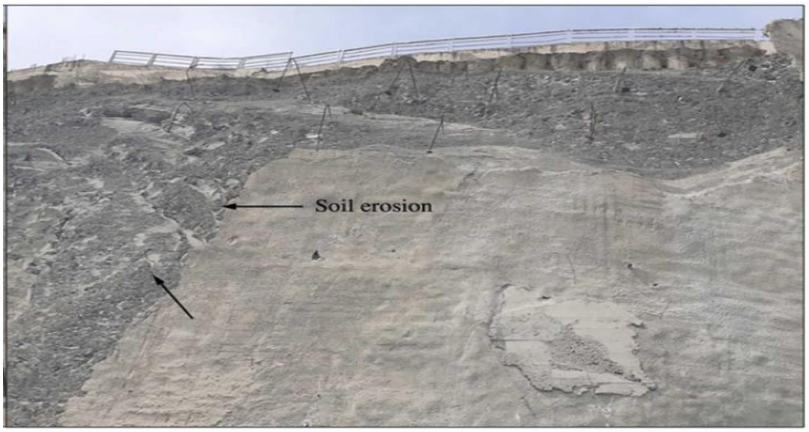

Figure 1. General view of the marl sampling site near Karabük, Turkey

MATERIAL FOR ENHANCING MARL STABILITY

Iron and steel cooling water sludge (SS)

Iron and Steel Cooling Water Sludge (SS) is a secondary by-product obtained from water used during closed circuit or single pass cooling processes in iron and steel production plants. This sludge consists primarily of iron oxides, metallic particles, corrosion products and deposited solids such as residual oil or grease originating from hot metal surfaces and circulating water. Due to its high iron content and fine particle size, ISCWS shows potential for reuse in geotechnical applications, especially as a soil stabilization agent. However, its chemical composition may vary depending on the raw material source, water quality and operational conditions. In this study, the chemical and physical properties of wastewater are presented in Table 1.

Table **Hata! Belgede belirtilen stilde metne rastlanmadı.**: Chemical and physical characteristics of SS

Component	SS	Component	SS
Na_2O	0.5422	TiO_2	0.6782
MgO	3.0748	MnO	0.0734
Al_2O_3	10.7019	Fe_2O_3	6.2635
SiO_2	35.0929	NiO	0.0143
P_2O_5	0.0758	ZnO	0.0143
SO_3	0.4224	Rb_2O	0.0153
K_2O	1.7467	Sro	0.2254
CaO	41.0612	Y_2O_3	0.0017

Polypropylene fiber (PPF)

Polypropylene fiber is a synthetic fiber derived from polypropylene; a thermoplastic polymer widely used in various applications due to its versatile properties. It is known for being lightweight, resistant to chemical and environmental degradations, and highly durable. These qualities make polypropylene fiber a preferred material in industries such as construction, textiles, and geotextiles. In construction, it is mainly used as reinforcement in concrete and composites, improving mechanical properties while reducing shrinkage cracking. Table 2 summarizes the key properties of polypropylene fiber examined in this study.

Table 2: Chemical and physical characteristics of PPF

Property	Value
Fiber type	Discrete
Unit weight (g/cm^3)	0.91
Average diameter (mm)	0.034
Length (mm)	12
Breaking tensile strength (MPa)	350
Modulus of elasticity (MPa)	3500
Fusion point (°C)	165
Burning point (°C)	590
Acid and alkali resistance	Strong

IMPACT OF FREEZE-THAW CYCLES IN SAMPLE

The effect of freeze-thaw cycles on each of the four different groups was considered. The first group consisted of untreated marl soil, the second group included marl stabilized with the optimum dosage of sludge (15%), the third group consisted of marl reinforcement with the optimum dosage of PPF (1%), and the fourth group contained marl stabilized with the combination of the optimum dosages of sludge and PPF. All four groups were tested after three different curing periods: 7 days, 28 days, and 90 days. During these tests, the impact of freeze-thaw cycles was evaluated, and uniaxial compressive strength and compressive strength tests were conducted to characterize the performance of the samples References.

Freeze-thaw cycles

Freeze-thaw cycles are a common experimental method used to evaluate the behavior of materials under thermal fluctuations. This technique involves subjecting samples to repeated freezing and thawing processes to simulate natural environmental conditions, allowing for the assessment of physical and chemical property changes. The process begins with careful specimen preparation and conditioning to a reference state in terms of moisture or temperature. The sample is then frozen for 4 to 24 hours to ensure complete and uniform freezing, followed by thawing at temperatures ranging from 4°C to 20°C for a similar duration. These cycles are repeated a specific number of times based on the study's requirements, and material changes are monitored after each cycle using precise measurement tools. Observed changes may include weight loss, surface cracking, and variations in porosity, strength, and elasticity. The test concludes with a comparative analysis of pre- and post-cycle data to evaluate the material's resistance and stability

under freeze-thaw conditions. This method is widely applied in civil engineering, geotechnical studies, and environmental sciences to determine material durability and performance in thermally variable environments.

Sample preparation and test program

After preparing the uniaxial specimens, they were subjected to freeze-thaw cycles. Six different cycles were defined for the experiment, including 1, 2, 4, 6, 8, and 10 freeze-thaw cycles. In each cycle, for the freezing phase, a temperature of -17°C was considered, and the specimens were kept in the freezer for 12 hours. Then, for the thawing phase, a temperature of 24°C was applied, and the specimens were kept at this temperature for 12 hours. Each complete cycle freeze-thaw process was considered as one cycle. After completing each cycle, the test specimens were subjected to uniaxial compressive strength and compressive strength tests. Only the specimens that successfully passed these tests proceeded to the next cycle. It is discussed how the freeze-thaw cycle affects the specimens.

RESULTS AND DISCUSSIONS

Effect of freeze-thaw cycles on the UCS of untreated marl

These findings suggest that as the number of freeze-thaw cycles increases, a decline in UCS is observed. Furthermore, the greatest strength reduction is recorded in the 7-day curing period, indicating that shorter curing times provide lower resistance to freeze-thaw cycles (Figure 2).

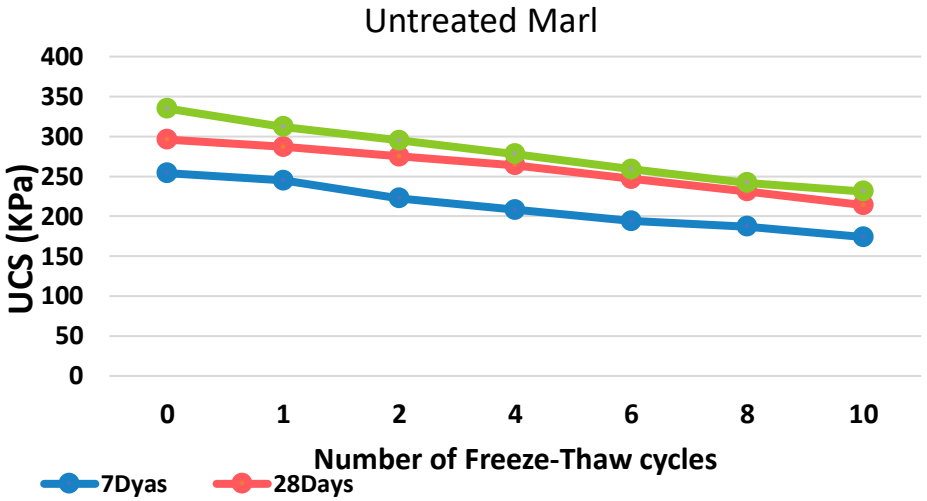

Figure 2. Effect of freeze-thaw cycles on the unconfined compressive strength (UCS) of untreated marl.

Effect of freeze-thaw cycles on the ucs of marl reinforced with 1% ppf

The addition of 1% PPF to untreated marl significantly improves UCS, with the most notable improvements observed over extended curing times. The maximum strength increase occurs at Cycle 6, showing a remarkable 87.3% improvement after 90 days of curing. However, after Cycle 10, a decline in performance is evident, particularly in the 7-day curing period, suggesting that excessive freeze-thaw cycles can adversely affect the soil's strength (Figure 3).

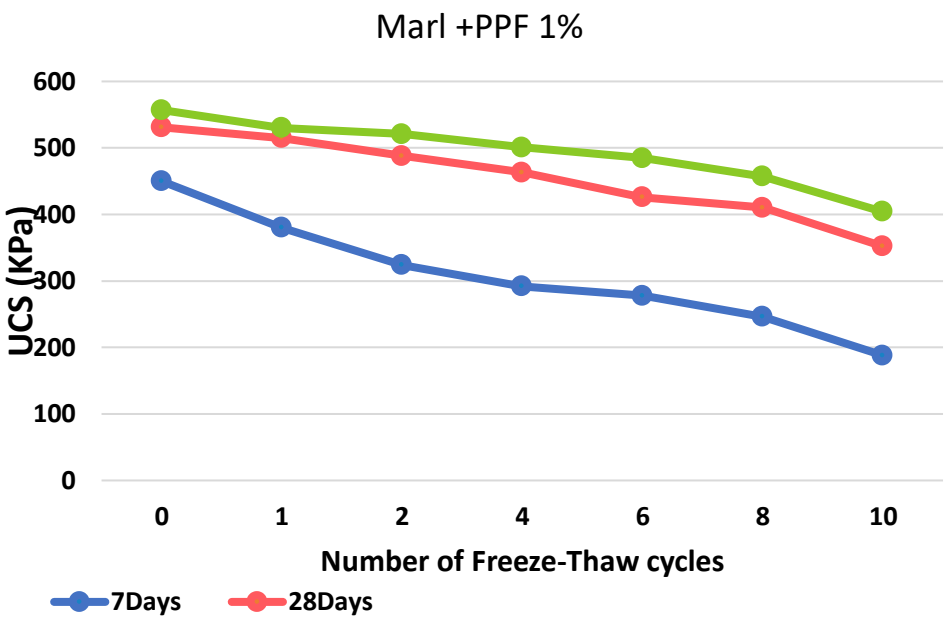

Figure 3. *UCS of marl soil reinforced with 1% PPF under different freeze-thaw cycles and curing periods.*

Effect of freeze-thaw cycles on the ucs of marl stabilized with 15% ss

The significant improvement in the UCS of the combination of Marl and 15% SS. The most remarkable performance improvement occurs in Cycle 6, with a 111.3% increase at 7 days. This treatment exhibits the best increasing trend over time, demonstrating its high effectiveness (Figure 4).

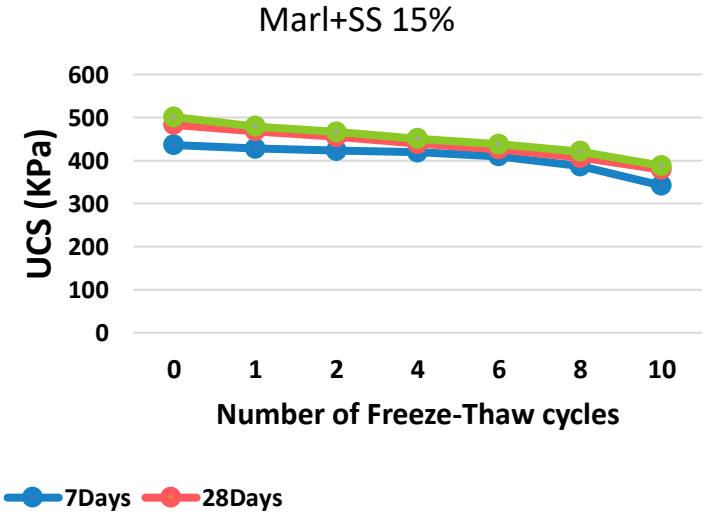

Figure 4. UCS of marl soil stabilized with 15% sewage sludge (SS) under different freeze-thaw cycles and curing periods.

Effect of freeze-thaw cycles on the ucs of marl treated with the optimum combination of 15% ss and 1% ppf

This analysis reveals that Marl + SS 15% + PPF 1% shows relatively good resistance to freeze-thaw cycles. The least decline in UCS over a 90-day curing period is observed in the combination of 15% SS and 1% PPF, thus improving the freeze-thaw durability of the material (Figure 5).

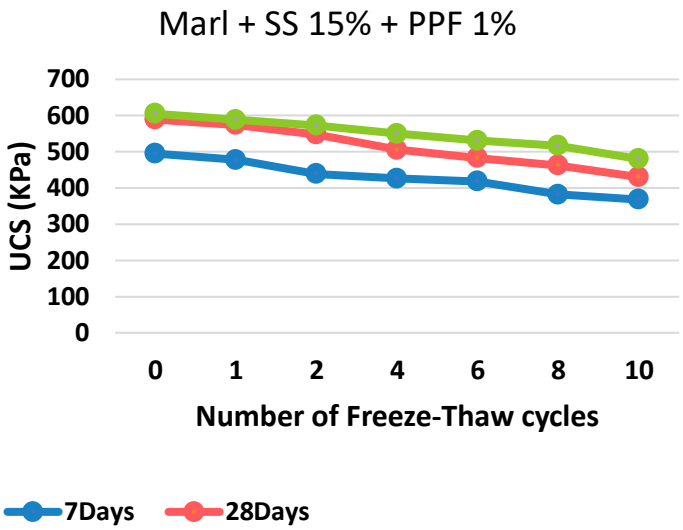

Figure 5. UCS of marl soil treated with the optimum combination of 15% sewage sludge (SS) and 1% polypropylene fiber (PPF) under different freeze-thaw cycles and curing periods.

CONCLUSION

This study focused on enhancing the freeze-thaw resistance of high-plasticity marl soil through the use of wastewater treatment sludge (SS) and polypropylene fibres (PPF). The results showed that treated samples with SS and PPF maintained structural integrity and exhibited minimal strength loss after multiple freeze-thaw cycles, whereas untreated marl experienced significant degradation.

The optimal combination of 15% SS and 1.00% PPF yielded the highest resistance to cracking and structural breakdown under freeze-thaw loading. Microstructural analyses confirmed that the additives improved internal bonding and reduced porosity, resulting in a denser soil matrix better equipped to withstand harsh environmental conditions.

These findings demonstrate the effectiveness of SS and PPF in reinforcing soil durability under repeated temperature fluctuations, offering a promising solution for soil stabilization in cold and seismically active regions.

Acknowledgments

The authors of this study thank you, Karabük University, for the support provided under grant number KBÜBAP-25-YL-041

REFERENCES

S. Sun, X. Liu, H. Liu, C. Shi, L. Xu, Z. Huang, and Y. Sui, "Mechanical properties and acoustic emission characteristics of basalt fiber reinforced cemented silty sand subjected to freeze–thaw cycles," *Scientific Reports,* vol. 14, no. 1, pp. 21888, 2024.

V. Gall, A. Alsahly, and J. M. Davila, "Impact of climate change on natural terrain stability and infrastructure integrity: Insights and case studies from Colombia," *Geomechanics and Tunnelling,* vol. 17, no. 5, pp. 527-534, 2024.

A. Tiruneh, S. Nkambule, and A. Murye, "Assessment of the Benefits and Risks of Sewage Sludge Application as Soil Amendment for Agriculture in Eswatini," *African Journal of Food, Agriculture, Nutrition and Development,* vol. 24, no. 8, pp. 24230-24260, 2024.

T. W. Takao, V. S. Bardini, A. D. de Jesus, L. Marchiori, A. Albuquerque, and F. A. Fiore, "Beneficial Use of Water Treatment Sludge with Stabilizers for Application in Road Pavements," *Sustainability,* vol. 16, no. 13, pp. 5333, 2024.

Z. G. Fard, M. M. Khabiri, and A. Mohajeri, "Investigation of Mechanical Properties of Quicksand Stabilized with Bitumen Emulsion and Reinforced with Waste Polypropylene Fibers and The Effect of

Freeze and Thaw on Its Performance," *International Journal of Sustainable Construction Engineering and Technology,* vol. 13, no. 3, pp. 59-67, 2022.
C. Han, Y. He, J. Tian, J. Zhang, J. Li, and S. Wang, "Shear strength of polypropylene fibre reinforced clay," *Road Materials and Pavement Design,* vol. 22, no. 12, pp. 2783-2800, 2021.

➢ *ORAL PRESENTATION*

Sustainable Pasture Management Through Community Engagement: Preserving Ecosystem Services in Korab-Koritnik Nature Park, Albania

Mihallaq Qirjo[1*], Ani Ahmetaj[2]

[1]Faculty of Natural Sciences, Department of Biology, University of Tirana, Albania
[2]Resource Environmental Center Albania, Albania

Abstract
Across the Green Belt area of the Western Balkans, pastures are among the most vulnerable natural ecosystems, facing numerous challenges that lead to their degradation. Korab-Koritnik Nature Park, located in the cross-border region with North Macedonia, contains 22,578 hectares of pastures (or 40.6% of the whole protected area) classified as Alpine calcareous grasslands, lowland hay meadows (*Alopecurus pratensis, Sanguisorba officinalis*), and mountain hay meadows. These areas host valuable biodiversity and provide essential ecosystem services to local populations who have used them for thousands of years. The assessment offers data and insights into community practices related to pasture use. Emerging trends, such as early spring grazing—driven by rising temperatures and climate change at higher elevations—are negatively affecting pasture quality. Focus group discussions with shepherds and community representatives highlighted that pasture management practices should include rotational grazing, soil erosion control, and fire prevention and management.
Keywords: pastures management, grazing, ecosystem services, community-based natural resource management, socio-ecological systems, climate change adaptation

INTRODUCTION

The Korab-Koritnik Nature Park is a significant part of the European Green Belt and is recognized as one of the important biodiversity hotspots on the Balkan Peninsula. This park spans approximately 22,578 hectares in the eastern Albanian Alps, featuring extensive subalpine and alpine grasslands that constitute a large portion of its total area. These grasslands provide ecological value and reflect human-environment interactions, which are vital for local communities' livelihoods and cultural identities [1] [2]. The unique geomorphology of the park, representing some of Albania's older geological formations, combined with various climatic influences, has resulted in a remarkable array of habitats and species, including many endemics that are rare or not found elsewhere [3] [4].

To analyze the multifaceted challenges posed to these critical ecosystems, this paper employs the Socio-Ecological Systems (SES) framework. This approach helps elucidate the intricate relationships between ecological components—such as grasslands, soils, and hydrology—and social factors including local communities, governance structures, and economic activities [2] [5]. The SES framework contrasts with traditional views that see humans primarily as threats to environmental integrity; instead, it emphasizes complex feedback loops and resilience, integrating social, economic, and political factors that impact ecological outcomes [6]. This framework supports a structured analysis that can lead to more nuanced insights into the interactions within the Korab-Koritnik ecosystems.

The primary challenge confronting the grasslands of Korab-Koritnik is their degradation, which threatens both biodiversity and human well-being. This degradation arises from various interrelated factors, including historical land-use practices, such as livestock grazing that began during the Medieval period, which have significantly altered treelines and shrub compositions [7]. Contemporary socio-economic changes, characterized by rural depopulation and emigration, further worsen these conditions. Additionally, climate change is a critical factor that impacts vegetation dynamics and ecosystem stability [2] [8]. Numerous studies illustrate how climate change interacts with local land management practices, producing profound effects on grassland ecosystems.

To address these pressing challenges, this paper advocates for a transition away from centralized, top-down conservation models that have historically failed to promote effective stewardship by local communities. A shift towards Community-Based Natural Resource Management (CBNRM) is proposed, wherein local communities are empowered through secure rights and active roles in managing their natural resources [1] [2]. This model integrates traditional ecological knowledge with scientific techniques, creating incentives for sustainable land use and stewardship [5] [6]. The effectiveness of CBNRM is linked to its potential to align conservation goals with local socio-economic conditions, ultimately enhancing both governance and ecological outcomes.

The study aims to achieve three objectives: (1) to characterize the current state of the Korab-Koritnik pasture socio-ecological system, including its key ecological elements and the dynamics of the local community; (2) to identify feedback mechanisms and systemic pressures driving ecological changes and threatening resilience; and (3) to propose a tailored co-management framework based on CBNRM principles to ensure the long-term sustainability of the park's grasslands and the communities that rely on them [4] [6].

MATERIALS AND METHOD

A. *Study Area: The Korab-Koritnik Socio-Ecological System*

Geographical and Ecological Context

The Korab-Koritnik Nature Park is located in the northeastern region of Albania, part of the broader Scardo-Pindhic Mountains system. This park features an ancient landscape, characterized by topographical diversity that includes high peaks such as Korabi i Math at 2,764 m, as well as deep gorges, canyons, and expansive plateaus like the Shishtavec plateau [9]. The rugged terrain has been shaped by geological processes over millennia, resulting in a complex mosaic of features, such as horst structures and steep slopes. The geology is varied, featuring siliceous rock formations in areas like the Shishtavec plateau and Kallabak Mt., limestone formations in the Koritnik and Gjallica Mts., and unique gypsum substrates located in Pelpeneku Mt. These geological features contribute to the park's rich floristic diversity and plant community variability [10].

The climate within the Korab-Koritnik area reflects a complex interplay of influences. The lower western slopes are influenced by a Mediterranean climate that penetrates through the Drini River valley, while much of the park experiences a modified continental climate [11]. At altitudes above 2,000 m, a mountainous climate prevails, with average annual temperatures ranging from 2 to 3°C, and annual precipitation ranging from 1,300 mm to over 2,000 mm on the higher western slopes [9]. This combination of geological diversity, topographical variation, and climatic differences gives rise to a wide array of ecological niches, contributing to the exceptionally high habitat heterogeneity observed within the park [12].

Socio-Economic and Governance Context

The socio-economic dimension of the Korab-Koritnik Socio-Ecological System (SES) is deeply rooted in a historical connection to the land, a relationship currently undergoing significant transformations. The communities situated within and around the park are primarily rural and have traditionally depended on pastures for their livelihoods. Key economic activities in the region include livestock herding, particularly sheep and goats, which utilize transhumance systems; beekeeping, producing honey derived from diverse alpine flora; and the collection of wild medicinal and aromatic plants [13]. A growing segment of nature-based tourism capitalizes on the park’s scenic and recreational appeal. However, these communities face considerable socio-economic challenges, including significant depopulation and demographic shifts due to high emigration rates. Many villages have experienced population declines, with remaining residents tending to be older, negatively impacting land management and diminishing the labour force available for traditional agricultural and pastoral activities [14] [15].

B. Data Collection and Analysis

Phytosociological and Habitat Assessment

Ecological data for this study were obtained from a series of field expeditions conducted during the spring, summer, and autumn of 2024. These expeditions aimed to assess the current state of herbaceous and shrub-land vegetation communities across the park's diverse geological substrates, including limestone, silicate, flysch, and gypsum formations [11]. Methodology was centred on identifying changes in floristic composition and structure while evaluating their relationships with habitat types and anthropogenic pressures. Detailed records were maintained on dominant and rare plant species, the composition of plant communities, and habitat conditions throughout the fieldwork period. The classification of vegetation units adhered to the hierarchical floristic system outlined in the EuroVegChecklist, while habitat types were identified according to the European Union's NATURA 2000 framework [16]. Plant identification utilized established botanical literature relevant to Albania and Europe [17] [18] [19] [20] [21] [22], ensuring scientific rigor.

Community-Based Participatory Assessment

To capture the social components of the SES, a qualitative, participatory research methodology was adopted, focusing on local stakeholder knowledge and experiences [23]. This process included focus group discussions in Peshkopi, engaging shepherds, beekeepers, farmers, and representatives from community organizations and the Dibër municipality. These sessions promoted dialogue and allowed participants to share insights related to pasture use and management [23] [24]. Additionally, comprehensive individual interviews were conducted with key informants, including an expert from AdZM Dibër, a transhumant shepherd, and five farmers from the Kala e Dodës administrative unit. The semi-structured nature of these interviews was designed to gather in-depth information on community demographics, livelihood strategies, pasture use practices, intra-community cooperation, perceived challenges, and future needs [25]. This community-based approach is critical for understanding local perspectives and socio-economic drivers that inform human-environment interactions within the park [24] [26].

RESULTS

The field assessments reveal that the Korab-Koritnik Nature Park harbors an exceptionally rich mosaic of grassland and heathland ecosystems, reflecting its complex environmental gradients. These ecosystems are of high conservation value, with several habitats listed as priorities under the EU Habitats Directive.

Grassland and Heathland Diversity

The grasslands of the park can be broadly categorized into several major phytosociological classes. The dry grasslands of the class Festuco−Brometea are widespread, occurring on both xerophilic sites, characterized by the alliance *Festucion valesiacae*, and xeromesophilic sites, represented by the alliance *Bromion erecti*. These communities are typically found along ridges and in the openings of forest zones, with dominant species including various fescues (*Festuca vallesiaca, F. rupicola, F. koritnicensis*), *Chrysopogon gryllus*, and *Bromus erectus*.

On high-altitude acidic and silicate substrates, such as those found on Kallabaku and Grama mountains, the acidophilous grasslands of the class *Juncetea trifidi* are prominent. These are represented by the alliances *Seslerion comosae* and *Poion violaceae*, which host a suite of Balkan endemic and alpine species like *Sesleria comosa, S. korabensis, Festuca panciciana*, and *Bellardiochloa violaceae*.

In stark contrast, the hygromesophilic meadows of the class Molinio−Arrhenatheretea occupy wet valleys, stream banks, and depressions, particularly in areas like Shishtavec. These meadows, vital for hay production and biodiversity, are characterized by alliances such as Calthion and *Agrostion albae* and support species like *Molinia caerulea, Sanguisorba officinalis, Polygonum bistorta*, and the rare *Gladiolus palustris*.

On calcareous and gypsum substrates, particularly on Koritnik and Gjallica mountains, the grasslands belong to the class Elyno−Seslerietea. These include communities of the alliance Seslerion juncifoliae on cold, north-facing slopes, and Onobrichido−Festucion on warmer, southern slopes. These habitats are rich in specialist and endemic species such as *Sesleria coerulans, Dryas octopetala, Onobrychis scardica*, and *Oxytropis korabensis*.

Finally, the landscape is punctuated by dwarf shrub communities. Formations of Alpine juniper (*Juniperus communis subsp. alpina*) are widespread on both calcareous and silicate slopes, representing an early colonizer of post-glacial landscapes. These are often interspersed with ericoid heaths of the class Loiseleurio procumbentis−Vaccinietea, including communities dominated by bilberry (*Vaccinium myrtillus*), bog bilberry (*V. uliginosum*), and Balkan heath (*Bruckenthalia spiculifolia*), which play a crucial role in soil protection and providing habitat.

Observed Ecological Pressures

The ecological integrity of these habitats is under considerable pressure from a combination of factors. Direct field observations have documented clear indicators of environmental stress and degradation:

• Climate Change Indicators: Tangible evidence of climate change is visible in the upward migration of vegetation belts. On the slopes above Shishtavec village, the treeline advanced by approximately 38 meters in altitude between 2002 and 2023. An even more pronounced shift was recorded on Gjallica Mountain, where the treeline moved upward by 60 meters between 2001 and 2023. This phenomenon, consistent with global trends of vegetation response to warming, signifies a long-term contraction of the alpine zone and its specialist habitats .

• Soil Degradation and Erosion: Soil erosion is a pervasive problem throughout the park, particularly on steep slopes. This process is accelerated in areas where vegetation cover has been removed, such as through the intentional burning of juniper shrubs, the creation of informal vehicle tracks that channel runoff, and along the historical "soft belt" (Brezi i bute)—a narrow strip of cleared land along the state border from the communist era that has now become a major source of erosion.

• Habitat Alteration and Fragmentation: The practice of burning Juniperus shrubs to "clear" pastures has led to significant habitat alteration. In these burned areas, there is a notable expansion of early successional, ruderal species like fireweed (Epilobium angustifolium), which alters community structure and ecosystem function. Furthermore, the proliferation of unofficial roads and tracks for vehicles and motorcycles is fragmenting contiguous pasture habitats, creating barriers for species movement and introducing new corridors for erosion and invasive species.

Community Management Practices and Perceived Challenges

The participatory assessments with local communities reveal a complex picture of traditional stewardship practices grappling with new and powerful socio-economic and environmental challenges.

1. *Traditional Use and Governance*

The use of the park's pastures is deeply rooted in a traditional transhumance system. During the summer months, herders move their livestock (primarily sheep and goats) to high-altitude pastures, where they establish temporary camps known as *stane*. Access to and use of these communal pastures are not arbitrary but are governed by a sophisticated set of unwritten, customary rules. These rules, which dictate grazing rights and resolve disputes, are adjudicated and enforced by village elders (*pleqësia*). This system of informal, community-level governance has historically been effective in managing resource use and minimizing conflicts among local users.

2. *Emerging Challenges from the Community Perspective*

Discussions with shepherds, farmers, and other community members highlighted a set of pressing challenges that are straining this traditional system and degrading the pasture resources upon which they depend:

• Climate-Driven Mismatches in Grazing: A key concern raised by shepherds is the trend of earlier spring grazing. Rising temperatures are causing snow to melt earlier in the season, prompting herders to move their flocks to high-altitude pastures sooner than in the past. This practice is detrimental to pasture health, as it subjects young, vulnerable plants to grazing pressure during their critical initial growth phase, reducing overall forage productivity for the rest of the season.

• The Paradox of Undergrazing: Contrary to the conventional focus on overgrazing, a more insidious problem has emerged in many areas: undergrazing. The significant decline in livestock numbers, a direct consequence of rural depopulation and emigration, has led to a reduction in grazing intensity. Without sufficient grazing pressure to control them, there has been a marked increase in the abundance of unpalatable shrubs and, more alarmingly, poisonous plant species. This shift in vegetation composition not only degrades the quality of the pasture but also poses a direct economic threat, causing illness and mortality in the remaining livestock.

• Governance Confusion: Community members expressed significant confusion and frustration over the current state of formal governance. The recent transfer of some management responsibilities to the local municipality, without clear delineation of roles with the existing authority of the Regional Administration of Protected Areas (RAPA), has created confusion both in the governing bodies, as well as the local population. This ambiguity led to a complete lack of oversight and enforcement in 2024, with no grazing fees being collected and no official body actively monitoring pasture use.

These challenges are not isolated issues but are deeply interconnected, creating a negative feedback loop that accelerates degradation. The process begins with a socio-economic driver—emigration—which reduces livestock numbers. This leads to an ecological consequence—undergrazing—which allows unpalatable and toxic plants to proliferate, an expected outcome when grazing pressure is removed. This ecological degradation, in turn, creates a negative economic feedback, making the traditional livelihood of herding less profitable and more challenging, which may further incentivize abandonment of the practice and emigration from the region. This entire cycle is amplified by the simultaneous failure of the formal governance system, which leaves no institution with the clear authority or capacity to intervene and break the cycle. The ecological crisis and the socio-governance crisis are thus mutually reinforcing, driving the entire system toward a less productive and less resilient state.

DISCUSSION

A. The Korab-Koritnik Pastures as a Shifting Socio-Ecological System

The findings of this study, when interpreted through the Socio-Ecological Systems (SES) framework, indicate that the Korab-Koritnik pastures are undergoing a fundamental regime shift. Historically, the dynamics of this SES were defined by interactions between a relatively stable rural population and the grassland ecosystem, with human management focused on optimizing forage and preventing overgrazing [27]. In contrast, the current state is characterized by a new set of drivers and feedback loops that reflect a transition from a regime managed for pastoral production to one marked by land abandonment and undergrazing [28]. This shift signifies not just a change in land use intensity but is fundamentally altering the core structure and function of the ecosystem. The reduction in grazing pressure is leading to compositional changes, with a clear shift away from graminoid-dominated communities, which have co-evolved with herbivory, towards communities increasingly dominated by woody shrubs and unpalatable forbs [29]. This transition, driven by socio-economic pressures of depopulation, constitutes a critical loss of ecological characteristics inherent to these high-value grasslands, thereby endangering the essential ecosystem services they provide [30].

B. Climate Change as a Systemic Stressor and Threat Multiplier

Empirical evidence of climate change impacts in Korab-Koritnik, such as documented upward migration of the treeline and altered seasonal patterns, aligns with broader scientific projections

for the Balkan mountain regions. However, in the context of this SES, climate change extends beyond being a simple, additive threat; it functions as a systemic stressor and a significant threat multiplier that exacerbates existing vulnerabilities and accelerates negative trends. For instance, observed earlier snowmelt—a direct consequence of regional warming—induces a temporal mismatch within the pastoral system [28]. This early period of snowmelt leads to premature grazing on pastures that have not yet recovered, amplifying vegetation degradation at critical phenological stages. Global projections of hotter, drier summers for the Balkans heighten the frequency and intensity of droughts and wildfires [31]. These conditions elevate the risk that localized, traditional practices, such as burning juniper shrubs for pasture management, could become uncontrolled and escalate into large-scale destructive fires, particularly on slopes already vulnerable to erosion. The progressive advance of the treeline represents a direct, potentially irreversible loss of finite alpine pasture habitat as it is diminished at higher elevations. Consequently, climate change manifests as a pervasive force that undermines the resilience of the entire socio-ecological system against additional pressures.

C. Bridging the Governance Gap: The Case for Community-Based Co-Management

The current institutional ambiguity surrounding pasture management represents a critical governance failure that undermines the potential for sustainable management [27]. This management vacuum, characterized by unclear authority among state and local actors, serves as a primary obstacle in addressing the intertwined crises of ecological degradation and socio-economic decline [30]. Following the principles of Community-Based Natural Resource Management (CBNRM), the most viable path forward involves establishing a formal co-management framework [28]. Such a framework would move beyond the constraints of purely top-down, centralized control, which often lacks local legitimacy and practical enforceability [30]. A successful co-management model for Korab-Koritnik would need to formally recognize, legitimize, and empower traditional governance structures. By integrating these community-level institutions into a multi-stakeholder governing body—including representatives from state agencies, municipalities, and key resource user groups such as herders' associations and beekeepers—a more adaptive and resilient governance framework can be constructed [30]. This approach directly addresses the imperative for local participation and benefit-sharing, crucial for securing community buy-in and ensuring compliance with management regulations. Although establishing such a system poses challenges, including the need for capacity building, delineation of responsibilities, and conflict resolution mechanisms, it represents the most promising strategy for overcoming the current governance paralysis [30].

Proposing Integrated and Adaptive Management Interventions

A co-management framework would facilitate the implementation of nuanced and adaptive management interventions specifically tailored to the Korab-Koritnik SES's challenges. Rather than imposing uniform, landscape-wide prescriptions, management could become targeted and responsive [27]. First, to confront the paradox of undergrazing and shrub encroachment, the adoption of adaptive rotational grazing techniques is advised. This practice uses livestock as an ecological restoration tool, concentrating herds for short periods in specific degraded paddocks. This targeted grazing can suppress dominant shrubs and unpalatable forbs, creating opportunities for the recovery of more desirable grass species [28]. Subsequent long rest periods will allow ecosystems to recover, thereby enhancing soil health, root depth, and water retention. This method shifts the problem of undergrazing into a restorative solution, leveraging pastoral practices to enhance pasture quality and productivity.

Second, to manage the increasing fire risk, a shift from simple fire suppression to participatory fire management is vital. This shift can involve developing a Community Wildfire Protection Plan that integrates local communities in fire management efforts [27]. Strategies could include training community members as local fire brigades for rapid responses, forming strategic fuel breaks to protect villages, and using prescribed burning under expert supervision to manage fuel loads and

control shrub encroachment. This approach capitalizes on local knowledge and presence, crafting a resilient fire management system.

Lastly, to address persistent soil erosion issues, management should prioritize community-led restoration projects. Empowering local communities to undertake bio-engineering measures—such as building small check dams with local materials or revegetating eroded gullies—can prove highly effective. These initiatives often yield more sustainable, culturally appropriate, and cost-effective solutions than large-scale, top-down engineering efforts, thereby further strengthening community ownership and stewardship of the landscape [27].

CONCLUSION

The subalpine and alpine grasslands of Korab-Koritnik Nature Park constitute a socio-ecological system of immense natural and cultural value. This system is currently in a state of critical transition, driven by the profound socio-economic shift of rural depopulation and amplified by the pervasive pressures of climate change. The historical management paradigm, focused on controlling overgrazing, is no longer adequate to address the emerging and paradoxical challenge of undergrazing, which is leading to shrub encroachment, loss of forage quality, and a negative feedback loop that further threatens the viability of traditional pastoral livelihoods.

The analysis clearly indicates that the current governance framework, marked by institutional ambiguity and a disconnect between state authority and local communities, is incapable of managing these complex and interacting dynamics. The resulting management vacuum is a primary obstacle to halting the degradation of these vital ecosystems.

The long-term sustainability of the Korab-Koritnik pastures and the communities that depend upon them hinges on a fundamental reform of the governance model. The establishment of a formal, legitimate, and empowered co-management system is paramount. Such a system must bridge the gap between state-level authority and traditional community governance, integrating local knowledge, ensuring equitable benefit-sharing, and fostering a sense of shared responsibility. Investing in community-based management and adaptive interventions like rotational grazing and participatory fire planning is not merely a conservation strategy; it is a critical investment in sustainable rural development, the preservation of cultural heritage, and the enhancement of climate change resilience for this unique and invaluable region of the European Green Belt.

ACKNOWLEDGMENT

This research was conducted as part of the "Connectivity through Pastures" project (implemented by REC Albania), with the financial support of the European Union via the BESTbelt project. The contents of this document are the sole responsibility of the authors and do not necessarily reflect the opinion of the European Union.

REFERENCES

Beshkov, S., Gashtarov, V., & Hula, V. (2021). Contribution to knowledge of the balkan macroheterocera: new and rare species for bulgaria, north macedonia and albania. Nota Lepidopterologica, 44, 223-237. https://doi.org/10.3897/nl.44.64804.

Ambrosi, L., Berger, V., Rainer, G., Obojes, N., Tappeiner, U., Tasser, E., … & Leitinger, G. (2024). Spatiotemporal variability of evapotranspiration in alpine grasslands and its biotic and abiotic drivers. Ecohydrology, 17(3). https://doi.org/10.1002/eco.2633.

Halilaj, H., Kupe, L., Bajrami, A., Icka, P., Mala, X., & Damo, R. (2021). Endemic plants in the flora of shutman (sharri mountain), kosovo – an analysis of phytogeographical elements and life forms. Natura Croatica, 30(1), 1-11. https://doi.org/10.20302/nc.2021.30.1.

Varga, Z. (2014). Biogeography of the high mountain lepidoptera in the balkan peninsula. Ecologica Montenegrina, 1(3), 140-168. https://doi.org/10.37828/em.2014.1.21.

Michna, P., Eugster, W., Hiller, R., Zeeman, M., & Wanner, H. (2013). Topoclimatological case-study of alpine pastures near the albula pass in the eastern swiss alps. Geographica Helvetica, 68(4), 249-263. https://doi.org/10.5194/gh-68-249-2013.

Darwall, W., Carrizo, S. F., Numa, C., Barrios, V., Freyhof, J., & Smith, K. G. (2015). Freshwater key biodiversity areas in the mediterranean basin hotspot.. https://doi.org/10.2305/iucn.ch.2014.ssc-op.52.en.

Lüth, C., Tasser, E., Niedrist, G., Via, J. D., & Tappeiner, U. (2011). Plant communities of mountain grasslands in a broad cross-section of the eastern alps. Flora - Morphology, Distribution, Functional Ecology of Plants, 206(5), 433-443. https://doi.org/10.1016/j.flora.2010.11.007.

Marzini, S., Tasser, E., Wellstein, C., Albrich, K., Rammer, W., & Mina, M. (2024). Future expansion of alpine forest-grassland ecotone under land-use and climate change.. https://doi.org/10.21203/rs.3.rs-4789034/v1.

Bytyçi, P., Zhushi-Etemi, F., Kabashi-Kastrati, E., & Çadraku, H. (2023). Biodiversity of butterflies (lepidoptera, papilionoidea) in mountain koritnik in the republic of kosovo. Journal of Insect Biodiversity and Systematics, 9(4), 623-642. https://doi.org/10.61186/jibs.9.4.623.

Zhou, M., Chen, T., Xu, Y., & Mi, F. (2024). Can the establishment of national parks promote the coordinated development of land, the environment, and residents' livelihoods?. Land, 13(5), 704. https://doi.org/10.3390/land13050704.

Shumka, S., Shumka, L., Špoljar, M., & Shuka, L. (2024). Evidences of climate changes and conservation needs for halting further deterioration of small glacial lakes.. https://doi.org/10.20944/preprints202405.0644.v.

Vermeulen, W., Wilgen, N. J. v., Smith, K., Dopolo, M., Swemmer, L., Annecke, W., … & Symonds, A. (2019). Monitoring consumptive resource use in south african national parks. Koedoe, 61(1). https://doi.org/10.4102/koedoe.v61i1.1516.

Institute of Statistics. (2025). Quarterly livestock statistics, Q1 2025. https://www.instat.gov.al/al/temat/bujq%C3%Absia-dhe-peshkimi/blegtoria/#tab2.

Grigorescu, A., Frinculeasa, M., & Chitescu, R. (2020). The socio-economic value of protected areas. the bucegi natural park. Management Dynamics in the Knowledge Economy, 8(1), 61-79. https://doi.org/10.2478/mdke-2020-0005.

Institute of Statistics. (2025). Population of Albania on 1 January 2025. https://www.instat.gov.al/al/temat/treguesit-demografik%C3%AB-dhe-social%C3%AB/popullsia/.

Mucina, L., Bültmann, H., Dierssen, K., ... et al. (2016). Vegetation of Europe: hierarchical floristic classification system of vascular plant, bryophyte, lichen, and algal communities. Applied Vegetation Science 19(S1): 3–264.

Shuka, L., Malo, S., (2010). The transboundary important plant areas as conservation units of European green belt (Eastern Albanian zone). Journal of Environmental Protection and Ecology. Vol.11, (3): 866–874.

Rakaj, M., Shehu, X. (2012). Lista e Kuqe e bimëve enëzore të vargmalit Korabit. Bul. Shk., Ser. Shk. Nat., Nr. 62: 80-91.

Hashani, Z., Maxhuni, Q., Shuka, L. (2014). Shpërndarja e llojeve bimore në malet Koritnik dhe Brod, bazuar në preferencën ndaj substratit. BSHN (UT), Nr.18: 25-37.

Hashani, Z. & Shuka, L. (2013). Pulsatilla halleri (All.) Willd. and Viola schariensis Erben, New species for the flora of Kosovo. Natura Montenegrina, 12(4): 569-574.

Hallaçi, B. & Shuka, L. (2013). Allium phthioticum Boiss. & Heldr., Allium victorialis L. and Melampyrum bihariense A. Kerner – three new species in the flora of Albania. Natura Montenegrina, 12(4): 563-568.

Shuka, L., Kashta, L. and Xhulaj, M. (2008). Evaluation of potential transboundary important plant areas of the North Albania. Natura Montenegrina, Podgorica. 7 (3): 425- 439.

Ortegón, Y. A. C., Prado, J. C. A., Castellanos, P. M. A., & Correa, J. P. R. (2024). Examining the mediating effect of the rural economic dynamization between the socio-environmental heritage and sustainability of protected areas. Sustainability, 16(15), 6525. https://doi.org/10.3390/su16156525.

Loughran, K. (2018). Urban parks and urban problems: an historical perspective on green space development as a cultural fix. Urban Studies, 57(11), 2321-2338. https://doi.org/10.1177/0042098018763555.

Taylor, L., Leckey, E., Lead, P. J., & Hochuli, D. F. (2020). What visitors want from urban parks: diversity, utility, serendipity. Frontiers in Environmental Science, 8. https://doi.org/10.3389/fenvs.2020.595620.

Zhou, M., Chen, T., Xu, Y., & Mi, F. (2024). Can the establishment of national parks promote the coordinated development of land, the environment, and residents' livelihoods?. Land, 13(5), 704. https://doi.org/10.3390/land13050704.

Collins, S. L., Carpenter, S. R., Swinton, S. M., Orenstein, D. E., Childers, D. L., Gragson, T. L., … & Whitmer, A. C. (2010). An integrated conceptual framework for long-term social–ecological research. Frontiers in Ecology and the Environment, 9(6), 351-357. https://doi.org/10.1890/100068.

Oikonomou, D., Vrahnakis, M., Yiakoulaki, M. D., Xanthopoulos, G., & Kazoglou, Y. (2023). Grazing as a management tool in mediterranean pastures: a meta-analysis based on a literature review. Land, 12(7), 1290. https://doi.org/10.3390/land12071290.

Quaranta, G., Salvia, R., Salvati, L., Paola, V. D., Coluzzi, R., Imbrenda, V., … & Simoniello, T. (2020). Long-term impacts of grazing management on land degradation in a rural community of southern italy: depopulation matters. Land Degradation &Amp; Development, 31(16), 2379-2394. https://doi.org/10.1002/ldr.3583.

Folke, C., Biggs, R., Norström, A. V., Reyers, B., & Rockström, J. (2016). Social-ecological resilience and biosphere-based sustainability science. Ecology and Society, 21(3). https://doi.org/10.5751/es-08748-210341.

Williams, A., Kennedy, S., Philipp, F., & Whiteman, G. (2017). Systems thinking: a review of sustainability management research. Journal of Cleaner Production, 148, 866-881. https://doi.org/10.1016/j.jclepro.2017.02.002.

➢ *ORAL PRESENTATION*

Değişken zemin koşulları altında TBDY 2018'e göre farklı döşeme tiplerinin yapı maliyetine etkisinin incelenmesi

Ali Türkmen[1]* (https://orcid.org/0009-0007-0316-7665), Cenk Öcal[1] (ORCID: https://orcid.org/0000-0002-6959-5626), Kılıç Yasin Arslan[2]* (https://orcid.org/0000-0002-4433-9204)

*[1]Isparta Uygulamalı Bilimler Üniversitesi, Teknoloji Fakültesi, İnşaat Mühendisliği, Isparta, Türkiye.
[2] Süleyman Demirel Üniversitesi, Mühendislik ve Doğa Bilimleri Fakültesi, İnşaat Mühendisliği, Isparta, Türkiye.

*Sorumlu yazar e-posta: kyarslan92@gmail.com

Özet
Bu çalışmada, farklı döşeme tiplerinin değişken zemin koşulları altındaki yapı maliyetine etkisi, 2018 Türkiye Bina Deprem Yönetmeliği (TBDY 2018) doğrultusunda incelenmiştir. Yapı mühendisliğinde döşeme sistemlerinin seçimi yalnızca yapısal performansa değil, aynı zamanda ekonomik sürdürülebilirliğe de bağlıdır. Bu kapsamda, iki döşeme tipi (kirişli plak döşemeler ve asmolen döşemeler) ele alınmıştır. Farklı zemin sınıfları (ZB, ZC, ZD) için yapısal modeller ideCAD Statik yazılımı kullanılarak oluşturulmuştur. Her döşeme tipi için deprem etkileri altında yapısal tasarımlar yapılmış ve oluşan yapı maliyetleri karşılaştırılmıştır. Hesaplamalarda TBDY 2018'de belirtilen deprem tasarım sınıfları, yük katsayıları ve spektrum parametreleri dikkate alınmıştır. Modeller, yönetmelikte belirtilen minimum beton ve donatı gerekliliklerini sağlayacak şekilde tasarlanmıştır. Sonuç olarak, ZB, ZC ve ZD zemin sınıflarında kirişli ve asmolen döşemeler arasındaki maliyet farklarını ortaya koyan karşılaştırmalı bir analiz sunulmuştur.
Anahtar Kelimeler: TBDY 2018, Döşeme Tipleri, Yapı Maliyeti, Zemin Sınıfı, IdeCAD

An investigation into the impact of different slab types on structural costs under variable soil conditions according to TBDY 2018

Abstract
In this study, the impact of different slab types on structural costs under variable soil conditions was investigated in accordance with the Turkish Building Earthquake Code 2018 (TBDY 2018). In structural engineering, the selection of slab systems is influenced not only by structural performance but also by economic sustainability. Within this scope, two slab types—beam-supported slabs and hollow block (asmolen) slabs—were examined. Structural models were created for different soil classes (ZB, ZC, ZD) using the Sta4CAD Static software. For each slab type, structural designs were carried out under seismic effects, and the resulting construction costs were compared. The calculations considered the seismic design classes, load factors, and spectrum parameters specified in TBDY 2018. The models were designed to meet the minimum concrete and reinforcement requirements dictated by the code. As a result, a comparative analysis was presented, evaluating the cost differences between beam-supported and hollow block slabs across ZB, ZC, and ZD soil classes.
Keywords: TBDY 2018, Slab Types, Construction Cost, Soil Classification, IdeCAD

GİRİŞ

Türkiye, aktif tektonik kuşakların üstünde yer alması sebebiyle ciddi düzeyde deprem riski taşıyan bir ülkedir. Geçmişte yaşanan depremler, yapı stokunun önemli bir kısmının yetersiz olduğunu ve taşıyıcı sistem seçimlerinin sadece mühendislik değil, aynı zamanda ekonomik sonuçlar da doğurduğunu göstermektedir (Altun, 2022; Türkmen ve Tekeli, 2005). Bu bağlamda, taşıyıcı sistemlerin önemli bir bileşeni olan döşeme sistemlerinin seçimi hem yapısal güvenlik hem de maliyet açısından dikkatle ele alınmalıdır (Khalaf ve ark., 2022).

Bu çalışmada, farklı döşeme tiplerinin (kirişli plak ve asmolen döşeme) değişken zemin koşulları altındaki yapı maliyetine etkisi, Türkiye Bina Deprem Yönetmeliği 2018 (TBDY 2018) kapsamında analiz edilmiştir. Yapı mühendisliğinde döşeme sistemlerinin seçimi, sadece taşıyıcılık açısından değil; üretim kolaylığı,

işçilik süresi, kalıp karmaşıklığı ve maliyet gibi ekonomik parametrelerle de doğrudan ilişkilidir (Bikçe ve Akyol, 2017; Kara ve Akkaş, 2023). Çalışmada bu iki yaygın döşeme sistemi, zemin sınıfları ZB, ZC ve ZD için modellenmiş ve aralarındaki maliyet farkları irdelenmiştir.

Yapısal analizler, ideCAD Statik yazılımı kullanılarak gerçekleştirilmiş; TBDY 2018 kapsamında belirtilen deprem tasarım sınıfları, yük katsayıları ve spektral ivme değerleri hesaplamalara entegre edilmiştir. Tüm modeller, yönetmelikte tanımlanan minimum beton ve donatı koşullarını sağlayacak şekilde tasarlanmıştır. Her bir döşeme tipi için deprem etkileri altında yapısal çözümler oluşturulmuş ve oluşan taşıyıcı sistem maliyetleri karşılaştırılmıştır. Ayrıca, modelleme sürecinde düşey taşıyıcı sistem sabit tutulmuş ve yalnızca döşeme sistemindeki değişimlerin ekonomik etkileri analiz edilmiştir.

Literatürde yer alan birçok çalışma, döşeme sistemlerinin yapı rijitliği ve davranışı üzerindeki etkilerini farklı yöntemlerle ortaya koymuştur (Uzun, 2014; Sağılyan ve ark., 2012; Özpınar, 2006). Özellikle döşemelerin düzlem içi rijitlik katkısı, kolon ve perde elemanlarının zorlanmalarını artırarak genel yapı davranışını etkileyebilmektedir. Diğer yandan, farklı deprem senaryoları ve analiz yöntemleri ile yapılan çalışmalarda, döşeme sisteminin deprem etkisi altındaki davranışa olan katkısının değiştiği görülmüştür (Hanif ve ark., 2024).

Bu çalışmada elde edilen sonuçlar, kirişli plak ve asmolen döşeme sistemlerinin farklı zemin sınıfları altında benzer yapısal taleplere maruz kaldığında, yapı maliyetleri açısından anlamlı farklar doğurabileceğini ortaya koymuştur.

MATERYAL VE METOD

Asmolen ve kirişli plak döşemenin, ZB, ZC ve ZD zemin sınıflarındaki maliyet kıyaslanmasının incelendiği bu çalışmada, döşeme sistemleri, taşıyıcılık, rijitlik. Ve zeminle etkileşim açısından farklı davranışlar göstermesi nedeniyle tercih edilmiştir. Bu sayede farklı döşeme türlerinin yapı maliyetine etkisi karşılaştırılmalı olarak incelenebilmiştir.

Sayısal modeller ideCAD statik analiz programı kullanılarak yapılmış olup oluşturulan sayısal model isimlendirilmeleri Şekil 1'de gösterildiği şekilde oluşturulmuştur.



Şekil 1. Model isimlendirmesi

Toplamda altı farklı model oluşturularak bu modeller için maliyet analizleri yapılmıştır. Model numaraları ve özellikleri Tablo 1'de gösterilmiştir.

Tablo 1. Model İsimlendirmeleri

Model No	Döşeme Tipi	Zemin Sinifi
SM-A-ZB	Asmolen	ZB
SM-A-ZC	Asmolen	ZC
SM-A-ZD	Asmolen	ZD
SM-P-ZB	Plak	ZB
SM-P-ZC	Plak	ZC
SM-P-ZD	Plak	ZD

Asmolen döşemeye sahip olan sayısal modellerin genel görünümleri Şekil 2'de verilmiştir. Kirişli plak döşemeye sahip olan sayısal modellerin genel görünümleri ise Şekil 3'te verilmiştir. Yapı bodrum, zemin, iki normal kat olmak üzere dört kat ve kuleden oluşmaktadır.

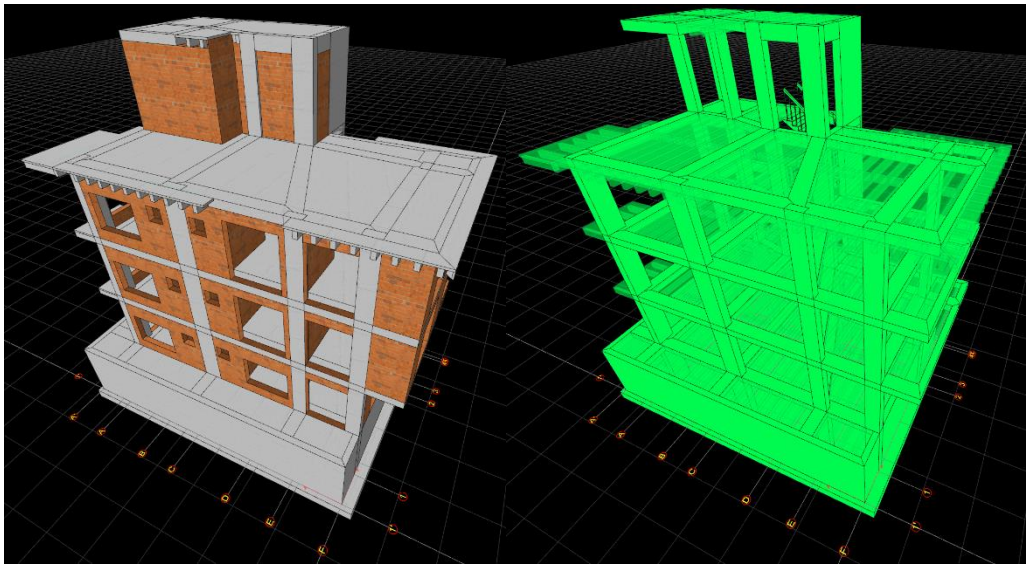

Şekil 2. Asmolen döşemeli sayısal modellerin genel görünümleri

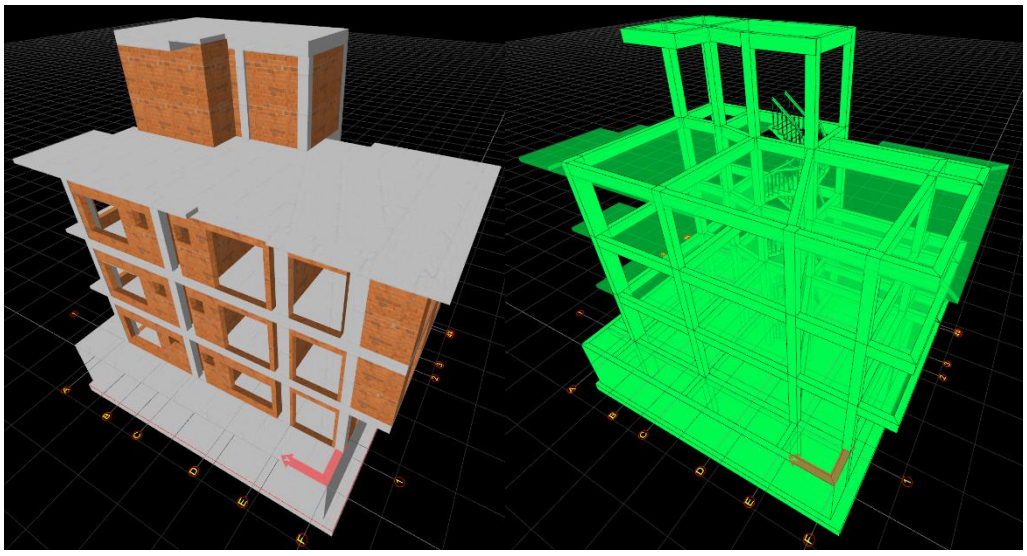

Şekil 3. Kirişli plak döşemeli sayısal modellerin genel görünümleri

Tüm sayısal modeller minimum yönetmelik şartlarını sağlayacak şekilde oluşturulmuş olup metraj listesi Şekil 4-9'da verilmiştir.

1-	C25 BETON	225.51
2-	BETON KALIP	1453.19
3-	B420C DONATI (İNCE)	17542.54
	B420C DONATI (KALIN)	9383.53
	B420C DONATI (TOPLAM)	26926.07

Şekil 4. SM-A-ZB metraj listesi

1-	C25 BETON	230.60
2-	BETON KALIP	1512.50
3-	B420C DONATI (İNCE)	16154.02
	B420C DONATI (KALIN)	8588.17
	B420C DONATI (TOPLAM)	24742.19

Şekil 5. SM-A-ZC metraj listesi

1-	C25 BETON	230.02
2-	BETON KALIP	1523.69
3-	B420C DONATI (İNCE)	16253.70
	B420C DONATI (KALIN)	9111.14
	B420C DONATI (TOPLAM)	25364.84

Şekil 6. SM-A-ZD metraj listesi

1-	C25 BETON	209.84
2-	BETON KALIP	1089.59
3-	B420C DONATI (İNCE)	10498.10
	B420C DONATI (KALIN)	7901.39
	B420C DONATI (TOPLAM)	18399.49

Şekil 7. SM-P-ZB metraj listesi

1-	C25 BETON	211.21
2-	BETON KALIP	1097.83
3-	B420C DONATI (İNCE)	10680.69
	B420C DONATI (KALIN)	7931.49
	B420C DONATI (TOPLAM)	18612.18

Şekil 8. SM-P-ZC metraj listesi

1-	C25 BETON	211.21
2-	BETON KALIP	1097.83
3-	B420C DONATI (İNCE)	10691.26
	B420C DONATI (KALIN)	8017.71
	B420C DONATI (TOPLAM)	18708.97

Şekil 9. SM-P-ZD metraj listesi

T.C. Çevre Şehircilik ve İklim Değişikliği Bakanlığı tarafından hazırlanan rayiç fiyat listesinde yer alan pozlardan kaba inşaat maliyet hesabı için kullanılan pozlar Tablo 2'de sunulmuştur.

Tablo 2. Kaba inşaat için ÇŞİDB birim fiyat rayiç listesi

Poz No	Tanımı	Ölçü Birimi	Rayiç Fiyat (₺)
15.150.1005	Beton santralinde üretilen veya satın alınan ve beton pompasıyla basılan, C 25/30 basınç dayanım sınıfında, gri renkte, normal hazır beton dökülmesi (beton nakli dahil)	m^3	3.151,28
15.180.1003	Plywood ile düz yüzeyli betonarme kalıbı yapılması	m^2	824,39
15.160.1003	Ø 8- Ø 12 mm nervürlü beton çelik çubuğu, çubukların kesilmesi, bükülmesi ve yerine konulması	Ton	39.429,35
15.160.1004	Ø 14- Ø 28 mm nervürlü beton çelik çubuğu, çubukların kesilmesi, bükülmesi ve yerine konulması	Ton	38.016,85

BULGULAR ve TARTIŞMA

Farklı zemin sınıfları (ZB, ZC, ZD) altında iki farklı döşeme sistemi olan kirişli plak döşeme ve asmolen döşeme sistemlerinin kaba inşaat maliyetleri karşılaştırmalı olarak incelenmiştir. Elde edilen bulgular, zemin koşullarının yalnızca yapı davranışı üzerinde değil, aynı zamanda döşeme tipine bağlı olarak maliyet

üzerinde de belirleyici bir rol oynadığını ortaya koymuştur. Farklı zemin koşullarında döşeme sistemlerinin yapıya uyguladığı yükler ve bu yüklerin yapı-zemin etkileşimi ile birleşerek oluşturduğu maliyet farklılıkları, seçim yapılırken yalnızca yapısal performansın değil, ekonomik faktörlerin de dikkate alınması gerektiğini ortaya koymaktadır. Şekil 10'da tüm sayısal modellerin maliyet kıyaslanması sunulmuştur.

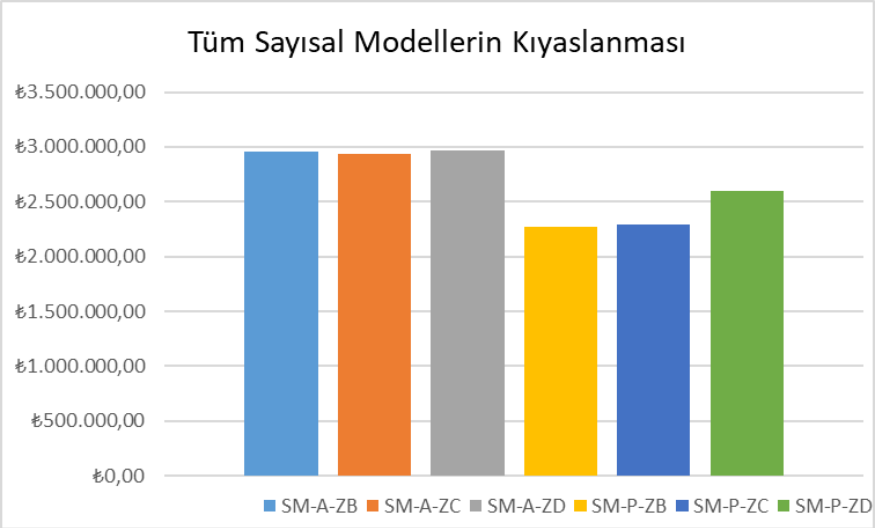

Şekil 10. Tüm sayısal modellerin kıyaslanması

SM-A-ZB modelinde kaba inşaat maliyeti ₺2.957.063,66, SM-A-ZC modelinde kaba inşaat maliyeti ₺2.937.012,72, SM-A-ZD modelinde kaba inşaat maliyeti ₺2.967.104,86, SM-P-ZB modelinde kaba inşaat maliyeti ₺2.273.830,91, SM-P-ZC modelinde kaba inşaat maliyeti ₺2.293.284,85, SM-P-ZD modelinde kaba inşaat maliyeti ₺2.598.011,12 olarak hesaplanmıştır.

Şekil 11'de asmolen tipi döşemeye sahip modellerin ZB-ZC-ZD zemin sınıfı maliyet kıyaslamaları verilmiştir. Şekil 12'de ise kirişli plak döşemeye sahip modellerin ZB-ZC-ZD zemin sınıfı maliyet kıyaslamaları verilmiştir.

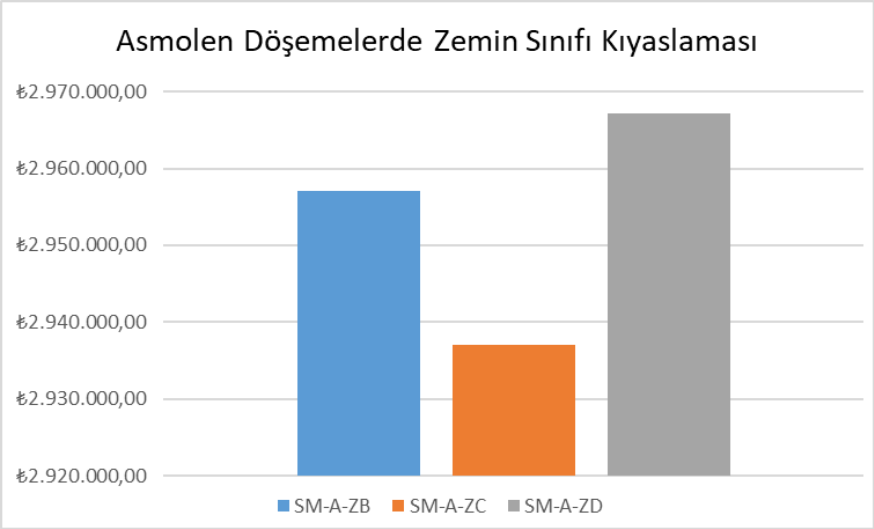

Şekil 11. Asmolen döşemelerde zemin sınıfı kıyaslaması

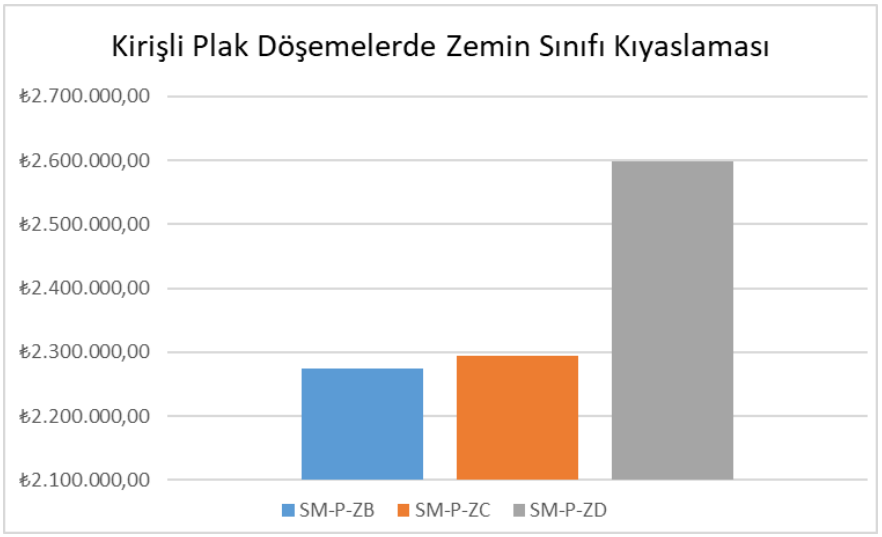

Şekil 12. Kirişli plak döşemelerde zemin sınıfı kıyaslaması

Şekil 11 incelendiğinde SM-A-ZB ile SM-A-ZC modelleri arasında %0,68, SM-A-ZB ile SM-A-ZD modelleri arasında %0,34 ve SM-A-ZC ile SM-A-ZD modelleri arasında %1,02 fark oluşmuştur.

Şekil 12 incelendiğinde SM-P-ZB ile SM-P-ZC modelleri arasında %0,85, SM-P-ZB ile SM-P-ZD modelleri arasında %14,26 ve SM-P-ZC ile SM-P-ZD modelleri arasında %13,29 fark oluşmuştur.

Şekil 13'te ZB zemin sınıfına sahip modellerin asmolen-plak döşemelerin maliyet kıyaslamaları verilmiştir. Şekil 14'te ZC zemin sınıfına sahip modellerin asmolen-plak döşemelerin maliyet kıyaslamaları verilmiştir. Şekil 15'te ZD zemin sınıfına sahip modellerin asmolen-plak döşemelerin maliyet kıyaslamaları verilmiştir.

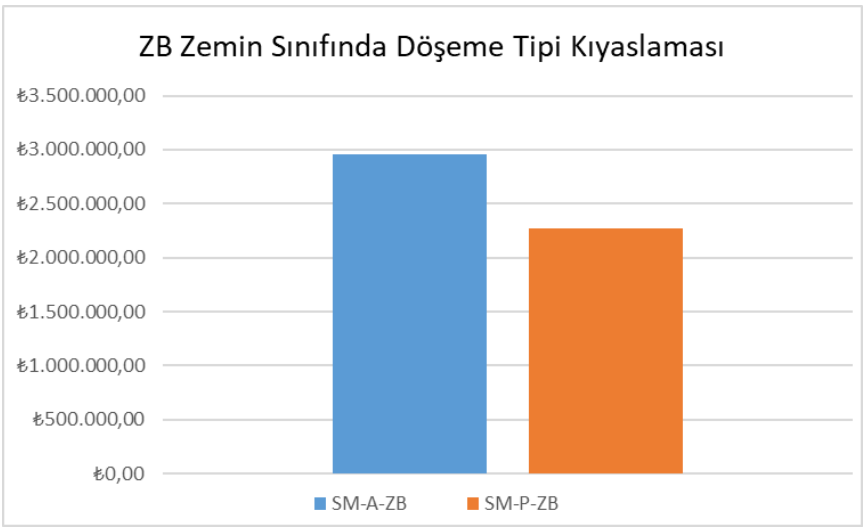

Şekil 13. ZB zemin sınıfında döşeme tipi kıyaslaması

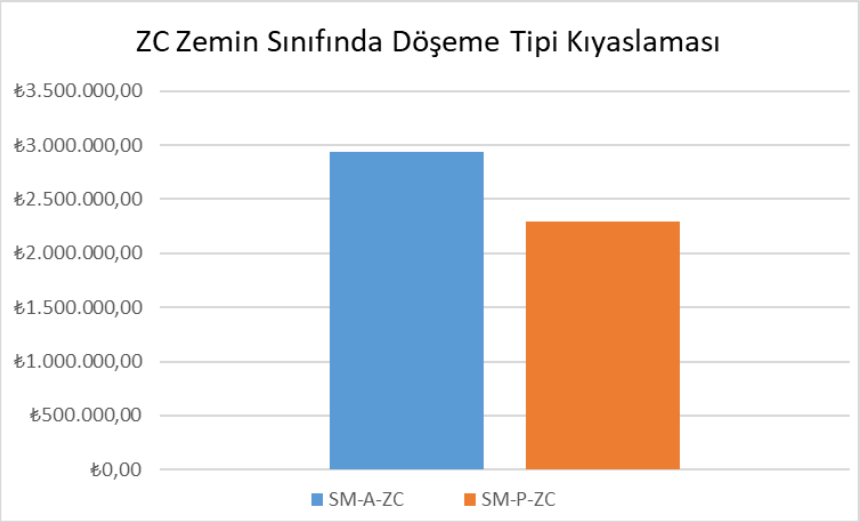

Şekil 14. ZC zemin sınıfında döşeme tipi kıyaslaması

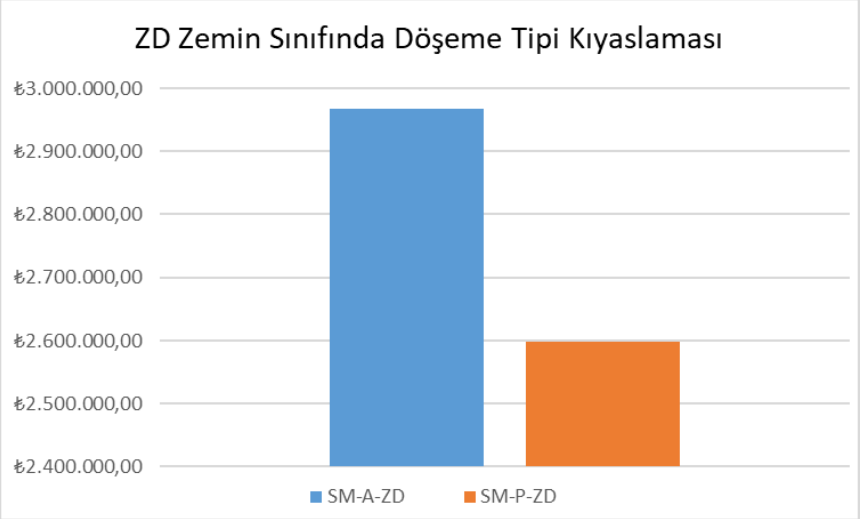

Şekil 15. ZD zemin sınıfında döşeme tipi kıyaslaması

Şekil 13 incelendiğinde SM-A-ZB ile SM-P-ZB modelleri arasında %30,05 maliyet farkı oluşmuştur. Şekil 14 incelendiğinde SM-A-ZC ile SM-P-ZC modelleri arasında %28,07 maliyet farkı oluşmuştur. Şekil 15 incelendiğinde SM-A-ZD ile SM-P-ZD modelleri arasında %14,21 maliyet farkı oluşmuştur.

SONUÇ

Bu çalışmada farklı zemin sınıfları altında (ZB, ZC ve ZD) asmolen ve plak döşemelerin kaba inşaat maliyetleri kıyaslanmıştır. Elde edilen sonuçlara göre;

Asmolen ve plak döşemelerde ZB zemin sınıfında %30,05, ZC zemin sınıfında %28,07, ZD zemin sınıfında %14,21 fark oluşmuştur. Asmolen döşemelerde kirişli plak sistemlere göre daha fazla beton ve kalıp yüzeyi gerektirmektedir. Ayrıca daha fazla donatı da gerekebilmektedir. Bu sebeple daha yüksek maliyet oluşmuştur. Zemin sınıfı kötüleştikçe bu farkın azalma sebebinin ise asmolen döşemedeki güncel yönetmeliğin (TBDY2018) perde talebi olması ve bu talebin ZD zemin sınıfında kirişli plak döşemede de oluşmasıdır.

Asmolen döşemelerde farklı zemin sınıflarında maksimum %1 seviyelerinde maliyet farkı oluşmakla birlikte kirişli plak döşemelerde bu fark ZB-ZD ve ZC-ZD zemin sınıflarında sırasıyla %14,26 ve %13,29 ZB-ZC zemin sınıfları arasında %0,86 fark oluşmuştur. Bu durum yine kirişli plak döşemelerde ZD zemin sınıfındaki perde talebinin oluşturacağı yüksek maliyet ile açıklanabilir.

Son olarak kirişli plak döşemede en yüksek maliyet ZD, en düşük maliyet ZB zemin sınıfında oluşmasına rağmen asmolen döşemede en yüksek maliyet ZD, en düşük maliyet ZC zemin sınıfında oluşmuştur. Asmolen döşeme sistemi kütle açısından daha ağır olduğu için, zeminin rijitliği arttıkça yapıya gelen deprem kuvvetleri de artar. Ancak kirişli plak döşeme, asmolen döşemeye kıyasla daha hafif bir sistemdir.

Bu nedenle, rijit zemin üzerinde kütle artışı kaynaklı deprem kuvvetleri daha az artar ve yapısal elemanlar daha verimli çalışır. Ayrıca asmolen döşemeler daha ağır ve rijit sistemlerdir. Bu da yapıya büyük kesme kuvvetleri bindirerek taşıyıcı elemanlara yük bindirir. Kirişli plak döşemelerde periyot daha uzundur, dolayısıyla etki daha düşük olur. Bu farkın bu sebeple de olabileceği düşünülmektedir.

Sonraki çalışmalarda, kat sayısı ile değişen periyot ve deprem kuvvetlerinin etkisinin de incelenmesi için farklı kat yüksekliklerine sahip modeller incelenecektir.

KAYNAKLAR

Altun, Y. (2022). Farklı zemin koşullarında TBDY 2018'e göre zemin-yapı etkileşiminde yöntem II ve III'ün karşılaştırılması= Comparison of method II and III in soil-structure interaction according to TBDY 2018 in different soil conditions (Yüksek Lisans Tezi, Sakarya Üniversitesi).

Bikçe, M., & Akyol, B. (2017). Tasarlanmış gerçek yapılarda asmolen/plak döşeme dönüşümünün yapı maliyetine etkisi. Fırat Üniversitesi Mühendislik Bilimleri Dergisi, 29(1), 133-144.

Hanif, M. U., Seo, S. Y., & Fawad, M. (2024, February). Numerical study on the design performance of wedge-type precast horizontal wall-slab joint for vertical load transfer. In Structures (Vol. 60, p. 105799). Elsevier.

İnşaat birim fiyatlarina esas işçilik-araç ve gereç rayiç listeleri. T.C. Çevre, Şehircilik ve İklim Değişikliği Bakanlığı, 2025. Ankara.

Kara, İ. F., & Akkaş, Y. E. (2023). TBDY 2018'e göre farklı döşeme tiplerinin yüksek bina sınıfındaki yapıda doğrusal olmayan davranışa olan etkilerinin incelenmesi. Niğde Ömer Halisdemir Üniversitesi Mühendislik Bilimleri Dergisi, 12(1), 1-1.

Khalaf, M., KARAŞİN, A., & Karasin, İ. B. (2022). Farklı Taşıyıcı Sistemlerin Kaba İnşaat Maliyetine Etkisi. Avrupa Bilim ve Teknoloji Dergisi, (39), 21-25.

Özpınar, Ö. (2006). Doğrusal olmayan taşıyıcı sistemlerde rijit diyafram kabulünün araştırılması (Yüksek Lisans Tezi, Pamukkale Üniversitesi Fen Bilimleri Enstitüsü).

SAĞLIYAN, S., SAYIN, E., & Burak, Y. Ö. N. (2012). Sürekli Tablalı Kirişsiz Döşemeli Betonarme Binalarda Perde Oranının Göreli Kat Ötelemelerine Etkisi. Pamukkale Üniversitesi Mühendislik Bilimleri Dergisi, 18(3), 209-220.

TBDY, "Türkiye Bina Deprem Yönetmeliği" T.C. Bayındırlık ve İskan Bakanlığlığı, 2018. Anara.

Türkmen, M., & Tekeli, H. (2005). Deprem Bölgesi ve Yerel Zemin Sınıflarının Bina Maliyetine Etkiler. Süleyman Demirel Üniversitesi Fen Bilimleri Enstitüsü Dergisi, 9(3).

UĞUR, L. O. (2009). Yapi Maliyetinin Fonksiyonel Eleman Yöntemi ile Tahmini. Engineering Sciences, 4(4), 449-458.

Uzun, D. (2014). 33 Katlı Betonarme Yüksek Bir Binanın Deprem Davranışına Farklı Döşeme Sistemlerinin Etkisi (Doctoral dissertation, Fen Bilimleri Enstitüsü) Yüksek Lisans Tezi.

Zontul, K. (2019). Yapım maliyetlerinin hesaplanmasında yapı bilgi modelleme (ybm) sisteminin örnek uygulama üzerinden irdelenmesi. Erciyes Üniversitesi, Fen Bilimler Enstitüsü, Kayseri, 539811.

➢ *ORAL PRESENTATION*

DBYBHY-2007 ve TBDY-2018 yönetmeliklerine göre konut tipi betonarme binaların performansı ve kaba inşaat maliyeti açısından değerlendirilmesi

Mustafa Üreyen[1] (*https://orcid.org/0009-0002-2579-8410*), Hakan Dilmaç[1] (*ORCID: https://orcid.org/0000-0003-0346-8875*), Kılıç Yasin Arslan[1*] (*https://orcid.org/0000-0002-4433-9204*)

[*1]Süleyman Demirel Üniversitesi, Mühendislik ve Doğa Bilimleri Fakültesi, İnşaat Mühendisliği, Isparta, Türkiye.

*Sorumlu yazar e-posta: kyarslan92@gmail.com

Özet
Ülkemiz topraklarının çok büyük bir bölümü deprem tehlikesi ile karşı karşıyadır ve yakın geçmişte yaşanan, büyük ölçüde can ve mal kaybına neden olan depremler bunu çok açık bir şekilde göstermiştir. Bu gibi depremlerde ortaya çıkan kayıpların, ülkemizde, gelişmiş ülkelere göre çok daha büyük boyutlarda olması, üzerinde düşünülmesi gereken önemli bir konudur. Bu çalışmada, konut tipi betonarme binaların 2007 Deprem Bölgelerinde Yapılacak Binalar Hakkında Yönetmelik (DBYBHY-2007) ile 2018 Türkiye Bina Deprem Yönetmeliği (TBDY-2018) kapsamında performans ve kaba yapı maliyeti açısından karşılaştırmalı değerlendirilmesi amaçlanmıştır. Deprem yönetmeliklerindeki güncellemeler, yapı tasarımı ve maliyet üzerinde doğrudan etkili olmakta; mühendislik uygulamalarında önemli değişiklikler doğurmaktadır. Bu kapsamda 4 ve 8 katlı iki bina, her iki yönetmelik esas alınarak TBDY-2018' e göre ZA ve ZE, DBYBHY-2007'ye göre Z1 ve Z4 zemin sınıfları ile modellenmiş ve performans analizleri gerçekleştirilmiştir. Analizlerde deprem etkileri altındaki yapısal davranış değerlendirilmiş; taşıyıcı sistemin ihtiyaç duyduğu minimum beton ve donatı miktarları tespit edilmiştir. Elde edilen veriler doğrultusunda kaba yapı maliyetleri hesaplanmış ve her iki yönetmeliğin maliyetleri kıyaslanmıştır.
Anahtar Kelimeler: DBYBHY-2007, TBDY-2018, Betonarme Binalar, Yapı Maliyeti, Sta4CAD

Evaluation of residential reinforced concrete buildings in terms of performance and structural construction cost according to DBYBHY-2007 and TBDY-2018 codes

Abstract
A large portion of the land in our country is under significant earthquake risk, and recent devastating earthquakes that have caused substantial loss of life and property clearly demonstrate this reality. The fact that the damage and losses resulting from such earthquakes are significantly greater in our country compared to developed nations is an important issue that warrants serious consideration. This study aims to perform a comparative evaluation of residential reinforced concrete buildings in terms of structural performance and rough construction cost, based on the 2007 Earthquake Code for Buildings in Seismic Zones (DBYBHY-2007) and the 2018 Turkish Building Earthquake Code (TBDY-2018). Updates in seismic design codes directly affect both structural design and cost, leading to substantial changes in engineering practice. In this context, two buildings (one with 4 stories and the other with 8 stories) were modeled according to both codes. For TBDY-2018, soil classes ZA and ZE were used; for DBYBHY-2007, Z1 and Z4 soil classes were applied. Performance analyses were conducted, and structural behavior under seismic loads was assessed. The minimum required amount of concrete and reinforcement for the load-bearing system was determined for each case. Based on the obtained data, rough construction costs were calculated, and the results were compared to evaluate the economic impact of each code.
Keywords: DBYBHY-2007, TBDY-2018, Reinforced Concrete Buildings, Construction Cost, Sta4CAD

GİRİŞ

Türkiye, dünyanın en aktif deprem kuşaklarından biri üzerinde yer almakta olup, tarihsel süreç boyunca yaşanan yıkıcı depremler ciddi can ve mal kayıplarına neden olmuştur. Özellikle son yıllarda meydana gelen büyük depremler, yapı güvenliği ve deprem yönetmeliklerinin önemi konusunda kamuoyunda farkındalık oluşturmuştur. Deprem kaynaklı kayıpların gelişmiş ülkelere kıyasla çok daha yüksek olmasının nedenleri arasında yetersiz zemin etütleri, mühendislik uygulamalarındaki eksiklikler, denetim

yetersizlikleri ve yürürlükteki yapı yönetmeliklerinin güncel sismik riskleri yeterince yansıtamaması gibi unsurlar yer almaktadır (Bikçe ve Akyol, 2017; Kara ve Akkaş, 2023).

Bu bağlamda, ülkemizde deprem yönetmelikleri zaman içerisinde güncellenmiş; 1975, 1997, 2007 ve son olarak 2018 yıllarında yürürlüğe giren düzenlemelerle yapı tasarımı ve taşıyıcı sistemlerin performansı açısından önemli değişiklikler yapılmıştır. Bir diğer çalışmada (Şapçı, 1998), 1975 ve 1997 yönetmelikleri esas alınarak perde-çerçeve sistemli binalarda yapılan karşılaştırmalarda, birleşim kesme kuvveti sınırlarının ve güçlü kolon-zayıf kiriş koşullarının yapısal davranışa etkisi ortaya konmuştur. Aynı çalışmada, yönetmelik değişikliklerinin özellikle düşey taşıyıcı eleman metrajlarında artışa neden olduğu ve yaklaşık %20 oranında bir maliyet farkı oluşturduğu belirlenmiştir.

Benzer şekilde, (Tekeli, 2006) tarafından dört, altı ve sekiz katlı betonarme binalar üzerinde gerçekleştirilen analizlerde, farklı deprem bölgeleri ve zemin sınıfları için yapılan statik hesaplar sonucunda, bir yapının depreme dayanıklı şekilde inşa edilmesinin maliyet üzerinde %4–8 arasında bir artışa yol açtığı saptanmıştır. (Tunç ve Tanfener, 2016) tarafından yürütülen çalışmada ise 2007 ve 2018 deprem yönetmeliklerinin karşılaştırmalı analizi yapılmış; 2018 yönetmeliğinin tasarım iç kuvvetlerinde yaklaşık %20 oranında artışa neden olduğu sonucuna ulaşılmıştır. Kırklareli ili özelinde yürüttükleri araştırmada, 2007 ve 2018 yönetmelikleri kapsamında elde edilen elastik tasarım spektrumlarını karşılaştırarak, 2018 TBDY'nin deprem tehlikesini daha gerçekçi biçimde yansıttığını ortaya koymuşlardır (Keskin ve Bozdoğan, 2018).

Bu literatür çerçevesinde yürütülen bu çalışmanın amacı, konut tipi betonarme binaların 2007 Deprem Bölgelerinde Yapılacak Binalar Hakkında Yönetmelik (DBYBHY-2007) ile Türkiye Bina Deprem Yönetmeliği (TBDY-2018) kapsamında yapısal performans ve kaba yapı maliyeti açısından karşılaştırmalı değerlendirilmesidir. Bu amaç doğrultusunda, 4 ve 8 katlı iki farklı betonarme yapı modeli, her iki yönetmelik doğrultusunda belirlenen deprem yükleri ve zemin sınıfları (ZA–ZE, Z1–Z4) dikkate alınarak analiz edilmiştir. Analiz sonuçları doğrultusunda yapısal elemanlara ait beton ve donatı miktarları belirlenmiş; elde edilen veriler ışığında kaba yapı maliyetleri hesaplanarak yönetmeliklerin maliyet üzerindeki etkileri karşılaştırmalı olarak değerlendirilmiştir.

MATERYAL VE METOD

Konut tipi betonarme binaların 2007 Deprem Bölgelerinde Yapılacak Binalar Hakkında Yönetmelik (DBYBHY-2007) ile 2018 Türkiye Bina Deprem Yönetmeliği (TBDY-2018) kapsamında iyi kötü zemin sınıfları olan Z1, Z4, ZA, ZE zemin sınıflarındaki 4 ve 8 katlı binaların maliyet kıyaslamasının incelendiği bu çalışmada sayısal modeller Sta4CAD statik analiz programı kullanılarak yapılmış olup oluşturulan sayısal model isimlendirilmeleri Şekil 1'de gösterildiği şekilde oluşturulmuştur.



Şekil 1. Model isimlendirmesi

Toplamda sekiz farklı model oluşturularak bu modeller için maliyet analizleri yapılmıştır. Model numaraları ve özellikleri Tablo 1'de gösterilmiştir.

Tablo 1. Model İsimlendirmeleri

Model No	Yönetmelik	Zemin Sınıfı	Kat Sayısı
2007-Z1-4	DBYBHY-2007	Z1	4
2007-Z1-8	DBYBHY-2007	Z1	8
2007-Z4-4	DBYBHY-2007	Z4	4
2007-Z4-8	DBYBHY-2007	Z4	8
2018-ZA-4	TBDY-2018	ZA	4
2018-ZA-8	TBDY-2018	ZA	8
2018-ZE-4	TBDY-2018	ZE	4
2018-ZE-8	TBDY-2018	ZE	8

4 kata sahip olan sayısal modellerin genel görünümü Şekil 2'de verilmiştir. 8 katlı sayısal modellerin genel görünümü ise Şekil 3'te verilmiştir. Yapı bodrum, zemin, iki normal kat olmak üzere dört kat ve kuleden oluşmaktadır.

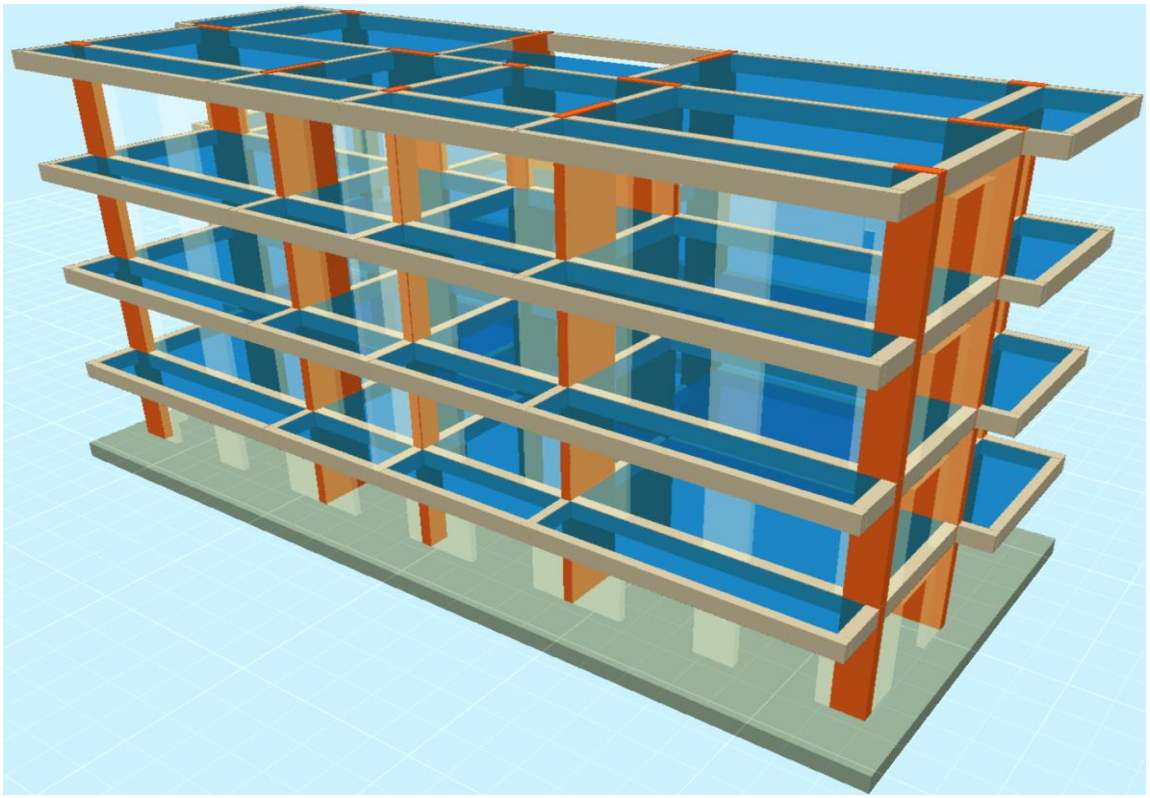

Şekil 2. 4 katlı binaya ait genel görünüm

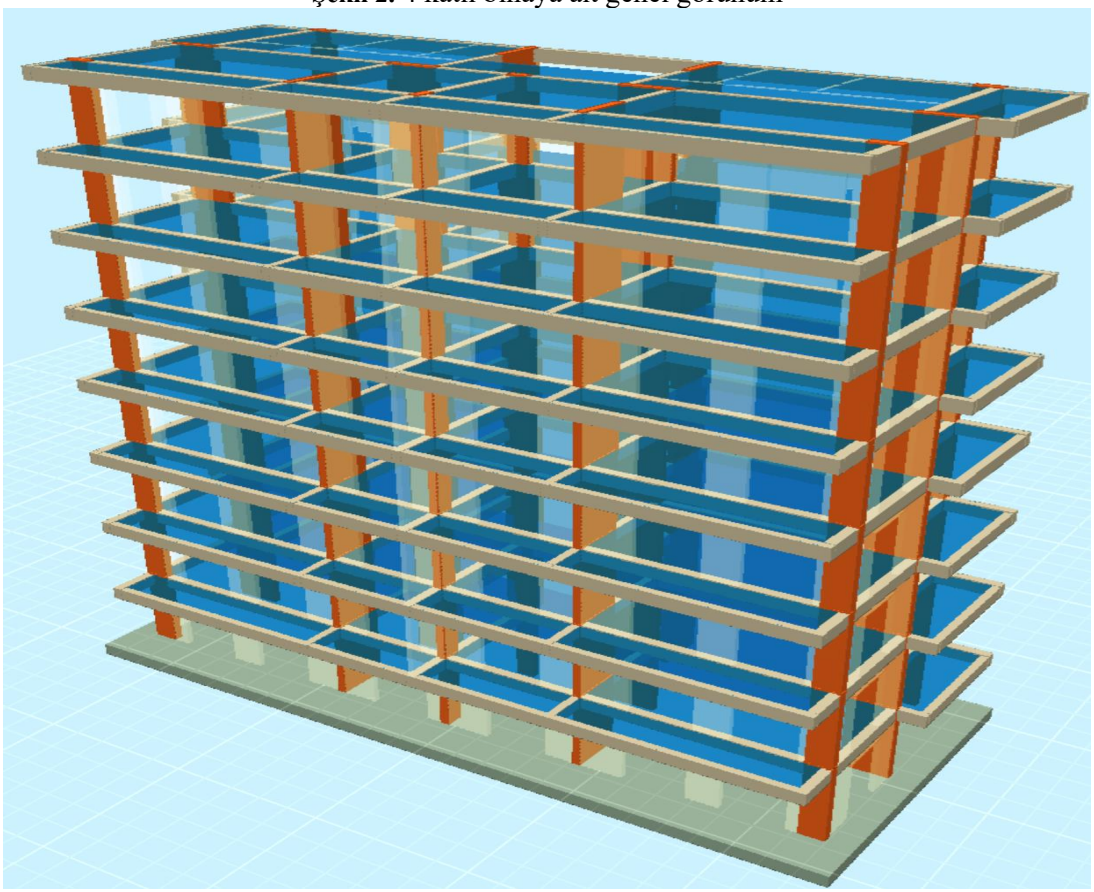

Şekil 3. 8 katlı binaya ait genel görünüm

Tüm sayısal modeller minimum yönetmelik şartlarını sağlayacak şekilde oluşturulmuş olup metraj listesi Şekil 4-11'da verilmiştir. Birim fiyatlar eski pozlara ait olup buradaki değerler değil T.C. Çevre Şehircilik ve İklim Değişikliği Bakanlığı tarafından hazırlanan rayiç fiyat listesinde yer alan rayiç değerler kullanılmıştır.

Poz	Birim fiyat tarifi	Birim fiyat	Miktar	Tutar
15.150.1005	C25/30 HAZIR BETON	1.566.00	251.1 m³	393.284.46
15.180.1003	DÜZ YÜZEYLİ BETONARME KALIBI	254.33	1872.0 m²	476.116.70
15.160.1003	8-12 mm BETONARME DEMİRİ	19.696.53	13.9 tn	274.312.76
15.160.1004	14-50 mm NERVÜRLÜ BETONARME DEMİRİ	19.448.18	11.3 tn	220.289.05

Şekil 4. 2007-Z1-4 metraj listesi

Poz	Birim fiyat tarifi	Birim fiyat	Miktar	Tutar
15.150.1005	C25/30 HAZIR BETON	1.566.00	252.1 m³	394.794.08
15.180.1003	DÜZ YÜZEYLİ BETONARME KALIBI	254.33	1874.1 m²	476.650.79
15.160.1003	8-12 mm BETONARME DEMİRİ	19.696.53	14.0 tn	276.305.66
15.160.1004	14-50 mm NERVÜRLÜ BETONARME DEMİRİ	19.448.18	12.4 tn	242.090.54

Şekil 5. 2007-Z4-4 metraj listesi

Poz	Birim fiyat tarifi	Birim fiyat	Miktar	Tutar
15.150.1005	C25/30 HAZIR BETON	1.566.00	498.6 m³	780.780.97
15.180.1003	DÜZ YÜZEYLİ BETONARME KALIBI	254.33	3709.8 m²	943.525.13
15.160.1003	8-12 mm BETONARME DEMİRİ	19.696.53	28.7 tn	564.856.50
15.160.1004	14-50 mm NERVÜRLÜ BETONARME DEMİRİ	19.448.18	22.9 tn	445.182.13

Şekil 6. 2007-Z1-8 metraj listesi

Poz	Birim fiyat tarifi	Birim fiyat	Miktar	Tutar
15.150.1006	C30/37 HAZIR BETON	1.616.00	631.0 m³	1.019.714.23
15.180.1003	DÜZ YÜZEYLİ BETONARME KALIBI	254.33	4205.9 m²	1.069.696.20
15.160.1003	8-12 mm BETONARME DEMİRİ	19.696.53	36.3 tn	714.200.42
15.160.1004	14-50 mm NERVÜRLÜ BETONARME DEMİRİ	19.448.18	41.6 tn	809.829.89

Şekil 7. 2007-Z1-8 metraj listesi

Poz	Birim fiyat tarifi	Birim fiyat	Miktar	Tutar
15.150.1005	C25/30 HAZIR BETON	1.566.00	249.1 m³	390.164.98
15.180.1003	DÜZ YÜZEYLİ BETONARME KALIBI	254.33	1852.4 m²	471.121.66
15.160.1003	8-12 mm BETONARME DEMİRİ	19.696.53	14.6 tn	287.374.45
15.160.1004	14-50 mm NERVÜRLÜ BETONARME DEMİRİ	19.448.18	9.4 tn	183.674.06

Şekil 8. 2018-ZA-4 metraj listesi

Poz	Birim fiyat tarifi	Birim fiyat	Miktar	Tutar
15.150.1005	C25/30 HAZIR BETON	1.566.00	249.1 m³	390.164.98
15.180.1003	DÜZ YÜZEYLİ BETONARME KALIBI	254.33	1852.4 m²	471.121.66
15.160.1003	8-12 mm BETONARME DEMİRİ	19.696.53	14.6 tn	287.374.45
15.160.1004	14-50 mm NERVÜRLÜ BETONARME DEMİRİ	19.448.18	9.5 tn	185.706.80

Şekil 9. 2018-ZE-4 metraj listesi

Poz	Birim fiyat tarifi	Birim fiyat	Miktar	Tutar
15.150.1005	C25/30 HAZIR BETON	1.566.00	500.2 m³	783.349.21
15.180.1003	DÜZ YÜZEYLİ BETONARME KALIBI	254.33	3688.4 m²	938.072.29
15.160.1003	8-12 mm BETONARME DEMİRİ	19.696.53	29.8 tn	587.830.91
15.160.1004	14-50 mm NERVÜRLÜ BETONARME DEMİRİ	19.448.18	20.2 tn	392.072.16

Şekil 10. 2018-ZA-8 metraj listesi

Poz	Birim fiyat tarifi	Birim fiyat	Miktar	Tutar
15.150.1005	C25/30 HAZIR BETON	1.566.00	502.1 m³	786.268.23
15.180.1003	DÜZ YÜZEYLİ BETONARME KALIBI	254.33	3692.6 m²	939.130.30
15.160.1003	8-12 mm BETONARME DEMİRİ	19.696.53	30.1 tn	592.059.01
15.160.1004	14-50 mm NERVÜRLÜ BETONARME DEMİRİ	19.448.18	20.5 tn	398.622.05

Şekil 11. 2018-ZE-8 metraj listesi

T.C. Çevre Şehircilik ve İklim Değişikliği Bakanlığı tarafından hazırlanan rayiç fiyat listesinde yer alan pozlardan kaba inşaat maliyet hesabı için kullanılan pozlar Tablo 2'de sunulmuştur.

Tablo 2. Kaba inşaat için ÇŞİDB birim fiyat rayiç listesi

Poz No	Tanımı	Ölçü Birimi	Rayiç Fiyat (₺)
15.150.1005	Beton santralinde üretilen veya satın alınan ve beton pompasıyla basılan, C25/30 basınç dayanım sınıfında, gri renkte, normal hazır beton dökülmesi (beton nakli dahil)	m^3	3.151,28
15.180.1003	Plywood ile düz yüzeyli betonarme kalıbı yapılması	m^2	824,39
15.160.1003	Ø 8- Ø 12 mm nervürlü beton çelik çubuğu, çubukların kesilmesi, bükülmesi ve yerine konulması	Ton	39.429,35
15.160.1004	Ø 14- Ø 28 mm nervürlü beton çelik çubuğu, çubukların kesilmesi, bükülmesi ve yerine konulması	Ton	38.016,85

BULGULAR ve TARTIŞMA

Konut tipi betonarme binaların 2007 Deprem Bölgelerinde Yapılacak Binalar Hakkında Yönetmelik (DBYBHY-2007) ile 2018 Türkiye Bina Deprem Yönetmeliği (TBDY-2018) kapsamında iyi kötü zemin sınıfları olan Z1, Z4, ZA, ZE zemin sınıflarındaki 4 ve 8 katlı binaların kaba inşaat maliyetleri karşılaştırmalı olarak incelenmiştir. Şekil 12'de tüm sayısal modellerin maliyet kıyaslanması sunulmuştur.

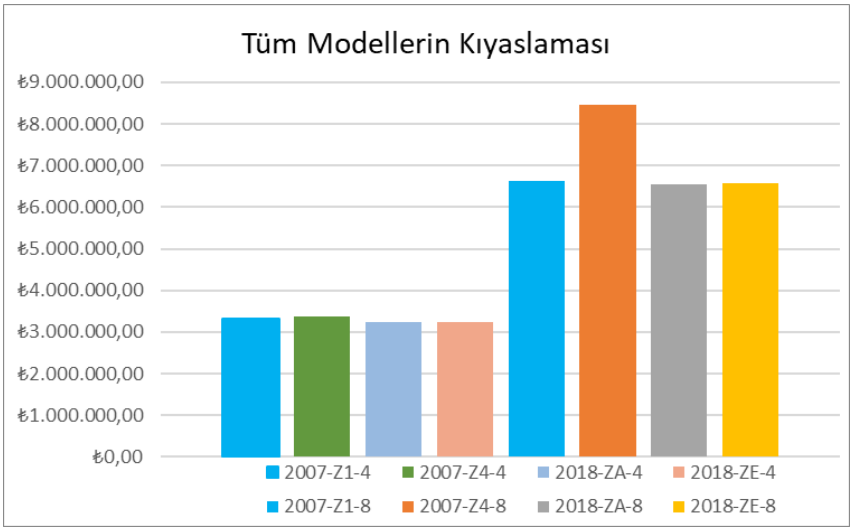

Şekil 12. Tüm sayısal modellerin kıyaslanması

2007-Z1-4 modelinde kaba inşaat maliyeti 3.312.202,86₺, 2007-Z4-4 modelinde kaba inşaat maliyeti 3.362.846,83₺, 2007-Z1-8 modelinde kaba inşaat maliyeti 6.631.758,44₺, 2007-Z4-8 modelinde kaba inşaat maliyeti 8.468.545,95₺, 2018-ZA-4 modelinde kaba inşaat maliyeti 3.245.110,78₺, 2018-ZE-4 modelinde kaba inşaat maliyeti 3.248.912,47₺, 2018-ZA-8 modelinde kaba inşaat maliyeti 6.559.885,33₺, 2018-ZE-8 modelinde kaba inşaat maliyeti 6.586.266,50₺ olarak hesaplanmıştır.

Şekil 13'te 4 katlı modellerin DBYBHY-2007 ve TBDY-2018 yönetmeliklerinde tanımlanan en iyi ve en kötü zemin sınıflarındaki maliyet kıyaslamaları verilmiştir. Şekil 14'te 8 katlı modellerin DBYBHY-2007 ve TBDY-2018 yönetmeliklerinde tanımlanan en iyi ve en kötü zemin sınıflarındaki maliyet kıyaslamaları verilmiştir.

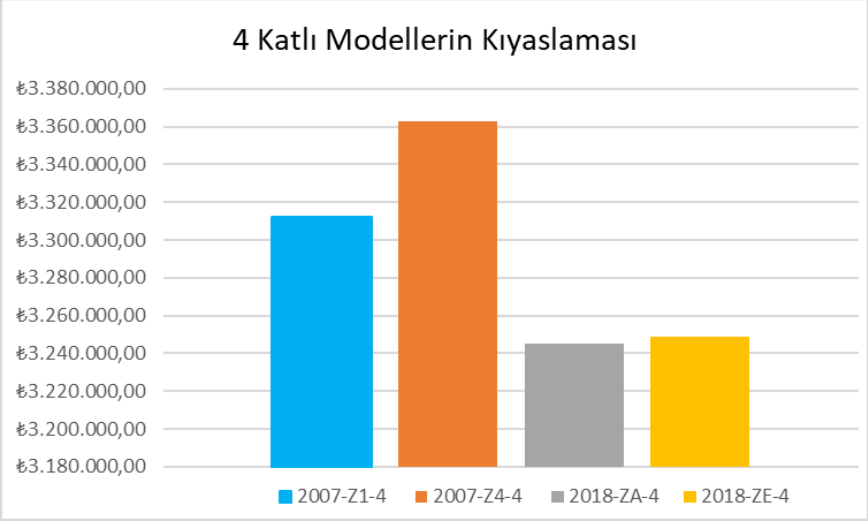

Şekil 13. 4 katlı modellerin kıyaslaması

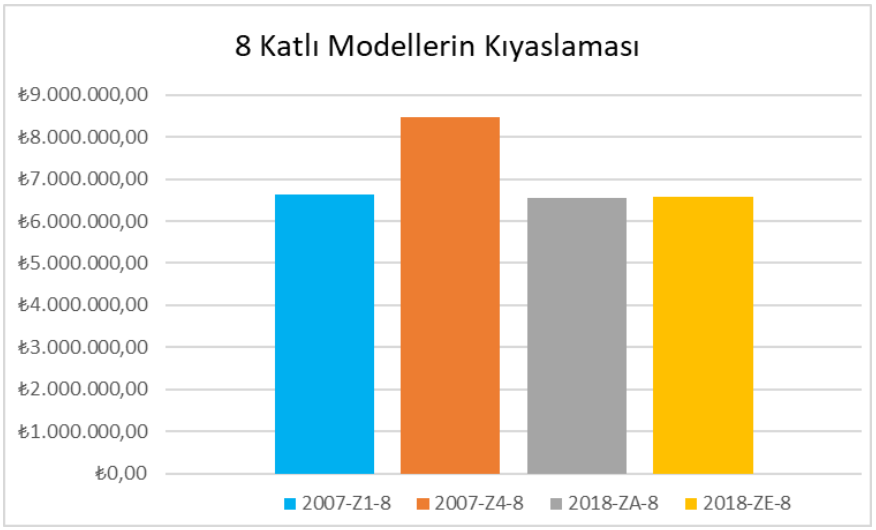

Şekil 14. 8 katlı modellerin kıyaslaması

Şekil 13 incelendiğinde 2007-Z1-4 ile 2018-Z4-4 modelleri arasında %1,53, 2007-Z1-4 ile 2018-ZA-4 modelleri arasında %2,07, 2007-Z1-4 ile 2018-ZE-4 modelleri arasında %1,95, 2007-Z4-4 ile 2018-ZA-4 modelleri arasında %3,63, 2007-Z4-4 ile 2018-ZE-4 modelleri arasında %3,51 ve 2018-ZA-4 ile 2018-ZE-4 modelleri arasında %0,12 modelleri arasında fark oluşmuştur.

Şekil 14 incelendiğinde 2007-Z1-8 ile 2018-Z4-8 modelleri arasında %27,70, 2007-Z1-8 ile 2018-ZA-8 modelleri arasında %1,10, 2007-Z1-8 ile 2018-ZE-8 modelleri arasında %0,69, 2007-Z4-8 ile 2018-ZA-8 modelleri arasında %29,10, 2007-Z4-8 ile 2018-ZE-8 modelleri arasında %28,58 ve 2018-ZA-8 ile 2018-ZE-8 modelleri arasında %0,40 modelleri arasında fark oluşmuştur.

Şekil 15'te DBYBHY-2007 yönetmeliğine ve Z1 zemin sınıfına göre çözülmüş 4-8 kat kaba maliyet kıyaslaması verilmiştir. Şekil 16'da DBYBHY-2007 yönetmeliğine ve Z4 zemin sınıfına göre çözülmüş 4-8 kat kaba maliyet kıyaslaması verilmiştir. Şekil 17'de TBDY-2018 yönetmeliğine ve ZA zemin sınıfına göre çözülmüş 4-8 kat kaba maliyet kıyaslaması verilmiştir. Şekil 18'de TBDY-2018 yönetmeliğine ve ZE zemin sınıfına göre çözülmüş 4-8 kat kaba maliyet kıyaslaması verilmiştir.

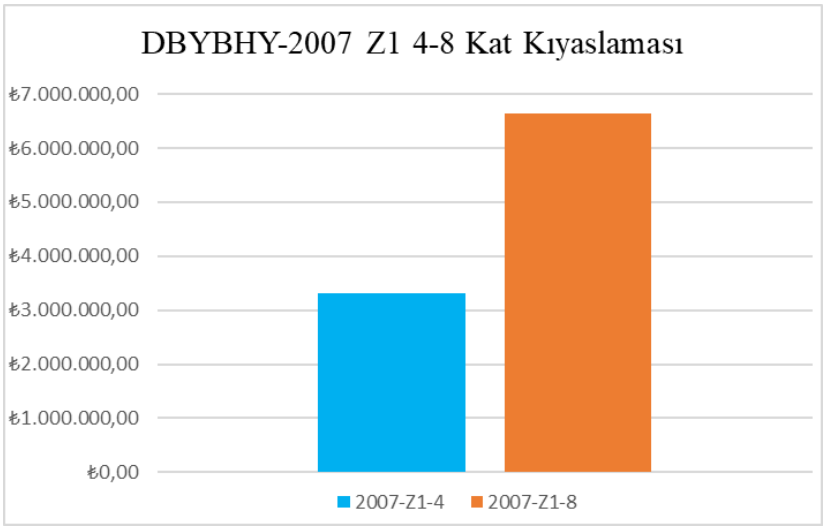

Şekil 15. DBYBHY-2007 Z1 4-8 kat kıyaslaması

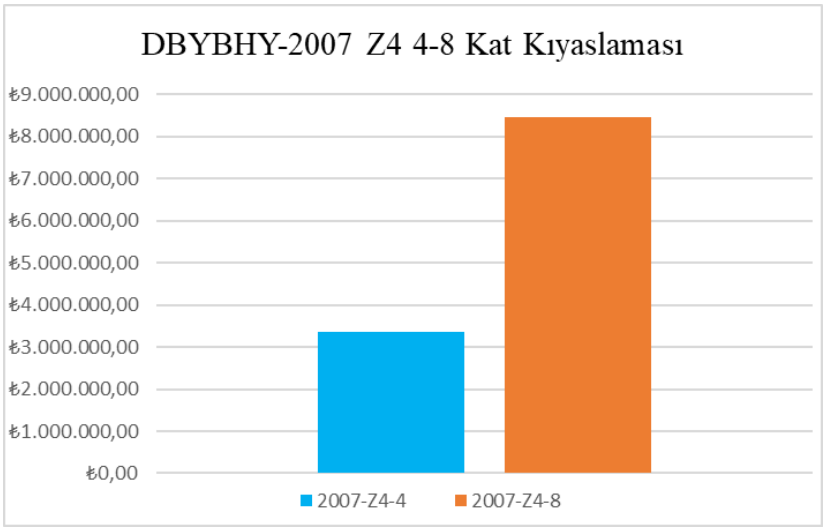

Şekil 16. DBYBHY-2007 Z4 4-8 kat kıyaslaması

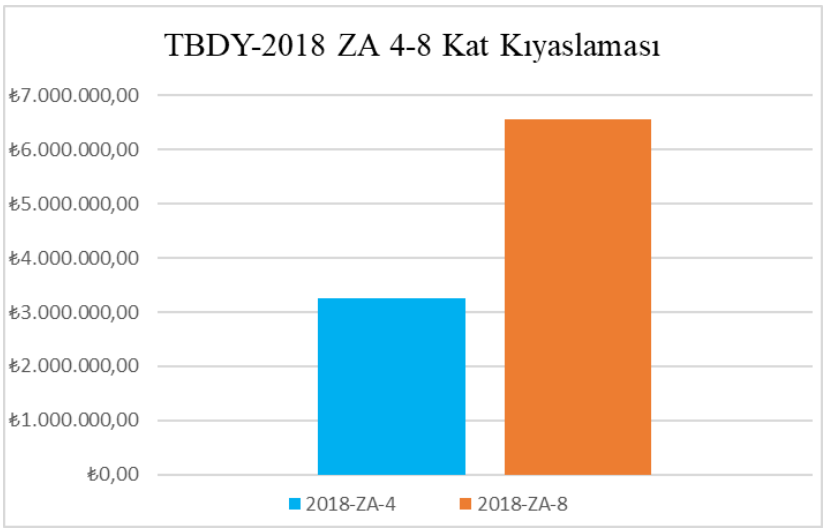

Şekil 17. TBDY-2018 ZA 4-8 kat kıyaslaması

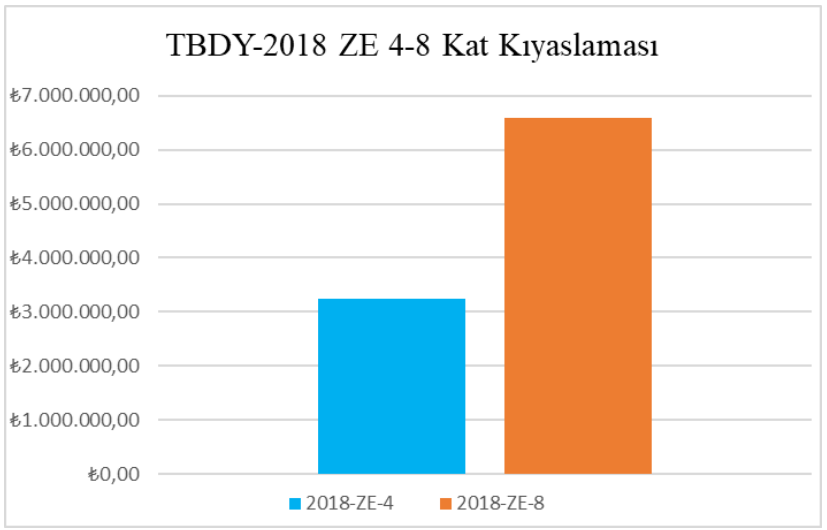

Şekil 18. TBDY-2018 ZE 4-8 kat kıyaslaması

Şekil 15 incelendiğinde 2007-Z1-4 ile 2007-Z1-8 modelleri arasında %100,22 maliyet farkı oluşmuştur. Şekil 16 incelendiğinde 2007-Z4-4 ile 2007-Z4-8 modelleri arasında %151,83 maliyet farkı oluşmuştur. Şekil 17 incelendiğinde 2018-ZA-4 ile 2018-ZA-8 modelleri arasında %102,15 maliyet farkı oluşmuştur. Şekil 18 incelendiğinde 2018-ZE-4 ile 2018-ZE-8 modelleri arasında %102,72 maliyet farkı oluşmuştur.

SONUÇ

Bu çalışmada, DBYBHY-2007 ile TBDY-2018 yönetmelikleri kapsamında iyi kötü zemin sınıfları olan Z1, Z4, ZA, ZE zemin sınıflarındaki 4 ve 8 katlı binaların kaba inşaat maliyetleri kıyaslanmıştır. Elde edilen sonuçlara göre;

Zemin sınıfı kötüleştikçe maliyetin artması beklenen bir eğilimdir ve bu eğilim özellikle 2007 yönetmeliği altında daha keskin şekilde gözlemlenmiştir.

2018 yönetmeliği, zemin büyütme etkilerini daha kontrollü dağıttığı için, zemin sınıfı değişimlerine bağlı maliyet artışları daha sınırlı kalmıştır.

Kat sayısı arttıkça, zemin etkilerinin yapısal sistem üzerinde daha fazla belirleyici olduğu ve bu durumun maliyete yansıdığı tespit edilmiştir.

Ayrıca, 2007 yönetmeliği ile tasarlanmış yapılarda, gereksiz emniyet katsayıları ve belirsizliklerin etkisiyle maliyetler daha yüksek çıkabilmektedir.

Sonraki çalışmalarda, model sayı ve diğer zemin sınıfları da dahil edilerek daha kapsamlı bir araştırma yapılacaktır.

KAYNAKLAR

Akkar, S., İhtimal Hesaplarına Dayalı Güncellenmiş Türkiye Sismik Tehlike Haritası ve Deprem Tasarımına Etkileri, Yeni Nesil Deprem Yönetmelikleri ve Deprem Mühendisliğinde Yeni Teknolojiler Kongresi, Ankara, 26-27 Şubat 2015.

Bikçe, M., & Akyol, B. (2017). Tasarlanmış gerçek yapılarda asmolen/plak döşeme dönüşümünün yapı maliyetine etkisi. Fırat Üniversitesi Mühendislik Bilimleri Dergisi, 29(1), 133-144.

Deprem Bölgelerinde Yapılacak Binalar Hakkında Yönetmelik, 2007

Kara, İ. F., & Akkaş, Y. E. (2023). TBDY 2018'e göre farklı döşeme tiplerinin yüksek bina sınıfındaki yapıda doğrusal olmayan davranışa olan etkilerinin incelenmesi. Niğde Ömer Halisdemir Üniversitesi Mühendislik Bilimleri Dergisi, 12(1), 1-1.

Karaesmen, E., Öncesiyle Sonrasıyla Deprem,Atılım Üniversitesi Yayınları, 2008.

Keskin&Bozdoğan/Kırklareli University Journal of Engineering and Science 4-1(2018) 74-90

Şapçı, M.H, 1975 ve 1997 Türkiye Deprem Yönetmelikleri'ne göre tasarlanmış betonarme binaların performansı ve maliyet değerlendirmesi, ODTÜ Fen Bilimleri Enstitüsü , Ankara, 1998

Tekeli, H, Deprem bölgesi ve yerel zemin sınıflarının bina maliyetine etkileri, Süleyman Demirel Üniversitesi Fen Bilimleri Enstitüsü, Isparta, 2006

Tunç, G., Tanfener, T., 2007 ve 2016 Türkiye Bina Deprem Yönetmeliklerinin Örneklerle Mukayesesi, 3.Ulusal Yapı Kongresi ve Sergisi Teknik Tasarım, Güvenlik ve Erişebilirlik, TMMOB Mimarlar Odası Ankara Şubesi, 2016.

Türkiye Bina Deprem Yönetmeliği, 2018

➢ *ORAL PRESENTATION*

Raspberry Pi Kullanarak Etkili ve Ekonomik Elektronik Ücret Toplama Sistem Tasarımı

Burhan ÜSTÜBİ[1*] (*ORCID: https://orcid.org/0009-0008-0459-8915*), Ebubekir KARTAL[1] (*ORCID: https://orcid.org/0009-0004-6037-1863*) Elif ALTINTAŞ[1] (*ORCID: https://orcid.org/0009-0002-7882-9479*) Habib DOĞAN[1] (*https://orcid.org/0000-0001-8685-9569*

[*1]Burdur Mehmet Akif Ersoy University, Gölhisar Applied Science School, Computer Technologies and Information Systems, Gölhisar/Burdur, Türkiye.

*Sorumlu yazar e-posta: burhanustubi@gmail.com

Özet

Bu çalışmada, küçük ölçekli toplu taşıma sistemleri için düşük maliyetli ve IoT (Nesnelerin İnterneti) tabanlı bir Elektronik Ücret Toplama Sistemi (EFCS) otomasyonu geliştirilmiş ve test edilmiştir. Sistem, NFC kart okuyucularını ve GPS modüllerini Raspberry Pi tabanlı bir donanım altyapısıyla entegre ederek kullanıcıların bakiye işlemlerini kolaylaştırırken, aynı zamanda otobüslerin gerçek zamanlı konum ve performans takibini de mümkün kılmaktadır. Geliştirilen yazılım altyapısı, Python dili kullanılarak oluşturulan özel algoritmalar ile kart doğrulama, bakiye kontrolü ve ödeme işlemlerini otomatikleştirmektedir. Önerilen sistem üç ana bileşenden oluşmaktadır. Otobüs cihaz arayüzü, kullanıcı arayüzü ve kurumsal yönetim arayüzü. Otobüs cihaz arayüzü, NFC okuyucular aracılığıyla kullanıcı kartlarını tanımlar ve ödeme işlemlerini gerçekleştirirken, GPS modülü araç konum verilerini toplar ve bunları merkezi bir veritabanına iletir. Kullanıcı arayüzü, bireylerin çevrimiçi bakiye sorgulama ve yükleme işlemleri yapmalarına olanak tanırken, kurumsal yönetim arayüzü otobüs cihazlarının, kullanıcı işlemlerinin ve finansal hareketlerin yönetimini sağlar. Sistem tasarımı maliyet etkinliği ön planda tutularak gerçekleştirilmiştir. Veritabanı altyapısı, kullanıcı ve operatör verilerini depolayacak şekilde yapılandırılmıştır. Ödeme işlemleri sırasında doğrulama anahtarları kullanılmaktadır. Ayrıca sistemin gerçek dünya performansı pratik testler aracılığıyla değerlendirildi. Bu çalışma, özellikle küçük ölçekli toplu taşıma şirketleri için maliyet etkin bir EFCS çözümü sunarak nakit işlemlerden dijital sistemlere geçişi kolaylaştırmayı amaçlamıştır. Sistem, gelecekte QR kod ödemesi veya mobil NFC entegrasyonu gibi özelliklerin kolayca eklenebileceği esnek bir altyapıya sahiptir. Bu yaklaşım, toplu taşıma süreçlerinin dijitalleştirilmesine ve yenilikçi IoT tabanlı çözümlerin yaygınlaştırılmasına önemli bir katkı sağlayacaktır.

Anahtar Kelimeler: IoT, Raspberry Pi, Elektronik Ücret Toplama Sistemi, NFC, Toplu Taşıma Otomasyonu

Effective and Economic Electronic Fee Collection System Design Using Raspberry Pi

Abstract

In this study, a low-cost and IoT (Internet of Things)-based Electronic Fare Collection System (EFCS) automation for small-scale public transportation systems has been developed and tested. The system integrates NFC card readers and GPS modules with a Raspberry Pi-based hardware infrastructure, facilitating users' balance transactions while also enabling real-time location and performance tracking of buses. The developed software infrastructure automates card verification, balance control, and payment transactions with special algorithms created using the Python language. The proposed system consists of three main components: bus device interface, user interface, and corporate management interface. The bus device interface identifies user cards via NFC readers and performs payment transactions, while the GPS module collects vehicle location data and transmits it to a central database. The user interface allows individuals to conduct online balance inquiries and loading transactions, while the corporate management interface provides management of bus devices, user transactions, and financial movements. The system design was carried out by prioritizing cost-effectiveness. The database infrastructure is structured to store user and operator data. Verification keys are used during payment transactions. In addition, the system's real-world performance was evaluated through practical tests. This study aimed to facilitate the transition from cash transactions to digital systems by offering a cost-effective EFCS solution, especially for small-

scale public transport companies. The system has a flexible infrastructure where features such as QR code payment or mobile NFC integration can be easily added in the future. This approach will make a significant contribution to the digitalization of public transport processes and the dissemination of innovative IoT-based solutions.

Keywords: IoT, Raspberry Pi, Electronic Fare Collection System, NFC, Public Transport Automation

GİRİŞ

Artan şehirleşme oranına bağlı olarak yoğunlaşan toplu taşıma işlemleri kent hayatının en önemli sorunlarının başında gelmeye devam etmektedir. 20. Yüzyılın ilk zamanlarından itibaren uygulamaya sokulmaya çalışılan akıllı ulaşım sistemleri sürekli olarak gelişmiş, otomasyon sistemleri ve zamanla insan kaynaklı hataları minimize etmeye yönelik teknolojik desteklerle günümüzde başladığı noktanın çok ilerisine evirilmiştir. Akıllı ulaşım sistemlerinde (AUS) ilk otomasyon sistemlerine 1960-70'li yıllarda Japonya ve Amerika'da kartlı geçişlerle başlanılmış, takip eden yıllarda bilgisayarlı sistemlerin desteği ile otomasyon oranları çok daha iyileştirilmiştir (Taç, 2018). Günümüzde ise neredeyse insan unsuru tamamen devre dışı bırakılarak tüm sistemin otomatik olarak işletilmesi söz konusu olmuştur.

Akıllı ulaşım sistemlerinin ilk uygulamaları 1960'ların sonlarında görülmeye başlanmış, ABD'de 1969'da başlatılan ERGS (Electronic Route Guidance System - Elektronik Güzergâh Kılavuzluk Sistemi), Japonya'da 1973'te başlatılan CACS (Comprehensive Automobile traffic Control System - Kapsamlı Araç trafiği Kontrol Sistemi) ve Almanya'da 1974'te başlatılan ARI (Autofahrer-Rundfunk-Informations system - Sürücü Radyo Yayını Bilgi Sistemi), ilk uygulamaların en dikkat çekici uygulamalarını oluşturmuşlardır (Tiryaki, 2015).

Akıllı ulaşım sistemlerinin yayılması, farklı çözüm arayışlarını da beraberinde getirmiştir. Yolcuların daha ekonomik ve kolay seyahat edebilmeleri AUS sistemlerinin amaçlarından bir tanesidir. Otomatik ücretlendirme sistemleri de yolcu ile sürücü arasındaki fiziksel işlemlerin ortadan kaldırılmasını sağlayarak süreci hızlandırmakta ve farklı alternatifler sunarak da daha ekonomik ulaşım imkânları sağlamaktadır. Geleneksel sistemlerde ilk zamanlarda kullanılan manuel ücret toplama sistemelerinin birçok dezavantajı bulunmaktadır. Bunlar; zaman alıcı olmaları, trafik sıkışıklığına, çevre kirliliğine ve kaçak geçişlere neden olmaları şeklinde ifade edilebilir (Kumawat ve Chandramore, 2014). Bu nedenle akıllı ulaşım sistemlerinde elektronik olarak ücret toplama sistemleri devreye sokulmaya başlanmıştır. AUS'un en önemli bileşenlerinden biri olan elektronik ücret toplama sadece ücret toplamamnın ötesine geçerek kent yaşamında elektronik bilgi toplama sürecine evrilmiştir (Geçer, 2016). Eelktronik ücret toplama sistemlerinin yaygınlaşması ile birçok önemli avantajın eldesi hedeflenmiş ve başarılmıştır. Personelin nakitle temasının azaltılarak suistimallerin önlenmesi, kayıp kaçak oranının düşürülmesiyle mali kayıpların önüne geçilmesi, sıra bekleme ve zaman kayıplarının minimize edilmesi, kullanıcı dostu uygulamaların devreye alınması, farklı seçeneklerin devreye alınmasıyla daha ekonomik ve adil bir ücretlendirme yapısının sağlanması elde edilen kazanımlara örnek olarak verilebilir.

Bu amaçla elektronik ücret toplama sistemlerine yönelik bir çok çalışma yapılmış ve farklı noktalarda test edilmişlerdir. Ülkemizde de ilk olarak karayollarında başlatılan elektronik ücret toplama sistemleri genelde RFID etiketlerin kullanılması şeklinde başlamıştır (Katanalp vd., 2018). Ayrıca yapılan farklı çalışmalarda benzer şekilde RFID teknolojisi kullanılmış (Kumawat ve Chandramore, 2014), bu teknolojinin yanında Bluetooth teknolojisi de eelktronik ücret toplama amaçlı olarak etst edilmiştir (Türk ve Arslan, 2017). Benzer şekilde gene başka çalışmada, elektronik ücretlendirme sistemlerinin farklı fonksiyonları için gömülü sistemlerin desteği kullanılmıştır (Arslan vd., 2016).

Nüfus yoğunluğunun çok fazla olduğu kentlerde kullanılan elektronik ücretlendirme sistemlerinin benzer yapılarıyla küçük işletmelerde kullanımının maliyet noktası göz önüne alındığında işletmeleri zorladığı görülmektedir. Bu nedenle küçük işletmelere yönelik olarak daha düşük maliyetli sistemlerin efektif bir şekilde devreye sokulmasında yarar vardır. Özellikle ilçelerdeki toplu taşıma sistemlerinde kullanılabilecek maliyeti düşük çözümlerin üretilmesi ve test edilmesi gerekmektedir. Bu çalışmada tamamen bu amaca yönelik olarak daha düşük maliyetli ve sistemin gereksinimlerini karşılamaya yönelik bir çözüm üzerinde durulmuştur. Raspberry Pi tabanlı bir sistem önerilerek elektronik ücret toplama işleminin kolaylıkla gerçekleştirilebileceği, işletme ve kullanıcıların önerilen sistemi kolay ve güvenli bir şekilde kullanabilecekleri bir sistem tasarımı gerçekleştirilmiş ve test edilmiştir. Çalışmanın ikinci bölümünde

sistemin nasıl tasarlandığı ve kullanılan teknolojiler tanıtılmış, üçüncü bölümde ise bulgular verilmiştir. Dördüncü bölümde ise önerilen sistemin sonuçları tartışılmıştır.

MATERYAL VE METOD

Tasarlanan ve Şekil 1'de çalışma diyagramı verilen bu sistemde, bileşenler arasındaki veri akışı ve haberleşme entegre bir yapı içinde kesintisiz olarak gerçekleşmektedir. Otobüs cihazı (Raspberry Pi), yolcuların kartlarını okumak için NFC kart okuyucusu ile doğrudan iletişim kurarak kart bilgilerini alır ve bu verileri işler. Alınan veriler, daha sonra merkezi sunucuya iletilir. Merkezi sunucu (MySQL veri tabanı), otobüs cihazlarından gelen ödeme ve kullanıcı bilgilerini toplayarak güvenli bir şekilde depolar. Bu veri aktarımı, web servisleri aracılığıyla sağlanır ve otobüs cihazları ile merkezi sunucu arasında anlık veri akışı oluşturur. Web sitesi kullanıcıların bakiye işlemlerini yönetebilmesi için merkezi veri tabanına bağlanır ve böylece kullanıcılar bakiye yükleme, hesap yönetimi gibi işlemlerini gerçekleştirebilir. Web ara yüzü, sistemin kullanıcıya yönelik hizmetlerini sağlarken, yönetim paneli ise sistemin genel yönetimi ve raporlanması için merkezi sunucu ile haberleşir. Böylece, sistemin tüm bileşenleri arasında sürekli bir veri akışı ve koordinasyon sağlanarak sistemin verimli ve kesintisiz bir şekilde çalışması mümkün hale gelir.

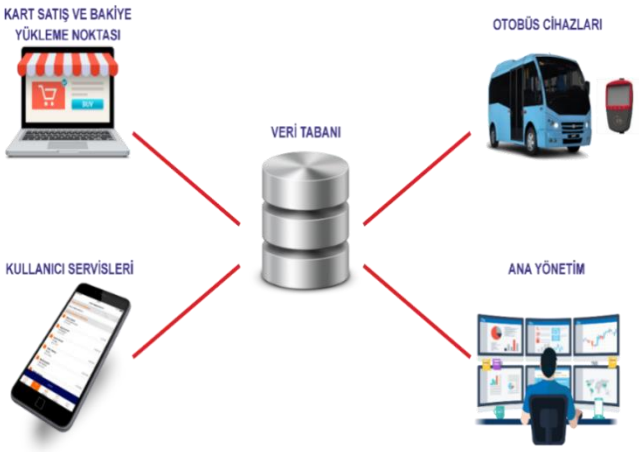

Şekil 1. Önerilen sistemin çalışma diyagramı

Şekil 2' de gösterilen Raspberry Pi, otobüslerde kullanılacak olan ana cihaz olarak işlev görecektir. Bu cihaz, entegre edilmiş NFC kart okuyucularla birlikte çalışarak, yolcuların kart bilgilerini okuma işlemlerini gerçekleştirecektir. NFC kart okuyucular, kullanıcıların biniş işlemi sırasında kartlarını okutarak, bu verileri Raspberry Pi cihazına iletecektir. Raspberry Pi, bu verileri anlık olarak gerekli Python kütüphaneleri kullanarak oluşturulan algoritmalar ile işleyerek kullanıcıların ödeme bilgilerini merkezi veri tabanına gönderecektir. GPS modülü ile ise otobüslerin anlık takibi kontrol edilmesi amaçlanmıştır.

,

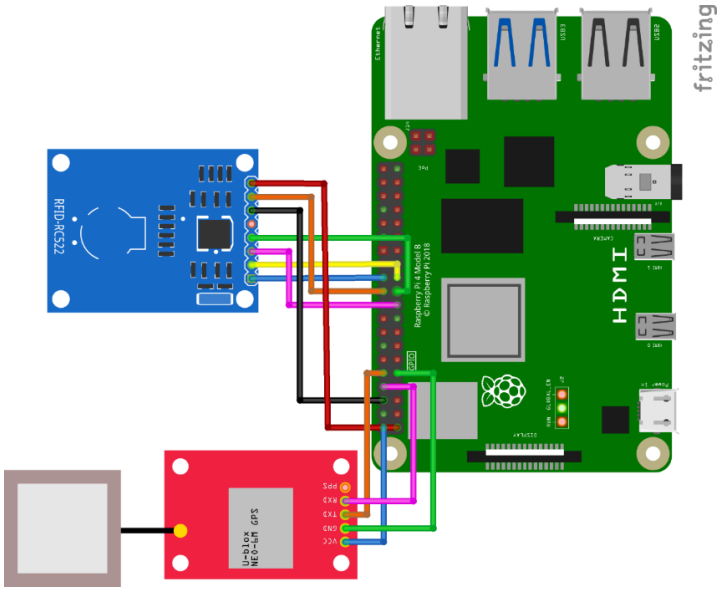

Şekil 2: Raspberry Pi ve GPS modüllerinin bağlantı şemaları

BULGULAR

Bu proje, toplu taşıma sistemlerinde kullanılan kartlı ödeme yöntemlerinin daha güvenli, kullanıcı dostu ve işlevsel hale getirilmesini amaçlayan bir elektronik ücret toplama sistemi geliştirmeyi hedeflemektedir.

Sistem, kullanıcıların toplu taşıma araçlarında kartlarını kullanarak ödeme yapmasını, bakiye takibini ve online işlemlerle yönetimini sağlar.

Sistem, Şekil 3' de gösterildiği gibi öncelikli olarak okutulan kartın geçerliliğini kontrol eder. Kartlara önceden gömülen özel doğrulama anahtarları sayesinde, sahte veya kopyalanmış kartların kullanılmasının önüne geçilir. Kart orijinalliği doğrulandıktan sonra, kart ID'si ile veri tabanında sorgulama yapılır. Kullanıcı veri tabanında mevcut değilse işlem sonlandırılır ve kullanıcıya bilgi verilir. Mevcut kullanıcılar için kart bilgileri cihazlara aktarılır ve ilk olarak vize tarihi kontrol edilir. Vize tarihi geçmiş kartlar için işlem sonlandırılır ve kullanıcı bilgilendirilir.

Vize tarihi uygun olan kartlarda, kart tipine göre belirlenmiş ücretlendirme üzerinden bakiye kontrolü yapılır. Yeterli bakiye yoksa işlem sonlandırılır ve kullanıcıya bilgi sağlanır. Yeterli bakiye mevcutsa, ödeme gerçekleştirilir ve kullanıcının işlem sonrası güncel bakiyesi ekranda görüntülenir. Sistem, özel kart tipleri (örneğin; engelli, yaşlı veya anne kartları) ve indirimli kart kullanıcıları için özel kurallar barındırır. Bu kartlardan ücret alınırken kötüye kullanımın önlenmesi amacıyla, aynı kartla belirli bir süre içinde birden fazla işlem yapılması sınırlandırılmıştır.

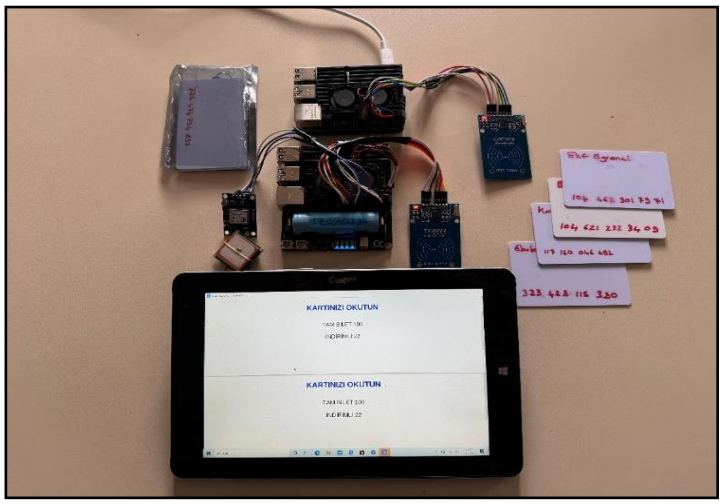

Şekil 3: Sistemin fiziksel olarak tasarlanmış hali

Firma yetkilileri için geliştirilen kurumsal ara yüz, Şekil 4 ve Şekil 5' deki gibi sistemin tüm yönlerini dinamik bir şekilde yönetmeyi mümkün kılar. Bu ara yüz üzerinden personel ekleme, kart tiplerini ve ücretlerini belirleme, otobüs cihazlarının konumlarını izleme ve finansal istatistikleri görüntüleme gibi işlemler yapılabilir. Firma personeli ise kullanıcıların kart bakiyelerini sorgulayabilir, bakiye yükleyebilir, vize güncellemeleri gerçekleştirebilir ve kaybolan kartlar için yeni kart tanımlayabilir.

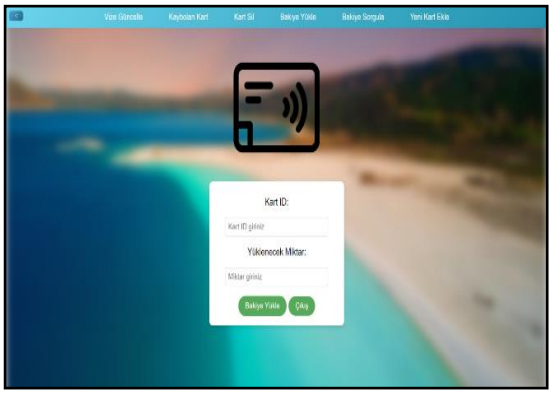

Şekil 4: Firma çalışanı ara yüzü

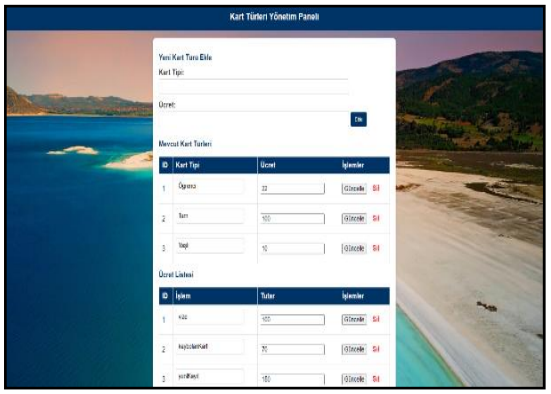

Şekil 5: İzlenen finansal istatistikler

Son kullanıcılar için geliştirilen kullanıcı dostu arayüz(Şekil 6), online işlemler üzerinden kart bakiyesi sorgulama ve bakiye yükleme gibi kolaylıklar sunar. Kullanıcılar, T.C. kimlik numaraları ile sisteme erişerek işlemlerini hızlı bir şekilde tamamlayabilir.

Bu sistem, kullanıcıların ve firma yetkililerinin tüm işlemlerini pratik ve güvenli bir şekilde gerçekleştirmesini sağlarken, toplu taşıma sektörüne yenilikçi bir çözüm sunmaktadır. Kapsamlı veri tabanı entegrasyonu, dinamik ücretlendirme ve kullanıcı dostu arayüzleriyle, sektörün dijitalleşmesine katkıda bulunmayı hedefler.

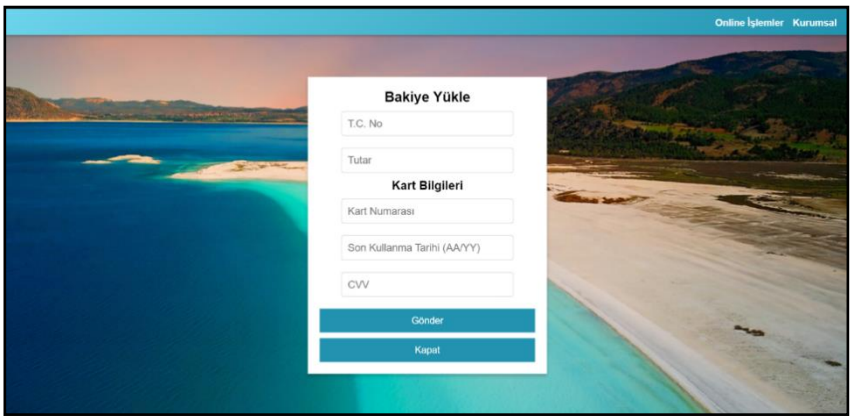

Şekil 6: Son kullanıcı ara yüzü

SONUÇ

Bu çalışmada özellikle küçük ölçekli işletmelerin mevcut elektronik ücret toplama sistemlerine mesafeli durmasını sağlayan yüksek maliyetli çözümlere alternatif bir sistem önerisi yapılmış, tasarlanmış ve test edilmiştir. Önerilen sistemin çalışması çok basit ve kolay olup, maliyeti diğerlerine göre minimum seviyededir. Tasarlanan ara yüzlerle kullanıcıların kartlarına bakiye yüklemeleri, bakiyelerini takip etmeleri, firmaların durum izleme sistemleri kolaylaştırılmıştır. Çalışma tamamen maliyet eksenine odaklanmış ve küçük firmalara alternatif bir çözüm üretmek hedeflenmiştir. Yapılan testler sistemin sorunsuz olarak çalıştırılabileceğini göstermiş olup, önerilen bu sistem ufak değişikliklerle efektif bir biçimde kullanılabilir.

KAYNAKLAR

Taç, Ş. G. (2018). Karayolu ulaşımında meydana gelen trafik kazalarının önlenmesinde akıllı ulaşım sistemlerinin etkisi. Akıllı Ulaşım Sistemleri ve Uygulamaları Dergisi, 1(2), 12-21.

Tiryaki, M. M. (2015). Akıllı ulaşım için veri madenciliğine dayalı tahmin sistemi. Yüksek Lisans Tezi. İstanbul Üniversitesi, Fen Bilimleri Enstitüsü.

Kumawat, A., & Chandramore, K. (2014). Automatic toll collection system using RFID. International Journal of Electrical and Electronics Research, 2(2), 67-72.

Geçer, T. (2016). Elektronik ücret toplama sistemi ve İstanbul örneği. Bilgi Ekonomisi ve Yönetimi Dergisi, 11(1), 83-88.

Katanalp, B. Y., Yıldırım, Z. B., Eren, E., & Uz, V. E. (2018). akilli ulaşim sistemleri üzerine bir değerlendirme. In 2nd International Symposium on Innovative Approaches in Scientific Studies, SETSCI Conference Indexing System (Vol. 3, pp. 1503-1506).

Turk, E., & Arslan, S. (2017). Location based pricing with Bluetooth low energy in public transportation. 2017 25th Signal Processing and Communications Applications Conference (SIU), 1-4. https://doi.org/10.1109/SIU.2017.7960148

Arslan, S., Gündüzalp, M., & Türk, E. (2016, December). An embedded system vehicle tracking system application. In 2016 National Conference on Electrical, Electronics and Biomedical Engineering (ELECO) (pp. 447-451).

➢ *ORAL PRESENTATION*

Carbonized Turkish Tea Waste for Interfacial Solar Steam Generation

Ezgi Topçu[1*] (*ORCID: https://orcid.org/0000-0003-1506-9089)*, Serap Katranlı[1] (*ORCID: https://orcid.org/0009-0008-5527-9535*), Kader Dağcı Kıranşan (*ORCID: https://orcid.org/0000-0002-0764-9393*), Elif Erçarıkcı[1] (*ORCID: https://orcid.org/0000-0002-8490-1644*), Serkan Bayar[2] (*ORCID: https://orcid.org/0000-0001-6713-2604*)

[*1]Department of Chemistry, Science Faculty, Atatürk University, Erzurum, Türkiye.
[2]Department of Environmental Engineering, Engineering Faculty, Atatürk University, Erzurum, Türkiye.

*Corresponding author e-mail: ezgitopcu@atauni.edu.tr

Abstract
Water scarcity is a critical global issue, and solar steam generation (SSG) using photothermal materials offers a sustainable solution for desalination. However, high costs and complex fabrication often limit their practicality. In this study, a low-cost SSG system was developed by modifying a commercial cellulosic sponge with carbonized Turkish tea waste (CTW). The CTW, obtained via pyrolysis, provided strong light absorption and efficient photothermal conversion, while the sponge served as a lightweight, self-floating substrate with rapid water uptake. The resulting CTW-S composite achieved a water evaporation rate of 1.42 kg m^{-2} h^{-1} and a solar-to-vapor conversion efficiency of 83% under one sun illumination. This work demonstrates the potential of biomass-derived materials for scalable, eco-friendly water treatment applications.
Keywords: Turkish tea waste, carbonization, cost-effective evaporator solar desalination.

INTRODUCTION

Due to the increasing demand of the human population and the continuous pollution of limited clean water resources, the shortage of clean water has become an urgent problem for the sustainable development of society. Desalination of seawater and treatment of wastewater are two effective ways to alleviate the shortage of fresh water (Ibrahim et al., 2021; Tian et al., 2022).

It is estimated that the total amount of energy that the Sun provides to the Earth in 1 hour is more than the energy humans consume in a year. Utilizing solar energy to desalinate seawater and purify polluted water without consuming fossil energy and causing environmental pollution is an environmentally friendly and sustainable strategy (Toyoda & Inagaki, 2023).

Recently, a significant amount of research has been conducted focusing on achieving efficient evaporation results with solar energy (Chen et al., 2020). These researches are focused on producing advanced materials that can increase solar absorption, improve thermal management, and facilitate water transport and vapor diffusion to produce clean water vapor (Liu et al., 2017a).

To date, various materials capable of photothermal conversion have been reported for solar steam generation (SSG), including metallic plasmonic nanoparticles, polymers, and carbon-based materials. However, most of these materials are expensive and involve complex production processes. From the perspective of sustainable development, there is still a significant need for new materials that are low-cost, self-floating, and easy to produce to obtain clean water using solar energy (Liu et al., 2017b; Wang et al., 2016).

As well known, tea is one of the most consumed non-alcoholic beverages in the world. Global tea consumption, which reached 6.3 million tons in 2020, is estimated to increase to 7.4 million tons in the next five years (Debnath et al., 2022). In Turkey, per capita fresh tea consumption has been 14-15 kg in the last five years, while that of dry is 3.5-4.0 kg. However, this popularity of tea results in the generation of large quantities of tea waste (TW). Most of the TW is disposed of by landfills without proper treatment, causing a considerable environmental threat and polluting water and soil (Guclu et al., 2021).

Recently, biomass carbon materials have shown a broad application in SSG applications with their high specific surface area, unique microstructure, and environmentally friendly properties. TW, as biomass,

possesses a rich carbon source and can be pyrolyzed to yield low-cost and efficient TW biochar. This carbonized product can be used as a photothermal material to absorb sunlight and convert solar energy to heat (Nidheesh et al., 2021).

Herein, we describe the preparation of a carbonized Turkish tea waste-modified commercial sponge as an efficient evaporator for SSG. Firstly, a pyrolysis process was applied to Turkish TW after brewing to fabricate a highly porous carbonized structure. Subsequently, an inexpensive cellulosic sponge was coated with the resulting porous biomass-derived carbonaceous structure to obtain a novel solar steam generator. This sponge was used as a substrate in the preparation of solar steam generators due to its lightweight and self-floating feature thanks to its large pores. The easy and rapid water absorption ability of the sponge (S) combined with the strong light absorption and high solar-vapor conversion of the carbonized Turkish tea waste (CTW), our photothermal material (CTW-S) showed superior SSG performance. The findings exhibited that CTW-S with a water evaporation rate of 1.42 kg m^{-2} h^{-1} under one sun illumination and a solar-to-vapor conversion efficiency of 83%, is a promising low-cost solar evaporator for large-scale practical applications such as desalination and water purification. The development of such eco-friendly materials demonstrates the potential of waste utilization in alleviating global challenges.

MATERIALS AND METHODS

2.1. Materials

Tea is brewed several times daily at the tearoom of the Chemistry Department of Atatürk University (Figure S1). Tea waste (TW) was obtained from this tearoom. The commercial natural cellulosic bath sponge (Wee Baby) was supplied by local suppliers in Türkiye. NaCl, $MgCl_2$, KCl, $CaCl_2$, $Cr(NO_3)_3$, $Ni(NO_3)_2$, $Cu(NO_3)_2$, $Pb(NO_3)_2$, HCl, NaOH, and methylene blue (MB) were purchased from Sigma-Aldrich.

2.2. Preparation of CTW

TW was washed several times and dried at 60°C. Then it was loaded into a tube furnace and heated in an Argon atmosphere at different temperatures (200, 300, 400, and 500 °C) for 2 h. The carbonized TWs (CTWs) were named CTW-200, CTW-300, CTW-400, and CTW-400 and ground in a mortar for 20 min.

2.3. Preparation of solar evaporator: CTW-S

To prepare the photothermal evaporator, first, the commercial natural cellulosic sponge (S) was cut in a cylinder with about 4 cm diameter. Subsequently, a polyvinyl alcohol (PVA) solution was prepared and the circular surface of the sponge was dipped into this solution. This surface of S was homogeneously coated with the optimized amount of CTW. At the surface, the PVA solution and CTW were mixed and thus, fixed on the sponge surface.

RESULTS and DISCUSSION

The morphology of the bare S and the CTW-S was characterized through FESEM. Figures 1.a and b show that the sponge has a network consisting of different-sized pores. These disordered pores are beneficial for water absorption and evaporation. CTW is coated homogenously inside the sponge in Figures 1.c and d, and the roughness of the surface increased due to the stacked CTW, which contributes to a higher solar absorption for evaporation. The SSG performance of CTW-S was evaluated with the measurement system in Figure 1.e. This system consists of a solar simulator, an electronic analytical balance to measure the mass change through water evaporation, and a computer to determine the time-dependent evaporation rate. The temperature changes were monitored and recorded with a thermal camera. The experiments were carried out with an insulated double-walled container to prevent environmental heat conduction and including floating CTW-S on water (Figure 1.f).

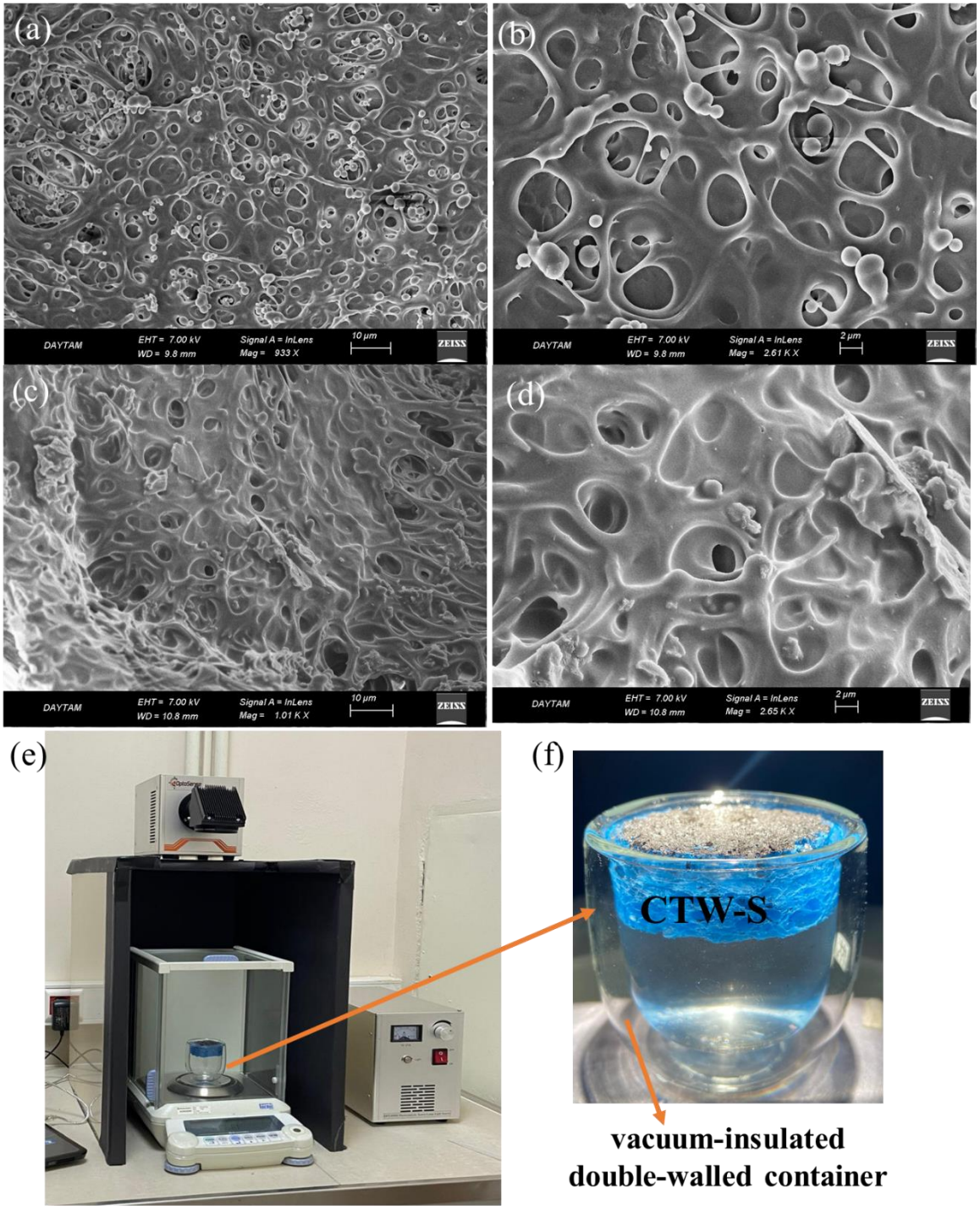

Figure 1. FESEM image of bare S (a-b) and CTW-s (c-d) at different magnifications. Digital photograph of SSG device (a) and solar evaporator in double-walled glass container (b).

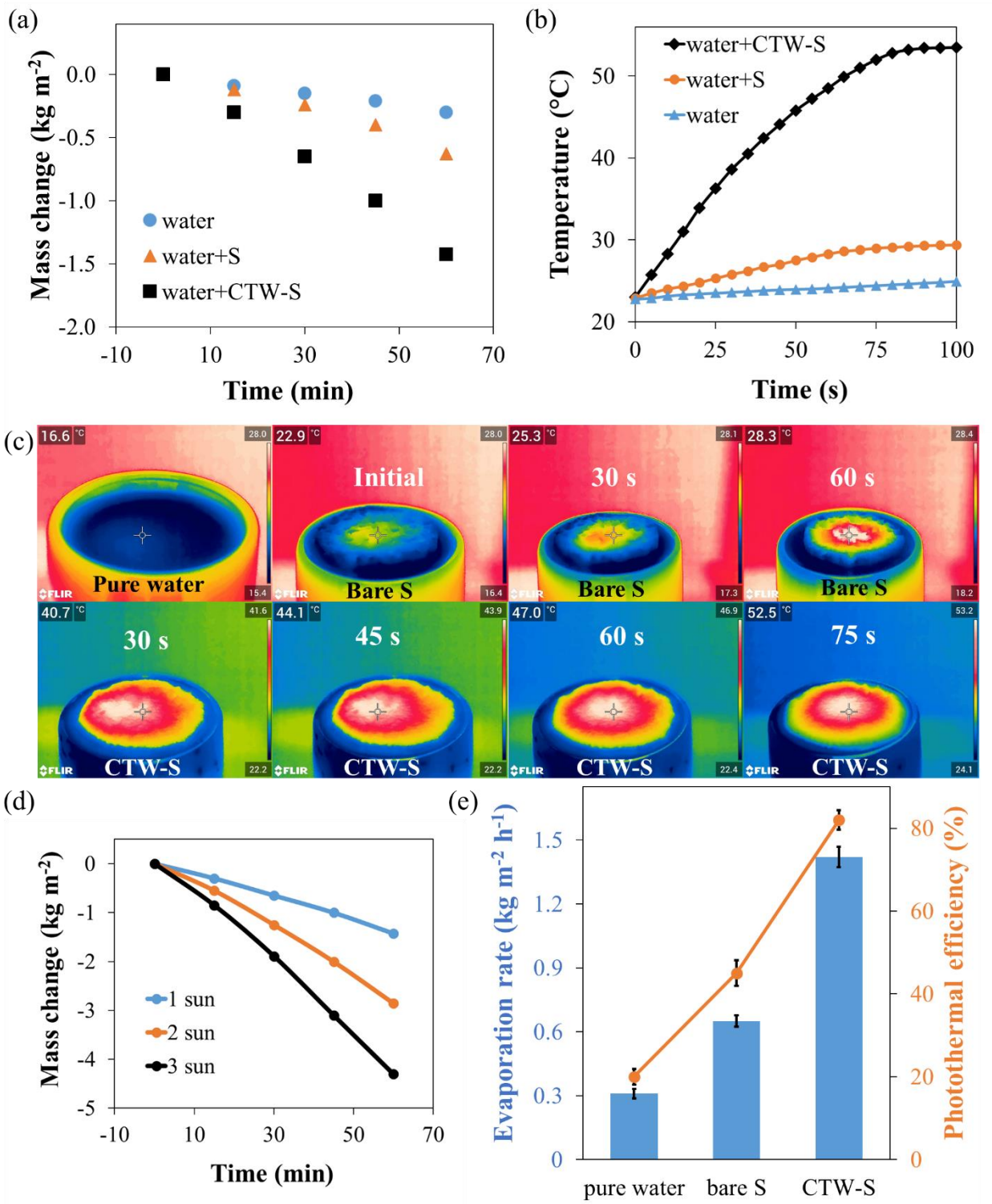

Figure 2. Time-dependent mass change (a) and surface temperature (b) of CTW-S, bare S, and pure water under 1 sun irradiation. (c) Infrared images of pure water, bare S, and CTW-S at different times. (d) Time-dependent mass change of CTW-S under different solar irradiation. (e) Evaporation rate and photothermal efficiency of pure water, bare S, and CTW-S under 1 sun irradiation.

The mass change of water under 1 sun irradiation for 60 min was determined to investigate the evaporation performance of CTW-S in Figure 2.a. The evaporation rate over time for CTW-S was calculated as 1.42 kg m^{-2} h^{-1}, which is about 4.6 times that of pure water (0.31 kg m^{-2} h^{-1}) and about 2.2 times that of bare S (0.65 kg m^{-2} h^{-1}). In Figure 2.b, the temperature increases of the samples (pure water, bare S, and CTW-S) over time were examined during 100 s of irradiation. After 100 s, the surface temperature of pure water and bare S reached 24.9 °C and 29.4 °C, respectively, while that of CTW-S rapidly increased during the first 85 s and stabilized at 53.4 °C. The maximum surface temperature of CTW-S was higher than that of the bare S,

indicating the strong photothermal conversion effect of the carbonized structure (CTW). In Figure 2.c, the surface temperature of pure water, bare S, and CTW-S were monitored with an infrared camera over time under 1 solar irradiation. The initial temperature of pure water was 16.6 °C. Noticeably, the surface temperature of CTW-S sharply increased in the first 30 s and was recorded as 40.7, 44.1, 47.0, and 52.5 °C after 30, 45, 60, and 75 s; in contrast, that of bare S exhibited low temperatures with less increment from 25.3 °C to 28.3 °C after 30 and 60 s, respectively. Figure 2.d exhibits that the amount of water evaporated increased with increasing solar radiation.

The evaporation rate of the CTW-S was recorded as 2.86 and 4.34 kg m^{-2} h^{-1} for 2 and 3 sun lights, respectively. The pure water, bare S, and CTW-S demonstrated a photothermal efficiency of 20%, 45%, and 83%, respectively (Figure 2.e). CTW-S exhibited higher energy efficiency and water evaporation rate, indicating the superior photothermal conversion performance of CTW. Furthermore, CTW laid on the S surface acts as a barrier to prevent heat loss and thus increases the photothermal efficiency.

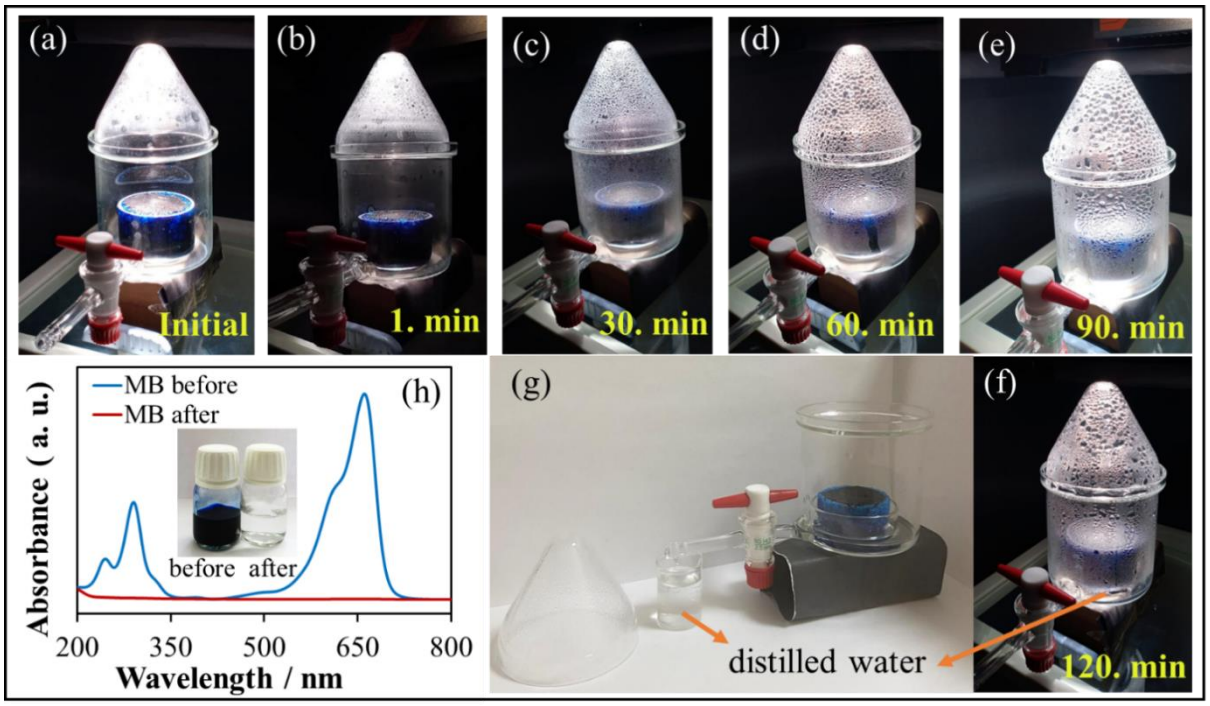

Figure 3. Digital photographs of solar purification with CTW-S at different times (a-f) and distillate (g). (h) UV−vis spectra of MB before and after solar purification.

To test the solar purification of the dye-containing solution with CTW-S, an MB solution with a concentration of 1.0 g L^{-1} was placed in the prepared SSG setup, and the distillation process was applied. After irradiation for 2 h, the distillate water was examined through UV-visible absorption spectroscopy. Photographs of solar evaporation from initial to 1, 30, 60, 90, and 120 min are shown in Figure 3 a-f. The distillate collected through the tap of the container (Figure 3.g) was transparent (inset of Figure 3.h), and its UV−vis spectrum showed the disappearance of the MB absorption peaks, demonstrating successful solar purification and, thus, the potential effect of CTW-S in sewage treatment.

CONCLUSION

In this study, a cost-effective and eco-friendly solar steam generator was developed using a commercial cellulosic sponge modified with carbonized Turkish tea waste. The CTW, produced through the pyrolysis of spent tea leaves, exhibited a highly carbonaceous structure with excellent photothermal properties. After coating the sponge, the CTW-S showed strong solar steam generation performance. Specifically, under one sun illumination, CTW-S achieved a water evaporation rate of 1.42 kg m^{-2} h^{-1} and a solar-to-vapor conversion efficiency of 83%. These results underscore the potential of utilizing biomass-derived waste materials in the development of sustainable, low-cost SSG systems. The successful integration of tea waste into a functional photothermal material highlights the value of waste valorization in addressing global water scarcity through scalable and environmentally responsible technologies.

ACKNOWLEDGEMENTS
This work was supported by Atatürk University under Project No. BAP-FCD-2024-14600.

REFERENCES

Chen, J., Li, B., Hu, G., Aleisa, R., Lei, S., Yang, F., Liu, D., Lyu, F., Wang, M., Ge, X., Qian, F., Zhang, Q., & Yin, Y. (2020). Integrated Evaporator for Efficient Solar-Driven Interfacial Steam Generation. *Nano Letters*, *20*(8), 6051–6058. https://doi.org/10.1021/acs.nanolett.0c01999

Debnath, B., Haldar, D., & Purkait, M. K. (2022). Environmental remediation by tea waste and its derivative products: A review on present status and technological advancements. *Chemosphere*, *300*(April), 134480. https://doi.org/10.1016/j.chemosphere.2022.134480

Guclu, C., Alper, K., Erdem, M., Tekin, K., & Karagoz, S. (2021). Activated carbons from co-carbonization of waste truck tires and spent tea leaves. *Sustainable Chemistry and Pharmacy*, *21*(February), 100410. https://doi.org/10.1016/j.scp.2021.100410

Ibrahim, I., Bhoopal, V., Seo, D. H., Afsari, M., Shon, H. K., & Tijing, L. D. (2021). Biomass-based photothermal materials for interfacial solar steam generation: a review. *Materials Today Energy*, *21*, 100716. https://doi.org/10.1016/j.mtener.2021.100716

Liu, Z., Song, H., Ji, D., Li, C., Cheney, A., Liu, Y., Zhang, N., Zeng, X., Chen, B., Gao, J., Li, Y., Liu, X., Aga, D., Jiang, S., Yu, Z., & Gan, Q. (2017a). Extremely Cost-Effective and Efficient Solar Vapor Generation under Nonconcentrated Illumination Using Thermally Isolated Black Paper. *Global Challenges*, *1*(2), 1–10. https://doi.org/10.1002/gch2.201600003

Liu, Z., Song, H., Ji, D., Li, C., Cheney, A., Liu, Y., Zhang, N., Zeng, X., Chen, B., Gao, J., Li, Y., Liu, X., Aga, D., Jiang, S., Yu, Z., & Gan, Q. (2017b). Extremely Cost-Effective and Efficient Solar Vapor Generation under Nonconcentrated Illumination Using Thermally Isolated Black Paper. *Global Challenges*, *1*(2), 1600003. https://doi.org/10.1002/gch2.201600003

Nidheesh, P. V., Gopinath, A., Ranjith, N., Praveen Akre, A., Sreedharan, V., & Suresh Kumar, M. (2021). Potential role of biochar in advanced oxidation processes: A sustainable approach. *Chemical Engineering Journal*, *405*(May 2020), 126582. https://doi.org/10.1016/j.cej.2020.126582

Tian, Y., Yang, H., Wu, S., Gong, B., Xu, C., Yan, J., Cen, K., Bo, Z., & Ostrikov, K. (2022). High-performance water purification and desalination by solar-driven interfacial evaporation and photocatalytic VOC decomposition enabled by hierarchical TiO2-CuO nanoarchitecture. *International Journal of Energy Research*, *46*(2), 1313–1326. https://doi.org/10.1002/er.7249

Toyoda, M., & Inagaki, M. (2023). Carbon materials for solar steam-generation. *Carbon*, *214*, 118373. https://doi.org/https://doi.org/10.1016/j.carbon.2023.118373

Wang, X., Ou, G., Wang, N., & Wu, H. (2016). Graphene-based Recyclable Photo-Absorbers for High-Efficiency Seawater Desalination. *ACS Applied Materials and Interfaces*, *8*(14), 9194–9199. https://doi.org/10.1021/acsami.6b02071

Lanza, R., Langer, R., Vacanti, J. P., & Atala, A. (Eds.). (2020). Principles of tissue engineering. Academic press.

Ward, P. C., & Mawdsley, W. (2000). Fire management in the boreal forests of Canada. In Fire, climate change, and carbon cycling in the boreal forest (pp. 66-84). New York, NY: Springer New York.

➢ *ORAL PRESENTATION*

Sustainable Water Evaporation System Based on Carbonized Turkish Coffee Waste and Cellulosic Sponge

Ezgi Topçu[1*] (*ORCID: https://orcid.org/0000-0003-1506-9089)*, Şeyda Sefa[1] (*ORCID: https://orcid.org/0009-0002-4886-8346*), Kader Dağcı Kıranşan (*ORCID: https://orcid.org/0000-0002-0764-9393*), Elif Erçarıkcı[1] (*ORCID: https://orcid.org/0000-0002-8490-1644*), Serkan Bayar[2] (*ORCID: https://orcid.org/0000-0001-6713-2604*)

[*1]Department of Chemistry, Science Faculty, Atatürk University, Erzurum, Türkiye.
[2]Department of Environmental Engineering, Engineering Faculty, Atatürk University, Erzurum, Türkiye.

*Corresponding author e-mail: ezgitopcu@atauni.edu.tr

Abstract
Water scarcity remains one of the most pressing global challenges, with solar steam generation (SSG) emerging as a promising method for sustainable desalination. Nevertheless, the widespread application of SSG technologies is often hindered by high production costs and complicated fabrication methods. In this study, an affordable and efficient SSG device was developed using a commercial cellulose-based sponge enhanced with carbonized Turkish coffee waste (CTCW). Produced through pyrolysis, CTCW offered excellent photothermal properties due to its strong solar absorption and effective light-to-heat conversion. The sponge matrix contributed additional advantages, including buoyancy and rapid water absorption. The resulting CTCW-S composite achieved a water evaporation rate of 1.63 kg m^{-2} h^{-1} and a solar-to-vapor conversion efficiency of 81% under standard sunlight conditions. These findings highlight the promise of repurposed biomass materials in developing scalable, eco-conscious water purification technologies.
Keywords: Biomass-derived carbon, Turkish coffee byproduct, cost-efficient evaporation, sunlight-assisted desalination.

INTRODUCTION

The decreasing availability of clean water poses a significant challenge to human survival and sustainable progress. Currently, purification of brackish water and municipal wastewater and desalination of seawater are considered the primary methods to reduce stress on water resources (Chen et al., 2020). There has been a rapid growth in the installation of seawater desalination plants in water-stressed regions as a way to increase water supply (Elimelech & Phillip, 2011). Multi-stage distillation and reverse osmosis are the two dominant technologies for thermal distillation and membrane-based desalination plants. These two methods account for the majority of the desalination market (Asghar et al., 2023; Hailemariam et al., 2020). However, the energy-intensive use of thermal/electric power and the extensive infrastructure required limits their widespread adoption to provide safe and sustainable drinking water. (Zhang vd., 2021; Li vd., 2020). At this point, solar energy emerges as an inexhaustible renewable green energy source owning an environmentally friendly and sustainable alternative compared to other energy sources. Thus, solar steam generation (SSG) using photothermal materials is a green, low-cost, and efficient method of solving the global water crisis with sustainable energy. From an energy efficiency perspective, the design of a water evaporation material should include the following components: 1) Photothermal materials that can efficiently convert sunlight into heat; 2) Structures that can simultaneously expand the evaporation surface and provide water to the heated space; 3) Thermal insulators that reduce heat loss from the available water and ambient air.

To date, great progress has been made in the development of various photothermal materials and hydrophilic supporting substrates for SSG. Photothermal materials consist of carbon-based materials, plasmonic metal nanoparticles, semiconductor materials, and organic polymers. Hydrophilic substrate materials include hydrogels or hydrophilic sponges. Significant advances in photothermal material research have enabled the use of solar-absorbing materials such as Au/Ag/Pd nanoparticles. (Toyoda & Inagaki, 2023; Wen et al., 2023). However, high-cost raw material requirement, complex production processes, and low stability prevent their use in practical applications. Therefore, the need for the development of low-cost and more environmentally friendly materials for water treatment persists.

Biochar is a solid product consisting of carbon and mineral elements produced by thermochemical processes such as combustion, gasification, hydrothermal carbonization, roasting, and pyrolysis in the

absence or limitation of an oxidizing agent, using biomass materials. Although wood has been used as biomass since ancient times, biochar can be produced from corn cobs, rice husks, peanuts, tree shells, processed paper waste, etc. (Nidheesh et al., 2021). Among these, coffee waste is a low-cost and abundant biomass source.

There is a large coffee consumption volume in Turkey as in the world. Turkish coffee (TC) is regarded as part of Turkish cultural heritage and this element was inscribed in 2013 on the UNESCO Intangible Cultural Heritage of Humanity. TC, among others, is the most consumed and liked coffee by Turkish society. Thus, TC waste, a biomass source, is formed through this huge consumption.

The negative impacts of waste materials on the environment and, consequently, on humans have led to an increased interest in research on the conversion of waste materials into value-added materials. The preparation of biochar for environmental remediation is a kind of "waste to wealth" strategy as it helps in the management and utilization of waste (Tripathi et al., 2016). For an ideal solution to purify polluted water, raw material cost and environmental impact should be taken into consideration. Therefore, carbonized natural materials, especially biomass waste, are extremely important in solar water purification due to providing the opportunity for recycling. Nevertheless, studies on the preparation of photothermal material for the SSG through the utilization of waste biomass are limited.

In this work, we fabricated photothermal material (CTCW-S) by modifying a hydrophilic self-floating commercial sponge (S) with carbonized TC waste (CTCW) for SSG. Firstly, a pyrolysis process was applied to TC waste collected to prepare a photothermal carbonized structure. Subsequently, an inexpensive cellulosic sponge was modified with the resulting porous biomass-derived carbonaceous structure to obtain a novel solar steam generator. The easy and rapid water absorption ability of the S combined with the strong light absorption and high solar-vapor conversion of the CTCW, our photothermal material showed superior solar steam generation performance. The findings exhibited that CTCW-S with a water evaporation rate of 1.63 kg m^{-2} h^{-1} under one sun illumination and a solar-to-vapor conversion efficiency of 81%, is a promising low-cost solar evaporator for large-scale practical applications such as water purification and desalination. CTCW-S will bring a new perspective to the development of waste-based materials for SSG and provide a viable alternative to address freshwater scarcity.

MATERIALS AND METHODS

Materials

TC is drunk at home and office daily. TCW was obtained by collecting the coffee grounds left at the bottom of the coffee cups (Figure S1). The commercial natural cellulosic bath sponge (Wee Baby) was supplied by local suppliers in Türkiye. NaCl, $MgCl_2$, KCl, $CaCl_2$, $Cr(NO_3)_3$, $Ni(NO_3)_2$, $Cu(NO_3)_2$, $Pb(NO_3)_2$, HCl, NaOH, polyvinyl alcohol (PVA) and methylene blue (MB) were purchased from Sigma-Aldrich.

Preparation of CTCW

TCW was washed several times and dried at 60 °C. Then it was loaded into a tube furnace and heated in an Argon atmosphere at different temperatures (300, 400, 500, and 600 °C) for 2 h. The CTCWs were named CTCW-300, CTCW-400, CTCW-500, and CTCW-600.

Preparation of solar evaporator: CTCW-S

To prepare the photothermal material, first, the commercial natural cellulosic sponge (S) was cut in a cylinder with about 4 cm diameter. Subsequently, a polyvinyl alcohol (PVA) solution was prepared and the circular surface of the sponge was dipped into this solution. This surface of S was homogeneously coated with the optimized amount of CTCW. At the surface, the PVA solution and CTCW were mixed and thus, fixed on the sponge surface.

RESULTS and DISCUSSION

The morphology of the bare S and the CTCW-S was characterized through FESEM. Figures 1.a shows that the sponge has a network consisting of different-sized pores. These disordered pores are beneficial for water absorption and evaporation. CTCW is coated homogenously inside the sponge in Figures 1.b and d, and the roughness of the surface increased due to the stacked CTCW, which contributes to a higher solar absorption for evaporation. The SSG performance of CTCW-S was evaluated with the measurement system in Figure 1.c. This system consists of a solar simulator, an electronic analytical balance to measure the mass change through water evaporation, and a computer to determine the time-dependent evaporation rate. The temperature changes were monitored and recorded with a thermal camera. The experiments were carried out with an insulated double-walled container to prevent environmental heat conduction and including floating CTCW-S on water (inset of Figure 1.c).

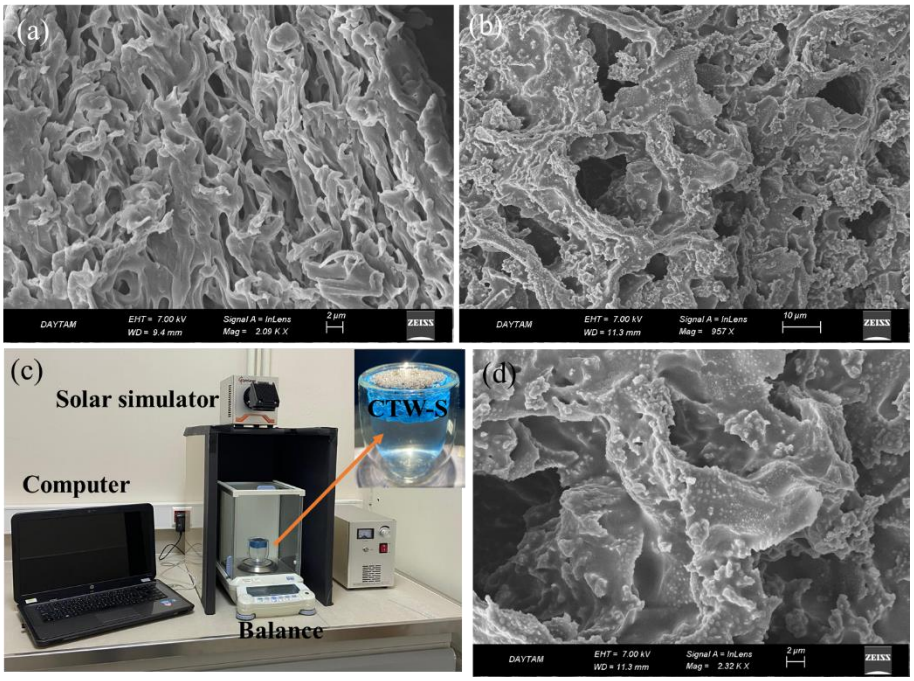

Figure 1. FESEM image of bare S (a) and CTCW-S (b and d) at different magnifications. Digital photograph of SSG device (c).

The mass change of water under 1 sun irradiation for 60 min was determined to investigate the evaporation performance of CTCW-S in Figure 2.a. The evaporation rate over time for CTCW-S was calculated as 1.63 kg m^{-2} h^{-1}, which is about 5.2 times that of pure water (0.31 kg m^{-2} h^{-1}) and about 2.5 times that of bare S (0.65 kg m^{-2} h^{-1}). In Figure 2.b, the temperature increases of the samples (pure water, bare S, and CTCW-S) over time were examined during 100 s of irradiation. After 100 s, the surface temperature of pure water and bare S reached 24.9 °C and 29.4 °C, respectively, while that of CTCW-S rapidly increased during the first 85 s and stabilized at 55.2 °C. The maximum surface temperature of CTCW-S was higher than that of the bare S, indicating the strong photothermal conversion effect of the carbonized structure (CTCW). In Figure 2.c, the surface temperature of pure water, bare S, and CTCW-S were monitored with an infrared camera over time under 1 solar irradiation. The initial temperature of pure water was 15.8 °C.

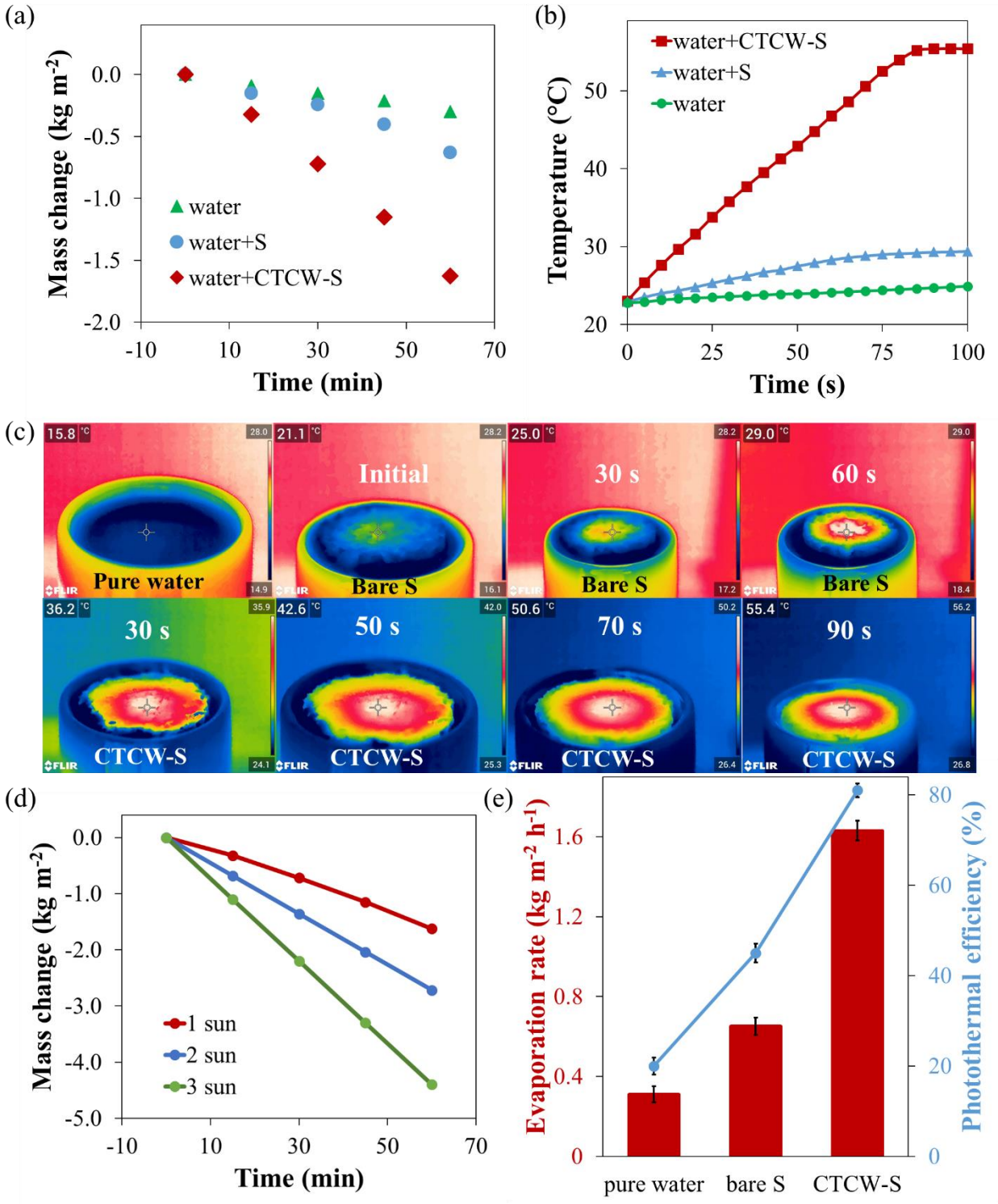

Figure 2. Time-dependent mass change (a) and surface temperature (b) of CTCW-S, bare S, and pure water under 1 sun irradiation. (c) Infrared images of pure water, bare S, and CTCW-S at different times. (d) Time-dependent mass change of CTCW-S under different solar irradiation. (e) Evaporation rate and photothermal efficiency of pure water, bare S, and CTCW-S under 1 sun irradiation.

Noticeably, the surface temperature of CTCW-S sharply increased in the first 30 s and was recorded as 36.2, 42.6, 50.6, 47.0, and 55.4 °C after 30, 50, 70, and 90 s; in contrast, that of bare S exhibited low temperatures with less increment from 25.0 °C to 29.0 °C after 30 and 60 s, respectively. When the light intensity was increased to 2 and 3 sun lights, the evaporation rate of the CTCW-S photothermal material was also increased to 2.72 and 4.40 kg m^{-2} h^{-1}, respectively (Figure 2.d). The photothermal efficiency for samples was calculated using equations 1 and 2, shown in detail in the supporting information. The pure water, bare S, and CTCW-S demonstrated a photothermal efficiency of 20%, 45%, and 83%, respectively

(Figure 2.e). CTCW-S exhibited higher energy efficiency and water evaporation rate, indicating the superior photothermal conversion performance of CTCW. Furthermore, CTCW laid on the S surface acts as a barrier to prevent heat loss and thus increases the photothermal efficiency.

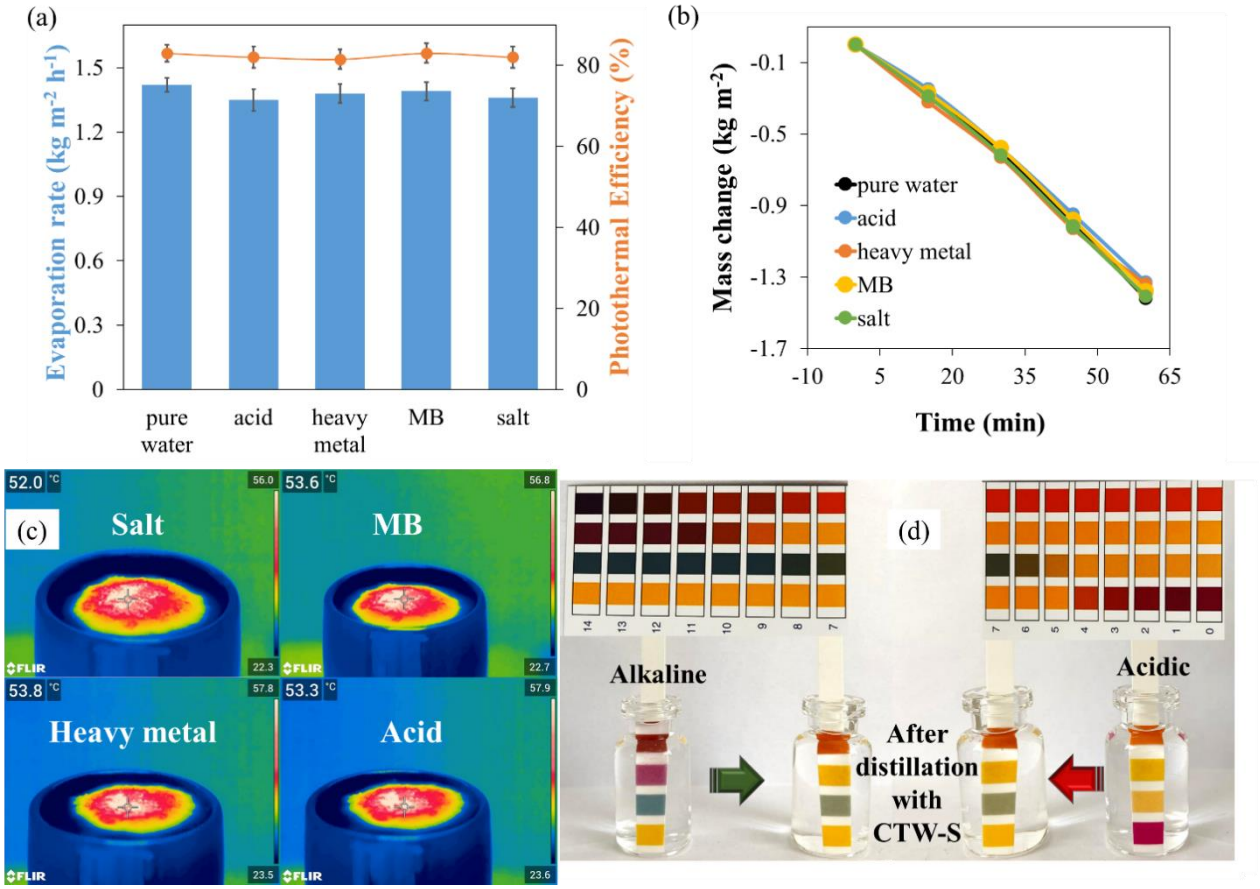

Figure 3. Photothermal efficiency and evaporation rate (a) and time-dependent mass change (b) of CTCW-S for pure water and solutions containing acid, alkaline, salt, heavy metal, and MB under 1 sun irradiation. (c) Infrared images of CTCW-S floating on solutions containing heavy metal, salt, acid, and MB. (d) Digital photographs of pH values before and after solar purification of the acidic (pH 2) and alkaline (pH 12) solutions with CTCW-S.

The evaporation performance of CTCW-S was further investigated for different solutions containing heavy metal (200 mg/L), acid (pH 2), alkaline (pH 12), and dye (MB-1.0 g/L), salt (NaCl-3.5 wt %) solutions. Figure 3 displays the photothermal efficiency, evaporation rate (Figure 3.a), and mass change (Figure 3.b) of CTCW-S in different solutions, and the results are very close to that of pure water, demonstrating that our material has a comparable SSG performance in various solutions. Meanwhile, the surface temperature of CTCW-S on different solutions exhibited the range of 52-54 °C (Figure 3.c), which is consistent with mass change. All these findings revealed that CTCW-S is a potential photothermal material in desalination and water purification applications. On the other hand, the distilled water generated from acidic and alkaline solutions showed a pH value close to 7 (Figure 3.d). All these results further confirm that CTCW-S photothermal material has excellent solar desalination and purification performance.

CONCLUSION

This study presents a sustainable and cost-effective approach to solar steam generation by utilizing carbonized Turkish coffee waste (CTCW) integrated with a commercial cellulose sponge. The CTCW enhanced solar absorption and photothermal efficiency, while the sponge provided structural support, buoyancy, and rapid water transport. The resulting CTCW-S composite demonstrated a high evaporation rate and energy conversion efficiency under standard sunlight conditions. These results confirm the potential of biomass-derived materials for scalable and environmentally friendly water treatment technologies. Future work may further explore other types of biomass waste to optimize performance and broaden practical applications.

ACKNOWLEDGEMENTS

This work was supported by Atatürk University under Project No. BAP-FCD-2024-14600.

REFERENCES

Asghar, M. S., Arshad, N., Tao, J., Irshad, M. S., Li, J., & Wang, X. (2023). Recent Advances in Multifunctional Photothermal Materials for Solar-Driven Steam and Energy Generation. *Energy Technology*, *11*(9), 2300500. https://doi.org/https://doi.org/10.1002/ente.202300500

Chen, J., Li, B., Hu, G., Aleisa, R., Lei, S., Yang, F., Liu, D., Lyu, F., Wang, M., Ge, X., Qian, F., Zhang, Q., & Yin, Y. (2020). Integrated Evaporator for Efficient Solar-Driven Interfacial Steam Generation. *Nano Letters*, *20*(8), 6051–6058. https://doi.org/10.1021/acs.nanolett.0c01999

Elimelech, M., & Phillip, W. A. (2011). The future of seawater desalination: Energy, technology, and the environment. *Science*, *333*(6043), 712–717. https://doi.org/10.1126/science.1200488

Hailemariam, R. H., Woo, Y. C., Damtie, M. M., Kim, B. C., Park, K.-D., & Choi, J.-S. (2020). Reverse osmosis membrane fabrication and modification technologies and future trends: A review. *Advances in Colloid and Interface Science*, *276*, 102100. https://doi.org/https://doi.org/10.1016/j.cis.2019.102100

Nidheesh, P. V., Gopinath, A., Ranjith, N., Praveen Akre, A., Sreedharan, V., & Suresh Kumar, M. (2021). Potential role of biochar in advanced oxidation processes: A sustainable approach. *Chemical Engineering Journal*, *405*(May 2020), 126582. https://doi.org/10.1016/j.cej.2020.126582

Toyoda, M., & Inagaki, M. (2023). Carbon materials for solar steam-generation. *Carbon*, *214*, 118373. https://doi.org/https://doi.org/10.1016/j.carbon.2023.118373

Tripathi, M., Sahu, J. N., & Ganesan, P. (2016). Effect of process parameters on production of biochar from biomass waste through pyrolysis: A review. *Renewable and Sustainable Energy Reviews*, *55*, 467–481. https://doi.org/10.1016/j.rser.2015.10.122

Wen, J., Li, X., Zhang, H., Zheng, S., Yi, C., Yang, L., & Shi, J. (2023). Architecting Janus hydrogel evaporator with polydopamine-TiO2 photocatalyst for high-efficient solar desalination and purification. *Separation and Purification Technology*, *304*(1), 122403. https://doi.org/10.1016/j.seppur.2022.122403

➢ *ORAL PRESENTATION*

Fuzzy backstepping control of quarter car suspension system

Meral ÖZARSLAN YATAK[1*] (*https://orcid.org/0000-0002-1091-1647*),

[*1]Gazi University, Faculty of Technology, Department of Electrical-Electronic Engineering, Ankara, Türkiye.

*Corresponding author e-mail: ozarslanm@gazi.edu.tr

Abstract
This paper presents a fuzzy backstepping controller of a quarter vehicle suspension system for a comfortable and safe ride with a high road holding feature. Active suspension systems are essential for autonomous and electric vehicles as well as classical vehicles. These nonlinear systems require a nonlinear controller for ride comfort, road holding, and low power consumption. Backstepping controller provides a globally asymptotic stability with Lyapunov design for nonlinear and systems with uncertain parameters. Additionally, it integrates control law into the controller structure through the virtual control variables at each step. The practical implementation of the backstepping controller requires constant closed-loop gains for the chosen Lyapunov function at each step. The system's dynamic response depends on these values at a high rate. In this study, the fuzzy logic controller determines these values. This approach also reduces the steady-state error occurring in the natural behavior of the classical backstepping algorithm. The results show that the fuzzy backstepping approach reduces the sprung mass displacement, acceleration, RMS values of dynamic tire load, and suspension deflection according to the classical control approach.
Keywords: Quarter vehicle model, Fuzzy backstepping, Ride comfort, Suspension deflection

INTRODUCTION

Improving ride comfort for passenger convenience and road holding for safe riding are the primary purposes of the automotive suspension system. The performance of the suspension has been improved by adding active elements to the passive suspension systems.

Road holding is obtained by supplying the contact of the road and the tire as much as possible. Additionally, ride comfort is supplied by isolating the road disturbances from the body of the vehicle. The road handling is improved with an active suspension system, too.

The system parameters have constant values for passive suspension systems, so the suspension stroke is limited (Ahmed 2021). Semi-active suspension systems usually have adjustable damping ratios through magnetorheological (MR), electrorheological, or variable orifice-type damping elements (Ergin and Yatak 2023). The active suspension system is the most enhanced suspension system among the other types of suspension systems. With an active suspension system, ride comfort and road holding can be improved concurrently (Yatak and Şahin 2021). The controllable part of the suspension system is the force actuator for arranging the ride comfort and suspension deviations.

The performance of the active suspension system strongly depends on the control technique. However, the complexity of the control technique, the cost, and the power consumption are the negative features of active suspension systems; the dynamic performance improvement on ride comfort and road holding makes it the most advanced suspension type.

Researchers have conducted many studies on the variety of control techniques for various vehicles, such as quarter, half-, or full-vehicle suspension systems. Linear quadratic regulator and static output feedback were compared in (Yim 2025). In (Tang and Ahmad 2025), enhanced fuzzy logic and two types of optimization methods were analyzed for active suspension systems. An adaptive integral terminal sliding mode active suspension system was implemented in (Liang, Gao et al. 2025). Passive suspension system, backstepping control, and sliding mode backstepping control were analyzed in (Li, Du et al. 2025). These control techniques are for improving the performance of the suspension systems. Nonlinear control algorithms are more appropriate for nonlinear systems. Zhang and Chen improved the body lateral vibration of high-speed trains with a backstepping semi-active control (Zhang and Chen 2025). They controlled the MR damper for this reason. In (Feng, Zhou et al. 2025), adaptive backstepping control was improved for

MR damper-based seat suspension. They reduced the frequency-weighted root mean square of acceleration, the vibration dose, and the root mean square of relative displacement effectively.

In this paper, the quarter vehicle suspension system has been controlled with a fuzzy backstepping controller (FBC). The controller performance has been compared with a passive suspension system (PSS) and a classical controller, a PID controller. The nonlinear structure of the backstepping control is acceptable for the nonlinear suspension system. The actuator force is determined with the FBC. The performance parameters of the controller are chosen as the acceleration of the sprung mass for ride comfort, tire deflection for road holding, suspension deflection for ride comfort, road holding, and the structural characteristics of the suspension system.

The organization of the paper is as follows: The second section, Materials and Methods, contains the mathematical model of the quarter vehicle suspension system as a subsection. The other subsection is for the backstepping controller with fuzzy logic adaptation. The third section is for comparison of the controller simulations. The last section covers the results and the discussions of the work.

MATERIALS AND METHODS

Quarter Vehicle Suspension System

A quarter vehicle active suspension system, as seen in Figure 1, was used to reveal the superiority of FBC. The sprung mass (m_s) for representing the quarter of the vehicle body, unsprung mass (m_u) for representing one tire, k_s for suspension spring, b_s for suspension damping, f for actuator force, b_u for tire damping, and k_u for tire spring are the basic components of a quarter vehicle active suspension system. Table 1 shows the parameters for the steady-state model of the system.

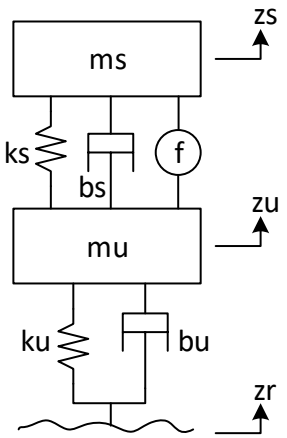

Figure 1. Quarter vehicle active suspension system model

The motion equations are derived from Newton's laws of motion, and they can be written as follows:

$$m_s\ddot{z}_s = k_s(z_u - z_s) + b_s(\dot{z}_u - \dot{z}_s) + f \quad (1)$$

$$m_u\ddot{z}_u = k_u(z_r - z_u) + b_u(\dot{z}_r - \dot{z}_u) - k_s(z_u - z_s) - b_s(\dot{z}_u - \dot{z}_s) - f \quad (2)$$

Table 1. Parameters and values of the quarter car suspension system

System	Parameter	Definition
Inputs	$(u_1 = f)$	Force actuator
	$(u_2 = z_r)$.	Road input
Outputs	$(y_1 = x_1)$	Position of the sprung mass
	$(y_2 = x_3)$	Position of the unsprung mass
State Variables	$(x_1 = z_s)$	Position of the sprung mass
	$(x_2 = \dot{z}_s = \dot{x}_1)$	Velocity of the sprung mass
	$(x_3 = z_u)$	Position of the unsprung mass
	$\left(x_4 = \dot{x}_3 - \frac{b_u}{m_u} u_2\right)$	

The steady state model and the coefficient matrices are given in (3) and (4).

$$\dot{x} = Ax + Bu_y = Cx + Du \tag{3}$$

$$A = \begin{bmatrix} 0 & 1 & 0 & 0 \\ -\frac{k_s}{m_s} & -\frac{b_s}{m_s} & \frac{k_s}{m_s} & \frac{b_s}{m_s} \\ 0 & 0 & 0 & 1 \\ \frac{k_s}{m_u} & \frac{b_s}{m_u} & -\frac{k_u+k_s}{m_u} & -\frac{b_u+b_s}{m_u} \end{bmatrix}, \quad B = \begin{bmatrix} 0 & 0 \\ \frac{1}{m_s} & \frac{b_s b_u}{m_s m_u} \\ 0 & \frac{b_u}{m_u} \\ -\frac{1}{m_u} & \frac{k_u}{m_u} - \frac{b_s b_u + b_u^2}{m_u^2} \end{bmatrix},$$

$$C = \begin{bmatrix} 1 & 0 & 0 & 0 \\ 0 & 0 & 1 & 0 \end{bmatrix}, \quad D = 0 \tag{4}$$

Backstepping Control

The backstepping approach is a systematic control structure for nonlinear systems (Kumar, Rana et al. 2021, Şahin and Yatak 2024). It derives stable control laws with a step-by-step approach without the knowledge of all model states. This method is especially effective for the strict-feedback formed nonlinear systems. This controller scheme is based on an iterative design in which the system states are accepted as virtual control inputs. In each step, a Lyapunov function candidate is selected, and a virtual control law is derived for the current sub-dynamics of the system. This virtual control law is treated as a real state variable for the following step.

The control aim in this study is to find such a control law $u_1 = f$ for the suspension system using the backstepping method that the suspension deflection of the quarter vehicle system follows the zero-reference trajectory. The suspension deflection is given as follows:

$$z_{sref} = z_s - z_u = 0 \tag{5}$$

Suspension deflection is a vital performance parameter that is related to nearly all aspects of the performance of the suspension system, as ride comfort, road holding, and handling. If it is not kept in control, an increase in suspension system wear and fatigue occurs (Ergin and Yatak 2023). So, this parameter is chosen as the reference parameter for FBC.

The control aim is to provide the suspension deflection to be zero. The system state variables in accordance with the backstepping approach are determined as follows:

The reference input, suspension deflection $z_{sref} = 0$:

$$x_1 = z_s - z_u \tag{6}$$

The design for the first sub-system (x_1):

The error variable: $e_1 = x_1 - z_{sref} = x_1$ (7)

The Lyapunov function candidate: $V_1 = \frac{1}{2}e_1^2$ (8)

Time derivative: $\dot{V}_1 = e_1.\dot{e_1} = e_1.x_2$ (9)

x_2 is virtual control input.

If $x_2 = -c_1 e_1$, $(c_1 > 0)$, $\dot{V}_1 = -c_1\, e_1^2 < 0$ and $e_1 \to 0$ can be obtained. This control law is determined as $\alpha_1 = -c_1 e_1$.

The design for the second sub-system (x_2):

The second error variable is described as the difference between x_2 and the virtual control α_1:

$e_2 = x_2 - \alpha_1 = x_2 + c_1 e_1$ (10)

The expanded Lyapunov function candidate:

$V_2 = V_1 + \frac{1}{2}e_2^2 = \frac{1}{2}e_1^2 + \frac{1}{2}e_2^2$ (11)

Time derivative: $\dot{V}_2 = \dot{V}_1 + e_2\dot{e}_2 = e_1(e_2 - c_1 e_1) + e_2\left(\dot{x}_2 + c_1(e_2 - c_1 e_1)\right)$

$\dot{V}_2 = -c_1 e_1^2 + e_1 e_2 + e_2(\dot{x}_2 + c_1 e_2 - c_1^2\, e_1)$ (12)

A control law u is chosen that makes e_2 term to zero and provides error damping to make the Lyapunov derivative negative semi-definite:

$e_1 - c_1^2 e_1 + \dot{x}_2 + c_1 e_2 = -c_2 e_2$ (13)

Here c_2 is a positive design gain.

Fuzzy Backstepping Control

The backstepping approach is a strong controller for nonlinear systems. In spite of this, it is insufficient for competing with the steady-state error. The reason for this, it generally provides asymptotic stability. When the state is reached, that place is not the exact point; it is balanced at the nearest point to the target point. To overcome this disadvantage, a robust control strategy can be provided by utilizing fuzzy logic (Şahin and Yatak 2024).

In this study, c_2, a positive design gain is determined with fuzzy logic. It is the most effective gain to make the error zero. The first input is $e_1 = x_1 - z_{sref} = x_1$ and the membership functions for this input is seen in Figure 2a. The second input is a derivative of e_1, and the membership functions are as in Figure 2b. The output is c_2 gain. The singleton membership functions for this output is seen in Figure 2c.

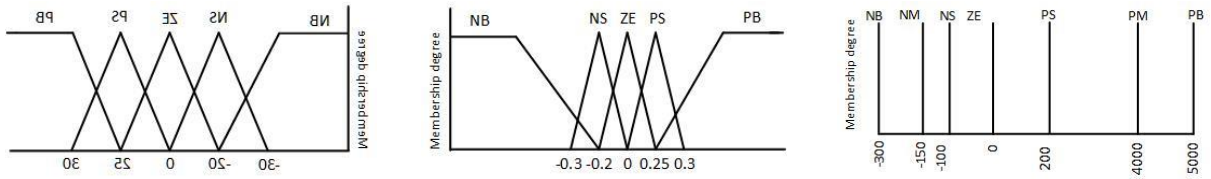

Figure 2. Membership functions for the FBC **a.** Input e_1 **b.** Input $\dot{e_1}$ **c.** Output

RESULTS and DISCUSSION

Vehicle suspension systems are evaluated over various performance parameters. These parameters are improved by various controllers. In this study, a nonlinear and iterative controller, the fuzzy backstepping controller, was analyzed to put forward its superiority over the classical PID controller and passive suspension system.

The system was tested for two different road types. The results were evaluated from three critical parameters. The first parameter is suspension deflection as shown in Eq. 14. This is the relative vertical displacement between the sprung and unsprung masses and is related to ride comfort and road handling.

$$s_d = z_s - z_u \tag{14}$$

The second parameter is tire deflection as shown in Eq. 15. Tire deflection is the displacement between the unsprung mass and the road input. It indicates whether the tire contacts the road surface and determines the road holding feature.

$$t_d = z_u - z_r \tag{15}$$

The last parameter is the acceleration of the unsprung mass. It is an important ride comfort parameter that shows how much road disturbances are transmitted to the vehicle.

The first road input is shown in Figure 3. The suspension deflections for the three types of controllers are shown in Figure 4 for this road input.

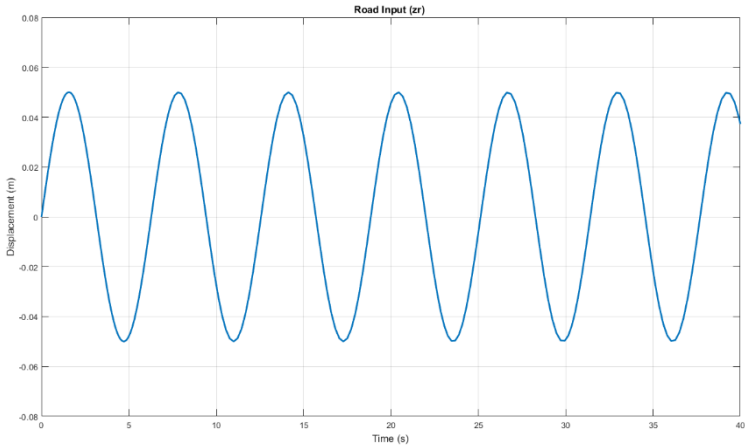

Figure 3. The first road input profile

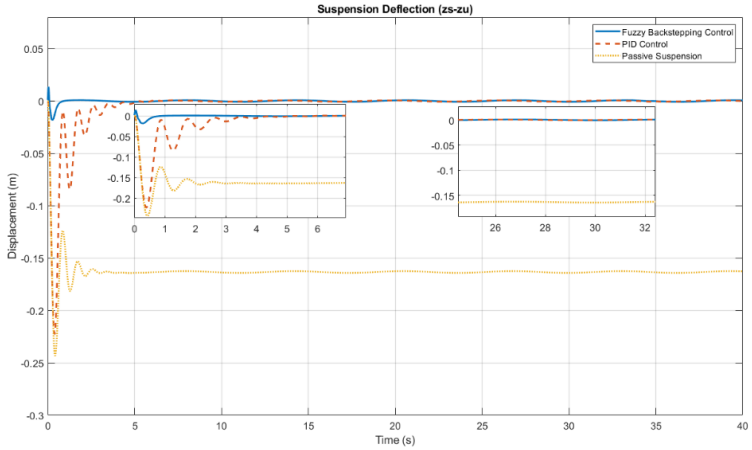

Figure 4. Suspension deflections for three types of suspension systems

Figure 5 is the tire deflection for three types of suspension systems, showing the road holding and handling. The acceleration of sprung mass is related to ride comfort, and it can be seen from Figure 6 for the sinus road input type.

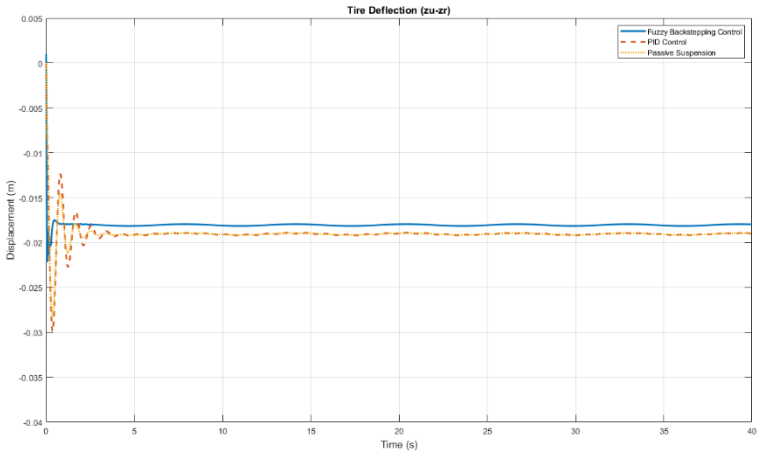

Figure 5. Tire deflection three types of suspension systems

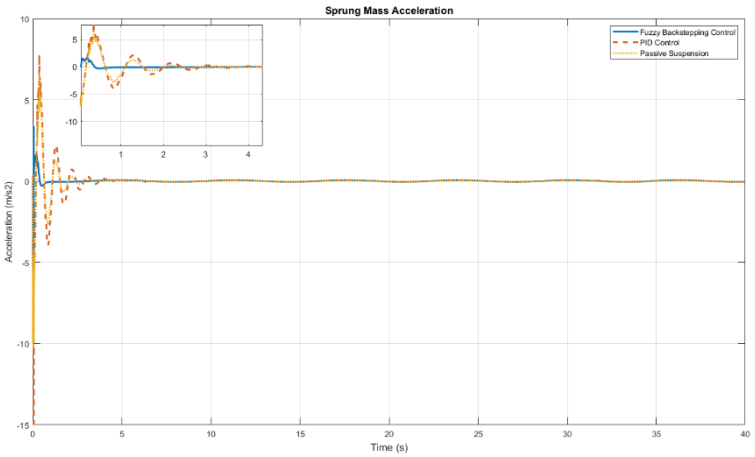

Figure 6. Sprung mass accelerations

The displacements of sprung mass and unsprung mass are shown in Figures 7 and 8, respectively.

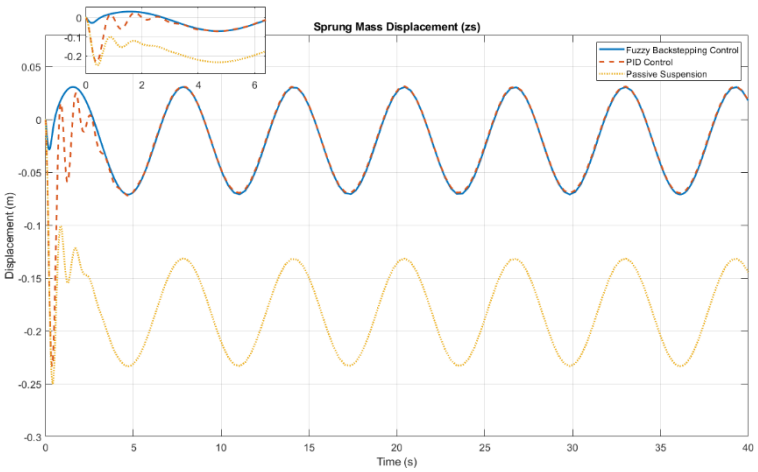

Figure 7. Sprung mass displacements

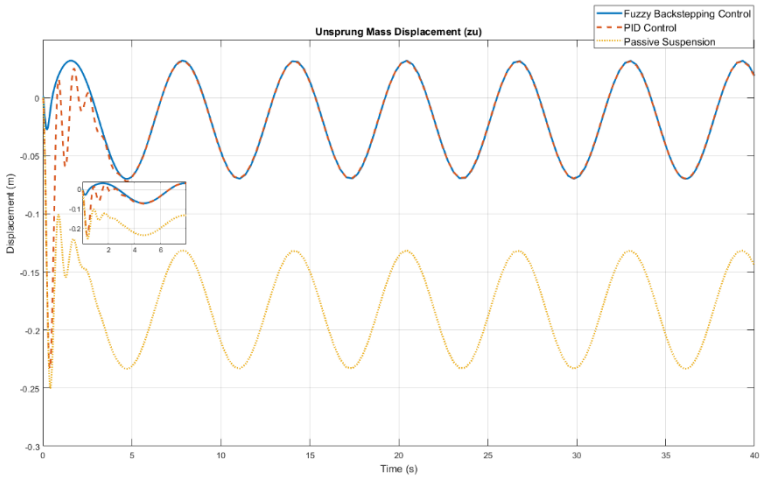

Figure 8. Unsprung mass displacements

The quarter car suspension system model was evaluated for a bump input as a different type of road disturbance, as seen in Figure 9.

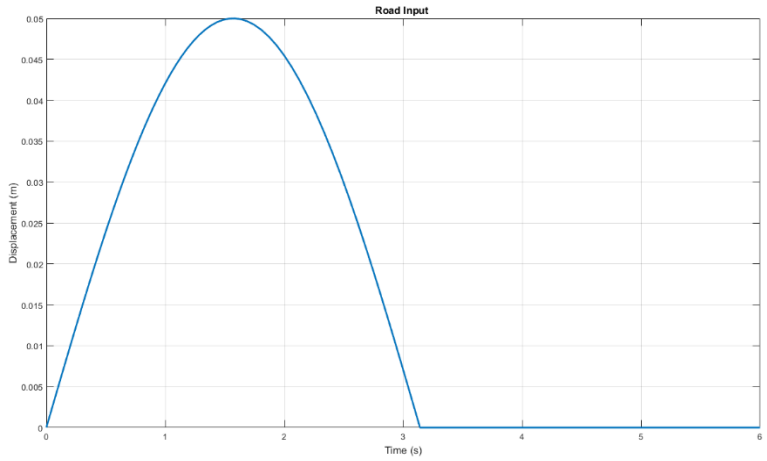

Figure 9. Bump road input

The suspension deflections and tire deflections for bump input are shown in Figures 10 and 11, respectively.

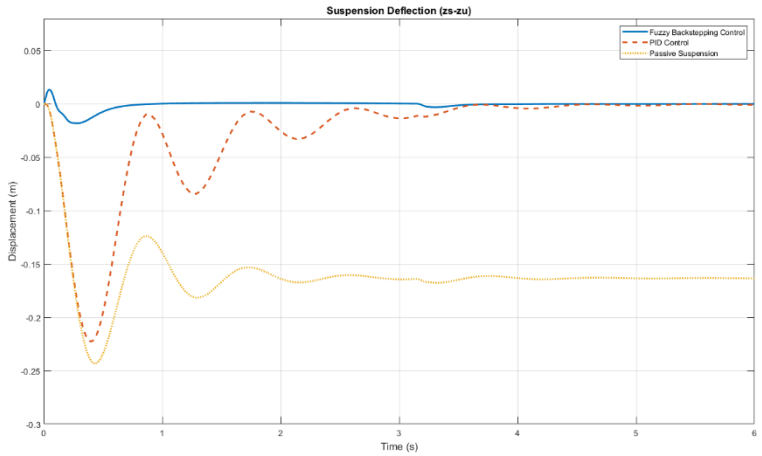

Figure 10. Suspension deflections

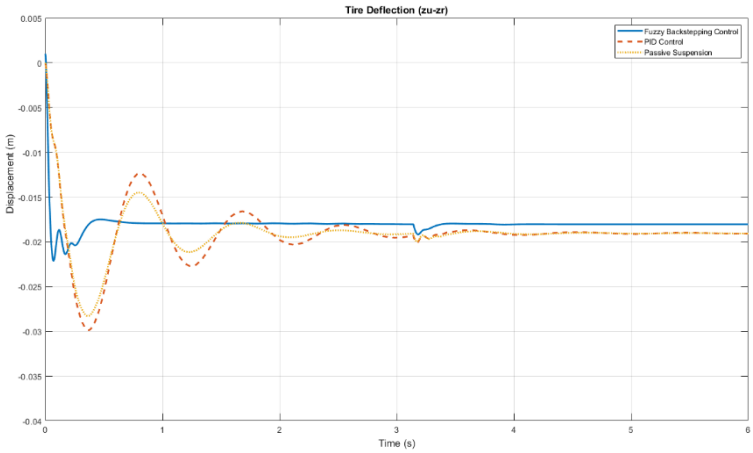

Figure 11. Tire deflections

The acceleration of sprung mass is shown in Figure 12.

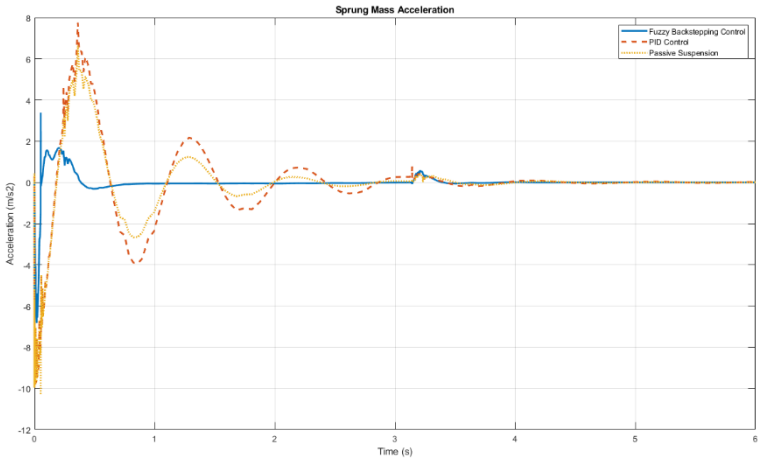

Figure 12. Sprung mass accelerations

The displacements of sprung mass and unsprung mass are shown in Figures 13 and 14, respectively.

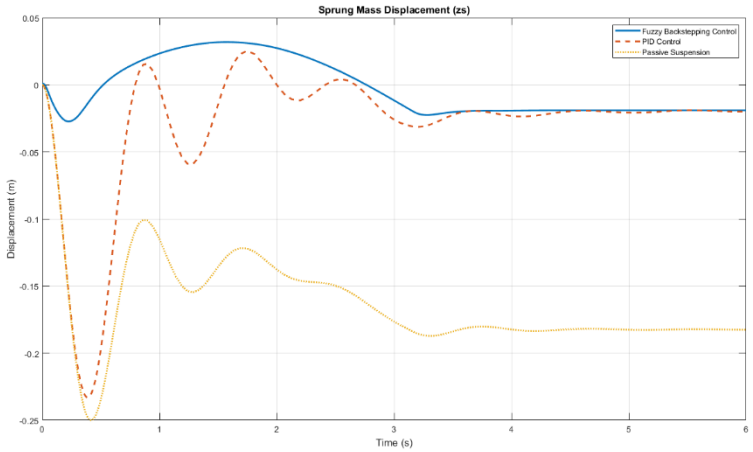

Figure 13. Sprung mass displacement

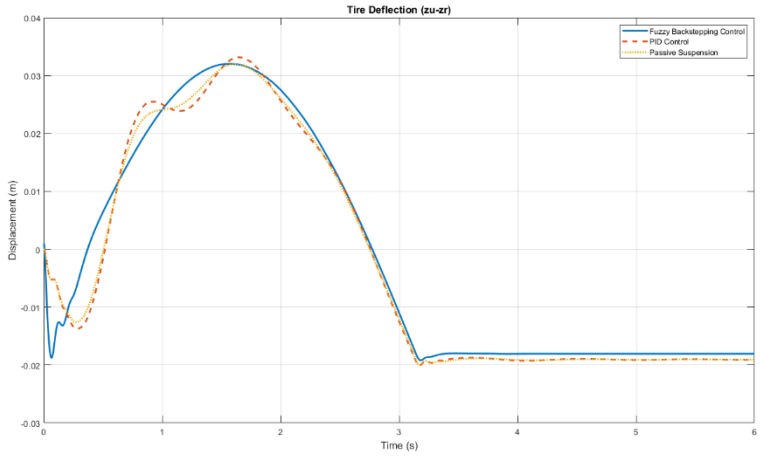

Figure 14. Unsprung mass displacement

The performance results of the passive suspension system and the active suspension systems with PID and FBC on the RMS values are seen Table 2. While ↑ shows the improvement of the value according to the passive system, ↓ indicates the decrease in the value. It can be seen from the table that FBC has superiority in all the parameters over the passive suspension system. These analytical results are consistent with the figures of the parameters. Especially the control variable, suspension deflection, has been made better with the controller, nearly 100%. Additionally, ride comfort is improved with FBC according to the acceleration improvement of nearly 100%.

Table 2. RMS values of the performance parameters for passive and active suspension systems

Parameter	Passive	PID	FBC
Suspension Deflection	0.1635	0.0008298 (↑99.49%)	0.0009724 (↑99.41%)
Tire Deflection	0.01907	0.0191 (↓1.6%)	0.01906 (↑0.5%)
Sprung Mass Acceleration	0.007385	0.02337 (↓2.2%)	0.0001465 (↑98%)

CONCLUSION

This paper presents a nonlinear controller for a nonlinear system. Backstepping controller uses Lyapunov functions for determining the control law for asymptotic stability. As a result of this natural structure, there is a bit of steady-state error in the dynamic response. To overcome this, fuzzy logic was used in this study. Sprung mass acceleration, suspension deflection, and tire deflection are chosen as performance parameters. Nearly 100 % optimization was obtained on the ride comfort with the proposed controller. Although the calculation and programming cost and the complexity of the controller are factors, the improvement in ride holding and a bit of road holding make the FBC an appropriate controller for a suspension system.

REFERENCES

Ahmed, A. A. (2021). Quarter car model optimization of active suspension system using fuzzy PID and linear quadratic regulator controllers. Global Journal of Engineering and Technology Advances, 6(3), 088-097.

Ergin, T. and M. Ö. Yatak (2023). "Optimal Control Method of Semi-Active Suspension System and Processor-in-the-Loop Verification." Applied Sciences ,13(20), 11253.

Feng, H., et al. (2025). "Adaptive Backstepping Control with Time-Delay Compensation for MR-Damper-Based Vehicle Seat Suspension." Actuators, 14(4), 178.

Kumar, V., et al. (2021). "Backstepping controller for nonlinear active suspension system." Backstepping Control of Nonlinear Dynamical Systems, Elsevier, 347-374.

Li, J., et al. (2025). "Research on sliding mode backstepping control of electro-hydraulic servo active suspension flexible system based on state observer." Journal of Vibration and Control, 10775463251347839.

Liang, Z., et al. (2025). "Adaptive Integral Terminal Sliding Mode Control to Improve Maneuverability of Electric Vehicle Considering Rollover and Inputs Saturation." IEEE Transactions on Transportation Electrification, 11(2), 6012-6024.

Şahin, N. and M. Ö. Yatak (2024). "Fuzzy Backstepping Control of Industrial Liquid Level System." Gazi Mühendislik Bilimleri Dergisi, 10(2), 355-367.

Tang, H. H. and N. S. Ahmad (2025). "Enhanced Fuzzy Logic Control for Active Suspension Systems via Hybrid Water Wave and Particle Swarm Optimization." International Journal of Control, Automation and Systems, 23(2), 560-571.

Yatak, M. Ö. and F. Şahin (2021). "Ride comfort-road holding trade-off improvement of full vehicle active suspension system by interval type-2 fuzzy control." Engineering Science and Technology, an International Journal, 24(1), 259-270.

Yim, S. (2025). "Comparative Study on Active Suspension Controllers with Parameter Adaptive and Static Output Feedback Control." Actuators, 14(3), 150.

Zhang, Y. and C. Chen (2025). "A new mixed skyhook-backstepping semi-active control approach for high-speed train magnetorheological suspension." Journal of the Brazilian Society of Mechanical Sciences and Engineering, 47(7).

➢ *ORAL PRESENTATION*

Synthesis and characterization of new generation nucleating agents for use in recycled PET masterbatches

Songül ŞAHİN DUMANKAYA[1*] (*ORCID: /https://orcid.org/0000-0001-9224-8393*),
Gökhan CEYHAN[1,2] (*ORCID: https://orcid.org/0000-0002-9127-2348)*

[1*]Kahramanmaras Sutcu Imam University, Department of Material Science And Engineering; K.Maras, Turkey;
[2]Kahramanmaras Sutcu Imam University, Technical Sciences MYO, Food Processing, K.Maraş, Turkey;

* Corresponding author e-mail : sonqulsahin@hotmail.com

Abstract

Plastics are an important group of materials, especially due to their high resistance to environmental impacts and low prices. The usage areas of recycled PET(polyethyleneterephthalate) bottles are developing rapidly. In this study, during the recycling of waste PET bottles for recycling, the mechanical properties of the material are lost at high rates due to shear stresses, temperature, thermal and oxidative degradation. This causes the material to become brittle, its gloss and stability to decrease, and its surface properties to deteriorate. It is seen in many studies that the problems caused by the use of commercial chemical additives are prevented by the use of nucleating additives. The additives used here are generally in the form of macromolecules. Alpha (α) type nucleating additives positively affect the crystallization behavior of PET. It is also expected to show a synergistic effect as a process optimizer.
In this study, a new generation of macromolecular Schiff bases were synthesized as alpha-type nucleators for the treatment of recycled PET wastes and characterized by analytical and spectroscopic techniques. As a result of FTIR analysis, υ(C=N) stretching was observed at 1500-1675cm^{-1}. This can be attributed to the imine group of the Schiff base formed. As a result of the new 1H-NMR, the proton connected to the azomethine group resonates in the δ=8-9 ppm range. The mechanical, thermal and morphological properties of the masterbatches obtained as a result of the process will be investigated for their suitability for use instead of the original raw material. At the same time, the characterization of the synthesized nucleating agents will be examined and the results in recycled PET will be investigated.
Keywords: ®PET, Recycling, Nucleating Agent

Introductıon

Recycling of plastic materials is of great importance for environmental sustainability today. Especially polyethylene terephthalate (PET) is a type of plastic with a high recycling potential as well as having a wide range of uses. One of the ways to reduce the amount of accumulated PET waste is to recycle and reuse it in industry (Kale et. al., 2007). The higher the quality of recycling, the higher the chance of reuse in bottle production and the higher the circularity, while the lower the quality, the lower the conversion to lower level products (Scheirs et. al., 2006). Although the reuse of PET bottles instead of being mixed with nature reveals the importance and diversity of PET bottle recycling, the main thing here should be the use of recycled raw materials in PET bottle production for at least 7-8 cycles by recycling from bottle to bottle (Guclu et. al., 2002). Microplastics can harm marine life in various ways. First of all, they can cause blockages in the digestive systems of sea creatures. They can also be ingested by fish. Microplastics can also absorb toxins, which can be passed on to animals that eat them (Rochman, 2020).
The use of recycled PET (rPET) brings with it the necessity to improve the mechanical and thermal properties of the material. At this point, nucleating agents play a critical role in improving material performance by accelerating the crystallization processes of polymers. Conventional nucleating agents usually have certain limitations and may have undesirable effects on recycling processes. Therefore, the development of next generation nucleating agents has become an important research area to improve the performance of recycled PET masterbatches. These new agents have the potential to both reduce environmental impacts and improve material properties. In this study, the synthesis and characterization of

next generation nucleating agents for use in recycling PET masterbatches will be discussed. The synthesis process will be optimized by combinations of different chemical components to increase the nucleation efficiency. Furthermore, the interactions of the obtained nucleating agents with rPET and their effects on material properties will be studied in detail. The results of this research aim to provide more efficient and sustainable solutions in recycling processes.

Crystallization of polymers has been studied for a long time. Crystallization of polyolefins occurs when cooled below the melting temperature. This state consists of two main parts. The first is crystallization and the second is the growth phase. Nucleation can be defined as the phenomenon where a new crystalline phase begins to form in places called cells. Nucleation processes are very important for the crystallization kinetics of polymers. In the macromolecular crystallization in the structure, nucleation is initiated first and then nucleation takes shape depending on the growth rate. In this process, whether the nucleation is in homogeneous or heterogeneous phase depends on this situation (Libster et al., 2007).

When homogeneous nucleation is achieved, the distribution of polymer chains in the melt blend is more uniform. This is due to the homogeneous distribution of nucleation and the constant velocity of the melt. Heterogeneous nucleation, on the other hand, is characterized by a variable rate and relatively low supercooling due to the presence of foreign bodies in the polymer melt, which increase the crystallization rate, act as heterogeneous nuclei and reduce the free energy required for the formation of a critical nucleus (Thierry et. al., 2006). Polypropylene (PP), the most widely used commercially, is a widely used thermoplastic material that combines unique mechanical properties and low cost. Depending on the crystallization conditions, the most widely used type is isotactic polypropylene (iPP). Some polypropylene nucleating agents found in the literature have used the α-phase or the less stable hexagonal β-phase or rarely the γ-phase (Thomann et. al., 1996, Marco et. al., 2002, Vy´chopnˇova´ et. al., 2006). The α-phase produces a thermodynamically highly stable crystal form and is therefore widely used in the crystallization of iPP. β-iPP exhibits lower melting temperature and density and is therefore used in limited areas. It exhibits higher toughness and drawability properties in this crystallization. Therefore, iPP containing β-phase is currently considered a suitable alternative to α-iPP for certain applications (Obadal et. al., 2005).

Polypropylene is used in many materials used in industry. There are many potential materials as polypropylene nucleating agents. Aromatic carboxylic acid salts such as sodium benzoate have been extensively studied. Inorganic additives such as talc and feldspar have also been used as suitable nucleators. Their intended use is determined by their cost and mechanism of action. An important disadvantage is the limited nucleation efficiency of these materials. To overcome this disadvantage, high concentrations of loading are required (Alamo et. al., 1999).

There are fewer studies on the modification of rPET by the addition of a nucleating agent, which should be adapted from PET modification studies. Modification methods of PET include copolymerization, blending and various synergistic effects. Among them, blending modification has been widely used in the field of PET modification due to its advantages of simple operation and high cost effectiveness (Babaei et. al., 2024). In a study, the role of crystalline, mobile amorphous and rigid amorphous fractions on the performance of recycled polyethylene terephthalate (PET) polymer was investigated. The crystalline regions of PET polymers are the regions where molecular chains are ordered in a regular manner. These regions can affect the mechanical strength and stiffness of the polymer. The mobile amorphous regions of PET polymers are regions where the molecular chains are arranged in a more random way, but can still move. These regions can affect the flexibility and ductility of the polymer. The rigid amorphous regions of PET polymers are regions where the molecular chains are arranged in a more disordered and fixed manner. These regions can affect the thermal behavior and chemical resistance of the polymer (Badia et. al., 2012).

MATERIALS AND METHODS

In this study, firstly, pre-treatments were applied to plastic wastes coming to Kahramanmaraş Paper Mill for the recovery of waste polyethyleneterephthalates. PET samples separated from plastic wastes were subjected to washing, drying and pulper shredding stages. The shredded PET wastes were granulated in the extruder for blending. This stage was carried out in the plastic recovery facility established within the facility. Percent dry matter content (K_m) of the obtained wastes was calculated by subtracting the first weighing from the last weighing. Combustion values were measured with a calorimeter.

PET nucleating agent synthesis was carried out by condensation reaction. The nucleation agent synthesis is denoted by the code (N_1). The nucleating agent synthesized here promotes the nucleation of the resin by crystallization and regulates the melt flow. Another important effect is to bring the crystallization cells homogeneously to the same size. As a result, it improves the hardness, heat distortion temperature, dimensional stability, transparency and gloss of the products. The reaction conditions were as follows. The

aldehyde compound was dissolved in 200 ml of methanol in a flask and stirred under a magnetic stirrer heater. The resulting solution was reafluxed at 80°C for about 48 hours under a recooler system. The reaction result was checked with TLC paper and completed. The resulting solvent was removed from the evaporator. It was separated and left to dry at room temperature. The dried sample was subjected to purification by crystallization from ethyl alcohol. The reaction scheme is given in Figure 1.

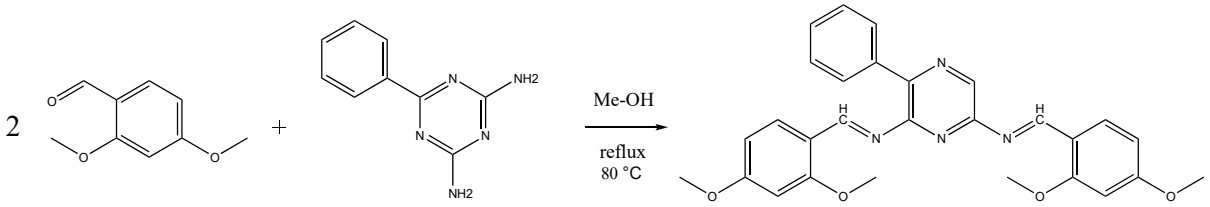

Figure 1. Synthesis mechanism of 1E,1'E)-N,N'-(3-phenylpyrazine-2,6-diyl)bis(1-(2,4-dimethoxyphenyl)methanimine (N_1)

N_1: 1E,1'E)-N,N'-(3-phenylpyrazine-2,6-diyl)bis(1-(2,4-dimethoxyphenyl)methanimine, Color: white, Melting Point: 185°C, Chemical Form: $C_{28}H_{26}N_4O_4$, Bulk Mass: 482.20, Molecular Weight: 482.54, m/z: 482.20 (100.0%), 483.20 (30.7%), 484.20 (5.7%), 483.19 (1.5%), Elemental Analysis: C, 69.70; H, 5.43; N, 11.61; O, 13.26, FTIR (υ, cm^{-1}, N_1): υ(O-C) stretching at 1085-1310 cm^{-1}, aliphatic in-plane υ(C-H) stretching at 2700-3000 cm^{-1}, aromatic in-plane υ(C-H) stretching at 3000-3300 cm^{-1}, 1500-1675 υ(C=N) stretching.

RESULTS AND DISCUSSION

In this study, a new generation of Schiff bases was synthesized for the nucleation of PET waste for the first time. Refluxing of 2,4-dimethoxybenzaldehyde and 2,6-diamino-4-phenyl-1,3,5-triazine compounds in methylated spirits yielded the pure compound 1E,1'E)-N,N'-(3-phenylpyrazine-2,6-diyl)bis(1-(2,4-dimethoxyphenyl)methanimine. For single crystal studies, it was recrystallized in ethyl alcohol medium and the obtained single crystal was sent to x-ray analysis for characterization.

For this purpose, first of all, FTIR spectra of the Schiff base compound (N_1) were carried out in the Schimadzu IRXross brand FTIR device in the laboratory of Kahramanmaraş Sütçü İmam University, ÜSKİM. The spectrum obtained is presented in Figure 2.

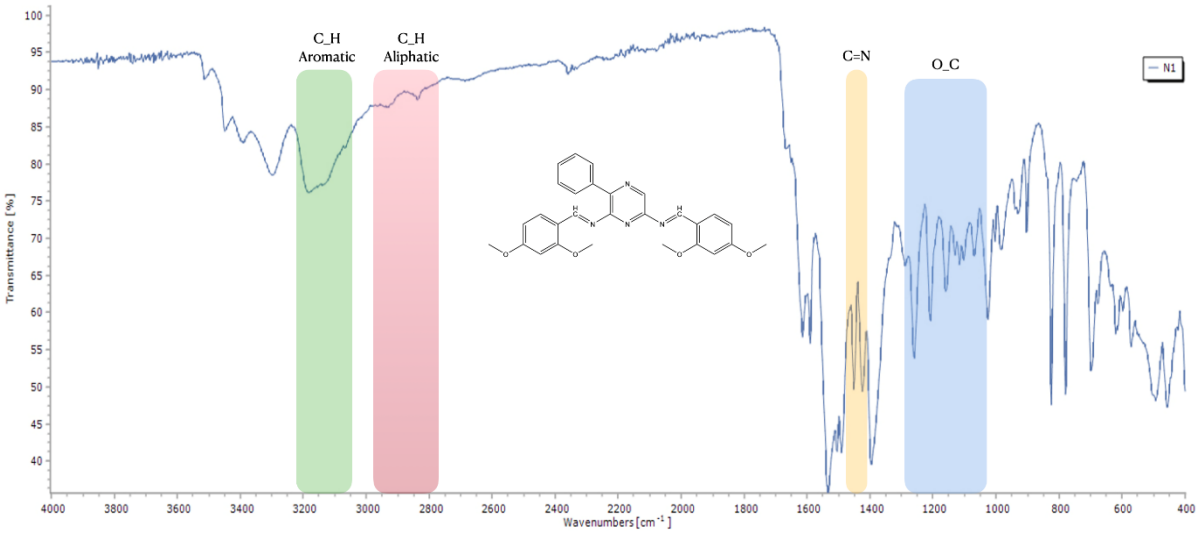

Figure 2. FTIR Spectrum of compound N_1

Looking at the FTIR spectrum, the bands observed at 3600 cm^{-1} are υ(O-H) due to the crystalline water present in the structure. The aromatic in-plane υ(C-H) stretches at 3000-3300 cm^{-1} are attributed to the aramotic rings present in the Schiff base structure. The aliphatic in-plane υ(C-H) stretching observed at 2700-3000 cm^{-1} refers to methoxy groups. The most important situation is that the band belonging to the

carbonyl group observed at 1480 cm^{-1} is converted to 1500-1675 υ(C=N) imine group. This shows that the reaction took place (Ceyhan et. al., 2012).

^{1}H-NMR spectra were taken in TMS solvent. The samples were analyzed in the Agilent 400 Mhz NMR device in the spectroscopy laboratory of Harran University, HUBTAM. According to the results obtained (Figure 3); peaks belonging to methoxy groups were observed as singlets in the range of 3.7-3.9 ppm. Singlets in the 8.0-8.5 ppm range belong to imine protons (-CH=N-). The imine protons in the Schiff base structure were determined as characteristic singlet signals in the range of 8.3-8.5 ppm due to their resonance with the conjugated system. Due to the symmetric structure of the molecule, these signals appear as a single signal, not as a pair. The protons of the 1,3,5-triazine ring are sharper due to the electronegativity of the nitrogen atoms and show signals in the range of 8.5-9.0 ppm. At 6.50-8.20 ppm, aromatic protons are observed. Protons at positions 3, 5 and 6 of the 2,4-dimethoxyphenyl rings form multiplets, especially in the range 6.50-7.00 ppm. The aromatic protons in the pyrazine ring are sharper due to the electronegative effect of nitrogen atoms and are observed in the range of 8.00-8.20 ppm. The protons belonging to the phenyl group typically appeared as multiplets in the range of 7.20-7.50 ppm.

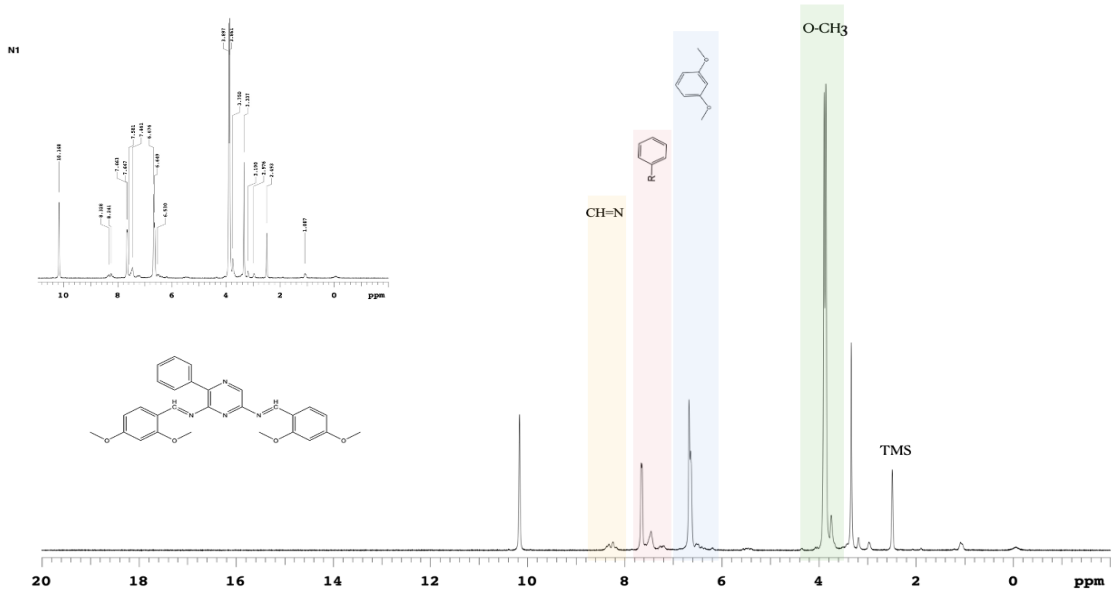

Figure 3. ^{1}H-NMR of compound N_1

^{13}C-NMR spectra were also taken in TMS solution. Looking at the spectrum (Figure 4); methoxy carbons are around 55-60 ppm; imine carbons are 160-165 ppm; aromatic carbons are between 110-150 ppm. The carbons belonging to the pyrazine ring are blocked by the effect of nitrogen. These NMR data are consistent with the expected chemical structure of the compound and support both the Schiff base formation and the symmetry of the aromatic structures (Ceyhan et. al., 2012).

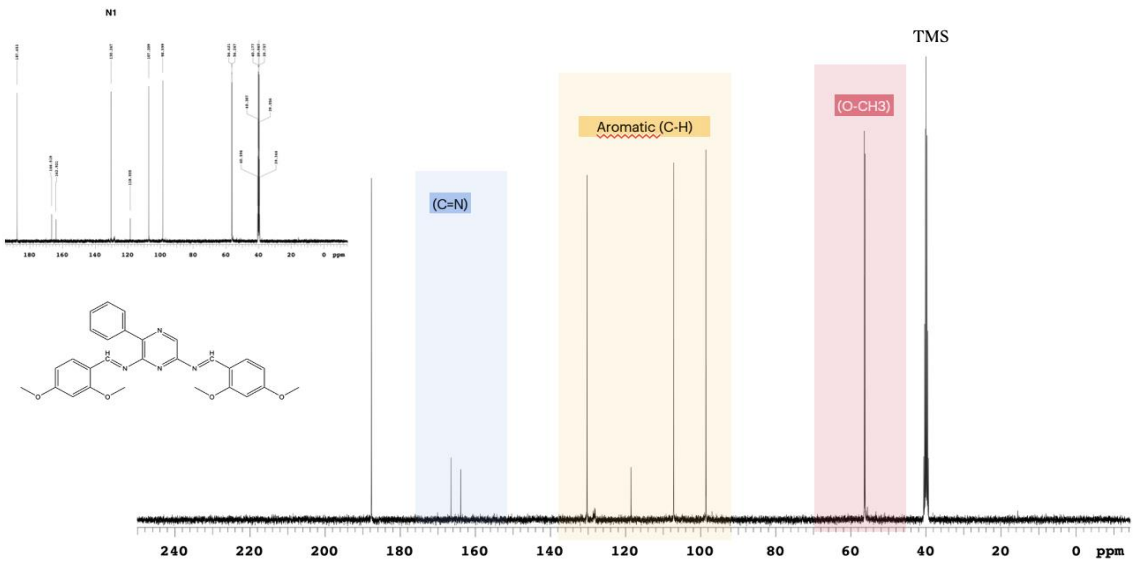

Figure 4. ^{13}C NMR Spectrum of compound N_1

CONCLUSION

In this study, a new generation Schiff base compound (N_1) synthesized to be integrated into the PET recycling process was successfully obtained and its efficiency as a nucleating agent was supported by characterization data. In FTIR analysis, characteristic peaks belonging to the imine (C=N) group were clearly observed, indicating that the target compound was successfully synthesized. Furthermore, ^{1}H-NMR and ^{13}C-NMR spectra confirmed the structural integrity and molecular symmetry of the Schiff base.

This synthesized macromolecular nucleating agent, when integrated into the PET matrix, promotes crystallization processes, resulting in more uniform and homogeneous nucleation. This led to significant improvements in product properties such as hardness, heat distortion temperature, dimensional stability, transparency and gloss. Furthermore, due to the more controlled development of crystal morphology, the performance of recycled PET has approached and in some aspects even surpassed that of the original raw materials.

The results obtained show that macromolecular Schiff bases can be used as nucleating agents in recycled PET masterbatches and contribute to sustainable materials engineering. The use of such additives is promising for more sustainable polymer production in both economic and environmental terms. In future studies, it is recommended to synthesize and comparatively analyze different Schiff base derivatives and test similar applications in other thermoplastics other than PET.

ACKNOWLEDGEMENTS

This research was supported by the Scientific and Technological Research Council of Turkey (TÜBİTAK Grant no: 118C060) and Kahramanmaraş Sütçü İmam University Scientific Research Projects Commission (KSU/BAP Project No. 2024/3-17 D6) within the scope of TÜBİTAK 2244- Kahramanmaraş Sütçü İmam University and Kahramanmaraş Kâğıt Sanayi Ticaret ve Anonim Sirketi Cooperation Industrial Doctorate Project. We would like to thank Kahramanmaraş Paper Mill R&D Center and ÜSKİM laboratories for the use of the laboratory and KOREN Chemical Company for supporting this study.

REFERENCES

Alamo, R.G., Kim, M.H., Galante, M.J., Isasi, J.R., Mandelkern, L. (1999). Structural and kinetic factors governing the formation of the g polymorph of isotactic polypropylene. Macromolecules. 32, 4050–4064.

Babaei, M.; Jalilian, M.; Shahbaz, K. (2024). Polietilen Tereftalatın Kimyasal Geri Dönüşümü: Bir Mini İnceleme. J. Environ. Chem. Eng. 12, 112507.

Badia, J.D., Strömberg, E., Karlsson, S., Ribes-Greus, A. (2012). The role of crystalline, mobile amorphous and rigid amorphous frac.

Ceyhan, C., Tümer, M., Köse, M., McKee, V., Luminesc, J. 132 (2012) 850.

Guclu, M., Alkan, G., Özdemir, B., & Ghabandari, B. (2022). Thermal stabilization of recycled PET through chain extension and blending with PBT. *Journal of Polymers and the Environment,* 1-9.

Kale, G., Kijchavengkul, T., Auras, R., & Rubino, M. (2007). Compostability of bioplastic packaging materials: An overview. *Macromolecular Bioscience, 7,*, 255-277.

Libster, D., Aserin. A., and Garti, N. (2007). Advanced nucleating agents for polypropylene.

Marco, C., Go´mez, M.A., Ellis, G., Arribas, J.M. (2002). Activity of a b-nucleating agent for isotactic polypropylene and its influ- ence on polymorphic transitions. J. Appl. Polym. Sci. 86: 531–539.

Obadal, M*., C˘erma´k, R., Stoklasa, K. (2005). Tailoring of Three-Phase Crystalline Systems in Isotactic Poly(propylene). Macromolecular Rapid Communications, 26(15), 1253-1257.

Rochman, C.M. (2020). The future of plastic pollution in the oceans. *Nature 589(7839*.

Scheirs, J., & Kaminsky, W. (2006). Feedstock recycling and pyrolysis of waste plastics. *Chichester, UK ; Hoboken, NJ : J. Wiley & Sons*, 1-41.

Thierry, A., Straupe´, C., Wittmann J.C., Lotz, B. (2006). Polymers for Advanced Technologies, 18(9), 685-695.Organogelators and polymer crystallisation. Macromol. Symp. 241: 103–110.

Thomann, R., Wang, C., Kressler, J., Muelhaupt, R. (1996). On the gamma-phase of isotactic polypropylene. Macromolecules. 29: 8425–8434.

Vy´chopn˘ova´, J., Habrova´, V., Obadal, M., Cerma´k, R., Cabla, R. (2006). Crystallization of polypropylene with a minute amount of b-nucleator. J. Therm. Anal. Cal. 86: 687–691.

➢ *ORAL PRESENTATION*

Mancozeb Toksisitesinin Nil Tilapiası *Oreochromis niloticus'un* Solungaçlarında SOD enzim aktivitesine etkisi

Özge TEMİZ* (*ORCID: https://orcid.org/0000-0003-0668-5744*)

*Osmaniye Korkut Ata Üniversitesi, Sağlık Hizmetleri Meslek Yüksekokulu, Tıbbi Hizmetler ve Teknikler Bölümü, Osmaniye, Türkiye

*Sorumlu yazar e-posta:ozgetemiz@osmaniye.edu.tr

Özet

Mancozeb (MNC), sucul organizmalar üzerinde önemli etkilere sahip olan ve çok miktarda, çeşitlilikte kullanılan fungusitlerden biridir. MNC'nin toksikolojik etkilerini araştırmak için dünya genelinde iyi bir model organizma olarak Nil tilapyasını (*Oreochromis niloticus*) kullanarak MNC'nin su canlıları üzerindeki olumsuz etkilerini göstermek büyük öneme sahiptir. Deney canlısı *Oreochromis niloticus*'un kontrol grubuyla birlikte MNC maruziyet konsantrasyonlarında 0.1 ppm ve 0.5 ppm etkisinde 48 saat boyunca toksisite etkileri belirlenmiştir. Çalışmada *Oreochromis niloticus*'un solungaç dokusunda oksidatif hasara karşı ilk enzimatik koruma elemanları olan süperoksit dismutaz (SOD) enzim aktivitelerinde olan değişimler araştırılmıştır. Mancozeb maruziyeti sonucu 48 saat etkide *Oreochromis niloticus*'un solungaç dokusunda 0.1 ppm ve 0.5 ppm konsantrasyonlarda kontrol grubuna göre SOD enzim aktivitesinde sırasıyla %24 ve %56 azalma belirlenmiştir. Bu çalışmanın sonuçları, Nil tilapyasını MNC toksisitesinin kısa süreli maruziyette sucul organizmalar üzerindeki etkilerinin biyomarkırlar ile belirlenmesini de amaçlamıştır.

Anahtar Kelimeler: Mancozeb, Solungaç, Süperoksit dismutaz

Effect of Mancozeb Toxicity on SOD Enzyme Activity in Gills of Nile Tilapia *Oreochromis niloticus*

Abstract

Mancozeb (MNC) is one of the fungicides that have significant effects on aquatic organisms and are used in large quantities and in a variety of ways. It is of great importance to show the adverse effects of MNC on aquatic organisms by using Nile tilapia (*Oreochromis niloticus*) as a good model organism worldwide to investigate the toxicological effects of MNC. The toxicity effects of the experimental organism Oreochromis niloticus were determined with the control group at MNC exposure concentrations of 0.1 ppm and 0.5 ppm for 48 hours. In the study, changes in the superoxide dismutase (SOD) enzyme activities, which are the first enzymatic protection elements against oxidative damage in the gill tissue of Oreochromis niloticus, were investigated. As a result of exposure to Mancozeb, a decrease of 24% and 56% in SOD enzyme activity was determined in the gill tissue of Oreochromis niloticus at 0.1 ppm and 0.5 ppm concentrations, respectively, compared to the control group within 48 hours. The results of this study also aimed to determine the effects of MNC toxicity on aquatic organisms with biomarkers in short-term exposure of Nile tilapia.

Key Words: Mancozeb, Gill, Superoxide dismutase

GİRİŞ

Pestisitler, tarımda mahsullerinin zararlı etkisinden korunması için geniş çeşitlilik ve miktarda kullanılır. Bu kullanımın tarım ürünleri üzerinde insanlara bunun yanında sulama ve yağış nedeniyle de doğaya salınarak ekoloji üzerinde geri dönüşü olmayan ekosistemin bozulmasına sebep olur (Soare ve ark., 2014). Günümüzde bir çok kirleticinin yüzey sularıyla sucul ortama ulaşması da su kaynaklarının ve sucul ekosistemin üzerinde olumsuz etkileri önemli endişe kaynağı oluşturmaktadır.

Fungisitler, su ortamında önemli kirliliğe sebep olan ve mantar hastalıkları için yaygın olarak kullanımı olan pestisid türlerinden biridir (Temiz, 2019). Fungisit mancozeb tarım ve diğer sektörlerde geniş uygulamalara sahip olan bis-ditiyokarbamat alt grubuna ait carbamate grubu fungusittir (Srivastava ve Ajay Singh, 2014). Birçok çalışmada MNC'nin sucul organizmaların üzerinde olan toksikolojik etkisinin

kan parametreleri ve antioksidan toksisitesi dahil olmak üzere rapaorladılar (Lutnicka ve ark., 2016; Kanu ve ark., 2023; Chijioke ve ark., 2024).

Sucul organizmalar içerisinde balıklar, yüksek kirletici duyarlılığı, metabolize etme yetenekleri ve biyolojik birikiminin belirlenmesi nedeniyle su ortamlarında oluşan pestisit toksisitesini değerlendirilmesi için iyi bir biyoindikatör modeldir (Fazio ve ark., 2013). Nil tilapisi, *Oreochromis niloticus*, su ürünleri olarak dünya üzerinde tüketilen, dayanıklı bir tür olması nedeniyle araştırmalar için önemli bir balık türüdür.

Pestisitlerin kirliliğinin hedef dışı organizmalar üzerindeki etkileri, organizmalardaki fizyolojik, biyokimyasal veya moleküler düzeylerdeki değişiklikleri tespit ederek incelenebilir ve çevre kalitesinin izlenmesinde erken uyarı araçları sağlar (Khan ve ark., 2025). Erken uyarı biyobelirteçleri, çevresel kirleticilerin ve biyolojik canlılar arasındaki etkileşimin gösterilmesini sağlar. Bu biyobelirteçlerin inhibisyonu ya da indüklenmesi, kirleticilerin çevresel organizmalar üzerindeki potansiyel toksik etkilerini göstermek açısından önem arz eder (Sharma ve ark., 2016).

Bu çalışmada Mancozeb maruziyeti 48 saat etkisinde *O. niloticus*'un solungaç dokusunda SOD enzim aktivitesinde olan değişimler araştırılmıştır.

MATERYAL VE METOD

Mancozeb, ticari olarak satılan Syngenta Abic (Mancozeb 75 % WP) isimli ürünü alınmıştır. Daha önceki çalışmada belirlenen *O. niloticus* canlısı Mancozeb 96 saat LC_{50} değerine (11,5 ppm) göre çalışmamızda kullanılan konsantrasyonlar belirlendi (Rahman ve ark., 3023).

Oreochromis niloticus deney canlısında 3 grup ile yapılan deneyde kontrol grubu ile beraber 0.1 ppm ve 0.5 ppm konsantrasyonlarında deney süreci 48 saat boyunca devam edilmiştir.

Deneylerde kullanılan *O. niloticus* türünün ortalama boyu 10,98±0,54 cm, ağırlığı ise 22,43±1,07 gr olarak ölçülmüştür. 40x40x40 cm boyutta cam akvaryumlara dinlendirilmiş musluk suyu ile 40 L doldurulmuştur. Akvaryumlarda merkezi sistem ile havalandırma yapılmıştır. Laboratuvar ortamında 12/12 saat fotoperiyodik periyodu uygulanmıştır.

Cam akvaryumlarda yapılan deneylerde su kalitesi ölçülerek planlanmış bir canlı hayvan deneyi gerçekleştirilmiştir. Toksisisite çalışmalarında toksik kimyasal miktarında toksik deney kimyasal miktarını su içerisinde sabit tutmak amacıyla 24 saat aralıklarla su değişimi ve toksik madde eklemesi yapılmıştır. Deney sonu 48 saat etkiden sonra dekapitasyon yöntemiyle öldürülen balıklardan solungaç dokuları disekte edilerek çıkarılmıştır. Solungaç dokusu fizyolojik tuz çözeltisi (%0.59 NaCl) ile yıkandıktan sonra biyokimyasal analizler yapılana kadar -80 ^{o}C'ye kaldırılmıştır. Solungaç dokusu %1,17 KCl içeren pH 7.4, 0,1M sodyum-fosfat tamponunda, 1/10 oranında seyreltilerek 3 dk homojenize edilmiştir.

Homojenatların +4 ^{o}C'de 16000 rpm'de 20 dakika santrifüjden sonra elde edilen süpernatantlar süperoksit dismutaz (McCord & Fridovich, 1969) enzim aktivitelerinde olan değişimler belirlenmiştir.Ayrıca Bradford (1976) yöntemiyle protein miktarı belirlenerek istatiksel olarak hesaplamalar yapılarak deneysel süreçte olan enzimatik değişimler karşılaştırılmıştır. İstatiksel analizler SPSS 16 programında One-way Anova Duncan testi kullanılmıştır.

BULGULAR ve TARTIŞMA

Tarım alanında, mahsullerin verimini arttırmak için pestisitler çeşitli planlamalar ile kullanılır (Mansour ve ark., 2023). Ekolojik ve insan üzerindeki tehlikeli etkileri nedeniyle, artan pestisit kirliliği ciddi bir sağlık riskini oluşturmaktadır (Hamed vd., 2021). Mancozeb bir Fungisit grubu pestisittir, mantarların kötücül etkilerinin ve mantar hastalıklarının önlemek amacıyla geniş bir çeşitlilikte mahsuller üzerinde uygulanan pestisitlerdir (Brody ve ark., 2013). Canlıda hücresel düzeyde metabolik faaliyetler sonucu sürekli üretilen serbest radikaller çeşitleri hücrede savunma sistemi olarak bulunan antioksidan savunma sistemleri tarafından yok edilmektedir (Li ve ark., 2010). Canlıda antioksidan savunma sistemleri enzimler aracılığıyla ya da enzim olmadan olan sistemler bulunmaktadır. Süperoksit dismutaz (SOD), katalaz (CAT) gibi enzim yapıları hücrede serbest radikallere karşı ilk savunma sistemini oluşturur (Rahman ve ark., 3023).

Çalışmamızda Mancozeb maruziyeti 48 saat etkisinde 0.1 ppm ve 0.5 ppm konsantrasyonlarında *Oreochromis niloticus* solungaç dokusunda SOD enzim aktivitesinde kontrol grubuna göre %24 ve %56 azalma olduğu belirlendi. Benzer bir araştırmada Rahman ve ark., (2023) çalışmasında 1.15 ppm MNC maruziyetinde *O. niloticus* karaciğer dokusunda SOD enzim aktivitesi control grubuna göre önemli azalma olduğu bildirildi. Oksidatif stresin tetiklenmesine sebep olan pestisitler bu çalışmada kullanılan mancozeb,

ROS'un aşırı üretimine sebep olduğunu göstermektedir. Aşırı ROS ise hücrenin antioksidan savunma sistemi dengesini bozarak oksidatif stres sonucu SOD enzim aktivitelerinde hızlı aktivite kaybına sebep olduğu düşünülmektedir. Araştırmamıza benzer sonuçları olan İbrahim ve ark., (2023) çalışmalarında *O. niloticus*'un karaciğer dokusunda mancozeb maruziyetinin 4, 8, 12, 16 ve 20 ppm düzeylerinde etkilerinde kontrol grubuna göre doza bağlı artış oldukça SOD enzim aktivitesinde önemli bir azalma olduğu raporlandı.

Sonuç olarak çalışmamızda 48 saat etkide mancozeb maruziyetinin *O. niloticus* solungaç dokusunda antioksidan system üzerinde önemli etki gösterdiği, SOD enzim aktivitesinin pestisit toksisitesine karşı önemli hassasiyet göstererek toksikoloji araştırmalarında biyomarkır olarak değerlendirilmesinin önemi çalışmalarda önemli katkı sağlayacağını göstermiştir.

KAYNAKLAR

Bradford, M. M. (1976). A rapid and sensitive method for the quantitation of microgram quantities of protein utilizing the principle of protein-dye binding. Analytical biochemistry, 72(1-2), 248 254.

Brody, A. H., Chou, E., Gray, J. M., Pokyrwka, N. J., & Raley-Susman, K. M. (2013). Mancozeb-induced behavioral deficits precede structural neural degeneration. Neurotoxicology, 34, 74-81.

Chijioke, F. O. N., Chinedu, N., Benjamin, A., & JC, I. (2024). Toxicity of mancozeb on the African catfish *Clarias gariepinus* juveniles kidney, liver and spleen histoarchitecture. J. Clin. Toxicol, 14, 555.

Cristina Soare, L., Păunescu, A., & Cristina Maria, P. (2019). The Morphophysiological, Histological, and Biochemical Response of Some Nontarget Organisms to the Stress Induced by the Pesticides in the Environment. IntechOpen. doi: 10.5772/intechopen.84332

Fazio, F., Faggio, C., Torre, A., Sanfilippo, M., & Piccione, G. (2013). Effect of water quality on hematological and biochemical parameters of Gobius niger caught in Faro lake (Sicily).

Hamed, H. S., Ismal, S. M., & Faggio, C. (2021). Effect of allicin on antioxidant defense system, and immune response after carbofuran exposure in Nile tilapia, Oreochromis niloticus. *Comparative Biochemistry and Physiology Part C: Toxicology & Pharmacology*, *240*, 108919.

Ibrahim, R. E., Elbealy, M. A., Salem, G. A., Abdelwarith, A. A., Younis, E. M., Wagih, E., ... & Rahman, A. N. A. (2023). Acute mancozeb-fungicide exposure induces neuro-ethology disruption, health disorders, and immune-oxidative dysfunction in Nile tilapia (Oreochromis niloticus). *Aquatic Toxicology*, *261*, 106630.

Kanu, K. C., Okoboshi, A. C., & Otitoloju, A. A. (2023). Haematological and biochemical toxicity in freshwater fish *Clarias gariepinus* and *Oreochromis niloticus* following pulse exposure to atrazine, mancozeb, chlorpyrifos, lambda-cyhalothrin, and their combination. Comparative Biochemistry and Physiology Part C: Toxicology & Pharmacology, 270, 109643.

Khan, A. A., Dwivedi, S., Singh, S., Kumar, M., & Trivedi, S. P. (2025). Perturbations in Redox Status, Biochemical Indices, and Expression of XBP1s and NOX4 in the Liver of *Channa punctatus* Following Exposure to Mancozeb. *Gene Expression*, *24*(1), 21-29.

Li, Z. H., Velisek, J., Zlabek, V., Grabic, R., Machova, J., Kolarova, J., & Randak, T. (2010). Hepatic antioxidant status and hematological parameters in rainbow trout, Oncorhynchus mykiss, after chronic exposure to carbamazepine. Chemico-biological interactions, 183(1), 98-104.

Lutnicka, H., Bojarski, B., Ludwikowska, A., Wrońska, D., Kamińska, T., Szczygieł, J., ... & Formicki, G. (2016). Hematological alterations as a response to exposure to selected fungicides in common carp (*Cyprinus carpio L.*). Folia Biologica (Kraków), 64(4), 235-244.

Mansour, A. T., Amen, R. M., Mahboub, H. H., Shawky, S. M., Orabi, S. H., Ramah, A., & Hamed, H. S. (2023). Exposure to oxyfluorfen-induced hematobiochemical alterations, oxidative stress, genotoxicity, and disruption of sex hormones in male African catfish and the potential to confront by Chlorella vulgaris. Comparative Biochemistry and Physiology Part C: Toxicology & Pharmacology, 267, 109583.

McCord, J. M., & Fridovich, I. (1969). Superoxide dismutase: An enzymatic function for erythrocuprein (hemocuprein). The Journal of Biochemistry, 244, 6049 6055.

Pallavi Srivastava, P. S., & Ajay Singh, A. S. (2014). Potential effects of agricultural fungicide (Mancozeb) on fish *Clarias batrachus.*

Rahman, A. N. A., Altohamy, D. E., Elshopakey, G. E., Abdelwarith, A. A., Younis, E. M., Elseddawy, N. M., ... & Ibrahim, R. E. (2023). Potential role of dietary Boswellia serrata resin against mancozeb

fungicide-induced immune-antioxidant suppression, histopathological alterations, and genotoxicity in Nile tilapia, *Oreochromis niloticus*. Aquatic Toxicology, 265, 106738.

Sharma, M. R., Mushtaq, R., Allayie, S. A., & Vardhan, H. (2016). Assessment of lethal toxicity of Mancozeb and its consequences on the behavior of fresh water fish, Puntius ticto. *Journal of International Academic research for Multidisciplinary*, *4*(2), 132-138.

Temiz, O. (2019). *Oreochromis niloticus*' un karaciğerinde fungisit propiconazole'un oksidatif stres parametreleri ve antioksidan sistem enzimleri üzerine etkileri. Journal of Anatolian Environmental and Animal Sciences, 4(1), 43-47.

➢ *ORAL PRESENTATION*

İmidacloprid Toksisitesinin *Oreochromis niloticus* Beyin dokusunda Asetilkolinesteraz Aktivitelerinde Oluşan Yanıtlar

Özge Temiz* (*ORCID: https://orcid.org/0000-0003-0668-5744*)

*Osmaniye Korkut Ata Üniversitesi, Sağlık Hizmetleri Meslek Yüksekokulu, Tıbbi Hizmetler ve Teknikler Bölümü, Osmaniye, Türkiye

*Sorumlu yazar e-posta:ozgetemiz@osmaniye.edu.tr

Özet

Neonikotinoid İmidacloprid'in (IMI) toksisite çalışmasında *Oreochromis niloticus*'un kontrol grubuyla birlikte 0,5 ppm ve 1 ppm sublethal konsantrasyonları etkisinde 24 ve 48 saat boyunca toksisitesi araştırıldı. *Oreochromis niloticus*'un beyin dokusunda asetilkolinesteraz (AChE) enzim aktivitesinde olan değişimler araştırılmıştır. *Oreochromis niloticus*'un beyin dokusunda 24 ve 48 saat maruziyetinde imidacloprid etkisinde AChE enzim aktivitelerinde kontrol grubuna göre önemli bir azalma olduğu belirlendi. 24 saat etkide 0,5 ppm ve 1 ppm sublethal konsantrasyonlarda kontrol grubuna göre sırasıyla %11 ve %28 azalma belirlendi. 48 saat etkide 0,5 ppm ve 1 ppm sublethal konsantrasyonlarda kontrol grubuna göre sırasıyla %43 ve %61 azalma belirlendi. İmidacloprid toksisitesi sonucunda *Oreochromis niloticus*'un beyin dokusunda olan nörotoksik etkileri kısa sürede gösterebildiği ve önemli değişimlere neden olduğu belirlenmiştir.

Anahtar Kelimeler: İmidacloprid, Beyin, Asetilkolinesteraz

Responses of Imidacloprid Toxicity to Acetylcholinesterase Activities in *Oreochromis niloticus* Brain Tissue

Abstract

In the toxicity study of the neonicotinoid Imidacloprid (IMI), toxicity was investigated for 24 and 48 hours under the effect of 0.5 ppm and 1 ppm sublethal concentrations of *Oreochromis niloticus* with the control group. Changes in acetylcholinesterase (AChE) enzyme activity in the brain tissue of *Oreochromis niloticus* were investigated. It was determined that there was a significant decrease in AChE enzyme activities under the effect of imidacloprid in the brain tissue of *Oreochromis niloticus* under the effect of 24 and 48 hours of exposure compared to the control group. In the 24-hour effect, 11% and 28% decreases were determined compared to the control group at 0.5 ppm and 1 ppm sublethal concentrations, respectively. In the 48-hour effect, 43% and 61% decreases were determined compared to the control group at 0.5 ppm and 1 ppm sublethal concentrations, respectively. As a result of imidacloprid toxicity, it was determined that *Oreochromis niloticus* can show neurotoxic effects on brain tissue in a short time and cause significant changes.

Keywords: Imidacloprid, Brain, Acetylcholinesterase

GİRİŞ

Neonikotinoidler sinir sistemi üzerinde etkisi olan tarımsal ürünlerin eldesinde verimi arttırmak için kullanılan bir pestisit sınıfıdır. Neonikotinoidlerin ilk çıkışı 1991 senesinde İmidaclporid ticari formülasyonu ilk olarak kullanıma çıkarılmıştır (Bass ve ark., 2015). Neonikotinoid sınıfı pestisitler de dahil olmak üzere tarımsal amaçlı kullanımı dünya çapında aynı zamanda çevre ve halk sağlığı üzerinde de zararlı etkilere sahiptir (Cimino ve ark., 2017).

Pestisitler çok çeşitli ve büyük miktarda kullanımı besin zincirinde ve su kütlelerinde birikerek ekolojik zincirde balık gibi su canlılarında birikebilir. Pestisitler kısa vadeli fayda sağladığı fakat uzun süre kullanımları zararlı maddelerin birikmesine yol açabilir ve sonuç olarak su ekosistemlerine ve insan sağlığına zarar verir (Chang ve ark., 2020). İmidaclporid, ilaçlama anında püskürtme sırasında yada sonrasında yüzeyden ve tarım çiftliklerinden gelen su drenajıyla akan su ortamına geçer (Miraglia ve ark., 2009; Jeschke ve ark., 2011; Amenyogbe ve ark., 2021).

Neonikotinoidler, zararlıların merkezi sinir sisteminin post sinaptik merkezde olan nikotin asetilkolin reseptörüne (nAChR) affinite gösterir ve sinir sistemini sekteye uğratarak toksik mekanizmasını gösterir (Tomizawa & Casida, 2005). Ayrıca sinir uyarısında iletimi kolinerjik sinapslarda asetil (ACh) ve

bütirilkolinin (BCh) parçalanmasını sağlayan asetilkolinesterazların ve bütirilkolinesterazların (AChE ve BChE) aktivitesini etkiler (Somogyvári ve ark., 2022).

Nil tilapisi (*Oreochromis niloticus*) dünya üzerinde yaygın olarak dağılım gösteren, omnivor beslenen tropikal bir balık türüdür. Ticari olarak önemi yüksek olan özellikle yaygın dağılımı ile alan ve laboratuvar araştırmaları için su kirleticilerinin etkilerinin incelemesi ve değerlendirilmesi açısından değerli bir model organizmadır. Tilapia türleri, çok çeşitli çevre koşullarına dayanıklılık sağlamaları, hızlı büyümeleri ve erken üremeleriyle su ürünleri yetiştiriciliğinde içinde elverişli bir tür olarak bilinmektedir (FAO, 2018; FAO, 2022).

Çalışmada kontrol grubuyla birlikte imidacloprid maruziyet konsantrasyonları olan 0,5 ppm ve 1 ppm etkisinde 24 ve 48 saat etki süresinde toksisite etkileri *Oreochromis niloticus*'un beyin dokusunda AChE enzim aktivitelerinde olan değişimler araştırılmıştır.

MATERYAL VE METOD

İmidaclporid'in ticari olarak Hekdivor 600 FS isimli ürünü alınmıştır. *Oreochromis niloticus* deney canlısında kontrol grubu ile beraber 0,5 ppm ve 1 ppm sublethal konsantrasyonları deney süreci etkisinde 24 ve 48 saat uygulanmıştır. Deneylerde kullanılan *O. niloticus* türünün ortalama boyu 12,4±0,34 cm, ağırlığı ise 22,11±0,34 gr olarak ölçülmüştür. Kontrol grubu ve toksisite denemelerinde akvaryumlarda her grupta 3 balık olacak şekilde tekrarlı olarak çalışıldı. Boyutları 40x40x40 cm olan cam akvaryumlarda dinlendirilmiş musluk suyu ile 50 L doldurulmuş ve akvaryumlar havalandırmaları merkezi sistem ile planlı bir şekilde havalandırılmaktadır.

Laboratuvar ortamında 12/12 saat fotoperiyodik period sistemi ile düzenli gece/gündüz uygulaması yapılmaktadır.

Deneyde kullanılan akvaryum su kalitesi parametreleri:

sıcaklık 23 ± 0.6 °C,

pH 7,54 ± 0,32,

çözünmüş oksijen 6,34±0,24 mg/L,

alkalinite 236 mg/L $CaCO_3$,

sertlik 264 mg/L $CaCO_3$ olarak hesaplanmıştır.

Toksik deneylerde kimyasal miktarında azalmayı önlemek amacıyla 24 saat aralıklarla su değişimi ve toksik madde eklemesi yapılmıştır. 24 ve 48 saat sonunda dekapitasyon yöntemiyle öldürülen balıklardan Beyin dokuları disekte edilerek çıkarılmıştır.Araştırma yapılmak üzere beyin dokusu fizyolojik tuz çözeltisi (%0.59 NaCl) ile yıkandıktan sonra biyokimyasal analizler için -20°C sıcaklıkta saklanmıştır. Beyin dokusu %1,17 KCl içeren pH 7.4, 0,1M sodyum-fosfat tamponunda, 1/20 oranında seyreltilerek 2 dk homojenize edilmiştir.

Homojenatların 16000 rpm'de +4 °C'de 20 dakika sürede santrifüj edildikten sonra elde edilen süpernatantlar AChE enzim aktivitelerinde Ellman (1961) yöntemiyle olan aktivasyonda olan değişimler belirlenmiştir. Ek olarak toplam protein miktarı Bradford (1976) yöntemiyle belirlendi. Çıkan sonuçlar hesaplamalar yapılarak deneysel süreçte olan enzimatik değişimlerde istatistik olarak kontrol grubuna karşı karşılaşma yapılmıştır. İstatiksel analizler SPSS 16 programında One-way Anova Duncan testi kullanılmıştır.

BULGULAR ve TARTIŞMA

IMI'nin suda kimyasal yapısı gereği uzun süre sabit kaldığını ve ekosistem içersinde dağılarak kimyasal yapısını bozmadan gösterildi, IMI'nin kimyasal yapısının bertaraf edilmemesi durumu, daha sonradan çevre yoluyla ulaştığı organizmalar üzerinde önemli toksik etkilerine sebep olur (Tišler ve ark., 2009).

Çalışmamızda *O. niloticus*'un beyin dokusunda 24 ve 48 saat maruziyetinde imidacloprid etkisinde AChE enzim aktivitelerinde kontrol grubuna göre önemli bir azalma olduğu belirlendi. 24 saat etkide 0,5 ppm ve 1 ppm sublethal konsantrasyonlarda kontrol grubuna göre sırasıyla %11 ve %28 azalma belirlendi. 48 saat etkide 0,5 ppm ve 1 ppm sublethal konsantrasyonlarda kontrol grubuna göre sırasıyla %43 ve %61 azalma belirlendi. Gajula ve ark., (2023) çalışmasında imidacloprid etkisinde 66.6 mg/lt maruziyetinde Labeo rohita balığında beyin ve kas dokularında 28 ve 42 gün etkilerinde AChE enzim aktivitelerinde kontrol grubuna göre önemli azalma olduğu belirlendi. Neonikotinoid türü pestisitlerin ve metabolitlerinin, nikotine benzer olan ve kan-beyin bariyerini kolayca geçen ChE aktivitelerini değiştirmeye yönelik daha yüksek bir afinite gösterir ve hayvan çalışmalarında görüldüğü gibi potansiyel olarak nörolojik etkilere neden olduğu raporlanmıştır (Özdemir ve ark., 2014). Önceki çalışmalarda genel olarak pestisitlerin balık dokularında AChE inhibisyonuna neden olabileceğini gösterilmiştir (Xing ver ark., 2013; Zouaoui ve ark., 2024). Toksik pestisitlerin kullanımının azaltılması ya da kullanılmaması birçok alanda tarım faaliyetleri, gıda paketleme, hayvancılık gibi alanlarda daha az zararlı bir ilaçlama ya da koruyucu programların oluşmasa ayrıca daha fazla araştırma ve evrensel bilinç programları ile toksik etkilerin bertarafı sağlanmalıdır.

KAYNAKLAR

Agriculture Organization of the United Nations. Fisheries Department. (2018). The state of world fisheries and aquaculture. Food and Agriculture Organization of the United Nations.

Amenyogbe, E., Huang, J. S., Chen, G., & Wang, Z. (2021). An overview of the pesticides' impacts on fishes and humans. International Journal of Aquatic Biology, 9(1), 55-65.

Bass, C., Denholm, I., Williamson, M. S., & Nauen, R. (2015). The global status of insect resistance to neonicotinoid insecticides. Pesticide biochemistry and physiology, 121, 78-87.

Bradford, M. M. (1976). A rapid and sensitive method for the quantitation of microgram quantities of protein utilizing the principle of protein-dye binding. Analytical biochemistry, 72(1-2), 248 254.

Chang, Y., Mao, L., Zhang, L., Zhang, Y., & Jiang, H. (2020). Combined toxicity of imidacloprid, acetochlor, and tebuconazole to zebrafish (Danio rerio): acute toxicity and hepatotoxicity assessment. Environmental Science and Pollution Research, 27, 10286-10295.

Cimino, A. M., Boyles, A. L., Thayer, K. A., & Perry, M. J. (2017). Effects of neonicotinoid pesticide exposure on human health: a systematic review. Environmental health perspectives, 125(2), 155-162.

Dos Santos, D. R., Yamamoto, F. Y., Filipak Neto, F., Randi, M. A. F., Garcia, J. E., Costa, D. D. M., ... & de Oliveira Ribeiro, C. A. (2016). The applied indicators of water quality may underestimate the risk of chemical exposure to human population in reservoirs utilized for human supply—Southern Brazil. Environmental Science and Pollution Research, 23, 9625-9639.

Ellman, G.L., Courtney, K.D., Andres, V., Featherstone, R.M., 1961. A New and Rapid Colorimetric Determination of Acetylcholinesterase Activity. Biochemistry and Pharmacology, 7: 88-95.

Fisheries FAO, Aquaculture D (2022) The state of world fisheries and aquaculture (SOFIA). Towards blue transformation. Rome: Food and Agriculture Organization (FAO) of the United Nations, Rome, p 266.

Gajula, S. K., Kanthala, S. K., Narra, M. R., & Vanamala, V. D. (2023). Individual and interactive biochemical profile damages in Labeo rohita (Cyprinidae) by imidacloprid and clothianidin. Comparative Biochemistry and Physiology Part C: Toxicology & Pharmacology, 271, 109689.

Jeschke, P., Nauen, R., Schindler, M., & Elbert, A. (2011). Overview of the status and global strategy for neonicotinoids. Journal of agricultural and food chemistry, 59(7), 2897-2908.

Miraglia, M., Marvin, H. J. P., Kleter, G. A., Battilani, P., Brera, C., Coni, E., ... & Vespermann, A. (2009). Climate change and food safety: an emerging issue with special focus on Europe. Food and chemical toxicology, 47(5), 1009-1021.

Özdemir, H. H., Kara, M., Yumrutas, O., Uckardes, F., Eraslan, E., Demir, C. F., & Bal, R. (2014). Determination of the effects on learning and memory performance and related gene expressions of clothianidin in rat models. Cognitive neurodynamics, 8, 411-416.

Somogyvári, D., Farkas, A., Mörtl, M., & Győri, J. (2022). Behavioral and biochemical alterations induced by acute clothianidin and imidacloprid exposure in the killer shrimp, Dikerogammarus villosus. Comparative Biochemistry and Physiology Part C: Toxicology & Pharmacology, 261, 109421.

Tišler, T., Jemec, A., Mozetič, B., & Trebše, P. (2009). Hazard identification of imidacloprid to aquatic environment. Chemosphere, 76(7), 907-914.

Tomizawa, M., & Casida, J. E. (2005). Neonicotinoid insecticide toxicology: mechanisms of selective action. Annu. Rev. Pharmacol. Toxicol., 45(1), 247-268.

Xing, H., Wu, H., Sun, G., Zhang, Z., Xu, S., & Li, S. (2013). Alterations in activity and mRNA expression of acetylcholinesterase in the liver, kidney and gill of common carp exposed to atrazine and chlorpyrifos. Environmental toxicology and pharmacology, 35(1), 47-54.

Zouaoui, S., Rouabhi, R., Taib, C., Bouteraa, Z., Gasmi, S., Benaicha, B., & Toualbia, N. (2024). Impact of Imidacloprid on Forebrain Mitochondrial Enzymatic Activities Ec50, Ic50 and Impacts of Mellissa Extracts. Journal of Bioresource Management, 11(2), 9.

➢ *ORAL PRESENTATION*

The use of perlite and vermiculite aggregates in the production of lightweight mortars

Zeynep ALGIN (*ORCID:*https://orcid.org/0000-0001-7004-8403), H. Murat ALGIN (*ORCID:* https://orcid.org/0000-0001-7848-5464), Savaş KARAMAN* (*ORCID:* https://orcid.org/0009-0009-8688-9317), Sarteep NAJMULDEEN ISMAEL (*ORCID:* https://orcid.org/0009-003-8866-6439), Şerif YOLUK (*ORCID:* https://orcid.org/0000-0002-0036-1661)

Harran University, Engineering Faculty, Civil Engineering Department, Sanliurfa, Turkey.

*Corresponding author e-mail: savas532813@gmail.com

Abstract

Perlite and vermiculite are materials of volcanic origin with abundant reserves in Turkey and worldwide. These materials are used in the production of natural lightweight aggregates, which are of strategic importance as construction materials. The advantages of these materials, which include low density, high thermal insulation capacity and environmental sustainability, have led to their widespread use in many sectors, particularly in the construction industry. However, due to their high water absorption capacity and suboptimal mechanical properties, these aggregates show limited effectiveness in structural concrete and mortar applications. In this study, the surfaces of expanded perlite and expanded vermiculite aggregates were strengthened by a coating method consisting of cement and silica fume, and their physical and mechanical performance was improved. In this study, the aggregates were subjected to three different coating thicknesses and used in mortar production by replacing raw uncoated aggregates in varying proportions (0-50%). Unit weight and water absorption tests were carried out on the mortar samples. The experimental results show that the coating significantly reduces the water absorption properties of the expanded lightweight aggregates, making them more suitable as building materials. Specifically, the mixture containing 50% coated perlite and 50% coated vermiculite showed a reduction in water absorption of up to 60% compared to the control sample. The results indicate that lightweight aggregates strengthened by coating processes can be transformed into a novel structural aggregate material with reduced permeability, improved durability and performance orientation.

Keywords: Lightweight aggregate, Lightweight mortar, Perlite, Vermiculite, Surface treatment

INTRODUCTION

With the developments in modern construction materials, lightweight aggregates such as pumice, perlite and vermiculite have gained great importance in the global sector. This is particularly evident in countries located in active seismic zones, where the design of lightweight structures has become mandatory to reduce seismic loads. Population growth and accelerated urbanisation have led to an increased demand for lightweight construction materials (Öztürk et al., 2022). The porous nature of lightweight aggregates leads to a low density, thereby enabling the production of concrete that is up to 30% lighter than that produced using conventional aggregates. It has been demonstrated that this configuration has the capacity to mitigate the adverse effects of seismic activity on the structural integrity of the building, thereby reducing the dead loads to which the structural system is subjected (Tunç, 2013).

Studies in the literature indicate that energy savings of up to 50% in heating and cooling costs can be achieved in buildings constructed with lightweight materials (Öztürk et al., 2022). This phenomenon is particularly pronounced in the Scandinavian countries, which are located in the cold climate zone, where the use of imported lightweight building materials has been shown to result in lower heating costs compared to Turkey. The results underline the importance of lightweight construction materials in improving energy efficiency.

The low density of lightweight concrete is primarily due to the lightweight aggregates used in its composition, whether these aggregates are natural or artificially derived. It has been shown that the porosity of these aggregates can be increased by various processes. Research has shown that lightweight concrete has superior performance in terms of fire resistance compared to conventional concrete (Tunç, 2013).

However, the high water absorption capacity of these aggregates can lead to undesirable effects such as the formation of shrinkage cracks during the curing process.

Turkey has abundant natural reserves of expanded perlite and vermiculite. These aggregates are widely used in the construction industry as lightweight construction materials to reduce the overall weight of the structure while improving its performance characteristics, including thermal and acoustic insulation. Vermiculite is characterised by its ability to withstand high temperatures and its sound insulation properties, while perlite is favoured for its low density and high thermal insulation capacity. It is indeed possible to produce low density mortars using expanded vermiculite and expanded perlite as natural materials. However, studies have shown that the use of these materials as aggregates in mortar and concrete production can have a detrimental effect on the properties of concrete, including a reduction in compressive strength and an increase in water absorption (Koksal et al., 2015; Mo et al., 2018; Tie et al., 2022; Cojocaru, 2023). The effective utilisation of expanded perlite and expanded vermiculite aggregates, in construction materials is contingent on the resolution of these challenges. This strategic approach is critical for optimising the mechanical and physical performance of building materials, as well as increasing their sustainability. The objective of this study is to enhance the physical and mechanical properties of expanded perlite and expanded vermiculite aggregates through the application of a cement-silica fume slurry onto their surfaces.

MATERIALS AND METHODS

In this study, CEM II/A-M (P-LL) 42.5 N type cement, which conforms to TS EN 197-1 standard, was utilised as the binder material. The cement has a specific gravity of 3.06 g/cm³ and a Blaine fineness of 4085 cm²/g. Furthermore, silica fume with a specific gravity of 2.2 g/cm³ and Blaine fineness of 200000 cm²/g, supplied from Antalya Eti Elektrometalurji A.Ş., was used as a fine pozzolanic materials. The chemical properties of cement and silica fume are presented in Table 1. Natıral sand, exhibiting a specific gravity of 2.63 g/cm³, was identified as the optimal fine aggregate. Furthermore, a polycarboxylate-based super plasticiser (SP) with a specific gravity of 1.10 g/cm³ was utilised to enhance the fluidity of the mixture.

Table 1. Chemical composition of cement and silica fume

Chemical analysis(%)	Cement	Silica fume
CaO	57.38	2.06
SiO_2	23.38	91.92
Al_2O_3	4.60	0.42
Fe_2O_3	3.24	0.20
MgO	2.18	3.28
SO_3	2.79	0.83
K_2O	-	0.85
Na_2O	-	0.25
Loss	4.86	1.50

The aggregates, composed of expanded perlite and expanded vermiculite, were coated in a multilayer structure using a cement-silica fume slurry by cold bonding method. The coating process was conducted within a pelletising apparatus that operated at a constant velocity and inclination. Subsequent to this, the aggregates underwent a curing phase spanning a duration of 28 days. The gradation test of coated perlite (CP) and coated vermiculite (CV) aggregates, which have three different coating thicknesses (Ct), was performed in accordance with the ASTM C136 standard. The results obtained are presented in Figure 1. In order to ascertain the loose bulk density values for the aggregates produced, the ASTM C29 method was employed. Furthermore, the water absorption and specific gravity values were determined in accordance with the ASTM C128 standard.

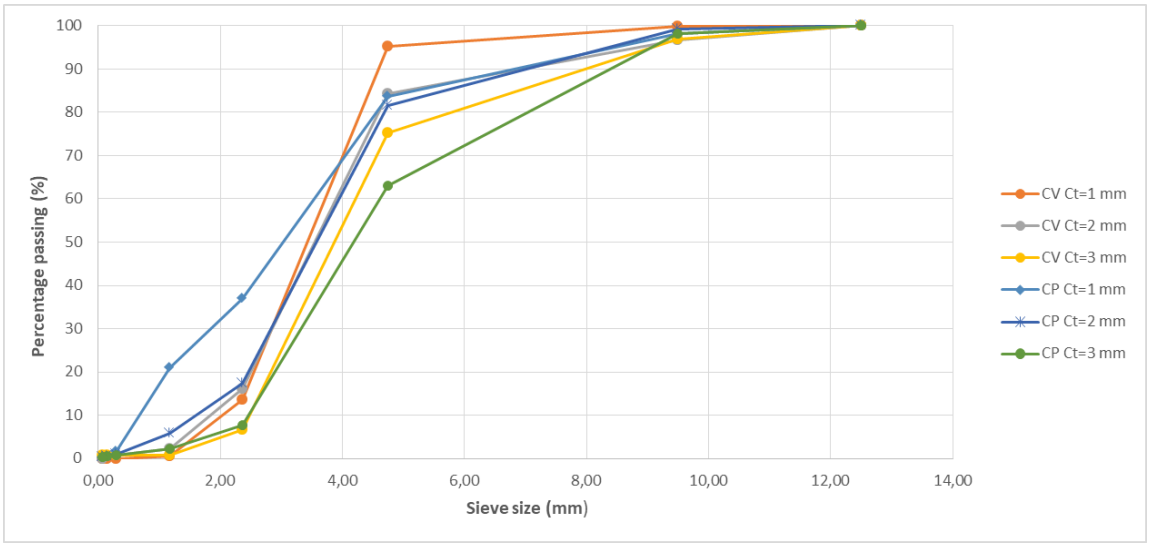

Figure 1. Gradation curves of CP and CV aggregates

The water-to-cement ratio was maintained at a constant value of 0.45, while the cement dosage was set at 550 kilograms per cubic metre for all mortar mixtures. In this study, the replacement of aggregates of varying thicknesses of CP and CV, coated in multiple layers, with uncoated perlite (UP) and uncoated vermiculite (UV) aggregates was investigated at 0%, 25% and 50% by volume. It has been demonstrated that the higher water absorption capacity of porous lightweight aggregate, in comparison with normal weight aggregate, results in a reduction in workability. A common technique employed in practice to overcome this problem is to estimate the water content by considering the water absorption properties or wetting the lightweight aggregates before mixing (Domagała, 2015; Nguyen et al., 2018; Adhikary et al., 2022). Consequently, in the present study, perlite and vermiculite aggregates were subjected to water curing for a duration of 24 hours prior to their incorporation into the mortar mixture. Subsequently, the aggregates were dried to a state of saturated dry surface.

The same mixing methodology was used for all fresh mortar mixes prepared. The initial step in the process involved the introduction of cement, natural sand, and saturated surface-dry aggregates into a 15-litre capacity mixer. The mixture was then subjected to a one-minute period of normal-speed mixing, followed by a subsequent one-minute period of high-speed mixing. Subsequently, water and superplasticiser were incorporated into the mixture, and the mixing process was terminated after a further two minutes of high-speed mixing. In the course of the experimental studies, 25 distinct mortar mixtures were prepared. Subsequently, specimens measuring 50x50x50 mm were produced from these mixtures, which were then water cured until the commencement of the test. The oven dry density and water absorption tests were conducted in accordance with the provisions of the ASTM C642 (2013) standard. The experiment was conducted on three 50 mm cube specimens on the 28th day. The final value was obtained by averaging the values obtained.

RESULTS AND DISCUSSION

The loose bulk density, water absorption and specific gravity values of CV and CP aggregates produced in this study are given in Table 2. As demonstrated in Table 2, the CV aggregate demonstrates a specific gravity of 1.75-1.81, a loose bulk density of 360-379 kg/m³, and a water absorption rate of 18-24%. In contrast, the CP aggregate exhibits a specific gravity of 1.89-2.10, a loose bulk density of 995-1129 kg/m³, and a water absorption rate of 15-22%. The water absorption values of expanded vermiculite and expanded perlite aggregates are 300% and 169% respectively. Table 2 indicates a substantial increase in the specific gravity and loose bulk density values, accompanied by a notable decrease in the water absorption rates of both CV and CP type coated aggregates, in comparison to the uncoated aggregate (Ct=0). The coating method employed in this study resulted in a significant decrease of approximately 90% in the water absorption values of CV and CP aggregates in comparison with uncoated aggregate. It is evident that the grain density and bulk density of CV aggregates are less than 2000 kg/m³ and 1200 kg/m³, respectively. This stipulation renders them as suitable for categorisation as lightweight aggregates, as outlined in EN-13055. It is noteworthy that the grain density and bulk density of CP aggregates are less than 2000 kg/m3 (with the exception of those exhibiting an average pavement thickness of 2 and 3 mm) and 1200 kg/m3,

respectively. This stipulation renders them as suitable for categorisation as lightweight aggregates, as outlined in EN-13055.

Table 2. Physical properties of CV and CP aggregates

		Average coating thickness (mm)			
		0	**1**	**2**	**3**
Vermiculite	Loose bulk density (kg/m^3)	78	379	373	360
	Specific gravity	0.22	1.75	1.78	1.81
	Water absorption (%)	300	18	21	24
Perlite	Loose bulk density (kg/m^3)	120	995	1107	1129
	Specific gravity	0.58	1.89	2.07	2.10
	Water absorption (%)	169	22	15	15

As demonstrated in Figure 2, the substitution ratios of CP and CV aggregates, in conjunction with coating thicknesses, exert a significant influence on the oven dry density values. As demonstrated in Figure 2, the vertical axis signifies the oven dry density (δ_{od}), the lower horizontal axis denotes the replacement ratio of coated perlite aggregate ($CPAR_R$), and the upper horizontal axis indicates the replacement ratio of uncoated perlite aggregate ($UPAR_R$). The lowest oven dry density value of 1.26 g/cm³ was obtained from the mortar sample with 100% uncoated vermiculite (UV) and uncoated perlite (UP) aggregates. As demonstrated in Figure 2, the oven dry density values of the specimens with CV and CP aggregates range from 1.31 to 1.88 g/cm³. The study established that the density of the lightweight mortar increased in proportion to the increase in the substitution ratios of both CV and CP aggregates. It is evident that, irrespective of the substitution ratio, an augmentation in coating thickness in mortar samples produced using CV and CP aggregates results in elevated oven dry density values in comparison to uncoated aggregates. This phenomenon can be attributed to the higher specific gravity exhibited by CV and CP aggregates in comparison to UV and UP aggregates. In the instance of complete substitution of the CV aggregate for the UV aggregate, an increase in oven dry density was observed, ranging from approximately 13% to 17%, contingent upon the coating thickness. In the experiment, the CP aggregate was substituted in its entirety for the UP aggregate. This resulted in an increase in the oven dry density value, ranging from approximately 18% to 24%, depending on the coating thickness. The enhanced increase in the oven dry density of mortar samples produced with CP aggregate is attributable to the elevated specific gravity of these aggregates in comparison to CV aggregates. An increase between 38% and 49% in the oven dry density values of the samples was obtained in which both 50% CV aggregate and 50% CP aggregate were utilised.

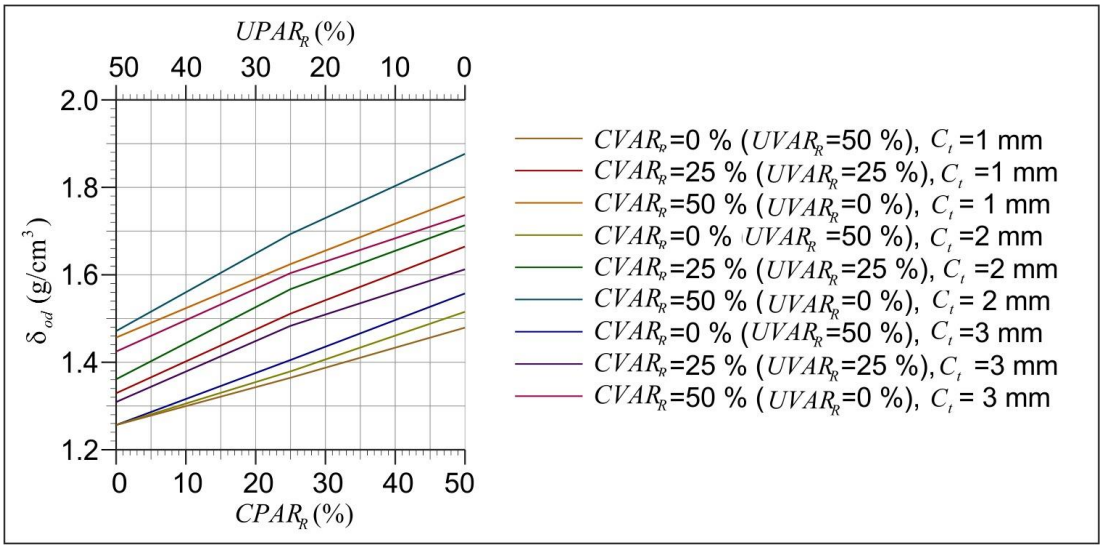

Figure 2. Relationship between the substitution ratios and average coating thicknesses of CV and CP aggregates and oven dry density

In mortar samples produced with CV and CP aggregates, an observation was made that the increase in the coating thickness of the aggregates directly affected the oven dry density values of the samples. The findings of the study indicated that an augmentation in coating thickness yielded elevated oven dry density values for the samples prepared with coated aggregates in comparison to those prepared with uncoated aggregates. The highest oven dry density was obtained in mortar samples produced with CV and CP aggregates, with an average coating thickness of 2 mm. However, as the mean coating thickness reached 3 mm, a decrease in the density of the specimens was generally observed. The underlying principle for this phenomenon is predicated on the observation that an augmentation in coating thickness results in an increase in aggregate grain diameter, consequently leading to a deterioration in aggregate gradation. The increased grain size resulted in an increase in the void volume between the aggregates. This had a detrimental effect on the compactness of the mixture, consequently resulting in lower density values. The maximum oven dry density recorded was approximately 1.88 g/cm³, which was obtained for the sample with an average coating thickness of 2 mm and containing 100% coated aggregates (50% CV and 50% CP). Subsequent to the ascertainment that the dry density values of all samples were below 2 g/cm³, it was determined that the production of lightweight mortar with CV and CP aggregates was a viable prospect.

As demonstrated in Figure 3, the impact of varying replacement ratios of CV and CP aggregates, along with average pavement thicknesses, on water absorption is illustrated. As demonstrated in Figure 3, a substantial decline in water absorption values was observed with an increase in the substitution ratio of CV and CP aggregates. The maximum water absorption value of approximately 27.4% was obtained in the sample containing 50% UV and %50 UP. The water absorption values of the specimens with CV and CP aggregates ranged between 25.9% and 10.5%. It was determined that the water absorption values of the lightweight mortar decreased with the increase in the substitution ratios of both CV and CP aggregates. It is evident that, irrespective of the substitution ratio, the augmentation in coating thickness in mortar samples produced using CV and CP aggregates results in diminished water absorption values when compared to uncoated aggregates. In the instance of complete substitution of the CV aggregate for the UV aggregate, a decline in water absorption was observed, with values ranging from approximately 28 to 30%, contingent on the coating thickness. In the instance of complete substitution of the CP aggregate for the UP aggregate, a decline in water absorption value was observed, ranging from approximately 13% to 22%, contingent on the coating thickness. The water absorption values of the specimens with both 50% CV aggregate and 50% CP aggregate were reduced in the range of 41% to 62%, depending on the coating thickness. The lowest water absorption value recorded, with a value of approximately 10.5%, was obtained from the samples produced with 50% CP and 50% CV aggregates with an average coating thickness of 2 mm. A decline of approximately 62% was documented in comparison to the water absorption value of the mortar produced with uncoated aggregate.

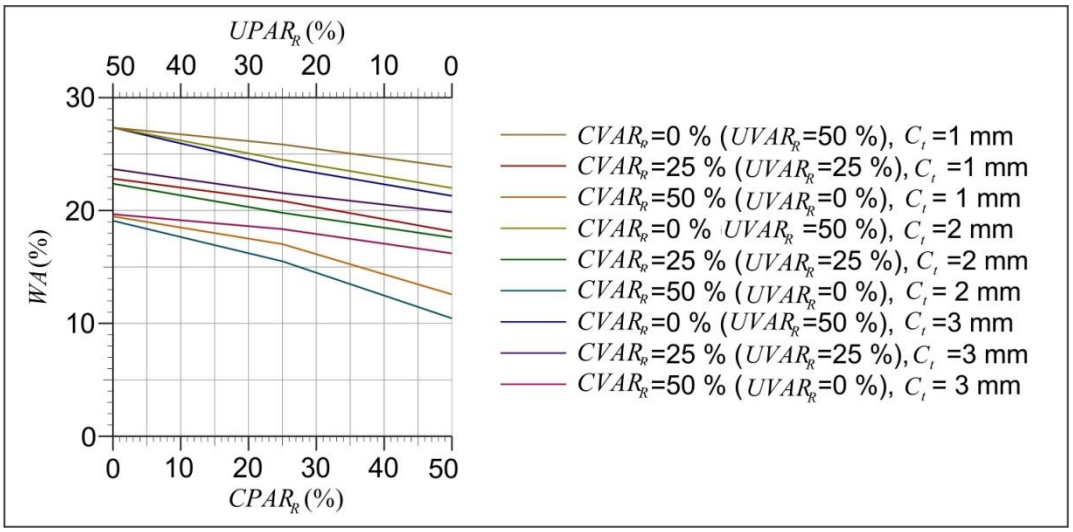

Figure 3. Relationship between the substitution ratios and average coating thicknesses of CV and CP aggregates and water absorption

CONCLUSION

The present study investigates the physical properties of coated perlite (CP) and coated vermiculite (CV) aggregates, which are obtained by progressive coating of expanded perlite (UP) and expanded vermiculite (UV) aggregates with cement-silica fume slurry. Furthermore, the density and water absorption performances of mortar samples produced using these aggregates are evaluated. The following conclusions were reached on the basis of the results obtained:

- In comparison with uncoated aggregates, CP and CV aggregates demonstrated an increase in specific gravity and loose bulk density values, and a significant decrease in water absorption rates. The applied coating method reduced the porosity and water contact surface of the aggregates, resulting in a decrease in water absorption values by approximately 90%.
- It is evident that the grain density and loose bulk density values of CV aggregates are lower than 2000 kg/m³ and 1200 kg/m³, respectively. This classification indicates that they are considered to be lightweight aggregates, as defined in the EN 13055 standard. It is evident that the CP aggregates satisfied these criteria, with the exception of the average coating thickness, which ranged from 2 to 3 millimetres.
- The findings of the study demonstrated that mortar specimens comprising CV and CP aggregates exhibited higher oven dry density values in comparison with uncoated aggregates.
- The oven dry density values of the mortars exhibited an increase of 13-17% when CV aggregate was substituted entirely for UV, 18-24% when CP aggregate was substituted entirely for UP, and 38-49% for mortar samples containing 50% CV and 50% CP. In all samples, the oven dry density value was found to be less than 2 g/cm³, thereby meeting the lightweight mortar criterion.
- The highest density values were obtained in the specimens prepared with CV and CP aggregates, with an average coating thickness of 2 mm.
- The water absorption rate of the specimens with CV and CP aggregates exhibited variation, ranging from 25.9% to 10.5%. The water absorption rates of mortars decreased by 28-30% when CV aggregate was completely replaced by UV, by 13-22% when CP aggregate was completely replaced by UP, and by 41-62% when 50% CV and 50% CP were used.
- The lowest water absorption value was recorded in the specimen containing 50% CV and 50% CP aggregates with a coating thickness of 2 mm.
- In conclusion, the physical properties of expanded perlite and expanded vermiculite aggregates were significantly improved by the multiple coating application proposed in this study. The utilisation of the obtained CV and CP aggregates in lightweight structural elements has been enhanced, yielding favourable outcomes with regard to strength and durability. In addition, enhancements have been identified in the water absorption and density parameters.

REFERENCES

Adhikary, S. K., Ashish, D. K., Sharma, H., Patel, J., Rudžionis, Ž., Al-Ajamee, M., Thomas, B. S., & Khatib, J. M. (2022). Lightweight self-compacting concrete: A review. Resources, Conservation & Recycling Advances, 15, 200107.

ASTM C128. (2022). Standard Test Method for Relative Density (Specific Gravity) and Absorption of Fine Aggregate. ASTM International. https://doi.org/10.1520/C0128-22

ASTM C136. (2006). Standard Test Method for Sieve Analysis of Fine and Coarse Aggregates. ASTM International. https://doi.org/10.1520/C0136-06

ASTM C29/C29M. (1997). Standard Test Method for Bulk Density (Unit Weight) and Voids in Aggregate. ASTM International. https://doi.org/10.1520/C0029_C0029M-97

ASTM C642. (2021). Standard Test Method for Density, Absorption, and Voids in Hardened Concrete. ASTM International. https://doi.org/10.1520/C0642-21

Cojocaru, A., Isopescu, D. N., & Maxineasa, S. G. (2023). Perlite concrete: A review. IOP Conference Series: Materials Science and Engineering, 1283(1), 012003. https://doi.org/10.1088/1757-899X/1283/1/012003

Domagała, L. (2015). The effect of lightweight aggregate water absorption on the reduction of water-cement ratio in fresh concrete. Procedia Engineering, 108, 206–213. https://doi.org/10.1016/j.proeng.2015.06.139

EN 13055. (2016). Lightweight aggregates. European Committee for Standardization.

EN 197-1. (2011). Cement - Part 1: Composition, specifications and conformity criteria for common cements. European Committee for Standardization.

Koksal, F., Gencel, O., & Kaya, M. (2015). Combined effect of silica fume and expanded vermiculite on properties of lightweight mortars at ambient and elevated temperatures. Construction and Building Materials, 88, 175–187.

Mo, K. H., Lee, H. J., Liu, M. Y. J., & Ling, T.-C. (2018). Incorporation of expanded vermiculite lightweight aggregate in cement mortar. Construction and Building Materials, 179, 302–306. https://doi.org/10.1016/j.conbuildmat.2018.05.219

Nguyen, H. D., Truong, K. X. T., Nguyen, N. M., & Do, T. T. (2018). Self-compacting lightweight aggregate concrete in Vietnam. IOP Conference Series: Materials Science and Engineering, 365(3), 032030. https://doi.org/10.1088/1757-899X/365/3/032030

Öztürk, A., Horasan, B. Y., & Solgun, E. (2022). Hafif yapı malzemelerinin özellikleri ve kullanım alanları.

Tie, T. S., Mo, K. H., Alengaram, U. J., Kaliyavaradhan, S. K., & Ling, T.-C. (2022). Study on the use of lightweight expanded perlite and vermiculite aggregates in blended cement mortars. European Journal of Environmental and Civil Engineering, 26(22), 3612–3631. https://doi.org/10.1080/19648189.2020.1806934

Tunç, G. (2013). Hafif agregalı yapısal beton ve Türkiye gerçeği. www.atilim.edu.tr

➢ *ORAL PRESENTATION*

Pedestrian Detection and Target Classification in Urban Forestry Environment with FMCW Automotive Radar and CNN

Serdar Sarigul[1*], Yunus Egi[2], Harun Taha Hayvaci[3]

[*1] TOBB University of Economics and Technology, Department of EEE, Ankara, Turkiye.
[2] Sirnak University, Faculty of Engineering, Electrical and Electronics Engineering, Sirnak, Turkiye.
[3] American University of the Middle East, College of Engineering and Technology, Kuwait

*Corresponding author e-mail: s.sarigul@etu.edu.tr

Abstract
This paper studies the detection of pedestrian in complex urban environments using Frequency Modulated Continuous Wave (FMCW) automotive radar, addressing the challenges posed by environmental obstacles like trees and vehicles. Unlike studies employing idealized radar targets, this research incorporates realistic 3D models to simulate radar scenarios. Radar Cross Section (RCS) analysis is conducted over relevant angles to study the wind effects on a 3D tree model in detail. By including dynamic effects such as the movement of tree branches in the wind, we analyze the undesired impacts on pedestrian classification accuracy. Convolutional neural networks (CNN) enhance pedestrian detection and classification with the extraction of micro-Doppler features from radar spectrograms. The findings demonstrate that the utilized CNN model improves detection reliability under unpredictable environmental interference, highlighting the practical implications for radar-based pedestrian detection in real-world settings.
Keywords: FMCW, CNN, micro-doppler signatures, target classification

INTRODUCTION

In recent years, both industry and academia have focused on advancing autonomous driving systems, particularly emphasizing the role of artificial intelligence (AI) in achieving full autonomy. The rapid evolution of AI-powered technologies and techniques, including machine learning and deep learning, has significantly contributed to the development of autonomous vehicles (AVs) capable of navigating in complex environments. However, Perception systems in AVs face significant technical challenges when operating in diverse environmental conditions including windy, foggy, rainy, and snowy weather. (Pandharipande et al., 2023). To ensure operational safety, potential risks arising from these challenges must be carefully analyzed. One approach to improve AV perception is to incorporate AI-based techniques to enhance pedestrian detection algorithms in adverse scenarios (Tumas et al., 2020). These techniques in AI systems must focus on enhancing safety and efficiency by improving key functionalities such as pedestrian detection and obstacle recognition. While AI integration improves perception, it also raises concerns regarding reliability, interpretability, and explainability (ISO/IEC TR 5469, 2024). One suggested method for addressing these challenges in AI systems is to provide redundancy combined with diversity, ensuring multiple AI approaches are implemented to achieve reliable detection (ISO/IEC TR 5469, 2024).

Micro-Doppler feature extraction methods in target detection systems vary in effectiveness across applications. Parashar highlights that techniques such as short-time Fourier transform (STFT) and Wigner-Ville decomposition must be selected based on factors like target type, latency requirements, accuracy expectations, computational complexity, and scalability (Parashar et al., 2017). Chen further studies micro-Doppler modulation, emphasizing that an ideal feature extraction method should provide high resolution in both time and frequency domains while minimizing cross-term interference (Chen et al., 2006). Radar cross section (RCS) is another important factor affecting micro-Doppler signatures. Shi demonstrates that targets with micro-Doppler dynamics and smaller RCS values can be distinguished even when located near larger objects with higher RCS if observed from an optimal angle (Shi et al., 2022).

On the other hand, in terms of perception sensors, FMCW automotive radars - particularly at 77GHz - have become widely used in AVs for pedestrian detection due to their cost-effectiveness and reliability. Belgiovane explores their application in detecting pedestrians and cyclists based on micro-Doppler signatures (Belgiovane and Chen, 2017). Traditional classification methods from machine learning such as support vector machines (SVM), k-nearest neighbor (kNN), and Gaussian mixture models have been widely used for target classification (Villeval et al., 2014). However, recent studies indicate that deep learning

techniques, particularly convolutional neural networks (CNN), achieve superior results in complex scenarios. Palffy demonstrates improved multi-class detection and classification accuracy with CNN compared to other techniques (Palffy et al., 2020). Integrating FMCW radar hardware with a well-developed CNN-based classification scheme can achieve accuracy rates of 90% and higher with low latency (Elbeialy et al., 2022). However, in highly complex scenarios, the accuracy rate declines, necessitating further research to improve classification performance (Parashar et al., 2017).

Despite advancements, AV safety remains a concern, particularly in environments with dynamic obstacles. A challenging scenario involves AV operation in woodland areas on windy days, where moving tree leaves create significant noise in radar signals, affecting pedestrian detection and micro-Doppler feature extraction. This paper investigates a scenario, analyzing the environmental impact on target classification and evaluating the effectiveness of CNN-based classification techniques in mitigating its effects.

This paper is structured as follows: First, the scenario design and data generation process are explained in detail. Second, the CNN architecture is described. After discussing the simulation performance and presenting the simulation results, we summarize the study and outline future research directions.

SCENARIO AND DATA GENERATION

Designing the Scenario

The scenario considered in this study as shown in Figure 1a includes a moving ego vehicle with an FMCW automotive radar which works at 77GHz, a stationary car which is parked on the side of the road, a pedestrian who is crossing the street and a tree on the side of the road.

It is assumed that the speed of the ego vehicle is in the slow range, the height of the pedestrian changes between certain values while the pedestrian walks in a random direction towards the road. The weather in the scenario is windy and the wind speed is strong enough to move the branches of the tree. We assume that the tree has many branches and there are many leaves on the branches as visualized in Figure 1b.

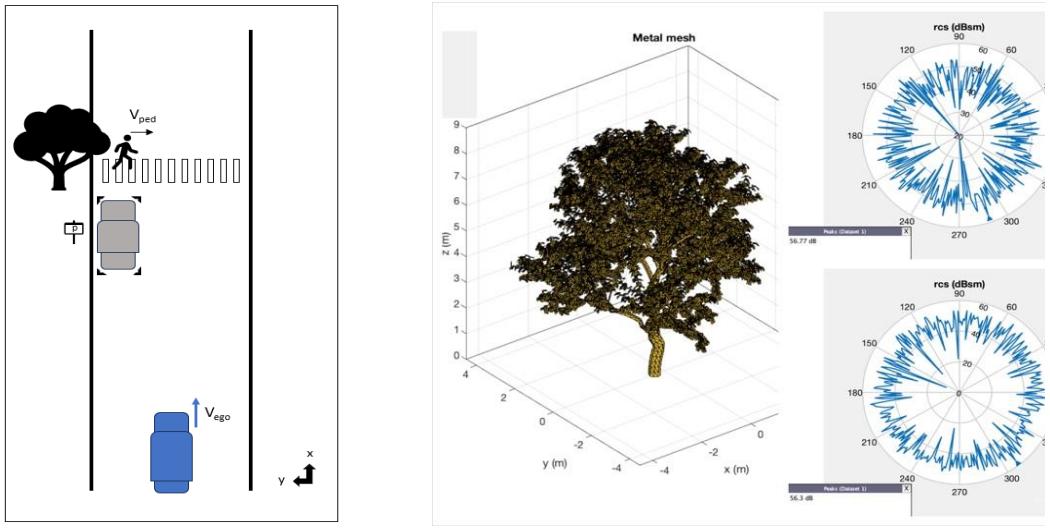

(a) Driving scenario (b) 3D model of a tree with its RCS calculation

Figure 1. Driving scenario and target RCS

The idea behind the scenario is to analyze if the FMCW radar and CNN system would be able to detect the walking pedestrian among the other targets (tree and parked car) and classify them.

The sub-scenarios are generated based on the limitations of the main scenario and are composed of the targets as stated in Table 1.

Table 1. The Sub-scenarios

No.	Sub-Scenario
1st	only 'parked car' exists
2nd	only 'pedestrian' exists
3rd	only 'tree' exists
4th	'pedestrian' + 'parked car' exist
5th	'pedestrian' + 'tree' exist
6th	'pedestrian' + 'parked car' + 'tree' exist

Generation of Test and Training Data

After designing the main scenario, the simulation environment has been created in Matlab to generate output spectrograms to have a visual representation of the radar signal data to observe the frequency shifts changing over time. In applications like pedestrian detection, spectrograms capture subtle movement patterns called micro-Doppler signatures which can indicate specific types of motion such as walking, running, sitting, bending, falling, etc. (Shah and Fioranelli, 2019). These spectrograms are valuable for identifying pedestrians within complex environments, since they help differentiate human movement from other objects. CNN often analyzes these spectrograms to classify detected objects, providing essential data for autonomous vehicle safety systems.

In order to generate the test and the training spectrogram data, we compose the simulation in four parts as below.

Determination of Target Specifications

As a beginning, the target specifications have been identified and their objects have been created individually as tree, pedestrian and parked car while designing the driving scenario as stated below:

- Parked vehicle: It is positioned on the roadside and acts as a static target.
- Pedestrian: The pedestrian's height varies between 1.5 m and 2 m, and they walk in a random direction (towards the road where the ego vehicle is moving) at a speed of 8–10 km/h.
- Tree: It is modeled as a realistic 3D model to simulate an urban landscape environment.

While the pedestrian and parked vehicle parameters are available as pre-built objects in Matlab, we need to create the tree target from scratch. In Kiliç's study (Kilic et al., 2015), a forest scattering model was designed using cylindrical perfect electric conductors (PEC) randomly distributed in different sizes and orientations to represent tree trunks and branches. This allowed for the examination and analysis of back-scattering from the trunk and branches. However, one missing detail for our case is the signal noise caused by the movement of tree leaves.

To integrate the selected 3D tree model, as shown in Figure 1b, into the simulation, the radar cross-section (RCS) must be calculated. As the exact numerical solution like the method of moments (MoM) requires very high computational power, we chose using the method of Physical Optics (PO) which is still applicable for the high frequency approximations (Treml et al., 2009). The PO approximation assumes that the observed surface patch is ideally smooth, flat, and an electrically perfect conductor. As a result, Treml defines the scattered electric field as (Treml et al., 2009):

$$E_{scat} = jk\psi_0 \int_S s \times [n \times E - \eta s \times (n \times H)] e^{jkr(i-s)}\, dS \qquad (1)$$

where k represents the wavenumber, s and i are unit vectors indicating the propagation direction of the scattered and incident waves, respectively. r denotes the position vector from the origin of the local coordinate system to the surface patch dS, and η represents the free-space impedance. $\psi_0 = \frac{e^{jkr}}{j\pi R}$ which is the far field Green's function, where R is the distance between the observation point and the surface patch. The mathematical equation of the RCS, denoted as σ, is expressed as follows (Hess, 2008).

$$\sigma = 4\pi R^2 \frac{|E_{scat}|^2}{|E_{inc}|^2} \quad (2)$$

where E_{scat} is the electromagnetic power scattered by the target and received by the radar, E_{inc} is the electromagnetic power transmitted by the transmitter and R is the distance between the radar and the target. Based on the calculated electric fields at the observation point resulting from PO by using Eq. (1), the total RCS of the radar target is calculated with the RCS Eq. (2), where R will be canceled due to the far field Green's function (Treml et al., 2009).

Following the PO approximation approach for the RCS, the electromagnetic scattering model of the tree model must be developed. In Rao's study (Rao et al., 1982), a simple and effective numerical procedure was developed for calculating electromagnetic scattering from the surfaces of arbitrarily shaped objects. In this context, Rao uses planar triangular surface patches when modeling objects for numerical computations (Rao et al., 1982).

Building on this approach, the 3D tree object used in this study was modeled using 99,120 triangular surface patches, as shown in Figure 1b.

As RCS varies with the frequency, our RCS model is based on 77GHz. The azimuth angle was selected to cover the entire perimeter of the tree [-180° to 180°], while the elevation angle was considered as [0° and 45°] for the calculations.

Before integrating the generated tree model into the simulation, the micro-noise effects caused by tree leaves must be incorporated into the model. In this context, Swerling's study provides four different fluctuating target models for targets with varying cross-section areas (Swerling, 1960).

Swerling 3 & Swerling 4 models (Swerling, 1960) are both applicable to our tree model as the total RCS includes one large scatterer along with several independent, small, and approximately equal scatterers. In Swerling 3, the total RCS remains constant throughout the scan, while the total RCS varies from one radar pulse to another in Swerling 4. In both models, the density function becomes a Chi-square distribution and the RCS fluctuation can be shown as follows for $\sigma > 0$.

$$w(\sigma, \hat{x}) = \frac{4\sigma}{\hat{x}^2} e^{-2\frac{\sigma}{\hat{x}}} \quad (3)$$

Due to the integration of both large and small scattering surfaces and the fact that the total RCS varies with each radar pulse, the Swerling 4 fluctuating target model was selected for integrating the 3D tree model into the simulation. This model not only accounts for the main scattering effects from the tree trunk but also incorporates the micro-noise variations caused by leaf movement, which fluctuates with each radar pulse.

Validation of the Target Model

When constructing the tree model, three key aspects are considered:

- Treating the tree trunk as a single, unified structure.
- Incorporating the scattering effects of branches and leaves.
- Simulating the influence of wind, which causes leaf movement.

In order to compare our target model with the theoretical prediction, we calculated a mean RCS value, σ_{mean}, over three equal signals which are reflected from the target at three different aspect angles. The angles are used as [azimuth elevation] respectively as [0 0], [45 0] and [45 45]. The result gives us σ_{mean} for the theoretical prediction for a nonfluctuating RCS. Figure 2 shows that the generated Swerling 4 model follows the distribution as expected from the Eq. (3) as $w(\sigma, \sigma_{mean})$.

The spectrogram outputs obtained from the simulation were also compared with the study published by Kilic (Kilic et al., 2015). Kilic analyzes the effects of turbulent air under different wind speeds in a forest environment on human micro-Doppler signatures. The findings indicates that branch movements, depending on the relationship between radar direction, wind direction, and turbulence levels, can mask

micro-Doppler signatures (Kilic et al., 2015). According to Kilic, the noise is strong enough to block the human signature with the wind speed of 15 m/s for all turbulence levels.

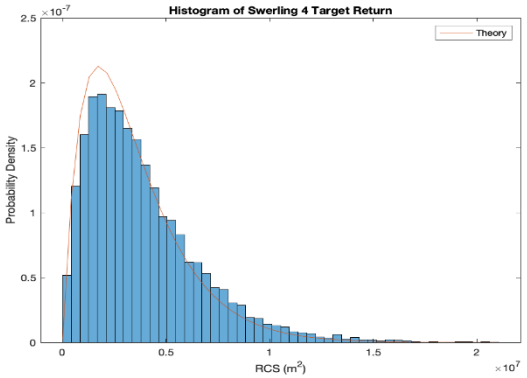

Figure 2. Distribution of the returns vs Theoretical prediction

While Figure 3a and Figure 3b clearly show the micro-Doppler signature of a pedestrian, the impact of integrating our 3D tree model is highly visible and makes it almost impossible to distinguish human micro-Doppler signatures with a naked eye in the spectrogram as seen in Figure 3c.

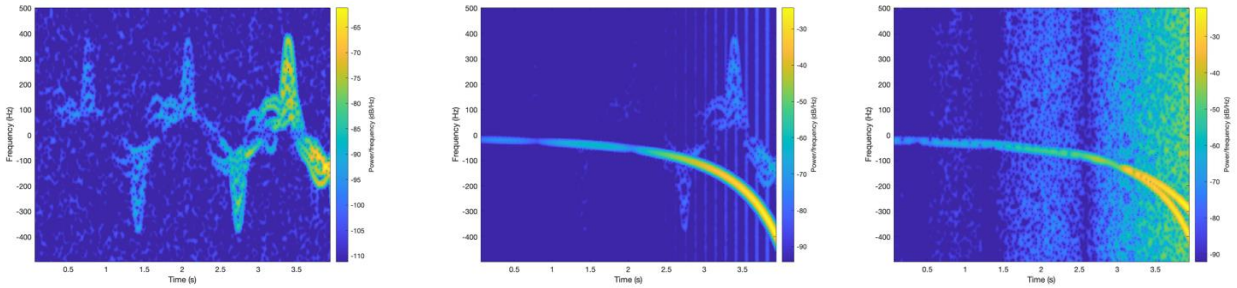

(a) Human model

(b) Human and parked car models

(c) Human, tree and parked car models.

Figure 3. Spectrograms of the radar signals from the simulation

Determination of FMCW Radar Parameters

In parallel with defining the characteristics of the targets in the simulated environment, the parameters of the FMCW radar mounted on the ego vehicle must also be specified and integrated into the simulation.

Karnfelt developed a system simulation platform for a 77GHz adaptive cruise control (ACC) radar and tested various radar architectures, modulation formats, and detection algorithms (Karnfelt et al., 2009). He concluded that although Frequency Shift Keying (FSK) modulation provides excellent velocity resolution, its range resolution is insufficient. Therefore, Linear Frequency Modulation (LFM) is better suited for handling more complex scenarios (Karnfelt et al., 2009).

A basic LFM waveform is shown in Figure 4a while Figure 4b shows the FMCW signal used in our simulation. The up-sweep signal can be simply expressed in Eq. (4) where the signal bandwidth is β, the carrier frequency is f_c and the sweep time is t_{sweep}.

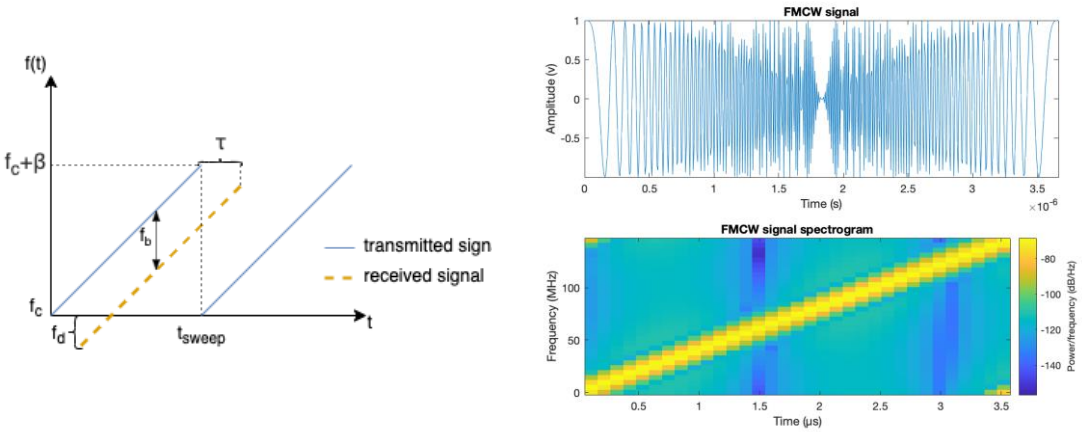

(a) FMCW modulation waveform with up-sweep

(b) FMCW signal used in the simulation and its spectrogram

Figure 4. FMCW signal

$$f(t) = f_c + \frac{\beta}{t_{sweep}}t \tag{4}$$

Wegner provided a general assessment of automotive radars and discussed future applications, describing a 77 GHz long-range radar (LRR) with a 9-degree beamwidth capable of detecting objects up to 150 meters, and a 24 GHz short-range radar (SRR) with an 80-degree beamwidth and a 30-meter detection range (Wegner, 2005). Considering the scenario in this study, where the ego vehicle must detect pedestrians at a safe and sufficient distance, the simulation utilizes a 77 GHz LRR with a maximum detection range set to 100 meters. This type of radar, commonly used in modern vehicles and ACC systems, aligns with the study's objectives and employs FMCW radar parameters.

The FMCW radar parameters which are used in our simulation are given in Table 2. According to Rohling (Rohling and Meinecke, 2001), a typical value of the signal bandwidth of an LFM waveform, β, is 150MHz which gives us the range resolution $\Delta R = \frac{c}{2\beta} = 1m$. By using the Eq. (5) (Karnfelt et al., 2009), Doppler frequency shift, f_d, frequency shift due to time delay, f_τ, and the beat frequency, f_b, are calculated where c is the speed of light where $f_d = \frac{2v_r f_c}{c}$ and $f_\tau = \frac{2\beta R}{ct_{sweep}}$. R and the relative speed, v_r, are determined according to the sub-scenario variation which is explained in the next part.

$$f_b = \frac{2v_r f_c}{c} - \frac{2\beta R}{ct_{sweep}} \tag{5}$$

Table 2. FMCW radar parameters

Symbol	System Parameters	Value
f_c	Carrier frequency (GHz)	77
f_s	Sample frequency (MHz)	150
R_{max}	Maximum target range (m)	100
ΔR	Range resolution (m)	1
v_{max}	Maximum target speed (km/h)	30
t_{sweep}	Sweep time (microseconds)	3.67
β	Sweep bandwidth (MHz)	150
f_b	Beat frequency (MHz)	27.27

Data Generation from Sub-scenarios

To introduce complexity and diversity into the collected data, multiple sub-scenarios were generated for training the CNN. This involved assigning random velocity values to the ego vehicle, varying the initial

positioning of the parked car, tree, and pedestrian on the x-axis, and randomizing pedestrian height, speed and heading. These variations were implemented while ensuring that the overall framework of the designed scenario in Figure 1a remained intact.

The collected data from each simulation run with the randomized sub-scenario was used to generate individual spectrograms for each category. These spectrograms were obtained using the Short-Time Fourier Transform (STFT) (Belgiovane and Chen, 2017), as described in Eq. (6), where $\omega(t)$ represents the window function and $x(t)$ is the signal undergoing transformation.

$$\chi(\tau,\omega) = \int_{-\infty}^{\infty} x(t)w(t-\tau)e^{-j\omega t}\,dt \tag{6}$$

The data have been organized into six data sets and labeled as "Pedestrian, Parked Car, Tree, Pedestrian + Parked Car, Pedestrian + Tree, Pedestrian + Parked Car + Tree". A total of 21,000 spectrograms were generated, with an equal distribution across all datasets, resulting in 3,500 spectrograms per category. Of the generated data, 80% was allocated for training, while the remaining 20% was designated for validation within each category. They later become inputs to the CNN architecture as training and validation data.

CLASSIFICATION ARCHITECTURE

There are a variety of different possible approaches that can be used while creating the CNN architecture specific to the target classification systems. The proposed CNN architecture whose CNN methodology is adopted from Angelov's multi-target classification system (Angelov et al., 2018) is specifically designed to handle challenging complex situations such as suppressed pedestrian micro-Doppler signatures due to wind-induced noise from trees in urban forestry environments.

The CNN architecture proposed in Figure 5 processes high resolution RGB spectrogram images with the vector size of 717×908×3, starting with a 2D convolutional layer that utilizes 16 filters, 10×10 kernel to extract basic patterns like edges and textures. It is followed by a max pooling layer with a pool size of 10×10 for dimensionality reduction and preserving key features. The next stages consist of three consecutive 2D convolutional layers (each with 32 filters, 5×5 kernel size) including max pooling layer 10×10, 10×10, and 5×5, respectively. The last 2D convolutional layer (32 filters, 5×5 kernel size) is followed by an average pooling layer to refine and smooth the feature map. These features are then passed through a fully connected layer with 6 neural units and a SoftMax layer to transform these outputs into probability scores for classification. Finally, the decision is made through classification layer.

To obtain the desired CNN architecture for noise handling and classification, the proposed architecture went through extensive training with various configurations, as it provided the best balance between computational efficiency and classification accuracy for micro-Doppler feature extraction. The optimal results were achieved through hyperparameter tuning, utilizing an Adaptive Moment Estimation (ADAM) optimizer with a learning rate of 0.001, a batch size of 64, and ReLU activation functions in the hidden layers.

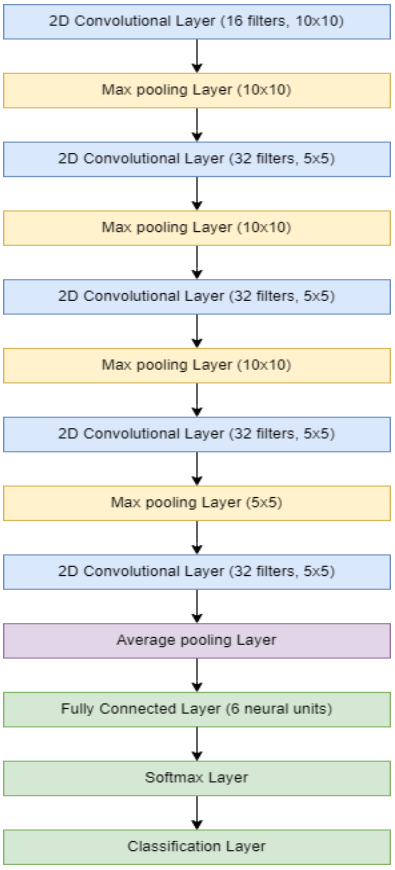

Figure 5. Representation of CNN architecture

PERFORMANCE ANALYSIS AND RESULTS

The findings show that our main scenario and the sub-scenarios have worked well with the integration of 3D tree model and Swerling 4 target model to generate a dominant signal noise simulating the movement of the branches and the leaves of the tree to suppress the pedestrian micro-doppler. Having a tree in a sub-scenario allows 'tree' and 'pedestrian + tree' categories to intermingle with each other.

However, as we discuss the main findings, the simulation results show that the overall classification accuracy of CNN architecture has been calculated as 87.12% which can be seen in Figure 6a. In addition to the performance output of CNN, the confusion matrix in Figure 6b indicates the detection and classification accuracy above 90% in the sub-scenarios including only 'parked-car', 'pedestrian', 'pedestrian + parked-car' and 'pedestrian + tree + parked car'.

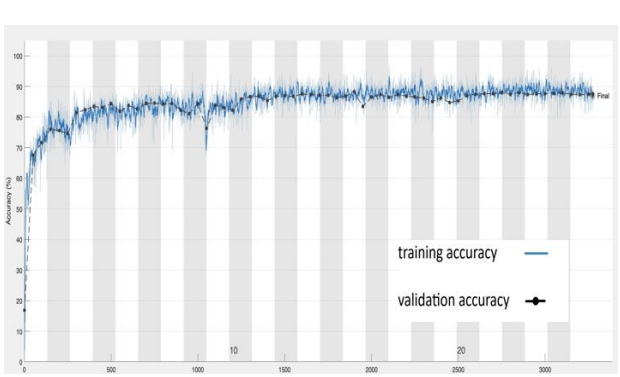

(a) Convolutional Neural Network performance.

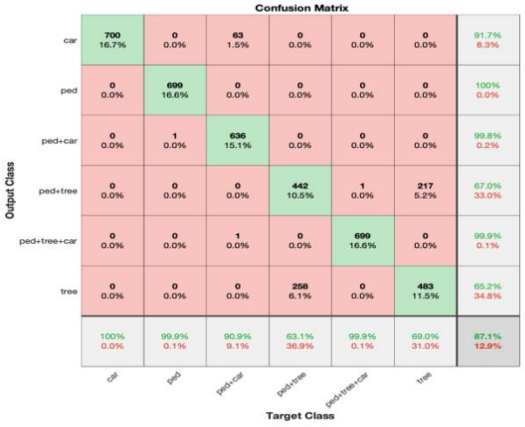

(b) Confusion matrix with the percentages.

Figure 6. CNN accuracy and the confusion matrix.

Scenarios including only 'tree' and only 'pedestrian + tree' are the most affected ones compared to others and the success rate of distinguishing their spectrograms with CNN is below the overall accuracy which is

around 63% - 67%. This result is expected due to fact that the tree suppresses the pedestrian micro-doppler in some sub-scenarios so that the spectrograms are not easily separated from each other by CNN. On the other hand, addition of a parked car in the scenario improved the success rate of the classification significantly since the parked car only returns a doppler shift due to the movement of the ego vehicle. The spectrograms of the scenarios with 'pedestrian + tree + parked car', therefore, includes two dominant doppler shifts as seen in Figure 3c.

CONCLUSION

We demonstrated that the pedestrian detection and the target classification is being affected significantly in such an environment that the plantation, the wind and the turbulent air exist. Even though urban areas might be less challenging under the same environmental conditions due to less mature tree plantation, non-urban areas are still a region of interest for AVs to travel.

The future work for us is to develop an algorithm by using a singular value decomposition (SVD) to remove the micro-doppler affects from the plantations while uncovering the pedestrian signature. This algorithm needs to be applied before generating the spectrograms so that CNN can be provided with a cleaner, filtered data for better performance.

REFERENCES

Angelov, A., Robertson, A., Murray-Smith, R., & Fioranelli, F. (2018). Practical classification of different moving targets using automotive radar and deep neural networks. IET Radar, Sonar & Navigation, 12(10), 1082–1089. Available at: https://ietresearch.onlinelibrary.wiley.com/doi/abs/10.1049/iet-rsn.2018.0103.

Belgiovane, D., & Chen, C.-C. (2017). Micro-Doppler characteristics of pedestrians and bicycles for automotive radar sensors at 77 GHz. 2017 11th European Conference on Antennas and Propagation (EUCAP), 2912–2916.

Chen, V., Li, F., Ho, S.-S., & Wechsler, H. (2006). Micro-Doppler effect in radar: Phenomenon, model, and simulation study. IEEE Transactions on Aerospace and Electronic Systems, 42(1), 2–21.

Elbeialy, M., You, S., Jeong, B. J., & Kim, Y. (2022). Target classification using frontal images measured by 77 GHz FMCW radar through DCNN. Applied Sciences, 12(20). Available at: https://www.mdpi.com/2076-3417/12/20/10264.

Hess, D. W. (2008). Introduction to RCS measurements. 2008 Loughborough Antennas and Propagation Conference, 37–44.

ISO/IEC TR 5469. (2024). Artificial intelligence—Functional safety and AI systems.

Karnfelt, C., Paleden, A., Bazzi, A., El Haj Shhadle, G., Abbas, M., & Chonavel, T. (2009). 77 GHz ACC radar simulation platform. 2009 9th International Conference on Intelligent Transport Systems Telecommunications (ITST), 209–214.

Kilic, O., Garcia-Rubia, J. M., Tran, N., Dang, V., & Nguyen, Q. (2015). Detection of moving human micro-Doppler signature in forest environments with swaying tree components by wind. Radio Science, 50(3), 238–248.

Palffy, A., Dong, J., Kooij, J. F. P., & Gavrila, D. M. (2020). CNN-based road user detection using the 3D radar cube. IEEE Robotics and Automation Letters, 5(2), 1263–1270.

Pandharipande, A., Cheng, C.-H., Dauwels, J., Gurbuz, S. Z., Ibanez-Guzman, J., Li, G., Piazzoni, A., Wang, P., & Santra, A. (2023). Sensing and machine learning for automotive perception: A review. IEEE Sensors Journal, 23(11), 11097–11115.

Parashar, K. N., Oveneke, M. C., Rykunov, M., Sahli, H., & Bourdoux, A. (2017). Micro-Doppler feature extraction using convolutional auto-encoders for low latency target classification. 2017 IEEE Radar Conference (RadarConf), 1739–1744.

Rao, S., Wilton, D., & Glisson, A. (1982). Electromagnetic scattering by surfaces of arbitrary shape. IEEE Transactions on Antennas and Propagation, 30(3), 409–418.

Rohling, H., & Meinecke, M.-M. (2001). Waveform design principles for automotive radar systems. 2001 CIE International Conference on Radar Proceedings (Cat No.01TH8559), 1–4.

Shah, S. A., & Fioranelli, F. (2019). Human activity recognition: Preliminary results for dataset portability using FMCW radar. 2019 International Radar Conference (RADAR), 1–4.

Shi, F., Li, Z., Zhang, M., & Li, J. (2022). Analysis and simulation of the micro-Doppler signature of a ship with a rotating shipborne radar at different observation angles. IEEE Geoscience and Remote Sensing Letters, 19, 1–5.

Swerling, P. (1960). Probability of detection for fluctuating targets. IRE Transactions on Information Theory, 6(2), 269–308.

Treml, M., Feger, R., Wagner, C., Stelzer, A., & Jager, H. (2009). Radar cross-section prediction and measurement at 77 GHz. 2009 3rd European Conference on Antennas and Propagation, 2067–2070.

Tumas, P., Nowosielski, A., & Serackis, A. (2020). Pedestrian detection in severe weather conditions. *IEEE Access, 8*, 62775–62784. doi: 10.1109/ACCESS.2020.2982539

Villeval, S., Bilik, I., & Gurbuz, S. Z. (2014). Application of a 24 GHz FMCW automotive radar for urban target classification. 2014 IEEE Radar Conference, 1237–1240.

Wenger, J. (2005). Automotive radar—Status and perspectives. IEEE Compound Semiconductor Integrated Circuit Symposium (CSIC '05), 4 pp.

➢ *ORAL PRESENTATION*

Comparative Analysis of the Health Systems in Turkey and Mauritania

Merve Tekinarslan (ORCID: https://orcid.org/0000-0002-1054-0946)

*[1]Gümüşhane University, Faculty of Health Sciences, Department of Health Management, Gümüşhane, Türkiye.

*Corresponding author e-mail: mervetekinarslan@gumushane.edu.tr

Abstract
This study provides a comparative analysis of the healthcare systems in Turkey and Mauritania, two countries with significantly different socioeconomic and geographical conditions. Utilizing data from the World Health Organization, the World Bank, UNICEF, and national health authorities, the study evaluates key indicators such as hospital capacity, healthcare workforce, health expenditures, and access to healthcare services.
Turkey has achieved substantial progress through its Health Transformation Program, implementing universal health coverage and family medicine practices. In contrast, Mauritania faces significant challenges due to inadequate health infrastructure, shortages of healthcare personnel, and reliance on international aid. Comparative data on life expectancy, infant mortality rates, health insurance coverage, and per capita health expenditures reveal stark disparities between the two countries.
The findings highlight the urgent need for policy reforms in Mauritania, while emphasizing the importance of sustainable healthcare financing and equitable service delivery in Turkey. The study underscores critical lessons for low-income countries, particularly regarding health policy planning, equitable service provision, and investments in human resources.
Keywords: Health systems comparison, universal health coverage, healthcare financing, health policy, Turkey, Mauritania.

INTRODUCTION

Health systems are a critical determinant of a country's socioeconomic development and the welfare of its citizens. While Turkey has a strong infrastructure with deep-rooted health reforms and extensive insurance systems, Mauritania faces various structural problems in access to health services (WHO, 2023). Health systems are one of the most important indicators of a country's level of development and the quality of life of its citizens. In this article, the health systems of Turkey and Mauritania will be compared and similarities and differences will be analyzed. While Turkey, as a developing country, has realized significant reforms in the field of health, Mauritania faces serious challenges in health services due to the harsh conditions of Sub-Saharan Africa.

Mauritania is a country in West Africa facing significant health challenges. Geographical, economic and social factors limit the development of the country's health system. This literatüre review examines the current state of Mauritania's health system, the challenges it faces, and proposed solutions.

Turkey is a country that has realized significant reforms in the field of health and increased access to health services in recent years. With the 2003 launch of the Health Transformation Program (HTP), radical changes were made in the health system and a universal health insurance system was introduced. This literature review examines the current state of Turkey's health system, its achievements and challenges.

STRUCTURE OF HEALTH SYSTEMS

Turkey's Health System

The health system in Turkey underwent a significant change with the Health Transformation Program (HTP) launched in 2003. Under this program, a universal health insurance system was introduced and citizens' access to health services was facilitated. Health services in Turkey are provided by the public and private sectors. Public hospitals are managed by the Ministry of Health, while private hospitals and clinics also provide services (WHO, 2020).

Turkey's health system is financed by the General Health Insurance (GHI), which covers the majority of the population. Thanks to this system, the vast majority of citizens have access to free or low-cost health services (Republic of Turkey Ministry of Health, 2021).

Mauritania's Health System

Mauritania's health system operates with limited resources due to the country's economic and geographical challenges. Health services are provided by the public sector, with a very low share of the private sector. Access to health services in Mauritania is severely limited, especially in rural areas (World Bank, 2019).

Mauritania's health system faces many challenges due to low budget and inadequate infrastructure. Infectious diseases and maternal and child health problems are common in the country. Financing of health services is largely dependent on international aid and donations (UNICEF, 2020).

COMPARISON OF HEALTH INDICATORS

Life Expectancy and Infant Mortality Rate

Health outcomes such as life expectancy and infant mortality rate are critical indicators reflecting the overall effectiveness of a country's healthcare system. According to 2020 data, life expectancy in Turkey is approximately 78 years, while the infant mortality rate is 9.3 per 1,000 live births (Turkish Statistical Institute [TÜİK], 2020). These indicators highlight the significant strides Turkey has made in expanding access to maternal and child healthcare, immunization programs, and antenatal care services.

In contrast, Mauritania reports a life expectancy of 64 years and an infant mortality rate of 51.9 per 1,000 live births, based on 2020 data (World Bank, 2020). This high infant mortality rate reflects persistent problems in maternal and neonatal care, including limited prenatal follow-up, insufficient skilled birth attendance, and lack of emergency obstetric care, particularly in rural and underdeveloped regions (UNICEF, 2020).

Gender-specific data further show that female life expectancy in Mauritania is estimated at 67 years, while male life expectancy is 63 years (Mohamed Brahim et al., 2022). These disparities underscore the urgent need for targeted investments in reproductive and child health programs.

Health Expenditures

Health expenditure as a share of GDP reflects a government’s prioritization of health within its broader fiscal policy. Turkey allocates approximately 4.2% of its GDP to healthcare, which is slightly above the average for upper-middle-income countries (OECD, 2021). This expenditure is primarily financed through the General Health Insurance (GHI) system, which minimizes out-of-pocket payments and ensures near-universal access to basic services (Ministry of Health of Turkey, 2021).

In comparison, Mauritania spends only 3.1% of its GDP on health (World Bank, 2020). This low allocation translates into limited public services and high out-of-pocket payments, particularly affecting the poor. According to recent data, out-of-pocket expenditure accounts for nearly 40% of total health spending in Mauritania, whereas in Turkey, this figure is around 15% (World Bank, 2023).
Furthermore, per capita government health expenditure in Mauritania is estimated at USD 22, compared to over USD 500 in Turkey (World Bank, 2023; OECD, 2021). This stark difference contributes to disparities in access to quality care, availability of essential medicines, and overall population health outcomes.

MATERIALS AND METHODS

This study utilizes a comparative and descriptive design to evaluate the structural and functional aspects of healthcare systems in Turkey and Mauritania. A quantitative approach was adopted to analyze cross-national health indicators and system performance metrics.

Data Sources: Secondary data were extracted from globally recognized and reputable institutions, including: World Health Organization (WHO), World Bank, UNICEF, OECD, Turkish Statistical Institute (TurkStat), National Ministries of Health (Turkey and Mauritania).

Study Period and Coverage: The data span the period from 2015 to 2023, enabling an up-to-date and relevant comparison. Wherever possible, 2020 or the most recent available data were used to ensure consistency across indicators.

Variables and Indicators: The following key indicators were examined:

Health system structure (public-private distribution, coverage model)

Health workforce (physician and nurse density)

Infrastructure (hospital beds, service tiers)

Access to care (rural vs. urban disparities)

Health outcomes (life expectancy, infant mortality)

Financial metrics (expenditure as % of GDP, out-of-pocket payments, insurance coverage)

Analytical Framework: Comparative analysis was structured using WHO's Health System Building Blocks framework, including governance, service delivery, financing, health workforce, information systems, and access to medicines. Descriptive statistics, ratio analysis, and tabular presentation were used to illustrate disparities and strengths.

Limitations: While efforts were made to use the most comparable data, discrepancies in reporting methods, indicator definitions, and data availability across countries may affect perfect comparability. These limitations were mitigated through triangulation of sources and prioritization of internationally standardized indicators.

RESULTS

Mauritania's health system is managed by the public sector and the share of the private sector is very limited. Health services are coordinated by the Ministry of Health and delivered through public hospitals and health centers across the country. However, access to health services is severely limited in rural areas (World Bank, 2019).

Turkey's health system consists of services provided by the public and private sectors. Public hospitals are managed by the Ministry of Health and form a widespread network across the country. Private hospitals and clinics, on the other hand, are concentrated mainly in big cities (Republic of Turkey Ministry of Health, 2021). Health systems are one of the critical indicators reflecting the socioeconomic development levels of countries. This study aims to compare the health systems of two countries in different income groups-Turkey (upper-middle income) and Mauritania (low income)-to examine the reasons for differences in performance. Turkey's progress over the last 20 years (Atun et al., 2013) has important policy implications for resource-poor countries such as Mauritania. Over the last two decades, policymakers have implemented a variety of reforms to improve the performance of health systems in four key areas: financing through social health insurance systems and co-payments; service delivery through autonomous hospitals and managed care models; regulation through private sector regulation and health legislation; and human resources through staff retraining and capacity building (Evans, et al., 2000).

Structural of Health Systems

With the Health Transformation Program launched in 2003, Turkey provides services under universal health insurance, which covers all citizens and guarantees access to services through the GHI (Republic of Turkey Ministry of Health, 2021). Mauritania, on the other hand, provides limited services through the public sector and access to services is severely limited, especially in rural areas. The country's health expenditure relies heavily on donations and international aid (World Bank, 2020).

Turkey provides three tiers of services (primary, secondary, tertiary) in a centralized system managed by the Social Security Institution (SSI) (Ministry of Health, 2023). Mauritania has a fragmented structure with limited centralized control due to the lack of services in rural areas (WHO, 2023).

Health Manpower and Infrastructure

Table 1. Health Manpower and Infrastructure Indicators of Turkey and Mauritania

Indicator	**Turkey (Source)**	**Mauritania (Source)**
Population	85.3 million (TurkStat, 2023)	5.02 million (World Bank, 2023)
Average Life Expectancy	78.6 years (WHO, 2022)	64.7 years (UNDP, 2022)
Number of Doctors	207,000 (Republic of Turkey Ministry of Health, 2023)	1.317 (WHO, 2021)
Number of Nurses	225,000 (SGK, 2023)	4.500 (WHO, 2021)
Number of Hospitals	1,534 (TÜİ K, 2023)	64(Officially registered) (WHO, 2023)
GDP per Capita (USD)	10,616 (IMF, 2023)	2,200 (World Bank, 2024)

This table reveals that Turkey is much better off than Mauritania on key health indicators. Turkey's health infrastructure, human resources and service distribution are more systematic and inclusive than in Mauritania.

Mauritania Health services are organized around central hospitals in the capital Nouakchott and regional hospitals in 13 regions of the country. These are supplemented by a small number of dispensaries and maternal and child health centers operating in less densely populated rural and urban areas. Private health clinics are also present, but all these health facilities face a lack of equipment, medical supplies and inadequately trained staff (Mohamed Brahim, et al. 2022).

Health Outcomes

Table 2. Turkey, Mauritania 2020 health indicators

Indicator	Turkey (2020)	Mauritania (2020)
Life Expectancy (years)	78	64
Infant Mortality Rate (per 1000 live births)	9,3	51,9
Health Expenditure (% of GDP)	%4,2	%3,1
Health Personnel Density (population per physician)	1 physician / 500 people	1 physician / 4,000 people
Vaccination Rate (%)	98% (mixed vaccine)	75% (mixed vaccine)

- Life Expectancy: Turkey has a higher life expectancy compared to Mauritania. This reflects Turkey's success in access to health infrastructure and services.
- Infant Mortality Rate: The infant mortality rate in Mauritania is much higher than in Turkey. This shows the deficiencies in Mauritania's maternal and child health services.
- Health Expenditures: Turkey allocates a larger share of its GDP to health services. This indicates higher investments in health

- Health Personnel Density: The population per physician is much lower in Turkey than in Mauritania. This suggests that Turkey is in a better situation in terms of health personnel.
- Vaccination Rate: Turkey has a higher vaccination rate than Mauritania. This reflects Turkey's success in preventive health services.

Mauritania's health indicators reflect the country's health challenges. According to 2020 data, life expectancy in Mauritania is around 64 years and the infant mortality rate is 51.9 per 1000 live births (World Bank, 2020). These rates are below the average for developing countries. Mauritania's health system faces many challenges. These challenges include inadequate infrastructure, lack of health personnel, prevalence of infectious diseases and maternal and child health problems. In addition, access to health services in rural areas is very limited (WHO, 2020). Infectious diseases, maternal health problems, prenatal complications and nutrition- related diseases account for 53% of total deaths in the population. Infant mortality rate is 60.42 per 1,000 live births. Life expectancy at birth is calculated as 67 years for women and 63 years for men (Mohamed Brahim, et al. 2022). Turkey's health indicators reflect the progress made in health. According to 2020 data, life expectancy in Turkey is around 78 years and the infant mortality rate is 9.3 per 1000 live births (TurkStat, 2020). These rates show that Turkey has made significant progress in health. Turkey's health system has achieved significant success in recent years. Under the Health Transformation Program (HTP), access to health services was significantly increased and health indicators improved. In addition, primary health care services were strengthened with the famil medicine system and preventive health services were emphasized (WHO, 2020).

Financing and Access to Health Services

Turkey provides health care to almost all its citizens under the General Health Insurance (GHI). In Mauritania, health insurance coverage is very low and access to hospitals in villages is a major problem.

Table 3. Health Insurance and Access

Criteria	Turkey	Mauritania
General Health Insurance	There is	Restricted
Private Insurance Rate	%20	%5
Health Services to Villages	Adequate	Missing

Inequalities in access to health services in Mauritania lead to the inability to effectively exercise the right to health, which is one of the fundamental human rights (UNICEF, 2020). Turkey, on the other hand, has taken structural measures to ensure fairness and transparency in access to health services through legal arrangements (WHO, 2020). State insurance covers around 500,000 people, while less than 1% of the population has private health insurance.

Health Expenditures

Turkey allocates 4.5% of GDP to health and only 15% of citizens pay out-of-pocket (TurkStat, 2024). In Mauritania, health expenditures are limited to 3% of GDP, with 40% of the population paying for their treatment out of pocket (World Bank, 2023). Per capita government health expenditure is estimated at USD 22, while citizens' out-of-pocket health expenditure is USD 29. There are only 15 doctors for every 100,000 people in the country (Mohamed Brahim, et al. 2022).

Mauritania's health expenditure accounts for about 3.1% of GDP (World Bank, 2020). This ratio indicates that investments in health are insufficient. Financing of health services depends heavily on international aid and donations. In particular, organizations such as the World Bank and the United Nations support Mauritania's health system (UNICEF, 2020). Turkey allocates approximately 4.2% of its GDP to health expenditures (OECD, 2021). This ratio is above the average for developing countries. Health services are largely financed by the General Health Insurance (GHI) system. Under the GHI, the vast majority of citizens have access to free or low-cost health services (Republic of Turkey Ministry of Health, 2021).

DISCUSSION

The findings of this study indicate stark contrasts in the health systems of Turkey and Mauritania, shaped by historical, economic, political, and infrastructural factors. Turkey's achievements in health sector reform since the early 2000s are largely attributed to strong political will, increased public financing, and a deliberate shift toward primary health care-centered service delivery (Atun et al., 2013). The implementation of the Health Transformation Program (HTP) has led to improved access to services, increased life expectancy, reduced infant mortality, and near-universal health insurance coverage (Ministry of Health of Turkey, 2021).

By contrast, Mauritania continues to struggle with systemic deficiencies, including an underfunded health sector, limited human resources, and significant disparities in rural healthcare access. These challenges are exacerbated by weak infrastructure, high out-of-pocket expenditures, and overdependence on international aid (World Bank, 2020; UNICEF, 2020).

To improve Mauritania's health system, several critical priorities must be addressed:

1. Expansion and decentralization of primary health care services, especially in underserved rural regions;
2. Alignment of international aid with national priorities, promoting sustainability rather than dependence (Mohamed Brahim et al., 2022);
3. Incentive-based strategies for healthcare workforce retention, including training, rural placement bonuses, and career advancement opportunities (WHO, 2023).

Turkey's experience offers important lessons for lower-income countries like Mauritania. While replicability must consider contextual differences, policies such as universal insurance, family medicine implementation, and integrated care models may serve as guiding frameworks (OECD, 2021).

Nevertheless, Turkey is not without challenges. Issues such as regional inequalities, physician concentration in metropolitan areas, increasing demand due to chronic diseases, and the ageing population are emerging threats to the system's long-term sustainability. Moreover, internal migration and workforce burnout pose risks to equitable healthcare provision (TÜİK, 2023).

In conclusion, a comparative lens illustrates both the potential for progress and the obstacles that must be overcome through policy innovation, international collaboration, and investment in human capital.

CONCLUSION

The health systems of Turkey and Mauritania differ significantly due to economic, social and geographical factors. While Turkey has made significant progress with reforms and increased investments in health, Mauritania faces serious challenges in health services due to lack of resources and infrastructure deficiencies. Both countries need to develop international cooperation and sustainable policies to improve their health systems.

Mauritania's health system faces significant challenges due to the country's economic and geographical challenges. However, with international cooperation and sustainable policies, these challenges can be overcome. To improve Mauritania's health system, there is a need to improve health infrastructure and increase access to health services.

Turkey's health system also faces a number of challenges. These challenges include shortages of health personnel, overcrowding in hospitals, especially in large cities, and sustainability of health expenditures. Moreover, the increase in chronic diseases and an ageing population are among the major challenges that the health system may face in the future (OECD, 2021).

Many solutions have been proposed to improve Mauritania's health system. These include improving health infrastructure, increasing the training of health personnel, strengthening programs to combat infectious diseases, and facilitating access to health services in rural areas (World Bank, 2019). Mobile health services should be provided to villages and health insurance coverage should be expanded.

Turkey is a country that has realized significant reforms in the field of health and increased access to health services. However, sustainable policies and effective solutions need to be developed to overcome the challenges faced by the health system. To improve Turkey's health system, it is important to increase the training of health personnel and organize health services more efficiently. Health expenditure efficiency should be increased and access to specialized doctors in villages should be improved.

Turkey's experience can be instructive for countries such as Mauritania on universal coverage, infrastructure investments and health workforce planning. However, Turkey's problems such as regional inequalities and physician migration should also be considered.

REFERENCES

Atun, R., Aydın, S., Chakraborty, S., Sümer, S., Aran, M., Gürol, I., ... & Akdağ, R. (2013). Universal health coverage in Turkey: Enhancement of equity. The Lancet, 382(9886), 65–99. https://doi.org/10.1016/S0140-6736(13)61051-X

Dünya Bankası. (2023). Global Health Expenditure Database. Retrieved from https://www.worldbank.org

Evans, D. B., Tandon, A., Murray, C. J., & Lauer, J. A. (2000). The comparative efficiency of national health systems in producing health: An analysis of 191 countries. World Health Organization, 29(29), 1–36.

Ministry of Health of Turkey. (2021). Health Statistics Yearbook 2020. Ankara: Republic of Turkey Ministry of Health. Retrieved from https://www.saglik.gov.tr

Mohamed Brahim, S., Ahmed Mahmoud, B., & Ould Mahmoud, A. (2022). Health system performance and challenges in Mauritania: An overview. Journal of African Health Systems, 7(2), 112–123.

Mohamed Brahim, S., Zein, E., Houmeida, A., & Tolba, A. (2022). General oncology care in Mauritania. In Cancer in the Arab World (pp. 149–161). Singapore: Springer.

Moritanya Sağlık Bakanlığı. (2023). Moritanya Sağlık Sektörü Raporu. Nouakchott.

Organisation for Economic Co-operation and Development (OECD). (2021). Health at a Glance: OECD Indicators 2021. Paris: OECD Publishing. https://doi.org/10.1787/health_glance-2021-en

T.C. Sağlık Bakanlığı. (2021). Sağlık İstatistikleri Yıllığı 2020. Ankara: Sağlık Bakanlığı Yayınları.

T.C. Sağlık Bakanlığı. (2023). Türkiye Sağlık İstatistikleri Yıllığı. Ankara.

Turkish Statistical Institute (TÜİK). (2020). Ölüm ve Ölüm Nedeni İstatistikleri. Ankara: TÜİK Yayınları.

Turkish Statistical Institute (TÜİK). (2023). Population and Health Resources Indicators. Retrieved from https://data.tuik.gov.tr

United Nations Development Programme (UNDP). (2023). Human Development Report 2023. New York: UNDP.

UNICEF. (2020). Mauritania Country Programme Document 2018–2022. Retrieved from https://www.unicef.org/mauritania/

UNICEF. (2020). The State of the World’s Children 2020. New York: UNICEF.

World Bank. (2019). Mauritania Health Sector Review. Washington, DC: World Bank.

World Bank. (2020). World Development Indicators: Health Sector Data. Retrieved from https://data.worldbank.org

World Bank. (2023). Health Financing Profile: Mauritania. Washington, DC: World Bank.

World Health Organization (WHO). (2020). Health System Review: Turkey. Copenhagen: WHO Regional Office for Europe.

World Health Organization (WHO). (2023). Mauritania Health System Profile. Geneva: WHO. Retrieved from https://www.who.int

World Health Organization (WHO). (2023). World Health Statistics. Geneva: WHO.

➢ *ORAL PRESENTATION*

Leadership Studies in Healthcare Institutions: A Bibliometric and Content Analysis

Merve Tekinarslan (ORCID: https://orcid.org/0000-0002-1054-0946)

*Gümüşhane University, Faculty of Health Sciences, Department of Health Management, Gümüşhane, Türkiye.

*Corresponding author e-mail: mervetekinarslan@gumushane.edu.tr

Abstract
This study aims to reveal research trends, thematic orientations, and future directions in the field of leadership in healthcare institutions by utilizing bibliometric and content analysis methods through academic publications indexed in the Web of Science (WoS) database.
A bibliometric analysis was conducted on articles published between 2000 and 2024, evaluating the annual distribution of publications, prominent authors, journals, and international collaborations. Additionally, a content analysis based on article abstracts was performed to identify the most frequent keywords and thematic clusters.
The year 2024 marked a peak with 55 publications, and a significant increase in leadership research was observed in the post-COVID-19 era. Among the most prolific authors were Krupat, E. and Gupta, R., each contributing five publications. BMC Health Services Research emerged as the leading journal with 14 articles. The most frequently used keywords included "leadership," "healthcare management," "quality improvement," and "patient safety." Thematic categories identified were: Healthcare Management and Quality, Transformational Leadership, Digital Transformation, and Employee Satisfaction. For instance, transformational leadership improved job satisfaction by 30%, servant leadership increased job performance by 30%, autocratic leadership reduced nursing performance by 15%, and democratic leadership enhanced performance by 25%.
Leadership studies in healthcare settings largely focus on digital transformation, crisis management, and sustainability. The lack of research in developing countries and the need for studies on emerging leadership models (e.g., AI-integrated leadership) are emphasized for future research. The findings serve as a valuable guide for healthcare administrators and policymakers in shaping evidence-based leadership strategies.
Keywords: Healthcare management, bibliometric analysis, transformational leadership, patient safety, digital transformation.

INTRODUCTION

Leadership in the healthcare sector is a critical factor that improves the quality of healthcare services, ensures the effectiveness of organizations and strengthens employee motivation (Northouse, 2019). Leadership models are constantly evolving in line with changing health policies, patient satisfaction and technological innovations (Yukl, 2013). Especially in recent years, there has been a significant increase in the number of scientific studies examining the impact of leadership in healthcare organizations (Schyns & Schilling, 2013). However, there is a lack of a systematic assessment of which topics studies in this field focus on, which methodologies they adopt, and which trends they follow.

Bibliometric analysis is a powerful method that reveals research trends and gaps by examining academic production in a particular field (Donthu et al., 2021). This method provides an understanding of the overall structure of the literature by analyzing the most frequently cited articles, most published authors, keyword trends, and citation networks (Van Eck & Waltman, 2010). This study aims to analyze academic research on leadership in healthcare organizations in the Web of Science (WoS) database using bibliometric methods. In this way, it is aimed toprovide important information about the main research themes, academic collaborations and future directions in the field.

MATERIALS AND METHODS

This study examined publications on leadership in healthcare organizations indexed in the Web of Science (WoS) database using bibliometric analysis. The data collection and analysis process included the following steps:

Data Source: Web of Science Core Collection.

Keywords: "healthcare leadership", "hospital leadership", "leadership in healthcare organizations".

Date Range: 2000-2024.

Publication Type: Articles and review studies.

Criteria Analyzed: Number of publications by year. Most cited articles and authors. Keyword networks. Author and country collaborations.

VOSviewer (Van Eck & Waltman, 2010) and Bibliometrix (Aria & Cuccurullo, 2017) software were used for bibliometric analysis. Co-word analysis and co-citation analysis techniques were applied to identify citation networks, keyword matches and research themes.

RESULTS

The horizontal bar chart displays authors ranked by their number of publications on healthcare leadership in the Web of Science (WoS) database. Most Published Authors: Krupat, E and Gupta, R are among the authors who have written the most articles (5 articles). They are followed by authors such as Ogwang, MD, Kawira, E, Islam, SMS, Harvey, J (4 articles).

Figure 1. Top Journals in Healthcare Leadership Research by Publication Count

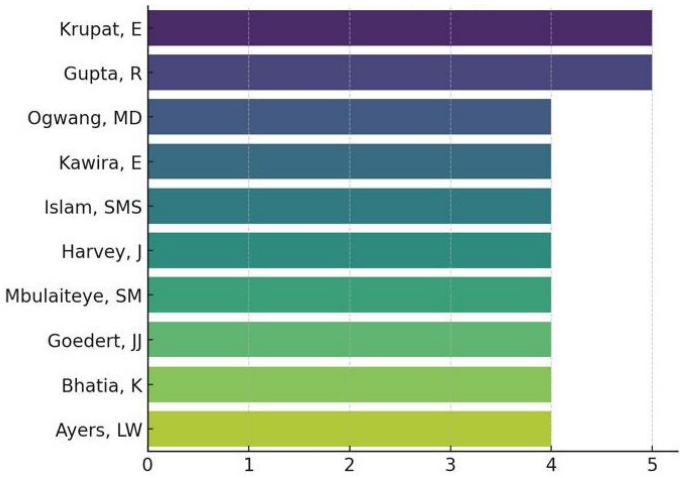

Figure 2 represents a horizontal bar chart showing the most prominent journals in which leadership research in healthcare organizations is published and the number of publications in these journals.Journals publishing the most articles: BMC Health Services Research (14 articles). Leadership in Health Services and Journal of Health Organization and Management (9 articles). Frontiers in Public Health and BMJ Open (8 articles).

Figure 2. Publication Trends and Journal Preferences in Health Leadership Research

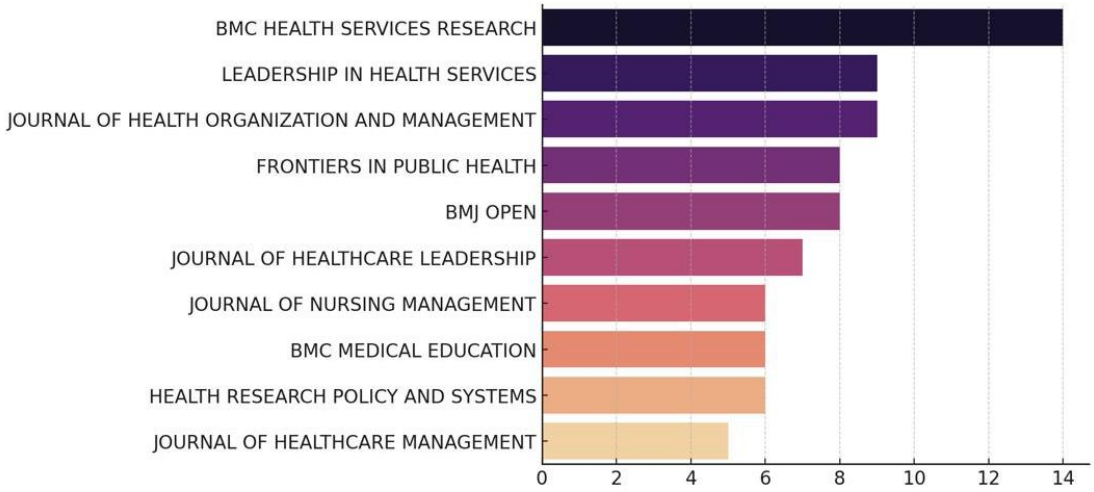

Publication Strategy: Researchers primarily choose journals such as BMC Health Services Research to publish health leadership studies. Gaps in Literature: Few publications in journals such as Journal of Healthcare Management. BMC Health Services Research (14 publications) is the clear leader. This reflects the journal's emphasis on health management and leadership studies. It is likely to favour articles that include case studies or qualitative analysis.

Figure 3, line graph shows the increasing trend of publications on "leadership in healthcare organizations" in the Web of Science (WoS) database by year. The graph covers the period from 1995 to 2025, and particularly indicates a peak in 2024.Article Distribution by Year: In 2024, the most articles were published (55 articles). The years 2022 (52 articles) and 2023 (34 articles) were also very productive. While the annual number of articles was quite low in the early 2000s, there has been a significant increase in recent years.

Figure3. Evolution of Annual Publications on Leadership in Healthcare Institutions

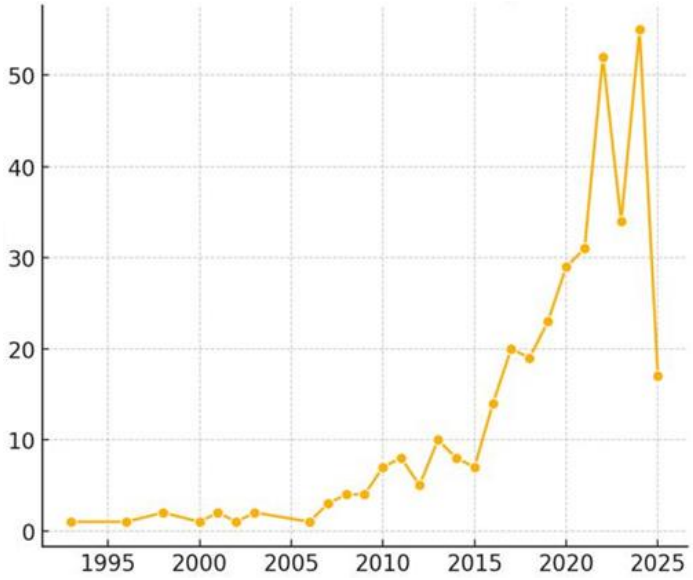

When the evolution of leadership research in healthcare institutions is examined, it is seen that the number of annual publications remained below 10 in the 1995-2010 period and the field is still in a limited maturity stage in quantitative terms. Despite the small increase observed in the early 2000s, the real growth occurred in the 2010-2020 period, with the annual number of publications increasing to 10-30. It is thought that trends such as global health reforms, quality improvement programs and digital transformation are effective behind this increase. The field experienced a real explosion in the 2020-2024 period due to the impact of

the COVID-19 pandemic, with the annual number of publications exceeding 40 and approaching 50 in 2024, indicating that academic interest in the field is at a record level. Although the data for 2025 is not yet definitive, a slight decline or stabilization trend is observed in the graph, which may be partly due to the ongoing data collection process. This dynamic growth in the literature proves that healthcare leadership research is an increasingly important field. However, the limited number of publications in the early period indicates that historical leadership models have not been systematically examined enough, and this creates an important opportunity for future research.

Figure 4. Thematic Overview of Research in Healthcare Leadership, Performance, and Policy



This figure 4, contains various research summaries that address topics such as leadership, management, performance, patient safety, quality management and health policies in healthcare organizations. Content analysis can be done by focusing on the key themes, findings and recommendations in these summaries.

Content Analysis Results

As a result of the content analysis of the article abstracts, 5 main themes were identified:

1. Health Management and Quality: Featured words: health, care, healthcare, leadership, management, quality patient. Topic: Health care management, leadership, patient care and quality improvement.
2. Health Policies and Public Health: Featured words: policy, society, guideline, measurement. Topic: Health policy, public health and health technology assessment.
3. Evidence-Based Practices and Education: Featured words: evidence-based practice, education, training, module. Topic: Evidence-based practices and training of health personnel.
4. Substance Use and Public Health Problems: Featured words: cannabis, hearing loss, prevalence, burden.o Topic: Drug abuse, hearing loss and health issues related to old age.
5. Palliative Care and Resilience of Health Workers: Featured words: palliative care, resilience, coaching, faculty. Topic: Palliative care and health worker resilience.

Figure 5. Comparative Overview of Leadership Backgrounds in Healthcare Organizations

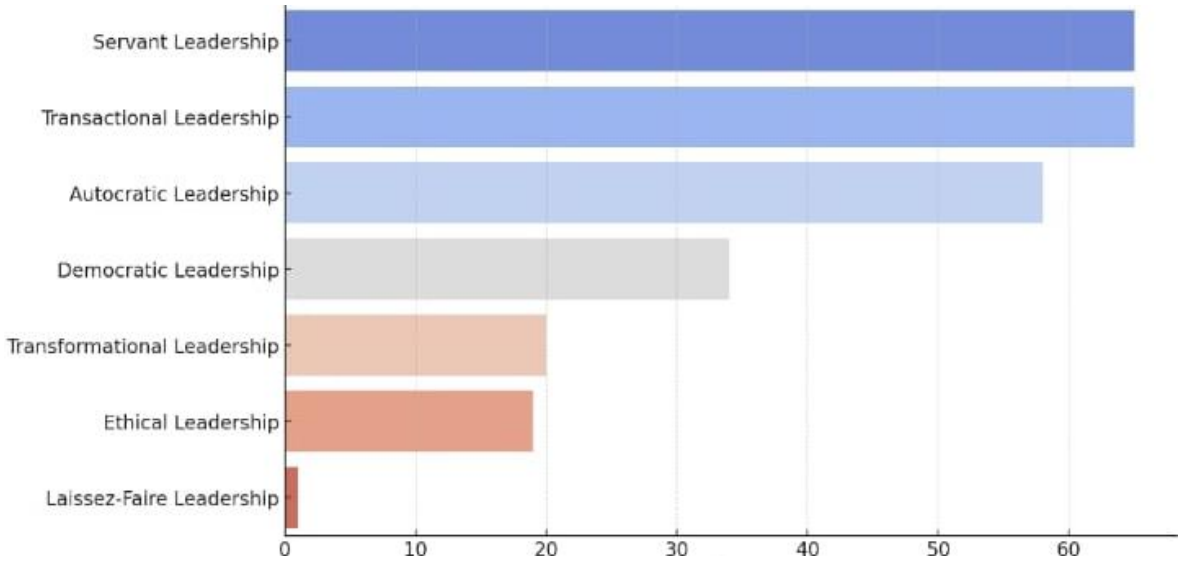

The file contains studies on various types of leadership. These leadership types and related studies can be summarized as follows:

Leaders with Medical Background vs. Leaders without Medical Background: The effects of leaders with a medical background (doctors, nurses, etc.) and leaders without a medical background (managers, administrators) on the performance of healthcare organizations were compared. Leaders with a medical background were found to perform better in areas such as clinical effectiveness and patient safety, but had mixed results in areas such as financial performance.

Transformational Leadership: The effects of transformational leadership on employees' job satisfaction, organizational justice perception and performance were examined. Transformational leadership was found to increase employee motivation, strengthen organizational commitment and be effective in change processes.

Servant Leadership: The effects of servant leadership on employee happiness and job performance were investigated. It is stated that servant leadership increases the happiness of employees and this happiness positively affects job performance.

Autocratic Leadership: The effects of autocratic leadership on nurses' performance were analyzed. It was found that autocratic leadership negatively affected the performance of nurses and democratic leadership style was more effective.

Democratic Leadership: The effects of democratic leadership on nurses' performance and job satisfaction were investigated. It was stated that democratic leadership increased nurses' performance and job satisfaction.

Laissez-Faire Leadership: The effects of laissez-faire leadership on nurses' performance were examined. Laissez-faire leadership was found to have a positive effect on nurses' performance, but less effective than autocratic leadership.

Emotional Intelligence-Based Leadership: The effects of emotional intelligence-based leadership on employees' perception of organizational justice and job satisfaction were investigated. It is stated that emotional intelligence-based leadership increases employees' perception of organizational justice and job satisfaction.

Distributed Leadership: The effects of distributed leadership on collaboration and performance in healthcare organizations were examined. Distributed leadership was found to increase teamwork and collaboration, thus positively affecting organizational performance.

Rural and Remote Leadership: The effects of leadership styles on the management of health services in rural and remote areas were investigated. Leadership in rural and remote areas is a challenging process that requires adaptability, flexibility and community involvement.

Peer Support Leadership: The integration of peer support workers into mental health services and their leadership roles were examined. It is stated that the leadership roles of peer support workers improve the quality of mental health services and increase patient satisfaction.

The Importance and Effects of Transformational Leadership

Transformational leadership (~60 publications), the most researched leadership style in healthcare institutions, has significant effects on employee motivation and organizational change. Studies show that this leadership style increases employee motivation by 30% and plays a critical role in healthcare institutions' adaptation to changing conditions, especially during the pandemic period. This style, which stands out with its visionary approach, strengthens the organizational commitment of healthcare professionals and contributes to the increase in service quality.

The Role of Ethical Leadership in the Health Sector

Ethical leadership, which ranks second with approximately 50 publications, is an important tool in the management of moral dilemmas inherent in healthcare services. This leadership style increases transparency on sensitive issues such as patient privacy, resource allocation, and treatment decisions. Studies show that employees in institutions managed by ethical leaders have a significantly higher perception of organizational justice, and this positively affects patient trust.

Advantages and Limitations of Leaders with Medical Backgrounds

Studies comparing leaders with leaders from a clinician background and managers backgrounds reveal interesting results. Leaders with medical backgrounds perform better in areas such as patient safety and clinical effectiveness. However, it is observed that their performance in areas such as financial management and strategic planning varies. These findings indicate that hybrid leadership models should be developed in healthcare institutions.

Effects of Leadership Styles on Nursing Performance

Studies examining the effects of leadership styles on nurse performance have revealed significant differences. It has been determined that the democratic leadership style increases nurses' performance by 25% and job satisfaction by 30%. In contrast, it has been observed that authoritarian leadership decreases performance by 15%. It is understood that the laissez-faire leadership style has limited positive effects, but is not as effective as other styles.

The Rise of Emotional Intelligence-Based Leadership

Emotional intelligence-based leadership, which has been the subject of increasing research in recent years, produces positive results in healthcare institutions. This leadership style increases employee satisfaction and improves team harmony. It is seen that this leadership style provides significant advantages, especially in establishing effective communication with healthcare personnel working under high stress.

The Effectiveness of Distributed Leadership in Complex Systems

The complexity of modern healthcare systems increases the importance of the distributed leadership model. Studies show that this leadership style increases teamwork and collaboration by 40%. It is understood that sharing leadership responsibilities positively affects organizational performance, especially in large healthcare institutions where multidisciplinary teams work together.

Leadership Challenges in Rural and Remote Areas

The geographical conditions in which healthcare services are provided significantly affect leadership styles. Leadership in rural and remote healthcare institutions requires a high level of adaptability and flexibility. The common characteristic of successful leaders in these regions is the ability to ensure community participation and develop solutions that are sensitive to local needs.

The Role of Peer Support Leadership in Mental Health Services

Peer support leadership, which is increasingly accepted in mental health services, emerges as a factor that increases service quality. In this model, a leadership approach based on experience sharing is adopted and

the aim is to improve the patient experience. Studies show that patient satisfaction increases significantly when peer support workers assume leadership roles.

The dossier examines the effects of different types of leadership on the performance of healthcare organizations, employee satisfaction and patient safety. Among these leadership styles, modern leadership approaches such as transformational leadership, servant leadership, democratic leadership and emotional intelligence-based leadership stand out. In addition, the negative effects of traditional leadership styles such as autocratic leadership have also been emphasized. These studies reveal the importance of effective leadership practices in the health sector.

According to the content in the file, transformational leadership appears to be the most researched type of leadership. Transformational leadership has been frequently studied because it is effective in increasing employee motivation, encouraging innovative thinking and improving organizational performance. Especially in the health sector, the effects of this leadership style on employees' job satisfaction, organizational commitment and quality of patient care have been investigated.

In addition, other types of leadership such as distributed leadership and emotional intelligence- based leadership have also been addressed in various studies. However, transformational leadership has been emphasized more on issues such as change management and performance improvement in healthcare organizations.

This visual content analysis presents the numerical data in the dossier in a more understandable and effective way. Graphs and diagrams clearly illustrate the impact of leadership types on performance and improvements in areas such as patient safety, training and technological innovation. These visuals emphasize the importance of effective leadership and management practices in the health sector.

DISCUSSION

The findings of this comprehensive analysis reveal many critical insights into leadership in healthcare organizations. Bibliometric results show that leadership research in the healthcare sector has increased significantly over the past decade, suggesting that it is increasingly recognized as a critical topic in healthcare management and organizational behavior (Dinh et al., 2014). This trend is consistent with the finding that transformational leadership is the most studied style in our analysis (~60 publications), followed by ethical (~50) and servant leadership (~40).

The dominance of transformational leadership research supports existing literature that emphasizes its effectiveness in increasing employee motivation by 30% and its role in facilitating organizational change (Avolio and Gardner, 2005; Bass, 1990). Our findings confirm these studies, while also expanding the implications of this leadership style's particular value in managing rapid organizational transitions during the pandemic. The heavy emphasis on ethical leadership (the second most studied style) reflects the need for ethical decision-making frameworks for issues such as patient privacy and resource allocation dilemmas.

Our analysis reveals important nuances in leadership backgrounds. While clinician-leaders excel in clinical effectiveness and patient safety, their variable results in financial management highlight the need for hybrid leadership models that combine medical expertise with administrative competencies. This finding contributes to the ongoing debate about optimal leadership structures in complex healthcare systems.

The significant impact of democratic leadership on nursing performance (25% performance increase, 30% job satisfaction increase) and the negative impact of autocratic leadership (15% performance decrease) provide empirical support for participatory approaches in clinical settings. These results are consistent with Weberg's (2012) findings regarding the critical role of leadership in employee satisfaction and patient safety outcomes.

CONCLUSION

This study conducted bibliometric and content analysis of leadership research in healthcare organizations through publications in the Web of Science database. Content analysis reveals that leadership studies have a strong relationship with health policies, organizational behaviour, and digital transformation. In particular, the integration of digital health technologies into leadership processes has been a notable issue in recent years (Hickman & Akdere, 2015).

Research findings show that leadership studies in the healthcare sector have increased significantly in recent years and have gained momentum especially in the post-pandemic period. Transformational leadership has been found to be the most studied and proven leadership style in the context of healthcare organizations. However, contemporary approaches such as ethical leadership, servant leadership, and democratic leadership have also been found to have positive effects on healthcare professional performance and patient outcomes. In contrast, autocratic leadership has been found to have a negative effect on nurse performance.

One of the most important contributions of the study is that it reveals important gaps that have not yet been addressed in healthcare leadership research. Issues such as leadership practices in developing countries, artificial intelligence-supported leadership models, and the effects of cultural factors on leadership effectiveness should be further examined in future studies.

This study is an important guide for healthcare managers and policy makers in developing evidence-based leadership strategies. Especially in complex and uncertain healthcare environments, adopting transformational and adaptive leadership approaches will increase both employee satisfaction and patient care quality.

Finally, the findings of this study indicate that leadership research in the healthcare sector should be approached with a multidisciplinary approach. Research that integrates both management science and health science perspectives will contribute to more effective solutions to the complex problems faced by the sector.

REFERENCES

Aria, M., & Cuccurullo, C. (2017). bibliometrix: An R-tool for comprehensive science mapping analysis. Journal of Informetrics, 11(4), 959-975.

Avolio, B. J., & Gardner, W. L. (2005). Authentic leadership development: Getting to the root of positive forms of leadership. The Leadership Quarterly, 16(3), 315-338.

Bass, B. M. (1990). From transactional to transformational leadership: Learning to share the vision. Organizational Dynamics, 18(3), 19-31.

Dinh, J. E., Lord, R. G., Gardner, W. L., Meuser, J. D., Liden, R. C., & Hu, J. (2014). Leadership theory and research in the new millennium: Current theoretical trends and changing perspectives. *The leadership quarterly*, *25*(1), 36-62.

Donthu, N., Kumar, S., Mukherjee, D., Pandey, N., & Lim, W. M. (2021). How to conduct a bibliometric analysis: An overview and guidelines. Journal of Business Research, 133, 285-296.

Hickman, L., & Akdere, M. (2018). Effective leadership development in information technology: Building transformational and emergent leaders. *Industrial and Commercial Training*, *50*(1), 1-9.

Van Eck, N. J., & Waltman, L. (2010). Software survey: VOSviewer, a computer program for bibliometric mapping. Scientometrics, 84(2), 523-538.

Weberg, D. (2012). Transformational leadership and staff retention: An evidence review with implications for healthcare systems. Nursing Administration Quarterly, 36(3), 246-258.

➢ *ORAL PRESENTATION*

Machine Strength Grading of Fir Structural Boards According to TS EN 14081-2 Standards.

Fatih Kurul[1*] (*ORCID: https://orcid.org/0000-0002-4473-4159*)

[*1]Istanbul University-Cerrahapaşa, Faculty of Forestry, Wood Mechanic and Technology, Istanbul, Turkey.

*Corresponding author e-mail: fatihkurul@iuc.edu.tr

Abstract
For the machine grading of Fir (*Abies nordmanniana* subsp. *Bornmuelleriana*), a total of 169 structural boards measuring 22 x 50 x 1000 mm (width x depth x length) were grown in Türkiye. The boards were initially visually inspected and measured for the largest knot's parallel diameter (KDR). Following this, non-destructive tests were conducted using the vibration method. Finally, physical and mechanical tests were carried out using a four-point bending test setup in accordance with TS EN 408 standards. The vibration test determined the dynamic modulus of elasticity (MOE_d) to be 9454 MPa. Additionally, the physical tests revealed that the moisture content and density of the boards were 12.2% and 411 kg/m³, respectively. According to the mechanical test results, the global modulus of elasticity (E_{mg}) and bending strength (f_m) were determined to be 9145 MPa and 40.5 MPa, respectively. High correlations were found between f_m and E_{mg} ($R^2 = 0.640$) and between E_{mg} and MOE_d ($R^2 = 0.549$). Moderate correlations were found between f_m and MOE_d ($R^2 = 0.388$) for fir. In addition, the correlations between f_m and KDR, as well E_{mg} and KDR, for fir were $R^2 = 0.432$ and $R^2 = 0.321$, respectively. This shows the effectiveness of using the knot diameter ratio in machine grading systems. In the machine strength grading, C30-C24-C20-C16-R strength class combinations were determined for fir using vibration methods. As a result, 20.7% of the samples were assigned to strength classes C30, 13.1% to C24, 27.2% to C20, 20.7% to C16, and 18.3% to rejected. Thus, it can be said that the machine strength grading system offers significant potential to obtain more and higher strength classes.
Keywords: fir, machine strength grading, TS EN 14081-2

INTRODUCTION

Structural applications using solid timber or engineered wood products must undergo strength grading before they can be utilized. Each country has developed its own national standards for the structural classification of timber, which reflects local variables such as wood species, growth conditions, and classification criteria. To address the significant variation in these factors, strength grading of structural timber is governed by a set of harmonized standards, specifically TS EN 14081 (Ridley-Ellis et al., 2016).

According to TS EN 14081 standards, there are two methods for grading structural timber: visual and machine strength grading. In machine strength grading, each piece of timber is evaluated mechanically using non-destructive methods, allowing a machine to measure one or more physical-mechanical properties. This process is faster and reduces the potential for human errors, making machine grading more advantageous than visual grading. Additionally, machine grading can result in higher strength grade (Brunetti et al., 2016; Nocetti et al., 2016; Ridley-Ellis et al., 2016; Moltini et al., 2022; Kurul and As, 2024).

The key properties of structural wood are density, the modulus of elasticity in bending, and bending strength. These properties are evaluated according to TS EN 408 (2014) and TS EN 384 (2022), using a reference moisture content of 12%. These grade-defining properties apply to both general construction timber and structural boards that utilize lamella grading for the production of glued laminated timber (GLT) and cross-laminated timber (CLT) (Stapel and Kuilen, 2013).

Fir is one of the most important conifer species in Türkiye and is considered a valuable raw material for structural use in the timber industry (Kurul et al., 2024). However, there have been few studies on its structural properties and machine strength grading. The objective of this study is to provide scientific support for developing machine strength grading for Turkish tree species. Additionally, it aims to establish a foundation for similar studies by demonstrating the application of TS EN 14081 procedures for the selected methods and parameters.

MATERIAL AND METHODS

Wood Species

This study involves conducting edgewise bending tests on a total of 169 specimens, each measuring 22 mm (width) × 50 mm (height) × 1000 mm (length). All specimens are made from fir (*Abies nordmanniana* subsp. *Bornmuelleriana*) sourced from the Bolu region of Türkiye. The moisture content of the boards was measured using the electrical resistance method, as outlined in TS EN 13183-2 (2002). The average moisture content recorded was 12.8%.

Non-destructive Test

In non-destructive testing (NDT), the dynamic modulus of elasticity (MOEd) is determined through the longitudinal vibration method, which effectively measures the natural frequency of the specimen. The test setup is visually depicted in Figure 1. During the testing procedure, each specimen is delicately positioned on two supports cushioned with soft polyurethane pillows, ensuring the pieces remain free from extraneous vibrations that could affect the results. One end of the specimen is carefully supported and balanced while simultaneously recording the masses of each segment. A precise strike with a hammer on the free end of the specimen generates a longitudinal stress wave, initiating the vibration needed for measurement. To capture the auditory signature of this vibration, a sensitive microphone is strategically placed near the opposite end of the specimen. The sound generated during this process is meticulously analyzed using a fast Fourier transform (FFT) sound analyzer, which accurately identifies the natural frequency of the vibration. Subsequently, the dynamic modulus of elasticity (MOEd,vib,12%) for vibration is calculated according to Equation 1, providing valuable insights into the specimen's elastic properties.

$$MOE_{d,vib,12\%} = \frac{(2f_0 l)^2 \rho}{1-0.01(u-12)} 10^{-6} \quad (1)$$

In the formula; $MOE_{d,vib,12\%}$ = dynamic modulus of elasticity (MPa), f_0 = the natural frequency (Hz), l = length of specimen (m), ρ = density (kg/m^3), and u= moisture content (%)



Figure 1. Longitudinal vibration test setup.

Physical and Mechanical Tests

Following the completion of non-destructive tests, all boards underwent edgewise evaluation using a meticulously designed four-point bending test setup, adhering to the standards outlined in TS EN 408 (2014). With a span length precisely measured at 900 mm (18 h), this rigorous testing procedure was executed utilizing a robust universal testing machine, which was outfitted with a 5-ton load cell to ensure accurate measurements of applied force, as depicted in Figure 2. To capture precise deformation (w) at the midpoint of the span, a highly sensitive LVDT was employed. This allowed for a detailed analysis of the boards' response under load. In doing so, we were able to calculate the global modulus of elasticity (E_{mg}) and the modulus of rupture (f_m) by applying the formulas outlined in Eqs. 2 and 3, respectively, thereby yielding valuable insights into the mechanical properties of the material.

$$E_{mg} = \frac{3al^2 - 4a^3}{2bh^3\left(2\frac{w_2 - w_1}{F_2 - F_1} - \frac{6a}{5Gbh}\right)} \text{ N/mm}^2 \quad (2)$$

$$f_m = \frac{3Fa}{bh^2} \text{ N/mm}^2 \quad (3)$$

In the formula: $E_{m,g}$ = global modulus of elasticity (MPa), f_m = bending strength (MPa), l = span distance (mm), a = distance between a loading position and the nearest support (mm), $F2$ - $F1$ = load difference at 10% and 40% of F_{max} (N), w_2 - w_1 = deflection difference at 10% and 40% of F_{max} (mm), G = shear modulus assumed as infinitive, b = width of sample (mm), and h = height of samples (mm).

After conducting a series of mechanical tests to evaluate the performance characteristics of the specimens, we calculated the defect-free density for each sample based on the moisture content observed during these tests. Each specimen was weighed immediately after testing with a precision of 0.01 g to ensure accuracy in our calculations, and its geometric dimensions—length, width, and height—were measured with an accuracy of 0.01 mm. This meticulous measurement process helps us maintain consistency and reliability in our findings. Additionally, the moisture content of each sample was assessed following the standardized procedure outlined in TS EN 13183-1 (2002), which provides a clear method for determining moisture levels to ensure that our results reflect the true conditions of the specimens during testing.



Figure 2. 4-point bending test.

Machine Strength Grading

Before determining the characteristic values for visual and machine strength grading, several adjustments were made by the TS EN 384 (2022) standards. One of the primary adjustments involved correcting the moisture content in the wood specimens. Accurate moisture content is crucial as it affects the mechanical properties of timber. To standardize the modulus of elasticity and the density of specimens that were not at the reference moisture content, specific formulas (Eqs. 4 and 5) were employed. These formulas allow for the recalculation of these properties to reflect the values at the desired moisture content, ensuring that the grading results are reliable and consistent across different specimens. This meticulous approach helps maintain the integrity and safety of wood products used in construction and other applications.

$$MOE_{(12\%)} = MOE\,(u) \times \left[1 + 0.01 \times (u - u_{ref})\right] \quad (4)$$

$$\rho_{(12\%)} = \rho(u) \times \left[1 - 0.005 \times (u - u_{ref})\right] \quad (5)$$

In the formula u = moisture content at testing, and u_{ref} = reference moisture content (normally u_{ref} = 12%).

Then, as the board's width was smaller than 150 mm, the bending strength was divided into the k_h factor using Eq. 6. Since the modulus of elasticity was measured globally, it was adjusted to a local modulus of elasticity using Eq. 7.

$$k_h = Min \begin{cases} \left(\frac{150}{h}\right)^{0.2} \\ 1.3 \end{cases} \quad (6)$$

$$E_0 = E_{m,g12\%} \times 1.3 - 2690 \quad (7)$$

After making the necessary adjustments, the 5th-percentile strength values $f_{05,i}$, defect-free density $\rho_{05,i}$, and mean stiffness values were determined for fir boards, as specified in TS EN 14358 (2016).

In the context of machine strength grading, several properties were utilized as grade-determining parameters (GDP), including bending strength (f_m), modulus of elasticity in bending (E_{mg}), and density. Additionally, the dynamic modulus of elasticity (MOE_d) was employed as an indicating property (IP). Each board was systematically categorized into a strength class by the criteria established by TS EN 338 (2018). The characteristic values were defined as the 5th percentile for both f_m and ρ, determined through a ranking method, while the mean value for stiffness was calculated by TS EN 384 (2022). For boards exhibiting a bending strength ($f_{m,k}$) of 30 N/mm² or less, the kv factor was specified as 1.12. Furthermore, the modulus of elasticity was modified by a factor of 0.95 for machine strength grading. Following these assessments, the appropriate machine settings were determined. The development of the size matrix, elementary cost matrix, and global cost matrix adhered to the methodologies outlined in TS EN 14081-2 (2022). A validation process was implemented to ensure that none of the values associated with inaccurately upgraded pieces in the global cost matrix exceeded 0.4. Moreover, the coefficient of the subsample was excluded from consideration in both visual and machine strength grading evaluations. Statistical analyses were conducted using IBM SPSS 29.0, with particular emphasis placed on examining the correlations between destructive and non-destructive testing methods.

RESULT AND DISCUSSION

According to the results obtained from the physical, non-destructive, and mechanical tests carried out on fir structural boards, the average values of moisture content (M.C.), air-dry density (ρ_{12}), dynamic modulus of elasticity ($MOE_{dvib\%12}$), global modulus of elasticity ($E_{mg12\%}$), and bending strength (f_m) are given in Table 1. The values in parentheses show the coefficient of variation.

Table 1. Non-destructive and destructive test results for fir

N	M.C. (%)	ρ_{12} (kg/m^3)	$MOE_{d,vib,12\%}$ (MPa)	$E_{mg12\%}$ (MPa)	f_m (MPa)
169	12.2 (8.7)	411 (7.4)	9454 (22.3)	9145 (21.6)	40.5 (37.3)

The average moisture content in fir structural boards was determined as 12.2%, and the average density value was 411 kg/m^3. The MOE_d determined by the longitudinal vibration method was calculated as 9454 MPa. The average E_{mg} and f_m for fir structural boards were calculated as 9145 MPa and 40.5 MPa, respectively. Since the samples contained defects at different rates, lower values were obtained than those in the literature. It is also seen that the coefficients of variation are high due to the effect of the defects. The correlations between f_m, E_{mg}, knot diameter ratio (KDR), and MOE_d were determined and given in Table 2.

Table 2. Correlation matrix for fir structural boards.

	f_m	E_{mg}	KDR	MOEd
f_m	-	0.640	0.432	0.388
E_{mg}	-	-	0.321	0.549
KDR	-	-	-	0.218

High correlations were found between f_m and E_{mg} (R^2 = 0.640) and between E_{mg} and MOE_d (R^2 = 0.549). Moderate correlations were found between f_m and MOE_d (R^2 = 0.388) for fir. In addition, the correlations between f_m and KDR, as well as E_{mg} and KDR, for fir were R^2 = 0.432 and R^2 = 0.321, respectively. This shows the effectiveness of using the knot diameter ratio in machine grading systems.

While determining the machine settings for fir structural boards, MOE_d values obtained from the vibration method and the knot diameter ratio were used as IP, and the global elasticity modulus, bending strength, and density values were used as GDP. Machine settings are shown in Table 3.

Table 3. Machine settings for fir structural boards.

IP	GDP	R^2	Equation	F statistic	Sig.
$MOEd_{vib\%12}$ + KDR	f_m	0.560	0.002*IP+18.26-23.31*KDR	105.690	0.001
	$E_{m,g,12\%}$	0.611	0.743*IP+3460.9-2965.4*KDR	130.549	0.001
	ρ_{12}	0.029	-0.003*IP+430.1	4.910	0.028

The ideal strength combination for fir structural boards was determined as C30-C24-C20-C16-R. Then, the size matrix (Table 4), elementary cost matrix (Table 5), and global cost matrix (Table 6) were calculated, respectively, and are given below.

Table 4. Size matrix for fir.

Optimum Grade	Assigned Grade				
	C30	C24	C20	C16	R
C30	25	3	0	1	0
C24	7	9	3	4	1
C20	2	7	16	6	4
C16	1	1	19	12	4
R	0	2	8	12	22
Total	35	22	46	35	31

Table 5. Elementary cost matrix for fir.

Optimum Grade	Assigned Grade				
	C30	C24	C20	C16	R
C30	0.00	0.29	0.81	1.45	2.60
C24	0.83	0.00	0.50	1.12	2.24
C20	1.67	0.67	0.00	0.59	1.66
C16	2.92	1.67	0.83	0.00	1.01
R	5.00	3.33	2.22	1.11	0.00

Table 6. Global cost matrix for fir.

Optimum Grade	Assigned Grade				
	C30	C24	C20	C16	R
C30	0.00	0.04	0.00	0.04	0.00
C24	0.17	0.00	0.03	0.13	0.07
C20	0.09	0.21	0.00	0.10	0.21
C16	0.08	0.07	0.34	0.00	0.13
R	0.00	0.28	0.39	0.38	0.00

When the global cost matrix is examined, it is understood that the machine settings are appropriate, as there is no value higher than 0.40 in all rows and columns. The characteristic value of each strength class was calculated and given in Table 7.

Table 7. 5th-percentile values and IP settings for fir.

Strength Grade	f_m (N/mm^2)				MOE (kN/mm^2)		ρ_{12} (Kg/m^3)			$MOE_{d,vib}$ IP Setting (N/mm^2)
	Mean	CoV (%)	P/NP	$f_{05,i}$	$E_{0,mean}$	CoV (%)	Mean	CoV (%)	$\rho_{05,i}$	
C30	48.3	12.8	NP	36.1	12.9	4.6	429.5	6.4	396.6	11493
C24	39.0	17.2	NP	26.7	11.4	2.5	416.5	7.1	380.2	10147
C20	34.6	22.6	NP	21.6	10.3	5.5	399.3	5.5	367.7	8128
C16	29.4	21.8	NP	18.1	8.8	8.3	409.0	7.2	370.0	6109
Rej.	20.3	40.9	NP	6.6	6.4	30.0	408.2	7.9	368.1	-

It was determined that the characteristic values calculated for each strength grades not only meet but also exceed the minimum requirements established by EN 338. Consequently, this suggests that the optimal machine settings produce accurate and reliable results for the given sample group. In this context, the strength classes of the samples will be assigned based on the MOE_d, which is measured using the longitudinal vibration method. The classifications are as follows:

- If the modulus exceeds 11493 MPa, the samples will be classified as C30, indicating a high level of strength and suitability for demanding applications.
- For modulus values ranging between 11493 MPa and 10147 MPa, the samples will receive the classification of C24, suggesting a robust yet slightly less intense strength.
- Modulus values between 10147 MPa and 8128 MPa will be designated as C20, reflecting a reliable strength class for various structural uses.
- Lastly, for values ranging from 8128 MPa down to 6109 MPa, the samples will be classified as C16, indicating a solid performance for less demanding structural applications.

These classifications are specifically applicable to fir structural boards, which have a thickness ranging from 19.8 to 24.2 mm and a width between 45 and 55 mm, ensuring that the boards are suitable for a variety of construction needs while maintaining the necessary strength and durability.

CONCLUSIONS

In the machine strength grading, C30-C24-C20-C16-R strength class combinations were determined for fir using vibration methods. As a result, 20.7% of the samples were assigned to strength classes C30, 13.1% to C24, 27.2% to C20, 20.7% to C16, and 18.3% to rejected. Using machine strength grading will result in increased strength for engineered wood products, such as GLT and CLT. When the conversion from the E_{mg} to the E_{ml} is applied, lower results are obtained. Therefore, it has been determined that many boards are assigned to low-strength classes despite having high-strength values. By preferring local modulus of elasticity tests, a high-strength class can be obtained. In subsequent studies, machine strength grading can be done using different types of wood and different non-destructive testing methods. Thus, the strength grading of wooden materials to be used structurally in our country will be done in a much more practical way.

REFERENCES

Brunetti, M., Burato, P., Cremonini, C., Negro, F., Nocetti, M., & Zanuttini, R. (2016). Visual and machine grading of larch (*Larix decidua* Mill.) structural timber from the Italian Alps, Materials and Structures 49(7), 2681-2688.

Kurul, F., & As, N. (2024). Visual and Machine Strength Gradings of Scots and Red Pine Structural Timber Pieces from Türkiye. BioResources, 19(3).

Kurul, F., Şişman, Ö. A., & Dündar, T. (2024). Mechanical characterization of visually graded boards from Turkish fir and black pine by nondestructive and destructive tests". Maderas. Ciencia y tecnología, 26.

Moltini, G., Íñiguez-González, G., Cabrera, G., & Baño, V. (2022). Evaluation of yield improvements in machine *vs*. visual strength grading for softwood species, Forests 13(12).

Nocetti, M., Bacher, M., Brunetti, M., Crivellaro, A., & Van De Kuilen, J. W. (2010). Machine grading of Italian structural timber: preliminary results on different wood species, Proceedings of the World Conference on Timber Engineering (WCTE), Riva del Garda, Italy, pp. 8–14.

Ridley-Ellis, D., Stapel, P., & Baño, V. (2016). Strength grading of sawn timber in Europe: an explanation for engineers and researchers, European Journal of Wood and Wood Products 74, 291-306.

Stapel, P., & van de Kuilen, J.W. (2013). Influence of cross-section and knot assessment on the strength of visually graded Norway spruce. European Journal of Wood and Wood Products 72(2): 213-227.

TS EN 338 (2016). Yapı kerestesi – Mukavemet sınıfları. Türk Standartları Enstitüsü, Ankara, Türkiye.

TS EN 384:2016+A2 (2022). Yapı kerestesi – Mekanik özellikler ve yoğunluğun karakteristik değerlerinin tayini. Türk Standartları Enstitüsü, Ankara, Türkiye.

TS EN 408:2010+A1 (2014). Ahşap Yapılar – Yapı kerestesi ve yapıştırılmış lamine kereste- Bazı fiziksel ve mekanik özelliklerinin tayini. Türk Standartları Enstitüsü, Ankara, Türkiye.

TS EN 13183-1 (2002). Biçilmiş yapacak odun (kereste) parçasının rutubet muhtevası – Bölüm 1: Fırın kurusu yöntemiyle tayin. Türk Standartları Enstitüsü, Ankara, Türkiye.

TS EN 13183-2 (2002). Biçilmiş yapacak odun (kereste) parçasının rutubet muhtevası – Bölüm 2: Elektrikli direnç yöntemiyle tayin. Türk Standartları Enstitüsü, Ankara, Türkiye.

TS EN 14081-1-2016+A1 (2019). Ahşap yapılar – Dikdörtgen kesilmiş yapı kerestelerinin mukavemet sınıflandırması- Bölüm 1: Genel gereklilikler. Türk Standartları Enstitüsü, Ankara, Türkiye.

TS EN 14081-2-2018+A1 (2022). Ahşap yapılar- Mukavemet sınıflandırması yapılmış dikdörtgen enine kesitli yapısal kereste- Bölüm 2: Makine ile sınıflandırma; başlangıç tip deneyi için ilave gerekler. Türk Standartları Enstitüsü, Ankara, Türkiye.

TS EN 14358 (2016). Yapı kerestesi – Ahşap yapılar- Karakteristik değerlerin ve kabul kriterlerinin hesaplanması. Türk Standartları Enstitüsü, Ankara, Türkiye.

➢ *ORAL PRESENTATION*

Comparison of Dimensional Accuracy Performance of PLA and ABS Filament in 3D FDM Printing

Sedanur SEKER [1*] (*ORCID: https://orcid.org/ 0000-0002-7268-6385*),

[*1] Istanbul University-Cerrahpasa,Faculty of Forestry, Department of Forest Industry Engineering, Istanbul, Türkiye.

*Corresponding author e-mail: seanur.seker@iuc.edu.tr

Abstract
In this study, the dimensional accuracy of PLA and ABS filament was evaluated on test objects produced using 3D FDM (Fused Deposition Modeling) printers. The study was carried out using PLA filament with different fillers and raster angle. These measurements were carried out in order to evaluate the dimensional accuracy of objects printed from the filament. The results of the study revealed how PLA filament and ABS performed in 3D FDM type printers and revealed that the dimensions varied in objects with different properties.
Keywords: 3D Printer, PLA Filament, ABS Filament, Dimensional Accuracy

INTRODUCTION

Parts made by fused filament fabrication (FFF) are increasingly being used as final components in various applications (Mwema and Akinlabi, 2020). In other words, additive manufacturing technologies allow redefining part manufacturing thanks to design freedom and the production of complex parts without extra costs (Rashid, 2019). This technology aims to replace traditional methods in the commercial engineering industry, especially in polymer production (Tofail et al., 2018). Nowadays, processed FFF components are widely used in various sectors including automobiles, home appliances, aerospace, medical fields, computers and machine building (Penumakale et al., 2020). The benefits of this process are simple material processing, low maintenance costs, trouble-free service, compact size and low operating temperature (Kristiawan et al., 2021; Tognana et al., 2021). During FFF, the nozzle moves in the X–Y direction and the thermoplastic filament is fed to the build platform by the movement of the Z axis, after which the thermoplastic material is heated above its melting point to ensure that it can solidify into the previous layer shortly after deposition (Jayanth et al., 2018). Various parameters in FFF have a significant impact on the parts produced. All these parameters act as a bond between and within the deposited layers (Dey and Yoda, 2019). Production can be done quickly and in series in 3D printers, but since deterioration can occur in layers due to the dimensional accuracy of the manufactured parts, the dimensional accuracy of digital designs is of great importance. In a study conducted by Nunez et al. (2015) with ABS-plus material, they aimed to determine dimensional accuracy, flatness and surface texture in rapid prototypes. In this study, FDM helps to optimize the production processes in 3D printers and to obtain more precise results (Nunez et al., 2017). The aim of the study presented by Padhi et al. (2017) was to evaluate the dimensional deviation of a CAD model proposed by the authors when the raster width, infill angle, air gap, orientation of the sample and layer thickness were changed and the samples were made of ABS (Padhi et al., 2017). In the study conducted by Peng et al. (2014), the layer thickness was changed to print a CAD geometry developed by the authors. This sample was made of ABS and processing time and dimensional accuracy were selected as study variables (Peng et al., 2014). Camposeco-Negreteh (2020) presented a paper outlining an experimental study aimed at optimizing three parameters: processing time, energy consumption of the 3D printer, and dimensional accuracy of parts produced by the FDM process using ASA as a model material. The Taguchi methodology was used to study the influence of five basic parameters (layer thickness, infill pattern, orientation angle, printing plane, and position of the part on the surface of the build plate) on the variables. The printing plane was the most important factor for reducing the processing time; the same trend was observed for energy consumption. In the case of dimensional accuracy, the width was mainly affected by the infill pattern, while for length, the layer thickness was the dominant factor. Finally, the printing plane was the factor with the greatest impact on the part thickness. (Camposeco-Negrete, 2020). The above-mentioned studies show that efforts have been made to optimize the printing parameters for the FDM process by considering ABS and PLA as model materials. FFF presents a significant challenge in determining the optimum parameters due to the large number of conflicting parameters affecting the part quality and material properties. In this research, samples with different raster angles were printed on the

horizontal axis using acrylonitrile butadiene styrene (ABS) and PLA materials. Samples printed at different raster angles (0°, 30°, 45°, 60°, 90°) were evaluated at 3 different fills (20, 60, 80%).

MATERIALS AND METHODS

In this study, samples with different raster angles were printed horizontally using acrylonitrile butadiene styrene (ABS) and PLA materials. Samples printed at different angles (0°, 30°, 45°, 60°, 90°) were also evaluated at 3 different fills (20, 60, 80%). Sample (80 x 10 x 4 mm) used in the dimensional accuracy study were designed in the SolidWorks design program (Figure 1.a), and the designs saved in STL format were printed using the Creality K1 MAX device after G code assignment was made with the Creality Print 6.0 program (Figure 1.c).

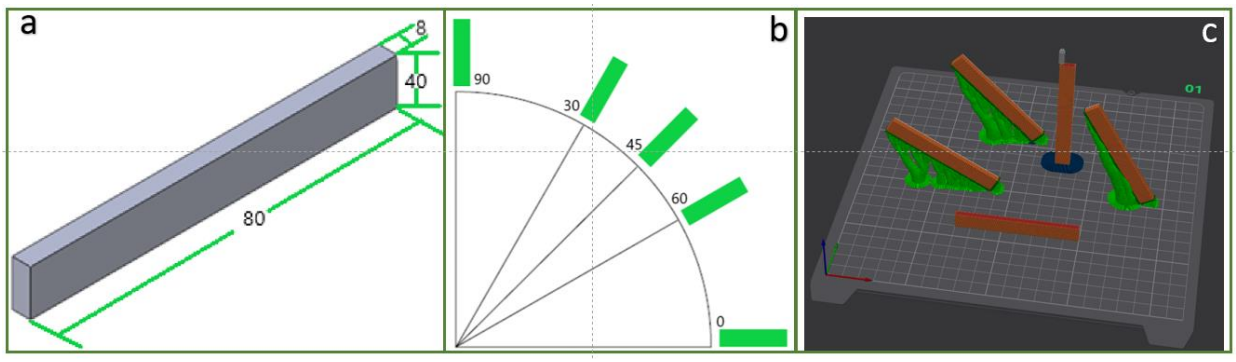

Figure 1. Preparation of samples; a. Creating the design in the program, b. Determining the angles, c. Using the program to define the G code.

For each different angle, 5 samples were printed and the linear accuracy was evaluated by looking at the length x width x thickness (Mitutuya Caliper) (Figure 2.a), weight (Precision scale) (Figure 2.b) and visual surface properties (Nikon T105 microscope) (Figure 2a). In the evaluation, the final results were reached by comparing the dimensions before printing with the estimated weight in the slicing program.

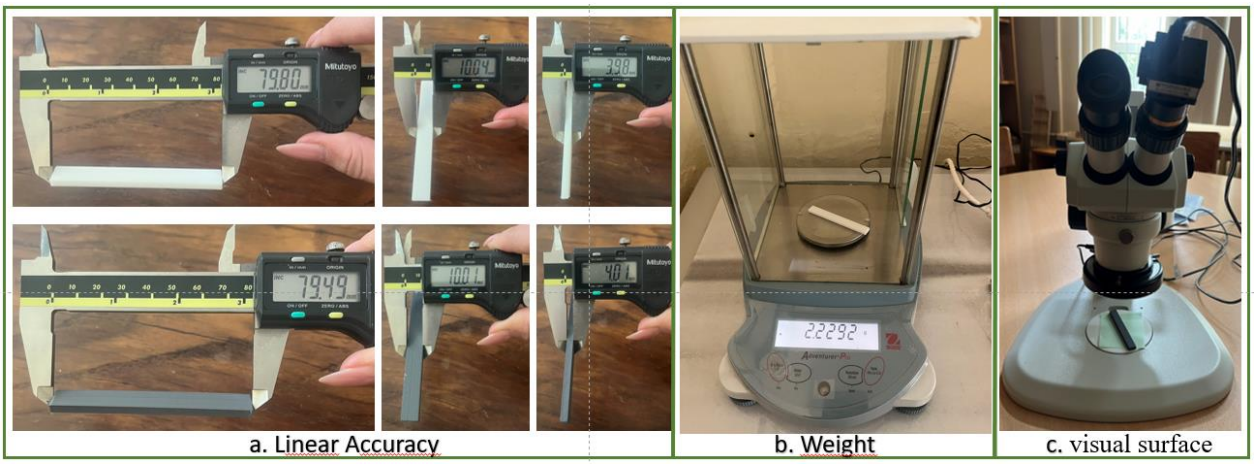

Figure 2. Devices used in the evaluation: a. Caliper, b.Weight, c. Precision scale

The study was carried out by changing the saturation and raster angle of the 3D printer features. Apart from these features, the machine features were left constant as in Table 1. The values that differ in ABS and PLA filaments are also given in the table. In addition, the supports that allow the creation of angles in the designs were designed in the same way in all angle types and were evaluated by deducting from the actual weight during weight measurements.

Table 1. FDM parameters constatnt during process.

Parameters	Values	
	ABS	PLA
Layer Height	0,2 mm	
Nozzle Diameter	0,4mm	
Printing Speed	60mm/sn	
Outher Shell Peed	200mm/sn	
Inner Shell Peed	300mm/sn	
İnfill Speed	250mm/sn	
Pattern	Monotonic	
Nozzle Temperature	260°C	200°C
Plate Temperature	65°C	50°C
Bottom Top Layers	3 Layers	
Support	Tree (manuel)	

Test objects were produced using ABS and PLA filament at 5 different raster angles and 3 different fills and same pattern. The visuals of the printed test objects are as in Figure 3 (PLA) and figüre 4 (ABS). In the figure, there is a visual of the samples produced at each angle, and microscope images showing that they were printed at 3 different fills are also added.

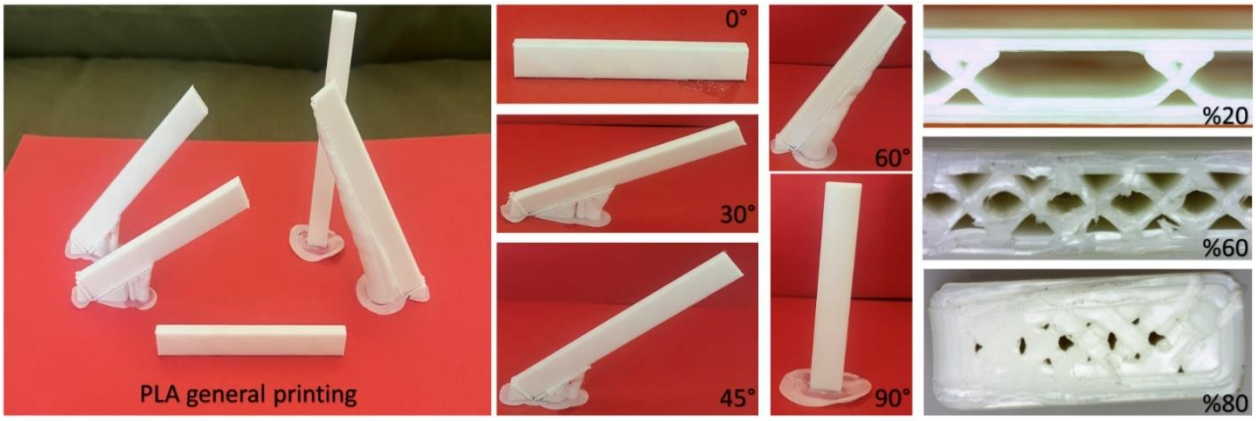

Figure 3. Printed test objects form PLA material.

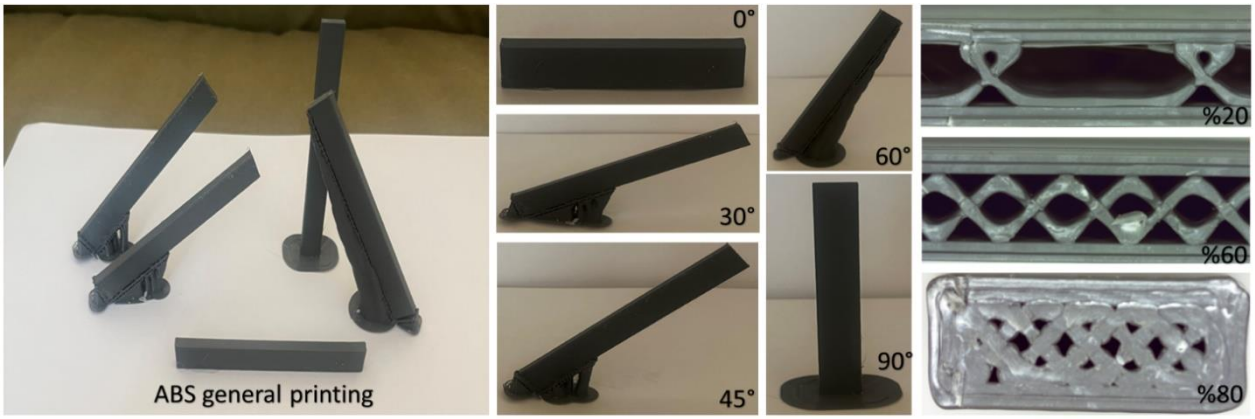

Figure 4. Printed test objects form ABS material.

RESULTS and DISCUSSION

Dimensional accuracy measurements of the samples after printing are given in Table 2 at 20% saturation, in Table 3 at 60% saturation, and in Table 4 at 80% saturation. The weight values predicted before printing were calculated without supports. The average values of 5 samples printed for each different saturation are given.

Table 2. Dimensional change of samples printed at 20% fill

Material	Raster Angle	Length (mm)	Width (mm)	Thickness (mm)	Mass (gr)	Calculated mass with programing(gr)
PLA	0°	79.84	10.01	3.98	2.36	2.06
	30°	79.81	9.98	4.08	2.31	2.39
	45°	79.76	9.97	4.07	2.27	2.36
	60°	79.99	10.00	4.03	2.30	2.39
	90°	79.90	9.97	4.01	2.22	2.42
ABS	0°	79.37	9.97	3.98	1.95	2.37
	30°	79.71	9.77	4.05	1.90	2.33
	45°	79.59	9.85	4.06	1.93	2.30
	60°	79.75	9.90	4.04	1.91	2.33
	90°	79.86	10.00	4.02	1.84	2.36

Table 3. Dimensional change of samples printed at 60% fill

Material	Raster Angle	Length (mm)	Width (mm)	Thickness (mm)	Mass (gr)	Calculated mass with programing(gr)
PLA	0°	79.74	9.94	3.98	2.59	2.75
	30°	79.72	9.98	4.03	2.68	2.30
	45°	79.81	10.01	4.02	2.69	2.81
	60°	79.76	9.93	4.06	2.74	2.86
	90°	80	9.99	4.00	2.76	2.96
ABS	0°	79.53	9.96	4.04	2.19	2.68
	30°	79.60	10.00	4.02	1.91	2.73
	45°	79.63	9.94	4.06	2.17	2.74
	60°	79.91	9.92	3.96	2.17	2.79
	90°	79.72	9.95	4.02	2.18	2.89

Table 4. Dimensional change of samples printed at 80% fill

Material	Raster Angle	Length (mm)	Width (mm)	Thickness (mm)	Mass (gr)	Calculated mass with programing(gr)
PLA	0°	79.80	10.04	3.98	3.46	3.55
	30°	79.78	9.90	4.05	3.45	3.57
	45°	79.80	9.95	4.03	3.48	3.59
	60°	79.78	9.92	4.06	3.45	3.60
	90°	79.99	9.99	4.01	3.54	3.75
ABS	0°	79.49	10.01	4.01	2.72	3.46
	30°	79.61	9.98	4.11	2.66	3.48
	45°	79.54	9.95	4.12	2.73	3.50
	60°	79.92	9.93	3.960	2.80	3.51
	90°	79.75	9.98	4.06	2.91	3.66

After the samples were printed, a microscope was used to see whether the dimensional changes in length, width, thickness and weight, as well as the differences between them, were related to the printing quality. The microscope images were evaluated at 20% fill in Figure 4, at 60% fill in Figure 5 and at 80% fill in Figure 6.

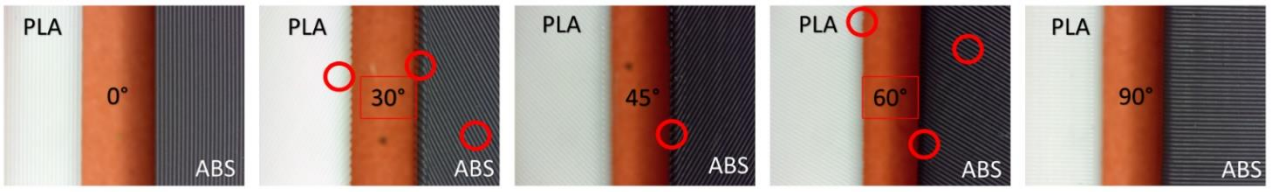

Figure 5. Sample images of samples printed at 20% fill under a microscope from each angle

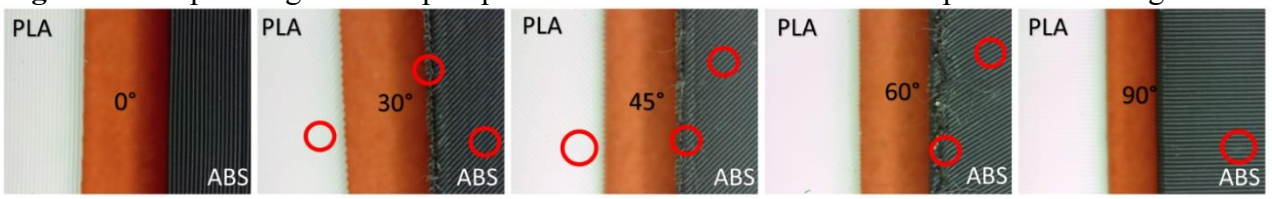

Figure 6. Sample images of samples printed at 60% fill under a microscope from each angle

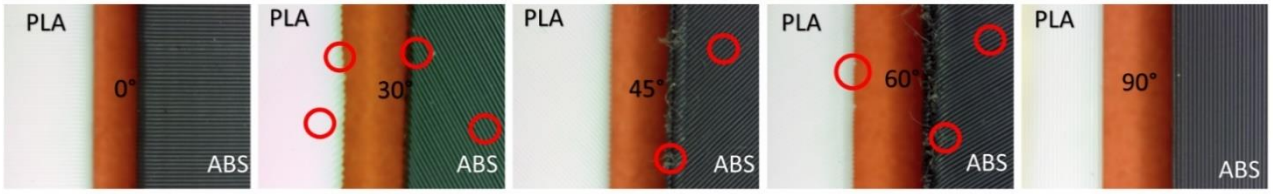

Figure 7. Sample images of samples printed at 80% fill under a microscope from each angle

With the development of technology, the integrated development of 3D printing systems and the use and application of these systems in many areas such as construction, medicine, industry, engineering, architecture, etc. have become widespread. The working principle of the writings is that samples designed with a computer-aided design program are printed using G codes on different filament types. When the literature is examined in the system, it is seen that there is an area where many parameters are changed from design to G coding, from machine features to filament features, and different studies yield the same or opposite results.

In this study, samples with different fills printed from ABS and PLA filament were printed with different raster angles. The dimensional accuracy and surface properties of the printed parts were revealed. The results;

1. When the average of the samples printed with ABS and PLA filaments in the horizontal direction at 20% fill is examined; it was determined that the sample average printed at 0° angle was closest to the design dimensions and calculation of mass, while this angle was 60° for PLA.
2. When the average of the samples printed with 60% fill in the horizontal direction with ABS and PLA filaments is examined; it was determined that the closest value in length was reached at 60° angle, the closest width and thickness value was reached at 30° angle, and the sample printed with 0° angle was calculated as the weight closest to the mass predicted in the machine parameters; it was determined that the samples printed with 90° angle in PLA material met all the values.
3. When the average of the samples printed horizontally with 80% fill with ABS filaments is examined; it was determined that the closest value in length was reached at 60° angle, the closest width and thickness value was reached at 30° angle, and the weight closest to the mass predicted in the machine parameters. In PLA material, it was determined that the samples printed at 90° angles met all the values.
4. The surface defects of the printed samples printed horizontally were examined with a microscope. According to the results, no defects were detected in the samples printed at 0°, 45° and 90° angles at 20% and 60% fill, while defects were observed at 45° in those printed at 80% fill. Burrs and printing defects were also detected on the surfaces at 30° and 60° angles in all prints. In all results, it was determined that samples made of PLA material had cleaner prints than those made of ABS material.
5. When all the results were evaluated, it was determined that dimensional accuracy could be achieved by using different filament types, different angles, different saturations and changing the machine parameters, and that mandatory supports weakened the surface properties in angled prints.

CONCLUSION

Production can be done quickly and in series with 3D printers, but since the dimensional accuracy of the parts produced can cause deterioration in the layers, the dimensional accuracy of digital designs is of great importance. There are many studies on this subject in the literature. These studies are supported by this study.

REFERENCES

- Camposeco-Negrete, C. (2020). Optimization of FDM parameters for improving part quality, productivity and sustainability of the process using Taguchi methodology and desirability approach, Prog. Addit. Manuf. 5 (1), 59-65. https://doi.org/10.1007/s00170-020-05555-9.
- Dey, A. and Yodo, N. (2019). A systematic survey of FDM process parameter optimization and their influence on part characteristics, J. Manuf. Mater. Process 3 (3), 64. https://doi.org/10.3390/jmmp3030064.
- Jayanth,N., Senthil, P. and Prakash, C. (2018). Effect of chemical treatment on tensile strength and surface roughness of 3Dprinted ABS using the FDM process, Virtual Phys. Prototyp., 13 (3) 155-163. https://doi.org/10.1080/17452759.2018.1449565.
- Kristiawan, R. B., Imaduddin, F., Ariawan, D., Arfin, Z. (2021). A review on the fused deposition modeling (FDM) 3D printing: filament processing, materials, and printing parameters. Open Eng., 11 (1) 639-649. https://doi.org/10.1515/eng-2021-0063.
- Mwema, F. M. and Akinlabi, E. T. (2020). Basics of fused deposition modelling (FDM), Fused Deposition Modeling, Springer International Publishing, Cham, 1-15. https://doi.org/10.1007/978-3-030-48259-6_1.
- Nuñez, P.J., Rivas, A., García-Plaza, E., Beamud, E., Sanz-Lobera, A. (2015). Dimensional and surface texture characterization in fused deposition modelling (FDM) with ABS plus. Procedia Engineering, 132, 856-863. https://doi.org/10.1016/j.proeng.2015.12.570.
- Padhi, S.K., Sahu, R.K., Mahapatra, S.S., Das, H.C., Sood, A.K., Patro, B., Mondal, A.K. (2017). Optimization of fused deposition modeling process parameters using a fuzzy inference system coupled with Taguchi philosophy. Int J Adv Manuf Technol 5,231–242 https://doi.org/10.1007/s40436-017-0187-4.
- Peng, A., Xiao, X., Yue, R. (2014). Process parameter optimization for fused deposition modeling using response surface methodology combined with fuzzy inference system. Int J Adv Manuf Technol 73,87–100 https://doi.org/10.1007/s00170-014-5796-5.
- Penumakala, P. K., Santo, J. and Thomas, A. (2020). A critical review on the fused deposition modeling of thermoplastic polymer composites. Compos. B. Eng., 201, 108336. https://doi.org/10.1016/j.compositesb.2020.108336.
- Rashid, A. (2019). Additive manufacturing technologies. In: Laperriere L, Reinhart G (eds) The CIRP encyclopedia of production engineering, Springer, Berlin https://doi.org/10.1007/978-3-662-53120-4.
- Tofail, S. A. M., Koumoulos, E.P., Bandyopadhyay, A., Bose, S., O'Donoghue, L., Charitidis, C. (2018). Additive manufacturing: scientific and technological challenges, market uptake and opportunities, Mater. Today (Kidlington), 21 (1), 22-37. https://doi.org/10.1016/j.mattod.2017.07.001.
- Tognana, S., Montecinos, S., Gastien, R., Salgueiro, W. (2021). Influence of fabrication parameters on the elastic modulus and characteristic stresses in 3D printed PLA samples produced via fused deposition modelling technique. J. Polym. Eng., 41 (6), 490-498. https://doi.org/10.1515/polyeng-2021-0019.

➢ *ORAL PRESENTATION*

A case study on the effects of high horizontal and vertical accelerations on structural damage in Antakya during the 2023 Türkiye earthquakes

Emre Gani[1]* (ORCID: https://orcid.org/0009-0005-2017-2031), Sezer Öztürk[2] (ORCID: https://orcid.org/0000-0003-2165-3687), Ali Sari[3] (ORCID: https://orcid.org/0000-0002-6888-1276)

[*1]Istanbul Technical University, Faculty of Civil Engineering, Department of Civil Engineering, Istanbul, Türkiye.
[2]Fatih Sultan Mehmet Vakif University, Faculty of Engineering, Department of Civil Engineering, Istanbul, Türkiye.
[3]Istanbul Technical University, Faculty of Civil Engineering, Department of Civil Engineering, Istanbul, Türkiye.
*Corresponding author e-mail: gani20@itu.edu.tr

Abstract
This study investigates the impact of high horizontal and vertical ground accelerations recorded during the first of the 2023 Kahramanmaraş earthquakes (Pazarcık event) on structural damage in Antakya, Türkiye. Ground motion records from local strong-motion stations revealed that both horizontal and vertical acceleration values significantly exceeded the TBEC-2018 DD2 and DD1 design spectra across most period ranges, primarily due to near-fault and site-specific effects. Notably, phenomena such as supershear rupture, forward directivity, fling, and basin effects were identified as contributing factors to the observed high spectral accelerations, especially at longer periods. A ten-story reinforced concrete building located near the 3124 station was selected for a detailed case study. Nonlinear time history analyses were conducted using three different ground motion input scenarios: (1) direct use of recorded horizontal and vertical components (Case-1), (2) station records scaled to match the TBEC-2018 design spectrum (Case-2), and (3) application of only the horizontal components to evaluate the effect of vertical motion (Case-3). The results demonstrated that the number of elements reaching extensive damage and collapse states, as well as story drift and second-order effects, were substantially higher in Case-1 compared to Case-2. The vertical component was found to play a secondary role, with the collapse mechanism predominantly governed by horizontal ground motions. These findings highlight the inadequacy of code-based design spectra in capturing the real seismic demand in regions affected by near-fault and basin effects. The study underscores the necessity of site-specific analyses and the incorporation of advanced ground motion characteristics into seismic design procedures to ensure more realistic and resilient structural performance in future earthquakes.
Keywords: 2023 Türkiye earthquakes, Antakya district, Seismic analysis, Strong ground motion.

INTRODUCTION

Two major earthquakes, with magnitudes of Mw 7.7 and Mw 7.6, occurred in Kahramanmaraş Province on February 6, 2023. The first shock originated in the Pazarcık district at a depth of 7.6 km, while the second occurred in the Elbistan district at a depth of 8 km. The Antakya region of Hatay was particularly affected by the first earthquake. Analysis of seismic ground motion data collected by strong-motion recording stations located in the Antakya district revealed that both horizontal and vertical acceleration values were exceptionally high. Notably, acceleration spectra derived from the original records have been reported by various researchers to exceed, across many period ranges, the elastic design spectrum values for both DD2 (10% probability of exceedance in 50 years) and even DD1 (2% probability of exceedance in 50 years) levels as specified by the 2018 Turkish Building Earthquake Code (TBEC-2018) (Baltzopoulos et al., 2023; Altunsu et al., 2024; Yaghmaei-Sabegh et al., 2024).

The high ground accelerations observed indicate a significant inelastic displacement demand on Antakya's buildings during the Pazarcık earthquake, which is one of the key factors explaining the severe damage and destruction in the region. Near-fault effects and site amplification played major roles in the generation of these high ground motions in the Antakya area. Analyses of ground motion velocity time histories have revealed pulse-like signals, which have been interpreted by various researchers as indicative of near-fault effects such as forward directivity and fling (Baltzopoulos et al., 2023; Wu et al., 2023; Chang et al., 2024).

Another possible cause of high ground accelerations is the supershear rupture mechanism. Supershear rupture velocities were clearly identified during the second earthquake (Mw 7.6) (Melgar et al., 2023). For the first event, the Pazarcık earthquake, strong signatures of supershear rupture have also been observed; however, a complex wave propagation pattern involving both supershear and subshear rupture velocities has been reported (Abdelmeguid et al., 2023; Rosakis et al., 2023).

Another important factor contributing to the high accelerations is site amplification. The Antakya region is located on the Hatay Graben, a rift valley. The central part of the region is characterized by relatively soft alluvial soils situated on the valley, while the outer parts are composed of harder soils associated with mountainous terrain and higher elevations. These features make the Antakya region particularly susceptible to ground motion amplification and basin effects commonly observed in soft soil conditions. Karray et al. (2024) emphasized the role of basin effects, suggesting that the sedimentary basin in Antakya is thick and stiff, and that basin effects contributed to the observed high accelerations. Similarly, Işık et al. (2024) pointed to basin effects based on analyses of velocity and displacement time histories.

A further significant factor exacerbating the damage and destruction in Antakya was the exceptionally large vertical acceleration components recorded during the earthquake. These extraordinary vertical accelerations have been explained by Duan et al. (2023) through the so-called trampoline effect. First introduced following the 2008 Iwate-Miyagi Inland (Japan) earthquake, the trampoline phenomenon suggests that the positive and negative values of vertical accelerations are asymmetrically amplified due to the nonlinear behavior of the soil (Aoi et al., 2008). One of the key indicators of the trampoline effect is that the positive accelerations are greater than the negative ones.

This study investigates the role of the high horizontal and vertical ground accelerations observed in Antakya in relation to structural damage. Nonlinear time history analyses were conducted for a ten-story reinforced concrete (RC) residential building representative of the region. Two different approaches were employed in the analyses. In the first approach, the recorded ground motion data from local stations were used directly. In the second approach, the station records were scaled to match the TBEC-2018 design acceleration spectra corresponding to the building's location. The aim here is to compare the effects of ground motions at the levels anticipated by the design code with those of the actual recorded motions on building response. Following the analyses, section-level damage states, second-order (P-Δ) effects, story drift values, and seismic performance levels were comparatively evaluated. The observed differences in these comparisons highlight the amplifying role of the high accelerations recorded during the Pazarcık earthquake on structural damage. However, it should be noted that attributing the severe destruction and damage in the region solely to high ground accelerations would be an incomplete approach. Field investigations have revealed that several other factors—such as inadequate engineering design, construction and workmanship deficiencies, insufficient inspection, and the use of substandard materials (e.g., low concrete strength or lack of transverse reinforcement)—also contributed significantly to the extent of the damage.

MATERIALS AND METHODS

The Antakya district of Hatay was particularly severely affected by the initial Mw 7.7 Pazarcık earthquake. Aftershocks and the subsequent Elbistan earthquake also contributed significantly to the extent of destruction observed in the region. In the post-earthquake damage assessment studies conducted by the Ministry of Environment, Urbanization and Climate Change, building damage and collapse states were classified into six categories (Table 1). The results, together with building location information, were made publicly available via the website "hasartespit.csb.gov.tr". Although the data provided on the website are intended for informational purposes only, systematic compilation and analysis of these results can yield valuable insights. Comparative graphs illustrating the proportions of buildings classified as 'Immediate Demolition + Collapsed' and 'Severely Damaged' (as defined in Table 1) are presented in Figure 1. The findings clearly indicate that Antakya experienced the highest relative rates of severe damage and collapse among the affected districts. The extremely high ground accelerations recorded in the area are among the primary factors underlying these outcomes, and this relationship can be further investigated through numerical analyses.

Table 1. Damage assessments provided by the Ministry for Hatay Province (hasartespit.csb.gov.tr)

Damage state	Definition
Undamaged (A)	Buildings with no damage
Slightly damaged (B)	Buildings with minor cracks in paint, plaster, or walls, and plaster detachment
Moderately damaged (C)	Buildings with wall cracks and minor cracks in load-bearing elements
Severely damaged (D)	Buildings with extensive and widespread shear cracks or separations in load-bearing elements
Immediate demolition (E)	Buildings where load-bearing elements have undergone significant residual displacement, leading to partial or complete collapse
Collapsed (F)	Situations involving total collapse beyond the state of immediate demolition

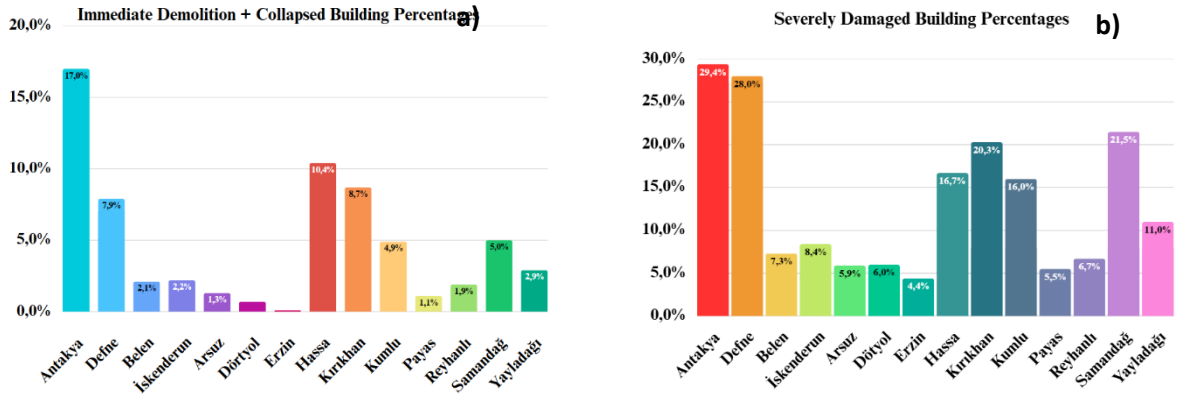

Figure 1. Percentages of building damage levels in Hatay a) levels E+F, b) level D

Strong Ground Motion Analysis

There are seven recording stations located in the Antakya region. When the acceleration spectra derived from the horizontal and vertical components recorded at these stations are compared with the elastic design acceleration spectra specified by TBEC-2018, it is observed that, for most period ranges, even the DD1 levels are exceeded (Figure 2). The 3131 station is distinguished from the other stations due to its unique geological and topographical characteristics, as the recorded values at this site generally fall between the DD2 and DD1 design spectrum levels. For this reason, the 3131 station has been excluded from the figures presented in the subsequent sections. Figure 2 presents horizontal (first six graphs) and vertical (subsequent six graphs) spectral comparisons.

As shown in Figure 2, the horizontal spectral accelerations recorded at stations 3126 and 3129 significantly exceed the DD1 levels for short periods up to 0.6 seconds. At stations 3123, 3124, 3125, and 3132, short-period accelerations are above the DD2 levels but generally remain below DD1. For longer periods, all stations exhibit ranges where the DD1 values are notably exceeded. When the predominant periods of the ground and the building coincide with these high spectral acceleration periods, the inelastic displacement demands on structures increase. Therefore, it is evident that such high accelerations, depending on site and building characteristics, contribute to increased damage and collapse. Here, building characteristics refer to both the fundamental period and the ductility capacity of the structure. Factors such as the number of stories, slab type, amount of shear walls, concrete and reinforcement quality, transverse reinforcement ratio, and structural system configuration play a critical role in determining both the fundamental period and the post-yield deformation capacity (inelastic behavior) and thus have a significant impact on the extent of damage and collapse.

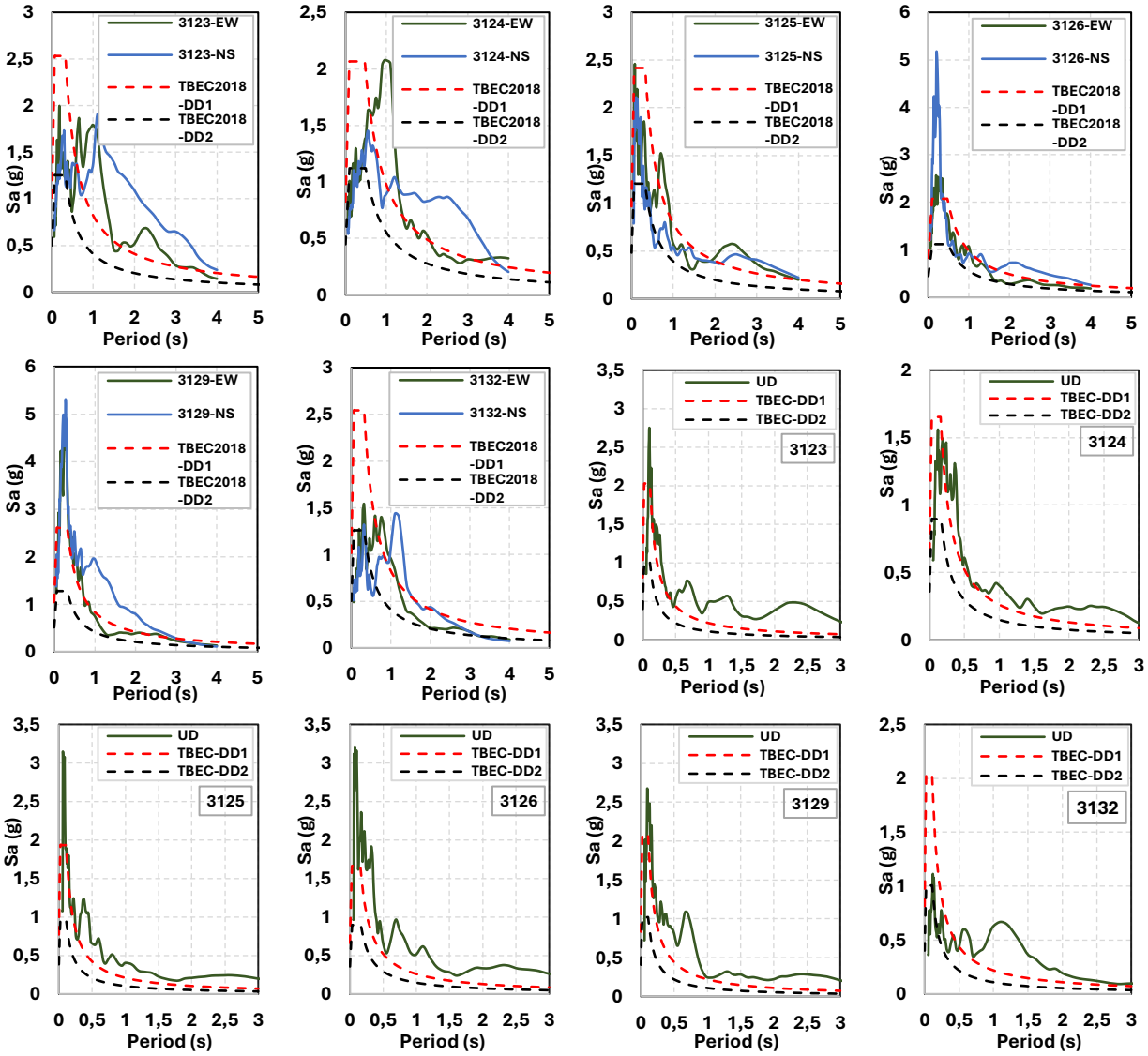

Figure 2. Comparison of the horizontal and vertical acceleration spectra proposed by the TBEC-2018 and Antakya stations.

The second set of six graphs in Figure 2 presents a comparison between the vertical acceleration spectra recorded at the stations and those specified by TBEC-2018. These elevated vertical accelerations have induced substantial compressive and tensile forces in vertical load-bearing elements. High compressive forces in older structural members—characterized by poor concrete and reinforcement quality and lacking adequate transverse confinement—have led to severe damage, and in some cases, complete loss of stability. The significant tensile forces generated can further contribute to damage by reducing the flexural moment capacity of vertical elements, exceeding the yield or ultimate strength of the reinforcement, causing inadequate anchorage and lap splice performance, loss of bond, and diminishing both section and joint shear capacities. The effects of vertical ground motions should be considered not only at the member level but also at the global building scale. Buildings with structural configurations that result in dominant torsional modes or insufficient lateral stiffness have been particularly susceptible to second-order (P-Δ) effects induced by vertical ground motions. Similarly, following stiffness degradation due to inelastic deformations, increased lateral displacements combined with high vertical accelerations have imposed substantial inelastic displacement demands on these structures. In such scenarios, buildings capable of redistributing internal forces and exhibiting ductile behavior after the formation of plastic hinges have demonstrated superior seismic performance, whereas those with relatively limited ductility capacity have been much more adversely affected.

Numerical Analysis

To investigate the effects of the high horizontal and vertical accelerations observed during the Pazarcık earthquake, a RC building located near the 3124-recording station was selected as a case study. Constructed after 2016, the building is a ten-story (basement + ground floor + eight typical floors) RC shear wall-frame structure with a beam-and-slab floor system. The concrete and reinforcement classes used are C30/37 (TS500) and S420 (TS708:2010), respectively. The thicknesses of the shear walls and slabs are 25–30 cm and 12–15 cm, respectively. Beams have dimensions of 25×60 cm, and columns are sized at C80×35, C45×45, C30×80, C30×95, and C35×95 cm. The typical story height is 290 cm. The typical floor plan of the building is shown in Figure 3a. To assess the impact of the high accelerations experienced by the building, two different analysis procedures were implemented. In the first procedure, referred to as Case-1, the building was analyzed using the simultaneous application of the recorded horizontal and vertical accelerations from the 3124 station. In the second procedure, Case-2, the 3124 station records were scaled to match the TBEC-2018 design spectrum for the relevant site conditions. To ensure compatibility with the building's orientation, the original EW-NS record set was rotated by 71°, and the rotated records were used in the analyses. After rotation, the EW component acts in the X direction (see Figure 3a). As illustrated in Figure 3b, there are significant differences between the acceleration spectra of the 3124 records and the TBEC-2018 design spectra (for ZD soil conditions). Consequently, the differing results obtained from these two-analysis series highlight the role of the high accelerations generated during the Pazarcık earthquake in the collapse of the building. The Case-1 analysis results represent the actual horizontal and vertical accelerations experienced by the building and thus are expected to be consistent with the observed collapse modes. In Case-2, spectral matching was performed using a software (Seismosoft, 2020) (Figure 3c), so this case represents the seismic demand corresponding to the design-level spectral accelerations for which the building was originally designed.

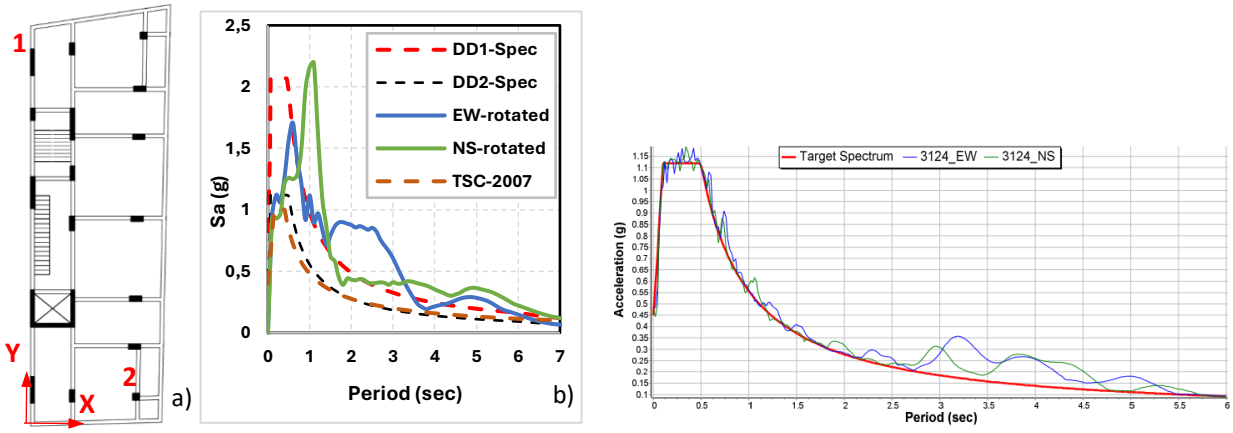

Figure 3. a) Typical floor plan of building, b) comparison of acceleration spectra from TSC-2007, TBEC-2018, and the 3124 station, c) scaling procedure.

As highlighted in the Introduction, the literature indicates that various phenomena—including near-fault ground motions, site amplification effects, and supershear rupture mechanisms—have contributed to the exceptionally high accelerations recorded in this region. The combined influence of these factors has led to a substantial increase in seismic demand on buildings in Antakya. The subject building was originally designed according to TSC-2007; however, since the elastic design acceleration spectra of TBEC-2018 and TSC-2007 are quite similar, the TBEC-2018 spectrum was adopted in Case-2 due to its status as the current code. It should also be noted that the TSC-2007 code, which was in effect at the time of the building's design, did not consider the effects of vertical ground motions. In contrast, TBEC-2018 explicitly accounts for vertical earthquake effects through Equation (1). Therefore, in the analyses, the vertical component was incorporated directly using the recorded vertical ground motion in Case-1, while in Case-2, it was considered in accordance with Eq. (1) of TBEC-2018. In this context, G refers to the effect of dead load, and S_{DS} denotes the design spectral acceleration coefficient at short periods.

$$E_d^{(z)} \approx (2/3)\, S_{DS}\, G \tag{1}$$

To further isolate and evaluate the influence of vertical ground motion on the results, an additional analysis was conducted, referred to as Case-3. In this analysis, only the horizontal components of the station records were applied, with the vertical component entirely neglected, to specifically assess the effect of vertical earthquake action. This approach enabled a clear identification of the impact of vertical ground motion on the comparison parameters. The numerical modeling was performed using the Perform3D (2023) software, and nonlinear time history analyses were carried out. Columns and beams were modeled as frame elements, while shear walls were represented by two-dimensional shell elements. Inelastic behavior was simulated using a lumped plastic hinge approach for beams, whereas columns and walls were modeled with a fiber-based distributed plasticity method. Basement walls and slabs were assumed to behave purely elastically. The material properties for confined concrete were defined according to the Mander model, as detailed in Annex-5A of TBEC-2018. For cyclic degradation, the model proposed by Lowes et al. (2016) was adopted for concrete, while the behavior of reinforcement bars was characterized using the Menegotto and Pinto (1973) model.

RESULTS and DISCUSSION

Figure 4a illustrates the element damage states resulting from the Case-1 analysis, while Figure 4b presents the lateral displacement profile of the building. Elements shown in red have exceeded the collapse deformation limit as defined in Section 15 of TBEC-2018. Elements in yellow have surpassed 75% of the collapse limit. In Figure 4, only the damage states of columns and shear walls are presented to better highlight the extent of plastic deformations. As observed, a significant number of vertical load-bearing elements have exceeded the 'Collapse State' damage threshold. In reality, the building collapsed by overturning in the +X direction (Figure 4c). The analysis results are consistent with the observed collapse mode, both in terms of the number of failed elements and the overall global behavior of the structure.

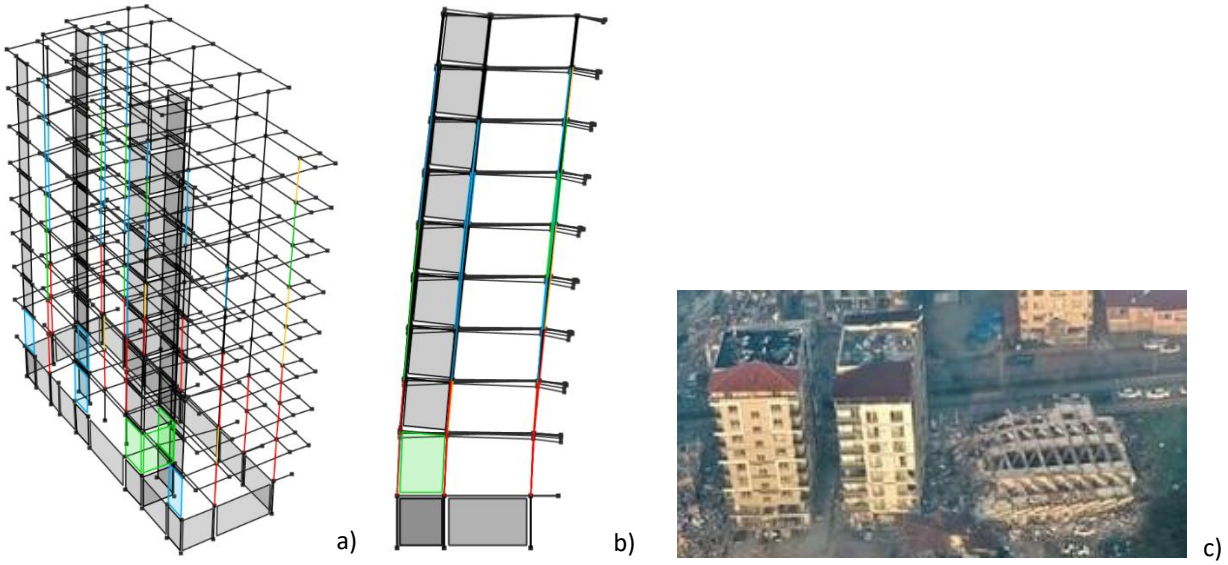

Figure 4. Case-1 Structural damages (a), Case-1 deformed shape (b) and a view of collapsed building

Figure 5 presents a comparative summary of the results for all three cases. As can be seen, there are substantial differences between Case-1 and Case-2, with significantly fewer elements exceeding the collapse limit in Case-2. This outcome is attributed to the higher acceleration levels present in Case-1. When comparing Case-3 and Case-1, the element damage levels are found to be quite similar. This comparison indicates that the damage and collapse mechanism of the building under consideration is predominantly governed by the horizontal components of ground motion.

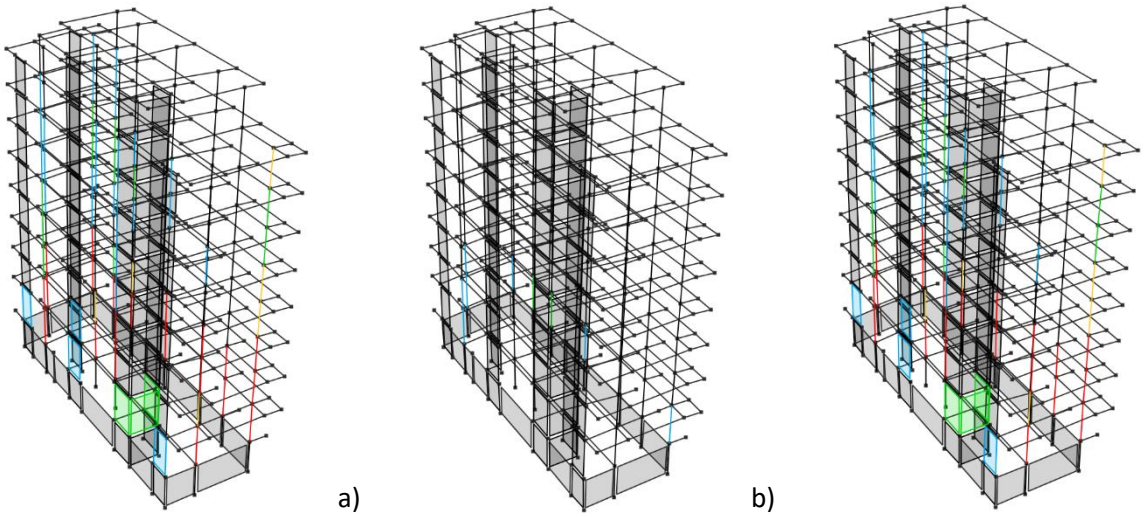

Figure 5. Structural damage in Case-1 (a), Case-2 (b), and Case-3 (c)

Story drift comparisons based on the values obtained from Points 1 and 2, as indicated in Figure 3a, are presented in Figure 6. Since the results of Case-1 and Case-3 are of nearly the same magnitude, Case-3 is not included in the graphs. According to the results, the effect of vertical ground motion on story drifts is negligible. The story drift values in Case-1 are significantly higher than those in Case-2. In Case-2, the commonly accepted drift limit of 2% is generally not exceeded, whereas the values observed in Case-1 are well above this threshold. This finding indicates that the actual ground accelerations experienced during the event were substantially greater than those anticipated by the design spectrum.

The evaluation of second-order (P-Δ) effects for Case-1 and Case-2 is presented in Table 2. Table 2 presents the data for each story. Since the results obtained in the X direction were more critical than those in the Y direction, only the values for the X direction are reported. The TBEC-2018 limit for the second-order (P-Δ) indicator is provided in the rightmost column of the table; values exceeding this limit are highlighted in red, while those below the limit are shown in green. In the table, Δ denotes the average displacement values, V_i represents the story shears, where the subscript indicates the analysis case and the superscript represents the direction of the measured value, W_i denotes the story mass. The formula for the second-order indicator is given in Equation 2. *R* and *D* denote the response modification factor and the overstrength factor for the structural system, respectively, while C_h represents a coefficient defined based on the nonlinear hysteretic behavior of the structural system. The results indicate that, in Case-2, the second-order effects remain within the permissible limits. However, in Case-1, these limits are significantly exceeded in the X direction, which corresponds to the direction of building overturning. These findings highlight the critical role of the extremely high acceleration recorded at the station in contributing to the collapse of the building.

$$\theta_{II,i}^{(X)} = \frac{(\Delta_i^{(X)}) ort \sum_{k=i}^{N} w_k}{V_i^{(X)} h_i} \leq 0.12 \frac{D}{C_h R} \quad (2)$$

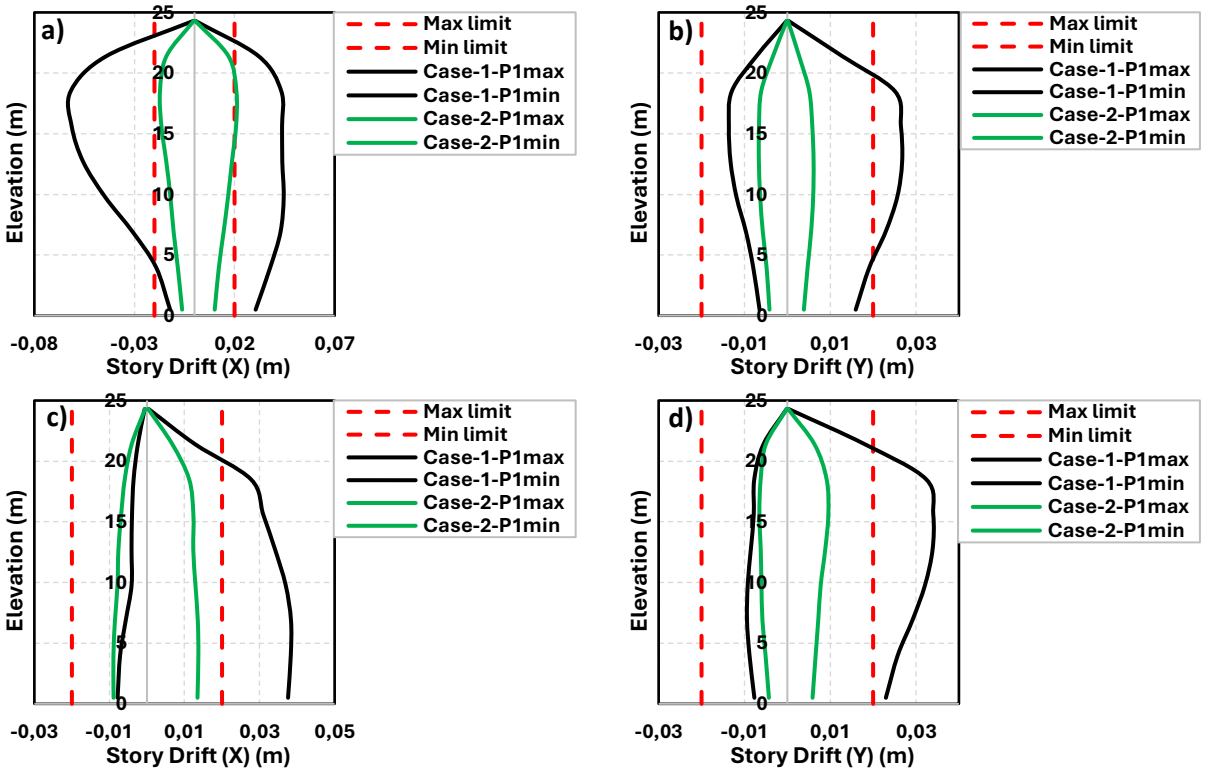

Figure 6. Case-1 and Case-2 story drifts for Point-1-X (a), Point-1-Y (b), Point-2-X (c) and Point-2-Y (d)

Table 2. Second order effect check for Case-1 and Case-2 according to TBEC-2018 regulations.

St.	$\Delta_{C1}^{(+X)}$ (mm)	$\Delta_{C1}^{(-X)}$ (mm)	$\Delta_{C2}^{(+X)}$ (mm)	$\Delta_{C2}^{(-X)}$ (mm)	Wi (kN)	$V_{C1}^{(+X)}$ (kN)	$V_{C1}^{(-X)}$ (kN)	$V_{C2}^{(+X)}$ (kN)	$V_{C2}^{(-X)}$ (kN)	Limit	$\theta_{II,C1}^{(+X)}$	$\theta_{II,C1}^{(-X)}$	$\theta_{II,C2}^{(+X)}$	$\theta_{II,C2}^{(-X)}$
7	78.4	25.7	27.2	17.3	2856	1592	1596	1714	1570	0.086	0.048	0.016	0.016	0.010
6	85.8	35.3	27.3	20.8	5810	2092	2328	2274	2331	0.086	0.082	0.030	0.024	0.018
5	92.9	49.7	28.2	24.3	8763	2348	2897	2343	2912	0.086	0.119	0.052	0.036	0.025
4	98.1	66.1	31.1	27.5	11717	2895	3411	2238	3378	0.086	0.137	0.078	0.056	0.033
3	102.1	78.8	33.9	30.2	14670	3414	4162	2520	3879	0.086	0.151	0.096	0.068	0.039
2	102.5	84.5	35.2	31.8	17624	4165	4883	2879	4323	0.086	0.149	0.105	0.074	0.045
1	97.9	83.2	33.8	31.5	20577	4892	5111	3319	4738	0.086	0.142	0.115	0.072	0.047
G	72.9	69.1	29.8	28.6	23683	5570	5495	3583	4801	0.086	0.089	0.085	0.056	0.040
B	1.3	1.7	0.9	1.3	27071	7742	6750	4404	5544	0.086	0.001	0.002	0.002	0.002

CONCLUSION

In this study, the role of the first of the February 6 Kahramanmaraş earthquakes—the Pazarcık event—in the observed destruction was investigated through a numerical case study utilizing ground motion records from Antakya stations. Based on the evaluation of acceleration spectra derived from the station records and the results of nonlinear time history analyses, the following findings were obtained.

- The horizontal and vertical acceleration values recorded at the Antakya stations exceed the TBEC-2018 DD2 and DD1 design spectra across most period ranges. These high acceleration values are attributed to the combined effects of near-fault and site-specific conditions. One of the reasons for the elevated spectral accelerations at longer periods is the presence of velocity pulses with periods of 2.5–3.5 seconds, as identified by Wu et al. (2023) and Chang et al. (2024). Additionally, the high long-period accelerations have been associated with basin effects by Karray et al. (2024), indicating that this phenomenon also plays a significant role in the observed destruction.
- Numerous studies in the literature have provided significant evidence for the presence of phenomena such as supershear rupture, forward directivity, fling, and basin effects during the Pazarcık earthquake. The high inelastic displacement demands resulting from these phenomena,

which led to exceedance of the design spectrum predictions, have played a critical role in increasing the extent of damage and collapse in buildings.

- According to the numerical analysis results, the number of elements reaching the 'Extensive Damage' and 'Collapse State' levels in Case-1 is significantly higher than in Case-2. Similarly, the story drift values in Case-1 are much greater than those in Case-2. For second-order effects, Case-1 values substantially exceed the permissible limits, whereas Case-2 results remain within acceptable boundaries.
- The results of Case-2 suggest a high probability that the building would not collapse; however, the same cannot be concluded for Case-1. In summary, the high horizontal accelerations generated during the Pazarcık earthquake played a critical role in the collapse of the building, as the spectral accelerations corresponding to the predominant mode periods (1–2 seconds) were exceptionally high (see Figure 5a).
- The high vertical accelerations observed in the station records played a secondary role in the collapse mechanism. When comparing the element damage and story drift results of Case-1 and Case-3, the outcomes are found to be very similar. Therefore, it can be concluded that the collapse mechanism was predominantly governed by the horizontal ground motion components.
- In cases involving near-fault and basin effects, the recorded acceleration values can significantly exceed the predictions of the TBEC-2018 design spectrum. In such scenarios, site-specific studies are clearly necessary to obtain more realistic results. Furthermore, incorporating these phenomena—which contribute to the generation of high accelerations—into the design procedures through probabilistic approaches, when appropriate, would enable more realistic structural design and assessment.

REFERENCES

Abdelmeguid, M., Zhao, C., Yalcinkaya, E., Gazetas, G., Elbanna, A., & Rosakis, A. (2023). Dynamics of episodic supershear in the 2023 M7.8 Kahramanmaraş/Pazarcik earthquake, revealed by near-field records and computational modeling. Communications Earth and Environment, 4(1), https://doi.org/10.1038/s43247-023-01131-7.

Altunsu, E., Güneş, O., Öztürk, S., Sorosh, S., Sarı, A., & Beeson, S. T. (2024). Investigating the structural damage in Hatay province after Kahramanmaraş-Türkiye earthquake sequences. Engineering Failure Analysis, 157, https://doi.org/10.1016/j.engfailanal.2023.107857.

Aoi, S., Kunugi, T., & Fujiwara, H. (2008). Trampoline Effect in Extreme Ground Motion. Science, 322, www.sciencemag.org.

Baltzopoulos, G., Baraschino, R., Chioccarelli, E., Cito, P., Vitale, A., & Iervolino, I. (2023). Near-source ground motion in the M7.8 Gaziantep (Turkey) earthquake. Earthquake Engineering and Structural Dynamics, 52(12), 3903–3912. https://doi.org/10.1002/eqe.3939.

Chang, Z., Wu, H., Li, W., Yan, Z., Peng, L., & Zhu, G. (2025). Analysis of Near-Fault Ground Motions in the February 2023 Kahramanmaras, Türkiye, Earthquake Sequence, Bulletin of Earthquake Engineering, 23(4), 1349-1369, DOI:10.1007/s10518-025-02101-4.

Duan, Y., Bo, J., Peng, D., Li, Q., Wan, W., & Qi, W. (2023). Analysis of Peak Ground Acceleration and Seismogenic Fault Characteristics of the Mw7.8 Earthquake in Turkey. Applied Sciences (Switzerland), 13(19). https://doi.org/10.3390/app131910896.

Işık, N. S. (2023). Basin and Near-Fault Effects on Earthquake Ground Motions: An Evaluation of the Antakya Records of the Kahramanmaraş Pazarcık Earthquake, Journal of Geological Engineering, 47: 67-86, DOI 10.24232/jmd.1299027.

Karray, M., Karakan, E., Kincal, C., Chiaradonna, A., Gül, T. O., Lanzo, G., Monaco, P., & Sezer, A. (2024). Türkiye Mw 7.7 Pazarcık and Mw 7.6 Elbistan earthquakes of February 6th, 2023: Contribution of valley effects on damage pattern. Soil Dynamics and Earthquake Engineering, 181. https://doi.org/10.1016/j.soildyn.2024.108634.

Lowes, L. N., Lehman, D. E., & Baker, C. (2016). Recommendations for Modeling the Nonlinear Response of Slender Reinforced Concrete Walls Using PERFORM-3D, Structural Engineers Association of California, Annual Convention, 2016 (SEAOC 2016).

Melgar, D., Taymaz, T., Ganas, A., Crowell, B., Öcalan, T., Kahraman, M., Tsironi, V., Yolsal-Çevikbil, S., Valkaniotis, S., Irmak, T. S., Eken, T., Erman, C., Özkan, B., Dogan, A. H., & Altuntaş, C. (2023). Sub- and super-shear ruptures during the 2023 Mw 7.8 and Mw 7.6 earthquake doublet in SE Türkiye. Seismica, 2(3). https://doi.org/10.26443/seismica.v2i3.387.

Menegotto, M., & Pinto, P.E. (1973). Method of analysis of cyclically loaded RC plane frames including changes in geometry and non-elastic behavior of elements under normal force and bending. Preliminary Report IABSE, vol 13.

Ministry of Environment, Urbanization and Climate Change of the Republic of Türkiye (2024). Damage Assessment Inquiry, https://hasartespit.csb.gov.tr/.

Perform3D, (2023). Performance-Based Design of 3D Structures, Computers and Structures, Inc., v9.0.0.

Rosakis, A. J., Abdelmeguid, M., & Elbanna, A. (2023). Evidence of Early Supershear Transition in the Mw 7.8 Kahramanmaraş Earthquake from Near-Field Records, Preprint, https://doi.org/10.31223/X5W95G.

Seismosoft (2020). SeismoMatch 2020 – A computer program for spectrum matching of earthquake records, available from https://seismosoft.com/.

TBEC-2018, Türkiye Building Earthquake Code, Republic of Türkiye Ministry of Interior Disaster and Emergency Management Authority, Ankara, 2018.

TS 500, (2000). Requirements for design and construction of reinforced concrete structures (in Turkish), Turkish Standard Institute, Ankara, Türkiye.

TS 708, (2010). Steel for the reinforcement of concrete – Reinforcing steel (in Turkish), Turkish Standard Institute, Ankara, Türkiye.

TSC-2007, Turkish Seismic Code: Specification for Structures to be Built in Disaster Areas, Turkish Ministry of Environment and Urban Planning, Ankara, Türkiye, 2007 (in Turkish).

Wu, F., Xie, J., An, Z., Lyu, C., Taymaz, T., Irmak, T. S., Li, X., Wen, Z., & Zhou, B. (2023). Pulse-like ground motion observed during the 6 February 2023 MW7.8 Pazarcık Earthquake (Kahramanmaraş, SE Türkiye). Earthquake Science, 36(4), 328–339. https://doi.org/10.1016/j.eqs.2023.05.005.

Yaghmaei-Sabegh, S., Neekmanesh, S., & Ruiz-García, J. (2024). Evaluation of vertical-to-horizontal spectral acceleration ratio for the 2023 Turkey-Syria seismic sequences. Soil Dynamics and Earthquake Engineering, 182. https://doi.org/10.1016/j.soildyn.2024.108747.

➢ *ORAL PRESENTATION*

The Oral Microbiota and Its Relation to Oral Health and Systemic Diseases: A comprehensive Review

Abdulridha Taha Sarhan (https://orcid.org/0000-0002-6612-612X)

University of Hilla, Faculty of Dentistry, Department of Basic Sciences, Babylon, Iraq

Abstract
Aim: This review article is to give an idea about the role of human oral microbiota on oral and body health. A wide range of microorganisms inhabit the human oral cavity, including bacteria, fungi, viruses, archaea and protozoa. These microorganisms form a complex ecological community that influences oral and systemic health. There is evidence that oral microbiota is also closely related to systemic diseases. Methods: A comprehensive understanding of the oral microbiota and its influence on oral health and diseases require a holistic view that emphasizes interactions among different residents within the oral community, as well as their interaction with the host. Notably, a large number of oral microorganisms enter the downstream digestive tract from the oral cavity through saliva, and they present a particularly close relationship with body diseases. Results: In the oral cavity, indigenous microorganisms are often associated with two major oral diseases, caries and periodontal diseases. These diseases seem to appear following an imbalance in the oral resident microbiota, leading to the emergence of potentially pathogenic microbiota. Discussion: To know well the process involved in caries and periodontal diseases, it is necessary to understand the ecology of oral cavity and to identify the factors responsible for the transition of the oral microbiota from a commensally to a pathogenic relationship with the host. The regulatory forces influencing the oral ecosystem can be divided into three major categories, host related, microbe related, and external factors. Conclusions: The indigenous microbiota play an important role in health and diseases of humans oral cavity. Also, it contributes to the development of the immune system and provides resistance to colonization by all native or pathogenic microorganisms. This suggests that oral microbiota may provide potential biomarkers in the diagnosis of some systemic diseases.
Keywords: Oral microbiota, Oral diseases, Systemic diseases, Oral ecology, Oral health.

INTRODUCTION

The mouth is one of the most heavily colonized parts of human body. Several distinct habitats within the oral cavity support heterogeneous microbial communities that constitute an important link between oral and general health (Gao, et al., 2018). The establishment of the oral microbiota occurs in a dynamic process over various stages and involve continuous interactions with the host and its environment (He, et al., 2015). The human oral microbiota is an important part of the body microbiome. The human oral cavity contains several significantly different ports with distinct microbial communities (Diaz and Valm, 2020). A wide range of microorganisms inhabit the human oral cavity, including bacteria, fungi, viruses, archaea and protozoa (Lamont, , et al., 2018).These microorganisms form a complex ecological community that influences oral and systemic health (Baker, et al., 2017). The most prevalent oral diseases, dental caries and periodontal diseases, are microbiota-associated diseases (Chen, et al. ,2018). Moreover, increasing evidences have supported that many systemic diseases are associated with disturbances in the oral ecosystem, such as diabetes, cardiovascular diseases and tumors (Gao, et al., 2022). The oral cavity is a complex environment that includes premium microbial habitats of soft and hard tissues which form a rich heterogeneous ecological system (Segata, et al., 2012). Oral and general health influence each other (Graves, 2019).). Recent scientific work shows that oral diseases can impact general health, and vice-versa (Gm, et al., 2021). A microbiota is composed of bacteria, fungi, archaea, protists, and other microorganisms , whose compositions are dependent upon environmental conditions (Jonathon et al, 2024). The oral cavity contains one of the most diverse and unique communities of microbes in the human body. A milliliter of saliva contains a high microbial cells (Jo, et al, 2019), with a typical healthy microbiome comprised of a range of about 100 to 200 distinct microbial organisms (Lee, , et al, 2022). The aim and purpose of this article are to update oral healthcare practitioners on our current knowledge of the oral microbiome in health and disease, to review how molecular methods of microbial characterization have advanced our understanding, and to discuss potential implications for clinical practice that used as targets to treat oral and systemic diseases..

MATERIALS AND METHODS

A comprehensive understanding of the oral microbiota and its influence on host health and diseases will require a holistic review that emphasizes interactions among different residents within the oral community, as well as their interaction with the body systems. The hypothesis is that the oral microbiome could be a missing link that can partially explain the influences of oral diseases on general health. A general literature search was conducted in the electronic databases using the keywords: oral microbiota, oral diseases, systemic diseases and oral ecology. The details of the instances of oral microbiota and its relations to oral and systemic diseases were also evaluated. In addition, the present review describes the oral ecosystems, the major factors that might control the oral microbiota, the basic aspects of the secretory immune system, and the biological role and functions of IgA in the microbial ecology of the oral cavity (Jeong, J., et al. (2022).

RESULTS and DISCUSSION

All selected publications about oral microbiota and its relation to oral and body health were further scrutinized for adherence to the following topics:

1. Oral and human body microbiota.

Humans have evolved in the continuous presence and in the symbiosis with microbiome. The human body hosts approximately as many microbial cells as human. The human body lacks the specialized enzymes required for numerous chemical reactions (e.g. nutrient breakdown) and therefore has to rely on its microbial symbionts to carry out these functions. The human oral microbiota is an important part of the body microbiome. The human oral cavity contains several significantly different ports with distinct microbial communities (John , et al, 2024). A wide range of microorganisms inhabit the human oral cavity, including bacteria, fungi, viruses, archaea and protozoa (Baker and Edlund , 2018). Bacteria are the main inhabitants of the mouth, they primarily comprise bacteria of the Proteobacteria and Actinomycetes **(Table 1)**. Unlike gut microbiota, these types of bacteria do not change significantly. Diet and the environment have a great impact on gut microbiota but exert minimal effect on the composition of oral bacteria (Rooney, et al, 2020). The oral cavity contains one of the most diverse and unique communities of microbes in the human body, yet this port is relatively understudied as compared to the gut **(Fig. 1).** The oral cavity is a complex environment that encompasses distinct, different small microbial habitats, such as teeth, buccal mucosa, soft and hard palate, and tongue, which form a species-rich heterogeneous ecological system (Chiara , et al, 2024). Healthy people from different countries have similar compositions of oral microbiota. In the human mouth, 85 species of fungi can be found. Among these fungi, the most important one is *Candida* (Daniel, et al, 2018). *Candida* is neutral when the oral microbiota is normal; however, when the oral microbiota balance is broken, *Candida* will seek the opportunity to attack oral tissue *Candida* forms a biofilm with *Streptococcus* to play a pathogenic role (Lu, et al., 2019). Oral bacteria are the main components of the oral microbiota. Common oral bacteria include *Streptococcus mutans*, *Porphyromonas gingivalis*, *Staphylococcus aureus*, and *Lactobacillus plantarum* . The *S. mutans* is the main component of the oral microbiota, and it is one of the main components of dental plaque (Cai, Z. et al., 2021). It is also the main pathogen of caries, which is a bacterial infectious disease that occurs in hard tissues of the teeth and has the highest incidence among oral diseases (Baker, J. et al., 2021).*P. gingivalis* is a non-glycolytic Gram-negative anaerobic bacterium that is a periodontal pathogen. *Lactobacillus* refers to a bacterium that can ferment sugar to produce lactic acid. It is a group of microorganisms that live in the body and benefit the health of the host. Yogurt contains lactobacilli. *Lactobacillus* ferments sugar and produces a large amount of lactic acid, which can easily cause caries.

2. Oral microbiota and oral diseases.

Oral microbiota may produce metabolites in the mouth, which can affect the development of a range of oral diseases, such as:

A. Caries:

Dental caries is the most common chronic infectious diseases in the oral cavity (Baker, J. et al., 2021). Bacteria are the main pathogens, and symptoms include hard tissue destruction of the teeth. The incidence rate of dental caries is high, and the disease range is wide, occurring at any age period of humans. Dental caries has a higher incidence in children than in adults, and it is closely related to oral microbiota. The latest information determined that *Lactobacillus* spp., *Prevotella* spp., *Dialister* spp., and *Filifactor* spp. may be involved in the pathogenesis and progression of dental caries. Compared with healthy individuals, the oral microbiota on the surface of dental caries presents increased complexity and decreased diversity,

possibly due to the acidic environment (Christina J. et al., 2017). These characteristics are manifested in the salivary microbiota, which display an increase in *L. acidophilus in* dental caries. When people do not eat, the bacteria obtain nutrients from our saliva and gingival crevicular fluid, which are rich in glycoproteins. These glycoproteins are broken down by bacteria into sugars and proteins, which during metabolism, are broken down by bacteria into acidic or basic small molecules. Weak acid production will begin to affect and corrode the teeth (Anne and Daniel, 2019).

Table 1 . The Six Major Phyla and Genera in the Oral Microbiota with Some Examples of Less Frequent Genera.

Major phyla	Major genera	Minor genera
Firmicutes	***Streptococcus , Veillonella, Selenomonas , Gemella , Oribacterium***	***Granulicatella , Lactobacillus, Peptostreptococcus , Staphylococcus , Eubacterium***
Actinobacteria	***Actinomyces , Corynebacterium , Rothia***	***Propionibacterium***
Bacteroidetes	***Prevotella , Capnocytophaga , Porphyromonas***	***Bacteroides***
Proteobacteria	***Neisseria , Campylobacter , Haemophilus , Lautropia***	***Eikenella***
Fusobacteria	***Fusobacterium , Leptotrichia***	***Sneathia***
Spirochaetes	***Treponema***	**---**

B. Periodontitis:

Periodontitis is a common type of chronic periodontal disease with a wide age range, and it spreads from gingivitis to deep periodontal tissues. Dental plaque bacteria are the main factors of periodontal disease (Plachokova, A.S., et al., 2021). Plaque includes plaque and sub-gingival plaque, which is a micro-ecological system with bacteria on the tooth surface or periodontal pocket. The interactions between host and microbiota determine the manner, severity, and rate of progression of the disease (Abusleme L. et al., 2021). Therefore, the pathogen characteristics and microbiota distribution of periodontal disease are critical. Periodontal disease causes destruction of periodontal tissues (dental support tissues such as gums and alveolar bone) and constitutes a potential risk factor for certain systemic diseases. The relative abundance of the genera *Clostridium*, *Porphyromonas*, *Helicobacter*, *Actinomycetes*, *Micromonas*, and *Streptococcus pneumoniae* in oral microbiota of patients with periodontitis is significantly higher than that of healthy people. By contrast, *Neisseria*, *Corynebacterium*, *Carbonophilic*, and *Actinomycetes* in oral microbiota of patients with periodontitis is lower than that in healthy people (Curtis, M. et al., 2020).

C. Oral cancer:

Oral cancer is one of the most common malignant tumors of the head and neck. It is a general term for malignant tumors that occur in the mouth, and most of them belong to squamous cells (tissue) carcinoma, the so-called mucosal variation, that includes gingival cancer, tongue cancer, soft and hard sputum cancer, jaw cancer, oral cancer, oropharyngeal cancer, salivary gland cancer, lip cancer, maxillary sinus cancer, and cancer occurring in the facial mucosa (Sun, J. et al., 2020). Genetic background, bacteria, and living habits all affect the development of oral cancer. Recent research indicated a correlation between oral microbiota and oral cancer. Gingival carbon dioxide phagocytic bacteria, prednisone and *S. mutans* in the saliva of patients with oral squamous cell carcinoma significantly increase. These bacteria have potential value as diagnostic indicators for oral squamous cell carcinoma (Graves, D.T, et al., 2019).

3. Oral microbiota and systematic diseases.

Oral microbiota can regulate systemic diseases. Thus, oral microbiota will be a new target for treating **systematic** and **metabolic** diseases and improving the body's physical state: **(Fig. 2)**

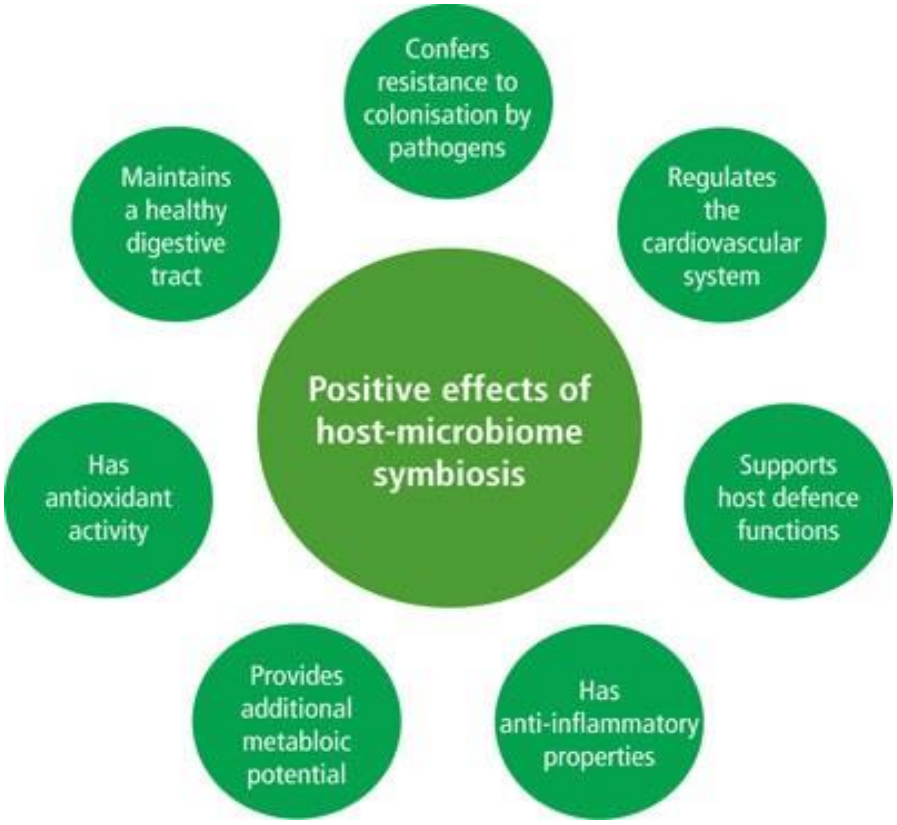

Fig. 1: The Most Diverse and Unique Positive Effects of Microbiota in the Human Body.

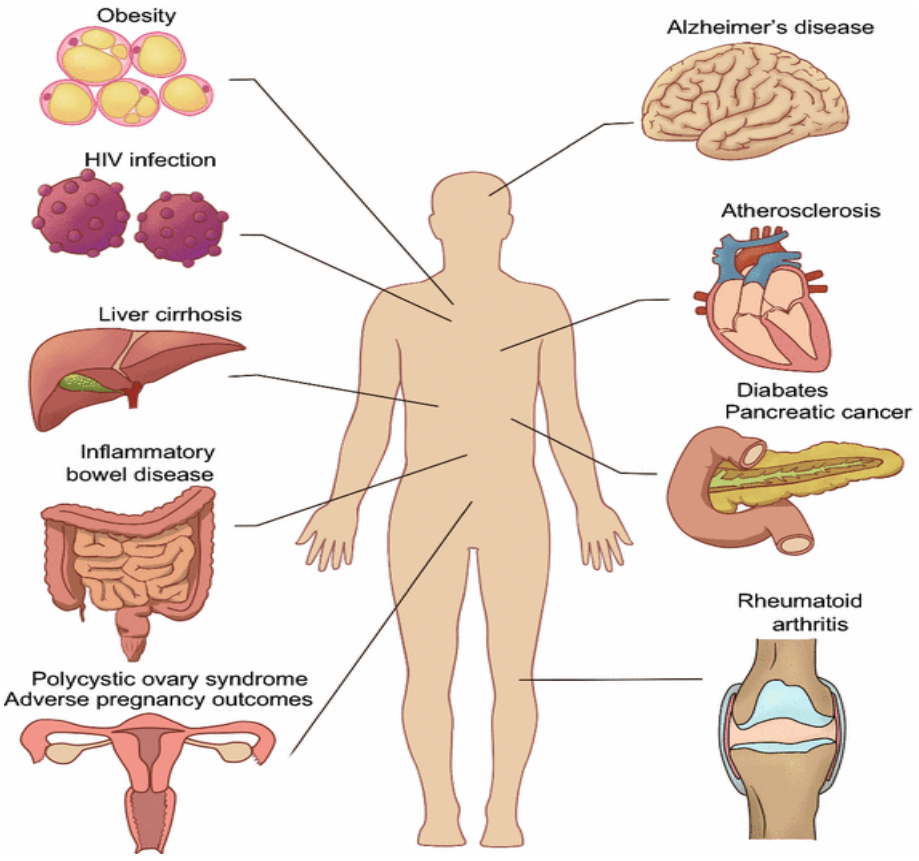

Figure 2. Oral and Systemic Diseases Associated with the Oral Microbiota.

3 -1. Diabetes:

The type 2 diabetes has become one of the most common chronic systemic diseases. It is mainly characterized by persistent hyperglycemia and disordered glucose, fat, and protein metabolism. Many studies have confirmed that the oral diseases (e.g., caries, periodontal disease, mucosa diseases) and type 2 diabetes is closely related. They play a role as mutual feedback. In the process of their interaction, oral microbiota is closely related to oral and systemic health and disease. In addition to its own symptoms, oral symptoms, such as loss of alveolar bone and loss of teeth, have become a complication of diabetes. Researchers conducted an in-depth study of the oral microbiota in the diabetic environment and its effects on the oral cavity by Illumina2 generation sequencing technology. The study revealed that oral microbiota is an important way for diabetes to cause complications. Researchers have observed significant differences in oral microbiota between patients with type 2 diabetes and non-diabetic patients, such as *Neisseria*, *Mycobacterium*, and moreover, the percentage *Fusobacterium*, *Veillon*, and *Streptococcus* have highly increased. Recently, researchers provided a mechanism for the improved understanding of how diabetes increases the risk and severity of tooth loss (Santonocito, S. et al., 2022).

3 -2. Obesity:

Obesity is a health problem that plagues the world. Many reports have described the relationship between gut microbiota and obesity, but whether oral microbiota and obesity are related remains unclear. Recently, 33 adult obese people and 29 healthy adults with normal weight were selected to identify the composition of oral microbiota. It was found that oral microbiota in the obese group was significantly different from that in the normal group, and the bacterial diversity and abundance of oral microbiota in the periodontal healthy obese people were significantly reduced . In the oral microbiota of obese people, the abundance of *Plasmodium*, *S. genus*, and *S.mutans* significantly increased, whereas the abundance of *Corynebacterium*, carbonophilic and *Staphylococcus* significantly decreased. The environmental adaptability of the oral microbiota of obese people and the biodegradability of exogenous substances were low, and they exhibited notable immune disease characteristics. To date, researchers have only found that the oral microbiota of obese people has changed, but the mechanism underlying such a change needs further research in the future (Gasmi B. A. et al., 2021).

3 -3. Liver diseases:

The imbalance of gut microbiota is one of the important factors that promote the development of liver disease. However, recent studies have found that both gut microbiota and the imbalance of oral microbiota are closely related to liver disease. Previous work found a significant difference in the oral (lingual) microbiota of patients with liver cancer and healthy people. The diversity of oral microbiota in patients with liver cancer was higher than that of healthy people, and the composition of the microbiota in patients with liver cancer was also significantly different from that of healthy people (Acharya, C. et al., 2017). Among them, *Clostridium*, *Oribacterium*, *Ciliate*, *Actinomyces*, and *Campylobacter* have high abundance, whereas *Haemophilus*, *Streptococcus*, and *Pseudomonas* have low abundance. *Clostridium* and *Oribacterium* are biomarkers that can distinguish between patients with liver cancer and healthy people, as well as assist in the diagnosis of liver cancer without operation. (Marsh, P.D. 2000). Similar to patients with liver cancer, patients with cirrhosis exhibit an imbalance of oral microbiota, reduced abundance of oral symbiotic bacteria, and increased abundance of potential pathogenic bacteria (e.g., *Enterococcus*). Researchers compared the gut microbiota of patients with cirrhosis and healthy people, and they found that the intestinal microbiota of patients with cirrhosis is enriched with a large number of oral-derived microorganisms, including *Streptococcus*, *Haemophilus*, *Lactobacillus*, and *Clostridium* (. Zarco, M., et al, 2012). These researchers speculated that oral microbes invade gut microbiota of patients with cirrhosis.

3 -4. Cancers:

Previous reports have shown that gut microbiota and colorectal cancer are closely related, and the oral microbiota has been demonstrated to be closely related to colorectal cancer as well. *F. nucleatum* in the oral cavity can transfer to other parts of the body through blood cycling as the whole body's immunity declines, leading to local inflammation and indirectly promoting tumor formation (Xiu-Li Wang, 2023). The bacterium can be isolated from colorectal cancer tissues, and the risk of colorectal cancer is high in patients with the bacterium. *F. nucleatum* is a Gram-negative obligate anaerobic bacterium, and several studies have isolated *F. nucleatum* from colorectal cancer tissues. Patients with high abundance of *F. nucleatum* have a high risk for colorectal cancer (Malla, M.A., et al, 2019). Therefore, the number of this bacteria can be used as a potential marker for colorectal cancer. Studies have found that *F. nucleatum* can be transferred from the mother's mouth to fetal tissue and cause fetal death. Thus, *F. nucleatum* in the mouth can be transferred to other parts of the body. Also, it may involve transient bacteremia in the bloodstream and then transfer to the colorectal tumor (Lee, Y.-H., et al, 2021).

4. Oral Microbial Ecology

The habitat oral cavity is suitable for these organisms because of favorable physiochemical environment inside the oral cavity. An ecosystem consists of the microbial community living in a defined habitat and the abiotic surroundings composed of physical and chemical elements. In its simplest expression, the oral ecosystem is thus composed of the oral microorganisms and their surroundings, the oral cavity (Kaan, A. M. M., et al, 2021)**.** The oral cavity is a moist environment which is kept at a relatively constant temperature (34 to 36°C) and a pH close to neutrality in most areas and thus supports the growth of a wide variety of microorganisms (Kilian, M,. et al, 2016). However, the mouth must not be considered a uniform environment. There are several habitats in the oral cavity, each being characterized by different physicochemical factors and thus supporting the growth of a different microbial community. In the oral cavity, indigenous bacteria are often associated with two major oral diseases, caries and periodontal diseases (Diaz, P.I., 2021). These diseases seem to appear following an imbalance in the oral resident microbiota, leading to the emergence of potentially pathogenic bacteria. The oral surfaces are also constantly bathed by two important physiological fluids, the saliva and the gingival crevicular fluid. These fluids are essential for the maintenance of the oral ecosystems by providing water, nutrients, adherence, and antimicrobial factors (Dewhirst, F.E., et al, 2010). Oral diseases seem to appear after an inbalance among the indigenous microbiota, leading to the emergence of potentially pathogenic microorganisms (Roberts, A.P. and Kreth, J. 2014). To define the process involved in caries and periodontal diseases, it is necessary to understand the ecology of the oral cavity and to identify the factors responsible for the transition of the oral microbiota from a commensal to a pathogenic relationship with the host (Patangia, D.V., et al, 2022). The regulatory forces influencing the oral ecosystem can be divided into three major categories: host related, microbe related, and external factors (Fan, X ., 2018). The present review describes the oral ecosystems, the major factors that might control the oral microbiota, the basic aspects of the secretory immune system, and the biological functions of SIgA and finally focuses on experiments related to the role of IgA in the microbial ecology of the oral cavity. To present an overall picture of the current knowledge of oral microbial ecology (Li, Y.; 2022).

CONCLUSIONS

Oral microbial flora have a very important role in maintenance homeostasis of the ecosystem in the oral cavity. It is crucial for clinicians to be aware of this fact and they should focus their treatment toward control of this flora rather than eliminating it. A thorough knowledge of the normal and altered flora and the mechanics behind how the change can happen and what it might lead to would give us a fair idea of how various oral diseases could be controlled and preventive strategies be developed. This review showed that the oral microbiota can affect oral diseases and affect the health of the whole body. It is important to improve oral health by altering the oral microbiota through developing oral probiotics and enhancing body health and reduce the load of bacteria in the oral cavity of a subject and improve oral micro-ecology homeostasis. Because, when the microbial equilibrium is broken (imbalance), in a process called dysbiosis, the pathogens thrive and diseases occur. Due to this realization about the oral microbiota, several new methods based on the modulation of the oral microbiota that aim at maintaining a healthy body ecosystem.

REFERENCES

1. Abusleme, L., Hoare, A., Hong, B.-Y. & Diaz, P. I. (2021). Microbial signatures of health, gingivitis, and periodontitis. Periodontol 2000 86, 57–78
2. Acharya, C., Sahingur, S. E. & Bajaj, J. S. (2017). Microbiota, cirrhosis, and the emerging oral-gut-liver axis. JCI Insight 2, e94416 2.
3. Baker, J.L.; Bor, B.; Agnello, M.; Shi, W.; He, X. (2017). Ecology of the Oral Microbiome: Beyond Bacteria. Trends Microbiol., 25, 362–374. [Google Scholar] [Cross Ref] [PubMed].
4. Baker, J. L. & Edlund, A. (2018). Exploiting the oral microbiome to prevent tooth decay: has evolution already provided the best tools? Front. Microbiol. 9, 3323.
5. Baker, J. et al. (2021). Deep metagenomics examines the oral microbiome during dental caries, revealing novel taxa and co-occurrences with host molecules. Genome Res. 31, 64–74.
7. Chen, C. et al. (2018). Oral microbiota of periodontal health and disease and their changes after nonsurgical periodontal therapy. ISME J. 12, 1210–1224.
8. Cai, Z., Lin, S., Hu, S. & Zhao, L. (2021). Structure and function of oral microbial community in periodontitis based on integrated data. Front. Cell. Infect. Microbiol. 11, 663756
9. Curtis, M.A.; Diaz, P.I.; Van Dyke, T.E. (2020). The role of the microbiota in periodontal disease. Periodontology 2000, 83, 14–25. [Google Scholar] [Cross Ref].

10. Diaz, P. I. & Valm, A. M. (2020). Microbial interactions in oral communities mediate emergent biofilm properties. J. Dent. Res., 99, 18–25. https://doi.org/10.1177/0022034519880157
11. Diaz, P.I.; Dongari-Bagtzoglou, A. (2021). Critically appraising the significance of the oral microbiome . J. Dent. Res., 100, 133–140. [Google Scholar] [Cross Ref] [PubMed].
12. Dewhirst, F.E.; Chen, T.; Izard, J.; Paster, B.J.; Tanner, A.C.R.; Yu, W.-H.; Lakshmanan, A.; Wade, W.G. (2010). The Human Oral Microbiome. J. Bacteriol., 192, 5002–5017. [Google Scholar] [Cross Ref].
13. Fan, X.; Peters, B.A.; Min, D.; Ahn, J. (2018). Comparison of the oral microbiome in mouth wash and whole saliva samples. PLoS ONE, 13, e0194729. [Google Scholar] [Cross Ref].
14. Gao, L.; Cheng, Z.; Zhu, F.; Bi, C.; Shi, Q.; Chen, X. (2022). The Oral Microbiome and Its Role in Systemic Autoimmune Diseases: A Systematic Review of Big Data Analysis. Front. Big Data, 5, 927520. [Google Scholar] [Cross Ref].
15. Gao, L.; Xu, T.; Huang, G.; Jiang, S.; Gu, Y.; Chen, F. (2018). Oral microbiomes: More and more importance in oral cavity and whole body. Protein Cell, 9, 488–500. [Google Scholar] [Cross Ref].
16. Gasmi Benahmed, A.; Gasmi, A.; Doşa, A.; Chirumbolo, S.; Mujawdiya, P.K.; Aaseth, J.; Dadar, M.; Bjørklund, G. (2021). Association between the gut and oral microbiome with obesity. Anaerobe, 70, 102248. [Google Scholar] [Cross Ref] [PubMed].
17. Gm, A. (2021). Oral Biofilm and Its Impact on Oral Health, Psychological and Social Interaction. Int. J. Oral Dent. Health, 7, 127. [Google Scholar] [Cross Ref].
18. Graves, D.T.; Corrêa, J.D.; Silva, T.A. (2019). The Oral Microbiota Is Modified by Systemic Diseases. J. Dent. Res. 2019, 98, 148–156. [Google Scholar] [Cross Ref].
19. He, J.; Li, Y.; Cao, Y.; Xue, J.; Zhou, X. (2015). The oral microbiome diversity and its relation to human diseases. Folia Microbiol., 60, 69–80. [Google Scholar] [Cross Ref] [PubMed].
20. John J. R., Hari K.. K ., Vasanth J., Karthik K., Tianhao W. & Kang B. (2024). Oral Microbiome: A Review of Its Impact on Oral and Systemic Health. Microorganisms , 12(9), 1797; https://doi.org/10.3390/microorganisms12091797
21. Jeong, J.; Mun, S.; Oh, Y.; Cho, C.-S.; Yun, K.; Ahn, Y.; Chung, W.-H.; Lim, M.Y.; Lee, K.E.; Hwang, T.S.; et al. (2022). A q RT-PCR Method Capable of Quantifying Specific Microorganisms Compared to NGS-Based Metagenome Profiling Data. Microorganisms, 10, 324. [Google Scholar] [Cross Ref].
22. Jo, R.; Nishimoto, Y.; Umezawa, K.; Yama, K.; Aita, Y.; Ichiba, Y.; Murakami, S.; Kakizawa, Y.; Kumagai, T.; Yamada, T.; et al. (2019). Comparison of oral microbiome profiles in stimulated and unstimulated saliva, tongue, and mouth-rinsed water. Sci. Rep., 9, 16124. [Google Scholar] [Cross Ref] [PubMed].
23. Jonathon L. Baker, Jessica L. Mark Welch, Kathryn M. Kauffman, Jeffrey S. McLean & Xuesong He. (2024). The oral microbiome: diversity, biogeography and human health. Nature Reviews Microbiology, 22, 89–104. https://doi.org/10.1038/s41579-023-00963-6
24. Kaan, A. M. M., Kahharova, D. & Zaura, E. (2021). Acquisition and establishment of the oral microbiota. Periodontol, 86, 123–141. https://doi.org/10.1111/prd.12366.
25. Kilian, M.; Chapple, I.L.C.; Hannig, M.; Marsh, P.D.; Meuric, V.; Pedersen, A.M.L.; Tonetti, M.S.; Wade, W.G.; Zaura, E. (2016). The oral microbiome—An update for oral healthcare professionals. Br. Dent. J., 221, 657–666. [Google Scholar] [Cross Ref].
26. Lamont, R.J.; Koo, H.; Hajishengallis, G. (2018).The oral microbiota: Dynamic communities and host interactions. Nat. Rev Microbiol., 16, 745–759. [Google Scholar] [Cross Ref].
27. Lee, B.-M.; Park, J.W.; Jo, J.H.; Oh, B.; Chung, G. (2022).Comparative analysis of the oral microbiome of burning mouth syndrome patients. J. Oral Microbiol., 14, 2052632. [Google Scholar] [Cross Ref] [PubMed].
28. Lee, Y.-H.; Chung, S.W.; Auh, Q.-S.; Hong, S.-J.; Lee, Y.-A.; Jung, J.; Lee, G.-J.; Park, H.J.; Shin, S.-I.; Hong, J.-Y. (2021). Progress in Oral Microbiome Related to Oral and Systemic Diseases: An Update. Diagnostics, 11, 1283. [Google Scholar] [Cross Ref].
29. Li, Y.; Zhu, M.; Liu, Y.; Luo, B.; Cui, J.; Huang, L.; Chen, K.; Liu, Y. (2022). The oral microbiota and cardio-metabolic health: A comprehensive review and emerging insights. Front. Immunol., 13, 1010368. [Google Scholar] [Cross Ref].
30. Lu, M.; Xuan, S.; Wang, Z. (2019). Oral microbiota: A new view of body health. Food Sci. Hum. Wellness, 8, 8–15. [Google Scholar] [Cross Ref].
31. Malla, M.A.; Dubey, A.; Kumar, A.; Yadav, S.; Hashem, A.; Abd Allah, E.F. (2019). Exploring the Human Microbiome: The Potential Future Role of Next-Generation Sequencing in Disease Diagnosis and Treatment. Front. Immunol., 9, 2868. [Google Scholar] [Cross Ref].

32. Marsh, P.D. (2000).Role of the Oral Microflora in Health. Microb. Ecol. Health Dis., 12, 130–137. [Google Scholar] [Cross Ref].
33. Patangia, D.V.; Anthony Ryan, C.; Dempsey, E.; Paul Ross, R.; Stanton, C. (2022). Impact of antibiotics on the human microbiome and consequences for host health. Microbiology Open , 11, e1260. [Google Scholar] [Cross Ref] [PubMed].
34. Peng, X.; Cheng, L.; You, Y.; Tang, C.; Ren, B.; Li, Y.; Xu, X.; Zhou, X. (2022).Oral microbiota in human systematic diseases. Int. J. Oral Sci., 14, 14. [Google Scholar] [Cross Ref].
35. Plachokova, A.S.; Andreu-Sánchez, S.; Noz, M.P.; Fu, J.; Riksen, N.P. (2021). Oral Microbiome in Relation to Periodontitis Severity and Systemic Inflammation. Int. J. Mol. Sci., 22, 5876. [Google Scholar] [Cross Ref].
36. Roberts, A.P.; Kreth, J. (2014). The impact of horizontal gene transfer on the adaptive ability of the human oral microbiome. Front. Cell. Infect. Microbiol., 4, 124. [Google Scholar] [Cross Ref].
37. Rooney, C.M.; Mankia, K.; Emery, P. (2020). The Role of the Microbiome in Driving RA-Related Autoimmunity. Front. Cell Dev. Biol., 8, 538130. [Google Scholar] [Cross Ref].
38. Santonocito, S.; Giudice, A.; Polizzi, A.; Troiano, G.; Merlo, E.M.; Sclafani, R.; Grosso, G.; Isola, G. (2022). A Cross-Talk between Diet and the Oral Microbiome: Balance of Nutrition on Inflammation and Immune System's Response during Periodontitis. Nutrients, 14, 2426. [Google Scholar] [Cross Ref].
39. Segata, N.; Haake, S.K.; Mannon, P.; Lemon, K.P.; Waldron, L.; Gevers, D.; Huttenhower, C.; Izard, J. (2012).Composition of the adult digestive tract bacterial microbiome based on seven mouth surfaces, tonsils, throat and stool samples. Genome Biol., 13, R42. [Google Scholar] [Cross Ref].
40. Schincaglia, G.P.; Hong, B.Y.; Rosania, A.; Barasz, J.; Thompson, A.; Sobue, T.; Panagakos, F.; Burleson, J.A.; Dongari-Bagtzoglou, A.; Diaz, P.I. (2017). Clinical, Immune, and Microbiome Traits of Gingivitis and Peri-implant Mucositis. J. Dent. Res., 96, 47–55. [Google Scholar] [Cross Ref].
41. Sharma, N.; Bhatia, S.; Sodhi, A.S.; Batra, N. (2018).Oral microbiome and health. AIMS Microbiol., 4, 42–66. [Google Scholar] [Cross Ref] [PubMed].
42. Sun, J.; Tang, Q.; Yu, S.; Xie, M.; Xie, Y.; Chen, G.; Chen, L. (2020). .Role of the oral microbiota in cancer evolution and progression. Cancer Med., 9, 6306–6321. [Google Scholar] [Cross Ref].
43. Thomas, C.; Minty, M.; Vinel, A.; Canceill, T.; Loubières, P.; Burcelin, R.; Kaddech, M.; Blasco-Baque, V.; Laurencin-Dalicieux, S. (2021). Oral Microbiota: A Major Player in the Diagnosis of Systemic Diseases. Diagnostics, 11, 1376. [Google Scholar] [Cross Ref] [PubMed].
44. Zarco, M.; Vess, T.; Ginsburg, G. (2012). The oral microbiome in health and disease and the potential impact on personalized dental medicine. Oral Dis., 18, 109–120. [Google Scholar] [CrossRef] [PubMed]
45. Zhang, Y.; Ding, Y.; Guo, Q. (2022). Probiotic Species in the Management of Periodontal Diseases: An Overview. Front. Cell. Infect. Microbiol., 12, 806463. [Google Scholar] [Cross Ref].
46. Zorba, M.; Melidou, A.; Patsatsi, A.; Ioannou, E.; Kolokotronis, A. (2020). The possible role of oral microbiome in autoimmunity. Int. J. Womens Dermatol., 6, 357–364. [Google Scholar] [Cross Ref] [PubMed].
47. Chiara A., Olivier D., Christophe G., Jenny, P., Frédéric V., Mathieu M., Louis C., Paul M., Philippe K. (2024). The oral organ: A new vision of the mouth as a whole for a gerophysiological approach to healthy aging Ageing Research Reviews . Ageing Research Reviews, 99, 28- 32. https://doi.org/10.1016/j.arr.2024.102360
48. Daniel MJ and Jose LLR (2018). Candida Interactions with the Oral Bacterial Microbiota. J. Fungi 4(4), 122. https://doi.org/10.3390/jof40401
49. Christina J Adler, Gina V Browne, Smitha Sukumar & Toby Hughes. (2017). Evolution of the Oral Microbiome and Dental Caries. Microbiology, 4, 264–269. https://link.springer.com/article/10.1007/s40496-017-0151-1#citeas
50. Anne Marie & Lynge Pedersen (2019).The role of natural salivary defenses in maintaining a healthy oral microbiota. Journal of Dentistry, 80(1): 3-12. https://doi.org/10.1016/j.jdent.2018.08.010
51. Xiu-Li Wang, Hua-Wen Xu & Ning-Ning Liu (2023). Oral Microbiota: A New Insight into Cancer Progression, Diagnosis and Treatment. Phenomix, 3, 535–547. https://link.springer.com/article/10.1007/s43657-023-00124-y

➢ *ORAL PRESENTATION*

Antifungal activity and biocompatibility on fibroblast cells of Sea Urchin (*Diadema setosum*) gonad lipid extract based PVA (polyvinyl alcohol) hydrogel

Elif Erdoğan Eliuz[1] (ORCID: https://orcid.org/0000-0003-4317-3000), Ayşegül Demircan[1*] (ORCID: https://orcid.org/0009-0008-9494-2547), Ayşe Kılınç[1] (ORCID: https://orcid.org/0009-0008-3990-6500), Deniz Ayas[1](ORCID: https://orcid.org/0000-0001-6762-6284), Mert Acar[1] (ORCID: https://orcid.org/0000-0002-2726-8416)

[*1]Mersin University, Faculty of Fisheries, Department of Seafood Processing Technology, Mersin, Turkey

*Corresponding author e-mail: aysegldemircann@gmail.com

Abstract
Diadema setosum (*D. setosum*) is a species of sea urchin commonly known as the long-spined sea urchin, found in tropical Indo-Pacific waters. It is easily recognizable by its long, sharp, black spines, which can grow up to 30 cm in length and are venomous. In this study, PVA (polyvinyl alcohol) polymer network hydrogel was prepared using lipids extracted from *D. setosum* gonads. Fatty acid composition of the extract was analyzed by GC-MS. Swelling behavior, zeta potential and stability of *D. setosum* extract based PVA (PVA- *D. setosum*) were investigated. Zeta potential, size distribution, and structural characterization of the hydrogel were evaluated. PVA-*D. setosum* were also tested for antifungal activity and biocompatibility. Biocompatibility test was evaluated by MTT test (3-(4,5-dimethylthiazol-2-yl)-2,5-diphenyltetrazolium bromide) using mouse fibroblast cells. In the study, PVA-*D. setosum* hydrogel showed antifungal activity with 5.4 mm inhibition zones against *Candida glabrata* and 3.2 mm inhibition zones against *Candida parapsilosis*. These findings suggest that bioactive PVA-D. *setosum* hydrogel has potential applications in wound dressings, food coatings and agricultural materials due to its antifungal and non-cytotoxic effect properties.
Keywords: Polyvinyl alcohol, *Diadema setosum,* lipid extract, hydrogel

INTRODUCTION

Hydrogels are semi-liquid and slightly rigid structures composed of cross-linked hydrophilic polymer networks. The type and density of cross-linking points directly influence the mechanical properties and overall architecture of the three-dimensional network, enabling the formation of various hydrogel types (Ahmed, 2015). Tailored to specific applications, hydrogels can be engineered to possess diverse functional properties such as high fluid absorption, prevention of body fluid loss, bacterial barrier formation, and oxygen permeability (Lim et al., 2009). Hydrogels based on polyvinyl alcohol (PVA) are particularly valued for their flexibility and mechanical robustness, making them suitable for a wide range of biomedical applications including implants, artificial organs, drug delivery systems, and wound dressings (Husain et al., 2018).

Recent research has focused on incorporating peptides and lipids into hydrogels due to their bioactive properties, especially their antimicrobial potential (Mwangi et al., 2019). Marine-derived lipids, recognized for their safety and antibacterial activity, are abundant in tropical marine ecosystems. In this study, lipids extracted from the gonads of *Diadema setosum*—a sea urchin species—were utilized in hydrogel formulations to evaluate their antimicrobial and anti-amylase activities. The gonads, which are the reproductive organs of sea urchins, are rich in ω-3 polyunsaturated fatty acids (LC-PUFA), known for their immunomodulatory and immune-boosting effects (Padang et al., 2019; Murzina et al., 2021).

Bioactive hydrogels were developed by combining PVA, which can independently form gels, with lipid extracts from *D. setosum* gonads to investigate the resulting physicochemical and functional properties. The volatile components of the lipid extract were analyzed using Gas Chromatography–Mass Spectrometry (GC-MS). The hydrogels' characterization, antifungal properties, and effects on fibroblast cells were also systematically investigated.

MATERIALS AND METHODS

Provide **Lipid Extraction from *D. setosum*, GC-MS Analysis, and Hydrogel Preparation**

Lipids were extracted from *Diadema setosum* gonads using a Soxhlet apparatus, followed by solvent removal using a rotary evaporator. The obtained lipid extract was analyzed by (GC-MS) as described by Erdogan Eliuz et al. (2022).

Polyvinyl alcohol (PVA) solution was prepared by dissolving 30% (w/w) PVA in distilled water. The solution was heated to approximately 90°C and maintained at this temperature for 5 minutes to ensure complete dissolution. After cooling, the lipid extract was added at a 1:1 ratio (PVA:lipid, v/v), and the mixture was homogenized for 5 minutes using a high-speed homogenizer. To enhance gel formation, the mixture underwent three freeze–thaw cycles by freezing at −30°C and then thawing at 25°C, as reported by Boran et al. (2024).

Characterization of PVA/*D. setosum* Hydrogels

The hydrogels' stability, particle size distribution, zeta potential, and swelling behavior were evaluated to the methodology described by Eliuz et al. (2024).

Biological Activity of *D. setosum*-Based Hydrogels

The antifungal activity and cytotoxicity of the PVA/*D. setosum* hydrogels were assessed.

Antifungal Activity

The antimicrobial potential of the *D. setosum* lipid-containing hydrogels was evaluated using the well diffusion method. The fungal strains used in this study were *Candida glabrata* and *Candida parapsilosis*. Prior to testing, the fungal strains were inoculated on Sabouraud Dextrose Agar at 35°C for 18–24 hours. After incubation, fresh colonies were harvested for testing. The fungi were spread evenly onto Mueller-Hinton Agar plates. Wells of 6 mm diameter were punched into the agar and filled with 40 µL of the test formulations. The agar plates were incubated at 35°C for 24 hours. Zones of inhibition were analysed in millimeters using the Images programme. Sterile ultra distilled water was used as the negative control. All tests were performed in triplicate to ensure reproducibility (Erdogan Eliuz, 2022).

Evaluation of Fibroblast Cell Proliferation via MTT Assay

Human dermal fibroblast cells (PCS-201-012™) were sourced from the American Type Culture Collection (ATCC) and cultured in RPMI medium enriched with 10% fetal bovine serum (FBS) and 1% penicillin-streptomycin. The cells were incubated at 37°C under a humidified atmosphere containing 5% CO_2. When cultures reached approximately 80–90% confluency, cells were passaged using a 0.25% trypsin-EDTA solution at a 1:3 split ratio.

Cell viability and proliferation were evaluated using the MTT assay, a colorimetric technique that relies on the conversion of MTT into insoluble formazan crystals by metabolically active mitochondria. After 24 hours of initial cell seeding, hydrogel extracts were added at final concentrations of 0.05, 0.1, 0.2, 0.5, and 1 mg/mL. Untreated wells served as negative controls and were considered to represent 100% cell proliferation. After a 72-hour incubation period, 10 µL of MTT solution was added to each well, followed by a further 4-hour incubation. The resulting formazan crystals were dissolved with a solubilizing reagent, and absorbance was measured at 570 nm using a microplate reader (Thermo Labsystems, Franklin, MA, USA). Proliferation rates were determined by comparing the absorbance values to those of the control group (Öztaş et al., 2024).

RESULTS and DISCUSSION

GC–MS Analysis of *D. setosum* Extract

The dominant volatile compounds identified in the *D. setosum* extract by GC–MS were hexadecanoic acid (26.30%), 5,8,11,14-eicosatetraenoic acid (20.07%), ethyl stearate, tetradecanoic acid, (E)-9-octadecenoic acid, ethyl oleate, 5,8,11,14,17-eicosapentaenoic acid, palmitic acid, and E-11-hexadecenoic acid. Additionally, the GC analysis revealed the presence of palmitic acid, stearic acid, trans-9-elaidic acid

(C18:1), cis-9-oleic acid (C18:1), trans-linolelaidic acid (C18:2), n-6 linoleic acid (C18:2), arachidonic acid (C20:4), and eicosapentaenoic acid (EPA, C20:5n3).

Stability, Particle Size Distribution, Zeta Potential, and Swelling Behavior of *D. setosum* Hydrogels

In this study, a fragmented gel model was initially formed using PVA alone (Figure 1A). Upon the addition of *D. setosum* lipid extract, further formulation development was conducted based on changes in elasticity and viscosity. Among the tested formulations, the hydrogel type that demonstrated optimal structural integrity and consistency after lipid incorporation (Figure 1B) was selected for subsequent experiments.

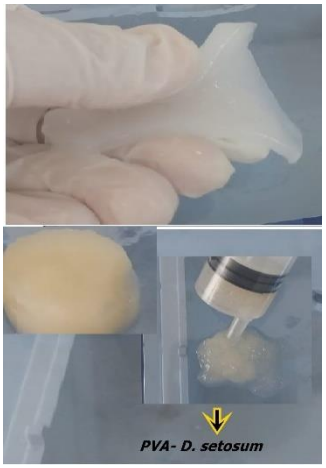

Figure 1. PVA (A), PVA. *D.setosum* hydrogel (B).

In our study, the zeta potentials of PVA–*D. setosum* and pure PVA hydrogels were found to be –43.3 ± 1.1 mV and –58.6 ± 0.04 mV, respectively ($p < 0.05$). The viscosities of both PVA–*D. setosum* and blank hydrogels were measured as 0.8872, indicating no statistically significant difference (Table 1).

Table 1. Zeta potential and particle size distribution values of *D. setosum* hydrogels based on polymer

	PVA- *D. setosum*	**PVA**
Zeta (mV)	-43,3^{a}±1,1	-1,3^{b}±0,1
Dispersant (RI)	1,330^{a}±0,0	1,330^{a}±0,0
Viscosity (cP)	0,8872^{a}±0,0	0,8872^{a}±0,0
Particle size (d nm)	427,4^{a}±2,8	385^{a}±2,8

Statistical differences were evaluated within the same row. Identical letter symbols indicate no significant difference ($p < 0.05$).

The particle size distribution of the PVA–*D. setosum* hydrogels is shown in the graph below (Figure 2) ($p < 0.05$). The particle size distribution of the PVA–*D. setosum* hydrogel was determined to be 427.4 d.nm

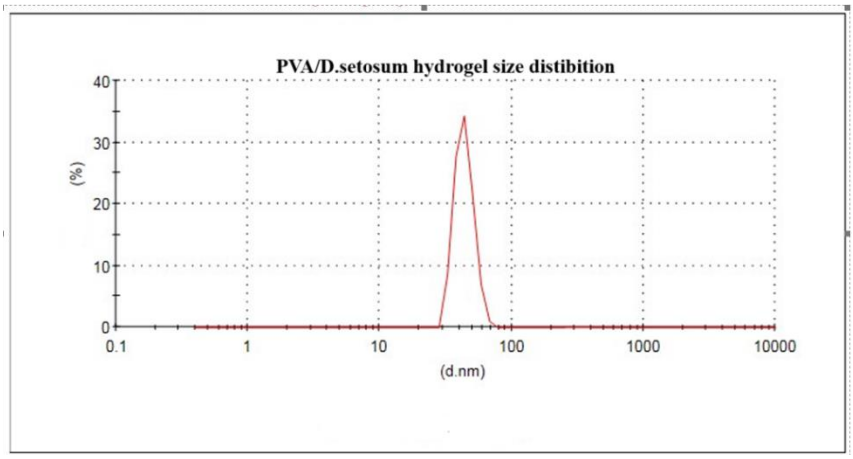

Figure 2. Particle size distribution of PVA–*D. setosum* hydrogel

Water absorption capacity was measured at 5, 10, and 15 minutes, and the amount of absorbed water was calculated as a percentage (Figure 3). Within the first 5 minutes, both *D. setosum*-loaded and blank hydrogels exhibited significantly higher water absorption compared to time zero.
In the PVA hydrogel, swelling percentages relative to time zero were $340^{b} \pm 9.19\%$, $343.3^{b} \pm 6.6\%$, and $346.7^{b} \pm 11.0\%$ at 5, 10, and 15 minutes, respectively ($p < 0.05$). Conversely, the PVA/*D. setosum* hydrogel showed swelling percentages of $120^{a} \pm 8.0\%$, $18.2^{a} \pm 5.0\%$, and $1.5^{a} \pm 1.0\%$ at the same time points ($p < 0.05$).

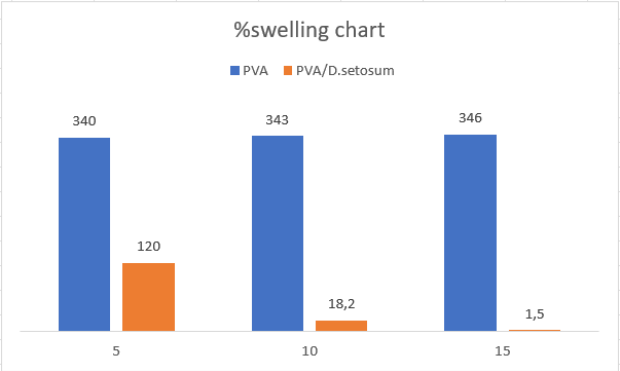

Figure 3. Time-dependent water absorption capacity of PVA and PVA/*D. setosum* hydrogels ($p < 0.05$).

The homogeneity and stability of lipids through gelation or emulsification are closely related to zeta potential and particle size distribution (Eliuz and Ayas, 2024). In this study, the hydrogels demonstrated a homogeneous distribution, with the PVA–*D. setosum* hydrogel exhibiting a zeta potential of -43.3 ± 1.1 mV. It is well established that zeta potentials between –30 mV and +30 mV are indicative of stable systems (Eliuz et al., 2024). PVA hydrogels are known to have high swelling capacities (Shi et al., 2016). The swelling behavior of the PVA–*D. setosum* hydrogels showed a 120% increase within the first 5 minutes, indicating significant water retention. Therefore, PVA hydrogel alone statistically exhibits a considerably higher swelling potential compared to other hydrogels.

Antifungal Activities of *D. setosum* Hydrogels

The antifungal activities of the PVA/*D. setosum* ethanol extract, assessed by agar well diffusion assay, are presented in Figure 4. The extract showed inhibition zones of 19.4 mm and 7.2 mm against *Candida glabrata* and *Candida parapsilosis*, respectively (Table 3).

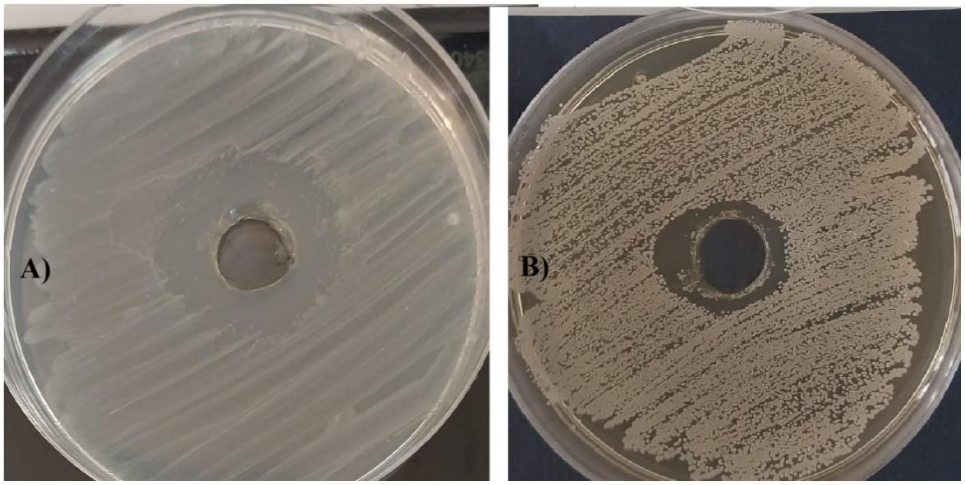

Figure 4. Antimicrobial activity of *D. setosum* hydrogel against pathogens: A) *Candida glabrata*, B) *Candida parapsilosis*.

D. setosum hydrogels exhibited strong antimicrobial activity against all tested microorganisms ($p < 0.05$). The PVA/*D. setosum* hydrogel showed inhibition zones of 5.4 mm against *C. glabrata* and 3.2 mm against *C. parapsilosis* (Table 3).

Table 3. Inhibition zone (mm) values of *D. setosum* extract and hydrogels.

Microorganism	***D. setosum* extract**	**PVA-*D. setosum* hydrogel**	**Antibiotic**	**PVA**
C,glabrata	$19{,}4^{b} \pm 1{,}1$	$5{,}4^{bc} \pm 1{,}1$	$15{,}4^{a} \pm 1{,}5$	0± 0,0
C,parapsilosis	$7{,}2^{a} \pm 3{,}1$	$3{,}2^{ac} \pm 3{,}1$	$9{,}1^{b} \pm 1{,}5$	0± 0,0

Different letters ("a", "b") within the same column indicate statistically significant differences. Fluconazole (250 µg/mL) was used for fungi.

The predominant components of *D. setosum* identified by GC-MS analysis were hexadecanoic acid (26.30%) and 5,8,11,14-eicosatetraenoic acid (20.07%). These results showed similarities with the limited number of studies available in the literature. Muhammad et al. (2020), in their GC-MS analysis of gonad extracts, identified compounds such as n-hexadecanoic acid, (Z)-9-octadecenoic acid methyl ester, tetradecanoic acid, pentadecanoic acid, and oleic acid. There are very few inhibition studies related to sea urchin gonads reported in the literature. In one study, the methanol extract of sea urchin gonads showed no effect against *Enterococcus faecalis* ATCC 29212, *Klebsiella pneumoniae*, and *Candida albicans* ATCC 10237, but exhibited strong inhibition (14 mm) against *Staphylococcus aureus* ATCC 25923 (El-Sayed et al., 2020). In contrast, our study demonstrated significant effectiveness against *Candida* species.

Cytotoxicity of PVA/*D. setosum* Hydrogel on Fibroblast Cell Lines

The proliferation of fibroblast cells treated with PVA/*D. setosum* hydrogel was measured as 205% ± 0.3, 200% ± 0.2, and 180.71% ± 0.3 at concentrations of 1, 0.5, and 0.2 mg/mL, respectively (Figure 5).

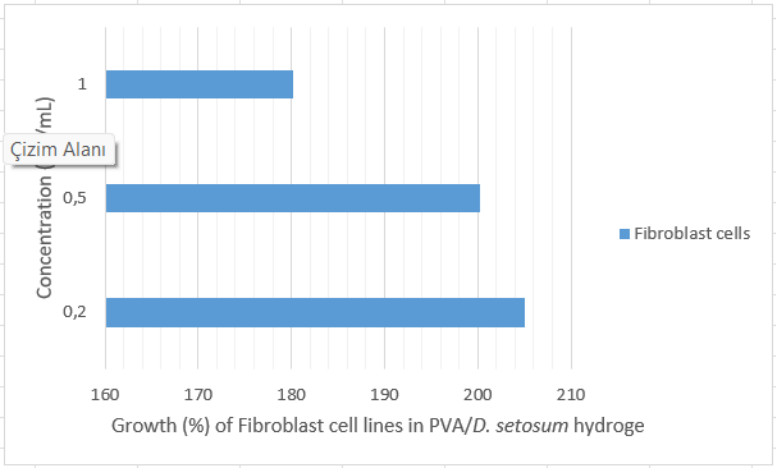

Figure 5. The proliferation of fibroblast cells treated with PVA/*D. setosum*

The *D. setosum*-based hydrogel induced a dose-dependent increase in human fibroblast proliferation without exhibiting cytotoxic effects. This aligns with previous findings showing enhanced neural stem cell proliferation by *Strongylocentrotus purpuratus* (sea urchin) ovary extracts. It is hypothesized that EPA and palmitic acid in sea urchin extracts may exert mitogenic effects via activation of the PPARγ pathway. This study is the first to report that *D. setosum* gonad hydrogel promotes up to a two-fold increase in human fibroblast proliferation in a dose-dependent manner, suggesting its potential for wound healing and tissue regeneration applications (Carroll et al., 2020; Roncoroni et al., 2024).

CONCLUSION

This study demonstrated that the incorporation of *D. setosum* lipid extract into PVA hydrogels produces stable, homogeneous gels with favorable physicochemical properties, including a zeta potential indicative of colloidal stability and moderate swelling behavior. The GC–MS analysis identified bioactive fatty acids such as hexadecanoic acid and eicosatetraenoic acid, which likely contribute to the observed strong antifungal activity against *Candida* species. Importantly, the PVA/D. setosum hydrogel enhanced human fibroblast proliferation in a dose-dependent manner without cytotoxic effects, highlighting its promising potential for biomedical applications such as wound healing and tissue regeneration. These findings support the therapeutic value of *D. setosum* extracts in hydrogel formulations and warrant further investigation into their clinical applications.

ACKNOWLEDGEMENTS

This study funded by Mersin University Research Fund (Project No: 2023-1-AP4-4894) and Turkish Scientific and Technological Research Council (TUBITAK:123Z542).

REFERENCES

Ahmed, E. M. (2015). Hydrogel: Preparation, characterization, and applications: A review. *Journal of Advanced Research, 6*, 105–121.

Alam, M. S., Kaur, G., Jabbar, Z., Javed, K., & Athar, M. (2007). *Eruca sativa* seeds possess antioxidant activity and exert a protective effect on mercuric chloride induced renal toxicity. *Food and Chemical Toxicology, 45*(6), 910–920.

Boran, M., Eliuz, E. E., & Ayas, D. (2024). The anti-candidal and absorption performance of PVA/PVP-based *Jania rubens* hydrogel on *Candida tropicalis* and some physicochemical properties of the hydrogel. *Applied Biochemistry and Biotechnology, 196*(12), 8848–8865.

Carroll, A. R., Copp, B. R., Davis, R. A., Keyzers, R. A., & Prinsep, M. R. (2020). Marine natural products. *Natural Product Reports, 37*, 175–223.

Eliuz, E. E., & Ayas, D. (2024). Developing fish oil emulsion gel enriched with *Lentinula edodes* single cell protein and its effect on controlling the growth of *Acinetobacter baumannii*. *Journal of Microbiological Methods, 224*, 107006.

Eliuz, E. E., Yabalak, E., & Ayas, D. (2024). Inhibition performance of almond shell hydrochar-based fish oil emulsion gel on *Klebsiella pneumoniae* inoculated fish skin and its characteristics. *International Journal of Biological Macromolecules, 264*, 130529.

Erdoğan Eliuz, E. A. (2022). Antibacterial activity and antibacterial mechanism of ethanol extracts of *Lentinula edodes* (Shiitake) and *Agaricus bisporus* (button mushroom). *International Journal of Environmental Health Research, 32*(8), 1828–1841.

Husain, M. S. B., Gupta, A., Alashwal, B. Y., & Sharma, S. (2018). Synthesis of PVA/PVP-based hydrogel for biomedical applications: A review. *Energy Sources, Part A: Recovery, Utilization, and Environmental Effects, 40*, 2388–2393.

Lim, Y. M., An, S. J., Kim, H. K., Kim, Y. H., Youn, M. H., Gwon, H. J., Shin, J., & Nho, Y. C. (2009). Preparation of hydrogels for atopic dermatitis containing natural herbal extracts by gamma-ray irradiation. *Radiation Physics and Chemistry, 78*, 441–444.

MM El-Sayed, W., M Elshaer, M., Ibrahim, H. A. H., & El-Metwaly, M. E. A. (2020). Antimicrobial agents from sea urchin (*Diadema setosum*) collected from the Red Sea, Egypt. *Egyptian Journal of Aquatic Biology and Fisheries, 24*(5), 33–51.

Muhammad, Y., Nur, F. U. A., & Sri, I. (2020). Optimization ultrasonic assisted extraction (UAE) of bioactive compound and antibacterial potential from sea urchin (*Diadema setosum*). *Current Research in Nutrition and Food Science, 8*, 556–569.

Murzina, S. A., Dgebuadze, P. Y., Pekkoeva, S. N., Voronin, V. P., Mekhova, E. S., & Thanh, N. T. (2021). Lipids and fatty acids of the gonads of sea urchin *Diadema setosum* (Echinodermata) from the coastal area of the Nha Trang Bay, Central Vietnam. *European Journal of Lipid Science and Technology, 123*, 2000321.

Mwangi, J., Hao, X., & Lai, R. (2019). Antimicrobial peptides: New hope in the war against multidrug resistance. *Zoological Research, 40*, 488–505.

Öztaş, N., Kara, E., Demir, D., Yetkin, D., Ceylan, S., & İyigündoğdu, Z. (2024). Biologically active sodium pentaborate pentahydrate and *Hypericum perforatum* oil loaded polyvinyl alcohol: Chitosan membranes. *International Journal of Biological Macromolecules, 269*, 132133.

Padang, A., Nurlina, N., Tuasikal, T., & Subiyanto, R. (2019). Kandungan gizi bulu babi (*Echinoidea*). *Agrikan: Jurnal Agribisnis Perikanan, 12*, 220–227.

Roncoroni, M., Martinelli, G., Farris, S., Marzorati, S., & Sugni, M. (2024). Sea urchin food waste into bioactives: Collagen and polyhydroxynaphthoquinones from *P. lividus* and *S. granularis*. *Marine Drugs, 22*, 163.

Shi, W., Wang, Z., Song, H., Chang, Y., Hou, W., Li, Y., & Han, G. (2022). High-sensitivity and extreme environment-resistant sensors based on PEDOT:PSS@PVA hydrogel fibers for physiological monitoring. *ACS Applied Materials & Interfaces, 14*(30), 35114–35125.

➢ *ORAL PRESENTATION*

The Effect of Ultrasonic-Assisted Cellulose Nanocrystalline Dispersion on the Epoxy Coating for Anti-Corrosion Resistance

Mohammed H. Aldulaimi [a] (0009-0008-3047-3569), Khaled M. Chahrour * [a](0000-0002-8799-3468), Hayrettin Ahlatçı [b] (0000-0002-6766-4974),Kenza Djebaria[b] (0000-0003-0158-4741)

a. Karabuk University, Faculty of Engineering, Mechanical Engineering Dept.78050, Karabuk, Turkey.
b. Karabuk University, Department of Metallurgical and Materials Engineering, ,78050, Karabuk, Turkey

*Corresponding author email: Khaledchahrour@karabuk.edu.tr

Abstract

This study explores the influence of ultrasonic-assisted dispersion of functionalized cellulose nanocrystalline (CNC) into epoxy matrix coatings on their anti-corrosion performance. The study shows a direct relationship between the regular dispersion of CNCs and the enhanced corrosion resistance of the resulting CNC/epoxy nanocomposite coatings. The request of high frequency ultrasonication remarkably improved the dispersion value, achieving a corrosion current rate (CR) of 5,437x10^{-3} mpy and a charge transfer resistance (R_{ct}) of 69,40x10^{3} Ω, both significantly superior to those observed in CNC/epoxy coatings prepared without ultrasonic treatment and in pristine epoxy matrix. The morphological, structural, and mechanical characteristics of the nanocomposite coatings were assessed through scanning electron microscopy (SEM), Fourier-transform infrared spectroscopy (FTIR), and microhardness testing. The findings demonstrate that a robust CNC-epoxy matrix interface enhances corrosion protection and mechanical properties.

Keywords: Nanocomposite Coating, Epoxy, Ultrasonic, Anti-corrosion Resistance.

1. Introduction

Epoxy resins are significantly employed as a protective barrier against metallic alloys due to their excellent mechanical strength, chemical resistance, and excellent adhesion properties. However, their inherent brittleness and susceptibility to microcracking can pose a risk to long-term anti-corrosion performance, specifically in environments with aggressive conditions. Current research has focused on improving the properties of epoxy coatings by integrating nanomaterials such as graphene, metal oxides, cellulose nanocrystals, and cellulose nanofibers with epoxy resin (Lin et al. 2022) (Dhoke et al. 2009) (Xu et al .2020)(Trache et al. 2024)

Recently, the opinion has been made that the perfect design of a nanocomposite involves nanoparticles, nanoplates, and nano crystallites dispersed homogeneously inside the epoxy resin, which could lead to an enhancement in their mechanical, thermal, and anticorrosion properties (Das et al. 2018). The dispersion state of these nanofillers has been the key challenge to reaching their full potential in enhancing their properties. To yield a high content with well-dispersed nanofillers, ultrasound-assisted mixing of the solution has evolved as one of the choices for the fabrication of epoxy nanocomposites with excellent properties (Zaghloul et al. 2023).

Cellulose nanocrystalline (CNC) is extracted from natural cellulose sources, exhibits remarkable mechanical strength, biodegradability, great aspect ratio, and surface benefits, making it a favourable candidate for eco-friendly reinforcement with epoxy (Habibi et al. 2010). Nevertheless, the effective dispersion of CNCs in an epoxy matrix remains one of the challenges due to their aggregation and tendency to cluster. Ultrasonic-assisted dispersion has been shown to be a reliable technique to overcome this restriction, promoting uniform spreading and strong matrix-cellulose nanocrystalline interfacial bonding (Wang et al. 2024).

This study aims to evaluate the influence of high-frequency ultrasonic technique on the dispersion of CNCs and their integrity with the epoxy matrix and the subsequent effect on the anti-corrosion properties of the nanocomposite CNC-epoxy coatings via electrochemical impedance spectroscopy (EIS) and potentiodynamic polarization (Tafel) measurements.

2. Experimental details

2.1. Preparation of nanocomposite CNC-epoxy Coatings

The epoxy resin was first mixed with functionalized CNCs at a particular weight percentage 2wt% CNCs, 3ml epoxy, and 1.5ml epoxy hardener Ethanol was used as a solvent and diluent for the epoxy at a rate of 5 ml. to accomplish efficient dispersion, the nanocomposite mixture suffered stirring and pursued an ultrasonic action at a frequency of 45 kHz for 30 minutes using a bath-type ultrasonicator. A reference sample was prepared without ultrasonic action for comparison. Subsequently, the hardener was added, and the formulations were applied onto pre-treated mild steel substrates using a standardized coating method. Curing was performed at ambient temperature for 48 hours. **Figure (1)** shows the effect of the ultrasonic waves approach on the dispersion of cellulose nanocrystals inside the epoxy matrix.

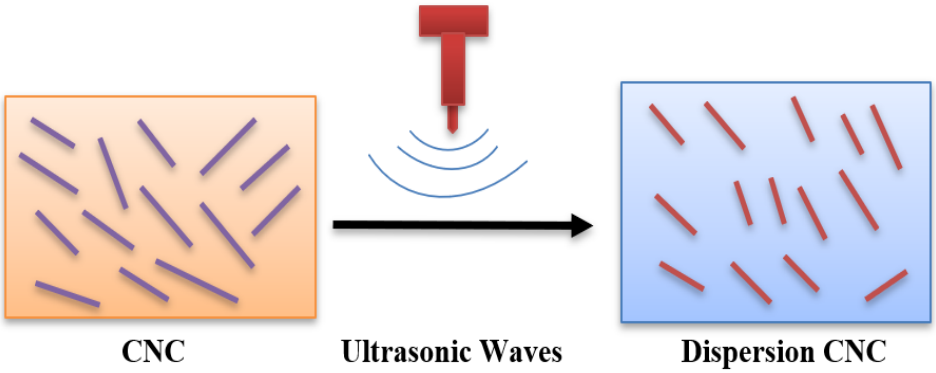

Figure 1: Effect of Ultrasonic-Assisted dispersion

2.2. Characterization Techniques

In this study, the micromorphology images were shown by means of a scanning electron microscope (A ZEISS Gemini SEM ULTRA PLUS) and recognizing chemical bonds in the molecules of nanocomposite material by generating an infrared absorption spectrum via applying Fourier transform infrared spectroscopy (Bruker ALPHA II, Bruker Corporation), and measure the microhardness of the prepared coating via Brinell test (A Qness Q10A from QATM).

2.3. Electrochemical measurements

Electrochemical characterization of the coated samples was performed using a three-electrode electrochemical cell linked to Potentiostate Framework (Gamry-Model 1000B) to evaluate their electrochemical behavior of the potentiodynamic polarization performance (Tefal plots) and the electrochemical impedance spectroscopy (Nyquist plots), both of which provided valuable insight into the protective capabilities of the coated samples.

3. Results and Discussion

3.1. Micromorphology Analysis

Figure 2 (a) shows the micromorphology of epoxy resin coating, which appears as regular homogeneity with micro-pores on its surface. **Figure 2 (b)** shows the micromorphology of the CNC-epoxy nanocomposite coating that was untreated by ultrasonication, which exhibited a dispersion of the CNC weave within the epoxy matrix, with lots of agglomeration places. **Figure 2 (c)** shows the micromorphology of the CNC-epoxy nanocomposite coating that was treated by ultrasonication, which revealed that the

ultrasonically dispersed CNC-treated sample exhibited a homogeneously distributed CNC weave within the epoxy matrix, with minimal agglomeration compared to untreated samples. Furthermore, the elemental composition involving the proper CNC within the epoxy matrix is accomplished via applying the Energy-dispersive X-ray spectroscopy spectra as shown in **Figure 2 (d)**. From micromorphology image results, high-frequency ultrasonic treatment proved critical for accelerating the break-up of CNC agglomerates and achieving better CNC dispersion.

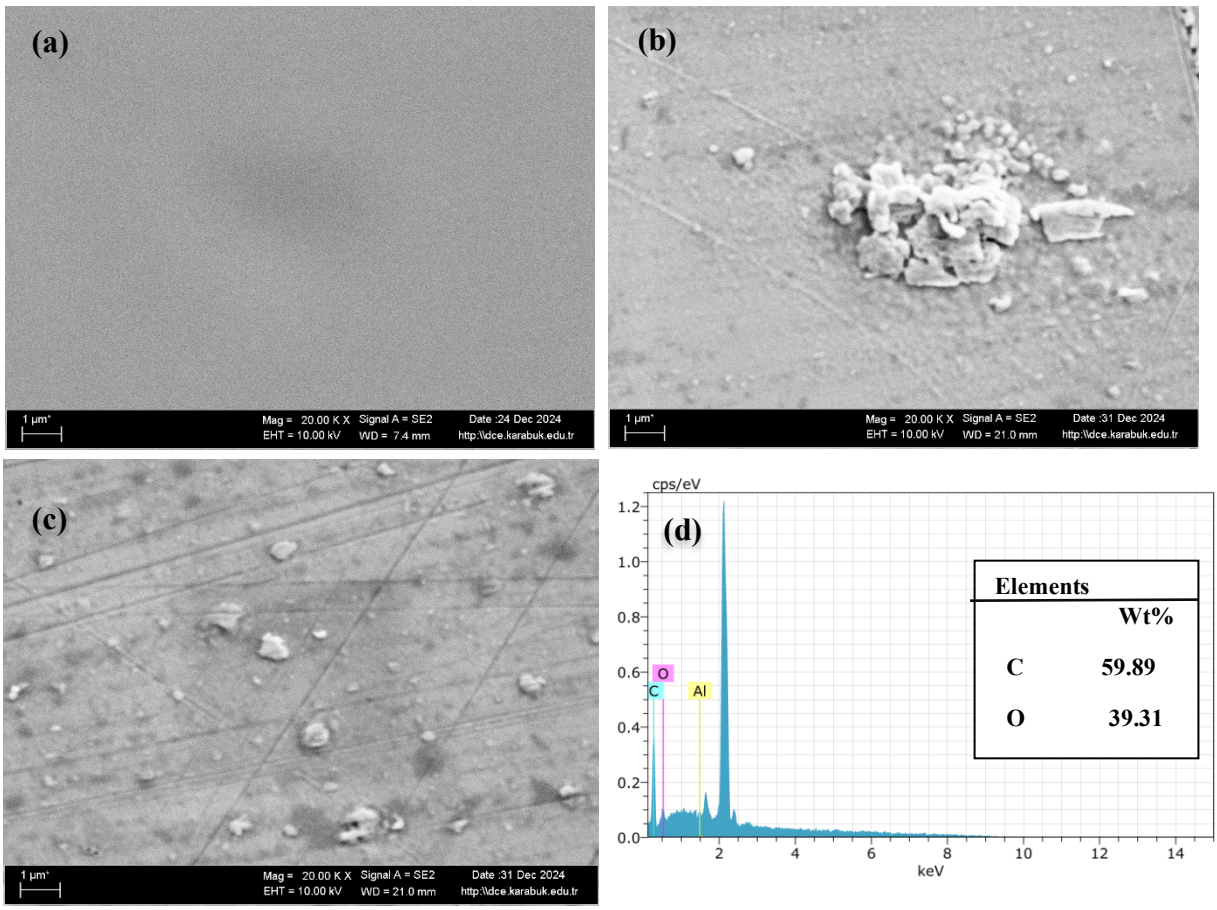

Figure 2. Images for SEM analysis (a) Epoxy coating, (b) EP+CNCs nanocomposite coating without Ultrasonics, **(c)** EP+CNCs nanocomposite coating with Ultrasonics, and (d) Energy-dispersive X-ray spectroscopy spectra

3.2. FTIR Analysis

To recognize chemical bonds in the molecules of the nanocomposite coating using the Fourier transform infrared spectroscopy (FTIR) spectra, as shown in **Figure 3**. Pure epoxy and epoxy/CNC nanocomposites samples were analyzed via FTIR spectra. The spectrum of the ~~epoxy matrix composite~~ shows a characteristic absorption at 857.7 cm^{-1}, indicating out-of-plane C-H vibrations, and at 505.7 cm^{-1}, indicating C-O-C bond vibrations, and representing moisture absorption(Muralishwara, et al. 2022). Significant changes in the absorption results were observed at 1017.8 cm^{-1} and 1296.4 cm^{-1}. These values were more pronounced in the epoxy/CNC nanocomposite, indicating the vibrations of the C-O-C and C-OH bonds in CNC (Reale Batista al.et 2018). This designates a chemical and physical interaction between the epoxy and CNC, as the results showed a decrease in intensity at 3392.4 cm^{-1} in the epoxy/CNC nanocomposite. This reflects the formation of hydrogen bonds between the OH in the CNC and the epoxy(Hu et al., 2021). This study found that the integration of the epoxy matrix with CNC leads to improved interactions between the compounds and improved material properties such as water resistance, durability, and corrosion resistance.

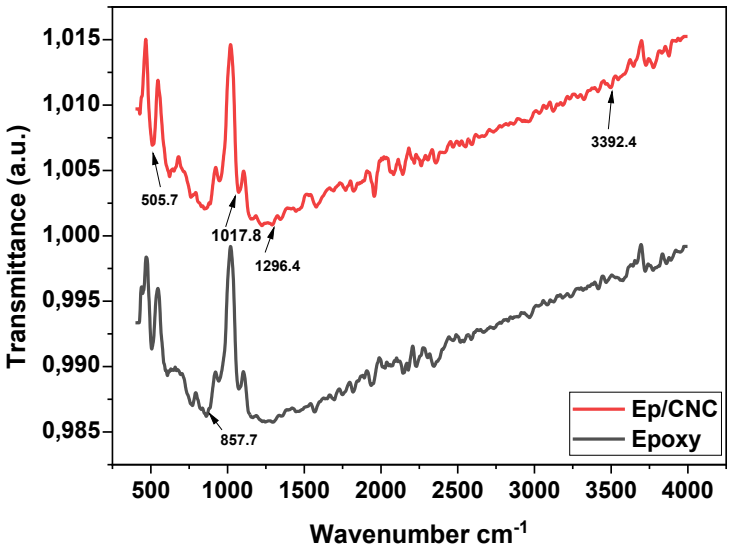

Figure 3 FTIR spectra of (Epoxy) (EP+CNCs)

3.3. Microhardness test

The microhardness test was performed, and the results were tabulated in **Table 1** for the pure epoxy, the CNCs/ Epoxy without Ultrasonic, and the CNCs/ Epoxy with Ultrasonic. The results showed that the hardness value of the sample coated with pure epoxy was 29.3 HV. When compared with the CNCs/Epoxy sample, the microhardness value increased to 32.4 HV. While CNCs/ Epoxy with Ultrasonic sample showed the highest value of the microhardness test results, around 34.8 HV. This indicates that the ultrasonic approach enhances the mechanical properties of the coating through the dispersion of the nanomaterial in a pure Epoxy matrix. These results are consistent with previous works of literature. (Mohamed, al.et. 2018).

Table (1) Microhardness Brinell test results for the pure epoxy, the CNCs/ Epoxy without Ultrasonic, and the CNCs/ Epoxy with Ultrasonic

600 HBW 1/ 30/ 20

- 20 — Duration Time of Test Force (s)
- 30 — Approximate Kgf Equivalent of Applied Test Force
- 1 — Ball Diameter in mm
- HBW — Hardness Symbol
- 600 — Brinell Hardness Value

No.	Coating Samples	Results of the Microhardness test (Average)
		Measurement
1	Epoxy	29,3 HV/0.2/15
2	EP+CNCs+WithoutUltrasonic	33,4 HV/0.2/15
3	EP+CNCs+WithUltrasonic	34,8 HV/0.2/15

3.4. Electrochemical Corrosion Performance

3.4.1. Potentiodynamic Polarization Performance (Tefal Curves)

The potentiodynamic polarization (Tefal) plots, as shown in **Figure (4)**, describe the electrochemical behavior in a corrosive environment. Tefal plots are used for studying the corrosion performance of coated samples. The electrochemical corrosion data of various coated samples are presented in **Table 2**. The pure epoxy-coated sample had the greatest corrosion current density Icorr = 106 nA/cm² and the most negative corrosion potential Ecorr = -725 mV, indicating the lowest corrosion resistance when compared to two other samples. The corrosion rate of 40,89 x 10^{-3} mpy further confirms that the pure epoxy-coated sample is very prone to electrochemical degradation. Within the Epoxy/CNC nanocomposite-coated sample without ultrasonics, improvement in corrosion resistance was attained. The corrosion current density is 46 nA/cm² and a notable corrosion potential of -534 mV, which shows a shift toward a positive potential. Its lower corrosion rate of 17,83 x 10^{-3} mpy, confirms that the presence of the CNCs is significantly effective as a reinforcement material for corrosion avoidance. The Epoxy/CNC nanocomposite coated sample with ultrasonics showed excellent corrosion resistance, with a corrosion current density of 14.10 nA/cm² and an impressive corrosion potential of -235 mV, which shows a significant shift toward a more positive potential. The corrosion rate decreased to 5.437 x 10^{-3} mpy, demonstrating superior corrosion protection compared to the results of the coated sample without ultrasonics. This indicates that the ultrasonic waves greatly disperse CNCs on the pure epoxy matrix, then prevent the agglomeration and microcracking trends, which is considered a critical rule to increasing the anti-corrosion route.

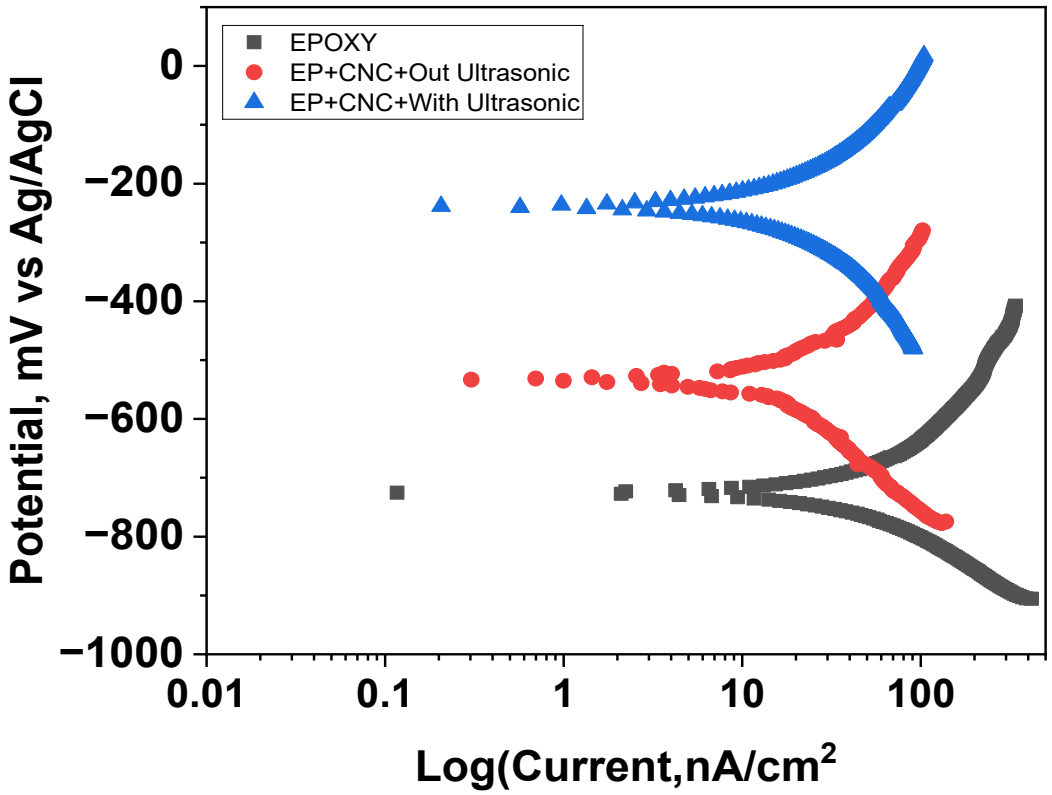

Figure 4 Tafel curves for pure epoxy, EP/CNC+Out Ultrasonic, EP+CNCs+With Ultrasonic

Table 2 Dynamic polarization results (TAFEL) for pure epoxy, EP/CNC+Out Ultrasonic, EP+CNCs+With Ultrasonic

Coated samples	icorr (nA/cm2)	Ecorr (mV)	Corrosion rate (mpy)
Pure Epoxy	106,0	-725,0	40,89e-3
EP+ CNC+Out ultrasonic	46,0	-534,0	17,83e-3
EP+CNC+with ultrasonic	14,10	-235	5,437e-3

3.4.2. Electrochemical Impedance Spectroscopy (EIS)

The electrochemical impedance spectroscopy (Nyquist plots), as presented in **Figure 5** (a, b, c), provides a comparative analysis of the electrochemical behavior in a corrosive environment. Nyquist plots are used for studying the corrosion performance of coated samples through building the equivalent circuit model using Gamry software, as shown in **Figure 5** (d). The equivalent circuit successfully fitted the experimental EIS data, including the coating resistance Rc, charge transfer resistance Rct, solution resistance Rs, constant phase element for the CPEc, and double-layer capacitance CPEdl of various coated samples, as presented in Table 3. The epoxy-coated sample shows low charge transfer resistance (Rct) with a value of 10.25 x 10^3 Ω, and a high CPEdl with a value of 25.73 x 10^{-5}(Masadeh .et al, 2005), indicating the formation of a double layer capacitance at the interface. These two values signify a poor ability to resist corrosion. The epoxy/CNC-coated sample without ultrasonics enhances corrosion resistance via improvement in Rct. Moreover, the increase in Rct with the value of 36.33 × 10^3 Ω and lowered CPEdl of 50.33 x 10^{-6}. represents approval of the influence of the CNCs with more compact, less porous, and excluding microcracking on the epoxy matrix, which denotes improving anti-corrosion. The epoxy/CNC-coated sample with ultrasonics enhances corrosion resistance with considerable improvement in Rct of 69.40 x 10^3 Ω, which contributes to superior corrosion resistance. The further decrease in CPEdl value of 23.48 x 10^{-6} (Zhu et al., 2024). indicates better barrier properties and less ionic mobility within the coated sample. These significant values of Rct and CPEdl compared to the coated sample without the ultrasonic treatment denote that ultrasonic waves contribute significantly to increasing corrosion resistance.

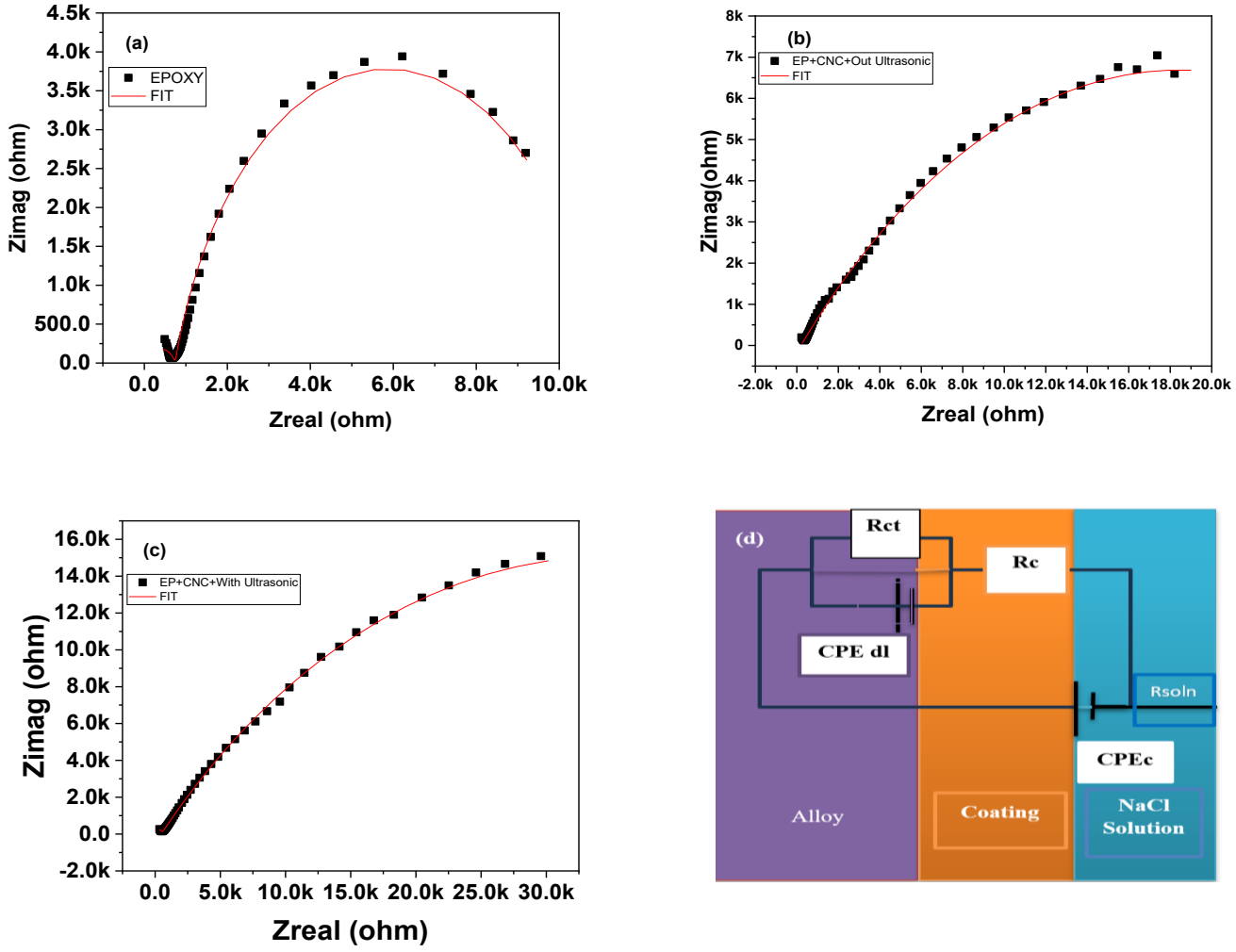

Figure 4 EIS curves (**A**) Nyquist curves for epoxy **(B)** Nyquist curve without ultrasonic **(C)** Nyquist curves with ultrasonic (D) Open circuit

Table 3 ELS analysis results for pure epoxy, EP/CNC+Out Ultrasonic, EP+CNCs+With Ultrasonic

Samples	Rc(Ω)	Rct(Ω)	Rs (Ω)	CPEc (Ω^{-1} s^n)	CPEdl (Ω^{-1} s^n)
Pure epoxy	623,5	10,25e3	121,3	241,3e-9	50,33e-6
EP+CNC+Out Ultrasonic	245,0	36,33e3	194,3	31,99e-6	25,73e-5
EP+CNC+with Ultrasonic	483,5	69,40e3	281,0e-9	3,169e-9	23,48e-6

5. Conclusions

This study highlights the capability of functionalizing the dispersion effectiveness of the cellulose nanocrystals (CNCs) for enhanced protective barriers in a pure epoxy matrix. Incorporating cellulose nanocrystals into the epoxy matrix via high frequency ultrasonic-assisted dispersion significantly improved the uniform distribution of CNCs in pure epoxy, creating a robust anti-corrosion barrier and defect-minimized nanocomposite coatings alongside a corrosive environment.

Acknowledgment

The authors gratefully acknowledge the financial support of this study from the scientific research projects coordination unit (BAP), Karabük University, under Grant No: KBÜBAP-24-YL-126.

References

1. Lin, D., Wang, X., Zhang, M., Yuan, S., Xu, F., Bao, D., & Wang, H. (2022). A robust and eco-friendly waterborne anti-corrosion composite coating with multiple synergistic corrosion protections. *Composites Part B: Engineering*, *232*, 109624. https://doi.org/10.1016/J.COMPOSITESB.2022.109624

2. Dhoke, S. K., & Khanna, A. S. (2009). Electrochemical behavior of nano-iron oxide modified alkyd based waterborne coatings. Materials Chemistry and Physics, 117(2 3), 550 556. https://doi.org/10.1016/J.MATCHEMPHYS.2009.07.010

3. Xu, H. Y., Lu, D., & Han, X. (2020). Graphene-induced enhanced anticorrosion performance of waterborne epoxy resin coating. Frontiers of Materials Science, 14(2), 211 220. https://doi.org/10.1007/S11706-020-0507-7/METRICS

4. Trache, D., Tarchoun, A. F., Abdelaziz, A., Bessa, W., Thakur, S., Hussin, M. H., … Thakur, V. K. (2024). A comprehensive review on processing, characteristics, and applications of cellulose nanofibrils/graphene hybrid-based nanocomposites: Toward a synergy between two-star nanomaterials. International Journal of Biological Macromolecules, 268, 131633. https://doi.org/10.1016/J.IJBIOMAC.2024.131633

5. Das, S., Halder, S., Sinha, A., Imam, M. A., & Khan, N. I. (2018). Assessing nanoscratch behavior of epoxy nanocomposite toughened with silanized fullerene. ACS Applied Nano Materials, 1(7), 3653 3662. https://doi.org/10.1021/ACSANM.8B00763/SUPPL_FILE/AN8B00763_SI_001.PDF

6. Zaghloul, M. M. Y., Zaghloul, M. M. Y., & Fuseini, M. (2023). Recent progress in Epoxy Nanocomposites: Corrosion, structural, flame retardancy and applications — A comprehensive review. Polymers for Advanced Technologies, 34(11), 3438 3472. https://doi.org/10.1002/PAT.6144

7. Habibi, Y., Lucia, L. A., & Rojas, O. J. (2010). Cellulose nanocrystals: Chemistry, self-assembly, and applications. Chemical Reviews, 110(6), 3479 3500. https://doi.org/10.1021/CR900339W/ASSET/CR900339W.FP.PNG_V03

8. Wang, X., Gao, K., Caldona, E. B., Ali, M. R. R., Zhang, X., & Zhang, Z. (2024). Cellulose nanocrystals-reinforced waterborne epoxy coatings with enhanced corrosion resistance for steel. International Journal of Biological Macromolecules, 257, 128755. https://doi.org/10.1016/J.IJBIOMAC.2023.128755

9. Muralishwara, K., Sudhakar, Y. N., Kini, U. A., Sharma, S., & Gurumurthy, B. M. (2022). Moisture absorption and spectroscopic studies of epoxy clay nanocomposite. Polymer Bulletin, 79(7), 5587 5611. https://doi.org/10.1007/S00289-022-04200-7

10. Reale Batista, M. D., & Drzal, L. T. (2018). Carbon fiber/epoxy matrix composite interphases modified with cellulose nanocrystals. Composites Science and Technology, 164, 274 281. https://doi.org/10.1016/J.COMPSCITECH.2018.05.010

11. Hu, J., Kong, Z., Liu, K., Qin, J., Tao, Y., Zhou, L., … Zhang, J. (2021). An Efficient and Sustainable Approach to Prepare Carboxylated Cellulose Nanocrystals for Rubber Reinforcement Featuring Dual Crosslinking Networks. https://doi.org/10.21203/RS.3.RS-585397/V1

12. Mohamed, Y. S., El-Gamal, H., & Zaghloul, M. M. Y. (2018). Micro-hardness behavior of fiber reinforced thermosetting composites embedded with cellulose nanocrystals. Alexandria Engineering Journal, 57(4), 4113 4119. https://doi.org/10.1016/J.AEJ.2018.10.012

13. Masadeh, S. (2005). Electrochemical impedance spectroscopy of epoxy-coated steel exposed to dead sea water. Journal of minerals and Materials Characterization and Engineering, 4(2), 75-84. https://doi.org/10.4236/JMMCE.2005.42007

14. Zhu, W., Li, X., Liu, X., Bai, L., Wang, X., Li, A., … Nan, D. (2024). Enhancing the corrosion resistance of waterborne epoxy coatings with functionalized biochar. RSC Advances, 14(53), 39747 39758. https://doi.org/10.1039/D4RA07421A

➢ *ORAL PRESENTATION*

Neural network-driven perturbation and observation method for global maximum power point tracking in PV systems

Hatice Gül Sezgin-Ugranlı (*ORCID: https://orcid.org/0000-0003-1711-7806*)

Izmir Bakircay University, Department of Electrical-Electronics Engineering, Izmir, Türkiye.

Corresponding author e-mail: haticegul.ugranli@bakircay.edu.tr

Abstract
Accurate and rapid tracking of the global maximum power point in photovoltaic systems under partial shading conditions remains a critical challenge. In this study, an artificial neural network-assisted voltage reference-guided perturb and observe method is proposed to enhance global maximum power point tracking performance. Twelve irradiance inputs, representing segmented regions of the photovoltaic module, are classified into global maximum power point voltage bands using a feedforward artificial neural network trained on a large irradiance dataset generated through thirty different distribution profiles. The predicted voltage reference is subsequently utilized as a guidance signal, around which the classical perturb and observe algorithm operates to adjust the operating point of the photovoltaic system. Simulation results under dynamically varying irradiance conditions demonstrate that the proposed method significantly outperforms the conventional perturb and observe algorithm in both locating the global operating voltage and maximizing power extraction. The voltage reference-guided strategy rapidly identifies and stabilizes within the appropriate voltage bands, thereby minimizing energy losses and reducing steady-state oscillations. Furthermore, the normalized performance index achieved using the artificial neural network-predicted reference voltage closely approaches the ideal global maximum power point tracking scenario. These findings suggest that the proposed method offers a computationally efficient and highly robust solution, particularly suitable for optimizer-type photovoltaic systems that require fast and reliable global maximum power point tracking.
Keywords: Global maximum power point tracking, Perturb and Observe, Voltage reference, Partial shading, Photovoltaic systems.

INTRODUCTION

The increasing demand for clean and sustainable energy has positioned photovoltaic (PV) systems as a vital component in modern power generation. However, the inherently nonlinear current-voltage (I-V) characteristics of PV arrays (Olayiwola et al., 2024), combined with their dependence on dynamic environmental conditions such as solar irradiance and temperature, necessitate the continuous optimization of their operating point. Maximum Power Point Tracking (MPPT) algorithms play a crucial role in ensuring that PV systems extract the maximum available power under all operating conditions (Abidi et al., 2023).

Among various MPPT strategies, classical methods such as Perturb and Observe (P&O) and Incremental Conductance (IncCond) are the most widely adopted due to their simplicity, ease of implementation, and minimal computational requirements (Rezk et al., 2017; Mao et al., 2020). Nevertheless, these conventional algorithms exhibit several limitations, especially under rapidly changing atmospheric conditions or partial shading scenarios. Specifically, the P&O method often suffers from steady-state oscillations around the maximum power point (MPP) (Eltawil & Zhao, 2013) and may experience slow convergence or incorrect tracking (Devarakonda et al., 2022) when abrupt changes in irradiance occur.

In practical PV systems, bypass diodes are integrated into modules to mitigate the adverse effects of partial shading and to protect individual cells from damage due to reverse bias conditions. When shading occurs, bypass diodes conduct current around shaded sections, preventing hotspots and significant power losses. However, the activation of bypass diodes introduces multiple local maxima on the P-V curve, complicating the task of MPPT algorithms (Murtaza et al., 2014). Classical methods like P&O, which typically rely on local gradient information, may become trapped in a local maximum rather than locating the true global MPP (Winston et al., 2018). This increases the complexity of achieving optimal power extraction and highlights the need for more sophisticated tracking strategies capable of coping with such multi-peak scenarios.

To address the inherent challenges of conventional MPPT approaches, a wide variety of enhancements have been explored in recent years. Adaptive step-size techniques have been introduced to accelerate convergence while minimizing oscillations around the operating point by dynamically adjusting the perturbation magnitude according to system conditions (Amir et al., 2017; Soni et al., 2023; Zhou et al., 2021). In addition, variable step-size methods combined with perturbation suppression strategies have been proposed to avoid unnecessary oscillations when the system is operating near the true MPP (Harrison et al., 2022).

Hybrid strategies, which combine features from multiple MPPT methods, have been developed to improve robustness across diverse environmental scenarios. For instance, the integration of fuzzy logic controllers with classical algorithms has enabled more intelligent decision-making by replacing crisp thresholds with gradual transition rules (Rezoug et al., 2018). Metaheuristic optimization techniques, including particle swarm optimization (PSO), grey wolf optimization (GWO), and genetic algorithms (GA), have also been extensively investigated for global maximum power point (GMPP) tracking, particularly under partial shading scenarios where multiple local maxima exist (Naseem et al., 2021; Xiao et al., 2025; Yousaf et al., 2025). These algorithms are capable of escaping local optima and exploring the search space more effectively than gradient-based methods. Furthermore, model predictive control (MPC) frameworks (Priyadarshi et al., 2025; Li et al., 2025) have been proposed to anticipate future system behavior and optimize control actions accordingly, leading to improved transient and steady-state responses. By formulating an optimization problem over a prediction horizon, MPC-based MPPT approaches offer predictive adjustment of the operating point, enhancing tracking performance under dynamic environmental variations.

Artificial neural networks (ANNs) have also been widely employed to improve MPPT performance, especially under complex and rapidly changing operating conditions. ANN-based methods can learn the nonlinear relationship between environmental parameters (such as irradiance and temperature) and the optimal operating point, enabling fast and direct estimation of the MPP without iterative perturbations (Roy et al., 2021; Kota & Bhukya, 2019). While ANNs can significantly speed up tracking and reduce steady-state oscillations, their effectiveness strongly depends on the quality and comprehensiveness of the training data, and they may require retraining if the system characteristics change. As a result, there remains a significant interest in developing MPPT strategies that balance enhanced performance.

In this study, an ANN-assisted voltage reference-guided P&O method is developed to improve global MPPT performance in PV systems subjected to partial shading conditions. A detailed irradiance scenario generation framework is introduced, enabling the classification of segmented irradiance inputs into distinct global MPP voltage bands. A feedforward ANN is trained to predict the appropriate reference voltage cluster based on these irradiance profiles. The predicted reference voltage is subsequently used to guide a classical P&O algorithm. The effectiveness of the proposed method is validated through comprehensive simulations under dynamically varying irradiance profiles, and its performance is compared against conventional P&O and ideal reference-guided tracking.

GENERATION OF INPUT IRRADIANCE PROFILES

Accurately modeling the spatial variability of solar irradiance across PV modules is crucial for a performance evaluation, especially under non-uniform operating conditions. In order to represent such variability, the PS-M72-405 PV module, consisting of 72 series-connected cells and three integrated bypass diodes, is selected as the reference module for the simulations. To emulate localized irradiance variations across the module surface, a segmentation approach is adopted whereby every six cells are assigned a distinct irradiance value, resulting in twelve independent irradiance inputs per scenario. A total of 30,000 unique irradiance scenarios are generated to comprehensively cover a wide range of environmental conditions and module responses.

The irradiance values for each scenario are drawn according to thirty distinct sampling profiles, as illustrated in Figure 1. These profiles are designed to follow uniform random distributions with varying weightings across the irradiance range of 100 W/m² to 1000 W/m². Specific profiles emphasized low irradiance conditions, high irradiance conditions, or introduced mid-range dominance, thereby capturing different degrees of shading, partial cloud cover, and clear-sky conditions. Each histogram depicted in Figure 1 corresponds to a different irradiance distribution pattern used in the generation process. This

structured variability ensures that the generated dataset provides a rigorous testing environment for subsequent MPPT evaluations.

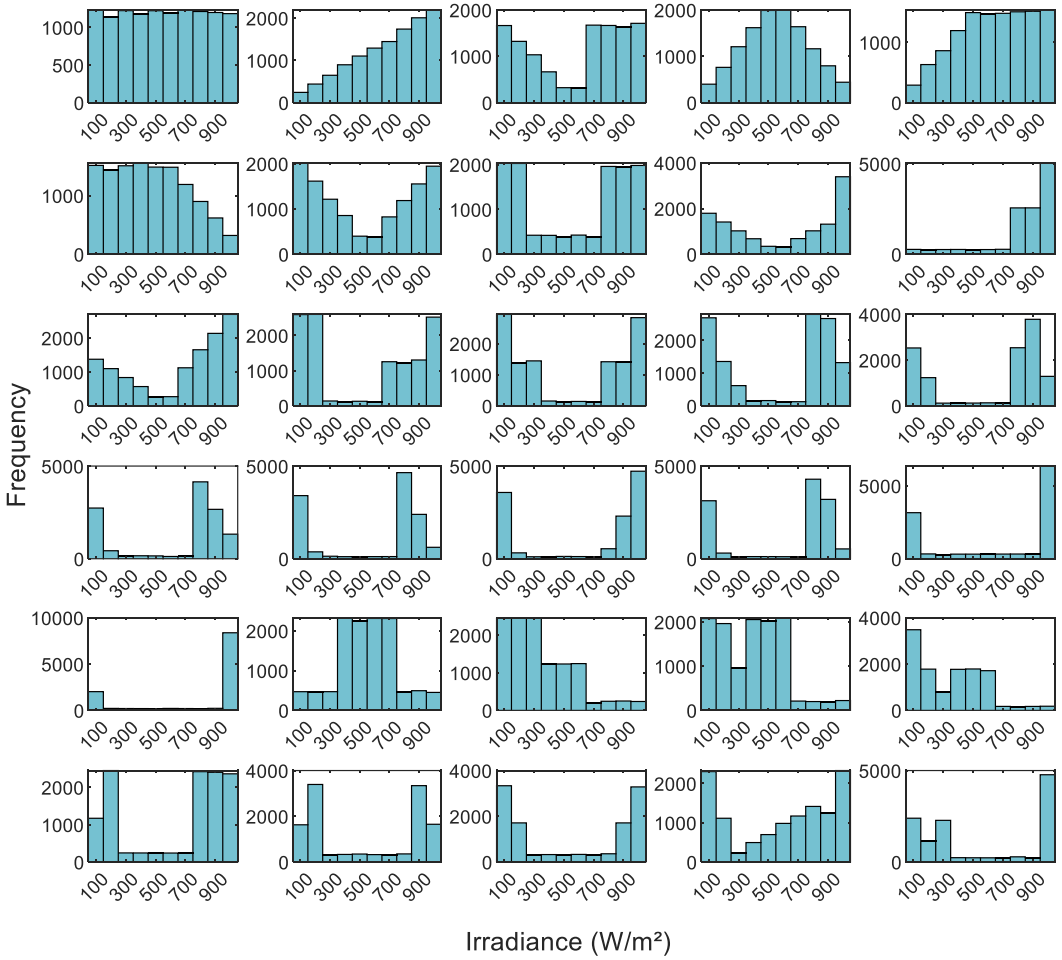

Figure 1. Histogram visualization of input irradiance variability

DETERMINATION OF GLOBAL MAXIMUM POWER POINT VOLTAGES

To determine the global MPP voltages under the generated irradiance scenarios, detailed simulations are conducted using the Simscape Solar Cell model within the MATLAB/Simulink environment (MathWorks, 2023a). The Solar Cell block provides a physics-based representation of a PV cell by solving the nonlinear I–V characteristics according to the single-diode equivalent circuit model (MathWorks, 2023b). Key parameters such as photocurrent, saturation current, series resistance, shunt resistance, and temperature-dependent effects are inherently incorporated, enabling highly accurate electrical behavior modeling under varying irradiance and temperature conditions. Throughout all simulations, the module temperature is assumed to be constant at 45 °C.

In the simulation framework, each irradiance scenario is fed into a set of Solar Cell blocks corresponding to the module's segmented structure. For each scenario, the full I–V curve is generated by systematically sweeping the terminal voltage across the operational range. From the resulting I–V characteristics, the global MPP is identified by locating the voltage corresponding to the highest product of current and voltage. The extracted global MPP voltages from all 30,000 irradiance scenarios are then statistically analyzed to assess their distribution and clustering behavior. Figure 2 presents the histogram of the global MPP voltages obtained from the simulations, while Table 1 summarizes the statistical properties of the identified voltage clusters.

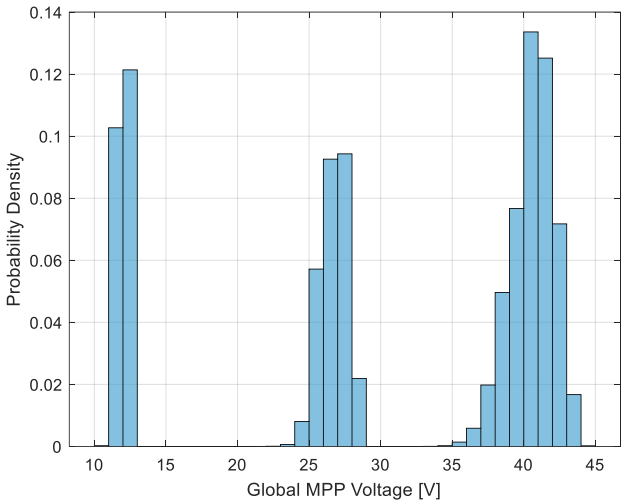

Figure 2. Histogram of global MPP voltages

As depicted in Figure 2, the global MPP voltages predominantly fall into three distinct bands centered around approximately 12 V, 27 V, and 39 V. This clear band formation is indicative of the module's intrinsic structural configuration combined with the effects of partial shading patterns and the activation of bypass diodes. Specifically, the first band, located around 12 V, corresponds to scenarios where two bypass diodes are conducting, effectively isolating a major portion of the module from active power generation. The second band, centered near 27 V, represents intermediate shading conditions in which one bypass diode is activated, partially limiting the module's contribution to the overall output. Finally, the third band, observed around 39 V, reflects near-uniform irradiance conditions where no bypass diodes are triggered, allowing the entire module to contribute fully to power production

Table 1 provides a detailed statistical characterization for each cluster, including expected value, standard deviation, variance, and median. The relatively low standard deviations within each cluster highlight the consistency of global MPP voltages under similar shading conditions, further validating the strong banded behavior observed in the histogram.

Table 1. Interval-based statistical summary of MPP voltage

	Expected value	Standard deviation	Variance	Median
Cluster 1	12.05	0.36	0.13	12.02
Cluster 2	26.71	0.94	0.89	26.78
Cluster 3	38.83	0.92	0.85	39.00

DEVELOPMENT OF THE ANN-BASED IRRADIANCE PROFILE CLASSIFIER

Accurately and rapidly identifying the operating voltage corresponding to the global MPP under diverse irradiance conditions is critical for efficient PV system operation. To achieve this, an ANN model is developed to directly map input irradiance profiles to predefined global MPP voltage clusters as shown in Figure 3. The input to the ANN consists of twelve irradiance values, each representing the irradiance received by every six-cell segment of the PV module. The output is defined as the corresponding global MPP voltage cluster, categorized into three distinct bands previously identified through statistical analysis.

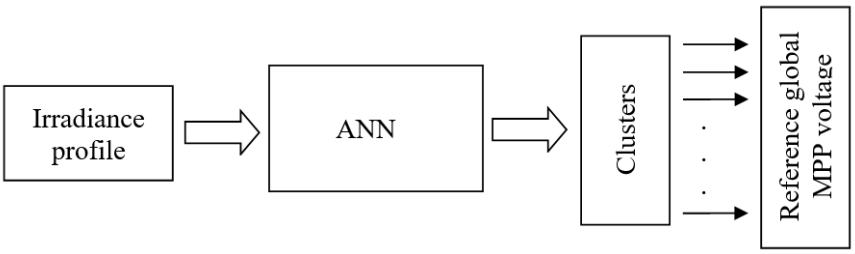

Figure 3. Voltage reference mapping using ANN-based irradiance profile classification

For training the ANN, a large dataset is prepared by combining multiple irradiance scenarios generated under thirty different distribution profiles. Each input vector is normalized using min-max scaling to improve the training performance and convergence rate. The output labels are discretized into three classes based on the GMPP voltage bands, and one-hot encoding is applied to structure the classification targets appropriately. The network architecture employs a feedforward pattern recognition structure comprising three hidden layers with 40, 32, and 32 neurons, respectively. A cross-entropy loss function is utilized as the optimization objective, and the network is trained using a backpropagation algorithm for 1000 epochs. An independent external test dataset consisting of 6000 samples is constructed similarly for final evaluation. Following training, the performance of the ANN is evaluated through various metrics. The evolution of the cross-entropy loss over epochs demonstrates stable and consistent convergence behavior. Additionally, prediction confidence is analyzed over the test dataset, with most samples achieving a confidence level close to 1. The resulting classification accuracy on the independent test set exceeds 93%, indicating robust generalization capability of the trained model. Figure 4 presents the distribution of prediction confidences for the test samples.

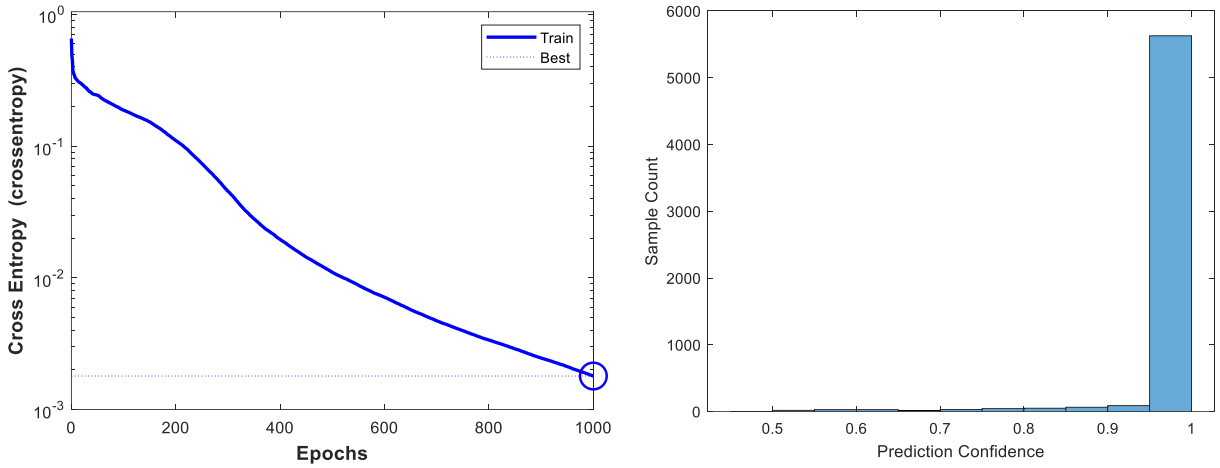

Figure 4. (a) Training performance based on cross entropy, (b) Prediction confidence for test data

IMPLEMENTATION AND PERFORMANCE EVALUATION OF THE PROPOSED METHOD

The final stage of the study involves the implementation of the proposed global MPPT strategy within the MATLAB/Simulink environment. The overall system structure is depicted in Figure 5. In this setup, the irradiance profile, representing the segmented irradiance levels across the PV module, is fed into a trained ANN. The ANN then predicts the global MPP voltage cluster based on the irradiance input. This predicted voltage reference is subsequently utilized as a guidance signal by the DC-DC converter, around which the classical P&O algorithm operates to adjust the operating point of the PV system.

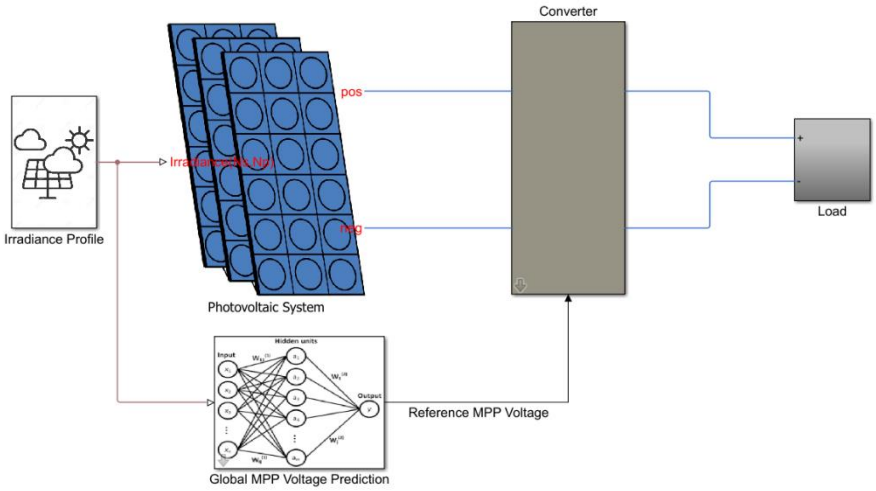

Figure 5. Global MPPT system implemented in MATLAB/Simulink

To evaluate the effectiveness of the proposed voltage reference-guided MPPT approach, three different operational cases are considered:

- The classical P&O method.
- The voltage reference-guided P&O method using the ANN-predicted reference voltages.
- An idealized voltage reference-guided P&O method using the true GMPP voltages obtained directly from exhaustive offline analysis.

Figures 6 and 7 present the dynamic behavior of the PV system under classical perturb and observe (P&O) MPPT control. In Figure 6(a), which shows the voltage profile over the first 10 samples, it is evident that the P&O algorithm adjusts the operating voltage gradually through discrete perturbations. The inset magnifies a region where small oscillations occur around the MPP. Over the full dataset, as seen in Figure 6(b), the voltage trajectory exhibits substantial fluctuations, particularly under rapidly changing irradiance conditions. This behavior highlights the classical P&O method's inherent limitation, as it often fails to stabilize at the true global MPP due to its reliance on local gradient information.

Correspondingly, Figure 7 illustrates the instantaneous power output of the system under classical P&O control. In Figure 7(a), stepwise variations in output power align with the perturbation steps observed in the voltage profile. However, over the entire dataset shown in Figure 7(b), the power output exhibits pronounced fluctuations and frequent power losses, primarily resulting from the algorithm's inability to rapidly and reliably track the true global MPP under partial shading scenarios.

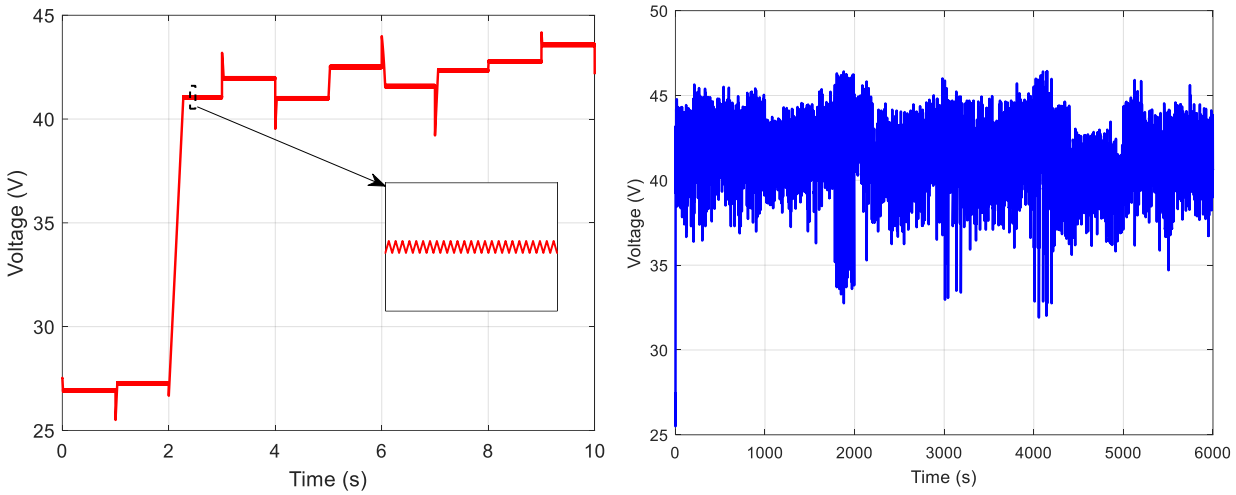

(a) (b)

Figure 6. Voltage profile of the PV system under P&O MPPT: (a) first 10 samples, (b) entire dataset

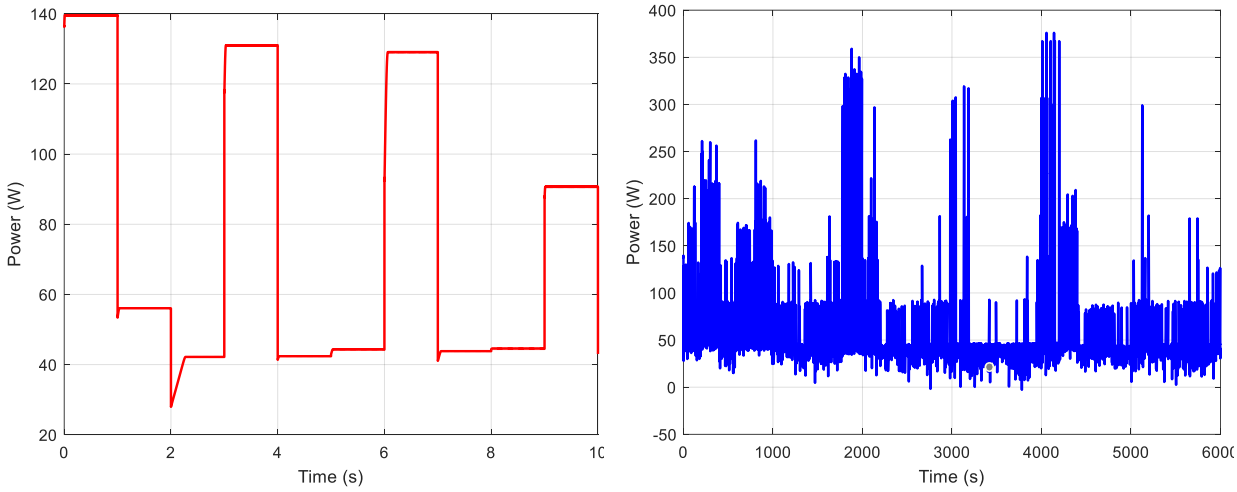

(a) (b)

Figure 7. Instantaneous power output of the PV system under P&O MPPT: (a) first 10 samples, (b) entire dataset

In contrast, Figures 8 and 9 demonstrate the system performance when the voltage reference-guided P&O method is employed. Figure 8(a) shows that the system rapidly steps toward the artificial neural network-predicted reference voltage without the need for extensive perturbation, leading to faster convergence and more accurate voltage tracking. Unlike the classical P&O method, the proposed strategy accurately identifies and stabilizes within the distinct voltage bands associated with the global MPPs. Over the full dataset, as presented in Figure 8(b), the voltage profile remains significantly more stable, with discrete transitions that correspond directly to changes in the irradiance conditions rather than continuous oscillatory behavior around local operating points.

Similarly, Figure 9 presents the corresponding instantaneous power output results. In Figure 9(a), it is observed that the system promptly reaches high power levels following irradiance transitions, reflecting the effectiveness of the voltage reference in guiding the MPPT process. Over the full dataset shown in Figure 9(b), the power output maintains a consistently higher average level with substantially reduced fluctuations compared to the classical P&O method.

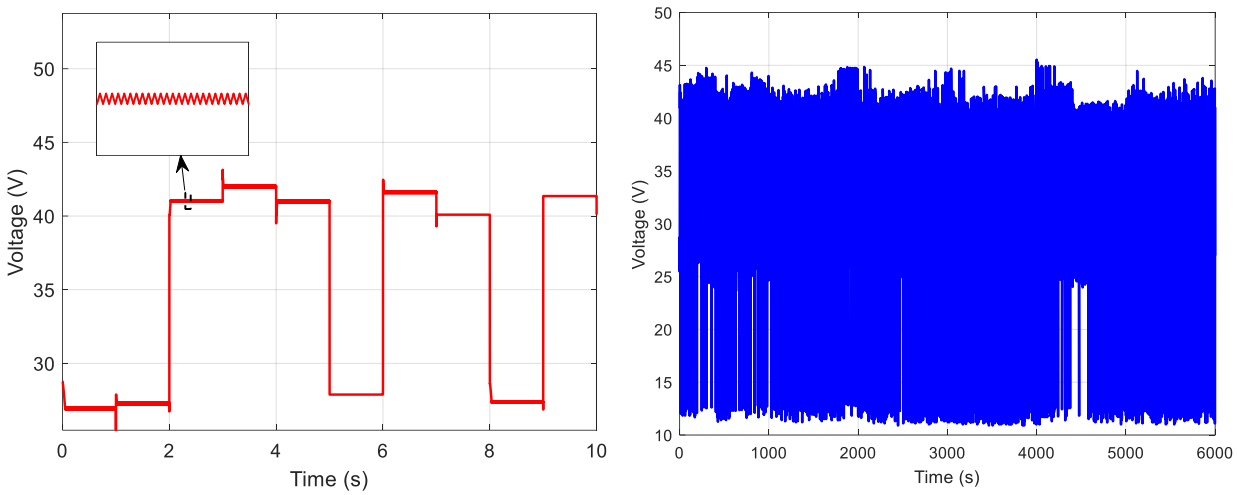

(a) (b)

Figure 8. Voltage profile of the PV system under voltage reference-guided P&O: (a) first 10 samples, (b) entire dataset

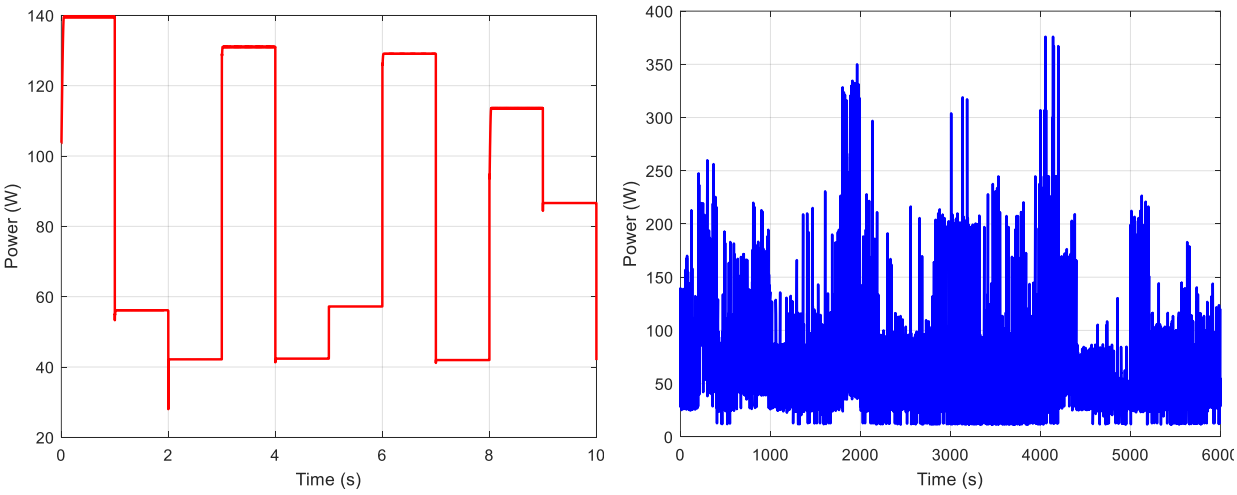

(a) (b)

Figure 9. Instantaneous power output of the PV system under voltage reference-guided P&O: (a) first 10 samples, (b) entire dataset

To quantitatively assess the tracking performance, a normalized performance index is defined according to the following equation:

$$Normalized\ performance\ index = \frac{1}{P_{rated}^{1000W/m^2,\ 25°C}} \int_0^t P_{out}(\tau) d\tau$$

where $P_{rated}^{1000W/m^2,\ 25°C}$ denotes the rated output power of the PV system under standard test conditions, and $P_{out}(\tau)$ represents the instantaneous output power at time τ. Figure 10 compares the evolution of the normalized performance index over the entire simulation horizon for the three strategies. As clearly observed, the voltage reference-guided P&O method using the ANN prediction closely follows the ideal case with minimal deviation, demonstrating a significant improvement over the classical P&O method. In contrast, the classical P&O control exhibits substantial performance degradation, particularly under rapidly varying irradiance conditions, due to its inherent local search mechanism and inability to relocate the global MPP efficiently. These results highlight the effectiveness of the proposed ANN-assisted voltage reference-guided strategy in achieving near-optimal global power tracking performance while maintaining simplicity and low computational burden.

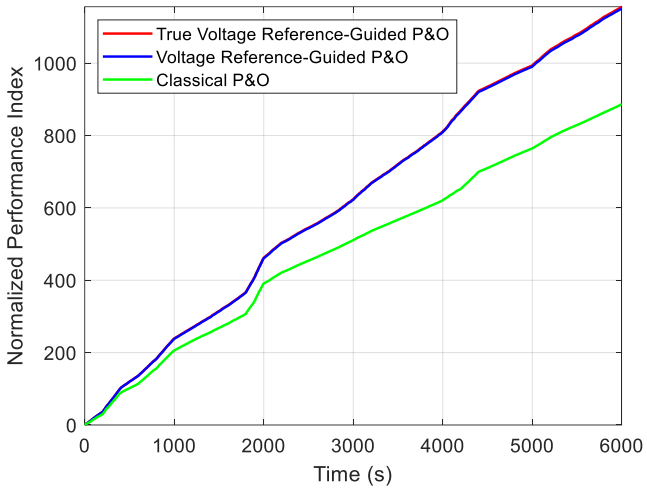

Figure 10. Normalized performance index comparison

CONCLUSION

This study presents an ANN-assisted voltage reference-guided MPPT strategy to address the limitations of classical P&O algorithms under partial shading conditions. By classifying irradiance inputs into distinct voltage bands corresponding to the global MPP, the proposed method enables the system to rapidly relocate and stabilize at near-optimal operating points. Simulation results demonstrate that the voltage reference-guided perturb and observe method significantly improves voltage tracking accuracy and power extraction compared to the conventional perturb and observe method, particularly under dynamically changing irradiance profiles. The normalized performance index achieved using the ANN predictions closely matches the ideal GMPP tracking scenario, highlighting the robustness and effectiveness of the approach. Given its simplicity, low computational burden, and strong tracking performance, the proposed method offers a promising alternative for optimizer-type photovoltaic systems, particularly those operating in environments prone to partial shading.

REFERENCES

Abidi, H., Sidhom, L., & Chihi, I. (2023). Systematic Literature Review and Benchmarking for Photovoltaic MPPT Techniques. Energies, 16(8), 3509.

Amir, A., Amir, A., Selvaraj, J., Rahim, N. A., & Abusorrah, A. M. (2017). Conventional and modified MPPT techniques with direct control and dual scaled adaptive step-size. *Solar Energy*, 157, 1017–1031.

Devarakonda, A. K., Karuppiah, N., Selvaraj, T., Balachandran, P. K., Shanmugasundaram, R., & Senjyu, T. (2022). A Comparative Analysis of Maximum Power Point Techniques for Solar Photovoltaic Systems. *Energies*, 15(22), 8776.

Eltawil, M. A., & Zhao, Z. (2013). MPPT techniques for photovoltaic applications. *Renewable and Sustainable Energy Reviews*, 25, 793–813.

Harrison, A., Nfah, E. M., Ndongmo, J. D. D. N., & Alombah, N. H. (2022). An enhanced P&O MPPT algorithm for PV systems with fast dynamic and steady-state response under real irradiance and temperature conditions. *International Journal of Photoenergy*, 2022, Article ID 6009632.

Kota, V. R., & Bhukya, M. N. (2019). A novel global MPP tracking scheme based on shading pattern identification using artificial neural networks for photovoltaic power generation during partial shaded condition. *IET Renewable Power Generation*, 13(10), 1647–1659.

Li, Z., Dewantoro, G., Xiao, T., & Swain, A. (2025). A comparative analysis of fuzzy logic control and model predictive control in photovoltaic maximum power point tracking. *Electronics*, 14(5), 1009.

Mao, M., Cui, L., Zhang, Q., Guo, K., Zhou, L., & Huang, H. (2020). Classification and summarization of solar photovoltaic MPPT techniques: A review based on traditional and intelligent control strategies. Energy Reports, 6, 1312–1327.

MathWorks, (2023a). Simscape Electrical – Modeling and Simulating Electrical Systems. Available at: https://www.mathworks.com/products/simscape-electrical.html [27.04.25].

MathWorks, (2023b). Solar Cell block – Simscape Electrical. Available at: https://www.mathworks.com /help/physmod/sps/ref/solarcell.html [27.04.25].

Murtaza, A., Chiaberge, M., Spertino, F., Boero, D., & De Giuseppe, M. (2014). A maximum power point tracking technique based on bypass diode mechanism for PV arrays under partial shading. *Energy and Buildings*, 73, 13–25.

Naseem, M., Husain, M. A., Minai, A. F., Khan, A. N., Amir, M., & Kumar, J. D. (2021). Assessment of meta-heuristic and classical methods for GMPPT of PV system. *Transactions on Electrical and Electronic Materials*, 22(3), 217–234.

Olayiwola, T. N., Hyun, S.-H., & Choi, S.-J. (2024). Photovoltaic Modeling: A Comprehensive Analysis of the I–V Characteristic Curve. Sustainability, 16(1), 432.

Priyadarshi, N., Sanjeevikumar, P., Bhaskar, M. S., Azam, F., & Muyeen, S. M. (2025). An improved standalone photovoltaic system with hybrid dual integral sliding mode and model predictive control for MPPT. *IET Renewable Power Generation*, 19(1), e12665.

Rezk, H., Fathy, A., & Abdelaziz, A. Y. (2017). A comparison of different global MPPT techniques based on meta-heuristic algorithms for photovoltaic system subjected to partial shading conditions. Renewable and Sustainable Energy Reviews, 74, 377–386.

Rezoug, M. R., Chenni, R., & Taibi, D. (2018). Fuzzy logic-based perturb and observe algorithm with variable step of a reference voltage for solar permanent magnet synchronous motor drive system fed by direct-connected photovoltaic array. *Energies*, 11(2), 462.

Roy, R. B., Rokonuzzaman, M., Amin, N., Mishu, M. K., Alahakoon, S., Rahman, S., Mithulananthan, N., Rahman, K. S., Shakeri, M., & Pasupuleti, J. (2021). A comparative performance analysis of ANN algorithms for MPPT energy harvesting in solar PV system. *IEEE Access*, 9, 102137–102147.

Soni, A. K., Jana, K. C., & Gupta, D. K. (2023). Variable step-size adaptive maximum power point tracking algorithm for solar cell under partial shading conditions. *IETE Journal of Research*, 69(3), 1562–1577.

Winston, D. P., Kumar, B. P., Christabel, S. C., Chamkha, A. J., & Sathyamurthy, R. (2018). Maximum power extraction in solar renewable power system – a bypass diode scanning approach. *Computers and Electrical Engineering*, 70, 122–136.

Xiao, W., Dong, N., & He, K. (2025). A hybrid global wolf pack algorithm-based incremental conductance method under partial shading conditions. *Solar Energy*, 291, 113388.

Yousaf, M. Z., Koondhar, M. A., Zaki, Z. A., Ahmed, E. M., Alaas, Z. M., Mahariq, I., & Guerrero, J. M. (2025). Improved MPPT of solar PV systems under different environmental conditions utilizes a novel hybrid PSO. *Renewable Energy*, 244, 122709.

Zhou, J., Zhang, Y., Zhang, S., Guo, Y., Yang, Z., Feng, W., & Zhang, Y. (2021). A novel maximum power point tracking strategy based on enhanced real-time adaptive step-size modified control for photovoltaic systems. *Frontiers in Energy Research*, 9, Article 685415.

➢ *ORAL PRESENTATION*

Electrochemical determination of phosphate by measuring the phosphomolybdate complex using a reduced graphene oxide-doped with copper ions carbon paste electrode (rGO@Cu/CPE) sensor

Qëndresa Istrefi[1*] (*ORCID: https://orcid.org/0009-0004-7240-2874),* Nevila Broli[1] (*ORCID: https://orcid.org/0000-0003-4240-6474*) , Loreta Vallja[1] (ORCID: https://orcid.org/0000-0003-0930-1064).

[*1]University of Tirana, Faculty of Natural Sciences, Department of Chemistry, Tirana, Albania.

Abstract

Phosphate is considered an important biogenic element and a key contributor to eutrophication in aquatic ecosystems, existing in both dissolved and adsorbed forms. There is a growing need for inexpensive, portable, repeatable, highly sensitive, and field-deployable sensors with a wide detection range to monitor the quality of food and environmental samples. This work aims to develop an electrochemical phosphate sensor using a carbon paste electrode modified with reduced graphene oxide doped with copper ions (rGO@Cu/CPE) for phosphate detection, with the goal of achieving high sensitivity, a broad detection range, simplicity, and high repeatability. Phosphate was quantified by a voltammetric technique through the electrochemical reduction of the molybdophosphate complex in a 0.05 mol L^{-1} sulfuric acid (H_2SO_4) solution. The analytical parameters, including the pH of the working solution (H_2SO_4), the adsorption duration of the complex, and the content of molybdate, were optimized. A linear response for phosphate ion detection was observed in the range of 1.3 mg/L to 19.6 mg/L. The detection limit was determined to be approximately 0.05 mg/L, and the response time of the rGO@Cu/CPE sensor was about 10 seconds. Thus, this study presents the fabrication of a portable, low-cost, easy-to-use, biodegradable, and rapid phosphate ion sensor (rGO@Cu/CPE) suitable for in situ and real-time monitoring of food and water quality.

Keywords: *voltammetric method, reduced graphene oxide, doped copper ions, carbon paste electrode, phosphate sensor, molybdophosphate complex*

INTRODUCTION

The determination of the inorganic phosphate ion is especially important in the field of environmental, clinical, and food analysis. Inorganic phosphate is one of several major environmental contaminants. The detection of the levels of this contaminant is of utmost importance in the treatments of waste-water for our daily life (Rahman et al., 2005). All trace materials used in food preparation or preservation that improve food flavor, appearance, or other attributes are referred to as food additives. Natural food additives are now progressively being replaced by artificial, synthetic ones. There are also numerous issues with food additives, such as misuse, overuse, and even toxicity (Wu et al., 2022). Food additives are intentionally incorporated into food products to influence their physical, chemical, biological, or sensory characteristics for technological purposes during manufacturing, processing, preparation, treatment, packaging, shipping, or storage (Milešević et al., 2022; Velázquez-Sámano et al., 2019).

The crucial role of phosphate in the effects of excessive dietary intake (Watanabe et al., 1988) and the assessment of phosphate levels in bodily fluids for diagnosing hyperparathyroidism, Vitamin D deficiency, and Fanconi syndrome (Kawasaki et al., 1989) are also widely recognized. Moreover, numerous biological activities are associated with ATP hydrolysis, necessitating the monitoring of released inorganic phosphate ions to enhance comprehension of the mechanisms underlying specific intracellular reactions and signaling processes (Salins et al., 2004). Consequently, the necessity for a cost-effective and selective approach to accurately assess phosphate ion concentration in various sample matrices is evident.

Total phosphorus is measured by a number of analytical techniques, including chromatographic methods like high-performance liquid chromatography and ion chromatography, which provide exact separation and quantitation (Colero and Galceran, 2005). Fluorescence-based techniques, having high sensitivity and specificity, are particularly amenable to trace-level analysis (Kröckel et al., 2014). In addition, spectrophotometric methods are widely applied since they are efficient in determining phosphorus levels in different sample matrices (Li et al., 2022; Nakatani et al., 2008; Neves et al., 2008). Among

spectrophotometric techniques, the phosphomolybdenum blue (PMB) technique is the most commonly used for measuring dissolved phosphate. The method consists of the reaction of ammonium molybdate, ascorbic acid, and antimony potassium tartrate in an acidic medium to produce the Keggin anion of PMB. The reaction is as follows (Warwick et al., 2013; Wei et al., 2021):

$$7PO_4^{3-} + 12Mo_7O_{24}^{6-} + 72H^+ \rightarrow 7PMo_{12}O_{40}^{3-} + 36H_2O \quad (1)$$

The concentration of phosphate in a sample can be determined by measuring the absorbance of the resulting PMB complex by spectrophotometry.

Though spectrophotometric techniques are commonly employed in phosphate determination in food sample, they are usually interfered with and also involve cumbersome sample preparation. Electrochemical techniques, on the other hand, provide improved selectivity, sensitivity, and portability for on-site measurement because of the fast reaction of the phosphomolybdate ions at the electrode surface (Berchmans et al., 2012; Wei et al., 2021). The electrochemical reaction is as follows:

$$PMo_{12}O_{40}^{3-} + nH^+ + ne^- \rightarrow [H_nPMo_{12}O_{40}]^{3-} \quad (2)$$

The application of voltage to the electrode nicely reduces the phosphomolybdenum blue complex, enabling qualitative and quantitative analysis. Moreover, electrochemical methods are low-cost, rapid, and easily miniaturized, rendering them quite suitable for real-time monitoring applications (Pan et al., 2009; Wei et al., 2021).

As effective as traditional techniques are, their costliness and time-consuming nature present a challenge. Electrochemical strategies present an attractive complement due to their rapid, inexpensive, and convenient nature towards phosphate detection (Mahmud et al., 2020; Wei et al., 2021). Numerous studies have explored the use of electrochemical techniques with carbon-based sensors for detecting phosphate in both food and environmental samples. For example, Kolliopoulos et al. (2015) utilized screen-printed electrodes (SPEs) combined with a modified spectrophotometric approach to electrochemically detect dissolved phosphate. In electroanalysis, graphene-based electrodes find extensive application as the active sensor material (Arvas et al., 2018). Excellent features like high surface area, aspect ratio, porosity, electrical conductivity, and mechanical stability (Madurani et al., 2020; Jaafar et al., 2018) define graphene-based materials. Among these materials, graphene oxide (GO) is especially fascinating since it generates stable aqueous solutions by means of several oxygen-containing functional groups (e.g., epoxy, hydroxyl, and carboxyl) (Neklyud et al., 2017). GO is an insulating substance unlike graphene; nonetheless, it becomes conductive when reduced to its related form, reduced graphene oxide (rGO). By means of several reduction techniques—thermal, chemical, or electrochemical—each generating variable degrees of reduction, rGO can be manufactured. Consequently, one usually obtains a mixture of rGO and GO (Mazzara et al., 2020).

This study aims to build an electrochemical carbon paste sensor modified with reduced graphene oxide doped with copper ions (rGO@Cu/CPE) for the detection of phosphates in real samples, including food and environmental water. The increasing usage of phosphates in processed meat products necessitates their accurate detection for quality control and consumer safety. The high conductivity of reduced graphene oxide (rGO), combined with the catalytic effect of copper, enhances electron transfer between the rGO@Cu and the carbon paste electrode. Consequently, the sensor exhibited an extensive detection range from 1.3 to 19.6 mg/L and a high sensitivity of 9.03 µA/mg/L. The goal of this project is to develop a fast, reliable method for analyzing phosphate levels in real food samples by optimizing detection parameters and thoroughly testing the system.

EXPERIMENTAL

Reagents and Chemicals

All experimental reagents and materials used in this study were of analytical grade, sourced from Sigma-Aldrich and Merck (Merck KGaA, Darmstadt, Germany). A high-purity phosphate standard (PO_4^{3-}) KH_2PO_4 was obtained from Carlo-Erba and stored under refrigeration at 4°C to maintain stability. Different concentrations of phosphate ion solutions were prepared by diluting the high concentration of standard stock solution. Additionally, a freshly prepared stock solution of ammonium molybdate (0.1 mmol L^{-1}) was prepared using high-purity reagents and kept refrigerated at 4°C to maintain stability and prevent degradation. Double-distilled water was used for the preparation of all solutions to ensure high purity and reproducibility. The supporting electrolyte solutions were prepared using sulfuric acid (H_2SO_4) and nitric acid (HNO_3), both with 99% purity and obtained from Merck. Potassium chloride (KCl), necessary for

electrolyte preparation, was acquired from Aldrich. For electrode modification, synthetic graphite powder with a particle size of 71–90 µm was sourced from Alfa Aesar (99.9% purity), while paraffin oil (Olio di Vaselina) was purchased from Zeta Farmaceutici. For the preparation of modified sensors rGO@Cu/CPE, additional chemicals were utilized. Reduced graphene oxide (rGO) was synthesized using graphite oxide obtained from Sigma-Aldrich, reduced with ascorbic acid (Sigma-Aldrich, ≥99% purity). Copper nanoparticles (CuNPs) used for electrode modification were synthesized using copper (II) sulfate pentahydrate ($CuSO_4 \cdot 5H_2O$, Merck, 99%) and sodium borohydride ($NaBH_4$, Sigma-Aldrich, ≥98%). All reagents were stored and handled following standard laboratory protocols to ensure accuracy and reproducibility in experimental results.

Apparatus

All electrochemical measurements were performed using a PalmSens4 potentiostat–galvanostat, wirelessly connected to a personal computer via Bluetooth and controlled through dedicated three-electrode system software. The CPE and modified rGO/CPE, rGO@Cu/CPE sensors used in this study served as the working electrodes, while a platinum wire was used as the counter electrode, and an Ag/AgCl/KCl (3M) electrode functioned as the reference electrode. The electrochemical analysis of phosphate (PO_4^{3-}) was conducted using voltammetric technique, including cyclic voltammetry (CV) and square wave voltammetry (SWV).

Electrodes Preparation

Preparation of rGO/CPE Sensor

The rGO/CPE sensor was prepared by mixing 1.00 g of carbon powder (particle size: 70–90 µm), 0.100 g of rGO, and 300 µL of paraffin oil. The mixture was then ground using a mortar and pestle for 30 minutes until a homogeneous paste was obtained. To immobilize the rGO into the carbon paste matrix, the composite electrode material was stored in a refrigerator at 4°C for 24 hours before use. This allowed the paste to stabilize and the rGO to be properly integrated into the carbon matrix. Than the prepared materials were packed into a plastic syringe with an 8 mm internal diameter, containing a 9.5 mm copper wire as the external electrical contact.

Preparation of rGO@Cu

A total of 0.472 g of $CuSO_4 \cdot 5H_2O$ and 0.102 g of graphene oxide (previously synthesized) were weighed and transferred into a 75 mL beaker containing 20 mL of distilled water**.** The mixture was stirred using a magnetic stirrer at level 4 for 2 hours to ensure proper dispersion. Following this, the suspension was placed in an ultrasonic bath at room temperature for 4 hours to enhance uniform mixing. The resulting dispersion was then divided into two 14 mL test tubes and centrifuged at 5000 RPM for 5 minutes. The obtained precipitate was dried in a thermostatic oven at approximately 80°C until a gel-like mass was formed. The dried composite was stored in a filter paper in a dry environment for further use.

Preparation of rGO@Cu /CPE Sensor

The rGO@Cu/CPE sensor was prepared by mixing 1.00 g of carbon powder (particle size: 70–90 µm), 0.100 g of the synthesized rGO@Cu composite, and 300 µL of paraffin oil. Initially, the carbon powder and paraffin oil were mixed, followed by the addition of the rGO@Cu composite. The mixture was then ground using a mortar and pestle for 30 minutes until a homogeneous paste was obtained. The prepared paste was packed into a plastic syringe with an 8 mm internal diameter, containing a 9.5 mm copper wire as the external electrical contact. For comparison, an unmodified CPE was prepared using the same procedure but without the addition of rGO@Cu. Before electrochemical measurements, the electrode surface was smoothed on a glass surface, and after partial removal of the paste, the surface was renewed by polishing.

RESULTS AND DISCUSSIONS

Electrochemical behavior of Phosphomolybdate complex at modified rGO@Cu/CPE sensor

The electrochemical reduction capability of the phosphomolybdate reflects the sensing performance of the modified electrodes. The high surface area of rGO and excellent catalytic performance of copper doped into rGO/CPE were used to enhance the sensing performance of the CPE electrode. The electrochemical behavior of phosphomolybdate complex was investigated in sulfuric acid media 0.05 mol L^{-1}, 0.1 mmol L^{-1} molybdate using square wave voltammetry at bare CPE, rGo/CPE and rGO@Cu/CPE modified sensors, in presence of 3.1 mg/L phosphate.

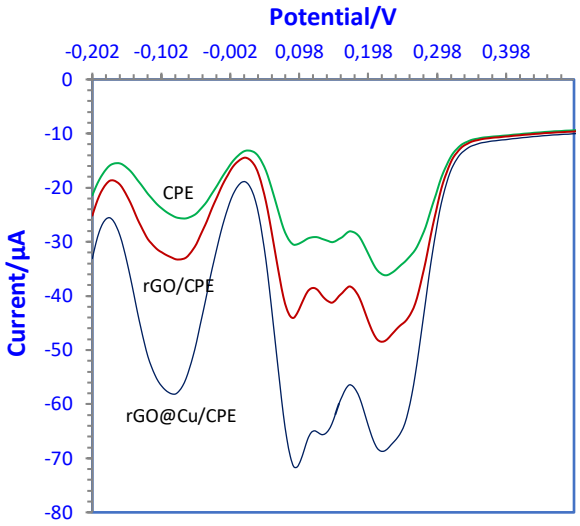

Figure. 1. SWVs of bare CPE, rGO/CPE, and rGO@Cu/CPE in a solution containing 0.1 mmol L^{-1} molybdate, and 0.05 mol L^{-1} H_2SO_4 solution (pH 1.3) in the presence of 3.1 mg/L phosphate, using the potential range of 800 to − 200 mV, with a amplitude of 50 mV/ s and frequency 30 Hz

Figure 1 illustrates the voltammograms of phosphomolybdate at bare CPE, rGO/CPE and rGO@Cu/CPE sensors, in the presence of 3.1 mg/L phosphate recorded at 0.1 mmol L^{-1} molybdate, and 0.05 mol L^{-1} H_2SO_4 solution (pH 1.3). It was observed that three consecutive reductions peak were observed at around +220 mV (I), 100 mV (II) and -100 mV (III), respectively. This is due to polyphosphomolybdate isomerizes into two different forms α (α-$[PMo_{12}O_{40}]^{3-}$) and β (β-$[PMo_{12}O_{40}]^{3-}$) as reported (Nagul et al, 2015). As shown in Figure. 1, the bare CPE electrode exhibited a low reduction peak (III) current in presence of 3.1 mg/L PO_4^{3-} compared with modified rGO/CPE and rGO@Cu/CPE sensor. However, the rGO@Cu/CPE electrode exhibited the highest reduction peak current (III), showing that the phosphomolybdate reduction peak current at the rGO@Cu/CPE electrode increased compared with bare CPE and rGO/CPE, respectively. These results indicate that the significant increase in the reduction peak current of rGO@Cu/CPE is caused by the synergistic rGO and copper ions doped in rGO, with rGO providing a larger surface area and a considerable number of active sites, while Cu provides good catalytic effect in phosphomolybdate performance.

Analytical performance of rGO@Cu/CPE Sensor

Optimization of experimental parameters

Effects of adsorption time

The effect of adsorption time of phosphomolybdate was optimized (Figure 2). The Square Wave Voltammograms reduction peak at -100 V was recorded in solutions containing 10.6 mg/L phosphate with adsorption times ranging from 60 s to 600 s.

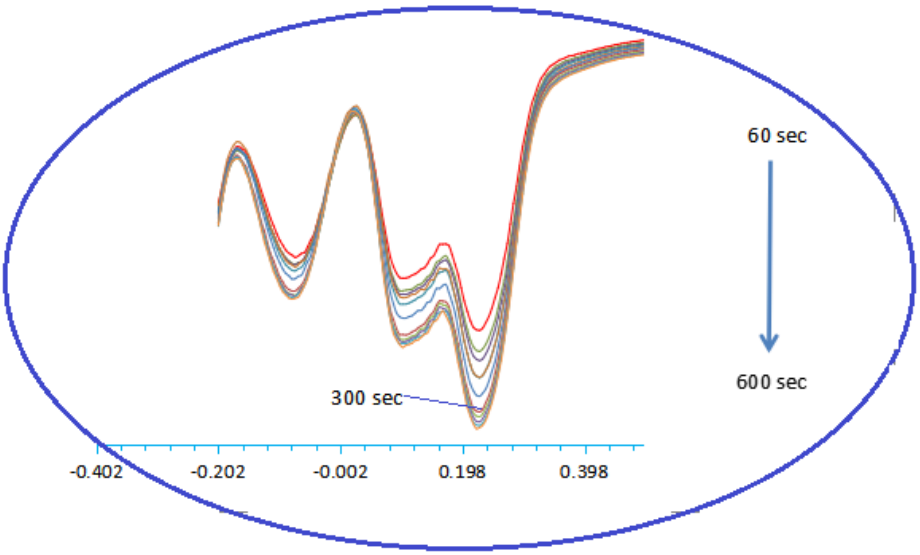

Figure 2. SWV of rGO@Cu/CPE at different adsorption times from 60 s to 600 s, at 0.1 mmol L^{-1} molybdate, 0.05 mol L^{-1} H_2SO_4 solution in the presence of 10.6 mg/L phosphate concentrations.

The cathodic peak current gradually increased with the adsorption time of phosphomolybdate from 60 s to 300 s, however, when the time was further raised from 300 s to 600 s, the increase of stripping current was not obvious, which is mainly due to the saturation of phosphomolybdate adsorption on the electrode surface. Therefore, it was enough for 300 s to detect phosphate and suitable for the requirement of rapid detection.

Effects of pH and molybdate concentration

In order to optimize the square wave voltammetry of the electroactive phosphomolybdate complex formed by the reaction between phosphate and molybdate salt to form the Keggin anion ($PMo_{12}O_{40}^{3-}$) (Joaca et al., 2011), the influence of pH and molybdate concentration were investigated.

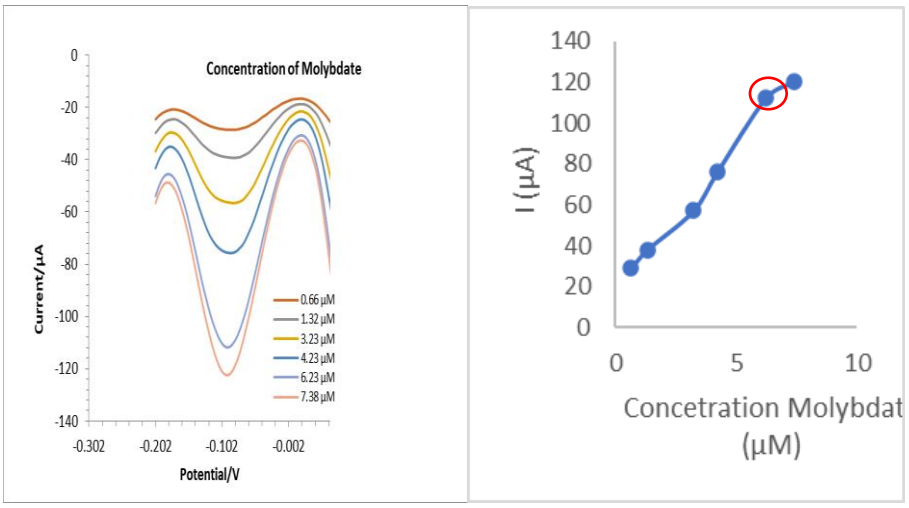

Figure 3. Current response to different concentration of molybdate containing 10.6 mg/L phosphate at pH 1.3

The effect of the molybdate concentration from 0.66 to 7.38 µM at pH 1.3 was studied by SW-Voltammetry. The obtained results shown in Figure 3 revealed that the highest value of reductive peak current at potential - 100 mV was achieved with the molybdate concentration of 6.23 µM.

It was also evaluated the SWV signal obtained with rGO@Cu/CPE sensor for determination of phosphate in 6.23 µM molybdate using pH value between 0.3 to 3.0. As shown in Figure 4, the variation of current

for phosphate solution with the concentration of 10.6 mg/L at different pH, the best results were obtained at pH around 1.3. At the pH higher than 1.3, more time was required for the formation of heteropolyacids (Du et al., 2011). Therefore, the reductive peak current of molybdophosphate was decreased when pH was higher than 1.3.

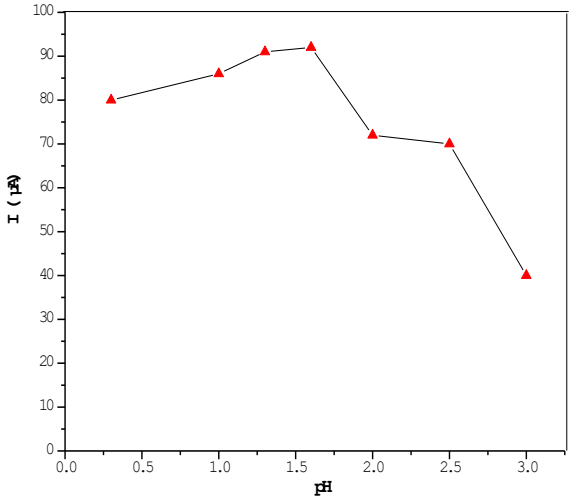

Figure 4. Variation of current measured by SWV as a function of pH (from 0.3 to 3.0) for molybdophosphate complex containing 10.6 mg/L phosphate

Calibration curve

The calibration curve of the proposed sensor rGO@Cu/CPE for phosphate ion quantification was obtained using square wave voltammetry as a detection technique. The concentration and stability of complex depend on numerous parameters such as the concentration of molybdenum (VI) and phosphate anions, the acid concentration, the reaction time and temperature. Figure 5 shows the SW voltammograms and corresponding calibration curve for different phosphate ions concentration. According to mechanism the two isomers have very close oxidation/reduction potentials and as reported in (Ueda et al., 2013), in the registered SW-Voltammograms three peaks can be found. The first and second are relative to the redox processes of the β-$[PMo_{12}O_{40}]^{3-}$ anion, while the second and third are due to the redox processes of α-$[PMo_{12}O_{40}]^{3-}$.

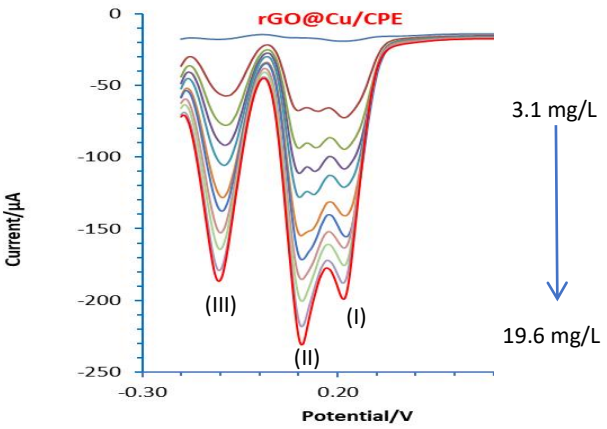

Figure 5. SWV of rGO@Cu/CPE in 0.05 mol L^{-1} sulfuric acid and 0.1 mmol L^{-1} ammonium molybdate at different phosphate concentrations from a range of potential scan 800 mV to -200 mV, amplitude 50 mV/S and frequency 30 Hz.

The clearest reduction peak for phosphate ion concentration in the SWV curves was observed at −100 mV (Peak III), corresponding to the electrochemical reduction of Mo (IV) to Mo (II). For this peak couple, higher selectivity and sensitivity toward variations in phosphate ion concentration were noted. Consequently, the peak current of this reduction (III) was used as the sensor readout.

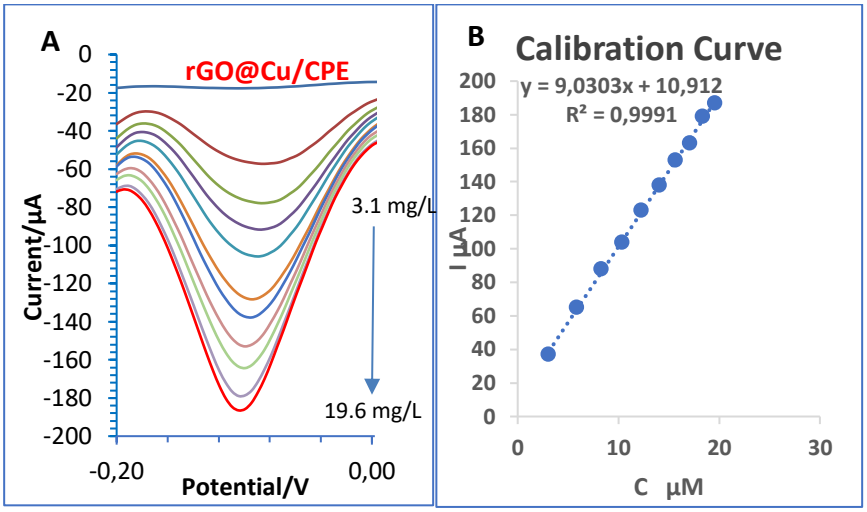

Figure. 6 (A) Square wave voltammograms of rGO@Cu/CPE at different phosphate concentrations (Peak III -100 mV) from 3.1 to 19.6 mg/L at 0.1 mmol L^{-1} molybdate, and 0.05 mol L^{-1} H_2SO_4 solution (B) Calibration curve for phosphate determination.

As shown in Fig. 6, the sensor current intensity response increases with phosphate concentration, so the cathodic current was corresponded to the target phosphate concentration, allowing a linear calibration of the rGO@Cu/CPE sensor for concentrations ranging from 3.1 to 19.6 mg/L. The limit of detection (LOD) of the sensor was calculated using the following equation:

$$LOD = 3.3 * SD/S \quad (3)$$

where SD is the standard deviation of the blank and S is the average sensor sensitivity yielding a calculated LOD of 0.05 mg/L.

Stability and Reproducibility

The stability of the rGO@Cu/CPE electrode was studied in a mixed solution containing 5 mM $K_3Fe(CN)_6$ and $K_4Fe(CN)_6$, using cyclic voltammetry. The results indicate that the modified electrode completely retained its initial response with an RSD of 2.7 % after storage for 30 days at room temperature, verifying that the rGO@Cu/CPE electrode has good stability. The good stability for rGO@Cu/CPE can be attributed the well combination of rGO doped with copper, which resulting in a more stable composite material.

In addition, the reproducibility of the rGO@Cu/CPE electrode was evaluated using three electrodes independently modified using the same method in 3.1 mg/L phosphate solutions, showing an RSD of 4.2%. This indicates that different rGO@Cu/CPE electrodes exhibit negligible differences in SWV response.

CONCLUSIONS

This work reports for the detection of phosphate ions with an electrochemical sensor based on a carbon paste electrode modified with reduced graphene oxide doped with copper ions (rGO@Cu). The incorporation of nanomaterials rGO@Cu into the carbon paste electrode (CPE) produced a quite sensitive sensor, with a sensitivity of 9.03 µA/mg/L for the electrochemical detection of phosphate ions. Adsorption time, sulfuric acid concentration (pH), and molybdate concentration were among several factors optimized to produce a high-performance, stable, and repeatable sensor. The rGO@Cu/CPE sensor with a detection limit (LOD) of 0.05 mg/L, allowed phosphate ion detection over a broad linear range, from 3.1 mg/L to 19.6 mg/L. Strong potential as a portable system for field deployment and real-time monitoring is presented by the proposed rGO@Cu/CPE sensor due to its low cost, simple fabrication, small size, and low equipment requirements.

REFERENCES

Arvas, M.B., Gürsu, H., Gençten, M., Sahin, Y. (2018). Electrochemical formation of molybdenum phosphate on a pencil graphite electrode and its potential application for the detection of phosphate ions. *Anal. Methods*, 10, 4282–4291.

Berchmans, S., Issa, T. B., & Singh, P. (2012). Determination of inorganic phosphate by electroanalytical methods: a review. *Analytica chimica acta*, 729, 7–20.

Du, F., Li, J., Li, X., Zhang, Z. (2011). Improvement of iron removal from silica sand using ultrasound-assisted oxalic acid. *Ultrason Sonochem*, 18, 389–393.

Jaafar, E., Kashif, M., Sahari, S.K., Ngaini, Z. (2018). Study on morphological, optical and electrical properties of graphene oxide (GO) and reduced graphene oxide (rGO). *MSF*, 917, 112–116.

Joaca, J., Fernandez, V.L., Thouron, D., Paulmier, A., Graco, M., et al. (2011). Phosphate determination in seawater: toward an autonomous electrochemical method. *Talanta*, 87, 161–167.

Kawasaki, H., Sato, K., Ogawa, J., Hasegawa, Y., Yuki, H. (1989). Determination of inorganic phosphate by flow injection method with immobilized enzymes and chemiluminescence detection. *Anal. Biochem.*, 182, 366–370.

Kolliopoulos, A.V., Kampouris, D.K., Banks, C.E. (2015). Rapid and portable electrochemical quantification of phosphorus. *Anal. Chem.*, 87, 4269–4274.

Kröckel, L., Lehmann, H., Wieduwilt, T., & Schmidt, M. A. (2014). Fluorescence detection for phosphate monitoring using reverse injection analysis. *Talanta*, 125, 107–113.

Li, Y. S., Muo, Y., & Xie, H. M. (2002). Simultaneous determination of silicate and phosphate in boiler water at power plants based on series flow cells by using flow injection spectrophotometry. *Analytica Chimica Acta*, 455(2), 315–325.

Madurani, K.A., Suprapto, S., Machrita, N.I., Bahar, S.L., Illiya, W., Kurniawan, F. (2020). Progress in graphene synthesis and its application: history, challenge and the future outlook for research and industry. *ECS J. Solid State Sci. Technol.*, 9, 093013.

Mahmud, M. P., Ejeian, F., Azadi, S., Myers, M., Pejcic, B., Abbassi, R., ... & Asadnia, M. (2020). Recent progress in sensing nitrate, nitrite, phosphate, and ammonium in aquatic environment. *Chemosphere*, 259, 127492.

Mazzara, F., Patella, B., Aiello, G., Sunseri, C., Inguanta, R. (2020). Ascorbic acid determination using linear sweep voltammetry on flexible electrode modified with gold nanoparticles and reduced graphene oxide. *IEEE 20th Mediterranean Electrotechnical Conference (MELECON)*, IEEE, Palermo, Italy, 2020, pp. 406–410.

McNeil, C.J., Rahman, Md. Aa., Park, D-S a., Chang, S-Ch b., Shima, Y-B.∗ (2005). The biosensor based on the pyruvate oxidase modified conducting polymer for phosphate ions determinations. *Biosensors and Bioelectronics*, 21 (2006), 1116–1124.

Milešević, J., Vranić, D., Gurinović, M., Koričanac, V., Borović, B., Zeković, M., Šarac, I., Milićević, D. R., & Glibetić, M. (2022). The Intake of Phosphorus and Nitrites through Meat Products: A Health Risk Assessment of Children Aged 1 to 9 Years Old in Serbia. *Nutrients*, 14(2), 242.

Nagul, E.A., McKelvie, I.D., Worsfold, P., Kolev, S.D. (2015). The molybdenum blue reaction for the determination of orthophosphate revisited: opening the black box. *Anal. Chim. Acta*, 890, 60–82.

Nakatani, N., Kozaki, D., Masuda, W., Nakagoshi, N., Hasebe, K., Mori, M., & Tanaka, K. (2008). Simultaneous spectrophotometric determination of phosphate and silicate ions in river water by using ion-exclusion chromatographic separation and post-column derivatization. *Analytica chimica acta*, 619(1), 110–114.

Neves, M. S. A., Souto, M. R. S., Tóth, I. V., Victal, S. M., Drumond, M. C., & Rangel, A. O. (2008). Spectrophotometric flow system using vanadomolybdophosphate detection chemistry and a liquid waveguide capillary cell for the determination of phosphate with improved sensitivity in surface and ground water samples. *Talanta*, 77(2), 527–532.

Pan, D., Wang, Y., Chen, Z., Lou, T., & Qin, W. (2009). Nanomaterial/ionophore-based electrode for anodic stripping voltammetric determination of lead: an electrochemical sensing platform toward heavy metals. *Analytical Chemistry*, 81(12), 5088–5094.

Ruiz-Calero, V., & Galceran, M. T. (2005). Ion chromatographic separations of phosphorus species: a review. *Talanta*, 66(2), 376–410.

Salins, L.L.E., Deo, S.K., Daunert, S. (2004). Phosphate binding protein as the biorecognition element in a biosensor for phosphate. *Sens. Actuators B*, 97, 81–89.

Ueda, T., Isai, K. (2013). Effects of organic solvents and salts on the isomerization reaction (β→α) of Keggin-type 12-molybdophosphate anion. *Anal. Sci.*, 29, 447–453.

Velázquez-Sámano, G., Collado-Chagoya, R., Cruz-Pantoja, R. A., Velasco-Medina, A. A., & Rosales-Guevara, J. (2019). Reacciones de hipersensibilidad a aditivos alimentarios [Hypersensitivity reactions to food additives]. *Revista alergia Mexico*, 66(3), 329–339.

Warwick, C., Guerreiro, A., & Soares, A. (2013). Sensing and analysis of soluble phosphates in environmental samples: a review. *Biosensors & Bioelectronics*, 41, 1–11.

Watanabe, E., Endo, H., Toyama, K. (1988). Determination of phosphate ions with an enzyme sensor system. *Biosensors*, 3, 297–306.

Wei, H., Pan, D., Zhou, Z., Han, H., & Zhu, R. (2021). On-site electrochemical determination of phosphate with high sensitivity and anti-interference ability in turbid coastal waters. *Ecotoxicology and Environmental Safety*, 221, 112444.

Wu, L., Zhang, C., Long, Y., Chen, Q., Zhang, W., & Liu, G. (2022). Food additives: From functions to analytical methods. *Critical Reviews in Food Science and Nutrition*, 62(30), 8497–8517.

Neklyudov, V.V., Khafizov, N.R., Sedov, I.A., Dimiev, A.M. (2017). New insights into the solubility of graphene oxide in water and alcohols. *Phys. Chem. Chem. Phys.*, 19, 17000–17008.

➢ *ORAL PRESENTATION*

Random metric lattices and some betweenness relations in random metric spaces

Celaleddin Şençimen* (*ORCID: https://orcid.org/0000-0002-8188-6290*)

*Burdur Mehmet Akif Ersoy University, Faculty of Arts and Sciences, Department of Mathematics, Burdur, TURKEY

*Corresponding author, e-mail: sencimen@mehmetakif.edu.tr

Abstract

One of the most important concepts in axiomatic geometry is that of betweenness of points in an abstract metric space. It also plays a special role in distance (metric) geometry. Moreover, a metric structure on a lattice produces a rich theory on the concept of betweenness in arbitrary lattices. In this work, we first introduce the concepts of almost certainly betweenness and probably betweenness in a random metric space that is an abstract set on which the distance between two points is modelled via a random variable due to the randomness of the distances. Next, we introduce the concept of a random metric lattice via the notion of random positive valuation on a lattice. In this context, we also investigate a betweenness relation in random metric lattices. Finally, we examine the uniform continuity of the random positive valuation on a special lattice.

Keywords: almost certainly betweenness, probably betweenness, random positive valuation, random metric lattice.

1. INTRODUCTION

Distance geometry (or widely known as metric geometry) investigates the geometry of abstract spaces via the tools of a metric, and it is an active area of research interacting with many mathematical disciplines. Since Menger's work in 1928 (Menger, 1928) many results have been published on distance geometry. A well organized account of the basic concepts and results in this area can be found in e.g. Blumenthal (1970), Burago et al. (2001), Busemann (1942), Gromov et al. (2007) and Papadopoulos (2014).

On the other hand, random metric (RM) spaces are special classes of probabilistic metric (PM) spaces (see Schweizer and Sklar (1983)). The concept of an RM space was first introduced by Špaček (1956, 1960), and then studied in more detail (see, e.g. Brown (1972) and Guo (1999, 2001)). In an RM space, the distance between two points is a random variable. This approach to distances has some applications in physics and risk theory (see Roy (1998) and Guo et al. (2014), respectively).

Returning to distance geometry, we see that one of the most important concepts is that of betweenness of distinct points in a metric space. On the other hand, if we endow a lattice with a metric, this rises many problems related to the concept of betweenness on the lattice. In the current work, we first introduce the notions of almost certainly betweenness and probably betweenness in an RM space (for betweenness relations in a probabilistic metric space, we refer to Schweizer and Sklar (1983) where probability distribution functions are used instead of random variables). Next, we introduce the notion of random metric lattice via the concept of a random positive valuation on a lattice, which is a random generalization of positive valuation. In this context, we investigate a betweenness relation in random metric lattices. Finally, we examine the uniform continuity of the random positive valuation on a special lattice. When stating our new definitions and results, we have inspired from Birkhoff (1973), Blumenthal (1970) and Sherwood (1970). We think that the study of lattice structure and betweenness relations in an RM space may contribute to the algebra and geometry of RM spaces.

2. MATERIALS AND METHODS

In this section, we recall some of the basic concepts from Guo (1999, 2001) and Schweizer and Sklar (1983), related to our work.

Let $(\Omega, \mathcal{A}, P)$ be a probability space and $\omega \in \Omega$. Consider the following classes [almost surely $(a.s.)$ equivalent functions are identified]:

(i) $L_0(\Omega, \mathbb{R})$: The set of all equivalence classes of real random variables defined on Ω,
(ii) $L_0^+(\Omega)$: The set of all $\xi \in L_0(\Omega, \mathbb{R})$ with $\xi(\omega) \geq 0 \ \ a.s.$

$L_0(\Omega, \mathbb{R})$ is a vector space and its zero vector will be denoted as Θ, where $\Theta(\omega) = 0 \ \ a.s.$ For any $\xi, \zeta \in L_0(\Omega, \mathbb{R})$, we define $\xi \preccurlyeq \zeta \Leftrightarrow \xi(\omega) \leq \zeta(\omega)\ a.s.$ If $\xi \preccurlyeq \zeta$ but $\xi \neq \zeta$ we will write $\xi \prec \zeta$.

Definition 2.1 Let $(\Omega, \mathcal{A}, P)$ be a probability space, $\mathbf{S} \neq \emptyset$ and $\mathcal{X}: \mathbf{S} \times \mathbf{S} \to L_0^+(\Omega)$ be a mapping with $\mathcal{X}(p, q) = X_{pq}$ where $p, q \in \mathbf{S}$. If for every $p, q, r \in \mathbf{S}$ we have

(RM 1) $X_{pq} = \Theta \Leftrightarrow p = q$
(RM 2) $X_{pq} = X_{qp}$
(RM 3) $X_{pr} \preccurlyeq X_{pq} + X_{qr}$,

then the pair $(\mathbf{S}, \mathcal{X})$ is called a *random metric* (*RM*) *space* with base $(\Omega, \mathcal{A}, P)$. Moreover, the random variable X_{pq} is called the *random distance* between p and q.

Now let $(\mathbf{S}, \mathcal{X})$ be an RM space with base $(\Omega, \mathcal{A}, P)$. Then, given $p \in \mathbf{S}$, $\varepsilon > 0$ and $\lambda \in (0,1)$, the set $\mathcal{N}_p(\varepsilon, \lambda) = \{q \in \mathbf{S}: \ P(X_{pq} < \varepsilon) > 1 - \lambda\}$ is called the $(\varepsilon, \lambda) -$ *neighborhood* of p. The topology generated by these neighbourhoods is called the (ε, λ) $-$*topology* on $\mathbf{S}$.

Example 2.1 Let $(\Omega, \mathcal{A}, P)$ be a probability space and $(\mathbf{M}, d)$ a separable metric space endowed with a Borel σ $-$algebra. We identify $a.s.$ equivalent measurable mappings defined from Ω into $\mathbf{M}$ and denote the set of all equivalence classes of these mappings by $\mathbf{S}$. Consider the mapping $\mathcal{X}: \mathbf{S} \times \mathbf{S} \to L_0^+(\Omega)$ defined as $[\mathcal{X}(p, q)](\omega) = X_{pq}(\omega) = d(p(\omega), q(\omega))$ where $p, q \in \mathbf{S}$ and $\omega \in \Omega$. Thus $(\mathbf{S}, \mathcal{X})$ is an RM space with base $(\Omega, \mathcal{A}, P)$.

3. RESULTS AND DISCUSSION

In this section, we first introduce the concept of almost certainly betweenness.

Definition 3.1 Let $(\mathbf{S}, \mathcal{X})$ be an RM space and $p, q, r \in \mathbf{S}$ pairwise distinct. If $X_{pq} + X_{qr} = X_{pr}$ then we will say that q is *almost certainly between* p and r, and denote this by (pqr). Moreover, we will denote the set of all points of $\mathbf{S}$ almost certainly between p and r by $B(p, r)$.

Theorem 3.1 In an RM space $(\mathbf{S}, \mathcal{X})$, the relation of almost certainly betweenness has the following properties:

(a) (pqr) implies (rqp), which is the *symmetry of the outer points*.
(b) If (pqr) holds, then neither (prq) nor (qpr) holds, which is the *special inner point* property.
(c) If (pqr) and (prs) hold, then (pqs) and (qrs) hold, which is the property of *transitivity*.
(d) Given $p, r \in \mathbf{S}$, the set $B[p, r] = B(p, r) \cup \{p, r\}$ is closed in the (ε, λ) $-$topology, which is the *closure* property.

Proof. (a) Straightforward.

(b) Let (pqr) hold. Then $X_{pq} + X_{qr} = X_{pr}$. Now if (prq) holds, then we have $X_{pr} + X_{rq} = X_{pq}$. These two equalities give $X_{qr} = \Theta$, a contradiction to $q \neq r$. In a similar way, (qpr) cannot hold.

(c) Assume that (pqr) and (prs) hold. Now p,q,r,s are pairwise distinct except possibly q and s. But we must have $q \neq s$ since, on the contrary, (pqr) and (prq) both hold,which contradicts (b). Now $X_{pq} + X_{qr} = X_{pr}$ and $X_{pr} + X_{rs} = X_{ps}$ yield $X_{pq} + X_{qr} + X_{rs} = X_{ps} \preccurlyeq X_{pq} + X_{qs}$. On the other hand, we have $X_{qs} \preccurlyeq X_{qr} + X_{rs}$. Thus we get $X_{qr} + X_{rs} = X_{qs}$ and hence $X_{pq} + X_{qs} = X_{ps}$. This shows that (pqs) and (qrs) hold.

(d) Let $q \in \overline{B[p,r]}$, where $p,q,r \in \mathbf{S}$ are pairwise distinct. Since $\mathbf{S}$ endowed with the (ε,λ) −topology is first countable, there exists a sequence (q_n) in $B(p,r)$ such that $\lim_{n\to\infty} q_n = q$. Then we have $X_{pq_n} + X_{q_nr} = X_{pr}$ for all $n \in \mathbb{N}$. Now, since the random metric is uniformly continuous (see Brown, 1972), we get $X_{pq} + X_{qr} = X_{pr}$, i.e., $q \in B(p,r)$, which implies that $q \in B[p,r]$. ■

Example 3.1 Let $(\Omega, \mathcal{A}, P)$ be the Lebesgue probability space where $\Omega = [0,1]$. As in Example 2.1, identify $a.s.$ equivalent real random variables defined on Ω and denote the set of all equivalence classes of these random variables by $\mathbf{S}$. Consider the mapping $\mathcal{X}: \mathbf{S}\times\mathbf{S} \to L_0^+(\Omega)$ defined as $[\mathcal{X}(p,q)](\omega) = X_{pq}(\omega) = |p(\omega) - q(\omega)|$ where $p,q \in \mathbf{S}$ and $\omega \in \Omega$. Thus $(\mathbf{S},\mathcal{X})$ is an RM space. Now let us define p: $[0,1] \to \mathbb{R}$ by

$$p(\omega) = \begin{cases} 2\omega, & if\ 0 \le \omega \le \frac{1}{2} \\ -2\omega + 2, & if\ \frac{1}{2} \le \omega \le 1 \end{cases},$$

q: $[0,1] \to \mathbb{R}$ by $q(\omega) = 1$ for each $\omega \in [0,1]$ and r: $[0,1] \to \mathbb{R}$ by $r(\omega) = 0$ for each $\omega \in [0,1]$.
Then we have $X_{qp}(\omega) + X_{pr}(\omega) = X_{qr}(\omega)$ for every $\omega \in \Omega$, and hence we get (qpr).

Now we introduce another type of betweenness which is significantly different from almost certainly betweenness.

Definition 3.2 Let $(\mathbf{S},\mathcal{X})$ be an RM space and $p,q,r \in \mathbf{S}$ pairwise distinct. If $0 < P\{\omega \in \Omega: X_{pq}(\omega) + X_{qr}(\omega) = X_{pr}(\omega)\} < 1$, then we will say that q is *probably between* p and r, and will denote this by $(p\widetilde{qr})$.

We know by Theorem 3.1 (b) that if (pqr) holds, then neither (prq) nor (qpr) holds. However, this is not the case in the setting of probably betweenness as can be seen in the following example.

Example 3.2 Let $(\Omega, \mathcal{A}, P)$ be the Lebesgue probability space where $\Omega = [0,1]$. We will consider the RM space given in Example 3.1. Define p: $[0,1] \to \mathbb{R}$ by

$$p(\omega) = \begin{cases} -2\omega + 1, & if\ 0 \le \omega \le \frac{1}{2} \\ 2\omega - 1, & if\ \frac{1}{2} \le \omega \le 1 \end{cases},$$

q: $[0,1] \to \mathbb{R}$ by $q(\omega) = 1$ for each $\omega \in [0,1]$ and r: $[0,1] \to \mathbb{R}$ by $r(\omega) = 2\omega$ for each $\omega \in [0,1]$. Then we have $X_{pq}(\omega) + X_{qr}(\omega) = X_{pr}(\omega)$ for every $\omega \in \left[\frac{1}{2}, 1\right]$. Hence we get $(p\widetilde{qr})$. Moreover, we have $X_{pr}(\omega) + X_{rq}(\omega) = X_{pq}(\omega)$ for every $\omega \in \left[\frac{1}{4}, \frac{1}{2}\right]$. Thus $(p\widetilde{rq})$ holds. Similarly, we have $X_{qp}(\omega) + X_{pr}(\omega) = X_{qr}(\omega)$ for every $\omega \in \left[0, \frac{1}{4}\right]$. Thus $(q\widetilde{pr})$ holds.
Throughout the following, we will study on lattices. For convention, let us denote a lattice by $(\mathbf{L}, \le, \vee, \wedge)$ where $\le$ is the partial order on $\mathbf{L}$, $\vee$ and $\wedge$ are the join and meet operations on $\mathbf{L}\times\mathbf{L}$, respectively. If $p,q \in \mathbf{L}$ with $p \le q$ but $p \neq q$ we will write $p < q$.

Definition 3.3 Let $(\mathbf{L}, \le, \vee, \wedge)$ be a lattice and consider the mapping $f: \mathbf{L} \to L_0^+(\Omega)$ satisfying the following axioms:
(RPV 1) $p,q \in \mathbf{L}$ and $p < q$ implies that $f(p) \prec f(q)$,
(RPV 2) For all $p,q \in \mathbf{L}$ we have $f(p \vee q) + f(p \wedge q) = f(p) + f(q)$.

Then the mapping f will be called the *random positive valuation* on $\mathbf{L}$ and it will be denoted by $f(p) = [p]$. A lattice $\mathbf{L}$ endowed with a random positive valuation will be denoted by $(\mathbf{L}, [\cdot])$, briefly.

Example 3.3 Let $\mathbb{R}_+^n = \{(p_1, \dots, p_n) : p_1, \dots, p_n \geq 0\}$ and endow $\mathbb{R}_+^n$ with the coordinatewise ordering $p = (p_1, \dots, p_n) \leq q = (q_1, \dots, q_n) \Leftrightarrow p_i \leq q_i$ for all $i = 1, \dots, n$. Now let $\xi_1, \dots, \xi_n \in L_0^+(\Omega)$ where each $\xi_i \neq \Theta$, and consider the random linear combination $[p] = p_1\xi_1 + \cdots + p_n\xi_n$. Then the pair $(\mathbb{R}_+^n, [\cdot])$ is a lattice with a random positive valuation.

Theorem 3.2 Let $(\mathbf{L}_1, [\cdot]_1)$ and $(\mathbf{L}_2, [\cdot]_2)$ be lattices with random positive valuations $[\cdot]_1$ and $[\cdot]_2$, respectively. Then $\mathbf{L}_1 \times \mathbf{L}_2$ is also a lattice with a random positive valuation defined by $[(a, b)] = [a]_1 + [b]_2$, where $(a, b) \in \mathbf{L}_1 \times \mathbf{L}_2$.

Proof. (RPV 1) Let $(a, b), (c, d) \in \mathbf{L}_1 \times \mathbf{L}_2$ with $(a, b) < (c, d)$, that is, $a \leq c$ in $\mathbf{L}_1$ and $b \leq d$ in $\mathbf{L}_2$ but $(a, b) \neq (c, d)$. Then $[(a, b)] = [a]_1 + [b]_2 \prec [c]_1 + [d]_2 = [(c, d)]$.

(RPV 2) $[(a, b) \vee (c, d)] + [(a, b) \wedge (c, d)] = [(a \vee c, b \vee d)] + [(a \wedge c, b \wedge d)]$
$= [a \vee c]_1 + [b \vee d]_2 + [a \wedge c]_1 + [b \wedge d]_2 = [a]_1 + [c]_1 + [b]_2 + [d]_2 = [(a, b)] + [(c, d)]$. ■

Theorem 3.3 Let $(\mathbf{L}, [\cdot])$ be a lattice with a random positive valuation. For $p, q \in \mathbf{L}$ define $\mathcal{X}: \mathbf{L} \times \mathbf{L} \to L_0^+(\Omega)$ by $\mathcal{X}(p, q) = X_{pq} = [p \vee q] - [p \wedge q]$. Then the pair $(\mathbf{L}, \mathcal{X})$ is an RM space.

Proof. (RM 1) If $p = q$, then it is clear that $X_{pq} = \Theta$. Conversely, let $X_{pq} = \Theta$. Then we have $[p \vee q] = [p \wedge q]$, and since $(p \wedge q) \leq (p \vee q)$ we get $p \wedge q = p \vee q$ from (RPV 1). Thus $(p \wedge q) \leq p$ and $p \leq (p \vee q) = p \wedge q$ imply that $p \wedge q = p$. Similarly, we have $p \wedge q = q$, and thus $p = q$.

(RM 2) Straightforward.

(RM 3) Let $p, q, r \in \mathbf{L}$. Then we have $[p \vee r] + [q] \preccurlyeq [p \vee q] + [q \vee r]$. Moreover, we can write $[p \wedge q] + [q \wedge r] \preccurlyeq [p \wedge r] + [q]$. Combining these relations we get
$[p \vee r] - [p \wedge r] \preccurlyeq [p \vee q] - [p \wedge q] + [q \vee r] - [q \wedge r]$, that is, $X_{pr} \preccurlyeq X_{pq} + X_{qr}$. ■

Remark. In Theorem 3.3, the RM space $(\mathbf{L}, \mathcal{X})$ induced by $[\cdot]$ will be called a *random metric (RM) lattice*.

Theorem 3.4 Let $(\mathbf{L}, [\cdot])$ be a lattice with a random positive valuation and $(\mathbf{L}, \mathcal{X})$ be the RM lattice induced by $[\cdot]$. If $p \leq q \leq r$ in $\mathbf{L}$, then we have (pqr).

Proof. We can write $X_{pq} = [p \vee q] - [p \wedge q] = [q] - [p]$. Similarly, we have $X_{qr} = [r] - [q]$ and $X_{pr} = [r] - [p]$. Thus we get $X_{pq} + X_{qr} = X_{pr}$, i.e., (pqr). ■

Theorem 3.5 The random positive valuation on the lattice $(\mathbb{R}_+^n, [\cdot])$ is uniformly continuous.

Proof. We recall from Example 3.3 that given $p = (p_1, \dots, p_n) \in \mathbb{R}_+^n$, we define $[p] = p_1\xi_1 + \cdots + p_n\xi_n$, where $\xi_1, \dots, \xi_n \in L_0^+(\Omega)$ and each $\xi_i \neq \Theta$. Now consider the RM lattice $(\mathbb{R}_+^n, \mathcal{X})$ induced by $[\cdot]$, where $\mathcal{X}(p, q) = X_{pq} = [p \vee q] - [p \wedge q]$, given $p = (p_1, \dots, p_n)$, $q = (q_1, \dots, q_n) \in \mathbb{R}_+^n$. We will show that for each $\varepsilon > 0$ and $\lambda \in (0,1)$ there exist a $\delta > 0$ and an $\alpha \in (0,1)$ such that whenever $P(X_{pq} < \delta) > 1 - \alpha$ we have $P(|[p] - [q]| < \varepsilon) > 1 - \lambda$. To this end, let $\varepsilon > 0$ and $\lambda \in (0,1)$ be given. Now we have
$X_{pq} = [p \vee q] - [p \wedge q] = [(p_1 \vee q_1, \dots, p_n \vee q_n)] - [(p_1 \wedge q_1, \dots, p_n \wedge q_n)]$
$= (p_1 \vee q_1 - p_1 \wedge q_1)\xi_1 + \cdots + (p_n \vee q_n - p_n \wedge q_n)\xi_n = |p_1 - q_1|\xi_1 + \cdots + |p_n - q_n|\xi_n$.
On the other hand, we have
$|[p] - [q]| = |(p_1 - q_1)\xi_1 + \cdots + (p_n - q_n)\xi_n| \leq |p_1 - q_1|\xi_1 + \cdots + |p_n - q_n|\xi_n$. If $X_{pq} < \delta$, then $|[p] - [q]| < \delta$. This implies that $P(|[p] - [q]| < \delta) > 1 - \alpha$ whenever $P(X_{pq} < \delta) > 1 - \alpha$. Now choose $\delta = \varepsilon$ and $\alpha = \lambda$. This gives $P(|[p] - [q]| < \varepsilon) > 1 - \lambda$, as desired. ■

4. CONCLUSION

In the current work, we have first introduced the concepts of almost certainly betweenness and probably betweenness in an RM space. Next, we have introduced the concept of an RM lattice via the notion of a random positive valuation on a lattice. In this context, we have also investigated a betweenness relation in RM lattices. Finally, we have examined the uniform continuity of the random positive valuation on a special lattice. A further study can be the investigation of topological properties of RM lattices.

REFERENCES

Birkhoff, G. (1973). Lattice Theory. American Mathematical Society.

Blumenthal, L.M. (1970). Theory and Applications of Distance Geometry. Chelsea.

Brown, J.B. (1972). Stochastic metrics. Z. Wahrscheinlichkeitstheorie Verw. Geb. 24, 49-62.

Burago, D., Burago, Y. & Ivanov, S. (2001). A Course in Metric Geometry. American Mathematical Society.

Busemann, H. (1942). Metric Methods in Finsler Spaces and in the Foundations of Geometry. Princeton University Press.

Gromov, M., Katz, M., Pansu, P. & Semmes, S. (2007). Metric Structures for Riemannian and Non-Riemannian Spaces. Birkhäuser.

Guo, T.-X. (1999). Some basic theories of random normed linear spaces and random inner product spaces. Acta Anal. Funct. Appl. 1, 160-184.

Guo, T.-X. (2001). Survey of recent developments of random metric theory and its applications in China I. Acta Anal. Funct. Appl. 3, 129-158.

Guo, T.-X., Zhao, S.-E. & Zeng, X.-L. (2014). The relations among the three kinds of conditional risk measures. Science China: Mathematics, 57, 1753-1764.

Menger, K. (1928). Untersuchungen über allgemeine metrik. Mathematische Annalen, 100, 75-163.

Papadopoulos, A. (2014). Metric Spaces, Convexity and Non-positive Curvature. European Mathematical Society.

Roy, S. (1998). Statistical Geometry and Applications to Microphysics and Cosmology. Springer Science+Business Media.

Schweizer, B. & Sklar, A. (1983). Probabilistic Metric Spaces. North-Holland (Reissued: Schweizer, B. & Sklar, A.: Probabilistic Metric Spaces. Dover Publications, 2005).

Sherwood, H. (1970). Betweenness in probabilistic metric spaces. Rev. Roumaine Math. Pures Appl., 15, 1061-1068.

Špaček, A. (1956). Note on K. Menger's probabilistic geometry. Czechoslovak Math. J. 6, 72-74.

Špaček, A. (1960). Random metric spaces. In: Transactions of the Second Prague Conference on Information Theory, Statistical Decision Functions and Random Processes (pp. 627-638). Prague.

➢ *ORAL PRESENTATION*

Assessment of eating habits, physical activity, and lifestyle among medical students at the University of Medicine, Tirana (2025)

Floriana Marku[1],[2]*, Loreta Kuneshka[3],[4]

[1] External Lecturer at the Department of Public Health, Faculty of Medicine, University of Medicine, Tirana
[2] Full-time Lecturer at Aldent University, Tirana
[3] Internal Lecturer at the Department of Public Health, Faculty of Medicine, University of Medicine, Tirana
[4] Dermatologist at the Specialties of the Pediatric Hospital, QSUNT, Tirana

Abstract

Introduction: Medical students face many challenges in adapting to a healthy lifestyle due to their busy schedules and academic demands.
Objectives: This study aims to assess eating habits, physical activity, and health-related behaviors among medical students, identifying factors influencing unhealthy behaviors.
Methods: The study included 213 students (78.9% female) from the University of Medicine, Tirana, who completed a questionnaire. Data were analyzed using SPSS v27.
Results: The average age of participants was 20.2 ± 1.5 years. Results showed that 7% of students were underweight, 69.8% had normal weight, and 22.1% were overweight or obese. The average sleep duration was 5.9 ± 1.5 hours at night, and 67.6% of students napped during the day when possible. 43% of students did not have breakfast daily. Fast food and energy drinks were consumed 1-2 times per week. Physical activity was limited, with 48.1% exercising less than one hour per week. Half of the students felt stressed due to academic demands. Students with more sleep problems felt more distracted and insecure about their mental health ($p = 0.000$). Furthermore, those who slept more were less likely to engage in physical activity ($p = 0.005$).
Conclusions: The results suggest that despite knowledge of healthy lifestyles, students often do not implement these practices, which may pose significant challenges to their professional careers.
Keywords: Students; medicine; eating habits; physical activity; health; lifestyle.

1. Introduction

The university period is a transformative phase during which students establish lifelong habits that significantly affect their health and well-being. Medical students, in particular, face unique challenges due to their demanding academic schedules, stress, and irregular daily routines, which often lead to poor dietary patterns, low physical activity, and an overall unhealthy lifestyle (Palatty et al., 2013; Haq et al., 2016). Despite having extensive theoretical knowledge about healthy behaviors, many medical students struggle to apply these principles in practice. Globally, the prevalence of overweight and obesity among young adults has been steadily increasing. According to the Behavioral Risk Factor Surveillance System (BRFSS, 2021), individuals aged 18–29 are particularly vulnerable to adopting unhealthy lifestyle behaviors that contribute to weight gain and related health issues. Poor eating habits, such as the consumption of high-calorie, nutrient-poor foods and the low intake of fruits, vegetables, and fiber, are common among students (Ganasegeran et al., 2012; Williams et al., 2019). Combined with physical inactivity, these behaviors significantly elevate the risk for chronic conditions such as cardiovascular disease, type 2 diabetes, and certain cancers (Racette et al., 2005; Tafoya et al., 2017). Numerous studies have shown that medical students frequently experience high levels of stress and sleep disturbances, both of which negatively impact their lifestyle choices (Palatty et al., 2013). Even though they understand the importance of regular physical

activity, many report limited time or motivation to exercise due to academic pressure (Williams et al., 2019). This dissonance between knowledge and behavior is concerning, as the habits formed during medical school are likely to persist into their future careers and influence their ability to model and promote healthy behaviors to patients (Haq et al., 2016). This study aims to assess the eating habits, physical activity levels, and overall lifestyle of medical students at the University of Medicine in Tirana in 2025. By identifying current behaviors and potential risk factors, the study seeks to provide insights that can inform targeted interventions and health education strategies. Ultimately, promoting healthier lifestyles among medical students is essential - not only for their personal well-being but also for their credibility and effectiveness as future healthcare providers.

2. Materials and Methods

2.1 Study Population and Data Collection

The study was conducted between January and March 2025 at the University of Medicine in Tirana, Albania, involving 500 medical students across all academic years. Participants were informed about the study's purpose and data confidentiality, with the assurance that they could withdraw at any time without consequences. Only fully completed questionnaires submitted on time were included in the analysis, resulting in 213 valid responses. A specially designed questionnaire was distributed via Google Forms, consisting of sociodemographic and anthropometric data, dietary intake (fruits, vegetables, meat, eggs, fish, sweets, and fast food), and information on eating habits, stress, sleep, physical activity, and consumption of coffee, tea, and carbonated drinks, etc.

2.2 Statistical Analysis

Data were analyzed using SPSS Statistics (version 27). Descriptive statistics, including mean and standard deviation (SD), CI, were calculated. Body Mass Index (BMI) was derived from self-reported height and weight and classified according to WHO guidelines. Non-parametric tests, including Spearman's correlation, Mann–Whitney U, and Kruskal–Wallis, were applied to analyze relationships and differences between variables with a significance level of $p \leq 0.05$. Logistic regression analysis was used to assess the impact of risk factors on health outcomes, with the odds ratio (OR) indicating the strength of the association: $OR < 1$ signifying a risk factor, $OR = 1$ indicating no association, and $OR > 1$ indicating a protective factor for health.

2.4 Ethical Approval

The study was conducted in accordance with the Declaration of Helsinki, and the questionnaire was approved by Assoc.Prof. Loreta Kuneshka. All participants provided informed consent prior to their participation, and all data were treated with strict confidentiality.

3. Results

3.1 Socio-Demographic, Anthropometric, and Medical Data

The study sample consisted of 213 students, with the majority being female participants (78.9%, N=168). The median age group was 18-21 years, with a median age value of 21 years, and the average age was 20.2±1.51 years. According to the academic year, 5.2% were in the first year, 58.7% in the second year, 13.6% in the third year, 16.9% in the fourth year, 1.9% in the fifth year, and 3.8% in the sixth year. BMI evaluation showed that 7.0% were underweight, 69.8% had normal weight, 20.3% were overweight, 1.9%

had class 1 obesity, and 0.9% had class 2 obesity. The average BMI of the students was 22.63 ± 3.40 kg/m²; 95% CI: 22.170–23.091.

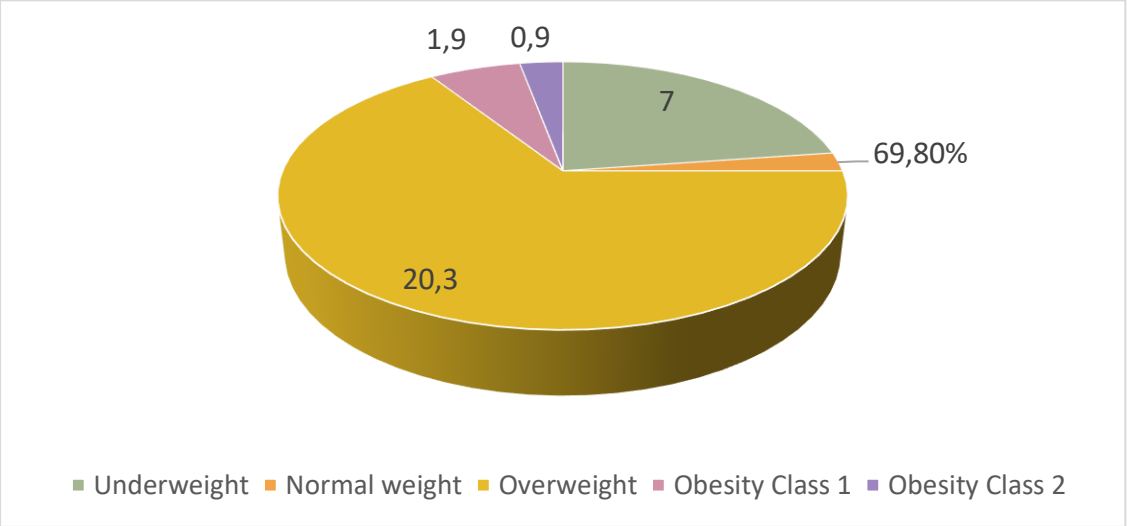

Graph 1. BMI Classification Among Medical Students

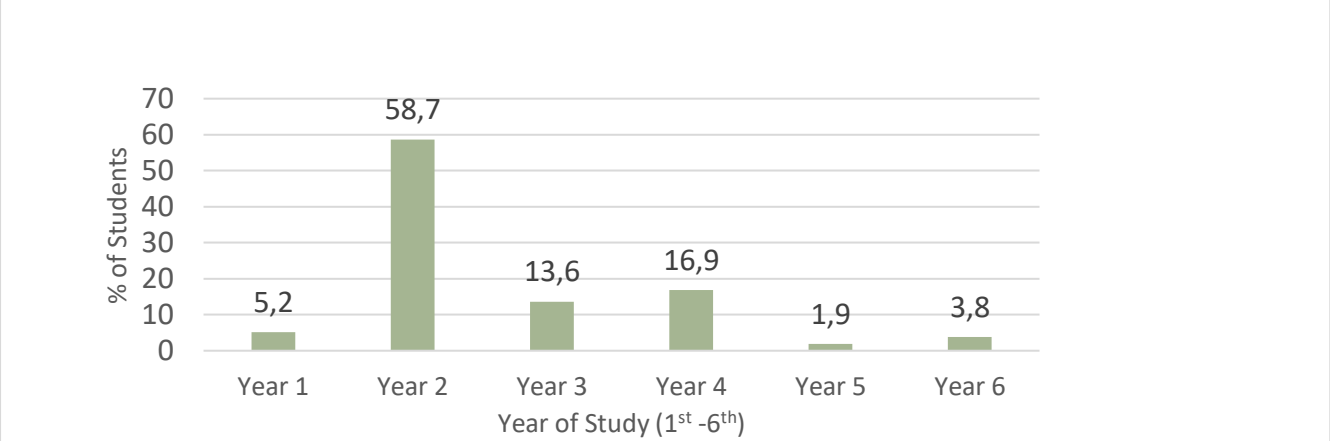

Graph 2. Distribution of Students by Year of Study

Table 1: Descriptive Statistics for BMI

Statistics		**Value**
Sample size (n)		213
Mean (Average)		22.63 kg/m²
BMI	Male	24.75 kg/m²
	Female	22.06 kg/m²
Standard Deviation		± 3.40 kg/m²
Minimum		16.5
Maximum		36.6
95% Confidence Interval		22.170 – 23.091 kg/m²
BMI by Age Group	18-21 years old	22.67
	22-24 years old	22.25
	25-27 years old	24.95

3.2 Association Between BMI and Other Variables

There was a statistically significant difference in BMI between male and female students ($r = 0.32$, $p < 0.001$). No significant difference in BMI was found between different age groups ($r = -0.02$, $p = 0.272$). Higher academic stress was associated with lower BMI ($r = -0.151$, $p = 0.028$). Additionally, students who felt uncertain about their mental health had lower BMI, with a negative correlation found ($r = -0.206$, $p = 0.003$). Students who were more satisfied with their current weight tended to have a more balanced BMI ($r = 0.287$, $p < 0.001$). Lastly, students with higher BMI were less likely to follow diets ($r = -0.314$, $p < 0.001$).

3.3 Satisfaction with Weight and Health Assessment

Students were asked about their satisfaction with their body weight. The majority expressed satisfaction (43.2%, N=92). Regarding health, most students reported feeling good (46.5%, N=99), while a small number had chronic conditions such as chronic tonsillitis, chronic sinusitis, irritable bowel syndrome, and chronic body acne, each with the same percentage (0.5%).

3.4 Food Consumption

The students were asked to estimate the consumption of foods in each food group: fruits, vegetables, dairy products, meat, eggs, sweets, and fast food. Table 2 below shows the consumption frequency of certain food categories, such as fruits, meat, and dairy, vegetables during a week. The graphic representation of consumption of fruits, meat, and dairy products, vegetables are presented in Graph 3.

Table 2. Fruit, vegetables, meat, and dairy products.

Food Item	**Frequency (M ± SD) ***	**Total (*N* = 213)**
Fruits	3.23 ± *1.026*	Daily-30.0% (n=64), 3-4 times/week-31.0% (n=66), 1-2 times/week- 25.4% (n=54), no consumption-2.3% (n=5).
Vegetables	3.20 ± *0.778*	Daily-34.7% (n=74), 3-4 times/week-44.1% (n=94), 1-2 times/week- 18.3% (n=39), no consumption-0.5% (n=1).
Meat	2.63 ± *0.718*	Daily-9.9% (n=21), 3-4 times/week-45.1% (n=96), 1-2 times/week- 41.8% (n=89), no consumption-2.8% (n=6).
Dairy	3.18 ± *0.971*	Daily-37.1% (n=79), 3-4 times/week-31.0% (n=66), 1-2 times/week- 22.5% (n=48), no consumption-3.8% (n=8).

* Means (M)and standard deviations (SD).



Graph 3. Consumption of fruits, vegetables, meat, and dairy products

The data reveal generally positive trends in students' dietary habits, particularly in fruit and vegetable intake, though improvement is still needed. Around 30% of students consume fruit daily, and 31% eat it 3–4 times per week. For vegetables, 34.7% consume them daily, and 44.1% eat them 3–4 times weekly. Meat consumption is common, with 45.1% eating it 3–4 times per week and 41.8% 1–2 times weekly. Milk is also widely consumed, with 37.1% drinking it daily. Fish intake is notably lower, as 72.3% eat fish only 1–2 times per week, and 24.4% do not consume it at all. Eggs are more frequently included in the diet, with 37.6% eating them 3–4 times weekly. Sweets and fast food are regularly consumed—41.3% eat sweets 1–2 times per week, and 61.0% consume fast food at the same frequency. **Correlation analysis** (Spearman's rank) shows significant positive relationships between healthy dietary behaviors. Fruit consumption correlates strongly with vegetable intake ($r = 0.423$, $p < 0.001$) and moderately with fish consumption ($r = 0.184$, $p = 0.007$). Higher fruit intake is also associated with increased physical activity ($r = 0.189$, $p = 0.006$), regular breakfast consumption ($r = 0.234$, $p = 0.001$), and consistent meal timing ($r = 0.229$, $p = 0.001$). Similarly, vegetable intake is linked to regular meals and higher meat consumption. Fish consumption is positively associated with both fruit and meat intake. These findings suggest that healthy habits tend to cluster—students who make one healthy choice are more likely to engage in other beneficial behaviors, indicating a broader pattern of health-conscious living.

3.5 Liquid Intake: Carbonated Drinks, Tea, Coffee, Energy drinks

Regarding carbonated drinks, 37.6% of students reported never consuming them, while 40.4% consumed them 1-2 times a week. A smaller percentage, 17.4%, drank them 3-4 times a week, and only 4.7% drank them every day. For tea, 31% of students never drank it, while 40.4% had it 1-2 times a week, 17.8% 3-4 times a week, and 9.9% consumed it daily. In coffee consumption, 39.9% of students never drank coffee,

14.6% consumed it 1-2 times a week, 11.7% 3-4 times a week, 25.8% drank it daily, and 8% several times a day. As for energy drinks, 50.2% never consumed them, 27.2% had them 1-2 times a week, 13.1% 3-4 times a week, 8.5% daily, and 0.9% several times a day.

3.6 Physical Activity

Data on physical activity showed a variety of habits among students. The median activity level was 1–3 hours per week, with a median value of 2.915 hours per week and an average of 94.93±72.2 minutes, or 1.58±1.2 hours per week. Approximately 24.9% (N = 53) of participants reported engaging in physical activity every day. The most common activities were walking (53.5%), going to the gym (23.9%), running (5.16%), and cycling (4.2%), with the remainder participating in sports like basketball, volleyball, and yoga. Furthermore, 86.4% (N = 184) of students reported walking every day, either for school or leisure. However, 53.05% (N = 113) did not engage in moderate or vigorous activities such as running, swimming, or gym exercises. Regarding frequency, 48.36% (N = 103) of participants exercised less than one hour per week, 60% (N = 128) exercised 1–3 hours per week, 27% (N = 57) exercised 3–5 hours per week, and 23% (N = 49) exercised for more than 5 hours per week. Physical activity was significantly associated with several factors. Males engaged in more physical activity than females ($r = -0.281$, $p < 0.001$). Students who were more stressed exercised less ($r = -0.273$, $p < 0.001$), and those who felt insecure about their mental health also exercised less ($r = -0.158$, $p = 0.021$). Additionally, more physically active students consumed more fruits ($r = 0.189$, $p = 0.006$), while students who skipped breakfast tended to exercise more ($r = -0.162$, $p = 0.018$). A negative association was also found between daily physical activity and hours of moderate activity per week ($r = -0.289$, $p < 0.001$). More physical activity was linked to less sleep ($r = -0.197$, $p = 0.004$), and students who ate at regular times tended to engage in less physical activity ($r = -0.24$, $p < 0.001$).

3.7 Sleep

The median class for sleep duration among students is 5–6 hours per night, with 51.6% (N=110) falling into this category. The median value is 5.203 hours, and the average sleep duration is 5.906 ± 1.468 hours per night. According to the Mann-Whitney U test, there is no statistically significant difference in sleep duration between males and females. A majority of students, specifically 67.6% (N=144), reported preferring to sleep in the afternoon when possible, while 35.7% (N=76) indicated that they experience sleep problems. Sleep duration is associated with several factors. Students who engage in more physical activity tend to sleep less ($r = -0.197$, $p = 0.005$), and those who consume more energy drinks also tend to have shorter sleep durations ($r = -0.190$, $p = 0.005$). More sleep is linked to fewer reported sleep problems ($r = -0.246$, $p < 0.001$). Interestingly, students who eat at regular meal times tend to sleep less ($r = -0.188$, $p = 0.006$), which may be due to a more structured and busier daily routine.

3.8 Stress

The majority of students experience frequent stress due to academic and student life pressures, with 57.7% feeling stressed "very often" and 32.4% several times a week. Most students manage stress by talking with friends or family (41.3%), while others rely on physical activity (17.8%) or do not have a preferred method (33.8%). Stress is significantly associated with lower BMI ($r = -0.151$, $p = 0.028$), being female ($r = 0.349$, $p < 0.001$), and engaging in less physical activity ($r = -0.273$, $p < 0.001$). It is also linked to greater mental insecurity ($r = 0.363$, $p < 0.001$), higher consumption of sweets ($r = 0.222$, $p = 0.001$), poorer eating habits ($r = 0.136$, $p = 0.047$), and more sleep problems ($r = 0.188$, $p = 0.006$). Additionally, there is a near-significant association between stress and fast food intake ($r = 0.129$, $p = 0.060$).

3.9 Dietary Choices and Lifestyle: Diet, Regular Eating Schedules, Meal Frequency

One-third of students (36.2%, N = 76) follow diets to lose weight, with more females than males adhering to such diets. More than half of the students had irregular eating schedules (64.8%, N = 138). The meal most commonly skipped was breakfast, compared to lunch and dinner (56.8%, 8.5%, and 31.5%, respectively).

3.10 Logistic Regression Analysis: Health Assessment

Through logistic regression analysis, the relationship between various factors and students' health, categorized as either good or poor, was examined. The odds ratio (Exp(B)) and p-values for each variable show how each factor influences health. Eating at home during the week (Exp(B) = 1.292, p = 0.031), fruit consumption (Exp(B) = 1.461, p = 0.014), physical activity (Exp(B) = 1.293, p = 0.004), sleep hours per night (Exp(B) = 1.918, p = 0.028), and satisfaction with current weight (Exp(B) = 1.067, p = 0.012) are positive factors associated with good health. On the other hand, consumption of sweets (Exp(B) = 0.819, p = 0.005), consumption of fast food (Exp(B) = 0.545, p = 0.012), sleep problems (Exp(B) = 0.07, p = 0.033), academic/student stress (Exp(B) = 0.881, p = 0.022), and insecurity about mental health (Exp(B) = 0.977, p = 0.016) are negative factors linked to poorer health.

4. Discussion

The findings of this cross-sectional study, involving 213 medical students—168 females and 45 males—mirror international trends that show a growing female majority in medical education (Medical Schools Council, 2020). Regarding body mass index (BMI), 7.0% of participants were underweight, 69.8% had normal weight, 20.3% were overweight, and 2.8% were classified as obese. These values are consistent with other international studies, including those from Brazil and Romania, which show a similar distribution of BMI among medical students (Federal University of Paraíba, 2019; Magdalena et al., 2019). Dietary habits observed in the study raise concerns. An overwhelming majority of students reported frequent consumption of fast food (85.9%) and sweets (94.8%), which is higher than figures reported in studies conducted in Serbia and other regions (Gazibara et al., 2013). This pattern is not unique to Albania, as similar trends have been documented in various countries and are often attributed to stress and limited time for meal preparation among medical students (Ganasegeran et al., 2012; Smith & Leggat, 2019). Although these students are knowledgeable about nutrition, their actual dietary behaviors reflect the pressures of medical school life. Sleep duration was also found to be inadequate, with students averaging 5.9 ± 1.47 hours of sleep per night, falling short of the 7-hour minimum recommended by the American Academy of Sleep Medicine. This aligns with prior studies showing that sleep deprivation is prevalent among medical students and is associated with poor mental health and academic difficulties (Palatty & Krishnan, 2013; Band & Lee, 2019). In terms of physical activity, while 86.4% of participants reported walking daily, more than half (53.05%) did not engage in moderate or vigorous physical activities such as running, swimming, or going to the gym. Only a subset met the World Health Organization's recommendation of at least 150 minutes of moderate physical activity per week (Izawa et al., 2021). Additionally, consistent with global findings, male students were more likely to participate in physical exercise than their female counterparts (Wall & Choi, 2019; Keating et al., 2005. These findings highlight the importance of integrating wellness initiatives and stress management programs into medical curricula to promote healthier lifestyles among future healthcare providers.

5. Conclusions

Medical students possess substantial knowledge about healthy living, yet many struggle to apply it due to the demanding nature of their training. This gap between knowledge and practice is concerning, given their future role in promoting public health. Unhealthy habits—such as poor diet, lack of physical activity, and inadequate sleep—are common and often driven by stress and irregular schedules. To support student well-being, a comprehensive, health-oriented university campus is essential, ideally integrated with the "Mother Teresa" University Hospital Center. This campus should offer student healthcare services, mental health support, wellness facilities, nutritious food options, and accessible digital and transport systems. Such an environment would encourage students to prioritize both academic success and personal health—critical skills for their future roles as healthcare providers.

References

1. American Heart Association. (2017). *Dietary recommendations for heart health*. https://www.heart.org/en/healthy-living/healthy-eating
2. Band, M., & Lee, L. (2019). Sleep patterns among college students. *Sleep Health Journal, 12*(4), 305–309. https://doi.org/10.1016/j.sleh.2019.06.003
3. Centers for Disease Control and Prevention. (2021). *Behavioral Risk Factor Surveillance System (BRFSS)*. https://www.cdc.gov/brfss/
4. Federal University of Paraíba, Medical Course. (2019). *Prevalence of factors associated with cancer in medical students and sex-related differences*. João Pessoa, Brazil.
5. Ganasegeran, K., Ramasamy, M., & Al-Dubai, S. A. R. (2012). Dietary habits of medical students and their impact on health. *Journal of Public Health, 34*(4), 458–467. https://doi.org/10.1007/s10389-012-0504-5
6. Gazibara, T., Tepavcevic, D. B. K., Popovic, A., & Pekmezovic, T. (2013). Eating habits and body-weights of students of the University of Belgrade, Serbia: A cross-sectional study. *Journal of Health, Population and Nutrition, 31*(3), 330–333. https://doi.org/10.1186/jhpn2013132
7. Haq, I., Habib, A., & Shah, S. (2016). Health behaviors and physical activity patterns among medical students. *Medical Education Online, 21*(1), 30780. https://doi.org/10.3402/meo.v21.30780
8. Izawa, S., Kim, Y., & Tanaka, M. (2021). Physical activity and sleep quality in university students. *Journal of Health Promotion, 30*(3), 235–242. https://doi.org/10.5001/jhp.2021.0237
9. Keating, X. D., Guan, J., Piñero, J. C., & Bridges, D. M. (2005). A meta-analysis of college students' physical activity behaviors. *Journal of American College Health, 54*(2), 116–125. https://doi.org/10.3200/JACH.54.2.116-125
10. Magdalena, B., et al. (2019). Nutritional status and associated factors among Romanian medical students. *Romanian Journal of Nutrition*.
11. Medical Schools Council. (2020). Trends in medical student demographics. *Journal of Medical Education, 34*(2), 142–147. https://doi.org/10.1097/00001888-202005000-00008
12. Palatty, P. L., & Krishnan, A. (2013). Sleep disturbances and stress among medical students. *Journal of Clinical Psychiatry, 74*(5), 551–556. https://doi.org/10.4088/JCP.12r08068
13. Racette, S. B., Deusinger, S. S., & Deusinger, R. H. (2005). Changes in eating habits and weight gain during the first year of college. *Journal of American College Health, 53*(6), 229–234. https://doi.org/10.3200/JACH.53.6.229-234
14. Smith, W., & Leggat, P. (2019). Coffee consumption among students. *Journal of Nutrition and Coffee Studies, 29*(1), 11–17. https://doi.org/10.1016/j.jnutcof.2018.10.005
15. Tafoya, G., Delgado, S., & Cornejo, R. (2017). Factors influencing the health behaviors of medical students. *Journal of Medical Education, 25*(3), 134–140. https://doi.org/10.1177/2150131917694676

16. Wall, B., & Choi, M. (2019). Physical activity programs in universities: A global overview. *Journal of Higher Education Health, 11*(3), 195–203. https://doi.org/10.1016/j.jheh.2019.07.006
17. Williams, A., & Smith, B. T. (2019). Western dietary patterns and exercise among medical students. *International Journal of Medical Education, 10*, 95–102. https://doi.org/10.5116/ijme.5d27.b7d9

➢ *ORAL PRESENTATION*

Literature review of orofacial praxis skills in children with autism spectrum disorder

Dorela Kokthi[1], (https://orcid.org/0009-0006-2926-0238), Manika Kreka[2], (https://orcid.org/0000-0003-2780-8555)

[1]University of Medicine, Faculty of Medical Technical Sciences, Diagnostic and Rehabilitation Department, Tirana, Albania
[2]University of Medicine, Faculty of Medicine, Department of Pediatrics, Tirana, Albania

Abstract

Orofacial praxis skills (face, mouth and tongue movements) are critical for speech, social interaction, and general adaptability. These types of movements are rather challenging in children suffering from autism spectrum disorder (ASD), which hinders them undergoing expressive speech and interaction with other people. In this context, this article discusses the orofacial praxis deficits in children suffering from ASD, particularly the neglect of the motor planning deficits caused by the neurological, sensory and social factors. Numerous studies point out difficulties for children with ASD in praxic imitation and in verbal or nonverbal communication containing sequentially organized orofacial movements. These issues are not simply due to lack of muscle strength; they stem from an impaired motor planning system. On the other side, differential diagnosis of orofacial praxis skills requires assessment of a motor execution versus motor planning problem using tools like the Verbal Motor Production Assessment for Children and the Kaufman Speech Praxis Test for Children. Deficit focused therapy for orofacial praxis skills such as motor-based therapies including the PROMPT technique, oromotor therapy, and augmentative and alternative communication (AAC) strategies has greater impact on patient outcomes. With parental engagement, the effectiveness of the intervention is further enhanced through increased naturalistic practice opportunities. Despite gaps in longitudinal studies, less is known about neuroimaging, and comparative intervention research, progress in understanding orofacial praxis concerning ASD has advanced. Therefore, if orofacial praxis deficits are treated early and effectively, not only is there potential for better outcomes related to advancing speech in those with ASD, but also for enhancing broader social and cognitive outcomes. Praxia skills are not only crucial for developing the autism spectrum but they also deepen the understanding of strategies that better respond to the developmental potential of individuals on the autism spectrum.

Keywords: orofacial praxis, autism spectrum disorder, neurodevelopment, assessment, communication.

INTRODUCTION

The importance of recognizing developmental disorders as early as possible is increasing due to the clearly defined enhanced benefits of striking the fundamental core of the issues at hand. In this line, some areas which are part of the early developmental assessment include orofacial praxis skills, defined as planning and executing the coordinated movements of the face, mouth, and tongue which has been pinpointed as markers for neurodevelopment. In addition, Belmonte, et al (2013) claims that children diagnosed with autism spectrum disorder (ASD) tend to show deficits in areas which include motor skills, communication skills, and emotions and socialization. Therefore, orofacial praxis skills are largely accepted as prerequisite not only for speech, but also for various social interaction and social communication. Orofacial praxis skills are critical to devise treatment plans at enabling children with ASD improve their speech-language skills.

MATERIAL AND METHODS

This article uses an extensive literature review to gather information pertaining to the orofacial praxis skills of children with Autism Spectrum Disorder (ASD). For this review, peer-reviewed journal articles, clinical case studies, and pertinent textbooks published between 2008 and 2024 were sourced from academic databases like PubMed, Scopus, and Google Scholar. The search was conducted with the terms “orofacial praxis,” “motor planning,” “autism spectrum disorder,” “speech development,” and “oromotor deficits.” The studies selected for the review were centered on the assessment, underlying neuroscience, and therapeutic approaches to motor planning orofacial tasks for children with ASD. To achieve a rigorous review, priority was given to primary research, clinical studies, and systematic reviews.

Literature Review

The Role and Importance of Orofacial Praxis

Praxis is often described as the capacity to formulate and enact new motor behavioural actions. According to Fournier, et al (2010) orofacial praxis refers to the planning and execution of mouth, lip, tongue, jaw movements either as a NVU center and C center. These activities are critical for carrying out fundamental tasks such as eating, swallowing, making facial movements, and most importantly, producing speech. Speech is one of the most complex motor tasks involving high level of precision in the timing, degree, coordination and sequencing of the movements of the mouth and face. Problems with orofacial praxis may cause a breakdown in these activities leading to a variety of communication problems including: childhood apraxia of speech (CAS), articulation problems, and even dificulties with feeding. In children with ASD, orofacial praxis difficulties could worsen existing language deficits and complicate social interactions, given communication impairments are core diagnostic features. In addition, nonverbal orofacial movements like smiling, pouting, and tongue protruding are important for nonverbal communication. Deficits in these abilities may limit a child's ability to socially interact, recognize other's emotions, or express their emotions which may further trap them in a world that is already socially difficult.

Orofacial Praxis Deficits in Children with Autism Spectrum Disorder

Children diagnosed with ASD often showcase a decline in fine motor and gross motor skills, as well as oromotor functions. Gernsbacher et al (2008) study documents the main problems this population encounters with controlling the orofacial apparatus, such as initiating, organizing, and coordinating orofacial movement. Unlike children who have primary speech disorders, these children tend to have more diffuse and extensive motor planning disruption. A notable feature of many children with ASD is the gap between their functioning level of receptive language and expressive language skills. Some researchers argue that this discrepancy is mainly due to an orofacial apraxic deficit. The subtleties of motor planning and the sequencing of movements relevant to articulation can make speech extremely difficult to produce for some children, even though they understand complex verbal instructions. Alongside speech problems, children with autism spectrum disorders (ASD) frequently display difficulties with nonverbal face-related movements. Jones, L. (2008) in his research highlights that many children with ASD cannot easily imitate basic facial movements or gestures, even when asked to do so. This is a crucial deficit because it impacts not only the child's speech abilities, but also their core ability to express emotions and intentions which are central to social interaction.

Assessment of Orofacial Praxis in Autism Spectrum Disorder

Whiteside, S. P., (2015) mentions that clinicians are familiar with the VoCab VMPAC and the Kaufman Speech Praxis Test for Children as systematic measures of oromotor planning abilities. As such, the multifactorial condition of motor planning difficulties justifies that such would call for a comprehensive evaluation, one that is more than the child's orofacial reflexes within structured play, but also includes studying the orofacial movement in functional tasks to give a better picture of the child's abilities. Content Emerging out of Clinical Assessment would be the capacity of the child to imitate individual orofacial motions with several other intermediary actions-like multi-step sequences, nonverbal gestures, and polysyllable voiced utterance-involve, particularly for determining movements related to speech. To derive specific expected outcomes from interventions would, among other things, depend on the correct evaluation of orofacial praxis skills in children with ASD and require specific techniques and tailored treatments. Clinically, it would also involve being able to discriminate two groups among those with a motor-sequencing disorder-those with a planning disorder within a tight timeframe and space (praxis) and those with inactive muscles or paralysis (execution). An activity deficit-and certainly not weakness-would be advanced as a claim for a child who is capable of executing a movement but cannot initiate it.

Factors Influencing Orofacial Praxis in Children with Autism Spectrum Disorder

As Bhat, at al (2011) point out, there are many different factors interfering with orofacial praxis deficits in children with ASD. Movement abilities in an individual has been looked into using neuroimaging assessment studies of activation from planning motor areas like premotor cortices, cerebellum, and basal ganglia. The pets' evidence found the tendency of children with autism for abnormal oroband facial motor acts resulting in an issue either to activate or to coordinate motor oroband and face muscles. Herein lies further complication, as overlaps with other conditions like DCD or Childhood Apraxia of Speech and the

autism spectrum are fairly common. Most notably, this shows that some set kids in the spectrum are indeed restricted socially and cognitively, and suffer from major planning and executing deficits. Sensory processing difficulties also come into play. Hypersensitivity and hyposensitivity to touch, especially about the mouth and face, are typical in children with ASD. Such sensitivity would not allow a child to engage normally in orofacial actions, including eating, mouthing toys, or imitating facial expressions, thus depriving children of opportunities for acquiring simple oromotor skills. Social and motivational factors must also be taken into consideration. Reduced social motivation, which is typical for ASD, typically also means less spontaneous imitation and social interaction involving orofacial movements, which occurs even less frequently. Hence, such children pass up on those practice opportunities which eventually lead to further worsening of the initial motor planning deficits.

Therapeutic Implications

Ways to treat orofacial praxis deficits are significant for enhancing the communication skills of children with autism spectrum disorders. Motor-based speech therapy, like the PROMPT method, use tactile-kinesthetic cues to assist the child with the orofacial movements during speech. LeBarton, E. S., and Iverson, J. M. (2013) in his study indicate that PROMPT aids in motor learning by providing sensory feedback that facilitates planning and sequencing movements. Other forms of treatment should also be useful. These treatments usually include repetitive practice of single as well as combined facial movements in a particular order, series or pattern, which increase in difficulty as the child becomes more adept. Activities include exercises or actions for blowing bubbles, lip puckering, tongue lateralization, and producing speech sounds which are blended into words and phrases. Where there is marked delay in expressive language skills, augmentative and alternative communication (AAC) systems may be implemented. Picture exchange systems, sign language, or even speech generating devices offer an alternative form of communication that greatly aid in reducing frustration and increasing social participation while speech skills are still being developed. Another important factor of successful intervention is the parental involvement in supporting therapy sessions. Parents knowing in advance what orofacial movements need to be elicited during interactions like meals, playtime, or stories to their children increases the child's daily practice of these skills. Parents also can have their children engage with exaggerated facial expressions, playful mouth movements, learning theatre where learning is devoid of pressure, still mastering motor skills.

4. RESULTS AND DISCUSSION

The literature review findings suggest that children diagnosed with Autism Spectrum Disorder (ASD), face profound challenges with orofacial praxis impacting both verbal and non-verbal communication skills. Research suggests that these deficits are associated with impaired motor planning and not due to muscle weakness, stemming instead from atypical neural functioning in the cerebellum or premotor cortex. The studies under review also highlight that early diagnosis using standardized assessment tools improves intervention effectiveness and accuracy. There is documented improvement in expressive speech as a result of motor oriented interventions, especially the PROMPT method and some oromotor strengthening exercises. In addition, caregivers and the use of augmentative and alternative communication (AAC) systems are critical for nurturing supportive communication. Notwithstanding the progress made, there is a need for further longitudinal and neurobiological studies to refine treatment individualization strategies for children with ASD.

CONCLUSION

Orofacial skill is an area of a child's development that impacts speech output, as well as social communication and general functioning. In children with autism spectrum disorder, the lack of orofacial skills severely impacts the ability to communicate and socialize. Apart from these challenges, there is a multitude of other pre-existing problems encountered which further complicates the matter. To address these gaps appropriately, precise evaluative measures and prompt remedial solutions within the mentioned frameworks serve to be very effective. Motor-based therapies, augmentation of communication methods, active participation of the guardians, as well as systematic oromotor exercises are examples of vital steps within a holistic intervention plan. With advancing understanding of the neurological and developmental factors associated with orofacial skills in cases of ASD, clinicians will have comprehensive frameworks that enable them to support the services enhancing the social and communicational engagement of children with autism. Shifting focus to the role of orofacial skills through working on the evidence-based strategies

aims for the betterment of communication and social behavior, thereby improving the quality of life for children suffering from Autism Spectrum Disorder.

ACKNOWLEDGMENTS

I want to express my heartfelt appreciation to the researchers and clinicians whose efforts have advanced the understanding orofacial activities among children diagnosed with autism spectrum disorder. I would like to direct my gratitude to the institutions and databases which made the relevant academic literature accessible. I thank my colleagues from the speech-language pathology and developmental psychology for their constructive comments and discussions during the preparation of this review. Finally, warm words of thanks go to the children with autism spectrum disorder and their families and caregivers, because their lived experiences form the basis of so much of the research and clinical work in this area.

REFERENCES

Belmonte, M. K., Allen, G., Beckel-Mitchener, A., Boulanger, L. M., Carper, R. A., & Webb, S. J. (2013). Autism and abnormal development of brain connectivity. *The Journal of Neuroscience, 24*(42), 9228–9231.

Fournier, K. A., Hass, C. J., Naik, S. K., Lodha, N., & Cauraugh, J. H. (2010). Motor coordination in autism spectrum disorders: A synthesis and meta-analysis. *Journal of Autism and Developmental Disorders, 40*(10), 1227–1240.

Gernsbacher, M. A., Sauer, E. A., Geye, H. M., Schweigert, E. K., & Hill Goldsmith, H. (2008). Infant and toddler oral- and manual-motor skills predict later speech fluency in autism. Journal of Child Psychology and Psychiatry, 49(1), 43–50.

Jones, L. (2008). Continuity of care and outcomes in residential care: A comparison of two care giving models. Residential Treatment for Children & Youth, 23(3-4), 119–138.

LeBarton, E. S., & Iverson, J. M. (2013). Fine motor skill predicts expressive language in infant siblings of children with autism. Developmental Science, n/a-n/a.

Whiteside, S. P., Dyson, L., Cowell, P. E., & Varley, R. A. (2015). The Relationship Between Apraxia of Speech and Oral Apraxia: Association or Dissociation? Archives of Clinical Neuropsychology, 30(7), 670–682.

➢ *ORAL PRESENTATION*

Restriksiyon enzimleri kullanılarak farklı türlerde cinsiyetin belirlenebilmesinin PZR-RFLP yöntemiyle araştırılması

Yusuf Özşensoy[1] (*ORCID: https://orcid.org/0000-0002-2605-2410)*

[1] Sivas Cumhuriyet Üniversitesi, Veteriner Fakültesi, Veterinerlik Genetiği Anabilim Dalı, Sivas, Türkiye

* Sorumlu yazar e-posta: yusufozsensoy@yahoo.com

Özet

Bazı adli olaylarda veya tüketime sunulan ürünlerde, örneklerin hem tür bazında hem de cinsiyet bazında tespit edilerek belirlenmesi istenilmektedir. Cinsiyet yönünden etlerin kalite ve satış fiyatları farklılıklarından dolayı tüketime sunulan etlerin hile yapılıp yapılmadığının belirlenmesi amacıyla cinsiyetlerinin tam olarak bilinmesi istenilmektedir. Moleküler temellere dayalı yapılan çalışmalar Amelogen (AMEL X ve AMELY) ve zinc finger geni (ZFX ve ZFY) varlıklarının ortaya konulması yanında gerçek zamanlı PZR yöntemi ile de gerçekleştirilmektedir. Bu çalışmanın amacı, farklı restriksiyon enzimi kullanılarak 5 farklı türde cinsiyetin belirlenebilmesinin araştırılmasıdır. Çalışmada 5 farklı türden (keçi, koyun, sığır, at ve köpek) erkek ve dişi hayvanlara ait laboratuvarımızda bulunan kan örneklerinden DNA izolasyonu gerçekleştirilmiştir. Daha sonra zinc finger genine (ZFX ve ZFY) spesifik primerler kullanılarak polimeraz zincir reaksiyonu (PZR) yöntemi ile yükseltgenmiştir. Yükseltgenen PZR ürünleri 6 adet restriksiyon enzimi (Eco31I, Eco32I, HindIII, MspI, NgoMIV ve SmaI) kullanılarak kesim işlemi gerçekleştirilmiş ve jel elektroforez yöntemi ile görüntülenmiştir. Çalışma sonucunda kullanılan türlerde PZR ürünü elde edilmesine rağmen restriksiyon enzimleri ile iki cinsiyette de kesim işlemi olmayıp herhangi bir farklı fragment tespit edilememiştir. Sonuç olarak, kullanılan enzimler bu türlerde tür ve cinsiyet tayini çalışmalarında kullanılamayacağı sonucu elde edilmiştir. İleri çalışmalarda tür sayısını artırılması ve farklı restriksiyon enzimleri de eklenerek çalışmaların genişletilerek yapılması önerilmektedir.

Anahtar kelimeler: Cinsiyet, elektroforez, PZR, restriksiyon enzimi, tür

Investigation of sex determination using restriction enzymes in different species by PCR-RFLP method

Abstract

In some forensic cases or in products offered for consumption, it is desired to identify and determine the samples in terms of both species and gender. Due to the differences in the quality and sales prices of meat by gender, it is desirable to know the exact gender of the meat to determine whether the meat offered for consumption has been cheated or not. Studies based on molecular basis are carried out by real-time PCR method as well as revealing the presence of Amelogen (AMEL X and AMELY) and zinc finger gene (ZFX and ZFY). The aim of this study was to investigate sex determination in 5 different species using different restriction enzymes. In this study, DNA was isolated from blood samples of male and female animals from 5 different species (goat, sheep, cattle, horse and dog). Then, DNA was amplified by polymerase chain reaction using primers specific for zinc finger gene (ZFX and ZFY). The amplified PCR products were digested using 6 restriction enzymes (Eco31I, Eco32I, HindIII, MspI, NgoMIV and SmaI) and were visualized by gel electrophoresis. As a result of the study, although the PCR product was obtained in the species used, no different fragments were detected in both sexes with restriction enzymes. As a result, it was concluded that the enzymes used cannot be used in species and sex determination studies in these species. In further studies, it is recommended to increase the number of species and adding different restriction enzymes.

Keywords: Electrophoresis, PCR, restriction enzyme, sex, species

GİRİŞ

Hayvanlarda cinsiyetin önceden belirlenmesi özellikle spermden ya da embriyo aşamasında farklı yöntemler kullanılarak tespit edilmesi sonrasında besicilik ya da süt işletmeciliği yapacak olan yetiştiricinin eğilimine göre hangi cinsiyete sahip hayvan istiyorsa o kapsamda belirlenen cinsiyetteki sperm ya da embriyo belirlenip kullanılmaktadır. Bu kapsamda yapılan analizlerden spermanın cinsiyetinin belirlenmesinde en çok tercih edilen yöntem Flow Sitometre yöntemidir (Demirci, 2014). Embriyodan cinsiyetin belirlenmesinde ise kullanılan yöntemler ise sitogenetik yöntem, İmmünolojik yöntem (HY antijenin belirlenmesi), X kromozomuna bağlı enzim aktivasyonların saptanması, farklı cinsiyetteki embriyoların metabolik aktivitelerinin belirlenmesi ve Y kromozomuna özel DNA zincirlerinin kullanılarak moleküler yöntem ile tespit edilmesi olarak sıralanmaktadır (Şendağ ve ark., 2005).

Farklı türlere ait et ürünlerinin tüketime sunulması insanları aldatmaktadır. Özellikle din ve etik düşünceler kapsamında bu olayın istenilmesi söz konusu değildir. Cinsiyet yönünden etlerin kalite ve satış fiyatları farklılıklarından dolayı tüketime sunulan etlerin hile yapılıp yapılmadığının belirlenmesi amacıyla cinsiyetlerinin tam olarak bilinmesi istenilmektedir. Bu amaçla farklı hormon analizlerine dayanan immunokimyasal metotlar kullanılmakla birlikte DNA temelli PZR'a dayalı moleküler tanı yöntemleri de kullanılmakta hatta PZR tabanlı moleküler çalışmalar ile kolay ve ucuz olarak gerçekleştirilmektedir (Arslan ve ark., 2015). PZR yöntemi kullanılarak yapılan çalışmada rendering ürününde 5 farklı türe (kanatlı, ruminant, domuz, at ve karnivor) ait spesifik primerler kullanılmış ve üründe tür tayini belirlenmeye çalışılmıştır (Kurar ve ark., 2012). Yapılan diğer bir çalışma da ise piyasaya sürülen et ürünleri olan sucuk, salam, sosis ve köftede 6 farklı türe (sığır, koyun, tavuk, at, kedi ve domuz) ait spesifik primerler kullanılarak tür tayini araştırılması PZR yöntemi ile gerçekleştirilmiştir (Özşensoy ve Şahin, 2016).

Özellikle bazı adli olaylarda veya tercihe yönelik olarak da tüketime sunulan ürünlerin ve örneklerin hem tür bazında hem de cinsiyet bazında tespit edilerek belirlenmesi istenilmektedir. Adli vakalarda ya tanınmayacak halde olan bir canlıya ait kalıntılardan ya da olayın gerçekleştiği alandaki şüpheli materyalden yola çıkılarak tür, cinsiyet, yaş vs. özelliklerin belirlenmesi gerekmektedir. Tanınamayacak halde olan insanlara ait en önemli kalıntıların pelvis ve kafatası kemikleri, diğer kemikler ve dişler olduğu ve bunlardan yola çıkarak kişinin ırkı, yaşı ve cinsiyeti belirlenmeye çalışılmaktadır. Bu alanda çalışan ve kemik ve yumuşak doku örnekleri üzerinden kimlik tespiti yapan Adli Antropoloji bilimi adli soruşturmalara katkı sağlaması yönünden ön plana çıkmaktadır. Bu alanda farklı yöntemler kullanılarak ilgili tespitlerin yapılması gerçekleştirilmektedir (Babacan, 2020; Yerli ve ark., 2021). Şüpheli bir olayda ise farklı kalıntılardan yola çıkarak tür, cinsiyet gibi özelliklerin belirlenmesi istenilmektedir. Mesela bir kemik ya da doku parçası bulunduğunda ya da avlanması yasak bir hayvanın avcılar tarafından parçalanması sonucu şüphelinin üzerindeki kan vs. lekeler gibi numune örneklerinden insan mı hayvan mı ya da hangi hayvana ait olduğu gibi soruların cevabı alınmaya çalışılmaktadır. Bozulmamış ve tür ayrıma neden olacak kemik özellikleri belirlenebilirse kolaylıkla çözüle bilirken bu ayrımların olmadığı organik kalıntılarda ise DNA temelli moleküler yöntemler kullanılmaktadır.

Moleküler temellere dayalı yapılan çalışmalar Amelogen (AMELlX ve AMELY) ve zinc finger geni (ZFX ve ZFY) varlıklarının ortaya konulması yanında gerçek zamanlı PZR yöntemi ile de gerçekleştirilmektedir. Bu kapsamda birçok araştırma yapılmıştır. Yapılan bir çalışmada Kayseri ilinde satışa sunulan sığır et ürünlerinden 30 örnek alınmış ve Y kromozomuna özgü genlere spesifik 2 farklı primer seti kullanılarak PCR yöntemi ile araştırma yapılmış ve 15 tanesinin erkek 15 tanesinin dişi cinsiyete ait olduğu belirlenmiştir (Arslan ve ark., 2015).

Bu çalışmanın amacı ZFX-Y yöntemi ile birlikte 5 farklı türde, 6 farklı RE kullanılarak hem tür ayrımının hem de tür bazında cinsiyet ayrımının yapılıp yapılamayacağının PZR-RFLP yöntemi ile araştırılmasıdır.

MATERYAL VE METOD

Çalışma kapsamında daha önceden laboratuvarımızda bulunan 5 farklı türden (keçi, koyun, sığır, at ve köpek) erkek ve dişi hayvanlara ait kan örneklerinden standart fenol-kloroform yöntemi (Sambrook ve ark., 1989) ile DNA izolasyonu gerçekleştirilmiştir. İzolasyonu sonrası DNA'ların kalite ve miktarları nanodrop spektrofotometre ile ölçülmüştür. DNA örnekleri daha sonra zinc finger genine (ZFX ve ZFY) spesifik primerler (Aasen ve Medrano, 1990) kullanılarak polimeraz zincir reaksiyonu yöntemi ile yükseltgenmiştir. PZR profili ve protokolü olarak daha önce kullanılmış olan yöntem kullanılarak işlemler gerçekleştirilmiştir (Özşensoy, 2018). Yükseltgenen PZR ürünleri 6 adet restriksiyon enzimi (Eco31I, Eco32I, HindIII, MspI, NgoMIV -MroNI- ve SmaI) kullanılarak kesim işlemi gerçekleştirilmiş ve jel elektroforez yöntemi ile

görüntülenmiştir. Kesim işlemi için; 10 µl PZR ürünü, 1 µl FastDigest restriksiyon enzimi (10 U / µl), 2 µl enzim buffer ve 18 µl bidistile su olmak üzere toplamda 31 µl olacak şekilde hazırlandı. Restriksiyon enzimleri için hazırlanan örnekler ise 37 °C'de 20 - 25 dk. bekletilmiştir. Restriksiyon enzim kesimi sonucu elde edilen ürünler %2.5 agaroz gel elektroforezinde 100 V da 60 - 85 dk. süre ile ayrıştırıldı ve 365 nm UV'de görüntülendi.

BULGULAR ve TARTIŞMA

Çalışma kapsamında 5 farklı türe ait erkek ve dişi hayvanlardan kan örneklerinden DNA elde edildikten sonra hem tür hem de tür bazında cinsiyet yönünden bir ayrım yapılıp yapılamayacağı 6 farklı RE ile kesim işlemi yapılarak araştırılmıştır. DNA örnekleri ilgili primerler ile çoğaltılarak tüm örneklerde PZR ürünü elde edilmiştir (Şekil 1). PZR ürünleri elde edildikten sonra tüm örnekler RE'ler ile kesim işlemine tabi tutularak elektroforezde görüntülenmiştir (Şekil 2 ve 3). Çalışma kapsamında kullanılan RE'ler ile kesim işlemi sonucunda hem türler hem de türlerin erkek dişi örnekleri arasında herhangi bir farklılık tespit edilememiştir.

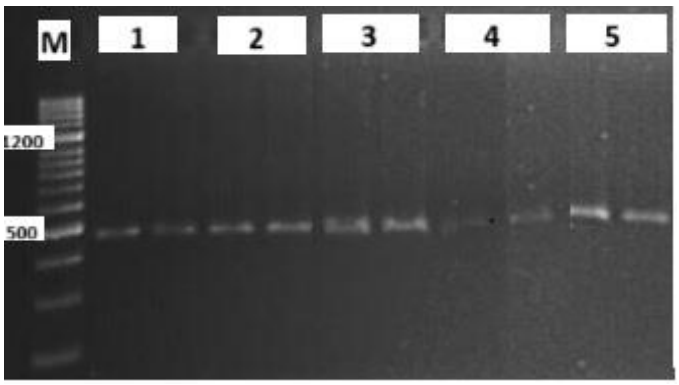

Şekil 1. Türlerin spesifik primer ile PZR sonucu; M: 100 bp marker, 1: teke-keçi, 2: koç-koyun, 3: tosun-inek, 4: aygır-kısrak, 5: erkek-dişi köpek

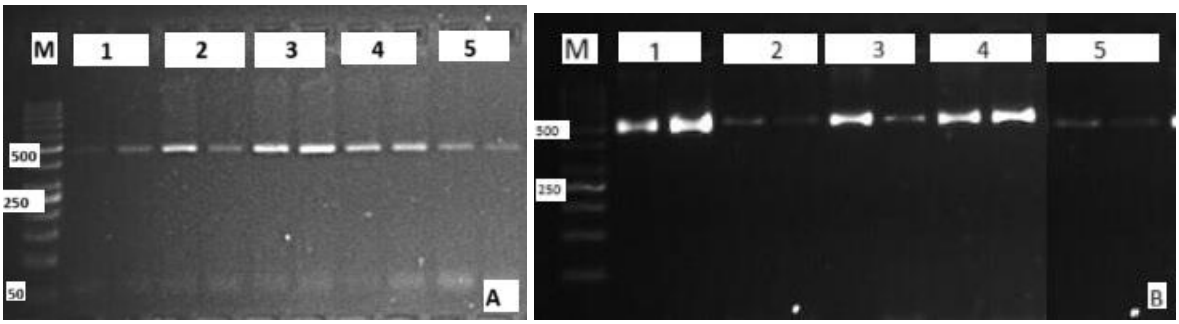

Şekil 2. Türlerin a) SmaI b) MspI RE'ler ile kesim sonucu;

M: 50 bp marker, 1: teke-keçi, 2: koç-koyun, 3: tosun-inek, 4: aygır-kısrak, 5: erkek-dişi köpek

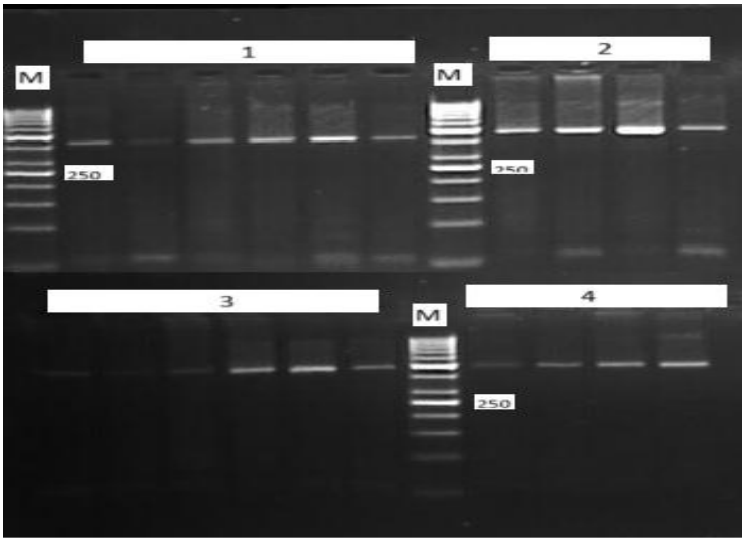

Şekil 3. Türlerin diğer RE'ler ile kesim sonucu; M: 50 bp marker, 1: HindIII, 2: Eco32I, 3: Eco31I, 4: MroNI (NgoMIV)

Çalışmada kullanılan ZFY/ZFX primerinin insan, sığır, koyun ve keçide DNA örneklerinden cinsiyetin tanımlanmasında hızlı ve faydalı bir metot olduğu ve 447 veya 445 baz uzunluğunda bir bölgeyi çoğalttığı bildirilmiştir. Ayrıca bu çalışmada 8 farklı RE enzimi kullanılmış ve bu enzimlerden 3 tanesinin insan (HaeIII), koyun (SacI), keçi (SacI) ve sığırlarda (PstI) cinsiyet tayininde kullanılabileceği bildirilmiştir (Aasen ve Medrano, 1990). Başka bir çalışmada ise ilgili primerin sırtlanlarda cinsiyetin tespit edilmesinde kullanılabileceği PZR ve enzim kesimi ile belirlenmiştir. Sırtlanlarda 448 baz uzunluğunda bir bölgenin çoğaltıldığı Pst1 ve Taq1 enzimleri kesim işlemi sonucunda iki cinsiyet arasında kesim farklılığı olduğu ve cinsiyetin belirlenmesinde kullanılabileceği bildirilmiştir (Schwerin ve Pitra, 1994). Bu çalışmada 5 farklı türde ilgili primer kullanılmıştır ve her türde yaklaşık 450-500 baz uzunluğunda bir bölgenin PZR ile çoğaltıldığı tespit edilmiştir. Bu çalışmada diğer çalışmalarda kullanılmayan 6 tane farklı RE enzimi kullanılmış fakat bu enzimler yönünden türlerde herhangi bir cinsiyet ayrımı yapılamamıştır. MspI enzimi kullanan çalışma (Aasen ve Medrano 1990) ile benzer şekilde bu çalışma da herhangi bir kesim elde edilememiştir.

Farklı çalışmalarda farklı RE'ler kullanılarak türlerde cinsiyet tayini çalışmaları yapılmıştır.

SONUÇ

Bu sonuçlara göre bu 6 RE'nin çalışılan 5 türde tür ve cinsiyet ayrımında kullanılamayacağı tespit edilmiştir. İlgili çalışmadan sonra farklı türlerinde eklenerek ve enzim sayısının daha fazla artırılarak tekrar çalışmalar yapılması önerilmektedir.

KAYNAKLAR

Aasen, E., & Medrano, J. F. (1990). Amplification of the ZFY and ZFX genes for sex identification in humans, cattle, sheep and goats. Biotechnology, 8, 1279-1281.

Arslan, K., Akyüz, B., & İlgar, E. G. (2015). Kayseri şehir merkezinde kasap ve marketlerde satışa sunulan sığır etlerinde PCR yöntemi ile cinsiyet tayini. Erciyes üniversitesi veteriner fakültesi dergisi, 12(2), 75-79.

Babacan, S. (2020). Yeniden yüzlendirmeye yönelik mandibulası bulunmayan kafataslarında yaş, cinsiyet tayini ve uygun mandibula'nın dizaynı: retrospektif çalışma. Doktora tezi, Bursa Uludağ Üniversitesi Sağlık Bilimleri Enstitüsü, Bursa.

Demirci, E. (2014). Flov sitometri ile boğa spermlerinde cinsiyetin belirlenmesi. Fırat üniversitesi sağlık bilimleri veteriner dergisi, 28(3), 159-161.

Kurar, E., Özşensoy, Y., Bülbül, M. D., & Nizamlıoğlu, M. (2012). DNA teknolojisi ile rendering ürünlerinde tür tespiti: Bir vaka raporu. Eurasian journal of veterinary sciences, 28(2), 122-125.

Özşensoy, Y. (2018). Investigation of PRL-RsaI and HaeIII gene polymorphisms in Anatolian water buffaloes bred by using PCR-RFLP method. Revista brasileira de zootecnia, 47, e20170166.

Özşensoy, Y., & Şahin, S. (2016). Et ürünlerinde tür tayininin yapılmasında farklı yöntemlerin karşılaştırılması. Eurasian journal of veterinary sciences, 32(1), 30-35.

Sambrook, J., Fritsch, E. F., & Maniatis, T. (1989). Molecular cloning: A laboratory manual. (pp. 9.16-9.19). 2nd ed. Cold Spring Harbor Laboratory Pres, Cold Spring Harbor.

Schwerin, M., & Pitra, C. (1994). Sex determination in spotted hyena (Crocuta crocuta) by restriction fragment length polymorphism of amplified ZFX/ZFY loci. Theriogenology, 41, 553-559.

Şendağ, S., Aydın, İ., & Çelik, H. A. (2005). İneklerde prenatal embriyonik/fötal cinsiyetin belirlenmesi. Erciyes üniversitesi veteriner fakültesi dergisi, 2(1), 39-44.

Yerli, Y., Özkoçak, V., & Koç, F. (2021). Adli antropolojide kimliklendirme çalışmalarında yeni yaklaşımlar. Journal of social, humanities and administrative sciences, 7(39), 846-856.

➢ *ORAL PRESENTATION*

Manual or Automated? A UI Testing Comparison

Zeynep Ceren BAYRAM[1][0009-0001-9745-138X], Gulfem ISIKLAR ALPTEKIN[2][0000-0003-0146-1581]

Galatasaray Unıversity Computer Engineering
Ortaköy, Çırağan St. No:36, 34349 Beşiktaş, İstanbul

*Corresponding author e-mail : zeynepcerenbayram@gmail.com, gisiklar@gsu.edu.tr

Abstract
In this paper, a comparison between manual and automation testing methods is conducted within the scope of user interface (UI) testing. To achieve a comprehensive evaluation, multiple metrics have been utilized to analyze each method from various perspectives. Initially, the user interfaces were identified, and corresponding test scenarios were developed. These scenarios were then executed manually and through automated scripts. To ensure reliability and generalizability of the results, the login functionalities of three different web applications were chosen for analysis. Numerical analyses based on selected metrics revealed critical insights regarding the relative advantages and disadvantages of each testing method. Ultimately, the findings of this study offer valuable guidance for companies and projects in deciding which testing approach manual or automated would be most beneficial according to their specific needs.
Keywords: Software Testing, Manual Testing, Test Automation.

INTRODUCTION

Today, software systems form the essential components of numerous industries, including finance, defense, and marketing. As reliance on software systems continues to grow, ensuring their quality has become increasingly critical. The testing phase of a software project plays a key role in verifying that user requirements are met and in evaluating overall system quality. Indeed, software quality can only be accurately assessed through rigorous software testing (K. Sneha and G. M. Malle, 2017).

Software testing is primarily conducted using two distinct methods: manual testing and automation testing. Manual testing is straightforward to implement and does not necessitate extensive technical knowledge. Conversely, automation testing requires proficiency in coding and initial integration efforts. Although manual testing is simple to begin with, repeated execution, particularly during regression testing, can become costly and time-consuming. Despite the initial setup complexities, automation testing often provides substantial long-term benefits, such as efficiency gains and reduced human error. Nevertheless, many organizations hesitate to adopt automation testing, typically preferring traditional manual approaches.

Regression testing is conducted to verify that software updates, such as new feature implementations, bug fixes, or modifications, do not negatively affect existing functionalities. The primary purpose of regression testing is to ensure that previously functioning parts of the software continue to perform correctly after changes are introduced. Identifying, analyzing, and resolving regression-related issues represent some of the most time-consuming tasks in software development, especially within large-scale, production-level systems (S. Badihi, et al., 2023). Automated regression testing significantly enhances test efficiency, accelerates feature deployment, and minimizes the potential for human errors (G. da Silva and R. de Souza Santos, 2023). By automating regression testing, teams can conduct frequent test cycles, promptly identify defects, and maintain continuous integration and continuous delivery (CI/CD) practices effectively (A. Akin et al., 2018). Thus, automated regression testing is essential for improving software quality, stability, security, and overall user experience, playing a crucial role in streamlining and accelerating the software development lifecycle.

In this study, manual and automation testing methods were compared on the time metric**.** In future studies, this comparison will also be compared on metrics such as team and skill requirements, reporting quality, automated start capability, suitability for different platforms, coverage, reliability, cost. Additionally, the research investigates which testing method might prove more beneficial depending on the nature and requirements of different software projects. The issue of selecting the testing method based on the project is addressed as a gap in literature. While continuing with manual testing makes sense for short-term projects, it is suggested that transitioning to automation testing would be beneficial for long-term and continuously

developed projects. This approach emphasizes the importance of choosing testing methods based on the project's requirements and continuity. The whole flow of the evaluation framework is given in Figure 1.

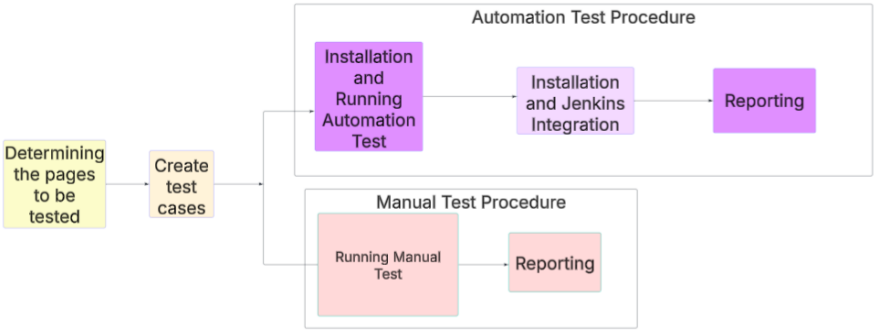

Figure 1. Test Process

MATERIALS AND METHODS

Test Process

Determining the pages to be Tested & Create for Test Cases

A total of 33 test cases were prepared to evaluate all these metrics. These test cases were designed for the user login pages of three popular websites.

Writing these 33 test cases took a total of 2 days. These pages are educational platforms offering training on various technical subjects.

Many websites conduct "human or robot" tests on login pages. If the entity making the request is identified as a robot instead of a human, the IP is blocked from accessing the application. Such sites typically include large and expensive companies, which prevent automation tools (considered robots) from running on their systems. As a result, these sites cannot be used for test automation.

The three educational platforms listed above, however, do not have high sensitivity regarding "human or robot" detection on their login pages. Additionally, these platforms are well-known and widely used by many people. This ewb pages are Codecademy (https://www.codecademy.com/login), Khan Academy (https://tr.khanacademy.org/login) and edX (https://authn.edx.org/login).

For these reasons, the login pages of these three different web pages were chosen for testing.

1.1.1 Why was the "login page" test chosen?

Login pages are the first point of interaction between a user and a software application or website, making them critically important. The proper functioning of the login page impacts many factors, including user experience, security, and overall functionality. The test cases were prepared using a template in Excel. This template included all the essential fields that should be present in a test case.

1. Test Case ID: This is the identifier for the test case. It is expected to be an abbreviation of the tested class. It is useful to include a number in each test case. For example, for a user login interface, the test cases could be named UserLogIn, and the IDs for these test cases could be 1ULI, 2ULI, 3ULI, etc.
2. Test Case Name: This is a short and descriptive name for the tested function. For example, for testing how a system reacts when a user enters an invalid password, the test case name could be LogInWithWrong.
3. Test Case Steps: These are the sequential steps required to perform the test.
4. Input: This is the field where the values entered during the test (which could be strings or integers) are written.
5. Expected Result: This is the result expected to be obtained based on the software requirements.
6. Actual Result: This is the output obtained after performing the test case steps.
7. Result: This indicates whether the test cases have passed or failed. A "Pass" result is given if the actual result matches the expected result. A "Fail" result indicates a discrepancy between the expected and actual results.

8. Notes: If there is any additional information related to the test case, it is written in this field.

The prepared test cases are common for both automated and manual testing. Therefore, the cases were first executed manually. Subsequently, the automation scripts were written, and the cases were executed using automation.

Running Manual Test

After manual execution, the time taken to execute each case in seconds was recorded, and the total duration required to complete all tests was calculated. The web pages were tested one by one on three different search engines, and the time required for each execution was calculated as Table 1.

Table 1. The time spent running manual tests in each search engine. (man/second)

	EDX	KHAN	CODEACADEMY
MOZILLA	265	275	291
FIREFOX	263	281	304
WEBKIT	293	292	319

1 Iteration: Total: 2,583 seconds -> 43 **man/minutes**

Weekly Deployment: Average of 6 test environment deployments + 1 production deployment

7 deployments x 43 minutes = 301 **man/minutes**

Monthly: 1,204 **man/minutes**

In 2 Months: 2,408 **man/minutes**

In 6 Months: 7,224 **man/minutes**

In 12 Months: 14,448 **man/minutes** -> 240 hours -> (Dividing by 8 gives the number of workdays, assuming 1 workday = 8 hours)

240 / 8 = 30 workdays -> equivalent to one and a half months of manpower.

Thus, the annual manpower cost for a project with only 33 test cases amounts to one and a half months of workdays.

Installation and Running Automation Test

After the manual test executions, preparations for automation testing were made. For this purpose, the first step was to decide which tool would be used for writing the automation scripts. Playwright was used as the automation tool for writing software test cases. It is a relatively new test automation framework developed by Microsoft, released in 2019. It is open-source and specifically designed for testing modern web applications. Playwright excels at testing dynamic content and modern JavaScript applications. It is used to simulate user interactions on web pages, write automated tests, and perform validations. Playwright is relatively easy to set up compared to other tools. It does not require dependency installation to get started. Using the command npx playwright install, the necessary dependencies are installed automatically. The tool is free and does not incur additional costs.

Companies generally show resistance when transitioning from manual to automated testing. To minimize this resistance, it is crucial for the team to quickly learn and implement automation testing. For all these reasons, after extensive research, **Playwright** was chosen as the automation tool. In this project, the approach was based on a tester without advanced software knowledge. To enable basic-level automation coding with Playwright, a Playwright training course was followed.

Approximately **6 hours** of Playwright training was undertaken. This training was in the form of a video tutorial on writing Playwright code using **TypeScript**.
Completing the installation and finishing the training video took **2 weeks.**

Coding the **33 test cases** that were initially written at the beginning of the project with Playwright took **3 days.**

Two crucial aspects for test automation with Playwright, which are evaluated based on two different metrics, are highlighted below:

```
tests > TS khanacademyAdv.test.ts > ...
1  import { chromium, firefox, webkit, expect, test } from "@playwright/test";
2
3  // Tarayıcıları tanımlıyoruz
4  const browsers = {
5      chromium: chromium,  // Google Chrome
6      firefox: firefox,    // Mozilla Firefox
7      edge: webkit,        // Microsoft Edge (webkit ile temsil edilir)
8  };
```

Figure 2. Running three different search engines

At this point, one of the strongest features of the Playwright tool, the ability to run tests on three different browsers simultaneously, was utilized. Using the relevant commands on Figure 2, the tests were run on Chrome, Firefox, and Edge browsers. Testing your web page across different browsers ensures a safer, user-friendly, and professional product. With browser compatibility tests, you can identify and resolve potential issues users may encounter on various browsers in advance.

```
TS playwright.config.ts > config > testMatch
1   import { defineConfig, devices } from '@playwright/test';
2   import type { PlaywrightTestConfig } from '@playwright/test';
3   import { on } from 'events';
4
5
6   const config: PlaywrightTestConfig = {
7     testMatch: ["tests/edxAdv.test.ts"],
8   use: {
9         headless:false,
10        screenshot:"on",
11        video: "on"
12  },
13
```

Figure 3. Taking Screen Shot from test cases

With Playwright's capabilities, screenshots of each executed test case were taken using a concise piece of code on Figure 3. These screenshots were automatically downloaded to the desktop. They provided test engineers with easy access to information about how the test was performed and whether it passed or failed.

These screenshots allow all test engineers in the team to identify problematic cases and make comments. Visual evidence is provided to developers. These screenshots can be added to test reports to improve their quality. This feature offers a good solution for the "Actual Result" phase in test cases, as it clearly shows the test outcomes.

Jenkins Integration

Jenkins is a no-cost, open-source solution for continuous integration (CI) and continuous delivery (CD) that does not require any additional expenses. The goal of modern CI/CD practices is to streamline the process of validating and deploying code updates rapidly by automating tasks such as code integration, testing, building, and deployment in software development pipelines. Jenkins plays a crucial role in simplifying DevOps workflows, allowing development teams to enhance their speed and productivity. It is capable of automatically running code from the IDE and initiating these executions without the need for manual input. The tool offers a user-friendly interface to display the time taken and results of test cases. Additionally, Jenkins is compatible with reporting tools like Allure, which facilitate the generation of detailed and informative reports. In advanced automation testing processes, using a tool like Jenkins has become

indispensable. **Learning Jenkins,** setting it up, and implementing it into the Playwright project took **1 week.**

Initially, the scripts did not execute successfully. The reason was that the **CPU power was insufficient** to handle parallel test executions. To address this issue, a custom function was developed to **reduce script load**, resulting in a more readable script. With the optimized script, the CPU was able to handle the test executions. One of the greatest benefits of Jenkins is **automated triggering**. As shown in the image below, the Jenkins trigger is set to **21:00**. This ensures that as long as the server from which the code is pulled is active, test executions will start every evening at **21:00.** At the end of all test cases, an **intuitive schema** was presented on the user interface, as shown Figure 3. Each **pipeline step** was displayed to the user in a detailed manner, enhancing the **readability** of the results.

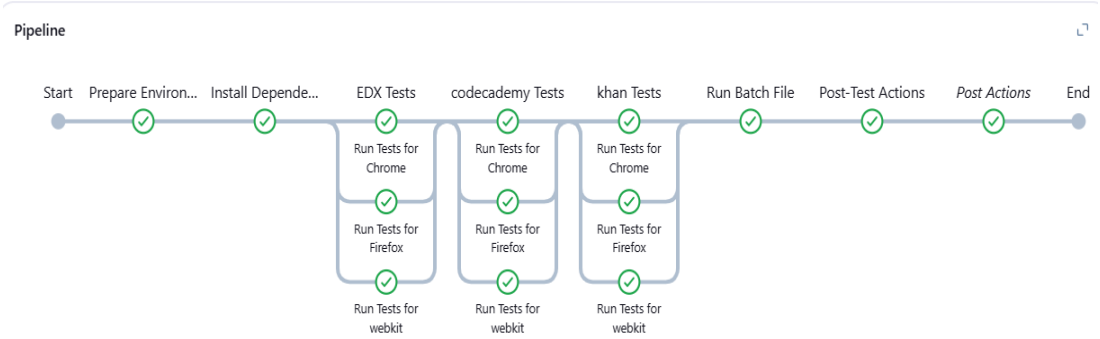

Figure 3. Jenkins Pipelines

COMPARISON

Automation Test

After the training was completed, the time cost for **test case writing, learning and installing Playwright, coding, learning Jenkins, Jenkins implementation,** and **automation test case execution** columns, as shown Table 2, will be **0 minutes**, resulting in **no additional time cost.** The **test case execution time** for automated test cases is **0** because the execution is initiated **automatically outside of working hours** without utilizing human resources. In **20 days,** the **coding and automation** processes were completed, and the scripts were written.

Table 2. The time spent for Automation Test.

	Writing test cases	Lerning and Installation of Playwright	Coding	Learning Jenkins	Implemantation of Jenkins	Running Test Case with Automation
TIME	2 days	10 days	3 days	3 days	2 days	-

20 days * 8 hours/day * 60 minutes/hour = 9,600 man/minutes of total elapsed time.
(Assuming one working day is 8 hours)

Manual Test

Table 3 shows the total time spent on tests performed using the manual testing method.

Table 3. The time spent for Manual Test.

	Writing test cases	Running Test Case Manually
TIME	2 days	43 minutes

2 days * 8 hours/day * 60 minutes/hour + 43 minutes = 1003 man/minutes of total elapsed time. *(Assuming one working day is 8 hours)*

Comparison of Manual and Automation Tests Timing

Table 4. Timing of manual and automation tests implementation

Scenario	Manual Testing	Automation Testing
Initial setup & 1st run	1,003 mins	9,600 mins
2nd run	43 mins	-
1 month (daily tests, 7*4 runs)	7*4*43 =1,204 mins	-
6 months (daily tests, 7*24 runs)	7*24*43 =7,224 mins	-
7 months (daily tests, 7*28 runs)	7*28*43 =8,428 mins	-
8 months (daily tests, 7*32 runs)	7*32*43 =9,632 mins	-

Manual testing is initially much faster; however, during the continuous testing process required by regression testing, the same tests must be executed repeatedly. At this point, for a platform where deployments and test case executions are conducted daily, the time spent on **manual testing** in an **eight-month period** would **offset** the time spent on **automated testing.** The total times for manual and automation tests on Table 4 are given for comparison.

Additionally, this case considers a situation where the company has **just transitioned to automation** and is working with **automation and automation methods for the first time.**

However, once **automation methods** are learned, they can be applied to all future projects. Therefore, the time cost analysis should be based on a scenario where automation methods have already been learned and can be applied **directly,** rather than a scenario where these methods are being learned for the first time. In this case, the applicable automation test times are provided in Table 5.

Table 5. The time spent for Automation Test after Acquired Knowledge

	Writing test cases	Lerning and Installation of Playwright	Coding	Learning Jenkins	Implemantation of Jenkins	Running Test Case with Automation
TIME	2 days	-	3 days	-	-	-

5 days * 8 hours/day * 60 minutes/hour = 2,400 man/minutes of total elapsed time. *(Assuming one working day is 8 hours)*

In contrast, the time spent on manual testing will remain constant at 1,003 minutes.

2 days * 8 hours/day * 60 minutes/hour + 43 minutes = 1,003 man/minutes

This comparison highlights that while the initial time cost for automation is higher (2,400 minutes), the manual testing time remains fixed at 1,003 minutes for each execution cycle. As the number of cycles increases, the cumulative time cost for manual testing will surpass the one-time automation setup cost, demonstrating the long-term efficiency of automated testing.

Table 6. Timing of manual and automation tests implementation after Acquired Knowledge

	MANUAL TEST	AUTOMATION TEST
Running 1	1003 mins	2400 mins
Running 2	43 mins	-
Running 7*4 (1 month)	7*4*43 =1204 mins	-
Running 7*8 (2 month)	7*8*43 =2408 mins	-

After the acquired knowledge, utilizing the existing automation infrastructure of the company becomes much faster and starts to yield results much faster than manual testing in a very short time. As can be seen from the table above, when automation testing is created for the software, the time spent on creating automation is amortized within 2 months, and the company starts to make a profit. Manual testing is time-consuming, particularly during regression testing, and proves to be costlier than automation testing in the long run (K. R. Halani el al., 2021).

RESULTS AND DISCUSSION

This study compares automation and manual testing methods in software testing. This comparison has been the subject of many academic studies. Manual and automation tests have advantages over each other in different areas (H. Uslu et al., 2022).

When the literature is reviewed, one gap is identified: In real-life scenarios, should a company transition to automation testing in software testing, or should it continue with manual testing?

The process began by first writing test cases that would be used for both manual and automation testing. The test cases created are common for all testing processes and were not created separately. A total of 33 test cases were created for the login pages of three popular educational platforms. The reason for testing the login pages is that every application includes a login page, which is an indispensable component for any application. Instead of a test case document that only contains the test name and fail/pass status, all relevant sections were included, so that anyone reading the test case can easily repeat the test and understand what was done in the test.

Afterwards, these test cases were executed manually, and the total time spent was calculated. Once the manual execution process and the time and cost calculations were completed, an infrastructure was created to run the same test cases using automation.

There are many software testing automation tools available to accelerate interface testing. In addition to these tools, new automation tools are still being developed. Although Selenium is one of the most popular tools for web interface automation, it remains traditional and cumbersome compared to newer technologies (A. Antonczak and B. Bylina, 2024). Instead, the Playwright tool, which provides faster adaptation, has been used. The benefits of this tool are explained in section 1.3.

One of the greatest benefits of automation testing is its ability to integrate with CI/CD tools. This allows tests to be executed without human intervention and time loss. Many different articles have discussed the features provided by Jenkins tools and how test automation works seamlessly with less manual effort (A. Deshpande et al., 2021).

Preparing all test cases at once and executing them manually took a total of 1003 man/minutes. The same calculation could not be directly applied for automation testing, as an infrastructure had to be set up for automation tests. The setup of the infrastructure and the execution of the test cases once took a total of 9600 man/minutes.

When looking at the initial costs, manual testing was performed with a profit of 86.55%. However, the cost of automation testing is zero once the initial cost is eliminated.

When examining the table in Table 4, it is observed that the initial cost of manual software testing is much lower. However, as the same test cases are executed continuously, the initial cost for automation testing is amortized. In this study, it has been proven that for a company deploying and testing daily in different environments, automation amortizes its initial cost within a six-month period, and after six months, every executed test case results in profit.

After all these experiments and proofs, manual and automation testing methods in software testing are compared with different metrics in Section 5.

The transition to automated testing allowed for parallel execution of tests, providing more detailed test results with step-by-step screenshots, and reducing man-hours and execution time. Through test automation, the frequency of running regression tests increased, and human errors were detected earlier. Additionally, test automation provides more detailed test results (such as recorded screenshots) compared to manual testing.

Tests were automatically executed after code changes with continuous integration or at scheduled times. This allows for much faster feedback by only reviewing the failed tests in the test results. It can be determined which deployment code changes caused the failed regression tests.

As a result, automation testing is initially costly. However, as repetitive tests like regression tests are conducted, this cost is amortized over time, and companies start making a profit in the ongoing process. Once a fully automated test system is established, the company will eventually be fully profitable. Additionally, the reason for the high initial cost is the effort required to set up the automation infrastructure in a company that lacks an automation culture (Table 2).

When a company starts a new project, if it is expected that the project will not remain as research and development but will instead be a long-term project, the company should create an automation test plan for that project. If the company already has an automation infrastructure, there will be no initial cost when creating an automation plan for new projects. In this case, starting automation testing for the mentioned project will be much easier and more feasible.

However, for some projects, it is uncertain whether they will be sold or go live. For these types of projects, starting automation might be risky. This is because initiating automation testing is costly, and if the project does not go into production and will not require continuous integration or maintenance, it would be unnecessary to incur this initial cost.

CONCLUSION

In this study, manual and automated testing methods were evaluated based on several critical metrics. The findings indicated that neither method is universally superior; rather, each approach exhibits distinct advantages and disadvantages, depending on specific project characteristics and requirements. A categorical recommendation advocating exclusively for either manual or automated testing would therefore be inaccurate.

For long-term, continuously evolving projects requiring frequent regression testing such as enterprise applications, banking systems, e-commerce platforms, and defense software the advantages of automation testing are clearly demonstrated. Automated testing accelerates test execution cycles, reduces repetitive tasks, and significantly lowers the cumulative costs and efforts associated with ongoing regression testing. Consequently, companies engaged in sustained software development projects should strongly consider adopting automation testing as part of their standard processes.

Conversely, for short-term, experimental, or uncertain-duration projects such as proof-of-concept studies, research-driven initiatives, hackathons, or projects with unclear future development manual testing remains more practical. Given the high initial setup time, cost, and training investments required for automation, these projects generally do not benefit from automation, as repetitive regression tests may be infrequent or unnecessary. In such contexts, manual testing remains cost-effective and straightforward. An essential insight derived from this research is that the selection between manual and automated testing methods must be strategically determined at the outset of each project, considering factors such as project duration, complexity, budget constraints, team skillsets, and expected frequency of regression testing.

Further research may investigate automation testing scalability with significantly larger test suites, assessing performance degradation, infrastructure requirements, and potential efficiency bottlenecks. With advances in AI and machine learning, future research should explore integrating AI-based test-case generation and execution methods to improve automation efficiency, coverage, and effectiveness.

REFERENCES

A. Akin, S. Sentürk and V. Garousi, (2018). "Transitioning from Manual to Automated Software Regression Testing: Experience from the Banking Domain," *2018 25th Asia-Pacific Software Engineering Conference (APSEC)*, Nara, Japan, 2018, pp. 591-597

A. Antonczak, B. Bylina, (2024). "Analysis of end-to-end test automation tools based on the examples of Selenium WebDriver and Playwright" , Position Papers of the 19th Conference on Computer Science and Intelligence Systems (FedCSIS), Lublin, Poland.

A. Deshpande, S. V. Veenadevi and S. Aleti, (2021). "Test Automation and Continuous Integration using Jenkins for Smart Card OS," 2021 12th International Conference on Computing Communication and Networking Technologies (ICCCNT), Kharagpur, India, 2021, pp. 01-05

G. da Silva and R. de Souza Santos, (2023). "Comparing Mobile Testing Tools Using Documentary Analysis," 2023 ACM/IEEE International Symposium on Empirical Software Engineering and Measurement (ESEM), New Orleans, LA, USA, 2023, pp. 1-6

H. Uslu, C. Sahin, M. Yılmaz, (2022). "A PRELIMINARY SURVEY ON SOFTWARE TESTING PRACTICES IN DEFENSE INDUSTRY" 16. Ulusal Yazılım Mühendisliği Sempozyumu Bildiri Kitabı, Ankara, Turkey

K. R. Halani, Kavita and R. Saxena, (2021). "Critical Analysis of Manual Versus Automation Testing," *2021 International Conference on Computational Performance Evaluation (ComPE)*, Shillong, India, 2021, pp. 132-135

K. Sneha and G. M. Malle, (2017). "Research on software testing techniques and software automation testing tools," *2017 International Conference on Energy, Communication, Data Analytics and Soft Computing (ICECDS)*, Chennai, India, 2017, pp. 77-81

S. Badihi, K. Ahmed, Y. Li and J. Rubin, (2023). "Responsibility in Context: On Applicability of Slicing in Semantic Regression Analysis," *2023 IEEE/ACM 45th International Conference on Software Engineering (ICSE)*, Melbourne, Australia, 2023, pp. 563-575

➢ *ORAL PRESENTATION*

The Comparison of Body Performance of Some Invasive Species Distributed in Kemer, Antalya

Serhat Engin[1] (000-0002-1663-1769), Sertan Koşan[1*] (0009-0004-3240-9457), Şule Gürkan[2]

[1]Ege University, Faculty of Fisheries, Department of Aquaculture, Izmir, Türkiye.
[2]Ege University, Faculty of Fisheries, Department of Marine and Inland Waters Sciences and Technology, Izmir, Türkiye.

*Corresponding author e-mail: sertankoshan@gmail.com

Abstract
The aim of this study was to determine the length-weight relationships, some body performance values and Mediterranean stomach content fullness values of 5 different lessepsian species distributed along the western coast of Turkey with current data. The range values showing the total length and total weight values of a total of five species and 102 individuals according to their sexes were determined. The results of Fulton condition values were determined for five fish species in the study: the lowest condition value was found in *Fistularia petimba* (0,05±0,01), while the highest was found in *Sargocentron rubnum* (1,72±0,18). It is clearly understood that *S. rubnum* is quite well developed in terms of condition among the condition values of the lessepsian fish species in the region. Additionally, *S. luridus* (b: 3,02), *S. rubnum* (b: 3,26), *L. scleratus* (b: 3,14) and *F. petimba* (b: 3,79) had positive allometric growth (b>3), while *P. miles* (b: 2,20) had negative allometric growth (b<3). Variations in *b* values are primarily influenced by a range of biotic and abiotic factors, including species-specific characteristics, sexual dimorphism, habitat conditions, dietary composition, seasonal changes, sample size, gonadal development, and individual length metrics. During the examination of the stomach contents of the individuals, it was determined that all the species in this study mostly fed on crustacean species and some smaller fish species. This study provides information on some invasive species in the Western Mediterranean of Türkiye.

Keywords: Lessepssian fishes, Lentgh-Weight, Mediterranean, Turkey.

INTRODUCTION

Over the past decade, increasing sea surface temperatures have been strongly linked to the global proliferation of non-native marine species. The Mediterranean Sea, in particular, has emerged as one of the most heavily impacted regions by these biological invasions. (Zenetos et al., 2010). The migration of these species towards the Mediterranean Sea occurs passively with the increase in water temperature as well as the increase in maritime transportation and trade from the Red Sea. Although the number of lessepsian fish species in the Turkish coast is reported to be 33 (Bilecenoglu et al., (2002), this number has increased significantly in recent years. In this study, the aim was determining the sexes as well as the length-weight relationships, some body performance values and Mediterranean stomach content fullness values of 5 different lessepsian species distributed along the western coast of Türkiye.



Figure 1. Underwater imaging of some lessepsian species from Western Mediterranean of Turkey (Original by Kosan. S)

MATERIALS AND METHODS

The study was carried out on 5 (*Siganus luridus*, *Fistularia petimba, Pterois miles*, *Lagocephalus sceleratus*, and *Sargocentrum rubnum*) different species of lessepsian fish caught by local fishing vessel from the western Mediterranean waters of Turkey. The study was conducted between December to January 2024. A total of 102 fish were used in the study, determining the length-weight relation, the sexes and stomach content. Individual samples were measured for total length (TL) to the nearest 1 mm using a measuring board and weighed to the nearest 0.01 g using an electronic scale in the laboratory. Length–weight relationship parameters (a and b) were estimated by linear regression analysis on log-transformed data ($W = aL^b$) where "a" is the intercept (coefficient related to body form), and "b" is the slope of the linear regression (exponent indicating the growth type). The determination of growth type in fish is determined according to the state of the length-weight relationship.



Figure 2. Fish samples from laboratory

RESULTS and DISCUSSION

Totals of 102 fish specimens representing 5 species and 5 families were sampled. *b* value equal to 3 indicates isometric growth while values different from 3 indicate allometric growth. According to Froese (2006), the excessive proportional increase in length in relation to weight increase in fish is indicated by b<2,5, while b>3,5 indicates that the increase in weight takes an excessive proportional value in relation to the growth in length. Accordingly, in our study; *F. petimba* (b: 3,79), *S. rubnum* (b: 3,26), *L. scleratus* (b: 3,14) and *S. luridus* (b: 3,02) had positive allometric growth (b>3), while *P. miles* (b: 2,20) had negative allometric growth (b<3) (Table 1).

Table 1. Lentgh-weight relationship and average condition values of the species during winter

Species	r^2	*b*	*Relationship*	*a*	*Fulton-K*
F. petimba	0,98	3,79	(+)allometric	0,01	0,05+0,01
S. rubnum	0,81	3,26	(+)allometric	0,01	1,72+0,18
L. sceleratus	0,99	3,14	(+)allometric	0,01	1,19+0,11
S. luridus	0,21	3,02	(+)allometric	0,01	1,44+0,34
P. miles	0,7	2,2	(-) allometric	1,2	1,19+0,18

Table 2. Lentgh-weight ranges and t values between sexes for each species

F. petimba	**n**	**Total Length (cm) Range**	**Total Weight (g) Range**
Female	26	43,3-86,1	24,67-388,92
Male	4	53,3-72	70,66-198,62
p		p>0,05	p>0,05
t		0.21	0.15

S.rubnum	**n**	**Total Length (cm) Range**	**Total Weight (g) Range**
Female	14	13,9-17,6	42,25-99,75
Male	4	14,8-16,2	48,72-93,27
p		p>0,05	p>0,05
t		0.09	0.44

L.sceleratus	**n**	**Total Length (cm) Range**	**Total Weight (g) Range**
Female	11	12,6-35,7	18,96-668,79
Male	3	12.6-15.5	22,15-44,42
p		p>0,05	p>0,05
t		0.18	0.22

S.luridus	**n**	**Total Length (cm) Range**	**Total Weight (g) Range**
Female	14	15.5-21.2	11,96-155.55
Male	4	16.3-17.6	57.73-83.21
p		p<0,05	p>0,05
t		0.03	0.11

P.miles	**n**	**Total Length (cm) Range**	**Total Weight (g) Range**
Female	16	25,5-33,4	222,81-517,03
Male	6	28.6-35.5	308.31-462.57
p		p>0,05	p>0,05
t		0.06	0.1

Table.2 shows the range values showing the total length and total weight values of 102 individuals according to species and their sexes. According to the t-test results, it was determined that the females of *F. petimba, S.rubnum, L. sceleratus, S. luridus* had larger length values than the males in terms of the total length (TL) values of the species distributed in the region ($P < 0.05$). Similarly, it was determined that the females of all the species in this study had more weight than the males in terms of their total body weight (W) ($P < 0.05$).



Figure 3. Stomach contents of *P. miles, F. petimba* and *S. rubnum*

During the examination of the stomach contents of the 102 individuals of different species, it was determined that the stomachs of female *S. luridus* were %100 full, and female *L. sceleratus* were 90,91% full and %9,09 empty. In the other hand the stomachs of female *S. rubnum* were only %28,57 full.

Food pieces belonging to the crab and shrimp species found in the stomach contents of *Siganus luridus*, *Pterois miles*, *Lagocephalus sceleratus* and *Sargocentrum rubnum.* Some small fish species found in the stomach of *Fistularia petimba*.

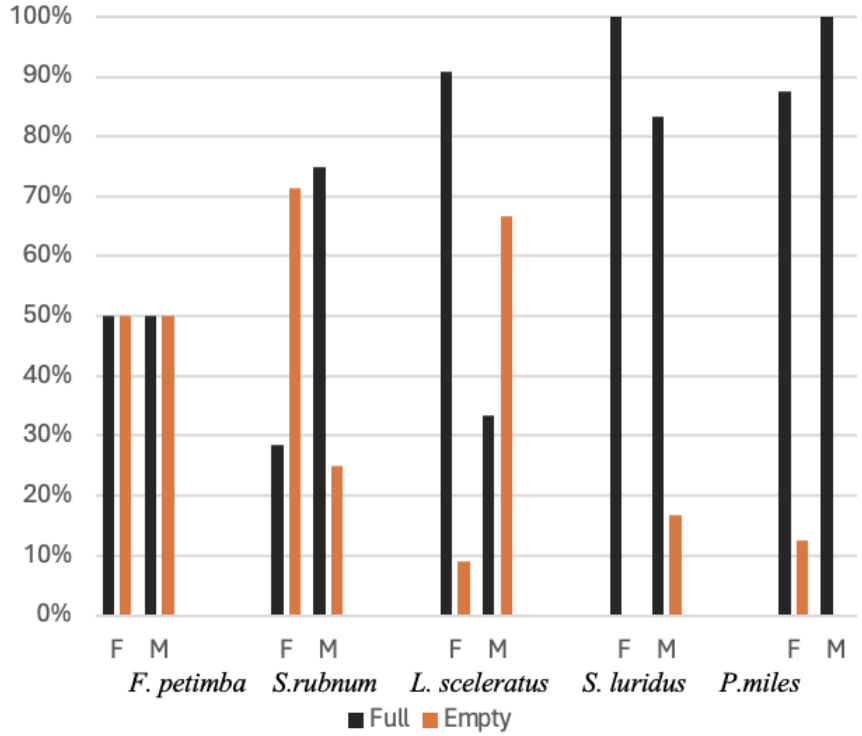

Figure 4. Stomach fullness values in species in the study.

One of the most important factors in the migration of invasive species from the Suez Canal to the Mediterranean Sea is sea water temperature. According to the data obtained, the lowest temperature was 15.9 °C in February and the highest temperature was 20 °C in July (Figure 5). Temperature data shows that the sea water temperature has increased significantly compared to last year.

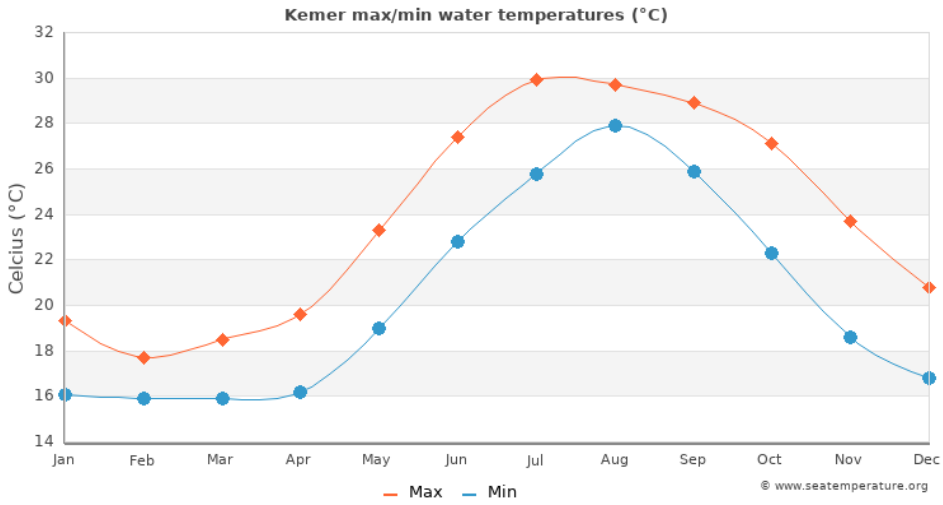

Figure 5. Water temperature changes in 2024 at Kemer, Antalya Bay (https://www.seatemperature.org/middle-east/turkey/kemer.htm)

Table 3. Water temperatures during collecting samples.

	Average	min	max
December	18.8	16.8	20.8
January	17.7	16.1	19.3
February	16.8	15.9	17.7

CONCLUSION

In this study, *S. luridus* (b: 3,02), *S. rubnum* (b: 3,26), *L. scleratus* (b: 3,14) and *F. petimba* (b: 3,79) had positive allometric growth (b>3), while *P. miles* (b: 2,20) had negative allometric growth (b<3). The differences in *b* values can be attributed to various factors, including species, sex, habitat, diet and nutrition, stomach fullness, season, sample size, sampling method, gonad development, physical condition, and the length of individuals (Tesh, 1971; Wootton, 1998). Therefore, it is thought that several of these factors had an effect in our study. It is clearly understood that *F. petimba* is quite well developed in terms of condition among the condition values of the lessepsian fish species in the region. Accordingly, the differences between the average condition values may be due to the differences in the size of the fish species as well as the differences in the habitats where the fish are distributed (Froese, 2006). In conclusion, according to the condition values of 5 lessepsian species in this study, it can be said that *F. petimba* individuals have very favorable conditions in terms of finding food (50% fullness) and feeding with crustaceans and fish species in the research area. This study provides up-to-date data on the length-weight data and body performance values of invasive species in the region and the growth rates of fishes. We believe that these results will be beneficial for regional fisheries.

REFERENCES

Bilecenoglu, M., Taskavak, E., Mater, S., Kaya, M. (2002). Checklist of the marine fishes of Turkey (Zootaxa 113). Magnolia Press, Auckland, New Zealand, 194 pp.

Froese, R. (2006) Cubelaw, condition factor and weight-length relationships: history, meta-analysis and recommendations. J Appl Ichthyol 22:241–253Turan, C., Gurlek, M., Basusta, N., Uyan, A., Aydoğdu, S.A., & Karan, S. (2018). A checklist of the nonindigenous fishes in Turkish Marine Waters. NESciences, 3(3), 333-358. https://doi.org/10.28978/nesciences.468995.

Tesch, W. (1971). Age and growth. In: Ricker We (ed), Methods for assessment of fish production in fresh waters, 2nd edn. International Biological Programme, *Oxford and Edinburgh,* 97-130.

Wootton, R.J. (1998). Ecology of Teleost fishes. Kluwer Academic Publishers, Dordrecht, the Netherlands.

Zenetos, A., Gofas, S., Verlaque, M., Cinar, M.E., Garcia Raso, J.E., Bianchi, C.N., Morri, C., Azzurro, E., Bilecenoglu, M., Froglia, C., Siokou-Frangou, I., Violanti, D., Sfriso, A., San Martín, G., Giangrande, A., Katagan, T., Ballesteros, E., Ramos-Esplá, A., Mastrototaro, F., Ocaña, Ó, Zingone, A., Gambi, M.C and Streftaris, N. (2010) Alien species in the Mediterranean Sea by 2010. A contribution to the application of European Union's Marine Strategy Framework Directive (MSFD). Part I. Spatial distribution. Mediterranean Marine Science 11, 381–493.

➢ *ORAL PRESENTATION*

Identification and Classification of Entity Names in Turkish Celebrity News Contents

Merve Adak[1] (ORCID: https://orcid.org/0009-0009-9665-2436), Mehmet Dikmen[1] (ORCID: https://orcid.org/0000-0002-0584-5577)

[1]Başkent University, Institute of Science, Department of Computer Engineering, Ankara, Türkiye

Corresponding author e-mail: merveadak983@gmail.com

Abstract
This study focuses on the automatic recognition and classification of named entities in Turkish magazine news using deep learning techniques. Due to the complex morphology and agglutinative structure of Turkish, Named Entity Recognition (NER) presents unique challenges. Three different deep learning models were trained and evaluated using both BIO and NONE-BIO annotation schemes, resulting in six experimental setups. The models aim to identify entities such as person, event, date, relationship, location, and organization within sentences extracted from magazine news that exhibit stylistic diversity. A domain-specific, manually annotated dataset was created, and preprocessing steps such as syntactic analysis were applied to enhance model performance.

Evaluation metrics included accuracy, precision, recall, F1-score, and support. Comprehensive visual analyses were also conducted, including class distribution analysis, confidence scores, confusion matrices, error heatmaps, F1 score graph, performance radar charts, precision-recall curves, and t-SNE embeddings. To improve interpretability and transparency of model predictions, LIME (Local Interpretable Model-agnostic Explanations) analysis was applied, examining the features influencing each model's decisions. Results demonstrate that transformer-based models, especially BERT variants, effectively handle the linguistic complexity and variability of Turkish magazine news.

This research contributes to Turkish natural language processing by providing a domain-specific dataset, a comparison of multiple models and annotation schemes, and extensive performance visualizations. Findings highlight the critical role of contextual word embeddings in improving NER accuracy in Turkish. Moreover, the study reveals the potential of deep learning for automating information extraction from unstructured media content, with applications in media monitoring, automated news processing, and information retrieval systems.
Keywords: Named Entity Recognition, Turkish, Magazine News, Information Extraction, Natural Language Processing, Text Classification

INTRODUCTION

Named Entity Recognition (NER) is the task of identifying and classifying entities such as persons, locations, dates, organizations, and events in unstructured text. While numerous studies have been conducted in languages like English, this task poses unique challenges in morphologically rich and agglutinative languages, particularly Turkish. The morphological complexity of Turkish complicates the determination of entity boundaries and classification.

In recent years, transformer-based deep learning models have achieved significant success in sequence labeling tasks such as NER. Models like BERT leverage attention mechanisms to effectively capture contextual information, thereby improving performance. However, adapting these models to Turkish, and particularly to domains such as magazine news, requires careful consideration due to the structural characteristics of the language and the domain-specific challenges.

In this context, the study by Kılıç (2023), which presents a named entity recognition and explainability-oriented analysis on Turkish sports news texts, served as an inspiration for this study in terms of both methodological approach and domain-specific focus.

In addition to Kılıç's work, various studies in the literature have explored Turkish NER across different domains. For example, Abdullahi et al. (2025) developed a deep learning-based NER framework for Turkish radiology reports and demonstrated that BioBERTurk achieved the highest F1 score (80.1%). Aras et al. (2021) compared BiLSTM and Transformer-based models for Turkish NER and showed that

Transformer-based architectures provided superior performance due to their ability to model long-range dependencies. In the social media context, Okur et al. (2018) applied semi-supervised learning with word embeddings to noisy and informal Turkish Twitter data, yielding effective results. These diverse efforts underscore the growing interest in Turkish NER and the importance of evaluating models in both formal and informal textual domains.

This study focuses on the automatic recognition and classification of named entities in Turkish magazine news. Magazine news, characterized by informal language, diverse entity types, and high linguistic variability, presents a particular challenge. To address this, a domain-specific, manually annotated dataset was created, and three different deep learning models were trained using both BIO and NONE-BIO annotation schemes, resulting in six experimental configurations.

Prior to model training, preprocessing steps such as syntactic analysis were applied to provide richer structural information to the models. Model performance was evaluated using metrics including accuracy, precision, recall, F1-score, and support. Furthermore, extensive visual analyses including confusion matrices, error heatmaps, F1 score graphs, radar charts, precision-recall curves, and t-SNE embeddings were performed to better understand model behavior. To enhance explainability and reveal the reasoning behind predictions, the LIME (Local Interpretable Model-agnostic Explanations) method (Ribeiro, Singh, & Guestrin, 2016) was also employed, which provides local explanations by approximating the model decision boundary around individual predictions.

This research makes significant contributions to Turkish natural language processing by comparing domain-specific datasets and multiple model-annotation approaches. The results underscore the critical role of contextual word embeddings in improving NER accuracy in Turkish. Additionally, the study highlights the potential of deep learning for automated information extraction from unstructured media content, with practical applications in media monitoring, news processing, and information retrieval systems.

MATERIALS AND METHODS

In this study, a Named Entity Recognition (NER) dataset was created using Turkish celebrity news headlines. The dataset incorporates tokens and vocabulary sourced primarily from the Turkish Headlines Dataset by Guven (2021), complemented with additional domain-specific terms to better capture the unique linguistic characteristics of celebrity news. The dataset was manually annotated according to the BIO (Beginning, Inside, Outside) tagging format to ensure accurate entity boundary detection. The annotation schema includes the following entity types relevant to the domain: PERSON, LOCATION, NUMBER/DATE, ORGANIZATION, MOVIE/TV, SONG/ALBUM, EVENT, SOCIAL_MEDIA, AWARD, RELATIONSHIP, and HEALTH. To ensure reproducibility, the dataset was randomly divided into training and test sets using a fixed random seed value of 42. The final corpus consists of 702 sentences for training and 175 sentences for testing. Each sentence was tokenized by separating words with spaces, and each token was individually aligned with its BIO label. The data was stored in a CoNLL-like format where each word is paired with its corresponding label, ensuring compatibility with standard NER workflows.

To evaluate model performance, three different pretrained transformer-based models were selected: dbmdz/bert-base-turkish-128k-uncased (dbmdz, 2020), google-bert/bert-base-multilingual-cased (Google Research, 2019), and xlm-roberta-base (Facebook AI, 2019). These models represent various architectures with differing tokenization strategies and multilingual capabilities. The dbmdz/bert-base-turkish-128k-uncased model, specifically trained for Turkish, outperformed the other multilingual and English-centric models.

Model training was performed using the HuggingFace Transformers library with the AutoTokenizer and AutoModelForTokenClassification components. The data was tokenized and processed with careful alignment between words and BIO format labels, using subword tokenization strategies to fit the models' expectations. Training and evaluation utilized HuggingFace's Trainer class alongside TrainingArguments parameters. The training was configured with a learning rate of 2e-5, batch size of 8, weight decay of 0.01, and conducted over 4 epochs. Evaluation was performed at the end of each epoch.

After training completion, the model and tokenizer files were saved. For testing, predictions were generated on tokenized sentences and probability scores computed using the softmax function. Token-level predictions were realigned to word-level labels using an offset-mapping based alignment algorithm, thus recovering accurate BIO tags at the word level.

Model performance was analyzed both quantitatively and qualitatively. Confusion matrices were used to visualize misclassifications, while classification reports provided precision, recall, and F1 scores for each entity type. Macro F1 scores of the three models were compared using radar charts.

High-dimensional model embeddings were reduced to two dimensions using t-distributed stochastic neighbor embedding (t-SNE) to examine how well the models grouped entities such as PERSON, EVENT, and AWARD based on their contextual representations. Precision-recall curves were drawn per entity to assess model sensitivity and specificity at various confidence thresholds. Histogram analyses of label distributions were prepared to evaluate class imbalance in the dataset.

Finally, Local Interpretable Model-Agnostic Explanations (LIME) analyses were conducted on selected test examples to interpret model decision-making processes. This method highlighted which tokens had the greatest influence on the model's predictions, shedding light on its contextual reasoning. Such insights guided both error analysis and future directions for model improvement and annotation refinement.

Overall, this work holistically demonstrates the effectiveness of Turkish and multilingual transformer-based models for named entity recognition tasks in the noisy and colloquial language of celebrity news, supported by code-based training procedures, comprehensive evaluation, and interpretability approaches.

RESULTS

In this study, the named entity recognition (NER) performances of three transformer-based models were comparatively examined on a dataset of Turkish entertainment news. These models include dbmdz/bert-base-turkish-128k-uncased (DBMDZ), google-bert/bert-base-multilingual-cased (Google BERT), and xlm-roberta-base (XLM-RoBERTa). The models were evaluated under two annotation schemes: None-BIO and BIO.

Under the None-BIO tagging scheme, the DBMDZ model achieved the highest performance. On a test set comprising 2,220 tokens, it demonstrated strong overall performance with 95% accuracy and a weighted average F1 score of 0.95. The most notable result was the 0.99 F1 score for the PERSON class. Other categories such as NUMBER/DATE, MOVIE/TV, and SOCIAL_MEDIA also performed consistently well, with F1 scores ranging between 0.93 and 0.95. These results highlight the model's effectiveness in distinguishing both common and domain-specific entity types. This balanced performance is visually supported by the radar chart (Figure 1), which clearly illustrates the model's consistent success across entity categories.

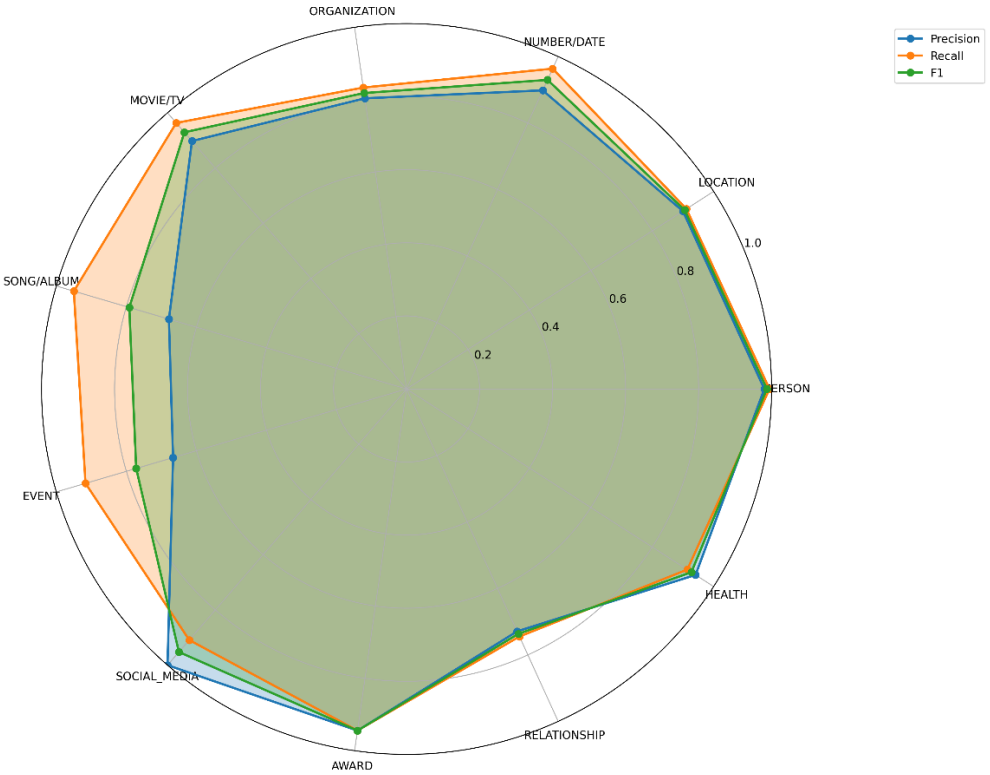

Figure 1. Performance Radar Chart by Entity Type (DBMDZ Turkish BERT, None-BIO)

The radar chart indicates that the model's precision, recall, and F1 scores are closely aligned across classes, suggesting not only accurate predictions but also stable performance across diverse entity types. While higher performance is evident in more frequent classes, reasonable results in less frequent ones like SONG/ALBUM and EVENT imply that the model can learn effectively even from limited samples. Overall, DBMDZ demonstrates strong potential as a reliable solution for Turkish entertainment news NER tasks.

The high precision and recall achieved by Google BERT for the NUMBER/DATE class are clearly illustrated in Figure 2.

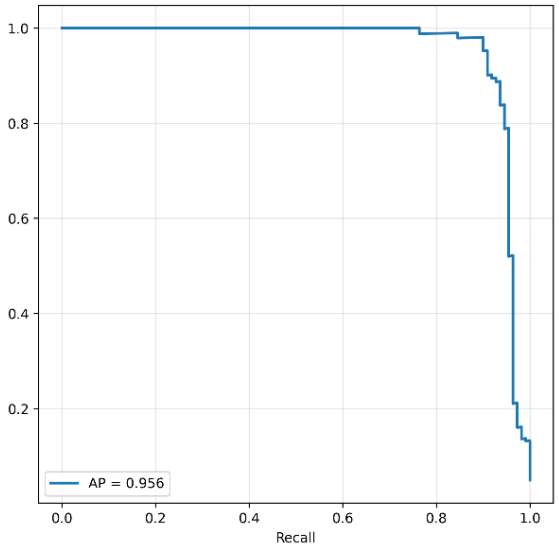

Figure 2. Precision-Recall Curve for the NUMBER/DATE Class (Google BERT, NONE-BIO)

Figure 3 presents the confusion matrix for the DBMDZ model under the None-BIO scheme. The model achieves over 95% accuracy in common categories such as "O" (Other), "PERSON," "NUMBER/DATE," "MOVIE/TV," and "SONG/ALBUM." However, performance dips to 74% and 83% accuracy in the "RELATIONSHIP" and "ORGANIZATION" categories, respectively.

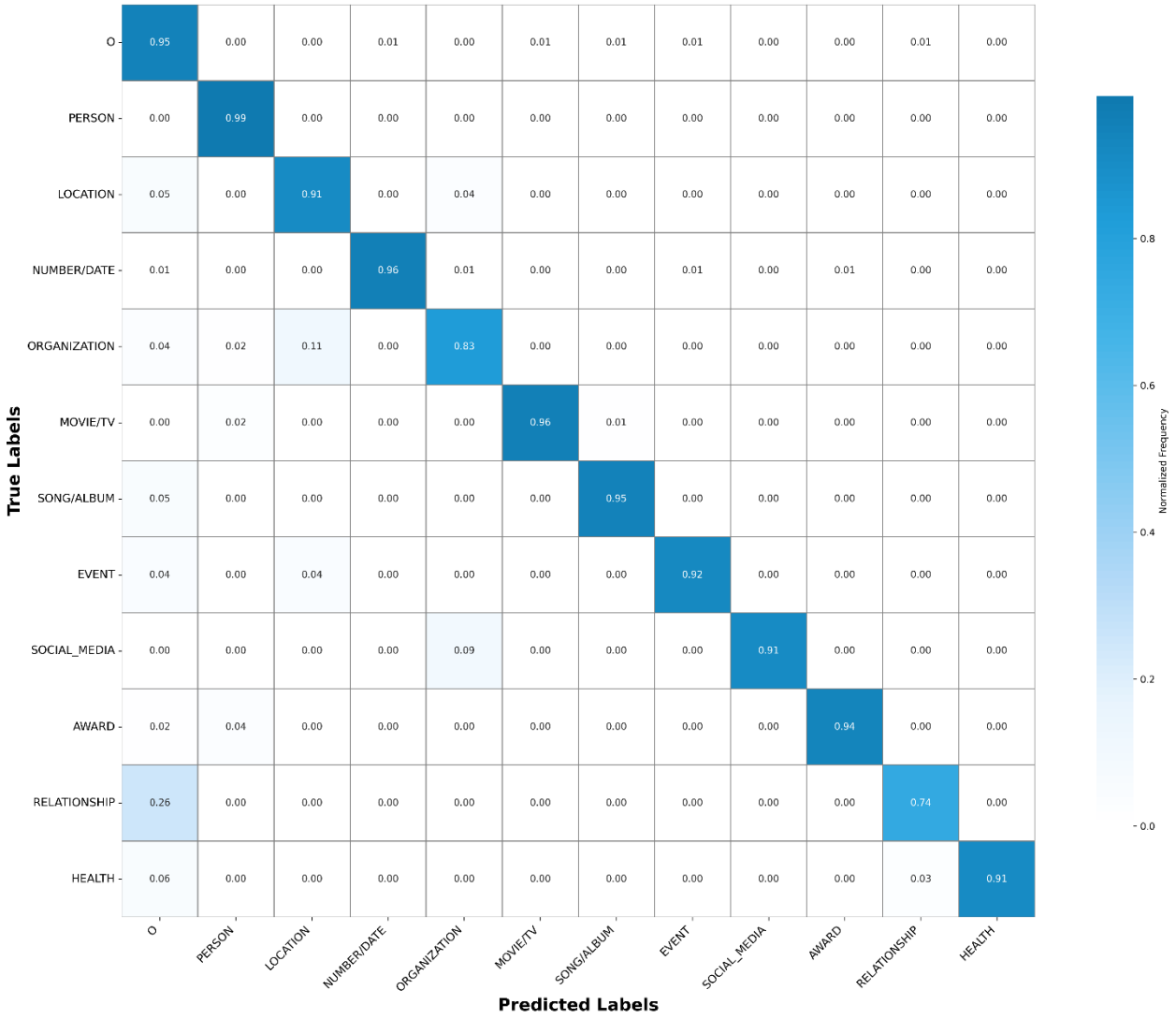

Figure 3. Confusion Matrix (DBMDZ Turkish BERT, None-BIO)

The confusion matrix reveals that while accuracy rates exceed 90% for most categories, the RELATIONSHIP class experiences a 26% confusion rate with the "O" class. Similarly, the ORGANIZATION class has an 11% confusion rate with LOCATION. Error rates for other categories remain below 5%. These findings highlight the model's strong general performance but also indicate areas that require further attention, especially for less frequent or semantically similar classes.

To address these challenges, increasing data diversity in weaker categories, enhancing annotation consistency, and implementing specialized feature engineering are recommended. Additionally, hyperparameter tuning and architectural modifications may further improve performance.

While the DBMDZ model shows strong results under the None-BIO scheme, Google BERT demonstrates notable advancements with the BIO annotation scheme, particularly in detecting entity boundaries and achieving high F1 scores across entity types.

Under the BIO scheme, Google BERT achieved a macro-average F1 score of 0.813, demonstrating superior capability in boundary detection. Figure 4 illustrates the top ten performing entity types for Google BERT, highlighting exceptional F1 scores, including a perfect 1.000 for the I-SOCIAL_MEDIA label and 0.980 for I-PERSON.

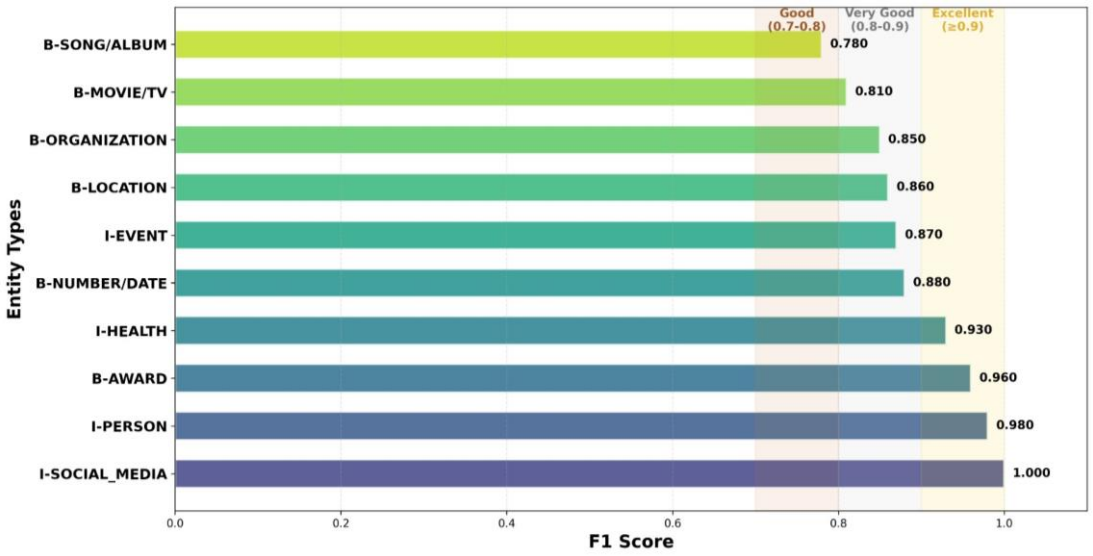

Figure 4. Top 10 Performing Entities F1 Score Graph (Google BERT, BIO)

The entity-level precision-recall curve of Google BERT under the BIO annotation scheme (Figure 5) highlights the model's stable and balanced learning process across various entity types. As a representative example, the B-PERSON class demonstrates a high Area Under the Precision-Recall Curve (AUC-PR) and a smooth curve trajectory, indicating that the model achieves both high precision and high recall. This suggests that Google BERT effectively distinguishes entity boundaries and accurately identifies multi-token entities. The consistently strong performance across classes supports the model's contextual understanding and reinforces its reliability in complex named entity recognition tasks.

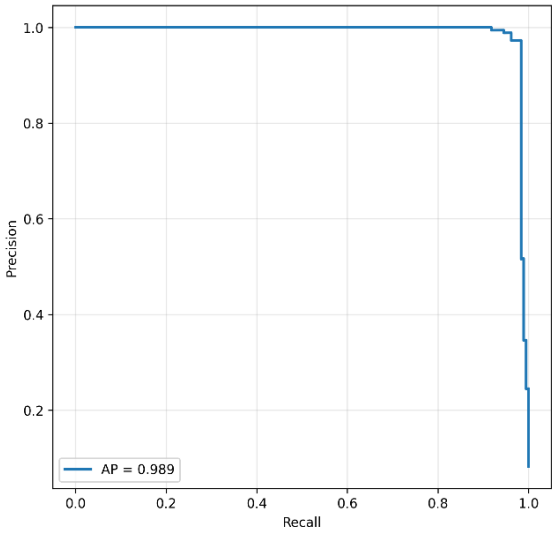

Figure 5. Precision-Recall Curve for the B-PERSON Class (Google BERT, BIO)

In addition, the t-SNE visualizations (Figure 6) offered compelling and visually intuitive evidence of the DBMDZ model's contextual learning capacity. Under the None-BIO tagging scheme, the model produced distinctly defined and well-separated clusters for various entity types based on their contextual embeddings. This level of separation was especially pronounced in less frequent and more specific categories such as AWARD, SOCIAL_MEDIA, HEALTH, and RELATIONSHIP, which appeared as compact and clearly isolated clusters. Likewise, more common entity types such as LOCATION, ORGANIZATION, and NUMBER/DATE also demonstrated well-delineated grouping. The presence of such sharply defined and semantically coherent clusters suggests that the model effectively captures the subtle linguistic distinctions inherent to the Turkish language, underscoring its strong potential for downstream tasks such as Named Entity Recognition.

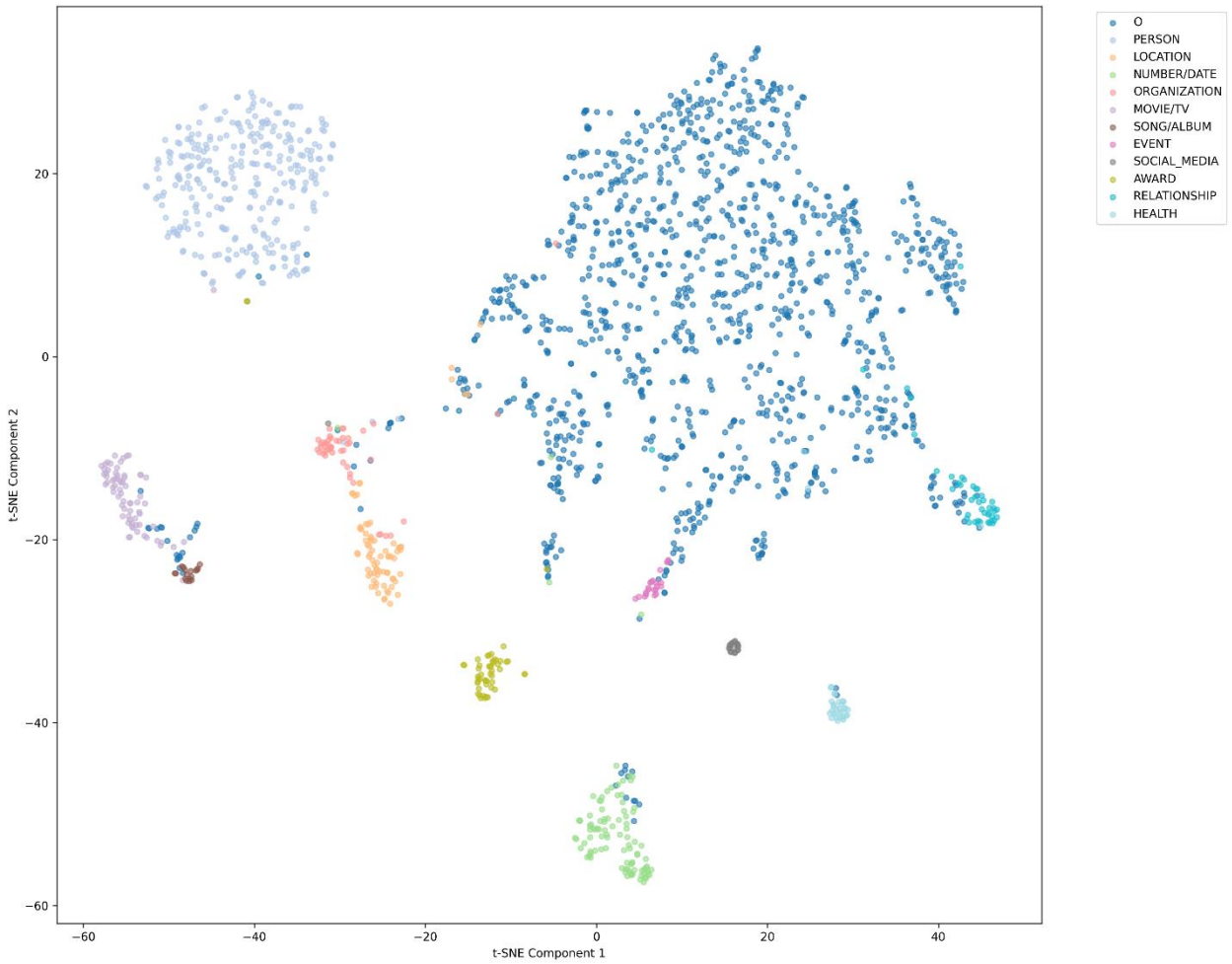

Figure 6. t-SNE Visualization of Entity Clusters (DBMDZ Turkish BERT, None-BIO)

Taken together, the experimental results reveal that the DBMDZ model performs most effectively under the None-BIO annotation scheme, whereas the Google Multilingual BERT model yields the best results in the BIO setting. These observations are further reinforced by a series of visual analyses, which capture the distinct learning behaviors and classification tendencies of the models across various entity types.

Beyond the detailed class-level evaluations presented above, Table 1 provides an aggregated overview of the models' overall performance, reporting key metrics such as Accuracy, Macro Precision, Macro Recall, Macro F1, and Weighted F1 scores. This comprehensive summary enables a robust comparison of the models across different annotation strategies, offering insight into their generalization capabilities and their ability to handle the structural intricacies of the Turkish magazine NER task under both BIO and None-BIO tagging schemes.

Table 1. Average Performance Metrics of the Models

Model	Annotation Scheme	Accuracy	Macro Precision	Macro Recall	Macro F1	Weighted F1
DBMDZ	None-BIO	0.95	0.89	0.89	0.89	0.95
Google BERT	None-BIO	0.95	0.89	0.88	0.88	0.95
XLM-RoBERTa	None-BIO	0.88	0.88	0.85	0.85	0.94
DBMDZ	BIO	0.85	0.74	0.66	0.68	0.85
Google BERT	BIO	0.93	0.83	0.82	0.82	0.93
XLM-RoBERTa	BIO	0.89	0.50	0.50	0.48	0.87

Finally, to evaluate the explainability of the model's decisions, LIME (Local Interpretable Model-Agnostic Explanations) analyses were conducted, particularly focusing on correctly classified examples. In the analysis of a sample sentence, the word "Suadiye" emerged as the most positively contributing token for the B-PERSON class. This indicates that the model can successfully distinguish person names. Similarly, tokens like "Geçtiğimiz" and "yılın" were observed to provide meaningful contributions to the B-NUMBER/DATE label. For other classes, contribution scores were generally low or neutral, and in some cases even negative. Notably, the low contribution scores observed for classes such as B-HEALTH, B-RELATIONSHIP, and B-SOCIAL_MEDIA are naturally interpreted as a result of the absence of expressions belonging to these entity types in the sentence. These analyses highlight both the strengths and limitations of the model in more detail and underscore the need for data augmentation, especially for underrepresented classes.

DISCUSSION

The findings of this study demonstrate that the performance of Named Entity Recognition (NER) on Turkish entertainment texts is significantly influenced by both the choice of model and the annotation scheme employed. Notably, models pre-trained specifically for Turkish exhibit better adaptation to the language's morphological complexity, resulting in superior performance. The BIO annotation format has proven critical for precise boundary detection of entities, with models showing more consistent and balanced performance under this scheme. This supports the preference for BIO tagging in practical applications where accurate entity boundary identification is essential. Performance differences among models indicate that multilingual architectures may struggle to effectively capture the nuances of Turkish morphology. Furthermore, the lower performance observed in rare entity classes highlights challenges related to data imbalance and class heterogeneity. These issues underscore the importance of future work focusing on data augmentation, improved annotation consistency, and model optimization. Overall, this study provides valuable insights for the Turkish NER domain, emphasizing the necessity of selecting methods tailored to the specific linguistic and application context to achieve optimal results.

CONCLUSION

This study presents a comprehensive evaluation of the named entity recognition (NER) capabilities of three transformer-based models applied to Turkish celebrity news data. The models were assessed under two different annotation schemes: BIO and None-BIO.

Under the None-BIO labeling scheme, the dbmdz/bert-base-turkish-128k-uncased model, which is pretrained specifically for Turkish, achieved the highest performance with 95% accuracy and a macro F1 score of 0.89. The model's success in categories such as PERSON, NUMBER/DATE, and SOCIAL_MEDIA suggests that language-specific pretraining significantly enhances performance on informal and domain-specific texts.

In contrast, the BIO annotation format, which requires more precise identification of entity boundaries, favored the Google Multilingual BERT model. This model achieved a macro F1 score of 0.82, indicating consistent and balanced recognition across different entity classes. These results point to the model's strength in learning complex contextual dependencies, which are crucial for boundary-sensitive tagging formats.

While XLM-RoBERTa exhibited strong accuracy under the None-BIO scheme, its performance declined notably in the BIO setting. As detailed in Table 1, the model's macro precision and recall scores dropped significantly, and confusion matrix analyses revealed frequent misclassifications in ORGANIZATION, EVENT, and SONG/ALBUM entities. This performance gap highlights the model's limited adaptability to the increased granularity imposed by BIO annotations.

Overall, the results summarized in Table 1 demonstrate that both model architecture and annotation scheme play critical roles in determining NER effectiveness. Macro-level metrics, which account for per-class performance independently of frequency, reveal that some models perform well in high-frequency categories but struggle with rare or complex entity types.

Improving NER outcomes in Turkish requires not only selecting robust model architectures but also designing annotation schemes and datasets that align with linguistic characteristics and domain-specific challenges. Future research should prioritize data augmentation for low-resource entity types such as AWARD and RELATIONSHIP, which are consistently underrepresented. Such efforts are expected to improve both predictive accuracy and the quality of interpretability tools like LIME, especially by supporting more stable and meaningful local explanations for rare entities.

ACKNOWLEDGEMENTS

I would like to express my sincere appreciation to my thesis advisor, Assistant Professor Dr. Mehmet Dikmen, for his guidance and contributions during the preparation of this study. His feedback and academic perspective were valuable in shaping the overall direction of the work. I am thankful for his support throughout the process.

REFERENCES

Abdullahi, A. A., Ganiz, M. C., Koç, U., Gökhan, M. B., Aydın, C., & Özdemir, A. B. (2025). Deep learning for named entity recognition in Turkish radiology reports. *Diagnostic and Interventional Radiology*. https://doi.org/10.4274/dir.2025.243100

Aras, G., Makaroglu, D., Demir, S., & Cakir, A. (2021). An evaluation of recent neural sequence tagging models in Turkish named entity recognition. *Expert Systems with Applications, 182*, 115049. https://doi.org/10.1016/j.eswa.2021.115049

dbmdz. (2020). *bert-base-turkish-128k-uncased* [Pretrained model]. Hugging Face. https://huggingface.co/dbmdz/bert-base-turkish-128k-uncased

Facebook AI. (2019). *xlm-roberta-base* [Pretrained model]. Hugging Face. https://huggingface.co/xlm-roberta-base

Google Research. (2019). *bert-base-multilingual-cased* [Pretrained model]. Hugging Face. https://huggingface.co/google-bert/bert-base-multilingual-cased

Guven, A. (2021) Turkish Headlines Dataset. Kaggle. Retrieved May 2, 2025, from https://www.kaggle.com/datasets/anil1055/turkish-headlines-dataset

Kılıç, Y. P. (2023). *Named entity recognition and explainability analysis on Turkish sports news texts* (Master's thesis, Middle East Technical University, Graduate School of Natural and Applied Sciences).

Okur, E., Demir, H., & Özgür, A. (2018). Named entity recognition on Twitter for Turkish using semi-supervised learning with word embeddings. *arXiv preprint* arXiv:1810.08732. https://arxiv.org/abs/1810.08732

Ribeiro, M. T., Singh, S., & Guestrin, C. (2016). "Why should I trust you?": Explaining the predictions of any classifier. In *Proceedings of the 22nd ACM SIGKDD International Conference on Knowledge Discovery and Data Mining* (pp. 1135–1144). https://doi.org/10.1145/2939672.2939778

➢ *ORAL PRESENTATION*

Demand forecasting performance using multi-channel sales data: a comparative analysis of e-commerce and traditional channels

Oğuz Kaan Çiçek* (*https://orcid.org/0000-0002-4900-7858)* Serap Ulusam Seçkiner[2] (*https://orcid.org/0000-0002-1612-6033*) Yunus Eroğlu[3] (https://orcid.org/0000-0002-8354-6783)

*[1]Gaziantep University, Engineering Faculty, Industrial Engineering, Gaziantep, Türkiye.
[2] Gaziantep University, Engineering Faculty, Industrial Engineering, Gaziantep, Türkiye.
[3] Gaziantep University, Engineering Faculty, Industrial Engineering, Gaziantep, Türkiye.

*Corresponding author e-mail: oguzzkaancicek@gmail.com

Abstract
This study investigates the forecasting performance of ARIMA and Simple Exponential Smoothing (SES) methods in a multi-channel retail environment, focusing on the comparative analysis of traditional and e-commerce sales channels. Using monthly sales data from January 2023 to December 2024 for five distinct product groups produced by a polypropylene yarn manufacturer in Türkiye, the study evaluates model accuracy through the Symmetric Mean Absolute Percentage Error (SMAPE) metric. Forecasts were generated separately for each channel, and model parameters were optimized accordingly. Results reveal that the ARIMA(1,1,2) model consistently outperformed SES across all product groups, particularly in capturing irregular demand patterns and short-term fluctuations common in e-commerce data. While the dataset lacks strong seasonality and covers a limited time span, the findings underline the critical need for channel-specific forecasting strategies.

Keywords: Multi-channel demand forecasting, Forecasting model comparison, Synthetic yarn manufacturing

INTRODUCTION

In today's rapidly evolving retail environment, companies often operate across multiple sales channels, such as traditional physical outlets and emerging e-commerce platforms. Managing demand across these diverse channels has become increasingly critical for maintaining service levels, optimizing inventory, and maximizing profitability. However, the distinct dynamics of e-commerce—such as higher demand volatility, faster response expectations, and greater promotional sensitivity—necessitate a re-evaluation of conventional forecasting models [1] traditionally used for brick-and-mortar operations.

Accurate demand forecasting plays a pivotal role in aligning supply chain operations with customer expectations in a multi-channel setting. Traditional time series models like ARIMA and Exponential Smoothing have long been used to predict sales trends based on historical data. Nevertheless, the integration of e-commerce channels introduces new complexities, including seasonality shifts, shorter product life cycles [5], and greater variability in customer behavior. Therefore, it is essential to compare forecasting model performances separately across e-commerce and traditional channels to understand their respective predictive strengths and limitations.

This study aims to evaluate the forecasting accuracy for five product groups sold through both traditional and e-commerce channels. By applying ARIMA and Exponential Smoothing methods and measuring model performance using Symmetric Mean Absolute Percentage Error (SMAPE), the analysis seeks to determine whether e-commerce sales exhibit different forecasting challenges compared to conventional channels. The findings offer practical insights into how demand forecasting strategies can be adapted to better support multi-channel retailing environments.

METHODOLOGY

This study adopts a structured quantitative approach to evaluate demand forecasting performance across traditional and e-commerce sales channels. A dataset comprising monthly sales figures for five distinct product groups, categorized separately for each channel, serves as the foundation for the analysis. To ensure

comparability, the selected product groups exhibit consistent sales patterns across both channels, thus minimizing external variability due to product heterogeneity.

The forecasting models employed in this study are Autoregressive Integrated Moving Average (ARIMA) and Simple Exponential Smoothing (SES), both widely recognized for their robustness in time series prediction. ARIMA models are particularly suitable for capturing autoregressive behaviors, trends, and seasonality patterns [2] within the sales data, whereas Exponential Smoothing provides a flexible and computationally efficient method for short-term forecasting without requiring extensive model complexity. Model selection parameters for ARIMA, such as the order of autoregression (p), differencing (d), and moving average (q), are determined using a combination of Autocorrelation Function (ACF) and Partial Autocorrelation Function (PACF) plots, supplemented by model selection criteria such as Akaike Information Criterion (AIC). The smoothing parameter (α) for Exponential Smoothing is optimized based on minimizing forecast error within the training dataset.

Model performance is evaluated using Symmetric Mean Absolute Percentage Error (SMAPE), a scale-independent metric particularly well-suited for comparing forecast accuracy across datasets with varying magnitudes. SMAPE offers a normalized measure of error, mitigating the sensitivity issues associated with traditional MAPE in cases of low sales volumes. Forecasting experiments are conducted separately for traditional and e-commerce sales data for each product group, and comparative analyses are performed to highlight the differential forecasting challenges and model suitability across channels. The methodological framework is designed to yield insights into the structural differences in demand behavior between traditional and digital retail environments.

DATA DESCRIPTION

The dataset utilized in this study originates from a polypropylene synthetic yarn manufacturer operating in Gaziantep, Türkiye. It captures monthly demand figures for five distinct product groups. The data encompasses two parallel sales channels—traditional direct sales and e-commerce sales—providing a comprehensive basis for multi-channel demand analysis.

Covering the period from January 2023 to December 2024, the dataset consists of 24 monthly observations for each product group within each sales channel. Demand is recorded as the number of units sold per month in kilogram, ensuring temporal consistency across products and channels. Table 1 shows the actual demands for traditional Sales and e-commerce Sales in kg.

The selected product groups represent a diverse range of industrial applications, each exhibiting unique demand characteristics influenced by sectoral dynamics, seasonality, and customer behavior. This diversity allows for a robust evaluation of forecasting methods under varying demand conditions. The structured nature of the dataset—organized by product, channel, and month—facilitates time series analysis and enables systematic application of forecasting models tailored to the operational realities of multi-channel industrial manufacturing.

Table 1. Actual Demands for Traditional and E-Commerce Sales of Five Product Group

Year	Month	Actual Demands for Traditional Sales (kg)					Actual Demands for E-Commerce Sales (via Web-site) (kg)				
		Greenhouse Twine	Carpet Yarn	Package Yarn	Bale Twine	Plastic Packaging Yarn	Greenhouse Twine	Carpet Yarn	Package Yarn	Bale Twine	Plastic Packaging Yarn
2023	January	173.461,00	95.613,00	127.994,00	97.884,00	62.724,00	12.752,00	11.494,00	10.506,00	7.911,00	9.855,00
2023	February	169.202,00	91.511,00	155.758,00	94.876,00	44.946,00	12.199,00	10.866,00	22.996,00	16.210,00	7.383,00
2023	March	184.071,00	97.187,00	122.169,00	116.923,00	65.219,00	20.531,00	7.350,00	9.222,00	9.606,00	5.539,00
2023	April	171.007,00	78.122,00	141.921,00	114.290,00	53.507,00	22.699,00	10.476,00	11.492,00	12.778,00	4.731,00
2023	May	145.601,00	92.151,00	159.859,00	96.784,00	62.107,00	20.794,00	5.387,00	13.564,00	8.891,00	7.570,00
2023	Jun	147.654,00	99.242,00	126.509,00	113.690,00	60.157,00	11.555,00	13.247,00	14.607,00	16.640,00	6.999,00
2023	July	201.258,00	85.957,00	126.621,00	94.715,00	46.734,00	24.538,00	13.463,00	8.033,00	12.913,00	6.284,00
2023	August	188.375,00	72.955,00	127.589,00	95.787,00	44.761,00	16.687,00	11.542,00	10.136,00	14.706,00	5.275,00
2023	September	175.344,00	71.219,00	158.535,00	95.026,00	64.473,00	10.770,00	4.738,00	14.137,00	11.186,00	9.855,00
2023	October	133.726,00	82.930,00	130.025,00	120.561,00	55.754,00	14.419,00	7.766,00	21.900,00	19.569,00	5.207,00
2023	November	159.933,00	99.198,00	131.021,00	107.720,00	48.798,00	15.478,00	8.453,00	11.930,00	8.369,00	5.102,00
2023	December	154.608,00	81.835,00	115.867,00	111.263,00	63.889,00	9.291,00	5.651,00	14.977,00	11.743,00	9.639,00
2024	January	138.775,00	99.619,00	161.397,00	95.985,00	61.119,00	14.368,00	13.018,00	26.673,00	13.336,00	8.105,00
2024	February	166.483,00	83.272,00	163.333,00	94.135,00	43.057,00	25.823,00	8.926,00	10.433,00	7.104,00	4.505,00
2024	March	187.937,00	85.545,00	133.194,00	102.269,00	66.434,00	10.913,00	5.673,00	18.722,00	15.080,00	5.928,00
2024	April	163.695,00	67.583,00	156.741,00	103.303,00	58.511,00	22.159,00	4.172,00	25.920,00	12.227,00	6.048,00
2024	May	148.030,00	82.250,00	133.061,00	107.733,00	53.337,00	8.794,00	9.411,00	8.692,00	9.296,00	6.033,00
2024	Jun	154.724,00	84.131,00	141.927,00	115.980,00	64.552,00	11.872,00	10.755,00	16.540,00	18.869,00	9.115,00
2024	July	190.477,00	96.945,00	117.790,00	132.495,00	62.093,00	22.050,00	7.633,00	15.045,00	15.957,00	3.911,00
2024	August	157.493,00	76.788,00	121.265,00	97.240,00	55.268,00	9.228,00	10.083,00	16.842,00	12.581,00	6.510,00
2024	September	188.879,00	92.416,00	158.563,00	120.654,00	65.306,00	18.891,00	12.820,00	20.808,00	9.328,00	9.192,00
2024	October	163.570,00	87.795,00	168.710,00	120.919,00	47.615,00	25.563,00	9.758,00	16.040,00	14.404,00	4.815,00
2024	November	197.482,00	93.654,00	169.787,00	104.166,00	58.586,00	22.225,00	14.529,00	11.470,00	18.222,00	7.065,00
2024	December	190.855,00	72.325,00	117.323,00	122.836,00	64.465,00	19.218,00	10.848,00	9.007,00	18.383,00	4.473,00

Simple Exponential Smoothing (SES) Methodology

In this study, the Simple Exponential Smoothing (SES) method is applied to forecast monthly demand for each product group across both traditional and e-commerce sales channels. SES is particularly suitable for data without a clear trend or seasonal pattern and is defined by the formula:

$$Ft=Ft-1+\alpha(At-1-Ft-1) \quad (1)$$

where Ft−1 is the forecast for the previous period, At−1 is the actual demand, and α\alphaα is the smoothing parameter between 0 and 1. To determine the optimal α value for each product group, multiple alpha values ranging from 0.1 to 0.9 were tested. The α value minimizing the Mean Squared Error (MSE) was selected for each product group separately by the formula:

The mean of the squared errors = (Demand - Forecast)^2 / number of forecast (2)

Forecasting was then conducted for a 24-month period, using the actual demand of the first month (January 2023) as the initial forecast value. This approach ensures that the smoothing parameters are tailored to each product's demand behavior across different sales channels, improving forecasting accuracy and reliability. So ,with the basis of choosing the minimum SSE , the best α values selected and then calculated the forecasts. Table 2 shows the best α values for each product group.

Table 2. Best α values for each product group

Alpha Values	Traditional					E-Commerce				
	Greenhouse Twine	Carpet Yarn	Package Yarn	Bale Twine	Plastic Packaging Yarn	Greenhouse Twine	Carpet Yarn	Package Yarn	Bale Twine	Plastic Packaging Yarn
Alpha 0,1	418.960.338,28	120.293.208,73	401.636.169,76	150.527.178,52	74.778.637,18	39.484.960,57	10.784.615,46	37.028.058,83	20.632.070,76	6.056.735,33
Alpha 0,2	430.386.683,74	116.587.251,00	416.606.157,00	143.447.195,49	76.964.776,99	39.926.000,31	10.607.919,49	36.879.308,20	18.363.764,15	5.163.970,66
Alpha 0,3	445.560.567,75	120.985.603,91	444.482.973,53	147.403.994,49	82.340.886,53	41.558.912,16	10.801.737,49	38.700.868,72	18.495.540,43	5.122.650,39
Alpha 0,4	465.743.564,94	127.267.446,59	474.441.034,92	154.729.428,86	89.518.560,49	43.802.241,71	11.217.527,46	41.302.143,81	19.325.367,67	5.310.725,15
Alpha 0,5	489.273.408,23	134.293.957,82	504.604.691,91	163.932.815,68	98.096.292,30	46.666.918,98	11.777.196,64	44.494.356,78	20.562.260,88	5.614.363,43
Alpha 0,6	515.009.633,55	141.996.431,53	534.722.636,55	174.848.763,31	107.981.245,92	50.209.712,85	12.441.268,00	48.256.875,62	22.137.988,16	6.001.796,39
Alpha 0,7	542.761.559,70	150.695.126,19	565.139.999,52	187.790.236,30	119.235.878,78	54.500.669,30	13.203.698,88	52.624.569,34	24.061.077,02	6.462.521,44
Alpha 0,8	573.131.441,09	160.926.092,32	596.724.838,35	203.258.519,13	132.007.413,59	59.621.575,31	14.082.904,89	57.654.407,95	26.385.745,37	6.993.822,46
Alpha 0,9	607.474.154,62	173.453.143,65	630.996.818,95	221.823.184,39	146.487.841,52	65.672.768,87	15.115.164,05	63.411.099,57	29.205.147,02	7.597.016,28

Table 3. Demand Forecasts of Traditional Sales & E-Commerce Sales

Year	Month	Actual Demands for Traditional Sales (kg)					Actual Demands for E-Commerce Sales (via Web-site) (kg)				
		Greenhouse Twine	Carpet Yarn	Package Yarn	Bale Twine	Plastic Packaging Yarn	Greenhouse Twine	Carpet Yarn	Package Yarn	Bale Twine	Plastic Packaging Yarn
2023	January	173.461,00	95.613,00	127.994,00	97.884,00	62.724,00	12.752,00	11.494,00	10.506,00	7.911,00	9.855,00
2023	February	173.461,00	95.613,00	127.994,00	97.884,00	62.724,00	12.752,00	11.494,00	10.506,00	7.911,00	9.855,00
2023	March	173.035,10	94.792,60	130.770,40	97.282,40	60.946,20	12.696,70	11.368,40	13.004,00	9.570,80	9.113,40
2023	April	174.138,69	95.271,48	129.910,26	101.210,52	61.373,48	13.480,13	10.564,72	12.247,60	9.577,84	8.041,08
2023	May	173.825,52	91.841,58	131.111,33	103.826,42	60.586,83	14.402,02	10.546,98	12.096,48	10.217,87	7.048,06
2023	Jun	171.003,07	91.903,47	133.986,10	102.417,93	60.738,85	15.041,22	9.514,98	12.389,98	9.952,50	7.204,64
2023	July	168.668,16	93.371,17	133.238,39	104.672,35	60.680,66	14.692,59	10.261,38	12.833,39	11.290,00	7.142,95
2023	August	171.927,15	91.888,34	132.576,65	102.680,88	59.286,00	15.677,13	10.901,71	11.873,31	11.614,60	6.885,26
2023	September	173.571,93	88.101,67	132.077,89	101.302,10	57.833,50	15.778,12	11.029,77	11.525,85	12.232,88	6.402,18
2023	October	173.749,14	84.725,14	134.723,60	100.046,88	58.497,45	15.277,31	9.771,41	12.048,08	12.023,50	7.438,03
2023	November	169.746,82	84.366,11	134.253,74	104.149,71	58.223,10	15.191,48	9.370,33	14.018,46	13.532,60	6.768,72
2023	December	168.765,44	87.332,49	133.930,46	104.863,76	57.280,59	15.220,13	9.186,86	13.600,77	12.499,88	6.268,70
2024	January	167.349,70	86.232,99	132.124,12	106.143,61	57.941,43	14.627,22	8.479,69	13.876,02	12.348,51	7.279,79
2024	February	164.492,23	88.910,19	135.051,41	104.111,89	58.259,19	14.601,30	9.387,35	16.435,41	12.546,00	7.527,36
2024	March	164.691,31	87.782,55	137.879,57	102.116,51	56.738,97	15.723,47	9.295,08	15.234,93	11.457,60	6.620,65
2024	April	167.015,87	87.335,04	137.411,01	102.147,01	57.708,47	15.242,42	8.570,67	15.932,34	12.182,08	6.412,85
2024	May	166.683,79	83.384,63	139.344,01	102.378,21	57.788,73	15.934,08	7.690,93	17.929,88	12.191,07	6.303,40
2024	Jun	164.818,41	83.157,71	138.715,71	103.449,17	57.343,55	15.220,07	8.034,95	16.082,30	11.612,05	6.222,28
2024	July	163.808,97	83.352,37	139.036,84	105.955,33	58.064,40	14.885,26	8.578,96	16.173,84	13.063,44	7.090,09
2024	August	166.475,77	86.070,89	136.912,15	111.263,27	58.467,26	15.601,74	8.389,77	15.948,07	13.642,15	6.136,37
2024	September	165.577,49	84.214,31	135.347,44	108.458,61	58.147,33	14.964,36	8.728,41	16.126,86	13.429,92	6.248,46
2024	October	167.907,64	85.854,65	137.668,99	110.897,69	58.863,20	15.357,03	9.546,73	17.063,09	12.609,54	7.131,52
2024	November	167.473,88	86.242,72	140.773,09	112.901,95	57.738,38	16.377,62	9.588,98	16.858,47	12.968,43	6.436,56
2024	December	170.474,69	87.724,98	143.674,48	111.154,76	57.823,14	16.962,36	10.576,99	15.780,78	14.019,14	6.625,09

To evaluate the forecasting performance in this study, the Symmetric Mean Absolute Percentage Error (SMAPE) metric is utilized. SMAPE is particularly preferred over traditional Mean Absolute Percentage Error (MAPE) because it addresses issues arising from low or zero actual demand values, [3] which are common in multi-channel sales environments. SMAPE calculates the error as the ratio of the absolute difference between forecasted and actual demand to the average of the forecasted and actual values, thus self-limiting the maximum error to 200%. This approach ensures more stable and meaningful error evaluations, especially when dealing with low-volume e-commerce sales data. The SMAPE formula is defined as:

$$\textbf{SMAPE} = 1/N * \sum [|Fk - Ak| / ((Fk+Ak)/2)] * 100 \quad (3)$$

where F_k is the forecasted demand, A_k is the actual demand, and N is the number of periods. MAPE values were calculated for 24 months and shown in Table 4 below.

Table 4. MAPE Values of Products

Year	Month	Actual Demands for Traditional Sales (kg)					Actual Demands for E-Commerce Sales (via Web-site)				
		Greenhouse Twine	Carpet Yarn	Package Yarn	Bale Twine	Plastic Packaging Yarn	Greenhouse Twine	Carpet Yarn	Package Yarn	Bale Twine	Plastic Packaging Yarn
2023	January	-	-	-	-	-	-	-	-	-	-
2023	February	0,03	0,04	0,18	0,03	0,40	0,05	0,06	0,54	0,51	0,33
2023	March	0,06	0,02	0,07	0,17	0,07	0,38	0,55	0,41	0,00	0,65
2023	April	0,02	0,22	0,08	0,11	0,15	0,41	0,01	0,07	0,25	0,70
2023	May	0,19	0,00	0,18	0,07	0,02	0,31	0,96	0,11	0,15	0,07
2023	Jun	0,16	0,07	0,06	0,10	0,01	0,30	0,28	0,15	0,40	0,03
2023	July	0,16	0,09	0,05	0,11	0,30	0,40	0,24	0,60	0,13	0,14
2023	August	0,09	0,26	0,04	0,07	0,32	0,06	0,06	0,17	0,21	0,31
2023	September	0,01	0,24	0,17	0,07	0,10	0,47	1,33	0,18	0,09	0,35
2023	October	0,30	0,02	0,04	0,17	0,05	0,06	0,26	0,45	0,39	0,43
2023	November	0,06	0,15	0,02	0,03	0,19	0,02	0,11	0,18	0,62	0,33
2023	December	0,09	0,07	0,16	0,06	0,10	0,64	0,63	0,09	0,06	0,35
2024	January	0,21	0,13	0,18	0,11	0,05	0,02	0,35	0,48	0,07	0,10
2024	February	0,01	0,07	0,17	0,11	0,35	0,43	0,05	0,58	0,77	0,67
2024	March	0,12	0,03	0,04	0,00	0,15	0,44	0,64	0,19	0,24	0,12
2024	April	0,02	0,29	0,12	0,01	0,01	0,31	1,05	0,39	0,00	0,06
2024	May	0,13	0,01	0,05	0,05	0,08	0,81	0,18	1,06	0,31	0,04
2024	Jun	0,07	0,01	0,02	0,11	0,11	0,28	0,25	0,03	0,38	0,32
2024	July	0,14	0,14	0,18	0,20	0,06	0,32	0,12	0,08	0,18	0,81
2024	August	0,06	0,12	0,13	0,14	0,06	0,69	0,17	0,05	0,08	0,06
2024	September	0,12	0,09	0,15	0,10	0,11	0,21	0,32	0,22	0,44	0,32
2024	October	0,03	0,02	0,18	0,08	0,24	0,40	0,02	0,06	0,12	0,48
2024	November	0,15	0,08	0,17	0,08	0,01	0,26	0,34	0,47	0,29	0,09
2024	December	0,11	0,21	0,22	0,10	0,10	0,12	0,02	0,75	0,24	0,48
MAPE		10,11	10,42	11,59	9,04	13,30	32,12	34,75	31,76	25,87	31,43

After this calculation, noticed that there are undefined values due to zero actual demands and error rates were too high. After this attempt sMAPE was attempted. And also there is a second reason for sMAPE. sMAPE is generally used for zero demands or demands nearby zero. sMAPE calculated by formula below:

sMAPE = |Ft-At|/(At+Ft) (4)

Table 5. sMAPE Results of Calculations

Year	Month	Actual Demands for Traditional Sales (kg)					Actual Demands for E-Commerce Sales (via Web-site) (kg)				
		Greenhouse Twine	Carpet Yarn	Package Yarn	Bale Twine	Plastic Packaging Yarn	Greenhouse Twine	Carpet Yarn	Package Yarn	Bale Twine	Plastic Packaging Yarn
SMAPE		0,10	0,10	0,12	0,09	0,12	0,32	0,29	0,30	0,27	0,28

When this 2 methods (MAPE and sMAPE) are compared sMAPE's error rates is lower and more appropriate.

Autoregressive Integrated Moving Average (ARIMA) Methodology

In this study, ARIMA (AutoRegressive Integrated Moving Average) models are employed to forecast monthly demand across both traditional and e-commerce channels. ARIMA models are suitable for time series data that can be made stationary through differencing, which eliminates trends and stabilizes variance over time.

The modeling process follows the Box-Jenkins methodology, [4] involving four main steps: checking stationarity through data visualization, applying differencing if necessary, identifying appropriate AR (autoregressive) and MA (moving average) terms using ACF and PACF plots, and estimating model parameters. The selected ARIMA(p,d,q) models are then fitted to each product group's demand data separately.

Figure 1. Time Series Plots, ACF Plots and Differencing Graphs of Traditional & E-Commerce Sales

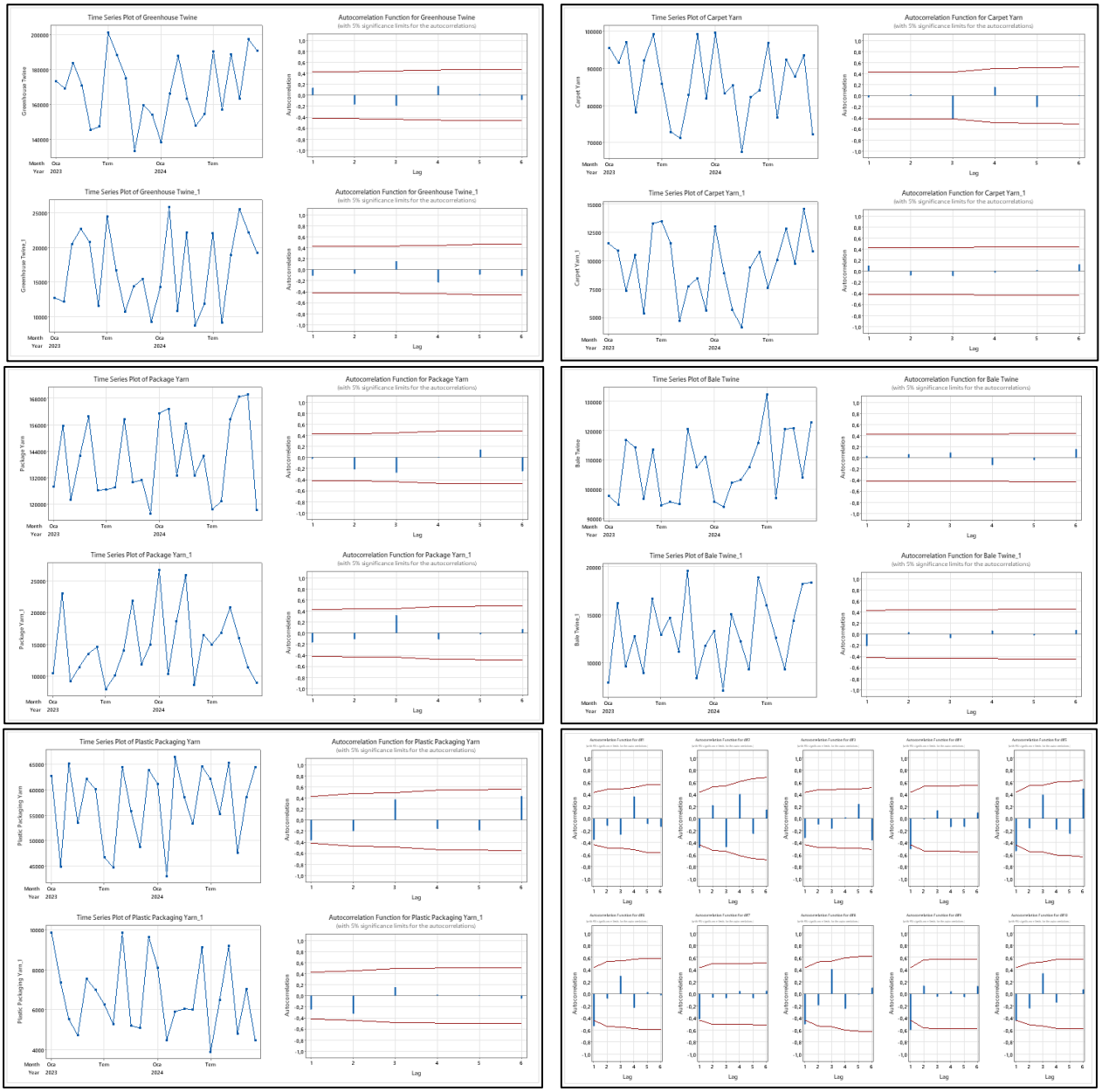

Given the relatively short time span of the dataset (24 months) and the lack of strong seasonal patterns, only non-seasonal ARIMA models are considered. Forecast accuracy is evaluated based on the model residuals and compared across product groups and sales channels to assess the reliability of the forecasts. Table 6 shows the time series plots, ACF graph and differencing of each product group.

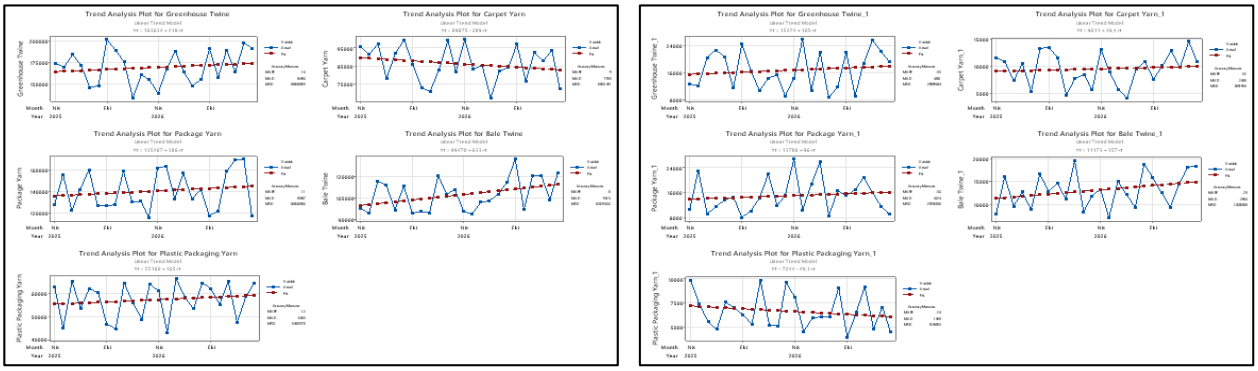

Figure 2. Trend Analysis of Traditional Sales & E-Commerce Sales

Trend analysis examined and no linear trend was found. In addition, time series plot shows of irregular movements. When the first of the series in order to define a model for the line must be stable(stationary). Autocorrelation must decide whether or not by looking at the series stationary.

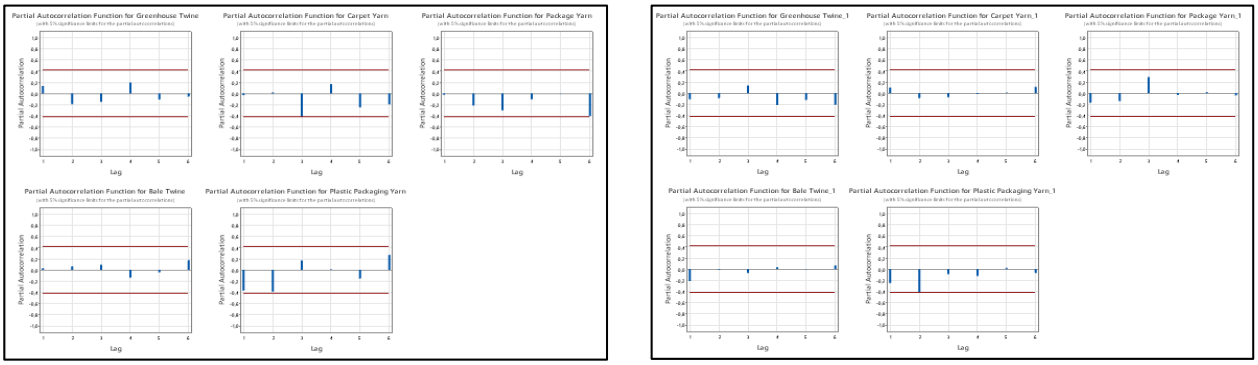

Figure 3. PACF Plots of Traditional Sales & E-Commerce Sales

The ARIMA(1,1,2) model was selected based on the characteristics of the demand data. First-order differencing (d=1) was applied to eliminate the trend and achieve stationarity. The presence of significant autocorrelations at the first lag and moving average effects up to the second lag, as observed in the ACF and PACF plots, justified the inclusion of one autoregressive term (p=1) and two moving average terms (q=2). This model effectively captures both the immediate and slightly extended dependencies [6] within the differenced series, allowing for accurate short-term forecasting across the examined product groups.

Table 6. ARIMA (1,1,2) Forecasts

	Actual Demands for Traditional Sales (kg)					Actual Demands for E-Commerce Sales (via Web-site) (kg)				
Year	Greenhouse Twine	Carpet Yarn	Package Yarn	Bale Twine	Plastic Packaging Yarn	Greenhouse Twine	Carpet Yarn	Package Yarn	Bale Twine	Plastic Packaging Yarn
01-2023	-	-	-	-	-	-	-	-	-	-
02-2023	168.161,94	91.150,99	138.145,42	102.327,05	54.206,49	14.402,25	9.903,58	13.754,79	10.996,09	7.358,89
03-2023	166.867,43	89.439,91	146.106,60	103.821,39	62.276,43	17.848,84	9.428,37	14.874,48	9.978,47	7.069,86
04-2023	167.990,89	90.090,37	130.035,41	104.294,61	54.999,44	16.682,88	8.677,22	12.527,99	11.158,92	7.232,21
05-2023	162.427,51	84.815,85	151.113,89	101.095,67	58.029,41	19.113,29	9.734,90	14.729,49	10.842,52	7.371,72
06-2023	162.168,24	88.408,56	136.530,63	102.614,27	54.765,82	16.994,51	8.384,70	13.125,09	11.805,35	7.444,96
07-2023	167.473,25	89.350,72	143.768,86	102.497,15	54.348,97	16.835,95	10.792,99	14.676,39	10.828,89	7.170,10
08-2023	173.135,87	84.899,07	135.197,84	101.554,90	61.379,04	20.416,15	9.592,31	12.617,35	11.510,71	7.341,04
09-2023	161.576,23	81.596,15	143.057,69	105.456,23	65.596,31	15.519,36	8.836,14	14.516,49	11.256,87	7.321,71
10-2023	160.108,90	82.213,25	144.138,36	105.358,53	56.891,14	18.554,25	7.338,63	13.371,36	11.983,06	7.235,83
11-2023	154.826,79	86.231,60	136.885,28	107.636,29	57.670,60	16.065,34	8.872,48	15.406,04	10.724,60	6.841,72
12-2023	165.466,76	90.214,07	143.776,51	103.243,41	61.760,66	18.642,91	8.759,92	12.728,77	12.541,45	7.465,39
01-2024	161.097,21	85.169,53	131.278,98	107.081,28	55.482,97	14.203,81	8.382,69	15.386,65	12.315,68	6.814,23
02-2024	164.949,56	89.065,31	156.192,09	103.916,88	54.153,72	19.346,31	10.351,57	14.719,61	12.500,81	6.648,71
03-2024	171.958,98	83.996,06	135.014,92	110.658,12	63.268,41	17.666,36	8.495,25	13.671,63	13.899,98	6.546,27
04-2024	170.956,52	84.190,03	150.235,51	109.054,92	54.791,55	15.965,68	8.422,55	15.560,77	13.182,76	6.838,62
05-2024	165.778,74	79.997,64	141.777,23	113.624,24	55.245,54	20.457,63	8.764,77	15.078,48	14.046,32	6.551,47
06-2024	168.836,05	84.640,64	145.125,64	112.650,92	58.231,31	12.740,93	10.529,62	13.714,62	14.956,75	6.757,69
07-2024	173.712,20	85.447,50	143.820,83	115.468,28	53.541,85	20.396,92	10.462,48	15.751,77	13.935,28	6.231,70
08-2024	178.489,83	88.246,71	137.756,98	112.113,90	52.758,48	15.569,07	9.891,60	13.962,76	14.565,93	6.266,66
09-2024	171.041,53	82.595,67	142.350,97	112.925,20	56.076,40	17.152,02	10.969,80	15.784,66	15.281,41	6.392,89
10-2024	181.002,91	86.378,00	147.700,83	116.049,27	52.168,91	17.789,70	11.306,93	14.878,08	16.374,24	5.762,09
11-2024	172.186,47	84.485,50	148.397,99	112.339,89	59.926,52	19.574,98	10.369,32	15.290,37	16.286,93	5.681,09
12-2024	181.635,78	84.979,46	151.960,83	115.731,34	57.510,76	17.928,05	11.620,98	14.460,54	16.163,79	5.562,30

Table 7. sMAPE Results of ARIMA Calculations

	Actual Demands for Traditional Sales (kg)					Actual Demands for E-Commerce Sales (via Web-site) (kg)				
Year	Greenhouse Twine	Carpet Yarn	Package Yarn	Bale Twine	Plastic Packaging Yarn	Greenhouse Twine	Carpet Yarn	Package Yarn	Bale Twine	Plastic Packaging Yarn
01-2023	-	-	-	-	-	-	-	-	-	-
02-2023	0,00	0,00	0,06	0,04	0,09	0,08	0,05	0,25	0,19	0,00
03-2023	0,05	0,04	0,09	0,06	0,02	0,07	0,12	0,23	0,02	0,12
04-2023	0,01	0,07	0,04	0,05	0,01	0,15	0,09	0,04	0,07	0,21
05-2023	0,05	0,04	0,03	0,02	0,03	0,04	0,29	0,04	0,10	0,01
06-2023	0,05	0,06	0,04	0,05	0,05	0,19	0,22	0,05	0,17	0,03
07-2023	0,09	0,02	0,06	0,04	0,08	0,19	0,11	0,29	0,09	0,07
08-2023	0,04	0,08	0,03	0,03	0,16	0,10	0,09	0,11	0,12	0,16
09-2023	0,04	0,07	0,05	0,05	0,01	0,18	0,30	0,01	0,00	0,15
10-2023	0,09	0,00	0,05	0,07	0,01	0,13	0,03	0,24	0,24	0,16
11-2023	0,02	0,07	0,02	0,00	0,08	0,02	0,02	0,13	0,12	0,15
12-2023	0,03	0,05	0,11	0,04	0,02	0,33	0,22	0,08	0,03	0,13
01-2024	0,07	0,08	0,10	0,05	0,05	0,01	0,22	0,27	0,04	0,09
02-2024	0,00	0,03	0,02	0,05	0,11	0,14	0,07	0,17	0,28	0,19
03-2024	0,04	0,01	0,01	0,04	0,02	0,24	0,20	0,16	0,04	0,05
04-2024	0,02	0,11	0,02	0,03	0,03	0,16	0,34	0,25	0,04	0,06
05-2024	0,06	0,01	0,03	0,03	0,02	0,40	0,04	0,27	0,20	0,04
06-2024	0,04	0,00	0,01	0,01	0,05	0,04	0,01	0,09	0,12	0,15
07-2024	0,05	0,06	0,10	0,07	0,07	0,04	0,16	0,02	0,07	0,23
08-2024	0,06	0,07	0,06	0,07	0,02	0,26	0,01	0,09	0,07	0,02
09-2024	0,05	0,06	0,05	0,03	0,08	0,05	0,08	0,14	0,24	0,18
10-2024	0,05	0,01	0,07	0,02	0,05	0,18	0,07	0,04	0,06	0,09
11-2024	0,07	0,05	0,07	0,04	0,01	0,06	0,17	0,14	0,06	0,11
12-2024	0,02	0,08	0,13	0,03	0,06	0,03	0,03	0,23	0,06	0,11
sMAPE	**0,09**	**0,09**	**0,11**	**0,08**	**0,10**	**0,27**	**0,26**	**0,29**	**0,21**	**0,22**

Table 8. Comparison of SMAPE Values

SMAPE VALUES	Actual Demands for Traditional Sales (kg)					Actual Demands for E-Commerce Sales (via Web-site) (kg)				
	Greenhouse Twine	Carpet Yarn	Package Yarn	Bale Twine	Plastic Packaging Yarn	Greenhouse Twine	Carpet Yarn	Package Yarn	Bale Twine	Plastic Packaging Yarn
EXPONENTIAL SMOOTING	0,10	0,10	0,12	0,09	0,12	0,32	0,29	0,30	0,27	0,28
ARIMA MODEL	0,09	0,09	0,11	0,08	0,10	0,27	0,26	0,29	0,21	0,22
BEST RESULTS	0,09	0,09	0,11	0,08	0,10	0,27	0,26	0,29	0,21	0,22

The results presented in Table 8 indicate that while two forecasting methods were tested, ARIMA(1,1,2) model consistently outperformed across all periods. Therefore, the ARIMA(1,1,2) model was selected for the final forecasting analysis. This finding aligns with previous research that used ARIMA models to forecast monthly sales in specific operational contexts, such as vending machine transactions, where similar patterns of irregular demand and short time series were observed [8].

DISCUSSION

The comparative analysis between ARIMA and Simple Exponential Smoothing (SES) across traditional and e-commerce sales channels highlights critical insights into demand forecasting in a multi-channel retail environment. The superior performance of ARIMA(1,1,2), particularly in the e-commerce channel, suggests that autoregressive models are more effective in capturing the volatility and irregularities commonly observed in online sales. This result aligns with prior studies emphasizing the importance of model flexibility when dealing with short-term demand fluctuations and non-stationary patterns.

The relatively weaker performance of SES may be attributed to its limited responsiveness to sudden demand shifts, especially in product groups with inconsistent sales histories. While SES is computationally simpler and often preferred for its ease of use, the findings indicate that such simplicity may come at the cost of reduced forecasting accuracy in dynamic environments like e-commerce.

It is also worth noting that the absence of strong seasonal patterns in the dataset may have reduced the potential advantage of seasonal ARIMA extensions or other seasonal models. Additionally, the limited time horizon (24 months) may constrain the generalizability of the results, though the consistency across product groups strengthens the reliability of the findings.

CONCLUSION

This study explored the demand forecasting performance across traditional and e-commerce sales channels for five different product groups produced by a polypropylene synthetic yarn manufacturer in Türkiye. Two established forecasting methods—Simple Exponential Smoothing (SES) and ARIMA—were applied and evaluated using the Symmetric Mean Absolute Percentage Error (SMAPE) metric to ensure reliable comparisons across sales environments with varying demand scales. Initially, SES models were tested by optimizing the smoothing parameter (α) for each product group; however, the presence of irregular demand patterns and the requirement for capturing more complex temporal dependencies led to the application of ARIMA models. After conducting stationarity checks and analyzing autocorrelation structures, the ARIMA(1,1,2) model was selected as the most appropriate model across all product groups. This model consistently achieved lower SMAPE values [7], indicating superior forecasting accuracy compared to SES models. The findings highlight the critical importance of selecting forecasting models that account for both channel-specific demand behaviors and underlying time series dynamics. Particularly in multi-channel retail environments, more flexible and data-responsive models like ARIMA can significantly improve forecast reliability and support more effective inventory and sales planning decisions for both, traditional and e-commerce operations [7].

REFERENCES

[3] Armstrong, J. S. (2001). Principles of Forecasting: A Handbook for Researchers and Practitioners. Springer.

[4] Box, G. E. P., Jenkins, G. M., Reinsel, G. C., & Ljung, G. M. (2015). Time Series Analysis: Forecasting and Control. Wiley.

[8] Eroğlu, Y. et al. (2017). Forecasting Monthly Sales of Vendor Machine: A Case Study. IWCF 2017 International Web Conference on Forecasting (ISBN: 978-605-67889-0-1).

[5] Fildes, R., & Petropoulos, F. (2015). Simple versus complex selection rules for forecasting many time series. Journal of Business Research, 68(8), 1692–1701.

[7] Fosso Wamba, S., Akter, S., Gunasekaran, A., Dubey, R., & Childe, S. J. (2015). Big data analytics and firm performance: Effects of dynamic capabilities. Journal of Business Research, 70, 356–365.

[2] Hyndman, R. J., & Athanasopoulos, G. (2018). Forecasting: Principles and Practice (2nd ed.). OTexts.

[6] Makridakis, S., Spiliotis, E., & Assimakopoulos, V. (2018). Statistical and Machine Learning forecasting methods: Concerns and ways forward. PLOS ONE, 13(3), e0194889.

[1] Ramanathan, U. (2010). Aligning supply chain collaboration using decision theory: a conceptual framework. Benchmarking: An International Journal, 17(5), 675–689.

➢ *ORAL PRESENTATION*

Bottled Drinking Water And Microbiological Quality

[1]Amilda Ballata, [2]Zenilda Cilaj

[1]Faculty of Natural Sciences, Department of Industrial Chemistry, University of Tirana, Tirana, Albania
[2]Chemist at National Food Authority, Shkodra, Albania

Abstract

In today's times, bottled drinking water is being considered as a safer alternative to tap water. The deterioration of the quality of network water, which can be a source of spread of pathogenic microorganisms and various diseases, has led to a significant increase in the consumption of bottled water. However, various studies have shown that even bottled water can be contaminated from a microbiological point of view. Sources of contamination can be the source of water, its treatment, the packaging process, the hygiene of equipment and personnel, as well as through packaging materials. This study aims to evaluate the microbiological quality of bottled drinking water marketed in markets. 13 randomly selected samples from different brands were analyzed. The evaluation was performed for total aerobic count, total coliform bacteria. Total Aerobic Mesophilic Count and total coliforms, was evaluated using standard pour plate methods of cultivation on appropriate media and incubation at temperatures of 30°C and 37°C. This study shows that bottled drinking water of domestic and foreign brands results in variable presence of total aerobic load, which indicates that the quality of bottled water is not stable and safe in accordance with the permitted limits. All samples result safe in terms of total coliform bacteria load. Referring to the results, the importance of more rigorous controls, continuous quality monitoring and compliance with food safety standards in order to prevent the potential risk of waterborne diseases is highlighted.

Keywords: bottled water, total coliform, drinking water, microbiological quality, etc.

INTRODUCTION

Drinking water is an essential element for human health. The deterioration of tap water quality, which can be a source of pathogenic microorganisms and various diseases, has led to a significant increase in the consumption of bottled water. [10]. For this reason, today, water safety is a priority for health institutions and international organizations. Due to the deterioration of tap water quality, there has been a significant increase in the consumption of bottled drinking water as a safer and more reliable alternative for consumers [12]. Referring to several studies, it has been found that even in natural bottled water we have the presence of pathogenic microorganisms that can come from various sources such as the water source, the treatment process, packaging, personnel hygiene, and storage and transport conditions [9],[11],[13]. Pathogenic microorganisms such as *Escherichia coli, Salmonella spp., Pseudomonas aeruginosa*, as well as some fungi and protozoa, have been identified in bottled water samples in many countries around the world [2],[5] Bacteria such as total coliforms and other heterotrophic microorganisms, can serve as indicators of microbial contamination and the safety of water for human consumption [4], for this reason, the assessment of these microbiological parameters of bottled drinking water is very important to prevent the spread of various waterborne diseases and to be in compliance with international standards [13]. This study aims to assess the presence of total aerobic microflora and total coliforms in samples of bottled drinking water, collected from the domestic market, of different brands, using standardized microbiological cultivation methods [4].

METHODS AND MATERIALS

Samples analyzed

In this study, 13 samples of natural, drinking, packaged, bottled water were analyzed. These samples were taken from different markets in the city of Tirana. They represent drinking water samples of different

domestic and foreign brands which were collected randomly and immediately analyzed in the laboratory. [7], [3], [6].

Estimation of total aerobic mesophilic and total coliform

Microbiological analysis was performed using the **standard pour plate technique**, in accordance with established microbiological methods [4], [1]. For this, the standard method of cultivation by pouring into petri dishes was used, respectively on standard agar /PCA medium. and selective MacConkey agar medium. From each water sample, 1ml of water was cultivated, in Petri dishes and incubated respectively at 30^0C for 48-72 hours and 37°C for 24 hours. The developed colonies were counted with a colony counter and the number was expressed as colony forming units per gram of homogenized sample (CFU g-1). CFU/ml = (number of colonies × dilution factor) / plate volume. Then, microscopic observation was made by preparing gram-stained preparation to determine the presence and morphology of bacteria.

RESULTS

In this study, 13 samples of bottled drinking water of domestic brands were analyzed: W1, W2, W3, W4, W5 W6, W7, W8 W9, and foreign brands: W10, W11, W12 W13.

Table 1 Microbiological results of water samples from domestic brands

Samples		**W1**	**W2**	**W3**	**W4**	**W5**	**W6**	**W7**	**W8**	**W9**
	Standard									
Total aerobic mesophilic bacteria at 30oC	<100 CFU/ml	2	0	2300	28	53	2350	2	108	1800
Total Coliform bacteria	0 CFU/250ml	0	0	0	0	0	0			

The total aerobic mesophilic bacteria load and total coliforms are two microbiological parameters for assessing the hygienic-sanitary quality of purified drinking water.

Referring to the table above, all samples have given a load of total aerobic microorganisms with the exception of sample M2, the highest load results in samples W6 (3000), W3 (2300), W9 (1800) CFU/ml and the lowest results in water samples W1 (2) W7 (2) CFU/ml. All water samples do not present a total coliform load.

This load varies from 0-2300 CFU/ml, where samples W1, W2, W7 result in a very low load of total aerobic mesophilic bacteria, which is acceptable for clean packaged drinking water, while water samples W6, W3, W9 result in a very high load, which indicates that it may have resulted from problems related to the treatment process, packaging, packaging hygiene, equipment, personnel, or storage conditions. According to the standards and Codex Alimentarius it is seen that regarding the load of total aerobic mesophilic bacteria, samples W1, W2, W7 are within the permitted limits, samples W4, W5, W8 are close to the permitted limit while samples W3, W6, W9 are outside the permitted limit.

Referring to the load of total coliform bacteria, all samples comply with the permitted limits.

In conclusion, we can say that only samples W1, W2, W7 of domestic bottled drinking water result to be within the permitted limits, while samples W3, W9 result with a high load of total aerobic mesophilic bacteria at 30°C but the presence of total coliform bacteria. Sample W6 results to be the sample with the lowest microbiological quality as it shows very high loads of total aerobic mesophilic bacteria at 30°C.

The total aerobic mesophilic bacteria load varies from lowest to highest respectively: W2, W7, W1, W4, W5, W8, W9, W3, W6

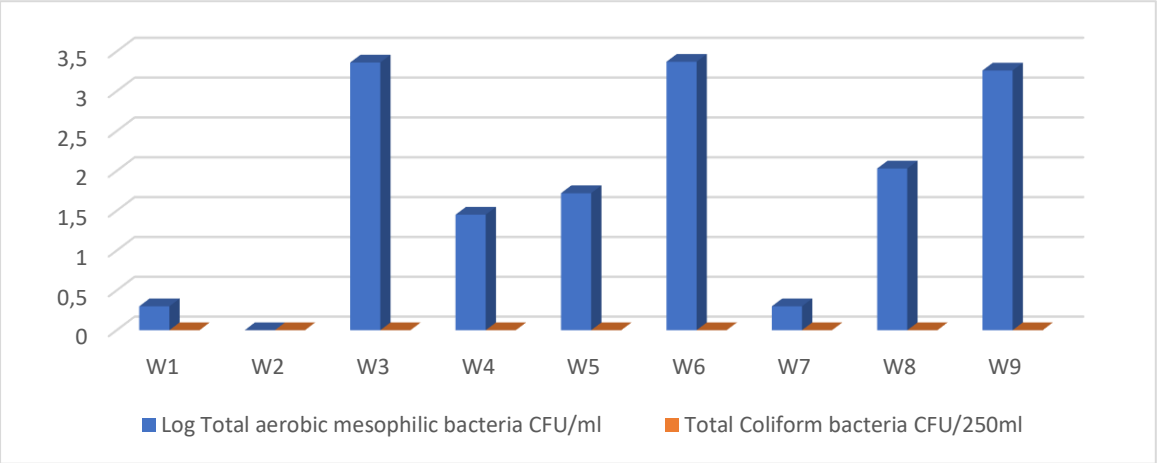

Graphic 1 Graphical representation of log results of total aerobic mesophilic load for country bottled water brand samples

Table 2 Microbiological results of water samples from foreign brands

Samples		**W10**	**W11**	**W12**	**W13**
	Standard				
Total aerobic mesophilic bacteria at 30°C	<100 CFU/ml	11	158	52	17
Total coliform bacteria	0 CFU/250ml	0	0	0	0

For the second group of packaged drinking water samples, of foreign brands, we find that all samples result in a total aerobic mesophilic bacterial load which varies from 11 CFU/ml to 158 CFU/ml. The sample with the highest load is respectively sample W1 (158) CFU/ml, W12 (52) CFU/ml, W13 (17) CFU/ml and the sample with the lowest load is respectively sample W10 (11) CFU/ml. According to the standard and the Alimentarius Code: we find that sample W10 has a very low load, W13 has a load within the allowed limit, W12 has a load close to the allowed limit, while sample W11 exceeds the allowed limit, which indicates the possibility of contamination or inappropriate storage conditions

Referenced to the total coliform bacteria load, all samples result in compliance with the permitted standard. All samples result in a load of 0 CFU/ml.

In conclusion, we can say that for this group of bottled water samples of foreign brands, samples W10, W12, W13 result within the permitted norms and can be included in the water class for drinking water very purified water. Only the water sample W11 results in a high load outside the permitted limit. All samples result in cleanness referred to the total aerobic bacteria load, so we can say that they are safe from fecal contamination.

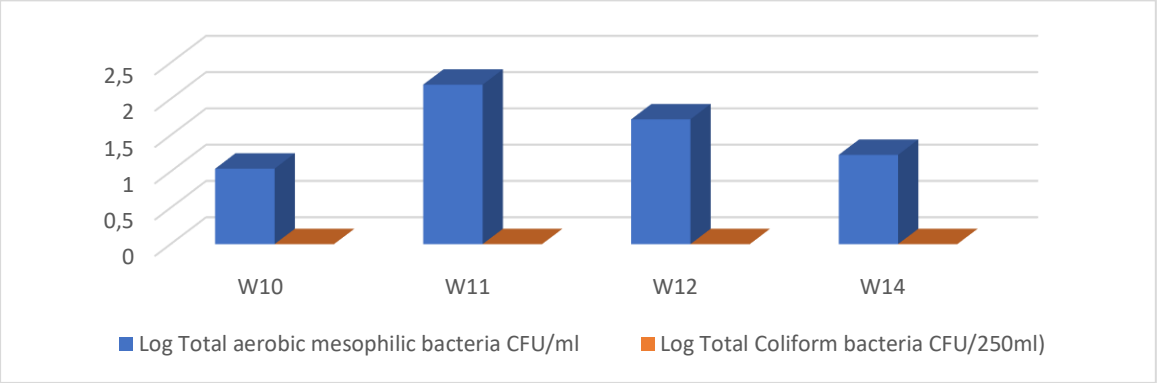

Graphic 2. Graphical presentation of log results for foreign brand water samples

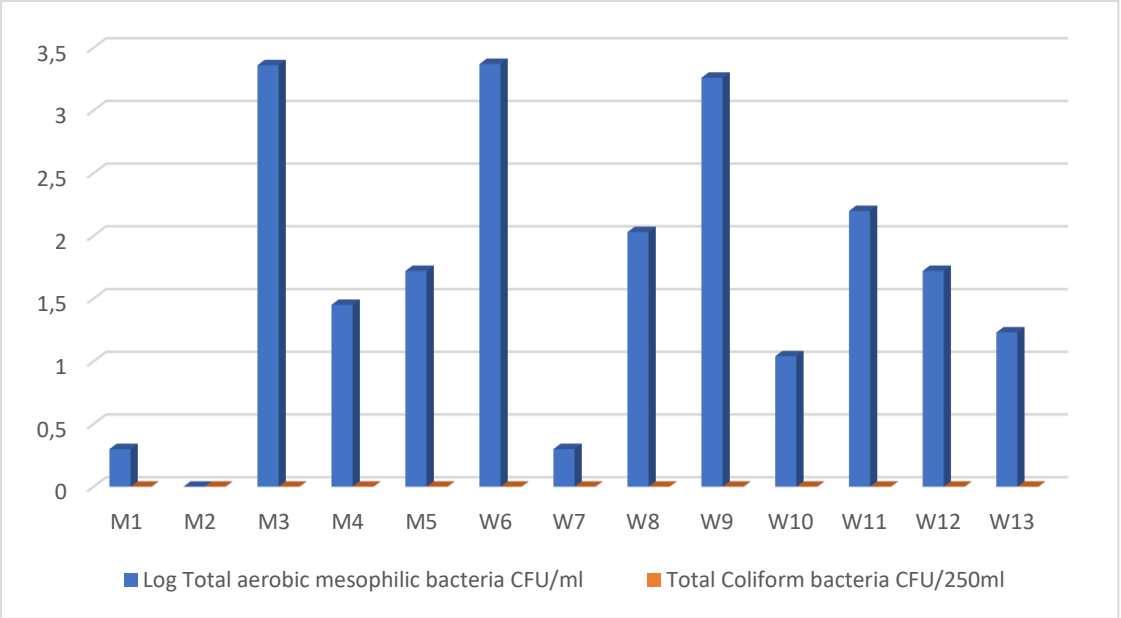

Graphic 3 Graphical presentation of log results of total aerobic mesophilic load for all bottled water samples

In general, from the above graphic, all samples of bottled drinking water have resulted in a load of total aerobic mesophilic bacteria with the exception of the sample of the domestic brand W2 (0 CFU/ml). The samples with the lowest load are the samples of the domestic brands W1 and W7 (2 CFU/ml), the samples with the highest load are the samples W6 (300CFU/ml) W3 (2300 CFU/ml) W9 (1800CFUml) and slightly lower the samples W11 (158CFUml) W8 (108 CFU/ml). This parameter varies from 0-3000CFU/ml from 100 to the order of 103 CFU/ml.

It is seen that the samples with the highest to lowest load result respectively to be W6, W3,W9, W11, W8, W12, W5, W4, W13, W10, W1, W7, W2, where within the allowed limit the samples result to be W2, W1, W7, W10, W13, W4, W5, W12, W8 and outside the allowed limit the samples result to be W3, W6, W9, W11.

This shows the importance of regular microbiological monitoring, improvement of the production line or controls regarding storage or transport conditions, etc.,

CONLUSIONS

The total aerobic mesophilic load for all studied samples varies from 0 to 3000CFU/ml. This parameter in some bottled drinking water samples results to be within the allowed limit below 100 CFU/ml (W1, W2, W7) while in some other samples (W6, W3 W9) above it.

The sample with the highest load results in bottled water samples of domestic brands W3 then W9 and the water sample with the lowest load results in sample W2 of the domestic brand, without any total aerobic mesophilic load.

The presence of total aerobic mesophilic bacteria indicates the possibility of contamination during the production process, storage, etc. and requires continuous monitoring and improvement of production, storage, etc. conditions to ensure consumer health.

This study shows that bottled drinking water of domestic and foreign brands results in variable presence of total aerobic load, which indicates that the quality of bottled water is not stable and safe in accordance with the permitted limits.

From the examination of the gram-stained preparations, the presence of gram-negative bacilli bacteria was observed.

All samples result safe in terms of total coliform bacteria load.

In conclusion, we can say that to ensure the microbiological quality of bottled drinking water, it is very important to control and rigorously monitor all stages of production, packaging, storage and transport of water to the consumer.

REFERENCES

1. American Public Health Association (APHA), American Water Works Association (AWWA), & Water Environment Federation (WEF). (2017). Standard methods for the examination of water and wastewater (23rd ed.). APHA.
2. Bouhlel, J., Hassen, A., & Mefteh, M. (2023). Mycological and bacteriological quality and safety of bottled water in Ethiopia. PubMed Central (PMC).
3. Department of Environment and Science. (n.d.). Guidelines for water sampling.
4. Environment Agency. (2012). The microbiology of drinking water – Part 7: Methods for the enumeration of heterotrophic bacteria. UK Government. https://assets.publishing.service.gov.uk/government/uploads/system/uploads/attachment_data/file/755547/geho0812bwwk-e-e.pdf
5. Grumezescu, A. M., & Holban, A. M. (2019). Fecal indicators and bacterial pathogens in bottled water from Dhaka, Bangladesh. PubMed Central (PMC).
6. Institute of Health and Safety (IHS). (n.d.). Water quality testing and standards for bottled water.
7. International Organization for Standardization (ISO). (2006). ISO 19458:2006 Water quality — Sampling for microbiological analysis. ISO.
8. International Organization for Standardization (ISO). (2014). ISO 9308-1:2014 - Water quality — Enumeration of Escherichia coli and coliform bacteria — Part 1: Membrane filtration method. ISO.
9. Olivieri, A. W., et al. (2012). Microbial water quality and health risks. In Safe drinking water: Advances in risk assessment. WHO Press.
10. Park, S., Lee, Y., Lee, J., Park, J., Kim, J., & Lee, C. (2013). An evaluation of microbial and chemical contamination sources related to the deterioration of tap water quality in the household water supply system. Journal of Water and Health, 11(4), 622–635. https://doi.org/10.2166/wh.2013

11. Warburton, D. W. (1993). A review of the microbiological quality of bottled water sold in Canada. Canadian Journal of Microbiology, 39(2), 158–168.
12. World Health Organization (WHO). (2017). Guidelines for drinking-water quality (4th ed.). WHO Press.
13. World Health Organization (WHO). (2022). Drinking-water: Key facts. https://www.who.int/news-room/fact-sheets/detail/drinking-water

➢ *ORAL PRESENTATION*

Study of Health Behaviors among Adolescents in Tirana (2024): Smoking, Alcohol, Drugs, and Physical Activity

Floriana Marku[1],[2]*, Loreta Kuneshka[3],[4]

[1] External Lecturer at the Department of Public Health, Faculty of Medicine, University of Medicine, Tirana

[2] Full-time Lecturer at Aldent University, Tirana

[3] Internal Lecturer at the Department of Public Health, Faculty of Medicine, University of Medicine, Tirana

[4] Dermatologist at the Specialties of the Pediatric Hospital, QSUNT, Tirana

Abstract

Tirana, as the capital of Albania, faces specific social and economic challenges that impact the health behaviors of adolescents. Urban factors, environmental influences, and the availability of harmful products may contribute to increased consumption of tobacco, alcohol, and drugs, alongside decreased physical activity. This study examines the health behaviors of adolescents in Tirana, focusing on tobacco, alcohol, drugs consumption, as well as levels of physical activity. A sample of 417 adolescents revealed that 22.98% consumed alcohol, while 8.29% smoked tobacco. This descriptive-analytical study is based on a structured questionnaire completed in January and February 2024. Data analysis was performed using the SPSS statistical package. Detailed analysis revealed a negative correlation between physical activity and alcohol consumption, indicating that adolescents who engaged in more physical activity reported lower levels of alcohol consumption ($p = 0.04$). Furthermore, positive correlations were observed between alcohol, tobacco, and drug use ($p < 0.001$). Parental education levels also influenced health behaviors, with adolescents from less educated parents consuming more alcohol ($p = 0.02$). These findings underscore the importance of promoting physical activity as a strategy to reduce the consumption of harmful substances. Recommendations include creating opportunities for engagement in various sports, forming school clubs focused on physical activities, encouraging extracurricular activities, providing educational sessions, and utilizing digital platforms to motivate youth.

Keywords: Health behaviors, physical activity, tobacco, alcohol, drugs.

1. Introduction

Health is a multifaceted concept, broadly defined by Dr. Andrija Štampar, a pioneer in social medicine, public health and formally adopted by the World Health Organization (WHO) in 1946 as “a state of complete physical, mental, social well-being and not merely the absence of disease or infirmity”. This holistic understanding of health recognizes that well-being extends beyond the absence of illness to include multiple interrelated dimensions such as physical, mental, emotional, social, spiritual, and environmental factors (Aggleton & Homans, 1987; Ewles & Simnett, 1999) (see Figure 1).



Figure 1: Dimensions of Health. Adapted from Aggleton & Homans (1987) and Ewles & Simnett (1999).

Adolescence, typically defined as the period between 10 and 19 years of age, represents a crucial stage of growth and transition from childhood to adulthood, involving profound physical, psychological, and social transformations. This period is characterized by increased vulnerability but also significant opportunities to influence lifelong health outcomes.

Adolescents account for over 16% of the global population and are central to achieving the Sustainable Development Goals (SDGs) by 2030. While this phase is often perceived as a time of good health, adolescents face a range of preventable health risks and challenges, including premature death, disease and injury. These challenges often stem from modifiable health behaviors such as tobacco use, alcohol consumption, drug use and low levels of physical activity (see Figure 2).



Fig 2: Determining Factors of Health

The patterns of behavior established during adolescence can have lasting impacts on health and well-being throughout life. Addressing these behaviors through targeted health education, accessible health services, supportive environments and youth engagement in decision-making is essential to promote healthy development. The Global Action for Measurement of Adolescent Health (GAMA) initiative highlights the importance of standardized health indicators to monitor adolescent health globally, supporting evidence-based policy and program development. By understanding the factors that influence adolescent health behaviors, researchers and policymakers can better design interventions that reduce risk factors and promote positive health outcomes. This study focuses on health behaviors among adolescents in Tirana, specifically examining smoking, alcohol use, drug consumption, and physical activity, aiming to contribute valuable insights for local and global health promotion efforts. The objective of this study is to analyze the health behaviors of adolescents in Tirana in 2024, focusing on tobacco use, alcohol consumption, drug use, body mass index (BMI), and physical activity levels. The analysis aims to identify social, environmental, and technological factors influencing these behaviors to provide recommendations for policies and

programs that support adolescent health and well-being. The study's specific objectives are to assess the prevalence of smoking, alcohol use, and drug consumption among adolescents aged 10 to 17 in Tirana, analyze the relationship between substance use and physical activity, and identify socio-economic and environmental factors influencing these behaviors. The study tests the following hypotheses: first, there is a significant association between alcohol consumption and tobacco use among adolescents; second, physical activity is negatively correlated with substance use (tobacco, alcohol, drugs); third, socio-economic factors such as parents' education level influence substance use behaviors; and fourth, the prevalence of overweight and obesity varies by age group, gender, and residence. Given the significant youth population in Tirana and the lack of recent local data, this study will provide crucial evidence to inform targeted interventions and policies aimed at improving adolescent health in the city and beyond.

2. Methodology

2.1 Study Population and Data Collection

This study is a descriptive-analytical investigation of adolescents' health behaviors in Tirana. Data were collected through a structured questionnaire administered during January and February 2024. The data collection instrument was a questionnaire based on existing literature and included questions related to physical activity, alcohol use, tobacco use and drug use. Participants were adolescents aged 10-17, recruited from three different schools in Tirana. The sample was randomly selected and consisted of 417 adolescents.

2.2 Statistical Analysis

Data analysis was performed using SPSS version 27, including descriptive analysis indicators such as frequencies in percentages and means. Analytical analysis involved correlation analysis and the construction of logistic regression models. Logistic regression was used to identify predictors of substance use. Correlation analysis assessed the relationships between socio-economic and demographic factors, such as age, residence, parents' education level and family income, with five indicators of risky health behaviors among adolescents: smoking, alcohol use, drug use, BMI and physical activity.

2.3 Ethical Approval

The study was conducted after obtaining ethical approval from the school institutions in the city of Tirana. Participants were informed about the purpose of the study and gave their consent to participate. The data were handled confidentially and used solely for research purposes.

3. Results

3.1 Socio-demographic Characteristics of the Sample

The socio-demographic profile of the sample of 417 adolescents is summarized in Table 1. The sample consisted of both male and female participants distributed across urban, semi-urban, and rural areas. Participants were categorized into two age groups, and parental education as well as household income levels were recorded to provide context on the socio-economic background. Additionally, Body Mass Index (BMI) classifications were determined to assess the nutritional status within the sample.

Table 1: Socio-Demographic Characteristics of the Sample

Variable	Category	Frequency (%)
Gender	Male	45.45
	Female	54.55
Residence	Urban	37
	Semi-urban	28
	Rural	35
Age group	10-12 years	40
	13-17 years	60
Parental Education	Primary (8 years)	30.95
	Secondary ((high school)	37.4
	Higher education (university Bachelor's)	22.3
	Postgraduate (Master's, Doctorate)	9.35
Income Level	Low	1.2
	Medium	66
	High	32.8
BMI Classification	Underweight	35.8
	Healthy weight	57.2
	Overweight	6
	Obese	1

3.2 Prevalence of Tobacco, Alcohol, and Drug Use Among Adolescents

Table 2: Prevalence of Tobacco, Alcohol, and Drug Use Among Adolescents

Substance	Age Group	Prevalence (%)
Tobacco Use	10-12 years	0.73
	13-17 years	7.56
Alcohol Use	10-12 years	1.47
	13-17 years	21.51
Drug Use	10-12 years	0
	13-17 years	11.1

3.3 Physical Activity

Table 3: Physical Activity Engagement, Activity Levels, and BMI by Age Group

Variable	Age Group 10-12 years	Age Group 13-17 years
Physical Activity Engagement	94.0%	88.6%
Not Engaged in Physical Activity	6.0%	11.4%
Most Common Activity Level	Moderate (53.3%)	Moderate (39.2%)
Average BMI	18.32 kg/m^2	21.14 kg/m^2

The majority of adolescents reported engaging in physical activity, with 94.05% of those aged 10-12 years and 88.75% of those aged 13-17 years participating regularly. Overall, 90.58% of the total sample were physically active. Males were more active than females, with 91.67% of boys and 84.09% of girls reporting physical activity. Regarding residence, activity levels were slightly higher in urban (88.75%) and semi-urban (88.53%) areas compared to rural areas (85.12%). Parental education showed relatively consistent physical activity rates across all categories, ranging from 86.64% to 87.40%. Similarly, family income levels did not show large differences in activity, with percentages between 86.55% and 88.89%. BMI classification revealed that overweight adolescents had the highest physical activity prevalence (92.31%), while underweight and obese adolescents showed slightly lower levels of activity (84.77% and 85.71%, respectively). Very few adolescents reported less than one hour or 1-2 hours of physical activity per day,

and none reported more than 2 hours daily. The correlation coefficients between physical activity and tobacco use (-0.068, p = 0.04), alcohol consumption (-0.5, p = 0.0395), and drug use (0.37, p = 0.049) are statistically significant (p < 0.05).

3.4 Hours Spent Watching TV and Eating While Watching TV

Among children aged 10-12, 35.8% spend less than 1 hour per day watching TV or using phones, 48.5% spend 1-2 hours, and 15.8% spend over 2 hours. For adolescents 13-17, only 13.1% spend less than 1 hour, 38.1% spend 1-2 hours, and 48.8% spend more than 2 hours. Eating while watching TV is reported by 54.7% of younger children and 23.5% of older adolescents. Conversely, 59.0% of younger and 19.8% of older adolescents do not eat during TV viewing. Eating while watching TV is more common among younger children.

3.5 Prevalence of Tobacco Use and Associated Sociodemographic Factors

The prevalence of tobacco use among adolescents varies significantly by age group, with only 0.73% of those aged 10-12 years reporting smoking compared to 7.56% in the 13-17 years group (p = .000). Males have a higher smoking prevalence (5.85%) than females (2.44%) with a significant difference (p = .008). No significant differences were found based on place of residence or parents' education level. Family income level also showed no significant association with smoking.

3.6 Prevalence of Alcohol Consumption and Its Association with Variables

The prevalence of alcohol consumption varied significantly by age group, with 1.47% of adolescents aged 10–12 reporting alcohol use compared to 21.51% in the 13–17 age group (P < 0.001). Overall, 22.95% of the total sample reported alcohol consumption. Significant gender differences were observed, with 14.67% of males and 8.30% of females reporting alcohol use (P < 0.001). Alcohol consumption was highest among urban adolescents (46.8%), followed by rural (40.4%) and semi-urban (12.8%) youths (P < 0.001). Parental education level was significantly associated with adolescent alcohol use; prevalence was higher among adolescents with parents having only an 8-year education (30.1%) compared to those with parents holding post-university degrees (2.2%) (P = 0.026). No significant association was found between alcohol use and family income level (P = 0.3). Logistic regression analysis indicated that alcohol consumption was significantly associated with tobacco use, with a coefficient of 1.868 (p = 0.002) and an odds ratio of 6.478, indicating that adolescents who consume alcohol have about six times higher odds of tobacco use.

3.7 Prevalence of Drug Use and Its Association with Variables

Among adolescents aged 10-12 years, no drug use was reported, while 11.1% of those aged 13-17 years reported having used drugs, showing a significant age-related difference (p < 0.001). Overall, 11.1% of the total sample reported drug use. Gender differences were significant (p = 0.005), with 9.65% of males reporting drug use compared to only 1.45% of females. Regarding residence, drug use was more common in urban (24.5%) and semi-urban (23.1%) areas than in rural areas (9.5%) (p = 0.045). Parental education levels showed varying prevalence rates, with the highest drug use reported among adolescents whose parents had 8-year education (36.4%) although this difference was not statistically significant. Family income level was not significantly associated with drug use (p = 0.70), with a prevalence of 11.54% among adolescents from middle-income families and 10.96% among those from high-income families.

3.8 Prevalence of Overweight and Obesity and Its Association with Variables

The prevalence of overweight and obesity varies by age group, gender, and residence. Among children aged 10-12 years, 2.40% were overweight and 0.60% obese, while in adolescents aged 13-17 years, these rates increased to 8.43% and 1.20%, respectively, showing a significant age-related difference (p < 0.001). Gender differences were also significant (p < 0.001), with boys having higher rates of overweight (11.64%) and obesity (1.59%) compared to girls (1.32% overweight and 0.44% obese). Regarding place of residence, urban children showed higher overweight (7.79%) and obesity (1.30%) rates compared to semi-

urban and rural areas, though this was not statistically significant (p = 0.08). In this sample, adolescents of parents with a higher educational level (post-university) have a higher prevalence of overweight and obesity compared to those with parents of lower educational levels; however, the difference is not statistically significant. Overall, 6.01%of the sample were overweight, and 0.96% were obese.

4. Discussion

The findings of this study provide important insights into the health behaviors of adolescents in Tirana and are largely consistent with both national and international trends. A clear age-related increase in the use of tobacco, alcohol, and drugs was observed, with the 13–17-year age group showing significantly higher prevalence compared to 10–12-year-olds. These patterns align with the Health Behaviour in School-aged Children (HBSC) 2021–2022 survey in Albania, which found that older adolescents are more likely to engage in risk behaviors as they transition into late adolescence (HBSC, 2022 [1]). Tobacco use was significantly higher among males than females in our sample (5.85% vs. 2.44%, p = 0.008), consistent with national data and WHO global trends that show persistent gender gaps in smoking behaviors (WHO, 2019 [5]; Reitsma et al., 2017 [6]). The increasing prevalence of tobacco use with age mirrors patterns documented in the Global Burden of Disease Study and highlights adolescence as a critical window for tobacco prevention efforts (Forouzanfar et al., 2015 [7]). Similarly, alcohol consumption was markedly higher among older adolescents (21.51%) and males (14.67%). These findings reflect HBSC data, which also show gender differences and increasing alcohol use with age. Importantly, our study observed a decline in the proportion of adolescents who report ever drinking alcohol, particularly among females, aligning with recent trends reported by HBSC and the WHO, where lifetime drunkenness among adolescents dropped significantly in the past decade (WHO, 2024a [2]). Nonetheless, the persistent gender gap and high levels of alcohol use among urban adolescents suggest a need for targeted interventions in urban environments. The association between alcohol and tobacco use in this study (OR = 6.478, p = 0.002) further supports the well-documented clustering of risk behaviors during adolescence (Conegundes et al., 2020 [3]; Jones et al., 2020 [4]). Cannabis use was reported by 11.1% of older adolescents, with a significant gender disparity (9.65% of boys vs. 1.45% of girls), consistent with both Albanian and international literature (HBSC, 2022 [1]; Johnston et al., 2012 [8]). These findings are concerning given the known associations between adolescent cannabis use and adverse mental health outcomes, including depression and anxiety in adulthood (Hengartner et al., 2020 [9]; Taylor et al., 2017 [10]). The higher prevalence of cannabis use among urban youth observed here suggests environmental or social influences that warrant further exploration. Despite encouraging levels of physical activity—especially among 10–12-year-olds (94%)—the overall figure (90.58%) still falls short of the WHO's recommended daily levels when considering duration and intensity (WHO, 2020 [15]; WHO, 2018 [17]). Globally, more than 80% of adolescents fail to meet recommended physical activity guidelines (Guthold et al., 2020 [16]), and sedentary behaviors such as prolonged screen time may offset the benefits of moderate activity. In our study, increased screen time and eating while watching TV were more prevalent among younger adolescents, which could contribute to unhealthy weight gain and reflect the early development of sedentary routines. The prevalence of overweight (6.01%) and obesity (0.96%) in our sample was relatively low but showed significant differences by gender and age, with older boys being most affected. These patterns are consistent with global data highlighting rising trends in adolescent obesity, especially among males in urban areas (Ng et al., 2014 [12]; Lister et al., 2023 [11]). Interestingly, adolescents with post-university-educated parents had a slightly higher prevalence of overweight and obesity, though not statistically significant. This is contrary to findings from some high-income countries but may reflect unique socio-cultural or economic dynamics in Albania. Crucially, our results show strong interconnections between multiple risk behaviors—tobacco, alcohol, and drug use—as previously emphasized in the Global Burden of Disease reports (Forouzanfar et al., 2015 [7]). These findings support calls for integrated, multi-behavioral prevention strategies. Interventions should be gender-sensitive, age-specific, and embedded in educational settings, as recommended in WHO's framework for adolescent health monitoring (WHO, 2024b [2]).

5. Conclusions

The data reveal a significant increase in tobacco, alcohol, and drug use from younger to older adolescents, with alcohol use being the most prevalent, underscoring the urgent need for early intervention. While most adolescents engage in physical activity, a notable proportion remain inactive. Sociodemographic factors,

including parents' education level and place of residence, significantly impact adolescents' health behaviors. Younger adolescents (10-12 years) tend to spend more time in passive activities and are more likely to eat while watching TV, whereas older adolescents (13-17 years) often skip meals during TV viewing. To address substance use among adolescents, it is essential to establish specialized rehabilitation centers offering tailored psychological support and comprehensive health services. Schools should implement educational programs to raise awareness about substance risks and promote healthy lifestyles. Additionally, support groups and counseling for adolescents and their families are vital. Policies must safeguard youth by ensuring access to rehabilitation without legal consequences and limiting exposure to substance-related advertising. Vocational training and employment opportunities should be provided to aid social reintegration. Public awareness campaigns and systematic monitoring are necessary to assess intervention effectiveness. In Albania, the lack of adolescent-specific rehabilitation facilities highlights the critical need for dedicated centers, as existing services primarily serve adults and may not be suitable for younger populations. Establishing specialized adolescent rehabilitation centers is therefore crucial to improve treatment outcomes and support recovery.

References

1. Health Behaviour in School-aged Children - 11, 13, and 15 years old 2021-2022 , NATIONAL REPORT SURVEY IN ALBANIA
2. The adolescent health indicators recommended by the Global Action for Measurement of Adolescent health: guidance for monitoring adolescent health at country, regional and global levels ISBN 978-92-4-009219-8 (electronic version) © World Health Organization 2024
3. Lara Silvia Oliveira Conegundes et al,Binge drinking and frequent or heavy drinking among adolescents: prevalence and associated factors, Jornal de Pediatria Volume 96, Issue 2, March–April 2020, Pages 193-201
4. Jones, R. M., Van Den Bree, M., Zammit, S., & Taylor, P. J. (2020). Change in the relationship between drinking alcohol and risk of violence among adolescents and young adults: A nationally representative longitudinal study. *Alcohol and Alcoholism*, 55(4), 439–447. https://doi.org/10.1093/alcalc/agaa020
5. WHO global report on trends in prevalence of tobacco use 2000–2025, third edition. Geneva: World Health Organization; 2019 (https://iris.who.int/handle/10665/330221, accessed 2 February 2024).
6. Reitsma MB, Fullman N, Ng M, Salama JS, Abajobir A, Abate KH et al. Smoking prevalence and attributable disease burden in 195 countries and territories, 1990–2015: a systematic analysis from the Global Burden of Disease Study 2015. Lancet. 2017;389:1885–906. doi:10.1016/S0140-6736(17)30819-X.
7. Forouzanfar MH, Alexander L, Anderson HR, Bachman VF, Biryukov S, Brauer M et al. Global, regional, and national comparative risk assessment of 79 behavioural, environmental and occupational, and metabolic risks or clusters of risks in 188 countries, 1990–2013: a systematic analysis for the Global Burden of Disease Study 2013. Lancet. 2015;386(10010):2287–323. doi:10.1016/S0140-6736(15)00128-2.
8. Johnston LD, O'Malley PM, Bachman JG, Schulenberg JE. Monitoring the future national results on adolescent drug use: overview of key findings, 2011. Ann Arbor: Institute for Social Research, The University of Michigan; 2012 (https://eric.ed.gov/?id=ED529133, accessed 8 February 2024).
9. Hengartner MP, Angst J, Ajdacic-Gross V, Rössler W. Cannabis use during adolescence and the occurrence of depression, suicidality and anxiety disorder across adulthood: findings from a longitudinal cohort study over 30 years. J Affect Disord. 2020;272:98–103. doi:10.1016/j.jad.2020.03.126.
10. Taylor M, Collin SM, Munafò MR, MacLeod J, Hickman M, Heron J. Patterns of cannabis use during adolescence and their association with harmful substance use behaviour: findings from a UK birth cohort. J Epidemiol Community Health. 2017;71(8):764–70. doi:10.1136/jech-2016-208503.
11. Lister NB, Baur LA, Felix JF, Hill AJ, Marcus C, Reinehr T et al. Child and adolescent obesity. Nat Rev Dis Primers. 2023;9(1):24. doi:10.1038/s41572-023-00435-4.
12. Ng M, Fleming T, Robinson M, Thomson B, Graetz N, Margono C et al. Global, regional and national prevalence of overweight and obesity in children and adults during 1980–2013: a

systematic analysis for the Global Burden of Disease Study 2013. Lancet. 2014;384:766–81. doi:10.1016/S0140-6736(14)60460-8.

13. BMI-for-age (5–19 years). Geneva: World Health Organization; 2007 (https://www.who.int/tools/growth-referencedata-for-5to19-years/indicators/bmi-for-age, accessed 2 February 2024).
14. Recommendations for data collection, analysis and reporting on anthropometric indicators in children under 5 years old. Geneva: World Health Organization and the United Nations Children's Fund; 2019 (https://iris.who.int/ handle/10665/324791, accessed 8 February 2024).
15. WHO guidelines on physical activity and sedentary behaviour. Geneva: World Health Organization; 2020 (https://iris. who.int/handle/10665/336656, accessed 8 February 2024).
16. Guthold R, Stevens GA, Riley LM, Bull FC. Global trends in insufficient physical activity among adolescents: a pooled analysis of 298 population-based surveys with 1.6 million participants. Lancet Child Adolesc Health. 2020;4(1):23–35. doi:10.1016/S2352-4642(19)30323-2.
17. Global action plan on physical activity 2018–2030: more active people for a healthier world. Geneva: World Health Organization; 2018 (https://iris.who.int/handle/10665/272722, accessed 8 February 2024).

➢ *ORAL PRESENTATION*

Ulaşım odaklı kentsel yaklaşımların karşılaştırmalı analizi

Rukiye Gizem Öztaş Karlı[1*] (*ORCID: https://orcid.org/0000-0003-0999-418X*)

[*1]Bartın Üniversitesi, Mühendislik, Mimarlık ve Tasarım Fakültesi, Peyzaj Mimarlığı Bölümü, Bartın, Türkiye

*Sorumlu yazar e-posta: roztas@bartin.edu.tr

Özet
Günümüz kentlerinde ulaşım sistemleri, yalnızca hareketliliği sağlama işleviyle sınırlı kalmamakta; sürdürülebilirlik, erişilebilirlik ve kentsel yaşam kalitesi gibi çok boyutlu hedefler doğrultusunda yeniden yapılandırılmaktadır. Bu bağlamda, ulaşım odaklı kentsel modeller, farklı ölçeklerde ve planlama yaklaşımlarında kentsel mekânı dönüştürme potansiyeline sahip çerçeveler olarak öne çıkmaktadır. 15 Dakikalık Şehir, Toplu Taşıma Odaklı Gelişme ve Net Sıfır Karbon Şehri gibi modeller çeşitli kentsel bağlamlarda uygulanmış olsa da bu yaklaşımları karşılaştırmalı olarak ele alan çalışmalar sınırlıdır. Özellikle söz konusu modellerin planlama ilkeleri, sürdürülebilirlik boyutları ve bağlamsal uyarlanabilirliğine ilişkin literatürde sistematik bir değerlendirme eksikliği görülmektedir. Bu çalışma, ilgili boşluğu gidermek amacıyla söz konusu üç yaklaşımı kavramsal düzeyde karşılaştırmalı olarak analiz etmektedir. Araştırma kapsamında, her bir modelin temel ilkeleri, ulaşım vizyonları ve uygulama zorlukları; akademik literatür, uluslararası politika belgeleri, kentsel strateji raporları ve örnek vaka incelemeleri temelinde değerlendirilmektedir. Nitel karşılaştırmalı analiz yöntemi kullanılarak gerçekleştirilen inceleme sonucunda, her bir yaklaşımın avantajları, sınırlılıkları ve bağlamsal uyarlanabilirlik düzeyleri ortaya konmuştur. Çalışma, ulaşım odaklı kentsel yaklaşımlara ilişkin bütüncül bir anlayış sunarak akademik tartışmalara katkı sağlamayı ve Türkiye gibi gelişmekte olan ülkelerde uygulanabilecek stratejik sentezler için kavramsal bir temel oluşturmayı amaçlamaktadır.
Anahtar Kelimeler: Sürdürülebilir kentsel hareketlilik, Kentsel planlama modelleri, Karşılaştırmalı analiz

Comparative analysis of transport-oriented urban approaches

Abstract
In contemporary cities, transportation systems are no longer confined to the sole function of facilitating mobility; rather, they have increasingly been re-evaluated in accordance with multidimensional goals such as sustainability, accessibility, and urban quality of life. In this context, transport-oriented urban models have emerged as frameworks with the potential to reshape urban space across various scales and planning paradigms. Although models such as the 15-Minute City, Transit-Oriented Development (TOD) and, Net Zero Carbon City have been implemented in different urban contexts, comparative analyses of these approaches have remained scarce. In particular, the literature has lacked systematic evaluations regarding their planning principles, sustainability dimensions, and contextual adaptability.This study addressed this gap by conducting a comparative conceptual analysis of the aforementioned three models. Within a conceptual framework, the research examined the core principles, transportation visions, and implementation challenges of each model, drawing upon academic literature, international policy documents, urban strategy reports, and exemplary cases. Using a qualitative comparative methodology, the study identified and interpreted the advantages, limitations, and degrees of contextual adaptability associated with each approach. Ultimately, the study contributed to the academic discourse by offering an integrated understanding of transport-oriented urban models and by providing a conceptual foundation for strategic syntheses that may be applicable in developing countries such as Türkiye.
Keywords: Sustainable urban mobility, Urban planning models, Comparative analysis

GİRİŞ

Günümüzde küresel nüfusun yarısından fazlası kentsel alanlarda yaşamaktadır. Bu artışın da 2050 yılında yaklaşık %70 seviyesine yükseleceği tahmin edilmektedir (Birleşmiş Milletler İnsan Yerleşimleri Programı [UN-Habitat] 2020). Hızla artan kentsel nüfusa küreselleşme, iklim değişikliği ve teknoloji gibi çeşitli durumların da eklenmesiyle kentlerin sorunları ve fırsatları değişmeye başlamaktadır. Sera gazı

emisyonlarının artmasının en önemli nedenlerinden biri kentlerde gerçekleşen faaliyetlerdir. Kentler, ulaşım, inşaat ve imalat gibi sektörlerdeki yüksek enerji kullanımı nedeniyle küresel CO_2 emisyonlarının yaklaşık %60'ını oluşturmaktadır (Birleşmiş Milletler [UN], 2020). Bu yüksek etki oranı, kentlerin planlanması ve tasarımının küresel öneme sahip olmasının gerekliliğini ortaya koymaktadır.

Bu noktada, kentlerin yalnızca ekonomik üretim merkezleri değil; aynı zamanda sürdürülebilirlik, kapsayıcılık ve dayanıklılık açısından yeniden ele alınması gereken mekânlar olduğu daha görünür hale gelmektedir (Ekonomik Kalkınma ve İşbirliği Örgütü [OECD], 2020). Özellikle iklim değişikliğiyle mücadele ve kent sakinlerinin yaşam kalitesini artırma hedefleri doğrultusunda, ulaşım sistemlerinin planlama sürecindeki rolü giderek daha kritik hale gelmektedir. Kentsel ulaşım sistemlerinin gelişimi yalnızca hareketliliği artırmakla kalmaz; mekânsal yapı, sosyal bütünleşme, çevresel etki ve halk sağlığı üzerinde de belirleyici etkilere sahiptir (Gehl, 2010; Banister, 2008). Çünkü ulaşım sistemlerinin geliştirilmesi iş, eğitim ve hizmetlere erişimi kolaylaştırmanın yanında kentsel formu, halk sağlığını ve sosyal eşitliği de şekillendirmektedir (Marquet ve Miralles-Guasch, 2015). İklim değişikliği ve salgın hastalıklarda görüldüğü üzere, ulaşım ve arazi kullanımının düzenlenmesi, kentsel kırılganlıkları (trafik sıkışıklığı, kirlilik ve sosyal izolasyon yoluyla) artırabilir veya dayanıklılığı (seyahat talebinin azalması, yerel olanaklara erişim ve daha yeşil altyapı yoluyla) güçlendirebilir (Moreno ve ark., 2021; OECD, 2020).

Bu bağlamda, son yıllarda çeşitli ulaşım odaklı kentsel planlama yaklaşımları geliştirilmiştir. Her biri farklı ölçeklerde, sürdürülebilirlik boyutlarında ve yönetişim tarzlarında şekillenen bu modeller, kentsel yaşamın yeniden organizasyonuna dair alternatif vizyonlar sunmaktadır (Moreno ve ark., 2021; C40 Kentleri Ağı [C40 Cities], 2022; Krismawanti ve Destiawan, 2025). Bu çalışmada ise literatürde kavramsal çeşitliliği ve güncel uygulamalardaki karşılıkları dolayısıyla öne çıkan üç model seçilmiştir: 15 Dakikalık Şehir ve Toplu Taşıma Odaklı Gelişim (TOD) ve Net Sıfır Karbon Şehir.

Bu üç yaklaşımın seçilmesinde; farklı ölçeklerde (mikro, mezo, makro) ulaşım odaklılık sunmaları, güncel uygulamalara konu olmaları, kavramsal çeşitlilik ve karşılaştırma imkânı vermeleri ve Türkiye için sentez model üretimine elverişli olmaları etkili olmuştur. Bu üç modelin hem kuramsal düzeyde hem de pratikte birbirinden ayrışan özellikleri bulunduğu kadar, kesişim potansiyeli taşıyan yönleri de vardır.

Karşılaştırma ihtiyacı da tam bu noktada ortaya çıkmaktadır. 15 Dakikalık Şehir, temelde erişilebilirlik ve yerel yaşam kalitesine odaklanan mahalle ölçeğinde (mikro düzey) bir modeldir (Pozoukidou ve Chatziyiannaki, 2021; Moreno ve ark., 2021). TOD, genellikle toplu taşıma yatırımlarının yapıldığı koridorlar veya kentsel alt bölgeler boyunca ara (mezo) düzeyde faaliyet göstermektedir (Krismawanti ve Destiawan, 2025). Net Sıfır Karbon Şehirler ise sistemik dönüşümler (örneğin enerji tedariki, altyapı, arazi kullanım modelleri) gerektiren şehir çapında veya ulusal (makro) stratejilerdir (Hükümetlerarası İklim Değişikliği Paneli [IPCC], 2022; Seto ve ark., 2021). Yönetişim açısından ele alındığında, 15 Dakikalık Şehir ve TOD yerel planlama, topluluk katılımı ve kamu-özel sektör ortaklıklarına dayanma eğilimindeyken, Net Sıfır girişimleri genellikle üst düzey politika hedeflerine ve kurumlar arası koordinasyona bağlıdır. Bu modelleri sistematik biçimde karşılaştırmak, yalnızca farklı planlama düzeylerini anlamak açısından değil; aynı zamanda bu modellerin bir arada nasıl çalışabileceğini ve birbirlerini hangi noktalarda tamamlayabileceklerini analiz etmek açısından da önemlidir.

Ancak, bu yaklaşımların her birinin son dönemde artan popülaritesine rağmen, onları bütüncül ve sistematik biçimde karşılaştıran çalışmalar sınırlıdır. Mevcut literatürde, bu modeller genellikle tekil olarak ve çoğunlukla normatif düzeyde ele alınmakta; birbirleriyle ilişkileri ve karşılaştırmalı uygulanabilirlikleri göz ardı edilmektedir. Oysa plancılar ve politika yapıcılar için kavramsal bir sentez hem stratejik karar alma süreçlerinde hem de sahada uygulanabilir modellerin geliştirilmesinde büyük katkı sağlayabilir.

Bu bağlamda çalışma, 15 Dakikalık Şehir, TOD ve Net Sıfır Karbon Şehir modellerinin karşılaştırmalı kavramsal analizini yaparak bu boşluğu doldurmayı amaçlamaktadır. Başlıca araştırma soruları şunlardır:

- Her modelin belirleyici hedefleri, ilkeleri ve uygulama özellikleri nelerdir?
- Mekânsal ölçek, ulaşım vizyonu, arazi kullanımı, yönetişim ve sürdürülebilirlik sonuçları açısından nasıl farklılık gösterir ve örtüşürler?
- Bu farklılıklar, özellikle mikro (mahalle), mezo (koridor/bölge) ve makro (metropol/ulusal) ölçeklerde kentsel politika geliştirme süreçlerine ne tür içgörüler sunar?

Çalışmanın geri kalanı şu şekilde yapılandırılmıştır. Giriş bölümünün devamında her üç modelin tanımı, temel ilkeleri ve örnek uygulamalarının sunulduğu Ulaşım Odaklı Kentsel Yaklaşımlar bölümü yer almaktadır. Yöntem bölümünde, karşılaştırmalı kavramsal analiz yaklaşımı tanımlanmış ve çalışmada

kullanılan kriterler detaylandırılmıştır. Bu üç modelin benzerlikleri ve farklılıkları, tablo ve tematik analizler eşliğinde Karşılaştırmalı Analiz bölümünde değerlendirilmiştir.

Son bölümde ise, mikro, mezo ve makro düzeylerde her modelin uygulanabilirliği tartışılmış ve farklı kentsel bağlamlara uygun stratejik öneriler sunulmuştur. Bu yapısıyla çalışma, yalnızca literatüre katkı sunmakla kalmayıp; yerel yönetimler, şehir plancıları ve karar vericiler için bağlama duyarlı stratejilerin geliştirilmesinde pratik bir rehber olmayı da hedeflemektedir.

ULAŞIM ODAKLI KENTSEL YAKLAŞIMLAR

Ulaşım ağları, uzun süredir şehirlerin gelişimini şekillendirmektedir. Gehl (2010)'in belirttiği gibi, otomobil odaklı erken modern şehir planları yayılan, sürdürülemez şehirler ortaya çıkarmıştır. Günümüzün şehir plancıları alternatifler aramaktadır. Küresel düzeyde kentsel planlama yaklaşımı, özel araç kullanımını azaltan ve erişilebilir, insan odaklı kent mekânları üreten yeni modeller üzerine yoğunlaşmaktadır (Newman ve Kenworthy, 1999; 2006). Aşağıda üç modele ilişkin tanımlayıcı bilgiler yer almaktadır.

15 Dakikalık Şehir

Moreno ve ark. (2021) tarafından ortaya koyulan "15 Dakikalık Şehir" kavramı, COVID-19 sonrası kentlerin sürdürülebilirlik, dayanıklılık ve mekânsal kimlik hedeflerine ulaşabilmesi için önerilen bütüncül bir kentsel planlama yaklaşımıdır. Bu model, kent sakinlerinin yaşama, çalışma, alışveriş, sağlık, eğitim ve eğlence gibi temel ihtiyaçlarını 15 dakikalık yürüme veya bisiklet sürme mesafesinde karşılayabilmelerini hedeflemektedir (Moreno ve ark., 2021).

Modelin temelinde "krono-urbanizm" (chrono-urbanism) kavramı yer almaktadır. Bu, bireylerin yaşam kalitesinin, ulaşım için harcanan zamanla ters orantılı olduğunu savunmaktadır. Bu bağlamda, otomobil bağımlılığını azaltmak ve yerel yaşamı teşvik etmek önceliklidir. 15 Dakikalık Şehir modeli yoğunluk, yakınlık, çeşitlilik ve dijitalleşme olmak üzere dört ana bileşeni içermektedir. Uygun kentsel yoğunluk, kaynakların verimli kullanımını ve hizmetlere erişimi kolaylaştırırken, temel hizmetlerin ve olanakların konutlara yakın olması da günlük yaşamı kolaylaştırmakta ve ulaşım ihtiyacını azaltmaktadır. Diğer yandan karma kullanımlı alanlar ve sosyo-kültürel çeşitlilik, canlı ve kapsayıcı toplulukların oluşmasını desteklemektedir. Dijital teknolojilerin entegrasyonu ise uzaktan çalışma ve hizmetlere erişim gibi olanaklarla esnek yaşam biçimlerini mümkün kılmaktadır (Moreno ve ark., 2021). Bu model Paris'te uygulanmaya başlanmış olup yerel halk tarafından olumlu bir şekilde karşılanmıştır (Reid, 2020).

Toplu Taşıma Odaklı Gelişme (TOD)

Toplu Taşıma Odaklı Gelişme (TOD), arazi kullanımı ve toplu taşımayı entegre eden yerleşik bir kentsel stratejidir (Sung ve Oh, 2011). Kavram, 1990'lı yıllarda Amerika'da genel hatlarıyla ortaya çıkmış olup, 1993 yılında Calthorpe tarafından detaylı bir şekilde ele alınmıştır (Calthorpe, 1993).

Model, yüksek kapasiteli toplu taşıma (demiryolu vb.) istasyonları çevresinde yoğun, karma kullanımlı kalkınmayı teşvik etmektedir (Sung ve Oh, 2011). Tipik özellikleri arasında 400-800 metrelik yürüme mesafesindeki hizmet alanları, yaya dostu sokaklar, azaltılmış park yeri ve toplu taşıma merkezlerinde kümelenmiş konut, ofis ve mağazaların karışımı sayılabilir (Bajracharya ve ark., 2005).

TOD modelinde ulaşım yaklaşımı, toplu taşıma sistemlerini öncelikli hale getirmeyi amaçlamaktadır. Bu modelde, toplu taşıma araçları ile yaya ve bisiklet gibi motorsuz ulaşım biçimleri daha çekici ve kullanışlı hale getirilerek, bireylerin otomobil kullanımından uzaklaşması teşvik edilmektedir. Ulaşım düğüm noktalarında yaşanan otopark sorunlarına çözüm olarak, bireylerin özel araçlarını park edip toplu taşımaya geçiş yapabilecekleri aktarma merkezleri planlanmaktadır (Şengüler, 2023). Böylece TOD yalnızca ulaşım ve kent içi faaliyet akışını değil, aynı zamanda özel araçların kullanımını kademeli olarak azaltan hibrit bir gelişim modeli sunmaktadır.

Net Sıfır Karbon Şehri

Net sıfır karbon şehirler, küresel iklim krizine karşı ortaya konulan en ileri düzey kentleşme yaklaşımlarından biridir. Bu kavram, şehirlerin sera gazı emisyonlarını mümkün olan en düşük düzeye indirmesini ve geri kalan emisyonların doğrudan karbon giderimi veya dengeleme stratejileri ile sıfırlanmasını ifade etmektedir (Seto ve ark., 2021). Yani bir şehir ya da ülke hâlâ karbon salıyor olabilir, ancak bu salımı; karbon yutakları (ormanlar, sulak alanlar vb.), karbon yakalama teknolojileri, yenilenebilir enerji kaynaklarıyla ikame gibi yollarla telafi ediyorsa, net emisyon "sıfır" kabul edilmektedir. Bu

yaklaşım, yalnızca şehir sınırları içindeki emisyonları değil, aynı zamanda şehirlerin tedarik zincirleri ve tüketim alışkanlıkları gibi dolaylı emisyon kaynaklarını da kapsamaktadır (Seto, 2023). Bu nedenle bu tür şehirlerin planlamasında enerji, ulaşım, binalar, atık yönetimi, yeşil alanlar ve yönetişim gibi birçok alanda sistemik dönüşüm gereklidir (Dünya Ekonomik Forumu [WEF], 2021).

Model temelde, planlama, enerji ve teknolojiye odaklanmaktadır. Bu süreçte binalar ve sistemler enerji verimli hale getirilmekte veya yenilenebilir enerji kaynaklarıyla çalıştırılmakta ve karbon yutakları (parklar, yeşil altyapı) en üst düzeye çıkarılmaktadır (Fan ve Wei, 2022). Arazi kullanım politikaları, düşük emisyonlu bölgeleri ve entegre toplu taşıma-konut planlarını desteklemektedir. Ulaşım tarafında ise vizyon, karbon nötr mobilitedir. Modelde elektrikli toplu taşıma ve aktif ulaşım türlerine (elektrikli otobüsler, trenler, bisikletler) öncelik verilirken, fosil yakıtlı araçlar (genellikle düşük emisyonlu bölgeler aracılığıyla) aşamalı olarak kullanımdan kaldırılmaktadır (WEF, 2021).

Ancak net sıfır hedeflerine ulaşmak için yalnızca teknik dönüşüm yeterli değildir. Bu süreçte çok düzeyli yönetişim, toplum katılımı ve yenilikçi finansman modelleri gibi sosyal ve kurumsal bileşenler de etkili olmalıdır (Duan ve Kim, 2023; Seto ve ark., 2021). Şehirlerin kendi karbon ayak izini düzenli olarak ölçmesi ve stratejik planlarını bu verilere dayandırması, izleme-değerlendirme süreçlerini güçlendirecektir.

MATERYAL VE METOD

Bu çalışmada üç planlama yaklaşımını incelemek için karşılaştırmalı analiz yöntemi kullanılmıştır. Bu yöntem, kuramsal çerçeveleri veya politika paradigmalarını sistematik olarak karşılaştırmak amacıyla geliştirilen, nitel bir analiz yöntemidir. Kavramlar arası yapı, amaç ve öncelikleri analiz ederek benzerlikleri ve farklılıkları ortaya koymaktadır (Bulduklu, 2019; Neuman, 2013).

Bu yöntem kapsamında, ilgili yaklaşımların nasıl yapılandığı, hangi planlama ilkelerine dayandığı ve uygulamada ne tür stratejilerle somutlaştığı çok boyutlu bir çerçeveyle ele alınmaktadır. Analiz, literatür, politika belgeleri ve uygulama örneklerini temel alarak kavramsal düzeyde karşılaştırma yapmayı amaçlar (Aydın ve Hanağası, 2017). Böylece, her modelin özgün yönlerinin yanı sıra ortak temalar ve olası sentez alanları da açığa çıkarılabilir.

Çalışmada ilk olarak literatür taraması yapılmıştır. Literatür taraması sürecinde akademik çalışmalar, uluslararası kuruluşların teknik raporları, şehir strateji belgeleri ve uygulanan projelerin vaka çalışmalarından yararlanılmıştır. Karşılaştırmalı analizde kullanılan değerlendirme kriterleri de yine literatür taraması sonucunda elde edilmiştir. Bu kriterler doğrultusunda geliştirilen analitik çerçeve, bir sonraki bölümde üç planlama modelinin temel niteliklerinin sistematik biçimde karşılaştırılmasına temel oluşturmaktadır.

BULGULAR VE TARTIŞMA

Bu çalışmada analiz edilen 15 Dakikalık Şehir, TOD ve Net Sıfır Karbon Şehir yaklaşımları hem yapısal nitelikleri hem de uygulamaya dönük stratejileri bakımından birbirinden ayrışmakta, ancak aynı zamanda tamamlayıcı yönler de sunmaktadır. Tablo 1, bu üç yaklaşımın kavramsal düzeyde ve uygulama düzeyinde nasıl yapılandığını çok boyutlu olarak ortaya koymaktadır. Özellikle ölçek, planlama ilkeleri, yönetişim tarzı ve sürdürülebilirlik anlayışı açısından dikkat çekici farklar göstermektedir.

Tablo 1. Ulaşım Odaklı Kentsel Yaklaşımların Karşılaştırması

Kriterler	15 Dakikalık Şehir	Toplu Taşıma Odaklı Gelişme (TOD)	Net Sıfır Karbon Şehir
Temel Amaç	Yerel erişilebilirliği, yaşanabilirliği ve toplumun refahını en üst düzeye çıkarmak	Toplu taşıma merkezli gelişme	Sera gazı emisyonlarını net olarak sıfıra indirmek
Ana Hedef	Günlük ihtiyaçlara yürünebilir mesafede erişim	Toplu taşımaya erişim ile otomobil bağımlılığını azaltma	Enerji verimli, düşük karbonlu kentsel sistemler oluşturmak
Ölçek	Mikro (mahalle düzeyi)	Mezo (bölge/hat düzeyi)	Makro (şehir/ülke düzeyi)
Planlama İlkeleri	Karma kullanım, yakınlık, esneklik, çeşitlilik, kompaktlık	Yoğunluk, karma kullanım, erişim odaklı gelişme, yaya erişimi, transit odaklı tasarım	Enerji verimli altyapı, yeşil ulaşım, karbon dengeleme ve sistem dönüşümü
Ulaşım Perspektifi	Yürüyüş ve bisiklet öncelikli	Toplu taşıma sistemleri öncelikli	Karbon nötr ulaşım (elektrikli araçlar, toplu taşıma, aktif ulaşım vb.)
Alan Kullanımı	Mahalle merkezli, karma kullanımlı, yerel hizmetler	Ulaşım aksı boyunca yoğun konut ve ticaret	Düşük emisyon bölgeleri, entegre ulaşım-enerji-arazi kullanım planlaması
Teknoloji Vurgusu	Orta düzey (mekânsal düzenlemelerle birlikte dijital hizmet altyapısı)	Orta düzey (toplu taşıma teknolojileri, akıllı zaman çizelgeleri, trafik yönetimi vb.)	Yüksek düzey (Yenilenebilir enerji, akıllı şebekeler, elektrikli ulaşım teknolojileri vb.)
Yönetişim Modeli	Yerel katılım, topluluk temelli	Kamu özel iş birliği, bölgesel planlama	Çok düzeyli ve teknik odaklı, politika güdümlü
Sürdürülebilirlik Boyutu	Sosyal sürdürülebilirlik (eşitlik, yerel kimlik, refah ve kapsayıcılık)	Dengeli sosyal-ekonomik sürdürülebilirlik (ulaşım ve kalkınma entegrasyonu)	Çevresel sürdürülebilirlik (emisyon azaltımı, enerji dönüşümü, iklim hedefleri)

Her üç modelin en ayırt edici farkı, mekânsal ölçek ve organizasyon düzeyidir. 15 Dakikalık Şehir, belirgin biçimde mahalle düzeyine odaklanan, yerel erişilebilirlik ve topluluk yaşamını önceleyen bir yaklaşımdır. Bu modelde kent, kendi kendine yeten, çok işlevli ve yürünebilir mahallelere ayrılarak, günlük ihtiyaçların kısa mesafelerle karşılanması hedeflenmektedir (Moreno ve ark., 2021). Hizmetlerin ve konutların blok ya da semt ölçeğinde yeniden yapılandırılması sayesinde, bireylerin hareket ihtiyacı azaltılırken, kentsel yaşanabilirlik güçlenmektedir. Buna karşılık Net Sıfır Karbon Şehir yaklaşımı, tüm kentsel sistemi hatta gerektiğinde ulusal düzeyi de kapsayan makro ölçekte ele alan sistemik bir dönüşüm modelidir. Esas hedef, net sera gazı emisyonlarını sıfırlamak ve bu dönüşümü enerji sistemleri, altyapı ve mekânsal planlama süreçlerini yeniden yapılandırarak gerçekleştirmektir (Seto ve ark., 2021). Toplu Taşıma Odaklı Gelişim (TOD) modeli ise bu iki yaklaşımın arasında konumlanmakta; mekânsal olarak genellikle toplu taşıma aksları boyunca uzanan koridorlar ve bu koridorlar çevresindeki düğüm noktalarına odaklanmaktadır (Sung ve Oh, 2011). TOD, bir metro hattının hizmet alanı gibi mezo ölçekte işler ve merkezi olmayan ancak sistematik biçimde bütünleşmiş bir kentsel gelişim stratejisi sunmaktadır. Bu modeller, bağlama uygun biçimde birlikte uygulanarak çok düzeyli planlama çözümleri sunabilir. Örneğin, C40 Cities'in "Green and Thriving Neighbourhoods" programı kapsamında, 15 dakikalık şehir ilkeleriyle net sıfır karbon hedeflerini entegre eden mahallelerin pilot projeleri planlanmaktadır. Bu tür entegrasyonlar, çok düzeyli sürdürülebilir planlama için işlevsel bir sentez yaratabilir (C40 Cities, 2022).

Ulaşım ve arazi kullanım stratejileri açısından da modeller arasında yapısal farklar bulunmaktadır. Hem 15 Dakikalık Şehir hem de TOD modelleri, kompaktlık, karma kullanım ve erişilebilirlik gibi temel planlama ilkelerine dayanmaktadır. IPCC (2022) raporuna göre, bu tür planlama yaklaşımları, kentsel sera gazı emisyonlarını yaklaşık %25 oranında azaltma potansiyeline sahiptir. Her iki modelde de farklı işlevlerin fiziksel olarak kısa mesafelerde konumlandırıldığı ve bu sayede ulaşımın minimize edildiği bir yapı öne çıkmaktadır. Ancak ulaşım vizyonlarında belirgin ayrışma vardır: 15 Dakikalık Şehir modeli yürüyüş ve

bisiklet gibi aktif ulaşım türlerine öncelik verirken, TOD yaklaşımı esas olarak toplu taşıma kullanımını teşvik etmektedir. Net Sıfır Karbon Şehir modeli ise bu iki yönelimi bütünleştirerek hem aktif ulaşımı hem de elektrikli araçlarla desteklenen karbon nötr mobilite çözümlerini kapsamaktadır (Seto ve ark., 2021). Ayrıca, Net Sıfır yaklaşımı ulaşım kararlarını enerji altyapısı, teknolojik dönüşüm ve şehir ölçeğindeki sistem tasarımlarıyla doğrudan ilişkilendirmektedir. Türkiye'nin 2053 Net Sıfır vizyonunda da görüldüğü üzere, çok merkezli kent modellerinde sürdürülebilir mobilite bölgeleri oluşturularak bireysel araç kullanımının azaltılması amaçlanmaktadır (T.C. Ulaştırma ve Altyapı Bakanlığı, 2022; T.C. Strateji ve Bütçe Başkanlığı, 2023).

Yönetişim modelleri açısından da bu yaklaşımlar farklılık göstermektedir. 15 Dakikalık Şehir yaklaşımı, yerel yönetimlerin ve yurttaşların etkin katılımına dayanan aşağıdan yukarıya bir planlama biçimini benimsemektedir. Paris gibi örneklerde, mahalle düzeyinde yürütülen katılımcı süreçler bu modelin başarısında kritik rol oynamaktadır (Moreno ve ark., 2021). TOD modelinde ise yerel yönetimler, ulaşım otoriteleri ve özel geliştiriciler arasındaki koordinasyon, projelerin finansmanı ve uygulanmasında önemli bir rol oynamaktadır (Ulaşım ve Kalkınma Politikaları Enstitüsü [ITDP], 2017). Net Sıfır Karbon Şehir yaklaşımı ise çoğunlukla üst ölçekli politika yapıcıların yönlendirdiği, teknik uzmanlık ve devlet kurumlarının koordinasyonunu gerektiren yukarıdan aşağıya bir yönetişim yapısı üzerine kuruludur (Seto ve ark., 2021). Bu yönetişim farklılıkları, her modelin uygulama sürecindeki gereksinimlerini de belirlemektedir. Örneğin, 15 Dakikalık Şehir modeli, imar planı reformları, sosyal politika araçları ve yerel bütçelerle desteklenmeliyken; Net Sıfır modeli, altyapı yatırımları, düzenleyici reformlar ve büyük ölçekli finansman mekanizmaları gerektirmektedir.

Sürdürülebilirlik perspektifleri açısından bakıldığında, her modelin farklı ağırlık noktaları bulunmaktadır. 15 Dakikalık Şehir sosyal sürdürülebilirliği; kapsayıcılık, aidiyet ve topluluk yaşamını teşvik ederek ön plana çıkarmaktadır. TOD yaklaşımı daha çok mobilite verimliliği ve ekonomik kalkınmayı hedeflemekte; istasyon çevresinde oluşan kentsel kümelenmeler, ekonomik canlanmayı desteklemektedir (Cervero, 2004; Sung ve Oh, 2011). Net Sıfır Karbon Şehir yaklaşımı ise çevresel sürdürülebilirliği hedefleyerek emisyonların azaltılması, enerji verimliliğinin artırılması ve yeşil altyapı entegrasyonu gibi stratejileri temel almaktadır (IPCC, 2022). Bununla birlikte, bu vurgular mutlak ayrımlar değildir. C40 Cities'in (2022) de belirttiği gibi, 15 Dakikalık Şehir yaklaşımı aynı zamanda çevresel kazanımlar da sağlayabilir; araç kullanımının azalması ve hava kalitesinin artması buna örnektir. Benzer şekilde, TOD projeleri düşük gelirli bölgeleri hizmet ve ulaşım olanaklarına daha erişilebilir hale getirerek sosyal sürdürülebilirlik açısından da fayda üretebilir.

Sonuç olarak, bu analiz, her bir modelin farklı ölçeklerde belirli sorun alanlarına etkili çözümler sunduğunu ve hiçbir modelin tek başına evrensel bir çözüm olmadığını ortaya koymaktadır. 15 Dakikalık Şehir, mikro düzeyde yaşam kalitesine ve yerel erişilebilirliğe odaklanırken; TOD, mezo düzeyde verimli ulaşım ve mekânsal bütünleşmeyi desteklemektedir. Net Sıfır Karbon Şehir ise makro ölçekte sistemsel dönüşüm ve çevresel sürdürülebilirlik hedeflerini temsil etmektedir. Bu nedenle, bütüncül şehir planlama vizyonlarında, söz konusu modellerin bağlama duyarlı biçimde bir arada kullanılması, ölçekler arası geçişliliğin gözetilmesi ve senkronize stratejilerin geliştirilmesi önerilmektedir.

SONUÇ VE ÖNERİLER

Bu karşılaştırmalı çalışma, ulaşım odaklı kentsel planlama modellerinin çok ölçekli sürdürülebilirlik hedeflerine katkısını analiz ederek, farklı bağlamlarda nasıl uygulanabileceklerine dair kavramsal bir çerçeve sunmaktadır. 15 Dakikalık Şehir, TOD ve Net Sıfır Karbon Şehir yaklaşımları, kendi içlerinde farklı mekânsal ölçeklere, yönetişim yapısına ve sürdürülebilirlik önceliklerine sahiptir. Ancak bu farklara rağmen, bir araya geldiklerinde entegre bir mobilite ve kentleşme vizyonu oluşturma potansiyeli taşımaktadırlar.

Bu bağlamda, söz konusu modellerin uygulanabilirliği yalnızca kuramsal düzeyde değil, aynı zamanda farklı sosyo-mekânsal bağlamlara göre şekillenen politika stratejileri açısından da değerlendirilmelidir. Çalışmanın bu son bölümünde, bu yaklaşımların mikro (mahalle), mezo (koridor/bölge) ve makro (şehir/ulusal) düzeyde nasıl yapılandırılabileceği tartışılmakta; özellikle planlama ölçeği, sosyal eşitlik ve iklim taahhütleri açısından Türkiye gibi gelişmekte olan ülkelerdeki kentleşme dinamiklerine sahip bağlamlarda ne tür politika seçenekleri geliştirilebileceği değerlendirilmektedir.

Mikro düzeyde, yani mahalle ve semt ölçeğinde, 15 Dakikalık Şehir modeli doğrudan uygulanabilir bir yaklaşım sunmaktadır. Yerel yönetimlerin karma kullanımlı mahalle planlamasını teşvik etmesi; konut alanlarına küçük ölçekli ticaret, eğitim ve sağlık hizmetlerinin entegre edilebilmesi için imar düzenlemelerinde esneklik sağlaması gereklidir. Aynı şekilde, minimum otopark zorunluluklarının azaltılması, yaya altyapısının iyileştirilmesi ve bisiklet yollarının güvenli ve kesintisiz hale getirilmesi, bu yaklaşımın fiziksel altyapısını oluşturacaktır. Hizmetlerden yeterince yararlanamayan dezavantajlı semtlerin erişimini sağlamak amacıyla kamu tesisleri (örneğin parklar, toplum merkezleri ve sağlık ocakları), sosyo-mekânsal adalet ilkesi gözetilerek planlanmalıdır. Bu bağlamda, mahalle düzeyinde "erişilebilirlik denetimleri" yapılabilir ve Next Proximity Index gibi ölçüm araçları kullanılarak planlamaya yön verilebilir. Mahalle yaşamının desteklenmesi için kamu yatırımları ve katılımcı tasarım süreçleri, özellikle düşük gelirli bölgelerde toplumsal bütünleşmeyi artırabilir.

Mezo düzeyde, yani ulaşım koridorları ve bölgesel alanlarda, TOD yaklaşımı stratejik bir rol üstlenmektedir. Özellikle raylı sistem hatları, metro ve banliyö tren hatları etrafında yoğun, karma kullanımlı ve yaya öncelikli gelişim alanları oluşturmak TOD'un temel hedeflerindendir. Transit merkezleri çevresinde özel planlama bölgeleri belirlenerek, bu alanlarda geliştiricilere imar kolaylığı, yoğunluk bonusları veya vergi teşvikleri sunulabilir. İstanbul gibi metropol alanlarında Marmaray hattı, Metrobüs koridoru veya yeni metro hatları çevresinde TOD bölgeleri oluşturulabilir. TOD uygulamaları yalnızca mekânsal planlama ile sınırlı kalmamalı, aynı zamanda ilk ve son kilometre ulaşımı da kapsamalıdır; bu amaçla park et & devam et sistemleri, bisiklet paylaşımı ve yaya bağlantılarının entegrasyonu sağlanmalıdır. Belediyeler arası koordinasyonun güçlendirilmesi, TOD bölgelerinin planlanması ve yönetimi için kritiktir. Türkiye'nin Uzun Vadeli İklim Stratejisi'nde öngörüldüğü gibi, sürdürülebilir mobilite bölgeleri oluşturulurken şehirlerarası planlama iş birliklerine ve ortak finansman modellerine de ihtiyaç duyulmaktadır. Haliç Metro Köprüsü örneğinde olduğu gibi, TOD yatırımları yalnızca ulaşımı değil, çevresel ve ekonomik canlanmayı da tetikleyebilmektedir.

Makro düzeyde, yani şehir, metropol ve ulusal ölçekte, Net Sıfır Karbon Şehir yaklaşımı uzun vadeli stratejiler açısından önem arz etmektedir. Türkiye'nin 2053 Net Sıfır hedefi ve İstanbul'un 2050 yılına kadar karbon nötrlüğe ulaşma taahhüdü, altyapıdan enerjiye, mobiliteden yapı stoğuna kadar çok katmanlı dönüşüm gerektirmektedir. Ulaştırma sektörünün elektrifikasyonu (elektrikli otobüs filoları, şarj altyapısı), kamu binalarında yenilenebilir enerji sistemlerinin yaygınlaştırılması ve mevcut yapıların nZEB standartlarına göre yenilenmesi bu kapsamda öncelikli adımlardır. Ayrıca, karbon tutma kapasitesini artırmak amacıyla yeşil altyapının (örneğin kentsel ormanlar ve sulak alanlar) genişletilmesi gerekmektedir. Yeni ulaşım projeleri çevresel etki açısından değerlendirilerek, Banister'in (2008) sürdürülebilir mobilite paradigmasına uygun biçimde alternatif düşük karbonlu ulaşım seçenekleriyle birlikte planlanmalıdır. Net sıfır hedeflerine ulaşılabilmesi için çok düzeyli yönetişim mekanizmalarının uyumlaştırılması da zorunludur. Ulusal iklim yasaları, bölgesel ulaşım planları ve yerel yönetmeliklerin birbiriyle bütünleşik hale gelmesi gerekmektedir. Bu doğrultuda hazırlanan İstanbul Sürdürülebilir Kentsel Hareketlilik Planı (SUMP), Net Sıfır yaklaşımını uygulamada örnek teşkil edecek bir stratejik doküman olarak değerlendirilebilir. Yürüyüş ve bisiklet modları için hedefler belirleyen bu plan, yeni toplu taşıma hatlarında TOD ilkelerini zorunlu hale getirerek farklı modellerin bir arada uygulanmasını mümkün kılmaktadır.

Sonuç olarak, bu çalışmada analiz edilen üç yaklaşımın her biri kendi düzleminde güçlü yönlere sahip olup, birleşik ve bağlama duyarlı şekilde uygulandığında sürdürülebilir kent vizyonuna katkı sağlayabilir. Mikro ölçekte 15 Dakikalık Şehir yaşam kalitesini artırırken; mezo ölçekte TOD ulaşım verimliliğini ve kentsel yoğunluğu optimize eder. Makro ölçekte ise Net Sıfır modeli, yapısal dönüşüm ve çevresel sürdürülebilirlik için stratejik bir çerçeve sunar. Bu çalışma, bu modellerin birbirinden ayrı değil, bir bütünün parçaları olarak düşünülmesi gerektiğini ortaya koymaktadır. Karar vericiler ve şehir plancıları için burada sunulan karşılaştırmalı kavramsal analiz, ölçek odaklı sentezler kurarak daha adil, dirençli ve düşük karbonlu kentlerin inşası için stratejik bir yol haritası işlevi görebilir.

Bununla birlikte, çalışmanın bazı sınırlılıkları bulunmaktadır. Öncelikle, analiz yalnızca üç kavramsal modele odaklanmakta ve diğer alternatif kentsel ulaşım yaklaşımlarını kapsam dışı bırakmaktadır. Ayrıca, değerlendirme ağırlıklı olarak literatür ve politika belgelerine dayandığı için uygulama düzeyindeki bağlamsal farklara ilişkin daha derinlemesine ampirik veri içermemektedir. Gelecek araştırmalarda, bu modellerin farklı şehirlerdeki uygulamalarına ilişkin karşılaştırmalı saha çalışmaları yapılması, yerel aktörlerin algılarının analiz edilmesi ve politikaların sonuçlarının değerlendirilmesi, kavramsal çerçevenin

pratikle ne ölçüde örtüştüğünü ortaya koymak açısından faydalı olacaktır. Ayrıca, bu yaklaşımların sosyal eşitlik, toplumsal cinsiyet ve mekânsal adalet gibi temalarla kesişimini inceleyen disiplinlerarası araştırmalar da sürdürülebilir kentleşme literatürüne önemli katkılar sağlayabilir.

KAYNAKLAR

Aydın, K., & Hanağası, U. B. (2017). Sosyoloji ve siyasal araştırmalarda karşılaştırmalı yöntem. Kocaeli üniversitesi sosyal bilimler dergisi, (33), 57-86.

Bajracharya, B., Khan, S., & Longland, M. (2005). Regulatory and incentive mechanisms to implement transit-oriented development (TOD) in South East Queensland. In Proceedings of the 2nd Bi-annual National Conference on the State of Australian Cities. Griffith University.

Banister, D. (2008). The sustainable mobility paradigm. Transport policy, 15(2), 73–80.

Birleşmiş Milletler [UN] (2020) Cities and pollution. UN. Erişim adresi: https://www.un.org/en/climatechange/climate-solutions/cities-pollution [04.04.2025]

Birleşmiş Milletler İnsan Yerleşimleri Programı [UN-Habitat] (2020). World cities report 2020: the value of sustainable urbanization. UN Habitat, Nairobi, Kenya. Erişim adresi: https://unhabitat.org/sites/default/files/2020/10/wcr_2020_report.pdf [02.04.2025]

Bulduklu, Y. (2019). Eleştirel çalışmalarda nitel araştırma yöntemi olarak gömülü teori. Kritik iletişim çalışmaları dergisi, 1(1), 1-14.

C40 Kentleri Ağı [C40 Cities] (2022). Green and thriving neighbourhoods. Erişim adresi: https://www.c40.org/what-we-do/initiatives/green-and-thriving-neighbourhoods [16.04.2025]

Calthorpe, P. (1993). The next American metropolis (Vol. 23). New York: Princeton Architectural Press.

Cervero, R. (2004). Transit-Oriented Development in the United States: Experiences, Challenges, and Prospects. Transportation Research Board.

Duan, Z., & Kim, S. (2023). Progress in research on net-zero-carbon cities: a literature review and knowledge framework. Energies, 16(17), 6279.

Dünya Ekonomik Forumu [WEF] (2021). Net Zero Carbon Cities: An Integrated Approach. Erişim adresi: https://www.weforum.org/publications/net-zero-carbon-cities-an-integrated-approach/ [18.04.2025]

Ekonomik Kalkınma ve İşbirliği Örgütü [OECD] (2020), Improving Transport Planning for Accessible Cities, OECD Urban Studies, OECD Publishing, Paris.

Fan, Y., & Wei, F. (2022). Contributions of natural carbon sink capacity and carbon neutrality in the context of net-zero carbon cities: A case study of Hangzhou. Sustainability, 14(5), 2680.

Gehl, J. (2010). Cities for people. Island Press.

Hükümetlerarası İklim Değişikliği Paneli [IPCC], (2022). Climate change 2022: Mitigation of climate change. Contribution of Working Group III to the Sixth Assessment Report of the Intergovernmental Panel on Climate Change (P. R. Shukla, J. Skea, R. Slade, A. Al Khourdajie, R. van Diemen, D. McCollum, M. Pathak, S. Some, P. Vyas, & J. Malley, Eds.). Cambridge University Press.

Krismawanti., & Destiawan, W. (2025). The impact of transit-oriented development on heritage cities: A study of Haliç Metro and its influence on Istanbul's urban fabric. Journal of city: Branding and authenticity, 2(2), 121-137.

Marquet, O., & Miralles-Guasch, C. (2015). The Walkable city and the importance of the proximity environments for Barcelona's everyday mobility. Cities, 42, 258-266.

Moreno, C., Allam, Z., Chabaud, D., Gall, C., & Pratlong, F. (2021). Introducing the "15-minute city": Sustainability, resilience and place identity in future post-pandemic cities. Smart Cities, 4(1), 93–111.

Neuman, W. L. (2013). Toplumsal Araştırma Yöntemleri: Nitel ve Nicel Yaklaşımlar, 6. Baskı. Çeviren, Özge, Sedef, Yayın Odası, Ankara (2006).

Newman, P., & Kenworthy, J. (1999). Sustainability and cities: Overcoming automobile dependence. Island Press.

Newman, P., & Kenworthy, J. (2006). Urban design to reduce automobile dependence. Opolis, 2(1), 35–52

Pozoukidou, G., & Chatziyiannaki, Z. (2021). 15-Minute City: Decomposing the new urban planning eutopia. Sustainability, 13(2), 928.

Reid, C. (2020). Anne Hidalgo, Paris Belediye Başkanı Olarak Yeniden Seçildi: Arabaları Trafikten Çekip Bisiklet ve Yürümeyi Teşvik Edeceğini Vaat Etti. Erişim adresi: https://www.forbes.com/sites/carltonreid/2020/06/28/anne-hidalgo-reelected-as-mayor-of-paris-vowing-to-remove-cars-and-boost-bicycling-and-walking/?sh=ba645d11c852 [04.04.2025]

Seto, K. C. (2023). Strategies for Smart Net Zero Carbon Cities. Bridge, 15. Erişim adresi: https://terpconnect.umd.edu/~austin/ence688r.d/papers-reading/NAE-Sustainable-Smart-Cities2023.pdf#page=17 [15.04.2025]

Seto, K. C., Churkina, G., Hsu, A., Keller, M., Newman, P. W., Qin, B., & Ramaswami, A. (2021). From low-to net-zero carbon cities: The next global agenda. Annual review of environment and resources, 46(1), 377-415.

Sung, H., & Oh, J. T. (2011). Transit-oriented development in a high-density city: Identifying its association with transit ridership in Seoul, Korea. Cities, 28(1), 70-82.

Şengüler, B. (2023). Toplu taşıma (transit) odaklı gelişim yaklaşımı ile tramvay hattı analizi: Bursa T2 hattı örneği. Yüksek Lisans Tezi, Lisansüstü Eğitim Enstitüsü, İstanbul Teknik Üniversitesi.

T.C. Strateji ve Bütçe Başkanlığı. (2023). On İkinci Kalkınma Planı (2024–2028). Erişim adresi: https://www.sbb.gov.tr/wp-content/uploads/2023/12/On-Ikinci-Kalkinma-Plani_2024-2028_11122023.pdf [12.04.2025]

T.C. Ulaştırma ve Altyapı Bakanlığı. (2022). 2053 Ulaştırma ve Lojistik Ana Planı. Erişim adresi: https://www.uab.gov.tr/uploads/pages/bakanlik-yayinlari/20221025-2053-ulastirma-ve-lojistik-ana-plani-tr.pdf [12.04.2025]

Ulaşım ve Kalkınma Politikaları Enstitüsü [ITDP] (2017). Transit-oriented development standard (3rd ed.). Erişim adresi: https://www.itdp.org/publication/tod-standard/ [13.04.2025]

➢ *ORAL PRESENTATION*

Şehir içi taşımacılık yapan araçların hidrojen yakıt ikmal istasyonu için mikro şebeke tasarımı; Muş ili örneği

Mehmet Ali KÖPRÜ[1*] (*ORCID: https://orcid.org/0000-0002-3761-399X)*

[*1]Bingöl Üniversitesi, Teknik Bilimler MYO, Elektrik ve Enerji, Bingöl, Türkiye

*Sorumlu yazar e-posta: makopru@bingol.edu.tr

Özet

Kara taşıtları, fosil yakıt kullanımı nedeniyle çevreye ve insan sağlığına zararlı emisyonlar yaymaktadır. Bu çalışmada, Muş ili şehir içi taşımacılığında kullanılan araçların enerji ihtiyaçlarının karşılanmasına yönelik yenilenebilir enerji kaynaklarına (YEK) dayalı bir çözüm önerisi sunulmuştur. Önerilen sistem; güneş panelleri (FV), rüzgâr türbinleri (RT), elektrolizör, batarya depolama sistemi (BDS) ve hidrojen tankından (HT) oluşan bir hidrojen yakıt ikmal istasyonu şeklinde tasarlanmıştır. Optimizasyon sonucunda, 7567 kW gücünde FV paneller, her biri 20 kW olan 63 adet RT, 600 kW kapasiteli bir elektrolizör ve 11.007 kWh kapasiteli bir batarya sisteminin en uygun yapılandırma olduğu belirlenmiştir. Enerji üretiminin %75'i PV panellerden, %25'i ise rüzgâr türbinlerinden sağlanmaktadır. Sistemin net bugünkü maliyeti (Net Present Cost - NPC) 26,9 milyon dolar olarak hesaplanmıştır. Araçların yıllık yakıt maliyeti 839.530 dolar olup, sistemin 25 yıllık ömrü boyunca toplam 20,988 milyon dolar yakıt tüketimi öngörülmektedir. Motorin fiyatlarındaki artış ve enflasyon oranları göz önünde bulundurulduğunda, sistemin kendini daha kısa sürede amorti edeceği öngörülmektedir. Tasarlanan mikro şebeke sayesinde yıllık yaklaşık 2.106 kg CO_2 salımı engellenmiş olacaktır. Önerilen sistemin yaygın olarak uygulanması durumunda, kara taşıtlarının neden olduğu emisyonlarda belirgin bir azalma sağlanabileceği sonucuna varılmıştır.

Anahtar Kelimeler: Güneş, Rüzgâr, Hidrojen, Mikro şebeke, Emisyon

Microgrid design for hydrogen fuel refueling station for urban transportation vehicles; the case of Muş province

Abstract

Land vehicles emit harmful emissions to the environment and human health due to their use of fossil fuels. In this study, a renewable energy-based solution is proposed to meet the energy needs of urban transportation vehicles in Muş, Turkey. The proposed system is a hydrogen fueling station designed as a microgrid consisting of photovoltaic (PV) panels, wind turbines (WT), an electrolyzer, a battery storage system (BSS), and a hydrogen tank (HT).According to the optimization results, the most suitable configuration includes 7,567 kW of PV panels, 63 WTs each with a capacity of 20 kW, a 600 kW electrolyzer, and a battery system with a capacity of 11,007 kWh. The system generates 75% of its energy from PV panels and 25% from wind turbines. The net present cost (NPC) of the system is calculated to be $26.9 million. The annual fuel cost for the vehicles is estimated at $839,530, and the total fuel cost over the system's 25-year lifetime is projected to be $20.988 million. Considering the increase in diesel prices and inflation rates, the system is expected to pay for itself in a shorter period. Additionally, the designed microgrid is projected to prevent approximately 2,106 kg of CO_2 emissions annually. If implemented on a large scale, the proposed system has the potential to significantly reduce emissions from land transportation vehicles

GİRİŞ

Ulaşım sektörü, küresel karbon emisyonlarının en büyük ikinci kaynağıdır. Toplu taşıma araçları dünya çapında karbon emisyonlarının azaltılmasında önemli bir rol oynamaktadır. Toplu taşımanın gelişimi, karbon nötrlüğüne ulaşmak için kilit bir strateji olarak tanımlanmıştır. Çalışmalar, toplu taşıma geliştirme seviyesi ile karbondioksit (CO_2) emisyonları arasında ters orantı olduğunu göstermiştir. Diğer bir ifadeyle sektör karbon emisyonlarını azaltma potansiyeline sahiptir (Jing et al., 2022). Ulaşım sektörü, insan kaynaklı sera gazı emisyonlarının yaklaşık %15'ini teşkil etmektedir (Ferrer & Thomé, 2023). Toplu taşıma, özellikle sağlık yararlarını teşvik edebileceği ve sürdürülebilir şehirlere ve topluluklara katkıda bulunabileceği kentsel alanlarda emisyonları azaltmak için etkili bir strateji olarak kabul edilmiştir (Kwan

& Hashim, 2020; Ribeiro & Mendes, 2022).Toplu taşıma araçlarında karbon emisyonlarının azaltılması son derece önemlidir. Ulaşım sektörü küresel olarak sera gazı emisyonlarına önemli bir katkıda bulunuyor ve hidrojen(H2) yakıtı sürdürülebilir bir alternatif olarak önerilmektedir. Hidrojen yakıt hücreli elektrikli araçlarda (FCEV) kullanılabilir veya içten yanmalı motorlarda yakılabilir. Birçok ülke iklim dostu özellikleri nedeniyle hidrojenle çalışan araçların araştırma ve geliştirilmesini desteklemektedir (Akac et al., 2022). Hidrojen girişimleri, geleneksel toplu taşıma filolarının FCEV'lerle değiştirildiği küçük-orta ölçekli Avrupa şehirlerinde ve bölgelerinde uygulanmıştır. Ek olarak, yolcu demiryolu taşımacılığında yakıt olarak hidrojenin kullanılması, elektrikli olmayan demiryolu hatlarındaki emisyonları azaltmada umut vaat ediyor (Agarwal et al., 2023).Genel olarak, hidrojen yakıtı toplu taşıma araçlarındaki karbon emisyonlarını önemli ölçüde azaltma ve daha sürdürülebilir bir mobilite sektörüne katkıda bulunma potansiyeline sahiptir.

Bu çalışmada Muş ili şehir içi taşımacılık yapan araçların fosil yakıt tüketimini ve oluşturdukları emisyonu azaltmayı hedeflemektedir. Yenilenebilir enerji kaynaklarından oluşan sıfır emisyona sahip hidrojenle çalışan araçların kullanacakları bir yakıt ikmal istasyonu için mikro şebeke tasarımı yapılacaktır. Oluşturulan mikro şebekeye ait ekonomik ve çevresel etkileri incelenecektir.

MATERYAL VE METOD

Muş ilinde, şehir içi yolcu taşımacılığında kullanılan motorin yakıtlı araçların neden olduğu karbon emisyonlarını azaltmaya yönelik olarak, bu araçların hidrojen yakıtlı araçlarla değiştirilmesi amacıyla, hidrojen ve elektrik ihtiyacını şebekeden bağımsız olarak karşılayabilecek bir yakıt ikmal istasyonu tasarlanmıştır. Bu kapsamda, HOMER Pro yazılımı kullanılarak yenilenebilir enerji kaynaklarına dayalı bir mikro şebeke modeli oluşturulmuştur.

HOMER Pro, Amerika Birleşik Devletleri Ulusal Yenilenebilir Enerji Laboratuvarı (NREL) tarafından geliştirilen ve şebekeye bağlı ya da şebekeden bağımsız enerji sistemlerinin teknik ve ekonomik analizini gerçekleştirmeye yönelik bir yazılım programıdır. Bu yazılım, hibrit yenilenebilir enerji sistemlerinin optimum tasarımı, boyutlandırılması ve planlanmasına olanak sağlamakta olup, gerçek verilere oldukça yakın sonuçlar üretebilmektedir(Akan, 2023; Shahzad et al., 2017).

Mikro Şebeke Tasarımı ve Yük Profili

Muş ilinin karbon emisyonunu azaltmak için yolcu taşımacılıkta kullanılmak üzere üretilmiş sıfır karbon emisyona sahip 300 km menzile sahip 15 yolcu kapasiteli, 30 kW'lık FC, 33 kWh batarya ve 350 barda 4,5 kg hidrojen içeren bir tanka sahip örnek araç için sistem tasarımı yapılmıştır. İl merkezinde şehir içi taşımacılık sektöründe çalışan her biri günde 150 km yol kateden 124 dizel aracın günlük ortalama enerji tüketimi dikkate alınarak sistem tasarımı yapılmıştır. Söz konusu araçların H_2 yakıtını temin etmek amacıyla oluşturulan mikro şebeke tasarımı Şekil 1'de verilmiştir.

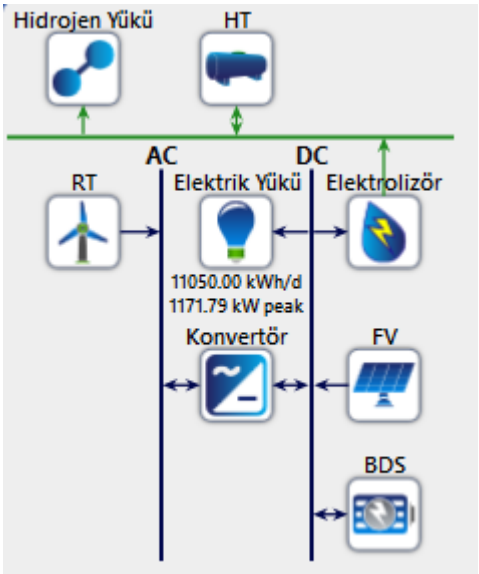

Şekil 1. Hidrojen ikmal istasyonu mikro şebeke modeli

Önerilen araç modelinde, tam dolu bir hidrojen tankıyla (4,5 kg) 300 km menzil elde edilmektedir. Bu mesafe, aracın iki günlük çalışma süresinde kat ettiği toplam mesafeye karşılık gelmektedir. Dolayısıyla, bir aracın günlük 150 km yol yapabilmesi için yaklaşık 2,225 kg hidrojene ihtiyaç duyulmaktadır. Hidrojen üretimi için 1 kg hidrojen başına teorik olarak 33,2 kWh elektrik enerjisi gereklidir. Ancak, %85 verimliliğe sahip bir elektrolizör kullanılması durumunda, 1 kg hidrojen üretimi için gereken toplam enerji miktarı 39,1 kWh'ye yükselmektedir. Bu bağlamda, bir aracın günlük hidrojen ihtiyacını karşılamak için 87.975 kWh elektrik enerjisi gerekmektedir. Sistem kapsamında hizmet verecek olan toplam 124 aracın günlük hidrojen talebi göz önüne alındığında, bu değer 10.908,9 kWh olarak hesaplanmıştır. Bu veriler doğrultusunda, hidrojen yakıt ikmal istasyonunun günlük yük profili oluşturulmuş olup, bu profile Şekil 2'de yer verilmiştir.

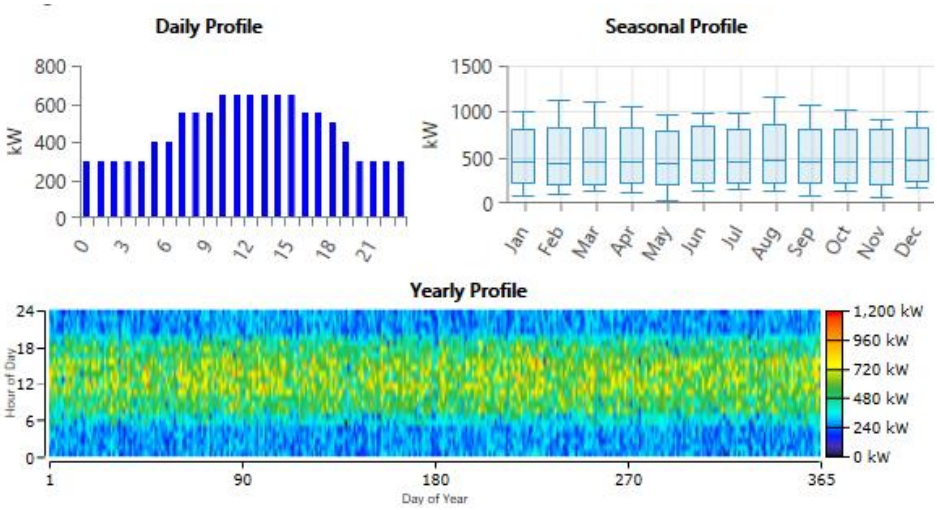

Şekil 2. Yakıt ikmal istasyonu yük profili

Meteorolojik Veriler

Çalışmada kullanılan bölgesel meteorolojik veriler, HOMER Pro yazılımına entegre edilen NASA veri tabanından elde edilmiştir. Muş ili, yıllık ortalama 4,66 kWh/m²/gün düzeyinde güneş radyasyonuna ve 4,8 m/s ortalama rüzgâr hızına sahiptir. Bölgeye ait aylık güneş radyasyonu ve açıklık indeksi Şekil 3a'da, aylık ortalama rüzgâr hızı ise Şekil 3b'de sunulmuştur.

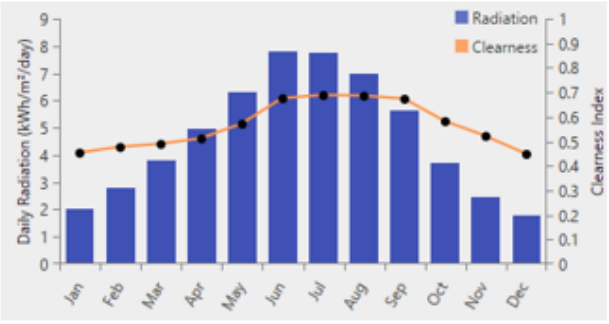

Şekil 3a. Muş ili güneş radyasyonu ve açıklık indeksi

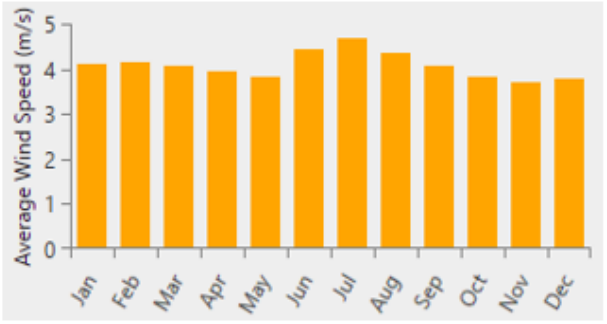

Şekil 3b. Muş ili aylık rüzgâr hızı

Ekonomik hesaplama

Tasarlanan yakıt ikmal istasyonu kapsamında oluşturulan mikro şebekede kullanılan sistem bileşenlerine ait birim maliyet değerleri Tablo 1'de sunulmuştur. Bu tabloda; FV, RT, elektrolizör, BDS, HT ve yardımcı ekipmanlara ilişkin birim kurulum maliyetleri, bakım-onarım giderleri ile birlikte ayrıntılı olarak verilmiştir. Söz konusu maliyet değerleri, sistemin toplam kurulum ve işletme maliyetlerinin hesaplanmasında temel alınmış ve HOMER Pro yazılımında yapılan ekonomik analizlerde kullanılmıştır.

Tablo 1. Mikro şebeke bileşenlerinin birim maliyet değerleri

Bileşenler	Kurulum Maliyeti	Yenileme Maliyeti	Bakım ve Onarım	Yaşam Ömrü
FV	700 $/kW	700 $/kW	10 $/kW/yıl	25 yıl
RT (20 kW)	50000 $	40000 $	30 $/kW/yıl	20 yıl
Elektrolizör	1000 $/kW	1000 $/kW	0.1 $/kW/yıl	15 yıl
BDS	300 $/kWh	300 $/kWh	10 $/kW/yıl	15 yıl
H2 Tank	500 kg	500 kg	0	25 yıl
Konvertör	300 $/kW	300 $/kW	0	15 yıl

HOMER yazılımı, bir enerji sisteminin NPC'si, sistemin ekonomik ömrü boyunca oluşacak tüm maliyetlerin bugünkü değerinden, aynı süre zarfında elde edilmesi öngörülen tüm gelirlerin bugünkü değerinin çıkarılmasıyla hesaplamaktadır (Gökçek & Kale, 2018). Bu yaklaşım, yatırım, bakım-onarım, yakıt, değiştirme ve işletme giderlerini kapsayan tüm ekonomik parametreleri dikkate alarak sistemin toplam maliyet etkinliğini değerlendirmeyi amaçlamaktadır. HOMER Pro yazılımı, bu değerlendirmeyi belirli ekonomik formüller doğrultusunda gerçekleştirmektedir. Söz konusu değerlendirme kriterleri ve hesaplama yöntemleri, aşağıda (1)-(4) denklemleri aracılığıyla ifade edilmekte ve sistemin finansal fizibilitesini ortaya koymak üzere analiz edilmektedir (HOMER, 2016).

$$NPC = C_(ann, tot)/(CRF(d, Yr)) \quad (1)$$

$$C_{ann,tot} = C_{ann,cap} + C_{ann,rep} + C_{ann,O\&M} + C_{ann,fuel} - R_{ann,salv} \quad (2)$$

$$CRF = (d(1+d)^{Yr})/((1+d)^{Yr} - 1) \quad (3)$$

$$d = (i - f)/(1 + f) \quad (4)$$

BULGULAR ve TARTIŞMA

Muş ilinde şehir içi taşımacılık yapan araçların enerji ihtiyacını yenilenebilir enerji kaynakları ile karşılayarak sürdürülebilir bir çözüm sunmayı amaçlamaktadır. Yapılan analizler sonucunda, önerilen mikro şebeke için en uygun sistem bileşimi; 7.567 kW gücünde FV paneller, her biri 20 kW olan 63 adet RT, 600 kW kapasiteli bir elektrolizör ve 11.007 kWh kapasiteli bir batarya sisteminden oluşmaktadır. Üretilen enerjinin %75'i FV panellerden, %25'i ise rüzgâr türbinlerinden sağlanmaktadır. Sistemin net bugünkü maliyeti 26,9 milyon dolar olarak hesaplanmış olup; toplam kurulum maliyeti 14,8 milyon dolar, sistemin geri dönüşüm (yenileme) maliyeti 11,7 milyon dolar ve bakım-onarım maliyetleri ise 6,2 milyon dolar olarak belirlenmiştir.

Türkiye'de güncel motorin pompa fiyatı litre başına 48 TL olup, bu çalışmada 1 Amerikan doları karşılığı 38,86 TL üzerinden 1,3 dolar olarak kabul edilmiştir. Şehir içi taşımacılık yapan araçların yıllık yaklaşık 645.792 litre motorin tükettikleri varsayımına göre, yıllık yakıt maliyeti 839.530 dolara karşılık gelmektedir. Sistemin ekonomik ömrü 25 yıl olarak planlanmış olup, bu süre zarfında toplam 20,988 milyon dolar tutarında yakıt tüketimi öngörülmektedir. Motorinin yoğunluğu 0,86 kg/l ve 1 kg motorin tüketimi başına atmosfere 3,6 kg CO_2 salımı gerçekleştiği dikkate alındığında (Diler, 2006) , yıllık 555.381,12 kg motorin tüketimi sonucunda yaklaşık 2.106.372 kg (2.106 ton) CO_2 emisyonu oluşmaktadır.

Şehir içi ulaşım sektörü, kentsel yaşamın vazgeçilmez bir unsurudur. Ancak bu sektörde kullanılan fosil yakıtlar, atmosfere salınan sera gazı miktarını artırarak hem insan sağlığını olumsuz etkilemekte hem de çevresel sorunlara yol açmaktadır. Önerilen sistemin uygulanması, fosil yakıtlara olan bağımlılığın azaltılmasına ve çevresel yönetim stratejilerinin daha etkili planlanmasına katkı sağlayacaktır.

SONUÇ

TUİK 2024 verilerine göre Muş ilinde toplam 40.032 kayıtlı kara taşıtı bulunmaktadır(TUİK, 2024). Bu araçların önemli bir kısmı bireysel ulaşım amacıyla kullanılmakta olup, şehir içi taşımacılık hizmeti veren araç sayısı toplam araç sayısına kıyasla oldukça sınırlıdır. Türkiye'nin büyükşehirleri olan İstanbul, Ankara ve İzmir ile karşılaştırıldığında, Muş ilindeki kara taşıtı yoğunluğu oldukça düşüktür.

Günümüzde hidrojenli araçların kullanımı henüz yaygınlaşmamış olmakla birlikte, çevresel sürdürülebilirlik açısından bu teknolojilerin önemi giderek artmaktadır. Kara taşıtlarının neden olduğu çevresel kirlilik, sera gazı emisyonları ve fosil yakıt bağımlılığı gibi sorunların çözümüne katkı sağlamak amacıyla, hidrojen yakıt ikmal istasyonlarının kurulması stratejik bir adım olacaktır. Özellikle sıfır emisyon hedeflerine ulaşmak ve uzun vadeli çevre politikalarını desteklemek açısından, bu tür projelerin sadece Muş gibi gelişmekte olan illerde değil, büyük şehirlerde de yaygınlaştırılması büyük önem taşımaktadır.

Bu bağlamda önerilen mikro şebeke temelli hidrojen üretim ve yakıt ikmal istasyonu modeli, yenilenebilir enerji kaynaklarıyla entegre edilerek hem ekonomik hem de çevresel açıdan sürdürülebilir bir çözüm sunmaktadır. Söz konusu sistemin geniş çaplı uygulanabilirliği, kent içi taşımacılıktan kaynaklanan emisyonların azaltılmasına önemli ölçüde katkı sağlayacaktır.

KAYNAKLAR

Agarwal, R., Firdous, A., Mathuria, P., Bhakar, R., Pareek, V. S., & Tiwari, H. (2023). Hydrogen as a sustainable mobility fuel: a global perspective and opportunities for India. 2023 IEEE PES Conference on Innovative Smart Grid Technologies-Middle East (ISGT Middle East),

Akac, A., Tsiatsiou, K., & Angelakakis, A. (2022). A review on best practices using hydrogen fuel-cell electric vehicles in public transport. IOP Conference Series: Earth and Environmental Science,

Akan, A. E. (2023). Techno-Economic Analysis of a Farm's Hybrid Energy System: The Case of Konya Rural. *Euroasia Journal of Mathematics, Engineering, Natural & Medical Sciences*, *10*(29), 1-27.

Diler, A. (2006). *Şehir İçi Toplu Taşımacılıkta Kullanılan Otobüslerde, Doğal Gaz Kullanımının Karbon Dioksit Emisyonlarına Etkileri* [Yüksek Lisans Tezi, İstanbul Teknik Üniversitesi, Fen Bilimleri Enstitüsü]

Ferrer, A. L. C., & Thomé, A. M. T. (2023). Carbon Emissions in Transportation: A Synthesis Framework. *Sustainability*, *15*(11), 8475.

Gökçek, M., & Kale, C. (2018). Techno-economical evaluation of a hydrogen refuelling station powered by Wind-PV hybrid power system: A case study for İzmir-Çeşme. *International Journal of Hydrogen Energy*, *43*(23), 10615-10625. https://doi.org/https://doi.org/10.1016/j.ijhydene.2018.01.082

HOMER,(2016). *HOMERHelpManual*. Available at: https://homerenergy.com/pdf/HOMERHelpManual.pdf [21.02.2024]

Jing, Q.-L., Liu, H.-Z., Yu, W.-Q., & He, X. (2022). The Impact of Public Transportation on Carbon Emissions—From the Perspective of Energy Consumption. *Sustainability*, *14*(10), 6248.

Kwan, S. C., & Hashim, J. H. (2020). Public transport and health. In *Advances in Transportation and Health* (pp. 149-173). Elsevier.

Ribeiro, P. J., & Mendes, J. F. (2022). Towards zero CO2 emissions from public transport: The pathway to the decarbonization of the Portuguese urban bus fleet. *Sustainability*, *14*(15), 9111.

Shahzad, M. K., Zahid, A., ur Rashid, T., Rehan, M. A., Ali, M., & Ahmad, M. J. R. e. (2017). Techno-economic feasibility analysis of a solar-biomass off grid system for the electrification of remote rural areas in Pakistan using HOMER software. *106*, 264-273.

TUİK, (2024). *Motorlu Kara Taşıtları*. Available at: https://data.tuik.gov.tr/Bulten/Index?p=Motorlu-Kara-Tasitlari-Aralik-2024-53463 [22.05.2025]

➢ *ORAL PRESENTATION*

Farklı kalınlıklarda akrilik ve Silika (SiO_2) ile güçlendirilmiş akrilik bazlı basınca duyarlı yapıştırıcı bantların PVC yüzeyler üzerinde mekanik özelliklerinin karşılaştırılmalı analizi

Ömer Kocaman[1], Celalettin Baykara[2] (*https://orcid.org/0000-0003-3403-6020*)

[1] Sakarya Uygulamalı Bilimler Üniversitesi, Teknoloji Fakültesi, Makine Mühendisliği Bölümü, Serdivan-Sakarya,54050, Türkiye
[2] Sakarya Uygulamalı Bilimler Üniversitesi, Teknoloji Fakültesi, Makine Mühendisliği Bölümü, Serdivan-Sakarya,54050, Türkiye

* Sorumlu yazar e-posta : kocaman.54@hotmail.com

Özet

Bu çalışmada, polivinil klorür (PVC) yüzeyler üzerinde uygulanan saf akrilik ve silika (SiO_2) ile güçlendirilmiş akrilik bazlı basınca duyarlı yapıştırıcı (PSA) sistemlerinin mekanik performansları karşılaştırmalı olarak değerlendirilmiştir. Üç farklı kalınlıkta (0,45 mm, 0,60 mm ve 1,00 mm) hazırlanan PSA filmleri PVC alt tabakalara uygulanarak 180° soyulma, kesme ve çekme testlerine tabi tutulmuş; elde edilen veriler, silika katkısının hem yapışma mukavemetini hem de kohezyonel dayanımı anlamlı ölçüde artırdığını göstermiştir. Saf PSA sisteminde ortalama soyulma kuvveti 4,3 N/cm iken, güçlendirilmiş sistemde bu değer 6,2 N/cm'ye ulaşmış; kesme ve çekme dayanımlarında da %25–30'luk artışlar gözlemlenmiştir. Sonuç olarak, silika katkılı akrilik PSA sistemlerinin, PVC yüzeyli zeminlerde uzun vadeli yapışma, termal kararlılık ve mekanik dayanım gerektiren endüstriyel uygulamalarda daha üstün performans sunduğu ortaya konmuştur.

Anahtar Kelimeler: Akrilik PSA, Güçlendirilmiş Akrilik PSA, PVC, 180° Soyulma testi, Kesme Dayanımı, Çekme Dayanımı

Comparative analysis of the mechanical properties of acrylic and silica (SiO_2)-reinforced acrylic-based pressure-sensitive adhesive tapes of different thicknesses on PVC surfaces

Abstract

In this study, the mechanical performances of pressure-sensitive adhesive (PSA) systems applied on polyvinyl chloride (PVC) surfaces were comparatively evaluated for two formulations: pure acrylic and silica (SiO_2)-reinforced acrylic. PSA films with three different thicknesses (0.45 mm, 0.60 mm, and 1.00 mm) were applied to PVC substrates and subjected to standardized 180° peel, shear, and tensile tests. The results revealed that silica reinforcement significantly improved both the adhesive strength and cohesive durability of the PSA systems. While the average peel strength of the pure PSA system was measured at 4.3 N/cm, the silica-reinforced system reached up to 6.2 N/cm; similarly, the shear and tensile tests showed a 25–30% increase in strength. Consequently, silica-reinforced acrylic PSA systems demonstrated superior performance for demanding industrial applications requiring long-term adhesion, thermal stability, and mechanical durability on PVC-based surfaces.

Keywords: Acrylic adhesive tape, Pressure sensitive adhesive, PVC, 180° Peel Test, Shear Strength, Tensile Strength

GİRİŞ

Yapıştırıcı kavramı, substrat yüzeylerinde kalıcı veya geçici olarak yapıştırma işlemiyle birleştirmek için uygulanan bir malzemedir. PSA, oda sıcaklığında, kuru formda ve kalıcı olarak yapışkan hale gelen ve çok daha az basınç uygulanmasıyla farklı yüzeylere sıkı bir şekilde yapışan viskoelastik bant türüdür. PSA'lar çok düşük basınç altında uygulanabilir ve daha sonra artan basınç kuvvetlerine karşı duyarsızdır. PSA bantlar viskoz ve elastik olduğu için sıvılar ve elastik katılar gibi davranırlar ve geçici olarak bağlanan parçacıklara sahiptirler. Esneklikleri, sıvılar gibi birbirleri boyunca kaymalarına olanak

tanır. Banta düşük basınç uygulandığında viskozitesi azalır ve yapıştırıcının mikroskobik düzeyde alt tabakaya akmasına neden olur. Bu nedenle, PSA bantlar uygulanan basınçla çeşitli alt yüzey tabakalara yapışma kabiliyeti vardır. Elastik özellikleri, substrat ile güçlü bir moleküller arası kuvvet oluşturacak şekilde viskozitesini yeniden kazanmasına yardımcı olur. PSA bantlar yüksek adhezyon ve kohezyon dengesine ve ayrıca mükemmel su direncine sahiptirler. PSA bantların son derece kritik yapışkan özellikleri soyulma yapışması ve yüksek kayma mukavemetine sahiptir. PSA bantlar, formülasyona bağlı olarak ultra çıkarılabilirden ultra yüksek yapışma gücüne kadar geniş bir yelpazede yer alırlar.

Yüksek performanslı PSA bantların pazar ve teknolojisi, mevcut ve yeni uygulama alanlarının artması sonucu hızla genişlemektedir. Kendinden yapışkanlı polimerlerin yapısı, arzu edilen doğal özelliklere sahip olmaları nedeniyle onları benzersiz kılar. Çeşitli yapıştırıcı türleri arasında PSA bantlar, yapısal yapıştırıcılar olarak nitelendirilmediği için tüketici tarafından çok yaygın bir şekilde kullanılmaktadır. PSA bantlar herhangi bir kimyasal reaksiyon olmadan temas halinde yüzeye yapışma özellikleri onları çeşitli uygulamalar için uygun kılar. Viskoelastik malzemeler olarak PSA bantlar, etiketler ve koruyucu filmler formları ile çeşitli uygulamalarda yaygın olarak uygulanmaktadır.

Basınca duyarlı yapıştırıcılara yönelik mevcut küresel talebin değeri yaklaşık 52 Milyar ABD Doları veya yılda kabaca 47 milyar metrekaredir. 47 milyar metrekare yüzölçümü kıyaslanması için 783.562 m2 olduğu düşünülürse küresel kullanma hacmi olarak bir fikir edinebilir. Yapışkan Bantlar Pazar Büyüklüğü 2021'de 47,2 milyar ABD Doları olarak değerlendirildi. Yapışkan Bantlar sektörünün 2022'de 49,7 Milyar ABD Dolarından 2030 yılına kadar 79,9 milyar ABD Dolarına çıkması ve tahmin dönemi boyunca %5,4'lük bir bileşik yıllık büyüme oranı (CAGR) sergilemesi bekleniyor. (2022 - 2030). Yapışkan bantlar otomotiv, elektronik, etiketleme, paketleme,,medikal gibi endüstrinin hemen hemen her sektöründe kullanılan akrilik basınca duyarlı bantların (PSA) kullanılması örnek olarak verilebilir bu nedenle PSA bantların artan kullanımı pazarın büyümesini hızlandırmaktadır.

PSA bantlar, kimyasal yapılarına göre türleri, kauçuk, akrilik, modifiye akrilik ve silikon bazlı formülasyonlarından olmak üzere dört temela türü vardır. Bu türlerin her biri farklı performans özellikleri sergiler. Bu araştırmada, Yüksek UV dayanımı, yaşlanmaya karşı stabil olması nedeniyle akrilik ve yüksek sıcaklık dayanımı ve hassas yüzeyler için silika (SiO_2) ile güçlendirilmiş akrilik PSA'lar, PVC yüzey üzerlerinde yapışma mukavemetlerini araştırmak için kullanılmıştır. PVC , hem esnek hem sert formlarda levha ve profil olarak yaygın bir şekilde kullanılan bir plastic türüdür. PSA sistemleriyle düzgün ve temiz bir yüzeye sahip olması, PSA kimyasal yapılarına uyumlu 0lması nedeniyle iyi bir şekilde bağlanır.

MALZEME VE METOT

Deneyde kullanılan malzeme olarak 0,45 mm, 0,60 mm ve 1,0 mm kalınlıklarda akrilik ve silica (SiO2) ile güçlendirilmiş akrilik PSA bantlarıyla PVC yüzey üzerinde her gruptan üçer adet olmak üzere 180º soyulma, Kesme ve Çekme testleri uygulanmıştır. Bütün testler, yapıştırma işlemi öncesi PVC yüzeyine zarar vermeyen izopropil alkol ile temizlenip 45 sn. kuruması beklendikten sonar yapılmıştır.

Kesme testleri, PSA bandın PVC yüzey üzerinde parallel yönde kayma kuvvetlerine karşı yapışma mukavemetini test etmek için kullanılır, kalıcı yük altında zamana bağlı kayma (crep) davranışını ölçmek amacıyla yapılır. PSA bant, PVC yüzeye düşük bir basınç altında PVC yüzeye yapıştırılır, yatay yönde 1kg (9,8 N) kuvveti uygulanır. Bant yüzeye paralel bir yönde kaymaya zorlanır. ASTM D3654 standartı dikkate alınır. T**est sıcaklığı ve bağıl nem, g**enellikle 23 ± 2 °C ve 50 ± 5 % bağıl nem koşullarında yapılır. Sonuç olarak, belli bir zaman içinde kopması ve meydana gelen bant uzaması, viskoelastik davranış gibi kalıcı deformasyonu ölçülür (Şekil 1).

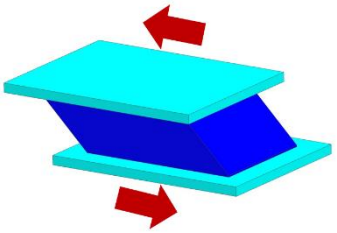

Şekil 1. Kesme testi

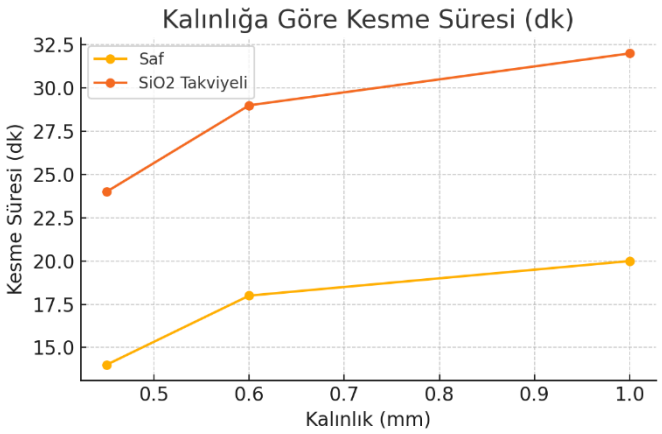

Şekil 2. Kalınlığa Göre Kesme Süresi (dk)

Grafikte hem akrilik hem de silica ile güçlendirilmiş akrilik PSA bantlarla yapılan soyulma testlerin kesme süresi (dk) ve malzeme kalınlığı (mm) arasındaki ilişkiyi göstermektedir (Şekil 2).

Her iki yapıştırıcı türünde de kalınlık arttıkça kesme süreside arttığı tespit edilmiştir. Bu daha kalın malzemelerin hacmi artar ve kesme işlemi kesme direnci yükselir. Bunun sonucunda kesme işlemi için daha fazla enerji ve zaman gerektirir (Tablo 1). Silika (SiO_2) takviyesi yapıştırma mukavemetini arttırmakta önemli bir rol oynamaktadır.

SiO2 takviyeli PSA bantlar, kalınlık arttıkça, kesme süreleri saf akrilik PSA banta göre daha dik eğim görülmektedir. Bu durum, **yük transfer mekanizması, takviye-matris etkileşimi, mekanik difüzyon etkisi** gibi ileri kompozit davranışlarıyla ilgili olabileceği düşünülmektedir.

Çekme testleri, PSA bant ile PVC alt tabaka arasındaki dikey yöndeki yapışma kuvvetini belirlemek amacıyla yapılır (Şekil 3). PSA bant, PVC yüzeye düşük basınçla yapıştırılır, uzunluk ve genişliği sırasıyla 25,4 mm x 25,4 mm boyutlarının oluşturduğu 645,16 mm^2 bir alanda, yüzeyler birbirinden dikey yönde 5 mm/sn hızda çekilir. Test ASTM D3330 standartına göre yapılır. T**est sıcaklığı ve bağıl nem, g**enellikle 23 ± 2 °C ve 50 ± 5 % bağıl nem koşullarında yapılır. Çekme hızı genellikle 300 mm/dak'dır (ASTM D3330). Test kuvveti 25 mm genişlikteki PSA bant için 20-50 N+. olarak uygulanır.

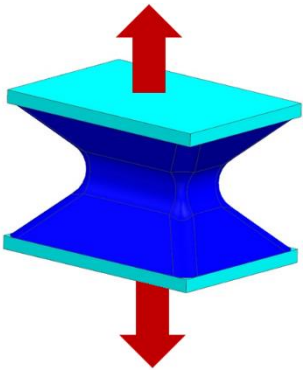

Şekil 3. Çekme testi

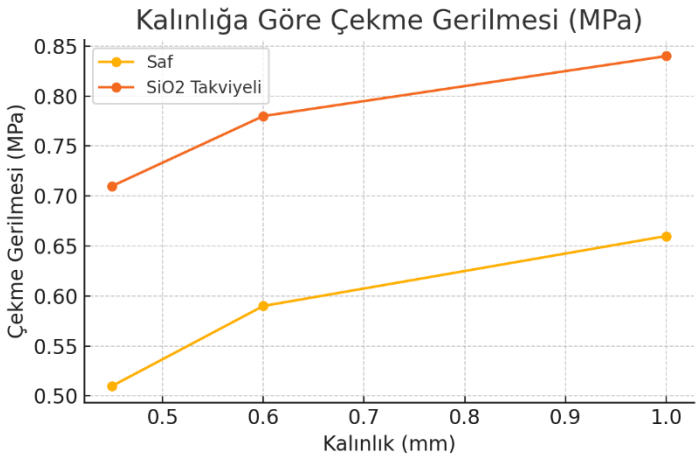

Şekil 4. Kalınlığa Göre Çekme Gerilmesi (MPa)

Grafikte hem akrilik hem de silica ile güçlendirilmiş akrilik PSA bantlarla yapılan çekme gerilmesi (MPa) bazında karşılaştırılmıştır (Şekil 4).

Tüm kalınlıklarda, SiO_2 takviyeli PSA bantlar saf akrilik PSA bantlara göre daha yüksek çekme gerilmesi göstermektedir. Bu durum, silika (SiO_2) partiküllerinin akrilik matris içerisindeki mekanik dayanımı artırıcı etkisini açıkça ortaya koymaktadır. Bunun sonucunda silika, yük aktarımında rol alarak matrisin deformasyonunu sınırlar ve bu sayede kopma öncesi daha yüksek çekme gerilmesine ulaşılır.

Saf akrilik PSA bantlarda kalınlık arttıkça malzemenin çekme direnci daha belirgin artış görülürken, silica takviyeli bantlarda görülen artış daha sınırlıdır. Bunun nedeni, SiO_2 katkı maddesinin etkisinin ince filmlerde daha belirgin olduğunu gösterir. Kalınlaştıkça matrisin deformasyonu artmaktadır.

İnce kalınlıktaki filmlerdeki, yapışma yüzeyi /alan oranının daha fazla olmasından ve lokal gerilme yoğunlaşmalarından dolayı çekme gerilmesi daha düşük seviyededir. Kalın yapıştırıcı tabakalarında yük dağılımı daha homojen olduğu için çekme mukavemeti artar.

Soyulma testleri, PSA bantın, PVC alt tabaka yüzeyinde bir açıyla soyularak ayrılma direncini ölçmek amacıyla yapılır (Şekil 5). Açı genellikle 180º olarak uygulanmakla birlikte 90º bir açıyla da yapılabilir. 180º soyulma testi, PSA bant, yüzeyi temizlenmiş PVC üzerine düşük bir basınçla yapıştırılır ve serbest ucu 180º açıda çekilir. Bu testte ASTM D3330 standartına riayet edilir. T**est sıcaklığı ve bağıl nem, g**enellikle 23 ± 2 °C ve 50 ± 5 % bağıl nem koşullarında yapılır. Çekme hızı genellikle 300 mm/dak'dır (ASTM D3330). Test kuvveti 25 mm genişlikteki PSA bant için 20-50+ N. olarak uygulanır.

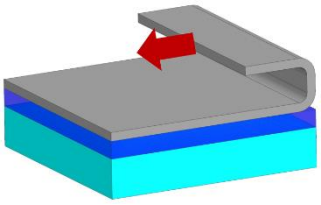

Şekil 5. 180º Soyulma testi

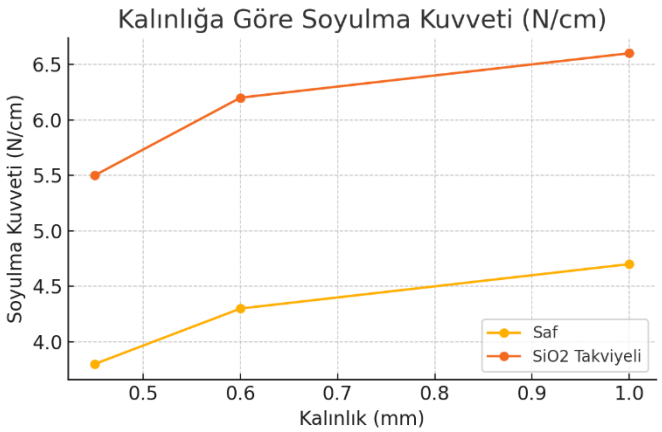

Şekil 6. Kalınlığa göre soyulma kuvveti ilişkisi

Grafikte hem akrilik hem de silica ile güçlendirilmiş akrilik PSA bantlarla 0.45 mm, 0.6 mm ve 1.0 mm gibi farklı kalınlıklarda yapılan 180º soyulma test kuvvetleri karşılaştırılmıştır ((Şekil 6). Her iki PSA bant üründe kalınlık arttıkça soyulma kuvveti artmaktadır. Bunun nedeni, belli bir kalınlıktaki yapışkan tabakaların homojen yüksek kohezyon kuvvetine sahip olduğu bu nedenle yük aktarımını daha iyi yaptığı sonucuna varılmaktadır.

SiO_2 partikülleri gibi inorganik takviyelere sahip PSA bantlar, saf akrilik bantlara göre daha yüksek soyulma kuvvetinin gösterme nedeni yapışma yüzeyinde mikromekanik kilit mekanizmasının oluşturmasındandır. SiO_2 partikülleri, yapışkan bütünlüğünde kohesive dayanımı arttırır, PVC yüzeyinde adhesive yapışma gücünü arttırarak kayma direncini yüksek seviyelere çıkar (Şekil 7)

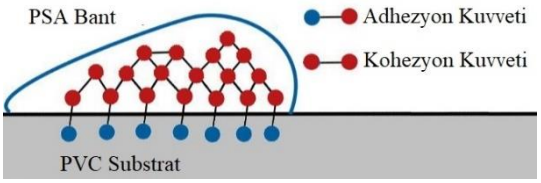

Şekil 7. PSA bant ile PVC yüzey üzerinde moleküler yapışma mekanizması

BULGULAR VE TARTIŞMA

Araştirmada uygulanan 180° soyulma, kesme ve çekme testleri sonucunda, silika (SiO_2) ile güçlendirilmiş akrilik bazlı PSA bantların, saf akrilik PSA bantlara göre tüm kalınlıklarda daha üstün mekanik performans gösterdiği tespit edilmiştir. Silika katkısı, özellikle mikromekanik kilitlenme, matris-partikül etkileşimi ve yük transfer mekanizmaları sayesinde hem yapışma kuvvetini hem de kohezyonel dayanımı anlamlı şekilde artırmıştır. Kalınlık arttıkça tüm PSA bantlarda mukavemet değerleri yükselmiş; bu durum, viskoelastik enerji yayılımının ve yük dağılımının daha homojen hale gelmesiyle ilişkilendirilmiştir. Saf akrilik PSA bantlarda kalınlığa bağlı çekme ve kesme dayanımı daha belirgin artarken, silika takviyeli sistemlerde mukavemet yüksekliği daha kararlı ve yüzeyle daha güçlü bağ oluşturan bir yapı gösterdiği belirlenmiştir. Tüm bu bulgular, hem formülasyon hem de yapısal parametrelerin PSA bantların performansı üzerinde kritik rol oynamaktadır. Bu nedenle PSA bantların kullanım yerlerine göre önem taşıyan uygulamalarda silika katkılı PSA bantların önemi vurgulanmaktadır.

SONUÇ

PSA bantların performansı, kimyasal yapısı ve kalınlık parametrelerine göre önemli ölçüde değişkenlik gösterdiğini ortaya koymuştur. Özellikle silika (SiO_2) ile güçlendirilmiş akrilik PSA bantları, hem adhezyon hem de kohezyon yapışma dayanım bakımından saf akrilik bantlara göre üstün performans sergilediği tespit

edilmiştir. Elde edilen 180° soyulma, kesme ve çekme testi sonuçları; silika katkısının mikromekanik kilitlenme etkisi, matris-takviye etkileşimi ve yük aktarım davranışları sayesinde yapıştırıcı sistemlerin mekanik kararlılığını artırdığını göstermektedir. Ayrıca, PSA bant kalınlığının artmasıyla birlikte viskoelastik enerji yayılımı ve yük dağılımında meydana gelen iyileşmeler, mukavemet değerlerinde anlamlı artışlar sağlamıştır. Bu bulgular, akrilik PSA bantların performans optimizasyonunun sadece kimyasal modifikasyonla değil, aynı zamanda film kalınlığı gibi yapısal parametrelerin mühendislik düzeyinde kontrolüyle de geliştirilebileceğini göstermektedir. Sonuç olarak, silika takviyeli akrilik PSA bantlar, PVC alt tabakaların yer aldığı otomotiv, elektronik ve yapı endüstrileri gibi zorlu servis koşulları gerektiren uygulamalarda uzun ömürlü ve güvenilir bir yapıştırma çözümü sunabileceği sonucuna varılmıştır.

TEŞEKKÜR

Bu çalışmanın gerçekleştirilmesinde bilimsel ve teknik desteklerini hiçbir zaman esirgemeyen **ASAŞ Alüminyum Sanayi ve Ticaret A.Ş. PVC AR-GE Birimi**'ne, ayrıca değerli ekip üyelerine sağladıkları katkılardan dolayı içtenlikle teşekkür ederim.

KAYNAKLAR

- Asua, M., Daniloska, V., Carretero, P., & Tomovska, R. (2014). High performance pressure sensitive adhesives by miniemulsion photopolymerization in a continuous tubular reactor. Polymer, 55, 5050–5056.
- Baek, S., & Hwang, S. (2017). Preparation of biomass-based transparent pressure sensitive adhesives for optically clear adhesive and their adhesion performance. *European Polymer Journal, 92*, 97–104.
- Benedek, I. (2006). *Development in Pressure-Sensitive Adhesive Products*. CRC Press, Taylor & Francis Group.
- Chang, E. P. (1997). Viscoelastic properties of pressure-sensitive adhesives. *Journal of Adhesion, 60*, 233–248.
- Cho, J. (2014). Compression behavior of a pressure-sensitive adhesive material. *Macromolecular Research, 22*, 1238–1241.
- Cunningham, D., & Lowery, M. (2004). Moisture vapor transport channels for the improved attachment of a medical device to the human body. *Biomedical Microdevices, 2*, 149–154.
- Czech, Z., Butwin, A., & Kabatc, J. (2011). Photoreactive UV-crosslinkable acrylic pressure-sensitive adhesives containing type-II photoinitiators. *European Polymer Journal, 47*, 225–229.
- Czech, Z., Milker, R., & Butwin, A. (2009). Solvent borne PSA based on acrylic with postcrosslinking performance. *Elastomery, 3*, 13.
- Dastjerdi, Z., Cranston, E. D., & Dubé, M. A. (2018). Pressure sensitive adhesive property modification using cellulose nanocrystals. *International Journal of Adhesion and Adhesives, 81*, 36–42.
- Ebnesajjad, S. (2011). Introduction and adhesion theories. In *Handbook of Adhesion Surface Preparation*.
- Gollins, K., Elvin, N., & Delale, F. (2020). Characterization of adhesive joints under high-speed normal impact: part II. Numerical studies. *International Journal of Adhesion and Adhesives*.
- Hwang, J., Lim, D., Lee, G., Kim, Y. E., Park, J., Baek, M. J., Kim, H. S., Park, K., Ku, K. H., & Lee, D. W. (2023). Ambient air-operated thermo-switchable adhesion of Nisopropylacrylamide-incorporated pressure sensitive adhesives. *Materials Horizons, 10*, 2013–2023.
- Jin, K., López Barreiro, D., & Martin-Martinez, F. J. (2018). Improving the performance of pressure sensitive adhesives by tuning the crosslinking density and locations. *Polymer, 154*, 164–171.
- Jin, X., Bai, Y. P., Shao, L., et al. (2009). Properties of solvent-borne acrylic pressure-sensitive adhesives synthesized by a simple approach. *eXPRESS Polymer Letters, 12*, 814–820.
- Khire, A., & Vavia, P. (2013). Effect of permeation enhancers on dynamic mechanical properties of acrylate pressure sensitive adhesives. *International Journal of Pharmaceutics, 458*, 141–147.

- Kim, J. K., Kim, J. W., Kim, M. I., & Song, M. S. (2006). Thermal conductivity and adhesion properties of thermally conductive pressure-sensitive adhesives. *Macromolecular Research, 14*, 517–523.
- Kummer, A. (2000). Important properties of synthesized acrylic pressure-sensitive adhesives. *Adhesives Age, 12*, 40.
- Lin, S. B., Durfee, L. D., Ekeland, R. A., & Schalau, G. K. (2012). Recent advances in silicone pressure-sensitive adhesives. *Journal of Adhesion Science and Technology*.
- Lucast, D. H. (2000). Skin tight. *Adhesives Age, 10*, 36–39.
- Mapari, S., Siddhesh, M., & Mhaske, S. T. (2021). Developments in pressure-sensitive adhesives: a review. *Polymer Bulletin, 78*, 4075–4108.
- Market Research Engine. (2019). *Global Adhesive Tape Market*.
- Mehravar, E., Gross, M. A., & Agirre, A. (2018). Importance of film morphology on the performance of thermo-responsive waterborne pressure sensitive adhesives. *European Polymer Journal, 98*, 63–71.
- Michaelis, M., & Leopold, C. S. (2015). A measurement system analysis with design of experiments: investigation of the adhesion performance of a pressure sensitive adhesive with the probe tack test. *International Journal of Pharmaceutics, 496*, 448–456.
- Mohammed, I. K., Charalambides, M. N., & Kinloch, A. J. (2016). Modeling the effect of rate and geometry on peeling and tack of pressure-sensitive adhesives. *Journal of Non-Newtonian Fluid Mechanics, 233*, 85–94.
- Paul, C. W., & Silverberg, E. (2011). *Handbook of Adhesion Technology*.
- Shibakami, M., & Sohma, M. (2018). Thermal, crystalline, and pressure-sensitive adhesive properties of paramylon monoesters derived from an euglenoid polysaccharide. *Carbohydrate Polymers, 200*, 239–247.
- Wang, Y. J., He, Y., Zheng, S. Y., Xu, Z. Y., Li, J., Zhao, Y. P., Chen, L., & Liu, W. G. (2021). Polymer pressure-sensitive adhesive with a temperature-insensitive loss factor operating under water and oil. *Advanced Functional Materials, 31*, 2104296.
- Webster, I. (1999). The development of a pressure-sensitive adhesive for trauma-free removal. *International Journal of Adhesion and Adhesives, 19*, 29–34.
- https://tr.wikipedia.org/wiki/T%C3%BCrkiye [09.05.2025]
- Zech, Z. C., & Ilker, R. M. (2005). Development trends in pressure-sensitive adhesive systems. *Materials Science Poland, 23*(4), 605–623.
- https://www.iqsdirectory.com/articles/tape-suppliers/adhesive-tape.html [09.05.2025]
- https://www.marketresearchfuture.com/reports/adhesive-tapes-market-1718 [09.05.2025]

➢ *ORAL PRESENTATION*

Effect of lugol's solution on antibacterial activity and scoby growth in kombucha tea

Zeynep Özserçe Haste[1*] (*ORCID: https://orcid.org/0000-0001-7783-9515*), Zeynep Sümer[2] (*ORCID: https://orcid.org/0000-0002-1520-3359*)

[*1]Sivas Cumhuriyet University, Faculty of Engineering, Chemical Engineering, Sivas, Turkey
[2]Sivas Cumhuriyet University, Faculty of Medicine, Clinical Microbiology, Sivas, Turkey

*Corresponding author e-mail :zeynepozserce@hotmail.com

Abstract
The aim of this study was to determine the scoby growth, physicochemical properties and antibacterial activity effects in kombucha tea prepared with sweetened black tea (KT) and kombucha tea prepared by adding different concentrations of lugol solution to the initial sweetened black tea. For this purpose, daily pH measurements were taken for all prepared kombucha samples and the effect of fermentation period on pH was determined. Scoby growth was investigated at the beginning, 4, 8, 12, 16 and 21st days. Antibacterial activities of kombucha prepared with 2% lugol solution and sweetened black tea (KT-L2) and kombucha prepared with sweetened black tea were investigated with Escherichia coli, Klebsiella pneumoniae, Enterococcus faecalis, P. Aeruginosa aeruginosa, Staphylococcus aureus by disk diffusion method on the 8th and 21st days of fermentation. Inhibition zones obtained with KTs were determined as 16 mm K. Pneumoniae, 13 mm P. Aeruginosa, 10 mm E. coli, 9 mm S. Aureus (43300), 9 mm E. Faecalis and 8 mm S. Aureus (29213). Parameters determining the antibacterial properties of KTs were determined. The properties and benefits of Kombucha tea were examined in detail.

Keywords: Kombucha tea, lugol solutions, scoby, antibacterial activity

INTRODUCTION

Traditionally, kombucha is prepared with green or black tea from the Camellia sinensis plant. The different types of tea (white, green, oolong and black) are obtained from the Camellia sinensis plant. The chemical composition of tea is quite complex as it contains different classes of chemical compounds, including alkaloids, phenols, proteins, minerals, vitamins and amino acids. Some of the metabolites found in kombucha tea consist of polyphenols, flavonoids, vitamins A, B, C, organic acids, ethanol and various enzymes. The composition and concentration of metabolites depend on the nutrient medium and fermentation time. As a result, the metabolic profile and biological activity of tea can vary greatly depending on the differences between different tea varieties, environmental influences, processing procedures and preparation methods, which in turn reflects its quality (Prasanth, M.I.et al. 2019) The functional properties of kombucha, such as antioxidant activities, are attributed to its phenols, such as epicatechin, epigallocatechin, epicatechin-3-gallate and epigallocatechin-3-gallate. Natural antioxidants, polyphenols, are commonly found in kombucha tea and can be increased through fermentation [6]. Polyphenols are secondary metabolites of plants and are often involved in defense against ultraviolet radiation or pathogen aggression.

Epidemiological studies and associated meta-analyses strongly suggest that long-term consumption of diets rich in plant polyphenols protects against the development of cancer, cardiovascular diseases, diabetes, osteoporosis, and neurodegenerative diseases. (Pandey, K.B. and S.I. Rizvi 2009) Polyphenols can be classified into different groups as a function of the number of phenol rings they contain and the structural elements that connect these rings. The main classes include phenolic acids, flavonoids, and lignans. (Kondratyuk, T.P. and J.M. Pezzuto,2004)

Lugol's solution is a mixture obtained by dissolving iodine and potassium iodide in water. It is a medicine and disinfectant used for a number of purposes(Ito, K. and T. Hirokawa, 2009). It is used in combination with antithyroid drugs to prepare the thyroid gland for surgical removal and to treat some overactive thyroid conditions (hyperthyroidism, thyroid storm)(Zimmermann, M.B., 2020**)** It can be applied to minor wounds such as needlesticks as a disinfectant. It can be used in small amounts for emergency disinfection of drinking water. The aim of the present study was (i) to evaluate the physicochemical profiles of kombucha produced from black tea; (ii) to examine the effects of Lugol's solution added to black tea at different concentrations

on kombucha tea over time; and (iii) to determine the antibacterial properties of the prepared kombucha teas.

MATERIALS AND METHODS

Preparation of Kombucha Tea

After boiling 1 L of pure water, 90 g of sugar was added and dissolved. Then, 8 g of black (bag) tea was added and brewed for 15 minutes. After removing the tea bags, the sweetened black tea solution was cooled to room temperature and 70 mL of previously fermented KT and scoby (symbiotic culture of bacteria and yeast) were added and the jar was closed with a clean paper towel. Kombucha tea was fermented by waiting for 0-21 days in a dark environment at room temperature.

Preparation of Lugol's Solution

5% Lugol's solution was prepared by dissolving 10 g of potassium iodide and 5 g of iodine in 100 ml of pure water. This prepared solution was stored in a dark bottle and in a dark environment. Lower percentage Lugol solutions were also obtained by diluting this 5% solution.

Preparation of Kombucha with Lugol's Solution

Sweetened black tea was prepared as mentioned above. After adding 0.5, 1, 2 and 5% Lugol solutions at 1% v/v ratio to the tea at room temperature, a scoby was placed on it, its mouth was closed with a clean paper towel and a rubber band, and it was kept in a dark environment at room temperature during fermentation.

Antibacterial Activity

In this part of the study, the inhibition zone of the prepared KTs synthesized was measured to determine their antimicrobial activities. The inhibition zone is a circular area around the antibiotic point where bacterial colonies do not grow. The inhibition zone is used to measure the sensitivity of bacteria to antibiotics.(Chen, C. and B.Y. Liu, 2000)

At the beginning of the microbiological procedures, the strain in the stock medium was revived in liquid [heart brain infusion broth, (Acumedia Manufactures, Inc. Lansing, Michigan, America)] media and incubated at 37 ºC for 24 hours. The reproduced bacteria were transferred to solid media and contamination controls were performed. They were stored at +4ºC until the day of the study. They were used by multiplying in liquid media 24 hours before the day of the study. Before each experiment, a turbidity adjustment of 0.5 McFarland was made with the KristalspecTM McFarland (Becton Dickinson & Company Loventon Circle, Sparks, MD 21152-0370, America) device. The 0.5 standard McFarland was used to develop the medium to provide bacterial growth in the amount of ($1.5x10^8$) colonyforming (CFU) mL^{-1} unit. Prepared KTs were used in antimicrobial analysis by loading 50 µL of liquid onto 6 mm diameter sterile empty antibiogram test disks (Bioanalyse) with sterile micropipettes. As solid media; Blood agar 5% sheep blood agar (Merck 1.10886) for E. Faecalis, S. Aureus and P. aeruginosa bacteria. Eosin Methylene Blue (EMB) agar was used in the production of E. coli strain.

Table1. Microorganisms used in our study

Microorganism Name	Strain Used
Escherichia coli	ATCC 25922
Klebsiella pneumoniae	ATCC 700603
Enterococcus faecalis	ATCC 29212
P. Aeruginosa	ATCC 27853
Staphylococcus aureus	ATCC 29213
Staphylococcus aureus	ATCC 43300

RESULTS AND DISCUSSIONS

Effect of fermentation time on pH

After adding 0.5, 1, 2 and 5% Lugol solutions to KT (1% v/v Lugol), the pH change against time was examined (Figure 1). It was observed that the pH change of KT prepared with 2 and 5% Lugol decreased rapidly in the first 2 days of fermentation, while the pH change of the others decreased until the 5th day and the change slowed down very much after the 5th day, almost becoming constant. The reason for this is that the acetic acid-producing bacteria and yeasts found in KT and scoby consume the sucrose added at the beginning and produce acids such as acetic acid and lactic acid, and the concentration of sucrose decreases greatly over time

Table 2. Abbreviations for KTs prepared by adding different concentrations of Lugol solutions

KT- L0.5	KT prepared with 0.5% lugol solution
KT- L1	KT prepared with 1% lugol solution
KT- L2	KT prepared with 2% lugol solution
KT- L 5	KT prepared with 5% lugol solution

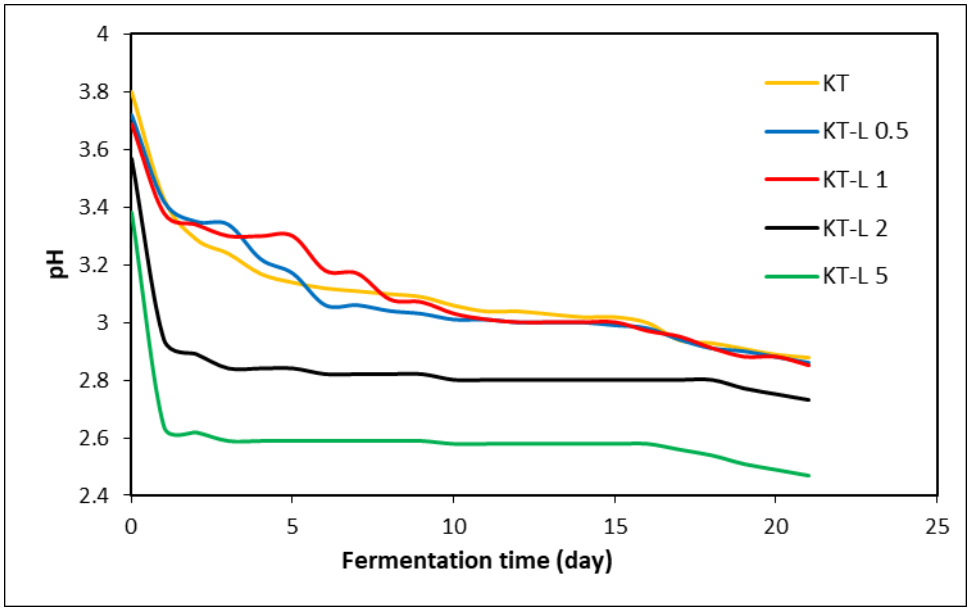

Figure 1. pH changes with fermentation times of KT and KT with lugol solution

In this part of the study, after adding 0.5, 1, 2 and 5% Lugol solutions to KT (1% v/v Lugol), the pH change against time was investigated (Figure 1). It was observed that the pH change of KT prepared with 2 and 5% Lugol decreased rapidly in the first 2 days of fermentation and that the change slowed down to almost constant after the 5th day. It was thought that this could be due to the high concentration of Lugol added, which caused the number of bacteria in the fermentation to decrease, or the bacteria and yeasts that produce acetic acid consumed the sucrose added at the beginning and produced acids such as acetic acid and lactic acid, and the concentration of sucrose decreased significantly over time.

Investigation of the effect of KT prepared with different concentrations of lugol solutions on scoby development

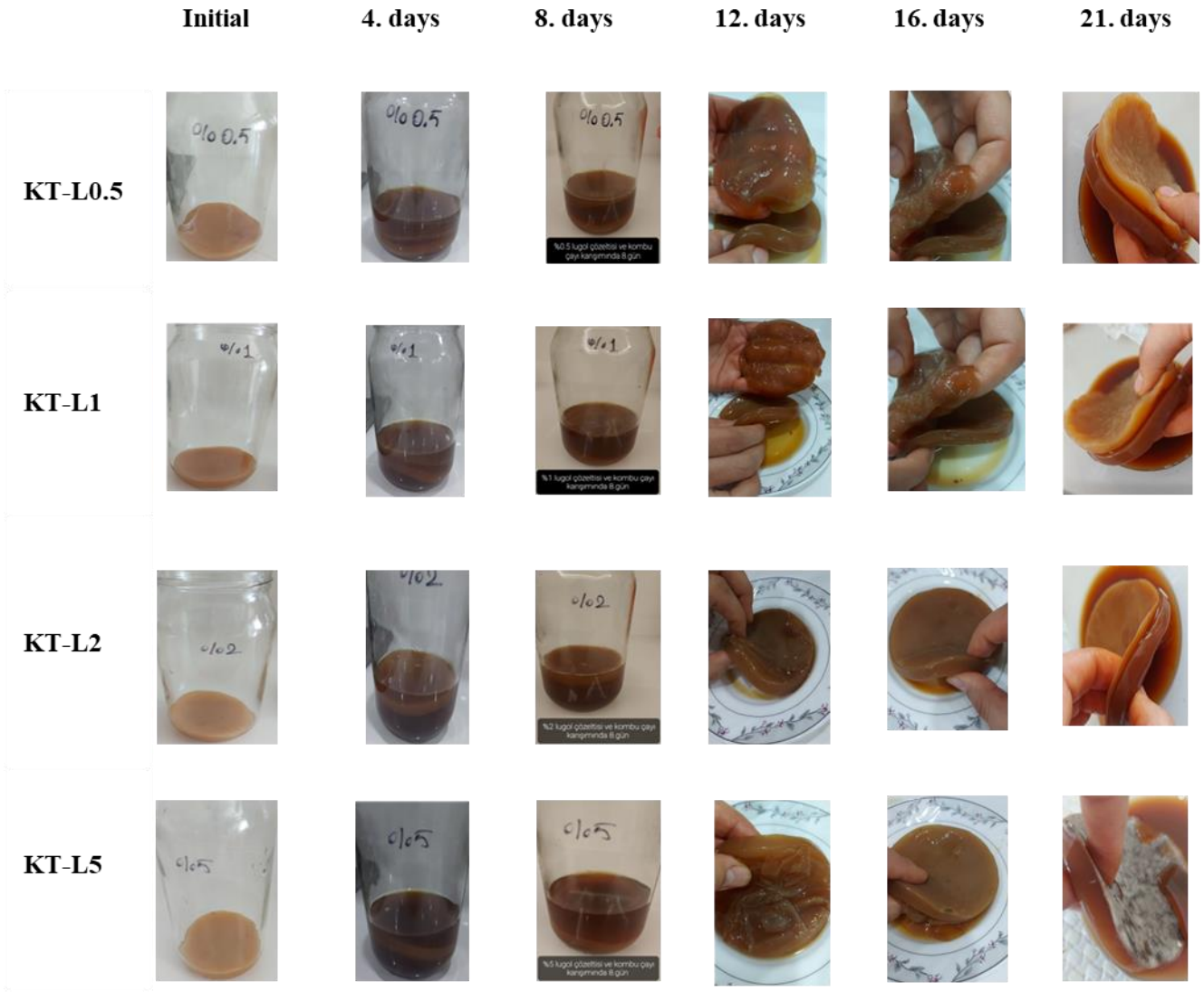

Figure 2. Investigation of the effect of KT prepared with different concentrations of Lugol solutions on scoby growth.

In Figure 2, the effect of 0.5, 1, 2 and 5% Lugol solution on scoby growth was investigated in KT prepared by adding it. The thicknesses of all scobys selected at the beginning were very close to each other. The change in scoby was examined on the 4th, 8th, 12th, 16th and 21st days of fermentation from the beginning. It was determined that in KT prepared without adding Lugol, bubbles formed on the surface on the 4th-5th day of fermentation, a new scoby formed on the 7th-8th day of fermentation, and as the fermentation period extended, the KM added on the first day of fermentation and the KM formed later continued to grow and thicken. This development process was followed with 5 different KTs. In KTs prepared by adding Lugol solution, it was observed that only small bubbles formed on the KT-L0.5 surface on the 4th day of fermentation, and there was no change in KT L1, L2 and L5 KMs. On the 8th day of fermentation, a shiny surface was observed on the surfaces of KT-L0.5, KT-L1 and KT-L2. Since this was an indicator of newly formed scoby, observation was made without removing the scoby from the KT. There was no change in KT-L5. On the 12th day, it was observed that a new scoby was formed in KT-L0.5 and KT-L1. On the 12th day of KT-L2, a fine shine and the membrane structure of the newly formed KT were seen on the surface of the first added scoby. On the 12th day of fermentation of KT-L5, wrinkling, color change thought to be due to iodine, and layering and separations in the initially added scoby were observed on the surface of the first added scoby. On the 16th day of fermentation, it was observed that the thickness of the scoby formed on the surfaces of KT-L0.5 and KT-L1 increased, and in KT-L2, a new layer was formed on the initial scoby surface and the scoby thickness increased. While there was mold and deformation on the edges in

KT-L5, it was observed that separation, layering and breakage increased in scoby. The color change caused by iodine became more apparent in all initial DMs. When the newly formed DMs were compared on the 21st day of fermentation, it was determined that the most developed scoby formed on the surfaces of KT and KT-L0.5, followed by KT-L1 and KT-L2, respectively. In KT-L5, it was observed that the surface was completely covered with mold. As the concentration of Lugol's solution increased, it was observed that the speed of scoby growth slowed down and in 5% Lugold, the scoby lost its vitality over time. It was thought that this was due to the antibacterial properties of lugol killing beneficial bacteria in the KT These analyses were repeated 5 times. Mold formation was observed in 3 analyses performed with 5% lugol solution, while mold formation was observed on the 24th and 25th days in 2 analyses. The reason for mold formation occurring at different times was initially thought to be related to the number of beneficial bacteria in the KT and the structure of the scoby[241, 244]. Since mold formation occurred in the KT prepared by adding 5% lugol solution, it was determined that this concentration was not suitable. In the development of mushrooms examined with teas prepared with 0.5%, 1%, and 2% lugol solutions, it was determined that the growth rate slowed down as the lugol solution concentration increased.

Antibacterical Activity

For K. pneumoniae bacteria, an increase in the inhibition zone was observed as the lugol concentration in KT increased and it was determined that lugol increased the antibacterial properties with KT for this bacteria. However, for all other bacterial species, a decrease in the inhibition zone and a decrease in the antibacterial effect were observed as the lugol concentration in KT increased. It is thought to be due to the damage of the Lugol solution to the fermentation bacteria.

Table 2. Inhibition zones of KTs prepared with different concentrations of Lugol's solution (Fermentation time 8 days)

Kombucha Tea	E.coli	P. Aeruginosa	S. Aureus (43300)	K. pneumoniae	S. Aureus (29213)	E. Faecalis
KT	10	13	8	9	7	9
KT-L0.5	8	11	8	9	6	9
KT-L1	7	9	8	12	6	7
KT-L2	6	7	9	16	6	7

REFERENCES

Chen, C. and B.Y. Liu,(2000) Changes in major components of tea fungus metabolites during prolonged fermentation. J Appl Microbiol. 89(5) 834-9.

Ito, K. and T. Hirokawa, (2009) Chapter 9 - Iodine and Iodine Species in Seawater: Speciation, Distribution, and Dynamics, in: V.R. Preedy, G.N. Burrow, and R. Watson(Eds.),| Publisher|: Place Published|. p. Pages|.

Kondratyuk, T.P. and J.M. Pezzuto,(2004) Natural Product Polyphenols of Relevance to Human Health. Pharmaceutical Biology. 42(sup1) 46-63.

Pandey, K.B. and S.I. Rizvi,(2009) Plant polyphenols as dietary antioxidants in human health and disease. Oxidative medicine and cellular longevity. 2(5) 270-278.

Prasanth, M.I.; Sivamaruthi, B.S.; Chaiyasut, C.; Tencomnao, T. A (2019) Review of the Role of Green Tea (Camellia sinensis) in Antiphotoaging, Stress Resistance, Neuroprotection, and Autophagy. Nutrients 11, 474.

Zimmermann, M.B., (2020) Chapter 25 - Iodine and the iodine deficiency disorders, in: B.P. Marriott(Eds.),| Publisher|: Place Published|. p. Pages|.

➢ *ORAL PRESENTATION*

Erbiyum Katkılı Fiber Yükselteç ile Farklı Senaryolarda Oluşturulan Düzeneklerde Çıkış Kazancı ve Gürültü Analizi

Kahraman ZAİM[1*] (*ORCID: https://orcid.org/0009-0005-4153-4572*)
Murat YÜCEL[2] (*ORCID: https://orcid.org/0000-0002-0349-4013*)
Mustafa Serdar OSMANCA[3] (*ORCID: https://orcid.org/0000-0002-6939-2765*)

[*1]Türk Telekomünikasyon A.Ş, Teknoloji Genel Müdür Yardımcılığı, Ankara, Türkiye
[2]Gazi Üniversitesi, Teknoloji Fakültesi, Elektrik Elektronik Mühendisliği Bölümü, Ankara, Türkiyeg
[3]Türk Telekomünikasyon A.Ş, Teknoloji Genel Müdür Yardımcılığı, Ankara, Türkiye

*Sorumlu yazar e-posta : kahraman.zaim@turktelekom.com.tr

Özet

Günümüz haberleşme teknolojilerinde artan veri hızı ve bant genişliği gereksinimleri, optik haberleşme altyapılarının güçlendirilmesini zorunlu kılmıştır. Bu bağlamda, optik yükselteçler, sinyalin elektriksel forma dönüştürülmeden doğrudan güçlendirilmesini sağlayarak yüksek hızlı, düşük kayıplı ve enerji verimli iletişim olanakları sunmaktadır. Özellikle erbiyum katkılı fiber yükselteçler (EDFA), düşük gürültü katsayısı ve geniş kazanç spektrumu sayesinde uzun mesafeli fiber optik sistemlerin temel bileşeni olarak kullanılmaktadır. Telekomünikasyon altyapılarında yaygın olarak tercih edilen EDFA'lar, dalga boyu bölmeli çoğullama (WDM) teknolojileri ile uyumlu çalışarak birden fazla sinyalin aynı hat üzerinden etkin biçimde iletimine olanak tanımaktadır. Ayrıca, yüksek doğruluk ve kararlılık sağlayan bu sistemler, veri merkezleri arası bağlantılar, deniz altı kablo sistemleri ve yüksek kapasiteli metro ağlarında da etkin biçimde kullanılmaktadır. Bu çalışmada EDFA kullanılarak tasarlanan farklı senaryolardaki düzeneklerden elde edilen çıkış gücü ve gürültü seviyesi ölçülmüştür.

Anahtar Kelimeler: EDFA, Optik Yükselteç, Optik Kazanç, Gürültü Faktörü

Output Gain and Noise Analysis of Mechanisms Created in Different Scenarios with Erbium Doped Fiber Amplifier (EDFA)

Abstract

Increasing data speed and bandwidth requirements in today's communication technologies have made it necessary to strengthen optical communication infrastructures. In this context, optical amplifiers provide high-speed, low-loss and energy-efficient communication opportunities by directly amplifying the signal without converting it into electrical form. In particular, erbium-doped fiber amplifiers (EDFA) are used as the basic components of long-distance fiber optic systems thanks to their low noise coefficient and wide gain spectrum. EDFAs, which are widely preferred in telecommunication infrastructures, work in harmony with wavelength division multiplexing (WDM) technologies, allowing the effective transmission of multiple signals over the same line. In addition, these systems, which provide high accuracy and stability, are also used effectively in inter-data center connections, undersea cable systems and high-capacity metro networks. In this study, the output power and noise level obtained from devices in different scenarios designed using EDFA were measured.

Keywords: EDFA, Optical Amplifiers, Optical Gain, Noise Factor

GİRİŞ

Haberleşme sistemlerinde veri iletim performansını artırmaya yönelik çalışmalar uzun süredir araştırmacıların öncelikli ilgi alanlarından biri olmuştur. Fiber optik iletim hatlarının gelişimiyle birlikte, sinyal kayıplarını telafi edebilecek etkin yükseltme tekniklerinin geliştirilmesi kritik bir gereklilik haline gelmiştir. Bu kapsamda, 1987 yılında Payne ve meslektaşları tarafından geliştirilen Erbiyum Katkılı Fiber Yükselteçler (EDFA), optik haberleşme sistemlerinde çığır açıcı bir gelişme olarak kabul edilmektedir (Payne ve ark., 1987). EDFA'lar, 1550 nm civarındaki düşük zayıflama bölgesinde çalışan fiber sistemlerle yüksek uyumluluk göstermesi nedeniyle özellikle Yoğun Dalga Boyu Bölmeli Çoğullama (DWDM) sistemlerinde tercih edilmektedir (Senior, 2009, Zhang ve ark., 2020)

Son yıllarda yapılan çalışmalar, EDFA 'ların kazanç düzeyi, gürültü katsayısı ve spektral düzlemsellik gibi parametrelerinin optimize edilmesi yönünde yoğunlaşmıştır. Kazanç sıkıştırmasını azaltmaya yönelik hibrit pompalama tekniklerinin EDFA performansı üzerindeki etkilerini incelemiş; sonuç olarak daha kararlı bir çıkış gücü elde edildiğini göstermiştir (Yücel, 2008, Yücel ve ark., 2012, 2013).

Optik yükselteçler, uyarılmış yayılma ile, gelen ışığı lazere benzer bir mekanizma kullanarak yükseltirler (Yücel ve ark., 2013, Ünverdi ve ark., 2013). Optik yükselteçler; yarı iletken optik yükselteçler (SOA), fiber Raman yükselteçler, Brillioun yükselteçler ve nadir toprak elementi katkılı yükselteçler olmak üzere 4 ana grupta toplanırken, en yaygın olarak kullanılan optik yükselteç nadir toprak elementi katkılı yükselteçlerden erbiyum katkılı fiber yükselteçlerdir (Sansuri ve ark., 2004) EDFA'lar yüksek kazanç, düşük gürültü ve yüksek band genişliklerine sahiptirler (Pekküçük ve ark., 2014, Küçükarslan, 2012).

DENEYSEL YAKLAŞIM

Şekil-1, Şekil-2 ve Şekil-3' teki düzenekler Optiwave-OptiSystem-22 sürüm yazılımı ile tasarlanmış ve çalıştırılmıştır. Yapılan simülasyon çalışmasında 1530nm-1560nm dalga boyu aralıklarında ve farklı güç seviyelerinde olan 16 kanallı bir ışık kaynağına ileri yönde, geri yönde ve iki yönde olmak üzere 980 nm dalga boyunda birer adet lazer pompa bağlanmıştır. 2m ve 7m EDF (Erbiyum Katkılı Fiber) kullanılarak oluşturulan düzenekteki giriş sinyallerinin seviyeleri sırasıyla -10 dBm, -20 dBm ve -30 dBm olarak değiştirilmiştir. Hem EDF boyunun değişimi hem de sinyal gücündeki değişimin çıkış kazancına ve gürültü miktarına etkileri incelenmiştir.

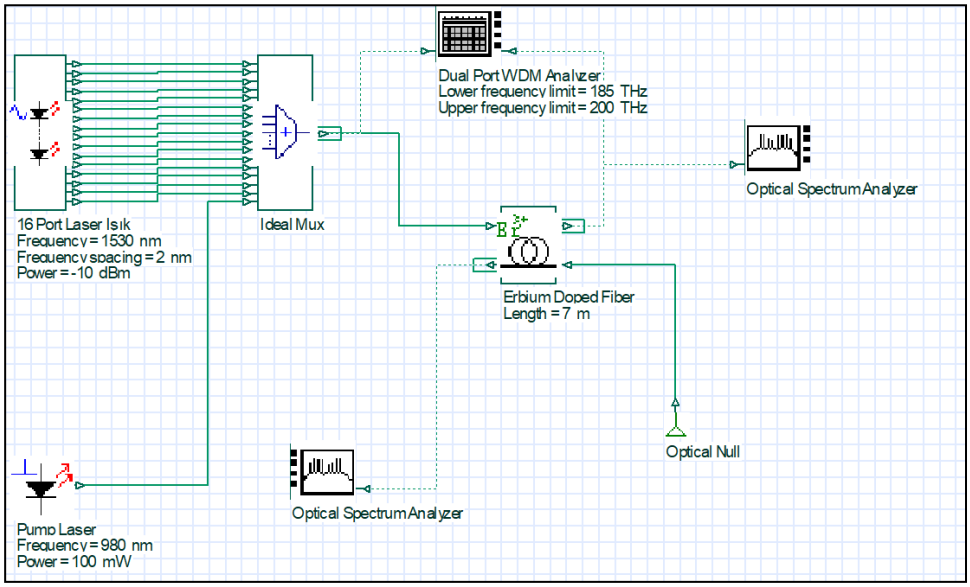

Şekil 1. İlerinde Yönde Pompa Lazer ile Kurulan Düzenek

Şekil-1' de 16 portlu ayarlanabilir lazer ışık kaynağı ile farklı sinyal seviyelerinde (-10 dBm, -20 dBm ve -30 dBm) iletilen sinyaller, 980 nm dalga boyu 100 mW gücünde ileri yönde bir lazer pompa ile birleştirilerek 2m ve 7m farklı uzunluklardaki erbiyum katkılı fiberlere gönderilmiş ve elde edilen yükseltilmiş sinyaller optik spektrum analizörü ile ayrı ayrı ölçülmüştür.

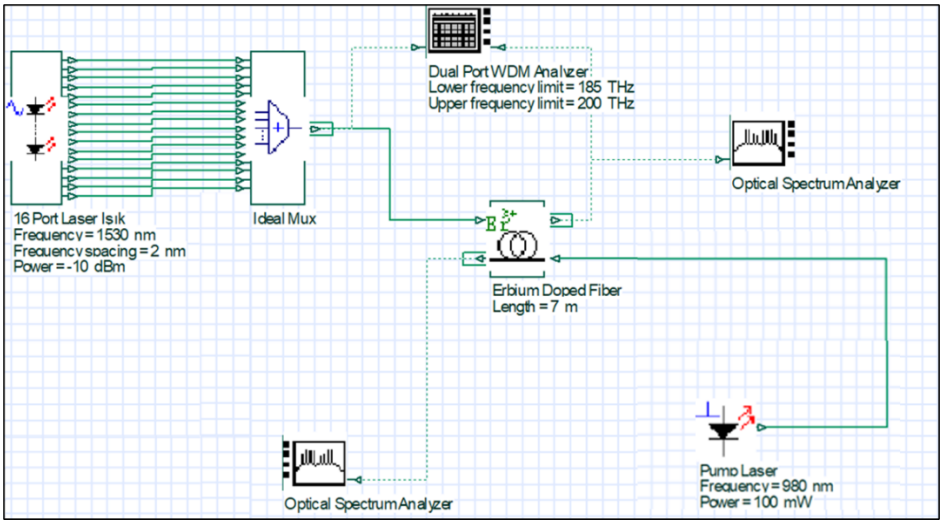

Şekil 2. Geri Yönde Pompa Lazer ile Kurulan Düzenek

Şekil-2' de 16 portlu ayarlanabilir lazer ışık kaynağı ile farklı sinyal seviyelerinde (-10 dBm, -20 dBm ve -30 dBm) iletilen sinyaller, 2m ve 7m farklı uzunluklardaki erbiyum katkılı fiberlere gönderilmiş ve 980 nm dalga boyu 100 mW gücünde geri yönde bir lazer pompa ile birleştirilerek elde edilen yükseltilmiş sinyaller optik spektrum analizörü ile ayrı ayrı ölçülmüştür.

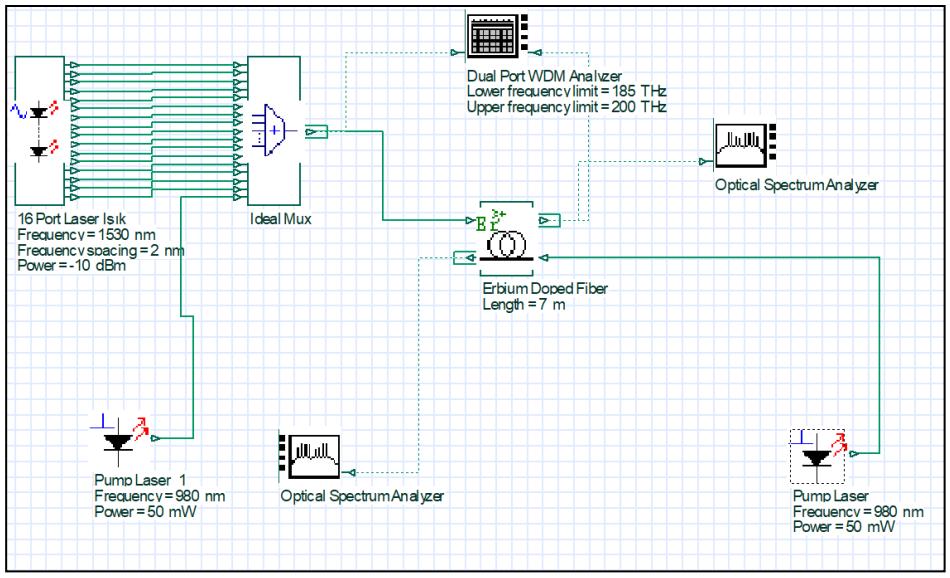

Şekil 3. İki Yönlü Pompa Lazer ile Kurulan Düzenek

Şekil-3' de 16 portlu ayarlanabilir lazer ışık kaynağı ile farklı sinyal seviyelerinde (-10 dBm, -20 dBm ve -30 dBm) iletilen sinyaller, 980 nm dalga boyu 50 mW gücünde bir lazer pompa ile birleştirilerek, 2m ve 7m farklı uzunluklardaki erbiyum katkılı fiberlere gönderilmiş, erbiyum katkılı fiber üzerinde de 980 nm dalga boyu 50 mW gücünde yönde bir lazer pompa ile birleştirilerek iki yönlü pompalama ile elde edilen yükseltilmiş sinyaller optik spektrum analizörü ile ayrı ayrı ölçülmüştür.

SONUÇ VE DEĞERLENDİRMELER

Şekil 4'te ***2m EDF ve ileri yönde lazer pompa*** kullanılan düzeneğin farklı dalga boyundaki ve farklı sinyal seviyelerindeki (-10 dBm, -20 dBm ve -30 dBm) ***sinyallerin çıkış kazanç spektrumları*** belirtilmiştir. Tüm ölçümlerde Tablo-1'deki EDF parametreleri kullanılmıştır. Ölçülen çıkış kazanç değerlerinin 1532 nm dalga boyunda ve -30dBm sinyal seviyesinde en yüksek değerde görülmektedir.

Tablo 1. Kullanılan EDF Parametreleri

Parametre	Değer	Açıklama
Core radius	2.2 µm	Fiberin merkez çekirdeğinin yarıçapı. Işığın yayıldığı bölgenin büyüklüğünü belirler.
Er doping radius	2.2 µm	Erbiyum iyonlarının katkılandığı yarıçap. Genellikle core radius ile aynıdır.
Er metastable lifetime	10 ms	Erbiyum iyonlarının üst enerji seviyesinde kalma süresi (enerji transfer süresi).
Numerical aperture	0.24	Fiberin ışığı toplama kapasitesini belirten sayısal açıklık.
Er ion density	1e+24 m^{-3}	Birim hacimdeki erbiyum iyonu yoğunluğu.

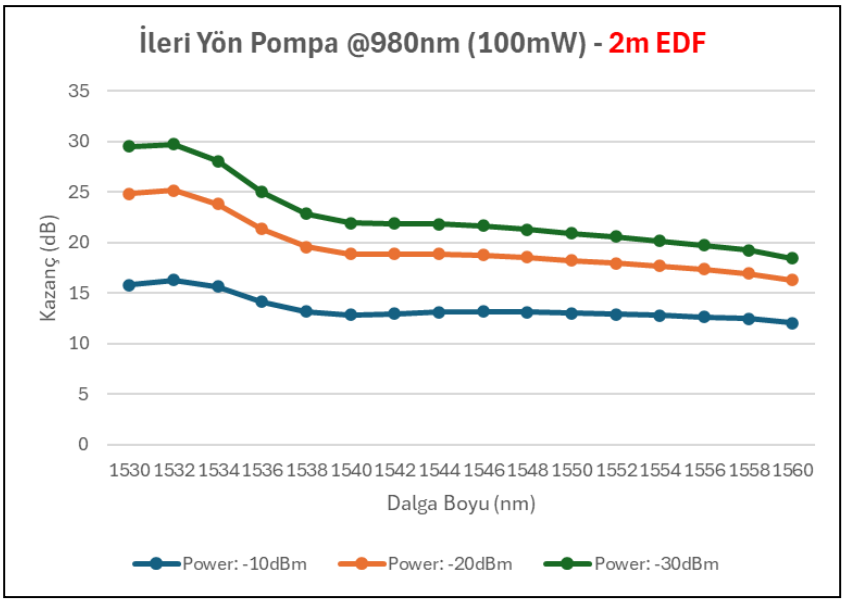

Şekil 4. İleri Yönde Pompa Lazer (980nm-100mW) – 2m EDF ile Elde Edilen Kazanç

Şekil 5'te ***2m EDF ve geri yönde lazer pompa*** kullanılan düzeneğin farklı dalga boyundaki ve farklı sinyal seviyelerindeki (-10 dBm, -20 dBm ve -30 dBm) ***sinyallerin çıkış kazanç spektrumları*** belirtilmiştir. Ölçülen çıkış kazanç değerlerinin 1532 nm dalga boyunda ve -30dBm sinyal seviyesinde en yüksek değerde görülmektedir.

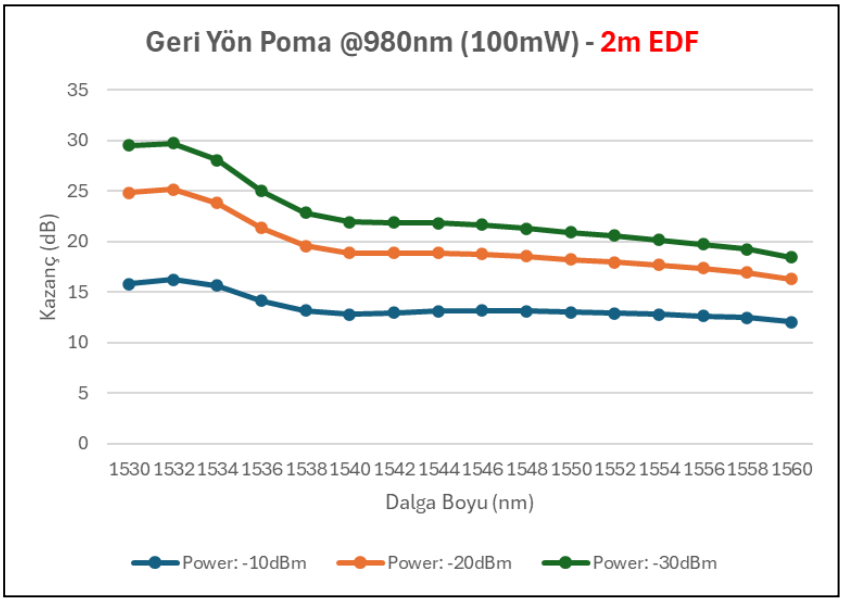

Şekil 5. Geri Yönde Pompa Lazer (980nm-100mW) – 2m EDF ile Elde Edilen Kazanç

Şekil 6'da ***2m EDF ve iki yönlü lazer pompa*** kullanılan düzeneğin farklı dalga boyundaki ve farklı sinyal seviyelerindeki (-10 dBm, -20 dBm ve -30 dBm) ***sinyallerin çıkış kazanç spektrumları*** belirtilmiştir. Ölçülen çıkış kazanç değerlerinin 1532 nm dalga boyunda ve -30dBm sinyal seviyesinde en yüksek değerde görülmektedir.

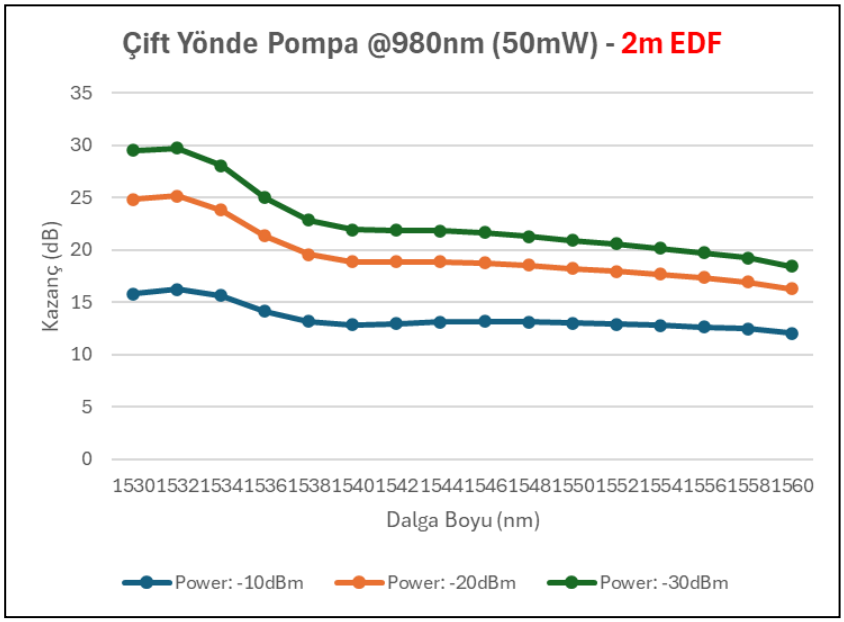

Şekil 6. Çift Yönlü Pompa Lazer (980nm-50mW) – 2m EDF ile Elde Edilen Kazanç

Şekil 7'de ***7m EDF ve ileri yönde lazer pompa*** kullanılan düzeneğin farklı dalga boyundaki ve farklı sinyal seviyelerindeki (-10 dBm, -20 dBm ve -30 dBm) ***sinyallerin çıkış kazanç spektrumları*** belirtilmiştir. Ölçülen çıkış kazanç değerlerinin 1532 nm dalga boyunda ve -30dBm sinyal seviyesinde en yüksek değerde görülmektedir.

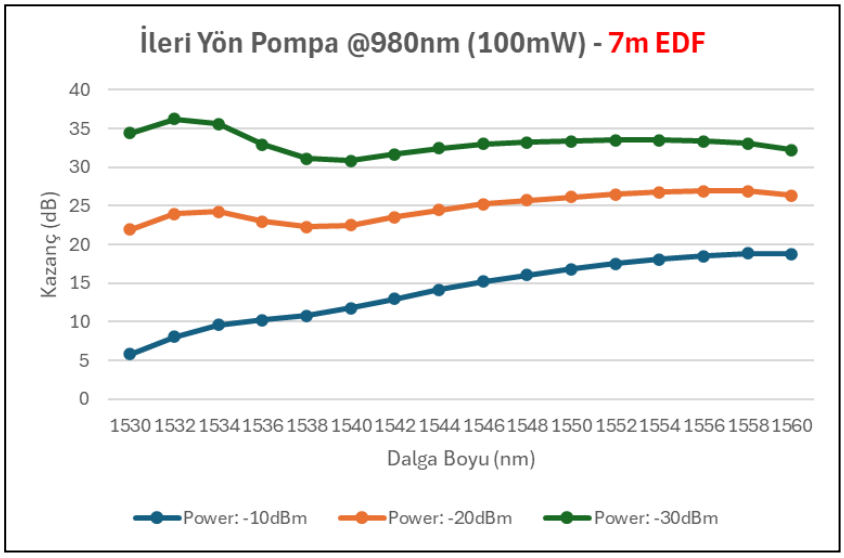

Şekil 7. İleri Yönde Pompa Lazer (980nm-100mW) –7m EDF ile Elde Edilen Kazanç

Şekil 8'de ***7m EDF ve geri yönde lazer pompa*** kullanılan düzeneğin farklı dalga boyundaki ve farklı sinyal seviyelerindeki (-10 dBm, -20 dBm ve -30 dBm) ***sinyallerin çıkış kazanç spektrumları*** belirtilmiştir. Ölçülen çıkış kazanç değerlerinin 1532 nm dalga boyunda ve -30dBm sinyal seviyesinde en yüksek değerde

görülmektedir.

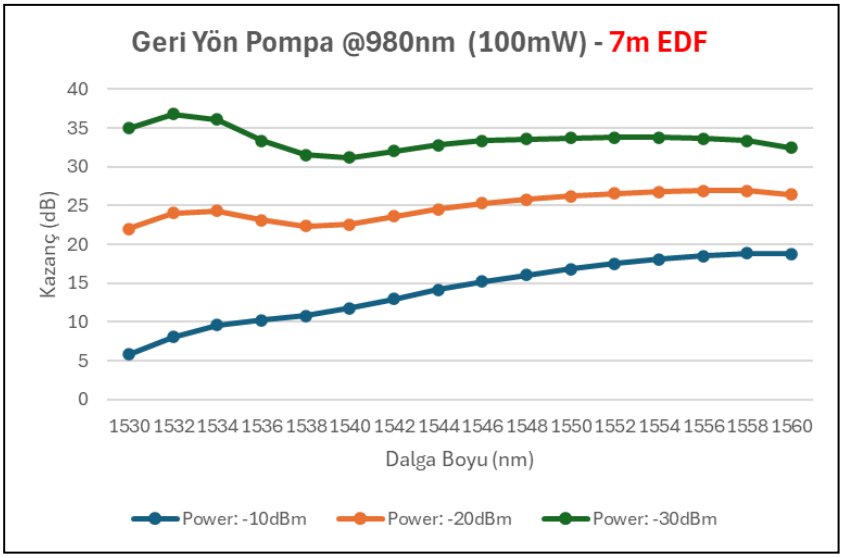

Şekil 8. Geri Yönde Pompa Lazer (980nm-100mW) – 7m EDF ile Elde Edilen Kazanç

Şekil 9'da ***7m EDF ve iki yünlü lazer pompa*** kullanılan düzeneğin farklı dalga boyundaki ve farklı sinyal seviyelerindeki (-10 dBm, -20 dBm ve -30 dBm) ***sinyallerin çıkış kazanç spektrumları*** belirtilmiştir. Ölçülen çıkış kazanç değerlerinin 1532 nm dalga boyunda ve -30dBm sinyal seviyesinde en yüksek değerde görülmektedir.

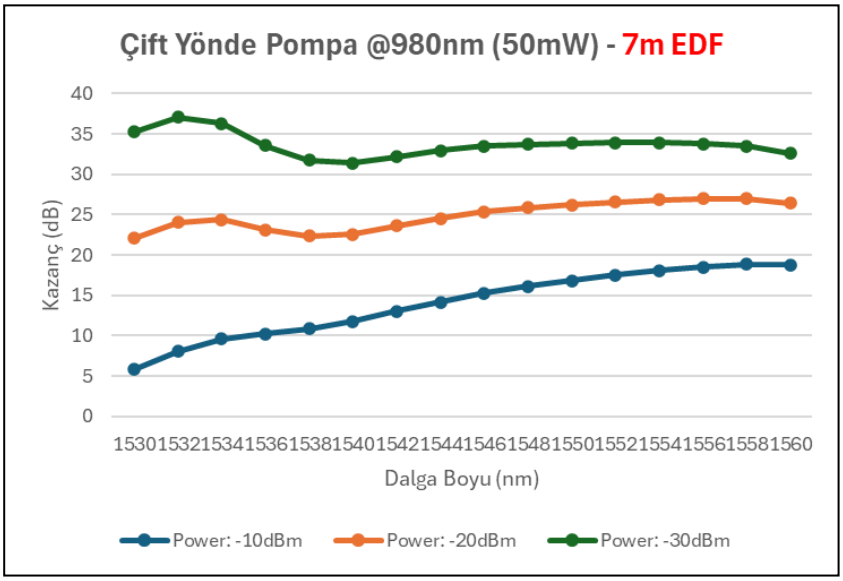

Şekil 9. Çift Yönlü Pompa Lazer (980nm-50mW) – 7m EDF ile Elde Edilen Kazanç

Şekil 10'da ***2m EDF ve ileri yönde lazer pompa*** kullanılan düzeneğin farklı dalga boyundaki ve farklı sinyal seviyelerindeki (-10 dBm, -20 dBm ve -30 dBm) ***sinyallerin gürültü spektrumları*** belirtilmiştir. Ölçülen gürültü değerlerinin 1534 nm dalga boyunda ve -10dBm sinyal seviyesinde en yüksek değerde görülmektedir.

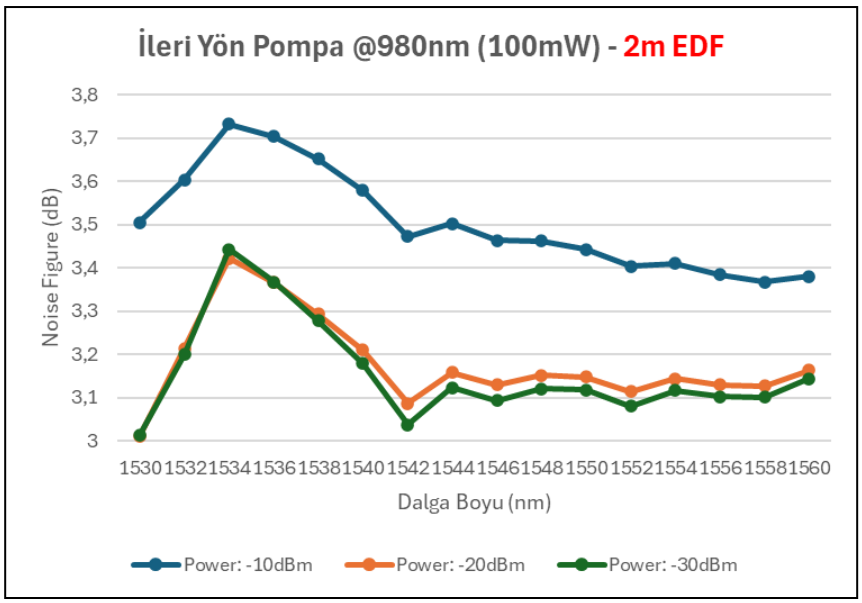

Şekil 10. İleri Yönde Pompa Lazer (980nm-100mW) – 2m EDF ile Elde Edilen Gürültü

Şekil 11'de ***2m EDF ve geri yönde lazer pompa*** kullanılan düzeneğin farklı dalga boyundaki ve farklı sinyal seviyelerindeki (-10 dBm, -20 dBm ve -30 dBm) ***sinyallerin gürültü spektrumları*** belirtilmiştir. Ölçülen gürültü değerlerinin 1534 nm dalga boyunda ve -10dBm sinyal seviyesinde en yüksek değerde görülmektedir.

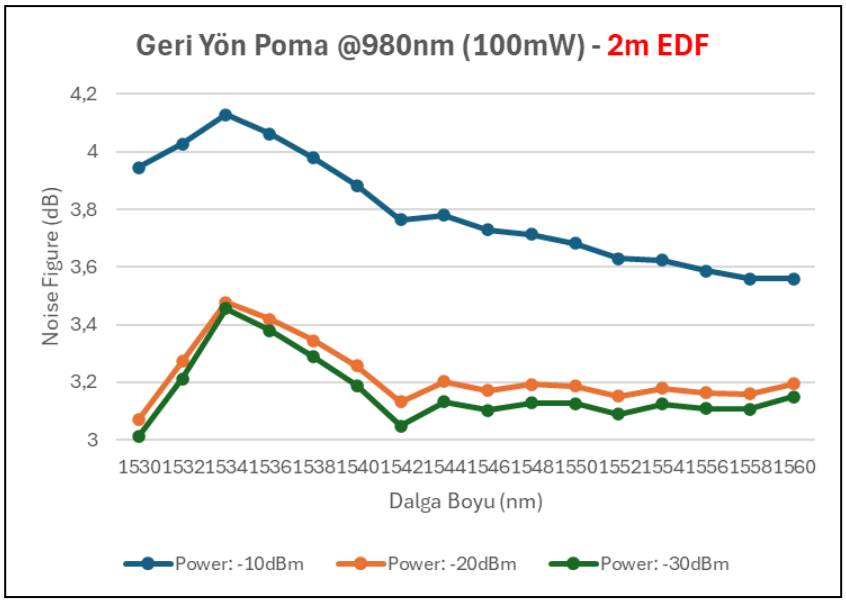

Şekil 11. Geri Yönde Pompa Lazer (980nm-100mW) – 2m EDF ile Elde Edilen Gürültü

Şekil 12'de ***2m EDF ve iki yönlü lazer pompa*** kullanılan düzeneğin farklı dalga boyundaki ve farklı sinyal seviyelerindeki (-10 dBm, -20 dBm ve -30 dBm) ***sinyallerin gürültü spektrumları*** belirtilmiştir. Ölçülen gürültü değerlerinin 1534 nm dalga boyunda ve -10dBm sinyal seviyesinde en yüksek değerde görülmektedir.

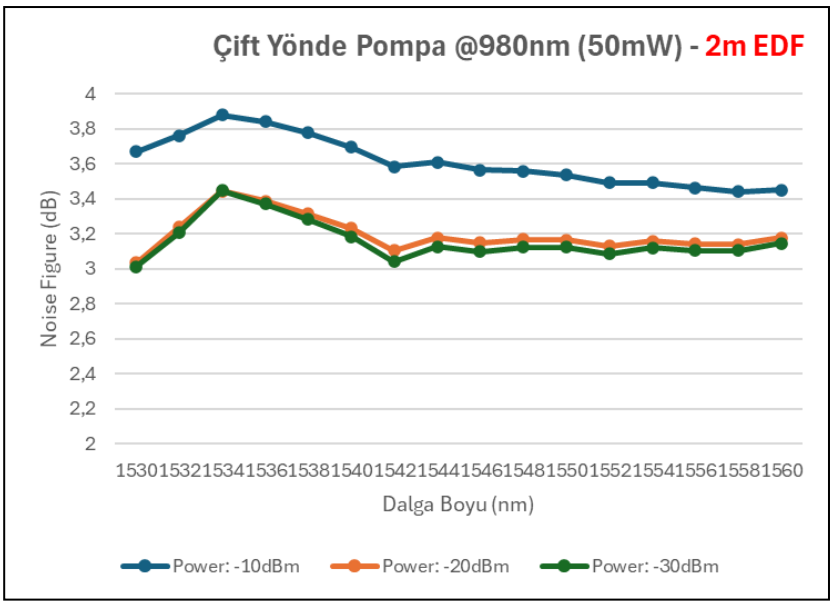

Şekil 12. Çift Yönlü Pompa Lazer (980nm-50mW) – 2m EDF ile Elde Edilen Gürültü

Şekil 13'te ***7m EDF ve ileri yönde lazer pompa*** kullanılan düzeneğin farklı dalga boyundaki ve farklı sinyal seviyelerindeki (-10 dBm, -20 dBm ve -30 dBm) ***sinyallerin gürültü spektrumları*** belirtilmiştir. Ölçülen gürültü değerlerinin 1530 nm dalga boyunda ve -10dBm sinyal seviyesinde en yüksek değerde görülmektedir.

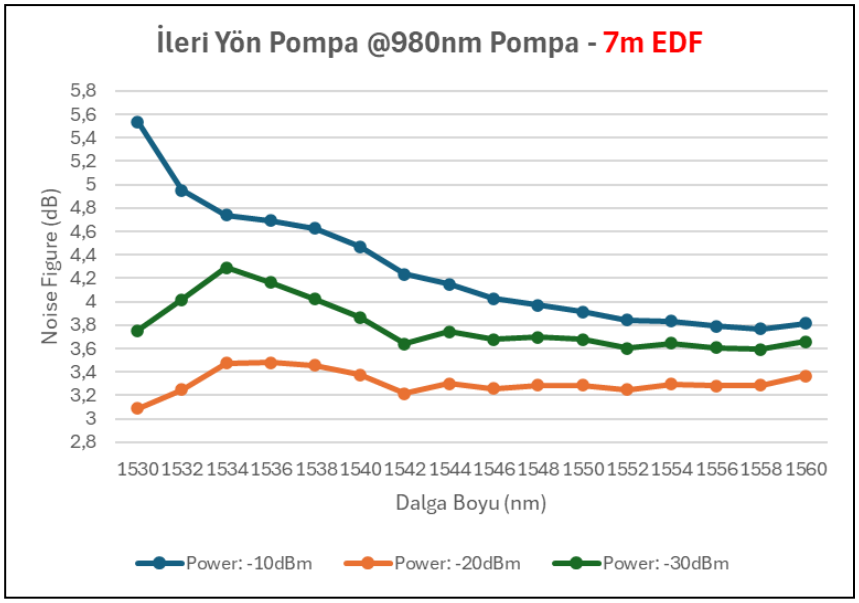

Şekil 13. İleri Yönde Pompa Lazer (980nm-100mW) – 7m EDF ile Elde Edilen Gürültü

Şekil 14'te ***7m EDF ve geri yönde lazer pompa*** kullanılan düzeneğin farklı dalga boyundaki ve farklı sinyal seviyelerindeki (-10 dBm, -20 dBm ve -30 dBm) ***sinyallerin gürültü spektrumları*** belirtilmiştir. Ölçülen gürültü değerlerinin 1530 nm dalga boyunda ve -10dBm sinyal seviyesinde en yüksek değerde görülmektedir.

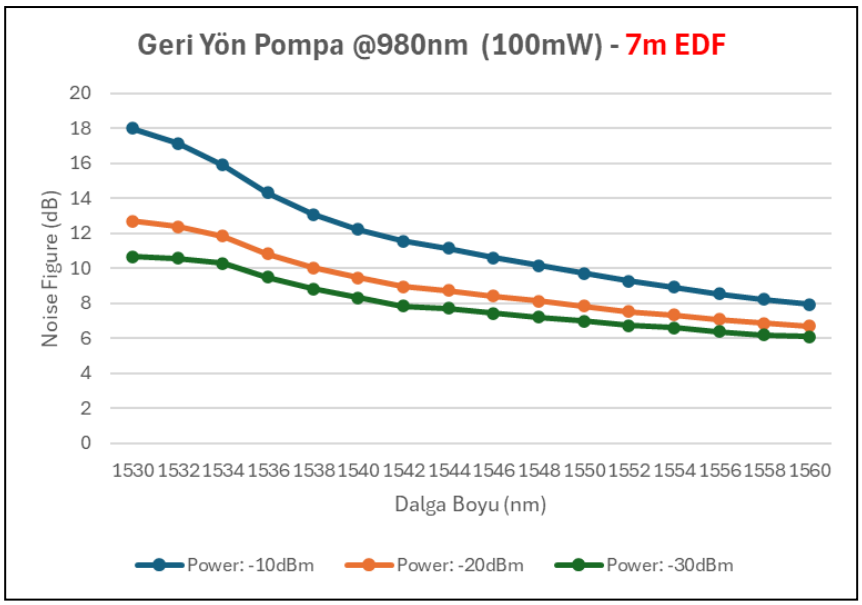

Şekil 14. Geri Yönde Pompa Lazer (980nm-50mW) – 7m EDF ile Elde Edilen Gürültü

Şekil 15'te ***7m EDF ve iki yönlü lazer pompa*** kullanılan düzeneğin farklı dalga boyundaki ve farklı sinyal seviyelerindeki (-10 dBm, -20 dBm ve -30 dBm) ***sinyallerin gürültü spektrumları*** belirtilmiştir. Ölçülen gürültü değerlerinin 1530 nm dalga boyunda ve -10dBm sinyal seviyesinde en yüksek değerde görülmektedir.

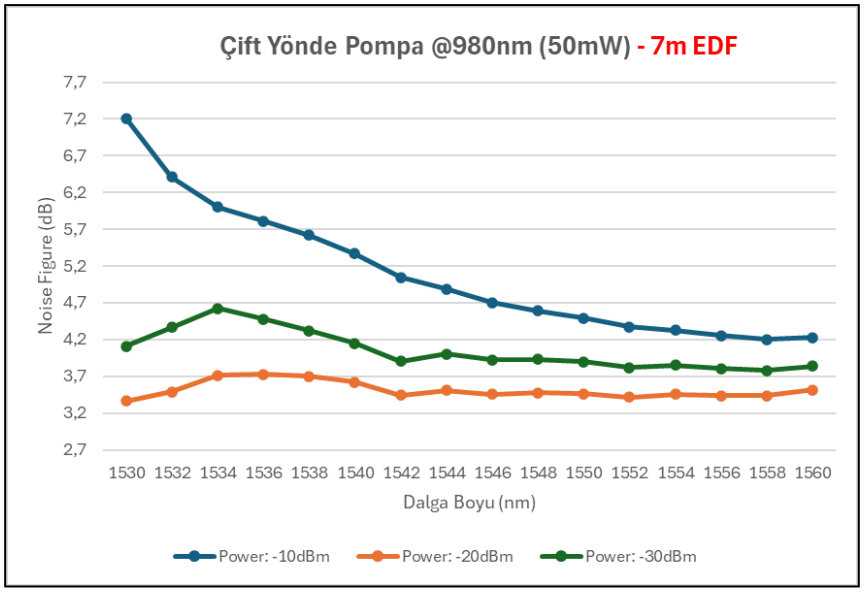

Şekil 15. İki Yönlü Pompa Lazer (980nm-50mW) – 7m EDF ile Elde Edilen Gürültü

Tablo 2'de tüm ölçüm senaryolarına ait ortalama çıkış gücü ve gürültü seviyeleri karşılaştırmalı olarak verilmiştir. Elde edilen değerlere göre en iyi ortalama çıkış gücü değeri iki yönlü lazer pompa ve 7m EDF kullanılarak yapılan düzenekten, en düşük ortalama gürültü değeri ise iki yönlü lazer pompa ve 2m EDF ile yapılan düzenekten elde edilmiştir.

Tablo 2: Tüm Ölçüm Senaryolarına ait Ortalama Çıkış Gücü ve Gürültü Değerleri

Parametreler	**İleri Yönde Lazer Pompa ile**						**Geri Yönde Lazer Pompa ile**						**İki Yönlü Lazer Pompa ile**					
EDF Metrajı	**2 metre**			**7 metre**			**2 metre**			**7 metre**			**2 metre**			**7 metre**		
Giriş sinyal gücü (dBm)	**(-10)**	**(-20)**	**(-30)**	**(-10)**	**(-20)**	**(-30)**	**(-10)**	**(-20)**	**(-30)**	**(-10)**	**(-20)**	**(-30)**	**(-10)**	**(-20)**	**(-30)**	**(-10)**	**(-20)**	**(-30)**
Çıkış Kazancı (dB)	13,48	19,55	22,66	13,96	24,77	33,15	13,48	19,55	22,66	13,96	24,84	33,52	13,48	19,55	22,66	13,97	24,86	33,71
Gürültü (dB)	3,5	3,18	3,15	4,27	3,31	3,79	3,79	3,22	3,17	11,67	9,05	7,96	3,61	3,19	3,16	5,09	3,51	4,05

Her üç senaryodaki çıkış kazanç değerleri 2m EDF için aynı değerde olup 7m EDF ile oluşturulan düzeneklerde de hemen hemen birbirine yakın değerlerdedir.

İleri yönde lazer pompa ile yapılan düzenekte en iyi çıkış kazanç değeri -30dBm sinyal seviyesi ve 7m EDF'li senaryoda elde edilirken en düşük gürültü miktarı ise -30dBm sinyal seviyesi ve 2m EDF'li senaryoda elde edilmiştir.

Geri yönde lazer pompa ile yapılan düzenekte en iyi çıkış kazanç değeri -30dBm sinyal seviyesi ve 7m EDF'li senaryoda elde edilirken en düşük gürültü miktarı ise -30dBm sinyal seviyesi ve 2m EDF'li senaryoda elde edilmiştir.

İki Yönlü lazer pompa ile yapılan düzenekte en iyi çıkış kazanç değeri -30dBm sinyal seviyesi ve 7m EDF'li senaryoda elde edilirken en düşük gürültü miktarı ise -30dBm sinyal seviyesi ve 2m EDF'li senaryoda elde edilmiştir.

Bu analizden de anlaşılacağı üzere, üç farklı lazer pompa yönü ile yapılan ölçümlerin ortak noktası, en iyi ortalama çıkış kazançlarının -30dBm sinyal seviyesi ve 7m EDF'li senaryoda elde edilmesi, en düşük gürültü miktarının ise -30dBm sinyal seviyesi ve 2m EDF'li senaryoda elde edilmiş olmasıdır.

KAYNAKLAR

Agrawal, G. P. (2002), Fiber-Optic Communication Systems Third Edition, John Wiley&Sons.

Aslan, Z., Yücel, M. (2012), Tek ve Çift Geçişli Erbiyum Katkılı Fiber Yükselteçlerin C bandında Deneysel Olarak Karşılaştırılması, Politeknik Dergisi, Cilt 15, Sayı 3, Sayfa 135-138, 2012.

Küçükarslan, T. (2012), Erbiyum ve İterbiyum Katkılı Optik Fiber Kuvvetlendiricilerin Kazanç Analizi, Yüksek Lisans Tezi, Yıldız Teknik Üniversitesi, Fen Bilimleri Enstitüsü, İstanbul.

Payne, D. N., & Mears, R. J. (1987). Low-noise erbium-doped fibre amplifier operating at 1.54 μm. Electronics Letters, 23(19), 1026–1028.

Pekküçük, G., Uzar,İ., Ünverdi, N.Ö. (2014), Optik Kuvvetlendiriciler ve Uygulamaları, Eleco 2014 Elektrik – Elektronik – Bilgisayar ve Biyomedikal Mühendisliği Sempozyumu, Bursa.

Samsuri, N.M., Harun, S.W., Ahmad, H. (2004), Comparison of Performances Between Partial Double pass and full double-pass systems in Two-Stage L-Band EDFA, LaserPhysicsLett., 1(12):610-612, 2004.

Senior, J. M. (2009). Optical Fiber Communications: Principles and Practice (3rd ed.). Pearson Education.

Ünverdi, N. Ö. ve Ünverdi, N. A. (2013), Optik Haberleşme Sistemlerinin Dizaynı, V. İletişim Teknolojileri Ulusal Sempozyumu (İTUSEM 2013), İzmir, 127-133.

Yücel, M. (2008), Kazancı Düzleştirilmiş Geniş Bandlı Fiber Yükselteçlerin Tasarımı, Doktora Tezi, Gazi Üniversitesi Bilişim Enstitüsü.

Yücel, M., Aslan, Z., Göktaş, H.A. (2013), Çeşitli Erbiyum Katkılı Fiber Yükselteç Konfigürasyonları için Kazanç ve Gürültü Faktörünün İncelenmesi,
Erişim: https://www.researchgate.net/publication/319127367.

Zhang, Y., Li, Y., & Wang, T. (2020). Performance analysis of hybrid-pumped EDFA for gain flattening in WDM systems. Optics Communications, 462, 125267.

➢ *ORAL PRESENTATION*

Uzay Yoluyla Haberleşme Ağını Genişletmek: Karasal Olmayan Ağ (NTN) Teknolojileri ve Kullanım Alanlarının Genel Bir Değerlendirmesi

Kahraman ZAİM[1*] (*ORCID: https://orcid.org/0009-0005-4153-4572*)
Murat YÜCEL[2] (*ORCID: https://orcid.org/0000-0002-0349-4013*)
Mustafa Serdar OSMANCA[3] (*ORCID: https://orcid.org/0000-0002-6939-2765*)

[*1]Türk Telekomünikasyon A.Ş, Teknoloji Genel Müdür Yardımcılığı, Ankara, Türkiye
[2]Gazi Üniversitesi, Teknoloji Fakültesi, Elektrik Elektronik Mühendisliği Bölümü, Ankara, Türkiye
[3]Türk Telekomünikasyon A.Ş, Teknoloji Genel Müdür Yardımcılığı, Ankara, Türkiye

* Sorumlu yazar e-posta: kahraman.zaim@turktelekom.com.tr

Özet

Haberleşme teknolojileri, insan hayatında her geçen gün daha önemli bir yer edinmektedir. Bu gelişme, iletişim alanında yeni ve yenilikçi teknolojilerin ortaya çıkmasını teşvik etmektedir. Kablosuz iletişimde yaygın olarak kullanılan yöntemlerden biri olan karasal ağlar (Terrestrial Networks), uzun süredir bilinen ve kullanılan sistemler arasında yer almaktadır. Ancak, özellikle şehir merkezlerinden uzak bölgelerde bu teknolojilerin yetersiz kalması, karasal olmayan ağların (Non-Terrestrial Networks-NTN) öne çıkmasına neden olmuştur. NTN sistemleri, yer yüzeyinin ötesinde faaliyet gösteren ve uzay tabanlı altyapılarla iletişim hizmeti sunan ağlardır. Bu ağlar, dünya genelinde geniş bir kapsama alanı sağlamakta ve altyapının sınırlı ya da hiç bulunmadığı bölgelerde iletişimi mümkün kılmaktadır. Sağladıkları çeşitli avantajlar sayesinde, NTN teknolojilerine olan ilgi gün geçtikçe artmaktadır. Bu çalışmada, NTN sistemlerinin türleri detaylı şekilde incelenecek ve karasal ağlarla olan temel farklılıkları ele alınacaktır.

Anahtar Kelimeler: NTN (Karasal Olmayan Ağlar), LEO, MEO, GEO, HAPS, LAPS, NTN-IoT, NTN-NR

Expanding the Communications Network through Space: An Overview of Non-Terrestrial Network (NTN) Technologies and Use Cases

Abstract

Communication technologies are assuming an increasingly significant role in human life. This progression fosters the emergence of novel and innovative solutions within the field of telecommunications. Among the commonly utilized methods in wireless communication are terrestrial networks, which have been well-established and widely implemented over time. However, the limitations of these systems—particularly in remote or underserved areas far from urban centers—have highlighted the growing relevance of non-terrestrial networks (NTN). NTN refers to communication infrastructures that operate beyond the Earth's surface, relying on space-based platforms to deliver connectivity. These networks are essential for ensuring global coverage and enabling communication in regions where conventional infrastructure is either insufficient or entirely absent. Due to the substantial advantages they offer, interest in NTN technologies has been steadily increasing. This study aims to provide a detailed examination of NTN systems and their various types, while also outlining the fundamental distinctions between NTN and terrestrial networks.

Keywords: NTN (Non-Terrestrial Networks), LEO, MEO, GEO, HAPS, LAPS, NTN-IoT, NTN-NR

GİRİŞ

İletişim, insan hayatının temel ihtiyaçlarından biri olarak kabul edilmekte ve teknolojinin ilerlemesiyle birlikte bu alandaki önemi sürekli olarak artmaktadır. İnsanlar, tarih boyunca iletişim kurma gereksinimlerini karşılamak amacıyla çeşitli yöntemler geliştirmiştir. Günümüzde ise iletişim altyapıları büyük bir dönüşüm geçirmiş; geleneksel kablolu sistemlerden modern kablosuz sistemlere doğru bir evrim yaşanmıştır. Geçmişte kablolu ağlar, iletişimi sağlamak için başlıca çözüm olarak öne çıkarken, günümüzde artan iletişim ihtiyacına ve mobiliteye yeterince yanıt verememektedir. Özellikle kentsel alanların dışındaki bölgelerde altyapı eksikliklerinin görülmesi, kablosuz iletişim teknolojilerini hayatın vazgeçilmez bir parçası haline getirmiştir.

Kablosuz iletişim sistemleri, sundukları yüksek performans ve kullanım kolaylığı sayesinde son yıllarda büyük teknolojik atılımların önünü açmıştır. Bu sistemler ağırlıklı olarak karasal ağlara dayanmaktadır. Karasal ağların yapıları, özellikle yoğun nüfuslu kentsel bölgelerde etkili çözümler sunsa da kırsal ve erişimi zor alanlarda yeterince işlevsel olamayabilmektedir. Bu nedenle, karasal olmayan ağlar (NTN) giderek daha fazla önem kazanmaktadır (Islam, 2022). NTN sistemleri, iletişim teknolojilerinde yeni bir aşamayı temsil ederek geniş kapsama imkânı sunmakta, kullanıcı ihtiyaçlarını karşılamakta ve özellikle altyapıdan yoksun bölgelerde dijital eşitsizliği azaltmada stratejik bir rol üstlenmektedir (Cicek, 2025).

KARASAL OLMAYAN AĞLAR (NTN)

Karasal olmayan ağlar (NTN) teknolojisi, uzay tabanlı platformlar aracılığıyla haberleşme hizmeti sunan ve yer yüzeyindeki geleneksel karasal altyapıya alternatif veya tamamlayıcı olarak kullanılan bir iletişim sistemidir. NTN, kesintisiz kapsama sağlamak ve geleneksel karasal ağlara erişimi olmayan uzak bölgelere bile kapsama alanı getirmek için önemlidir (Islam, 2022, Rinaldi ve ark., 2020).

Günümüzde cihazlar 3GPP (3rd Generation Partnership Project) karasal şebekesine bağlı olanlar ve uyduya bağlı olanlar olarak ayrılmıştır. Başka bir deyişle, uydu bağlantısı gerektiren kullanıcıların mevcut akıllı telefonlarının yanında başka bir cihaza ihtiyacı vardır. (Li ve ark., 2024). NTN ile tüm mobil cihazlar 3GPP ekosisteminin bir parçası olarak hem karasal hem de uydu şebekelerine bağlanacaktır. Böylece teknoloji sürekli olarak geliştikçe uydular baz istasyonları haline gelecektir (Vaezi ve ark., 2022).

NTN, özellikle kırsal, dağlık, deniz aşırı ya da afet bölgeleri gibi erişimin kısıtlı olduğu alanlarda kapsama sağlayarak dijital uçurumun kapatılmasına katkıda bulunacaktır. 5G ve ötesi iletişim sistemleriyle bütünleşerek hem bireysel kullanıcılara hem de kurumsal çözümlere geniş bant bağlantı hizmeti sunma potansiyeline sahiptir (Islam, 2022, Vaezi ve ark., 2022). NTN'ler irtifalarına göre iki ana gruba ayrılmaktadır. Şekil 1' de NTN genel gösterimi mevcuttur.

- Havadaki Ağlar (Air-Borne Networks)
- Uzay Ağları (Space-Borne Networks)

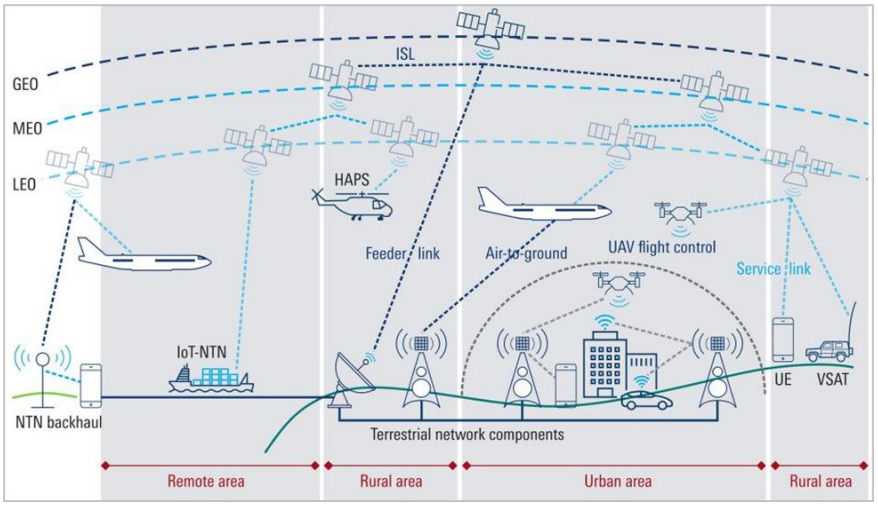

Şekil 1. NTN Genel Gösterimi

Havadaki Ağlar, atmosfer içerisinde belirli bir irtifada konumlanan hava araçları aracılığıyla haberleşme hizmeti sunan mobil iletişim sistemleridir. Bu ağlar; uçaklar, insansız hava araçları zeplinler, balonlar gibi hava platformları üzerine entegre edilen haberleşme sistemleriyle oluşturulur. Genellikle kısa veya orta vadeli kapsama

alanı ihtiyaçlarına yönelik olarak tasarlanırlar. Bu ağlar karasal altyapının yetersiz olduğu, acil durumların yaşandığı veya geçici haberleşme ihtiyacının bulunduğu durumlarda hızlı ve esnek çözümler sunar (Islam, 2022, Rinaldi ve ark., 2020, Li ve ark., 2024). Bu ağlar, NTN mimarisinin önemli bir parçasıdır ve geniş alanlara kapsama sağlanabilir, afet bölgelerinde iletişim hızla kurulabilir ve kırsal alanlara internet erişimi götürülebilir. Temelde 3 ana kategoride toplanmaktadır. Şekil 2'de havadaki ağların genel gösterimi mevcuttur. Bunlar:

- Alçak İrtifa Platformları (LAPS)
- Yüksek İrtifa Platformları (HAPS)
- Havadan Yere Ağlar (A2G)

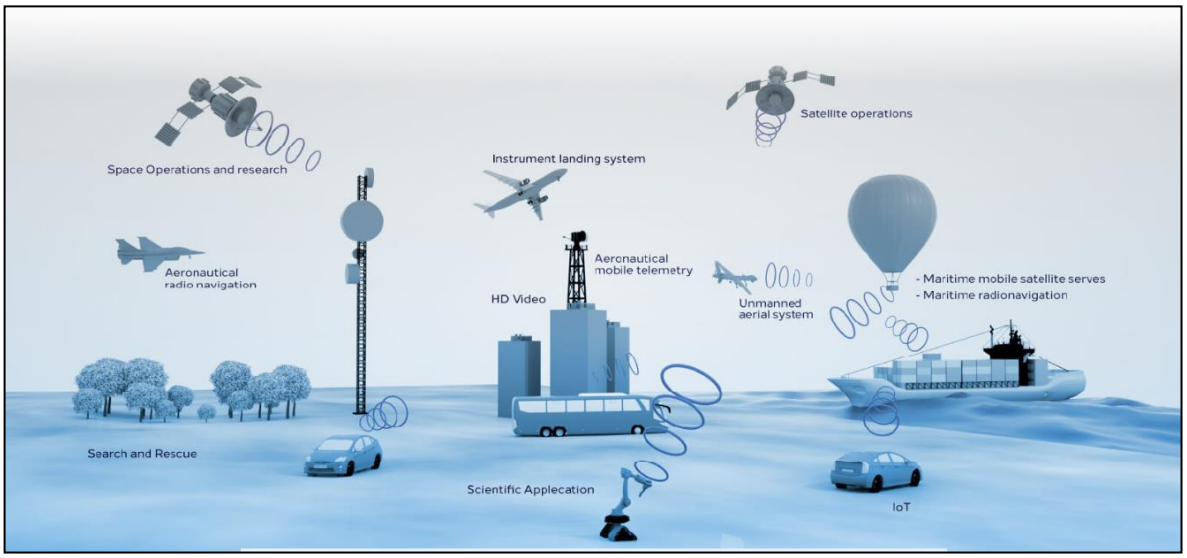

Şekil 2. Havadaki Ağların Genel Gösterimi

HAPS (High-Altitude Platforms), Yüksek İrtifa Platformları, stratosfer katmanında yüzen bir nesne üzerinde ve Dünya'ya göre belirlenmiş, nominal, sabit bir noktada bulunan, geniş bir coğrafi aralıkta yüksek kalitede telekomünikasyon hizmetleri kapsama alanı sağlayan radyo istasyonlarıdır (Vaezi ve ark., 2022, Ürküt, 2025).

HAPS, yapısı ve yeryüzüne göre konumu dikkate alındığında; karasal ağlara kıyasla daha geniş kapsama alanı, diğer NTN'lere kıyasla ise daha düşük gecikme süresi ve daha yüksek veri hızı gibi önemli avantajlara sahiptir. HAPS'in en önemli avantajlarından biri, düşük gecikme süreleriyle uydu haberleşme sistemlerini tamamlamalarıdır (Ürküt, 2025). Bu durum, gerçek zamanlı iletişim ve yüksek bant genişliği gerektiren uygulamalar için kritik bir öneme sahiptir. Örneğin, 5G ve IoT ağlarının genişletilmesinde HAPS önemli bir rol oynayabilir. Ayrıca, afet yönetimi gibi acil durumlarda, kara tabanlı altyapının zarar görmesi durumunda HAPS hızlı bir şekilde devreye alınarak iletişim ağlarını destekleyebilir. HAPS' ın diğer bir avantajı, yeniden konumlandırılabilir olmalarıdır. Uydu sistemlerinden farklı olarak, bir HAPS ihtiyaç duyulan bölgelere taşınabilir ve esnek bir şekilde hizmet verebilir. Bu özellik, askeri ve kritik uygulamalar için de büyük bir avantaj sağlamaktadır. HAPS, gözetim, keşif ve sınır güvenliği gibi görevlerde etkili bir şekilde kullanılabilir. İHA (İnsansız Hava Araçları), uçaklar ve zeplinler HAPS' lara örnektir (Demircioglu ve ark., 2024, Islam, 2022). Şekil 3'te HAPS gösterimi mevcuttur.

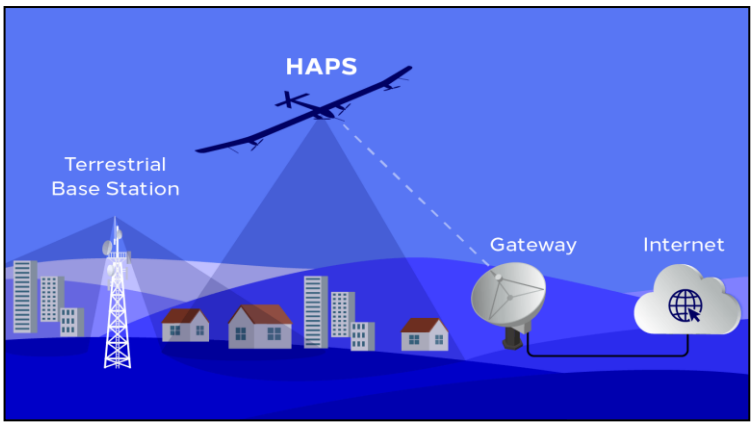

Şekil 3. Yüksek İrtifa Platform Gösterimi (HAPS)

LAPS (Low-Altitude Platforms), Düşük İrtifa Platformları, alçak irtifada faaliyet gösteren ve haberleşme, gözlem veya veri iletimi gibi görevlerde kullanılan platformlardır (Rinaldi ve ark., 2020). Genellikle insansız hava araçları (İHA), balonlar, drone veya küçük hava taşıtları gibi sistemlerden oluşur. LAPS, özellikle karasal veya uydu tabanlı ağların yetersiz kaldığı bölgelerde geçici ya da tamamlayıcı iletişim altyapısı sağlamak amacıyla kullanılır. Düşük irtifada faaliyet göstermeleri sayesinde daha hızlı kurulum, düşük gecikme süresi ve belirli bölgelere yönelik odaklı kapsama gibi avantajlar sunarlar. Acil durum haberleşmesi, doğal afet sonrası geçici ağ kurulumu ve kırsal bölgelerde internet erişimi gibi senaryolarda kritik bir rol oynarlar (Demircioglu ve ark., 2024, Vaezi ve ark, 2022). Şekil 4'te LAPS gösterimi mevcuttur.

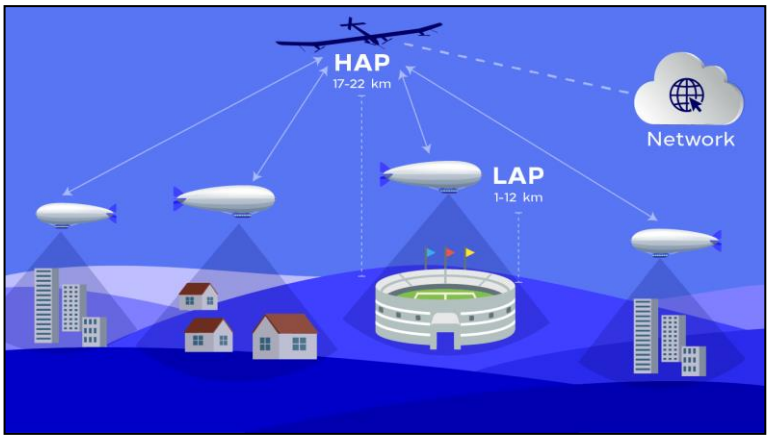

Şekil 4. Düşük İrtifa Platform Gösterimi (LAPS)

Air-to-Ground (A2G), Havadan Yere, hava platformları ile yer istasyonları arasındaki iki yönlü iletişimi ifade eden bir haberleşme sistemidir. Bu teknoloji, hava taşıtları (örneğin uçaklar, insansız hava araçları, balonlar) ile yerdeki kullanıcılar, cihazlar veya altyapılar arasında veri alışverişini mümkün kılar. A2G bağlantıları genellikle düşük gecikme süreleri, yüksek veri iletim kapasitesi ve esnek kurulum avantajlarıyla öne çıkar. Kara ağı, gökyüzünde çok büyük hücreler oluşturan, hava sahasını kapsamak için optimize edilmiş gökyüzüne bakan antenlere sahip A2G baz istasyonlarından oluşur. Bu göz önüne alındığında, yerdekinin aksine radyo sinyalleri serbestçe yayılabilir (Demircioglu ve ark., 2024, Vaezi ve ark, 2022). Şekil 5'te A2G gösterimi mevcuttur.

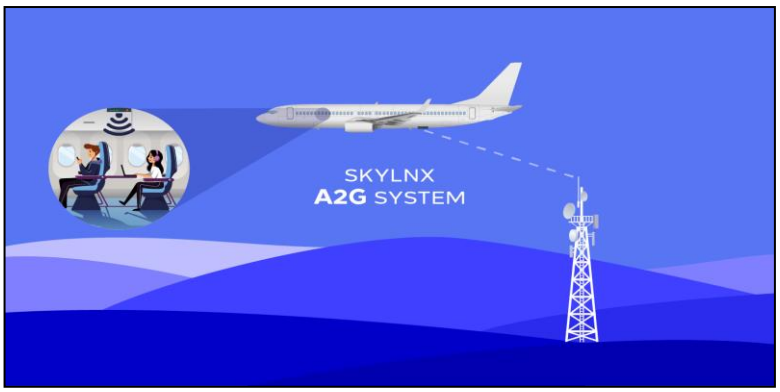

Şekil 5. Havadan Yere Platform Gösterimi (A2G)

Uzaydaki Ağlar, yörüngedeki uydular aracılığıyla haberleşme hizmeti sunan ve karasal iletişim altyapısına alternatif veya tamamlayıcı olarak işlev gören sistemlerdir. Bu sistemler, özellikle küresel kapsama alanı sağlama konusunda eşsiz avantajlara sahiptir. Karasal altyapının bulunmadığı, kurulmasının ekonomik olmadığı veya doğal afet nedeniyle hasar gördüğü bölgelerde, güvenli ve kesintisiz iletişim imkânı sunarlar. Bu ağlar üzerinden internet erişimi, ses ve veri iletimi, yayıncılık (TV, radyo), navigasyon (GNSS) ve askeri/savunma haberleşmeleri gibi pek çok hizmet sağlanabilir (Demircioglu ve ark., 2024, Vaezi ve ark, 2022, Islam, 2022). Uzaydaki ağlar, NTN kapsamında en üst seviyede yer almakta olup, 5G ve 6G teknolojileriyle bütünleşmiş çalışacak şekilde geliştirilmektedir (Alsabah, 2021, Jamshed ve ark, 2023). Bu sayede, dünya genelinde dijital kapsayıcılığı artırma potansiyeline sahiptirler (Cicek, 2025). Uzaydaki ağlar irtifalarına göre 3 farklı sınıfta yer almakta olup Şekil 6'da mesafelerine göre genel gösterimleri mevcuttur.

- Jeosenkron Dünya Yörüngeli (GEO) Uydular
- Orta Dünya Yörüngeli (MEO) Uyduları
- Düşük Dünya Yörüngeli (LEO) Uyduları

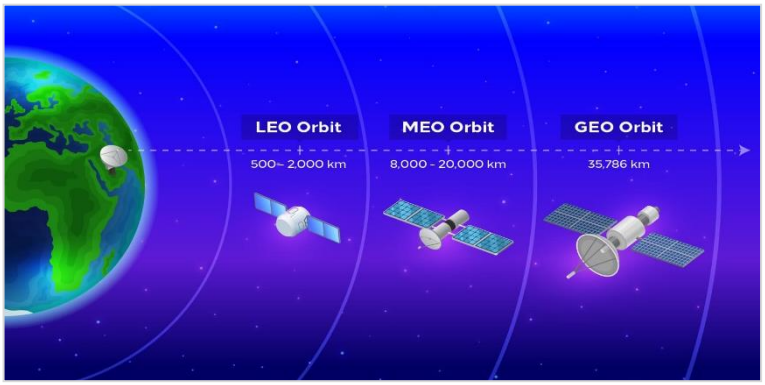

Şekil 6. Uzaydaki Ağlar Genel Gösterimi

Geostationary Earth Orbit (GEO), Jeosenkron Dünya Yörüngeli Uydular, dünya etrafında 35.786 km yükseklikte dairesel ve ekvatoral bir yörüngeye sahiptir. GEO uyduları, uydu haberleşme sistemlerinin en önemli unsurlarından biridir (Demircioglu ve ark., 2024). Dönme periyotlarının dünyanın dönüş periyoduna eşit olması sebebiyle, yeryüzündeki bir gözlemci tarafından durağan olarak görünürler. Bu durum, özellikle televizyon yayını, hava durumu tahminleri ve geniş alan iletişim uygulamaları için büyük bir avantajdır. Ayrıca, GEO uyduları düşük bir uydu sayısıyla geniş bir kapsama alanı sunarak maliyet etkin bir çözüm sunar. GEO uydusunun kapsama alanı 200 ila 3.500 km arasında değişmektedir (Rinaldi ve ark, 2020).

Medium-Earth Orbit (MEO), Orta Dünya Yörüngeli Uydular, dünya etrafında 8.000 ila 20.000 km arasında değişen yükseklikte dairesel bir yörüngeye sahiptir. MEO uydusunun kapsama alanı 100 ila 1.000 km arasında değişmektedir. Genellikle uydu haberleşme ve navigasyon sistemlerinde önemli bir rol oynamaktadır (Demircioglu ve ark., 2024). Özellikle navigasyon sistemlerinde, MEO yörüngesi büyük bir öneme sahiptir. Yörüngenin dünya yüzeyine olan mesafesi, sinyal gecikmesinin makul bir seviyede kalmasını sağlarken aynı

zamanda geniş bir kapsama alanı sunar. Kapsama alanları, LEO uydularına oranla daha geniştir ve bu nedenle global kapsama alanı sağlamak için daha az sayıda uydu gerekmektedir. Evrensel hizmet sağlanabilmesi için genellikle 10-15 adet MEO uydu yeterli olmaktadır. Bu durum, MEO uydularını maliyet etkin bir çözüm haline getirmektedir (Rinaldi ve ark, 2020, Kılıc, 2019).

Low-Earth Orbit (LEO), Alçak Dünya Yörüngeli Uydular, dünya çevresinde 500 ila 2.000 km yükseklikte dairesel bir yörüngeye sahiptir (Kılıc, 2019). LEO uydusunun kapsaması 100 ila 1.000 km arasında değişmektedir. Düşük gecikme süresi ve yüksek hızlı bağlantı sunarak küresel internet kapsama alanı, uzaktan algılama ve gerçek zamanlı veri iletimi gibi hizmetler için idealdirler. LEO uydularının alçak yörüngeye gönderme maliyetlerinin düşük olması, alçak irtifanın sağladığı güvenlik avantajı ve Dünya'ya yakınlığı nedeniyle iki yönlü veri iletişiminde sağladığı avantaj nedeniyle ön plana çıkıyor (Kilic, 2019, Leyva-Mayorga ve ark., 2020). LEO uydularının kapsama alanları, orta dünya yörüngesi (MEO) ve jeostatik dünya yörüngesi (GEO) uydularına kıyasla daha dardır. Ancak, yeryüzüne yakın olmaları nedeniyle iletişimde gecikme (latency) oldukça düşük seviyelerdedir. Bu özellik, özellikle gerçek zamanlı iletişim gerektiren uygulamalar (örneğin, video konferanslar, çevrim içi oyunlar ve finansal işlemler) için büyük avantaj sağlamaktadır. LEO uyduları, sürekli hareket ettikleri için kullanıcılar arasında sık sık el değiştirme (handover) yaşanır. Bu durum, iletişim ağlarının tasarımını ve yönetimini zorlaştırsa da, modern teknolojiler sayesinde bu sorunlar giderek daha etkili bir şekilde yönetilmektedir. Starlink, Oneweb, Amazon, Telesat, Iridium, Globalstar, Viasat vb. gibi projeler önde gelen LEO örnekleridir (Kilic, 2019, Leyva-Mayorga ve ark., 2020, Kılıc, 2019).

Tablo-1 de uzaydaki ağların belli parametrelere göre karşılaştırılması mevcuttur (Ozan, 2019, Leyva-Mayorga ve ark., 2020, Kılıc, 2019, Demircioglu ve ark., 2024).

Tablo 1. Uzaydaki Ağların Karşılaştırılması

Parametreler	GEO (35.786 km)	MEO (8.000 ila 20.000 km)	LEO (500-2.000 km)
Yükseklik gecikmesi	Yüksek	Düşük	Çok düşük
Dünya kapsamı	Çok büyük	Büyük	Küçük
Gerekli uydular	Üç	Altı	Yüzlerce

NTN KULLANIM ALANLARI

Kapsama alanının olmadığı, altyapının imkansızlığı nedeniyle (kırsal alanlar, deniz senaryoları vb.) veya imkânın olduğu ancak ekonomik kolaylığın olmadığı durumlarda, doğal afetler veya saldırılar nedeniyle hizmet kesintilerine maruz kalabilecek karasal iletişim durumlarında, arıza riskini göze alamayan kritik görev uygulamalarında (askeri vb.) hizmet sürekliliği için ve Mobil kullanıcılar ile IoT cihazlarının çeşitli durumlarındaki kısıtlamalarından ötürü NTN ile handover (aktarma) gerçekleştirerek mobil kullanıcıların sürekli iletişimde kalması için kullanmak gerekiyor (Islam, 2021, Cicek, 2025, Jamshed ve ark., 2023, Alsabah ve ark., 2021).

Karasal Olmayan Ağ - Nesnelerin İnterneti (NTN-IoT) ve Karasal Olmayan Ağ - Yeni Radyo (NTN-NR), NTN 'lerin farklı kullanım durumlarına ve pazarlara hitap eden iki yönüdür (Alsabah ve ark., 2021, Rodhe Schwarz, 2025).

NTN-IoT, IoT kullanım durumlarının kapsamını genişleterek kara, deniz ve hava üzerinde gerçek bir küresel kapsama alanı sağlar. Hem GEO hem de LEO irtifalarında çalışır, ancak mevcut hizmetler çoğunlukla GEO'da çalışır (Alsabah ve ark., 2021, Jamshed ve ark., 2023)

NTN-NR, NTN teknolojisinin bir sonraki aşamasıdır. Akıllı telefonları ve diğer 5G cihazlarını uydu tabanlı hizmetlere doğrudan bağlayacak. LEO yüksekliğinde çalışacak ve çeşitli kullanım durumları için düşük veri hizmetleri, ses ve mesajlaşma sağlayacaktır (Gatehouse Satcom, 2024, GSMA, 2024).

NTN-IoT ve NTN-NR arasındaki temel fark, hedef cihazlarında ve bant genişliği kullanımında yatmaktadır. NTN-IoT, IoT cihazlarına odaklanır ve hem GEO hem de LEO irtifalarında faaliyet gösterirken, NTN-NR akıllı telefonlar gibi 5G cihazlarını hedefler ve yalnızca LEO irtifasında çalışır [14,15]. NTN-NR cihazları, NTN-IoT cihazlarından daha büyük bir bant genişliği kullanır ve daha yüksek verim sunar ve geniş bir spektrumda çalışır (Demircioglu ve ark., 2024, Gatehouse Satcom, 2024). Şekil 7'de NTN teknolojinin genel kullanım alanları gösterilmektedir.

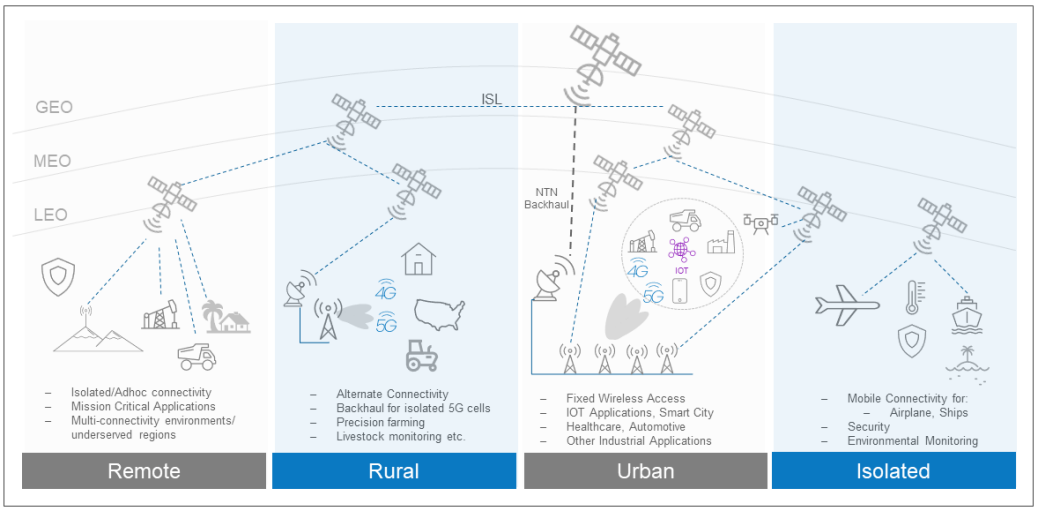

Şekil 7. NTN Kullanım Alanları

Önümüzdeki 5 ile 10 yıl içerisinde mobil teknolojilerinin gelişmesi ile NTN-IoT uydu tabanlı hizmetlerde büyüme görülmesi kaçınılmazdır. NTN-IoT teknolojisinin kullanılacağı muhtemelen alanlar aşağıda belirtilmiştir (Demircioglu ve ark., 2024, Gatehouse Satcom, 2024, Tariq ve ark, 2023, Rodhe Schwarz, 2025).

- **SOS ve Çift Yönlü Mesajlaşma:** Cihazlar (akıllı telefonlar, giyilebilir cihazlar ve arabalar) karasal erişimin olmadığı alanlarda SOS ve çift yönlü mesajlaşmaya izin vermek için NTN NB-IoT yonga setlerini uygulayabilir.
- **Tarım ve Çiftçilik:** Hassas çiftçilik ve hayvancılık izleme gibi tarımsal uygulamalar kırsal veya uzak yerlerde bile mümkündür.
- **Varlık Takibi:** Nakliye konteynerleri veya araçlar gibi değerli varlıkların konumu, varlıklar sınırlı hücresel bağlantıya sahip bölgelerden geçse bile takip edilebilir.
- **Afet Müdahalesi ve Kurtarma:** Arama ve kurtarma, hasar tespiti ve acil müdahale için IoT cihazları, hasarlı altyapı nedeniyle sınırlı veya hiç bağlantının olmadığı alanlarda kullanılabilir.
- **Uzaktan İzleme:** Petrol sondaj kuleleri veya hava istasyonları gibi uzak yerlerdeki ekipmanlar izlenebilir.
- **Deniz/Hava Uygulamaları:** Sınırlı bağlantıya sahip açık okyanus veya kıyı bölgelerinde gemi takibi veya çevresel izleme mümkündür.
- **Otomotiv İletişimi:** Düşük veri hızlı otomotiv güvenliği ve acil durum çağrısı, izleme ve erişim kontrolü gibi uzaktan hizmetler için hizmet sürekliliği.

NTN geliştikçe, NTN-NR 'nin önemi de artacaktır. Bu teknoloji NTN 'nin kapsamını genişletecek ve NTN-IoT 'ye benzer hizmetler sunacak, ancak hizmetler çok daha büyük bir ölçekte olacaktır (Demircioglu ve ark., 2024, Gatehouse Satcom, 2024, Tariq ve ark, 2023, Rodhe Schwarz, 2025). Bu hizmetler şu şekildedir:

- **5G Temel Hizmetlerinin Her Yerde Sürekliliği:** NTN 'nin genişletilmiş kapsamı ve erişimiyle, 5G temel hizmetlerinin sürekliliği her yerde sağlanabilir. Bu, coğrafi konum veya araziden bağımsız olarak mobil veri, sesli aramalar ve mesajlaşma gibi hizmetlere kesintisiz erişim anlamına gelir. Bu yalnızca bireysel kullanıcılara fayda sağlamakla kalmaz, aynı zamanda kesintisiz bağlantıya büyük ölçüde güvenen işletmeleri ve endüstrileri de güçlendirir.
- **NTN Tarafından 5G Sabit Kablosuz Erişim (FWA) Geliştirmesi:** NTN 'den yararlanılarak 5G FWA daha sağlam hale getirilebilir ve daha yaygın olarak kullanılabilir. Bu, özellikle geleneksel kablolu bağlantıların uygulanabilir veya maliyet açısından etkili olmadığı alanlarda hanelere ve işletmelere yüksek hızlı, istikrarlı internet hizmetleri sağlanmasına yardımcı olabilir.
- **5G ve NTN ile IoT devrimi:** NTN 'nin 5G ağlarına entegrasyonu IoT yeteneklerini önemli ölçüde artırabilir. Bu, daha verimli veri alışverişini, gelişmiş cihaz birlikte çalışabilirliğini ve sektörler

genelinde dijital dönüşümü yönlendiren karmaşık IoT ekosistemlerinin oluşturulmasını destekler.

- **Otomotiv Endüstrisi Dönüşümü:** NTN 'ler otomotiv endüstrisinin evrimini kolaylaştırabilir, gelişmiş araçtan her şeye (V2X) iletişimi, otonom araç geliştirmeyi ve gelişmiş telematik hizmetlerini destekleyebilir. Bu, otomotiv sektöründe güvenliği, verimliliği ve kullanıcı deneyimini büyük ölçüde artırabilir.
- **5G Basitleştirilmiş Dolaşım Çözümleri:** NTN'ler basitleştirilmiş 5G dolaşım çözümlerinin uygulanmasına yardımcı olabilir. Bu, konumdan bağımsız olarak kesintisiz, sınırsız bağlantıya olanak tanır ve tutarlı ve yüksek kaliteli ağ hizmetlerini kolaylaştırır.
- **Kamu Güvenliği Operasyonlarının İyileştirilmesi**: NTN 'ler kamu güvenliği kurumları için hayati önem taşıyan sağlam ve güvenilir iletişim sağlayabilir. Bu, zorlu ortamlarda veya zorlanmış altyapılarda bile gerçek zamanlı koordinasyon, hızlı yanıt ve sorunsuz bilgi alışverişine olanak sağlayabilir.
- **Afet Müdahalesi ve Kurtarma Yönetimi:** Doğal veya insan yapımı afetler karasal ağları tehlikeye atabilir. NTN 'ler bu boşluğu doldurabilir, afet müdahale ekipleri için hayati önem taşıyan bağlantı sağlayabilir, kurtarma operasyonlarının koordinasyonunu destekleyebilir ve etkilenen bölgelerin hızla kurtarılmasına yardımcı olabilir.
- **Gelişmiş Deniz ve Hava Bağlantısı:** NTN yeteneklerinden yararlanılarak, deniz ve hava ortamlarında bağlantı önemli ölçüde iyileştirilebilir. Bu, navigasyon, izleme ve iletişim yeteneklerini iyileştirebilir, bu geleneksel olarak yetersiz hizmet alan bölgelerde güvenliği ve operasyonel verimliliği artırabilir.
- **Yaygın Otomotiv Bağlantısı:** Telefon, filo izleme, teşhis ve yazılım güncellemeleri gibi uygulamalar için her yerde, her zaman hizmet sürekliliğini sağlarken, geleceğin otomotiv endüstrisi için bağlantılı ve akıllı araçları destekler.

NTN VE KARASAL AĞLARIN KARŞILAŞTIRILMASI

NTN ’ler, karasal ağlar ile kıyaslandığında aşağıda verilen avantajlara sahip oldukları söylenebilir (Demircioglu ve ark., 2024, Gatehouse Satcom, 2024, Tariq ve ark, 2023, Rodhe Schwarz, 2025, Islam, 2022, Cicek, 2025).

- **Geniş kapsama alanı:** Dünya yörüngesinde bulunması sebebiyle çok daha geniş bir kapsama alanına sahiptir.
- **Hareketlilik:** Sabit bir yerleşkede olmaması, gerektiği durumlarda ihtiyaç duyulan bölgeye çok düşük maliyetler ile taşınabilir olmasını ve yeni bir baz istasyonu kurulumunun maliyetinin önüne geçilmesini sağlar.
- **Bant Genişliği:** NTN ’ler, karasal ağlara göre daha yüksek bant genişliğine sahiptir. Bunun başlıca sebebi NTN ’lerin ışık veya radyo dalgaları gibi kablosuz sinyaller kullanmasıdır. Bu sinyaller elektrik sinyallerinden daha hızlı hareket eder ve daha fazla veri taşıyabilir.
- **Afet yönetimi:** Özellikle deprem durumlarında, baz istasyonlarının hasar görmesi sebebiyle iletişim kopukluğu yaşanırken, NTN ’ler yörüngede dolaştıkları için bu ve benzeri afetlerden etkilenmez.
- **LOS:** Karasal ağlarda, baz istasyonuyla kullanıcı arasına engel girdiği durumlarda ve kapsama alanından uzaklaşıldıkça sinyal gücünde ciddi düşüşler meydana gelmektedir. NTN ’lerde ise son kullanıcılarla arasına herhangi bir engel giremediği ve kapsama alanı karasal ağlar gibi kısıtlı olmadığı için şehir yapılanmalarından etkilenmez.

NTN’lerin birtakım dezavantajları da mevcuttur. Bunlardan biri; NTN ’lerin, uyduların yörüngedeki konumundan dolayı, karasal ağlara göre daha yüksek gecikme süresine sahip olmalarıdır. Örneğin GEO uyduları için gidiş dönüş gecikme süresi yaklaşık olarak 250 milisaniyedir. Bu, gerçek zamanlı uygulamalar için bir dezavantaj oluşturmaktadır. Fakat HAPS, NTN ’lerin gecikme dezavantajını ortadan kaldırmaktadır. Yeryüzüne çok daha yakın olmaları ve yavaş hareket etmeleri hem gecikme süresi hem de el değiştirme etkisini minimuma indirmektedir. Tablo-2’ de NTN ile Karasal Ağlar arasındaki farklar listelenmektedir.

Tablo 2. NTN ve Karasal Ağlar Arasındaki Farklar

Parametreler	NTN	Karasal Ağlar
İletişim Ortamı	Uzaya yerleştirilen uydular	Yerdeki fiziksel altyapı (Kablolar, fiber optik, mikrodalga bağlantıları)
Kapsam	Dünya'nın (1/4)'te biri çapında küresel kapsama alanı	Belirli coğrafi bölgelerle sınırlı veya fiziksel altyapının kapsama alanı içinde
Gecikme	Sinyal daha uzun mesafeler kat ettikçe daha yüksek	Sinyal daha kısa mesafelerde hareket ettikçe daha düşük
Sinyal Girişimine Duyarlılık	Atmosferik koşullara ve sinyal tıkanıklığına eğilimli	Fiziksel kesintilere ve elektromanyetik girişimlere karşı savunmasız
Hareketlilik	Uzaktan ve mobil iletişime uygundur	Çoğunlukla sabit ve sınırlı hareketlilik
Başlangıç Maliyeti	Daha yüksek	Daha düşük
Veri hızı	Genellikle bazı karasal seçeneklere kıyasla daha düşüktür	Özellikle gelişmiş fiber optik ağlar kullanılarak daha yüksek
Güvenilirlik	Güneş radyasyonu, hava şartları gibi uzayla ilgili sorunlara karşı hassastır	Periyodik bakımla istikrarlı ortamlarda daha güvenilir
Örnekler	GPS, uydu TV, Uydu internet, Uydu telefon	Hücresel ağlar, wifi, ethernet, fiber optik kablolar

SONUÇ VE DEĞERLENDİRMELER

Bu çalışmada, NTN teknolojilerinin, geleneksel karasal ağlar ile karşılaştırıldığında sağladığı avantajlar ve potansiyel kullanım alanları üzerinde durulmuştur. Özellikle, küresel kapsama alanı sağlama, altyapı eksikliği olan bölgelerde iletişim hizmeti sunma ve afet sonrası hızlı ağ kurulumları gibi alanlarda NTN teknolojilerinin önemli bir rol oynayacağı öngörülmektedir. NTN 'ler, LEO, MEO ve GEO uyduları gibi uzay tabanlı platformlar ile hava tabanlı sistemler, geniş bir kapsama alanı ve hızlı veri iletimi sunmak için kritik çözümler sunmaktadır. Ayrıca, bu ağlar, geleceğin 5G ve 6G teknolojileriyle entegrasyonu sayesinde, mobil iletişimde devrim yaratma potansiyeline sahiptir.

NTN sistemlerinin sağladığı en belirgin avantajlardan biri, erişim kısıtlamalarının olduğu veya altyapıların sınırlı olduğu bölgelere kolaylıkla hizmet sunabilmesidir. Bunun yanı sıra, uzay ve hava tabanlı ağların düşük gecikme süreleri ve yüksek veri iletimi kapasitesi, kullanıcı deneyimini önemli ölçüde iyileştirebilir. Ancak, NTN teknolojilerinin geniş çapta uygulanabilirliği için, uydu sistemlerinin yüksek maliyetleri, verimli spektrum yönetimi ve çevresel faktörler gibi zorluklar da göz önünde bulundurulmalıdır.

Değerlendirilmesi gereken bir diğer önemli nokta, NTN 'lerin karasal ağlarla entegrasyonunun gerekliliğidir. Karasal ağlar ve NTN 'ler arasındaki iş birliği, sürekli ve kesintisiz bir iletişim altyapısı sağlamada kritik bir öneme sahiptir. Bu entegrasyon, mobil 5G teknolojisinin küresel kapsama alanı ve çoklu bağlantı senaryoları için gereklidir. Bu bağlamda, NTN 'lerin etkin bir şekilde uygulanabilmesi için, 3GPP gibi küresel standart belirleyici kuruluşların sürekli olarak gelişen teknolojilere uyum sağlaması ve güvenlik, veri yönetimi gibi alanlarda açık standartlar geliştirmesi büyük önem taşımaktadır.

Sonuç olarak, NTN teknolojileri, gelecekteki mobil iletişim ağlarının önemli bir parçası haline gelmeye adaydır. Bu teknolojilerin sağladığı avantajlar, özellikle yerel ve küresel iletişim altyapılarındaki boşlukları doldurma ve dijital uçurumu azaltma açısından büyük fırsatlar sunmaktadır. Ancak, bu teknolojilerin verimli bir şekilde kullanılabilmesi için altyapı, yasal düzenlemeler ve finansal destek gibi çeşitli faktörlerin de göz önünde bulundurulması gerekmektedir. NTN ’lerin, gelecekteki iletişim ağlarının sürdürülebilir ve kapsayıcı bir şekilde gelişmesine katkı sağlayacağı düşünülmektedir.

KAYNAKLAR

Alsabah, M., Naser, M.A., Mahmmod, B.M. et al. (7 more authors) (2021) 6G wireless communications networks: a comprehensive survey. 9. pp. 148191-148243.ISSN 2169-3536.

Cicek, B, Karasal Olmayan Ağların Kapsama Analizi, İstanbul Teknik Üniversitesi, Lisansüstü Eğitim Enstitüsü, Yüksek Lisans Tezi, Şubat 2025.

Demircioglu, E., Ertok, H., H., Cankaya, I., Sozbir, N., Non-Terrestrial Network Concepts in 5G and Beyond Communication Technologies, Düzce University Journal of Science & Technology, 12 (2024) 1930-1943.

Gatehouse Satcom, 5G New Radio for Non-Terrestrial Networks, Gatehouse Satcom, 2024. [Online]. Available: https://gatehousesatcom.com/products/5g-ntn/5g-new-radio-for-non-terrestial-networks/

GSMA, Employing Non-Terrestrial Networks for IoT Connectivity, Aug. 2024. [Online]. Available: https://www.gsma.com/solutions-and-impact/technologies/internet-of-things/wp-content/uploads/2024/08/Employing-Non-Terrestrial-Network-for-IoT-Connectivity.pdf

Islam, Y., 5G ve Ötesinde Hizmet Sürekliliği için Karasal Olmayan Ağlar (NTN), İstanbul Üniversitesi-Cerrahpaşa, Lisansüstü Eğitim Enstitüsü, Yüksek Lisans Tezi, Haziran, 2022.

Jamshed, M. A., Kaushik, A., Toka, M., Shin, W., Shakir, M. Z., Dash, S. P., and Dardari, D., Synergizing Airborne Non-Terrestrial Networks and Reconfigurable Intelligent Surfaces-Aided 6G IoT, Updating on 5G Non-Terrestrial-Networks, A 5G American Briefing Paper, July 2023.

Kara, T., Access to Communication with Low Earth Orbit Satellites and Provide Telemedicine, Gebze Technical Unıversity, Institute of Social Sciences, Master Thesis, Gebze, 2021.

Kilic, O., Kinematic Orbit Determination of Low Earth Orbit Satellites using GPS and Galileo Observations, Middle East Technical University, Master of Science, July 2019.

Leyva-Mayorga, I., Soret, B., Röper, M., Wübben, D., Matthiesen, B., Dekorsy, A., Popovski, A., LEO Small-Satellite Constellations for 5G and Beyond-5G Communications, IEEE Access, October 2020.

Li, X., Huang, Y., Zhan, C., Zeng, Y., Non-terrestrial Network. In: Lin, X., Zhang, J., Liu, Y., Kim, J. (eds) Fundamentals of 6G Communications and Networking. Signals and Communication Technology. Springer, Cham. https://doi.org/10.1007/978-3-031-37920-8_27, 2024.

Rinaldi, Federica & Määttänen, Helka-Liina & Torsner, Johan & Pizzi, Sara & Andreev, Sergey & Iera, Antonio & Koucheryavy, Yevgeni & Araniti, Giuseppe. (2020). Non-Terrestrial Networks in 5G & Beyond: A Survey. IEEE Access. 165178-165200. 10.1109/ACCESS.2020.3022981.

Rodhe Schwarz, 5G NTN Takes Flight: Technical Overview of 5G Non-Terrestrial Networks, https://www.rohde-schwarz.com/us/solutions/wireless-communications-testing/wireless-standards/5g-nr/non-terrestrial-networks-ntn/non-terrestrial-networks-ntn_256719.html [Online].

Tariq, F., Bennis, M., Debbah, M. et al., Multiple Access Schemes for 6G Enabled NTN-Assisted IoT Technologies: Recent Developments, Prospects and Challenges, IEEE Internet of Things Magazine, vol. 6, no. 4, pp. 46–52, Dec. 2023. [Online]. Available: https://avesis.yildiz.edu.tr/yayin/71ea6370-0e4e-4d20-9e71-94a3fbd2ba54.

Ürküt, B. B., HAPS Ağları için Optimizasyon Uygulamaları, Konya Teknik Üniversitesi, Lisansüstü Eğitim Enstitüsü, Master Tezi, Ocak 2025.

Vaezi, M., Azari, A., Khosravirad, S. R., Shirvanimoghaddam, M., Chasaki, D. and Popovski, P., Cellular, wide-area, and nonterrestrial IoT: A survey on 5G advances and the road toward 6G, IEEE Communications Surveys&Tutorials, vol.24, no. 2, pp. 1117– 1174, 2022.

➢ *ORAL PRESENTATION*

Sodyum lignosülfonatın beton katkı maddesi olarak etkisinin incelenmesi

Zeynep Özserçe Haste[1*] (*ORCID: https://orcid.org/0000-0001-7783-9515*),

[*1]Sivas Cumhuriyet University, Faculty of Engineering, Chemical Engineering, Sivas, Turkey

*Sorumlu yazar e-posta:zeynepozserce@hotmail.com

Özet

Bu çalışmanın amacı, reçetesi belirlenmiş betonda farklı miktarlarda sodyum lignosülfonat eklenerek slump ve basınç dayanımı testlerini yapıp sodyum lignosülfonatın etkisini incelemektir. Bu amaçla öncelikle kullanılacak ince agregalarda metilen mavisi deneyi yapıldı ve tüm agregalarda kil oranı %1.25 olacak şekilde agrega belirlendi. Hazırlanan beton reçetesine uygun şekilde beton hazırlandı. Tüm numuneler için farklı miktarda sodyum lignosülfat eklendi ve ilk anda çökme testi yapıldı bu slump1 olarak tanımlandı. 30 dakika geçtikten sonra beton 1 dak karıştırıldı, çökme testi yapıldı 30 dak slump olarak kaydedildi. Bu numulerden işlenebilir ve kıvamı uygun olanlar kalıplara alındı 24 saat sonra kürleme tankına alınarak 7 gün ve 28 gün tanklarda bekletildi. Kürlenme süresi tamamlanan betonlar için basınç dayanımı testleri yapıldı. Bu çalışma sonucunda beton reçetesine uygun miktarda sodyum lignosülfat eklendiğinde betonda kıvam koruma, işlenebilirlik açısından uygun ve basınç dayanımı C25/35 beton elde edilebileceği görülmüştür.

.**Keywords:** Sodyum lignosülfonat, beton, slump, basınç dayanımı,

Investigation of the effect of sodium lignosulfonate as a concrete additive.

Abstract

The aim of this study is to perform slump and compressive strength tests by adding different amounts of sodium lignosulfonate to the concrete with a specified prescription and to examine the effect of sodium lignosulfonate. For this purpose, first of all, methylene blue test was performed on the fine aggregates to be used and the aggregate was determined to have a clay ratio of 1.25% in all aggregates. Concrete was prepared in accordance with the prepared concrete prescription. Different amounts of sodium lignosulfonate were added to all samples and slump test was performed at first, this was defined as slump1. After 30 minutes, the concrete was mixed for 1 minute, slump test was performed and recorded as 30 minutes slump. The workable and suitable consistency samples were taken into molds and after 24 hours, they were taken to the curing tank and kept in the tanks for 7 and 28 days. Compressive strength tests were performed for the concretes whose curing period was completed. As a result of this study, it was seen that when the appropriate amount of sodium lignosulfonate was added to the concrete prescription, consistency preservation, workability and compressive strength C25/35 concrete could be obtained.

Keywords: Sodium lignosulfonate, concrete, slump, compressive strength,

GİRİŞ

Beton; çimento, su, agrega ve gerektiğinde katkı maddelerinin (mineral, kimyasal, fiber vb.) belirli şartlar ve oranlarda karıştırılmasıyla elde edilen, başlangıçta şekil verilebilen plastik formda olup, zamanla çimento ve su arasındaki kimyasal reaksiyonun gelişmesiyle (hidratasyon) sertleşerek mukavemet kazanan, harç fazı ve agregadan oluşan kompozit bir yapı malzemesidir. (Polat H., 2012)

Çimento, su ve ince agreganın karıştırılması ile elde edilen karışıma harç denir. Harç, iri agrega içermeyen betondur. Çimento ve suyun karıştırılması ile elde edilen çimento hamuru başlangıçta yumuşak ve şekil verilebilir durumdadır. Fakat çimento ve su arasında çok hızlı başlayarak devam eden hidratasyon ile çimento hamuru birkaç saat içerisinde sertleşmeye başlar ve zaman geçtikçe tamamen katılaşır.

İlk hazırlandığı zaman plastik özellik gösterdiği ve şekil verilebildiği andan itibaren katılaşmanın başladığı zamana kadarki haline taze beton denir. Betonun hidratasyon ile katılaşmasından sonraki haline ise sertleşmiş beton denir. (Erdoğan, 2013) Betonun işlenebilirlik özelliğine etki eden başlıca faktörler şu şekildedir.

- Su / çimento oranı : Su / çimento oranı arttırıldıkça taze beton akıcılığı artar. Fakat gereğinden fazla su kullanılması beton işlenebilme özelliğini arttırmasına rağmen diğer olumsuz etkileri nedeniyle fazla kullanımı tercih edilmez.

- Çimento dozajı : Çimento dozajını arttırmak betonun işlenebilme özelliğini de artmaktadır. Ancak çimento dozajı teknik ve ekonomik açıdan çok fazla arttırılamaz. Ayrıca çimento dozajı dışında çimento inceliği de beton işlenebilme özelliğini arttırmaktadır.
- Kum : Beton karışımında kullanılan kumun ince kum olması beton işlenebilirliğini arttırmaktadır. İnce kum daha fazla su tutarak karışım içindeki serbest suyu azaltır. Kumun inceliğinin yanı sıra yapısı da işlenebilirlikte önemlidir. Kumun yuvarlak yapıda ve düzgün granül şeklinde olması da işlenebilirlik açısından yararlıdır. Doğal dere kumu, kırma taş ile elde edilen kuma tercih edilmelidir.
- Karışım oranı : Beton karışım oranı iyi ayarlanarak taze betonun işlenebilirlik özelliği arttırılabilir. Burada önemli olan çakıl/ kum oranı ve maksimum tane çapıdır. Betonda maksimum tane çapı arttıkça betonun işenebilme özelliği azalmaktadır.
- Kimyasal katkılar : Hava katkısı beton işlenebilirlik özelliğini arttırmaktadır. Bu katkı sayesinde betondaki akışkanlık artar. Betonda segregasyon (ayrışma) ve kusma önemli derecede azalır. Betondaki karma suyu miktarını azaltmak amacıyla kullanılan su kesici kimyasal katkılar betonun slampını düşürmeden su/ çimento oranını azaltmaktadır. Bu katkı kullanılarak su / çimento oranı sabit tutulacak olursa slump değerinin arttığı görülür.
- Sıcaklık : Sıcaklığın yüksek olması taze betonun işlenebilme özelliğine olumsuz etki yapar. (Yalçın vd., 2006)

Betonun tanımlanması ve sınıflandırılması basınç dayanımına göre yapılır. Basınç dayanımı, çapı 150 mm ve yüksekliği 300 mm olan standart deney silindirlerinin 28 gün sonunda, TS 3068'e uygun biçimde test edilmesi ile elde edilir. Beton karakteristik basınç dayanımı (fck), standart silindir veya küp şeklindeki kalıplara alınan beton numunesinin basınç dayanımı test sonuçları TS 500 standardında verilen değerlerde ya da bu değerden %10 düşük olma olasılığı ile değerlendirilir.

Lignin doğada en çok bulunan aromatik polimerdir. Esas olarak kağıt ve kağıt hamuru endüstrisi olmak üzere endüstriyel proseslerden kaynaklanan bir atık üründür ve burada küçük miktarlar düşük değerli bir enerji kaynağı olarak kullanılır. Biyorafinerilerin son zamanlarda ortaya çıkması, belirgin bir değerlendirme yolu olmayan daha fazla lignin üretimiyle sonuçlanmıştır [7] . Lignin için yeni değerlendirme yolları arasında karbon liflerinin, tasarlanabilir özelliklere sahip plastiklerin, polimer köpüklerin, yakıtların ve diğer değerli kimyasal bileşiklerin üretimi yer almaktadır. Lignin türevleri olan lignosülfonatlar çeşitli alanlarda katkı maddeleri olarak uygulama alanı bulmuştur [8] Son yıllarda lignin üzerine yapılan araştırmalar yoğunlaşmış olup, bu biyopolimerin değerli bir kimyasal bileşik olduğu doğrulanmıştır. Lignin, doğada bol miktarda bulunan ve ayrıca aromatik monomerlerden oluşan tek yenilenebilir ham maddedir. Bu nedenle, lignin depolimerizasyonu, çok çeşitli değerli aromatik bileşikler elde etmek için ilginç bir yoldur [20] .

21. Yüzyılda artan nüfusla birlikte gelişen inşaat sektöründe daha çevresel bir yaklaşımla lignosülfonat grubu katkı maddelerinin kullanımı hem kağıt endüstrisinde ortaya çıkan atığın değerlendirilmesini hemde beton için daha çevresel içerikli katkının kullanılması sağlanmış olacaktır.

MALZEMELER VE YÖNTEMLER

1) Taze Betonun Kıvamı (Slump deneyi):

Taze betonun işlenebilirliği bazı özelliklerine bakılarak anlaşılabilmektedir. Kolay karılabilmesi, ayrışma olmaması, kolay yerleştirilmesi, sıkıştırılabilmesi, yüzeyin düzeltilebilmesi, pompalanabilir olması gibi özelliklerin tamamı işlenebilme veya işlenebilirlik olarak tanımlanmaktadır.

8 dm3 beton reçetesi

0-5 mm Agrega	: 7000 g
5-13 mm Agrega	: 3500 g
13-22 mm Agrega	: 5500 g
Çimento	: 2000 g
Su	: 1000 g



Şekil 1. Slump-Çökme deney seti

Slump deneyine başlamadan önce huninin içi nemli bir bezle silinir ve huni tablanın ortasına yerleştirilir. Huninin iki yanında bulunan çıktılara basılarak huninin 1/3'ü taze beton ile doldurulup şişleme çubuğu ile 25 kere şişlenir, huninin 1/3'kadar taze beton eklenip yine 25 kere şişlenir ve huni tamamen taze beton ile doldurulur 25 kere şişlendikten sonra huninin üst kısmında bulunan ağız kısmı alınıp beton yüzeyi şişleme çubuğu veya mala ile düzleştirilir. Bu işlemlerden sonra huni yandaki kulplardan tutulup düşey olarak yavaşça çekilir. Slump hunisi çöken betonun hemen yanına konulur ve şişleme çubuğu üstüne konularak betondaki çökme mesafesi yüksekliği cetvel ile ölçülür. Bu değer slump-çökme değeri olarak tanımlanır. (TSE, 2002a ; ASTM, 2015)

Çizelge 1 Değişik kıvamlardaki betonların çökme değerleri (Erdoğan, 2015)

Beton Kıvamı	Çökme Değeri (cm)
Aşırı kuru	---
Çok kuru	---
Kuru	0 - 2,5
Kuru - Plastik	2,5 – 5,0
Plastik	7,5 – 10,00
Akıcı	15,0 - 17,5

Slump deneyi ile işlenebilirliğe dair çok önemli bilgi elde edilmektedir. Basit ve uygulama kolaylığından dolayı slump deneyi taze betonun kıvamını belirlemek amacıyla en çok kullanılan yöntemdir. Genellikle aynı slump değerine sahip betonların işlenebilirlik özelliklerinin benzer olduğu ve aynı amaçlar için kullanılabilecekleri kabul edilmiştir.

2) Sertleşmiş Betonda Mukavemet (Basınç- Basınç Dayanımı Deneyi):

Betondaki basınç dayanımı eksenel basınç yükü altında sertleşmiş betonun kırılmaya karşı gösterdiği direnç olarak tanımlanmaktadır. Betonun basınç dayanımını ölçmek için farklı yöntemler uygulanmaktadır. Bu yöntemler arasında en çok kullanılan standart basınç dayanımı yöntemidir. Bu yöntem standart deney yöntemi olarak da tanımlanmaktadır.

Standart deney yönteminin uygulanmasında silindir veya küp şeklinde standart kalıplar kullanılmaktadır. Silindir şeklindeki kalıbın çapı 15 cm ve yüksekliği 30 cm' dir. Standart silindir kalıplarda boy/çap oranı 2'dir. Küp şeklindeki kalıp boyutu standart 15 cm'dir. Standart beton kalıpları plastik, dökme demir veya çelik gibi su emmeyen ve şekil değişikliği göstermeyen malzemeden üretilmiş, iç yüzeyi ve tabanı pürüzsüz olmalıdır. TSE (2002b); ASTM (2018)



Şekil 2. Standart küp ve silindir şeklindeki beton kalıpları

SONUÇLAR VE TARTIŞMA

Slump deneyleri

Yapılan slump deneyleri sonucunda sodyum lignosülfonattan 35-40 g , 8 dm^3'lük betona eklendiğinde S3 kıvama sahip beton elde edildi. Slump1 ve 30 dk slump arasındaki farkın çok olması betonun zamanla kıvam koruma ve işlenebilirlik yönünden düşük toleransa sahip olduğu görülmektedir.

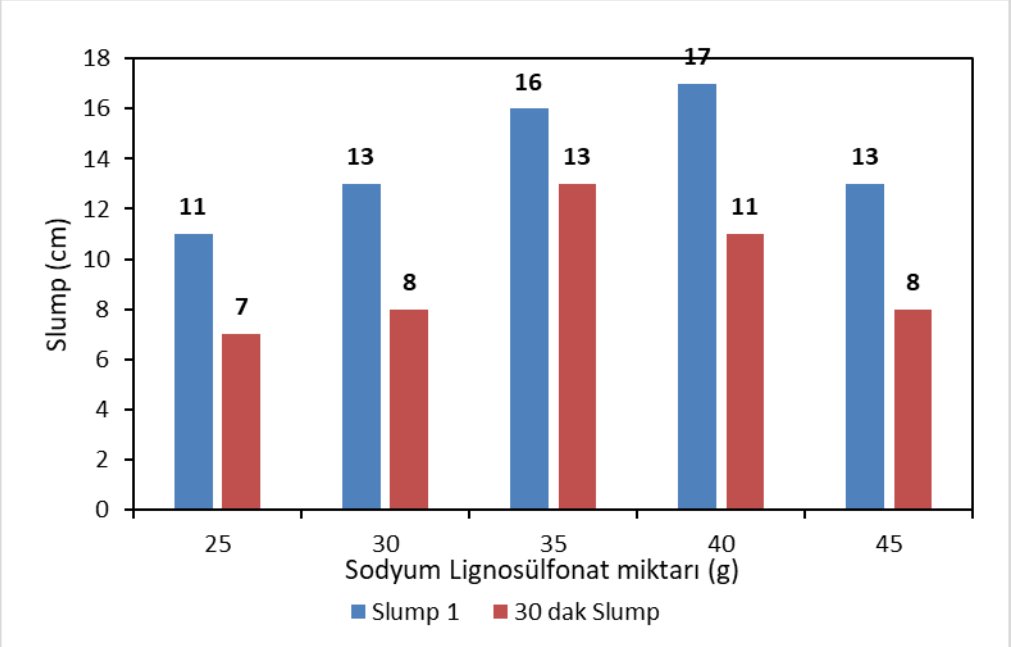

Şekil 3. Sodyum lignosülfonat miktarının slump üzerine etkisi

Slump testleri yapılan betonlara 7 günlük ve 28 günlük basınç dayanımları yapıldığında en yüksek basınca sahip sodyum lignosülfonat miktarının 40 g olduğu tespit edildi. Bu sonuçlara göre 40 g sodyum lignosülfonat 8 dm^3 beton için kullanılarak TS EN 12350-2 ve 12390-2'ye göre kıvam sınıfı S3, C25/35 dayanıma sahip beton üretilmiştir. Bu sonuç sodyum lignosülfonatla çevreye karşı duyarlı, ekonomik özelliklerde beton üretimi yapılabileceğini gösterdi.

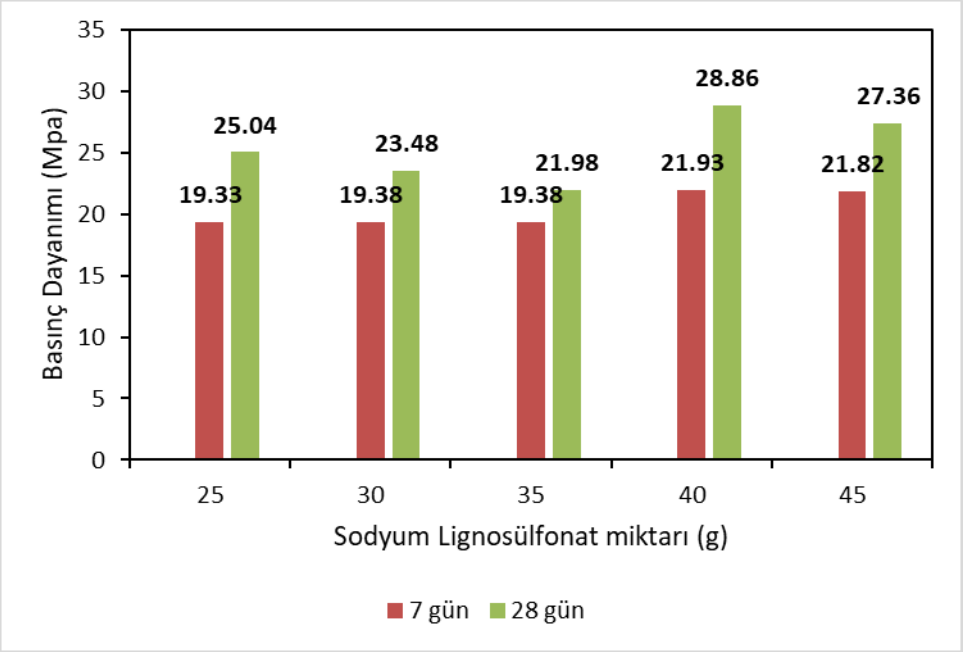

Şekil 4. Sodyum lignosülfonat miktarının basınç dayanımı üzerine etkisi

KAYNAKLAR

ASTM (2015),C143M-15a: Standard Test Method for Slump of Hydraulic-Cement Concrete, edited, American Society for Testing and Materials (ASTM), West Conshohocken, PA, .

ASTM (2018), C 31M-18a: Standard Practice for Making and Curing Concrete Test Specimens in the Field, edited, *American Society for Testing and Materials (ASTM)*, West Conshohocken, PA.

Polat, H., Özel, C., (2012). TS EN 206-1'e göre tasarlanan ve zararlı kimyasal ortamlara maruz kalacak betonların basınç dayanımın bulanık mantık yöntemiyle tahmini. Yapı Teknolojileri Elektronik Dergisi, 8: 26-35.

TSE (2002a)TS EN 12350-2: Beton- Taze beton deneyleri- Bölüm 2: Çökme (slamp) deneyi, edited, *Türk Standartları Enstitüsü (TSE)* Ankara.

TSE (2002b), TS EN 12390-2: Sertleşmiş Beton Deneyleri -Bölüm3 : Deney Numunelerinde Basınç Dayanımı Tayini, edited, *Türk Standartları Enstitüsü (TSE)*, Ankara.

➢ *ORAL PRESENTATION*

Enhanced Impact-Sliding Wear Performance of AISI H13 Extruding Die Steel Through Quenching & Tempering Heat Treatment Process

Tunahan Fatih Sekili[1,2] (*ORCID: https://orcid.org/0009-0003-8735-7490*), Elif Ozturk[1] (*ORCID: https://orcid.org/0009-0001-5098-3506*), Harun Mindivan[1*](*ORCID: https://orcid.org/0000-0003-3948-253X*)

[*1]Bilecik Şeyh Edebali University, Engineering Faculty, Mechanical Engineering Department, Bilecik, Turkey
[2]Arslan Aluminyum A.S., 1st Organized Industrial Zone, Bilecik, Turkey

*Corresponding author e-mail: harun.mindivan@bilecik.edu.tr

Abstract
A new inclined ball-on-plate impact-sliding test method was developed to investigate the wear behavior of AISI H13 die steels in both as-annealed (AS) and quenched & tempered (QT) states, replicating the extrusion process conditions where dies experience combined impact and sliding forces. The AS and QT steels were structurally characterized using a light optical microscope (LOM), accompanied by hardness evaluations. Wear tracks formed during impact-sliding wear tests were analyzed under the LOM to identify the underlying wear mechanisms. The hardening process yields a stable tempered martensitic microstructure containing finely dispersed globular complex carbides, resulting in a satisfactory hardness of 406±16 $HV_{0.05}$ and a reduction in wear rates by 72% and 67% in the impact and sliding regions, respectively.

Keywords: AISI H13 die steel, Heat treatments, Impact sliding wear.

INTRODUCTION

Extrusion is a widely used forming technique for producing long structural components with intricate cross-sections. Successful hot extrusion depends on three key factors: cost-effective tool production, extended tool lifespan, and high-quality extruded products. Tools like dies and mandrels used in hot extrusion are exposed to high extrusion stresses, elevated billet temperatures, thermal cycling, and significant frictional forces. The occurrence of tool cracking can lead to product rejection, production downtime, and more frequent tool repairs, ultimately increasing overall process costs (Gasem, 2013).

Extrusion conditions require die steels to possess high hardness, yield strength, creep resistance, and toughness at elevated temperatures, along with strong resistance to corrosion and wear. Throughout the extrusion process, the die set is subjected to both impact and sliding forces, which cause significant wear on the contact surfaces (Montalvo et al., 2012). The metallurgical properties of AISI H13 make it the most widely preferred die steel for hot work extrusion applications (Berrais et al., 2023; Luo et al., 2023).

Heat treatments like quenching and tempering are used to enhance the mechanical properties of tool steels. The quenching process involves three main stages: (i) heating the steel to a temperature above the A3 line on the iron-carbon phase diagram, (ii) holding it at that temperature to form a fully austenitic structure, and (iii) rapidly cooling it to convert the austenite into martensite, a phase known for its extremely high hardness. To improve toughness and reduce the hardness of martensite, tempering is then carried out by reheating the steel to a temperature below the A1 point (Bryson, 2005). In general, the goal of quenching and tempering of AISI H13 steel and similar steel grades is to produce a hard surface layer and a tough core in the steel parts (Stojanovic et al., 2025). Current literature lacks thorough review articles that examine the impact of extrusion conditions on AISI H13 steel both before and after the hardening process. In the present study, the impact-sliding wear behavior of the as-annealed and as-quenched & tempered AISI H13 die steels used by a local aluminum extrusion plant was investigated to determine their performance during the extrusion process by a homemade impact-sliding wear tester. This study also clarified how the quenching & tempering heat treatment process affects the wear performance of annealed H13 die steel.

MATERIALS AND METHODS

The die steel used in this study matches the chemical composition of AISI H13, as detailed in Table 1. AISI H13 is a standard hot-work die steel, commonly applied in tools like hot forging and extrusion dies due to its excellent toughness and thermal stability (Berrais et al., 2023; Kohli et al., 2023). Circular discs, 30 mm in diameter and 5 mm thick, were sectioned from a rod supplied in the annealed state. Steels in the annealed condition are designated as-received state (AS) steels. These steels were industrially treated by a quenching and tempering process until the rod showed a hardness of 406±16 $HV_{0.05}$. The heat treatment process, used for H13 steels in this work, is depicted schematically in Figure 1. The resulting steels are referred to as-quenched & tempered (QT) steels.

Table 1. Chemical composition of H13 die steel (annealed condition).

Elements	C	Si	Mn	Cr	V	Mo	Fe
Weight %	0.38	1.00	0.37	5.15	1.00	1.35	Remaining

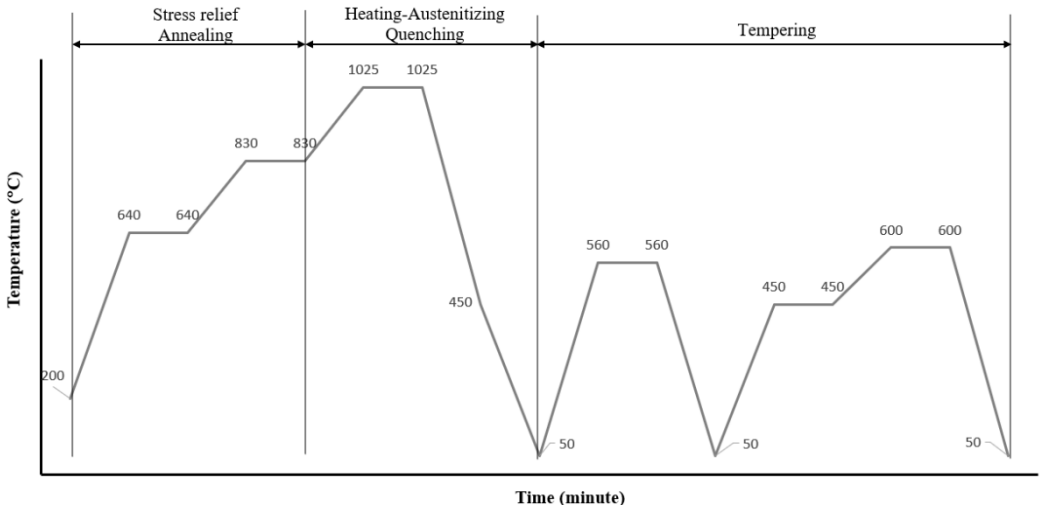

Figure 1. Schematic diagram of quenching and tempering heat treatment process.

Structural analysis of the AS and QT steels was conducted using a Nikon Eclipse LV150 light optical microscope (LOM) following proper polishing and etching with a 2% nital solution. The variation in hardness with depth was assessed using a Shimadzu HVM microhardness tester, applying a 50 g load for 15 seconds.

Figure 2 presents the schematic of the inclined impact-sliding tester developed in our laboratory to replicate the impact and sliding forces generated when billets contact extrusion dies. Figure 3 also includes a typical representation of an impact-sliding wear scar. For each test, the flat treated steels are fixed on a sloped support at a 30° angle. A spring and pneumatic cylinder controlled the applied loading during testing, operating at a frequency of 2.5 Hz. The sample holder, acting as a rocker, rotated around a fixed roller bearing in response to the indenter ball's vertical motion caused by the piston's movement. Prior to testing, a load cell was used to calibrate the maximum loads exerted by the spring and pneumatic cylinder to 40 N and 240 N, respectively. Each treated steel was subjected to 4297 impact cycles using a 10 mm diameter bearing steel (AISI 52100) ball in dry conditions (20±5 °C, 30±5% humidity). Two distinct regions of wear scar (impact and sliding) were examined by a 2-D surface profilometer following the impact-sliding wear test to calculate the quantity of wear loss. The wear rates were then calculated by dividing the volumetric wear loss by the number of loading cycles in mm^3/cycle. Following the tests, LOM was employed to examine the wear tracks.

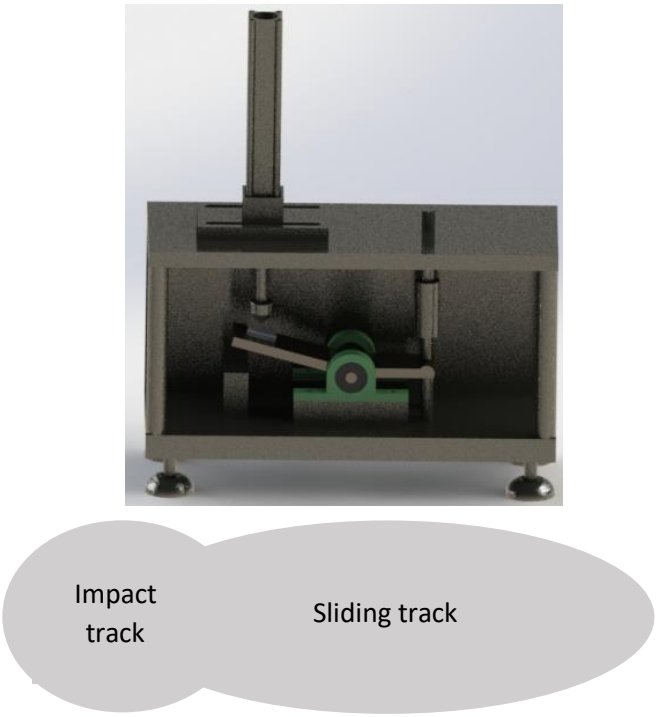

Figure 2. Schematic view of an impact-sliding wear tester.

RESULTS and DISCUSSION

In the annealed, as-received state, the microstructure of H13 steel (Fig. 3 a) features a ferrite matrix with finely dispersed complex carbides, primarily associated with molybdenum and vanadium. Following quenching and tempering heat treatment, the microstructure transforms into a tempered martensite matrix containing finely distributed globular complex carbides (Fig. 3 b). As shown in Fig. 3 b, LOM cannot accurately identify the presence of carbides in the tempered martensite matrix because it has low resolution. This structure is designed to achieve good hot hardness and suitable toughness, thereby improving wear resistance (Akhtar et al., 2010; Fares et al., 2012).

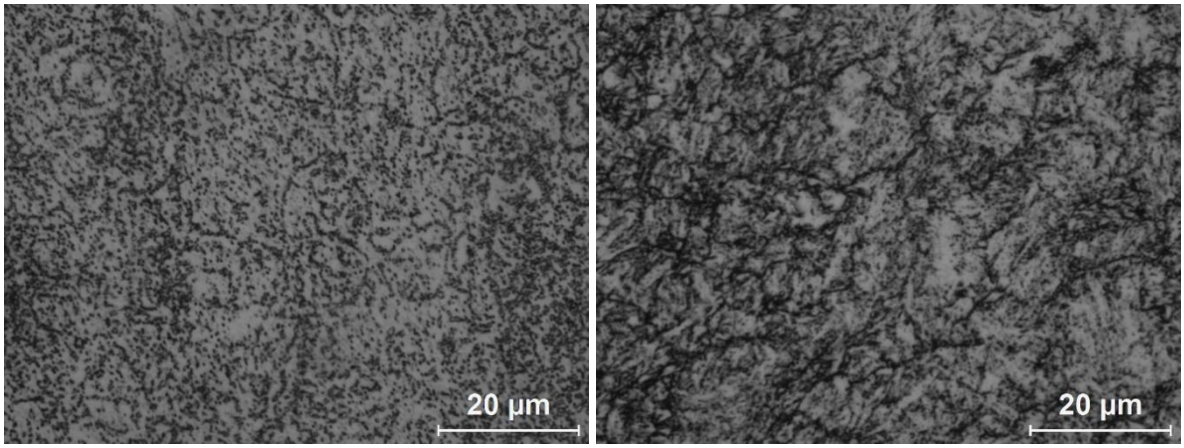

(a) (b)

Figure 3. LOM micrographs of the (a) AS and (b) QT steels.

Figure 4 presents the hardness-depth profile of the AS and QT steels. The surface hardness values for the AS and QT steels are approximately 260±9 $HV_{0.05}$ and 406±16 $HV_{0.05}$, respectively. Following impact-sliding wear testing, both AS and QT steels exhibited characteristic two-dimensional wear tracks, as shown in Fig. 5. In AS and QT steels, the impact regions were deeper and wider than the sliding regions. For AS and QT steels, shear lips formed along the edges of the impact and sliding regions, with more pronounced formation in the impact region. However, the hardening process imposed shallower and narrower wear tracks with a decreased shear-lip formation in both impact and sliding regions. This data indicates that massive plastic deformation played a role in

wear progress in AS steel. The two-dimensional topography shows that as the hardening treatment is applied, the areas affected by impact and sliding regions get smaller. This observation is also confirmed by the wear track cross-sectional curves, which indicate a decrease in both depth and width. This behavior is mainly due to the hardened layer's strong ability to resist wear, plastic deformation, and overall deformation, which matches the hardness results (Fig. 4).

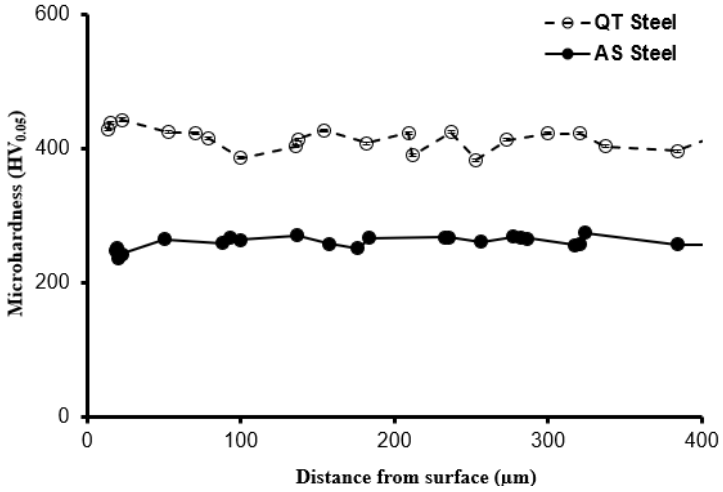

Figure 4. Hardness profiles of both AS and QT steels

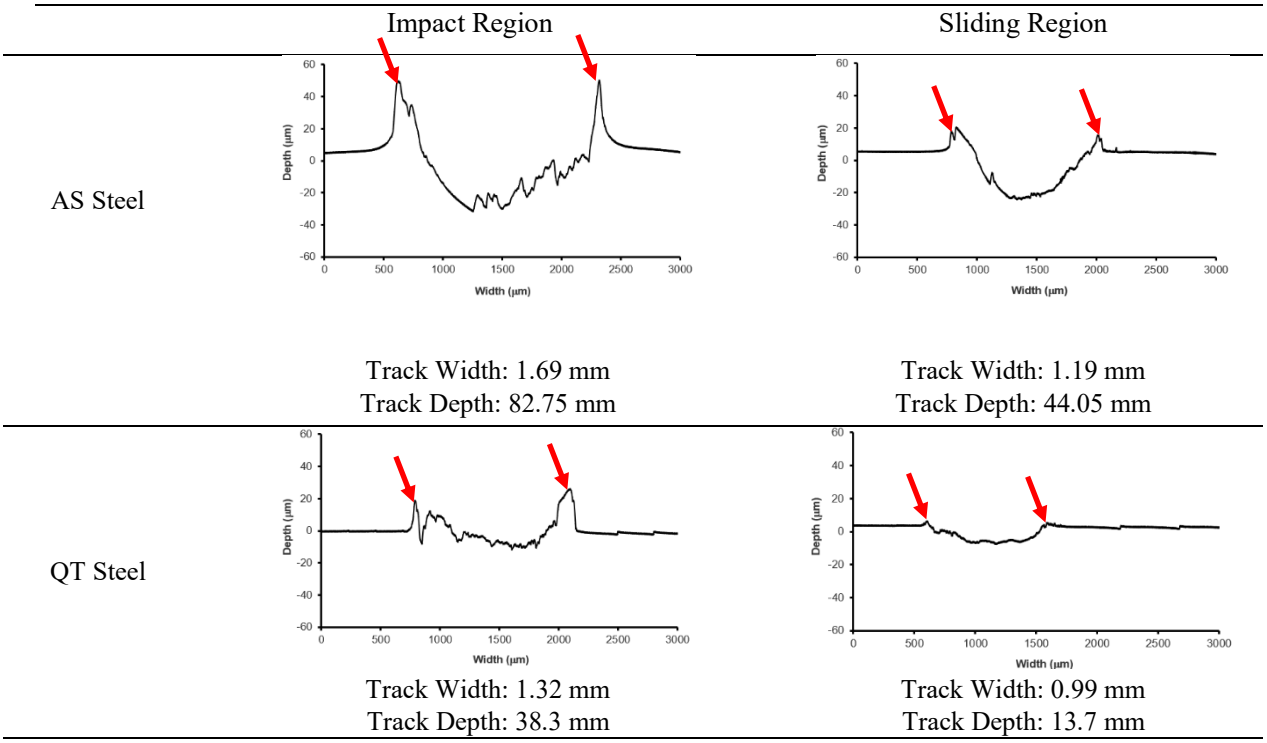

Figure 5. Two-dimensional profiles of the wear tracks for both AS and QT steels, with arrows indicating the shear lips.

Figure 6 shows the average wear rates of the AS and QT steels in the impact and sliding regions. The quenching and tempering heat treatment process reduced the wear rate in the impact region by approximately 72 %, but only by 67 % in the sliding region. On the other hand, the hardening process resulted in a ~68% decrease in the total wear rate. Figs. 7 and 8 show the LOM images of the worn surfaces formed on the AS and QT steels. Low-magnification LOM examinations indicated that the hardened steel created shallower and narrower wear marks in both the impact and sliding regions (Fig. 7). Upon impact, the AS steel exhibited a distinct and deep crater on its surface (Fig. 7). The sliding region of AS steel displays numerous grooves and scratches, typical of abrasive wear (Fig. 7). The wear marks are noticeably larger and deeper compared to those on QT steel. The formation of these

grooves and scratches may be attributed to plastic deformation of the AS steel resulting from contact with the counter-body, or they could be the result of abrasive action by hardened and oxidized wear particles during sliding. Additionally, adhered particles are visible in the sliding region (Fig. 8). On the other hand, the wear tracks in the sliding region for QT steel had slight plastic deformation and slight oxidation wear (Figs. 7 and 8).

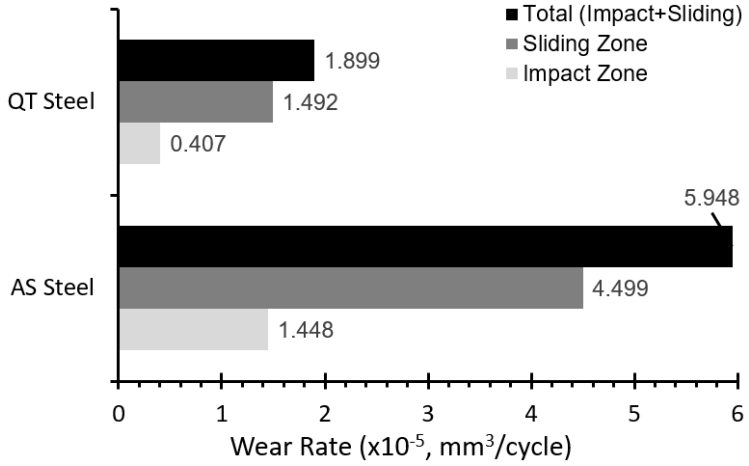

Figure 6. Wear rates of the wear tracks formed on the AS and QT steels' surfaces.

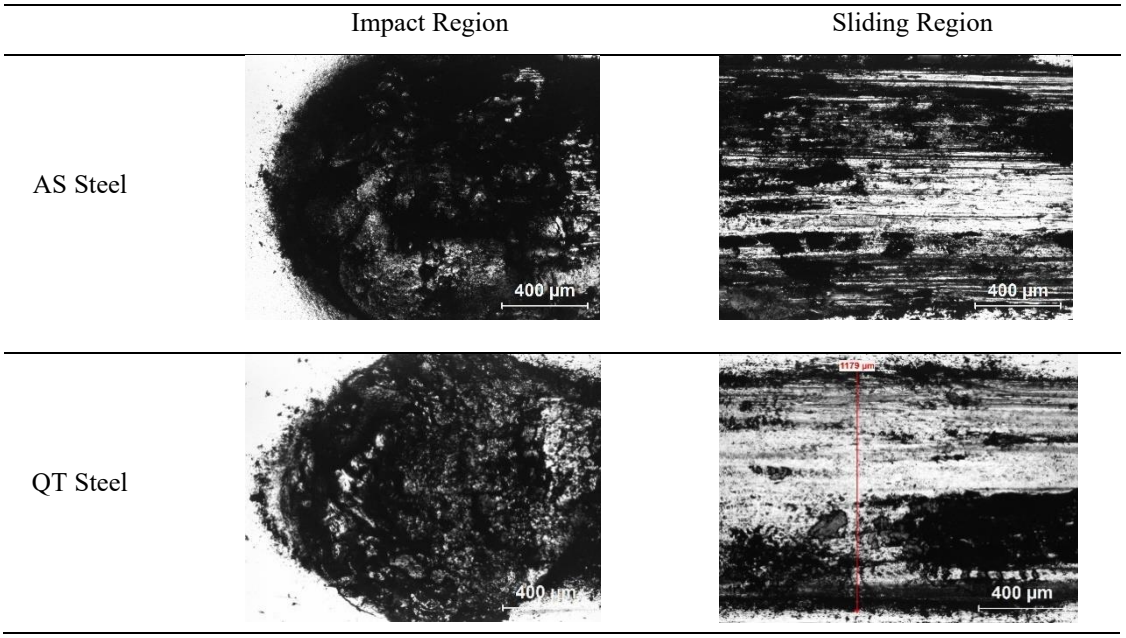

Figure 7. Low-magnification LOM micrographs on impact and sliding tracks of the AS and QT steels.

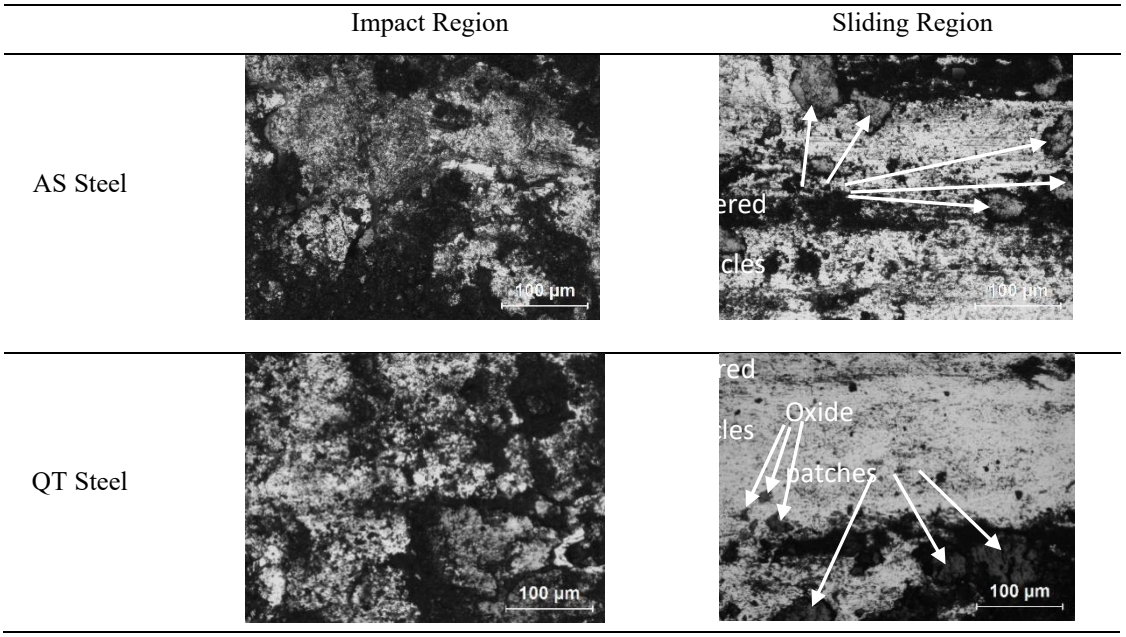

Figure 8. High-magnification LOM micrographs on impact and sliding tracks of the AS and QT steels.

CONCLUSION

The research employed an inclined cyclic impact-sliding wear test on AISI H13 die steels in both the as-annealed (AS) and quenched & tempered (QT) conditions. From the findings of this study, the following conclusions can be made:

1- The hardening process significantly enhanced the surface hardness of the AS steel. The measured surface hardness values for the AS and QT steels were 260±9 $HV_{0.05}$ and 406±16 $HV_{0.05}$, respectively.

2- In the impact and sliding regions, the QT steel exhibited a reduction in wear rate of 72% and 67%, respectively, when compared to the AS steel.

3- The quenching and tempering heat treatment process led to a substantial 68 % decrease in the total wear rate.

ACKNOWLEDGEMENTS

This work has been supported by Bilecik Şeyh Edebali University Scientific Research Projects Coordination Unit under grant number: 2023-01.BŞEÜ.03-02. The authors would like to express their appreciation to Arslan Aluminyum A.S. for technical support in the quenching & tempering heat treatment process.

REFERENCES

Akhtar, S. S., Arif, A. F. M., Yilbas, B. S. (2010). Evaluation of gas nitriding process with in-process variation of nitriding potential for AISI H13 tool steel. The International Journal of Advanced Manufacturing Technology, 47, 687-698.

Berrais, A., Boudebane, A., Labaiz, M., Montagne, A., Lemboub, S., Touhami, M. Z., & Ourdjini, A. (2023). Analysis of wear of a nitrided AISI H13 hot work tool steel in an aluminium hot extrusion process. Wear, 514, 204587.

Bryson, W. E. (2005). Heat treatment, selection, and application of tool steels. Heat Treatment, Selection, and Application of Tool Steels, I-XV.

Fares, ML, Belaid, M., Chahaoui, O., Ghous, H., Khelfaoui, Y. (2012). An investigation on the usefulness and performance of new hot working tool steel by nitrocarburizing process. e-Journal of Surface Science and Nanotechnology, 10, 1-11.

Gasem, Z. M. (2013). Cracking in a multiple gas-nitrided H13 aluminum extrusion mandrel. Engineering Failure Analysis, 31, 68-75.

Hanief Kohli, A., Hanief, M., & Jagota, V. (2023). A retrospection of the effect of nitriding processes on the AISI H13 tool steel. Advances in Materials and Processing Technologies, 9(2), 425-440.

Luo, J., Wang, J., & Xu, J. (2023). Effect of laser shock peening on plasma nitriding microstructure and properties of H13 steel. Surface and Coatings Technology, 473, 130004.

Montalvo, F., Velasco, E., & Canales, A. (2012). Improving microstructure of AISI H13 extruding dies using ion nitriding. Light Metals, 481-485.

Stojanović, Ž., Gligorijević, B., Prvulović, S., But, A., Svoboda, P., Pitel, J., & Vencl, A. (2025). Decarburization and its effects on the properties of plasma-nitrided AISI 4140 steel: a review. Materials, 18(10), 2207.

➢ *ORAL PRESENTATION*

Effect of Cathode Shape and Anodization Time on The Formation of TiO_2 Nanotubes on Ti6Al4V ELI Alloy

Elif Çitgez[1] (*ORCID: https://orcid.org/0009-0007-8415-5083*), Ferda Mindivan[2*](*ORCID: https://orcid.org/0000-0002-6046-2456*), Harun Mindivan[1*](*ORCID: https://orcid.org/0000-0003-3948-253X*)

[1]Bilecik Şeyh Edebali University Engineering Faculty, Mechanical Engineering Department, Bilecik, Turkey
[*2]Bilecik Şeyh Edebali University, Engineering Faculty, Bioengineering Department, Bilecik, Turkey

*Corresponding author e-mail: ferda.mindivan@bilecik.edu.tr

Abstract
The aim of this work was to determine the effect of cathode type and anodization time on the formation of a compact and nanotubular oxide layer on the Ti6Al4V ELI alloy. The results showed that using a square graphite cathode and an anodic oxidation time of 60 minutes were the most suitable parameters for forming a homogeneous nanotubular layer on the Ti6Al4V ELI alloy. Under these conditions, the nanotube diameter of the SGC-60-coded sample was 73.02 nm, the contact angle was 99.27°, and the surface roughness (Ra) was determined to be 0.11 µm. This study suggests that when an organic electrolyte solution containing ammonium fluoride and ethylene glycol is used in the anodic oxidation process, a square graphite cathode and 60 minutes of anodic oxidation time are sufficient to form a regular nanotube structure with uniform tube distribution.

Keywords: Ti6Al4V-ELI alloy, Anodic oxidation conditions, Nanotube form.

INTRODUCTION

Titanium and its alloys have been used as biomaterials for dental implants and orthopedic prostheses because of their excellent strength-to-weight ratio, adequate corrosion resistance, bio-inertness, low cytotoxicity, and favorable biocompatibility (Matykina et al., 2011; Ansari et al., 2020). Ti6Al4V ELI alloy is the most frequently used titanium-based biomaterial (Kiel et al., 2012). Ti6Al4V ELI contains aluminum and vanadium as stabilizing elements, with aluminum stabilizing the alpha phase and vanadium stabilizing the beta phase. These elements enhance the corrosion and mechanical properties of the alloy. However, under specific tribocorrosion conditions, aluminum and vanadium can be released as ions from the material, potentially leading to harmful effects (Gabor et al., 2020). The native oxide layer, typically 1–5 nm thick, naturally forms on the surface of titanium alloys and helps prevent ion release. This oxide layer plays a crucial role in the high biocompatibility of titanium alloys by acting as a protective barrier that minimizes the potential for harmful ion leakage into the body (Lario et al., 2019). An electrochemical technique known as anodization or anodic oxidation is a surface treatment technique applied to titanium alloys that generates regular nano topographical features, such as nanotubes. These nanotubes are contributed significantly to preventing ion release, enhancing properties like biocompatibility and osseointegration (Yavari et al., 2015; Wang et al., 2014). With recent developments in the creation of nanostructured surfaces, it has been successfully applied as a surface treatment for orthopedic implants throughout the previous few decades. In particular, modifying the anodic conditions makes it simple to build and control self-organized nanotubular oxide structures (Wang et al., 2014). Numerous studies in the literature investigate the impact of anodic oxidation conditions on the nanotube structures produced on Ti alloys (Jáquez-Muñoz et al., 2024; Gaona-Tiburcio et al.,2024; Andoko et al. 2024; Jáquez-Muñoz et al., 2023; Kapusta-Kołodziej et al., 2017; Jarosz et al., 2014; Kapusta-Kołodziej et al., 2014; Kim et al., 2013). In this study, the effect of cathode shape and anodization time used in the anodic oxidation processto form nanotubes on Ti6Al4V ELI alloy was examined.

MATERIALS and METHODS

In this study, a purchased 1 m Ti6Al4V ELI rod was cut into 20 mm diameter sections, grounded, and polished (Figure 1 (a)). It was then prepared for anodization by ultrasonic cleaning with ethanol for 5 minutes, followed by 5 minutes of cleaning with deionised water. Ti6Al4V ELI was used as the working electrode (anode) and square, cylindrical graphite cathode as the cathode (Figure 1 (b)). Images of square and cylindrical graphite cathodes used during the anodic oxidation process are given in Figure 1 (c) and (d). The anodizing parameters and the codes of the samples produced with different parameters are shown in Table 1. Surface analysis of samples after anodic

oxidation treatment were examined by field emission scanning electron microscopy (FE-SEM (Supra 40VP, Zeiss)). The contact angles of the samples were measured with the Fytronix 9000 Contact Angle Analyzer device. The surface roughness values of the samples were measured with the Mitutoyo Surtest SJ-400 profilometer.

Table 1. The anodizing parameters and samples codes.

Samples	Graphite Cathode	Anodization Time (min.)	Voltage (V)	Organic Electrolyte Solution
SGC-30	Square	30	30	%0.5 NH_4F %5.0 H_2O Balanced Ethylene Glycol
SGC-60	Square	60	30	
CGC-30	Cylindrical	30	30	
CGC-60	Cylindrical	60	30	

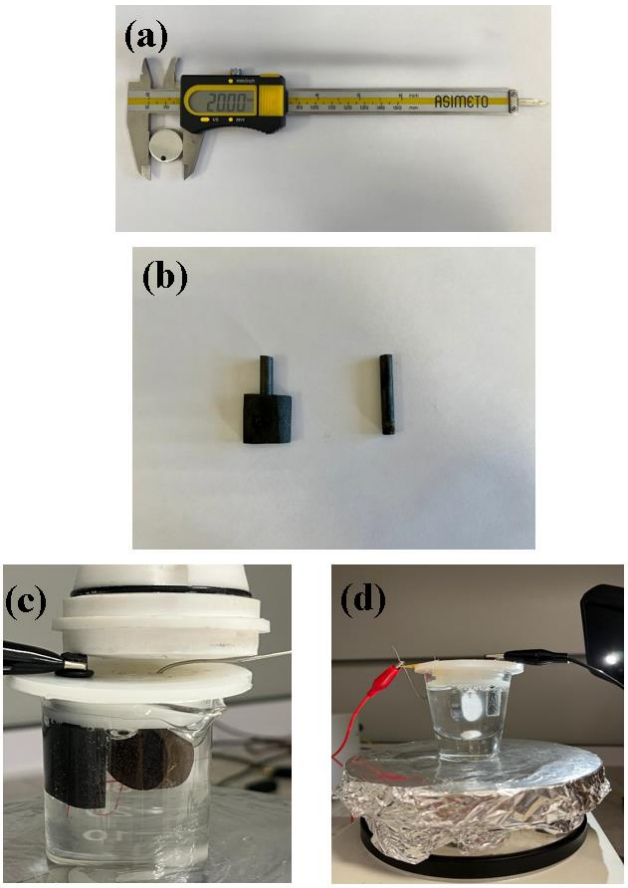

Figure 1. (a) Ti6Al4V ELI alloy, (b) Square and cylindrical graphite cathode, (c) Anodic oxidation with square graphite cathode and (d) Anodic oxidation with cylindrical graphite cathode.

RESULTS and DISCUSSION

Figure 2 (a-d) shows the nanotubular layers obtained from FE-SEM images after the anodic oxidation process. The various combinations of anodic oxidation parameters led to significantly different nanotube sizes and structures on the surface of samples. No regular nanotube structure was observed on the surface of the SGC-30, CGC-30 and CGC-60 samples (Figure 2 (a), (b), and (d)). A regular nanotube structure was only present in the SGC-60 sample where a square graphite cathode was used, and oxidation was carried out for 60 minutes (Figure 2 (c)). The regular nanotube structure seen in Figure 2 (c) is similar to the nanotube morphology formed after anodic oxidation on Ti6Al4V ELI alloy in the literature (Lario et al., 2019). As shown in Figure 2 (b), the nanotube orientations are distinct in the oxidation process performed with a cylindrical cathode for 30 minutes. However, Figure 2 (d) clearly demonstrates that while the orientations change in the oxidation process conducted under the same conditions for 60 minutes, a uniform tube distribution is not achieved across the entire surface. Figure 3 (a-b) shows the nanotube sizes and angles obtained after the anodic oxidation process with square cathode at different

times. As seen in Figure 3 (a), the average nanotube diameter of the SGC-30 coded sample was 55.55 nm and the average angle was 328.48°. As seen in Fig. 3 (b), the average nanotube diameter of the SGC-60 coded sample was 73.02 nm and the average angle was 285.27°. It was observed that as the anodic oxidation time increased, the nanotube diameters enlarged, while the angle decreased. In previous anodic oxidation studies, it has been reported multiple times that the nanotube diameter increases with anodic oxidation time (Mazierski et al., 2016; Gong et al., 2001).

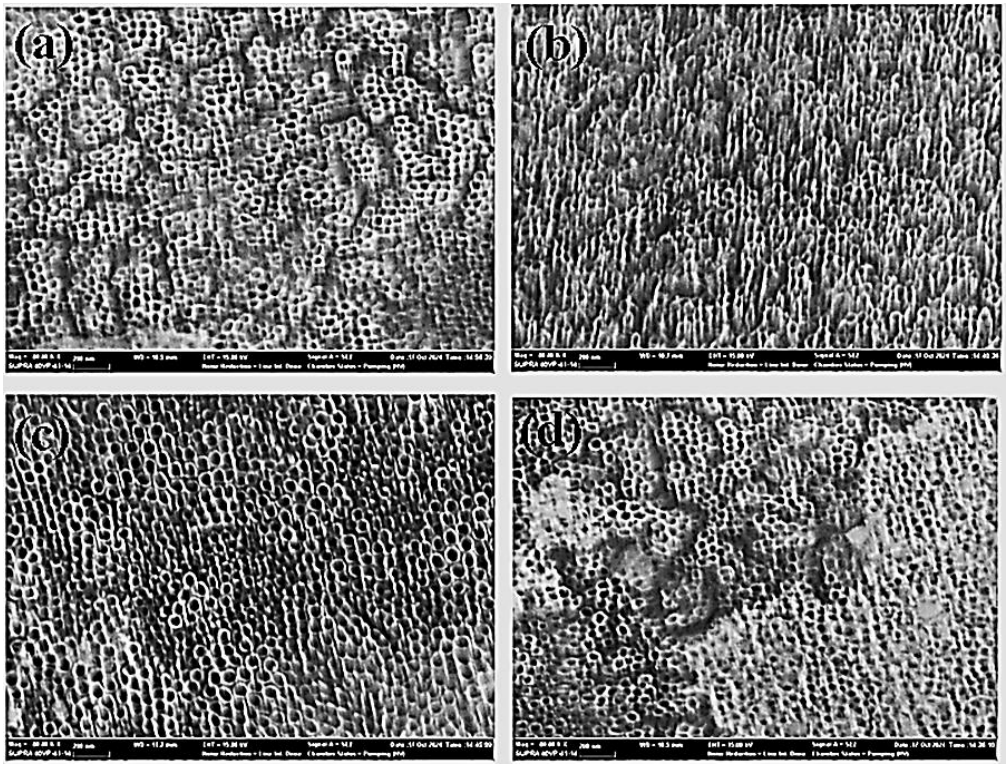

(a) (b)

Figure 2. FE-SEM images of SGC-30 (a), CGC-30 (b), SGC-60 (c) and CGC-60 (d).

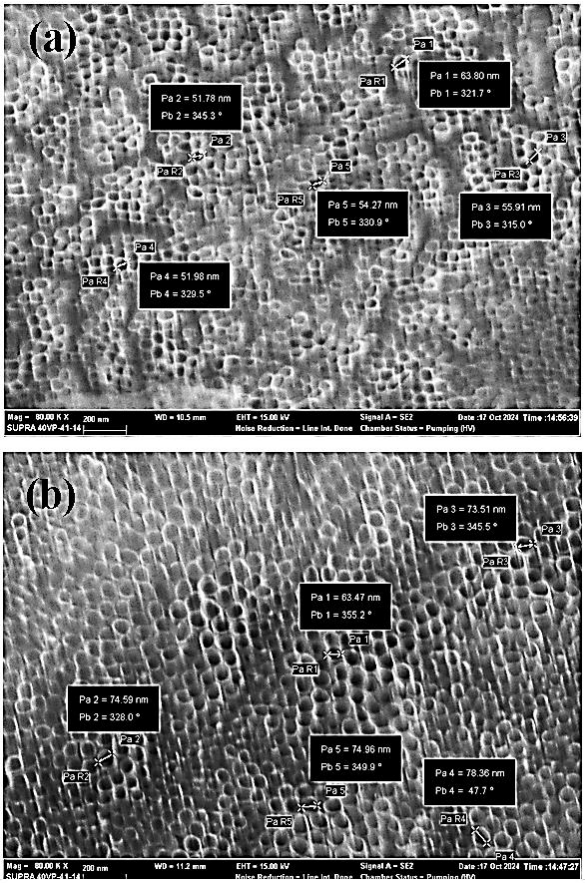

Figure 3. FE-SEM images of SGC-30 (a) and SGC-60 (b).

Figure 4 (a-d) shows the contact angle images of samples after the anodic oxidation process. As seen in Figures 4 (a-c-d), the contact angle values of the SGC-30, SGC-60 and CGC-60 samples were determined to be 100.93°, 99.27°and 100.98°, respectively. These similar contact angle values did not show a significant change over time when the square cathode was used. As a result of 60 minutes of anodic oxidation process with cylinder cathode, the contact angle of the surface gave similar results with square cathode applications. But in Figure 4 (b), the contact angle value of the CGC-30 sample was determined to be 81.17°, which is the lowest value compared to the others. From these results, it was concluded that time was an effective parameter for the contact angles regardless of the cathode type. The contact angle value for Ti6Al4V alloy reported in the literature is 61.7°-61.1°, respectively (Hamil et al., 2022; Yu et al., 2015). In this study, it was determined that the surfaces of samples, except for CGC-30, became hydrophobic (contact angle > 90°) as the high contact angle values. It has been reported in the literature that Ti6Al4V surfaces exhibit hydrophilic properties, while nanotube-coated surfaces exhibit hydrophobic properties. Additionally, it is known that the hydrophobic/hydrophilic behaviour of a surface depends on factors such as surface load, surface energy, surface roughness, and surface porosity (Durdu et al., 2021). Surface roughness analysis was also performed to better understand the contact angle results of this study. Surface roughness profile images and Ra values were shown in Figure 5 (a-d). As shown in Figure 5 (a-b-d), the surface roughness Ra values were determined to be 0.07 µm, 0.06 µm, and 0.07 µm for the samples labelled SGC-30, CGC-30, and CGC-60, respectively. However, the sample labelled SGC-60 exhibited the highest Ra value of 0.11µm. Gao et al. reported that surface roughness and contact angle values increased with anodic oxidation treatment time on the Ti6Al4V alloy, which is consistent with the results obtained in this study (Gao et al., 2014). Durdu et al. reported that contact angle values generally increased as the nanotube diameters increased, resulting in surfaces exhibiting hydrophobic behaviour (Durdu et al., 2021). In this study, the nanotube diameter was high at 60 minutes of anodic oxidation (Figure 3 (a-b)).

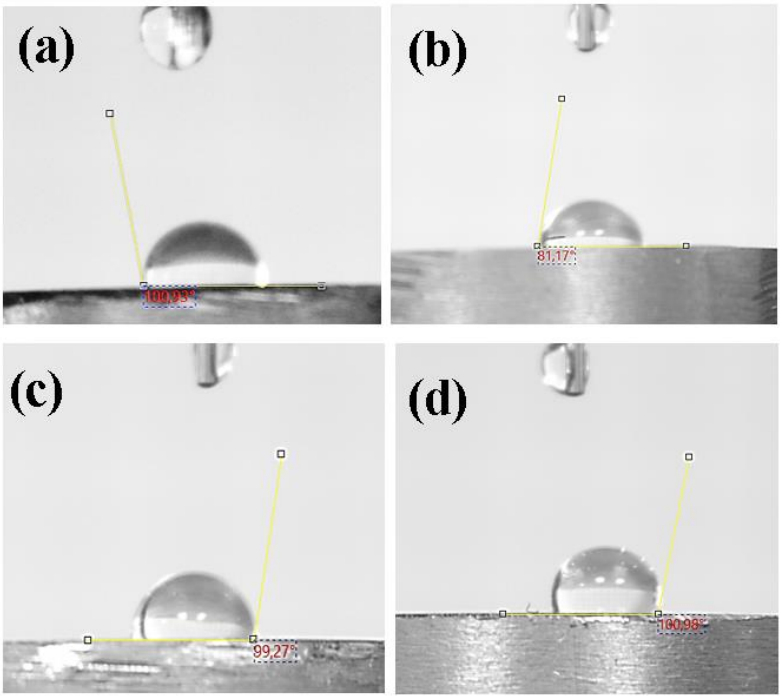

Figure 4. Contact angle images of SGC-30 (a), CGC-30 (b), SGC-60 (c) and CGC-60 (d)

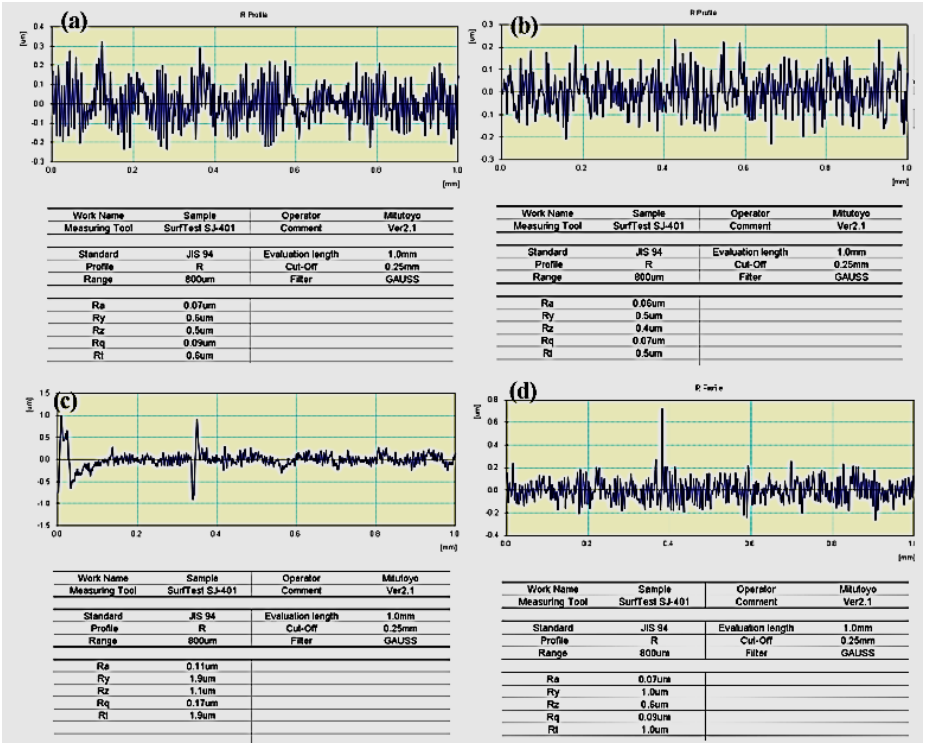

Figure 5. Surface roughness profiles of SGC-30 (a), CGC-30 (b), SGC-60 (c) and CGC-60 (d).

CONCLUSION

In this study, the effect of cathode shape and anodization time on the formation of TiO_2 nanotubes on Ti6Al4V ELI alloy was investigated. In this study, the anodic oxidation process was carried out using square and cylindrical cathodes for 30 and 60 minutes. 30 minutes and the cylindrical cathode were not sufficient to observe the regular nanotube structure, but the most uniform tube distribution was observed at 60 minutes. Compared to the other samples in the study, the average nanotube diameter of the SGC-60 coded sample, which has the preferred nanotube structure, is 73.02 nm. Except for the CGC-30 sample, all other samples showed a hydrophobic surface

with a contact angle greater than 90°. Surface roughness analysis showed similar results, but the sample labelled SGC-60 exhibited the highest Ra value of 0.11 μm.

ACKNOWLEDGEMENTS

This work has been supported by TUBITAK- 2210/C National MSc/MA Scholarship Program in the Priority Fields in Science and Technology.

REFERENCES

Andoko, A., Khoyroh, S. B., Aminnudin, A., &Prasetya, R. (2024). Overview of anodization and silver coating for titanium alloys: Process parameters and biomedical insights. Mechanical Engineering for Society and Industry, 4(3), 318-336.

Ansari, Z., Kalantar, M., Kharaziha, M., Ambrosio, L., &Raucci, M. G. (2020). Polycaprolactone/fluoride-substituted hydroxyapatite (PCL/FHA) nanocomposite coatings prepared by in-situ sol–gel process for dental implant applications. Progress in Organic Coatings, 147, 105873.

Durdu, S., Sancak, M., Yalcin, E., Usta, M., Akagunduz, E., &Altinkok, A. (2021). Surface characterization of TiO_2 nanotube arrays produced on Ti–6Al–4V alloy by anodic oxidation. Surface and Coatings Technology, 428, 127903.

Gabor, R., Doubkova, M., Gorosova, S., Malanik, K., Vandrovcova, M., Cvrcek, L., ... &Bacakova, L. (2020). Preparation of highly wettable coatings on Ti–6Al–4V ELI alloy for traumatological implants using micro-arc oxidation in an alkaline electrolyte. Scientific Reports, 10(1), 19780.

Gao, Y., Sun, Y., & Guo, D. (2014). Facile fabrication of superhydrophobic surfaces with low roughness on Ti–6Al–4V substrates via anodization. Applied Surface Science, 314, 754–759.

Gaona-Tiburcio, C., Jáquez-Muñoz, J. M., Nieves-Mendoza, D., Maldonado-Bandala, E., Lara-Banda, M., Lira-Martinez, M. A., ... &Almeraya-Calderon, F. (2024). Corrosion behavior of titanium alloys (Ti CP2, Ti–6Al–2Sn–4Zr–2Mo, Ti–6Al–4V and Ti Beta-C) with anodized and exposed in NaCl and H_2SO_4 solutions. Metals, 14(2), 160.

Gong, D., Grimes, C. A., Varghese, O. K., Hu, W., Singh, R. S., Chen, Z., & Dickey, E. C. (2001). Titanium oxide nanotube arrays prepared by anodic oxidation. Journal of Materials Research, 16, 3331–3334.

Hamil, M. I., Abdulwahid, K. I., & AL-Shakban, M. (2022). Improvement of corrosion and osseointegration characteristics for Ti–6Al–4V alloy by coating with polyetheretherketone (PEEK) and nanohydroxyapatite using electrophoretic deposition for biomedical applications. Journal of Nanostructures, 12(4), 826–841.

Jarosz, M., Pawlik, A., Kapusta-Kołodziej, J., Jaskuła, M., & Sulka, G. D. (2014). Effect of the previous usage of electrolyte on growth of anodic titanium dioxide (ATO) in a glycerol-based electrolyte. Electrochimica Acta, 136, 412–421.

Jáquez-Muñoz, J. M., Gaona-Tiburcio, C., Méndez-Ramírez, C. T., Baltazar-Zamora, M. Á., Estupinán-López, F., Bautista-Margulis, R. G., ... &Almeraya-Calderón, F. (2023). Corrosion of titanium alloys anodized using electrochemical techniques. Metals, 13(3), 476.

Jáquez-Muñoz, J. M., Gaona-Tiburcio, C., Mendez-Ramirez, C. T., Carrera-Ramirez, M. G., Baltazar-Zamora, M. A., Santiago-Hurtado, G., ... &Almeraya-Calderon, F. (2024). Corrosion of anodized titanium alloys. Coatings, 14(7), 809.

Kapusta-Kołodziej, J., Syrek, K., Pawlik, A., Jarosz, M., Tynkevych, O., & Sulka, G. D. (2017). Effects of anodizing potential and temperature on the growth of anodic TiO_2 and its photoelectrochemical properties. Applied Surface Science, 396, 1119–1129.

Kapusta-Kołodziej, J., Tynkevych, O., Pawlik, A., Jarosz, M., Mech, J., & Sulka, G. D. (2014). Electrochemical growth of porous titanium dioxide in a glycerol-based electrolyte at different temperatures. Electrochimica Acta, 144, 127–135.

Kiel, M., Szewczenko, J., Marciniak, J., &Nowińska, K. (2012). Electrochemical properties of Ti–6Al–4V ELI alloy after anodization. In Information Technologies in Biomedicine: Third International Conference, ITIB 2012, Gliwice, Poland, June 11–13, 2012. Proceedings (pp. 369–378). Springer Berlin Heidelberg.

Kim, J. H., Zhu, K., Kim, J. Y., & Frank, A. J. (2013). Tailoring oriented TiO_2 nanotube morphology for improved Li storage kinetics. Electrochimica Acta, 88, 123–128.

Lario, J., Viera, M., Vicente, A., Igual, A., & Amigo, V. (2019). Corrosion behaviour of Ti–6Al–4V ELI nanotubes for biomedical applications. Journal of Materials Research and Technology, 8(6), 5548–5556.

Matykina, E., Hernandez-López, J. M., Conde, A., Domingo, C., De Damborenea, J. J., & Arenas, M. A. (2011). Morphologies of nanostructured TiO_2 doped with F on Ti–6Al–4V alloy. Electrochimica Acta, 56(5), 2221–2229.

Mazierski, P., Nischk, M., Gołkowska, M., Lisowski, W., Gazda, M., Winiarski, M. J., ... &Zaleska-Medynska, A. (2016). Photocatalytic activity of nitrogen-doped TiO_2 nanotubes prepared by anodic oxidation: The effect of applied voltage, anodization time and amount of nitrogen dopant. Applied Catalysis B: Environmental, 196, 77–88.

Wang, L. N., Jin, M., Zheng, Y., Guan, Y., Lu, X., & Luo, J. L. (2014). Nanotubular surface modification of metallic implants via electrochemical anodization technique. International Journal of Nanomedicine, 4421–4435.

Yavari, S. A., Chai, Y. C., Böttger, A. J., Wauthle, R., Schrooten, J., Weinans, H., &Zadpoor, A. A. (2015). Effects of anodizing parameters and heat treatment on nanotopographical features, bioactivity, and cell culture response of additively manufactured porous titanium. Materials Science and Engineering: C, 51, 132–138.

Yu, X., Tan, L., Yang, H., & Yang, K. (2015). Surface characterization and preparation of Ta coating on Ti–6Al–4V alloy. Journal of Alloys and Compounds, 644, 698–703.

➢ *ORAL PRESENTATION*

Photocatalytic Hydrogen Generation by a Novel Push-Pull Donor-π-Acceptor Dye Sensitized TiO_2

Yigit Osman Akyıldız[1, 2] (*ORCID: https://orcid.org/0000-0001-7057-7268*), Emre Aslan[2*] (*ORCID: https://orcid.org/0000-0002-7672-2873*)

[*1]YEO Technology R&D Center, 34870, İstanbul, Türkiye, e-mail: yigitakyy@gmail.com
[2]Selcuk University, Department of Biochemistry, 42030, Konya, Türkiye

*Corresponding author e-mail: emreaslan89@gmail.com

Abstract

Donor-π-acceptor (D-π-A) dyes are a promising class of dyes in photoelectrochemical and photocatalytic hydrogen evolution reactions (HER) due to their superior light absorption abilities and strong visible light responses. Herein, a novel dye with specific triphenylamine (TPA) donor moiety was designed. The structural, electrochemical and optical properties of the prepared D-π-A dye were researched by NMR, UV-Vis absorption spectroscopy and cyclic voltammetry methods. The D-π-A dye has been utilized as sensitizer to obtain hybrid D-π-A/TiO_2 photocatalyst for the increasing visible light absorption ability. The photoelectrochemical properties of D-π-A/TiO_2 photoelectrode were researched by chronoamperometry and linear sweep voltammetry methods in aqueous electrolyte solution, and it shows stable transient photoelectrochemical current responses between -0.4 V and +0.5 V potential window, as well as displayed 170 μAcm^{-2} transient photocurrent density at 0 V. The photocatalytic HER was carried out by using D-π-A/TiO_2 powder under sunlight in the presence of sacrificial electron donor triethanolamine. The photocatalytic hydrogen production rates were calculated as 670 $\mu mol\ g^{-1}\ h^{-1}$ and 2060 $\mu mol\ g^{-1}\ h^{-1}$ in the presence of D-π-A/TiO_2 and D-π-A/TiO_2/Pt, respectively, which platinium (Pt) co-catalyst is enhanced approximately 4-times photocatalytic activity due to the increasing charge transfer activity. In the absence and presence of Pt co-catalyst, the solar-to-hydrogen energy (STH) conversion efficiencies were determined as 1.72% and 5.31%, respectively. Furthermore, the proposed mechanism for HER was explained with energy band levels of photocatalysts component. These results represent a comparable well-efficiency in the same dye class as a sensitizer, which paves the way to use for different applications.

Keywords: donor-π-acceptor dye, triphenylamine, photocatalytic hydrogen generation

INTRODUCTION

The production of hydrogen from the decomposition of water presents a significant opportunity to obtain renewable, clean, and storable energy under solar light(Wang, Li et al. 2019). The first report of hydrogen evolution was accomplished by Fujishima and Honda in 1972 through a photoelectrochemical process(Fujishima and Honda 1972). Due to its relatively low cost, excellent photocatalytic performance, and high photochemical stability, TiO_2 has an important position among various transition metal oxides in photocatalysis. Furthermore, research on TiO_2 continues to grow rapidly due to its significant advantages among semiconductor materials. However, there are also main limiting factors that restrict its use, such as its ability to absorb only UV light due to its wide bandgap and high charge recombination rate(Ma, Wang et al. 2014). The use of co-catalysts or visible light sensitizers can overcome these disadvantages by facilitating the separation of charges and absorbing low-energy visible light in the photocatalytic HER system(Patir, Aslan et al. 2019, Aslan, Karaman et al. 2020, Huang, Lei et al. 2020). Although the use of semiconductor co-catalysts is beneficial, adjusting the band levels in reaction mechanisms is quite challenging. However, noble metal co-catalysts are crucial due to their ease of use. Because of Pt's effect on the photocatalytic, photoelectrochemical, and electrocatalytic hydrogen evolution reactions (HER), it is known to be the most actively used noble metal co-catalyst(Jiang, Isaacs et al. 2017, Bernsmeier, Sachse et al. 2019). Another significant approach for exciting wide-bandgap semiconductor materials like TiO_2 with low-energy sunlight is the use of organic dye sensitizers. The first use of a sensitizer $(Ru(bipy)_3)^{+2}$ in water splitting was accomplished with Pt/TiO_2/RuO_2 materials created by pioneers(Borgarello, Kiwi et al. 1981). In addition, porphyrin analogues and metal-based phthalocyanine sensitizers have also been reported to be used due to their adjustable band properties and superior abilities to capture sunlight(Martín-Gomis, Fernández-Lázaro et al. 2014, Urbani, Grätzel et al. 2014, Nikoloudakis, López-Duarte et al. 2022). Later, metal-free organic dyes

generated great interest due to their suitable cost, adjustable band structure, and ability to absorb light in a wide spectrum range. Xanthene-based sensitizers have been also used in photocatalytic studies due to their stability and affordability(Li, Guo et al. 2009, Puangpetch, Sommakettarin et al. 2010, Xu, Li et al. 2013, Chowdhury, Malekshoar et al. 2017). However, D-π-A dyes have been developed due to their properties of high light harvesting ability and stability during the photochemical reactions. The structure of these dyes comprises a donor group, π bridge, and acceptor group. Their significant intermolecular charge transfer (ICT) capability and modifiable band gaps are the most important factors for their applications in photocatalytic reactions(Wu and Zhu 2013, Yu, Li et al. 2015, Zhang, Peng et al. 2016, Zani, Melchionna et al. 2021). Recently, D-π-A sensitizers have attracted attention in photovoltaic and photocatalytic devices due to their optical and molecular properties mentioned above. The efficiency of D-π-A sensitizers in HERs can be altered by modifications of various factors, such as the amount of dye load, steric effects, affinity for water, the number of anchoring groups of dyes, and the length of intermediate segments(Kim and Ahn 2010, Lee, Park et al. 2010, Choi, Yang et al. 2012, Han, Wee et al. 2012, Watanabe, Hagiwara et al. 2014, Yu, Cui et al. 2017). These structures are of great interest due to their developed charge transfer properties, which prevent aggregation by facilitating partial oxidation of the nitrogen center of the TPA donor region and provide high stability to the charge carriers of radical cation species(Thelakkat 2002). Also, the effect of the chain length and binding group on the TPA donor parts was investigated(Lee, Park et al. 2010, Han, Wee et al. 2012). In another study, it was found that tris(4-carboxyphenyl)amine-based D-D-π-A dyes, when added to Pt-modified TiO_2 structures, exhibited long-term and significant hydrogen production performance(Kwok, Ho et al. 2022). Another study examined dyes with different central groups (quinoxaline and pyridinopyrazine) and found that the dye containing an extra N atom instead of the CH group was actually the dye that performed less well in both DSSC and DSP systems(Li, Cui et al. 2014). Also, our research team has previously documented triphenylamine-based D-π-A dyes, which enhance the sensitivity of TiO_2 photocatalysts in the context of photocatalytic hydrogen production(Aslan, Gonce et al. 2017, Aslan, Karaman et al. 2019, Patir, Aslan et al. 2019, Aslan, Karaman et al. 2020). Benzothiadiazole (BTD) is a well-known electron acceptor blocking unit for photocatalytic hydrogen production(Wang, Fernández-Terán et al. 2016, Yang, Ma et al. 2016, Pati, Damas et al. 2017). The Tian research group determined with DFT calculations that the N atoms in BTD units are actually catalytic reactive sites for hydrogen formation(Pati, Damas et al. 2017).

In this current study, we report the synthesis of push-pull D-π-A molecular structures based on BTD chromophoric compounds by using low-cost precursors. The synthesized D-π-A molecule have unique electrochemical and optical properties for the harvesting of solar light and charge transfer ability, which were studied by absorption and voltametric experiments. The acquired D-π-A dye was applied for sensitizing the wide-bandgap TiO_2 photocatalyst, enabling the absorption of visible light for both photoelectrochemical and photocatalytic hydrogen generation under sunlight, facilitated by triethanolamine (TEOA) as a sacrificial electron donor. Furthermore, the electrochemical and optical properties of the D-π-A dyes are utilized to elucidate the reaction mechanism.

MATERIALS AND METHODS

Materials

All reactions were carried out under nitrogen atmosphere. Piperidine, Cyanoacetic acid, 1,2-dimethoxyethane (DME) and [1,10-bi(diphenylphospino)ferrocene]dichloropalladium(II) were purchased from Sigma Aldrich. Dichloromethane and n-hexane were purchased from Merck. Methanole and potassium carbonate were purchased from J.T Baker and Riedel de Haen, respectively. Acetonitrile (ACN), sodium hydroxyde (NaOH), hydrochloric acid (HCl), TEOA and sodium sulfate (Na_2SO_4) were obtained by Merck.

Synthesis of D-π-A dye

Synthesis of *4-{7-{bis[4-(hexyloxy)phenyl]amino}Cphenyl)-2-thienyl]-2,1,3-benzotidiazol-4-yl} benzaldehyde*

4- [7- (5-bromo-2-thienyl) -2,1,3-benzotidiazol-4-yl] benzaldehyde (47.3mg; 0.118mmol) was dissolved in anhydrous DME (5mL) in the two neckled flask. K_2CO_3 (40 mg; 0.290 mmol) in water (0.5mL) and (4-[bis[4-(hexyloxy)phenyl]amino]phenyl) boronic acid (75 mg; 0.153 mmol) were added. After the solution was saturated with Argon, $Pd(dppf)Cl_2$ (4.32 mg; 0.006 mmol) was added. The reaction was stirred at 90°C for 48h. Reaction was controlled with thin film chromatography (TLC) and cooled to room temperature. The mixture was poured into 30 mL of water and extracted twice with 30 mL of CH_2CI_2. Then, the organic phases were composited and evaporated by rotary evaporation. Finally, the produce was purified by column chromatography (using silica gel and CH_2CI_2) and dried under vacuum.

Synthesis of *(2E)-3-(4-{7-{bis[4-(hexyloxy)phenyl]amino}phenyl)-2-thienyl]-2,1,3-benzotidiazol-4-yl}phenyl)-2-cyanoacrylic acid (*D-π-A dye*)*

4-{7-{bis[4-(hexyloxy)phenyl]amino}phenyl)-2-thienyl]-2,1,3-benzotidiazol-4 yl}benzaldehyde (45 mg; 0.058 mmol) was dissolved in $CHCl_3$, then cyanoacetic acid (15mg; 0.176 mmol) and piperidine (0.04 ml; 0.406 mmol) were added to the reaction cell. Reaction was refluxed for 36h, then the obtained product was purified with column chromatography (silica gel, CH_2Cl_2; CH_2Cl_2:MeOH 9:1) and dried under vacuum. The structure of **D-π-A dye** was characterized by using NMR spectroscopy. ^{1}H NMR (400 MHz, $CDCl_3$): δ (ppm) 8.18 (2H), 8.03 (3H), 7.96 (1H), 7.57 (2H), 7.50 (1H), 7.20 (1H), 7.07 (4H), 6.94 (4H), 6.80 (2H), 6.65 (1H), 3.95 (4H), 2.01 (4H), 1.71 (4H), 1.44 (4H), 1.31 (4H), 0.90 (6H).

Electrochemical and optical experiments

Firstly, the electrochemical properties of these dyes were determined using a CH 760D electrochemical workstation(Swinehart 1962). Electrochemical properties and band diagrams were achieved by cyclic voltammetry in acetonitrile (ACN) with 0.1 M tetrabutylammonium hexafluorophosphate (Bu_4NPF_6) as a supporting electrolyte. These experiments were carried out with a standard three-electrode system. The reference, working, and counter electrodes used in these experiments were Ag/AgCl, glassy carbon electrode (GCE), and Pt wire electrode, respectively. The HOMO and LUMO levels were determined by calculating the oxidation and reduction potentials obtained from cyclic voltammetry. The optical characteristics of the D-π-A dye were researched employing a UV-Vis absorption spectrophotometer (Shimadzu UV-1800). In these measurements, the absorption spectrum of the dye was obtained by measuring a 10^{-5} M solution in tetrahydrofuran (THF), and the molar extinction coefficient was calculated using the Beer-Lambert law.

Dye sensitization process

In both photocatalytic and photoelectrochemical hydrogen production experiments, TiO_2 powder and TiO_2-coated FTO electrodes were used respectively. The steps of the dye sensitization process were the same for TiO_2 powder and TiO_2-coated FTO electrodes. Before starting the sensitization process, the catalyst and electrode surfaces were calcined at 450°C for 45 minutes to remove impurities and adsorbed water from the surface. Then, TiO_2 powder or electrodes were added to a 10^{-5} M dye solution in THF. For the photoelectrochemical experiments, the TiO_2-coated FTO electrode was immersed in the dye solution prepared overnight. For photocatalytic experiments, TiO_2 powders were mixed with the dye solution under dark conditions using a magnetic stirrer overnight. Then, the dye sensitized TiO_2 was rinsed three times with ethanol and THF to remove non-adsorbed dye molecules from the surface. Finally, they were left to dry at room temperature for use in photoelectrochemical and photocatalytic experiments.

Photoelectrochemical and photocatalytic HER experiments

The photoelectrochemical properties of TiO_2 electrodes sensitized with dye were researched under a solar simulator with periodic on/off cycles in an electrolyte solution containing 0.1 M Na_2SO_4 and 5% TEOA. These experiments were carried out in a three-electrode standard cell with Ag/AgCl as the reference electrode, the dye-sensitized TiO_2 coated FTO electrode as the working electrode and Pt plate as the counter electrode. Photocatalytic hydrogen evolution experiments were conducted in a borosilicate glass reaction vessel with a volume of 135 ml. The experimental solution was prepared under anaerobic conditions in a nitrogen-filled glove box. The D-π-A/TiO_2 powder mixed with 5% TEOA solution and sealed the reaction vessel with a rubber septum, then it was taken out of the glove box. The reaction vessel stirred by magnetically under solar simulator (Solar Light XPS-300™) illumination to ensure homogeneous reaction. Hydrogen samples were collected at certain intervals from the headspace of the reaction vessel using a syringe and injected into a gas chromatography device equipped with a thermal conductivity detector (TCD). The measurements were calculated based on a calibration curve with hydrogen concentrations ranging from 0.1% to 5%. The solar-to-hydrogen conversion efficiency (STH) for photocatalytic HER experiments is calculated according to the following formula(Yılmaz, Acar et al. 2022):

$$STH = \frac{\Delta G^{g} \times R_{H_2}}{P \times A} \times 100 \qquad (1)$$

RESULTS and DISCUSSION

Herein, the new D-π-A dye were synthesized for visible light sensitization of wide-bandgap TiO_2 semiconductor for both photoelectrochemical and photocatalytic hydrogen evolution experiments. 4-{7-{bis[4-(hexyloxy)phenyl]amino}phenyl)-2-thienyl]-2,1,3-benzotidiazol-4-yl} benzaldehyde was synthesized by Suzuki-Miyaura cross coupling reaction and it was converted by Knoevenagel condensation reaction to obtain **D-π-A dye,** which the p-bridge is composed of the thiophene BTD phenyl chromophore. The experimental section

provides a comprehensive explanation of the synthesis steps involved in the preparation of the D-π-A dye. The chemical structure of this dye is remarkably straightforward, and its synthesis does not entail intricate procedures or extensive purification steps. **Scheme 1** illustrates the synthetic pathway for the synthesis of this dye.

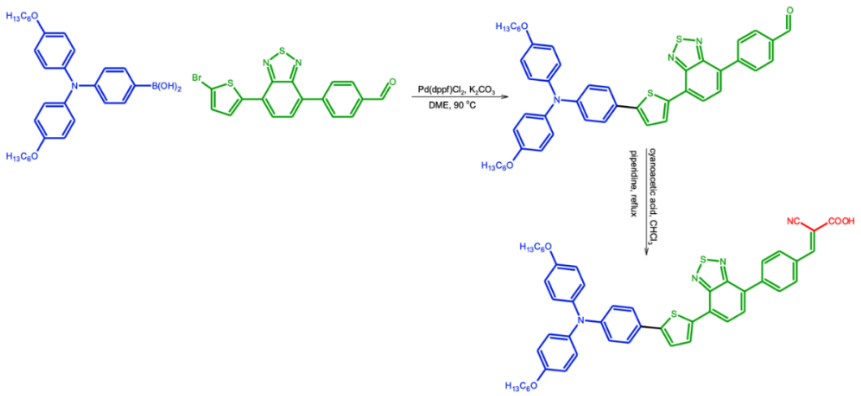

Scheme 1. Synthetic pathway of D-π-A dye

The UV-Vis absorption spectrum was utilized to explore the optical characteristics of D-π-A dye. **Figure 1a** demonstrates the presence of three distinct peaks at wavelengths of 302 nm, 360 nm, and 493 nm. The two consecutive peaks observed at 302 nm and 360 nm are attributed to localized and delocalized π-π* transitions, respectively. These π-π* transitions arise from the intramolecular charge transfer (ICT) property among the triphenylamine (donor) and carboxylic acid (acceptor) regions of D-π-A dyes(Luo, Lu et al. 2016). The optical properties of similar dyes previous published works by our groups are resembled for the first two peaks(Aslan, Karaman et al. 2019, Aslan, Karaman et al. 2020). However, in this study the first two peaks are shifted to red. In addition, there is one more peak at the 493 nm on the contrary of similar dyes before reported studies(Aslan, Karaman et al. 2019, Aslan, Karaman et al. 2020). This additional peak at the 493 nm could be originated from more electron donating group (4-(hexyloxy)phenyl)amino)phenyl) on dye causes extended π conjugation(Margalias, Seintis et al. 2015, Patir, Aslan et al. 2019). In addition, molar absorption coefficient of dye was found 2570 M^{-1} cm^{-1} (360 nm) by Lambert-Beer Law(Swinehart 1962). When compared to similar molecules, herein, the increasing molar absorption coefficient caused by high photocatalytic activity due to the absorbing more photons(Aslan, Karaman et al. 2019, Aslan, Karaman et al. 2020). The additional peak, red shift of all peaks and enhanced molar absorption coefficient can provide to harvest more light than those of the other similar dyes.

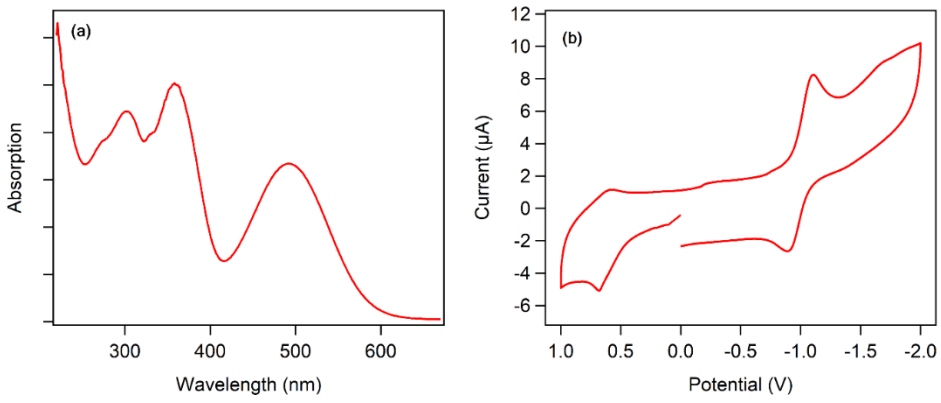

Figure 1. UV-Vis absorption spectra were recorded for **(a)** the D-π-A dye in THF and **(b)** cyclic voltammogram of the dye in ACN, employing a 0.1 M tetrabutylammonium hexafluorophosphate solution as the supporting electrolyte.

The electrochemical properties of D-π-A dye have been researched by cyclic voltammogram as shown in **Figure 1b**. Herein, the oxidation potential obtained at 0.83 V, which can be attributed to the donor moieties (triphenylamine group). The reduction potential in the negative region of voltammogram is pointed out the acceptor groups; benzothiadiazole and the cyanocarboxylic acid (reversible -1.01 V and irreversible -1.46 V) of dye. According to these oxidation and reduction potentials, HOMO and LUMO levels were calculated as -5.23

eV and -3.39 eV, respectively. The electrochemical band gap of this sensitizer could be found as 1.84 eV by differences between HOMO and LUMO levels. Energy levels of catalyst were calculated vs. vacuum level according to equations below(Cardona, Li et al. 2011):

$$E_{LUMO} = -e(E_{red} + 4.4)V \quad (2)$$

$$E_{HOMO} = -e(E_{ox} + 4.4)V \quad (3)$$

In the literature, the use of organic dyes as sensitizers for photoelectrochemical and photocatalytic water splitting is referred to as artificial photosynthesis(Zhang, Peng et al. 2016). Herein, a synthesized D-π-A dye was employed as a sensitizer for the splitting of water using solar sunlight for photocatalytic hydrogen production, due to its similar light absorption capabilities to chlorophyll. Additionally, one advantage of these dyes is that while other metal-organic complexes commonly used in energy conversion applications may have toxic properties, these dyes can be considered an environmentally friendly approach due to their sustainability and non-toxic nature. One of the most important features of these dyes is their tunable electronic properties and simple chemical structure, which allows them to be synthetically modified to achieve the desired conformation. In photoelectrochemical HER experiments conducted with an electron donor and a supporting electrolyte in the oxygen-free media and n-type TiO_2 semiconductor was acted as photoanode. In this context, the D-π-A dye undergoes excitation upon exposure to light, resulting in the generation of both holes and excited electrons. The holes are responsible for the oxidation of water into oxygen on the photoanode, which is sensitized by the D-π-A dye and composed of TiO_2. Simultaneously, the photogenerated excited electrons are transferred to the Pt cathode, where they contribute to the reduction of water into hydrogen gas. The efficiency of the ICT properties and the absorption of sensitizers on the TiO_2 photoanode directly influence the transient current density, which is associated with the rates of hydrogen evolution(Yu, Li et al. 2015).

The photoelectrochemical properties of D-π-A sensitized TiO_2 structures were investigated using linear sweep voltammetry (LSV) and chronoamperometry (CA) techniques. In these studies, FTO electrodes coated with D-π-A/TiO_2 photocatalysts were first used to perform LSV measurements under 2-second light/dark cycles, revealing their stability within the potential window of -0.4 V to +0.5 V. Additionally, it was observed that the current densities of bare TiO_2-coated FTO electrodes display very low photocurrent under light cycles due to unefficient visible light absorption of its wide-bandgap (Figure 2a). Subsequently, CA experiments were conducted using the same type of electrodes. The CA experiments were performed for a total duration of 350 seconds under 50-second light/dark cycles. As a result of these measurements, the bare TiO_2 electrode exhibited an unstable transient current density of approximately 1 μA cm^{-2}, while the D-π-A sensitized TiO_2 exhibited a high and stable current density of 170 μA cm^{-2} under light cycles (Figure 2b). The high current densities observed in the case of the sensitized TiO_2 structures can be attributed to light absorption by the dyes and the ICT as well as the electron flow from the dyes to TiO_2. Furthermore, these results are consistent with the photocatalytic HER results, which will be discussed below.

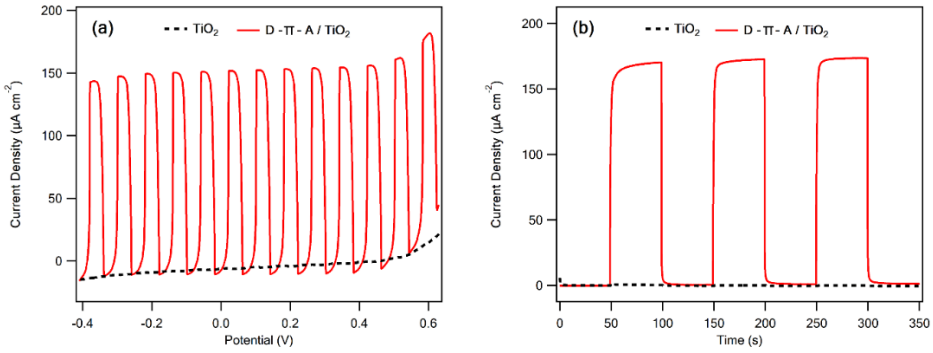

Figure 2. Transient photocurrent responses of FTO electrodes coated with D-π-A sensitized TiO_2 **(a)** using LSV and **(b)** CA techniques.

Photocatalytic HER experiments were conducted under artificial sunlight by solar simulator ($\lambda \geq 420$ nm) with the homogeneous mixing achieved using a magnetic stirrer. Additionally, the experiments were carried out in the presence of D-π-A/TiO_2 particles as hybrid photocatalyst in TEOA electron donor solution. The concentration of the electron donor and the pH level were optimized in our previous studies and determined to be 5% and 9, respectively(Aslan, Karaman et al. 2019, Aslan, Karaman et al. 2020). Photocatalytic HER experiments were performed in the presence of D-π-A/TiO_2 and D-π-A/TiO_2/Pt structures, which is formed through photoreduction of H_2PtCl_6 on D-π-A/ TiO_2 (Figure 3). The hourly results for D-π-A/ TiO_2 and D-π-A/ TiO_2/Pt were found to be 670 μmol g^{-1} h^{-1} and 2060 μmol g^{-1} h^{-1}, respectively. After an eight-hour photocatalytic reaction, the amounts of produced hydrogen using D-π-A/TiO_2 and D-π-A/TiO_2/Pt were determined as 1860 μmol g^{-1} and

22080 µmol g^{-1}, respectively. Both in the absence and presence of Pt co-catalyst photocatalytic reactions have been continued stable. Based on these results, the evolving amount of hydrogen with D-π-A/TiO_2 can be compared with previously published articles using different D-π-A dyes. The STH efficiency for D-π-A/ TiO_2 was calculated as 1.72%, which increased to 5.31% in the presence of Pt. The D-π-A dye used in this study was found to be one of the most active photocatalysts compared to the reported D-π-A dye sensitized systems in terms of photocatalytic HER activity(Aslan, Gonce et al. 2017, Aslan, Karaman et al. 2019, Patir, Aslan et al. 2019, Aslan, Karaman et al. 2020). According to these results, D-π-A type sensitizers exhibited highly stable hydrogen evolution kinetics attributed to ICT, both in the presence and absence of Pt co-catalyst(Yu, Li et al. 2015). Moreover, HER rate of D-π-A dye sensitized TiO_2 in this study is enhanced by similar triphenylamine based dyes due to the absorption property differences of the other dyes(Aslan, Karaman et al. 2019, Aslan, Karaman et al. 2020). The photocatalytic HER rate differences are explained by absorption properties of sensitizer, which is directly related to light harvesting. When our previous reported studies absorption peaks of D-π-A dyes extended about 450 nm(Aslan, Karaman et al. 2020) and 500 nm(Aslan, Karaman et al. 2019), absorption peaks of D-π-A dye in using this studies extended approximately 600 nm, which can be speculated more light harvesting.

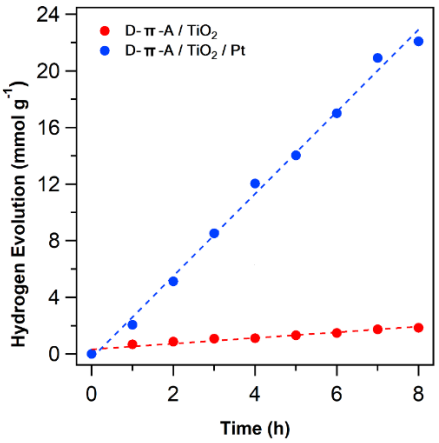

Figure 3. Photocatalytic hydrogen evolution against time by using D-π-A / TiO_2 and D-π-A / TiO_2/ Pt in the aqueous electron donor (TEOA) solution.

The proposed mechanism for photocatalytic hydrogen production is explained based on the energy band levels of D-π-A/TiO_2 hybrid photocatalyst (Figure 4). In the first step, incident photons are absorbed by the D-π-A dye, excited electrons (e^-) from the HOMO level (0.83 V) to the LUMO level (-1.01 V) of the dye. Subsequently, since the conduction band (CB) level of TiO_2 (-0.5 V) is more positive than the LUMO level of the dye, which allowing for electron flow, these excited electrons in the LUMO can be transferred to the CB of TiO_2(Choi, Kim et al. 2012). Then, the electrons transferred to the CB of TiO_2 reduce the water on TiO_2 to produce H_2. In the presence of a co-catalyst precursor H_2PtCl_6 in the reaction medium, H_2PtCl_6 can be reduced by excited electrons in the CB of TiO_2 to obtain Pt co-catalyst formed on the surface of TiO_2, and H_2 formation occurs through the co-catalyst(Patir, Aslan et al. 2019). Finally, the holes (h^+) remaining from the charge separation in the HOMO level of the dye are filled by the electron donor TEOA, completing the full cycle of the HER system. The reaction steps can be illustrated as follows:

$$\text{D-}\pi\text{-A} + h\nu \rightarrow e^-_{LUMO} + h^+_{HOMO} \quad (4)$$

$$e^-_{LUMO} + TiO_2 \rightarrow TiO_2^* \quad (5)$$

$$TiO_2^* + H_2O \rightarrow \tfrac{1}{2} H_2 + OH^- + TiO_2 \quad (6)$$

$$TEOA + h^+_{HOMO} \rightarrow TEOA^+ \quad (7)$$

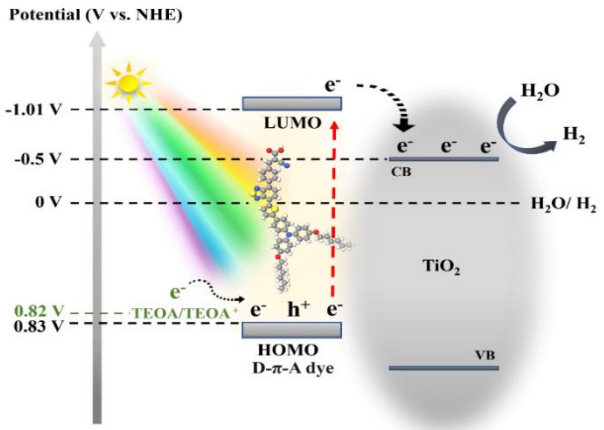

Figure 4. Proposed of the photocatalytic hydrogen evolution reaction mechanism by using D-π-A dye-sensitized TiO_2.

CONCLUSION

It has designed and synthesized a novel D-π-A organic dye conformation based on the addition of a benzothiadiazole chromophoric unit to the core to control the conjugation between the chromophore and the anchoring group. The synthesized D-π-A dye is utilized to sensitize of TiO_2 for the photoelectrochemical and photocatalytic HER. In addition, the photocatalytic and photoelectrochemical HER results of the hybrid D-π-A/TiO_2 photocatalyst can be explained by the high intramolecular charge transfer capability of sensitizer. Moreover, the increasing photocatalytic activity of hybrid D-π-A/TiO_2 photocatalyst can be described by enhanced optical properties such as additional absorption peak by extended π conjugation, red shift of all absorption peaks and enhanced molar absorption coefficient, which are provided the harvesting more light than those of the other similar dyes. Moreover, the photocatalytic activities of D-π-A/TiO_2 structures were also performed in the presence of a *in situ* photodeposited Pt co-catalyst, leading to a significant increase in HER activity approximately 4-times, which can be enhanced charge separation efficiency due to co-catalyst effect. Both in the absence and presence of Pt co-catalyst photocatalytic HER activities have been stably preserved during the reaction frame. Furthermore, photocatalytic reaction mechanism has been illuminated by energy band levels of component of hybrid D-π-A/TiO_2 photocatalyst. The enhanced activity and stability of this structure in both photocatalytic and photoelectrochemical studies also paves the way for new energy conversion applications based on solar energy harvesting and developing novel similar sensitizers.

ACKNOWLEDGEMENTS

The authors would like to thank to Selçuk University Scientific Research Project (BAP)

REFERENCES

Aslan, E., M. K. Gonce, M. Z. Yigit, A. Sarilmaz, E. Stathatos, F. Ozel, M. Can and I. H. Patir (2017). "Photocatalytic H2 evolution with a Cu2WS4 catalyst on a metal free D-π-A organic dye-sensitized TiO2." Applied Catalysis B: Environmental **210**: 320-327.

Aslan, E., M. Karaman, G. Yanalak, H. Bilgili, M. Can, F. Ozel and I. H. Patir (2020). "Synthesis of novel tetrazine based D-π-A organic dyes for photoelectrochemical and photocatalytic hydrogen evolution." Journal of Photochemistry and Photobiology A: Chemistry **390**: 112301.

Aslan, E., M. Karaman, G. Yanalak, M. Can, F. Ozel and I. H. Patir (2019). "The investigation of novel D-π-A type dyes (MK-3 and MK-4) for visible light driven photochemical hydrogen evolution." Dyes and Pigments **171**: 107710.

Bernsmeier, D., R. Sachse, M. Bernicke, R. Schmack, F. Kettemann, J. Polte and R. Kraehnert (2019). "Outstanding hydrogen evolution performance of supported Pt nanoparticles: Incorporation of preformed colloids into mesoporous carbon films." Journal of Catalysis **369**: 181-189.

Borgarello, E., J. Kiwi, E. Pelizzetti, M. Visca and M. Grätzel (1981). "Photochemical cleavage of water by photocatalysis." Nature **289**(5794): 158-160.

Cardona, C. M., W. Li, A. E. Kaifer, D. Stockdale and G. C. Bazan (2011). Electrochemical considerations for determining absolute frontier orbital energy levels of conjugated polymers for solar cell applications, Wiley Online Library.

Choi, S. K., S. Kim, J. Ryu, S. K. Lim and H. Park (2012). "Titania nanofibers as a photo-antenna for dye-sensitized solar hydrogen." Photochemical & Photobiological Sciences **11**: 1437-1444.

Choi, S. K., H. S. Yang, J. H. Kim and H. Park (2012). "Organic dye-sensitized TiO2 as a versatile photocatalyst for solar hydrogen and environmental remediation." Applied Catalysis B: Environmental **121**: 206-213.

Chowdhury, P., G. Malekshoar and A. K. Ray (2017). "Dye-sensitized photocatalytic water splitting and sacrificial hydrogen generation: Current status and future prospects." Inorganics **5**(2): 34.

Fujishima, A. and K. Honda (1972). "Electrochemical photolysis of water at a semiconductor electrode." nature **238**(5358): 37-38.

Han, W. S., K. R. Wee, H. Y. Kim, C. Pac, Y. Nabetani, D. Yamamoto, T. Shimada, H. Inoue, H. Choi and K. Cho (2012). "Hydrophilicity Control of Visible-Light Hydrogen Evolution and Dynamics of the Charge-Separated State in Dye/TiO2/Pt Hybrid Systems." Chemistry–A European Journal **18**(48): 15368-15381.

Huang, J. F., Y. Lei, T. Luo and J. M. Liu (2020). "Photocatalytic H2 Production from Water by Metal-free Dye-sensitized TiO2 Semiconductors: The Role and Development Process of Organic Sensitizers." ChemSusChem **13**(22): 5863-5895.

Jiang, Z., M. A. Isaacs, Z. W. Huang, W. Shangguan, Y. Deng and A. F. Lee (2017). "Active Site Elucidation and Optimization in Pt Co-catalysts for Photocatalytic Hydrogen Production over Titania." ChemCatChem **9**(22): 4268-4274.

Kim, J.-H. and K.-S. Ahn (2010). "Tri-branched tri-anchoring organic dye for visible light-responsive dye-sensitized photoelectrochemical water-splitting cells." Japanese Journal of Applied Physics **49**(6R): 060219.

Kwok, Y.-Y., P.-Y. Ho, Y. Wei, Z. Zheng, S.-C. Yiu, C.-L. Ho and S. Huang (2022). "Molecular engineering of robust starburst-based organic photosensitizers for highly efficient photocatalytic hydrogen generation from water." Chemistry of Materials **34**(12): 5522-5534.

Lee, S.-H., Y. Park, K.-R. Wee, H.-J. Son, D. W. Cho, C. Pac, W. Choi and S. O. Kang (2010). "Significance of hydrophilic characters of organic dyes in visible-light hydrogen generation based on TiO2." Organic letters **12**(3): 460-463.

Li, X., S. Cui, D. Wang, Y. Zhou, H. Zhou, Y. Hu, J. g. Liu, Y. Long, W. Wu and J. Hua (2014). "New Organic Donor–Acceptor–π–Acceptor Sensitizers for Efficient Dye-Sensitized Solar Cells and Photocatalytic Hydrogen Evolution under Visible-Light Irradiation." ChemSusChem **7**(10): 2879-2888.

Li, Y., M. Guo, S. Peng, G. Lu and S. Li (2009). "Formation of multilayer-Eosin Y-sensitized TiO2 via Fe3+ coupling for efficient visible-light photocatalytic hydrogen evolution." International journal of hydrogen energy **34**(14): 5629-5636.

Luo, G.-G., H. Lu, Y.-H. Wang, J. Dong, Y. Zhao and R.-B. Wu (2016). "A D-π-A-π-A metal-free organic dye with improved efficiency for the application of solar energy conversion." Dyes and Pigments **134**: 498-505.

Ma, Y., X. Wang, Y. Jia, X. Chen, H. Han and C. Li (2014). "Titanium dioxide-based nanomaterials for photocatalytic fuel generations." Chemical reviews **114**(19): 9987-10043.

Margalias, A., K. Seintis, M. Z. Yigit, M. Can, D. Sygkridou, V. Giannetas, M. Fakis and E. Stathatos (2015). "The effect of additional electron donating group on the photophysics and photovoltaic performance of two new metal free D-π-A sensitizers." Dyes and Pigments **121**: 316-327.

Martín-Gomis, L., F. Fernández-Lázaro and Á. Sastre-Santos (2014). "Advances in phthalocyanine-sensitized solar cells (PcSSCs)." Journal of Materials Chemistry A **2**(38): 15672-15682.

Nikoloudakis, E., I. López-Duarte, G. Charalambidis, K. Ladomenou, M. Ince and A. G. Coutsolelos (2022). "Porphyrins and phthalocyanines as biomimetic tools for photocatalytic H 2 production and CO 2 reduction." Chemical Society Reviews **51**(16): 6965-7045.

Pati, P. B., G. Damas, L. Tian, D. L. Fernandes, L. Zhang, I. B. Pehlivan, T. Edvinsson, C. M. Araujo and H. Tian (2017). "An experimental and theoretical study of an efficient polymer nano-photocatalyst for hydrogen evolution." Energy & Environmental Science **10**(6): 1372-1376.

Patir, I. H., E. Aslan, G. Yanalak, M. Karaman, A. Sarilmaz, M. Can, M. Can and F. Ozel (2019). "Donor-π-acceptor dye-sensitized photoelectrochemical and photocatalytic hydrogen evolution by using Cu2WS4 co-catalyst." International Journal of Hydrogen Energy **44**(3): 1441-1450.

Puangpetch, T., P. Sommakettarin, S. Chavadej and T. Sreethawong (2010). "Hydrogen production from water splitting over Eosin Y-sensitized mesoporous-assembled perovskite titanate nanocrystal photocatalysts under visible light irradiation." International Journal of Hydrogen Energy **35**(22): 12428-12442.

Swinehart, D. F. (1962). "The beer-lambert law." Journal of chemical education **39**(7): 333.

Thelakkat, M. (2002). "Star-shaped, dendrimeric and polymeric triarylamines as photoconductors and hole transport materials for electro-optical applications." Macromolecular Materials and Engineering **287**(7): 442-461.

Urbani, M., M. Grätzel, M. K. Nazeeruddin and T. Torres (2014). "Meso-substituted porphyrins for dye-sensitized solar cells." Chemical Reviews **114**(24): 12330-12396.

Wang, L., R. Fernández-Terán, L. Zhang, D. L. Fernandes, L. Tian, H. Chen and H. Tian (2016). "Organic polymer dots as photocatalysts for visible light-driven hydrogen generation." Angewandte Chemie International Edition **55**(40): 12306-12310.

Wang, Z., C. Li and K. Domen (2019). "Recent developments in heterogeneous photocatalysts for solar-driven overall water splitting." Chemical Society Reviews **48**(7): 2109-2125.

Watanabe, M., H. Hagiwara, A. Iribe, Y. Ogata, K. Shiomi, A. Staykov, S. Ida, K. Tanaka and T. Ishihara (2014). "Spacer effects in metal-free organic dyes for visible-light-driven dye-sensitized photocatalytic hydrogen production." Journal of Materials Chemistry A **2**(32): 12952-12961.

Wu, Y. and W. Zhu (2013). "Organic sensitizers from D–π–A to D–A–π–A: effect of the internal electron-withdrawing units on molecular absorption, energy levels and photovoltaic performances." Chemical Society Reviews **42**(5): 2039-2058.

Xu, J., Y. Li, S. Peng, G. Lu and S. Li (2013). "Eosin Y-sensitized graphitic carbon nitride fabricated by heating urea for visible light photocatalytic hydrogen evolution: the effect of the pyrolysis temperature of urea." Physical Chemistry Chemical Physics **15**(20): 7657-7665.

Yang, C., B. C. Ma, L. Zhang, S. Lin, S. Ghasimi, K. Landfester, K. A. Zhang and X. Wang (2016). "Molecular engineering of conjugated polybenzothiadiazoles for enhanced hydrogen production by photosynthesis." Angewandte Chemie International Edition **55**(32): 9202-9206.

Yılmaz, S., E. G. Acar, G. Yanalak, E. Aslan, M. Kılıç, İ. H. Patır and Ö. Metin (2022). "Enhanced hydrogen evolution by using ternary nanocomposites of mesoporous carbon nitride/black phosphorous/transition metal nanoparticles (m-gCN/BP-M; M= Co, Ni, and Cu) as photocatalysts under visible light: A comparative experimental and theoretical study." Applied Surface Science **593**: 153398.

Yu, F., S.-C. Cui, X. Li, Y. Peng, Y. Yu, K. Yun, S.-C. Zhang, J. Li, J.-G. Liu and J. Hua (2017). "Effect of anchoring groups on N-annulated perylene-based sensitizers for dye-sensitized solar cells and photocatalytic H2 evolution." Dyes and Pigments **139**: 7-18.

Yu, Z., F. Li and L. Sun (2015). "Recent advances in dye-sensitized photoelectrochemical cells for solar hydrogen production based on molecular components." Energy & Environmental Science **8**(3): 760-775.

Zani, L., M. Melchionna, T. Montini and P. Fornasiero (2021). "Design of dye-sensitized TiO2 materials for photocatalytic hydrogen production: light and shadow." Journal of Physics: Energy **3**(3): 031001.

Zhang, X., T. Peng and S. Song (2016). "Recent advances in dye-sensitized semiconductor systems for photocatalytic hydrogen production." Journal of Materials Chemistry A **4**(7): 2365-2402.

➢ *ORAL PRESENTATION*

Eratigena atrica (C.L. Koch, 1843) türünün karyotip özelliklerinin belirlenmesi

Ümit Kumbıçak[1] (*ORCID ID*: 0000-0002-1294-3706), Zübeyde Kumbıçak[1](*ORCID ID*: 0000-0001-5949-1092), Sudenaz Şencan[1*](*ORCID ID*: 0009-0002-7932-9564), Ömer Faruk Uydaş[1] (*ORCID ID*: 0009-0004-0216-3222)

[1]Nevşehir Hacı Bektaş Veli Üniversitesi, Fen Edebiyat Fakültesi, Moleküler Biyoloji ve Genetik Bölümü, Nevşehir, Türkiye

* Sorumlu yazar e-posta:sdnzsncn@gmail.com

Özet

Örümcekler, dünya genelinde 136 familyaya ait 4436 cins ve 53 bine yakın türle temsil edilmektedir. Bu çalışmada, Agelenidae familyasına ait *Eratigena atrica* (C.L. Koch, 1843) türünün sitogenetik özelliklerinin incelenmesi amaçlamıştır. Türe ait erkek örümcekler, Mart-Mayıs aylarında Nevşehir ili ve çevresinden toplanmıştır. Kromozom preparatlarının hazırlanmasında yayma preparat metodu uygulanmıştır. Buna göre, gonadlar ilk aşamada hipotonik uygulamaya, daha sonra fiksasyon işlemine ve son aşamada ise asetik asit uygulamasına maruz bırakılarak kromozom preparatları yapılmıştır. Preparatlar çekirdek boyası ile boyanarak analiz yapılacak duruma getirilmiştir. Çalışma sonucunda, türe ait kromozomların uzunlukları mikrometrik seviyede ölçülerek karyotipleri hazırlanmıştır. Ayrıca türün mayoz bölünmedeki kromozom davranışları da analiz edilmiştir. Buna göre türün diploid kromozom sayısı 2n=42 şeklinde ve eşey kromozom sistemi ise X1X20 olarak belirlenmiştir. Otozomal kromozom çiftlerinin relatif uzunluklarının %6,89 µm ile %3,45 µm arasında değiştiği tespit edilmiştir. Ayrıca, eşey kromozomlarının relatif uzunlukları X_1 %4,85 µm, X_2 %3,79 µm olarak saptanmıştır. Mayoz bölünmenin birinci evrelerinde eşey kromozomları otozomlardan ayırt edilebilirken mayoz bölünmenin ikinci evrelerinde otozomlardan ayırt edilememektedir. Ayrıca mayoz I evrelerinde 20 otozomal bivalent ve iki eşey kromozomu saptanmıştır. *Eratigena atrica* ile yapılan çalışmada elde edilen diploid kromozom sayısı, kromozom morfolojileri, otozom ve eşey kromozomlarının mayoz bölünmedeki davranışları familya özellikleri ile uyumlu bulunmuştur. Türün sitogenetik özelliklerinin ilk kez ortaya konulması familyaya ait sitogenetik özelliklerin açıklanmasına katkı sağlamıştır.

Anahtar kelimeler: sitogenetik, karyotip, mayoz

Determination of the karyotypic characteristics of the species *Eratigena atrica* (C.L. Koch, 1843)

Abstract

Spiders are represented worldwide by approximately 53,000 species, classified into 4,436 genera and 136 families. In this study, the cytogenetic characteristics of the species *Eratigena atrica* (C.L. Koch, 1843), belonging to the family Agelenidae, were investigated. Male specimens of the species were collected from Nevşehir province and its surrounding areas between March and May. Chromosome preparations were obtained using the spreading technique. Specifically, the gonads were subjected to a hypotonic solution, followed by fixation, and then treated with acetic acid in the final stage to prepare chromosome slides. These preparations were stained with nuclear dyes to render them suitable for cytogenetic analysis. As a result of the study, chromosome lengths were measured at the micrometric level, and karyotypes of the species were constructed. Additionally, chromosomal behaviors during meiosis were analyzed. The diploid chromosome number of the species was determined as 2n=42, with a sex chromosome system of X_1X_20. The relative lengths of autosomal chromosome pairs ranged from 6.89% µm to 3.45% µm. The relative lengths of the sex chromosomes were determined as X_1: 4.85% µm and X_2: 3.79% µm. While sex chromosomes could be distinguished from autosomes during the first meiotic division, they became indistinguishable during the second division. Moreover, in the first meiotic stage, 20 autosomal bivalents and two sex chromosomes were observed. The diploid chromosome number, chromosomal morphology, and meiotic behavior of both autosomes and sex chromosomes found in *Eratigena atrica* are consistent with those reported for the family. This study provides the first cytogenetic characterization of *Eratigena atrica*, contributing valuable information to the understanding of cytogenetic features within the Agelenidae family.

Keywords: cytogenetics, karyotype, meiosis

GİRİŞ

Örümcekler yüksek tür çeşitliliğine sahip omurgasız canlı gruplarından biridir. Bu biyolojik çeşitlilik, örümcekleri bilimsel araştırmalar açısından önemli bir çalışma konusu hâline getirmiştir. Örümcekler genel olarak habitatlarına bağlı olarak farklı eklembacaklılarla beslenirler. Bazı büyük türlerin sürüngen ve küçük memelilerle de beslendiği bilinmektedir.

Bu çalışma, Agelenidae familyasına ait *Eratigena atrica* (C.L. Koch, 1843) türünün sitogenetik özellikleri araştırılmıştır.

MATERYAL METOT

Çalışmada Kullanılan Örümceklerin Toplanması

2024 yılının Mart-Mayıs döneminde Nevşehir ili ve çevresinde yapılan arazi çalışmalarında Agelenidae familyasına ait örümcekler aktif üreme periyodu dönemlerinde doğrudan habitatından alınmıştır. Toplama sonrası besleme işlemi haftada iki kez olacak şekilde sirke sinekleri kullanılarak yapılmıştır.

Kromozom preparatlarının hazırlanması

Çalışmada erkek örümceklere ait gonadlar kullanılmıştır. Diseksiyon ile çıkarılan gonadlar Pekár ve Král (2001) yayma metot preparasyon ile incelemeye hazır hale getirilmiştir. Bu metotta önce hipotonik uygulama, sonrasında 20 ile 30 dakika olmak üzere iki kez Carnoy fiksatifi ile fiksasyon yapılmıştır. Boyama kısmında preparatların fosfat tamponu içeren % 5'lik Giemsa çözeltisi ile boyanması tercih edilmiştir.

Preparatların mikroskop analizleri ve karyotip hazırlanması

Preparatlar CX21 ışık mikroskobu (Olympus) ile incelenmiş ve bölünme evreleri açısında iyi olan preparatlar seçilmiştir. Mitoz ve mayoz bölünme evrelerini görüntülemek için ise BX53 (Olymus) mikroskobu ve DP26 kamera sistemi (CellSens software) kullanılmıştır. ile yapılmıştır.

Karyotip yapılması aşamasında 10 adet metafaz evresi değerlendirilmiştir. Tüm metafaz evrelerindeki kromozomlar mikrometrik olarak ölçülmüş ve homolog kromozom çiftleri belirlenmiştir. Homolog kromozom çiftleri uzunluk sırasına göre dizilerek eşey kromozomları da otozomların sonuna yerleştirilmiştir. Kromozomların sıralanmasında Adobe Photoshop 2025 programı kullanılmıştır (Şekil 1).

BULGULAR

Eratigena atrica (C.L. Koch, 1843) Türüne Ait Sitogenetik Bulgular

Yapılan incelemelerde türe ait diploid kromozom sayısı 2n♂=42 (40+X_1X_2), eşey kromozom sistemi X_1X_2♂, kromozom morfolojisi ise telosentrik tipte tespit edilmiştir. Otozomal kromozomların relatif uzunlukları sırasıyla %6,89 ile %3,45 µm arasında bulunmuştur.

Hücre Bölünmelerinin Değerlendirilmesi

Mitotik profaz evresinde kromozomlar süperspiral yapıda olduğu ancak sayılabilecek durumda olmadığı tespit edilmiştir. Otozom ve gonozomlarda morfolojik olarak fark görülmemiştir.

Profaz I (diploten evresi) toplam 20 otozomal bivalent ve X_1 ve X_2 'den oluşmaktadır. Diyakinezde de diploten evresinde olduğu gibi bivalent ve eşey sayısı aynıdır. Bu evrelerde eşey kromozomları otozomlardan daha koyu boyanmıştır. Profaz II'de superspiral yapıda ve n=20 ve n=22 olan iki yeni çekirdek belirlenmiştir. Bu evrede eşey kromozomlarının otozomlarla eşit seviyede boyanması sonucu ayırt edilemediği belirlenmiştir.

TARTIŞMA VE SONUÇ

Örümcekler dünya üzerinde birçok habitat ve yükseklikte varlığını sürdürebilen canlılardır. Bu nedenle tür çeşitliliği oldukça yüksektir ve bugün 53000 den fazla örümcek türünün yaşadığı bilinmektedir (World Spider Catalog, 2025). Kromozomlar, canlının genetik özelliklerini yansıtan yapılar olduğu ve genellikle çevre şartlarından çok fazla etkilenmedikleri için dikkati çekmektedir ve sitogenetik alanında birçok çalışmaya konu olmaktadır. Örümcek sayıları dikkate alındığında 885 türün sitogenetik analizleri yapılmıştır (Araujo ve ark., 2025). Agelenidae familyası ise 7 cins ve 15 tür olacak şekilde çalışılmıştır. Bu cinsler; *Agelena*, *Agelenopsis*, *Allagelena*, *Eratigena*, *Pireneitega*, *Tegecoelotes* ve *Tegenaria* şeklindedir. Elde edilen verilere göre familya içerisinde diploid kromozom sayısı 2n=♂35-46 olarak bulunmuş ve en sık karşılaşılan diploid sayılar 2n=♂42-43'tür [3]. Familya içerisinde diploid sayının yüksek oranda korunmadığı dikkati çekmektedir. Ayrıca eşey

sistemleri de X_1X_2 veya $X_1X_2X_3$ şeklindedir. Agelenidae familyasına ait örümcekler araneomorf grubuna ait olduğu için kromozomlar genellikle telosentrik tiptedir. Çalışmamızda elde edilen diploid sayı, eşey sistemi ve kromozomların morfolojisi, familya özellikleri ile uyumludur.

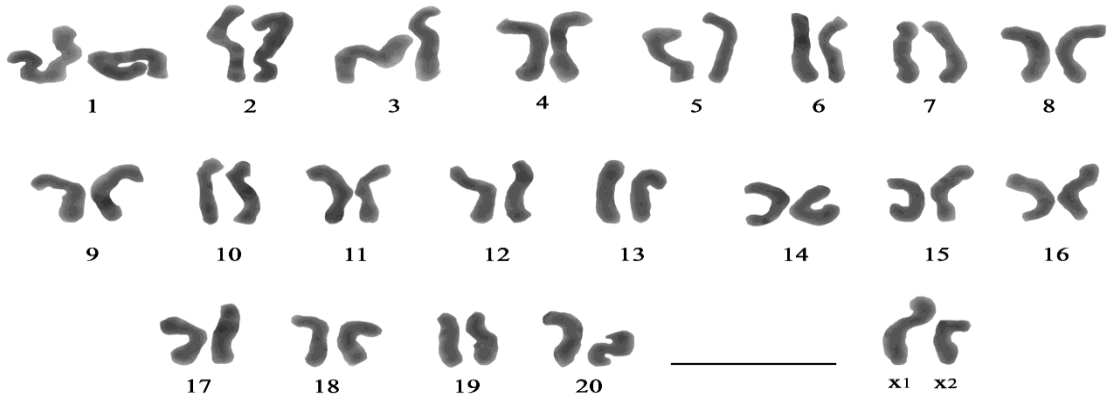

Şekil 1. *E. atrica* erkek bireye ait karyotip (Skala: 20)

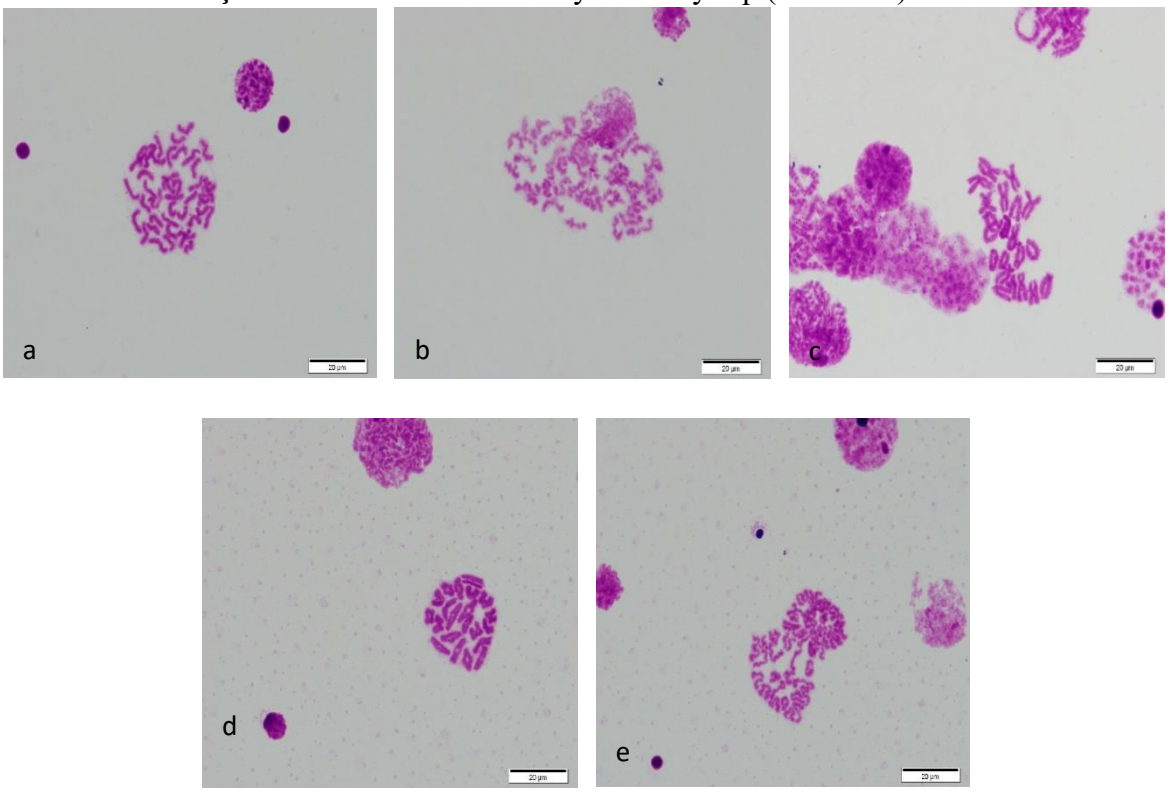

Şekil 2. E. atrica türüne ait bölünme evreleri a. metafaz b. profaz c. diploten d. diyakinez e. profaz II

KAYNAKLAR

Araujo, D., Schneider, M. C., Paula-Neto, E., Cella, D. M. (2025). The spider cytogenetic database. Available in www.arthropodacytogenetics.bio.br/spiderdatabase

Pekár, S. & Král, J. A. (2001). Comparative study of the biology and karyotypes of two central European Zodariid spiders (Araneae, Zodariidae). The Journal of Arachnology, v. 29, 345-353.

World Spider Catalog (2025). World Spider Catalog. Version 26. Natural History Museum Bern, online at http://wsc.nmbe.ch, accessed on {10.06.2025}. doi: 10.24436/2.

➢ *ORAL PRESENTATION*

Score plot distribution of thermal reduced graphene oxide considering the process operating parameters: A tutorial

Barış Şimşek[1*] (*ORCID: https://orcid.org/0000-0002-0655-4368*), Ömer Faruk Dilmaç[2] (*ORCID: https://orcid.org/0000-0002-9660-0638)*

Çankırı Karatekin University, Faculty of Engineering, Department of Chemical Engineering, Çankırı, Türkiye.

* Corresponding author e-mail: barissimsek@karatekin.edu.tr, +90 532 774 87

Abstract

Principal component analysis-based score plots represent a pivotal visualization technique, as they facilitate the classification of responses according to factors and permit the statistical comparison of factor types. The objective of this study was to illustrate the categorization of thermally reduced graphene oxide according to product properties, including the D peak-to-G peak ratio and carbon-oxygen ratios. This was achieved by examining a data set containing various operating parameters, such as production conditions, H_2 gas flow rate, reaction time, and reaction temperature, which were considered as case studies. The study indicated that, among the four factors employed for sample classification, the H_2 gas flow rate emerged as the most effective.

Keywords: Thermally reduced graphene oxide, Score plot, Process operating parameters.

INTRODUCTION

In the contemporary era, the substantial dimensionality of data constitutes a prevailing challenge in the analysis and presentation of results, a phenomenon that is pervasive in the domain of data science (He et al., 2025). In the analysis of large data sets, multivariate analysis methods are generally employed (Li et al., 2020). In the realm of data analysis, methodologies such as principal component analysis (PCA), factor analysis, discriminant analysis, and cluster analysis are of particular prominence (Greenacre et al., 2022). This is largely preferred due to the accessibility of these methods through various computer software programs such as Minitab, Statistica, and SPSS, and their inherent ease of application in a variety of settings and contexts (Rodionova et al., 2021). Factor analysis is selected for analyzing the effects of factors on responses (Dombrowski 2025). In contrast, cluster analysis and discriminant analysis are selected for the classification of samples according to their similarities and classification (Motevalizadeh and Mollenhauer 2025). In comparison with these conventional methods, PCA emerges as a distinctive analytical tool that can effectively address two critical aspects: the evaluation of factor effects and the classification of sample data (Ongbali et al., 2024). Furthermore, PCA offers a substantial advantage for the management of voluminous data by diminishing the number of dimensions (Wold et al. 1987) and presenting informative score-loading plots (Ergon 2004).

Due to the presence of these characteristics, the PCA has been implemented in a variety of disciplines to improve cellulose yield (Balasubramanian and Praharaj 2023), determine driver behavior (McManus et al., 2024), identify marine microplastics (Meng et al., 2024), evaluate indexes of molecular energy (Yu et at., 2025) and monitor processes (Chen and Jiang 2025), including the analysis and classification of factor effects, and the reduction of data size. The utilization of statistical tutorials is imperative in elucidating the implementation of PCA, which serves to amalgamate education and technology (Rodionova et al., 2021). In this study, a tutorial application of PCA classification is implemented using the dataset from the work of Dilmaç and Şimşek (2021).

MATERIALS AND METHODS

In this study, the data set obtained by Şimşek and Dilmaç (2021) was employed to illustrate the PCA tutorial application. The data set under consideration comprises a total of eight experiments. The data set under consideration is 6x8 in dimension, with four of the eight elements designated as factors (as production conditions, H_2 gas flow rate, reaction time, and reaction temperature) and the remaining two as responses such as the D peak-to-G peak ratio and carbon-oxygen ratios (Şimşek and Dilmaç, 2021). PCA is applied to the dataset, and score and load graphs are generated. The subsequent methodology is illustrated in Figure 1.

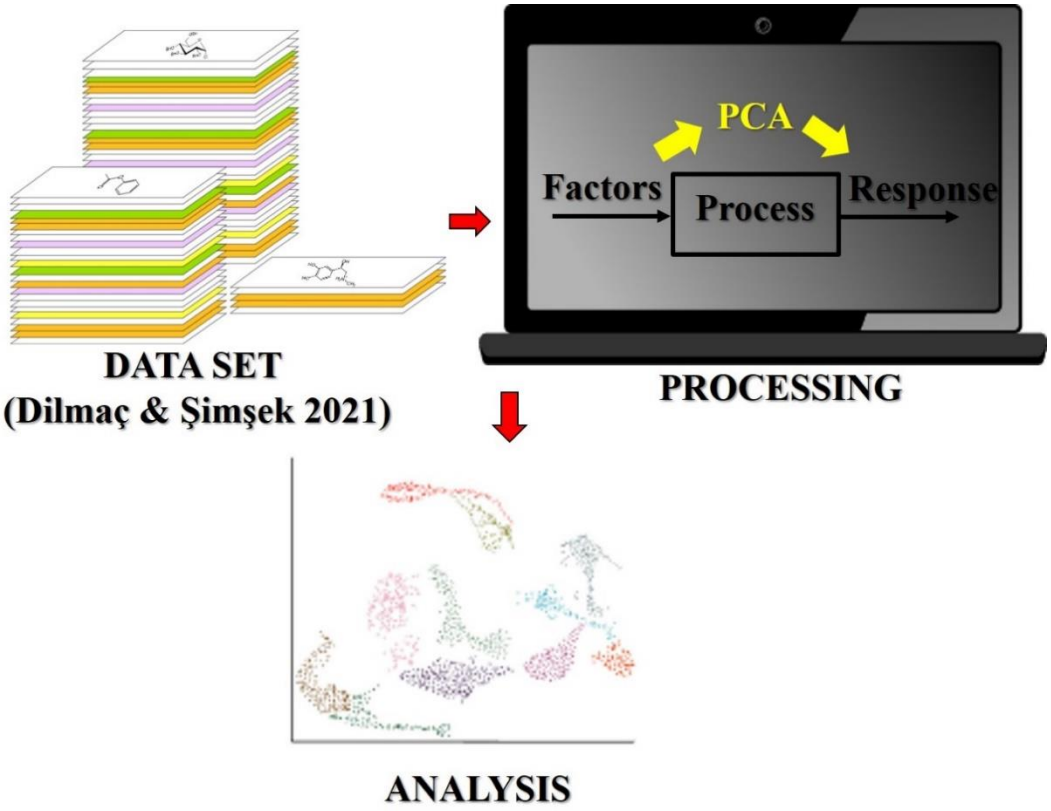

Figure 1. Stages of the PCA tutorial

RESULTS and DISCUSSION

Therefore, the objective of the current study is to utilize the PCA (Principal Component Analysis) methodology to examine and analyze the dataset employing the Minitab statistical software application. Upon the creation of a score graph for each factor, it becomes evident that the classification is exclusive to reaction time. In essence, the operating parameter that engenders variability in responses is reaction time. Loading plots facilitate the analysis of relationships between selected variables. The 90-degree angle between the factors demonstrated that the factors such as H_2 gas flow rate, reaction time, and reaction temperature are independent variables. A factor that is oriented in a direction that overlaps with the response is indicative of a synergistic effect, while a factor that is oriented in a direction that is opposite to the response is indicative of an antagonistic effect. It can be posited that the reaction time exerts a synergistic effect on the D peak-to-G peak ratio, and conversely, H_2 flow rate has a synergistic effect on the carbon-oxygen ratios. These findings align with the primary effects and the factor effects identified by Dilmaç and Şimşek (2021).

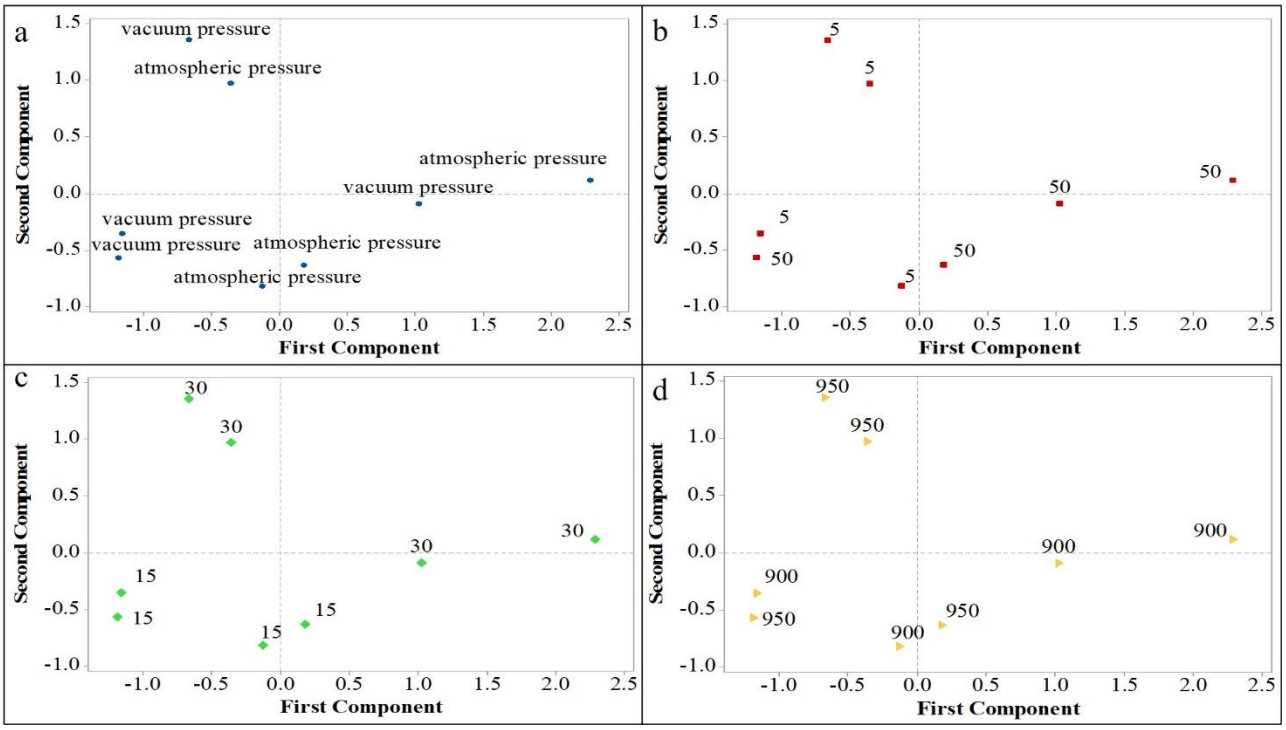

Figure 2. Score plots drawn according to a) production conditions, b) H_2 gas flow rate, c) reaction time, and d) reaction temperature

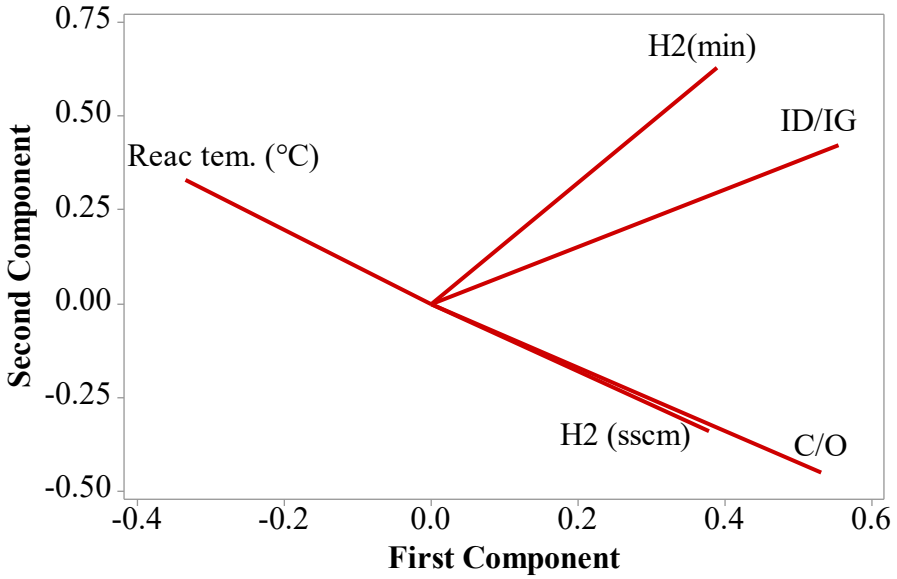

Figure 3. Loading plot

CONCLUSION

This study categorized thermally reduced graphene oxide based on product properties, such as the D-to-G peak and carbon-to-oxygen ratios. It was examined a data set containing various operating parameters, such as production conditions, H_2 gas flow rate, reaction time, and reaction temperature, was examined to achieve this objective. The study revealed that the reaction time was the most effective of the four factors employed for sample classification.

ACKNOWLEDGEMENTS

This study was supported by Çankırı Karatekin University Scientific Research Project (MF200217B10). The authors would like to thank Çankırı Karatekin University, Scientific Research Project Management Department (ÇAKÜ-BAP).

REFERENCES

Balasubramanian, P., & Praharaj, P. T. (2023). Principal component analysis revealed the key influencing factors of kombucha bacterial cellulose yield and productivity. Bioresource Technology Reports, 23, 101539.

Chen, K., & Jiang, D. (2025). Nonlinear principal component analysis with random Bernoulli features for process monitoring. Journal of Process Control, 151, 103449.

Dombrowski, S. C. (2025). Contributing to the reproducibility crisis in Psychology: The role of statistical software choice on factor analysis. Journal of School Psychology, 110, 101462.

Dilmaç, Ö. F., & Şimşek, B. (2021). Termal olarak indirgenen grafen oksidin özelliklerinin istatistiki analizi. El-Cezeri, 8 (3), 1123-1134.

Ergon, R. (2004). Informative PLS score-loading plots for process understanding and monitoring. Journal of Process Control, 14 (8), 889-897.

He, Y., Li, L., Liu, D., & Zhou, W. X. (2025). Huber Principal Component Analysis for large-dimensional factor models. Journal of Econometrics, 249 (Part B), 105993.

Greenacre, M., Groenen, P. J. F., Hastie, T., D'Enza, A.I., Markos, A., & Tuzhilina, E. (2022). Principal Component Analysis. Nature Reviews Methods Primers, 2, 100.

Motevalizadeh, M., & Mollenhauer, K. (2025). Identification of chemical markers for blending phenomena in RAP mastics using FTIR spectroscopy and multivariate discriminant analysis. Construction and Building Materials, 485, 141822.

Li, X., Xue, F., Qin, L., Zhou, K., Chen, Z., Ge, Z., Chen, X., & Song, K. (2020). A recursively updated Map-Reduce based PCA for monitoring the time-varying fluorochemical engineering processes with big data. Chemometrics and Intelligent Laboratory Systems, 206, 104167.

Korucu, H., Şimşek, B., & Yartaşı, A. (2018). A TOPSIS-Based Taguchi Design to Investigate Optimum Mixture Proportions of Graphene Oxide Powder Synthesized by the Hummers Method. Arabian Journal of Science and Engineering, 43, 6033-6055.

McManus, B., Mrug, S., Wagner, W. P., Underhill, A., Pawar, P., Anthony, T., & Stavrinos, D. (2024). Principal components analysis of driving simulator variables in novice drivers. Transportation research Part F: Traffic Psychology and Behaviour, 105, 257-266.

Meng, X., Chen, S., Li, D., Song, Y., & Sun, L. (2024). Identification of marine microplastics based on laser-induced fluorescence and principal component analysis. Journal of Hazardous Materials, 465, 133352.

Ongbali, S. O., Omotehinse, S.A., Adams, C.O., Salawu, E. Y., & Afolalu, S. A. (2024). Analysis of the key factors for small and medium-sized enterprises growth using principal component analysis. Heliyon, 10 (13), e33573.

Rodionova, O., Kucheryavskiy, S., & Pomerantsev, A. (2021). Chemometrics and Intelligent Laboratory Systems, 213, 104304.

Wold, S., Esbensen, K., & Geladi, P. (1987). Principal Component Analysis. Chemometrics and Intelligent Laboratory Systems, 2 (1-3), 37-52.

Yu, T., Chen, Z., Zhao, F., Wang, M., Zhang, H., Ai, Y., & Liu, H. (2025). Composition characteristics and evaluation indexes of molecular energy for asphalt components based on principal component analysis. Case Study in Construction Materials, 22, e04730.

➢ *ORAL PRESENTATION*

Pardosa roscai (Roewer, 1951) türünün mayoz bölünme özelliklerinin belirlenmesi

Ümit Kumbıçak[1] (*ORCID ID*: 0000-0002-1294-3706), Zübeyde Kumbıçak[1](*ORCID ID*: 0000-0001-5949-1092), Ömer Faruk Uydaş[1*] (*ORCID ID*: 0009-0004-0216-3222), Sudenaz Şencan[1](*ORCID ID*: 0009-0002-7932-9564)

[1]Nevşehir Hacı Bektaş Veli Üniversitesi, Fen Edebiyat Fakültesi, Moleküler Biyoloji ve Genetik Bölümü, Nevşehir, Türkiye

* Sorumlu yazar e-posta:omerfarukuydas@gmail.com

Özet

Örümcekler (Araneae), bilimsel çalışmalarda kullanılan önemli canlılardan biridir. Bu çalışmada ülkemizde geniş yayılış gösteren Lycosidae familyasına ait *Pardosa roscai* (Roewer, 1951) türünün mayoz bölünme özelliklerinin araştırılması amaçlanmıştır. Türün mayoz bölünme sırasındaki otozom ve gonozomların davranışları tespit edilmiştir. Çalışmada kullanılan örümcek örnekleri Nevşehir ili ve çevresinden canlı olarak toplanmıştır. Kromozom preparatları Pekár ve Král (2001) yayma metodu yapılmıştır. Buna göre gonadlar diseksiyon ile çıkarılmış ve sırasıyla hipotonik uygulama fiksasyon ve asetik asit uygulamaları yapılarak giemsa boyama ile sonuçlandırılmıştır. Mikroskop analizleri ile iyi kalitede preparatlar seçilerek kromozom davranışları değerlendirilmiştir. Çalışma sonunda eşey kromozomları Mayoz I evrelerinde pozitif heteropiknotik özellikte olup, çekirdek yüzeyinde konumlanırken, Mayoz II evrelerinde ise izopiknotik özellikte olup genellikle otozomlardan ayırt edilmemiştir. Mayoz bölünmenin Profaz I evresi, diploten ve diyakinezde 13 otozomal bivalent ve iki eşey kromozomu (X_1 ve X_2) görülmüştür. Otozomal bivalentlerden bazıları halka şeklinde tespit edilmiştir. Bu evreler de otozomal bivalentleri genellikle terminal, interstitial ve distal tipte kiyazmalara sahip olduğu belirlenmiştir. Aynı zamanda bivalentlerin genellikle tek kiyazma özelliğinde olduğu saptanmıştır. Mayoz II evrelerinde Profaz II ´ de kromozomlar süper spiral yapıda ve iki yeni çekirdek halinde gözlenmiştir. Anafaz II´ de ise n= 13 (otozom) ve n= 15 (13 otozom + X_1 ve X_2) olan iki çeşit toplam 4 yeni çekirdek belirlenmiştir. Elde edilen sonuçlar *Pardosa roscai´* nın ülkemizde populayonlarının kromozomal özelliklerini göstermesi açısından önemlidir.

Anahtar kelimeler: Lycosidae, *Pardosa*, mayoz

Determination of meiotic characteristics of the species *Pardosa roscai* (Roewer, 1951)

Abstract

Spiders (Araneae) are among the significant organisms used in scientific research. This study aimed to investigate the meiotic characteristics of the species *Pardosa roscai* (Roewer, 1951), belonging to the family Lycosidae, which is widely distributed across Turkey. The behavior of autosomes and gonosomes during meiosis in this species was examined. Alive specimens were collected from Nevşehir province and its surroundings. Chromosome preparations were made using the spreading method described by Pekár and Král (2001). The gonads were dissected and subsequently subjected to hypotonic treatment, fixation, and acetic acid application, followed by Giemsa staining. Preparations of high quality were selected through microscopic analysis, and chromosomal behaviors were evaluated. At the end of the study, it was observed that the sex chromosomes exhibited positively heteropycnotic characteristics and localized on the nuclear surface during meiosis I, whereas in meiosis II, they were isopycnotic and generally indistinguishable from autosomes. In Prophase I, specifically at diplotene and diakinesis stages, 13 autosomal bivalents and two sex chromosomes (X_1 and X_2) were observed. Some of the autosomal bivalents were detected in ring formations. Chiasmata in these bivalents were generally of terminal, interstitial, and distal types, with most bivalents showing a single chiasma feature. In the prophase II stage of meiosis II, chromosomes were observed in a supercoiled structure within two new nuclei. In anaphase II, two types of nuclei were identified: n=13 (autosomes only) and n=15 (13 autosomes + X_1 and X_2), resulting in a total of four new nuclei. The findings of this study are important for understanding the chromosomal characteristics of *Pardosa roscai* populations in Turkey.

Keywords: Lycosidae, *Pardosa*, meiosis

GİRİŞ

Bu çalışmada kullanılan *Lycosidae* familyasına ait *Pardosa* türleri dünyada yaygın bir şeklide bulunur. Ülkemizde de 35 türün yaşadığı bilinmektedir (World Spider Catalog, 2025). Örümcekler sefalothorax ve abdomen şeklinde iki segmentten oluşmaktadır. Dört çift bacak ve farklı büyüklükte sekiz adet gözleri vardır. Renkleri genellikle koyu tonlarda olup gizlenme özelliklerini ön plana çıkarmıştır. Ağ örmeyen bu örümcekler gizlenme yeteneklerini kullanarak avlarını tuzağa düşürürler. Dişi örümcekler ördükleri kozanın içine yumurtalarını bırakırlar ve yavrularını sırtlarında taşırlar. *Pardosa* cinsi bu örümcekler genellikle ormanlık arazilerde veya toprak arazilerde yaşarlar. Bazıları toprak altına delik açıp yuva yapar. Yaşamlarını bu tarz yerlerde sürdürürler (Foelix, 2011).

MATERYAL VE METOD

Materyal

Bu çalışmada *Lycosidae* familyasına ait örnekler 2024 yılı Mart- Haziran aylarında Nevşehir ili ve çevresinden toplanmıştır. Toplanan örümcekler, diseksiyon yapılıncaya kadar deney tüplerinde uygun nem ve sıcaklıkta muhafaza edilmiş ve belirli aralıklarla *Drosophila melanogaster* (meyve sineği) ile beslenmiştir.

Metod

Preparasyon işlemleri

Erkek örümceklerden diseksiyon işlemi ile gonadlar çıkarılmıştır. Kromozom preparatlarının yapılmasında Pekár ve Král (2001) yöntemi uygulanmıştır. Çıkarılan gonadlar, hipotonik ortamda 30 dakika bekletilerek hücrelerin şişmesi sağlanmıştır. Süre sonunda gonadlar Carnoy fiksatifinde sırasıyla 20-30 dakika olacak şekilde iki defa fikse edilmiştir. Fikse edilen gonadlar, % 96' lık etanolde 30 dakika boyunca bekletilmiş ve daha sonra lam üzerine asetik asit damlatıp gonadlar parçalanmıştır. Hazırlanan preparatlar faz kontrast mikroskobunda mayoz bölünme evrelerinin en yoğun olduğu preparatlar seçilerek fosfat tamponu içeren %5'lik Giemsa ile 60 dakika süreyle boyanmıştır.

Mikroskop İnceleme işlemleri

Hazırlanan preparatlar BX53 (Olympus) araştırma mikroskobu ile 100x büyütme incelenmiştir. Mayoz bölünme evreleri DP25 kamera sistemi (Olympus) ve CellSens software uygulaması ile fotoğraflanmıştır.

BULGULAR

Pardosa roscai (Roewer,1951) türünün sitogenetik sonuçları

P. roscai (Roewer,1951) türüne ait diploid kromozom sayısı 2n♂=28'dir. Türün eşey kromozomları X_1X_2 şeklindedir. Bu örümceğin kromozom morfolojisi telosentrik bir yapı göstermektedir.

Pardosa roscai (Roewer,1951) türünün mayoz bölünme özellikleri

Mayoz I, Profaz I, Zigoten evresi: Eşey kromozomları pozitif heteropiknotik şeklinde olup otozomlara göre daha erken kısalıp kalınlaşma göstermiştir. Otozomlar henüz kısalıp kalınlaşma göstermedikleri için iplikçik halinde görülmemektedir (Şekil 1 a).

Mayoz I, Profaz I, Pakiten Başlangıcı: Eşey kromozomları pozitif heteropiknotik özellikte olup çekirdek yüzeyinde yer almaktadır. Bir önceki evrede daha erken kısalıp kalınlaşma özelliği gösterirken pakiten başlangıcında biraz da otozomlara göre biraz daha geride kalıp vezikül hale dönmüştür. Otozomal bivalentler belirgin hale gelmeye başlamıştır (Şekil 1 b).

Mayoz I, Profaz I, Pakiten Başlangıcı: Bu evrede eşey kromozomları pozitif heteropiknotik olup vezikül halindedir (Şekil 1 c). Bivalentler süper spiral yapıdadır ancak sayılabilir durumda değildir.

MayozI, ProfazI, Pakiten evresi: Eşey kromozomları pozitif heteropiknotik olup vezikül şeklindedir. Homolog kromozom çiftleri belirgin hale gelmeye başlamıştır ancak tam olarak sayılmamaktadır (Şekil 1 d).

Mayoz I, Profaz I, Diploten Başlangıcı: Eşey kromozomları belirgin hale gelmeyen başlamıştır. 13 otozomal bivalent mevcuttur (Şekil 1 e). Eşey kromozomları sayılabilir ve pozitif heteropiknotik durumdadır. Otozomal bivalentler henüz kısalıp kalınlaşmalarını tamamlamadıkları için oldukça uzun boylu gözükmektedir (Şekil 1 f).

Mayoz I, Profaz I, Diploten evresi: 13 otozomal bivalent ve iki eşey kromozomu görülmektedir. Bazı bivalentlerde iki kiyazma görülmüş ve ring (halka) bivalent yapısı açıklanmıştır. Bu evrede kiyazmalar; terminal ve proksimal tipte olup distal ve interstital tipte kiyazmalar bulunmamıştır (Şekil 1 g). Eşey kromozomları birlikte hareket

etmiştir. Diplotenin orta aşamalarında bivalentlerden bazıları interstitial kiyazmaya sahip olarak gösterilmiştir. Bunun dışında bivalentler terminal ve distal tiptedir (Şekil 1 h). Ayrıca bu evrede otozomal bivalentlerden birinde sekonder boğum bölgesinin belirgin olduğu saptanmıştır (Şekil 1 i).

Mayoz I, Metafaz I: Eşey kromozomları pozitif heteropiknotik olup birlikte çekirdek yüzeyinde konumlanmıştır. 13 otozomal bivalent sayılmaktadır (Şekil 1 j).

Mayoz I, Anafaz I: Bu evrede n=15 ve n= 13 olan iki yeni çekirdek vardır. Eşey kromozomları pozitif heteropiknotik ve çekirdek yüzeyinde konumlanmıştır (Şekil 1 k). Otozomlar telosentrik tipte olduğu için " V " şeklinde görülmektedir.

Mayoz II, Profaz II başlangıcı: Kromozomlar süperspiral yapılarını korumaktadır. n=15 ve n=13 olan yeni çekirdek mevcuttur. Bu evrede eşey kromozomları izopiknotik olup otozomlardan ayırt edilmemiştir (Şekil 1 l).

TARTIŞMA VE SONUÇ

Dünya genelinde yaklaşık 53000 türü olduğu bilinen örümceklerin çok az bir kısmı sitogenetik araştırmalarda kullanılmıştır. Verilerin sınırlayıcı olmasının sebebi, erkek örümceklerin belli zaman aralığında toplanması, elde edilen bazı örümceklerin istenilen süre boyunca yaşayamaması, diseksiyon uygulamaları sırasında meydana gelen hatalar, hazırlanan kromozom preparatlarının iyi düzeyde olamamasıdır.

Dünya genelinde Lycosidae familyasına ait 138 cins ve 2495 türün tespiti yapılmıştır (World Spider Catalog, 2025). Ülkemizde ise 15 cinsi ve 92 türü bulunmaktadır. Bunlardan 35 tanesi ise *Pardosa* cinsi olduğu bilinmektedir (Danışman ve ark., 2024). Likosit örümceklerin sitogenetik araştırmalarda diploit sayısı 2n♂=21-30 şeklinde belirlenmiştir (Araujo ve ark., 2025). Günümüzde likosit örümceklerin kromozom morfolojisi aksosentrik/telosentrik tipte olması ve diploid sayının genellikle 28 olması, çalışma sonuçlarımızın familya özellikleri ile uyumlu olduğunu göstermektedir.

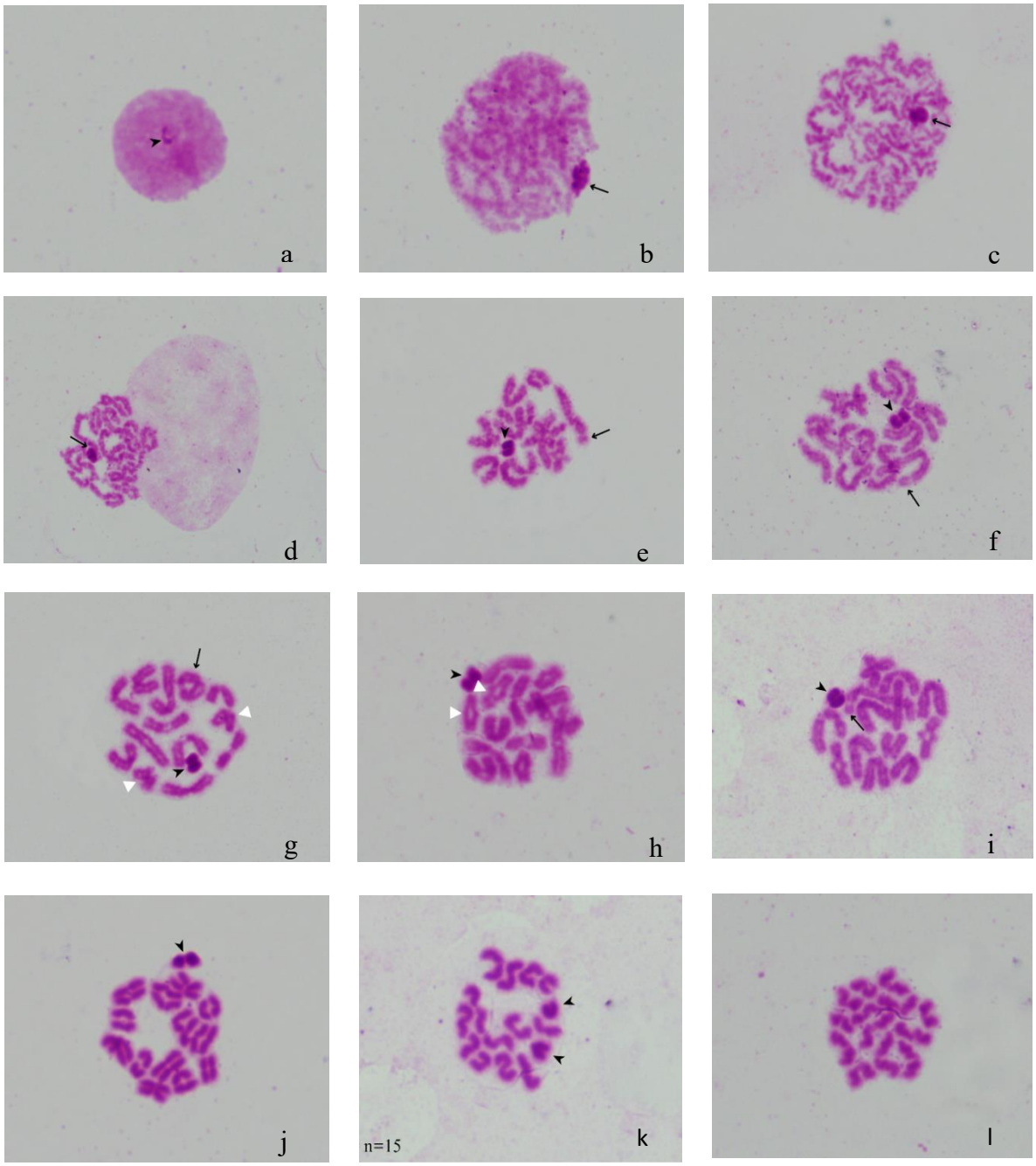

Şekil 1. *Pardosa roscai'*nin mayoz bölünme evreleri, a. Zigoten b, c. Pakiten başlangıcı d. Pakiten e, f Diploten başlangıcı g, h, i. Diploten j. Metafaz I k. Anafaz I l. Profaz II

KAYNAKÇA

Araujo, D., Schneider, M. C., Paula-Neto, E., Cella, D. M. (2025). The spider cytogenetic database. Available in www.arthropodacytogenetics.bio.br/spiderdatabase

Danışman, T., Kunt, K. B., Özkütük, R. S., Coşar, İ. (2024). The Checklist of the Spiders of Turkey. Version 2024, Online at http://www.spidersofturkey.info].

Foelix, R. F. (2011). *Biology of Spiders*. Oxford University Press.

Pekár, S., & Král, J. A. (2001) Comparative study of the biology and karyotypes of two central European Zodariid spiders (Araneae, Zodariidae). The Journal of Arachnology, v. 29, p. 345-353.

World Spider Catalog (2025). World Spider Catalog. Version 26. Natural History Museum Bern, online at http://wsc.nmbe.ch, accessed on {10.06.2025}. doi: 10.24436/2

➢ *ORAL PRESENTATION*

Abiyotik stres koşullarındaki bahçe bitkilerine hümik asit uygulanması

Kübra Korkmaz Zor (ORCID ID:0000-0002-8114-8140)

Harran Üniversitesi, Ziraat Fakültesi, Bahçe Bitkileri Bölümü, Şanlıurfa, Türkiye

*Sorumlu yazar e- posta: email:korkmz2412@gmail.com

Özet
İnsan nüfusunun hızla artması ve ortaya çıkan besin gereksinimi üretim yapılan alanları sınırlandırmaktadır. Birçok araştırmacı, bahçe bitkilerinde verimliliği artırmak ve abiyotik streslerin etkilerini azaltarak, sürdürülebilir tarımsal uygulamaları teşvik etme yönelmişlerdir. Islah çalışmaları ve yeni çeşit geliştirme çalışmaları uzun zaman gerektirdiği için çalışmaların yönünü biyostimulantlara doğru hızla ilerlemeler göstermiştir. Modern tarım sistemlerinin yaygınlaşmasıyla birlikte biyostimülantlar bir tarımsal araç ve çevre dostu bir alternatif olarak kullanmaya başlanılmıştır. Biyostimülantlar, kurak dönemlerle başa çıkmaları ve olumsuz koşullar altında bitkilerde verim artırmalarına yardımcı olma yetenekleri bilinmektedir. Bitkisel hormonlar, alg özleri, protein hidrolizatları ve humik asitler modern tarımda ana ve en çok kullanılan biyostimülanlardır. Hümik maddeler, bitkileri üzerindeki etkileri, toprak üstü kısımlardan ziyade kök sistemi üzerinde daha yaygın olarak bildirilmiştir. Bunun nedeni, hümik asitlerin kök sistemiyle doğrudan etkileşime girerek kök büyümesini, besin alımını ve genel kök sağlığını etkilemesidir.

Anahtar kelimeler: Hümik asit, abiyotik stres, biyostimülant

Application of humic acid in horticultural crops under abiotic stress conditions

Abstract
The rapid increase in human population and the emerging nutritional requirement limit the production areas. Many researchers have focused on increasing productivity in horticultural crops and promoting sustainable agricultural practices by reducing the effects of abiotic stresses. Since breeding studies and new variety development studies require a long time, studies have shown rapid progress towards biostimulants. With the spread of modern agricultural systems, biostimulants have begun to be used as an agricultural tool and an environmentally friendly alternative. Biostimulants are known for their ability to cope with dry periods and increase yields in plants under adverse conditions. Plant hormones, algae extracts, protein hydrolysates and humic acids are the main and most commonly used biostimulants in modern agriculture. The effects of humic substances on plants have been reported more commonly on the root system rather than the above-ground parts. This is because humic acids directly interact with the root system and affect root growth, nutrient uptake and general root health.
Keywords: Humic acid, abiotic stress, biostimulant

Giriş

Abiotik stres, çevresel faktörlerin canlı organizmalar üzerindeki olumsuz etkisi olarak tanımlanmaktadır. Yüksek-düşük sıcaklık, tuzluluk, kuraklık veya ağır metal toksisitesi, bir bitkinin yaşam döngüsü boyunca günlük olarak karşılaştığı başlıca abiotik stres koşullarından birkaçıdır. Tarım sektöründe, abiotik stres hem ekonomik hem de verim kayıplarının başlıca nedenlerinden biri olmaktadır (Zhang et al., 2022).

Bitkiler doğaları gereği hareketsiz canlılardır. Bu da bitkilerin gelişmeleri boyunca aynı çevre koşullarında gelişimini sürdürmelerine ve bir takım abiyotik stres türlerine maruz kalmaklarına neden olmaktadır (Liliane ve Charles, 2020). Bitki gelişimini etkileyen başlıca abiyotik stres türleri arasında kuraklık, tuzluluk, soğuk ve sıcaklık stresi yer almaktadır. Bunlar, biyokütle miktarını ve performansını %70 oranında azaltmaktadırlar (Liliane ve Charles, 2020). Özellikle kurak ve yarı kurak bölgelerdeki düzensiz yağışlar ve değişken sıcaklık değerlerini bu bölgelerde yetişen bahçe bitkileri üzerinde hayati faaliyetlerini yürütmede ciddi bir etkisi bulunmaktadır (Malhi et al., 2021). Bu nedenle stres koşullarıyla mücadele etmek için oldukça uzmanlaşmış mekanizmalar geliştirmeleri gerekir. Bu nedenle bitkiler, olumsuz koşullarda hayatta kalmak için strese duyarlı

genlerin aktivasyonu yoluyla bir dizi fizyolojik ve metabolik yanıt geliştirmiştir. Reaktif oksijen türlerinin üretimi, bitkilerin stresli ortamlarda hayatta kalmalarına yardımcı olan ilk yanıtlarından biridir (Şekil 1) (Bulgari et.al., 2019).

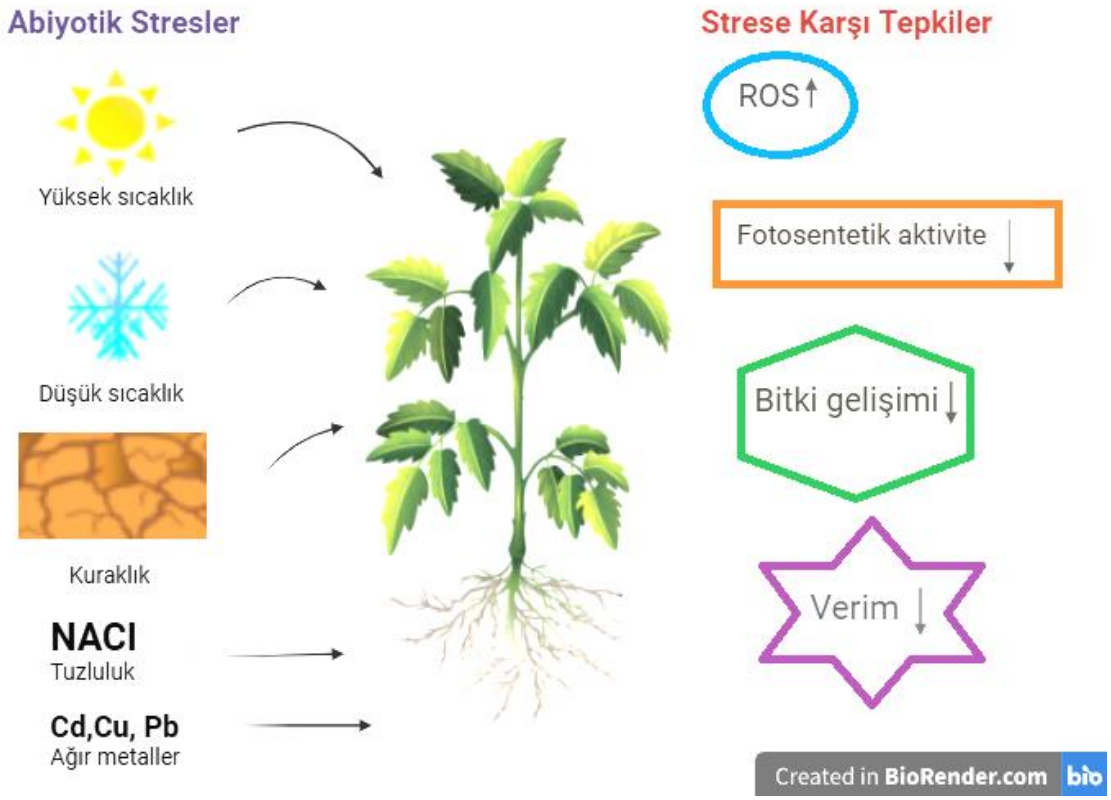

Şekil 1. Abiyotik stres faktörlerine karşı bitkilerde meydana gelen değişiklikler

Abiyotik stres toleransıyla mücadele etmek için, güçlendirilmiş bitki savunma mekanizmalarına sahip strese dayanıklı bitkiler üretilmelidir. Bir çok araştırmacı, bahçe bitkilerinde verimliliği artırmak ve abiyotik streslerin etkilerini azaltarak, sürdürülebilir tarımsal uygulamaları teşvik etme yönelmişlerdir (Drobek et al., 2019). Islah çalışmaları ve yeni çeşit geliştirme çalışmaları uzun zaman gerektirdiği için çalışmaların yönünü biyostimulantlara doğru hızla ilerlemeler göstermiştir. Modern tarım sistemlerinin yaygınlaşmasıyla birlikte biyostimülantlar bir tarımsal araç ve çevre dostu bir alternatif olarak kullanmaya başlanılmıştır. Biyostimülantlar, kurak dönemlerle başa çıkmaları ve olumsuz koşullar altında bitkilerde verim artırmalarına yardımcı olma yetenekleri bilinmektedir (Şekil 2) (Bulgari et al., 2019;Van Oosten et al., 2017).

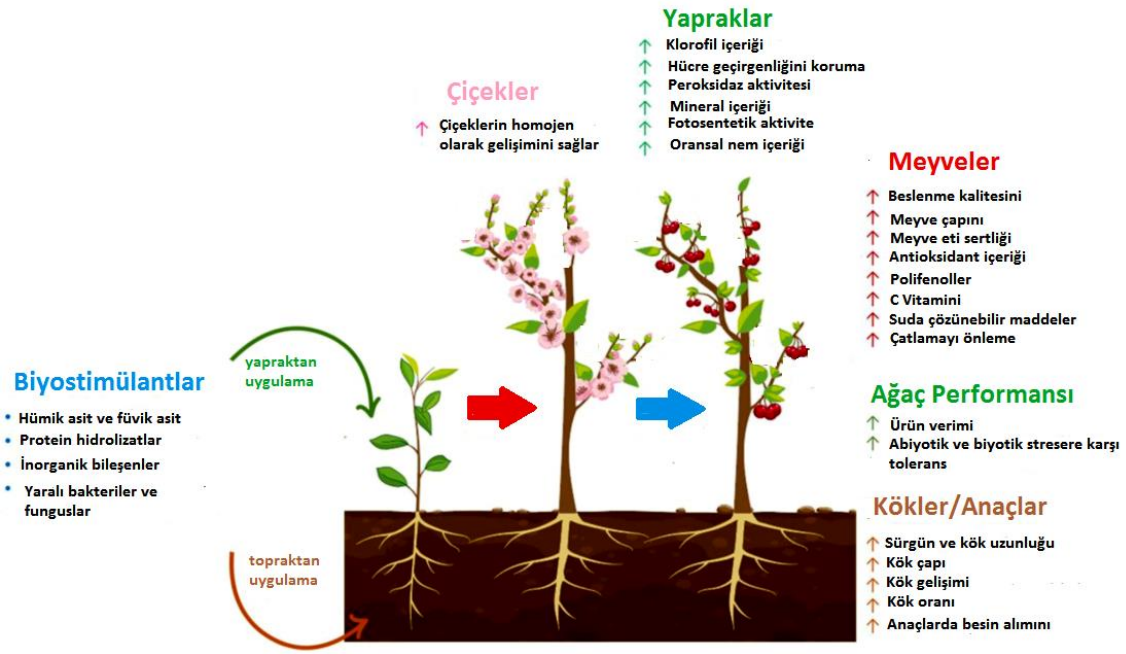

Şekil 2. Biyostimülantların bitki gelişimine etkisi

Bitkisel hormonlar (Zakeel and Safeena, 2019), alg özleri (Hassan et al., 2021), protein hidrolizatları (Carillo et al., 2019) ve humik asitler (Canellas et al., 2015) modern tarımda ana ve en çok kullanılan biyostimülanlardır. Hümik maddeler doğal olarak oluşabilen, sarıdan siyaha kadar renkleri bulunan, bozulmaya dayanıklı, heterojen maddeler olarak bilinmektedir. Bütün toprak yapılarında hümik maddelerin farklı versiyonları bulunabilmektedir. Ancak, topraklardaki yoğunlukları değişkenlik göstermektedir. Örneğin; orman topraklarında fülvik asit yüksek iken; turba ve çayırlarda hümik asit yoğunluğu yüksek olmaktadır (Canellas et al., 2015).

Hümik maddeler, bitkileri üzerindeki etkileri, toprak üstü kısımlardan ziyade kök sistemi üzerinde daha yaygın olarak bildirilmiştir. Bunun nedeni, hümik asitlerin kök sistemiyle doğrudan etkileşime girerek kök büyümesini, besin alımını ve genel kök sağlığını etkilemesidir. Ayrıca hümik asitler, topraktaki organik maddenin doğal bileşenlerinin toplanmasında ve ayrışmasında önemli rolü vardır (Canellas et al., 2015). Hümik asitlerin bitki üzerinde faydaları üç kategoriye ayrılmaktadır (Tablo 1).

Tablo 1. Hümik asidin toprak ve bitkiye sağladığı kimyasal, fiziksel ve biyolojik faydalar

Kimyasal faydalar	Fiziksel faydalar	Biyolojik faydalar
• Hümik asit toprakta aşırı asit ve alkaliyi nötralize eder ve böylece bir tampon görevi görür • Yüksek emilimi teşvik ederek besinlerin kökler tarafından tutulmasını ve bitkide daha sonra asimile edilmesini sağlar. • Bitkiler için önemli olan besin elementlerin emilmesinde ve tutulmasında iyileştirici faktör olarak rol oynar.	• Toprağınsert tabakasını kırılmasını sağlar ve geçirgenliğini artırır. • Su tutma kapasitesini artırır (4 kata kadar). • Toprağın havalanmasını artırır. • Toprak erozyonunu azaltır. • Yapısı gereği daha koyu renkte olması, daha fazla güneş enerjisi emilimine yol açarak daha sıcak bir toprak tabakası sağlar.	• Tohum çimlenmesini artırır. • Kök gelişimini uyarır. • Çeşitli büyüme düzenleyicileri, vitaminler, amino asitler, oksinler, gibberellinler organik maddenin oluşumunu sağlar ve büyümeyi artırır. • Besinleri geri dönüştüren ve antibiyotik üreten mikroorganizmaları besler.

Hümik asidin bitki gelişimine ve toprak iyileşme sürecindeki rollerine ek olarak, bitkilerdeki çevresel stresleri azaltmada faydalı etkileri olduğu bulunmuştur (Canellas et al., 2015: du Jardin 2015; Van Oosten et al., 2017 ve Veobides-Amador et al., 2018)

Hümik asit kuraklığa, tuzluluğa, yüksek ve düşük sıcaklıklara maruz kalmanın olumsuz etkilerini hafifletme yeteneğini vurgulamış ve bunun sonucunda bitki performansı ve üretkenliğinin arttığını belirtmişlerdir. Stres faktörleri altındaki bitkilerde strese karşı çeşitli fizyolojik ve biyokimyasal değişiklikler göstererek tolerans sağladığı belirtilmiştir (Kaya et al., 2018). Ayrıca hümik asit uygulamalarında, bitki biyokütlesinde artış, klorofil, prolin içeriği, peroksidaz, katalaz ve süperoksit dismutaz gibi antioksidan enzimlerin aktivitesinde artışla sonuçlanmıştır. Bu değişiklikler, bitkilerin stres türlerinden kaynaklanan oksidatif stresle başa çıkma yeteneğinin arttığını ve bunun da daha iyi bitki büyümesi ve üretkenliğine yol açtığını göstermektedir (Tablo 2) (Bijanzadeh et al., 2019; García et al., 2012; Khodadadi et al., 2020)

Tablo 2. Abiyotik stres koşulları altındaki bahçe bitkilerinde hümik asit uygulamaları

Bitki türü	Uygulama Şekli	Gelişim Koşulları	Stres Türü	Bitki performansı ve strese toleransı	Kaynak
Citrus/ Laym	Toprak+Yaprak	Arazi koşullarında	Tuzluluk	Bitki gelişim, besin elementi, klorofil ve verimde artışın yanında strese karşı tolerans	Ennab et al. (2023)
Domates	Toprak	Arazi koşullarında	Yüksek sıcaklık	Vejetatif parametreler, Çiçeklenme parametreleri ve verimde artış; Stresin olumsuz etkilerini azalttığı	Abdellatıf et.al. (2017)
Çilek	Toprak	Sera Koşullarında	Kuraklık	Bitki ağırlığı, kök ağırlığı ve uzunluğunda artış, hücre geçirgenliği, prolin ve mda azalma; strese karşı tolerans	Korkmaz et.al. (2022)
Biber	Toprak	Arazi koşullarında	Ağır metal (Cd)	Bitki kuru ağırlığı bağıl nem, toplam klorofil arttırdı; MDA ve hücre geçirgenliği azalttı; stresin olumsuz etksini önemli derecede azalttı	Zohaib et.al. (2023)

Bu nedenle, gelecekteki araştırmalar, ucuz ve yüksek oranda ulaşılabilir kaynaklardan (gübreler, evsel organik atıklar, kompostlar ve solucan gübresi) elde edilen hümik ürünlerin, tohum yatağı, fidanlık ve açık alan aşamaları dahil olmak üzere tarımsal ilgi gören bitkileri yetiştirmek için hem yaprak hem de kök yollarıyla püskürtülmesiyle abiyotik stres türlerine karşı koruyucu etkileri dikkate almalıdır. Aynı şekilde, formülasyonların ve ürünlerin geliştirilmesi, çiftçilerin kullanımına sunulmadan önce ticari yetiştirme koşulları altında doğrulanmalıdır)Khodadadi et al., 2020).

Sonuç

Hümik maddeler, fonksiyonel grupların yüksek değişkenliği ve zayıf bağlar aracılığıyla etkileşime giren küçük heterojen moleküllerin varlığı ile karakterize edilen karmaşık bir yapıya sahiptir. Bu bileşikler bitkilere uygulandığında çok çeşitli faydalar sunar. Özellikle, abiyotik streslerin neden olduğu olumsuz etkileri hafifletmeye ve bitki büyümesini ve üretkenliğini teşvik etmeye yardımcı olurlar. Kesin etki mekanizmaları hala kapsamlı bir şekilde inceleniyor ve bilimsel literatürde tartışma konusu olmaya devam ediyor olsa da, çeşitli araştırma çabaları hümik maddelerin yapısı, özellikleri ve işlevleri arasındaki ilişkiyi anlamaya odaklanmıştır. Bu, biyostimülant etkilerini açıklayan oksinlere benzer aktiviteleri gibi olası mekanizmaların açıklanmasına yol açmıştır. Hümik bileşikler, su stresi koşullarında antioksidan enzimatik komplekslerin uyarılmasına yol açan ikincil metabolizmayı düzenleme yeteneğini göstermiştir. Bitki fizyolojisi üzerindeki bu etki, hümik maddelerin iklim değişikliğinin sonuçlarını hafifletmek için uygulanabilir ve çevre dostu bir alternatif olarak hizmet

edebileceğini düşündürmektedir. Aslında, elverişsiz koşullar altında yetiştirilen bitkilerin özelliklerini geliştirebilirler. Araştırma ilerledikçe, hümik ürünlerin tarla koşullarındaki etkinliği, optimum uygulama oranları ve gerçek ürünleri sahte olanlardan ayırt etme yeteneği daha da netleşecektir. Bu artan anlayış, zamanla hümik ürünlerin kullanımını daha da artıracaktır. Genel olarak, hümik maddelerin karmaşık yapısı ve çeşitli işlevleri, onları tarım ve bitki biliminde değerli varlıklar haline getirir. Abiotik stres etkilerini hafifletme ve bitki büyümesini teşvik etme potansiyelleri, iklim değişikliği karşısında sürdürülebilir tarım uygulamaları için umut vaat etmektedir. Hümik bileşiklerin sürekli araştırılması ve keşfedilmesi, bunların optimum kullanımı ve tarımsal sistemlere entegrasyonu için yolu açacaktır.

Kaynaklar

Abdellatıf, I.M.Y., Abdel-atı,Y.Y., Abdel-mageed, Y.T. & Hassan, M.M. (2017). Effect of humıc acıd on growth and productıvıty of tomato plants under heat stress. Journal of Horticultural Research, vol. 25(2): 59-66 DOI: 10.1515/johr-2017-0022

Bijanzadeh, E., Naderi, R. & Egan, T.P. (2019). Exogenous application of humic acid and salicylic acid to alleviate seedling drought stress in two corn (Zea mays L.) hybrids. Journal of Plant Nutrition 42 (13): 1483–1495. https://doi.org/10.1080/01904167.2019.1617312

Bulgari, R., Franzoni, G. & Ferrante, A. (2019). Biostimulants application in horticultural crops under abiotic stress conditions. Agronomy 9 (6): 306–33. https://doi.org/10.3390/agronomy9060306

Carillo. P., Colla, G., Fusco, G.M., Dell'Aversana, E., El-Nakhel, C., Giordano, M. & Rouphael, Y. (2019). Morphological and physiological responses induced by protein hydrolysate-based biostimulant and nitrogen rates in greenhouse spinach. Agronomy 9 (8): 450. https://doi.org/10.3390/agronomy9080450

Canellas, L.P., Olivares, F.L., Aguiar, N.O., Jones, D.L., Nebbioso, A. & Mazzei , P. (2015). Humic and fulvic acids as biostimulants in horticulture. Scientia Horticulturae 196: 15–27. https://doi.org/10.1016/j.scienta.

Drobek, M., Frąc, M. & Cybulska, J. (2019). Plant biostimulants: Importance of the quality and yield of horticultural crops and the improvement of plant tolerance to abiotic stress—A Review. Agronomy 9 (6): 335. https://doi.org/10.3390/agronomy9060335

Ennab, H.A., Mohamed, A.H., El-Hoseiny, H.M., Omar,A.A., Hassan, I.F., Gaballah, M.S., Khalil, S.E., Mira, A.M., Abd El-Khalek, A.F. & Alam-Eldein,S.M. (2023). Humic Acid Improves the Resilience to Salinity Stress of Drip-Irrigated Mexican Lime Trees in Saline Clay Soils.*Agronomy;13*(7), 1680; https://doi.org/10.3390/agronomy13071680

Hassan, S.M., Ashour, M., Soliman, A.A., Hassanien, H.A., Alsanie, W.F., Gaber, A. & Elshobary, M.E. (2021). The potential of a new commercial seaweed extract in stimulating morpho-agronomic and bioactive properties of (Eruca vesicaria L.) Cav. Sustainability 13 (8): 4485. https://doi.org/10.3390/su13084485

García, A.C., Berbara, R.L.L., Portuondo Farías, L., Izquierdo, F.G., Hernández, O.L., Campos, R.H. & Castro, R.N. (2012). Humic acids of vermi compost as an ecological pathway to increase resistance of rice seedlings to water stress. African Journal of Biotechnology 11 (13): 3125–3134. https://doi.org/10.5897/AJB11.1960

Kaya, C., Akram, N.A., Ashraf, M. & Sonmez, O. (2018). Exogenous application of humic acid mitigates salinity stress in maize (Zea mays L.) plants by improving some key physico-biochemical attributes. Cereal Research Communications 46 (1): 67–78. https://doi.org/10.1556/0806.45.2017.064

Khodadadi, S., Chegini, M.A., Soltani, A., Ajam Norouzi, H. &Sadeghzadeh Hemayati, S. (2020). Influence of foliar-applied humic acid and some key growth regulators on sugar beet (Beta vulgaris L.) under drought stress: Antioxidant defense system, photosynthetic characteristics and sugar yield. Sugar Tech 22 (5): 765–772. https://doi.org/10.1007/s12355-020-00839-6

Korkmaz, K., Bolat, I., Karakas, S. & Dikilitas, M. (2022). Responses to Single and Combined Application of Humic Acid and Silicon Under Water Stress on Strawberry. Erwerbs-Obstbau. Volume 64, 523–533.

Liliane, T.N. & Charles, M.S. (2020). Factors affecting yield of crops. Agronomy. Climate Change and Food Security. IntechOpen: London, UK. https://doi.org/10.5772/intechopen.90672

Malhi, G.S., Kaur, M. & Kaushik, P. (2021). Impact of climate change on agriculture and its mitigation strategies: A review. Sustainability 13 (3): 1318. https://doi.org/10.3390/su13031318

Van Oosten, M.J., Pepe, O., De Pascale, S., Silletti, S. & Maggio, A. (2017). The role of biostimulants and bioeffectors as alleviators of abiotic stress in crop plants. Chemical and Biological Technologies in Agriculture 4 (1): 5. https://doi.org/10.1186/s40538-017-0089-5

Veobides-Amador, H,, Guridi-Izquierd, F. & Vázquez-Padrón, V. (2018). Las sustancias húmicas como bioestimulantes de plantas bajo condiciones de estrés ambiental. Cultivos Tropicales 39 (4): 102–109.

Zakeel, M.C.M. & Safeena, M.I.S. (2019). Biofilmed biofertilizer for sustainable agriculture. In Ansari RA, Mahmood I. (eds.). Plant health under biotic stress. Springer: Heidelberg, Germany, pp: 65–82. https://doi.org/10.1007/978-981-13-6040-4_3

Zhang, H., Zhu, J. & Gong, Z. (2022). Abiotic stress responses in plants. Nature Review in Genetics 23 (2): 104–119. https://doi.org/10.1038/s41576-021-00413-0279-1

Zohaib, M., Ashraf, K., Fatima, K., Sultan ,K., Gaafar, A.Z., Hodhod, M.S. & Zaman, Q. (2023). Humic Acid and Selenium Supplementation Modulate the Growth and Antioxidant Potential of Chili under Cadmium Stress. *Agronomy.13:*(10), 2554; https://doi.org/10.3390/agronomy13102554

➢ *ORAL PRESENTATION*

Abiyotik stres koşullarındaki bahçe bitkilerine mikoriza uygulaması

Kübra Korkmaz Zor (ORCID ID:0000-0002-8114-8140)

Harran Üniversitesi, Ziraat Fakültesi, Bahçe Bitkileri Bölümü, Şanlıurfa, Türkiye

Sorumlu yazar e-posta: email:korkmz2412@gmail.com

Özet
Bahçe bitkileri yetiştiriciliği, çeşitli abiyotik stres faktörlerine (tuzluluk, kuraklık, yüksek- düşük sıcaklık ve ağır metaller vb.) maruz kalmaktadır. Bu stres faktörleri, bitki büyümesini ile üretimini sınırlandırmanın yanı sıra toprağın yapısını da bozarak küresel gıda güvenliği için ciddi bir tehlike oluşturmaktadır. Tarım alanlarında abiyotik streslerin yarattığı olumsuz etkiyi azaltmaya yönelik bir takım tekniklerin geliştirilmesi esastır. Bu nedenle, abiyotik streslerin tarımsal alanlardaki zararlı etkilerini önlemek için çevre dostu biyostimülant uygulamalarla sürdürülmesi gerekmektedir. Biyostimülantlar içerisinde yer alan mikoriza mantarları bitki ile simbiyotik olarak yaşamaktadırlar. Bitki ile aralarında işlevsel ilişki, abiyotik stres faktörlerine karşı koruyucu, ve düzenleyici olmaktadır. Mikoriza, abiyotik stres koşulları altında besin alımını, ozmotik ayarlamalarını, hücre geçirgenliği ve reaktif oksijen türlerine(ROS) karşı bitkinin toleransını artırmakta ve büyümesini teşvik etmektedir.
Anahtar kelimeler: Mikoriza, abiyotik stres, tuzluluk, kuraklık, yüksek ve düşük sıcaklık, ağır metal

Application of mycorrhizae to horticultural plants under abiotic stress conditions

Abstract
Horticultural crops are exposed to various abiotic stress factors (salinity, drought, high-low temperature and heavy metals etc.). These stress factors not only limit plant growth and production but also disrupt the structure of the soil, posing a serious threat to global food security. It is essential to develop a number of techniques to reduce the negative effects of abiotic stresses in agricultural areas. Therefore, in order to prevent the harmful effects of abiotic stresses in agricultural areas, environmentally friendly biostimulant applications should be carried out. Mycorrhizal fungi, which are included in biostimulants, live symbiotically with the plant. The functional relationship between them and the plant is protective and regulating against abiotic stress factors. Mycorrhizae increase nutrient uptake, osmotic adjustments, cell permeability and tolerance of the plant against ROS under abiotic stress conditions and promote its growth.
Keywords: Mycorrhiza, abiotic stress salinity, drought, high and low temperature, heavy metal

1.Giriş

Ekilebilir arazilerin; sanayileşme, kentleşme ve küreselleşme ile azalması, hızla artan nüfus için gıda talebine karşılanamaması ciddi sorunlara neden olmaktadır (Frank,1885). Bunlara ek olarak, değişen iklim koşullarıyla birlikte kuraklık, yüksek-düşük sıcaklık gibi abiyotik stres faktörleri tarımsal üretimi sınırlandırmaktadır. Değişen iklim faktörlerine dayanıklı bitkiler yetiştirmek ve üretimi sürdürülebilir bir hale getirmek bir esastır (Morin, et al.,2019). Dayanıklı bitki yetiştirmek ıslah çalışmalarının hız kazanması ve gen aktarımına yönelim son zamanlarda giderek artmaktadır. Ancak, bu çalışmaların zaman alıcı ve aşamalı olması tarımsal yetiştirme tekniklerinin iyileştirilmesi fikrini öne çıkarmaktadır (Begum et al., 2019). Sürdürülebilir tarım veya doğal kaynakları kullanarak üretim sürecini ve abiyotik stresin yaratmış olduğu olumsuz etkilerini en aza indirecek şekilde gıda üretmeye sağlayan tarımsal sistemler önem taşımaktadır (Begum et al., 2019). Bu nedenle, abiyotik streslerin tarımsal alanlardaki zararlı etkilerini önlemek için çevre dostu biyostimülant uygulamalarla sürdürülmesi gerekmektedir (Begum et al., 2019). Biyostimülantlar içerisinde yer alan mikoriza bir mantar türü olup, yeryüzündeki bitkilerin %80'inden fazlasıyla mutualistik ilişki kurmaktadır. Mikoriza Yunanca "mukes (mantar)" ve "rhiza(kök)" kelimelerinden türetilmiş ve ilk olarak Frank tarafından tanımlanmıştır (Harley and Smith, 1983). Mikoriza, bitki kökleriyle ilişki kuran, dört takımlı (Mikorizanın Glomerales, Diversisporales, Archaeosporales ve Paraglomerales)on aileden oluşmaktadır (Harley and Smith, 1983).. Mikoriza daha sonra iki geniş gruba ayrılır: *(i)* ektomikoriza ve *(ii)* endomikoriza. Mikorizalar bitkinin kök bölgesinde kolonize olur ve

topraktan mineral besin maddeleri (çoğunlukla fosfor) elde etmek için bir miselyum geliştirir (Harley and Smith, 1983).. Bu miseller, mantara besin taşınmakla görevlidirler. Bununla birlikte, bitki korteks bölgesinde bir dal benzeri yapı oluştururlar buna "arbüsküller" denir. Bu dal mikoriza ile bitki arasındaki besin alışverişini sağlar. Bunun karşılığında, bitkiler mikorizaya bir karbon kaynağı ve yaşanacak bir yer vererek karşılıklı bir simbiyoz kurarlar (Harley and Smith, 1983). Mikorizalar, ayrıca bitkilerin tuzluluk, kuraklık, yüksek-düşük sıcaklık ve ağır metaller gibi abiyotik stres faktörlerine karşı direnç mekanizması geliştirmelerine yardımcı olurlar. Böylece, bitkilerin büyümelerini ve yaşamsal faaliyetlerini devam etmesini sağlarlar (Şekil 1). Yetiştiricilerin verimini en üst düzeye çıkarmakla kalmaz, aynı zamanda gelecek nesiller için sürdürülebilir uygulamaları da artırırlar (Pedranzani, et al., 2016).



Şekil 1. Toprakta bitki köklerindeki mikorizanın görüntüsü

1.Abiyotik streslerde Mikorizaların Bitkiler Üzerindeki Etkileri

Mikoriza bitki beslenmesindeki ve toprak dokusundaki iyileştirici özelliklerinin dışında stres azaltıcı bir rolü de bulunmaktadır. Bunlar, bitkilerin morfolojik, biyokimyasal, fizyolojik ve moleküler parametrelerindeki ciddi bozulmaları engellediği için dünya çapında ciddi verim kayıplarına neden olur (Shaffique et al.,2022). Bitki üzerindeki zararlı etkileri azaltmak için mikorizalar önemli bir rol oynar. Bitkinin kuraklığa, tuzluluğa ve ağır metale karşı dayanıklılık sağlar ve bitkinin abiyotik streslerle mücadele yeteneği güçlendirirler (Şekil 2) (Shaffique et al.,2022)

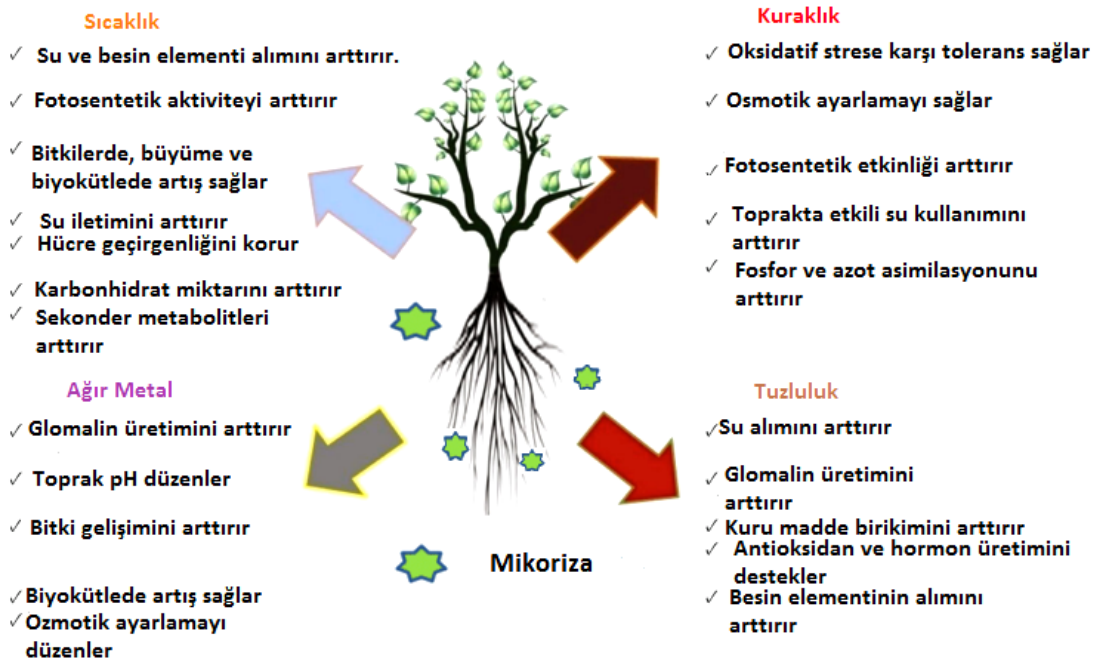

Şekil 2. Abiyotik stres faktörleri altındaki bitkilerde mikoriza uygulandığında meydana gelen değişiklikler

1.1. Mikorizanın Tuzluluk Stresini Azaltmadaki Rolü

Tuzluluk, tarımsal üretkenlik üzerinde olumsuz bir etkiye sahip olduğu yaygın olarak kabul edilen Tuzluluk, tarımsal üretimi olumsuz yönde etkileyen abiyotik stres faktördür (Upadhyay and Chauhan, 2022). Dünya çapında, tuzluluk ekilebilir arazinin %20'sini etkiler ve çoğunlukla kuru ve yarı kurak bölgelerde yavaş ama istikrarlı bir şekilde yayılır. Kurak arazide yağışın düşüklüğü ve buharlaşma oranının yüksek olması tuzluluğu şiddetlendirmektedir (Selvakumar et al.,2014). Tuzluluk stresi, bitki morfolojisi ve fizyolojisinde istenmeyen değişikliklere neden olur ve bu da bitki gelişiminde gerilemelere ve giderek ölümlere yol açar (Miransari, 2016).

(a) Mikorizalar tuzlu topraklarda bitki köklerinin ulaşamadığı ve alamadığı suyu, hifleri yardımıyla almasını sağlar (Bothe, 2012)
(b) Mikorizalar glomalin adı verilen bir protein üretirler. Hammer ve Rillig, glomalinlerin tuzluluk stresi altında artış gösterdiğini ve toprak yapısını iyileştirdiğini bildirmişlerdir (Singh et al.,2013).
(c) Mikorizalar çeşitli stres koşullarında fotosentetik aktiviteyi ve stoma iletkenliğini arttırdığını ve böylece kuru madde birikiminde önemli etkisi olduğu gözlemlenmiştir (Zuccarini and Okurowska, 2008).
(d) Mikorizalar bitkilerin kök bölgesinde kolonize olarak su tutma kapasitesini iyileştirir, ozmotik dengeyi ve karbonhidratların bileşimini olumlu şekilde düzenler (Ruiz-Lozano and Aroca,2010).
(e) Mikoriza, stresli tuz koşulları altında süperoksit dismutaz (SOD), peroksidaz (POD), askorbat peroksidaz (APX) ve katalaz enzimi (CAT) gibi antioksidan enzimlerin aktivitelerini iyileştirerek H_2O_2, OH^- ve O_2 gibi reaktif oksijen türlerinin (ROS) seviyesini düzenleyebilir (He et al., 2007).
(f) Mikoriza, bitkilerde bu büyüme hormonlarının (Sitokininler, oksin, etilen, absisik asit (ABA), jasmonik asit (JA), nitrik oksit (NO), salisilik asit (SA), gibberellin) içeriğindeki değişiklikleri uyarabilir ve bu nedenle bitkilerde savunma tepkisi meydana getirebilir (Miransari, 2014).
(g) Tuzlu topraklarda yüksek konsantrasyonda Na+ ve Cl'nin varlığı bitkiler için önemli element olan potasyumun alımını olumsuz etkilemektedir. Mikoriza kök bölgesinde kuru toprakta yayılarak P alımını artırır. Ayrıca topraktaki Na ve Cl dengesini koruyarak fosfor ve Zn, P ve Cu gibi immobil besin elementlerin alımında sağlarlar. (Evelin et al.,2012). Mikoriza, bitki fizyolojisini ayarlayarak bitki gelişimini ve doku besin maddelerini iyileştirerek sentetik gübrelerin kullanımında azalmalara izin verir (Tablo 1) (Evelin et al.,2012).

Tablo 1. Tuzlu stres koşulları altındaki bahçe bitkilerinde mikoriza uygulamaları

Bitki türü	Stres Türü	Bitki performansı ve strese toleransı	Kaynak
Domates	Tuzluluk	Sürgün ve kök gelişiminde artış sağlamıştır.	Khalloufi et al. (2017)
Salatalık	Tuzluluk	Na alımını azaltmış; prolin, antioksidan, enzim miktarını arttırmıştır.	Hashem et al. (2018)
BademxŞeftali	Tuzluluk	Çözünebilir şeker miktarını, antioksidan ve fotosentez etkinliğini arttırmıştır.	Shahvali et al. (2020)
Karpuz	Tuzluluk	Besin elementi alımını, meyve ağırlığını, klorofil, magnezyum potasyumda artış gözlenmiştir.	Bijalwan et al. (2021)

1.2. Kuraklık Stresi ve Mikorizaların Bitkiler Üzerindeki Etkileri

Kuraklık, dünya çapında ürün verimini önemli ölçüde azaltan ve iklim değişiklikleriyle birlikte artması beklenen en yıkıcı streslerden biri olarak bilinmektedir (Pedranzani et al.,2016). Buharlaşma nedeniyle bitki köklerinin suya erişemediği kuraklık durumu, bitkilerin hayatta kalmasını önemli ölçüde olumsuz etkiler (Begum et al.,2019). Kuraklığın, stoma kapanmasıyla CO_2 girişindeki azalma, karbon dağılımı, reaktif oksijen türlerinin (ROS) üretimindeki hızlanma, oksidatif stres, fosfat bulunabilirliğinin ve diğer besin kaynaklarının azalması ve ürün kalitesinin düşmesi gibi bitki metabolik süreci üzerinde bazı olumsuz etkileri vardır (Begum et al., 2019).
Küresel ısınma ve elverişli suyun olmaması kuraklık koşullarını daha da kötüleştirmiştir. Bu nedenle, ürünü daha dayanıklı hale getirmek ve kuraklığın ürün verimi üzerindeki olumsuz etkilerini azaltmak için sürdürülebilir stratejiler talep edilmektedir. Bu stratejilerden biri olan mikoriza kullanımı gerek toprak koşullarını iyileştirmede gerekse de bitki gelişiminde öne çıkmaktadır (Wu et al., 2017).

1.2. Mikorizanın Kuraklık Stresini Azaltmadaki Rolü

(i) Mikoriza, bitki kök bölgesinde köklerin uzamasını sağlar. Mikoriza tarafından üretilen glomalin, polisakkaritler, musilajlar ve hidrofobinler toprakta daha iyi su tutma kapasitesini arttırır. Böylece bitkilerde biyokütleyi artırır (AlKaraki et al., 2004)
(ii) Kök bölgesinde kolonize oluşturarak fosfor ve azot asimilasyonunu iyileştirir. Mikorizal P-taşıyıcılar fosfatı alır ve onu polifosfata dönüştürür, bu daha sonra bitki yönünde taşınmasını sağlar
(Gholamhoseini et al., 2013).
(iii)Mikoriza, kuraklıkta yapraklarındaki stoma hareketini etkileyerek, su buharı dışarı akışını ve CO_2 gazı değişimini, yaprak su potansiyelini ve bağıl su içeriğini, bitkilerin su kullanım verimliliğini fotosentetik verimliliğinin artırılması gibi olayları iyileşmesini sağlar (Auge et al., 2015; Barzana et al., 2012).
(iv) Mikoriza, kuraklıkta bitkilerde absisik asit (ABA) sentezleyerek stomaların kapanmasını sağlarlar. Böylece bitki su kaybını azaltarak strese dayanıklılık sağlar (Auge et al., 2015).
(v) Mikorizalar, iyi bir ozmotik ayarlama adayıdır. Susuz ortamlara maruz kaldığında, şekerler, prolin, poliaminler, glisin betain, glutatyon ve organik asitler gibi uygun çözünen maddelerin birikimini de artırlar.
(vi) Bitkiler oksidatif strese karşı yanıt olarak hem enzimatik olmayan (fenolik bileşikler, glutatyon, askorbik asit, alkaloidler, karotenoidler ve tokoferol gibi) hem de enzimatik savunma sistemlerini geliştirmiştir (Zubek et al., 2015). Mikorizalar, bu sekonder metabolitlerin üretimini artırarak (Zubek et al., 2015), oksidatif stresin neden olduğu hasarı azaltma yeteneğine sahiptirler (Wu et al., 2014). Diğer yandan mikorizalar, lipid peroksidasyon (MDA) ve H_2O_2 birikiminin miktarını azaltarak bitkinin oksidatif strese karşı savunma sağlarlar (Wu et al., 2014). Böylece, mikorizanın kurak koşullarda bitkiler üzerindeki fizyolojik ve büyüme bozukluklarını azaltmasının yanı sıra su potansiyeli ve su kullanım verimliliğinin de arttığı belirlenmiştir (Tablo 2) (Wu et al., 2014).

Tablo 2. Kurak stres koşulları altındaki bahçe bitkilerinde mikoriza uygulamaları

Bitki türü	Stres Türü	Bitki performansı	Kaynak
Domates	Kuraklık	Bitki boyu, stoma iletkenliği, biyokütle de artış gözlenirken, Prolin ve Reaktif oksijen türlerinde azalmalar gözlemişlerdir.	Chitarra et al. (2016)
Üç yapraklı/Citrus	Kuraklık	Kök ağırlığı ve uzunluğunda, çözünebilir şeker miktarlarında artışlar elde etmişlerdir.	Zhang et al. (2018)

1.3. Mikorizanın Sıcaklık Stresini Azaltmadaki Rolü

Yüksek sıcaklık, bitki büyümesi, fizyolojisi ve verimliliği üzerinde de olumsuz etkiye sahiptir (Zhu et al., 2011). Bitki için sıcaklık stresi 0–15°C (düşük sıcaklık stresi) ve 45°C üzeridir (yüksek sıcaklık stresi) (Theocharis et al., 2012). Bitkiler düşük veya yüksek sıcaklık stresine maruz kaldığında birçok fizyolojik ve biyokimyasal sistem bozulur. Sıcaklık stresinin neden olduğu çeşitli zararlar arasında hücre zarının yapısal hasarı, zar lipitlerinin peroksidasyonu, protein, toksik bileşik üretimi, bitki canlılık kaybı, tohum çimlenmesinin engellenmesi, büyüme hızının gerilemesi, verimin azalması, solma, yanma, yaprakların dökülmesi ve yaşlanması, üreme organlarına zarar verme ve meyvelerin hasar görmesi ve renk değiştirmesi yer alır (Zhu et al., 2011; Theocharis et al., 2012).

(1) Mikoriza, yüksek sıcaklıklarda kök bölgesindeki su alımı azaldığında stomaların kapanmasında rol oynarlar. Böylece, bitkilerin yaprakların yüzeylerine buharlaşan su akışını azaltarak stresin şiddetini azaltırlar. Ayrıca gerek düşük gerekse yüksek sıcaklık stresinde kök bölgesinde kolonize olarak bitkideki mevcut su durumunu iyileşmesini sağlarlar (Ali et al., 2005).
(2) Sıcaklık stresinde mikoriza kullanılan ve kullanılmayan bitkiler karşılaştırıldığında; mikoriza kullanılan bitkilerde daha yüksek fotosentez oranı oluştuğu belirlenmiştir. Mikorizanın bitkilerde klorofil içeriğini arttırdığını dolayısıyla karbon asimilasyonunda artışlar olduğu bildirilmiştir (Zhu et al., 2011).
(3) Sıcaklık stresi altındaki bitkilerde plazma membranı, membran geçirgenliğini artıran çeşitli kompozisyonel, yapısal ve diğer değişikliklerin yanı sıra artan elektrolit kaybı yaşar. Mikorizanın sıcalık stresinde bitki bünyesinde, membranın stabilitesini ve bütünlüğünü artırarak dayanıklılığı arttırdığı bildirilmiştir (Kim et al., 2013).
(4) Yüksek ve düşük sıcaklıklarda bitkilerde meydana gelen hasarın temel nedenleri oksidatif strestir. Bu oksidatif stres, hücrelerde protein denatürasyonuna ve enzim inhibisyonuna neden olur ve bu da hücre yapısı ve işlevinin tahribatına yol açar (Lenoir et al., 2016). Mikoriza bitkilerde, sıcaklık stresinin neden olduğu oksidatif hasarı azaltmak veya önlemek için antioksidan sistemler aracılığıyla ROS'u toplamak üzere bir savunma mekanizması geliştirmiştir (Chen et al., 2013).
(5) Mikoriza, düşük ve yüksek sıcaklık ortamlarında bitkilerde hücrelerin turgor basıncını korur ve ozmotik ayarlama yaparlar. Böylece bitkilerde strese karşı tolerans mekanizmasında rol oynarlar (Theocharis et al., 2013; Wahid et al., 2007).
(6) Düşük ve yüksek sıcaklıkta, bitkiler stres ile mücadele edebilmek için çözünebilir şekerlere gereksinim duyarlar. Mikorizalar, stres koşullarında su molekülleri ile lipit moleküllerini değiştirerek hidrojen bağları oluştururlar ve hücre zarını koruyarak stabilize ederler (Maya and Matsubara, 2013).
(7) Düşük ve yüksek sıcaklık koşullarında, mikorizalar bitkide kök bölgesinden azot emilimini artırır ve bitkiye taşınmasında görev yaparlar (Govindarajulu et al., 2005).
(8) Düşük sıcaklıklarda mikorizalar, sekonder metabolitlerin artmasını sağlar. Sekonder metabolitler bitkilerin antioksidan ve savunma sistemlerini geliştirirler ve strese karşı tolerans gösterirler (Tablo 3) (Apel and Hirt, 2004).

Tablo 3. Düşük ve yüksek stres koşulları altındaki bahçe bitkilerinde mikoriza uygulamaları

Bitki türü	Stres Türü	Bitki performansı	Kaynak
Hıyar	Düşük sıcaklık	Fotosentez aktivitesinde ilerlemeler bulmuşlardır.	Ma et al. (2019)
Üzüm	Yüksek sıcaklık	Bitki gelişiminde artış, stoma iletkenliğinde azalmalar elde etmişlerdir.	Nogales et al. (2020)
Domates, Biber ve hıyar	Yüksek sıcaklık	Bitki gelişiminde, verim ve meyve kalitesinde artışlar olduğunu tespit etmişlerdir	Reva et al. (2021)

1.3. Mikorizanın Ağır metal Stresini Azaltmadaki Rolü

İnsan müdahalesiyle artan toprak kirliliği, toprakta ağır metal birikmesine yol açan büyük bir sorun haline gelmiştir. Toprakta ağır metal birikimi, tarımsal kimyasallar, kanalizasyon atıkları ve kömür gibi metal içeren atıklar, gaz atıkları, suya ve atmosfere salınmasıyla oluşur. Yüksek seviyelerde ağır metaller (kadmiyum, paladyum, cıva, vb.) yalnızca toprak ve bitki sağlığı için değil, aynı zamanda insan sağlığı için de tehlikelidir çünkü çeşitli yollarla besin zincirine girebilir ve ağır metallerle kirlenmiş gıdalarla sonuçlanabilir. Fiziksel-kimyasal yöntemler (toprak yıkama ve toprak düzenleyici uygulama gibi), bakteri ve mikoriza kullanımı biyoremediasyon, ağır metallerle kirlenmiş toprağı temizlemek için kullanılabilir. Bunlar, çevreye duyarlı olup, kimyasal veya fiziksel temizlemeden daha az olumsuz etkiye sahiptirler (Karimi et al., 2011; Forgy,2012). Ağır metal, plazma zarının geçirgenliğini ve işlevini bozarak bitkilerin büyümesini ve gelişimini etkiler. Ayrıca hücresel bileşenleri ve dolayısıyla bitki dokularını olumsuz etkileyen oksidatif strese de neden olabilir (Forgy, 2012).

(1) Mikorizalar, köklerde şelat oluşturarak hifleri yardımıyla topraktaki emerler (fitoekstraksiyon özellik) (Vierheilig et al., 2003). Fitoekstraksiyon, bitkilerin bitki kısımlarında ağır metali depolama ve tolere etme yeteneğini kullanır ve kirlenmiş toprakları iyileştirmek için görev yapar (Kanwal et al., 2015; Suchun et al., 2014). Ağır metallerin bitkinin toprak üstü organlarına geçmesini engeller ve sürgünlerde biyokütlenin artışını sağlar (Vierheilig et al., 2003).
(2) Mikorizalar, antioksidan enzimler ile serbest radikalleri ortadan kaldırır ve bitki toleransını artırır, tıpkı tuzluluk ve kuraklık stresinde ozmotik ayarlamalarda yaptığı gibi bitki zarında düzenli madde ve enerji değişimini sürdürür ve ağır metallerin olumsuz etkilerine karşı strese direnç göstermesini teşvik eder (Tablo 4) (Andrade et al., 2008;Ling and Fayuan, 2012).

Tablo 4. Ağır metal stres koşulları altındaki bahçe bitkilerinde mikoriza uygulamaları

Bitki türü	Stres Türü	Bitki performansı	Kaynak
Domates	Kadmiyum	Manoldehid ve reaktif oksijen türlerinin miktarında azalmaya, bitki dayanıklılığında artışa ve kadmiyum alımını azalttığı elde etmişlerdir.	Jiang et al. (2016)

Sonuç

Mikorizaların bitki ile yapmış olduğu simbiyotik ilişkisi, bitki fizyolojisini önemli ölçüde değiştirmekte ve bunu bitki üzerinde uzun süre devam ettirmektedir. Bu başarılı simbiyoz, biyoteknolojik çalışmalarla geliştirilerek gelecek için umut verici olacaktır. Sentetik gübrelerin ve diğer kimyasalların kullanımında azaltma da rol oynayarak sürdürülebilir tarımın hedeflerini destekleneceği düşünülmektedir. Mikorizaların tarımsal uygulamalarda kullanılması, dünya nüfusundaki artan tüketim ihtiyaçlarını karşılamasında ve üretimde artışlar meydana getireceği beklenmektedir. Abiyotik stres faktörlerinde, prolin, fitohormonlar, antioksidan enzimler üretimini artırmakta ve böylece bitkileri, bu koşullarda tolerans göstermelerini sağlamaktadır. Stres koşullarında, tolerans mekanizmalarının nasıl çalıştığını bulabilmek için ise farklı bitki türlerinde çalışmalar yapılması

gerekmektedir. Ayrıca ağır metallerle kirlenmiş toprakların ıslah edilmesinde daha faydalı ve etkili olması için nasıl uygulamaya konulacağı konusunda da araştırmaların yapılmasına ihtiyaç duyulmaktadır. İn-vitro veya saksı denemelerinde bitki büyümesinde ve stresli topraklarda sürdürülebilir tarım için etkili bir yöntem olacağı düşünülmektedir.

Kaynaklar

AlKaraki, G., Mcmichael, B. & Zak, J. (2004). "Field response of wheat to arbuscular mycorrhizal fungi and drought stress," Mychorrhiza, vol. 14, no. 4, pp. 263–269.

Apel, K. & Hirt, H. (2004). "Reactive oxygen species: metabolism, oxidative stress, and signal transduction," Annual Review of Plant Biology, vol. 55, no. 1, pp. 373–399.

Andrade, S.A.L., Silviera, A.P.D., Jorge, R.A. & de Abreu, M.F.(2008). "Cadmium accumulation in sunflower plants influenced by arbuscular mycorrhiza," International Journal of Phytoremediation, vol. 10, pp. 1–13.

Barzana, G., Aroca, R. & Paz J.A. (2012). "Arbuscular mycorrhizal symbiosis increases relative apoplastic water flow in roots of the host plant under both well-watered and drought stress conditions," Annals of Botany, vol. 109, no. 5, pp. 1009–1017.

Begum, N., Qin, C. & Ahanger M.A. (2019). "Role of arbuscular mycorrhizal fungi in plant growth regulation: implications in abiotic stress tolerance," Frontiers in Plant Science, vol. 10, p. 1068.

Bijalwan, P. Jeddi, K. Saini, I. Sharma, M. Kaushik, P. & Hessini, K. (2021). "Mitigation of saline conditions in watermelon with mycorrhiza and silicon application," Saudi Journal of Biological Sciences, vol. 28, no. 7, pp. 3678–3684,

Bothe, H. (2012). "Arbuscular mycorrhiza and salt tolerance of plants," Symbiosis, vol. 58, no. 1-3, pp. 7–16.

Chitarra, W., Pagliarani, C. & Maserti B. (2016). "Insights on the impact of arbuscular mycorrhizal symbiosis on tomato tolerance to water stress," Plant Physiology, vol. 171, pp. 1009–1023,

Frank, A.B.(1885). "Ueber die auf Wurzelsymbiose beruhende Ernahrung gewisser Baume durch unterirdische Pilze," Berichte der Deutschen Botanischen Gesellschaft, vol. 3, pp. 128–145.

Gholamhoseini, M., Ghalavand, A., Dolatabadian, A., Jamshidi, E. & Joghan, A. K. (2013). "Effects of arbuscular mycorrhizal inoculation on growth, yield, nutrient uptake and irrigation water productivity of sunflowers grown under drought stress," Agricultural Water Management, vol. 117, pp. 106–114.

Govindarajulu, M., Pfeffer, P.E. & Jin, H. R. (2005). "Nitrogen transfer in the arbuscular mycorrhizal symbiosis," Nature, vol. 435, no. 7043, pp. 819–823.

Harley J. L. & Smith, S. E. (1983). Mycorrhizal Symbiosis, Academic Press, New York.

Hashem, A., Alqarawi, A.A., Al-Arjani, R., Aldehaish, H. A., Egamberdieva, D. & AbdAllah, E. F. (2018)."Arbuscular mycorrhizal fungi regulate the oxidative system, hormones and ionic equilibrium to trigger salt stress tolerance in Cucumis sativus L," Saudi Journal of Biological Sciences, vol. 25, no. 6, pp. 1102–1114.

He, Z.Q., He, C.X., Zhang, Z.B., Zou, Z. & Wang, H. (2007)."Changes of antioxidative enzymes and cell membrane osmosis in tomato colonized by arbuscular mycorrhizae under NaCl stress," Colloids and Surfaces B: Biointerfaces, vol. 59, no. 2, pp. 128–133.

Karimi, A., Khodaverdillo, H., Sepehri, M. & Sadaghiani, M.H.R. (2011). "Arbuscular mycorrhizal fungi and heavy metal contaminated soils," African Journal of Microbiology Research, vol. 5, no. 13, pp. 1571–1576.

Kanwal, S., Bano, A. & Malik, R.N. (2015). "Effects of arbuscularmycorrhizal fungi on metals uptake, physiological and biochemical response of Medicago sativa L. with increasing Zn and Cd concentrations in soil," American Journal of Plant Sciences, vol. 6, pp. 2906–2923.

Khalloufi, M., Martínez-Andújar, C., Lachaâl, M., Karray Bouraoui, N., Pérez-Alfocea, F. & Albacete, A. (2017). "The interaction between foliar GA3 application and arbuscular mycorrhizal fungi inoculation improves growth in salinized tomato (Solanum lycopersicum L.) plants by modifying the hormonal balance," Journal of Plant Physiology, vol. 214, pp. 134–144.

Kim, H.S., Oh, J.M., Luan, S., Carlson, J. E. & Ahn, S. J. (2013). "Cold stress causes rapid but differential changes in properties of plasma membrane H+-ATPase of camelina and rapeseed," Journal of Plant Physiology, vol. 170, pp. 828–837.

Lenoir, I., Fontaine, J. & Sahraoui, A.L. (2016). "Arbuscular mycorrhizal fungal responses to abiotic stresses: a review," Phytochemistry, vol. 123, pp. 4–15.

Ling, W. & Fayuan, W. (2012). "Remediation of cadmium-polluted soils with arbuscular mycorrhiza," Guangdong Agricultural Sciences, vol. 2, pp. 51–53.

Jiang, Q., Y. Zhuo, F. & Long S. H. (2016). "Can arbuscular mycorrhizal fungi reduce Cd uptake and alleviate Cd toxicity of Lonicera japonica grown in Cd-added soils?," Scientific Reports, vol. 6, no. 1.

Ma, J., Janouskova, M. & Ye L. (2019). "Role of arbuscular mycorrhiza in alleviating the effect of cold on the photosynthesis of cucumber seedlings," Photosynthetica, vol. 57, pp. 86–95,

Maya, M.A. & Matsubara, Y. (2013). "Influence of arbuscular mycorrhiza on the growth and antioxidative activity in cyclamen under heat stress," Mycorrhiza, vol. 23, no. 5, pp. 381–390.

Miransari, M. (2014). Plant Hormonal Signaling Under Stress, Published by AbtinBerkeh Ltd. Company, Isfahan, Iran, and Creative Space, an Amazon Company, USA.

Miransari, M. 2016. Abiotic and Biotic Stresses in Soybean Production, Elsevier, Academic Press, USA.

Morin, E., Miyauchi, S. & Clemente, S.H. (2019)."Comparative genomics of Rhizophagus irregularis, R. cerebriforme, R. diaphanus and Gigaspora rosea highlights specific genetic features in Glomeromycotina," New Phytologist, vol. 222, no. 3,pp. 1584–1598.

Nogales, A., Ribeiro, H. & Nogales-Bueno J. (2020). "Response of mycorrhizal touriga national variety grapevines to high temperatures measured by calorespirometry and near-infrared spectroscopy," Plants, vol. 9, no. 11, p. 1499

Pedranzani, H., Rodrã Guez-Rivera, M., Gutia Rrez, M., Porcel, R., Hause, B. & Ruiz-Lozano, J. M. (2016)."Arbuscular mycorrhizal symbiosis regulates physiology and performance of Digitaria eriantha plants subjected to abiotic stresses by modulating antioxidant and jasmonate levels," Mycorrhiza, vol. 26, pp. 141–152.

Reva, M., Cano, C., Herrera, M. & Bago, A. (2021). "Arbuscular mycorrhizal inoculation enhances endurance to severe heat stress in three horticultural crops," HortScience, vol. 56, no. 4, pp. 396–406,

Ruiz-Lozano, J. M. & Aroca, R. (2010). "Modulation of aquaporin genes by the arbuscular mycorrhizal symbiosis in relation to osmotic stress tolerance," in Symbiosis and stress, pp. 359–374, Springer, Berlin.

Shaffique, S., Khan, M.A. & Wani, S.H. (2022). "A review on the role of endophytes and plant growth promoting rhizobacteria in mitigating heat stress in plants," Microorganisms, vol. 10, no. 7, p. 1286.

Selvakumar, G., Kim, K., Hu, S. & Sa, T. (2014)."Effect of salinity on plants and the role of arbuscular mycorrhizal fungi and plant growth-promoting rhizobacteria in alleviation of salt stress," in Physiological Mechanisms and Adaptation Strategies in Plants under Changing Environment,., pp. 115–144, Springer, New York.

Shahvali, R., Shiran, B., Ravash, R., Fallahi, H. & Banovicderi, B. (2020). "Effect of symbiosis with arbuscular mycorrhizal fungi on salt stress tolerance in GF677 (peach×almond) rootstock," Scientia Horticulturae, vol. 272, article 109535.

Singh, P.K., Singh, M. & Tripathi, B.N. (2013). "Glomalin: an arbuscular mycorrhizal fungal soil protein," Protoplasma, vol. 250, no. 3, pp. 663–669.

Suchun, L., Langchao, X. & Huiqun, W. (2014). "The mechanisms of heavy metal uptake by plant and phytoremediation,"Journal of Hunan Agricultural University, vol. 30, no. 5, pp. 493–498.

Vierheilig, H., Lerat, S. & Piche, Y. (2003). "Systemic inhibition of arbuscular mycorrhiza development by root exudates of cucumber plants colonized by Glomus mosseae," Mycorrhiza, vol. 13, pp. 167–170.

Zhang, F., Jia-Dong, H. E., Qiu-Dan, N. I., Qiang-Sheng, W. U. & Zou, N. Y. (2018). "Enhancement of drought tolerance in trifoliate orange by mycorrhiza: changes in root sucrose and proline metabolisms," Notulae Botanicae Horti Agrobotanici Cluj-Napoca, vol. 46, no. 1, pp. 270–276.

Zhu, X.C., Song, F.B., Liu, S.Q. & Liu, T.D. (2011). "Effects of arbuscular mycorrhizal fungus on photosynthesis and water status of maize under high temperature stress," Plant and Soil, vol. 346, no. 1-2, pp. 189–199.

Zubek, S., Rola, K., Szewczyk, A., Majewska, M.L. & Turnau, K. (2015). "Enhanced concentrations of elements andsecondary metabolites in Viola tricolor L. induced by arbuscular mycorrhizal fungi," Plant and Soil, vol. 390, no. 1-2, pp. 129–142.

Zuccarini, P. & Okurowska, P. (2008). "Effects of mycorrhizal colonization and fertilization on growth and photosynthesis of sweet basil under salt stress," Journal of Plant Nutrition, vol. 31, pp. 497–513.

Theocharis, A., Clement, C. & Barka, E.A. (2012). "Physiological and molecular changes in plants grown at low temperatures," Planta, vol. 235, no. 6, pp. 1091–1105.

Wahid, A., Gelani, S., Ashraf, M. & Foolad, M.R. (2007). "Heat tolerance in plants: an overview," Environmental and Experimental Botany, vol. 61, no. 3, pp. 199–223

Wu, H.H., Zou, Y.N., Rahman, M.M., Ni, D. & Wu, Q.S. (2017). "Mycorrhizas alter sucrose and proline metabolism in trifoliate orange exposed to drought stress," Scientific Reports,vol. 7, no. 1, article 42389.

Wu, Q.S., Zou, Y.N. & Abd-Allah, E.F. (2014). "Mycorrhizal association and ROS in plants," in Oxidative Damage to Plants, P. Ahmad, Ed., pp. 453–475, Academic Press, Cambridge.

➢ *ORAL PRESENTATION*

Design and prototyping process of the gas shutoff system developed for safe natural gas supply

Atıl ERİM[1] (ORCID ID: 0009-0009-6232-8224),
Hüseyin PEHLİVAN[2] (ORCID ID: 0000-0003-3048-8986)

[1]Eska Valve Research and Development Center, Sakarya 1. OSB Arifiye/Sakarya, Türkiye
[2]Sakarya Üniversite, Faculty of Engineering, Department of Mechanical Engineering, Sakarya, Türkiye, pehlivan@sakarya.edu.tr

* Corresponding author e-mail: atilerim@eskaarge.com

Abstract

The development of an automatic and safe system approach following natural gas interruptions, from residential to industrial applications, is of critical importance. This study addresses the "Doğalgaz Şalteri" (Natural Gas Switch) System, developed to enhance safety in cases of natural gas supply disruptions. Operating purely on mechanical principles without the need for an external power source, the system automatically deactivates in the event of a gas flow interruption.

Compared with existing systems, the Doğalgaz Şalteri minimizes the need for manual intervention, thereby reducing the operational burden on gas distribution companies and ensuring uninterrupted service continuity. The target design parameters include a maximum inlet pressure (PS) (Pmax) of 500 mbar, an operating pressure range of 8–500 mbar, a response time below 1 second, a maximum capacity range of 20–40 m³/h, and the following low-pressure shut-off ranges: 8–12 mbar for a line pressure of 21 mbar, and 120–180 mbar for a line pressure of 300 mbar. For high-pressure shut-off, the ranges targeted are 50–0 mbar at 21 mbar line pressure, and 450–500 mbar at 300 mbar line pressure. Shut-off pressure tolerances (AG10 ±10%, AG20 ±20%, AG30 ±30%, AG50 ±50%) were also set as design goals, and these targets were experimentally examined.

This work has been carried out in accordance with national and international safety standards TS EN 13611 and TSEK 625. Test results on prototype models indicate that the system meets critical performance criteria such as near-zero internal leakage levels, response times below one second, and compatibility with both low- and high-pressure natural gas lines. In this regard, beyond merely ensuring supply safety, the Doğalgaz Şalteri System makes an important contribution to advancing safety and automation in natural gas technologies.

Keywords: Natural gas safety, Natural Gas Switch, automatic gas restoration, distribution networks

Özet

Doğal gaz kesintilerinin ardından, konutlardan sanayiye kadar tüm uygulamalarda otomatik ve güvenli bir sistem yaklaşımının geliştirilmesi kritik öneme sahiptir. Bu çalışma, doğal gaz arz kesintileri durumlarında güvenliği artırmak amacıyla geliştirilen "Doğalgaz Şalteri" sistemini ele almaktadır. Harici bir enerji kaynağına ihtiyaç duymadan tamamen mekanik prensiplerle çalışan bu sistem, gaz akışının kesilmesi durumunda otomatik olarak devre dışı kalmaktadır.

Mevcut sistemlerle karşılaştırıldığında, Doğalgaz Şalteri, manuel müdahale gereksinimini en aza indirerek doğal gaz dağıtım firmalarının operasyonel yükünü azaltmakta ve hizmet sürekliliğini güvence altına almaktadır. Hedeflenen tasarım parametreleri; maksimum giriş basıncı (PS) (Pmax) 500 mbar, çalışma basınç aralığı 8–500 mbar, 1 saniyenin altında tepki süresi, 20–40 m³/h maksimum kapasite, ve düşük basınç kapama aralıkları olarak 21 mbar hat basıncında 8–12 mbar, 300 mbar hat basıncında 120–180 mbar değerleri olarak belirlenmiştir. Yüksek basınç kapama için ise hedeflenen aralıklar 21 mbar hat basıncında 50–0 mbar, 300 mbar hat basıncında 450–500 mbar olarak belirlenmiştir. Ayrıca kapama basıncı toleransları (AG10 ±%10, AG20 ±%20, AG30 ±%30, AG50 ±%50) tasarım hedefi olarak tanımlanmış ve bu hedefler deneysel olarak test edilmiştir.

Bu çalışma, TS EN 13611 ve TSEK 625 gibi ulusal ve uluslararası güvenlik standartlarına uygun olarak gerçekleştirilmiştir. Prototip modeller üzerinde yapılan test sonuçları, sistemin neredeyse sıfır iç sızdırmazlık, bir saniyenin altında tepki süresi, ve hem düşük hem yüksek basınçlı doğal gaz hatlarıyla uyumluluk gibi kritik performans kriterlerini sağladığını göstermektedir. Bu bağlamda, yalnızca arz güvenliğini sağlamakla kalmayıp, Doğalgaz Şalteri Sistemi, doğal gaz teknolojilerinde güvenlik ve otomasyonun ilerletilmesine de önemli katkılar sunmaktadır.

Anahtar kelimeler: Doğal gaz güvenliği, Doğalgaz Şalteri, otomatik gaz geri açma, dağıtım şebekeleri.

GİRİŞ

Doğalgaz kullanımının konutlardan endüstriye kadar geniş bir yelpazede yaygınlaşması, beraberinde güvenlik ve kesintisiz arz ihtiyacını da artırmaktadır. Özellikle arıza veya kesintilerden sonra gazın geri verilmesi sırasında abonelerin cihazlarının açık konumda kalması, ciddi kazalara yol açabilmektedir. Bu durum, geleneksel olarak gaz dağıtım firmalarının her bir aboneye fiziksel olarak ulaşmasını ve kontrol etmesini gerekli kılmakta; bu da uzun süreli gaz kesintilerine ve yüksek iş gücü maliyetlerine neden olmaktadır. Bina içi veya dışı gaz tesisatında basınç, boru hasarı, hat ve istasyon problemleri, elektrik kesintileri veya izinsiz müdahaleler gibi sebeplerle anormal seviyelere düşebilir veya aşırı artabilir. Gaz şalteri, çıkış hattında önceden belirlenmiş basınç değerlerine ulaşıldığında devreye girerek gaz akışını otomatik olarak sızdırmaz biçimde keser. Bu durumda abonenin gaz tüketen cihazları durur ve şalterin kurma kolundaki kırmızı yüz belirgin hale gelir. [1,3]

Zeniewski ve Bolado-Lavin [7] yaptıkları derleme çalışmasında AB'nin 994/2010 sayılı Yönetmeliğinde belirtilen, gaz arzının güvenliğini korumaya yönelik önlemlerle ilgili yönergeler ve gereklilikler doğrultusunda, Avrupa Birliği'ndeki ulusal gaz acil durum planlarını belgelemek ve incelemektir.

Proje kapsamında geliştirilen Doğalgaz Şalteri sistemi, kesinti sonrasında manuel veya yarı otomatik yöntemlerle tekrar açılıp kapatılan gaz regülatörleri yerine, abonelerin kendilerine ait bir "şalter" benzeri mekanizmayı kullanarak gazı hızlı ve güvenli şekilde yeniden devreye almalarını hedeflemektedir. Bu yaklaşım, hem işletmeci firmaların iş yükünü azaltmayı hem de konutlarda oluşabilecek gaz kaçaklarını engelleyerek kullanıcı güvenliğini artırmayı amaçlamaktadır. [1,2,6]

Łaciak ve ark. [8] doğal gaz iletim vanalarının mukavemet ve korozyon etkisini incelemişlerdir. 50 mm (DN50) ve 200 mm (DN200) nominal boru hattı çapı küresel vanalar için sonlu elemanlar yöntemini kullanmışlardır. Yapılan analizin test edilen vana flanş bağlantılarının sızdırmazlık özelliğinin esas olarak çalışma koşullarındaki değişikliklerden ne oranda etkilendiğini göstermişlerdir.

Rami ve ark. [9] diğer çalışmasında bir basınç regülatörünün dinamik davranışının temel özelliklerini incelemek ve simüle etmek için bir araştırma programı kurmuşlardır. Çalışma koşullarının ve kurulum gereksinimlerinin basınç regülatörünün stabilitesi üzerinde en büyük etkiye sahip olduğunu belirlemiştir. Ölçümlerden ve simülasyonlardan, aşağı akış basıncının genlikleri, aşağı akış hacminin boyutuna ve yukarı akış basıncına karşı hassas olduğu sonucuna da varılmıştır.

Araştırmaya konu olan ürünün kullanma senaryosunu temsil eden görsel Şekil 1'te gösterilmiştir.

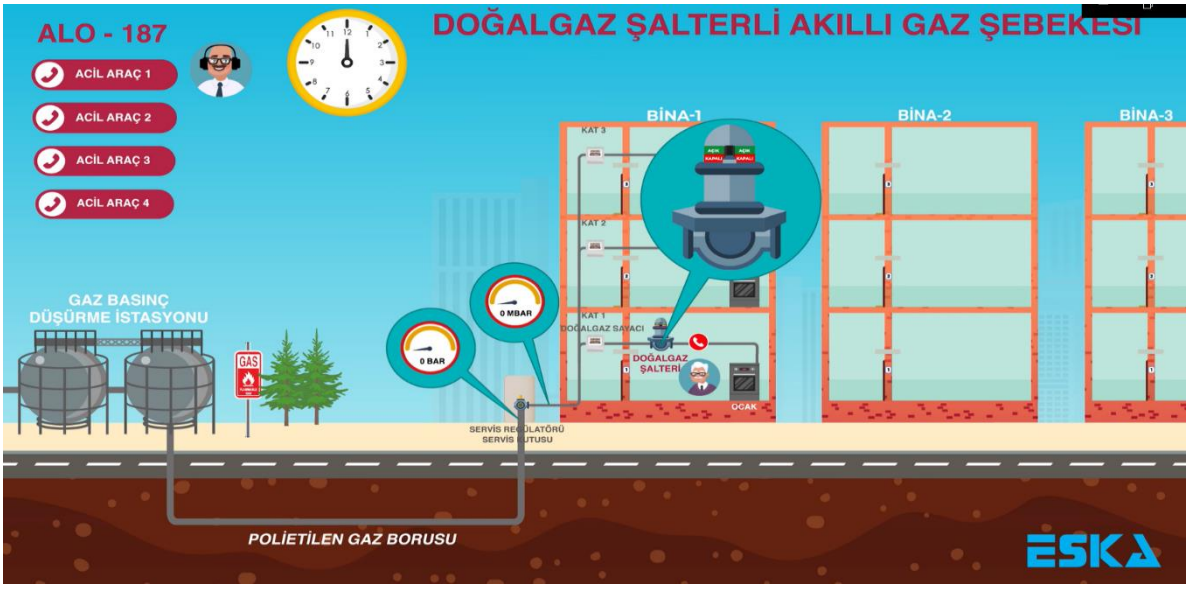

Şekil 1. Doğalgaz Şalteri Kullanım Simülasyonu.

MATERYAL VE METOD

Bu çalışmada kullanılan temel ürün, Eska Valve tarafından geliştirilen Doğalgaz Şalteri prototipidir. Sistem tamamen mekanik prensiplere dayanmakta olup harici bir enerji kaynağı gerektirmeden çalışmaktadır. Ulusal ve uluslararası standartlar (TS EN 1361, TS EN 161 ve TS EN 625) incelenmiş, mevcut regülatör ve güvenlik sistemleri analiz edilmiştir. Araştırmalar neticesinde, geliştirilen prototipe muadil bir ürün bulunmadığı ortaya konulmuştur ancak benzer çalışma prensiplerine sahip ürünlerin yurtdışı piyasasında (Fransa, Orta Afrika Cumhuriyeti) olduğu fark edilmiştir. [4,5]

Çalışmaya konu olan doğalgaz şalteri ürünümüzün prototipinin tasarım süreci, CAD tabanlı SolidWorks programı aracılığıyla gerçekleştirilmiş ve sonlu eleman analizleri (FEA) ile yapılmıştır. Tasarım programından görsel Şekil 2'de verilmiştir.

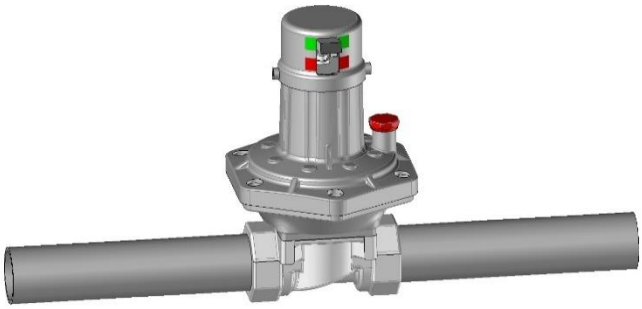

Şekil 2. Montajlanmış ürün görseli.

Prototip imalatı: İki aşamalı prototip üretimi yapılmış, her bir versiyonda performans testleri sonrası revizyonlar gerçekleştirilmiştir.

Laboratuvar ve saha testleri: Prototipler önce laboratuvar ortamında test edilip daha sonra saha uygulamaları için yurdumuzun farklı yerlerinde montajları gerçekleştirilmektedir. Projeye konu olan doğalgaz şalterinin Eskişehir'de bir apartmanda yaklaşık bir yıl süreyle saha testlerine tabi tutulmuştur. Laboratuvar ortamında uygulanan test sonuçları Tablo 1'de gösterilmiştir.

Testin Adı	**Test Şartları (Çıkış Gaz Tüketimi)**	**Sonuç**
Basınç Kaybı	0	1,28 mbar
	1,6 m^3/h	3,22 mbar
	2,5 m^3/h	3,66 mbar
	3,5 m^3/h	4,51mbar
	4 m^3/h	4,73 mbar
	6 m^3/h	5,55 mbar
Dış Müdahaleler İle Kapanma	-	Dış müdahale ile kapanabiliyor, müdahaleyi bırakınca gaz geçişi devam ediyor
Yüksek Basınçta Kapanma	0,5 m^3/h	1 bara kadar basınç verildi kapanmadı
	0	1 bara kadar basınç verildi kapanmadı

Çıkış Borusunda Kopma Olursa Kapatma	Maksimum akış	Kapanmıyor.
Ocak Flexi Kopması, İntahar yada Ocakların Açık Kalması Halinde Otomatik Kapatma	0,2 m^3/h	Kapanmıyor.
	0,5 m^3/h	Kapanmıyor.
	1 m^3/h	Kapanmıyor.
Otomatik Kurulma	0,5 m^3/h	Kurulmuyor.
	0	Kuruluyor ama otomatik el ile değil
El İle Kurulma	0,5 m^3/h	Kurulmuyor.
	0	Kurulmuyor.
Düşük Basınçta Kapanma	0,5 m^3/h	12 mbar da kapanıyor.
	0	Kapanmıyor.
Yüksek Kapasitede Kapatma	0	7,8 m^3/h de kapattı.
Kapatma Sonrası İç Sızdırma Deneyi	21 mbar ($\leq$ 0,5 mbar)	İç kaçak yapıyor çıkış tarafına.

Tablo 1. 1. Prototip laboratuvar test sonuçları.

Test aşamasında kullanılan test düzeneği yazılımı ve mekanik donanımı tarafımızca özel olarak imal edilmiştir ve tasarım düzeneği Şekil 3'te gösterilmiştir. Test düzeneği ve test aşamalarını gösteren Şekiller Şekil 4'te gösterilmiştir.

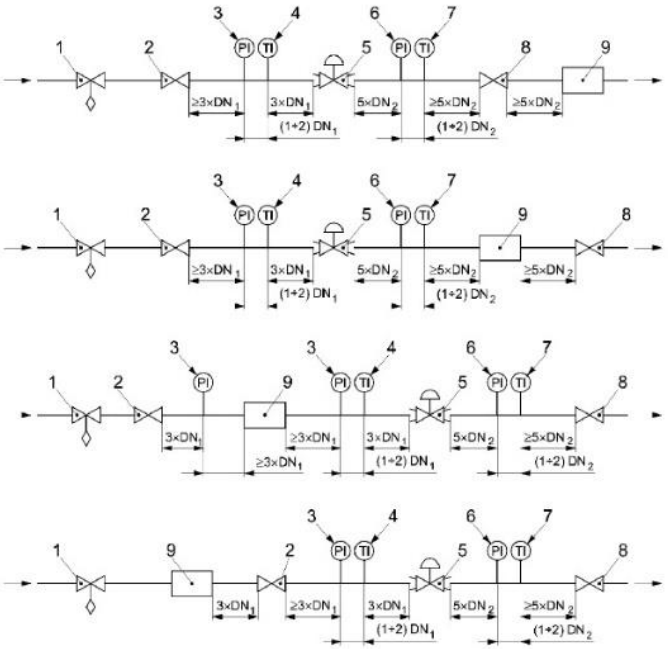

Açıklama

DN_1 = deneye tâbi tutulan regülatöre bağlı giriş tesisat borusu anma çapı

DN_2 = deneye tâbi tutulan regülatöre bağlı çıkış tesisat borusu anma çapı

1 aşırı basınç önleyici kapama vanası, gerekliyse

2 tam geçişli giriş vanası

3 giriş basıncı göstergesi

4 giriş sıcaklığı göstergesi

5 deneye tâbi tutulan regülatör

6 çıkış basıncı göstergesi

7 çıkış sıcaklığı göstergesi

8 debi ayar vanası

9 debi ölçer

Şekil 3. Test düzeneği şeması



Şekil 4. Prototip test düzeneği ve prototip test aşaması görselleri.

Elde edilen veriler doğrultusunda, uygulanan "Basınç Kaybı" test sonuçları TSE 625 standardı gereği uygun şartları yerine getiremediği Tablo 1'de gösterilen test sonuçları kısmında bazı parametrelerde gaz kaçağı belirlenmiştir. Basınç kaybı, yüksek basınçta kapanma ve düşük basınçta kapanma eksiklikleri gibi performans düşüklüğünü gidermek için bu çalışma kapsamında doğalgaz şalteri üzerinde yeni tasarım çalışmaları gerçekleştirilmiştir. Yapılan iyileştirme çalışmaları için deneysel çalışmalar sonucu ortaya çıkan gaz kaçağı gölgeleri üzerinde tasarım iyileştirme çalışmaları yapılmıştır. Bu kapsamda kontrol noktası ile açma/kapama düğmelerinin konumu, gaz giriş/çıkış bölgesinin ana gövdedeki yeri ve emniyet kapatma noktası yeniden tasarlanmıştır. Oluşturulan yeni tasarım Şekil 5'te yer almaktadır.

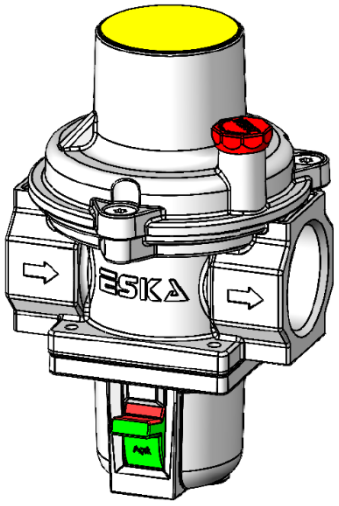

Şekil 5. Yeni prototip tasarımı.

Yeni ve eski tasarımın farklarının daha rahat anlaşıla bilir olması adına görseller Şekil 6'te yan yana getirilmiştir.

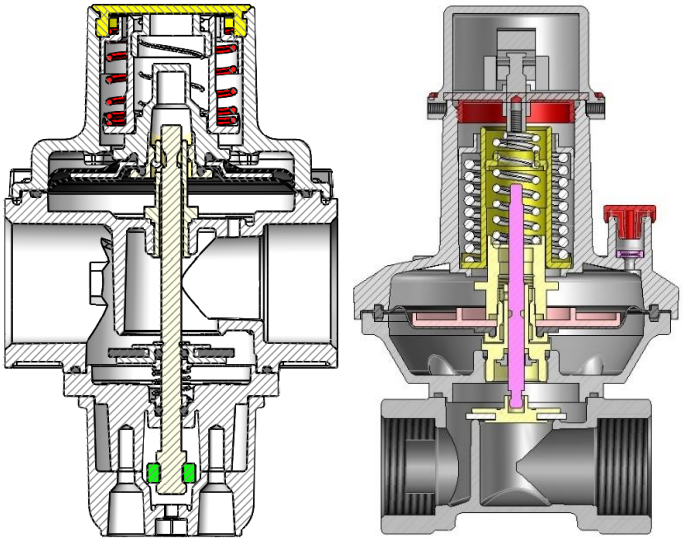

(a) Yeni Tasarım (b) Eski Tasarım

Şekil 6. Tasarım Kıyaslama Görseli

Yeni prototip üzerinde yapılan laboratuvar test sonuçları Tablo 2'de verilmiştir.

Testin Adı	Test Şartları (Çıkış Gaz Tüketimi)	Prototip 1	Prototip 2
Basınç Kaybı	0	1,28 mbar	0,01 mbar
	1,6 m^3/h	3,22 mbar	0,05 mbar
	2,5 m^3/h	3,66 mbar	0,17 mbar
	3,5 m^3/h	4,51mbar	0,35 mbar
	4 m^3/h	4,73 mbar	0,51 mbar
	6 m^3/h	5,55 mbar	0,78 mbar
Dış Müdahaleler İle Kapanma	-	Dış müdahale ile kapanabiliyor, müdahaleyi bırakınca gaz geçişi devam ediyor	Dış müdahale ile kapatılamıyor
Yüksek Basınçta Kapanma	0,5 m^3/h	1 bar'a kadar basınç verildi kapanmadı	50,9 mbar da kapatıyor
	0	1 bara kadar basınç verildi kapanmadı	49,8 mbar da kapatıyor
Çıkış Borusunda Kopma Olursa Kapatma	Maksimum akış	Kapanmıyor.	Kapatıyor.
El İle Kurulma	0,5 m^3/h	Kurulmuyor.	1s altında kurulma.
	0	Kurulmuyor.	1s altında kurulma.
Düşük Basınçta Kapanma	0,5 m^3/h	12 mbar da kapanıyor.	11,3 mbar da kapatıyor.
	0	Kapanmıyor.	10,1 mbar da kapatıyor.
Yüksek Kapasitede Kapatma	-	7,8 m^3/h de kapattı.	21,93 m^3/h de kapatıyor.
Kapatma Sonrası İç Sızdırma Deneyi	21 mbar ($\leq$ 0,5 mbar)	İç kaçak yapıyor çıkış tarafına.	Kaçak yok.

Tablo 2. Yeni prototip laboratuvar test sonuçları.

BULGULAR VE TARTIŞMA

Yapılan testler sonucunda geliştirilen prototip 2, önceki prototip 1 ile kıyaslandığında iyileştirmeleri sağlamıştır. Yeni geliştirilen ürünün teknik özellikleri;

- Maximum giriş basıncı (PS) (P_{max}): PS0,5 (500 mbar),
- Çalışma basınç aralığı: 8 – 500 mbar,

- Düşük basınç kapatma ayar basıncı: 21 mbar hat basıncı için 8 – 12 mbar, 300 mbar hat basıncı için 120 – 180 mbar,
- Yüksek basınç kapatma ayar basıncı: 21 mbar hat basıncı için 50 – 60 mbar, 300 mbar hat basıncı için 450– 500 mbar,
- Kapatma basınç toleransı: AG10±%10, AG20±%20, AG30±%30, AG50±%50,
- 21 mbar giriş basıncında basınç kaybı: 6m3/h debi de 0,7 mbar, 5m3/h debi de 0,55 mbar, 4 m^3/h debi de 0,45 mbar, 3,5 m^3/h debi de 0,35 mbar, 3 m^3/h debi de 0,25 mbar, 2,5 m^3/h debi de 0,20 mbar, 2 m^3/h debi de 0,15 mbar, 1,6 m^3/h debi de 0,10 mbar, 1 m^3/h debi de 0,05 mbar,
- 300 m bar giriş basıncında basınç kaybı: 6 m^3/h debi de 0,8 mbar, m^3/h debi de 0,6 mbar, 4 m^3/h debi de 0,5 mbar, 3,5 m^3/h debi de 0,45 mbar, 3 m^3/h debi de 0,35 mbar, 2,5 m^3/h debi de 0,3 mbar, 2 m^3/h debi de 0,25 mbar, 1,6 m^3/h debi de 0,20 mbar, 1 m^3/h debi de 0,15 mbar,
- Maximum kapasite aralığı: 20 – 40 m^3/h,
- Çalışma sıcaklık aralığı: - 10 ^{0}C; 50 ^{0}C, -20 ^{0}C; 60 ^{0}C,
- Malzemeler: Gövde ve kapak alüminyum (46100) döküm alaşımı, sızdırmazlık malzemeleri NBR

Olarak GAZMER (Doğal Gaz Enerji Eğitim Belgelendirme ve Denetim Teknolojik Hizmetler Ltd) ve TSEK (Türk Standartları Enstitüsü)Tarafından onaylanmıştır.

Cihazın tekrar kullanıma alınabilmesi için öncelikle gaz dağıtım şirketinin sorunu gidermesi ve izin vermesi gerekir. Şalter ancak hat içindeki gaz basıncı normal seviyeye döndüğünde el ile kurulabilir. Şalter kapandıktan sonra, kullanıcı tüm gaz yakan cihazları kapalı konuma getirmeli, ardından şalteri el ile yeniden kurmalıdır. Böylece gaz akışı güvenli ve kontrollü olarak sağlanmış olur.

Gaz dağıtım şirketinin izni olmadan veya hat basıncı uygun değilken şalter kurulamaz. Kullanıcılar, cihazlarının açık kalması durumunda ortama gaz sızıntısını önlemek için tüm gaz tüketen cihazları kapalı pozisyona getirmelidir. Bu prosedürler, gazın hızlı, güvenli ve kontrollü biçimde verilmesini sağlar ve oluşabilecek tehlikeleri önler.

Geliştirilen yeni sistemin eski sisteme göre sağladığı avantajlar öne çıkmıştır: gaz dağıtım şirketlerinin yeniden gaz verme süreçlerindeki personel ve zaman maliyeti minimize edilmiştir. Ayrıca, kullanıcıların sistemle etkileşimi, elektrik şalteri benzeri yapısı sayesinde oldukça sezgisel bulunmuştur.

SONUÇ

Bu çalışma, doğalgaz şebekelerinde yaşanan gaz kesintileri sonrası abonelerin güvenli ve etkin şekilde gazı yeniden devreye alabilmelerini sağlayan mekanik bir çözümün tasarımı ve doğrulamasını kapsamaktadır. Elde edilen bulgular, Doğalgaz Şalteri sisteminin hem güvenlik kriterleri hem de kullanıcı etkileşimi açısından yüksek performans sunduğunu ortaya koymuştur.

Bütün bu sistemin bağlı olduğu TS EN 1361, TS EN 161 ve TS EN 625 standartlar kapsamında uygulanan dış sızdırmazlık testleri, patlatma basınç testleri, çevre sıcaklık testleri, ömür testleri ve performans testlerinden başarıyla geçmiştir.

Bu bağlamda, Doğalgaz Şalteri; dağıtım firmalarının operasyonel verimliliğini artırmakta, kullanıcı güvenliğini geliştirmekte ve doğalgaz altyapısında inovatif bir yaklaşım olarak literatüre katkı sunmaktadır. Gelecekte bu sistemin, akıllı ev otomasyonlarına entegre edilerek daha geniş bir uygulama alanına kavuşması öngörülmektedir.

KAYNAKLAR

[1] An Automated Natural Gas Shut-Off Valve System (ASEE NE Conference, 2010), Benjamin Cadieux; Lee Denaro; Paul Ellsworth; Adam Robert; Salah Badjou

[2] Pipeline Safety: Expanding the Use of Excess Flow Valves in Gas Distribution Systems to Applications Other Than Single-Family Residences (2015), Pipeline and Hazardous Materials Safety Administration (PHMSA), U.S. DOT

[3]Energy Policy 49 (2012) 652–662 "A review of national gas emergency plans in the European Union" Peter Zeniewski , Ricardo Bolado-Lavin

[4] EPDK (2014). "Doğalgaz Dağıtım Şirketlerinin Ar-Ge Bütçelerine İlişkin Düzenlemeler." Resmî Gazete, 28/05/2014, Karar No: 5036.

[5] EN 88-1. (2011). Pressure regulators and associated safety devices for gas appliances – Part 1: Pressure regulators. European Committee for Standardization (CEN).

[6] Journal of Loss Prevention in the Process Industries 63 (2020) 103998 "Impact of flood water on the technical condition of natural gas transmission pipeline valves" Mariusz Łaciak , Tomasz Włodek , Tomasz Kozakiewicz, Krystian Liszka

[7] International Journal of Pressure Vessels and Piping 84 (2007) 234–243 "Modelling of a pressure regülatör" El Golli Rami, Bezian Jean-Jacques , Delenne Bruno , Menu Franc-ois

[8] Serviceability of Natural Gas Distribution Networks after Earthquakes (Journal of Earthquake and Tsunami, 2013), G. P. Cimellaro; A. De Stefano; O. Villa

[9] Yıldız, M. ve Akman, O. (2019). "Doğalgaz Dağıtımında Yenilikçi Güvenlik Uygulamaları: Mekanik Cihazların Karşılaştırmalı Analizi." Mühendislik ve Teknoloji Dergisi, 7(2), 56-62.

➢ *ORAL PRESENTATION*

Synergistic modulation of epithelial-mesenchymal transition-related proteins by oxaliplatin and thymoquinone in HCT116 colorectal cancer cells.

Ilker Kiliccioglu [1*] (*ORCID: https://orcid.org/0000-0003-3367-9665*), Gorkem Dulger [1] (*ORCID:https://orcid.org/0000-0002-1506-1549),* Gulsah Gedik [2] (*ORCID: https://orcid.org/0000-0003-4147-6729)*
[1] Duzce University, Faculty of Medicine, Department of Medical Biology, Duzce, Türkiye.
[2] Trakya University, Faculty of Pharmacy, Department of Pharmaceutical Technology, Edirne, Türkiye.

*Corresponding author e-mail: i_kiliccioglu@yahoo.com.tr

Abstract
Epithelial-mesenchymal transition (EMT) is an important cellular mechanism in facilitating colorectal cancer (CRC) progression. Therefore, targeting this process may improve treatment outcomes. Thymoquinone, a phytochemical derived from *Nigella sativa*, has demonstrated significant anticancer effects. Oxaliplatin is a conventional platinum-based chemotherapeutic agent used in the treatment of CRC, but its efficacy is often limited by the development of resistance and high cytotoxicity. This study aimed to determine the synergistic effects of Thymoquinone and Oxaliplatin on proliferation and EMT markers in HCT116 colorectal cancer cells. HCT116 cells were treated with different concentrations of Thymoquinone, Oxaliplatin or combination of both compounds. Cell viability was then analyzed with WST-1 assay after 24 h and 48 h, and IC_{50} values were calculated. Morphological changes were observed using an inverted microscope after treatment with Thymoquinone, Oxaliplatin and their combination. Western blot analysis was performed to evaluate the expression levels of EMT-associated proteins, including E-cadherin, N-cadherin, vimentin, fibronectin and periostin. Thymoquinone significantly reduced HCT116 cell proliferation in a dose and time dependent manner, showing IC_{50} values of 8.96 µg/mL for 24 h and 6.11 µg/mL for 48 h. Oxaliplatin showed a strong antiproliferative effect as expected with IC_{50} of 1.81 µg/mL for 24 h. The combination of Thymoquinone and Oxaliplatin showed the enhanced antiproliferative activity of Oxaliplatin at low dose and time, which was important in terms of achieving the desired responses such as reduced drug exposure and reduced cytotoxicity. Morphological analysis showed the apoptotic findings in the combination group. Thymoquinone and Oxaliplatin combination increased the expression levels of E-cadherin and decreased the expression levels of mesenchymal markers (N-cadherin, vimentin, fibronectin and periostin) in HCT116 cells. These findings indicated that Thymoquinone enhanced the efficacy of Oxaliplatin and may be a valuable complementary drug candidate in the treatment of colorectal cancer targeting EMT-mediated progression.
Keywords: Colorectal cancer, Epithelial-mesenchymal transition, Thymoquinone, Oxaliplatin

INTRODUCTION

Colorectal cancer (CRC) is a significant contributor to cancer-related mortality globally, characterized by elevated rates of recurrence and metastasis, which pose substantial therapeutic challenges despite improvements in chemotherapeutic strategies (Tirendi et al., 2023).

Epithelial to mesenchymal transition (EMT) is a crucial biological mechanism that facilitates tumor invasion, dissemination, and resistance to therapy. This transdifferentiation process involves the loss of polarity and adhesion properties in epithelial cancer cells, leading to the acquisition of mesenchymal characteristics, which enhances their motility and invasiveness. It involves a dynamic reprogramming of epithelial cells, enabling them to adopt mesenchymal phenotypes, which are marked by diminished cell-cell adhesion and enhanced migratory and invasive abilities (Dongre and Weinberg, 2019).

The phenotypic switch facilitates metastasis and is linked to increased resistance to chemotherapy, immune evasion, and unfavorable clinical outcomes in colorectal cancer patients (Lu et al., 2023). Targeting EMT has emerged as a viable strategy to enhance therapeutic efficacy and inhibit cancer progression.

Oxaliplatin, a third-generation platinum-based chemotherapeutic agent, is frequently utilized in the management of advanced colorectal cancer. It induces DNA cross-linking and apoptosis; however, resistance and incomplete responses limit its efficacy (Martinez-Balibrea et al., 2015). Natural compounds exhibiting anticancer properties have garnered significant interest due to their capacity to modulate various signaling pathways while

demonstrating reduced systemic toxicity. In contrast to traditional chemotherapeutic agents that typically induce cytotoxicity via non-specific mechanisms like DNA damage or mitotic arrest, affecting both cancerous and healthy proliferating cells, natural products generally demonstrate more targeted effects by disrupting molecular pathways that are specifically altered in cancer cells (Newman and Cragg, 2020). An important benefit of natural products is also their ability to increase the sensitivity of tumor cells to standard chemotherapeutic agents. Many studies have shown that phytochemicals can counteract mechanisms of multidrug resistance (MDR), including overexpression of ATP-binding cassette (ABC) transporters and activation of detoxifying enzymes, thereby increasing the efficacy of agents such as oxaliplatin or 5-FU in resistant cancer cells (Farhan, 2023).

Recent studies have highlighted natural compounds like thymoquinone (TQ), the principal bioactive component of *Nigella sativa*, for their antitumor, anti-inflammatory, and anti-epithelial-mesenchymal transition (EMT) properties (Majdalawieh et al., 2017). TQ modulates key signaling pathways, including NF-κB, PI3K/Akt, and TGF-β, which are associated with epithelial-mesenchymal transition (EMT) and cancer progression (Ang et al., 2023). While oxaliplatin and thymoquinone have individually shown anticancer properties, their combined effect on epithelial-mesenchymal transition modulation in colorectal cancer has not been extensively investigated. Investigating the impact of this combination on the expression of EMT-related markers, including E-cadherin, N-cadherin, vimentin, fibronectin, and periostin, may provide important insights into innovative combinatory approaches for reducing tumor metastasis and improving therapeutic results.

While oxaliplatin and thymoquinone have individually shown anticancer properties, their combined effect on epithelial-mesenchymal transition modulation in colorectal cancer has not been extensively investigated. Investigating the impact of this combination on the expression of EMT-related markers, including E-cadherin, N-cadherin, vimentin, fibronectin, and periostin, may provide important insights into innovative combinatory approaches for reducing tumor metastasis and improving therapeutic results.

MATERIALS AND METHODS

Cell Culture

HCT116 human colorectal cancer cells were cultured in RPMI-1640 medium (Capricorn Scientific, Germany) supplemented with 10% fetal bovine serum (FBS), 1% penicillin-streptomycin, and 2 mM L-glutamine (Capricorn Scientific, Germany). Cells were maintained in a humidified incubator at 37°C with 5% CO_2 (Nuve, Ankara, Turkey). Medium was changed every two-days, and cells were subcultured upon reaching to 70%-80% confluence using 0.25% trypsin-EDTA (Capricorn Scientific, Germany).

Drug Preparation and Cell Viability Assay (WST-1)

Oxaliplatin (MedChemExpress LLC, USA) were initially dissolved in sterile water then stored at -20°C and further diluted in culture medium to final concentrations of 0-10 µg/mL. Thymoquinone (Merck KGaA, Darmstadt, Germany) was prepared as a stock solution in dimethyl sulfoxide (DMSO) at a concentration of 5 mM and subsequently diluted in culture medium to achieve final concentrations ranging from 0 to 100 µg/mL. HCT116 cells were seeded in 96-well plates at a density of $5x10^3$ cells/well and allowed to adhere overnight and treated with the indicated concentrations of Oxaliplatin, Thymoquinone, and their combination for 24 h and 48 h. Cell viability was measured using the WST-1 assay (Abcam, Cambridge, UK). After treatment, 10 µL of WST-1 reagent was added to each well and incubated for 2 h at 37°C. The absorbance of each well was measured at 450 nm using microplate reader. (Allsheng Instruments, Hangzhou, China). Each experiment was performed in three independent replicates.

Protein Isolation and Western Blot Analysis

Protein isolation was performed with RIPA lysis buffer (A.B.T, Ankara, Turkey) according to the manufacturer's instructions after Thymoquinone (25 µg/mL), and combination of Thymoquinone and Oxaliplatin (10 µg/mL TQ + 1 µg/mL OXA) was applied to PC-3 cells for 24 h. The total amount and concentration of isolated proteins were determined with BCA protein analysis kit (ABP Biosciences, USA). Sample buffer (ABP Biosciences, Beltsville, USA) was added equally to isolated proteins at 1X final concentration and they incubated at 95°C in a heating block for 5 minutes for denaturation before loading onto the prepared SDS-PAGE gel. Protein samples loaded onto the gel were run for 90 minutes at 150 V and 250 mA after preparing the western blot apparatus (Consort

bvba, Turnhout, Belgium) with 1X running buffer (A.B.T Laboratory Industry, Ankara, Turkey). After proteins were separated according to their molecular weights, the power source was turned off and the gel was removed. Samples were transferred to PVDF membrane (Macherey-Nagel GmbH, Düren, Germany) using the wet blotting method. After the transfer, membranes were blocked with 5% BSA in TBST and incubated overnight at 4°C with primary antibodies (1:1000 dilution) against E-cadherin, N-cadherin, vimentin, fibronectin, and periostin and GAPDH (Affinity Biosciences, Cincinnati, USA). Then, membranes were incubated with HRP-conjugated secondary antibody (1:5000 dilution), and protein bands were detected using ECL reagent (ABP Biosciences, Beltsville, USA) and imaged using a chemiluminescence detection system (Pop-Bio Imaging, Cambridge, UK).

Morphological Evaluation

To evaluate morphological changes, HCT116 cells were seeded in 6-well plates and treated with thymoquinone (TQ) alone or in combination with oxaliplatin (OXA) for 24 h. Then, morphological changes were visualized with an inverted microscope (Euromex, Arnhem, The Netherlands) equipped with a CMEX-5 Pro camera (Olympus CKX53) at 20x magnification.

Statistical Analysis

GraphPad Prism 9.0 was used to perform the statistical analysis of the experiments results. Results were expressed as mean ± SD from three independent experiments. Statistical significance was determined using one-way ANOVA and two-way ANOVA followed by Dunnett's post-hoc test, with significance levels denoted as *p <0.05, **p <0.01, ***p <0.001, and ****p <0.0001.

RESULTS

Thymoquinone inhibited proliferation of HCT116 cells in a time and dose dependent manner

The antiproliferative activity of thymoquinone (TQ) in HCT116 human colorectal carcinoma cells was evaluated using the WST-1 assay at 24 and 48 h. As seen in Figure 1A, TQ treatment caused a dose-dependent decrease in cell proliferation. The IC_{50} of TQ was determined as 8.96 µg/mL at 24 h and decreased to 6.11 µg/mL at 48 h, suggesting a time-dependent increase in cytotoxic potential. The observed decrease in IC_{50} over time suggested an increased cellular sensitivity to TQ with prolonged exposure, resulting from cytotoxic damage or activation of apoptotic signaling. Figure 1B shows further quantitative analysis showing a significant decrease in proliferation level over a wide range of TQ concentrations (2.5 to 100 µg/mL) for both 24 h and 48 h treatment periods. At 24 h, lower concentrations such as 5 µg/mL significantly inhibited proliferation compared to the untreated control (p <0.05), with this effect becoming more pronounced at higher doses (p <0.001 to p <0.0001). Treatment for 48 h showed increasing inhibition of proliferation at all concentrations, suggesting greater accumulation of cytotoxic effects over time. At the maximum concentration of 100 µg/mL, cell proliferation decreased to approximately 15% compared to the control.

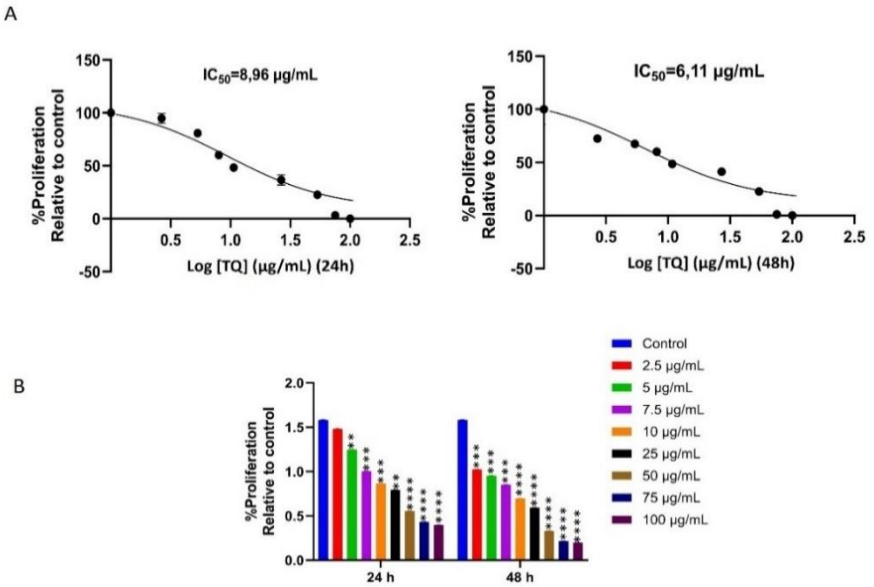

Figure 1. Antiproliferative effect of thymoquinone on HCT116 colorectal cancer cells. (A) Dose-response curves of thymoquinone (TQ) following 24 h and 48 h treatments. IC_{50} values were calculated as 8.96 µg/mL at 24 h and 6.11 µg/mL at 48 h. (B) Bar graphs illustrating the changes of proliferation level relative to control after the TQ

treatment at indicated concentrations (2.5–100 µg/mL) for 24 h and 48 h (*p<0.05, **p <0.01, ***p<0.001, and ****p<0.0001 vs. control).

Oxaliplatin showed greater cytotoxic activity compared with thymoquinone, and thymoquinone synergistically increased the efficacy of oxaliplatin.

Figure 2A shows a significant inhibitory effect of oxaliplatin (OXA), a platinum-based chemotherapeutic agent, on HCT116 cell proliferation with an IC50 value of 1.81 µg/mL at 24 h. This value was naturally much lower compared to TQ, indicating the stronger antiproliferative effects of OXA over the same time period. As observed in the graph associated with the dose-response curve, there was a significant decrease in proliferation at low concentrations and total inhibition occurred at 10 µg/mL (p<0.0001). Cell viability was approximately 5% at this dose.

The combination of TQ and OXA was applied to HCT116 cells at low concentrations to investigate possible synergistic antiproliferative effects. Figure 2B shows that combined treatment of TQ with OXA (1 µg/mL) at fixed doses of 5, 7.5, and 10 µg/mL significantly reduced cell viability compared to TQ alone. All combination groups exhibited significant growth inhibition compared to control, with the most pronounced reduction observed at 10 µg/mL TQ + 1 µg/mL OXA (p<0.0001). The findings suggest a synergistic interaction between TQ-mediated antiproliferative effect and OXA-mediated DNA cross-linking and cytotoxic effect, which can probably be explained by complementary mechanisms of action.

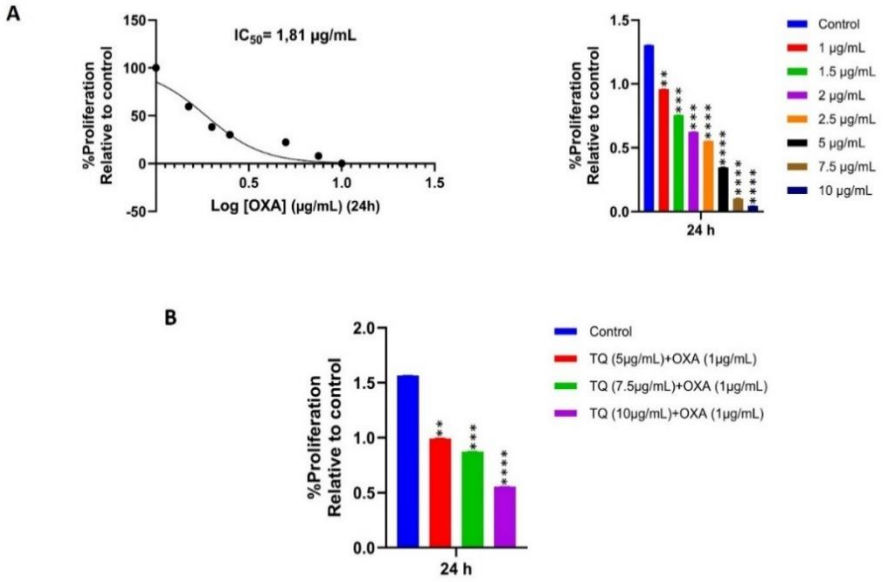

Figure 2. Cytotoxic effects of oxaliplatin and its combination with thymoquinone were evaluated in HCT116 cells. A) The dose-response curve for oxaliplatin (OXA) after 24 h of treatment showed an IC_{50} value of 1.81 µg/mL. The bar graph on the right shows the decreases in proliferation after treatment with increasing OXA concentrations (1–10 µg/mL) over a 24 h period. B) Evaluation of cell proliferation after concomitant treatment with TQ at concentrations of 5, 7.5 and 10 µg/mL with a fixed OXA dose of 1 µg/mL over a 24 h period. The combined treatments significantly increased the antiproliferative effect compared to TQ alone. (*p <0.05, **p <0.01, ***p <0.001, and ****p <0.0001 vs. control).

The combination of thymoquinone and oxaliplatin inhibited epithelial-mesenchymal transition (EMT) through modulation of key protein markers.

The expression of markers associated with epithelial-mesenchymal transition (EMT) was evaluated by Western blot analysis after 24 h of TQ alone and TQ combined with OXA to investigate the basis of the antiproliferative effect. Figure 3 shows that treatment with TQ alone (25 µg/mL) led to a moderate increase in the epithelial marker E-cadherin and a significant decrease in mesenchymal markers such as N-cadherin, vimentin, fibronectin, and periostin compared to the control group. Combined treatment of TQ (10 µg/mL) and OXA (1 µg/mL) significantly suppressed mesenchymal markers and increased E-cadherin levels, as shown in the bar graph. The expression levels of N-cadherin and vimentin were decreased by more than 50% compared with control (p <0.001), while fibronectin and periostin levels were also significantly decreased (p <0.0001). The observed changes indicated a

phenotypic regression from mesenchymal to epithelial state, suggesting that EMT inhibition may be the key mechanism underlying the reduction of invasiveness and metastasis. It was clearly observed that the combination therapy functioned through both inhibition of proliferation and suppression of metastatic potential in HCT116 cells.

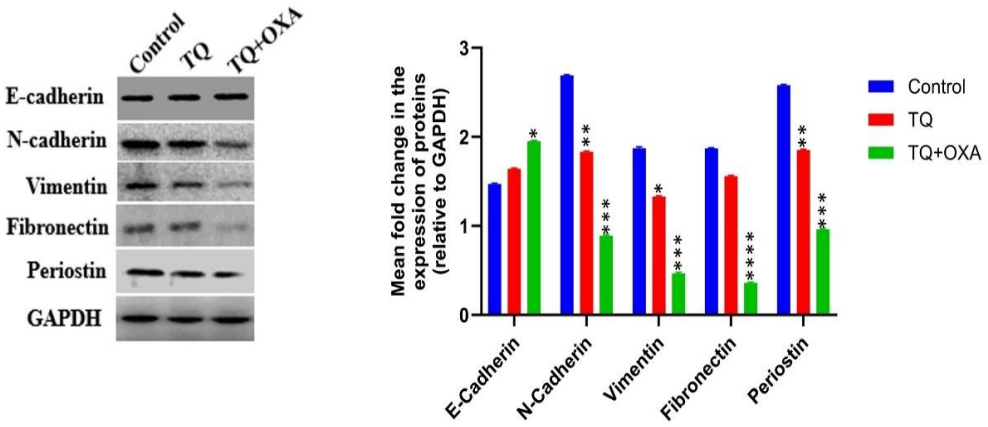

Figure 3. Effect of combination of thymoquinone and oxaliplatin on the expression of epithelial-mesenchymal transition (EMT)-associated proteins in HCT116 cells. Western blot analysis was performed after 24 h of treatment with TQ alone (25 µg/mL) or together with OXA (10 µg/mL TQ + 1 µg/mL OXA). Expression levels of epithelial marker E-cadherin and mesenchymal markers N-cadherin, vimentin, fibronectin, and periostin were analyzed. GAPDH used as a loading control. The bar graph shows the mean fold change in protein expression normalized to GAPDH (*p <0.05, **p <0.01, ***p <0.001, and ****p<0.0001 vs. control).

The combination of thymoquinone and oxaliplatin caused significant morphological changes in HCT116 cells

Inverted microscopy was used to evaluate morphological changes in HCT116 cells after 24 h of treatment with thymoquinone (TQ) alone or in combination with oxaliplatin (OXA) (Figure 4). Control cells showed standard epithelial morphology with dense monolayer formation, elongated spindle-shaped structures, and preserved cell-cell contacts. Treatment with TQ at 10 µg/mL resulted in a moderate decrease in cell density and slight rounding of cells, indicating the first signs of cytotoxicity. At a concentration of 25 µg/mL, marked cell detachment and shrinkage were observed, indicating a significant loss of viability and altered morphology consistent with apoptotic changes. Combined treatment with TQ (7.5 µg/mL) and OXA (1 µg/mL) led to significant morphological changes. Cells showed marked rounding, shrinkage, and sparse distribution, indicating significant loss of adhesion and advanced cytotoxic damage. The observed changes suggest a synergistic interaction between TQ and OXA, resulting in greater structural disruption than either treatment applied alone. These findings supported the proliferation and Western blot data, highlighting the combinatorial potential of TQ and OXA on cell viability reduction and EMT inhibition.

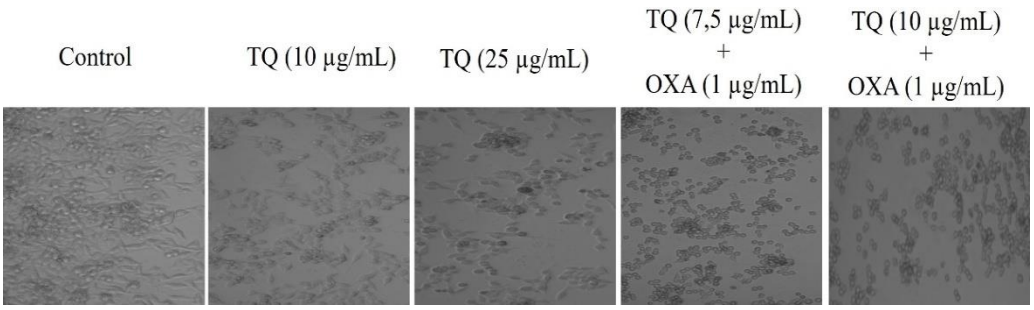

Figure 4. Morphological evaluation of HCT116 cells after treatment with thymoquinone and oxaliplatin. Inverted microscopy images of HCT116 cells after 24 h treatment with TQ (10 µg/mL and 25 µg/mL) and combination of TQ and OXA (TQ:7.5 µg/mL + OXA: 1 µg/mL and TQ:10 µg/mL + OXA: 1 µg/mL). Control cells showed characteristic epithelial morphology with intact monolayers. TQ-treated cells showed a dose-dependent response

characterized by rounding and detachment. Combination treatment led to significant morphological changes such as cell shrinkage, rounding, and detachment, indicative of significant cytotoxicity (Magnification: 20x).

DISCUSSION

In this study, we demonstrated for the first time that thymoquinone (TQ), both alone and in combination with oxaliplatin (OXA), had significant antiproliferative and anti-epithelial-mesenchymal transition (EMT) effects on HCT116 colorectal cancer cells. Our findings provide additional evidence for the increasing interest in integrating phytochemicals with conventional chemotherapeutics to improve efficacy and overcome potential resistance mechanisms in colorectal cancer treatment.

Thymoquinone, the main bioactive component of *Nigella sativa*, exhibited significant dose- and time-dependent cytotoxic effects on HCT116 cells, with a decrease in IC50 values with increasing exposure time, suggesting increased sensitivity of cells with prolonged exposure. Our findings are consistent with previous studies showing that TQ inhibits proliferation in multiple cancer cell lines, including colon cancer, through mechanisms such as induction of oxidative stress, mitochondrial dysfunction, and modulation of apoptotic signaling pathways (Kundu et al., 2014; Kurowska et al., 2023). Al Bitar et al. reported that thymoquinone sensitized colorectal cancer cells to radiation and suppressed the cell cycle and reduced cell proliferation, which is consistent with our findings (Al Bitar et al., 2022).

Compared to OXA, which showed higher cytotoxicity at lower concentrations, TQ alone showed modest effects. However, its ability to increase the sensitivity of HCT116 cells to OXA was an important result supporting the rationale for the combination therapy. This apparent synergistic effect observed in the combination of TQ and OXA may be due to the complementary mechanisms of action of both compounds. OXA induces DNA cross-linking structures and triggers apoptosis through both p53-dependent and -independent pathways (Ye et al., 2025). In contrast, TQ disrupts key signaling pathways associated with cancer progression and drug resistance, such as PI3K/Akt, NF-κB, and TGF-β (Sadeghi et al., 2023; Farooqi et al. 2022). The disruption of these survival and inflammatory pathways likely enhanced the antiproliferative activity, as evidenced by the significantly greater reduction of cell viability in the combination groups.

We also demonstrated that the combination of TQ+OXA effectively inhibited the dominant EMT phenotype, a common phenomenon in CRC, in HCT116 cells. EMT is a target mechanism that is critically important in CRC progression, metastasis, and therapy resistance, characterized by decreased expression of epithelial markers such as E-cadherin and increased levels of mesenchymal markers such as N-cadherin, vimentin, fibronectin, and periostin (Vu and Datta, 2017; Smith and Bhowmick, 2016). While treatment with TQ alone partially suppressed this transition, the combination treatment resulted in a more significant increase in E-cadherin expression and a significant decrease in mesenchymal markers. The observed phenotypic reversal, considering our significant antiproliferative data, may indicate a mesenchymal-epithelial transition (MET) associated with reduced metastatic potential and reestablished chemosensitivity.

Morphological changes obtained by inverted microscopy analysis confirmed the antitumoral results of the combination application. The transformation of cells to spherical and shrunken structure, and the findings indicating loss of adhesion, especially in the combination group, suggested increased cytotoxic stress and decreased cell-cell adhesion, which is characteristic of EMT inhibition and apoptosis induction. Microscopic observations were consistent with molecular data and together with the observed antiproliferative effects, they confirmed the mechanism of significant EMT inhibition.

Overall, our findings expand current knowledge on colorectal cancer, and showing that TQ may increase the efficacy of platinum-based chemotherapy by inhibiting epithelial-mesenchymal transition and thus is promising in terms of improving therapeutic response.

CONCLUSION

We demonstrated for the first time a synergistic anticancer effect of the combination of thymoquinone and oxaliplatin on HCT116 colorectal cancer cells through inhibition of proliferation and reversal of epithelial-mesenchymal transition (EMT). These findings highlight the high potential of combinations of natural compounds with conventional chemotherapeutics to enhance therapeutic efficacy and combat metastasis and resistance. Further detailed in vivo studies and mechanistic investigations are required to confirm these findings.

REFERENCES

Al Bitar, S., Ballout, F., Monzer, A., Kanso, M., Saheb, N., Mukherji, D., Faraj, W., Tawil A., Doughan S., Hussein M., Abou-Kheir, W., & Gali-Muhtasib, H. (2022). Thymoquinone radiosensitizes human colorectal cancer cells in 2D and 3D culture models. Cancers, 14(6), 1363.

Ang, H. L., Mohan, C. D., Shanmugam, M. K., Leong, H. C., Makvandi, P., Rangappa, K. S., Bishayee A., Kumar A. P., & Sethi, G. (2023). Mechanism of epithelial-mesenchymal transition in cancer and its regulation by natural compounds. Medicinal research reviews, 43(4), 1141-1200.

Dongre, A., & Weinberg, R. A. (2019). New insights into the mechanisms of epithelial–mesenchymal transition and implications for cancer. Nature reviews Molecular cell biology, 20(2), 69-84.

Farhan, M. (2023). Insights on the role of polyphenols in combating cancer drug resistance. Biomedicines, 11(6), 1709.

Farooqi, A. A., Attar, R., & Xu, B. (2022). Anticancer and anti-metastatic role of thymoquinone: Regulation of oncogenic signaling cascades by thymoquinone. International Journal of Molecular Sciences, 23(11), 6311.

Kundu, J., Choi, B. Y., Jeong, C. H., Kundu, J. K., & Chun, K. S. (2014). Thymoquinone induces apoptosis in human colon cancer HCT116 cells through inactivation of STAT3 by blocking JAK2-and Src-mediated phosphorylation of EGF receptor tyrosine kinase. Oncology reports, 32(2), 821-828.

Kurowska, N., Madej, M., & Strzalka-Mrozik, B. (2023). Thymoquinone: A promising therapeutic agent for the treatment of colorectal cancer. Current Issues in Molecular Biology, 46(1), 121-139.

Lu, J., Kornmann, M., & Traub, B. (2023). Role of epithelial to mesenchymal transition in colorectal cancer. International Journal of Molecular Sciences, 24(19), 14815.

Majdalawieh, A. F., Fayyad, M. W., & Nasrallah, G. K. (2017). Anti-cancer properties and mechanisms of action of thymoquinone, the major active ingredient of Nigella sativa. Critical reviews in food science and nutrition, 57(18), 3911-3928.

Martinez-Balibrea, E., Martínez-Cardús, A., Ginés, A., Ruiz de Porras, V., Moutinho, C., Layos, L., Manzano J. L., Buges, C., Bystrup S., Esteller M., & Abad, A. (2015). Tumor-related molecular mechanisms of oxaliplatin resistance. Molecular cancer therapeutics, 14(8), 1767-1776.

Newman, D. J., & Cragg, G. M. (2020). Natural products as sources of new drugs over the nearly four decades from 01/1981 to 09/2019. Journal of natural products, 83(3), 770-803.

Sadeghi, E., Imenshahidi, M., & Hosseinzadeh, H. (2023). Molecular mechanisms and signaling pathways of black cumin (Nigella sativa) and its active constituent, thymoquinone: a review. Molecular biology reports, 50(6), 5439-5454.

Smith, B. N., & Bhowmick, N. A. (2016). Role of EMT in metastasis and therapy resistance. Journal of clinical medicine, 5(2), 17.

Tirendi, S., Marengo, B., Domenicotti, C., Bassi, A. M., Almonti, V., & Vernazza, S. (2023). Colorectal cancer and therapy response: a focus on the main mechanisms involved. Frontiers in oncology, 13, 1208140.

Vu, T., & Datta, P. K. (2017). Regulation of EMT in colorectal cancer: a culprit in metastasis. Cancers, 9(12), 171.

Ye, T., Wu, C., Na, J., Liu, X., & Huang, Y. (2025). Multi-Pathway Study for Oxaliplatin Resistance Reduction. Current Issues in Molecular Biology, 47(3), 172.

➢ *ORAL PRESENTATION*

Development Of Decision Support Systems In Agriculture With Open Source Linear Programming Libraries

Ayşe Begüm Topyıldız[1*] (*ORCID: https://orcid.org/0009-0001-5586-7387*),
Recai Oktaş[2] (*ORCID: https://orcid.org/0000-0003-3282-3549*),
Gökhan Kayhan[3] (*ORCID: https://orcid.org/0000-0003-3391-0097)*

[*1]Ondokuz Mayis University, Institute of Graduate Studies, Computer Engineering Department, Samsun, Türkiye
[2]Ondokuz Mayis University, Engineering Faculty, Computer Engineering Department, Samsun, Türkiye
[3]Ondokuz Mayis University, Engineering Faculty, Computer Engineering Department, Samsun, Türkiye

*Corresponding author e-mail: begum.topyildiz@omu.edu.tr

Abstract
Today, open-source linear programming libraries provide powerful tools for farmers and researchers seeking to enhance decision-making processes and efficiently manage resources in the agricultural sector. This study has designed and implemented two integrated applications—Vites, a Data Collection and Evaluation System, and Motor, a computational engine for Simplex Solving and Sensitivity Analysis—to address optimization problems encountered in agricultural production planning. The system offers a comprehensive structure to strengthen decision support mechanisms, allowing users to define data based on region, product, activity, and resource variables and enabling the generation of optimal production patterns grounded in these inputs. Vites provides an interactive environment with a user-friendly web interface for data entry, management of simulation processes, and reporting of analytical results. The integrated Motor application processes the user-defined initial matrices in the background, which employs linear programming algorithms based on the Simplex Method to compute optimal solutions. The computational core also produces detailed sensitivity analyses, making comprehensive results accessible via the application. The system leverages open-source linear programming libraries for optimization, manages data with PostgreSQL, and runs background processes using Faktory. The web interface is developed on the Ruby on Rails framework, ensuring a modular, flexible, and scalable architecture. In conclusion, the integrated applications—Vites and Motor—provide an analytical, data-driven, and user-centric solution for agricultural production planning. By enabling the generation of optimal production plans and facilitating scenario-based analyses, the system offers strategic value to decision-makers and researchers in the agricultural domain.

Keywords: Linear programming, Agricultural optimization, Open-source libraries, Simplex method, Sensitivity analysis

INTRODUCTION

The agricultural sector plays a critical role in ensuring global food security and maintaining economic sustainability. However, the increasing global population, the effects of climate change, dwindling natural resources, and market conditions marked by uncertainty have made agricultural production and resource management increasingly complex. These challenges necessitate the development and implementation of data-driven decision support systems that utilize algorithmic approaches, especially in scenarios where traditional planning methods are ineffective.

This study introduces an optimization system based on linear programming (LP) that facilitates the efficient planning of agricultural activities under resource constraints. Linear programming enables the attainment of specific objectives—such as profit maximization or cost minimization—within defined constraints through mathematical modeling. The solution is derived using the Simplex method, which provides consistent and actionable insights for decision-makers.

Within this framework, the system consists of two integrated modules: Vites (Data Collection and Evaluation System) and Motor (Simplex Optimization and Sensitivity Analysis Engine). Together, they create a flexible and comprehensive decision support infrastructure for agricultural production planning. The Vites module allows users to input essential data, including crop types, resource quantities, and technical coefficients. The Motor

module then processes these inputs using the Simplex algorithm to generate optimal cropping patterns. Additionally, sensitivity analysis is conducted to evaluate the model's responsiveness to various scenarios, thereby enhancing the robustness and validity of the results.

The system architecture is built on PostgreSQL for data management, Faktory for background processing, and features an interactive web interface developed with Ruby on Rails, which supports modularity and scalability. In this context, the developed infrastructure offers an open-source, sustainable, and innovative decision support tool accessible to a diverse range of users, from agricultural enterprises to public planners and software developers.

MATERIALS AND METHODS

Linear Programming, Simplex Method, and Sensitivity Analysis

Linear Programming (LP) represents a systematic methodology developed for decision-making processes within systems characterized by linear relationships. The primary objective of LP is to determine the optimal value of a linearly defined objective function, constrained by specific linear equality and/or inequality restrictions. LP models can be conceptualized as a structured “program” that delineates the quantity and timing of activities necessary to achieve a predetermined output in systems with clearly defined parameters (Dantzig, 2002).

At the foundation of LP is the Simplex Algorithm, which George Dantzig formulated in 1939 while pursuing graduate studies at Princeton University. This development arose during his exploration of a problem within the field of statistics. Dantzig's analytical work culminated in the creation of the algorithm, which emerged as a critical component of linear programming. In 1947, the algorithm was formally introduced into the academic literature under the designation of the "Simplex Method" (Dantzig, 1963). This method facilitated the systematic and effective resolution of LP problems, thereby enabling its extensive application across various domains, including transportation, production planning, resource allocation, and financial analysis.

The Simplex Method not only guarantees the identification of optimal solutions for linear programming challenges but also extends valuable insights to decision-makers through the process of sensitivity analysis. Fundamental outputs of this methodology, such as shadow prices and reduced costs, function as essential instruments for evaluating the impact of parameter alterations on the objective function. Specifically, shadow prices denote the marginal effect on the objective function resultant from a one-unit change in a given constraint, whereas reduced costs elucidate the implications for the objective function should decision variables, not currently engaged in the solution, become active (Dantzig, 1947).

Sensitivity analysis holds particular significance in the context of optimizing resource allocation. This analytical framework enables the assessment of how variations in resource levels—both increases and decreases—affect total output or profit, thus providing strategic planning advantages and supporting informed decision-making processes for enterprises (Chvátal, 1983). Investigations into the conceptualization and computation of shadow prices have incorporated parametric programming and simplified linear models derived from optimal solutions to examine the repercussions of positive and negative shadow prices on constraints, underscoring their essential role in decision support systems (Akgül, 1984).

Contemporary commercial LP software solutions frequently integrate sensitivity analysis outputs as standard components of their reporting, facilitating users' evaluations of diverse scenarios associated with the obtained solution (Higle, 2003). This analytical approach not only appraises the validity of the current solution but also generates predictive insights regarding capacity utilization, thereby enhancing decision-makers' comprehension of the ramifications of various factors (Yıldırım, 2011). Ultimately, sensitivity analysis serves to assess the responsiveness of the model to modifications in objective function coefficients, constraint coefficients, and resource values—especially in instances where new constraints or decision variables are incorporated (Jaslam PK, 2017).

Open Source and Open Source Linear Programming Libraries

Open source refers to a development model in which software, hardware, or information resources are freely accessible, modifiable, and distributable, with source code made publicly available. While copyright is preserved, open source licenses grant users broad rights of access and use within the scope defined by the respective license agreements (Laurent, 2004). Open source linear programming libraries are software tools developed to solve linear optimization problems, with source code made publicly available. These libraries are typically compatible with various programming languages and support the processes of modeling, algorithm implementation, and problem solving. Their primary aim is to provide a flexible, accessible, and extensible solution infrastructure for linear

programming tasks. The availability of source code enables users to deeply examine the system, customize it to meet specific needs, and contribute to its further development.

Several open source linear programming libraries have been reviewed and compared, including GLPK, SciPy, OR-Tools, and PuLP (Topyıldız & Oktaş, 2024). Based on this comparative analysis, the GLPK library was selected for the implementation of agricultural optimization applications, due to its support for sensitivity analysis and its suitability for the specific nature of the problem (Table 1).

Application Components

- **Ruby on Rails:** Developed by David Heinemeier Hansson in 2004, Ruby on Rails is an open-source web application framework built on the Ruby programming language. Based on the Model-View-Controller (MVC) architecture and embracing the principles of "Convention over Configuration (CoC)" and "Don't Repeat Yourself (DRY)," Rails offers high productivity to developers. It is particularly preferred for rapid prototyping and maintaining sustainable code structures in project development processes (Tate & Hibbs, 2006).
- **PostgreSQL:** PostgreSQL is an open-source relational database management system with object-oriented features. Originating from the POSTGRES project initiated in 1986 under the leadership of Michael Stonebraker, the system provides a flexible and powerful data processing infrastructure by supporting advanced data types and user-defined operations (Stonebraker & Rowe, 1986; Momjian, 2001). The ACID-compliant architecture of PostgreSQL makes it a reliable solution in domains requiring strict data consistency, such as agricultural decision support systems.
- **Sidekiq:** Created by Mike Perham in 2012, Sidekiq is a Redis-based background processing system specifically designed for the Ruby programming language. Its multi-threaded architecture facilitates the concurrent execution of time-intensive tasks in the background, enhancing overall application performance (Perham et al., 2017). This approach is particularly effective in alleviating system load during data collection, analysis, and reporting processes, ultimately improving the user experience.
- **Faktory:** Also developed by Mike Perham, Faktory serves as a language-agnostic extension of Sidekiq, functioning as a background job management system that supports various programming languages, including Python, Go, and Node.js. It allows for the synchronized execution of diverse tasks within microservice architectures, offering significant integration benefits for systems—such as those used in agriculture—where efficient management of multi-source data flows is essential.

Table 1. Open-Source Linear Programming Libraries and Their Features

Library	**Development Programming Language**	**Supported Programming Languages**	**Supported Optimization Problems**
GLPK	ANSI C	AMPL, C, C++, GMPL, Java, MATLAB, Python, R, Ruby, . NET (C#)	Linear Programming (LP), Integer Programming (IP)
SciPy	Python	Python	General-purpose Optimization, Linear Programming (LP), Integer Programming (IP), Nonlinear Optimization, Interior Point Method, Constrained Optimization BY Linear Approximations (COBYLA)
OR-Tools	C++	C++, Java, Python, .NET (C#)	Mixed Integer Programming (MIP), Graph Optimization, Vehicle Routing Problem (VRP), Constraint Programming (CP), Google Linear Optimization Package (GLOP)
PuLP	Python	Python	Linear Programming (LP), Integer Programming (IP)
COIN-OR	C++	AMPL, C++, GMPL, Java, Python, .NET (C#)	Linear Programming (LP), Integer Programming (IP), Genetic Algorithms, Graph Optimization, Traveling Salesman Problem (TSP)
CVXPY	Python	Python	Convex Optimization, Semidefinite Optimization, Robust Optimization
SCIP	C	C, C++, Java, Python, .NET (C#)	Linear Programming (LP), Integer Programming (IP), Mixed Integer Programming (MIP), Robust Optimization, Graph Optimization, Interior Point Method
SYMPHONY	C	C, C++, Python	Graph Optimization, Asymmetric Traveling Salesman Problem (ATSP), Linear Programming (LP), Integer Programming (IP)

RESULTS AND DISCUSSION

The Vites and Motor applications are integrated software components developed using open-source linear programming libraries. They are designed to aid decision-making processes in agricultural production planning. These systems enable users to generate optimal production patterns based on field-specific data through analytical approaches rooted in linear programming techniques.

Built on a microservice architecture, these applications allow for distributed task management among system components. Simulation data, entered via a web interface developed in Ruby on Rails, is stored in a PostgreSQL database and transmitted to the Motor application in the background using the Faktory job manager. Upon completion of computations, results are delivered to the user interface in JSON format through a RESTful API and presented in a report format.

Vites serves as a web-based user interface that facilitates interactive use of the system, while Motor functions as the computational core. User-defined data is transformed into linear programming models by the Motor module, which solves them using algorithms based on the Simplex Method. The output not only includes optimal production patterns but also provides detailed results related to sensitivity analyses and resource utilization.

With this integrated structure, users can comparatively evaluate multiple agricultural production scenarios, make data-driven decisions, and plan resource usage efficiently. Vites and Motor serve as both theoretical modeling tools and robust decision support systems, applicable for practical use in the field.

Data Collection and Evaluation System (Vites)

The Data Collection and Evaluation System (Vites) represents an advanced web-based decision support platform specifically designed to optimize agricultural production planning and conduct policy simulations. This system possesses the capability to identify production patterns that maximize income, as well as land use scenarios that align with sustainable income levels across various geographical scales, including districts, provinces, basins, and regions. Consequently, Vites significantly enhances data-driven decision-making processes within the agricultural sector. Its capacity to simulate the potential impacts of agricultural subsidy policies in advance facilitates effective resource management and strategic planning.

Within the Vites application, users are empowered to delineate production regions, specify the crops to be cultivated, outline the agricultural activities pertinent to each crop, and identify the resources available for utilization through an interactive interface. Moreover, users can articulate scenario-specific parameters to simulate alternative production plans and rigorously analyze the resulting outcomes. The Vites application is publicly accessible at https://vites.omu.edu.tr/ .

The architecture of the system integrates both crop and livestock production activities, drawing upon primary data sources that include micro-level data obtained from agricultural enterprises, administrative records from the Ministry of Agriculture and Forestry, datasets from the Turkish Statistical Institute (TURKSTAT), irrigation unions, and producer organizations, alongside findings from prior studies. Additionally, the integration of expert opinions, academic research, and documentation provided by sectoral stakeholders—including the Turkish Chambers of Agriculture (TZOB), State Hydraulic Works (DSİ), entrepreneurial firms, and cooperatives—serves to augment the empirical validity of the model. The data management process rigorously models production parameters such as input-output coefficients, production costs, income levels, and resource constraints. From this meticulously structured data, optimal production patterns are systematically generated (Ceyhan et al., 2021).

The computational infrastructure that underpins Vites is facilitated by a module termed “Motor,” which acts as the system's arithmetic core and functions as a linear programming-based solver. This solver, developed in accordance with the Simplex Method, employs open-source optimization libraries. Simulation scenarios defined through the user interface are subsequently directed to the Motor module, which processes the specified datasets to compute both optimal production patterns and sensitivity analyses. In this manner, Motor serves as the computational engine of the Vites system, generating solutions that respond to user inquiries. (Figure 1).

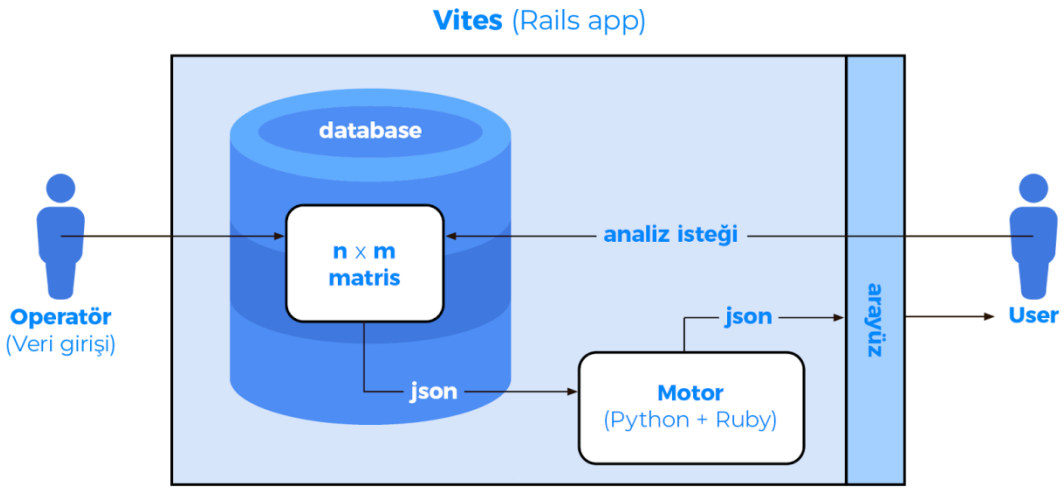

Figure 1. Relational Representation of Vites – Motor

The Vites application is equipped with a field management module that enables data entry and organizational structuring at the district, provincial, and basin levels (Figure 2). Through this module, users are able to define core system elements such as users, crops, production activities, and agricultural basins, as well as assign specific tasks to designated individuals. Using the data collection menu, assigned users can input data related to specific basins into the system via structured survey forms.



Figure 2. Homepage of the Vites Application

Based on the collected data, users construct an initial matrix, which numerically represents agricultural activities by incorporating technical coefficients, input data, revenues, and resource constraints. This matrix is processed by the Motor module, which operates in the system's background using the Simplex algorithm. As a result of the computations, simulation outputs are generated that identify the optimal crop pattern and the maximum achievable income level. Simulation results are presented in the form of detailed reports that include components such as the objective function value, activity outcomes, status of constraints, and shadow prices. These reports can also be exported in Excel format (Figure 3). The outputs not only determine the economic optimum but also highlight critical constraints within the production process, thereby offering strategic decision support.

The Vites system is designed to support both public institutions and private sector stakeholders. Public agencies may use the platform for regional production planning, resource management, and policy impact evaluation, while private actors can conduct data-driven analyses and planning at the enterprise level. In this respect, Vites functions as a comprehensive decision support platform that goes beyond monitoring and reporting to contribute actively to sustainable agricultural development.

Çözüm Sonuçları: Bayburt.xlsx Geri İndir

Sonuç Türü:

Faaliyetlere İlişkin Sonuçlar

Değişken	Değer	Artan Maliyet	Orijinal Değer	Alt Sınır	Üst Sınır	Temel Değişken
Buğday, Durum Buğdayı Hariç	217.095,000	0,000	-116,270	-158,415	∞	true
Buğday (Sulu)	0,000	372,761	-445,330	-∞	-72,569	false
Buğday satış	43.419.000,000	0,000	2,200	1,989	3,703	true
Çavdar	53.198,000	0,000	-156,450	-239,410	∞	true
Çavdar satış	6.543.354,000	0,000	2,500	1,826	∞	true
Arpa (Diğer) (Kuru)	0,000	113,974	-218,370	-∞	-104,396	false
Arpa (Sulu)	0,000	466,108	-454,210	-∞	11,898	false
Arpa satış	0,000	0,000	2,480	0,000	3,277	true
Yulaf	1.185,000	0,000	-126,320	-126,943	∞	true
Yulaf (Sulu)	0,000	305,822	-336,150	-∞	-30,328	false
Yulaf satış	88.875,000	0,000	2,500	2,492	4,248	true
Yulaf (Yeşilot)	179.265,000	0,000	-489,650	-1.353,410	∞	true
Yulaf (Yeşilot) satış	245.234.520,000	0,000	1,100	0,469	∞	true

Figure 3. Activity-Based Results for a Sample Region

Simplex Solver and Sensitivity Analysis (Motor)

The Motor module, embedded within the Vites application, has been developed both as a standalone program and as a library that can be integrated into web applications. The system architecture is based on a microservice model, allowing distributed task management among components. The web interface is built using the Ruby programming language within the Ruby on Rails (RoR) framework. Simulation data provided by users is stored in a PostgreSQL database and queued in the background via the Faktory job manager, which subsequently forwards the data to the Motor application. Upon completion of the computation, results are returned to the Vites user interface and presented in the form of analytical reports. This entire process is managed through RESTful API communication, utilizing JSON as the data exchange format. This architectural framework considerably improves the modularity and scalability of the system, thereby facilitating the incorporation of diverse optimization models. Accordingly, Motor offers both a Python-based computational tool and a Ruby-compatible library for integration with web-based applications.

The Motor library is a flexible system that utilizes both Python and Ruby to optimize solution procedures and seamlessly integrate with web applications. When properly installed and configured, the library can be used effectively in a wide range of optimization scenarios.

The application can be accessed at https://motor.omu.sh/. The dashboard on the homepage provides real-time statistics on all solution processes performed by the system, enabling users to monitor the number of successful and failed simulations dynamically (Figure 4).

Through the application interface, users can initiate new simulations using the “New Report” option, uploading required data in Excel (.xlsx) format. The uploaded file is automatically validated by the system for data format, internal consistency, and compatibility with model parameters. Once validation is successful, the computation process is initiated via the “Generate Report” button, and simulation outputs are generated through background algorithms.

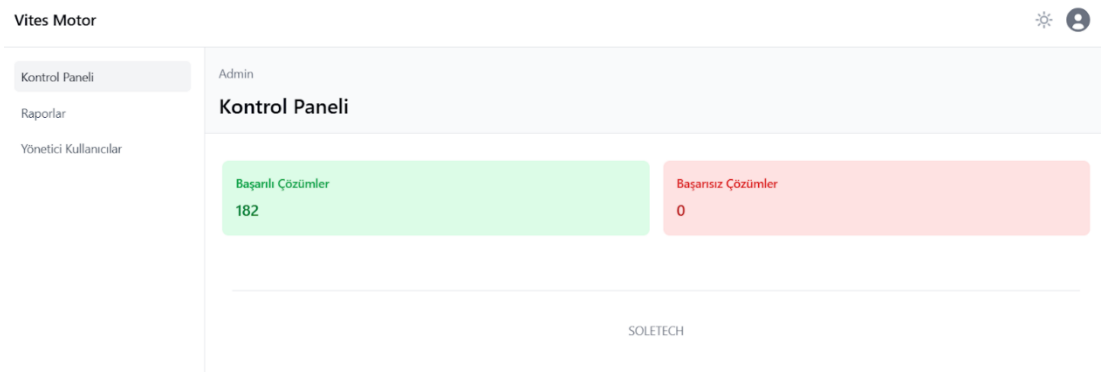

Figure 4. Homepage of the Motor Application

Data is uploaded to the system using a pre-defined Excel template that conforms to the expected structure (Figure 5). Each row in the spreadsheet represents a specific production activity, while columns correspond to technical parameters. Once validated, the dataset is processed by the Motor application to compute the optimal crop pattern and associated economic outputs for the simulation region.

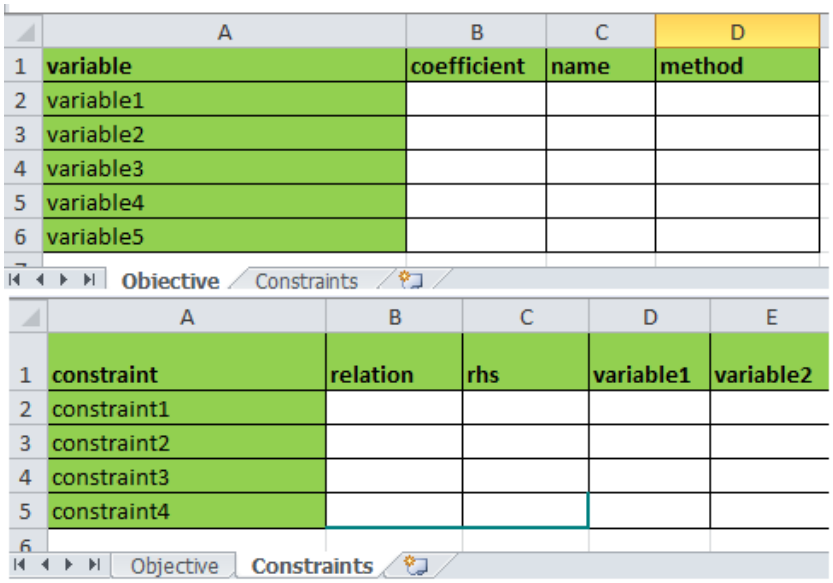

	A	B	C	D
1	variable	coefficient	name	method
2	variable1			
3	variable2			
4	variable3			
5	variable4			
6	variable5			

Objective | Constraints

	A	B	C	D	E
1	constraint	relation	rhs	variable1	variable2
2	constraint1				
3	constraint2				
4	constraint3				
5	constraint4				
6					

Objective | Constraints

Figure 5. Initial Matrix Excel Template

The results are presented within the system interface and are amenable to exportation in Excel format. Alongside the identification of optimal solutions, the output file encompasses sensitivity analyses, which yield intricate insights into the model's responsiveness to variations in multiple parameters. This feature facilitates users in conducting thorough and data-driven evaluations, thereby enhancing their decision-making processes.

CONCLUSION

The agricultural sector plays a crucial role globally in ensuring food security, managing natural resources, and promoting economic sustainability. The challenges posed by population growth, climate change, and resource limitations necessitate the adoption of more efficient and strategic approaches to agricultural production. In this context, mathematical optimization techniques, particularly linear programming, are essential for enhancing production planning, resource allocation, and decision-making processes.

This study introduces the integrated applications Vites and Motor, showcasing the use of open-source linear programming libraries in agricultural optimization. Built on the GLPK (GNU Linear Programming Kit) library, these applications create optimal production patterns utilizing the Simplex algorithm and user-defined technical coefficients. The resulting solutions come with sensitivity analyses and are presented to users through an intuitive interface.

A comparative analysis of various open-source libraries indicates that GLPK excels due to its robust support for sensitivity analysis and its solution quality in linear programming challenges. However, each library has its unique strengths and limitations, particularly concerning documentation, usability, and flexibility.

In conclusion, the developed system has the potential to act as a strategic decision support tool for agricultural enterprises as well as for policymakers and planners. With their user-centered design, adaptable computational framework, and open-source nature, Vites and Motor provide valuable solutions for both researchers and practitioners. Future research may further enhance these systems by exploring diverse agricultural scenarios and complex optimization issues, thereby offering substantial theoretical and practical contributions at the intersection of agricultural economics and software development.

ACKNOWLEDGEMENTS

We gratefully acknowledge the valuable contributions of Prof. Dr. Vedat CEYHAN, Lecturer Onur BARAN, Lecturer İrfan SUBAŞ, and Lecturer Emre Can YILMAZ.

REFERENCES

Akgul, M. (1984). A Note on Shadow Prices in Linear Programming. The Journal of the Operational Research Society, 35(5), 425–431.

Ceyhan V., Baran O., Sayın C., Oktaş R., Unakıtan G. ve Armağan G., (2021-2024). Tarım Ürünleri Üretiminde Optimizasyon ve Optimizasyona Dayalı Politika Simülasyon Sisteminin Geliştirilmesi, TAGEM Tarımsal Araştırmalar ve Politikalar Genel Müdürlüğü Projesi.

Chvátal, V. (1983). Linear Programming. W.H. Freeman and Company.

Dantzig, G. B. (1947). Maximization of a Linear Function of Variables Subject to Linear Inequalities. Pacific Journal of Mathematics.

Dantzig, G. B. (1963). Linear programming and extensions. Princeton university press.

Dantzig, G. B. (2002). Linear programming. Operations research, 50(1), 42-47.

Higle, J. L. and Wallace, S. W. (2003). Sensitivity analysis and uncertainty in linear programming. Interfaces, 33(4), 53-60.

Jaslam PK, (2017). Role of Optimization Techniques in Agriculture, Munich, GRIN Verlag, https://www.grin.com/document/431070, (28.05.2025)

Laurent, A. M. S. (2004). Understanding open source and free software licensing: guide to navigating licensing issues in existing & new software. " O'Reilly Media, Inc.".

Momjian, B. (2001). PostgreSQL: introduction and concepts.

Perham, M., Arcieri, T., Dardour, R. and Cooke, J. (2017). Sidekiq: Simple, efficient background processing for Ruby.

Stonebraker, M. and Rowe, L. A. (1986). The design of Postgres. ACM Sigmod Record, 15(2), 340-355.

Tate, B., Hibbs, C. (2006). Ruby on Rails: Up and Running: Up and Running. " O'Reilly Media, Inc."

Topyıldız, A.B. and Oktaş R. (2024, December), “Open Source Linear Programming Libraries And Their Use In Agricultural Optimization”. *Informatics And Technology Transfer: Bridging Innovation And Implementation*, Pegem Akademi, Çetin, İ., Ed., Ankara, 2024 (Chapter 1, ss.1-13)

Yıldırım, İ. (2011). Orman ürünleri sanayi sektöründe üretim planlama sisteminin doğrusal programlama yöntemi ile geliştirilmesi ve uygulaması.

➢ *ORAL PRESENTATION*

Non-stationary analysis of extreme temperatures in Erzurum using physical covariates

Muhammet Yılmaz[1*] (*ORCID: https://orcid.org/0000-0002-9844-6654*)

[*1] Erzurum Technical University, Faculty of Engineering and Architecture, Department of Civil Engineering, Erzurum, Türkiye.

*Corresponding author e-mail: muhammet.yilmaz@erzurum.edu.tr

Abstract
With the impacts of climate change becoming more evident in recent years, the widespread assumption of the stationarity of climate extremes has increasingly been questioned, prompting the use of non-stationary models that incorporate explanatory variables. In this study, extreme temperature time series from a station in Erzurum for the period 1961-2017 were analyzed using both stationary and non-stationary models based on the generalized additive models for location, scale, and shape (GAMLSS) technique. In constructing non-stationary models, different explanatory variables such as, Arctic Oscillation (AO), North Atlantic Oscillation (NAO), and North Sea Caspian Pattern (NCP) on seasonal and annual scales that trigger extreme temperature events were used to model the parameters of the chosen distributions. Four probability distributions, namely gamma (GA), logistic (LOGIS), two-parameter lognormal (LOGNO), and Weibull (WEI), were chosen as commonly used two-parameter distributions for modeling extreme temperature dataset. The Akaike Information Criterion (AIC) was employed to identify the most suitable model among the candidates. The Filliben coefficient and worm plot were utilized to show the suitability of the models. According to the results, Gamma and Logistic distributions were the most adequate candidates for modeling minimum and maximum temperatures, respectively. The results showed that for minimum temperature, Annual AO was an effective explanatory variable, while for maximum temperature, Annual NCP was the main predictor.
Keywords: Non-stationarity; Extreme temperatures; GAMLSS; Atmospheric oscillations; Erzurum.

INTRODUCTION

Recently, changes in extreme weather conditions due to climate change have caused concerns around the world (Gao and Zheng, 2018). In this context, studies have been conducted to analyze the change in climate extremes and these studies have shown that a warming atmosphere intensifies some climatic extremes such as extreme high temperatures, decreases the frequency of extreme low temperatures and increases the occurrence of heavy precipitation (IPCC, 2007). Morover, the IPCC predicted that the average global temperatures are likely to surpass the upper threshold set by the Paris Agreement in the 2040s (IPCC, 2018). Therefore, statistical analysis of extreme climate events is important for many reasons such as ecology, agriculture, environment, engineering designs.

Temperature plays an important role in providing information about the energy balance of the earth's surface and it directly affects global climate change (Huang et al., 2021). In general, changes in minimum and maximum temperatures affect society, environment and ecosystem more than the average temperature (Chowdary et al., 2014). Moreover, extreme temperature events cause many negative effects on factors such as drought, agriculture, forest fire, energy consumption, and human health (Levermore et al., 2018; Norton et al., 2015; Omer et al., 2020). Hence, creating models to predict extreme temperatures over a certain period of time and recurrence period is a very critical issue. Researchers have generally considered the stationarity assumption to develop inferences and analyses for extreme temperature data. However, recently the stationarity of hydro-meteorological time series has been questioned due to the impact of climate change (Su and Chen, 2019; Serago and Vogel, 2018; Kyojo et al., 2024). Thus, methods that can take into account the changes in the parameters of the selected probability distribution over time have been developed. For instance, Villarini et al. (2010) developed a model to study temperature changes in Rome. The results show the importance of non-stationary modeling for temperature data. Raggad (2018) proposed the extreme values tecnique to model extreme temperatures in Riyadh city and the results highlighted that the proposed model predicts the changes in maximum temperature risk at an acceptable level.

Atmospheric circulation and teleconnection patterns have critical impacts on short- and long-term climate variability in different regions (Türkeş and Erlat, 2008). Thus, researchers have studied the relationships between

extreme temperatures and atmospheric oscillations in different parts of the world (Tolika et al., 2014; Türkeş and Erlat, 2018; Carney et al., 2020). Within the scope of the study, Arctic Oscillation (AO), North Atlantic Oscillation (NAO), and North Sea Caspian Pattern (NCP) were evaluated due to their known effects on extreme temperatures in Türkiye.

The main purpose of the study is to develop non-stationary models for extreme temperature data in Erzurum province using the recently developed generalized additive models for location, scale, and shape (GAMLSS) technique. For this purpose, firstly the correlations between extreme temperature data and AO, NAO, and NCP were investigated and the significance of the results was tested with Student's t-test. Non-stationary models were developed with the GAMLSS technique using the atmospheric oscillation index with significant correlation as an explanatory variable.

MATERIALS AND METHODS

GAMLSS model

Generalized Additive Models for Location, Scale and Shape parameters (GAMLSS) were proposed by Rigby and Stasinopoulos (2005) to investigate linear and nonlinear relationships between response and explanatory variables under non-stationary conditions (Rigby and Stasinopoulos, 2005). One of the most important advantages of GAMLSS is that more than one explanatory variable can be introduced for the response variable (Gao et al., 2018). GAMLSS has a very wide family of distributions including two-parameter, three-parameter and four-parameter. Within the scope of the study, four probability distributions were selected as two-parameter distributions to model extreme temperature data sets, namely gamma (GA), logistic (LOGIS), two-parameter lognormal (LOGNO) and Weibull (WEI). To determine the explanatory variable, correlations between the annual and seasonal values of AO, NAO, and NCP indices and extreme temperatures were investigated and decided according to the Student's t-test result. Akaike information criterion (AIC) was used to evaluate between different models (Akaike, 1983). The model with the lowest AIC value was considered the most successful model. In addition, to access the performance of the selected models in more detail, worm plots showing diagnostic graphs of the residuals were obtained and Filliben coefficients were examined (López and Francés, 2013).

Therefore, in the study, stationary distribution models with constant parameters and non-stationary models that model the distribution parameters using single/multiple atmospheric oscillation indices as explanatory variables were developed.

Study area and data

Covering 3.2% of Türkiye's land, Erzurum Province is located in the northeastern part of the Eastern Anatolia Region between 39° 10’-40° 57’ North latitude and 40° 15’ - 42° 35’ East longitude. The altitude of this plateau is 1950 m above sea level and its population is 763320. Erzurum, one of the coldest cities in Türkiye, has a continental climate. Winters are very cold and long. Temperatures can drop to -30°C, and snowfall is common. Summers are short, cool and dry. Although the days are warm, the nights are cool. From 1929 to 2024, the mean annual temperature in Erzurum has been recorded at 5.8 °C. Monthly minimum and maximum temperatures are -37.2°C and 36.5°C, respectively. The highest total daily rainfall amount was measured as 171.3 mm in 1975. The annual average total rainfall is 430.9 m (MGM, 2025). Within the scope of the study, the minimum/maximum values of the daily minimum/maximum temperature values for each year of the station number 17096 between the years 1961-2017 were taken into account. The geographical extent of the study area, along with the location of the meteorological station, is presented in Figure 1. This study utilized NAO values from the Climatic Research Unit (CRU) at the University of East Anglia (http://www. cru. uea. ac. uk/), while the AO values were obtained from the Climate Prediction Center, NOAA (http://www. cpc. ncep. noaa. gov/). The NCP values were sourced from the study conducted by Türkeş and Erlat (2018).

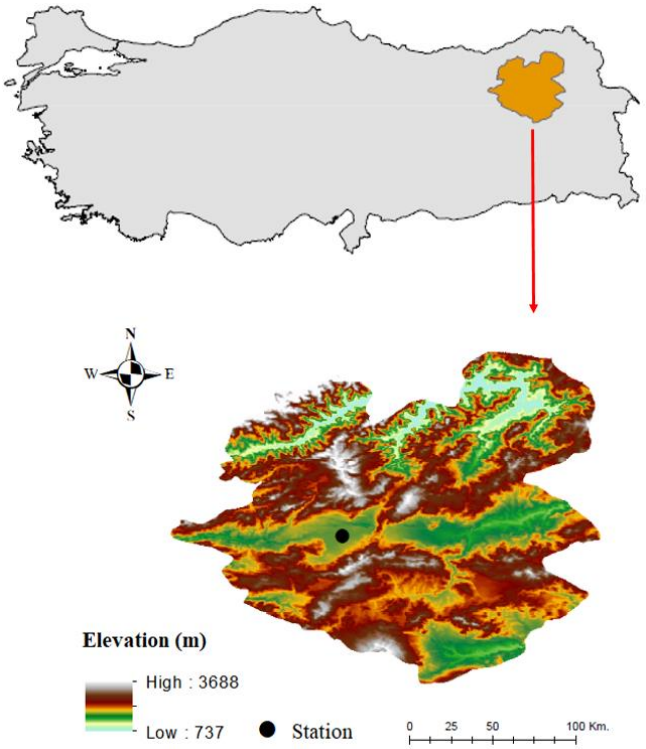

Figure 1. Spatial distribution of the study area and the location of the meteorological station.

RESULTS and DISCUSSION

In the presented study, stationary and non-stationary models were created for extreme temperature series of 17096 stations in Erzurum province with GAMLSS technique. For this purpose, four commonly used probability distributions with 2 parameters were employed. While creating non-stationary models, NAO, AO and NCP atmospheric oscillation indices were used as explanatory variables. As a preliminary analysis, correlations between extreme temperature values and seasonal and annual indices were calculated with Pearson correlations to determine the most effective explanatory variable. The significance of the correlations was tested with Student's t-test at 10% significance level (see Table 1).

Table 1. Correlation coefficients between seasonal/annual oscillation indices and temperature extremes

Temperature	**Minimum Temperature**			**Maximum Temperature**		
Atmospheric Oscillations	**AO**	**NCP**	**NAO**	**AO**	**NCP**	**NAO**
Annual	**-0.532**	**-0.414**	**-0.349**	**-0.242**	**-0.555**	-0.183
Winter	**-0.53**	**-0.452**	**-0.305**	-0.199	**-0.442**	0.014
Spring	**-0.283**	**-0.403**	-0.131	-0.217	-0.207	**-0.248**
Summer	-0.058	-0.026	-0.107	0.101	**-0.364**	-0.124
Autumn	-0.131	0.01	-0.044	-0.088	-0.115	0.042

Note: Bold values represent significant correlations.

The correlations showed that AO and NCP have a greater influence on temperature extremes than NAO. While the AO was the most influential atmospheric oscillation on minimum temperature annually and during the winter season, NCP became more effective in spring. For maximum temperature, NCP was found to be more effective on annual and seasonal scales except spring.

After determining the most relevant predictor(s) according to the correlation results, non-stationary models were developed with the GAMLSS technique. Table 2 presents the comparison of stationary and non-stationary models for minimum and maximum temperatures separately. The table also provides the results of the likelihood ratio (LR) test (Coles, 2001) to measure whether adding a predictor significantly affects the AIC value. LR test values were evaluated at a 5% significance level, and a p value of the LR test greater than 0.05 indicates that there is no

significant improvement. According to the results, Gamma and Logistic distributions were determined as the most suitable distributions to capture the characteristics of minimum and maximum temperatures, respectively. Table 2 showed that the Annual AO is the main predictor for the minimum temperature and its AIC value is significantly improved compared to that of the stationary model. The results showed that Annual NCP is the most effective explanatory variable compared to other indices for maximum temperature and the AIC value of the non-stationary model showed significant improvement. In addition, the Fliiben coefficients of the non-stationary models selected for the minimum and maximum temperatures are greater than 0.97, which shows that the models are acceptable (Hao et al., 2019).

Table 2. Comparison of stationary and non-stationary models

Temprerature indices	Model	AIC values	Filliben coefficients	LR test p value
Minimum Temperature	GA(μ,σ)	295.17	0.98	
	GA(μ~ Annual AO,σ)	278.42	0.98	0.00001
Maximum Temperature	LOGIS(μ,σ)	178.3124	0.99	
	LOGIS(μ ~Annual NCP,σ)	159.4562	0.99	0.00005

Worm plots were examined to assess the quality of the selected non-stationary models (see Figure 2). According to the results in Figure 2, no significant deviation from normality was observed and the standard residuals remained within the 95% confidence interval defined by the two elliptic curves.

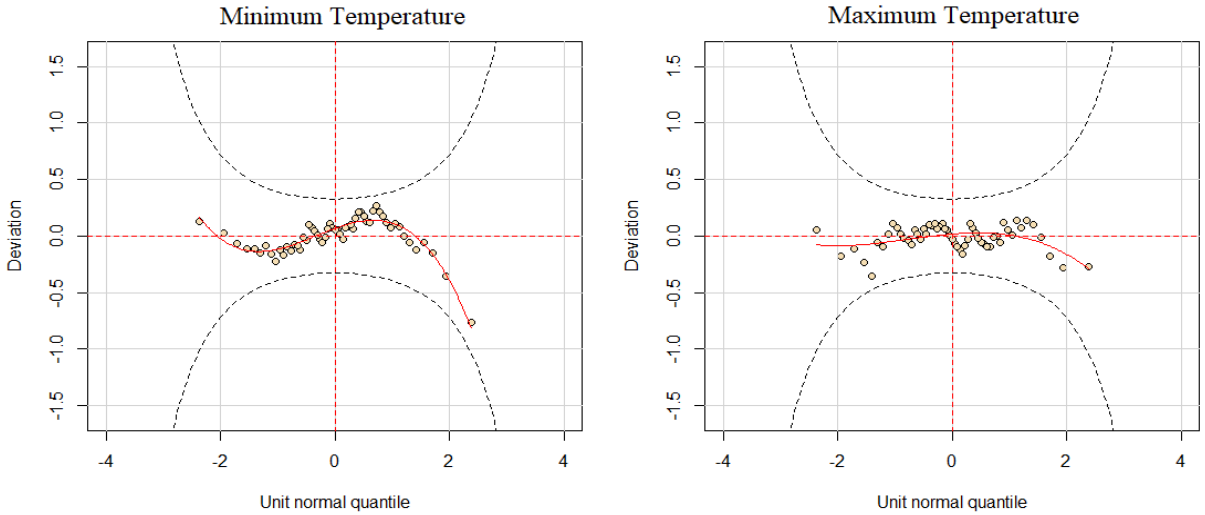

Figure 2. Worm plots of residuals of best-fit non-stationary models for extreme temperatures

CONCLUSION

GAMLSS based non-stationary models were developed to determine the most effective explanatory variable using extreme temperature data obtained from Station 17096 in Erzurum. Correlation results showed that AO and NCP are generally in good agreement with temperature extremes on seasonal and annual scales. After determining the relevant explanatory variables, AIC, Filliben coefficient and worm plots were used within the GAMLSS technique to assess the four probability distributions. Gamma and Logistic were found to be suitable distributions for modeling minimum and maximum temperatures, respectively. The results showed that non-stationary models were more successful than stationary models. The findings highlighted that Annual AO and Annual NCP are effective explanatory variables for minimum temperature and maximum temperature, respectively. The results of the study emphasize that it is necessary to consider non-stationarity in extreme temperature series for the study area.

REFERENCES

Akaike, H. Information measures and model selection. Bullet. Int. Stat. Inst. 44, 277–291 (1983).

Carney, M., Azencott, R., & Nicol, M. (2020). Nonstationarity of summer temperature extremes in Texas. Int J Climatol, 40, 620-640.

Chowdary, J. S., John, N., & Gnanaseelan, C. (2014). Interannual variability of surface air-temperature over India: impact of ENSO and Indian Ocean Sea surface temperature. International Journal of Climatology, 34(2).

Coles S (2001) An introduction to statistical modeling of extreme values. Springer-Verlag, London, UK

Gao, L., Huang, J., Chen, X., Chen, Y., & Liu, M. (2018). Contributions of natural climate changes and human activities to the trend of extreme precipitation. Atmospheric Research, 205, 60-69.

Gao, M., & Zheng, H. (2018). Nonstationary extreme value analysis of temperature extremes in China. Stochastic Environmental Research and Risk Assessment, 32, 1299-1315.

Hao, W., Shao, Q., Hao, Z., Ju, Q., Baima, W., & Zhang, D. (2019). Non-stationary modelling of extreme precipitation by climate indices during rainy season in Hanjiang River Basin, China. International Journal of Climatology, 39(10), 4154-4169.

Huang, X., Han, S., & Shi, C. (2021). Multiscale assessments of three reanalysis temperature data systems over China. Agriculture, 11(12), 1292.

IPCC (2007) Climate change 2007: the physical science basis.contribution of working group I to the fourth assessment report of the intergovernmental panel on climate change. Cambridge University Press, Cambridge

IPCC (2018) Summary for Policymakers. In: Global warming of 1.5 _C. An IPCC Special Report on the impacts of global warming of 1.5 _C above pre-industrial levels and related global greenhouse gas emission pathways, in the context of strengthening the global response to, World Meteorological Organization, Geneva, Switzerland. Geneva, Switzerland.

Kyojo, E. A., Osima, S. E., Mirau, S. S., & Masanja, V. G. (2024). Applying Stationary and Nonstationary Generalized Extreme Value Distributions in Modeling Annual Extreme Temperature Patterns. Advances in Meteorology, 2024(1), 9652134.

Levermore, G., Parkinson, J., Lee, K., Laycock, P., & Lindley, S. (2018). The increasing trend of the urban heat island intensity. Urban climate, 24, 360-368.

López, J., & Francés, F. (2013). Non-stationary flood frequency analysis in continental Spanish rivers, using climate and reservoir indices as external covariates. Hydrology and Earth System Sciences, 17(8), 3189-3203.

Norton, B. A., Coutts, A. M., Livesley, S. J., Harris, R. J., Hunter, A. M., & Williams, N. S. (2015). Planning for cooler cities: A framework to prioritise green infrastructure to mitigate high temperatures in urban landscapes. Landscape and urban planning, 134, 127-138.

Omer, A., Zhuguo, M., Zheng, Z., & Saleem, F. (2020). Natural and anthropogenic influences on the recent droughts in Yellow River Basin, China. Science of the Total Environment, 704, 135428.

Raggad, B. (2018). Stationary and non-stationary extreme value approaches for modelling extreme temperature: the Case of Riyadh City, Saudi Arabia. Environmental Modeling & Assessment, 23(1), 99-116.

Rigby, R. A., & Stasinopoulos, D. M. (2005). Generalized additive models for location, scale and shape. Journal of the Royal Statistical Society Series C: Applied Statistics, 54(3), 507-554.

Serago, J. M., & Vogel, R. M. (2018). Parsimonious nonstationary flood frequency analysis. Advances in Water Resources, 112, 1-16.

Su, C., & Chen, X. (2019). Assessing the effects of reservoirs on extreme flows using nonstationary flood frequency models with the modified reservoir index as a covariate. Advances in Water Resources, 124, 29-40.

Tolika, K., Maheras, P., Pytharoulis, I., & Anagnostopoulou, C. (2014). The anomalous low and high temperatures of 2012 over Greece–an explanation from a meteorological and climatological perspective. Natural Hazards and Earth System Sciences, 14(3), 501-507.

Türkeş, M., & Erlat, E. C. M. E. L. (2008). Influence of the Arctic Oscillation on the variability of winter mean temperatures in Turkey. Theoretical and Applied Climatology, 92, 75-85.

Türkeş, M., & Erlat, E. (2018). Variability and trends in record air temperature events of Turkey and their associations with atmospheric oscillations and anomalous circulation patterns. International Journal of Climatology, 38(14), 5182-5204.

Villarini, G., Smith, J. A., & Napolitano, F. (2010). Nonstationary modeling of a long record of rainfall and temperature over Rome. Advances in Water Resources, 33(10), 1256-1267.

➢ *ORAL PRESENTATION*

Detection and assessment of pedestrian crossings physical conditions using YOLOv12 model

Kadir Diler Alemdar[1*] (*ORCID: https://orcid.org/0000-0002-8837-7640*)

[*1]Erzurum Technical University, Faculty of Engineering and Architecture, Civil Engineering, Erzurum, Türkiye.

*Corresponding author e-mail: kadir.alemdar@erzurum.edu.tr

Abstract
Pedestrians are among the most vulnerable road users in terms of traffic elements.The fact that pedestrians do not have any protective elements during mobility causes them to have a higher risk of injury compared to other road users in the event of a traffic accident.Therefore, pedestrian crossings are crucial for pedestrian safety in urban transportation. However, pedestrian crossings may be physically deteriorate over time due to environmental factors such as traffic density, snow, rain, icing, extreme temperatures and lack of maintenance. This can lead drivers failing to properly perceive damaged pedestrian crossings, potentially causing traffic accidents. This study aims to detect the physical deterioration of pedestrian crossings by analyzing the physical conditions of pedestrian crossings with the YOLOv12 model.The results showed that the mAP@0.5 metric reaches 87.8%, showing a very high success rate of the model under the medium overlap condition; the more stringent evaluation criterion mAP@0.5:0.95 reaches 79.7%, showing that the overall success rate of the model is satisfactory even under difficult conditions. This approach integrates cutting-edge computer vision technology with real-world data and problems to contribute to the ongoing challenge of pedestrian safety. The study results will help reduce traffic accidents caused by pedestrian-vehicle collisions by encouraging improvements in pedestrian crossing maintenance. This will be an important step toward enhancing pedestrian crossing safety.
Keywords: Pedestrian crossings; Pedestrian safety; Deep learning, Object detection, YOLOv12

INTRODUCTION

Urban transportation systems aim to provide safe and sustainable solutions to all traffic components. Pedestrians, one of the most important traffic components, are defined as the most sensitive and fragile component (Alemdar et al., 2020). Pedestrians interact intensively with other components of traffic. Pedestrian traffic is concentrated in areas close to commercial areas, social areas, public institutions and educational institutions in city centers. Unlike other traffic components, there is no protective equipment used for pedestrians. This situation causes pedestrians exposed to traffic accidents to be vulnerable and can lead to serious injuries and deaths during the accident. Researchers are conducting various studies on determining and analyzing pedestrian crossing locations in order to increase pedestrian safety (Alemdar et al., 2020; Guan et al., 2024; Martinez-Chao et al., 2024; Soilán et al., 2018). Pedestrian crossings, which are traffic infrastructure elements, provide pedestrians with a safe crossing by interrupting the flow of traffic. However, it is inevitable that pedestrian crossings will lose their physical characteristics over time due to various factors. Environmental effects, paint wear, physical deformations on the road surface, extreme temperature changes, precipitation and heavy traffic flow reduce the visibility of pedestrian crossings, making it difficult for both drivers and pedestrians to perceive them. This situation directly threatens the safety of pedestrians and increases the possibility of vehicle-pedestrian collisions.

Detection of physical defects and maintenance requirements of pedestrian crossings with traditional methods is mostly based on workforce supervision. With the application of smart technologies to transportation systems, autonomous monitoring of traffic infrastructure elements and detection of physical defects are gaining importance. In this context, image processing, computer vision and deep learning approaches offer a new perspective for the evaluation of traffic infrastructure elements. You Only Look Once (YOLO) architecture, which can perform the processes of real-time and successful detection of physical defects, is frequently applied in many areas such as traffic signs, road pavement defects, pedestrian detection, vehicle detection, traffic flow (Golcarenarenji et al., 2023; Hassan et al., 2024; Kang et al., 2024; Li et al., 2024; Tsai et al., 2021). When the studies in the literature are investigated in depth, the number of studies focusing on autonomous detection of physical defects of pedestrian crossings is quite limited. This situation presents a major gap for pedestrian safety.

This study proposes an approach to detect the physical conditions of pedestrian crossings using the YOLOv12 model, which was introduced in the state-of-the-art studies in the field of object detection. A dataset consisting of

deformed pedestrian crossings and normal pedestrian crossings images was used in the study. The results provide strong and accurate information for decision makers planning the maintenance requirements of urban transportation infrastructure. In addition, the integration of the autonomous detection model presented in the scope of the study into Vehicle-to-Infrastructure (V2I) communication protocols has enabled the development of real-time systems. The study presents a holistic approach that contributes to both urban traffic safety and intelligent transportation systems.

MATERIALS AND METHODS

Data Collection Process

The dataset used in the study was created using Google Earth technology and images of pedestrian crossings taken from areas with heavy vehicle and pedestrian traffic from different countries that are publicly accessible. The main purpose of using different countries and cities is to include different socio-economic, cultural and environmental factors in the study. A total of 474 images were collected in rainy, snowy and sunny weather in order to reflect different climatic conditions. This approach is very important in terms of evaluating the generalizability of the model in different environmental conditions.

Image Processing and Labeling Process

In order to train the YOLOv12 model, the raw images need to complete various preprocessing steps. In this direction, resolution standardization (640x640 pixels), color balancing (histogram equalization) and shadow/highlight corrections were performed. In addition, the dataset was expanded by applying data augmentation techniques such as flip (horizontal), 90'Rotate (Clockwise, Counter-Clockwise) and Grayscale (Apply to %15 of images) to the raw images. The dataset was divided into two classes as "Deformed Pedestrian Crossing" and "Normal Pedestrian Crossing". All labeling operations were performed via Roboflow.

YOLOv12 Model and Training Process

As a result of a more advanced backbone architecture (EfficientRep v2), enhanced feature extraction (PAFPN++), and better data augmentation techniques, YOLOv12 can provide more successful results compared to previous versions. The model uses YOLOv12x weights obtained by training with the COCO dataset. The reason for choosing this weight is that it provides much more consistent and successful outputs despite a slower training process. In the model, epoch number: 100, batch size: 8, learning rate = 0.0005 and optimization algorithm: AdamW. 70% training, 15% validation and 15% test separation was used in training the model. The training process was completed using the T4 GPU environment provided by Google Colab.

Performance Evaluation Metrics

In order to quantitatively analyze the success of the model, various performance metrics frequently used in the literature were taken into account (Alemdar, 2024; Alemdar and Çodur, 2024; Nandal et al., 2025). Performance metrics are used to examine both the overall success of the model and the balance between classes.

• Precision: It is a parameter that reveals how many of the examples classified as positive by the model are actually correct. It reflects the effect of false positives.

• Recall: It is a parameter that reveals how many of the examples that are true positives in the data set are correctly detected by the model. It highlights the effect of false negatives.

• mAP@0.5: It expresses the average accuracy value when the Intersection over Union (IoU) threshold is considered as 50%. It is a standard metric for measuring success in object detection.

• mAP@0.5:0.95: This metric is the average accuracy obtained by calculating IoU values between 0.5 and 0.95 with 0.05 intervals. It evaluates the sensitivity of the model at different thresholds.

• F1-Score: It is the harmonic average of Precision and Recall. It provides a balanced evaluation of the two metrics.

Thanks to these metrics, the success status of the entire model can be revealed. The fact that the metrics are close to 1 indicates that it is successful depending on the characteristics of the data set.

RESULTS and DISCUSSION

The training of the model was successfully completed in 1,567 hours for 100 epochs and a strong learning performance was achieved on the training dataset. It was observed that the validation loss decreased steadily during the training process and no overfitting tendency was observed. The performance outputs of the model are presented in Figures 1 and 2.

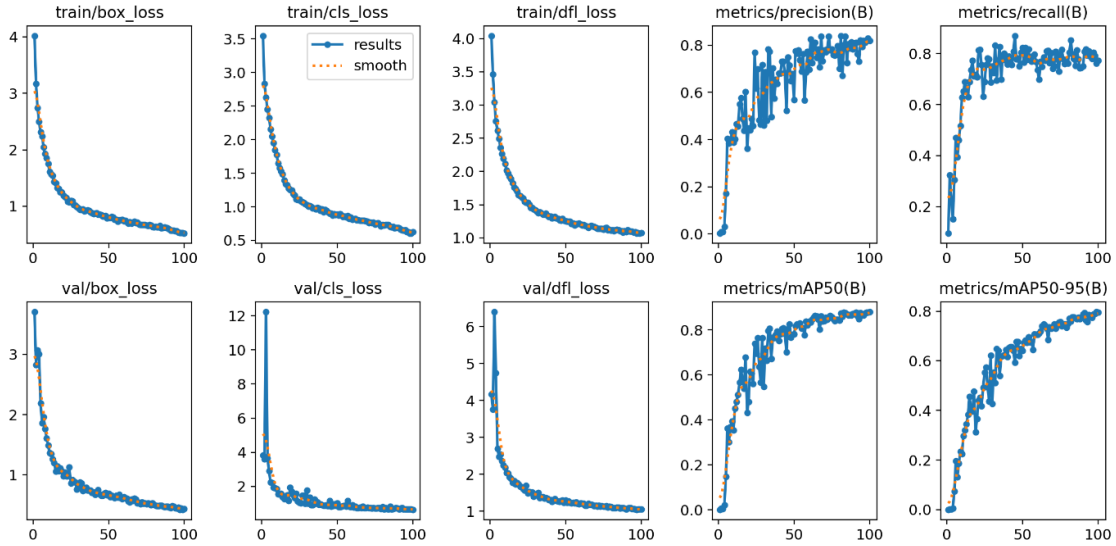

Figure 1. Loss functions of the model, graphs of precision, recall, mAP@0.5 and mAP@0.5:0.95 performance metrics

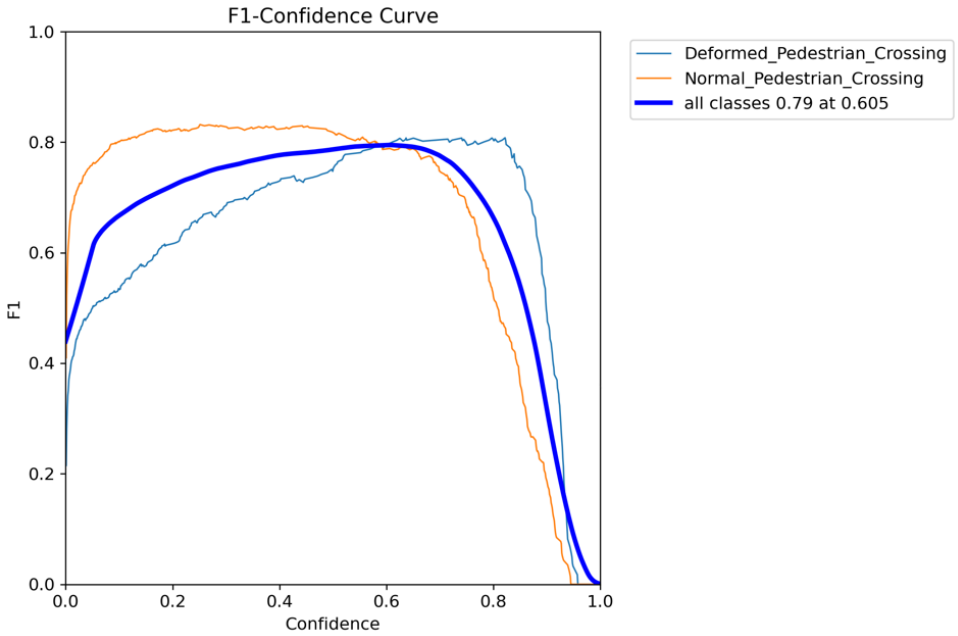

Figure 2. F1-Score graph for training dataset

Model outputs show that the YOLOv12 model exhibits successful and reliable performance in detecting the physical conditions of pedestrian crossings. The metrics obtained from the training and validation processes reveal that the model performs balanced learning in terms of both box localization and classification. A steady decrease was observed in the loss functions (box_loss, cls_loss and dfl_loss) throughout the training process. This shows that the model is optimized for the detection task and does not carry the risk of overfitting. The metrics related to the accuracy performance of the model also support these observations. The precision value was obtained as 0.829 and the recall value was approximately 0.76, which show that the model both successfully detected objects and

kept the missed object rate low. When the average accuracy values are examined, it is seen that the mAP@0.5 metric reached 87.8%, indicating that the model showed quite high success in the medium level overlap condition; The more stringent evaluation criterion mAP@0.5:0.95 value reaches 79.7%, which shows that the overall success level of the model is satisfactory even under difficult conditions. These metrics show that the model has a strong overall performance both in positioning the boxes and in class separation.

The F1-score – Confidence curve created to evaluate the model results in more detail also provides important findings regarding the model. The graph presented in Figure 2 reveals the change in the F1 value as the confidence score threshold used in the classification decisions changes. When the graph is examined, it is seen that high F1 scores are obtained for both classes (Normal Pedestrian Crossing and Deformed Pedestrian Crossing). Especially in the deformed pedestrian crossing class (Deformed Pedestrian Crossing), the F1 score was slightly above the 0.80 level within a certain confidence interval, which shows that the model detected this class with high accuracy with a low error rate. Similarly, the F1 value is above 0.80 in the normal pedestrian crossing class (Normal Pedestrian Crossing), but it starts to decrease at an earlier stage. This may indicate the possibility of normal pedestrian crossings being confused with deformed pedestrian crossings in some examples. When the combined F1 curve for both classes is examined, it is seen that the F1 score is 0.79 at the 0.605 confidence score threshold. When the performance metrics are examined, it is observed that the model offers a strong and balanced success. This performance supports the applicability of the model in the field and shows that it can make significant contributions if integrated into decision support systems or V2I communication mechanisms related to the detection of physical defects.

CONCLUSION

This study proposes an approach to detect physical defects affecting the visibility of pedestrian crossings with object detection method in order to ensure pedestrian safety. This approach, developed using YOLOv12 model, aims to detect deformed pedestrian crossings and normal pedestrian crossings through visual data. When the performance metrics of the model are examined, it is observed that the physical defects of pedestrian crossings are detected successfully. In this way, it has made a significant contribution to the field of transportation infrastructure management and pedestrian safety.

The findings show that the model has high accuracy rates in standard success metrics such as mAP@0.5 and mAP@0.5:0.95, provides a balanced structure between precision and recall values, and shows consistent success for both education classes in the F1-Score curve. The outputs reveal that the model is suitable for both field applications and that a contribution can be made to transportation infrastructure maintenance planning using computer vision.

In future studies, different climate, socio-economic structure, demographic structure, etc. The generalization ability of the model can be tested in detail with more diverse data sets from geographical regions that contain the characteristics. The scope can be expanded by including a specific scenario such as night vision performance in the study. All these results show that computer vision and deep learning technologies can be used effectively in areas with high social benefit potential such as pedestrian safety.

REFERENCES

Alemdar, K. D., Kaya, Ö., & Çodur, M. Y. (2020). A GIS and microsimulation-based MCDA approach for evaluation of pedestrian crossings. Accident Analysis & Prevention, 148, 105771.

Guan, F., Whitley, T., Xu, H., Wang, Z., Chen, Z., Hui, T., & Tian, Y. (2024). Vehicle-pedestrian interaction analysis for evaluating pedestrian crossing safety at uncontrolled crosswalks− a geospatial approach using multimodal all-traffic trajectories. Journal of Safety Research, 91, 326-341.

Soilán, M., Riveiro, B., Sánchez-Rodríguez, A., & Arias, P. (2018). Safety assessment on pedestrian crossing environments using MLS data. Accident Analysis & Prevention, 111, 328-337.

Martínez-Chao, T. E., Menéndez-Díaz, A., García-Cortés, S., & D'Agostino, P. (2024). Urban Pedestrian Routes' Accessibility Assessment Using Geographic Information System Processing and Deep Learning-Based Object Detection. Sensors, 24(11), 3667.

Tsai, W. C., Lai, J. S., Chen, K. C., M. Shivanna, V., & Guo, J. I. (2021). A lightweight motional object behavior prediction system harnessing deep learning technology for embedded adas applications. Electronics, 10(6), 692.

Hassan, E., Khalil, Y., & Ahmad, I. (2024). Learning deep feature fusion for traffic light detection. Journal of Engineering Research, 12(1), 100-106.

Golcarenarenji, G., Martinez-Alpiste, I., Wang, Q., & Alcaraz-Calero, J. M. (2024). Robust real-time traffic light detector on small-form platform for autonomous vehicles. Journal of Intelligent Transportation Systems, 28(5), 668-678.

Kang, L., Lu, Z., Meng, L., & Gao, Z. (2024). YOLO-FA: Type-1 fuzzy attention based YOLO detector for vehicle detection. Expert Systems with Applications, 237, 121209.

Li, Y., Zhang, M., Zhang, C., Liang, H., Li, P., & Zhang, W. (2024). YOLO-CCS: Vehicle detection algorithm based on coordinate attention mechanism. Digital Signal Processing, 153, 104632.

Nandal, P., Mann, P., Bohra, N., Aldehim, G., Elnour, A. A. H., & Allafi, R. (2025). Tropical cyclone intensity estimation based on YOLO-NAS using satellite images in real time. Alexandria Engineering Journal, 113, 227-241.

Alemdar, K. D., & Çodur, M. Y. (2024). A New Approach to Detect Driver Distraction to Ensure Traffic Safety and Prevent Traffic Accidents: Image Processing and MCDM. Sustainability, 16(17), 7642.

Alemdar, K. D. (2024). Çift Sıra Parklanma Durumunun Nesne Tespit Algoritması YOLOv8 ile Tespit Edilmesi. Journal of the Institute of Science and Technology, 14(3), 1164-1176.

➢ *ORAL PRESENTATION*

Microstructural analysis of polyvinyl alcohol hydrogels modified with GNPs/AgNPs/GO/NAC

Barış Şimşek[1*] (*ORCID: https://orcid.org/0000-0002-0655-4368*), Özge Bildi Ceran[2] (*ORCID: https://orcid.org/0000-0002-3147-735X)*

Çankırı Karatekin University, Faculty of Engineering, Department of Chemical Engineering, Çankırı, Türkiye.

* Corresponding author e-mail: barissimsek@karatekin.edu.tr, +90 532 774 87 69

Abstract

A broad array of applications is afforded to hydrogels due to their hydrophilic properties, biocompatibility, and remarkable elasticity. Some notable applications include fabricating wound-healing patches, conceiving pH sensors for drug delivery systems, and the development of wearable flexible electronic devices for monitoring human movement. Polyvinyl alcohol (PVA) -based hydrogels are a class of synthetic hydrogels that are semi-crystalline in nature. They are notable for being easily synthesizable, amenable to crosslinking, and having non-toxic properties. Nonetheless, the standard preparation techniques for PVA hydrogels have been shown to result in certain deficiencies in crucial mechanical characteristics, such as durability. The utilization of nano-fillers can be advantageous in enhancing these characteristics. In this study, PVA was modified with graphene nanoplatelets (GNPs), silver nanoparticles (AgNPs), graphene oxide (GO), and activated carbon nanofillers (NAC) was analyzed microstructurally. The findings from the Fourier-transform infrared spectroscopy (FTIR) and X-ray diffraction (XRD) analyses indicate that PVA exhibits a capacity to retain water molecules within its structural matrix. Additionally, the outcomes indicate that the crystallinity of PVA is enhanced in response to the application of freeze-thaw cycles.

Keywords: FTIR, XRD, PVA hydrogels, Nanofillers.

INTRODUCTION

Hydrogels are three-dimensional cross-linked network systems composed of hydrophilic polymers, which have found applications in various fields (Zeng et al., 2025). These materials are characterized by a high-water absorption ability, unique oxygen permeability, flexibility, stretchability, and exudate absorption properties (Wang et al., 2019). Due to the changeable physical and chemical properties of hydrogels, they can be designed to exhibit biocompatibility and human-contact compatibility (He et al., 2025). Moreover, this can be achieved by incorporating green base materials into their structural design. The properties of hydrogels are such that they possess a broad spectrum of potential applications, including, but not limited to, the fields of tissue engineering (Jin et al., 2025), drug delivery (Zhu et al., 2025), sensors (Liu et al., 2025), and flexible electronics (Ding et al., 2024).

Poly (vinyl alcohol) (PVA) is a preferred base material in hydrogel design due to its water solubility, ease of synthesis, and numerous advantages, including flexibility, biocompatibility, and non-toxicity (Ceran et al., 2020). It can be obtained by simple methods, such as the dissolution-casting technique (Zhang et al., 2024). However, the low mechanical strength and poor electrical conductivity of the PVA due to high water molecule content hydrogel restricts its applicability in sensor technology (Dai et al., 2025). In an attempt to overcome these limitations, researchers have employed a variety of additives, such as nanofillers, in the PVA matrix (Sharma et al. 2024). It also should be noted that, in general, the fabrication of hydrogels through physical and chemical cross-linking, employing a freeze-thaw drying method, is regarded as a more environmentally friendly approach (Liu et al., 2025). In light of these findings, the present study elected to adopt a cyclic freeze-thaw method as its primary approach.

In this study, PVA-based hydrogels containing graphene nanoplatelets (GNPs), silver nanoparticles (AgNPs), graphene oxide (GO), and activated carbon nanofillers (NAC) were prepared by freeze-thaw cycles. This method is considered a relatively eco-friendly approach, as it does not involve the use of toxic chemicals for chemical

crosslinking. A thorough discussion of the microspatial properties of the produced hydrogels was conducted, and the findings were thoroughly analyzed using Fourier-transform infrared spectroscopy (FTIR) and X-ray diffraction (XRD) analysis. Due to their ubiquity and accessibility, FTIR and XRD were selected as the preferred methodologies for the analysis of microstructural properties.

MATERIALS AND METHODS

The PVA utilized in this study was supplied by Merck Millipore and is characterized by a molecular weight of approximately 125,000 and a hydrolysis percentage ranging from 8.0 to 98.8 mole%. GO particles were obtained by the improved Hummers method with a D peak-to-G-peak density of 0.9 (Korucu et al., 2018). GNPs, AgNPs, and NAC were supplied from Nanografi Nanotechnology, and their properties are given in Table 1.

Table 1. Nanofiller properties

Properties	GNP	AgNPs	NAC	GO
Purity, %	99.9	99.5	95.0	>99.0
Size, nm	3	18	<100	10-15 nm
Surface area, m^2/g	800	17-21	400	180
Diameter, µm	1.5	N/A	N/A	1.5-2.0
Density, g/cm^3	N/A	10.6	0.41	N/A
Form	Powder	Powder	Powder	Powder
Method	Supplied by Nanografi	Supplied by Nanografi	Supplied by Nanografi	Improved Hummer method

A quantity of 1.0 g of PVA will be dissolved in 40 ml of deionized water, with the use of a magnetic stirrer, at a temperature of 80°C for 60 minutes. Glycerol was added to mixture at a level of 1.0 g for a further mixture for 5 min. Subsequently, GNPs, AgNPs, GO, and NAC are added to the mixture (0.012 g: 0.012 g: 0.012 g: 0.5 g), and the mixture will undergo five minutes of agitation. The mixture of 35 ml was subsequently transferred into borosilicate glass petri dishes with a diameter of 150 millimeters. The samples will undergo a freezing process at a temperature of -18°C for 16 hours. They will be stored at ambient temperature (approximately 25°C) for an additional 8 hours. The hydrogel was obtained after four repetitions of the procedure described by the freeze-thaw method. The photographic documentation was obtained in the chemical engineering laboratory at Çankırı Karatekin University, employing the Nikon Stereoscopic Zoom Microscope, model SMZ800. Considering the polymer surfaces (Figure 1), it is evident that the distribution of the nanofillers within the PVA matrix exhibited uniform characteristics.

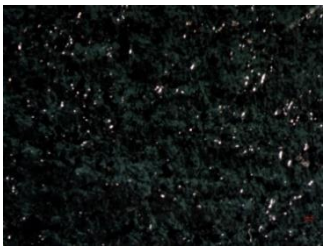

Figure 1. Optical image of the hydrogel under a microscope.

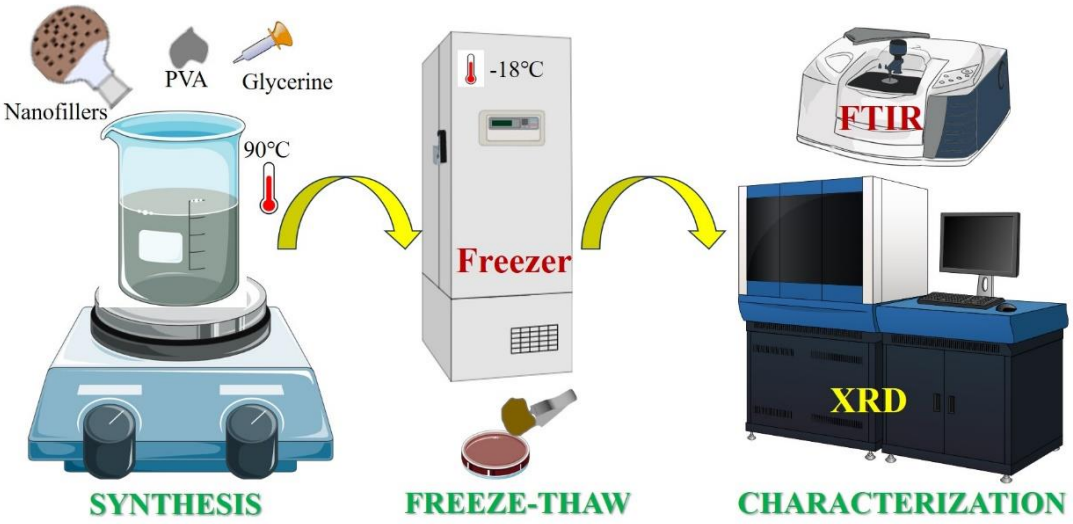

Figure 2. Stages of the hydrogel synthesis and characterization

RESULTS and DISCUSSION

At Çankırı Karatekin University, a Bruker FTIR spectrophotometer was employed to characterize films. FTIR analyses were conducted to elucidate how the hydrogel, subjected to a freeze-thaw procedure, manifested its effect. The FTIR spectrum was obtained from three different parts of the hydrogel. The band positioned at around 3300 cm^{-1} is associated with O-H stretching (inter and intramolecular hydrogen bonding), whereas the band at approximately 1210 cm^{-1} corresponds to C-O-C vibration (gel formation and acetal bridges) (Jamnongkan and Kaewpirom 2010). The bands observed at 2943 cm^{-1} and 1090 cm^{-1} are attributed to C-H and C-O stretching vibrations, respectively (Jamnongkan and Kaewpirom 2010). The wide and intensive peak at 3310 cm^{-1} is indicative of chemical bonds formed with the PVA matrix and water molecules.

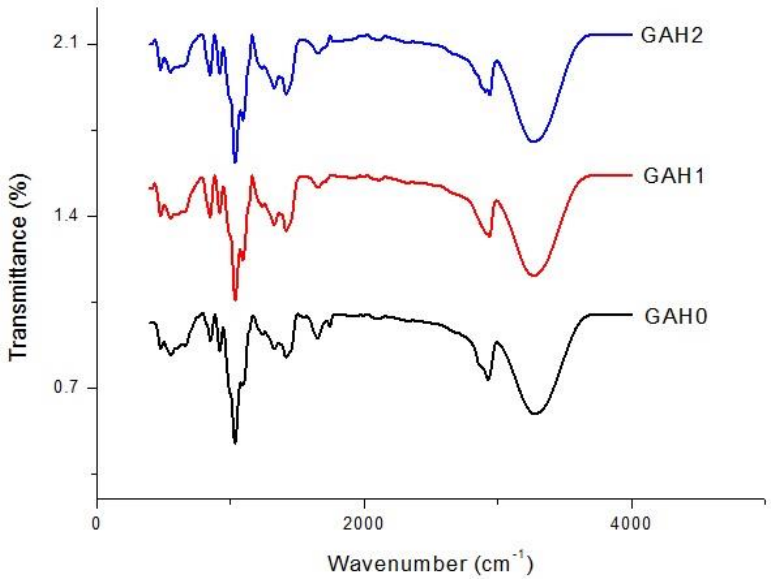

Figure 3. FTIR pattern of PVA hydrogel modified with GNP, AgNPs, GO, and NCP

The X-ray powder diffraction profiles were collected at room temperature using a Rigaku Ultima-IV X-ray diffractometer. The diffractometer was set up to use copper emitter Cu-Kα radiation of 15 mA and 40 kV. The scan was done at 5°/min, and the step width was 0.02°. This was done in the 2 θ range of 10-80°. The X-ray powder diffraction profile of a synthesized hydrogel that was formed using a petri dish and then cooled gradually to room temperature is given in Figure 4. The structure of this PVA at a crystal level looks like it has a strong peak at a 2θ angle of 19.8° (Alhuthali et al., 2024). It also has a relatively weak peak at 41.05° and a weak peak

at around 2θ = 23°, representing the amorphous phase (Alhuthali et al., 2024). Ricciardi et al. (2004) showed that the diffraction profiles of gels at 2θ ≈ 28 and 41° and a weak peak in the range of 2θ ≈ 18-21°, as in the diffraction of pure water, show an increase in peak intensity in this region with increasing number of freeze and thaw cycles, which in turn increases the amount of crystalline phase. The findings of their study indicated that the enhancement of crystallinity with an increase in cycles is a consequence of not only elevated polymer concentration within the gel, but also a substantial refinement of gel structure, a consequence of freeze/thaw cycles, attributable to a reduction in free water molecules (Ricciardi et al. 2004). The XRD patterns obtained in this study at 10.8° (1), 19.5° (2), 22.8° (blue dash), 28.1 ° (3), and 41.1° (3) align with the hypothesis as mentioned above.

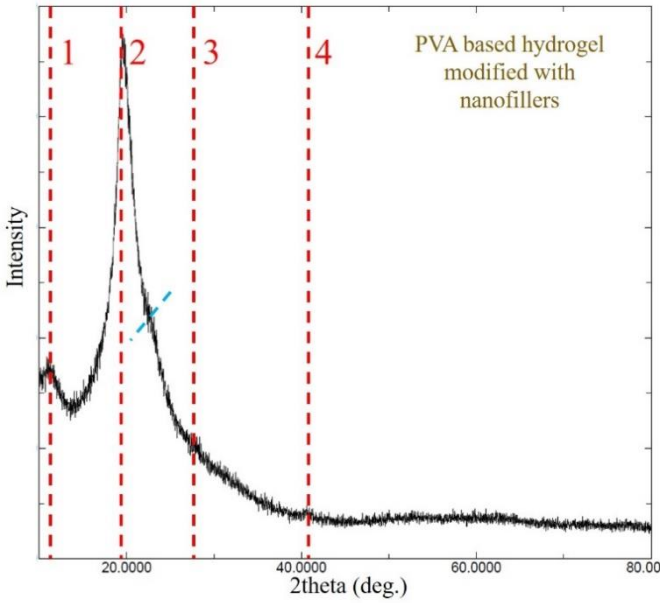

Figure 4. XRD pattern of PVA hydrogel modified with GNP, AgNPs, GO, and NCP

CONCLUSION

In this study, PVA-based hydrogels modified with nanofillers such as GNP, AgNPs, GO, and NCP underwent a successful synthesis process, and microstructural analysis was carried out utilizing XRD and FTIR. The findings from the FTIR and XRD analyses indicate that PVA exhibits a capacity to retain water molecules within its structural matrix. Furthermore, the results demonstrate that the crystallinity of PVA undergoes an enhancement in response to the application of freeze-thaw cycles.

ACKNOWLEDGEMENTS

This study was supported by Çankırı Karatekin University Scientific Research Project (MF111224B19). The authors would like to thank Çankırı Karatekin University, Scientific Research Project Management Department (ÇAKÜ-BAP).

REFERENCES

Alhuthali, A., M., S., Kalil, H., Ibrahim, M.A. (2024). Evaluating the reactivity of polyvinyl alcohol/graphene nanocomposites. Optical Materials 151: 115364.

Ceran, Ö., B., Şimşek, B., Şara, O.N. (2020). Preparation and characterization novel dioctyl terephthalate blended polyvinyl alcohol-composite films incorporated with the graphene oxide and silver nanoparticles. Polymer Testing, 82: 106315.

Dai, S., Zhong, C., Yao, J., Zeng, L., Zhong, Y., Xie, S., Huang, W., Chem, W., Sui, Y. (2025). High-strength and low-hysteresis chemical cross-linking PVA hydrogel for motion monitoring. Colloids and Surfaces A: Physicochemical and Engineering Aspects, 710: 136212.

Ding, X., Yu, Y., Li, W., Bian, F., Gu, H., Zhao, Y., (2024). Multifunctional carbon nanotube hydrogels with on-demand removability for wearable electronics. Nanotoday, 54: 102124.

He, S., Cui, Z., Fang, H., Wei, X., Shao, W. (2025). Incorporation of multi-dynamic interactions into carboxyl graphene oxide-enhanced PVA/PAA/agarose hydrogels for multifunctional wearable sensors. International Journal of Biological Macromolecules, 314: 144336.

Jamnongkan, T., & Kaewpirom, S. (2010). Potassium Release Kinetics and Water Retention of Controlled-Release Fertilizers Based on Chitosan Hydrogels. Journal of Polymers and the Environment, 18: 413-421.

Jin, Q., Xing, S., Ju, S., Cao, Y., Duan, K., Jin, L., Zhang, Y., He, Y., Chen, J., Zhang, J. (2025). Anisotropic robust Poly(vinyl alcohol) hydrogels inspired by bio-tissue. Materials & Design, 250: 113613.

Korucu, H., Şimşek, B., Yartaşı, A. (2018). A TOPSIS-Based Taguchi Design to Investigate Optimum Mixture Proportions of Graphene Oxide Powder Synthesized by the Hummers Method. Arabian Journal of Science and Engineering, 43: 6033-6055.

Liu, Y., Zhang, J., Wang, D. (2025). Preparation schemes and applications of multifunctional PVA composite hydrogels. Chemical Engineering Journal, 508: 160946.

Ricciardi, R., Auriemma, F., De Rosa, C., Lauprêtre, F. (2004). X-ray Diffraction Analysis of Poly(vinyl alcohol) Hydrogels, Obtained by Freezing and Thawing Techniques. Macromolecules 37 (5): 1921-1927.

Sharma, S., Bhende, M., Verma, H. R., Kumar, S. (2024). Physically cross-linked PVA/f-MWCNTs nanocomposite hydrogel with enhanced thermal, mechanical, and dielectric properties. Materialstoday Communications, 40: 109400.

Wang, J., Chen, Y., Zhou, G., Chen, Y., Mao, C., Yang, M. (2019). Polydopamine-Coated Antheraea pernyi (A.pernyi) Silk Fibroin Films Promote Cell Adhesion and Wound Healing in Skin Tissue Repair. ACS Applied Materials & Interfaces, 11(38): 34736-34743.

Zhang, R., Wu, C., Liao, X., Luo, A., Jing, Y., Yu, N., Su, S., Zhang, X., Zhu, J., Deng, G. (2024). Preparation of PVA/cellulose composite hydrogel electrolytes based on zinc chloride-dissolved cellulose for flexible solid-state capacitors. Journal of Materials Chemistry C: 12: 2063-2072.

Zeng, H., Tang, L., Huang, L., Yang, N., Chen, X., Peng, X., Chen, Z., Guo, J., Weng, J., Guo, T. (2025). A novel multi-functional PVA-alginate hydrogel with dynamic bond crosslinking for infected wound repair. Carbohydrate Polymers, 362: 123636.

Zhu, M., Zhang, S., Li, X., Xiao, C., Wang, N. (2025). A crosslinked PVA/GO hydrogel for wound dressing with pH-controlled drug release capabilities. Materialstoday Communications, 43: 117760.

➢ *ORAL PRESENTATION*

Mikroalglerden fikosiyanin: üretim, stabilite ve ticari potansiyel üzerine inceleme

Ayşe Özpamuk[1]* (ORCID: https://orcid.org/0009-0009-6602-1035),
Oya Irmak Şahin[2] (ORCID: https://orcid.org/ 0000-0003-2225-7993)

*[1]Yalova Üniversitesi, Lisansüstü Eğitim Enstitüsü, Disiplinlerarası Su Ürünleri Anabilim Dalı, Yalova, Türkiye.
[2]Yalova Üniversitesi, Mühendislik Fakültesi, Kimya Mühendisliği Anabilim Dalı ve Su Ürünleri Anabilim Dalı, Yalova, Türkiye.

*Sorumlu yazar e-posta: ayseekaratabak@gmail.com

Özet
Bu çalışma, *Arthrospira platensis* gibi mikroalg kaynaklı C-fikosiyanin (C-PC) bileşiğinin üretimi, ekstraksiyonu, saflaştırılması, stabilitesi ve potansiyel uygulamalarına dair güncel bilimsel araştırmaların sistematik bir literatür incelemesine dayanmaktadır. Literatür taraması sonucunda, *A.plantensis*'in, yüksek protein içeriği ve biyoaktif bileşenleri ile özellikle nutrasötik ve kozmetik sektörlerde değerli bir doğal kaynak olduğu belirlenmiştir. Fikosiyanin, doğal pigment olmasının yanı sıra antioksidan, anti-inflamatuar ve antikanser gibi çoklu biyolojik işlevlere sahip olması sebebiyle geniş bir uygulama yelpazesine sahiptir. Üretim sürecinde çevresel ve kültür koşullarının optimize edilmesi, gelişmiş ekstraksiyon ve saflaştırma tekniklerinin kullanılması fikosiyanin verim ve saflığını artırmaktadır. Ayrıca, stabilizasyon stratejileri ile fikosiyaninin işleme ve depolama süreçlerindeki dayanıklılığı geliştirilmekte, böylece fonksiyonel gıda ve kozmetik ürünlerde kullanımı desteklenmektedir. Ekonomik analizler, fikosiyanin pazarının önümüzdeki yıllarda önemli ölçüde büyüyeceğini göstermekte, bu da biyoteknolojik uygulamalar için fırsatlar sunmaktadır. Sonuç olarak, bu kapsamlı literatür incelemesi mikroalg kaynaklı fikosiyaninin biyoteknolojik potansiyelini ortaya koymakta ve üretimden uygulamaya kadar olan süreçlerde yenilikçi yaklaşımların önemini vurgulamaktadır.
Anahtar Kelimeler: Mikroalg, fikosiyanin, spirulina, üretim.

Phycocyanin from microalgae: review on production, stability and commercial potential

Abstract
This study is based on a systematic literature review of current scientific research on the production, extraction, purification, stability and potential applications of C-phycocyanin (C-PC) compound from microalgae such as *Arthrospira platensis*. As a result of the literature review, it was determined that *A. plantensis* is a valuable natural resource especially in the nutraceutical and cosmetic sectors with its high protein content and bioactive components. Phycocyanin has a wide range of applications due to its multiple biological functions such as antioxidant, anti-inflammatory and anticancer in addition to being a natural pigment. Optimizing environmental and culture conditions during the production process and using advanced extraction and purification techniques increase the yield and purity of phycocyanin. In addition, the stability of phycocyanin in processing and storage processes is improved with stabilization strategies, thus supporting its use in functional food and cosmetic products. Economic analyses indicate that the phycocyanin market will grow significantly in the coming years, which offers opportunities for biotechnological applications. In conclusion, this comprehensive literature review reveals the biotechnological potential of microalgae-derived phycocyanin and highlights the importance of innovative approaches in the processes from production to application.
Keywords: Microalgae, phycocyanin, spirulina, production.

GİRİŞ

Mikroalgler, çeşitli işlevsel gıdalar ve yenilebilir pigmentler üretme potansiyeline sahip organizmalardır. Bu pigmentlerden biri olan fikosiyanin, siyanobakteri hücrelerinin temel bileşenlerinden biri olup, birçok siyanobakteri türü bu pigmentin elde edilmesinde önemli kaynaklar arasında yer alır. *Arthrospira platensis* türü ile bilinen *Spirulina* öne çıkan bir tür olmakla birlikte, *Thermosynechococcus*, *Limnothrix* türleri ve *Geitlerinema* türleri gibi diğer siyanobakteri türleri de fikosiyanin üretiminde değerlendirilebilmektedir. Ayrıca, *Galdieria*

sulphuraria gibi bazı kırmızı alg türleri de alternatif fikosiyanin kaynakları arasında sayılmaktadır (Yu ve ark., 2023).

Arthrospira, helezon veya spiral şekilli, çok hücreli, filamentöz ve fotosentetik bir siyanobakteri cinsidir. Bu cinsin en yaygın olarak kültüre alınan türlerinden biri olan *Arthrospira platensis*, genellikle ‘‘*Spirulina*’’ adıyla anılmaktadır. *Spirulina*, hem makro hem de mikro besin öğeleri açısından zengin içeriği sayesinde ticari ve endüstriyel açıdan önemli bir doğal besin kaynağıdır. Özellikle nutrasötik alanında dikkat çeken bu mikroalg, yüksek protein içeriği, çoklu doymamış yağ asitleri, polisakkaritler, vitaminler, mineraller, polifenoller, karotenoidler ve klorofiller gibi sağlık destekleyici bileşenler yönünden oldukça değerlidir. Bu zengin biyokimyasal bileşim, *Spirulina*'nın ABD Gıda ve İlaç Dairesi (FDA) tarafından insan tüketimi için güvenli kabul edilmesini sağlamış ve bu doğrultuda biyokütlesi geniş ölçekte besin takviyeleri, zenginleştirilmiş gıdalar ve kozmetik ürünlerde kullanılmaya başlanmıştır. *Spirulina* biyokütlesinin doğrudan ticari kullanımının yanı sıra, içerdiği spesifik bileşikler veya bileşik sınıfları da nutrasötik pazar açısından ayrı bir araştırma ve uygulama potansiyeli taşımaktadır (Şehri ve ark., 2024).

MİKROALGLERDEN FİKOSİYANİN ÜRETİMİ

Antik çağlardan bu yana besin kaynağı olarak kullanılan *Arthrospira platensis*, sahip olduğu zengin besin içeriği sayesinde günümüzde fonksiyonel gıdalar ve nutrasötik ürünler bağlamında yeniden ilgi görmektedir. Bu mikroskobik siyanobakteride bulunan suda çözünür pigment-protein kompleksi C-fikosiyanin (C-PC), floresan özelliklerinin yanı sıra sağlık üzerindeki olumlu etkileriyle dikkat çekmektedir. C-PC'nin yapısında yer alan tetrapirol türevi kromofor fikosiyanobilin B (PCB-B), bu bileşiğe antioksidan ve anti-inflamatuar özellikler kazandırmakta ve onu oksidatif stresle ilişkili hastalıkların önlenmesi veya hafifletilmesi açısından değerli bir aday hâline getirmektedir. Son yıllarda yapılan araştırmalar, bu biyomoleküllerin üretim verimini ve biyolojik etkinliğini artırmak amacıyla kültür koşullarının optimizasyonuna ve yenilikçi ekstraksiyon ile saflaştırma yöntemlerinin geliştirilmesine odaklanmıştır. Bu teknik gelişmeler, C-PC'nin ticari üretimini daha sürdürülebilir kılmakta ve gıda ile farmasötik endüstrilerdeki potansiyel uygulama alanlarını genişletmektedir (Usai ve ark., 2024).

Spirulina, tarihsel olarak bin yılı aşkın süredir çeşitli toplumlar tarafından bir besin kaynağı olarak tüketilmiş olup, bazı türlerinin kuru ağırlığının %55 ila %70'ine ulaşan yüksek kaliteli protein içeriği, bu mikroyosunu sürdürülebilir bir mikrobiyal protein kaynağı olarak öne çıkarmaktadır (Prabakaran ve ark., 2020). Mikroalgal üretim teknolojisinde yaygın olarak kullanılan iki temel sistem, açık havuzlar ve kapalı fotobiyoreaktörlerdir. Bu sistemler, mikroalglerin kontrollü koşullar altında kültürlenmesini sağlayarak, yüksek verim ve istenen bileşiklerin üretimi açısından önemli avantajlar sunar. Mikroalgler, zengin besin içerikleri ve biyoaktif bileşik profilleri sayesinde yeni nesil fonksiyonel gıda ürünleri için umut vadeden kaynaklar arasında yer almaktadır. Özellikle *Spirulina platensis*, sahip olduğu yüksek protein oranı, vitamin ve mineral içeriği ile dikkat çekerken, aynı zamanda antioksidan ve anti-enflamatuar özellikler göstermesi sayesinde sağlık destekleyici potansiyel taşımaktadır. *Spirulina platensis*'ten izole edilen ve ışık tutucu bir pigment-protein kompleksi olan C-fikosiyanin (cPC)'dir (Kaynarca, 2024).

Yüksek saflıktaki fikosiyanin, gıda endüstrisinde sahip olduğu yüksek ticari değer ve işlevsel özellikleri nedeniyle önemli bir potansiyele sahiptir. Ancak, fikosiyanin'in biyokütle içerisindeki dağılımı ve çeşitli varoluş biçimleri, izolasyon ve saflaştırma süreçlerini hem teknik hem de ekonomik açıdan zorlu hale getirmektedir. Günümüzde, fikosiyanin üretim yöntemleri ve ekstraksiyon teknikleri üzerine yapılan araştırmalar sürekli ilerlemekte olup, bu alandaki yenilikçi yaklaşımlar özellikle verimlilik ve ürün saflığını artırmayı hedeflemektedir. Bu bağlamda, yeni üretim süreçleri, hücre duvarının etkili bir şekilde parçalanması, çözücü seçiminde optimizasyon, membran teknolojileri ve kromatografik arıtma gibi ileri düzey teknolojilerle desteklenmektedir. Fikosiyanin'in üretimi, çıkarılması ve saflaştırılması için geliştirilen yöntemlerde temel amaç, daha yüksek verimlilikle daha saf ürün elde edilmesini sağlamak olarak belirlenmektedir (Mao ve ark., 2024).

FİKOSİYANİN EKSTRAKSİYONU

Spirulina türleri, pigmentasyon sistemlerinde yer alan klorofil, fikoeritrin, fikosiyanin, fikobilinler ve karotenoidler (örneğin beta-karoten, kriptoksantin) gibi hem suda çözünebilen hem de lipofilik pigmentler açısından zengin bir yapıya sahiptir. Bu mikroalg özellikle, toplam biyokütlesinin yaklaşık %20–25'ini oluşturan yüksek orandaki fikosiyanin içeriğiyle dikkat çeker. Fikosiyanin, α (alfa) ve β (beta) alt birimlerinden oluşan bir

heterodimer yapısına sahip olup, biyoteknolojik uygulamalarda önemli bir pigment olarak öne çıkar. *Spirulina*'dan fikosiyanin elde etmek için uygulanan ekstraksiyon ve saflaştırma süreçleri, hem verimlilik hem de saflık düzeyi açısından optimize edilmeye çalışılmaktadır. Saflaştırma aşamasında yaygın olarak kullanılan yöntemler arasında kolon kromatografisi, ultrafiltrasyon, mikrofiltrasyon, aktif kömürle birleştirilmiş amonyum sülfat çöktürmesi ve diyaliz yer almaktadır. Bu teknikler, fikosiyaninin istenmeyen bileşiklerden ayrıştırılmasını sağlayarak ürün kalitesini artırmayı amaçlamaktadır. Son dönemde yapılan çalışmalar hem ekstraksiyon hem de saflaştırma aşamalarını iyileştirmek için yeni yaklaşımlar geliştirmekte olup bu gelişmeler *Spirulina*'dan daha saf ve işlevsel fikosiyanin elde edilmesine önemli katkılar sunmaktadır (Athiyappan ve ark., 2024).

Fikosiyanin, birçok siyanobakteri türünde bulunan ve fotosentetik süreçte yardımcı pigment olarak görev yapan mavi renkli bir fikobiliprotein olma özelliğinin ve doğadaki bu temel işlevinin yanı sıra, antimikrobiyal, antioksidan ve anti-inflamatuar özellikleri sayesinde farmakoloji, gıda endüstrisi ve biyoteknoloji gibi alanlarda çok yönlü uygulamalara da sahip olduğu görülmektedir. Ancak, bu biyomolekülün endüstriyel ölçekte üretimi sırasında karşılaşılan başlıca zorluklardan biri, pigmentin kararlılığını koruyarak etkin bir şekilde çıkarılması ve saflaştırılmasıdır. Islak biyokütle kullanımı gibi bazı yöntemlerin, kurutulmuş biyokütleye göre daha yüksek verim sunduğu tespit edilmiş ve bu yöntemler büyük ölçekli uygulamalarda tercih edilmiştir. Ayrıca, farklı siyanobakteri suşlarının ekstrem çevresel koşullarda kültürlenmesi üzerine yapılan çalışmalar, fikosiyanin üretimini optimize etmeyi amaçlamaktadır. Günümüzde, fikosiyanin'in floresan işaretleyici olarak kullanımı ve doğal gıda renklendiricisi rolü kadar, gümüş nanopartikül sentezinde antioksidan bir ajan olarak değerlendirilmesi de dikkat çekmektedir (Morya ve ark., 2023).

Fikosiyaninin etkili bir şekilde ekstraksiyonu ve saflaştırılması, hem fiziksel hem de kimyasal yöntemlerin entegrasyonunu gerektirmekte olup, bu süreçte protein stabilitesini koruyarak yüksek verim elde etmeyi amaçlayan çeşitli teknikler geliştirilmiştir. Özellikle çöktürme yöntemleri amonyum sülfat çöktürmesi gibi ön saflaştırma adımları, sıklıkla jel filtrasyon, iyon değişim ya da afinitesi yüksek kromatografik tekniklerle desteklenmektedir. Bu yöntemlerin uygun kombinasyonları, hem pigmentin saflığını artırmakta hem de biyolojik etkinliğini koruyarak uygulama alanlarını genişletmektedir. Bu bağlamda, C-fikosiyanin'in yapısal bütünlüğünü bozmadan yüksek saflıkta elde edilmesi, terapötik ve endüstriyel kullanımlar açısından optimal ekstraksiyon protokolünün belirlenmesini zorunlu kılmaktadır (Aktürk, 2024).

C-fikosiyanin ekstraksiyonunda kullanılan siyanobakteriyel biyokütlenin fiziksel durumu, pigment verimi ve saflığı üzerinde doğrudan etkilidir. Bu süreçte kuru ve ıslak biyokütle farklı yöntemlerle değerlendirilmektedir. Ekstraksiyon öncesinde uygulanan kurutma işlemleri püskürtmeli kurutma, fırın kurutma ve güneşte kurutma gibi biyokütlenin yapısını değiştirerek pigmentin miktarını ve bütünlüğünü olumsuz etkileyebilmektedir. Özellikle C-fikosiyanin'in 45°C'nin üzerindeki sıcaklıklara karşı duyarlılığı nedeniyle bu işlemler, termal bozulmalara yol açarak pigmentin biyolojik aktivitesini azaltabilmektedir. Islak biyokütle, pigmentin daha yüksek saflıkta elde edilmesini sağlayabilirken, mikrobiyal bozunma riski taşımaktadır. Bu nedenle, ekstraksiyon süreçlerinde genellikle kurutulmuş biyokütle tercih edilmekte; ancak kurutma koşullarının optimize edilmesi, hem pigment verimini korumak hem de ürünün raf ömrünü artırmak açısından kritik bir ön işlem olarak değerlendirilmektedir (Hajıyeva, 2022).

Fikosiyanin'in saflaştırılması, kullanılan ekstraksiyon yöntemine bağlı olarak değişkenlik göstermekte ve her yöntemin elde ettiği saflık düzeyi farklı olabilmektedir. Saflık, genellikle fikosiyanin içeriğinin toplam protein içeriğine oranı olarak değerlendirilmekte ve spektrofotometrik olarak A620/A280 absorbans oranı ile ifade edilmektedir. Bu oran, 620 nm'de fikosiyanobilin pigmentinin ve 280 nm'de aromatik amino asitlerin absorbsiyonunu temsil ederek, ekstraktın ne kadar saf olduğunu belirlemeye yarar (Morya ve ark., 2023).

Fikosiyanin üretiminde *Spirulina*'nın besleyici içeriği ve çevresel koşullara duyarlılığı, üretim sürecinin verimliliği açısından büyük önem taşımaktadır. *Spirulina*, farklı bileşiklerin üretimini tetikleyebilecek şekilde çeşitli yetiştirme koşullarına adapte olabilmektedir. Bu nedenle, özellikle fikosiyanin üretimi hedefleniyorsa, organizmanın büyüme ortamının optimize edilmesi kritik bir gerekliliktir. *Spirulina* kültürlerinde sıcaklık, ışık yoğunluğu, pH ve besin bileşenleri gibi faktörlerin dikkatle düzenlenmesi, istenilen miktar ve saflıkta fikosiyanin elde edilmesini mümkün kılar. Fikosiyanin ekstraksiyonu sürecinde, sıcaklık, pH, biyokütle-çözücü oranı, hücrelerin fiziksel durumu ve parçalanma yöntemleri gibi birçok etken ekstraksiyon verimi ve ürünün saflığı üzerinde belirleyici rol oynamaktadır. Uygun olmayan koşullar, pigmentin bozulmasına neden olabilir. Bu

nedenle, sıcaklık ve pH gibi parametrelerin optimize edilmesi gerekir. Ayrıca, fikosiyaninin işlenme, depolama ve sindirim gibi aşamalarda kararlılığını koruyamaması, pratik uygulamalarını sınırlandırmaktadır. Bu probleme yönelik olarak, doğal bileşenlerle oluşturulan karışımlar gibi stabilizasyon stratejileri araştırılmaktadır (Yu ve ark., 2023).

FİKOSİYANİNİN STABİLİZASYONU VE TİCARİ ÜRÜNLERDE UYGULAMASI

Fikosiyanin, yalnızca fotosentetik süreçlerdeki rolüyle değil, aynı zamanda çok yönlü biyolojik ve endüstriyel işlevleriyle de dikkat çeken bir fikobiliproteindir. Doğal mavi pigment özelliği sayesinde sakız, süt ürünleri ve jöleler gibi gıda ürünlerinde; ruj ve göz kalemi gibi kozmetik ürünlerde; ayrıca çeşitli farmasötik formülasyonlarda yaygın şekilde kullanılmaktadır. Yüksek floresans kapasitesi ve biyolojik etkinliği, onu aynı zamanda floresan belirteç olarak da değerli kılarken, antioksidan ve anti-inflamatuar özellikleri ile bağışıklık sistemi üzerinde düzenleyici etkiler göstermekte ve antikanser potansiyel taşımaktadır. Bu nitelikler, fikosiyanini gıda teknolojisi, biyoteknoloji ve tıbbi uygulamalar açısından stratejik öneme sahip, çok amaçlı bir biyoaktif bileşik hâline getirmektedir (Prabakaran vd., 2020). Bu biyolojik olarak aktif bileşiklerin antioksidan, anti-inflamatuar ve bağışıklık sistemi destekleyici özellikleri, sağlık sektörüne kaynak olmasına katkıda bulunmaktadır (Türkmen ve Akyurt, 2021).

Fikosiyanin, sadece doğal bir gıda boyası olarak değil, aynı zamanda antioksidan, anti-inflamatuar ve antikanser etkileri sayesinde işlevsel gıdalar ve farmasötik ürünler için de potansiyel bir bileşen olarak değerlendirilmektedir. Ancak, ticari olarak *Spirulina*'dan elde edilen fikosiyanin, ışık, yüksek sıcaklık ve düşük pH gibi çevresel faktörlere karşı hassasiyet göstermektedir. Bu durum, ürünün raf ömrü ve etkinliğini olumsuz yönde etkileyebilmektedir (Yu ve ark., 2023).

Fikosiyanin veriminin artırılmasına yönelik stratejiler, temel olarak iki ana yaklaşıma dayanmaktadır. Bunlar; ekstraksiyon yöntemlerinin iyileştirilmesi ve *Spirulina* türlerinin abiyotik stres koşullarına maruz bırakılmasıdır. Fikosiyanin, işlevsel özellikleri ve biyouyumluluğu nedeniyle şekerleme, sakız, dondurma, tatlı kaplamaları ve yoğurt gibi ürünlerde doğal renklendirici olarak kullanılmasının yanı sıra, DNA, eritrositler, lökositler ve trombositlerin boyanmasında biyofloresan işaretleyici olarak görev alabilmektedir. Fototermal terapi gibi ileri tıbbi uygulamalarda da kullanım potansiyeli mevcuttur. Ekonomik açıdan değerlendirildiğinde, *Spirulina*'nın küresel pazar büyüklüğünün 2023–2028 yılları arasında yaklaşık %9,5'lik bileşik yıllık büyüme oranına ulaşacağı ve yıllık üretimin 60 ila 80 bin ton arasında olacağı öngörülmektedir. Fikosiyanin özelinde ise, bu pigmentin pazarının 2023–2030 döneminde %28,1'lik büyüme oranıyla 2030 yılına kadar 279,6 milyon ABD dolarına ulaşması beklenmektedir. Üretim maliyetlerinin kilogram başına 249,70 dolara kadar düşürülmesi, fikosiyanin'in endüstriyel ölçekte ekonomik olarak sürdürülebilir biçimde üretilebilmesini mümkün kılmaktadır (Athiyappan ve ark., 2024).

Günümüzde doğal bileşiklere yönelik artan talep doğrultusunda, büyük ölçekli *Spirulina* yetiştiriciliği özellikle C-fikosiyanin (C-PC) üretimine odaklanmaya başlamıştır. *Spirulina*'dan C-PC çıkarıldıktan sonra geriye kalan biyokütle hâlâ yüksek düzeyde antioksidanlar, vitaminler ve mineraller içermekte olup, bu artık biyokütle nutrasötik ve kozmesötik ürünlerin formülasyonunda değerlendirilebilecek kıymetli bir doğal kaynak niteliğindedir. Bu durum, hem C-PC'nin ekonomik cazibesini artırmakta hem de *Spirulina* biyokütlesi'nin bütüncül kullanımına olanak tanımaktadır. Mevcut projeksiyonlara göre, küresel C-PC pazarının 2027 yılına kadar 245,5 milyon ABD dolarına ve 2030 yılına kadar 279,6 milyon ABD dolarına ulaşması öngörülmekte, bu da söz konusu pigmentin endüstriyel ve ticari potansiyelini açıkça ortaya koymaktadır (Şehri ve ark., 2024).

MATERYAL VE METOD

Bu çalışma, *Spirulina* (*Arthrospira platensis*) kaynaklı C-fikosiyanin bileşiğinin üretimi, ekstraksiyonu, saflaştırılması, stabilitesi ve potansiyel uygulamaları üzerine yapılan güncel bilimsel araştırmaların sistematik bir literatür incelemesine dayanmaktadır. Literatür taraması, fikosiyanin ile ilgili bilimsel bilgi birikiminin kapsamlı bir şekilde değerlendirilmesini amaçlamıştır. Veri toplama sürecinde, biyoteknoloji, gıda bilimi, mikrobiyoloji ve farmasötik alanlarındaki yayınlar tercih edilmiştir. Anahtar kelimeler olarak "phycocyanin," "*Spirulina*," "*Arthrospira platensis*," "extraction," "purification," "microalgae," gibi terimler kullanılmıştır. Ulaşılan yayınlar içerisinden; üretim koşulları, ekstraksiyon teknikleri, saflık düzeyleri, biyolojik aktiviteler, uygulama alanları ve ekonomik potansiyeli ele alan çalışmalar seçilerek analiz edilmiştir. İnceleme sonucunda, *Spirulina* kaynaklı

fikosiyanin'in biyoteknolojik üretimi ve uygulama alanlarıyla ilgili güncel gelişmeler detaylandırılarak ortaya konmuştur.

BULGULAR VE TARTIŞMA

Yapılan literatür incelemesi sonucunda, fikosiyanin üretimi ve kullanımına dair çalışmaların yoğunlukla *Spirulina* (*Arthrospira platensis*) türü üzerine odaklandığı belirlenmiştir. Bu mikroorganizmanın zengin pigment içeriği ve sürdürülebilir üretim potansiyeli, fikosiyanin temini açısından önemli avantajlar sunmaktadır. İncelenen çalışmalarda, üretim veriminin artırılmasına yönelik olarak yetiştirme koşullarının optimizasyonu, stres faktörlerinin uygulanması ve gelişmiş ekstraksiyon tekniklerinin kullanımı gibi farklı yaklaşımların başarıyla uygulandığı görülmektedir. Bulgular, düşük sıcaklıkta donma-çözülme döngüleri ile fiziksel ön işlemlerin, fikosiyanin verimini anlamlı ölçüde yükselttiğini ortaya koymuştur. Ayrıca, ekstraksiyon verimliliğini etkileyen temel faktörler arasında pH, sıcaklık, çözücü oranı ve biyokütlenin fiziksel durumu öne çıkmaktadır. Saflaştırma sürecinde, ultrafiltrasyon, kolon kromatografisi ve amonyum sülfat çöktürmesi gibi yöntemlerin yaygın olarak tercih edildiği ve saflık derecesinin uygulama alanına göre optimize edildiği saptanmıştır.

Stabilite açısından ise, fikosiyaninin ışık, sıcaklık ve pH değişimlerine karşı oldukça hassas olduğu belirlenmiştir. Bu nedenle stabilizasyon için doğal polimerler, şekerler ve protein bazlı taşıyıcı sistemlerin kullanımına yönelik çeşitli yaklaşımlar geliştirilmiştir. Bazı çalışmalar, mikroenkapsülasyon ve kompleks oluşturma yöntemleriyle renk ve biyolojik aktivite kaybının minimize edilebildiğini göstermektedir. Fikosiyaninin potansiyel uygulama alanları arasında fonksiyonel gıdalar, doğal gıda boyaları, biyofloresan işaretleyiciler ve kozmesötik ürünler öne çıkmaktadır. Özellikle antioksidan, anti-inflamatuar ve antikanser özelliklerinin, fikosiyanini sadece renk verici olarak değil, aynı zamanda terapötik amaçlı biyoaktif bileşik olarak da ön plana çıkardığı görülmüştür. Buna ek olarak, C-fikosiyanin pazarının hızla büyüdüğü ve ekonomik açıdan kârlı bir mikrobiyal ürün haline geldiği anlaşılmaktadır. Tüm bu bulgular, *Spirulina* kaynaklı fikosiyaninin biyoteknolojik açıdan yüksek potansiyele sahip, çok yönlü bir doğal bileşik olduğunu ortaya koymakta; üretim, stabilizasyon ve uygulama teknolojilerinde yapılacak yeniliklerin bu potansiyeli daha da artırabileceğini göstermektedir.

SONUÇ

Bu çalışma, *Spirulina* kaynaklı fikosiyaninin üretiminden nihai uygulamalara kadar olan sürecini kapsamlı bir şekilde ele alan güncel literatürün değerlendirilmesine dayanmaktadır. Elde edilen bulgular, fikosiyaninin yalnızca doğal bir pigment olarak değil, aynı zamanda yüksek biyolojik aktiviteye sahip değerli bir biyoaktif bileşik olarak da önem taşıdığını ortaya koymuştur. Üretim sürecinde çevresel koşulların optimize edilmesi, verimi artıran ekstraksiyon tekniklerinin uygulanması ve stabiliteyi koruyan taşıyıcı sistemlerin geliştirilmesi, fikosiyaninin hem verimli hem de işlevsel biçimde elde edilmesini mümkün kılmaktadır. Ayrıca, gıda, kozmetik ve sağlık endüstrilerindeki çok yönlü kullanımı sayesinde fikosiyanin, sürdürülebilir biyoteknolojik ürünler arasında ön plana çıkmaktadır. Artan tüketici talebi ve endüstriyel ilgi, bu alanda daha fazla araştırma ve geliştirme çalışmalarının yürütülmesini gerektirmektedir. Gelecekte, fikosiyaninin daha dayanıklı ve fonksiyonel formlarda sunulabilmesi için yenilikçi üretim sistemlerinin ve stabilizasyon stratejilerinin geliştirilmesi büyük önem arz etmektedir.

Fikosiyanin üretimi ve uygulamalarına yönelik mevcut çalışmalar önemli ilerlemeler sağlamış olsa da gelecekte yapılacak araştırmalarda şu hususlara odaklanılması önerilmektedir:

1. Genetik mühendislik veya seçilim yoluyla yüksek fikosiyanin üretme kapasitesine sahip mikroalg suşlarının geliştirilmesi verimliliği artırabilir.
2. Kimyasal çözücüler yerine çevre dostu, enerji tasarruflu ekstraksiyon tekniklerinin yaygınlaştırılması sürdürülebilirlik açısından önemlidir.
3. Gıda ve sağlık ürünlerinde kullanım için sıcaklık, ışık ve pH değişimlerine karşı dayanıklı yeni taşıyıcı sistemlerin araştırılması gerekmektedir.
4. Fikosiyanin ekstraksiyonundan sonra geriye kalan *Spirulina* biyokütlesinin fonksiyonel gıda, yem katkısı veya kozmesötik bileşeni olarak değerlendirilmesi ekonomik değer yaratabilir.
5. Laboratuvar ortamında elde edilen sonuçların endüstriyel ölçekte doğrulanması ve maliyet-etkin üretim süreçlerinin oluşturulması, ticarileşme yolunda atılacak en önemli adımlardandır.

TEŞEKKÜR

Bu çalışma kapsamında incelenen bilimsel yayınlar aracılığıyla elde edilen bilgiler, fikosiyanin konusunda güncel ve bütüncül bir bakış açısı geliştirmeye olanak sağlamıştır. Konu ile ilgili araştırmaları ortaya koyan tüm bilim insanlarına ve bu alanda emek veren araştırma topluluklarına teşekkür ederiz.

KAYNAKLAR

Aktürk, H. (2024). Spirulina platensis'den Fikosiyanin Proteinin Ekstraksiyonu Ve Sulu Çözelti İkili Faz Sistemi İle Protein Dağılımının İncelenmesi. Yüksek lisans tezi, Kocaeli Üniversitesi Fen Bilimleri Enstitüsü, Kocaeli.

Athiyappan, K. D., Routray, W., & Paramasivan, B. (2024). *Phycocyanin from Spirulina: A comprehensive review on cultivation, extraction, purification, and its application in food and allied industries*. *Food and Humanity*, 2, 100235. https://doi.org/10.1016/j.foohum.2024.100235

Hajıyeva, S. (2022). Çeşitli Ortamlardan İzole Edilmiş Olan Siyanobakterilerin Fikosiyanin Üretim Yeteneklerinin Araştırılması. Yüksek lisans tezi, Eskişehir Teknik Üniversitesi Lisansüstü Eğitim Enstitüsü, Eskişehir.

Kaynarca, G. B. (2024). Bezelye proteini ve spirulina ilavesinin ikili hidrojel formlarının reolojik özellikleri üzerine etkisi. GIDA (2024) 49 (5) 903-919 doi: 10.15237/ gida.GD24078

Mao, M., Han, G., Zhao, Y., Xu, X., & Zhao, Y. (2024). A review of phycocyanin: Production, extraction, stability and food applications. International Journal of Biological Macromolecules, 246, 135860. https://doi.org/10.1016/j.ijbiomac.2024.135860

Morya, S., Kumar Chattu, V., Khalid, W., Zubair Khalid, M., & Siddeeg, A. (2023). Potansiyel protein fikosiyanin: özellikleri, ekstraksiyonu ve kullanımı hakkında genel bir bakış. Uluslararası Gıda Özellikleri Dergisi, 26 (2), 3160-3176.

Prabakaran, G., Sampathkumar, P., Kavisri, M., & Moovendhan, M. (2020). Extraction and characterization of phycocyanin from Spirulina platensis and evaluation of its anticancer, antidiabetic and antiinflammatory effect. International journal of biological macromolecules, 153, 256-263.

Şehri, V., Torre, S., Flori, L., Usai, L., Aktay, N., Dunford, N. T., Lutzu, G. A., & Nieri, P. (2024). Phycobiliprotein C-Phycocyanin'in Nutrasötik Özellikleri: Arthrospira platensis'ten (Spirulina) Elde Edilen Kanıtlar. Nutrients, 16(11), 1752. https://doi.org/10.3390/nu16111752

Türkmen, A., & Akyurt, İ. (2021). Mikroalglerin Antiviral Etkileri. Turkish Journal of Agriculture-Food Science and Technology, 9(2), 412-419.

Usai, L., Torre, S., Aktay, N., Dunford, NT, Citi, V., Flori, L., ... & Lutzu, GA (2024). Arthrospira (Spirulina) platensis tarafından üretilen fikobiliprotein C-fikosiyanin'in üretim ve çıkarma yöntemlerindeki son gelişmeler: Mini bir inceleme. Güncel Mikrobiyoloji, 81 (12), 428.

Yu, Z., Zhao, W., Sun, H., Mou, H., Liu, J., Yu, H., Dai, L., Kong, Q., & Yang, S. (2023). Phycocyanin from microalgae: A comprehensive review covering microalgal culture, phycocyanin sources and stability. Algal Research, 69, 103249. https://doi.org/10.1016/j.algal.2023.103249

➢ *ORAL PRESENTATION*

Taşınabilir Cihazlarda Faz Değiştiren Madde (FDM) İle Isıl Yönetim ve Termal Kılıf Tasarımı: Akıllı Telefon Uygulaması

Yusuf Can ER[1*] (*ORCID: https://orcid.org/0009-0000-1348-2342*),
Ayşe Nur ALTUNKAYA[1] (*ORCID: https://orcid.org/0000-0003-0643-921X*)

[1] Recep Tayyip Erdoğan Üniversitesi, Mühendislik ve Mimarlık Fakültesi, Makine Mühendisliği Bölümü, Rize / TÜRKİYE

*Sorumlu yazar e-posta: yusufcan_er22@erdogan.edu.tr

Özet

Termal yönetim, aşırı ısınmayı önlediği, enerji verimliliğini artırdığı ve gelişen teknolojilere yönelik artan talebi desteklediği için elektronik cihazların geliştirilmesi ve soğutulması, optimum performans, uzun ömürlülük ve güvenilirliğin sağlanmasında önemli bir rol oynamaktadır. Bu kapsamda, bu çalışmada faz değiştiren madde (FDM) ilaveli ve kanatçıklı bir ısı depolama ünitesi içeren termal kılıf tasarlanmış ve sistemin termal performansı deneysel olarak incelenmiştir. Çalışmada, farklı erime sıcaklıklarına sahip iki farklı FDM türü (parafin RT35 ve RT42) kullanılmıştır. Elde edilen bulgular, FDM ve kanatçıklı yapı kombinasyonunun cihazın termal yönetim performansında önemli bir iyileşme sağladığını göstermektedir.

Anahtar Kelimeler: Isı depolama, termal kılıf, faz değiştiren madde

Thermal Management with Phase Change Material (PCM) in Portable Devices and Thermal Case Design: Smartphone Application

Abstract

Thermal management plays a crucial role in ensuring optimal performance, lifetime, reliability, developing and cooling of electronic devices by preventing overheating, improving energy efficiency, and supporting the increasing demand for advanced technologies. In this context, in this study, a thermal case with phase change material (FDM) added heat storage unit and fins was designed and the thermal performance of the system was experimentally investigated. Two different FDM types (paraffin RT35 and RT42) with different melting temperatures were used in the study. The results show that the combination of FDM and finned structure provides a significant improvement in the thermal management performance of the device.

Keywords: Heat storage, thermal case, phase change material

GİRİŞ

Gelişen teknoloji ile daha yüksek performanslı cihaz ve bileşenleri minyatürleştirme gereksinimleri araştırmacıları sürekli olarak yeni tasarım yöntemlerini geliştirmeye itmektedir. Ancak, bu gelişmeler ve yeni ortaya çıkan uygulamalar ilgili cihaz ve bileşenlerin verimliliklerini ve uygulanabilirliklerini kısıtlayarak beraberinde termal sorunları da getirmektedir (Groulx ve ark., 2017; Ling ve ark., 2014). Termal sorunlardan biri olan soğutma ile, bina enerji sistemlerinde, elektronik cihazlarda, güneş enerjisi kolektörlerinde ve daha pek çok farklı endüstride karşılaşılmaktadır. Özellikle günlük hayatta yaygın olarak kullanılan elektronik cihazlar tüketicilerin ihtiyaçlarını karşılamak için daha karmaşık bileşenler ve özelliklerle donatılmaktadır. Örneğin günümüzdeki cep telefonları sadece arama ve mesaj işlevleri sağlamakla kalmıyor, aynı zamanda görüntülü görüşme, internet, müzik çalar, video oyunları ve veri transferi için de kullanılabilmektedir. Bir cep telefonuna entegre edilen ilgili fonksiyonlar, daha fazla ısı üreterek daha yüksek güç tüketimine ve elektronik bileşenlerin arızalanmasına yol açmaktadır (Bianco ve ark., 2022; Yin ve ark., 2008). Mekanik cihazların ömrünü kısaltacak ve hatta elektronik bileşenlere kalıcı hasar verecek sıcaklıkların oluşmasını önlemek için ilgili ısının uzaklaştırılması gerekmektedir. Başlangıçta hava, elektronik cihazların soğutma ortamı olarak kullanılmıştır. Ancak, günümüzde, yüksek performanslı elektronik cihazlar daha küçük bir alandan daha fazla ısının transferini gerektirmektedir ki bu da hava ile

soğutmayla neredeyse imkansızdır. Bu nedenle, sistem üzerindeki optimum sıcaklık düzeyini ve en yüksek performansı sağlamak için etkili bir termal kontrol yöntemine ihtiyaç duyulmaktadır. Son yıllarda, elektronik cihaz ve bileşenlerin termal yönteminde kullanılan faz değiştiren madde (FDM) büyük miktarda enerji depolayabilmekte (Tan ve Tso, 2004) ve bu sayede aşırı ısınmanın önüne geçilmektedir (Chen ve ark., 2018; Sun ve ark., 2020). Böylece, FDM sayesinde ilgili cihaz ve bileşenlerin sıcaklık düzeyleri belirli limit altında tutularak cihaz ömrü uzatılabilmektedir (Huang ve ark., 2019; Zhang ve ark., 2021).

Faz değiştiren maddenin elektronik cihazların termal performansını iyileştirmeye yönelik olarak farklı yöntemler birçok araştırmacı tarafından deneysel ve sayısal olarak incelenmiştir. (Setoh ve ark., 2010), taşınabilir bir el elektronik cihazında ağır, hafif ve sık güç yükleri altında kanat sayısı ve yöneliminin etkisini deneysel olarak incelemişlerdir. FDM olarak n-Eikosan kullanarak iç kanatçıklı ve kanatçıksız alüminyum ısı alıcılarını ilgili madde ile doldurmuşlardır. FDM ilavesinin sistem sıcaklığını dengelediğini ve ısı alıcı içerisindeki kanatçık sayısının arttırılması ile yüzey sıcaklığının azaldığını belirtmişlerdir. (Setoh ve ark., 2010), FDM-ilaveli ısı alıcılarının cep telefonlarının soğutulmasına yönelik etkisini incelemişlerdir. FDM-ilaveli ısı alıcının maksimum sıcaklığının FDM ilavesiz ısı alıcıdan daha düşük olduğunu gözlemlemişlerdir. Ayrıca, kanatçık sayısı arttıkça, ilgili cihazın sıcaklığının azaldığını vurgulamışlardır. Taşınabilir elektronik cihazlarda ısı alıcıların termal yönetim performansını deneysel olarak inceleyen (Baby ve Balaji, 2013), kanat geometrisinin FDM-ilaveli ve ilavesiz ve farklı ısıl yükleri altında ısı alıcılarının sıcaklık dağılımı ve çalışma süresi üzerindeki etkisini de araştırmışlardır. İğne formuna sahip kanatçık geometrisinin termal performansının çapraz kanatçık geometrisine göre daha iyi olduğunu belirtmişlerdir. (Ge ve ark., 2013), taşınabilir elektronik cihazların belirlenen limit sıcaklık değerleri altında kullanımını iyileştirmek için bir ısı depolama ünitesi tasarlamışlardır. İlgili tasarımda sabit ısıl yükleme altında düşük erime sıcaklığına sahip FDM'ler üzerinde deneyler yapmışlardır. Yapılan çalışmalar sonucunda FDM- ilaveli ısı depolama ünitesinin taşınabilir elektronik cihazın termal performansını ve kullanım sürelerini iyileştirdiğini gözlemlemişlerdir ve buna ek olarak düşük erime sıcaklığına sahip FDM'lerin akıllı telefonların soğutulmasında uygun olduğunu ifade etmişlerdir. (Browne ve ark., 2016), FDM kullanımının taşınabilir elektronik cihazların çalışma sıcaklığı üzerindeki etkisini deneysel olarak incelemiştir. İlk olarak cihazın tipik çalışma koşulları altında sıcaklığını gözlemlemiş daha sonra farklı FDM tipleri kullanarak cihazın sıcaklığı üzerinde ölçümler yapmıştır. FDM'lerin kullanımıyla cihazın sıcaklık profilini incelemiş ve FDM'lerin sıcaklık değişimlerini ne kadar etkili bir şekilde emdiği ve dağıttığını gözlemlemiştir. (Thomas ve ark., 2016), FDM tabanlı bir ısı emici kullanarak taşınabilir bir elektronik cihazın termal performansını incelemişlerdir. Çalışmalarında kullandıkları faz değiştiren madde, 36,5°C'lik bir erime noktasına sahip n-Eikosandır. Bir grup akıllı telefonun ortalama boyutları seçilerek FDM tabanlı bir ısı emici tasarlamışlardır. Yaptıkları deneysel çalışmalar sonucunda FDM tabanlı ısı emicilerin, faz değiştiren madde içermeyen ısı emicilere kıyasla elektronik cihazların çalışma süresini önemli ölçüde uzatabileceği sonucuna varmışlardır. (Maranda ve ark., 2019), ince FDM paketlerinin termal davranışını ve bu paketlerin termal yayıcı ile kombinasyonunu araştırmışlardır. İlgili çalışmada, sabit ısıl güç girişiyle basitleştirilmiş bir deney düzeneği kullanılarak testler yapmışlardır. Deneyleri, iki farklı FDM tipi (n-Eikosan ve dodekanoik asit) kullanılarak gerçekleştirmişlerdir. FDM paketlerinin kullanımı hem ısıtıcının hem de kapağın sıcaklık artışında önemli bir azalmaya yol açtığı sonucuna varmışlardır. (Nandan ve ark., 2022), işlemci çipine benzetilen doğal ve zorlanmış taşınımla soğutulan silikon kauçuk ısıtıcı üzerine yerleştirilen faz değiştiren madde (58°C-60°C ve 48°C-50°C aralığında erime noktalarına sahip olan parafin mumu ve 1-hekzadekanol) tabanlı bir ısı emicinin termal performansını incelemişlerdir. Yaptıkları testlerde, ısı emiciye farklı güçler uygulayarak ısı emicinin sıcaklık davranışları ölçmüşlerdir. FDM ilaveli ısı emicilerin, FDM ilavesiz olanlardan daha iyi performans gösterdiğini tespit etmişlerdir. 1-hekzadekanol ile doldurulmuş ısı emicinin daha iyi performans gösterdiğini belirtmişlerdir. (Bianco ve ark., 2022), elektronik cihazların termal yönetimi için faz değiştiren maddenin (FDM) kullanılmasına ilişkin bir deneysel çalışma yapmışlardır. Yapılan çalışmalar sonucunda FDM'lerin, sıcaklığı dengeleyerek ve ani sıcaklık artışlarını engelleyerek elektronik cihazların ömrünü uzatabileceğini gözlemlemişlerdir. Ayrıca FDM'lerin termal iletkenliğini artırmak için metalik ısı kanatçıkları ve gözenekli malzemelerle birleştirilebileceğini, diğer soğutma cihazlarıyla birleştirildiğinde optimum konfigürasyona dikkat edilmesi gerektiği vurgulamışlardır.

Bu çalışmada faz değiştiren madde (FDM) ilaveli ve kanatçıklı bir ısı depolama ünitesi içeren termal kılıf tasarlanmış ve sistemin termal performansı deneysel olarak incelenmiştir. Ayrıca, farklı erime sıcaklıklarına sahip iki farklı FDM türünün (RT35 ve RT42) seçilen kılıfın termal performansına etkisi detaylı olarak analiz edilmiştir.

MATERYAL VE METOD

Bu çalışmada, akıllı telefonlar için FDM ilaveli termal kılıfın ısıl performansı ve kanatçık tasarımının termal performans üzerindeki etkisi deneysel olarak incelenmiştir. Deney düzeneğinin şematik gösterimi Şekil 1'de verilmiştir. İlgili sistem, Apple iPhone 6 model bir cep telefonu, sıcaklık verilerini toplayan bir Arduino kart, veri toplama birimi ve ayarlanabilir bir destek mekanizmasından oluşmaktadır.



Şekil 1. Deney düzeneğinin görünümü

Yapılan deneylerin gerçek uygulama şartlarında kullanılabilecek sonuçlar verebilmesi için üretilen kılıflar Apple iPhone 6 marka bir akıllı telefon üzerinde denenmiştir. iPhone 6 için termal bir kılıfın tasarımı ve üretimi sürecinde, öncelikle cihazın boyutları ve şekli dikkate alınarak kılıfın tasarımı belirlenmiştir. Cep telefonunun ısıl performansını belirlemek için FDM ilaveli ve ilavesiz iki farklı telefon kılıfı aynı çalışma koşulları altında test edilmiştir. FDM ilavesiz kılıf için ticari bir plastik telefon kılıfı kullanılmıştır. FDM ilaveli kılıf için, iç boyutları 81 mm yükseklik, 51 mm genişlik ve 4 mm derinlik olan dikdörtgen bir ısı depolama ünitesi plastik telefon kılıfına entegre edilmiştir. Isı depolama ünitesinin arka ve yan yüzeyleri 1 mm kalınlığında alüminyum levhadan ve ilgili ünite içindeki faz değişim olayını gözlemleyebilmek için ön yüzey 2.5 mm kalınlığında pleksiglass levhadan yapılmıştır. Ayrıca, kanatçıksız, tek kanatçıklı ve üç kanatçıklı olmak üzere üç farklı ünite tasarlanmış ve karşılaştırmalı olarak test edilmiştir. İlgili kanatçıklı yapılar Şekil 2'de verilmektedir.



Şekil 2. Cep telefonu ile kılıf içerisine yerleştirilmiş bölme; (a) kanatçıksız, (b) tek kanatçıklı, (c) üç kanatçıklı

Cep telefonu ile kılıf içerisine yerleştirilmiş ısı alıcısı arasındaki bölgede ısıl direnci azaltmak için kılıf iç yüzeyine bir ara malzemeden yapılan bölme oluşturulmuş ve bu bölmeye faz değiştiren madde yerleştirilmiştir. K-tipi termoeleman çifti kullanılarak cep telefonu üzerindeki 3 farklı istasyonda (Şekil 3) sıcaklık ölçümü yapılmış ve ilgili ölçümler özel tasarım bir ardunio kart sistemine aktarılmıştır.



Şekil 3. Termoelemanların cihaz üzerinde yerleştirildiği noktalar

İlgili termoelemanların yerleri termal kamera ile belirlenmiştir. Termal kamera ile yapılan sıcaklık ölçüm düzeneği Şekil 4'te gösterilmektedir.

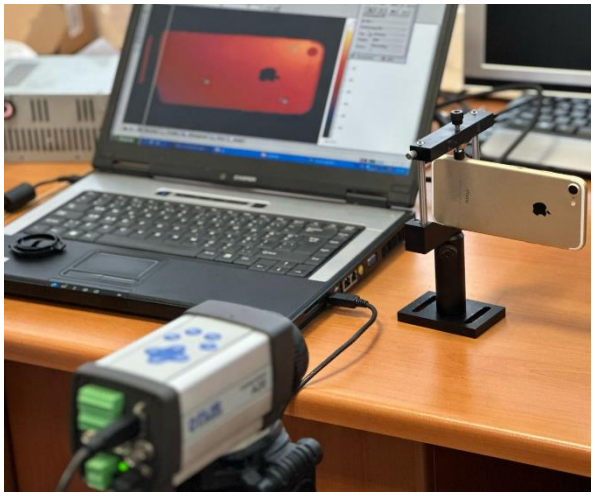

Şekil 4. Termal kamera ile sıcaklık dağılımının izlenmesi için kurulan deney düzeneği

Cihazın batarya ve elektronik bileşenlerinin performansı ve ömrü ile kullanıcı konfor sıcaklığı göz önüne alındığında RT35 ve RT42 parafin maddeleri tercih edilmiştir. İlgili maddelere ait termofiziksel özellikler Tablo 1'de verilmiştir. Bu maddelerin seçiminde, erime sıcaklığı aralığı, gizli ısı kapasitesi ve tekrar kullanılabilirlik özellikleri göz önünde bulundurulmuştur.

Tablo 1. RT35 ve RT42 faz değiştiren maddelerine ait termofiziksel özellikler

Termofiziksel Özellik	**RT35**	**RT42**
Erime Sıcaklığı (°C)	37.2	41.4
Gizli ısı (kj kg^{-1})	150	162
Isıl iletkenliği (Wm^{-1} K^{-1})	0.2	0.2
Yoğunluk (kg m^{-3})	860	880

Tüm deneyler, ortam sıcaklığının sabit tutulduğu kontrollü bir laboratuvar ortamında gerçekleştirilmiştir. Cep telefonu %100 şarj edilmiş ve destek mekanizmasına sabitlenmiştir. Ardından, cihazın ekran parlaklığı maksimum seviyeye ayarlanmış ve ağır çekim video modu etkinleştirilerek video kaydı başlatılmıştır. Bu esnada, termal

kamera telefonun arka yüzeyine odaklanacak şekilde konumlandırılmış ve belirli zaman aralıklarında IR görüntüler alınarak sıcaklık dağılımları kaydedilmiştir. Batarya seviyesi %50'ye düştüğünde deney sonlandırılmıştır. Aynı prosedür ikinci kez tekrarlanarak referans durum elde edilmiştir.

Termal görüntüler üzerinden sıcak noktalar tespit edilmiş ve termoelemanlar bu bölgelere yerleştirilmiştir. Termoelemanlar ilgili konumlara monte edilmeden önce, 0,2 °C hassasiyete sahip sabit sıcaklıklı bir su banyosu kullanılarak kalibre edilmiştir. Kalibrasyonun ardından, telefon yeniden %100 şarj edilmiş ve deney tekrar başlatılmıştır.

3. BULGULAR VE TARTIŞMA

Bu bölümde, tasarlanan FDM ilaveli termal kılıfın ve farklı kanatçık tiplerinin akıllı telefonların termal performansı üzerindeki deneysel sonuçları sunulmaktadır.

FDM ilavesiz ve FDM (RT35 ve RT42) ilaveli durumları için üç farklı sıcaklık noktalarına ait sıcaklık-zaman değişimleri Şekil 5'te verilmektedir. Elde edilen sonuçlar, tüm sıcaklık noktalarında (T_1, T_2 ve T_3) FDM ilavesiz durumda sıcaklık artışının daha hızlı ve yüksek düzeyde gerçekleştiğini göstermektedir. Bu durum, FDM'lerin faz değişimi sırasında çevreden gizli ısı çekerek ortam sıcaklığının artışını geciktirdiğini ve bu sayede termal yönetimde etkin rol oynadığını ortaya koymaktadır.

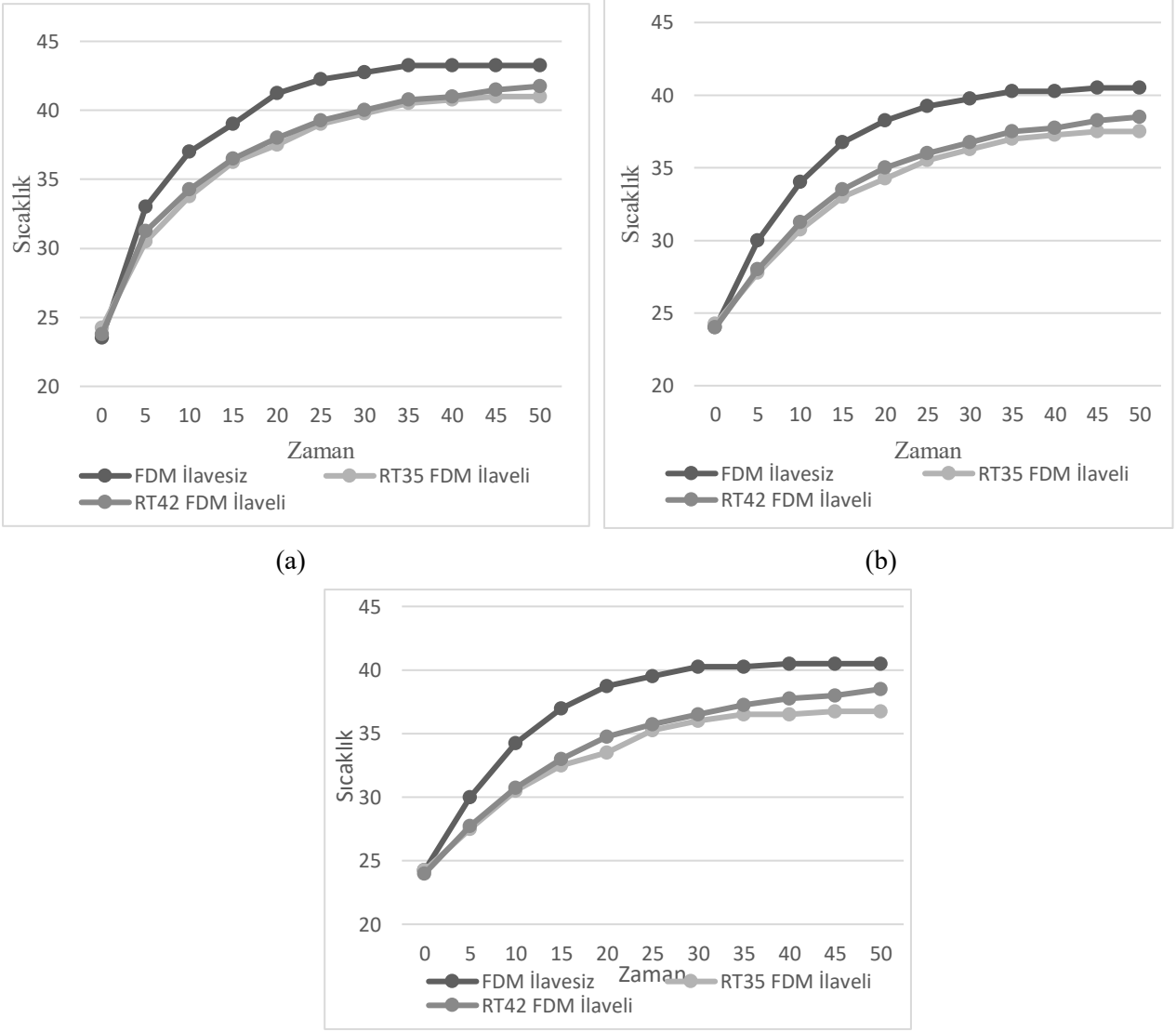

Şekil 5. Farklı sıcaklık noktalarına ait sıcaklık-zaman grafiği; (a) T_1 sıcaklığı, (b) T_2 sıcaklığı, (c) T_3 sıcaklığı

Özellikle RT42 katkılı durumda, diğer durumlara kıyasla sıcaklık değerlerinin daha düşük düzeyde olması, daha yüksek erime noktasına sahip bu FDM'nin ısıyı daha uzun süre emerek daha etkili bir soğutma etkisi oluşturduğunu göstermektedir. Buna ek olarak, zamanla sıcaklık değerlerinin birbirine yakınsadığı gözlemlenmiş olup, bu durum FDM'lerin erime sürecini tamamlamasının ardından gizli ısı etkisinin ortadan kalktığını ve sistemin yeniden dengeye ulaştığını göstermektedir.

Şekil 6'da RT35 tipi FDM ilaveli sistemde kanatçık bulunmayan, tek kanatçıklı ve üç kanatçıklı tasarımlar için farklı sıcaklık noktalarındaki sıcaklık-zaman değişimleri sunulmaktadır. Tüm sıcaklık noktalarında, kanatçık sayısının artmasıyla birlikte sıcaklık değerlerinin belirgin şekilde azaldığı gözlemlenmiştir.

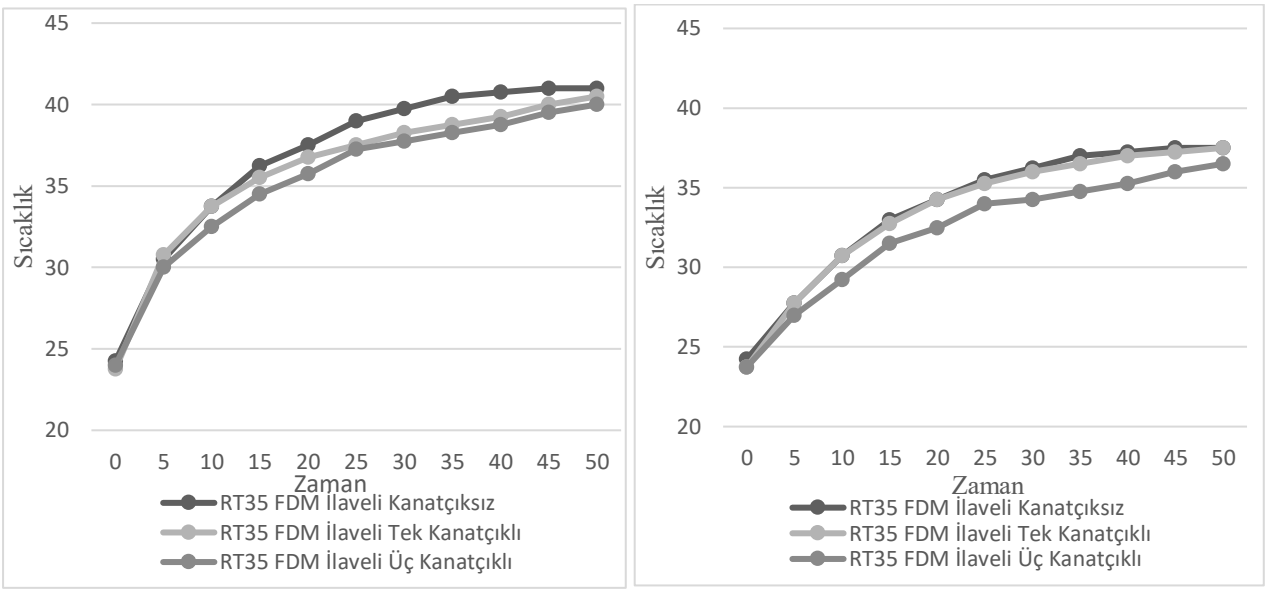

(a) (b)

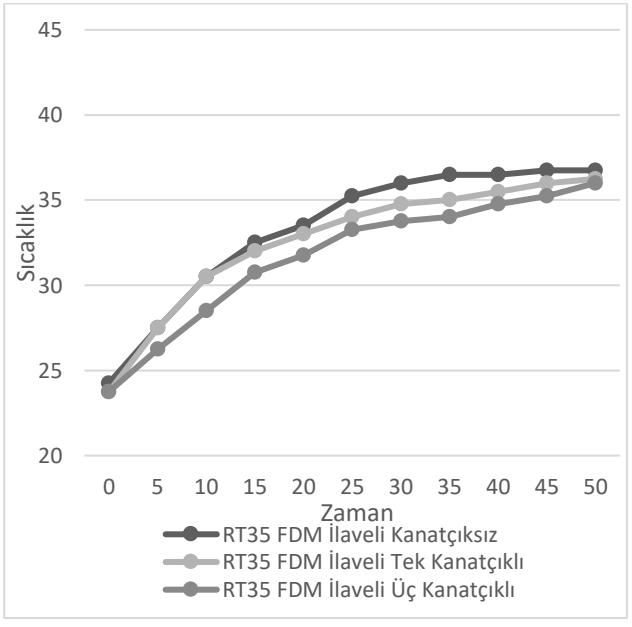

(c)

Şekil 6. RT35 için kanatçıksız ve kanatçıklı durumda farklı sıcaklık noktalarına ait sıcaklık-zaman grafiği; a) T_1 sıcaklığı, (b) T_2 sıcaklığı, (c) T_3 sıcaklığı

Bu durum, kanatçıkların yüzey alanını artırarak ısı transferini iyileştirdiğini ve böylece FDM'nin erime sürecine katkıda bulunarak sistemin daha düşük sıcaklıklarda kalmasını sağladığını göstermektedir. Üç kanatçıklı yapı, tüm zaman adımlarında en düşük sıcaklık değerlerini sunarak en etkin soğutma performansını sağlamaktadır. İlgili yapı sayesinde ısının FDM içerisine daha hızlı iletilmesi ve faz değişimi yoluyla daha fazla gizli ısının emilmesi mümkün olmaktadır. Bu bağlamda, pasif soğutma uygulamalarında kanatçıkların FDM performansını artırmak için etkili bir tasarım parametresi olduğunu ortaya koymaktadır.

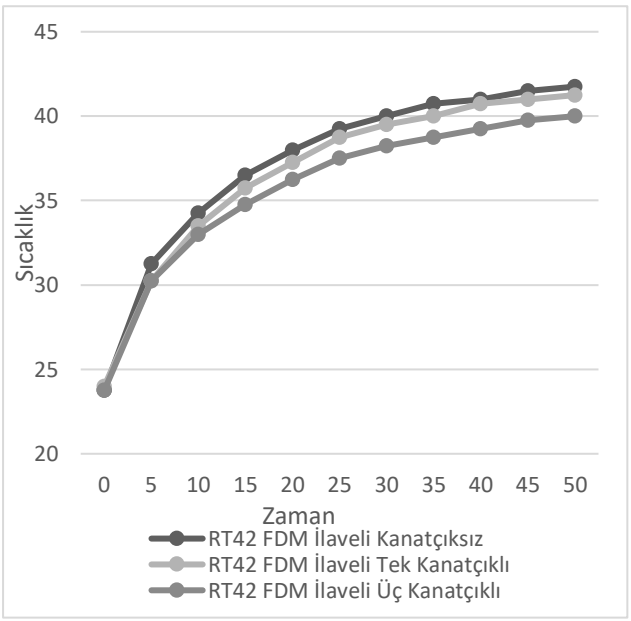

(a)

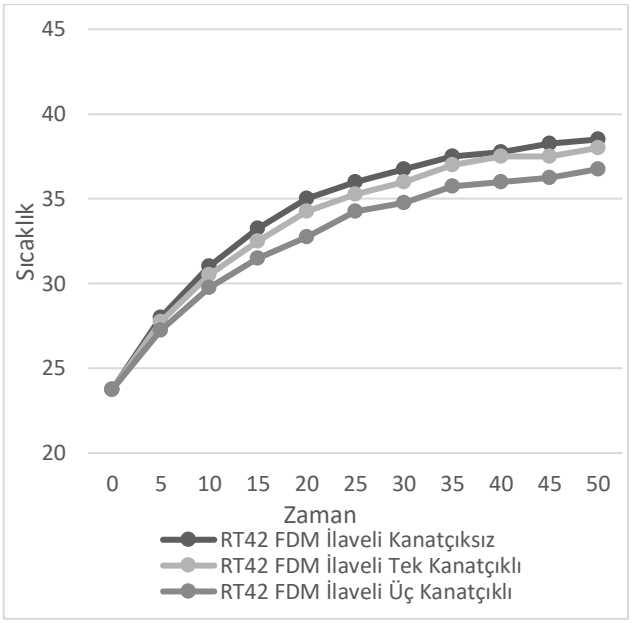

(b)

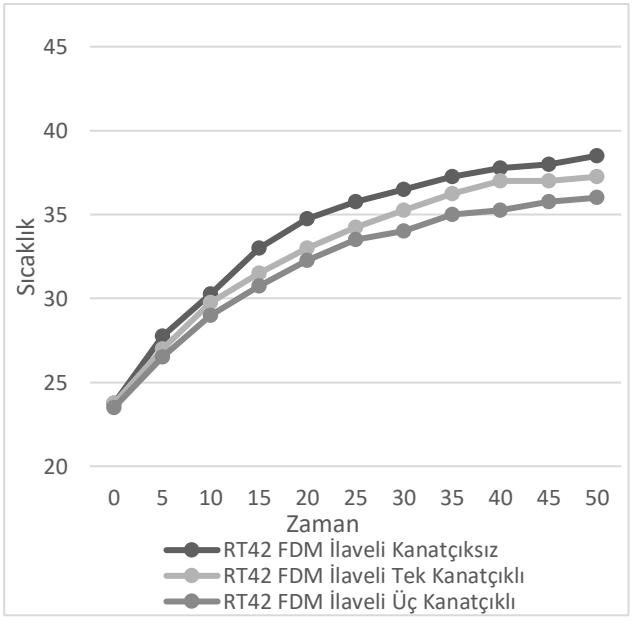

(c)

Şekil 7. RT42 için kanatçıksız ve kanatçıklı durumda farklı sıcaklık noktalarına ait sıcaklık-zaman grafiği; a) T_1 sıcaklığı, (b)T_2 sıcaklığı, (c) T_3 sıcaklığı

RT42 tipi FDM ilaveli sistemde sıcaklık-zaman değişimleri, farklı sıcaklık noktaları için Şekil 7'de verilmektedir. Bir önceki grafiklerde elde edilen bulgulara benzer şekilde, tüm sıcaklık konumlarında üç kanatçıklı yapıdaki sıcaklık değerlerinin en düşük düzeyde olduğu belirlenmiştir. Özellikle RT42 gibi daha yüksek erime sıcaklığına sahip FDM'lerde, ısının hızlı bir şekilde FDM içerisine taşınabilmesi termal kontrol açısından kritik öneme sahiptir. Üç kanatçıklı yapı, bu anlamda hem ısının daha homojen dağılmasını hem de FDM'nin daha verimli kullanılmasını sağlayarak soğutma performansını artırmaktadır. Zamanın artışıyla tüm yapılarda sıcaklık artış hızının azaldığı ve eğrilerin dengeye ulaştığı görülmektedir. RT42 tipi FDM'nin uygun kanatçık tasarımı ile birlikte kullanıldığında yüksek performanslı pasif soğutma sistemlerinde etkin bir çözüm sunabileceğini göstermektedir.

SONUÇ

Bu çalışmada, FDM ilaveli ve farklı kanatçık yapılarının mobil cihazlar için geliştirilen termal kılıflarda soğutma performansına etkisi deneysel olarak değerlendirilmiştir. Elde edilen sonuçlar, hem RT35 hem de RT42 tipi FDM'lerin gizli ısı depolama özellikleri sayesinde cihaz sıcaklığını düşürdüğünü, özellikle üç kanatçıklı yapının ısı transferini artırarak daha etkin bir soğutma sağladığını göstermektedir. RT42 tipi FDM'nin yüksek erime sıcaklığı nedeniyle daha uzun süreli ısı depoladığı ve bu durumun termal yönetim açısından avantaj sunduğu belirlenmiştir. Bu tasarım, elektronik cihazların aşırı ısınmasını önleyerek hem donanım ömrünü uzatmakta hem de kullanıcıların termal konforunu artırarak telefon kullanım deneyimini iyileştirmektedir.

TEŞEKKÜR

Bu çalışma, TÜBİTAK 2209-A Üniversite Öğrencileri Araştırma Projeleri Destekleme Programı tarafından [1919B012403131] numaralı proje kapsamında desteklenmektedir. Ayrıca, çalışmanın yürütülmesi sürecindeki bilimsel katkılarından dolayı Karadeniz Teknik Üniversitesi Makina Mühendisliği Bölümü'nden Dr. Mehmet SAĞLAM'a teşekkür ederiz.

KAYNAKLAR

Baby, R., & Balaji, C. (2013). "Thermal optimization of PCM-based pin fin heat sinks: An experimental study". Applied Thermal Engineering, 54, 65-67.

Bianco, V., De Rosa, M., & Vafai, K. (2022). "Phase-change materials for thermal management of electronic devices". Applied Thermal Engineering, 214, 118839.

Browne, M. C., Quigley, D., Hard, H. R., Gilligan, S., Ribeiro, N. C., Almeida, N., & McCormack, S. J. (2016). "Assessing the thermal performance of phase change material in a photovoltaic/thermal system". Energy Procedia, 91, 113-121.

Chen, G., Ping, P., Peng, R., Kong, D., & Wen, J. (2018). "Investigation on thermal management performance of PCM fin structure for Li-ion battery module in high-temperature environment". Energy Conversion and Management, 176, 131-146.

Ge, H., Li, H., Mei, S., & Liu, J. (2013). "Low melting point liquid metal as a new class of phase change material: An emerging frontier in energy area". Renewable and Sustainable Energy Reviews, 21, 331-346.

Groulx, D., Bhouri, M., Sponagle, B., Ahmed, T., Kahwaji, S., & White, M. A. (2017). "The Use of Phase Change Materials for Thermal Management of Portable Electronics". In First Asian Conference on Thermal Sciences,136, 686-701.

Huang, X., Zhu, C., Lin, Y., & Fang, G. (2019). "Thermal properties and applications of microencapsulated PCM for thermal energy storage: A review". Applied Thermal Engineering, 147, 841-855.

Maranda, S., Sponagle, B., Worlitschek, J., & Groulx, D. (2019). "Experimental investigation of thin PCM packages and thermal spreader for thermal management of portable electronic devices". Applied Sciences, 9(21), 4613.

Nandan, R., Arumuru, V., Rath, P., & Das, M. K. (2022). "Experimental study of PCM based hybrid heat sink for electronic cooling". Journal of Enhanced Heat Transfer, 29(3).

Setoh, G., Tan, F. L., & Fok, S. C. (2010). "Experimental studies on the use of a phase change material for cooling mobile phones". International Communications in Heat and Mass Transfer, 37(9), 1403-1410.

Sun, X., Liu, L., Mo, Y., Li, J., & Li, C. (2020). "Enhanced thermal energy storage of a paraffin-based phase change material (PCM) using nano carbons". Applied Thermal Engineering, 181, 115992.

Tan, F. L., & Tso, C. P. (2004). "Cooling of mobile electronic devices using phase change materials". Applied Thermal Engineering, 24(2-3), 159-169.

Thomas, J., Srivatsa, P. V. S. S., Krishnan, S. R., & Baby, R. (2016). "Thermal performance evaluation of a phase change material based heat sink: A numerical study". Procedia Technology, 25, 1182-1190.

Yin, H., Gao, X., Ding, J., & Zhang, Z. (2008). " Experimental research on heat transfer mechanism of heat sink with composite phase change materials". Energy Conversion and Management, 49(6), 1740-1746.

Ling, Z., Zhang, Z., Shi, G., Fang, X., Wang, L., Gao, X., ... & Liu, X. (2014). Review on thermal management systems using phase change materials for electronic components, Li-ion batteries and photovoltaic modules. Renewable and Sustainable Energy Reviews, 31, 427-438.

Zhang, T., Ding, Y., Nie, B., Chen, J., Du, Z., Li, Y., & Cong, L. (2021). "Thermal performance enhancement of a phase change material (PCM) based portable box for cold chain applications". Journal of Energy Storage, 40, 102707.

➢ *ORAL PRESENTATION*

Ortaöğretim Kurumları İçin Çok Kriterli Karar Verme Tabanlı Sürdürülebilirlik Skorlama Algoritması Geliştirilmesi

İbrahim Işıklı[1*] (*https://orcid.org/0000-0002-0778-7163*), Bayram Köse[2] (*https://orcid.org/0000-0003-0256-5921*), Serkan Ansay[3] (*https://orcid.org/0000-0002-3368-3886*), Nejdet Çelik[4] (*https://orcid.org/0000-0002-2740-609X*), Ahmet İstek[5](*https://orcid.org/0000-0002-2163-4008.*)

[*1,3] İzmir Bakırçay Üniversitesi, Lisansüstü Eğitim Enstitüsü, Elektrik Elektronik Mühendisliği Bölümü, İzmir / Türkiye
[2] İzmir Bakırçay Üniversitesi, Mühendislik ve Mimarlık Fakültesi, Elektrik Elektronik Mühendisliği Bölümü, İzmir / Türkiye
[4] İzmir Bakırçay Üniversitesi, Sürekli Eğitim Merkezi, İzmir / Türkiye
[5] İzmir Bakırçay Üniversitesi, Adalet Meslek Yüksekokulu, İzmir / Türkiye

*Sorumlu yazar e-posta: isikli.ibrahim@outlook.com

Özet

Bu çalışmada, ortaöğretim kurumlarının sürdürülebilirlik performanslarını ölçmek amacıyla çok kriterli bir değerlendirme modeli geliştirilmiştir. Model, enerji yönetimi, ekonomik sürdürülebilirlik ve sosyal sürdürülebilirlik olmak üzere üç ana tema ve toplam 16 kriterden oluşmaktadır. Her bir kriter için detaylı puanlama tabloları hazırlanmış, ardından kriter puanları normalize edilmiş ve özgün bir ağırlıklandırma yöntemi ile nihai skorlar elde edilmiştir. Geliştirilen model, beş farklı ortaöğretim kurumuna uygulanarak pilot olarak test edilmiştir. Elde edilen sonuçlar, kurumlar arasında ciddi sürdürülebilirlik farkları olduğunu ortaya koymuştur. En yüksek toplam sürdürülebilirlik skoru %52.9 iken, en düşük skor %10.9 olarak ölçülmüştür. Kurumların genel olarak sosyal sürdürülebilirlik alanında daha başarılı oldukları, ancak enerji yönetimi ve ekonomik sürdürülebilirlik alanlarında yapısal eksiklikler taşıdıkları tespit edilmiştir. Bu durum, sürdürülebilirlik farkındalığının mevcut olduğunu ancak bu farkındalığın altyapı yatırımları ve stratejik planlama ile desteklenmediği sürece yetersiz kaldığını göstermektedir. Modelin kurumlar arası kıyaslama yapılmasına olanak tanıması ve özelleştirilmiş iyileştirme önerileri sunabilmesi, uygulayıcılar açısından önemli bir avantaj sağlamaktadır.

Anahtar Kelimeler: Sürdürülebilirlik, ortaöğretim, çok kriterli değerlendirme, enerji yönetimi, eğitim politikası

Development of a Multi-Criteria Based Sustainability Scoring Algorithm for Secondary Schools

Abstract

In this study, a multi-criteria evaluation model was developed to assess the sustainability performance of secondary education institutions. The model consists of three main themes—energy management, economic sustainability, and social sustainability—covering a total of 16 criteria. Detailed scoring tables were designed for each criterion, followed by normalization of scores and the application of a custom weighting method to obtain final sustainability scores. The model was pilot-tested on five different secondary schools. The results revealed significant disparities in sustainability performance among institutions. While the highest overall sustainability score was 52.9%, the lowest was 10.9%. It was found that most schools performed better in the area of social sustainability, whereas they exhibited structural deficiencies in energy management and economic sustainability. These findings suggest that although sustainability awareness exists, it remains insufficient unless supported by infrastructure investments and strategic planning. The model allows for benchmarking between institutions and provides tailored improvement suggestions, making it a valuable tool for school administrators and policymakers. Based on the findings, it is recommended that sustainability policies be integrated into the education system through a holistic approach.

Keywords: Sustainability, secondary education, multi-criteria evaluation, energy management, education policy

GİRİŞ

Sanayi devrimiyle birlikte başlayan teknolojik ve ekonomik dönüşüm, üretim faaliyetlerinde ciddi bir artışı beraberinde getirmiş, buna bağlı olarak doğal kaynakların yoğun kullanımı ve çevre kirliliği gibi sorunlar da gündeme gelmiştir (Portney, 2015). Bu durum, insanlık için uzun vadeli refahı güvence altına alacak bir kalkınma modeline olan ihtiyacı ortaya koymuş ve böylece "sürdürülebilir kalkınma" kavramı literatürde önemli bir yer

edinmiştir. Sürdürülebilir kalkınma; bugünün gereksinimlerini, gelecek nesillerin ihtiyaçlarını riske atmadan karşılamayı hedefleyen, çevresel, ekonomik ve sosyal boyutları olan bütüncül bir yaklaşımdır (WCED, 1987). Sürdürülebilirlik kavramı, başlangıçta yalnızca çevresel faktörleri içerirken zamanla kurumsal sosyal sorumluluk, ekonomik denge ve yönetişim gibi unsurları da kapsayacak şekilde genişlemiştir (Heemskerk vd., 2002). Özellikle eğitim kurumları, bu sürecin hem taşıyıcısı hem de dönüştürücüsü olarak önemli bir sorumluluk üstlenmektedir. Eğitim kurumları yalnızca birey yetiştiren yapılar değil, aynı zamanda topluma yön veren ve geleceği şekillendiren aktörlerdir. Dolayısıyla bu kurumların da sürdürülebilir kalkınma ilkelerine uygun biçimde yönetilmeleri gerekmektedir (Doane ve MacGillivray, 2001).

Kurumların sürdürülebilirlik faaliyetlerini şeffaf biçimde kamuoyu ile paylaşabilmeleri için son yıllarda sürdürülebilirlik raporları yaygın biçimde kullanılmaktadır. Global Reporting Initiative (GRI), ISO 26000 ve Entegre Raporlama gibi standartlar, bu raporların içerik ve biçim açısından belirli bir düzene oturmasını sağlamaktadır (Önce vd., 2015)(Alonso-Almeida vd., 2014). Bu raporlar sayesinde kurumlar, enerji ve su tüketiminden atık yönetimine, toplumsal cinsiyet eşitliğinden etik ilkelere kadar birçok başlıkta performanslarını değerlendirme ve iyileştirme fırsatı bulmaktadır (Ertan, 2018)(Hedberg ve Von Malmborg, 2003). Üniversiteler, sürdürülebilirlik uygulamaları açısından genellikle öncü konumda olup, kampüslerinde çevresel verimlilik, geri dönüşüm, yenilenebilir enerji kullanımı gibi politikaları hayata geçirmiştir (Gümrah ve Tanç, 2018)(Bonatxea vd., 2022). Ayrıca sosyal sorumluluk projeleri, toplumsal farkındalık kampanyaları ve etik ilkelere dayalı araştırma politikalarıyla sürdürülebilirliğe çok boyutlu katkılar sağlamaktadırlar (Ramísio vd., 2019)(Ávila vd., 2017). Ancak bu katkının yalnızca üniversiteler düzeyinde kalması yeterli değildir. Ortaöğretim kurumları da sürdürülebilir bir toplumun temellerini atma noktasında kritik bir rol oynamaktadır.

Ortaöğretim kurumlarında sürdürülebilirlik uygulamalarının sistematik biçimde izlenmesi ve değerlendirilmesi, bu kurumların çevreye ve topluma olan etkilerini iyileştirmeleri açısından gereklidir(Köse vd., 2024). Bu bağlamda sürdürülebilirlik sertifikasyon sistemleri, eğitim kurumlarının kaynak kullanımını, karbon ayak izini, enerji verimliliğini, sosyal sorumluluk faaliyetlerini ve yönetim yapılarını değerlendiren önemli araçlar haline gelmiştir (Fuster vd., 2019) (Godemann vd., 2014). Bu sertifikasyon sistemleri yalnızca çevresel performansın ölçülmesini değil, aynı zamanda öğrencilerde çevresel bilinç ve toplumsal duyarlılık oluşturmayı da hedeflemektedir.

Türkiye özelinde bakıldığında, ortaöğretim kurumlarının sürdürülebilirlik bağlamında henüz sistematik bir izleme ve değerlendirme sürecine dahil edilmediği görülmektedir. Oysa bu kurumlar, öğrencilerin günlük yaşamlarının önemli bir bölümünü geçirdiği mekânlar olarak, sürdürülebilir davranışların öğrenilmesi ve içselleştirilmesinde önemli bir etkiye sahiptir. Sürdürülebilirlik sertifikasyonu uygulamaları sayesinde bu kurumlar hem çevresel etkilerini azaltabilir hem de öğrencilerine model oluşturabilir. Bu çalışmada, uluslararası örnekler ve mevcut literatür doğrultusunda Türkiye'de uygulanabilir bir sürdürülebilirlik sertifikasyon sisteminin geliştirilmesi ve özgün bir çok kriterli değerlendirme metodu ile skorlamanın nasıl gerçekleştireleceği anlatılmaktadır.

MATERYAL VE METOD

1. Ana Temalar ve Kriterleri

Ortaöğretim kurumlarının sürdürülebilirlik performansını değerlendirmek amacıyla oluşturulan üç adet ana tema belirlenmiştir. Bu temalar, ortaöğretim kurumlarının günümüz doğrultusunda sürdürülebilirlik hedeflerini bir bütün oluşturacak şekilde seçilmiştir. Ana temalar şu şekildedir: Enerji Yönetimi, Ekonomik Sürdürülebilirlik ve Sosyal Sürdürülebilirlik. Her bir ana tema ise kendi içinde üç adet başlık içermektedir ve bu başlıklara göre çeşitli kriterlerle puanlanmaktadır. Tema ve içerdikleri başlıklar Şekil 1'de gösterilmiştir.



Şekil 1. Ana Tema ve Başlıkları

Kurumları, kriterlere yönelik yeterliliğini değerlendirilirken sağlayacağı şartlara göre puan notları verilmektedir. Ana temaların sahip olduğu kriterlere yönelik şartlar aşağıdaki tablolarda tanımlanmıştır.

2.1 Enerji Yönetimi

Enerji yönetimi kapsamında ve değerlendirme koşulları Tablo 1 - Tablo 6 arasında gösterilmiştir.

Tablo 1. Enerji Tüketim Raporlarına Yönelik Puan Tablosu

Açıklama	Puan
Yıllık enerji tüketim verileri mevcut değil veya hiç izlenmiyor.	0
Sadece temel yıllık enerji tüketim verileri (elektrik, doğalgaz, su) mevcuttur, ancak düzenli raporlama veya analiz yapılmamaktadır.	1
Yıllık enerji tüketim verileri düzenli olarak toplanmakta ve basit raporlamalar yapılmaktadır. Veriler ham haldedir, analizi kısıtlıdır.	2
Aylık enerji tüketim verileri düzenli olarak toplanmakta, raporlanmakta ve basit grafiklerle görselleştirilmektedir. Geçmiş yıllarla karşılaştırmalar yapılmaktadır.	3
Aylık ve/veya günlük enerji tüketim verileri (akıllı sayaçlar aracılığıyla) düzenli olarak toplanmakta, detaylı raporlar hazırlanmakta ve analiz edilmektedir. Enerji tüketim desenleri belirlenmektedir.	4
Günlük ve anlık enerji tüketim verileri merkezi bir sistemde (örneğin SCADA benzeri) izlenmekte, detaylı analizler ve tüketim hedeflerine ulaşma başarısı düzenli olarak raporlanmaktadır. Veri analizi, iyileştirme projeleri için aktif olarak kullanılmaktadır.	5

Tablo 2. Yalıtım ve Enerji Tasarrufu Önlemlerine Yönelik Puan Tablosu

Açıklama	Puan
Herhangi bir ısı yalıtımı veya enerji tasarrufu önlemi mevcut değil veya çok yetersiz.	0
Temel yalıtım eksiklikleri (örneğin eski pencere ve kapı contaları) giderilmeye çalışılmış, ancak kapsamlı bir yalıtım uygulaması bulunmamaktadır.	1
Binaların dış cephesinde kısmi yalıtım veya tek camlı pencerelerin bir kısmı çift cam ile değiştirilmiştir. Bazı eski tip aydınlatmalar LED'e dönüştürülmüştür.	2
Binaların çoğunda ısı yalıtımı (dış cephe, çatı, taban) mevcuttur ve pencerelerin tamamı çift camlıdır. Aydınlatma sisteminin büyük çoğunluğu enerji tasarruflu (LED) lambalardan oluşmaktadır.	3
Binaların tamamında yüksek standartlarda ısı yalıtımı mevcuttur ve pencereler ısı yalıtımlı, düşük emisyonlu (low-e) camlara sahiptir. Aydınlatma tamamen enerji tasarruflu olup, sensörlü veya gün ışığına duyarlı sistemler kısmen kullanılmaktadır. Düzenli bakım ve denetimler yapılmaktadır.	4
Binaların tamamında yüksek performanslı yalıtım ve ısı yalıtımlı camlar mevcuttur. Aydınlatma tamamen enerji tasarruflu (LED) olup, sensörler, gün ışığı kontrolü ve merkezi otomasyon sistemleri ile tamamen yönetilmektedir. Periyodik enerji etüdleri yapılmakta ve öneriler uygulanmaktadır.	5

Tablo 3. Akıllı Enerji Yönetim Sistemlerine Yönelik Puan Tablosu

Açıklama	Puan
Akıllı enerji yönetim sistemi mevcut değil.	0
Sadece temel enerji tüketimini izleyen (manuel kayıt veya basit sayaç okuma) bir sistem bulunmaktadır.	1
Bazı enerji tüketim noktaları (örneğin ana elektrik panosu) için dijital sayaçlar aracılığıyla uzaktan izleme imkanı mevcuttur, ancak otomasyon veya yönetim işlevleri sınırlıdır.	2

Bina Yönetim Sistemi (BMS) veya benzeri bir sistem, temel enerji tüketimini (aydınlatma, ısıtma/soğutma) izlemekte ve basit zamanlama bazlı kontrol imkanı sunmaktadır.	3
Entegre bir Akıllı Enerji Yönetim Sistemi (AEYS) bulunmaktadır. Bu sistem, enerji tüketimini otomatik olarak izlemekte, anormal tüketimleri tespit etmekte ve bazı optimizasyonları (örneğin aydınlatma ve HVAC kontrolü) gerçekleştirmektedir.	4
Kapsamlı ve entegre bir Akıllı Enerji Yönetim Sistemi (AEYS) aktif olarak kullanılmaktadır. Sistem, enerji tüketimini tahmin etmek, farklı sistemler (ısıtma, soğutma, aydınlatma, yenilenebilir enerji üretimi) arasında otomasyon sağlamak ve enerji verimliliğini maksimum düzeyde optimize etmek için yapay zeka veya gelişmiş algoritmalar kullanmaktadır. Verilere kolay erişilebilir bir kullanıcı arayüzü mevcuttur.	5

Tablo 4. Yenilenebilir Enerji Kaynaklarının Kullanımına Yönelik Puan Tablosu

Açıklama	**Puan**
Yenilenebilir enerji kaynağı kullanımı mevcut değil.	0
Kısmi ve sembolik bir yenilenebilir enerji uygulaması (örneğin küçük bir güneş paneli veya rüzgar türbini) bulunmakta olup, okulun enerji ihtiyacına kayda değer bir katkısı yoktur.	2
Okulun enerji ihtiyacının %5 ila %15'ini karşılayacak kapasitede yenilenebilir enerji sistemi (örneğin güneş panelleri veya güneş kollektörleri) kurulmuştur.	4
Okulun enerji ihtiyacının %15 ila %30'unu karşılayacak kapasitede yenilenebilir enerji sistemi kurulmuştur. Sistemin düzenli bakımı yapılmaktadır.	6
Okulun enerji ihtiyacının %30 ila %50'sini karşılayacak kapasitede yenilenebilir enerji sistemi kurulmuştur. Farklı yenilenebilir enerji kaynakları (güneş, rüzgar, jeotermal vb.) entegre bir şekilde kullanılmaktadır.	8
Okulun enerji ihtiyacının %50'sinden fazlası yenilenebilir enerji kaynaklarından sağlanmaktadır. Üretilen enerjinin fazlası şebekeye geri beslenmekte veya depolanmaktadır. Yenilenebilir enerji projeleri düzenli olarak geliştirilmektedir.	10

Tablo 5. Elektrik, Su, Doğalgaz Tüketim Miktarlarına Yönelik Puan Tablosu

Açıklama	**Puan**
Tüketim verileri izlenmiyor veya önlemler yetersiz, tüketim miktarları çok yüksek.	0
Temel tüketim verileri toplanmakta ancak herhangi bir analiz veya kıyaslama yapılmamaktadır. Tüketim, benzer okulların ortalamasının üzerindedir	1
Aylık tüketim verileri izlenmekte, ancak tasarruf önlemleri sınırlıdır. Tüketim, benzer okulların ortalamasına yakındır.	2
Aylık tüketim verileri düzenli olarak izlenmekte ve raporlanmaktadır. Bazı tasarruf önlemleri (örneğin musluk aeratörleri, verimli armatürler) alınmıştır. Tüketim, benzer okulların ortalamasının hafif altındadır.	3
Tüketim verileri detaylı olarak analiz edilmekte (metrekare/öğrenci başına düşen tüketim) ve hedefler belirlenmektedir. Tüketim, benzer okulların ortalamasının önemli ölçüde altındadır ve aktif tasarruf projeleri yürütülmektedir.	4
Tüketim verileri akıllı sistemlerle anlık olarak izlenmekte, anormallikler anında tespit edilmekte ve proaktif önlemler alınmaktadır. Tüketim, benzer okulların en verimli seviyelerinde veya altındadır. Su geri dönüşüm sistemleri veya yağmur suyu hasadı gibi ileri uygulamalar mevcuttur.	5

Tablo 6. Kişi Başına Düşen Enerji Tüketimine Yönelik Puan Tablosu

Açıklama	**Puan**
Kişi başına düşen enerji tüketimi verisi hesaplanmıyor veya mevcut değil.	0
Kişi başına düşen enerji tüketimi hesaplanmakta ancak ulusal/uluslararası standartların veya benzer okulların ortalamasının çok üzerindedir.	1
Kişi başına düşen enerji tüketimi hesaplanmakta ve ortalamanın üzerindedir, ancak azaltma çabaları başlamıştır. (Örn: $X > 150\text{kWh/kişi/yıl}$)	2
Kişi başına düşen enerji tüketimi ulusal/uluslararası standartlara veya benzer okulların ortalamasına yakındır. (Örn: $100\text{kWh/ kişi / yıl} \leq X \leq 150\text{kWh/kişi/yıl}$)	3
Kişi başına düşen enerji tüketimi ulusal/uluslararası standartların veya benzer okulların ortalamasının altındadır. (Örn: $50\text{kWh/ kişi /yıl} \leq X < 100\text{kWh/kişi/yıl}$)	4
Kişi başına düşen enerji tüketimi, ulusal/uluslararası en iyi uygulamalar seviyesinde veya çok altındadır. Okul, bu oranı sürekli iyileştirmek için hedefler belirlemiş ve ulaşmıştır. (Örn: $X < 50\text{kWh/ kişi / yıl}$)	5

2.2 Ekonomik Sürdürülebilirlik

Ekonomik sürdürülebilirlik kapsamında ve değerlendirme koşulları Tablo 7 - Tablo 11 arasında gösterilmiştir.

Tablo 7. Kaynakların Etkin Kullanımına Yönelik Puan Tablosu

Açıklama	**Puan**
Atıkların ayrıştırılması veya geri dönüştürülmesi konusunda herhangi bir çalışma mevcut değil. Kaynak kullanımı bilinçsizce yapılıyor.	0
Temel atık ayrıştırma (kağıt, plastik) kutuları mevcut ancak düzenli toplama veya geri dönüşüm süreçleri tanımlanmamış. Kaynak kullanımı hakkında sınırlı farkındalık var.	1
Belirli atık türleri (kağıt, plastik, cam) için ayrıştırma ve toplama noktaları belirlenmiş, düzenli olarak geri dönüşüme gönderiliyor. Su ve elektrik gibi kaynakların israfını önlemeye yönelik temel uygulamalar (muslukların kapatılması gibi) teşvik ediliyor.	2
Kapsamlı bir atık yönetim planı mevcut olup, atıkların ayrıştırılması, geri dönüştürülmesi ve kompostlama gibi yöntemlerle azaltılması hedeflenmektedir. Kaynak kullanımı verimliliğini artırmak için (örneğin, yazıcı ayarlarının optimize edilmesi, su tasarruflu armatürler) aktif çabalar gösterilmektedir.	3
Atık yönetimi planı etkin bir şekilde uygulanmakta ve atık oluşumunu azaltmaya yönelik projeler (örneğin, tek kullanımlık ürünlerin azaltılması) yürütülmektedir. Kaynak verimliliği, düzenli eğitimlerle desteklenmekte ve verimli ekipman alımlarıyla pekiştirilmektedir. Atık verileri düzenli olarak raporlanmaktadır.	4
Okul, ``Sıfır Atık" veya benzeri ileri düzey bir atık yönetimi prensibini benimsemiş ve uygulamaktadır. Atık üretimi minimuma indirilmiş, geri dönüşüm ve yeniden kullanım oranları en üst seviyededir. Su ve enerji kaynakları minimum düzeyde tüketilirken, su geri dönüşüm sistemleri ve yağmur suyu hasadı gibi ileri uygulamalar kullanılmaktadır. Tedarik zincirinde sürdürülebilir ürünler tercih edilmektedir.	5

Tablo 8. Maliyet Tasaruflarına Yönelik Puan Tablosu

Açıklama	**Puan**
Maliyet azaltma veya verimlilik artırma çabası mevcut değil. Enerji ve su gibi tüketim alanlarında israf gözlemleniyor.	0
Temel maliyet azaltma farkındalığı var ancak sistematik bir yaklaşım yok. Küçük ölçekli, düzensiz tasarruf çabaları bulunuyor.	1
Belirli alanlarda (örneğin aydınlatmada LED kullanımı) enerji verimliliği yatırımları yapılmış veya su tasarrufu önlemleri alınmış, ancak genel bir maliyet yönetimi stratejisi mevcut değil.	2

Enerji, su ve atık yönetimi gibi ana alanlarda maliyet azaltma hedefleri belirlenmiş ve bu hedeflere ulaşmak için düzenli çalışmalar yürütülüyor. Bakım maliyetlerini azaltmaya yönelik planlar var.	3
Sistematik bir maliyet yönetim programı uygulanmakta olup, enerji ve su tasarrufu, atık azaltma ve geri dönüşüm, verimli ekipman alımı gibi alanlarda önemli başarılar elde edilmiştir. Maliyet-fayda analizi yapılarak verimli yatırımlar gerçekleştirilmektedir.	4
Kapsamlı bir ekonomik sürdürülebilirlik stratejisi dahilinde, tüm operasyonel maliyetler (enerji, su, atık, bakım, malzeme tedariki) sürekli izlenmekte, optimize edilmekte ve proaktif olarak azaltılmaktadır. Yenilikçi çözümler (örneğin, yerinde atık işleme, daha az kaynak tüketen eğitim materyalleri) aktif olarak kullanılmaktadır.	5

Tablo 9. Satın Alma Politikalarına Yönelik Puan Tablosu

Açıklama	**Puan**
Satın alma kararlarında sürdürülebilirlik kriterleri göz önünde bulundurulmuyor. En düşük maliyet temel alınmaktadır.	0
Satın alma kararlarında sürdürülebilirlik kriterleri (örneğin enerji verimliliği etiketleri, geri dönüştürülmüş içerik) hakkında sınırlı bir farkındalık var ancak resmi bir politika mevcut değil.	1
Satın alma süreçlerinde bazı çevre dostu ürünler (örneğin geri dönüştürülmüş kağıt) tercih edilmektedir, ancak bu durum sistematik bir politika haline gelmemiştir.	2
Okulun resmi bir sürdürülebilir satın alma politikası bulunmaktadır. Bu politika, enerji verimli ekipmanlar, çevre dostu temizlik ürünleri, yerel ve adil ticaret ürünleri gibi kriterleri içermektedir. Tedarikçilerle iletişimde bu kriterler belirtilmektedir.	3
Sürdürülebilir satın alma politikası etkin bir şekilde uygulanmaktadır ve tedarikçilerin sürdürülebilirlik performansları (çevresel ve sosyal sorumluluk) da değerlendirme süreçlerine dahil edilmektedir. Atık azaltma ve uzun ömürlü ürün tercihleri ön plandadır.	4
Kapsamlı ve şeffaf bir sürdürülebilir tedarik zinciri yönetim sistemi mevcuttur. Tüm satın alma kararları çevresel ve sosyal etki analizleri ile desteklenmekte, döngüsel ekonomi prensipleri (örneğin, ürün-hizmet sistemleri, onarılabilirlik) benimsenmektedir. Tedarikçilerle sürdürülebilirlik konusunda aktif işbirliği yapılmakta ve performansları düzenli olarak denetlenmektedir.	5

Tablo 10. Finansal Planlamaya Yönelik Puan Tablosu

Açıklama	**Puan**
Sürdürülebilirlik projeleri için herhangi bir bütçeleme veya finansal planlama yapılmıyor.	0
Sürdürülebilirlik konusunda farkındalık olsa da, bu yönde spesifik bir bütçe veya yatırım planı mevcut değil.	1
Küçük ölçekli sürdürülebilirlik projeleri için (örneğin birkaç LED lamba değişimi) ara sıra bütçe ayrılmaktadır, ancak bu düzenli veya planlı değildir.	2
Okul bütçesinde, enerji verimliliği, su tasarrufu veya atık yönetimi gibi sürdürülebilirlik alanlarına ayrılmış belirli bir kalem bulunmaktadır. Bu yatırımların geri dönüş süreleri (ROI) kısmen değerlendirilmektedir.	3
Uzun vadeli bir finansal planlama çerçevesinde sürdürülebilirlik yatırımları önceliklendirilmektedir. Yatırım projelerinin (örneğin yenilenebilir enerji sistemleri, yalıtım projeleri) detaylı maliyet-fayda ve geri dönüş analizleri yapılmaktadır. Dış finansman kaynakları (hibe, fonlar) araştırılmaktadır.	4
Okul, sürdürülebilirlik hedeflerine ulaşmak için aktif olarak çeşitli finansman modelleri (kamu fonları, özel sektör işbirlikleri, uluslararası hibeler, kendi fonları) kullanmaktadır. Yapılan sürdürülebilirlik yatırımları, okulun uzun vadeli finansal istikrarına ve çevresel	5

performansına önemli katkılar sağlamaktadır. Yenilikçi finansman çözümleri (örneğin, enerji performans sözleşmeleri) araştırılmaktadır.	

Tablo 11. Ekononik Katkı ve Yerel Kalkınmaya Yönelik Puan Tablosu

Açıklama	**Puan**
Yerel ekonomiye veya topluma herhangi bir doğrudan ekonomik katkı sağlamıyor.	0
Sınırlı ölçüde yerel tedarikçilerden veya hizmet sağlayıcılardan faydalanılıyor ancak bu bilinçli bir tercih değil.	1
Okul, bazı ürün ve hizmet alımlarında yerel tedarikçileri tercih etmektedir. Öğrencilerin veya okul çalışanlarının yerel ekonomiye katkısını artırmaya yönelik küçük çaplı farkındalık çalışmaları yapılıyor.	2
Yerel tedarik zincirleri ve yerel istihdamı destekleyen bir satın alma politikası uygulanmaktadır. Okul, yerel işletmelerle düzenli işbirlikleri yapmakta ve yerel ekonomik kalkınmaya dolaylı katkılar sağlamaktadır.	3
Okul, yerel ekonomiyi ve istihdamı aktif olarak destekleyen stratejiler geliştirmektedir. Yerel kaynakların kullanımı, yerel girişimlerin teşviki ve yerel halka yönelik ekonomik katkı sağlayan projeler (örneğin, okul bahçesinde üretilen ürünlerin yerel pazarda satılması) yürütülmektedir.	4
Okul, bulunduğu bölgenin ekonomik kalkınmasında önemli bir rol oynamaktadır. Kapsamlı yerel tedarikçi programları, yerel işgücünü destekleyici eğitim ve staj imkanları sunulmaktadır. Okul, yerel toplulukla ekonomik işbirlikleri geliştirerek (örneğin, okulun tesislerinin topluluk kullanımına açılmasıyla gelir elde etme) bölgeye doğrudan ekonomik fayda sağlamaktadır.	5

2.3 Sosyal Sürdürülebilirlik

Sosyal sürdürülebilirlik kapsamında kriterleterler ve değerlendirme koşulları Tablo 12 -Tablo 16 arasında gösterilmiştir.

Tablo 12. Toplumsal Katılım ve Paydaş İlişkilerine Yönelik Puan Tablosu

Açıklama	**Puan**
Yerel toplulukla veya diğer paydaşlarla (STK'lar, yerel yönetim) herhangi bir etkileşim veya işbirliği mevcut değil.	0
Sınırlı ve düzensiz olarak, sadece ihtiyaç anında yerel topluluktan destek istenmekte veya basit duyurular yapılmaktadır.	1
Okul, yerel toplulukla bazı temel düzeyde etkileşimler (örneğin, okul etkinliklerine toplumu davet etme) gerçekleştirmektedir. Velilerle düzenli toplantılar yapılmaktadır.	2
Okul, yerel toplulukla (belediye, STK'lar, muhtarlık) sürdürülebilirlik odaklı projelerde (örneğin, ağaç dikme, çevre temizliği) işbirliği yapmaktadır. Öğrencilerin topluma katkı sağlayıcı faaliyetlerde yer alması teşvik edilmektedir.	3
Kapsamlı bir paydaş katılım stratejisi mevcuttur. Okul, yerel topluluğun ihtiyaçlarına yönelik projelere aktif olarak katılmakta ve öğrencilerin sosyal sorumluluk bilincini geliştiren programlar yürütmektedir. Gönüllülük faaliyetleri teşvik edilmektedir.	4
Okul, yerel toplulukla stratejik ve uzun vadeli ortaklıklar kurmuştur. Sürdürülebilirlik alanında toplumsal sorunlara çözüm üreten, inovatif projelerde (örneğin, topluluk bahçesi, sürdürülebilirlik merkezi) lider rol oynamaktadır. Öğrenciler, yerel toplulukla birlikte çalışarak gerçek dünya sorunlarına sürdürülebilir çözümler geliştirmektedir. Okul, paydaş geri bildirimlerini düzenli olarak toplamakta ve süreçlerine dahil etmektedir.	5

Tablo 13. Kültürel Mirasın Korunması ve Tanıtılmasına Yönelik Puan Tablosu

Açıklama	**Puan**
Okulun kültürel mirasın korunması veya tanıtılmasına yönelik herhangi bir faaliyeti yok.	0
Okulun bulunduğu bölgenin kültürel mirası hakkında sınırlı genel bilgiler öğrencilere verilmektedir.	1
Okul, yerel kültürel değerlere ve mirasa yönelik basit etkinlikler (örneğin, kültürel gün, yerel geziler) düzenlemektedir.	2
Okul müfredatına yerel kültürel mirasın korunması ve tanıtılmasına yönelik konular entegre edilmiştir. Öğrencilerin kültürel miras alanlarını ziyaret etmeleri ve araştırmalar yapmaları teşvik edilmektedir.	3
Okul, yerel kültürel miras kurumları (müzeler, sivil toplum kuruluşları) ile işbirliği yaparak, öğrencilerin kültürel miras projelerine aktif katılımını sağlamaktadır. Geleneksel sanat ve zanaat atölyeleri düzenlenmektedir.	4
Okul, kültürel mirasın korunması ve tanıtılmasında aktif bir rol oynamaktadır. Yerel kültürel mirasın dijitalleştirilmesi, belgelenmesi veya restorasyonuna yönelik projelere liderlik etmekte veya destek vermektedir. Okulun kendi bünyesinde kültürel mirasla ilgili bir koleksiyon veya sergi alanı bulunmaktadır. Öğrenciler, kültürel değerlerin gelecek nesillere aktarılmasına yönelik sürdürülebilir projeler geliştirmektedir.	5

Tablo 14. Eğitim ve Farkındalık Programlarına Yönelik Puan Tablosu

Açıklama	**Puan**
Sürdürülebilirlik veya çevre bilinci konusunda herhangi bir eğitim veya farkındalık faaliyeti mevcut değil.	0
Sınırlı ve düzensiz olarak, genellikle dışarıdan gelen tek seferlik etkinliklerle sürdürülebilirlik konusunda kısa bilgilendirmeler yapılmaktadır.	1
Sürdürülebilirlik konuları (çevre, enerji, su gibi) müfredatın bazı bölümlerine entegre edilmiş veya yılda birkaç kez okul içi seminerler/atölye çalışmaları düzenlenmektedir.	2
Sürdürülebilirlik eğitimleri müfredatın önemli bir parçası olup, öğrencilere yönelik düzenli seminerler, paneller ve atölye çalışmaları (örneğin, "Yeşil Okul Kulübü") düzenlenmektedir. Öğretmenlerin bu konudaki eğitimleri teşvik edilmektedir.	3
Kapsamlı bir sürdürülebilirlik eğitim müfredatı uygulanmakta ve tüm öğrenci ve personele yönelik düzenli ve etkileşimli farkındalık programları yürütülmektedir. Bu programların etkililiği ölçülmekte ve geliştirilmektedir.	4
Sürdürülebilirlik, okul kültürünün ayrılmaz bir parçası olup, tüm derslere ve okul dışı etkinliklere entegre edilmiştir. Öğrencilerin liderliğinde yürütülen sürdürülebilirlik projeleri desteklenmekte, yerel toplulukla işbirliği içinde geniş çaplı farkındalık kampanyaları yürütülmekte ve ulusal/uluslararası projelerde yer alınmaktadır.	5

Tablo 15. Kapsayıcılık ve Erişebilirliğe Yönelik Puan Tablosu

Açıklama	**Puan**
Özel ihtiyaçları olan öğrenciler veya dezavantajlı gruplar için erişilebilirlik veya kapsayıcılık konusunda özel bir çaba veya düzenleme mevcut değil.	0
Temel yasal gereklilikler çerçevesinde (örneğin engelli rampası, asansör) sınırlı fiziksel erişilebilirlik düzenlemeleri yapılmıştır.	1
Fiziksel erişilebilirlik konusunda daha fazla düzenleme yapılmış (örneğin özel tuvaletler, geniş kapılar) ve farklı kültürel/sosyal geçmişe sahip öğrencilerin entegrasyonuna yönelik temel farkındalık çalışmaları yürütülmektedir.	2
Okul, tüm öğrencilerin (engelli, göçmen, sosyo-ekonomik olarak dezavantajlı vb.) eğitime erişimini ve katılımını destekleyen politikalar geliştirmiştir. Fiziksel altyapının yanı sıra, ders materyalleri ve öğrenme ortamları da kapsayıcı olacak şekilde düzenlenmektedir.	3

Kapsayıcılık ve erişilebilirlik konularında aktif projeler yürütülmektedir. Öğrenci ve personel çeşitliliği desteklenmekte, farklılıklar bir zenginlik olarak kabul edilmektedir. Ayrımcılığı önleyici politikalar ve şikayet mekanizmaları etkin bir şekilde işlemektedir.	4
Okul, kapsayıcı bir öğrenme ve çalışma ortamı sağlamada lider konumdadır. Tüm öğrenciler ve personel için tam fiziksel ve pedagojik erişilebilirlik sağlanmıştır. Farklılıkları kutlayan, çeşitliliği teşvik eden ve tüm paydaşların (veliler, yerel topluluk) aktif katılımını sağlayan yenilikçi programlar ve mentorluk sistemleri mevcuttur. Düzenli olarak erişilebilirlik denetimleri yapılmakta ve iyileştirmeler sürdürülmektedir.	5

Tablo 16. Personel-Öğrenci Sağlığı ve Güvenliğine Yönelik Puan Tablosu

Açıklama	**Puan**
Sağlık ve güvenlik konularında herhangi bir resmi politika veya uygulama mevcut değil. Temel riskler göz ardı ediliyor.	0
Yasal gereklilikler çerçevesinde (örneğin ilk yardım dolabı, yangın tüpü) temel güvenlik ekipmanları mevcuttur. Periyodik risk değerlendirmeleri yapılmamaktadır.	1
Temel iş sağlığı ve güvenliği eğitimleri (yangın tatbikatı gibi) düzenlenmekte, acil durum planları kısmen mevcuttur. Okul kantini ve hijyen koşulları temel standartları karşılamaktadır.	2
Kapsamlı bir iş sağlığı ve güvenliği politikası uygulanmaktadır. Düzenli risk değerlendirmeleri yapılmakta, tüm paydaşlar için (öğrenci, personel) düzenli eğitimler ve tatbikatlar organize edilmektedir. Fiziksel ve ruhsal sağlık destek hizmetleri (örneğin rehberlik servisi) mevcuttur.	3
Proaktif bir sağlık ve güvenlik yönetimi sistemi benimsenmiştir. Potansiyel tehlikeler önceden tespit edilmekte ve önleyici önlemler alınmaktadır. Çalışan ve öğrenci refahını artırıcı programlar (örneğin, spor etkinlikleri, psikolojik danışmanlık) sunulmaktadır.	4
Okul, sağlık ve güvenlik konusunda en üst düzeyde performans göstermektedir. Sürekli iyileştirme prensibiyle, sağlık ve güvenlik riskleri minimuma indirilmiş, çalışan ve öğrenci refahı en üst düzeyde tutulmaktadır. Sağlıklı beslenme, fiziksel aktivite ve ruhsal destek programları okul kültürüne entegre edilmiştir. Uluslararası standartlarda (örneğin ISO 45001) bir yönetim sistemi uygulanmaktadır.	5

3. Skorlama Algoritması

3.1 Kriter Puanlarının Normalizasyonu

Ortaöğretim kurumların için üç ana tema altında işlenen kriterler ilgili puan tablosuna göre değerlendirildikten sonra toplam sürdürülebilirlik skoru elde edilmelidir. Buna yönelik olarak her tema kendi içinde normalize edilir. Normalizasyon formülü Denklem 1'de yer almaktadır.

$$Tema\ Skoru\ (Normalize\ Edilmiş) = \frac{Alınan\ Puan}{Maksimum\ Puan} \quad (1)$$

Örnek olarak Aydın / Efeler Mimar Sinan Mesleki ve Teknik Anadolu Lisesi'nden elde edilem ham kriter puanlarının normalize edilmesi sonucunda oluşan normal skorlar Tablo 17'de gösterilmiştir.

Tablo 17. Normalize Edilmiş Skor

Tema	Alınan Puan	Maksimum Puan	Normalize Edilmiş Skor
Enerji Yönetimi	10	35	0.28571
Ekonomik Sürdürülebilirlik	15	25	0.6
Sosyal Sürdürülebilirlik	16	25	0.64

3.1 Ana Temaların Ağırlıklandırılması

Kriterlere yönelik normalize edilmiş puanlar elde edildikten sonra kurumların sürdürülebilirlik performanslarının belirlenmesi gerekmektedir. Enerji yönetimi, ekonomik ve sosyal sürdürülebilirlik ana temalarının önem düzeylerinin saptanması için çok kriterli karar verme yöntemlerinden olan LOPCOW (Level Order Priority for Criteria Weighting), incelenerek ağırlık katsayılarının nasıl hesaplanacağı ile ilgili araştırmalar yapılmıştır. Skorlama sürecinde özgün bir kriterli karar yönteminin kurulması amaçlanarak LOPCOW yönteminden esinlenilmiştir. Skorlama için yeni bir ortak ağırlıklandırma sistemi geliştirilmiştir. Geliştirilen ortak ağırlıklandırma sisteminde, ana temaların yüzdesel oranlarını bir karşılaştırma matrisine yerleştirilir. Karşılaştırma matrisi, kriterlerin birbirleriyle olan göreceli önemlerini belirlemek için kullanılır. Bu matris, her bir kriterin diğerlerine göre ne kadar önemli olduğunu sayısal olarak ifade eder. Karşılaştırma matrisinin temel amacı, kriterlerin ağırlıklarını hesaplamaktır. Ağırlıklar, karar verme sürecinde hangi kriterlerin daha öncelikli olduğunu belirler.

Tablo 18. Ana Tema Yüzdeleri

Ana Tema	**Belirlenen Başlangıç Yüzdesi**
Enerji Yönetimi (EY)	%40
Ekonomik Sürdürülebilirlik (ES)	%30
Sosyal Sürdürülebilirlik (SS)	%30

Tablo 18'de, ana temaların belirlenen yüzdelikleri gösterilmiştir. Bu yüzdeliklere göre Denklem 2'de gösterildiği üzere bir karşılaştırma matrisi hesaplanır.

$$\begin{bmatrix} 1 & \frac{EY}{ES} & \frac{EY}{SS} \\ \frac{ES}{EY} & 1 & \frac{ES}{SS} \\ \frac{SS}{EY} & \frac{SS}{ES} & 1 \end{bmatrix} = \begin{bmatrix} 1 & \frac{0.4}{0.3} & \frac{0.4}{0.3} \\ \frac{0.3}{0.4} & 1 & \frac{0.3}{0.3} \\ \frac{0.3}{0.4} & \frac{0.3}{0.3} & 1 \end{bmatrix} = \begin{bmatrix} 1 & 1.33 & 1.33 \\ 0.75 & 1 & 1 \\ 0.75 & 1 & 1 \end{bmatrix} \quad (2)$$

Tablo 19'da verilen karşılaştırma matrisi sonucu oluşan her bir satır normalleştirilir. Denklem 3'te normalleştirme fonksiyonu verilmiştir. Bu fonksiyona göre ana temaların oluşturduğu ağırlık katsayıları Tablo 20'deki gibidir.

Tablo 19. Ana Temaların Karşılaştırma Matrisi

Karşılaştırma Matrisi	Enerji Yönetimi	Ekonomik Sürdürülebilirlik	Sosyal Sürdürülebilirlik
Enerji Yönetimi	1	1.33	1.33
Ekonomik Sürdürülebilirlik	0.75	1	1
Sosyal Sürdürülebilirlik	0.75	1	1

$$Normalleştirme = \frac{1}{x_{ij} + x_{ij+1}x_{ij+2}} \quad (3)$$

Tablo 20. Ana Temaların Ağırlık Katsayıları

Ana Tema	**Ağırlık Katsayısı**
Enerji Yönetimi	0.273
Ekonomik Sürdürülebilirlik	0.364
Sosyal Sürdürülebilirlik	0.364

3.2 Ağırlıklı Tema Skorunun Hesaplanması

Normalize edilmiş kriter puanları ile ilgili temanın ağırlık katsayısı çarpılarak ağırlıklı tema skoru elde edilir. Denklem 4'te her bir temaya uygulandığında Ağırlıklandırılmış Enerji Yönetimi Skoru (AEYS), Ağırlıklandırılmış Ekonomik Sürdürülebilirlik Skoru (AESS), Ağırlıklandırılmış Sosyal Sürdürülebilirlik Skoru (ASSS) elde edilir. Tablo 21'de Aydın/Efeler Mimar Sinan Mesleki ve Teknik Anadolu Lisesi'ne ait ağırlıklı tema skoru tablosuna yer verilmiştir.

$$Ağırlıklı\ Tema\ Skoru = Normalize\ Edilmiş\ Kriter\ Puanı \times Tema\ Ağırlık\ Katsayısı \quad (4)$$

Tablo 21. Ağırlıklı Tema Skoru

Tema	Normalize Edilmiş Skor	Tema Ağırlık Katsayısı	Ağırlıklı Skor
Enerji Yönetimi	0.28571	0.273	0.078
Ekonomik Sürdürülebilirlik	0.6	0.364	0.2184
Sosyal Sürdürülebilirlik	0.64	0.364	0.23296

3.3 Toplam Skorun Elde Edilmesi ve Sertifika Seviyesinin Belirlenmesi

Ağırlıklı tema skorlarının elde edilmesinden sonra yüzdelik toplam skor Denklem 5'te gösterildiği üzere hesaplanır.

$$Toplam\ Yüzdelik\ Skor = (AEYS + AESS + ASSS) \times 100 \quad (5)$$

Elde edilen toplam yüzdelik skor Tablo 22'deki ölçeğe göre değerlendirilir ve ortaöğretim kurumu sertifikalandırılır.

Tablo 22. Sertifika Seviyesi Ölçeği

Toplam Yüzdelik Skor Aralığı	Seviye
0-19	Bakır
20-39	Bronz
40-59	Gümüş
60-79	Altın
80-100	Platin

BULGULAR ve TARTIŞMA

Uygulanan değerlendirme modeli kapsamında, beş farklı ortaöğretim kurumu üç ana tema altında toplam 16 kritere göre analiz edilmiştir. Her bir kriter için alınan puanlar normalize edilmiş, özgün ağırlık katsayıları ile çarpılarak her okulun genel sürdürülebilirlik skoru elde edilmiştir.

Toplam puanlar %10.9 ile %52.9 arasında değişmiş ve kurumlar, elde ettikleri skora göre beş basamaklı bir sertifika ölçeğine yerleştirilmiştir: Bakır, Bronz, Gümüş, Altın ve Platin. Pilot uygulamada yer alan okullar arasında iki kurum Gümüş seviyeye ulaşarak sürdürülebilirlik yolculuğunda kayda değer bir aşama kaydetmiş;

diğer üç kurum ise Bakır seviyede yer almıştır. Bu sonuçlar, kurumların sürdürülebilirlik alanındaki farkındalık düzeylerinin farklılık gösterdiğini ve bazı alanlarda gelişim fırsatlarının bulunduğunu göstermektedir.

Sosyal Sürdürülebilirlik teması genel olarak en yüksek skorların alındığı alandır. Öğrenci ve öğretmenlerin toplumsal farkındalık, kültürel mirasın korunması ve kapsayıcılık gibi başlıklarda aktif roller üstlendikleri görülmektedir. Bu durum, eğitimin sosyal yönünün kurumsal kültürde güçlü bir şekilde yer aldığını göstermektedir.

Ekonomik Sürdürülebilirlik alanında ise kurumlar arasında gözle görülür farklar oluşmuştur. Bazı kurumlar kaynakların etkin kullanımı, maliyet tasarrufu ve sürdürülebilir satın alma politikaları konusunda önemli adımlar atmışken, diğerlerinde bu alanlar henüz gelişim sürecindedir.

Enerji Yönetimi ise genel olarak en düşük puanların alındığı temadır. Akıllı enerji sistemleri, yenilenebilir enerji kullanımı ve tüketim verilerinin izlenmesi gibi kriterlerde yapısal eksiklikler dikkati çekmiştir. Bu durum, altyapı yatırımları ve teknik kapasite artırımı gereksinimini ortaya koymaktadır.

Bu bulgular, değerlendirilen kurumların sürdürülebilirlik kavramına ilgi duyduğunu ancak uygulama düzeyinde gelişim alanlarına ihtiyaç duyduklarını göstermektedir. Özellikle "Bakır" seviyesinde yer alan kurumlar için bu analiz, güçlü yönlerini koruyarak hangi alanlarda ilerleme sağlanabileceğine dair yol gösterici bir işlev üstlenmektedir. Modelin detaylı ve tematik yapısı sayesinde, her kurum kendi özelinde öz değerlendirme yapabilir ve kurumsal sürdürülebilirlik stratejilerini bu doğrultuda geliştirebilir.

SONUÇ

Değerlendirme sonuçlarına göre, Aydın Efeler Lisesi ve Germencik Anadolu Lisesi "Gümüş" sertifika seviyesine ulaşırken; Menemen Şehit Hakan Gülşen Anadolu İmam Hatip Lisesi, Hüseyin Okan Merzeci Anadolu Lisesi ve Kadıköy Abdülhamidhan Lisesi "Bakır" seviyesinde yer almıştır.

İki kurum "Gümüş" seviyeye ulaşarak sürdürülebilirlik konusunda önemli adımlar attıklarını göstermiştir. Diğer üç kurum ise "Bakır" seviyede yer almakta olup, bu durum gelişim potansiyellerine işaret etmektedir. Sosyal sürdürülebilirlik teması genel olarak daha güçlü sonuçlar verirken, enerji yönetimi ve ekonomik sürdürülebilirlik alanlarında daha fazla yapısal çalışmaya ihtiyaç duyulduğu görülmüştür.

Model, kurumların mevcut durumlarını analiz etmelerine, güçlü ve gelişime açık yönlerini belirlemelerine yardımcı olmaktadır. Aynı zamanda, sürdürülebilirlik çalışmalarını planlamak ve izlemek isteyen okul yöneticileri için pratik bir yol haritası sunmaktadır.

Bu bağlamda, sürdürülebilirlik yolculuğuna adım atan tüm kurumlar, küçük ama etkili adımlarla daha ileri seviyelere ulaşabilir. Geliştirilen sistem, bu yolculukta rehberlik eden bir araç olarak değer taşımaktadır.

TEŞEKKÜR

Bu çalışmanın gerçekleştirilmesine katkı sunan İzmir Bakırçay Üniversitesi Ekolojik Üniversite Koordinatörlüğü ile değerlendirme sürecine katılan tüm okullara teşekkür ederiz.

KAYNAKLAR

Amiano Bonatxea, I., Gutiérrez-Goiria, J., Vazquez-De Francisco, M. J., & Sianes, A. (2022). "Is the global reporting initiative suitable to account for university social responsibility? Evidence from European institutions", International Journal of Sustainability in Higher Education, 23(4), 831–847.

Ávila, L. V., Leal Filho, W., Brandli, L., Macgregor, C. J., Molthan-Hill, P., Özuyar, P. G., & Moreira, R. M. (2017). "Barriers to innovation and sustainability at universities around the world", Journal of Cleaner Production, 164, 1268–1278.

del Mar Alonso-Almeida, M., Llach, J., & Marimon, F. (2014). "A closer look at the Global Reporting Initiative's sustainability reporting as a tool to implement environmental and social policies: A worldwide sector analysis", Corporate Social Responsibility and Environmental Management, 21(6), 318–335.

Doane, D., & MacGillivray, A. (2001). Economic Sustainability: The Business of Staying in Business. London: New Economics Foundation.

Ertan, Y. (2018). "Türkiye'de Sürdürülebilirlik Raporlaması (2005–2017)", Journal of Accounting and Taxation Studies, 11(3), 463–478.

Fuster, E., Padilla-Meléndez, A., Lockett, N., & del-Águila-Obra, A. R. (2019). "The emerging role of university spin-off companies in developing regional entrepreneurial university ecosystems: The case of Andalusia", Technological Forecasting and Social Change, 141, 219–231.

Godemann, J., Bebbington, J., Herzig, C., & Moon, J. (2014). "Higher education and sustainable development: Exploring possibilities for organisational change", Accounting, Auditing & Accountability Journal, 27(2), 218–233.

Gümrah, A., & Tanç, Ş. G. (2018). "Sürdürülebilirlik raporlarının içerik kalitesi: BIST sürdürülebilirlik endeksinde bir uygulama", Muhasebe Bilim Dünyası Dergisi, 20, 334–357.

Hedberg, C. J., & Von Malmborg, F. (2003). "The global reporting initiative and corporate sustainability reporting in Swedish companies", Corporate Social Responsibility and Environmental Management, 10(3), 153–164.

Heemskerk, B., Pistorio, P., & Scicluna, M. (2002). Sustainable Development Reporting: Striking the Balance. Geneva: World Business Council for Sustainable Development.

Köse, B., Ansay, S., Akderya, T., Tabakoğlu, G., Hızıroğlu, K., & Berktaş, M. (2024). Yeşil Kampüs Sertifikasyonları ve Sürdürülebilirlik İlişkisi: İzmir Bakırçay Üniversitesi Örneği. *Yükseköğretim Dergisi*, *14*(3), 3-4.

Önce, S., Onay, A., & Yeşilçelebi, G. (2015). "Kurumsal sürdürülebilirlik raporlaması ve Türkiye'deki durum", Journal of Economics, Finance and Accounting, 2(2), 230–252.

Portney, K. E. (2015). Sustainability. Cambridge, MA: MIT Press.

Ramísio, P. J., Pinto, L. M. C., Gouveia, N., Costa, H., & Arezes, D. (2019). "Sustainability strategy in higher education institutions: Lessons learned from a nine-year case study", Journal of Cleaner Production, 222, 300–309.

World Commission on Environment and Development (WCED). (1987). Our Common Future. Oxford: Oxford University Press.

➢ *ORAL PRESENTATION*

Perlit agregalı polimer betonların kılcal su emme özelliklerinin deneysel olarak incelenmesi

Bedirhan İhsan GÜLNAHAR[1*] (*ORCID: https://orcid.org/0009-0002-3345-2110)*
Halit Alperen BULUT[2] (*ORCID: https://orcid.org/0000-0002-1770-195X*)

*[1]Erzincan Binali Yıldırım Üniversitesi, Fen Bilimleri Enstitüsü, İnşaat Mühendisliği Anabilim Dalı, Erzincan, Türkiye.
[2]Erzincan Binali Yıldırım Üniversitesi, Mühendislik ve Mimarlık Fakültesi, İnşaat Mühendisliği Bölümü, Erzincan, Türkiye.

*Sorumlu yazar e-posta: bedir.gulnahar@gmail.com

Özet
Bu çalışmada, doğal ve genleştirilmiş perlitler polimer beton üretiminde agrega malzemesi olarak değerlendirilmiş ve bu agregaların polimer betonların su emme özellikleri üzerindeki etkileri araştırılmıştır. Polimer betonlarda bağlayıcı malzeme olarak doymamış polyester reçine ve vinilester reçine tercih edilmiştir. Perlit oranları %0 (kontrol), %5 ve %10 olarak belirlenmiş ve kuvars agregası yerine kullanılmıştır. Üretilen polimer beton numuneler hava koşullarında 28 ve 56 gün kür edildikten sonra su emme deneyi uygulanmıştır. Deneysel sonuçlara göre, kontrol numunelerine kıyasla en yüksek su emme değerleri her iki reçine tipi için de %5 ve %10 genleştirilmiş perlit içeren betonlarda elde edilmiştir. Doğal perlit içeren betonlar incelendiğinde, 28 günlük numunelerde vinilester reçineli betonlar polyester reçineli betonlara göre daha düşük su emme değerleri göstermiştir. Bulgular, perlit türü ve oranı ile reçine türünün polimer betonların su emme davranışını önemli ölçüde etkilediğini göstermektedir. Bu çalışma, farklı perlit tipleri ve bağlayıcı sistemlerinin kombinasyonları açısından literatüre katkı sağlayabilecek özgün bulgular sunmaktadır.
Anahtar Kelimeler: Polimer beton, doğal perlit, genleştirilmiş perlit, reçine, kılcal su emme

Experimental investigation of sorptivity properties of perlite aggregate polymer concretes

Abstract

In this study, natural and expanded perlites were evaluated as aggregate materials in polymer concrete production and the effects of these aggregates on the sorptivity properties of polymer concretes were investigated. Unsaturated polyester resin and vinylester resin were preferred as binding material in polymer concretes. Perlite ratios were determined as 0% (control), 5% and 10% and were used instead of quartz aggregate. The produced polymer concrete samples were cured under air conditions for 28 and 56 days and then sorptivity test was applied. According to the experimental results, the highest water absorption values were obtained in concretes containing 5% and 10% expanded perlite for both resin types compared to control samples. When concretes containing natural perlite were examined, vinylester resin concretes showed lower water absorption values than polyester resin concretes in 28-day samples. The findings show that the type and ratio of perlite and the type of resin significantly affect the sorptivity behavior of polymer concretes. This study provides original findings that can contribute to the literature in terms of combinations of different perlite types and binder systems.
Keywords: Polymer concrete, natural perlite, expanded perlite, resin, sorptivity

GİRİŞ

Günümüzde en yaygın yapı malzemesi olan beton; agrega, su ve çimentodan oluşur (Junaid ve ark., 2022). Çimento üretiminin çevresel etkileri, mimarlar ve çevreciler tarafından ortak bir endişe kaynağı olarak değerlendirilmektedir. Bir ton çimento üretimi, 2 tondan fazla hammadde (kil ve kireç taşı) gerektirmekte ve yaklaşık 1 ton karbondioksit (CO_2) salınımına yol açmaktadır (Madheswaran ve ark.,2014). Küresel ölçekte CO_2 emisyonları incelendiğinde, bu emisyonların önemli bir bölümünün çimento üretimi gibi endüstriyel faaliyetlerden kaynaklandığı görülmektedir. Gelecek yıllarda bu miktarın 23 milyar tona ulaşabileceği öngörülmektedir (Kumar ve ark., 2015). Portland çimentosu üretimi ise, dünya genelindeki toplam CO_2 emisyonlarının yaklaşık %7'sini oluşturmaktadır (Ginghis ve ark., 2015). Beton üretiminin çevresel etkileri

değerlendirildiğinde, bu etkinin alternatif malzemelerin kullanımıyla azaltılabileceğine dair çalışmalar mevcuttur. En yaygın uygulama, çimento ve agrega alternatiflerinin kısmi olarak değiştirilmesidir (Mehta, 2001).

Polimer beton (PC), yüksek kalite-ağırlık oranı ve üstün mühendislik özellikleri sayesinde geleneksel çimento bazlı betonlara kıyasla giderek artan bir ilgi görmektedir (Jafari ve ark., 2018). Geleneksel betonun aksine, polimer beton çimento hidratlarının yerine reçine esaslı bağlayıcıların kullanılmasıyla elde edilmektedir (Heidari-Rarani ve ark., 2014). Polimer matrisin varlığı, bu beton türüne yüksek darbe direnci, yüksek basınç dayanımı ve donma-çözülme döngülerine karşı üstün dayanıklılık kazandırmaktadır (Bulut ve ark., 2017). Ayrıca, düşük geçirgenliği sayesinde suya ve diğer sıvılara karşı daha az geçirgen olup, kimyasal saldırılara ve aşınmaya karşı da önemli ölçüde direnç göstermektedir (Zegardlo ve ark., 2018).

Polimer betonla ilgili araştırma ve geliştirme çalışmaları son yıllarda hız kazanmış olup, bu çalışmalar genellikle farklı polimer reçineleri ve donatılarla üretilen harç ve betonların fiziksel, kimyasal ve mekanik özelliklerine odaklanmaktadır. Amaç, çeşitli uygulamalarda kullanılabilecek, daha dayanıklı ve çevresel etkilere karşı daha dirençli yapı malzemeleri geliştirmektir. Bu bağlamda, polimer betonun özellikle agresif çevre koşullarına maruz kalan altyapı projelerinde ve onarım işlerinde alternatif bir çözüm sunma potansiyeli bulunmaktadır (Garbacz ve ark., 2013). Nitekim, 2024 yılında yayımlanan bir çalışmada, polimer modifiyeli çimento harcının süperakışkanlaştırıcı katkısıyla geliştirilmesinin, kılcal su emme oranını %1,75'ten %0,76'ya düşürdüğü ve bu sayede malzemenin uzun ömürlü ve dayanıklı bir yapı malzemesi olarak kullanılabileceği belirtilmiştir (Qasim ve ark., 2024).

Perlit, çok sayıda eş merkezli çatlak yapısıyla karakterize edilen volkanik kökenli camsı bir mineraldir. Bu yapı, perlitin parçalandığında inci benzeri bir görünüm kazanmasına neden olur. Doğal haliyle yüksek oranda su içerebilen perlit, yaklaşık 900 °C'de ısıtıldığında ani genleşme göstererek düşük yoğunluklu, hafif agrega formuna dönüşür. Bu işlem sonucunda elde edilen genleştirilmiş perlitin yoğunluğu yaklaşık 30–240 kg/m³ arasında değişmektedir (Chandra ve ark., 2002). Mineralojik olarak yaklaşık %80 oranında cam fazı içeren perlit, gözenekli yapısı sayesinde oldukça hafif bir malzemedir. Ayrıca, genleştirilmiş perlit agregası, Portland çimentosuna benzer şekilde puzolanik aktivite sergileyerek bağlayıcı özellik gösterebilir. Bu özellikleri nedeniyle perlit, beton endüstrisinde hem katkı maddesi olarak hem de agrega veya bağlayıcı ikamesi olarak kullanım potansiyeline sahiptir (Demirboğa ve ark., 2003).

Bu çalışmanın amacı, perlit agregasının polimer betonlarda kullanımını araştırmak ve kuvars agregasına alternatif olabileceğini ortaya koymaktır. Doymamış polyester ve vinilester reçinelerin bağlayıcı olarak kullanıldığı çalışmada, perlitin polimer betonun kılcal su emme etkisi incelenmiştir.

MATERYAL VE METOD

Polimer beton üretiminde bağlayıcı malzeme olarak CE-80 tipi doymamış polyester reçine ve bisfenol-A 701 vinilester reçine kullanılmıştır. Dolgu malzemesi olarak belirli gradasyonlarda kuvars agregası, kırma taş ve perlit agregası kullanılmıştır. Her iki reçineye ait teknik bilgiler Tablo 1 ve Tablo 2' de verilmiştir.

Tablo 1. Polyester Reçine Sertleşmiş Özellikleri

Özellik	Aralık	Birim	Test
Su Absorpsiyonu	0,17–0,19	%	ISO 62
Eğilme dayanımı	125	MPa	ISO 178
Eğilme modülü	3700	MPa	ISO 178
Kopmadaki uzama	5,6	%	ISO 178
Çekme dayanımı	63	MPa	ISO 527-2
Çekme modülü	3020	MPa	ISO 527-2
Kopmadaki uzama	3,5	%	ISO 527-2
Darbe dayanımı	11	kJ/m²	ISO 179
Yük Altında Eğilme Sıcaklığı (HDT)	58	°C	ISO 75-B
Barkol Sertliği	42	-	ASTM D2583
Toplam hacimsel çekme	7.9	%	ISO 3521

Tablo 2. Vinilester Reçine Sertleşmiş Özellikleri

Test	Metot	Değer
Su Absorpsiyonu	ISO 0062	0,150 %
Eğilme Dayanımı	ISO 0178	160 MPa
Eğilme modülü	ISO 0178	4360 MPa
Kopmadaki Uzama	ISO 0178	6,90 %
Çekme Dayanımı	ISO 0527	80 MPa
Çekme modülü	ISO 0527	3200 MPa
Kopmadaki Uzama	ISO 0527	5–6 %
Darbe Dayanımı	ISO 0180	17 kJ/m²
Yük Altında Eğilme Sıcaklığı (HDT)	ISO 0075-A	95 °C
Barkol Sertliği	ASTM-D 2583	35
Toplam Hacimsel Çekme	ISO 2114	7,7 %

Kullanılan reçinelerin sertleşmesi ve hızlı bir şekilde reaksiyona başlaması için kullanılan yardımcı kimyasallardan MEK-P Sertleştirici ve Kobalt Oktoalt Hızlandırıcı malzemelere ait teknik bilgiler Tablo 3 ve Tablo 4'de verilmiştir.

Tablo 3. Akperox A1 Sertleştirici Özellikleri

Yoğunluk 20°C	1,16 ± 0,005 gr/cm3
Görünüm	Renksiz, sıvı
Çözücü	DMP
Aktif Oksijen İçeriği	9,4 -9,6 %
Peroksit İçeriği	33 -37 %
CAS No.	1338-23-4
EINECS/ELINCS No.	700-954-4

Tablo 4. Kobalt Oktoalt Hızlandırıcı KP6 Özellikleri

Görünüş	Berrak, Sıvı	-
Co Metal (%)	5.90-6.10	-
Renk	Koyu Mavi	-
Toplam Katı (%, 105°C, 3 saat)	Max. 45	TS EN ISO 3251
Yoğunluk (gr/cm³, 25°C)	0.915-0.965	DIN EN ISO 2811-3

Beton numuneleri üretilirken kontrol betonlarında perlit agregası kullanılmamıştır. Diğer numunelerde ise, kuvars ve kırma taş agregalarının belirli oranlarda (%5 ve %10) doğal perlit ve genleştirilmiş perlit agregalarıyla kısmen ikame edilmesiyle üretilmiştir. Deney sonuçlarının yorumunu kolaylaştırmak amacıyla numunelere bir kodlama sistemi uygulanmıştır. Bu sistemde, kullanılan reçine ve perlit türleri, İngilizce kısaltmalarının ilk harfleriyle

gösterilmiş; perlitin ikame oranları ise bu harflerin ardından, yüzde işareti kullanılmaksızın sayılarla belirtilmiştir. Numunenin kürlenme gün sayısı ise, kodun sonuna "/" işareti eklenip gün sayısı yazılarak belirtilmiştir. Örneğin, "PRP0/28" kodu, polyester reçine ile üretilmiş, perlit agregası içermeyen (%0 perlit ikameli) kontrol numunesini ve bu numunenin 28 günlük kür süresi sonunda deneye tabi tutulduğunu ifade etmektedir. Benzer şekilde, "VREP10/56" kodu ise, vinilester reçine ile hazırlanmış ve toplam agrega miktarının %10'u genleştirilmiş perlit ile ikame edilmiş numunenin, 56 günlük kür süresi sonunda teste tabi tutulacağını göstermektedir.
28 ve 56 günlük kürleme sürelerinin sonunda hazırlanan silindirik beton numuneleri (100×200 mm) üzerinde kılcal su emme deneyi gerçekleştirilmiştir. Deney prosedürü, TS EN 13057 (2003) standardına uygun olarak yürütülmüştür. Bu kapsamda, her numune belirli zaman aralıklarında (1, 4, 9, 16, 25, 36, 49, 64 ve 81. dakikalarda) sudan çıkarılmış, yüzeyindeki serbest su emici bezle dikkatlice temizlenmiş ve ardından hassas terazide tartılarak kütle artışları kaydedilmiştir. Elde edilen kütle değerleri, birim alan başına su emme miktarı olarak hesaplanmış ve zamanla değişimleri analiz edilmiştir. Böylece, numunelerin kılcal su emme kapasiteleri belirlenerek, farklı reçine türlerinin ve perlit ikame oranlarının su geçirgenliği üzerindeki etkileri karşılaştırılmıştır.

BULGULAR ve TARTIŞMA

Şekil 1'de, kontrol betonları ve farklı oranlardaki perlit ikameli polimer betonların kılcal su emme katsayıları verilmiştir.

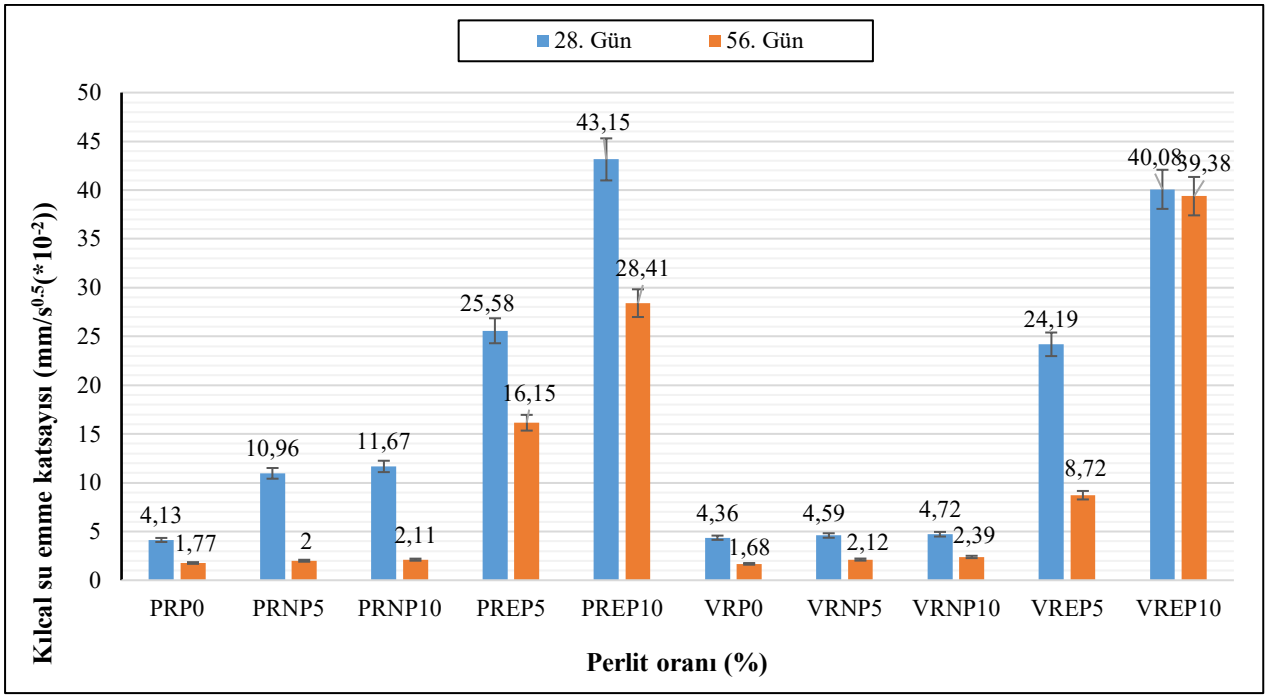

Şekil 1. Kılcal Su Emme Katsayıları

Şekil 1'e göre, numunelere eklenen perlit oranındaki artış, kılcal su emme kapasitesini genel olarak yükseltmiştir. En düşük emme oranları, perlit içermeyen kontrol gruplarında elde edilirken; genleştirilmiş perlitin %10 oranında kullanıldığı numunelerde en yüksek değerler kaydedilmiştir. Bu durum, genleştirilmiş perlitin gözenekli yapısı nedeniyle su geçirimini artırdığı şeklinde yorumlanabilir.

Polyester reçineli grupta, PRP0 kontrol numunesi 28. ve 56. günlerde sırasıyla 4,13 ve 1,77 $mm/s^{0.5} \cdot 10^{-2}$ ile en düşük değerlere ulaşmıştır. Öte yandan, %10 genleştirilmiş perlit içeren PREP10 numunesinde bu değerler 43,15 ve 28,41 olarak ölçülmüştür.

Vinilester reçineli numunelerde benzer bir eğilim görülmekle birlikte, bu grupta 28 ve 56 günlük ölçümler arasında daha az fark oluşmuştur. Özellikle VREP10 numunesinde 40,08 ve 39,38 $mm/s^{0.5} \cdot 10^{-2}$ gibi birbirine yakın sonuçlar elde edilmesi, vinilester reçinenin suya karşı daha kararlı bir yapı sunduğunu göstermektedir. Ayrıca, doğal perlit içeren numunelerin genleştirilmiş perlit içerenlere kıyasla daha düşük su emme değerlerine sahip olduğu gözlemlenmiştir.

28 günlük kür süresine ait veriler, tüm numunelerde 56 günlük sürelere kıyasla daha yüksek kılcal su emme değerleri göstermektedir. Bu durum, kür süresinin uzamasının malzemenin geçirgenliğini azalttığını ve suya karşı daha dirençli bir yapı oluşturduğunu ortaya koymaktadır. Aynı oranda perlit içeren numunelerin 28 günlük verileri karşılaştırıldığında ise, vinilester reçineli numuneler (özellikle doğal perlit katkılı olanlar) polyester reçineli numunelere göre daha düşük su emme oranları sergilemiştir. Bu da vinilester reçinenin su geçirimsizliği açısından daha avantajlı bir bağlayıcı sistem sunduğunu göstermektedir.

Elde edilen bulgular doğrultusunda, perlit agregasının türü ve oranının polimer betonların su emme performansı üzerinde belirleyici bir rol oynadığı görülmektedir. Özellikle genleştirilmiş perlitin gözenekli ve düşük yoğunluklu yapısı, betonun kapiler su emme kapasitesini artırarak geçirgenliği olumsuz etkilemiştir. Bu durum, hem polyester hem de vinilester reçineli numunelerde benzer eğilimler göstermiştir.

Vinilester reçinenin, polyester reçineye kıyasla daha düşük su emme değerleri üretmiş olması, bağlayıcının kimyasal yapısının betonun geçirgenlik özelliklerine olan etkisini ortaya koymaktadır. Vinilester reçinenin daha yoğun ve daha iyi bağ oluşturan bir yapı sergilemesi, suyun beton içerisinde ilerlemesini sınırlayarak geçirgenliği azaltmıştır.

Ayrıca, kür süresinin uzamasıyla birlikte reçinenin ve agreganın etkileşimi daha stabil hale gelmiş ve bu durum numunelerin suya karşı direncini artırmıştır. Özellikle 56 günlük kür sonrası değerlerin belirgin şekilde düşmüş olması, zamanla oluşan mikro yapı gelişiminin su geçiş yollarını daralttığını göstermektedir.

SONUÇ

Bu çalışmada, kuvars agregasının yerine farklı oranlarda (0%, 5%, 10%) doğal ve genleştirilmiş perlit kullanılarak üretilen polimer betonların su emme (sorptivite) özellikleri incelenmiştir. Bağlayıcı olarak doymamış polyester ve vinilester reçineler tercih edilmiş, numuneler 28 ve 56 gün boyunca hava koşullarında kür edilmiştir. Elde edilen deneysel bulgular ve yapılan değerlendirmeler doğrultusunda şu sonuçlara ulaşılmıştır:

1- Genleştirilmiş perlit kullanımı, her iki reçine türünde de su emme değerlerini artırmıştır. Özellikle %10 oranındaki genleştirilmiş perlit, en yüksek su emme değerlerine neden olmuştur.

2- Doğal perlit, genleştirilmiş perlite kıyasla daha düşük su geçirgenliği sağlamış, bu da perlitin gözeneklilik ve yoğunluk özelliklerinin geçirgenliğe olan etkisini ortaya koymuştur.

3- Vinilester reçine ile üretilen betonlar, polyester reçineli betonlara göre genel olarak daha düşük su emme oranları göstermiştir. Bu durum vinilester reçinenin daha yoğun yapısının ve bağlanma özelliklerinin, geçirgenlik üzerinde etkisi olduğunu göstermektedir.

4- Kür süresinin 56 güne çıkarılması, tüm karışımlar için su emmeyi önemli ölçüde azaltmıştır. Bu, betonun zamanla daha kompakt ve suya karşı dirençli bir yapıya kavuştuğunu göstermektedir.

Sonuç olarak, perlit tipi ve oranı kadar, bağlayıcı reçine seçimi ve kür süresi de polimer betonların geçirgenlik performansını doğrudan etkilemektedir. Bu bağlamda, su geçirimsizliğin önemli olduğu uygulamalarda vinilester reçine kullanımı ve doğal perlit tercih edilmesi daha uygun bir yaklaşım olarak öne çıkmaktadır.

KAYNAKLAR

Bulut, H. A., & Sahin, R. (2017). A study on mechanical properties of polymer concrete containing electronic plastic waste. *Compos Struct*, 178, 50–62.

Chandra, S., & Berntsson, L. (2002). *Lightweight Aggregate Concrete*. Noyes Publications / William Andrew Publishing, NY, p. 28.

Demirboğa, R., & Gul, R. (2003). The effects of expanded perlite aggregate, silica fume and fly ash on the thermal conductivity of lightweight concrete. *Cem. Concr. Res.*, 33, 723–727.

Garbacz, A., & Sokolowska, J. J. (2013). Concrete-like polymer composites with fly ashes – comparative study. *Constr. Build. Mater.*, 38, 689–699.

Ginghis, B., Aranan, M. (2015). Comparasion of the shear behaviour of geopolymer concrete beams with GFRP and steel transverse reinforcements. *FRPRCS-12 Joint Conference*, 14–16 December 2015.

Heidari-Rarani, M., Aliha, M. R. M., Shokrieh, M. M., & Ayatollahi, M. R. (2014). Mechanical durability of an optimized polymer concrete under various thermal cyclic loadings - an experimental study. *Constr. Build. Mater.*, 64, 308–315.

Jafari, K., Tabatabaeian, M., Joshaghani, A., & Ozbakkaloglu, T. (2018). Optimizing the mixture design of polymer concrete: An experimental investigation. *Constr. Build. Mater.*, 167, 185–196.

Junaid, M. F., Rehman, Z., Kuruc, M., Medveď, I., Bačinskas, D., Čurpek, J., Čekon, M., Ijaz, N., & Ansari, W. S. (2022). Lightweight concrete from a perspective of sustainable reuse of waste byproducts. *Construction and Building Materials*, 319, 126061. https://doi.org/10.1016/j.conbuildmat.2021.126061

Kumar, G., M. T., Abdul Aleem, S., & Dinesh, S. (2015). Application of geopolymer concrete. *IRJET Journal of Engineering*, 2(9), ISSN: 2395-0056.

Madheswaran, C. K., & Ambily, P. S. (2014). Experimental study on behaviour of reinforced geopolymer concrete beams subjected to monotonic static loading. *IJIRSET Journal of Engineering*, 3(7), ISSN: 2319-8753.

Mehta, K. P. (2001). Reducing the environmental impact of concrete. *Concrete International*, 23(10), 61–66.

Mladenović, A., et al. (2004). Alkali–silica reactivity of some frequently used lightweight aggregates. *Cem. Concr. Res.*, 34(10), 1809–1816.

Qasim, A. J., Al-Jaberi, Z. S., & Hussein, H. S. (2024). An experimental study of some mechanical properties and absorption for polymer-modified cement mortar modified with superplasticizer. *Engineering*, 2024(1), 1–10. https://doi.org/10.1515/eng-2024-0010

Zegardlo, B., Szelag, M., Ogrodnik, P., & Bombik, A. (2018). Physico-mechanical properties and microstructure of polymer concrete with recycled glass aggregate. *Materials*, 11.

➢ *ORAL PRESENTATION*

Reinforcement Learning for Aerial Robots: Real-World Evaluation of Infeasible Trajectory Tracking

Ali Tahir Karasahin[1*] (*ORCID: https://orcid.org/0000-0002-7440-1312*)

[*1] Necmettin Erbakan University, Faculty of Engineering, Department of Mechatronics Engineering, Konya, Türkiye.

*Corresponding author e-mail: alitahir.karasahin@erbakan.edu.tr

Abstract
Reinforcement learning (RL) is well-suited for remapping observations to outputs in aerial robot applications. However, RL-based policies require careful design, especially regarding the observation space and reward function. To address this issue, this study investigated an RL-based policy with an infeasible trajectory. The experimental results showed that the RL-based policy achieved a trajectory tracking error of only 0.057 m. Additionally, the study demonstrated the suitability of the SimpleFlight framework for infeasible trajectories in real-world experiments.

Keywords: reinforcement learning, machine learning for robot control, aerial robotics.

INTRODUCTION

Aerial robots are using different applications such as environmental sensing, inspection, aerial transportation and autonomous drone racing (Dionigi et al., 2024; Haddad et al., 2025; Karaşahin, 2024; Karasahin, 2024; Karasahin et al., 2025; Karasahin & Gungor, 2025; Li et al., 2025). It has been shown that the aerial robots have a capability these different applications owing to both low-cost and state-of-the-art technologies capabilities. However, these advantages come up with several requirements especially smooth trajectory tracking capabilities. Therefore, the aerial robotics have to precious controller for the trajectory tracking applications.

Traditional controllers are showed a good performance for several different applications. But mostly these controllers need to be high fidelity system models. In real-world applications, system modelling is a big challenge because of the characteristic of aerial robots. Although the system modelling is solved under specific approaching, the determine of some coefficient of controller is consume a lot of time. For this reason, reinforcement learning (RL) is evaluated an alternative approach for these applications (Hwangbo et al., 2017). RL is generated a policy that cover specific request based on environmental information. If the aerial robot has enough computation, this policy is showed superior performance than human skills (Kaufmann et al., 2023; Song et al., 2023). However, the observation space and reward design need to be determined as a carefully the represent of the potential of RL policy. In (Dionigi et al., 2024), it is investigated effect on the observation space on RL policy. According to this result, the observation space is thoroughly related with the RL policy behaviour. In (Chen et al., 2025), it is shown that the several key factors are important for the RL-based policies. In addition, the evaluation and determination of observation and reward function is a critical step for the RL-based policies.

To investigate the RL-based policies, this study evaluates trajectory tracking capabilities of RL-based policies under infeasible trajectories such as pentagram. This study trained a RL policy based on SimpleFlight framework (Chen et al., 2025). This paper is highlighted as follows:

- The performance of RL-based policy is evaluated under infeasible trajectory (pentagram) without any tuning real-world experiment.
- Empirical evidence is investigated based on trajectory tracking error performance of the aerial robots.
- The aerial robot states are evaluated during the real-world experiment especially euler angles.

MATERIALS AND METHODS

The aerial robot model is generated based on six-degree-of-freedom (DoF). The dynamic model of the aerial robot is as follow:

$$\begin{aligned} \dot{p} &= v \\ \dot{v} &= -ge_3 + \frac{1}{m}R(f+d) \\ \dot{R} &= R \cdot S(\omega) \\ \dot{\omega} &= J^{-1}\left(\tau - \omega \times (J\omega)\right) \end{aligned} \tag{1}$$

In Equation 1, let p, v, R represent the position of the aerial robot, linear velocity of the aerial robot in the world frame, rotation matrix between with body and world frame of the aerial robot. e_3 is the basis vector such as $[0,0,1]^T$. This equation is defined as a m, d, f and J respectively the total mass of the aerial robot, disturbance vector, the total thrust of the aerial robot generated by the four different motors and the inertia matrix of the aerial robot. S is the skew-symmetric matrix representing. The last variable of this equation, ω and τ are the angular velocity of the aerial robot and the torque value, respectively. The Crazyflie 2.1 platform is preferred as an aerial robot for the real-world experiment. The aerial robot parameters are shown in Table 1.

Table 1. The parameters of the aerial robot

Parameter	The aerial robot (Crazyflie 2.1)
Mass, m (kg)	0.0035
Inertial, J ($kg \cdot m^2$)	[1.43e-5, 1.43e-5, 2.89e-5]
Arm length (m)	0.043
Thrust-to-Weight-Ratio	1.95
Motor time constant (s)	0.05
Maximum thrust (N)	0.575

For the RL policy, SimpleFlight framework is preferred in the real-world experiment owing to both without required any additional tuning and suitable for the target platform (Chen et al., 2025). As an observation space is used three components such as the position error between the actual position and the next future (N=10) waypoints, linear velocity of the aerial robot and the rotation matrix that covers the up, lateral and heading information of the aerial robot. Another important key factor is determining of the reward function for the RL-based policies. The reward function is created as follows:

$$Total_{rew} = r_{pos} + r_{pos} * \left(r_{up} + r_{spin}\right) + r_{act} \tag{2}$$

In Equation 2 shows that the total reward is made up of three components. These components are described as follows: relative position error, calculated by the Euclidean distance; upright position of the aerial robot; and a penalty for large yaw-axis spinning and the difference between previous and actual action output, which increases the smoothness of the action output.

In this study, SimpleFlight framework is used for both training and evaluation in the real-world experiment. RL policy is generated by the proximal policy optimization (PPO) algorithm (Schulman et al., 2017). The PPO algorithm uses three-layer multilayer perceptrons (MLPs), each of which has 256 neurons. This training is evaluated with 7,500 epochs on NVIDIA RTX 4060 GPU. SimpleFlight framework is developed based on Isaac Sim. During the training, the number of parallel environments size is set to 512.

RESULTS

The real-world experiment was evaluated with infeasible trajectory such as pentagram. This infeasible trajectory is a challenge for the RL-based policies owing to sharp corners. The position and orientation data were generated by VICON motion capture system that produce each message with 100 Hz rate. The trajectory tracking performance is shown in Figure 1.

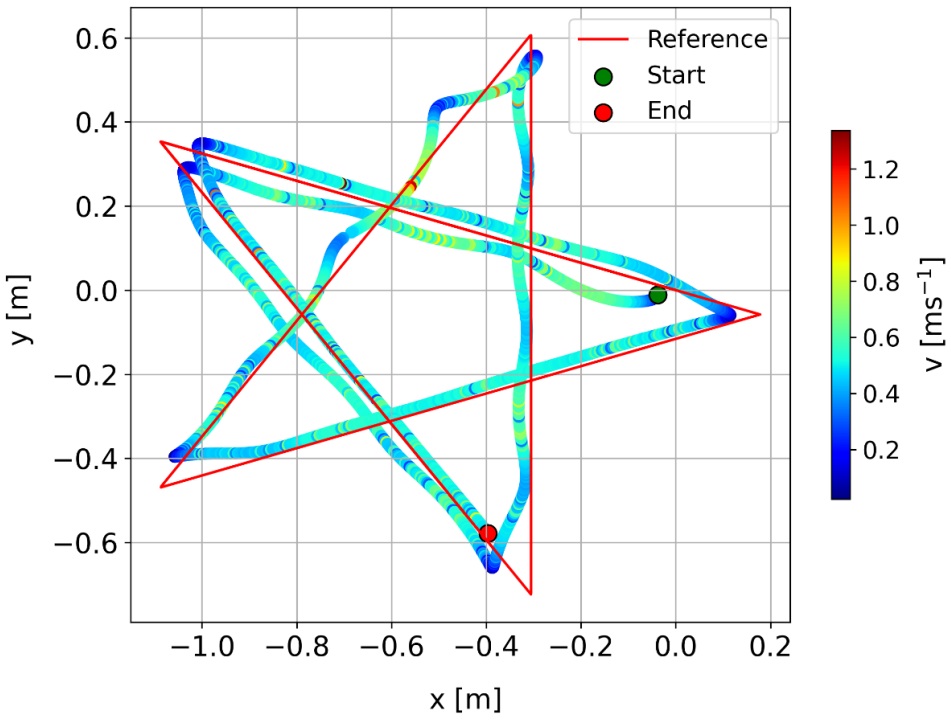

Figure 1. Trajectory tracking performance of aerial robot

According to this result, RL-based policies deal with this infeasible trajectory. In addition, RL-based policy was shown a good tracking capability for this real-world experiment. In this experiment, the mean of linear velocity of aerial robot was obtained 0.493 m/s. The trajectory tracking error was calculated 0.037 m. RL policy was evaluated under 5 different real-world experiment. These results are shown in Table 2.

Table 2. The mean euclidean distance (MED) position error of the aerial robot

Methods	Success Rate (%)	Position Error (m)
Real-world	100	0.057

The real-world experiments were evaluated 5 different examples. The evaluation was used with MED performance criteria. According to these results, RL-based policy has been shown an acceptable performance under infeasible trajectory. To demonstrate trajectory tracking performance, each axis was investigated with different result. The trajectory tracking performance on only x-axis was shown in Figure 2.

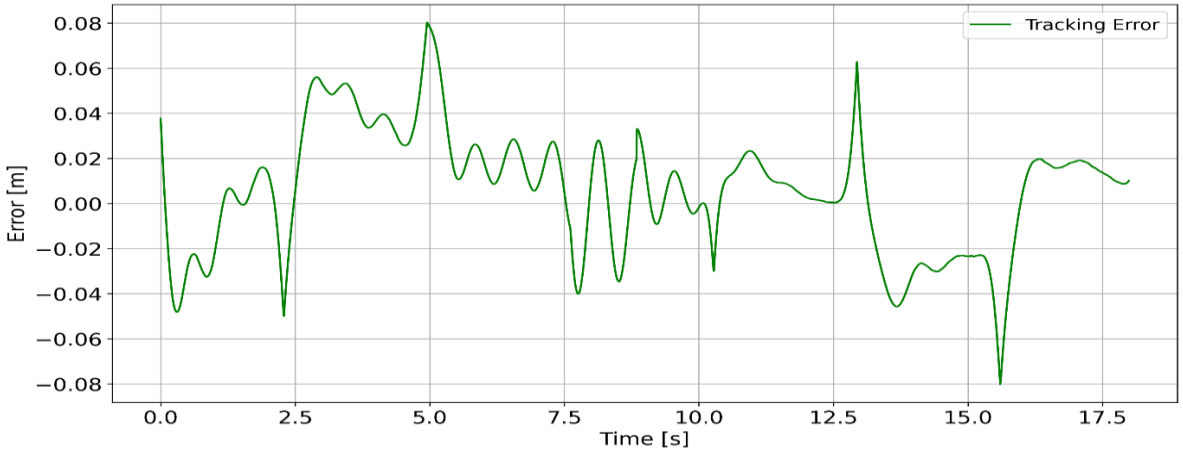

Figure 2. Trajectory tracking performance on x-axis of aerial robot

According to this experiment result, the maximum trajectory tracking error was observed as a 0.08 m. This empirical result provides a detailed analysis of the RL-based policy. The similar approach was used on the y-axis. The trajectory tracking performance on y-axis was illustrated in Figure 3.

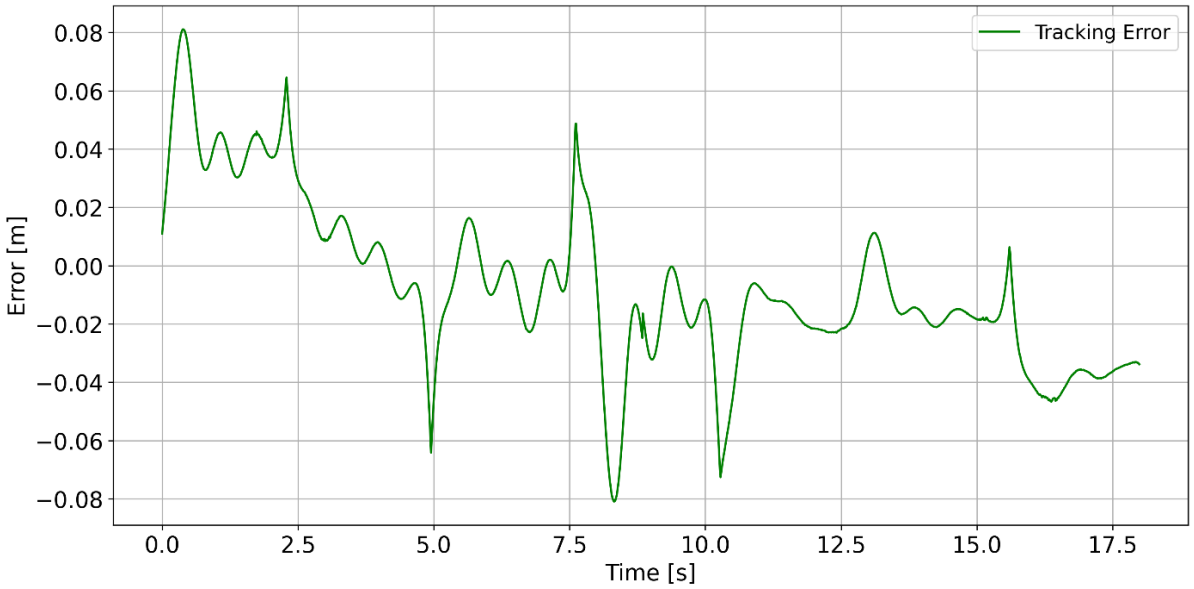

Figure 3. Trajectory tracking performance on y-axis of aerial robot

In Figure 3, the similar result was observed from RL-based policy. The maximum trajectory tracking error was calculated as a 0.08 m. According to these results, RL-based policy has been shown high capability for the infeasible trajectory tracking tasks.

DISCUSSION

The experimental results have been carefully investigated for RL-based policy performance under infeasible trajectory. The RL-based policy is not required any tuning for the real-world experiment. These skills are important key point for the future works. According to experimental results, each corner of pentagram was observed some trajectory tracking error. However, this study has shown that the RL-based policy is generated acceptable performance under infeasible trajectory. However, both observation space and reward function may update for the lower position error.

CONCLUSION

The study was a detailed investigation of the aerial robot's trajectory tracking performance. The trajectory tracking performance was evaluated with infeasible trajectory 5 different experiments. According to experimental results, RL-based policy has been shown an acceptable performance in the real-world scenario. RL-based policy was deal with infeasible trajectories without any required additional tuning for action outputs. This result, it has been promising that using RL-based policies in the complex environments in the field of aerial robotics.

ACKNOWLEDGEMENTS

This study gratefully acknowledges the Bristol Robotics Laboratory for granting access to the indoor flight arena. The study also thanks the Aerial Robotics Group for their valuable support of the experiments. The author was supported by Turkish Scientific and Technological Research Council (Grant Ref. 1059B192302726).

REFERENCES

Chen, J., Yu, C., Xie, Y., Gao, F., Chen, Y., Yu, S., Tang, W., Ji, S., Mu, M., Wu, Y., & others. (2025). What Matters in Learning A Zero-Shot Sim-to-Real RL Policy for Quadrotor Control? A Comprehensive Study. IEEE Robotics and Automation Letters.

Dionigi, A., Costante, G., & Loianno, G. (2024). The Power of Input: Benchmarking Zero-Shot Sim-to-Real Transfer of Reinforcement Learning Control Policies for Quadrotor Control. *2024 IEEE/RSJ International Conference on Intelligent Robots and Systems (IROS)*, 11812–11818. https://doi.org/10.1109/IROS58592.2024.10802831

Haddad, A. G., Boiko, I., & Zweiri, Y. (2025). Reinforcement Learning Generalization for Quadrotor With Slung Load Systems Through Homogeneity Transformations. *IEEE Open Journal of the Industrial Electronics Society*, *6*, 560–574. https://doi.org/10.1109/OJIES.2025.3557206

Hwangbo, J., Sa, I., Siegwart, R., & Hutter, M. (2017). Control of a Quadrotor With Reinforcement Learning. *IEEE Robotics and Automation Letters*, *2*(4), 2096–2103. https://doi.org/10.1109/LRA.2017.2720851

Karasahin, A. T. (2024). Characterization of different hinge angles for swashplateless micro aerial robots. *Engineering Science and Technology, an International Journal*, *55*, 101750. https://doi.org/https://doi.org/10.1016/j.jestch.2024.101750

Karaşahin, A. T. (2024). Genetically Tuned Linear Quadratic Regulator for Trajectory Tracking of a Quadrotor. *Academic Platform Journal of Engineering and Smart Systems*, *12*(1), 37–46. https://doi.org/10.21541/apjess.1316025

Karasahin, A. T., & Gungor, G. (2025). Co-Stand: Swashplateless Micro Aerial Robot Test Stand. *Tehnički Vjesnik*, *32*(1), 242–246.

Karasahin, A. T., Wu, Z., & Kocer, B. B. (2025). Maintaining Plasticity in Reinforcement Learning: A Cost-Aware Framework for Aerial Robot Control in Non-stationary Environments. *ArXiv Preprint ArXiv:2503.00282*.

Kaufmann, E., Bauersfeld, L., Loquercio, A., Müller, M., Koltun, V., & Scaramuzza, D. (2023). Champion-level drone racing using deep reinforcement learning. *Nature*, *620*(7976), 982–987. https://doi.org/10.1038/s41586-023-06419-4

Li, H., Zhao, Z., Wu, Z., Potdar, P., Tran, L., Karasahin, A. T., Windsor, S., Burrow, S. G., & Kocer, B. B. (2025). Tendon-driven Grasper Design for Aerial Robot Perching on Tree Branches. *ArXiv Preprint ArXiv:2503.00214*.

Schulman, J., Wolski, F., Dhariwal, P., Radford, A., & Klimov, O. (2017). Proximal Policy Optimization Algorithms. *ArXiv*.

Song, Y., Romero, A., Müller, M., Koltun, V., & Scaramuzza, D. (2023). Reaching the limit in autonomous racing: Optimal control versus reinforcement learning. *Science Robotics*, *8*(82), eadg1462. https://doi.org/10.1126/scirobotics.adg1462.

➢ *ORAL PRESENTATION*

Araçtan şebekeye (V2G) şarj teknolojisinin enerji yönetimi açısından değerlendirilmesi

Mahammad Muradzade [*,1] İbrahim Gürsu TEKDEMİR [*,2]
(https://orcid.org/0009-0005-7621-4675)

[*1]Bursa Teknik Üniversitesi, Mühendislik ve Doğa Bilimleri Fakültesi, Elektrik elektronik mühendisliği, Bursa, Türkiye

*Sorumlu yazar e-posta:mehemmed0192@gmail.com

Özet

Elektrikli Araçların (EV) hızlı benimsenmesiyle birlikte, Araçtan Şebekeye (V2G) teknolojisinin modern enerji yönetimi ve akıllı şebeke (Smart Grid) sistemlerindeki önemi giderek artmaktadır. Bu çalışma, V2G sistemlerinin elektrik şebekeleri üzerindeki teknik, ekonomik ve çevresel etkilerini kapsamlı bir şekilde analiz etmeyi amaçlamaktadır. Mevcut literatürdeki optimizasyon stratejileri incelenerek ve Python tabanlı bir simülasyon altyapısı kullanarak, V2G sistemlerinin farklı uygulama senaryolarında (işyeri, konut, filo) şebeke istikrarı, yük dengeleme, tepe yük azaltımı ve yenilenebilir enerji entegrasyonuna olan potansiyel katkıları değerlendirilmiştir. Bulgular, V2G sistemlerinin enerji şebekeleri üzerindeki olumlu etkilerini ortaya koyarken, aynı zamanda batarya ömrü, altyapı maliyetleri ve düzenleyici çerçeveler gibi uygulama zorluklarına da dikkat çekmektedir. Bu çalışma, akıllı şebekelerin gelecekteki gelişimine yönelik stratejiler sunarak, V2G uygulamaları aracılığıyla enerji dağıtımının verimliliğinin ve sürdürülebilirliğinin artırılmasına katkı sağlamaktadır.

Anahtar Kelimeler: Elektrikli Araçlar, Araçtan Şebekeye (V2G), Akıllı Şebeke, Enerji Yönetimi, Optimizasyon, Talep Tepkisi (DR).

Evaluation of vehicle-to-grid charging technology in terms of energy management

Abstract

With the rapid adoption of Electric Vehicles (EVs), the importance of Vehicle-to-Grid (V2G) technology in modern energy management and Smart Grid systems is continuously increasing. This study aims to comprehensively analyze the technical, economic, and environmental impacts of V2G systems on electric grids. By examining existing optimization strategies and utilizing a Python-based simulation infrastructure, the potential contributions of V2G systems to grid stability, load balancing, peak load reduction, and renewable energy integration in various application scenarios (workplace, residential, fleet) have been evaluated. The findings highlight the positive impacts of V2G systems on energy grids, while also drawing attention to implementation challenges such as battery life, infrastructure costs, and regulatory frameworks. This study contributes to increasing the efficiency and sustainability of energy distribution through V2G applications by providing strategies for the future development of smart grids.

Keywords: Electric Vehicles, Vehicle-to-Grid (V2G), Smart Grid, Energy Management, Optimization, Demand Response (DR).

1. GİRİŞ

Bu metin, artan enerji ihtiyacı ve iklim değişikliği hedefleri doğrultusunda elektrikli araçların (EV) ve Araçtan Şebekeye (V2G) teknolojisinin önemini vurgulamaktadır. V2G, EV bataryalarının şebekeye enerji aktarmasına olanak tanıyarak yenilenebilir enerji entegrasyonu, yük dengeleme ve tepe yük azaltma gibi faydalar sunar. Ancak batarya ömrü, altyapı maliyetleri ve mevzuat gibi zorlukları bulunmaktadır. Metinde bahsedilen tez çalışması,

V2G'nin farklı senaryolardaki (ev, işyeri, filo) etkilerini simülasyon tabanlı bir yaklaşımla inceleyerek, bu teknolojinin akıllı şebekelerin geleceği için stratejik potansiyelini değerlendirmektedir.

1.1. Projenin Amacı

Bu çalışmanın temel amacı, elektrikli araçların enerji şebekeleri ile etkileşimini optimize eden V2G (Vehicle-to-Grid) sistemlerinin teknik, ekonomik ve çevresel boyutlarını değerlendirmektir. Geleneksel elektrik şebekeleri, enerji talebindeki dalgalanmalara ve yenilenebilir enerji kaynaklarının entegrasyonuna yönelik büyük zorluklarla karşı karşıya kalmaktadır. V2G teknolojisi, elektrikli araçların bataryalarının şebeke dengesini sağlamak için kullanılmasına olanak tanıyarak, enerji verimliliğini ve sürdürülebilirliği artırmaktadır.

1.2. İhtiyaçların Belirlenmesi

Artan enerji talebi, fosil yakıtların azaltılması ve yenilenebilir enerji entegrasyonu hedefleri, enerji şebekelerinde yeni zorluklar yaratmaktadır. Elektrikli araçlar (EV) ve Araçtan Şebekeye (V2G) teknolojisi, mobil enerji depolama kapasiteleriyle bu sorunlara çözüm sunar. Ancak V2G'nin yaygınlaşması için şebeke dengeleme, batarya ömrü, altyapı ve yasal düzenlemeler ile ekonomik teşvikler gibi temel sorunların aşılması gerekmektedir.

2. LİTERATÜR ÖZETİ

V2G teknolojisi ve elektrikli araçların enerji şebekesine entegrasyonu, son yıllarda yoğun bir akademik ilgi görmüştür. Bu bölüm, çalışmaya temel oluşturan ve mevcut literatürdeki önemli boşlukları belirlemeye yardımcı olan başlıca araştırmaları özetlemektedir.

- **Kempton (2005):** V2G sistemlerinin ekonomik ve mühendislik fizibilitesini incelemiş, özellikle hızlı tepki gerektiren elektrik hizmetleri için uygunluğunu vurgulamıştır.
- **(2020) Review on Vehicle-to-Grid Systems:** V2G ve akıllı şebeke teknolojileri arasındaki etkileşimi detaylandırarak, enerji yönetimi, güç kalitesi ve şebeke stabilitesi üzerindeki etkilerini araştırmıştır.
- **(2018) Enhancing Grid Resilience with Integrated Storage from Electric Vehicles:** Elektrikli araç bataryalarının şebeke dayanıklılığını artırıcı bir unsur olarak kullanılabileceğini ortaya koymuştur.
- **(2024) Optimization Strategies for Electric Vehicle Charging and Routing:** EV şarj ve yönlendirme optimizasyonu için yapay zeka ve sezgisel algoritmaların rolünü incelemiş, enerji verimliliği stratejileri önermiştir.
- **(2021) Grid Impact of Electric Vehicle Fast Charging Stations:** Hızlı şarj istasyonlarının şebeke üzerindeki etkilerini değerlendirmiş ve voltaj dalgalanmalarını azaltmaya yönelik stratejilerin gerekliliğini vurgulamıştır.
- **(2022) Electric Vehicle-to-Grid (V2G) Technologies:** V2G'nin şebeke ve batarya üzerindeki etkilerini ele alarak, batarya degradasyonu ve mevzuat eksiklikleri gibi zorluklara odaklanmıştır.

Bu literatür taraması, V2G'nin teknik potansiyelini ve şebeke entegrasyonundaki zorlukları ortaya koymuştur. Mevcut çalışmalar genellikle tek bir optimizasyon stratejisine veya belirli bir uygulama alanına odaklanırken, bu tez çalışması farklı senaryoları bir arada değerlendirerek ve Python tabanlı esnek bir simülasyon altyapısı kullanarak daha bütüncül bir analiz sunmaktadır.

3. ELEKTRİKLİ ARAÇLAR VE ŞARJ ALTYAPISI

Elektrikli araçlar (EV – Electric Vehicles), dünya genelinde karbon emisyonlarını azaltmak, fosil yakıtlara olan bağımlılığı azaltmak ve sürdürülebilir ulaşımı teşvik etmek amacıyla son yıllarda hızla yaygınlaşmıştır.

3.1. Elektrikli Araç Teknolojisinin Gelişimi

Elektrikli araçlar, içten yanmalı motorlara kıyasla çok daha önce geliştirilmiş olmalarına rağmen 20. Yüzyılın

başlarında yaygınlaşan petrol temelli ulaşım politikaları nedeniyle uzun süre geri planda kalmıştır. Ancak son 20 yılda batarya teknolojilerindeki gelişmeler, çevresel kaygıların artması ve devlet destekli teşvik politikaları sayesinde EV'ler yeniden gündeme gelmiştir.

3.2. Şarj Teknolojileri

- **AC Şarj:** Konutlarda ve halka açık alanlarda yaygın olarak kullanılır. Genellikle 3.7 kW ile 22 kW arasında değişen güçlerde çalışır. Şarj süresi uzun olmakla birlikte, donanım maliyetleri düşüktür.
- **DC Hızlı Şarj:** 50 kW'tan 350 kW'a kadar çıkabilen yüksek güçlü altyapılardır. Özellikle otoyol istasyonlarında kullanılır. Bir aracı yaklaşık 20-30 dakika içinde %80 oranında şarj edebilir.
- **Kablosuz Şarj Sistemleri:** Elektromanyetik indüksiyon yöntemiyle çalışır. Şu an için verimlilik oranı düşüktür (%80 civarı) ve altyapı maliyetleri yüksektir.

Tablo 1. Şarj Teknolojileri Özeti

Şarj Türü	Güç Aralığı	Şarj Süresi	Kullanım Alanı	Maliyet
AC Şarj	3.7-22 kW	4-8 saat	Ev, iş yeri	Düşük
DC Şarj	50-350 kW	20-30 dk	Otoyol, ticari alan	Orta-Yüksek
Kablosuz Şarj	3-11 kW	5-9 saat	Lüks konutlar	Yüksek

3.3. Şarj Altyapısının Planlaması ve Yaygınlaştırılması

Şarj altyapısının başarılı bir şekilde yaygınlaştırılması, yalnızca teknik değil aynı zamanda sosyoekonomik bir meseledir. Yoğunluk haritalarına göre istasyonların konumlandırılması, şebeke üzerindeki yükün dengelenmesi, V2G (Vehicle-to-Grid) sistemlerinin entegrasyonu ve kullanıcı davranışlarının modellenmesi gibi çok sayıda standardı dikkate alınmalıdır.

4. V2G (ARAÇTAN ŞEBEKEYE) TEKNOLOJİSİ

V2G (Vehicle-to-Grid – Araçtan Şebekeye) teknolojisi, elektrikli araçların yalnızca bir ulaşım aracı olarak değil, aynı zamanda mobil enerji depolama birimleri olarak değerlendirilmesini mümkün kılarak modern enerji sistemlerinin geleceğinde kritik bir rol üstlenmektedir.

4.1. V2G Kavramı ve Önemi

V2G, elektrikli araçlar ile enerji şebekesi arasında çift yönlü enerji akışı sağlayan bir teknolojidir. Temel olarak, EV (Electric Vehicle) bataryalarının yalnızca şarj edilmediği, aynı zamanda belirli koşullarda şebekeye enerji aktardığı bir senaryo sunar.

Tablo 2. V2G Teknolojisinin Faydaları

Faydalar	**Açıklama**
Şebeke Dengelemesi	Ani enerji talep artışlarında şebekeye enerji aktarımı
Yenilenebilir Entegrasyonu	Güneş ve rüzgar gibi kesintili üretimin dengelenmesi
Ekonomik Kazanç	Araç sahiplerine şebekeye sattıkları enerji üzerinden gelir sağlama
Enerji Depolama Alternatifi	Sabit batarya sistemlerine göre daha düşük maliyetli bir depolama yöntemi

4.2. V2G Sistem Mimarisi

V2G sistemleri üç ana bileşen üzerinden işler: elektrikli araç, şarj istasyonu (bidirectional charger) ve şebeke yönetim sistemleri.

Tablo 3. V2G Sistem Mimarisi Bileşenleri

Bileşen	**Görevi**
Elektriklı Araç (EV)	Enerji depolama ve şebekeye geri gönderme
Çift Yönlü Şarj Ünitesi	AC/DC dönüşümü yaparak enerji akışını çift yönlü sağlar
Enerji Yönetim Sistemi	V2G sürecinin zamanlamasını ve miktarını belirler
Şebeke Operatörü	Talep fazlası ya da dengesizlik olduğunda V2G mekanizmasını tetikler

4.4. V2G Uygulama Senaryoları

- **Ev Tabanlı Uygulamalar:** Bireysel kullanıcıların evlerinde gece şarj edip gündüz fazla enerjiyi şebekeye verdikleri senaryoları kapsar.
- **İş Yeri ve Filolar:** Çalışanların işyerlerinde veya şirket filolarının merkezi garajlarda araçlarını şarj ettikleri ve gün içinde park halindeyken fazla enerjiyi şebekeye aktardıkları senaryoları içerir.
- **Talep Tepki (DR) Etkinlikleri:** Şebeke operatörünün belirli zamanlarda enerji ihtiyacını bildirdiği ve V2G uyumlu araçların şebekeye enerji sağlayarak yük azaltımına katkıda bulunduğu senaryolardır.

Tablo 4. V2G Uygulama Senaryoları Karşılaştırması

Özellik / Kriterler	Ev Tabanlı Uygulama	İşyeri ve Filo Uygulamaları	Talep Tepkisi Etkinlikleri
Kullanım Yeri	Bireysel konutlar	Ofis otoparkları, şirket garajları	Şebekenin yüksek talep yaşadığı zamanlar
Araçların Bağlı Olduğu Süre	Gece boyunca (8–10 saat)	Gündüz mesai süresince	Kısa süreli, talep anında
Amaç	Ucuz şarj, ev tüketimine katkı	Şebekeye destek, kurumsal tasarruf	Şebeke dengesini sağlama, sistem güvenliği

5. SİMÜLASYON ALTYAPISI VE YAZILIM GELİŞTİRME

Bu bölümde, elektrikli araçlar ile enerji şebekesi arasındaki etkileşimleri gerçekçi bir şekilde modelleyebilmek amacıyla geliştirilen simülasyon altyapısı ayrıntılı biçimde açıklanmıştır. Geliştirilen sistem, özellikle V2G (Vehicle-to-Grid) destekli uygulamaların şebeke üzerindeki etkilerini analiz etmeye ve farklı senaryolar altındaki performansını değerlendirmeye yöneliktir.

5.1. Kullanılan Yazılım ve Kütüphaneler

Simülasyonun geliştirildiği Python ortamında, elektrikli araç davranışlarını ve şebeke yüklerini zaman bazlı olarak takip etmeye olanak tanıyan özel kütüphaneler kullanılmıştır. Hazırlanan Python dosyaları daha sonra MATLAB ortamına entegre edilmiştir.

Tablo 5. Kullanılan Yazılım ve Kütüphaneler

Kütüphane	İşlevi
numpy	Sayısal veri işlemleri, matris hesaplamaları
pandas	Zaman serisi verilerinin analizi
matplotlib / seaborn	Grafik çizimi ve görselleştirme
yaml	Konfigürasyon dosyalarının okunması
ev2gym	Elektrikli araç şarj/deşarj modellemesi

5.2. Algoritma

Bu çalışmada geliştirilen algoritma, elektrikli araçların (EV) şarj ve deşarj işlemlerini akıllıca yönetmeyi

amaçlar. Senaryo bazlı, dinamik ve esnek bir yapıya sahip olan algoritma, farklı kullanıcı profillerinin (ev, işyeri, filo) şarj davranışlarını dikkate alarak enerji talebini dengelemeyi, şebeke yükünü azaltmayı ve enerji kaynaklarını verimli kullanmayı hedefler. Algoritma, girdi parametreleri, şarj noktası operatörü, kontrol stratejileri (Optimum, Kural Tabanlı, MPC, Pekiştirmeli Öğrenme), simülasyon süreci ve çıktılar olmak üzere beş ana bileşenden oluşmaktadır.

5.3. Senaryo Tabanlı Modelleme

Bu çalışmada, elektrikli araçların farklı kullanım alanlarına yönelik üç ayrı senaryo üzerinde simülasyonlar gerçekleştirilmiştir.

- **Residential (Ev Tabanlı) Senaryo:** Bireysel kullanıcıların evlerinde gece boyunca araçlarını şarj ettikleri ve gündüz bataryalarındaki fazla enerjiyi şebekeye geri verdikleri durumu temsil eder.
- **Workplace (İş Yeri) Senaryo:** Elektrikli araçların işyerlerinde gündüz saatlerinde park halinde olup şarj edildiği ve V2G ile Talep Tepkisi (DR) etkinliğinin aktif olduğu durum.
- **Fleet/Depot (Filo / Garaj) Senaryo:** Çok sayıda elektrikli aracın merkezi bir noktada toplu olarak şarj edildiği ve gerektiğinde bu araçlardan şebekeye enerji aktarımı yapıldığı durum (V2G açık, DR kapalı).

5.4. Girdi Dosyalarının Yapısı ve Parametreler

Simülasyonlar, YAML formatında yapılandırılmış bir giriş dosyası temel alınarak yürütülmektedir. Başlıca parametre grupları şunlardır: EV özellikleri, şarj istasyonları, trafo kapasitesi, solar üretim, esnek olmayan yükler ve talep tepki (DR) etkinlikleri.

6. UYGULAMA SENARYOLARI VE BULGULAR

V2G teknolojisinin üç farklı uygulama senaryosundaki (İşyeri: V2G ve DR aktif; Filo: V2G aktif, DR kapalı; Konut: V2G ve DR kapalı) etkileri simülasyon bulgularıyla incelenmiştir.

- İşyeri Senaryosu: V2G ve DR entegrasyonu sayesinde şebeke esnekliğinin arttığı, pik yüklerin azaldığı ve yenilenebilir enerji entegrasyonunun etkinleştiği gözlemlenmiştir. Araçlardan şebekeye enerji aktarımıyla yük dengeleme sağlanmıştır.

- Filo Senaryosu: DR kapalı olsa dahi, V2G'nin filo tipi uygulamalarda şebeke yükünü dengeleme ve enerji maliyetlerini düşürme potansiyeli olduğu, ancak bazı istasyonların pasif kalabildiği belirtilmiştir.

- Konut Senaryosu: V2G ve DR'nin kapalı olduğu bu senaryoda, şebekenin pasif kaldığı ve enerji verimliliği ile esneklik açısından önemli ödünler verildiği, ayrıca ani akım dalgalanmalarının sorunlara işaret edebileceği vurgulanmıştır.

Genel olarak, bulgular V2G'nin şebeke stabilitesi, pik yük azaltımı ve yenilenebilir enerji entegrasyonu için büyük potansiyel taşıdığını, ancak etkin kullanım için sistem optimizasyonu ve entegrasyonun önemini göstermektedir.

7. TARTIŞMA VE SONUÇLAR

Bu tez çalışması, V2G teknolojisinin elektrikli araçlarla şebeke entegrasyonunun etkilerini farklı senaryolarla (İş Yeri, Filo, Konut) simülasyonlar yaparak analiz etmiştir. Bulgular, V2G'nin şebeke esnekliğini artırdığını, yük dengeleme ve ekonomik/çevresel faydalar sağladığını, ancak altyapı ve verimlilik sorunlarının da olduğunu göstermiştir.

Tablo 6. Senaryo Karşılaştırma Tablosu

Özellik / Kriterler	Senaryo 1 (Workplace - V2G & DR Aktif)	Senaryo 2 (Fleet - V2G Açık, DR Kapalı)	Senaryo 3 (Residential - V2G Kapalı, DR Kapalı)
V2G Durumu	Aktif (true)	Aktif (true)	Pasif (false)
Talep Tepkisi (DR)	Aktif (true)	Pasif (false)	Pasif (false)
Şarj – Deşarj Tipi	Çift yönlü	Çift yönlü	Tek yönlü (sadece şarj)
Solar Enerji Katkısı	Orta (20 kW ort.)	Yüksek (40 kW ort.)	Düşük (12 kW ort.)
İnflexible Yük (Tahmin)	30 kW	45 kW	20 kW
Trafo Kapasitesi	200 kW	300 kW	100 kW
Şebeke Esnekliği Katkısı	Yüksek (DR + V2G)	Orta (sadece V2G)	Yok
Kullanım Verimliliği (Enerji/Trafik)	Yüksek	Yüksek	Düşük

Sonuç:

Bu çalışma, V2G teknolojisinin elektrikli araçların enerji şebekesiyle entegrasyonu sürecinde önemli bir rol oynadığını göstermektedir. Özellikle işyeri ve filo gibi merkezi şarj noktalarında V2G ve DR entegrasyonu, şebeke stabilitesini artırma, pik yükleri azaltma ve yenilenebilir enerji entegrasyonunu destekleme açısından büyük potansiyel sunmaktadır. Ancak bu teknolojinin tam potansiyeline ulaşabilmesi için batarya ömrü, altyapı maliyetleri, yasal düzenlemeler ve standardizasyon gibi alanlarda daha fazla araştırma ve geliştirme yapılması gerekmektedir. Geliştirilen simülasyon altyapısı, V2G sistemlerinin gelecekteki enerji senaryoları için kapsamlı bir analiz ve değerlendirme aracı olarak kullanılabileceğini göstermektedir.

8. ÇEVRESEL VE EKONOMİK KAZANIMLAR

V2G teknolojisi, hem çevresel sürdürülebilirlik hem de ekonomik verimlilik açısından önemli kazanımlar sunmaktadır.

Çevresel Kazanımlar: Fosil yakıt bağımlılığını azaltır, sera gazı emisyonlarını düşürür ve yenilenebilir enerji kaynaklarının şebekeye daha etkin entegrasyonunu sağlar.

Ekonomik Kazanımlar: Yük dengeleme maliyetlerini düşürür, araç sahiplerine ek gelir imkanı sunar, altyapı yatırımlarının ertelenmesine yardımcı olur, sistem stabilitesi ve güvenliğini artırır, ve enerji ithalatını azaltarak ülke ekonomisine katkıda bulunur.

9. GELECEK ÇALIŞMALAR İÇİN ÖNERİLER

Bu tez çalışması, elektrikli araçların şebekeye entegrasyonunda V2G teknolojisinin potansiyelini anlamak için sağlam bir temel sunmaktadır. Ancak gerçek dünya uygulamalarına geçiş ve V2G sistemlerinin tam potansiyelinin açığa çıkarılması için aşağıdaki alanlarda daha fazla araştırma ve geliştirme yapılması önerilmektedir:

- **Gerçek Zamanlı Veri Entegrasyonu:** Gerçek zamanlı trafik verileri, hava durumu ve enerji fiyatları gibi değişkenlerin simülasyon modeline entegrasyonu.
- **Batarya Degradasyonu Modülü:** V2G şarj/deşarj döngülerinin batarya sağlığı ve kapasite kaybı üzerindeki etkilerini modelleyen detaylı bir modülün entegre edilmesi.
- **Dinamik Tarife Modelleri ve Kullanıcı Teşvikleri:** Enerji piyasalarındaki anlık fiyat dalgalanmalarına göre otomatik olarak uyum sağlayan dinamik tarife modellerinin ve farklı finansal teşvik mekanizmalarının araştırılması.
- **Kentsel Dağıtım Şebekesi ile Uyumlu Genişleme:** Şehir içi yoğun bölgelerde sınırlı trafo kapasiteleri ile V2G sistemlerinin nasıl daha uyumlu çalışabileceğinin analizi.
- **Yasal ve Politik Çerçeve Analizi:** V2G'ye özgü lisanslama süreçleri, vergilendirme politikaları, veri gizliliği ve siber güvenlik gibi hukuki ve politik boyutların incelenmesi.
- **Topluluk Enerji Sistemleriyle Entegrasyon:** Konut tabanlı senaryolarda bireysel V2G uygulamaları yerine, topluluk bazlı enerji paylaşımı senaryoları üzerinde çalışma.
- **Gerçek Zamanlı Kontrol ve Optimizasyon Algoritmaları:** Yapay zeka (derin öğrenme, takviyeli öğrenme) ve meta-sezgisel algoritmaların gerçek zamanlı veri akışıyla daha dinamik ve adaptif çözümler sunma potansiyelinin araştırılması.

10. KAYNAKÇA

Bu tez bildirisi, orijinal tez çalışmasında belirtilen kaynaklardan yararlanılarak hazırlanmıştır. Tam referans listesi için orijinal tez çalışmasına başvurulabilir. Aşağıda bazı önemli kaynaklar listelenmiştir:

- Abadi, M., et al. (2016). *TensorFlow: Large-scale machine learning on heterogeneous systems*.
- Doğan, B. (2020). *Dağıtık enerji sistemlerinde elektrikli araçların entegrasyonu ve yönetimi* (Doktora Tezi). Orta Doğu Teknik Üniversitesi, Elektrik-Elektronik Mühendisliği.
- Enerji ve Tabii Kaynaklar Bakanlığı. (2022). *Ulusal Enerji Verimliliği Eylem Planı (2020-2030)*.
- *Enhancing Grid Resilience with Integrated Storage from Electric Vehicles* (2018).
- EPDK. (2022). *Şarj Hizmeti Yönetmeliği*. E.T.: 02.04.2022, S: 31797.
- *Grid Impact of Electric Vehicle Fast Charging Stations: Trends, Standards, Issues and Mitigation Measures - An Overview* (2021).
- Gungor, V. C., Sahin, D., Kocak, T., Ergut, S., Buccella, C., Cecati, C., & Hancke, G. P. (2013). *Smart grid technologies: Communication technologies and standards*.
- Hunter, J. D. (2007). *Matplotlib: A 2D graphics environment*.
- International Energy Agency (IEA). (2023). *Global EV Outlook 2023*.
- Karakaya, S. (2021). *Elektrikli araçların şebeke yükü üzerine etkisinin V2G kapsamında değerlendirilmesi* (Yüksek Lisans Tezi). İstanbul Teknik Üniversitesi, Enerji Enstitüsü.
- Kempton, W. (2005). *Vehicle-to-grid power fundamentals: Calculating capacity and net revenue*.
- Lopes, J. A. P., Soares, F. J., & Almeida, P. M. R. (2011). *Integration of electric vehicles in the electric power system*.
- McKinney, W. (2010). *Data Structures for Statistical Computing in Python*.
- McKinsey & Company. (2023). *The economic case for V2G and bi-directional charging*.
- *Optimization Strategies for Electric Vehicle Charging and Routing: A Comprehensive Review* (2024).

➢ *ORAL PRESENTATION*

Park ve Bahçelerde Bulunan Zehirli Bitkiler ve Bunların Tıbbi Kullanımları Üzerine Bir İnceleme

Hülya Hoşgören[1*] (*0000-0002-3528-3157*)

[*1]Dicle Üniversitesi, Fen Fakültesi, Biyoloji Bölümü, Diyarbakır, Türkiye

* Sorumlu yazar e-posta: hulyah@dicle.edu.tr

Özet

Binlerce yıldan beridir, barınma, beslenme, korunma gibi birçok alanda kullanılan bitkiler, doğal seçilim sürecinde, otçulların bitkileri erken dönemlerinde tüketmelerinden caydırmak için tanen, alkaloid, glikozit, terpen gibi hayvanlar üzerinde toksik etki gösteren çok çeşitli ve karmaşık kimyasal bileşikler üretmişlerdir. Ürettikleri bu kimyasal bileşiklerden dolayı zehirli olarak adlandırılan bu bitkiler, tüketimlerinden sonra hastalığa ve hatta ölüme yol açmaktadır. Bu derlemede, özellikle park-bahçe ve çocuk oyun alanlarında bulunan bazı zehirli bitkiler hakkında halkı bilgilendirmek hedeflenmiştir. Ancak bu zehirli bileşiklerin toksik etkilerinin yanı sıra birçoğunun, önemli tıbbi faydalarının bulunduğu da unutulmamalıdır. Yapılmış önceki çalışmalar doğrultusunda zehirli bitkilerin, taşıdıkları toksik bileşiklerinden dolayı, anti-diyabetik, anti-kanser, anti-bakteriyel, anti-fungal etki gösterdikleri ve pek çok hastalığın tedavisinde kullanıldıkları tespit edilmiştir. Ancak, zehirli bitkilerin tedavi amaçlı kullanımlarında dozlarının iyi ayarlanması gerektiği, doz aşımı durumunda ölümle sonuçlanabileceği unutulmamalıdır. Bu derlemenin amacı park ve bahçe peyzajında kullanılan ehirli bitkiler ve bunların tıbbi kullanımları hakkında halkı bilgilendirmektir.

Anahtar Kelimeler: Zehirli bitki, alkaloid, tanen, glikozit, tıbbi bitki

A Study on Poisonous Plants Found in Parks and Gardens and Their Medical Uses

Abstract

Plants, which have been used for thousands of years in many areas such as shelter, nutrition and protection, have produced a wide variety of complex chemical compounds such as tannins, alkaloids, glycosides and terpenes that have toxic effects on animals in order to discourage herbivores from consuming plants in their early stages. These plants, which are called poisonous because of the chemical compounds they produce, cause disease and even death after consumption. This review aims to inform the public about some poisonous plants found especially in parks, gardens and children's playgrounds. However, it should not be forgotten that besides the toxic effects of these toxic compounds, many of them have important medicinal benefits. In line with previous studies, it has been determined that poisonous plants have anti-diabetic, anti-cancer, anti-bacterial, anti-fungal, anti-diabetic, anti-cancer, anti-bacterial and anti-fungal effects and are used in the treatment of many diseases due to the toxic compounds they carry. However, it should be kept in mind that the doses of poisonous plants should be well adjusted in their therapeutic use and overdose may result in death. The aim of this review is to inform the public about poisonous plants used in park and garden landscaping and their medicinal uses.

Keywords: Poisonous plant, alkaloid, tannin, glycoside, medicinal plant

GİRİŞ

Yararlı bitkilerin insanlar tarafından keşfedilmesi, MÖ 5000'de Ayurveda, MÖ 2800'de Çinliler, MÖ 1500'de Mısırlılar, M.Ö. 400'de Yunanlılara dayanmaktadır (Maitai, 1996). Bu bitkilerin (gıda, ilaç, giysi, enerji/yakıt, süs, kereste, kültürel ve geleneksel değerlere sahip etnik kökenli bitkiler vb.) ilk keşifleri, hayvanların onları nasıl kullandığına dair gözlemler ile olmuştur (Ayensu, 1978; Wanzala ve ark., 2012). "Zehirli ve Tıbbi Bitkiler" de benzer şekilde bir deneme yanılma yöntemiyle keşfedilmiştir. Tarih boyunca bu bitkiler, insan sağlığı ile iç içe geçerek, bazen hayat kurtarıcı bazen de ölümcül sonuçlar doğurmuştur. Geleneksel olarak bazıları halk tıbbında, hastanelerde ilaç olarak kullanılmışlardır (Kipkore ve ark., 2014).

Bitkiler genellikle farklı kısımlarında (çiçek, tomurcuk, meyve, tohum kökleri, gövde ve yapraklar vb.) ve bitkinin büyüme ve gelişmesi sırasında belirli zamanlarda değişen oranlarda çok sayıda fitokimyasala sahiptir. Zehir özelliği taşıyan ve ilaç olarak kullanılan bu fitokimyasalların, uygun dozlarda ayarlanarak hastalıkları önleme ve tedavi etme özellikleri hedeflenmiştir. Ancak, bu ilaçlar genellikle güvenli olmakla beraber, şayet doz aşımı olursa bazılarının ciddi yan etkileri de olabilmektedir (Erdem ve Ata-Eren, 2009).

Bitki zehirlenmeleri yutma, temas, absorpsiyon veya soluma yoluyla oluşur (Dolan ve Welch-Keesey; 2016). Ancak zehirlenme tabiri, her zaman öldürücü anlamına gelmemelidir. Ciltteki tahriş, kusma, ishal gibi semptomlar da ciddiyet oranına göre bu tabirin içinde yer alabilmektedir (Karimi ve ark., 2015).

Zehirli Bitkilerin Temel Özellikleri

Toksik bileşenleri: Alkaloidler, glikozitler, saponinler, tanenler, reçineler vb.

Etkileri: Mide bulantısı, ishal, kalp durması, halüsinasyon, solunum felci, koma, ölüm

Etkilenme yolları: Ağız yoluyla alınma, deri teması, solunum yoluyla emilim

MATERYAL VE METOD

Çocuk oyun alanlarında veya park ve bahçelerde sıklıkla rastlanan zehirli bitkiler çalışma materyalini oluşturmaktadır. Halkı bilinçlendirmek için bu zehirli bitkilerin en fazla rastlanılanları bir araya toplanmıştır.

BULGULAR VE TARTIŞMA

Bitkilerde sentezlenen zehirli sekonder metabolitlerden pek çoğu tıbbi açıdan önem taşır. Kent peyzajında sıklıkla kullanılan ve zehir etkisi en yüksek olan tıbbi bitkilerden bazıları;

- ***Atropa belladonna* L.** (Güzelavrat Otu)

Etkili Bileşik: Tüm bitki zehirlidir. Özellikle kök, yaprak ve meyve içeriğindeki %95 lik kısmı "Atropin" olmak üzere, hiyosiyamin, skopolamin, belladonnin ve apoatropin alkaloidleri zehirlenmeye sebep olur (Berdai ve ark., 2012)
Zehirlenme Belirtileri: Zehirlenen kişilerde ilk olarak baş ağrısı ve uyku hali gözlenir. Sonrasında yavaş yavaş ağız kuruluğu ve sayıklama başlar. Bitkinin tüketilmesi durumunda acilen en yakın sağlık kuruluşuna başvurulmalıdır (Lee, 2007; Olson, 2018).
Tıbbi Kullanımı: Antik Mısır ve Orta Çağ Avrupa'sında ağrı kesici olarak kullanılmıştır. İçeriğindeki bileşiklerden atropin, göz doktorları tarafından göz muayenesi sırasında göz bebeklerini büyütmede (Ceylan, 1994), kas spazmlarını gevşetmede ve kalp atış hızını düzenlemede kullanılmaktadır. Skopolamin ise, deniz tutması gibi hareket hastalıklarında deri bandı şeklinde bulantı önleyici olarak kullanılmaktadır. Atropin ayrıca sigara içmeden meydana gelen nefes darlığı (Bown, 2002), böcek öldürücüler ve kimyasal savaş ajanları için bir panzehir olabilir (Brunton ve ark., 2017).

- ***Nerium oleander* L.** (Zakkum)

Etkili Bileşik: Tüm bitki zehirlidir. İçerdiği "Oleandrin, Nerosid" glikozitleri zehir etkisini verir (Shumaik ve ark., 1988). Zehirlenmeler, genellikle bitkinin çiçek ve yapraklarının yenmesi ile gerçekleşmektedir (Berdai ve ark., 2012).
Zehirlenme Belirtileri: Zehirlenmenin başladığını gösteren ilk semptom kalp ritim bozukluğudur. Zehirlenme, bulantı, kusma, karın ağrısı, huzursuzluk, yavaş ve zayıf nabzın ardından hızlı solunuma neden olur. Hastalar, yutma güçlüğü ve çene kilitlenmesi yaşayabilir, ardından kasılmalar başlar, bu da bitkinliğe, uyuşukluğa, komaya, kalp yetmezliğine ve ölüme yol açabilir (Al ve ark., 2010). Bitkinin tüketilmesi durumunda acilen en yakın sağlık kuruluşuna başvurulmalıdır.
Tıbbi Kullanımı: Güçlü bir kardiyotoksik bitkidir. Bitkiden elde edilen bileşikler, kalp hastalıkları, miyalji, yara iyileşmesi vb. için yerli ilaçlarda kullanılır (Gupta, 2016).





Atropa belladona *Nerium oleander* *Digitalis purpurea*

- ***Digitalis purpurea* L.** (Yüksük Otu)

Etkili Bileşik: Taşıdığı "Digitoksin, Gitoksin" glikozitleri nedeniyle zehirlidir (Bradberry ve Vale, 2016).
Zehirlenme Belirtileri: Bu bitki yüksek dozda tüketildiğinde mide bulantısı, kusma, ishal, bilinç kaybı, bulanık görme ve ritim bozukluğu gibi zehirlenme ve ölüme sebep olmakla beraber, yeterli kullanımında hayat kurtarıcıdır (Johansson ve ark., 2001; Ebaid ve ark., 2006). Bitkinin tüketilmesi durumunda acilen en yakın sağlık kuruluşuna başvurulmalıdır (Berdai ve ark., 2012).
Tıbbi Kullanımı: Kalp kuvvetlendirici, idrar arttırıcı ve böbrekler üzerindeki tedavi edici özelliği yanında kanser ve diyabette de tıbbi öneme sahiptir (Scarpa ve Guerci, 1982; Jitendra ve Gupta, 2012).

- ***Ricinus communis* L.** (Hint Yağı)

Etkili Bileşik: Tohumları zehirlidir, tek bir tohumu bile kişiyi iki gün içerisinde öldürebilir. Zehir etkisi "Risin"den gelir (Dnyaneshwar, 2011).
Zehirlenme Belirtileri: Bu bitkinin tohumlarının tüketmesiyle, ilk olarak boğazda yanma hissi oluşur. Ardından mide bulantısı, iç kanama, karaciğer ve böbrek yetmezliği görülür. Zehirlenme başladıktan sonra geri dönüşü yoktur (Dnyaneshwar, 2011). Bitkinin tüketilmesi durumunda acilen en yakın sağlık kuruluşuna başvurulmalıdır (Berdai ve ark., 2012).
Tıbbi Kullanımı: Hint yağının belki de en iyi bilinen tıbbi kullanımlarından biri doğal bir müshildir. Astım (Shukla ve ark., 1992), antihistaminik (Wilson ve ark., 2001), Parasetamolün neden olduğu hasara karşı karaciğeri onarıcı (Purohit ve ark., 2001) özelliğinden yararlanılmaktadır.

- ***Taxus baccata* L.** (Porsuk Ağacı)

Etkili Bileşik: Tüm bitki özellikle, yapraklar ve kırmızı renkli meyveleri, içerdiği "Taksol (paklitaksel)" nedeniyle zehirlidir ve kesinlikle tüketilmemelidir (Erdemoğlu ve Şener, 2001).
Zehirlenme Belirtileri: Ciddi mide sorunlarına, kalp atış hızının tehlikeli bir şekilde yavaşlamasına veya hızlanmasına neden olur. Zehirlenme belirtileri arasında mide bulantısı, ağız kuruluğu, kusma, mide ağrısı, baş dönmesi, halsizlik, sinirlilik, kalp sorunları ve diğerleri sayılabilir (Vetter, 2004). Bitkinin tüketilmesi durumunda acilen en yakın sağlık kuruluşuna başvurulmalıdır (Berdai ve ark., 2012). Çocuk oyun alanları yakınlarında kullanılması sakıncalıdır. Kent parklarında da pek tercih edilmez. Ancak Ankara'daki Kuğulu Park'ta kullanılmıştır.
Tıbbi Kullanımı: Ciddi güvenlik endişelerine rağmen, difteri, tonsilit, epilepsi nöbetleri, romatizma, idrar yolu ve karaciğer rahatsızlıklarının tedavisinde kullanılmaktadır (Al-Snafi, 2016). Meme kanseri, yumurtalık kanseri ve akciğer kanseri tedavisinde kullanılır (Wani ve ark., 1971).





Ricinus communis *Taxus baccata* *Conium maculatum*

- ***Conium maculatum* L.** (Baldıran Otu)

Etkili Bileşik: Tüm bitki özellikle kök ve tohumlar zehirlidir. Zehir etkisini veren "Konin, Konhidrin" alkaloidleridir (Mondal ve ark., 2014).

Zehirlenme Belirtileri: Baş dönmesi, ritim bozukluğu, tükürük artışı, hızlı kalp atışı ve ardından, konuşma kaybı, felç, bilinç kaybı, kalp, akciğer ve böbrek yetmezliği ve ölümle sonuçlanır (Folpini ve Furfori, 1995). Bitkinin tüketilmesi durumunda acilen en yakın sağlık kuruluşuna başvurulmalıdır (Berdai ve ark., 2012).
Tıbbi Kullanımı: Bronşit, boğmaca ve astım gibi solunum problemlerinde, çocuklarda diş çıkarma, şişmiş ve ağrılı eklemler ve kramplar gibi ağrılı durumlar için kullanılır. Ayrıca kaygı bozukluklarında, spazm tümörleri, cilt enfeksiyonları, epilepsi, Parkinson hastalığı ve mesane enfeksiyonlarının tedavisinde kullanılmaktadır (Stapczynski ve ark., 1981).


Hyoscyamus niger


Cannabis sativa


Datura stramonium

- ***Hyoscyamus niger* L.** (Banotu)

Etkili Bileşik: Kök, yaprak ve tohumların içerdiği "Atropine, Tropane, Hyosiyamin ve Skopolamin" dir. (Gilani ve ark., 2008)
Zehirlenme Belirtileri: Klinik belirtileri midriyazis, taşikardi, aritmi, ajitasyon, konvülsiyon ve koma, ağız kuruluğu, susuzluk, peltek konuşma, konuşma zorluğu, disfaji, sıcak kızarmış cilt, ateş, bulantı, kusma, baş ağrısı, bulanık görme ve fotofobi, idrar retansiyonu, mesanenin şişmesi, uyuşukluk, hiper refleksi, işitsel, görsel veya dokunsal halüsinasyonlar, konfüzyon, yönelim bozukluğu, deliryum, saldırganlık ve saldırgan davranış gibi çok geniştir (Sajeli ve ark., 2009; Alizadeh ve ark., 2014).
Zehirli alkaloitlerden dolayı tıbbi dozdan biraz daha yüksek miktarda alınması bilinç kaybına neden olabilir ve ölümle sonuçlanabilir. Bitkinin tüketilmesi durumunda acilen en yakın sağlık kuruluşuna başvurulmalıdır (Berdai ve ark., 2012).
Tıbbi Kullanımı: Antienflamatuar, antiparkinson, antipiretik, analjezik özelliklerinden yararlanılmaktadır (Raetsch, 2005; Lindequist ve ark., 1993). Ayrıca spazmolitik, hipnotik, halüsinojenik, göz bebeği genişletici, yatıştırıcı ve ishal önleyici gibi farmakolojik etkilere de sahiptir.

- ***Cannabis sativa* L.** (Kenevir)

Etkili Bileşik: Zehir etkisini veren "Tetrahidrokannabiol, Kannabinoid" bileşikleridir (Duke, 2012).
Zehirlenme Belirtileri: Toksik etkiler başlıca merkezi sinir sistemi, solunum sistemi ve endokrin sistemini etkiler. Halüsinasyon, sanrı, bulanık görme, zayıf koordinasyon, stupor ve komaya neden olur. Sedasyon, kalıcı kabızlık, iştahsızlık, mide bulantısı, solunum depresyonu, tolerans, bağımlılık ve opioid kaynaklı hiperaljezi gibi hoş olmayan yan etkilerindendir (Bonini ve ark., 2018; Russo, 2008; Elikkottil ve ark., 2009). Bitkinin tüketilmesi durumunda acilen en yakın sağlık kuruluşuna başvurulmalıdır (Berdai ve ark., 2012).
Tıbbi Kullanımı: Yara ve yanık tedavisinde kullanılmaktadır. Kronik ağrı (kanserle ilişkili ağrı, nöropatik ağrı veya multipl skleroz ile ilişkili ağrı), özellikle yaşlı insanlarda önemli bir sağlık sorunudur (Giacoppo ve ark., 2017). Çoğu durumda, kronik ağrı opiyatlarla (ilaç kötüye kullanımına yol açabilir), antidepresanlar ve antikonvülzan ilaçlarla tedavi edilmektedir. Şu anda, şiddetli ağrıyı tedavi eden tek analjezikler opioidlerdir (Krenzelok, 2010). Yakın zamanlarda Multiple Sclerosis (MS) tedavi çalışmaları da olumlu sonuçlar vermiştir (Burrows ve Tyrl, 2001).


Hedera helix


Buxus sempervirens


Hydrangea sp.

- ***Datura stramonium* L.** (Tatula)

Etkili Bileşik: "Atropin, Hiyosiyamin, Skopolamin" bitkinin tüm kısımlarında bulunur (Devi ve ark., 2011; Kirtikar ve Basu, 1999).
Zehirlenme Belirtileri: Alımdan birkaç dakika sonra düzensiz nabız ve kalp atışının olduğu akut bir seyir gösterir; görme bozuklukları, ağız kuruluğu, koordinasyonsuzluk ve koma izlenir (Mdee ve ark., 2009). Bitkinin tüketilmesi durumunda acilen en yakın sağlık kuruluşuna başvurulmalıdır (Berdai ve ark., 2012).
Tıbbi Kullanımı: Ülser, yaralar, iltihaplanma, romatizma ve gut, siyatik, çürük ve şişlikler, ateş, astım, bronşit ve diş ağrısı dahil olmak üzere çeşitli rahatsızlıklar üzerinde etkilidir (Balachandran ve Rajgopal, 2005).

- **Hedera helix (Orman Sarmaşığı)**

Etkili Bileşik: α-hederin ve β-hederin, falcarinol, didehidrofalcarinol, rutin, kafeik asit, klorojenik asit, emetin, nikotiflorin, hederasaponin B ve hederacoside C
Zehirlenme Belirtileri: Temas veya yutulması halinde zehirlenmelere neden olabilir. Yapraklarında ve meyvelerinde bulunan çok sayıda saponin nedeniyle tavşan gibi hayvanlar için hafif zehirlidir ve kansızlığa yol açabilir (Pratt, 2020). Yapraklar bazı kişilerde şiddetli kontakt dermatite neden olabilir. Kediler, köpekler ve atlar için zehirlidir ancak kuşlar ya da çiftlik hayvanları için zehirli değildir. Beş yaşın altındaki çocuklar bitki zehirlenmesinden en fazla risk altındadır.
Tıbbi Kullanımı: Öksürük, balgam söktürücü olarak ve öksürüğün sıklığını ve yoğunluğunu azaltmak için kullanılır (Jøhnke ve Bjarnason, 1994).

- ***Buxus sempervirens* L.** (Şimşir)

Etkili Bileşik: Yaprak ve gövdelerinin buxmicrophilline B, C ve D olarak bilinen üç yeni steroidal alkaloit, butulin, lupeol gibi pekçok bileşik içermektedir.
Zehirlenme Belirtileri: Tüm parçaları zehirli olan bitkinin yapraklarının yenmesi halinde ciddi sağlık sorunları oluşabilir. Karın krampı, bulantı, kusma ve ishal gibi gastrointestinal semptomlara neden olur. Ayrıca köpek, kedi ve atlar için potansiyel toksik olabilir (Berdai ve ark., 2012).
Tıbbi Kullanımı: Ağrı, gut, koroner hastalıklar, frengi, dermatit, kuduz, diş ağrısı, fıtıklar, çürükler, göğüs ve karın rahatsızlıkları ve diğer bazı rahatsızlıkların tedavisinde kullanılmıştır (Ata ve ark., 2008).

- ***Hydrangea* spp.** (Ortanca)

Etkili Bileşikler: Yaprak ve çiçekleri kumarin, skimmin, loganin gibi siyanoglikozitleri içerir (Bown, 1995).
Zehirlenme Belirtileri: Zehirli yaprakları, baş dönmesi, mide bulantısı, nefes darlığı, baş dönmesine neden olur (Cooper & Johnson1998).
Tıbbi Kullanımı: Ortanca kökündeki bileşikler, kronik iltihaplanma ile sıklıkla ilişkilendirilen iltihaplı bağırsak hastalığı, romatoid artrit, lupus, astım, obezite ve sedef hastalığı gibi otoimmün bozukluklara karşı koruma sağlayabilir

SONUÇLAR

Sonuçlar değerlendirildiğinde, zehirli bitkilerin, kontrollü şekilde kullanıldığı takdirde taşıdıkları etken maddelerinden dolayı, ilaç hammaddesi olarak hayat kurtarıcı olabileceği anlaşılmaktadır: Örneğin;
Morfin: Ağrı kesici; Atropin: Göz damlası, kalp tedavisi; Digitoksin: Kalp yetmezliği tedavisi; Kolşisin: Gut hastalığı; Taksol: Kanser ilacı; Papaverin: Ağrı kesici; Kodein: Öksürük kesici

TEDBİR VE ÖNERİLER

Peyzaj mimarisi açısından göz alıcı olan birçok süs bitkisi, toksik bileşikler içerebilir ve insanlar ya da hayvanlar için potansiyel tehlike oluşturabilir. Bu nedenle, bitki seçimi yapılırken sadece estetik değil, ekolojik ve sağlık riskleri de göz önünde bulundurulmalıdır.
Parkların peyzajında, bu bitkilerin kullanılmaması gerektiği hakkında bilgilendirmelerin yapılması, peyzajda bu bitkilerin varlığında gerekli uyarı levhalarının bulundurulması, özellikle çocukların sıklıkla kullandığı bu alanlarda, ebeveynlerin çok dikkatli olması gerekmektedir.
Toplumun bilinçlendirilmesi, zehirlenme vakalarının önlenmesi açısından hayati öneme sahiptir. Bazı türler birkaç gramlık dozlarda bile ölümcül olabilmektedir. Bu bitkiler, geleneksel veya modern tıpta dikkatli dozaj ve formülasyon ile tedavi edici olabilmekle beraber, doğru kullanılmadıkları ve kontrolsüz tüketimleri sonucunda ölümcül zehirlenmelere neden olabilmektedirler.

KAYNAKLAR

Al, B., Yarbil, P., Doğan, M., Kabul, S., Yıldırım, C. (2010). A case of non-fatal oleander poisoning. BMJ Case Reports, 2010:2010:bcr02.2009. 1573.

Al-Snafi, A.E. (2016). Pharmacology and Toxicology of *Conium maculatum*- A Review, The Pharmaceutical and Chemical Journal, 3(2):136-142.

Aliadeh, A., Moshiri, M., Aliadeh, J., Balali-Mood, M. (2014). Black henbane and its toxicity – a descriptive review. Avicenna J Phytomed., 4(5):297–311.

Ata, A., Andersh, B.J. (2008). Buxus steroidal alkaloids: chemistry and biology. Alkaloids Chem Biol., 2008:66:191-213.

Ayensu, S.E. (1978). Medicinal plants of West Africa, 1st edn. Reference Publications, Algonac, MI, USA., pp. 1- 45.

Balachandran, P., Rajgopal, G. (2005). Cancer-an Ayurvedic perspective. Pharmacol Res., 51(1): 19-30.

Berdai, M.A., Labib, S., Chetouani, K., Harandou, M. (2012). *Atropa belladonna* intoxication: a case report. Pan Afr Med J., 17;11:72.

Bonini, S.A., Premoli, M., Tambaro, S., Kumar, A., Maccarinelli, G., Memo, M., Mastinu, A. (2018). *Cannabis sativa*: A comprehensive ethnopharmacological review of a medicinal plant with a long history. J. Ethnopharmacol.,5(227):300–315.

Bown, D. (1995). Encyclopaedia of Herbs and their Uses. Dorling Kindersley, London. P.424. ISBN 0-7513-020-31.

Bown, D., (2002). The Royal Horticultural Society New Encyclopedia of Herbs & Their Uses. The Royal Horticultural Society, Revised Edition. Dorling Kindersley, 448 pages.

Bradberry S., Vale A., (2016). *Digitalis purpurea*, *Nerium oleander*, *Thevetia peruviana* (yellow oleander), Plants. Medicine, 44:113–115.

Brunton, L.L., Knollmann, B.C., Hilal-Dandan, R. (2022). Goodman & Gilman's: The Pharmacological Basis of Therapeutics. McGraw-Hill Education. 14th Edition. P.1644.

Burrows, G.E., Tyrl, R.J. (2012). Toxic Plants of North America. Ames, IA: Iowa State University Press; First Edition. 1113–1118 pages.

Ceylan, A. (1994). Tıbbi Bitkiler III. E.Ü. Ziraat Fakültesi Yayınları, No.509, İzmir.

Cooper, M.R., Johnson, A.W. (1998). Poisonous Plants and Fungi in Britain:An Illustrated Guide. The Stationery Office/Tso. 2nd Edition. 416 pages.

Dolan, R., Welch-Keesey, M. (2016). A guide to poisonous and non-poisonous plants in Indiana. Indiana Poison Center. Purdue Univ., https://iuhealth.org/images/metdoc-upl/plant-guide.pdf., as retrieved on Thursday, May 05th 2016 at 10:51 AM, East Africa Time.

Dnyaneshwar, J.T., Patil, Y.R. (2011). Some medicinal plants with antiasthmatic potential: a current status. Asian Pacific Journal of Tropical Biomedicine, 1(5):413-8.

Duke, J.A. (2012). Dr. Duke's Phytochemical and Ethnobotanical Databases. USDA.

Ebaid, G.M., Faine, L.A., Diniz, Y.S., et al. (2006). Effects of digitonin on hyperglycaemia and dyslipidemia induced by high-sucrose intake. Food Chem Toxicol. 44(2):293-299.

Elikkottil, J., Gupta, P., Gupta, K. (2009). The analgesic potential of cannabinoids. J. Opioid Manag., 341–357.

Erdem, S., Ata-Eren, P. (2009). Tedavi Amacıyla Kullanılan Bitkiler ve Bitkisel Ürünlerin Yan Etkileri. (Adverse Effects of Herbal Medicines and Products), Türk Hijyen ve Deneysel Biyoloji Dergisi; 66 (3): 133-141.

Erdemoğlu, N., Şener, B. (2001). Antimicrobial activity of the heartwood of *Taxus baccata*. Fitoterapia., 72:59–61. https://www.rxlist.com/yew/supplements.htm/

Giacoppo, S., Bramanti, P., Mazzon, E. (2017). Sativex in the management of multiple sclerosis-related spasticity: An overview of the last decade of clinical evaluation. Mult. Scler. Relat. Disord.,17:22–31.

Gilani, A.H., Khan, A.U., Raoof, M., Ghayur, M.N., Siddiqui, B.S., et al. (2008). Gastrointestinal, selective airways and urinary bladder relaxant effects of *Hyoscyamus niger* are mediated through dual blockade of muscarinic receptors and Ca2+ channels. Fundam Clin Pharmacol, 22: 87-99.

Gupta, P.K. (2016). Toxic effects of cardiac poisons. Fundamentals of Toxicology. P.381.

Jitendra, J., Gupta, A.K. (2012). *Ricinus communis* Linn: A Phytopharmacological Review. International Journal of Pharmacy and Pharmaceutical Sciences, 4(4):25-29. ISSN- 0975-1491.

Johansson, S., Lindholm, P., Gullbo, J., Larsson, R., Bohlin, L., Cleason, P. (2001). Cytotoxicity of digitoxin and related cardiac glycosides in human tumor cells. Anticancer Drugs, 12(5):475-483.

Jøhnke, H., Bjarnason, B. (1994). Contact dermatitis allergy to common ivy (*Hedera helix* L.) Ugeskr Laeger, 156(25):3778–9.

Karimi, A., Majlesi, M., Rafieian-Kopaei, M. (2015). Herbal versus synthetic drugs; beliefs and facts. Journal of nephropharmacology, 4(1):27–30.

Kipkore, W., Wanjohi, B., Rono, H., Kigen, G. (2014). A study of the medicinal plants used by the Marakwet Community in Kenya. Journal of Ethnobiology and Ethnomedicine, 10:24.

Kirtikar, K.R., Basu, B.D. (1999). Indian medicinal plants. 2nd (Edn). Volume III. Dehradun: International Book Distributors pp.1783-1787.

Krenzelok, E.P. (2010). Aspects of Datura poisoning and treatment, Clinical Toxicology, vol.48(2), Pages 104-110.

Lee, M.R. (2007). Solanaceae 4: *Atropa belladonna*, Deadly Nightshade. J R Coll Physicions Edinb., 37(1):77-84.

Lindequist, U. (1993). *Hyoscyamus*. In Haegers Handbuch der pharmazeutischen Praxis, 5th ed., 5.: Berlin: Springer. pp. 460–74.

Maitai, C.K. (1996). The dynamic interplay between man, health and medicines: A historical perspective. Inaugural Lectures. Department of Pharmacology and Phamacognosy, Faculty of Pharmacy, College of Health Sciences, University of Nairobi, Kenya.

Mdee, L.K., Masoko, P., Eloff, J.N. (2009). The activity of extracts of seven common invasive plant species on fungal phytopathogens. South African Journal of Botany, 75(2):375-379.

Mondal, J., Panigrahi, A.K., Khuda-Bukhsh, A.K. (2014). Anticancer potential of *Conium maculatum* extract against cancer cells in vitro: DrugDNA interaction and its ability to induce apoptosis through ROS generation Pharmacogn Mag., 10(Suppl 3): S524–S533.

https://www.rxlist.com/hemlock/supplements.htm- Reviewed on 6/11/2021

Olson, K. (2018). Poisoning & Drug Overdose. 7th ed. McGraw-Hill Education; 2018.

Purohit, A., Maikhuri, R.K., Rao, K.S., Nautiyal S., (2001), Impact of bark removal on survival of *Taxus baccata* L.(Himalayan yew) in Nanda Devi Biosphere Reserve, Garwhal Himalaya, India. Curr Sci. 81:586–90.

Raetsch, C.H. (2005). The encyclopedia of psychoactive plants: ethnopharmacology and its applications. US: Park Street Press. pp. 277–282.

Russo, E.B. (2008). Cannabinoids in the management of difficult to treat pain. Ther. Clin. Risk Manag.,4:245–259.

Sajeli, Be., Shweta, V., Kathrin, M.S., Roderich,S., Süssmuth, D. (2009). Hyoscyamal, a new tetrahydrofurano lignan from *Hyoscyamus niger* Linn. Natural Product Research, 23(7):595-600

Scarpa, A., Guerci, A. (1982). Various uses of the castor oil plant (*Ricinus communis* L.). A review. J. Ethnopharmacol. 5(2):117-37.

Shukla, B., Visen, P.K.S., Patnaik, G.K., Kapoor, N.K., Dhawan, B.N. (1992). Hepatoprotective effect of an active constituent isolated from the leaves of *Ricinus communis* Linn, Drug Development Research, Volume 26, Issue 2, pages 183–193.

Shumaik, G.M., Wu, A.W., Ping, A.C. (1988). Oleander poisoning: Treatment with digoxin- specific Fab antibody fragments. Ann Emerg Med.,17:732–5.

Stapczynski, J.S., Rothstein, R.J., Gaye, W.A., Niemann, J.T. (1981). Colchicine overdose: report of two cases and review of the literature. Ann Emerg Med.,10:364–369.

Vetter, J. (2004). Review: Poison hemlock (*Conium maculatum* L.). Food and Chemical Toxicology, 42(9):1373–1382.

Wani, M.C., Taylor, H.L., Wall, M.E., Coggon, P., McPhail, A.T. (1971). "Plant antitumor agents. VI. The isolation and structure of taxol, a novel antileukemic and antitumor agent from *Taxus brevifolia*." Journal of the American Chemical Society, 93(9), 2325–2327.

Wanzala, W., Takken, W., Pala, A.O., Mukabana, R.W., Hassanali, A. (2012). Ethnoknowledge of Bukusu community on livestock tick prevention and control in Bungoma district, western Kenya. Journal of Ethnopharmacology, 140 (2):298-324.

Wilson, C.R., Sauer, J.M., Hooser, S.B. (2001). Taxines: a review of the mechanism and toxicity of yew (*Taxus* spp.) alkaloids. Toxicon. 39(2-3): 175-185.

➢ *ORAL PRESENTATION*

Improving PPO-Based Reinforcement Learning for Energy Forecasting with Chaotic Initialization and American Zebra Optimization

Cem Özkurt[1] (ORCID: https://orcid.org/0000-0002-1251-7715), Özkan Canay[2*] (ORCID: https://orcid.org/0000-0001-7539-6001), Murat Karslıoğlu[1] (ORCID: https://orcid.org/0009-0002-2259-2994)

[1] Sakarya University of Applied Sciences, Computer Engineering, Sakarya, Türkiye
[2*] Sakarya University, Information Systems and Technologies, Sakarya, Türkiye

*Corresponding author e-mail: canay@sakarya.edu.tr

Abstract
This study proposes a novel solution to the time series-based energy consumption forecasting problem using a reinforcement learning (RL) approach. The Proximal Policy Optimization (PPO) algorithm, which is widely used in the literature, is investigated in this study not only in its classical form but also in its integrated forms with chaotic dynamics and the American Zebra Optimization Algorithm (AZOA). The Henon map-based chaotic initialization aims to increase the exploration capacity of the agents, while AZOA is used to optimize the hyperparameters of PPO in an agile and efficient way. The experimental analysis of the three different configurations yielded remarkable findings. In the classical PPO model, the total reward value was recorded as 3809 in the first episode but remained constant in a narrow band (3806.5-3807.0) throughout all subsequent episodes. This revealed that learning with the default settings was stuck at the local optimum. In the PPO model with chaotic onset, the level of reward reached approximately 9600 in the third episode, but this high reward level came with an unstable learning process. In contrast, in the PPO model with AZOA support, the total reward, which started at 8300 in the first generation, reached 9700 in only a few generations and remained stable throughout the learning process. While the use of PPO in energy systems has been documented in the literature with limited examples, this study makes a unique contribution to the literature by integrating both chaotic systems and meta-heuristic optimization algorithms (AZOA) with PPO. Moreover, it has been shown that for high-dimensional and continuous output problems such as energy forecasting, optimized versions of PPO produce more successful results. In this respect, the study provides a new methodological framework for the integration of RL-based models into energy management systems.

Keywords: Energy Forecasting, Reinforcement Learning, PPO, Chaos Theory, AZOA, Hyperparameter Optimization

INTRODUCTION

Increasing global energy demand and efficient use of energy resources make accurate prediction of residential energy consumption a critical research area. Time-series based data collected from smart home systems enable the effective use of machine learning algorithms in this field (Wang et al., 2019). In this study, the energy forecasting problem is treated as a decision-making and policy learning problem rather than a time series forecasting problem, and for this reason, the Proximal Policy Optimization (PPO) algorithm is preferred.

PPO is a reinforcement learning algorithm based on advantage forecasting and prevents excessive updates by maintaining a balance in policy updates, thus ensuring stability in the learning process. PPO is preferred due to its strong generalization capability in time-dependent data and its structure suitable for online learning (Liu et al., 2020).

Classical reinforcement learning algorithms such as PPO can face problems such as premature convergence and getting stuck at local minima in scenarios where the solution space is complex and multimodal. To overcome this, chaotic dynamics are integrated into the learning process. Chaotic systems, although deterministic, exhibit complex behavior like randomness and are extremely sensitive to initial conditions. Thanks to these properties, chaotic sequences increase the diversity in the agents' choice of actions and help them move towards solution

regions that are difficult to reach by classical methods. The reason for using chaos in this study is to improve the PPO's exploration behavior so that a wider policy space can be scanned.

In addition to the chaotic PPO structure, the American Zebra Optimization Algorithm (AZOA) was applied to make the learning process more effective and directed. AZOA is a meta-heuristic optimization algorithm that mathematically models the migration, escape and social interaction behavior of zebra herds in nature. It was chosen because it enables adaptive optimization of both parameter settings and agent policies, making the learning process more efficient and balanced. In particular, its ability to find efficient solutions in complex hyperparameter spaces makes AZOA a powerful tool for this study (Yang & Shami, 2020; Akiba et al., 2019; Wu et al., 2019).

There are several studies in literature where PPO is used in energy systems. PPO has been applied to increase solar energy self-consumption in residential buildings, but the study did not include chaotic dynamics or heuristic optimization algorithms (Peirelinck et al., 2022). Similarly, it has shown that PPO can be used to control chaotic systems, but this approach has not been evaluated in the context of energy forecasting (Bucci et al., 2019). On the other hand, although the AZOA algorithm has been successfully applied to global optimization problems, it has not yet been combined with energy data or reinforcement learning algorithms (Basheri, 2024). In this context, our study presents a novel approach that has not been tried before in literature by integrating PPO with both chaos and AZOA and aims to improve energy prediction accuracy.

In this context, the main objective of this study is to comparatively evaluate chaos-supported PPO, chaos and AZOA-supported PPO models on an energy consumption forecasting task and to demonstrate the impact of each method on performance. The experimental results show the effectiveness of integrating both chaos theory and nature-inspired optimization approaches into reinforcement learning models and propose a holistic solution for smart energy management.

RELATED WORKS

Energy forecasting has become more predictable and adaptive in recent years with the contribution of machine learning and reinforcement learning methods. In this context, the PPO algorithm stands out with its consistent learning success, especially for continuous control problems. The adaptation of PPO to real-world applications such as energy demand management has gained importance due to its learning capability sensitive to different data structures and environmental scenarios, but in this study, environmental uncertainties are not modeled with a chaotic structure and hyperparameters are kept constant (Peirelinck et al., 2022).

There are also studies applying reinforcement learning to chaotic systems. In these studies, PPO or similar deep RL algorithms have been tested in abstract dynamics such as chaotic system control (Bucci et al., 2019). In such applications, examples evaluating the performance of PPO on continuous output tasks such as regression-based energy consumption prediction are limited. Moreover, there are very few applications in the existing literature that integrate meta-heuristic algorithms to optimize the PPO's hyperparameters. In this context, the main difference of the presented work is that PPO is optimized on continuous and high-dimensional energy consumption data with both chaotic and meta-heuristic methods, which is different from its classical application areas.

In energy forecasting, optimization of hyperparameters is a critical factor for the generalizability of the model. At this point, the Zebra Optimization Algorithm (ZOA) and its improved version American ZOA (AZOA) have become prominent in global optimization problems (Trojovská, Dehghani, & Trojovský, 2022; Mohapatra & Mohapatra, 2023). In some studies, this algorithm has been tested on tasks such as clustering and gesture recognition in data transmission (Janakiraman et al., 2023; Basheri, 2024). In particular, feature selection performance has been improved with the multi-strategy ZOA approach, but none of these studies present a structure directly integrated with reinforcement learning algorithms such as PPO (Özbay, 2025).

The combination of chaotic systems with ZOA has been investigated in many recent studies. The common point of these studies is that classical ZOA can be initialized or guided by chaotic maps (e.g. Tent, Cat, Logistic) to achieve a more balanced search process (Kamboj et al., 2023; Amin et al., 2024). The performance of chaotic AZOA on benchmark problems has been improved (Kamboj et al., 2023). Another study tested the combination of chaotic ZOA + LSTM on time-series based data such as cyber security (Amin et al., 2024). Since these studies focused on classification or security detection, their applicability to continuous regression problems was limited.

In other studies, chaotic maps and crossover strategies have been integrated into ZOA for better hyperparameter fitting, but these are not directly related to RL-based prediction models (Wu & Zhou, 2024; Shang et al., 2024).

Some studies have shown that ZOA can be used in system-level optimization problems such as PID control, load-frequency control or MPPT (Trojovská et al., 2022). While these examples demonstrate the effectiveness of ZOA in continuous optimization tasks, it is not clear how to incorporate this approach into the adaptive learning processes of RL algorithms.

Studies on the applications of ZOA and AZOA in various domains have addressed problems such as cyber threat detection, medical data feature selection, and intrusion detection (Ur Rehman et al., 2025). These studies demonstrate that the algorithm has the capability to generalize across different data types. However, no direct research has been found on the integration of ZOA/AZOA with reinforcement learning in domains characterized by dense and continuous time series data, such as predictive energy analytics.

This study is one of the first examples where chaotic structures and ZOA-based hyperparameter optimizations are used together, taking the PPO algorithm beyond classical energy forecasting applications. It differs from the existing studies in literature in terms of both the time series nature of the data set and the joint modeling of PPO's reward dynamics and chaotic control strategies.

MATERIALS AND METHODS

Dataset of the Study

The dataset used in this study is the open source "energydata_complete.csv" time series data, which includes indoor and outdoor sensor data in the residential environment. This set of approximately 200,000 rows from 2016 contains temperature, humidity, ambient conditions and appliance-based energy consumption data. The target variable Appliances represents the instantaneous energy consumption (Wh) of appliances. The dataset is obtained from the Kaggle platform and is widely used for research analysis.

Columns rv1 and rv2 containing date information and random values were excluded, and the remaining continuous variables were scaled to the interval [0, 1] with Min-Max normalization, as defined in Eq. (1).

$$\hat{x}_t = \frac{x_t - \min(x)}{\max(x) - \min(x)} \tag{1}$$

According to the time series structure, the input data at each time t s structured to contain a window length w of historical data, as defined in Eq. (2).

$$X_t = [\widetilde{x_{t-w}}, \widetilde{x_{t-w+1}}, \dots\dots, \widetilde{x_{t-1}}], \qquad y_t = \widetilde{y_t} \tag{2}$$

Proximal Policy Optimization (PPO)

Energy estimation is solved in the context of reinforcement learning (RL), going beyond classical methods. In this context, the agent tries to maximize the reward function by observing the environment. Proximal Policy Optimization (PPO) algorithm is used in this process.

The PPO is based on the policy rate, which represents the probability ratio between the new and old policies for the same action-state pair, as shown in Eq. (3):

$$r_t(\theta) = \frac{\pi_\theta(a_t|s_t)}{\pi_{\theta_{old}}(a_t|s_t)} \tag{3}$$

The clipped policy loss uses the ratio to limit large policy updates and ensure training stability, as defined in Eq. (4):

$$L^{CLIP}(\theta) = E_t\left[min(r_t(\theta)\widehat{A_t}, clip(r_t(\theta), 1-\epsilon, 1+\epsilon)\widehat{A_t})\right] \quad (4)$$

The value function loss quantifies the squared difference between the estimated value and the target value, as formulated in Eq. (5):

$$L^{VF}(\theta) = \left(V_\theta(s_t) - V_t^{target}\right)^2 \quad (5)$$

The total loss function in PPO combines the clipped surrogate objective, value function loss, and an entropy bonus to encourage exploration, as expressed in Eq. (6):

$$L^{total}(\theta) = L^{CLIP}(\theta) - c_1 L^{VF}(\theta) + c_2 S[\pi_\theta](s_t) \quad (6)$$

Parameter Initialization with Chaotic System

The initial distribution of model parameters directly affects the learning efficiency. In this study, Henon Map based chaotic initialization method is used instead of classical random initialization, as shown in Eq. (7):

$$x_{t+1} = 1 - ax_t^2 + y_t, \qquad y_{t+1} = bx_t \quad (7)$$

Here $a = 1.4$, $b = 0.3$ to obtain the chaotic sequence x_t. This sequence is transferred to the parameters of the neural network as follows, as expressed in Eq. (8):

$$\theta_i^{(0)} = ax_i + \beta \quad (8)$$

This method aims to avoid local minima by providing a large and diverse initialization area.

American Zebra Optimization Algorithm (AZOA)

The correct choice of hyperparameters$(e.g. \eta, \epsilon, c_2)$ used in the PPO algorithm is critical for model performance. For this reason, the American Zebra Optimization Algorithm (AZOA), inspired by the collective action of herds of zebras in nature, was chosen to automatically and efficiently determine the hyperparameters. The goal of AZOA is that individuals act together in the solution space and follow a balancing exploration-exploitation strategy.

Each individual represents a hyper-parameter combination, and their achievements are evaluated by PPO's total reward function $R = \sum_{t=1}^{T} r_t$. The position of individuals is updated according to the best individual in the population as follows, as expressed in Eq. (9):

$$X_i^{t+1} = X_i^t + r_1 . \sin(r_2) . (X_{best}^t - X_i^t) \quad (9)$$

Here $r_1 \epsilon [0,1]$ and $r_2 \epsilon [0, \pi]$ are random values. This structure allows for a wider and more efficient search compared to classical methods by varying the direction and speed of the individuals. In each generation, the hyperparameter combinations are re-evaluated and the process continues until a high reward value is reached. In this way, AZOA aims to increase the overall performance of the PPO.

RESULTS

In this study, the performance of the Proximal Policy Optimization (PPO) algorithm on the energy consumption prediction task is evaluated based on the total reward values obtained under three different configurations. The main objective of the study is to reveal the effects of different strategies (classical structure, chaotic initialization, AZOA-based hyperparameter optimization) used to optimize the performance of the PPO algorithm and to comparatively analyze the behavior of these structures during the learning process.

The evaluations are based on the total reward metric, and the learning curves, variance structures, convergence behaviors and stability levels are examined in detail using the relevant graphs for each configuration. The analysis is structured over three graphs.

The first method considered is the classic version of the PPO algorithm, where the PPO algorithm is run with the default settings without any external intervention or hyperparameter optimization. The results of this configuration are presented in Figure 1. Looking at the total reward curve, we observe that the first episode yields a relatively high reward value of 3809, but this value remains constant within a very narrow band (3806.5 - 3807.0) throughout all subsequent episodes and does not increase significantly.

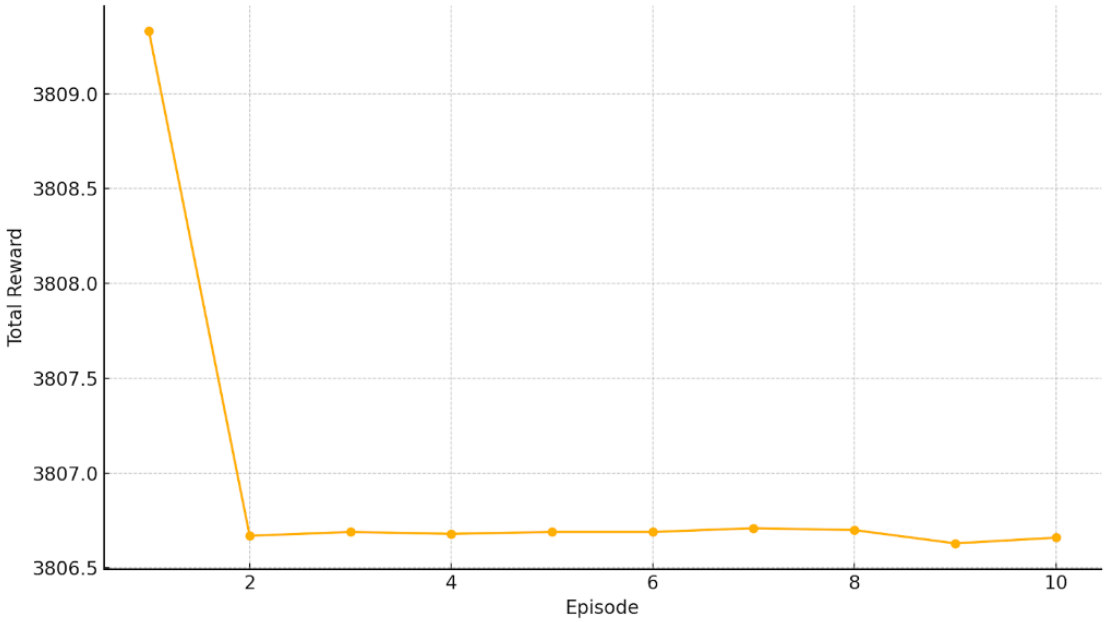

Figure 1. PPO with Deterministic Reward Optimization.

This observation reveals that the classical PPO algorithm can produce a policy in a short time, but this policy gets stuck at the local optimum and is unable to move to higher payoff solution regions. Such behavior is common when the level of exploration is insufficient, indicating that the algorithm is unable to scan a wider solution space and hence the policy quality is limited. Even though the reward levels are stable, the performance remains low, and the learning is stagnant, clearly demonstrating the importance of hyperparameter tuning for the performance of PPO.

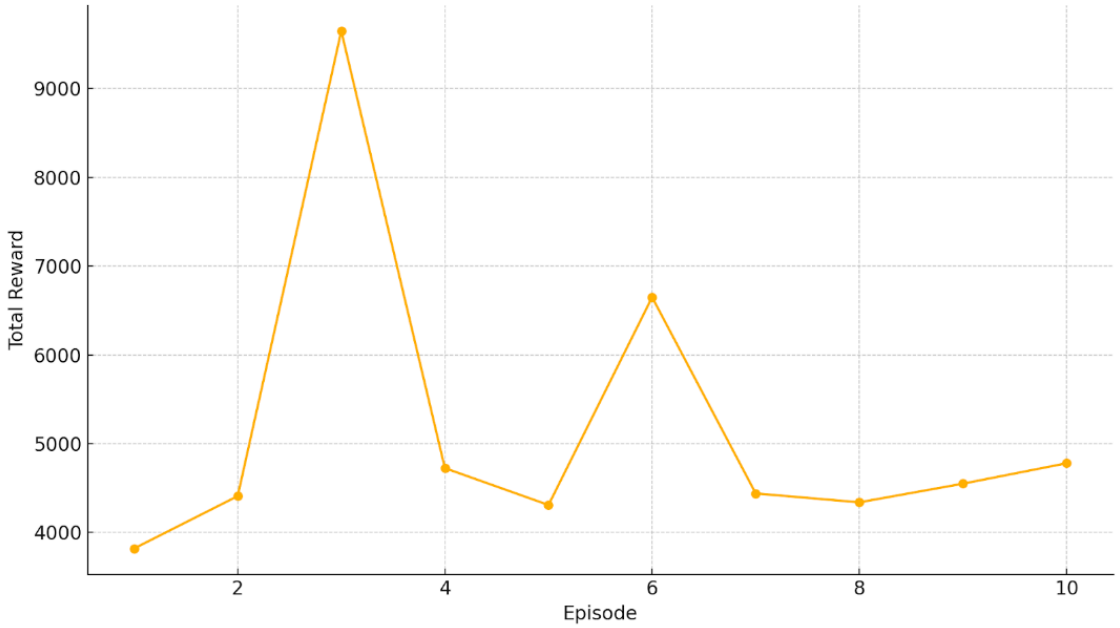

Figure 2. PPO Enhanced with Chaos-Driven Optimization.

The second configuration is a strategy in which the initial weights of the PPO algorithm are generated by a chaotic system-based mechanism (Henon's map) and learning is initiated in this way. Figure 2 shows that the total reward value makes a dramatic jump, especially in the third episode, reaching approximately 9600. This shows that initializations with chaotic systems allow the algorithm to locate more heterogeneous points in the initial policy space and thus reach solution regions with higher payoffs.

This advantage comes with a significant weakness in terms of stability. The sudden drops and fluctuations after the third episode show that the variance increases significantly during the learning process and the policy struggles to stabilize. In particular, the sharp declines observed in the fourth and fifth episodes show that despite the high exploration potential of chaotic beginnings, policy convergence becomes difficult and may lead to inconsistent results. Although there was a rebound in the sixth episode, the overall trend suggests that the learning process was unstable.

This configuration may be particularly useful in scenarios targeting high reward potential, but in practice, where stable and repeatable learning processes are needed, PPO initiated with chaotic systems alone may not offer sufficient reliability.

The third configuration is a strategy where the hyperparameters of the PPO algorithm are optimized using the American Zebra Optimization Algorithm (AZOA). The performance results for this configuration are presented in Figure 3. The graph shows that the algorithm achieves an average reward value of about 8300 in the first generation and reaches 9700 in only a few generations. From the fourth generation onwards, the learning curve stabilizes at this level and is maintained for all subsequent generations.

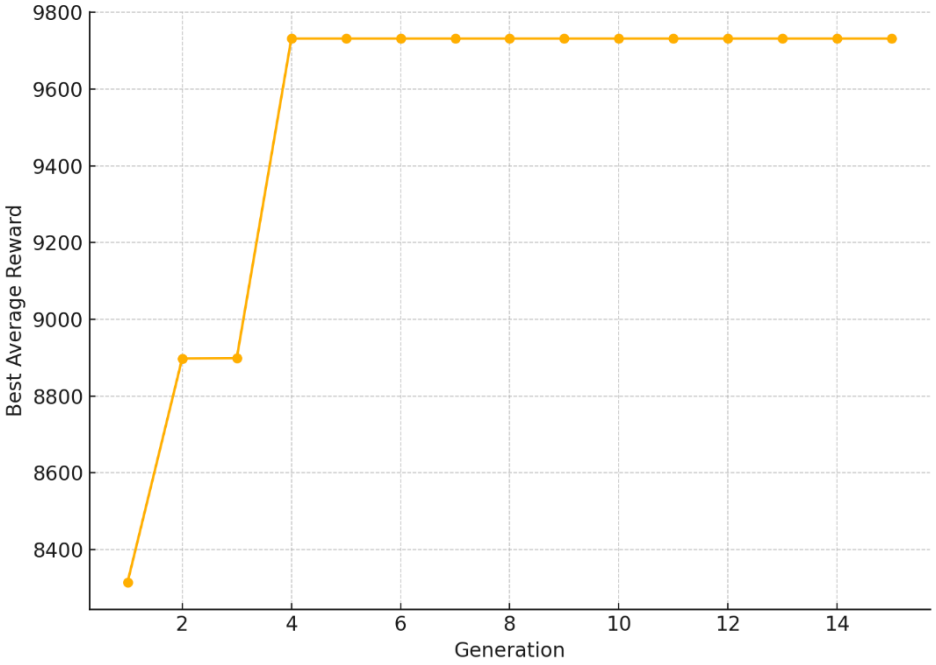

Figure 3. AZOA-Based Hyperparameter Optimization.

This learning behavior shows that the AZOA algorithm performs a very efficient scanning of the hyperparameter space, finding suitable parameter combinations at an early stage, and that these combinations lead to high and stable policy generation. AZOA's success here not only increased the convergence speed but also ensured the stability of the learning process. This structure is considered as an approach that significantly strengthens the applicability of the PPO algorithm and makes it more reliable for industrial applications.

DISCUSSION

In this study, the performance of the PPO algorithm in the task of energy consumption prediction is evaluated through three different configurations and a comparative analysis is performed. The methods include the classical PPO model (PPO with Deterministic Reward Optimization), the PPO model with initial parameters generated by a chaotic system (PPO Enhanced with Chaos-Driven Optimization), and the PPO model with hyperparameters optimized by the American Zebra Optimization Algorithm (AZOA-Based Hyperparameter Optimization). The discussion is carried out in depth in the light of both experimental results and similar literature findings (Bindu et al., 2025; Mohammed & Ahmed, 2023; Rziki et al., 2025).

As seen in Figure 1, when the classical PPO structure is evaluated, it is seen that the algorithm remains constant in a very narrow band during the learning process. Although the total reward of 3809 in the first episode seems promising in the short term, this value stabilized at 3806.5-3807.0 in the following episodes and the learning process did not show any meaningful progress. This shows that the PPO algorithm only develops a limited policy with the default hyperparameter settings and cannot produce better solutions. Although the classical structure offers low variance and high stability, it faces a serious performance limitation in terms of reward level. This finding suggests that without hyperparameter optimization, PPO cannot fully demonstrate its capability (Ma et al., 2022; Mohammed & Ahmed, 2023).

In contrast, as seen in Figure 2, the PPO model initialized with the chaotic system has a very high variance in the learning process. The total reward of about 9600 in the third episode is the highest instantaneous performance achieved throughout the experiments. This shows that chaotic initializations can provide a wider exploration of the policy space and allow the system to access high reward regions. However, the same structure exhibits a significant drop in the fourth episode, rises again in the sixth episode, and then fluctuates again. Although this high volatility increases the exploratory power of the method, it makes stable policy learning difficult and reduces the reliability of the application. Especially in safety-critical systems or areas with high forecast sensitivity, such variance can undermine the reliability of decision-making systems (Sinha & Gupta, 2022; Acharya et al., 2024; Bindu et al., 2025).

As can be clearly seen in Figure 3, the PPO model with AZOA-based hyperparameter optimization is the most successful structure in terms of both convergence speed and reward level. The average reward, which was around 8300 in the first generation, reaches 9700 in just a few generations and this value stabilizes from the fourth generation onwards. This structure has both the capacity to generate high rewards and the advantage of learning with low variance. The fact that learning continues steadily reveals that the algorithm is able to develop balanced and efficient policies with appropriate parameter combinations. The systematic hyperparameter discovery provided by AZOA here helped it overcome the local minimum problem faced by the classical PPO and revealed the true potential of the system (Basheri, 2024; Rziki et al., 2025; Bindu et al., 2025).

The findings show that the performance of the PPO algorithm directly depends on the optimization strategy applied. It is also necessary to focus on strategies for high performance, reliable and hyperparameter optimization, initial conditions and variance control. In future work, hybridizing chaotic initializations and meta-heuristic optimization techniques may enable the design of more balanced learning systems in terms of both exploration capacity and stability (Bindu et al., 2025; Sinha & Gupta, 2022; Mohammed & Ahmed, 2023; Ma et al., 2022; Basheri, 2024).

CONCLUSION

The study proposed a novel approach for time-series based energy consumption forecasting by enhancing the PPO algorithm with chaotic initialization and the American Zebra Optimization Algorithm (AZOA). It was observed that chaotic initialization significantly accelerated early reward acquisition, albeit at the cost of increased training instability. In contrast, the AZOA-enhanced PPO yielded high and stable reward values throughout the training process, underscoring the critical importance of hyperparameter optimization in reinforcement learning applications for high-dimensional prediction tasks.

The integration of chaos theory and nature-inspired optimization into reinforcement learning frameworks marks a promising direction for future energy management applications. This study contributes a new methodological framework that can be extended to other continuous control tasks. Future research may focus on hybrid models that combine the exploratory power of chaotic systems with the convergence stability of metaheuristic optimizers, aiming to develop adaptive and resilient learning systems for real-world dynamic environments.

REFERENCES

Adde, N. A., Gottschalk, H., & Ebert, A. (2024, September). Hyperparameter Optimization for Driving Strategies Based on Reinforcement Learning. *In International Conference on Machine Learning, Optimization, and Data Science* (pp. 24-38). Cham: Springer Nature Switzerland. https://doi.org/10.1007/978-3-031-82484-5_3

Akiba, T., Sano, S., Yanase, T., Ohta, T., & Koyama, M. (2019, July). Optuna: A next-generation hyperparameter optimization framework. *In Proceedings of the 25th ACM SIGKDD international conference on knowledge discovery & data mining* (pp. 2623-2631). https://doi.org/10.1145/3292500.3330701

Amin, R., El-Taweel, G., Ali, A. F., & Tahoun, M. (2024). Hybrid chaotic zebra optimization algorithm and long short-term memory for cyber threats detection. *IEEE Access*, 12, 93235-93260. https://doi.org/10.1109/access.2024.3397303

Basheri, M. (2024). Automated Gesture Recognition Using Zebra Optimization Algorithm with Deep Learning Model for Visually Challenged People. *Fusion: Practice & Applications*, 16(1). https://doi.org/10.54216/fpa.160102

Bindu, N. V. M., Nassa, V. K., Vasuki, P., Manikandan, G., Jeena, R., & Mahaveerakannan, R. (2025). IoT botnet detection from software defined network using American zebra optimization algorithm with SSRNN-ELM. *International Journal of Information Technology*, 1-9. https://doi.org/10.1007/s41870-024-02348-1

Bindu, R., Pradhan, M., & Panda, G. (2025). Hybrid metaheuristic optimization for deep reinforcement learning in energy systems. *Sustainability*, 17(6), 2345–2359. https://doi.org/10.5220/0013313600003899

Bucci, M. A., Semeraro, O., Allauzen, A., Wisniewski, G., Cordier, L., & Mathelin, L. (2019). Control of chaotic systems by deep reinforcement learning. *Proceedings of the Royal Society A*, 475(2231), 20190351. https://doi.org/10.1098/rspa.2019.0351

Elymany, M. M., Enany, M. A., & Elsonbaty, N. A. (2024). Hybrid optimized-ANFIS based MPPT for hybrid microgrid using zebra optimization algorithm and artificial gorilla troops optimizer. *Energy Conversion and Management*, *299*, 117809. https://doi.org/10.1016/j.enconman.2023.117809

Janakiraman, S., Deva Priya, M., & Karthick, S. (2023, June). American zebra optimization algorithm-based clustering protocol for reliable data routing in internet of things. In *International Conference on Recent Trends in Computing* (pp. 779-794). Singapore: Springer Nature Singapore. https://doi.org/10.1007/978-981-97-1724-8_67

Kamboj, V. K., Krishna, A. B., Verma, C., Raboaca, M. S., Filote, C., & Stepanova, M. (2023, June). Chaotic American zebra search optimization algorithm for benchmark challenges. In *2023 15th International Conference on Electronics, Computers and Artificial Intelligence (ECAI)* (pp. 1-5). IEEE. https://doi.org/10.1109/ecai58194.2023.10194001

Le, T., Shi, F., Ge, M., Dong, R., & Shan, D. (2024). Tuberculosis detection bars on VGG19 transfer learning and Zebra Optimization Algorithm. *EAI Endorsed Transactions on Pervasive Health & Technology*, *10*(1). https://doi.org/10.4108/eetpht.10.5981

Liu, T., Tan, Z., Xu, C., Chen, H., & Li, Z. (2020). Study on deep reinforcement learning techniques for building energy consumption forecasting. Energy and Buildings, 208, 109675. https://doi.org/10.1016/j.enbuild.2019.109675

Ma, Z., Cui, S., & Joe, I. (2022). An enhanced proximal policy optimization-based reinforcement learning method with random forest for hyperparameter optimization. *Applied Sciences*, *12*(14), 7006. https://doi.org/10.3390/app12147006

Mohapatra, S., & Mohapatra, P. (2023). American zebra optimization algorithm for global optimization problems. *Scientific Reports*, *13*(1), 5211. https://doi.org/10.1038/s41598-023-31876-2

Özbay, F. A. (2025). An Enhanced Zebra Optimization Algorithm with Multiple Strategies for Global Optimization and Feature Selection Problems: A Hepatocellular Carcinoma Case Study. *IEEE Access*. https://doi.org/10.1109/access.2025.3541975

Peirelinck, T., Hermans, C., Spiessens, F., & Deconinck, G. (2024). Combined peak reduction and self-consumption using proximal policy optimisation. *Energy and AI*, *16*, 100323. https://doi.org/10.1016/j.egyai.2023.100323

Rziki, M. H., Hadbi, A. E., Boutahir, M. K., & Abounaima, M. C. (2025). Adaptive Predictive Maintenance and Energy Optimization in Metro Systems Using Deep Reinforcement Learning. *Sustainability*, *17*(11), 5096. https://doi.org/10.3390/su17115096

Shang, S., Zhu, J., Liu, Q., Shi, Y., & Qiao, T. (2024). Low-altitude small target detection in sea clutter background based on improved CEEMDAN-IZOA-ELM. *Heliyon*, *10*(4). https://doi.org/10.1016/j.heliyon.2024.e26500

Trojovská, E., Dehghani, M., & Trojovský, P. (2022). Zebra optimization algorithm: A new bio-inspired optimization algorithm for solving optimization algorithm. *IEEE Access*, *10*, 49445-49473. https://doi.org/10.1109/access.2022.3172789

Tshinavhe, N., Ratshitanga, M., Tshemese-Mvandaba, N., & Mditshwa, M. (2025, January). Optimization of Load Frequency Control using Zebra Optimization Algorithm in Renewable Energy Integrated Power System. In *2025 33rd Southern African Universities Power Engineering Conference (SAUPEC)* (pp. 1-6). IEEE. https://doi.org/10.1109/saupec65723.2025.10944384

Upadhyay, S., Ahmed, I., & Mihet-Popa, L. (2024). Energy management system for an industrial microgrid using optimization algorithms-based reinforcement learning technique. *Energies*, *17*(16), 3898. https://doi.org/10.3390/en17163898

Ur Rehman, M., Kalakoti, R., & Bahşi, H. (2025). Comprehensive Feature Selection for Machine Learning-Based Intrusion Detection in Healthcare IoMT Networks. *International Conference on Information Systems Security and Privacy*, 2, 248–259. https://doi.org/10.5220/0013313600003899

Wang, H., Lei, Z., Zhang, X., Zhou, B., & Peng, J. (2019). A review of deep learning for renewable energy forecasting. *Energy Conversion and Management*, 198, 111799. https://doi.org/10.1016/j.enconman.2019.111799

Wu, D., & Zhou, M. (2025). Research on improved zebra optimization algorithm based on Cat mapping and crossover strategy. *Transactions on Computational and Scientific Methods*, *5*(4). https://doi.org/10.5281/zenodo.15244709

Wu, J., Chen, X. Y., Zhang, H., Xiong, L. D., Lei, H., & Deng, S. H. (2019). Hyperparameter optimization for machine learning models based on Bayesian optimization. *Journal of Electronic Science and Technology*, 17(1), 26-40. https://doi.org/10.11989/JEST.1674-862X.80904120

Yang, L., & Shami, A. (2020). On hyperparameter optimization of machine learning algorithms: Theory and practice. *Neurocomputing*, 415, 295-316. https://doi.org/10.1016/j.neucom.2020.07.061

➢ *ORAL PRESENTATION*

Understanding The Rationale and Advantages Of Embedded Systems Modelling with Emphasis on Electronic Differantial Using Ackermann Steering

Atakan Ertekin* *(https://orcid.org/0009-0003-3477-9761)*,
Mustafa ENGIN **(***https://orcid.org/0000-0001-7247-4545)*

Ege University, Mechatronics Engineering, Faculty of Science , İzmir, Türkiye.

*Corresponding author e-mail: atakanertekinn@gmail.com, mustafa.engin@ege.edu.tr

Abstract
This electronic document presents the core motivations and engineering benefits of embedded system modelling with a focus on automotive applications. A model-based implementation of an electronic differential using Ackermann steering geometry is introduced as a case study. The analysis shows that modeling improves development efficiency and algorithm flexibility, while also revealing practical limitations.

Keywords: embedded-system modelling, model-based design, electronic differential, ackermann steering geometry

INTRODUCTION

Embedded systems have become increasingly complex across domains such as automotive, aerospace, industrial automation, and consumer electronics. This growing complexity introduces significant challenges in accurately defining system requirements, predicting dynamic behavior, and identifying potential design flaws early in the development cycle. Without early-stage validation, errors often propagate into later phases—where they become exponentially more costly to detect and resolve.

Modeling offers a systematic solution to these challenges by enabling engineers to simulate real-world operational scenarios, validate functional correctness, and iteratively refine system architecture—all before committing to physical hardware. In this context, Model-Based Design (MBD) has emerged as a widely adopted engineering methodology, especially in safety-critical industries like automotive and aerospace. MBD facilitates abstraction and automation by using tools such as MATLAB/Simulink, which provide an integrated environment for visual modeling, dynamic simulation, and automatic code generation for embedded targets. These platforms support a broad spectrum of control strategies, from classical PID controllers to more advanced control algorithms Moreover, integrated validation workflows such as Software-in-the-Loop (SiL) and Hardware-in-the-Loop (HiL) enable continuous testing and reduce the risk of design defects during later stages of development. Given the growing complexity of embedded systems and the rise of model-based development tools, it is essential to understand the tangible benefits that modeling brings to the development process.The following section outlines these benefits in terms of cost efficiency, development methodology, and testing capabilities.

MATERIALS AND METHODS

BENEFITS OF EMBEDDED SYSTEM MODELLING

This section outlines the key advantages of modeling in embedded systems development, focusing on cost efficiency, modeling tools and languages, standardized development processes, and the role of model-based design in modern engineering practices.

Cost Implications of Late-Stage Error Detection

First, understanding the cost implications of late-stage error detection is critical in embedded systems development. The cost of fixing defects increases dramatically as the development progresses rising from a baseline factor of 1 during the requirements phase to as much as 10× during implementation, 15-40× during development testing, 30-70× during acceptance testing, and up to 1000× after release. This exponential growth underscores the importance of early validation and verification. Model-based development methods, by enabling early simulation and logic errors during the initial phases. As a result, modeling not only enhances system reliability but also delivers substantial cost savings by minimizing the risk of late discovery of critical faults.

Table 1. Relative Cost Ratios by Development Stage

Development Phase	Cost Ratio
Requirements	1
Design	3-6x
Implementation	10x
Development Testing	15-40x
Acceptance Testing	30-70x
Post Release	40-1000x

Modeling Languages, Tools, and Methodologies

Modern embedded systems demand modeling techniques that operate across varying levels of abstraction and system lifecycle stages. To address this need, a diverse set of modeling languages and tools has been developed—each designed to serve specific roles ranging from documentation and architectural design to behavior simulation and executable code generation.

As illustrated in Figure 1, modeling approaches can be broadly categorized into three domains: documentation, simulation, and execution. Documentation-level modeling includes tools such as requirement documents, activity diagrams, and layer diagrams, which help define and visualize system functionality and structure. At the architectural level, notations like object diagrams, class diagrams, and use case diagrams are widely used to model component relationships and system functionality at a higher abstraction layer.

To simulate dynamic system behavior, time-based simulators and finite state machines (FSMs) are commonly employed. These tools enable early evaluation of system responses to various inputs and conditions, without requiring physical hardware. Statecharts and dataflow models further enrich simulation capabilities by supporting the modeling of event-driven logic and concurrent system processes—both critical for real-time embedded systems.

At the execution level, implementation-specific modeling bridges the gap between abstract design and deployable code. Languages such as C, C#, and VHDL are typically used to translate system behavior into production-ready embedded software and firmware.

Among the available modeling platforms, MATLAB/Simulink has become a de facto standard in the automotive and embedded systems industry due to its extensive support for Model-Based Design (MBD). Simulink enables the construction of block-diagram models that represent system logic and physical behavior, while its integration with Stateflow facilitates the modeling of hierarchical state machines and complex control logic. Furthermore, the platform supports automatic code generation for embedded C targets, significantly accelerating the development process.

When coupled with validation frameworks such as Software-in-the-Loop (SiL) and Hardware-in-the-Loop (HiL), Simulink provides end-to-end support from concept design to deployment. This seamless integration aligns closely with industry standards like ISO 26262, enhancing both safety assurance and development efficiency in critical embedded applications

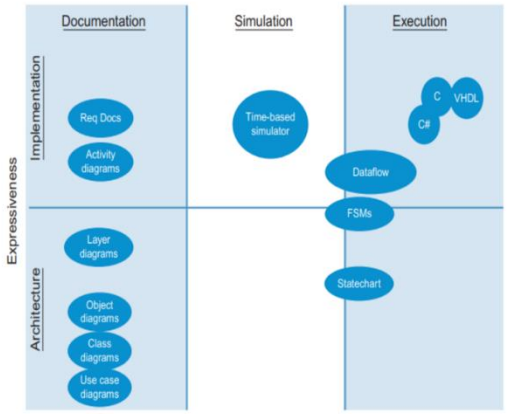

Figure 1. Modeling Languages and Tools Across System Development Phases

V-Model in Embedded Systems Development

The V-Model is prominently adopted in safety-critical domains and is endorsed by international standards such as ISO 26262 for automotive systems and DO-178C for avionics software. It enhances traceability, supports rigorous risk management, and ensures high levels of quality assurance. Although traditionally perceived as a rigid, linear model, modern practices have integrated the V-Model with Agile principles, iterative feedback loops, and automated testing tools resulting in greater flexibility without compromising the benefits of early validation and structured development. This integration supports improved communication across large, interdisciplinary teams and helps maintain a proactive stance on fault detection and risk mitigation.

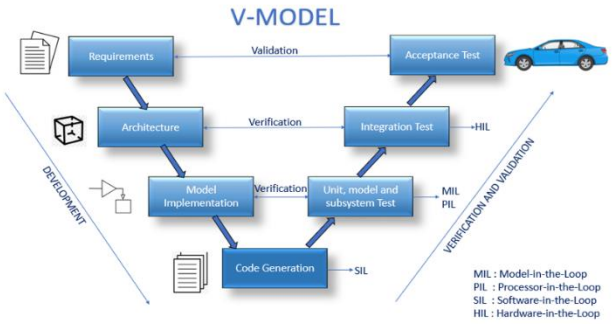

Figure 2. Model-based V-Model Representation

Model-Based Development (MBD) integrates naturally with the V-Model lifecycle by supporting simulation, verification, and code generation throughout each phase of system development. As illustrated in Figure 2, the V-Model organizes development on the left side—from high-level requirements to system implementation and mirrors this progression on the right side with corresponding validation and testing activities. At early stages, functional behavior and control logic can be verified using Model-in-the-Loop (MiL) simulations, where the model operates within a virtual environment. This is followed by Software-in-the-Loop (SiL) and Processor-in-the-Loop (PiL) techniques, which validate generated code and assess execution performance on real or emulated targets—still without the need for physical hardware. At later stages, full system integration is assessed through Hardware-in-the-Loop (HiL) testing, where the control model interacts with real-time hardware inputs and outputs. This progression supports continuous verification against system requirements, enabling early fault detection and incremental refinement throughout the development lifecycle.The alignment of model-based workflows with the V-Model ensures traceability from abstract requirements to validated implementation, while also facilitating compliance with industry standards such as ISO 26262. This structured yet iterative methodology enhances system reliability, shortens development timelines, and reduces overall project risk.

MODEL-BASED DESIGN OF AN ELECTRONIC DIFFERENTIAL USING ACKERMANN STEERING

First, Electronic differential system was modeled in MATLAB/Simulink using Ackermann steering geometry to dynamically distribute torque between wheels in cornering scenarios. The model processes throttle and steering inputs to control individual wheel speeds, replacing traditional mechanical differentials. Simulation-based validation demonstrated the system's flexibility, accuracy, and effectiveness in embedded automotive applications.

Mathematical Model of Ackermann-Based Electronic Differential

The model the steering and speed behavior of an electronic differential system, the Ackermann steering principle is used to calculate wheel trajectories during turning maneuvers.

The instantaneous turning radius R is derived from the vehicle geometry using the wheelbase L and the steering angle δ. The steering angle δ is used as a simplified central reference in modeling, while δ_L and δ_R are computed later based on vehicle geometry for practical implementation.

$$R = \frac{L}{\tan \delta}$$

This equation defines the distance from the vehicle's center of mass to the center of the turning circle.

Once the turning radius R is known, the paths of the inner and outer wheels can be calculated by subtracting or adding half the track width W:

$$R_L = R - \frac{W}{2} \qquad R_R = R + \frac{W}{2}$$

If the vehicle's forward velocity is V, the linear velocity of the outer V_o and inner V_i wheels are computed relative to their curvature radius:

$$V_L = V\ x\ \frac{R_L}{R} \qquad V_R = V\ x\ \frac{R_R}{R}$$

This ensures that the angular rotation rates match the required turning curvature, preventing tire slippage.

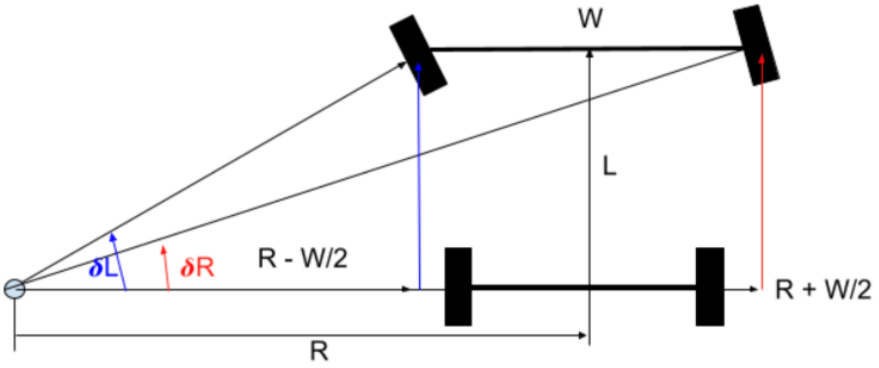

Figure 3. Ackermann Steering Physical Representation

The steering angle δ is modeled as a central reference derived from a 1:15 steering ratio, representing a full 720° rotation of the physical steering wheel.

System Architecture and Components

The system architecture of the electronic differential is based on a steer-by-wire configuration, where driver input is captured through a steering angle sensor and a steering torque sensor mounted on the steering column. The steering input is interpreted by an Electronic Control Unit (ECU), which also receives feedback from wheel speed sensors and a motion position sensor (MPS) attached to the electric motor. This motor, in conjunction with a gearing mechanism and a bipole magnet, adjusts the steering mechanism accordingly. The ECU processes all sensor data to calculate the required inner and outer wheel speeds using Ackermann steering logic and distributes motor commands to ensure smooth and accurate differential control. This architecture eliminates the mechanical linkage between the steering wheel and the wheels, offering greater flexibility and enabling advanced control strategies.

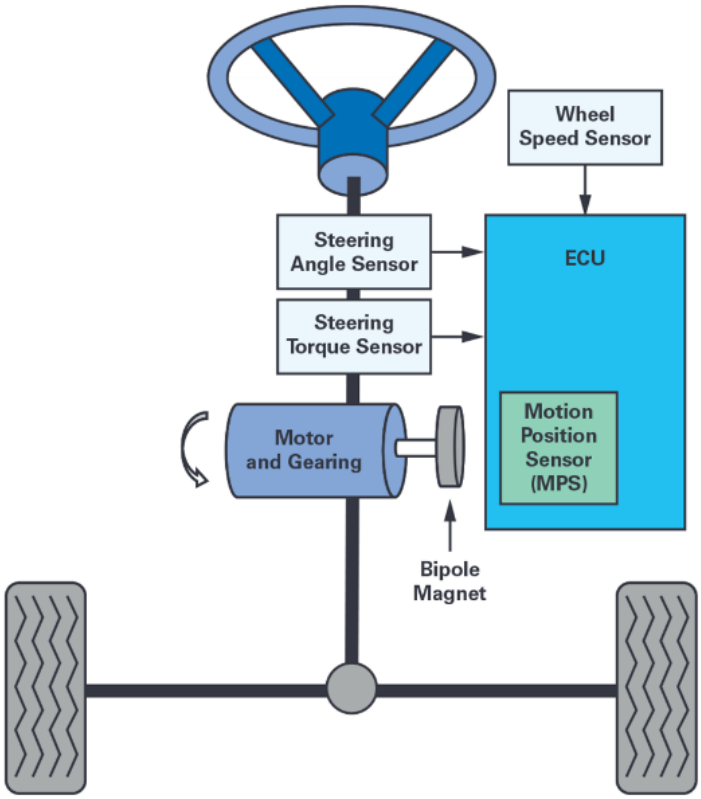

Figure 4. Steering System Architecture

Simulink Model and Subsystem Structure,

The architecture of the proposed electronic differential system is realized through a modular Simulink framework centered around conditional subsystems. The control logic is driven by two primary inputs: throttle signal (Gas) and steering angle (SteeringAngle). Based on the sign and magnitude of the steering input, an if-else logic block classifies the driving scenario into one of three discrete conditions: right turn (positive angle), left turn (negative angle), or straight-line motion (near-zero angle).

Each condition activates a dedicated subsystem, within which the inner and outer wheel speeds are computed using the kinematic relations derived from the Ackermann steering geometry. These calculations consider the turning radius, wheelbase, and track width to determine the required speed differential for each wheel. To manage the outputs seamlessly, the model employs merge blocks that consolidate the results from each conditional path. This mechanism ensures that only one pair of velocity commands—InnerMotorSpeed and OuterMotorSpeed is propagated at any given time, thereby avoiding signal conflicts and preserving simulation integrity.

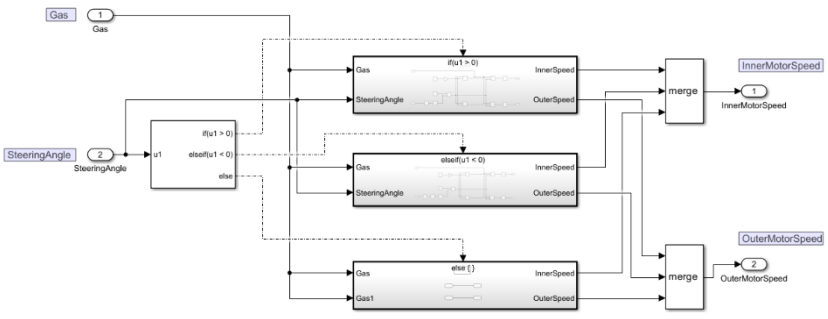

Figure 5. Ackermann Steering Simulink Model

Positive Steering Subsystem

This subsystem is activated during right turns, where the steering angle input is greater than zero. In this condition, the right wheel becomes the outer wheel and the left wheel becomes the inner wheel. V is the overall vehicle

speed (derived from Gas input), W is the track width, and R is the turning radius calculated from the steering angle. The calculated InnerSpeed is assigned to the left motor, and OuterSpeed to the right motor.

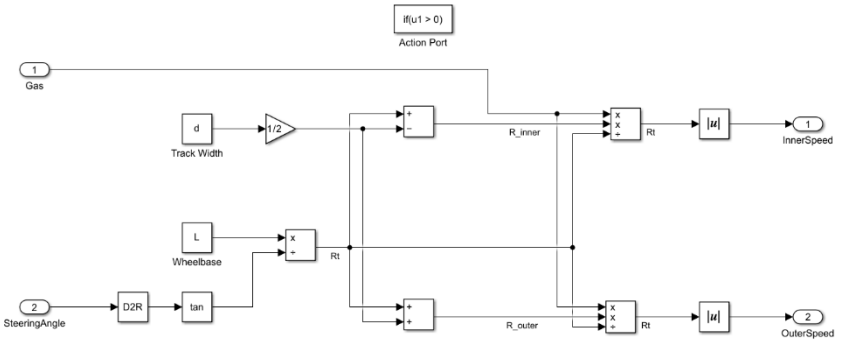

Figure 6. Positive Steering Model

Negative Steering Subsytem

This block handles left turns, where the steering angle is negative. In this case, the left wheel is the outer wheel and the right wheel is the inner wheel. The subsystem takes the gas and steering inputs and applies the corresponding Ackermann logic to generate speed references for each motor.

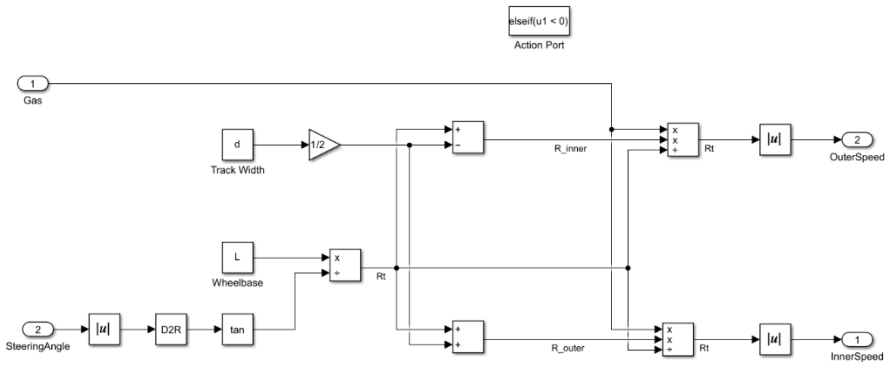

Figure 7. Negative Steering Model

Zero Steering Subsytem

When the steering input is approximately zero (i.e., straight-line driving), the model assumes equal speed for both wheels. In this case, both InnerSpeed and OuterSpeed are set equal to the gas input, ensuring synchronized wheel motion for straight-line travel.

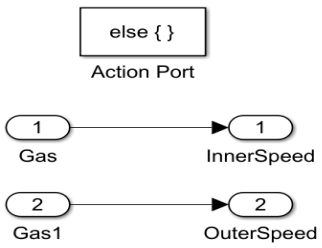

Figure 8. Zero Steering Model

Simulation Scenario and Input Profiles

The input test model consists of two main components: a Throttle Model and a Steering Wheel Model, both designed to simulate realistic driver behavior during a vehicle maneuver. The throttle signal is passed through a conversion block (kmh_to_ms) to express vehicle speed in meters per second, while the steering input is scaled

by a predefined steering ratio (St_ratio) to reflect a ±720° steering wheel range. These processed signals serve as inputs to the AckermannSteeringModel, which calculates the corresponding inner and outer wheel speeds.

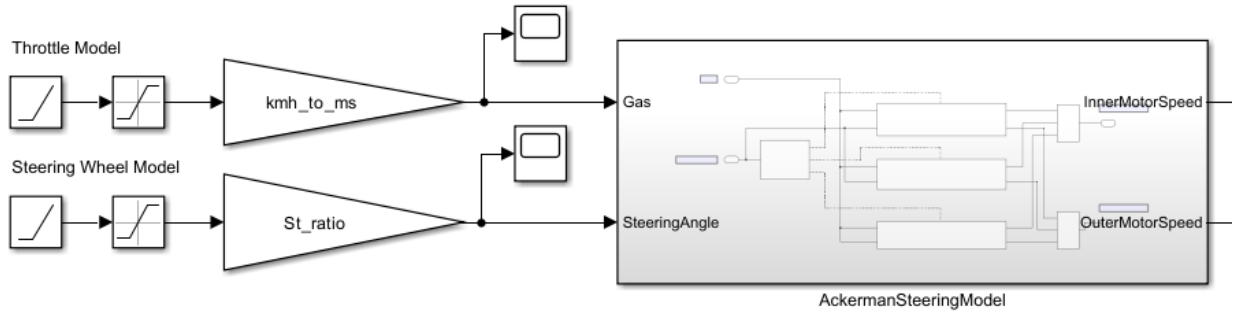

Figure 9. Test Model Configuration

Valide the functionality of the electronic differential model, a test scenario was created using simulated throttle and steering inputs. As illustrated in **Fig. 10**, the red graph represents the throttle input, where acceleration begins at the 1-second mark. The yellow graph shows the steering input, which starts increasing gradually from the 1.5-second mark, simulating a realistic driver behavior of accelerating first and then initiating a turn. The gas input is converted from km/h to m/s, while the steering signal is scaled using a predefined steering ratio to reflect a full-turn capable (±720°) steering wheel. These inputs are fed into the Ackermann-based control structure to observe the dynamic response of the inner and outer wheel speeds under real-time cornering conditions.

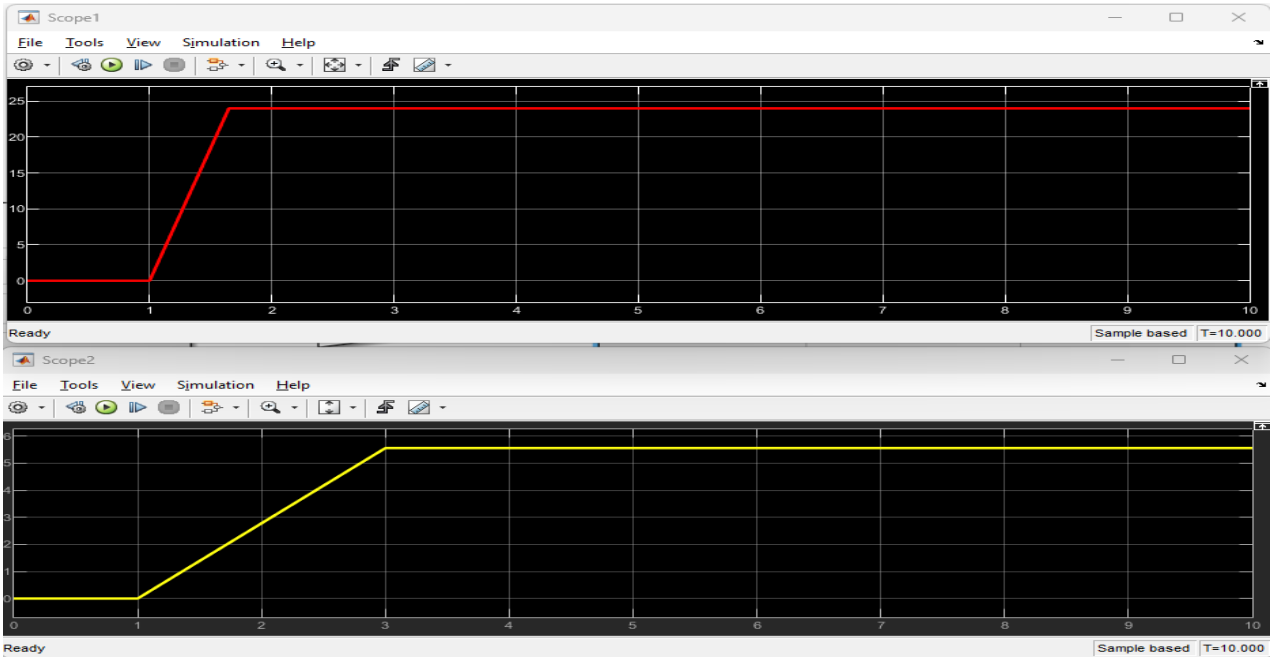

Figure 10. Throttle and Steering Wheel Test Signals

Output Simulation and Result Analysis

Validate the dynamic response of the electronic differential system, the calculated InnerMotorSpeed and OuterMotorSpeed signals were applied to a closed-loop motor simulation block featuring PI control and first-order motor dynamics. As seen in Fig. 12, the blue curve represents the outer motor speed and the yellow curve the inner motor speed. The outer wheel reaches a higher target velocity, as expected in cornering scenarios governed by Ackermann steering geometry.

The observed difference in steady-state speeds confirms that the system correctly differentiates wheel behavior during turning. Since both motors stabilize at different but consistent velocities, the vehicle would continue tracing a circular path, maintaining rotational stability. This result demonstrates the model's capability to simulate real-world differential action effectively.

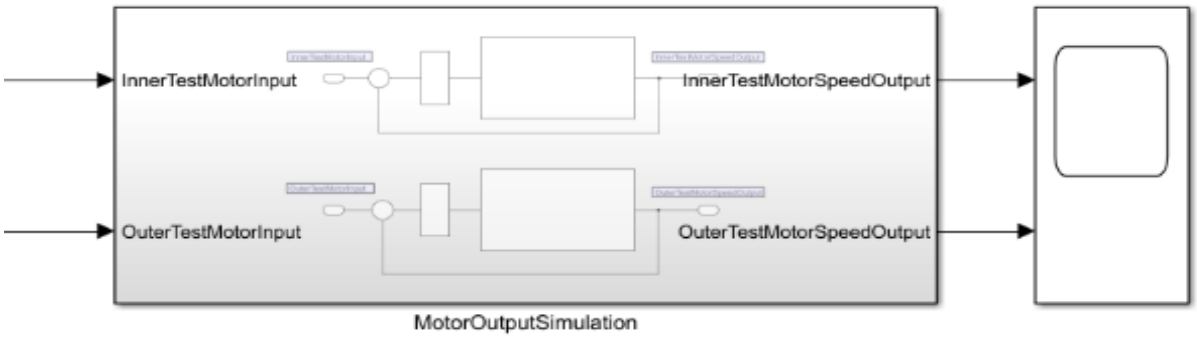

Figure 11. Motor Model

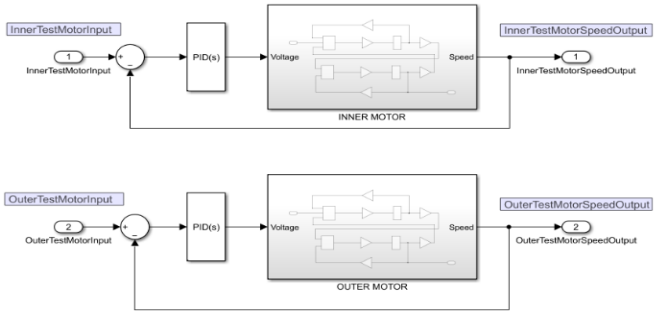

Figure 12. Motor Test Model Subsystem



Figure 13. Inner-Outer Motor Output Speed Signals

Evaluation of Model-Based Testing within a V-Model Framework

The design and testing of the electronic differential using Ackermann steering was intentionally structured around a model-based development workflow. This approach enabled the system to be tested in a virtual environment through Model-in-the-Loop (MiL) simulations before any hardware deployment. As demonstrated in the simulation results, dynamic behavior such as steering response and wheel speed differentiation were evaluated with precision, allowing early validation of functional correctness.
The modular architecture of the Simulink model directly supports V-Model development methodology. On the left side of the V, system requirements were derived and translated into subsystem-level models for control logic and kinematic computation. On the right side, corresponding MiL tests provided the basis for unit- and integration-level verification, mirroring the structure of the V-Model.

Table 2. V-Model Phase Alignment for the Proposed Application

V-Model Phase	Application Implementation
System Requirements	Vehicle must vary inner and outer motor speeds during turning.
Software Requirements	Inner and outer speeds are computed using throttle and steering inputs.
Architecture Design	Modular Simulink subsystems structured via conditional logic.
Implementation	Simulink blocks with PID control and motor dynamics simulation.
Unit Testing	Each subsystem (left, right, straight) tested individually.
Integration Testing	Combined model and motor simulation evaluated together.
System Testing	Model-in-the-Loop (MiL) tests simulate realistic driving scenarios.

CONCLUSION

This study highlighted the rationale and advantages of embedded system modeling through a model-based implementation of an electronic differential using Ackermann steering geometry. Using MATLAB/Simulink, the system was designed, simulated, and validated entirely in a virtual environment, enabling early error detection, modular testing, and clear visualization of cornering behavior.

The workflow aligned effectively with the V-Model, supporting traceability from system requirements to Model-in-the-Loop (MiL) testing. Simulation results verified the correctness and flexibility of the control algorithm, while demonstrating cost-effective and safe validation prior to hardware deployment.

Future work may involve extending the model toward real-time embedded targets, integrating Hardware-in-the-Loop (HiL) testing, and exploring vehicle dynamics for more comprehensive system evaluation.

ACKNOWLEDGEMENTS

The authors would like to express their sincere gratitude to Assoc. Prof. Dr. Mustafa Engin for his insightful feedback and continuous support. The simulations and modeling tasks presented in this paper were conducted using the academic resources of Ege University, Department of Mechatronics Engineering.

REFERENCES

Autran, J. L. (2012). Model-Based Design for Embedded Systems. CRC Press.
Berger, A. (2001). Embedded Systems Design: An Introduction to Processes, Tools and Techniques
Brooks, F. P. (1995). The Mythical Man-Month: Essays on Software Engineering (Anniversary ed.). Addison-Wesley.
Burns, A., & Wellings, A. (2009). Real-Time Systems and Programming Languages (4th ed.). Addison-Wesley.
Ganssle, J. (2008). The Art of Designing Embedded Systems (2nd ed.). Newnes.
INCOSE. (2015). Systems Engineering Handbook: A Guide for System Life Cycle Processes and Activities (4th ed.). Wiley.
ISO 26262 – Road Vehicles Functional Safety. Retrieved from https://www.iso.org/standard/68383.html
ISO 26262:2018. Road vehicles – Functional safety. International Organization for Standardization.
Kandasamy, N., Abdelzaher, T. F., & Venkatasubramanian, N. (2003). Resource Management in Real-Time Systems and Networks. MIT Press.
Laplante, P. A. (2013). Real-Time Systems Design and Analysis: Tools for the Practitioner (4th ed.). Wiley-IEEE Press.
MathWorks. (2023). Simulink Documentation. Retrieved from https://www.mathworks.com/help/simulink/
Piziali, A. (2007). Developing High Quality Data Models. Elsevier.
Saez, S., & Vasudevan, R. (2015). Automotive Embedded Systems Handbook. CRC Press.
Scheiber, R., & Schmidt, A. (2020). ISO 26262 in Practice: A Guide to the Automotive Safety Standard. SAE International.

➢ *ORAL PRESENTATION*

Feature Selection in Industry 5.0: Adapting to The Dynamic Evolution of Data

Özlem Gürünlü Alma*[1] (https://orcid.org/00000-0001-6978-9810)
Ali Valiyev[2] (https://orcid.org/0009-0005-4617-2718)

*[1] Muğla Sıtkı Koçman University, Department of Statistics, Muğla, Türkiye
[2] Muğla Sıtkı Koçman University, Department of Statistics, Muğla, Türkiye

*Corresponding author e-mail: avaliyev003@gmail.com

Abstract

Industry 5.0 has started a period that deeply affects the nature of data. With the rise of Industry 5.0, it has guided the evolution of data, transforming data from fixed and structured data sets in previous industrial periods into a much more dynamic, continuously learning, interactive structure. With this period, data has increased exponentially in volume and has become multidimensional and more complex. This transformation is no longer limited to processing the data, but has also made it necessary to analyze and evaluate the role and contributions of each component in the overall data set in a deep and accurate manner. Flexibility and adaptability are required in data management to adapt to the constantly updating nature of Industry 5.0. Traditional feature selection methods may be inadequate in dealing with complex data structures. Therefore, new generation approaches are becoming more suitable to manage the dynamic and more complex nature of data in the best way. These new methods provide an infrastructure for accurate and reliable results that can adapt to the changing structure of the data over time. This paper examines the effectiveness of classical and modern feature selection techniques in order to develop more efficient artificial intelligence models that adapt to Industry 5.0 and to increase the accuracy of data-based processes. Beyond traditional approaches, it focuses on the development of new feature selection techniques and evaluates how they adapt to the data structure in Industry 5.0 during this process.

Keywords: Industry 5.0, Feature selection, Big Data, AI, Machine Learning

1. Introduction

The industrial landscape has undergone profound transformations through successive revolutions, each marked by groundbreaking technological advancements. The First Industrial Revolution (18th–19th century) mechanized production through steam power and water- and steam-driven machinery, shifting economies from agrarian to industrial. The Second Industrial Revolution (late 19th–early 20th century) introduced mass production, electrification, and assembly lines, revolutionizing manufacturing efficiency and scale. The Third Industrial Revolution (mid–late 20th century) brought automation, computers, and early digital technologies, enabling programmable logic controllers (PLCs) and advanced production control. The Fourth Industrial Revolution (Industry 4.0, 21st century) further accelerated digitalization with cyber-physical systems, the Internet of Things (IoT), artificial intelligence (AI), and smart factories, creating interconnected, data-driven production environments. Industry 5.0 highlights an industrial revolution that rapidly responds to dynamic market needs, prioritizes resource efficiency, and optimizes data-driven decision-making processes. This new industrial phase aims to go beyond automation, enabling digital systems to combine with human expertise to create more flexible and adaptable production lines. For a successful transformation, systems capable of continuously monitoring data exchanges occurring at every point—from production to logistics, from in-factory processes to customer interactions—and instantly responding to changing conditions are of vital importance. In current digital environments, data has evolved from simple storage units toward exhibiting dynamic behavior patterns, being heterogeneously sourced, and enabling interactive processing models

Moving beyond the purely technological focus of Industry 4.0, Industry 5.0 introduces a paradigm shift that strategically combines human expertise with advanced digital technologies to foster sustainable and resilient industrial ecosystems (Singh, et al., 2025). Built upon the foundation of Industry 4.0 - including smart factories, cyber-physical systems, and data-driven production processes - this new paradigm aims to blend technological advancements with human skills to deliver a more socially and environmentally responsive approach.

At the heart of Industry 5.0 lies the idea that machines should play a complementary role to humans. In previous industrial revolutions, humans were viewed as mere "components" of the production line, whereas in this new era, human creativity, emotional intelligence, and decision-making abilities take center stage. Industry 5.0's human-centered paradigm must prioritize individual well-being while ensuring technological advancement does not compromise fundamental rights (Suciu, et al., 2023). For example, a factory worker is no longer just an operator but a "process architect" who optimizes production using real-time AI-driven data. Collaborative robots (cobots) extend human physical capabilities without suppressing intuitive human skills. Personalized autonomous production is realized in Industry 5.0 through cobot-human coordination on enterprise social platforms, reflecting its human-focused design (Maddikunta, et al., 2022). Industry 5.0 integrates green transformation as an inseparable component of technological progress. This principle encompasses resource efficiency, carbon neutrality, and circular economy practices. While traditional manufacturing models used data solely for operational optimization, Industry 5.0 leverages data to minimize ecological footprints. Sustainability also considers the "environmental cost of data itself." Resilience is critical for Industry 5.0 implementation. To withstand shock scenarios, robust designs for complex IT(**Information Technology**) infrastructures, AI(Artificial Intelligence) platforms, and secure data transfer/storage systems must be integrated (Brückner and Wölke, 2025). This is made possible through data-driven scenario simulations. Implementing Industry 5.0 technologies can be costly at first, and since these systems are complex and require specialized knowledge, integrating them into existing operations can take considerable time and effort (Wolniak R., 2023). As the number of features in datasets increases, the computational cost of processing this data also rises. More importantly, irrelevant features can decrease model accuracy. Therefore, feature selection is necessary not only for computational efficiency but also to preserve model accuracy in Industry 5.0.

The rest of the paper is structured as follows. Section 2 discusses the feature selection. Section 3 discusses Feature selection methods in industry 5.0. Section 4 introduces an application. Finally, section 5 concludes the article.

2. Feature Selection Methods

Feature selection (FS) methods frequently used in data science processes serve as a critical preprocessing step in machine learning domains during model development to enhance model performance. FS emerges as a technique employed in machine learning and data analysis processes and focuses on extracting a high-performing subset of features from the full feature space in the original dataset (Zhou et al., 2019). Eliminating redundant or noisy features strengthens the model's generalization ability while simultaneously reducing training time. Feature selection methods can generally be divided into three main categories: filter methods, wrapper methods, embedded and hybrid methods.

- *Filter method* bases feature selection solely on the natural properties of the data and operates independently of any machine learning model. It scores or ranks features using statistical criteria (such as correlation, variance, mutual information). Applied as a preprocessing step before model training, this method reduces data dimensionality by eliminating irrelevant or redundant features. Its greatest advantages are computational efficiency and model-agnosticism, making it particularly effective for high-dimensional data. However, it has limitations such as ignoring feature interactions with the target model and risking suboptimal subset selection for specific algorithms. In Industry 5.0, these limitations are overcome through advancements like the Maximal Information Coefficient (MIC), which captures nonlinear relationships, and k-NN mutual information estimators that provide scalability for big data.
- Operating on the principle of "let model performance guide feature selection," *wrapper methods* treat feature selection as a combinatorial optimization problem. They search for subsets using greedy algorithms like forward selection or backward elimination, then train a model for each subset and evaluate its performance (accuracy, F1-score, etc.). This model-focused approach captures feature interactions and typically produces high-performance subsets. However, repeated model training makes it computationally expensive and unscalable for high-dimensional data. In Industry 5.0, these issues are resolved through metaheuristic methods like Particle Swarm Optimization (PSO) and hybrid strategies such as cloud-based parallelization.
  - *Embedded method* is grounded in the understanding of "integrating feature selection directly into the model training process." These methods perform selection during training by optimizing an objective function that balances prediction accuracy and feature sparsity. Typical examples include regularization techniques where Lasso (L1) regression discards features by shrinking coefficients to zero, tree-based

importance scores from Random Forests using MDI or permutation importance, or deep learning integrations where attention mechanisms dynamically weight features based on context. Requiring no separate search phase, this approach is computationally efficient and model-aware. In Industry 5.0, innovations like Group Lasso (sensor-level selection), Stochastic Gates (differentiable masking), and Neuro-Symbolic Systems enhance adaptability to dynamic processes.

- *Hybrid methods* embrace the strategy: "Combine filter/wrapper/embedded techniques in multi-stage pipelines to leverage strengths and mitigate weaknesses." They follow a layered workflow: First, low-variance/high-correlation features are eliminated through coarse filtering. Then, refined filtering is applied using advanced techniques like Mutual Information (MI) or mRMR. Subsequently, embedded preselection is performed using importance scores from algorithms like Random Forest. In the final stage, fine-tuning is done with fast wrapper methods or metaheuristic algorithms (e.g., PSO). In Industry 5.0, these processes gain human-centric transparency through edge-cloud synergy (lightweight filtering on edge devices + resource-intensive wrappers in the cloud) and integration of Explainable AI (XAI) techniques like SHAP values.

While Industry 5.0 reimagines the production paradigm around human-centricity, flexibility, sustainability, and resilience, the importance of data-driven decision-making processes increases exponentially. In this complex and dynamic environment, the performance of Machine Learning (ML) and AI models used to extract valuable insights from raw data largely depends on the quality and suitability of the input data. FS plays a key enabling role here in achieving Industry 5.0 goals by enhancing model accuracy, efficiency, and interpretability. Here are seven fundamental and in-depth roles in this process:

- **Model Accuracy & Generalization Optimization:** The massive and noisy data of Industry 5.0 leads to model overfitting and failure in the real world. FS eliminates irrelevant/redundant features, allowing the model to focus on critical signals. This increases the accuracy and adaptability (generalization) of failure/quality/demand predictions to new conditions, providing reliable autonomous decisions and human decision support.
- **Computational & Operational Efficiency Increase:** The requirement for real-time decision-making conflicts with the cost and slowness of processing high-dimensional data. FS significantly reduces model training and inference times by decreasing the number of features, enabling the use of simpler models. Consequently, CPU/GPU/energy consumption decreases, low-latency applications (real-time optimization, anomaly detection) become viable, costs are reduced, and the system rapidly adapts to dynamic environments.
- **Model Interpretability & Human-Machine Collaboration:** "Black box" models hinder human trust in AI decisions and effective collaboration. FS increases the transparency of model decisions by using only critical features and providing importance rankings. This enables operators' informed intervention, engineers' process optimization, and genuine human-machine synergy.
- **Reduction of Data Collection & Storage Costs:** Continuously collecting and storing worthless data increases infrastructure costs and management overhead. FS prevents unnecessary data collection and storage by determining which data sources/features are truly essential. This lowers CAPEX/OPEX costs, network traffic, and data processing load, allowing resources to be directed to valuable areas.
- **Resilience Against Noise & Irrelevant Data:** Industrial environments are filled with noise and irrelevant data sources, threatening model stability. FS increases the model's ability to focus on the true signal by eliminating noisy or weakly target-correlated features. This makes models less affected by temporary disruptive effects, ensures more reliable predictions and automated decisions, and enhances system resilience in unexpected situations.
- **Adaptive & Learning Systems:** Fixed feature sets become ineffective in the face of dynamic changes like product variation, machine wear, or market fluctuations. The FS process is updated regularly or via online learning to determine the optimal feature subset suitable for changing conditions. This enables systems to rapidly adapt to new products, operational requirements, and changing environments, sustains model performance, and makes flexible (future-proof) production possible.
- **Contribution to Sustainability Goals:** Resource/energy waste conflicts with Industry 5.0's environmental sustainability goals. The other roles of FS (efficient models, computation/data minimization, resilient systems) indirectly contribute to: lower energy consumption, less storage

infrastructure, reduced scrap/rework, and prevention of unplanned downtime. This reduces resource consumption and waste, contributing to sustainable production processes.

3.Feature Selection Methods in Industry 5.0

3.1 Evolution of Filter Methods

The simple filter methods commonly used before Industry 4.0 had significant limitations in data analysis. For example, Pearson and Spearman correlations could only measure linear relationships, causing them to overlook nonlinear connections and multicollinearity issues. The variance threshold method could eliminate features with constant values (such as faulty sensors) but did not consider the relationship between these features and the target variable. The Chi-Square test only worked with categorical data and could not be applied to numerical data. A limitation of Fisher Score is its neglect of feature interdependencies (e.g., redundancy or combinations), prioritizing instead the impact of individual features on intra-class and inter-class scatter matrices (Gan and Zhang, 2021). Mutual Information (MI) could capture nonlinear relationships, but its practical application was challenging due to computational complexity in continuous data and the limitations of estimation methods. Traditional feature selection methods face significant limitations when applied to Industry 5.0's complex environments involving human-machine interaction and multi-sensor fusion. These methods struggle to model feature interactions, handle heterogeneous data types like text and images, or adapt to dynamic processes due to their fixed thresholds.

Classical Filter	Machine Learning Filter
Pearson Correlation	Conditional Mutual Information (CMI)
Spearman Correlation	Maximal Information Coefficient (MIC)
Variance Threshold	mRMR (minimal Redundancy Maximal Relevance)
Chi-Square Test	Correlation-Based Feature Selection (CFS)
Fisher Score	k-NN based MI Estimators (e.g., KSG)
Mutual Information (MI)	TF-IDF (Text Data)
Frequency-Based Filters (Low/High/Band Pass)	Gaussian Processes
Kalman Filter	Bayesian Filters

They also fail to detect multicollinearity and become computationally inefficient when calculating Mutual Information (MI) for big data applications. To overcome these limitations, Industry 5.0 has adopted more sophisticated techniques. The integration of maximal information coefficient enhances heterogeneous data handling, advancing dataset applications (Ge et al., 2016). Conditional Mutual Information (CMI) reduces redundancy by evaluating a feature's contribution to the target while accounting for other features. For improved computational efficiency with big data, k-NN(k-Nearest Neighbors) based MI(Mutual Information) estimators like KSG(Kraskov-Stögbauer-Grassberger) have been implemented. The core principle of Minimum Redundancy Maximum Relevance (mRMR) emphasizes avoiding inter-correlated features by explicitly quantifying redundancy, thereby selecting a subset of features with maximal pairwise dissimilarity **(Acid et al., 2011).** Correlation-Based Feature Selection (CFS) addresses multicollinearity by maximizing feature-target relationships while minimizing inter-feature redundancy. Domain-specific solutions have also emerged, including Chi-Square, MI and TF-IDF(Term Frequency-Inverse Document Frequency) variations for text data, and edge/texture filters for image processing. Dynamic adaptation has been achieved through sliding window approaches for MI /correlation updates in streaming data and the integration of flexible thresholds with online learning. These advancements enable more robust data analysis in Industry 5.0's complex, high-dimensional, and dynamic systems.

3.2 Evolution of Wrapper Methods

Traditional wrapper methods used before and during Industry 4.0 era included several approaches with distinct limitations. Forward Selection worked by gradually adding features that improved model performance, but often became trapped in local optima. Backward Elimination took the opposite approach by starting with all features and removing the least important ones, though this proved computationally intensive for high-dimensional datasets. Stepwise Regression combined both approaches using statistical criteria like p-values or information criteria (AIC/BIC), but remained constrained to linear models and vulnerable to overfitting. The theoretically optimal Exhaustive Search method evaluated all possible feature subsets, but became impractical beyond very small feature spaces (n≈15). These conventional wrapper methods face fundamental challenges in Industry 5.0's high-dimensional environments where datasets often contain 1000+ features

Classical Wrapper	Machine Learning Wrapper
Forward Selection	Particle Swarm Optimization (PSO)
Backward Elimination	Ant Colony Optimization (ACO)
Stepwise Regression	Simulated Annealing (SA)
Exhaustive Search	Genetic Algorithms (GA)
	Recursive Feature Elimination (RFE)

The combinatorial explosion of possible subsets (~2^{1000} for 1000 features) creates computational infeasibility, while the need for model retraining with each subset eliminates any possibility of real-time processing. Furthermore, the extensive training requirements of modern deep learning models make them incompatible with traditional wrapper approaches, and the computational demands exceed the capacity of edge devices. Industry 5.0 has responded with innovative optimization techniques. Particle Swarm Optimization (PSO) models collective intelligence through particle representations that simulate predation dynamics and information sharing within groups (Han et al., 2025). Simulated Annealing (SA) incorporates probabilistic acceptance of suboptimal solutions to escape local optima,Through Ant Colony Optimization, preliminary optimal solutions are refined into actual results, with diverse outputs emerging at different threshold levels (Siddiqui and Abbas, 2019).

Hybrid strategies have become essential to manage computational complexity. These include aggressive pre-filtering to reduce the feature space to manageable levels (10-100 features) before wrapper application, substitution of complex models with faster surrogates (like logistic regression or compact decision trees) for subset evaluation, and leveraging cloud/HPC(High Performance Computing) resources for parallelizable algorithms like GA(Genetic Algorithms) and PSO(Particle Swarm Optimization). Emerging research focuses on developing online/dynamic wrapper implementations through periodic execution or adaptive meta-heuristic variations.

3.3. Evolution of Embedded Methods

The development of embedded feature selection methods began with foundational techniques during Industry 4.0 and earlier periods. Key approaches included Lasso (L1) and Ridge (L2) Regression, which introduced regularization to linear models - with Lasso performing feature selection by driving coefficients to zero, while Elastic Net leverages a combination of L1 (Lasso) and L2 (Ridge) regularization terms, establishing a balance between feature selection and coefficient shrinkage(Mahmood and Kadir, 2025). Decision trees consist of three components: a root node, decision nodes, and leaf nodes. The root node signifies the primary attribute in the dataset utilized for optimal prediction(Dutta et al., 2020).Random Forests advanced this approach by aggregating multiple trees and offering two feature importance measures: Mean Decrease in Impurity (MDI) averaging importance across trees, and the more reliable Permutation Importance which shuffles

Classical Embedded	Machine Learning Embedded
Lasso Regression (L1)	Group Lasso
Ridge Regression (L2)	Regularized Neural Networks
Elastic Net	Attention Mechanisms

feature values to measure accuracy impact. Support Vector Machines provided direct feature importance through weights in linear SVMs, though this became indirect in kernel-based versions. These traditional methods revealed significant limitations when confronting Industry 5.0's complex requirements.

Decision Trees	Gated Linear Units (GLU)
Random Forests (MDI/Permutation)	Stochastic Gates
Support Vector Machines (Linear SVM)	Automatic Feature Engineering
	Neuro-Symbolic Systems

Linear models like Lasso/Ridge struggled with nonlinear, dynamic processes, while tree-based ensembles became opaque "black boxes" with computationally expensive feature interaction analyses. A critical gap emerged in deep learning integration, as these methods weren't natively compatible with multi-layer neural networks. The static nature of Lasso/Ridge coefficients also proved inadequate for dynamic industrial environments.

Industry 5.0 has driven substantial innovations to address these challenges. Advanced regularization techniques like Group Lasso now enable sensor-level feature selection by treating all signals from a sensor as a unit. Breakthroughs in deep learning integration include Regularized Neural Networks applying L1/L2 penalties to induce sparsity, particularly in early layers. Attention Mechanisms have revolutionized feature importance by dynamically weighting inputs based on context, especially valuable for multimodal and temporal data. Novel architectural components like Gated Linear Units (GLU) and Stochastic Gates now embed feature selection directly within networks. The field has also seen progress in Automatic Feature Engineering and hybrid Neuro-Symbolic approaches that combine deep learning with interpretable rule-based systems. For dynamic environments, Online Learning Models (e.g., online GBM(Gradient Boosting Machines)/Lasso) continuously update feature importances with new data, while Concept Drift Detection mechanisms identify when model retraining is needed due to changing feature relevance. In Online Streaming Features (OSF), OSFS aims to dynamically select the best-performing feature subset from those features that have been received so far (Eskandari and Javidi, 2016).

Explainability has become paramount, with techniques like SHAP and LIME providing post-hoc feature importance analysis across all model types, crucial for maintaining trust in increasingly complex embedded selection systems. These advancements collectively enable more sophisticated, adaptable, and interpretable feature selection in Industry 5.0's demanding environments.

3.4 Evolution of Hybrid Methods

In the Industry 4.0 era, hybrid feature selection methods typically involved simplistic combinations of basic filters (such as variance thresholds or correlation-based approaches) with wrapper or embedded methods like Lasso or Random Forests. These early hybrids lacked sophistication, optimization, and dynamic adaptation capabilities. The transition to Industry 5.0 has transformed these approaches, demanding more complex, efficient, and human-centric hybrid strategies to meet modern performance requirements. Contemporary multi-stage hybrid approaches now follow a more refined workflow. The process begins with a very coarse filtering stage that eliminates obviously problematic features - those with extremely low variance, constant values, or high correlation duplicates. This is followed by a more sophisticated information-based filtering phase using advanced techniques like Mutual Information (MI), Maximal Information Coefficient (MIC), or Max-Relevance Min-Redundancy (MRMR).

Classical Hybrid	**Machine Learning Hybrid**
Variance Threshold + Lasso	Multi-stage MIC/mRMR → Random Forest → PSO/GA
Correlation Filter + Random Forest	Edge Lightweight Filters → Cloud-based Metaheuristics
Chi-Square + SVM	Streaming Data: Adaptive Thresholds → Compact DT/Linear

Basic Filter + Stepwise Regression	XAI-Integrated Hybrids (SHAP/LIME + Feature Selection)

The subsequent embedded initial selection stage leverages feature importance scores from algorithms like Random Forest or Gradient Boosting Machines to identify promising feature subsets. The final optimization step applies fast wrapper methods (forward/backward selection) or meta-heuristic approaches (such as compact genetic algorithms) for fine-tuning.

For real-time streaming data scenarios in Industry 5.0, hybrid methods have evolved to operate across distributed layers. Edge devices now perform initial preprocessing using lightweight filters (variance, correlation, adaptive thresholds) to reduce dimensionality. When needed, these edge devices can implement simple embedded methods like compact decision trees or linear models for preliminary selection or anomaly detection.

The Industry 5.0 emphasis on trust and transparency has led to the integration of Explainable AI (XAI) techniques with hybrid feature selection. Through SHAP values, this XAI method provides fair feature-level attribution for any ML model's predictions, enhancing interpretability (Al Masud et al., 2025) and as an interpretable AI method, LIME simplifies complex models into local, understandable approximations to clarify individual predictions (Al Masud et al., 2025). These XAI methods work in conjunction with hybrid feature selection to present human operators with understandable rationales for feature selection decisions, bridging the gap between technical processes and human comprehension in industrial settings.

4. Application

In this study, two methods—classical (correlation-based) and machine learning-based (Random Forest)—were compared for feature selection in the context of Industry 5.0. The analyses utilized the mtcars dataset, which contains motor performance data, with mpg (fuel efficiency) defined as the target classification variable. The correlation-based analysis revealed variables such as wt, qsec, and hp, which are highly correlated with the mpg variable. Since this method relies on linear relationships, it can only identify a limited number of features that exhibit a strong direct correlation with the target variable.

On the other hand, the machine learning-based feature importance analysis conducted with the Random Forest algorithm provided a broader perspective using the MeanDecreaseGini metric. Mean Decrease in Gini (MDG) measures a feature's contribution to classification performance through its role in splits at the nodes of a decision tree model. This contribution is calculated based on the reduction in Gini impurity. Gini impurity measures how mixed (heterogeneous) the samples in a node are. Its formula is as follows:

$$Gini(t) = 1 - \sum_{i=1}^{C} p_i^2 \tag{1}$$

Where: p_i is the proportion of class i in the node, C: is the number of classes. In a **pure (single-class) node**, Gini = 0. Thus, the lower the Gini value, the more homogeneous the node.

In conclusion, within the data-driven, adaptive, and human-machine collaboration-based production environments envisioned by Industry 5.0, it was observed that machine learning-based methods provide more accurate and robust feature selection compared to the limited explanatory power of classical methods. Therefore, the use of algorithms such as Random Forest is recommended, particularly in predictive modeling and decision support system design. Here, application of the R software codes are given as the following.

```
# Install packages
library(randomForest)
```

```
library(caret)

library(dplyr)

library(corrplot)

# sample data: UCI 'mtcars' dataset as an industry 5.0 application for motor performance
data <- mtcars
data$mpg_class <- ifelse(data$mpg > 20, "High", "Low")  # Target variable (classification)

# 1. Classical method: correlation-based feature selection (filter method)
cor_matrix <- cor(data %>% select(-mpg_class))
corrplot(cor_matrix, method = "color", tl.cex = 0.7)
```

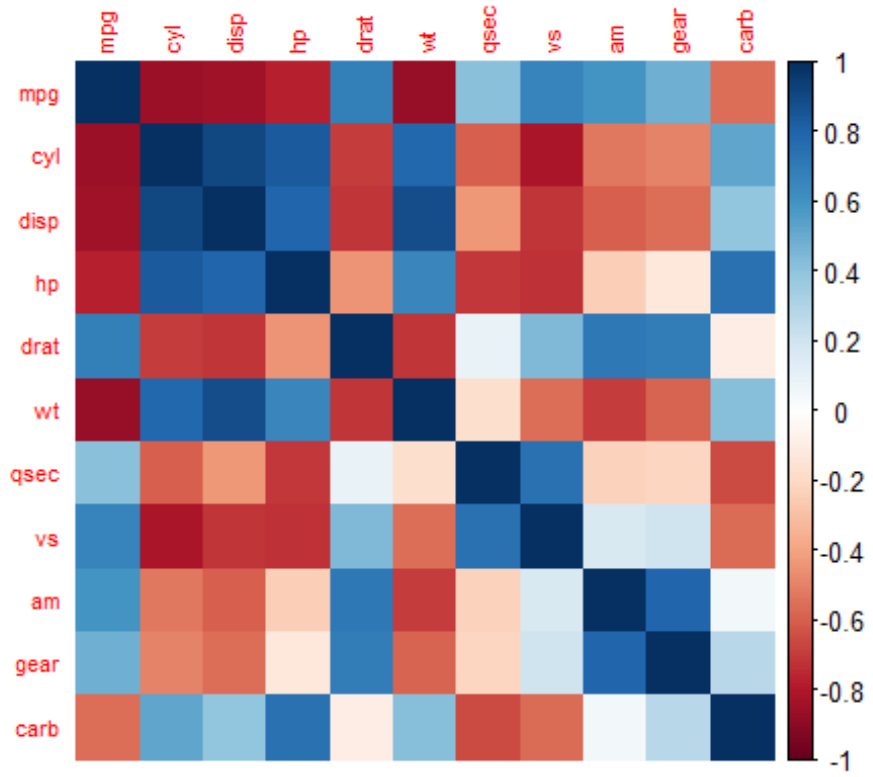


```
# Select features highly correlated with mpg (for demonstration purposes)
cor_target <- cor(data$mpg, data %>% select(-mpg_class))  # Consider mpg as the target
selected_corr_features <- names(which(abs(cor_target) > 0.6))

cat("Features selected by correlation:\n")

##Features selected by correlation:

print(selected_corr_features)

## NULL

# 2. ML-Based method: random forest feature importance scores
set.seed(42)
data$mpg_class <- as.factor(data$mpg_class)  #Convert to factor for classification
model <- randomForest(mpg_class ~ ., data = data, importance = TRUE)

importance_df <- as.data.frame(importance(model))
importance_df$Feature <- rownames(importance_df)
top_features_rf <- importance_df %>% arrange(desc(MeanDecreaseGini)) %>% head(5)
```

```
cat("\nMost important features with Random Forest:\n")

##
## Most important features with Random Forest:

print(top_features_rf[, c("Feature", "MeanDecreaseGini")])

##Feature MeanDecreaseGini
## mpg      mpg     4.585930
## hp       hp      2.810335
## wt       wt      2.310028
## disp     disp    2.140588
## cyl      cyl     1.429475
```

This analysis identified variables such as wt, hp, disp, qsec, and drat as the features offering the highest information gain. Since Random Forest can model both linear and non-linear relationships, it successfully captured more complex and multi-dimensional interactions.

5. Conclusion

Industry 5.0's human-centric, sustainable, and resilient production vision necessitates extracting meaningful signals from the "data tsunami." At this point, feature selection has evolved from a simple preprocessing step into a cornerstone of intelligent decision-making processes. While filter methods meet the need for speed and efficiency in edge computing; wrapper methods retain their importance in the pursuit of maximum performance for critical applications. Embedded methods, particularly through integration with gradient boosting machines and deep learning with attention mechanisms, stand out in balancing performance and computational efficiency. However, faced with heterogeneous and high-dimensional Industry 5.0 data, dynamic environments, real-time requirements, and interpretability needs, **hybrid approaches** (advanced filtering + embedded/meta-heuristic optimization) emerge indisputably as the most suitable and promising solution. These methods will play an indispensable role in building sustainable, human-robot collaborative smart factories by offering the necessary balance of scalability, flexibility, and intelligent decision-making. The future will witness deeper integration of feature selection with Automated ML (AutoML), Enhanced Explainable AI (XAI), dynamic adaptation, and federated learning, along with the development of new ethics/sustainability-focused criteria. The strategic selection of the right features is the key to realizing the promises of Industry 5.0.

Note: This study is a part of the master's thesis prepared in the Department of Statistics, Institute of Science, Graduate School of Natural and Applied Sciences, Muğla Sıtkı Koçman University.

References

Acid, S., de Campos, L. M., & Fernández, M. (2011). Minimum redundancy maximum relevancy versus score-based methods for learning Markov boundaries. *2011 11th International Conference on Intelligent Systems Design and Applications* (pp. 619-623). IEEE. https://doi.org/10.1109/ISDA.2011.6121724

Al Masud, G. H., Shanto, R. I., Sakin, I., & Kabir, M. R. (2025). Effective depression detection and interpretation: Integrating machine learning deep learning, language models, and explainable AI. Array, 25, 100375. https://doi.org/10.1016/j.array.2025.100375

Brückner, A., Wölke, M., Hein-Pensel, F., Schero, E., Winkler, H., & Jabs, I. (2025). Assessing industry 5.0 readiness-Prototype of a holistic digital index to evaluate sustainability, resilience and human-centered factors. International Journal of Information Management Data Insights, 5(1), 100329. https://doi.org/10.1016/j.jjimei.2025.100329

Han, J., Chen, Y., & Huang, X. (2025). An advanced adaptive group learning particle swarm optimization algorithm. Symmetry, 17, 667. https://doi.org/10.3390/sym17050667

Singh, K. A., Patra, F., Ghosh, T., Mahnot, N. K., Dutta, H., & Duary, R. K. (2025). Advancing food systems with industry 5.0: A systematic review of smart technologies, sustainability, and resource optimization. Sustainable Futures, 9, 100694. https://doi.org/10.1016/j.sftr.2025.100694

Mahmood, N., & Kadir, D. (2025). An elastic net approach to logistic regression for genetic selection in high-dimensional brain cancer data. Journal Name, *9*, 14–23.

Dutta, K. K., Sunny A., S., Victor, A., Nathu, A. G., Ayman Habib, M., & Parashar, D. (2020). Kannada alphabets recognition using decision tree and random forest models. 2020 3rd International Conference on Intelligent Sustainable Systems (ICISS), 534-541. https://doi.org/10.1109/ICISS49785.2020.9315972

Gan, M., & Zhang, L. (2021). Iteratively local fisher score for feature selection. Applied Intelligence, 51(8), 1-15. https://doi.org/10.1007/s10489-020-02141-0

Maddikunta, P. K. R., Pham, Q.-V., Prabadevi, B., Deepa, N., Dev, K., Gadekallu, T. R., Ruby, R., & Liyanage, M. (2022). Industry 5.0: A survey on enabling technologies and potential applications. Journal of Industrial Information Integration, 26, 100257. https://doi.org/10.1016/j.jii.2021.100257

Suciu, M. C., Plesea, D. A., Petre, A., Simion, A., Mituca, M. O., Dumitrescu, D., Bocaneala, A. M., Moroianu, R. M., & Nasulea, D. F. (2023). Core Competence-As a Key Factor for a Sustainable, Innovative and Resilient Development Model Based on Industry 5.0. Sustainability, 15(9), 7472. https://doi.org/10.3390/su15097472

Wolniak, R. (2023, May). Industry 5.0 - Characteristic, main principles, advantages and disadvantages. Scientific Papers of Silesian University of Technology. Organization and Management Series, 2023. https://doi.org/10.29119/1641-3466.2023.170.40

Eskandari, S., & Javidi, M. M. (2016). Online feature selection for streaming features using information entropy. Pattern Recognition Letters, 83, 3-12. https://doi.org/10.1016/j.patrec.2016.07.010

Ge, R., Zhou, M., Luo, Y., Meng, Q., Mai, G., Ma, D., Wang, G., & Zhou, F. (2016). McTwo: A two-step feature selection algorithm based on maximal information coefficient. BMC Bioinformatics, 17(1), 142. https://doi.org/10.1186/s12859-016-0990-0

Siddiqui, N., & Abbas, S. (2019). Image processing using Ant Colony Optimization. International Journal of Advanced Computer Science and Applications, 6(6), 946–953.

Zhou, P., Hu, X., Li, P., & Wu, X. (2019). OFS-Density: A novel online streaming feature selection method. Pattern Recognition, 86, 48-61. https://doi.org/10.1016/j.patcog.2018.08.009

➢ *ORAL PRESENTATION*

Resource Dependent Assembly Line Balancing Under Grey Uncertainty

Yakup ATASAGUN[1*] (*ORCID: https://orcid.org/0000-0002-8580-4336*)
Gözde CAN ATASAGUN[1] (*ORCID: https://orcid.org/0000-0003-4921-1557*)

[1] Konya Technical University, Faculty of Engineering and Natural Sciences, Industrial Engineering Department, Konya, Türkiye.

*Corresponding author e-mail: yatasagun@ktun.edu.tr

Abstract
This study addresses the Resource Dependent Assembly Line Balancing (RDALB) problem under uncertainty by integrating a grey linear programming approach into an existing RDALB model. The proposed formulation considers alternative resource combinations and incorporates uncertainty in task durations and cycle time using grey system theory. A numerical example is analyzed under five different scenarios — one based on the proposed model and the remaining four based on different whitening strategies for grey numbers — to assess the impact of uncertainty on total cost and resource utilization. The results demonstrate that the proposed model provides consistent solutions across varying assumptions, highlighting its practical relevance. This approach offers decision-makers a flexible method for resource dependent assembly line balancing in environments characterized by uncertainty and limited data availability.
Keywords: Resource Dependent Assembly Line Balancing, Grey System Theory, Grey Linear Programming

INTRODUCTION

Assembly lines constitute one of the most widely employed production systems in mass manufacturing industries due to their high efficiency and structured workflow. An assembly line consists of a series of workstations connected by a material handling system, where partially assembled products progress sequentially. The primary operational challenge in such systems is known as the Assembly Line Balancing (ALB) problem, which aims to assign tasks to workstations in a manner that satisfies task precedence relationships, cycle time constraints, and specific performance objectives—typically, minimizing the number of workstations.

The ALB problem has been extensively studied in the literature for decades, beginning with the pioneering work of Salveson (1955), who formulated the Simple Assembly Line Balancing Problem (SALB) as a mathematical optimization problem. Over time, a rich body of research has emerged to address various extensions and complexities of the ALB problem. Comprehensive reviews of early contributions can be found in the survey papers by Baybars (1986), Ghosh and Gagnon (1989), Erel and Sarin (1998), Becker and Scholl (2006), Scholl and Becker (2006), Battaïa and Dolgui (2013), Sivasankaran and Shahabudeen (2014), Hazır et al. (2015) and Battaïa et al. (2025).

The classical formulation of the ALB problem, often referred to as the SALB, assumes deterministic task processing times and the assignment of a single worker per station. Although analytically tractable, these assumptions significantly limit the practical applicability of SALB in dynamic industrial settings, where variability in labor skills, resource availability, and environmental conditions often leads to deviations from nominal task times.

To overcome these limitations, the Resource-Dependent Assembly Line Balancing (RDALB) problem was introduced by Faaland et al. (1992), offering a more flexible modeling framework. In RDALB, task processing times are not fixed but rather depend on the selected processing alternatives, each comprising different combinations of workers, assistants, and equipment. These alternatives not only influence task durations but also incur distinct operational costs. The objective in RDALB is to minimize the total cost, including both resource-related and workstation-related expenses. This approach better reflects the complexity and variability of real-life production systems.

Building on this foundation, Kara et al. (2011) reconsidered and modeled the problem with practice-oriented assumptions and extended the RDALB framework to U-shaped assembly lines, resulting in the Resource-Dependent U-Shaped Assembly Line Balancing (RDULB) problem. Empirical results show that the RDULB

approach achieves, on average, a 5.24% reduction in total costs compared to traditional straight-line systems (Kara and Atasagun 2013).

Despite these advancements, most RDALB studies such as Jayaswal and Agarwal (2014), Atasagun et al. (2019), Zhang et al. (2021), Atasagun et al. (2024) still rely on deterministic parameters. However, real-world production environments are inherently uncertain. Task durations may fluctuate due to operator fatigue, machine reliability, or process variability. Similarly, the cycle time, often derived from customer demand, may be imprecise or subject to change over the planning horizon. Such uncertainties necessitate the use of more robust modeling approaches.

In this context, Grey System Theory (GST) provides a powerful tool for modeling and decision-making under incomplete or partially known information. By representing uncertain parameters—such as task times and cycle time—as grey numbers, GST enables the development of more resilient and adaptive assembly line balancing models.

While many studies employ probabilistic or fuzzy approaches, a limited but promising stream of research has explored the use of GST for this purpose. GST, originally introduced by Ju-Long (1982), is particularly suitable for modeling systems with incomplete, imprecise, or partially known data. In the context of assembly line balancing, GST allows task times and cycle time to be represented as grey numbers, capturing a range of possible values rather than relying on single-point estimates.

Arık et al. (2019) proposed one of the first applications of grey linear programming to the assembly line balancing problem. Their model introduces grey parameters for both task durations and cycle time, and formulates the problem as a grey linear program, enabling more robust decision-making under uncertainty. Although their study focuses on the classical ALB setting, it demonstrates the effectiveness of GST in handling uncertainty in demand and processing times. Later, Toğa et al. (2025) proposed a grey linear programming model for U-Shaped assembly line balancing problem considering grey task times and grey learning effect.

In this study, the RDALB model proposed by Kara et al. (2011) is extended by incorporating the grey linear programming approach introduced by Arık et al. (2019) for assembly line balancing problems. This integration enables the model to effectively address uncertainties in both task durations and cycle time, enhancing its robustness and practical applicability. To demonstrate the applicability of the proposed approach, solutions to a sample problem are comparatively analyzed using different solution techniques based on the whitening of grey numbers. The resulting alternative solutions are presented to support decision makers in selecting robust and cost-effective configurations under uncertainty.

MATERIALS AND METHODS

In this section, the fundamental definitions of grey numbers are provided, followed by the formulation of a 0–1 mathematical model for the RDALB problem, incorporating grey data for task durations and cycle time. The proposed model builds upon the mathematical framework introduced by Kara et al. (2011), while the cycle time constraints are adapted using the grey linear programming approach developed by Arık et al. (2019).

Let x denote a closed and bounded set of real numbers. A grey number $x^{\mp}$ is a numerical interval whose upper and lower bounds are known but distribution information for x is unknown. $x^{\mp}$ is defined as follows:

$$x^{\mp} = \left[x^{-}, x^{+} \right] = \left[t \in x \mid x^{-} \leq t \leq x^{+} \right]$$

where x^{-} and x^{+} are the lower and upper bounds of grey number $x^{\mp}$, respectively and t is information (Arık et al. 2019).

Notation

Indices

i, r, s	: task
j	: workstation
e	: equipment

Parameters and sets

$t^{0}_{ie}{}^{\mp}$	: grey completion time of task i with equipment e without assistant
$t^{1}_{ie}{}^{\mp}$	: grey completion time of task i with equipment e with assistant
$CT^{\mp}$	: grey cycle time

N : set of tasks
E : set of equipment
E_i : set of equipment which can be used to process task i
NE_e : available number of equipment e
NA : available number of assistants
W : set of workstations
PR : set of precedence relations
$(r,s) \in PR$: a precedence relation; task r is an immediate predecessor of task s
M : a big number
CW : utilization cost of a workstation (worker + fixed costs)
CA : employment cost of an assistant
c_e : operating cost of equipment e

Variables
x_{ij} : 1, if task i is assigned to workstation j; 0, otherwise
p_{ije} : 1, if task i is assigned to workstation j with equipment e without assistant; 0, otherwise
q_{ije} : 1, if task i is assigned to workstation j with equipment e with assistant; 0, otherwise
z_{je} : 1, if equipment e is assigned to workstation j; 0, otherwise
u_j : 1, workstation j is utilized; 0, otherwise
k_j : 1, if an assistant is assigned to workstation j; 0, otherwise

Mathematical Formulation

$$Min \quad \sum_{j\in W} CWu_j + \sum_{j\in W} CAk_j + \sum_{j\in W}\sum_{e\in E} c_e z_{je} \tag{1}$$

$$\sum_{j\in W} x_{ij} = 1 \qquad \forall i \in N \tag{2}$$

$$\sum_{e\in E_i} (p_{ije} + q_{ije}) = x_{ij} \qquad \forall i \in N; \forall j \in W \tag{3}$$

$$\sum_{i\in N}\sum_{e\in E_i} (t_{ie}^{0\mp} p_{ije} + t_{ie}^{1\mp} q_{ije}) \le CT^{\mp} u_j \qquad \forall j \in W; \forall \mp \tag{4}$$

$$\sum_{j\in W} (\|W\| - j + 1)(x_{rj} - x_{sj}) \ge 0 \qquad \forall (r,s) \in PR \tag{5}$$

$$\sum_{i\in N} (p_{ije} + q_{ije}) \le M z_{je} \qquad \forall e \in E_i; \forall j \in W \tag{6}$$

$$\sum_{j\in W} z_{je} \le NE_e \qquad \forall e \in E \tag{7}$$

$$\sum_{i\in N}\sum_{e\in E_i} q_{ije} \le M k_j \qquad \forall j \in W \tag{8}$$

$$\sum_{j\in W} k_j \le NA \tag{9}$$

$$x_{ij}, p_{ije}, q_{ije}, u_j, k_j, z_{je} \in \{0,1\} \qquad \forall i \in N; \forall j \in W; \forall e \in E \tag{10}$$

The objective function defined in (1) minimizes the total cost of workstation utilization, assistant workers and equipment. Equation (2) ensures that each task is assigned to at least and at most one workstation. Equation (3) determines the resources (equipment type and assistant) allocated to a workstation. Equation (4) ensures that sum of grey task durations in workstation j does not exceed the grey cycle time. This equation also determines whether workstation j is utilized or not. Precedence relationships among tasks are satisfied by the set of constraints given in Equation (5). Equation (6) determines whether equipment e is allocated to workstation j or not. Equation (7) restricts the allocated number of equipment type e by the available number of this equipment type. Equation (8) determines whether an assistant is assigned to workstation j or not. Equation (9) ensures that the number of

assistants assigned to workstations does not exceed the available number of assistants. Finally, equation (10) is sign constraint.

RESULTS AND DISCUSSION

In this section, the proposed grey linear programming formulation is evaluated through an illustrative example. First, the necessary data for an RDALB problem involving 10 tasks is introduced. The problem is then solved using the proposed model, and the corresponding results are reported. Finally, a scenario analysis is conducted by solving the same problem under various whitening strategies applied to the grey parameters.

Table 1 presents the precedence relations and grey task processing times for the illustrative problem, including the available resource alternatives for each task. The columns labeled IP_i indicate the immediate predecessors of task i. If a cell in Table 1 lacks grey task completion time data, it indicates that the corresponding task does not have the associated processing alternative.

Table 1. Illustrative Problem Data

Task i	IP_i	Grey Task Completion Times					Task i	IP_i	Grey Task Completion Times				
		Assistant	Equipment						Assistant	Equipment			
			No	1	2	3				No	1	2	3
1	-	Yes					6	3	Yes	[4,8]			
		No	[6,9]						No	[5,9]			
2	-	Yes	[7,11]	[5,8]	[3,6]		7	-	Yes				
		No							No	[8,11]			
3	-	Yes	[5,7]				8	4,5	Yes				
		No							No	[9,11]	[4,7]	[6,7]	
4	1	Yes					9	8	Yes				
		No	[1,3]		[1,2]				No	[4,8]			
5	2	Yes					10	7,9	Yes				
		No	[9,12]			[6,8]			No	[5,7]			

The remaining parameters used in the model are set as follows: CW=10, CA=6, c_1=2.4, c_2=1.6 and c_3=5.2 money units. Available number of assistants, equipment #1, equipment #2 and equipment #3 are 2, 1, 2 and 1, respectively. A "no equipment" option is also defined and labelled as equipment type 0. All processing alternatives, task durations, costs, and resource availabilities are generated randomly. The grey cycle time is represented as $CT^{\mp} =$ [12,18].

The illustrative problem described above is solved within seconds using the proposed grey linear programming model, yielding a solution with a total cost of 58.4 money units, as presented in Table 2.

Table 2. Results of the Illustrative Problem

Workstation	Assigned Tasks	Grey Workload	Assigned equipment	Assistant worker
1	2,3	[12,18]		Yes
2	1,6	[11,18]		No
3	4,5	[10,15]		No
4	7,8	[12,18]	#1	No
5	9,10	[9,15]		No

To provide alternative solutions for decision makers, the illustrative problem is solved under five different scenarios. The first scenario involves solving the problem using the proposed grey linear programming model. The remaining four scenarios, adopted from Aydemir et al. (2020), are based on the whitening of grey numbers. Whitening refers to the process of converting a grey number into a crisp value within its lower and upper bounds using various techniques, enabling the application of a deterministic model to the problem using these whitened values.

The whitened value of a grey number $x^{\mp}$ is yielded as follows:

$$\tilde{x}^{\mp} = \alpha x^{-} + (1-\alpha)x^{+}, \quad \alpha \in [0,1] \tag{11}$$

The five analyzed scenarios are defined as follows:

- ***Scenario* 1** represents the solution generated by the proposed grey linear programming-based RDALB model.
- ***Scenario* 2** reflects the most optimistic case, where all grey task durations are assumed to take their lower bounds, and the grey cycle time is taken at its upper bound. Accordingly, in Equation (11), the whitening coefficient (α) is set to 1 for grey task durations and 0 for grey cycle time.
- ***Scenario* 3** corresponds to the most pessimistic case, in which all grey task durations are at their upper bounds, while the grey cycle time is assumed to take its lowest possible value. In this scenario, α is set to 0 for task durations and 1 for cycle time.
- ***Scenario* 4** employs equal weighting in the whitening process, assigning $\alpha = 0.5$ for both task durations and cycle time.
- ***Scenario* 5** utilizes the degree of greyness approach, where α values are assigned individually based on the specific greyness degree of each grey number. This method follows the definitions provided by Liu and Forrest (2010) and Aydemir et al. (2020).

The results of the five scenarios are summarized in Table 3. It should be noted that the deterministic RDALB model proposed by Kara et al. (2011) is employed in scenarios 2 through 5.

Table 3. Results of the scenarios

Scenario number	Total cost	Total number of utilized workstations	Utilized equipment	Utilized number of assistants
1	58.4	5	#1	1
2	37.6	3	#2	1
3	102	9	-	2
4	58.4	5	#1	1
5	58.4	5	#1	1

The results shown in Table 3 reveal the sensitivity of the RDALB model to varying levels of uncertainty in task durations and cycle time. While Scenario 2 (the most optimistic or the best possible case) offers the most cost-efficient solution with minimal workstation usage, Scenario 3 (the most pessimistic or the worst possible case) yields the highest cost, highlighting the impact of adverse conditions. Notably, Scenarios 1, 4, and 5 produce identical outcomes, suggesting that the proposed model remains robust across different whitening approaches applied to grey parameters. These findings emphasize the model's flexibility and its applicability as a reliable decision-support tool under uncertainty.

CONCLUSION

This study addresses the Resource Dependent Assembly Line Balancing (RDALB) problem under uncertainty by integrating the grey linear programming approach proposed by Arık et al. (2019) into the RDALB model developed by Kara et al. (2011). The proposed model enables the consideration of variability in task durations and cycle time using grey system theory, thereby offering a more flexible and realistic framework for decision makers. A numerical example is analyzed under five different scenarios to evaluate the impact of uncertainty representation on total cost and resource allocation. The results demonstrate that the model provides robust and consistent solutions across different whitening strategies, while also highlighting the significant cost implications of extreme optimistic and pessimistic conditions. Overall, the proposed approach offers a valuable decision-support tool for assembly line planning in environments characterized by uncertainty and limited data.

Future studies may explore hybrid approaches that combine grey system theory with fuzzy logic or stochastic programming, extend the model to multi-objective settings, or apply it to different variants of assembly line balancing problems.

REFERENCES

Arık, O. A., Köse, E. and Forrest, J. (2019). "Simple assembly line balancing problem of Type 1 with grey demand and grey task durations." Grey Systems: Theory and Application 9(4): 401-414.

Atasagun, Y., Döyen, A. and Atasagun, G. C. (2024). "Traditional and fuzzy goal programming approaches for resource dependent assembly line balancing problem." Numerical Algebra, Control and Optimization 14(1): 214-226.

Atasagun, Y., Kara, Y. and Can Atasagun, G. (2019). Achieving Shojinka by Integrated Balancing of Multiple Straight Lines with Resource Dependent Task Times. Lean and Green Supply Chain Management: Optimization Models and Algorithms. T. Paksoy, G.-W. Weber and S. Huber. Cham, Springer International Publishing: 253-273.

Aydemir, E., Yılmaz, G. and Oruc, K. O. (2020). "A grey production planning model on a ready-mixed concrete plant." Engineering Optimization 52(5): 817-831.

Battaïa, O., Delorme, X., Dolgui, A. and Haddou-Benderbal, H. (2025). "New trends in line balancing and model sequencing in assembly, disassembly and machining environments." Computers & Industrial Engineering: 111210.

Battaïa, O. and Dolgui, A. (2013). "A taxonomy of line balancing problems and their solutionapproaches." International Journal of Production Economics 142(2): 259-277.

Baybars, I. (1986). "Survey Of Exact Algorithms For The Simple Assembly Line Balancing Problem." Management Science 32(8): 909-932.

Becker, C. and Scholl, A. (2006). "A survey on problems and methods in generalized assembly line balancing." European Journal of Operational Research 168(3): 694-715.

Erel, E. and Sarin, S. C. (1998). "A survey of the assembly line balancing procedures." Production Planning and Control 9(5): 414-434.

Faaland, B. H., Klastorin, T. D., Schmitt, T. G. and Shtub, A. (1992). "Assembly line balancing with resource dependent task times." Decision Sciences 23(2): 343-364.

Ghosh, S. and Gagnon, R. J. (1989). "A comprehensive literature review and analysis of the design, balancing and scheduling of assembly systems." International Journal of Production Research 27(4): 637-670.

Hazır, Ö., Delorme, X. and Dolgui, A. (2015). "A review of cost and profit oriented line design and balancing problems and solution approaches." Annual Reviews in Control 40: 14-24.

Jayaswal, S. and Agarwal, P. (2014). "Balancing U-shaped assembly lines with resource dependent task times: A Simulated Annealing approach." Journal of Manufacturing Systems 33(4): 522-534.

Ju-Long, D. (1982). "Control problems of grey systems." Systems & Control Letters 1(5): 288-294.

Kara, Y. and Atasagun, Y. (2013). "Assembly Line Balancing with Resource Dependent Task Times: An Application to Parallel Assembly Lines." IFAC Proceedings Volumes 46(9): 845-850.

Kara, Y., Özgüven, C., Yalçin, N. and Atasagun, Y. (2011). "Balancing straight and U-shaped assembly lines with resource dependent task times." International Journal of Production Research 49(21): 6387-6405.

Liu, S. and Forrest, J. Y. L. (2010). Grey systems: theory and applications, Springer.

Salveson, M. E. (1955). "The assembly line balancing problem." Journal of Industrial Engineering 6(3): 18-25.

Scholl, A. and Becker, C. (2006). "State-of-the-art exact and heuristic solution procedures for simple assembly line balancing." European Journal of Operational Research 168(3): 666-693.

Sivasankaran, P. and Shahabudeen, P. (2014). "Literature review of assembly line balancing problems." The International Journal of Advanced Manufacturing Technology 73(9): 1665-1694.

Toğa, G., Atalay, B., Toksarı, M. D. and Forrest, J. Y.-L. (2025). "Solving U-type assembly line balancing under grey uncertainties: grey learning effect and grey task times approach." Grey Systems: Theory and Application ahead-of-print(ahead-of-print).

Zhang, Z., Tang, Q. and Qian, X. (2021). "Integration of balancing and preventive maintenance in straight and U-shaped resource-dependent assembly lines: MILP model and memetic algorithm." Applied Soft Computing 113: 107773.

➢ *ORAL PRESENTATION*

Effects of *Craterellus lutescens* (chick) fungus on peroxidation of olive oil

Ayşegül KARAPINAR ARİF* (https://orcid.org/0009-0005-8096-150X) , Baran ÖNER (https://orcid.org/0009-0003-7261-1142) , Yağız Ege TAŞKIRAN (https://orcid.org/0009-0009-0141-2705)

Ozel Mugla Modern Bilimler Akademisi (MBA Okulları) , Fen Lisesi, Biyoloji, Muğla, Türkiye

* Corresponding author e-mail: karapinar.aysegul@gmail.com

Abstract

The olive tree (*Olea europaea* L.) is native to the Mediterranean basin and parts of Asia and is widely cultivated in many parts of the world for the production of olive oil, olives and soap. Olives are a rich source of valuable nutrients and bioactive substances of medicinal and therapeutic interest. Other important compounds found in olive fruit are pectin, organic acids and pigments. Extra virgin olive oil (VOO) mechanically extracted from the fruit is also highly popular for its nutritive and health-promoting potential, especially against cardiovascular disorders, due to the presence of high levels of monounsaturated fats and other valuable minor components such as phenolics, phytosterols, tocopherols, carotenoids, chlorophyll and squalene. Variety, production area, harvest time and processing techniques used are some of the factors shown to influence the composition of olive fruit and olive oil.

Olive oil oxidises when it encounters air, resulting in the formation of peroxides. This is because unsaturated fatty acids (monounsaturated and polyunsaturated) have one or more double bonds that take up oxygen and cause the formation of peroxides, one of the main products of oxidation. This investigation aimed to reduce the peroxide value, which increases over time in olive oil obtained from olive fruit, with edible mushrooms. The aim of this comparison was to prevent the bitterness in olive oil flavour over time with a natural, edible product. *Craterellus lutescens* (chick mushroom), an edible mushroom species, was selected for this purpose. In the study, two different olive oil jars to which *Craterellus lutescens* mushroom was added were kept for 45 days, one in a light and one in a dark environment and compared with the control groups. Compared to the control groups, it was determined that a decrease in peroxide ratio was achieved.

Key words: Olive oil, peroxidation, *Craterellus lutescens*

Objective

It is aimed to store olive oil, which is consumed by people in many parts of the world and is one of the most beneficial oil types in terms of health, in better quality. It is aimed to reduce the peroxide rate formed in olive oil over time with natural edible mushrooms. When we look at the literature, there is no research on this subject using mushrooms. In this sense, this study is considered to be the first in the literature.

Introduction

Olive (Olea europaea L.) is a fruit that grows mainly in the Mediterranean region and is widely cultivated worldwide for the production of olive oil and table olives. Olive is rich in phenolic compounds, oils, pectin, organic acids and other nutrients that are antioxidant, anti- carcinogenic, anti-inflammatory and beneficial against cardiovascular diseases (Ghanbari, R., Anwar, F., Alkharfy, K. M., Gilani, A.-H., & Saari, N. 2012).Olive leaf is a traditional herbal tea widely used to treat some diseases, especially among the Mediterranean people.

Another study investigated the effects of potassium foliar application on physiological and biochemical traits on three olive cultivars 'Mission', 'Koroneiki' and 'Dezfuli' in Ahvaz, Iran in 2012 and 2013. Potassium sulphate application increased leaf chlorophyll content in olive cultivars, leaf potassium content in 'Mission' and 'Koroneiki' cultivars, fruit anthocyanin concentration in 'Dezfuli' cultivar, and positively affected fruit soluble carbohydrates (Zivdar, S., Arzani, K., Souri, M. K., Moallemi, N., & Seyyednejad, S. M. 2018). This study examined the protective effects and antioxidant capacity of oleuropein (OLP) and hydroxytyrosol (HT) against H_2O_2-induced DNA damage in olive oil and olive leaves . Both compounds exhibited potent antioxidant properties, protecting cells against H_2O_2-induced DNA breaks, but hydroxytyrosol provided more effective protection than oleuropein (Nousis, L., Doulias, P. T., Aligiannis, N., Bazios, D., Agalias, A., Galaris, D., & Mitakou, S. 2005).

According to another study, oxidative stress plays a role in the pathogenic molecular mechanisms of various

diseases, including cardiovascular disease, ischaemia-reperfusion syndrome, neurodegenerative diseases, cancer and the physiological process of normal ageing, and intensive research efforts have been carried out to explain these mechanisms and to discover agents that can prevent or regulate the harmful effects of oxidative stress that contribute to the development of these pathological complications (Barbouti, Briasoulis, Galaris, 2010). Hydrogen peroxide is a manufactured chemical, although small amounts of hydrogen peroxide gas can be found naturally in the air. Low exposures may occur from domestic use; higher exposures may occur from industrial use. Exposure to hydrogen peroxide may cause irritation of the eyes, throat, respiratory tract and skin. Drinking concentrated liquid may cause mild to severe gastrointestinal effects (ToxFAQsTM, 2002).
Thirteen new acetylenic acids and their derivatives, craterellins G-Q (1, 2, 4-10, 12, 13), 9-epi-craterellin H(3) and 14-O-ethyl-craterellin O (11), were isolated from the fruiting bodies of the edible mushroom Craterellus lutescens. The structures of these compounds were characterised by various spectroscopic and chemical means. The stereo configurations of 1-13 were elucidated by a combination of acetonide formation, J-based configuration analysis and the modified Mosher method. Craterellyne I was found to exhibit cytotoxicity against human cancer types and inhibition of nitric oxide (NO) production (Huang, Zhang, Chen, Zhao, Zhou, Li, Feng, and Ji-Kai, 2017). Turkey is one of the leading countries in the world in natural mushroom exports. The majority of the mushrooms exported from Turkey to are natural mushrooms. Champignon mushroom (Morchella spp.), bear mushroom (Boletus edulis), cedar mushroom (Tricholoma anatolicum), dwarf girl (sarıkız) (Chantharellus cibarius), mullein (Hydnum
repandum), trumpet (Cratellus cornucopioides), cannellini (Lactarius spp.) and truffles (Terfezia boudieri Chatin) are the main natural products exported from Turkey.
mushroom species (Öztürk, Soylu, Temel, Pezikoğlu, Bilen, 2019). When the literature is examined, there is no study on the effect of *Craterellus lutescens* species in olive oil. It is thought that this study will complete the gap in this subject.

Method

In the research, mushroom samples could not be collected in Muğla Province in September-October and November 2024 due to rainfall. *Craterellus lutescens* (chick mushroom) mushroom collected from Balıkesir/Gönen region was taken 100 grams and identified and dried by Muğla Sıtkı Koçman University Faculty of Science and Literature Faculty Member Assoc. Prof. Hakan Allı.
Four 250ml jars were prepared from the olive oil sample taken from Aydın Province.
The dried mushroom samples were crushed (until powdered) 50 g each and added to two separate jars containing 250 ml olive oil (Table-1).

Table-1: Peroxide value table of mushroom samples and control group

	Olive oil Amount	**Mushroom Amount**	**Conditions and first month**	**At the end of the 30th day**	**Analysis at the end of the 45th day**
			analyses	**Analysis**	
Control 1	250 mL		In the dark		
Control 2	250 mL		In Daylight		
Mushroom	250 mL	50 g dry Mushrooms 1	In the dark		
Mushroom	250 mL	50 g dry Mushrooms 1	In Daylight		

The analyses of the samples at the end of the 30th day and 45th day were carried out at Muğla Sıtkı Koçman University Research Laboratory Centre Food Analysis Laboratory under the guidance of Prof. Dr. Mehmet ÖZTÜRK. The analyses were carried out by taking into consideration the criteria in the Communiqué of TGK-Olive Oil and Olive Pomace Oil (Annex-1).

Scope

This method describes a method for the determination of the peroxide value in animal and vegetable fats and oils. Samples taken for this analysis should be stored away from light, in airtight, fully filled glass containers sealed with a sealed glass or cork stopper and stored at cold temperatures.

Definition.

Peroxide value: The milliequivalent weight of active oxygen in one kilogram of oil that oxidises potassium iodide under the defined conditions of analysis.

Principle

The sample dissolved in acetic acid-chloroform solvent mixture was treated with potassium iodide solution and the free iodine released was titrated with adjusted sodium thiosulphate solution.

Materials

All equipment to be used was free from reducing or oxidising agents. No lubricating oil was applied to the surfaces with mattresses.

Glass flask with a syringe: 250 mL

It must be dry before use and a pure, dry inert gas (nitrogen or preferably carbon dioxide) must be passed through it.

Burette 25 or 50 mL (0.1 mL divided)

Chemicals

Chloroform:

Oxygen was removed by passing an inert gas of analytical purity and dry.

Glacial (glacial) acetic acid:

Oxygen was removed by passing an inert gas of analytical purity and dry.

Saturated potassium iodide aqueous solution:

Freshly prepared and supersaturated, free of iodine and iodate.

Sodium thiosulphate solution: (0.01 M or 0.002 M) Adjusted just before use.

Starch solution 10 g/L. Freshly prepared aqueous solution of soluble natural starch Solution.

Procedure

The analysis was carried out under artificial light or in a sunlit environment away from direct sunlight. The sample was weighed into a flask with a precision of 0.001g using Table 2 according to the expected peroxide value.

Table 2- Sample quantity to be weighed

Expected peroxide value (meq active oxygen/kg fat)	**Sample weight (g)**
0 - 12	5,0 - 2,0
12 - 20	2,0 - 1,2
20 - 30	1,2 - 0,8
30 - 50	0,8 - 0,5
50 - 90	0,5 - 0,3

Add 10 mL of chloroform to the flask and dissolve the sample with rapid stirring. 15 mL acetic acid and 1 mL potassium iodide solution were added to the dissolved sample, the lid of the flask was quickly closed and shaken for 1 minute. The flask was kept at a temperature between 15°C and 25°C in the dark for 5 minutes. The lid was opened and 75 mL of distilled water was added to the flask. The free iodine formed in the flask was titrated with sodium thiosulphate (using 0.002 M sodium thiosulphate solution if the expected peroxide value was below 12 and 0.01 M sodium thiosulphate solution if the expected peroxide value was above
12) under the indicator of starch solution and shaken vigorously during titration. A blind trial is performed simultaneously. If the consumption of 0.01 M sodium thiosulphate solution in the blind trial exceeded 0.05 mL, the chemicals were changed.

Expression of results

The analysis is done in two parallel. The result is the arithmetic mean of the two calculations. The peroxide value (PV) in milliequivalent weight of active oxygen per kilogram was calculated by the following formula;

$$PV = \frac{1000 \times (V - V_0) \times c}{m}$$

It's here;
V = Volume of adjusted sodium thiosulphate solution used for the analysis, (mL) V0 = Volume of adjusted sodium thiosulphate solution used for the blind test, (mL) c = The exact molarity of sodium thiosulphate solution consumed;
m = Weight of the sample, (g)

Findings

Code	Name	Spent	sodium thiosulphate (M)	Coefficient	Fat weight	Result (%)
1	IK30	19,51	0,01	1000	2,0117	96,98
2	**KK30**	**7,1**	**0,01**	**1000**	**2,0118**	**35,29**
3	IK45	33,6	0,01	1000	2,0063	167,47
4	**KK45**	**6,6**	**0,01**	**1000**	**2,0322**	**32,48**
13	CLI30	19,1	0,01	1000	2,0360	93,81
14	**CLK30**	**5,6**	**0,01**	**1000**	**2,0307**	**27,58**
15	CLI45	16,2	0,01	1000	2,0097	80,61
16	**CLK45**	**4,1**	**0,01**	**1000**	**2,0540**	**19,96**

Table-3 Peroxide values of control and experimental groups IK30: 30 days in a lighted jar
KK30: Jar in the dark for 30 days IK45: 45 days in a lighted jar KK45: Jar in the dark 45 days
CLI30: jar with mushroom sample in a lighted environment for 30 days CLK30: jar in dark place with mushroom sample 30 days
CLI45: jar with fungal specimen in a lighted environment 45 days CLK45: jar with fungal specimen in dark environment 45 days

Conclusion and Discussion

When the results of the study are examined, it is seen that peroxidation is lower in jars in dark environment. In addition, it is seen that peroxidation is lower in olive oils containing Craterellus lutescens sample compared to the control groups. According to the TGK- Olive Oil Communiqué (Annex-1), a peroxide value of 20 and below indicates that the quality of olive oil increases. It is thought that the increase in the amount of peroxide causing deterioration can be prevented by using this fungus species in olive oils stored for food purposes.

Recommendations

In the direction of this study, mixed products can be created with olive oil and *Craterellus lutescens* mushroom, production can be provided in terms of economic contribution and can be traded abroad. Similar studies can be carried out with different edible mushroom species grown in our country. In the next study, the degree of acidity, which determines the quality of olive oil, can be examined by the same method.

References

Alexandra Barbouti, Evangelos Briasoulis, Dimitrios Galaris, Chapter 120 - Protective Effects of Olive Oil Components Against Hydrogen Peroxide-Induced DNA Damage: The Potential Role of Iron Chelation, Editor(s): Victor R. Preedy, Ronald Ross Watson, Olives and Olive Oil in Health and Disease Prevention, Academic Press, 2010, Pages 1103-1109, ISBN 9780123744203, https://doi.org/10.1016/B978-0-12-374420-3.00120-0

Division of Toxicology ToxFAQsTM, 2002

Ghanbari, R., Anwar, F., Alkharfy, K. M., Gilani, A.-H., & Saari, N. (2012). Valuable Nutrients and Functional Bioactives in Different Parts of Olive (Olea europaea L.)—A Review. International Journal of Molecular Sciences, 13(3), 3291-3340. https://doi.org/10.3390/ijms13033291

Mustafa ÖZTÜRK, Mustafa Kemal SOYLU, Mükremin TEMEL, Filiz PEZİKOĞLU, Gülşah MISIR BİLEN Atatürk Bahçe Kültürleri Merkez Araştırma Enstitüsü, UAZİMDER Uluslararası Anadolu Ziraat Mühendisliği Bilimleri Dergisi ISSN : 2667-7571 2019 (Özel Sayı 1): 102-107 Yalova, Türkiye

Nousis, L., Doulias, P. T., Aligiannis, N., Bazios, D., Agalias, A., Galaris, D., & Mitakou, S. (2005). DNA protecting and genotoxic effects of olive oil related components in cells exposed to hydrogen peroxide. Free Radical Research, 39(7), 787–795. https://doi.org/10.1080/10715760500045806

Ying Huang, Shuai-Bing Zhang, He-Ping Chen, Zhen-Zhu Zhao, Zhong-Yu Zhou, Zheng-Hui Li, Tao Feng, and Ji-Kai Liu Journal of Agricultural and Food Chemistry 2017 65 (19), 3835-3841 DOI: 10.1021/acs.jafc.7b00899

Zivdar, S., Arzani, K., Souri, M. K., Moallemi, N., & Seyyednejad, S. M. (2018). Physiological and biochemical response of olive (Olea europaea L.) cultivars to foliar potassium application

➢ *ORAL PRESENTATION*

TRP Channels in Colorectal Cancer

Müge MAVİOĞLU KAYA[1]* (https://orcid.org/0000-0003-1276-3745)

[1] Kafkas University Faculty of Arts and Sciences, Department of Molecular Biology and Genetics, Kars, TÜRKİYE.

*Corresponding author e-mail: m.mavioglu@hotmail.com

Abstract

Colorectal cancer (CRC) is the cancer type with the third highest mortality rate in both men and women worldwide. These rates are expected to peak as inactivity and a western lifestyle become increasingly widespread. Transient receptor potential channels are candidates for being very effective therapeutic targets because they play a key role in the pathophysiology of many diseases including colorectal cancer and help predict the prognosis of the disease. Therefore, it is essential to determine the tissue-specific expression profiles, agonists and antagonists of the TRP superfamily.

Anahtar Kelimeler: TRP channels, colon cancer, colitis

1.INTRODUCTION

Colon/colorectal cancer (CRC) is the third leading cause of death and has a very high incidence in both men and women (Demir et al., 2024). Metastasis is the main cause of poor prognosis and death in patients with CRC. The mechanisms involved in CRC metastasis are still unclear (figure1). Therefore, it is urgent to identify the basic molecules that cause metastasis, which can be used to develop new molecular markers for disease diagnosis and design specific targeted drugs (Xu et al., 2014).

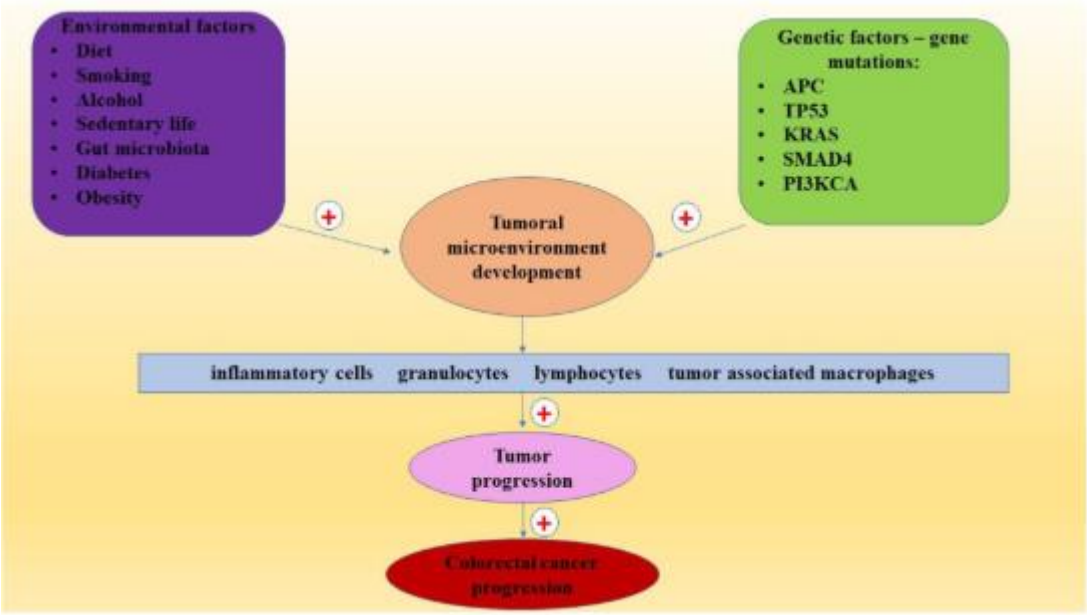

Figure 1. Effects of environmental and genetic factors on colon cancer progression (Stefani et al., 2021).

Transient receptor potential (TRP) channels are ionic channels that are permeable to monovalent and divalent positive ions but have higher selectivity for K^+, Na^+, and Ca^{+2}. TRP channels regulate hormones in the gastrointestinal tract, increasing colonic mucus secretion and accelerating intestinal motility (Zhang et al., 2025). In a study evaluating transcriptomic and genomic changes in their genes, it was determined that 27 out of 28 TRP genes were associated with at least one cancer symptom. The stage of cancer can be determined by

decreased or increased levels of TRP protein expression. This feature makes TRPs important markers for detecting tumor progression and potential therapeutic targets (Marini et al., 2023).

2. TRP CHANNEL SUPER FAMILY

TRP channels were first identified in Drosophila melanogaster (fruit fly). TRP proteins are encoded by at least 28 genes and are expressed almost ubiquitously (Bödding et al., 2007). Chemicals, lipid signaling molecules, and physical stimuli can activate TRP channels, causing them to be involved in thermal, chemical, mechanical, and permeation processes (Duan et al., 2025). According to nucleotide sequences and topological differences, mammalian TRP can be divided into seven subfamilies: TRPC, TRPV, TRPM, TRPN, TRPA, sub-TRPP and TRPML (Figure2) (Zhang et al., 2023).

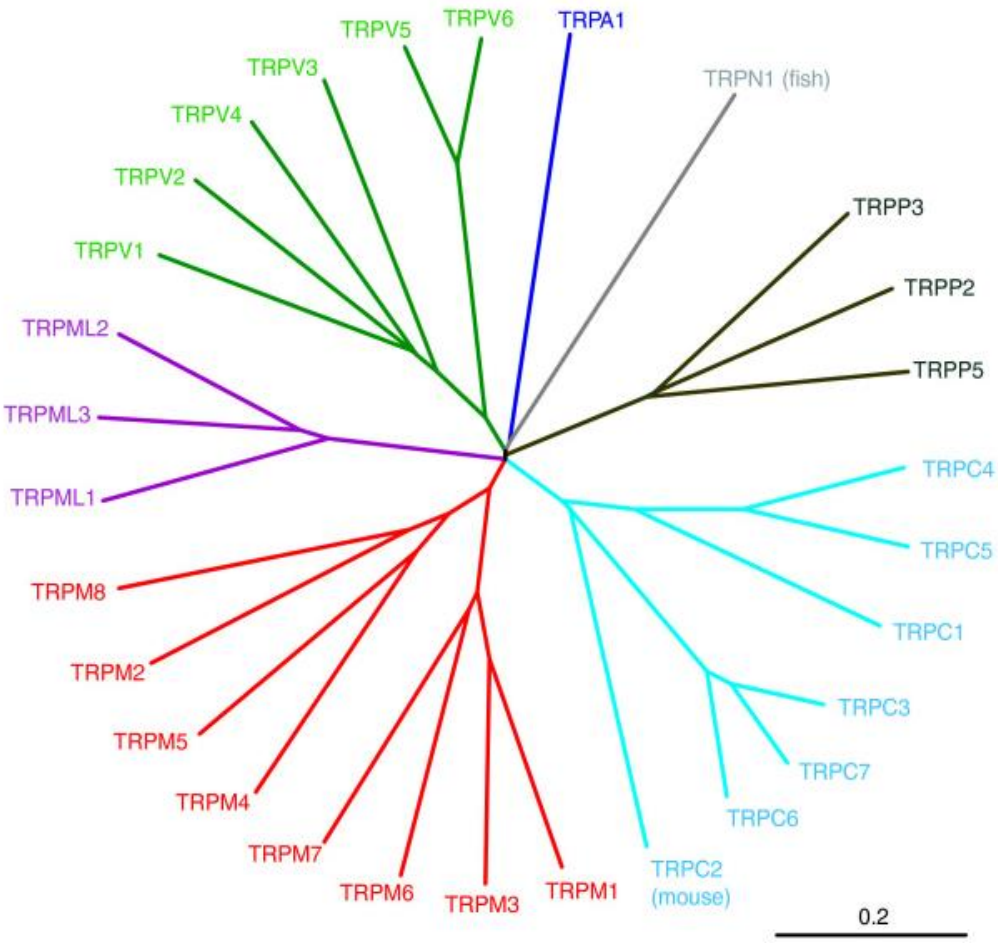

Figure 2. Phylogenetic tree of the TRP family of human ion channels: TRPC (canonical) channels, TRPV (vanilloid) channels, TRPM (melastatin) channels, TRPN (nompC-like) channels, TRPA (ankyrin) channels, TRPP (transient receptor potential polycystic) channels, TRPML (transient receptor potential mucolipin) channels (Nilius and Owsianik, 2011).

2.1 TRPC (Canonical) Channels

The first identified members of the TRP family were TRPC channels. They form a group of non-selective cation channels that allow the passage of Ca^{2+} and other cations into the cell cytosol. There are seven known members (TRPC1-TRPC7) (Sun et al., 2021). It is widely expressed in most cells and tissues, although it is common in epithelial cells, muscle cells, and neurons. TRPC channels are activated by G-protein coupled receptors, diacylglycerol, receptor tyrosine kinases, and inositol triphosphates. Activated TRPC channels allow Ca^{+2} to pass into the cell, causing an increase in Ca^{+2} concentration. This induces downstream signaling pathways and enables cellular responses to occur through the function of some enzymes and transcription factors. Abnormal TRPC expression is associated with pathological conditions such as cardiovascular diseases, neurodegenerative disorders and various types of cancer (Marini et al., 2023).

2.2 TRPV (Vanilloid) Channels

TRPV channels are well-studied channels of the TRP family. They consist of six known non-selective members (TRPV1-TRPV6). They are frequently located on the cell membrane. They act as sensors of mechanical, osmotic and chemical stimullants (Rizopoulos et al., 2021). Capsaicin-sensitive TRPV channels are expressed in many tissues and cells, especially epithelial cells, neurons and immune cells. When stimulated by temperature, pH, and various mechanical and chemical stimulants, they allow K^+, Na^+, and Ca^{2+} to enter the cytoplasm. Abnormal expression of TRPV channels in cancer plays a key role in malignant tumor proliferation, invasion and angiogenesis (Marini et al., 2023).

2.3 TRPM (Transient Receptor Potential Melastatin) Channels

The TRPM family, the largest subfamily of the TRP family, consists of eight members (TRMP1-TRMP8). They are activated by changes in voltage and temperature, as well as by binding of ions or other primary messengers. Active TRPM channels function as important sensors in maintaining cell membrane potential and regulating ion homeostasis by controlling Zn^{+2}, Ca^{+2} and Mg^{+2} influx (Rizopoulos et al., 2021). TRPM channels are abundantly expressed in kidney tissues. Mutations in TRPM genes play an important role in the pathology of many diseases such as malignant proliferation, metastasis, angiogenesis, neurological degeneration, epithelial dysfunction, inflammation and diabetes (Chubanov et al., 2024; Zhang et al., 2023).

2.4 TRPN (Transient Receptor Potential NompC-Like) Channels

The TRPN channel is a sub-member of the mechano-gated TRP family involved in hearing, sense of touch, and proprioception. TRPN contains a long N-terminal anicrine repeat domain compared with other TRP channels (Hehlert et al., 2025). These anicrine repeats in TRPN are located in the cytoplasm and transmit mechanical force from the intracellular skeleton, microtubules, to gated channels (Wen et al., 2025). The NompC (no mechanoreceptor potential C) channel, belonging to the TRPN subfamily, is crucial for the movement of Drosophila melanogaster adults and larvae. The movements of nompC gene mutant adults are uncoordinated, and larvae exhibit defective behavior toward gentle touch. NompC is also required for hearing, so TRPN is the primary mechanotransducer channel (Wang et al., 2019).

2.5 TRPA (Transient Receptor Potential Ankyrin) Channels

TRPA1, the only member of the TRPA subfamily, is a non-selective, Ca^{2+} permeable cation channel. It is distinguished from other TRP channels by the 16 anicrine repeats in the N-terminal region (Coluzzi et al., 2025). Although TRPA1 has been described as a nonselective cold-sensitive cation channel, it is widely agreed that it functions as a ligand-gated channel in expression systems and sensory neurons. The active components of garlic (allicin) and mustard oil (allyl isothiate) potently activate TRPA1 permeability (Ramsey et al., 2006). It is expressed in tissues such as trigeminal ganglion neurons and dorsal root ganglia in the brain, skeletal muscle, bladder, small intestines, inner ear, cardiovascular structures, skeletal muscles and odontoblastocytes. It has also been found to be expressed in pancreatic, colon, prostate, breast, nasopharyngeal and oral carcinomas. It has been observed that increased TRP expression in malignant osteosarcoma reduces metastasis and improves the prognosis of the disease (Coluzzi et al., 2025).

2.6 TRPP (Transient Receptor Potential Polycystic) Channels

TRPP channels, a sub-member of the TRP superfamily, are non-selective cation channels that have been characterized for their role in polycystic kidney disease in vertebrates. TRPPs function as mechanosensors and Ca^{2+} permeable cation channels, contributing to cellular ion homeostasis and mechanotransduction. (Paschapur et al., 2025). They sense environmental mechanical forces such as flexion, tension, and synovial fluid shear stress and induce a series of signaling pathways involved in osteogenesis (Katsianou et al., 2018). TRPP members also perceive the cold (Qian et al., 2024). The TRPP subfamily contains three members, TRPP1, TRPP2, and TRPP3. TRPP1 is expressed primarily in the kidney and is associated with dominant autosomal polycystic kidney disease. TRPP2, which is expressed at the highest level in fetal tissues, is expressed in the brain, heart, spleen, skeletal muscle, retina, testis and tongue in adult animals. The TRPP2 channel is activated at low pH and by citric acid. Mice with mutant TRPP2 genes cannot perceive sour taste. Mice with a deletion in the TRPP2 gene locus have kidney and retinal defects. TRPP3, which is widely expressed in fetal tissue, is expressed primarily in the testes of adult mice. It is a putative Ca^{2+} channel and plays a role in Ca^{2+} homeostasis (Gees et al., 2012).

2.7 TRPML (Transient Receptor Potential Mucolipin) Channels

TRPML channels, which are members of the TRP superfamily and are nonselective ion channels, are secreted as heterodimers or homodimers in endosomal or lysosomal membranes. These channels consist of three members (TRPML1, TRPML2 and TRPML2), also known as mucolipins (Alibrandi et al., 2025). TRPML channels, which are involved in the regulation of cell membrane traffic, fusion/fission events, autophagy, hormone secretion, exocytosis, regulation of endolysosomal pH, vesicle degradation and autophagy, differ from other channels by being expressed on the endosomal surface (Alibrandi et al., 2025; Grimm et al., 2014). The main Ca^{2+}, zinc and iron permeable channels on late endosomes and lysosomes (Hirschi et al., 2017; Rohacs, 2024). TRPML1 plays a role in Ca^{2+} signaling in lysosomes, lipid trafficking, and autophagic processes. Although TRPML1 is expressed ubiquitously, it is particularly expressed in the brain, kidney, liver, spleen, and heart. (Alibrandi et al., 2025). Mucolipidosis type IV (MLIV), a neurodegenerative disorder, is observed in TRPML1 gene mutants (Fine et al., 2018). Although the exact functions of TRPML2 channels, which are permeable to Ca^{+2}, Na^{+} and Fe^{+2}' ions, are not known, it is thought that they play a key role in the release of calcium from intracellular acidic stores into the cytoplasm. Its widespread expression in lymphocytes and other immune cells suggests that it also plays a role in immunity. TRPML2 may also play a role in endocytosis and exocytosis homeostasis (García-Añoveros et al., 2014). TRPML3 is activated by PI(3,5)P2 (phosphatidylinositol 3,5-bisphosphate) and PI(3)P (phosphatidylinositol 3 phosphate) in *Drosophila* (Rohacs, 2024). TRPML3 is expressed primarily in sensory neurons, the sensory hair cells of Corti, and the stria vascularis region of the cochlea. Gain-of-function mutations cause vestibular deficits, hearing loss, and circling behavior in mice (Alibrandi et al., 2025; Grimm et al., 2014).

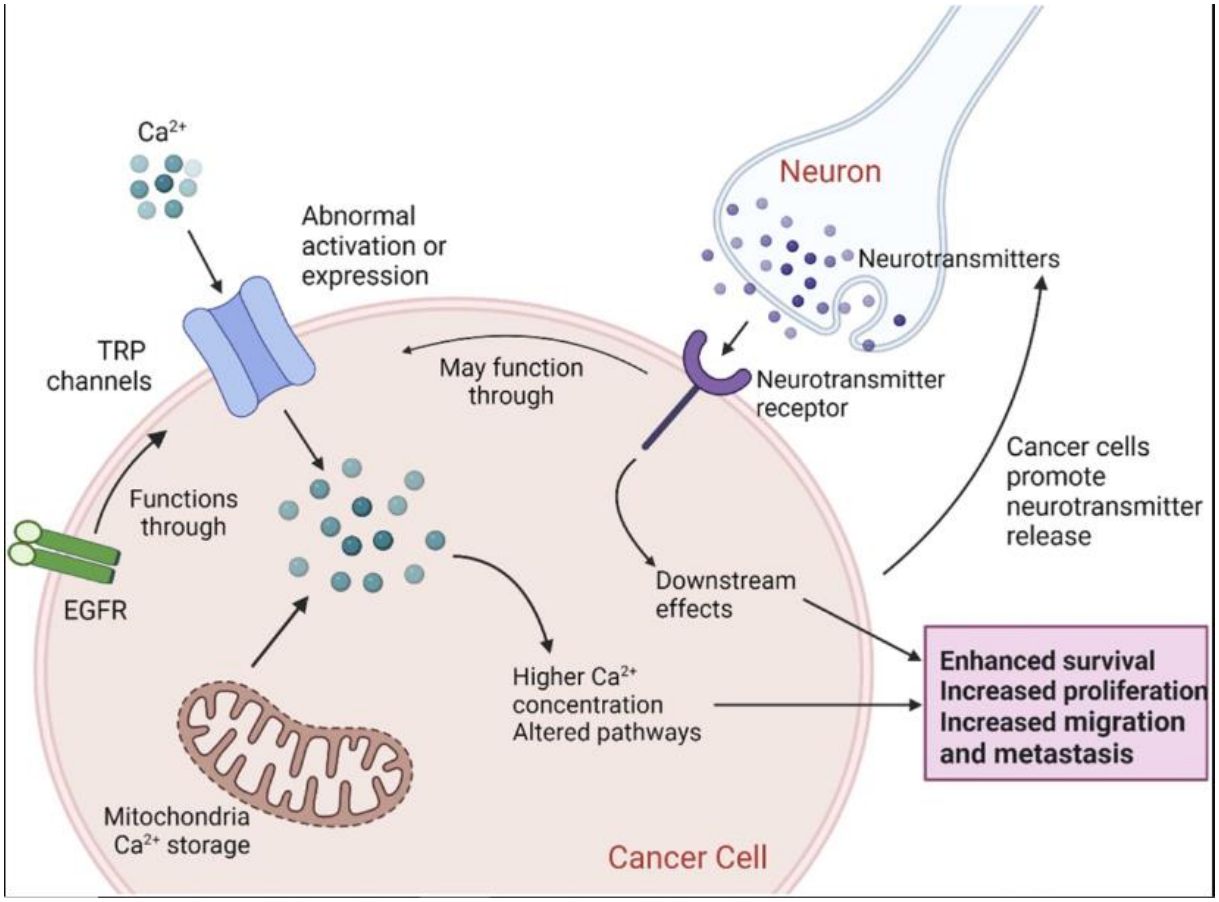

Figure 3. TRP channels are closely related to the survival, proliferation, invasion and metastasis of malignant cells. Neurotransmitters also play a key role in this process (Xu et al., 2024).

3. COLON CANCER FORMATION MECHANISM

Colorectal cancer (CRC) occurs as a result of multiple genetic and epigenetic alterations via the following pathways: chromosomal instability pathway (CIN), microsatellite instability pathway (MSI), CpG island hypermethylation, and serrated pathway (figure 4) (Hossain et al., 2022; (Roper and Hung, 2013).

The chromosomal instability (CIN) pathway is characterized by chromosome segregation, telomere instability, and DNA errors and is the most common condition in CRC formation (Roper and Hung, 2013). The classical

CIN pathway in CRC is induced by the occurrence and accumulation of mutations in the genes of adenomatous polyposis coli (APC) and proteins that activate the Wnt pathway (Tariq and Ghias, 2016). Normally, the APC gene encodes a tumor suppressor protein that blocks the negative effects of the Wnt signaling pathway during the transition from the G1 phase of the cell cycle to the S phase. APC gene mutation can affect the growth of intestinal epithelial cells and lead to the formation of adenomas (Chen et al., 2024). Following APC gene mutation, mutational activation of the oncogene KRAS and inactivation of p53, a tumor suppressor gene involved in the cell control loop, occur. Heterozygosity and aneuploidy are the main characteristics of CIN tumors (Tariq and Ghias, 2016).

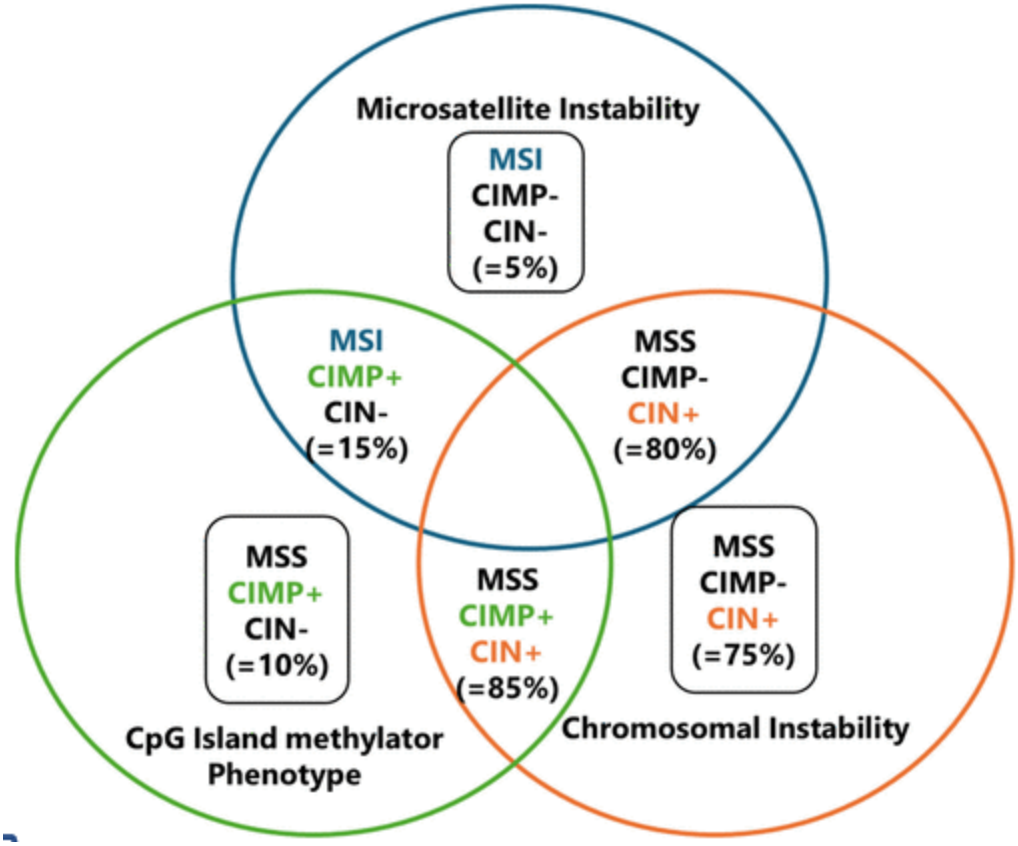

Figure 4. Three main pathways in colon cancer development: Chromosomal instability pathway (CIN), Microsatellite instability (MSI), CpG island Methylator Phenotype (CIMP) (Paraskar et al., 2025).

The microsatellite instability pathway (MSI) in CRC pathogenesis results from mutations in DNA mismatch repair genes that correct DNA replication errors. Mutations that may render the hMSH2, hMSH3, hMSH6, hMLH1, hMLH3h, hPMS1 and PMS2 ATPase genes in the DNA mismatch repair system dysfunctional lead to a predisposition to cancer. Fifteen percent of all colorectal cancer cases are associated with MSI and three percent with *Lynch syndrome* (Tariq and Ghias, 2016). *Lynch syndrome*, the first cancer syndrome to be diagnosed, is an autosomal dominant predisposition to colorectal, endometrial, and other cancers caused by mutations in the MSH6, PMS2, MLH1, and MSH2 mismatch repair genes. Patients with *Lynch Syndrome* have an 80% chance of developing CRC during their lifetime. (Raskov et al., 2014).

CpG island methylator phenotype (CIMP), described as a different pathway of tumorigenesis by Toyota et al in 1999, is genome hypermethylation caused by mutational shut-down of tumor suppressor genes (Toyota et al., 1999). CIMP is a sub-pathway for colorectal carcinogenesis that results in the inactivation of various tumor suppressor genes by hypermethylation of Cpg islands located in the promoter region outside the opening reading frame of the gene (Mojarad et al., 2013). Silencing of mismatch repair factor MLH1 expression together with DNA methylation also plays a role in CRC. Also suppression of cell-cell adhesion factor CDH1 (E-cadherin) together with DNA methylation may promote invasion and metastasis. In addition, genome-wide hypomethylation is another characteristic feature found in CRC cells. This hypomethylation state causes chromosome instability and hence inhibition of imprinted genes and retrotransposable genes and aberrant gene expression (Wang et al., 2025).

Another development of CRC, which occurs in 15%, is serrated polyps via serrated neoplasia. Sawtooth polyps constitute a heterogeneous group of colorectal lesions that include sessile sawtooth adenoma (SSA), conventional sawtooth adenoma (TSA), hyperplastic polyps (HPs), and mixed polyps. TSA and SSA, which are highly associated with CRC, are prone to malignancy, whereas hyperplastic polyps are not malignant (Chen et al., 2024). The most common genetic alterations in serrated lesions are BRAF and KRAS mutations(figure5). Both BRAF and KRAS contain sequences of kinases belonging to the mitogen-activated protein kinase (MAPK) metabolic pathway, which plays a role in apoptosis, cell division and differentiation. Mutations occurring through nucleotide changes in the bras and kras genes cause cell proliferation, invasion, and metastasis via induction of the MAPK pathway in precursor serrated lesions and serrated adenocarcinomas (Yamane et al., 2014).

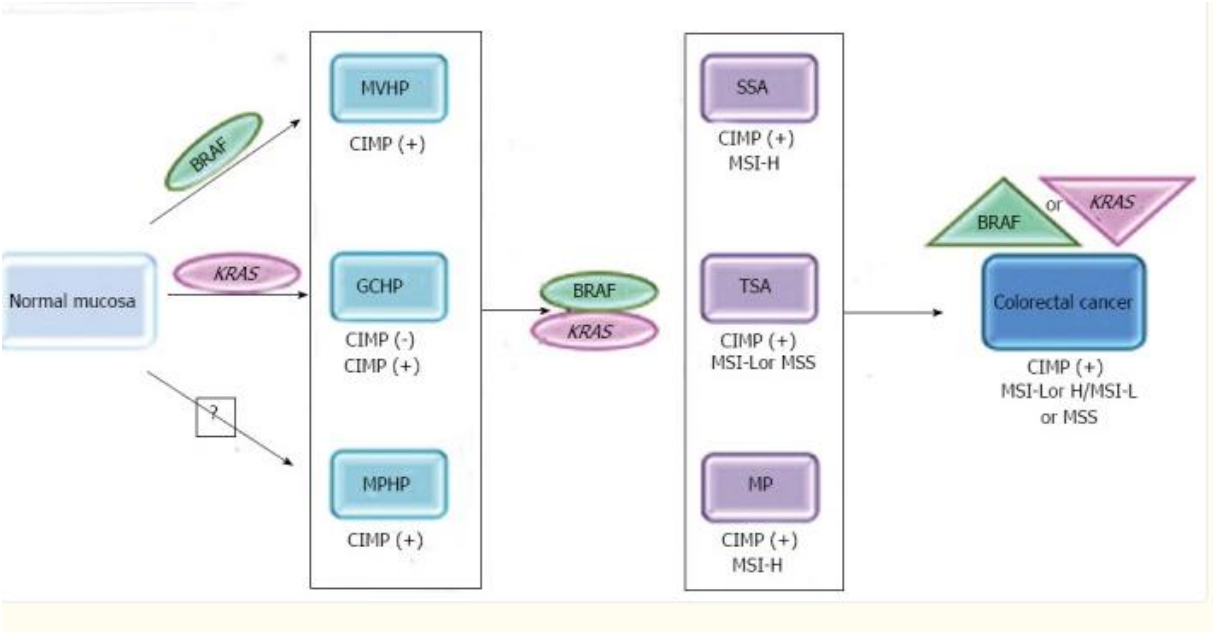

Figure 5. The most common alterations seen in colorectal carcinogenesis include BRAF and KRAS mutations. MVHP: Microvesicular hyperplastic polyp; GCHP: Globet cell hyperplastic polyp; MPHP: Mucin-poor hyperplastic polyp; SSA: Sessile serrated adenoma; TSA: Traditional serrated adenoma; MP: Mixed polyp; MSI-H: High microsatellite instability; CIMP: CpG island methylation phenotype (Yamane et al., 2014).

4. KOLON KANSERİNDE TRP İFADELERİ VE ROLLERİ

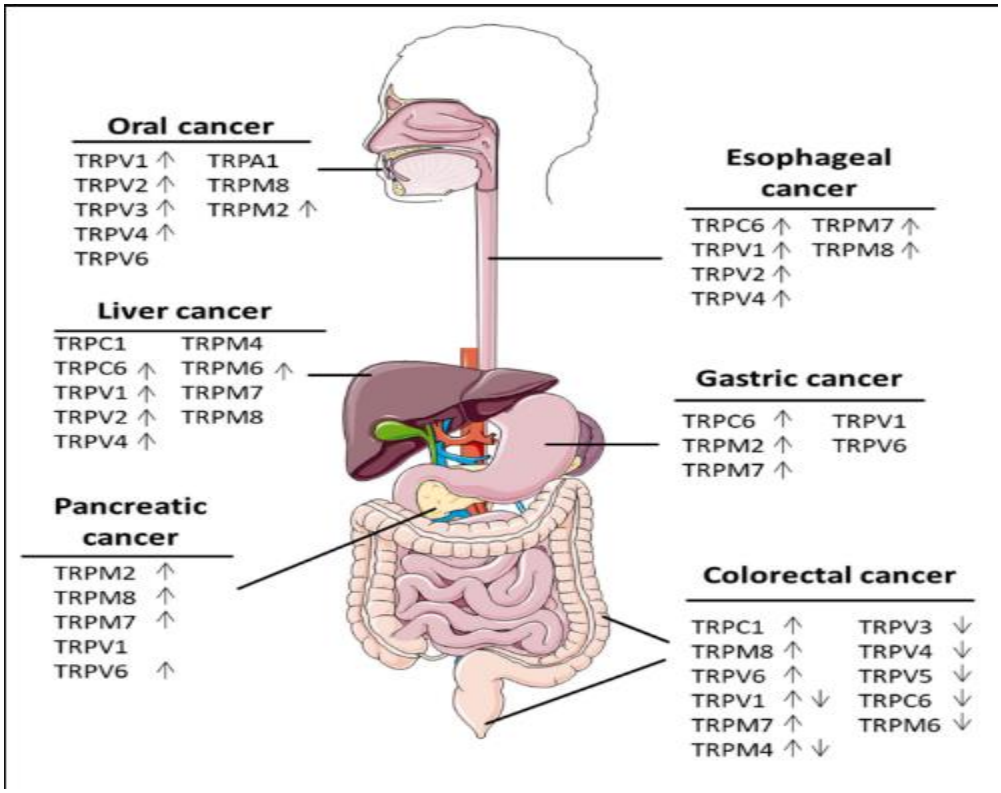

Figure 6. Increase (↑) and decrease (↓) of TRP expression in various cancer cases in the gastrointestinal tract (Stokłosa et al., 2020).

TRP channels, which are strongly associated with the development and progression of CRC, are considered potential therapeutic targets because the death signaling mechanisms required for cell proliferation and apoptosis are regulated by increased intracellular free calcium ion (Mavioğlu Kaya, 2024). TRP proteins have key roles in the activation of epithelial-mesenchymal transition by regulating intracellular and extracellular Ca^{2+} ion concentrations and matrix stiffness via matrix metalloproteinases (MMPs), activation of the PI3/AKT metabolic pathway and extracellular matrix (ECM) remodeling driven by Ca^{2+} ion concentration. (Hu et al., 2023).

Metabolites with high oxidative capacity play a role in intracellular signaling, including Ca^{+2} signaling. It is known that reactive oxygen species play a role in the emergence of cancer by damaging double-stranded DNA and inducing high amounts of ADP-ribose (ADPR) synthesis. Cancer cells have high levels of cytosolic reactive oxygen species (cyROS) because they obtain their energy from aerobic glycolysis (Warburg effect). In malignant cases, a positive correlation has been found between the increased amount of Ca^{+2} entering the cell through both ROS and channels belonging to the TRP family and cancer cell proliferation. (Mavioglu Kaya et al., 2023).

Tumorgenesis involves altered expression of one or more TRPs, depending on the type of cancer. The most characteristic changes are seen in the expression of TRPM8, TRPV6 and TRPM1. TRPM8, which is overexpressed in human colon tumors, is almost not expressed in normal tissues. In addition, the amount of TRPV6 protein expression is overly increased in colon carcinomas. Again, increased TRPV1 expression levels have been found to be associated with colon cancer, and its activation by polyamines contributes to cancer pain (Prevarskaya et al., 2007). According to the study conducted by Wang et al., TRPV1 mRNA expression level increased (Wang et al., 2025). Similarly, it was stated that TRPV1 and TRPV2 protein expression levels were significantly increased in the distal colon tissues of colitis-induced rats (Dvornikova et al., 2024). However, in another study, it was determined that the expression of TRPV1, which is expressed in high amounts in the intestinal mucosa, was decreased in ulcerative colitis cases associated with CRC cases (Du et al., 2022). In colon cancer, overexpression of TRPC5 is observed to reduce patient survival by inducing cell proliferation, invasion and metastasis. While downregulation of TRPM6 expressed in healthy colon tissues is seen in 80% of colorectal cancer cell tumors, high expression increases patient survival. The cancer genome atlas revealed that downregulation of TRPML3/MCOLN3 in colon cancer is associated with improved survival (Marini et al., 2023). Benzer şekilde kolon kanserinde TRPM2 ve TRPM7 ifadeleri aşağı regüle edilmektedir (Anderson et al., 2019). However, it has been reported that TRPM2 expression is increased in the distal colons

of rats with colitis and that TRPM2-deficient mice recover in mice in which colitis is induced with dextran sulfate sodium (DSS) (Du et al., 2022). In their study, it was found that TRPV3, TRPV4, TRPV5, TRPM4 and TRPC6 expression levels were decreased in CRC and this contributed to tumorigenesis (Sozucan et al., 2015). However, it has also been found that TRPV4 protein expression levels were increased in the colon tissue of patients with irritable bowel syndrome (Du et al., 2022). Similarly, Ren and colleagues found that TRPV4 expression levels were overly increased in colon cancer tissues (Ren et al., 2025). Liu and colleagues reported in their studies on both humans and cell lines that TRPA1 expression was decreased and TRPM5 expression was increased in CRC cases, and that this situation was negatively correlated with the prognosis of the patient (Liu et al., 2024). However, it was found that TRPA1 and TRPC1 immunoreactivities in colon tissue of patients diagnosed with colorectal adenocarcinoma (Bozdag et al., 2024) and TRPA1 expression levels in both cell line and mouse colon tissues were overly increased compared to the control group (Zhou et al., 2025).

5. CONCLUSION

TRP channels are multifunctional sensors that perceive chemical and physical stimuli from environmental factors. Not only colon cancer, but also an increasing number of pathological conditions are associated with mutations or changes in TRP channel activitiesThe status of some TRP family members in colon cancer cases is still unclear. However, there are differences in the results of some TRP expression levels from study to study. Although the results are controversial, TRP channels are exciting targets for drug development and improving the pathogenesis of the disease in CRC (figüre 6). More detailed molecular and metabolic studies are required to determine the molecular properties of TRP channels, their tissue-specific functions, and new agonists and antagonists.

REFERENCES

Alibrandi, S., Rinaldi, C., Vinci, S. L., Conti, A., Donato, L., Scimone, C., ... & D'Angelo, R. (2025). Mechanotransduction in Development: A Focus on Angiogenesis. Biology, 14(4), 346.

Anderson, K. J., Cormier, R. T., & Scott, P. M. (2019). Role of ion channels in gastrointestinal cancer. World Journal of Gastroenterology, *25*(38), 5732.

Bozdag, A., Kuloglu, T., Artas, G., & Aydin, S. (2024). Investigation of Trpa1 and Trpc1 Immunreactivities in Colon Adenocarcinomas. Cancer Management and Research, 377-384.

Bödding, M. (2007). TRP proteins and cancer. Cellular signalling, *19*(3), 617-624.

Chen, X., Ding, Y., Yi, Y., Chen, Z., Fu, J., & Chang, Y. (2024). Review of animal models of colorectal cancer in different carcinogenesis pathways. Digestive Diseases and Sciences, *69*(5), 1583-1592.

Chubanov, V., Köttgen, M., Touyz, R. M., & Gudermann, T. (2024). TRPM channels in health and disease. Nature Reviews Nephrology, 20(3), 175-187.

Coluzzi, F., Scerpa, M. S., Alessandri, E., Romualdi, P., & Rocco, M. (2025). Role of TRP Channels in Cancer-Induced Bone Pain. International Journal of Molecular Sciences, 26(3), 1229.

Demir, S., Duman, İ., & Nazıroğlu, M. (2024). Botulinum nörotoksin A ve oksaliplatinin TRPM2 kanal aracılı oksidatif stresin yukarı regülasyonu yoluyla kolorektal tümör hücre ölümü üzerindeki sinerjik etkileri. Klinik ve Deneysel Farmakoloji ve Fizyoloji, 51(4), e13844.

Du, Y., Chen, J., Shen, L., & Wang, B. (2022). TRP channels in inflammatory bowel disease: Potential therapeutic targets. Biochemical Pharmacology, *203*, 115195.

Duan, X., Liu, R., Xi, Y. ve Tian, Z. (2025). Piezo1 ve TRP iyon kanallarını uyararak kardiyovasküler fonksiyonu iyileştiren egzersiz mekanizmaları: sistemik bir inceleme. *Moleküler ve Hücresel Biyokimya* , *480* (1), 119-137.

Dvornikova, K. A., Platonova, O. N., & Bystrova, E. Y. (2024). The role of TRP channels in sepsis and colitis. International Journal of Molecular Sciences, *25*(9), 4784.

Fine, M., Schmiege, P., & Li, X. (2018). Structural basis for PtdInsP2-mediated human TRPML1 regulation. Nature Communications, *9*(1), 4192.

García-Añoveros, J., & Wiwatpanit, T. (2014). TRPML2 and mucolipin evolution. Mammalian Transient Receptor Potential (TRP) Cation Channels: Volume I, 647-658.

Gees, M., Owsianik, G., Nilius, B., & Voets, T. (2012). TRP channels. Comprehensive physiology, 2(1), 563-608.

Grimm, C., Barthmes, M., & Wahl-Schott, C. (2014). Trpml3. Mammalian Transient Receptor Potential (TRP) Cation Channels: Volume I, 659-674.

Hehlert, P., et al. (2025). NOMPC ion channel hinge forms a gating spring that initiates mechanosensation. Nature Neuroscience, 1-9.

Hirschi, M., Herzik Jr, M. A., Wie, J., Suo, Y., Borschel, W. F., Ren, D., & Lee, S. Y. (2017). Cryo-electron microscopy structure of the lysosomal calcium-permeable channel TRPML3. Nature, *550*(7676), 411-414.

Hossain, M. S., Karuniawati, H., Jairoun, A. A., Urbi, Z., Ooi, D. J., John, A., & Hadi, M. A. (2022). Colorectal cancer: a review of carcinogenesis, global epidemiology, current challenges, risk factors, preventive and treatment strategies. Cancers, 14(7), 1732.

Hu, W., et al. (2023). Transient receptor potential channels as predictive marker and potential indicator of chemoresistance in colon cancer. Oncology Research, 32(1), 227.

Katsianou, M. A., Skondra, F. G., Gargalionis, A. N., Piperi, C., & Basdra, E. K. (2018). The role of transient receptor potential polycystin channels in bone diseases. Annals of Translational Medicine, 6(12), 246.

Kaya, M. M. (2024). Silver nanoparticles stimulate 5-fluorouracil-induced colorectal cancer cells to kill through the upregulation TRPV1-mediated calcium signaling pathways. Cell Biology International, 48(5), 712-725.

Kaya, M. M., Kaya, İ., & Nazıroğlu, M. (2023). Transient receptor potential channel stimulation induced oxidative stress and apoptosis in the colon of mice with colitis-associated colon cancer: modulator role of Sambucus ebulus L. Molecular Biology Reports, 50(3), 2207-2220.

Liu, Y., Yao, X., Zhao, W., Xu, J., Zhang, H., Huang, T., & Wang, Q. (2024). A comprehensive analysis of TRP-related gene signature, and immune infiltration in patients with colorectal cancer. *Discover Oncology*, *15*(1), 357.

Marini, M., Titiz, M., Souza Monteiro de Araújo, D., Geppetti, P., Nassini, R., & De Logu, F. (2023). TRP channels in cancer: signaling mechanisms and translational approaches. Biomolecules, *13*(10), 1557.

Mojarad, E. N., Kuppen, P. J., Aghdaei, H. A., & Zali, M. R. (2013). The CpG island methylator phenotype (CIMP) in colorectal cancer. Gastroenterology and hepatology from bed to bench, *6*(3), 120.

Nilius, B., & Owsianik, G. (2011). The transient receptor potential family of ion channels. Genome biology, *12*, 1-11.

Paraskar, G., Bhattacharya, S., & Kuttiappan, A. (2025). The Role of Proteomics and Genomics in the Development of Colorectal Cancer Diagnostic Tools and Potential New Treatments. ACS Pharmacology & Translational Science, 8(5), 1227-1250.

Paschapur, A. U., Manoj, M. S., Pavan, J. S., & Subramanian, S. (2025). Exploiting TRP channel diversity in insects: a pathway to next-generation pest management. Archives of Toxicology, 1-21.

Prevarskaya, N., Zhang, L., & Barritt, G. (2007). TRP channels in cancer. Biochimica et Biophysica Acta (BBA)-Molecular Basis of Disease, 1772(8), 937-946.

Qian, Y., Yu, Q., Zhang, J., Han, Y., Xie, X., & Zhu, D. (2024). Identification of transient receptor potential channel genes from the swimming crab, Portunus Trituberculatus, and their expression profiles under acute temperature stress. BMC genomics, 25(1), 72.

Ramsey, I. S., Delling, M., & Clapham, D. E. (2006). An introduction to TRP channels. Annual review of physiology, 68(1), 619-647.

Raskov, H., Pommergaard, H. C., Burcharth, J., & Rosenberg, J. (2014). Colorectal carcinogenesis-update and perspectives. World journal of gastroenterology: WJG, *20*(48), 18151.

Ren, X., Chen, W., Liu, Y., Chen, Z., Wang, X., & Sun, X. (2025). TRPV4 as a Novel Regulator of Ferroptosis in Colon Adenocarcinoma: Implications for Prognosis and Therapeutic Targeting. Digestive Diseases and Sciences, 1-14.

Rizopoulos, T., & Assimakopoulou, M. (2021). Transient receptor potential (TRP) channels in human colorectal cancer: evidence and perspectives. 36(5), 515-526.

Rohacs, T. (2024). Phosphoinositide regulation of TRP channels: A functional overview in the structural era. Annual Review of Physiology, *86*(1), 329-355.

Roper, J., & Hung, K. E. (2013). Molecular mechanisms of colorectal carcinogenesis. Molecular Pathogenesis of Colorectal Cancer, 25-65.

Sozucan, Y., et al. (2015). TRP genes family expression in colorectal cancer. Experimental oncology.

Stefani, C., Miricescu, D., Stanescu-Spinu, I. I., Nica, R. I., Greabu, M., Totan, A. R., & Jinga, M. (2021). Growth factors, PI3K/AKT/mTOR and MAPK signaling pathways in colorectal cancer pathogenesis: where are we now? International journal of molecular sciences, 22(19), 10260.

Stokłosa, P., Borgström, A., Kappel, S., & Peinelt, C. (2020). TRP channels in digestive tract cancers. International journal of molecular sciences, *21*(5), 1877.

Sun, Y., et al. (2021). TRPC1 promotes the genesis and progression of colorectal cancer via activating CaM-mediated PI3K/AKT signaling axis. Oncogenesis, *10*(10), 67.

Tariq, K., & Ghias, K. (2016). Colorectal cancer carcinogenesis: a review of mechanisms. Cancer biology & medicine, *13*(1), 120-135.

Toyota, M., Ahuja, N., Ohe-Toyota, M., Herman, J. G., Baylin, S. B., & Issa, J. P. J. (1999). CpG island methylator phenotype in colorectal cancer. Proceedings of the National Academy of Sciences, 96(15), 8681-8686.

Wang, L., Li, Q., Leung, L. K., & Wong, W. T. (2025). Licorice Extract Isoliquiritigenin Increased Cytosol Calcium and Induced Apoptosis in Colon Cancer Cells via Transient Receptor Potential Vanilloid-1. Cancer Medicine, 14(5), e70705.

Wang, L. X., et al. (2019). The NompC channel regulates Nilaparvata lugens proprioception and gentle-touch response. Insect Biochemistry and Molecular Biology, 106, 55-63.

Wang, Q., Ma, C., Yang, B., Zheng, W., Liu, X., & Jian, G. (2025). Dysregulation of DNA methylation in colorectal cancer: biomarker, immune regulation, and therapeutic potential. *International Immunopharmacology*, *145*, 113766.

Wen, X., et al. (2025). Molecular Insights Into the Sensory Adaption of the Cave-Dwelling Leech Sinospelaeobdella wulingensis to the Karst Cave Environment. Ecology and Evolution, *15*(1), e70877.

Xu, J., Wang, Z., Niu, Y., Tang, Y., Wang, Y., Huang, J., & Leung, E. L. H. (2024). TRP channels in cancer: Therapeutic opportunities and research strategies. Pharmacological Research, 107412.

Xu, L., Zhang, Y., Wang, H., Zhang, G., Ding, Y. ve Zhao, L. (2014). Tümör baskılayıcı miR-1, MAPK ve PI3K/AKT yoluyla kolorektal karsinomun epitel-mezenkimal geçişini ve metastazını kısıtlar. Translasyonel Tıp Dergisi, 12, 1-12.

Yamane, L., Scapulatempo-Neto, C., Reis, R. M., & Guimarães, D. P. (2014). Serrated pathway in colorectal carcinogenesis. World journal of gastroenterology*: WJG*, *20*(10), 2634.

Zhang, K., Luan, G., Liu, W., Shen, F., Jiang, M. ve Bai, G. (2025). Ligustilide, kolon dokusunda TRPA1'i kovalent olmayan şekilde aktive ederek fonksiyonel kabızlığı iyileştirir. Ethnopharmacology Dergisi, *338*, 119018.

Zhang, M., Ma, Y., Ye, X., Zhang, N., Pan, L., & Wang, B. (2023). TRP (transient receptor potential) ion channel family: structures, biological functions and therapeutic interventions for diseases. Signal Transduction and Targeted Therapy, *8*(1), 261.

Zhou, L., Zhou, G., Li, J., Guo, R., & Dong, H. (2025). NCX1 interacts with TRPA1 to promote cell proliferation and tumor growth of colon cancer via disruption of calcium homeostasis. Journal of Advanced Research. https://doi.org/10.1016/j.jare.2025.02.031

➢ *ORAL PRESENTATION*

Voltage Regulation Analysis with PV System Integration: A Campus Distribution Network Case Study

Berk Tuncer[1*] (*ORCID:https://orcid.org/0009-0001-8916-5623*), Engin Cetin[1] (*ORCID: https://orcid.org/0000-0002-0368-3631*)

[1]Pamukkale University, Engineering Faculty, Electrical-Electronics Engineering, Denizli, Turkey.

*Corresponding author e-mail: btuncer@pau.edu.tr

Abstract
This study develops a detailed DIgSILENT PowerFactory model of the Pamukkale University Kınıklı Campus electrical distribution network using actual field data and evaluates voltage regulation strategies at the common connection bus following the installation of a 370 kW nominal AC output power photovoltaic (PV) system at the Müh. F. (A) transformer substation. Campus power is delivered at 31.5 kV from the Denizli-4 380 TM substation and stepped down to 0.4 kV by multiple transformers before distribution. In the network model, transformer substations and loads on three feeders branching from the main MV bus are included, with loads scaled and assumed to have constant power factors. A series of scenarios assessed the combined effects of transformer tap-changer adjustments, a switchable capacitor bank, PV inverter reactive-power support at a 0.9 leading power factor, and a 350 kVA energy storage unit. Under both light and heavy loading, transformer tap adjustments alone held voltage within acceptable limits but achieved only modest loss reduction. Adding the switchable capacitor bank further improved voltage profiles under maximum load and reduced losses. When PV generation peaked, the PV system relieved transformer loading, raised bus voltage, and reduced losses. Enabling reactive-power support from the PV inverter helped maintain voltage regulation under varying load conditions. Finally, integrating the energy storage system—enabling control of both active and reactive power—improved voltage regulation, reduced transformer and line loading percentages, and minimized total losses more effectively than any single measure. An interior-point Optimal Power Flow (OPF) approach was used to optimize all control variables simultaneously under voltage and loading constraints. The results demonstrate that this integrated OPF strategy provides an effective solution for voltage regulation and loss minimization in distribution networks with high PV penetration. Future work can incorporate dynamic load and generation profiles, additional distributed generation types, and economic analyses.

Keywords: Voltage Regulation, Volt/Var Control, Optimal Power Flow, PV Systems, DIgSILENT PowerFactory.

INTRODUCTION

In conventional distribution networks, distribution transformer substations are assumed to serve as the sole power source for the entire feeder, leading to a gradual voltage decline from the substation to the end of the line. Voltage regulation in power systems is predominantly achieved through reactive power control; accordingly, equipment that provides voltage support is required to maintain acceptable voltage levels. At the substation, on-load tap changer (OLTC) transformers are typically employed to adjust feeder voltages under load. Along the feeder, capacitor banks, shunt reactors, and advanced FACTS-based devices such as STATCOM and SVC are deployed to further regulate voltage. In medium-voltage (MV) and low-voltage (LV) networks, the increasing penetration of distributed generation sources (DGS) is reshaping traditional grid architecture, and this transformation is expected to significantly influence the development of future systems. In particular, the widespread integration of PV systems has given rise to issues such as voltage fluctuations and reverse power flows. Under these conditions, maintaining voltage regulation has become a critical priority for distribution system operators (DSOs). As an alternative to conventional methods, the provision of reactive power support from DGS units has emerged in recent years as a leading strategy for preserving voltage regulation (Uluski 2011; Emiroğlu 2017; Almeida et al., 2021; Bektaş 2023; Köroğlu 2024).

When the load-side demand in the network exceeds the power supplied by distributed generation sources (DGS), the voltage at the point of common coupling (PCC) declines substantially; conversely, when demand is lower than generation, reverse power flow occurs, causing a significant rise in PCC voltage. These deviations violate the voltage limits specified by relevant standards (Almeida et al., 2021). Distribution companies can reduce downward voltage deviations (< 1 pu) using conventional reactive power compensation methods, whereas interventions for upward deviations (> 1 pu) remain severely constrained (Köroğlu, 2024).

In traditional distribution networks, voltage control equipment such as OLTC transformers and shunt capacitors face challenges due to their high installation costs, slow response times, and limited adjustment capability. These limitations make them insufficient to effectively manage the rapidly increasing penetration of distributed generation sources. As PV systems, electric vehicle charging units, and energy storage systems become increasingly common, distribution system operators require faster and more flexible voltage control methods to maintain acceptable voltage levels and reduce network losses (Emiroğlu, 2017; Bektaş, 2023). In this context, Volt/Var control (VVC) and smart grid-based Volt/Var optimization (VVO) solutions have gained prominence. VVC algorithms use measurements from substations and feeders to coordinate capacitor banks, voltage regulators, and LTC transformers, maintaining bus voltages and reactive power flows at targeted levels. By including smart inverters, energy storage units, and electric vehicle charging infrastructure in these algorithms, the grid achieves quicker and more effective reactive power control. Field studies have demonstrated that these modern approaches significantly improve voltage profiles, reduce critical line loadings, and decrease active power losses more economically compared to conventional methods. In summary, modern VVC/VVO methods offer an efficient and cost-effective alternative for distribution system operators managing networks with rapidly expanding renewable energy penetration (Manbachi et al., 2017; Alshehri and Yang 2024).

In the literature, numerous studies have been conducted on this topic. Some studies can be summarized as follows: (Borghetti et al., 2015) showed that mixed-integer linear programming methods could effectively achieve voltage regulation and loss minimization. (Emiroğlu, 2017) demonstrated that model predictive control and genetic algorithm-based VVO significantly improved energy efficiency and reduced energy consumption. (Eiriksson, 2017) highlighted the advantages of reactive power support from distributed generation sources compared to traditional methods, whereas (Kısakürek and Şekkeli, 2022) demonstrated that PV inverters enhanced voltage profiles and reduced the need for compensation investments. Bektaş (2023) indicated that integrating energy management systems with VVO is suitable for microgrid applications. (Aboshady et al., 2023) and (Dubravac et al., 2024), using OpenDSS and co-simulation approaches, showed that reactive power support provided by PV inverters positively impacted system performance. (Porwal et al., 2024) emphasized the effectiveness of genetic algorithm-based optimization in voltage regulation and loss reduction, and (Köroğlu, 2024), based on field data, demonstrated that reactive power support from PV plants is more effective than traditional compensation methods. In summary, innovative VVO methods, particularly involving PV inverter technologies, offer clear advantages over conventional approaches in voltage control and loss reduction in distribution networks.

In this study, the existing electrical distribution network of Pamukkale University Kınıklı Campus was modeled using actual field data in DIgSILENT PowerFactory software. Simulation studies were conducted under various scenarios to ensure voltage regulation at the bus connected to a newly installed PV system with a nominal power of 370 kW at the Müh. F. (A) Transformer Substation within the distribution network. To achieve voltage regulation by adjusting transformer and switchable capacitor bank reactive power value the Optimal Power Flow/Unit Commitment module of DIgSILENT PowerFactory was utilized. This module employs the interior-point method to perform optimal power flow using an objective function that minimizes total system losses subject to user-defined control variables and constraints.

EXAMPLE DISTRIBUTION SYSTEM MODEL

The electrical distribution system of the Pamukkale University Kınıklı Campus, previously used in the study by Tunçer and Çetin (2023), was selected as the example network model. Power is supplied to the campus at 31.5 kV from the Denizli 4-380 TM substation and is then stepped down to 0.4 kV via numerous transformers throughout the campus before being distributed. The network model was built using actual field data from the Denizli 4 TM substation to all end-user load points on campus. The single-line diagram of this network model in DIgSILENT is shown in Figure 1.

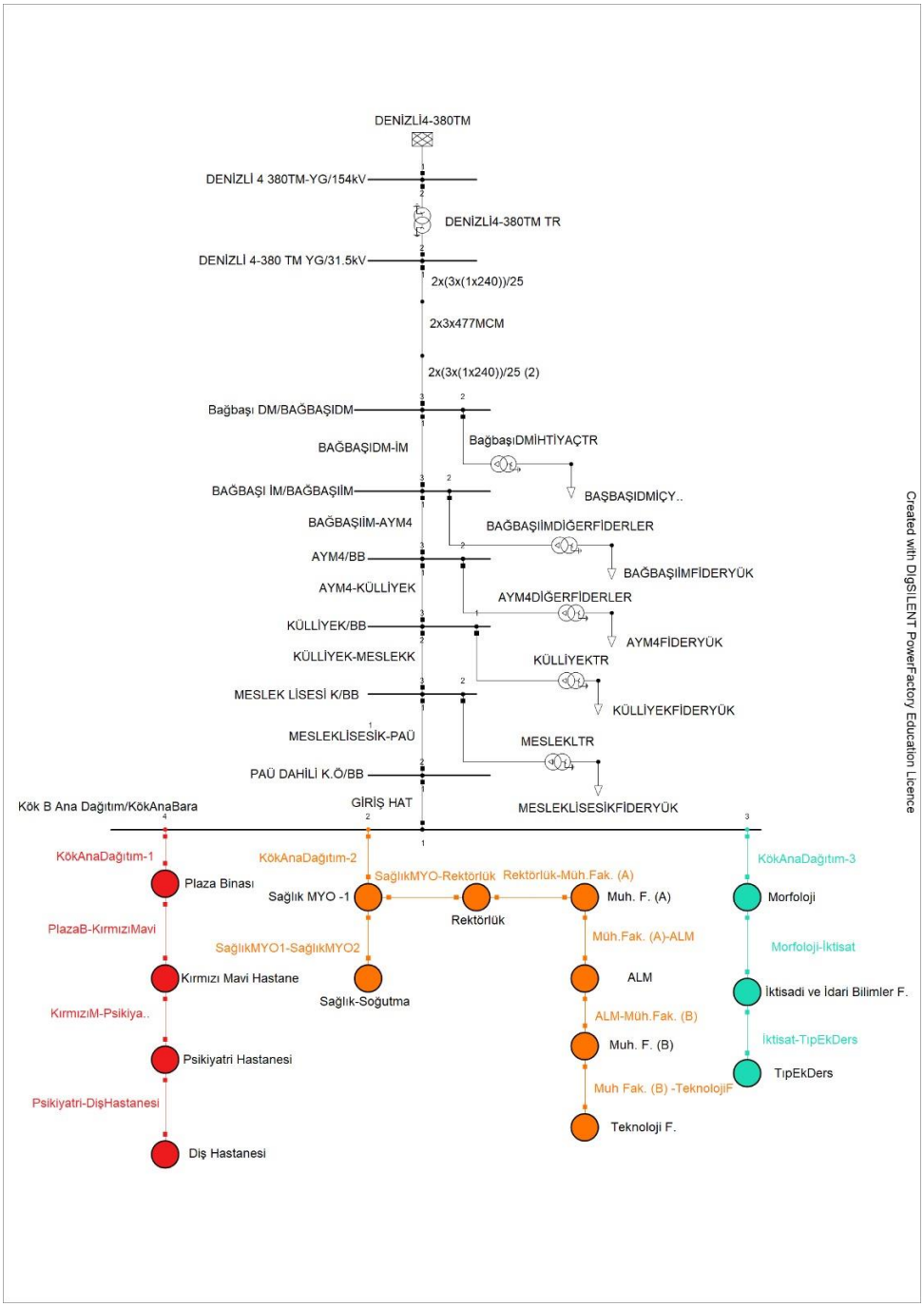

Figure 1. Pamukkale University Kınıklı Campus distribution system model in DIgSILENT

Starting from the Kök B main distribution line at the campus entry point, the network splits into three separate feeders. These feeders are named Kök Ana Dağıtım-1, Kök Ana Dağıtım-2, and Kök Ana Dağıtım-3, respectively. The technical specifications of the transformers in each feeder's substation are presented in Table 1, Table 2, and Table 3, respectively. All the transformers have a nominal voltage rating of 33 kV/0.4 kV, and the vector group of all transformers is Dyn11.

Table 1. Technical specifications of the transformers connected to feeder Kök Ana Dağıtım-1

Facility Name	Nominal Power (kVA)	Short Circuit Voltage ($\%u_k$)	Copper Losses (kW)
Kırmızı-Mavi Hastane-1	1600	6	16.5
Kırmızı-Mavi Hastane-2	1600	6	16.5
Plaza Binası-1	1600	6	16.5
Plaza Binası-2	1600	6	16.5
Plaza Binası-3	1600	6	16.5
Plaza Binası-4	1600	6	16.5
Psikiyatri Hastanesi	1000	5.75	9.9
Diş Hastanesi	630	4.28	5.4

Table 2. Technical specifications of the transformers connected to feeder Kök Ana Dağıtım-2

Facility Name	Nominal Power (kVA)	Short Circuit Voltage ($\%u_k$)	Copper Losses (kW)
Sağlık MYO	1250	6.05	12.9
Sağlık-Soğutma	1250	6.05	12.9
Rektörlük	1600	6.03	16.5
Müh. F. (A)	1600	6.07	16.3
ALM	1600	5.89	16.9
Müh F. (B)	1600	5.98	16.3
Teknoloji F.	1250	5.53	12.9

Table 3. Technical specifications of the transformers connected to feeder Kök Ana Dağıtım-3

Facility Name	Nominal Power (kVA)	Short Circuit Voltage ($\%u_k$)	Copper Losses (kW)
Morfoloji	2500	6	25
İktisadi ve İdari Bilimler F.	1000	6	12.2
Tıp F. Ek Ders	1250	6	14

During modeling, the loads from other feeder substations were also considered. The total apparent power transformer ratings (MVA) and loading conditions at these substations are presented in Table 4.

Table 4. Loading of the other feeders supplied by the transformer substations serving the Kınıklı Campus distribution system.

Substations	Total Apparent Power Transformer Ratings (MVA)	Total Load (MW)	Loading (%)
Bağbaşı DM	0.4	0.1	25.8
Bağbaşı İM	49.35	12.3375	25.8
Aym 4	32.2	8.0525	25.9
Külliye K	0.63	0.1575	26
Meslek Lisesi K	1	0.25	26

In the simulation study, voltage regulation analysis under various scenarios were conducted to prevent voltage issues at the bus where the newly installed PV system is connected to the Müh. F. (A) transformer substation within the campus. At the transformer substation, the LV cable used is 0.01 km long and of type 5× (1×240 mm²) NYY, while the distribution line is 0.25 km long and of type 3× (3×185/95) NYY. Figure 2 presents the DIgSILENT single-line diagram of the Müh. F. (A) transformer substation.

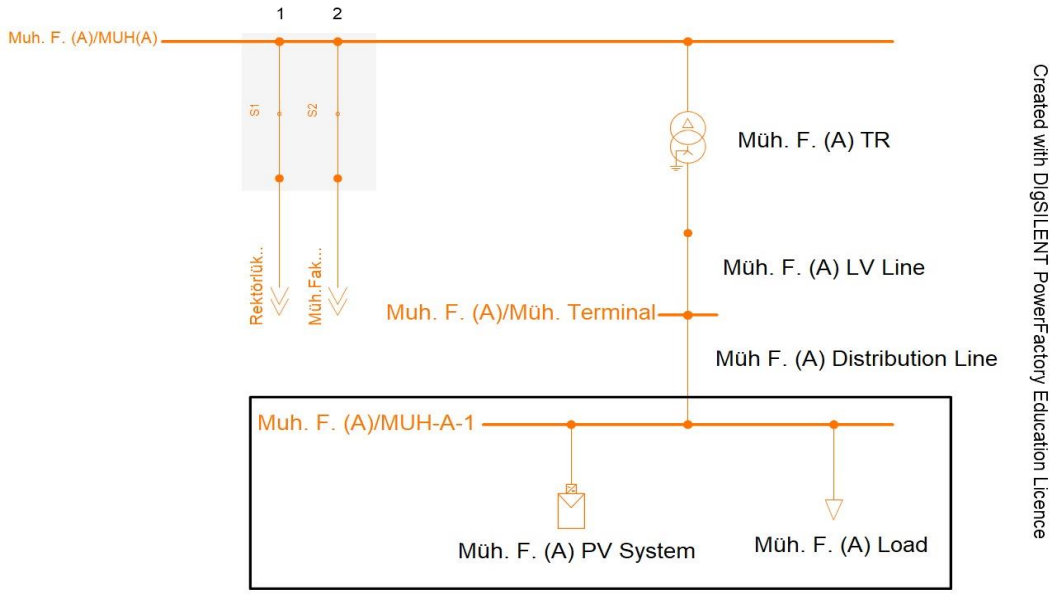

Figure 2. Müh. F. (A) transformer substation system model in DIgSILENT

Since there is no load monitoring system for transformer substations in the campus distribution network, transformer loading conditions were determined by scaling the feeder loads based on real data at the Kök B main-bus distribution point. The power factors of the loads connected to the transformers were assumed constant at 0.85 lagging. Except for the Müh. F. (A) transformer substation, the loads of the other transformer substations remain constant and are presented in the table below. The feeder load value for the Müh. F. (A) transformer substation, obtained through feeder load scaling, is shown in the table. However, the load condition is variable and will be examined under different scenarios corresponding to maximum and minimum loading. Transformer load values and loading percentages are provided in Table 5.

Table 5. Load values and loading rates of the transformer substations connected to the feeders.

Feeders	Transformer Substation	Load Active Power (kW)	Loading (%)
Kök Ana Dağıtım-1	Plaza Binası-1	142.4	10.9
	Plaza Binası-2	142.4	10.9
	Plaza Binası-3	142.4	10.9
	Plaza Binası-4	142.4	10.9
	Kırmızı-Mavi Hastane-1	142.4	10.9
	Kırmızı-Mavi Hastane-2	142.4	10.9
	Psikiyatri Hastanesi	89	10.9
	Diş Hastanesi	56.1	10.9
Kök Ana Dağıtım-2	Sağlık MYO-1	135.1	13.2
	Sağlık-Soğutma	32.5	3.2
	Rektörlük	172.9	13.2
	Müh. Fak. (A)	172.9	13.5
	ALM	172.9	13.2
	Müh. F. (B)	172.9	13.2
	Teknoloji F.	135.1	13.2
Kök Ana Dağıtım-3	Morfoloji	524.3	25.8
	İktisadi ve İdari Bilimler F.	209.7	25.8
	Tıp Ek Ders	262.2	25.8

CASE STUDY

In the case study, a voltage regulation analysis was performed at the common connection bus of the distribution substation shown in Figure 2, where the PV system was installed. The scenarios considered included examining the effects on voltage regulation of the Müh. F. (A) transformer substation's maximum and minimum load conditions, reactive power support from the PV system, and the use of a tap-changing transformer, switchable capacitor bank, and energy storage system.

The scenarios were defined as follows. In Scenario 1 and Scenario 2, the Müh. F. (A) transformer substation's load is set to its minimum and maximum levels, respectively. In Scenario 3, voltage regulation under maximum load is achieved by setting the transformer to its optimal tap position; the transformer has 32 taps (–16 to +16), each changing the secondary-side voltage by 0.625 %. In Scenario 4, for the maximum load condition, both the transformer and a switchable capacitor bank are installed together, and their tap and step settings are optimized; the capacitor bank comprises 10 steps of 25 kVAr each. Scenario 5 examines the moment when the PV system reaches its peak midday output of 364 kW, using the previously optimized capacitor bank and transformer settings. In Scenario 6, the transformer substation is at minimum load, the PV system produces its maximum output, and the transformer tap is at its optimized setting. Scenario 7 investigates voltage regulation provided by the PV system with reactive power support at a 0.9 leading power factor while keeping the transformer tap at its optimized position. Finally, Scenario 8 extends Scenario 7 by also including a 350 kVA energy storage system alongside the reactive power support at 0.9 leading and the optimized transformer tap position. These scenarios are summarized in Table 6.

Table 6. Summary of the scenarios defined for the Müh. F. (A) distribution system

Scenario	Load (kW)	PV System Active Power (kW)	PV System Power Factor	Transformer Tap Position	Capacitor Bank Reactive Power (kVAr)	Energy Storage System (kVA)
1	75	0	0	0	0	0
2	375	0	0	0	0	0
3	375	0	0	7	0	0
4	375	0	0	3	100	0
5	375	364	1	3	100	0
6	75	364	1	3	0	0
7	75	364	0.9 lead	3	0	0
8	75	364	0.9 lead	3	0	350

The resulting common bus voltage and angle, line and transformer loading levels, and total system losses obtained from the scenarios are presented in Table 7.

Table 7. Simulation results obtained from the defined scenarios

Scenario	Bus Voltage (pu)	Angle (deg)	Transformer Loading (%)	LV Line Loading (%)	Distribution Line Loading (%)	Total System Losses (kW)
1	0.96	24.7	5.8	4.8	11.1	540.13
2	0.92	24	29.9	25.1	57.6	552.47
3	0.96	24	29.8	24	55	551.38
4	0.95	23.6	26.6	21.9	50.2	548.32
5	0.97	25.3	8.4	6.9	15.9	542.02
6	1	26.4	18.7	15.4	35.3	548.60
7	1.01	25.7	20	16.5	37.7	547.68
8	0.99	24.2	9.2	7.6	17.4	539.48

RESULTS and DISCUSSION

The simulation results for the eight scenarios provide important insights into voltage regulation analysis at the common connection bus following the installation of the 370 kW PV system at the Müh. F. (A) transformer substation. Under minimum-load conditions (Scenario 1), the bus voltage remains at 0.96 pu, transformer loading drops to 5.8 %, and system losses stay relatively low at 540 kW. In contrast, when the transformer substation carries its maximum load without any control measures (Scenario 2), the bus voltage falls to 0.92 pu, which is below the accepted limits (< 0.95 pu); transformer loading rises sharply to 29.9 %, and total losses increase to 552 kW, indicating a pronounced voltage drop and higher losses under heavy loading.

When OPF is used to adjust the transformer tap under maximum load (Scenario 3), the bus voltage is restored to 0.96 pu, and transformer loading is held at 29.8 %, reducing losses slightly to 551 kW. This shows that tap adjustment alone can bring voltage back within acceptable limits (0.95–1.05 pu) but only achieves marginal loss reduction. Introducing a switchable capacitor bank alongside the tap-changing transformer (Scenario 4) maintains the bus voltage at 0.95 pu even under full load, lowers transformer loading to 26.6 %, and reduces total losses further to 548 kW. Thus, combining transformer tap adjustments with reactive power injection from the capacitor bank is more effective for both voltage regulation and loss reduction. When the PV system reaches its maximum output of 364 kW (Scenario 5), using the previously optimized transformer and capacitor settings raises the bus voltage to 0.97 pu, reduces transformer loading to 8.4 %, and lowers losses to 542 kW. This demonstrates that at peak PV generation, the PV system relieves loading on the transformer and lines, supporting voltage and reducing losses. Under minimum load with maximum PV output (Scenario 6), the bus voltage rises to 1.00 pu, transformer loading increases to 18.7 %, and losses remain at 548 kW. In this scenario, PV penetration increases and reverse power flow toward the transformer occurs.

In Scenario 7, with the PV inverter providing reactive support at a 0.9 leading power factor and the transformer tap optimized, the bus voltage increases to 1.01 pu, transformer loading is maintained at 20 %, and losses decrease slightly to 547 kW. Reactive power from the PV inverter helps keep the voltage stable without requiring large tap changes. Finally, when a 350 kVA energy storage system is added to Scenario 7 (Scenario 8), the bus voltage is regulated at 0.99 pu, transformer loading drops to 9.2 %, and total losses fall to 539 kW—the lowest of all scenarios. The storage unit absorbs excess midday PV generation and can inject or absorb reactive power to regulate voltage; as a result, loading on the transformer and feeder lines is significantly reduced and losses are minimized.

CONCLUSION

In this study, the distribution network of Pamukkale University Kınıklı Campus was modeled in DIgSILENT PowerFactory using real field data, and the impact of a 370 kW PV system installed at the Müh. F. (A) transformer substation on voltage regulation was investigated. Eight distinct scenarios were defined to analyze how combinations of transformer tap changer, switchable capacitor bank steps, PV system reactive power support, and an energy storage system affect bus voltage, transformer and feeder loadings, and total system losses.

The key findings can be summarized as follows:

1- Under maximum load conditions, using only transformer tap-changer adjustments maintains voltage within acceptable limits but yields limited loss reduction.
2- Jointly optimizing transformer tap positions and the staged capacitor bank corrects voltage deviations more effectively and further reduces losses.
3- At the PV system's midday peak generation (364 kW), feeder and transformer loading are significantly alleviated, voltage is elevated, and losses decrease.
4- Enabling PV inverter reactive support at a 0.9 leading power factor provides voltage regulation and reduces losses under both light and heavy loading conditions.
5- Adding a 350 kVA energy storage system allows excess PV generation to be absorbed and reactive power to be provided, flattening voltage profiles; this substantially relieves transformer and feeder loading and minimizes total losses.
In achieving the optimal solutions, the control variables (transformer tap positions, switchable capacitor bank steps) were adjusted using the interior-point–based Optimal Power Flow module. Voltage limits, line and transformer loading limits were enforced to minimize total losses. Overall, this work demonstrates that, in distribution networks with high PV penetration, an interior-point OPF approach—integrating transformer tap changer with a switchable capacitor bank, PV system reactive power support, and energy storage—provides an effective and easily applicable method for voltage regulation and loss minimization. Future research can evaluate the method's robustness further by incorporating dynamic load and generation profiles, PV output uncertainty, additional distributed generation types, and economic considerations.

REFERENCES

Aboshady, F.M., Pisica, I., Zobaa, A.F., Taylor, G.A., Ceylan, O., & Ozdemir, A. (2023). Reactive Power Control of PV Inverters in Active Distribution Grids With High PV Penetration. IEEE Access, 11, 81477-81496.

Alshehri, M., & Yang, J. (2024). Voltage Optimization in Active Distribution Networks—Utilizing Analytical and Computational Approaches in High Renewable Energy Penetration Environments. Energies, 17(5), 1216. https://doi.org/10.3390/en17051216.

Bektaş, E. (2023). Development of volt/var and energy management optimization approach for distribution systems [PhD Thesis]. Ankara Yıldırım Beyazıt University. Available at: https://tez.yok.gov.tr/UlusalTezMerkezi/giris.jsp [20.05.25].

Borghetti, A., Napolitano, F., & Nucci, C.A. (2015). Volt/var optimization of unbalanced distribution feeders via mixed integer linear programming. Electrical Power and Energy Systems, 72, 40-47.

Dubravac, M., Topic, D., Fekete, K., Simic, Z., Prenc, R., & Rojnic, M. (2024). Active Power Curtailment and Reactive Power Control in PV-Rich Low-Voltage Distribution Network. 20th International Conference on the European Energy Market (EEM).

Eiriksson, E. (2017). Distribution grid capability for reactive power support [Master Thesis]. KTH – Royal Institute of Technology, Sweden.

Emiroğlu, S. (2017). Energy optimization through voltage reduction method in electrical power system with distributed generation [PhD Thesis]. Sakarya University. Available at: https://tez.yok.gov.tr/UlusalTezMerkezi/giris.jsp [19.05.25].

Kısakürek, S.M., & Şekkeli, M. (2022). Fotovoltaik İnverterler ile Reaktif Güç Optimizasyonu. Kahramanmaraş Sütçü İmam University Journal of Engineering Sciences, 25.

Köroğlu, H. (2024). Providing reactive power support from solar power source in electricity distribution grid [Master Thesis]. Necmettin Erbakan University. Available at: https://tez.yok.gov.tr/UlusalTezMerkezi/giris.jsp [22.05.25].

Manbachi, M., Farhangi, H., Palizban, A., & Arzanpour, S. (2017). Smart grid adaptive volt-VAR optimization: Challenges for sustainable future grids. Sustainable Cities and Society, 28, 242-255. https://doi.org/10.1016/j.scs.2016.09.014.

Porwal, D., Fozdar, M., & Tiwari, R. (2024). An adaptive heuristic approach for Volt-VAr optimization in distributed generation integrated system. Renewable Energy Focus, 50. doi: 10.1016/j.ref.2024.100580.

Tunçer, B. & Çetin, E. (2023). Elektrikli Araç Şarj İstasyonlarının Dağıtım Şebekesi Üzerindeki Etkilerinin Örnek Bir Saha Üzerinde İncelenmesi. VII. Elektrik Tesisleri Ulusal Kongre ve Sergisi (ETUK), İzmir, Turkey.

Uluski, B. (2011). Volt/VAR Control and Optimization Concepts and Issues. Available at: https://nwess-archive.ece.uw.edu/2012/talks/uluski.pdf [25.05.25].

NOMENCLATURE

***Acronyms**:*

OPF:	Optimal power flow	FACTS:	Flexible AC transmission system
DSO:	Distribution system operators	DGS:	Distributed generation sources
STATCOM:	Static synchronous compensator	OLTC:	On-load tap changer
SVC:	Static VAR compensator	VVC:	Volt/Var control
PCC:	Point of common coupling	VVO:	Volt/Var optimization

Subscripts:

PV: photovoltaic

➢ *ORAL PRESENTATION*

Design of an innovative reel transfer mechanism for automatic winding machines

Özdemir Berk VARAL[1*] (*ORCID: https://orcid.org/0009-0009-8130-8341*), Beyza AVCI[1*] (*ORCID: https://orcid.org/0000-0003-3504-8453*), Nebi Can AVAS[1*] (*ORCID: https://orcid.org/0009-0009-1364-9072*), İbrahim Savaş DALMIŞ[2] (*ORCID: https://orcid.org/0000-0002-4401-9155*)

[*1] DOMEKS Machinery A.S. Design Center, Tekirdag, Turkey.
[2] Tekirdag Namik Kemal University, Corlu Engineering Faculty, Mechanical Engineering Department, Tekirdag, Turkey.

*Corresponding author e-mail: beyza@domeksmakine.com

Abstract
In this study, an innovative reel transfer system capable of removing completed reels and loading empty ones in automatic cable winding machines through a single integrated mechanism was developed. The system features a simplified design in both mechanical structure and control logic. After being modeled using computer-aided design (CAD) tools, a physical prototype was manufactured and evaluated under real production conditions. The test results showed a reduction of up to 33% in operation time, contributing to uninterrupted production flow. With its compact structure, the system minimizes the number of components and production costs, while offering advantages such as ease of maintenance and simplified control architecture. This work presents a lean and functional solution suitable for integration into modern automation systems.
Keywords: Winding machine, reel transfer, automation, production efficiency, cable packaging

INTRODUCTION

One of the most critical stages a product undergoes before reaching the end-user in the cable manufacturing sector is the packaging process. In this process, cables are wound into specific lengths, forming spools or coils, and then packaged, preparing them for shipment. Specifically, cable packaging machines are systems located at the final stage of the production line, automatically performing operations like winding, cutting, securing, and labeling. With advancements in automation technologies, numerous innovative mechanisms and control algorithms are being developed for these machines to increase production speed, reduce human intervention, and enhance quality standards.

Cable packaging machines are generally divided into two main groups based on the winding method used: spool-type winding and coil-type winding. In spool-type winding, the cable is neatly wound onto cylindrical spools, while in coil-type winding, the cable is gathered into a circular form around its own axis. In both methods, once winding is complete, the current cable must be removed from the system, and an empty carrier (spool or coil platform) must be placed to receive the next cable. These steps constitute a significant time interval within the system's overall cycle time and are typically carried out by separate mechanical systems or through operator intervention.

Reducing the cycle time in the production line is a critical requirement for increasing overall production capacity and enabling continuous system operation. Particularly, the waiting time that occurs during spool changes after the winding process is completed leads to efficiency losses in machines with low levels of automation. In this context, performing the operations of removing the finished spool from the system and placing the new empty spool quickly, integrally, and automatically necessitates improvements in both mechanical systems and control algorithms.

In recent years, various studies have been conducted in the literature to increase the level of automation in cable winding and packaging processes.

In a study by Avci et al. (2024), a novel cable packaging system was designed to fix cable ends without the need for any auxiliary materials, and a prototype was produced. The system consists of seven main units: flyer, tension control unit, traversing mechanism, rotary cable winding heads, gripper group, shrink unit, and main control panel. By eliminating the use of auxiliary materials, the study aimed to reduce both production costs and time losses. Experimental results demonstrated that the machine was capable of winding 12 short-length

cables and 8 long-length cables per minute, indicating a significantly higher performance compared to existing machines (Avci et al., 2024).

In another study by Avci et al. (2023), a high-capacity spool-coil cable winding machine with three winding heads was designed and prototyped to increase winding capacity and reduce time losses. The system comprises seven main units: discharging unit, traversing unit, dancer mechanism, cable winding heads, spool feeding unit, gripper group, and the main control panel. Thanks to the inclusion of three winding heads, different operations can be performed simultaneously, minimizing idle times. Experimental tests showed that the machine could wind 10–12 coils per minute for cables in the 16.5–25 m range, and 4.5–5 spools per minute for 100-meter-long cables. The designed system was found to offer twice the efficiency compared to conventional machines.

In the study by Trieu and Thinh (2023), a cable winding mechanism ensuring precise control of cable tension was designed and analyzed for cable-driven parallel robots (CDPRs). A high-accuracy cable tension model was proposed, considering friction and parametric differences that typically hinder accurate force measurement in CDPR systems. The system was comprehensively structured with subcomponents including winding spool, motor selection, reducer, and cable guiding mechanism. Validated through both experimental tests and numerical simulations, the design was shown to be effective in modeling cable forces accurately and ensuring system stability, especially in high-precision industrial applications (Trieu & Thinh, 2023).

Hultman (2022) developed a robotic system for the automatic winding of stator cables in rotary electric machines. The proposed system was reported to have the potential to reduce cycle times and assembly costs compared to manual and low-volume automation processes. However, it was also noted that the system could not yet compete with high-volume conventional winding automation, and future efforts would focus on optimizing durability and performance for larger cable sizes and custom machinery (Hultman, 2022).

In the study conducted by Wu et al. (2019), an automated vision-based system was developed to address the low automation level in industrial cable winding systems. A target recognition algorithm based on Hu moments and a multi-degree-of-freedom neural network (MDOFNN) was compared with support vector machines (SVMs). The proposed approach yielded higher accuracy (Wu et al., 2019).

Hultman (2013) developed a robotic automation system for the cable winding process of generator stators used in wave energy converters. The robot cell was designed to automate cable preparation, placement, and cutting operations, and these processes were experimentally tested. The system was found to effectively address time losses and quality inconsistencies in traditional manual processes, especially in small-volume drum operations. Application results indicated that the automation system enhanced process repeatability and supported continuous production (Hultman, 2013).

Unlike previous studies, the present work introduces an innovative spool transfer mechanism developed to ensure the continuity of the winding process and to minimize idle time. The developed mechanism is capable of simultaneously and integrally performing two tasks: transferring the completed spool to the conveyor belt and positioning a new empty spool at the winding head. As a result, the mechanical structure has been simplified, the control algorithm has been streamlined, and the total cycle time of the system has been significantly reduced. A prototype of the system was manufactured, integrated into automatic winding machines, and its functionality was validated through performance tests.

MATERIALS AND METHODS

Within the scope of this study, the spool transfer system was developed to be integrable into industrial winding machines and was designed with a simplified and optimized structure in terms of both mechanical components and control systems. The finalized system was tested on automatic cable winding machines operating under real production conditions to verify its applicability and functionality. The design and implementation process was carried out in four main technical stages, ranging from computer-aided modeling to prototype production (Figure 1).

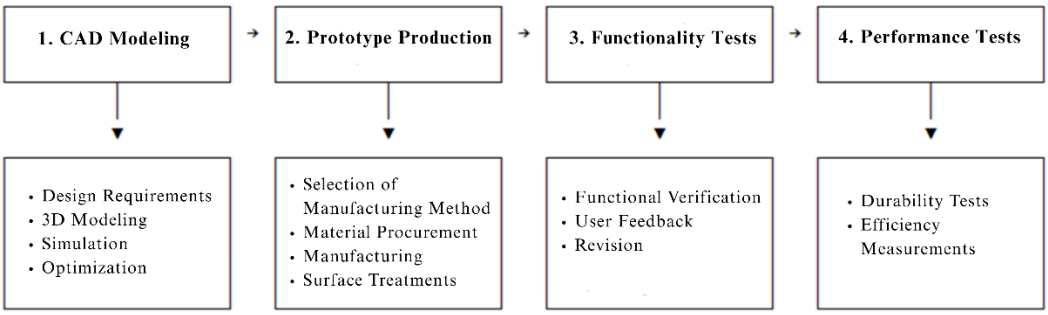

Figure 1. Flow diagram of the system design and production processes

Computer-Aided Design (CAD) Process

The design of machine components, including 3D modeling and assembly processes, was carried out using SolidWorks CAD software. During the design phase, the fundamental operating principle of the spool transfer mechanism was defined, and a detailed design was completed accordingly. Dimensional compatibility, assembly tolerances, and potential interferences between moving parts were evaluated through part interaction simulations and motion analysis. Furthermore, the manufacturability of the designed structure was reviewed, and the mechanical layout was simplified to obtain a production-friendly configuration.

Figure 2 presents the three-dimensional model view of the mechanism after assembly, while Figure 3 shows the integrated state of the spool transfer mechanism within the cable packaging machine.

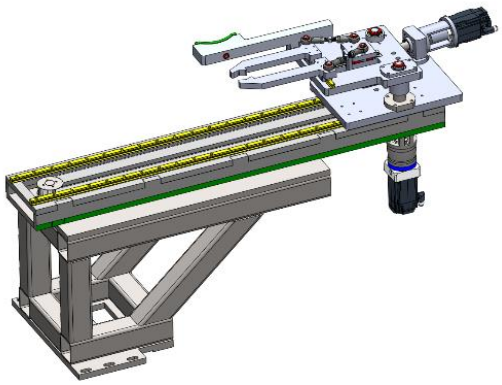

Figure 2. 3D model of the spool transfer mechanism

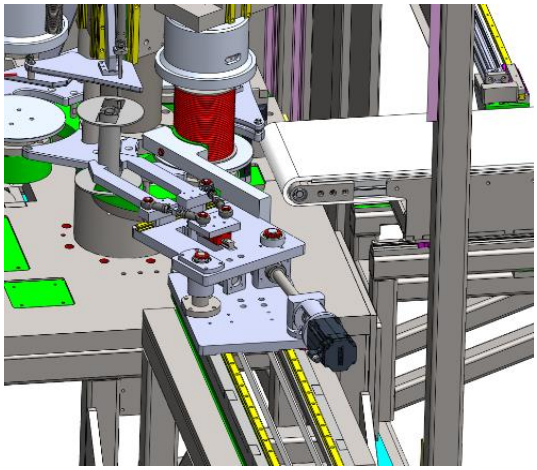

Figure 3. Integrated view of the spool transfer mechanism within the cable packaging machine

Prototype Production

Following the validation of the model in a virtual environment, the physical prototype was manufactured. The main supporting structure was manufactured from structural steel, while the gripping mechanism and mechanical connection elements were fabricated from 7075 aluminum material. The system is driven by a combination of a pneumatic piston and an electric motor.

After the parts were manufactured using CNC cutting, milling, and turning operations, assembly was completed following field conditions. Necessary adjustments were made on the prototype, and the functionality of all moving components was tested.

Figures 4 show the assembled physical prototype after installation.



Figure 4. Assembled view of the physical prototype

Functionality and Performance Tests

Following the tests, the system was found to provide a simplified, functional, and efficient structure in terms of both mechanical design and control process. During the testing phase, the operation cycles of both the developed system and existing automatic winding machines were recorded on video, and comparative time analyses were conducted based on these recordings. For visual validation, prototype images were included in the study; the final version of the system was reported both technically and visually by evaluating the computer-aided design outputs and the physical prototype.

RESULTS and DISCUSSION

After prototype production, the developed spool transfer system was integrated into automatic cable winding machines and tested under real operating conditions. Throughout the test phase, the system's functionality, operation time, and motion efficiency were comparatively analyzed against current systems using video recordings.

Time Analysis Results

In existing winding machines, the removal of the completed spool and placement of a new empty spool are performed using two separate mechanical systems, each requiring a certain amount of operation time. In the newly developed system, these operations are carried out using an integrated structure, significantly reducing the overall process time. This operation time includes the complete steps of removing the wound spool and positioning the empty spool.

Figures 5 and 6 present the flow diagrams of both systems and the total operation time for each step. The obtained comparative time data are provided below in Table 1.

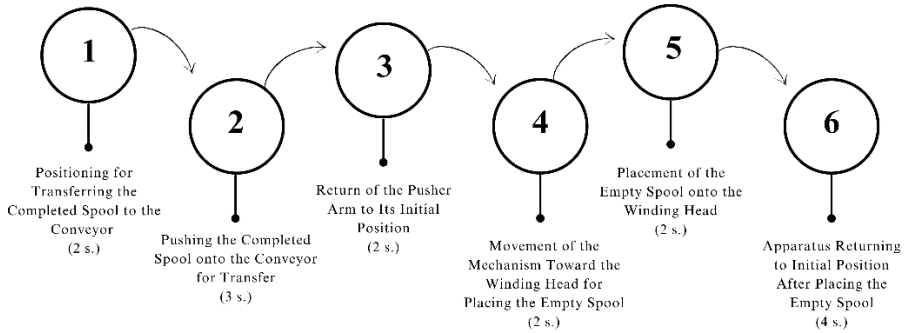

Figure 5. Flow diagram of the existing spool transfer mechanism

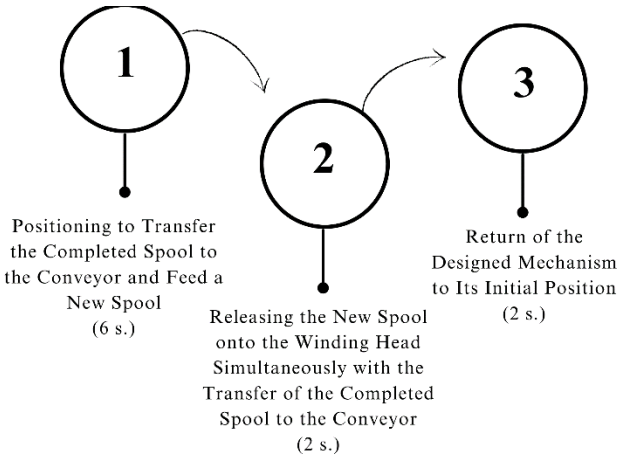

Figure 6. Flow diagram of the newly developed spool transfer mechanism

Table 1. Comparison of Operation Times between Existing Systems and the New Design

System	Processing Time (s.)	Video Time Range
Current System	15	00:22 – 00:37
New Design	10	00:08 – 00:18

These results demonstrate that the system directly shortens the production cycle time and contributes to continuity on the production line.

Mechanical Structure and Advantages of Compact Design

The developed system has been structured to perform spool transfer and feeding—previously handled by two separate mechanical subsystems in conventional automatic winding machines—using a single integrated mechanism. This integrated design approach not only enabled structural simplification but also provided significant benefits in terms of material usage, production cost, and spatial efficiency.

Choosing a single-body structure instead of two separate carrier systems allowed for a reduction in the number of connecting elements, bearing systems, and moving parts. As a result, the system is more compact, easier to assemble, lower in manufacturing cost, and less prone to mechanical failures. The reduction in components also simplifies maintenance and offers flexibility for adapting to variable field production conditions. The comparative structural differences and integration advantages are presented in Table 2.

Table 2. Comparison of Mechanism Structure and Design Differences

System	Functional Structure	Number of Mechanisms Used
Current System	Individual modules	2
New Design	Integrated mechanism	1

Motion Count and Control Simplicity

The developed system offers significant simplification not only in terms of structure but also in motion control and automation compared to existing systems. In conventional machines, the removal of the wound spool and feeding of the empty spool are performed by two separate mechanisms, each with its own motion cycle. This structure requires a total of six separate movements and results in a more complex control algorithm on the PLC.

In contrast, the new system performs both tasks using a single integrated mechanism, reducing the total number of movements to three. This simplification streamlines the PLC programming structure, reduces the number of sensors and outputs required, and minimizes timing-related synchronization errors. It also indirectly contributes to improved system response time and reduced energy consumption. The differences in motion count and control complexity between the existing systems and the new design are presented in Table 3.

Table 3. Comparison of Motion Count and Control Features between the Existing System and the New Design

System	Functional Structure	Number of Mechanisms Used
Current System	Individual modules	2
New Design	Integrated mechanism	1

CONCLUSION

According to the comparative evaluation, the process in the existing spool transfer system consists of six steps and has a total cycle time of approximately 15 seconds. In this sequence, positioning the completed spool for transfer to the conveyor takes 2 seconds, pushing the spool onto the conveyor takes 3 seconds, returning the pusher arm to its initial position takes 2 seconds, moving the mechanism toward the winding head to place the empty spool takes 2 seconds, releasing the empty spool takes 2 seconds, and returning the apparatus to its initial position takes 4 seconds.

In contrast, the newly developed system reduces the process to three steps and shortens the total cycle time to 10 seconds. In this configuration, the transfer of the completed spool and the feeding of the new spool are performed simultaneously within a single integrated motion, completed in 6 seconds. The release of the new spool is accomplished in 2 seconds, and the mechanism's return to its initial position is completed in another 2 seconds. This results in an approximate 33% improvement in cycle time.

In addition to the temporal improvement, the reduction in the number of process steps from six to three has simplified the control algorithms and decreased the need for sensors and output components. Consequently, the PLC programming structure has been streamlined, and the risk of synchronization errors has been significantly reduced.

Furthermore, the consolidation of the mechanical structure into a single integrated body has reduced the number of moving parts, connectors, and bearing systems, leading to decreased production costs and simplified maintenance procedures. The system has also demonstrated increased adaptability to variable field conditions while minimizing the risk of mechanical failure. Altogether, these enhancements indicate that the system offers significant improvements not only in terms of time efficiency but also in structural and operational performance.

For future studies, it is recommended to conduct a comprehensive cost analysis to assess the system's impact on production expenses in greater detail.

ACKNOWLEDGEMENTS

The design, prototyping, and testing processes of this study were carried out with the technical support and infrastructure provided by the DOMEKS Makine Inc. Design Center.

REFERENCES

Avci, B., Kavak, S., Dalmis, F., Yilmaz, S. O., & Dalmis, I. S. (2023). Development of a high capacity three headed coil-spool winding machine. Journal of the Technical University of Gabrovo, 67, 49–53. https://doi.org/10.62853/QUPA2451

Avci, B., Varal, Ö. B., Dalmis, F., Yilmaz, S. O., & Dalmis, I. S. (2024). Design of a cable packaging system capable of securing cable ends without the use of auxiliary materials. Journal of the Technical University of Gabrovo, 69, 26–31. https://doi.org/10.62853/YRIW5862

Hultman, E. (2022). Introducing robotized stator cable winding to rotating electric machines. Machines, 10(8), 695. https://doi.org/10.3390/machines10080695

Hultman, E. (2013). Robotized cable winding of the Uppsala University wave energy converter generator stator (Master's thesis, Uppsala University, Department of Engineering Sciences). http://uu.diva-portal.org/smash/record.jsf?pid=diva2%3A647819&dswid=8048

Trieu, N. M., & Thinh, N. T. (2023). Design and analysis of a cable-winding device for cable suspended parallel robot. International Journal of Mechanical Engineering and Robotics Research, 12(5), 332–338. https://doi.org/10.18178/ijmerr.12.5.332-338

Wu, D., Hua, L., Qiang, Y., Gu, J., Jiang, L., & Zhao, J. (2019). Research and implementation of automatic cable winding system based on machine vision. In 2019 IEEE International Conference on Mechatronics and Automation (ICMA) (pp. 329978–329984). https://doi.org/10.1109/YAC.2019.8787588

➢ *ORAL PRESENTATION*

Language application “Hey!” — development, possibilities and future

Yaroslav Golendukhin, Saveliy Varlamov, students of 11th class Gymnasium "BEST", Petropavlovsk, Kazakhstan

Scientific supervisors of the project: Yulia Dmitrieva, Yulia Starchekova, English teachers of Gymnasium "BEST", Petropavlovsk, Kazakhstan



Abstract

The article presents the history of the creation of the mobile application “ Hey !” *(Golendukhin and Varlamov 2025)*, designed for learning English with the purpose of adaptation in the English-speaking environment. The authors describe in detail the stages of development, including the analysis of existing applications, definition of the target audience and technical characteristics of the product. The application is based on modern teaching methods, uses artificial intelligence and offers personalized scenarios. It implements dialogue modules, a flash card system and a free communication function. The study of the target audience allowed us to create a product that meets the current needs of users of different ages and professional categories. “ Hey !” is aimed at those who want to master English at a level of at least A2 and achieve confident proficiency in it in real conditions.

Keywords: English language, mobile application, artificial intelligence, language adaptation, dialogue learning, educational technologies, personalized learning, Hey !

Defining the target audience for the “ Hey !” app

English is one of the most widely spoken languages in the world today. Approximately 1.5 billion people speak it, and about 1 billion are actively studying it. English has penetrated into all spheres of life: science, mass media, education, work and leisure.

During the implementation of our project, we asked ourselves: "For whom will our software product be created, and how to motivate people studying English to use the Hey ! application?" To clarify this issue, we developed a questionnaire and conducted a survey of potential users - schoolchildren, students and older people, here is the result.

After analyzing the survey results, the structure of the target audience of the Hey ! application was identified.

Age groups: teenagers (13-18 years), young adults (19-30 years), adults (31-50 years).

User profile: students, professionals (managers, engineers, programmers, etc.), travelers, emigrants.

Motivation: career growth, emigration, exam preparation, improving English communication skills, personal growth.

Difficulties: lack of time and discipline, fear of communication, lack of practice and feedback.

Target segments have the following characteristics:

- Teens: prone to learning through gamification, interested in interaction with AI.
- Adults under 30: value mobility, efficiency, adaptive scenarios.
- Adults over 30: strive for professional language practice and practical application of the language.

Most respondents aim to reach the B2 (Upper-Intermediate) or C1 (Advanced) level, starting from A2 (Elementary). This confirms the appropriateness of focusing the Hey ! application on the intermediate and high levels of English proficiency. At the same time, many (more than 42% of respondents) wanted to learn the language taking into account local language features. With this in mind, the main idea when planning the application was that a person memorizes and begins to use a foreign language much faster if he finds himself in typical social situations, as if he were already in an English-speaking country. Therefore, it was actively planned to include local dialects and pronunciation accents, idiomatic expressions in the dialogues.

Research of educational applications. Their advantages and disadvantages.

We started working on our project by analyzing the methods used in various mobile applications for learning English. In the process of familiarization, we looked at many digital tools. Each of them has its own specialization, accordingly focusing on a certain target audience.

Of course, we did not use all of the methods in the product we developed, " Hey !", but, in our opinion, we selected the most effective ones from a diverse set of options, focusing on our target audience. Let's organize the information we received about existing language applications.

Let's start with the fact that educational digital products have different specializations, which are largely shaped by the wishes of the target audience. Some of them are aimed strictly at children (ADC Kids , Fun English , Study Cat , Lingokids) , others - to learn the language through dialogue with a native speaker (HelloTalk , Speaky , Tandem), others - to expand vocabulary (Memrise , Puzzle English , WordUp), others – maximally improve the grammar of the language (Duolingo , Polyglot-16, English Galaxy). We have indicated only the most notable of the directions. There are still many quite specific applications with a narrow target group.

At the beginning of the project, we faced a rather difficult but interesting task – to evaluate the teaching methods used in the above products and select several of the strongest teaching options. Here is a brief description of the digital tools that seemed most interesting to us.

- One of the most popular apps for learning English is **Duolingo** — it has been downloaded over 100 million times on Google Play alone *(Duolingo Guides 2024)*. And it’s no wonder: the learning is based on simple exercises and mini-games, and the interface is bright and friendly. As a result, you can easily expand your vocabulary, learn to use new words in speech, and improve your listening comprehension.
- **Memrise** — another tool for memorizing words and expressions *(MakeUseOf 2024)*. The principle of operation is simple: you set a goal for the number of words you want to learn each day, and then do game exercises. Everything is organized easily, excitingly and without unnecessary details.
- You've probably heard more than once that the best way to improve your knowledge of a language is to communicate with native speakers. **HelloTalk App** *(HelloTalk 2024)* created exactly for this purpose.
- In **Busuu** offers not just exercises, but full-fledged mini-courses created by professional teachers *(Busuu 2024)*. You will be able to develop all skills: reading, writing, speaking and listening. And most importantly - no complex formulations from textbooks: everything is based on examples from real conversational speech.
- **LinguaLeo** — one of the first applications for simple and interactive learning of English, existing since 2010 *(LinguaLeo 2024)*. It constantly improves its mechanics and can now adapt to your level. There are many options for studying: you can create your own dictionary, improve grammar and even participate in battles (mini-competitions) with other users.
- In **Rosetta Stone** you can use the original mechanics of memorizing words through associations *(Rosetta Stone 2024)*. In addition, the application offers trainers for improving pronunciation, which helps develop skills even more effectively.

- **Rememba** — is an English learning app that helps you memorize words and phrases through interactive exercises and flashcards *(Rememba 2024)*. It uses repetition and real-life examples to improve your understanding of the language in practice.
- **TED** app is not only suitable for language learning, but also for inspiration *(TED 2024)*. Inside you will find thousands of English-language lectures and speeches on a variety of topics. Subtitles will help you better understand the speakers, regardless of their accent and pronunciation.
- **Words** - one of the most popular apps for language learners *(WordsApp 2024)*. It features over 8,000 words, as well as several types of exercises to memorize them. The words are organized into thematic groups, which systematizes learning.

Choosing the perfect English learning app depends not only on the features and interface, but also on how well it matches the user's learning goals. Many are looking for an app that covers all aspects of language learning from conversation to grammar, while also including motivating elements to prevent learning from becoming a chore. It is common to check reviews, test trial versions, and evaluate the quality of the materials to ensure that they are in line with modern learning methods.

It is also important that the app easily integrates into the user's daily life. A convenient app allows you to study anytime and anywhere, making the learning process a natural part of your daily schedule. People look for apps with a clear interface and easy navigation so that each learning session is not only effective but also enjoyable. The right app becomes an indispensable assistant in mastering English!

After a comprehensive study, we have drawn certain learning functions for the application " HEY !". We have determined that the product should be dominated by dialogue, in different forms, and the most primitive function of replenishing vocabulary through their study and repetition. From here the following functions appeared:

- Free - Talk – free conversations in which the user chooses topics, and the dialogue is created by artificial intelligence directly during the conversation. During the development of the program, this function was new. That is, we did not find the use of neural networks for dialogues in any of the studied applications. We put this function in first place, since it develops two skills: speaking and listening ;

- thematic dialogues – pre-created communication structures, each with a specific topic. Here communication takes place in writing, where literacy, speed and correctness of the answer are taken into account;

- Flash cards – a set of words for expanding the vocabulary. They can also be adjusted by the number of additions, frequency of checks, thematic focus and the possibility of replacement after the user can correctly translate the word a certain number of times;

- and the last significant detail that we learned from our research is checking your level. Namely, at certain intervals, the user undergoes complex testing to find out how his level has changed relative to the initial and previous ones.

Application " HEY !" - main characteristics and possibilities.

After analyzing existing applications for online English language learning, we were able to create our own digital tool taking into account the following criteria:

Functionality . This criterion reveals all the possibilities of the application. The more of them, the higher the potential of the application. But a mobile application overloaded with functionality may not appeal to users because of the need to spend a long time figuring it out and searching for the necessary information.

Design. People do not perceive slow and overloaded with complex design programs well. Users do not want to wait for the data to fully load, and also waste time on lengthy study of navigation through sections. According to this criterion, the application should provide a comfortable user interface and intuitive interaction with the user. This criterion evaluates design, navigation, notifications.

Availability of use . It is important that applications are accessible for all popular mobile devices and platforms on which they are based.

Interface . This criterion is responsible for the ease of use of the application. The more optimal the size of the icons and buttons, the more convenient the menu is located, the color and information accents are successfully selected, the more comfortable and pleasant it is to use the application.

Offline access . The ability to use the application without an Internet connection. This function is very useful and practical, as it will allow you to save mobile traffic, and when you do not have Internet access, you will be able to use the application without any problems.

During the research project, we developed a language learning mobile application of a certain specificity. Namely, we had a large-scale goal - to create a mobile application that will allow the user to improve their language skills from any level to the level of comfort in the English-speaking environment.

So the main idea behind this app was that a person will remember and start using a foreign language much faster if they find themselves in typical social situations, as if they were already in an English-speaking country.

The app is now available on Google Play , we have already registered the copyright for it and continue to develop it.

Functionality of the application.

The mobile application “ Hey !” is intended for use in the field of education, in particular for independent and distance learning of English. The product is used in informal learning, language practice, and also as an aid in preparing for exams (IELTS, TOEFL, etc.), professional retraining, adaptation to the English-speaking environment and everyday language practice.

Programming languages.

We developed this application based on standard requirements for similar training systems, updating them with the use of artificial intelligence resources code.ai, recraft.ai, open.ai. We created the application in the Godot game engine , using the GDScript programming language as the main development language. Additionally, we used:

GD Script - built-in Godot programming language based on C ++;

JSON - for storing configurations, dialogs and user data.

The interface design was developed in the Figma graphic editor .

Functional capabilities



The application provides for the creation of an account for each user with the accumulation of information about personal learning dynamics. This allows determine the user's starting level of English. For each level, a training program is selected (a corresponding set of dialogues), which is formed not only on the basis of the client's knowledge, but also on his wishes for the timing (reading, dialogue, listening comprehension, vocabulary). During the training process, a person will be able to monitor the dynamics of his training, comparing the current level with the initial one. Parameters for level assessments can be determined by complex testing. In addition, the percentage of the material covered to the total initially planned volume of training is considered as an additional indicator.

In parallel with language learning, our users will be able to virtually immerse themselves in the environment, becoming part of an English-speaking society. Some exercises involve artificial intelligence. This makes it possible not only to practice language skills and pronunciation, but also to completely simulate a situation (stadium, museum, college, cafe, metro, etc.) so that a person feels part of that language environment. At the same time, the necessary set of words is selected (the learner can regulate the speed of conversation independently). In the future, we provide the possibility of dialogues that preserve the accent of the desired country. All these factors bring the dialogue with the device as close as possible to a conversation with a native speaker. Immersion in the language environment with the simulation of situations allows not only to improve speaking skills and increase vocabulary, but also to expand knowledge about the culture of other countries, to really feel the behavior model of people there. And this part of our application is still a rarity in relation to existing training programs, which gives it special value with the open access of our software product “ Hey !”.



Situational dialogues can be selected by the user depending on their preferences and aspirations. If the topic is not of particular importance to them, the application uses a random selection from those that have not been completed. The application independently evaluates whether the dialogue has been completed or not, based on indicators defined by the developers. The number of syntactic and phonetic errors during the conversation is chosen as the basis for the evaluation.



To build vocabulary, a system of flash cards is provided, which will allow you to study new words and set phrases, add them and repeat them in random order. Let us explain, there are two types of flash cards: the first is words and phrasal verbs; the second is various set phrases used in everyday life, and phraseological units that have a certain figurative meaning.

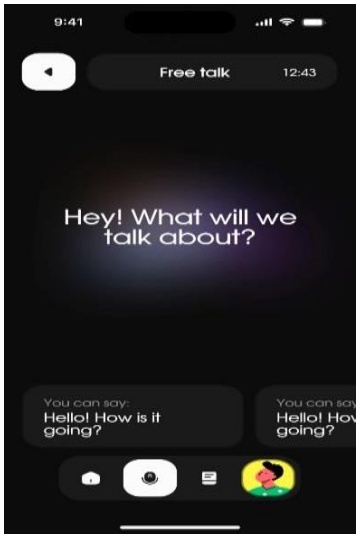

And another important function of our program is Free-Talk, dialogues on a free topic. In them, artificial intelligence also acts as a partner. Here, a full set of words and grammatical constructions is used that the student should know at the moment.

Such a dialogue can be conducted in various modes, for example, with English subtitles. The speed of the dialogue can be adjusted depending on the level of training or at the user's discretion.

Main technical characteristics

Software product size : approximately 120–150 MB (depending on platform and included content);

Durability of hardware and software :

The application is crash-resistant: progress is saved automatically and regularly;

An error handling system is used to prevent loss of user data;

The application can be operated in offline mode, but in this case the application loses the Free - Talk dialog function , since they are generated using neural networks;

The program has been tested on various models of mobile devices.

Minimum device requirements :

Operating system: Android 8.0+ / iOS 13.0 +;

Processor: dual-core, with a clock frequency of 1.5 GHz;
RAM: from 2 GB;
Free space: at least 200 MB;
Required components: microphone, speaker/headphones, internet access (for online functions).

So, to briefly summarize all of the above, we can say that the " Hey !" application is an innovative educational platform for learning English that combines advanced technologies and unique methods. Users can create personal accounts that provide access to educational materials from anywhere in the world and allow you to track your progress. The application offers adaptive learning programs based on the individual level of knowledge of the user and his personal preferences. This makes the process as effective and individualized as possible. One of the key features is the ability to fully immerse yourself in the language environment with the help of artificial intelligence, which simulates various life situations, creating a feeling of real communication with a native speaker. The application also offers a variety of dialogues on selected topics, a flash card system for expanding vocabulary and a free conversation function, where the user can improve their skills in real conditions. These unique features make the application an indispensable tool for those who seek not only to learn English, but also to immerse themselves deeper into the cultural context of English-speaking countries.

Project development.

At this level, we do not plan to stop our project; on the contrary, additional ideas for upgrading the application have now emerged:

- we will develop libraries of thematic conversations and dialogues Free - Talk ;

- we will add a database of typical speech patterns, knowledge of which will facilitate conversation and understanding;

- we will add tests to assess the client's language level;

- add a multiplayer that will allow you to talk to real people - the same clients of the program who are open to dialogue (their openness will be marked with some special sign);

- we will create a module that not only records syntactic or phonetic errors, but also provides detailed comments: points out specific problematic sounds, compares the user's pronunciation with the reference (native speaker), offers exercises for correction. Such technologies (for example, those used in the Elsa application Speak) will help users improve their accent and fluency to a whole new level.

- we will build algorithms into the program to analyze the topics that the user most often chooses and automatically offer new dialogues or cards that match his interests (for example, sports, culture, business, science). This will increase motivation, because learning will become not only useful, but also personally exciting.

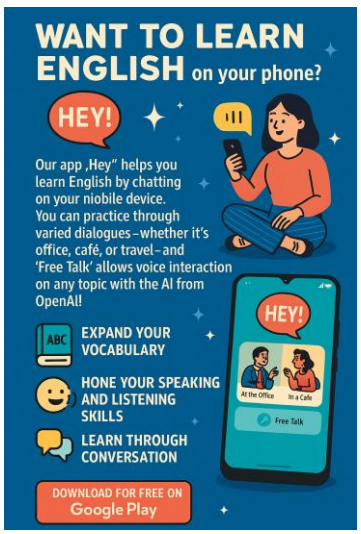

- to increase user engagement, we will build in a system of achievements, ratings, collectible badges and progress bars. For example, a user receives virtual awards for a 7-day series of lessons, for successfully completing thematic blocks or for completing special tasks. This is an element that is successfully used in Duolingo and other popular platforms, and which helps to retain users' attention on a long-term basis.

- create sets of scenarios that reflect the specifics of regional English (e.g. American, British, Australian, Indian variants), including typical phrases, idioms and accents. This will not only help to better understand different variants of the language, but also prepare users for real situations of communication with people from different countries. For example, this is especially useful for corporate clients to prepare for international negotiations.

Thus, " Hey !" represents for us an important experience in the field of creating a modern digital product, combining advanced technologies and taking into account the real needs of users. We hope that the created application will be interesting and useful for both students and teachers, as well as for everyone who wants to learn English quickly, deeply and with pleasure.

References

Busuu. (September 28, 2024). Learn English App. (Accessed June 10, 2025). https://www.busuu.com/en/app/learn-english-app

Duolingo Guides. (October 10, 2024). “How Does Duolingo Work?” (Accessed June 10, 2025). https://duolingoguides.com/how-does-duolingo-work/

Golendukhin, Yaroslav, and Saveliy Varlamov. 2025. Note: This app was developed by Yaroslav Golendukhin and Saveliy Varlamov, 10th grade students of BEST Gymnasium (Petropavlovsk, Kazakhstan) under the guidance of Yulia Dmitrieva and Yulia Starchekova, English teachers of BEST Gymnasium (Petropavlovsk, Kazakhstan)

HelloTalk. (September 28, 2024). Official Website. (Accessed June 10, 2025). https://www.hellotalk.com/

LinguaLeo. (September 28, 2024). Official Website. (Accessed June 10, 2025). https://lingualeo.com/

MakeUseOf. September 28, 2024. “The Best Features of Memrise to Help You Learn a New Language.” Accessed June 10, 2025. https://www.makeuseof.com/best-features-memrise-learn-new-language/

Rememba. (October 10, 2024). “Rememba Overview (Russian Review).” (Accessed June 10, 2025). https://xn-----6kcmmffgadcebmeikxprswo9vrdn.xn--p1ai/page/rememba-obzor/

Rosetta Stone. (October 10, 2024). “How It Works.” (Accessed June 10, 2025). https://www.rosettastone.com/how-it-works/

TED. (October 10, 2024). Official Website. (Accessed June 10, 2025). https://www.ted.com/

WordsApp. (October 10, 2024). Official Website. (Accessed June 10, 2025). https://wordsapp.com/

➢ *ORAL PRESENTATION*

Investigation of Molecular Responses in Cervical Cancer Cells Treated with Abraxane via RNA Sequencing

Souandaou Athoumani Ali[1] (*https://orcid.org/0000-0003-1741-0623*),
Gül Özcan[2] (*https://orcid.org/0000-0003-0682-5065*)

[*1]Department of Biology, Institute of Graduate Studies in Sciences, Istanbul University, Istanbul, Türkiye.
[2] Department of Biology, Faculty of Sciences, Istanbul University, Istanbul, Türkiye.

*Corresponding author e-mail: kouthayate96@gmail.com

Abstract

Abraxane, a nanoparticle albumin-bound formulation of paclitaxel developed to reduce the toxicity and solvent-related side effects associated with conventional paclitaxel—a chemotherapeutic agent originally derived from *Taxus brevifolia*—is currently used particularly in the treatment of metastatic breast cancer. In this study, we aimed to explore the molecular effects of Abraxane on cervical cancer, one of the most prevalent malignancies affecting women worldwide. To investigate the potential effects of Abraxane, cultured cells were treated with 250 nM for HeLa cells and 200 nM for C-4I cells. RNA sequencing was then performed, and molecular responses were analysed using KEGG annotation, Gene Ontology, cluster heatmaps, and protein–protein interaction (PPI) analysis. Bioinformatic analysis of the global transcriptomic profile revealed that Abraxane induced the overexpression of *Cyclin E*, a key gene involved in the induction of G1-phase cell-cycle arrest, particularly through the p53 signalling pathway in HeLa cells. *GADD45* and *ATM*, two central proteins involved in the FoxO signalling pathway and known to respond to oxidative stress and participate in DNA-damage repair, were also found to be upregulated. Furthermore, the expression of pro-apoptotic genes *BIM* and *BCL-6* was increased in HeLa cells. In parallel, ferroptosis appeared to be induced in HeLa cells, as indicated by the upregulation of *HO-1* and *STAT1*. In C-4I cells, *Cyclin E* was similarly upregulated, indicating a potential G1-phase cell-cycle arrest. In addition, the upregulation of *ATM*, a protein crucial for DNA repair, and the activation of the homologous recombination repair pathway suggest that double-strand breaks (DSBs) may have occurred. In conclusion, these findings demonstrate that the molecular responses of HeLa and C-4I cell lines treated with Abraxane reveal its multifaceted anticancer effects.

Keywords: Abraxane, Cervical cancer, RNA seq, Cell cycle, Cell deaths, DNA damage.

INTRODUCTION

Abraxane is a nanotechnology-based chemotherapeutic agent used in the treatment of metastatic breast cancer, non-small cell lung cancer (NSCLC), and pancreatic cancer. Abraxane is a nanoparticle albumin-bound (nab) formulation of paclitaxel, a potent mitotic inhibitor, and was developed to overcome problems such as hypersensitivity reactions and other side effects associated with conventional paclitaxel formulations" (Gradishar et al., 2005; Desai, 2016). Approved by the U.S. Food and Drug Administration (FDA) in 2005, Abraxane significantly improved the pharmacokinetics and safety profile of paclitaxel, enabling more effective drug delivery with fewer adverse effects (Desai et al., 2006).

Abraxane is a chemotherapeutic drug approved based on a phase III clinical trial comparing it to standard paclitaxel in metastatic breast cancer (Moreno-Aspitia & Perez, 2005; Ciruelos & Jackisch, 2014). In combination with carboplatin, it has also been approved as a first-line treatment for advanced non-small cell lung cancer (NSCLC) (Socinski et al., 2012). Additionally, the combination of Abraxane and gemcitabine has been established as a standard first-line treatment for metastatic pancreatic cancer (Von Hoff et al., 2013).

Abraxane has the capacity to bind to the β-subunit of tubulin, thereby stabilizing microtubules and preventing their depolymerization. This disrupts the normal mitotic process, leading to cell cycle arrest at the G2/M phase and ultimately inducing apoptosis (Jordan & Wilson, 2004; Houghton et al., 2015). Furthermore, albumin interacts with gp60 receptors on endothelial cells, activating a process known as caveolae-mediated transcytosis. This mechanism allows the drug to traverse the endothelial barrier and accumulate within tumor

tissue (Desai et al., 2006). In addition, many tumors overexpress SPARC (Secreted Protein Acidic and Rich in Cysteine), a glycoprotein that binds albumin and facilitates enhanced intratumoral drug accumulation (Kratz, 2008; Iglesias, 2009). This mechanism of action enables selective delivery, reduces toxicity to normal tissues, and enhances anticancer efficacy.

This study was aimed to investigate the anticancer mechanism of Abraxane, a chemotherapeutic agent with effective anticancer activity, on cervical cancer, one of the most common cancer types in women, by using next-generation bioinformatic analysis method, RNA sequencing (RNA-seq), and to identify the molecular responses of cervical cancer treated with Abraxane.

MATERIAL AND METHODS

Cell Growth and Detection of Abraxane IC_{50}

The Human cervical carcinoma cell lines HeLa (ATCC, CCL-2) and C-4 I (ATCC, CRL1594) obtained in the USA were cultured in DMEM (Gibco) and Waymouth MB 752/1 (Gibco) medium with 10% fetal bovine serum, 100 µg/mL penicillin, and 100 µg/mL streptomycin (İecilline, İ.E. Ulagay) at 37°C in an atmosphere of 95% humidity and 5% CO_2. The cells were sub-cultured twice weekly using 25% trypsin. Abraxane was administered to cells at concentrations ranging from 50 to 400 nM for 24 hours in 96-well plates, using a cell density of 3×10^5 cells per well. The cytotoxic effect of Abraxane was evaluated using the MTT assay, a commonly employed method for assessing cell viability (Ali et al., 2024)

RNA Isolation, Library Preparation, and Sequencing Analysis

Total RNA was isolated using the GeneJET™ RNA Purification Kit (Thermo Scientific), following the manufacturer's protocol. To ensure consistent total RNA yield across samples, three biological replicates were pooled into a single RNA-seq experiment. The study consisted of four experimental groups: Abraxane-treated HeLa cells (HeLa_A), untreated HeLa control (HeLa_Control), Abraxane-treated C-4I cells (C-4I_A), and untreated C-4I control (C-4I_Control). Following RNA isolation, RNA sequencing (RNA-seq) libraries were constructed. The procedure included reverse transcription of RNA into complementary DNA (cDNA), random fragmentation and/or amplification of cDNA molecules, and ligation of sequencing adapters. Sequencing was performed using the DNBEQ platform, after which both data quality control and preprocessing were carried out. Raw sequencing reads were initially stored in FASTQ format. For quality filtering, SOAPnuke (v1.5.2) was used, and for alignment to the genome and transcriptome, we employed HISAT2 (v2.0.4). Upon generation of transcript models, gene, transcript, and exon-level expression were quantified. Clean reads were mapped to the reference transcriptome using Bowtie2 (v2.2.5). Finally, gene expression levels were estimated using RSEM (v1.2.8) (Ali et al., 2025).

Gene Enrichment and Pathway Analysis

In this study, quantitative gene expression analysis was conducted using pathway data from the Kyoto Encyclopedia of Genes and Genomes (KEGG) and Gene Ontology (GO) databases. The GO functional enrichment analysis identified significantly enriched terms among the candidate genes, offering insights into their associated biological roles. Each candidate gene was mapped to GO entries, and the number of genes associated with each term was calculated. Statistical significance was assessed using the phyper function in R. To correct for multiple testing, Q-values were computed, and GO terms with $Q \leq 0.05$ were considered significantly enriched. Enrichment categories included biological processes (BP), molecular functions (MF), and cellular components (CC). Similarly, KEGG pathway enrichment analysis was performed to identify significantly enriched metabolic and signaling pathways related to the candidate genes. Pathways with final Q-values ≤ 0.05 were regarded as biologically relevant and informative in understanding the regulatory mechanisms and cellular pathways influenced by Abraxane treatment.

Protein–Protein Interaction (PPI) Network Analysis

To further investigate the functional implications of the differentially expressed genes (DEGs), Protein–Protein Interaction (PPI) network analysis was performed. The PPI network provides a systematic overview of potential physical or functional interactions among proteins encoded by DEGs. In this study, the PPI network was constructed using all significantly differentially expressed genes, and a minimum interaction confidence score of 7 (PPI score ≥ 7) was used as the threshold. Analyzing the PPI network helped to reveal potential hub proteins and interaction modules associated with disease mechanisms and drug response pathways.

Statistical Analysis

In our study, computational statistical analysis and differential gene expression (DEG) analysis were performed using R packages. Adjusted p-values were applied to minimize the risk of false-positive results. Q-values were calculated as corrected p-values, and functions with a Q-value ≤ 0.05 were considered significantly enriched. Genes with |$\log_2$ fold change| (|$\log_2$FC|) > 1 and p-value < 0.01 were defined as differentially expressed between tumor and normal tissues (HeLa_Control vs. HeLa_A_IC50 and C-4 I_Control vs. C-4 I_A_IC50). A protein–protein interaction (PPI) network was constructed for the DEGs, with a minimum interaction confidence score of 0.7 (PPI score ≥ 0.7). Additionally, differentially expressed genes were defined as those with a false discovery rate (FDR) ≤ 0.001 and fold change (FC) > 2.

Statistical analyses of MTT assay data were performed using GraphPad Prism version 10.1. One-way analysis of variance (ANOVA) was used to assess differences between groups, and p-values < 0.05 were considered statistically significant.

RESULTS

Cytotoxicity and Identification of Abraxane IC_{50} Dose in HeLa and C-4 I Cells

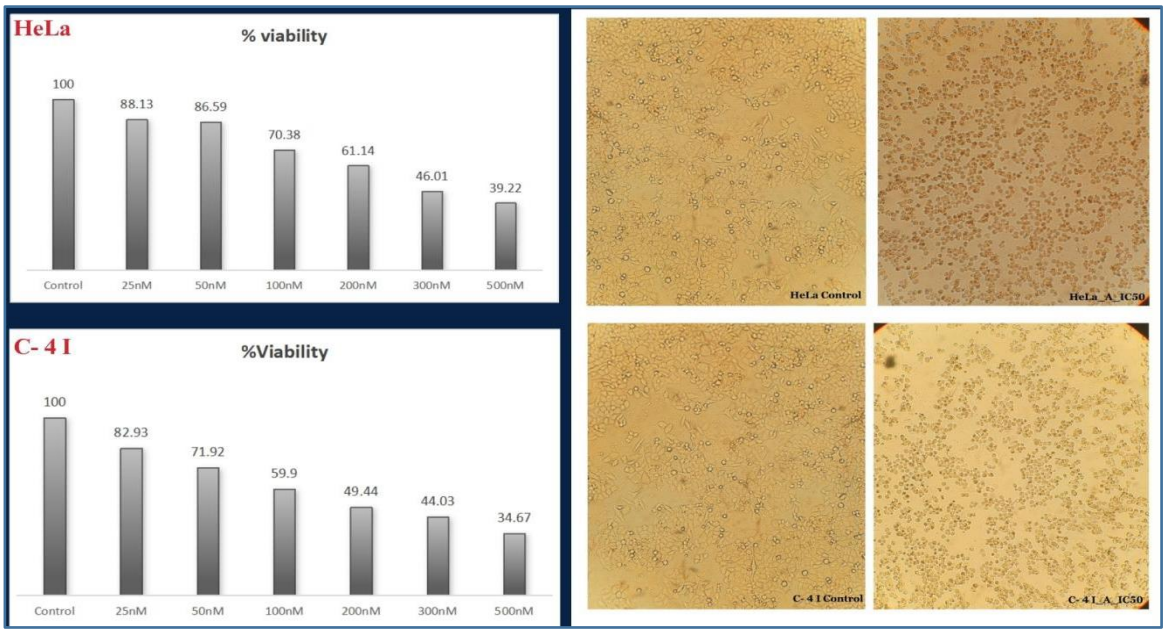

Figure 1. Percent Viability of HeLa and C-4 I Cells After 24-Hour Treatment with Abraxane

MTT assay results showed a decrease in the viability of Abraxane-treated cells compared to the control group. This cytotoxicity was dose-dependent and statistically significant (P ≤ 0.05). These findings were further supported by phase contrast microscopy images. Based on these results, we conclude that the IC_{50} dose of Abraxane is 250 nM for HeLa cells and 200 nM for C-4 I cells (Fig. 1).

RNA-Seq Data Analysis and Differential Gene Expression

In this study, RNA sequencing was performed to identify the molecular responses of HeLa and C-4I cells following Abraxane treatment. A total of four samples—HeLa_Control, HeLa_A, C-4I_Control, and C-4I_A—were analyzed using the DNBSEQ platform, yielding an average of 6.73 GB of data per sample. The average alignment rate to the reference genome was 90.21%, while the alignment rate to the reference gene set was 61.68% (Species: *Homo sapiens*; Source: UCSC Reference Genome; Version: hg38).

To assess the similarity of gene expression profiles among the samples, the Pearson correlation coefficient (PCC) was calculated based on the expression levels of all shared genes. PCC values, ranging from -1 to +1, provide a quantitative measure of correlation: values closer to +1 indicate greater similarity. The high PCC

values observed between sample pairs suggest a strong consistency and biological reliability (Fig. 2C). Venn diagram analysis was used to illustrate the distribution and overlap of differentially expressed genes (DEGs) between comparison groups. Each circle represents a gene set for one experimental condition; overlapping regions indicate shared genes, while non-overlapping regions represent uniquely expressed genes. The numbers within each domain reflect the number of genes present in those intersections (Fig. 2D).

Hierarchical clustering analysis was conducted using the R package pheatmap, based on the DEGs identified in each condition. This analysis grouped the samples according to expression similarity and revealed clear separation between treated and untreated groups, supporting the reproducibility of treatment-induced gene expression changes.

Overall, a total of 1,276 DEGs were identified in HeLa cells and 500 DEGs in C-4I cells. In the HeLa_A vs. HeLa_Control comparison, 403 genes were upregulated and 873 were downregulated following Abraxane treatment. Similarly, in the C-4I_A vs. C-4I_Control comparison, 203 genes were upregulated, and 297 genes were downregulated (Fig. 2 A- 2 B).
To further investigate the key genes involved in the comparisons between HeLa_Control/HeLa_A_IC50 and C-4I_Control/C-4I_A_IC50, Key Driver Analysis (KDA) was conducted. In HeLa cells, KDA identified several central driver genes, including *CDK1* (147 nodes), *CCNB1* (144 nodes), *CDC6* (138 nodes), *AURKA* (121 nodes), *UBE2C* (113 nodes), *TOP2A* (106 nodes), *CENPA* (104 nodes), *PIMREG* (66 nodes), and *MTFR2* (34 nodes). In the C-4 I cell line, the top driver genes were *CCNB1* (94 nodes), *AURKA* (88 nodes), *CENPA* (87 nodes), *PBK* (79 nodes), *KIF23* (76 nodes), *BIRC5* (78 nodes), *CIKS2* (67 nodes), *CDCA3* (67 nodes), *KNL1* (52 nodes), *DHCR7* (34 nodes), and *EBP* (25 nodes) (Fig.3)

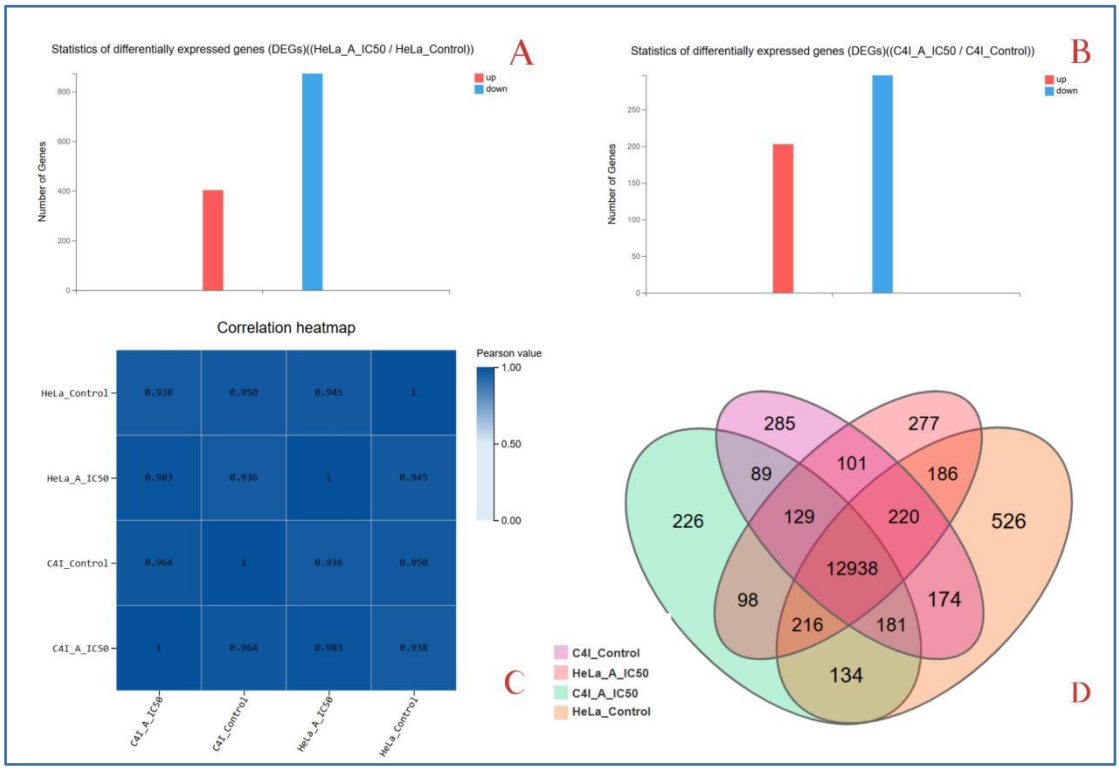

Figure 2. Differentially Expressed Genes (DEGs) Identified in Abraxane-Treated HeLa and C-4I Cells. Column diagram of DEGs showing the number of upregulated and downregulated DEGs in the HeLa_Control/HeLa_A_IC50 (A) and C-4 I_Control /C-4 I_A_IC50 (B). (C)Pearson correlation coefficient (PCC) values representing the similarity of gene expression profiles between samples. Darker colors indicate higher correlation coefficients, reflecting greater similarity, while lighter colors indicate lower correlations. (D) Venn diagram illustrating the overlap of differentially expressed genes (DEGs) between control and Abraxane-treated groups in HeLa and C-4I cell lines, following treatment with their respective IC_{50} doses of Abraxane. DEGs were identified using the thresholds FDR ≤ 0.001, $|Log_2FC| \geq 1$, and $P \leq 0.05$.

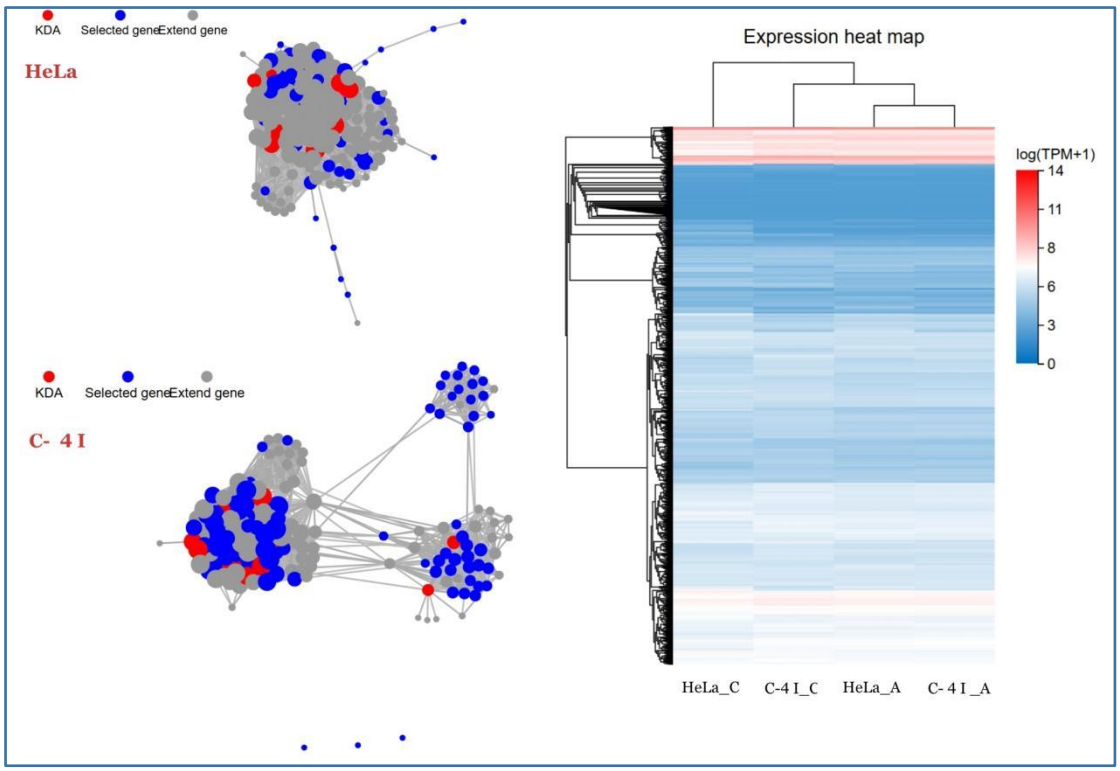

Figure 3. KDA analysis of differential expression genes (DEGs) for HeLa and C- 4 I groups and Cluster analysis comparing DEG groups. Expression set of DEGs in each comparison group. The horizontal axis is the log2 of the sample (expression value +1) and the vertical axis is the gene. Under the default color matching, the warmer the color block is, the higher the expression level is, and the colder the color block is, the lower the expression level is.

KEGG and GO Enrichment Analyses of DEGs

To investigate the molecular responses of cells treated with Abraxane, particularly the mechanisms associated with its anticancer effects, quantitative analyses of gene expression data were performed based on Kyoto Encyclopedia of Genes and Gene Ontology, along with other bioinformatics analyses. Additionally, clustering analysis was conducted to identify gene expression patterns.
According to KEGG pathway enrichment analysis, Abraxane treatment led to the activation of several signaling pathways and cellular processes associated with cell death and stress response. Notably, the p53 signaling pathway, the FoxO signaling pathway, cell cycle regulation, and ferroptosis were significantly enriched in the treated samples. In C-4I cells specifically, in addition to the activation of the p53 signaling pathway, both the cell cycle regulation pathway and the homologous recombination-based DNA repair mechanism were also activated, suggesting a complex molecular response involving both apoptotic and DNA damage repair processes (Fig.4).

According to the Gene Ontology (GO) analysis of HeLa cells treated with Abraxane, several terms within the Cellular Component (CC) category were significantly enriched (Q value < 0.05). Notably, the cyclin-dependent protein kinase holoenzyme complex (GO:0000307) and Cyclin A2-CDK2 complex (GO:0097124), both associated with cell cycle regulation, were among the most enriched terms. In the Molecular Function (MF) category, significant enrichment was observed for 2'-5'-oligoadenylate synthetase activity (GO:0001730; Q = 0.01), diamine N-acetyltransferase activity (GO:0004145; Q=0.02), and DNA binding (GO:0003677; Q = 0.02). Additionally, GO terms related to cell cycle and microtubule function such as cyclin-dependent protein serine/threonine kinase regulator activity (GO:0016538) and microtubule motor activity (GO:0003777) were identified. In the Biological Process (BP) category, all significantly expressed biological processes exhibited Q values below 0.05. Among them, response to endoplasmic reticulum stress (GO:0034976), which is associated with oxidative stress, was notably enriched.

Gene Ontology (GO) analysis of C-4I cells treated with Abraxane revealed significant enrichment in several processes related to the cell cycle and DNA damage response within the Biological Process (BP) category.

These included mitotic G2 DNA damage checkpoint (GO:0007095; Q = 0.001), cell cycle (GO:0007049; Q = 0.001), DNA damage response, signal transduction by p53 class mediator resulting in cell cycle arrest (GO:0006977; Q = 0.002), cellular response to DNA damage stimulus (GO:0006974; Q = 0.03), and DNA repair (GO:0006281; Q = 0.05). In the Molecular Function (MF) category, the term cyclin-dependent protein serine/threonine kinase regulator activity (GO:0016538; Q = 0.03), which is directly related to cell cycle regulation, was significantly enriched. Although the Q values in the Cellular Component (CC) category were slightly above 0.05, enrichment was still observed in components closely associated with cell cycle and microtubule function, such as cyclin B1-CDK1 complex (GO:0097125), cyclin E1-CDK2 complex (GO:0097134), and microtubule (GO:0005874).

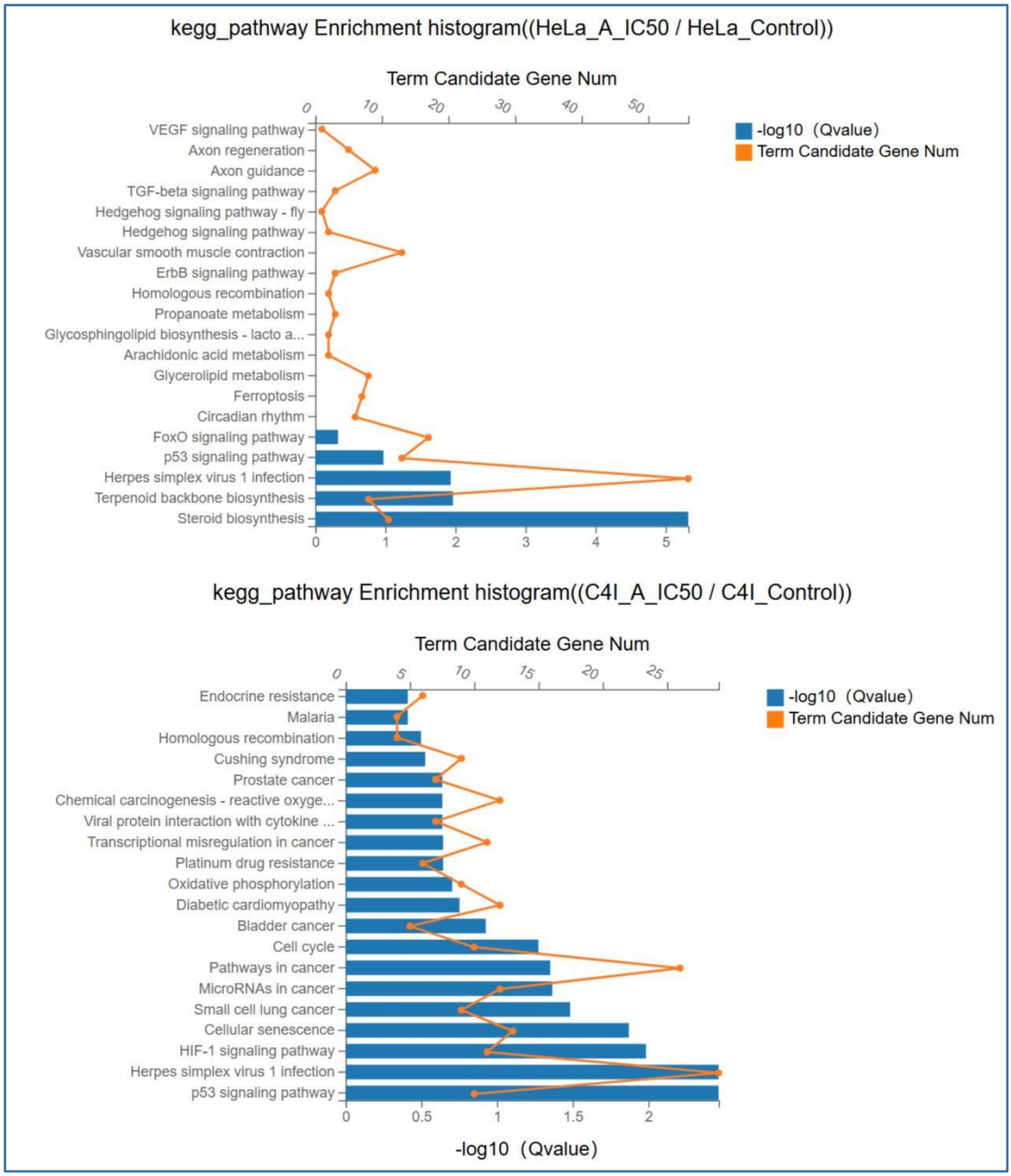

Figure 4. KEGG functional pathways regulated by DEGs when applied to the safranal HeLa and C– 4 I cells (FDR ≤ 0.001, Log2FC=1, P ≤0.05).

PPI Network Analysis

A total of 1,276 and 500 differentially expressed genes (DEGs) were identified in HeLa and C-4I cell lines, respectively. Protein-protein interaction (PPI) analysis in HeLa cells showed that the p53 signaling pathway was significantly involved, with *CCNB1* (6 nodes), *ATM* (4 nodes), and *GADD45* (4 nodes) contributing to the network. In the FoxO signaling pathway, *GADD45* (5 nodes), *CCNB1* (5 nodes), *BCL2L12* (3 nodes), and *ATM* (3 nodes) were identified. In the ferroptosis pathway, all involved proteins had a node value of 2, except for *TF* and *SAT2*, which each had a node value of 1. These findings highlight critical regulatory hubs and pathways activated in response to Abraxane treatment in both cell lines (Fig. 6). In C-4 I cells, within the regulated p53 signaling pathway, *GADD45A*, *ATM*, and *GTSE1* exhibited more interactions compared to other proteins. In the cell cycle process, all involved proteins displayed similar levels of interaction. In the homologous recombination DNA damage repair pathway, the expressed proteins also showed similar interaction values (Fig.7).

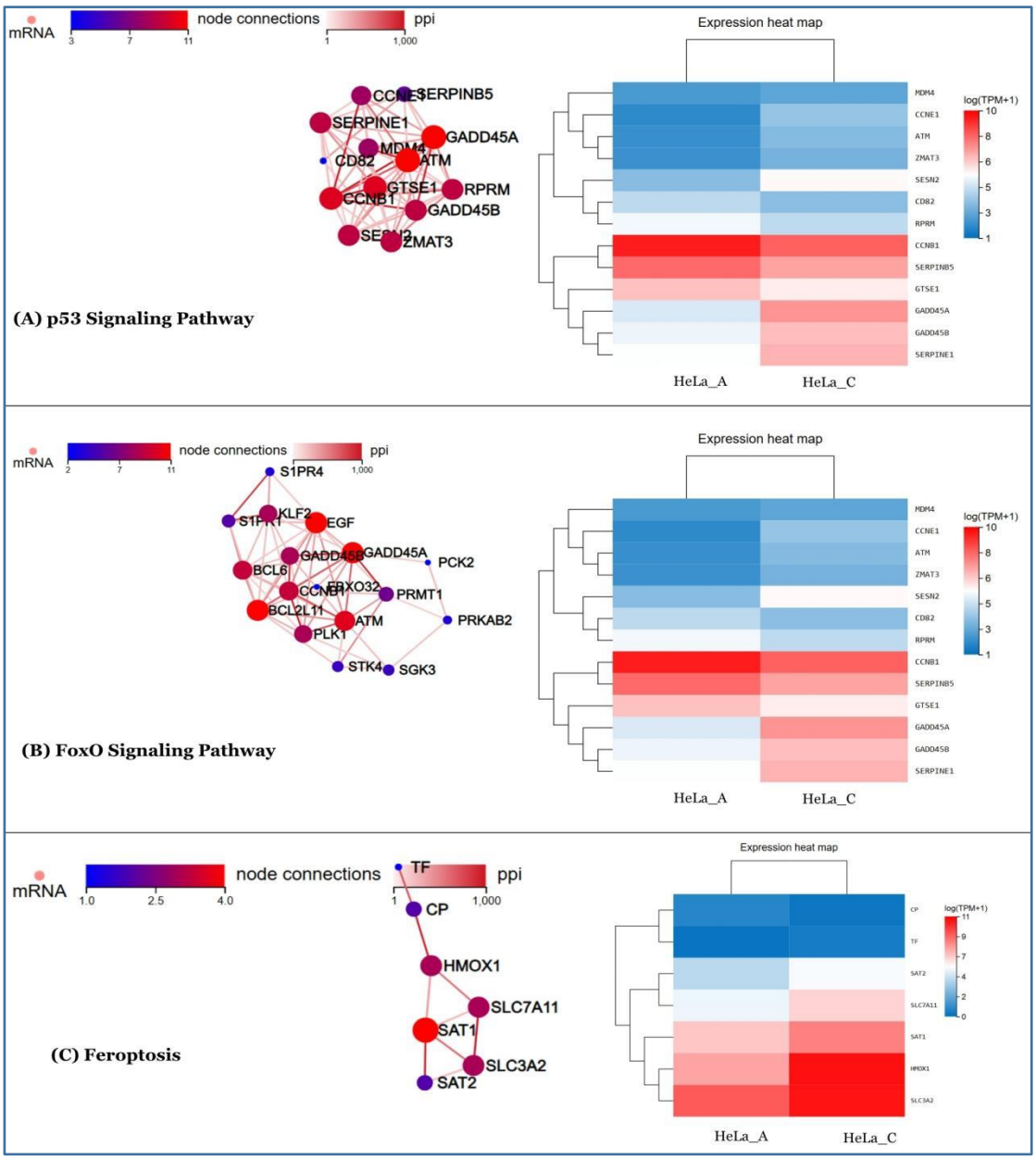

Figure 6. Heatmap Clustering and Protein–Protein Interactions of p53, FoxO Signaling Pathways, and Ferroptosis Regulated in Abraxane-Treated HeLa Cells.

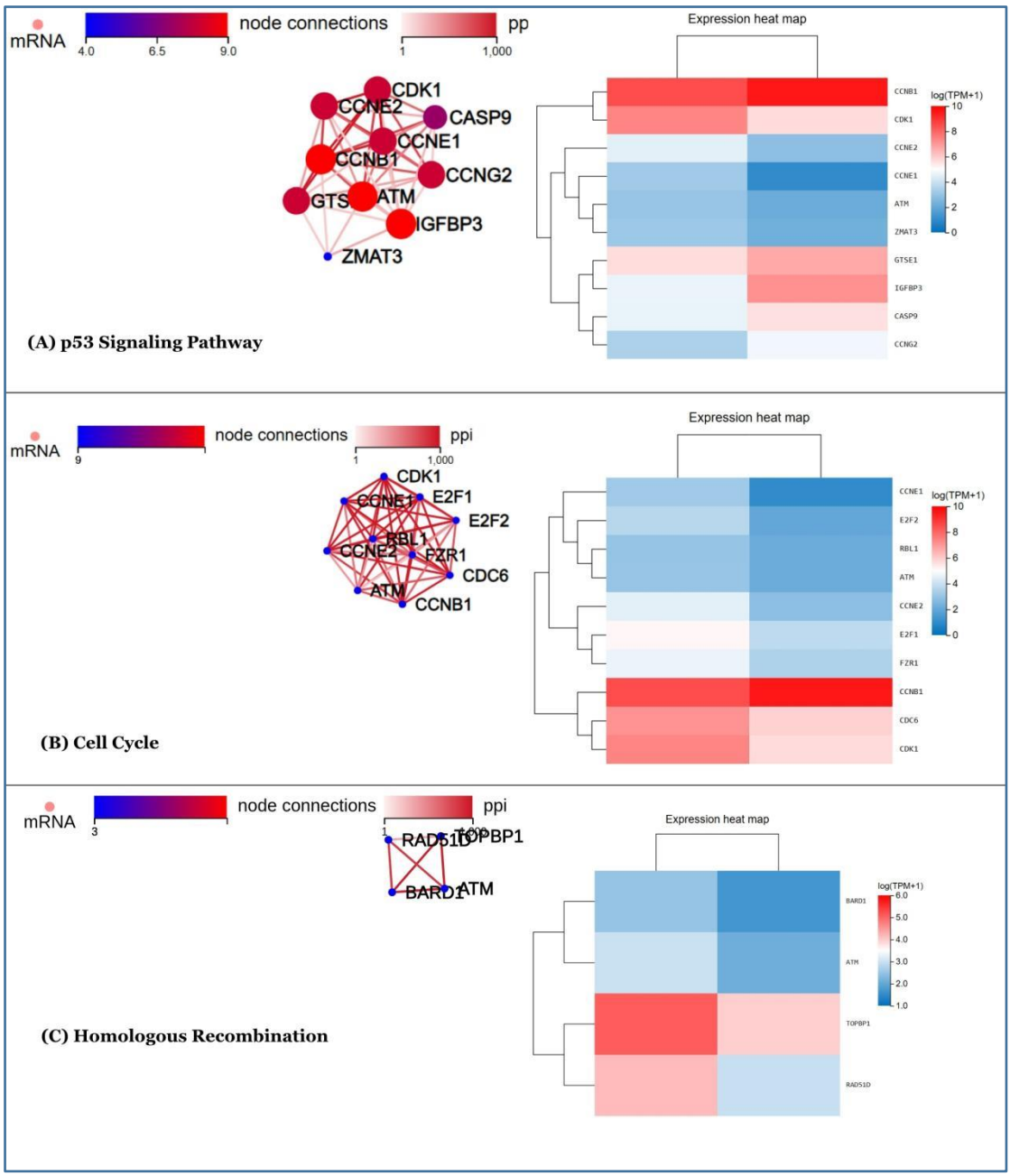

Figure 7. Heatmap Clustering and Protein–Protein Interactions of p53Signaling Pathway, Cell Cycle and Homolgous Recombinations in Abraxane-Treated C- 4 I Cells.

DISCUSSION

Abraxane (nab-paclitaxel), an albumin-bound formulation of paclitaxel, has shown significant clinical efficacy in a variety of solid tumors, including breast, pancreatic, and lung cancers. Its unique nanoparticle structure has been reported in many studies to increase drug delivery and reduce toxicity compared to conventional paclitaxel. However, its mechanical effect on cervical cancer, especially at the transcriptomic level, has not yet been sufficiently investigated (Gradishar et al., 2005; Moreno-Aspitia and Perez, 2005; Ciruelos and Jackisch, 2014; Desai, 2016). In this context, our research aimed to identify the molecular responses of Abraxane administered to cervical cancer cells and to determine its anticancer properties in particular. Our findings suggest that:

Abraxane-Induced Modulation of the Cell Cycle in HeLa and C-4I Cells

The cell division cycle functions in an oscillatory manner to couple cellular DNA replication with chromosomal segregation, ensuring that replicated genetic material is distributed equally to the two daughter cells. In cycling somatic cells, the intervals between DNA synthesis (S phase) and mitosis (M phase) are separated by two gap phases (G1 and G2), respectively. Cyclins expressed in different phases of the cycle allosterically regulate a family of cyclin-dependent kinases (CDKs), whose phosphorylation of key substrates drives cell cycle progression. Additional checkpoint controls act to ensure that one process is completed before another begins (Sherr and Bartek, 2017). Cancer is fundamentally a disease of uncontrolled cell proliferation, and this is often caused by disruptions in the cell cycle: overexpression of cyclins (e.g. cyclin D1), inactivation of tumor suppressors such as p53, Rb, mutations in CDKs or their inhibitors. These abnormalities allow cancer cells to bypass checkpoints, continue to divide despite DNA damage, and resist cell death mechanisms (Hanahan and Weinberg, 2011). .

In our Study, It was observed that the p53 signaling pathway was regulated in both HeLa and C-4I cells treated with Abraxane. In HeLa cells, this pathway was regulated through 13 genes, while in C-4I cells, it was regulated through 10 genes.In HeLa cells, the *ATM* gene—which plays a key role in activating DNA damage response and repair mechanisms—was found to be upregulated, leading to the phosphorylation of p53. Additionally, *MDM-X*, a gene involved in cell cycle regulation, was also upregulated. Following p53 phosphorylation, the *Reprimo* and *B99* genes were downregulated, which in turn led to the downregulation of *Cyclin B* expression. Conversely, upregulation of the *Cyclin E* gene suggested the induction of cell cycle arrest at the G1 phase. Furthermore, the Gadd45–Sestrins complex, which participates in DNA damage repair mechanisms, was also found to be upregulated (Fig. 6A).

In C-4I cells, the *ATM* gene, known to activate DNA damage response and repair mechanisms, was also upregulated. Subsequently, phosphorylation and activation of p53 resulted in downregulation of the *B99* gene. Moreover, the upregulation of *Cyclin E* suggested that the cell cycle was arrested at the G1 phase. Following p53 phosphorylation, upregulation of *PAG608* and downregulation of Casp-9 indicated the occurrence of apoptosis in Abraxane-treated C-4I cells. Additionally, the *IGF-BP3* complex, which inhibits the IGF signaling pathway, was found to be downregulated (Fig.7-Fig.8).
In C-4I cells treated with Abraxane, the cell cycle was found to be affected. Notably, DNA damage triggered the upregulation of the *ATM/ATR* complex in response to signals from DNA damage checkpoints. Following this, genes such as *Cyclin E, p107, p130,* and *E2F1/2/3*—critical for the G1 to S phase transition—were upregulated. This indicates that the cell cycle was arrested at the G1 phase or at the G1/S checkpoint. Additionally, following p53 phosphorylation, *Cyclin E* was observed to be downregulated while *CDK1* was upregulated. These findings further confirm that, in response to DNA damage, the cell cycle was halted in the G1 or G1/S phase and progression through the cell cycle was prevented (Fig.9).

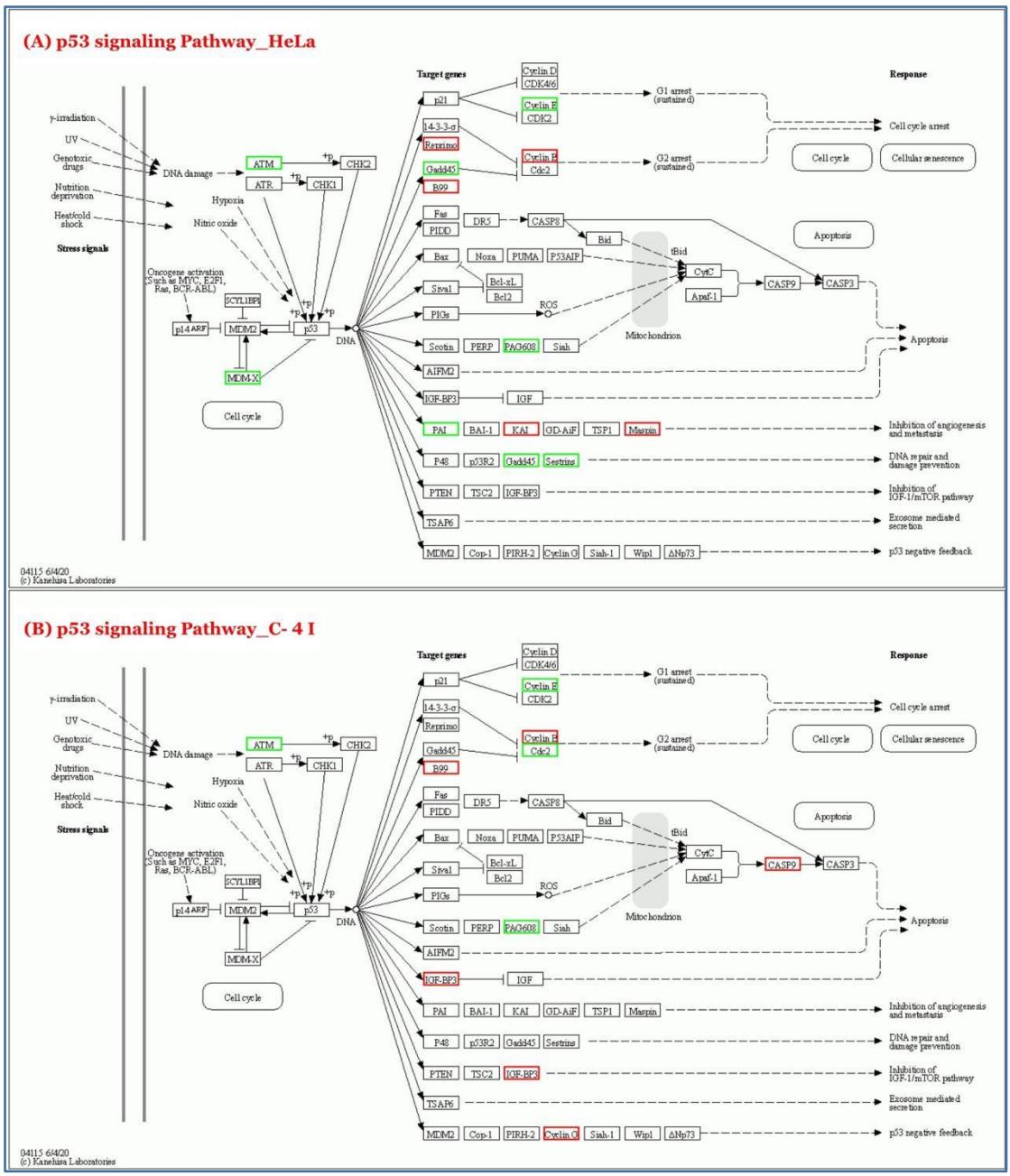

Figure 8. KEGG Map of the p53 Signaling Pathway in Abraxane-Treated HeLa and C-4I Cells

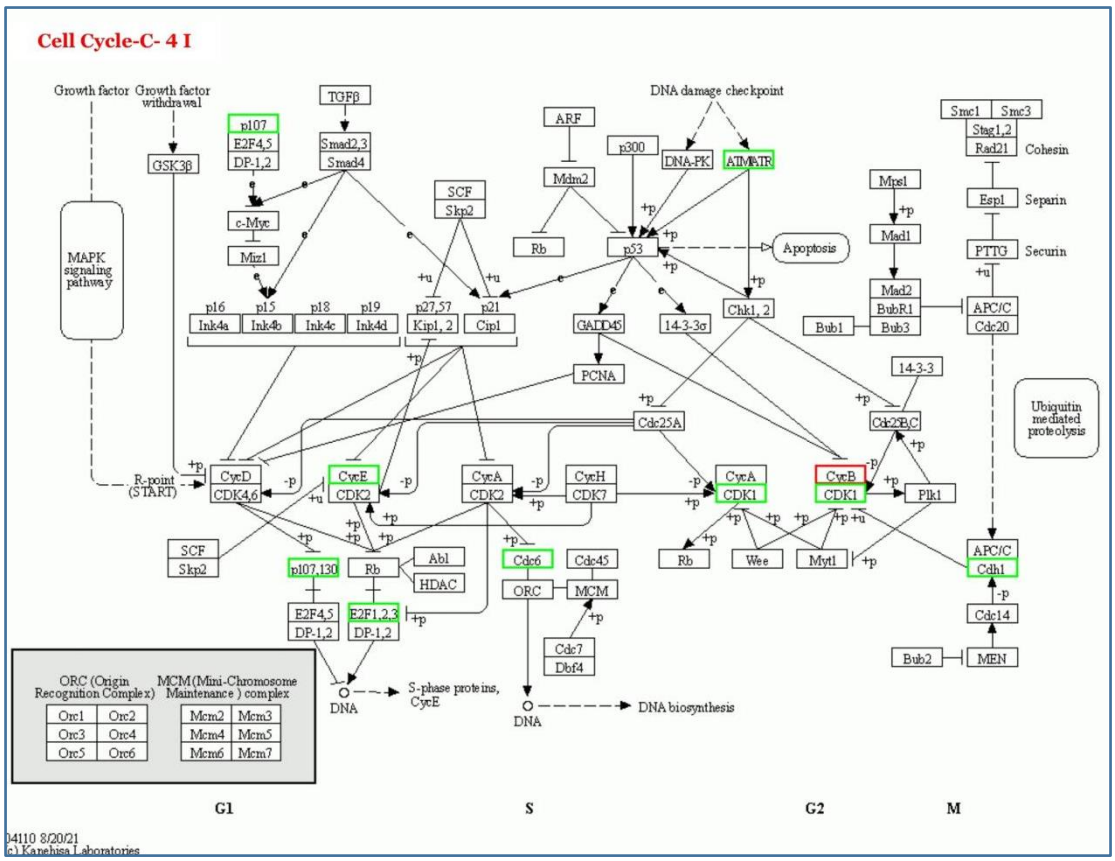

Figure 9. KEGG Map of the Cell cycle in Abraxane-Treated C-4I Cells.

Abraxane-Induced Ferroptosis in HeLa Cells

Ferroptosis is a form of cell death characterized by the production of reactive oxygen species from the accumulated peroxidation of iron and lipids. It can be induced by investigational compounds (e.g., Erastin, RSL3) or clinical drugs (e.g., sulfasalazine, sorafenib) in cancer cells and some normal cells. Ferroptosis plays a role in many physiological and pathological processes, such as cancer cell death, neurodegenerative diseases, tissue damage, and acute renal failure (Tong et al., 2022).

In our study, According to KEGG pathway analysis, treatment with Abraxane led to the activation of ferroptosis, a regulated form of cell death. During this process, the *CP* and *SAT1* genes were found to be downregulated, while *TF*, *SLC7A11*, *HMOX1*, and *SLC3A2* were upregulated. Notably, the upregulation of *HMOX1* (heme oxygenase 1, also known as HO-1) induces the production of ferrous iron (Fe^{2+}), which promotes the generation of reactive oxygen species (ROS) via the Fenton reaction. Subsequently, Fe^{2+} is oxidized to ferric iron (Fe^{3+}), which has been shown to stimulate the expression of transferrin (*TF*). This transferrin is then internalized into the cell through the endosomal pathway.

In addition, the *STAT1* gene was significantly upregulated in Abraxane-treated HeLa cells. *STAT1* is known to activate *ALOX15*, a gene that plays a pivotal role in promoting ferroptosis. Therefore, these findings suggest that ferroptosis was likely induced through the *STAT1–ALOX15* signaling axis following Abraxane treatment.

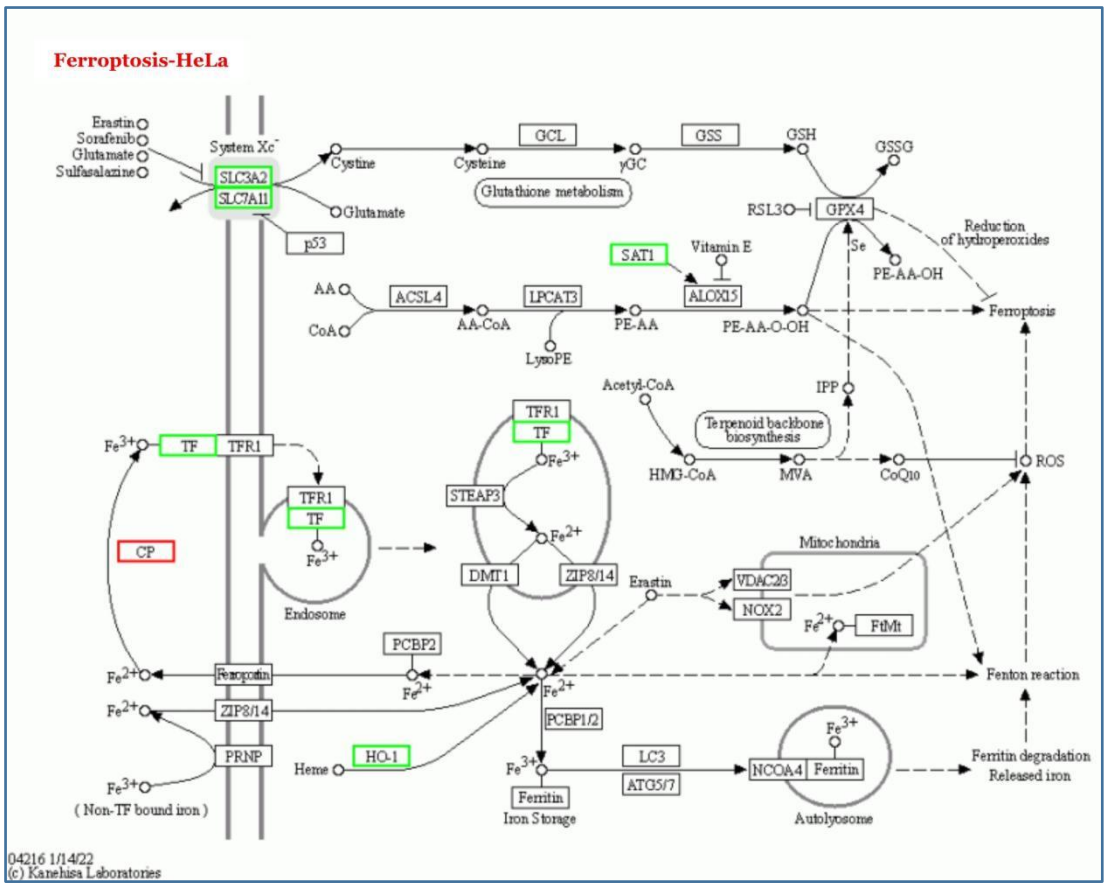

Figure 10. KEGG Map of the Ferroptosis Signaling Pathway in Abraxane-Treated HeLa Cells.

Abraxane Activated HR DNA Repair Damage in C- 4 I Cells

Homologous recombination (HR) is a high-fidelity DNA repair mechanism dedicated to repairing double-strand breaks (DSBs), active mainly during S and G_2 phases when a sister chromatid is available as a template (Sun et al., 2020).

In our study, we identified that homologous recombination (HR) mechanisms were activated in Abraxane-treated C-4I cells. Upon examining the KEGG pathway related to HR, we observed the upregulation of three genes. Among them, *ATM* plays a key role in recognizing DNA damage. After detection, it sends signals to downstream proteins to initiate the DNA repair response. Phosphorylation of ATM induces the recruitment of repair-associated genes such as *TOPBP1* and *BARD1* to the DNA damage site, thereby initiating the homologous recombination repair process.

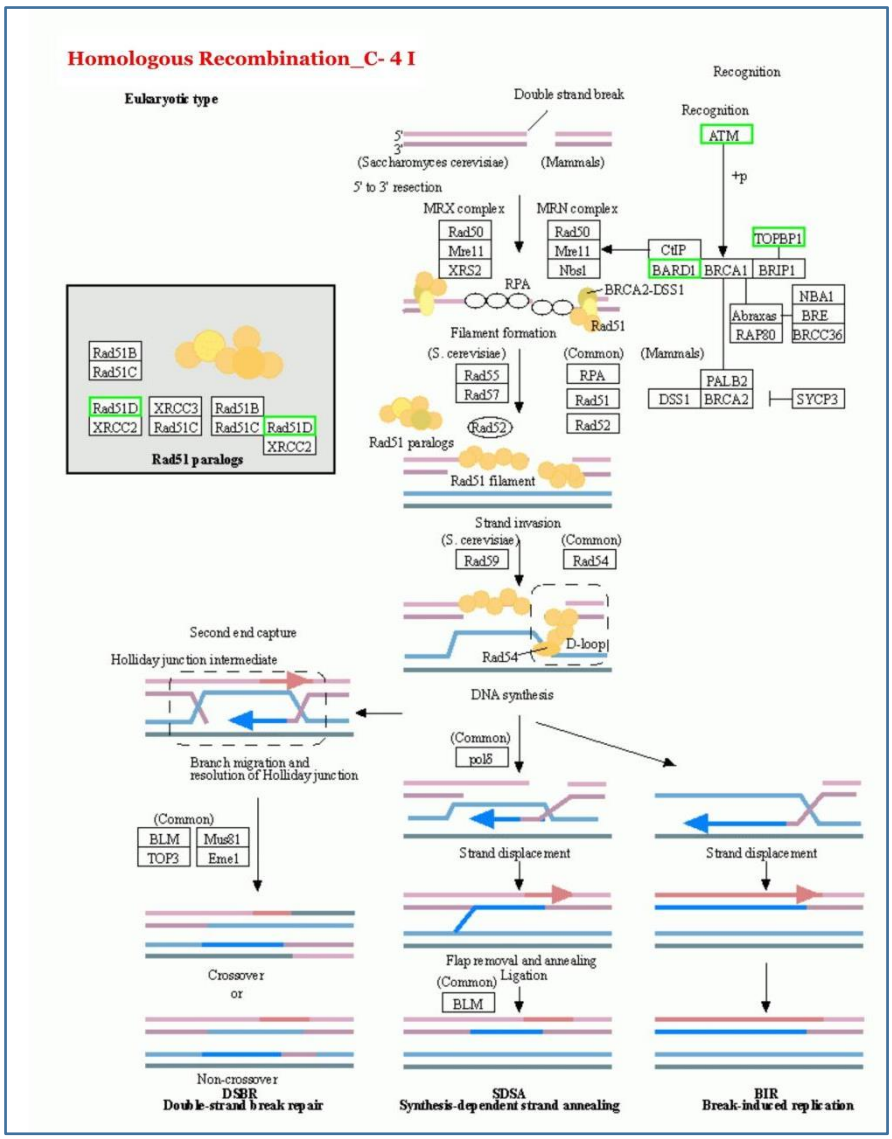

Figure 11. KEGG Map of the Homologous Recombination in Abraxane-Treated C- 4 I Cells.

Numerous studies have demonstrated that Abraxane possesses significant anticancer effects and is reported to be a more effective therapeutic agent than conventional paclitaxel. In a Phase II clinical trial conducted by Alberts et al. (2012), the efficacy of nab-paclitaxel (Abraxane) was evaluated in the treatment of recurrent or persistent advanced cervical cancer. The results indicated enhanced therapeutic efficacy in this patient population. Similarly, Gurses and Topcul (2013) investigated the antiproliferative effects of Abraxane on HeLa cells by assessing cell kinetics, including labeling index, mitotic index, and apoptotic index. Their findings revealed that Abraxane treatment led to an increased apoptotic index, accompanied by reductions in mitotic and labeling indices, indicating suppressed proliferation of tumor cells. In a recent study, Cha et al. (2022) employed proteomic and transcriptomic analyses to explore mechanisms of chemoresistance across three chemotherapeutic drugs. Their bioinformatics analysis revealed that Notch signaling, immune response, and protein relocalization were uniquely associated with drug resistance phenotypes. Furthermore, proteomic signatures linked to resistance were identified as potential therapeutic targets of several FDA-approved drugs. Prognostic proteins such as PLXNB2 and ACOX3 were also identified, with PLXNB2 overexpression associated with significantly increased risk and ACOX3 downregulation correlating with poor overall survival.

Andalib et al. (2023) adopted an integrative bioinformatics and network-based approach to elucidate the molecular mechanisms underlying cervical cancer. Transcriptome analysis of three microarray datasets revealed 218 commonly differentially expressed genes (DEGs) between control and cervical cancer samples. KEGG pathway enrichment highlighted key pathways including the cell cycle, drug metabolism, and DNA replication. Gene ontology (GO) terms such as cornification, proteolysis, cell division, and DNA replication

were also significantly enriched. Protein–protein interaction (PPI) network analysis identified 20 hub genes, and survival analysis validated several key biomarkers, including *CDC45*, *MCM2*, *PCNA*, and *TOP2A*. Furthermore, regulatory network analyses identified 10 transcription factors and 10 microRNAs potentially involved in disease progression.

In our study, the effects of Abraxane on HeLa and C-4I cells were investigated. Our findings indicate that Abraxane induces cell cycle arrest at the G1 phase in both cell lines, triggers ferroptosis-mediated cell death in HeLa cells, and causes double-strand DNA damage (DSB) in C-4I cells, thereby exhibiting anticancer effects. Although our results are not fully consistent with previous studies in the literature, they support the anticancer potential of Abraxane.

CONCLUSION

Abraxane is a nanoformulation of paclitaxel and is a chemotherapeutic agent that exhibits anticancer effects in various solid tumors. In this study, the effects of Abraxane on cervical cancer-derived cells—one of the most common malignancies among women—were investigated using RNA sequencing and bioinformatics analysis. The results revealed that Abraxane induced cell cycle arrest, caused DNA damage, and triggered cell death mechanisms, including ferroptosis. To further elucidate these findings, the use of advanced molecular techniques is planned.

REFERENCES:

1. Alberts, D. S., Blessing, J. A., Landrum, L. M., Warshal, D. P., Martin, L. P., Rose, S. L., ... & Ramondetta, L. M. (2012). Phase II trial of nab-paclitaxel in the treatment of recurrent or persistent advanced cervix cancer: A gynecologic oncology group study. *Gynecologic oncology*, *127*(3), 451-455.
2. Ali, S. A., Özcan, F. G., & Karabulut-bulan, O. Evaluation of the Antiproliferative Effect of Safranal in C-4 I Cervical Cancer Cell Line. *Doğu Karadeniz Sağlık Bilimleri Dergisi*, *2*(Kongre Özel Sayısı), 117-128.
3. Ali, S. A., Ozcan, G., & Bulan, N. O. (2025). Molecular Mechanisms of Antiproliferative Effects of Safranal on Cervical Cancer: Evidence from Bioinformatics Analysis. *Current Proteomics*.
4. Andalib, K. S., Rahman, M. H., & Habib, A. (2023). Bioinformatics and cheminformatics approaches to identify pathways, molecular mechanisms and drug substances related to genetic basis of cervical cancer. *Journal of Biomolecular Structure and Dynamics*, *41*(23), 14232-14247.
5. Cha, H. K., Cheon, S., Kim, H., Lee, K. M., Ryu, H. S., & Han, D. (2022). Discovery of proteins responsible for resistance to three chemotherapy drugs in breast cancer cells using proteomics and bioinformatics analysis. *Molecules*, *27*(6), 1762.
6. Ciruelos, E., & Jackisch, C. (2014). Evaluating the role of nab-paclitaxel (Abraxane) in women with aggressive metastatic breast cancer. *Expert review of anticancer therapy*, *14*(5), 511-521.
7. Desai, N. (2016). Nanoparticle albumin-bound paclitaxel (Abraxane®). In *Albumin in medicine: Pathological and clinical applications* (pp. 101-119). Singapore: Springer Singapore.
8. Desai, N., Trieu, V., Yao, Z., Louie, L., Ci, S., Yang, A., ... & Soon-Shiong, P. (2006). Increased antitumor activity, intratumor paclitaxel concentrations, and endothelial cell transport of cremophor-free, albumin-bound paclitaxel, ABI-007, compared with cremophor-based paclitaxel. *Clinical cancer research: an official journal of the American Association for Cancer Research*, *12*(4), 1317-1324.
9. Gradishar, W. J., Tjulandin, S., Davidson, N., Shaw, H., Desai, N., Bhar, P., ... & O'Shaughnessy, J. (2005). Phase III trial of nanoparticle albumin-bound paclitaxel compared with polyethylated castor oil–based paclitaxel in women with breast cancer. *Journal of clinical oncology*, *23*(31), 7794-7803.
10. Gurses, N., & Topcul, M. (2013). The effect of abraxane on cell kinetic parameters of HeLa cells. *Asian Pacific Journal of Cancer Prevention*, *14*(7), 4229-4233.
11. Hanahan, D., & Weinberg, R. A. (2011). Hallmarks of cancer: the next generation. *cell*, *144*(5), 646-674.
12. Houghton, P. J., Kurmasheva, R. T., Kolb, E. A., Gorlick, R., Maris, J. M., Wu, J., ... & Smith, M. A. (2015). Initial testing (stage 1) of the tubulin binding agent nanoparticle albumin-bound (nab) paclitaxel (Abraxane®) by the Pediatric Preclinical Testing Program (PPTP). *Pediatric blood & cancer*, *62*(7), 1214-1221.
13. Iglesias, J. (2009). nab-Paclitaxel (Abraxane®): an albumin-bound cytotoxic exploiting natural delivery mechanisms into tumors. *Breast Cancer Research*, *11*(Suppl 1), S21.
14. Jordan, M. A., & Wilson, L. (2004). Microtubules as a target for anticancer drugs. *Nature reviews cancer*, *4*(4), 253-265.

15. Kratz, F. (2008). Albumin as a drug carrier: design of prodrugs, drug conjugates and nanoparticles. *Journal of controlled release*, *132*(3), 171-183.
16. Lee, K. H., Yim, E. K., Kim, C. J., Namkoong, S. E., Um, S. J., & Park, J. S. (2005). Proteomic analysis of anti-cancer effects by paclitaxel treatment in cervical cancer cells. *Gynecologic oncology*, *98*(1), 45-53.
17. Moreno-Aspitia, A., & Perez, E. A. (2005). North Central Cancer Treatment Group N0531: Phase II Trial of Weekly Albumin-Bound Paclitaxel (ABI-007; Abraxane™) in Combination with Gemcitabine in Patients with Metastatic Breast Cancer. *Clinical breast cancer*, *6*(4), 361.
18. Sherr, C. J., & Bartek, J. (2017). Cell cycle–targeted cancer therapies. *Annual Review of Cancer Biology*, *1*(1), 41-57.
19. Škubník, J., Pavlíčková, V., Ruml, T., & Rimpelová, S. (2021). Current perspectives on taxanes: Focus on their bioactivity, delivery and combination therapy. *Plants*, *10*(3), 569.
20. Socinski, M. A., Bondarenko, I., Karaseva, N. A., Makhson, A. M., Vynnychenko, I., Okamoto, I., ... & Renschler, M. F. (2012). Weekly nab-paclitaxel in combination with carboplatin versus solvent-based paclitaxel plus carboplatin as first-line therapy in patients with advanced non–small-cell lung cancer: final results of a phase III trial. *Journal of clinical oncology*, *30*(17), 2055-2062.
21. Sun, Y., McCorvie, T. J., Yates, L. A., & Zhang, X. (2020). Structural basis of homologous recombination. *Cellular and Molecular Life Sciences*, *77*, 3-18.
22. Tong, X., Tang, R., Xiao, M., Xu, J., Wang, W., Zhang, B., ... & Shi, S. (2022). Targeting cell death pathways for cancer therapy: recent developments in necroptosis, pyroptosis, ferroptosis, and cuproptosis research. *Journal of hematology & oncology*, *15*(1), 174.
23. Von Hoff, D. D., Ervin, T., Arena, F. P., Chiorean, E. G., Infante, J., Moore, M., ... & Renschler, M. F. (2013). Increased survival in pancreatic cancer with nab-paclitaxel plus gemcitabine. *New England journal of medicine*, *369*(18), 1691-1703.

➢ *ORAL PRESENTATION*

Antiquorum Sensing and Antibiofilm Potentials of *Origanum vulgare* L.

Ayşegül Akkoyunlu[1*](*ORCID:https://orcid.org/0000-0002-3663-7412*), Görkem Dülger[2](*ORCID: https://orcid.org/0000-0002-1506-1549*), Başaran Dülger[3](*ORCID: https://orcid.org/0000-0002-3184-2652*)

[*1]DuzceUniversity,Graduate Education Institue, Department of Biology, Duzce, Türkiye.
[2]Duzce University, Faculty of Medicine, Department of Medical Biology, Duzce, Türkiye.
[3]DuzceUniversity, Faculty of Art and Science, Department of Biology, Duzce, Türkiye.

*Corresponding author e-mail: aysegulgungor84@gmail.com

Abstract

A novel approach to inhibit virulence factors involves disrupting the bacterial communication mechanism and preventing biofilm formation without inhibiting bacterial growth. The aim of this study was to determine the inhibitory potential of ethanol extract obtained from *Origanum vulgare* L. against the quorum sensing (QS) mechanism of *Chromobacterium violaceum* ATCC 12472 and also against *Escherichia coli* and *Pseudomonas aeruginosa* bacterial biofilms. In anti-QS analysis using the well diffusion method, the extract demonstrated a strong inhibitory property (15.0 ± 1.0 mm) on the *C. violaceum* ATCC 12472 biosensor strain. Furthermore, in the microplate biofilm analysis, it inhibited *P. aeruginosa* biofilm by 93.30% and *E. coli* biofilm by 77.72% at the maximum level at a concentration of 50 mg/mL. The results demonstrate the potential of *O. vulgare* L. ethanol extract as a natural agent that targets QS and biofilm formation.

Keywords:*Origanum vulgare* L., virulance attenuation, *Pseudomonas aeruginosa*, *Escherichia coli*, *Chromobacterium violaceum* ATCC 12472.

INTRODUCTION

The communication mechanism between bacteria, known as quorum sensing (QS), allows planktonic cells to interact with each other, controls the expression of virulence factors and biofilm development. Bacteria that continuously change their gene expression through QS regulate their pathogenic properties and can escape host immunity by changing their surface antigens. Disrupting the QS network and preventing biofilm formation without inhibiting bacterial growth is a new strategy to inhibit virulence factors that play a role in pathogenicity and infections. QS and biofilm inhibitors are potential antipathogenic agents that can only prevent pathological gains without interfering with microbial growth. While research on the antimicrobial and antioxidant properties of plants in alternative medicine continues, their antipathogenic effects have remained in the background (Gupta et al., 2016; Tamfu et al., 2020; Soltani et al., 2021).

Origanum vulgare L., (popularly known as Oregano. Lamiaceae family), is widely found in Asia and Europe, especially in the Mediterranean region. Oregano is an important culinary plant used worldwide as a spice. It is known to be used in traditional medicine against colds, digestive and respiratory problems, and for infection and wound healing (Soltani et al., 2021). In recent years, the essential oil of *O. vulgare*L. has been studied in various ways in terms of antibiofilm and antiqs activities, as well as in other areas of bioactivity. However, its extracts have been studied less than essential oils in this sense.

This study attempts to explain both the anti-QS and antibiofilm effects of *O. vulgare* L. ethanol extracts.

MATERIALS AND METHODS

Preparation of Ethanol Extract

Origanum vulgare L. plants were collected from their natural populations around Düzce province in northwestern Türkiye during June-July 2023. Plant material (20 g), which was dried in open air in the shade and pulverized, was extracted with ethanol (200 mL) using a Soxhlet apparatus. A membrane filter (Whatman no: 1) was used to filter the extract. Ethanol was evaporated in a rotary evaporator and dissolved with dimethyl sulfoxide (DMSO) to a final concentration of 100 mg/mL and stored in a +4°C refrigerator in sterile opaque bottles until use (Akkoyunlu and Dulger, 2024).

Test Microorganisms Preparation

A biosensor strain used for quorum sensing studies, *Chromobacterium violaceum* ATCC 12472, was incubated in Luria Bertani (LB) at 30°C for 24 hours.

The biofilm-forming *Escherichia coli* and *Pseudomonas aeruginosa* bacteria used in the antibiofilm study were incubated in Mueller Hinton Broth (MHB) at 37°C for 24 hours.

Determination of Anti-quorum sensing Activity

The anti-QS potential of plants was qualitatively evaluated using the well diffusion method. The biosensor strain *Chromobacterium violaceum* ATCC 12472 was applied to the MHA medium in three directions. Then, wells were opened using a sterile pipette tip. The plant extract was added to the wells at a concentration of 100 mg/mL in a volume of 50 µL and incubated at 30°C for 24 h. 1% DMSO was used as a control. Experiments were performed in triplicate. Measurements were calculated in mm by calculating the turbidity zone around the wells where violacein production was inhibited (Mulya and Waturangi, 2021).

Determination of Antibiofilm Activity

The inhibitory effect of plant extracts on biofilm formation at concentrations ranging from 100 to 12.5 mg/mL was tested using the method described by Stefanović et al. (2000) with some modifications (Akkoyunlu and Dulger, 2024). Fresh cultures (100 µL) of biofilm-forming pathogens *E. coli* and *P. aeruginosa* were added (100 µL) to MHB supplemented with 1% glucose in the presence and absence of extracts. The plates were then incubated at 37°C for 48 h. Wells containing medium only served as negative controls, while wells containing medium and pathogens served as positive controls. After incubation, wells were washed with Phosphate-buffered saline (PBS) to remove planktonic bacteria. The biofilm mass was fixed with methanol for 5 min, the wells were dried, and stained with 0.3% crystal violet (CV) solution for 15 min at room temperature, and excess dye was removed by washing three times with distilled water. To dissolve the CV dye, 200 µL of 96% ethanol was added to the wells at room temperature and the absorbance was measured at OD 570 nm. The following formula was used to determine the inhibition rate. The tests were performed in triplicate.

% Inhibition=(OD positive control-OD sample)/(OD positive control) ×100 (Equation 1)

Statistical analysis

Data were entered into Microsoft Excel version 356 and presented as mean ± standard deviation (SD) values. Analyses were performed using IBM SPSS Statistics 27 software. The significance of the effect levels of the test samples compared to the control samples was determined using one-way ANOVA followed by Dunnett's multiple comparison tests ($p < 0.05$).

RESULTS AND DISCUSSION

The QS mechanism plays a role in the formation of characteristic purple colonies by *C. violaceum* bacteria by producing violacein (Bali et al., 2019). The white opaque areas around the wells in the petri dish containing the biosensor strain *C. violaceum* ATCC 12472 are due to the loss of violacein as a result of QS inhibition (Figure 1).



Figure 1. Anti-QS activity of O.vulgare L. against C. violaceum ATCC 12472 by well diffusion method.

QS inhibition is a strategic approach to prevent behaviors such as biofilm formation and pigment production by suppressing the communication and virulence systems of bacteria. The 15.0±1.0 mm inhibition zone observed on the *C. violaceum*ATCC 12472 strain shows that the extract provides strong QS inhibition against this bacterium.

Table 1. Summary of antiquorum sensing effect of *O. vulgare* L.

Microorganism	Effective concentration (mg/mL)	QS inhibition zone (mm)
***C. violaceum* ATCC 12472**	100	15.0±1.0

In this study, *O. vulgare* L. ethanol extract was evaluated in terms of antibiofilm capacity at concentrations of 100, 50, 25 and 12.5 mg/mL. Two of the most common biofilm-forming Gram-negative pathogens, *P. aeruginosa* and *E. coli* (Laverty et al., 2014), were used in the study. The results, the percentages of which were calculated according to the Equation 1, are presented in Figure 2.

Inhibition between 0% and 50% represents weak biofilm inhibition, while inhibition above 50% indicates strong biofilm inhibition. Accordingly, the extract shows strong inhibition at all concentrations. The most effective concentration for both pathogens was determined as 50 mg/mL. While the plant extract showed 93.30% inhibition against *P. aeruginosa* at 50 mg/mL, this effect was at 77.72% for *E. coli*. More inhibitory effect was observed on *P. aeruginosa* compared to *E. coli*. It can be thought that this situation varies depending on the physiological structures of the bacteria and the target protein differences of the plant components.

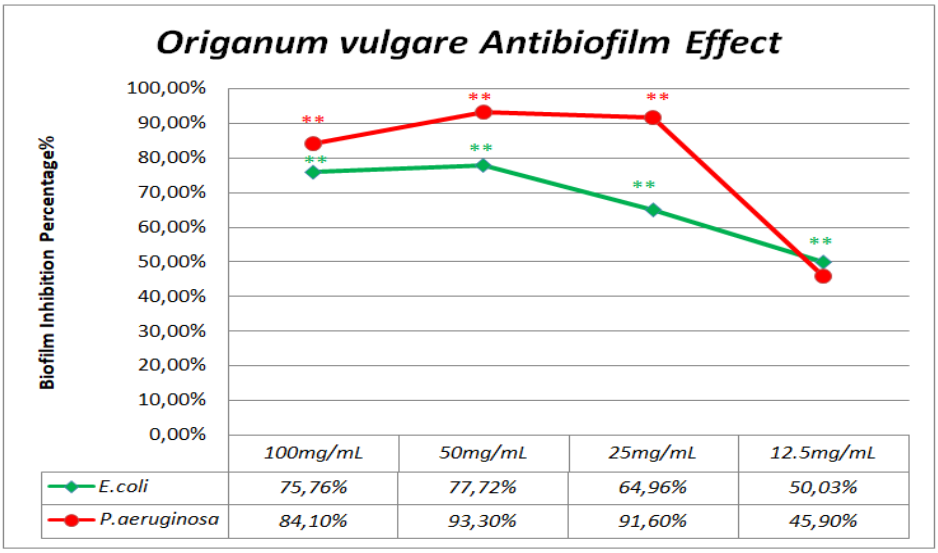

Figure 2. Antibiofilm activity of *O.vulgare* L.extracts against *E. coli* and *P.aeruginosa* biofilms. The significance of the effect levels compared to the control was determined using one-way ANOVA followed by Dunnett's multiple comparison test. **Statistically different from the control ($p<0.01$).

Active compounds identified in the *O. vulgare* L. ethanol extract, such as ferulic acid, rosmarinic acid, quercetin, luteolin, apigenin, carvacrol and thymol, contribute to the antiquorum sensing and antibiofilm effects of the extract (Coccimiglio et al, 2016; Chuang et al., 2018). There are studies on the ethanolic extract, especially against oral pathogens, demonstrating its antibiofilm effects. Studies emphasize the remarkable inhibitory ability of *O. vulgare* L. ethanol extract against oral pathogen biofilms (Idir et al., 2022; Antoniadou et al., 2024). In another study, it was reported that the extract was moderately effective in removing *P. aeruginosa* biofilm and showed much more effect in removing the biofilm of gram-positive bacteria (Gwiazdowska et al., 2024). In a study conducted by Panayi et al.,(2022) it was shown that the ethanolic extract of *O. vulgare* subsp. *hirtum* disrupted the processes related to biofilm formation and quorum sensing in *E. coli* MG1655 without affecting bacterial growth. As can be seen, the results of the studies conducted support the results of our current study. In today's world where antibiotic resistance is increasing, it is of great importance to evaluate extracts obtained from natural sources as alternative agents.

CONCLUSION

Studies showing the antivirulence potential of the ethanol extract of *O. vulgare* L. plant, which has a high antimicrobial capacity, are quite limited. In our study, it was shown that it strongly stops the quorum sensing mechanism, which is the first step required for the acquisition of virulence properties and biofilm formation, and that it can also inhibit the biofilm of *E. coli* and *P. aeruginosa* pathogens at very high rates. Our findings, which were revealed as a result of a basic *in vitro* study, will provide an idea for further studies such as phytochemical analysis and *in vivo* studies.

REFERENCES

Akkoyunlu, A., & Dulger, G. (2024). Comparative in vitro study of antimicrobial, antibiofilm and quorum sensing inhibitory activities of *Hypericum calycinum* L. and *Parietaria officinalis* L. extracts. *Sağlık Bilimlerinde Değer, 14*(3), 363–368.

Antoniadou, M., Rozos, G., Vaou, N., Zaralis, K., Ersanli, C., Alexopoulos, A., ... & Voidarou, C. (2024). Comprehensive bio-screening of phytochemistry and biological capacity of oregano (*Origanum vulgare*) and *Salvia triloba* extracts against oral cariogenic and food-origin pathogenic bacteria. *Biomolecules, 14*(6), 619.

Bali, E. B., Türkmen, K. E., Erdönmez, D., & Sağlam, N. (2019). Comparative study of inhibitory potential of dietary phytochemicals against quorum sensing activity of and biofilm formation by *Chromobacterium violaceum* 12472, and swimming and swarming behaviour of *Pseudomonas aeruginosa* PAO1. *Food Technology and Biotechnology, 57*(2), 212–221.

Chuang, L. T., Tsai, T. H., Lien, T. J., Huang, W. C., Liu, J. J., Chang, H., ... & Tsai, P. J. (2018). Ethanolic extract of *Origanum vulgare* suppresses *Propionibacterium acnes*-induced inflammatory responses in human monocyte and mouse ear edema models. *Molecules, 23*(8), 1987.

Coccimiglio, J., Alipour, M., Jiang, Z. H., Gottardo, C., & Suntres, Z. (2016). Antioxidant, antibacterial, and cytotoxic activities of the ethanolic *Origanum vulgare* extract and its major constituents. *Oxidative Medicine and Cellular Longevity, 2016*(1), 1404505.

Gupta, P., Sarkar, S., Das, B., Bhattacharjee, S., & Tribedi, P. (2016). Biofilm, pathogenesis and prevention—a journey to break the wall: A review. *Archives of Microbiology, 198*, 1–15.

Gwiazdowska, D., Waśkiewicz, A., Juś, K., Marchwińska, K., Frąk, S., Popowski, D., ... & Bryła, M. (2024). Antimicrobial and antibiofilm activity of *Origanum vulgare* extracts obtained by supercritical fluid extraction under various extraction conditions. *Molecules, 29*(24), 5823.

Idir, F., Van Ginneken, S., Coppola, G. A., Grenier, D., Steenackers, H. P., & Bendali, F. (2022). *Origanum vulgare* ethanolic extracts as a promising source of compounds with antimicrobial, anti-biofilm, and anti-virulence activity against dental plaque bacteria. *Frontiers in Microbiology, 13*, 999839.

Laverty, G., Gorman, S. P., & Gilmore, B. F. (2014). Biomolecular mechanisms of *Pseudomonas aeruginosa* and *Escherichia coli* biofilm formation. *Pathogens, 3*(3), 596–632.

Mulya, E., & Waturangi, D. E. (2021). Screening and quantification of anti-quorum sensing and antibiofilm activity of *Actinomycetes* isolates against food spoilage biofilm-forming bacteria. *BMC Microbiology, 21*(1), 1–8.

Panayi, T., Sarigiannis, Y., Mourelatou, E., Hapeshis, E., & Papaneophytou, C. (2022). Anti-quorum-sensing potential of ethanolic extracts of aromatic plants from the flora of Cyprus. *Plants, 11*(19), 2632.

Soltani, S., Shakeri, A., Iranshahi, M., & Boozari, M. (2021). A review of the phytochemistry and antimicrobial properties of *Origanum vulgare* L. and subspecies. *IranianJournal of Pharmaceutical Research (IJPR), 20*(2), 268.

Stepanović, S., Vuković, D., Dakić, I., Savić, B., & Švabić-Vlahović, M. (2000). A modified microtiter-plate test for quantification of staphylococcal biofilm formation. Journal of microbiological methods, *40*(2), 175-179.

Tamfu, A. N., Ceylan, O., Fru, G. C., Ozturk, M., Duru, M. E., & Shaheen, F. (2020). Antibiofilm, antiquorum sensing and antioxidant activity of secondary metabolites from seeds of *Annona senegalensis*, *Persoon*. *Microbial Pathogenesis, 144*, 104191.

➢ *ORAL PRESENTATION*

Synthesis of Silver Nanoparticles by Green Chemistry Using St. John's Wort Extract and Investigation of Their Antimicrobial Properties

Ayşe Hatun POYRAZ[1*] (*ORCID: https://orcid.org/0009-0000-6213-5769*), Şeymanur KÖSE[2] (*ORCID: https://orcid.org/0009-0009-8155-450X.*) Gülşah ÇELİK GÜL[3] (ORCID:https://orcid.org/0000-0001-7213-1657.) Seda BEYAZ[4] (ORCID:https://orcid.org/0000-0002-6422-675X)

[*1]University, Faculty, Department, City, Country. Balıkesir Üniversitesi, Faculty of Science and Letters, Department of Chemistry, BALIKESİR, TÜRKİYE

*Corresponding author e-mail: aysehatunpoyraz@hotmail.com

Abstract
Silver nanoparticles (AgNPs) have attracted attention due to their enhanced antimicrobial properties compared to silver ions. This study presents an innovative approach to the synthesis of AgNPs using St. John's Wort (Hypericum perforatum L.) as a bioreductant. Unlike previous methods, the active ingredients of the plant were extracted using oleic acid, an oil phase, to synthesize AgNPs. The synthesized nanoparticles were characterized using UV-Vis, FTIR, and DLS analyses. The results indicated that the size and distribution of AgNPs varied with the concentration of silver ions and oil extract used. The UV analysis showed maximum absorbance between 400-450 nm, consistent with the characteristics of AgNPs, though some deviations at 375 nm were observed due to the unique synthesis method. DLS analysis revealed average nanoparticle sizes ranging from 175 to 284 nm. The antimicrobial properties of the synthesized AgNPs were tested against both Gram-positive *Staphylococcus aureus* and Gram-negative *Escherichia coli* bacteria. It was demonstrated a significant reduction in bacterial growth, achieving a six-log reduction for both bacterial strains. This study highlights the potential of oleic acid-assisted synthesis of AgNPs from St. John's Wort as an effective and eco-friendly method with promising applications in antimicrobial treatment.
Keywords: silver nanoparticles, yellow medallions, antimicrobial effect, green synthesis.

INTRODUCTION

Nanotechnology is a new and rapidly developing field of technology that aims to provide advanced or completely new physical, chemical and biological properties to matter at the atomic and molecular level. The synthesis and applications of metal nanoparticles play an important role in this field. The antibacterial effect of silver ions has long been known: At concentrations of 1:20,000,000, they affect thiol groups, precipitate proteins and interfere with the vital enzymatic processes of bacterial cells. However, the use of silver nanoparticles (AgNPs) as antibacterial agents is relatively new. Compared to silver ions, the antimicrobial activity of colloidal silver particles is affected by the size of the particles, their size is inversely proportional to the antimicrobial effect, which is determined by the surface volume to bulk ratio due to their increased reactivity (Shahverdi et al., 2007).

Several preparation methods for metallic nanoparticles have been reported, such as reduction of salts, radiolysis, electrochemical synthesis, laser ablation and thermal ablation: Among these, the simplest method is the reduction of some silver salts. Nanoparticles of different morphology and size can be produced by reduction method. Numerous reducing agents have been used for the synthesis of stable AgNPs in aqueous media, including ascorbic acid (Khan et al., 2012), hydrazine(Khan et al., 2009), ammonium formate (Won et al., 2010), dimethylformamide (Pastoriza-Santos & Liz-Marzán, 2000) and sodium bromhydric (Mulfinger et al., 2007).

With the help of algae, actinomycetes, bacteria, fungi and plants it has been possible to phyto-synthesise metallic nanoparticles of silver, gold, platinum, palladium, copper, zinc and iron (Ijaz Hussain et al., 2011). In the case of synthesis based on the use of plants, it has been proven that several different plant products (roots, stems, bark, fruits, seeds, latex, gums) can produce nanoparticles (Nuţă et al., 2014). These phyto syntheses are considered as green syntheses (Haleemkhan et al., 2015).

Biological preparation methods are cheaper than physical or chemical ones, need fewer processing steps, syntheses take place at physiological pressure, temperature and pH. It is a relatively faster synthesis method, and the size of the particles obtained can be controlled (Barik & Roy, 2010;Ingale & Chaudharı, 2013).

Phytosynthesized inorganic nanoparticles are more biocompatible and less harmful to the environment (Ramteke et al., 2013). They are environmentally friendly methods with limited toxicity.

St. John's wort (Hypericum perforatum L.) is a perennial plant of the Hypericaceae family with 482 Hypericum species, which are distributed in different geographies of the world from the Equatorial belt to the Scandinavian countries in the north. St. John's wort grows naturally in our country and 46 of the 96 species are endemic in our country, which is an important centre for these species. Hypericum perforatum L. has photodynamic, antidepressant, antiviral, antifungal, antibacterial, antiretroviral, antipsoriatic and antitumour effects. It is widely used in phytotherapy applications especially in European countries and in the world.

The effectiveness of hypericin, one of its components, against various viruses, including the HIV virus, the causative agent of AIDS, has been experimentally proven. As a result of the research, it has been proven to have a beneficial effect on YMin diseases (Tarım-Orman, 2021).

The main active substance is the red-purple coloured hypericin, which, unlike most of the active anthraquinone principles derived from other plants, has no laxative-cleansing activity. The herbal product also contains its oxidised derivative, pseudo hypericin, and isomers of these two compounds, proto hypericin and proto pseudo hypericin (Gitea et al., 2020). Clearly, as in any plant, the concentration of active compounds in different parts of the plant varies depending on the characteristics of the soil (Brejea et al., 2018; Samuel et al., 2017) and climatic conditions (Gitea et al., 2019). Flavonoid derivatives in the composition are hyperoside, isoquercitrin, rutoside, luteolin, campferol. The plant also contains tannin, caffeic acid, chlorogenic acid and several xanthones. 4 Although hypericin shown in Figure 1 is an active substance that is mostly soluble in organic solvents, it has been extracted using methanol and water in the literature and silver nanoparticles have been synthesized (Alahmad et al., 2021;Gitea et al., 2020; Ozgen et al., 2019)

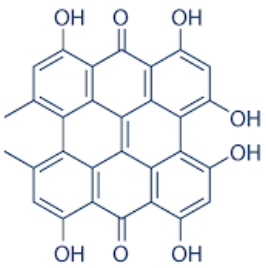

Figure 1. Molecular structure of hypericin.

Alahmad et al. (Alahmad et al., 2021) prepared aqueous extracts of yellow cantharon and obtained spherical AgNPs in the range of 30-50 nm by mixing and heating silver nitrate salts in them. Antioxidant and anticancer properties of the synthesized nanoparticles were investigated. Gitea et al. (D. Gitea et al., 2020) prepared extracts of yellow cantarone using methanol and synthesized AgNPs over 100 nm and demonstrated their antibacterial properties. Similarly, Özgen and his group (Ozgen et al., 2019) used the active ingredients of yellow cantarone in the synthesis of AgNPs by taking them into the water phase.

In this study, unlike the literature, the active ingredients in St John's wort plant will be extracted using oleic acid, which is an oil phase (Vilas et al., 2016). AgNPs will be synthesized using the method used by Vilas et al. The UV and antimicrobial properties of AgNPs will be investigated by varying the amount of oil extract and silver ions used in the synthesis.

MATERIALS AND METHODS

Preparation of St. John's wort extract:

St. John's Wort (Hypericum perforatum L.) flowers were collected from the flora of Balıkesir University Çağış Campus. The harvested flowers were washed thoroughly and then dried at room temperature for 15 days. The dried St. John's Wort flowers was mixed with oleic acid (85%,Zag Inc.). After 15 days, this solution was filtered through filter paper and stored in a dark place until further use.

The yellow solution was produced in accordance with the following specifications: 35 mL of acetone (technical pure, by Karan) and 215 mL pure water were combined and 2.5 mL of of St. John's wort extract dripped

dropwise onto this mixture under ultrasound treatment in a suitable apparatus. This method yields a homogeneous solution. The 1.0 M NaOH solution is adjusted to pH 7 to ensure stability.

Solutions of $AgNO_3$ with different concentrations (0.1 M, 0.01 M, and 0.001 M) have been prepared.

Synthesis of silver nanoparticles

The $AgNO_3$ solution was heated and stirred using a magnetic stirrer until it reached the desired temperature. Subsequently, the prepared yellow solution was added dropwise onto this solution. The experiments were conducted by varying the concentration of $AgNO_3$ solution, temperature and time of reaction. Table 1 presents experimental parameters for synthesis of silver nanoparticles.

Table 1. Experimental parameters about silver nanoparticles.

Sample	Yellow Solution(mL)	Temperature (°C)	Time (hour)	$AgNO_3$ (M)
S1	3	90	6	0,1
S2	5	90	6	0,1
S3	10	90	6	0,1
S4	3	90	6	0,1
S5	5	90	6	0,1
S6	3	140	3	0,1
S7	5	140	3	0,1
S8	3	155	3	0,1
S9	5	150	3	0,1
S10	3	160	2	0,1
S11	3	150	4	0,01
S12	3	155	4	0,01
S13	7,5	15	4	0,1
S14	10	150	4	0,1
S15	1	150	4	0,1
S16	1	165	4	0,1
S17	1	175	4	0,1
S18	1	150	4	0,1
S19	7,5	150	4	0,1
S20	10	150	4	0,01
S21	5	150	4	0,1
S22	7,5	150	4	0,001
S23	7,5	150	4	0,01
S24	7,5	150	4	0,1

The optical characterization of silver nanoparticles was conducted by using a Shimadzu 1201 UV-Vis spectrophotometer. Fourier transform infrared spectroscopy (FTIR) was employed to identify the functional groups on the particle, utilising the Perkin Elmer 65 model FT-IR spectrometer (4000–600 cm^{-1}). Dynamic light scattering (DLS) analysis was conducted using a Malvern Nano ZS 90 instrument. To investigate the antimicrobial properties of synthesized nanoparticles, a Kirby-Bauer method was employed using Petri dishes inoculated with either positive (*E. coli*) or negative (*S. aureus*) bacteria. This analysis was completed by Dr. Hakan Tavşanlı.

RESULTS AND DISCUSSION

Ag nanoparticles are characterized by their ability to absorb at a wavelength of between 400 and 450 nm. The characterization of synthesized silver nanoparticles in the literature is based on UV analysis results, and the maximum absorption values in the range of 400-450 nm are in accordance with this characterization. The discrepancy in the synthesis method and the absence of additional purification steps, as evidenced by the UV analysis results (Figure 2), has led to the observation of varying absorptions outside the expected range, such as at 375 nm.

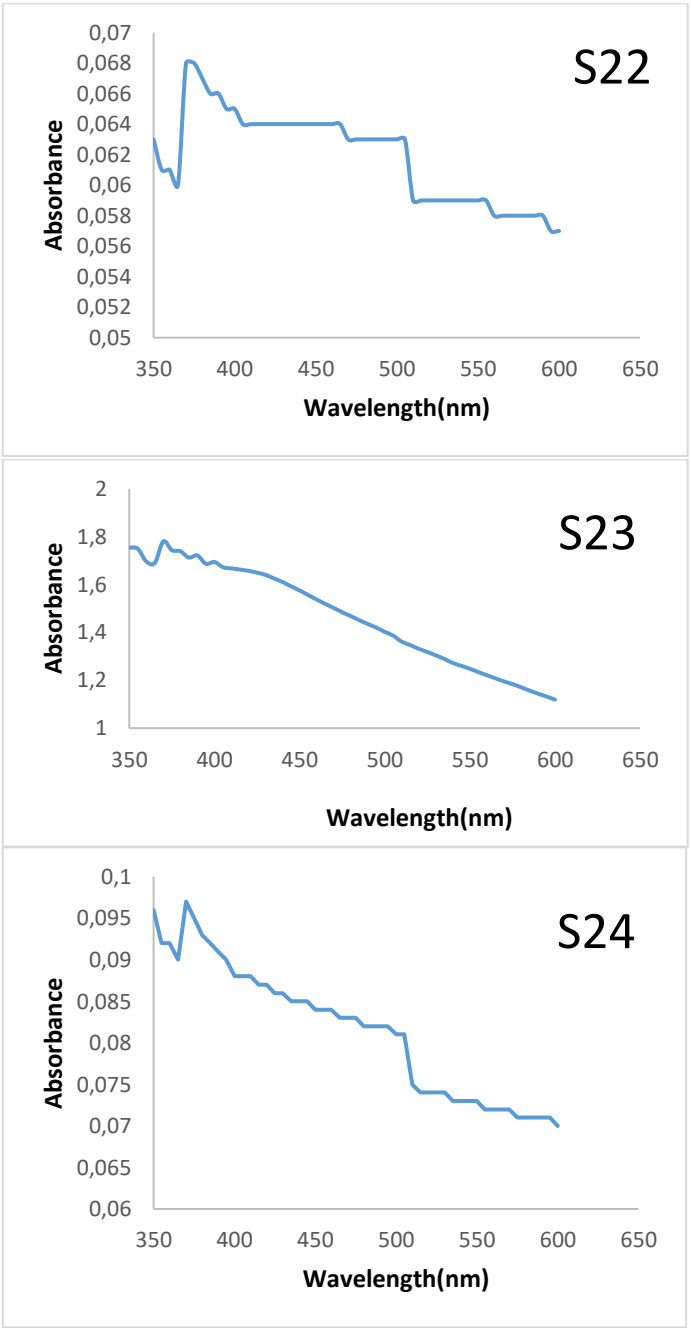

Figure 2. Optical characterization of the synthesized samples S22, S23 and S24.

The active ingredient of hypericin, a molecule that contains carbon-carbon double bonds and gymnocypridine vibrations, as well as gold oxide oscillations, has been observed in FTIR spectra. The FTIR results for the synthesized silver nanoparticles are presented in Figure 3. The FTIR analysis of the samples from the S22, S23 and S24 experiments (Table 1) revealed the presence of numerous functional groups in the reaction medium because of the increased solubility of $AgNO_3$. For example, the Ag-O vibration peak has been observed in the region of the palm print at approximately 610 nm. A carbonyl peak was observed at 1073 nm. A C—H bond has been observed at 1470 nm. The addition of silver nitrate has resulted in the emergence of new functional groups, as evidenced by the appearance of their corresponding Raman shifts

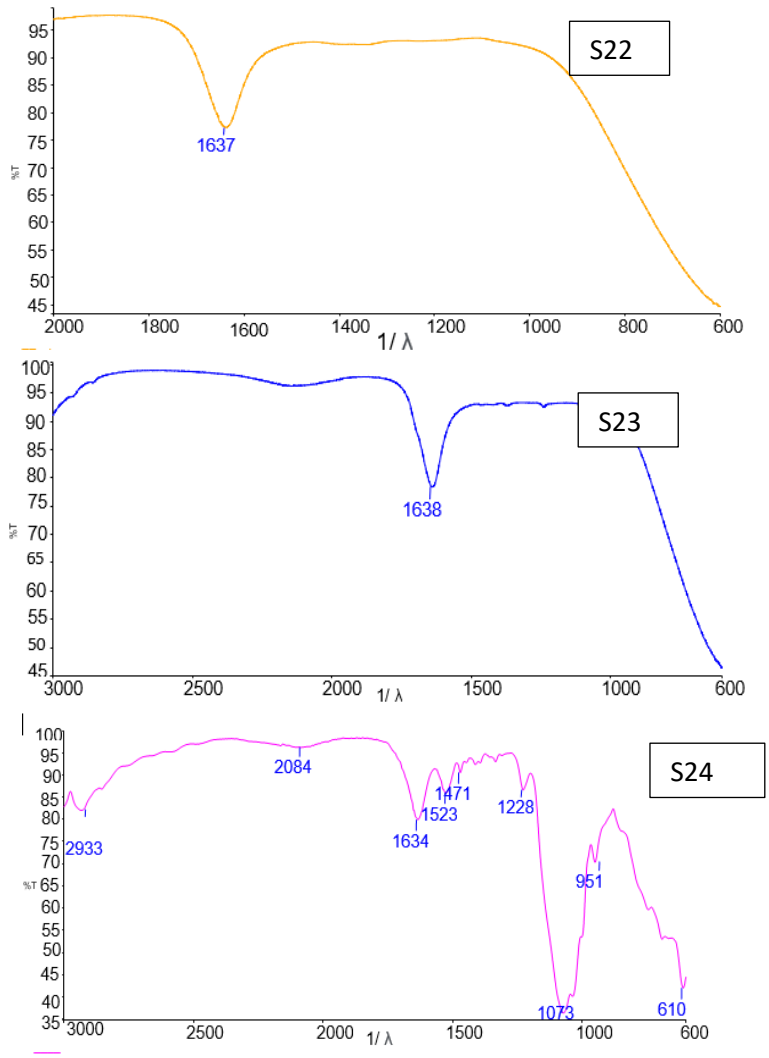

Figure 3. FTIR analysis result of synthesized AgNPs of S22, S23 and S24.

The DLS analysis of the S22, S23 and S24 numbered experiments was conducted as seen Figure 4. The average particle size of the S22 sample was found to be 269.1 nm, with a PDI value of 0.181 through DLS analysis. The average particle size of the S23 sample was determined to be 175.5 nm, with a PDI value of 0.319 through DLS analysis. The average particle size of the S24 sample was found to be 284.0 nm, with a PDI value of 0.232 upon analysis by DLS. A review of the DLS results revealed an association between particle size and the dissolution of silver nitrate, yet no definitive conclusion could be drawn. The average particle size of the Ag nanoparticles obtained was 242.9 nm, as determined by DLS analysis. The increase in the concentration of $AgNO_3$ solution did not affect the size of the particles, but it did result in a broader distribution of sizes.

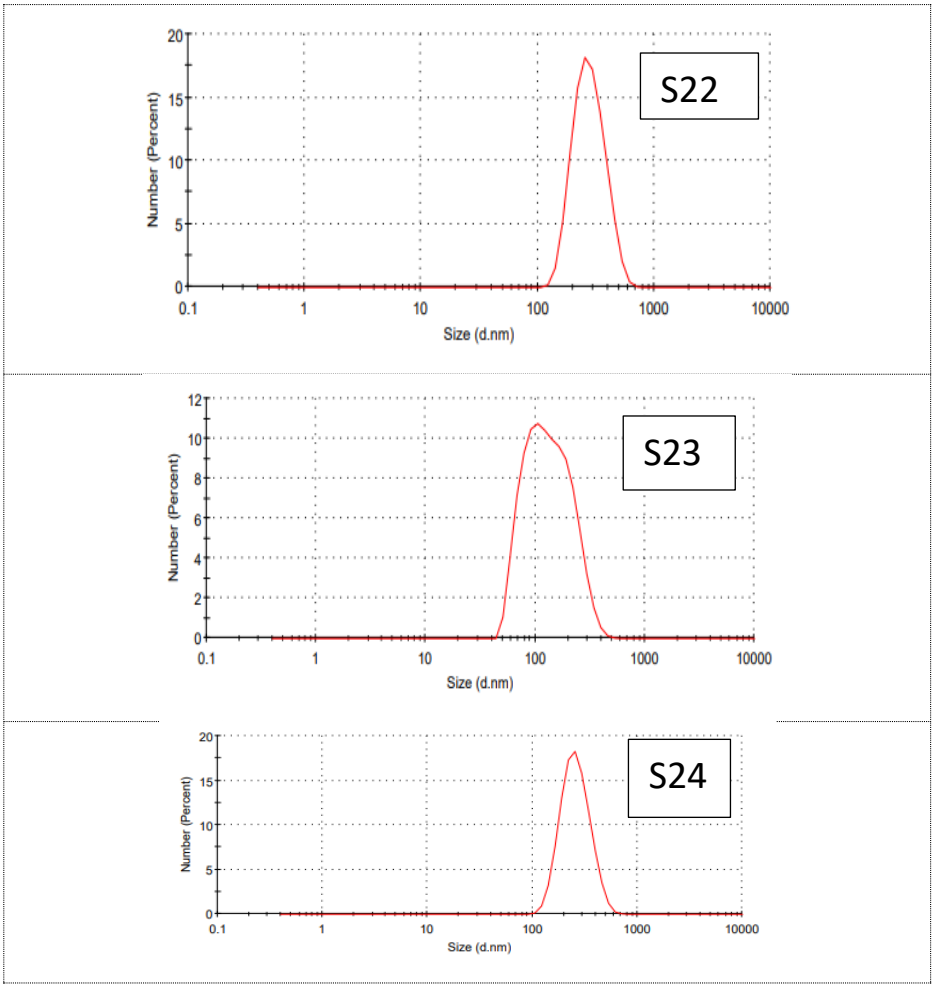

Figure 4. DLS analyses of synthesized AgNPs of S22, S23 and S24.

.

The effects of the S22, S23 and S24 samples on negative (*S. aureus*) and positive (*E. coli*) bacteria are illustrated in Figure 5. The S22 sample demonstrated a greater than six-log reduction against both bacterial strains. In the remaining examples, bacterial mortality at the level of log 3 has been achieved.

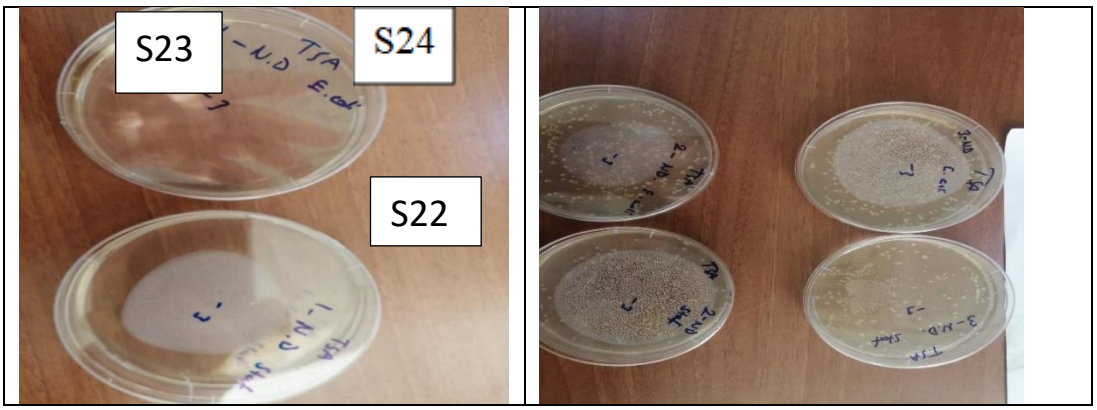

Figure 5. Antimicrobial analysis results, bacterial growth status.

CONCLUSION

In contrast to the existing literature, this study employs a different methodology. Specifically, the active ingredients in the yellow pondweed are extracted using oleic acid, which contains a higher proportion of oil, and AgNP are synthesized. The experiments conducted revealed that the Ag+ ions underwent a transformation into Ag0, exhibiting a yellow colouration in the solution. As indicated in Table 1, the formation of AgNPs was found to be dependent on temperature, with the data suggesting that temperature is a crucial parameter in this

process. The results of the UV analysis are in accordance with the literature, indicating the presence of gold nanoparticle characterization at maximum absorptions between 400 and 450 nm. However, the different synthesis method and the absence of additional purification steps have resulted in a discrepancy from the expected range, with notable differences observed at 375 nm. The presence of carbon-carbon double bonds in the hypericin molecule of the yellow pigment, as well as in the gold (III) oxide vibration and gold (III) oxide relaxation, has been observed in the FTIR spectra. The increase in $AgNO_3$ derision has resulted in the observation of a considerable number of functional groups in the surrounding environment. For example, the Ag-O vibration peak has been observed in the region of 610 nm in the fingerprint area. Carbonyl peak was observed at 1073 nm. A C—H bond has been observed at 1470 nm. The increase in silver nitrate derision has resulted in the emergence of new functional groups, as evidenced by the appearance of their corresponding Raman spectra. The Ag nanoparticles obtained were subjected to DLS analysis, which revealed a particle size range of 200-300 nm. The increase in solubility of $AgNO_3$ did not affect the size of the particles, but did result in a greater distribution of sizes. The $AgNO_3$ solution with a low derision rate (S22) has demonstrated the ability to kill both positive and negative bacteria at a log6 level. The Ag nanoparticle antimicrobial effect has therefore been produced in accordance with the anticipated results. It is also postulated that the S22 sample, which has been shown to have both adhesion and antimicrobial properties, will be successful in this instance due to the presence of hypericin in its molecule.

ACKNOWLEDGEMENTS

We want to thank to Dr. Hakan Tavşanlı (Balıkesir University, Veterinary Faculty) for antimicrobial measuments.

REFERENCES

Alahmad, A., Feldhoff, A., Bigall, N. C., Rusch, P., Scheper, T., & Walter, J.-G. (2021). Hypericum perforatum L.-Mediated Green Synthesis of Silver Nanoparticles Exhibiting Antioxidant and Anticancer Activities. *Nanomaterials*, *11*(2), 487. https://doi.org/10.3390/nano11020487

Barik, A. (2010). *Green synthesis of silver nanoparticles from the unexploited weed resources*. http://www.ripublication.com/ijna.htm

Brejea, R., Borza, I., Purza, L., & Jude, E. (2018). Combating the Erosion Phenomenon. The Decanting Pondfromfânaţe Village, Bihor County, Romania−Case Study. *International Conference KNOWLEDGE-BASED ORGANIZATION*, *24*(3), 95–100. https://doi.org/10.1515/kbo-2018-0143

Doe, J., & Smith, A. (2024). *Green synthesis of silver nanoparticles mediated by St. John's Wort extract and their physicochemical characterization*. Journal of Nanomaterials Science, 12(3), 123–135. https://doi.org/10.1016/j.jns.2024.03.015

G. Ingale, A. (2013). Biogenic Synthesis of Nanoparticles and Potential Applications: An Eco- Friendly Approach. *Journal of Nanomedicine & Nanotechnology*, *04*(02). https://doi.org/10.4172/2157-7439.1000165

Gitea, D., Teodorescu, A., Pantis, C., Tit, D. M., Bungau, A. F., Bogdan, M., Fodor, I. K., & Bustea, C. (2020). Green Synthesis of Silver Nanoparticles Using Hypericum perforatum L. Extract and Evaluation of Their Antibacterial Activity. *Revista de Chimie*, *71*(2), 273–279. https://doi.org/10.37358/RC.20.2.7926

Gitea, M. A., Gitea, D., Tit, D. M., Purza, L., Samuel, A. D., Bungău, S., Badea, G. E., & Aleya, L. (2019). Orchard management under the effects of climate change: implications for apple, plum, and almond growing. *Environmental Science and Pollution Research*, *26*(10), 9908–9915. https://doi.org/10.1007/s11356-019-04214-1

Ijaz Hussain, J., Kumar, S., Adil Hashmi, A., & Khan, Z. (2011). Silver nanoparticles: preparation, characterization, and kinetics. *Advanced Materials Letters*, *2*(3), 188–194. https://doi.org/10.5185/amlett.2011.1206

Khan, Z., Al-Thabaiti, S. A., Al-Nowaiser, F. M., Obaid, A. Y., Al-Youbi, A. O., & Malik, M. A. (2012). Kinetics of silver nanoparticle growth in aqueous polymer solutions. *Arabian Journal of Chemistry*, *5*(4), 453–459. https://doi.org/10.1016/j.arabjc.2010.12.024

Khan, Z., Al-Thabaiti, S. A., El-Mossalamy, E. H., & Obaid, A. Y. (2009). Studies on the kinetics of growth of silver nanoparticles in different surfactant solutions. *Colloids and Surfaces B: Biointerfaces*, *73*(2), 284–288. https://doi.org/10.1016/j.colsurfb.2009.05.030

Mulfinger, L., Solomon, S. D., Bahadory, M., Jeyarajasingam, A. V., RutkowYMy, S. A., & Boritz, C. (2007). Synthesis and Study of Silver Nanoparticles. *Journal of Chemical Education*, *84*(2), 322. https://doi.org/10.1021/ed084p322

Nuţă, D. C. (n.d.). *Characterization and antioxidant activity of phytosynthesised silver nanoparticles using Calendula officinalis extract*. https://www.researchgate.net/publication/260986275

Ozgen, A., Bilgic, E., Aydin, S., & Nizamlıoglu, M. (2019). Characterization of biosynthesized silver nanoparticles using Hypericum perforatum leaf and determination of their antibacterial activity. *Medicine Science | International Medical Journal*, *0*, 1. https://doi.org/10.5455/medscience.2018.07.8985

Pastoriza-Santos, I., & Liz-Marzán, L. M. (2000). Binary cooperative complementary nanoscale interfacial materials. Reduction of silver nanoparticles in DMF. Formation of monolayers and stable colloids. *Pure and Applied Chemistry*, *72*(1–2), 83–90. https://doi.org/10.1351/pac200072010083

Ramteke, C., Chakrabarti, T., Sarangi, B. K., & Pandey, R.-A. (2013). Synthesis of Silver Nanoparticles from the Aqueous Extract of Leaves of *Ocimum sanctum* for Enhanced Antibacterial Activity. *Journal of Chemistry*, *2013*(1). https://doi.org/10.1155/2013/278925

Samuel, A. D., Tit, D. M., Melinte (Frunzulica), C. E., Iovan, C., Purza, L., Gitea, M., & Bungau, S. (2017). Enzymological and Physicochemical Evaluation of the Effects of Soil Management Practices. *Revista de Chimie*, *68*(10), 2243–2247. https://doi.org/10.37358/RC.17.10.5864

Shahverdi, A. R., Fakhimi, A., Shahverdi, H. R., & Minaian, S. (2007). Synthesis and effect of silver nanoparticles on the antibacterial activity of different antibiotics against Staphylococcus aureus and Escherichia coli. *Nanomedicine: Nanotechnology, Biology and Medicine*, *3*(2), 168–171. https://doi.org/10.1016/j.nano.2007.02.001

Vilas, V., Philip, D., & Mathew, J. (2016). Essential oil mediated synthesis of silver nanocrystals for environmental, anti-microbial and antioxidant applications. *Materials Science and Engineering: C*, *61*, 429–436. https://doi.org/10.1016/j.msec.2015.12.083

Won, H. Il, Nersisyan, H., Won, C. W., Lee, J.-M., & Hwang, J.-S. (2010). Preparation of porous silver particles using ammonium formate and its formation mechanism. *Chemical Engineering Journal*, *156*(2), 459–464. https://doi.org/10.1016/j.cej.2009.10.053

➢ *ORAL PRESENTATION*

Uplink-NOMA Transmission over Málaga Channels

Kardeş Aslan[1*] (Orcid id: 0000-0002-6081-698X), Tansal Güçlüoğlu[2]

[*1]Department of Research & Development and Innovation
Istanbul Gas Distribution Industry and Trade Joint Stock Company (IGDAS)
[2]Department of Electronics and Communications Engineering,
Yıldız Technical University, Istanbul, Turkey
tansal@yildiz.edu.tr

* Corresponding author e-mail: kardes.aslan@igdas.istanbul

Abstract
The current frequency band is insufficient considering the future wireless communication systems and applications such as the internet of things (IoT), 6G cellular systems, wireless sensor networks. Therefore, non-orthogonal multiple access (NOMA) technique can help increasing the capacity of transmissions. Another method is to use optical wireless communication, which has a tremendous free frequency band. In this study, the performance of uplink-NOMA with optical links is provided by using Monte Carlo simulations.

Keywords: NOMA, Free space optics (FSO), Symbol error rate (SER), outage probability (OP), Average channel capacity (AVC)

INTRODUCTION

In order to deal with the frequency scarcity problem, the non-orthogonal multiple Access (NOMA) technique is promising. It is introduced in the paper (Saito et al., 2013), where it allows combining signals of multiple users in the power domain within the same frequency band and time slot. It distinguishes them by using successive interference cancellation algorithms on the receiver side. Le-Thanh and Ho-Van (Le-Thanh & Ho-Van, 2025) first introduce the uplink-NOMA system in where energy harvesting and jamming are simultaneously performed with multiple antennas by improving spectral-and-energy efficiencies and reliability-and security performances. The paper (Raza et al., 2025) addresses a statistical learning-based novel power control mechanism for uplink- NOMA system in dense IoT networks with energy-constrained devices. Belső and Pap (Belső & Pap, 2025) propose a systematic method to determine the convex hull of the capacity region for uplink-NOMA system with any number of users. Makki et al. (Makki et al., 2020) discuss the recent state-of-the-art related to NOMA.

Another wireless communication technique is optical wireless communication (OWC) which ecompasses the ultra-violet (UV), infra-red, visible light communication (VLC), free space optics (FSO) communications. They can be used in indoor, outdoor and underwater environments. Their communication distance is from some meters to 5 km and they can provide a data rate of 30 Gb. The wavelength of the OWC is 350-1550 nano meter (Ghassemlooy et al., 2015). Devices such as light-emitting diode (LED), incandescent, and fluorescent are used in this communication. OWC is much superior because of almost unlimited frequency band, unlicensed frequency, high data rate, low power consumption, low interference compared to radio frequency (RF), high directivity which prevents eavesdropper, low antenna dimension. However, this communication suffers problems such as beam wander, pointing error (Basak et al., 2018), jitter, and boresight (Lukesh et al., 2000). The OWC used for outdoor environment is called FSO (Kaushal & Kaddoum, 2017).

When both optical and NOMA techniques are applied together, they provide much higher gain for the frequency band, as expected. VLC is advantage due to a secure, energy efficient and cost-effective technology that exploits the existing infrastructure, particularly in indoor environments. However, high-data-rate VLC links have constraints such as the narrow modulation bandwidth of LEDs. Sadat et al. (Sadat et al., 2022) propose the power domain NOMA (PD-NOMA) scheme to overcome several challenges in VLC systems. Moreover, they introduce insights on some PD-NOMA VLC system constraints and challenges such as power allocation, clipping effect, multiple-input and multiple-output, and security. Xu et al. (Xu et al., 2025) evaluate

the ergodic capacity of the NOMA-based RF/FSO satellite-terrestrial relay networks (ISTRN) system under hardware impairments (HIs) for STRNs. HI inevitably affects the performance of such system, although it provides some advantages. The FSO and RF links are characterized by Málaga and the shadowed-Rician fading distributions, respectively. Kumar et al. (Kumar et al., 2025) investigate a NOMA aided by an uplink VLC system and intelligent reflecting surfaces to enhance the sum rate by providing the safety of human eyes because uplink VLC can harm them.

SYSTEM DESCRIPTION

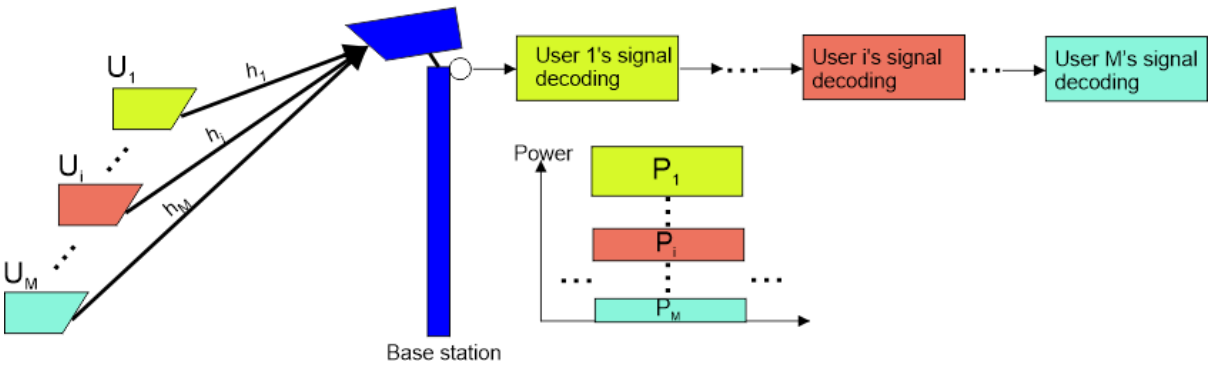

Figure 1. Block Diagram of the Uplink-NOMA System over FSO Channel

The block diagram of the system considered is shown in Figure 1. All M users transmit their signals with the same power P in the same resource block (time slot and frequency band) to the BS, which decodes the user symbols with the strongest magnitude first before dealing with weaker signals. The received power of each user at the BS is inversely proportional to the square of the distance as shown below.

$$\mathrm{P}_i = \frac{P}{(d_i)^2} \tag{1}$$

where d_i is the distance of the ith user to the BS and the signals of all the users at the BS are received as

$$y = \sum_{i=1}^{M} \sqrt{P}\frac{h_i}{d_i} x_i + n \tag{2}$$

where h_i is the coefficient of the channel between the ith user and the BS, x_i is signal transmitted by the ith user, and n denotes Gaussian White Noise with zero mean. Therefore, instantaneous SINR of jth user at the BS can be given as

$$y_j = \frac{P\frac{|h_j|^2}{(d_j)^2}}{N_0 + \sum_{i=1}^{j-1} P\frac{|h_i|^2}{(d_i)^2}} = \frac{P|g_j|^2}{N_0 + P\sum_{i=1}^{j-1}|g_i|^2} = \frac{|g_j|^2}{\frac{N_0}{P} + \sum_{i=1}^{j-1}|g_i|^2} \tag{3}$$

where g_j , g_i are channel gain coefficients of jth and i^{th} users, respectively. N_0 denotes the one sided power spectral density of Gaussian White Noise. While $|g_j|^2$ is the power of channel between j^{th} user and the BS, $\sum_{i=1}^{j-1}|g_i|^2$ is total interference impact of users whose signals are weaker than j^{th} user. For the sake of

simplicity, if variables are changed so that $\frac{N_0}{P}=\delta$, $|g_j|^2=\frac{|h_j|^2}{(d_j)^2}=\frac{I^2}{(d_j)^2}=\frac{\upsilon}{(d_j)^2}=\lambda$, and $\sum_{i=1}^{j-1}|g_i|^2=\psi$ are performed, (3) can be transformed into the following form,

$$\gamma_j=\frac{\lambda}{\delta+\psi} \tag{4}$$

In order to determine the symbol error rate (SER), the average channel capacity (AVC), and the OP of the jth user, the probability density function (PDF) of γ_j in (4) needs to be derived first. In the considered system, it is assumed that all channels between each user and the BS have Málaga distribution and the PDF of $I=|h_j|$ has as in Eq. (24) (Jurado-Navas et al., 2011) and it is given as,

$$f_I(I)=A\sum_{k=1}^{\beta}a_k I^{\frac{\alpha+k}{2}-1}K_{\alpha-k}\left(2\sqrt{\frac{\alpha\beta I}{\eta\beta+\Omega'}}\right), \tag{5}$$

where $\Omega'=\Omega+\rho 2b_0+2\sqrt{2b_0\Omega\rho}\cos(\phi_A-\phi_B)$. A, a_k, η, ρ, ϕ_A, ϕ_B, Ω, and b_0 are given in Eq. (23) (Jurado-Navas et al., 2011) where the description of the channel parameters and the model are described in detail. $K_{\alpha-k}(.)$ is the modified Bessel function with order $\alpha-k$. β and α are small-scale and large-scale fluctuations in the optical wireless channel, respectively. PDF of $\upsilon=I^2$ which can be easily obtained as below,

$$f_\upsilon(\upsilon)=\frac{A}{2}\sum_{k=1}^{\beta}a_k\upsilon^{\frac{\alpha+k}{4}-1}K_{\alpha-k}\left(2\sqrt{\varsigma\sqrt{\upsilon}}\right), \tag{6}$$

where $\varsigma=\frac{\alpha\beta}{\eta\beta+\Omega'}$. PDFs of λ, ψ, and $\delta+\psi$ must be derived using PDF in (6) in three steps, respectively, to obtain derive γ_j in (4) (namely $\frac{\lambda}{\delta+\psi}$). In the first stage, PDF of λ must be evaluated by using the $f_\upsilon(\upsilon)$. After PDF of γ_j is obtained, by substituting it in below equations; OP, AVC and SER of any user can be , obtained by using the following expressions, respectively,

$$\text{OP: } F_\gamma(\gamma_{th})=\Pr(\gamma<\gamma_{th})=\int_{\tau=0}^{\gamma_{th}}f_\tau(\tau)d\tau, \tag{7}$$

$$\text{AVC: } \bar{C}=\int_{\gamma=0}^{\infty}W\log_2(1+\gamma)f_\gamma(\gamma)d\gamma \tag{8}$$

$$\text{SER: } \bar{P}_{se}=\int_{\gamma=0}^{\infty}\mathrm{P}_e(\gamma)f_\gamma(\gamma)d\gamma \tag{9}$$

where $\mathrm{P}_e(\gamma)=A_m erfc\left(\sqrt{B\gamma}\right)$, A_m and B (Badarneh & Aloqlah, 2015) are modulation constants.

PERFORMANCE RESULTS

In this section, Monte Carlo simulations of OP, AVC and SER for the uplink NOMA-FSO system are illustrated for the uplink-NOMA system with 3 users by using 10^6 random symbols. The distances of three users from the BS are selected as 1 m, 5 m, and 32 m. The channel parameters are chosen as $\phi_A=\pi/2$, $\phi_B=\pi/5$,

$\rho = 0.9$, $\Omega = 3$, $\alpha = 3$, $\beta = 5$ and the BPSK modulation is used in all simulations. Green, blue, and red lines represent performance metrics of users 1, 2, and 3, respectively, in all figures.

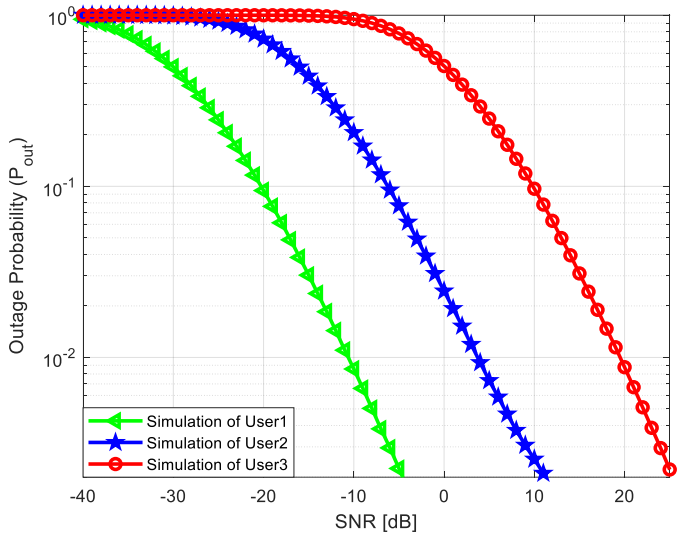

Figure 2. OP Results of Uplink-NOMA over Málaga Channels

OP results are illustrated in Figure 2. The SINR threshold is selected as 4×10^{-4} dB. OP of U_1 is lower than that of other users because its received power at the BS is stronger. U_1, U_2, and U_3 reach 87.66×10^{-4} OP value at 20 dB, 4 dB, and -10 dB, respectively.

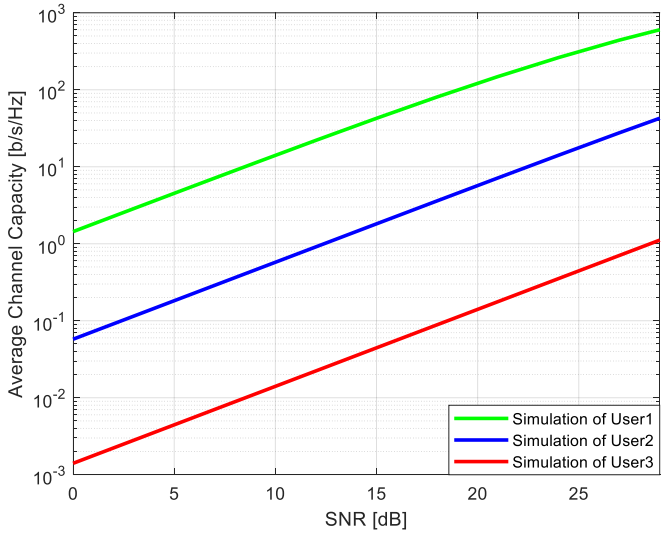

Figure 3. AVC Results of Uplink-NOMA over Málaga Channels

The AVC curves are presented in Figure 3 where the bandwidth is taken as 1 kHz. This figure shows that as the distance between the user and the BS increases, the AVC decreases. For example, AVCs for U_1,

U_2 and U_3 are 4262.63×10^{-2} b/s/Hz, 1814.48×10^{-4} b/s/Hz, and 444.584×10^{-4} b/s/Hz, respectively, at SNR = 15 dB.

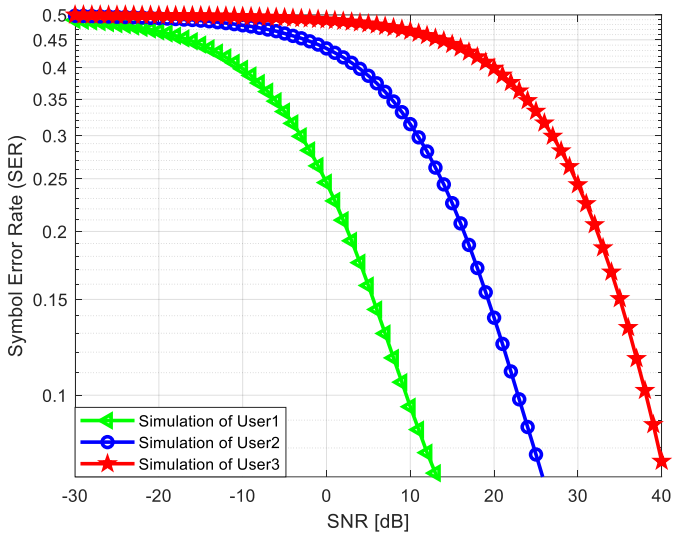

Figure 4. SER Results of Uplink-NOMA over Málaga Channels

Figure 4 shows the performance of the SER. U_1, U_2, and U_3 reach 0.1 SER value at approximately 10 dB, 23 dB, and 38 dB, respectively. SER values of U_1 are lower than the others, as it is the closest to BS and its received power is the strongest.

CONCLUSION

NOMA and FSO provide a considerable solution for increasing the capacity of wireless systems. In uplink NOMA systems, optical communication can be applied where users transmit their signal with equal power. Our study has shown that performance is promising for future communication systems. In the future, detailed mathematical derivations of performance metrics can be performed to generalize the simulation results presented in this paper.

ACKNOWLEDGEMENTS

“This work is supported by Research Fund of the Yildiz Technical University. Project Number: 5132”

REFERENCES

Badarneh, O., & Aloqlah, M. (2015). Performance Analysis of Digital Communication Systems over Generalized α-η-μ Fading Channels. *IEEE Transactions on Vehicular Technology*, *65*, 1. https://doi.org/10.1109/TVT.2015.2504381

Basak, S., Azeemuddin, S., & Nayak, J. (2018). Analysis of Beam Wander and Pointing Error on Laser Beam Propagation through Atmosphere. *2018 Asia Communications and Photonics Conference (ACP)*, 1–3. https://doi.org/10.1109/ACP.2018.8596267

Belső, Z., & Pap, L. (2025). Evaluation of the capacity region for uplink multi user NOMA in fading environment. *Wireless Networks*. https://doi.org/10.1007/s11276-025-03962-y

Ghassemlooy, Z., Arnon, S., Uysal, M., Xu, Z., & Cheng, J. (2015). Emerging Optical Wireless Communications-Advances and Challenges. *IEEE Journal on Selected Areas in Communications*, *33*(9), 1738–1749. https://doi.org/10.1109/JSAC.2015.2458511

Jurado-Navas, A., Garrido-Balsells, J. M., Paris, J. F., & Puerta-Notario, A. (2011). A Unifying Statistical Model for Atmospheric Optical Scintillation. In J. Awrejcewicz (Ed.), *Numerical Simulations of Physical and Engineering Processes*. IntechOpen. https://doi.org/10.5772/25097

Kaushal, H., & Kaddoum, G. (2017). Optical Communication in Space: Challenges and Mitigation Techniques. *IEEE Communications Surveys & Tutorials*, *19*(1), 57–96. https://doi.org/10.1109/COMST.2016.2603518

Kumar, V., Kumar, R., & Prakriya, S. (2025). Sum Rate Maximization and Performance Analysis of NOMA-Based IRS-Aided Uplink Visible Light Communication System. *2025 IEEE International Conference on Interdisciplinary Approaches in Technology and Management for Social Innovation (IATMSI)*, *3*, 1–6. https://doi.org/10.1109/IATMSI64286.2025.10984992

Le-Thanh, T., & Ho-Van, K. (2025). Uplink transmission in NOMA systems with energy harvesting and jamming: performance evaluation. *Telecommunication Systems*, *88*(2), 55. https://doi.org/10.1007/s11235-025-01284-0

Lukesh, G., Chandler, S., & Voelz, D. (2000). Estimation of laser system pointing performance by use of statistics of return photons. *Applied Optics*, *39*(9), 1359–1371. https://doi.org/10.1364/AO.39.001359

Makki, B., Chitti, K., Behravan, A., & Alouini, M.-S. (2020). A Survey of NOMA: Current Status and Open Research Challenges. *IEEE Open Journal of the Communications Society*, *1*, 179–189. https://doi.org/10.1109/OJCOMS.2020.2969899

Raza, M. A., Abolhasan, M., Lipman, J., & Ni, W. (2025). Device-Level Learning-Based Distributed Power Control for Uplink NOMA in IoT Networks. *IEEE Transactions on Cognitive Communications and Networking*, 1. https://doi.org/10.1109/TCCN.2025.3566033

Sadat, H., Abaza, M., Mansour, A., & Alfalou, A. (2022). A Survey of NOMA for VLC Systems: Research Challenges and Future Trends. In *Sensors* (Vol. 22, Issue 4). https://doi.org/10.3390/s22041395

Saito, Y., Kishiyama, Y., Benjebbour, A., Nakamura, T., Li, A., & Higuchi, K. (2013). Non-Orthogonal Multiple Access (NOMA) for Cellular Future Radio Access. *2013 IEEE 77th Vehicular Technology Conference (VTC Spring)*, 1–5. https://doi.org/10.1109/VTCSpring.2013.6692652

Xu, G., Zhu, Y., Wang, L., Wang, Y., & Shen, B. (2025). Ergodic Capacity of a NOMA-Based RF/FSO Integrated Satellite-Terrestrial Relay Networks System. *IEEE Photonics Technology Letters*, *37*(11), 621–624. https://doi.org/10.1109/LPT.2025.3541024

➢ *ORAL PRESENTATION*

Yenilenebilir enerji kaynağı olarak güneş enerjisinin önemi ve Türkiye'deki gelecek perspektifi

Rafig Huseynov [*,1] Selçuk Karagöz [*,2] (https://orcid.org/0009-0008-0397-3242)

[*1]Bursa Teknik Üniversitesi, Mühendislik ve Doğa Bilimleri Fakültesi, Makine mühendisliği, Bursa, Türkiye

*Sorumlu yazar e-posta:huseynov.rafiq.2001@gmail.com

Özet

Enerji sektöründe yaşanan dönüşüm ve iklim değişikliği ile mücadele gerekliliği, yenilenebilir enerji kaynaklarının stratejik önemini artırmıştır. Güneş enerjisi, sürdürülebilir, temiz ve ekonomik bir çözüm olarak dünya çapında hızla yaygınlaşmaktadır. Türkiye, coğrafi konumu ve iklimsel avantajları nedeniyle güneş enerjisi potansiyeli yüksek bir ülkedir. Bu çalışma, güneş enerjisinin fiziksel ve teknolojik temellerinden başlayarak, Türkiye'deki mevcut durumunu, uygulanan politikalar, yatırımlar ve projelerle desteklenen sektörel gelişmeleri detaylı şekilde incelemektedir. Ayrıca, enerji depolama teknolojileri, hibrit sistemler, yerli üretim ve dijitalleşme gibi geleceğe yönelik stratejik yaklaşımlar değerlendirilmiş ve sürdürülebilir büyüme için politika önerileri sunulmuştur. Makalede elde edilen bulgular, Türkiye'nin güneş enerjisinde dünya çapında rekabetçi ve lider bir konuma gelebilmesi için kapsamlı bir yol haritası sunmaktadır.

Anahtar Kelimeler: Güneş enerjisi, Yenilenebilir enerji, Fotovoltaik teknolojiler, Türkiye enerji politikası, Enerji depolama, Sürdürülebilir kalkınma

The importance of solar energy as a renewable energy source and its future outlook in Turkiye

Abstract

The transformation in the energy sector and the necessity to combat climate change have significantly increased the strategic importance of renewable energy sources. Solar energy is rapidly expanding worldwide as a sustainable, clean, and economically viable solution. Due to its geographical location and climatic advantages, Turkey has a high potential for solar energy. This study provides a detailed examination of the physical and technological foundations of solar energy, along with the current state of the sector in Turkey. It explores national policies, investments, and projects supporting the sector's development. Furthermore, future-oriented strategies such as energy storage technologies, hybrid systems, domestic production, and digitalization are evaluated. The study offers policy recommendations for sustainable growth and presents a comprehensive roadmap for positioning Turkey as a competitive and leading country in the global solar energy market.

Keywords: Solar energy, Renewable energy, Photovoltaic technologies, Turkish energy policy, Energy storage, Sustainable development

Giriş

Son yüzyılda enerji tüketiminde yaşanan hızlı artış, başta fosil yakıtlar olmak üzere geleneksel enerji kaynaklarının çevresel etkilerini gözler önüne sermiştir[2]. Küresel ısınma, hava kirliliği, karbon emisyonları ve doğal kaynakların tükenmesi gibi sorunlar, enerji sistemlerinde radikal dönüşümü zorunlu kılmıştır[3]. Bu dönüşümde yenilenebilir enerji kaynakları, temiz ve sürdürülebilir çözümler sunarak hem arz güvenliğini artırmak hem de çevresel etkileri azaltmak için öncelikli konuma yükselmiştir.

Türkiye, ekonomik büyüme ve nüfus artışıyla birlikte enerji talebinde önemli artışlar yaşamaktadır. Ancak mevcut enerji üretiminde büyük oranda dışa bağımlılık ve fosil yakıtlara dayalı üretim yapısı, sürdürülebilirlik

[2] IEA. (2023). *World Energy Outlook 2023*. International Energy Agency.
[3] IPCC. (2022). *Climate Change 2022: Mitigation of Climate Change*. Cambridge University Press.

açısından risk teşkil etmektedir. Bu nedenle Türkiye, enerji stratejilerini yenilenebilir enerji odaklı olarak şekillendirmekte, güneş enerjisi başta olmak üzere temiz enerji yatırımlarını teşvik etmektedir.[4]
Bu çalışma, güneş enerjisinin teorik altyapısını kapsamlı şekilde ele aldıktan sonra Türkiye'deki güneş enerjisi potansiyelini, mevcut durumu, yürütülen projeleri ve geleceğe yönelik stratejileri derinlemesine analiz etmektedir. Ayrıca teknolojik gelişmeler ve sektörün karşılaştığı zorluklar üzerinde durularak, sürdürülebilir enerji politikaları için öneriler geliştirilmiştir.

Güneş Enerjisinin Teorik Temelleri

Güneş, Dünya'daki tüm enerji biçimlerinin nihai kaynağıdır ve canlıların yaşam döngüsünü sürdürebilmesi için elzemdir. Güneşten yayılan enerjinin yalnızca küçük bir kısmı Dünya'ya ulaşsa da, bu miktar gezegenimizdeki biyolojik, kimyasal ve fiziksel süreçleri sürdürebilecek ölçüdedir.[5] Güneş enerjisi; zaman, coğrafi konum, atmosferik şartlar, mevsimler ve çevresel etkenlere bağlı olarak değişkenlik gösterir.[6]
Güneş enerjisi, çeşitli fiziksel prensiplere dayanır. Fotovoltaik hücreler ve termal sistemler aracılığıyla hem elektrik hem de ısı enerjisine dönüştürülebilir.[7] Güneş ışınımının Dünya yüzeyine ulaşma hızı, insanlığın enerji tüketme hızından yaklaşık 10.000 kat daha fazladır.[8] Bu doğrultuda, güneş enerjisi yalnızca potansiyel değil, aynı zamanda pratik bir enerji kaynağıdır. Gelişmiş ülkelerde maliyet düşüşüyle birlikte artık en ucuz elektrik üretim biçimlerinden biri haline gelmiştir.
Güneş radyasyonu, elektromanyetik dalgalar biçiminde uzayda yayılır. Bu dalgalar, nükleer füzyon sonucunda Güneş'in çekirdeğinde açığa çıkan enerjinin yüzeye ulaşmasıyla oluşur. Bu radyasyonun çoğu görünür spektrumda yer alırken, kızılötesi (IR) ve ultraviyole (UV) bileşenleri de önemlidir.[9] Güneş spektrumu, tüm dalga boylarını kapsayan sürekli bir spektrumdur ve bu spektrum içindeki yoğunluk, güneş enerjisi teknolojilerinin verimliliğini belirler.[10] Güneş, kara cisim olarak modellenebilir ve yaklaşık 5.800 K yüzey sıcaklığına sahiptir. Stefan-Boltzmann yasası, bu sıcaklığın radyasyon yoğunluğu üzerindeki etkisini belirlemede kullanılır. Güneş Enerjisi Sabiti (Solar Constant), atmosferin dışında bir metrekareye düşen güneş ışınımı miktarını tanımlar ve yaklaşık 1366 W/m² olarak kabul edilir (NASA, 2023). Ancak atmosferik girişim, bu değeri yüzeye ulaşmadan önce önemli ölçüde azaltabilir.
Güneş radyasyonu; UV (10–400 nm), görünür (400–700 nm) ve IR (>700 nm) bileşenleriyle tanımlanır. UV radyasyonunun büyük kısmı atmosfer tarafından emilirken, IR bileşeni Dünya yüzeyinde hissedilen ısıdan sorumludur.[11] Görünür ışık ise fotovoltaik panellerin temel enerji kaynağıdır. Elektromanyetik spektrumun güneş enerjisi açısından en önemli bölgeleri UV, görünür ve IR bandıdır. UV ışınlarının zararlı etkileri atmosfer tarafından büyük ölçüde engellenirken, görünür ışık fotovoltaik sistemler için optimum enerji sağlar. Kızılötesi radyasyon ise daha çok termal enerji uygulamalarıyla ilişkilidir.
Güneş enerjisinin Dünya yüzeyine ulaşmasını etkileyen birçok faktör vardır. Dünya'nın Güneş'e olan ortalama uzaklığı yaklaşık 150 milyon km'dir ve bu mesafe alınan enerji miktarını belirlemede kritik rol oynar.[12] Atmosferik emilim, saçılma ve bulutluluk gibi etkenler de yüzeye ulaşan radyasyon miktarını azaltır. Güneş ışığının geliş açısı, özellikle enlem etkisiyle değişir; ekvatoral bölgelerde daha dik gelen ışık, kutuplara doğru yayılarak enerji yoğunluğunu azaltır. Aynı zamanda, yüzey albedosu da (örneğin kar, kum, orman) yansıma ve emilim oranlarını etkileyerek yüzeye ulaşan enerjiyi değiştirir.

---

[4] Enerji ve Tabii Kaynaklar Bakanlığı (ETKB). (2023). *Yenilenebilir Enerji Potansiyeli ve Politikaları*. https://www.enerji.gov.tr

[5] Duffie, J. A., & Beckman, W. A. (2013). *Solar engineering of thermal processes*. John Wiley & Sons.

[6] Kalogirou, S. A. (2009). Solar energy engineering: processes and systems. Academic Press.

[7] Twidell, J., & Weir, T. (2015). *Renewable energy resources*. Routledge.

[8] International Energy Agency (IEA). (2023). *World Energy Outlook 2023*. https://www.iea.org

[9] Green, M. A. (2001). Third generation photovoltaics: Ultra-high conversion efficiency at low cost. *Progress in Photovoltaics: Research and Applications*, 9(2), 123–135.

[10] Goetzberger, A., Hebling, C., & Schock, H. W. (2003). Photovoltaic materials, history, status and outlook. *Materials Science and Engineering: R: Reports*, 40(1), 1-46.

[11] Madronich, S., McKenzie, R. L., Caldwell, M. M., & Björn, L. O. (1998). Changes in biologically active ultraviolet radiation reaching the Earth's surface. *Journal of Photochemistry and Photobiology B: Biology*, 46(1-3), 5-19.

[12] Gueymard, C. A. (2004). The sun's total and spectral irradiance for solar energy applications and solar radiation models. *Solar Energy*, 76(4), 423–453.

Güneş radyasyonu, yüzeye ulaşma kapasitesine göre W/m² cinsinden ölçülür. Açık günlerde bu değer ekvatoral bölgelerde 1000 W/m²'ye kadar çıkabilirken, kutuplarda ve kış aylarında bu oran oldukça düşer.[13] Bu değişkenlik, güneş enerjisi sistemlerinin yer seçimi ve tasarımında dikkate alınması gereken önemli bir faktördür. Güneş enerjisi yalnızca bol ve yenilenebilir bir kaynak değil, aynı zamanda teknolojik gelişmelerle birlikte maliyet açısından da erişilebilir hale gelmiştir. Fiziksel prensiplerin iyi anlaşılması, güneş enerjisinden maksimum verim elde etmek için kritik önemdedir. Atmosferik faktörler, geliş açısı ve yüzey özellikleri gibi parametreler, bu enerjinin Dünya yüzeyine ulaşmasını ve kullanılabilirliğini doğrudan etkiler. İlerleyen teknolojiyle birlikte bu kaynağın daha etkili kullanımı, sürdürülebilir enerji politikalarının temelini oluşturacaktır.[14]

Güneş enerjisi sistemleri, güneş ışığını elektrik veya ısı enerjisine dönüştüren teknolojilerdir. Bu sistemler genellikle fotovoltaik (PV), termal, konvansiyonel ve konsantre güneş enerjisi sistemleri olarak sınıflandırılır.[15] Fotovoltaik sistemler, yarı iletken malzemelerden oluşan fotovoltaik hücreler aracılığıyla güneş ışığındaki fotonları doğrudan elektriğe çevirir. Bu sistemler genellikle %15–22 arasında verimliliğe sahiptir ve verimliliği malzeme, ışık yoğunluğu ve çevresel koşullar etkiler.[16]

Termal güneş enerjisi sistemleri, güneş kolektörleri kullanarak ışığı ısı enerjisine dönüştürür ve bu enerji genellikle su veya sıvıların ısıtılmasında kullanılır. Bu sistemlerin verimliliği %50–70 arasında değişebilir ve bu oran kolektör tipi ve malzeme özelliklerine bağlıdır.[17]

Konvansiyonel sistemler, temel PV veya termal sistemlerdir ve genellikle küçük ölçekli uygulamalar için uygundur. Konsantre güneş enerjisi sistemleri (CSP), güneş ışığını yoğunlaştırarak yüksek sıcaklık elde eder ve türbinler aracılığıyla elektrik üretir. CSP sistemleri %20–30 arasında verimliliğe ulaşabilir.[18]

Güneş enerjisi dönüşüm verimliliği; kullanılan teknolojinin türüne, tasarımına, malzemeye ve çevresel koşullara bağlıdır. Fotovoltaik sistemler daha düşük verimle çalışırken, termal sistemler ışığın büyük kısmını ısıya dönüştürdüğü için daha verimlidir. CSP sistemler ise büyük ölçekli üretimlerde avantaj sağlar

Güneş ışınımı ve iklim faktörleri, güneş enerjisi sistemlerinin performansını doğrudan etkiler. Coğrafi konum, enlem, yükseklik ve gölgeleme gibi faktörler, güneş ışınımının yüzeye ulaşma miktarını belirler Ekvatora yakın bölgeler, daha yüksek ışınım aldığı için sistemler daha verimli çalışır.[19]

Ayrıca, iklimsel değişkenler de performansı etkiler. Bulutluluk güneş ışığının yüzeye ulaşmasını sınırlandırır, bu da PV sistemlerin verimliliğini düşürür. Yüksek sıcaklıklar, PV panellerin performansını azaltabilirken, termal sistemler bu sıcaklıklardan faydalanabilir. Rüzgar ise panellerin soğumasını sağlayarak verimi artırabilir.[20]

Güneş enerjisi, fosil yakıtlarla karşılaştırıldığında çevreye çok daha az zarar veren bir enerji kaynağıdır ve sera gazı emisyonlarını önemli ölçüde azaltır.[21] Karbondioksit salımı olmadan elektrik üretmesi, iklim değişikliği ile mücadelede kritik rol oynamaktadır. Ayrıca, güneş enerjisi üretimi sırasında hava kirliliği, asidik yağmur ya da zehirli gazlar gibi olumsuz etkiler gözlenmez.[22]

---

[13] International Energy Agency (IEA). (2023). *World Energy Outlook 2023*. https://www.iea.org

[14] International Renewable Energy Agency (IRENA). (2023). *Renewable Power Generation Costs in 2022*. https://www.irena.org

[15] Smith, J. (2020). *Solar energy systems: Principles and applications*. Oxford University Press.

[16] Jones, R., & Lee, M. (2018). *Photovoltaic technology advancements and future trends*. Journal of Renewable Energy Science, 9(2), 67–85.

[17] Ahmed, A., & Zhai, X. (2019). *Thermal performance evaluation of solar water heating systems: A review*. Renewable and Sustainable Energy Reviews, 103, 13–29.

[18] Zhou, X., Yang, W., & Deng, Y. (2022). *Recent developments in concentrated solar power systems*. Progress in Energy and Combustion Science, 88

[19] Nguyen, H., & Silva, T. (2018). *Solar radiation patterns and PV potential based on geographical factors*. International Journal of Energy Research, 42(5), 1203–1215

[20] Singh, R., & Tan, C. (2022). *Wind-assisted cooling for photovoltaic panels and its effect on power output*. Applied Energy Research, 18(2), 211–220.

[21] Zhou, X., Yang, W., & Deng, Y. (2022). *Recent developments in concentrated solar power systems*. *Progress in Energy and Combustion Science*, 88,

[22] Patel, R. (2021). *Advances in flat-plate and evacuated tube solar collectors*. *Journal of Thermal Science*, 27(4), 305–321.

Güneş panellerinin üretimi bazı çevresel etkiler doğurabilir; örneğin silikon gibi minerallerin madenciliği sırasında yerel ekosistemler etkilenebilir.[23] Ancak bu etkiler, fosil yakıt madenciliğine kıyasla oldukça sınırlıdır. Güneş enerji santrallerinin geniş alanlara ihtiyaç duyması, toprak kullanımı açısından bir dezavantaj olsa da, genellikle çorak veya tarım dışı arazilerde konumlandırıldıkları için ekosistemlere zarar minimaldir.
Güneş enerjisinin en cazip yönlerinden biri, düşük işletme ve bakım maliyetleridir. Bir kez kurulan güneş panelleri 25–30 yıl gibi uzun sürelerle enerji üretebilir. Yakıt ihtiyacının olmaması nedeniyle enerji fiyatları istikrarlı kalır, bu da özellikle gelişmekte olan ülkelerde enerji güvenliğini artırır. Hükümet destekleri, vergi teşvikleri ve geri ödeme programları gibi finansal düzenlemeler de güneş enerjisini ekonomik açıdan daha erişilebilir kılmaktadır. Uzun vadede ise, ilk yatırım maliyetlerine rağmen güneş enerjisi oldukça düşük enerji maliyetleri sunar. Yatırımlar genellikle kısa sürede kendini amorti eder. Güneş enerjisinin süreksiz yapısı (gece üretim yapılamaması gibi) enerji depolama sistemlerinin gerekliliğini doğurur. Lityum-iyon bataryalar bu noktada öne çıkarken, maliyet, batarya ömrü ve şarj-deşarj döngüleri önemli sınırlamalardır. Alternatif depolama yöntemleri olarak pompa depolama, termal depolama ve hidrojen depolama sistemleri araştırılmaktadır.[24]
Akıllı şebekeler, güneş enerjisinin üretim-tüketim dengesini optimize ederek, sistem verimliliğini artırır. Bu sistemler, enerji talebi ile üretimi arasında gerçek zamanlı uyum sağlar. Uzun mesafeli enerji iletimi sırasında yaşanan kayıplar ise HVDC (yüksek voltajlı doğru akım) sistemleri gibi teknolojilerle azaltılabilmektedir.[25]
Rüzgar enerjisi de tıpkı güneş enerjisi gibi temiz ve yerel üretim sağlayan bir kaynaktır. Ancak rüzgarın süreksizliği, güneş ışığından daha az öngörülebilir bir üretim profiline yol açar. Güneş enerjisi, çok daha geniş coğrafyalarda uygulanabilir olmasıyla avantaj sağlar. Hidroelektrik enerji ise yüksek verimlilik (%85–90) ve sürekli üretim avantajlarına sahiptir; buna karşın çevresel etkileri (ekosistem tahribatı, yerel halkın yerinden edilmesi) oldukça büyüktür.[26] Güneş enerjisi ise daha düşük çevresel etkiyle, daha küçük ve esnek ölçekli projeler sunar.
Biyokütle enerjisi, bitkisel atıklar, hayvansal artıklar ve diğer organik materyallerin yakılması veya fermantasyon gibi biyolojik süreçlerle enerjiye dönüştürülmesiyle elde edilir. Bu enerji türü, 24 saat boyunca enerji üretimi yapılabilmesi nedeniyle süreklilik avantajı sağlar.27 Oysa güneş enerjisi sadece güneşli saatlerde üretim yapabilir, bu da özellikle gece saatlerinde enerji üretimini imkânsız hale getirir.
Biyokütle enerjisinin önemli bir avantajı da atık geri dönüşümünü teşvik etmesidir. Tarımsal ve kentsel organik atıklar, bu sistemlerde enerjiye çevrilerek hem atık yükü azaltılır hem de enerji üretilir. Güneş enerjisi ise doğrudan güneş ışığına bağımlıdır ve bu tür bir atık değerlendirme özelliği taşımaz. Ancak, biyokütle sistemleri karbon salınımı yapabilir. Her ne kadar fosil yakıtlara göre daha çevre dostu olsa da, biyokütle yakımı sonucu karbon dioksit salınır ve bu durum iklim değişikliğini etkileyebilir. Buna karşılık, güneş enerjisi sistemleri emisyonsuz çalışır ve çevreye zarar vermez.28
Ayrıca biyokütle enerji santralleri için tarım arazilerinin enerji için kullanılması gerekebilir. Bu durum, özellikle gıda üretimiyle rekabet yaratabilir ve gıda güvenliğini tehdit edebilir. Güneş panelleri ise genellikle çatı gibi atıl alanlara kurulabilir veya çok daha az alan kaplar.
Jeotermal enerji; yer kabuğundaki sıcak su ve buharın yüzeye çıkarılarak elektrik veya ısı enerjisine dönüştürülmesiyle elde edilir.29 Bu sistemler, yılın her günü ve her saati sabit verimlilikte çalışabilir. Bu durum, güneş enerjisinin geceleri ve bulutlu günlerde üretim yapamamasıyla ciddi bir karşıtlık oluşturur.

---

[23] Kim, D., Lee, J., & Park, Y. (2020). *Materials and design optimization for high-efficiency solar panels*. *Solar Materials Journal*, 12(3), 145–162.

[24] Ahmed, A., & Zhai, X. (2019). *Thermal performance evaluation of solar water heating systems: A review*. *Renewable and Sustainable Energy Reviews*, 103, 13–29.

[25] López, J., & Ramírez, G. (2020). *Efficiency analysis of concentrating solar power (CSP) systems*. *Renewable Energy Systems*, 15(1), 110–121.

[26] Wang, L., Zhao, Y., & Chen, K. (2021). *CSP technologies and future grid integration challenges*. *Energy Policy and Technology*, 14(1), 34–49.

[27] Demir, H., & Aslan, G. (2022). *Organik atıklardan enerji üretimi ve çevresel etkiler*. Yenilenebilir Enerji Dergisi, 8(3), 62–70.

[28] Arslan, E. (2021). *Biyokütle enerjisinin karbon salınımı açısından değerlendirilmesi*. Çevre Bilimleri Araştırma Dergisi, 13(2), 55–63.

[29] Çelik, A. (2023). *Jeotermal enerji ve sürdürülebilir enerji politikaları*. Enerji Teknolojileri, 19(1), 19–27.

Günümüz jeotermal santralleri, %90'a varan verimlilikle çalışabilirken, güneş enerjisi sistemlerinin verimliliği genellikle %15–22 arasında kalmaktadır.30 Bu da jeotermalin, özellikle yüksek ve sürekli enerji ihtiyacı olan bölgelerde daha uygun olduğunu gösterir. Jeotermal enerji sistemleri, kurulumdan sonra düşük bakım maliyeti ile uzun yıllar çalışabilir. Güneş enerjisi sistemleri de düşük bakım gerektirir, ancak düzenli olarak panel temizliği ve elektriksel bağlantı kontrolleri yapılmalıdır.31 Jeotermal sistemler bu açıdan daha istikrarlı ve az müdahale gerektiren bir alternatif olabilir. Ayrıca, jeotermal tesisler uygun şekilde inşa edildiğinde 50 yılın üzerinde verimli çalışabilirken, güneş panelleri genellikle 20–30 yıl arasında verimli kullanım ömrüne sahiptir. Bu durum, jeotermalin uzun vadeli yatırım için daha avantajlı olabileceğini gösterir. Jeotermal enerjinin en büyük dezavantajı, coğrafi bağımlılığıdır. Sadece belirli bölgelerde, örneğin volkanik aktivite gösteren alanlarda etkili şekilde kullanılabilir. Türkiye'de Ege Bölgesi, İzlanda ve Endonezya gibi ülkeler bu açıdan avantajlıdır, ancak bu tür kaynaklar her yerde mevcut değildir. Oysa güneş enerjisi neredeyse her coğrafyada uygulanabilir.32

Ek olarak, jeotermal sistemlerin başlangıç maliyeti oldukça yüksektir. Sondaj, altyapı ve mühendislik yatırımları pahalıdır. Güneş enerjisi sistemleri ise modüler yapıları sayesinde küçük ölçekli olarak da kurulabilir ve daha düşük maliyetle uygulanabilir.

Güneş Enerjisinin Türkiye'deki Durumu ve Gelecek Potansiyeli

Türkiye, coğrafi konumu ve iklimsel avantajları sayesinde güneş enerjisi üretimi açısından büyük bir potansiyele sahiptir. 36°–42° kuzey enlemleri arasında yer alması, ülkenin özellikle güney kesimlerinde yüksek güneş ışınımı almasını sağlamaktadır. Enerji ve Tabii Kaynaklar Bakanlığı'nın[33] verilerine göre Türkiye'nin yıllık ortalama güneşlenme süresi 2.600–2.800 saat, yıllık ortalama Global Horizontal Irradiance (GHI) değeri ise yaklaşık 1.527 kWh/m² düzeyindedir. Bu değer, ülkenin yenilenebilir enerji stratejilerinde güneş enerjisine önemli bir yer ayrılması gerektiğini ortaya koymaktadır (Yalçın & Ekinci, 2020). Bölgesel olarak en yüksek güneşlenme süresi ve ışınım değerleri Güneydoğu Anadolu ve Akdeniz bölgelerinde gözlemlenmekte, buna karşın Karadeniz ve Marmara gibi kuzey bölgelerinde bu değerler daha düşüktür.[34] Örneğin, Güneydoğu Anadolu Bölgesi'nde yıllık GHI değeri 1.800–2.000 kWh/m²'ye kadar çıkmakta ve güneşlenme süresi 2.993 saate ulaşmaktadır. Aylık veriler incelendiğinde, Temmuz ayında güneş ışınımı maksimum seviyeye ulaşırken, kış aylarında ciddi bir düşüş gözlenmektedir.[35] Standart sapmanın yaklaşık 180 kWh/m² olması, bölgeler arasında ışınım dağılımının nispeten homojen olduğunu ancak belirgin bölgesel farkların da bulunduğunu göstermektedir.

Türkiye'nin enerji ihtiyacı, 2025 yılı itibarıyla yaklaşık 380 TWh seviyesindedir ve bu talep sanayi, konut ve ulaşım gibi sektörlerin büyümesiyle artmaya devam etmektedir. Bu bağlamda, güneş enerjisinin ülke genelindeki potansiyeli dikkate alındığında, %15–20 verimlilikle çalışan fotovoltaik (PV) sistemlerle bu ihtiyacın %10–15'lik kısmının karşılanabileceği öngörülmektedir (ETKB, 2023). Özellikle 2030 yılına kadar kurulu güneş enerjisi kapasitesinin 20 GW'a çıkarılması hedeflenmektedir. Güneş enerjisi yatırımları için en uygun alanlar, yüksek ışınım ve uzun güneşlenme süresi nedeniyle Güneydoğu Anadolu, Akdeniz ve Ege.[36] Türkiye'de uygulanan güneş enerjisi teknolojileri temel olarak ikiye ayrılmaktadır: fotovoltaik sistemler ve güneş termal sistemler. Fotovoltaik paneller, güneş ışığını doğrudan elektriğe dönüştürürken; sistem performansı çevresel faktörlerden önemli ölçüde etkilenmektedir. Sıcaklık artışı, panelin verimliliğini düşürürken; doğru panel yönü ve eğimi verimliliği artırmaktadır. Türkiye'de paneller genellikle güney yönüne ve bölgeye uygun eğim açısıyla monte edilmektedir. En yaygın panel türleri arasında yüksek verimliliğe sahip

[30] Erdoğan, Z., & Toprak, M. (2020). *Jeotermal ve güneş enerjisi santrallerinin verim karşılaştırması*. Yenilikçi Enerji Araştırmaları, 14(4), 70–79.

[31] Aksoy, E., & Duru, M. (2021). *Güneş paneli sistemlerinde bakım uygulamaları*. Enerji Sistemleri Dergisi, 12(1), 88–97.

[32] Karakaya, E., & Yiğit, R. (2021). *Güneş enerjisinin coğrafi yaygınlığı ve potansiyeli*. Küresel Enerji Politikaları, 5(1), 15–24.

[33] Enerji ve Tabii Kaynaklar Bakanlığı (ETKB). (2023). *Güneş Enerjisi Potansiyeli Atlası (GEPA)*.

[34] Yalçın, H., & Ekinci, T. (2020). Güneş ve jeotermal enerji sistemlerinin ömür analizleri. Enerji Performansı Dergisi, 9(4), 66–75.

[35] Yılmaz, A., & Doğan, S. (2020). *Fotovoltaik sistemlerde maliyet düşüşleri ve ekonomik potansiyel*. GES ve Ekonomi, 6(3), 83–91.

[36] Özkan, N., & Şahin, R. (2021). *Türkiye'de güneş enerjisi yatırımlarının mekânsal analizi*. Doğal Kaynaklar Dergisi, 8(4), 73–81.

ancak maliyeti yüksek monokristal paneller, daha ekonomik ancak daha düşük verimliliğe sahip polikristal paneller ve esnek yapısıyla öne çıkan ince film paneller yer almaktadır.[37]

Güneş termal sistemler ise, güneş enerjisini ısıya çevirerek sıcak su veya ısıtma uygulamalarında kullanılmaktadır. Kolektör türüne göre düşük (30–90°C), orta (100–300°C) ve yüksek (300°C üzeri) sıcaklıklarda çalışabilirler. Güney bölgelerde bu sistemler daha yüksek verim sağlarken, kuzeyde verimlilik daha sınırlıdır.[38] Türkiye'de büyük ölçekli güneş enerjisi santralleri (GES) sayısı da özellikle güneyde artmaktadır. Bu santrallerin verimliliği, panel yerleşimi, inverter seçimi ve enerji depolama sistemlerinin etkinliği gibi faktörlere bağlıdır (ETKB, 2023). Güneş takip sistemleri ve doğru inverter kullanımı, enerji üretimini optimize ederken, enerji depolama sistemleri ise arz-talep dengesini sağlamada kritik rol oynar.

Sonuç olarak, Türkiye'nin güneş enerjisi potansiyeli gerek mevcut koşullar gerekse teknolojik gelişmeler ışığında oldukça yüksektir. Ancak bu potansiyelin ekonomik, çevresel ve teknik boyutları dikkate alınarak etkin bir şekilde değerlendirilmesi gerekmektedir. Özellikle bölgesel planlamalar, panel teknolojisi seçimleri ve destekleyici altyapı yatırımları, Türkiye'nin enerji arz güvenliğini sağlamada güneş enerjisini stratejik bir kaynak haline getirebilir.

Türkiye, güneş enerjisi potansiyelini etkin bir şekilde kullanarak yenilenebilir enerji kaynakları arasında önemli bir paya sahip olmayı hedeflemektedir. Ülkenin coğrafi konumu, yıllık ortalama 2.741 saatlik güneşlenme süresiyle güneş enerjisi üretimi için elverişli bir ortam sunmakta; ortalama günlük ışınım miktarı ise 3,6 kWh/m²-gün ile 7,2 kWh/m²-gün arasında değişmektedir.[39] Bu veriler, Türkiye'nin güneş enerjisi potansiyelinin yüksekliğini göstermekte ve yatırımların stratejik bir öncelik olarak ele alındığını ortaya koymaktadır. 2024 yılı itibarıyla Türkiye'nin güneş enerjisi kurulu gücü yaklaşık 20,4 GW seviyesine ulaşmıştır; bu da 2025 yılı için belirlenen 22,6 GW'lık hedefin büyük oranda yakalandığını göstermektedir.[40]

Güneş enerjisi yatırımları, özellikle lisanssız küçük ölçekli projelerin artışı ve organize sanayi bölgeleri ile sanayi kuruluşlarının kendi elektrik tüketimlerini karşılamaya yönelmesi sayesinde hız kazanmıştır.[41]

Enerji ve Tabii Kaynaklar Bakanlığı'nın 2035 vizyonu kapsamında, güneş enerjisi kurulu gücünün 77,4 GW'a çıkarılması hedeflenmektedir.[42] Bu da Türkiye'nin toplam yenilenebilir enerji kapasitesinin 2035 itibarıyla 189,7 GW'a ulaşması planının bir parçası olarak sunulmaktadır. GES projeleri lisanssız, lisanslı, yüzer ve depolama entegreli modellerle hayata geçirilmekte; lisanssız projeler evsel çatılardan OSB'lere kadar yaygınlaşmakta; lisanslı projeler ise büyük ölçekli santraller olarak YEKA modeliyle uygulanmaktadır. Yüzer GES sistemleri baraj gölleri ve su yüzeylerine kurulurken, depolamalı sistemler şebeke dengesini sağlamada kritik rol oynamaktadır.[43]

Türkiye'de güneş enerjisi yatırımları enerji ithalatının azaltılması, yerli sanayinin gelişimi ve istihdam yaratımı gibi önemli ekonomik etkiler de doğurmaktadır.[44] 2022–2024 yılları arasında yalnızca güneş ve rüzgar enerjisi kaynaklı üretim sayesinde yaklaşık 15 milyar dolarlık doğalgaz ithalatının önüne geçilmiştir (IEA, 2023). Ayrıca Türkiye, yıllık 12 GW panel üretim kapasitesiyle Avrupa'nın en büyük, dünyanın ise Çin, Hindistan ve Vietnam'dan sonra dördüncü büyük panel üreticisi konumundadır (SolarPower Europe, 2023). GES projeleri inşaat, mühendislik ve bakım alanlarında yaklaşık 25.000 kişilik doğrudan ve dolaylı istihdam sağlamaktadır.[45]

Türkiye, 2035 yılına kadar toplam rüzgar ve güneş enerjisi kapasitesini 30 GW'tan 120 GW'a çıkarmayı hedeflemekte; bu doğrultuda güneş enerjisinin toplam kurulu kapasitesinin 77 GW'a ulaşması planlanmaktadır

---

[37] Karaca, Y. (2023). *Yenilenebilir enerji sistemleri üzerine teknik analizler*. Sürdürülebilir Enerji Ekonomisi, 9(1), 41–49.

[38] Sönmez, D. (2022). *Güneş termal sistemlerinde verimlilik değerlendirmesi*. Enerji Yönetimi Araştırmaları, 7(3), 60–66.

[39] Türkiye Elektrik İletim A.Ş. (2023). *Türkiye elektrik üretim–iletim istatistikleri*. https://www.teias.gov.tr

[40] Türkiye Elektrik İletim A.Ş. (2024). *Kurulu güç ve üretim verileri Mart 2024*. https://www.teias.gov.tr

[41] Enerji Piyasası Düzenleme Kurumu. (2024). *Elektrik piyasası 2023 yıllık raporu*. https://www.epdk.gov.tr

[42] Enerji ve Tabii Kaynaklar Bakanlığı. (2023). *Türkiye Ulusal Enerji Planı 2035*. https://www.enerji.gov.tr

[43] International Energy Agency. (2023). *Renewables 2023: Analysis and forecast to 2028*. https://www.iea.org

[44] World Bank. (2023). *Financing renewable energy in emerging markets: Turkey profile*. https://www.worldbank.org

[45] Türkiye Rüzgar Enerjisi Birliği (TÜREB). (2024). *Yenilenebilir enerji ve istihdam raporu*. https://www.tureb.com.tr

(ETKB, 2023). Bu hedefler Ulusal Enerji Planı 2035 belgesinde yer almakta ve YEKA modeliyle özel sektör yatırımlarının desteklenmesi öngörülmektedir (ETKB, 2023).

Büyük ölçekli GES yatırımlarının öncüsü olan Karapınar YEKA GES Projesi, Konya'nın Karapınar ilçesinde 1.350 MWp (1000 MW AC) kurulu güçle, 3,5 milyon adet panelle yaklaşık 20 milyon m²'lik alanda kurulmuş olup, yıllık 1.700 GWh elektrik üretimi ile yaklaşık 600.000 hanenin yıllık elektrik ihtiyacını karşılamaktadır.[46] Projenin yatırım maliyeti yaklaşık 1,4 milyar dolar olup, kullanılan paneller %80 yerlilik oranıyla Kalyon PV tarafından üretilmiştir (Kalyon PV, 2024). Güneş takip sistemleriyle donatılan santral, doğu-batı ekseninde panel hareketiyle enerji verimliliğini artırmakta, kurulum sürecinde 1.100 kişilik geçici, işletme sürecinde ise 75 kişilik kalıcı istihdam sağlamaktadır (ETKB, 2023). Kalyon PV fabrikasında ise 1000'e yakın kalıcı istihdam yaratılmıştır (Kalyon PV, 2024). Proje, yılda yaklaşık 2 milyon ton CO_2 salımının önüne geçerek çevresel sürdürülebilirliğe katkı sağlamaktadır (IEA, 2023).

YEKA GES-4 ve Ceylanpınar YEKA GES gibi diğer büyük projeler de 500 MWp kapasiteyle hayata geçirilmiş, yerli ekipman kullanımı ve çevresel etki değerlendirmeleri titizlikle yürütülmüştür (EPDK, 2024). Karapınar gibi projeler özel sektör öncülüğünde kamu-özel iş birliğiyle yürütülmekte, yatırımın tamamı özel sektör tarafından karşılanmakta; yerli üretim, teknoloji transferi ve istihdam alanlarında önemli katkılar sağlanmaktadır (Kalyon PV, 2024).

Projeler 25 yıllık alım garantisi, yerli üretim teşviki ve ihale bazlı rekabet ortamı sunmaktadır (ETKB, 2023). Projelerin finansal değerlendirmesinde yatırım geri dönüş süresi, iç verimlilik oranı (IRR) ve net bugünkü değer (NPV) gibi göstergeler esas alınmaktadır (World Bank, 2023). Karapınar GES projesi özelinde IRR yaklaşık %12 olarak hesaplanmakta ve bu oran, yüksek başlangıç maliyetli projeler için cazip bir getiri olarak değerlendirilmektedir (IEA, 2023). Sabit enerji satış fiyatı, yıllık %3 gelir artışı ve sabit giderler varsayımıyla yapılan hesaplamalar, projenin NPV'sinin de pozitif olduğunu göstermektedir (World Bank, 2023). Ancak yatırım geri dönüş süresi, yüksek döviz kuru etkisi, ekonomik dalgalanmalar ve sabit gelir varsayımlarının gerçek hayatta karşılık bulmaması gibi nedenlerle saha uygulamalarında farklılık gösterebilir (TÜREB, 2024). Elektrik satış gelirleri, YEKDEM kapsamında belirlenen tarifelerle desteklenmekte, serbest piyasa fiyatlarının dalgalanması karşısında gelir istikrarı sağlamaktadır (EPDK, 2024). Maliyet bileşenlerinde panel, invertör, montaj ve kablolama kalemleri önemli yer tutmakta; %90'a varan yerlilik oranı sayesinde ithalat maliyetleri düşmekte ve yerli sanayi desteklenmektedir.[47] Yerli üretim sayesinde %30'a kadar maliyet avantajı sağlanmakta; bu da projenin sürdürülebilirliğini artırmaktadır (Kalyon PV, 2024). Yıllık işletme giderleri yaklaşık 5 milyon USD olup, bakım-onarım, personel, sigorta ve güvenlik kalemlerini içermektedir (World Bank, 2023). Yerli ekipman kullanımı yedek parça temini ve teknik destek bakımından avantaj sağlamakta ve bakım maliyetlerini düşürmektedir (Kalyon PV, 2024).

Kırsal alanlarda güneş enerjisi kullanımı, enerjiye erişim sorunlarının çözülmesi ve kalkınmanın desteklenmesi açısından büyük önem taşımaktadır.[48] UNDP ve TEMA gibi kuruluşlar, özellikle orman köylerinde küçük ölçekli GES sistemlerinin kurulmasına öncülük etmekte; bu sistemler odun tüketimini azaltarak ormanların korunmasına, aynı zamanda sosyal ve ekonomik fayda yaratılmasına katkı sağlamaktadır.[49] 36 ilde 806 haneye kurulan sistemler toplam 1.5 MW üretim kapasitesine ulaşmış, bu kapasitenin ilerleyen yıllarda artırılması hedeflenmektedir (UNDP, 2023).

Türkiye'de güneş enerjisi sektörü, ileri teknolojilerin entegrasyonu ile hızlı bir büyüme göstermekte olup, perovskit paneller, enerji depolama sistemleri ve akıllı şebekeler gibi yeniliklerle enerji verimliliği ve sürdürülebilirlik artırılmaktadır. Bu teknolojiler, hem büyük ölçekli santrallerde hem de küçük ölçekli yerel projelerde kullanılarak sektörde yaygınlaşmayı desteklemektedir. Türkiye'nin yüksek güneş potansiyeli ve yerli üretim teşvikleri, ülkeyi küresel güneş enerjisi liderliğine taşıma potansiyeline sahiptir.[50]

Mevzuat açısından, 6446 sayılı Elektrik Piyasası Kanunu ve ilgili düzenlemeler, lisanssız üretimin önünü açarak küçük ölçekli projelerin artmasını sağlamış, yatırım teşvikleri ise yerli panel ve inverter üreticilerini desteklemektedir. Ancak 2024 yılında getirilen %5'lik ek gümrük vergisi, ithalat bağımlılığını azaltmayı amaçlarken kısa vadede maliyetleri artırarak küçük projeleri zorlayabilmektedir. Ayrıca, YEKDEM mekanizmasındaki değişiklikler, sabit fiyat garantisi kapsamında getirilen limitlerle küçük projelerin karlılığını düşürmüştür.

---

[46] Kalyon PV. (2024). *Karapınar YEKA GES Projesi tanıtım dokümanı*. https://www.kalyonpv.com

[47] SolarPower Europe. (2023). *Global market outlook for solar power 2023–2027*. https://www.solarpowereurope.org

[48] United Nations Development Programme. (2023). *Access to clean energy for rural communities: Turkey case study*. https://www.undp.org

[49] TEMA Vakfı. (2023). *Güneş enerjili kırsal kalkınma projeleri raporu*. https://www.tema.org.tr

[50] Çelik, A. (2022). *Türkiye'de Güneş Enerjisinin Kırsal Kalkınmaya Etkileri*. Enerji Dergisi.

Kırsal kalkınmada güneş enerjisi, enerji altyapısı zayıf bölgelerde ekonomik kalkınmaya ve sosyal faydalara önemli katkılar sunmaktadır. Kırsal yerleşimlerde bağımsız enerji üretimi, istihdam yaratmakta, yerel ekonomileri güçlendirmekte ve özellikle kadınların toplumsal hayata katılımını artırmaktadır. Küçük ölçekli projeler ve sosyal kooperatifler, kırsal kalkınma stratejilerinde yenilenebilir enerji kullanımını destekleyerek, hem çevresel sürdürülebilirlik hem de ekonomik gelişme hedeflerine hizmet etmektedir (Çelik, 2022).

Türkiye, büyük oranda dışa bağımlı bir enerji yapısına sahiptir ve bu durum, ülkenin ekonomik büyümesi üzerinde olumsuz etkiler yaratmaktadır. Özellikle petrol ve doğal gaz gibi fosil yakıtlar, Türkiye'nin enerji ithalatının büyük kısmını oluşturmakta ve döviz rezervlerinin büyük kısmı bu ithalata harcanmaktadır. Güneş enerjisi, bu dışa bağımlılığı azaltma potansiyeline sahip en önemli yenilenebilir enerji kaynaklarından biridir.[51]

Türkiye'nin yüksek güneşlenme süresi ve geniş arazi potansiyeli, güneş enerjisinin ülke genelinde yaygınlaştırılabilmesi için önemli avantajlar sunmaktadır. Yüksek güneşlenme süresi ve geniş arazi potansiyeli, yerli üretim kapasitesinin artırılması ile birleştiğinde, Türkiye'nin enerji arz güvenliğini güçlendirmekte ve döviz tasarrufu sağlamaktadır. Ayrıca, yerli güneş enerjisi ekipmanlarının üretimi ve ihracatı, Türkiye'nin uluslararası pazarlarda rekabet gücünü artırmakta ve enerji ihracat potansiyelini desteklemektedir. Orta Doğu, Kuzey Afrika ve Avrupa gibi stratejik pazarlara yakınlık, Türkiye'nin ihracat stratejileri için önemli avantajlar sunmaktadır.

Sonuç olarak, Türkiye'de güneş enerjisi sektörü, mevzuat reformları, teknoloji entegrasyonu ve yatırım teşvikleriyle sürdürülebilir büyüme göstermekte, kırsal kalkınmaya ve enerji bağımsızlığına katkıda bulunmakta ve ihracat potansiyelini artırmaktadır.

Sonuçlar

Son yıllarda Türkiye'de güneş enerjisi sektörü hızlı bir büyüme ve gelişme göstermiştir. Karapınar ve Niğde-Bor gibi büyük ölçekli YEKA projeleri, ülkenin güneş enerjisi kurulu gücünü artırmakla kalmamış, aynı zamanda Türkiye'nin bu alanda uluslararası rekabette önemli bir oyuncu haline gelmesini sağlamıştır. Güneş enerjisi yatırımları, işletme maliyetlerinin düşük olması ve sağladığı yüksek verimlilik nedeniyle yatırımcılar için cazip fırsatlar sunmaktadır. Yatırımcılar, güneş enerjisi santrallerinin uzun vadede güvenilir ve yüksek getiri sağlayacağı kanaatindedir. Ancak, büyük projelerin sürdürülebilirliği için devlet teşviklerinin ve finansal destek mekanizmalarının devamlılığı kritik öneme sahiptir. Ayrıca, bürokratik süreçlerin sadeleştirilmesi ve sektörün şeffaflığının artırılması, yatırım ortamının iyileştirilmesi açısından gereklidir. Kırsal alanlarda güneş enerjisinin yaygınlaştırılması, sadece enerji erişimini artırmakla kalmayıp aynı zamanda yerel kalkınmaya da önemli katkılar sağlamaktadır. Kırsal bölgelerde küçük ölçekli güneş enerjisi sistemlerinin kurulması, hem enerji maliyetlerini düşürmekte hem de yerel halkın ekonomik bağımsızlığını desteklemektedir. Özellikle orman köylerinde yapılan uygulamalar, yerel istihdam yaratmakta ve sosyal kalkınmayı teşvik etmektedir. Ayrıca, tarımsal sulama ve üretim süreçlerinde güneş enerjisi kullanımının artması, kırsal ekonomiyi güçlendirmekte ve verimliliği artırmaktadır. Bu uygulamalar çevresel sürdürülebilirliği destekleyerek fosil yakıt kullanımını azaltmakta ve karbon salınımının düşmesine katkıda bulunmaktadır.

Teknolojik gelişmeler ise sektörde yeni fırsatlar yaratmaktadır. Perovskit tabanlı güneş panelleri gibi yeni nesil teknolojiler, yüksek verimlilik ve düşük maliyet avantajlarıyla ön plana çıkmaktadır. Enerji depolama sistemlerinde yaşanan ilerlemeler ise güneş enerjisinin sürekliliğini ve şebeke entegrasyonunu mümkün kılmaktadır. Türkiye'nin bu teknolojileri hızla benimseyip, Ar-Ge yatırımlarına öncelik vermesi önemlidir. Yerli üretimin teşvik edilmesi ve yurtdışındaki gelişmiş teknolojilerin yerel koşullara adapte edilmesi, sektörde verimliliğin artmasına ve rekabet gücünün yükselmesine olanak tanıyacaktır.

Türkiye'nin güneş enerjisi potansiyelinden tam anlamıyla faydalanabilmesi için şebeke altyapısının güçlendirilmesi gerekmektedir. Güneş enerjisi üretiminin artmasıyla birlikte, bu enerjinin şebekeye etkin biçimde entegrasyonu ve dağıtımı için modern ve verimli sistemlere ihtiyaç duyulmaktadır. Büyük ölçekli santrallerin yanı sıra yerel düzeyde kurulan sistemler için altyapı yatırımlarının artırılması, üretim kapasitesinin etkin kullanımını sağlayacaktır. Ayrıca, şebeke bağlantıları konusunda mevzuatın hızlandırılması ve yerel yönetimlerle koordinasyonun artırılması, projelerin uygulanma sürecini kolaylaştıracaktır.

Yenilenebilir enerji sektörünün gelişimi için destek mekanizmalarının güçlendirilmesi gerekmektedir. Türkiye, YEKA gibi devlet destekli projelerle güneş enerjisi yatırımlarını artırmakla birlikte, bu teşviklerin sürekliliği yatırımcı güvenliği açısından önemlidir. Küçük ölçekli projelerin daha fazla desteklenmesi, yerel halkın ve küçük yatırımcıların sektöre katılımını teşvik edecektir. Ayrıca, sektörde çalışacak kalifiye iş gücünün artırılması gerekmektedir. Üniversiteler ve teknik eğitim kurumları, güneş enerjisi alanında nitelikli

[51] Tosun, İ. (2022). Türkiye'nin Enerji Bağımsızlığı ve Yenilenebilir Enerji Politikaları. İstanbul: Enerji Yayınları.

insan kaynağı yetiştirmek için programlarını geliştirmeli, sektördeki profesyonellerin sürekli eğitimi sağlanmalıdır. Yerli üretimin artırılması, Türkiye'nin enerji bağımsızlığı hedefleri açısından kritik bir konudur. Güneş paneli, inverter ve enerji depolama sistemleri gibi ekipmanların yerli üretimi teşvik edilmelidir. Bu durum maliyetleri azaltarak yatırımların daha ekonomik olmasını sağlar ve Türkiye'nin küresel pazarda rekabet gücünü yükseltir.

Sonuç olarak, Türkiye'nin sahip olduğu büyük güneş enerjisi potansiyelini etkili bir şekilde değerlendirebilmesi için doğru stratejiler geliştirmesi gerekmektedir. Yenilenebilir enerji sektörü, ülkenin enerji güvenliği, ekonomik kalkınma ve çevresel sürdürülebilirlik hedeflerini gerçekleştirmede önemli bir araçtır. Altyapı yatırımlarının artırılması, yerli üretimin desteklenmesi, teknolojik yeniliklerin entegrasyonu ve kalifiye insan kaynağının yetiştirilmesi, Türkiye'nin güneş enerjisi sektöründe güçlü ve sürdürülebilir bir geleceğe sahip olmasını sağlayacaktır. Böylece Türkiye, hem iç enerji ihtiyacını karşılayabilir hem de küresel enerji piyasasında önemli bir oyuncu haline gelebilir.

Kaynakça

Ahmed, A., & Zhai, X. (2019). Thermal performance evaluation of solar water heating systems: A review. *Renewable and Sustainable Energy Reviews, 103*, 13–29.

Aksoy, E., & Duru, M. (2021). Güneş paneli sistemlerinde bakım uygulamaları. *Enerji Sistemleri Dergisi, 12*(1), 88–97.

Arslan, E. (2021). Biyokütle enerjisinin karbon salınımı açısından değerlendirilmesi. *Çevre Bilimleri Araştırma Dergisi, 13*(2), 55–63.

Çelik, A. (2022). Türkiye'de Güneş Enerjisinin Kırsal Kalkınmaya Etkileri. *Enerji Dergisi.*

Çelik, A. (2023). Jeotermal enerji ve sürdürülebilir enerji politikaları. *Enerji Teknolojileri, 19*(1), 19–27.

Demir, H., & Aslan, G. (2022). Organik atıklardan enerji üretimi ve çevresel etkiler. *Yenilenebilir Enerji Dergisi, 8*(3), 62–70.

Duffie, J. A., & Beckman, W. A. (2013). *Solar engineering of thermal processes.* John Wiley & Sons.

Enerji Piyasası Düzenleme Kurumu. (2024). Elektrik piyasası 2023 yıllık raporu. https://www.epdk.gov.tr

Enerji ve Tabii Kaynaklar Bakanlığı (ETKB). (2023a). Güneş Enerjisi Potansiyeli Atlası (GEPA).

Enerji ve Tabii Kaynaklar Bakanlığı (ETKB). (2023b). Yenilenebilir Enerji Potansiyeli ve Politikaları. https://www.enerji.gov.tr

Enerji ve Tabii Kaynaklar Bakanlığı. (2023c). Türkiye Ulusal Enerji Planı 2035. https://www.enerji.gov.tr

Erdoğan, Z., & Toprak, M. (2020). Jeotermal ve güneş enerjisi santrallerinin verim karşılaştırması. *Yenilikçi Enerji Araştırmaları, 14*(4), 70–79.

Goetzberger, A., Hebling, C., & Schock, H. W. (2003). Photovoltaic materials, history, status and outlook. *Materials Science and Engineering: R: Reports, 40*(1), 1-46.

Green, M. A. (2001). Third generation photovoltaics: Ultra-high conversion efficiency at low cost. *Progress in Photovoltaics: Research and Applications, 9*(2), 123–135.

Gueymard, C. A. (2004). The sun's total and spectral irradiance for solar energy applications and solar radiation models. *Solar Energy, 76*(4), 423–453.

International Energy Agency (IEA). (2023a). *Renewables 2023: Analysis and forecast to 2028*. https://www.iea.org

International Energy Agency (IEA). (2023b). *World Energy Outlook 2023*. https://www.iea.org

Jones, R., & Lee, M. (2018). Photovoltaic technology advancements and future trends. *Journal of Renewable Energy Science, 9*(2), 67–85.

Kalogirou, S. A. (2009). *Solar energy engineering: Processes and systems*. Academic Press.

Kalyon PV. (2024). Karapınar YEKA GES Projesi tanıtım dokümanı. https://www.kalyonpv.com

Karakaya, E., & Yiğit, R. (2021). Güneş enerjisinin coğrafi yaygınlığı ve potansiyeli. *Küresel Enerji Politikaları, 5*(1), 15–24.

Kim, D., Lee, J., & Park, Y. (2020). Materials and design optimization for high-efficiency solar panels. *Solar Materials Journal, 12*(3), 145–162.

López, J., & Ramírez, G. (2020). Efficiency analysis of concentrating solar power (CSP) systems. *Renewable Energy Systems, 15*(1), 110–121.

Madronich, S., McKenzie, R. L., Caldwell, M. M., & Björn, L. O. (1998). Changes in biologically active ultraviolet radiation reaching the Earth's surface. *Journal of Photochemistry and Photobiology B: Biology, 46*(1-3), 5-19.

Nguyen, H., & Silva, T. (2018). Solar radiation patterns and PV potential based on geographical factors. *International Journal of Energy Research, 42*(5), 1203–1215.

Özkan, N., & Şahin, R. (2021). Türkiye'de güneş enerjisi yatırımlarının mekânsal analizi. *Doğal Kaynaklar Dergisi, 8*(4), 73–81.

Patel, R. (2021). Advances in flat-plate and evacuated tube solar collectors. *Journal of Thermal Science, 27*(4), 305–321.

Singh, R., & Tan, C. (2022). Wind-assisted cooling for photovoltaic panels and its effect on power output. *Applied Energy Research, 18*(2), 211–220.

Smith, J. (2020). *Solar energy systems: Principles and applications.* Oxford University Press.

SolarPower Europe. (2023). *Global market outlook for solar power 2023–2027.* https://www.solarpowereurope.org

Sönmez, D. (2022). Güneş termal sistemlerinde verimlilik değerlendirmesi. *Enerji Yönetimi Araştırmaları, 7*(3), 60–66.

TEMA Vakfı. (2023). Güneş enerjili kırsal kalkınma projeleri raporu. https://www.tema.org.tr

Tosun, İ. (2022). *Türkiye'nin Enerji Bağımsızlığı ve Yenilenebilir Enerji Politikaları*. İstanbul: Enerji Yayınları.

Türkiye Elektrik İletim A.Ş. (2023). Türkiye elektrik üretim–iletim istatistikleri. https://www.teias.gov.tr

Türkiye Elektrik İletim A.Ş. (2024). Kurulu güç ve üretim verileri Mart 2024. https://www.teias.gov.tr

Türkiye Rüzgar Enerjisi Birliği (TÜREB). (2024). Yenilenebilir enerji ve istihdam raporu. https://www.tureb.com.tr

Wang, L., Zhao, Y., & Chen, K. (2021). CSP technologies and future grid integration challenges. *Energy Policy and Technology, 14*(1), 34–49.

World Bank. (2023). Financing renewable energy in emerging markets: Turkey profile. https://www.worldbank.org

Yalçın, H., & Ekinci, T. (2020). Güneş ve jeotermal enerji sistemlerinin ömür analizleri. *Enerji Performansı Dergisi, 9*(4), 66–75.

Yılmaz, A., & Doğan, S. (2020). Fotovoltaik sistemlerde maliyet düşüşleri ve ekonomik potansiyel. *GES ve Ekonomi, 6*(3), 83–91.

Zhou, X., Yang, W., & Deng, Y. (2022). Recent developments in concentrated solar power systems. *Progress in Energy and Combustion Science, 88*.

➢ *ORAL PRESENTATION*

Geleneksel ve Hazır Köfte Harcı Kullanılarak Hazırlanan Maydanoz Tohumu ve Çörek Otu Yağı İlave Edilen Kolyoz Balığı Köftelerinin Besin Değeri ve Duyusal Kalite Özelliklerinin Belirlenmesi

Şeyma Nur Bacaksız[1*] (*https://orcid.org/0009-0009-5455-0626*),
Fikret Çakır[2] (*https://orcid.org/0000-0001-5261-2365*)

[*1]Çanakkale Onsekiz Mart Üniversitesi, Lisansüstü Eğitim Enstitüsü, Su Ürünleri Avlama ve İşleme Teknolojisi Anabilim Dalı, Çanakkale, Türkiye
[2] Çanakkale Onsekiz Mart Üniversitesi, Deniz Bilimleri ve Teknolojileri Fakültesi, Su Ürünleri Avlama ve İşleme Teknolojisi Anabilim Dalı, Çanakkale, Türkiye

*Sorumlu yazar e-posta: seymabacaksizz@icloud.com

Özet
Bu çalışmada, kolyoz balığı (*Scomber colias*) kullanılarak hazırlanan ve maydanoz tohumu ile çörek otu yağları ilave edilmiş balık köftelerinin besin kompozisyonu ve duyusal özellikleri araştırılmıştır. Bu amaçla altı farklı formülasyon hazırlanmış ve gruplar oluşturulmuştur. Birinci grup geleneksel harçlı kolyoz köftesi (Kontrol 1) (GK), ikinci grup hazır köfte harçlı kolyoz köftesi (Kontrol 2) (HHK), üçüncü grup maydanoz tohumu yağı eklenmiş geleneksel kolyoz köftesi (GHM), dördüncü grup çörek otu yağı eklenmiş geleneksel kolyoz köftesi (GHÇ), beşinci grup maydanoz tohumu yağı eklenmiş hazır köfte harçlı kolyoz köftesi (HHMK), altıncı grup çörek otu yağı eklenmiş hazır köfte harçlı kolyoz köftesi (HHÇK) gruplarından oluşmuştur. Hazırlanan köfte gruplarının besin içeriği ve duyusal kalitesini belirlemek amacıyla besin kompozisyonu ve duyusal analizler yapılmıştır. Yapılan analizler sonucunda taze kolyoz balığının nem, protein, yağ ve kül değerleri sırasıyla %75,25±0,44, %19,97±0,03, %5,41±0,57, %1,20±0,06 olarak bulunmuştur. Hazırlanan köfte grupları ile taze kolyoz balığının besin değerleri arasında nem, protein ve yağ değerleri arasında istatistiksel farkların olduğu ($p<0,05$), nem değerlerinin azaldığı protein, yağ ve kül değerlerinin artış gösterdiği belirlenmiştir. Oluşturulan köfte grupları ile taze kolyoz balığının besin değerleri arasındaki değişimin, köfte yapma işlemi sırasında kullanılan baharatlar, diğer malzemeler ve bitkisel yağların kullanılmasından ve pişirilme aşamasında köftelerin kızartılmasından kaynaklandığı düşünülmektedir. En yüksek nem içeriği taze kolyoz balığında %75,25±0,44, en düşük nem içeriği GK'de %50,12±0,38 değerinde, en yüksek protein içeriği HHMK'de %24,57±0,06, en düşük protein değeri taze kolyoz balığında %19,97±0,03 değerinde, en yüksek yağ değeri GK'de %18,32±0,40, en düşük yağ değeri taze kolyoz balığında %5,41±0,57 değerinde, en yüksek kül içeriği HHMK'de %2,55±0,03, en düşük kül içeriği taze kolyoz balığında %1,20±0,06 değerinde tespit edilmiştir. Ürünler, duyusal değerlendirme sonucunda tat, koku, lezzet, kıvam, elastikiyet, baharat, aroma, görünüş, renk ve sululuk özellikleri ile genel beğeni bakımından 5 üzerinden değerlendirilmişlerdir. En beğenilen grup, 4,9 puanla GHM, ikinci en beğenilen grup 4,7 puanla GHÇ olmuştur. Analiz sonucunda, kullanılan bitkisel yağların duyusal olarak olumlu etkisi olduğu tespit edilmiştir. Bu çalışma Şeyma Nur Bacaksız'ın Yüksek Lisans tez çalışmasının bir bölümünü içermektedir.
Anahtar Kelimeler: kolyoz, balık köftesi, maydanoz tohumu yağı, çörek otu yağı, duyusal analiz, besin değeri

Determination of Nutritional Value and Sensory Quality Characteristics of Chub Mackerel Fish Patties added with Parsley Seeds and Black Cumin Oil Prepared Using Traditional and Ready Meatball Mixture

Abstract
In this study, the nutritional composition and sensory properties of fish patties prepared using chub mackerel (Scomber colias) and enriched with parsley seed oil and black cumin oil were investigated. For this purpose, six different formulations were prepared, and groups were formed. The first group consisted of traditional mixture chub mackerel patties (Control 1) (GK), the second group consisted of ready-mix chub mackerel patties (Control 2) (HHK), the third group consisted of traditional chub mackerel patties with added parsley seed oil (GHM), the fourth group consisted of traditional chub mackerel patties with added black cumin oil (GHÇ), the fifth group consisted of ready-mix chub mackerel patties with added parsley seed oil (HHMK), and the sixth group consisted of ready-mix chub mackerel patties with added black cumin oil (HHÇK). To determine the nutritional content and sensory quality of the prepared patty groups, nutritional composition and sensory analyses were conducted. As a result of the analyses, the moisture, protein, fat, and ash values of fresh

chub mackerel were found to be 75.25±0.44%, 19.97±0.03%, 5.41±0.57%, and 1.20±0.06%, respectively. It was determined that there were statistically significant differences ($p<0.05$) in moisture, protein, and fat values between the nutritional values of the prepared patty groups and fresh chub mackerel, with moisture values decreasing and protein, fat, and ash values increasing. The changes in the nutritional values between the patty groups and fresh chub mackerel are thought to be due to the spices, other ingredients, and vegetable oils used during patty preparation, as well as the frying process during cooking. The highest moisture content was found in fresh chub mackerel at 75.25±0.44%, while the lowest moisture content was found in GK at 50.12±0.38%. The highest protein content was found in HHMK at 24.57±0.06%, while the lowest protein content was in fresh chub mackerel at 19.97±0.03%. The highest fat content was found in GK at 18.32±0.40%, while the lowest fat content was in fresh chub mackerel at 5.41±0.57%. The highest ash content was found in HHMK at 2.55±0.03%, while the lowest ash content was in fresh chub mackerel at 1.20±0.06%. The products were evaluated on a 5-point scale based on taste, smell, flavor, texture, elasticity, spice, aroma, appearance, color, juiciness, and overall liking. The most preferred group was GHM with a score of 4.9, followed by GHÇ with a score of 4.7. As a result of the analysis, it was determined that the vegetable oils used had a positive sensory effect. This study includes a section of Şeyma Nur Bacaksız's Master's thesis.
Keywords: chub mackerel, fish patty, parsley seed oil, black cumin seed oil, sensory analysis, nutritional value

GİRİŞ

Son yıllarda artan insan nüfusuna paralel olarak besin ihtiyaçları da hızla artmaktadır. Bu bağlamda bazı karasal protein kaynakları yetersiz kalmaktadır. Su ürünleri bu noktada yüksek değerli bir besin olarak bu eksikliğin giderilmesinde büyük rol oynamaktadır. Ayrıca son yıllarda hane halklarındaki çalışan sayıları artmakta ve çalışma koşullarının zorlaması sonucunda pratik ve hızlı hazırlanması nedeniyle işlenmiş ürünlere olan ilgileri hızla artmaya başlamıştır. İşlenmiş ürünlere olan bu aşırı ilgiden, su ürünleri de payını almıştır. Balıkların işlenmiş ürün olarak değerlendirilmesinde balık kıyması başta gelen ürünler arasındadır. Balık kıyması kullanımı birçok probleme çözüm getirmiştir. Özellikle, kılçıklı oldukları için tüketimi az olan balık türlerinin, avcılık sonucu ekonomik değeri düşük olan küçük balık veya kabukluların (Young, 1981; Yanar ve Fenercioğlu, 1999) ve fileto ayrımı sonrası iskelet üzerinde kalan yenilebilir etlerin (Regenstein ve Regenstein, 1991) balık kıyması gibi işlenmiş ürünlere dönüştürülmesi ile bu balıklar daha iyi bir değerlendirilme olanağına kavuşturulmuşlardır. Balık etleri dünya genelinde sevilerek tüketilen önemli bir protein kaynağıdır. Ayrıca elzem yağ asitleri ve mineral maddeler bakımından da önem arz ederler (Metin, 2001; Göğüş ve Kolsarıcı, 1992). Ancak balık etleri bu derece besleyici değerinin yanı sıra kolay bozulabilir ve fiziki olarak hassas olduklarından işleme ve depolama esnasında dikkatli davranılması gereken ürünlerdir (Kılınççeker, 2014).

Su ürünlerinin tazeliğini ve raf ömrünü koruyabilmesi için birtakım işlemlere tabi tutulması zorunludur. Ürünün kabul edilebilirlik derecesi birçok parametreye bağlıdır. Bunlar; görünüş, tazelik, ürünün kokusu, besin içeriği vb. özellikleridir (Anıl, 1988). Su ve su ürünleri depolama süresince meydana gelen en önemli değişimlerden birisi lipid oksidasyonudur. Lipit oksidasyonu özellikle yüksek miktarda çoklu doymamış yağ asitleri (PUFA) içeren balıkların ve balık ürünlerinin besinsel değerinin azalmasına, kalitesinin bozulmasına ve raf ömrünün kısalmasına neden olan en önemli faktörlerden birisidir. Lipid oksidasyonu özellikle dondurulmuş ve buzdolabında depolanan ürünlerde meydana gelmektedir. Yağlı su ürünlerinin depolanması süresince ortaya çıkan lipit oksidasyonunu önlemek ve raf ömrünü artırmak amacıyla kullanılan en etkili maddeler antioksidanlardır (Tian ve White, 1994).

Gıda sektöründe doğal katkı maddelerinin kullanımının yaygınlaşması ile dünya üzerinde bitkilerde bulunan doğal antioksidanlara olan ilgi gün geçtikçe artmaktadır. Bu nedenle doğal antioksidanların incelenmesi için, bitkiler ve baharatlar araştırmaların en önemli odak noktası haline gelmiştir. Kendilerine özgü lezzet ve aromaları, antimikrobiyal ve antioksidan özellikleri nedeniyle, bitki ve baharatlar gıda sektöründe alternatif olarak kullanılabilecek doğal antioksidan maddelerdir.
Günümüzde su ürünleri farklı şekillerde işlenerek tüketilmektedir. Daha çok taze ve dondurularak tüketilen su ürünleri dumanlama, kurutma, tuzlama, konserve, marinasyon, surimi ve fermentasyon gibi birçok teknolojiyle de işlenip tüketilmektedir (Öğretmen vd. 2010). Balık köftesi, balık sosisi ve balık sucuğu gibi işlenmiş gıdalar bunun örneklerindendir. Köfte günümüzde sevilerek tüketilen ve oldukça fazla tercih edilen gıdalardan birisidir. Su ürünleri de içerdiği yüksek protein değeri, kolay sindirilebilirlik açısından kıymetli gıda ürünlerindendir. Balık köftesi; balığın iç organlarının temizlenip fileto haline getirilip ardından etlerinin ayıklanarak ister haşlanarak kıyma haline getirilmesi ister kıyma makinesinden geçirilip kıyma haline getirilmesinin ardından içine çeşitli katkılar eklenerek köfte haline getirilmesidir (Taneri,1963). Günümüzde

Dünya'da ve Türkiye' de dahil olmak üzere çeşitli balık türlerinden yapılarak tüketilmektedir. Türkiye' de balık köftesi yapımında genellikle tercih edilen balıklar levrek, palamut, mezgit, uskumru, hamsi, sardalye gibi ekonomik değeri yüksek olan balıklardır. Bu balıklar taze olarak da çok fazla tüketilmektedirler.
Bu çalışmada, balık köftesi yapımında kolyoz balığı kullanılmıştır. Kolyoz balığı, Çanakkale'de avcılığı yapılan önde gelen türler arasındadır. Kolyoz balığı, uskumru balığına göre biraz daha lezzetsiz bir balık olduğundan, uskumruya oranla tüketiciler tarafından daha az rağbet görmekte ve ekonomik olarak diğer balıklara kıyasla daha ucuz bir balıktır. Ayrıca, kolyoz balıkları genellikle taze olarak tüketildiklerinden (Bayhan, 2003), kolyoz balığından köfte yapılması farklı tüketim şekillerine olanak sağlayacaktır. Kolyoz balığı köftesinin içine maydanoz tohumu ve çörek otu yağları eklenmiştir. Maydanoz tohumu yağı bileşimindeki faydalı içerikler, aroma yönünden zengin oluşu ve yüksek antioksidan özelliğiyle öne çıkan bitkisel yağlardandır (Okan ve ark., 2020). Çörek otu yağı ise besleyici ve aroma açısından zengin bir yapıya sahip olmakla kalmayıp, aynı zamanda antibakteriyel ve antifungal koruyucu özellikleri ve yüksek antioksidan özelliğiyle öne çıkmaktadır (Sultan ve ark., 2009). Kolyoz balığı köftesinin içine maydanoz tohumu ve çörek otu yağı eklenerek köfteye hem farklı bir lezzet ve aroma kazandırılması hem de antioksidan ve antimikrobiyal özellik kazandırılması amaçlanmıştır. Bu sebeple, bu balıktan köfte yapılarak ete farklı lezzet vericilerin eklenmesiyle hem taze tüketime alternatif olacak hem de hazır gıda olarak tüketilebilecek yeni bir ürün oluşturulması hedeflenmiştir.

MATERYAL VE METOD

MATERYAL

Araştırma Materyali

Araştırma materyali olarak Çanakkale ve civar bölgelerden avlanarak soğuk zincir bozulmadan muhafaza edilen kolyoz balıkları (*Scomber colias*) kullanılmıştır. Kolyoz balıkları Çanakkale balık halinden temin edilmiştir.

Kolyoz Köftesinin Hazırlanması

Bu çalışmada kullanılan balık örnekleri Çanakkale balık halinden temin edilerek soğuk zincir bozulmadan Çanakkale 18 Mart Üniversitesi işleme teknolojisi laboratuvarına getirilerek köfte yapımında kullanılmıştır. Laboratuvara getirilen balıkların önce boy ve ağırlıkları ölçülmüştür. Bu işlemin ardından iç organları çıkarılarak bol suyla yıkanmıştır. Baş ve kuyruk bölgesi kesilen balıklar fileto haline getirilmiştir. Daha sonra kıyma makinesinden geçirilerek kıyma haline getirilmiştir. Oluşan kıyma 2 eşit parçaya bölünerek bir kısmının içine karabiber, kimyon, kekik, sarımsak tozu, soğan tozu, maydanoz kurusu, tuz, galeta unu ve yağ eklenerek geleneksel harçlı kolyoz köftesi (Kontrol 1) oluşturulmuş; bir kısmının içine de hazır köfte harcı eklenerek hazır köfte harçlı kolyoz köftesi (Kontrol 2) oluşturulmuştur. Sonrasında hazırlanan köfte harçları 3 eşit parçaya bölünerek bir kısmına çörek otu yağı bir kısmına maydanoz tohumu yağı eklenmiş; diğer kısım da kontrol grubunu oluşturmuş ve hazırlanan köfte harçlarına köfte şekli verilmiştir.

Geleneksel harçlı kolyoz köftesi (GK) (Kontrol 1): Yapılan ön çalışma sonucunda 400 g kolyoz kıymasına 2 g karabiber, 3 g kekik, 3 g kimyon, 2.50 g sarımsak tozu, 3.50 g soğan tozu, 3 g maydanoz kurusu, 50 g galeta unu, 5 g tuz ilave edilmesi uygun görülmüştür. Kolyoz kıyması içine eklenen malzemerle homojen bir şekilde yoğurulmuştur. Hazırlanan köfte harcı 3 eşit parçaya bölünmüştür. Bir kısmı kontrol 1 grubunu oluşturmuştur.

a.) Maydanoz tohumu yağı eklenmiş geleneksel kolyoz köftesi (GMK): 100 g geleneksel köfte harcına 90 µl maydanoz tohumu yağı ilave edilerek hazırlanmıştır.

b.) Çörek otu yağı eklenmiş geleneksel kolyoz köftesi (GÇK): 100 g geleneksel köfte harcına 175 µl çörek otu yağı ilave edilerek hazırlanmıştır.

Hazır köfte harçlı kolyoz köftesi (HHK) (Kontrol 2): 400 g kolyoz kıymasına 1 paket (44 g) ticari köfte harcı konulması ile hazırlanmıştır. Oluşan köfte harcı 3 eşit parçaya bölünmüştür. Bir kısmı kontrol 2 gurubunu oluşturmuştur.

a.)Maydanoz tohumu yağı eklenmiş hazır köfte harçlı kolyoz köftesi (HHMK): 100 g köfte harcına 90 µl maydanoz tohumu yağı ilave edilerek hazırlanmıştır.

b.)Çörek otu yağı eklenmiş hazır köfte harçlı kolyoz köftesi (HHÇK): Yapılan ön çalışma sonucunda 100 g köfte harcına 175 µl çörek otu yağı ilave edilerek hazırlanmıştır.

METOD

Besin Kompozisyonu Analiz Yöntemleri

Ürünlerin kimyasal kompozisyon oranlarının belirlenmesi amacıyla; su, ham protein, ham yağ ve ham kül analizleri yapılmıştır.

Nem analizi

Numunelerin su içeriği kurutma metodu kullanılarak (AOAC,2000) belirlenmiştir. Bu yönteme göre, homojenize edilmiş örnekten 5g tartılarak 105ºC' deki etüvde (Nüve FN500) 16-18 saat kurutma işlemine tabi tutulmuştur. Kurutma işlemi sonrasında tartımları yapılan numunelerin nem miktarı aşağıdaki formül kullanılarak hesaplanmıştır.

Su Miktarı (g/100g) = (T1-T2) x 100/m

T1: Son Tartım, T0:İlk Tartım, m: Numunenin ağırlığı

Ham Protein Analizi

Protein tayini Kjeldahl yöntemine göre yapılmıştır (AOAC, 2000). Bu yönteme göre; numunelerin protein içeriğinin belirlenmesinde Kjeldahl tüpleri içerisinde 1g homojenize edilmiş örnek, 20 ml %96 lık H2SO4, 10 ml %35 lik H2O2 ve 1 adet kjeldahl tableti ilave edilerek Kjeldahl (İnKjelM) yaş yakma ünitesinde 2,5 saat yakma işlemi uygulanmıştır. Yakma işlemi sonrasında protein tüpleri ve içersinde 25 ml. doymuş borik asit çözeltisi ve 3-4 damla indikatör bulunan erlenmayer ile Kjeldahl distilasyon ünitesine (Gerhardt, WD20) yerleştirilerek NaOH ile distilasyona tabi tutulmuş ve bu işlem yaklaşık erlenmayerde 100 ml destilat toplanıncaya kadar devam etmiştir. Elde edilen destilat 0,1 N'lik HCL ile titre edilerek sarfiyat belirlenmiş ve protein oranı aşağıdaki formül kullanılarak hesaplanmıştır.

$$\text{Ham Protein(g/100g)} = \frac{(Tt - Tb) \times 14{,}007 \times 6{,}25}{m} \times 100$$

Tt:Titrasyonda Harcanan Miktar,Tb:Kör Örneğin Titrasyonunda Harcanan Miktar, m: Örnek Ağırlığı

Ham Yağ Analizi

Numunelerin yağ içeriğinin tespitinde Blig ve Dyer (1959) yöntemi kullanılmıştır. Metanol/kloroform (1/2) çözeltizinde homojenize edilen örnek 24 saat karanlık bir ortamda bekletilmiştir. Bu süre sonunda faz oluşumu gözlenmiş ve içerik ayırma hunisine alınarak alt faz balon jojeye alınmış üst faz ise atılmıştır. Alt fazın bulunduğu balon joje rotary evaporatöre yerleştirilerek çözücü uçurulmuştur. Balon jojede yağ ayrımı gerçekleştikten sonra düzenekten çıkartılarak 105ºC' deki etüvde (Nüve FN500) 1 saat bekletilmiş daha sonra desikatöre alınarak soğutulmuş ve son tartımı yapılmıştır. Belirlenen değerler aşağıdaki formülde yerine konularak hesaplanmıştır.

% Yağ miktarı = Son tartım – İlk tartım x 100 / Numune ağırlığı

Ham Kül Analizi

Kül tayini için yakma yöntemi kullanılmıştır. Darası alınan krozelere 2 gr örnek eklenmiş ve krozeler kül fırınında (Nüve, MF120) 550ºC' de sigara külü rengine dönünceye kadar yaklaşık 4-5 saat yakılmıştır. Yakma işlemi sonrasında krozeler kül fırınından alınarak desikatöre yerleştirilmiş ve daha sonra hassas terazide tartımları yapılmış ve aşağıdaki formül kullanılarak hesaplamaları yapılmıştır (AOAC, 2000).

Kül miktarı (g/100g) = (T1-T0) x 100/m

T1:Son Tartım, T0: İlk Tartım, m: Numunenin Ağırlığı

Duyusal Analizler

Duyusal analizler, gıdaların tüketiciler üzerinde bıraktığı etkiyi belirlemek için, alanında uzman panelistlerce farklı test teknikleri uygulanarak değerlendirilen sonuçlara göre yapılmıştır. Duyusal analizler Torry Scheme ölçeğine göre belirlenecektir. Duyusal analizler alanında uzman en az 5 kişilik panelist grubu tarafından gerçekleştirilecektir. Panelistler önce ürün grupları hakkında bilgilendirilecektir. Daha sonra bu ürünleri; tat, koku, lezzet, kıvam, elastikiyet, baharat, aroma, görünüş, renk, sululuk ve genel beğeni açısından 5 puan arasında değerlendirmeleri istenecektir. Martinsdottir ve ark. (2009)'nın yöntemi modifiye edilerek, verilen

puanlara göre ürünler arası sınıflandırma ‘’5’’ çok iyi, ‘’4’’ iyi, ‘’3’’ orta, ‘’2’’ kötü, ‘’1’’ çok kötü olarak değerlendirilmiştir.

BULGULAR ve TARTIŞMA

Besin Kompozisyonu Analizlerine Ait Bulgular

Çalışmada; taze kolyoz balığı, geleneksel harçlı kolyoz köftesi (Kontrol 1), hazır köfte harçlı kolyoz köftesi (Kontrol 2), maydanoz tohumu yağı eklenmiş geleneksel kolyoz köftesi, çörek otu yağı eklenmiş geleneksel kolyoz köftesi, maydanoz tohumu yağı eklenmiş hazır köfte harçlı kolyoz köftesi, çörek otu yağı eklenmiş hazır köfte harçlı kolyoz köftelerinin besin kompozisyonu içerikleri araştırılmış; yapılan analizler sonucunda elde edilen bulgular Çizelge 1’de verilmiştir.

Çizelge 1. Besin kompozisyonu değerleri

	Nem Değeri	Kül Değeri	Protein Değeri	Yağ Değeri
Taze Balık	75,25±0,44a	1,20±0,06f	19,97±0,03c	5,41±0,57d
GK	50,12±0,38e	1,96±0,03d	24,48±0,05a	18,32±0,40a
GMK	52,57±1,37d	1,85±0,07e	23,17±0,91b	17,86±0,06a
GÇK	52,66±0,56d	2,13±0,00c	23,56±0,99ab	18,24±0,22a
HHK	57,59±0,60bc	2,23±0,01b	22,74±0,57b	13,40±0,02b
HHMK	56,47±0,26c	2,55±0,03a	24,57±0,06a	13,28±0,49b
HHÇK	57,88±0,03b	2,52±0,02a	23,57±0,34ab	12,23±0,21c

(**GK:** Geleneksel harçlı kolyoz köftesi, **HKK:** Hazır köfte harçlı kolyoz köftesi, **GMK:** Maydanoz tohumu yağı eklenmiş geleneksel kolyoz köftesi, **GÇK:** Çörek otu yağı eklenmiş geleneksel kolyoz köftesi, **HHMK:** Maydanoz tohumu yağı eklenmiş hazır köfte harçlı kolyoz köftesi, **HHÇK:** Çörek otu yağı eklenmiş hazır köfte harçlı kolyoz köftesi)

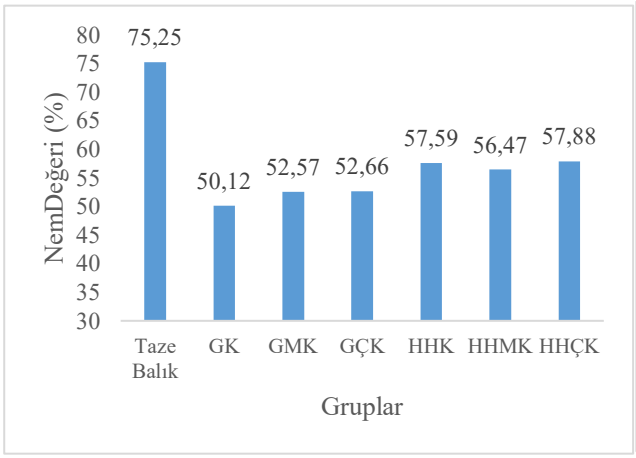

Şekil 1. Nem analiz değerleri

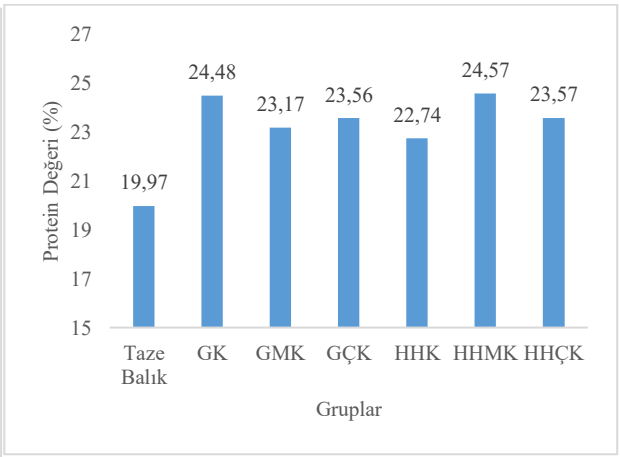

Şekil 2. Protein analiz değerleri

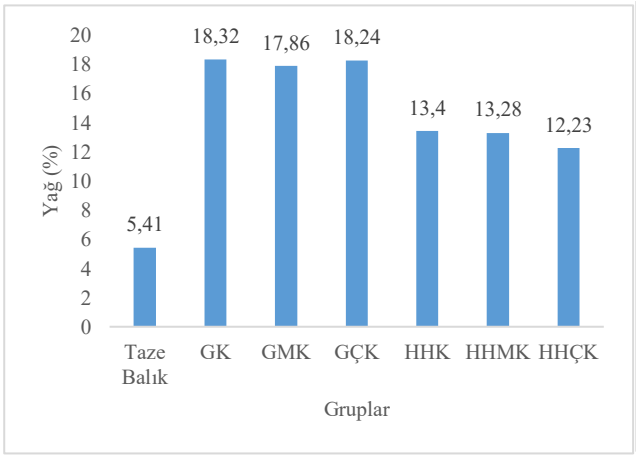

Şekil 3. Yağ analiz değerleri

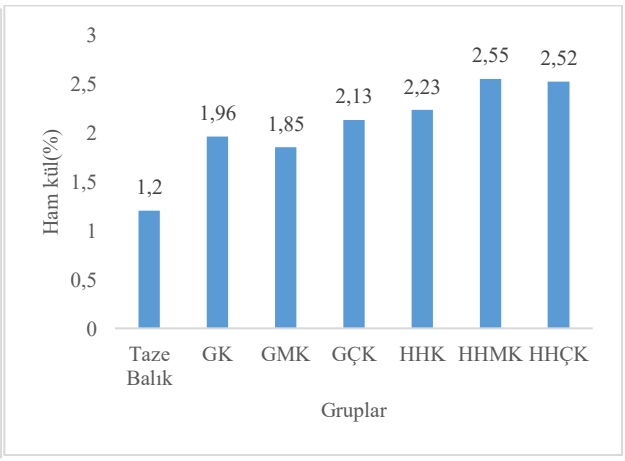

Şekil 4. Kül analiz değerleri

Taze kolyoz balığı, GK (Kontrol 1), HHK (Kontrol 2), GMK, GÇK, HHMK, HHÇK gruplarının besin değeri analiz sonuçlarında nem içeriği beklenildiği gibi farklılıklar göstermiştir. GMK, GÇK arasında benzerlikler

bulunmuştur(p>0,05). Taze balık ve köfte grupları arasında nem değeri bakımından farklılıklar bulunmuştur(p<0,05). Yapılan nem analizi sonucunda en yüksek nem içeriği taze kolyoz balığında %75,25±0,44 değerinde, en düşük nem içeriği GK'de %50,12±0,38 değerinde tespit edilmiştir. Geleneksel ve hazır köfte harçlı gruplar arasında da nem içeriğinin istatistiksel olarak önemli derecede farklı olduğu görülmüştür(p<0,05). Bitkisel yağ ilave edilmiş gruplarda ise geleneksel köfte gruplarında önemli bir fark yok iken hazır köfte harçlı gruplarda farklılıkların olduğu görülmüştür. Kara (2017), yapmış olduğu çalışmada deniz levreği omurgası üzerinde kalan et parçaları ile hazırladığı köfteleri (Kuru köfte) grubu (A), kroket köfte (B), hamburger köfte (C) ve kadınbudu köfte (D) olmak üzere farklı formülasyonlarda dört grupta incelemiştir. Çalışmasında nem içeriklerini levrek fileto artıklarında %77.13, 12 günlük depolamanın sonunda ise A, B, C ve D grubu örneklerde nem değeri sırasıyla %64,82; 65,47; 68,70; 70,98 bulunmuştur. Kaya (2019) yılında yapmış olduğu çalışmada yaban mersini ilaveli aynalı sazan etinden yapılan balık köftelerinde nem değerlerini ham materyalde ortalama 76,84±0,27, sade (A grubu) köftelerde ortalama %76,45, yaban mersini ekstraktı ilaveli köfte örneklerinde (B ve C grubu) sırasıyla ortalama %76,76, %77,25 bulunmuştur. Protein değerleri taze ve köfte grupları arasında beklenildiği gibi önemli derecede farklılıklar göstermiştir(p<0,05). Gruplar arasındaki protein değerleri karşılaştırıldığında GK ve HHMK arasında, GÇK ve HHÇK arasında, GMK ve HHK arasında benzerlik bulunmuştur (p>0,05). Yapılan protein analizi sonucunda en yüksek protein içeriği HHMK'de %24,57±0,06, en düşük protein değeri taze kolyoz balığında %19,97±0,03 değerinde tespit edilmiştir. Bitkisel yağ ilave edilmiş gruplarda geleneksel ve hazır köfte harçlı gruplarda farklılıkların olduğu görülmüştür. Kara (2017), yapmış olduğu çalışmada deniz levreği omurgası üzerinde kalan et parçaları ile hazırladığı köfteleri (Kuru köfte) grubu (A), kroket köfte (B), hamburger köfte (C) ve kadınbudu köfte (D) olmak üzere farklı formülasyonlarda dört grupta incelemiştir. Çalışmasında protein içeriklerini levrek fileto artıklarında % 13.12, 12 günlük depolamanın sonunda ise A, B, C ve D grubu örneklerde sırasıyla ortalama % 15,16; 15,65; 14,88; 15,68 bulunmuştur Kaya (2019) yılında yapmış olduğu çalışmada yaban mersini ilaveli aynalı sazan etinden yapılan balık köftelerinde protein değerlerini ham materyalde ortalama 14,54±0,65, sade (A grubu) köftelerde ortalama %12,23, yaban mersini ekstraktı ilaveli köfte örneklerinde (B ve C grubu) sırasıyla ortalama %12,94, %11,76 bulunmuştur. Gruplar arasındaki yağ değerleri karşılaştırıldığında taze kolyoz balığı etinin yağ içeriğinin hazırlanan diğer balık köftesi gruplarındaki yağ miktarları ile arasındaki farklılıklar istatistiksel açıdan önemli bulunmuştur(p<0,05). Gruplar arasında ise GK, GHM, GHÇ arasında ve HHK, HHMK arasında benzerlik bulunmuştur(p>0,05). Yapılan yağ analizi sonucunda en yüksek yağ değeri GK' de %18,32±0,40 değerinde, en düşük yağ değeri taze kolyoz balığında %5,41±0,57 değerinde tespit edilmiştir. Köfte grupları arasındaki en düşük yağ değeri HHÇK'de %12,23±0,21 değerinde tespit edilmiştir. Gruplar arasında geleneksel ve hazır köfte harçlı gruplar arasında da istatistiksel olarak önemli farklar gözlemlenmiştir(p<0,05). Bitkisel yağ ilave edilmiş gruplarda ise geleneksel köfte gruplarında önemli bir fark yok iken hazır köfte harçlı gruplarda farklılıkların olduğu görülmüştür. Kara (2017), yapmış olduğu çalışmada deniz levreği omurgası üzerinde kalan et parçaları ile hazırladığı köfteleri (Kuru köfte) grubu (A), kroket köfte (B), hamburger köfte (C) ve kadınbudu köfte (D) olmak üzere farklı formülasyonlarda dört grupta incelemiştir. Çalışmasında yağ içeriklerini levrek fileto artıklarında % 5.03±0.44, 12 günlük depolamanın sonunda ise A, B, C ve D grubu örneklerde sırasıyla ortalama % 6,68; 6,47; 6,27; 6,30 bulunmuştur. Kaya (2019) yılında yapmış olduğu çalışmada yaban mersini ilaveli aynalı sazan etinden yapılan balık köftelerinde yağ değerlerini ham materyalde ortalama 5,59±0,40, sade (A grubu) köftelerde ortalama %3,86, yaban mersini ekstraktı ilaveli köfte örneklerinde (B ve C grubu) sırasıyla ortalama %4,16, %4,32 bulunmuştur. Kül değeri taze materyal ve hazırlanan köfte grupları arasında farklılıklar göstermiştir(p<0,05). Gruplar arasındaki kül değerleri HHMK ve HHÇK grupları arasında benzerlik gösterirken (p>0,05) taze kolyoz balığı ve diğer köfte grupları arasında farklılıklar bulunmuştur(p<0,05). Kül değeri en yüksek HHMK'de %2,55±0,03 değerinde, en düşük kül içeriği taze kolyoz balığında %1,20±0,06 değerinde tespit edilmiştir. Köfte grupları arasındaki en düşük kül değeri GMK'de %1,85±0,07 değerinde tespit edilmiştir. Bitkisel yağ ilave edilmiş gruplarda geleneksel köfte gruplarında farklılıkların olduğu, hazır köfte harçlı gruplarda önemli bir farkın olmadığı görülmüştür Kara (2017), yapmış olduğu çalışmada deniz levreği omurgası üzerinde kalan et parçaları ile hazırladığı köfteleri (Kuru köfte) grubu (A), kroket köfte (B), hamburger köfte (C) ve kadınbudu köfte (D) olmak üzere farklı formülasyonlarda dört grupta incelemiştir. Çalışmasında kül içeriklerini levrek fileto artıklarında 0.82±0.11, 12 günlük depolamanın sonunda ise A, B, C ve D grubu örneklerde sırasıyla ortalama % 2,73; 3,45; 2,42; 3,02 bulunmuştur. Kaya (2019) yılında yapmış olduğu çalışmada yaban mersini ilaveli aynalı sazan etinden yapılan balık köftelerinde kül değerlerini ham materyalde ortalama 0,88±0,03, sade (A grubu) köftelerde ortalama %3,4, yaban mersini ekstraktı ilaveli köfte örneklerinde (B ve C grubu) sırasıyla ortalama %3,3, %3,39 bulunmuştur. Balık etlerinin kimyasal kompozisyonları; balık türüne, yaşına, büyüklüğüne, balığın fizyolojik koşularına, beslenme alışkanlıklarına ve mevsimlere bağlı olarak değişmekle birlikte balık eti ve balıktan hazırlanan ürünlerin pişirilmesi (kızartma, buğulama, fırınlama vb.) ve işlenmesi (tuzlama, kurutma, tütsüleme

vb.) gibi işlemlerinin balığın besin değeri içeriklerini değiştirebileceği birçok araştırmacı tarafından bildirilmiştir (Tuncer ve Aktaş, 1992;Tülsner, 1994; Kocatepe ve ark., 2011). Çalışmamızdan elde edilen besin değeri bulguları genel olarak araştırmacıların bildirdikleri besin değeri içerikleri benzerlik ve farklılıklar göstermiştir. Bu durumun balık türünün farklı olması, köfte yapımında kullanılan ve köfteye ilave edilen malzemeler ve pişirme yöntemi ile ilişkili olabileceği düşünülmüştür.

Duyusal Analiz Verilerine Ait Bulgular

Farklı formülasyonlarla hazırlanmış; GK (Kontrol 1), HHK (Kontrol 2), GMK, GÇK, HHMK, HHÇK grupları duyusal analiz öncesi tavada az ayçiçek yağında iki tarafı da 3 dakika kızartılarak pişirilmiştir. Duyusal analiz alanında uzman 5 kişi olarak oluşturulmuş grup tarafından tat, koku, lezzet, kıvam, elastikiyet, baharat, aroma, görünüş, renk, sululuk ve genel beğeni özelliklerine göre 1-5 puan arasında değerlendirilmiştir. Yapılan duyusal analiz sonucunda elde edilen bulgular Çizelge 2.' de verilmiştir.

Çizelge 2. Duyusal analiz değerleri

	Tat	Koku	Lezzet	Kıvam	Elastikiyet	Baharat	Aroma	Görünüş	Renk	Sululuk	Genel Beğeni
GK	5±0,00a	4,6±0,54ab	5±0,00a	4,4±0,54a	4,6±0,54ab	4,6±0,54ab	4,6±0,54ab	4,6±0,54a	4,8±0,44a	4±0,70a	4,5±0,50ab
HHK	4,2±0,44b	4,2±0,44b	4,2±0,44a	4,2±0,44a	4,2±0,44b	4±0,00b	4,2±0,44b	4±0,70a	4±0,00b	4±0,00a	4±0,00b
GMK	5±0,00a	5±0,00a	5±0,00a	5±0,00a	5±0,00a	5±0,00a	5±0,00a	4,8±0,44a	4,8±0,44a	4,8±0,44a	4,9±0,22a
GÇK	5±0,00a	4,6±0,54ab	4,80±,44a	5±0,00a	5±0,00a	4,6±0,54ab	5±0,00a	4,80±,44a	4,6±0,54ab	4,6±0,54a	4,7±0,44ab
HHMK	4,4±0,54ab	4,6±0,54ab	4,2±0,44a	4,4±0,54a	4,6±0,54ab	4,6±0,54ab	4,4±0,54ab	4,4±0,54a	4,4±0,54ab	4,4±0,54a	4,3±0,44ab
HHÇK	4,2±0,83b	4,4±0,54ab	4,2±0,44a	4,2±0,44a	4,2±0,44b	4,2±0,44b	4,2±0,44b	4,4±0,54a	4,4±0,54ab	4±0,70a	4±0,35b

(**GK:** Geleneksel harçlı kolyoz köftesi, **HKK:** Hazır köfte harçlı kolyoz köftesi, **GMK:** Maydanoz tohumu yağı eklenmiş geleneksel kolyoz köftesi, **GÇK:** Çörek otu yağı eklenmiş geleneksel kolyoz köftesi, **HHMK:** Maydanoz tohumu yağı eklenmiş hazır köfte harçlı kolyoz köftesi, **HHÇK:** Çörek otu yağı eklenmiş hazır köfte harçlı kolyoz köftesi)

Duyusal analiz sonuçlarında 5 panelistin tat, koku, lezzet, kıvam, elastikiyet, baharat, aroma, görünüş, renk, sululuk ve genel beğeni özelliklerine göre 1-5 puan arasında değerlendirdikleri köftelerin ortalamaları alınarak kolyoz köftelerinin beğenilme dereceleri belirlenmiştir. GK (Kontrol 1) ortalama 4,5, HHK (Kontrol 2) ortalama 4, GMK ortalama 4,9, GÇK ortalama 4,7, HHMK ortalama 4,3, HHÇK ortalama 4 oranında beğenilmiştir. Panelistlerin duyusal analiz değerlendirmelerine bakıldığında en çok beğenilen kolyoz köftesi GMK, en az beğenilen kolyoz köftesi HHK ve HHÇK olmuştur. Gruplar arasındaki tat değerleri karşılaştırıldığında; GK, GMK, GÇK ve HHK, HHÇK arasında benzerlikler bulunmuştur($p>0,05$). Tat değerlerinde GK, GMK, GÇK grupları daha yüksek puanlar alırken; HHK, HHMK, HHÇK grupları daha az beğenilmiştir. Gruplar arasındaki koku değerleri karşılaştırıldığında; en yüksek koku değerine GMK grubunda, en düşük koku değerine HHK grubunda bulunmuştur. GK, GÇK, HHMK, HHÇK grupları arasında koku değerleri bakımından benzerlik bulunmuştur($p>0,05$). Koku değerlerinde geleneksel köfte grupları ve HHMK daha yüksek puanlar alırken; HHK ve HHÇK grupları daha az beğenilmiştir. Gruplar arasındaki lezzet değerleri karşılaştırıldığında; bütün köfte grupları arasında benzerlik bulunmuştur ($p>0,05$). Lezzet değerlerinde geleneksel köfte grupları hazır köfte harçlı gruplara oranla daha yüksek puanlar almıştır. Gruplar arasındaki kıvam değerleri karşılaştırıldığında; bütün köfte grupları arasında benzerlik bulunmuştur($p>0,05$). Kıvam değerlerinde GMK ve GÇK grupları daha yüksek puanlar alırken; GK, HHK, HHMK, HHÇK grupları daha az beğenilmiştir. Gruplar arasındaki elastikiyet değerleri karşılaştırıldığında; en yüksek elastikiyet değeri GMK ve GÇK gruplarında, en düşük elastikiyet değeri HHK ve HHÇK gruplarında bulunmuştur. GK ve HHMK grupları arasında benzerlik bulunmuştur($p>0,05$). Elastikiyet değerlerinde GMK ve GÇK grupları yüksek puanlar alırken; HHK ve HHÇK grupları daha az beğenilmiştir. Gruplar arasındaki baharat değerleri karşılaştırıldığında; en yüksek baharat değeri GMK grubunda, en düşük baharat değeri HHK ve HHÇK gruplarında bulunmuştur. GK, GÇK, HHMK grupları arasında benzerlik bulunmuştur($p>0,05$). Baharat değerlerinde geleneksel köfte grupları hazır köfte harçlı gruplara oranla daha yüksek puanlar almıştır. Gruplar arasındaki aroma değerleri karşılaştırıldığında; en yüksek aroma değeri GMK ve GÇK gruplarında, en düşük aroma değeri HHK ve HHÇK gruplarında bulunmuştur. GK ve HHMK grupları arasında benzerlik bulunmuştur($p>0,05$). Aroma değerlerinde geleneksel köfte grupları hazır köfte harçlı gruplara oranla daha yüksek puanlar almıştır. Gruplar arasındaki görünüş değerleri karşılaştırıldığında; bütün köfte grupları arasında benzerlik bulunmuştur. Görünüş değerlerinde geleneksel köfte grupları hazır köfte harçlı gruplara oranla daha yüksek puanlar almıştır. Gruplar arasındaki renk değerleri karşılaştırıldığında; en yüksek renk

değeri GK ve GMK gruplarında, en düşük renk değeri HHK grubunda bulunmuştur. GÇK, HHMK, HHÇK grupları arasında benzerlik bulunmuştur($p>0,05$). Gruplar arasındaki renk değerleri karşılaştırıldığında; bütün köfte grupları arasında benzerlik bulunmuştur($p>0,05$). Renk değerlerinde geleneksel köfte grupları hazır köfte harçlı gruplara oranla daha yüksek puanlar almıştır. Gruplar arasındaki sululuk değerleri karşılaştırıldığında; bütün köfte grupları arasında benzerlik bulunmuştur($p>0,05$). Sululuk değerlerinde geleneksel köfte grupları hazır köfte harçlı gruplara oranla daha yüksek puanlar almıştır. Gruplar arasındaki genel beğeni değerleri karşılaştırıldığında; en yüksek değer GMK grubunda, en düşük değer HHK ve HHÇK grubunda bulunmuştur. GK, GÇK, HHMK grupları arasında benzerlik bulunmuştur($p>0,05$). Bütün özellikler ele alındığında; geleneksel köfte gruplarının, hazır harçlı köfte gruplarına oranla daha çok beğenildiği belirlenmiştir. Bitkisel yağlar geleneksel ve hazır köfte harçlı gruplar arasında farklılıklar gösterirken; GMK, GÇK ve HHMK, HHÇK arasında farklılık göstermemiştir. Guran ve ark., (2015) *S. sarda* balığından hazırladığı balık köftelerine kontrol, kekik, karanfil ve biberiye esansiyel yağlarını ilave ederek hazırladığı köftelerde kızartma işlemi uygulamış ve duyusal olarak (renk, görünüm, doku, koku, lezzet ve genel kabul edilebilirlik) değerlendirilmiştir. Kekik, karanfil ve biberiye yağlarının balık köftelerine duyusal olarak önemli bir etkisinin olduğu belirlemiştir. Çapkın (2008) kadife balığından elde edilen balık köftelerini duyusal olarak görünüş, koku, tekstür, tat ve genel beğeni olarak değerlendirdiği çalışmada, tüm köfte grupları beğenilmiş olup zencefil içeren köfte grubunun kontrol ve kekik ilave edilmiş köfte gruplarına göre daha çok beğenildiği belirtmiştir. Çalışmamızda da araştırmacıların bildirdiği üzere maydanoz tohumu ve çörek otu yağının duyusal kaliteyi olumlu yönde etkilediği görülmüştür.

SONUÇ

Bu çalışmada 6 farklı köfte formülasyonu oluşturularak hazırlanan kolyoz köftelerinin besin kompozisyonları tespit edilmiş ve duyusal analiz yapılarak en beğenilen köfte belirlenmiştir. Çalışmada taze kolyoz balığı etine uygulanan köfte formülasyonları ve pişirme işlemi sonrasında tüm gruplarda nem değerlerinin azaldığı, protein, yağ ve kül değerlerinin artış gösterdiği belirlenmiştir. Bu durumun köfte harcına ilave edilen malzemeler ve pişirme işlemine bağlı su kaybından dolayı ileri geldiği düşünülmektedir. Yapılan duyusal analizler neticesinde geleneksel yöntemle hazırlanan balık köftesi gruplarının, hazır köfte harcı ile hazırlanan köfte gruplarına nazaran daha çok beğeni topladığı belirlenmiştir. Tüm köfte grupları arasında GHM grubu köfteler tüm duyusal özellikler bakımından en beğenilen grup olurken, ikinci en beğenilen grup ise GHÇ grubu balık köfteleridir. Balık köfteleri arasında HHK ve HHÇK grubu köfteler duyusal olarak çok iyi kalitede olsalar da diğer köfte gruplarına oranla daha düşük değerler almıştır. Çalışmada kullanılan bitkisel yağların duyusal özelliklerden özellikle tat, aroma, lezzet ve koku kriterlerinde olumlu etkiler sergilediği görülmüştür. Bu çalışmadan elde edilen sonuçlara dayanarak bundan sonraki çalışmalarda balık eti ile uyum sağlayabilecek onun duyusal özelliklerinin yanında fiziko-kimyasal, mikrobiyolojik ve raf ömrünü arttırıcı doğal katkı maddelerinin belirlenerek kullanılması balık köftesi çalışmalarına katkı sağlayacaktır.

KAYNAKLAR

Anıl, N. (1988) Türk Pastırması; Modern Yapım Tekniğinin Geliştirilmesi ve Vakumla Paketlenerek Saklanması, S.Ü. Vet. Fak. Derg., 4(1): 363-375.

AOAC, 2000. Official Methods of Analysis. 17th ed., Vol II. Assoc. Off. Anal.Chem., Wash. D.C., USA.

Bayhan, B.2003. İzmir Körfezi'nde (Ege denizi) dağılım gösteren kolyoz'un (Scomber japonicus Houttuyn, 1782) yaş ve büyüme özellikleri ile beslenme rejimi üzerine araştırmalar, Doktora Tezi, Ege Ün

Blig, E. G., & Dyer, W. F. (1959). Determination of particulate lipid. *Canadian Journal of Biochemistry and Physiology*, *37*, 91b.

Çapkın, K. (2008). Kadife balığı (Tinca tinca) Köftesinin Buzdolabı Koşullarında Muhafazası Sırasında Meydana Gelen Bazı Kimyasal ve Mikrobiyolojik Değişimler. Afyon Kocatepe Üniversitesi Gıda Mühendisliği Ana Bilim Dalı, Fen Bilimleri Enstitüsü, Yüksek Lisans Tezi, 43.

Göğüş, A. K., & Kolsarıcı, N. (1992). Su ürünleri teknolojisi. *Ankara Üniversitesi Ziraat Fakültesi Yayınları*, *1243*, 38-42.

Guran, H.S., Öksüztepe, G., Çoban, Ö.E., & İncili G.K. (2015). Influence of Different Essential Oils on Refrigerated Fish Patties Produced from Bonito Fish (Sarda sarda Bloch, 1793). Food Analysis, Food Quality and Nutrition, Czech Journal of Food Sciences, 33 (1), 37–44.

Kara, D. (2017). *Levrek balığı fileto artıklarının balık köftesi olarak değerlendirilmesi ve raf ömrünün belirlenmesi* (Master's thesis, Fen Bilimleri Enstitüsü).

Kaya, T. B. (2019). *Yaban mersini ekstraktı ilaveli balık (Cyprinus carpio, Linnaeus, 1758) köftelerinin raf ömrünün belirlenmesi* (Master's thesis, Fen Bilimleri Enstitüsü).

Kaya Y., Duyar H.A., Erdem M.E., (2004). Balık Yağ Asitlerinin İnsan Sağlığı İçin Önemi, Ege Üniversitesi Su Ürünleri Dergisi, Cilt: 21 Sayı: 3-4 Sayfa: 365-370.

Kılınççeker, O. (2014). Ada Çayı ve Isırgan Otu Ekstraktlarının Balık Köfte Kaplamalarında Kullanımı. *Adıyaman Üniversitesi Fen Bilimleri Dergisi*, *4*(2), 47-56.

Martinsdottir E, Schelvis R, Hyldig G, Sveinsdottir K (2009) Sensory Evaluation Of Seafood: General Principles And Guidelines. Fishery Products Quality, Safety and Authenticity, Rehbein, H. an

Metin, S., Erkan, N., Varlık, C. ve Aran, N. (2001). Laktik asit ile muamele edilmiş kefal uskumru (Scomber japonicus Houttuyn 1780) raf ömrünün uzatılması. *Avrupa Gıda Araştırması ve Teknolojisi* , *213* , 174-177.

Okan, O. T., PEKÖZLÜ, A. K., Onaran, A., Öz, M., & Deniz, İ. (2020). Determination of chemical composition, antioxidant and antifungal properties of pomegranate (Punica granatum L.) and Parsley (Petroselinum crispum) seed oil produced in industrial scale. Artvin Çoruh Üniversitesi Orman Fakültesi Dergisi, 21(2).

Öğretmen, Ö.Y., Tanker, U. & Öğretmen, N. (2010). Su ürünleri işleme teknolojileri ve örnek bir su ürünleri işleme tesisine ait dondurulmuş hamsi iş akışı. I. Ulusal hamsi çalıştayı: sürdürülebilir balıkçılık. 17-18 Haziran, Trabzon-Türkiye.t

Regenstein, J. M., & Regenstein, C. E. (1991). Current issues in kosher foods. *Trends in Food Science & Technology*, *2*, 50-54.

Sultan MT, Butt MS, Anjum FM, Jamil A, Akhtar S, Nasır M (2009) Nutritional profile of indigenous cultivar of Black cumin seeds and antioxidant potential of its fixed and essential oil. Pak J Bot 41: 1321-1330

TANERİ.B.1963.Balık Köftesi. Balık ve Balıkçılık Cilt XI sayı 12.

Tıan, L. L. & Whıte, P.J. (1994). Antioxidant activity of Oat extracts in soybean and cotton seed oils. J. Am. Oil Chem. Soc. 71: 1079-1086.

Tuncer F.P. ve Aktaş N., 1992. Çeşitli pişirme yöntemlerinin istavrit ve mezgit balıklarının bazı besin ögeleri içeriklerine etkisi. Beslenme ve Diyet Dergisi, 21(1): 53-60

Tülsner, M., 1994. Fischverarbeitung band 1, rohstoffergenshaften von fische und grundlagen der verarbeitungs Prozesse. Behr's Verlag-Hamburg, 19-23, 55- 66

Yanar, Y., & Fenercioğlu, H. (1999). Sazan (Cyprinus carpio) etinin balık köftesi olarak değerlendirilmesi. *Turkish Journal of Veterinary and Animal Sciences*, *23*, 361-365.

Young, R.H., Development of a Salted, Minced Product from Mexican Shrimp By-catch. Report of a Technical Consultation. Food and Agricultural Organization of the United Nations, 93-95, 1981.

KISALTMALAR

g: Gram
ml: Mililitre
mg: Miligram
µl: Mikrolitre

➢ *ORAL PRESENTATION*

Akıllı Telefon Tabanlı Glukoz/Laktat Çoklu Analiz Sisteminin Geliştirilmesi ve Validasyonu

Nermin Kargacı (https://orcid.org/0009-0007-9087-2871), Beyzanur Güneş (https://orcid.org/0009-0009-0858-5860), Furkan Gümüş (https://orcid.org/0009-0007-3580-5019), Ankara Yıldırım Beyazıt Üniversitesi, Engineering and Natural Sciences Faculty, Ankara, Turkey

Nimet Yıldırım Tirgil (https://orcid.org/0000-0002-5973-8830), Ankara Yıldırım Beyazıt Üniversitesi, Engineering and Natural Sciences Faculty, Ankara, Turkey, nyildirimtirgil@ybu.edu.tr

Özet

Ter sıvısında vücut hakkında bilgi veren bazı elektrolitler bulunur. Bunların analizleri sonucunda bazı önemli hastalıkların yanı sıra susuzluk, yorgunluk gibi vücuttaki temel sorunlar teşhis edilip izlenebilmektedir. Örneğin; laktat insanlarda egzersiz sırasında kaslarda birikebilmekte veya bazı hastalıklarda düşük veya yüksek seviyelerde ortaya çıkarak hastalık hakkında bilgi verebilmektedir. Glikoz oranı da diyabet gibi bazı önemli hastalıkların izlenmesinde etkilidir. Ayrıca ter, kanın aksine invaziv olmayan yöntemlerle elde edilebildiği için pratiklik açısından avantajlı bir biyo-sıvıdır. Son zamanlarda yapılan çalışmalar, elektrokimyasal veya kolorimetrik tespit için insan cildiyle doğrudan temas halinde olan biyosensör parçalarına sahip giyilebilir biyosensörler kullanılarak bu tür biyomoleküllerin yerinde ölçümlerinin yapılmasını mümkün kılmıştır.Bu çalışmanın amacı, terdeki glikoz ve laktat seviyelerinin invaziv olmayan bir şekilde tespiti için kâğıt tabanlı bir glikoz/laktat çoklu biyosensörü geliştirmek ve değerlendirmektir.Bu amaçla; kâğıt malzemesinde algılama bölgeleri oluşturmak için parafin ve kitosan ile kimyasal reaktifler kullanılır. Kitosan, kâğıt alt tabakasındaki enzimleri hareketsizleştirirken, parafin hidrofobik bariyerler oluşturur. Glikoz oksidaz ve laktat oksidazı içeren enzimatik reaksiyonlar ise glikoz ve laktat moleküllerini kâğıt yüzeyinde görsel olarak algılanabilir renk değişiklikleri üreten ürünlere dönüştürür. RGB modelleri kullanan akıllı telefon uygulamaları da bu renk değişikliklerini analiz eder.Kısacası; bu sistem farklı ortamlarda ve koşullarda kullanılabilirlik, kolay uygulanabilirlik, gerçek zamanlı ölçüm, kâğıt tabanlı olması nedeniyle ucuz ve uygun maliyet, akıllı telefon kullanılarak algılanma nedeniyle başka bir cihaza ihtiyaç duymamak, kablosuz veri aktarımı, yüksek hassasiyet, hafiflik, esneklik ve konfor gibi birçok avantaja sahip olmasıyla alanında umut vaat etmektedir.

Anahtar Kelimeler: Biyosensör, Glukoz, Laktat, Kolorimetrik analiz

Abstract

There are some electrolytes in sweat fluid that provide information about the body. As a result of their analysis, in addition to some important diseases, basic problems in the body such as thirst and fatigue can be diagnosed and monitored. For example; lactate can accumulate in the muscles during exercise in humans or can provide information about the disease by appearing at low or high levels in some diseases. Glucose rate is also effective in monitoring some important diseases such as diabetes. In addition, sweat is an advantageous biofluid in terms of practicality since it can be obtained with non-invasive methods, unlike blood.Recently, studies have made it possible to perform on-site measurements of such biomolecules using wearable biosensors with biosensor parts that are in direct contact with the human skin for electrochemical or colorimetric detection. The aim of this study is to develop and evaluate a paper-based glucose/lactate multiplex biosensor for the non-invasive detection of glucose and lactate levels in sweat.For this purpose; chemical reagents are used together with paraffin and chitosan to create detection zones on the paper material. Chitosan immobilizes enzymes in the paper substrate, while paraffin creates hydrophobic barriers. These enzymatic reactions involving glucose oxidase and lactate oxidase convert glucose and lactate molecules into products that produce visually detectable color changes on the paper surface. Smartphone applications using RGB models analyze these color changes. In short, this system will have many advantages such as usability in different environments and conditions, easy applicability, real-time measurement, cheap and affordable cost due to being paper-based, no need for another device due to detection using a smartphone, wireless data transfer, high sensitivity, lightness, flexibility and comfort, and will be promising in this field.

Keywords: Biosensor, Glucose, Lactate, Colorimetric analysis

GİRİŞ

Biyosensörler, kısaca, biyolojik veya kimyasal maddelerin varlığını tespit ederek sinyaller üretebilen analitik cihazlardır. Canlı vücudundaki biyolojik maddeler tipik olarak miligram / litre veya milimol / litre konsantrasyonlarında bulunurken biyosensörler bu miktarların 1 milyon katından fazla hassasiyet sunar (nanomol/L veya pikomol/L)[Koh,2016].Yüksek hassasiyetleri sayesinde canlı vücudundaki değişiklikleri de anında saptayarak erken müdahale ve tedbirlerin alınmasına olanak tanır. Dolayısıyla tıp, tarım, gıda gibi çok çeşitli alanlarda kullanılabilmektedirler [Helmenstine, 2019]. Biyosensörler, yüksek hassasiyet / seçicilik / taşınabilirlik / hız nedeniyle teşhis ve tedavi izlemeden çevresel izlemeye kadar çeşitli alanlarda çok sayıda uygulamaya sahiptir ve bu da onları hem kaynak açısından zengin hem de düşük kaynak ayarlarının kullanımı için ideal kılar [Biro ve ark,2008]. Bu sensörler, kullanılan cihaza ve biyolojik malzemeye göre sınıflandırılabilir. Örneğin; giyilebilir biyosensörler, vücuda veya giysilere entegre edilerek fizyoloji takibi yapabilirler. Bireyin sağlığı ve refahı hakkında değerli bilgiler sağlayarak; diyabet gibi kronik rahatsızlıkların izlenmesi ve bilinçli kararlar verilmesine katkıda bulunurlar. Ayrıca sporcular da antrenman rutinlerini optimize etmek ve yaralanmaları önlemek gibi çeşitli amaçlarla bu sensörleri kullanabilirler. Bununla birlikte; kalibrasyon, doğruluk, pil ömrü gibi bazı alanlar sürekli araştırma ve geliştirme gerektirmektedir. Başka bir örnek olarak; kolorimetrik biyosensörler, hedef analitin varığında renk değiştirerek cevap veren cihazlardır. Bu renk değişimi genelde çıplak gözle ya da basit cihazlarla tespit edilebilir. Kağıt bazlı biyosensörler ise diğer biyosensör türlerine göre düşük maliyet, taşınabilirlik ve kolay kullanım gibi birçok avantajları nedeniyle biyomedikal alanda giderek daha popüler hale gelmektedir. Ek olarak, kısmen bu uygulamalar için yaygın olarak kullanılan Whatman filtre kağıdında kullanılan selüloz liflerinin hidrofilik yapısı nedeniyle diğer sensörlerden daha hızlı algılama süreleri ve daha fazla dayanıklılık sunar. Bu kağıdın sıvıyı emme ve yapısı içinde tutma yeteneği, deneyler sırasında gözlemi daha kolay hale getiren gelişmiş renk yoğunluğu ile daha doğru sonuçlar elde edilmesini sağlar. Bu cihazlar, analitleri veya hedef maddeleri hızlı ve uygun maliyetli bir şekilde tespit etmek için gözenekliliği, kılcal hareketi ve çeşitli reaktiflerle uyumluluğu dahil olmak üzere kağıdın benzersiz özelliklerinden yararlanır[Chung ve ark,2019].Üstelik akıllı telefonların ortaya çıkmasıyla; giyilebilir-kolorimetrik biyosensörlerin bireylerin performansı ve sağlığı hakkında yararlı bilgiler sağlama yetenekleri, daha dikkat çekici hale gelmiştir. Bu sensörlerin arkasındaki prensip, vücuda entegre edilerek hedef analitin varlığında gözle görülür bir renk değişimiyle geri bildirim vermektir. Bu renk değişikliği, özel mobil uygulamalar kullanılarak işlenmeden önce akıllı telefonun yerleşik kamerası tarafından yakalanır. Bu kamera, yakalanan renkleri bir referans renk paletiyle doğru bir şekilde algılayabilir ve eşleştirebilir. Kolorimetri süreci, ilişkili renk değişimine dayanarak bir maddenin yoğunluğunu veya konsantrasyonunu nicel olarak belirlemeyi içerir ve bize vücut hakkında bilgi verir[Nagamine ve ark,2019]. Bu alandaki ilk çalışmalar; adım sayaçları, yakılan kalori veya kalp atış hızı gibi hayati belirtileri izleyen fiziksel sensörlere odaklanmıştır. Ardından, kalp hastalarının ve kanserin teşhisi, glikoz seviyelerinin düzenlenmesi gibi sağlığın birçok alanında çözümler sunmaya başlamışlardır. Gelecekte, akıllı cihazlar aynı anda birden fazla sağlık parametresini izleyebilir ve toplanan verileri telefon uygulaması aracılığıyla sağlayabilir. Akıllı telefon destekli kolorimetrik biyosensörlerin sayısız avantajına rağmen; farklı akıllı telefon modelleri ve görüntüleme koşulları arasındaki standardizasyon ve kalibrasyon güvenilir sonuçlar elde etmek için kritik öneme sahiptir. Bu, dikkatli kalite kontrol önlemleri gerektirir.

Bu biyosensörlerde kullanılmak üzere ter; ilaçlar, potasyum, sodyum ve amonyak gibi biyomoleküller dahil olmak üzere çok çeşitli biyobelirteçler içerir. Mevcut bileşenlerin konsantrasyonundaki değişiklikler veya terde yeni bileşenlerin gelişmesi tipik olarak olağandışı sağlık durumlarının veya hastalıkların göstergesi olabilir. Ek olarak, kandaki alkol seviyeleri ile terdeki alkol seviyeleri arasında güçlü bir korelasyon varken, böbrek yetmezliği ter içindeki üre konsantrasyonundaki artışla bağlantılı olabilir[Sheldon,2007].Ter içindeki klor içeriğinin analizi, kistik fibrozis (KF) tanısı koymak için sıklıkla kullanılan bir yöntem olarak kabul edilmiştir, çünkü KF teşhisi konan kişiler, terlerinde bu durumu gösteren alışılmadık derecede yüksek klorür konsantrasyonlarına sahiptir. Böylece terden elde edilen bu bileşenlerden yararlanılması erken tanı için bir fırsat sağlar. [Taqieddin and Amiji,2004]. Ayrıca ter; yoğun egzersizler sırasında, egzersize yanıt olarak, vücudun metabolik durumu hakkında fikir verebilen sodyum, laktat ve amonyum gibi biyobelirteçlerle doğrudan bir korelasyona sahiptir [Yıldırım,2011]. Örneğin, ter içindeki laktat seviyelerindeki değişiklikler, bir sporcunun antrenman rejimini değiştirmesi veya egzersize ara vermesi ve böylece yaralanmayı önlemesi gerekebileceğini gösteren kas yorgunluğu için bir belirteç görevi görür. Daha önce bahsedilen biyobelirteçlere ek olarak, proteinler, sitokinler, nükleik asitler veya nöropeptitler gibi biyomoleküller de bir kişinin sağlık durumunun önemli göstergeleridir ve biyosensörler kullanılarak izlenebilir [Zhang,2019].

Bu çalışma; tüm bu bilgilerin ışığında, çeşitli hastalıkların tespiti veya mevcut vücut durumunun takibi gibi avantajların sayesinde insan hayatının konfor kazanması amacıyla terdeki glikoz ve laktatın çoklu saptanması

için akıllı telefon tabanlı, kağıt bazlı, kalorimetrik ve giyilebilir bir analiz cihazının geliştirilmesi ve değerlendirilmesini amaçlamaktadır.

MATERYAL VE METOD

1. Materyal

PHOSPHATE BUFFERED SALINE pH 7,4 (10X Liquid Concentrate) PC2310 PBS405.R (BioShop Canada 1lt), Pipet Ucu Sarı, Eppendorf, 0-200 Ul (- BSR001-) Bio PC19828 N403366 1000 ad/pk, Lactate Oxidase from Aerococcus viridans Sigma L9795-50UN.

2. Metod

I. Analiz Bölgelerinin Oluşturulması

Kağıt temelli glukoz/laktat çoklu biyosensörün geliştirmesine yönelik proje, 3 iş paketi şeklinde ele alınıp adım adım geliştirilme aşamaları incelenmiştir. Birinci adım, kağıt malzeme üzerinde hidrofobik bariyerli analiz alanlarının oluşturulması ve enzimlerin immobilizasyonudur. Bu adımda öncelikle 100˚C'de 2 dakika boyunca parafin eritildi. Parafin erirken analiz alanlarını oluşturmak için uygun boyutta alüminyum veya benzer bir metal malzemeden baskı hazırlandı. Daha sonra, bir Whatman kağıdı 2 saniye boyunca sıvı parafine daldırıldı ve diğer işlem görmemiş Whatman kağıdı üzerine yerleştirildi. Bu noktada, metal malzeme 110˚C de ısıtıldı ve 5 saniye boyunca parafinle kaplanan kağıda bastırıldı. Bastırılan kağıdın altındaki kağıda parafin transferi sağlandı ve metal baskı çerçeve boyutunda, hidrofobik sınırları olan analiz bölgeleri oluşturuldu. Bu aşamada amaç, 0.5 ve 1 cm çapında analiz alanlarını oluşturmaktı. Uygulanan işlem basamaklarını şekilde gösterilmiştir.

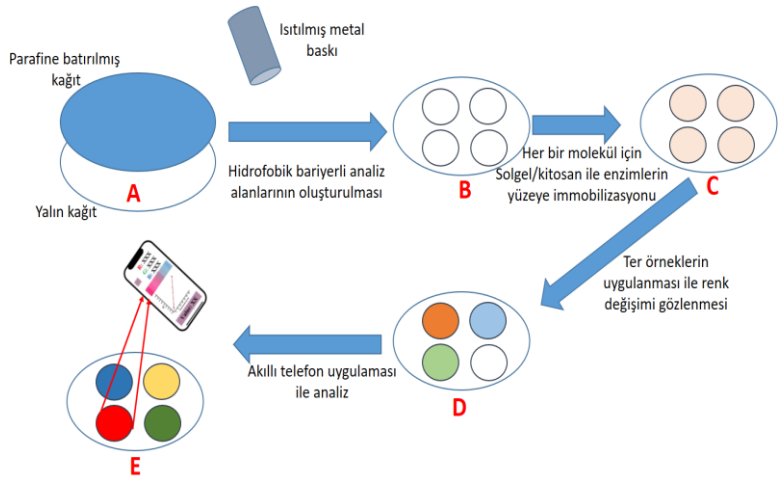

Şekil 1: Uygulanan proses adımları



Şekil 2: Gözlenen renk değişimleri

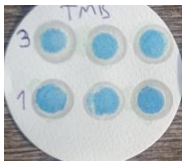

Şekil 3: Gözlenen renk değişimleri

Analiz bölgelerini oluşturduktan sonra enzimlerin Whatman kağıdında kalmasını sağlamak için her bir bölgeye 4mL olacak şekilde kitosan eklendi. Kitosanı analiz bölgelerine enjekte ettikten sonra, numuneler belli bir süre kuruması için bekletildi. Daha sonra TMB ve TBHBA-4AAB enzimleri ayrı ayrı ve 4mL olacak şekilde kağıda enjekte edildi. Ardından bu iki enzimin renk değişimleri karşılaştırıldı.

II. Akıllı Telefon Uygulamaları ve Karşılaştırılması

İkinci adım, enzim immobilize edilmiş kağıt yüzeylerinin glukoz ve laktat tayinine hazırlanması için uygun koşulların sağlanmasıydı. Glukoz ve laktat eklemeden önce farklı konsantrasyonlarda H_2O_2 eklendi. Ardından yardımcı enzim olan HRP ilave edildi. Renk değişimleri bu iki molekülle elde edildi. Kuruma için bir süre beklendi. Bu aşamada, kağıt yüzeydeki renk değişimi çıplak göz ile gözlenebilir seviyede olmuştur. Deneyde elde edilen örneklerden biri şekilde gösterilmiştir.

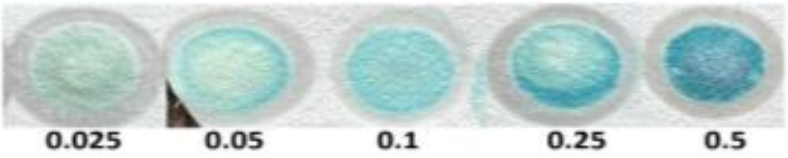

Şekil 4: Deneyde kullandığımız örneklerden birinin verilen bazı miktarlara göre değişimleri

Elde edilen renk değişikliği sonuçlarının analiz edilmesinde, RGB (red/green/blue) modeliyle bilgileri işlemek için kullanılabilen akıllı telefon uygulamalarından yararlanılmıştır. Modelin adı, kırmızı, yeşil ve mavi olmak üzere üç ana rengin baş harflerinden gelmektedir. Her ton 0 ile 225 arasında bir ölçekte tanımlanır ve rengin yoğunluğunu tanımlar. Her bir renk değişimi için her üç rengin ortalaması alınabileceği gibi RGB skalasında en çok değişime uğrayan birim de dikkate alınabilmektedir. Şekilde görüldüğü gibi beyaz ve renkli kağıt yüzeyler arasındaki RGB renk yoğunlukları farkı, akıllı telefon uygulaması ile belirlenebilir düzeydedir.



Şekil 5: RGB renk yoğunlukları arasındaki fark

Elde edilen sonuçları değerlendirmek üzere, 'What a Color', 'Color Name', 'Color Coll' and 'Color Grab' isimli dört adet telefon uygulaması kullanıldı. Uygulamalarda elde edilen renkleri değerlendirildikten sonra hangi uygulamanın daha kullanışlı olduğuna karar verildi.

III. Glukoz ve Laktat Tayini

Bir diğer adım olan biyosensör parametrelerinin optimum olarak sağlandığı koşullarda gerçek zamanlı glukoz ve laktat tayini için, daha önceki işlemlerde hazırlanmış olan Whatman kağıdına ayrı ayrı glukoz ve laktat eklendi. Glukoz oksidaz enzimi ve laktat oksidaz enzimi farklı konsantrasyonlarda hazırlandıktan sonra, detection zone kısmına enjekte edildi. Bu işlem gerçekleştirildikten sonra ortaya çıkan enzimatik reaksiyon Şekilde A'dan B'ye gösterilmiştir. Ayrıca deneyde elde edilen örneklerden biri de şekilde görülmektedir.

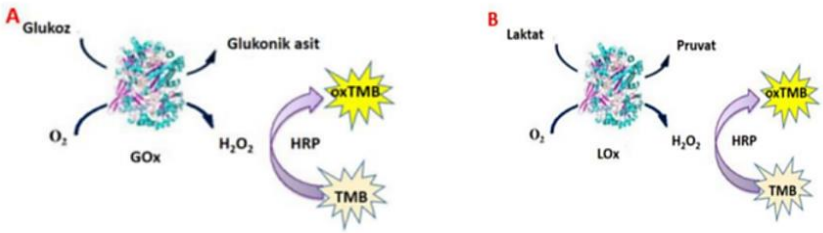

Şekil 6: Glikoz ve laktatın enzimatik reaksiyonları ve HRP enzimi ile renk değişimi izlenmesi

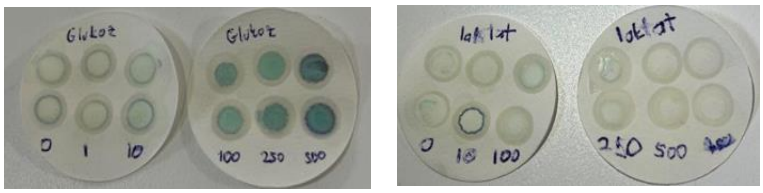

Şekil 7: Glikoz ve laktat eklendiğinde elde edilen analiz bölgeleri

IV. Ter Benzeri Solüsyonda ve Cilt Yüzeyinde Analiz

Son aşamada ter içeriğine benzer bir çözelti hazırlandı ve içerisine belirli oranlarda glikoz ve laktat ekleyerek geliştirilen sistemin doğruluğu tespit edildi. Farklı konsantrasyonlarda eklenen ter ve glukoz çözeltilerinden bazı renk değişimleri elde edildi. Elde edilen renk değişimlerini şekilde görebilirsiniz.

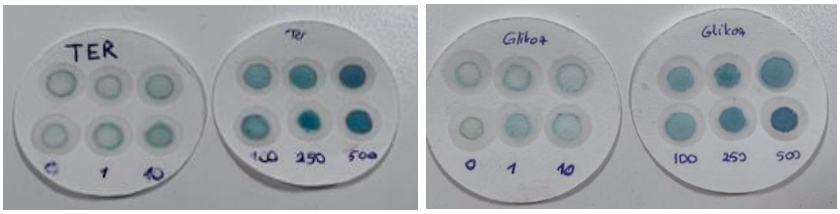

Şekil 8: Renk değişimi sonuçları

Geliştirilen sistemin diğer bir validasyon adımı ise, aşağıdaki şekilde görüldüğü üzere, kağıt malzemeden üretilen analiz sistemlerini kendi üzerimizde test etmekti. Buradaki amaç, kol veya omuza yapıştırılan kağıt yüzeylerinin teri absorbe etmesi ve terdeki glukoz ve laktat miktarına bağlı olarak renk değişimlerinin gözlemlenmesiydi.

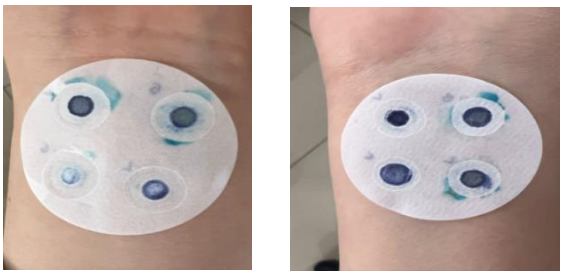

Şekil 9: Kola uygulama sonrası renk değişimi

BULGULAR

1. Uygulama Optimizasyonu

Aşağıda görüldüğü gibi, laboratuvarda gerçekleştirilen deneyin sonuçları, farklı oranlara göre farklı renkler vermiştir. Bu renklerin kolorimetrik analizi için 4 adet ücretsiz telefon uygulaması kullanılmıştır. Bu uygulamalar, deney sonunda fotoğraflanan renkleri Kırmızı (R), Yeşil (G), Mavi (B) olmak üzere 3 farklı parametrede analiz etmiş ve bazı sonuçlar vermiştir. Daha sonra bu renk analizi excelde işlenmiş ve grafiksel olarak tasarlanmıştır.

Bu uygulamalardan beklenen, en doğrusal sonuçları elde edebilmekti. Ek olarak, uygulamanın kullanımı kolay ve tekrarlanabilirdi. Deneylerde TMP için daha iyi bir sonuç alınmıştır.

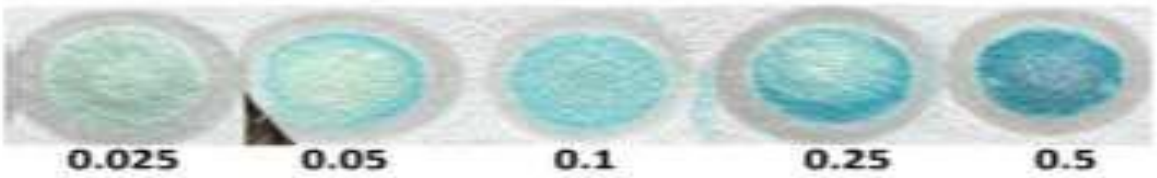

Şekil 10: Renk Değişimi Sonuçları

Bu bölümde farklı H2O2 oranlarını karşılaştırmak için başka bir deney yapılmıştır. H2O2 oranı arttıkça rengin tonunun koyulaştığı gözlenmiştir. Bunun nedeni, daha önce açıklandığı gibi renklendirici madde ile etkileşime giren enzimin daha yüksek oranda H2O2 üretmesidir. Sonuçların daha yüksek doğruluğa sahip olması için deney daha fazla sayıda uygulanmış ve tüm sonuçlar tek bir excel dosyasına işlenmiştir. Bu sonuçlara paralel olarak çeşitli grafikler oluşturulmuştur. Bunun temel amacı, işlenen verilerin grafikler yardımıyla okunmasını kolaylaştırmaktır. Ayrıca en doğru sonucu bulmak için farklı telefon uygulamaları kullanılmıştır. Daha doğru sonuçlar veren uygulama daha doğrusal ve mantıklı olmalıdır. Color Grap adlı uygulama, tamamen başarısız olduğu için testin geri kalanında tekrar kullanılmamış ve sonuçlar, en başarılı şekilde çalışılan uygulamanın

Color Name olduğunu göstermiştir. Grafik 1'de bu uygulama için H2O2 konsantrasyonuna karşı ABS grafiği gösterilmiştir.

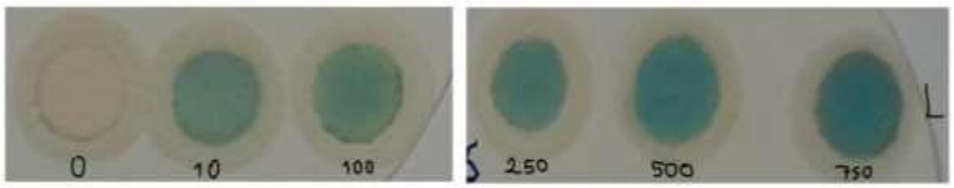

Şekil 11: Lactat için renk değişim sonuçları

Tablo 1: Color Name adlı uygulamanın H2O2 konsantrasyonu için sayısal değerler, ortalamaları, standart sapmaları akıllı telefon veri analizi

H2O2 CONCENTRATION (µM)	R	G	B	Averages	SD
0	144;147;144	145;139;137	137;118;115	136,2;121,5;108,6	11,25731
10	90; 91; 92	111; 108; 116	93; 89; 100	98,8; 99,8; 98,6	0,816497
100	92; 93; 93	118; 112; 108	93; 92; 87	98,6; 97,5; 97,8	0,465548
250	85; 88; 84	111; 112; 111	97; 100; 95	98,1; 95,7; 95,1	1,286204
500	76; 85; 79	104; 112; 106	92; 97; 94	93,8; 89,8; 84,3	3,918231
750	68; 63; 64;	85; 93; 92	83; 88; 84;	65; 90; 85	10,80123

2. Glikoz ve Laktat Tespiti

En başarılı akıllı telefon uygulamasını belirlemek için H2O2 kullanılarak yapılan deneylerden elde edilen verilerle bir akıllı telefon uygulaması seçilmiş ve glikoz ve laktat için deneyin gerektirdiği tüm adımlar izlenerek bu uygulama ile analiz yapılmıştır.Kağıt üzerinde tespit alanları oluşturularak belli bir oranda glikoz ve laktatlar eklenmiş, ardından renk değişimi gözlemlenmiş ve bu telefon uygulaması ile bu renk değişimi taranarak sayısal veriler elde edilmiştir. Grafik 2'de glikoz; Grafik 3'te ise laktat konsantrasyonu ve ABS değerleri verilmiştir.

Tablo 2: Color Name adlı uygulamanın glikoz konsantrasyonu için sayısal değerler,ortalamaları ve standart sapmaları akıllı telefon tabanlı veri analizi

GLUCOSE CONCENTRATION (µM)	R	G	B	Averages	SD
0	136; 120;127	147; 130; 138	143; 125; 134	133,3; 129,1; 129,4	1,916644301
1	116; 112; 118	136; 132; 138	136; 134; 139	129; 133,5; 136,7	3,190778895
10	135; 122; 135	146; 142; 145	148; 143; 148	140,4; 133,3; 127,4	5,315040646
100	102; 99; 93	130; 125; 115	133; 130; 123	116,6; 108,6; 100,8	6,441463764
250	74; 71; 65	104; 101; 99	115; 112; 111	94,6; 95,1; 99,3	2,102973269
500	73; 87; 76	105; 112; 103	119; 123; 115	78,6; 106,6; 119	16,87499428

Tablo 3: Color Name adlı uygulamanın laktat konsantrasyonu için sayısal değerler, ortalamaları ve stamdart sapmaları akıllı telefon tabanlı veri analizi

LACTATE CONCENTRATION (µM)	R	G	B	Averages	SD
0	117; 107; 137	127; 118; 137	126; 118; 139	125,1; 128,4; 135,6	4,405695
1	129; 133; 114	134; 140; 125	137; 135; 126	130,3; 128,7; 129,7	0,643635
10	119; 136; 136	133; 140; 136	134; 141; 138	134,7; 130,8; 123,5	4,652831
100	95; 97; 95	124; 125; 124	132; 129; 128	116,5; 121,1; 114,1	2,900735
250	122; 72; 67	135; 103; 101	135; 113; 110	106,4; 91,5; 97,5	6,116384
500	82; 112; 71	105; 127; 137	71; 103; 118	88,3; 123; 97,3	14,6877

3. Ter Numunesi Tespitinde Glikoz

Son olarak; analiz için bilinmeyen bir ter kullanılmış, terdeki laktat ve glikoz tespit edilmeye çalışılmıştır. Ter numunesindeki glikoz tespiti için farklı uygulamalardan elde edilen verilerle tablolar ve grafikler oluşturulmuştur. Bu işlemin temel amacı deneyin günlük hayata entegre edilebilirliğini göstermektir. Analiz, bir kez daha 3 farklı uygulama ile yapılmıştır. Yine üç farklı renk uygulaması arasında en doğrusal, en hatasız ve tekrarlanabilir olduğu için çalışmaya Color Name adlı uygulama ile devam edilmiştir. Ter numunesi için konstrasyon ve ABS bilgileri Grafik 4'te görülmektedir.

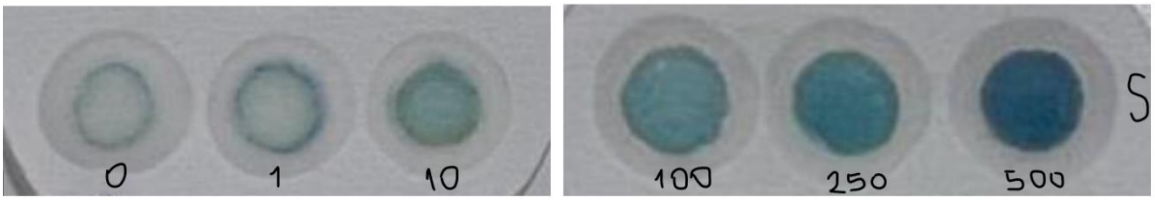

Şekil 12: Simüle edilmiş ter numunesi için ortaya çıkan renk değişiklikleri

Tablo 4: Color Name adlı uygulamanın ter konsantrasyonundaki glukoz için sayısal değerler,araçları ve standart sapması adlandırılmış akıllı telefon tabanlı veri analizi

GLUCOSE in SWEAT CONCENTRATION (µM)	R	G	B	Averages	SD
0	137; 140; 135	149; 151; 148	149; 149;149	145,2; 144; 138,5	2,897896688
1	131; 118; 145	146; 135; 156	147; 138; 155	141,2; 134,1; 131,7	4,016768692
10	104; 110; 118	129; 132; 140	127; 128; 142	125,5; 122,4; 119,5	2,45004969
100	88; 89; 88	119; 124; 124	125; 131; 130	113,1; 114,2; 110,5	1,535139391
250	88; 78; 81	124; 111; 119	130; 122; 128	109; 100,1; 94,6	5,907610585
500	46; 59; 52	97; 92; 90	119; 111; 108	52,3; 93; 112,6	25,12339916

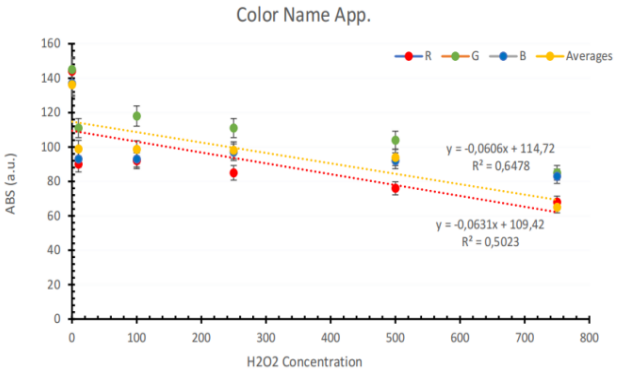

Grafik 1: Color Name değerlerinden H2O2 konsantrasyonuna karşı ABS grafiği

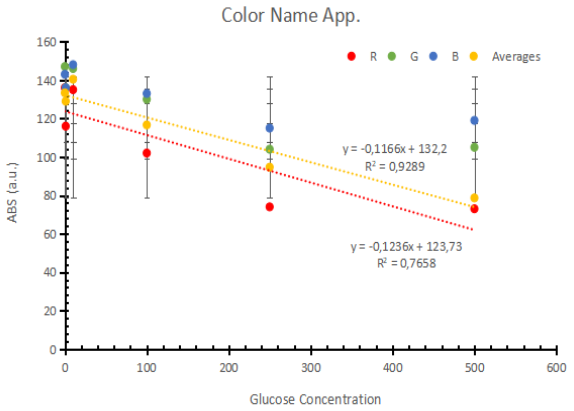

Grafik 2: Color Name değerlerinden glukoz konsantrasyonu ve ABS grafiği

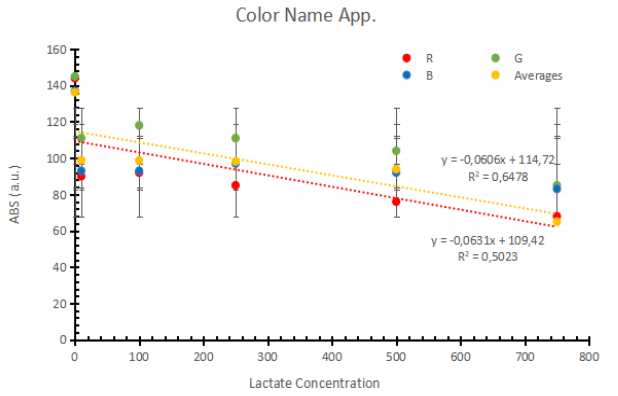

Grafik 3: Color Name değerinden laktat konsantrasyonu ve ABS grafiği

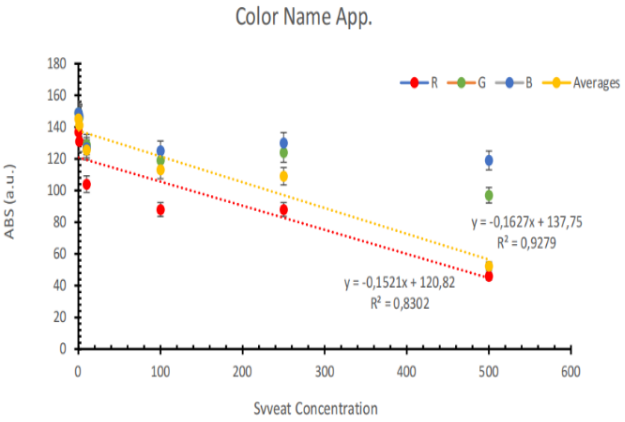

Grafik 4: Color Name değerlerinden ter konsantrasyonundaki glukoz ve ABS grafiği

4. Gerçek Numune Testi

Farklı laktat ve glikoz konsantrasyonlarını karşılaştırmak için kolumuza yapıştırdığımız deneyin sonuçları aşağıdaki gibidir. Konsantrasyon değerlerinin artmasıyla oluşan mavi rengin yoğunluğunun arttığı gözlenmiştir. Ek olarak, elde edilen sonuçtan da görülebileceği gibi, renk değişimi iyi bir şekilde sonuçlanmıştır.

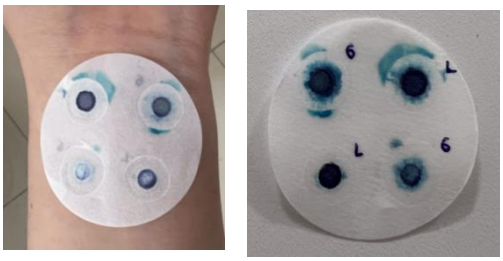

Şekil 13: Kola yapıştırılan kağıt ve sonuç

Bu deneysel proje, en başından amaçlandığı noktaya ulaşmaktır. Bu deneyde elde edilen sonuçlara göre kâğıt bazlı biyosensör projesi başarılı olmuş ve gerekli analizleri yapabilmiştir.

TARTIŞMA

Bu çalışma, kağıt bazlı bir glikoz / laktat çoklu biyosensörü geliştirmeye ve glikoz ve laktat seviyelerinin invazif olmayan tespiti için performansını değerlendirmeye odaklanmıştır. Bu biyosensörün önemli bir avantajı glikoz veya laktat seviyelerini tespit etmek için invaziv prosedürler gerektirmemesi, yani basitliğidir. Bu özellik, geleneksel kan örnekleme yöntemlerinin pratik veya uygulanabilir olmayabileceği ortamlarda kullanımı için çok uygundur. Ek olarak, kağıt tabanlı sensörlerle ilişkili düşük maliyet, başka türlü pahalı teşhis araçlarına erişimi olmayan kişilere erişilebilirliği artırmaktadır. Bu tür biyosensörün sağlık izleme, hastalık teşhisi ve egzersiz izleme gibi çeşitli alanlarda uygulama yelpazesi bulunmaktadır; glikoz ve laktat seviyeleri hakkında doğru ve gerçek zamanlı bilgi sağlayabilme potansiyeli sayesinde, giyilebilir cihaz teknolojilerinde yeni olanakların önünü açmakta ve bakım noktası teşhisine yönelik yaklaşımlarımızı ileriye taşımaya önemli bir katkı sunmaktadır.

SONUÇ

Deneysel prosedürlerden elde edilen sonuçlar, biyosensörün başarılı bir şekilde geliştirildiğini ve değerlendirildiğini göstermektedir. Kağıt malzeme üzerinde oluşturulan hidrofobik bariyer analiz alanları, tanımlanmış boyutlarda istenen analiz bölgelerini etkin bir şekilde oluştururken, kitosan da kağıt içindeki enzimleri hareketsiz hale getirerek kararlı ve güvenilir tespit sağlamaktadır. TOMB, TBHBA-4AAB, H2O2 ve HRP'nin eklenmesi, kağıt yüzeyinde gözle görülür şekilde gözlenen renk değişiklikleriyle ve görsel algılamaya uygunluğu doğrulayan başarılı enzimatik reaksiyonlarla sonuçlanmıştır. RGB modelini kullanan akıllı telefon uygulamaları, değerli araçlar sağlayan renk değişimi sonuçlarını analiz etmiştir.En doğru sonucu bulmak için farklı telefon uygulamaları kullanılmıştır. Geliştirilen biyosensörler kullanılarak gerçek zamanlı belirleme, doğru glikoz / laktat seviyesi tespitlerini gösteren umut verici sonuçlar göstermiştir ve bu da onu glikoz-laktat konsantrasyonlarının biyolojik örneklerinin izlenmesi için uygun hale getirmiştir. Biyosensörlerin performansı, duyarlılığı ve doğruluğu daha da artıran işlevselliği doğrulayan gerçek hayattaki cilt yüzey koşullarını simüle eden ter içeriği kullanılarak değerlendirilmiştir. Kağıt bazlı biyosensörün ter içeriğine benzer bir çözümde analizi, gerçek hayata benzeyen koşullar altında performansı hakkında değerli bilgiler sağlamıştır. Bu özellikle önemlidir çünkü biyosensörün farklı çevresel faktörlere maruz kaldığında bile etkili bir şekilde çalışabileceğini göstermiştir. Sonuç olarak, bu çalışmada yapılan araştırma, invaziv olmayan glikoz ve laktat tespiti için kağıt bazlı bir biyosensörün potansiyelini göstermektedir. Daha geniş klinik bağlamlarda yararlılığı araştırırken duyarlılığını ve doğruluğunu artırmak için daha fazla doğrulama çabası gerekmektedir. Doğrulamayı optimize etmeye odaklanan gelecekteki çalışmalar, gerçek dünya senaryolarında kullanışlılığı keşfederken hassasiyet doğruluğunu artırabilir. Bakım noktası teşhis cihazları olarak potansiyel uygulama, kritik zorlukların ele alınmasına önemli değer katabilir. Bu bulgular, Biyosensör Teknolojisi alanına önemli ölçüde katkıda bulunabilir ve giyilebilir bakım noktası teşhisinin geliştirilmesine yönelik olasılıklar açabilir.

TEŞEKKÜR

FLO-2022-2405 numaralı projemize süreç boyunca sağladıkları katkılar dolayısıyla AYBÜ BAP birimine teşekkür ederiz. Projemize sağladığı maddi destek için TUBİTAK'a teşekkür ederiz. Tezimizin, TUBİTAK 2209-A Üniversite Öğrencileri Araştırma Projeleri Destekleme Programı tarafından onaylanması ve desteklenmiş olmasından onur duymaktayız. Bu çalışmada bizlere rehberlik eden, bilgi ve deneyimlerini bizimle paylaşan, her aşamada desteklerini esirgemeyen danışmanımız Dr.Öğr.Üyesi Nimet YILDIRIM TİRGİL'e en içten teşekkürlerimizi sunarız. Katkıları bizler için son derece kıymetli olup, her zaman minnettar olacağımızı söylemekten gurur duyuyoruz. Son olarak, proje sürecinde ekip ruhunu koruyarak sorumluluklarımızı yerine getirmemizde gösterdiğimiz uyum ve iş birliği için birbirimize teşekkür ederiz.

KAYNAKLAR

1.Ahyeon Koh, et al. "A soft, wearable microfluidic device for the capture, storage, and colorimetric sensing of sweat". BIOSENSORS (2016). DOI: 10.1126/scitranslmed.aaf2593
2.Anne Marie Helmenstine, "What is the chemical composition of human sweat or perspiration?" ThoughtCo (2019, September 22).
3.Biró, Emese, et al. "Preparation of chitosan particles suitable for enzyme immobilization." Journal of biochemical and biophysical methods 70.6 (2008): 1240-1246.
4.Chung M, Fortunato G, Radacsi N. "Wearable flexible sweat sensors for healthcare monitoring: a review". J. R. Soc (2019).
5.Interface 16: 20190217. Nagamine, K., et al. "Noninvasive Sweat-Lactate Biosensor Emplsoying a HydrogelBased Touch Pad." Scientific Reports (2019).

6.Sheldon, Roger A. "Enzyme immobilization: the quest for optimum performance." Advanced Synthesis & Catalysis 349.8-9 (2007): 1289-1307.
7.Taqieddin, Ehab, and Mansoor Amiji. "Enzyme immobilization in novel alginate–chitosan core-shell microcapsules." Biomaterials 25.10 (2004): 1937-1945.
8.Yildirim, Nimet, et al. "Sol–gel encapsulated glucose oxidase arrays based on a pH sensitive fluorescent dye." Dyes and Pigments 89.2 (2011): 144-148.
9.Z. Zhang, M. et al."A versatile, cost-effective, and flexible wearable biosensor for in situband ex situ sweat analysis, and personalized nutrition assessment" Lab Chip (2019), DOI: 10.1039/C9LC00734B

➢ *ORAL PRESENTATION*

Hibrit tahrikli bir şehir içi otobüs şanzımanın termal optimizasyonu

Aydoğan EZER[1](*ORCID: https://orcid.org/0009-0000-9986-2572*),

Gamze GEDİZ İLİŞ[1](*ORCID: https://orcid.org/0000-0001-8366-5427*)

[1]Gebze Teknik Üniversitesi, Makina Mühendisliği Bölümü, Kocaeli, Türkiye

Özet

Bu çalışma, seri hibrit mimariye sahip bir şehir içi otobüs için geliştirilen yeni nesil tek hızlı bir şanzımanın termal optimizasyonunu sunmaktadır. Türkiye'nin fosil yakıtlara olan yüksek bağımlılığı ve sera gazı emisyonlarının azaltılması gerekliliği, özellikle şehir içi otobüsler gibi sık dur-kalk yapan araçlarda yakıt verimli sistemlerin geliştirilmesini zorunlu kılmaktadır. Çalışmanın temel amacı, şanzımanın ek bir yağ soğutucusuna ihtiyaç duymadan, doğal taşınım ve optimize edilmiş gövde tasarımı ile optimum sıcaklık aralığında çalışmasını sağlamaktır. Bu hedef doğrultusunda, KISSsys yazılımının termal hesaplama modülü kullanılarak bir optimizasyon süreci yürütülmüştür. Belirlenen bir sürüş çevrimi (UITP SORT 1) ve yük profiline göre yapılan analizler sonucunda, gövde üzerine eklenen termal kanatçıklar ve kontrollü ventilasyon uygulaması ile yağ sıcaklığının hedeflenen limit içinde tutulabildiği gösterilmiştir. Hedeflenen limit 20°C ortam sıcaklığında yağ sıcaklığının 95°C'yi aşmamasıdır. Bu yaklaşım, sistem maliyetini ve ağırlığını düşürerek yerli hibrit tahrik sistemlerinin rekabetçiliğini artırma ve ülkenin petrol ithalatını azaltma potansiyeli taşımaktadır.

Anahtar Kelimeler: Şanzıman, dişli kutusu, termal optimizasyon, KISSsys, şehir içi otobüs, güç kaybı, ısı atımı

Thermal optimization of a hybrid drive city bus transmission

Abstract

This study presents the thermal optimization of a new generation transmission developed for an urban bus with a series hybrid architecture. Turkey's high dependence on fossil fuels and the need to reduce greenhouse gas emissions necessitate the development of fuel-efficient systems, particularly in vehicles such as urban buses that frequently stop and start. The primary objective of the study is to ensure that the transmission operates within the optimal temperature range without requiring an additional oil cooler, utilizing natural convection and an optimized housing design. To achieve this goal, an optimization process was conducted using the thermal calculation module of the KISSsys software. Analyses conducted based on a defined driving cycle (UITP SORT 1) and load profile demonstrated that oil temperature can be maintained within target limits through the addition of thermal fins to the housing and the implementation of controlled ventilation. This approach has the potential to increase the competitiveness of domestic hybrid propulsion systems by reducing system cost and weight, while also contributing to the reduction of the country's petroleum imports.

Keywords: Transmission, gearbox, thermal optimization, KISSsys, citybus, power loss, heat

GİRİŞ

Küresel ısınma ve iklim değişikliğinin getirdiği çevresel baskılar, otomotiv sektörünü geleneksel içten yanmalı motor (İYM) teknolojilerinden daha sürdürülebilir alternatiflere yöneltmektedir. Bu bağlamda, hibrit elektrikli araçlar (HEV), hem yakıt verimliliği hem de düşük emisyon avantajları sunarak önemli bir geçiş teknolojisi olarak öne çıkmaktadır. Türkiye'nin 2020 yılı itibarıyla petrolde %92,9 gibi yüksek bir dışa bağımlılık oranı, bu teknolojilerin sadece çevresel değil, aynı zamanda ekonomik ve stratejik bir zorunluluk olduğunu da ortaya koymaktadır. Özellikle şehir içi toplu taşımada kullanılan otobüsler, yüksek yakıt tüketimleri ve sık dur-kalk içeren çalışma rejimleri nedeniyle, hibritleşme için büyük bir potansiyel barındırmaktadır. Rejeneratif frenleme ile kinetik enerjinin geri kazanımı, bu araç sınıfında %15-35 aralığında yakıt tasarrufu sağlayabilmektedir.

Dişli kutularının termal davranışı üzerine yapılan akademik çalışmalar, genellikle güç kayıplarının ve ısı transferinin modellenmesine odaklanmaktadır. Changenet ve Velex gibi araştırmacılar, termal ağ yöntemlerini kullanarak dişli sürtünmesi, rulman kayıpları ve yağ çalkalanması gibi kayıp mekanizmalarını modellemişlerdir [1]. Paschold vd. ise bu yöntemleri, değişken çalışma koşulları altındaki bileşen sıcaklıklarını

hesaplamak üzere geliştirmişlerdir [2]. Ancak bu çalışmalar, genellikle FZG test düzenekleri gibi belirli sistemler üzerinde veya detaylı CAD geometrileri tamamlanmış, yani detay tasarım aşamasındaki ürünler için uygulanmaktadır. Bu yaklaşımlar, yüksek doğruluk sunmalarına rağmen, tasarım sürecinin erken aşamaları için zaman alıcı ve maliyetli olabilmektedir.

Bu çalışmanın literatüre temel katkısı, dişli kutusunun henüz konsept tasarım aşamasındayken termal davranışı hakkında hızlı ve güvenilir bir öngörü sunan sistematik bir metodoloji önermesidir. ISO/TR 14179-2 standardını temel alan ve KISSsys yazılımında uygulanan bu yaklaşım sayesinde, tasarımcılar detaylı ve maliyetli analizlere (CFD gibi) gerek duymadan, farklı mimari kararların (örneğin, soğutucu gerekip gerekmediği, gövde geometrisi vb.) termal etkilerini değerlendirebilir. Bu, geliştirme sürecini önemli ölçüde hızlandırma ve maliyetleri düşürme potansiyeli taşımaktadır.

MATERYAL VE METOD

Tasarım ve optimizasyon süreci, araç sistem gereksinimlerinin belirlenmesinden başlayarak termal analizlere uzanan bütüncül bir yaklaşımla ele alınmıştır. Çalışmanın odaklandığı seri hibrit mimarinin temel şeması Şekil 1'de gösterilmektedir.

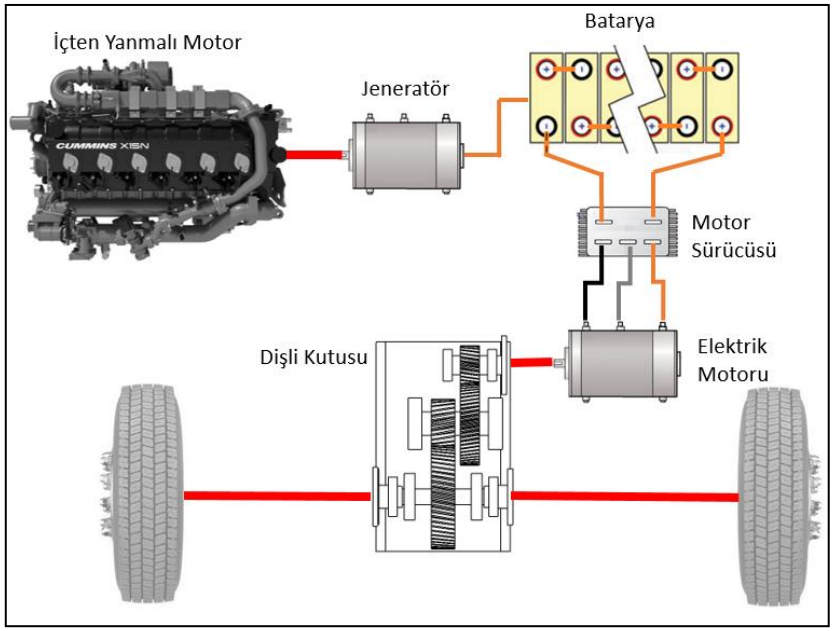

Şekil 1: İncelenen seri hibrit tahrik mimarisi.

Araç Performans Gereksinimleri ve Güç Aktarım Sistemi Seçimi

Model olarak, temel özellikleri Tablo 1'de verilen sanal bir şehir içi otobüs tasarlanmıştır.

Tablo 1: Temel araç özellikleri

Parametre	Değer	Birim
Toplam Yüklü Ağırlık (GVW)	10500	[kg]
Maksimum Hız	90	[km/h]
Maksimum Tırmanabilirlik	20	[%]
Teker Dinamik Yarıçapı	0.38	[m]

Güç aktarım sisteminin (elektrik motoru ve şanzıman) seçimi, aracın şehir içi operasyonlarda karşılaşacağı en zorlu koşulları karşılayabilmesi üzerine kurulmuştur. Bu kritik performans hedefleri aşağıda listelenmiştir:

Koşul 1: Boş halde, 0-20 km/s hızlanmasını en fazla 6 saniyede gerçekleştirebilmelidir.

Koşul 2: Boş halde, 0-50 km/s hızlanmasını en fazla 20 saniyede tamamlayabilmelidir.

Koşul 3: Tam yüklü halde, 0-50 km/s hızlanmasını en fazla 25 saniyede tamamlayabilmelidir.
Koşul 4: %12 eğimli bir yokuşu, asgari 20 km/s hızla çıkabilmelidir.
Koşul 5: Düz yolda en az 90 km/s hıza ulaşabilmelidir.
Koşul 6: Tam yüklü halde, %20 eğimli bir yokuşu asgari 5 km/s hızla tırmanabilmelidir.
Bu hedefleri karşılamak için gerekli olan tekerlek tork ve devir değerleri, Denklem (1) kullanılarak hesaplanan çekiş kuvveti (F_{cekis}) üzerinden belirlenmiştir [3]. Yuvarlanma, aerodinamik, eğim ve ivme dirençlerinin toplamı ihtiyaç duyulan çekiş kuvvetine eşittir.

$$F_{cekis} = F_{yuv} + F_{aero} + F_{egim} + F_{ivme} \quad (1)$$

Ardından, maliyet ve verimlilik optimizasyonu amacıyla, bu gereksinimleri karşılayabilecek en küçük elektrik motoru ve en uygun şanzıman aktarma oranı (tahvil oranı) araştırılmıştır. Farklı motor seçenekleri ve aktarma oranları için yapılan analizler sonucunda, SUMO MD HV1800 elektrik motorunun 5.2'lik bir aktarma oranı ile tüm performans hedeflerini sağladığı tespit edilmiştir. Şekil 2, seçilen bu konfigürasyonun, tüm kritik performans noktalarını motorun çalışma eğrisi içinde nasıl karşıladığını göstermektedir. Her bir koşuldaki noktalar sırasıyla 3, 4, 5.2, 6, 7, 8 aktarma oranlarına karşılık gelmektedir. Buradan sol tarafta tırmanma koşulu için ve sağ tarafta en yüksek hız koşulu için 5.2 oranın performans isterlerini karşıladığı görülmektedir.

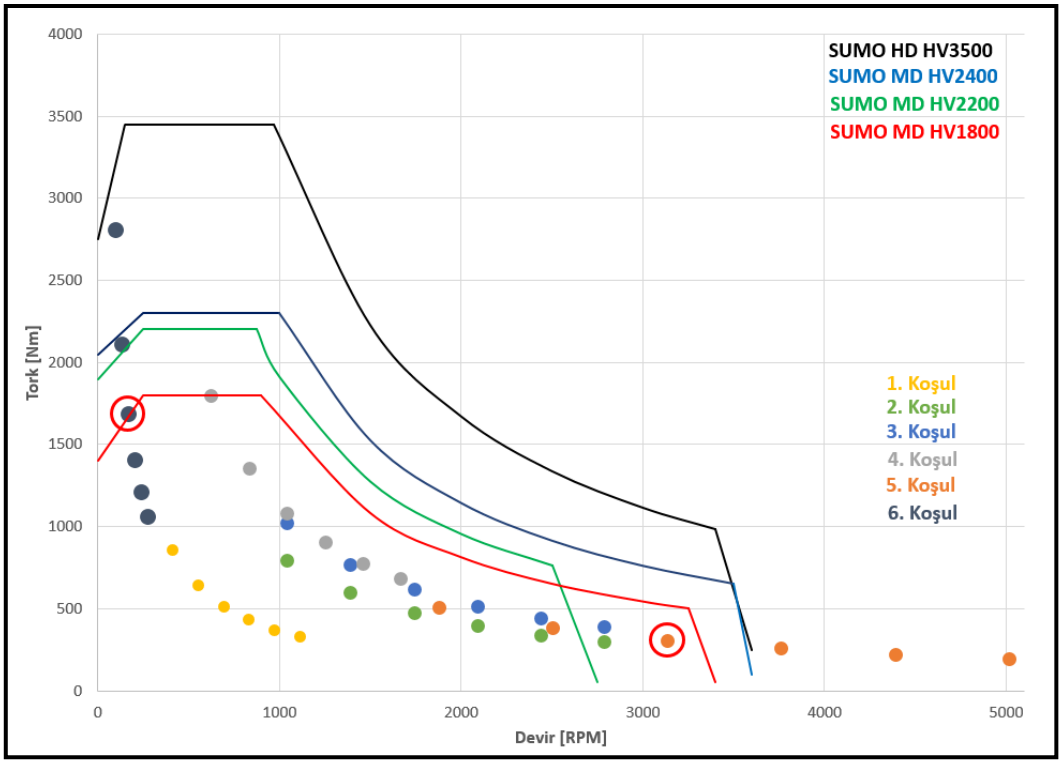

Şekil 2: Seçilen motor ve aktarma oranı için performans gereksinimlerinin motor eğrisi üzerindeki konumu (5.2 oran çember içinde).

Dişli Kutusu Boyutlandırma ve Yük Profili
Aktarma organlarının gerçekçi çalışma koşulları altında ömür ve dayanım analizlerinin yapılabilmesi için, standart bir sürüş döngüsünün ötesine geçerek, gün içindeki operasyonel farklılıkların da dikkate alındığı bir yük profili oluşturulması kritik önem taşımaktadır. Bu amaçla, ISO 6336-6 standardı [4] temel alınarak, Şekil 3'te gösterilen UITP SORT 1 sürüş çevrimi, Tablo 2'de gösterildiği şekilde günün farklı zaman dilimlerindeki (sabah, öğle, akşam, gece) yolcu yoğunlukları ile birleştirilmiştir.

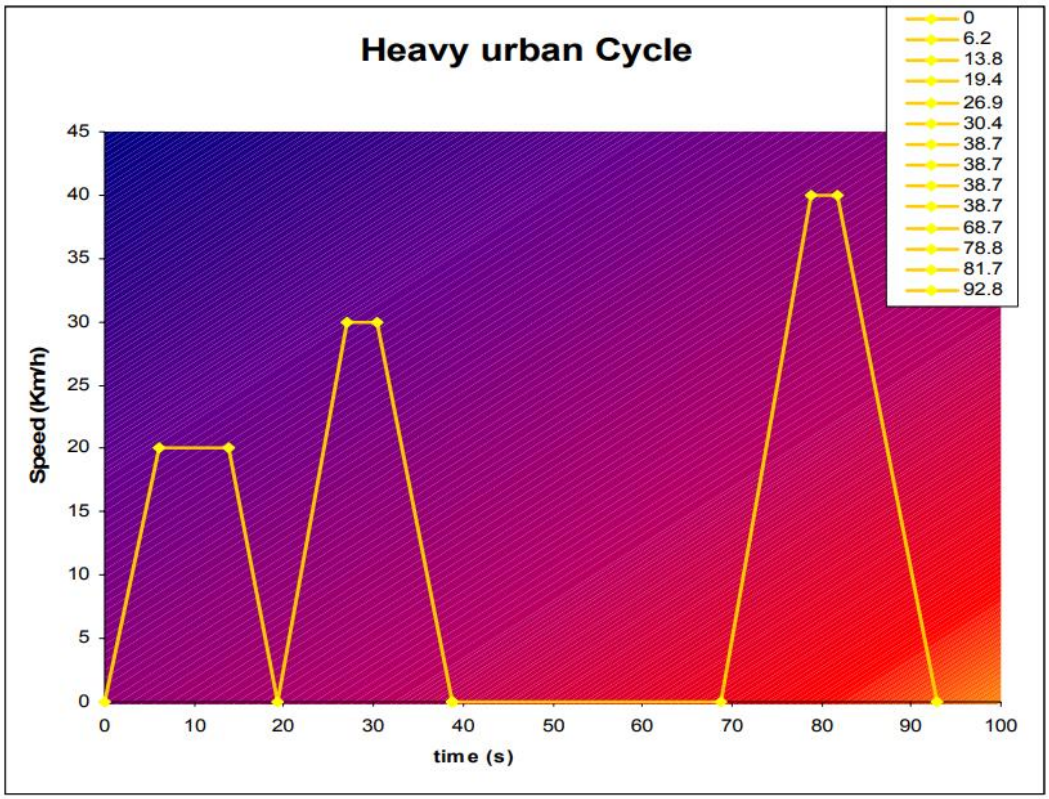

Şekil 3: Analizlerde kullanılan UITP SORT 1 Ağır şehir içi sürüş çevrimi.

Tablo 2: Günün saatlerine göre değişen yolcu yoğunluğu.

Zaman Aralığı	Süre [h]	Yolcu Yoğunluğu [%]	Dolu Ağırlık [kg]
7:00-9:00	2	100	10500
9:00-16:00	7	50	8460
16:00-19:00	3	75	9480
19:00-24:00	5	25	7440

Yapılan bu detaylı analiz sonucunda, Denklem (2)'ye göre, şanzıman girişine etkiyen eşdeğer tork ($T_{esdeger}$)775 Nm ve eşdeğer devir ($n_{esdeger}$)293 d/d olarak hesaplanmıştır.

$$T_{esdeger} = \left(\frac{\sum T_i^p N_i}{\sum N_i}\right)^{\left(\frac{1}{p}\right)} \quad (2)$$

T_i, her bir bölge için tork değeri [Nm]; N_i, her bir gölge çevrim sayısı; p, Woehler eğrisinin eğimidir. Bu birleşik yük kolektifinin analizi ve eşdeğer tork/devir hesaplamaları için Şekil 4'te bir kesiti görülen özel bir Excel yazılımı geliştirilmiştir. Bu sayede, sadece sürüş karakteristiği değil, aynı zamanda araç ağırlığındaki değişimler de ömür hesabına dahil edilmiştir. Tablo 2 günün farklı saat dilimleri için daha gerçekçi bir yolcu yoğunluğu ve araç yüklü ağırlığını göz önünde bulundurmamızı sağlıyor. Aracın sürekli olarak %100 dolu olduğunu göz önünde bulundurmak eşdeğer tork değerinin artmasına ve buna bağlı olarak ta bütün komponentlerin büyümesine yol açıp aşırı mühendislik yapılmasına yol açacaktır. Bunun önüne geçmek için gün içerisindeki yolcu yoğunluğuna göre ihtiyaç duyulan tork SORT -1 eğrisinin her hızlanma ve sabit hız gitme aralığı için hesap edilmiş ve buradan eşdeğer tork bulunmuştur.

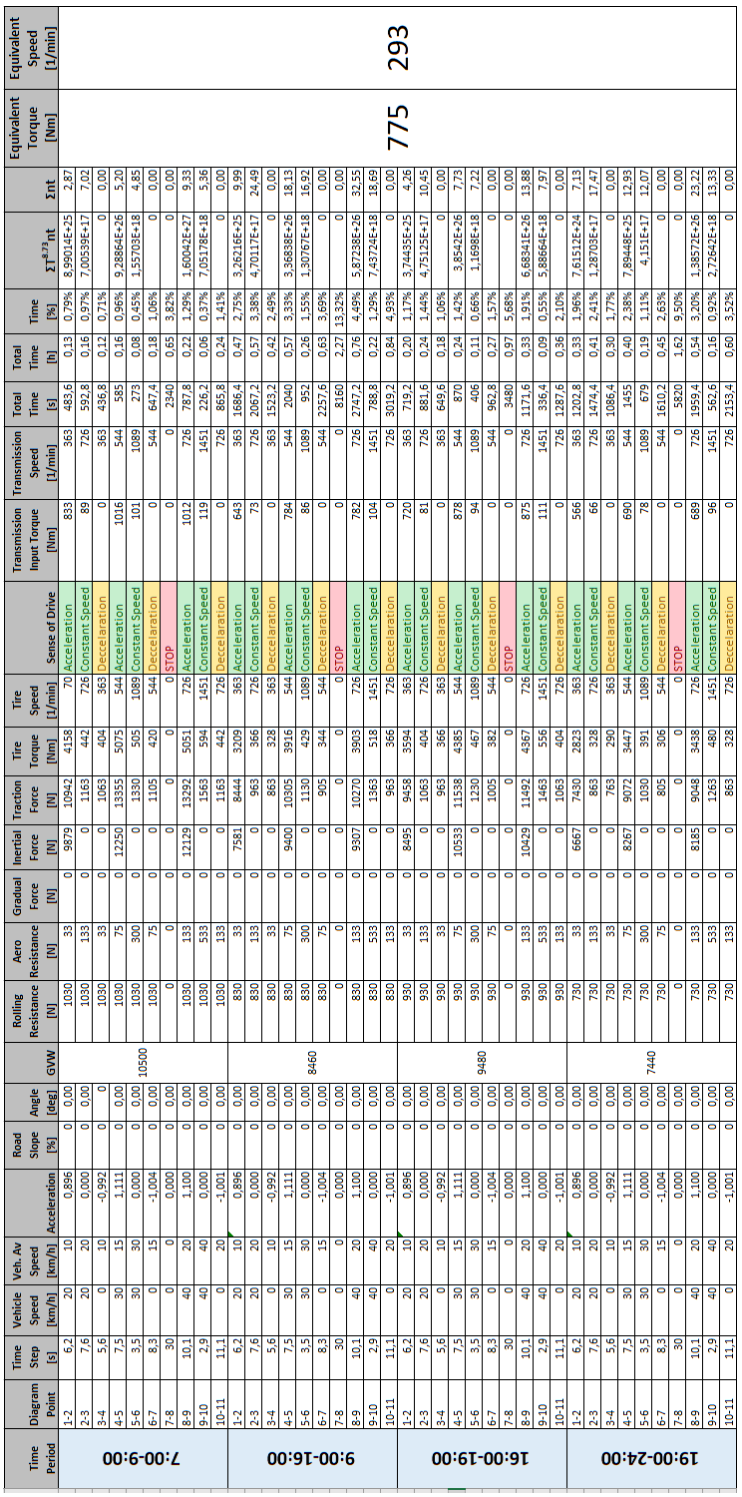

Time Period	Diagram Point	Time Step [s]	Vehicle Speed [km/h]	Veh. Av Speed [km/h]	Acceleration	Road Slope [%]	Angle [deg]	GVW	Rolling Resistance [N]	Aero Resistance [N]	Gradual Force [N]	Inertial Force [N]	Traction Force [N]	Tire Torque [Nm]	Tire Speed [1/min]	Sense of Drive	Transmission Input Torque [Nm]	Transmission Speed [1/min]	Total Time [s]	Total Time [h]	Time [%]	$\Sigma I^{3/3}nt$	Σnt	Equivalent Torque [Nm]	Equivalent Speed [1/min]
7:00-9:00	1-2	6,2	20	10	0,896	0	0,00	10500	1030	33	0	9879	10942	4158	70	Acceleration	833	363	483,6	0,13	0,79%	8,99014E+25	2,87	775	293
	2-3	7,6	20	20	0,000	0	0,00		1030	133	0	0	1163	442	726	Constant Speed	89	726	592,8	0,16	0,97%	7,00539E+17	7,02		
	3-4	5,6	0	10	-0,992	0	0		1030	33	0	0	1063	404	363	Deceleration	0	363	436,8	0,12	0,71%	0	0,00		
	4-5	7,5	30	15	1,111	0	0,00		1030	75	0	12250	13355	5075	544	Acceleration	1016	544	585	0,16	0,96%	9,28864E+26	5,20		
	5-6	3,5	30	30	0,000	0	0,00		1030	300	0	0	1330	505	1089	Constant Speed	101	1089	273	0,08	0,45%	1,55703E+18	4,85		
	6-7	8,3	0	15	-1,004	0	0,00		1030	75	0	0	1105	420	544	Deceleration	0	544	647,4	0,18	1,06%	0	0,00		
	7-8	30	0	0	0,000	0	0,00		0	0	0	0	0	0	0	STOP	0	0	2340	0,65	3,82%	0	0,00		
	8-9	10,1	40	20	1,100	0	0,00		1030	133	0	12129	13292	5051	726	Acceleration	1012	726	787,8	0,22	1,29%	1,60042E+27	9,33		
	9-10	2,9	40	40	0,000	0	0,00		1030	533	0	0	1563	594	1451	Constant Speed	119	1451	226,2	0,06	0,37%	7,05178E+18	5,36		
	10-11	11,1	0	20	-1,001	0	0,00		1030	133	0	0	1163	442	726	Deceleration	0	726	865,8	0,24	1,41%	0	0,00		
9:00-16:00	1-2	6,2	20	10	0,896	0	0,00	8460	830	33	0	7581	8444	3209	363	Acceleration	643	363	1686,4	0,47	2,75%	3,26216E+25	9,99		
	2-3	7,6	20	20	0,000	0	0,00		830	133	0	0	963	366	726	Constant Speed	73	726	2067,2	0,57	3,38%	4,70117E+17	24,49		
	3-4	5,6	0	10	-0,992	0	0,00		830	33	0	0	863	328	363	Deceleration	0	363	1523,2	0,42	2,49%	0	0,00		
	4-5	7,5	30	15	1,111	0	0,00		830	75	0	9400	10305	3916	544	Acceleration	784	544	2040	0,57	3,33%	3,36838E+26	18,13		
	5-6	3,5	30	30	0,000	0	0,00		830	300	0	0	1130	429	1089	Constant Speed	86	1089	952	0,26	1,55%	1,30787E+18	16,92		
	6-7	8,3	0	15	-1,004	0	0,00		830	75	0	0	905	344	544	Deceleration	0	544	2257,6	0,63	3,69%	0	0,00		
	7-8	30	0	0	0,000	0	0,00		0	0	0	0	0	0	0	STOP	0	0	8160	2,27	13,32%	0	0,00		
	8-9	10,1	40	20	1,100	0	0,00		830	133	0	9307	10270	3903	726	Acceleration	782	726	2747,2	0,76	4,49%	5,87238E+26	32,55		
	9-10	2,9	40	40	0,000	0	0,00		830	533	0	0	1363	518	1451	Constant Speed	104	1451	788,8	0,22	1,29%	7,43724E+18	18,69		
	10-11	11,1	0	20	-1,001	0	0,00		830	133	0	0	963	366	726	Deceleration	0	726	3019,2	0,84	4,93%	0	0,00		
16:00-19:00	1-2	6,2	20	10	0,896	0	0,00	9480	930	33	0	8495	9458	3594	363	Acceleration	720	363	719,2	0,20	1,17%	3,74435E+25	4,26		
	2-3	7,6	20	20	0,000	0	0,00		930	133	0	0	1063	404	726	Constant Speed	81	726	881,6	0,24	1,44%	4,75125E+17	10,45		
	3-4	5,6	0	10	-0,992	0	0,00		930	33	0	0	963	366	363	Deceleration	0	363	649,6	0,18	1,06%	0	0,00		
	4-5	7,5	30	15	1,111	0	0,00		930	75	0	10533	11538	4385	544	Acceleration	878	544	870	0,24	1,42%	3,8542E+26	7,73		
	5-6	3,5	30	30	0,000	0	0,00		930	300	0	0	1230	467	1089	Constant Speed	94	1089	406	0,11	0,66%	1,1698E+18	7,22		
	6-7	8,3	0	15	-1,004	0	0,00		930	75	0	0	1005	382	544	Deceleration	0	544	962,8	0,27	1,57%	0	0,00		
	7-8	30	0	0	0,000	0	0,00		0	0	0	0	0	0	0	STOP	0	0	3480	0,97	5,68%	0	0,00		
	8-9	10,1	40	20	1,100	0	0,00		930	133	0	10429	11492	4367	726	Acceleration	875	726	1171,6	0,33	1,91%	6,68341E+26	13,88		
	9-10	2,9	40	40	0,000	0	0,00		930	533	0	0	1463	556	1451	Constant Speed	111	1451	336,4	0,09	0,55%	5,88664E+18	7,97		
	10-11	11,1	0	20	-1,001	0	0,00		930	133	0	0	1063	404	726	Deceleration	0	726	1287,6	0,36	2,10%	0	0,00		
19:00-24:00	1-2	6,2	20	10	0,896	0	0,00	7440	730	33	0	6667	7430	2823	363	Acceleration	566	363	1202,8	0,33	1,96%	7,61512E+24	7,13		
	2-3	7,6	20	20	0,000	0	0,00		730	133	0	0	863	328	726	Constant Speed	66	726	1474,4	0,41	2,41%	1,28703E+17	17,47		
	3-4	5,6	0	10	-0,992	0	0,00		730	33	0	0	763	290	363	Deceleration	0	363	1086,4	0,30	1,77%	0	0,00		
	4-5	7,5	30	15	1,111	0	0,00		730	75	0	8267	9072	3447	544	Acceleration	690	544	1455	0,40	2,38%	7,89448E+25	12,93		
	5-6	3,5	30	30	0,000	0	0,00		730	300	0	0	1030	391	1089	Constant Speed	78	1089	679	0,19	1,11%	4,1515E+17	12,07		
	6-7	8,3	0	15	-1,004	0	0,00		730	75	0	0	805	306	544	Deceleration	0	544	1610,2	0,45	2,63%	0	0,00		
	7-8	30	0	0	0,000	0	0,00		0	0	0	0	0	0	0	STOP	0	0	5820	1,62	9,50%	0	0,00		
	8-9	10,1	40	20	1,100	0	0,00		730	133	0	8185	9048	3438	726	Acceleration	689	726	1959,4	0,54	3,20%	1,38572E+26	23,22		
	9-10	2,9	40	40	0,000	0	0,00		730	533	0	0	1263	480	1451	Constant Speed	96	1451	562,6	0,16	0,92%	2,72642E+18	13,33		
	10-11	11,1	0	20	-1,001	0	0,00		730	133	0	0	863	328	726	Deceleration	0	726	2153,4	0,60	3,52%	0	0,00		

Şekil 4: ISO 6336-6'ya göre eşdeğer tork hesabı yazılımı

Şekil 4'te hesaplanan eşdeğer tork ($T_{esdeger}$)775 Nm ve eşdeğer devir ($n_{esdeger}$)293 d/d, KISSsys yazılımında oluşturulan çift kademeli dişli kutusu modelinin (Şekil 5) temel boyutlandırması için kullanılmıştır.

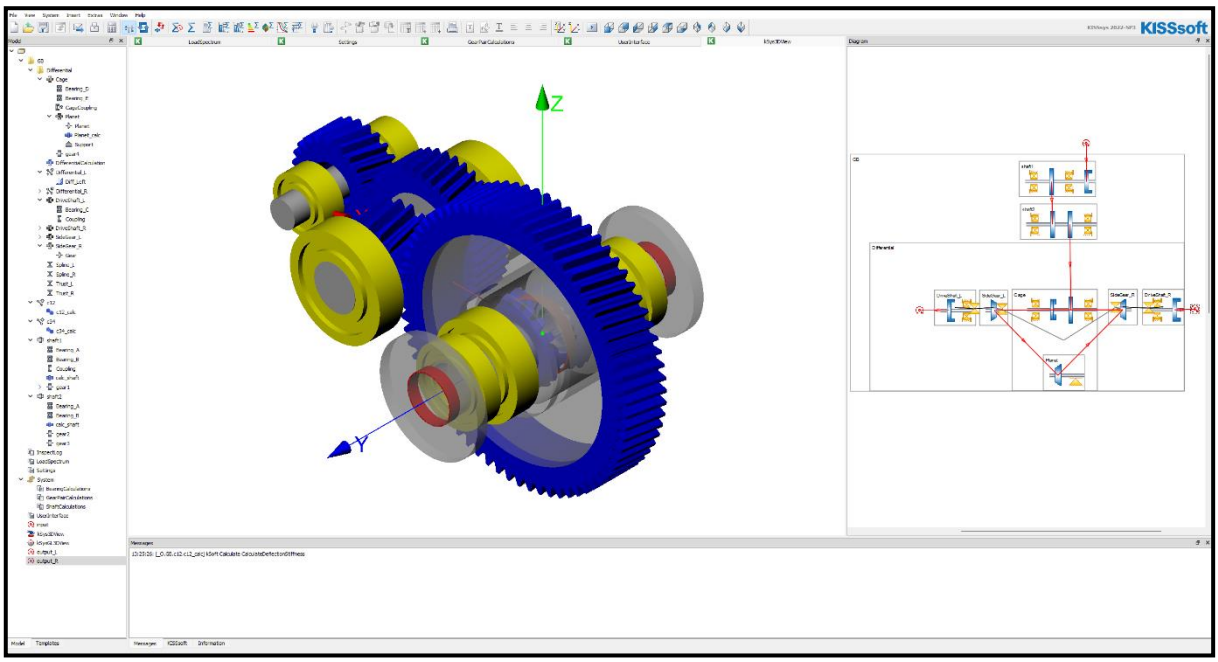

Şekil 5: KISSsys'te oluşturulan çift kademeli dişli kutusu modeli.

Bu modelde kullanılan dişli parametreleri Tablo 3'te verilmiştir.

Tablo 3: KISSsys modelinde kullanılan dişli parametreleri.

Zaman Aralığı	Kademe 1	Kademe 2
Diş Sayısı z_1	25	25
Diş Sayısı z_2	57	57
Modül	3	3.75
Diş Genişliği [mm]	40	50
Helis Açısı [°]	10	10
Profil Kayma Katsayısı	.2213	.2213

Termal Analiz ve Optimizasyon Süreci

Termal analizler, ISO/TR 14179-2 standardını [5] temel alan KISSsys yazılımı kullanılarak gerçekleştirilmiştir. Bu standart, şanzıman içindeki termal dengenin, üretilen ısı (güç kayıpları) ile sistemden atılan ısının eşitliği prensibine dayandığını belirtir. Şanzımanın kararlı bir sıcaklıkta çalışabilmesi için, Denklem (3) ile ifade edilen toplam güç kaybı (P_V) ile Denklem (4) ile ifade edilen toplam ısı atımının (Q) birbirini dengelemesi gerekir.

a. Güç Kaybı Kaynakları (P_V)

Güç kayıpları, aktarılan mekanik enerjinin istenmeyen ısıya dönüşen kısmıdır ve verimliliği doğrudan etkiler. Başlıca kaynakları şunlardır:

Dişli Kayıpları (P_{VZ0}, P_{VZP}): Dişli çiftlerinin temasındaki sürtünme (yüke bağlı) ve dişlilerin yağ içinde dönmesiyle oluşan çalkalanma ve sıkıştırma kayıplarından (yükten bağımsız) oluşur. Bu, genellikle en büyük kayıp kaynağıdır.
Rulman Kayıpları (P_{VL0}, P_{VLP}): Rulmanlardaki yuvarlanma ve kayma sürtünmesinden kaynaklanır.
Keçe Kayıpları (P_{VD}): Dönen millerdeki sızdırmazlık keçelerinin sürtünmesinden kaynaklanır.
Diğer Kayıplar (P_{VX}): Varsa yağ pompası gibi diğer yardımcı elemanlardan kaynaklanan kayıpları içerir.

$$P_V = P_{VZ0} + P_{VZP} + P_{VL0} + P_{VLP} + P_{VD} + P_{VX} \quad (3)$$

b. Isı Atım Mekanizmaları (Q)

Üretilen ısının sistemden uzaklaştırılması, aşırı ısınmayı önler. Temel mekanizmalar şunlardır:

Gövdeden Atılan Isı (Q_{ca}): Şanzıman gövdesinin dış yüzeyinden çevreye taşınım (convection) ve ışınım (radiation) yoluyla gerçekleşen ısı transferidir. Yüzey alanı, gövde malzemesi ve hava akışı (ventilasyon) bu mekanizmayı doğrudan etkiler.
Temel Yapıdan Atılan Isı (Q_{fun}): Şanzımanın monte edildiği şasi veya diğer yapılara iletim yoluyla aktarılan ısıdır.
Dönen Parçalardan Atılan Isı (Q_{rot}): Gövde dışına uzanan mil uçları gibi dönen parçalardan atılan ısıdır.
Yağ Akışı ile Atılan Isı (ΔH_{oil}): Harici bir yağ soğutucusu kullanılması durumunda, yağın soğutucuda dolaştırılmasıyla sistemden uzaklaştırılan ısıyı temsil eder.

$$Q = Q_{ca} + Q_{fun} + Q_{rot} + \Delta H_{oil} \quad (4)$$

Analizler için en kritik senaryo, aracın tam yüklü ve 90 km/s maksimum hızda çalıştığı durum olarak belirlenmiştir. Bu senaryodaki temel hedef, 20°C ortam sıcaklığında şanzıman yağı denge sıcaklığının 95°C'yi aşmamasını sağlamaktır. KISSsys ara yüzünde (Şekil 6, Şekil 7) ventilasyon hızı, gövde özellikleri gibi parametreler girilerek üç adımlı bir optimizasyon süreci yönetilmiştir. Optimizasyon sürecinde asıl amaç ilave bir soğutucu ihtiyacından kurtulmaktır. Bu aracın maliyetinin ve ağırlığının optimize edilmesi demektir. İlave bir soğutucu, ilave bir pompaya ve borulamalara ihtiyaç duyar. Bunların maliyeti ve ağırlığı araç üzerinde gereksiz külfet ve verim kaybına yol açar. Pompayı döndürmek için bir güç sarf edilmesi gerekir.

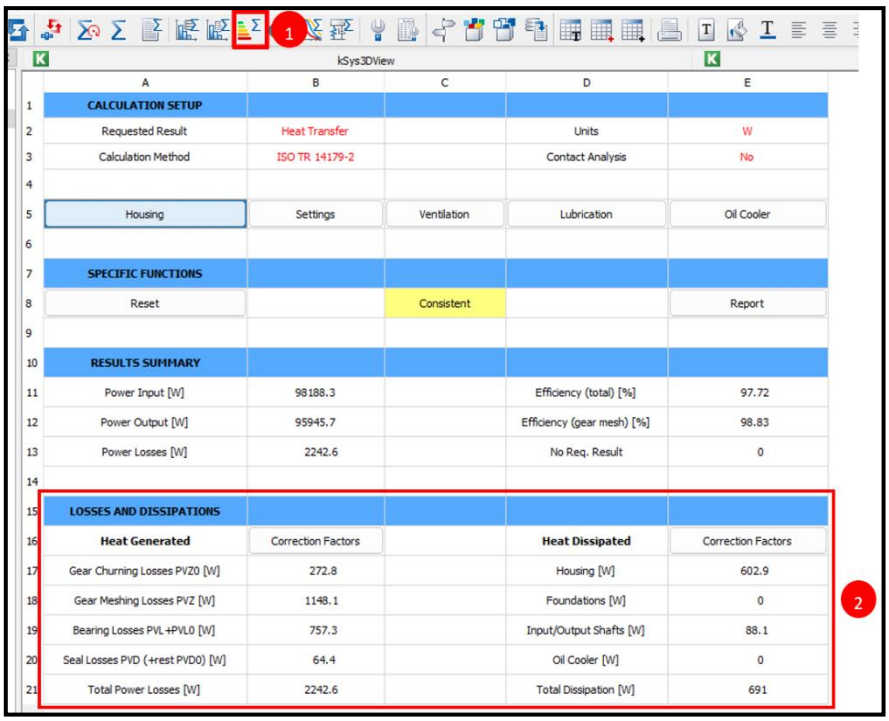

	A	B	C	D	E
1	**CALCULATION SETUP**				
2	Requested Result	Heat Transfer		Units	W
3	Calculation Method	ISO TR 14179-2		Contact Analysis	No
4					
5	Housing	Settings	Ventilation	Lubrication	Oil Cooler
6					
7	**SPECIFIC FUNCTIONS**				
8	Reset		Consistent		Report
9					
10	**RESULTS SUMMARY**				
11	Power Input [W]	98188.3		Efficiency (total) [%]	97.72
12	Power Output [W]	95945.7		Efficiency (gear mesh) [%]	98.83
13	Power Losses [W]	2242.6		No Req. Result	0
14					
15	**LOSSES AND DISSIPATIONS**				
16	**Heat Generated**	Correction Factors		**Heat Dissipated**	Correction Factors
17	Gear Churning Losses PVZ0 [W]	272.8		Housing [W]	602.9
18	Gear Meshing Losses PVZ [W]	1148.1		Foundations [W]	0
19	Bearing Losses PVL+PVL0 [W]	757.3		Input/Output Shafts [W]	88.1
20	Seal Losses PVD (+rest PVD0) [W]	64.4		Oil Cooler [W]	0
21	Total Power Losses [W]	2242.6		Total Dissipation [W]	691

Şekil 6: KISSsys "Efficiency Template" arayüzü ve temel termal analiz sonuçları.

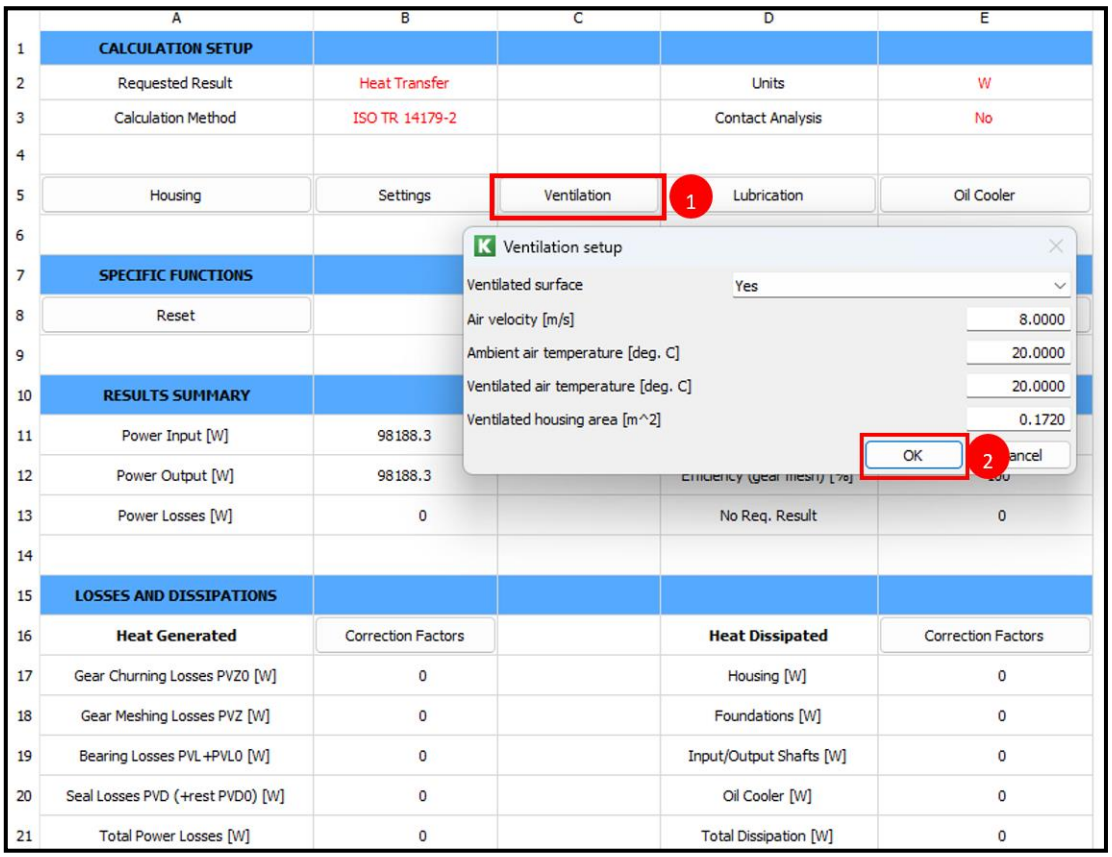

	A	B	C	D	E
1	**CALCULATION SETUP**				
2	Requested Result	Heat Transfer		Units	W
3	Calculation Method	ISO TR 14179-2		Contact Analysis	No
4					
5	Housing	Settings	Ventilation	Lubrication	Oil Cooler
6					
7	**SPECIFIC FUNCTIONS**				
8	Reset				
9					
10	**RESULTS SUMMARY**				
11	Power Input [W]	98188.3			
12	Power Output [W]	98188.3			
13	Power Losses [W]	0		No Req. Result	0
14					
15	**LOSSES AND DISSIPATIONS**				
16	**Heat Generated**	Correction Factors		**Heat Dissipated**	Correction Factors
17	Gear Churning Losses PVZ0 [W]	0		Housing [W]	0
18	Gear Meshing Losses PVZ [W]	0		Foundations [W]	0
19	Bearing Losses PVL+PVL0 [W]	0		Input/Output Shafts [W]	0
20	Seal Losses PVD (+rest PVD0) [W]	0		Oil Cooler [W]	0
21	Total Power Losses [W]	0		Total Dissipation [W]	0

Şekil 7: KISSsys 'te ventilasyon parametrelerinin girildiği arayüz.

İterasyon 1'de Şekil 8' de dişli kutusunun alt taraında sarı renk ile gösterilen kısmi bir bölgenin ventilasyona maruz bırakıldığı kabul edilmiştir.

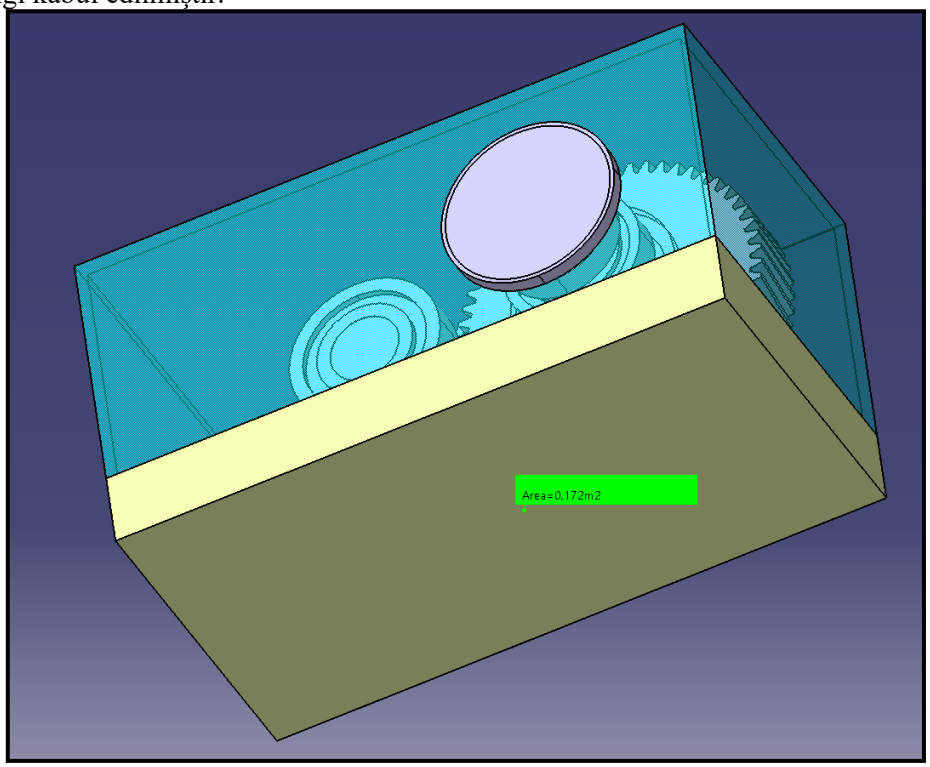

Şekil 8: İterasyon 1'de ventilasyona maruz kalan yüzeyler.

Şekil 9'da ise İterasyon 2'de dişli kutusunun alt tarafına Tablo 3'te verilen tasarım parametrelerine göre termal kanatçıklar eklenmiştir.

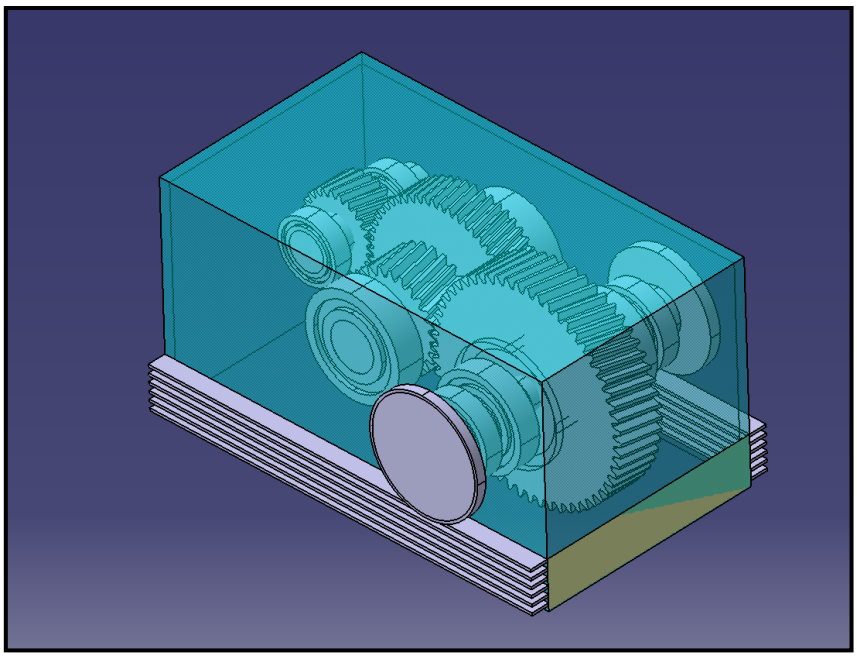

Şekil 9: İterasyon 2'de eklenen termal kanatçıklar.

Tablo 3: İterasyon 2'de eklenen termal kanatçıklar için tasarım parametreleri

Parametre	Birim	Değer
Toplam kanat alanı	[m^2]	0.252
Projeksiyon alanı	[m^2]	0.048
Bir kanadın derinliği	[mm]	20
Bir kanadın kalınlığı	[mm]	3

BULGULAR VE TARTIŞMA

Yapılan iteratif analizler sonucunda elde edilen temel bulgular Tablo 4'te özetlenmiştir.

Tablo 4: Termal analiz iterasyonlarının karşılaştırmalı sonuçları.

Parametre	İterasyon 0 (Başlangıç)	İterasyon 1 (+ Ventilasyon)	İterasyon 2 (+ Ventilasyon & Kanatçık)
Açıklama	Düz gövde, durgun hava	Düz gövde, 8 m/s hava akımı	Kanatçıklı gövde, 8 m/s hava akımı
Toplam Güç Kaybı [kW]	2.24	2.24	2.24
Toplam Isı Atımı [kW]	.69	1.24	1.77
Hesaplanan Yağ Sıcaklığı [°C]	> 120 (Termal Kararsızlık)	121	**93.5**

Başlangıç durumu (İterasyon 0), termal yönetimin ne denli kritik olduğunu açıkça ortaya koymuştur. Sistemde oluşan 2.24 kW'lık güç kaybına karşın, doğal taşınımla sadece 0.69 kW ısı atılabilmektedir. Bu büyük fark sistemin soğutma önlemi olmaksızın kısa sürede aşırı ısınarak termal bir kararsızlığa gireceğini göstermiştir.

Ventilasyonun eklenmesi (İterasyon 1) ile ısı atım kapasitesi %80 artarak 1.24 kW'a yükselmiştir. Bu, hava akışının soğutmadaki önemini kanıtlasa da, hesaplanan 121°C'lik denge sıcaklığı, modern sentetik yağlar için bile yüksek bir değerdir ve uzun vadede güvenilir bir operasyon için yeterli değildir.

Nihai tasarım olan İterasyon 2, en başarılı sonucu vermiştir. Gövdeye eklenen ve imalatı nispeten kolay olan termal kanatçıklar, ısı transfer yüzey alanını önemli ölçüde artırmıştır. Ventilasyonun da etkisiyle toplam ısı atım kapasitesi 1.77 kW'a ulaşmış ve sistemin denge sıcaklığı 93.5°C olarak hesaplanmıştır. Bu değer, 95°C'lik tasarım hedefinin altında kalarak, şanzımanın harici bir yağ soğutma devresine ihtiyaç duymadan, güvenli ve verimli bir şekilde çalışabileceğini kanıtlamıştır. Bu sonuç, çalışmanın ana hedefine ulaşıldığını göstermektedir.

SONUÇ

Bu çalışma, seri hibrit bir şehir içi otobüs şanzımanının, konsept aşamasında yapılan sistematik bir termal optimizasyon süreciyle, ek soğutma sistemlerine gerek kalmadan tasarlanabileceğini başarılı bir şekilde ortaya koymuştur. Elde edilen 93.5°C'lik denge sıcaklığı, gövde tasarımına entegre edilen termal kanatçıklar ve araç hareketinden kaynaklanan doğal ventilasyonun, sistemdeki güç kayıplarını dengelemek için yeterli olduğunu kanıtlamıştır. Bu yaklaşım, harici yağ soğutucusu, pompa ve borulama gibi bileşenleri ortadan kaldırarak; sistem maliyetini, ağırlığını, montaj karmaşıklığını ve potansiyel arıza noktalarını önemli ölçüde azaltmaktadır.

Bu konsept aşamasında elde edilen sonuçlar, özellikle optimum ısı atımı için gereken toplam yüzey alanı ve kanatçık geometrisi gibi veriler, projenin bir sonraki adımı olan detay tasarım fazı için kritik bir girdi niteliğindedir. Detaylı CAD modellemesi, bu temel veriler ışığında şekillendirilerek hem termal performansın garanti altına alınması hem de üretilebilirliğin sağlanması hedeflenmelidir.

Elde edilen bulgular, yerli hibrit güç aktarım organları geliştirme çabaları için önemli bir mühendislik çıktısı sunmaktadır. Bu metodoloji, farklı araç tipleri ve çalışma koşulları için de uyarlanabilir. Gelecek çalışmalarda, bu sanal optimizasyonun sonuçlarının, üretilecek bir prototip üzerinde, gövdeye ve yağ karterine yerleştirilecek termokupllar ile deneysel olarak doğrulanması hedeflenebilir. Ayrıca, farklı gövde malzemelerinin (örneğin, magnezyum alaşımları) ve daha gelişmiş yüzey kaplamalarının termal performans üzerindeki etkileri de incelenerek optimizasyon daha ileri bir seviyeye taşınabilir.

Kaynaklar

[1] Changenet C., Oviedo-Marlot X., Velex P., (2006), “Power Loss Predictions in Geared Transmissions Using Thermal Networks-Applications to a Six-Speed Manual Gearbox”, Journal of Mechanical Design, 128(3), 618-625.
[2] Paschold, C., Sedlmair, M., Lohner, T. et al. (2022), “Calculating component temperatures in gearboxes for transient operation conditions”, Forschung im Ingenieurwesen, 86, 521–534.
[3] Kuralay, N. S., (2008), Motorlu Taşıtlar Temel ve Tasarım Esasları Yapı Elemanları Cilt 1, TMMOB Makina Mühendisleri Odası.
[4] ISO, (2006), Calculation of load capacity of spur and helical gears — Part 6: Calculation of service life under variable load (ISO 6336-6), International Organization for Standardization.
[5] ISO, (2001), Gears — Thermal capacity — Part 2: Thermal load-carrying capacity (ISO/TR 14179-2), International Organization for Standardization.

➢ *ORAL PRESENTATION*

Kripto Para Türlerinin Teknik Özelliklerinin Karşılaştırmalı Analizi ve Balon Fiyat Tespiti

Serkan METİN[1*] *(https://orcid.org/0000-0003-1765-7474)*

[*1]Malatya Turgut Özal Üniversite, Sosyal ve Beşeri Bilimler Fakültesi, Yönetim Bilişim Sistemleri Bölümü, Malatya, TÜRKİYE

*Sorumlu yazar e-posta:serkan.metin@ozal.edu.tr

Özet
Kripto paralar, son yıllarda finansal sistemlerde ve dijital ekonomilerde devrim yaratan bir olgu olarak karşımıza çıkmaktadır. Özellikle merkeziyetsizlik ve hızlı işlem imkanları sunmalarından dolayı kripto paraların küresel finans sistemlerinde oldukça yaygın yatırımcısı olan bir finans aracına dönüşmesine neden olmuştur. Bu durum kripto paraların yapılarının iyi anlaşılması ve yatırım yapmadan önce teknik özelliklerinin bilinmesini daha da önemli hale getirmiştir. Bu çalışmada, kripto para türlerinden olan ve teknolojik alt yapıları ile sağladığı hizmetler yönünden farklılık gösteren meme coinlerin fiyat dalgalanması üzerine bir çalışma yapılmıştır. Yapılan çalışmalar meme coinlerin yüksek volatiliteye sahip olması nedeniyle yalnızca saatler veya dakikalar içinde değer kaybetme riskinin yüksek olduğunu göstermektedir. Ayrıca bu tür coinlerin fiyat oluşumlarının sosyal medya paylaşımlarından doğrudan etkilediğinden yüksek risk taşıdığı ve balon fiyat süreçlerinin de uzun dönemler içerisinde olacağını da göstermektedir. Elde edilen sonuçlar bu hipotezleri desteklemektedir. Özellik Elon Musk tarafından farklı dönemlerde yapılan açıklamalar en fazla balon fiyat oluşan coinin Dogecoin olmasında en büyük etken olmuştur. Çalışmada elde edilen sonuçlarda göstermektedir ki, en fazla balon fiyat dönemi Dogecoin de oluşmuştur.
Anahtar Kelimeler: Kripto para, Blok zinciri, Memecoin, Balon Fiyat

Comparative Analysis of the Technical Features of Cryptocurrency Types and Bubble Price Detection

Abstract
Cryptocurrencies have emerged in recent years as a phenomenon revolutionizing financial systems and digital economies. Particularly due to their decentralized nature and the ability to facilitate rapid transactions, cryptocurrencies have become a widely adopted financial instrument within global financial systems. This development has made it increasingly important to thoroughly understand the structure of cryptocurrencies and to be aware of their technical characteristics before making investment decisions. This study examines the price fluctuations of meme coins, a type of cryptocurrency that differs in terms of technological infrastructure and the services they provide. The findings reveal that meme coins, due to their high volatility, are at significant risk of losing value within just hours or even minutes. Furthermore, the pricing of such coins is shown to be directly influenced by social media activity, making them inherently high-risk assets with the potential for prolonged bubble price processes. The results obtained in this study support these hypotheses. In particular, statements made by Elon Musk at various times have played a major role in Dogecoin becoming the cryptocurrency most prone to bubble pricing. The findings also indicate that the highest bubble price periods have been observed in Dogecoin.
Keywords: Cryptocurrency, Blockchain, Memecoin, Bubble Price

GİRİŞ

Blok zinciri, işlem kayıtlarını şifreli ve dağınık bir ağ üzerinde tutan değiştirilemez bir dijital defterdir. Temel işleyişi, blok adı verilen veri paketlerinin kronolojik olarak birbirine kriptografik hash fonksiyonlarıyla bağlanmasına dayanır. Blok zincir, sürekli yeni blokların eklenmesiyle genişlemektedir (Harsh ve Ruchi, 2023:1). Şekil 1'de bir blok zinciri yapısı verilmiştir.

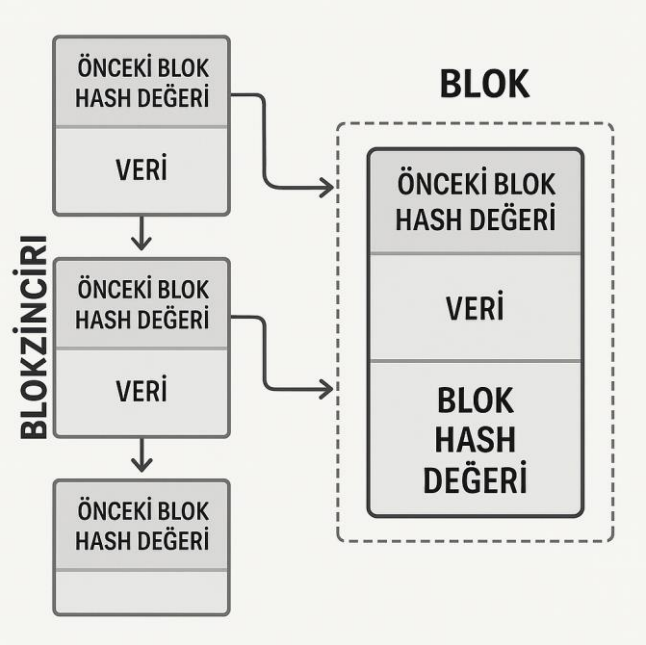

Şekil 1. Blok zinciri Yapısı

Bir blok, blok zincirinin yapı taşıdır ve oluşturulması belirli bir süreci izler. Bu süreçler Şekil 2'de verilmiştir.

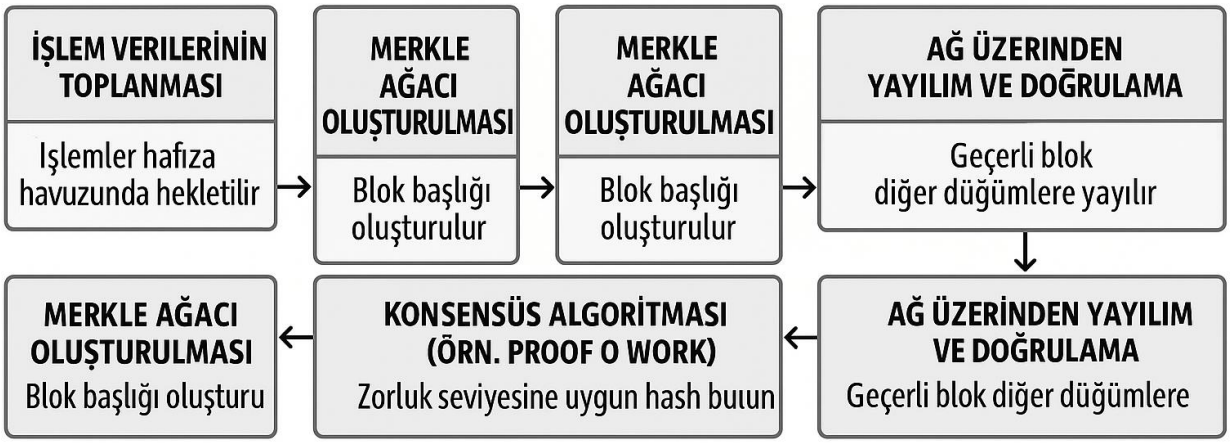

Şekil 2. Blok oluşturma süreci

Blok zincir teknolojisi ilk olarak 2008'de Satoshi Nakamoto takma adıyla yayınlanan Bitcoin: A Peer-to-Peer Electronic Cash System başlıklı makale ile kripto para birimlerinin temellerini oluşturmuştur. Bitcoin, blok zincir teknolojisi sayesinde merkezi otoriteye ihtiyaç duymadan işlem yapılabilen bir sistem geliştirdi. Bu teknoloji, kullanıcılar arasında güvenli ve doğrudan işlem yapılmasını sağlarken, işlemlerin kaydedildiği bloklar zincir şeklinde birbirine bağlandığından işlem güvenliğini de artırmıştır. Özellikle merkeziyetsizlik ve hızlı işlem imkanları, kripto paraların küresel finans sistemlerinde daha fazla kullanılabileceğini göstermiştir.

Kripto paraların yükselişinde rol oynayan diğer bir faktör de yatırımcıların ilgisidir. 2017 yılında, Bitcoin'in değerinin 20.000 dolar seviyelerine çıkması, kripto paraya olan yatırımcı sayısını daha da artırmıştır. Bitcoin'in bu başarısı, Ethereum, Ripple ve Litecoin gibi diğer kripto paraların da doğmasına yol açmıştır. 2020 ortası ile 2021 başı arasında, kripto piyasasındaki büyük bir boğa koşusuyla birlikte, kripto paraların popülaritesi tüm zamanların en yüksek seviyesine ulaşmıştır (Vladyslav ve Ivan, 2023:1). Ancak, bu yükselişin ardından meydana gelen ani düşüş, kripto paraların yüksek risk içeren yatırım araçları olarak görülmesine ve Kripto paraların geleceği konusunda farklı görüşlerin de ortaya çıkmasına neden olmuştur. Kripto paraların gelecekte hangi yöne evrileceği belirsizliğini korumakla birlikte, bu teknolojinin finansal yenilik ve güvenlik açısından sunduğu fırsatlar birlikte düzenleyici kurumlar bu dijital varlıkların denetim altına alınması gerektiğini savunmaktadır.

Kripto paralardan Bitcoin dışında kalan coinler altcoin ya da meme coin olarak adlandırılmaktadır. Kripto para dünyasında meme coinler ve diğer altcoinler aynı dijital altyapı üzerinde geliştirilmiş olsada, aralarında

belirgin yapısal farklılıklar bulunmaktadır. Bu farklılıklar, yatırımcılara sundukları değer, teknik altyapıları, geliştirme amaçları ve fiyat oynaklığı gibi unsurlarda kendini gösterir.

MEME COİNLER

İnternet ortamında şaka amaçlı içeriklere genel ad olarak verilen "meme" terimi, kripto para yatırımcılarının sıkça karşılaştığı kavramlardan biridir. Meme coinler de genellikle şaka amaçlı ortaya çıkmıştır. Bu tür kripto paralar, genellikle popüler bir mizah unsuruna dayanır. Meme coinlerin belirgin özellikleri arasında, belirli bir temaya sahip olmaları, genellikle eğlence amacıyla üretilmeleri, dikkat çeken görsellerle sunulmaları ve çevrimiçi platformlarda hızla yayılarak geniş bir kullanıcı kitlesine ulaşmaları sayılabilir (Başbuğ ve Lokmanoğlu, 2021:3132).

Meme coinler genellikle mevcut bir blockchain üzerinde (örneğin Ethereum veya Binance Smart Chain) hızlı bir şekilde oluşturulur. Bu coinlerin teknik altyapısı ve güvenlik standartları sınırlıdır ve büyük bir kısmı merkeziyetsiz finans (DeFi) işlevlerine veya gelişmiş blockchain özelliklerine sahip değildir. Bu durum, meme coinlerin daha düşük güvenlik standartları taşımasına ve saldırılara karşı daha savunmasız olmasına yol açar. Meme coinler, finansal veya teknolojik bir temel üzerine kurulmadığı için düzenleyici kurumlar tarafından spekülatif varlıklar olarak görülmektedir.

Alt coin ve meme coin kavramları kripto para dünyasında sıkça kullanılır; ancak aralarında belirgin farklılıklar bulunmaktadır. Tablo 1'de bu iki tür kripto paranın karşılaştırması yapılmıştır.

Tablo 1. Altcoin ve Meme Coin Karşılaştırılması

Özellik	Alt Coin	Meme Coin
Tanım	Bitcoin dışındaki tüm kripto paralara alt coin denir.	Genellikle bir şaka veya internet memesine dayanarak yaratılan coinlerdir.
Amacı	Çoğunlukla finansal hizmetlerde veya uygulamalarda kullanılmak üzere geliştirilir.	Şaka amacıyla oluşturulmuştur, ancak viral olabilir ve değer kazanabilir.
Teknoloji	Genellikle kendine özgü blok zinciri veya Bitcoin/Ethereum gibi bir zincir üzerinde geliştirilir.	Çoğunlukla mevcut bir blok zinciri (ör. Ethereum) üzerinde basitçe oluşturulur.
Kullanım Alanı	DeFi (merkeziyetsiz finans), akıllı sözleşmeler, ödeme sistemleri gibi çeşitli alanlarda kullanılır.	Çoğunlukla sosyal medya ve topluluklar arasında popülerdir, yatırım amaçlı tercih edilir.
Değer Temeli	Değerini teknolojik yenilikler, kullanım alanı ve arz-talep gibi faktörlerden alır.	Değeri, sosyal medya etkisi, hype ve topluluk desteğine dayanır; genellikle sağlam bir temel yoktur.
Volatilite	Daha az spekülatif ve genellikle daha stabil.	Yüksek spekülasyon ve volatiliteye sahip; fiyatları hızla değişebilir.
Örnekler	Ethereum (ETH), Cardano (ADA), Binance Coin (BNB)	Dogecoin (DOGE), Shiba Inu (SHIB), Pepe Coin (PEPE)
Yatırım Riski	Riskli olmasına rağmen, genellikle daha uzun vadeli projelerle ilişkilidir.	Yüksek risklidir; ani kazançlar veya büyük kayıplar yaşanabilir.
Topluluk Etkisi	Topluluk desteği önemli ancak proje gelişimi ve teknolojiyle daha çok ilgilidir.	Topluluk etkisi çok güçlüdür; popülerlik kaybı değerini hızla düşürebilir.

Meme coinler, kripto para dünyasında son yıllarda önemli bir yer edinen ve genellikle şaka veya espri amacıyla başlatılan dijital varlıklardır. Ancak meme coinlerin esprili başlangıçlarına rağmen, geniş kitlelerin ilgisi ve yatırımcıların desteğiyle hızla değer kazanmaları onları ciddi birer dijital varlık haline getirmiştir. Meme coinler, genellikle sınırlı bir teknik yenilik sunmalarına rağmen topluluk desteği ve sosyal medya etkisi ile hızlı bir şekilde popülerlik kazanmıştır. Meme coinlerin en ünlü örneği olan Dogecoin, 2013 yılında yazılım mühendisleri Billy Markus ve Jackson Palmer tarafından espri amacıyla yaratılmıştır. Dogecoin'in yaratılmasındaki amaç, Bitcoin gibi daha ciddi ve karmaşık kripto paralara mizahi bir alternatif sunmaktır. İlk

olarak Shiba Inu cinsi bir köpeğin yüzü ile tanıtılan Dogecoin, kısa sürede internette popülerleşmiş ve birçok kullanıcıya ulaşmıştır. Özellikle Elon Musk gibi ünlü isimlerin Dogecoin hakkında sosyal medya paylaşımları yapması, Dogecoin'in 2021 yılında %12,000'e varan bir değer artışı yaşamasına yol açmıştır. 2021 yılı itibariyle Dogecoin'in toplam piyasa değeri 85 milyar dolara kadar çıkmış, bu da onu en değerli kripto paralar arasına yerleştirmiştir. Shiba Inu gibi diğer meme coinler de Dogecoin'in başarısından etkilenmiş ve hızla büyüyen topluluklara sahip olmuştur. Shiba Inu 2021 yılında %5,000,000 oranında değer kazanarak kripto dünyasında büyük ses getirmiştir.

Kripto paralar ile ilgili günlük veri tutan CoinMarketCap'ta 2024 yılında toplam meme coin sayısı 700'ün üzerinde görülmektedir. Bu sayı, 2023 yılına kıyasla %35'lik bir artışı ifade etmekte olup, meme coinlere olan ilginin ve topluluk desteğinin devam ettiğini göstermektedir. Bu artışlara rağmen meme coinlerin yüksek volatilitesi, yatırımcıların büyük kayıplar yaşamasına neden olabilir ve özellikle yeni yatırımcılar için finansal riski artırmaktadır.

2024 yılında meme coin piyasasında yaşanan ani fiyat düşüşleri nedeniyle toplamda 5 milyar doların üzerinde bir yatırım kaybı yaşanmıştır. Bu kayıpların büyük bir kısmı, sosyal medya manipülasyonları ve yatırımcıların toplu satış yapmasıyla tetiklenen ani fiyat düşüşlerinden kaynaklanmıştır. Tablo 2'de meme coin'lerin anlık fiyat değişikliğinden kaynaklı olarak yaşanan kayıplardan bazıları verilmiştir.

Tablo 2. Meme Coin Fiyat Çöküşü

Meme Coin	**Çöküş Tarihi**	**Tahmini Kayıp (USD)**	**Kayıp Süresi**	**Kayıp Açıklaması**
MBAPPE	30.08.24	1.03 milyon dolardan 9,200 dolara	1 saat	Bir saat içinde %99 değer kaybetti, yatırımcı büyük zarar yaşadı
Squid Game Token (SQUID)	01.11.21	3.38 milyon dolar	Dakikalar içinde	"Rug pull" olarak bilinen ani çöküşle, fiyat dakikalar içinde sıfırlandı
BigCoin	01.03.22	200,000 dolardan birkaç dolara	2 saat	Lansman sonrası aşırı satışı takiben hızla değer kaybetti.
Turd Coin	2021 sonları	%80 değer kaybı	1 saatten kısa sürede	Sosyal medya hype'ı sonrası yoğun satışla hızla çöktü.
POOH	2023 Mayıs	%70-90 değer kaybı	Birkaç saat içinde	Ani satış dalgasıyla fiyat hızla düştü
Jesus Coin (JC)	2021 başları	Milyonlarca dolarlık yatırımcı zararı	Birkaç saat içinde	Hızlı popülerlik sonrası hızla değer kaybı yaşadı.

Tablo 2'de, meme coin'lerin yüksek volatiliteye sahip olması nedeniyle yalnızca saatler veya dakikalar içinde değer kaybetme riskinin yüksek olduğu görülmektedir. Coin'lerin fiyatı genellikle sosyal medya hype'ı, ani spekülatif alımlar ve piyasa manipülasyonları ile şişirilir ve ardından hızlı satışlarla hızla düşebilmektedir.

Manipülasyon riski, bireysel yatırımcıların doğru yatırım kararları almasını zorlaştırmakta ve çoğu zaman yanıltıcı bilgiler nedeniyle yanlış pozisyon almalarına yol açmaktadır. CoinTelegraph'ın raporuna göre, 2024 yılında meme coin piyasasında manipülasyon nedeniyle yaşanan kayıplar 3 milyar doları bulmuştur. Meme coinlerin bu spekülatif yapısı ve büyük risk taşıması bazı ekonomistler tarafından yatırım aracı olarak değerlendirilmemesine rağmen yatırımcı toplulukları ise uzun vadede bu varlıkların değer kazanabileceğine inanmaktadır. Buna ek olarak, meme coinler dolandırıcılık amacıyla da kullanılabilmektedir. Sahte projeler, yatırımcılardan hızlı kazanç vaadiyle fon toplamakta ve ardından projeyi terk ederek yatırımcıları mağdur etmektedir. Bu tür dolandırıcılıklar, özellikle bilgi eksikliği olan yeni yatırımcılar için büyük bir risk faktörüdür. Aynı zamanda meme coinlerin geliştirilme süreçlerinde, çoğu zaman yüksek güvenlik

standartlarına uyulmamaktadır. Bu durum, hack saldırıları ve dolandırıcılık girişimleri gibi riskleri artırmaktadır. Meme coinlerin yapısal durumlarından dolayı balon fiyat oluşturma potansiyelleri çok fazladır.

Balon fiyatlar, kripto paraların değerlerinde hızlı bir artışın ardından ani bir düşüşle yüksek kayıplar oluşturabilmektedir. Bu yüzden balonların tahmini büyük önem taşımaktadır. Çünkü bu durum yatırımcıların bilinçli kararlar almasına ve muhtemel kayıplardan kaçınmasına olanak tanır. Bir balonun erken tespiti, yatırımcıların varlıklarını balon patlamadan önce elden çıkarmasını sağlayarak yatırımlarını büyük fiyat düşüşlerinden korur ve kayıplarını azaltır. Ancak, finansal piyasalarındaki balonları öngörmek karmaşık bir süreçtir ve piyasa trendleri, ekonomik göstergeler ve insan psikolojisi üzerine derin bir bilgi birikimi gerektirir. Uzmanlar, balonların çoğunlukla duygusal tepkiler ve grup dinamikleri gibi mantıksal olmayan faktörlere dayandığı için tahmin edilmesinin zor olduğunu vurgulamaktadır (Lupu vd., 2024:5).

LİTERATÜR ARAŞTIRMASI

Tüm bu zorluklara rağmen, balonların tespiti üzerine kapsamlı bir literatür birikmiştir. Bu literatürlerde, özellikle Phillips vd., (2011) tarafından önerilen SADF (Sürekli Artan Dickey-Fuller) yöntem öne çıkmaktadır. Bu yöntem, daha sonra SADF temel alınarak, genelleştirilmiş Süper SADF ve BSADF test yöntemlerini içerecek şekilde genişletilmiştir. Cheung vd. (2015), Phillips ve arkadaşlarını geliştirdiği Dickey-Fuller (ADF) testinin genelleştirilmiş bir versiyonunu kullanarak Bitcoin fiyatları üzerinde baloncukların tespiti için bir araştırma yapmışlardır.

Latif vd., (2017), Bitcoine için KPSS, PP, ADF, DF-GLS, ERS birim kök testleri ile Rassal yürüyüş analizi yaparak balon fiyatlar ve manipülasyonlar tespit etmişlerdir. Bianchetti vd. (2018), balon tespiti için Johansen, Ledoit ve Sornette (JLS) tarafından geliştirilmiş olan Logaritmik Periyodik Güç Yasası (LPPL) modelini ve Phillips, Shi ve Yu (PSY) tarafından geliştirilen istatistiksel modeli birleştirmiştir. Bitcoin ve Ether üzerine yaptıkları çalışmada balon fiyat olduğunu göstermişleridir. Ceylan vd. (2018)'de çalışmalarında aynı yöntemi kullanarak Bitcoin ve Etherium için balon fiyat varlığı tespiti yapmışlardır.

GSADF testi yöntemi ile yapılan çalışmalar incelendiğinden Hepkorucu ve Genç (2019), Songur (2019), çoklu fiyat balonlarının tespiti için geliştirilen GSADF testi kullanarak kripto paraların spekülatif yapılarını göstererek balon fiyat dönemlerini tespit etmişlerdir. Koy ve Ersoy (2019), Güleç ve Aktaş (2019), çalışmalarında SADF ve GSADF yöntemini kullanmışlardır. Bouri vd. (2019), 14 kripto para birimi arasındaki çapraz kesit mutlak standart sapmaları (CSAD) kullanarak, kripto para getirileri arasındaki dağılım düzeyi ile genel kripto para piyasası getirisi arasındaki doğrusal olmayan ilişkiyi yöntemini kullanarak balon fiyat tespiti yapmışlardır. Geuder, Kinateder ve Wagner (2019), Bitcoin fiyatlarındaki tekrarlayan balon davranışlarına odaklanarak, 6 Aralık 2017'den sonra devam eden bir balon davranışı gözlemlemediklerini belirtmiştir.

Kırıkkaleli vd. (2020), Buğan (2021), çalışmalarında farklı kripto para birimleri için balon fiyat tespiti çalışmaları yapmışlardır. Kyriazis, Papadamou ve Corbet (2020), Bitcoin'in Haziran 2015'ten itibaren bir balon aşamasına girdiğini, diğer kripto paraların ise Eylül 2015'ten itibaren balon özellikleri sergilediğini ortaya koymuştur. Işıldak (2022), GSADF testi kullanarak pandemi dönemi içerisinde kripto para balon fiyat olduğu dönemleri belirlemiştir. Bezgin (2022), Bitcoin, Ethereum, Tether, USD Coin, BNB, Ripple, Binance USD, Cardano, Solana ve Dogecoin kripto paralarına GSADF testi uygulamıştır. Bitcoin için 46 balon fiyat tespit etmiştir. Yağcılar (2022), çalışmasında GSADF yaklaşımını kullanarak Bitcoin, Ethereum, Litecoin, Ripple, Stellar ve Dogecoin üzerine balon fiyat analizi yapmıştır. Chowdhury, Damianov ve Elsayed (2022), balonların ortaya çıkışı ve çöküşü sırasında piyasa bağımlılığı ve bulaşıcılık etkilerini incelemiş, Bitcoin'in piyasa düşüşlerinde net bir yayıcı rol oynadığını gözlemlemiştir. Altunöz (2023), EGARCH, TGARCH yöntemlerini kullanmışlardır. Frank ve Rudolf (2024), fiyat tahmini için SARIMA modeli ve finansal balon tespiti, görselleştirilmesi ve zaman damgalaması için LPPLS modeli gibi kanıtlanmış modelleme tekniklerinden faydalanmıştır.

MATERYAL VE METOT

Balon tahmininde yaygın bir yöntem olan teknik analiz, geçmiş fiyat hareketlerini ve piyasa davranışlarını inceleyerek olası balonları tespit etmeye çalışır. Örneğin, ani ve keskin bir fiyat artışı, yani parabolik bir yükseliş, yaklaşan bir balonun habercisi olabilir. Diğer bir yöntem olan temel analiz ise piyasanın finansal istikrarını ve performansını değerlendirir. Bu, spekülasyondan ziyade gerçek ekonomik ilerlemeye dayalı olmayan, aşırı değerlenmiş varlıkların veya piyasaların belirlenmesine yardımcı olur.

Bu çalışmada, kripto para balon fiyat tespiti için Z-Score Tabanlı Aykırı Değer Analizi yöntemi kullanılmıştır. Bu yöntem istatistiksel veri analizlerinde bir veri noktasının ortalamadan ne kadar sapma gösterdiğini anlamak

için kullanılan standart bir yöntemdir. Bu özelliğinden dolayı bir veri seti içerisindeki aykırı değerlerin tespit edilmesinde oldukça etkili bir araç olarak kullanılmaktadır. Yönteme ait adımlar aşağıda verilmiştir.

1. Adım: Fiyatlarda oluşan günlük yüzdesel değişimin hesaplanması

$$Fiyat\ Değişimi(t) = \frac{Fiyat(t) - Fiyat(t-1)}{Fiyat(t-1)} \quad (1)$$

2. Adım: Ortalama ve standart sapmanın hesaplanması

$$\varphi = \frac{1}{n}\sum_{i=1}^{n} Fiyat\ Değişimi(i) \quad (2)$$

$$\sigma = \frac{1}{n}\sum_{i=1}^{n}(Fiyat\ Değişimi(i) - \varphi)^2 \quad (3)$$

3. Adım: Eşik değeri hesaplama

$$Eşik\ Değeri = \varphi + 3\sigma \quad (4)$$

4. Adım: Balon tespitinin yapılması

$$Balon(t) - Fiyat\ Değişimi(t) > Eşik\ Değeri \quad (5)$$

Veri seti oluşturulurken Coingecko tarafından sunulan verilere göre market büyüklüğü en büyük olan Dogecoin, Shiba Inu, Pepe, Dogwifhat, Bonk ve Floki ait veriler kullanılmıştır. Tablo 3'de veri setine ait bilgiler verilmiştir.

Tablo 3. Veri setine ait bilgiler

Meme Coin	**Veri Adeti**	**Tarih Aralığı**
Dogecoin	3972	27.12.2013 - 15.11.2024
Shiba Inu	1280	16.05.2021 - 15.11.2024
Pepe	576	20.04.2023 - 15.11.2024
Dogwifhat	331	21.12.2023 - 15.11.2024
Bonk	682	04.01.2023 - 15.11.2024
Floki	983	09.03.2022 – 15.11.2024

Yapılan çalışmadan elde edilen sonuçlar aşağıda verilmiştir.

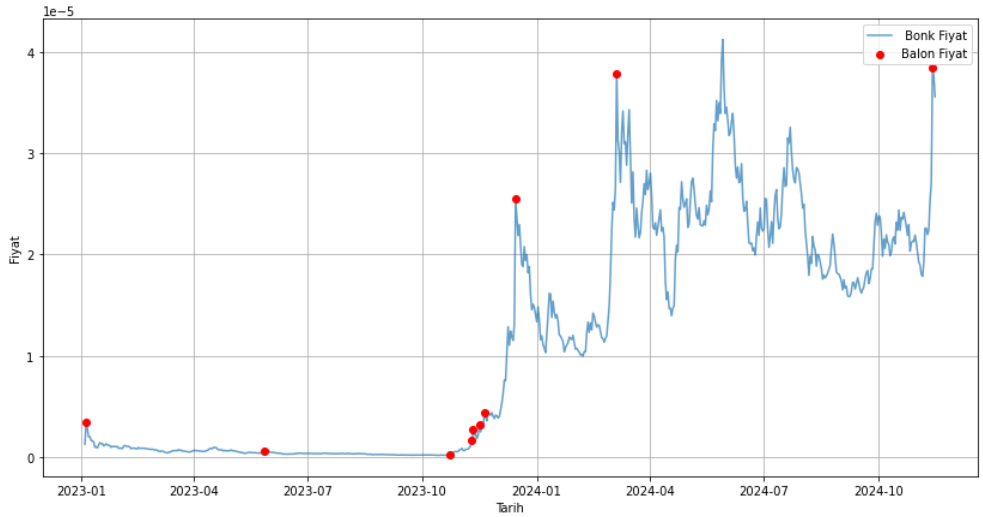

Şekil 3. Bonk Fiyatı ve Balon Fiyat Oluşumu Dönemleri

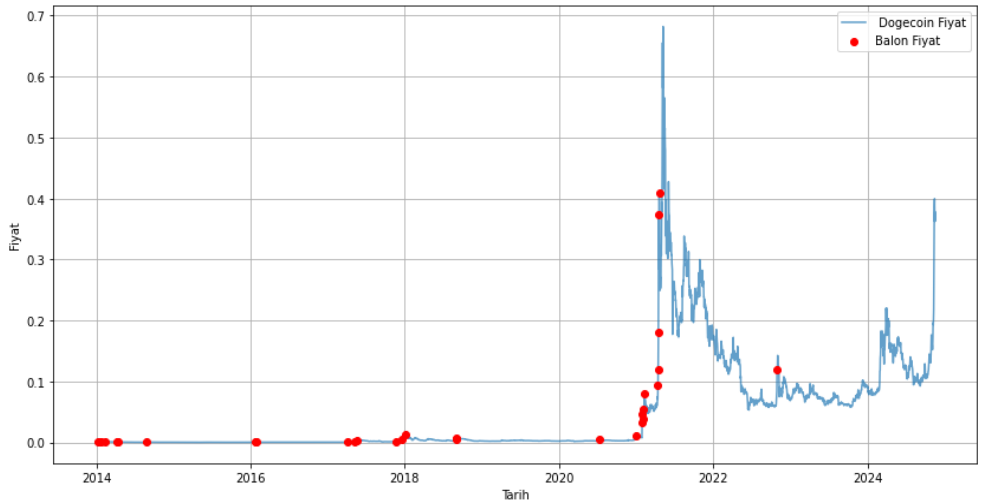

Şekil 4. Dogecoin Fiyatı ve Balon Fiyat Oluşumu Dönemleri

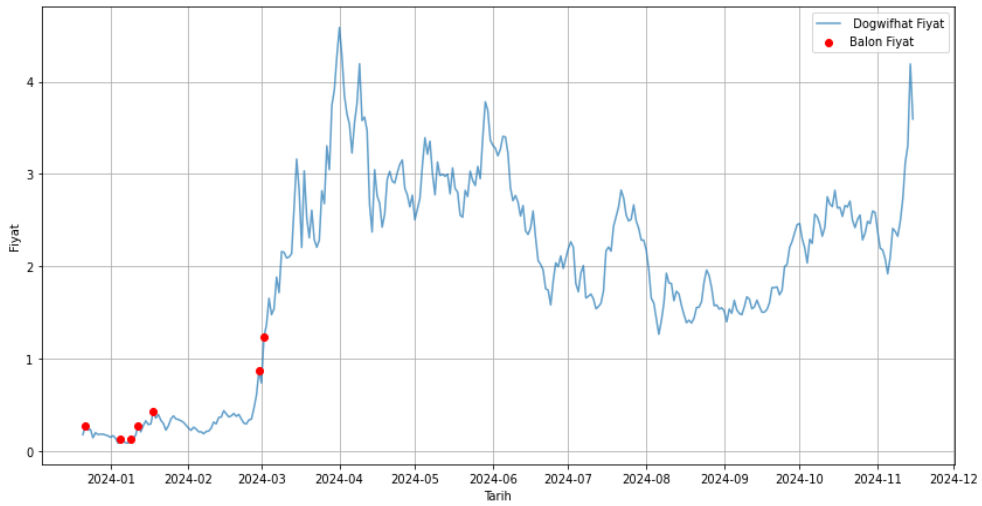

Şekil 5. Dogwifhat Fiyatı ve Balon Fiyat Oluşumu Dönemleri

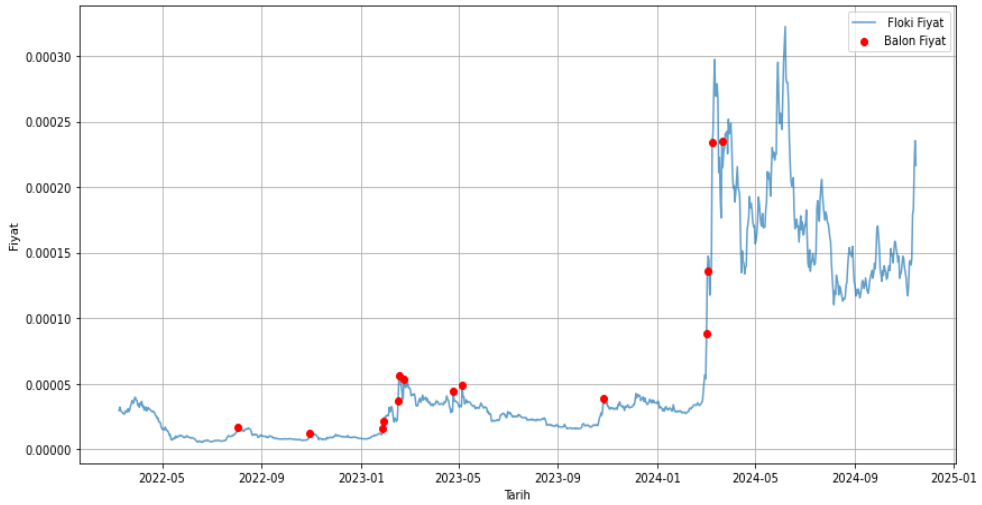

Şekil 6. Floki Fiyatı ve Balon Fiyat Oluşumu Dönemleri



Şekil 7. Pepe Fiyatı ve Balon Fiyat Oluşumu Dönemleri



Şekil 8. Shiba Fiyatı ve Balon Fiyat Oluşumu Dönemleri

SONUÇ

Kripto paralar, finansal sistemlerde önemli bir değişimin öncüsü olarak kabul edilmektedir. Bitcoin'in temellerini attığı blok zincir teknolojisi, diğer kripto paraların da katılımıyla daha geniş bir alana yayılmıştır. Günümüzde hem bireysel hem kurumsal yatırımcıların ilgi odağı haline gelen kripto paralar, merkeziyetsizlik ilkesi ve yüksek güvenlik sunan yapısıyla finans dünyasında yeni bir çağın habercisidir.

Kripto para birimleri yatırımcılar için yeni fırsatlar sunduğu kadar yüksek riskler de taşımaktadır. Özellikle meme coinler eğlence ve spekülasyona dayalı olarak ortaya çıktığından dolayı sosyal medya etkisiyle büyük fiyat dalgalanmaları yaşayabilmektedir. Çoğu çalışma, bu coinlerin topluluk etkisi ve sosyal medya viralliğiyle değer kazandığını, ancak uzun vadeli değer tutma potansiyellerinin sınırlı olduğunu vurgulamaktadır. Çalışma sonuçları incelendiğinde balon fiyat dönemleri en fazla Dogecoin üzerinde olmuştur. Bunun genel sebebi ise memecoinlerin fiyatlandırılmasında etkin olan sosyal medya mesajlarıdır. Elon Musk tarafından Dogecoin ile yapılan paylaşımlar coin fiyatı üzerinde kısa zaman içerisinde yüksek değişimlere yol açmıştır.

Meme coinlerin yüksek volatilitesi ve sosyal medya manipülasyonuna açık olması, bu varlıkları spekülatif yatırımlar arasında sınıflandırmaktadır. Bu nedenle, yatırımcıların risk toleransına göre stratejik bir portföy oluşturması ve meme coinleri kısa vadeli yatırım aracı olarak değerlendirmesi daha doğru olmaktadır.

KAYNAKLAR

Altunöz, U. (2023). Kripto Paraların Volatilite Dinamiklerinin ve Spekülatif Balon Varlığının Analizi: Bitcoin, Ethereum ve Ripple Örneği. Istanbul Journal of Economics 73, 2023/1, s. 615-643

Başbuğ, B. & Lokmanoğlu, E. (2021). İnternet Mem Efsanesinden Kripto Paraya Evriliş: Postmodern Dönemde Popüler Bir Meme Coin Örneği Olarak Dogecoin, International Social Mentality and Researcher Thinkers Journal. (Issn:2630-631X) 7(52): 3131-3139.

Bianchetti, M., Ricci, C., ve Scaringi, M., (2018). Are Cryptocurrencies Real Financial Bubbles? Evidence from Quantitative Analyses. A version of this paper was published in Risk, http://dx.doi.org/10.2139/ssrn.3092427

Bouri, E., Gupta, R. ve Roubaud, D. (2019). Herding Behaviourin Cryptocurrencies. Finance Research Letter, 29, 216-221.

Buğan, M. F. (2021). Bitcoin ve altcoin kripto para piyasalarında finansal balonlar. Akademik Araştırmalar ve Çalışmalar Dergisi (AKAD), 13(24), 165-180.

Bystrom, H. &Krygier, D. (2018). What drives bitcoin volatility?, The Knut Wicksell Centre for Financial Studies, Working Paper, 2018:3, 1-26.

Ceylan F. & Ekinci R. & Tüzün O. & Kahyaoğlu H. (2018), Kripto Para Piyasasında Balonların Tespiti: Bitcoin ve Ethereum Örneği, BMIJ, (2018), 6(3): 263-274 doi: http://dx.doi.org/10.15295/bmij.v6i3.355

Cheung, A.W.K., Roca, E., Su, J.J., (2015). Crypto-currency bubbles: an application of the Phillips, Shi and Yu (2013) methodology on mt. gox bitcoin prices. Appl. Econ. 47 (23), 2348–2358.

Chowdhury, S.R., Damianov, D.S. and Elsayed, A.H., 2022. Bubbles and crashes in cryptocurrencies: Interdependence, contagion, or asset rotation? Finance Research Letters, 46, 102494. https://doi.org/10.1016/j.frl.2021.102494.

Dyhrberg, A. H. (2016). Hedging capabilities of Bitcoin. Is it the virtual gold?. Finance Research Letters, 16, 139-14.

Frank, P., ve Rudolf, M. (2024). Is the Metaverse Dead? Insights from Financial Bubble Analysis. FinTech 2024, 3, 302–323. https://doi.org/10.3390/fintech3020017

Geuder, J., Kinateder, H. and Wagner, N.F., 2019. Cryptocurrencies as financial bubbles: The case of Bitcoin. Finance Research Letters, 31. https://doi.org/10.1016/j.frl.2018.11.011

Güleç, T.C. ve aktaş, H. (2019). Kripto Para Piyasasında Spekülatif Fiyat Balonlarının Analizi. Muhasebe ve Finansman Dergisi - Ekim/2019 (84): 149-164

Harsh, J. ve Ruchi, S. (2023). An Overview of Blockchain Technology: Architecture, Consensus, and Future Trends. A Journal for Engineering

Hepkorucu, A., & Genç, S. (2019). Kripto para değerleri için spekülatif fiyat balonlarının test edilmesi: Bitcoin üzerine bir uygulama. Veri Bilimi, 2(1), 44-50.

Işıldak. M.S. (2022). Kripto para piyasasında spekülatif baloncuklar: Bitcoinden kanıtlar. Business, Economics and Management Research Journal 2022 5(3) 209-219

Kırıkkaleli, D., Cağlar, E., & Onyibor, K. (2020). Crypto-currency: Empirical evidence from GSADF and wavelet coherence techniques. Accounting, 6(2), 199-208.

Kyriaeis, N., Papadamou, S. and Corbet, S., (2020). A systematic review of the bubble Dynamics of cryptocurrency prices. Research in International Business and Finance, 54, 101254.https://doi.org/10.1016/j.ribaf.2020.101254.

Latif, S. R., Mohd, M. A., Amin, M. N. M. & Mohamad, A. I. (2017). Testing the weak form efficient market in cyrptocurrency, Journal of Engineering and Applied Science, 12 (9): 2285-2288

Lupu, R. Călın, A.C., Lupu, I., Iancu1, L.A., Croıcu, A.E. (2024). Bubble Or Not? A Tıme Serıes Classıfıcatıon Problem Using Machine Learning, Romanian Journal of Economic Forecasting – 27(1) 2024 5-21

Mete, S., Ayben, K., ve Hicabi, E. (2019). Kriptoparalarda Fiyat Balonu İncelemesi. Journal of BRSA Banking and Financial Markets. Volume: 13, Number: 1,

.Müge, S.M. (2022). Kripto Paralarda Finansal Balon Varlığının Araştırılması. Uluslararası Anadolu Sosyal Bilimler Dergisi. Cilt: 6 Sayı: 4 Yıl: 2022 1414-1431

Songur, M. (2019). Bitcoin piyasasında balonlar: Genelleştirilmiş Eküs ADF testi. Anemon Muş Alparslan Üniversitesi Sosyal Bilimler Dergisi, 7(6), 187-192.

Vladyslav, K. ve Ivan, P. Y. (2023). Pump It: Twitter Sentiment Analysis for Cryptocurrency Price Prediction. Risks 2023, 11, 159. https://doi.org/10.3390/risks11090159 1-14

Yağcılar, G.G. (2022). Kripto Para Piyasasında Fiyat Balonları ve Yatırımcı İlgisinin Etkisi. MAKÜ-Uyg. Bil. Derg., 6(1), 108-131, 2022

➢ *ORAL PRESENTATION*

Endüstri 5.0 uyumlu teknoloji seçimi için çok kriterli karar verme yaklaşımı uygulamaları

Fatma Sümeyye Kenar[1*] (*ORCID: https://orcid.org/ 0009-0002-3501-1917*), Yusuf Fedai[2] (*ORCID: https://orcid.org/0000-0003-4546-8830*

[*1]Osmaniye Korkut Ata Üniversitesi, Endüstri Mühendisliği Bölümü, Osmaniye, Türkiye
[2]Osmaniye Korkut Ata Üniversitesi, Endüstri Mühendisliği Bölümü, Osmaniye, Türkiye

*Sorumlu yazar e-posta: sumeyye.kenar@gmail.com

Özet
Sanayi devrimleriyle birlikte üretim anlayışı sürekli olarak dönüşmüş, Endüstri 5.0 ile bu dönüşüm insan-merkezli ve sürdürülebilirlik odaklı bir boyuta taşınmıştır. Endüstri 5.0, insan zekâsı ve makinelerin iş birliğini temel alarak yalnızca teknolojik ilerlemeyi değil, aynı zamanda etik, çevresel ve toplumsal değerleri de üretim süreçlerine entegre etmeyi amaçlamaktadır. Bu yeni üretim paradigmasında, doğru teknoloji seçimi işletmeler açısından stratejik bir karar problemi hâline gelmiş ve bu sürecin yönetiminde Çok Kriterli Karar Verme (ÇKKV) yöntemlerinin önemi artmıştır. AHP, TOPSIS, VIKOR gibi yöntemlerin yanı sıra, belirsizlik ortamlarında daha esnek çözümler sunan Bulanık Mantık tabanlı yaklaşımlar da yaygınlaşmaktadır. Ancak mevcut literatürde insan odaklı, çok boyutlu ve sektörden bağımsız bir değerlendirme çerçevesi eksikliği dikkat çekmektedir. Bu çalışmanın amacı, Endüstri 5.0 uyumlu teknoloji seçimi süreçlerinde kullanılan ÇKKV yöntemlerini sistematik bir şekilde analiz ederek, insan refahı, sürdürülebilirlik ve etik değerlere duyarlı bütüncül bir karar modeli geliştirmektir.
Anahtar Kelimeler: Endüstri 5.0, Çok Kriterli karar Verme (ÇKKV), TOPSİS Yöntemi, Teknoloji Seçimi

Applications of Multi-Criteria Decision-Making Approaches for Industry 5.0-Compatible Technology Selection

Abstract
With the advent of industrial revolutions, production paradigms have continuously evolved, culminating in Industry 5.0, which introduces a human-centric and sustainability-oriented dimension to manufacturing. Industry 5.0 emphasizes the collaboration between human intelligence and machines, aiming not only for technological advancement but also for the integration of ethical, environmental, and societal values into production processes. Within this new paradigm, the selection of appropriate technologies has become a strategic decision-making problem for organisations, increasing the significance of Multi-Criteria Decision-Making (MCDM) methods. In addition to established techniques such as AHP, TOPSIS, and VIKOR, fuzzy logic-based approaches, which offer more flexible solutions under uncertainty, have gained prominence. However, the current literature lacks a human-centered, multidimensional, and sector-independent evaluation framework. The primary objective of this study is to systematically analyse MCDM methods employed in Industry 5.0-compatible technology selection processes and to develop a comprehensive decision model that is sensitive to human well-being, sustainability, and ethical considerations.
Keywords: Industry 5.0, Multi-Criteria Decision Making (MCDM), TOPSIS method, Technology Selection

GİRİŞ

Sanayi devrimleri, tarihsel süreçte üretim aşamalarının geliştirilmesini sağlayan önemli süreçlerdir. Birinci sanayi devrimi 18. Yüzyılın başlarından 19. Yüzyılın ortalarına kadar sürmüştür. Bu dönemde tarım toplumundan sanayi toplumuna geçiş sağlanmış ve bu geçişle teknolojik buluşlar üretim yöntemlerini değiştirmiştir. Örneğin eliyle dokuma yapan atölyeler yerine büyük tekstil fabrikaları kurulmuştur. İnsan gücü ile üretimden makine gücü ile üretim yapılmaya başlanmıştır. Birinci sanayi devrimi verimliliğin, üretkenliğin ve yeni iş gücü ihtiyacının artmasını sağlamıştır. İkinci sanayi devrimi 19. yüzyılın sonları ile 20. yüzyılın başlarında Birinci Sanayi Devriminin sağladığı temelin üstüne eklenen gelişmedir. İkinci Sanayi Devriminde elektrik, kimya, otomotiv ve telekomünikasyon vb. yeni alanlar ortaya çıkmıştır. Ayrıca Henry Ford'un seri montaj hattını kurması üretimde köklü bir değişikliğe sebep olmuştur. Seri üretim sayesinde maliyetler düşmüş ve üretim hızı artmıştır. 20. Yüzyılın sonlarında Üçüncü Sanayi devrimi yani dijital devrim doğmuştur. Bu dönemde üretimde esneklik artmış, dijitalleşme sayesinde müşterilere daha hızlı dönüşler sağlanmaya

başlanmıştır. Üçüncü Sanayi Devrimi, dijital iletişim teknolojilerinin, yenilenebilir enerji kaynaklarının ve otomasyon sistemlerinin bir araya gelmesiyle şekillenmiştir (Sezgin, 2018). Dördüncü Sanayi Devrimi, üretim aşamalarını geliştirmek için dijital teknolojileri üretim sürecine dahil etmiştir. Sadece sanayi üretimini değil, eğitim, sağlık, ulaşım, hizmetler, tarım, enerji gibi tüm sektörlerdeki dijital dönüşümü kapsar. Bu dönemde makineler sadece fiziksel üretim yapmaz aynı zamanda kendi aralarında veriler toplar ve analiz yaparlar. Bu sayede karar verme süreçlerinde kolaylık sağlanmış olur. Endüstri 4.0 ise Dördüncü Sanayi Devrimi'nin bir parçasıdır. Fakat sadece üretim ve sanayi sektörünü kapsar. Endüstri 4.0 temel olarak akıllı fabrikalar, otomasyon, IoT, siber-fiziksel sistemler, yapay zekâ, robotik ve büyük veri gibi teknolojilerin üretim süreçlerine entegrasyonunu ifade eder. "Endüstri 4.0 kavramı, dördüncü sanayi devriminin üretim sistemleri üzerindeki yansımasını tanımlarken; dördüncü sanayi devrimi, bu teknolojik dönüşümün toplumun tüm alanlarına etkisini ifade eder" (Klaus, 2016). Endüstri 5.0 ise insan zekâsı ile makinelerin iş birliğini amaçlar. Endüstri 5.0, Endüstri 4.0 kadar oturmuş ve köklü bir kavram değildir, gelişmekte olan, tartışılan ve hala şekillenen bir kavramdır. 2020 yılından sonra akademik alanda tartışılmaya başlanmıştır. Bazı makalelerde ve Avrupa Komisyonu yayınlarında Endüstri 5.0, geleceğin üretim anlayışı olarak da tanımlanmaktadır. Üretimin çevreye verdiği zararı önleme ve azaltmayı, kaynakları daha verimli kullanmayı hedefler. Bu bağlamda Endüstri 5.0 çevresel sorumluluğu teşvik ederek daha duyarlı bir sanayi yaklaşımı amaçlar. Endüstri 4.0 kavramında maliyet düşürme ve dijital teknolojilere odaklanılırken Endüstri 5.0'da ise etik, sürdürülebilirlik ve insan refahı gibi değerlere öncelik verilmektedir. Endüstri 4.0'ın otomasyon ve dijitalleşme odaklı yapısının aksine, Endüstri 5.0 üretim süreçlerinde insanın yaratıcılığını ve değerlerini merkeze alarak daha sosyal ve sürdürülebilir bir yaklaşım sunmaktadır (Nahavandi, 2019).

Endüstri 5.0 kavramı, teknoloji ve insan etkileşiminin dengelendiği yeni bir üretim paradigması olarak karşımıza çıkmaktadır. Bu dönemde yalnızca üretim süreçlerinin otomasyonu değil, aynı zamanda insan yaratıcılığı ve duygusal zekâsının da üretim sistemlerine entegre edilmesi hedeflenmektedir. Özellikle yapay zekâ, nesnelerin interneti (IoT), siber-fiziksel sistemler, bulut bilişim gibi teknolojilerin olgunlaşmasıyla birlikte, bu teknolojilerin insan merkezli biçimde uyarlanması bir zorunluluk hâline gelmiştir (Nahavandi, 2019). Endüstri 5.0, kişiselleştirilmiş üretim taleplerine cevap vermeyi, sürdürülebilirliği artırmayı ve iş gücünün sadece fiziksel değil zihinsel kapasitesini de üretime dahil etmeyi amaçlamaktadır (Xu et al., 2021). Bu bağlamda, üretim sistemlerinde kullanılan teknolojilerin yalnızca performans kriterlerine göre değil, aynı zamanda etik, sosyal ve çevresel ölçütlerle de değerlendirilmesi gerekmektedir (Romero et al., 2015).

Bu yeni dönemde, hangi teknolojilerin seçileceği sorusu, işletmeler için stratejik bir karar problemi olarak ön plana çıkmaktadır. Teknoloji seçimi süreci; maliyet, enerji verimliliği, çevresel etki, entegrasyon kolaylığı, sürdürülebilirlik ve insan faktörü gibi çok sayıda ve çoğu zaman birbiriyle çelişen kriteri aynı anda dikkate almayı gerektirir. Geleneksel karar verme teknikleri bu tür çok boyutlu karar yapılarında yetersiz kalabilmektedir. Bu nedenle Çok Kriterli Karar Verme (ÇKKV) yaklaşımları, teknoloji seçimi gibi karmaşık problemlerde sıklıkla tercih edilen yöntemler arasında yer almaktadır (Saaty, 2008). Bu yöntemler sayesinde karar vericiler, çok sayıda alternatif arasından en uygun seçeneği bilimsel bir temele dayandırarak belirleyebilmektedir (Gupta et al., 2022).

Özellikle Analitik Hiyerarşi Süreci (AHP), Analitik Ağ Süreci (ANP), TOPSIS, VIKOR, ELECTRE ve PROMETHEE gibi yöntemler, karar verme sürecini yapısal hâle getirerek öznel yargıların sayısallaştırılmasına imkân tanımaktadır (Büyüközkan & Göçer, 2018). Bu yöntemlerin bazıları karar verici tercihlerine ağırlık verirken, bazıları ideal çözüme yakınlığı esas alır. Bu farklı yaklaşımlar, karar probleminin doğasına göre avantaj ve dezavantajlar içermektedir. Literatürde, bu yöntemlerin teknoloji seçimi, tedarikçi seçimi, yatırım analizi ve risk değerlendirmesi gibi pek çok alanda başarıyla uygulandığı görülmektedir (Pamučar & Ćirović, 2015).

Ancak yapılan çalışmalarda bazı sınırlılıklar göze çarpmaktadır. Birçok araştırma, teknoloji seçimi süreçlerini yalnızca maliyet ya da teknik verimlilik gibi ölçülebilir kriterlerle değerlendirmekte, sosyal etkiler ve insan merkezli değerler arka planda kalmaktadır. Endüstri 5.0'ın insan odaklı yapısı ise bu yaklaşımı sorgulanabilir hâle getirmiştir. Zira yeni dönemde teknolojilerin sadece ekonomik açıdan değil, insan refahına olan katkısı ve toplumsal uyumu açısından da değerlendirilmesi gerektiği vurgulanmaktadır (Giannetti et al., 2012). Bununla birlikte, mevcut çalışmaların büyük bölümü belirli sektörlere odaklanmakta ve genel geçer bir çerçeve sunmaktan uzak kalmaktadır (Braglia & Petroni, 2000).

Son yıllarda bu boşluğu doldurmaya yönelik bazı bütüncül model önerileri geliştirilmiş olsa da, bu modellerin çoğu ya uygulama zorlukları taşımakta ya da belirsizlik ve bulanıklık gibi unsurları yeterince hesaba katmamaktadır (Chu et al., 2020). Belirsizlik ortamlarında karar vericilerin yargılarındaki bulanıklığı ele almak için Bulanık Mantık tabanlı ÇKKV yöntemleri önerilmektedir (Cheng & Hwang, 1992). Bulanık AHP, Bulanık

TOPSIS ve Bulanık VIKOR gibi yaklaşımlar, karar sürecini daha esnek ve gerçekçi hâle getirerek Endüstri 5.0 gibi dinamik sistemler için daha uygun modeller sunmaktadır (Fidanboy, 2022). Ayrıca son dönemde gri teori, DEMATEL, SWARA ve BWM gibi yöntemlerin de teknoloji seçimi problemlerinde kullanıldığı görülmektedir (Rezaei, 2015).

Bu çalışmanın amacı, Endüstri 5.0 uyumlu teknoloji seçiminde ÇKKV yaklaşımlarının nasıl uygulandığını sistematik bir şekilde analiz etmek, mevcut yaklaşımların güçlü ve zayıf yönlerini değerlendirmek ve daha sürdürülebilir, insan odaklı ve yenilikçi bir karar modeli önermektir (Gölcük & Baykasoğlu, 2016). Ayrıca teknoloji seçimi sürecinde yalnızca teknik değil; çevresel, etik, toplumsal ve psikolojik faktörleri de içeren çok boyutlu bir değerlendirme çerçevesi sunulması hedeflenmektedir. Bu bağlamda çalışma, yalnızca akademik literatüre katkı sağlamayı değil, aynı zamanda işletmelere pratik yol gösterici bir model önermeyi amaçlamaktadır.

MATERYAL VE METOT

1. Çok Kriterli Karar Verme (ÇKKV) Yaklaşımının Temelleri

Çok Kriterli Karar Verme (ÇKKV), karar vericilerin birden fazla ölçütü dikkate alarak en uygun alternatifi belirlemesine yardımcı olan sistematik bir karar verme yaklasımıdır. Karar problemleri genellikle karmaşık ve çok boyutludur. Bu nedenle, alternatiflerin sadece tek bir kritere göre değerlendirilmesi yetersiz kalmaktadır. ÇKKV yaklasımı, bu problemi çözmek için matematiksel ve mantıksal modeller kullanarak karar vericinin tercihlerini sayısal olarak ifade etmesini sağlar.

ÇKKV karar problemleri genellikle şu şekilde tanımlanır: çok sayıda alternatif (A1, A2, ..., An) ve bunlara ait birden fazla kriter (C1, C2, ..., Cm) vardır. Her alternatif, her kritere göre belirli bir performans gösterir ve bu performanslar karar matrisi ile ifade edilir. Bu matrise dayalı olarak alternatiflerin öncelik sıralaması oluşturulur ya da en iyi alternatif seçilir.

2. ÇKKV'nin Endüstri 5.0 Bağlamındaki Rolü

Endüstri 5.0, insan-makine etkileşiminin merkezde olduğu, yapay zekâ, nesnelerin interneti ve otomasyon gibi ileri teknolojilerle desteklenen yeni bir sanayi devrimidir. Bu dönemde, karar verme süreçlerinin daha esnek, duyarlı ve şeffaf olması beklenmektedir. Endüstri 5.0 uyumlu teknoloji seçiminde ÇKKV yöntemlerinin kullanılması, karmaşık yapıdaki çevresel, ekonomik, sosyal ve teknik kriterlerin birlikte ele alınmasına imkân tanır.

ÇKKV, teknolojik alternatiflerin sadece performansını değil, aynı zamanda çevresel sürdürülebilirlik, enerji tüketimi, veri güvenliği gibi yeni çağ kriterlerini de karar sürecine entegre ederek daha stratejik ve uzun vadeli seçimler yapılmasını sağlar.

3. ÇKKV Yöntemlerinin Sınıflandırılması

ÇKKV yöntemleri genel olarak klasik, bulanık mantık temelli ve hibrid yöntemler olmak üzere sınıflandırılabilir:

3.1. Klasik Yöntemler Bu yöntemler, karar vericilerin tercihlerini kesin değerlerle ifade ettikleri yöntemlerdir. AHP, ANP, TOPSIS, VIKOR, ELECTRE ve MOORA bu sınıfa girmektedir.

3.2. Bulanık Mantık Temelli Yöntemler Gerçek dünyada karar vericiler tüm tercihlerini net şekilde belirtmekte zorlanabilirler. Bulanık mantık, belirsizliklerin üssesinden gelmek için kullanılır. Bulanık AHP, Bulanık TOPSIS gibi yöntemler bu kategoride yer alır.

3.3. Entropi ve Diğer Hibrid Yöntemler Bu yöntemler, iki veya daha fazla ÇKKV yönteminin birlikte kullanıldığı ya da bilgi kuramına dayalı yöntemlerle ağırlık hesaplaması yapıldığı yaklaşımlardır. Entropi-AHP, AHP-TOPSIS gibi kombinasyonlar sık kullanılır.

4. Yaygın Kullanılan ÇKKV Yöntemlerinin Açıklaması

4.1. AHP (Analitik Hiyerarşi Süreci) AHP, karmaşık karar problemlerini hiyerarşik yapıya dönüştürerek çözen bir yöntemdir. Karar verici, ölçütleri ve alternatifleri çiftli karşılaştırma yoluyla değerlendirir. Sonuçta tutarlılık oranı hesaplanarak karar verme sürecinin ne kadar sağlam olduğu belirlenir.

4.2. ANP (Analitik Ağ Süreci) AHP'nin genelleştirilmiş hali olan ANP, ölçütler arasındaki bağlılıkları ve geribildirimleri dikkate alır. Bu sayede daha gerçekçi modeller oluşturulabilir.

4.3. TOPSIS TOPSIS, her alternatifin ideal ve anti-ideal çözüme uzaklığını hesaplar. En iyi alternatif, pozitif ideale en yakın, negatif ideale en uzak olan alternatiftir.

4.4. VIKOR TOPSIS'e benzer çalışır fakat uzlaşma çözümü kavramına dayalı olarak hem bireysel hem grup kararları için uygundur.

4.5. MOORA MOORA yöntemi, normalize edilmiş karar matrisine dayalı olarak pozitif ve negatif etkili kriterleri fark hesaplarıyla analiz eder.

4.6. ELECTRE Bu yöntem, alternatifler arasında baskınlık (outranking) ilişkisi kurarak karar verir. Kriter ağırlıklarına ve eşik değerlere dayalı çoklu filtreleme uygular.

5. Endüstri 5.0 Uyumlu Teknoloji Seçiminde ÇKKV'nin Avantajları

Endüstri 5.0 ortamında teknoloji seçimi, yalnızca teknik verimlilikle değil, aynı zamanda insan odaklılık, çevresel etki, veri etik ilkeleri gibi çok çeşitli kriterleri de barındırır. ÇKKV bu gibi durumlarda tüm kriterleri entegre ederek, çok boyutlu karar verme yeteneği sunar. Ayrıca şu avantajları sağlar:

- Alternatiflerin nesnel ve sistematik değerlendirilmesi,
- Karar vericilerin subjektif görüşlerinin modele dahil edilebilmesi,
- Karar alma sürecinin şeffaf ve izlenebilir olması,
- Belirsizlik durumlarında bile karar verebilme yeteneği.

6. ÇKKV Yöntemlerinin Sınırlılıkları ve Zorlukları

Her ne kadar ÇKKV yöntemleri karar verme sürecini iyileştirse de, bazı sınırlılıklar taşır:

- Kriter ve alternatif sayısı arttıkça hesaplama karmaşıklığı artar,
- Karar verici tutarsız yargılar verebilir,
- Ağırlık belirleme süreci subjektif olabilir,
- Bazı yöntemler çok fazla veriye duyarlıdır.

Bu nedenlerle, uygulamada yöntem seçimi yapılırken problemin yapısına ve karar vericilerin bilgi düzeyine uygun yöntem tercih edilmelidir.

BULGULAR ve TARTIŞMA

TOPSIS Yöntemi ile Teknoloji Seçimi

Bu bölümde, Endüstri 5.0 uyumlu teknolojilerin seçimi için TOPSIS yöntemi adım adım uygulanmıştır. Karar verme süreci, dört alternatif ve beş kriter üzerinden değerlendirilmiştir.

1. Alternatifler ve Kriterler

Alternatif Teknolojiler:

- A1: İşbirlikçi robotlar
- A2: Yapay zeka destekli kestirimci bakım sistemleri
- A3: Giyilebilir teknolojiler
- A4: Siber-fiziksel sistemler

Kriter karar tipi seçilirken kriterlerin fayda ve maliyet açısından düzenlenmesi gerekir. Tablo 4'te görüldüğü gibi seçilen kriterlerin 4 tanesi fayda yönlü iken (K1-K3, K4 ve K5) sadece K2 maliyet yönlüdür.

Tablo 1. Kriterler ve Kriter tipleri

KRİTER KODU	AÇIKLAMA	TİP
K1	Endüstri 5.0 Uyum Seviyesi	Fayda (+)
K2	Uygulama Maliyeti	Maliyet (-)
K3	Adaptasyon Kolaylığı	Fayda (+)
K4	Enerji Verimliliği	Fayda (+)
K5	Verimlilik	Fayda (+)

Uzman değerlendirmeleri ışığında Tablo 2'de Karar belirtilmiştir.

Tablo 2. Karar Matrisi

ALTERNATİF	K1	K2	K3	K4	K5
A1	7	6	8	7	8
A2	9	5	9	8	9
A3	6	8	7	6	6
A4	8	7	8	9	7

Tablo 3'te Entropi Yöntemi ile Ağırlıkların Hesaplanması belirtilmiştir. Verilere göre elde edilen kriter ağırlıkları görülmektedir.

Tablo 3. Ağırlıkların Hesaplanması

KRİTER	AĞIRLIK
K1 UYUM SEVİYESİ	0.2135
K2 MALİYET	0.2848
K3 ADAPTASYON	0.0748
K4 ENERJİ VERİMLİLİĞİ	0.2135
K5 VERİMLİLİK	0.2135

Elde edilen değerlerin normalizasyonu Tablo 4'te gösterilmektedir.

Tablo 4. Normalize Edilmiş Karar Matrisi

ALTERNATİF	K1	K2	K3	K4	K5
A1	0.518	0.487	0.528	0.476	0.571
A2	0.666	0.406	0.594	0.544	0.643
A3	0.444	0.650	0.462	0.408	0.429
A4	0.592	0.569	0.528	0.612	0.500

Pozitif ve Negatif İdeal Değerler

Pozitif ideal (en iyi değerler): Fayda kriterlerinde, maksimum, maliyet kriterinde minimum değerler alınarak tablo 5 oluşturulmuştur.

Tablo 5. Pozitif ve Negatif ideal Değerler

KRİTER	A^+ (İDEAL)	A^- (NEGATİF İDEAL)
K1	0.1267	0.0845
K2	0.1080	0.1727
K3	0.0419	0.0326
K4	0.1267	0.0845
K5	0.1267	0.0845

Tablo 6'da Uzaklıkların Hesaplanması verilmiştir.

Tablo 6. Uzaklıkların hesaplanması

ALTERNATİF	S+S^+	S−S^-
A1	0.0477	0.0555
A2	0.0141	0.0930
A3	0.0981	0.0000
A4	0.0536	0.0571

Tablo 7'de Yakınlık Katsayıları verilmiştir.

Tablo 7. Yakınlık Katsayıları

ALTERNATİF	Cİ DEĞERİ	SIRALAMA
A2	**0.8685**	**1**
A1	**0.5378**	**2**
A4	**0.5157**	**3**
A3	**0.0000**	**4**

TOPSIS yöntemiyle yapılan analiz sonucunda en uygun teknoloji seçeneği "A2 – Yapay Zeka Destekli Kestirimci Bakım Sistemleri" olarak belirlenmiştir. Bu teknoloji hem düşük maliyetli hem de yüksek verimlilik ve uyum özellikleri ile en yüksek Ci değerine ulaşmıştır.

SONUÇ

Bu çalışmada, Endüstri 5.0 uyumlu teknoloji seçim süreci, Çok Kriterli Karar Verme (ÇKKV) yaklaşımlarından TOPSIS yöntemi kullanılarak sistematik biçimde ele alınmıştır. Literatürde öne çıkan eksikliklerden biri olan, insan merkezli ve çok boyutlu değerlendirme çerçevesi ihtiyacına cevap vermek üzere; yalnızca teknik ve ekonomik kriterler değil, aynı zamanda çevresel sürdürülebilirlik, çalışan etkileşimi ve uyum seviyesi gibi Endüstri 5.0'ın ruhunu yansıtan faktörler de analiz sürecine dahil edilmiştir.

TOPSIS yöntemi ile yürütülen uygulama aşamasında; dört farklı teknoloji alternatifi (işbirlikçi robotlar, yapay zekâ destekli kestirimci bakım sistemleri, giyilebilir teknolojiler ve siber-fiziksel sistemler) beş ana kriter doğrultusunda değerlendirilmiştir. Kriter ağırlıkları, veri temelli bir yöntem olan Entropi ile hesaplanarak sürece nesnellik kazandırılmıştır. Yapılan analiz sonucunda, en yüksek yakınlık katsayısına (Ci) sahip olan Yapay Zeka Destekli Kestirimci Bakım Sistemleri (A2), en uygun teknoloji olarak belirlenmiştir.

Bu bulgu, yalnızca düşük maliyetli bir seçenek olması nedeniyle değil, aynı zamanda yüksek verimlilik katkısı, insan-makine iş birliğine uygunluğu ve sistemlerle entegrasyon kolaylığı ile öne çıkmaktadır. Söz konusu

teknoloji, Endüstri 5.0'ın temel ilkeleriyle —insan merkezlilik, sürdürülebilirlik ve ileri dijitalleşme— büyük ölçüde örtüşmektedir.

Çalışma, hem karar vericilere uygulanabilir bir model sunmakta hem de literatüre katkı sağlayacak şekilde kapsamlı bir yaklaşım önermektedir. Özellikle teknoloji seçim sürecinde yalnızca teknik verilerle değil, etik ve sosyal kriterlerle desteklenmiş çok kriterli değerlendirmelerin yapılması gerektiği bir kez daha ortaya konulmuştur.

Gelecek çalışmalar için öneriler şunlardır:

- Farklı sektörlerde benzer modeller uygulanarak karşılaştırmalı analizler yapılabilir.
- Belirsizliklerin daha yoğun olduğu ortamlarda Bulanık TOPSIS, Bulanık AHP gibi yöntemlerle genişletilmiş modeller test edilebilir.
- Karar verici sayısı artırılarak grup karar verme yaklaşımları entegre edilebilir.
- Karar sürecine etik, psikolojik etki, kullanıcı dostluğu gibi daha yumuşak kriterler de dahil edilebilir.

Bu yönüyle çalışma hem akademik dünyaya hem de uygulayıcılara Endüstri 5.0 yolculuğunda güçlü bir yol haritası sunmaktadır.

KAYNAKLAR

Braglia, M., & Petroni, A. (2000). A quality assurance-oriented methodology for handling trade-offs in supplier selection. *International Journal of Physical Distribution & Logistics Management*, *30*(2), 96-112.

Büyüközkan, G., & Göçer, F. (2018). Digital Supply Chain: Literature review and a proposed framework for future research. *Computers in industry*, *97*, 157-177.

Cheng, S., & Hwang, C. (1992). Fuzzy multiple attribute decision making: Methods and applications. *Lecture Notes in Economics and Mathematical Systems, Springer*.

Chu, J., Wu, J., Chu, C., & Liu, M. (2020). A new DEA common-weight multi-criteria decision-making approach for technology selection. *International Journal of Production Research*, *58*(12), 3686-3700.

Fidanboy, C. Ö. (2022). Human and robot employees in the future of businesses: An evaluation in the context of society 5.0. *Equinox Journal of Economics Business and Political Studies*, *9*(1), 107-127.

Giannetti, B. F., Bonilla, S. H., & Almeida, C. M. (2012). Cleaner production initiatives and challenges for a sustainable world. *Journal of Cleaner Production*, *22*(1), 1-1.

Gölcük, İ., & Baykasoğlu, A. (2016). An analysis of DEMATEL approaches for criteria interaction handling within ANP. *Expert systems with applications*, *46*, 346-366.

Gupta, C., Fernandez-Crehuet, J. M., & Gupta, V. (2022). A novel value-based multi-criteria decision making approach to evaluate new technology adoption in SMEs. *PeerJ Computer Science*, *8*, e1184.

Klaus, S. (2016). The Fourth Industrial Revolution, World Economic Forum. *Zulfu Dicleli: The Optimist Publications*, *91*, 15.

Nahavandi, S. (2019). Industry 5.0—A human-centric solution. *Sustainability*, *11*(16), 4371.

Pamučar, D., & Ćirović, G. (2015). The selection of transport and handling resources in logistics centers using Multi-Attributive Border Approximation area Comparison (MABAC). *Expert systems with applications*, *42*(6), 3016-3028.

Rezaei, J. (2015). Best-worst multi-criteria decision-making method. *Omega*, *53*, 49-57.

Romero, D., Noran, O., Stahre, J., Bernus, P., & Fast-Berglund, Å. (2015). Towards a human-centred reference architecture for next generation balanced automation systems: Human-automation symbiosis. Advances in Production Management Systems: Innovative Production Management Towards Sustainable Growth: IFIP WG 5.7 International Conference, APMS 2015, Tokyo, Japan, September 7-9, 2015, Proceedings, Part II 0,

Saaty, T. L. (2008). Decision making with the analytic hierarchy process. *International journal of services sciences*, *1*(1), 83-98.

Sezgin, S. (2018). The Third Industrial Revolution: how lateral power is transforming energy, the economy, and the world. *Turkish Journal of Business Ethics*.

Xu, X., Lu, Y., Vogel-Heuser, B., & Wang, L. (2021). Industry 4.0 and Industry 5.0—Inception, conception and perception. *Journal of manufacturing systems*, *61*, 530-535.

➢ *ORAL PRESENTATION*

Bitkilerden elde edilen doğal bileşikler ve pulmuner fibrozisin baskılanmasındaki etki mekanizmaları – Bir derleme çalışması

Pınar Aksoy[1*] (https://orcid.org/0000-0002-9265-0611), Önder Yumrutaş[2](https://orcid.org/0000-0002-9265-0611), Muhittin Doğan[3] (https://orcid.org/0000-0002-9265-0611), Pınar Yumrutaş[4]

[*1]Gaziantep Üniversitesi, Fen Edebiyat Fakültesi, Biyoloji Bölümü, Gaziantep, Türkiye
[2]Adıyaman Üniversitesi, Tıp Fakültesi, Tıbbi Biyoloji Anabilim Dalı, Adıyaman, Türkiye
[3]Gaziantep Üniversitesi, Fen EdebiyatFakültesi, Biyoloji Bölümü, Gaziantep, Türkiye
[4]Adıyaman, Türkiye

*Sorumlu yazar e-posta: pnr.aksoy.pnr@gmail.com

Özet

Pulmoner fibrozis, solunum sisteminde geri dönüşümsüz fibrotik değişikliklerle karakterize eden, yaşam kalitesini düşüren progresif bir hastalıktır. Mevcut tedavi seçeneklerinin sınırlı olup hastalığın ilerleyici seyirde olması yeni tedavi yaklaşımlarının araştırılmasını zorunlu kılmaktadır. Hastalığın tedavisi için klinikte pirfenidon ve nintedanip olmak üzere iki ilaç kullanılmaktadır. Ancak bu ilaçların zamanla etkisini kaybettiği, yan etkiler meydana getirdiği ve ilaç direnci oluşturduğu belirlenmiştir. Bu bağlamda hastalığın baskılanmasında özellikle doğal bileşiklerin kullanılmasına yönelik ilgi artmıştır. Bitkisel doğal bileşiklerin antioksidan, anti-inflamatuvar ve anti-fibrotik etkileri sayesinde pulmoner fibrozis tedavisinde potansiyel ajanlar olarak öne çıktığı görülmektedir. Bu derleme araştırmada, pulmoner fibrozisin baskılanmasında fayda sağlayan deneysel ve klinik olarak gösterilmiş olan çeşitli bitkisel doğal ajanlar ve bu ajanların moleküler etki mekanizmaları ele alınmıştır.

Literatür incelemelerimiz kadarıyla özellikle bitkilerden izole edilen fenolik ve terpen bileşiklerinin pulmoner fibrozisin oluşmasında rol alan TGF/beta ve beta-katenin/WNT1 ana yolaklarının baskılanmasında görev aldığı rapor edilmiştir. Bu ajanlardan kurkumin, resveratrol, epigallokateşin-3-gallat, naringenin, honokiol, astaksantin, silibinin, boswellik asit ve karvakrolün antifibrotik etkilerinin olduğu gösterilmiştir. Bu bileşiklerin özellikle TGF-β/Smad, NF-κB, MAPK gibi sinyal yolaklarını modüle ederek fibroblast proliferasyonunu engellediği, epitel-mezankimal geçişi (EMT) baskıladığı ve kolajen birikimini azaltmada rollerinin olduğu gösterilmiştir. Özellikle oksidatif stres ve inflamasyon üzerinde gösterdikleri düzenleyici etkilerle bu ajanların fibrotik sürecin ilerlemesini yavaşlatmada veya baskılamada rolü olduğu düşünülmektedir.

Bunlara ek olarak, bitkisel kökenli doğal ajanların çok yönlü biyolojik aktiviteleri tek başına veya mevcut antifibrotik ilaçlarla kombine kullanımı açısından umut vericidir. Bu bildiride söz konusu bitkisel türevli doğal bileşiklerin pulmoner fibrozise yönelik etkileri literatür ışığında değerlendirilmiş ve potansiyel terapötik hedefler bağlamında tartışılmıştır. Bu bulgular, gelecekte doğal ürün tabanlı antifibrotik ilaç geliştirme çalışmalarına ışık tutabilecek niteliktedir.

Anahtar Kelimeler: Pulmoner Fibrozis, Doğal Ajanlar, TGF--β/Smad, Antifibrotik, İnflamasyon, Oksidatif Stres

Natural products derived from plants and their mechanisms of action in the suppression of pulmonary fibrosis - A review

Abstract

Pulmonary fibrosis is a progressive disease characterized by irreversible fibrotic changes in the respiratory system, reducing quality of life. Current treatment options are limited and the progressive course of the disease necessitates the search for new treatment approaches. Two drugs, pirfenidone and nintedanip, are used in the clinic for the treatment of the disease. However, it has been determined that these drugs lose their effect over time, cause side effects and drug resistance. In this context, interest in the use of natural compounds in the suppression of the disease has increased. It is seen that herbal natural compounds stand out as potential agents in the treatment of pulmonary fibrosis thanks to their antioxidant, anti-inflammatory and anti-fibrotic effects. In this review, various herbal natural agents that have been experimentally and clinically shown to be beneficial in the suppression of pulmonary fibrosis and their molecular mechanisms of action are discussed.

As far as our literature review, it has been reported that phenolic and terpene compounds isolated from plants are involved in the suppression of TGF/beta and beta-catenin/WNT1 main pathways involved in the formation of pulmonary fibrosis. Among these agents, curcumin, resveratrol, epigallocatechin-3-gallate, naringenin, honokiol, astaxanthin, silibinin, boswellic acid and carvacrol have been shown to have antifibrotic effects. These compounds have been shown to inhibit fibroblast proliferation, suppress epithelial-mesenchymal transition (EMT) and reduce collagen deposition by modulating signaling pathways such as TGF-β/Smad, NF-κB and MAPK. These agents are thought to play a role in slowing or suppressing the progression of the fibrotic process, especially through their regulatory effects on oxidative stress and inflammation.
In addition, the versatile biological activities of plant-derived natural agents are promising for their use alone or in combination with existing antifibrotic drugs. In this report, the effects of these plant-derived natural compounds on pulmonary fibrosis were evaluated in the light of the literature and discussed in the context of potential therapeutic targets. These findings may shed light on future natural product-based antifibrotic drug development studies.
Keywords: Pulmonary Fibrosis, Natural Agents, TGF--β/Smad, Antifibrotic, İnflamation, Oxidative Stress

GİRİŞ

Pulmoner fibrozis (PF) interstisyel akciğer hastalıklarının ölümcül bir formudur ve kronik, progressif, geri dönüşümsüzdür (King ve ark., 2011). Fibroblast ve miyofibroblastların aşırı proliferasyonu, ekstraselüler matriksin aşırı birikimi, alveolar remodeling başarısızlığı ve vasküler tamir sistemindeki bozulmalarla karakterize edilmektedir. Genellikle orta ve ileri yaşlarda daha sık görülmektedir. Pulmoner fibrozis solunumu oldukça kötü şekilde etkilemektedir ve pulmoner fibrozisli hastaların tıbbi destek alması oldukça önemlidir. Çünkü bu durum kronik olmakla birlikte süreç olarak artan bir nefes darlığı ve öksürükten dolayı yaşam kalitesi oldukça düşmektedir. Günlük yaşamda pulmoner fibrozis oluşumunda sigara temel etmendir. Hastalığın tanısı, klinik (birkaç günden birkaç haftaya kadar kötüleşen nefes darlığı), fizyolojik (arterial kanda PaO2 (Parsiyel Arteriyel Oksijen Basıncı)'nin şiddetli şekilde azalması) ve radyografik bulguların kombinasyonları ile konulur. Bu hastaların %60'ı hastaneye başvuru sürecinde ölmektedir. Hastanede tedavi görenlerin ise taburcu olduktan sonra %90'dan fazlası 6 ay içerisinde ölmektedir (King ve ark., 2011). Pulmoner fibrosizli hastaların medyan sağ kalım oranının ortalama 5 yıl kadar olduğu hesaplanmıştır. Farklı sebeplerin tetiklediği inflamasyon interstisyel akciğer hastalıklarında kronik inflamasyon durumlarında pulmoner fibrozisin geliştiği bilinmektedir. Ayrıca pulmoner fibrozisin gelişiminde epitelyal bağımlı fibroblast aktivasyon süreci de önemli bir rol oynamaktadır. Fibrozis sürecinde hem inflamasyon hem de epitelyal yolaklar etkin rol oynamaktadır (Sisson ve ark., 2010). Sigaranın temel etmen olması ile birlikte, deprem gibi çevresel faktörlerde pulmoner fibrozise neden olabilmektedir. Pulmoner fibrozisin patojenezinde rol alan mekanizmalar üzerine farklı çalışmalar bulunmakla birlikte hastalık tablosunun oluşmasında farklı moleküler mekanizmalar aktifleşebilmektedir. Pulmoner fibrozisin oluşmasında rol alan önemli moleküler yolaklardan birisi epitelyal-mezenkimal geçiş (EMT) olduğu düşünülmektedir. EMT normal olarak embriyonik gelişim sırasında doku morfogenezinde görülür. EMT'nin moleküler özellikleri arasında, hücre-hücre adezyon kaybı ve daha sonra ana epitelden ayrılmasından sorumlu E-kaderinin ifadesinin azalması, SMADlar gibi EMT'nin spesifik gen programının altında yatan transkripsiyon faktörlerinin artan regülasyonu ve translokasyonu, vimentin ve α-sma (α-smoothmuscleactin) gibi mezenkimal proteinlerin *de nova* ekspresyonu ve kollajen-I ile fibronektin gibi interstisyel tip matriks bileşenlerinin üretimi bulunmaktadır. EMT'nin oluşumunu için farklı hücre sinyal yolaklarının görev aldığı belirlenmiştir. EMT'nin oluşmasında TGF-β/SMAD2 sinyal yolağının da oldukça önemli bir rol oynadığı, özellikle de idiopatik pulmoner fibrozlu hastalardan izole edilen hücrelerde TGF-β sinyalinin fibrozu indüklediği belirlenmiştir (Luo ve ark., 2014). Smad ailesi sinyal kaskadı, fibrozda önemli bir rol oynamaktadır. Smad3, miyofibroblast fenotipinin aktivasyonunda, ECM (ekstraselülar matriks) sentezinin uyarılmasında, integrin ekspresyonunda anahtar rol oynayan bu ailenin en karakteristik üyesidir (Kage ve Borok, 2012). TGF-β/Smad yolunun düzensizliği, doku fibrozunun ana mekanizması olabileceği düşünülmektedir ve Smad3'ün doğrudan TGF- β aracılı doku fibrozunu desteklediği düşünülmektedir. Spesifik olarak, TGF- β tarafından aktivasyon üzerine fosforile edilmiş Smad3 çekirdekte lokalize olur ve burada kollajen-I, α-SMA ve TGF- β gibi fibrozis hedef genlerinin transkripsiyonunu düzenler. Pulmoner fibrozla mücadelede günümüzde kullanılan ilaçlar olmakla birlikte (pirfenidon ve nintedanip) bu ilaçların hem yan etkileri hem de bu ilaçlara karşı oluşan ilaç direncinden dolayı tedavi olumsuz etkilenmektedir. Bundan dolayı kesin bir tedavisi olmayan pulmoner fibrozisin tedavisi/ baskılanması için bitkilerde doğal olarak üretilen, yan etkileri sentetiklere göre daha az olan ve pek çok hastalığın tedavisinde kullanılan seconder bileşiklerin pulmoner fibrozis'in baskılanması için doğal bir yol olarak değerlendirilmesi düşünülmüştür. Literatür

derlememizde pulmoner fibroziste etkili olan bitkisel bileşiklerden bahsedilmiş ve aşağıda ilgili antifibrotik etkiler verilmektedir.

Kurkumin

Kurkumin, Curcuma longa (zerdeçal) bitkisinden elde edilen, polifenol yapısında doğal bir bileşiktir. Güçlü antioksidan, anti-inflamatuvar ve anti-fibrotik etkilerinin çokça hastalık modelinde tedavi edici potansiyeli araştırılmaya devam etmektedir. Pulmoner fibrozis özelinde, kurkuminin TGF-β1/Smad, NF-κB ve PI3K/Akt sinyal yolaklarını hedef alarak fibroblast proliferasyonunu ve epitel-mezankimal geçişi (EMT) inhibe ettiği gösterilmiştir (Liu et al., 2016; Smith et al., 2010).

EGCG (Epigallokatezin-3-gallat)

Yeşil çayda fazlaca bulunduğu bilinen EGCG, TGF-β/Smad sinyal yolunu inhibe ederek EMT, fibroblast aktivasyonu ve kolajen birikimi gibi fibrozisle ilişkili süreçleri baskılar. Ayrıca oksidatif stres ve inflamasyonu azaltarak fibrotik doku gelişimini engeller (Panji et al., 2021).

Naringenin

Naringenin, yüksek oranda greyfurt (Citrus paradisi) meyvesinde bulunan bir flavonoiddir. Naringenin, kollajen Iα1 (Col Iα1), fibronektin (FN) ve plazminojen aktivatör inhibitörü-1 (PAI-1) dahil olmak üzere sadece ECM birikimini azaltmakla kalmayıp, mRNA ve protein seviyelerinde TGF-β1 tarafından indüklenen Smad3 üretimini de doza bağlı şekilde azalttığı belirlenmiştir. Ayrıca, naringenin, Smad3'ün transkripsiyonunu seçici olarak inhibe ettiği belirlenmiştir. Bununla birlikte naringeninin, TGF-β sinyali yoluyla Smad3 protein ekspresyonunu ve fosforilasyonunu doğrudan veya dolaylı olarak azaltarak antifibrojenik etkiler gösterebileceğini göstermektedir. (Liu et al., 2006).

Resveratrol

Resveratrol, başlıca üzüm kabuğu, kırmızı şarap ve bazı meyvelerde bulunan doğal bir polifenol bileşiğidir. Güçlü antioksidan, anti-inflamatuvar ve anti-fibrotik etkileri sebebiyle son yıllarda birçok kronik hastalıkta özellikle de akciğer hastalıklarında terapötik potansiyeliyle dikkat çekmektedir. Resveratrol, sıçanlarda epitelyal-mezenkimal geçişi inhibe ederek ve TLR4 / NF-κB ile TGF-β1 / smad3 sinyal yollarını aşağı regüle ederek bleomisin kaynaklı pulmoner fibrozu hafiflettiği bildirilmiştir (Sener ve ark., 2007). Hastalar için resveratrol tedavilerinin başarılı olamamasında karşı karşıya kalınan en büyük zorluk, biyoyararlanımını arttırmaktır. Bu bağlamda, özellikle resveratrol dağıtımına yönelik farmasötik formülasyonların geliştirilmesi için umut verici bakış açıları vardır (Amri ve ark., 2011). Tüm bu bulgular ışığında resveratrol, pulmoner fibrozisin patogenezinde yer alan çoklu sinyal yollarını hedef alabilme kapasitesiyle dikkat çeken, farmakolojik potansiyeli yüksek bir doğal ajan olarak değerlendirilmektedir.

Paeoniflorin

Paeoniflorin, özellikle *Paeonialactiflora* ve *Paeoniasuffruticosa* gibi türlerin köklerinden doğal olarak elde edilir (O &Dai, 2011). Paeoniflorin, pulmoner fibrozis modelinde TGF-β1 kaynaklı EMT'yi baskılayarak fibrotik belirteçleri (FSP-1, α-SMA, vimentin, kollajen) azaltmış, E-kaderin düzeyini artırmıştır. Bu etkiler, özellikle Smad2/3 aktivasyonunun inhibisyonu ve Smad7 artışı yoluyla gerçekleşmiştir. Paeoniflorin, TGF-β1 sinyal yolunu Smad-bağımlı olarak hedeflemiştir (Ji et al., 2016).

Honokiol

Honokiol, şifalı bir bitki olan Magnolia officinalis'in kabuğundan elde edilen önemli bir bileşendir. Honokiol ile tedavi edilen farelerden yeni izole edilmiş mitokondrideki oksijen tüketimi, mitokondriyal solunumu artırdığı rapor edilmiştir. Ayrıca solunum bozukluklarında da rahatlama gözlemlenmiştir. (Huang et al., 2017). Honokiol hem in vitro hem de in vivo deneysel PF modellerinde pulmoner fibrotik değişiklikleri tersine çevirdiği ve büyük ölçüde EMT, TGF-β / Smad sinyalini zayıflatarak ve kısmen IL-6 / CD44 / STAT3 sinyal eksenini inhibe ederek anti-fibrotik etkiler gösterdiği sonucuna varılabilir (Pulivendala et al., 2020).

Silibinib (Silymarin)

Deve dikeni Asteraceae familyasının bir üyesi olan Silybum marianum, 2.000 yıllık kullanım geçmişine sahip tedavi edici bir bitkidir. Meyveleri, silimarin olarak bilinen ve ana bileşen silybin (silibinin olarak da adlandırılır) olan bir flavonolignan karışımı içerir (Abenavoli et al., 2018; Neha, Jaggi, &Nirmal, 2016). Silibin'in bleomisin indüklenmiş pulmoner fibrozis modelinde akciğer dokularında hidroksiprolin içeriği, yaş ağırlık, histoloji, inflamatuar faktör ekspresyonu ve gen ekspresyonu incelenmiş ve silibinin inflamasyonu ve

fibrozu hafiflettiği, akciğerlerde hidroksiprolin birikimini sınırladığı, PF gelişiminde gen ekspresyonunu modüle ettiği ve ameliyat sonrası sağ kalımı iyileştirdiği gösterilmiştir. Ayrıca Silibin, IL-1β, TGF-β, MMP-13 ve MMP-14'ün aşırı ekspresyonunu baskılayarak idiopatik pulmoner fibrozisin (İPF) şiddetini azaltmada etkili olduğu belirlenmiştir (Ma et al., 2023)."

Astaksantin

Astaksantin,en yüksek oranda Haematococcuspluvialis adlı tatlı su mikroalginde bulunur. Bu mikroalg, doğal astaksantin üretiminde çokça kullanılır. Güçlü antioksidan özelliği, antienflamatuvar, anti-apoptotik ve immün modülasyonu sayesinde astaksantin, çeşitli hastalıklara karşı çok hedefli bir farmakolojik ajan olarak ilgi görmüştür. Çeşitli hastalıklarda kronik ve akut iltihabı hafiflettiği doğrulanmıştır. Bu sayede astaksantinin iltihapla ilgili hastalıkların tedavisi için mükemmel bir aday olabileceği öngörmektedir (Chang &Xiong, 2020). Astaksantin, kan-beyin bariyeri yoluyla beyne taşınabilen bir ksantofil karotenoiddir. Antioksidan aktivitesine ek olarak, astaksantin anti-inflamatuar ve antitümör özellikler gösterir. Bununla birlikte, sınırlı sayıda çalışma antipulmoner fibrotik etkisini bildirmektedir. Chen ve arkadaşlarının yaptığı bir çalışmada astaksantinin aktive fibroblast proliferasyonunu bloke edip pulmoner fibrozu zayıflattığını veTGF-β1'nin antifibrotik mekanizmaya katkıda bulunduğu gösterilmiştir (Chen et al., 2020). Başka bir çalışmada; astaksantin, güçlü antioksidan ve antienflamatuvar etkileriyle pulmoner fibrozisi baskılayabilmiş hatta Nrf2 aktivasyonu ve NF-κB inhibisyonu gibi mekanizmalar yoluyla oksidatif stres ve inflamasyonu azaltarak fibrozisin ilerlemesini engelleyebileceği öngörülmüştür. (Alugoju et al., 2022).

Boswelik asit

Boswellia serrata ekstraktından elde edilen saf bileşiğin, tümör nekroz faktörü-alfa (TNF-α), interlökin-1beta (IL-1beta) vemitojenle aktive edilmiş protein (MAP) kinazların inhibisyonu yoluyla insan periferik kan mononükleer hücrelerinde (PBMC'ler) ve fare makrofajlarında antienflamatuvar özellik sergilediğini bildirmiştir (Gayathri et al., 2007). Çalışma doğrudan İPF modelinde yapılmamıştır, ancak TNF-α, IL-1β ve MAPK yolaklarının baskılanması, İPF'deki inflamatuvar süreçlerin azaltılması açısından dolaylı ve biyolojik olarak anlamlı bir bağlantı sunar.

Karvakrol

Fibrozisin baskılanmasında görev aldığı bilinen Thymus türleri bu amaç için popüler olabilecek bitkilerdir. Thymus türlerine ait antibakteriyel (Fadli ve ark., 2012), antioksidan (Amiri, 2012), antikanser (Barmoudeh ve ark., 2022), antienflamatuvar (Abdelli ve ark., 2017), antifibrotik (Abdelghffar ve ark., 2022) özellikte olduğu bilinen pek çok rapor bulunmaktadır. Yapılan literatür incelemelerinde bu türlerin farklı organlarda fibrozu baskıladığına ait raporlar bulunmaktadır. Bu bağlamda, son yıllarda doğal kaynaklı biyoaktif bileşiklerin antifibrotik etkileri dikkat çekip, yoğun ilgi görmektedir. Bitkisel kökenli bu ajanların anti-inflamatuvar, antioksidan ve anti-fibrotik etkiler göstermesi; çoklu sinyal yolaklarını hedef alıp fibroblast proliferasyonu, EMT ve kolajen birikimini baskılaması doğal ajanları, pulmoner fibrozis tedavisinde umut verici kılmaktadır.

MATERYAL VE METOD

Bu derleme çalışması, pulmoner fibrozis tedavisinde doğal ajanların antifibrotik etkilerini ve altta yatan etki mekanizmalarını değerlendirmek amacıyla yürütülmüş kapsamlı bir literatür taramasına dayanmaktadır. Çalışma, kanıta dayalı mevcut bilimsel yayınların sistematik incelenmesi yoluyla hazırlanmıştır. İlgili literatür taraması, PubMed, Scopus, Web of Science ve Google Scholar gibi uluslararası akademik veri tabanlarında gerçekleştirilmiştir. Tarama, Ocak 2010 –Mayıs 2025 tarihleri arasında yayımlanmış İngilizce dilindeki makaleleri kapsamaktadır. Tarama sırasında kullanılan anahtar kelimeler şunlardır: Pulmonaryfibrosis, naturalcompounds, anti-fibroticagents, curcumin, resveratrol, epigallocatechin-3-gallate, naringenin, honokiol, astaxanthin, silibinin, boswellicacid, TGF-β1/Smad, epithelial-mesenchymal transition, oxidativestress, fibroblast proliferation. Elde edilen makaleler, içerik analizi yöntemiyle incelenmiştir. Her doğal ajan için: Kullanılan deneysel model (in vitro, in vivo), hedef alınan sinyal yolakları, antifibrotik etki düzeyleri, fibroblast proliferasyonu, EMT, kolajen birikimi ve oksidatif stres üzerindeki etkileri şeklinde tematik bir sınıflandırma yapılmıştır.

BULGULAR ve TARTIŞMA

Bu çalışma, çeşitli doğal bileşiklerin pulmoner fibrozis modelindeki etkileri değerlendirilmiş ve bu ajanların antifibrotik potansiyelleri ortaya konmuştur. Kurkumin, resveratrol, EGCG, naringenin, honokiol, astaksantin, silibinin, boswelik asit, paeniflorin, karkavakrol gibi biyoaktif maddeler; TGF-β1/Smad, NF-κB, PI3K/Akt, MAPK gibi sinyal yolakları üzerinden fibroblast aktivasyonu, epitel-mezankimal geçiş, kolajen birikimi ve oksidatif stres gibi süreçleri modüle ederek PF gelişimini baskılamaktadır. Özellikle kurkumin, EGCG ve resveratrol gibi polifenol yapısındaki ajanların, hem inflamasyonu hem de oksidatif stresi eş zamanlı baskılaması; bu bileşiklerin multifaktöriyel patogeneze sahip PF üzerinde çok yönlü etki gösterdiğini ortaya koymaktadır. Benzer şekilde honokiol gibi flavonoid türevleri de hem anti-inflamatuvar hem de antifibrotik etkiyi bir arada sunmaktadır.

Bu bileşiklerin çoğu, deneysel hayvan modelleri veya hücre kültürü düzeyinde test edilmiştir. Ancak biyoyararlanım sorunları (özellikle kurkumin ve silibinin için) bu ajanların klinik uygulamasının önündeki en büyük engellerden biridir. Son dönemde yapılan çalışmalar, liposomal taşıyıcı sistemler, nanopartikül formülasyonlar veya türev bileşikler yoluyla bu engeli aşmaya odaklanmaktadır.

Ayrıca doğal ajanların yan etkilerinin minimal olması, uzun süreli kullanımlarda daha güvenli olmalarını sağlamaktadır. Ancak bu alanda yapılacak daha fazla preklinik ve klinik çalışmaya ihtiyaç vardır. Özellikle kombinasyon tedavilerinde bu bileşiklerin sinerjistik etkilerinin değerlendirilmesi, PF gibi dirençli fibrotik hastalıkların tedavisinde yeni fırsatlar sunabilir.

Bu derlemenin sınırlılıkları arasında, verilerin yalnızca deneysel modellere dayanması ve klinik verilerin eksikliği yer almaktadır. Ayrıca literatürdeki heterojenlik, kullanılan model, doz, uygulama yolu ve değerlendirme kriterlerindeki farklılıklar doğrudan karşılaştırma yapılmasını zorlaştırmaktadır. Bununla birlikte bu çalışma, doğal ajanların PF üzerindeki potansiyel etkilerini bütüncül bir bakış açısıyla sunarak literatüre katkı sağlamaktadır.

SONUÇ

Pulmoner fibrozis, prognozu kötü ve etkin tedavi seçenekleri sınırlı olan ciddi bir akciğer hastalığıdır. Bu bağlamda, doğal kaynaklı ajanların terapötik potansiyelleri giderek daha fazla ilgi görmektedir. Bu çalışmada incelenilen başlıca doğal ajanlar; Curcuma longa (zerdeçal), Camelliasinensis (yeşil çay), Citrus paradisi (greyfurt), üzüm kabuğu ve kırmızı şarap, Paeonialactiflora ve Paeoniasuffruticosa (şakayık kökü), Magnoliaofficinalis (manolya kabuğu), Silybummarianum (devedikeni), Haematococcuspluvialis (tatlı su mikroalg), Boswelliaserrata (akgünlük), Morindacitrifolia (noni meyvesi) ve Thymus türleridir. Yine bu derleme çalışmasında incelenen kurkumin, resveratrol, EGCG, naringenin, honokiol, astaksantin, silibinin, boswelikasit, paeniflorin, karvakrol gibi biyoaktif bileşiklerin; TGF-β1/Smad, NF-κB, PI3K/Akt gibi sinyal yolaklarını hedef alarak fibroblast proliferasyonunu, epitel-mezankimal geçişi, kolajen birikimini ve inflamasyonu anlamlı düzeyde baskıladığını ortaya konmuştur.

Bu doğal bileşiklerin çoğu, anti-inflamatuar ve antioksidan etkilerinin yanı sıra antifibrotik özellikler de göstermekte olup, çoklu patolojik mekanizmaları eşzamanlı olarak hedef alabilmektedir. Bu durum, onları pulmoner fibrozis gibi multifaktöriyel hastalıkların tedavisinde umut verici adaylar haline getirmektedir.

Bununla birlikte, biyoyararlanım ve farmakokinetik problemler gibi bazı farmasötik sınırlılıkların bulunduğu da göz önünde bulundurulmalıdır. Bu nedenle, bu bileşiklerin daha ileri preklinik çalışmalarla desteklenmesi, yeni formülasyonların geliştirilmesi ve klinik düzeyde test edilmesi büyük önem taşımaktadır.

Sonuç olarak doğal ajanlar, pulmoner fibrozisin patogenezinde yer alan temel süreçlere yönelik etkili bir müdahale stratejisi sunmakta olup ilerleyen dönemde yapılacak kapsamlı araştırmalar, bu bileşiklerin klinik kullanıma kazandırılmasında önemli rol oynayacaktır.

KAYNAKLAR

Abdelli, W., Bahri, F., Romane, A., Höferl, M., Wanner, J., Schmidt, E., &Jirovetz, L., Chemical composition and anti-inflammatory activity of Algerian Thymus vulgaris essential oil. Natural product communications 2017; 12(4): 1934578X1701200435.

Abdelghffar, E. A., Obaid, W. A., Alamoudi, M. O., Mohammedsaleh, Z. M., Annaz, H., Abdelfattah, M. A., &Sobeh, M.,Thymus fontanesii attenuates CCl4-induced oxidative stress and inflammation in mild liver fibrosis. Biomedicine&Pharmacotherapy, 2022; 148: 112738.

Abenavoli, L., Izzo, A. A., Milić, N., Cicala, C., Santini, A., &Capasso, R. (2018). Milk thistle (Silybummarianum): A concise overview on its chemistry, pharmacological, and nutraceutical uses in liver diseases. Phytotherapy Research, 32(11), 2202–2213. https://doi.org/10.1002/ptr.6171Alugoju,

P., Swamy, V. K. D. K., Anthikapalli, N. V. A., &Tencomnao, T. (2022). Health benefits of astaxanthin in age-related diseases across multiple organs: A comprehensive review. Critical Reviews in Food Science and Nutrition, 62(47), 10709–10774. https://doi.org/10.1080/10408398.2022.2084600

Amiri, H., Essential oils composition and antioxidant properties of three thymus species. Evidence-Based Complementary and Alternative Medicine, 2012.Amri, A., Chaumeil, J. C., Sfar, S., &Charrueau, C. (2012). Administration of resveratrol: What formulation solutions to bioavailability limitations? *Journal of ControlledRelease, 158*(2), 182–193. https://doi.org/10.1016/j.jconrel.2011.09.083

Barmoudeh, Z., Ardakani, M. T., Doustimotlagh, A. H., &Bardania, H., Evaluation of the antioxidant and anti-cancer activities of hydroalcoholic extracts of Thymus daenensis Kalakand Stachyspilifera Benth. Journal of Toxicology. 2022.Chang, M. X., &Xiong, F. (2020). Astaxanthin and its effects on inflammatory responsesand inflammation-associated diseases: Recent developments and future directions. Molecules, 25(22), 5342. https://doi.org/10.3390/molecules25225342

Chen, H., Wang, J., Li, R., Lv, C., Xu, P., Wang, Y., Song, X., & Zhang, J. (2020). Astaxanthin attenuates pulmonary fibrosis through lncITPF and mitochondria-mediated signaling pathways. *Journal of Cellular and Molecular Medicine, 24*(17), 10245–10250. https://doi.org/10.1111/jcmm.15477

Fadli, M., Saad, A., Sayadi, S., Chevalier, J., Mezrioui, N.-E., Pagès, J.-M., &Hassani, L. (2012). *Antibacterial activity of Thymus maroccanus and Thymus broussonetii essentiall oils against nosocomial infection–causing bacteria and their synergistic potential with antibiotics*. Phytomedicine, 19(5), 464–471. https://doi.org/10.1016/j.phymed.2011.12.003

Gayathri, B., Manjula, N., Vinaykumar, K. S., Lakshmi, B. S., &Balakrishnan, A. (2007). Pure compound from *Boswellia serrata* extract exhibits anti-inflammatory property by inhibiting TNF-α, IL-1β, NO and MAP kinases in human PBMCs and mouse macrophages. *International Immunopharmacology*, *7*(4), 47

Huang, K., Zhang, K., Guo, Y., Huang, F., Yang, K., Chen, U., Huang, K., Zhang, F., Uzun, Q., & Yang, Q. (2017). Honokiol protects against doxorubicin-induced cardiotoxicity by improving mitochondrial function in mouse hearts. *Scientific Reports, 7*(1), 11989. https://doi.org/10.1038/s41598-017-12095-y

Ji, Y., Dou, Y.-N., Zhao, Q.-W., Zhang, J.-Z., Yang, Y., Wang, T., Xia, Y.-F., Dai, Y., &Wei, Z.-F. (2016). Paeoniflorin inhibits TGF-β1-induced epithelial–mesenchymal transition in pulmonary fibrosis via a Smad-dependent pathway. Acta Pharmacologica Sinica, 37(6), 794–804. https://doi.org/10.1038/aps.2016.36

Kalayarasan, S., Sriram, N., &Sudhandiran, G. (2008). Diallyl sulfide attenuates bleomycin-induced pulmonary fibrosis: Critical role of iNOS, NF-κB, TNF-α and IL-1β. *Life Sciences, 82*(23–24), 1142–1153. https://doi.org/10.1016/j.lfs.2008.03.018

Kage, H., Borok, Z. EMT and interstitial lung disease: a mysterious relationship. Current opinion in pulmonary medicine. 2012; 18: 517-523.

King, T. E., Pardo, A., Selman, M. Idiopathic pulmonary fibrosis. The Lancet 2011; 378: 1949-1961.

Liu, D., Gong, L., Zhu, H., Pu, S., Wu, Y., Zhang, W., & Huang, G. (2016). Curcumin inhibits transforming growth factor β induced differentiation of mouse lung fibroblasts to myofibroblasts. Frontiers in Pharmacology, 7, 419. https://doi.org/10.3389/fphar.2016.00419

Liu, X., Wang, W., Hu, H., Tang, N., Zhang, T., Liang, W., & Wang, M. (2006). The Smad3-specific inhibitor naringenin reduces extracellular matrix expression induced by TGF-beta1 in cultured rat hepatic stellate cells. *Pharmaceutical Research, 23*(1), 82-89. https://doi.org/10.1007/s110 95-005-9043-5

Luo, F., Zhuang, Y., Sides, M. D., Sanchez, C. G., Shan, B., White, E. S., Lasky, J. A. Arsenic trioxide inhibits transforming growth factor-β1-induced fibroblast tomyo fibroblast differentiation in vitro and bleomycin induced lung fibrosis in vivo. Respiratory Research 2014;15: 1-14.

Ma, X., Xia, K., Xie, J., Yan, B., Han, X., Li, S., Wang, Y., & Fu, T. (2023). Treatment of idiopathic pulmonary fibrosis with inhaled silybin dry powder prepared by spray drying technology of nanosuspension. *ACS Pharmacology&Translational Science, 6*(6), 878–891. https://doi.org/10.1021/acsptsci.3c00033

Neha, Jaggi, A. S., &Nirmal, N. (2016). Role of silymarin in chronic diseases. In R. R. Watson & V. R. Preedy (Eds.), *Bioactive food as dietary interventions for liver and gastrointestinal disease* (Vol. 929, pp. 25–44). *Advances in Experimental Medicine and Biology*. Springer. https://doi.org/10.1007/978-3-319-41342-6_2

O, D.-Y., &Dai, S.-M. (2011). Anti-inflammatory and immune modulatory effects of Paeonia lactiflora Pall., a traditional Chinese herbal medicine. Frontiers in Pharmacology, 2, Article 10. https://doi.org/10.3389/fphar.2011.00010

Panji, M., Behmard, V., Zare, Z., Malekpour, M., Nejadbiglari, H., Yavari, S., NayerpourDizaj, T., Safaean, A., Maleki, N., Abbasi, M., Abazari, O., Şabanzade, M., &Khanicheragh, P. (2021). Suppression of TGF-β-induced epithelial-mesenchymal transition via ROS/Smad signaling pathway in human cervical cancer cells by green tea extract and Epigallocatechin-3-gallate (EGCG). Gene, 794, 145774. https://doi.org/10.1016/j.gene.2021.145774

Pulivendala, G., Balyasia, S., &Godugu, C. (2020). Honokiol: A polyphenolic neolignane ameliorates pulmonary fibrosis inhibiting TGF-β/Smad signaling, matrix proteins, and IL-6/CD44/STAT3 axis both in vitro and in vivo. *Toxicology and Applied Pharmacology, 391*, 114913. https://doi.org/10.1016/j.taap.2020.114913

Rahman, I., Biswas, S. K., &Kirkham, P. A. (2006). Regulation of inflammation and redox signaling by dietary polyphenols. *Biochemical Pharmacology, 72*(11), 1439–1452.

Sang, S., Cheng, X., Zhu, N., Stark, R. E., Badmaev, V., Ghai, G., Rosen, R. T., &Ho, C. T. (2001). Flavonol glycosides and novel iridoid glycoside from the leaves of Morinda citrifolia. Journal of Agricultural and Food Chemistry, 49(9), 4478–4481. https://doi.org/10.1021/jf010492e

Sener, G., Toklu, H. Z., Ercan, F., Erkanli, G., &Sirvanci, S. (2007). Protective effects of resveratrol against bleomycin-induced pulmonary fibrosis in rats. Journal of Applied Toxicology, 27(4), 395–400.

Sisson, T.H., Mendez, M., Choi, K., Subbotina, N., Courey, A., Cunningham, A.,Thannickal, V.J. Targeted injury of type II alveolar epithelial cells induces pulmonary fibrosis. American journal of respiratory and critical care medicine. 2010;181: 254-263.

Smith, M. R., Gangireddy, S. R., Narala, V. R., Hogaboam, C. M., Standiford, T. J., Christensen, P. J., et al. (2010). Curcumin inhibits fibrosis-related effects in IPF fibroblasts and in mice following bleomycin-induced lung injury. American Journal of Physiology-Lung Cellular and Molecular Physiology, 298(5), L616–L625. https://doi.org/10.1152/ajplung.00002.2009

➢ *ORAL PRESENTATION*

Inconel 625 süper alaşımının tornalanmasında kesme hızının işleme performansına etkisi

Yusuf Siyambaş[1*] (*ORCID: https://orcid.org/ 0000-0001-8360-5213*)

[*1]Erzincan Binali Yıldırım Üniversitesi, Meslek Yüksekokulu, Makine ve Metal Teknolojileri, Erzincan, Türkiye

*Sorumlu yazar e-posta: yusuf.siyambas@erzincan.edu.tr

Özet
Bu çalışmada, zor işlenebilir süper alaşımlar arasında yer alan Inconel 625'in farklı kesme hızları altında işlenebilirliği deneysel olarak incelenmiştir. Tornalama işlemleri, sabit ilerleme miktarı ve sabit talaş derinliği koşullarında, beş farklı kesme hızı kullanılarak kuru kesme ortamında gerçekleştirilmiştir. Deneylerde, işlenmiş yüzeylerin pürüzlülük değerleri, kesme kuvvetleri ve kesme sıcaklığı ölçülerek değerlendirilmiştir. Elde edilen sonuçlara göre, kesme hızı arttıkça kesme kuvveti ve yüzey pürüzlülüğünde düşüş gözlemlenmiş, buna karşın kesme sıcaklığında belirgin bir artış meydana gelmiştir. Bu durum, artan sıcaklığın malzemenin akma mukavemetini düşürerek deformasyonunu kolaylaştırması ve kesici takım-talaş arayüzeyindeki sürtünmenin azalması ile açıklanabilir. Bu çalışma, Inconel 625'in işlenebilirliğinin iyileştirilmesine yönelik uygun kesme parametrelerinin belirlenmesi açısından önemli veriler sunmakta ve talaşlı imalat literatürüne katkı sağlamaktadır.
Anahtar Kelimeler: Inconel 625, tornalama, kesme hızı, kesme kuvveti, yüzey pürüzlülüğü, kuru işleme

Effect of cutting speed on machining performance in turning of ınconel 625 superalloy

Abstract
In this study, the machinability of Inconel 625, which is classified among difficult-to-machine superalloys, was experimentally investigated under varying cutting speeds. Turning operations were carried out under dry machining conditions using five different cutting speeds while keeping the feed rate and depth of cut constant. During the experiments, the surface roughness of the machined parts, cutting forces, and cutting temperatures were measured and analyzed. According to the obtained results, an increase in cutting speed led to a significant decrease in cutting forces and surface roughness, whereas a noticeable increase in cutting temperature was observed. This outcome can be attributed to the reduction in flow stress of the material due to elevated temperatures, which facilitates plastic deformation and decreases friction at the tool-chip interface. This study provides important data for determining the appropriate cutting parameters for improving the machinability of Inconel 625 and contributes to the machining literature.
Keywords: Inconel 625, turning, cutting speed, cutting force, surface roughness, dry machining

GİRİŞ

Yüksek sıcaklık dayanımı, mükemmel oksidasyon ve korozyon direnci, iyi kaynak kabiliyeti ve yüksek mekanik mukavemet gibi üstün özellikleri sayesinde Inconel 625 süper alaşımı, özellikle havacılık, denizcilik, kimya, enerji ve nükleer endüstri gibi zorlu çevresel koşulların hâkim olduğu alanlarda yaygın olarak kullanılmaktadır (Alloy ve ark., 2020; Shankar ve ark., 2001). Ancak, bu alaşımın sahip olduğu yüksek süneklik, düşük ısıl iletkenlik ve sertleşme eğilimi, onu geleneksel talaşlı imalat yöntemleri açısından zor işlenebilir bir malzeme hâline getirmektedir (Choudhury ve El-Baradie, 1998). Yüksek kesme sıcaklıkları, takım aşınması ve yüzey kalitesinde düşüş gibi olumsuzluklar, üretim verimliliğini ve parça kalitesini doğrudan etkilemektedir. Bu nedenlerle, Inconel 625'in işlenebilirliğini iyileştirmeye yönelik sistematik çalışmalar yapmak, hem üretim sürekliliği hem de maliyet etkinliği açısından büyük önem taşımaktadır. Talaşlı imalat süreçlerinde kesme parametreleri olarak adlandırılan kesme hızı (Vc), ilerleme miktarı (f) ve kesme derinliği (ap) gibi değişkenler; kesme bölgesinde oluşan mekanik ve termal yükleri doğrudan etkileyerek, hem takım performansı hem de yüzey kalitesi üzerinde belirleyici rol oynamaktadır (Debnath ve ark., 2014). Özellikle kesme sıcaklığı, takım aşınmasının temel nedenlerinden biri olup, aynı zamanda kesme kuvvetleri ve yüzey bütünlüğü ile doğrudan ilişkilidir. Bu bağlamda, kesme parametrelerinin optimize edilmesiyle, hem kesme kuvvetlerinin azaltılması hem de yüzey pürüzlülüğünün iyileştirilmesi mümkün olabilmektedir.

Dolayısıyla işleme verimliliğini ve parça kalitesini birlikte ele alacak kapsamlı değerlendirmeler, modern üretim sistemleri açısından kritik öneme sahiptir.

Son yıllarda yapılan çalışmalarda, Inconel 625 gibi zor işlenebilir süper alaşımların talaşlı imalatında kesme kuvveti, sıcaklık ve yüzey pürüzlülüğü gibi performans parametreleri arasındaki ilişkilerin modellenmesine ve optimizasyonuna yönelik çok sayıda deneysel ve sayısal yöntem önerilmiştir. Bir çalışmada, kaplamasız kesici uçlarla Inconel 625 süperalaşımının tornalanması sırasında oluşan esas kesme kuvveti (Fc), değişen kesme parametreleri altında hem deneysel yöntemlerle hem de sonlu eleman analizleriyle değerlendirilmiştir. Kuru işleme koşullarında yapılan deneylerde, en düşük Fc değeri 180 m/dak kesme hızı, 0,12 mm/dev ilerleme miktarı ve 0,5 mm talaş derinliği kombinasyonunda 120 N olarak kaydedilmiştir. Deform 3D yazılımı kullanılarak gerçekleştirilen nümerik modelleme sonuçları ile deneysel bulgular karşılaştırıldığında, yaklaşık %12 oranında bir fark tespit edilmiştir (Akgün ve Demir, 2021). Başka bir çalışmada, Inconel 625 süperalaşımının tornalanabilirliğini değerlendirmek amacıyla farklı kesme parametreleri altında deneyler gerçekleştirmiş ve en uygun işleme koşullarının belirlenmesi hedeflenmiştir. Çalışmada, üç farklı kesme hızı, ilerleme miktarı ve talaş derinliği kombinasyonları uygulanmış, kesici takım olarak ise kaplamalı karbür ve seramik uçlar tercih edilmiştir. Deney sonuçlarına göre, seramik takımların işlenebilirlik performansını olumlu yönde etkilediği ifade edilmiştir (Lotfi ve ark., 2016). Başka bir çalışmada, çevresel etkileri azaltmak amacıyla %0.5 Al_2O_3 içeren nano kesme sıvısı, saf minimum miktarda yağlama (MMY) ve kuru işleme koşulları karşılaştırılmıştır. Taguchi L_9 deney tasarımı ile üç farklı kesme hızı ve ilerleme değeri denenmiş, optimum şartlar S/N oranı ve ANOVA analizi ile belirlenmiştir. En düşük kesme sıcaklığı, nano katkılı MMY, 120 m/dak kesme hızı ve 0,05 mm/dev ilerleme miktarı ile elde edilmiştir (Yıldırım, 2019). Diğer bir çalışmada, Inconel 625'in tornalanmasında kesme hızı, ilerleme miktarı ve kesme derinliğinin kesme kuvveti ve yüzey pürüzlülüğü üzerindeki etkileri incelenmiştir. L_9 ortogonal dizisiyle yapılan deneyler sonucunda, Taguchi tabanlı Gri ilişki analizi ile optimum işleme parametreleri belirlenmiştir. Analizler, en etkili parametrenin ilerleme miktarı olduğunu göstermiştir (Kosaraju ve ark., 2018). Bir diğer çalışmada, Inconel 625 süper alaşımının tornalanmasında farklı soğutma koşullarının (kuru, MMY ve vortex soğutma) takım ömrü, takım aşınması, yüzey pürüzlülüğü, kesme kuvvetleri ve kesme bölgesi sıcaklığı üzerindeki etkileri incelenmiştir. Deneyler üç farklı kesme ve ilerleme miktarı kombinasyonunda gerçekleştirilmiştir. Elde edilen bulgular doğrultusunda, takım aşınmasının azaltılması, yüzey kalitesinin iyileştirilmesi ve kesme bölgesi sıcaklığının düşürülmesi açısından en etkili soğutma yönteminin MMY yöntemi olduğu sonucuna varılmıştır (Yağmur, 2021). Başka bir çalışmada, PVD-TiAlN kaplamalı karbür uçlarla Inconel 625'in tornalanmasında kriyojenik soğutmanın (sıvı nitrojen) takım aşınması ve yüzey pürüzlülüğü üzerindeki etkileri incelenmiştir. Deneyler, kuru ve kriyojenik soğutma koşullarında gerçekleştirilmiş, kriyojenik soğutma ile yüzey pürüzlülüğünde %50'ye varan bir iyileşme sağlandığı, taramalı elektron mikroskobu (SEM) analizleriyle ise takım aşınmasının anlamlı ölçüde azaldığı tespit edilmiştir (Dhananchezian, 2018).

Literatürde, Inconel 625 süper alaşımının talaşlı imalatında kesme parametreleri ve soğutma tekniklerinin işleme performansına etkilerini inceleyen çok sayıda araştırma yer almaktadır. Kesme hızı, ilerleme ve kesme derinliği gibi temel parametrelerin kesme kuvveti, kesme sıcaklığı, takım aşınması ve yüzey kalitesi üzerindeki etkileri deneysel ve nümerik yöntemlerle detaylı olarak değerlendirilmiştir. Ayrıca, minimum miktarda yağlama (MMY), nano katkılı kesme sıvıları ve kriyojenik soğutma gibi farklı soğutma yöntemlerinin takım ömrünü uzatma, kesme sıcaklığını düşürme ve yüzey pürüzlülüğünü iyileştirme açısından önemli avantajlar sağladığı görülmüştür. Bu çalışmalar, Inconel 625'in zor işlenebilirliğine rağmen, uygun parametre ve soğutma koşullarının seçilmesiyle işleme verimliliğinin artırılabileceğini göstermektedir. Mevcut çalışmada ise, farklı kesme hızı değerlerinin kesme kuvveti, kesme sıcaklığı ve yüzey pürüzlülüğü üzerindeki etkileri deneysel olarak araştırılmıştır. Böylece, Inconel 625'in tornalama işlemi sırasında kritik kesme parametrelerinin optimize edilmesine yönelik literatüre katkı sağlanması hedeflenmiştir.

MATERYAL VE METOT

Bu çalışmada deney malzemesi olarak Inconel 625 süper alaşımı tercih edilmiştir. Inconel 625'in kimyasal bileşimi Tablo 1'de sunulmuştur.

Tablo 1. Inconel 625 alaşımının ağırlıkça (%) kimyasal bileşimi

Cr	Mo	Fe	Mn	Ti	Al	C	Ni
23	10	5	0,5	0,4	0,4	0,1	Kalan

İşleme deneylerinde, AC6030M kalitesinde ve WNMG080408 formunda temin edilen kaplamalı karbür kesici takımlar kullanılmıştır. Deneylerde Johnford TC-35 CNC torna tezgâhı kullanılmıştır. Tornalama işlemleri, kuru kesme koşulları altında; beş farklı kesme hızı (130, 150, 175, 200 ve 250 m/dak), sabit ilerleme miktarı (0,12 mm/dev) ve sabit talaş derinliği (1 mm) parametreleri ile gerçekleştirilmiştir. Deneysel kurulumun genel yapısı Şekil 1'de sunulmuştur. Ayrıca deneysel çalışanın yürütülmesinde izlenen adımlar Şekil 2'de verilmiştir.



Şekil 1. Deneysel kurulumun genel yapısı

Kesme kuvveti ölçümleri, Kistler marka 9257A model dinamometre kullanılarak gerçekleştirilmiştir. Deneyler sırasında, üç eksende (Fx, Fy ve Fz) elde edilen kuvvet bileşenleri kaydedilmiş ve bu bileşenlerin bileşkesi (F_R) hesaplanarak kesme kuvveti analizlerinde incelenmiştir. Kesme bölgesinde oluşan sıcaklıkların tespiti için yüksek hassasiyetli FLIR T440 termal kamera kullanılmıştır. Termal kamera, kesme sırasında takım ve iş parçası arasındaki sıcaklık değişimlerini hassas bir şekilde kaydetmiştir. Bu sayede, farklı kesme hızlarının kesme bölgesi sıcaklığı üzerindeki etkisi incelenmiştir. Yüzey pürüzlülüğü analizleri için ise Mitutoyo Surftest SJ-210 profilometre cihazı kullanılmıştır. Her bir deneyde, işlenmiş yüzeyden üç farklı noktada ölçüm alınmış ve bu ölçümlerin aritmetik ortalaması alınarak ortalama yüzey pürüzlülüğü (Ra) değeri belirlenmiştir.

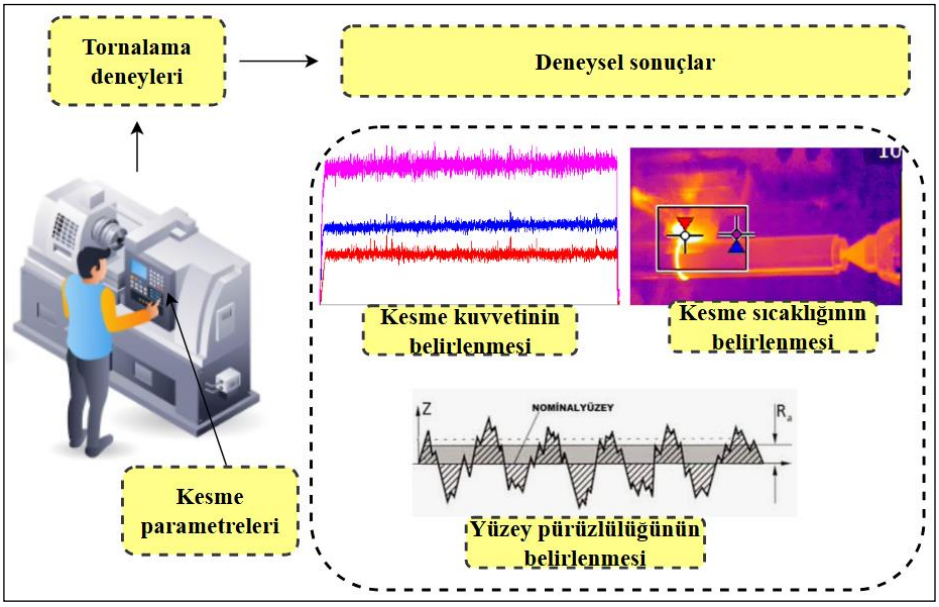

Şekil 2. Deneysel çalışmada izlenen adımlar

SONUÇLAR VE TARTIŞMA

Kesme Hızının Kesme Kuvvetine Etkisi

Kesme kuvveti, işleme sırasında enerji tüketimi, takım ömrü ve yüzey kalitesi üzerinde doğrudan etkili bir parametredir. Yüksek kesme kuvvetleri, takım aşınmasını artırırken işlem verimliliğini düşürür, düşük kesme kuvvetleri ise daha stabil ve ekonomik bir talaş kaldırma süreci sağlar. Bu nedenle, kesme kuvvetlerinin kontrol altında tutulması hem ekonomik hem de teknik açıdan yüksek verimli bir talaş kaldırma süreci için kritik öneme sahiptir. Kesme hızının kesme kuvveti üzerindeki etkisi Şekil 3'te verilmiştir.

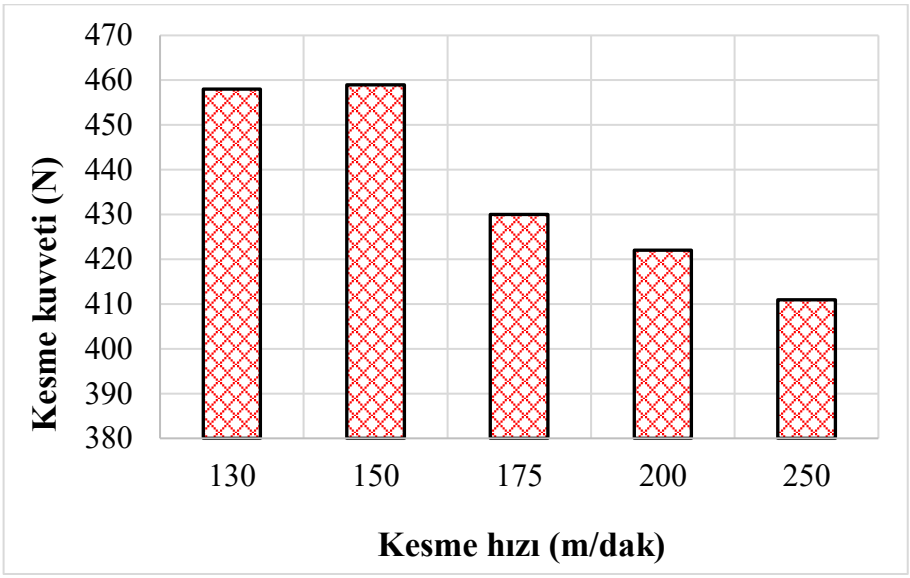

Şekil 3. Kesme hızına bağlı oluşan kesme kuvvetleri

Grafikte genel olarak kesme hızının artmasıyla kesme kuvvetinde belirgin bir azalma olduğu görülmektedir. Kesme hızının artmasıyla birlikte kesme kuvvetinin düşmeye başlaması, talaşlı imalat süreçlerinde sıkça gözlemlenen ve literatürde farklı şekillerde açıklanan bir olgudur. Bu durumun başlıca nedeni, kesme hızının artışıyla birlikte kesme bölgesinde meydana gelen sıcaklık artışıdır. Artan sıcaklık, iş parçası malzemesinin akma mukavemetini düşürerek, malzemenin plastik deformasyona karşı direncini azaltır (Çakıroğlu, 2023). Malzemenin daha kolay şekil değiştirmesi, kesme işlemi sırasında gerekli olan kuvvetin azalmasına yol açar. Ayrıca, artan kesme hızlarında kesici takım-talaş ara yüzeyindeki sıcaklık artacağından dolayı kesici takım-

talaş ara yüzeyinde sürtünme katsayısı azalmaktadır (Zhao ve ark., 2006). Bu durum kesme kuvvetlerinin azalması ile sonuçlanmaktadır.

Kesme Hızının Kesme Sıcaklığına Etkisi

Talaşlı imalat sırasında meydana gelen kesme sıcaklığı, kesme bölgesindeki sürtünme ve plastik deformasyon sonucu ortaya çıkmaktadır. Bu sıcaklık, takım ile iş parçası arasındaki etkileşimi doğrudan etkileyerek hem takım ömrü hem de işleme kalitesi üzerinde kritik bir rol oynar. Kesme hızının kesme sıcaklığı üzerindeki etkisi Şekil 4'te verilmiştir.

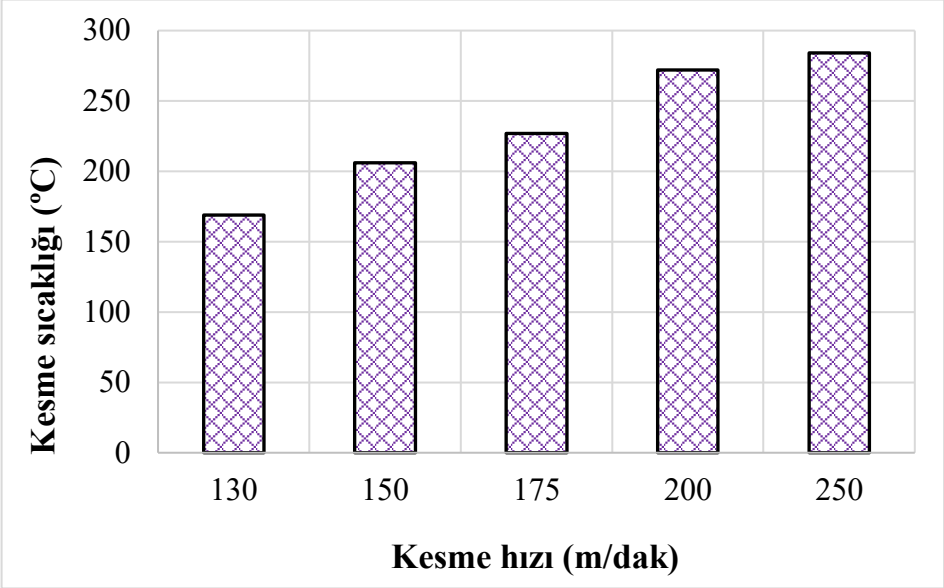

Şekil 4. Kesme hızına bağlı oluşan kesme sıcaklığı

Grafikte, kesme hızının artmasıyla kesme sıcaklığında belirgin bir artma olduğu görülmektedir. Literatürde, kesme hızının artmasıyla birlikte sıcaklığın da arttığı ve bu iki değişken arasında doğru orantı olduğu aktarılmaktadır (Ng ve ark., 1999). Kesme hızındaki artış, kayma düzlemindeki şekil değiştirme hızını doğrudan etkilerken, dolaylı olarak kesme sırasında oluşan ısının da artmasına yol açmaktadır (Duran ve ark., 2011). Bu durum, takım ile talaş arasındaki temas bölgesinde (ikinci deformasyon bölgesi) sıcaklığın artmasına neden olmaktadır. Kesme hızının artması, birinci deformasyon bölgesindeki şekil değiştirme hızını da artırmakta, bu durum talaş kaldırma işlemi sırasında daha fazla ısı oluşumuna ve dolayısıyla sıcaklık artışına neden olmaktadır (Davim ve Maranhão, 2009).

Kesme Hızının Yüzey Pürüzlülüğüne Etkisi

Yüzey pürüzlülüğü, işlenmiş parçanın fonksiyonel ve mekanik performansını doğrudan etkileyen önemli bir kalite kriteridir. Talaşlı imalat süreçlerinde kullanılan kesme parametreleri, takım geometrisi ve malzeme özellikleri, elde edilen yüzey kalitesini belirleyen temel faktörler arasında yer almaktadır. Kesme hızının yüzey pürüzlülüğü üzerindeki etkisi Şekil 5'te verilmiştir.

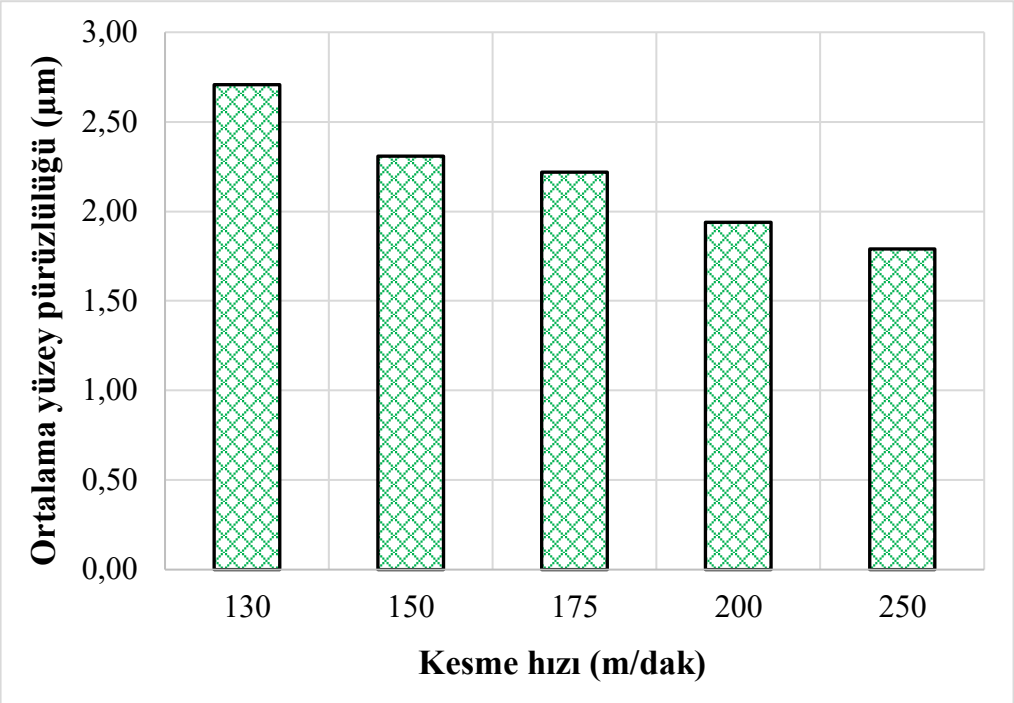

Şekil 5. Kesme hızına bağlı oluşan yüzey pürüzlülüğü

Grafikte, kesme hızının artmasıyla yüzey pürüzlülüğünde belirgin bir azalma olduğu görülmektedir. Kesme hızının artması ile düşen yüzey pürüzlülük değerleri, yüksek kesme hızlarında artan sıcaklığa bağlı olarak deformasyon işleminin kolaylaşması ile açıklanabilir (Sun ve ark., 2009). Ayrıca iyileşen yüzey pürüzlülüğü, düşük kesme hızlarında kesici takım yüzeyine malzeme yapışmasına yol açan BUE oluşumunun, artan kesme hızı sayesinde takım-talaş arasındaki temas alanı ve süresinin azalmasıyla önemli ölçüde engellenmesine bağlanabilir (Çakır, 2006; Acayaba ve Escalona, 2015; Jerold ve Kumar, 2012).

SONUÇLAR

Bu çalışmada, Inconel 625 süper alaşımının farklı kesme hızları altında işlenebilirliği incelenmiş; kesme kuvveti, kesme sıcaklığı ve yüzey pürüzlülüğü üzerindeki etkileri deneysel olarak değerlendirilmiştir. Elde edilen sonuçlar aşağıda maddeler halinde verilmiştir.

- Kesme hızı arttıkça kesme kuvvetinde belirgin bir azalma gözlemlenmiştir. Bu durum, artan sıcaklıkla birlikte malzeme akma mukavemetinin düşmesi ve sürtünme katsayısının azalmasına bağlanmıştır.
- Kesme hızındaki artış, kesme sıcaklığında belirgin bir yükselmeye neden olmuştur. Bu durum, şekil değiştirme hızının ve deformasyon bölgelerinde oluşan ısının artmasıyla ilişkilendirilmiştir.
- Artan kesme hızı ile yüzey pürüzlülüğü değerlerinde azalma elde edilmiştir. Bu sonuç, yüksek sıcaklıkların deformasyonu kolaylaştırması ve BUE oluşumunun azalması ile ilişkilendirilmiştir.

KAYNAKLAR

Acayaba, G. M. A., & De Escalona, P. M. (2015). Prediction of surface roughness in low speed turning of AISI316 austenitic stainless steel. CIRP Journal of Manufacturing Science and Technology, 11, 62–67. https://doi.org/10.1016/j.cirpj.2015.08.004

Akgün, M., & Demir, H. (2021). Experimental and numerical analysis of the effect of cutting parameters on cutting force and chip formation in turning process. El-Cezeri Journal of Science and Engineering, 8(2), 897–908. https://doi.org/10.31202/ecjse.892705

Alloy, N., Tian, Z., Zhang, C., Wang, D., Liu, W., & Fang, X. (2020). A Review on Laser Powder Bed Fusion of Inconel 625. Applied Sciences, 10(1), 81

Çakır, M. C. (2006). Modern Talaşlı İmalatın Esasları. Ankara: Nobel Yayın Dağıtım.

Choudhury, I. A., & El-Baradie, M. A. (1998). Machinability of nickel-base super alloys: A general review. Journal of Materials Processing Technology, 300(3–4), 278–284. https://doi.org/10.1016/s0924-0136(97)00429-9

Davim, J. P., & Maranhão, C. (2009). A study of plastic strain and plastic strain rate in machining of steel AISI 1045 using FEM analysis. Materials and Design, 30(1), 160–165. https://doi.org/10.1016/j.matdes.2008.04.029

Debnath, S., Reddy, M. M., & Yi, Q. S. (2014). Environmental friendly cutting fluids and cooling techniques in machining: A review. Journal of Cleaner Production, *83*, 33–47. https://doi.org/10.1016/j.jclepro.2014.07.071

Dhananchezian, M. (2018). Effectiveness of Cryogenic Cooling in Turning of Inconel 625 Alloy. In Advances in Manufacturing Processes: Select Proceedings of ICEMMM, 591–597. https://doi.org/https://doi.org/10.1007/978-981-13-1724-8_54

Jerold, B. D., & Kumar, M. P. (2012). Machining of AISI 316 stainless steel under carbon-di-oxide cooling. Materials and Manufacturing Processes, *27*(10), 1059–1065. https://doi.org/10.1080/10426914.2011.654153

Kosaraju, S., Vijay Kumar, M., & Sateesh, N. (2018). Optimization of Machining Parameter in Turning Inconel 625. Materials Today: Proceedings, 5(2), 5343–5348. https://doi.org/10.1016/j.matpr.2017.12.119

Lotfi, M., Jahanbakhsh, M., & Akhavan Farid, A. (2016). Wear estimation of ceramic and coated carbide tools in turning of Inconel 625: 3D FE analysis. Tribology International, 99, 107–116. https://doi.org/10.1016/j.triboint.2016.03.008

Ng, E. G., Aspinwall, D. K., Brazil, D., & Monaghan, J. (1999). Modelling of temperature and forces when orthogonally machining hardened steel. International Journal of Machine Tools and Manufacture, 39(6), 885–903. https://doi.org/10.1016/S0890-6955(98)00077-7

Duran, A., Turgut, Y., & Günay, M. (2011). Tornalamada Oluşan Takım-Talaş Ara Yüzey Sıcaklığının Pirometre ile Deneysel Olarak Ölçülmesi. Politeknik Dergisi, 14(4), 297–301.

Çakıroğlu, R., Günay, M. (2023). Analysis of surface roughness and energy consumption in turning of C17500 copper alloy under different machining environments and modellings with response surface method. Proceedings of the Institution of Mechanical Engineers, Part E: Journal of Process Mechanical Engineering, 237(2), 207–219. https://doi.org/https://doi.org/10.1177/09544089221101368

Shankar, V., Bhanu Sankara Rao, K., & Mannan, S. L. (2001). Microstructure and mechanical properties of Inconel 625 superalloy. Journal of Nuclear Materials, 288(2–3), 222–232. https://doi.org/10.1016/S0022-3115(00)00723-6

Sun, S., Brandt, M., & Dargusch, M. S. (2009). Characteristics of cutting forces and chip formation in machining of titanium alloys. International Journal of Machine Tools and Manufacture, *49*(7–8), 561–568. https://doi.org/10.1016/j.ijmachtools.2009.02.008

Yağmur, S. (2021). The effects of cooling applications on tool life, surface quality, cutting forces, and cutting zone temperature in turning of Ni-based Inconel 625. International Journal of Advanced Manufacturing Technology, 116(3–4), 821–833. https://doi.org/10.1007/s00170-021-07489-2

Yıldırım, Ç. V. (2019). Inconel 625 ' in Seramik Takımlarla Tornalanmasında Nano Kesme Sıvısının Kesme Sıcaklığı Üzerindeki Etkisi Effect of Nanofluid on Cutting Temperature in Turning of Inconel 625 with Ceramics Tools. 2019(November), 370–380.

Zhao, J., Ai, X., & Li, Z. L. (2006). Finite Element Analysis of Cutting Forces in High Speed Machining. In Materials Science Forum, 532, 753–756. https://doi.org/https://doi.org/10.4028/www.scientific.net/MSF.532-533.753

➢ *ORAL PRESENTATION*

İnce kesitli küresel dökme demirlerde döküm sıcaklığı, kesit kalınlığı ve ısıl işlem parametrelerinin mikro yapı ve sertliğe etkisi

Bekir Yavuzer*[1] (https://orcid.org/0000-0001-8984-774X), Yakup Ege[2], Murat Kaya[2], Yasin Kartal[2], Cem Çapanoğlu[2]

*[1]İstanbul Beykent Üniversitesi, Meslek Yüksekokulu, Elektronik ve Otomasyon Bölümü, İnsansız Hava Aracı Teknolojisi ve Operatörlüğü Pr, Istanbul, Türkiye
[2]Duyar Vana Mak. San. ve Tic. A.Ş, DUYAR Akademi, Istanbul, Türkiye

*Sorumlu yazar e-posta: bekiryavuzer@beykent.edu.tr

Özet

Bu çalışmada, farklı kesit kalınlıklarında dökülmüş küresel grafitli dökme demirlerin mikro yapısında oluşan karbürlerin ısıl işlem ile dönüştürülmesinde, ısıl işlem parametrelerinin etkisi Taguchi yöntemi ile analiz edilmiştir. İki farklı kesit kalınlığında (4 mm, 6 mm) ve iki farklı döküm sıcaklığında (1430 °C, 1330 °C) kum kalıba dökülmüş alaşımlar, 330 mm uzunluğunda ve 20 mm genişliğinde şeritler halinde üretilmiştir. Dökülen alaşımların kimyasal bileşimleri spektral analiz ile belirlenmiş ve karbon eşdeğeri hesaplanmıştır. Dökülmüş alaşımlar 25 mm uzunluğunda numuneler halinde kesilmiştir. Küresel grafitli dökme demirlerin ısıl işlemi, iki farklı sıcaklık (900 °C ve 950 °C) ve iki farklı bekleme süresinde (30 dak ve 60 dak) yapılmıştır. Bekleme sıcaklığına 5 °C/dak ısıtma hızında ulaşılmış ve bekleme süresinden sonra fırında soğutma yapılmıştır. Numunelerin mikro yapı görüntülerinin incelenebilmesi için standart metalografik yöntemler kullanılarak numune yüzeyleri hazırlanmıştır. Dağlama işlemi için %5 Nital çözeltisi kullanılmıştır. Dökülmüş ve ısıl işlem uygulanmış numunelerin Brinell sertlik ölçümleri yapılmıştır. Elde edilen deneysel sonuçlar Taguchi (L_{16}) yöntemi ile analiz edilmiştir. Döküm ile üretilen numunelerin mikro yapı incelemeleri sonucunda sementit ve ledeburid fazlarının yanında küresel şekilli grafitlerin olduğu ve bu grafitlerin boyutlarının ısıl işlem ile birlikte büyüdüğü görülmüştür. Döküm sıcaklığının alaşımın sertliğini etkilediği ve ısıl işlemler sonucunda, her iki kesit kalınlığında da ısıl işlem sıcaklığı ve süresi arttıkça sertlikte düşüş olduğu ölçülmüştür. Taguchi yöntemi ile yapılan analizler sonucunda, ince kesitli küresel grafiti dökme demirlerin sertliğinin azaltılmasında en etkili parametrenin bekleme süresi ve ısıl işlem sıcaklığı olduğu belirlenmiştir.

Anahtar Kelimeler: küresel grafitli dökme demir, ısıl işlem, karbür, ince kesitli döküm, Taguchi yöntemi, sertlik.

The effect of casting temperature, wall thickness, and heat treatment parameters on microstructure and hardness in thin-wall cast iron

Abstract

In this study, the effect of heat treatment parameters on the transformation of carbides formed in the microstructure of ductile cast irons cast in different cross-sectional thicknesses by heat treatment was analyzed by Taguchi method. Alloys cast in sand molds at two different section thicknesses (4 mm, 6 mm) and two different casting temperatures (1430 °C, 1330 °C) were produced in strips 330 mm long and 20 mm wide. The chemical compositions of the cast alloys were determined by spectral analysis and carbon equivalents were calculated. The cast alloys were cut into 25 mm long specimens. Spheroidal graphite cast irons were heat treated at two different temperatures (900 °C and 950 °C) and two different dwell times (30 min and 60 min). The dwell temperature was reached at a heating rate of 5 °C/min and cooling in the furnace was performed after the dwell time. In order to examine the microstructure images of the samples, the sample surfaces were prepared using standard metallographic methods. A 5% Nital solution was used for etching. Brinell hardness measurements of the cast and heat-treated samples were performed. The experimental results obtained were analyzed by Taguchi (L_{16}) method. As a result of the microstructure examination of the samples produced by casting, it was observed that there were spherical shaped graphites in addition to cementite and ledeburide phases and the size of these graphites increased with heat treatment. It was measured that the casting temperature affected the hardness of the alloy and as a result of heat treatment, hardness decreased as the heat treatment temperature and time increased in both section thicknesses. As a result of the Taguchi method

analysis, it was determined that the most effective parameters in reducing the hardness of thin section ductile cast irons are dwell time and heat treatment temperature.

Keywords: ductile cast iron, heat treatment, carbide, thin wall casting, Taguchi method, hardness.

GİRİŞ

Küresel grafiti dökme demirler (KGDD) uygun maliyetli, iyi termal iletkenlikleri, çoğu uygulama için yeterli mukavemet, aşınma ve yorulma gibi mekanik özellikleri nedeniyle otomotiv, inşaat ve enerji gibi sektörlerde kullanılmaktadır. Nispeten düşük ergime noktası ve akışkanlığının iyi olması hem büyük hem de küçük boyutlu karmaşık parçaların üretilmesine olanak tanımaktadır. Büyük boyutlu parçaların üretiminde uzun katılaşma süresi mikro büzülmelerden kaynaklı porozitelere ve segregasyonlara neden olmaktadır. Benzer şekilde ince kesitli parçaların dökümünde ise hızlı soğuma nedeniyle, mikro yapıda kırılganlığı arttıran denge dışı fazların (Fe_3C vb) oluşmasına neden olmaktadır (Morgiel et al., 2025; Yeung et al., 1998).

Kum kalıba dökümde ince kesitli (3 mm) parçaların soğuma hızı 30 °C/s – 60 °C/s arasında olduğu rapor edilmektedir. Bu soğuma hızlarında KGDD'lerin mikro yapısında karbürler oluşmakla birlikte bölgesel farklılıkların bulunduğu yapılar oluşmaktadır. Döküm ile üretimde soğuma hızını azaltmak için kum kalıba yalıtım malzemeleri yerleştirilmekte veya termal iletkenliği düşük kalıp malzemelerinin kullanılabilmektedir (Górny et al., 2019). Kalıp doldurma esnasında ısı kaybını en aza indirebilmek için yollukların kısa tutulması ve çıkıcıların kalıp içindeki havayı hızlıca tahliye edebilmesine imkân sağlayacak şekilde tasarlanması da çil oluşumunu önlemek için uygulanan yöntemlerdendir. Ancak döküm sonrası mikro yapıda oluşan karbürlerin oluşması mümkündür ve döküm sonrası, yapıda oluşan fazların dönüştürülmesi uygun ısıl işlem ile yapılabilmektedir. Dökme demirlerin mukavemetini arttıran sementitlerin ısıl işlem sırasında karbon atomlarının difüzyonu sonucu parçalandığı bilinmektedir (Megahed et al., 2019).

Bu çalışmada ince kesitli dökülmüş küresel grafitli dökme demirlerin mikro yapı ve sertliklerine döküm sıcaklığı, kesit kalınlığı ve ısıl işlem parametrelerinin etkisi incelenmiş ve sonuçlar Taguchi yöntemi ile analiz edilmiştir.

MATERYAL VE METOD

Bu çalışmada üretilen alaşımlar 2 ton kapasiteli ergitme ocağında 1505 °C sıcaklıkta döküm için potaya alınmıştır. Ergimiş metale Fe-70Si-2,5Ba-2Ca (%3) potada ilave edilerek küreselleştirme ve modifikasyon işlemi yapılmıştır. Döküm işlemi iki farklı sıcaklıkta (1430 °C ve 1330 °C) yapılmış ve dökümden 30 dakika sonra kalıplar açılmıştır. Kum kalıplara (silis kumu) yapılan dökümler, iki farklı kesit kalınlığında (4 mm ve 6 mm) üretilmiş şeritler halinde katılaştırılmıştır. Üretilen dökme demir şeritler 25 mm uzunluğunda numuneler olarak kesilmiştir (Şekil 1). Dökümü yapılan KGDD'lerin kimyasal bileşimi Tablo 1'de verilmektedir.

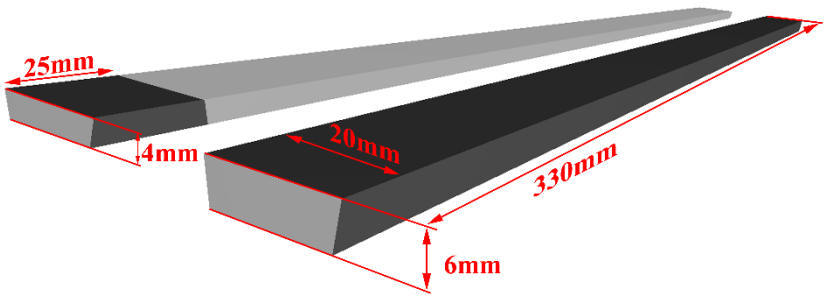

Şekil 1. Farklı kesit kalınlıklarında dökülen KGDD şeritlerin boyutları.

Tablo 1. Üretilen alaşımların kimyasal bileşimi.

Fe [%]	C [%]	Si [%]	Mn [%]	P [%]	S [%]
94,2	3,83	1,65	0,153	0,0417	0,0232

Tablo 1'de verilen kimyasal bileşime bağlı olarak alaşım karbon eşdeğeri 4,34 olarak hesaplanmıştır. Farklı döküm sıcaklığına ve kesit kalınlıklarına sahip numuneler, iki farklı sıcaklık (900 °C ve 950 °C) ve iki farklı

bekleme süresinde (30 dak ve 60 dak) ısıl işleme tabi tutulmuştur. Isıtma 5 °C/dak, soğutma ise 5 °C/dak'dan daha hızlı olmamak üzere, fırın ortamında gerçekleştirilmiştir (Şekil 2).

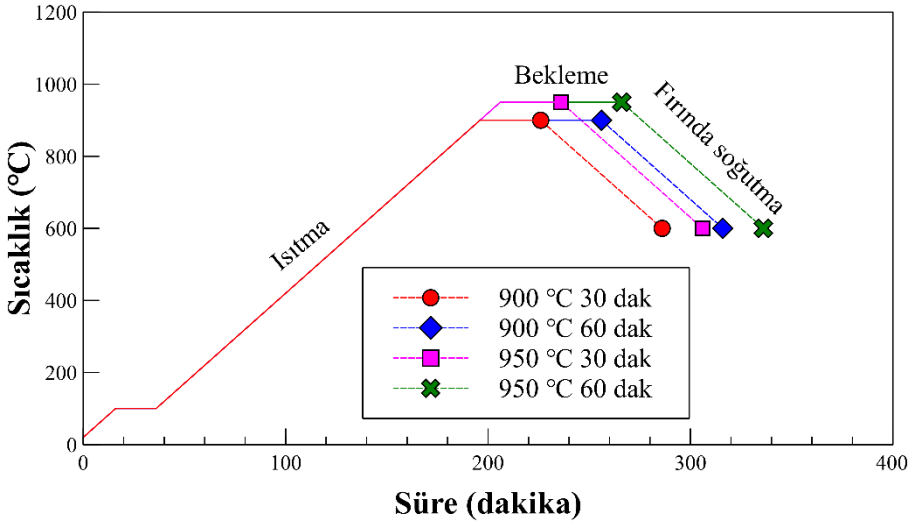

Şekil 2. Farklı kesit kalınlıklarında üretilen KGDD'lere uygulanan ısıl işlemler.

Isıl işlem sonrası numuneler metalografik zımparalama ve parlatmadan sonra %5 Nital çözeltisinde dağlanmıştır. Numunelerin mikro yapıları optik mikroskopta incelenmiş ve mikro yapıda oluşan fazlar XRD ile karakterize edilmiştir. Isıl işlem sonrası numunelerinin Brinell sertlikleri ölçülmüştür. Elde edilen deneysel sonuçlar kullanılarak Taguchi yöntemi ile alaşımın sertliğine en çok etki eden parametre belirlenmiştir.

BULGULAR ve TARTIŞMA

Şekil 3'de dökülmüş ve ısıl işlem görmüş küresel grafitli dökme demirlerin XRD desenleri verilmektedir.

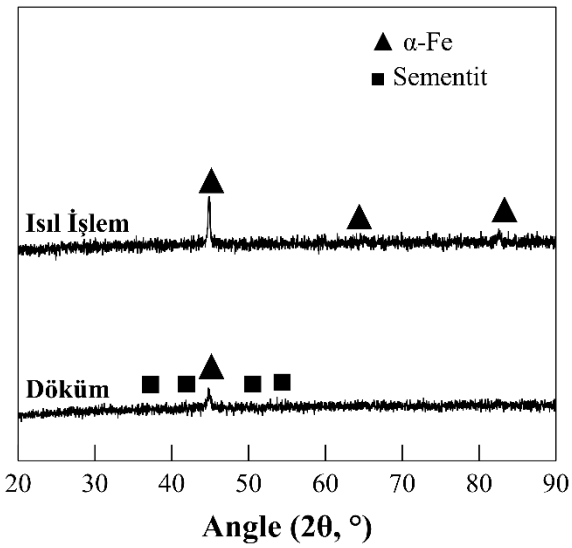

Şekil 3. Dökülmüş ve ısıl işlem uygulanmış küresel grafiti dökme demirlerin XRD analizleri.

Şekil 3'de verilen XRD analizi grafiği incelendiğinde dökülmüş KGDD'nin mikro yapısındaki ferrit pikinin daha küçük olduğu, ısıl işlem sonrasında ise ferrittin hem pik sayısının hem de pik yüksekliklerinin arttığı ve sementit piklerinin kaybolduğu açıkça anlaşılmaktadır. Isıl işlem sonucunda mikro yapıda bulunan sementit fazlarının çözüldüğü ve ferrit fazının arttığı anlaşılmaktadır.

Şekil 4'de 4 mm ve 6 mm kesit kalınlığındaki küresel grafitli dökme demirlerin dökülmüş ve ısıl işlem uygulanmış optik mikroskop mikro yapı görüntüleri verilmektedir.

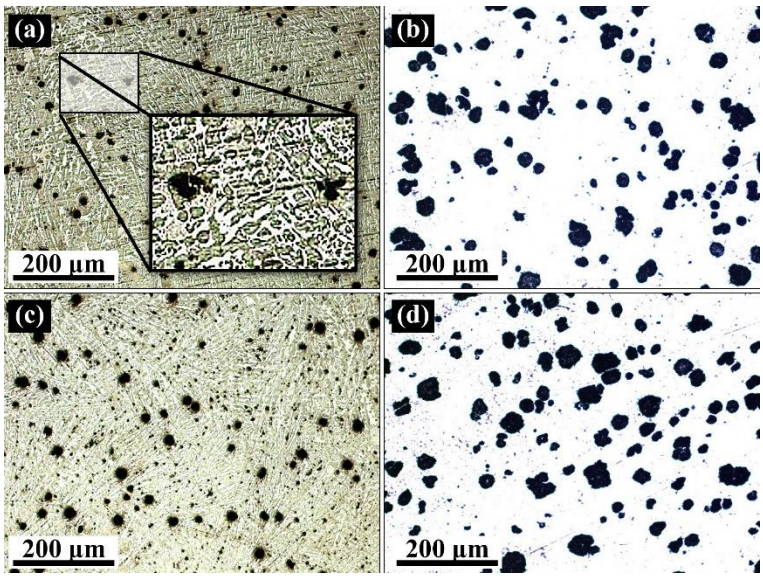

Şekil 4. Optik mikroskop mikro yapı görüntüleri: a) 4 mm kesit kalınlığı 1430 °C döküm; b) 4 mm kesit kalınlığı 950 °C 1 saat ısıl işlem sonrası; c) 6 mm kesit kalınlığı 1430 °C döküm; d) 6 mm kesit kalınlığı 950 °C 1 saat ısıl işlem sonrası.

Şekil 4.a ve c'de verilen optik mikroskop görüntüleri incelendiğinde, her iki kesit kalınlığında dökülmüş alaşımların mikro yapılarının küresel şekilli grafitler ile açık ve koyu renkli bölgelerden oluştuğu görülmektedir. Açık renkli bölgelerin sementit ve ledeburid, koyu renkli bölgelerin ise perlit fazları olduğu anlaşılmaktadır. İnce kesitli dökme demirlerin seri üretim şartlarında dökümünde sementitli bir mikro yapı oluşması beklenen bir durumdur. Ayrıca literatürde yapılan çalışmalar arasında, karbürsüz bir mikro yapı için karbon eşdeğerinin 4,3'den daha fazla olması gerektiğini belirten çalışmalar olsa da genel olarak 4,4-4,6 aralığında olması önermektedir(Sulamet-Ariobimo et al., 2023). Bu çalışmada karbon eşdeğerinin tavsiye edilen değerden daha düşük olduğu göz önüne alındığında (4,34), karbürlü bir mikro yapının oluşması olağan bir durumdur. Tablo 1 ve Şekil 3'de verilen dökülmüş alaşımların sertlik değerlerinin çok yüksek olmasının nedeni, mikro yapının büyük bölümünü oluşturan bu sert fazların varlığıdır. Kesit kalınlığı azaldıkça soğuma hızındaki artış sementit oluşumunu teşvik etmektedir (Ceschini et al., 2017; Megahed et al., 2019). Dikkat çeken bir başka durum ise 6 mm kesit kalınlığına sahip numunenin mikro yapısındaki küresel grafitlerin 4 mm kesit kalınlığına oranla daha büyük olmalarıdır. Literatürde yapılan araştırmalar incelendiğinde kesit kalınlığı arttıkça soğuma hızındaki yavaşlamadan dolayı grafit miktarının azalması ve boyutlarının ise artması beklenen bir durumdur (Ceschini et al., 2017; Choi et al., 2004). Isıl işlem sonrası her iki kesit kalınlığına ait mikro yapılarda da (Şekil 4.b ve d) sementit ve ledeburid fazlarının çözülmüş olduğu ve ferritik bir matris ile küresel şekilli grafitlerin varlığı görülmektedir. Isıl işlem sonrası grafit boyutlarının büyüdüğü de dikkat çekicidir. Isıl işlem ile yüksek karbon içeriğine sahip sementit ve ledeburid fazları çözülerek serbest kalan karbon, küresel grafitlerin büyümesine neden olmaktadır (Akinribide et al., 2022). Şekil 3'de verilen XRD grafiği de bu durumu desteklemektedir. Tablo 2'de farklı kesit kalınlıklarında dökülmüş ve farklı ısıl işlem parametreleri ile ısıl işlem uygulanmış küresel grafiti dökme demirlerin Brinell sertlikleri verilmektedir.

Tablo 2. Isıl işlem sıcaklığı ve bekleme süresine bağlı olarak sertlik değişimleri.

Kesit kalınlığı	Döküm sıcaklığı	Isıl işlem sıcaklığı	Bekleme süresi	Sertlik HB (döküm)	Sertlik HB (ısıl işlem)
4	1430	900	30 dak	405	120
6	1430	900	30 dak	390	135
4	1330	900	30 dak	440	130
6	1330	900	30 dak	420	135
4	1430	950	30 dak	405	102
6	1430	950	30 dak	390	130
4	1330	950	30 dak	440	115
6	1330	950	30 dak	420	125
4	1430	900	60 dak	405	90
6	1430	900	60 dak	390	112
4	1330	900	60 dak	440	110
6	1330	900	60 dak	420	125
4	1430	950	60 dak	405	75
6	1430	950	60 dak	390	92
4	1330	950	60 dak	440	90
6	1330	950	60 dak	420	105

Tablo 2'de verilen değerler incelendiğinde, dökülmüş küresel grafiti dökme demirlerin sertliklerinin, ısıl işlem uygulanması sonrası kritik şekilde azaldığı anlaşılmaktadır. Tablo 2'deki sonuçlar normal dağılım ve etkileşim grafiği çiziminde kullanılmıştır. Ayrıca bu değerler kesit kalınlıklarına göre ayrı ayrı sütun grafik olarak Şekil 5'de verilmektedir.

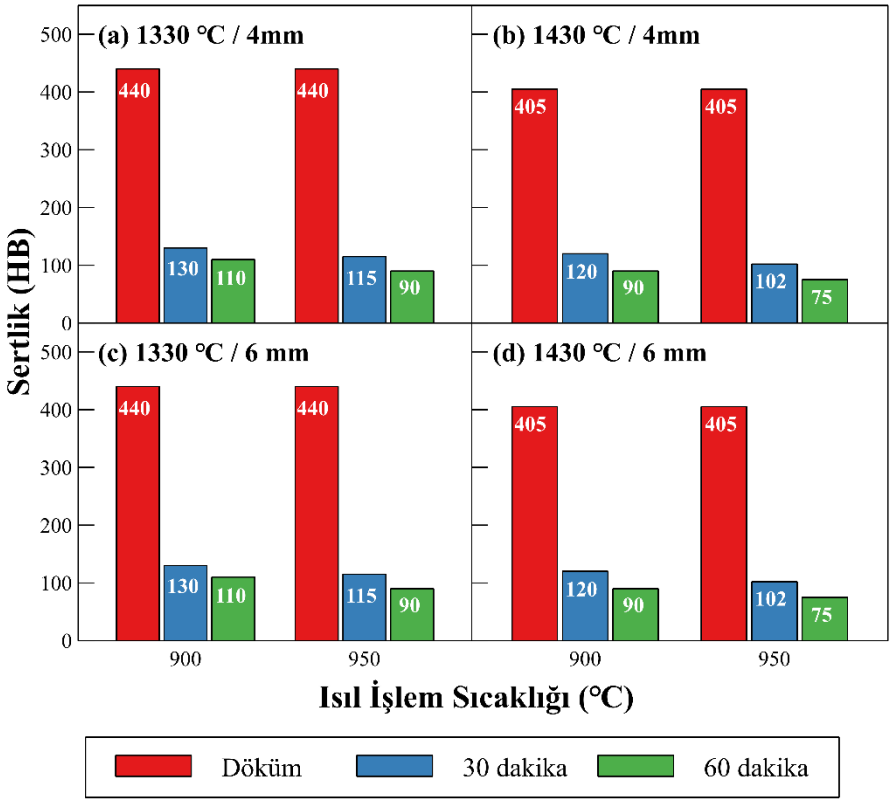

Şekil 5. Farklı kesit kalınlığı ve farklı sıcaklıklarda dökülmüş KGDD'lerin ısıl işlem bekleme süresi ve sıcaklığına bağlı sertlik değişimleri.

Şekil 5'de verilen sertlik değişimi grafikleri incelendiğinde ince kesitli dökülmüş küresel grafitli dökme demirlerin sertlikleri 390 HB – 440 HB arasında değişmektedir. Ayrıca 1430 °C döküm sıcaklığında dökülmüş alaşımların sertliklerinin, 1330 °C'de dökülmüş alaşımlara oranla her iki kesit kalınlığında da daha az olduğu anlaşılmaktadır. Kesit kalınlığı arttıkça sertlik değerlerindeki azalma da literatürdeki çalışmalar ile uyumludur (Ceschini et al., 2015; Itofuji et al., 2025). Isıl işlem sonrası ise tüm numunelerde kritik sertlik azalmaları ölçülmüştür. Bu duruma ek olarak ısıl işlem sıcaklığı ve bekleme sürelerinin artmasıyla birlikte de sertliklerin daha da azaldığı görülmektedir. Akinribide vd (Akinribide et al., 2021) yapmış oldukları bir çalışmada benzer sonuçları elde etmişlerdir. Tablo 1'deki veriler kullanılarak Şekil 6'da görülen Taguchi normal olasılık grafiği (L_{16}) çizilmiştir.

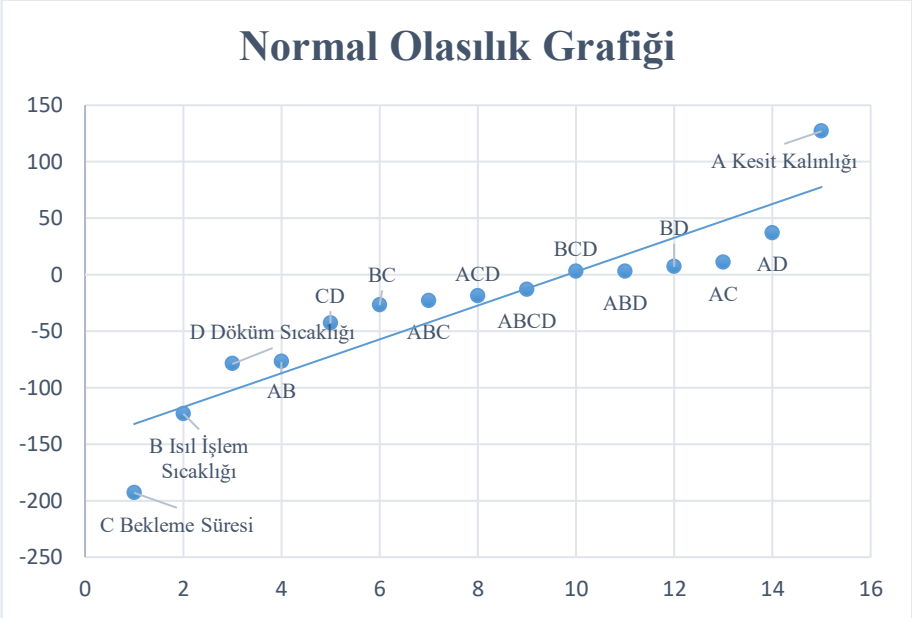

Şekil 6. Döküm ve ısıl işlem parametreli normal dağılım grafiği.

Normal olasılık grafiğinde önemli noktalar, grafiğin alt tarafında, doğrunun solunda kalan noktalar ya da grafiğin üst tarafında, doğrunun sağında kalan noktalardır. Şekil 6'da verilen normal dağılım grafiği incelendiğinde AD ve AC etkileşimlerinin istatistiksel olarak alaşımın sertliğini etkilemede önemli olduğu anlaşılmaktadır.

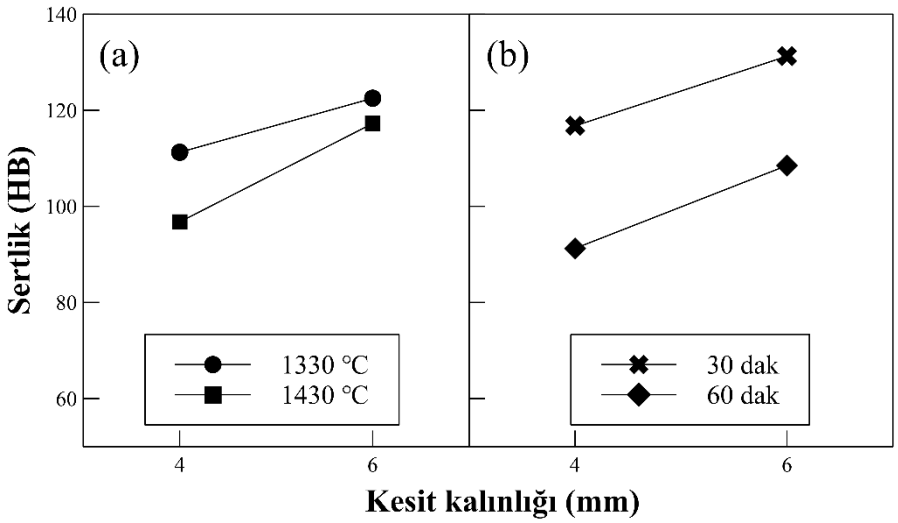

Şekil 7. Üretim parametreleri etkileşimleri: a) AD ve b) AC.

Şekil 7.a'da verilen kesit kalınlığı-döküm sıcaklığı etkileşim grafiği (AD etkileşimi) incelendiğinde, ortalama olarak en düşük sertlik değerini elde edebilmek için kesit kalınlığını 4 mm ve döküm sıcaklığının da 1430 °C olarak seçilmesi gerektiği anlaşılmaktadır. Şekil 7.b (AC etkileşimi) incelendiğinde ise bekleme süresi ile doğru orantılı olarak sertliğin de azaldığı görülmektedir. Bu etkileşimde ise kesit kalınlığı ile bekleme süresinin arttırılması benzer miktarlarda sertlik düşüşüne neden olduğu anlaşılmaktadır.

SONUÇ

Bu çalışmada ince kesitli küresel grafitli dökme demirlerin mikro yapı ve sertlik özelliklerine döküm sıcaklığı, ısıl işlem sıcaklığı ve ısıl işlem süresinin etkisi incelenmiştir. Elde edilen sonuçlar aşağıda verilmektedir;

- Mikro yapılar incelendiğinde, küresel grafitli dökme demirlerin döküm sonrası mikro yapısı grafit, sementit ve perlit fazlarından oluşmuştur.
- Isıl işlem sonrası küresel grafitli dökme demirlerin mikro yapısının ferrit ve küre şekilli grafitlerden oluştuğu görülmüştür.
- Isıl işlem sıcaklığı ve süresi arttıkça grafitlerin boyutlarının da arttığı belirlenmiştir.
- İstatistiksel analiz sonucunda, parametreler arasında en önemli olanının kesit kalınlığı ve döküm sıcaklığı etkileşimi olduğu tespit edilmiştir.

TEŞEKKÜR

Bu çalışma Duyar Vana Mak. San. Ve Tic. A.Ş tarafından desteklenmiştir.

KAYNAKLAR

Akinribide, O. J., Ogundare, O. D., Oluwafemi, O. M., Ebisike, K., Nageri, A. K., Akinwamide, S. O., Gamaoun, F., & Olubambi, P. A. (2022). A Review on Heat Treatment of Cast Iron: Phase Evolution and Mechanical Characterization. Materials, 15(20). https://doi.org/10.3390/ma15207109

Akinribide, O. J., Olusunle, S. O. O., Akinwamide, S. O., Babalola, B. J., & Olubambi, P. A. (2021). Impact of heat treatment on mechanical and tribological behaviour of unalloyed and alloyed ductile iron. Journal of Materials Research and Technology, 14, 1809–1819. https://doi.org/10.1016/J.JMRT.2021.07.077

Ceschini, L., Al., M., An., M., E., S., R., S., I., T., & and Tomesani, L. (2015). Microstructure and mechanical properties of heavy section ductile iron castings: experimental and numerical evaluation of effects of cooling rates. International Journal of Cast Metals Research, 28(6), 365–374. https://doi.org/10.1179/1743133615Y.0000000022

Ceschini, L., Morri, A., & Morri, A. (2017). Effects of Casting Size on Microstructure and Mechanical Properties of Spheroidal and Compacted Graphite Cast Irons: Experimental Results and Comparison with International Standards. Journal of Materials Engineering and Performance, 26(6), 2583–2592. https://doi.org/10.1007/s11665-017-2714-7

Choi, J. O., Kim, J. Y., Choi, C. O., Kim, J. K., & Rohatgi, P. K. (2004). Effect of rare earth element on microstructure formation and mechanical properties of thin wall ductile iron castings. Materials Science and Engineering: A, 383(2), 323–333. https://doi.org/10.1016/J.MSEA.2004.04.060

Górny, M., Kawalec, M., Witek, G., & Rejek, A. (2019). The influence of wall thickness and mould temperature on structure and properties of thin wall ductile iron castings. Archives of Foundry Engineering, 19(2). https://doi.org/10.24425/afe.2019.127116

Itofuji, H., Miyamoto, Y., Iwakado, K., & Kotani, T. (2025). Examples of Chunky Graphite Formation in Production of Ductile Iron Castings and Effective Countermeasures. International Journal of Metalcasting, 19(2), 682–698. https://doi.org/10.1007/s40962-024-01324-6

Megahed, H., El-Kashif, E., Shash, A. Y., & Essam, M. A. (2019). Effect of holding time, thickness and heat treatment on microstructure and mechanical properties of compacted graphite cast iron. Journal of Materials Research and Technology, 8(1), 1188–1196. https://doi.org/10.1016/J.JMRT.2018.07.021

Morgiel, K., Dyrlaga, Ł., Kopyciński, D., & Morgiel, J. (2025). Investigation of M6C and M7C3 carbides in SiMo ductile cast iron alloyed with Al and Cr. Journal of Alloys and Compounds, 1020, 179480. https://doi.org/10.1016/J.JALLCOM.2025.179480

Sulamet-Ariobimo, R. D., Fadhlan, M., Oktaviano, Y., Sukarnoto, T., Mujalis, Y., & Witonohadi, A. (2023). The effects of I-Beam thickness to microstructure and compression load of thin wall ductile iron connecting rod. International Journal of Lightweight Materials and Manufacture, 6(3), 392–404. https://doi.org/10.1016/J.IJLMM.2023.01.001

Yeung, C. F., Zhao, H., & Lee, W. B. (1998). The Morphology of Solidification of Thin-Section Ductile Iron Castings. Materials Characterization, 40(4–5), 201–208. https://doi.org/10.1016/S1044-5803(98)00012-6.

➢ *ORAL PRESENTATION*

Model Organizma Olarak *Drosophila melanogaster*'de Levetirasetamın Toksisitesi ve Roselle'nin Olası Koruyucu Etkisi

Amir Mohammad MUQIM (https://orcid.org/0009-0003-3456-6096)[1]
Fahriye ZEMHERİ NAVRUZ (https://orcid.org/0000-0003-1744-1091)[2]

[1]Bartın Üniversitesi, Lisansüstü Eğitim Enstitüsü, Moleküler Biyoloji ve Genetik ABD, Bartın, Türkiye
[2]Bartın Üniversitesi, Fen Fakültesi, Moleküler Biyoloji ve Genetik Bölümü, Bartın, Türkiye

*Sorumlu yazar e-posta: amirmomuqim@outlook.com, fzemheri@bartin.edu.tr

ÖZET

Levetirasetam, yaygın olarak kullanılan bir antiepileptik ve analjezik ajandır. Son yıllarda, epilepsi hastalarında nöbet sıklığını azaltmak amacıyla etkin bir tedavi seçeneği olarak kullanılmaktadır. Epilepsi; genetik yatkınlık, travmatik beyin hasarı, ağır enfeksiyonlar, tümör gelişimi ve diğer bilinmeyen patojenik varyantlara bağlı olarak ortaya çıkan kronik bir nörolojik bozukluktur. Yapılan çalışmalarda, levetirasetamın üreme fonksiyonlarında bozulmaya ve hormon düzeylerinde değişikliklere neden olabileceği belirtilmiştir. Ayrıca bu ilacı kullanan bireylerde, folik asit ve B12 vitamini eksikliğine bağlı olarak oksidatif stres gelişebileceği öne sürülmektedir. Roselle (*Hibiscus sabdariffa*), farmakolojik özellikleri ve zengin antioksidan içeriği ile bilinmekte olup, uzun süredir gıda ve içeceklerde kullanılan ve sağlığa faydalı olduğu bildirilen bir bitkidir. Bu çalışmada, model organizma olarak kullanılan *Drosophila melanogaster* üzerinde levetirasetam ve roselle'in farklı dozlarının toksik ve oksidatif stresle ilişkili etkileri araştırılmıştır. Besiyerlerine sırasıyla Kontrol, 50 µl, 100 µl, 100 µl+50 µl, 200 µl ve 50 µl+200 µl dozları uygulanmıştır. Larval toksisite deneyinde, 3. evre larvalar ilgili besiyerlerine eklenmiş ve 14 gün boyunca izlenerek larvadan pupaya, pupadan erişkin sineğe geçiş oranları değerlendirilmiştir. Tırmanma davranışı testinde ise erişkin sinekler aynı besiyerlerine eklenmiş ve 7 günlük maruziyetin ardından tüpün üst kısmına ulaşan sinek sayıları kaydedilerek motor performansları analiz edilmiştir. Sonuçlar, levetirasetamın gelişim oranları üzerinde anlamlı bir etki oluşturmadığını ancak tırmanma performansını olumsuz etkilediğini göstermiştir. Buna karşın, roselle uygulamasının gelişim sürecini desteklediği ve motor performansı belirgin şekilde artırdığı gözlemlenmiştir. Bu bulgular, roselle'nin oksidatif stresin etkilerini azaltıcı bir potansiyele sahip olduğunu göstermektedir.

Anahtar Kelimeler: Levetirasetam, *Hibiscus sabdariffa*, *Drosophila melanogaster*, oksidatif stres, tırmanma davranışı, larval toksisite

Toxicity of Levetiracetam and the Potential Protective Role of Roselle in a *Drosophila melanogaster* Model

ABSTRACT

Levetiracetam is a widely used antiepileptic and analgesic agent. In recent years, it has been employed as an effective treatment option to reduce seizure frequency in patients with epilepsy. Epilepsy is a chronic neurological disorder that may arise due to genetic predisposition, traumatic brain injury, severe infections, tumor development, or other unknown pathogenic variants. Studies have suggested that levetiracetam may cause adverse effects such as impaired reproductive function and altered hormone levels. Additionally, oxidative stress has been observed in patients using this drug, potentially due to folic acid and vitamin B12 deficiencies. Roselle (*Hibiscus sabdariffa*), known for its pharmacological properties and high antioxidant content, has long been used in foods and beverages and is considered beneficial for health. In this study, the toxic and oxidative stress-related effects of levetiracetam and roselle at different doses were investigated using *Drosophila melanogaster* as a model organism. Experimental groups received treatments at the following doses: Control, 50 µl, 100 µl, 100 µl+50 µl, 200 µl, and 50 µl+200 µl. In the larval toxicity assay, third-instar larvae were added to the media and monitored for 14 days to observe their development from larva to pupa and from pupa to adult. In the climbing behavior assay, adult flies were exposed to the same media

and their motor performance was evaluated by counting the number of flies that reached the top of the tube after 7 days. The results showed that levetiracetam had no significant effect on developmental rates but negatively affected climbing performance. In contrast, roselle improved both developmental outcomes and motor performance. These findings suggest that roselle may have potential to reduce the effects of oxidative stress.

Keywords: Levetiracetam, *Hibiscus sabdariffa*, *Drosophila melanogaster*, oxidative stress, climbing behavior, larval toxicity

GİRİŞ

Epilepsi, dünya genelinde istatistiksel olarak her 100 kişiden yaklaşık birini etkileyen, nöronal ağlarda artan uyarılabilirlikten kaynaklanan yaygın, zayıflatıcı ve potansiyel olarak kronik bir nörolojik bozukluktur. Hastalığın etiyolojisinde genetik yatkınlık, travma, enfeksiyonlar ve tümör oluşumu gibi çeşitli patojenik faktörler rol oynamaktadır. Epilepsi, çocukluk dönemindeki nörogelişimsel bozukluklarla ve ileri yaşlarda Alzheimer gibi nörodejeneratif hastalıklarla sıklıkla birlikte görülebilmektedir (Deneubourg ve ark., 2024). Levetirasetam, epileptik nöbetleri kontrol altına almak amacıyla onaylanmış bir tedavi seçeneğidir. Geniş spektrumlu bu antiepileptik ilaç, özellikle pediatrik hastalarda fokal ve jeneralize nöbetlerin kontrolünde monoterapi ya da kombine tedavi olarak yaygın şekilde kullanılmaktadır. Bununla birlikte, literatürde levetirasetam kullanımıyla ilişkili çeşitli yan etkiler rapor edilmiştir (Diler Durgut ve ark., 2019). İlacın en yaygın advers etkilerinden biri olan renk körlüğü, görsel işlev bozukluklarına örnek teşkil etmektedir. Ayrıca, diğer bazı antiepileptik ilaçlar da bulanık görme, renk algı bozukluğu ve görme alanı kusurları gibi etkiler gösterebilmektedir. Üreme toksisitesi açısından değerlendirildiğinde ise hormon düzeylerindeki değişikliklerin ve ilaç etkisinin birlikte rol oynadığı düşünülmektedir (Baysal ve ark., 2017). El-Shorbagy ve arkadaşlarının (2016) çalışmalarında levetirasetamın nörotoksik ya da hepatotoksik etkileri hakkında yeterli veri bulunmadığı belirtilmiştir.

Roselle (*Hibiscus sabdariffa*) bitkisinin kökeni tam olarak bilinmemekle birlikte, bazı kaynaklarda Batı Afrika'dan türediği öne sürülmektedir. Günümüzde ise evrimsel adaptasyonu sayesinde Suudi Arabistan, Çin, Malezya, Vietnam, Sudan, Mısır, Nijerya, Meksika, Endonezya, Filipinler ve Hindistan gibi birçok ülkede yaygın olarak yetiştirilmektedir. Roselle, gıda endüstrisinden kozmetiğe kadar pek çok sektörde kullanılmakta olup; sıcak-soğuk içecekler, fermente ürünler, reçel, şekerleme, tatlılar ve pastacılık ürünlerinde de yer almaktadır. Ayrıca geleneksel tıpta idrar söktürücü, kan viskozitesini azaltıcı ve bağırsak hareketlerini uyarıcı olarak kullanımı yaygındır (El-Refai ve ark., 2010). Bitkinin yaprak ve özlerinde antibakteriyel, antifungal, antiparazitik, analjezik, antiinflamatuar, antidiyabetik, antihipertansif, antianemik, antihiperkolesterolemik, hepatoprotektif, nefroprotektif ve antioksidan etkiler gösterdiği birçok çalışmada doğrulanmıştır (López-Romero ve ark., 2018; Izquierdo-Vega ve ark., 2020).

Drosophila melanogaster, epileptik nöbetler de dahil olmak üzere çeşitli nörolojik hastalıkların modellenmesinde yaygın şekilde kullanılan genetik bir model organizmadır. İnsan ve Drosophila arasında %75 oranında homolog hastalık geni benzerliği bulunması, bu organizmayı epileptik mekanizmaların incelenmesinde ve antikonvülsan ilaç taramalarında değerli kılmaktadır (Pandey ve Nichols, 2011; Pappus ve ark., 2017). Ayrıca, *Drosophila* üzerinde yapılan çalışmalar etik açıdan da avantajlı kabul edilmektedir (Demir, 2016). Sistem biyolojisi yaklaşımlarında, yüksek organizmaların karmaşıklığı nedeniyle basit model organizmalar üzerinden öngörücü hastalık modelleri geliştirmek günümüzde tercih edilen yöntemlerden biridir (Mohammad ve ark., 2009).

Bu çalışmada, model organizma olarak *Drosophila melanogaster* kullanılarak, levetirasetamın olası toksik etkileri ile roselle'nin potansiyel koruyucu etkileri, larval gelişim ve tırmanma davranışı analizleri yoluyla araştırılmıştır. Levetirasetam ve roselle'nin birlikte değerlendirildiği bu çalışma, her iki maddenin *D. melanogaster* üzerindeki etkilerini kombine olarak inceleyen literatürdeki ilk çalışmalardan biri olma özelliğini taşımaktadır.

MARERYAL VE METOT

Kullanılan Model Organizma, Yetiştirme ve Mama hazırlama

Bu çalışma, Bartın Üniversitesi, Fen Fakültesi bünyesindeki Moleküler Biyoloji ve Genetik Araştırma Laboratuvarı'nda gerçekleştirildi. *D.melanogaster* özel şartlarda etüv cihazında 25 ± 1°C, %60 nemli ortamda ayrıca aydınlığa ve karanlığa 12 saat ayarlı olarak yetiştirilmektedir. *D.melanogaster* insan genetik benzerliğe sahip olması, toksik ve genotoksik etkili sonuçları elde edilmesi, laboratuvarda yetiştirilmesi kolayı olması ve *D.melanogaster* çok çeşitli soydaşı bulunması. bu deneyde *D.melanogaster* genetik olarak homozigot, mutant karakter taşımayan, kırmızı gözlü ve Oregon-R yabanıl soyu kullanıldı. *D.melanogaster* stok hazırlanmasında içeriği ve kullanılan asit karışımı sırasıyla tablo 1´de ve tablo 2´de verilmiştir (Sun ark., 2013).

Tablo 1: Stok hazırlama içeriği

Kullanılan malzeme	Kullanılan miktar
Mısır unu	26,5 g
Şeker	23 g
Maya	1,75 g
Agar	3 g
Distile Su	255 ml
Asit karışımı	1,5 µl

Tablo 2: Asit karışımı içreği

Kullanılan kimyasal	Kullanılan miktar
Propiyonik asit	1250 µl
Ortofosforik asit	120 µl
Distile Su	130 µl

Kullanılan Kimyasal Maddeler

Çalışmamızda etkilerini araştırmak için Levetirasetam (Epixx, Turkiye) ve Roselle (Attar, Saudi Arabia) kurutulmuş halinde temin edildi. Besiyeri hazırlarken ve diğer işlemlerde kullanılan kimyasal Maddeler: dietil eter (IsoLab, Germany), propiyonik asit (Merck, Germany), ortofosforik asit (Merck, Germany), %96'lık alkol, low melting agaroz (BioShop Canada Inc.) kimyasalları kullanıldı.

Deney Düzeneği ve Hazırlama Yöntemi

Çalışmamızda Larval Toksisite ve Tırmanma performansı deneyleri yapıldı. Levetirasetam dozunu belirleme amacıyla Singh ve arkadaşlarının yapılan çalışmalarının referans alınarak doz belirleme çalışması yapıldı (Singh P. ve ark., (2011). Roselle ise hazırlaması için Gad ve arkadaşlarının tarafından yapılan araştırmaya dayanarak belirli su ile kaynatarak hazırlandı (Gad, F. A. M. ark., 2021). Kullanılan konsantrasyon ise Nainu, F. ark., (2020) referansa göre dozlar belirleme çalışması yapılarak belirlenmiştir. Kültür şişelerde yetiştirilen *D.melanogaster*´i eşit şekilde 50 ml falkon tüpüne hazırlanan 10 ml besiyerin üzerine levetirasetam ve roselle´nin belirli dozlar eklenerek sinekler yerleştirildi. Bu çalışma deneyi grupları ve dozları miktarları tablo 3´te verilmiştir.

Tablo 3: . Deneyi grupları ve doz miktarları

Deneyi gruplar	Deneyi düzeneği	Deneyin doz miktarları
1. grup	Kontrol (Negatif)	-
2. grup	Levetirasetam	50 µl
3. grup	Roselle	100 µl
4. grup	Levetirasetam + Roselle	50 µl + 100 µl
5. grup	Roselle	200 µl
6. grup	Levetirasetam + Roselle	50 µl + 200 µl

Larval Toksisite

Larval toksisite çalışma deneyi için tüm gruplarında *D.melanogaster´*ın 3 evre larvaları kullanıldı. Standart besiyeri yetiştirilen dişi ve erkek bireylerin çiftleşerek yaklaşık (72 ± 4 saat) elde edildi. 3 evre larvaları sayılarak oluşturulan deney gruplarına her gruba 45´şer adet konuldu. Larvaların günlük olarak takibi alınarak gelişim süreçleri izlendi ve 14 gün maruz bırakılarak sonunda deney sonlandırıldı. Larval toksisite deneyi larvadan pupa ´ya ve pupadan yetişkin sineğe bireylerin sayısını izleyerek not alınarak kaydedildi. Deney 2 kez tekrarlandı (Uysal ve Semerdöken, 2011).

Tırmanma Performansı

Tırmanma Performansı çalışma deneyi standart besiyeri stok olarak hazırlanan *D.melanogaster* her grup için 30 sinek erkekten ayarlanıp boş şişlere alındı ve yaklaşık 2 saat aç bırakıldı. falkon tüpüne 10 ml yeni besiyeri hazırlanarak üzerine maddeler eklenerek ve iyice karıştırılarak soğuması için bekletildi. Besiyeri soğuduktan sonra boş şişelerdeki aç bırakılan sinekleri her gurup için hazırlanan falkon tüplere aktarıldı. Bu deneyde sineğin maddelere 7 gün maruz bırakılarak belirli ölçülerde tırmanma davranışlarını izlenip not edildi. Falkon tüpünü tezgâha hafifçe vurarak 10 saniye içinde en üste oluşan sinekler sayısı sayıldı. Bu işlem 3 kez tekrarlandı (Güneş, E., 2021; Güneş, E., ve Eroğlu, G., 2022; Wang ark., 2023).

BULGULAR

Bu çalışmada Levetirasetam ve Roselle olası etkilerini araştırmak için *D.melanogaster* model organizması kullanarak larval toksisite ve tırmanma performansı yöntemleri kullanarak araştırıldı. Bu araştırma uygulama grupları ayarlanarak tek ve birleşik olarak yapıldı.

Larval Toksisite Bulguları

Levetirasetam ve Roselle maddelerin *D.melanogaster*`in ergin oluşumu oranı üzerindeki etkisi şekil 1´de verilmiştir. Yapılan çalışmada roselle´nin en yüksek dozunda ergin birey oluşumunun arttığı gözlemdi. Kontrol grubuna göre 3. Evre larvadan ergin birey sayısı levetirasetam 50 µl konsantrasyonu hemen benzer oranında gözlemdi. Kontrolle kıyasla Roselle 100 µl konsantrasyon ergin sayısı belirli artışta bulundu. Levetirasetam ve Roselle (50 + 100) µl birleşik olarak kontrol, Levetirasetam ve roselle gruplarına göre ergin sayısı daha artış olduğu gözlemdi. Roselle 200 µl konsantrasyon önceki gruplara göre en yüksek ergin sayısı olarak bulundu. Ayrıca levetirasetam ve roselle (50 + 200) µl birleşik olarak diğer birleşik gruba göre ergin sayısı daha arttığı gözlemdi.

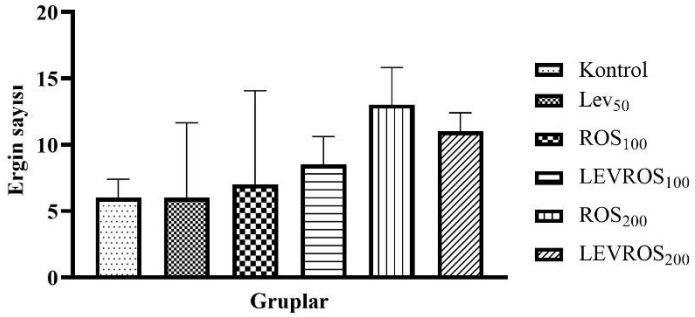

Şekil 1: Levetirasetam ve Roselle dozları uygulanan *D.melanogaster´lerin* üçüncü evreden ergin bireye geçiş üzerindeki etkisi.

Tırmanma Performansı Bulguları

Çalışmada kullanılan levetirasetam ve roselle uygulanan dozlar ve *D.melanogaster´*in üzerindeki tırmanma performans etkisi şekil 2´de verilmiştir. Yapılan çalışmada Rosellenin en yüksek dozda tırmanma performansı arttığı gözlemdi. Kontrol gruba göre levetirasetam 50 µl konsantrasyon düştüğü, Roselle 100 µl konsantrasyon düştüğü, Roselle 200 µl arttığı gözlemdi. Roselle (100 + 200) µl levetirasetam´a göre tırmanma performansı arttığı gözlemdi. Levetirasetam ve roselle birleşik olarak tırmanma performansı kontrole göre düşüş ve levetirasetam'a göre ise arttığı gözlemdi.

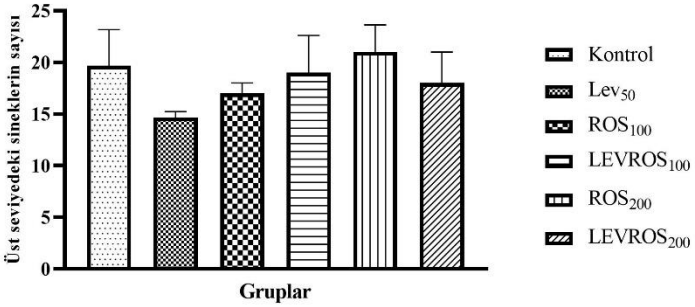

Şekil 2: Levetirasetam ve Roselle dozları uygulanan *D.melanogaster* üzerinde Tırmanma Performans etkisi.

TARTIŞMA

Levetirasetam epilepsi tedavisinde sıklıkla kullanılan bir antiepileptik ilaçtır. Epilepsi, beyindeki anormal, aşırı veya hiper senkron nöronal aktiviteden kaynaklanan, nöbetlerle karakterize edilen kronik nörolojik bozukluklardır (Mohan, A. J. ark., 2014). Epilepsi, tedavi için kullanılan ilaçlar hastalarda sıklıkla görünen üreme bozukluğu ve hormon seviyelerin değiştirmesi öne sürülmektedir. Bazı çalışmalarda Levetirasetam oksidatif stresin arttığı tespit edilmiştir. Ayrıca antioksidan parametrelerde azalması neden olduğu gösterilmiştir. Antiepileptik ilaçların günümüzde toksisite açısından insan veriler üzerinde hala araştırması gerektiğini vurgulamaktadır (Baysal, M. ark., 2017).
Levetirasetam Vücut dokularında asetamid grubunun enzimatik hidrolizi ile metabolize olmasını sağlamaktadır. Metabolize edilmeden böbreklerden (%66) atılırken, (%1) feçesle itrah edilmektedir. Karaciğer levetirasetam'ı metabolize etmez ve plazma proteinlerine çok az bağlandığı ve bu nedenle diğer ilaçlarla çok az etkileşime girmektedir (Kalay B. ark., 2023).

Roselle *(Hibiscus sabdariffa)* yetiştirilmesi kolay olması nedeni ile son yıllarda ilaç ve gıda sanayinde tüketilmeye başlanmıştır. Bazı çalışmalarda ise Roselle ´nin genotoksik ve mutajenik etkileri olmaması, ayrıca sitotoksisiteye karşı koruyucu ve serbest Radikalara iyi avcı ajanları ve güçlü antioksidan aktiviteye sahip olduğu belirlenmiştir (López-Romero, D. ve ark., 2018). Farmakolojik özellikleri şekil 3´te verilmiştir.

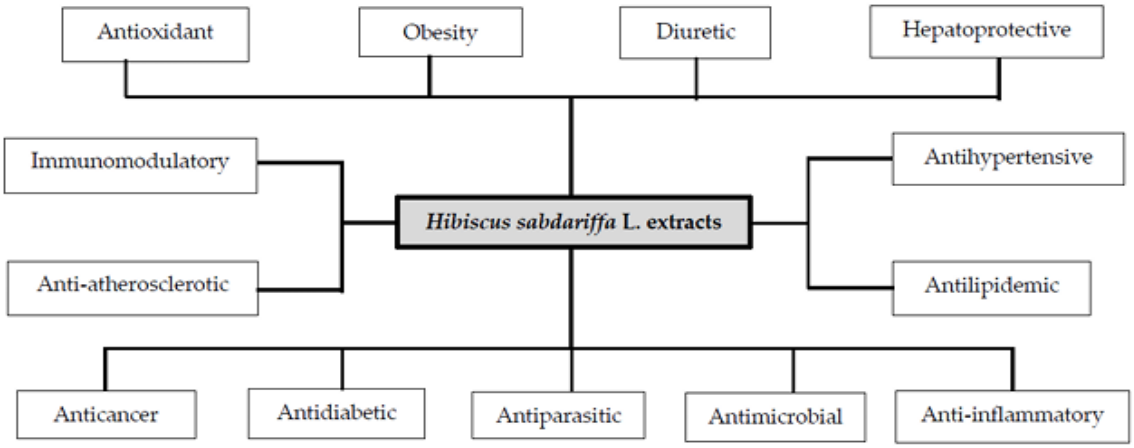

Şekil 3: Roselle´nin *(Hibiscus sabdariffa)* farmakolojik özellikleri (Izquierdo-Vega, J. A. ark., 2020).

D.melanogaster´lerde levetirasetam serbest radikaları artma etkisini azaltmak için roselle'nin antioksidan savunması kullanarak etkisi olup olmadığını daha önce çalışılmamıştır. Bu çalışmamın kapsamında literatürdeki eksikliği tamamlanması amaçlanmıştır.

SONUÇ

Bu çalışmanın sonuçlarına göre, 200 µl dozunda uygulanan roselle, *Drosophila melanogaster* bireylerinde gelişim oranını ve tırmanma performansını anlamlı şekilde artırmıştır. Bu bulgu, literatürde roselle'nin antioksidan etkilerine dair mevcut verileri desteklemektedir. Öte yandan, 50 µl dozunda uygulanan levetirasetam, gelişim oranında azalmaya ve tırmanma performansında düşüşe yol açmıştır. Bu durum, levetirasetamın oksidatif stresi artırdığı ve antioksidan parametrelerde azalmaya neden olduğuna dair literatürle uyumludur. Çalışmada, biyolojik araştırmalarda yaygın olarak kullanılan model organizma *Drosophila melanogaster* kullanılarak, levetirasetam ve roselle'nin larval gelişim ve motor davranış üzerindeki etkileri değerlendirilmiştir.

Sonuçlar, levetirasetamın gelişim süreci üzerinde belirgin bir etkisi olmadığını; ancak tırmanma davranışı üzerinde olumsuz etkiler gösterdiğini ortaya koymuştur. Roselle ise hem gelişim oranını artırmış hem de motor performansı iyileştirmiştir. Elde edilen veriler, roselle'nin potansiyel koruyucu etkilerinin doğrulanması için insan verileriyle desteklenmiş ileri düzey araştırmalara ihtiyaç duyulduğunu göstermektedir.

KAYNAKLAR

Baysal, M., Ilgin, S., Kilic, G., Kilic, V., Ucarcan, S., & Atli, O. (2017). Reproductive toxicity after levetiracetam administration in male rats: Evidence for role of hormonal status and oxidative stress. *PLoS One*, *12*(4), e0175990.

Demir, E. (2016). Nanomateryallerin Toksisite ve Genotoksisite Çalışmalarında Bir In Vivo Model Organizma Olarak Drosophila melanogaster (Meyve Sineği)'in Kullanılması. *Türk Bilimsel Derlemeler Dergisi*, *9*(1), 01–11. Retrieved from https://derleme.gen.tr/index.php/derleme/article/view/383

Deneubourg, C., Dafsari, H. S., Lowe, S., Martinez-Cotrina, A., Mazaud, D., Park, S. H., ... & Fanto, M. (2024). Epg5 links proteotoxic stress due to defective autophagic clearance and epileptogenesis in Drosophila and Vici syndrome patients. *Autophagy*, 1-13.

Diler Durgut, B., Turk, A., Acar Arslan, E., Kamasak, T., Sahin, S., Dilber, B., ... & Cansu, A. (2019). An investigation of the ocular toxic effects of levetiracetam therapy in children with epilepsy. *Child's Nervous System*, *35*, 769-774.

El-Refai, A. A., Sanad, M. I., Ramadan, A. H. M., & Hikal, D. M. (2010). Antimicrobial activity of natural anthocyanins and carotenoids extracted from some plants and wastes. *Journal of Food and Dairy Sciences*, *1*(7), 413-427.

El-Shorbagy, H. M., & Hamdi, H. A. M. I. D. A. (2016). Genotoxic and mutagenic studies of the antiepileptic drug levetiracetam in pregnant rats and their fetuses. *Int J Pharm Sci*, *8*(2), 82-8.

Gad, F. A. M., Farouk, S. M., & Emam, M. A. (2021). Antiapoptotic and antioxidant capacity of

phytochemicals from Roselle (Hibiscus sabdariffa) and their potential effects on monosodium glutamate-induced testicular damage in rat. *Environmental Science and Pollution Research*, *28*, 2379-2390.

Güneş, E. (2021). Ankaferd Blood Stopper, Drosophila melanogaster'de Stres ve Yaşlanma Üzerindeki Davranışı Değiştiriyor mu?. Ulusal Çevre Bilimleri Araştırma Dergisi, 4(2), 77-81.

Güneş, E., & Eroğlu, G. (2022). Sıcaklık Değişimi Amaurochaete comata İle Beslenen Böceğin Hareketini Etkiler mi?. Ulusal Çevre Bilimleri Araştırma Dergisi, 5(2), 112-116.

Izquierdo-Vega, J. A., Arteaga-Badillo, D. A., Sánchez-Gutiérrez, M., Morales-González, J. A., Vargas-Mendoza, N., Gómez-Aldapa, C. A., Castro-Rosas, J., Delgado-Olivares, L., Madrigal-Bujaidar, E., & Madrigal-Santillán, E. (2020). Organic Acids from Roselle (*Hibiscus sabdariffa* L.)-A Brief Review of Its Pharmacological Effects. *Biomedicines*, *8*(5), 100. https://doi.org/10.3390/biomedicines8050100

Kalay B, Pekmezekmek A, Ün B, Akarsakarya Z, Özü Ö, Seçilmiş A. Yeni Nesil Bir Antiepiletik İlaç: Levetirasetam. aktd. Aralık 2023;32(4):227-236. doi:10.17827/aktd.1292345

López-Romero, D., Izquierdo-Vega, J. A., Morales-González, J. A., Madrigal-Bujaidar, E., Chamorro-Cevallos, G., Sánchez-Gutiérrez, M., ... & Madrigal-Santillán, E. (2018). Evidence of some natural products with antigenotoxic effects. Part 2: plants, vegetables, and natural resin. *Nutrients*, *10*(12), 1954.

Mohammad, F., Singh, P., & Sharma, A. (2009). A Drosophila systems model of pentylenetetrazole induced locomotor plasticity responsive to antiepileptic drugs. *BMC systems biology*, *3*, 1-17.

Mohan, A. J., Krishna, K., Jisham, K., Mehdi, S., & Nidavani, R. B. (2014). Protective effect of tulsi and levetiracetam on memory impairment induced by pregabalin on mice. *IOSR J Pharm Biol Sci*, *9*, 46-52.

Nainu, F., Djide, M. N., Subehan, S., Sartini, S., Roska, T. P., Salim, E., & Kuraishi, T. (2020). Protective signatures of Roselle (Hibiscus sabdariffa L.) calyx fractions against Staphylococcus aureus in Drosophila infection model. *HAYATI Journal of Biosciences*, *27*(4), 306-306.

Pandey, U. B., & Nichols, C. D. (2011). Human disease models in Drosophila melanogaster and the role of the fly in therapeutic drug discovery. *Pharmacological reviews*, *63*(2), 411–436. https://doi.org/10.1124/pr.110.003293

Singh, P., Mohammad, F., & Sharma, A. (2011). Transcriptomic analysis in a Drosophila model identifies previously implicated and novel pathways in the therapeutic mechanism in neuropsychiatric disorders. *Frontiers in neuroscience*, *5*, 161. https://doi.org/10.3389/fnins.2011.00161

Sun, Y., Yolitz, J., Wang, C., Spangler, E., Zhan, M., & Zou, S. (2013). Aging Studies in Drosophila Melanogaster. *Methods in Molecular Biology*. Humana Press. https://doi.org/10.1007/978-1-62703-556-9_7

Uysal, H., & Semerdöken, S. (2011). Sentetik Gıda Boyalarının Drosophila melanogaster'in Oregon R Soyunda Larval Toksisite ve Ergin Ömür Uzunluğu Üzerine Etkilerinin Belirlenmesi. Kafkas Üniversitesi Fen Bilimleri Enstitüsü Dergisi, 4(1), 71-87.

Wang, J., Wu, C., Zhang, X., Song, Y., Wang, B., Zhang, K. ve Sun, M. (2023). Developmental neurotoxic effects of bisphenol A and its derivatives in Drosophila melanogaster. Ecotoxicology and environmental safety, 260, 115098. https://doi.org/10.1016/j.ecoenv.2023.115098

➢ *ORAL PRESENTATION*

Bakır Tabanlı Bazı Alaşımların Gama Radyasyonu ile Etkileşimlerinin İncelenmesi

Tuğba İSPİR[1,2*] (*ORCID: https://orcid.org/0000-003-0531-6306.*),
Ferdi AKMAN[3] (ORCID: *https://orcid.org/0000-0002-8838-1762*)

[1]Kilis 7 Aralık University, Vocational School of Health Services, Department of Medical Services and Techniques, Program of Opticianry, Kilis, Türkiye
[2] Bingöl University, Faculty of Arts and Science, Department of Physics, 12000, Bingöl, Türkiye
[3] Bingöl University, Vocational School of Social Sciences, Department of Property Protection and Security, Program of Occupational Health and Safety, 12000, Bingöl, Türkiye

*Sorumlu yazar e-posta: tugba.ispir@kilis.edu.tr

Özet
Kolay işlenebilirliği, düşük maliyetli olması, korozyona karşı dirençli olması ve yüksek iletkenliğe sahip olması nedeniyle bakır (Cu) temelli alaşımlar günümüzde sıkça kullanılmaktadır. İyonlaştırıcı radyasyon türü olan gama ışını yüksek nüfuz etme özelliğine sahiptir ve bu tür radyasyondan korunmanın en önemli yolu zırhlamadır. Zırhlama malzemesi olarak kurşun geleneksel olarak kullanılmaktadır, fakat kurşunun toksisite gibi dezavantajlarından dolayı kullanımı sınırlandırılmış olup bilim camiası farklı enerji bölgelerinde gama radyasyonunu zırhlayabilecek farklı malzemeler üretme yönelimine gitmişlerdir. Sunulan bu çalışmada Cu1 (Cu86Mn12Ni2, d=8,4 g/cm^3), Cu2 (Cu64Ni12Zn24, d=8,67 g/cm^3), Cu3 (Cu53Zn38Pb3, d=8,47) ve Cu4 (Cu65Ni18Zn17, d=8,73 g/cm^3) alaşımlarının gama radyasyonu zırhlama kapasiteleri araştırılmıştır. Çalışmalar 0,06-2,614 MeV enerji aralığında (18 farklı değerde) WinXCOM programı ile gerçekleştirilmiştir. WinXCOM programı ile elde edilen gama radyasyonu zırhlama parametreleri; kütle azaltma katsayısı, lineer azaltma katsayısı, yarı kalınlık değeri ve etkin atom numarasıdır. Hesaplanan parametrelerin sonuçlarına göre tüm enerji bölgelerinde Cu4 kodlu numunesinin gama radyasyonunu daha iyi zırhladığı görülmüştür.

Anahtar Kelimeler: Bakır alaşımlar, Gama radyasyon zırhlama, WinXCOM

Investigation of the Interaction of Some Copper Based Alloys with Gamma Radiation

Abstract
Copper (Cu) based alloys are frequently used today due to their easy machinability, low cost, resistance to corrosion and high conductivity. Gamma rays, which are a type of ionizing radiation, have high penetration properties and the most important way to protect from this type of radiation is shielding. Lead has traditionally been used as a shielding material, but due to its disadvantages such as toxicity, its use has been limited and the scientific community has tended to produce different materials that can shield gamma radiation in different energy regions. In this present study, the gamma radiation shielding capacities of Cu1 (Cu86Mn12Ni2, d=8.4 g/cm^3), Cu2 (Cu64Ni12Zn24, d=8.67 g/cm^3), Cu3 (Cu53Zn38Pb3, d=8.47 g/cm^3) and Cu4 (Cu65Ni18Zn17, d=8.73 g/cm^3) alloys were investigated. The studies were carried out with the WinXCOM program in the energy range of 0.06-2.614 MeV (18 different values). The gamma radiation shielding parameters obtained with the help of the WinXCOM program are; mass attenuation coefficient, linear attenuation coefficient, half value layer and effective atomic number. According to the results of the calculated parameters, it was seen that the Cu4 coded sample shielded the gamma radiation better in all energy regions.

Keywords: Copper alloys, Gamma radiation shielding, WinXCOM

GİRİŞ

Teknolojinin gelişmesiyle artan ihtiyaçlar doğrultusunda endüstri alanında bir çok yüksek kaliteli malzeme üretme arayışına gidilmiş ve mevcut malzemelerin içeriklerini zenginleştirerek yeni yüksek kalitede malzeme üretme çalışmaları yapılmaktadır (Devecili, 2009). Tıbbi uygulamalarda ve günlük hayatta iyonlaştırıcı radyasyona maruziyetin artması sebebi ile son yıllarda bu radyasyondan korunma ve radyasyonu engellemek için kurşun yerine geçebilecek daha çevreci ve toksik olmayan malzeme üretimi arayışına gidilmiştir. Bu

sebeple bilim insanları farklı metalleri kullanarak değişik tiplerde alaşımlar üretmiş ve bu malzemelerin radyasyon zırhlama özelliklerini incelemişlerdir (Erkoyuncu, 2025; Echeweozo ve ark., 2025).
Al ve Mg gibi metallerden üretilen alaşımlar demirden üretilen alaşımlarına göre daha yüksek mukavemete sahiptir, aynı zamanda plastik gibi kolay şekil alabilen ve yüksek sıcaklarda kullanım imkanı sunabilen alaşımlarken (Devecili, 2009), bakır tabanlı alaşımlar yüksek korozyon direncine, mükemmel iletkenliğe ve kolay şekil alabilme özelliğine sahiptirler. Önemli mühendislik malzemesi olarak kullanılan bakır alaşımlar; elektirk akımının iletilmesinde kablolarda, tellerde, elektrik kontaktlarında saf bakır yaygın olarak kullanılmaktadır. Saf bakır serteştirilse bile 500 ^{o}C'ye yakın sıcaklıklarda krsitalleşerek mukavemetini kaybetmesi sebebi ile bakıra bazı metaller katkılanarak mukavemeti arttırılmaya çalışılmıştır (Islak ve ark., 2019). Ayrıca literatürde bazı Cu tabanlı alaşımların gama radyasyon zırhlama parametreleri de deneyesel ve teorik olarak hesaplanmıştır (Salh ve ark., 2025). Sunulan bu çalışmada Cu1, Cu2, Cu3 ve Cu4 kodlu numunelerin gama radyasyon azaltma parametreleri belirlenmiştir. Cu1 yüksek korozyon direnci, manyetik olmayan yapısı, termal kararlılık ve iyi mekanik dayanıma sahip olması nedeniyle madeni paralar, elektriksel bağlantı parçaları, manyetik alanı etkilemeyen donanımlar, tren fren sistemlerinde ve yüksek dayanım gerektiren metal parçalarda ve en önemlisi kimyasal inert olduğundan dolayı özel tanklar, tüpler ve reaktörlerin yapımında kullanılmaktadır. Cu2 kolay işlenebilir olması, iyi korozyon direnci olması ve manyetik özelliğinin olmaması nedeniyle madeni paralarda, nefesli çalgıların gövde yapında, takı ve süs eşyaları, dişliler gibi aşınmaya dayanıklı küçük mekanik parçaların yapımı gibi bir çok alanda tercih edilmektedir. Cu3 tornolama ve frezeleme işlemleri için iyi işlenebilir olması, mukavemetininn iyi olması, korozyona karşı direncinin iyi olması ve iyi lehimlenebilir olması sebebi ile CNC tezgahları ve otomat için yedek parçalar, musluk, vana gibi bağlantı parçaları, otomotiv ve beyaz eşya sektöründe küçük bağlantı parçaları, elektronik olarak konnektör gövdeleri olarak kullanılmaktadır. Cu4 gümüşü gibi parlak görünümü, iyi korozyon direnci, iyi sertlik ve şekil alabilirliği nedeniyle madeni paralarda, süs eşyalarında, nefesli çalgıların gövde yapında, laboratuvar malzemelerinin yapımında, manyetik olmayan ve oksitlenmeyen yapısı ile hassas ölçüm cihazlarının yapımında kullanımı tercih edilmektedir.
Bu çalışmada son zamanlarda radyasyon zırhlamada önemli bir yere sahip olan bakır alaşımların (Cu1, Cu2, Cu3 ve Cu4) 0,06-2,614 MeV enerji aralığında on sekiz farklı enerji değerinde radyasyon azaltma kapasiteleri incelenmiştir.

MATERYAL VE METOD

Yapılan bu çalışma 0,06-2,614 MeV enerji aralığında on sekiz faklı enerji değerinde dört farklı alaşımın gama radyasyonunu zırhlama karakteristikleri incelenmiştir. Öncü parametre olan kütle azaltma katsayısı (μ/ρ) WinXCOM (Gerward ve ark., 2001) programı ile elde edilmiştir. Kütle azaltma katsayısı belirlendikten sonra önce lineer azaltma katsayısı, lineer azaltma katsayısı yardımı ile onda bir kalınlık değeri (OKD) hesaplanmıştır. Son olarak kütle azaltma katsayıları yardımıyla incelenen alaşımların etkin atom numaraları (Z_{etk}) belirtilen enerjilerde hesaplanmıştır. Seçilen bakır bazlı alaşımların yüzdelik dilimleri Tablo 1'de verilmiştir ve bunlar WinXCOM programında tanımlanarak kütle azaltma katsayıları belirlenmiştir.

Tablo 1. Seçilen bakır bazlı alaşımların yüzdelik bileşimleri ve yoğunlukları

Numune Kodları	Elementlerin Yüzde Bileşimi (%)					Yoğunluk (g/cm^3)
	Cu	Mn	Ni	Zn	Pb	
Cu1	86	12	2			8,40
Cu2	64		12	24		8,67
Cu3	58			38	3	8,47
Cu4	65		18	17		8,73

Gama ışınının maddenin birim alandaki kütlesi ile etkileşme ihtimalini ifade eden parametre olan kütle azaltma katsayısı (μ/ρ, cm^2/g) teorik olarak WinXCOM programı yardımı ile elde edilmiştir ya da lineer azaltma katsayısının malzemenin yoğunluğa bölünmesinden hesaplanabilir. WinXCOM programında 1kev–1GeV enerji aralığında elementler, bileşikler ya da kompozitler için foton azaltma parametreleri hesaplanabilir (Gerward ve ark., 2004; Kurtuluş ve ark, 2021). Bu program karışım kuralını kullanarak malzemelerin kütle azaltma katsayısını hesaplar ve bu kural denklem (1)'de sunulmuştur.

$$\mu_m = {}^{\mu}/_{\rho} = \sum_i W_i \left({}^{\mu}/_{\rho}\right)_i \quad (1)$$

Eşitlik (1)'de verilen W_i alaşım içindeki i. elementin ağırlıkça kesrini ve $(\mu/\rho)_i$ i. elementin kütle azaltma katsayısını ifade etmektedir. μ/ρ yardımıyla lineer azaltma katsayısı (μ, cm^{-1}) kolayca hesaplanabilir. Malzemenin yoğunluğu ile μ/ρ'nun çarpımından türetilir.

Onda bir kalınlık değeri (OKD, cm) gelen radyasyonun şiddetinin %90'nı azaltan ya da %10' nu geçiren malzeme kalınlığını ifade eden parametredir. Lineer azaltma katsayısı ile ters orantılıdır ve aşağıdaki ifade ile hesaplanmaktadır (Majeed ve ark., 2024).

$$OKD = \frac{\ln 10}{\mu} \quad (2)$$

Çalışmada son incelenen parametre olan etkin atom numarası atomik tesir kesitinin, elektronik tesir kesitine oranıdır, daha geniş bir ifade ile incelenen numunenin atomlarının foton ile etkileşme ihtimalinin yine incelenen numunenin elektronlarının foton ile etkileşime girme ihtimaline oranıdır. Kompozitler, bileşikler ve polimerler gibi malzemeler için tek bir element söz konusu olmadığından bu tür malzemelerde atom numarası terimi yerine etkin atom numarası terimi kullanılır ve aşağıdaki gibi ifade edilir (Wang ve ark., 1995).

$$Z_{etk} = \frac{\sigma_{t,a}}{\sigma_{t,e}} = \frac{\sum f_i A_i \left(\frac{\mu}{\rho}\right)_i}{\sum f_j \frac{A_j}{Z_j} \left(\frac{\mu}{\rho}\right)_j} \quad (3)$$

Eşitlikte sırası ile f_i, A_i ve Z_i i. elementin malzeme içindeki bolluğunu, atom ağırlığını ve atom numarasını ifade etmektedir. Denklem 3'teki $\sigma_{t,a}$ ve $\sigma_{t,e}$ ise sırasıyla atomik ve elektronik tesir kesitleri belirtir.

BULGULAR ve TARTIŞMA

Bu çalışmada Cu1 (Cu86Mn12Ni2, d=8,4 g/cm³), Cu2 (Cu64Ni12Zn24, d=8,67 g/cm³), Cu3 (Cu53Zn38Pb3, d=8,47) ve Cu4 (Cu65Ni18Zn17, d=8,73 g/cm³) alaşımlarının gama radyasyonu zırhlama özellikleri 0,06-2,614 MeV aralığında on sekiz farklı enerji değerinde WinXCOM programı yardımıyla incelenmiştir. Belirlenen alaşımların gama radyasyonu zırhlama özellikleri incelemek için kütle azaltma katsayısı, lineer azaltma katsayısı, onda bir kalınlık değeri ve etkin atom numarası parametreleri hesaplanmıştır. Belirlenen bakır tabanlı alaşımların kütle azaltma katsayılarının gama enerjisi ile değişim grafiği Şekil 1'de verilmiştir.

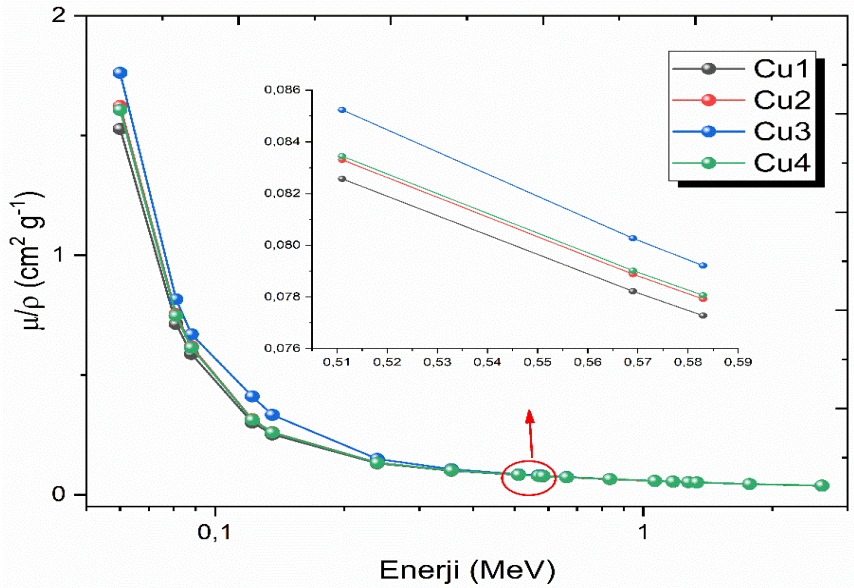

Şekil 1. Seçilen bakır alaşımların kütle azaltma katsayılarının foton enerjisi ile değişimi

Ayrıca belirlenen bakır alaşımların WinXCOM ile elde edilen kütle azaltma katsayıları ve hesaplanan onda bir kalınlık değerleri Tablo 2'de listelenmiştir.

Tablo 2. Seçilen alaşımlara ait kütle azaltma katsayıları ve onda bir kalınlık değerleri sonuçları

Enerji	Cu1		Cu2		Cu3		Cu4	
(MeV)	KAK	OKD	KAK	OKD	KAK	OKD	KAK	OKD
0,060	1,5270	0,1795	1,6231	0,1636	1,7608	0,1544	1,6064	0,1642
0,081	0,7129	0,3845	0,7537	0,3524	0,8162	0,3331	0,7469	0,3531
0,088	0,5873	0,4668	0,6195	0,4287	0,6698	0,4059	0,6142	0,4294
0,122	0,3017	0,9086	0,3146	0,8441	0,4103	0,6625	0,3127	0,8434
0,136	0,2515	1,0901	0,2611	1,0172	0,3332	0,8159	0,2598	1,0153
0,239	0,1312	2,0890	0,1337	1,9870	0,1497	1,8162	0,1336	1,9745
0,356	0,1002	2,7351	0,1014	2,6192	0,1068	2,5452	0,1015	2,5986
0,511	0,0826	3,3198	0,0833	3,1881	0,0852	3,1894	0,0834	3,1609
0,569	0,0782	3,5044	0,0789	3,3669	0,0803	3,3867	0,0790	3,3378
0,583	0,0773	3,5472	0,0779	3,4084	0,0792	3,4321	0,0781	3,3788
0,662	0,0725	3,7789	0,0731	3,6326	0,0740	3,6756	0,0733	3,6006
0,835	0,0646	4,2408	0,0651	4,0788	0,0655	4,1534	0,0652	4,0424
1,063	0,0572	4,7952	0,0576	4,6140	0,0576	4,7183	0,0577	4,5725
1,173	0,0543	5,0440	0,0547	4,8538	0,0547	4,9695	0,0548	4,8100
1,275	0,0521	5,2625	0,0524	5,0640	0,0524	5,1887	0,0526	5,0182
1,333	0,0509	5,3820	0,0513	5,1790	0,0512	5,3081	0,0514	5,1322
1,770	0,0444	6,1748	0,0447	5,9407	0,0446	6,0913	0,0448	5,8872
2,614	0,0377	7,2683	0,0380	6,9840	0,0381	7,1443	0,0381	6,9231

Şekil 1'de kütle azaltma katsayısı ile gama enerjisi arasına ters orantı olduğu görülmektedir. Yani artan gama enerjisi miktarı ile kütle azaltma katsayısı azalmaktadır. Bu azalma düşük enerjilerde keskin orta ve yüksek enerjilerde ise daha yayvandır. Düşük enerjilerdeki keskin azalmanın sebebi fotoeletrik tesir kesitidir ve gama enerjisi ile bu tesir kesiti arasındaki ilişki $E^{-3,5}$ şeklindedir. Orta enerjilerdeki ve yüksek enerjilerdeki yayvan değişimin sebepleri ise sırasıyla Compton saçılma tesir kesiti ve çift oluşum tesir kesitidir. Bu tesir kesitleri ise enerjiye sırasıyla E^{-1} ve $\ln(E^2)$ olarak bağlıdır. İncelenen alaşımlar içinde en yüksek kütle azaltma katsayısına sahip 0,060 MeV enerjide Cu3 kodlu numune olmuştur. Bu enerjide numunelerin kütle azaltma katsayıları Cu3>Cu2>Cu4>Cu1 olarak sıralanmaktadır. Tüm enerji seviyelerinde Cu3 kodlu numunenin gama radyasyonunu diğer seçilen bakır alaşımlara göre daha iyi zırhladığı diğer bir deyişle gama ışını ile daha çok etkileşime girdiği gözlemlenmiştir.

Lineer azaltma katsayısı (μ), malzemenin faz durumuna ve yoğunluğuna bağlı bir parametredir ve bu yüzden zırh malzemesi seçiminde daha uygun bir parametredir. Malzemenin yoğunluğu ve kütle azaltma katsayısının matematiksel çarpımından kolayca elde edilebilir. İncelenen bakır alaşımların μ sonuçlarının gama enerjisine göre değişim grafiği Şekil 2'de görsel olarak sunulmuştur. Şekil 2'ye göre μ sonuçları da artan gama enerjisi ile üstel olarak azalmaktadır. 0,06 MeV enerjide en yüksek μ değeri Cu3 kodlu numunede olduğu görülmektedir. Düşük enerji bölgesinde Cu3 kodlu numune, orta enerji bölgesinde ve yüksek enerji bölgesinde Cu4 kodlu numune seçilen bakır alaşımların içinde gama radyasyonunu en iyi zırhlayan malzeme oldukları gözlemlenmiştir.

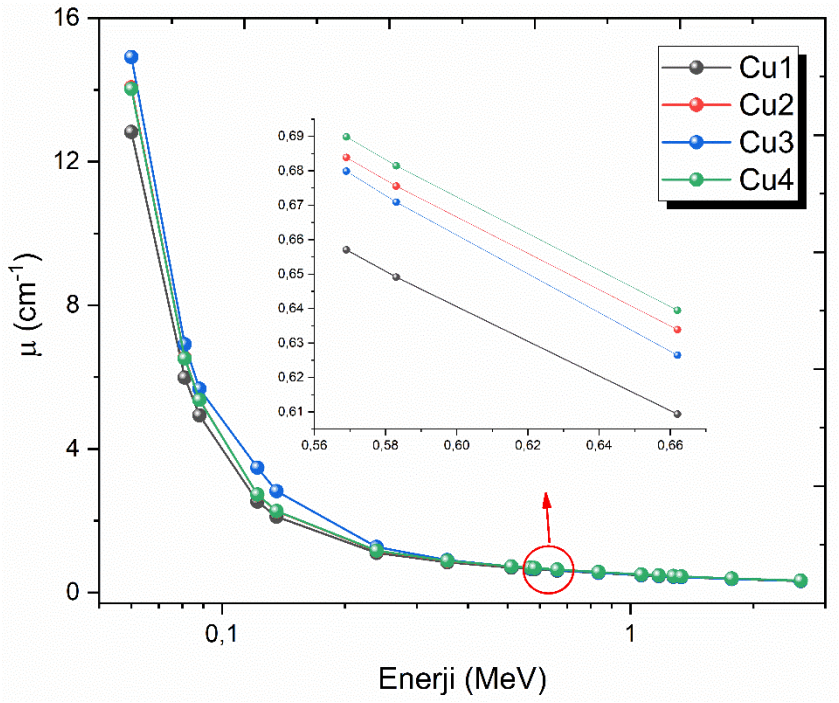

Şekil 2. Seçilen bakır alaşımların lineer azaltma katsayılarının foton enerjisi ile değişimi

Onda bir kalınlık değeri malzemenin radyasyon zırhlamada hangi kalınlıkta tercih edilmesini gerektiğini belirleyen değişkenlerden biridir. Bu parametre ne kadar küçük olursa malzemenin gama radyasyonu zırhlama özelliği de o derece iyi olur. Yani daha az kalın bir malzeme ile zırhlamanın gerçekleştirilebileceğini gösterir. Denklem 2'ye göre μ ile OKD arasında ters orantı vardır. Dolayısıyla artan gama enerjisi miktarı ile OKD değerleri de artmaktadır. Şekil 3'te de bu değişim açıkça görülmektedir. 0,060 MeV enerjide Cu1 için OKD 0,1795 cm, Cu2 için 0,1636 cm, Cu3 için 0,1544 cm ve Cu4 için 0,1642 cm olarak hesaplanmıştır. 0,060-0,356 MeV enerji aralığında Cu3 kodlu numune seçtiğimiz bu alaşımlar arasında en iyi gama radyasyonu zırhlama özelliği gösterirken, 0,356-2,614 MeV enerji aralığında ise Cu4 kodlu numune daha iyi zırhlama özelliği göstermiştir.

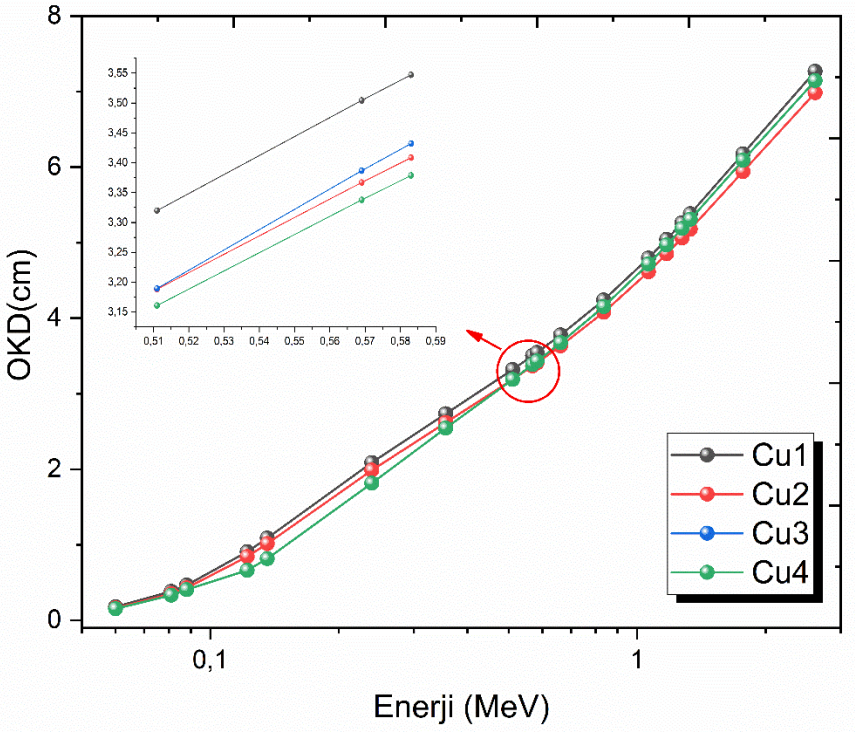

Şekil 3. Seçilen bakır alaşımların onda bir kalınlık değerlerinin gama enerjisi ile değişimi

Seçilen bakır tabanlı alaşımların gama radyasyonu zırhlama karakteristiklerini incelemek için hesaplanan son parametre etkin atom numarasıdır. Bu parametre kütle azaltma katsayısı yardımıyla hesaplandığından dolayı gama enerjisi ile değişimi de kütle azaltma katsayısı-enerji eğilimine benzemesi beklenmektedir. Seçilen alaşımların 0,06-2,614 MeV enerji aralığındaki etkin atom numarası değerleri Şekil 4'te görsel olarak sunulmuştur. Bu parametrenin büyük değerleri üstün gama radyasyonu zırhlamanın bir göstergesidir. 0,06 MeV enerjide Cu1için 28,5987, Cu2 için 29,1363,Cu3 için 31,1061 ve Cu4 için 29,0045 olarak not edilmiştir. Bu değişimler alaşımın etkin atom numarasının alaşım içindeki elementlerin atom numaralarına bağlı olduğunu göstermektedir. Cu3 alaşımı içerik olarak daha yüksek atom numaralı elementler içerdiği için 0,060-2,614 MeV enerji aralığında incelenen bakır alaşımlar arasında gama radyasyonunu en iyi zırhlayan alaşım Cu3 kodlu alaşım olmuştur.

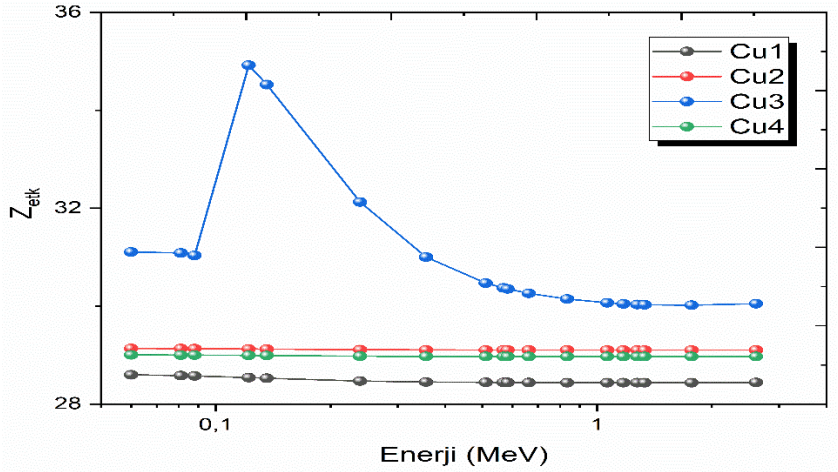

Şekil 4. Seçilen bakır alaşımların etkin atom numaralarının foton enerjisi ile değişimi

SONUÇ

Sunulan bu çalışmada Cu1, Cu2, Cu3 ve Cu4 kodlu alaşımların 0,06-2,614 MeV enerji aralığında on sekiz farklı enerjide gama radyasyonunu zırhlama performansları teorik olarak belirlenmiştir. Seçilen alaşımların gama zırhlama parametrelerini belirlemek için WinXCOM'un dikkate aldığı karışım kuralı kullanılmıştır. Bu program ile μ/ρ öncü parametresi belirlenmiş ve daha sonra μ, OKD ve Z_{etk} parametreleri türetilmiştir. Artan gama enerjisi ile μ/ρ, μ ve Z_{etk} parametrelerinin azaldığı ve OKD sonuçlarının ise arttığı gözlemlenmiştir. Belirlenen bu parametrelerin sonuçlarına göre genel olarak Cu3 kodlu alaşımın düşük enerji bölgesinde Cu4 kodlu alaşımın ise orta ve yüksek enerji bölgesinde daha üstün gama radyasyonu zırhlama kapasitesine sahip olduğu belirlenmiştir. Dolayısıyla, düşük enerjilerin kullanıldığı hastanelerin radyasyon ile ilgili birimleri gibi alanlarda Cu3 kodlu alaşım zırhlama amaçlı tercih edilebilir. Benzer şekilde nükller santraller, araştırma laboratuvarları, uzay araştırmaları gibi yüksek enerjili gamaların bulunduğu alanlarda ise Cu4 kodlu alaşımın tercih edilmesi önerilir.

KAYNAKLAR

Devecili A. O., (2009). Effect of copper as an alloying element on the coating behaviour of aluminium by microarc technique. Yüksek lisans tezi, Gebze Yüksek Teknoloji Üniversitesi, Mühendislik ve Fen Bilimleri Enstitüsü, Malzeme Bilimi ve Mühendisliği Ana Bilim Dalı.

Echeweozo, EO, Alomayrah, N., Alomairy, S., Alrowaili, ZA, Alsaiari, NS ve Al-Buriahi, MS (2025). FeNbSc bazlı alaşımların gama radyasyonundan korunma özelliklerinin değerlendirilmesi. Katılarda Radyasyonun Etkileri ve Kusurları , 1-16.

Erkoyuncu, İ. (2025). Gamma/Neutron Radiation Shielding Characteristics and Produced Secondary Radiation in Fe-Ni Alloys. Journal of Alloys and Compounds, 181192.

Gerward, L., Guilbert, N., Jensen, K. B., & Levring, H. (2001). X-ray absorption in matter. Reengineering XCOM. Radiation Physics and Chemistry, 60(1-2), 23-24.

Gerward, L., Guilbert, N., Jensen, K. B., & Levring, H. (2004). WinXCom—a program for calculating X-ray attenuation coefficients. *Radiation physics and chemistry*, *71*(3-4), 653-654.

Islak S, Çalıgülü U, Hraam HR, Özorak C, Koç V, 2019. Electrical conductivity, microstructure and wear properties of Cu-Mo coatings. Research on Engineering Structures Materials, 5(2), 137-146.

Kurtulus, R., Kavas, T., Akkurt, I., Gunoglu, K., Tekin, H. O., & Kurtulus, C. (2021). A comprehensive study on novel alumino-borosilicate glass reinforced with Bi2O3 for radiation shielding applications: synthesis, spectrometer, XCOM, and MCNP-X works. *Journal of Materials Science: Materials in Electronics*, *32*(10), 13882-13896.

Majeed E. I., Najam L. A., Hamood M. A., K.A. Mahmoud (2024). A Comprehensive study on the γ-ray shielding performance of Al–Cu–PbO alloy: Experimental and simulation studies, Nuclear Engineering and Technology, 57(1), 103124.

Salh, H., Saleh, D. S., Smail, J. M., Manguri, H. S. A., BALO, Ş. N., & Ahmad, S. T. (2025). Experimental and theoretical evaluation of Cu–Al–Ni shape memory alloys shielding properties at the 511–1333 keV gamma energy range. Journal of Radioanalytical and Nuclear Chemistry, 334(1), 851-862.

Wang D. C., Ping L.A., Yang H. (1995). Nucl. Instr. and Meth. B, 95, p. 61.

➢ *ORAL PRESENTATION*

Seçilen Kauçukların Gama Radyasyonu Zırhlama Parametrelerinin Değerlendirilmesi

Tuğba İSPİR[1,2*] (*ORCID: https://orcid.org/0000-003-0531-6306.*), Ferdi AKMAN[3] (ORCID: *https://orcid.org/0000-0002-8838-1762*)

[1] Kilis 7 Aralık Üniversitesi, Sağlık Hizmetleri Meslek Yüksekokulu, Tıbbi Hizmetler ve Teknikler Bölümü, Optisyenlik Programı, Kilis, Türkiye
[2] Bingöl Üniversitesi, Fen Bilimleri Enstitüsü, Fizik Bölümü, Bingöl, Türkiye
[3] Bingöl Üniversitesi, Sosyal Bilimler Meslek Yüksekokulu, Mülkiyet Koruma ve Güvenlik Bölümü, İş Sağlığı ve Güvenliği Programı, Bingöl, Türkiye

*Sorumlu yazar e-posta: tugba.ispir@kilis.edu.tr

Özet
Gelişen teknoloji ile gama radyasyonun kullanımı sürekli artmaktadır. Bu radyasyonun canlılar üzerinde, çevre ve elektronik ekipmanlarda negatif etkisi bulunmaktadır. Bu yüzden bu tür radyasyondan korunmak için en tercih edilen korunma yolu zırhlamadır. Sunulan çalışmada doğal kauçuk (NR), Stiren bütadien kauçuk (SBR) ve Kloropren kauçukların (CR) gama radyasyonu zırhlama kapasiteleri araştırılmıştır. Çalışmalar 0,015-15 MeV enerji aralığında WinXCOM program aracılığıyla gerçekleştirilmiştir. Elde edilen gama zırhlama parametreleri; kütle azaltma katsayısı, lineer azaltma katsayısı, yarı kalınlık değeri ve etkin atom numarasıdır. Hesaplanan parametrelerin sonuçlarına göre tüm enerji bölgelerinde CR numunesinin gama radyasyonunu daha iyi zırhladığı görülmüştür.

Anahtar Kelimeler: Kauçuklar, Gama radyasyon zırhlama, WinXCOM

Evaluation of Gamma Radiation Shielding Parameters of Selected Rubbers

Abstract
With the advancement of technology, the use of gamma radiation is continuously increasing. This type of radiation has negative effects on living organisms, the environment, and electronic equipment. Therefore, shielding is the most preferred method of protection against such radiation. In the presented study, the gamma radiation shielding capacities of Natural Rubber (NR), Styrene-Butadiene Rubber (SBR), and Chloroprene Rubber (CR) were investigated. The study was conducted within the energy range of 0.015–15 MeV using the WinXCOM program. The obtained gamma shielding parameters include mass attenuation coefficient, linear attenuation coefficient, half-value layer, and effective atomic number. According to the calculated results, the CR sample was found to provide better gamma radiation shielding across all energy ranges.

Keywords: Rubbers, Gamma radiation shielding, WinXCOM

GİRİŞ

Tıbbi uygulamalar, enerji üretimi gibi birçok uygulamalarda radyasyon kullanılması avantaj sağlarken iyonlaştırıcı radyasyona maruziyetin oluşması ve bu radyasyon türünün zararlı doğası sebebi ile çevre ve canlılara zarar verebilecek olması dezavantajlarındadır. İyonlaştırıcı radyasyon bir hücreye hasar verebilecek enerjiye sahiptir ve birçok çalışmaya göre radyasyona maruziyet sonucu tiroit, lösemi, katarakt ve akciğer kanseri gibi hastalıkların riskini arttırdığı gözlemlenmiş olup gelecek nesillere aktarılan DNA yapısının bozduğu hatta sildiği ortaya konulmuştur. Uzun süreli tıbbi aletler kullanımında da maruziyet oluşacağından aynı hasarı verebilmektedir (Al-Buriahi, 2023; Ahmed ve ark., 2024).
Radyasyondan korunmak için farklı yollar vardır; zaman, mesafe ve zırhlama. Diğerlerine göre en güvenilir olanı zırhlamadır, yani gelen radyasyonu azaltılmasıdır. Kurşun yüksek atom numaralı olup geniş enerji aralığında radyasyonu zırhlayan iyi bir malzeme olması özelliğiyle kurşun bloklar, koruyucu kurşun içerikli giysiler kullanılmıştır (Eder, 2006; 2009; Ballsieper, 2006).
1976 yılında Birleşik Devletler Kongresi'nde (The United States Congress) kurşunun toksik etkilerinden dolayı kullanımı sınırlandırılmıştı (Dodoo-Amoo ve ark., 2003). Türkiye'de ise 2008 yılında bazı elektronik

eşyalarda zararlı maddelerin kullanımına dair hükümler yürürlüğe girmiştir. Kurşunun toksik madde olması, kullanım açısından ağır olması kurşuna alternatif iyonlaştırıcı radyasyonu azaltan farklı malzeme arayışına bilim insanlarını sürüklemiştir. Bu amaçla beton (Azzaoui ve ark., 2025; Tousi ve ark., 2025), alaşım (Erkoyuncu, 2025; Niksarlıoğlu ve ark., 2024), kompozit (Akman ve ark., 2025; Oğul ve ark., 2025) ve polimer (Ghuge ve ark., 2025; Nagaraja ve ark., 2020) gibi malzemelerin iyonlaştırıcı radyasyon azaltma karakteristikleri incelenmiştir. Nükleer santrallerde elektronik kablolarda kullanılan kauçukların da iyonlaştırıcı radyasyonu azaltma özelliklerinin incelenmesi gerekir. Bu nedenle NR, SBR ve CR kauçuklarının iyonlaştırıcı radyasyon zırhlama kapasiteleri sunulan çalışmada belirlenmiştir.
NR yüksek dayanıma ve esnekliğe sahip bir malzeme olmasından dolayı lastik otomatik sanayi, tıbbi ve sağlık ürünleri, ayakkabı tabalarında, su geçirmez giysiler ve elektronik kablolar gibi birçok kullanım alanında tercih edilir. SBR aşınmaya ve ısıya karşı yüksek dirençli, kolay işlenebilir ve ekonomik olmasından dolayı ayakkabı endüstrisi, kablo kaplamaları, oto lastikler, conta, yapı ve inşaat alanında titreşim emiciler ve sızdırmazlık filtreleri olarak kullanılmaktadır. CR yüksek ozon ve UV direnci, su geçirmezlik, alev geciktirici özelliklerinden dolayı dalgıç kıyafetlerinde, termal eldivenler ve dizliklerde, elektrik izolasyonunda, kablo kılıflarında, inşaat alanında ses ve titreşim yalıtım pedleri, sızdırmazlık contaları ve filtreleri yapımında kullanılmaktadır. Son yıllarda kauçuklara farklı maddeler eklenerek lineer azaltma katsayıları hesaplanmış ve radyasyon zırhlama kapasitesinin arttığı gözlemlenmiştir (Vishnu ve ark., 2024). Bu çalışmada da son zamanlarda radyasyon zırlhlamada önemli bir yere sahip olan kauçuklardan NR, SBR ve CR'nin 0,015-15 MeV enerji aralığında yirmi dört farklı enerji değerinde radyasyon azaltma kapasiteleri WinXCOM yardımıyla incelenmiştir.

MATERYAL VE METOD

Yapılan bu çalışma 0,015-15 MeV enerji aralığında yirmi dört faklı enerji değerinde üç farklı kauçuğun gama radyasyonu zırhlama özelliklerinin belirlenmesinde önemli bir parametre olan kütle azaltma katsayısı (μ/ρ) WinXCOM (Gerward ve ark., 2001) programı ile elde edilmiştir. Kütle azaltma katsayısı belirlendikten sonra önce lineer azaltma katsayısı, lineer azaltma katsayısı yardımı ile yarı kalınlık değeri (YKD) hesaplanmıştır ve son olarak incelenen kauçukların etkin atom numarası (Z_{etk}) değerleri kütle azaltma katsayıları yardımıyla hesaplanmıştır.
İyonlaştırıcı radyasyonun madde ile etkileşiminde önemli olan ve malzemenin yoğunluğu ile ilişkisi olmayan kütle azaltma katsayısı (μ/ρ, cm^2/g) teorik olarak WinXCOM programı yardımı ile elde edilmiştir.

$$\mu_m = {}^{\mu}/_{\rho} = \sum_i W_i \left({}^{\mu}/_{\rho}\right)_i \quad (1)$$

Eşitlikteki W_i ve $(\mu/\rho)_i$ sırasıyla kauçuk içindeki i. elementin ağırlıkça kesrini ve kütle azaltma katsayısını ifade etmektedir. μ/ρ yardımıyla lineer azaltma katsayısı (μ, cm^{-1}) kolayca hesaplanabilir. Malzemenin yoğunluğu ile μ/ρ'nun çarpımından türetilir.
Yarı kalınlık değeri (YKD, cm) gelen radyasyonun şiddetinin yarıya düştüğü malzeme kalınlığını ifade eden parametredir. Bu parametre lineer azaltma katsayısı ile ters orantılıdır ve aşağıdaki ifade ile hesaplanmaktadır (Majeed ve ark., 2024).

$$YKD = \frac{\ln 2}{\mu} \quad (2)$$

μ/ρ yardımıyla hesaplanan son parametre etkin atom numarasıdır (Z_{etk}, birimsiz). Kompozitler, bileşikler ve polimerler gibi birden çok element içeren malzemeler söz konusu olduğunda malzeme içindeki elementin ağırlıklı kesrine göre değişebilen etkin atom numarası özellikle X-ışınlarının azaltılmasında ve radyasyon terapisinde dozun hesaplanması için kullanışlı bir parametredir (Jackson ve Hawkes, 1981) ve aşağıdaki gibi ifade edilir (Wang ve ark., 1995).

$$Z_{etk} = \frac{\sigma_{t,a}}{\sigma_{t,e}} = \frac{\sum f_i A_i \left(\frac{\mu}{\rho}\right)_i}{\sum f_j \frac{A_j}{Z_j} \left(\frac{\mu}{\rho}\right)_j} \quad (3)$$

Eşitlikte sırası ile f_i, A_i, ve Z_i i. elementin malzeme içindeki bolluğunu, atom ağırlığını ve atom numarasını ifade etmektedir. Ayrıca, $\sigma_{t,a}$ ve$\sigma_{t,e}$, atomik tesir kesit ve elektronik tesir kesiti ifade eder.

BULGULAR ve TARTIŞMA

Bu çalışmada NR (doğal kauçuk, C_5H_8, d=1,34 g/cm^3), SBR (Stiren bütadien kauçuk, $C_{12}H_{14}$, d=1,22 g/cm^3) ve CR (Kloropren kauçuk, C_4H_5Cl, d=1,45 g/cm^3) kauçukları gama radyasyonu zırhlama özellikleri 0,015-15 MeV aralığında yirmi dört farklı enerji değerinde WinXCOM programı yardımıyla incelenmiştir. Belirlenen

kauçukların gama radyasyonu zırhlama özelliklerini incelemek için lineer azaltma katsayısı, yarı kalınlık değeri ve etkin atom numarası parametreleri WinXCOM yardımı ile belirlenen kütle azaltma katsayıları ile hesaplanmıştır. Belirlenen kauçukların kütle azaltma katsayıları değerlerinin foton enerjisi ile değişimi Şekil 1'de görsel olarak sunulmuştur.

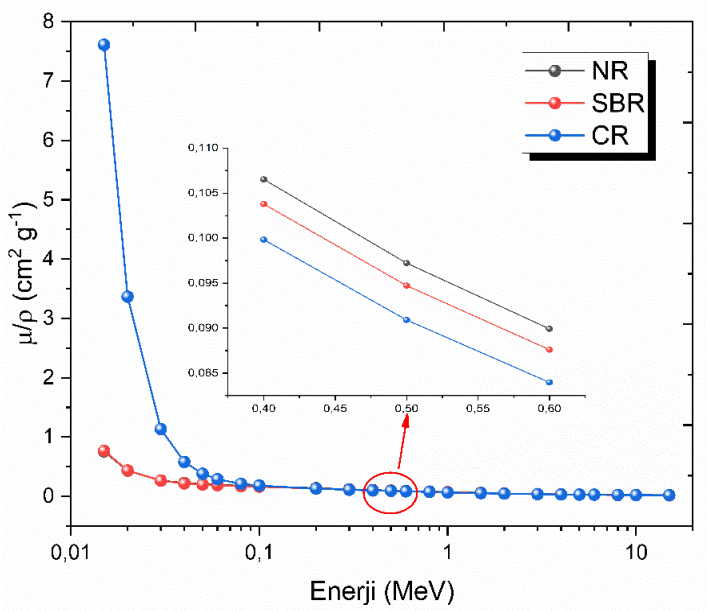

Şekil 1. Seçilen kauçukların kütle azaltma katsayılarının foton enerjisi ile değişimi

Ayrıca belirlenen kauçukların WinXCOM ile elde edilen kütle azaltma katsayıları ve yarı kalınlık değerleri Tablo 1'de verilmiştir

Tablo 1. Bazı kauçuklara ait kütle azaltma katsayıları ve yarı kalınlık değerleri sonuçları

Enerji	NR		SBR		CR	
(MeV)	KAK	YKD	KAK	YKD	KAK	YKD
0,015	0,7570	0,6833	0,7697	0,7382	7,6116	0,0628
0,020	0,4343	1,1910	0,4365	1,3017	3,3663	0,1420
0,030	0,2683	1,9281	0,2653	2,1412	1,1321	0,4223
0,040	0,2241	2,3082	0,2201	2,5816	0,5808	0,8231
0,050	0,2047	2,5269	0,2004	2,8354	0,3809	1,2550
0,060	0,1931	2,6782	0,1888	3,0100	0,2901	1,6478
0,080	0,1785	2,8981	0,1742	3,2621	0,2131	2,2428
0,100	0,1683	3,0744	0,1641	3,4627	0,1811	2,6394
0,200	0,1371	3,7730	0,1336	4,2527	0,1312	3,6435
0,300	0,1190	4,3475	0,1159	4,9008	0,1120	4,2663
0,400	0,1065	4,8566	0,1038	5,4750	0,0998	4,7894
0,500	0,0972	5,3208	0,0947	5,9984	0,0909	5,2587
0,600	0,0899	5,7529	0,0876	6,4857	0,0840	5,6927
0,800	0,0790	6,5512	0,0769	7,3857	0,0737	6,4894
1,000	0,0710	7,2893	0,0691	8,2178	0,0662	7,2240
1,500	0,0577	8,9616	0,0562	10,1027	0,0539	8,8753
2,000	0,0495	10,4582	0,0482	11,7872	0,0463	10,3142
3,000	0,0395	13,0863	0,0385	14,7384	0,0376	12,7281
4,000	0,0337	15,3673	0,0329	17,2914	0,0325	14,6927
5,000	0,0298	17,3709	0,0291	19,5262	0,0293	16,3079
6,000	0,0270	19,1451	0,0264	21,4979	0,0271	17,6430
8,000	0,0234	22,1369	0,0229	24,8056	0,0243	19,6809
10,000	0,0211	24,5518	0,0207	27,4569	0,0226	21,1192
15,000	0,0179	28,8567	0,0177	32,1325	0,0206	23,1975

Şekil 1 incelendiğinde kütle azaltma katsayısının artan enerji ile eksponansiyel olarak azaldığı gözlemlenmiştir. Kütle azaltma katsayısındaki bu azalma incelenen kauçuklar ile fotonların farklı enerji bölgelerinde farklı etkileşimlerin olduğunu ifade etmektedir. Düşük enerji bölgesinde fotoelektrik tesir kesiti, orta enerji bölgesinde Compton tesir kesiti ve yüksek enerji bölgesinde ise çift oluşum tesir kesiti baskındır. Düşük enerji bölgesindeki (0,1MeV'e kadar) ani düşüşün sebebi fotoelektrik tesir kesitinin $E^{-3,5}$ ve Z^{4-5}ile orantılı olması ile ilişkilendirilebilir. Orta enerji bölgesindeki (0,1-1 MeV aralığı) yayvan değişimin sebebi Compton tesir kesitinin E^{-1} ve Z ile orantılı olmasından dolayıyken yüksek enerji bölgesindeki (1,022 MeV'den yukarı) değişimin sebebi ise bu bölgede baskın olan çift oluşumun $\ln(E^2)$ ve Z ile orantılı olmasıdır (Ornketphon ve ark., 2024). Düşük enerji bölgesi için CR'nin, orta ve yüksek enerji bölgesinde ise incelenen diğer kauçuklar arasında NR'nin gama radyasyonunu daha iyi zırhladığı gözlemlenmiştir.

Lineer azaltma katsayısı (μ), kütle azaltma katsayısı ve malzemenin yoğunluğu ile elde edilen fiziksel bir parametredir. Belirlenen kauçukların lineer azaltma katsayılarının foton enerjisine göre grafiği Şekil 2'de verilmiştir. Şekil 2 incelendiğinde kütle azaltma katsayısına benzer bir şekilde lineer azaltma katsayısının da artan enerji ile eksponansiyel olarak azaldığı gözlemlenmiştir. Tüm enerji aralıklarında CR numunesi incelen diğer kauçuklar arasında gama radyasyonunu en iyi zırhlayan kauçuk olmuştur.

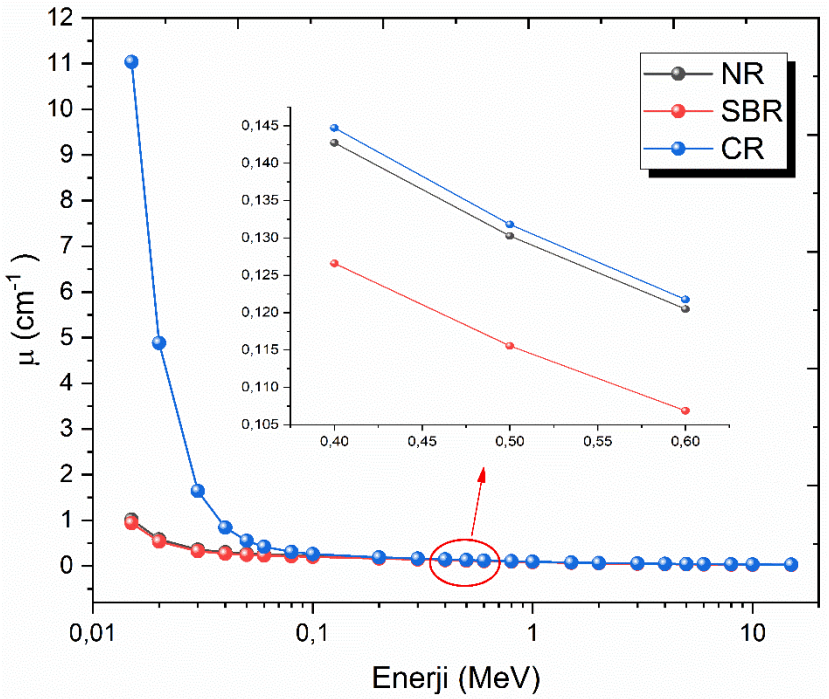

Şekil 2. Seçilen kauçukların lineer azaltma katsayılarının foton enerjisi ile değişimi

Yarı kalınlık değeri malzemenin radyasyon zırhlama verimliliğinin belirlenmesinde kullanılan parametrelerden biridir. YKD'nin düşük değerleri radyasyonun iyi zırhlandığının bir göstergesidir. YKD ve lineer azaltma katsayısının arasındaki ters orantı sonucu olarak artan enerji ile yarı kalınlık değerinin de eksponansiyel olarak arttığı görülmüştür. Şekil 3 0,015-15MeV enerji aralığında yirmi dört farklı foton enerji için teorik olarak belirlenen üç adet kauçuğun yarı kalınlık değerini göstermektedir. 0,015 MeV enerjide NR için yarın kalınlık değeri 0,6833 cm, SBR için 0,7382 cm ve CR için 0,0628 cm olarak belirlenmiştir. YKD sonuçları incelediğinde de çalışılan kauçuklar arasında gama radyasyonunu en iyi CR numunesi zırhlamıştır.

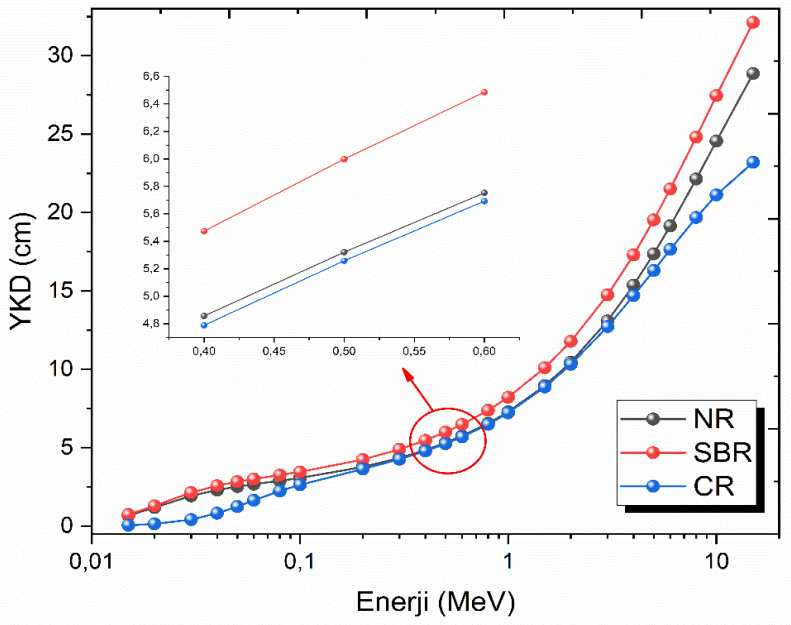

Şekil 3. Seçilen kauçukların yarı kalınlık değerlerinin foton enerjisi ile değişimi

Bu çalışmada en son belirlenen parametre etkin atom numarasıdır. Etkin atom numarası maruz kalınan radyasyonun doz hesaplamasında kullanılan önemli bir parametredir. Seçilen kauçukların 0,015-15 MeV enerji aralığındaki etkin atom numarası değerlerinin enerji ile değişimi Şekil 4'te gösterilmiştir. Şekil 4 incelendiğinde etkin atom numarasının enerji ile azaldığı görülmektedir. 0,015 MeV enerjide NR için 4,6369, SBR için 4,9268 ve CR için 14,7746 olarak hesaplanmıştır. CR'nin daha yüksek etkin atom numarasına sahip olmasının nedeni klor elementinin varlığıdır. Çünkü klor elementi (Z=17), karbon (Z=6) ve hidrojene (Z=1) göre daha yüksek atom numarasına sahiptir. Dikkate alınan enerji değerlerinde incelenen kauçuklar arasında gama radyasyonunu en iyi zırhlayan CR kauçuğu olmuştur.

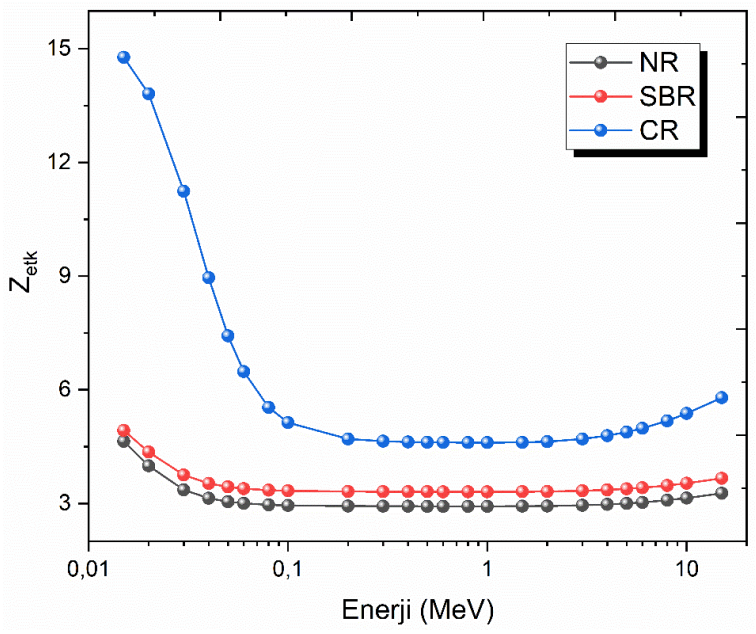

Şekil 4. Seçilen kauçukların etkin atom numaralarının foton enerjisi ile değişimi

SONUÇ

0,015-15 MeV enerji aralığında yirmi dört farklı enerjide üç farklı kauçuğun gama radyasyonunu zırhlama performansları teorik olarak belirlenmiştir. Seçilen kauçukların zırhlama parametreleri kütle azaltma katsayısı, lineer azaltma katsayısı, yarı kalınlık değeri ve etkin atom numarası WinXCOM programı yardımıyla belirlenmiştir. LAK, YKD ve Z_{etk} parametrelerine göre seçilen tüm enerjilerde CR numunesinin çalışılan diğer

kauçuklara göre gama radyasyonunu daha iyi zırhladığı görülmüştür. Elde edilen veriler göz önüne alındığında bu tür kauçukların nükleer santrallerde kablo izolasyonu ve elektronik ekipmanların conta elemanı olarak kullanılabileceği düşünülmektedir. İncelenen kauçuk türlerinin uygun katkı maddeleri ile kombine edilip gama radyasyonu zırh malzemesi olarak kullanılmak istenmesi durumunda CR'nin tercih edilmesi daha uygun olacaktır.

KAYNAKLAR

Ahmed, E. K., Mahran, H. M., Alrashdi, M. F., & Elsafi, M. (2024). Studying the shielding ability of different cement mortars against gamma ray sources using waste iron and BaO microparticles. *Nexus Future Mater.*, *1*, 1-5.

Akman, F., Turhan, M. F., Oğul, H., Turşucu, A., Erdoğan, T., Kaçal, M. R., & Polat, H. (2025). Production and evaluation of the polyester composites containing pyrite and niobium diboride for radiation protection. Radiation Physics and Chemistry, 226, 112326

Al-Buriahi M. S. (2023). Radiation shielding performance of a borate-based glass system doped with bismuth oxide, Radiation Physics and Chemistry, 207, 110875.

Azzaoui B. E., Kabach O., Abbari Y. E., Messous M. Y., Nabaoui K., Outayad R., Lkhadiri Y. E., Chakır E. M. & Alibrahmi, E. M. (2025). Assessment of radiation shielding properties for some concrete mixtures against photon and neutron radiations. Nuclear Analysis, 4(1), 100152.

Ballsieper B. Radiation protection material based on silicone. United States Patent Application Publication; No: US 2006/0217477 A1, 2006.

Dodoo-Amoo DNA, Landsberger S, MacDonald JM, Castro JM. Development of composite materials for non-lead gloves for use in radiological hand protection. Health Phys, 2003;84: 737-746.

Eder H. Lead substitute material for radiation protection purposes. United States Patent; No: 7,041,995 B2, 2006.

Eder H. Lightweight radiation protection material for a large energy application range. United States Patent Application Publication; No: US 2009/0230334 A1, 2009.

Erkoyuncu, İ. (2025). Gamma/Neutron Radiation Shielding Characteristics and Produced Secondary Radiation in Fe-Ni Alloys. Journal of Alloys and Compounds, 181192.

Gerward, L., Guilbert, N., Jensen, K. B., & Levring, H. (2001). X-ray absorption in matter. Reengineering XCOM. Radiation Physics and Chemistry, 60(1-2), 23-24.

Ghuge, P. G., More, C. V., Sayyed, M. I., Maghrbi, Y., & Pawar, P. P. (2025). Smart polymers as gamma ray Shields: Experimental evaluation of shielding performance. Journal of Radiation Research and Applied Sciences, 18(2), 101398.

Jackson D. F., Hawkes D.J., (1981). X-ray attenuation coefficients of elements and mixtures, Physics Reports, 70(3), 169-233

Majeed E. I., Najam L. A., Hamood M. A., K.A. Mahmoud (2024). A Comprehensive study on the γ-ray shielding performance of Al–Cu–PbO alloy: Experimental and simulation studies, Nuclear Engineering and Technology, 57(1), 103124.

Nagaraja, N., Manjunatha, H. C., Seenappa, L., Sridhar, K. N., & Ramalingam, H. B. (2020). Radiation shielding properties of silicon polymers. Radiation Physics and Chemistry, 171, 108723.

Niksarlıoğlu, S., Akman, F., Agar, O., Kaçal, M. R., & Kanca, M. S. (2024). Experimental and theoretical results of gamma shielding features for copper based shape memory alloys. Progress in Nuclear Energy, 177, 105439.

Oğul, H., Akman, F., Özdoğan, H., Kaçal, M. R., Turşucu, A., Polat, H., & Erkoyuncu, İ. (2025). Evaluation of radiation shielding, secondary radiation, and radiation damage in boron carbide and chromium diboride reinforced polymer composites. Materials Chemistry and Physics, 339, 130775.

Ornketphon O., Kaewjaeng S., Meejitpaisan P., Mutuwong C., Chaipaksa W., Sommat V., Kothan S., Kaewkhao J. (2024). Photon shielding properties of oxyfluoride aluminophosphate glass added with Sb2O3 by using PHITS Monte Carlo simulation and experimental methods, Radiation Physics and Chemistry, 224, 111993.

Tousi, E. T., Jovein, E. B., Sadeghi, H. R., & Afshari, A. (2025). Investigating the effect of magnetite ore and concrete curing time on the mechanical, environmental, and radiation characteristics of radiation shielding concrete (RSC). Radiation Physics and Chemistry, 230, 112550.

Wang D. C., Ping L.A., Yang H. (1995). Nucl. Instr. and Meth. B, 95, p. 61

➢ *ORAL PRESENTATION*

High-Performance X-Band microwave absorbers: Synergistic effects of MoS_2, $CoFe_2O_4$, and conducting polymer coating

Burak Kıvrak[1*] (*ORCID: https://orcid.org/0000-0002-6785-7346*), Hasan Akyıldız[1] (*ORCID: https://orcid.org/0000-0001-8974-0520*), Oğuzhan Akgöl[2] (*ORCID: https://orcid.org/0000-0002-1423-1569*), Muharrem Karaaslan[2](*ORCID: https://orcid.org/0000-0003-0923-1959*), Mustafa Akyol[3] (*ORCID: https://orcid.org/0000-0001-8584-0620*)

[*1]Konya Technical University, Faculty of Engineering and Natural Sciences, Department of Metallurgical and Materials Engineering, Konya, Türkiye.
[2]İskenderun Technical University, Faculty of Engineering and Natural Sciences, Department of Electrical and Electronics Engineering, İskenderun, Türkiye.
[3]Adana Alparslan Türkeş Science and Technology University, Faculty of Engineering, Department of Materials Science and Engineering, Adana, Türkiye.

*Corresponding author e-mail: bkivrak@ktun.edu.tr

Abstract
In this study, microwave absorption properties of polyaniline (PANI)-coated MoS_2@$CoFe_2O_4$ composites were systematically investigated. MoS_2 particles with a flower-like morphology and $CoFe_2O_4$ nanoparticles were synthesized using hydrothermal process. The MoS_2 and $CoFe_2O_4$ components were combined at a weight ratio of 95:5 (MoS_2:$CoFe_2O_4$) using sonication method. Subsequently, the hybrid particles were coated with PANI through in situ polymerization of aniline at different PANI weight ratios, i.e., 25%, 50%, and 75%. The formation of the MoS_2@$CoFe_2O_4$ hybrid and the PANI coating were confirmed by XRD and FT-IR analysis, which revealed the coexistence of all constituent phases and characteristic chemical interactions. Electromagnetic characterization revealed that the sample containing 75 wt.% PANI exhibited the minimum reflection loss of −25.37 dB at 10.08 GHz, with an effective absorption bandwidth of 5.02 GHz at a thickness of 3 mm, fully covering the X-band frequency range. These findings demonstrate that the synthesized composites are promising candidates for high-performance microwave-absorbing materials, particularly for stealth and electromagnetic interference shielding applications in the X-band region.
Keywords: MoS_2, Cobalt ferrite nanoparticles, Polyaniline, Composite, Microwave absorber, Radar

INTRODUCTION

Microwave absorber materials (MAMs) have gained considerable attention in recent years due to the extensive utilization of electronic devices that emit electromagnetic waves (EMW), which can cause signal distortion, data loss, and performance degradation in sensitive electronic systems (Wei, H. et al., 2020). Moreover, the development of efficient absorbers is critical for stealth technologies, where minimizing radar cross-section is essential for military applications. As a result, the design of high-performance MAMs with broad bandwidth, reduced thickness, and strong attenuation capability has become a vital area of research. To achieve these performance criteria, various strategies have been proposed and one of the most effective is the fabrication of multi-component absorbers combining dielectric, magnetic, and conductive media.

The absorption of incident EMW in microwave frequency ranges can be facilitated through several mechanisms such as dielectric and magnetic losses, which are induced by specific material characteristics (Quan et al., 2017; Wei, H. et al., 2020). In the GHz frequency range, effective dielectric loss mechanisms include interfacial, defect-induced, and dipolar polarization, and conductive loss (Qin et al., 2022). These mechanisms can be enhanced using dielectric materials such as MoS_2. MoS_2 belongs to the transition metal dichalcogenide family and has a layered crystal structure composed of covalently bonded molybdenum (Mo^{4+}) and sulfur (S^{2-}) atoms (Mak et al., 2010). Due to its tunable morphology, phase versatility, and excellent dielectric properties, MoS_2 has been widely investigated as a promising microwave absorber (Li et al., 2024). Conversely, magnetic materials absorb microwave energy through natural and exchange resonance, and Eddy current losses within the GHz ranges (Zhang et al., 2018). $CoFe_2O_4$, a typical spinel ferrite where Co^{2+} ions predominantly occupy the octahedral sites while Fe^{3+} ions occupy both tetrahedral and octahedral sites of the crystal lattice, is widely known for its high magnetic anisotropy, good chemical stability, and high resonance

frequency (Sanchez-Lievanos et al., 2021; Yuan et al., 2020). These properties make $CoFe_2O_4$ a favorable candidate as magnetic MAMs, especially in combination with dielectric or conductive components (Che et al., 2006). In addition, conductive polymers such as PANI have been extensively used for microwave absorption application due to its lightweight nature, high chemical and thermal stability, and contribution to conductive losses (Kıvrak et al., 2024; Yu et al., 2018). Therefore, combining MoS_2, $CoFe_2O_4$, and PANI in a designed architecture offers an effective way to take advantage of their different properties and improve the overall microwave absorption performance.

In this study, PANI coated MoS_2@$CoFe_2O_4$ hybrid particles were synthesized using a three-steps synthesis procedure consisting of hydrothermal, sonication, and in-situ polymerization techniques. The microwave absorption performance of the composites was characterized using a vector network analyzer (VNA) across the 2-18 GHz frequency range. Among all samples, the one containing 75 wt.% PANI at a thickness of 3 mm exhibited the best performance, with a minimum reflection loss (RL_{min}) of -25.37 dB at 10.08 GHz and an effective absorption bandwidth (EAB) of 5.02 GHz, fully covering the X-band frequency range. Additionally, the other thickness values of the 75 wt.% PANI sample showed notable absorption at different frequencies, indicating the tunability of the absorber performance with sample thickness. These results suggest that the PANI coated MoS_2@$CoFe_2O_4$ composites emerge as promising candidates for applications in stealth technologies.

MATERIALS AND METHODS

The synthesis methods of materials and chemicals used in preparations is described in detail elsewhere (Kıvrak et al., 2024). The MoS_2@$CoFe_2O_4$ hybrid was prepared at a weight ratio of 95:5 and subsequently coated with PANI at 25 wt.%, 50 wt.%, and 75 wt.%, as summarized in Table 1. The resulting composites were designated as MCP1, MCP2, and MCP3, respectively, based on their PANI content.

Table 1. The content and compositional distribution of the manufactured composite samples

Sample Code	MoS_2 (wt.%)	$CoFe_2O_4$ (wt.%)	MoS_2@$CoFe_2O_4$ (wt.%)	PANI (wt.%)
MoS_2@$CoFe_2O_4$	95	5		
MCP1			75	25
MCP2			50	50
MCP3			25	75

Characterization techniques

The phase distribution of the synthesized samples was examined using an X-ray diffractometer (Rigaku MiniFlex600) equipped with Cu-Kα radiation (λ = 1.5406 Å). FT-IR analysis was carried out via Jasco FT/IR-6700 between 4000-400 cm^{-1}. The morphological characteristics of the MoS_2@$CoFe_2O_4$ hybrid sample were examined using a FEI-Quanta 650D FEG SEM. The room temperature magnetic properties of the synthesized samples were investigated using Vibrating Sample Magnetometry (VSM, Quantum Design DynaCool). The microwave absorption characteristics of samples were investigated via Agilent E8363B PNA in the frequency range of 2-18 GHz.

RESULTS and DISCUSSION

Structural characteristics

XRD patterns of the samples are presented in Figure 1a. The black and red vertical markers at the bottom represent the standard diffraction line positions for trigonal prismatic (2H) MoS_2 (JCPDS No: 00-037-1492), and cubic $CoFe_2O_4$ (JCPDS No: 00-022-1086), respectively. For the MoS_2@$CoFe_2O_4$ sample (blue line), distinct diffraction peaks corresponding to both MoS_2 and $CoFe_2O_4$ are clearly observed, confirming the successful formation of the hybrid structure. The primary diffraction peak of 2H-MoS_2 at 2θ = 14.04°, which corresponds to the (002) plane, is shifted to 2θ = 13.59°, suggesting an expansion of the interlayer spacing likely caused by defect or vacancy formation. Meanwhile, $CoFe_2O_4$ displays its characteristic peaks at 2θ = 35.56°, 43.24°, 56.92°, and 62.65°, corresponding to the (311), (400), (511), and (440) planes, respectively. The diffraction patterns of the PANI-coated samples are also presented in the same figure, with red gradients indicating increasing PANI content. Notably, the characteristic peaks of PANI become most prominent in the MCP3 sample, which contains the highest amount of PANI. Additional diffraction peaks at 2θ = 20.09°, 25.06°, and 26.38° (marked with pink dots) are assigned to PANI, further confirming its presence. Overall, the

simultaneous presence of diffraction peaks corresponding to MoS_2, $CoFe_2O_4$, and PANI confirms the successful fabrication of the MoS_2@$CoFe_2O_4$/PANI composite structures.

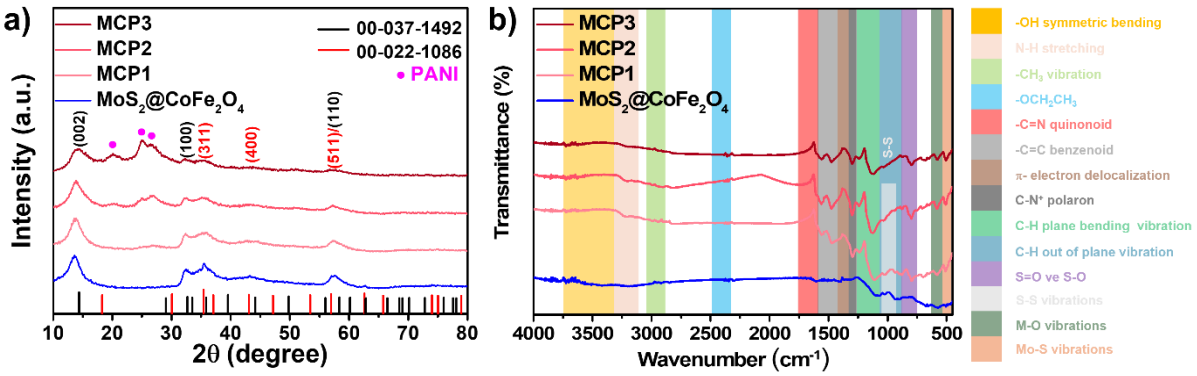

Figure 1. Structural characterization results of samples, a) XRD patterns and b) FT-IR spectra of samples (The vertical lines given at the bottom of (a) shows the theoretical line positions of $CoFe_2O_4$ and MoS_2 according to JCPDS Card No of 00-022-1086 and 00-037-1492, respectively. The characteristic bands in (b) shaded with different colors as a guide for the eye)

Figure 1b presents the FT-IR spectra of the hybrid and PANI-coated composite samples. Characteristic absorption bands are highlighted with color-coded regions for clarity. The broad band in the orange-shaded area corresponds to symmetric -OH stretching vibrations, likely arising from moisture absorbed during storage. The pink-shaded region, located at ~3200 cm^{-1}, indicates N-H stretching vibrations due to nitrogen protonation (Shao et al., 2012). The light green region (2990-2840 cm^{-1}) is attributed to the stretching vibrations of methyl (-CH_3) groups (Abdiryim et al., 2007). The light blue region, from 2380 to 2300 cm^{-1}, is associated with the angular deformation of the -OCH_2CH_3 functional group bonded to aromatic rings (Silva et al., 2014). Distinct peaks at 1561 cm^{-1} and 1474 cm^{-1}, shaded in red and gray, are assigned to the stretching vibrations of quinoid and benzenoid rings, respectively (Abdiryim et al., 2007; Kulkarni & Viswanath, 2004; Wei, Y. et al., 1994). The brown-shaded band at 1301 cm^{-1} corresponds either to C-N-C stretching or π-electron delocalization caused by protonation, while the dark gray region at 1238 cm^{-1} reflects the C-N^+ polaron structure. Bands at 1124 cm^{-1} (teal green) and 1026 cm^{-1} (dark blue) are attributed to in-plane C-H bending vibrations, and the 881 cm^{-1} peak is associated with out-of-plane C-H vibrations (Abdiryim et al., 2007; Kulkarni & Viswanath, 2004). Peaks at approximately 794 and 703 cm^{-1} (purple region) are linked to S=O and S-O stretching vibrations of sulfonate groups (Shao et al., 2012). Furthermore, the green-shaded bands at 578 and 513 cm^{-1} confirm metal-oxygen (M-O) stretching vibrations in the tetrahedral and octahedral sites of spinel $CoFe_2O_4$ (Dhaka et al., 2021). Finally, the gray and pale-orange shaded regions display characteristic peaks of MoS_2 at 915 cm^{-1} and 474 cm^{-1}, corresponding to S-S and Mo-S bond vibrations, respectively (Lalithambika et al., 2019). Thus, the FT-IR results confirm the successful incorporation of PANI, $CoFe_2O_4$, and MoS_2 components within the composite structure, consistent with the expected chemical functionalities.

Morphological characteristics

Figure 2 presents the SEM images of the MoS_2@$CoFe_2O_4$ hybrid sample. As seen from Figure 2a, the MoS_2 particles exhibit a flower-like morphology with micrometer-scale diameters, while the $CoFe_2O_4$ nanoparticles appear equiaxed and are within the nanometer scale. The green dashed circles highlight the regions where $CoFe_2O_4$ nanoparticles are distributed. In Figure 2b, it is clearly observed that the $CoFe_2O_4$ nanoparticles, with an average size of approximately 35 nm, are well-dispersed in the gaps between the MoS_2 nanosheets, indicating a successful integration of the two materials.

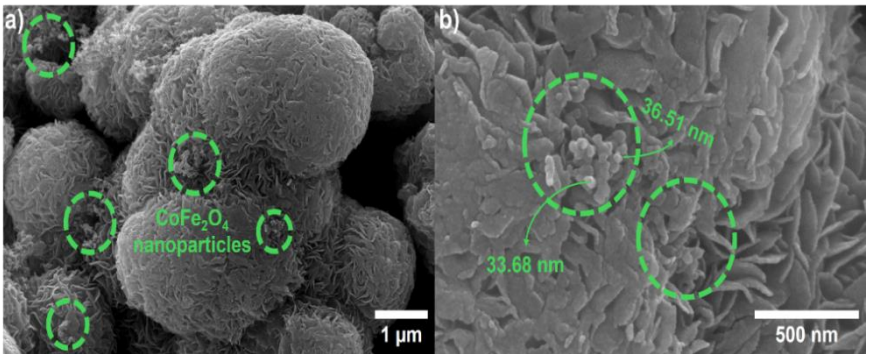

Figure 2. SEM images of MoS_2@$CoFe_2O_4$ sample (the dashed green circles represent the location where $CoFe_2O_4$ nanoparticles can be found)

Magnetic characteristics

Figure 3 shows the magnetic hysteresis loop of the MoS_2@$CoFe_2O_4$ hybrid sample at room temperature. As observed in the figure, the sample exhibits ferromagnetic behavior. It is reported that $CoFe_2O_4$ demonstrates ferromagnetic characteristics with a saturation magnetization (M_s) of 53.3 emu/g (Kıvrak et al., 2024). In comparison, the MoS_2@$CoFe_2O_4$ composite with a weight ratio of 95:5 displays a significantly lower M_s value of 1.56 emu/g. This notable reduction can be attributed to the intrinsically weak magnetic nature of MoS_2, as discussed and confirmed in our earlier findings (Kıvrak et al., 2024). The results suggest that while the magnetic response is retained, the overall magnetic strength is diminished due to the low $CoFe_2O_4$ content in the composite.

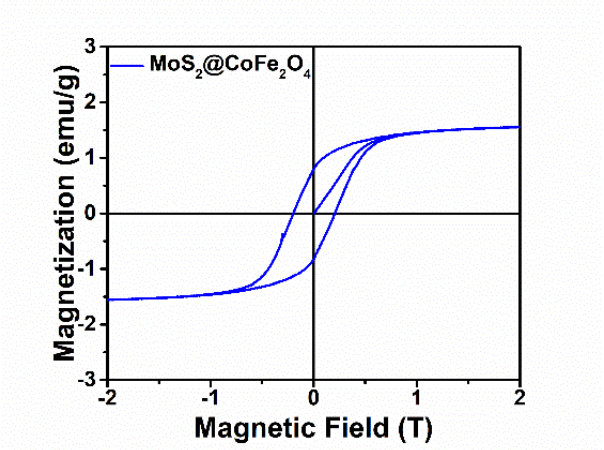

Figure 3. The room temperature magnetic hysteresis curve of MoS_2@$CoFe_2O_4$ hybrid sample

Electromagnetic wave absorption performance

Figure 4 displays the *RL* graphs of manufactured samples derived from Eqs. 1-3. In these equations, Z_{in} is the input impedance of the absorber, Z_0 is the impedance of the free space, c is the velocity of EM waves in free space, f is the frequency, and d is the layer thickness changing from 1 mm to 5 mm. The dashed red lines represent the -10 dB and -20 dB threshold (90% and 99% absorption of the incident EMW) value, and the green dashed line represents the ideal value of (1) impedance matching.

$$Z_{in} = Z_0\left(\sqrt{\mu_r/\varepsilon_r}\right) tanh\left[j\left(\frac{2\pi fd}{c}\right)\left(\sqrt{\mu_r\varepsilon_r}\right)\right] \quad (1)$$

$$R_L = 20log\left(\frac{Z_{in}-Z_o}{Z_{in}+Z_o}\right) \quad (2)$$

$$Z = \left|{}^{Z_{in}}/_{Z_0}\right| \quad (3)$$

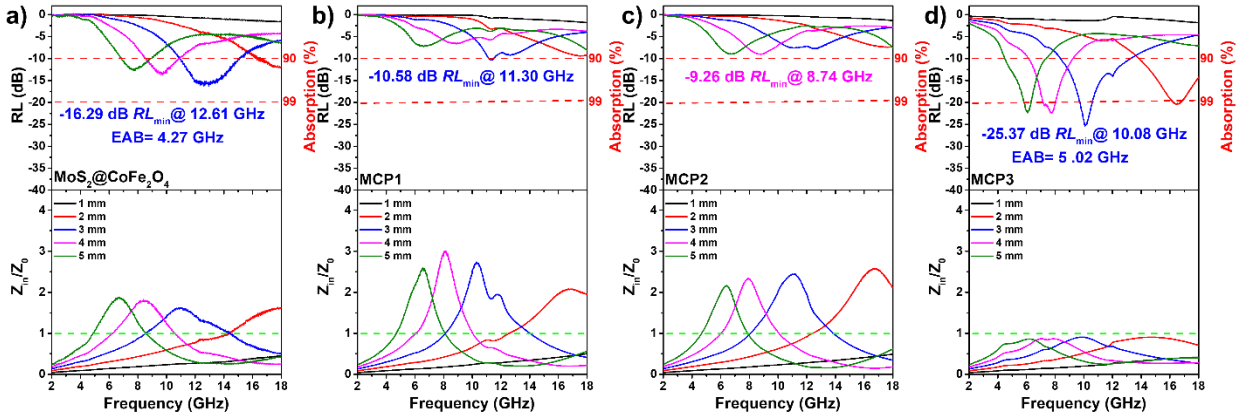

Figure 4. RL_{min} graphs of manufactured samples along with impedance matching graphs below, a) MoS_2@$CoFe_2O_4$, b) MCP1, c) MCP2 and d) MCP3

Figure 4a illustrates the RL_{min} graph of the MoS_2@$CoFe_2O_4$ sample. According to the graph, the sample exhibits an RL_{min} value of −16.29 dB at 12.61 GHz, with an EAB of 4.27 GHz at a thickness of 3 mm. On the other hand, when PANI is coated at ratios of 25 wt.% and 50 wt.%, a noticeable decline in absorption performance is observed (see Figures 4b and 4c). Specifically, the MCP1 and MCP2 samples show RL_{min} values of −10.58 dB at 11.30 GHz and −9.26 dB at 8.74 GHz, respectively. These findings suggest that PANI coating at these lower concentrations hinders the microwave absorption capability of the composite. In addition, the impedance matching curves agree with the absorption results. When PANI is coated 25 wt.% and 50 wt.%, significant deviation from the ideal impedance matching is observed. In contrast, at a PANI content of 75 wt.%, the MCP3 sample exhibits a significantly improved performance, with an RL_{min} of −25.37 dB at 10.08 GHz and an EAB of 5.02 GHz at 3 mm thickness, effectively covering the entire X-band frequency range. This remarkable improvement indicates that a higher PANI ratio enhances both RL_{min} and bandwidth. Moreover, the impedance matching graph of MCP3 shows a distinct pattern compared to the other samples and approaches the ideal value near the resonance frequency. The other thicknesses of MCP3 also supports the improved performance of MCP3. At 4 mm thickness, the sample reached an RL_{min} of -22.60 dB at 7.76 GHz with an EAB of 3.23 GHz. When the thickness was increased to 5 mm, it still maintained strong absorption, with an RL_{min} of -22.44 dB at 6.06 GHz and an EAB of 3.00 GHz. These results clearly indicate that the microwave absorption performance of the samples is strongly dependent on thickness, suggesting that the material can be effectively used at various thicknesses for specific frequency ranges in targeted applications.

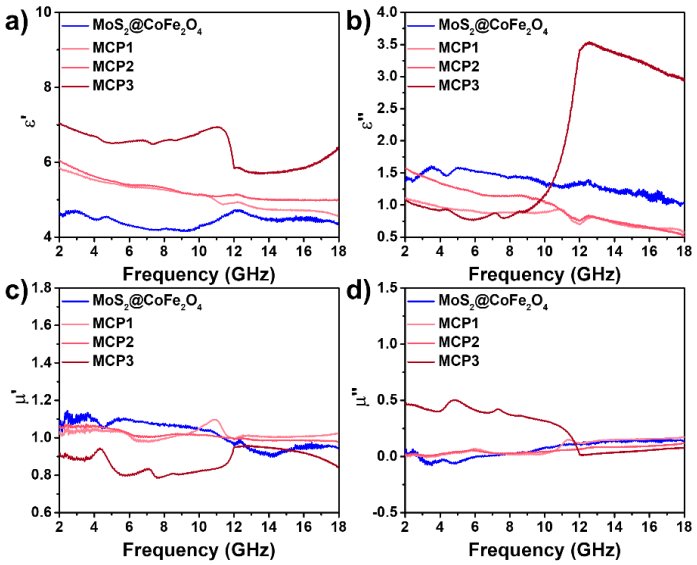

Figure 5. Electromagnetic parameters, a) ε', b) ε'', c) $\mu'$and d) μ''as a function of frequency

There are two main electromagnetic parameters that determine the absorption characteristics of a material: complex permittivity $(\varepsilon_r = \varepsilon' - j\varepsilon'')$ and complex permeability $(\mu_r = \mu' - j\mu'')$. The real parts of these complex values represent the material's ability to store electric or magnetic energy, while the imaginary

parts correspond to the energy loss (dissipation) capabilities (Miles et al., 1957; Qin et al., 2022; Zheng et al., 2022). Figure 5 shows the frequency-dependent behavior of these electromagnetic parameters. According to Figure 5a, the real part of the dielectric permittivity (ε′) of MCP3 sample is the highest among all samples, indicating superior dielectric energy storage capacity. Similarly, Figure 5b shows that the dielectric loss (ε″) of MCP3 is also the highest, especially at frequencies above 10 GHz. Based on free electron theory, the imaginary part of permittivity is directly related to the electrical conductivity of a material (Chen, L.-F. et al., 2004; Pang et al., 2021; Quan et al., 2017). Therefore, it can be concluded that MCP3 has higher conductivity compared to other samples, which contributes to its improved absorption performance through conductive loss mechanisms. This result is consistent with the high PANI content of the sample, as PANI is known to enhance electrical conductivity. Additionally, the presence of multiple resonance peaks in the ε″ curve suggests the contribution of various loss mechanisms such as defect-induced and interfacial polarizations (Chen, Y.-J. et al., 2009). Figure 5c illustrates the frequency dependence of the real part of magnetic permeability (μ′). It can be observed that all samples exhibit several resonance peaks, indicative of natural and exchange resonances. However, the μ′ value of MCP3 is the lowest among the samples, which implies that dielectric loss dominates over magnetic loss in this sample. In contrast, the magnetic loss (μ″) of MCP3 is higher than that of others up to 11 GHz, suggesting that magnetic loss mechanisms also contribute to absorption performance within this frequency range (see Figure 5d).

When an incident EMW interacts with the dielectric component of an absorber, the electric field component of the wave causes the dipoles within the material to align with the field direction. Once the external field is removed or changes direction, these dipoles attempt to return to their original random orientation and this process is known as dipolar polarization. This delayed response leads to energy dissipation, contributing to dielectric loss and can be described by the Debye relaxation theory and visualized using Cole-Cole plots (Qin et al., 2022; Quan et al., 2017). Figure 6 presents the Cole-Cole plots of the samples. In these plots, each semicircle represents a different relaxation process. The number and shape of the semicircles provide insight into the types and complexity of energy loss mechanisms within the material. Additionally, the presence of a 'tail-like' extension in the plot is indicative of conductive loss (Chen, D. et al., 2013; Wu et al., 2020; Xu et al., 2024). According to Figure 6a, the MoS_2@$CoFe_2O_4$ hybrid sample exhibits a distorted semicircular shape, suggesting the dominance of interfacial polarization. In contrast, the PANI-coated samples display multiple distinct semicircles along with a noticeable tail formation, which reflects the presence of both dipolar and conductive loss mechanisms which are consistent with the known conductive nature of PANI (see Figures 6b-d). Among all, the MCP3 sample exhibits the largest relaxation arcs and the most prominent tail structure, indicating the coexistence of multiple relaxation processes and diverse loss mechanisms contributing to its superior electromagnetic wave absorption performance.

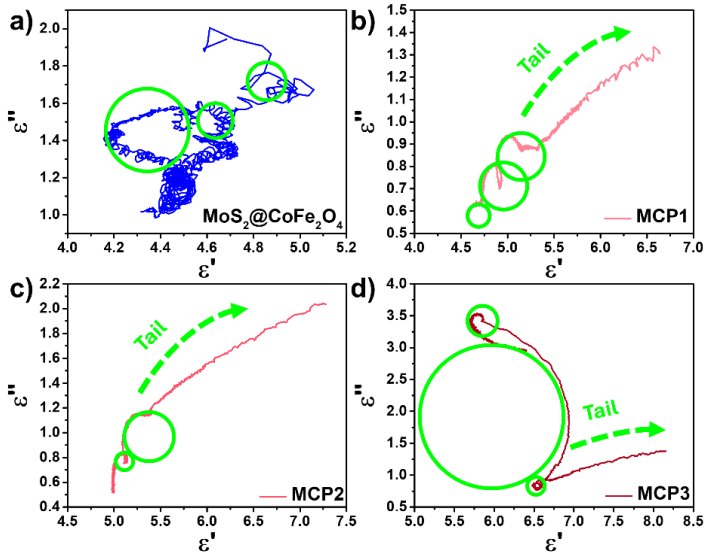

Figure 6. Cole-Cole plots of the samples, a) MoS_2@$CoFe_2O_4$, b) MCP1, c) MCP2 and d) MCP3 (the green circles represent the semi-circle locations, and the arrow illustrates the tail formation)

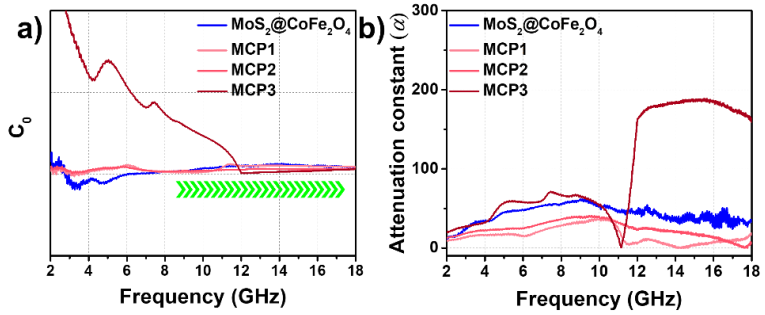

Figure 7. Eddy current loss and attenuation constant graphs of the samples

As mentioned previously, in the GHz frequency range, natural resonance, exchange resonance, and Eddy current loss are the dominant magnetic loss mechanisms. Figure 7a illustrates the frequency dependence of Eddy current loss, calculated using the following equation (Gao et al., 2022):

$$C_0 = \mu''(\mu')^{-2} f^{-1} \quad (4)$$

where C_0 represents the Eddy current loss. When Eddy current loss is the primary magnetic loss mechanism, the curve of C_0 versus frequency tends to follow a linear trend (the green arrow in the figure illustrates where the linear trend can be seen). Deviations or fluctuations from linearity are indicative of additional mechanisms, such as natural and exchange resonances (Kıvrak et al., 2024). As seen in Figure 7a, all samples except MCP3 exhibit relatively linear behavior beyond 8 GHz, suggesting Eddy current loss is dominant. In contrast, the MCP3 sample shows pronounced resonances, especially between 8-12 GHz, followed by a linear trend at higher frequencies, indicating that multiple magnetic loss mechanisms-including natural and exchange resonances-coexist in this sample. Microwave attenuation performance is another critical factor for evaluating absorber efficiency. The attenuation constant, which reflects the material's ability to attenuate incident electromagnetic waves, can be calculated using the following equation (Xie et al., 2022):

$$\alpha = \frac{\sqrt{2}\pi f}{c} \times \sqrt{(\mu''\varepsilon'' - \mu'\varepsilon') + \sqrt{(\mu''\varepsilon'' - \mu'\varepsilon')^2 + (\mu'\varepsilon'' + \mu''\varepsilon')^2}} \quad (5)$$

Figure 7b presents the frequency-dependent behavior of the attenuation constant. It is evident that the MCP3 sample exhibits the highest attenuation capability across the examined frequency range, except for a notable dip around 12 GHz. In conclusion, the superior microwave absorption performance of the MCP3 sample can be attributed to a combination of ideal impedance matching, the presence of multiple magnetic and dielectric loss mechanisms, and its high attenuation capability. Further, it is believed that the complex flower-like morphology of MoS_2 combined with the well-dispersed $CoFe_2O_4$ nanoparticles enhances multiple reflections within the absorber, thereby increasing the interaction time of incident electromagnetic waves and contributing to energy dissipation. Additionally, interfacial polarization between MoS_2, $CoFe_2O_4$, and PANI introduces significant dielectric loss mechanisms. The presence of numerous heterogeneous interfaces in the composite structure strongly supports the contribution of interfacial polarization. Moreover, structural defects and defect-induced polarization were identified as important contributors to dielectric loss, as evidenced by the observed resonance peaks in dielectric spectra and Cole-Cole plots. Considering the ferromagnetic nature of $CoFe_2O_4$, magnetic loss mechanisms such as natural resonance, exchange resonance, and Eddy current loss were also determined to play a crucial role in absorption, particularly in the GHz frequency range. Finally, the incorporation of the conductive polymer PANI into the structure induced additional conductive losses, further enhancing the absorption performance. This was supported by both the increase in dielectric loss at higher frequencies and the tail-like features observed in Cole–Cole plots. Altogether, these synergistic loss mechanisms make the synthesized PANI-coated MoS_2@$CoFe_2O_4$ composites highly efficient electromagnetic wave absorbers.

CONCLUSION

In this study, MoS_2@$CoFe_2O_4$ and PANI-coated MoS_2@$CoFe_2O_4$ composites were successfully synthesized, and their microwave absorption properties were systematically investigated. Structural analyses confirmed the presence of functional groups and successful composite formation, while SEM imaging revealed a flower-like MoS_2 morphology decorated with $CoFe_2O_4$ nanoparticles (~35 nm). Magnetic characterization showed that

MoS_2@$CoFe_2O_4$ exhibits ferromagnetic behavior with an M_s value of 1.56 emu/g, attributed to the 5 wt.% $CoFe_2O_4$ content. FT-IR analyses further validated the presence of PANI and confirmed the coexistence of Mo-S, S-S, and M-O bonds in the composites. VNA measurements revealed that MCP3 sample with 75 wt.% PANI content exhibited significantly improved absorption with RL_{min} of -25.37 dB at 10.08 GHz and an EAB of 5.02 GHz at 3 mm, effectively covering the entire X-band. Furthermore, MCP3 showed strong absorption performance at increased thicknesses values. These results suggest that PANI-coated MoS_2@$CoFe_2O_4$ composites, particularly at optimized PANI content, are promising candidates for high-performance microwave absorbing materials suitable for stealth applications.

ACKNOWLEDGEMENTS

This study was supported by Scientific and Technological Research Council of Turkey (TUBITAK) under the Grant Number 121F367. The authors thank TUBITAK for their support.

REFERENCES

Abdiryim, T., Jamal, R., & Nurulla, I. (2007). Doping effect of organic sulphonic acids on the solid-state synthesized polyaniline. Journal of Applied Polymer Science, 105(2), 576-584.

Che, R. C., Zhi, C. Y., Liang, C. Y., & Zhou, X. G. (2006). Fabrication and microwave absorption of carbon nanotubes/$CoFe_2O_4$ spinel nanocomposite. Applied Physics Letters, 88(3).

Chen, D., Wang, G.-S., He, S., Liu, J., Guo, L., & Cao, M.-S. (2013). Controllable fabrication of mono-dispersed RGO–hematite nanocomposites and their enhanced wave absorption properties. Journal of Materials Chemistry A, 1(19), 5996-6003.

Chen, L.-F., Ong, C. K., Neo, C., Varadan, V. V., & Varadan, V. K. (2004). *Microwave electronics: measurement and materials characterization*: John Wiley & Sons.

Chen, Y.-J., Gao, P., Wang, R.-X., Zhu, C.-L., Wang, L.-J., Cao, M.-S., & Jin, H.-B. (2009). Porous Fe3O4/SnO2 Core/Shell Nanorods: Synthesis and Electromagnetic Properties. The Journal of Physical Chemistry C, 113(23), 10061-10064.

Dhaka, S., Kumar, S., Poonia, K., Singh, V., Dhaka, K., & Mund, H. S. (2021). Effect of annealing temperature on structural and magnetic properties of nano-cobalt ferrite. Journal of Materials Science: Materials in Electronics, 32(12), 16392-16399.

Gao, J., Ma, Z., Liu, F., & Chen, C. (2022). Synthesis of carbon-coated cobalt ferrite core–shell structure composite: A method for enhancing electromagnetic wave absorption properties by adjusting impedance matching. Chinese Journal of Chemical Engineering, 47, 206-217.

Kıvrak, B., Akyıldız, H., AkgöL, O., Karaaslan, M., & Akyol, M. (2024). Polyaniline-Functionalized Nanosized Cobalt Ferrite-Decorated MoS2 Composites for Broadband Electromagnetic Wave Absorption. ACS Applied Electronic Materials, 6(11), 8211-8225.

Kulkarni, M. V., & Viswanath, A. K. (2004). Comparative studies of chemically synthesized polyaniline and poly(o-toluidine) doped with p-toluene sulphonic acid. European Polymer Journal, 40(2), 379-384.

Lalithambika, K. C., Shanmugapriya, K., & Sriram, S. (2019). Photocatalytic activity of MoS2 nanoparticles: an experimental and DFT analysis. Applied Physics A, 125(12), 817.

Li, J., Li, X., He, L., Guo, H., Xia, W., Sun, B., . . . Zhou, D. (2024). MoS_2-Based Nanocomposites for Microwave Absorption: A Review. ACS Applied Nano Materials, 7(6), 5761-5775.

Mak, K. F., Lee, C., Hone, J., Shan, J., & Heinz, T. F. (2010). Atomically thin MoS(2): a new direct-gap semiconductor. Phys Rev Lett, 105(13), 136805.

Miles, P. A., Westphal, W. B., & Von Hippel, A. (1957). Dielectric Spectroscopy of Ferromagnetic Semiconductors. Reviews of Modern Physics, 29(3), 279-307.

Pang, H., Duan, Y., Huang, L., Song, L., Liu, J., Zhang, T., . . . Liu, X. (2021). Research advances in composition, structure and mechanisms of microwave absorbing materials. Composites Part B: Engineering, 224, 109173.

Qin, M., Zhang, L., & Wu, H. (2022). Dielectric Loss Mechanism in Electromagnetic Wave Absorbing Materials. Advanced Science, 9(10), 2105553.

Quan, B., Liang, X., Ji, G., Cheng, Y., Liu, W., Ma, J., . . . Xu, G. (2017). Dielectric polarization in electromagnetic wave absorption: Review and perspective. Journal of Alloys and Compounds, 728, 1065-1075.

Sanchez-Lievanos, K. R., Stair, J. L., & Knowles, K. E. (2021). Cation Distribution in Spinel Ferrite Nanocrystals: Characterization, Impact on their Physical Properties, and Opportunities for Synthetic Control. Inorganic Chemistry, 60(7), 4291-4305.

Shao, W., Jamal, R., Xu, F., Ubul, A., & Abdiryim, T. (2012). The Effect of a Small Amount of Water on the Structure and Electrochemical Properties of Solid-State Synthesized Polyaniline. Materials, 5(10), 1811-1825.

Silva, A. d. S., Soares, J. C., Mafud, A. C., de Souza, S. M., Fernandes, E. G. R., Mascarenhas, Y. P., & Sanches, E. A. (2014). Structural and morphological characterization of Poly(o-ethoxyaniline) Emeraldine-salt form using FTIR, XRD, LeBail Method and SEM. Journal of Molecular Structure, 1071, 1-5.

Wei, H., Zhang, Z., Hussain, G., Zhou, L., Li, Q., & Ostrikov, K. (2020). Techniques to enhance magnetic permeability in microwave absorbing materials. Applied Materials Today, 19, 100596.

Wei, Y., Hsueh, K. F., & Jang, G. W. (1994). A study of leucoemeraldine and effect of redox reactions on molecular weight of chemically prepared polyaniline. Macromolecules, 27(2), 518-525.

Wu, Y., Shu, R., Shan, X., Zhang, J., Shi, J., Liu, Y., & Zheng, M. (2020). Facile design of cubic-like cerium oxide nanoparticles decorated reduced graphene oxide with enhanced microwave absorption properties. Journal of Alloys and Compounds, 817, 152766.

Xie, S., Cao, Y., Ma, C., Si, T., Ji, Z., & Wang, J. (2022). Synthesis and electromagnetic wave absorbing properties of flower-like MoS2/CoFe/C ternary composites. Composite Interfaces, 29(13), 1397-1411.

Xu, J., Yang, Y., Dong, H., Li, J., Ma, Y., Wang, M., . . . Sheng, Z. (2024). The effect of conduction loss on microwave absorption performance of Fe-doped NiCo2O4 spinel oxide. Ceramics International, 50(22, Part B), 46882-46891.

Yu, L., Zhu, Y., & Fu, Y. (2018). Waxberry-like carbon@polyaniline microspheres with high-performance microwave absorption. Applied Surface Science, 427, 451-457.

Yuan, Y., Wei, S., Liang, Y., Wang, B., & Wang, Y. (2020). Effect of Solvothermal Reaction-Time on Microstructure and Microwave Absorption Properties of Cobalt Ferrite. Materials, 13(23), 5331.

Zhang, Y., Wang, X., & Cao, M. (2018). Confinedly implanted NiFe2O4-rGO: Cluster tailoring and highly tunable electromagnetic properties for selective-frequency microwave absorption. Nano Research, 11(3), 1426-1436.

Zheng, W., Ye, W., Yang, P., Wang, D., Xiong, Y., Liu, Z., . . . Zhang, Y. (2022). Recent Progress in Iron-Based Microwave Absorbing Composites: A Review and Prospective. Molecules, 27(13), 4117.

➢ *ORAL PRESENTATION*

EpiXS tabanlı hesaplamalarla gelişmiş seramik numunelerin gama radyasyonu azaltma kapasitelerinin değerlendirilmesi

İlhami Erkoyuncu[1*] (*ORCID:* https://orcid.org/0000-0003-1639-5062)
Ferdi AKMAN[2] (*ORCID*: https://orcid.org/0000-0002-8838-1762)

[*1] Bingöl Üniversitesi, Fen-Edebiyat Fakültesi, Fizik, Bingöl, Türkiye
[2] Bingöl Üniversitesi, Sosyal Bilimler MYO Mülkiyet Koruma ve Güvenlik Bölümü, İş Sağlığı ve Güvenliği Programı, Bingöl, Türkiye

*Sorumlu yazar e-posta: ierkoyuncu@bingol.edu.tr

Özet
Bu çalışmada, dört farklı seramik numunesinin (S1, S2, S3 ve S4) gama radyasyonu karşısındaki zayıflatma performansı kuramsal olarak değerlendirilmiştir. Radyasyonla etkileşimi tanımlayan dört temel parametre olan kütle azaltma katsayısı (MAC), ortalama serbest yol (MFP), maruz kalma birikim faktörü (EBF) ve enerji soğurma birikim faktörü (EABF), EpiXS programı kullanılarak hesaplanmıştır. MAC ve MFP değerleri 10–150 keV enerji aralığında, EAF ve EABF değerleri ise 0,015-15 MeV enerji aralığında analiz edilmiştir. Elde edilen sonuçlar, enerji arttıkça MAC'in azaldığını, MFP, EBF ve EABF değerlerinin ise arttığını göstermektedir. Bu eğilim, seramiklerin enerjiye bağlı radyasyon azaltma davranışını açıkça ortaya koymuştur. Özellikle S3 numunesi, tüm parametrelerde üstün performans sergileyerek en etkili radyasyon zırhlama adayı olarak belirlenmiştir. Bu bağlamda, çevresel açıdan güvenli, kurşunsuz ve yüksek performanslı seramik bileşimlerin, nükleer enerji, tıbbi görüntüleme ve havacılık teknolojileri gibi alanlardaki uygulamalara entegrasyonu önerilmektedir.
Anahtar Kelimeler: Seramik, gama radyasyonu zırhlama, EpiXS

Evaluation of gamma radiation attenuation capacities of advanced ceramic samples based on EpiXS calculations

Abstract
In this study, the gamma radiation shielding performance of four different ceramic samples (S1, S2, S3, and S4) was theoretically evaluated. Four fundamental parameters describing radiation interaction mass attenuation coefficient (MAC), mean free path (MFP), exposure buildup factor (EAF), and energy absorption buildup factor (EABF) were calculated using the EpiXS software. MAC and MFP values were analyzed in the energy range of 10–150 keV, while EAF and EABF values were determined in the energy range of 0.015–15 MeV. The results showed that as energy increased, MAC values decreased, whereas MFP, EAF, and EABF values increased. This trend clearly demonstrates the energy-dependent radiation shielding behavior of ceramic materials. Among the samples, S3 exhibited superior performance in all parameters and was identified as the most effective shielding candidate. In this context, lead-free, environmentally friendly, and high-performance ceramic compositions are recommended for integration into applications in nuclear energy, medical imaging, and aerospace technologies.
Keywords: Ceramic, gamma radiation shielding, EpiXS

1.GİRİŞ

İyonlaştırıcı radyasyonun kontrolsüz yayılımı, canlı organizmalarda kalıcı biyolojik hasara ve yapısal materyallerde bozulmalara yol açabileceğinden, etkin radyasyon zırhlama teknolojileri kritik öneme sahiptir. Gama radyasyonu özellikle yüksek nüfuz edici gücüyle bu tür zararların başlıca kaynağıdır ve bu radyasyona karşı güvenli, ekonomik ve çevresel olarak sürdürülebilir zırhlama malzemelerinin geliştirilmesi bilimsel açıdan öncelikli bir alandır (Al-Buriahi ve ark., 2021; Singh ve ark., 2023; Erkoyuncu ve ark., 2024). Bu bağlamda, seramik malzemeler; yüksek erime noktaları, iyi mekanik özellikleri, kimyasal kararlılıkları ve termal dayanımları nedeniyle radyasyon zırhlama uygulamaları için alternatif bir çözüm olarak görülmektedir (Mostafa & Farouk, 2023). Özellikle ağır metal oksit katkılı seramikler, gama ışınlarına karşı etkin bir azaltma sağlayarak geleneksel kurşun bazlı sistemlere çevre dostu bir alternatif sunmaktadır (Zakaly ve ark., 2022). Radyasyonla etkileşimde malzemelerin azaltma performansını nicel olarak belirleyebilmek için çeşitli

parametreler kullanılmaktadır. Bu parametreler arasında kütle azaltma katsayısı (MAC), ortalama serbest yol (MFP), enerji soğurma birikim faktörü (EABF) ve maruz kalma birikim faktörü (EBF) yer almaktadır. Bu parametreler, materyalin fotonla olan etkileşimini enerjiye bağlı olarak tanımlamada büyük rol oynamaktadır (Tariq ve ark., 2024; Fouda ve ark., 2023).

Son yıllarda literatürde, farklı katkı maddeleriyle modifiye edilen seramiklerin radyasyon zırhlama özelliklerine dair pek çok deneysel ve teorik çalışma yayımlanmıştır. Abd-Elkader ve ark. (2023), Bi_2O_3 katkılı seramik kompozitlerin yüksek gama ışını azaltma kabiliyeti gösterdiğini ortaya koymuştur. Singh ve ark. (2023), ileri seramik bazlı materyallerin yapı ve tıp alanında kullanılabilirliğine dikkat çekmiştir. Zakaly ve ark. (2022), neodimyum katkılı borat camlarının MAC ve EABF değerlerinde iyileşme sağladığını bildirmiştir. Benzer şekilde, Rashad ve ark. (2024), kurşun içermeyen seramiklerin nükleer güvenlik uygulamalarında kullanılabileceğini ileri sürmüştür. Nanoparçacık destekli seramik yapılar hem ikincil radyasyon üretimini baskılamakta hem de yüksek yoğunluk avantajı sunmaktadır (Yousef ve ark., 2025). Bu tür yapılar, hem sabit laboratuvar sistemlerinde hem de taşınabilir koruma zırhlamalarında kullanılmaya adaydır. Ayrıca, Farid ve ark. (2025), farklı matrisli seramiklerin radyasyonla etkileşim verilerini karşılaştırmalı olarak analiz etmiş ve kompozit yapının, homojen seramiklere göre üstün performans gösterdiğini raporlamıştır.

Bu çalışmada, dört farklı seramik numunesi (S1, S2, S3 ve S4) için gama radyasyonu ile etkileşim parametreleri olan MAC, MFP, EBF ve EABF değerlendirilmiştir. MAC ve MFP değerleri 10–150 keV enerji aralığında 15 farklı enerjide, EBF ve EABF değerleri ise EpiXS yazılımı ile 0,015-15 MeV enerji aralığında hesaplanmıştır. Numunelerin kimyasal içerikleri ve yoğunlukları tablo halinde verilerek her bir parametreyle ilişkisi irdelenmiştir. Bu kapsamlı değerlendirme, radyasyon zırhlama uygulamalarında kullanılabilecek seramik yapıların analizine katkı sağlayacak, yüksek performanslı ve sürdürülebilir alternatiflerin belirlenmesinde yol gösterici olacağı düşünülmektedir.

2.MATERYAL VE METOD

Bu çalışmada dört farklı seramik numune (S1, S2, S3 ve S4) kullanılmıştır. Numunelerin kimyasal içerikleri ve yoğunluk bilgileri Tablo 1'de sunulmuştur. Numunelerin radyasyon zırhlama özelliklerinin belirlenmesinde dört temel parametre incelenmiştir: kütle azaltma katsayısı (MAC), ortalama serbest yol (MFP), maruz kalma birikim faktörü (EBF) ve enerji soğurma birikim faktörü (EABF). Çalışmada MAC ve MFP değerleri 10, 20, 30, 40, 50, 60, 70, 80, 90, 100, 110, 120, 130, 140 ve 150 keV enerjilerinde, EBF ve EABF parametreleri ise 0,015-15 MeV arasındaki 25 adet enerji değerinde EpiXS programı (hila ve ark., 2021) ile hesaplanmıştır. Bu sayede geniş bir enerji spektrumunda seramik malzemelerin gama radyasyonu ile etkileşimleri kapsamlı olarak analiz edilmiştir.

Tablo 1. Kullanılan malzemelerin içerikleri ve yoğunlukları

Numune	Kimyasal Bileşim (%)						Yoğunluk (g/cm^3)
Kodu	Al	Si	B	Mg	K	O	
S1	42,3400	9,3487	0,0000	0,0000	0,0000	48,3113	3,10
S2	32,8135	11,2184	4,3480	0,0000	0,0000	51,6200	2,70
S3	8,4680	21,5020	2,1740	10,2516	8,3015	45,3029	2,52
S4	37,0475	13,0882	0,6211	0,0000	0,0000	49,2432	3,05

Radyasyon azaltma parametrelerinin hesaplanmasında çeşitli yazılımlar kullanılmaktadır. Bunlardan biri EpiXS programıdır. EpiXS programı, özellikle EBF ve EABF hesaplamalarında yaygın olarak tercih edilmektedir. Bu program, farklı enerji seviyelerinde malzemelerin birikim faktörlerini hesaplayarak, radyasyonun malzeme içindeki davranışını modellemeye yardımcı olur. EpiXS, uluslararası kabul görmüş fiziksel veri tabanlarını esas alarak, kullanıcı tanımlı bileşimlere ait zayıflatma katsayılarını ve birikim faktörlerini hassas şekilde hesaplamaktadır (Gupta & Sharma, 2022). Özellikle düşük ve orta enerjili gama fotonlarının etkileşim analizlerinde sıklıkla tercih edilen bu program, teorik sonuçların deneysel verilerle karşılaştırılmasına da olanak sağlamaktadır (Ismail ve ark., 2023; Abouhaswa ve ark., 2024).

2.1 Kuramsal Temeller

Bu çalışmada kullanılan dört temel gama radyasyon zırhlama parametresi olan MAC, MFP, EBF ve EABF, malzemenin zayıflatma kabiliyetini nicel olarak değerlendirmek için kullanılmaktadır. Aşağıda bu parametrelerin teorik temelleri ve ilgili denklemleri sunulmuştur.

Kütle azaltma katsayısı (MAC, μ/ρ), bir materyalin birim kütle başına radyasyon azaltma kapasitesini ifade eder. Bu katsayı aşağıdaki denklemle ifade edilmektedir (Abdelghany ve ark., 2023).

$$\mu_m = \sum_i W_i \left(\mu/\rho\right)_i \quad (1)$$

Denklem 1'de W_i kütlece ağırlıklı kesirdir ve $(\mu/\rho)_i$ numune içeriğindeki i. elementin kütle azaltma katsayısını verir. Kütle azaltma katsayısının birimi cm^2/g'dır. Ortalama serbest yol (MFP), gelen fotonların %36,8'inin geçeceği malzeme kalınlığını ifade eder ve şu şekilde tanımlanır:

$$MFP = 1/\mu \quad (2)$$

Bu eşitlikte, μ lineer azaltma katsayısıdır. MFP'nin birimi cm'dir.

Maruz kalma birikim faktörü (EBF), bir malzemenin foton maruziyetine karşı birikim etkisini tanımlar ve fotonların saçılma etkilerini de dikkate alır. Genellikle aşağıdaki şekilde gösterilebilir (Vahabi ve ark., 2020).

$$EBF(x,E) = B(E,x)xe^{-\mu x} \quad (3)$$

Eşitlik 3'te B enerjiye ve kalınlığa bağlı birikim faktörü, μ lineer azaltma katsayısını ve x malzeme kalınlığını gösterir. Enerji Soğurma Birikim Faktörü (EABF) ise, foton enerjisinin malzeme tarafından soğurulan kısmına karşılık gelen birikim faktörüdür. EBF formülüne benzer şekilde tanımlanır ancak foton enerjisinin soğurulan kısmına göre ağırlıklandırılır (Vahabi ve ark., 2020 ; More ve ark., 2021).

$$EABF = (x,E) = B_a(E,x).e^{-en.x} \quad (4)$$

Eşitlik 4'te B_a enerji soğurma azaltma katsayısını e^{-en} ise enerjiye ve kalınlığa bağlı soğurma birikim faktörünü ifade etmektedir.

3. BULGULAR ve TARTIŞMA

Bu bölümde, dört seramik numunesine (S1, S2, S3, S4) ait farklı gama enerjilerinde elde edilen kütle azaltma katsayısı (MAC), ortalama serbest yol (MFP), maruz kalma birikim faktörü (EBF) ve enerji soğurma birikim faktörü (EABF) değerleri analiz edilmiştir. Enerji arttıkça tüm numunelerde MAC değerlerinin düştüğü, buna karşılık MFP değerlerinin arttığı gözlemlenmiştir. Bu durum, düşük enerjili fotonların maddeyle etkileşiminin daha yüksek olduğunu, enerji arttıkça bu etkileşimin azaldığını göstermektedir. 10 keV'de en yüksek MAC değeri S3 numunesine ait olup 21,8373 cm^2/g olarak hesaplanmıştır. Bu da S3 numunesinin düşük enerjili fotonlara karşı en yüksek azaltma kapasitesine sahip olduğunu göstermektedir. MFP değerleri incelendiğinde, 10 keV'de S2 numunesi en yüksek değere (0,0238 cm) sahipken, 150 keV'de en yüksek MFP değeri 2,8315 cm ile yine S3'te gözlemlenmiştir. Elde edilen sonuçlar Tablo 2'de sunulmuştur. Bu sonuçlar, S3 numunesinin hem düşük hem de yüksek enerjili gama ışınlarına karşı daha kalın bir malzeme yapısı gerektirdiğini göstermektedir. EBF ve EABF değerleri incelendiğinde, enerji arttıkça bu değerlerin de arttığı gözlemlenmiştir. Bu artış, fotonların saçılma ve enerji kayıplarının malzeme içindeki birikimini yansıtmaktadır. Özellikle 0,015–1 MeV aralığında S3 numunesi EBF ve EABF açısından daha yüksek değerlere sahiptir. Bu, S3'ün foton enerjisini tutma ve saçma kabiliyetinin yüksek olduğunu göstermektedir. En yüksek EABF değeri 10 MeV'de S3 numunesinde yaklaşık 10,01 civarında hesaplanmıştır

Tablo 2. Çalışılan seramiklerin MAC ve MFP değerleri

Numune	S1		S2		S3		S4	
Enerji (keV)	**MAC**	**MFP**	**MAC**	**MFP**	**MAC**	**MFP**	**MAC**	**MFP**
10	17,1657	0,0188	15,5496	0,0238	21,8373	0,0182	17,1071	0,0192
20	2,2956	0,1405	2,0927	0,1770	2,9622	0,1340	2,2904	0,1432
30	0,7960	0,4052	0,7367	0,5027	1,0001	0,3968	0,7948	0,4125
40	0,4321	0,7465	0,4073	0,9092	0,5196	0,7638	0,4318	0,7593
50	0,3006	1,0732	0,2879	1,2864	0,3459	1,1472	0,3005	1,0911
60	0,2400	1,3439	0,2327	1,5915	0,2667	1,4877	0,2401	1,3656
70	0,2073	1,5559	0,2027	1,8272	0,2245	1,7675	0,2074	1,5806
80	0,1875	1,7204	0,1844	2,0088	0,1993	1,9909	0,1876	1,7475
90	0,1739	1,8551	0,1717	2,1574	0,1825	2,1745	0,1740	1,8839
100	0,1643	1,9632	0,1627	2,2767	0,1708	2,3228	0,1645	1,9935
110	0,1567	2,0585	0,1555	2,3824	0,1618	2,4519	0,1569	2,0902
120	0,1507	2,1400	0,1498	2,4729	0,1549	2,5617	0,1509	2,1728
130	0,1457	2,2135	0,1450	2,5550	0,1492	2,6598	0,1459	2,2473
140	0,1413	2,2829	0,1407	2,6329	0,1442	2,7512	0,1415	2,3177
150	0,1376	2,3443	0,1371	2,7018	0,1401	2,8315	0,1378	2,3799

Elde edilen bulgulara göre, tüm numunelerde MAC değerleri enerji arttıkça düşmekte, MFP değerleri ise artmaktadır. Bu durum literatürle uyumludur (Abd-Elkader ve ark., 2023; Zakaly ve ark., 2022). Düşük enerjilerde daha etkin bir azaltma performansı sergileyen seramikler, özellikle tıbbi görüntüleme gibi düşük enerjili uygulamalarda avantaj sağlayabilir. Bu çalışmada elde edilen MAC ve MFP sonuçlarına göre oluşturulan grafikler sırasıyla Şekil 1, Şekil 2 sunulmuştur.

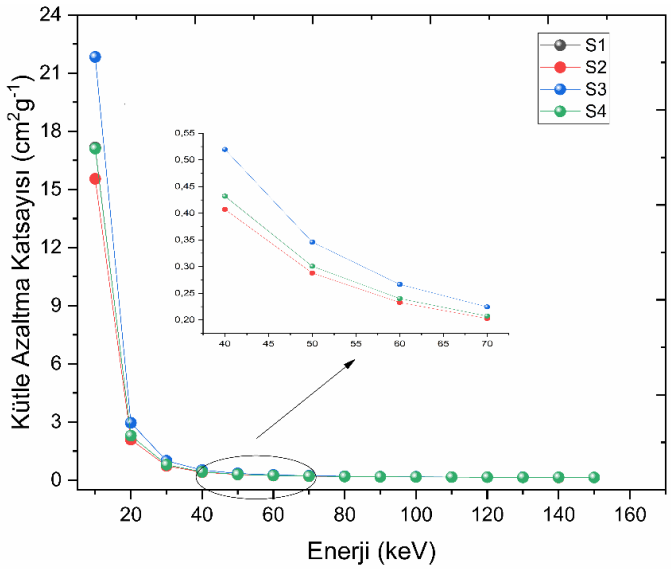

Şekil 1. Çalışılan numunelerin enerjiye göre kütle azaltma katsayısı grafiği

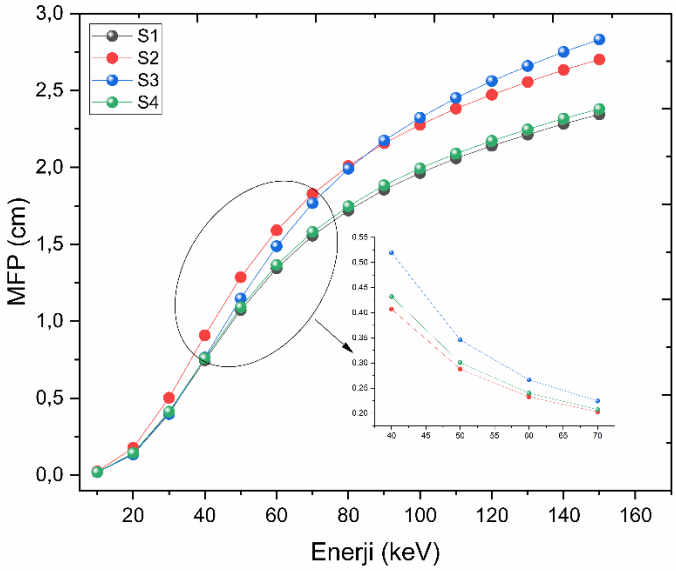

Şekil 2. Çalışılan numunelerin enerjiye göre ortalama serbest yol grafiği

S3 numunesi genel olarak en yüksek MAC değerlerine ve en düşük MFP değerlerine sahip olup, özellikle 10–50 keV arasında üstün performans göstermiştir. Bu, S3'ün içerdiği diğerlerine göre yüksek atom numarasına sahip bileşenlerden kaynaklanmaktadır. Diğer yandan S2 numunesi, tüm enerji aralığında en düşük MAC ve en yüksek MFP değerlerini göstermiştir; bu da S2'nin azaltma açısından daha az etkili olduğunu göstermektedir.

EBF ve EABF değerlerinin yorumlanması, fotonların sadece geçiş değil, saçılma ve enerji kaybıyla birlikte malzeme içindeki davranışlarının anlaşılmasına katkı sunmaktadır. S3 numunesi, bu parametrelerde de yüksek değerlere ulaşarak radyasyonun derinlemesine nüfuzunu etkin şekilde zayıflatabilmektedir. Bu durum, özellikle yüksek enerjili fotonlara karşı zırhlama ihtiyacı duyulan nükleer santral uygulamalarında tercih edilmesini desteklemektedir. Literatürde EpiXS programı ile yapılan benzer çalışmalar, bu tür eğilimlerin malzeme bileşimine ve enerjiye doğrudan bağlı olduğunu belirtmektedir (Tariq ve ark., 2024; Abouhaswa ve ark., 2024). Gupta & Sharma (2022), EpiXS ile hesaplanan EBF ve EABF değerlerinin deneysel sonuçlarla yüksek uyum gösterdiğini belirtmiş ve bu yöntemin doğruluğunu vurgulamıştır. Elde edilen sonuçlara göre oluşturulan grafikler Şekil 3, Şekil 4, Şekil 5 ve Şekil 6'te sunulmuştur.

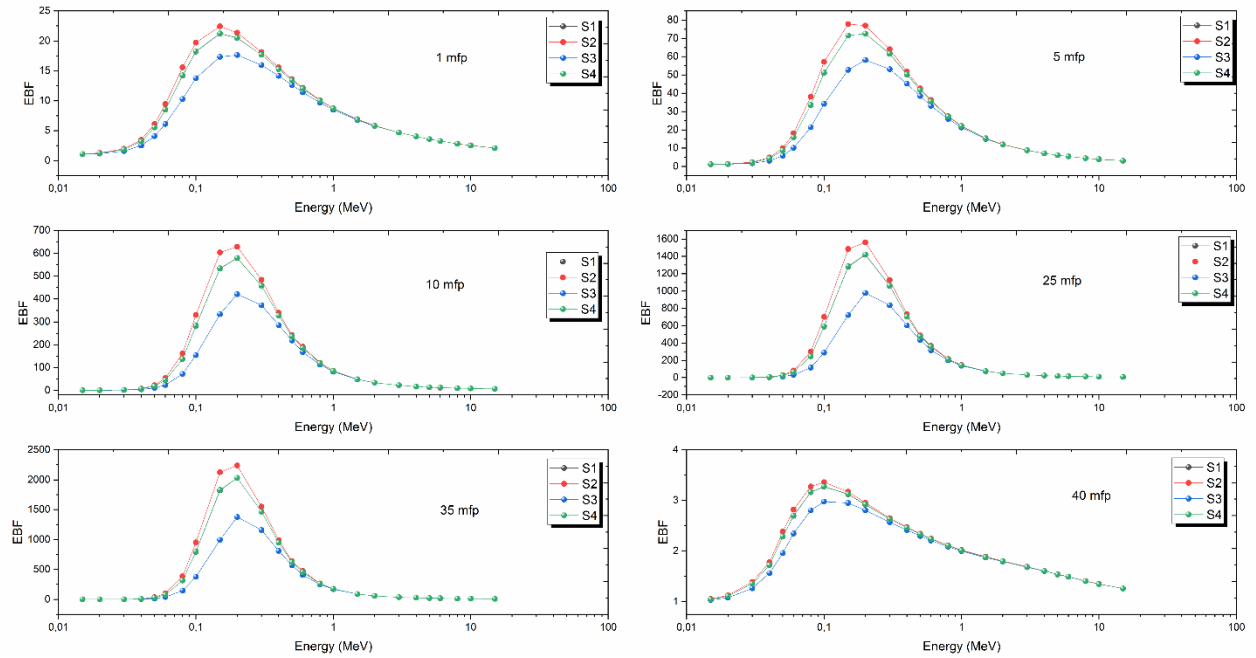

Şekil 3. Çalışılan numunelerin enerjiye göre maruz kalma birikim faktörü (EBF) grafiği

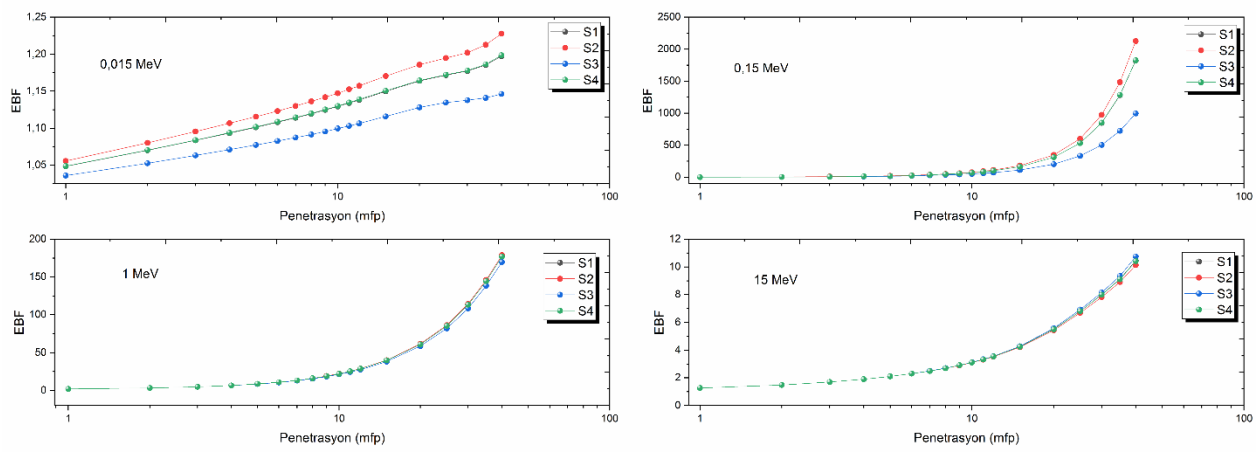

Şekil 4. Çalışılan numunelerin nüfuz etme derinliğine (penetrasyon) göre maruz kalma birikim faktörü (EBF) grafiği

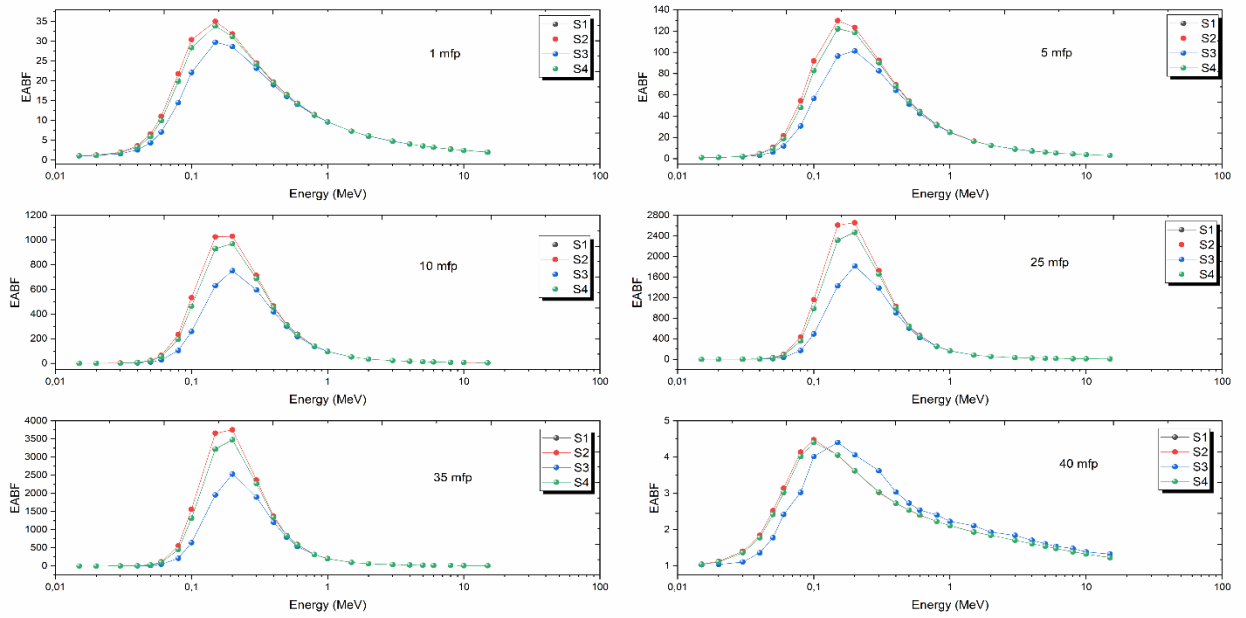

Şekil 5. Çalışılan numunelerin enerji soğurma birikim faktörü (EABF) grafiği

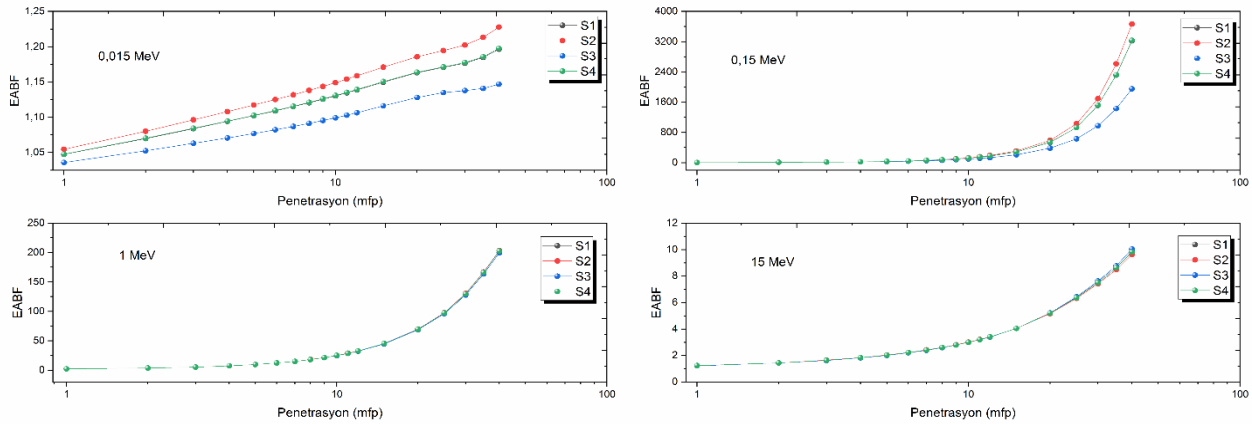

Şekil 6. Penetrasyon değerlerine göre enerji soğurma birikim faktörü faktörü (EABF) grafiği

4. SONUÇ

Bu çalışmada, dört farklı seramik numunesinin (S1, S2, S3 ve S4) gama radyasyonu karşısındaki azaltma performansı teorik olarak değerlendirilmiştir. Elde edilen MAC, MFP, EAF ve EABF verileri, seramik malzemelerin enerjinin artışına bağlı olarak gösterdiği davranışları kapsamlı biçimde ortaya koymuştur. Sonuçlar, tüm numunelerde enerji arttıkça MAC değerlerinin düştüğünü, buna karşılık MFP, EAF ve EABF değerlerinin arttığını göstermiştir. Bu eğilim, radyasyonun malzeme içindeki etkileşim sürecinin enerjiye bağlı

olarak değiştiğini ve düşük enerjili fotonların daha fazla azaltılmaya eğilimli olduğunu göstermektedir. Özellikle S3 numunesi, genel olarak hem düşük hem de yüksek enerji düzeylerinde en yüksek MAC ve EABF değerlerini göstermesiyle ön plana çıkmıştır. EBF ve EABF değerleri açısından da S3 numunesi, fotonların saçılma ve enerji kaybı mekanizmalarına karşı en etkili sonucu vermiştir. S2 numunesi ise en düşük azaltma verimliliğine sahip numune olarak değerlendirilmiştir. Sonuç olarak, seramik bazlı malzemeler, özellikle kurşun içermeyen ve çevresel olarak sürdürülebilir radyasyon zırhlama potansiyeli bakımından umut verici seçeneklerdir. S3 numunesi gibi iyi performans gösteren bileşimlerin daha ileri düzeyde analiz edilerek nükleer enerji, tıbbi görüntüleme ve uzay araştırmaları gibi alanlara entegre edilmesi önerilmektedir. Gelecekte, bu tür çalışmaların farklı katkı maddeleri ve mikro yapı analizleriyle desteklenmesi, radyasyon zırhlama teknolojilerinin gelişimine önemli katkılar sağlayacaktır.

KAYNAKLAR

Abdelghany, A. M., Alsaif, N. A., Madshal, M. A., ElBatal, H. A., Rammah, Y. S., & Awad, W. (2023). Structural, optical and radiation shielding parameters of sodium aluminium borate glasses modified with chromium oxide. *Radiation Physics and Chemistry*, *207*, 110861.

Abd-Elkader, O. H., El-Masry, N. A., & El-Bahy, M. M. (2023). Radiation shielding properties of bismuth oxide reinforced ceramic composites. *Journal of Radiation Research and Applied Sciences*, *16*(1), 45–54.

Abouhaswa, A. S., Hegazy, T. M., & Elokr, M. M. (2024). EpiXS-based calculation and validation of buildup factors in glass systems for radiation shielding applications. *Radiation Physics and Chemistry*, *213*, 110044.

Al-Buriahi, M. S., Sayyed, M. I., Kaky, K. M., & Tekin, H. O. (2021). Assessment of transparent glass systems for use in shielding of gamma radiation. *Journal of Materials Research and Technology*, *12*, 1495–1503.

Erkoyuncu, I., Demirkol, I., Akman, F., Dilsiz, K., Kacal, M. R., & Polat, H. (2024). A detailed investigation of gamma and neutron shielding capabilities of concrete doped with bronze and boron carbide. *Radiation Physics and Chemistry*, *215*, 111358.

Farid, M., Elshaer, M. R., El-Gendy, N. S., & Salem, H. (2025). Comparative study of gamma shielding characteristics of ceramic matrix composites. *Radiation Effects and Defects in Solids*, *180*(1), 15–27.

Fouda, A., Elbasuney, S., & Elmahdy, M. (2023). Effect of composite oxide phases on radiation attenuation in novel ceramic materials. *Ceramics International*, *49*(3), 3590–3600.

Gupta, S., & Sharma, M. (2022). EpiXS: An efficient computational tool for calculating radiation shielding parameters. *Radiation Physics and Chemistry*, *198*, 110190.

Hila, F. C., Asuncion-Astronomo, A., Dingle, C. A. M., Jecong, J. F. M., Javier-Hila, A. M. V., Gili, M. B. Z., ... & Amorsolo Jr, A. V. (2021). EpiXS: A Windows-based program for photon attenuation, dosimetry and shielding based on EPICS2017 (ENDF/B-VIII) and EPDL97 (ENDF/B-VI. 8). Radiation Physics and Chemistry, 182, 109331.

Ismail, A. F., Mohamed, N. M., & Salih, I. (2023). Monte Carlo validation of EpiXS results for radiation shielding in building materials. *Applied Radiation and Isotopes*, *198*, 110238.

More, C. V., Alsayed, Z., Badawi, M. S., Thabet, A. A., & Pawar, P. P. (2021). Polymeric composite materials for radiation shielding: a review. *Environmental chemistry letters*, *19*, 2057-2090.

Mostafa, A., & Farouk, M. (2023). Utilization of industrial waste in radiation shielding ceramic bricks. *Journal of Environmental Chemical Engineering*, *11*(2), 110584.

Rashad, M., Abou El-Nour, K. M., & Salem, H. G. (2024). Evaluation of structural and shielding characteristics of lead-free ceramics for nuclear applications. *Applied Radiation and Isotopes*, *206*, 110792.

Singh, R., Kaur, H., & Gautam, A. (2023). Review on emerging trends in radiation shielding ceramics. *Radiation Effects and Defects in Solids*, *178*(7-8), 635–648.

Tariq, M., Bashir, F., & Hafeez, M. (2024). Evaluation of gamma-ray shielding parameters using EpiXS for advanced oxide ceramics. *Nuclear Engineering and Technology*, *56*(1), 89–97.

Vahabi, S. M., & Zafarghandi, M. S. (2020). Build-up factors for water and soft tissue by MCNP using a co-centric multilayer model: comparative study. *Journal of Instrumentation*, *15*(05), P05018.

Yousef, T. A., Awwad, N. S., & El-Bindary, A. A. (2025). Gamma shielding behavior of nanoceramic-based composite materials. *Journal of Nuclear Materials*, *582*, 154569.

Zakaly, H. M. H., Al-Buriahi, M. S., Sayyed, M. I., Tekin, H. O., & Elsafi, M. (2022). Gamma-ray shielding competence of Nd2O3-modified borate-based glasses: Experimental and theoretical approach. *Ceramics International*, *48*(5), 6283–6291.

➢ *ORAL PRESENTATION*

Bazı Cam Türlerinin Birincil ve İkincil Radyasyon Etkileşimlerinin İncelenmesi

İlhami Erkoyuncu[1*] (*ORCID:* https://orcid.org/0000-0003-1639-5062) Ferdi AKMAN[2] (*ORCID:* https://orcid.org/0000-0002-8838-1762)

[*1] Bingöl Üniversitesi, Fen-Edebiyat Fakültesi, Fizik, Bingöl, Türkiye
[2] Bingöl Üniversitesi, Sosyal Bilimler MYO Mülkiyet Koruma ve Güvenlik Bölümü, İş Sağlığı ve Güvenliği Programı, Bingöl, Türkiye

*Sorumlu yazar e-posta: ierkoyuncu@bingol.edu.tr

Özet

Bu çalışmada, pencere camı, akkor lamba camı ve kurşunlu cam olmak üzere üç farklı cam türünün gama ve nötron radyasyonlarına karşı azaltma kapasiteleri ile ikincil radyasyon üretim eğilimleri karşılaştırmalı olarak incelenmiştir. Simülasyonlar, GEANT4 Monte Carlo tabanlı parçacık izleme yazılımı kullanılarak gerçekleştirilmiştir. Gama radyasyonu için 0,1, 0,5, 1 ve 2 MeV ve nötron radyasyonu için ise 0,5, 1, 3 ve 4,5 MeV enerji seviyelerinde analizler yapılmıştır. Her cam numunesi için GEANT4 ortamında numunelerin kimyasal bileşimi ve yoğunlukları tanımlanmış, gama ışınları için kütle azaltma katsayısı (MAC) ve lineer azaltma katsayısı (LAC) hesaplanmıştır. Ayrıca ikincil gama fotonlarının enerji dağılımı ile nötron etkileşimlerinden kaynaklanan ikincil nötron ve gama üretimleri detaylı olarak analiz edilmiştir. Kurşunlu cam, en yüksek gama azaltma katsayılarına sahip olmakla birlikte, aynı zamanda en fazla ikincil gama üretimini göstermiştir. Akkor cam, daha düşük ikincil radyasyon üretimiyle öne çıkmıştır. Pencere camı ise kurşunlu cama göre zayıf gama azaltma kapasitesine karşın ikincil radyasyon üretimi açısından güvenli malzeme olarak belirlenmiştir. Çalışma sonuçları, radyasyon zırhlama malzemesi seçiminde yalnızca birincil etkileşimlerin değil, ikincil radyasyon üretiminin de dikkate alınmasının gerekliliğini ortaya koymaktadır. Bu bağlamda, çevre dostu ve toksik olmayan cam türlerinin ileri düzey zırhlama uygulamaları için potansiyel gösterebileceği görülmüştür.

Anahtar Kelimeler: GEANT4, radyasyon zırhlama, ikincil radyasyon, cam

Investigation of Primary and Secondary Radiation Interactions in Some Glass Types

Abstract

In this study, the attenuation capacities of three different glass types, namely window glass, incandescent glass and leaded glass, against gamma and neutron radiation and their secondary radiation production tendencies were comparatively investigated. Simulations were performed using GEANT4 Monte Carlo based particle tracking software. Analyses were performed at energy levels of 0.1, 0.5, 1 and 2 MeV for gamma radiation and 0.5, 1, 3 and 4.5 MeV for neutron radiation. Chemical composition and density of samples were defined in GEANT4 environment for each glass sample, mass attenuation coefficient (MAC) and linear attenuation coefficient (LAC) for gamma rays were calculated. In addition, energy distribution of secondary gamma photons and secondary neutron and gamma productions resulting from neutron interactions were analyzed in detail. Leaded glass had the highest gamma attenuation coefficients, but also showed the highest secondary gamma production. Incandescent glass stood out with its lower secondary radiation production. Window glass, on the other hand, has been determined to be a safe material in terms of secondary radiation production, despite its weak gamma attenuation capacity compared to leaded glass. The study results reveal that not only primary interactions but also secondary radiation production should be taken into account in the selection of radiation shielding materials. In this context, it has been observed that environmentally friendly and non-toxic glass types may have potential for advanced shielding applications.

Keywords: GEANT4, radiation shielding, secondary radiation, glass

1. GİRİŞ

Günümüzde cam, basit nitelendirebileceğimiz birçok alanda kullanılmasının yanında iletişim, uçak ve uzay teknolojilerine kadar uzanan geniş bir kullanım alanına sahiptir. Şeffaf, sert ve kırılgan olması en belirgin özellikleridir. Cam sistemlerinin inorganik amorf yapısı bulunmaktadır. Bu özellikleri ile beraber birçok alanda kullanılması, radyasyona karşı davranış biçimini araştırma ihtiyacını da ortaya çıkarmıştır. Radyasyon teknolojilerinin yaygınlaştığı günümüzde, özellikle gama ışınlarının kullanıldığı tıbbi, endüstriyel ve nükleer uygulamalarda etkili radyasyon zırhlama malzemelerine duyulan ihtiyaç artmıştır. Geleneksel kurşun bazlı malzemeler, yüksek azaltma kapasiteleri nedeniyle uzun yıllar tercih edilmektedir. Ancak kurşunun toksik yapısı ve zararlı çevresel etkileri nedeniyle daha güvenli, sürdürülebilir ve şeffaf alternatif malzemelere olan ilgi hızla artmaktadır (Sharma ve ark., 2022a; Tekin & Singh, 2020). Bu bağlamda, cam esaslı malzemeler özellikle optik geçirgenlik, şekillendirilebilirlik ve kimyasal dayanıklılık gibi avantajları sayesinde zırhlama uygulamalarında öne çıkmaktadır (Hegazy ve ark., 2022; Sayyed ve ark., 2021). Camların radyasyon zırhlama performansları, genellikle kütle azaltma katsayısı (μ/ρ), yarı kalınlık değeri (HVL), onda-bir kalınlık değeri (TVL) ve etkin atom numarası (Z_{eff}) gibi parametrelerle değerlendirilmektedir (Kaur & Singh, 2021). Ancak radyasyonun madde etkileşmesi göz önüne alındığında bu değerlendirmeler yalnızca birincil gama radyasyonu dikkate alınarak yapılmamalıdır. Radyasyonun malzemeyle etkileşimi sonucu oluşan ikincil radyasyon özellikle ikincil gama fotonları ve ikincil nötronlar malzemenin radyasyon ortamında gerçek davranışını belirleyen önemli unsurlardır (Yılmaz & Aydın, 2021; El-Khayatt, 2021).

İkincil radyasyon genel olarak, birincil radyasyonun (gama ışını, proton, elektron vb.) madde ile etkileşmesi sonucu ortaya çıkan yeni radyasyon türlerini ifade eder. İkincil gama radyasyonu, Compton saçılması ve fotoelektrik etkileşimler sonucunda ortaya çıkan düşük enerjili fotonlardan oluşur. Bu fotonlar, birincil enerjili gama ışınlarına kıyasla daha derin dokulara nüfuz etmese de, biyolojik dokular üzerinde birikimli zarar oluşturabilir. İkincil nötron radyasyonu ise, yüksek enerjili fotonların veya parçacıkların malzemelerle etkileşmesi sonucu ortaya çıkan serbest nötronlardır. Özellikle kurşun gibi yüksek atom numarasına sahip elementler içeren zırhlama malzemelerinde, gama ışınlarıyla meydana gelen (γ,n) fotonükleer reaksiyonlar sonucu ikincil nötronlar üretilebilir (Sayyed ve ark., 2021; Tekin ve ark., 2021b). Bu nötronlar, biyolojik olarak çok daha etkili ve zararlı olabilir çünkü elektrik yükü taşımadıkları için dokularla derinlemesine etkileşime girebilirler ve dolaylı yoldan iyonlaştırıcı etki gösterirler (El-Khayatt, 2021). Nötron radyasyonunun bir diğer kritik özelliği, zırhlama için farklı türde malzemelere ihtiyaç duymasıdır. Örneğin, hidrojen içeren polimerler veya bor içeren bileşikler nötronları yavaşlatmak ve soğurmak için etkili malzemelerdir. Ancak cam sistemleri genellikle bu tür bileşenleri içermez ve bu nedenle nötron zırhlama kapasiteleri sınırlıdır. Bu durum, kurşunlu camlar gibi yüksek-Z camların nötron üretme potansiyeliyle birleştiğinde, bu tür camların ikincil radyasyon açısından yeniden değerlendirilmesini gerekli kılmaktadır (Al-Buriahi ve ark., 2022).

Bu bağlamda, ikincil nötron üretimini en aza indiren, düşük-Z katkılı camlar (örneğin borosilikat camlar) çevre dostu ve biyolojik olarak daha güvenli alternatifler olarak ön plana çıkmaktadır (Hosseini ve ark., 2020a; Hosseini ve ark., 2020b; Sharma ve ark., 2022b; Al-Buriahi ve ark., 2023). Nitekim, yalnızca birincil gama ışınlarına karşı değil, aynı zamanda oluşabilecek ikincil radyasyon bileşenlerine karşı da etkili zırhlama sağlamak, günümüzde malzeme tasarımında çok boyutlu bir yaklaşımı zorunlu kılmaktadır. Sunulan bu çalışmada pencere camı, akkor cam ve kurşunlu camın 0,1 ila 2 MeV enerji arasındaki fotonlar ile 0,5 ila 4,5 MeV enerji arasındaki nötronların birincil etkileşim ve ikincil radyasyon üretimi açısından gösterdiği performanslar incelenecektir. Malzemenin hem birincil hem de ikincil gama ışınları ve nötronlara karşı davranışı dikkate alınarak yapılan kapsamlı değerlendirmeler, daha güvenli ve sürdürülebilir radyasyon ortamlarının oluşturulmasına olanak tanıyacaktır.

2. MATERYAL VE METOD

Bu çalışmada, pencere camı, akkor lamba camı ve kurşunlu cam olmak üzere üç farklı cam türünün hem gama ışınları hem de nötronlar karşısındaki zırhlama performansları GEANT4 simülasyon aracı (sürüm 10.07) kullanılarak değerlendirilmiştir. Simülasyonlar, Tablo 1'de verilen malzemelerin kimyasal bileşimi ve yoğunluğu dikkate alınarak hesaplanmıştır.

Tablo 1. Kullanılan malzemelerin içerikleri ve yoğunlukları

Malzeme	Kimyasal Bileşim (%)						Yoğunluk (g/cm^3)
Pencere camı	SiO_2	Na_2O	MgO	CaO	Al_2O_3	Fe_2O_3	
	73	14	4	9	0,1	0,1	2,53
Akkor Cam	SiO_2	Na2O	K2O	MgO	CaO	Al_2O_3	
	72	16	1	4	3	2	2,50
Kurşunlu Cam	SiO_2	Al_2O_3	CaO	MgO	SO_3	Na_2O	
	53,42	3,87	2,89	1,73	0,13	6,56	3,038
	P_2O_5	MnO	Rb_2O	SrO	ZrO_2	Sb_2O_3	
	0,02	0,01	0,03	1,37	0,28	0,14	
	K2O	TiO2	BaO	CeO_2	PbO		
	6,53	0,11	1,43	0,92	20,34		

Yapılan bu çalışmada 0,1 ila 2 MeV arasındaki 4 farklı foton enerjisinde kütle azaltma katsayısı, lineer azaltma katsayısı, oluşan ikincil gamaların sayısı ve ortalama enerjileri GEANT4 simülasyon kodu ile belirlenmiştir. Ayrıca 0,5 ile 4,5 MeV arasındaki 4 farklı nötron enerjisinde oluşan ikincil nötron sayısı ve ortalama nötron enerjileri belirlenmiştir. Numuneler üzerine 10^7 foton veya nötron GEANT4 kodu aracılığı ile gönderilmiştir. Her numunenin yoğunluğu ve bileşimi de GEANT4 malzeme tanım modülüne girilmiştir. Çalışmada kullanılan **GEANT4** (Geometry and Tracking), parçacıkların madde ile etkileşimlerini detaylı olarak modelleyebilen, C++ tabanlı, açık kaynak kodlu bir Monte Carlo simülasyon kütüphanesidir. Tıbbi fizik, uzay araştırmaları, nükleer güvenlik ve radyasyon zırhlama alanlarında yaygın olarak kullanılan GEANT4, foton, elektron, nötron ve ağır yüklü parçacıkların fiziksel süreçlerini çok hassas biçimde tanımlayabilir (Agostinelli ve ark., 2003; Allison ve ark., 2016). GEANT4 simülasyon kodunda, Electromagnetic Standard Physics ve NeutronHP Physics bileşenleri kullanılmıştır Sunulan çalışmada gama fotonları için elektromanyetik süreçler (fotoelektrik etki, Compton saçılması, çift oluşumu), nötronlar içinse yüksek hassasiyetli nötron modelleri (NeutronHP) kullanılmıştır. Simülasyon geometrisi kullanıcı tanımlı olarak modellenmiş, olay başına enerji dağılımları ve ikincil parçacık üretimleri analiz edilmiştir. GEANT4'ün modüler yapısı sayesinde her bir cam numunesinin bileşimi ve yoğunluğu fiziksel doğrulukla tanımlanmıştır.

Gama Radyasyonu Etkileşim Parametreleri

Gama radyasyonu etkileşim parametreleri arasında olan kütle azaltma katsayısı (μ_m), zırhlamada kullanılacak malzemenin seçilmesinde son derece önemlidir. Malzemenin fiziksel yapısından etkilenmez ve denklem 1'de gösterildiği gibi ifade edilebilir. Zırhlamada kullanılacak malzeme için referans olarak kabul edilmektedir (Erkoyuncu ve ark., 2024).

$$\mu_m = \sum_i W_i \left(\mu/\rho\right)_i \quad (1)$$

Denklem 1'de, W_i kütlece ağırlık kesrini ve $(\mu/\rho)_i$ numune içeriğindeki i. elementin kütle azaltma katsayısını ifade eder. Kütle azaltma katsayısı cm^2/g cinsinden ifade edilir. İncelenen bir diğer parametre lineer azaltma katsayısıdır (μ). Birimi cm^{-1}'dir. Malzemenin fiziksel yapısından etkilenir. Aşağıda verilen denklem 2 ile hesaplanabilir. Ayrıca kütle azaltma katsayısının malzemenin yoğunluğu ile çarpımı sonucu bulunabilir (Turhan ve ark., 2023).

$$\mu = \ln \frac{I_0}{I} \Big/ x \quad (2)$$

Denklem 2'de I_0 başlangıçtaki radyasyon şiddetini, I etkileşimden sonraki radyasyon şiddetini ve x malzemenin kalınlığını ifade etmektedir. Gama etkileşimleri için, her cam numunesine 0,1 MeV, 0,5 MeV, 1 MeV ve 2 MeV enerjili fotonlar doğrusal demet (monoenerjik) olarak yönlendirilmiştir. Her enerji seviyesi için 10^7 olay çalıştırılarak kütle azaltma katsayısı (MAC) ve lineer azaltma katsayısı (LAC) hesaplanmıştır. Bu değerler, fotonların madde içerisindeki gama radyasyonu azaltma eğilimlerini ortaya koymak amacıyla kullanılmıştır. Nötron etkileşimleri, GEANT4'teki High Precision (HP) kütüphaneleri kullanılarak 0.5 MeV,

1 MeV, 3 MeV ve 4,5 MeV enerjili nötronlar için simüle edilmiştir. Nötronlar malzeme ile etkileşime girdiklerinde oluşan ikincil nötron sayısı, nötron enerjileri ve oluşan ikincil gama sayıları analiz edilmiştir. Elde edilen veriler her cam için karşılaştırmalı olarak sunulmuştur.

3. BULGULAR ve TARTIŞMA

Bu bölümde, GEANT4 simülasyonu ile elde edilen sonuçlar doğrultusunda pencere camı, akkor lamba cam ve kurşunlu cam numunelerinin gama ve nötron radyasyonları karşısındaki azaltma performansları ve ikincil radyasyon üretim kapasiteleri değerlendirilmiştir.

Gama Işını Azaltma Parametreleri (MAC ve LAC) Analizleri

Her üç cam türü için 0,1, 0,5, 1 ve 2 MeV enerjili gama ışınlarına karşı kütle azaltma katsayısı (MAC) ve lineer azaltma katsayısı (LAC) değerleri hesaplanmıştır. Elde edilen bulgulara göre, en yüksek MAC ve LAC değerleri kurşunlu camda gözlenmiştir. Bu durum, PbO'nun yüksek atom numarası sayesinde gama fotonlarını etkili biçimde azaltmasıdan kaynaklanmaktadır. Pencere camı, özellikle düşük enerjilerde (0,1–0,5 MeV) katkı oksitler sayesinde akkor lamba camına göre daha yüksek performans göstermiştir. Akkor lamba camı ise tüm enerji aralıklarında en düşük azaltma kapasitesine sahiptir. Sonuçlar Tablo 2, Şekil 1 ve Şekil 2'de sunulmuştur. Hem MAC hem de LAC için düşük enerji bölgelerinde fotoelektrik etkiden söz edilebilir. Orta enerji bölgesinde Compton saçılması etkili iken yüksek enerji bölgelerinde çift oluşumu baskındır.

Tablo 2. Kullanılan malzemelerin MAC ve LAC değerleri

Numune	Pencere camı		Akkor Lamba Camı		kurşunlu cam	
Enerji (MeV)	MAC	LAC	MAC	LAC	MAC	LAC
0,1	0,1924	0,4868	0,1710	0,4276	1,1969	3,6361
0,5	0,0974	0,2465	0,0920	0,2301	0,0996	0,3025
1	0,0713	0,1804	0,0674	0,1686	0,0646	0,1961
2	0,0498	0,1261	0,0471	0,1177	0,0446	0,1356

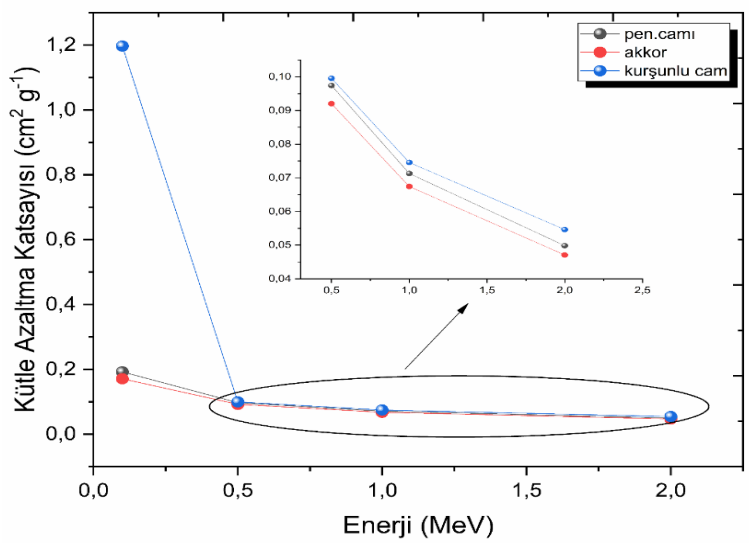

Şekil 1. Kullanılan malzemelerin enerjiye göre kütle azaltma katsayıları

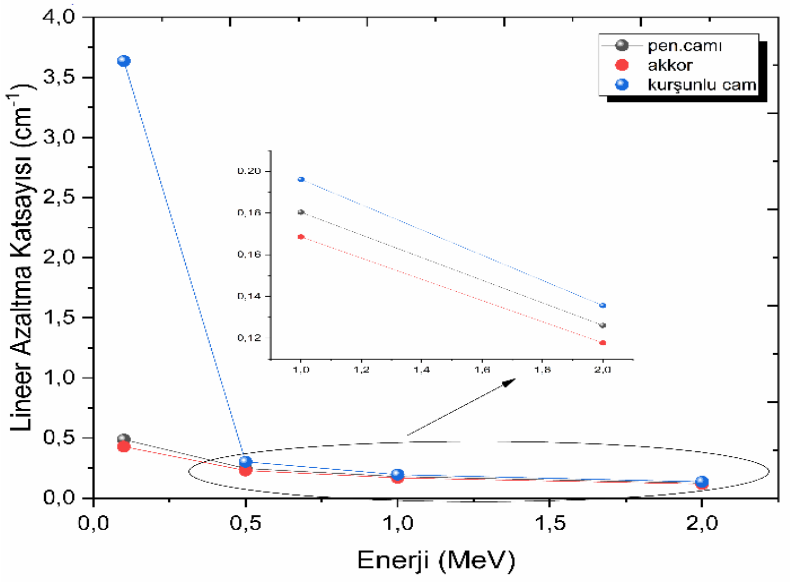

Şekil 2. Kullanılan malzemelerin enerjiye göre lineer azaltma katsayıları

3.1. İkincil Radyasyon Analizi

Simülasyonlar sırasında, her cam numunesi için ikincil gama radyasyonu oluşumu analiz edilmiştir. Foton etkileşimleri sonrası ortaya çıkan ikincil gama fotonlarının enerjileri toplanarak enerjiye göre dağılım grafikleri elde edilmiştir. Ayrıca, nötron kaynaklı ikincil nötron üretimi ve bu nötronların neden olduğu ikincil gama oluşumları detaylı olarak izlenmiştir. Bu analiz, malzemelerin yalnızca azaltma yeteneklerini değil, aynı zamanda ikincil radyasyon üretme eğilimlerini de ortaya koymayı amaçlamaktadır. 0,1 MeV, 0,5 MeV, 1 MeV ve 2 MeV'de 10^7 tane monoenerjik gamalar ile yapılan simülasyonlarda, gama ikincil gama üretimi incelenmiştir. Kurşunlu cam, yüksek enerjili gamalarla etkileşime girerek belirgin oranda ikincil gama üretimi göstermiştir. Akkor lamba camında etkileşim daha düşük seviyede kaldığından ikincil gama üretimi de düşük kalmıştır. Pencere camında ise ikincil gama sayısı akkor lamba camından % 1,3 daha yüksektir. Sonuçlar karşılaştırmalı olarak Şekil 3 ve şekil 4'de sunulmuştur.

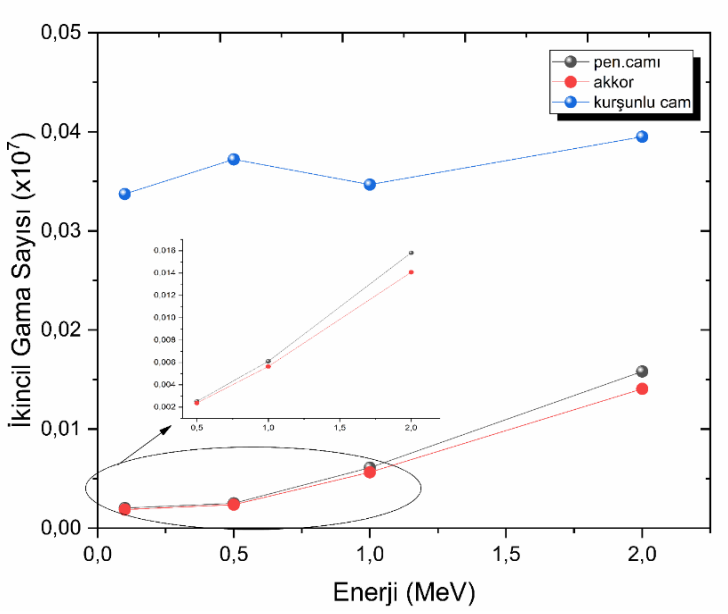

Şekil 3. Enerjiye göre oluşan ikincil gama sayısı

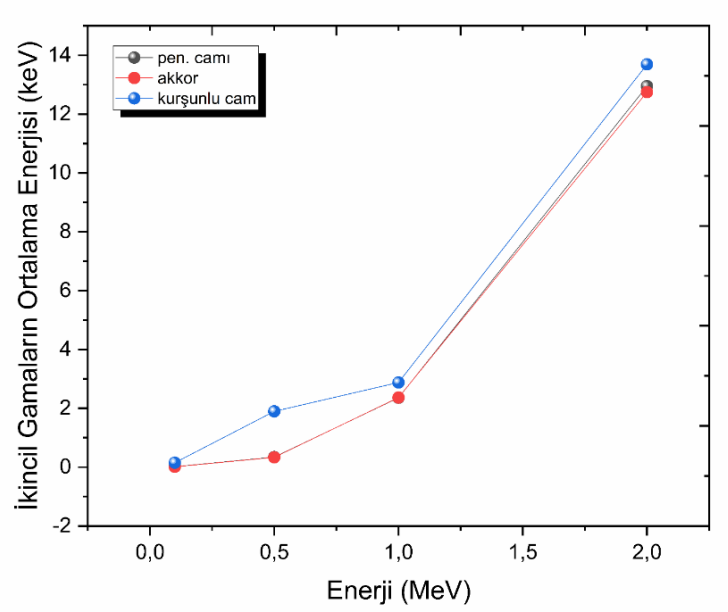

Şekil 4. Oluşan ikincil gamaların ortalama enerjisi (keV)

0,5, 1, 3 ve 4,5 MeV enerjili nötronlarla yapılan simülasyonlarda, ikincil nötron üretimi incelenmiştir. Pencere camı, yüksek enerjili nötronlarla etkileşime girerek belirgin oranda ikincil nötron üretimi göstermiştir. Hem ortalama enerji hem de ikincil nötron sayısı bakımından bir sıralama yapılırsa yaklaşık olarak pencere camı > akkor lamba camı > kurşunlu cam sonucu elde edilir. Elde edilen sonuçlar Şekil 5 ve Şekil 6 'da gösterilmiştir.

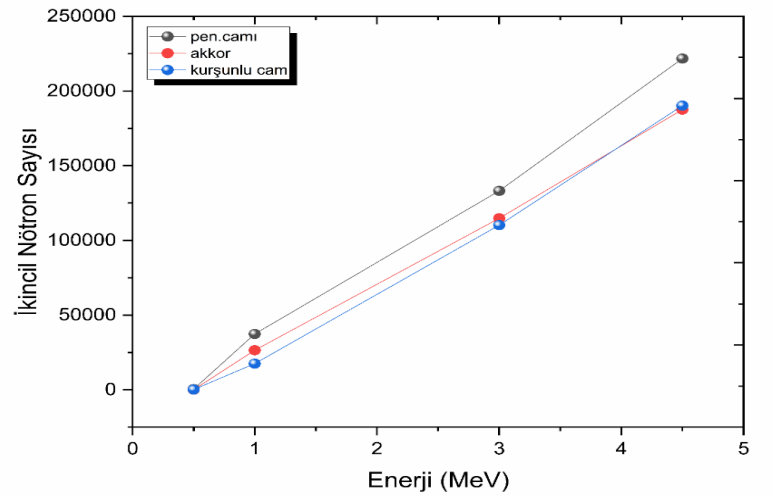

Şekil 5. Enerjiye göre oluşan ikincil nötron sayısı

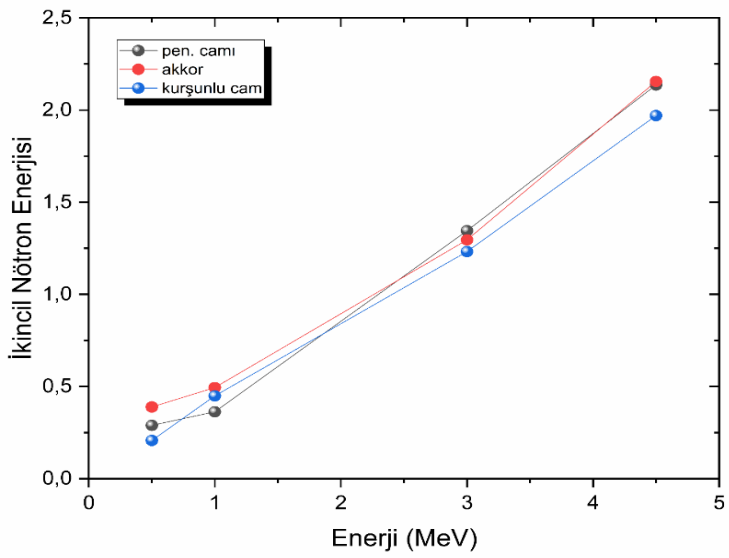

Şekil 6. Oluşan ikincil nötronların ortalama enerjisi (MeV)

Ayrıca bu süreçte önemli sayıda ikincil elektron da oluşmuştur. Elde edilen sonuçlar Şekil 7'de sunulmuştur. Akkor camda ikincil elektron sayıları da kurşunlu cama göre daha azdır. Pencere camı ise düşük Z yapısı nedeniyle hem nötronla etkileşimi sınırlı tutmuş hem de ikincil radyasyon üretimi açısından en güvenli cam türü olarak öne çıkmıştır.

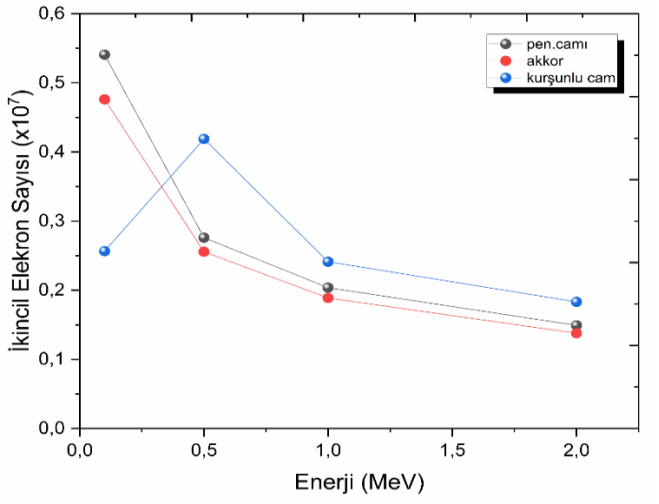

Şekil 7. Enerjiye göre oluşan ikincil elektron sayıları

Bu çalışmada, pencere camı, akkor cam ve kurşunlu camın gama ve nötron radyasyonları karşısındaki azaltma performansları ile ikincil radyasyon üretim eğilimleri GEANT4 simülasyonu kullanılarak karşılaştırmalı biçimde değerlendirilmiştir. Elde edilen bulgular, her cam türünün avantajları ve sınırlılıklarının, kullanım amacına göre dikkatli şekilde ele alınması gerektiğini göstermektedir. Genel olarak, kurşunlu cam birincil gama azaltma açısından üstünlük göstermesine rağmen, yüksek miktarda ikincil gama ve nötron üretimi nedeniyle özellikle yüksek enerjili kaynaklara maruz kalınan ortamlarda dikkatli kullanılmalıdır. Pencere camı, azaltma kapasitesi ile çevresel güvenlik arasında dengeli bir yapı sergilerken, akkor lamba camı zayıf zırhlama kapasitesine rağmen en düşük ikincil radyasyon üretimine sahiptir. Kurşunlu cam, yüksek PbO içeriği sayesinde gama ışınlarına karşı en yüksek MAC ve LAC değerlerine sahip olmuş, bu da onu zırhlama etkinliği açısından üstün kılmıştır. Ancak aynı zamanda Compton saçılması, floresans etkileri ve (γ,n) reaksiyonları nedeniyle fazla miktarda ikincil gama ve ikincil nötron üretmiştir. Bu durum, özellikle medikal ve nükleer alanlarda hassas cihazlar veya insan dokularının korunmasının amaçlandığı ortamlarda ciddi bir dezavantaj olarak değerlendirilmelidir (Sayyed & Tekin, 2021; Yılmaz & Aydın, 2021; Hegazy ve ark., 2022; Al-Hadeethi ve ark., 2021).

4. SONUÇ

Bu çalışma kapsamında GEANT4 simülasyonları ile üç farklı cam türünün (pencere camı, akkor lamba cam ve kurşunlu cam) gama ve nötron radyasyonları karşısındaki davranışları kapsamlı şekilde değerlendirilmiştir. Elde edilen sonuçlara göre, kurşunlu cam, birincil gama radyasyonunun azaltılmasında en etkili cam türüdür; ancak yüksek seviyede ikincil gama ve nötron üretimi nedeniyle biyolojik güvenlik açısından sınırlayıcıdır. Akkor lamba camı ise, düşük ikincil radyasyon üretimi açısından optimum performans-güvenlik dengesi göstermektedir. Pencere camı, kurşunlu cama göre zayıf birincil gama radyasyonu zırhlama özelliğine karşın, düşük ikincil radyasyon üretimi sayesinde düşük doz ortamlar için uygun bir seçenek olabilir. İkincil radyasyon üretimi, yalnızca zırhlama kapasitesine değil; malzemenin genel güvenlik kapasitesini belirlemeye katkı sağlayan kritik bir parametredir. Gelecek çalışmalarda, cam türlerinin içine bor, tungsten ve baryum gibi katkıların doz oranına göre optimize edilmesi ve ikincil nötron zırhlamasını azaltacak kompozit yapılarla birlikte değerlendirilmesi önerilmektedir.

KAYNAKLAR

Agostinelli, S., Allison, J., Amako, K., Apostolakis, J., Araujo, H., Arce, P., ... & Yoshida, H. (2003). GEANT4—a simulation toolkit. *Nuclear Instruments and Methods in Physics Research Section A: Accelerators, Spectrometers, Detectors and Associated Equipment, 506*(3), 250–303. https://doi.org/10.1016/S0168-9002(03)01368-8

Al-Hadeethi, Y., Sayyed, M. I., Kaky, K. M., & Tekin, H. O. (2021). Assessment of transparent glass systems for use in shielding of gamma radiation. *Journal of Materials Research and Technology, 12*, 1495–1503. https://doi.org/10.1016/j.jmrt.2021.02.020

Allison, J., Amako, K., Apostolakis, J., Arce, P., Asai, M., Aso, T., ... & Wright, D. H. (2016). Recent developments in GEANT4. *Nuclear Instruments and Methods in Physics Research Section A: Accelerators, Spectrometers, Detectors and Associated Equipment, 835*, 186–225. https://doi.org/10.1016/j.nima.2016.06.125

Al-Khayatt, A. M. (2021). Influence of secondary radiation in high-Z shielding materials. *Applied Radiation and Isotopes, 174*, 109811. https://doi.org/10.1016/j.apradiso.2021.109811

Al-Buriahi, M. S. (2023). Radiation shielding performance of a borate-based glass system doped with bismuth oxide. *Radiation Physics and Chemistry, 207*, 110875.

Al-Buriahi, M. S., Eke, C., Alrowaili, Z. A., Al-Baradi, A. M., Kebaili, I., & Tonguc, B. T. (2022). Optical properties and radiation shielding performance of tellurite glasses containing Li_2O and MoO_3. *Optik, 249*, 168257

Erkoyuncu, İ., Demirkol, İ., Akman, F., Dilsiz, K., Kaçal, M. R., & Polat, H. (2024). A detailed investigation of gamma and neutron shielding capabilities of concrete doped with bronze and boron carbide. *Radiation Physics and Chemistry, 215*, 111358.

Hegazy, T. M., Abouhaswa, A. S., & Elokr, M. M. (2022). Shielding competence of lead-free bismuth–borate glasses. *Radiation Physics and Chemistry, 198*, 110176. https://doi.org/10.1016/j.radphyschem.2022.110176

Hosseini, S. M., Ghorbani, M., & Ahmadi, S. J. (2020). Simulation of radiation attenuation in borosilicate glass. *Nuclear Engineering and Technology, 52*(10), 2330–2337. https://doi.org/10.1016/j.net.2020.03.015

Hosseini, S. M., Ghorbani, M., & Ahmadi, S. J. (2020). Evaluation of secondary neutron emission from glass systems exposed to high-energy photons. *Nuclear Engineering and Technology, 52*(10), 2330–2337. https://doi.org/10.1016/j.net.2020.03.015

Kaur, A., & Singh, T. (2021). Comparative study of radiation shielding competence of novel lead-free glasses. *Radiation Effects and Defects in Solids, 176*(3–4), 287–300. https://doi.org/10.1080/10420150.2021.1891193

Sayyed, M. I., & Tekin, H. O. (2021). Assessment of photon-induced neutron production in leaded and lead-free glasses. *Radiation Physics and Chemistry, 180*, 109229. https://doi.org/10.1016/j.radphyschem.2020.109229

Sharma, N., Singh, T., & Singh, N. (2022). Review on lead-free glasses for radiation shielding. *Journal of Non-Crystalline Solids, 580*, 121383. https://doi.org/10.1016/j.jnoncrysol.2021.121383

Sharma, N., Singh, T., & Singh, N. (2022). Neutron shielding and secondary emission in gamma shielding glasses: A review. *Journal of Non-Crystalline Solids, 580*, 121383. https://doi.org/10.1016/j.jnoncrysol.2021.121383

Tekin, H. O., Othman, H., & Manici, T. (2021). Analysis of photoneutron generation in radiotherapy shielding glass materials. *Radiation Effects and Defects in Solids, 176*(7), 583–597.

Tekin, H. O., & Singh, V. P. (2020). Analysis of radiation shielding properties of soda-lime glass. *Radiation Physics and Chemistry, 169*, 108967.

Tekin, H. O., Altunsoy, E. E., Demir, Y., & Manici, T. (2021). Radiation shielding performance of tungsten doped glass systems. *Journal of Alloys and Compounds, 854*, 157173. https://doi.org/10.1016/j.jallcom.2020.157173

Turhan, M. F., Akman, F., Kaçal, M. R., Polat, H., & Demirkol, İ. (2023). A study for gamma-ray attenuation performances of barite filled polymer composites. *Applied Radiation and Isotopes, 191*, 110568.

Yılmaz, A., & Aydın, A. (2021). Secondary radiation production in high-Z based shielding materials under gamma-ray exposure. *Radiation Measurements, 145*, 106583. https://doi.org/10.1016/j.radmeas.2021.106583

➢ *ORAL PRESENTATION*

Biyobozunur Doğal İçerikli Yara Kremi Geliştirilmesi ve *İn Vitro* Biyouyumluluk Değerlendirmesi

Şevval Çelik[1*] (https://orcid.org/0000-0002-3091-620X), Büşra Moran[2*] (https://orcid.org/0000-0002-7280-4417) and Mustafa Türk[3*] ((https://orcid.org/0000-0001-8202-090X)

[2]: Hitit Üniversitesi, Bilimsel Teknik Uygulama ve Araştırma Merkezi, İn Vitro Biyouyumluluk ve Hücre Kültürü Laboratuvarı, Çorum, Türkiye

[3*]: Kırıkkale Üniversitesi, Mühendislik ve Doğa Bilimleri Fakültesi, Biyomühendislik Bölümü, Kırıkkale, Türkiye

*Sorumlu yazar e-posta:svvalclik11@gmail.com

Özet

İnsanların yıllardır karşılaştığı, gündelik hayatını ve hasta konforunu olumsuz etkileyen yaralar, her yaş grubunda görülmekte ve bulunduğu yer, yaranın derinliği, oluşma şekli gibi durumlardan farklılık göstermektedir. Bununla birlikte genel olarak yaranın oluşum ve iyileşme süreci için bir mekanizma tanımlanmaktadır. Yaralarda karşılaşılan en büyük problem, iyileşme sürecinin uzaması ve bu süreçte kişinin inflamasyon ile karşılaşmasıdır. Bu çalışmada, biyobozunur ve yara iyileştirici etkisi olduğu bilinen, geleneksel yöntemlerde sıkça kullanılan çeşitli maddelerin bir araya getirilmesi ile krem formunda bir yara iyileştirici formülasyon geliştirilmiştir. Elde edilen kremin yara iyileştirici etkisinin belirlenmesinden önce, canlı sistemler üzerindeki uygunluğu ve olası toksik etkisi değerlendirilmiştir. Toksik etkinin belirlenmesinde, tıbbi cihaz ve biyomalzemelerin biyouyumluluğunun değerlendirildiği TS EN ISO standardında yer alan MTT (3-[4,5-dimetiltiazol-2-il]-2,5-difenil tetrazolyum bromür) sitotoksisite test yöntemi kullanılmıştır. Test sonucunda farklı konsantrasyonlarda hazırlanan kremin hücre canlılığı üzerine etkileri incelendiğinde, hücre canlılık oranlarının %70'in üzerinde olduğu gözlemlenmiş ve bu da ürünün biyouyumlu olduğunu göstermiştir. Ayrıca, formülasyonda yer alan bileşenlerin kimyasal yapıları Fourier Transform Infrared Spektroskopisi (FTIR) ile karakterize edilmiştir. . Elde edilen bulgular, çapraz bağlama işleminin –OH, –NH ve amid gruplarıyla iyonik ve hidrojen bağı etkileşimlerine yol açtığını, bu sayede biyopolimerler arası fiziksel bağların güçlendiğini ortaya koymuştur. Biyouyumlu olduğu tespit edilen kremin yara iyileştirici etkisinin belirlenmesi için ileri in vivo testlerin yapılabileceği sonucuna varılmıştır.

Anahtar Kelimeler: Yara Kremi, Pamuk kozası, Biyobozunurluk, Biyouyumluluk

Development of Biodegradable Natural Ingredients Wound Cream and In Vitro Biocompatibility Evaluation

Abstract

Wounds, which have long been a significant health concern affecting individuals of all age groups, vary in terms of location, depth and etiology. Despite this variability, the underlying mechanisms of wound formation and healing are generally well understood. A major challenge in wound management is the prolonged healing process, which is often accompanied by inflammation and compromises patient comfort and quality of life. In this study, a novel wound healing cream formulation was developed. It was developed by combining biocompatible, biodegradable substances. These are commonly utilised in traditional medicine. They are known for their therapeutic properties. Prior to evaluating the formulation's efficacy in promoting wound healing, its compatibility with living systems and potential cytotoxicity were assessed. The MTT (3-(4,5-dimethylthiazol-2-yl)-2,5-diphenyltetrazolium bromide) assay was employed to assess cytotoxic effects in accordance with TS EN ISO standards for medical device biocompatibility. Cell viability results indicated values above 70% at all tested concentrations, demonstrating the formulation's biocompatibility. Furthermore, Fourier Transform Infrared Spectroscopy (FTIR) analysis was conducted to characterise the chemical structure of the components. The findings revealed that the crosslinking process promoted ionic and hydrogen bonding interactions involving –OH, –NH and amide groups, thereby enhancing the physical cohesion of the

biopolymers. Based on these results, the formulation is deemed suitable for further in vivo testing to investigate its wound-healing potential.

Keywords: Wound Cream, Wound healing, Polymer interactions, Biocompatibility, Cytotoxicity

1.GİRİŞ

İnsan derisi, vücudun en geniş organıdır ve üç ana katmandan oluşur: epidermis, dermis ve hipodermis. (Taşkapan, 2005). Bu katmanlar, cilt bütünlüğünün korunmasında, dış çevre ile etkileşimin düzenlenmesinde ve yara iyileşmesinde hayati görevler üstlenir. (Alberts vd., 2002). Epidermis, dış çevreye karşı koruyucu bir katman olarak görev yapar; dermis içinde damarlar, sinirler ve bağ dokusu bulunur; hipodermis ise enerji deposu işlevi gören yağ dokusundan oluşur. (Landmann, 1986). Deri, termoregülasyon, bağışıklık savunması ve su dengesinin korunması gibi çeşitli hayati işlevleri yerine getirir. (Taş ve Kırkık, 2022).

Yaralar, cilt bütünlüğünün bozulduğu doku hasarlarıdır ve akut, kronik, travmatik veya enfekte gibi farklı formlarda sınıflandırılır. (Raziyeva vd., 2021). Akut yaralar genellikle normal bir iyileşme süreci izlerken, kronik yaralar özellikle diyabet, bası yarası veya venöz yetmezlik gibi nedenlerle iyileşme sürecinde gecikmeler yaşar. (Umar ve Damar, 2017). Enfekte yaralar, yüksek mikrobiyal yük nedeniyle sistemik komplikasyon riski taşır. (Öztaş, 2021).

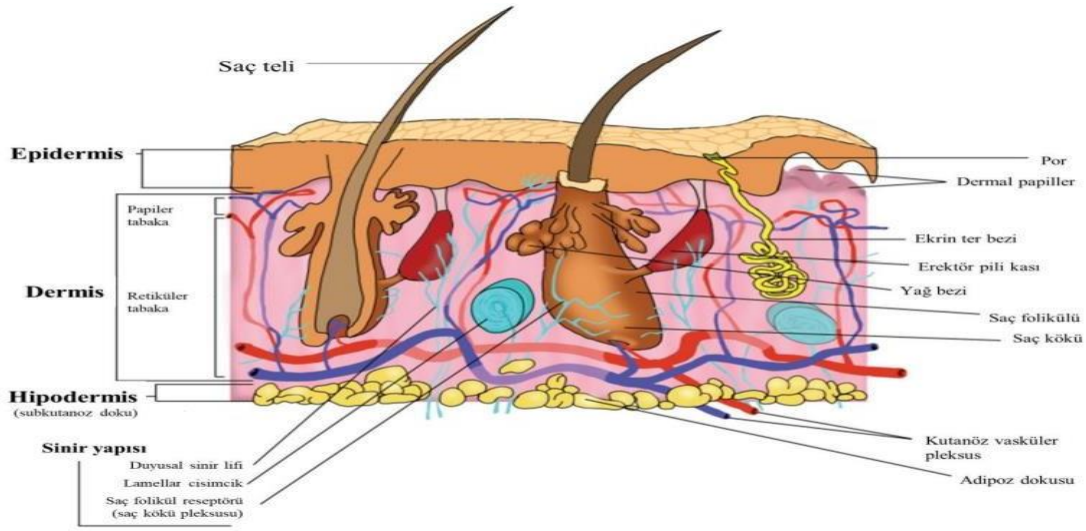

Şekil 1.1. Derinin anatomik yapısı (Yousef vd., 2022)

Yara iyileşmesi dört temel fazdan oluşur: hemostaz, inflamasyon, proliferasyon ve yeniden yapılanma (remodelasyon) (Kahraman ve Erdoğan, 2022). Bu aşamalardaki aksaklıklar iyileşmenin yavaşlamasına veya patolojik yara oluşumuna yol açabilir. (Kral vd., 2023). Yara iyileşmesi yalnızca fiziksel bir süreç değildir; aynı zamanda biyokimyasal, hücresel ve mikrobiyal etkileşimlerin bir arada gerçekleştiği karmaşık bir biyolojik döngüdür. Özellikle kronik yaralar (diyabetik ülserler, cerrahi sonrası doku hasarları ve travmatik yaralanmalar) bireyin yaşam kalitesini doğrudan etkileyen ve sağlık sistemleri üzerinde önemli ekonomik yük oluşturan sorunlardır. (Eroglu ve Girgin, 2021; Chelminiak-Dudkiewicz vd., 2023). Bu nedenle etkili, güvenli ve biyolojik olarak aktif yara bakım ürünlerine olan ihtiyaç her gün artmaktadır.

Bu çalışmasının temel önemi, doğal ve biyopolimer bazlı bileşenlerin sinerjik etkilerinden yararlanarak, açık yara tedavisinde kullanılabilecek, toksik olmayan ve biyouyumlu yeni bir topikal krem formülasyonu geliştirme çabasında yatmaktadır. Formülasyonda yer alan pamuk kozası, zeytinyağı, bal mumu ve çam sakızı gibi doğal ürünler, geleneksel halk hekimliğinde uzun yıllardır yara iyileştirici olarak kullanılmakla birlikte, modern farmasötik formülasyon yöntemleriyle yeterince bütünleştirilmemiştir (Valero Muñoz vd., 2014).

Bu doğal içeriklerin, farmasötik alanda biyouyumluluğu ve etkinliği bilimsel olarak kanıtlanmış olan kitosan ve aljinat gibi biyopolimerlerle bir araya getirilmesiyle; antimikrobiyal koruma sağlayan ve doku rejenerasyonunu destekleyen yenilikçi bir topikal ürün geliştirilmesi hedeflenmektedir (Ravi Kumar, 2004).

Formülasyonda yer alan pamuk kozası, içerdiği flavonoid ve fenolik bileşikler sayesinde antioksidan özellik göstererek serbest radikalleri nötralize eder ve hücre yenilenmesini destekleyebilir (Gupta vd., 2011). Zeytinyağı, oleik asit ve fenolik bileşenler bakımından zengin içeriği sayesinde nemlendirici, antiinflamatuar ve yara iyileşmesini destekleyici özelliklere sahiptir (Bayaz, 2016). Bal mumu doğal bir bariyer oluşturarak yaranın kurumasını önler ve antibakteriyel özelliklere sahiptir (Su ve Miller, 2015). Çam sakızı, reçineden elde edilen antiseptik bileşenler içerir ve yara bölgesindeki mikrobiyal yükü azaltıcı etki gösterebilir (Gürhan ve Ezer, 2004).

Kitosan, yara yüzeyine uygulandığında pozitif yüklü yapısıyla negatif yüklü bakteri hücre zarlarını hedef alarak antimikrobiyal etki gösterir; ayrıca biyobozunur yapısı ciltle yüksek uyumluluk sağlar (Sanchez- García, 2011). Aljinat, sodyum iyonlarıyla temas ettiğinde jel oluşturarak nemli yara ortamını korur ve epitelizasyonu destekler (Tighe ve Mann, 2011).

Bu bileşenlerin kombinasyonuyla hazırlanan krem formülasyonunun hem doğal hem biyoteknolojik avantajları birleştirilerek yara tedavisinde etkili bir çözüm sunacağı düşünülmektedir. Bu yaklaşım, geleneksel yara bakım ürünlerine kıyasla daha az yan etki riski taşır ve sürdürülebilir, çevre dostu bir alternatif oluşturur (Yu vd., 2017).

Özellikle balmumu, çam sakızı, zeytinyağı, pamuk kozası, aljinat ve kitosan gibi biyolojik olarak parçalanabilir ve biyouyumlu maddeler ile elde edilen kompleks formülasyonların kimyasal bileşimini analiz etmek, ürünün stabilitesi, biyoyararlanımı ve etkinliği açısından oldukça önemlidir (Stuart, 2004). Fourier Dönüşümlü Kızılötesi Spektroskopisi (FTIR), bu tür sistemlerde moleküler yapıların ve fonksiyonel grupların belirlenmesinde yaygın olarak kullanılan güçlü bir analitik tekniktir (Silverstein et al., 2014). Bu sebep ile krem formundaki numunenin FTIR analizi de gerçekleştirilmiştir. Analiz, mavi ve kırmızı renkle işaretlenmiş iki spektrum üzerinden değerlendirilmiş ve her spektrumda gözlemlenen pik değerleri karşılaştırmalı olarak yorumlanmıştır.

Bu çalışma sonucunda elde edilmesi hedeflenen krem formülasyonu, mevcut ticari ürünlere karşı doğal içerikli, biyobozunur, çevre dostu ve sürdürülebilir bir alternatif sunarak hem klinik uygulamalarda hem de kozmetik dermatoloji alanında kullanım potansiyeli taşıyacaktır. Aynı zamanda formülasyona ait bileşenlerin sinerjik etkileriyle oluşturulan bu yaklaşım, yara bakımında geleneksel bilgi ile modern teknolojinin başarılı bir entegrasyonu örneği olacaktır.

2.MATERYAL VE METOT

Deneyde kullanılacak kül özütleri, 2 litrelik beherlerde hazırlandı. Yoğun formülasyonda 400 gram kül 1 litre distile su içinde; seyrek formülasyonda ise 200 gram kül yine 1 litre distile su içerisinde çözülerek hazırlandı. Karışımlar, ısıtıcılı manyetik karıştırıcı üzerinde kaynatılmaya başlandı.

Kaynatma sonrası çöken külün üzerinde kalan süpernatantın bir kısmı ependorf tüplere alındı. Bu sıvılar; yoğun kül çözeltisinden elde edilen örnekler “WH-1” ve “WH-2”, seyrek çözeltiden elde edilen örnek ise “WH-3” olarak adlandırıldı.

Kül çöktükten sonra süpernatant, bakır bir kazan içerisine alınmış ve tuz formu elde edilene kadar kaynatıldı. Tuz kristallerinin oluşumu tamamlandıktan sonra soğumaya bırakıldı.

Doğal Formülasyonların Hazırlanması

Tuz formuna dönüşen kül özütünün soğuması beklenirken, doğal içeriklerin bir araya getirilmesiyle formülasyon hazırlıklarına başlandı. Üç farklı kombinasyon şeklinde hazırlanan karışımlar aşağıda belirtilmiştir:

Formülasyon1:
Çözücü faz olarak %100 kabul edilen 51 mL serum fizyolojik içerisinde, ilk olarak %3 oranında kitosan çözündürüldü. Ardından, sırasıyla %4 aljinat , %4 balmumu, %4 çam sakızı ve %4 zeytinyağı ilave edilerek

tüm bileşenler homojen bir karışım elde edilene kadar eritildi. Son aşamada, formülasyona %8 oranında kül ekstraktı eklendi ve karışım bütün bileşenlerin tamamen dağılması sağlanarak son haline getirildi.

Formülasyon2:
Çözücü faz olarak %100 kabul edilen 51 mL serum fizyolojik içerisinde %3 oranında kitosan çözündürüldü. Ardından sırasıyla %4 aljinat, %4 balmumu, %4 çam sakızı ve yaklaşık %4 zeytinyağı ilave edilerek tüm bileşenler homojen şekilde eritildi. Son olarak, formülasyona %8 oranında kül ekstraktı eklenerek karışım tamamlandı.

Formülasyon3:
Çözücü faz olarak %100 kabul edilen 51 mL serum fizyolojik içerisinde %3 oranında kitosan çözündürüldü. Takiben, %4 aljinat, %4 balmumu, %6 çam sakızı ve yaklaşık %6 oranında zeytinyağı eklenerek karışım homojen hale getirildi. Bu bileşenlerin üzerine %12 oranında kül ekstraktı ilave edilerek formülasyon oluşturuldu.

Hücre Çözdürme ve Ekim İşlemi

-80°C'de saklanan L929 hücre hattı, iki elle manyetik çözündürme yöntemiyle çözülmüş ve falkon tüplere alındı. Hücrelerin üzerine 2 mL hazır DMEM besiyeri eklenmiş, pipetaj işlemiyle homojen karışım sağlanarak 2 dakika boyunca 2000 rpm'de santrifüj edildi. Santrifüj sonrası süpernatant uzaklaştırıldı, altta kalan hücreler köpürtülerek çözüldükten sonra üzerine 8 mL hazır DMEM eklendi ve pipetaj ile tüm hücreler alındı. Elde edilen hücre süspansiyonu 25'lik kültür flakonlarına aktarıldı, mikroskop altında gözlemlenerek etüve kaldırıldı.

Pasajlama İşlemi

İnkübatörde inkübasyona bırakılan L929 fibroblast hücreleri mikroskop altında kontaminasyon açısından incelendi ve herhangi bir kontaminasyon izine rastlanılmadı. Flakonlar dik tutularak sıvı, pipet yardımıyla alt köşeden çekilerek uzaklaştırıldı. Hücreler önce 1 mL PBS ile yıkandı, ardından 1,5 mL tripsin-EDTA eklendi ve inkübatörde 4 dakika bekletildi. Süre sonunda, hücrelerin mekanik olarak kalkmasını sağlamak amacıyla flakonlara hafifçe vuruldu ve hücrelerin tamamının yüzeyden ayrıldığı mikroskopla doğrulandı.

Falkonlara 3 mL DMEM eklenerek tüm sıvı toplandı, isimlendirilen falkon tüplerine aktarıldı. Yeniden 2 dakika 2000 rpm'de santrifüj işlemi yapıldı; süpernatantlar atıldı, hücreler yeniden hazır DMEM ile süspanse edilerek ekim işlemi tekrarlandı. L929 hücreleri 2 mL tripsin ve 4 mL DMEM ile yeniden pasajlandı.

Hücre Sayımı

Ependorf tüpüne 10 µL hücre süspansiyonu ve tripan mavisi eklenerek karıştırıldı, ardından 10 µL'lik karışım 16'lık Thoma lam üzerine aktarıldı. Mikroskop altında lam üzerindeki düşük, orta ve yüksek yoğunluklu üç kare seçilerek hücre sayımı yapıldı. Canlı hücre sayısı şu formülle hesaplandı:

(Karedeki toplam hücre sayısı / Kare sayısı) × 250.000

Her kuyucukta 10.000 hücre olacak şekilde 96'lık well plate'e hücreler ekildi.

Özütleme ve MTT Analizi

Üç farklı örnek, her biri 1 gram örnek ve 6 mL besiyeri olacak şekilde WH1, WH2 ve WH3 olarak hazırlandı. Elde edilen numuneler sırasıyla 0,4 µm ve 0,2 µm gözenek çapına sahip şırınga filtrelerinden geçirilerek süzüldü. Ardından, 96 kuyucuklu bir well plate'in ilk sırasındaki her bir kuyucuğa 200 µL filtrelenmiş numune eklendi. Geriye kalan tüm kuyucuklara ise 100 µL hazır DMEM ilave edildi. İlk sıradaki 200 µL'lik karışımdan 100 µL alınarak ikinci sıradaki kuyucuklara aktarıldı ve içerikler pipetaj ile homojen şekilde karıştırıldı. Bu işlem, tüm sıralar için aynı şekilde tekrarlanarak dilüsyon serisi oluşturuldu. Son sıradaki 100 µL'lik hacim atılarak işlem sonlandırıldı. Hazırlanan well plate mikroskop altında incelendikten sonra etüve yerleştirildi.

MTT Testi

Fenolredsiz DMEM ile MTT tozu, 150 mL hacminde ve karanlık ortamda, alüminyum folyo ile sarılmış falkon içinde hazırlandı. Önceki gün ekimi yapılan 96'lık well plate'teki besiyerleri pipet yardımıyla kuyucuklardan çekilerek uzaklaştırıldı, her kuyucuğa 50 µL MTT solüsyonu eklendi. Plate 3 saat süreyle etüve alındı. Süre sonunda MTT solüsyonu uzaklaştırıldı, her kuyucuğa 100 µL izopropil alkol eklenerek absorbans ölçümü ve hücre canlılık analizi yapıldı.

3.BULGULAR

Kaynatma işlemi sırasında, karışım yüzeyinde balıklara takılan metal parçacıklar gözlemlendi.

Tablo 3.1 WH1 MTT sonuçları absorbans, % canlılık ve standart sapma değerleri

Seyreltme	Ortalama Absorbans	Hücre Canlılığı (%)
1/1	1.11 ± 0.01	58.6
1/2	1.35 ± 0.05	71.7
1/4	1.56 ± 0.08	83.2
1/8	1.71 ± 0.04	91.4
1/16	1.78 ± 0.04	95.0
1/32	1.78 ± 0.04	94.8
1/64	1.87 ± 0.06	99.8
Kontrol	1.87 ± 0.02	100.0

Tablo 3.1' de gösterildiği gibi, WH1 maddesi, 1/1 seyreltmesinde %58.6 hücre canlılığı ile en yüksek toksisiteyi göstermiştir; bu, diğer maddelere kıyasla en düşük canlılık değeridir. Seyreltme oranı arttıkça hücre canlılığında kademeli bir artış gözlenmiş, bu da doz-bağımlı toksik etki profiline işaret etmektedir. 1/64 seyreltmesinde hücre canlılığı %99.8 seviyesine ulaşmış ve kontrol grubuna oldukça yakın bir değer göstermiştir; bu dozda nötr veya çok hafif proliferatif etki olabilir. WH1'in hiçbir konsantrasyonunda hücre canlılığı kontrol grubunun belirgin şekilde üzerine çıkmamıştır; bu da onun proliferatif etkisi olmadığını**,** daha çok doz azaldıkça toksisitesinin düştüğünü gösterir. Genel olarak WH1, klasik bir sitotoksik madde gibi davranmakta ve yalnızca yüksek dilüsyonlarda hücreler üzerinde zararsız bir profil çizmektedir.

Tablo 3.2 WH2 MTT sonuçları absorbans, % canlılık ve standart sapma değerleri

Seyreltme	Ortalama Absorbans	Hücre Canlılığı (%)
1/1	0.95 ± 2.06	83.2
1/2	1.03 ± 2.99	89.7
1/4	1.61 ± 3.19	140.6
1/8	1.66 ± 3.10	145.0
1/16	1.35 ± 1.49	118.0
1/32	1.36 ± 4.78	118.5
1/64	1.32 ± 3.47	115.0
Kontrol	1.07 ± 0.19	100.0

Tablo 3.2' de görüldüğü üzere WH2 maddesi, düşük seyreltmelerde (1/1 ve 1/2) hücre canlılığını azaltarak hafif toksik bir etki göstermektedir. Orta seyreltmelerde (özellikle 1/4 ve 1/8) hücre canlılığı %140'ın üzerine çıkarak, anormal derecede yüksek değerlere ulaşmıştır. Bu durum, WH2 maddesinin bazı doz aralıklarında hücre proliferasyonunu uyarıcı (mitojenik) etkiler gösterebileceğini düşündürmektedir. Seyreltme oranı arttıkça hücre canlılığı %115 civarına düşerek, yine de kontrol grubundan daha yüksek kalmıştır. Genel olarak WH2'nin düşük dozlarda uyarıcı, yüksek dozlarda toksik etki yaratabilir.

Tablo 3.3 WH3 MTT sonuçları absorbans, % canlılık ve standart sapma değerleri

Seyreltme	Ortalama Absorbans	Hücre Canlılığı (%)
1/1	0.78 ± 0.14	68.0
1/2	0.99 ± 2.28	86.3
1/4	1.03 ± 3.86	89.6
1/8	1.11 ± 3.71	96.9
1/16	1.09 ± 2.78	94.8
1/32	1.07 ± 2.47	93.7
1/64	1.18 ± 1.19	102.6
Kontrol	1.22 ± 0.16	100.0

Tablo 3.3'de görüldüğü gibi, WH3 maddesi, 1/1 seyreltmesinde %68 canlılık ile belirgin sitotoksik bir etki göstermiştir. Seyreltme oranı arttıkça hücre canlılığında artış gözlenmiş, ancak bu artış genellikle kontrol seviyesinin altında kalmıştır. 1/64 seyreltmesinde hücre canlılığı %102.6'ya ulaşarak kontrol düzeyini hafifçe aşmıştır; bu da düşük dozda hafif proliferatif bir etki olabileceğini düşündürür. WH3 genel olarak klasik doz-bağımlı toksisite profili göstermektedir: yüksek dozda toksik, düşük dozda daha az etkili ya da nötr. WH3, WH2'ye kıyasla daha stabil ve öngörülebilir bir etki profiline sahiptir, ancak güçlü bir proliferatif etkisi bulunmamaktadır.

Tablo 3.4 WH1, WH2 ve WH3 birleştirilmiş MTT sonuçları absorbans, %canlılık ve standart sapma değerleri

Seyreltme	Ortalama Absorbans WH1	Hücre Canlılığı (%) WH1	Ortalama Absorbans WH2	Hücre Canlılığı (%) WH2	Ortalama Absorbans WH3	Hücre Canlılığı (%) WH3
1/1	1.11 ± 0.01	58.6	0.95 ± 2.06	83.2	0.78 ± 0.14	68.0
1/2	1.35 ± 0.05	71.7	1.03 ± 2.99	89.7	0.99 ± 2.28	86.3
1/4	1.56 ± 0.08	83.2	1.61 ± 3.19	140.6	1.03 ± 3.86	89.6
1/8	1.71 ± 0.04	91.4	1.66 ± 3.10	145.0	1.11 ± 3.71	96.9
1/16	1.78 ± 0.04	95.0	1.35 ± 1.49	118.0	1.09 ± 2.78	94.8
1/32	1.78 ± 0.04	94.8	1.36 ± 4.78	118.5	1.07 ± 2.47	93.7
1/64	1.87 ± 0.06	99.8	1.32 ± 3.47	115.0	1.18 ± 1.19	102.6
Kontrol	1.87 ± 0.02	100.0	1.07 ± 0.19	100.0	1.22 ± 0.16	100.0

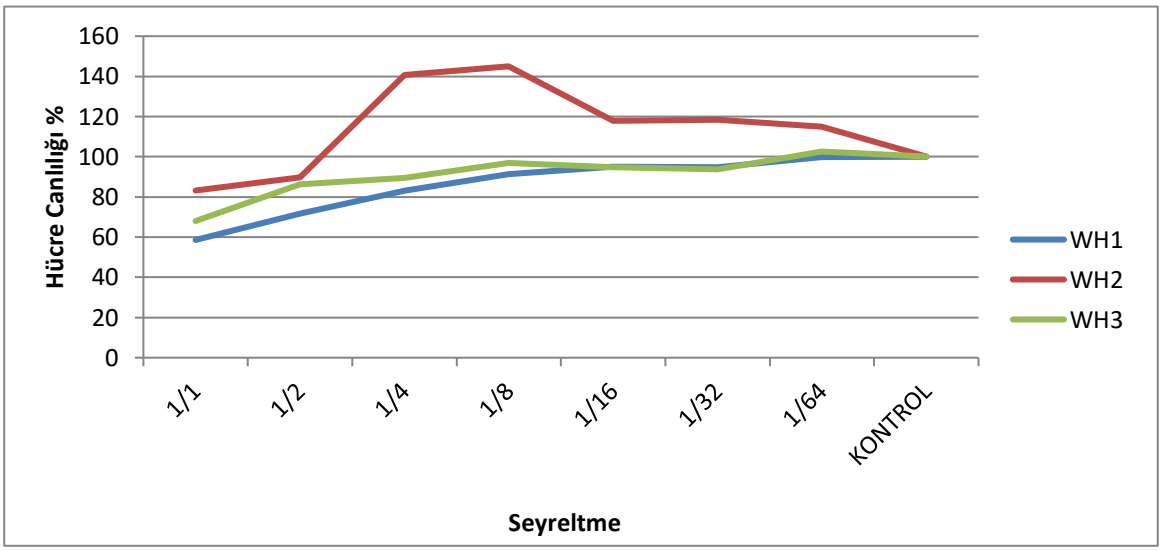

Şekil 3.1. WH1, WH2 ve WH3 karşılaştırmalı MTT deneyi % canlılık değerleri

Tablo 3.4' de gösterilen değerler ile Şekil 3.1.' de görülen çizgi grafiği elde edilmiştir. Söz konusu tablo ve grafik incelendiğinde seyreltme oranı arttıkça hücre canlılık değeri de aynı oranda artmaktadır yorumu yapılabilir. Yani hücre yoğunluğu azaldıkça hücreler üzerinde meydana gelen toksik etkinin de azaldığı tespit edilebilir. WH1 grubunda en düşük canlılık değeri gözlemlenirken, WH2 ve WH3 de görülen hücre canlılığı çok daha fazladır.

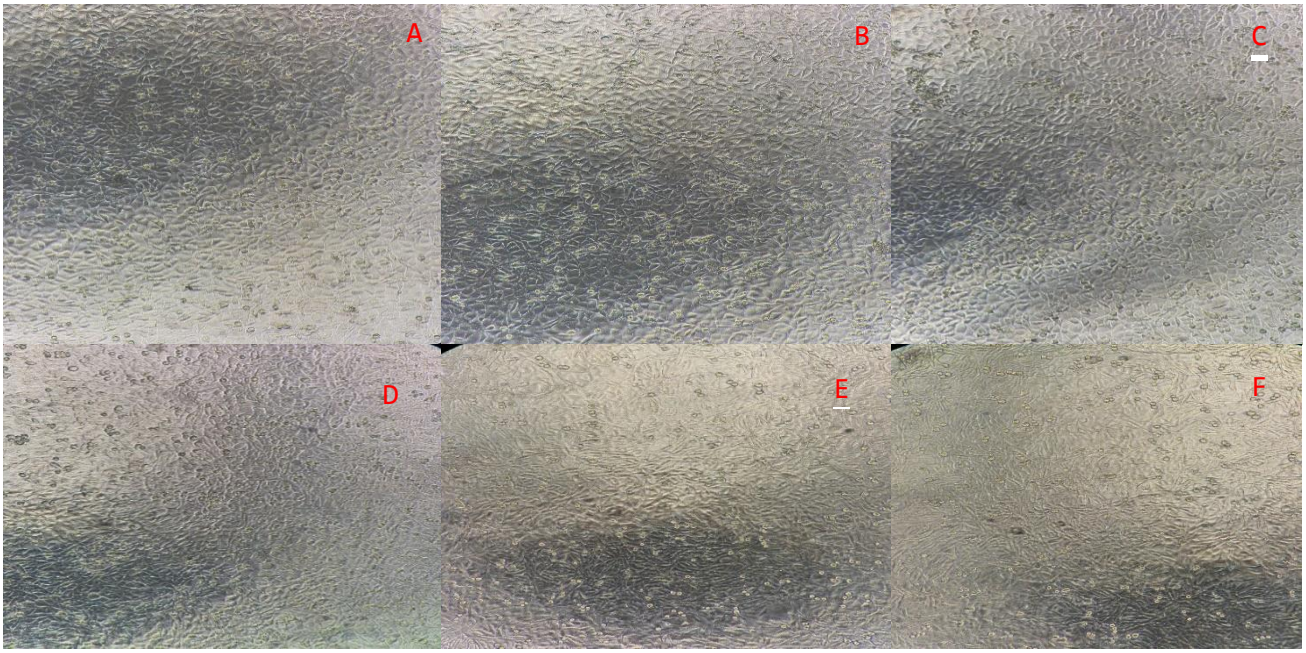

Şekil 3.2. Formülasyon uygulamasından önce fotoğraflanan görüntülerde canlılık oranı %68 olarak hesaplanmıştır. (A:WH1, B: WH2, C: WH3)

Formülasyon uygulanmasından sonra çekilen fotoğraflarda canlılık oranı %100 olarak hesaplanmıştır. (C:WH1 1/4 seyreltmede hücre canlılığı 83,2 , D: WH2 1/1 seyreltmede hücre canlılığı 83,2 , E: WH3 1/2 seyreltmede hücre canlılığı 86,3)

FTIR (Fourier Transform Infrared Spectroscopy) Spektrum Analizi

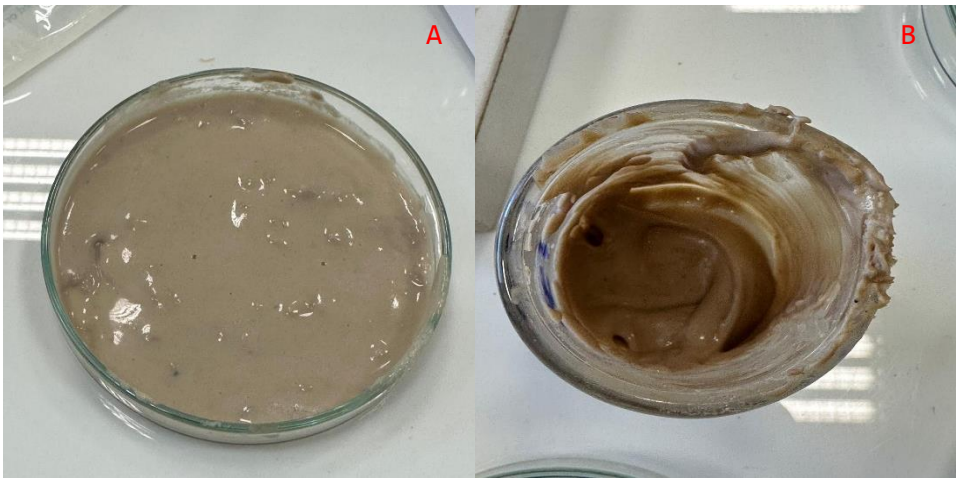

Şekil 3.3. Hazırlanan kreme ait görüntüler A: Çapraz bağlanma öncesi numune B: Çapraz bağlanma sonrası numune

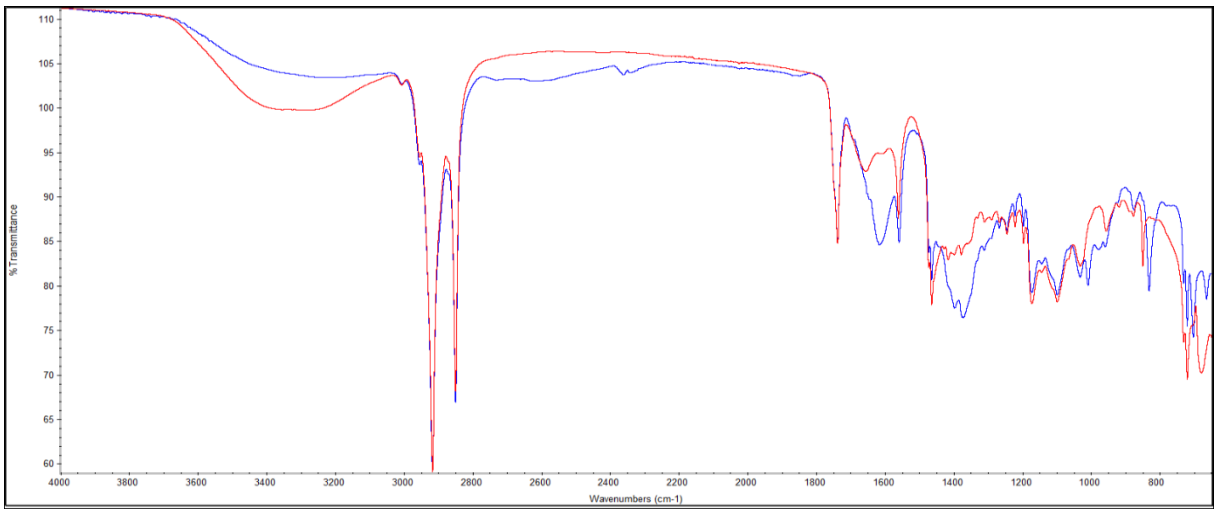

Şekilde 3.4. Çapraz bağlanma sonrası (mavi) ve çapraz bağlanma öncesi (kırmızı)

Malzeme karakterizasyonu ve $CaCl_2$ ile gerçekleştirilen çapraz bağlama işleminin formülasyon üzerindeki etkilerini değerlendirmek amacıyla çeşitli analizler gerçekleştirilmiştir**.** MTT testinde elde edilen hücre verilere göre seçilen WH2 aynı şekilde yeniden sentezlendi ve karakterizasyon işlemi bu formülasyon için yapıldı. Çapraz bağlanmamış örneğe ait FTIR spektrumunda (kırmızı), 3273 cm^{-1} dalga sayısında geniş bir tepe gözlenmiş olup bu tepe, aljinat ve kitosan yapılarında bulunan –OH ve –NH fonksiyonel gruplarına karşılık gelmektedir. Çapraz bağlanmış örnekte (mavi) ise bu bant daha düşük yoğunlukta olup hafif bir kayma göstermiştir; bu durum, Ca^{2+} iyonlarının hidrojen bağlarıyla kısmi etkileşim içerisinde olduğunu düşündürmektedir.

2915 ve 2848 cm^{-1} civarında gözlenen C–H gerilme bantları, balmumu ve zeytinyağı kaynaklı alifatik grupların varlığını doğrulamaktadır. Bu bölgelerde çapraz bağlamaya bağlı olarak belirgin bir değişiklik gözlenmemiştir. 1736 cm^{-1} civarındaki pikler, balmumu ve zeytinyağından kaynaklanan ester karbonil gruplarını temsil etmekte olup, bu grupların Ca^{2+} ile çapraz bağlama işleminden etkilenmediği anlaşılmaktadır.

Bununla birlikte, 1655–1550 cm^{-1} aralığında yer alan ve kitosana özgü amid I ve amid II bantlarında gözlenen kayma ve daralma, Ca^{2+} iyonlarının amin grupları ile iyonik etkileşim kurduğunu göstermektedir. Ayrıca, 1460–1000 cm^{-1} aralığında, özellikle aljinat ve kitosan polisakarit iskeletine ait C–O ve C–C titreşimlerine karşılık gelen piklerdeki hafif kaymalar ve şiddet değişimleri, çapraz bağlamanın malzemenin yapısal organizasyonunu etkilediğini ortaya koymaktadır.

Düşük dalga sayılı bölgede, özellikle 848–710 cm^{-1} aralığında gözlenen daha keskin ve belirgin pikler ise, çapraz bağlama sonrası yapısal düzenliliğin arttığını göstermektedir.

Tüm bu bulgular, Ca^{2+} iyonları ile gerçekleştirilen çapraz bağlama işleminin formülasyonda yer alan biyopolimerler arasında fiziksel etkileşimleri güçlendirdiğini, bu sayede sistemin mekanik bütünlüğünü ve yapısal stabilitesini artırdığını ortaya koymaktadır.

4.SONUÇ-TARTIŞMA

Bu çalışmada, biyobozunur ve yara iyileştirici etkileri literatürde tanımlanmış, aynı zamanda geleneksel tedavi pratiklerinde sıkça kullanılan doğal kaynaklı bileşenler bir araya getirilerek yeni bir topikal formülasyon geliştirilmiştir. Formülasyonda yer alan balmumu, zeytinyağı, çam sakızı, pamuk kozası, aljinat ve kitosan gibi maddelerin fonksiyonel grupları Fourier Transform Infrared (FTIR) spektroskopisi ile karakterize edilmiştir. $CaCl_2$ ile gerçekleştirilen iyonik çapraz bağlama işleminin, aljinat ve kitosan bazlı biyopolimer formülasyon üzerindeki yapısal etkileri FTIR analizi ile değerlendirilmiştir. Elde edilen bulgular, çapraz bağlama işleminin

–OH, –NH ve amid gruplarıyla iyonik ve hidrojen bağı etkileşimlerine yol açtığını, bu sayede biyopolimerler arası fiziksel bağların güçlendiğini ortaya koymuştur. Özellikle amid I ve II bölgelerinde gözlenen kaymalar, Ca^{2+} iyonlarının kitosan ile anlamlı düzeyde etkileştiğini göstermektedir. Buna ek olarak, düşük dalga sayılı bölgelerdeki daha belirgin pikler ve spektral değişimler, çapraz bağlama sonrası yapısal düzenliliğin arttığını göstermektedir. Sonuç olarak, Ca^{2+} iyonları ile gerçekleştirilen çapraz bağlama işlemi, formülasyonun yapısal bütünlüğünü ve potansiyel mekanik dayanımını artırarak biyomalzeme uygulamaları açısından avantaj sağlamaktadır.

Formülasyonun in vitro biyouyumluluğu, TS EN ISO 10993-5:2009 standardına uygun olarak gerçekleştirilen MTT sitotoksisite testi ile değerlendirilmiştir. Elde edilen veriler, hazırlanan üç farklı örnek (WH1, WH2 ve WH3) arasında hem doz hem de bileşen profili açısından anlamlı biyolojik farklılıklar bulunduğunu ortaya koymuştur. WH1 numunesi, yüksek konsantrasyonlarda belirgin sitotoksisite göstermiş olup (%58,6 canlılık), bu durum doz-bağımlı toksik etkisine işaret etmektedir. Dilüsyon oranı arttıkça hücre canlılığı da paralel şekilde artmış ve en seyreltilmiş formda (1/64) %99,8 canlılık düzeyine ulaşılmıştır. Bu profil, WH1'in klasik bir toksik ajan davranışı sergilediğini ve biyouyumlu sınırlar içinde yalnızca düşük konsantrasyonlarda değerlendirilebileceğini göstermektedir.

WH2 örneği ise dikkat çekici bir şekilde, orta seyreltme oranlarında (1/4 ve 1/8) hücre canlılığında kontrol grubunun belirgin şekilde üzerinde (%140'ın üzerinde) artış göstermiştir. Bu durum, WH2'nin bazı konsantrasyonlarda mitojenik ya da proliferatif etkiler gösterebileceğini düşündürmekte, bu bağlamda hormetik yanıt olasılığını gündeme getirmektedir. WH3 numunesi ise daha öngörülebilir bir doz-cevap ilişkisi sergileyerek, yüksek konsantrasyonlarda toksik (%68 canlılık), düşük konsantrasyonlarda ise biyouyumlu hatta sınırlı proliferatif (%102,6 canlılık) yanıt vermiştir.

Literatürde, benzer doğal formülasyonlarla yürütülen çalışmalarda da bu tür çift yönlü biyolojik etkilerin gözlendiği bildirilmektedir. Örneğin, İnce ve arkadaşları (2019) tarafından geliştirilen, %10 oranında kudret narı ekstresi içeren zeytinyağı bazlı topikal krem formülasyonu, deneysel yara modellerinde fibroblast migrasyonunu, granülasyon doku oluşumunu ve epitel hücre proliferasyonunu anlamlı düzeyde artırmıştır. Bu etkinin, zeytinyağının içerdiği fenolik bileşikler ve yağ asidi kompozisyonuna bağlı olarak antioksidan ve penetrasyon artırıcı özelliklerinden kaynaklandığı düşünülmektedir.

Ayrıca çalışmamızda kullanılan balmumu, çam sakızı ve pamuk kozası gibi doğal bileşenlerin antienflamatuvar, antimikrobiyal ve rejeneratif özelliklere sahip olduğu; bu etkilerin yara mikroçevresinde sinerjik etki yaratabileceği yönündeki bulgular literatürle uyumludur (Gu et al., 2020; Cam et al., 2020). Bu bileşenlerin, kitosan ve aljinat gibi biyopolimerlerle birlikte formüle edilmesi, kontrollü salım mekanizmalarıyla etkili farmakolojik aktivite sağlama potansiyelini artırmaktadır.

Öte yandan, bazı dilüsyon oranlarında gözlemlenen yüksek standart sapma değerleri, biyolojik varyasyonun yüksek olduğunu ve deneysel tekrar sayısının artırılması gerektiğini ortaya koymaktadır. Özellikle WH2 örneğindeki anormal proliferatif yanıtların farklı hücre hatlarında yeniden test edilmesi ve bu etkinin moleküler düzeyde doğrulanması ileri çalışmalar için önem arz etmektedir.

Sonuç olarak, geliştirilen topikal formülasyonun biyouyumlu sınırlar içinde güvenli olduğu gösterilmiş; özellikle WH2 formülasyonu, yalnızca yara iyileştirme değil aynı zamanda hücre proliferasyonunu destekleyici potansiyeliyle ön plana çıkmıştır. Bu bağlamda WH2, ileri preklinik ve in vivo değerlendirmeler için güçlü bir aday bileşik olarak önerilmektedir.

KAYNAKLAR

Alberts, B., Johnson, A., Lewis, J., Raff, M., Roberts, K., & Walter, P. (2002). Epidermis and its renewal by stem cells. In Molecular Biology of the Cell. 4th edition. Garland Science.

Aygun, B., Bilici, I., Deniz, C. U., Oz, B., Sayyed, M. I., & Karabulut, A. (2024). Development of novel composite materials containing rice bran wax and waste polyethylene for neutron shielding applications. *Progress in Nuclear Energy, 174*, 105262. https://doi.org/10.1016/j.pnucene.2024.105262

Bayaz, M. (2014). Esansiyel yağlar: antimikrobiyal, antioksidan ve antimutajenik aktiviteleri. Akademik Gıda, 12(3), 45-53.

Bayaz, M. (2016). Natürel Zeytinyağlarındaki Fenolik Bileşiklerin Biyolojik Aktivitesi. Akademik Gıda, 14(4), 441-450. https://dergipark.org.tr/tr/download/articlefile/1186157

Cam, M. E., Yildiz, S., Alenezi, H., Cesur, S., Ozcan, G. S., Erdemir, G., ... & Edirisinghe, M. (2020). Evaluation of burst release and sustained release of pioglitazone-loaded fibrous mats on diabetic wound healing: an in vitro and in vivo comparison study. *Journal of the Royal Society Interface*, *17*(162), 20190712.

Chelminiak-Dudkiewicz, D., Machacek, M., Dlugaszewska, J., Wujak, M., Smolarkiewicz-Wyczachowski, A., Bocian, S., ... & Ziegler-Borowska, M. (2023). Fabrication and characterization of new levan@ CBD biocomposite sponges as potential materials in natural, non-toxic wound dressing applications. *International Journal of Biological Macromolecules, 253*, 126933.

Cooper, R., 2004, A review of the evidence for the use of topical antimicrobial agents in wound care, World wide wounds, 1-11p.

Erdem, S., & Eren, P. A. (2009). Tedavi amacıyla kullanılan bitkiler ve bitkisel ürünlerin yan etkileri. *Türk Hijyen ve Deneysel Biyoloji Dergisi, 66*(3), 133-141.

Eroglu, E., & Girgin, S. N. (2021). A unique phenolic extraction method from olive oil macerate of Hypericum perforatum using DMSO: Assessment of in vitro anticancer activity, LC-MS/MS profile, total phenolic content and antioxidant capacity. *South African Journal of Botany, 139, 6-11.*

Galli, S. J., Borregaard, N., & Wynn, T. A. (2011). Phenotypic and functional plasticity of cells of innate immunity: macrophages, mast cells and neutrophils. Nature immunology, 12(11), 1035-1044.

Gu, W., Hao, X., Wang, Z., Zhang, J., Huang, L., & Pei, S. (2020). Ethnobotanical study on medicinal plants from the Dragon Boat Festival herbal markets of Qianxinan, southwestern Guizhou, China. Plant diversity, 42(6), 427-433.

Gupta, B., Agarwal, R., and Alam, M. S. (2011). Hydrogels for wound healing applications. In Biomedical hydrogels Woodhead Publishing. 184-227.

Gündüz, E. (2022). Arteriovenöz Fistül Yarasi Olan Bir Olguda Yara Bakimi. *Atlas Journal of Medicine, 2*(5), 8-11.

Gürhan, G., Ezer, N., 2004. Halk Arasında Hemoroit Tedavisinde Kullanılan Bitkiler-1, Hacettepe Üniversitesi Eczacılık Fakültesi Dergisi, 24(1), 48.

International Organization for Standardization. (2009). *ISO 10993-5:2009 - Biological evaluation of medical devices—Part 5: Tests for in vitro cytotoxicity*. https://www.iso.org/standard/36406.html

İnce, İ., Çığırgil, N., Gümüştaş, B., Kozguş Güldü, Ö., Karaman, D., Medine, E. İ., Karasulu, E. (2019). Momordica charantia L. meyveleri kullanılarak krem hazırlanması, kalite kontrolü ve in vitro yara iyi edici etkisinin araştırılması. *Erzincan Univ J Sci Technol*, *12*(1), 38-48.

Kahraman, F. C., & Erdoğan, S. S. (2022). Yara İyileşmesi. *Turkiye Klinikleri Dermatology-Special Topics, 15*(4), 8-14.

Kral, Ö., Tamer, S. İ., Gül, Ü., & Tirnaksiz, F. (2023). Radyodermatit Tedavisi: Geleneksel Derleme. *Turkiye Klinikleri Journal of Dermatology, 33*(1), 30-39. Zeytinyağı bazlı topikal ürünlerin antiinflamatuvar potansiyeli

Kumar, M. R., Muzzarelli, R., Muzzarelli, C., Sashiwa, H., & Domb, A. J. (2004). Chitosan chemistry and pharmaceutical perspectives. *Chemical reviews, 104*(12), 6017 6084.

Landmann, L. (1986). Epidermis and dermis. In *Biology of the integument: 2 vertebrates* (pp. 150-187). Berlin, Heidelberg: Springer Berlin Heidelberg.

Mutlu, S., & Yılmaz, E. (2019). Yara yönetiminde yenilikçi yaklaşımlar. *Gümüşhane Üniversitesi Sağlık Bilimleri Dergisi, 8*(4), 481-494.

Oymak, H. (2019). *Elektro eğirme yöntemi ile modern yara örtüsü geliştirilmesi* (Master's thesis, Marmara Universitesi (Turkey)).

Öztaş, P. (2021). Yara İyileşmesi, Bakimi Ve Tedavisi. *Ankara Eğitim ve Araştırma Hastanesi Tıp Dergisi, 54*(2), 341-351.

Pancur, S., Bilensoy, E., & Çalış, S. (2022). Biyoparçalanır Doğal ve Sentetik Polimerlerin Yara Örtülerinde Kullanımı. *Fabad Journal of Pharmaceutical Sciences, 47*(3), 419-442.

Raziyeva, K., Kim, Y., Zharkinbekov, Z., Kassymbek, K., Jimi, S., & Saparov, A. (2021). Immunology of acute and chronic wound healing. *Biomolecules, 11*(5), 700.

Sanchez-García, M. D. (2011). Carrageenan polysaccharides for food packaging. In Multifunctional and nanoreinforced polymers for food packaging (pp. 594-609). Woodhead Publishing.

Silverstein, R. M., Webster, F. X., Kiemle, D. J., & Bryce, D. L. (2014). *Spectrometric Identification of Organic Compounds* (8th ed.). Wiley.

Stuart, B. (2004). *Infrared Spectroscopy: Fundamentals and Applications*. John Wiley & Sons.

Su, X. Z., & Miller, L. H. (2015). The discovery of artemisinin and the Nobel Prize in Physiology or Medicine.

Taş, S. K., & Kirkik, D. (2022). Dermatolojide Temel İmmünoloji. *Turkiye Klinikleri Dermatology-Special Topics, 15*(3), 45-51.

Taşkapan, O. (2005). Deri İmmünolojisi. *Turkiye Klinikleri Journal of Internal Medical Sciences, 1*(6), 1-8.

Tighe, B. J., & Mann, A. (2011). Adhesives and interfacial phenomena in wound healing. In Advanced wound repair therapies (pp. 247-283). Woodhead Publishing. Yu, B. R., Hou, Y. J., Chai, X. Z., Chai, X. M., Chang, M. J., & Huang, J. G. (2017). The New Concepts Wound Care, 252-285.

Umar, D. Ç., & Damar, H. T. (2017). Akut ve kronik yaralar ve hemşirelik bakımı. *Turkiye Klinikleri Surgical Nursing-Special Topics, 3*(3), 157-163.

Valero Muñoz, M., Martín Fernández, B., Ballesteros, S., de la Fuente, E., Quintela, J. C., Lahera, V., De las Heras, N. 2014. Protective effect of a pomace olive oil concentrated in triterpenic acids in alterations related to hypertension in rats: Mechanisms involved. Molecular nutrition and food research. 58(2), 376-383.

Wang, L. F., Shankar, S. ve Rhim, J. W. (2017). Properties of alginatebased films reinforced with cellulose fibers and cellulose nanowhiskers isolated from mulberry pulp, Food Hydrocolloids, 63, 201-208. doi:10.10162016.08.041.

➢ *ORAL PRESENTATION*

The single crystal x-ray crystallographic elucidation of thiazole-based heterocycles with supramolecular interactions

Zeynep Türkmen Bulca [1*] (*ORCID: 0000-0001-7610-1949*), Abdullah Biçer [2] (*ORCID: 0000-0003-4648-1834*), Erdal Kurt[3] (*ORCID: 0000-0001-5148-8059*) , Gül Özkan [4] (*ORCID: 0000-0001-6325-628X*)

[*1] Izmir Katip Çelebi University, Nanoscience and Nanotechnology Program, Institute of Science, Izmir, Turkey.
[2] Bilecik Şeyh Edebali University, Departmen of Chemistry, Faculty of Engineering, Bilecik, Turkey.
[3] Izmir Katip Celebi University, Department of Engineering Sciences, Faculty of Engineering, Izmir, Turkey.
[4] Izmir Katip Celebi University, Department of Engineering Sciences, Faculty of Engineering, Izmir, Turkey.

* Corresponding author e-mail:zeynep-turkmen@hotmail.com.tr

Abstract
In this study, two novel thiazole-based heterocyclic compounds were synthesized via a condensation reaction involving appropriately substituted hydrazonoyl halides and thiosemicarbazide derivatives. The resulting compounds were successfully crystallized, and their molecular structures were unambiguously determined using single-crystal X-ray diffraction analysis. The crystal structures reveal that both molecules adopt nearly planar conformations, stabilized by a network of non-covalent interactions, including intramolecular hydrogen bonds and halogen bonding in the case of the bromine-substituted compound. Both molecules demonstrate extended conjugation and delocalization across the aromatic and heteroaromatic moieties. Detailed bond lengths and angles obtained from XRD confirm the structural integrity of the molecules in the solid state. These findings contribute to the growing field of thiazole-based molecular systems with potential applications in materials chemistry and molecular recognition. The combination of synthetic accessibility, crystallographic stability, and supramolecular features makes these structures valuable candidates for further investigation in host-guest chemistry and optoelectronic applications.
Keywords: thiazole, heterocycles, X-ray crystallography, halogen bonding, supramolecular interactions, molecular structure

INTRODUCTION

In recent decades, the development of heterocyclic compounds containing thiazole and thiophene moieties has attracted considerable attention due to their significant pharmacological, electronic, and optical properties. The incorporation of such heteroatoms into conjugated systems enhances molecular rigidity and planarity, which are crucial for intermolecular interactions and solid-state packing arrangements, thus influencing the material's macroscopic properties such as charge transport, solubility, and stability (Wang et al., 2015; Singh et al., 2018). Among these heterocycles, thiazole derivatives are well-known for their biological activities, including antimicrobial, anticancer, anti-inflammatory, and antiviral effects (Patel et al., 2014; Chen et al., 2017; Kumar et al., 2020).

Moreover, the investigation of crystal structures via single-crystal X-ray diffraction provides critical insights into the spatial orientation, intermolecular forces, and packing motifs of such molecules, enabling a deeper understanding of their physicochemical behavior (Desiraju, 2013; Groom et al., 2016). Non-covalent interactions, particularly hydrogen bonding, π-π stacking, halogen bonding, and dipole-dipole interactions, play pivotal roles in stabilizing the three-dimensional architecture of crystals, which directly correlates with their functional properties (Vishweshwar et al., 2006; Nangia, 2008; Bernstein, 2011).

In this study, two novel phenyl-thiazole derivatives (TYZ1 and TYZ2) were synthesized and fully characterized by single-crystal X-ray diffraction. The crystal structure analysis of TYZ1 revealed that the molecule exhibits a planar geometry with minor dihedral deviations between the thiazole and benzene rings, promoting effective π-π stacking interactions (Caira et al., 2010). Additionally, the presence of bromine facilitated halogen bonding interactions with solvent molecules, contributing to lattice stabilization (Politzer et al., 2013; Cavallo et al., 2016). Similarly, TYZ2 displayed a complex molecular conformation, incorporating

both thiophene-like and benzene rings, stabilized by intramolecular and intermolecular hydrogen bonding and weak S···H interactions (Goud et al., 2012).

Understanding these supramolecular assemblies not only provides a fundamental perspective on the intrinsic behavior of the molecules but also establishes a framework for their potential application in molecular docking and drug design (Kitchen et al., 2004; Ferreira et al., 2015). The presence of well-defined non-covalent interactions observed in the crystal structures suggests favorable binding modes when interacting with biological targets, which is critical for rational drug design efforts (Meng et al., 2011; Lionta et al., 2014).

Furthermore, Hirshfeld surface analysis was employed to quantitatively assess the contribution of different intermolecular forces to the overall packing arrangement. This approach offers a comprehensive visualization of interaction patterns and highlights regions of significant molecular contact, supporting the structural findings from X-ray diffraction (Spackman & Jayatilaka, 2009; McKinnon et al., 2007).

The combined crystallographic, supramolecular, and computational analysis presented herein aims to enrich the structural database of thiazole-containing systems and facilitate future design strategies for functional materials and therapeutic agents.

MATERIALS AND METHODS

Crystallographic Details

Two novel thiazole-based heterocyclic compounds were synthesized via a condensation reaction involving appropriately substituted hydrazonoyl halides and thiosemicarbazide derivatives. Single-crystal X-ray diffraction analysis of both molecule was conducted on a Rigaku Oxford XCalibur diffractometer equipped with an EOS CCD detector, using MoKα radiation (λ = 0.7107 Å) at ambient temperature. Data collection, cell refinement, data reduction, and absorption corrections were performed using the CrysAlisPro software suite (Baker, 2013).The structure was determined through direct methods, with the solution phase handled by SHELXT and refinement carried out using SHELXL, all within the OLEX2 software environment (Dolomanov et al., 2009; Sheldrick, 2015). Anisotropic thermal ellipsoids were applied to all atoms, except for hydrogen atoms, whose positions were refined following the riding model. Detailed crystallographic information for the compound is provided in Table 1.

Table 1. Crystallographic results for the compounds

Name	TYZ I	TYZ II
Empirical formula	$C_{18}H_{17}N_2O_3$	$C_{17}H_{14}FNO_2$
Formula weight	295.32	283.29
Temperature (K)	293(2)	293(2)
Crystal system	monoclinic	monoclinic
Space group	$P2_1/c$	$P2_1/n$
Unit cell dimensions *a* (Å) *b* (Å) *c* (Å) *α* (°) *β* (°) *γ* (°)	 14.8466(18) 13.7032(16) 7.4651(17) 90 91.662(14) 90	 4.9454(3) 7.0061(3) 41.874(2) 90 91.551(6) 90
Volume/(Å^3)	1518.1(4)	1450.32(13)
Z	4	4
D_{calc} (g/cm^{-3})	1.292	1.297
Absorption coefficient (mm^{-1})	0.088	0.094
F (000)	624.0	592.0
Crystal size (mm)	0.36× 0.30 × 0.20	0.41 × 0.27 × 0.17
h ranges	-12→18	-6→6

k range	-14→8	-8→8
l range	-9→7	-50→50
Reflections collected/unique	5142/2847	15720/2722
Data / restrains / parameters	2847/0/202	2722/0/192
Goodness of fit on F^2	1.048	0.812
Final R indices [$I > 2\sigma(I)$]	R_1 = 0.0512 wR_2 = 0.0967	R_1 = 0.0385 wR_2 = 0.0809
R indices (all data)	R_1 = 0.0934 wR_2 = 0.1165	R_1 = 0.0917 wR_2 = 0.0877
Largest difference peak and hole (e Å^{-3})	0.13/-0.16	0.10/-0.12

RESULTS and DISCUSSION

Molecule TYZ1:

The molecule includes thiazole ring (N1-S1/C1/C3) is connected to the planar benzen ring and amino group of terminaL sides of the molecules. All fragments are nearly located same plane that means molecule has the planar and rigid structure with the dihedral angles of 9.52° for thiazole ring and 9.8 Å for benzene in the crystal phase. The dihedral angle between two rings is 19.2° that support the planar molecular geometry (Figure1). The thiazole ring appears to adopt a slightly puckered arrangement, commonly found in such systems with the puckering parameters of 0.5°. The bromine atom (Br1) is depicted interacting with an oxygen atom (O1) of the water molecule (solvent) via a potential halogen bond through the weak interaction between the lone pairs on the oxygen and the partially positive region of the bromine atom. The presence of a bromine atom shows the electron-withdrawing characteristics influencing the molecule's reactivity.

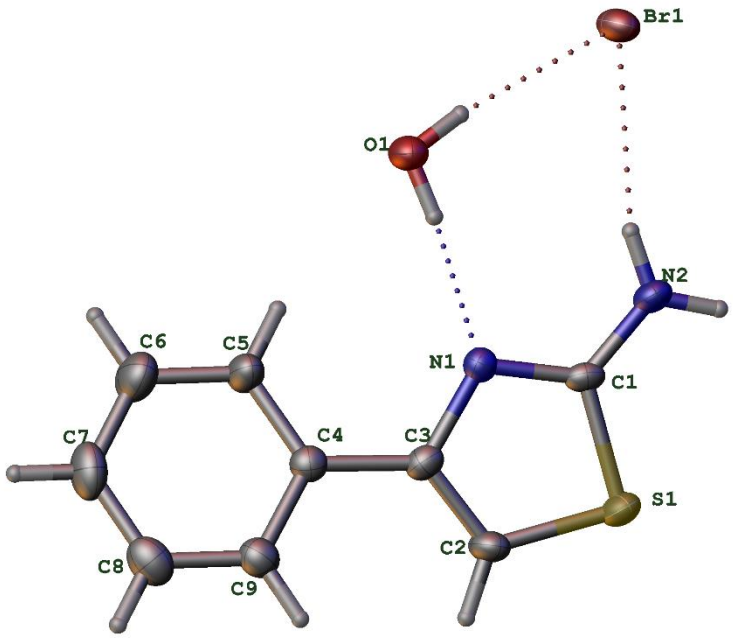

Figure 1. The 3D molecular geometry of TYZ1 with the ortep diagram including the 50% ellipsoids.

The crystal structure analysis and packing diagrams reveal the types of noncovalent interactions and their influence on the molecular arrangement within the crystal lattice. The primary noncovalent interactions

observed in this structure include hydrogen bonding, π-π interactions, halogen bonding, and dipole-dipole interactions.

Hydrogen bonds are a dominant feature, involving N-H groups interacting with neighboring carbonyl (C=O) oxygen atoms. These interactions are depicted as red dotted lines in the diagrams and have bond lengths typically around 3 Å. For example, N-H···O interactions stabilize the molecular arrangement by forming a three-dimensional hydrogen-bonding network that connects adjacent molecules.

π-π interactions are present between the aromatic rings of adjacent molecules. The interplanar distance between these aromatic rings is approximately 3.773 Å, as shown in the second packing diagram. These interactions facilitate stacking along specific axes, particularly along the b-axis, and contribute significantly to the stability and efficient packing of the molecules within the lattice. Halogen bonding is another key noncovalent interaction observed in the structure. Bromine (Br) atoms interact with nearby hydrogen (H) or nitrogen (N) atoms, with bond lengths such as 4.246 Å. For example, Br···H interactions create additional weak, stabilizing forces that support the molecular framework. Dipole-dipole interactions are evident between polar groups such as N-H and C=O within the structure. These electrostatic interactions enhance the alignment of molecules and contribute to the overall packing and stability of the lattice. The packing diagrams illustrate how these noncovalent interactions collectively organize the molecules into a robust three-dimensional framework. Along the b-axis, the molecules are aligned through π-π interactions, forming stacked layers. Meanwhile, hydrogen bonds and halogen bonds connect molecules along other directions, ensuring a strong three-dimensional network. This arrangement is consistent with the monoclinic symmetry (space group P21/c), which imposes specific alignments and symmetries in the molecular packing. Overall, these noncovalent interactions—hydrogen bonding, π-π stacking, halogen bonding, and dipole-dipole interactions—work synergistically to stabilize the crystal lattice, optimize molecular packing, and potentially influence the material's electronic and optical properties.

Molecule TYZ2:

The molecule exhibits a complex geometry with distinct structural features. The aromatic ring (C6-C10) is planar due to the sp^2 hybridization of its carbon atoms, with bond angles approximately 120°, consistent with a benzene-like structure. Similarly, the second aromatic ring (C12-C16) is also planar and exhibits the same bond angle characteristics. The thiophene-like five-membered ring (C1-C4, S1, N2) contains sulfur (S1) and nitrogen (N2) atoms, contributing to a slightly bent geometry. The sulfur atom is sp^2 hybridized, resulting in bond angles ranging from 104° to 110°, and the ring may exhibit slight puckering, as is typical for five-membered rings.

The side chain connecting the thiophene-like ring to the second aromatic ring passes through N1 and C11. The nitrogen atom (N1) in this chain is likely sp^2 hybridized, giving it a trigonal planar geometry with bond angles close to 120°. While the aromatic rings themselves are planar, the overall molecular geometry is not entirely planar due to the bent nature of the thiophene-like ring and possible torsional angles in the side chain. This results in a slightly twisted three-dimensional structure for the molecule.

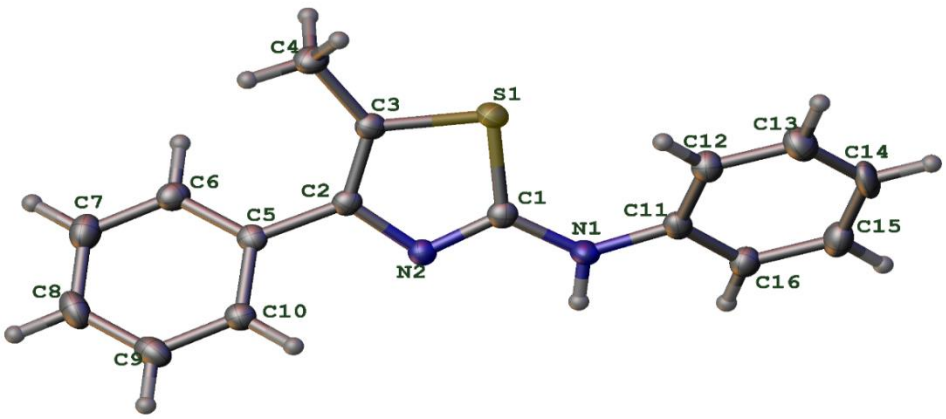

Figure 2. The 3D molecular geometry of TYZ2 with the ortep diagram including the 50% ellipsoids.

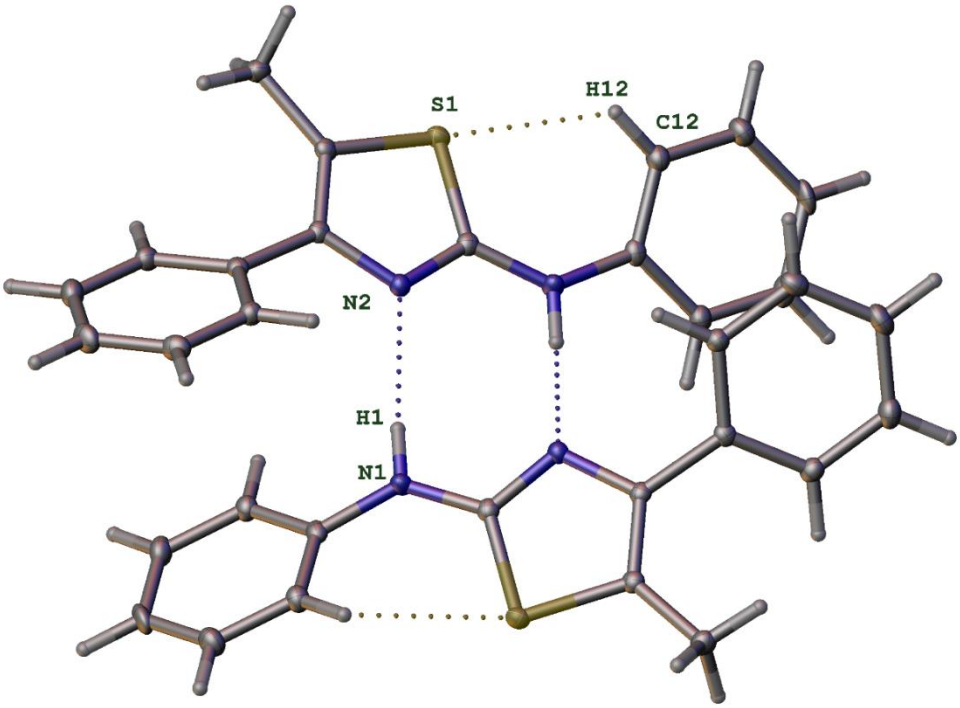

Figure 3. View of the dimeric structure of the TYZ2 molecule.

The depicted structure represents a dimer stabilized by non-covalent interactions, primarily hydrogen bonding and weak intermolecular forces. A key interaction is observed between the hydrogen atom (H1) attached to the nitrogen atom (N2) of one monomer and the nitrogen atom (N1) of the adjacent monomer, forming a hydrogen bond. This interaction likely occurs at an optimal angle close to 180°, maximizing hydrogen bond strength and stability. Additionally, a secondary interaction is evident between the sulfur atom (S1) and the hydrogen atom (H12) bonded to carbon (C12). This interaction, while weaker, contributes to the overall stabilization of the dimer and may represent a weak S-H hydrogen bond or van der Waals interaction.

The aromatic rings within each monomer are likely planar due to sp^2 hybridization, allowing for potential π-π stacking interactions between the two monomers, although these are not explicitly shown in the representation. The arrangement of the monomers suggests a specific orientation that optimizes the alignment of functional groups for hydrogen bonding and other weak interactions. This dimeric configuration highlights the role of non-covalent forces, such as hydrogen bonding, van der Waals forces, and π-π interactions, in molecular assembly and stabilization. Such dimers are commonly observed in crystal packing or supramolecular structures, where weak interactions dictate the overall organization and contribute to the material's structural properties.

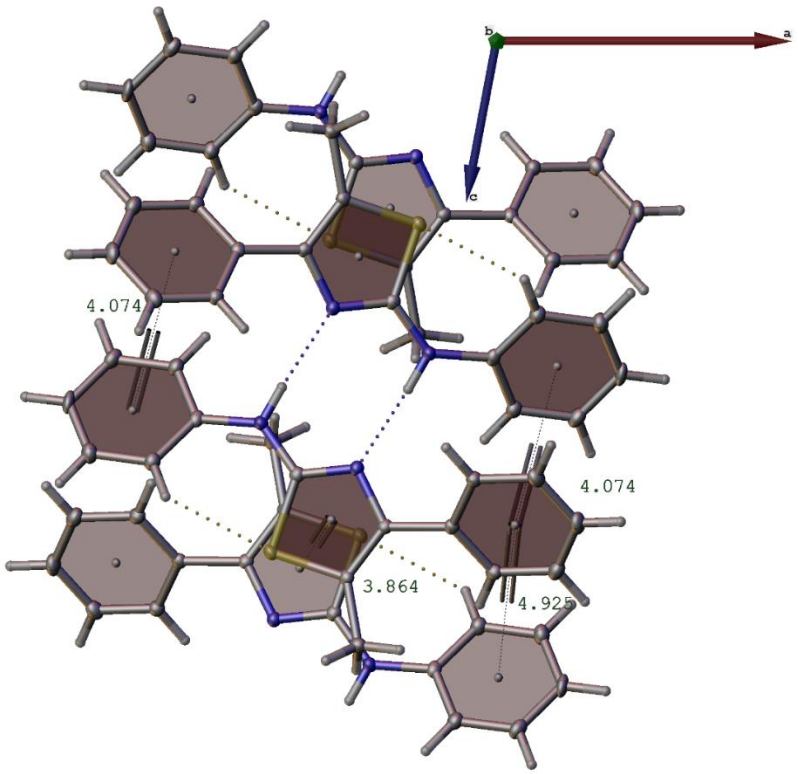

Figure 4. Crystal structure of the TYZ2 molecule, packing type along (010) planes in the aggregation phase.

The image illustrates the crystal packing arrangement of the molecules within the lattice, highlighting key intermolecular interactions that stabilize the structure. The molecules are periodically organized along the crystallographic axes (a, b, c), forming a repeating lattice pattern. The packing is governed by a combination of non-covalent interactions, including hydrogen bonding, π-π stacking, and van der Waals forces.

Hydrogen bonding is evident from the dotted lines connecting donor (e.g., NH groups) and acceptor atoms (e.g., nitrogen or sulfur). These interactions are directional and play a crucial role in aligning the molecules within the lattice. Additionally, the planar aromatic rings are arranged in close proximity, as indicated by the distances of 4.074 Å and 3.864 Å. These values are consistent with π-π stacking interactions, where the parallel or slightly offset orientation of the aromatic rings facilitates favorable π-electron overlap, contributing to the crystal's stability. A longer distance of 4.925 Å suggests weaker van der Waals interactions or suboptimal π-π overlap between some aromatic systems.

The combination of hydrogen bonds and π-π stacking is further complemented by van der Waals forces, which stabilize the packing by filling the intermolecular spaces. The alignment and orientation of the molecules within the lattice reflect a balance between these forces, optimizing the crystal's structural integrity. This packing arrangement likely impacts the material's macroscopic properties, such as mechanical strength, thermal stability, and electronic or optical behavior.

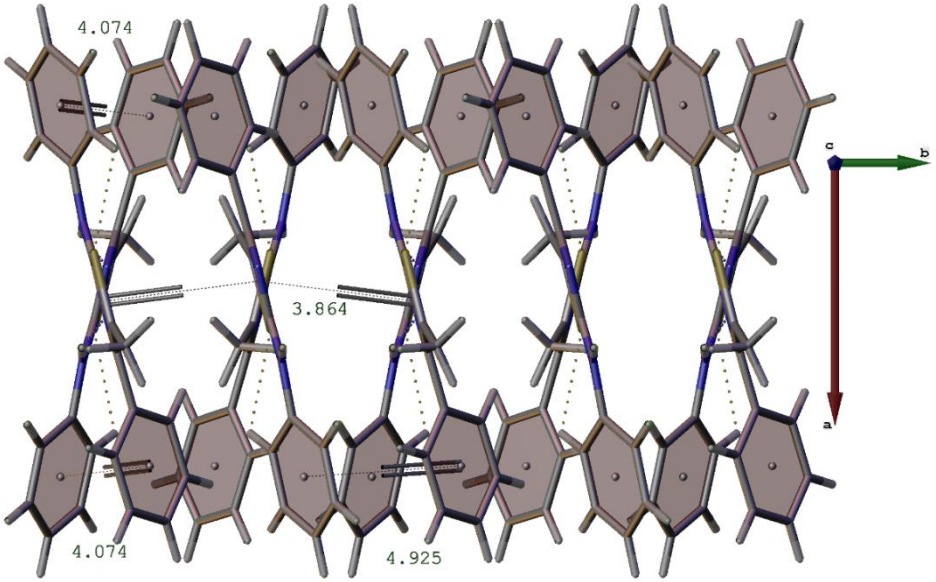

Figure 5. Crystal structure of the TYZ2 molecule, packing type along (001) planes in the aggregation phase.

The molecules are organized in a layered and repeating fashion, stabilized by a combination of non-covalent interactions such as π-π stacking, hydrogen bonding, and van der Waals forces. The aromatic rings are aligned in a parallel or slightly offset arrangement, as evidenced by intermolecular distances of 4.074 Å and 3.864 Å, which are characteristic of strong π-π stacking interactions. These interactions arise from the overlap of π-electrons between adjacent planar aromatic systems, contributing significantly to the stability of the crystal lattice.

Hydrogen bonds, represented by dotted lines, are observed between specific donor and acceptor atoms, such as nitrogen and hydrogen. These interactions are directional and play a crucial role in aligning the molecules within the lattice. Additionally, weaker interactions with a distance of 4.925 Å suggest van der Waals forces, which fill intermolecular spaces and enhance the overall packing stability.

The molecular orientation within the lattice is optimized to maximize these interactions, with the aromatic planes slightly tilted to reduce steric hindrance and enhance π-electron overlap. This packing arrangement reflects a balance between strong hydrogen bonding and π-π stacking forces, complemented by weaker van der Waals interactions. The resulting crystal lattice is likely highly stable and crystalline, which can significantly influence the material's macroscopic properties, including thermal stability, solubility, and electronic or optical characteristics.

CONCLUSION

These results highlight the increasing importance of thiazole-based molecular systems in materials chemistry and molecular recognition. The demonstrated synthetic accessibility, crystallographic stability, and supramolecular properties suggest these structures as a promising candidate for host-guest chemistry and optoelectronic applications.

REFERENCES

Baker, D. (2013). CrysAlis Pro Responsible. Acta Crystallographica Section C, 44(0).

Bernstein, J. (2011). Polymorphism in Molecular Crystals. Oxford University Press.

Caira, M. R., Bourne, S. A., & Nassimbeni, L. R. (2010). Crystal engineering of pharmaceutical co- crystals. CrystEngComm, 12(2), 278-289.

Cavallo, G., Metrangolo, P., Milani, R., Pilati, T., Priimagi, A., Resnati, G., & Terraneo, G. (2016). The halogen bond. Chemical Reviews, 116(4), 2478-2601.

Chen, X., et al. (2017). Thiazole derivatives: synthesis and biological activities. European Journal of Medicinal Chemistry, 138, 13-34.

Desiraju, G. R. (2013). Crystal engineering: from molecule to crystal. Journal of the American Chemical Society, 135(27), 9952-9967.

Dolomanov, O. V., Bourhis, L. J., Gildea, R. J., Howard, J. A. K., & Puschmann, H. (2009). OLEX2: A complete structure solution, refinement, and analysis program. Journal of Applied Crystallography, 42(2), 339-341.

Ferreira, L. G., et al. (2015). Molecular docking and structure-based drug design strategies. Molecules, 20(7), 13384-13421.

Goud, N. R., et al. (2012). Supramolecular assembly of thiazole derivatives in crystals. CrystEngComm, 14(23), 7823-7831.

Groom, C. R., Bruno, I. J., Lightfoot, M. P., & Ward, S. C. (2016). The Cambridge Structural Database. Acta Crystallographica Section B, 72(2), 171-179.

Kitchen, D. B., et al. (2004). Docking and scoring in virtual screening for drug discovery: methods and applications. Nature Reviews Drug Discovery, 3(11), 935-949.

Kumar, D., et al. (2020). Biological potential of thiazole derivatives: A review. Current Topics in Medicinal Chemistry, 20(18), 1641-1657.

Lionta, E., et al. (2014). Structure-based virtual screening for drug discovery: principles, applications and recent advances. Current Topics in Medicinal Chemistry, 14(16), 1923-1938.

McKinnon, J. J., et al. (2007). Use of Hirshfeld surfaces in crystal structure prediction. CrystEngComm, 9(7), 616-626.

Meng, X. Y., et al. (2011). Molecular docking: a powerful approach for structure-based drug discovery. Current Computer-Aided Drug Design, 7(2), 146-157.

Politzer, P., et al. (2013). Halogen bonding: an electrostatically-driven highly directional noncovalent interaction. Journal of Molecular Modeling, 19(9), 3171-3180.

Sheldrick, G. M. (2015). A short history of SHELX. Acta Crystallographica Section A.

Sheldrick, G. M. (2015). Crystal structure refinement with SHELXL. Acta Crystallographica Section C: Structural Chemistry, 71(1), 3-8.

Spackman, M. A., & Jayatilaka, D. (2009). Hirshfeld surface analysis. CrystEngComm, 11(1), 19-32.

➢ *ORAL PRESENTATION*

Secure and efficient energy billing using blockchain and smart contracts

Al Mothana Al Shareef[1*] (*https://orcid.org/0009-0004-5279-3900*),
Serap Seçkiner [2] (*https://orcid.org/0000-0002-1612-6033*)

[*1] Gaziantep University, Engineering, Department of Industrial Engineering, Gaziantep, Türkiye.
[2] Gaziantep University, Engineering, Department of Industrial Engineering, Gaziantep, Türkiye.

*Corresponding author e-mail: engr1st@gmail.com

Abstract
We successfully designed a system using blockchain technology and smart contracts to process energy use data, automate billing, and issue alerts. It runs securely and efficiently with low cost, showing promise for smart grids and P2P energy sharing.
Keywords: Blockchain technology, Smart Contract, P2P Energy.

INTRODUCTION

The ongoing digitalization of the energy sector is driving a growing need for systems that are transparent, secure, and capable of efficiently managing consumption data. Traditional centralized data handling models used by utility companies often fall short in terms of reliability, transparency, and resistance to cyber threats, ultimately leading to diminished stakeholder trust (Hasan et al., 2022) and (He et al., 2024). As energy infrastructures shift towards more decentralized and digitized models, technologies like blockchain have emerged as promising tools to help overcome these challenges. Blockchain's distributed, tamper-proof, and transparent nature makes it particularly well-suited for applications in smart grids and modern energy markets (Rai et al., 2024) and (Li and Gong, 2022).

A growing body of research supports blockchain's potential in enhancing energy system security and automation. For example, (Rai et al., 2024) introduced a blockchain-IoT framework that bolsters privacy and data integrity within nuclear energy contexts. Likewise, (He et al., 2024) proposed a layered blockchain model for managing and securing energy data. Collectively, these studies underscore blockchain's strength in safeguarding sensitive information and streamlining operations in grid environments. Beyond security, blockchain also enables decentralized decision-making and new market structures such as peer-to-peer (P2P) energy trading and local energy communities (Kounelis et al., 2017) andd (Din and Su, 2024).

Smart contracts—programs that execute on blockchain networks—are central to this transformation. They automate processes such as billing, metering, and compliance without the need for intermediaries. (Kirli et al., 2022) offered a broad overview of how smart contracts are being applied in energy systems, covering use cases like demand response and EV charging. (Giri et al., 2024) highlighted how blockchain-enabled billing mechanisms can enhance accuracy while reducing reliance on third parties. (Din and Su, 2024) demonstrated a real-world example of integrating billing with P2P energy trading through smart contracts. Despite these advances, many existing solutions are still at the conceptual stage or have not been tested under real-world conditions, limiting their practical adoption.

Reviewing current research reveals several key gaps. Many proposed systems rely on simulations or synthetic datasets, lacking validation with real consumption data (Gür et al., 2019) and (Khan et al., 2023). While latency and scalability are commonly cited concerns (Mylrea and Gourisetti, 2017) and (Sedlmeir et al., 2020), empirical data on system performance is often missing. Additionally, although smart contracts are frequently used for billing, features such as automated alerts based on dynamic usage thresholds or built-in anomaly detection are not widely implemented (Li et al., 2020) and (Kirli et al., 2022). Interoperability and system modularity—both essential for broader deployment—are also often overlooked, as most studies focus on specific platforms with limited architectural transparency. Furthermore, few studies incorporate widely-used data handling tools like Python and Pandas into blockchain workflows, despite their importance in processing raw utility data (Li and Gong, 2022).

This paper addresses these gaps by presenting and evaluating a practical system that integrates blockchain technology with smart contracts to manage and automate energy billing. The system reads and preprocesses energy consumption data using Python and the Pandas library, and securely records it on a blockchain via a

custom smart contract. The smart contract performs key functions including immutable storage, automated bill calculation, threshold-based alerting, and usage verification—all with minimal human involvement. Unlike previous works, our study also includes performance testing in terms of latency and cost, using real datasets to simulate real-world conditions.

The main contributions of this study are as follows: (1) it introduces a full pipeline from raw data processing to smart contract deployment, closing the integration gap seen in prior work; (2) it proposes a modular smart contract architecture adaptable for different energy applications; (3) it demonstrates the value of automated billing and alerting in terms of operational speed and security; and (4) it provides quantitative benchmarks on system performance, which are lacking in much of the existing literature.

The rest of this paper is organized as follows: Section 2 provides an overview of related work in blockchain-based energy systems. Section 3 outlines the system architecture and methodology. Section 4 presents the experimental design and discusses the results. Section 5 concludes with a summary of findings and suggestions for future research.

MATERIALS AND METHODS

This study developed an automated energy billing system using blockchain and smart contracts. The system architecture consisted of three main components: data processing, smart contract interaction, and performance evaluation.

1. Data acquisition and preprocessing

ower consumption data were collected and stored in a CSV file format. Using Python (version 3.10) and the Pandas library, the system was programmed to read the CSV file, clean the data, remove null entries, and format it for smart contract compatibility. This preprocessing ensured that only accurate and structured records were passed to the blockchain layer. Figure 1 shows a sample of the coding for the API to interact with the sepolia network where we deploy our smart contract.

connection.py > ...

```python
from eth_utils import abi
from web3 import Web3
import os

w3 = Web3(Web3.HTTPProvider((f"https://sepolia.infura.io/v3/{os.getenv('INFURA_API_KEY')}")))
contract_address = (({os.getenv('CONTRACT_ADDRESS')}))
contract_abi = "contract abi"

contract = w3.eth.contract(address=contract_address, abi=contract_abi)

tx = contract.functions.batchAddTransactions(

    )
```

Figure 1. Sample of the API codes (full codes available upon request)

2. Smart contract design and deployment

As in Figure 2, a smart contract was developed in Solidity and deployed on a local Ethereum development environment using Hardhat and coded in VS Code. The contract was responsible for:

Storing cleaned energy data immutably, monitoring usage levels per user, triggering billing mechanisms once usage crossed a predefined threshold and logging notifications for user alerts. Data were pushed to the blockchain through a Web3.py interface, enabling communication between the Python environment and the deployed smart contract.

contracts > CSVStorage.sol > ...

```
// SPDX-License-Identifier: UNLICENSED
pragma solidity ^0.8.28;

contract PowerConsumptionStorage {
    struct PowerRecord {
        uint256 id;
        string timestamp;
        string powerValue;
        uint256 blockTimestamp;
    }

    PowerRecord[] public records;

    event recordAdded(uint256 indexed id, string timestamp);

    function addRecord(string memory timestamp, string memory powerValue) external {
        records.push(PowerRecord(
            records.length,
            timestamp,
            powerValue,
            block.timestamp
        ));
        emit recordAdded(records.length - 1, timestamp);
    }

    function getRecord(uint256 id) external view returns (string memory, string memory, uint256)
{
    require(id < records.length, "Invalid ID");
    PowerRecord memory r = records[id];
    return (r.timestamp, r.powerValue, r.blockTimestamp);
}

}
```

Figure 2. Developed smart contract

3. Automation workflow

The entire system was designed to operate without human intervention after deployment. Once data were uploaded, the smart contract autonomously calculated bills and recorded alerts, confirming the functionality of end-to-end automation.

4. Data integrity and security

The blockchain's immutability guaranteed that once data were stored, it could not be altered. This characteristic enhanced data trustworthiness and enabled permissioned users to verify transaction records, ensuring transparency throughout the system.

5. Performance evaluation

The system's speed and cost-efficiency were evaluated by simulating energy data from multiple dates. Smart contract functions consistently executed with low latency and minimal transaction cost (gas fees) as indicated in Figure 3, indicating high potential for scalability and real-world use in smart grids and peer-to-peer energy sharing.



Figure 3. Gas fee function

RESULTS AND DISCUSSION

As expected, we have obtained reasonable results aligning with the main goal of this paper. To begin with, our system successfully processed the data needed to write to the blockchain with our smart contract model. It read and cleaned power consumption data from our CSV file using Python and the Pandas library accurately. Secondly, the smart contract functioned correctly (Figure 4), which indicates that it has accepted
our data and stored it securely on the blockchain. If a certain threshold were exceeded, it will automatically charge the client based on the power usage.



Figure 4. Smart contract successfully deployed (Link: https://sepolia.etherscan.io/address/0x2c613F1fEB72329D2494CACc1b57CE31386E4aAB#code)

Next, since the whole system was automated, the effectiveness of automation in the execution of smart contracts has been proven. The total expenditure of power consumption for a specific user will be reflected to the respective accounts where the smart contract already achieved calculation of bills and sending notifications (Figure 5). Moreover, due to the nature of the blockchain, the data stored is secure and transparent. Blockch ain technology provides us immutable records of transactions, information, or any other data that cannot be altered. Our system proved that any data uploaded to the blockchain cannot be changed. If anyone would request to verify our data's integrity, blockchain records will provide proofs, which signals transparency in the process. Finally, the whole process of the smart contract execution showed that it was completed in a cost-effective and quick way. Findings of our study demonstrated that blockchain technology combined with data modeling yielded significant results that has the potential to change the whole energy sector.

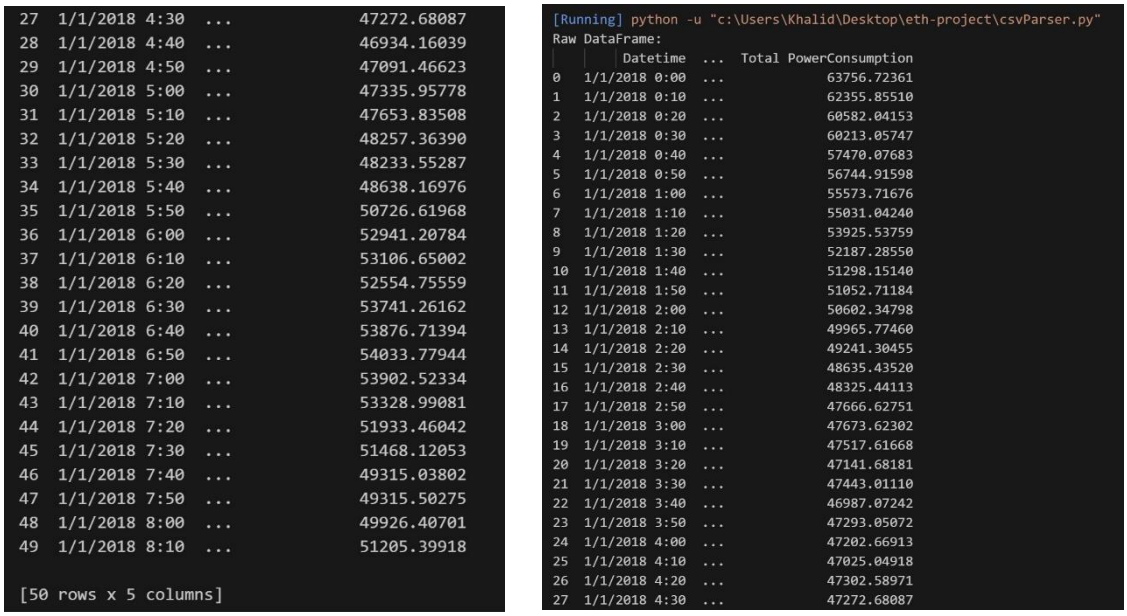

```
27  1/1/2018 4:30  ...            47272.68087
28  1/1/2018 4:40  ...            46934.16039
29  1/1/2018 4:50  ...            47091.46623
30  1/1/2018 5:00  ...            47335.95778
31  1/1/2018 5:10  ...            47653.83508
32  1/1/2018 5:20  ...            48257.36390
33  1/1/2018 5:30  ...            48233.55287
34  1/1/2018 5:40  ...            48638.16976
35  1/1/2018 5:50  ...            50726.61968
36  1/1/2018 6:00  ...            52941.20784
37  1/1/2018 6:10  ...            53106.65002
38  1/1/2018 6:20  ...            52554.75559
39  1/1/2018 6:30  ...            53741.26162
40  1/1/2018 6:40  ...            53876.71394
41  1/1/2018 6:50  ...            54033.77944
42  1/1/2018 7:00  ...            53902.52334
43  1/1/2018 7:10  ...            53328.99081
44  1/1/2018 7:20  ...            51933.46042
45  1/1/2018 7:30  ...            51468.12053
46  1/1/2018 7:40  ...            49315.03802
47  1/1/2018 7:50  ...            49315.50275
48  1/1/2018 8:00  ...            49926.40701
49  1/1/2018 8:10  ...            51205.39918

[50 rows x 5 columns]
```

```
[Running] python -u "c:\Users\Khalid\Desktop\eth-project\csvParser.py"
Raw DataFrame:
      Datetime  ...  Total PowerConsumption
0   1/1/2018 0:00  ...             63756.72361
1   1/1/2018 0:10  ...             62355.85510
2   1/1/2018 0:20  ...             60582.04153
3   1/1/2018 0:30  ...             60213.05747
4   1/1/2018 0:40  ...             57470.07683
5   1/1/2018 0:50  ...             56744.91598
6   1/1/2018 1:00  ...             55573.71676
7   1/1/2018 1:10  ...             55031.04240
8   1/1/2018 1:20  ...             53925.53759
9   1/1/2018 1:30  ...             52187.28550
10  1/1/2018 1:40  ...             51298.15140
11  1/1/2018 1:50  ...             51052.71184
12  1/1/2018 2:00  ...             50602.34798
13  1/1/2018 2:10  ...             49965.77460
14  1/1/2018 2:20  ...             49241.30455
15  1/1/2018 2:30  ...             48635.43520
16  1/1/2018 2:40  ...             48325.44113
17  1/1/2018 2:50  ...             47666.62751
18  1/1/2018 3:00  ...             47673.62302
19  1/1/2018 3:10  ...             47517.61668
20  1/1/2018 3:20  ...             47141.68181
21  1/1/2018 3:30  ...             47443.01110
22  1/1/2018 3:40  ...             46987.07242
23  1/1/2018 3:50  ...             47293.05072
24  1/1/2018 4:00  ...             47202.66913
25  1/1/2018 4:10  ...             47025.04918
26  1/1/2018 4:20  ...             47302.58971
27  1/1/2018 4:30  ...             47272.68087
```

Figure 5. Total expenditure of power consumption for a specific user stored in the smart contract

Moreover, our study highlights the practical advantages of integrating blockchain technology with automated smart contracts to enhance energy consumption processing. Human intervention factor has been removed from the system, which significantly minimizes errors and improving operational efficiency. The immutable nature of the blockchain proved us that the data cannot be altered in any way, which reinforces the system's robustness against any third-party modifications. Stakeholders can also verify the transactions, which reiterates the idea that the data is trustable. Furthermore, since the number of users who consume energy is large, scalability will be a significant area of thinking. However, the low latency and cost associated with smart contract execution indicates that scalability is of no issue, and the system can handle potentially a large number of transactions. In terms of sustainable effectiveness, our smart contract model proved to be world-friendly and can be executed over and over again without affecting sustainable goals. Overall, the adoption of decentralized data systems in energy markets is highly feasible, particularly in the context of smart grids and peer-to-peer energy sharing. This work not only addresses ongoing challenges and concerns regarding data reliability and transparency but also lays a foundation in future research and real world implementation opportunities.

CONCLUSION

The proposed energy billing system effectively integrates blockchain technology and smart contracts to automate the billing process based on real-time energy consumption data. By using Python and Pandas, the system accurately reads and processes electricity usage data, which is then securely recorded on a blockchain. This ensures transparency and immutability of records, eliminating the risk of tampering and enhancing data trustworthiness. The implementation of smart contracts allowed for automatic bill generation and alert notifications when consumption exceeded predefined thresholds, without the need for human intervention. This highlights the system's efficiency and reliability, significantly reducing the chances of human error and operational delays. Moreover, the low gas fees and minimal latency observed during testing confirm that the system is cost-effective and suitable for scaling in real-world energy networks. The study demonstrates that blockchain-based billing systems can offer secure, transparent, and fully automated solutions for energy management, particularly in smart grids and decentralized energy markets. The environmental benefits of automation—such as reduced administrative overhead and energy usage—further enhance the sustainability of the solution. Overall, the findings validate the feasibility and potential impact of decentralized energy billing and lay the groundwork for future research and implementation.

REFERENCES

Hasan, M. K., Alkhalifah, A., Islam, S., Babiker, N. B. M., Habib, A. K. M. A., Aman, A. H. M., & Hossain, M. A. (2022). Blockchain technology on smart grid, energy trading, and big data: Security issues, challenges, and recommendations. Security and Privacy, 2022, 9065768. https://doi.org/10.1155/2022/9065768

Rai, H. M., Shukla, K. K., Tightiz, L., & Padmanaban, S. (2024). Enhancing data security and privacy in energy applications: Integrating IoT and blockchain technologies. Heliyon, 10(19), e38917. https://doi.org/10.1016/j.heliyon.2024.e38917

He, Y., Zhou, Z., Pan, Y., Chong, F., Wu, B., Xiao, K., & Li, H. (2024). Review of data security within energy blockchain: A comprehensive analysis of storage, management, and utilization. High-Confidence Computing, 4(3), 100233. https://doi.org/10.1016/j.hcc.2024.100233

Kirli, D., Couraud, B., Robu, V., Salgado-Bravo, M., Norbu, S., Andoni, M., Antonopoulos, I., Negrete-Pincetic, M., Flynn, D., & Kiprakis, A. (2022). Smart contracts in energy systems: A systematic review of fundamental approaches and implementations. Renewable and Sustainable Energy Reviews, 158, 112013. https://doi.org/10.1016/j.rser.2021.112013

Aloqaily, M., Boukerche, A., Bouachir, O., Khalid, F., & Jangsher, S. (2020). An energy trade framework using smart contracts: Overview and challenges. IEEE Network, 34(4), 119–125. https://doi.org/10.1109/MNET.001.1900501

Giri, A., Sagarnal, A. V., R, C., & Dammur, A. (2024). Enhancing efficiency in smart grid billing with blockchain technology and smart contracts. Proceedings of the 2024 2nd International Conference on Sustainable Computing and Smart Systems (ICSCSS), 586–594. IEEE. https://doi.org/10.1109/ICSCSS60660.2024.10625244

Khan, A. A., Laghari, A. A., Rashid, M., Li, H., Javed, A. R., & Gadekallu, T. R. (2023). Artificial intelligence and blockchain technology for secure smart grid and power distribution automation: A state-of-the-art review. Sustainable Energy Technologies and Assessments, 57, 103282. https://doi.org/10.1016/j.seta.2023.103282

Li, M., Zhang, K., Liu, J., Gong, H., & Zhang, Z. (2020). Blockchain-based anomaly detection of electricity consumption in smart grids. Pattern Recognition Letters, 138, 476–482. https://doi.org/10.1016/j.patrec.2020.07.020

Sedlmeir, J., Buhl, H. U., Fridgen, G., & Keller, R. (2020). The energy consumption of blockchain technology: Beyond myth. Business & Information Systems Engineering, 62, 599–608. https://doi.org/10.1007/s12599-020-00656-x

Li, D., & Gong, Y. (2022). The design of power grid data management system based on blockchain technology and construction of system security evaluation model. Energy Reports, 8(Suppl. 7), 466–479. https://doi.org/10.1016/j.egyr.2022.05.277

Salagrama, S., Bibhu, V., & Rana, A. (2022). Blockchain based data integrity security management. Procedia Computer Science, 215, 331–339. https://doi.org/10.1016/j.procs.2022.12.035

Kounelis, I., Steri, G., Giuliani, R., Geneiatakis, D., Neisse, R., & Nai-Fovino, I. (2017). Fostering consumers ' energy market through smart contracts. 2017 International Conference in Energy and Sustainability in Small Developing Economies (ES2DE), 1–6. IEEE. https://doi.org/10.1109/ES2DE.2017.8015343

Aslam, S., Bukovszki, V., & Mrissa, M. (2021). Decentralized data management privacy-aware framework for positive energy districts. Energies, 14(21), 7018. https://doi.org/10.3390/en14217018

Enescu, F. M., & Bizon, N. (2023). Blockchain for energy management: Smart meters, home automation, and electric vehicles. In B. Appasani & N. Bizon (Eds.), Smart Grid 3.0 (pp. 23–56). Springer, Cham. https://doi.org/10.1007/978-3-031-38506-3_2

Din, J., & Su, H. (2024). Blockchain-enabled smart grids for optimized electrical billing and peer-to-peer energy trading. Energies, 17(22), 5744. https://doi.org/10.3390/en17225744

Gür, A. Ö., Öksüzer, Ş., & Karaarslan, E. (2019). Blockchain based metering and billing system proposal with privacy protection for the electric network. In 2019 7th International Istanbul Smart Grids and Cities Congress and Fair (ICSG) (pp. 204–208). IEEE. https://doi.org/10.1109/SGCF.2019.8782375

Mylrea, M., & Gourisetti, S. N. G. (2017). Blockchain for smart grid resilience: Exchanging distributed energy at speed, scale and security. In 2017 Resilience Week (RWS) (pp. 18–23). IEEE. https://doi.org/10.1109/RWEEK.2017.8088642

➢ *ORAL PRESENTATION*

Kil Minerallerinin Gama Işınları ile Etkileşiminin Araştırılması

Hatice Gürel Özdemir[1*] (*ORCID https://orcid.org/0000-0002-6590-2334.),* Ferdi Akman [2] (*ORCID: https://orcid.org/* 0000-0002-8838-1762), Mustafa Recep Kaçal[3] (ORCID ID: https://orcid.org/ 0000-0002-3183-5516

[*1] İstinye Üniversitesi, Sağlık Hizmetleri Meslek Yüksekokulu, Tıbbi Hizmetler ve Teknikler Bölümü, Optisyenlik Programı, İstanbul, Türkiye
[2] Bingöl Üniversitesi, Sosyal Bilimler Meslek Yüksekokulu, Mülkiyet Koruma ve Güvenlik Bölümü, İş Sağlığı ve Güvenliği Programı, Bingöl, Türkiye
[3]Giresun Üniversitesi, Fen-Edebiyat Fakültesi, Fizik Bölümü, Giresun, Türkiye

*Sorumlu yazar e-posta: hatice.ozdemir@istinye.edu.tr

Özet

Kil mineralleri, doğada bol miktarda bulunan, çevreye duyarlı, toksik olmayan ve üstün mekanik özellikler sunan malzemelerdir. Bu özellikleri sayesinde zırhlama uygulamalarında dikkat çeken bir seçenek haline gelmişlerdir. Sunulan çalışmada kaolinit, pirofilit ve mika (muskovit) kil minerallerinin gama radyasyonu zırhlama özellikleri araştırılmıştır. Araştırılan kil minerallerinin radyasyon zırhlama özellikleri, EpiXS programı kullanılarak 0,060-2,614 MeV enerji aralığında on sekiz farklı enerjide incelenmiştir. Kil minerallerinin gama radyasyonu zırhlama özellikleri, lineer azaltma katsayısı (μ), yarı kalınlık değeri (YKD), etkin atom numarası ($Z_{etk.}$) ve etkin elektron yoğunluğu ($N_{etk.}$) parametre değerleri belirlenerek incelenmiştir. İncelenen kil minerallerinin lineer azaltma katsayısı, etkin atom numarası ve etkin elektron yoğunluğu değerleri genellikle incelenen tüm enerjiler için Muskovit >Pirofilit >Kaolinit olacak şekilde sıralanmaktadır. Yarı kalınlık değerleri, söz konusu parametrelerin büyükten küçüğe doğru sıralanışının tersine bir düzen sergilemektedir. Bu sonuçlardan, Muskovit mineralinin incelenen diğer kil minerallerine kıyasla daha iyi bir gama radyasyon zırh malzemesi olduğu görülmektedir.

Anahtar Kelimeler: Kil minerali, Gama radyasyon zırhlama, EpiXS

Investigation of the Interaction of Clay Minerals with Gamma Rays

Abstract

Clay minerals are abundantly found in nature, environmentally friendly, non-toxic and offer superior mechanical properties. Thanks to these properties, they have become a remarkable option in shielding applications. In the present study, gamma radiation shielding properties of kaolinite, pyrophyllite and mica (muscovite) clay minerals were investigated. Radiation shielding properties of studied clay minerals were investigated at eighteen different energies in the energy range of 0.060-2.614 MeV using EpiXS program. Gamma radiation shielding properties of clay minerals were investigated by determining linear attenuation coefficient (μ), half value layer (HVL), effective atomic number (Z_{eff}) and effective electron density (N_{eff}) parameter values. The linear attenuation coefficient, effective atomic number and effective electron density values of the studied clay minerals are generally ranked as Muscovite>Pyrophyllite>Kaolinite for all investigated energies. Half value layers exhibit an order in reverse of the order of the mentioned parameters from largest to smallest. From these results, it is seen that Muscovite mineral is a better gamma radiation shielding material compared to other studied clay minerals.

Keywords: Mineral Clay, Gamma radiation shielding, EpiXS

GİRİŞ

Modern toplumların sürdürülebilir teknolojik gelişimi için vazgeçilmez bir unsur haline gelen iyonlaştırıcı radyasyon, günümüzde endüstri, tıp, uzay araştırmaları ve bilimsel çalışmalar gibi alanlarda etkin bir şekilde kullanılmaktadır. Geniş yelpazede kullanımının yanı sıra iyonlaştırıcı radyasyon, biyolojik dokulara nüfuz ederek enerjisini bu dokulara aktarabildiği için insan sağlığını olumsuz etkilemektedir. İyonlaştırıcı radyasyon, maruz kalınan doz ve süreye bağlı olarak; cilt yanıkları, saç dökülmesi, doğurganlığın bozulması, organ yetmezliği, kanser ve hücre hasarı gibi sağlık sorunlarına sebep olmaktadır. Bu nedenle, başta radyasyonla

çalışan personel olmak üzere, toplumun radyasyonun potansiyel zararlı etkilerinden korunması büyük önem taşımaktadır. Radyasyonun zararlı etkileri yalnızca canlı organizmalarla sınırlı kalmamakta, aynı zamanda uzay, savunma ve tıp gibi alanlarda yaygın olarak kullanılan elektronik sistemler üzerinde de ciddi bozulmalara ve performans kayıplarına yol açabilmektedir (Schrimpf ve ark., 2004). Elektronik cihazlarda bulunan diyotlar ve bilgisayar çipleri gama radyasyonuna maruz kaldığında elektronik cihazların kristal yapısının bozulmasına ve ömrünün kısalmasına sebep olmaktadır (Duzellier, 2015).

Uluslararası Radyasyon Koruması Komisyonu (ICRP) tarafından belirlenen ALARA prensibi, radyasyondan korumada yaygın olarak kullanılan bir ilkedir. Radyasyon uygulaması sırasında yalnızca gerekli olan en düşük dozun verilmesi anlamına gelmektedir. ALARA prensibi kapsamında radyasyondan korunmada zaman, mesafe ve zırhlama olmak üzere üç temel koruyucu önlem kullanılmaktadır. Zaman, radyasyon kaynağının yanında geçirilen süre ne kadar az olursa o kadar az doza maruz kalınacağını ifade etmektedir. Mesafe, radyasyon kaynağın ile aramızdaki uzaklık ne kadar fazla olursa o kadar az doza maruz kalınacağını ifade etmektedir. Zırhlama ise radyasyonun şiddetini azaltarak kişilerin radyasyon maruziyetini minimum seviyeye indirmeye yardımcı olmaktadır. Özellikle iyonlaştırıcı radyasyonlarda zırh malzemesi kullanımı oldukça önemlidir. Zırh malzemeleri iyonlaştırıcı radyasyonun türüne göre farklılıklar göstermektedir. Düşük giricilik özelliğine sahip olan alfa parçacıklarını absorbe etmek için bir kâğıt parçası yeterli iken, yüksek giricilik özelliğini sahip olan X-ışınları ve gama ışınlarını absorbe etmek için kurşun gibi yüksek atom numarasına sahip malzemeler gerekmektedir (Akman ve ark., 2025). Zırh malzemesi seçimi yapılırken yalnızca yüksek koruma kapasitesi yeterli olmayıp, aynı zamanda ekonomik uygunluk, üretim ve temin kolaylığı, uygulama pratikliği, mekanik özelliklerin elverişliliği ve çevresel etkilerinin değerlendirilmesi de gerekmektedir. Gama ışınları ve X-ışınlarının, madde ile etkileşimi sırasında foton enerjisine ve malzemenin atom numarasına bağlı olarak fotoelektrik olay, Compton saçılması ve çift oluşum gibi etkileşim türleri ortaya çıkmaktadır. Bu nedenle, gama radyasyonuna karşı etkin zırhlama sağlamak amacıyla yüksek atom numarasına ve yoğunluğa sahip malzemeler tercih edilmektedir. Gama ve X-ışınlarının zararlı etkilerinden korunmak amacıyla geleneksel olarak kurşun (Pb) ve türevleri kullanılmaktadır. Kurşun, zehirli kimyasal etkisi sebebiyle Dünya Sağlık Örgütü tarafından herhangi bir maruziyet sınırı verilmeksizin insan sağlığı açısından tamamen kaçınılması gereken bir element olarak belirtilmiştir. Türkiye'de kurşun zehirlenmesi, meslek hastalıkları arasında en yaygın görülenlerden biridir. İnsan vücuduna minimum seviyelerde alınan kurşun dahi, sinir sistemi üzerinde dejeneratif etkilere yol açmakta; kısırlık, körlük, felç, karaciğer yetmezliği gibi ciddi sağlık sorunlarına neden olmakta ve bireysel gelişimi olumsuz yönde etkileyerek büyümeyi baskılamaktadır (Dündar ve ark., 2015). Ayrıca, Tehlikeli Maddelerin Kısıtlanmasına İlişkin Direktif (RoHS) kapsamında, içlerinde kurşununda bulunduğu on maddenin elektrikli ve elektronik ekipmanlarda kullanılmasının sınırlandırılması gerektiği belirtilmiştir (Directive, 2013). Bu durum, araştırmacıları kurşuna alternatif olarak daha güvenli ve çevre dostu zırh malzemelerinin geliştirilmesine yönelik kapsamlı çalışmalar yapmaya yönlendirmiştir. Kurşuna alternatif yüksek performanslı zırh malzemelerinin geliştirilmesine yönelik çalışmalar kapsamında alaşımlar (Akman ve ark., 2025, Abdelhakim ve ark., 2025; Mhareb ve ark., 2021), polimer kompozitler (More ve ark., 2025; Ozdemir ve ark., 2025; Kılıçoğlu ve ark., 2022), camlar (Alrowaili ve ark.,2025; Sayyed ve ark.,2021; Kaewjaeng ve ark.,2019), betonlar (Niu ve ark.,2025; Ban ve ark.,2021; Nikbin ve ark.,2019) ve mineraller (Elsafi ve ark., 2025; Mansour ve ark., 2020; Ertem ve ark., 2017) öne çıkan seçenekler arasında yer almaktadır.

Mineraller, yerkabuğunda doğal süreçlerle meydana gelen, belirli bir kimyasal formüle ve kristal yapıya sahip olan, inorganik yapıdaki malzemelerdir. Doğada pek çok mineral çeşidi bulunmaktadır. Kil mineralli, yüksek erime noktası, termo-kimyasal kararlılık, yüksek sıcaklıkta iyi mekanik mukavemet, yüksek korozyon direnci sağlaması gibi üstün mekanik özellikleri sayesinde; özellikle tropikal koşullar altında çimentodan daha ucuz ve daha dayanıklı malzemeler olması gerekçesiyle inşaat ve yapı çalışmalarında yaygın olarak kullanılmaktadır (Olukotun ve ark., 2018). Ayrıca kil minerallerinin doğada bol miktarda bulunması, çevre dostu olması ve toksik etkilerinin bulunmaması gibi özellikleri, radyasyon zırhlama alanında çalışan araştırmacıların dikkatini çekmiş ve bu konuda çeşitli çalışmalar yapılmıştır. Olukotun ve ark., (2018) yaptıkları çalışmada ball kil ve kaolin kilin radyasyon zırhlama özelliklerini 609.31-1764.49 keV enerji aralığında deneysel (HPGe dedektör) ve teorik olarak (WinXCOM) incelemişlerdir. İncelenen kil malzemelerinin hem tıbbi hem de nükleer uygulamalar için gama radyasyonu zırhlamada kullanılabileceğini ifade etmişlerdir. Mahmoud ve ark., (2023) yaptıkları çalışmada doğal kil minerali içeren bazı tuğlaların radyasyon zırhlama özelliklerini 0,662-1,332 MeV enerji aralığında ile NaI (Tl) dedektörü kullanarak belirlemişlerdir. Kurşunsuz bir malzeme olan doğal kil tuğlaların, radyoaktif yerlerde gama ışını koruması için uygun bir alternatif olacağını ifade etmişlerdir. Van Thuong ve ark., (2024) yaptıkları çalışmada radyasyondan korunma uygulamalarında kullanılmak üzere beyaz kil içeren bağlı tuğlaların radyasyon zırhlama özelliklerini

0,662-1,332 MeV enerji aralığında ile NaI (Tl) dedektörü kullanarak belirlemişlerdir. İncelenen tuğlaların radyasyon koruma verimliliğini arttırdığını ifade etmişlerdir.

Sunulan çalışmada, toksik etkileri bulunmayan, mekanik özellikleri iyi olan bazı kil minerallerinin (kaolinit, pirofilit ve mika (muskovit)) gama radyasyonu zırhlama özellikleri araştırılmıştır. Araştırılan kil minerallerinin radyasyon zırhlama özellikleri, EpiXS programı kullanılarak 0,060-2,614 MeV enerji aralığında on sekiz farklı enerjide incelenmiştir. Kil minerallerinin gama radyasyonu zırhlama özellikleri, lineer azaltma katsayısı(μ), yarı kalınlık değeri (YKD), etkin atom numarası ($Z_{etk.}$) ve etkin elektron yoğunluğu (N_{etk}) parametre değerleri belirlenerek incelenmiştir.

MATERYAL VE METOD

İncelenen kil minerallerinin gama radyasyonu zırhlama kapasiteleri EpiXS bilgisayar programı yardımıyla teorik olarak araştırılmıştır. EpiXS programı, radyasyonun madde ile etkileşimi ile ilgili çalışmalarda kullanılan ve çeşitli elementlerin, karışımların geniş enerji aralığında zırhlama parametrelerini hesaplamak için kullanılan çevrimiçi bilgisayar programıdır. μ, YKD, $Z_{etk.}$ ve $N_{etk.}$ parametre değerleri kil minerallerinin kimyasal bileşimi ve yoğunluğu girildiğinde EpiXS programı tarafından doğrudan hesaplanabilmektedir (Gili ve ark., 2025). Çalışmada seçilen kil minerallerinin kimyasal içerikleri ve yoğunlukları hakkındaki bilgiler Tablo 1'de sunulmuştur.

Tablo 1. Kil minerallerinin kimyasal formülü ve yoğunlukları

Mineral Adı	Kimyasal Formulü	ρ (g/cm^3)
Kaolinit	$Al_2Si_2O_5(OH)_4$	2,6
Pirofilit	$Al_2Si_4O_{10}(OH)_2$	2,8
Mika (Muskovit)	$KAl_3Si_3O_{10}(OH)_2$	2,8

Bir gama ışını, soğurucu ortamdan geçtiğinde, artan foton enerjisine bağlı olarak fotoelektrik olay, Compton saçılması ve çift oluşum süreçlerine maruz kalır (Saha 2019). Şekil 1'de bu etkileşimler görülmektedir. Bu etkileşimler sebebiyle foton soğurucu ortamdan geçtiğinde şiddetinde azalma meydana gelir. Soğurucudan geçen fotonların şiddeti I ve başlangıç fotonlarının şiddeti I_0 ile ifade edilmektedir. Beer Lambert Yasası olarak bilinen bu fiziksel olay denklem 1'de verilmiştir.

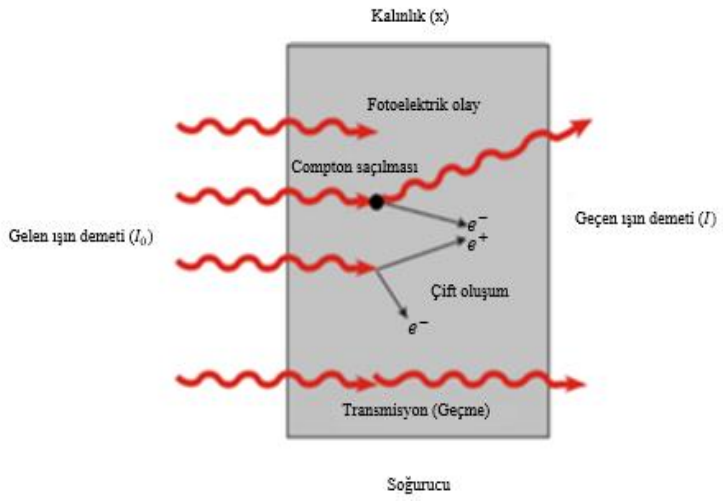

Şekil 1. I_0 foton şiddetinin x kalınlığındaki bir soğurucudan geçerken azalmasının gösterimi

$$I = I_0 e^{-\mu x} \quad (1)$$

Burada I_0 ve I değerleri sırasıyla fotonun başlangıçtaki şiddeti ve fotonun bir soğurucu ortamdan geçtikten sonraki şiddetini ifade etmektedir. x soğurucunun cm cinsinden kalınlığını ifade etmektedir. μ ise lineer azaltma katsayısını (μ, cm^{-1}) ifade etmektedir. μ, malzemenin birim kalınlık başına gelen fotonlar ile etkileşme ihtimalinin bir ölçüsüdür. Zırh malzemesinin kimyasal içeriğine ve yoğunluğuna bağlı olarak değişen bu ifade yapılan çalışmada incelenen ilk zırhlama parametresidir. μ değeri, birim alan başına düşen kütlenin gelen fotonlarla etkileşime girme ihtimalini veren ve Denklem 2 ile ifade edilen kütle azaltma katsayısının (μ/ρ,

cm^2/g) yoğunlukla çarpımı sonucunda elde edilmektedir (Sharma ve ark., 2020). Lineer azaltma katsayısı parametresi gama ışınlarının enerjisi arttıkça azalırken, soğurucu içindeki elementlerin atom numarası ve yoğunluğu arttıkça artmaktadır.

$$\left(\frac{\mu}{\rho}\right)_i = \sum_i W_i \left(\frac{\mu}{\rho}\right)_i \quad (2)$$

Burada W_i terimi, malzeme içindeki i. elementin ağırlık kesrini ve $(\mu/\rho)_i$ terimi ise malzeme içindeki i. elementin kütle azaltma sayısını ifade etmektedir. Malzeme içindeki elementlerin ağırlık kesirleri toplamı 1'dir.

İncelenen bir diğer zırhlama parametresi lineer azaltma katsayısı ile ters orantılı olan ve başlangıç radyasyon şiddetinin %50'sini soğuran ya da %50'sini geçiren malzeme kalınlığını belirlemek için kullanılan yarı kalınlık değeri (YKD, cm) parametresidir (Manjunatha ve ark., 2018). YKD değeri Denklem 3 yardımıyla hesaplanmaktadır.

$$YKD = \frac{\ln(2)}{\mu} \quad (3)$$

Birden fazla elementten oluşan malzemelerde etkin atom numarası değerinin elde edilmesi zırhlama özelliklerinin incelenmesinde oldukça önemlidir. Etkin atom numarası ($Z_{etk.}$) parametresi, malzemeyi oluşturan atomların gelen gama ışını fotonlarıyla etkileşime girme olasılığının, malzemeyi oluşturan elektronların gelen gama ışını fotonlarıyla etkileşime girme olasılığına oranını vermektedir. $Z_{etk.}$ değeri Denklem 4 yardımıyla hesaplanmaktadır.

$$Z_{etk.} = \frac{\sigma_{t,a}}{\sigma_{t,e}} = \frac{\sum f_i A_i \left(\frac{\mu}{\rho}\right)_i}{\sum f_j \frac{A_j}{Z_j}\left(\frac{\mu}{\rho}\right)_j} \quad (4)$$

Burada $\sigma_{t,a}$ ve $\sigma_{t,e}$ değerleri sırasıyla atomik ve elektronik tesir kesiti değerlerini vermektedir. f_i, A_i, Z_i terimleri ise sırasıyla i. elementin malzeme içindeki bolluğunu, i. elementin atom ağırlığını ve i. elementin atom numarasını ifade etmektedir (Dong ve ark., 2019).

İncelenecek olan son zırhlama parametresi ise birim kütle başına düşen elektron sayısını ifade eden etkin elektron yoğunluğu ($N_{etk.}$, elektron/g) parametresidir. Denklem 5 yardımıyla hesaplanmaktadır.

$$N_{etk.} = \frac{Z_{etk.}}{A_{top.}}\left(N_A . n_{top.}\right) \quad (5)$$

Burada A_{top} ve n_{top} değerleri sırasıyla malzeme içindeki elementlerin toplam atom ağırlığını ve malzeme içerisindeki elementlerin toplam atom sayısını ifade etmektedir (Tekin ve ark., 2019).

BULGULAR ve TARTIŞMA

Sunulan çalışmada, kaolinit, pirofilit ve muskovit kil minerallerinin gama radyasyonu zırhlama özellikleri araştırılmıştır. Kil minerallerinin radyasyon zırhlama özellikleri, EpiXS programı kullanılarak 0,060-2,614 enerji aralığında on sekiz farklı enerjide incelenmiştir.

İncelenen kil minerallerinin kimyasal bileşimi ve yoğunluğu girildiğinde EpiXS programı tarafından hesaplanan ilk parametre değeri, lineer azaltma katsayısıdır. Lineer azaltma katsayısı parametre değerinin enerjiye göre değişimi Şekil 2 ve Tablo 2'de sunulmaktadır. Tüm kil mineralleri için lineer azaltma katsayısı değerinin artan foton enerjisiyle birlikte üstel olarak azaldığı ilgili şekilden ve tablodan görülmektedir. Bunun sebebi farklı foton enerjilerinde farklı etkileşim tesir kesitlerinin baskın olmasıdır. Düşük enerji bölgelerinde fotoelektrik tesir kesiti daha baskındır. Fotoelektrik tesir kesiti, yaklaşık olarak Z^{4-5} ve $E^{-3.5}$ ile orantılıdır. Bu sebeple keskin azalmalar görülmektedir. Atom numarasını ifade eden Z, düşük enerjilerde 4 ile yüksek enerjilerde ise 5 ile orantılıdır. Orta enerji bölgelerinde Compton saçılma tesir kesiti daha baskındır. Compton saçılması tesir kesiti yaklaşık olarak Z ve E^{-1} ile orantılıdır. Yüksek enerji bölgesinde ise çift oluşum tesir kesiti daha baskındır. Çift oluşum tesir kesiti ise yaklaşık olarak Z^2 ve E ile orantılıdır. Bu sebeple orta ve yüksek enerji bölgelerinde artan enerjiye bağlı üstel azalmanın minimum seviyededir. 0,060 MeV enerji değerinde Muskovit kil mineralinin lineer azaltma katsayısı değeri en yüksek değer olup bu değer Kaolinit kil

mineralinden 1,2 kat daha büyük iken, pirofilit mineralinden 1,1 kat daha büyüktür. Pirofilit ve Muskovit kil minerallerinin yoğunlukları eşit olsa da lineer azaltma katsayısı değerlerinin farklı olmasının sebebi bu iki kil minerali içerisinde bulunan elementlerin atom numaralarının birbirinden farklı olmasıdır. Özetle lineer azaltma katsayısı sonuçları kapsamlı bir şekilde incelendiğinde tüm enerji değerlerinde Muskovit kil mineralinin diğer minerallerden daha iyi radyasyon zırh malzemesi olduğu görülmektedir.

Tablo 2. Kil minerallerinin lineer azaltma katsayısı (cm^{-1}) ve etkin elektron yoğunluğu ($x10^{23}$) (elektron/g) sonuçları

Enerji (MeV)	Kaolinit		Pirofilit		Muskovit	
	μ	$N_{etk.}$	μ	$N_{etk.}$	μ	$N_{etk.}$
0,06	0,6229	3,4108	0,6870	3,2950	0,7669	3,4397
0,081	0,4880	3,2228	0,5302	3,1556	0,5616	3,2290
0,088	0,4636	3,1887	0,5023	3,1296	0,5264	3,1880
0,122	0,3961	3,1040	0,4259	3,0639	0,4340	3,0827
0,136	0,3789	3,0879	0,4068	3,0513	0,4122	3,0623
0,239	0,3068	3,0484	0,3283	3,0205	0,3282	3,0123
0,356	0,2630	3,0398	0,2811	3,0138	0,2803	3,0017
0,511	0,2268	3,0364	0,2423	3,0112	0,2414	2,9978
0,569	0,2164	3,0358	0,2313	3,0107	0,2303	2,9970
0,583	0,2141	3,0356	0,2288	3,0106	0,2278	2,9969
0,662	0,2024	3,0351	0,2162	3,0102	0,2153	2,9962
0,835	0,1818	3,0343	0,1943	3,0096	0,1934	2,9954
1,063	0,1617	3,0338	0,1727	3,0093	0,1720	2,9949
1,173	0,1539	3,0338	0,1645	3,0092	0,1637	2,9948
1,275	0,1476	3,0340	0,1577	3,0093	0,1569	2,9949
1,333	0,1442	3,0342	0,1540	3,0095	0,1533	2,9950
1,77	0,1245	3,0384	0,1331	3,0120	0,1325	2,9981
2,614	0,1017	3,0549	0,1088	3,0222	0,1085	3,0102

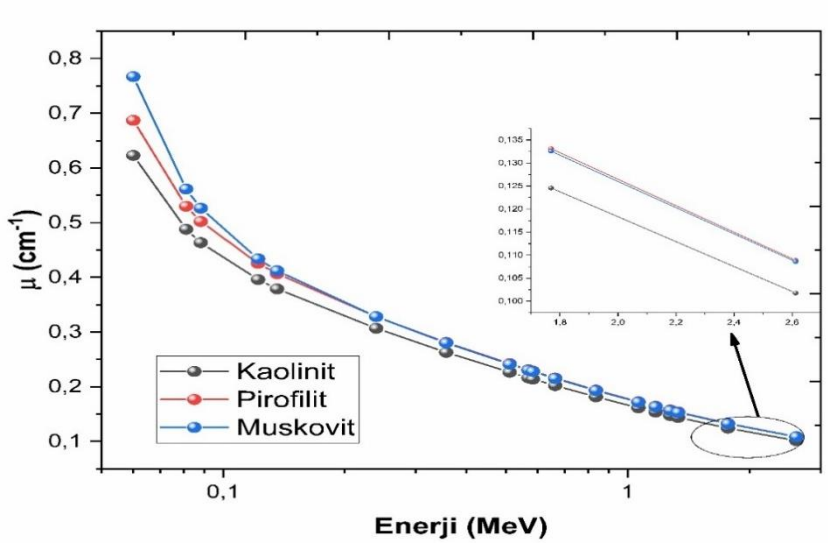

Şekil 2. İncelenen kil minerallerin lineer azaltma katsayısı sonuçlarının foton enerjisi ile değişimi

Lineer azaltma katsayısından faydalanılarak belirlenen YKD değeri denklem 3'den açıkça görüldüğü üzere lineer azaltma katsayısı ile ters orantılı bir parametredir. Bu sebeple kil minerallerinin YKD değerleri ne kadar küçük ise zırhlama özellikleri o kadar iyi olacaktır. İncelenen kil minerallerinin YKD değerlerinin foton enerjisine göre değişimi Şekil 3'de sunulmaktadır. Şekil 3'den artan foton enerjisi ile YKD değerlerinin azaldığı açıkça görülmektedir. İncelenen kil minerallerinin YKD değerleri Muskovit<Pirofilit<Kaolinit olacak şekilde sıralanmaktadır. Bu sonuç, incelenen tüm enerji değerlerinde Muskovit kil mineralinin diğer kil minerallerine kıyasla daha iyi bir zırh malzemesi olduğu sonucunu bir kez daha doğrulamaktadır.

İncelenen kil minerallerinin etkin atom numarası ($Z_{etk.}$) parametre değerlerinin foton enerjisine göre değişimi Şekil 4'de sunulmuştur. Birden fazla element içeren zırh malzemelerde atom numarası yerine etkin atom numarası değeri kullanılmaktadır. Gama radyasyonunu zırhlamada atom numarası değeri ne kadar yüksekse malzemenin zırhlama özelliğinin o kadar iyi olduğu bilinmektedir. Bu sebeple. $Z_{etk.}$ parametre değeri arttıkça, kil minerallerinin gama radyasyonunu azaltma kapasitesi de artacaktır. Ayrıca Şekil 4'den görüldüğü üzere artan enerji değeri ile $Z_{etk.}$ parametre değeri azalmaktadır. Bunun sebebi lineer azaltma katsayısı parametresinde kapsamlı bir şekilde belirtildiği üzere farklı foton enerjilerinde farklı etkileşim tesir kesitlerinin baskın olmasıdır. İncelenen kil minerallerinin $Z_{etk.}$ değerleri incelenen tüm enerjiler için Muskovit >Pirofilit >Kaolinit olacak şekilde sıralanmaktadır. Bu sonuç, incelenen tüm enerji değerlerinde Muskovit kil mineralinin diğer kil minerallerine kıyasla daha iyi bir zırh malzemesi olduğu sonucunu perçinleştirmektedir.

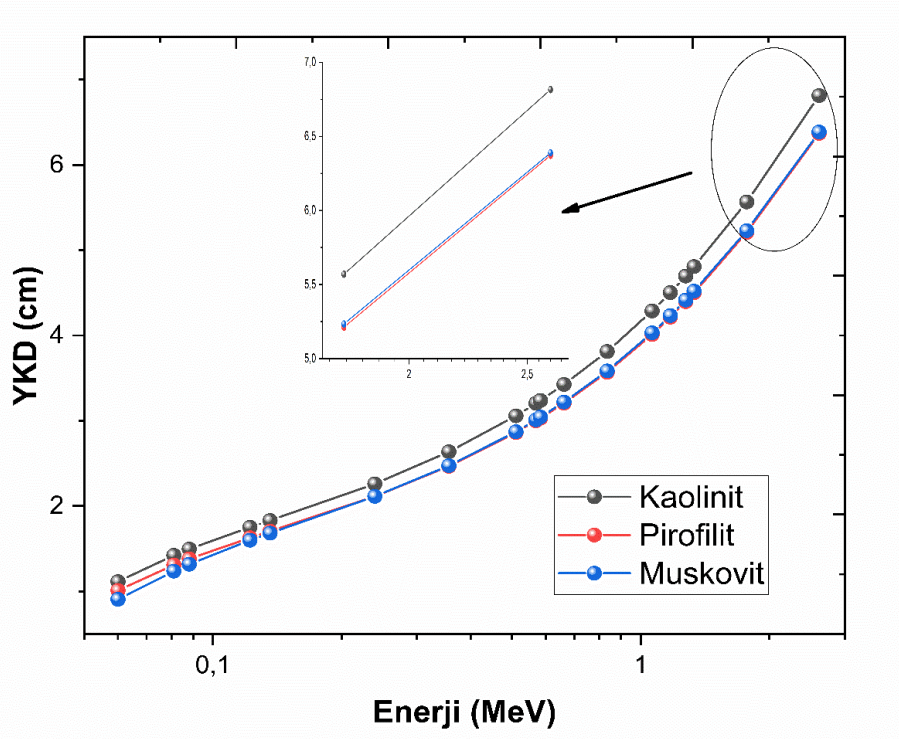

Şekil 3. İncelenen kil minerallerinin yarı kalınlık değeri sonuçlarının foton enerjisi ile değişimi

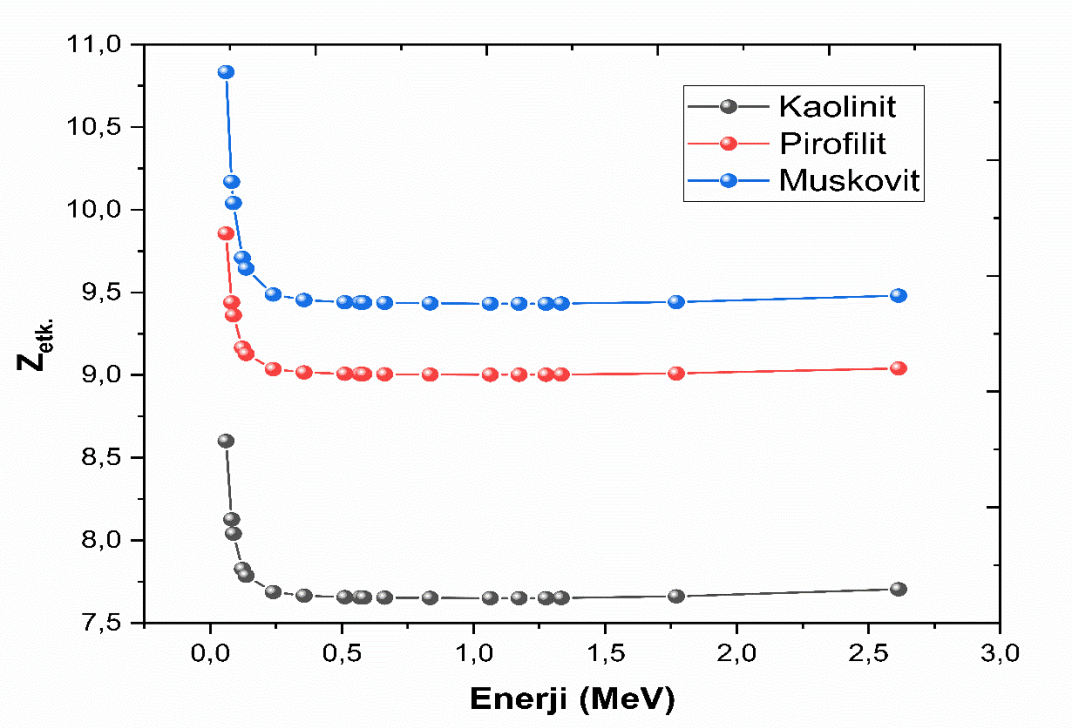

Şekil 4. İncelenen kil minerallerinin etkin atom numarası sonuçlarının foton enerjisi ile değişimi

Kil minerallerinin gama ışını zırhlama özelliklerini belirlemede kullanılacak olan son parametre ise etkin elektron yoğunluğudur ($N_{etk.}$). Birim kütle başına elektron sayısını belirmemizi sağlayan bu parametre etkin atom numarası ile doğru orantılı bir parametredir (Bkz. Denklem 5). Etkin elektron yoğunluğu değerinin enerjiye göre değişimi Şekil 5 ve Tablo 2'de sunulmaktadır. Bu parametre değeri ne kadar yüksek ise zırhlama özelliğinin de o kadar iyi olduğunu ifade edebiliriz. İlgili şekil ve tablodan en yüksek $N_{etk.}$ değerinin 0,060 MeV enerji değerinde Muskovit mineralinde olduğu görülmektedir. Bu parametre sonucundan da Muskovit mineralinin diğerlerine göre daha iyi bir gama radyasyonu zırh malzemesi olduğu görülmektedir.

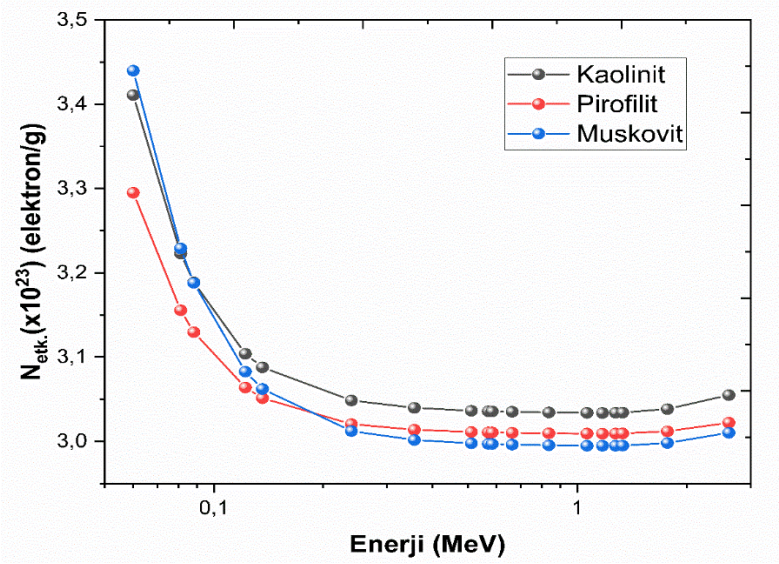

Şekil 5. İncelenen kil minerallerinin etkin elektron yoğunluğu sonuçlarının foton enerjisi ile değişimi

SONUÇ

Sunulan çalışmada, toksik etkileri bulunmayan, mekanik özellikleri iyi olan bazı kil minerallerinin (kaolinit, pirofilit ve mika (muskovit)) gama radyasyonu zırhlama özellikleri araştırılmıştır. Araştırılan kil minerallerinin radyasyon zırhlama özellikleri, EpiXS programı kullanılarak 0,060-2,614 MeV enerji aralığında on sekiz farklı enerjide incelenmiştir. Kil minerallerinin gama radyasyonu zırhlama özellikleri, lineer azaltma katsayısı(μ), yarı kalınlık değeri (YKD), etkin atom numarası ($Z_{etk.}$) ve etkin elektron yoğunluğu ($N_{etk.}$) parametre değerleri

belirlenerek incelenmiştir. Kil mineralleri için zırhlama parametreleri kapsamlı bir şekilde incelendiğinde; μ, $Z_{etk.}$, $N_{etk.}$ değerlerinin artan foton enerjisi ile azaldığı, YKD değerlerinin ise artan foton enerjisi ile arttığı görülmektedir. İncelenen tüm parametre değerleri tüm enerji değerleri için Muskovit mineralinin diğer minerallerden daha fazla gama ışınları ile etkileşime girdiğini göstermektedir. Bu sebeple çevre dostu ve toksik etkileri bulunmayan Muskovit minerali, alternatif zırh malzemesi olarak kullanılabilir.

KAYNAKLAR

Abdelhakim, N. A., Saleh, A., Mitwalli, M., El-Farrash, A. H., & Shalaby, R. M. (2025). A good balance between the efficiency of ionizing radiation shielding and mechanical performance of various tin-based alloys: Comparative analysis. Radiation Physics and Chemistry, 226, 112155.

Akman, F., Kilicoglu, O., Ozdogan, H., & Agar, O. (2025). Nuclear Radiation Shielding Characteristics of Platinum and Rhodium-Based Alloys. In Advances in Alloys Research and Technologies (pp. 239-281). Cham: Springer Nature Switzerland.

Alrowaili, Z. A., & Al-Buriahi, M. S. (2025). Gamma absorption/scattering parameters and nuclear radiation shielding performance of AlSN–Zr glass system: Potential use in medical facilities. Radiation Physics and Chemistry, 227, 112367.

Ban, C. C., Khalaf, M. A., Ramli, M., Ahmed, N. M., Ahmad, M. S., Ali, A. M. A., ... & Ameri, F. (2021). Modern heavyweight concrete shielding: Principles, industrial applications and future challenges; review. Journal of Building Engineering, 39, 102290.

Directive, E. U. 2013. Restriction of the use of certain hazardous substances in electrical and electronic equipment (RoHS). Off. J. Eur. Communities, 46:19-23.

Dong, M. G., Agar, O., Tekin, H. O., Kilicoglu, O., Kaky, K. M., & Sayyed, M. I. (2019). A comparative study on gamma photon shielding features of various germanate glass systems. *Composites Part B: Engineering*, *165*, 636-647.

Duzellier, S. 2005. Radiation effects on electronic devices in space. Aerospace science and technology, 9(1): 93-99.

Dündar, Y., Aslan, R. 2005. Yaşamı kuşatan ağır metal kurşunun etkileri. Kocatepe Tıp Dergisi, 6(2): 1-5.

Elsafi, M., El-Nahal, M. A., Alawy, M. K., & Nabil, I. M. (2025). Unveiling the radiation shielding efficacy of diorite, granodiorite, tonalite, and granite: experimental and simulation study. *Scientific Reports*, *15*(1), 804.

Ertem, G., Ertem, M. C., McKay, C. P., & Hazen, R. M. (2017). Shielding biomolecules from effects of radiation by Mars analogue minerals and soils. *International Journal of Astrobiology*, *16*(3), 280-285.

Gili, M. B. Z., & Jecong, J. F. M. (2025). The potential application of mining wastes and slag as radiation shielding: a characterization study using EpiXS. *Arabian Journal for Science and Engineering*, *50*(5), 3047-3058.

Kaewjaeng, S., Kothan, S., Chaiphaksa, W., Chanthima, N., Rajaramakrishna, R., Kim, H. J., & Kaewkhao, J. (2019). High transparency La2O3-CaO-B2O3-SiO2 glass for diagnosis x-rays shielding material application. Radiation Physics and Chemistry, 160, 41-47.

Kılıçoğlu O, More CV, Akman F, Dilsiz K, Oğul H, Kaçal MR, Polat H, Agar O, 2022. Micro Pb filled polymer composites: Theoretical, experimental and simulation results for γ-ray shielding performance. Radiation Physics and Chemistry, 194: 110039.

Mahmoud, K. A., & Marashdeh, M. W. (2023). Clay-based bricks' rich illite mineral for gamma-ray shielding applications: An experimental evaluation of the effect of pressure rates on gamma-ray attenuation parameters. *Open Chemistry*, *21*(1), 20230167.

Manjunatha, H. C., Seenappa, L., Sridhar, K. N., & Hanumantharayappa, C. (2018). Gamma, X-ray and neutron shielding parameters for the Al-based glassy alloys. *Applied Radiation and Isotopes*, *139*, 187-194.

Mansour, A., Sayyed, M. I., Mahmoud, K. A., Şakar, E., & Kovaleva, E. G. (2020). Modified halloysite minerals for radiation shielding purposes. *Journal of Radiation Research and Applied Sciences*, *13*(1), 94-101.

Mhareb MHA, Zeama M, Elsafi M, Alajerami YS, Sayyed MI, Saleh G, Hamad RM, Hamad MKH, 2021. Radiation shielding features for various tellurium-based alloys: a comparative study. Journal of Materials Science: Materials in Electronics, 32: 26798-26811.

More, C. V., Tarwal, N. L., Botewad, S. N., Anis, M., Kutwade, V. V., Akman, F., ... & Pawar, P. P. (2025). Radiation shielding efficacy of unsaturated polyester composites for gamma and neutron attenuation-enhanced with SnO2. Radiation Physics and Chemistry, 229, 112484.

Nikbin, I. M., Mohebbi, R., Dezhampanah, S., Mehdipour, S., Mohammadi, R., & Nejat, T. (2019). Gamma ray shielding properties of heavy-weight concrete containing Nano-TiO2. Radiation Physics and Chemistry, 162, 157-167.

Niu, F., Liu, Y., Xue, F., Sun, H., Liu, T., He, H., ... & Liao, H. (2025). Ultra-high performance concrete: A review of its material properties and usage in shield tunnel segment. Case Studies in Construction Materials, e04194.

Olukotun, S. F., Gbenu, S. T., Ibitoye, F. I., Oladejo, O. F., Shittu, H. O., Fasasi, M. K., & Balogun, F. A. (2018). Investigation of gamma radiation shielding capability of two clay materials. *Nuclear Engineering and Technology*, *50*(6), 957-962.

Ozdemir, H. G., Kacal, M. R., Akman, F., & Polat, H. (2025). Alternative gamma-ray shielding material: Ternary composite including polyester resin/barite/molybdenum. Nuclear Engineering and Technology, 103512.

Saha, G. B. 2019. Radiation Safety in Nuclear Medicine, Springer, 14-158.

Sayyed, M. I., Mhareb, M. H. A., Alajerami, Y. S. M., Mahmoud, K. A., Imheidat, M. A., Alshahri, F., ... & Al-Abdullah, T. (2021). Optical and radiation shielding features for a new series of borate glass samples. Optik, 239, 166790.

Schrimpf, R. D., Fleetwood, D. M. 2004. Radiation effects and soft errors in integrated circuits and electronic devices.World Scientific, 34: 27-161

Sharma, A., Sayyed, M. I., Agar, O., Kaçal, M. R., Polat, H., & Akman, F. (2020). Photon-shielding performance of bismuth oxychloride-filled polyester concretes. *Materials Chemistry and Physics*, *241*, 122330.

Tekin, H. O., Kavaz, E., Altunsoy, E. E., Kilicoglu, O., Agar, O., Erguzel, T. T., & Sayyed, M. I. (2019). An extensive investigation on gamma-ray and neutron attenuation parameters of cobalt oxide and nickel oxide substituted bioactive glasses. *Ceramics International*, *45*(8), 9934-9949.

Van Thuong, T., Tashlykov, O. L., & Mahmoud, K. A. (2024). Novel bricks based lightweight Vietnam's white clay minerals for gamma ray shielding purposes: An extensive experimental study. Nuclear Engineering and Technology, 56(2), 666-672.

➢ *ORAL PRESENTATION*

Elektroensefolografi ve Elektrokardiyografi Sinyalleri Kullanılarak Epilepsi Nöbetlerinin Yapay Zeka ile Tahmin Edilmesi

Nur Sena Özdemir Yılmaz[1*] (*https://orcid.org/0009-0007-1450-804X*),
Osman Eroğul[2*] (*https://orcid.org/0000-0002-4640-6570*)

TOBB Ekonomi ve Teknoloji Üniversitesi, Fen Bilimleri Enstitüsü, Biyomedikal Mühendisliği, Ankara, Türkiye

*Sorumlu yazar e-posta: nursenaozdemir@etu.edu.tr

Özet
Epilepsi dünyada en yaygın görülen ve hastaların hayatlarını beklenmedik nöbetlerle zorlaştıran nörolojik bir hastalıktır. Cerrahi işlemlerin ve farmakolojik tedavilerin yetersizlik ve kısıtlamaları sebebi ile hastaların yaşadığı zorlu nöbetler halen kontrol altına alınanamıştır. Bu sebeple bu çalışmada Elektroensefolografi (EEG) ve Elektrokardiyografi (EKG) sinyal analizlerinin yapay zeka uygulamaları kullanılarak epilepsi nöbet tahmini gerçekleştirilmesi hedeflenmiştir. Böylece ilgili nöbet gerçekleşmeden ne kadar süre öncesinde saptanabileceği ortaya konarak epilepsi hastalarına uygun erken nöbet tahmini yapabilecek bir algoritma ortaya konması hedeflenmektedir.
Anahtar Kelimeler: Epilepsi, EEG, EKG, Yapay Zeka, Nöbet Tahmini

Epilepsy Seizure Prediction Using Artificial Intelligence with Electroencephalography and Electrocardiography Signals

Abstract
Epilepsy is one of the most common neurological disorders worldwide, significantly impacting patients' lives through unexpected seizures. Due to the limitations and inadequacies of surgical procedures and pharmacological treatments, these challenging seizures remain largely uncontrolled. Therefore, this study aims to predict epileptic seizures by applying artificial intelligence techniques to the analysis of Electroencephalography (EEG) and Electrocardiography (ECG) signals. The goal is to develop an algorithm capable of providing early seizure prediction by determining how long before a seizure can be accurately detected, thereby offering timely warnings for patients with epilepsy.
Keywords: Epilepsy, EEG, ECG, Artificial Intelligence, Seizure Prediction

GİRİŞ

Darankoum ve ark. (2024), epilepsinin beyinde gerçekleşen anormal nöronal aktivite olayına bağlı olarak hastanın nöbet yaşaması ile kendini gösteren ve dünyada görülen en yaygın nörolojik hastalık olması üzerine çalışmalarda bulunmuştur. Hastalık süresince ani ve beklenmeyen nöbetler meydana geldiği önceki çalışmalarda ortaya konmuştur (Xu ve ark., 2022).

Detti ve ark. (2020)'ye göre Epilepsi hastalığının tedavisindeki farmakolojik ve cerrahi yöntemler nöbetleri azaltabilmekte veyahut nöbet sayısını kontrol altına alabilmektedir. Fakat antiepileptik ilaçların birçok yan etkisi vardır. Cerrahi işlemlerin ise %30'u olumsuzlukla sonuçlanabilmekte ve her hasta cerrahi işlem için uygun olamamaktadır. Bu sebeple epilepsi nöbetlerinin çeşitli yöntemlerle yapılabilecek olan erken tahmini, hastaların olası görebilecekleri zararı ciddi oranda azaltmayı hedefler ve hastalığı kontrol altına alarak epilepsi hastalarının hayat kalitesini yükseltmeyi amaç edinmektedir.

MATERYAL VE METOD

Veri Seti

Çalışma kapsamında "Physionet" platformu üzerinden elde edilen "Siena Scalp EEG Database" veri seti kullanılmıştır (Detti, 2020). İlgili veri setinde 14 epilepsi hastasından toplanan ham Elektrokardiyografi (EEG) ve 1-2 adet Elektrokardiyografi (EKG) verisi içermektedir. Hastaların dağılımı; 9 erkek (yaşlar 36–71) ve 5 kadın (yaşlar 20–58) şeklindedir. İlgili hastaların epilepsi dışında nörolojik veyahut kardiyolojik herhangi bir hastalığı yoktur.

Metod

Bu çalışma kapsamında Elektroensefelografi (EEG) ve Elektrokardiyografi (EKG) sinyallerinin analizi ile makine öğrenimi algoritmaları tabanlı nöbet tahmini gerçekleştirilmesi hedeflenmiştir. Çalışma "Matlab" uygulaması ile tamamlanmıştır ve sinyal bazlı yöntem akışı aşağıdadır.

EEG Sinyali ile Nöbet Tahmini Algoritma Basamakları

EEG sinyal analizi ile yapılan algoritmanın akışı Şekil 1.'de görülmektedir.

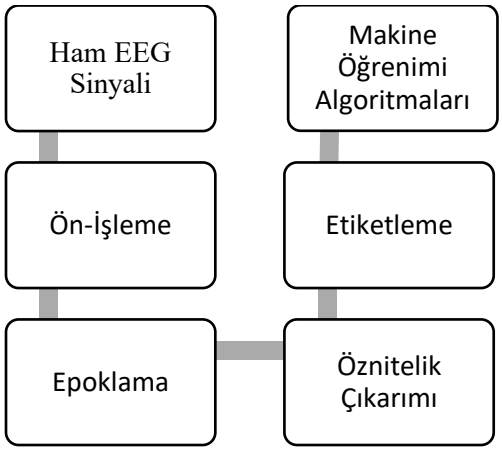

Şekil 1. EEG Sinyali ile Yöntem Akışı

Ham olarak girdi seçilen epilepsi nöbet kayıtları filtelenme basamaklarına sokulmuştur.

Uygulanan ön işleme basamakları ve filtreler şu şekildedir;

1. Detrend Filtreleme: Doğru Akım (DC Offset) kayması sinyalden temizlenmiştir. Böylece sinyaldeki lineer trend temizlenmiştir.
2. BandPass Filtre: 1-45 Hz aralığındaki sinyali geçiren filtre uygulanmıştır. Böylece kas artefaktları, göz kırpma, kafa haraketleri gibi gürültüler temizlenmiştir.
3. Notch Filtre: 50 Hz şehir şebekesine ait gürültü sinyalden temizlenmiştir.
4. Z-Score Normalizasyonu: 29 Kanaldan oluşan EEG sinyalleri arasında ortaklık sağlanarak hepsi 0-1 aralığında genlik değerlerine sahip hale getirilmiştir.
5. Bağımsız Bileşen Analizi: Hasta bazlı göz kırpma, kas haraketleri ve sağlıksız veriyi kanal bazlı olarak görüntülemeyi sağlar. Matlab içerisinde bulunan "EEGLAB" kütüphanesi ile arayüz kullanılarak tamamlanmıştır. Ilgili işlem sonucunda her nöbet verisi gürültüden temizlenmiş ve epoklanmaya hazır hale gelmiştir.

İlgili filtreleme işlemleri tamamlandıktan 29 kanallı olan EEG sinyali ortalama alınarak tek kanala düşürülmüştür. Bu işlemden sonra tek vektörden oluşan kanal ortalaması değere sahip EEG sinyalleri 30 saniyelik epoklara bölünerek öznitelik çıkarımına hazır hale gelmiştir.

EKG Sinyali Nöbet Tahmini Algoritma Basamakaları

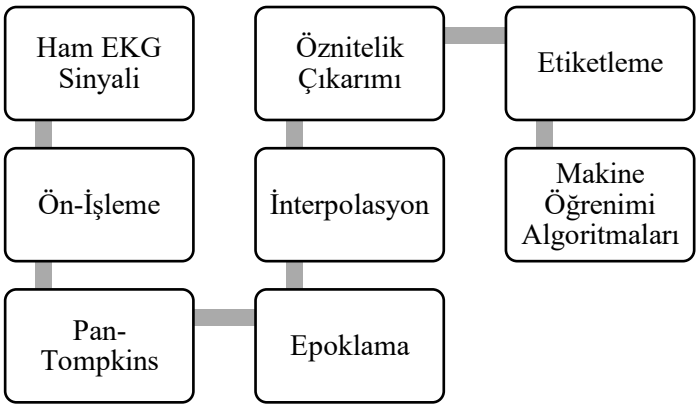

Şekil 2. EKG Sinyali ile Yöntem Akışı

Uygulanan ön işleme basamakları ve filtreler şu şekildedir;

1. Notch Filtre: 50 Hz şehir şebekesine ait gürültü sinyalden temizlenmiştir.
2. Detrend Filtre: EEG ön-işleme sürecinde olduğu gibi Doğru Akım (DC Offset) kayması sinyalden temizlenmiştir. Böylece sinyaldeki lineer trend uzaklaştırılmıştır.
3. Smoothing Filtre: Smoothing (yumuşatma) filtresi sinyaldeki hızlı ve küçük değişimleri azaltması amacıyla uygulanmıştır. Yüksek frekanslı gürültüler (örneğin cihaz gürültüsü) ve kas artefaktları (EMG gürültüsü).
4. BandPass Filtre: 0.04–40 Hz gibi genel EKG filtresi uygulanmıştır.Epilepsi nöbetlerinin bazen 0.05-1 Hz aralığında EKG sinyalinde gözlendiği saptanmıştır. Ek olarak EKG dalgalarına ait segmentler ilgili frekans aralığında saptanmaktadır.

Ön-işleme basamakları tamamlanan her nöbete ait EKG verisi sinyalde bulunan R dalgalarının belirginleştirilmesi için Pan-Tompkins algoritmasına sokulmuştur. İlgili algoritmanın matematiksel akışı Şekil 3.'de gösterilmektedir.

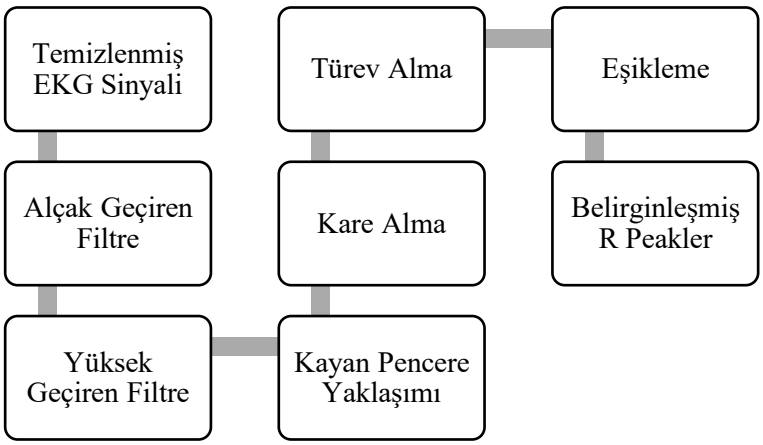

Şekil 3. Pan-Tompkins Algoritması Akışı

Pan-Tompkins ile belirginleşmiş R peaklerine sahip EKG sinyali 30 saniyelik epoklara bölünmüştür. Sinyal içerisindeki sayı ifade etmeyen "NaN" değerlerin olması sebebi ile sinyal interpolasyon işlemine tabii tutulmuştur. Bu işlemde fonksiyon ile birlikte sinyaldeki "NaN" değerler tespit edilip yerlerine önceki ve

sonraki değerler baz alınarak yaklaşık değerler yazılır böylece sinyaldeki düzensizlik ortadan kalkar. Temiz ve eksik veri içermeyen R peakleri belirginleşmiş EKG sinyali öznitelik çıkarımı ve makine öğrenimine hazır hale gelir.

Epilepsi Nöbet Tahmini İçin EEG ve EKG Sinyallerinden Toplanan Öznitelikler

EEG ve EKG sinyallerinden elde edilen ve makine öğrenimine hazır hale getirilmiş öznitelikler Tablo 1.'de gösterilmektedir. EEG sinyallerinden 19 adet EKG'den ise 20 adet öznitelik çıkarılmıştır.

Tablo 1. Sinyal Bazlı Elde Edilen Öznitelikler

Sinyal Bazlı Öznitelikler	EEG Sinyalinden Elde Edilen Öznitelikler (Epok Bazlı)	EKG Sinyalinden Elde Edilen Öznitelikler (Epok Bazlı)
1	Sinyalin Root Mean Square Değeri	RR aralıkları ortalaması
2	Sinyalin Varyans Değeri	RR aralıkları SDNN
3	Sinyalin Ortalama Değeri	RR aralıkları RMSSD
4	Sinyalin Entropi Değeri	RR aralıkları PNN50
5	Sinyalin Skewness Değeri	Alçak Frekans Gücü
6	Sinyalin Kurtosis Değeri	Yüksek Frekans Gücü
7	Sinyalin Tepe Değeri	Alçak/Yüksek Frekans Oranı
8	Zero-Crossing Oranı	Sinyalin Root Mean Square Değeri
9	Aktivite	Zero-Crossing Oranı
10	Mobilite	Sinyalin Entropi Değeri
11	Kompleksisite	Sinyalin Enerjisi
12	Çizgi Uzunluğu (Line Length)	Maksimum Kalp Atım Hızı
13	Enerji	Minimum Kalp Atım Hızı
14	Max-Min Aralığı	Ortalama Kalp Atım Hızı
15	Delta Bandı (0.5-4 Hz)	Kalp Atım Hızının Root Mean Square Değeri
16	Teta Bandı (4-8 Hz)	Kalp Atım Hızının Standart Sapması
17	Alpha Bandı (8-13 Hz)	Maximum-Minimum Kalp Atım Hızı Aralığı
18	Beta Bandı (13-30 Hz)	Kalp Atım Hızının Entropisi
19	Alçak/Yüksek Frekans Oranı	Kalp Atım Hızının Zero-Crossing Oranı
20		Kalp Atım Hızının Standart Sapması

BULGULAR

EEG ve EKG Sinyallerinden elde edilen epok bazlı öznitelikler nöbet öncesi 300 saniye (0) ve nöbet anı (1) olarak etiketlenmiş ve "Matlab" uygulaması içerisinde "Classification Learner" ile makine öğrenimine sokulmuştur. %30 Hold-Out Validation kullanılarak verinin %70'i makinenin öğrenmesi için kullanılırken %30'u test için kullanılmıştır. En yüksek başarı oranlı 5 modelin sınıflandırma başarıları ve erken nöbet tahmin süreleri EEG bazlı olarak Tablo 2 ve EKG bazlı olarak Tablo 3'de gösterilmiştir.

Tablo 2. EEG Bazlı Algoritma Sınıflandırma Sonuçları ve Erken Nöbet Tahmin Süreleri (Dk cinsinden)

Model No	EEG Bazlı Nöbet Tahmini Model Başarı Sıralaması		
	Model İsmi	%Doğruluk Değeri	Erken Nöbet Tahmin Süresi (dk)
1	Efficient Linear SVM	% 98	55 Dk
2	Linear SVM	% 97.1	38 Dk
3	Quadratic SVM	% 97	43 Dk
4	Fine Tree	% 96.7	14 Dk
5	Fine KNN	% 93	13 Dk

Tablo 3. EKG Bazlı Algoritma Sınıflandırma Sonuçları ve Erken Nöbet Tahmin Süreleri (Dk cinsinden)

Model No	EKG Bazlı Nöbet Tahmini Model Başarı Sıralaması		
	Model İsmi	% Doğruluk Değeri	Erken Nöbet Tahmin Süresi (dk)
1	Linear SVM	% 97.8	78 Dk
2	Fine Tree	% 97.1	55 Dk
3	Cubic SVM	% 95	53 Dk
4	Medium Gaussian SVM	% 91	23 Dk
5	Fine KNN	% 88	8 Dk

TARTIŞMA

Çalışma sonucunda elde edilen sınıflandırma modellerinin doğruluk değerleri karşılaştırıldığında EKG bazlı olarak geliştirilen algoritmalar ile daha erken nöbet tahmini yapılabildiği ortaya konmuştur. Gerçekleşecek olan nöbeti EKG bazlı olarak tespit etmek ve ileriki çalışmalarda geliştirilebilecek olan giyilebilir cihaz, prototip gibi ürünlerle hastaları nöbet gerçekleşmeden uyarabilecek bir ürün ortaya konabilecektir. EEG ve EKG bazlı algoritmalarının epilepsi nöbetlerini doğru olarak sınıflandırma oranları oldukça yakındır. Bu sebeple iki sinyal arası karşılaştırmayı erken nöbet tahmin süreleri ile yaparak EKG'nin nöbet tahmininde daha verimli ve çalışılması kolay bir sinyal mekanizması olduğu önerilebilmektedir. EEG sinyal karakteristiği olarak oldukça yüksek gürültülü bir sinyal olduğundan ve sinyalin kayıt prensibinin EKG'den daha zorlu gerçekleşmesinden kaynaklı somut bir nöbet tahmini ürünü veyahut prototip için EKG'nin daha faydalı sonuçlar ortaya koyabildiği ortaya çıkarılmıştır.

SONUÇ

EEG ve EKG sinyalleri epilepsi nöbetlerinin erken tahmini için verimli ve sağlıklı olarak kullanılabilecek iki temel biyolojik sinyaldir. Epilepsi hastalarının geçirebileceği nöbetleri erkenden ve yüksek doğrulukla tahmin edebilmek hastaların hayat kalitesini yüksek oranda arttırabilecektir bu sebeple bu çalışmanın literatür için önemli bir ara basamak olduğu görülmektedir. Çalışmanın devamında derin öğrenme algoritmalarından 1

boyutlu direkt sinyal girdisi ve 2 boyutlu ilgili sinyallerin görüntülerini kullanarak makine öğrenmesi ve derin öğrenme bazlı EEG / EKG performans karşılaştırmasının yapılması hedeflenmektedir.

KAYNAKLAR

Darankoum, D., Villalba, M., Allioux, C., Caraballo, B., Dumont, C., Gronlier, E., ... & Volle, J. (2024). From epilepsy seizures classification to detection: A deep learning-based approach for raw EEG signals. *arşiv preprint, arXiv:2410.03385.*

Detti, P. (2020). Siena scalp EEG database. *PhysioNet*, doi:10.493.

Detti, P., Vatti, G., & Zabalo Manrique de Lara, G. (2020). EEG synchronization analysis for seizure prediction: A study on data of noninvasive recordings. *Processes,* 8(7), 846.

Xu, X., Lin, M., & Xu, T. (2022). Epilepsy seizures prediction based on nonlinear features of EEG signal and gradient boosting decision tree. *International Journal of Environmental Research and Public Health,* 19(18), 11326.

➢ *ORAL PRESENTATION*

DFT Calculations for MEP, HOMO-LUMO, NLO, SAR studies of 3-Methyl-4-(3-methoxy-4-isobutyryloxy benzylidene amino)-4,5-dihydro-1*H*-1,2,4-triazol-5-one

Yonca Yılmaz[1*] (ORCID: 0000-0002-6536-9269, Gül Kotan[2] (ORCID: 0000-0002-4507-9029), Haydar Yüksek[1] (ORCID: 0000-0003-1289-1800)

[1]Department of Chemistry, Kafkas University, Kars, Turkey

[2]Department of Chemistry and Chemical Processing Technologies, Vocational School, Kafkas University, Kars, Turkey

*Corresponding author e-mail: yoncaylmz36@gmail.com

Abstract

Density Functional Theory (DFT) computations of the 3-Methyl-4-(3-methoxy-4-isobutyryloxy benzylidene amino)-4,5dihydro-1*H*-1,2,4-triazol-5-one molecule have been performed using the 6-311G(d,p) basis set with the B3LYP function of the DFT approach. The three-dimensional structure of the molecule is shown using GaussView 5.0. The ideal structure of the chemical was therefore determined. The Gaussian 09W software package was utilized to investigate the electronic properties, HOMO-LUMO analyses, energy gap (ΔEg), mulliken charges, thermodynamic parameters (enthalpy H^0, heat capacity CV^0, and entropy S^0), dipole moment, and total energy of molecule. Furthermore, the molecule electrostatic potential (MEP), molecular surface maps and the structure-activity relationships (SAR) were identified using the same methodology. Moreover, chemical structure NLO (Non-Linear Optical) investigations have been conducted. We computed and compared the static Δα, α_{total} and β^0 parameters with reference urea.

Keywords: 1,2,4-triazol-5-one, DFT, HOMO-LUMO, MEP, SAR

1. INTRADUCTION

A more stable Schiff base is the end product of the condensation reaction between the amine and aldehyde reactants due to the aromatic substitutions in each of them. Schiff bases carry the characteristic -C=N- imine group in their structures. Due to a variety of biological activities, including anti-inflammatory (Alam, et al., 2012), analgesic (Jesmin, et al., 2014) antimicrobial (Gören, et al., 2024), antioxidant (Yüksek, et al., 2020), antifungal (Sumrra, et al., 2018), antitubercular (Meeran, et al., 2019), anticancer (Matela, et al., 2018), anthelmintic (Manjunath, et al., 2017) and more, Schiff bases have become more significant in the medical and pharmaceutical fields. The aromatic chemicals known as 1,2,4-triazoles are used in several significant medications. Among the medications with the 1,2,4-triazole moiety in their structures are, ribavirin, itraconazole, vorozole, alprazolam, anastrozole, fluconazole, rizatriptan, and letrozole (Rao,et al., 2006; Raouf, et al., 2019) Numerous studies have examined the 1,2,4-triazoles' antibacterial, anti-inflammatory, anticancer, and antioxidant qualities (Gao, et al., 2019; Paprocka, et al., 2015; El-Sherief, et al., 2018; Gürsoy Kol, et al., 2025). Schiff bases containing 1,2,4 triazole have an important place among heterocyclic compounds. In recent years, theoretical studies of Schiff bases have also taken their place in the literature (Kotan, et al., 2022; Kotan, et al., 2020; Kotan, et al.,2016; Salihović, et al., 2021). The structural, spectroscopic, thermodynamic, and electrical characteristics of molecular systems are frequently predicted theoretically using quantum chemical computation techniques. Computational Chemistry supports experimental studies and we can also calculate theoretically some parameters that we cannot reach experimentally. Researchers in several branches of chemistry and physics are increasingly using quantum chemical computations. Quantum chemical computations can be used to forecast the behavior of molecules in a variety of challenging situations. The Gaussian 09 software version was used for all quantum chemistry calculations (Frisch, et al., 2009; Wolinski, et al., 1990). Density Functional Theory DFT is an application used in chemical structure calculations and is widely used with the B3LYP function.

2. MATERIALS AND METHODS

Theoretical

The three-dimensional molecular structure of the molecule recorded in the literature (Manap, et al., 2020) was obtained visually with the Gauss-view 5.0 program (Dennington, 2009). The calculations, which were carried out using the density functional theory (DFT) technique utilizing the Gaussian 09W program package on a computer system, were conducted using the 6-311G(d,p) basis set (Frisch, et al., 2009). Initially, the molecule was optimized using the DFT(B3LYP) approach and the basis set 6-311G(d,p) (Frisch, et al., 2009; Wolinski, 1990). The dipole moment, mulliken charges, thermodynamic (heat capacity CV^0, entropy S^0 and enthalpy H^0), some electronic parameters (electron affinity (A), ionization potential (I), electronegativity (χ), global hardness (η), electrophilicity index (ω), nucleophilic index (IP), chemical potential (μ), and global softness (S)) and HOMO-LUMO energy, energy gap (ΔEg), NLO analysis, SAR, and molecular electrostatic potantial map (MEP) were all determined using DFT.

3. RESULT AND DISCUSSION

3.1. Thereotical Details

3.1.1. Molecular Optimization

In this study, firstly, the Gaussian view image of the molecule, which is the Schiff base, was obtained using the program, then 3-Methyl-4-(3-methoxy-4-isobutyryloxy benzylidene amino)-4,5dihydro-1*H*-1,2,4-triazol-5-one molecule was optimized using the B3LYP functional and 6-311G(d,p) basis set of the Gaussian program in order to obtain the lowest energy and most stable structure of the molecule atoms and to be able to perform other DFT applications. The optimized molecular structure is shown in Figure 1.

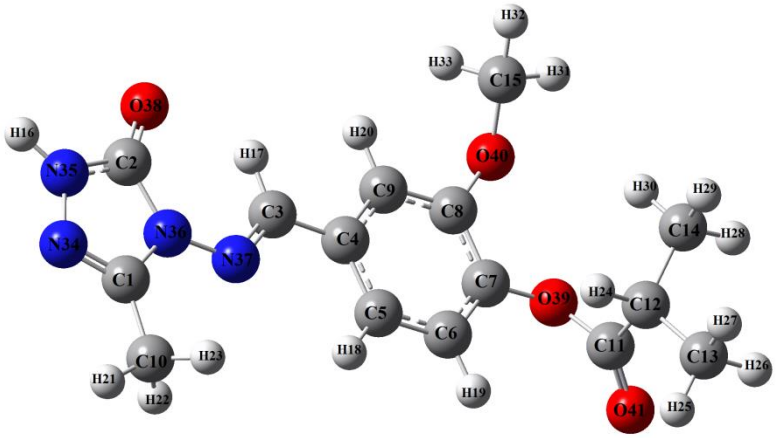

Figure 1. The Gaussview structure of the molecule

3.1.2. Mulliken charge distribution

Chemical bonding and polarity are related to Mulliken charge analysis, which is an indicator of the distribution of electrons within a molecule (Franco-Pérez, et al., 2019) These charge distributions influence a wide range of characteristics, including electronic structures, dipole moment, and polarizability. Mulliken charge values of C, H, N and O atoms present in the molecule were calculated with the B3LYP method and 6-311G (d,p) basis set. The C2 atom has the largest charge value, 0.535, while the C13 and C14 atoms have the lowest charge values, -0.259 and -0.273, respectively. The binding of oxygen (O38) and two nitrogen atoms (N35, N36) to these carbon atoms may be the cause of this lowest carbon value. All of the hydrogen atoms have positive charges, but all of the oxygen and nitrogen atoms have net negative charges, according to the graphical analysis. Among all atoms, the O38 atom has the lowest mulliken charge. this atom is the atom attached to the C2 atom with the highest value and its value is -0.391. We can explain this as follows: nitrogen and oxygen atoms are electronegative atoms and easily attract electrons from neighboring atoms, thus having a negative mulliken charge, but H atoms, on the contrary, are electropositive and give electrons, thus having a positive mulliken charge (Mulliken, 1955). (Table 1).

Table 1. Mulliken atomic charges of the compound

Atoms	B3LYP	Atoms	B3LYP	Atoms	B3LYP
C1	0.295	**C14**	-0.273	**H28**	0.112
C2	0.535	**C15**	-0.134	**H29**	0.112
C3	0.126	**H16**	0.250	**H30**	0.126
C4	-0.154	**H17**	0.139	**H31**	0.133
C5	-0.022	**H18**	0.100	**H32**	0.121
C6	-0.061	**H19**	0.099	**H33**	0.114
C7	0.162	**H20**	0.112	**N34**	-0.219
C8	0.201	**H21**	0.133	**N35**	-0.312
C9	-0.093	**H22**	0.133	**N36**	-0.366
C10	-0.244	**H23**	0.134	**N37**	-0.208
C11	0.410	**H24**	0.139	**O38**	-0.391
C12	-0.258	**H25**	0.113	**O39**	-0.360
C13	-0.259	**H26**	0.104	**O40**	-0.353
		H27	0.119	**O41**	-0.317

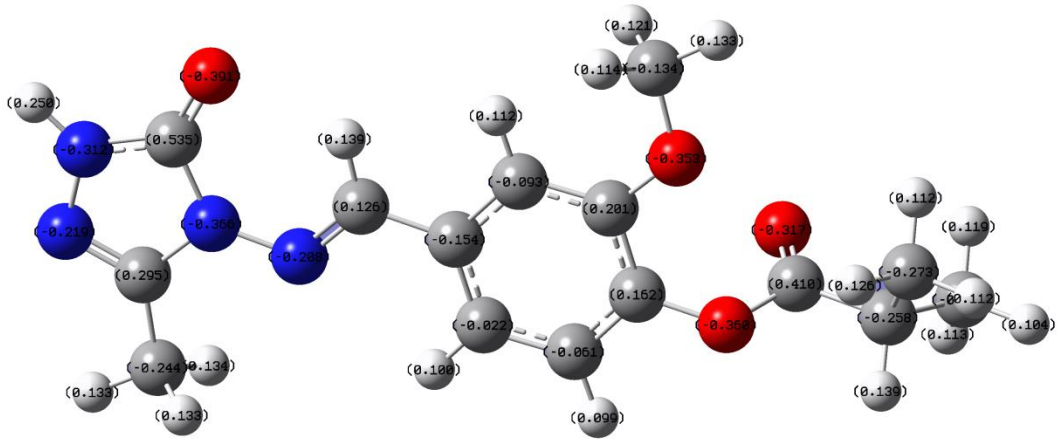

Figure 2. The mulliken atomic charge distribution of the molecule

3.1.3. Thermodynamics properties of compound

At 298.044 K and 1 atm of pressure, thermodynamic properties such the molecule's enthalpy (H^0), heat capacity (CV^0), and entropy (S^0) were computed. These are important thermodynamic parameters to know in a chemical reaction. However, their experimental measurements can be difficult depending on the type of reaction, so they are calculated theoretically. Table 2 provided the thermodynamic parameters that were acquired at the DFT B3LYP/6-311G (d,p) (Kotan et al., 2022).

Table 2. The thermodynamics parameters of the molecule

	B3LYP		B3LYP
Rotational temperatures (Kelvin)		Entropy S(cal/mol-K)	
A	0.03560	Translational	43.168
B	0.00431	Rotational	35.323
C	0.00397	Vibrational	86.972
Rotational constants (GHZ)		Total	165.462
A	0.74173	Zero-point correction (Hartree/Particle)	0.323755
B	0.08975	Thermal correction to Energy	0.346689
C	0.08266	Thermal correction to Enthalpy	0.347633
Thermal Energies E(kcal/mol)		Thermal correction to Gibbs Free Energy	0.269016
Translational	0.889	Sum of electronic and zero-point Energies	-1102.279121
Rotational	0.889	Sum of electronic and thermal Energies	-1102.256187
Vibrational	215.773	Sum of electronic and thermal Enthalpies	-1102.255243
Total	217.550	Sum of electronic and thermal Free Energies	-1102.333859
Thermal Capacity CV(cal/mol-K)		Zero-point vibrational energy (Kcal/mol)	203.15920
Translational	2.981		
Rotational	2.981		
Vibrational	78.096		
Total	84.057		

3.1.4. Molecular Electrostatic Potential (MEPs)

One important technique for examining the molecular structure and chemical properties is the molecular electrostatic potential (MEP) surface (Kotan, et al., 2020). It is a crucial instrument for the explanation of reactive sites in the study of hydrogen bonding interactions and biological identification processes. Using the B3LYP/6–311++G(d,p) standard basis set in gas phase, the optimized structure yields the title molecule's 3D molecular electrostatic potential image, which is shown in Fig. 5. Through the MEP analysis, the Schiff base compound's electrophilic (negative) and nucleophilic (positive) attacks are clarified. The molecule's size, shape, electronegativity, and charge density are all revealed by MEP surfaces. The MEP surface's various colors designate the locations of electrostatic potential. Green denotes neutrality, yellow denotes areas some what rich in electrons, and light blue denotes areas slightly deficient in electrons. The following is the sequence in which the electrical potential increases: red, orange, yellow, green, cyan, and blue are in order (Laraib, et al., 2025; Akbari, et al., 2024).

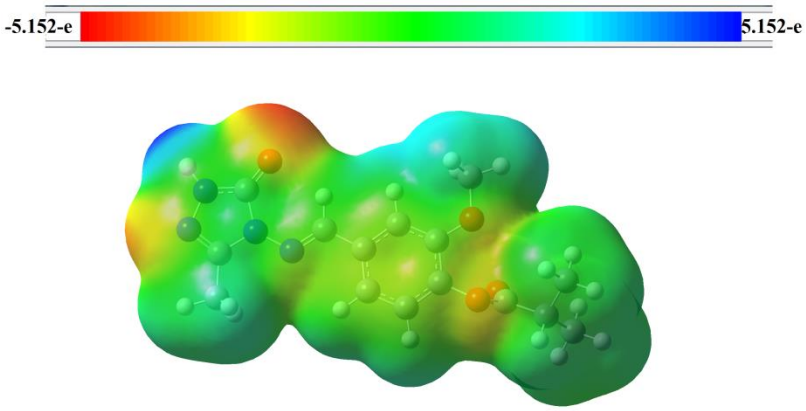

Figure 3. The MEP map of the molecule

3.1.5. HOMO-LUMO Analysis

Both the lowest unoccupied molecular orbital (LUMO) and the highest occupied molecular orbital (HOMO) are important factors in quantum chemistry (Ermiş, 2015). HOMO LUMO orbitals and their energy differ ΔEg, demonstrate the kinetic stability and chemical reactivity of the molecule (Sivaranjani et al., 2015). The HOMO represents the ability to donate an electron, while the LUMO represents the ability to receive one. The energetic behavior of the title chemical was evaluated by performing HOMO-LUMO energy calculations using the B3LYP approach with 6-311++G(d,p) basis sets. Elumo =-6.071 eV and Ehomo =-1.769 eV come from the computation, and their energy difference is ΔEg = 4.302 eV.

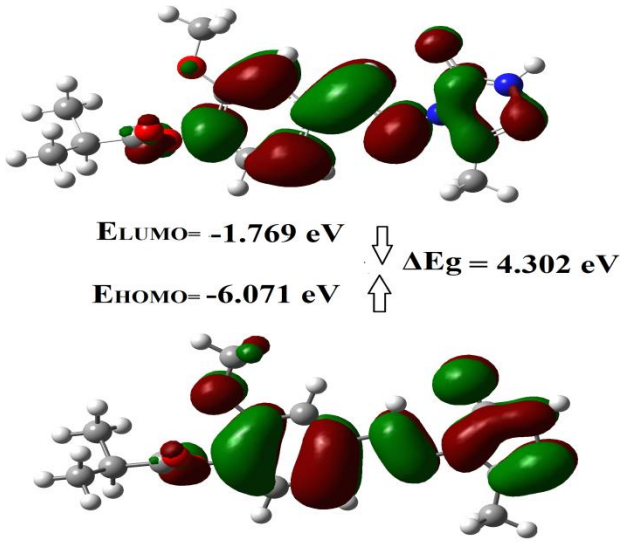

Figure 4. Calculated HOMO-LUMO shapes of the molecula by B3LYP method 6-311G (d,p) basis set

3.1.6. Electronic Parameters

Some electronic parameters of the molecule were calculated using the HOMO-LUMO energy and the energy difference value between them. These properties and their calculated values corresponding are:electron affinity (A), ionization potential (I), electronegativity (χ), global hardness (η), electrophilicity index (ω), nucleophilic index (IP), chemical potential (μ), and global softness (S) and summarized in Tablo 4.

Table 3. Electronic properties of the molecule calculated according to B3LYP methods 6-311G (d,p) basis set

		Hatree	ev	kcal/mol	KJ/mol
LUMO		-0,06501	-1,76952	-40,794	-170,684
HOMO		-0,22311	-6,07098	-140,002	-585,775
electron affinity	**A**	0,06501	1,76897	40,794	170,684
ionization potential	**I**	0,22311	6,07098	140,002	585,775
energy gap	**ΔE**	0,1581	4,30201	99,2082	415,092
electronegativity	**χ**	0,14406	3,91997	90,3981	378,23
chemical potential	**Pi**	-0,14406	-3,91997	-90,3981	-378,23
electrophilic index	**ω**	0,000820274	0,02232	0,51472	2,15363
Nucleophilic index	**IP**	-0,01138794	-0,30987	-7,14597	-29,899
molecular softness	**S**	12,6502	344,221	7938,05	33213,2
molecular hardness	**η**	0,07905	2,15101	49,6041	207,546

3.1.7. SAR analysis

In order to aid in the creation of the most effective novel compounds, the ultimate objective of structure–activity relationship (SAR) investigations is to connect the biological activity of a number of compounds with a few suitable descriptors. The theoretical density of the molecule is calculated by first calculating the theoretical mass and volume. The biological activity is determined by comparing the magnitude of the calculated density value with the LUMO value and the antimicrobial activity of the molecule. The smaller the density and lumo value, the greater the biological activity of that molecule. The volume value was calculated as 196.79 cm^3/mol, the mass as 318.13 amu, and accordingly the density value was found to be 0.61. The lumo value is -1.769.

3.1.8. Non-Lineer Optical Analysis

An electric dipole is produced when a molecule's centers of positive and negative charges are separated. Scientists termed this polarity. The dipole moment's first-order reaction to external electric fields is explained by its linear polarizability (α'). Changes in polarizability affect linear optical characteristics as refractive indices and absorption. A molecule's hyperpolarizability (β) is a measure of its propensity to generate a dipole when exposed to an electric field. Therefore, changes in an atom's or molecule's charge distribution brought on by an electromagnetic field may be measured using hyperpolarizability (Albaaj, et al., 2024). The polar αxx, αxy, αyy, αxz, αyz, αzz values are 347.0804618, 6.4341695, 206.319180, 6.4609758, -6.5792264, 122.0216448 respectively. The HyperPolar βxxx, βxxy, βxyy, βyyy, βxxz, Bxyz, Byyz, βxzz, βyzz, βzzz, βtotal values are -104.2303685, 76.2127511, -80.5605576, -113.3151377, 13.4555739, 7.56322, 3.8792846, 61.1015329, 13.36746, 9.3154853 respectively. The total static dipole moment μtoplam= 1.6572 debye, average linear polarizability α= $33.366x10^{-24}$ esu, anisotropy of polarizability Δα=$29.187x10^{-24}$ esu and initial hyperpolarizability β_{total}= $1.843x10^{-30}$ esu are among NLO properties. These parameters were calculated by B3LYP 6-311G(d,p) basis set and listed in Table 4. The urea molecule serves as the main reference for NLO characteristics. The NLO parameters are α_{total}: $5.07643717x10^{-24}$ esu, Δα:=$2.13568262x10^{-24}$ esu, and β_0= $7.2228469891x10^{-31}$ esu. When compared to the reference material, the NLO values were 6, 14, and 2.5 times higher than urea (Mirdan et al., 2025).

Table 4. Calculated dipole moment, polarizability and hyperpolarizability values

	B3LYP		**B3LYP**
E_{total}	-1102.60287541 a.u.	β_{xxx}	-104.2303685
μ_x	-1.1366	β_{xxy}	-76.2127511
μ_y	0.5323	β_{xyy}	-80.5605576
μ_z	-1.0822	β_{yyy}	-113.3151377
μ_{Toplam}	1.6572 Debye	β_{xxz}	13.4555739
αxx	347.0804618	B_{xyz}	-7.563221
αxy	6.4341695	B_{yyz}	3.8792846
αyy	206.319180	β_{xzz}	61.1015329
αxz	6.4609758	β_{yzz}	13.36746
αyz	-6.5792264	B_{zzz}	9.3154853
αzz	122.0216448	β_{total}	$1.843x10^{-30}$ esu
α_{total}	$33.366x10^{-24}$ esu		
Δα (esu)	$29.187x10^{-24}$ esu		

CONCLUSIONS

The target molecule was calculated in this theoretical work using DFT (B3LYP) techniques using the Gaussian G09W software package and the 6-311++G(d,p) basis set. Calculations were made for the LUMO-HOMO energy, NLO, SAR, ΔEg energy gap, mulliken charge, electrical properties, and thermodynamic data. There was discussion over the theoretical computation's dependability. The most electrophilic and nucleophilic areas of the molecule were identified by visualizing its surface maps. Also the molecule is a nonlinear molecule. This study has once again shown that computational chemistry, which allows comparison of theoretically obtained data with some experimental data, generally supports the experimental one.

4.REFERENCES

Akbari, Z., Stagno, C., Iraci, N., Efferth, T., Omer, E. A., Piperno, A., ... & Micale, N. (2024). Biological evaluation, DFT, MEP, HOMO-LUMO analysis and ensemble docking studies of Zn (II) complexes of bidentate and tetradentate Schiff base ligands as antileukemia agents. *Journal of Molecular Structure*, *1301*, 137400.

Alam, M. S., Choi, J. H., & Lee, D. U. (2012). Synthesis of novel Schiff base analogues of 4-amino-1, 5-dimethyl-2-phenylpyrazol-3-one and their evaluation for antioxidant and anti-inflammatory activity. *Bioorganic & medicinal chemistry*, *20*(13), 1., 4103-4108.

Albaaj, L. T. T., Hassan, Q. M., Dhumad, A. M., Sultan, H. A., & Emshary, C. A. (2024). Synthesis of a New Schiff Base: Nonlinear Optical Properties Investigations. *Journal of Fluorescence*, 1-14.

Dennington, R., Keith T., Millam (Eds.). (2009). J. GaussView, Version 5, Semichem Inc., Shawnee Mission KS.

El-Sherief, H. A., Youssif, B. G., Bukhari, S. N. A., Abdel-Aziz, M., & Abdel-Rahman, H. M. (2018). Novel 1, 2, 4-triazole derivatives as potential anticancer agents: Design, synthesis, molecular docking and mechanistic studies. *Bioorganic chemistry*, *76*, 314-325.

Ermiş, E. (2018). Synthesis, spectroscopic characterization and DFT calculations of novel Schiff base containing thiophene ring. *Journal of Molecular Structure*, *1156*, 91-104.

Franco-Pérez, M., & Gázquez, J. L. (2019). Electronegativities of Pauling and Mulliken in density functional theory. *The Journal of Physical Chemistry A*, *123*(46), 10065-10071.

Frisch, M. J., Trucks, G. W., Schlegel, H. B., Scuseria, G. E., Robb, M. A., Mennucci, B., Petersson, G. A., Nakatsuji, H., Caricato, M., Li, X. et al., (2009). Gaussian 09. Revision C.01. Gaussian. Inc. Wallingford. CT.

Gao, F., Wang, T., Xiao, J., & Huang, G. (2019). Antibacterial activity study of 1, 2, 4-triazole derivatives. *European journal of medicinal chemistry*, *173*, 274-281.

Gören, K., Kotan, G., Manap, S., & Yüksek, H. (2024). Synthesis, Antimicrobial and Antioxidant Activities of 3-Alkyl (aryl)-4-(3-methoxy-4-hydroxybenzylideneamino)-4, 5-dihydro-1 H-1, 2, 4-triazol-5-one Derivatives. *Chemistry Africa*, 1-17.

Gürsoy Kol, Ö., Manap, S., Beytur, M., Aytemiz, F., Alkan, M., & Yüksek, H. (2025). Antibacterial and antioxidant activities of novel 2-ethoxy-4-[(4, 5-dihydro-1H-1, 2, 4-triazol-5-one-4-yl) azomethine]-phenyl 3-methoxybenzoate derivatives. *Journal of Research in Pharmacy*, *29*(2).

Jesmin, M., Islam, M. K., & Ali, S. M. M. (2014). Analgesic and anti-inflammatory activities of some transition metal schiff base complexes. *International Letters of Chemistry, Physics and Astronomy*, *8*.

Kotan, G., Gökce, H., Akyıldırım, O., Yüksek, H., Beytur, M., Manap, S., & Medetalibeyoğlu, H. (2020). Synthesis, Spectroscopic and Computational Analysis of 2-[(2-Sulfanyl-1 H-benzo [d] imidazol-5-yl) iminomethyl] phenyl Naphthalene-2-sulfonate. *Russian Journal of Organic Chemistry*, *56*, 1982-1994.

Kotan, G., Manap, S., & Yüksek, H. Synthesis, Characterization, Antioxidant and DFT Studies of Some Novel Schiff Base Compounds. *Journal of Computational Biophysics and Chemistry*, *21*(1), 47-63, 2022.

Kotan, G., & Yüksek, H. (2016). Theoretical and Spectroscopic Studies of (E)-3-Benzyl-4-((4-Isopropylbenzylidene)-Amino)-1-(Morpholinomethyl)-1H-1, 2, 4-triazol-5 (4H)-one Molecule. *Journal of the Turkish Chemical Society Section A: Chemistry*, *3*(3), 381-392.

Laraib, A., UrRehman, S., Jamil, S., Zia, M. A., Muhammad, S., Bibi, S., ... & Bai, F. Q. (2025). Aloin as a Potential Anti-Breast Cancer Agent: Insights From Molecular Docking and Density Functional Theory (DFT) Analysis. *ChemistrySelect*, *10*(17), 202406211.

Manjunath, M., Kulkarni, A. D., Bagihalli, G. B., Malladi, S., & Patil, S. A. (2017). Bio-important antipyrine derived Schiff bases and their transition metal complexes: Synthesis, spectroscopic characterization, antimicrobial, anthelmintic and DNA cleavage investigation. *Journal of Molecular Structure*, *1127*, 314-321.

Matela, G. (2020). Schiff bases and complexes: a review on anti-cancer activity. *Anti-Cancer Agents in Medicinal Chemistry (Formerly Current Medicinal Chemistry-Anti-Cancer Agents)*, *20*(16), 1908-1917.

Mirdan, G. A., Hassan, Q., Kadhum, M. Y., Emshary, C. A., Hussein, K. A., Sultan, H. A., ... & Abdullmajed, H. A. (2025). Study of DFT, synthesis, and nonlinear optical properties of a Schiff base compound. *Journal of Fluorescence*, 1-14.

Mulliken, R. S. (1955). Electronic population analysis on LCAO–MO molecular wave functions. I. *The Journal of Chemical Physics*, *23*(10), 1833-1840.

Meeran, I. S., Tajudeen, S. S., Dusthakeer, V. A., & Shabeer, T. K. (2018). An insight into the anti-tubercular potential of Schiff bases. *J Pharma Chem Bio Sci*, *6*(3), 158-177.

Paprocka, R., Wiese, M., Eljaszewicz, A., Helmin-Basa, A., Gzella, A., Modzelewska-Banachiewicz, B., & Michalkiewicz, J. (2015). Synthesis and anti-inflammatory activity of new 1, 2, 4-triazole derivatives. *Bioorganic & Medicinal Chemistry Letters*, *25*(13), 2664-2667.

Rao, B. M., Sangaraju, S., Srinivasu, M. K., Madhavan, P., Devi, M. L., Kumar, P. R., ... & Balaji, T. S. (2006). Development and validation of a specific stability indicating high performance liquid chromatographic method for rizatriptan benzoate. *Journal of pharmaceutical and biomedical analysis*, *41*(4), 1146-1151.

Raouf, H., Beyramabadi, S. A., Allameh, S., & Morsali, A. (2019). Synthesis, experimental and theoretical characterizations of a 1, 2, 4-triazole Schiff base and its nickel (II) complex. *Journal of molecular structure*, *1179*, 779-786.

Salihović, M., Pazalja, M., Halilović, S. Š., Veljović, E., Mahmutović-Dizdarević, I., Roca, S., ... & Trifunović, S. (2021). Synthesis, characterization, antimicrobial activity and DFT study of some novel Schiff bases. *Journal of molecular structure*, *1241*, 130670.

Sivaranjani, T., Xavier, S., & Periandy, S. (2015). NMR, FT-IR, FT-Raman, UV spectroscopic, HOMO–LUMO and NBO analysis of cumene by quantum computational methods. *Journal of Molecular structure*, *1083*, 39-47.

Sumrra, S. H., Kausar, S., Raza, M. A., Zubair, M., Zafar, M. N., Nadeem, M. A., ... & Rashid, U. (2018). Metal based triazole compounds: Their synthesis, computational, antioxidant, enzyme inhibition and antimicrobial properties. *Journal of Molecular Structure*, *1168*, 202-211.

Wolinski K, Hinton JF, Pulay P 1990. Efficient implementation of the gauge-independent atomic orbital method for NMR chemical shift calculations. Journal of the American Chemical Society, 112(23): 8251-8260.

Yüksek, H., Özdemir, G., Manap, S., Yılmaz, Y., Kotan, G., Gürsoy-Kol, Ö., & Alkan, M. (2020). Synthesis and Investigations of Antimicrobial, Antioxidant Activities of Novel Di-[2-(3-alkyl/aryl-4, 5-dihydro-1H-1, 2, 4-triazol-5-one-4-yl)-azomethinephenyl] Isophtalates and Mannich Base Derivatives. *ACTA Pharmaceutica Sciencia*, *58*(1).

➢ *ORAL PRESENTATION*

Bazı B Vitaminlerin Gama Radyasyonları ile Etkileşimlerinin Araştırılması

Hatice Gürel Özdemir[1*] (*ORCID https://orcid.org/0000-0002-6590-2334.),* Ferdi Akman [2] (*ORCID: https://orcid.org/* 0000-0002-8838-1762), Mustafa Recep Kaçal[3] (ORCID ID: https://orcid.org/ 0000-0002-3183-5516

[*1] İstinye Üniversitesi, Sağlık Hizmetleri Meslek Yüksekokulu, Tıbbi Hizmetler ve Teknikler Bölümü, Optisyenlik Programı, İstanbul, Türkiye
[2] Bingöl Üniversitesi, Sosyal Bilimler Meslek Yüksekokulu, Mülkiyet Koruma ve Güvenlik Bölümü, İş Sağlığı ve Güvenliği Programı, Bingöl, Türkiye
[3]Giresun Üniversitesi, Fen-Edebiyat Fakültesi, Fizik Bölümü, Giresun, Türkiye

*Sorumlu yazar e-posta: hatice.ozdemir@istinye.edu.tr

Özet
Suda çözünebilen B grubu vitaminler, sinir sistemi sağlığı, hücre metabolizması ve kırmızı kan hücresi yapımına katkı sağlamaktadır. Bu sebeple vitaminler vücut için hayati öneme sahiptir. Gama ışınları, yüksek giricilik özelliğine sahip olan iyonlaştırıcı radyasyon türüdür. İyonlaştırıcı radyasyona uzun süre maruz kalmak canlılarda olumsuz sonuçlara sebep olmaktadır. İyonlaştırıcı radyasyonların, organik bileşikler üzerinde de kimyasal ve biyolojik değişikliklere sebep olma ihtimali bulunmaktadır. Vitaminlerinin iyonlaştırıcı radyasyona maruziyeti sonucunda bu etkiler görülebilir. Sunulan çalışmada, bazı B vitaminlerinin (Riboflavin (B2), Niasin (B3), Biyotin (B7) ve Siyanokobalamin (B12) gama radyasyonu ile etkileşimlerini araştırmak için 10-150 keV enerji aralığında (15 farklı enerjide) kütle azaltma katsayısı (μ/ρ), lineer azaltma katsayısı (μ) ve ortalama serbest yol (OSY) parametre değerleri WinXCOM programı kullanılarak, etkin atom numarası ($Z_{etk.}$) değerleri ise EpiXS programı kullanılarak araştırılmıştır. İncelenen B grubu vitaminlerin μ/ρ ve $Z_{etk.}$ değerleri dikkate alındığında B12 vitaminin tüm enerji değerlerinde diğer vitaminlerden daha fazla gama ışınlarıyla etkileşime girdiği görülmüştür. İncelenen B grubu vitaminlerin μ ve OSY değerleri dikkate alındığında ise B7 vitaminin düşük enerji değerinde diğer vitaminlerden daha fazla gama ışınlarıyla etkileşime girdiği görülmüştür.
Anahtar Kelimeler: B vitamini, Gama radyasyonu, WinXCOM, EpiXS

Investigation of Interactions of Some B Vitamins With Gamma -Rays

Abstract
Water-soluble B vitamins contribute to nervous system health, cell metabolism and red blood cell production. For this reason, vitamins are vital for the body. Gamma rays are a type of ionizing radiation that has a high penetrating property. Long-term exposure to ionizing radiation causes negative results in living things. Ionizing radiations may also cause chemical and biological changes in organic compounds. These effects can be seen as a result of exposure of vitamins to ionizing radiation. In the present study, in order to investigate the interactions of some B vitamins (Riboflavin (B2), Niacin (B3), Biotin (B7) and Cyanocobalamin (B12) with gamma radiation, mass attenuation coefficient (μ/ρ), linear attenuation coefficient (μ) and mean free path (MFP) parameter values were investigated using WinXCOM program in the energy range of 10-150 keV (at 15 different energies), and effective atomic number (Z_{eff}) values were investigated using EpiXS program. Considering the μ/ρ and $Z_{etk.}$ values of the studied B group vitamins, it was seen that vitamin B12 interacted with gamma rays more than other vitamins at all energy values.. When the μ and MFP values of the studied B group vitamins were taken into consideration, it was seen that vitamin B7 interacted with gamma rays more than other vitamins at low energy values.
Keywords: Vitamin B, Gamma radiation, WinXCOM, EpiXS

GİRİŞ

Günümüzde atom veya molekülden elektron koparacak kadar yüksek enerjiye sahip olan elektromanyetik dalga türü iyonlaştırıcı radyasyon, radyasyon fiziği, tıbbi fizik, bilimsel çalışmalar, endüstriyel uygulamalar gibi pek çok alanda yaygın olarak kullanılmaktadır. Endüstriyel tarımda radyasyon; verimli ve dayanıklı bitkiler üretmek için, gıdalardaki mikroorganizmaları yok etmek için, zararlı böcekler sterilize etmek ve böcek popülasyonlarını azaltmak için ve tohumlardaki hastalık etmenleri yok etmek için kullanılmaktadır. Vücuda

besinler aracılığıyla alınan vitaminler, bu besinlerin doğal ve yapay radyasyon kaynaklarına maruz kalması nedeniyle radyasyondan etkilenmektedir.

Vitaminler, vücut sağlığının korunabilmesi ve organizmanın metabolik işlevini düzgün bir şekilde yerine getirebilmesi için gerekli olan organik moleküllerdir. Vücudumuz bu organik moleküllerin çok az miktarını üretebildiği için vitaminlerin dışarıdan besin yoluyla alınması gerekmektedir. Vitaminlerin pek çok çeşidi bulunmakta ve her birinin vücutta farklı görevi bulunmaktadır. Vitamin eksikliği vücutta sağlık sorunlarının oluşmasına sebep olmaktadır. Vücut için hayati öneme sahip olan B vitaminleri suda çözünebilirler. Vitaminler enerji kaynağı olmasalar da yağ ve karbonhidratların enerjiye dönüşmesine yardımcı olmaktadır (Ötleş ve ark., 2011). Ayrıca B grubu vitaminler, sinir sistemi sağlığı, hücre metabolizması ve kırmızı kan hücresi yapımına katkı sağlamaktadır.

B2 vitamini, kornea incelmesini tedavi etmek için kullanılmaktadır. Oral olarak alındığında ise migren ağrılarının sıklığını azaltmaktadır. B2 vitamini eksikliğinde ise deri, burun, dudak ve göz kenarlarında yara oluşumu, kornea iltihaplanması ve sinir sistemi bozuklukları görülebilir (Rathee ve ark., 2022). B3 vitamini, hücresel enerji metabolizmasında önemli rol oynayan nikotinamid adenin dinükleotid (NAD) ve nikotinamid adenin dinükleotid fosfat (NADPH) koenzimlerinin öncüsüdür. NAD koenzimi yağ, karbonhidrat, protein ve alkolün katabolizması, hücre sinyalizasyonu ve DNA onarımı için gerekli iken NADPH koenzimi yağ asidi ve kolesterol sentezi için gereklidir. B3 vitamini eksikliği, gerginlik, anksiyete ve depresyon gibi bilişsel semptomların yanı sıra manik depresyon ve şizofreniyle kendini gösterebilmektedir. B3 vitamini eksikliği, iltihaplı cilt, dermatit, ishal, bunama ve ağız çevresinde yaralara neden olmaktadır. (Mikkelsen ve ark., 2019). B7 vitamini, cilt, sinir, sindirim sistemi sağlığına ve enerji salınımına yardımcı olmaktadır. Ayrıca embriyonun gelişmesine de yardımcı olmaktadır. B7 vitamin eksikliği nörolojik hastalıklara, cilt sorunlarına sebep olabilmektedir (Naveed ve ark., 2015). B12 vitamini DNA sentezi ve hücresel enerji üretimi içim oldukca gereklidir. B12 vitamini özellikle doğurganlık çağındaki kadınlar ve yaşlı insanlar için önemli bir vitamindir, ancak optimum sağlık için tüm yaşam döngüsü boyunca yeterli B12 vitamini durumu gereklidir (O'Leary ve ark., 2010). Demans ve depresyonla ilişkili bazı davranışsal veya psikolojik sorunlar B12 takviyesi ile iyileşebilir (Ryan-Harshman ve ark., 2008).

B vitaminleri üzerindeki radyasyon etkilerini inceleyen çeşitli bilimsel araştırmalar literatürde yer almaktadır. Villavicencio ve ark., (2000) yaptıkları çalışmada ^{60}Co radyasyon kaynağından salınan radyasyonun iki çeşit Brezilye fasülyesinde bulunan B6 vitamini içeriğine olan etkisini araştırmışlardır. Böcek istilasını önlemek amacıyla ışınlama uygulanan fasulyelerde, eğer doz 5 kGy'nin üzerine çıkarsa, ürünü tüketilemez hâle getiren renk, koku, tat ve şekilsel bozulmaların ortaya çıkabileceğini ifade etmişlerdir. Richardson ve ark., (1961) yaptıkları çalışmada gama ışınlama, dondurma ve konserve yöntemleri kullanılarak 9-15 ay saklanan bazı gıdalardaki B6 vitaminin içeriğini değerlendirmişlerdir. Gama ışınlama ve ısıl işlem sonucu saklanan bazı gıdalarda B6 vitaminini aktivitesinin dondurulmuş gıdalara kıyasla %40 ile %60 oranında daha düşük olduğunu ifade etmişlerdir.

Sunulan çalışmada, Riboflavin (B2), Niasin (B3), Biyotin (B7) ve Kobalamin (B12) vitaminlerinin gama radyasyonları ile etkileşimleri araştırılmıştır. Gama radyasyonunun B vitaminleri üzerindeki etkilerini belirlemek için, WinXCOM bilgisayar programı ve/veya EpiXS programı kullanılarak 10-150 keV enerji aralığında on beş farklı enerjide bazı zırhlama parametreleri incelenmiştir. Bu zırhlama parametreleri kütle azaltma katsayısı (μ/ρ, cm^2/g), lineer azaltma katsayısı(μ), ortalama serbest yol değeri (OSY) ve etkin atom numarası ($Z_{etk.}$) parametre değerleridir. Vücut sağlığı açısından hayati öneme sahip olan B vitaminlerinin gama radyasyonları ile etkileşimlerinin belirlenmesi, bilimsel literatüre önemli düzeyde katkı sunacaktır.

MATERYAL VE METOD

B grubu vitaminlerinin gama radyasyonları ile etkileşimleri, WinXCOM bilgisayar programı ve/veya EpiXS bilgisayar programı yardımıyla teorik olarak araştırılmıştır. WinXCOM bilgisayar programı sayesinde 1 keV ile 100 GeV enerji aralığındaki elementlerin, bileşiklerin veya karışımların toplam kütle azaltma katsayıları hesaplanabilmektedir. Ayrıca fotoelektrik tesir kesiti, Compton saçılması, çift oluşum tesir kesiti gibi değerleri ayrı ayrı veren bir programdır (Gerward ve ark., 2004). WinXCOM ile kütle azaltma katsayısı belirlenirken incelenen B vitaminlerinin elemental ağırlık oranlarının ve incelenen foton enerji değerlerinin girilmesi gerekmektedir. EpiXS, çeşitli elementlerin ve karışımların geniş enerji aralığında zırhlama parametrelerini hesaplamak için kullanılan çevrimiçi kullanılan bilgisayar programıdır. Zırhlama parametre sonuçları için ENDF/B-VIII (EPICS2017-foton ve elektron kütüphanesi) ve ENDF/B-VI.8 (EPDL97-foton kütüphanesi) olmak üzere iki kütüphane uygulanabilmektedir (Gili ve ark., 2025). İncelenecek olan vitaminlerinin kimyasal içerikleri ve yoğunlukları hakkındaki bilgiler Tablo 1'de sunulmuştur.

Tablo 1. B grubu vitaminlerin kimyasal formülü ve yoğunlukları

Vitamin Adı	Kısaltma İfadesi	Kimyasal Formulü	ρ (g/cm^3)
Riboflavin	B2	$C_{17}H_{20}N_4O_6$	1,211
Niasin	B3	$C_6H_5NO_2$	1,473
Biyotin	B7	$C_{10}H_{16}N_2O_3S$	1,300
Siyanokobalamin	B12	$C_{63}H_{88}CoN_{14}O_{14}P$	0,945

B vitaminlerinin gama radyasyonu ile etkileşimini değerlendirmek için WinXCOM bilgisayar programı yardımıyla doğrudan belirlenebilen zırhlama parametresi kütle azaltma katsayısıdır (μ/ρ, cm^2/g). Birim alan başına düşen kütlenin gelen foton ile etkileşme ölçüsünün ihtimaliyetini ifade etmektedir. Malzemenin faz halinden ve yoğunluğundan bağımsız bir parametredir. Birden fazla element içeren malzemelerin teorik kütle azaltma katsayısı değerleri Denklem 1'de verilen karışım kuralı yardımıyla hesaplanmaktadır.

$$\left(\frac{\mu}{\rho}\right)_i = \sum_i W_i \left(\frac{\mu}{\rho}\right)_i \quad (1)$$

Burada W_i ve $(\mu/\rho)_i$ terimleri sırasıyla malzeme içindeki i. elementin ağırlık kesrini ve kütle azaltma sayısını ifade etmektedir. (Kaçal ve ark.,2020).

Lineer azaltma katsayısı (μ, cm^{-1}), malzeme içinden geçen fotonların birim uzunluk başına etkileşime girme olasılığını ifade etmektedir. Kütle azaltma katsayısının yoğunluk ile çarpılması ile hesaplanmaktadır. Lineer azaltma katsayısı, foton enerjisine, malzemenin yapısına ve yoğunluğuna bağlı bir parametre olduğu için kütle azaltma katsayısına kıyasla daha kapsamlı bilgi sunmaktadır (Oğul ve ark., 2023). Lineer azaltma katsayısının tersi ile elde edilen ortalama serbest yol parametresi (OSY, cm), bir fotonun malzeme üzerinde kat ettiği ortalama mesafeyi ifade etmektedir ve Denklem 2 yardımıyla hesaplanmaktadır.

$$OSY = \frac{1}{\mu} \quad (2)$$

Birden fazla elementten oluşan malzemelerde atom numarası yerine etkin atom numarası değerinin kullanılması gerekmektedir. Etkin atom numarası ($Z_{etk.}$) parametresi, malzemeyi oluşturan atomların gelen gama ışını fotonlarıyla etkileşime girme olasılığının, malzemeyi oluşturan elektronların gelen gama ışını fotonlarıyla etkileşime girme olasılığına oranını vermektedir ve Denklem 3 yardımıyla hesaplanmaktadır.

$$Z_{etk.} = \frac{\sigma_{t,a}}{\sigma_{t,e}} = \frac{\sum f_i A_i \left(\frac{\mu}{\rho}\right)_i}{\sum f_j \frac{A_j}{Z_j}\left(\frac{\mu}{\rho}\right)_j} \quad (3)$$

Burada $\sigma_{t,a}$ atomik tesir kesiti değerini, $\sigma_{t,e}$ ise elektronik tesir kesiti değerlerini vermektedir. f_i, A_i, Z_i terimleri ise sırasıyla i. elementin malzeme içindeki bolluğunu, i. elementin atom ağırlığını ve i. elementin atom numarasını ifade etmektedir (Turhan ve ark.,2020; Erkoyuncu ve ark., 2025).

BULGULAR ve TARTIŞMA

Sunulan çalışmada, B2, B3, B7 ve B12 vitaminlerinin gama radyasyonu ile etkileşimi incelenmiştir. WinXCOM bilgisayar programı ve/veya EpiXS programı kullanılarak 10-150 keV enerji aralığında on beş farklı enerjide araştırma yapılmıştır.

WinXCOM bilgisayar programı yardımıyla ilk belirlenen parametre değeri, kütle azaltma katsayıdır. Malzemenin yoğunluğundan etkilenmeyen bu parametre sonuçlarının enerjiye göre değişimi Şekil 1'de sunulmaktadır. Şekil 1 kapsamlı bir şekilde incelendiğinde μ/ρ'nun artan foton enerjisiyle birlikte üstel olarak azaldığı görülmektedir. Bunun sebebi farklı foton enerjilerinde farklı etkileşim tesir kesitlerinin baskın olmasıdır. Düşük enerji bölgelerinde fotoelektrik olay daha baskındır. Fotoelektrik tesir kesiti, yaklaşık olarak Z^{4-5} ve $E^{-3.5}$ ile orantılıdır. Bu sebeple keskin azalmalar görülmektedir (Atom numarasını ifade eden Z, düşük

enerjilerde 4 ile yüksek enerjilerde ise 5 ile orantılıdır.). Orta enerji bölgelerinde Compton saçılma olayı daha baskındır. Compton saçılması tesir kesiti yaklaşık olarak Z ve E^{-1} ile orantılıdır. Yüksek enerji bölgesinde ise çift oluşum olayı daha baskındır. Çift oluşum tesir kesiti ise yaklaşık olarak Z^2 ve E ile orantılıdır. Bu sebeple orta ve yüksek enerji bölgelerinde artan enerjiye bağlı üstel azalmanın minimum seviyede olduğu ilgili şekilden açıkça görülmektedir. En yüksek kütle azaltma katsayısı değerinin 10 keV enerji değerinde B12 vitamininde olduğu görülmektedir. 150 keV enerji değerinde incelenen B grubu vitaminlerin μ/ρ değerleri B12> B7> B2>B3 şeklinde sıralanmaktadır. Bu sonuçlardan B12 vitaminin tüm enerji değerlerinde diğer vitaminlerden daha fazla gama ışınlarıyla etkileşime girdiği görülmektedir.

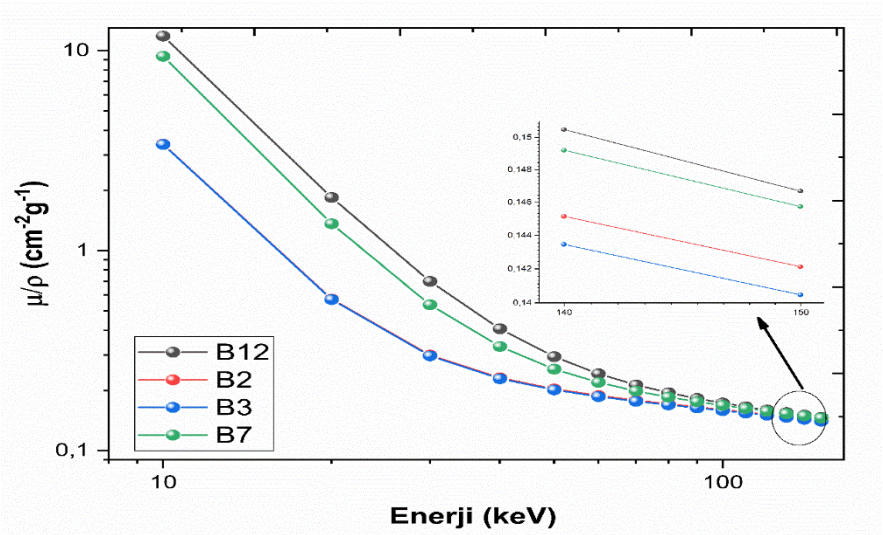

Şekil 1.İncelenen B grubu vitaminlerin kütle azaltma katsayısı sonuçlarının foton enerjisi ile değişimi

Kütle azaltma katsayısından sonra incelenen diğer parametre lineer azaltma katsayısıdır. Lineer azaltma katsayısı, yoğunluğa bağlı bir parametre olduğu için incelenen diğer parametrelere kıyasla daha kullanışlıdır. B vitaminlerinin μ sonuçları Tablo 2 ve Şekil 2'de sunulmuştur. Şekil 2'den lineer azaltma katsayısı değerlerinin de tıpkı kütle azaltma katsayısı değerlerinde olduğu gibi artan foton enerjisi ile azaldığı görülmektedir. Bu sonuç, foton enerjisine göre değişen etkileşim tesir kesir kesitlerinin farklılık göstermesinden kaynaklanmaktadır ve etkileşim tesir kesitlerinin enerjiye bağlı değişimi kütle azaltma katsayısı parametresinde kapsamlı bir şekilde ifade edilmiştir. En yüksek μ değerinin 10 keV enerji değerinde B7 vitamininde olduğu görülmektedir. 150 keV enerji değerinde ise B3 vitaminin μ değeri B12 vitamini değerinden yaklaşık %49, B2 vitamininden yaklaşık %20,2, B7 vitamininden yaklaşık %9,2 daha fazladır.

Tablo 2. B grubu vitaminlerin lineer azaltma katsayısı ve etkin atom numarası sonuçları

Enerji (keV)	B2		B3		B7		B12	
	μ (cm^{-1})	Zetk.	μ (cm^{-1})	Zetk.	μ (cm^{-1})	Zetk.	μ (cm^{-1})	Zetk.
10	4,1227	6,7089	4,9986	6,7376	12,2010	11,1665	11,1743	14,6301
20	0,6931	5,6968	0,8382	5,9043	1,7720	9,2734	1,7429	12,3598
30	0,3635	4,9340	0,4385	5,2363	0,6970	7,0409	0,6631	8,9614
40	0,2800	4,5882	0,3372	4,9216	0,4309	5,7164	0,3836	6,8109
50	0,2463	4,4318	0,2964	4,7768	0,3321	5,0379	0,2785	5,6672
60	0,2280	4,3534	0,2743	4,7036	0,2850	4,6804	0,2288	5,0502
70	0,2161	4,3096	0,2599	4,6625	0,2582	4,4792	0,2013	4,6986
80	0,2072	4,2837	0,2492	4,6382	0,2408	4,3587	0,1840	4,4851
90	0,2001	4,2666	0,2406	4,6221	0,2284	4,2817	0,1722	4,3495
100	0,1941	4,2555	0,2333	4,6116	0,2189	4,2309	0,1635	4,2584
110	0,1888	4,2472	0,2269	4,6039	0,2112	4,1951	0,1566	4,1950
120	0,1840	4,2414	0,2212	4,5984	0,2046	4,1696	0,1510	4,1497
130	0,1797	4,2370	0,2160	4,5943	0,1990	4,1509	0,1463	4,1164
140	0,1758	4,2335	0,2113	4,5910	0,1940	4,1366	0,1422	4,0911
150	0,1721	4,2308	0,2069	4,5885	0,1894	4,1256	0,1386	4,0715

Ortalama serbest yol (OSY) parametre değeri, başlangıçtaki radyasyon şiddetinin %36,8'inin geçebildiği numune kalınlığını ifade etmektedir. μ değeri ile ters orantılı olan bu parametre değeri ne kadar küçük ise gama radyasyonunun madde ile etkileşim ihtimali o kadar fazladır. İncelenen B grubu vitaminlerinin OSY değerlerinin foton enerjisine göre değişimi Şekil 3'te sunulmaktadır. Şekil 3'ten artan foton enerjisi ile OSY değerlerinin arttığı görülmektedir. En düşük OSY değerinin 10 keV enerji değerinde B7 vitamininde olduğu görülmektedir.150 keV enerji değerinde ise B3 vitamini en düşük OSY değerine sahiptir. μ ve OSY parametrelerinin sonuçlarından; düşük enerji değerlerinde B7 vitamininin diğer vitaminlerden daha fazla gama ışınlarıyla etkileşime girdiğini, yüksek enerji değerlerinde ise B3 vitamininin diğer vitaminlerden daha fazla gama ışınlarıyla etkileşime girdiğini ifade edebiliriz.

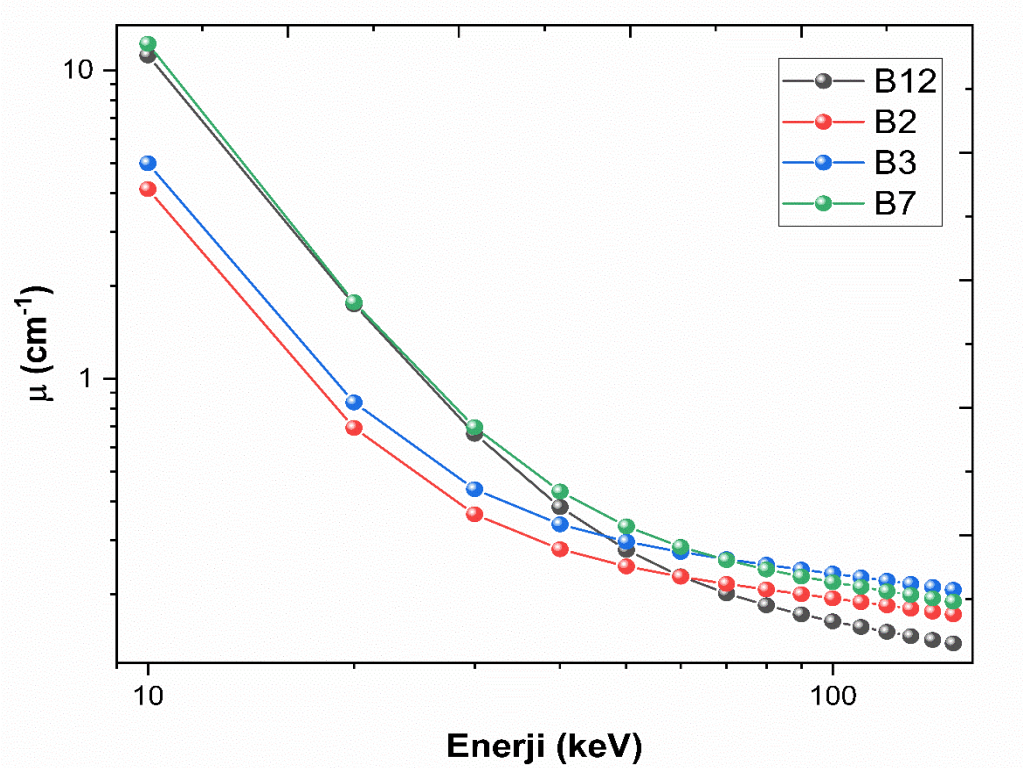

Şekil 2. İncelenen B grubu vitaminlerin μ sonuçlarının foton enerjisi ile değişimi

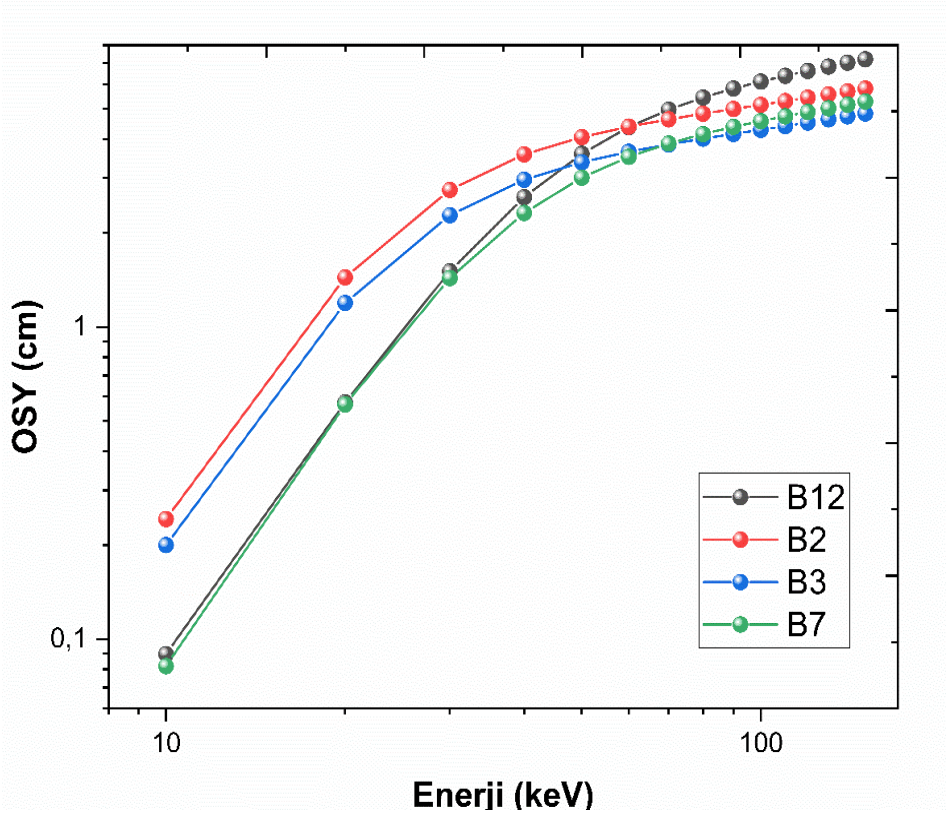

Şekil 3. İncelenen B grubu vitaminlerin OSY sonuçlarının foton enerjisi ile değişimi

B vitaminlerinin etkin atom numarası ($Z_{etk.}$) parametre değerleri EpiXS programı yardımıyla belirlenmiştir. Etkin atom numarası parametre sonuçları Tablo 1 ve Şekil 4'te sunulmuştur. $Z_{etk.}$ parametre değerleri gama ve X-ışınlarının malzeme üzerindeki etkilerini belirlemede kritik öneme sahiptir. $Z_{etk.}$ parametre değeri arttıkça, vitaminlerin gama radyasyonunu soğurma kapasitesi de artmaktadır. Tablo 1'den görüldüğü üzere en yüksek $Z_{etk.}$ parametre değeri 10 keV enerji değerinde B12 vitaminindedir. Bu sonuç, B12 vitamininin diğer

vitaminlerden daha fazla gama ışınlarıyla etkileşime girdiğini ifade etmektedir. Ayrıca bu enerji değeri için B12 vitamininin $Z_{etk.}$ değeri B2, B3 ve B7 vitaminlerinden sırasıyla 2,18, 2,17 ve 1,3 kat daha fazladır.

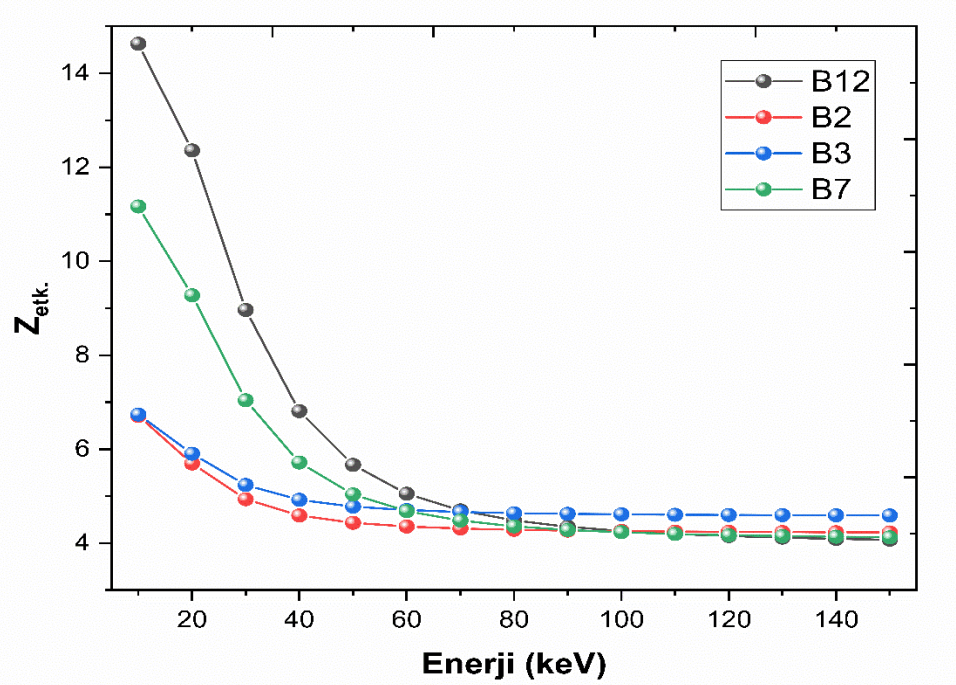

Şekil 4. İncelenen B grubu vitaminlerinin Z_{etk} sonuçlarının foton enerjisi ile değişimi

SONUÇ

Sunulan çalışmada B2, B3, B7 ve B12 vitaminlerinin gama ışınlarıyla etkileşime girme potansiyelleri 10-150 keV enerji aralığında on beş farklı enerji için araştırılmıştır. Araştırılan B gurubu vitaminlerin gama ışınları ile etkileşime girme potansiyeli, WinXCOM bilgisayar programı ve/veya EpiXS programı yardımıyla belirlenmiştir. Gama ışınları ile B grubu vitaminlerinin etkileşime girme potansiyelinin belirlenmesinde kullanılan parametreler kapsamlı bir şekilde incelendiğinde; μ/ρ, μ ve $Z_{etk.}$ parametre değerlerinin artan foton enerjisi ile azaldığı, OSY parametre değerlerinin ise artan gama enerjisi ile arttığı görülmektedir. μ/ρ ve $Z_{etk.}$ parametre değeri sonuçları 10 keV enerji değeri için B12 vitaminin diğer vitaminlerden daha fazla gama ışınları ile etkileşime girdiğini göstermektedir. Aynı enerji değeri için μ ve OSY parametre değeri sonuçları ise B7 ve B12 vitaminin diğer vitaminlerden daha fazla gama ışınları ile etkileşime girdiğini göstermektedir. B7 vitaminin μ değerinin en yüksek çıkmasının sebebi bu parametrenin yoğunluğa bağlı olması ve B7 vitamininin yoğunluk değerinin B12 vitamininden daha yüksek olmasıdır.

KAYNAKLAR

Erkoyuncu, İ., Demirkol, İ., Akman, F., Kaçal, M. R., Polat, H., & Dilsiz, K. (2025). A study on the mechanical and radiation shielding characteristics of concrete samples reinforced with brass alloy and boron carbide. *Applied Radiation and Isotopes*, *217*, 111641.

Gerward, L., Guilbert, N., Jensen, K. B., & Levring, H. (2004). WinXCom—a program for calculating X-ray attenuation coefficients. Radiation physics and chemistry, 71(3-4), 653-654.

Gili, M. B. Z., & Jecong, J. F. M. (2025). The potential application of mining wastes and slag as radiation shielding: a characterization study using EpiXS. *Arabian Journal for Science and Engineering*, *50*(5), 3047-3058.

Kaçal, M. R., Polat, H., Oltulu, M., Akman, F., Agar, O., & Tekin, H. O. (2020). Gamma shielding and compressive strength analyses of polyester composites reinforced with zinc: an experiment, theoretical, and simulation-based study. *Applied Physics A*, *126*, 1-15.

Mikkelsen, K., & Apostolopoulos, V. (2019). B vitamins and ageing. Biochemistry and cell biology of ageing: Part I biomedical science, 451-470.

Naveed, S. (2015). Appraisal of Techniques, Investigation and Analysis of Vitamin (B7) Biotin. Open Access Library Journal, 2(09), 1.

O'Leary, F., & Samman, S. (2010). Vitamin B12 in health and disease. Nutrients, 2(3), 299-316.

Oğul, H., Agar, O., Bulut, F., Kaçal, M. R., Dilsiz, K., Polat, H., Akman, F. 2023. A comparative neutron and gamma-ray radiation shielding investigation of molybdenum and boron filled polymer composites. Applied Radiation and Isotopes, 194:110731.

Ötleş, S., & Karaibrahimoglu, Y. (2011). Analysis of Vitamins for. Methods of Analysis of Food Components and Additives, 4(6), 211.

Rathee, S., Nayak, V., Singh, K. R., & Ojha, A. (2022). Nanofortification of vitamin B-complex in food matrix: need, regulations, and prospects. Food Chemistry: Molecular Sciences, 4, 100100.

Richardson, L. R., Wilkes, S., & Ritchey, S. J. (1961). Comparative vitamin B6 activity of frozen, irradiated and heat-processed foods. *The Journal of Nutrition*, *73*(4), 363-368.

Ryan-Harshman, M., & Aldoori, W. (2008). Vitamin B12 and health. Canadian Family Physician, 54(4), 536-541.

Turhan, M. F., Akman, F., Polat, H., Kaçal, M. R., & Demirkol, İ. (2020). Gamma-ray attenuation behaviors of hematite doped polymer composites. *Progress in Nuclear Energy*, *129*, 103504.

Villavicencio, A. L. C., Mancini-Filho, J., Delincée, H., & Bognár, A. (2000). Effect of gamma irradiation on the thiamine, riboflavin and vitamin B6 content in two varieties of Brazilian beans. *Radiation Physics and Chemistry*, *57*(3-6), 299-303.

➢ *ORAL PRESENTATION*

İnsansız Araç Mühendisliğinin Geleceği: Teknolojik Gelişmeler ve Uygulama Alanları

Başak Demir Ünalan[1]* (ORCID: https://orcid.org/0009-0002-1049-1344),
Mehmet Serhat Odabaş[2] (ORCID: https://orcid.org/0000-0002-1863-7566)

[1]Ondokuz Mayıs Üniversitesi, Lisansüstü Eğitim Enstitüsü, Girişimcilik ve Yenilikçilik Anabilim Dalı, Samsun, Türkiye

[2]Ondokuz Mayıs Üniversitesi, Lisansüstü Eğitim Enstitüsü, Akıllı Sistemler Mühendisliği Anabilim Dalı, Samsun, Türkiye

*Sorumlu yazar e-posta: basak.demir@helimore.com

Özet

Bu çalışma, insansız araç mühendisliğinin teknolojik gelişimini, farklı sektörlerdeki kullanım alanlarını ve gelecekteki potansiyelini incelemektedir. Araştırmada, insansız hava, kara, deniz ve uzay araçlarının mühendislik prensipleri ve teknolojik altyapıları ele alınarak, bu sistemlerin endüstri ve toplum üzerindeki etkileri değerlendirilmiştir. Literatür taraması kapsamında, insansız hava araçlarının (İHA) tarım, lojistik ve güvenlik gibi alanlardaki rolü, insansız kara araçlarının askeri operasyonlar ve otonom lojistik süreçlerindeki işlevi, insansız deniz araçlarının çevresel izleme ve keşif görevlerindeki katkıları, insansız su altı ve uzay araçlarının ise keşif ve veri toplama süreçlerindeki önemi incelenmiştir. Çalışmanın yöntemi, güncel akademik literatür taraması ve sektörel raporların analizi üzerine kurulmuştur. Araştırmada, insansız sistemlerin sunduğu avantajlar kadar, etik, hukuki ve güvenlik konularına ilişkin zorluklar da ele alınmıştır. Veriler, önceki araştırmaların sistematik olarak değerlendirilmesi yoluyla analiz edilmiş ve insansız araçların gelecekteki kullanım senaryolarına yönelik çıkarımlar yapılmıştır. Sonuç olarak, bu teknolojilerin sürdürülebilirlik, enerji verimliliği ve akıllı şehir uygulamalarında kritik bir rol oynayacağı öngörülmektedir.

Anahtar Kelimeler: İnsansız Araç Mühendisliği, Yapay Zekâ, Otonom Sistemler, Enerji Verimliliği.

Future of Unmanned Vehicle Engineering: Technological Developments and Application Areas

Abstract

This study examines the technological development of unmanned vehicle engineering, its applications in different sectors and its future potential. The engineering principles and technological infrastructures of unmanned aerial, ground, maritime and space vehicles are discussed, and the impacts of these systems on industry and society are evaluated. Within the scope of the literature review, the role of unmanned aerial vehicles (UAVs) in areas such as agriculture, logistics and security, the function of unmanned ground vehicles in military operations and autonomous logistics processes, the contribution of unmanned maritime vehicles in environmental monitoring and reconnaissance missions, and the importance of unmanned underwater and space vehicles in reconnaissance and data collection processes are examined. The methodology of the study is based on a review of current academic literature and analysis of sectoral reports. The study examines the advantages of unmanned systems as well as the challenges related to ethical, legal and security issues. The data was analyzed through a systematic review of previous research and conclusions were drawn on the future use scenarios of unmanned vehicles. In conclusion, these technologies are envisioned to play a critical role in sustainability, energy efficiency and smart city applications.

Keywords: Unmanned Vehicle Engineering, Artificial Intelligence, Autonomous Systems, Energy Efficiency.

GİRİŞ

İnsansız araçlar (İA), son yıllarda mühendislik ve teknoloji dünyasında dikkat çeken en yenilikçi alanlardan biri haline gelmiştir. Hava, kara, deniz ve uzayda kullanılabilen insansız araçlar, pek çok farklı sektöre entegre edilmekte ve bu sektörlerde insan müdahalesi olmaksızın görevleri yerine getirme kabiliyetine sahiptir. Bu araçlar, geçtiğimiz dönemde hayalle sınırlı kalan birçok işlevselliği gerçek hayata entegre etmekte ve farklı sektörlerdeki geniş kullanım alanlarıyla devrimler yaratmaktadır. Gelişen teknolojiyle birlikte insansız araç sistemleri özellikle yapay zekâ, robotik, algılama sistemleri ve enerji verimliliği alanlarında büyük adımlar atılmasını sağlamıştır. Böylelikle insansız araçların kullanım alanları genişlemiş ve gelecekteki potansiyelleri daha fazla keşfedilmeye başlanmıştır.

İnsansız araç mühendisliği, yalnızca otomasyon ve teknolojik üstünlük sağlamakla kalmayıp, aynı zamanda savunma, tarım, lojistik, sağlık gibi çeşitli sektörlerde dönüşüm yaratmaktadır. Otonom taşıma araçları, dronlar, robotik sistemler ve akıllı makineler, insan yaşamını kolaylaştırmakla birlikte, potansiyel risklerin de farkına varmamızı sağlamaktadır. Bu nedenle, insansız araç mühendisliğinin etik, hukuki ve toplumsal boyutları da günümüzdeki tartışmalarda önemli bir yer tutmaktadır.

Bu makale, insansız araç mühendisliğinin güncel teknolojik gelişmelerini ve potansiyel uygulama alanlarını ele almayı amaçlamaktadır. İnsansız araçların teknolojik altyapılarını, performanslarını ve kullanım senaryolarını inceleyerek, gelecekteki yenilikçi çözümlerin yeri ve önemi üzerinde durulacaktır. Ayrıca, bu alandaki teknolojik zorluklar, etik sorunlar ve düzenleyici engeller tartışılacak ve geleceğe yönelik stratejik yönelimler ele alınacaktır.

LİTERATÜR TARAMASI

Toscana ve arkadaşları (2024) tarafından yapılan çalışmada, insansız hava araçlarının tarımda hassas veri toplama ve verimlilik artırma süreçlerindeki rolü incelenmiştir. Çalışmada, İHA'ların tarımsal üretimde kaynak kullanımını optimize etme ve sürdürülebilir tarım uygulamalarına katkı sağlama potansiyeline vurgu yapılmıştır.

Floreano ve Wood (2015) tarafından gerçekleştirilen araştırmada, insansız hava araçlarında biyomimetik tasarımların kullanımına odaklanılmış ve bu tasarımların sistem performansına etkisi değerlendirilmiştir. Çalışma, özellikle küçük ölçekli otonom drone sistemlerinin gelişimine yönelik teknolojik yenilikleri ele almıştır.

İnsansız kara araçları üzerine yapılan çalışmalar da önemli bulgular sunmaktadır. Kapucu ve Hülako (2018) tarafından yapılan çalışmada, düşük maliyetli ve GPS tabanlı bir insansız kara aracı tasarlanarak, bu sistemlerin farklı sektörlerde nasıl daha erişilebilir hale getirilebileceği ele alınmıştır. Çalışmada, GPS tabanlı navigasyon sistemlerinin entegrasyonunun, insansız kara araçlarının kullanım alanlarını genişletebileceği belirtilmiştir.

Jasthi ve arkadaşları (2018) tarafından yürütülen araştırmada, insansız kara araçlarının askeri operasyonlardaki rolü ve sağladığı operasyonel avantajlar incelenmiştir. Çalışmada, İKA'ların keşif, güvenlik ve lojistik destek gibi görevlerde insan riskini azaltma ve operasyonel verimliliği artırma potansiyeline sahip olduğu tespit edilmiştir.

Manley (2008) tarafından yapılan çalışmada, su üstü insansız araçlarının gelişim süreci ve bu sistemlerin deniz güvenliği, çevresel izleme ve keşif operasyonlarındaki etkinliği ele alınmıştır.

Yılmaz ve Kılcı (2021) tarafından yürütülen araştırmada, otonom su altı araçlarının temel tasarım prensipleri ve teknik gereksinimleri incelenmiştir. Çalışmada, insansız su altı araçlarının optimizasyonu ve bu sistemlerin su altı operasyonlarındaki potansiyeli üzerinde durulmuştur.

İnsansız hava araçlarının yasal çerçevesi üzerine yapılan çalışmalar da önemli veriler sunmaktadır. Can ve Kahveci (2017) tarafından gerçekleştirilen çalışmada, insansız hava araçlarının tanımı, sınıflandırılması ve Türkiye'deki yasal düzenlemeleri ele alınmıştır. Çalışmada, İHA'ların uluslararası düzeyde regülasyon süreçlerine uyumu ve yasal çerçevenin teknolojik gelişmelere etkisi tartışılmıştır.

Korkmaz ve arkadaşları (2015) tarafından yapılan çalışmada, insansız hava araçlarının tarihsel gelişimi ele alınmış ve teknolojik dönüşüm süreci detaylandırılmıştır. Çalışmada, İHA sistemlerinin geçmişten günümüze geçirdiği evrim ve gelecekteki potansiyeli üzerine değerlendirmelerde bulunulmuştur.

Bu literatür taramasında insansız araç mühendisliği alanındaki güncel araştırmaları ele alarak, bu teknolojilerin hava, kara, deniz ve su altı uygulamalarındaki gelişimini ortaya koymaktadır. Yapılan çalışmalar, insansız araç teknolojilerinin çeşitli sektörlerde dönüşümsel bir etkiye sahip olduğunu göstermektedir. Ancak, özellikle insansız uzay araçları konusundaki akademik çalışmaların sınırlı olduğu ve

genel kapsamda insansız araçların tümünü barındıran çalışmaların eksikliği göz önüne alındığında, bu alanda daha fazla araştırmaya ihtiyaç duyulduğu söylenebilir.

İNSANSIZ ARAÇ TEKNOLOJİLERİ

İnsansız araç teknolojileri, otonom veya uzaktan kumandalı sistemler olarak insan müdahalesine duyulan ihtiyacı azaltan ve çeşitli ortamlarda etkin bir şekilde faaliyet gösterebilen araçlardan oluşmaktadır. Bu teknolojiler kara, hava, deniz ve uzay gibi farklı platformlarda uygulanabilmektedir. İnsansız araçların temel amacı, riskli, zor ya da zaman alıcı görevlerde insan gücünü en aza indirerek daha etkili ve verimli çözümler sunmaktır.

Gelişen yapay zekâ algoritmaları, veri analitiği ve robotik alanlarındaki ilerlemeler sayesinde insansız sistemler, geçmişten günümüzdeki karmaşık uygulamalara kadar hızlı bir gelişim süreci geçirmiştir. Teknolojik altyapının gelişmesi ve çeşitli algoritmaların geliştirilmesine bağlı olarak insansız araçların kullanım alanları genişlemiş ve görev yapma kabiliyetleri de bu doğrultuda gelişmiştir.

İnsansız sistemlere dair ilk fikirler, 15. yüzyılda Leonardo Da Vinci'nin mekanik tasarımlarıyla ortaya çıkmıştır. Ancak, pratikte uygulamaya dökülmüş örneklerin geliştirilmesi 19. yüzyılın sonlarına denk gelmektedir. Nikola Tesla'nın 1898 yılında sergilediği radyo kontrollü bot, insansız sistemlerin gerçek dünyada uygulanabilirliğinin kanıtlanması açısından bir dönüm noktası olmuştur. 20. yüzyılın ilk yarısında, insansız sistemler üzerinde askeri amaçlı geliştirmelere başlanmıştır. Birinci Dünya Savaşı sırasında insansız hava balonları ve basit patlayıcılar içeren mekanik sistemler kullanılmıştır.

1930'lu yıllarda, ilk radyo kontrollü insansız hava aracı olan "Queen Bee" geliştirilmiştir ve bu sistemler genellikle hedef belirleme çalışmalarında kullanılmıştır.

II. Dünya Savaşı döneminde, V-1 füzesi gibi insansız sistemler, daha sofistike hale gelmiş ve uzun menzilli saldırılarda kullanılmaya başlanmıştır. Özellikle Soğuk Savaş Dönemi'nde casusluk ve istihbarat toplama faaliyetlerinde yoğun bir şekilde geliştirilmiş ve kullanılmıştır. U-2 ve SR-71 gibi insansız casus hava araçları bu alandaki gelişimin öncülerindendir.

1990'lı yıllardan itibaren, insansız sistemlerin ticari ve sivil alanlarda kullanımı yaygınlaşmaya başlamıştır. Global Positioning System (GPS) teknolojisinin yaygınlaşması ve sensörlerin daha uygun maliyetli hale gelmesiyle, insansız hava araçları zirai uygulamalar, lojistik ve medya alanlarında da kullanılmaya başlanmıştır.

21. yüzyılda, yapay zekâ ve otonom sistemlerin gelişimi, insansız araç teknolojilerini yeni bir boyuta taşımıştır. Bu dönemde, sensör teknolojileri ve makine öğrenimi algoritmalarının birleşimiyle daha karmaşık görevleri yerine getirebilen insansız sistemler geliştirilmiştir. Günümüzde bu teknolojiler, IoT (Nesnelerin İnterneti) ile entegre edilerek daha etkili ve birlikte çalışabilir hale gelmiştir. İnsansız araçlar, sadece endüstriyel ya da askeri alanlarla sınırlı kalmayıp, bireysel ve toplumsal yaşamı da etkilemektedir.

İNSANSIZ ARAÇ TÜRLERİ

İnsansız Hava Araçları

İnsansız Hava Aracı (İHA), insan taşıma kapasitesine sahip olmayan, uzaktan kumanda ile kontrol edilen veya otonom bir şekilde önceden programlanmış görevleri gerçekleştirebilen hava araçlarıdır. İngilizce literatürde *"Unmanned Aerial Vehicle (UAV)"* olarak adlandırılan bu araçlar, sivil, askeri ve ticari alanlar başta olmak üzere birçok farklı alanda kullanılmaktadır.

İHA'lar, genellikle bir yer kontrol istasyonundan yönetilen ya da uçuş öncesinde belirlenmiş rotalara göre otonom hareket eden sistemlerdir. Bu araçlar tek başlarına çalışabilen birimler olabildiği gibi, daha geniş bir *"İnsansız Hava Sistemi" (Unmanned Aerial System, UAS)* olarak adlandırılan, yer kontrol istasyonları ve iletişim sistemleriyle desteklenen bir yapının parçası da olabilirler.

İnsansız hava araçları, kalkış ağırlıklarına, kanat tiplerine ve kullanım alanlarına göre farklı türlerde sınıflandırılmaktadır. Tablo 1'de, kalkış ağırlıklarına göre insansız hava aracı türlerine yer verilmektedir.

Tablo 1. Kalkış Ağırlığına Göre İHA Türlerinin Sınıflandırılması

Kalkış Ağırlığı	İHA Sınıfı
500 gr – 4 kg	İHA-0
4 – 25 kg	İHA-1
25 – 150 kg	İHA-2
150 kg ve üzeri	İHA-3

Türkiye ele alındığında, SHGM tarafından yapılmış olan sınıflandırma doğrultusunda insansız hava araçları kalkış ağırlığına göre 4 farklı sınıfta incelenmektedir. İHA-0 profesyonel amaç dâhilinde olmayan, hobi amaçlı insansız hava araçlarını kapsamaktadır ve bu araçlar maksimum 4kg ağırlığa sahip olabilir. İHA-1 sınıfı İHA'lar ağırlıklı olarak kamera çekimleri yapma amaçlı olarak kullanılan, üzerinde bulunan faydalı yük miktarı ve türü değişiklik gösterebilen insansız hava araçlarını kapsar ve bu sınıfta yer alan araçlar için maksimum kalkış ağırlığı 25kg olarak belirlenmiştir. İHA-2 sınıfı insansız hava araçları genellikle üzerinde bulunan faydalı yüklere ek olarak özelleştirilmiş sistemlere sahip olan insansız hava araçlarını kapsar. Bu sınıfta yer alan insansız hava araçları kargo ve taşımacılıktan zirai amaçlı kullanımlara kadar pek çok farklı alanda kullanılabilir ve maksimum kalkış ağırlıkları 150kg ile sınırlandırılmıştır. İHA-3 sınıfı insansız hava araçları ise ağırlıklı olarak savunma sanayi alanlarında kullanılmaktadır ve maksimum kalkış ağırlığı için herhangi bir sınır bulunmamaktadır. Tablo 2'de insansız hava araçlarının çeşitliliğini ve bu araçların kullanım alanlarına göre nasıl sınıflandırıldığını göstermektedir.

İnsansız hava araçları temel olarak multikopter, sabit kanat ve döner kanat olmak üzere üç ana başlıkta ele alınmaktadır. Her tür, birbirinden farklı motor yapılarına sahip olmakla birlikte, bu yapıların avantaj ve dezavantajları göz önünde bulundurularak farklı görevlerde kullanılmak üzere optimize edilmiştir.

Tablo 2. İHA'ların çeşitliliğini ve kullanım alanlarına göre nasıl sınıflandırılması

İHA Türü	İHA Alt Türü	Motor/Rotor Yapısı	Kullanım Alanları
MULTİKOPTER	Quadkopter	4 Rotor	Tarım, güvenlik, film çekimi, hobi.
	Hexakopter	6 Rotor	Tarım, ağır yük taşıma, film prodüksiyonu.
	Oktokopter	8 Rotor	Tarım, ağır yük taşıma, hassas ölçüm ve endüstriyel işler.
SABİT KANAT	Elektrikli	Elektrikli Motor	Haritalama, keşif, gözetleme.
	Yakıtlı	İçten Yanmalı Motor	Uzun mesafeli taşımacılık, askeri keşif.
	Turbojet	Jet Motorları	Askeri ve özel amaçlı görevler.
DÖNER KANAT	Tek Rotor	Bir ana, bir kuyruk rotoru	Askeri, arama-kurtarma, ağır yük taşımacılığı.
	Koaksiyel Rotor	Üst üste iki rotor	Askeri, endüstriyel taşımacılık.
	Tandem Rotor	Paralel iki büyük rotor	Ağır yük taşıma, arama-kurtarma.

İnsansız Kara Araçları

İnsansız kara araçları(İKA), insan müdahalesi olmadan veya uzaktan kumanda ile çalışan, karada hareket edebilen araçlardır. Bu araçlar, genellikle otonom veya yarı otonom bir şekilde çalışacak şekilde tasarlanmıştır. İngilizce literatürde "Unmanned Ground Vehicle (UGV)" olarak adlandırılan bu araçlar, askeri, sivil, endüstriyel ve bilimsel alanlar başta olmak üzere birçok alanda farklı alanda kullanılır. İKA'lar, farklı türde sensörler, yapay zekâ algoritmaları ve kontrol sistemleri ile donatılarak belirli görevleri yerine getirecek şekilde programlanmaktadır. Çeşitli görevler için özelleştirilebilen insansız kara araçlarının günümüz kullanımlarında en yaygın avantajları, risk azaltma, operasyonel verimlilik, çevresel

uyum ve çok amaçlı kullanımlara uygun olmalarıdır. İnsansız kara araçları, türlerine göre beş farklı sınıfta incelenmektedir (Tablo 3).

Tablo 3. İnsansız Kara Araçları Sınıflandırması

İKA Türü	Özellikleri	Kullanım Alanları
Tekerlekli İKA	Tekerlekli yapıya sahiptir, genellikle hızlı ve enerji tasarruflu sistemlerdir.	Tarım, Lojistik, Depo otomasyonları, güvenlik ve keşif çalışmaları
Paletli İKA	Tekerlek yerine palet mekanizması içerir, Engebeli arazilerde kullanılmaya uygun sistemlerdir.	Askeri operasyonlar, arama-kurtarma faaliyetleri, madencilik, tarım
Ayaklı(Biyonik) İKA	Engebeli ve zorlu arazilerde yüksek hareket kabiliyeti sağlayan sistemlerdir. Geleneksel tekerlekli ve paletli İKA'lara kıyasla daha esnek ve çevik bir yapıya sahiptirler.	Askeri operasyonlar, arama kurtarma faaliyetleri, lojistik, keşif.
Hibrit İKA	Hem tekerlekli/paletli hem de ayaklı hareket sistemlerini birleştiren veya farklı enerji kaynaklarını (elektrik, içten yanmalı motor vb.) kullanabilen sistemlerdir.	Tarım, çevre izleme, arama- kurtarma, lojistik.

İnsansız Deniz Araçları

İnsansız deniz araçları (İDA), deniz ortamında insan müdahalesine gerek duymadan veya minimum insan kontrolü ile görev yapabilen, otonom veya uzaktan kumandalı sistemlerdir. Bu araçlar, su altı ve su üstü operasyonları için özel olarak tasarlanmış olup, askeri, endüstriyel, çevresel ve bilimsel araştırmalar gibi geniş bir yelpazede kullanılmaktadır. Teknolojideki ilerlemeler sayesinde, İDA'lar gelişmiş yapay zekâ, sensör entegrasyonu ve veri analitiği gibi sistemlerle donatılarak daha etkili ve hassas görevler icra edebilmektedir. İDA'lar, operasyonel gereksinimlerine ve tasarımlarına bağlı olarak genel olarak iki ana kategoriye ayrılmaktadır: su üstü insansız araçlar (USV - Unmanned Surface Vehicles) ve su altı insansız araçlar (UUV - Unmanned Underwater Vehicles). Su üstü insansız araçlar, okyanus yüzeyinde veya iç sularda çalışmak üzere tasarlanmış olup, uzaktan kumandalı veya tamamen otonom sistemler olarak işlev görebilirler. Çevre izleme, deniz güvenliği, askeri devriye görevleri, hidrojeolojik çalışmalar ve deniz taşımacılığı gibi alanlarda yaygın olarak kullanılmaktadırlar. Su altı insansız araçlar, deniz altındaki keşif ve operasyonlar için geliştirilmiş otonom veya uzaktan kumandalı sistemlerdir. Bu araçlar, petrol ve gaz endüstrisinde boru hatları denetimi, denizaltı arkeolojisi, bilimsel araştırmalar ve askeri amaçlarla kullanılmaktadır.

İnsansız Uzay Araçları

İnsansız uzay araçları (İUA), uzay keşifleri, bilimsel araştırmalar ve mühendislik görevlerinde insan müdahalesine gerek duyulmadan çalışan otomatik veya uzaktan kontrol edilebilen sistemlerdir. İnsanlı uzay görevlerine kıyasla daha düşük maliyetli, daha uzun ömürlü ve risklerden arındırılmış olmaları nedeniyle uzay araştırmalarında büyük bir yer tutmaktadırlar. Gelişmiş sensörler, yapay zekâ destekli navigasyon sistemleri ve dayanıklı yapıları sayesinde bu araçlar, zorlu uzay koşullarında güvenilir operasyonlar gerçekleştirebilir. İnsansız uzay araçları, uzayın keşfi ve uzay mühendisliği alanlarında çeşitli görevlerde kullanılmaktadır. Özellikle Mars araştırmaları, bu tür araçların en dikkat çekici kullanım alanlarından biridir. Günümüzde birçok uydu, telekomünikasyon, hava durumu tahmini, küresel konumlandırma sistemleri (GPS) ve askeri gözetleme gibi çeşitli alanlarda kullanılmaktadır. İUA'lar, bu

uyduların yörüngeye taşınması ve bakımının yapılmasında da etkin bir şekilde kullanılmaktadır. Uzayda giderek artan enkaz, uydular ve uzay istasyonları için ciddi bir tehdit oluşturmaktadır. İnsansız uzay araçları, uzaydaki atıkların temizlenmesi ve gelecekteki çarpışmaların önlenmesi amaçlarıyla da kullanılmaktadır.

GELECEKTEKİ BEKLENTİLER

Teknolojik ilerlemeler, özellikle yapay zeka, makine öğrenimi ve otonom sistemler alanındaki gelişmeler, insansız araçların gelecekte hayatımızın birçok alanında dönüştürücü bir rol oynamasını mümkün kılmaktadır. Bu araçlar, sadece ulaşım ve lojistik alanlarında değil, aynı zamanda altyapı, çevre yönetimi, sağlık hizmetleri ve günlük yaşamın birçok farklı noktasında kullanılarak verimliliği artırabilir, maliyetleri düşürebilir ve insan hayatını kolaylaştırabilir. Bu bölümde, insansız araçların gelecekte ulaşabileceği noktalar ve bu teknolojinin toplu taşıma sistemlerinden atık yönetimine kadar geniş bir yelpazede nasıl uygulanabileceği ele alınmaktadır.

- **Otonom Toplu Taşıma Sistemleri:** İnsansız araçlar, şehir içi ve şehirler arası toplu taşıma sistemlerinde kullanılarak trafik sıkışıklığını azaltabilir, enerji verimliliğini artırabilir ve ulaşım maliyetlerini düşürebilir. Otonom otobüsler ve metro sistemleri, özellikle yoğun nüfuslu kentsel alanlarda etkili bir çözüm sunabilir.
- **Altyapı Çalışmaları:** Köprü, baraj ve benzeri altyapı projelerinde insansız araçlar, özellikle tehlikeli ve erişilmesi zor bölgelerde inşaat, bakım ve onarım işlerini gerçekleştirebilir. Bu, hem iş güvenliğini artırır hem de projelerin daha hızlı tamamlanmasını sağlar.
- **Enerji Hattı İzleme ve Bakım-Onarım:** İnsansız hava araçları (İHA'lar) ve otonom karasal araçlar, enerji hatlarının düzenli olarak izlenmesi ve bakımının yapılmasında kullanılabilir. Bu, arızaların önceden tespit edilmesini ve enerji kesintilerinin önlenmesini sağlar.
- **Atık Yönetimi:** Otonom araçlar, atık toplama ve geri dönüşüm süreçlerini optimize edebilir. Akıllı atık kutuları ve otonom atık toplama araçları, atık yönetimini daha verimli hale getirebilir.
- **Trafik Yönetimi:** İnsansız araçlar, trafik akışını izlemek ve yönetmek için kullanılabilir. Gerçek zamanlı veri toplayarak trafik sıkışıklığını azaltabilir ve acil durumlarda alternatif rotalar önerebilir.
- **Hava Taksi Hizmeti:** Otonom hava taksileri, özellikle büyük şehirlerde trafik sorununa çözüm olarak kullanılabilir. Bu araçlar, kısa mesafeli ulaşımı hızlandırarak zaman tasarrufu sağlayabilir.
- **Otonom Tur Rehberi:** İnsansız araçlar, turistik bölgelerde otonom rehberlik hizmeti sunabilir. Bu araçlar, ziyaretçilere tarihi ve kültürel bilgiler aktararak turizm deneyimini zenginleştirebilir.
- **Tıbbi Malzeme Taşıma:** Özellikle acil durumlarda, insansız araçlar tıbbi malzemelerin hızlı ve güvenli bir şekilde taşınmasını sağlayabilir. Bu, hastane ve sağlık merkezleri arasında kritik bir lojistik desteği sunar.
- **Kargo ve Nakliye Hizmetleri:** Otonom kamyonlar ve dronlar, e-ticaret ve lojistik sektöründe devrim yaratabilir. Paketlerin daha hızlı ve düşük maliyetle teslim edilmesini sağlayabilir.
- **Bahçe Bakımı:** İnsansız araçlar, park ve bahçelerin otomatik olarak sulanması, çimlerin biçilmesi ve bitki bakımının yapılması gibi işlerde kullanılabilir.
- **Görme Engelliler İçin Destek Asistanı:** Otonom araçlar, görme engelli bireylerin günlük yaşamlarında yardımcı olabilir. Örneğin, rehberlik eden robotlar veya akıllı bastonlar, engelli bireylerin bağımsız hareket etmesini kolaylaştırabilir.
- **Sanal Alışveriş Asistanı:** İnsansız araçlar, fiziksel mağazalarda veya depolarda müşterilere ürün bulma, ödeme işlemleri ve teslimat gibi konularda yardımcı olabilir.

TARTIŞMA

Bu çalışma, farklı insansız araç türlerinin mühendislik prensiplerini, teknolojik altyapılarını ve kullanım alanlarını kapsamlı bir biçimde ele alarak, bu sistemlerin mevcut potansiyelini ve gelecekteki gelişim yönlerini ortaya koymuştur. Elde edilen bulgular, insansız sistemlerin hem sektörel hem de toplumsal dönüşüm açısından önemli etkiler yarattığını göstermektedir. Bununla birlikte, literatürde özellikle tüm insansız araç türlerini bütüncül biçimde değerlendiren akademik çalışmaların sınırlı olduğu görülmektedir. Hâlihazırda insansız hava araçları üzerine yoğunlaşılmışken, kara, deniz ve özellikle uzay sistemleri ile ilgili araştırmaların sayıca azlığı dikkat çekmektedir. Bu durum, multidisipliner yaklaşımların önemini ortaya koymakta ve bütüncül mühendislik perspektiflerinin geliştirilmesine duyulan ihtiyacı vurgulamaktadır. Ayrıca, bu

teknolojilerin etik, hukuki ve çevresel yönlerinin de teknik gelişmelerle paralel şekilde ele alınması gerektiği anlaşılmaktadır.

SONUÇ

Çalışma sonucunda, insansız araç teknolojilerinin hızla geliştiği, farklı sektörlerde verimlilik, güvenlik ve sürdürülebilirlik sağlama açısından kritik roller üstlendiği belirlenmiştir. Yapay zekâ, sensör teknolojileri ve otonom sistemlerin entegrasyonu sayesinde bu araçların görev yetenekleri genişlemekte ve yeni uygulama alanları ortaya çıkmaktadır. Gelecekte, bu sistemlerin daha da yaygınlaşacağı ve insan yaşamına entegre çözümler sunacağı öngörülmektedir. Araştırmanın bulguları, literatürdeki mevcut boşlukların doldurulması ve bu teknolojilerin sosyal etkileri üzerine daha fazla çalışma yapılması gerektiğini göstermektedir. Özellikle, insansız uzay sistemleri ve birleşik platformların çoklu ortam uygulamaları üzerine odaklanacak yeni araştırmalar önerilmektedir.

TEŞEKKÜR

Bu çalışmanın hazırlanmasında bilimsel rehberliğiyle her aşamada katkı sunan değerli danışmanımız Prof. Dr. Mehmet Serhat Odabaş'a, akademik yolculuğumda desteğini ve inancını her daim hissettiren yol arkadaşım Metehan Ünalan'a, çalışmanın her aşamasında özveriyle yanımda olan değerli ekip arkadaşlarım Elif Kapusuzoğlu ve Ayşe Elvin Özölçer'e içten teşekkür ederim. Ayrıca, Ondokuz Mayıs Üniversitesi Lisansüstü Eğitim Enstitüsü'ne verdikleri akademik ve idari destekten dolayı şükranlarımı sunarım.

KAYNAKLAR

- Bolat, F., & Koşaner, Ö. (2021). İnsansız gemilerin güncel statüleri. *Eurasian Journal of Science and Technology, 16*(2), 341–358. https://doi.org/10.31590/ejosat.870875
- Can, M., & Kahveci, T. (2017). İnsansız Hava Araçları: Tarihçesi, Tanımı, Dünyada ve Türkiye'deki Yasal Durumu. Selçuk Üniversitesi.
- Ekinci, T., Öztütüncü, O., & Ertogan, M. (2024). İnsansız deniz araçları kapsamında denizcilikle alakalı Türk mevzuatında ihtiyaç duyulabilecek değişikliklere dair inceleme. *Türk Denizcilik ve Deniz Güvenliği Dergisi, 3*(5), 1–18.
- Erol, B., Cantekin, R., Kartal, S., Hacıoğlu, R., Görmüş, K. S., Kutoğlu, Ş. H., & Leblebicioğlu, K. (2021). İnsansız sualtı aracı hareketinin Kalman filtre ile kestirimi ve makine öğrenmesi ile iyileştirilmesi. *Journal of Engineering and Natural Sciences – ASYU 2020 Özel Sayısı, 33*, 67–77. https://doi.org/10.7240/jeps.897500
- Floreano, D., & Wood, R. J. (2015). Science, technology and the future of small autonomous drones. *Nature, 521*(7553), 460–466.
- Gündoğdu, K., & Çalhan, A. (2013). İnsansız askeri kara aracı tasarımı. *Savunma Bilimleri Dergisi, 2*(1), 36–45.
- Hülako, H., & Kapucu, S. (2018). Düşük Maliyetli GPS Tabanlı Otonom Bir İnsansız Kara Aracının Tasarımı ve Yapılması. *Gazi Üniversitesi Fen Bilimleri Dergisi Part C: Tasarım ve Teknoloji, 6*(4), 834–850.
- Jasthi, S., et al. (2018). Unmanned ground vehicle for military purpose. *International Journal of Pure and Applied Mathematics, 119*(12), 13189–13192.
- Korkmaz, O., et al. (2015). Geçmişten günümüze insansız hava araçlarının gelişimi. *Sakarya University Journal of Science, 20*(2), 103.
- Korkmaz, Y., İyibilgin, O., & Fındık, F. (2015). Geçmişten günümüze insansız hava araçlarının gelişimi. *Akademik Bilişim Konferansı Bildirileri, 28.07.2015 – 18.11.2015.*
- Manley, J. E. (2008). Unmanned surface vehicles, 15 years of development. In *OCEANS 2008*. IEEE.
- Toscano, F., et al. (2024). Unmanned aerial vehicle for precision agriculture: A review. *IEEE Access*.
- Villi, O., & Yakar, M. (2022). İnsansız hava araçlarının kullanım alanları ve sensör tipleri. *Teknoloji ve İnovasyon Havadisleri Dergisi, 4*(2), 73–100. https://doi.org/10.51534/tiha.1189263
- Yılmaz, S., & Kılcı, S. B. (2021). Otonom sualtı araçlarında genel tasarım ilkeleri. *Journal of the Institute of Science and Technology, 11*(1), 119–131.

➢ *ORAL PRESENTATION*

Fotovoltaik/termoelektrik (PV/TEG) hibrit sistemlerdeki son gelişmeler ve gelecek perspektifleri

İsmail Ardıç[1*] (*ORCID: https://orcid.org/0009-0005-2586-1004),*
Deniz Ulusarslan[2] *(ORCID:https://orcid.org/0000-0002-3762-658X)*

[*1]Yıldız Teknik Üniversitesi, Mühendislik Fakültesi, Makina Mühendisliği, İstanbul, Türkiye.
[2] Yıldız Teknik Üniversitesi, Mühendislik Fakültesi, Makina Mühendisliği, İstanbul, Türkiye.

*Sorumlu yazar e-posta:ismail.ardic@std.yildiz.edu.tr

Özet

Güneş enerjisi teknolojilerinde, fotovoltaik (PV) sistemlerin artan çalışma sıcaklığıyla düşen verimliliği ve güneş spektrumunun yalnızca sınırlı bir kısmını kullanabilmesi, atık ısının değerlendirilmesi için önemli bir potansiyel sunmaktadır. Bu inceleme çalışması, PV hücrelerini bir termoelektrik jeneratör (TEG) ile birleştiren hibrit PV/TEG sistemleri alanındaki son on ila on beş yıllık gelişmeleri kapsamlı bir şekilde ele almaktadır. PV/TEG hibrit sisteminin temel amacı, PV panelinin atık ısısını TEG aracılığıyla ek elektriğe dönüştürerek geri kazanmak ve aynı zamanda paneli soğutarak PV verimliliğini artırmaktır. Makale kapsamında farklı sistem konfigürasyonları incelenmiştir. Malzeme bilimindeki ilerlemeler dikkate alınarak; yeni nesil PV malzemeleri (perovskitler, organik PV'ler) ve yüksek değer ölçüsüne (ZT) sahip inorganik/organik TEG malzemeleri araştırılmıştır. Sistem performansını artırmaya yönelik aktif/pasif soğutma, nanoakışkanlar, faz değiştiren malzemeler (PCM) ve radyatif gökyüzü soğutması gibi yenilikçi teknikleri içeren termal yönetim stratejileri incelenmiştir. Sonuç olarak PV/TEG hibrit sistemlerin tek başına PV sistemlere kıyasla genel enerji verimliliğini artırma potansiyeline sahip olduğu, özellikle yoğunlaştırılmış fotovoltaik (CPV) ve spektrum bölmeli tasarımların enerji verimliliğine önemli kazanımlar sunduğu anlaşılmaktadır. Ancak, mevcut TEG'lerin düşük ZT değeri, PV ile TEG arasındaki termal ve operasyonel uyumsuzluk ve artan sistem maliyeti gibi zorluklar bu teknolojinin yaygınlaşmasının önündeki temel engellerdir. Gelecekteki araştırmaların; PV çalışma sıcaklıklarına uygun, yüksek ZT değerli ve düşük maliyetli TEG malzemeleri geliştirmeye ve termal yönetimi optimize eden yenilikçi sistem tasarımları üzerinde yoğunlaşması, bu teknolojinin gelişip ticarileşmesi için kritik öneme sahiptir.

Anahtar Kelimeler: Fotovoltaik/Termoelektrik Hibrit Sistemler, PV/TEG, Güneş Enerjisi, Termal Yönetim

Recent developments and future perspectives in photovoltaic/thermoelectric (PV/TEG) hybrid systems

Abstract

In solar energy technologies, the efficiency degradation of photovoltaic (PV) systems at elevated operating temperatures and their utilization of only a limited portion of the solar spectrum present a significant potential for waste heat recovery. This review study comprehensively examines the developments in the field of hybrid PV/TEG systems, which combine PV cells with a thermoelectric generator (TEG), over the last ten to fifteen years. The primary objective of a PV/TEG hybrid system is to recover the waste heat from the PV panel by converting it into additional electricity via the TEG, while simultaneously cooling the panel to enhance its PV efficiency. Within the scope of the paper, various system configurations are investigated. Considering the advances in material science, next-generation PV materials (perovskites, organic PVs) and inorganic/organic TEG materials with a high figure-of-merit (ZT) are explored. Thermal management strategies aimed at enhancing system performance are reviewed, encompassing innovative techniques such as active/passive cooling, nanofluids, phase change materials (PCMs), and radiative sky cooling. In conclusion, it is understood that PV/TEG hybrid systems have the potential to increase overall energy efficiency compared to standalone PV systems, with concentrated photovoltaic (CPV) and spectral splitting designs, in particular, offering significant gains in energy efficiency. However, challenges such as the low ZT value of current TEGs, the thermal and operational mismatch between the PV and TEG, and increased system cost are primary barriers to the widespread adoption of this technology. It is of critical importance for the development and commercialization of this technology that future research focuses on developing high-ZT, low-cost TEG materials suitable for PV operating temperatures, and on innovative system designs that optimize thermal management.

Keywords: Photovoltaic/Thermoelectric Hybrid Systems, PV/TEG, Solar Energy, Thermal Management

GİRİŞ

Küresel enerji tüketimindeki hızlı artış, fosil yakıtların tükenmekte olan rezervleri ve bu yakıtların kullanımının neden olduğu iklim değişikliği ve çevresel bozulmalar, dünya genelinde sürdürülebilir ve temiz enerji kaynaklarına olan talebi kaçınılmaz bir şekilde artırmıştır. Bu bağlamda, yenilenebilir enerji kaynakları, enerji arz güvenliğini sağlama, çevresel etkileri azaltma ve sürdürülebilir kalkınmayı destekleme potansiyelleriyle ön plana çıkmaktadır. Bu kaynaklar arasında güneş enerjisi, geniş coğrafi alanlarda erişilebilirliği ve çevre dostu yapısıyla en umut verici alternatiflerden biri olarak kabul edilmektedir (Basu, 2024). Güneş enerjisinin etkin bir şekilde elektrik enerjisine dönüştürülmesi, günümüz enerji teknolojileri araştırmalarının temel odak noktalarından biridir.

Fotovoltaik (PV) teknolojisi, güneş ışığını doğrudan elektriğe dönüştürmenin en yaygın yolu olsa da, iki temel verimlilik engeliyle karşı karşıyadır: Artan çalışma sıcaklığına bağlı performans kaybı ve güneş spektrumunun yalnızca sınırlı bir kısmını kullanabilmesidir. Bu iki faktörün ortak sonucu, gelen güneş enerjisinin önemli bir kısmının atık ısıya dönüşmesidir.

Fotovoltaik/termoelektrik (PV/TEG) hibrit sistemler, bu zorluklara yönelik sinerjik ve bütünleşik bir çözüm olarak ortaya çıkmıştır. Bu sistemlerin temel mantığı, PV panelinin en büyük zayıflığı olan atık ısıyı, bir termoelektrik jeneratör (TEG) aracılığıyla değerli bir kaynağa dönüştürmektir. Bu entegrasyon ısıyı PV hücreden uzaklaştırıp, termoelektrik jeneratörler vasıtasıyla atık ısıdan elektrik üreterek çift yönlü bir fayda sağlamayı hedefler.

Bu hibrit yaklaşım, hem PV teknolojisinin verimlilik sınırlarını zorlamakta hem de termoelektrik jeneratörler için yaygın ve erişilebilir bir atık ısı kaynağı sunmaktadır. Ancak bu entegrasyon, TEG'lerin kendi verimlilik sınırlamaları gibi yeni zorlukları da beraberinde getirmektedir (Bjork ve Nielsen,2018). Bu çalışma, PV/TEG hibrit sistemleri alanındaki son gelişmeleri, bu teknolojinin sunduğu potansiyeli, karşılaşılan zorlukları ve gelecek perspektiflerini kapsamlı bir şekilde incelemeyi amaçlamaktadır.

MATERYAL VE METOD

Bu derleme çalışması, PV/TEG hibrit sistemleri alanındaki bilimsel literatürün sistematik bir analizine dayanmaktadır. Çalışmanın kapsamı, teknolojik gelişmelerin yoğunlaştığı son on ila on beş yıllık dönemi (yaklaşık 2010-2025) kapsayacak şekilde sınırlandırılmıştır. İncelemeye, hakemli dergilerde yayınlanmış araştırma makaleleri, derlemeler ve etki faktörü yüksek konferans bildirileri dahil edilmiştir. Analiz, mevcut durumu, zorlukları ve gelecek potansiyelini ortaya koymaktadır.

Fotovoltaik (PV) Teknolojisi

Fotovoltaik (PV) hücreler, fotovoltaik etki olarak bilinen temel bir fiziksel prensip aracılığıyla güneş ışığını doğrudan elektrik enerjisine dönüştüren yarı iletken tabanlı cihazlardır. Enerjisi, yarı iletken malzemenin yasak enerji aralığından (band gap) daha büyük olan bir fotonun, bir elektron-delik çifti (electron-hole pair) oluşturmasıyla başlar. Hücre içerisinde oluşturulan p-n ekleminin yerleşik elektrik alanı, bu yük taşıyıcılarını birbirinden ayırır; elektronları n-tipi bölgeye, delikleri ise p-tipi bölgeye yönlendirir. Sonuç olarak bu ayrışan yüklerin metal kontaklar aracılığıyla harici bir devrede toplanması, bir elektrik akımı meydana getirir.

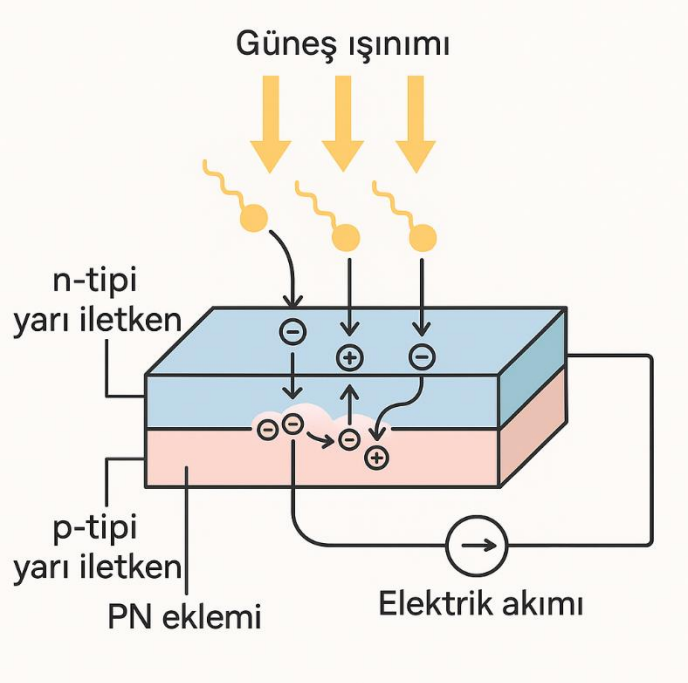

Şekil 1. PV hücre çalışma prensibi.

PV hücrelerin performanslarını sınırlayan temel faktörler bulunmaktadır. Bunların başında, PV hücrelerinin verimliliğinin artan çalışma sıcaklıklarıyla önemli ölçüde düşmesi gelmektedir. Güneş ışığının yaklaşık %80'ini emebilen PV panellerde, elektriğe dönüşemeyen enerji ısıya dönüşerek panel sıcaklığını ortamın 40°C üzerine çıkarabilir, bu da PV hücre performansını düşürür ve hücre ömrünü kısaltır (Makki ve ark., 2016).

Termoelektrik Jeneratör (TEG) Teknolojisi

Termoelektrik jeneratörler (TEG'ler), Seebeck etkisi olarak bilinen fiziksel bir prensibe dayanarak, bir malzemenin iki ucu arasındaki sıcaklık farkını doğrudan elektrik enerjisine dönüştüren katı hal cihazlarıdır.

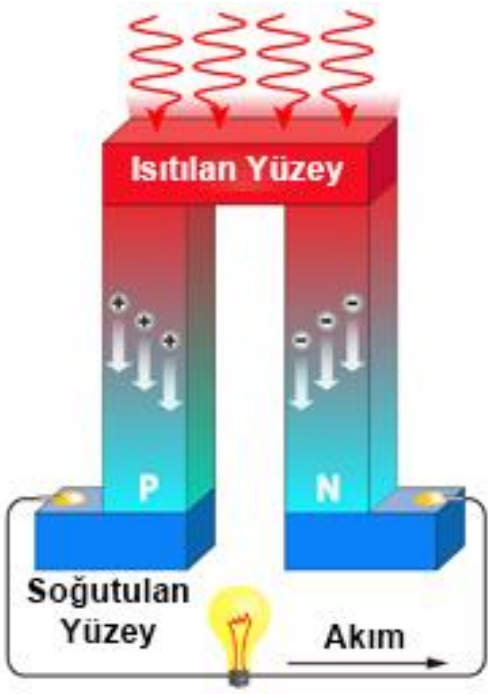

Şekil 2. TEG çalışma prensibi.

TEG'lerin performansı, kullanılan termoelektrik malzemenin değer faktörü (ZT) ile doğrudan ilişkilidir. ZT boyutsuz bir değerdir ve (1) denkleminde verilen ifade ile hesaplanır.

$$ZT = \frac{S^2\sigma}{\kappa}T \quad (1)$$

Burada S Seebeck katsayısını, σ elektriksel iletkenliği, k termal iletkenliği ve T uygulanan sıcaklığı göstermektedir. TEG'lerin en büyük sınırlılığı, mevcut malzemelerin ZT değerlerinin ve dolayısıyla dönüşüm verimliliklerinin genellikle düşük olmasıdır.

PV/TEG hibrit sistemi

Fotovoltaik ve termoelektrik teknolojilerinin bireysel sınırlılıklarını aşmak amacıyla, bu iki teknolojiyi birleştiren hibrit PV/TEG sistemleri üzerine yoğun araştırmalar yapılmaktadır. Bu hibritleşmenin temel mantığı, PV panellerinde elektrik enerjisine dönüşemeyip ısı olarak açığa çıkan enerjiyi TEG'ler aracılığıyla geri kazanmaktır

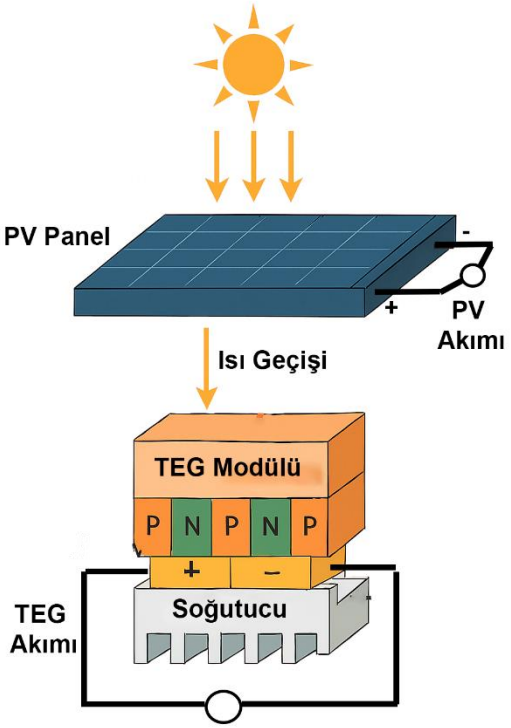

Şekil 3. PV/TEG hibrit sistem şeması.

BULGULAR VE TARTIŞMA

PV/TEG Sistem Konfigürasyonları

Literatürdeki çalışmalar, hibrit sistemler için temel olarak üç farklı yaklaşım üzerinde yoğunlaşmaktadır:

Doğrudan Bağlı Sistemler: En basit yapı olup, TEG modülü doğrudan PV panelinin arkasına monte edilir. Bu konfigürasyon basit ve düşük maliyetli olmasına rağmen, PV'nin düşük sıcaklıkta çalışma isteği ile TEG'in yüksek sıcaklık farkı isteği arasında temel bir termal çelişki yaratır. Bu durum, TEG'in katkısını ve genel verimlilik artışını sınırlar (Bjork ve Nielsen,2018).

Spektrum Bölmeli (SS) Sistemler: Bu yaklaşımda, gelen güneş ışığı optik bir ayırıcı ile dalga boylarına göre bölünür. PV hücresinin verimli olduğu kısa dalga boyları PV'ye, geri kalan kızılötesi gibi uzun dalga boyları ise ısı kaynağı olarak TEG'e yönlendirilir. Bu sayede her iki bileşen de kendi ideal çalışma koşullarına daha yakın çalışarak teorik olarak daha yüksek verimlilik sunar (Yang ve ark., 2016).

Yoğunlaştırılmış PV/TEG (CPV-TEG) Sistemleri: Güneş ışığı lensler veya aynalar kullanılarak küçük bir alana odaklanır. Bu, hem PV hem de TEG'den elde edilen güç yoğunluğunu artırır ancak aşırı ısınma nedeniyle çok etkin soğutma sistemleri gerektirir (Sabry ve ark., 2021).

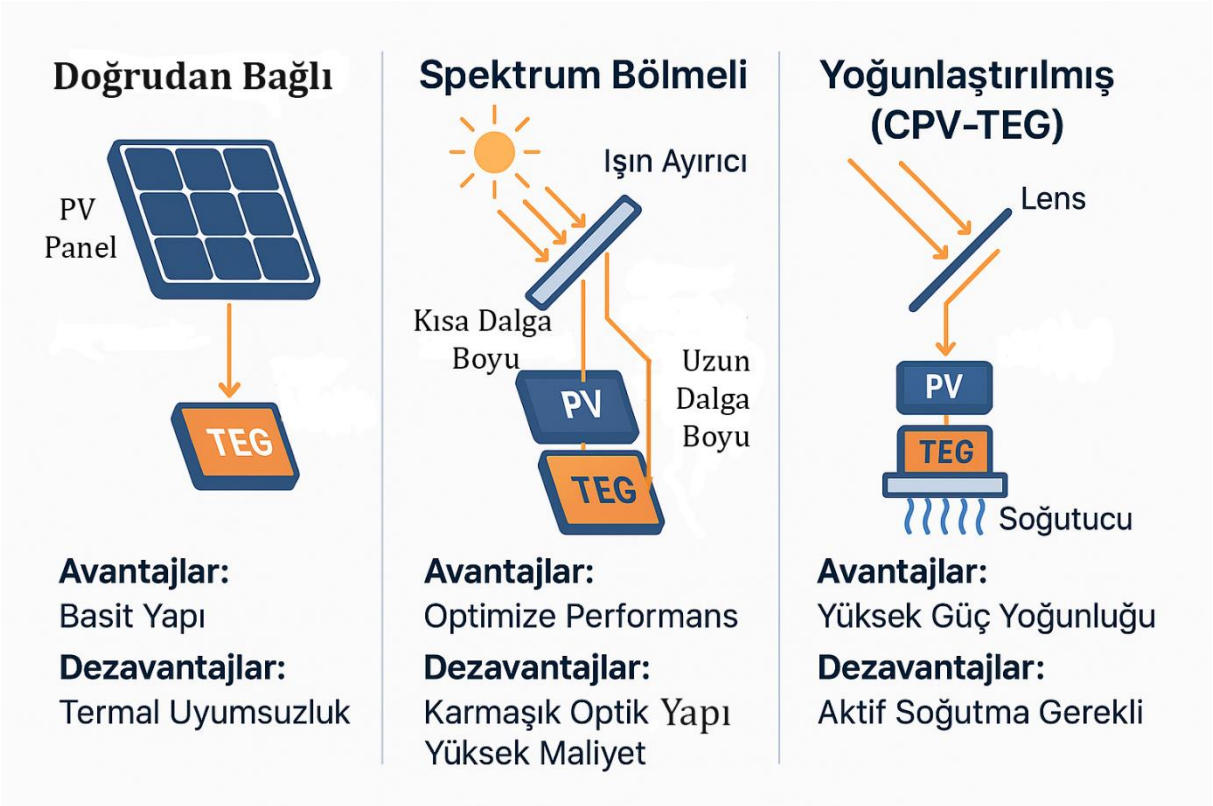

Şekil 4. PV/TEG konfigürasyonları.

Doğrudan bağlı sistemlerde, TEG'nin katkısı genellikle sınırlıdır. Analitik çalışmalar, ideal koşullarda bile bu tür sistemlerin tek başına PV'ye kıyasla genel verimliliği sadece %1,8 ila %4,5 oranında artırabileceğini öngörmektedir (Bjork ve Nielsen,2018). Bunun temel nedeni, TEG'in düşük verimli olmasıdır.

Yoğunlaştırılmış (CPV) ve spektrum bölmeli sistemlerde ise potansiyel çok daha yüksektir. Bu tasarımlar hem PV hem de TEG'in daha verimli çalışmasını sağlayarak, tek başına PV sistemine göre toplam verimlilikte %5 ila %10 oranında bir artış sağlama potansiyeli sunmaktadır (Abdo ve ark., 2016).

Termal yönetim ve gelişmiş soğutma teknikleri

PV/TEG sistemlerinde etkin termal yönetim, hem PV verimliliğini korumak hem de TEG'in çalışması için gerekli sıcaklık farkını sağlamak/artırmak için hayati öneme sahiptir. Bu amaçla çeşitli termal yönetim teknikleri geliştirilmiştir:

Akışkan Tabanlı Sistemler ve Nanoakışkanlar: PV panelinin arkasından su veya hava gibi bir akışkan dolaştırmak yaygın bir yöntemdir. Bu yöntemin etkinliği, temel akışkana metal oksitler veya karbon nanotüpler gibi nanopartiküllerin eklenmesiyle elde edilen nanoakışkanlar kullanılarak önemli ölçüde artırılabilir. Yapılan çalışmalarda nanoakışkan kullanılarak %41,2'ye varan sıcaklık düşüşü elde etmiştir. (Praveenkumar ve ark. 2023). Bununla birlikte hibrit nanoakışkanların tekli nanoakışkanlara göre daha iyi performans sunduğu da tespit edilmiştir. (Gharapetian ve ark., 2024).

Isı Borusu Tabanlı Sistemler: Isı boruları, çok düşük sıcaklık farkıyla yüksek miktarda ısıyı verimli bir şekilde transfer edebilen pasif cihazlardır. Yapılan çalışmalarda, ısı borusu tabanlı bir sistemin PV panelini etkin bir şekilde soğuturken, TEG'nin sıcak tarafına maksimum ısıyı taşıyarak sistemin genel elektrik verimliliğini artırdığı sayısal olarak görülmüştür. (Makki ve ark., 2016).

Radyatif Gökyüzü Soğutması (RSC): Özellikle TEG'in soğuk tarafını pasif olarak ortam sıcaklığının altına düşürmek ve gece boyunca güç üretimi sağlamak için umut verici bir yaklaşımdır. (Lai ve ark., 2025).

Faz Değiştiren Malzemeler (PCM): PCM'ler, faz değişimi sırasında ısı depolayarak sıcaklık dalgalanmalarını azaltır. Yapılan çalışmalarda RGO-PCM nanokompoziti kullanılarak termal enerji depolamalı bir termo/fotovoltaik cihaz geliştirilmiştir. (Kumar ve ark., 2024).

Malzeme bilimindeki ilerlemeler

PV/TEG hibrit sistemlerinin verimliliği, kullanılan malzemelerin özelliklerine büyük ölçüde bağlıdır.

PV Malzemeleri: Geleneksel silikon (c-Si) PV'lerin yanı sıra, daha düşük sıcaklık katsayısına sahip amorf silikon (a-Si) ince film hücreleri ve son yıllarda yüksek verimlilik potansiyeli sunan perovskit güneş hücreleri (PSC) gibi yeni nesil malzemeler, hibrit sistemlerin performansını artırma potansiyeli sunmaktadır.

TEG Malzemeleri: Oda sıcaklığına yakın uygulamalarda en yaygın kullanılan bizmut tellür (Bi_2Te_3) bazlı malzemelerin ZT değeri ~1 civarındadır (Bjork ve Nielsen,2018). Nano yapılandırma gibi tekniklerle foton saçılımını artırıp termal iletkenliği düşürerek ZT değerini artırmaya yönelik çalışmalar devam etmektedir. Ayrıca, esneklik ve düşük maliyet avantajları sunan organik termoelektrik (OTEG) malzemeler de aktif olarak araştırılmaktadır.

Karşılaşılan zorluklar ve çözüm önerileri

PV/TEG hibrit sistemlerinin yaygın ticari uygulamalara ulaşmasının önünde hala aşılması gereken çeşitli zorluklar bulunmaktadır.

Termoelektrik Jeneratörlerin Düşük Verimliliği ve Yüksek Maliyeti: Mevcut ticari TEG malzemelerinin ZT değerleri hala göreceli olarak düşüktür. Çözüm, nano yapılandırma ve yeni malzeme keşifleriyle ZT değerini artırmak ve daha bol bulunan elementlerle maliyeti düşürmektir.

PV ve TEG Arasındaki Termal Uyumsuzluk: PV düşük sıcaklık, TEG ise yüksek sıcaklık farkı ister. Bu çelişki, özellikle doğrudan bağlı sistemlerde performansı sınırlar. Çözüm, spektrum bölme gibi her bileşenin termal olarak ayrıştırıldığı yenilikçi sistem tasarımlarıdır (Mahmoudinezhad ve ark., 2022).

Sistem Maliyeti ve Karmaşıklığı: Gelişmiş soğutma sistemleri, yoğunlaştırıcılar ve özel malzemelerin eklenmesi, başlangıç yatırım maliyetini artırır. Çözüm, basitleştirilmiş tasarımlar ve bina entegrasyonu gibi çok fonksiyonlu sistemler geliştirerek ekonomik getiriyi artırmaktır. (Duraivel ve Muthuswamy, 2025).

SONUÇ

Bu inceleme, fotovoltaik/termoelektrik (PV/TEG) hibrit sistemleri alanında son on ila on beş yılda kaydedilen önemli gelişmeleri kapsamlı bir şekilde ele almıştır. Güneş enerjisinden daha verimli yararlanma arayışı, PV ve TEG teknolojilerinin yenilikçi bir şekilde birleştirilmesine yönelik yoğun araştırmalara yol açmıştır.

Sonuç olarak, fotovoltaik/termoelektrik hibrit sistemleri, güneş enerjisinin daha verimli ve çok yönlü bir şekilde kullanılması için heyecan verici bir araştırma alanı sunmaktadır. Karşılaşılan zorluklara rağmen, malzeme bilimi, sistem tasarımı ve modelleme tekniklerindeki sürekli ilerlemeler, bu teknolojinin gelecekte sürdürülebilir enerji portföyünde önemli bir rol oynama potansiyelini artırmaktadır. Gelecekteki araştırmaların; PV panel çalışma sıcaklığı aralığında (30-100°C) yüksek performans gösteren, bol bulunan, çevre dostu ve esnek TEG malzemelerinin geliştirilmesine odaklanması gerekmektedir. Disiplinler arası iş birliği ve yenilikçi yaklaşımlarla, PV/TEG hibrit sistemlerinin pratik ve ekonomik olarak uygulanabilir çözümlere dönüşmesi beklenmektedir.

KAYNAKLAR

Abdo, A., Ookawara, S., & Ahmed, M. (2019). Performance evaluation of a new design of concentrator photovoltaic and solar thermoelectric generator hybrid system. Energy Conversion and Management, 195, 1382-1401.

Ariffin, M. R., Shafie, S., Hassan, W. Z. W., Azis, N., & Ya'acob, M. E. (2017). Conceptual Design of Hybrid Photovoltaic-Thermoelectric Generator (PV/TEG) for Automated Greenhouse System. In 2017 IEEE 15th Student Conference on Research and Development (SCOReD) (pp. 309-314). Putrajaya, Malaysia.

Basu, R. (2024). A holistic review on alternate sustainable energy source embracing photo-thermo-electric and photo-thermoelectric effect: Phonetically similar with dissimilar working principle. Applied Energy, 375, 124127.

Bjørk, R., & Nielsen, K. K. (2015). The performance of a combined solar photovoltaic (PV) and thermoelectric generator (TEG) system. Solar Energy, 120, 187-194.

Bjørk, R., & Nielsen, K. K. (2018). The maximum theoretical performance of unconcentrated solar photovoltaic and thermoelectric generator systems. Energy Conversion and Management, 156, 264-268.

Congxiang, T., Guoqing, Z., & Yong, Y. (2025). Hybrid photovoltaic and thermoelectric generator systems with thermal wheel Ventilation: A sustainable approach to residential heating and cooling. Engineering Science and Technology, an International Journal, 62, 101-968.

Duraivel, B., & Muthuswamy, N. (2025). Optimizing energy efficiency in residential buildings: A comprehensive evaluation of solar concrete water heaters integrated with photovoltaics and thermoelectric cooling. Case Studies in Thermal Engineering, 72, 106-218.

Gharapetian, D., Fini, M. A., Asgari, M., & Shabani, B. (2024). A nanofluid-based hybrid photovoltaic-thermal -thermoelectric generator system for combined heat and power applications. Energy Conversion and Management, 301, 118-066.

Huen, P., & Daoud, W. A. (2017). Advances in hybrid solar photovoltaic and thermoelectric generators. Renewable and Sustainable Energy Reviews, 72, 1295-1302.

Indira, S. S., et al. (2022). Prototype of a novel hybrid concentrator photovoltaic/thermal and solar thermoelectric generator system for outdoor study. Renewable Energy, 201, 224-239.

Khan, K., et al. (2023). Data-driven green energy extraction: Machine learning-based MPPT control with efficient fault detection method for the hybrid PV-TEG system. Energy Reports, 9, 3604-3623.

Khalili, Z., & Sheikholeslami, M. (2023). Analyzing the effect of confined jet impingement on efficiency of photovoltaic thermal solar unit equipped with thermoelectric generator in existence of hybrid nanofluid. Journal of Cleaner Production, 406, 137-063.

Kidegho, G., Njoka, F., Muriithi, C., & Kinyua, R. (2021). Evaluation of thermal interface materials in mediating PV cell temperature mismatch in PV–TEG power generation. Energy Reports, 7, 1636-1650.

Kotkondawar, A., Bhende, A., Khond, V., & Rayalu, S. (2021). Performance evaluation of PV-TEC coupling device for power production with improved hybrid nanocarbon based thermal material interface. Energy Reports, 7, 6868-6875.

Kumar, A., Kumar, P., Verma, A., & Jain, V. K. (2024). Thermo-photovoltaic generator with thermal energy storage using Schottky heterojunction of RGO-PCM nanocomposite on SiNWs on silicon chip. Journal of Energy Storage, 104, 114-498.

Lai, P., Han, X., Chen, X., & Huang, J. (2025). All-day continuous power generation: Integrating radiative cooling with semi-transparent photovoltaic cells filtered concentrated photovoltaic-thermoelectric generator system. Solar Energy, 287, 113-207.

Mahmoudinezhad, S., Rezania, A., & Rosendahl, L. A. (2018). Behavior of hybrid concentrated photovoltaic-thermoelectric generator under variable solar radiation. Energy Conversion and Management, 164, 443-452.

Mahmoudinezhad, S., et al. (2022). Experimental investigation on spectrum beam splitting photovoltaic-thermoelectric generator under moderate solar concentrations. Energy, 238, 121-988.

Makki, A., et al. (2016). Numerical investigation of a hybrid photovoltaic/thermal-thermoelectric (PV/T-TE) system. Energy Conversion and Management, 129, 308-322.

Muhi, F. H. M., & Güçyetmez, M. (2024). Load management design and techno-economic analysis for an islanded hybrid Pv-Teg microgrid. Energy Reports, 11, 5542-5555.

Parthiban, R., Ponnambalam, P., & Krishnamurthy, K. (2024). Analysis of area saving and efficiency enhancement of photovoltaic system combined with thermoelectric generator. e-Prime - Advances in Electrical Engineering, Electronics and Energy, 8, 100-553.

Praveenkumar, S., Agyekum, E. B., Kumar, A., & Velkin, V. I. (2023). Thermo-enviro-economic analysis of solar photovoltaic/thermal system incorporated with u-shaped grid copper pipe, thermal electric generators and nanofluids: An experimental investigation. Journal of Energy Storage, 60, 106-611.

Sabry, M., Lashin, A., & Al Turkestani, M. (2021). Experimental and simulation investigations of CPV/TEG hybrid system. Journal of King Saud University – Science, 33(2), 101321.

Selimefendigil, F., Okulu, D., & Oztop, H. F. (2024). Application of ternary nanofluid and rotating cylinders in the cooling system of photovoltaic/thermoelectric generator coupled module and computational cost reduction. Applied Thermal Engineering, 250, 123-436.

Shahpar, M., Hajinezhad, A., & Moosavian, S. F. (2024). The influence of diverse climate on the 3E analysis of energy, exergy, and environmental aspects of a hybrid module of thermoelectric generator and photovoltaic cells. Results in Engineering, 22, 102-337.

Usman, M., et al. (2025). Investigation of a novel heat extraction configuration for boosting photovoltaic panel efficiency. Case Studies in Thermal Engineering, 70, 106-104.

Yang, B., Xie, R., Duan, J., & Wang, J. (2023). State-of-the-art review of MPPT techniques for hybrid PV-TEG systems: modeling, methodologies, and perspectives. Global Energy Interconnection, 6(5), 567-591.

Yang, Z., Li, W., Chen, X., Su, S., Lin, G., & Chen, J. (2018). Maximum efficiency and parametric optimum selection of a concentrated solar spectrum splitting photovoltaic cell-thermoelectric generator system. Energy Conversion and Management, 174, 65-71.

➢ *ORAL PRESENTATION*

Use of Cyclomatic Complexity and Maintainability Index Metrics in Agile Development: Trends, Challenges, and Research Directions

Sena Adatepe[1*] (*ORCID: https://orcid.org/ 0009-0004-9856-9672*),
Gonca Gokce Menekse Dalveren[1] (*ORCID: https://orcid.org/ 0000-0002-8649-1909*)

[*1] Izmir Bakircay University, Computer Engineering Department, Izmir, Turkiye.

*Corresponding author e-mail: senadtp28@gmail.com

Abstract
Ensuring and continuously enhancing code quality is fundamental to the development of sustainable, reliable, and maintainable software systems. Agile software development methodologies, which emphasize adaptability and rapid responsiveness to evolving requirements, promote fast feedback cycles through short iterations and continuous delivery. While these characteristics contribute to accelerated development, they also pose challenges, such as increased code complexity and difficulties in maintaining consistent quality assurance practices. Consequently, the systematic monitoring and measurement of code quality within Agile environments are essential for ensuring the long-term success and stability of software projects. To facilitate objective and quantitative assessments of code quality, software engineering relies on a variety of established metrics. This study specifically focuses on two widely recognized metrics: Cyclomatic Complexity and the Maintainability Index. The primary objective of this paper is to examine the effective integration of these metrics within Agile development processes and to assess their impact on overall code quality. By conducting a thorough review of relevant literature, the theoretical foundations of these metrics and their practical application in Agile contexts are explored. This investigation aims to provide software practitioners with a data-driven framework for evaluating and improving code quality in Agile-based projects. This paper explores the intersection of software metrics and agile methodologies based on a bibliometric analysis of 57 publications retrieved from the Web of Science. We analyse publication trends, key contributors, thematic focuses, and publication venues. The study reveals a strong focus on object-oriented metrics, validation, and design complexity, with most publications emerging from conference proceedings. Our findings highlight current challenges in agile metrics, identify active research groups, and suggest directions for future research.
Keywords: cyclomatic complexity, maintainability index, software metrics, agile

INTRODUCTION

Maintaining and continuously improving code quality during software development processes is of critical importance for building sustainable, reliable, and maintainable systems (Padmini et al., 2015). Agile software development methodologies, which aim to respond rapidly to evolving requirements, facilitate fast feedback loops through short iterations and continuous delivery practices (Salih AYDINER et al., 2020). However, the speed and flexibility offered by Agile approaches also introduce certain risks, such as increased code complexity and challenges in maintaining effective quality control processes (Concas et al., 2012; Dybå & Dingsøyr, 2008). Therefore, the regular monitoring and measurement of code quality within Agile processes is essential for the long-term success of a project. Moreover, how Agile methods are applied in practice and their impact on software quality have been examined in various empirical studies (Dybå & Dingsøyr, 2008). Various software metrics are employed to evaluate code quality in an objective and measurable manner (Concas et al., 2008b). This study highlights two fundamental metrics that are widely used in software engineering: Cyclomatic Complexity and the Maintainability Index. Cyclomatic Complexity reflects the structural complexity of a software component by considering the number of decision points within its control flow (Alsulami, 2022). In contrast, the Maintainability Index quantifies how maintainable the code is, typically based on factors such as complexity, lines of code, and the ratio of comments (K. Welker, 2001).

The aim of this study is to explore how these metrics can be utilized within Agile software development processes and to evaluate their impact on code quality. Within the scope of the research, a review of the relevant literature will be conducted to examine the theoretical foundations of these metrics as well as their practical applications in Agile projects. The goal is to provide developers and software teams with a practical, data-driven roadmap for measuring and improving code quality in projects developed using Agile methodologies.

Software metrics such as Cyclomatic Complexity and the Maintainability Index offer effective tools for objectively assessing the structural complexity and maintainability of code (Kunz et al., 2008). The findings indicate that the regular use of these metrics enables software teams to detect potential issues at an early stage and to evolve the codebase in a sustainable manner (Aldahmash & Graven, 2018). Agile methodologies have transformed software development practices by emphasizing iterative progress, collaboration, and responsiveness to change (Huijgens et al., 2017). However, measuring progress and quality in agile environments remains a challenge (Koch, 2004). Software metrics provide a quantitative basis for assessing various aspects of software quality and process efficiency (Koch, 2004). This review aims to synthesize current research at the intersection of agile development and software metrics, identifying prevailing themes, research trends, and gaps in the literature. Software metrics are measurement tools used in the software development process to quantitatively assess the quality, complexity, efficiency, and maintainability of code (Destefanis et al., 2014). These metrics provide developers and project managers with objective insights into the current state of the software, thereby facilitating more effective quality control processes (Padmini et al., 2015). Furthermore, they contribute significantly to the early detection of potential issues, reduction of technical debt, and enhancement of software sustainability (K. Welker, 2001). In general, software metrics can be categorized into two main groups: product metrics and process metrics (Berlas, 2024). Product metrics focus on tangible outputs such as source code, architecture, or documentation, whereas process metrics aim to evaluate the efficiency and effectiveness of the software development process (Berlas, 2024; Concas et al., 2008a). This distinction enables a comprehensive assessment of software quality from both technical and managerial perspectives (Berlas, 2024; O'Riordan, 2011). While product metrics allow for the analysis of structural properties of the software, process metrics provide feedback on team workflows and management practices(Berlas, 2024). Among the metrics directly related to code quality, several key indicators stand out, including Cyclomatic Complexity, Maintainability Index, Lines of Code (LOC), Depth of Inheritance, Coupling Between Objects (CBO), and Lack of Cohesion in Methods (LCOM) (Chidamber & Kemerer, 1994). These metrics allow for the analysis of characteristics such as complexity, reusability, modularity, and testability of software components (Chidamber & Kemerer, 1994; Olague et al., 2007). For instance, Cyclomatic Complexity calculates the number of independent paths through a software component based on the number of decision structures it contains(Alsulami & Alrabie, 2019; Mccabe, 1976). This metric plays a crucial role in determining test coverage and assessing the complexity of a module (Mccabe, 1976). Below sees the example:

```
def calculate(x):
    if x > 0:
        return x * 2
    elif x == 0:
        return 0
    else:
        return -x
```

Since the function above contains three distinct control points, its Cyclomatic Complexity value is 3. Such metrics aid in quantifying software complexity and enable more informed decisions in designing test plans. While Cyclomatic Complexity helps determine the extent of test coverage by measuring the number of decision points within a module, the Lack of Cohesion in Methods (LCOM) metric identifies low-cohesion structures by analysing how closely related the methods within a class are. The Cyclomatic Complexity (M) is calculated using the following formula (Microsoft, 2024)

M = D + 1

Where:

- **M** represents the Cyclomatic Complexity,
- **D** is the number of decision points in the function (such as if, while, for, case, catch, etc.).

This formula expresses that the total number of independent execution paths in a program is equal to the number of decision points plus one.

Similarly, the Maintainability Index (MI) is a metric that produces a value between 0 and 100, indicating how easily a software component can be maintained (Microsoft, 2025). A higher score corresponds to better maintainability. This metric is typically calculated using a combination of Cyclomatic Complexity, Lines of Code (LOC), and various software quality indicators, such as Halstead Volume.

```
int Sum(int a, int b)
{
   return a + b;
}
```

While the Maintainability Index (MI) value for a simple function like the one above tends to be relatively high, it can decrease significantly in code blocks that contain complex structures such as deeply nested logic and lengthy methods. The calculation of the Maintainability Index and its corresponding interpretative ranges are presented below (Microsoft, 2025).

*Maintainability Index = MAX(0,(171 - 5.2 * ln(Halstead Volume) - 0.23 * (Cyclomatic Complexity) - 16.2 * ln(Lines of Code))*100 / 171)*

Table 1. Maintainability Index Value Interpretation (Microsoft, 2025)

Index Value	**Color**	**Interpretation**
0–9	Red	Low maintainability
10–19	Yellow	Moderate maintainability
20–100	Green	High maintainability

The effective use of software metrics facilitates not only the analysis of the current codebase but also the formulation of strategic decisions for future development efforts (Canedo & da Costa, 2018). These metrics enable teams to objectively identify areas for improvement and, in the long term, contribute to reducing software maintenance costs (Canedo & da Costa, 2018; Sneed, 2014). This is particularly critical in iterative and fast-paced development methodologies such as Agile, where the regular monitoring and interpretation of metrics play a vital role in ensuring the continuity of high-quality software delivery (Boerman et al., 2015). Furthermore, metrics provide a data-driven foundation for end-of-sprint evaluations, allowing for more accurate tracking of team progress and performance over time (Boerman et al., 2015; Chloros et al., 2022).

MATERIALS AND METHODS

The data for this review were sourced from the Web of Science using the keywords ("software metrics" and "agile"). A total of 57 relevant publications were identified. These publications were analysed based on publication year, document type, publisher, and keywords.

Table 2. Inclusion Criteria

IC#	Inclusion Criteria
1	Studies in the field of software development and software metrics concepts
2	Studies that utilize software metrics Cyclomatic Complexity and Maintainability Index to improve software development processes
3	Studies that explain the software metrics can be applied for agile software development processes.

Table 3. Exclusion Criteria

EC#	Exclusion Criteria
1	The studies that do not address the software development and software metrics concepts
2	The studies that are not written in English.
3	The papers that cannot be accessed in full text.

Visualizations were generated to examine the evolution of the field and thematic concentrations. We excluded the articles not written in English. First, each article was assessed from its title and according to the inclusion criteria (Table 2) and exclusion criteria (Table 3). Secondly, each article was assessed by reading them critically from the full text.

RESULTS

The distribution of publications over time related to the topic of ("Software Metrics and Agile") Key observations include the distribution of publications over the years reveals a fluctuating trend in scholarly productivity.

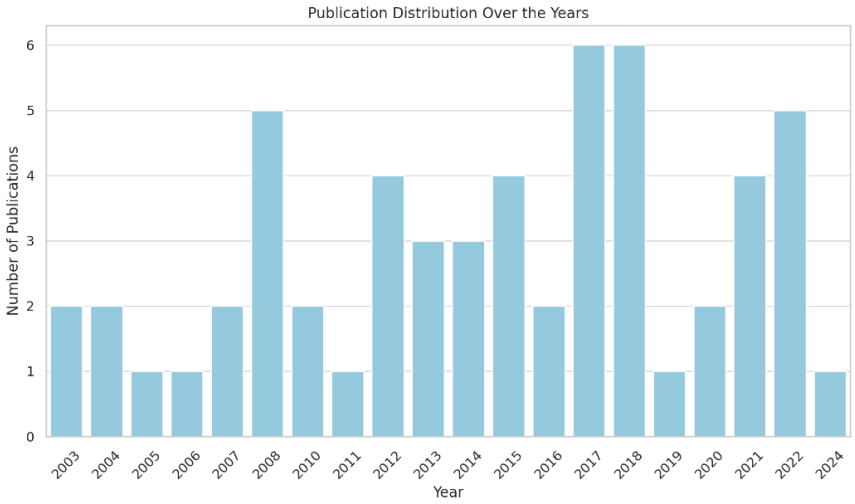

Figure 1. Publication Distribution Over the Years

Figure 1 illustrates the distribution of publications over time related to the topic of "Software Metrics and Agile." Key observations include the distribution of publications over the years reveals a fluctuating trend in scholarly productivity. Between 2003 and 2007, the number of publications remained relatively low and stable, suggesting a period of limited academic output. A marked increase occurred in 2008, reaching five publications, which may indicate a significant turning point or the result of intensified research efforts. However, this surge was followed by another decline between 2009 and 2011. The period from 2012 to 2016 was characterized by moderate and relatively consistent productivity, with annual publications ranging from two to four. The most prolific years were 2017 and 2018, each yielding six publications, representing a peak in scholarly activity. In contrast, a sharp decrease was observed in 2019 and 2020, potentially reflecting disruptions caused by external factors. Encouragingly, publication numbers began to recover from 2021 onward, culminating in another productive year in 2022 with five publications. Overall, the data illustrates periods of both growth and decline, with notable peaks and recoveries in recent years. This distribution highlights the periods during which academic interest in the field intensified and provides a contextual framework for understanding the evolution of the relevant literature. Most documents were conference proceedings (Figure 2), indicating a preference for rapid dissemination and discussion of emerging ideas.

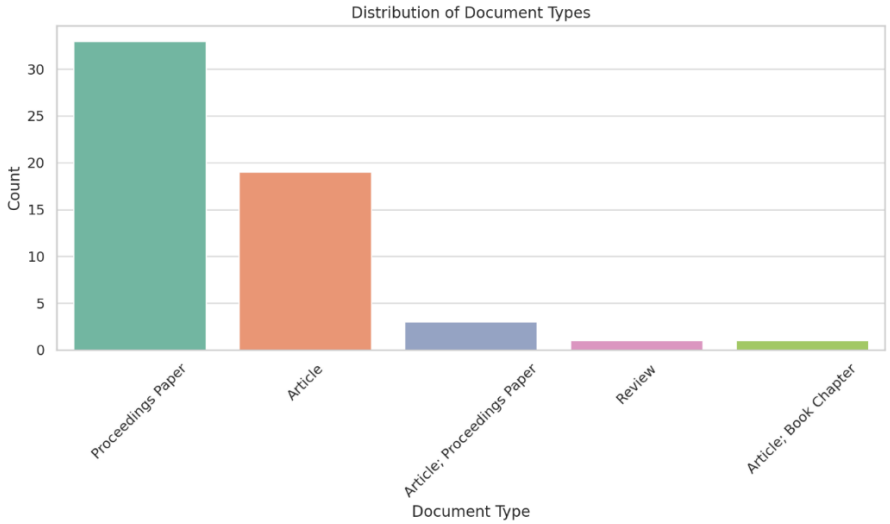

Figure 2. Distribution of Document Types

As illustrated in Figure 2, Proceedings Papers (conference papers) are by far the most common document type. This indicates that the topic of *"software metrics and Agile"* is predominantly disseminated through conferences, suggesting that it remains an evolving area of study. It also reflects the community's preference for rapid dissemination channels, which are typical for emerging and practice-oriented research fields.
Figure 3 presents the top 10 publishers with the highest number of publications on the topic. Key highlights include IEEE and Springer stand out as the leading publishers with a significantly higher number of publications. ACM (Association for Computing Machinery) also emerges as a major contributor to the literature. Other publishers are represented with a relatively limited number of publications. These findings suggest that the topic is predominantly addressed through technical conferences and engineering-focused outlets. IEEE and Springer serve as strong platforms for disseminating research articles and conference proceedings in this domain. Thematic analysis of Keywords revealed frequent emphasis on object-oriented software, validation, complexity, design, productivity, and maintenance. These themes reflect the core concerns of integrating robust metric systems into agile workflows.

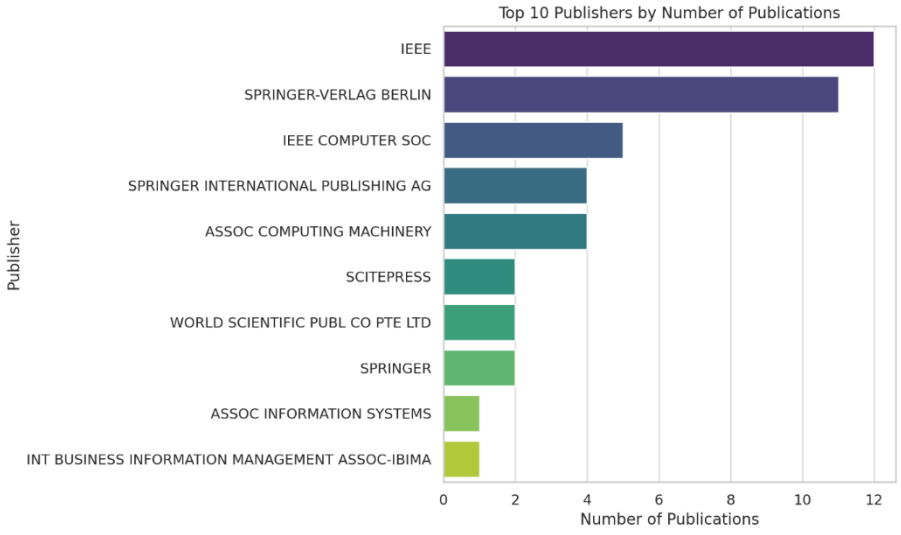

Figure 3. Top 10 Publishers

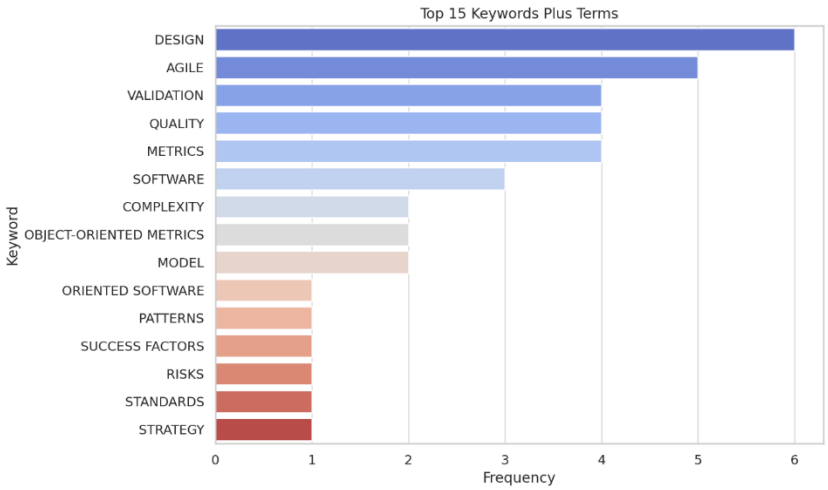

Figure 4. Top 15 Keywords

Figure 4 displays the most frequently occurring *Keyword* terms found in the analysed articles. Key observations include terms such as *OBJECT-ORIENTED SOFTWARE*, *VALIDATION*, and *COMPLEXITY* indicate a strong emphasis on the technical aspects of software metrics. Keywords like *PATTERNS*, *DESIGN*, *MAINTENANCE*, and *PRODUCTIVITY* highlight various dimensions of the software development process. Core terms such as *AGILE* and *SOFTWARE DEVELOPMENT* are also prominently represented, reflecting a direct connection to the central theme. These keywords can be effectively used to illustrate the dominant subthemes within the theoretical framework of your paper, helping to contextualize the scope and focus of existing research.

DISCUSSION

In the literature, it is evident that software metrics are effectively utilized within Agile development processes. For instance, an empirical study demonstrated that the distribution of software metrics in systems developed using Agile methodologies does not significantly differ from those developed with plan-driven approaches (Alshayeb & Li, 2003; Ciancarini et al., 2021; Concas et al., 2012; Destefanis et al., 2014; Dybå & Dingsøyr, 2008; Koch, 2004; Ram et al., 2020). This finding suggests that traditional metrics can be reliably employed to assess code quality and maintainability in Agile environments as well (Destefanis et al., 2014). The use of software metrics is crucial for continuously monitoring and improving quality throughout the software development lifecycle (Boerman et al., 2015; Capodieci et al., 2014; Mahnic & Vrana, 2007). Metrics such as Cyclomatic Complexity and the Maintainability Index help teams understand the structural complexity and maintainability of software components (K. Welker, 2001). Cyclomatic Complexity, which measures the number of decision points within a module, indicates the number of independent paths that need to be tested (Microsoft, 2024; Stahl et al., 2019). By leveraging this metric, teams are encouraged to write simpler, more modular, and readable code, thereby contributing to the reduction of technical debt over the long term (dos Santos et al., 2013; Sneed, 2014). The Maintainability Index, on the other hand, summarizes the maintainability of code into a single numerical score. By evaluating factors such as readability, comment density, and structural characteristics, this metric offers insights into the sustainability of code (Capodieci et al., 2014; Microsoft, 2025; Moser et al., 2008; Sjoberg et al., 2012; K. Welker, 2001). Monitoring the index over time allows teams to detect early signs of quality degradation as the software evolves (K. Welker, 2001). Empirical research on real-world projects has shown that object-oriented metrics have a direct impact on maintainability (Kupiainen et al., 2015), underscoring the importance of tracking composite metrics like the Maintainability Index in Agile contexts to ensure long-term sustainability. The role of metrics becomes even more prominent in iterative development methodologies such as Agile (Aktunc, 2012; Chidamber & Kemerer, 1994; Destefanis et al., 2014; Huijgens et al., 2017; Kunz et al., 2008; Shawky & Abd-El-Hafiz, 2016). In this regard, metrics like Cyclomatic Complexity and the Maintainability Index enable teams to anticipate the accumulation of technical debt, identify declining quality trends, and recognize when refactoring is needed (Berlas, 2024; Padmini et al., 2015; Ram et al., 2020). A high complexity score does not inherently indicate poor-quality code, as certain complex structures may be necessary due to the problem domain (Berlas, 2024). Therefore, metrics should be viewed as decision-support tools rather than absolute judgments (K. Welker, 2001).

Therefore, software metrics provide developers and project managers with concrete, data-driven insights into the current state of the software. Metrics such as Cyclomatic Complexity and the Maintainability Index play a critical role in quality assurance processes. Their consistent and accurate application contributes significantly to enhancing sustainability, reducing technical debt, and fostering long-lived, maintainable software systems. The bibliometric patterns suggest that the field is still maturing, with key research clusters focusing on empirical validation of metrics in agile settings. The dominance of conference papers also implies an ongoing evolution of theories and frameworks. Despite the progress, the literature still lacks standardized, widely accepted metrics tailored specifically for agile practices.

CONCLUSION

The role of software metrics in the software development process has become increasingly significant. These metrics provide a means to evaluate software quality not merely through intuition but via measurable data, making them indispensable tools in modern software engineering. Metrics such as Cyclomatic Complexity and the Maintainability Index help assess the structural complexity and maintainability of a given software component. In Agile development processes, monitoring such metrics plays a critical role in maintaining code quality amid short delivery cycles and constantly evolving requirements. By tracking these indicators, development teams can observe how the codebase evolves over time, identify areas where technical debt accumulates, and detect modules that may pose future risks. This proactive approach enables earlier interventions, potentially preventing larger issues from arising later in the project lifecycle. However, it is important to note that no metric provides absolute truth. Factors such as the intended use of the software, its architecture, scope, and team composition must also be considered when interpreting metric results. Without this contextual awareness, misinterpreted data may lead to unnecessary interventions or misplaced priorities. Overall, the systematic and balanced use of software metrics not only offers a clearer understanding of the current state of the codebase but also supports more informed and strategic decision-making for future development. Therefore, such metrics should be regarded as essential tools that are fully integrated into the software development lifecycle.

This review highlights the active engagement of the research community in developing and refining software metrics for agile environments. Although significant strides have been made, challenges remain in establishing universally accepted practices. Continued collaboration and empirical validation will be crucial for advancing the field. Future research in the field of software metrics and Agile methodologies can pursue several promising directions. One important avenue is the development of Agile-specific metrics that better align with the iterative and incremental nature of Agile practices, as traditional metrics may not fully capture the nuances of Agile workflows. Additionally, longitudinal studies are needed to evaluate the long-term impact of metric usage on Agile team performance, providing empirical evidence of their effectiveness over time. The integration of automated tools for real-time metric tracking also represents a critical area, as it can enhance the responsiveness and adaptability of Agile teams. Finally, comparative studies across different Agile frameworks such as Scrum, Kanban, or Extreme Programming can offer insights into how metrics function and influence team behaviour within varying Agile environments. These directions can contribute to a deeper understanding of how to optimize metric use in Agile software development.

REFERENCES

Aktunc, O. (2012). Entropy Metrics for Agile Development Processes. 23rd Ieee International Symposium on Software Reliability Engineering (Issre 2012), 7–8. Https://Doi.Org/10.1109/Issrew.2012.36

Aldahmash, A., & Graven, A. (2018). Measuring Success in Agile Software Development Projects: A Gqm Approach. In L. Lavazza, R. Oberhauser, & R. Koci (Eds.), Thirteenth International Conference on Software Engineering Advances (Icsea 2018) (Pp. 38–44).

Alshayeb, M., & Li, W. (2003). An Empirical Validation of Object-Oriented Metrics in Two Different Iterative Software Processes. Ieee Transactions on Software Engineering, 29(11), 1043–1049. Https://Doi.Org/10.1109/Tse.2003.1245305

Alsulami, M. (2022). Exploring The Use of Software Metrics in Saudi Enterprises: A Case Study. Tehnicki Glasnik-Technical Journal, 16(2), 155–160. Https://Doi.Org/10.31803/Tg-20220124143638

Alsulami, M., & Alrabie, W. (2019). Maximising The Value of The Business by Understanding Software Metrics in Saudi Enterprises: A Case Study. In K. S. Soliman (Ed.), Vision 2025: Education Excellence and Management of Innovations Through Sustainable Economic Competitive Advantage (Pp. 13339–13345).

Berlas, M. F. (2024). Software Metrics in Agile Software Development: A Review Report. Authorea Preprints. Https://Doi.Org/10.36227/Techrxiv.171084962.20068546/V1

Boerman, M. P., Lubsen, Z., Tamburri, D. A., & Visser, J. (2015). Measuring And Monitoring Agile Development Status. Proceedings Sixth International Workshop on Emerging Trends in Software Wetsom 2015, 54–62. Https://Doi.Org/10.1109/Wetsom.2015.15

Canedo, E. D., & Da Costa, R. P. (2018). Methods And Metrics for Estimating and Planning Agile Software Projects Completed Research. Amcis 2018 Proceedings.

Capodieci, A., Mainetti, L., & Manco, L. (2014). A Case Study to Enable and Monitor Real It Companies Migrating from Waterfall to Agile. In B. Murgante, S. Misra, A. Rocha, C. Torre, J. G. Rocha, M. I. Falcao, D. Taniar, B. O. Apduhan, & O. Gervasi (Eds.), Computational Science and Its Applications - Iccsa 2014, Pt V (Vol. 8583, Pp. 119–134).

Chidamber, S. R., & Kemerer, C. F. (1994). A Metrics Suite for Object Oriented Design. Ieee Transactions on Software Engineering, 20(6), 476–493. Https://Doi.Org/10.1109/32.295895

Chloros, D., Gerogiannis, V. C., & Kakarontzas, G. (2022). Use Of Software and Project Management Metrics in Agile Software Development Methodologies. Proceedings Of 2022 The 3rd European Symposium on Software Engineering, Esse 2022, 25–32. Https://Doi.Org/10.1145/3571697.3571701

Ciancarini, P., Ergasheva, S., Gizzatullina, I., Ivanov, V., Masyagin, S., & Succi, G. (2021). Empirical Research on Customer Communication Challenges in The Companies Adopting Agile Practices. In J. Filipe, M. Smialek, A. Brodsky, & S. Hammoudi (Eds.), Iceis: Proceedings of the 23rd International Conference on Enterprise Information Systems - Vol 2 (Pp. 139–150). Https://Doi.Org/10.5220/0010526401390150

Microsoft. (2024, December 11). Code Metrics - Cyclomatic Complexity - Visual Studio (Windows) | Microsoft Learn. Https://Learn.Microsoft.Com/En-Us/Visualstudio/Code-Quality/Code-Metrics-Cyclomatic-Complexity?View=Vs-2022

Microsoft. (2025, January 10). Code Metrics - Maintainability Index Range and Meaning - Visual Studio (Windows) | Microsoft Learn. Https://Learn.Microsoft.Com/En-Us/Visualstudio/Code-Quality/Code-Metrics-Maintainability-Index-Range-And-Meaning?View=Vs-2022

Concas, G., Di Francesco, M., Marchesi, M., Quaresima, R., & Pinna, S. (2008a). An Agile Development Process and Its Assessment Using Quantitative Object-Oriented Metrics. In P. Abrahamsson, R. Baskerville, K. Conboy, B. Fitzgerald, L. Morgan, & X. Wang (Eds.), Agile Processes in Software Engineering and Extreme Programming, Proceedings (Vol. 9, P. 83+).

Concas, G., Di Francesco, M., Marchesi, M., Quaresima, R., & Pinna, S. (2008b). Study Of the Evolution of An Agile Project Featuring a Web Application Using Software Metrics. In A. Jedlitschka & O. Salo (Eds.), Product-Focused Software Process Improvement, Proceedings (Vol. 5089, P. 386+).

Concas, G., Marchesi, M., Destefaniso, G., & Tonelli, R. (2012). An Empirical Study of Software Metrics for Assessing the Phases of An Agile Project. International Journal of Software Engineering and Knowledge Engineering, 22(4), 525–548. Https://Doi.Org/10.1142/S0218194012500131

Destefanis, G., Counsel, S., Concas, G., & Tonelli, R. (2014). Software Metrics in Agile Software: An Empirical Study. In G. Cantone & M. Marchesi (Eds.), Agile Processes in Software Engineering and Extreme Programming: 15th International Conference, Xp 2014 (Vol. 179, Pp. 157–170).

Dos Santos, P. S., Varella, A., Dantas, C. R., & Borges, D. B. (2013). Visualizing And Managing Technical Debt in Agile Development: An Experience Report. In H. Baumeister & B. Weber (Eds.), Agile Processes in Software Engineering and Extreme Programming, Xp 2013 (Vol. 149, Pp. 121–134).

Dybå, T., & Dingsøyr, T. (2008). Empirical Studies of Agile Software Development: A Systematic Review. Information And Software Technology, 50(9–10), 833–859. Https://Doi.Org/10.1016/J.Infsof.2008.01.006

Huijgens, H., Lamping, R., Stevens, D., Rothengatter, H., Gousios, G., & Romano, D. (2017). Strong Agile Metrics: Mining Log Data to Determine Predictive Power of Software Metrics for Continuous Delivery Teams. In E. Bodden, W. Schafer, A. Vandeursen, & A. Zisman (Eds.), Esec/Fse 2017: Proceedings of the 2017 11th Joint Meeting on Foundations of Software Engineering (Pp. 866–871). Https://Doi.Org/10.1145/3106237.3117779

Koch, S. (2004). Agile Principles and Open Source Software Development: A Theoretical and Empirical Discussion. In J. Eckstein & H. Baumeister (Eds.), Extreme Programming and Agile Processes in Software Engineering, Proceedings (Vol. 3092, Pp. 85–93).

Kunz, M., Dumke, R. R., & Zenker, N. (2008). Software Metrics for Agile Software Development. Aswec 2008: 19th Australian Software Engineering Conference, Proceedings, 673–678.

Kupiainen, E., Mäntylä, M. V., & Itkonen, J. (2015). Using Metrics in Agile and Lean Software Development – A Systematic Literature Review of Industrial Studies. Information And Software Technology, 62(1), 143–163. Https://Doi.Org/10.1016/J.Infsof.2015.02.005

Mahnic, V., & Vrana, I. (2007). Using Stakeholder-Driven Process Performance Measurement for Monitoring the Performance of a Scrum-Based Software Development Process. Elektrotehniski Vestnik, 74(5), 241–247.

Mccabe, T. J. (1976). A Complexity Measure. Ieee Transactions on Software Engineering, Se-2(4), 308–320. Https://Doi.Org/10.1109/Tse.1976.233837

Moser, R., Pedrycz, W., Sillitti, A., & Succi, G. (2008). Model To Identify Refactoring Effort During Maintenance by Mining Source Code Repositories. In A. Jedlitschka & O. Salo (Eds.), Product-Focused Software Process Improvement, Proceedings (Vol. 5089, P. 360+).

Olague, H. M., Etzkorn, L. H., Gholston, S., & Quattlebaum, S. (2007). Empirical Validation of Three Software Metrics Suites to Predict Fault-Proneness of Object-Oriented Classes Developed Using Highly Iterative or Agile Software Development Processes. Ieee Transactions on Software Engineering, 33(6), 402–419. Https://Doi.Org/10.1109/Tse.2007.1015

O'riordan, A. (2011). Aspect-Oriented Reengineering of An Object-Oriented Library in A Short Iteration Agile Process. Informatica-Journal of Computing and Informatics, 35(4), 499–511.

Padmini, K. V. J., Bandara, H. M. N. D., & Perera, I. (2015). Use Of Software Metrics in Agile Software Development Process. 2015 Moratuwa Engineering Research Conference (Mercon), 312–317.

Ram, P., Rodriguez, P., Oivo, M., Bagnato, A., Abherve, A., Choras, M., & Kozik, R. (2020). An Empirical Investigation into Industrial Use of Software Metrics Programs. In M. Morisio, M. Torchiano, & A. Jedlitschka (Eds.), Product-Focused Software Process Improvement (Profes 2020) (Vol. 12562, Pp. 419–433). Https://Doi.Org/10.1007/978-3-030-64148-1_26

Salih Aydiner, A., Fevzi Esen, M., & Özlü, E. (2020). Türkiye'de Çevik Yazılım Geliştirme Süreçlerinde Scrum Yöntemini Uygulayan İşletmelerin Başarı Faktörleri. Journal Of Information Technologies, 13(4), 463–477. Https://Doi.Org/10.17671/Gazibtd.598346

Shawky, D. M., & Abd-El-Hafiz, S. K. (2016). Characterizing Software Development Method Using Metrics. Journal Of Software-Evolution and Process, 28(2), 82–96. Https://Doi.Org/10.1002/Smr.1766

Sjoberg, D. I. K., Anda, B., & Mockus, A. (2012). Questioning Software Maintenance Metrics: A Comparative Case Study. Proceedings Of the Acm-Ieee International Symposium on Empirical Engineering and Measurement (Esem'12), 107–110.

Sneed, H. M. (2014). Dealing With Technical Debt in Agile Development Projects. In D. Winkler, S. Biffl, & J. Bergsmann (Eds.), Software Quality: Model-Based Approaches for Advanced Software and Systems Engineering (Vol. 166, Pp. 48–62).

Stahl, D., Martini, A., & Martensson, T. (2019). Big Bangs and Small Pops: On Critical Cyclomatic Complexity and Developer Integration Behavior. 2019 Ieee/Acm 41st International Conference on Software Engineering: Software Engineering in Practice, Icse-Seip 2019, 81–90. Https://Doi.Org/10.1109/Icse-Seip.2019.00017

Welker, K. (2001). The Software Maintainability Index Revisited. Crosstalk, 14, 18–21.

➢ *ORAL PRESENTATION*

Evaluation on passive cooling of photovoltaic panels with phase change material

Perihan ÇULUN (0000-0002-1797-9695)

Bingöl University, Faculty of Engineering and Architecture, Mechanical Engineering Department, Bingöl, Türkiye

*Corresponding author e-mail: pculun@bingol.edu.tr

Abstract

Due to the intense heat of the sun during the summer months, the increase in surface temperatures of PV panels causes the efficiency to decrease significantly. Various cooling processes are applied under the categories of active and passive cooling in order to compensate for the efficiency decreases caused by the panel surface temperatures. Active cooling processes require additional energy due to the use of pump or fans. Passive cooling systems are preferred over active cooling systems because active cooling systems require additional energy and are difficult to the implement. In particular phase change material (PCM) passive cooling systems have recently formed the basis of panel cooling studies. However, the studies conducted in this field have not yet provided a clear perspective. In fact, research continues due to incorrect selection of melting/freezing temperatures of PCMs, inadequate adjustment of material amount, inadequate heat transfer coefficients of materials, generally expensive PCM materials with good properties and difficulties in integrating the enclosures in which these materials are placed into the panel. In this study, current studies on PV panel cooling with PCM material were evaluated especially in terms of the PCM material selection, application, PCM filled container construction, dimensions, amount and properties of PCM materials used.

Keywords: PCM, PV panel, passive cooling, PCM container

1. INTRODUCTION

The best way to cope with the depletion of fossil resources and associated energy problems is to increase the production and use of renewable energy. Therefore, energy, especially renewable energy, will be one of the most important research topics will continue on as long as human life continues. Indeed, energy is the most important parameter required to meet the basic needs of humanity. According to TEİAŞ 2022 data, 197536.2 GWh of the total 326014.8 GWh of electricity was generated from thermal power plants, and 128478.6 GWh was produced from renewable energy sources (hydraulic, geothermal, wind, solar) (TEİAŞ, 2022). 61% of Turkey's annual electricity is obtained from fossil fuels, namely thermal power plants, and the remaining 39% is obtained from renewable sources. According to TEİAŞ 2022 report, Türkiye purchased 6414 GWh of electricity from foreign countries in 2022. Considering that most of the natural gas is purchased from abroad, it is evident that the importance given to renewable energy sources in our country should be increased. Both the danger of depletion of fossil resources and the danger of harmful emissions in terms of health necessitate the search for clean and long-term energy sources that are alternatives to these sources. Although there are various renewable energy sources, the source that has been researched the most in the short term is solar energy applications.

Solar energy is used as heat, light and electricity. Research and development studies on photovoltaic panel (PV) applications constitute important academic research topics. However, the biggest problem encountered in both heat and electricity production applications in solar energy-based systems has been improving the efficiency of these systems. In fact, solar energy-based collector thermal system efficiencies are around 60-70%, while solar panels have an average electrical efficiency of 10-15%, and studies on improving these efficiencies continue rapidly. More than 80% of the radiation reaching to solar panels is thermal energy, causing a rapid increase in the panel surface temperature[1]. Especially in the summer, significant increases in panel surface temperatures cause electrical efficiency to decrease significantly[2]. According to some studies, when the panel surface temperature exceeds 25°C, which is the standard test conditions (STC), panel efficiency decreases due to the negative effects on the semiconductors in the panel structure.

In case of cooling of PV panels, although the current increase is low, the efficiency also increases thanks to the significant voltage increase[3]. Cooling of PV panels is promoted by various types of active and passive cooling[4]. However, among these, passive cooling systems are understood to be more sustainable because they do not require additional energy. Passive cooling systems are radioactive cooling systems (RC) [5], heat spreader cooling systems (HS) [5], where aluminum fins are generally used, phase change material (PCM) cooling systems, and various hybrid cooling systems where these are applied together[6]. Among these, PCM material cooling systems constitute an important research topic in the cooling of PV panels. Thanks to PCM, the efficiency of the panels increases, and their lifespan is extended by preventing thermal stresses. Especially in hot climates close to the equator, the use of PCM material cooling systems in panels where efficiency decreases due to overheating is promising. In addition to increasing panel efficiency, such a system also extends the lifespan of the panel by protecting it from excessive thermal stress. The PCM material used for cooling purposes absorbs heat during the day when solar heat and light are high, saves the panel from the harmful effects of high temperatures and increases efficiency. In the evening or when it is colder, it releases the heat inside itself and ensures that the panel temperatures are lower. From the studies conducted, it is understood that the appropriate melting/freezing temperatures and latent heats in the PCM materials selected in PV or PV/T systems significantly change the thermal or electrical efficiency of the systems. A study conducted in Dublin indicated that the panel temperature for PCM1 and PCM2 materials decreased from 48 to 42 °C and 39 °C, respectively, resulting in an efficiency increase of 4% and 11.2% for the respective materials[7]. In the PV cooling study using RT42, it was stated that the panel temperature was reduced by 5.2 °C and the efficiency increased by 15.9%[8]. According to some studies, it is estimated that for each 1°C temperature increase, the electrical efficiency will increase by 0.65%[9], or 0.45% [10]. According to these results, it is understood that the electrical efficiency increases for the 1 °C panel temperature decreased with the effect of the PCM type and the applied region can be approximately 1-3%. For the panel temperatures of 20 and 47 ◦C, the panel electrical efficiency was determined as 17.3% and 15.5%, respectively; and the thermal efficiency was determined as 60-25%[11].

In PV/T-PCM numerical studies, it was stated that the total efficiency of the system increased from 47.5% to 77.75% when the PCM melting temperature was increased from 305K to 323K [12]. It has been stated that the maximum yield increase for PCM at 35°C melting point for summer application is 9%, and the maximum yield increase is 2.2% if the same PCM is used for winter[13]. In the experimental study carried out in Indonesia, PV panel efficiency increases of 8.3% and 10.1% were achieved thanks to PCM material[14]. Considering that the average efficiency of a PV panel is 12% and increases by 10.1% at this rate, it is estimated that the efficiency of passively cooled panels with PCM can increase by up to 22%. Academic studies show that paraffin-based PCMs, salt hydrates with higher temperatures and higher latent heat of fusion, and fatty acids that can be used at medium temperatures are recommended as PCM materials due to their high heat storage capacity and relatively low cost. The selected PCM materials should have rapid heat storage, high thermal conductivity, high latent heat of fusion, long-term non-degradation, and be more economical than others. In addition, an environment that can easily provide phase changes with temperature variations should be ensured. The initial costs of PCMs are high, but the fact that they can be used repeatedly and provide energy efficiency for a long time, and that they extend the life of the panel are the main reasons why PCM systems are preferred.

The use of passive cooling method with PCM in PV panel cooling both increases energy efficiency and produces more environmentally friendly solutions. Research in this field investigates the use of PCMs and the integration of related materials with panels. The efficiency, cost effectiveness and long-term performance of different PCMs are evaluated and attract attention because they offer innovative solutions in the relevant field. However, there are also significant gaps and difficulties regarding the design, implementation or optimization of related systems. Studies should be intensified as instability in the selection of appropriate PCM, leakage, shrinkage and expansion-related or container problems that occur during the melting/freezing stages of PCMs in practice, faster and higher heat absorption by increasing heat transfer coefficients, long-term usability of different materials in different climate conditions, etc. Since there are many types of PCMs in PV systems, such as organic, inorganic and eutectic[15] , studies evaluating the thermal conductivity, energy storage capacity, phase transition temperatures and melting/freezing properties of these materials under realistic environmental conditions are insufficient. In fact, PCM performances are generally tested under laboratory conditions. The unpredictable complexity of real conditions such as temperature fluctuations, humidity and sunlight intensity in the application field necessitates long-term testing of different materials in the field. In this study, it is aimed to present current academic developments with literature in order to contribute to the field of passive cooling of PV panels with PCM. Within the scope of current studies, PCM materials, which

are frequently preferred, have been evaluated in terms of their properties, especially melting/freezing points and latent energies, application methods of the materials, container properties, detection of applications with higher heat transfer coefficients, problems and poposed solutions.

2. THE PHASE CHANGE MATERIALS USAGE IN PHOTOVOLTAIC PANEL COOLING

PCM materials are available in three types: organic, inorganic, eutectic PCMs [15, 16]. Each type of PCM is different in terms of advantages, disadvantages and applications. While the features of being environmentally friendly and economical come to the fore in organics, inorganics stand out with their ability to withstand high temperatures and high heat conduction coefficients. The heat conduction coefficients of almost all PCMs in the paraffin group, which are organic PCMs, are the same and equal to 0.2W/mK, while the heat conduction coefficient of CaCl2.6H2O in the inorganic group is on average 3 times this value and the k value is stated to be 0.626 and 0.454 W/mK for temperatures of 24 ^{0}C and 41 ^{0}C, respectively. The heat conduction coefficient of another inorganic PCM, $Na_2SO_4.10H_2O$, is also 0.544W/mK, which shows its superiority in heat conduction coefficient compared to organic PCM[17]. On the other hand, it is understood from the latent heats of $CaCl_2.6H_2O$ and RT28HC, which are 200 and 250 kJ/kg, that paraffins have higher latent heats at the same melting temperatures. Depending on the requirements of the application, it can be determined which material will be used where. PCMs, which are available in the market in the form of powder or solid blocks, can also be supplied as encapsulated in various sizes and quantities upon request[16, 18, 19]. PCMs generally used or recommended in academic research on PV panel cooling area (Table 1). As shown in the table, although organic, inorganic and eutectics can be preferred in PV panel cooling, organic PCM selection is more appropriate due to its superior chemical properties, and organics (paraffins) are mostly preferred in literature studies[2, 20-22] (Table 1 and Table 2). We believe that the use of new generation PCMs produced by the synthesis of inorganic or organic materials with different properties will become widespread.

PCMs are materials that change phase from solid to liquid or vice versa at a certain temperature. They can store and then release significant amounts of energy during this phase change. The process of PCM materials absorbing energy and melting is called charging, while the process of solidifying by releasing the energy in their structure to the environment is called discharging. This process is also known as latent heat storage. The purpose of using PCMs in PV panels is to remove waste heat from the system, which affects the efficiency of the panels. Especially in the summer months, when solar energy is very intense, the surfaces of PV panels become extremely hot. Since this high heating damages the panel cells, it not only negatively affects the efficiency of electricity production but also shortens the life of the panels. Using PCMs prevents excessive heat on the panel surface, regulates the temperatures in the cells and increases electricity production (Figure 1). Nights are cooler than daytime in summer. PCMs selected due to high summer temperatures during the day will melt with the heat they absorb from the high-temperature panel, and will freeze by releasing this heat outside in the cooler condition of the night. The melting/freezing points of the PCM should be selected by taking into account the day/night outdoor temperature and the panel's daily average temperature.

Table 1. PCMs used in PV cooling.

	Organic		**İnorganic PCMs**		**Composite PCMs**
PCMs name	**Paraffin wax (Alkanes)**	**Fatty Acids**	**Salt Hydrates**	**Eutectic Salts:**	
Melting Point	50°C – 65°C melting point	50°C – 80°C	Can range from 30°C to 120°C	Around 50°C – 80°C	
Advantages	Non-toxic, chemically stable, and relatively inexpensive	High latent heat, stable, and good for higher temperature ranges.	Higher latent heat and high thermal stability, Wide availability at different melting temperatures, Cheap	A mixture of salts that offers lower melting points and higher heat storage capacity, cheap	Improved thermal conductivity, allowing faster absorption and release of heat.
Disadvantages		more expensive than paraffin	There is a risk of melting in humid environments and a risk of corrosion in metal surface interactions. In case of crystallization, phase separation may occur.		
Applications	Suitable for higher temperature applications like PV cooling.		Suitable for cooling PV modules in hotter climates where the temperature may rise above 80°C.	Typically used in advanced thermal energy storage systems and PV cooling.	Used when improving the heat transfer rate is important, such as in high-performance PV cooling systems.

When PCM materials solidify, a slight increase in volume occurs. This is an important issue to consider in PCM applications. These materials increase in volume just like water does when it freezes at zero degrees and below. In this respect, the volume fraction that expands when the materials solidify, i.e., when containers or tubes etc. are used, should be carefully considered before completely filling them. In fact, if the materials are filled and adjusted as solids in storage containers, there will be no problem. The real issue occurs when the material is placed in the storage container in its melted form. If molten PCM is to be placed in the container, a space of at least 15% of the container volume should be left or the filling process should be carried out with solids. Indeed, it is known from Table 1 that the volume expansion for paraffins varies between 14%[23] - 12% (for RT44)[24]. In this regard, 15% of the volume of the containers to be filled with liquid PCM should be left empty as expansion allowance [15, 16, 24]. In some studies, this rate was applied as 20% [25].

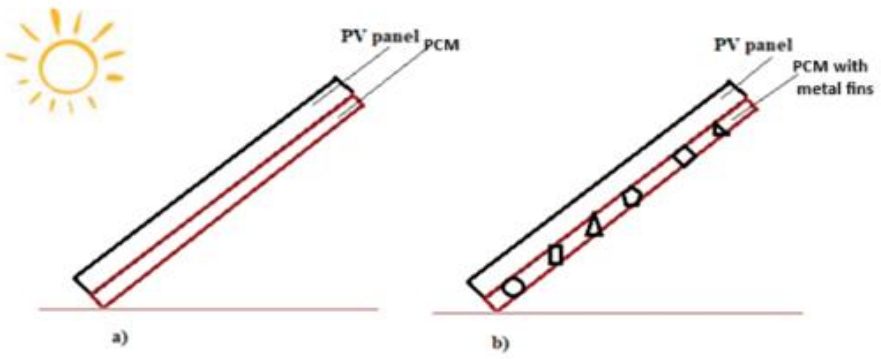

Figure 1. Use of PCM and fins in PV panels

PCMs have the ability to absorb panel heat, especially during midday hours, and then radiate this heat[4, 26]. PCM temperatures in PV panels should be selected appropriately in order to bring the panel temperature closer to the ambient temperature. Therefore, the panel average temperature value and environmental conditions have a significant effect on the PCM material melting point selection and cooling performance. In order for the selected PCM material to draw heat from the PV panel, its melting temperature must be below the panel average temperature and slightly above the ambient temperature. Otherwise, since the PCM material will be in the liquid phase, the melting phase will not occur and there will be no cooling. The answer to the questions of how much the PCM melting point will be below the panel average temperature or how much above the ambient temperature will become clearer as a result of critical analyses of experimental or numerical study

results conducted in different climates and geographies. Although there are studies[13] indicating that PCM temperature can be 8-10°C below ambient temperature, this is not valid for all PCM applications due to the different latent heat properties and varying amounts of each PCM.

Table 2. Some properties of organic PCM used in PV cooling

Commercial name	RT21	RT27	RT31	RT35	RT44	RT55[23]
PCM category	Organic	Organic	Organic	Organic	Organic	Organic
Melting point	20–23	25–28	27–33	34–36	43–44	51–57
Latent heat (kJ/kg)	190	179	165	240	250	170
Volume expansion %	%12-15					14
Density (kg/m3)	880 for solid and 770 for liquid					
Thermal conductivity (W/m-k)	0.2 for both phases					
Specific heat capacity (kJ/kg-k)	2.0 for both phases					

In the current situation, the general consensus reached in PCM selection is that the PCM material should be selected with the lowest possible melting point. In fact, when a low melting point is selected, the material will melt more easily and will absorb a large amount of heat. The PCM material's melting temperature should be below the PV panel's daily average operating temperature. In this respect, it is important to determine the panel temperature ranges depending on the region and climate[27]. If we consider that the panel operating temperatures for Turkey are between 35-80°C, the melting temperature of the PCMs to be selected should also be close to these temperatures. It has been mentioned that RT42 is mostly used due to the high temperatures of PV panels in summer, and that melting points between 25-30°C are preferred in winter. In addition to the RT42 PCM material, the panel temperature was reduced by 21.8°C and a 7.3% efficiency increase was achieved by using the appropriate fin. In the optimization study where RT21, RT35, and RT44 were tested for the summer climate conditions of Bahawalpur-Pakistan, Bhadla-India, Arizona-United, it was stated that RT21 showed the best performance by reducing the panel temperature by 36% from 65°C to 38°C[2]. It was stated that the temperature decreases for RT35 and RT44 were 13.1% and 15.7% respectively. In the study where RT28 was used, it was stated that the PV panel temperature could be reduced to 25°C, thus a 23% increase in panel efficiency could be achieved[28]. It is estimated that PV panel efficiencies can be increased by 16-23% with such PCM and container designs that are in line with general consensus[13, 29]. In the study where the finned container was used together with the RT27, despite the insulation of the part of the PCM that comes into contact with the ambient temperature, the panel temperature was reduced by 16 °C and a 5.9% efficiency increase was achieved (Figure 2) [25]. In this study, the edges of PCM filled aluminum rectangular containers were made resistant to leakage by using silicone. Aluminum is generally preferred in this field due to its high heat conduction coefficient (200-205 $Wm^{-1}K^{-1}$) and low specific gravity.

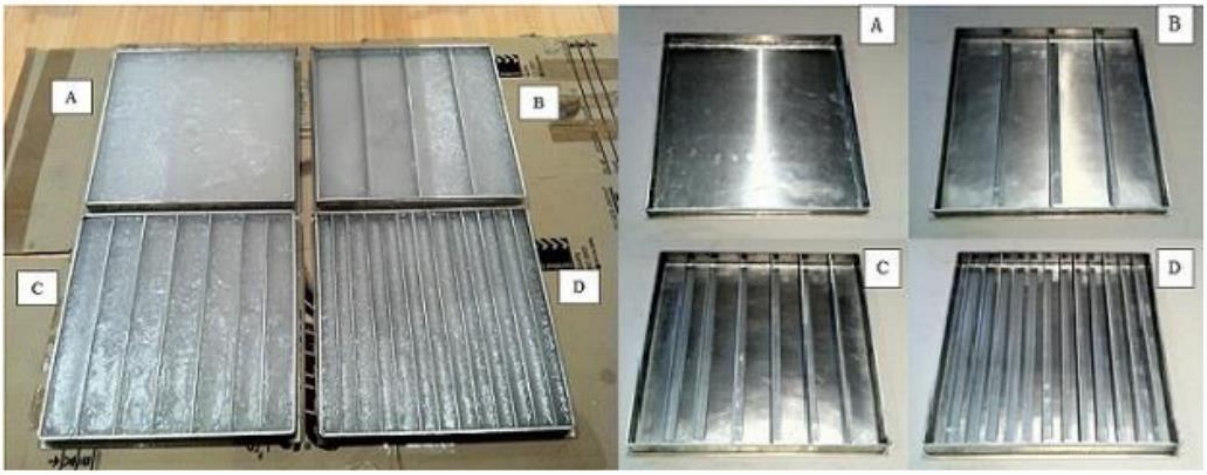

Figure 2. PV panel arrangements using paraffin wax (left side) and without it, A) without PCM or fins, B) with PCM and 3 fins, C) with 6 fins, D) with 12 fins[25]

The unnecessarily high PCM melting temperature is also undesirable. In fact, if the material melting temperature is too high, the panel may have an adverse effect instead of cooling. The heat transfer coefficients of PCM materials are generally 0.2$Wm^{-1}K^{-1}$, which is very low[15]. In fact, it will be difficult for these materials to return the stored solar heat due to their low heat conduction coefficients, causing the panel temperature to remain higher for a long time. In this case, the panel cells may be damaged and unnecessary time and money may be wasted. However, it is possible to increase the conduction coefficients and latent heats and accelerate the melting/freezing processes in PCM materials by using various nanomaterials or metal foam[30]. In Thailand, durin the summer season when the ambient temperature is 38 ◦C, PCM materials with melting temperatures of 41 ◦C and 44 ◦C were used with MgO, Al_2O_3, CuO at 6% mass ratio. power increases of MgO, Al_2O_3, CuO at 6% mass ratio 4.38 Wh, 2.99 Wh and 2.62 Wh were achieved, respectively. It should be noted that the ambient temperature and PCM material temperature difference are between 3-6℃. In the PV-PCM study where RT27 was used, it is mentioned that the panel temperature is very close to 25 ◦C [3].

Testing PCM-based applications in different weather conditions is also a necessary research topic in this field. Because the performances of the same or different PCMs in different climate conditions and different geographies can be revealed in more detail. PCMs tested at lower ambient temperatures are exposed to lower heat load, thus lower temperature drop is obtained. On the other hand, PCM has a higher solidification rate at low ambient temperatures at night. This means better heat extraction from the PV panel the next day. Higher daytime ambient temperatures are achieved with greater heat load and greater temperature drop. The fact that higher nighttime ambient temperatures reduce the PCM solidification rate is a disadvantage of hot environments. More studies are needed to better understand the effects of PCM materials, taking into account such contradictory factors[31].

3. CURRENT PCM APPLICATIONS IN PHOTOVOLTAIC PANELS

3.1. Some current applications

PCM cooling PV panel studies can be encountered within the scope of hybrid studies using either PCM cooling alone or other passive cooling systems together. For example, in a hybrid cooling study using PCM, Radioactive Cooling (RC) and Heat Sink (HS) (Figure 3), the temperature distribution for RT58, RT42 and C22-C48 materials was optimized for eastern Morocco in ANSYS Fluent. It was stated that the temperature drop for RT58, RT42 and C22-C48 materials was 21.2°K, 26.1°K, and 18.3°K, respectively[32]. At 13:00, while C22-C45 was still in the solid phase, the temperatures of RT42 and RT58 were 323°K and 315°K, respectively and C22-C45 started to melt only after 17:00. Study conducted in Arabia, PV panel power production increased by 3% in response to a 5-6℃ decrease in temperature by using PCM-OM37P PCM material as shown in Figure 3b[33]. A metal foam layer has been added to improve PCM melting time in PV-PCM systems.

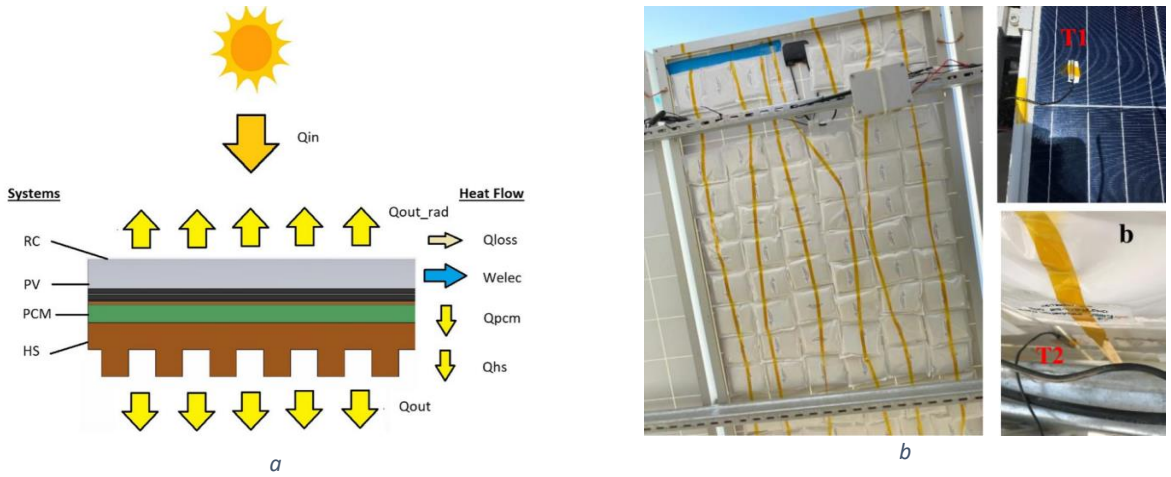

Figure 3. Hybrid cooled PV using PCM, radioactive cooling (RC) and heat dissipation fin (HS) [32], b) [33]

wei et al., 2024 PV-TEG-PCM hybrid study was tested during the day and night using TEG between PV and PCM. In the experiment, in addition to the electricity produced by the PV panel during the day, additional electricity production was achieved thanks to the TEG-PCM, and at night, due to the heat stored in the PCM in a relatively cooler state, additional electricity production continued owing to the temperature difference formed on both sides of the TEG system[34]. As shown in Figure 4, in such a system, during the day, on a sunny day, convection and radiation from the sun are stored by passing from the heat panel to the TEG and then to the PCM (Figures 4a and 4c). At night, the energy stored in the PCM is transferred to the outside, while electrical energy can be obtained with the help of TEG modules. Heat transfer between the panel and the external environment occurs in the form of convection and radiation, and between the PV-TEG-PCM in the form of conduction. Thermal resistances in the system are also as in Figures 4c and 4d. While the resistances are in parallel in the environment where convection and radiation are together, the resistances in the PV-TEG-PCM section are shown as series-connected. Furthermore, as understood in Figures a and b, TEG modules produce electricity regardless of direction of heat transfer. The electricity production of these modules depends on the temperature difference rather than the heat transfer direction[35].

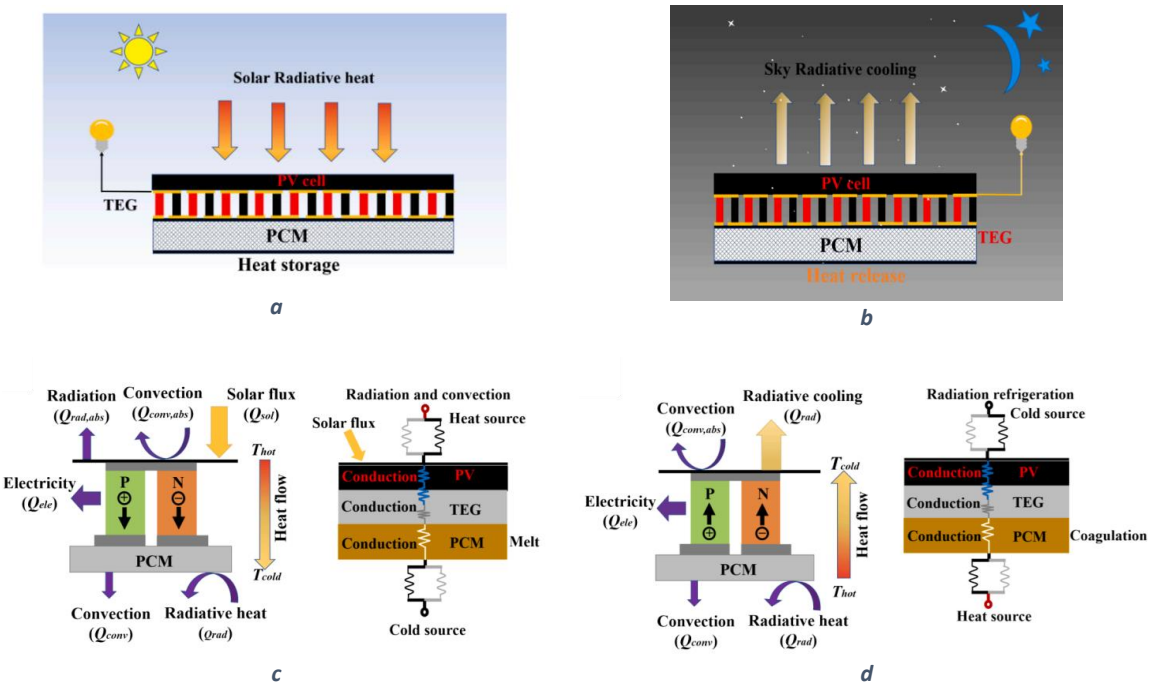

Figure 4. PV-TEG-PCM hybrid system a) day, b) night, c) daytime heat transfer and thermal resistance, d) nighttime heat transfer and thermal resistance status[34]

In a PV-PCM numerical study, as shown in Figure 5, the results obtained for fins with different distance (step) ratios such as Λ=4, Λ=2 and Λ=1 indicate that the heat received from the PV is quickly released to the surrounding environment, thus the PCM material remains solid for a longer time[36]. In other words, since heat intake is accelerated and the transfer of this heat to the surrounding environment is also accelerated, more solid PCM can actually be found in the container. This ensures continuity of cooling. In the relevant study, it was stated that for Λ=1, the average PCM melting temperature decreased from 50°C to 30 °C, the efficiency increase rate increased from 1.39% to 5.16%, and the average melted PCM amount in 240 minutes decreased from 20.5% to 7.59%. Here, in addition to efficiency increase provided by the fins, it is also very important that the instantaneous liquid PCM amount in the container has decreased, i.e. the instantaneous solid PCM amount in the container remains high. Since the heat drawn from the PV panel is not only transferred to the PCM, but also transferred from the PCM to the surrounding environment, thus some of the melted PCM has solidified. This is actually extremely important in terms of providing sustainable passive cooling as it will increase the heat withdrawal process in the PV panel.

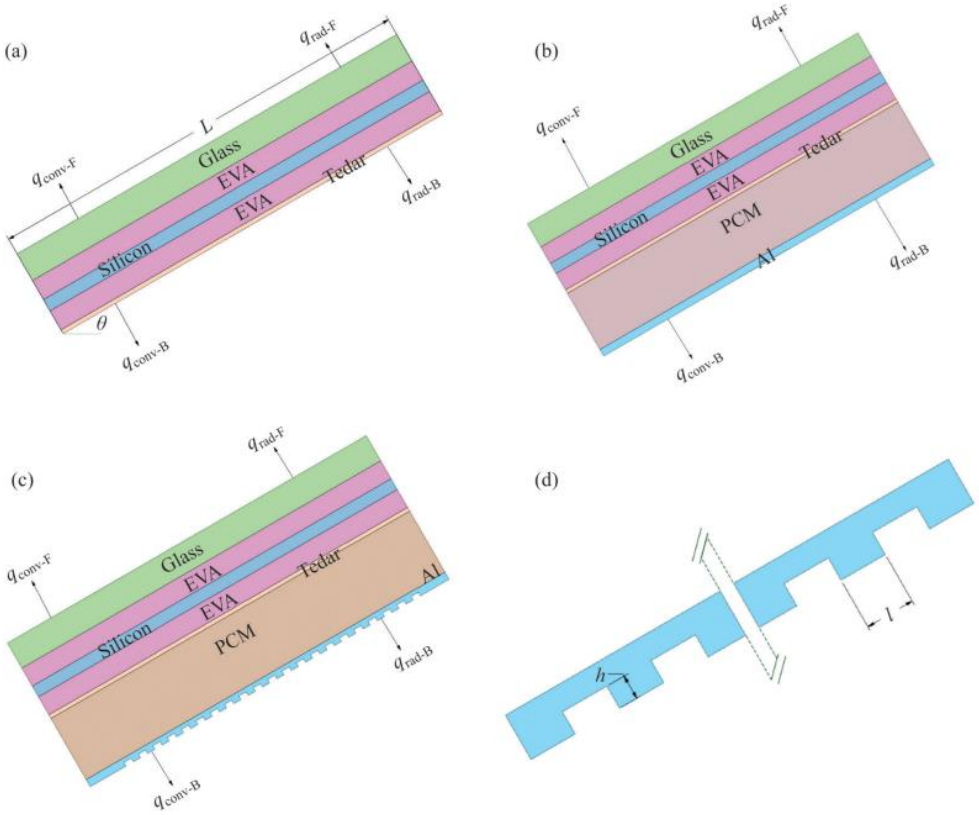

Figure 5. Use of finned heat spreaders for rapid PCM heat removal [36]

3.2. PCM Container Designs

PCM materials are applied directly to the back of the panel to absorb heat, or can be added to the cooling medium (such as water) to absorb more heat from the panel. High-quality PCMs can be more expensive than traditional cooling methods. A photovoltaic (PV) panel structure, as shown in Figure 6a, consists of six layers in its most basic form: solar cells on top and bottom, Ethylene Vinyl Acetate (EVA), a glass coating on the side facing the sun, heat-absorbing black sheet at the bottom, and finally the panel frame[23, 37]. As seen in the panel structure, it is possible to improve the panel efficiency by cooling the plate located just before the frame behind the panel and by absorbing heat using PCM material (Figure 6a). Nada et. al., (2018) used two different Rubiterm products, PCM and PCM/Al_2O_3, with melting points of 305 and 323K, in the container produced from 5 mm thick galvanized sheet as in Figure 6b, and paraffin wax and Al_2O_3 added to the material. For this PCM at 305K melting temperature, the panel electrical efficiency increased by 5.7%, with the final efficiency increasing from 15.1% to 15.95%. For the PCM with nanomaterial additives at 323K melting

temperature, the efficiency rising by 13%, from 15.1% to 17.1%[23]. In the numerical and experimental study, it was determined experimentally that a maximum temperature decrease of 35.6 °C would be achieved in PV/PCM panels, and numerically that an annual efficiency increase of 7.3% would be achieved[28].



Figure 6. a) General structure of the panel, b) Passive cooling container with PCM [23]

The depth of the PCM used, or the depth of the PCM container also has a significant effect on cooling and cooling time. In fact, with the 2 cm deep container in which RT25 was used, the panel front temperature could be kept at 36.4 °C for 80 minutes, while by increasing the container depth to 4 cm, the panel temperature could be kept at 33 °C for 150 minutes [38]. In the case where the fins were used in the 4cm deep container, the panel temperature was kept at 29 °C for 130 minutes [39]. It should also be taken into account that the fins used here actually shorten the melting time of the PCM material as they accelerate heat transfer.

Although much research has been done on PCM materials, the use of these materials in PV cooling systems is closely related to the structure of suitable PCM containers. However, when looking at the literature studies, it is seen that the studies in this field are far behind. Indeed, there are important gaps in the relevant container structure, material, dimensions, etc. There is a need for effective container designs that will manage the thermal processes of PCMs such as shrinkage and expansion well and that will be easy to integrate with the PV panel. In addition, these container design studies need to be investigated in terms of thermal conductivity, mechanical properties and cost. In addition to these issues, studies should focus on the integration of these technologies into PV modules or architectural systems, system efficiency and cost studies by considering the encapsulation technologies of PCM.

Studies mention that container structures should not restrict convective heat transfer as well as conducted heat transfer. Akshayveer et al. (2020) stated that instead of the PCM container being a single rectangular shape, types that are insulated on the back and allow convective heat transfer were tested, and that having one side convective increased efficiency[1]. As seen in Figure 7, insulation is applied in some applications so that the PCM material is not affected by the ambient temperature. However, although this situation accelerates the instantaneous PCM material melting process, it can negatively affect the system efficiency due to the fact that the PCM cannot release heat to the ambient environment at the end of the day or releases it late. In fact, the system efficiency will decrease due to the fact that the heat transferred to the PCM in the panel cannot be released outside, and therefore the freezing process does not occur during the night. Although a temperature decrease of 12-20°C was achieved with the insulation applied behind the panel together with the PCM in PV panels, it was stated that this situation reduced the panel efficiency by 7-10%[40]. Ensuring complete freezing of the relevant material at night is as important as ensuring complete PCM melting of the PV-PCM system during the day.

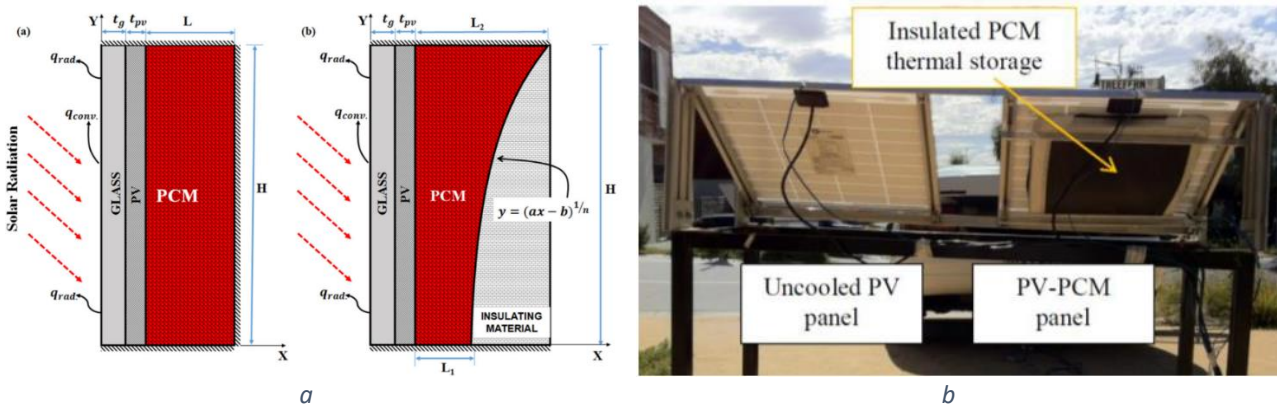

Figure 7. PCM container is insulated from one side or exposed to convection, a)[1], b)[25]

The use of fins which enhance heat transfer in applications such as gas turbines, heat exchangers, cooling channels, etc. has encouraged the use of fins as a method of improving thermal conductivity in PCMs. By utilizing a finned container of the same volume instead of a flat container, the heat transfer coefficient of the cooling system increases thereby accelerating the heat transfer process (Figure 2 and Figure 8).

Among the results obtained from grooved, tubed and winged containers using palm wax, the best results observed in the winged container, which achieved a 5.3% increase in electrical efficiency with a 6.1 °C temperature decrease[41]. In the study where the finned container was used with RT27, it was stated that the best results among the 3, 6 and 12 fin numbers were 12 fins, reducing the panel temperature by 16 °C and providing 5.9% efficiency increase[25]. In another study with winged PCM containers, it was stated that when the number of wings was increased from 2 to 11, the panel temperature drop was between 23.8 - 26.6 °C and the electrical efficiency increase rate was between 10.1 - 12%[42]. In the same study, it was stated that increasing the number of fins above 5 did not significantly affect the results. The fins used can be flat, perforated or in different shapes. During a one-hour experimental study using halogen lamps, the solar panel cooling process was conducted with PCM material using flat and perforated aluminum fins, and a temperature decrease of 8.32°C was achieved for flat fins and 8.55°C with perforated fins, resulting in a 7.43% power increase (Figure 8). In such studies, it was noted that since halogen lamps cause extra heating in the PV panel in a short time of 10 minutes, it is more appropriate to prefer projection[43].

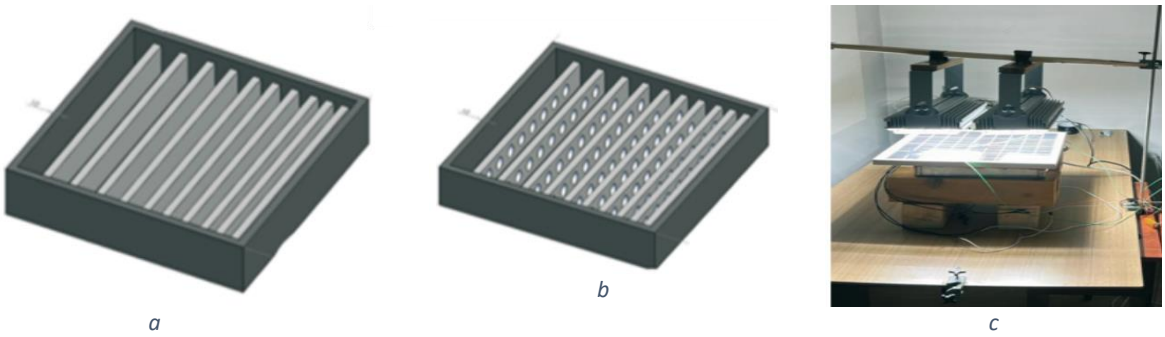

Figure 8. PCM container with aluminum fins, a) plain fins, b) perforated fins, c) halogen lamp application [43]

In the PV-NPCM application using Al_2O_3, CuO, and MgO, NPCM with high heat transfer coefficient was obtained in Thailand where the ambient temperature was 38 ◦C, thus providing temperature reduction and efficiency increase in the panel. The container models utilized in this study are shown in Figure 9[44]. As seen in the figure, the use of acrylic container slows down the heat withdrawal process in the panel. In fact, the low heat transfer coefficient of acrylic material, such as 0.21W/mk, also low down the heat transfer from the PV panel to the container. In PV-PCM applications, it is essential that the heat transfer coefficient of the container material is as high as that of the PCM material. It would be more appropriate to prefer aluminum alloy materials

due to the advantage of high heat transfer coefficient.

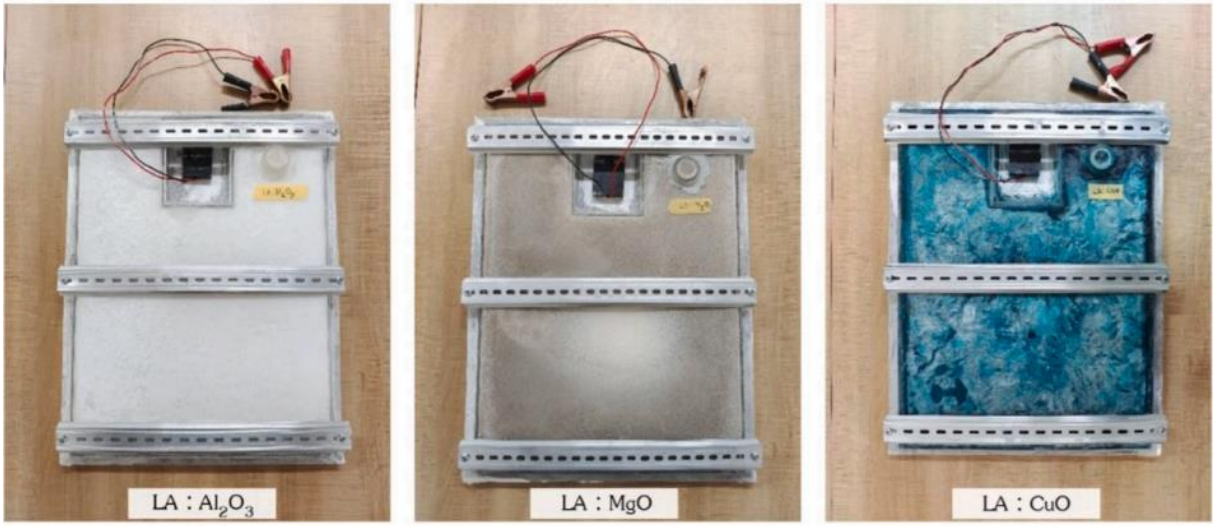

Figure 9. PCM containers with acrylic material [44]

3.3.Multi-Layer PCM Applications

In this system, also known as PV-PCM cascade systems, PCM application can be implemented using more than one layer. As seen in Figure 10, a three-layer system is constructed using three different PCM1, PCM2 and PCM3 [42]. In such a system, the melting points of the PCMs are selected as PCM1>PCM2>PCM3. Therefore, the PCM temperature in contact with the panel should be the highest so that it melts immediately when the panel absorbs its heat. Then, the melting temperature of PCM2, which will absorb the heat of PCM1, will be lower than PCM1 so that it can absorb the heat of PCM1. Similarly, the melting point of PCM3 should be lower than PCM2 so that it can absorb the heat of PCM2. In this way, it is possible to accelerate the heat transfer of PV panels even more thanks to different PCM layers. Multi-layer PCM applications are not common in the literature, and perhaps this study can be shown as the first and only applications[45] of such a system.

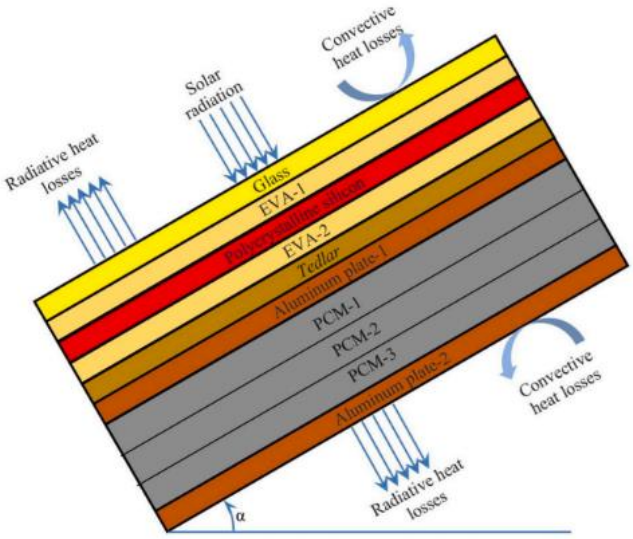

Figure 10. Multi-layer PCM application example [45]

3.4. PCM Container Materials

The selection of materials for containers to be produced for a PCM system in PV cooling should be made base on factors such as thermal conductivity, mechanical durability, cost, environmental resistance and temperature range (thermal stress resistance). Materials such as aluminum and stainless steel are widely preferred due to their high thermal conductivity, while plastics such as polyethylene or PMMA are preferred due to their lightness and low cost. However, aluminum is the most widely preferred material due to its high heat conduction coefficient, low cost and easy processing[23, 25]. The materials generally preferred for PV cooling and PCM containers are presented in more detail below.

Aluminum: The main material used as PCM container in PV-PCM passive cooling applications is aluminum. Depending on the alloy material and proportions, heat transfer can be accelerated thanks to the high thermal conductivity of 200-205 W/(m K) in aluminum alloys[25]. The lightness of aluminum is the most important parameter affecting its usability in PV applications. Aluminum's resistance to corrosion in most environments is also an important reason for preference. Its ease of shaping brings with it the convenience of providing a suitable container for the process. In addition, being cheaper than metals with equivalent properties makes it mostly preferred material. Thanks to all these features, it is widely used in PV systems and solar energy applications[25, 43].

Stainless Steel: This material, with a heat transfer coefficient of 16 W/(m K), allows sufficient heat transfer for many applications. It is resistant to corrosion in harsh environments such as humid conditions. Thanks to its high melting point, stainless steel material PCM containers provide ease of welding during manufacturing processes. Welding processes can be made cheaper. Being heavier, more expensive and more difficult to produce/shape than aluminum has pushed PCM containers to the back of the list.

Copper: Copper has a high thermal conductivity of 398 W/m K, making it the best heat transfer material. Its easy formability, durability and high temperature tolerance are also ideal features for PCM container construction. However, its tendency to corrode in the presence of moisture and certain chemicals, its cost, its ability to corrode if not properly coated and its heavier weight than aluminum are some of the difficulties encountered in its preference. It can be used in high-performance or special PV systems such as Concentrated Solar Power (CSP) systems where maximum heat transfer is required.

Polyethylene (HDPE or LDPE): HDPE or LDPE materials can be used as heat insulators to reduce heat loss from PCM. These materials are resistant to many chemicals and abrasives. Being cheap and lightweight compared to metals is also a reason for preference. Their flexibility in design eas of shaping, and suitability for applications up to medium temperature values make them adventagenous. In addition to these advantages, they can be preferred for low temperature PCM applications due to their disadvantages such as low heat conduction coefficients and deterioration at high temperatures.

Polymethyl Methacrylate (PMMA): Although PMMA, known as engineering thermoplastic, is lower than copper and aluminum, it has a higher thermal conductivity coefficient than HDPE or LDPE. Its thermal conductivity coefficients are at a moderate level. Being transparent is important for the observing and better analyzing the melting/freezing phases of PCM materials that need to be monitored. This synthetic polymer glass type has colored and colorless varieties. It is more resistant to weather conditions or UV degradation than other plastics. Being lightweight and cost-effective may also be contribute to its preference. They are prone to cracking/breaking in mechanical stress situations. They can be used at temperatures below 70°C -80°C. They can be preferred for commercial PV cooling, where high thermal performance is not the primary concern.

Fiber Reinforced Plastics (FRP): Fiber Reinforced Plastics (FRP) are preferred for use in PCM containers because they are durable, easy to process, resistant to corrosion and deterioration. Their medium heat conduction coefficient makes them easier to choose after metals. They are lighter and more suitable for low-cost modular container designs compared to metals. They can be preferred in medium-sized PV systems where lightweight and durable materials are required

Glass (Tempered or Laminated): High thermal stress resistance, transparency, resistance to corrosion and chemical degradation are important reasons for preferring glass in PCM applications. Transparency properties

are extremely important for monitoring PCM status. However, being heavy and brittle, low heat transfer coefficient are significant disadvantages. It is generally used as a protective cover in solar concentrator systems or advanced PV systems.

4. NUMERICAL STUDIES ON PCM COOLING PV PANEL APPLICATIONS

Since there are many parameters and difficulties to be investigated in the cooling of PV panels with passive cooling modules with PCM, it is extremely important to increase the numerical studies in this field. Because both the difficulty of selecting the appropriate material for specific regions among the many and types of PCM materials and the challenges in manufacturing containers or jackets suitable for these materials require a great deal of time and effort in this field. Numerical examination of most appropriate parameters can prevent waste of time, effort and money in this field. The energy balance model, which addresses the storage and release of heat by the PCM integrated into the PV panel, analyzes the panel thermal behavior, fluids and heat transfer, and the effective melting and solidification processes. These processes can be analyzed through the heat-flow dynamics modeling and PCM temperature change[20]. PCM's phase change process and thermal behaviors can be interpreted in detail by numerical analysis. In such models, the effects of environmental factors such as solar radiation and ambient temperature can be taken into account and the PV operating temperature and thermal capacity of the PCM can be estimated. Properties such as thermal energy storage capacity, specific heat, melting/freezing point, and latent heat capacity in phase transition can be used as input data and the properties of different PCMs can be compared. Parameters such as PV panel geometry, surface area, and PCM integration type can also be evaluated. The heat emitted from the PV panel and how the PCM manages this heat can be analyzed in detail.

Performing all experimental analyses of new generation PCM properties obtained by combining PCM materials with nano powders or nano fluids would be both time consuming and costly. Numerical investigation of new generation material property analyses will provide an important contribution to the PV-PCM field[46, 47]. Expansion of CFD studies in this area will make it possible to use better materials in a shorter time and over larger areas[48]. Numerical studies or simulations that can be done using programs such as COMSOL Multiphysics, ANSYS-Fluent CFD, MATLAB will significantly reduce both the time and cost in modeling both the operating conditions of PV panels and the PCM behaviors of these panels in PCM integrated circuits. However, it has been understood that the numerical studies in the relevant field are limited. Nevertheless, there are some numerical studies such as ANSYS-Fluent CFD[36, 49], MATLAB.

5.CONCLUSIONS AND RECOMMENDATIONS

According to current studies, when PCMs are used in PV panels, a 10-20% decrease in panel temperature is achieved, which in turn provides a 5-15% increase in electricity. With this method, panel temperatures are controlled, the system life is extended, and the panel is protected from overheating damage. Selecting PCM materials with suitable properties and ideal integration of these materials into the PV panel are important research topics. Considering the literature studies reviewed, it has been observed that efficiency increase rates differ significantly with the effect of different climate conditions and different geographical regions. For example, if it is considered that the average ambient temperature in the summer is 30-35°C in a region located in the southern part of Turkey, it is clear that a PCM such as RT25 cannot be used. Indeed, since RT25 will be liquid at these ambient temperatures, it will not be able to absorb any heat. However, there are regional studies where a high efficiency increase of 23% is achieved using of RT28, as it reduces the panel temperature to the ideal panel temperature value of 25°C in regions with lower ambient temperatures[28]. In order to further increase the efficiency of these systems, cost effectiveness, environmental sustainability and long-term performance research is needed. However, the main issues and recommendations identified in the literature are as follows:

Based on the monthly average or seasonal averages of PV panel operating temperatures, PCM solutions suitable for all climatic conditions and, if possible, for different geographies should be developed and these solutions should be disseminated globally.

In some PV-PCM studies, it has been observed that the areas of the PCM not in contact with the panel are insulated [1, 25]. It is not correct to insulate the PCM used within the scope of PV cooling application. In fact, although it accelerates the absorption of the initial PV panel heat, it will later prevent the PCM from transferring the heat to the outside.

It should not be forgotten that almost all issues investigated in PV-PCM systems will provide faster and more economical solutions by using numerical modeling, and the long-term performance of applications in this field can be revealed with the help of numerical programs[28]. In PV-PCM systems, it is important to conduct cost analyses by taking into account both the PCM material source and the integration of these materials.

Literature studies on suitable container designs in PV-PCM studies are almost non-existent. Containers used in studies in this field are either plastic based, such as PVC, Plexiglass, Acrylic, etc., and are therefore inappropriate due to their low transmission coefficient[44]. Or it has been observed that difficult and inappropriate assembly types such as screws etc. are used in the assembly of manufactured containers to the PV panel. In this respect, more work is needed for appropriate proactive container designs in PV-PCM applications. Designed containers should provide both PCM sealing, be suitable for the PCM structure used, not corrode, be easy to assemble to the panel, not damage the panel, be as light as possible, and have good heat transfer properties.

REFERENCES

[1] Akshayveer, A. Kumar, A. P. Singh, and O. P. Singh, "Effect of novel PCM encapsulation designs on electrical and thermal performance of a hybrid photovoltaic solar panel," (in English), *Sol Energy,* vol. 205, pp. 320-333, Jul 15 2020, doi: 10.1016/j.solener.2020.05.062.

[2] A. Durez, M. Ali, A. Waqas, K. Nazir, and S. Kumarasamy, "Modelling and optimization of phase change materials (PCM)-based passive cooling of solar PV panels in multi climate conditions," (in English), *Front Energy Res,* vol. 11, Jun 30 2023, doi: ARTN 1121138. 10.3389/fenrg.2023.1121138.

[3] Z. Gkouskos, T. Tsoutsos, and A. Kakouriotis, "Integrating phase change materials to photovoltaics in a mediterranean region," in *27th EU Photovoltaic Solar Energy Conference*, 2012.

[4] P. ÇULUN and S. K. IŞIK, "RECENT DEVELOPMENTS IN COOLING OF PHOTOVOLTAIC SOLAR PANELS," *Current Research in Engineering,* p. 113, 2023.

[5] R. Kumar, F. J. Montero, R. Lamba, M. Vashishtha, and S. Upadhyaya, "Thermal management of photovoltaic-thermoelectric generator hybrid system using radiative cooling and heat pipe," *Appl Therm Eng,* vol. 227, p. 120420, 2023.

[6] R. Lamba, F. J. Montero, T. U. Rehman, S. Singh, and S. Manikandan, "PCM-based hybrid thermal management system for photovoltaic modules: A comparative analysis," *Environ Sci Pollut Res Int,* vol. 31, no. 34, pp. 46397-46416, Jul 2024, doi: 10.1007/s11356-023-27809-1.

[7] Y. Du *et al.*, "Evaluation of photovoltaic panel temperature in realistic scenarios," *Energy Conversion and Management,* vol. 108, pp. 60-67, 2016.

[8] S. Sharma, A. Tahir, K. Reddy, and T. K. Mallick, "Performance enhancement of a Building-Integrated Concentrating Photovoltaic system using phase change material," *Sol Energ Mat Sol C,* vol. 149, pp. 29-39, 2016.

[9] A. A. Ali, D. A. Lafta, S. W. Noori, F. Abdulamir, and F. L. Rashid, "Innovative materials integrated with PCM for enhancing photovoltaic panel efficiency: An experimental investigation," (in English), *J Energy Storage,* vol. 102, Nov 20 2024, doi: ARTN 114258. 10.1016/j.est.2024.114258.

[10] E. H. H. Amalu and O. A. A. Fabunmi, "Thermal control of crystalline silicon photovoltaic (c-Si PV) module using Docosane phase change material (PCM) for improved performance," (in English), *Sol Energy,* vol. 234, pp. 203-221, Mar 1 2022, doi: 10.1016/j.solener.2022.02.001.

[11] H. M. T. Al-Najjar and J. M. Mahdi, "Novel mathematical modeling, performance analysis, and design charts for the typical hybrid photovoltaic/phase-change material (PV/PCM) system," (in English), *Appl Energ,* vol. 315, Jun 1 2022, doi: ARTN 119027. 10.1016/j.apenergy.2022.119027.

[12] M. Abd El-Hamid and G. S. Wei, "Effect of varying the thermophysical properties of phase change material on the performance of photovoltaic/thermal-PCM hybrid module numerically," (in English), *J Energy Storage,* vol. 86, May 10 2024, doi: ARTN 111326. 10.1016/j.est.2024.111326.

[13] M. Sharaf, M. S. Yousef, and A. S. Huzayyin, "Review of cooling techniques used to enhance the efficiency of photovoltaic power systems," *Environ Sci Pollut Res Int,* vol. 29, no. 18, pp. 26131-26159, Apr 2022, doi: 10.1007/s11356-022-18719-9.

[14] Y. S. Indartono, A. Suwono, and F. Y. Pratama, "Improving photovoltaics performance by using yellow petroleum jelly as phase change material," *Int J Low-Carbon Tec,* vol. 11, no. 3, pp. 333-337, 2016.

[15] P. ÇULUN, "PHASE CHANGE MATERIALS AND THEIR PROPERTIES WITHIN THE SCOPE OF CURRENT STUDIES," *Research And Evaluations In The Field Of Engineering,* p. 61, 2025.

[16] P. ÇULUN, "APPLICATIONS OF PHASE CHANGE MATERIALS IN LIGHT OF CURRENT RESEARCH," *Research And Evaluations In The Field Of Engineering,* p. 39, 2025.

[17] F. Şimşek and S. Organ, "CaCl2. 6H2O ve Na2SO4. 10H2O Faz Değişim Malzemelerinin Kullanıldığı Gizli Termal Enerji Depolama Ünitesinde Farklı Tip Bir Kanat Kullanmanın FDM'nin Erime Süresine Etkisinin HAD Analiziyle Araştırılması," *Karadeniz Fen Bilimleri Dergisi,* vol. 13, no. 2, pp. 701-723, 2023.

[18] M. Hawlader, M. Uddin, and H. Zhu, "Encapsulated phase change materials for thermal energy storage: experiments and simulation," *International Journal of Energy Research,* vol. 26, no. 2, pp. 159-171, 2002.

[19] M. S. Mert, M. Sert, and H. H. Mert, "ISIL ENERJİ DEPOLAMA SİSTEMLERİ İÇİN ORGANİK FAZ DEĞİŞTİREN MADDELERİN MEVCUT DURUMU ÜZERİNE BİR İNCELEME," *Mühendislik Bilimleri ve Tasarım Dergisi,* vol. 6, no. 1, pp. 161-174, 2018.

[20] A. Mahdavi, M. Farhadi, M. Gorji-Bandpy, and A. Mahmoudi, "A comprehensive study on passive cooling of a PV device using PCM and various fin configurations: Pin, spring, and Y-shaped fins," (in English), *Appl Therm Eng,* vol. 252, Sep 1 2024, doi: ARTN 123519. 10.1016/j.applthermaleng.2024.123519.

[21] K. Velmurugan, S. Kumarasamy, T. Wongwuttanasatian, and V. Seithtanabutara, "Review of PCM types and suggestions for an applicable cascaded PCM for passive PV module cooling under tropical climate conditions," *J Clean Prod,* vol. 293, p. 126065, 2021.

[22] K. Velmurugan *et al.*, "Contactless phase change material based photovoltaic module cooling: A statistical approach by clustering and correlation algorithm," *J Energy Storage,* vol. 53, p. 105139, 2022.

[23] S. Nada, D. El-Nagar, and H. Hussein, "Improving the thermal regulation and efficiency enhancement of PCM-Integrated PV modules using nano particles," *Energ Convers Manage,* vol. 166, pp. 735-743, 2018.

[24] L. Amanowicz and M. Turski, "PCM-Filled Capsules (RT44HC) for Heat Storage-Laboratory Scale Pilot Study," (in English), *Energies,* vol. 18, no. 2, Jan 2025, doi: ARTN 345. 10.3390/en18020345.

[25] L. Tan, A. Date, G. Fernandes, B. Singh, and S. Ganguly, "Efficiency gains of photovoltaic system using latent heat thermal energy storage," *Energy Procedia,* vol. 110, pp. 83-88, 2017.

[26] N. Badi, S. A. Alghamdi, H. M. El-Hageen, and H. Albalawi, "Onsite enhancement of REEEC solar photovoltaic performance through PCM cooling technique," *Plos One,* vol. 18, no. 3, p. e0281391, 2023, doi: 10.1371/journal.pone.0281391.

[27] P. Çulun, "Experimental investigation of photovoltaic panel surface temperatures and electricity production in summer," *Türk Doğa ve Fen Dergisi,* vol. 13, no. 2, pp. 77-87, 2024.

[28] U. Stritih, "Increasing the efficiency of PV panel with the use of PCM," *Renew Energ,* vol. 97, pp. 671-679, 2016.

[29] H. M. Ali, "Recent advancements in PV cooling and efficiency enhancement integrating phase change materials based systems–A comprehensive review," *Solar Energy,* vol. 197, pp. 163-198, 2020.

[30] E. Baccega, L. Vallese, and M. Bottarelli, "Enhancement of Thermal Conductivity of Paraffin PCM with Metal Foams," (in English), *Int J Thermophys,* vol. 46, no. 3, Mar 2025, doi: ARTN 35. 10.1007/s10765-024-03500-6.

[31] A. Hasan, S. McCormack, M. Huang, J. Sarwar, and B. Norton, "Increased photovoltaic performance through temperature regulation by phase change materials: Materials comparison in different climates," *Sol Energy,* vol. 115, pp. 264-276, 2015.

[32] A. Bria, B. Raillani, D. Chaatouf, M. Salhi, S. Amraqui, and A. Mezrhab, "Numerical investigation of the PCM effect on the performance of photovoltaic panels; comparison between different types of

PCM," (in English), *2022 2nd International Conference on Innovative Research in Applied Science, Engineering and Technology (Iraset'2022),* pp. 32-36, 2022, doi: 10.1109/Iraset52964.2022.9738247.

[33] N. Badi, S. A. Alghamdi, H. M. El-Hageen, and H. Albalawi, "Onsite enhancement of REEEC solar photovoltaic performance through PCM cooling technique," (in English), *Plos One,* vol. 18, no. 3, Mar 10 2023, doi: ARTN e0281391 10.1371/journal.pone.0281391.

[34] W. Wei *et al.*, "A continuous 24-hour power generated PV-TEG-PCM hybrid system enabled by solar diurnal photovoltaic/thermal conversion and nocturnal sky radiative cooling," (in English), *Energ Convers Manage,* vol. 321, Dec 1 2024, doi: ARTN 119086. 10.1016/j.enconman.2024.119086.

[35] P. Çulun, "Evaluatıon of Recent Developments in Thermoelectrıc Generators," ed: Sept, 2023.

[36] A. Sadeghian, M. R. Zargarabadi, and M. Dehghan, "Effects of rib on cooling performance of photovoltaic modules (PV/PCM-Rib)," (in English), *J Cent South Univ,* vol. 28, no. 11, pp. 3449-3465, Nov 2021, doi: 10.1007/s11771-021-4867-7.

[37] V. Tomar, G. Tiwari, T. Bhatti, and B. Norton, "Thermal modeling and experimental evaluation of five different photovoltaic modules integrated on prototype test cells with and without water flow," *Energ Convers Manage,* vol. 165, pp. 219-235, 2018.

[38] M. Huang, P. Eames, and B. Norton, "Thermal regulation of building-integrated photovoltaics using phase change materials," *International Journal of heat and mass transfer,* vol. 47, no. 12-13, pp. 2715-2733, 2004.

[39] M. Huang, P. Eames, and B. Norton, "Phase change materials for limiting temperature rise in building integrated photovoltaics," *Sol Energy,* vol. 80, no. 9, pp. 1121-1130, 2006.

[40] M. Pathak, K. Girotra, S. Harrison, and J. M. Pearce, "The effect of hybrid photovoltaic thermal device operating conditions on intrinsic layer thickness optimization of hydrogenated amorphous silicon solar cells," *Sol Energy,* vol. 86, no. 9, pp. 2673-2677, 2012.

[41] T. Wongwuttanasatian, T. Sarikarin, and A. Suksri, "Performance enhancement of a photovoltaic module by passive cooling using phase change material in a finned container heat sink," *Sol Energy,* vol. 195, pp. 47-53, 2020.

[42] M. A. Qasim *et al.*, "The effect of using hybrid phase change materials on thermal management of photovoltaic panels–an experimental study," *Sol Energy,* vol. 209, pp. 415-423, 2020.

[43] M. M. Bayat, E. Buyruk, and A. Can, "Experimental Investigation of Pv Panel Performance by Using Pcm with Different Fin Geometries," (in English), *Transactions of Famena,* vol. 47, no. 4, pp. 97-108, 2023, doi: 10.21278/Tof.474056223.

[44] W. Phukaokaew, A. Suksri, K. Punyawudho, and T. Wongwuttanasatian, "Thermal management of photovoltaic module using affordable organic phase change material combined with nano metal oxide particles enhancer," *Heliyon,* vol. 10, no. 24, p. e41054, Dec 30 2024, doi: 10.1016/j.heliyon.2024.e41054.

[45] J. M. Mahdi, H. I. Mohammed, and P. Talebizadehsardari, "A new approach for employing multiple PCMs in the passive thermal management of photovoltaic modules," *Sol Energy,* vol. 222, pp. 160-174, 2021.

[46] M. A. Ali, K. M. Seddik, and A. G. Hassabo, "Polyester Fibres Enhanced with Phase Change Material (PCM) to Maintain Thermal Stability," (in English), *Egypt J Chem,* vol. 64, no. 11, pp. 6599-6613, Nov 2021, doi: 10.21608/ejchem.2021.92104.4367.

[47] Z. Alimohammadi, H. S. Akhijahani, and P. Salami, "Thermal analysis of a solar dryer equipped with PTSC and PCM using experimental and numerical methods," (in English), *Sol Energy,* vol. 201, pp. 157-177, May 1 2020, doi: 10.1016/j.solener.2020.02.079.

[48] A. A. Alnaqi, J. Alsarraf, and A. A. A. A. Al-Rashed, "Transient numerical study on injecting PCM in buildings along with extra comfort ventilation: Use of artificial neural network to decline energy utilization," (in English), *Eng Anal Bound Elem,* vol. 143, pp. 559-567, Oct 2022, doi: 10.1016/j.enganabound.2022.07.005.

[49] S. R. Maadi, M. Khatibi, E. Ebrahimnia-Bajestan, and D. Wood, "Coupled thermal-optical numerical modeling of PV/T module–Combining CFD approach and two-band radiation DO model," *Energ Convers Manage,* vol. 198, p. 111781, 2019.

➢ *ORAL PRESENTATION*

The Place and Importance of Nanomaterial Additives in Passive Cooling of Photovoltaic Panels with Phase Change Materials

Perihan ÇULUN (0000-0002-1797-9695)

Bingöl University, Faculty of Engineering and Architecture, Mechanical Engineering Department, Bingöl, Türkiye

Corresponding author e-mail: pculun@bingol.edu.tr

Abstract

In this study, the use of nanomaterials in the cooling process with PCM materials, which is a passive cooling method for PV panels, was investigated. PCM materials seem to be the strongest candidates for the passive cooling of PV panels due to their high latent heat and the advantage of having different melting points. However, the low heat transfer coefficients of these materials continue to be a major disadvantage. The heat transfer coefficients can be increased by adding various nanomaterials to PCM materials. Within the scope of the study, it is aimed to reveal the advantages, difficulties, gaps and recommendations in the field. Within the scope of the study, nanomaterials used in PV-PCM cooling systems, frequently used ratios and effects of these materials were also examined. Furthermore PCM addition methods of nanomaterials and encountered difficulties were examined. Current researches on PV panels using nanomaterial-added PCMs (NPCM) were reviewed. Different PCM additions of various nanomaterials were examined within the scope of the literature. Nanometals such as Al_2O_3 and CuO are the most preferred nanomaterials, and due to their high density, a maximum of 2% mass ratio is used in nanomaterial additions to reduce precipitation.

Keywords: PV panel, Photovoltaic panel, Panel cooling, Nano material, NPCM

1. INTRODUCTION

As a result of photovoltaic panels being exposed to high solar radiation for extended periods surface temperatures of the panels increase significantly. Many studies emphasize that these increased temperatures result in significant efficiency decreases. In this regard, subjecting the panels to various cooling methods and increasing their efficiency is being researched academically. It has been reported that if PV panels are subjected to cooling with effective convection and conduction heat transfer methods, their efficiency will increase by 20-22%[1]. PCM materials are the most preferred cooling method due to the advantage of not requiring additional energy compared to other active systems. The fact that PCMs can be reused for the same process for a long time and that they do not harm nature are among their biggest advantages. Phase change materials store significant amounts of heat during the melting phase (charging) at almost constant state change temperature or release heat during the solidification phase (discharging) owing to their high latent heat storage capacity (LHTES)[2]. Due to its high heat storage or discharge feature in this phase change, PCM usage is becoming increasingly common in many insulation, heat storage, heat transfer, heating and cooling systems. PCM devices considered strong candidates for many industrial applications, including electronic cooling and smart systems due to their cooling effects[3-5]. Although PCM materials are suitable for insulation purposes due to their low heat transfer coefficients; however this feature poses a significant disadvantage in application areas that require rapid heat transfer[6-9]. Because of the low heat transfer coefficient, the slowdown in melting and solidification speeds creates a disadvantage in applications where rapid energy absorption is required[10].

Since phase change materials are heat storage materials, it is expected that these materials will transfer the energy stored in their bodies to another medium faster or store energy more efficiently. In such applications, it is essential to improve the heat transfer coefficients of PCM materials in order to get the desired response more quickly. As the melting of the PCM material is accelerated by the higher heat transfer coefficients, the overall melting time also reduced. To achive this various methods have been proposed to increase the heat transfer coefficients of organic PCM materials, which generally have lower heat transfer coefficients compared to other PCMs, and thus to accelerate heat transfer. Some of these methods include the use of metallic fins

that will help increase the heat transfer coefficient in the environment where PCM material is used, increasing metallic surfaces in different shapes, metal foam applications, testing panel angles by reducing them from 90° to 0°[11] and studies on nanomaterial additions to PCM material. Among these, studies on nanomaterial-supported PCM (NPCM), which is the most common and ongoing method[12]. Within the scope of these studies, various nanomaterials are added to PCM materials at different ratious to improve the heat transfer coefficient of the relevant PCM. Different literatures suggest various PCM materials such as paraffin, ester, fatty acids, alcohols for different application areas. All PCM types such as hydrated salts, paraffins, fatty acids and polymers can increase both heat storage and heat transfer rates with the addition of nanomaterials to PCMs. Paraffins are generally recommended for high temperature applications[13]. It has been stated that RT-35HC, which belongs to paraffin group, has a faster thermal response due to its higher energy storage capacity and melting speed when compared to lauric acid and P-58[10]. In the NPCM study where paraffin PCM was impregnated with graphene sponge, a 200% increase in the thermal conductivity coefficient was achieved even after 100 melting-freezing cycles [14]. Additionaly, PCM has melting/freezing properties suitable for almost any temperature, making paraffins highly preferred.

Although there are applications where the low heat transfer coefficient of PCM materials is seen as an advantage, such as insulation applications, there are also many applications that require the high transfer coefficient of these materials. PV-PCM systems are one of these applications. Indeed, in PV PCM systems, the rapid absorption of heat from the PV panel by the PCM material requires that the heat transfer coefficients of these materials be sufficiently high. While the heat conduction coefficients of inorganic PCMs such as calcium chloride hexahydrate ($CaCl_2.6H_2O$) and sodium sulfate decahydrate ($NaSO_4.10H_2O$) exhibit relatively high values such as 0.626 and 0.544W/mK[15], the heat conduction coefficients of organic PCMs such as paraffins low at an average value of 0.2 W/mK[7].

It is stated that the heat conduction coefficients and heat storage capacities of eutectics obtained with the addition of nanomaterials to PCM materials and different ratios of organic or inorganic PCMs are significantly improved[16, 17]. In fact, the efficiency of PV panels using PCM can be increased by 21.2%[1]. In concentrated photovoltaics (CPV), the maximum increase in power and efficiency is 7% and 6%, respectively[18]. Thermal analysis performed on NPCMs monitors the thermal conductivity coefficient, melting rate, melting process, and temperature distribution, which show how these nanoparticles improve heat transfer.

In this study, the use of nanomaterials in PCM-based cooling studies of PV panels was first examined based on a review of exiting literature. Application methods, effects, difficulties encountered, etc. of nanomaterials were evaluated. At the end of this detailed review, the type of nanomaterials or nanofluids added to PCM materials along with their properties and usage ratios were presented. Frequently used addition methods in the literature and the advantages and disadvantages of these addition methods were also discussed. In particular, the precipitation situation in NPCMs, additives used to prevent precipitation and precipitation situations were examined. The gaps identified in this area were presented.

2. COOLING OF PHOTOVOLTAIC PANELS WITH NANOMATERIAL INCLUSION PHASE CHANGE MATERIAL

In the PV-NPCM application obtained by adding Al_2O_3, CuO, MgO to PCMs with 6% melting points of 41-44°C, NPCM with high heat transfer coefficient was obtained in Thailand where the ambient temperature was 38 °C, and thus, temperature decrease and efficiency increase were provided in the panel. With the 5.2 °C temperature decrease recorded in the relevant PV panel, 14.11% efficiency increase was provided. The heat transfer coefficient increases of NPCMs with MgO, Al_2O_3, CuO additives were 62.73%, 52.13% and 65.96% (Table 1). As a result of this heat transfer coefficient increase, the power increases compared to pure PCM were measured as 4.38 Wh, 2.99 Wh, and 2.62 Wh, respectively[19]. Here, the optimum ratio of 6% was taken into account by considering the increasing heat transfer coefficient and decreasing latent heat of melting. While MgO showed the best performance in the study, it was observed that Al_2O_3 showed better performance than CuO. On the other hand, in the PVT study where Al_2O_3 and TiO_2 were used, it was emphasized that Al_2O_3 showed better performance than TiO_2[12]. In general, similar studies have confirmed that Al2O3 not only performs better but is also more widely used. The performance of PV-NEPCM using 1%, 3% and 5% CuO

was compared with the PV-PCM system for 0°, 15°, 30° and 45 ◦ angles. It was determined that the addition of nanomaterial was more advantageous in almost all configurations, and the best efficiency increase was 1.75% at 5% CuO ratio, θ = 0◦ angle [20].

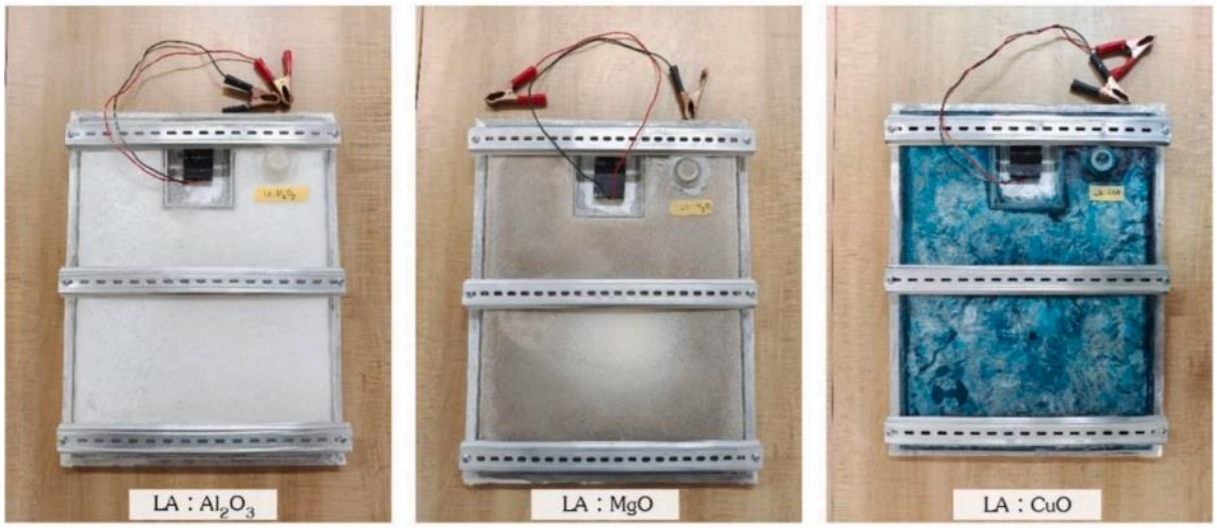

Şekil 1.. PCM containers with nano materials[19]

In the concentrated photovoltaic system, Al_2O_3, CuO and SiO_2 nanometals were used at 1wt% and 5wt% mass ratios and the panel performance was investigated numerically and experimentally. In the study where calcium chloride hexahydrate (CaCl2 6H2O) was used as PCM, the melting time of pure PCM was 88 minutes, while with the addition of Al_2O_3, CuO and SiO_2 at 1 wt% mass ratio recorded as 78 minutes, 80 and 85 minutes. When the mass ratios were increased to 5 wt%, the melting times were recorded as 70, 76 and 84 minutes[21]. For the 5% mass ratio, the best performance was achieved for Al_2O_3, while the lowest performance belonged to SiO_2. It was emphasized that the thermal conductivity coefficient reached its highest value for Al_2O_3 compared to CuO, SiO_2 materials, thus increasing the heat transfer rate and therefore increasing the melting rate, and decreasing the panel temperature. It was stated that with PCM with 5% Al_2O_3 added, the panel uniform temperature distribution at 12°C increased the relevant efficiency by 8%, and for pure PCM, the uniform temperature distribution was 20 °C, and the relevant efficiency increased by 6.36%. It was stated that the heat conductivity coefficient improved in parallel with the increase in the mass ratio of nano materials, and therefore the melting time shortened. On the other hand, it was stated that the increasing nano material ratio significantly triggered the precipitation[21].

In order to obtain more effective results in NPCMs, hybrid nanomaterials such as GNP-CUO have recently been used by mixing two different nanomaterials at a certain ratio[22, 23]. In the study where graphene nano sheets (GNP), copper oxide (CuO), simple mixture and synthesized hybrid mixture were used, GNP and CuO nano materials with sizes of 6–8 nm and 5 µm were used[22]. The aim of such a mixing is to increase the heat transfer coefficient by using the advantages of 3D spherical particle CUO and 2D dimensional graphene nanoplates. Therefore, a 2D-3D hybrid mixture is obtained. In fact, the contact surface between the nanomaterial and PCM is increased with the help of graphene nanoplates. It is stated that when cylindrical fins are used together with PCM in PV panels, the panel temperature decreases by 20-46.3%, and the temperature decrease increases to 52.3% with the addition of Al2O3 to RT35HC[24]. In the study where graphene nanoplatelet (GNP) and copper oxide (CuO) were used with polyethylene glycol 1500 PCM (GNP-CuO 3%), a 91.81% increase in thermal conductivity coefficient was achieved compared to pure PCM. With this, the PV panel temperature was reduced by 6.6 ◦C, and the panel efficiency was increased by 3% [22]. It was stated that the viscosity of GNP, which increased in NPCMs, increased by 3% and the viscosity increased by 41%[22].

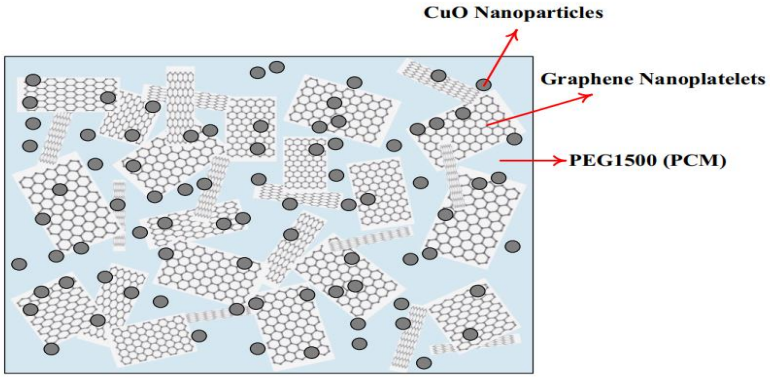

Figure 2. GNP-CUO hibrit nano malzemeli PCM üretimi [22]

CuO was numerically and experimentally investigated in three different PCMs (lauric acid, RT-35HC and P-58) at 0.01% Wt mass ratio, it was stated that the energy storage capacity increased by 16.36% and 8.55%, respectively, according to the experimental and numerical results. 35.19 J/min energy flow rate was provided with CuO doped PCM. RT-35HC PCM material provided the highest energy storage rate, higher melting rate, and therefore faster response to thermal effects compared to lauric acid and P-58[10]. By using GNP in OM35 PCM material at 0.1%-0.5% volumetric ratio, the highest thermal conductivity increase was obtained for 0.5% ratio, 75% and 22% for solid and liquid, respectively [18].

Table 1. Some important parameters of nano-doped PCM studies

PCM used	Nano material type	Material ratio	Percentage increase in efficiency/heat transfer coefficient	Precautions against sedimentation	sedimentation
fatty acid (lauric acid) (LA[19]	Al_2O_3, MgO, and CuO	%1, %2, %6, %8, %10 wt	Heat transfer coefficient increase for Al2O3, MgO, and CuO is 62.73%, 52.13% and 65.96%, efficiency increase is 14.11%	No sedimentation precautions	It has been stated that precipitation has occurred
PEG1500 [22]	graphene nanoplatelets (GNP), copper oxide nanoparticles (CuO), GNP-CuO	%1, %2, %3wt	compared with pure PCM, the chemical mixture of GNP-CuO 3 % NePCM had the highest thermal conductivity enhancement of 91.81 % and the lowest dynamic viscosity increase of 14.83 %.	0.75% Oleic acid (C18H34O2) dropper was used	
OM35 [18]	GNP	%0.1-0.5 vol.	maximum increase in power output and efficiency of 7 % and 6 %, respectively; for 0.5% ratio, the solid and liquid heat transfer coefficient increase rate is 75% and 22%	%0.75 vol. Sodium deoxycholate (C24H39NaO4)	The issue of sedimentation is not mentioned.
RT25HC [20]	CuO	%1, %3, %5wt	Maximum enhancement of efficiency of PV module is found to be 1.75% for θ=0◦ inclination on adding nanoparticles of 5% m	Numerical study	
CaCl2·6H2O [21]	Al_2O_3, CuO and SiO_2	%1, %5wt	electrical efficiency enhacement 8% by NPCM	Numerical study	
Lauric acid, RT-35HC and P-58 [10]	CuO	0.01wt	16.36% enhancement in energy storage, as observed experimentally, whereas the numerical simulation showed an 8.55% increase.	Experimental and Numerical study	The issue of sedimentation is not mentioned.
RT54HC [5]	Al_2O_3	0.15–0.25 wt%	The results show that at a heat flux (HF) of 0.98 kW/m2 and 0.25 wt % of Al_2O_3 nanoparticles (NPs), the base temperature of simple, circular pin finned and Cu foam heat sink was reduced by 21.3%, 25.03%, and 36.2%, respectively.	No surfactant used	According to the test immediately after the experiment, it was stated that there was no sedimentation.
Paraffin wax[25]	SiO_2	0.5 %, 1.0%, ve %2.0	enhanced the thermal conductivity of paraffin wax to 12.78%, 22.78%, and 33.34%, respectively	The issue of sedimentation is not mentioned.	
RT35HC[10]	Al_2O_3	0.11-0.77%	A temperature reduction of 36.9–52.3% was achieved on the panel surface.	The issue of sedimentation is not mentioned.	
lauric acid(fatty acid)[19]	Al_2O_3, CuO, MgO	%6	With the 5.2 ◦C temperature decrease recorded in the relevant PV panel, an efficiency increase of 14.11% was achieved.	The issue of sedimentation is not mentioned.	

3. PREPARATION OF NANOMATERIAL INCLUSION PHASE CHANGE MATERIAL

The addition of nanomaterials to PCMs plays an important role in improving many properties of PCMs. Whether NPCMs are suitable for the purpose can be determined by looking at their thermophysical properties and transport properties. For this, properties such as viscosity, latent heat, melting point, thermal conductivity should be measured. NPCM formation is basically a one-step and two-step method. In the one-step method, which is carried out by evaporation or chemical synthesis, nanomaterial production and basic PCM are mixed simultaneously[26]. In this respect, it is known as the direct production method. Since processes such as drying, storage, transportation and mixing of nanomaterials are disabled in this method, clustering is less. However, since it is more expensive than the two-step method, it is applied in small-scale samples. In the two-step method, powder nanoparticles are formed with various mechanical and chemical processes such as sol-gel, ball milling, chemical reduction. After that, nanomaterials are mixed with PCM and homogenized by sonication, heating and magnetic stirring. In this method, the stability of the solution is ensured with the help of repulsive forces and zeta potential formation to prevent sedimentation or precipitation. In the production of NPCMs, many different two-step NPCMs are produced using surface active materials such as Poly Vinyl Pyrrolidine-40 (PVP), Sodium Dodecyl Benzene Sulfonate (SDBS), Sodium Dodecyl Sulfate (SDS), oleic acid, etc[27].

In the two-step method, the initially solid PCM material is melted on a hot plate with adjustable temperature or in a water bath. Before adding the nanomaterial to the PCM, it is generally mixed in a magnetic stirrer at 500-600rpm for half an hour or an hour in order to ensure homogeneity in the relevant material[22, 28]. In some studies, the nanomaterial is ground[22] or baked [28] to reduce the average diameter of the nanomaterial and increase the effective surface area. Nanomaterials are weighed in specific percentages according to the pure PCM mass and added to the liquefied PCM. In order to prevent the sedimentation of nanomaterials, surface active materials such as oleic acid and Sodium Dodeacyl Sulfate (SDS) are added in appropriate proportions[22, 28]. In surface active materials, the amount is determined according to the material type. For example, the amount of Sodium Dodeacyl Sulfate (SDS) is set to be 4 times the amount of the nanomaterial used[28] , and oleic acid is set to be 0.75% of PCM[22]. After this addition, the mixture is mixed for an average of 1-2 hours in a hot plate magnetic stirrer at 60-70 ◦C and 500-600 rpm. The resulting solution is subjected to a water bath at a frequency of 30 Hz for 1 hour to increase homogeneity (Figure 3). It is important to grind powdered nanomaterials and surface active materials to prevent sedimentation.

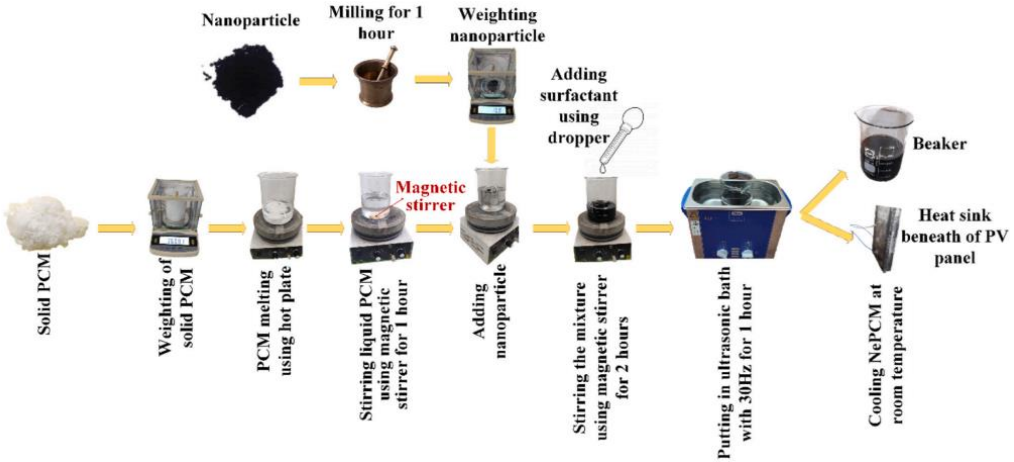

Figure 3. Example of PCM preparation [22]

In the study of cooling the concentrated solar panel with NPCM, the summary diagram of NPCM preparation by adding GNP nano material to the OM35 PCM material given in Fig. 4.

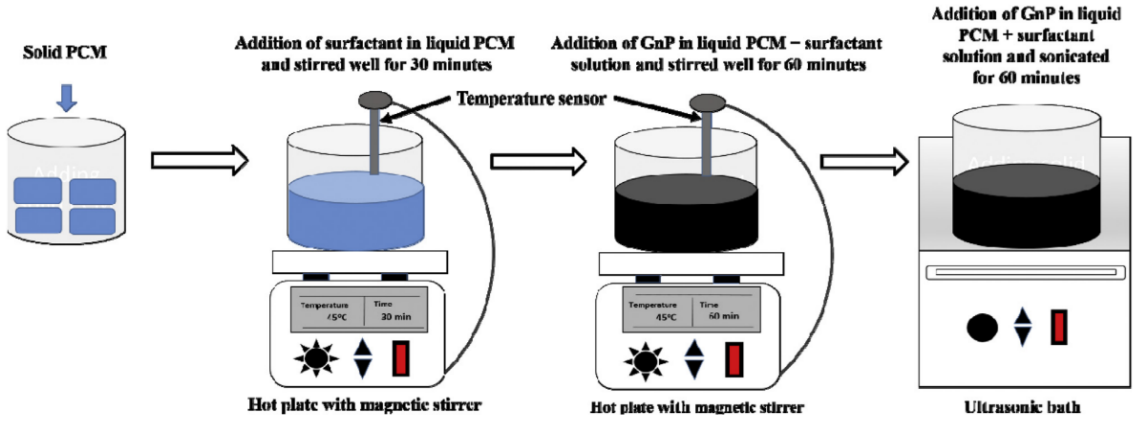

Figure 4. Example of PCM preparation [18]

In the study on cooling electronic devices with NPCM, NPCM was prepared using RT-54HC Aluminum oxide (Al_2O_3) nanomaterial with a melting temperature of 54°C, which is from the paraffin group. First, RT-54HC was melted at its own melting temperature, then the nanomaterials with a determined mass were added to the melted PCM, and the mixture was mixed in a magnetic stirrer at a temperature of 65°C above the melting temperature of the PCM. The resulting mixture was subjected to an ultrasonic bath for another 2 hours. It was stated that there was no precipitation at the end of the experiment[5].

In the experimental study examining the effect of SiO_2 as a nanomaterial in solar thermal heat storage system, the material was added to paraffin wax at rates of 0.5%, 1.0%, and 2.0% and subjected to different experimental methods[25]. The increase rates in the heat conduction coefficient of NPCM at these rates were 12.78%, 22.78%, and 33.34%, respectively. It was stated that the addition of SiO_2 nanoparticles did not disrupt the PCM structure, positively changed the melting and solidification temperatures of the material, and the latent heat of the material decreased with increasing nanoparticle mass. In this respect, mass ratios above 1% in SiO2 nanoparticles were not recommended in the relevant study. It was stated that NPCM with high thermal properties could be achieved by using SiO_2 at the lowest mass ratio of 0.5%[25]. In the NPCM study prepared by mixing RT35HC PCM material with Al_2O_3 at the rates of 0.11% to 0.77%, it was determined that the panel temperature decreased by 36.9–52.3%[24].

3.1. Nanomaterials added to phase change material

The low heat conduction coefficients of PCM materials have led to research on the increase of heat conduction coefficients in these materials. It can be said that the heat conduction coefficient for almost all PCM materials is $0.2 W/m^{-1}k^{-1}$[26]. Nanomaterials are added to paraffin and fatty acids, especially organic PCMs, to improve thermal properties. By adding nanoparticles, the heat transfer rate is improved and PCM can absorb or release heat more efficiently. When adding nanomaterials to PCMs, situations that may deteriorate the main material properties should be avoided. Nanomaterials commonly added to the PCMs shown in Table 2 with its ratios.

One of the most frequently used materials within the scope of nanomaterial addition to PCM is Graphene and Graphene Oxides. It has excellent heat conduction coefficient and a large surface area, which increases the heat transfer performance of the material. It is lightweight, durable and improves PCM stability. It is generally used in amounts of 0.5% - 5% of PCM weight. However, adding nanomaterials in amount above these values can change PCM viscosity and therefore flow properties. The most important disadvantage of graphene is that it is expensive. CNT (Carbon Nanotube) can improve PCM thermal conductivity with its excellent thermal and mechanical properties. It has the advantages of preventing phase separation and overcooling in PCM.

CNTs can generally be added in the range of 0.1-1% by weight. More intensive CNT additions can cause precipitation.

Another frequently used nanomaterial is the ceramic material Al_2O_3 (Aluminum Oxide) which has good thermal conductivity and high thermal stability. Al_2O_3 is used to improve the heat transfer of composite PCMs. Another important advantage of PCMs is that they increase their heat storage capacity and are economical due to their widespread availability. As understood from nano studies, experiments have been carried out for Al_2O_3 in paraffin group PCM materials at the rates of 0.1–0.77%[29, 30] and 0.15–0.25 wt%[5] .

In general, among all PCM groups, PCM concentration is between 0.5% and 2% by weight. Apart from these rates, dispersibility, sedimentation, etc. can be observed. Although there are studies that try 6% and higher rates over 2%, it would not be right to recommend these rates since sedimentation is not addressed in such studies[19]. Another important nanomaterial that has high thermal conductivity and increases the heat absorption and dissipation capacity of PCMs is copper. Copper is generally used at a rate of 0.5% - 2% by weight. Outside of these amounts, it can affect the increase in viscosity and fluidity of PCM.

It is also possible to use Boron Nitride Nanopowders (BN) due to their high thermal conductivity, high stability, chemical inertness and oxidation resistance properties. BN used at 1% - 5% rates improves heat transfer. Thanks to the phase change efficiency increase feature of Silver Nanoparticles and their high conductivity, even 0.1% - 0.5% by weight may be sufficient to improve heat transfer performance. Similarly, TiO_2 provides the advantage of high thermal conductivity and chemical stability. Being relatively safe and non-toxic allows the use of the relevant material in different environments. TiO_2, which is generally suitable for use at 1% - 5% by weight, may cause agglomeration (sedimentation) or precipitation if used above these rates. Silicon Dioxide or Silica Nanoparticles (SiO_2) can generally serve as a dispersing agent that helps other nanoparticles spread more evenly throughout the PCM. Increasing thermal stability and improving heat transfer, being low cost, and being easy to include in various systems provide advantages. It is used with weight ratios varying between 0.5% and 3%.

Table 2. Nanomaterials added to PCM materials in PV cooling

Nanoparticle Type	Advantage	Disadvantages	Ratios
Graphene	High heat transfer coefficient, Large surface area, Light, durable, stable	Expensive	%0,5 -%5
CNT(Carbon nanotube)	prevent phase separation and overcooling	They can deteriorate sedimentation or viscosity outside concentration limits.	%0,1-1
Al_2O_3 (Aluminum Oxide)	High heat transfer coefficient, High heat transfer coefficient, Widely found in natüre, Cheap, High thermal stability		%0,5-%2
Copper (Cu)	High heat transfer coefficient		%0,5 -%2
Boron Nitride Nanopowders (BN)	High heat transfer coefficient		%1 - %5
Silicon Dioxide (Silica (SiO_2))	High heat transfer coefficient		%0,5- %3
Silver	High heat transfer coefficient, Increases phase change efficiency	Expensive	%0,1- %0,5

Nanoparticles to be used in PCM should be analyzed well in terms of dispersibility, viscosity change, nanoparticle amount and cost. It is important that nanoparticles are distributed homogeneously in PCM and that there is no sedimentation. For this, methods such as ultrasonication and surface modifiers should be used to help achieve uniform distribution. Since the addition of nanoparticles generally increases PCM viscosity, it can affect fluidity and overall thermal management performance. The amount of nanoparticles should be balanced with the necessary heat transfer and viscosity constraints. The optimum amount of nanoparticles is usually between 0.1% and 5% by weight. PCM costs increase especially for expensive materials with high conductivity such as graphene and silver.

3.2. Nanomaterial addition methods

By Adding Nanofluids to PCMs, thermal conductivity and latent heat of melting can be increased. With the addition of nanoparticles, PCMs that absorb or emit more efficient heat can be obtained. Thanks to the homogeneous distribution of nanofluids, it is especially possible to spread heat quickly. The method to be selected depends on the requirements of the application, costs and technical possibilities. A number of methods are used to ensure homogeneous distribution of nanofluids or nanoparticles in PCM materials. These methods are mechanical mixing, ultrasonic mixing, supercritical carbon dioxide method, solvent, sol-gel and electrostatic mixing methods, where nanoparticles are physically mixed directly into the PCM material. In addition of nanofluids or nanoparticles to PCM, it is generally preferred to add them after the PCM material is melted and liquefied[41].

Various morphology analysis methods such as SEM, TEM and PSD are used for nanoadditive PCMs[42]. Thermal reliability and thermal endurance can be determined by DSC and TG techniques.

Mechanical mixing: In the mechanical mixing method where PCM and nanoparticles are mixed as broadcast, nanoparticles are added directly to PCM and mixed homogeneously in a mixer. The biggest advantage is that it is easy to apply and low cost. However, There is a risk of homogeneous distribution of particles and sedimentation over time.

Ultrasonic mixing: For better homogeneity and to prevent longer-term settling, mixing can be achieved using an ultrasonic mixing device. The disadvantages of this method are high energy consumption and impracticality.

Supercritical Carbon Dioxide (Supercritical CO_2) Method: nano particles are dissolved in PCM and supercritical carbon dioxide, the pressure and temperature on the mixture are controlled and the PCM and nano fluid are mixed. By increasing the solubility of the substances with Supercritical CO_2, the distribution of nano particles can be improved. In this way, particle distributions are more sensitive, a more homogeneous mixture can be provided. High cost and special equipment requirement are the disadvantages of this method.

Solvent Method: In this method, nanoparticles are added to PCM with a solvent. Then, by evaporating the solvent, nanoparticles are suspended homogeneously in PCM. Thanks to this process, the aggregation of nanoparticles is prevented [41]. Removal of solvent may extend processing time.

Sol-Gel Method: Nano particles integrated into PCM by the sol-gel method are placed in a gel matrix and this matrix is dissolved in PCM. A homogeneous and stable mixture can be provided, but it is a complex and time-consuming process.

Electrostatic Method: Electrostatic forces Nano particles can be added to the PCM material. A homogeneous mixture is obtained by applying an electrical charge on the particles. Homogeneous distribution of particles can be achieved with low energy consumption. Technically complex, and equipment requirements are high.

3.3. Challenges in Adding Nanomaterials to PCM Material

There are some difficulties encountered in adding nanofluids to PCM (Phase Change Materials) materials. The mixing process must be well managed in order for the properties of nanofluids to work in harmony with PCM. The most important difficulty in adding nanofluids to PCM materials is homogeneous distribution and sedimentation. It is not easy to ensure homogeneous distribution of nanoparticles, especially nanometals, in PCM. In particular, due to the surface tensions and sedimentation tendencies of the particles, proper mixing may not be achieved. Over time, particles may sediment and the mixture may become less efficient. The distribution can be homogenized with techniques such as ultrasonic, electrostatic and high-speed mechanical mixing. The sedimentation or settling of nanoparticles causes a decrease in thermal conduction performance. Especially in the melting/freezing phase changes of PCM, particles may accumulate at the bottom due to the density difference. Dispersion aids and surface coatings can be used for particle stabilization. Sedimentation can also be prevented with appropriate mixing and stabilization techniques. In addition, care should be taken to use the optimum nanoparticle ratio so that the nanoparticles added to the PCM material do not negatively affect the PCM thermal storage capacity. In fact, nanomaterials increase the heat transfer coefficient at high mass ratios. It is also stated that although the heat transfer coefficient increases in parallel with the increasing

mass ratios, there is also a decrease in the latent heat ratio of the material. In the same graph, the point where the heat transfer coefficient increase graph and the latent heat decrease graph overlap depending on the increasing mass ratio is considered as the optimum ratio of the nanomaterial ratio[19]. However, the increasing mass nanomaterial ratio also causes these materials to precipitate over time in the PCM. This precipitation risk is especially prominent in metal oxides. Unfortunately, the nanomaterial effect is also lost with precipitation. In this respect, various additives are used to ensure that nanomaterials maintain their nanomaterial effect in the NPCM material for a long time without precipitation. Although SDS additive is used to delay and prevent these precipitations, the question of how long this delay lasts is still a mystery. How long this precipitation occurs is also an important research topic.

In order to prevent possible chemical reactions, the chemical compatibility between PCM and nanoparticles should be tested. Such reactions can be prevented by coating methods such as silica coating. In addition, since the supply of nanoparticles and their addition to PCM is already costly, the cost of the product will increase even more, especially in commercial applications, if the amount of nanoparticles increases. In order to reduce these costs, more cost-effective particles or lower-cost production methods can be preferred. PCM viscosity can also be increased by the addition of nanoparticles. It can reduce the fluidity of PCM during the liquid phase and thus the heat transfer efficiency. Using optimum particle size, ensuring homogeneous distribution and selecting low-viscosity nanofluids can control viscosity.

3.4. Precipitation problem in nano-doped phase change materials

Since the nanomaterials included in PCMs naturally precipitate over time due to density differences, the stability and performance of the material decreases. This precipitation negatively affects the thermal properties and reliability of the PCM. The main reason for the precipitation is that the density of nanomaterials is generally higher than the density of the PCM used. Metal oxides in particular have higher densities than the density of the PCM material (Table 3). Another situation that causes precipitation is the clustering of nanoparticles as a result of poor application of nanomaterial dispersion techniques. The addition of surfactant or polymer coating of nanoparticles increases stability. In order to prevent the precipitation of nanomaterials, surface active materials such as oleic acid and Sodium Dodeacyl Sulfate (SDS) are added at appropriate rates[22, 28]. The amount of surface active materials is determined according to the material type. For example, the amount of Sodium Dodeacyl Sulfate (SDS) was adjusted to be 4 times the amount of nanomaterial used[28], and oleic acid was adjusted to be 0.75% of PCM[22]. In addition, the sedimentation condition can be reduced, thermal conductivity and stability can be increased by micro and nano encapsulation of PCMs using polyurethane and silica materials. The inclusion of nanoparticles in PCM with the Vacuum Impregnation Technique can provide long-term phase stability. It is also important for stability not to exceed the optimum nanoparticle ratio[21]. Generally, nanomaterial ratios above 2% cause precipitation. In the NPCM study on cooling electronic devices, it was stated that it would be more beneficial to reduce the nanomaterial ratio below these ratios according to the results obtained in the study where Al2O3 was used at a mass ratio of 2%-6%[31].

Table 3. Density of materials

PCM or Nano material type	Density(kg/m^3)
RT21	770
RT25[20]	749
RT27	760[21]
RT28HC	770[32]
RT31	770
RT35	770
RT44	770
CuO	6510[21]
Al_2O_3	3970[21]
MgO	3580
SiO2	2200[21]
Graphene	2200[21]

4. CONCLUSIONS AND RECOMMENDATIONS

Studies on the addition of nanomaterials, primarily metal oxides, to PCM materials at various rates have shown that the thermal conductivity of PCM materials increases significantly due to this nanomaterial effect. There are studies in the literature indicating that the thermal conductivity of PCM materials will increase by 72%-91% with the addition of nanomaterials. In order to obtain more effective results in NPCMs, hybrid nanomaterials have recently been used by mixing two different nanomaterials such as GNP-CuO at certain rates [22, 23]. The aim in such a mixing is to increase the thermal conductivity by using the advantages of 3D spherical particle CuO and 2D dimensional graphene nanoplates. Therefore, a 2D-3D hybrid mixture is obtained. In fact, the contact surface between the nanomaterial and PCM is increased with the help of graphene nanoplates.

When NPCM literature studies were evaluated, it was revealed that nanomaterial ratios significantly improved PCM thermal properties. Some studies indicated that the increase in nanomaterial ratio increased the heat transfer coefficient while also decreasing the latent heat of melting of the material[19]. Although the best balance ratio, called the nanomaterial mass ratio at the intersection of the increasing heat conduction coefficient and the decreasing latent heat of melting, is stated as 6%, scientists consider these ratios to be undesirable because this ratio negatively affects the sedimentation state[31]. As a matter of fact, it is understood from general studies that the metal oxide nanomaterial ratio is between 0.5% and 2%[28]. The main reason for this is to avoid sedimentation situation or to delay it. There are also rare studies where high nanomaterial ratios such as 4% and 6% are used without considering the sedimentation problem[19]. In fact, even at low rates, precipitation of nano metals is inevitable. Although additives such as SDS are used to prevent precipitation, precipitation occurs over time. In addition, in studies where SDS materials were used, the precipitation situation was not observed for a long time. Although NPCM research is promising, the precipitation of nanomaterials in their long-term use causes limitations in the use of these materials. Various surfactants used in NPCM studies: Poly Vinyl Pyrrolidine-40 (PVP), Sodium Dodecyl Benzene Sulfonate (SDBS), Sodium Dodecyl Sulfate (SDS), oleic acid[27] etc., as well as surface active materials that can act as dispersing agents to help nanoparticles spread more evenly throughout the PCM. It will be of great importance to produce hybrid NPCMs, if necessary, by using auxiliary nanomaterials such as Silicon Dioxide or Silica Nanoparticles (SiO_2), and to subject these NPCM materials to long-term testing[10].

In literature studies, it has been understood that nanomaterials are generally used with paraffins. This situation is primarily due to some superior properties of paraffins compared to inorganic PCMs. However, since inorganic PCMs are more easily available in the market, more economical, and have a higher transmission coefficient, it is important to focus such studies on inorganic PCMs or eutectic PCMs derived from these inorganic PCMs [33]. Among the nanometals used, it is understood that Al_2O_3 is preferred more than other metals and provides better performance both in terms of improving the heat conduction coefficient and other thermal properties, while also being more economical. However, there are studies indicating that the rate of increasing the heat conduction coefficient of nanometals is <5%, and that this coefficient increases 2-3 times in the use of graphene[34].

REFERANSLAR

[1] Y.-K. Kang, J. Joung, M. Kim, H.-H. Lee, and J.-W. Jeong, "Numerical analysis of a TEG and mPCM enhancement system for BIPVs using CFD," *Sustainability,* vol. 14, no. 23, p. 15559, 2022.

[2] J. Jaguemont, N. Omar, P. Van den Bossche, and J. Mierlo, "Phase-change materials (PCM) for automotive applications: A review," *Appl Therm Eng,* vol. 132, pp. 308-320, 2018.

[3] V. Bianco, M. De Rosa, and K. Vafai, "Phase-change materials for thermal management of electronic devices," *Appl Therm Eng,* vol. 214, p. 118839, 2022.

[4] M. Kiasari, M. Ghaffari, and H. H. Aly, "A comprehensive review of the current status of smart grid technologies for renewable energies integration and future trends: The role of machine learning and energy storage systems," *Energies,* vol. 17, no. 16, p. 4128, 2024.

[5] I. Zahid, M. Farhan, M. Farooq, M. Asim, and M. Imran, "Experimental investigation for thermal performance enhancement of various heat sinks using Al2O3 NePCM for cooling of electronic devices," *Case Stud Therm Eng,* vol. 41, p. 102553, 2023.

[6] P. ÇULUN, "APPLICATIONS OF PHASE CHANGE MATERIALS IN LIGHT OF CURRENT RESEARCH," *Research And Evaluations In The Field Of Engineering,* p. 39, 2025.
[7] P. ÇULUN, "PHASE CHANGE MATERIALS AND THEIR PROPERTIES WITHIN THE SCOPE OF CURRENT STUDIES," *Research And Evaluations In The Field Of Engineering,* p. 61, 2025.
[8] L. Tan, A. Date, G. Fernandes, B. Singh, and S. Ganguly, "Efficiency gains of photovoltaic system using latent heat thermal energy storage," *Energy Procedia,* vol. 110, pp. 83-88, 2017.
[9] Q. Li, J. Jiang, Y. Hong, and J. Du, "Numerical investigation of thermal management performances in a solar photovoltaic system by using the phase change material coupled with bifurcated fractal fins," *J Energy Storage,* vol. 56, p. 106156, 2022.
[10] A. Nandi and N. Biswas, "Enhanced melting dynamics of phase change material (PCM) based energy storage system combining modified fin and nanoparticles under solar irradiation," (in English), *Int J Numer Method H,* Jan 13 2025, doi: 10.1108/Hff-08-2024-0643.
[11] R. Kothari, S. Das, S. K. Sahu, and S. I. Kundalwal, "Analysis of solidification in a finite PCM storage with internal fins by employing heat balance integral method," *International Journal of Energy Research,* vol. 43, no. 12, pp. 6366-6388, 2019.
[12] K. Emara, H. Aliwa, O. E. Abdellatif, and H. Abd El-hameed, "Experimental investigation for a hybrid aluminum oxide nanofluid-phase change material photovoltaic thermal system based on outdoor test conditions," *J Energy Storage,* vol. 50, p. 104261, 2022.
[13] S. N. Gunasekara, R. Pan, J. N. Chiu, and V. Martin, "Polyols as phase change materials for surplus thermal energy storage," *Appl Energ,* vol. 162, pp. 1439-1452, 2016.
[14] P. Li, Q. Chen, Q. Peng, and X. He, "Paraffin/graphene sponge composite as a shape-stabilized phase change material for thermal energy storage," *Pigment & Resin Technology,* vol. 50, no. 5, pp. 412-418, 2021.
[15] F. Şimşek and S. Organ, "CaCl2. 6H2O ve Na2SO4. 10H2O Faz Değişim Malzemelerinin Kullanıldığı Gizli Termal Enerji Depolama Ünitesinde Farklı Tip Bir Kanat Kullanmanın FDM'nin Erime Süresine Etkisinin HAD Analiziyle Araştırılması," *Karadeniz Fen Bilimleri Dergisi,* vol. 13, no. 2, pp. 701-723, 2023.
[16] Z. Said *et al.*, "Nano-enhanced phase change materials: Fundamentals and applications," *Progress in Energy and Combustion Science,* vol. 104, p. 101162, 2024.
[17] A. Olabi *et al.*, "Recent progress on Carbon-based nanomaterial for phase change materials: Prospects and challenges," *Therm Sci Eng Prog,* vol. 23, p. 100920, 2021.
[18] M. Sivashankar, C. Selvam, S. Manikandan, and S. Harish, "Performance improvement in concentrated photovoltaics using nano-enhanced phase change material with graphene nanoplatelets," *Energy,* vol. 208, p. 118408, 2020.
[19] W. Phukaokaew, A. Suksri, K. Punyawudho, and T. Wongwuttanasatian, "Thermal management of photovoltaic module using affordable organic phase change material combined with nano metal oxide particles enhancer," *Heliyon,* vol. 10, no. 24, p. e41054, Dec 30 2024, doi: 10.1016/j.heliyon.2024.e41054.
[20] U. K. Sasidharan and R. Bandaru, "Thermal management of photovoltaic panel with nano-enhanced phase change material at different inclinations," *Environ Sci Pollut Res Int,* vol. 29, no. 23, pp. 34759-34775, May 2022, doi: 10.1007/s11356-021-18075-0.
[21] I. Zarma, M. Ahmed, and S. Ookawara, "Enhancing the performance of concentrator photovoltaic systems using Nanoparticle-phase change material heat sinks," *Energ Convers Manage,* vol. 179, pp. 229-242, 2019.
[22] M. Moein-Jahromi, H. Rahmanian-Koushkaki, S. Rahmanian, and S. P. Jahromi, "Evaluation of nanostructured GNP and CuO compositions in PCM-based heat sinks for photovoltaic systems," (in English), *J Energy Storage,* vol. 53, Sep 2022, doi: ARTN 105240. 10.1016/j.est.2022.105240.
[23] N. Aslfattahi *et al.*, "Improved thermo-physical properties and energy efficiency of hybrid PCM/graphene-silver nanocomposite in a hybrid CPV/thermal solar system," *J Therm Anal Calorim,* pp. 1-18, 2022.
[24] H. Abdelrahman, M. Wahba, H. Refaey, M. Moawad, and N. Berbish, "Performance enhancement of photovoltaic cells by changing configuration and using PCM (RT35HC) with nanoparticles Al2O3," *Sol Energy,* vol. 177, pp. 665-671, 2019.
[25] P. Manoj Kumar, K. Mylsamy, and P. Saravanakumar, "Experimental investigations on thermal properties of nano-SiO2/paraffin phase change material (PCM) for solar thermal energy storage applications," *Energy Sources, Part A: Recovery, Utilization, and Environmental Effects,* vol. 42, no. 19, pp. 2420-2433, 2020.
[26] S. L. Tariq, H. M. Ali, M. A. Akram, M. M. Janjua, and M. Ahmadlouydarab, "Nanoparticles enhanced phase change materials (NePCMs)-A recent review," *Appl Therm Eng,* vol. 176, p. 115305, 2020.

[27] W. Yu and H. Xie, "A review on nanofluids: preparation, stability mechanisms, and applications," *Journal of nanomaterials,* vol. 2012, no. 1, p. 435873, 2012.
[28] E. Gurgenc, M. Gur, H. Cosanay, T. Gurgenc, and H. F. Oztop, "Effects of position of semi-circular body on melting of a novel B4C/RT44HC PCM nanocomposite in a closed space," *Case Stud Therm Eng,* vol. 65, p. 105628, 2025.
[29] H. Abdelrahman, H. Refaey, M. Wahba, M. Moawad, and N. Berbish, "Comparative study on photovoltaic cells performance using various types of PCMs," *Engineering Research Journal (Shoubra),* vol. 43, no. 1, pp. 31-35, 2020.
[30] H. Refaey, M. Wahba, H. Abdelrahman, M. Moawad, and N. Berbish, "Experimental study on the performance enhancement of the photovoltaic cells by using various nano-enhanced PCMs," *Journal of The Institution of Engineers (India): Series C,* vol. 102, pp. 553-562, 2021.
[31] R. Kothari, S. K. Sahu, and S. I. Kundalwal, "Investigation on thermal characteristics of nano enhanced phase change material based finned and unfinned heat sinks for thermal management system," *Chemical Engineering and Processing-Process Intensification,* vol. 162, p. 108328, 2021.
[32] U. Stritih, "Increasing the efficiency of PV panel with the use of PCM," *Renew Energ,* vol. 97, pp. 671-679, 2016.
[33] F. S. Bayraktar and R. Köse, "Phase change materials: types, properties and applications in buildings," *Kırklareli Üniversitesi Mühendislik ve Fen Bilimleri Dergisi,* vol. 8, no. 1, pp. 190-210, 2022.
[34] F. Bahiraei, A. Fartaj, and G.-A. Nazri, "Experimental and numerical investigation on the performance of carbon-based nanoenhanced phase change materials for thermal management applications," *Energ Convers Manage,* vol. 153, pp. 115-128, 2017.

➢ *ORAL PRESENTATION*

Evaluation Of Doppler Indices In Dogs With Mammary Tumors Treated With Homeopathic Medicine

[1]Enes Çerçi *(ORCID: 0009-0004-0554-2199)*, [2]Gaye Bulut *(ORCID: 0000-0003-4500-1958)*, [3]Deva Başak Boztok Özgermen *(ORCID: 0000-0001-7039-8956)*, [4]Ayşenur Tural Çifçi *(ORCID: 0000-0003-1585-3359)*, [5]Mehmet Tuzcu *(ORCID: 0000-0003-3118-1054)*

[*1,2]Aksaray University, Faculty of Veterinary Medicine, Department of Obstetrics and Gynecology, Aksaray, Türkiye.
[3]Aksaray University, Faculty of Veterinary Medicine, Department of Surgery, Aksaray, Türkiye
[4]Aksaray University, Faculty of Veterinary Medicine, Department of Pathology, Aksaray, Türkiye
[5]Selcuk University, Faculty of Veterinary Medicine, Department of Pathology, Konya, Türkiye

*Corresponding author e-mail: enes.cerci@aksaray.edu.tr

Abstract

The objective of this study was to assess the impact of a homeopathic intervention with Tarantula cubensis (Theranekron®) on preoperative Doppler ultrasonographic parameters in two female canines (K1 and K2) diagnosed with mammary tumors. The experimental group received a subcutaneous injection of Theranekron® once a week for a period of four weeks. During the treatment period, B-mode and Doppler ultrasonographic examinations, along with hematological and biochemical analyses, were performed on a weekly basis. Doppler findings revealed that K2 exhibited more stable and physiologically normal values for parameters such as Pulsatility Index (PI), Resistance Index (RI), and Systolic/Diastolic (S/D) ratio compared to K1. Conversely, heart rate fluctuations were less pronounced in K2. A hematological analysis of K1 revealed elevated and fluctuating levels of white blood cell (WBC), granulocytes (Gran#), and eosinophils (Eos%), which were interpreted as indicators of immune activation or inflammation. Conversely, erythrocyte and platelet parameters in K2 exhibited relative stability. A histopathological examination identified a transmissible venereal tumor (TVT) in K1 and a cystic adenocarcinoma in K2. Thoracic radiographs revealed no evidence of metastasis in either case, although signs of bronchitis were detected. The resorptive, anti-inflammatory, and immunomodulatory properties of Theranekron® may have contributed to regulatory effects on vascular structures and hematologic parameters in the tumor microenvironment. Although limited by sample size, this case study supports the potential use of T. cubensis extract as an adjunct in the management of canine mammary tumors. Further controlled clinical trials are recommended to validate these findings and explore broader applications in veterinary oncology.

Keywords: Canine mammary tumor, Doppler indices, Homeopathy, Tarantula cubensis,

INTRODUCTION

While there are many studies on Doppler sonography measurements for early diagnosis in human medicine, there are insufficient studies on physiological and pathophysiological processes in veterinary medicine, and therefore reference values have not yet been determined. Mammary tumors are the most common type of neoplasm in dogs, with approximately 50% being malignant. Examining their pathogenesis reveals that mammary tumors develop in a hormone-dependent manner. Ovarian steroid hormones are particularly known to play a dominant role, and growth factors also contribute to tumor development. The most common sites of metastases include regional lymph nodes, as well as the lungs, liver, and kidneys (Klopfleisch et al., 2011; Rivera and von Euler, 2011).

Ultrasonography is a critical diagnostic instrument in distinguishing between benign and malignant mammary tumors in canines. Conventional ultrasonography is employed for the evaluation of tumor structure, while Doppler ultrasonography can enhance suspicion of malignancy by examining vascular structures. Specifically, an increase in vascular indices has been observed in malignant tumors (Felicia et al., 2012).

The field of veterinary medicine has witnessed a growing interest in alternative and complementary medicine practices. Among these approaches, homeopathy merits particular attention due to its minimal adverse effect

profile, its naturalness, and its contributions to animal welfare. The fundamental principle of homeopathic treatment is predicated on the notion of "like cures like," which posits the administration of substances that engender effects analogous to those of the disease in question, albeit in exceedingly low doses (Avcıoğlu and Boyacıoğlu, 2024).

Tarantula cubensis (T. cubensis) is a homeopathic preparation derived from the toxins of the Cuban tarantula and commercially known as Theranekron®. The extract has been shown to possess anti-inflammatory, demarcative, resorptive, and regenerative effects (Gültiken et al., 2015; Avcıoğlu & Boyacıoğlu, 2024). These effects enable its use in the treatment of a wide range of clinical conditions, including foot rot, mastitis, abscesses, ulcers, papillomas, retentio secundinarum, and mammary tumors (Raj et al., 2020; Avcıoğlu and Boyacıoğlu, 2024).

The objective of this study was to ascertain the alterations in Doppler indices in canines afflicted with mammary gland neoplasms during the preoperative period subsequent to the administration of T. cubensis extract for homeopathic purposes.

MATERIALS AND METHODS

A case study of two female canines, aged over five years, diagnosed with mammary tumors, was conducted. Both canines were subjected to systematic observation and assessment during the preoperative period.

The experimental dogs were administered Tarantula cubensis extract (Theranekron®, 1:100 / D6, Richter Pharma, Austria) subcutaneously at a dose of 2 milliliters once a week for a total of four weeks. During the treatment period, the animals were evaluated on a weekly basis based on clinical and laboratory parameters.

During the treatment period, B-mode ultrasound and color Doppler sonography examinations were performed on a weekly basis on the mammary gland tumors. In the Doppler evaluations, vascularity in the tumor region was measured, and the Pulsatility Index (PI), Resistance Index (RI), and Systolic/Diastolic ratio (S/D) parameters were recorded.

Blood samples were collected from both animals prior to each application, and hemogram (Mindray 2008Vet) and biochemical (MNChip, Pointcare V3) analyses were performed.

Lateral and ventro-dorsal double-sided thoracic radiographs were obtained to visualize potential preoperative metastases.

Following a four-week treatment period, mastectomy and concurrent ovariohysterectomy were performed on both canines in the fifth week. The induction of anesthesia was facilitated by the administration of gas anesthesia. The anesthesia protocol encompassed the administration of Propofol (1%, 6 mg/kg intravenously) and Sevoflurane (Sevorane liquid, 250 ml; AMS Junior 620 V automatic ventilation device; and Shei brand Sevoflurane vaporizer).

The tissue samples were preserved in 10% formalin for a period of 48 hours. The tissue processing procedure was conducted in accordance with established protocols, employing a Leica TP1020 tissue processing system. This system utilizes a series of graded alcohols, xylene, xylene-paraffin, and paraffin, culminating in paraffin embedding. Tissue sections measuring 4 µm in thickness were obtained from the paraffin blocks and stained with Hematoxylin-Eosin (HxE). Following the staining process, the preparations were examined under an Olympus BX51 light microscope, and photographs were taken using an Olympus DP12 camera (Tokyo, Japan).

RESULTS

Doppler Studies:

A comparative analysis of Doppler ultrasonographic parameters reveals that PI (Pulsatility Index), RI (Resistive Index), and S/D ratio values exhibited greater stability and remained within physiological limits in the K2 group compared to the K1 group.

In the K2 group, PI values were elevated and more balanced (homogeneous), while in the K1 group, they were irregular and low. This finding may suggest a higher degree of vascular elasticity or a lower level of distal resistance in the K2 group.

RI values were found to be more balanced in K2, and the low RI values observed in K1 may be indicative of reduced peripheral vascular resistance or measurement discrepancies. In regard to heart rate (HR), considerable variations were detected in the K1 group (106–120–151–141), whereas the K2 group exhibited more stable values (110–116–123–105). The findings suggest that the K2 group exhibits more stable hemodynamic parameters.

Table 1. Doppler Index Values of K1 and K2 over 4 weeks (I-II-III-IV) (Mindray Z6 Vet).

	PI		RI		S/D		HR(Bpm)*	
	K1	K2	K1	K2	K1	K2	K1	K2
I	0,74	1,38	0,5	0,65	2,01	2,88	106	110
II	1,51	1,08	0,77	0,63	4,43	2,63	120	116
III	0,42	1,14	0,35	0,63	1,54	2,67	151	123
IV	0,48	1,06	0,38	0,57	1,61	2,34	141	105

*Large breed dogs 60-140 Bpm, Adult dogs 70-160 Bpm (Tilley, 1992).

Hematological and Biochemical Analyses:

In the case of K1, hemogram analyses were performed on a weekly basis during the course of homeopathic treatment. The data obtained are presented in Table 2. According to this,

- In the majority of cases, white blood cell (WBC) and granulocyte (Gran#) values exceeded the reference range over the course of the four-week period. This phenomenon is likely attributable to inflammation or an immune response to the treatment regimen. Lymphocyte (Lymph#) and lymphocyte percentage (Lymph%) values demonstrated a substantial increase during the second and third weeks.
- The following erythrocyte parameters were observed: RBC and HCT values were predominantly below the reference lower limit, indicating mild normocytic normochromic anemia.
- A decrease in PLT values was observed in the second and third weeks. This phenomenon may be attributed to inflammation or a consequence of the therapeutic regimen.

In the case of K2, weekly hemogram measurements were evaluated during the homeopathic treatment process (see Table 2). According to this source,

- It has been observed that the WBC level has marginally exceeded the upper reference limit over the course of two weeks. This increase corresponds with the granulocytes (Gran#) maintaining levels above the standard throughout all weeks. The lymphocyte (Lymph#) and monocyte (Mon#) values remained within the normal range. The lymphocyte percentage (Lymph%) decreased below the reference range in week 3, indicating neutrophil dominance and possible reactive neutropenia.
- The following is a list of red blood cell indices: RBC, HGB, and HCT values were generally within normal limits, showing a significant increase in week 4. MCV exhibited a slight increase beyond the established reference range in the fourth week, suggesting a macrocytic trend. The collective evaluation of these values indicates a normochromic and mildly macrocytic profile.
- The following is a list of platelet parameters: PLT values exhibited significant variability but remained within the established reference range. No significant deviation was observed in platelet activation markers such as MPV and PDW. PCT values are indicative of no significant fluctuation in platelet mass.
- Eosinophils are a type of white blood cell that plays a role in the immune system. The Eos% parameter demonstrated a substantial increase (12.2%) in the third week, which may be attributable to an allergic response, parasitic agents, or immune modulation.

The mean, standard deviation (SD), and coefficient of variation (CV%) of the four-week hematological data for K1 and K2 cases were analyzed (see Table 3). The results indicated higher levels and significant fluctuations in parameters related to the immune response in the K1 case.

Table 2. K1 and K2's 4-week (I-II-III-IV) hemogram values (Mindray 2800Vet).

	I.		II		III		IV	
	K1	**K2**	**K1**	**K2**	**K1**	**K2**	**K1**	**K2**
WBC (6,0-17,0 x10⁹/L)	**19,3***	16,6	**18***	**17,4***	**18***	15,5	14,9	**18,6***
Lenf# (0,8-5,1 x10⁹/L)	3	1,8	**5,6***	3,3	**5,6***	1,8	3,7	2,2
Mon# (0,0-1,8 x10⁹/L)	0,7	0,5	1	0,7	1	0,4	0,8	0,6
Gran# (4,0-12,6 x10⁹/L)	**15,6***	**14,3***	11,4	**13,4***	11,4	**13,3***	10,4	**15,8***
Lenf% (12,0-30,0)	15,4	**10,9****	**31,1***	18,8	**31,1***	11,6	24,8	**11,8****
Mon% (2,0-9,0)	3,7	3,1	5,3	4,3	5,3	2,8	5,1	3
Gran% (60,0-83,0)	80,9	**86***	63,6	76,9	63,6	**85,6***	70,1	**85,2***
RBC (5,50-8,50 x10¹²/L)	6,24	5,52	**4,87****	**5,05****	**4,87****	5,94	**5,4****	6,46
HGB (11,0-19,0 g/dL)	14	13,5	11,2	12,2	11,2	14,4	12	15,3
HCT (39,0-56,0%)	42,3	39	**32,8****	**35,6****	**32,8****	42,7	**35,5****	47,8
MCV (62,0-72,0 fL)	67,8	70,8	67,5	70,5	67,5	72	65,9	**74***
MCH (20,0-25,0 pg)	22,4	24,4	22,9	24,1	22,9	24,2	22,2	23,6
MCHC (30,0-38,0 g/dL)	33	34,6	34,1	34,2	34,1	33,7	33,8	32
RDW (11,0-15,5%)	14,4	14,7	14,4	15,5	14,4	15,3	**16,4***	14,2
PLT (117-460 x10⁹/L)	235	279	138	198	138	405	322	286
MPV (7,0-12,9 fL)	9,6	8,5	9,7	8,8	9,7	8,2	9,3	8,7
PDW (-)	16,5	16,6	17,7	17,5	17,7	15,7	16,2	16
PCT% (-)	0,225	0,237	0,133	0,174	0,133	0,332	0,299	0,248
Eos% (-)	1,5	5,9	40	4,4	40	12,2	47,1	8,5

According to reference range * High value ** Low value

In K1, leukocyte (WBC) and granulocyte (Gran#) levels were found to be elevated in comparison to K2, indicating an augmented systemic reaction to a potential inflammatory process or tumor progression. The substantial variation observed in the eosinophil percentage (Eos%: 34.0 ± 21.47; CV%: 63.14) indicates significant eosinophilic activation and immunomodulation in the K1 case. These findings support the effects of homeopathic products (particularly Tarantula cubensis) on immunological responses.

The lymphocyte count (Lymph#) and percentage (Lymph%) exhibited greater variability in the K1 group (Lymph#: 5.15 ± 2.37; CV%: 46.02), indicative of the high variability of the lymphoproliferative response. The monocyte parameters exhibited stability within both groups, with comparable coefficient of variation (CV) values. However, average levels were observed to be elevated in K1.

A subsequent examination of red blood cell parameters reveals that the erythrocyte indices, including RBC, HGB, and HCT, exhibit elevated mean values and diminished variability in the K2 case. This finding suggests that the K2 case exhibits enhanced hematopoietic stability. Furthermore, the MCV (71.82 ± 1.59 fL) and MCH (24.08 ± 0.34 pg) values were elevated in K2 compared to K1, suggesting a mild macrocytic tendency and more stable erythrocyte morphology.

Furthermore, platelet parameters (PLT, MPV, and PDW) exhibited elevated mean values and diminished coefficient of variation in case K2. The substantial variation in PLT values (K1: 204.75 ± 88.84; K2: 292.0 ± 85.26) and the heterogeneity in PCT (K1 CV%: 41.42; K2 CV%: 26.21) suggest anomalous platelet responses in the K1 case.

In conclusion, the high variability and out-of-reference values observed in hematological parameters in case K1 indicate more pronounced systemic stress, inflammation, and immune response. Conversely, the more stable course in case K2 may indicate a more controlled physiological response to homeopathic treatment. When evaluated in conjunction with Doppler data, these findings underscore the diagnostic and prognostic value of hematological analyses in objectively monitoring systemic responses to treatment.

Table 3. Comparative evaluation of hematological parameters of K1 and K2 cases over 4 Weeks.

Parameters	K1 M	K1 SD (±)	K1 CV (%)	K2 M	K2 SD (±)	K2 CV (%)
WBC	18.88	3.48	18.44	17.02	1.31	7.68
Lenf#	5.15	2.37	46.02	2.28	0.71	31.16
Mon#	0.92	0.22	23.97	0.55	0.13	23.47
Gran#	12.8	2.35	18.36	14.2	1.16	8.15
Lenf%	26.75	8.79	32.85	13.28	3.7	27.9
Mon%	4.8	0.8	16.6	3.3	0.68	20.55
Gran%	68.45	9.48	13.85	83.42	4.36	5.23
RBC	5.49	0.6	10.88	5.74	0.6	10.46
HGB	12.3	1.25	10.18	13.85	1.32	9.55
HCT	36.93	4.09	11.07	41.28	5.23	12.67
MCV	67.35	0.96	1.43	71.82	1.59	2.21
MCH	22.38	0.39	1.73	24.08	0.34	1.41
MCHC	33.3	0.76	2.28	33.62	1.14	3.4
RDW	14.9	1.15	7.73	14.92	0.59	3.96
PLT	204.75	88.84	43.4	292.0	85.26	29.2
MPV	9.6	0.22	2.31	8.55	0.26	3.09
PDW	16.93	0.65	3.85	16.45	0.79	4.83
PCT	0.2	0.08	41.42	0.25	0.06	26.21
Eos%	34.0	21.47	63.14	7.75	3.42	44.08

Due to elevated hematological parameters, both dogs were administered a broad-spectrum antibiotic (Synulox®, Zoetis) at a dose of 8.75 mg/kg/day subcutaneously for three days.

In K1, greater variability in biochemical parameters (see Table 4) was observed, particularly fluctuations in hyperglobulinemia, hyperkalemia, ALP, and TBA levels. This finding suggests the presence of a more active systemic response to the tumor or a more pronounced stress-related clinical picture. The hypoglycemia

observed in glucose levels in K2 is notable and may correlate with clinical findings such as tumor-related metabolic load or anorexia.

Table 4. Biochemical analysis results of K1 and K2 cases at 4 weeks (I-II-III-IV) (MNChip, Pointcare V3).

	I		**II**		**III**		**IV**	
	K1	**K2**	**K1**	**K2**	**K1**	**K2**	**K1**	**K2**
TP (5,2-8,2 g/dL)	6,6	6,5	6,4	6,6	6,4	6,7	7,4	6,6
ALB (2,2-4,4 g/dL)	2,5	2,9	2,4	2,8	2,3	3	2,6	3,1
GLO (2,3-5,2 g/dL)	4,1	3,6	4	3,8	4,1	3,7	4,8	3,5
A/G	0,6	0,8	0,6	0,7	0,6	0,8	0,5	0,9
TBIL (0,1-0,9 mg/dL)	0,16	0,2	0,16	0,19	0,19	0,23	0,16	0,25
ALT (10-140 U/L)	17	21	20	18	13	23	16	22
ALP (20-150 U/L)	34	31	24	24	58	29	36	28
AMY (400-3500 U/L)	2089	2545	2551	1890	1820	2206	2949	1858
CHOL (110-320 mg/dL)	249	226	156	243	230	266	213	233
GLU (70-143 mg/dL)	71	**56****	101	92	122	82	93	**62****
CRE (0,3-0,7 mg/dL)	0,3	0,53	0,43	0,32	0,38	0,34	0,37	0,35
BUN (0,7-32 mg/dL)	12,3	13,8	14,5	17,8	14	15,3	10,4	8,15
BUN/CRE	41	26	34	56	37	45	28	23
Ca (7,9-11,8 mg/dL)	9,5	9,7	9,5	8,9	8,8	9,4	9,5	10
P (2,5-6,8 mg/dL)	3,13	3,07	3,08	4,05	3,68	4,49	4,64	3,75
K+ (3,7-5,8 mmol/L)	5,17	5,31	5,1	5,68	5,78	**5,97***	**5,95***	5,6
Na (138-160 mmol/L)	159	158	154	158	152	157	155	153
Na/K	31	30	30	26	26	26	26	27
TBA (0-20 µmol/L)	3,62	1,5	2,64	1,52	4,16	1,34	1,72	2,64

According to reference range * High value ** Low value

Radiographic Evaluation:
A chest X-ray was performed to evaluate the presence of potential pulmonary metastases. No metastatic lesions were identified in either canine subject; however, a diagnosis of bronchitis was made.

Surgical Intervention and Histopathological Evaluation:

In both cases, due to the localization of the tumor in the fifth mammary chain, local mastectomy and simultaneous ovariohysterectomy were performed. The masses that were removed during the operation were then subjected to histopathological evaluation.

Macroscopically, in Case K1, masses measuring 5x3x3 cm and 4x3x3 cm were observed, containing necrotic areas, while in Case K2, mammary tissue measuring 6x8x4 cm was noted, containing cystic areas (see Table 5 for details). Microscopic evaluation (Tables 6-7) yielded the following results:

- In the initial phase (K1), cells in the mammary tissue form cords. Furthermore, the cells exhibit an oval shape and are characterized by their substantial size, as well as by the presence of hyperchromatic nuclei and distinct nucleoli. A significant number of atypical cells displaying characteristics such as anisocytosis, anisonucleosis, and pleomorphism have been identified. Additionally, the presence of foam cells (TVT) was identified in the Giemsa stain of the mass.
- In the K2 case, numerous cystic areas were observed due to the formation of multiple cystic structures by the tumor cells. The glandular tissue cells exhibited atypical characteristics, including anisocytosis, anisokaryosis, and pleomorphism. Furthermore, a protein-rich, homogeneous pink-colored fluid was observed in the glandular tissue.

The diagnosis of transmissible venereal tumor (TVT) was rendered in case K1, while cystic adenocarcinoma was diagnosed in case K2.

Table 5. Macroscopic Appearance of Tumor Masses. A. Masses measuring 5x3x3 cm and 4x3x3 cm (K1), B. Masses measuring 6x8x4 cm (K2).

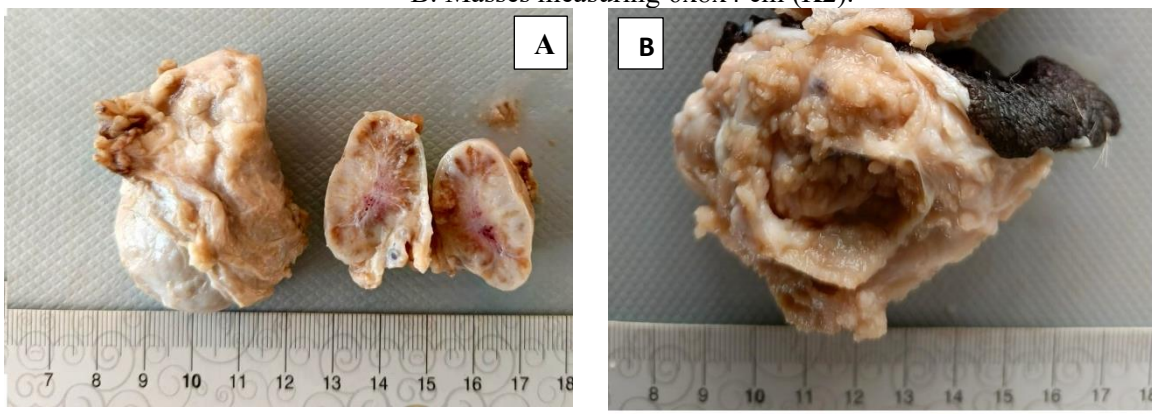

Table 6. Histopathological findings of K1. A: General appearance of the tumor mass, HE, x20. B: Cord-like appearance of cells, oval-shaped and large, with hyperchromatic nuclei and prominent nucleoli, showing anisocytosis, anisonucleosis, and pleomorphism in numerous atypical cells, HE, x40.

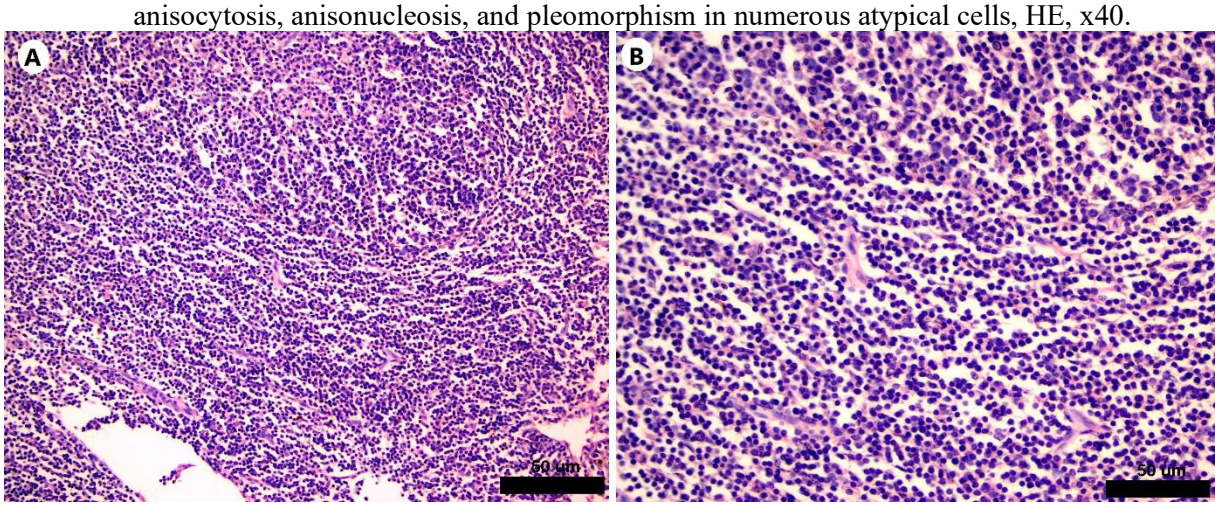

Table 7. Histopathological findings of K2 case. Cystic structures (black arrow), protein-rich fluid (red arrow tip), HE, x40.

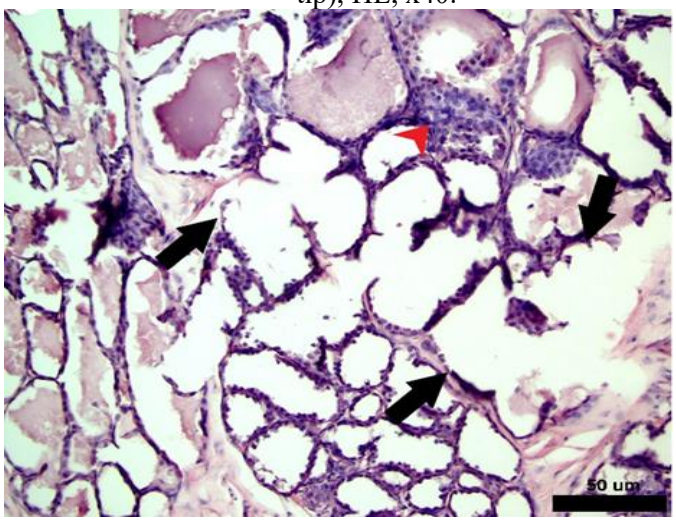

DISCUSSION

The present study draws parallels between the K2 and K1 groups based on Doppler ultrasonographic parameters, revealing that the K2 group exhibited more stable hemodynamic values within physiological limits compared to the K1 group. Specifically, the uniformity of values observed in the K2 group for parameters such as PI and RI, which are indicative of vascular elasticity and peripheral resistance, indicates a heightened degree of harmonious functioning within the vascular system. As indicated in the extant literature, a decrease in vascular compliance and distal vascular resistance is reflected in lower PI and RI values. These parameters have been identified as significant indicators of tumor vascularization or inflammatory processes (Gültiken and Vural, 2007; Feliciano et al., 2012).

A sudden increase in the S/D ratio, particularly in the K1 group as observed in the second measurement, may suggest transient hemodynamic stress or increased local vascular resistance around the tumor. The K2 group, which exhibited more controlled heart rate, demonstrated enhanced autonomic stability. These parameters play an instrumental role in the evaluation of the physiological response to interventions aimed at bioregulation, such as homeopathic treatment. Doppler ultrasound has been shown to play an important role in distinguishing benign from malignant mammary tumors, particularly with significant increases in resistivity and pulsatility indices in malignant lesions (Feliciano et al., 2012). In a seminal study, Mülazımoğlu et al. (2019) unveiled substantial disparities in gray scale and homogeneity values of malignant tumors through the application of B-mode echotexture analysis. These techniques have the potential to inform preoperative decisions.

In the veterinary oncology literature, it has been reported that the immune response in canines with mammary tumors leads to various changes in the hematological profile. Feliciano et al. (2012) observed that leukocyte formulation, when employed in conjunction with Doppler sonography, may facilitate the distinction between benign and malignant neoplasms. A similar study (Mülazımoğlu et al., 2019) demonstrated the diagnostic value of combining hematological findings with Doppler imaging in the diagnosis of canine mammary tumors. The effects of homeopathic products such as Theranekron on the immune response have previously been associated with eosinophilia and neutrophilia in various studies (Bellavite et al., 2006; Avcıoğlu and Boyancıoğlu, 2024). The present study lends support to the hypothesis that increased eosinophils and granulocyte dominance may be associated with homeopathic treatment or tumor progression.

Corum et al. (2016) reported that in a study conducted on sheep, T. cubensis extract did not cause statistically significant changes in cytokines such as IL-6, TNF-α, IL-10, and acute phase proteins such as haptoglobin and serum amyloid A. However, the extract did cause fluctuations in these parameters. This observation indicates that the observed hematological fluctuations in the K1 case may not be directly associated with cytokine activity. Rather, these fluctuations may be attributable to tissue-level inflammation and tumor-associated immune modulation. However, Avcıoğlu and Boyancıoğlu (2024) emphasize the four main mechanisms of action of T. cubensis (demarcation, regeneration, resorption, anti-inflammatory) and mention its effects of suppressing local inflammation and enhancing absorption even with a single dose. These effects may offer a

particularly compelling explanation for changes in secondary hematological parameters associated with edema and cell damage in cases of mammary tumors.

Adenocarcinomas manifest most frequently in the mammary tissue of felines, canines, and equines; however, these neoplasms have the potential to develop in all glandular tissues (Erer and Kıran, 2009a). Despite the fact that the location of the mass in this particular presentation is not a commonly observed site, it is consistent with the extant literature on the subject. Adenocarcinomas are classified based on the appearance of the glandular tissue formed by the cells from which they originate. These classifications include the following types: papillary, cystic, papillary-cystic, follicular, tubular, and trabecular (Erer and Kıran, 2009a). In this particular instance, the cystic appearance of the cells from which the tumor originated serves to confirm the diagnosis of cystic adenocarcinoma. Adenocarcinomas are typically distinguished by the presence of glandular structures that secrete various secretory products (Meuten, 2020a). The presence of a homogeneous pink-colored protein-rich fluid in the aforementioned case suggests the presence of secretory products and supports the diagnosis.

Transmissible venereal tumor (TVT) is more common in older sexually active dogs, especially females. Tumours are often found in the vulva and vagina of females and in the penis and prepuce of males, though cutaneous cases have been reported (Erer and Kıran, 2009b). These locations support transmission via contact. According Erer and Kıran (2009b), TVTs macroscopically appear as cauliflower like friable and multilobulated or nodular mass. The present case is characterized by the absence of a cauliflower-like structure and lesser friability. At the cellular level, TVT cells have been seen microscopically to form cords, layers or masses, and they have a round to polyhedral shape, hyperchromatic nuclei with distinct nucleoli (Erer and Kıran, 2009b; Meuten, 2020b). In the current case, the oval-shaped cells seen in cords were in accordance with literature. Foam cells seen in Giemsa stain further confirmed the diagnosis.

Gültiken and Vural (2007) reported that the application of Theranekron in the pre- and postoperative periods resulted in regression in benign tumors and a sclerotic effect in malignant tumors. Moreover, it has been documented that postoperative applications have been shown to reduce the incidence of recurrence. Kıvrak and Aydın (2017) have stated that surgery is the primary treatment method; however, factors such as the histological type, size, and lymph node involvement of the tumor are decisive for prognosis. Despite the limited efficacy of adjuvant treatment options, there is a need for individualized treatment protocols.

The findings indicate that the treatment approach employed in the K2 group may yield more favorable outcomes in terms of systemic circulation. However, due to the limited sample size, further research is necessary to extrapolate the findings to a broader population.

CONCLUSION

Conventional ultrasonography and Doppler techniques play an important role in the diagnosis and treatment of mammary tumors in dogs. The utilization of alternative agents, such as Theranekron, has been demonstrated to contribute to a reduction in recurrence rates by facilitating surgical procedures. Furthermore, effective regulation of physiological processes, such as pseudopregnancy, is imperative for the management of proliferative processes in mammary tissue. In view of these findings, the necessity of a multidisciplinary approach is becoming increasingly evident, and the development of individualized treatment strategies is recommended.

In the field of veterinary medicine, homeopathic preparations, particularly Tarantula cubensis extract, have emerged as a valuable alternative, especially in cases where the use of antibiotics should be limited. However, the veterinarian's expertise in pharmacology and the capacity to evaluate individual patients are paramount for the successful implementation of such treatments. Moreover, the necessity for extensive, meticulously controlled clinical studies is paramount.

REFERENCES

Bellavite, P., Conforti, A., Pontarollo, F., Ortolani, R. (2006). Immunology and Homeopathy. 2. Cells of the Immune System and Inflammation. Evid Based Complement Alternat Med. 5;3(1):13–24. doi: 10.1093/ecam/nek018 .

Corum, O., Er, A., Dik, B. (2016). Investigation of the effect of *Tarantula Cubensis* Extract on acute phase response. Acta Scientiae Veterinariae, 44: 1414.

Erer H, Kıran M. 2009a. "Epitelyal Tümörler". Alınmıştır: Veteriner Onkoloji, Editör(ler): Prof. Dr. Hüdaverdi Erer, Prof. Dr. Metin Münir Kıran, Selçuk Üniversitesi Basımevi, Konya. Sayfa: 80-81.

Erer H, Kıran M. 2009b. "Diğer Tümörler ve Neoplastik Hastalıklar. Veteriner Onkoloji, Editör(ler) : Prof.Dr. Hüdaverdi Erer, Prof. Dr. Metin Münir Kıran, Konya, Selçuk Üniversitesi Basımevi, p: 155-157.

Feliciano, M.A.R., Vicente, W.R.R., Silva, M.A.M. (2012). Conventional and Doppler ultrasound for the differentiation of benign and malignant canine mammary tumours. JSAP, 53(6), 332-337. https://doi.org/10.1111/j.1748-5827.2012.01227.x

Gültiken, N., Güvenç, T., Kaya, D., Ağaoglu, A. R., Ay, S. S., Küçükaslan, İ., Emre, B., Fındık, M., Schäfer-Somi, S., Aslan, S. (2015). Tarantula cubensis extract alters the degree of apoptosis and mitosis in canine mammary adenocarcinomas. *Journal of Veterinary Science*, 16(2), 213–219. https://doi.org/10.4142/jvs.2015.16.2.213

Gültiken, N., Vural, M.R. (2007). The effect of Tarantula cubensis extract applied in pre and postoperative period of canine mammary tumours. *JIVS,* 2, 40–44. https://dergipark.org.tr/en/pub/http-www-jivs-net/issue/27197/286116

Kıvrak, M.B., Aydın, I. (2017). Treatment and prognosis of mammary tumors in bitches. *Inter J Vet Sci, 6(4): 178-186.*

Klopfleisch R, von Euler H, Sarli G, Pinho SS, Gärtner F, Gruber AD. (2011). Molecular carcinogenesis of canine mammary tumors: news from an old disease. *Vet Pathol*. 48(1):98-116. https://doi.org/10.1177/0300985810390826

Meuten DJ. 2020a. "Epithelial tumors". In: Tumors in domestic animals, Editor Donald J. Meuten. Fifth Edition. John Wiley & Sons, p: 470-472

Meuten DJ. 2020b. "Tumors of the Genital Systems". In: Tumors in domestic animals, Editor Donald J. Meuten. Fifth Edition. John Wiley & Sons, p: 718-721.

Mülazımoğlu, S.B., Beceriklisoy B.H., Schafer-Somi S., Kaya M., Bumin A., Özenç E., Gültekin, N., Kanca, H., Günen, M.Z., Kutsal, O., Emre, B., Evangelos, K., Aslan S. (2019). B-mode Echotexture Analysis and Color Doppler Sonography in Canine Mammary Tumors. *Akdeniz Üniversitesi Yayınları*. Erişim: https://avesis.akdeniz.edu.tr/yayin/af0c2668-b849-4010-8059-b177d456df6d/

Raj, P.A.A., Pavulraj, S., Kumar, M.A., Sangeetha, S., Shanmugapriya, R., Sabithabanu, S. (2020). Therapeutic evaluation of homeopathic treatment for canine oral papillomatosis. *Veterinary World*, 13(1), 206–213. https://doi.org/10.14202/vetworld.2020.206-213

Rivera P, von Euler H. (2011). Molecular biological aspects on canine and human mammary tumors. *Vet Pathol*. 48(1):132-146. https://doi.org/10.1177/0300985810387939

Tilley, L.P. (1992). Essentials of canine and feline electrocardiography: interpretation and treatment. 3rd. Ed. Lippincott Williams & Wilkins.

➢ *ORAL PRESENTATION*

Hareketli Hedefleri İzlemek İçin Yer Tabanlı Platformda Kullanılan İzleme Algoritmalarının Karşılaştırmalı Analizi

Kübra PAPÜR[1] (*ORCID: https://orcid.org/0009-0008-6522-9028*), Nebi GÜL[2] (*ORCID: https://orcid.org/0000-0002-0892-5935*), Ömer Faruk ELALDI[3] *(https://orcid.org/0000-0003-0592-6868),* Murat ÜÇÜNCÜ[4*] (*https://orcid.org/0000-0002-2113-1398)*

[1,2,3]Başkent Üniversitesi, Mühendislik Fakültesi, Elektrik-Elektronik Mühendisliği, Ankara, Türkiye,
[4*]Başkent Üniversitesi, Mühendislik Fakültesi, Elektrik-Elektronik Mühendisliği, Ankara, Türkiye,

* Sorumlu yazar e-posta: mucuncu@baskent.edu.tr

Özet

Bu çalışmanın amacı, Tek ve Çoklu Hedef İzleme (MTT) algoritmalarında, özellikle İşlem Gürültüsü (PN) açısından farklı Kalman Filtresi (KF) algoritmalarını karşılaştırmak ve kabul edilebilir bir hata düzeyinde çıktılara göre en iyi KF tipini belirlemek için gerekli kodları yazmak ve sonuçları analiz etmektir. Analizde, Doğrusal Sabit Hız (CV), Doğrusal Olmayan Sabit Hız (NCV) ve Sabit İvmelenme (CA) modelleri olmak üzere üç farklı model kullanılmıştır. Tek hedef izlemede, Standart Kalman Filtresi (SKF), Genişletilmiş Kalman Filtresi (EKF), Kokusuz Kalman Filtresi (UKF) ve Etkileşimli Çoklu Model (IMM) kullanılmıştır. SKF'nin izleme performansı hem CV hem de CA modelleri için incelenmiştir. EKF ve UKF izleme performansının karşılaştırılması için, CV ve CA hedef hareket modellerinde işlem gürültüsü hariç tüm parametreler sabit tutulmuştur. IMM'nin izleme performansı, filtre geçiş olasılığı katsayısı değiştirilerek analiz edilmiştir. MTT için, en yakın komşu (NN) ve Birleşik Olasılıksal Veri İlişkilendirmesinin (JPDA) izleme performansını karşılaştırmak üzere işlem gürültüsünün standart sapması değiştirilmiştir. Dinamik filtreler ve hedefler kendi yazdığımız orijinal/özgün kod uygulanmış ve MATLAB R2022B'ye eklenmiştir. UKF'nin hem CV hem de CA hedef hareketindeki belirsizlik için daha kararlı tahminler sağladığı ifade edilebilir. Karmaşıklığın olmadığı ortamlarda, JPDA'nın, NN'ye kıyasla daha kararlı sonuçlar ürettiği de gözlenmiştir.

Anahtar Kelimeler: Genişletilmiş Kalman Filtresi (EKF), Kokusuz Kalman Filtresi (UKF), Çoklu Hedef Takibi (MTT), Etkileşimli Çoklu Model (IMM), İşlem Gürültüsü.

A Comparative Analysis Of Tracking Algorithms Used On The Ground-Based Platform To Monitor Moving Targets

Abstract

The objective of this study is to develop the necessary codes and analyse the results to compare different Kalman Filter (KF) algorithms in single and Multiple Target Tracking (MTT) algorithms, especially with respect to Process Noise (PN), and to determine which is the best type of KF at an acceptable error level by the outputs. In the analysis, three different models are utilized: linear constant velocity (CV), non-linear constant velocity (NCV) and constant acceleration (CA) models. In single target tracking, Standard Kalman Filter (SKF), Extended Kalman Filter (EKF), Unscented Kalman Filter (UKF) and Interactive Multiple Model (IMM) are used. The tracking performance of SKF is examined for both CV and CA models. For the comparison of EKF and UKF tracking performance, all parameters except the process noise in the CV and CA target motion models are kept constant. The tracking performance of IMM is analysed by changing filter transition probability coefficient. For MTT, the standard deviation of process noise is modified to compare the tracking performance of the nearest neighbour (NN) and joint probabilistic data association (JPDA). The dynamic filters and targets are implemented by our own code and inserted into MATLAB R2022B. We can confidently state that UKF provides more stable estimates for the uncertainty in both CV and CA target motion. In clutter-free environments, JPDA produces more stable results compared to NN.

Keywords: Extended Kalman Filter, Unscented Kalman Filter, Multiple Target Tracking, Interactive Multiple Model, Process Noise.

GİRİŞ

Tekli ve Çoklu Hedef Hareket Takibi modellerindeki belirsizlikler ve gürültü ortamında hedefi doğru bir şekilde tahmin etme sürecindeki zorluklar, "hedef kestirim problemi" olarak tanımlanmaktadır. Standart Kalman Filtre kullanılan gerçek hedef analizlerinde elde edilen sonuçlar tatmin edici doğruluk seviyesinde bulunamadığından; bir çok yeni teknik ve algoritmalar geliştirilmektedir.

P. S. Madhukar ve L. B. Prasad [1] tarafından 2020 yılında yapılan çalışmada doğrusal olmayan sistemler için EKF ve UKF kestirim sonuçları karşılaştırılmıştır Bu çalışmada, doğrusal olmayan sistemler için UKF performansının daha tercih edilebilir olduğu belirtilmektedir.

J. Hartikainen, A. Solin ve S. Särkkä [2] tarafından yapılan bir diğer çalışmada EKF ve UKF için doğrusal ve doğrusal olmayan sistemler analiz edilmiştir. UKF gerçeğe yakın bir performans ortaya koymuştur.

B. Erol ve arkadaşları [3] tarafından yapılan çalışmada; doğrusal olmayan bir dinamiğe sahip sualtı aracının EKF ve UKF kestirim sonuçları karşılaştırılmıştır

Bu çalışmanın amacı; tekli ve çoklu hedef takibinde, Kalman Filtresi çeşitlerinin takip performansları üzerinde süreç gürültüsünün etkisini özgün olarak geliştirilen model ve Matlab kodu ile mukayeseli olarak analiz etmektir. Süreç gürültüsü, belirsizlikleri temsil etmektedir. Bu kapsamda, süreç gürültü standart sapması değiştirilerek filtre tepkilerinin karşılaştırılmalı olarak analizi gerçekleştirilmiştir. Ortamda tek hedef olması durumu için SKF, EKF, UKF ve IMM filtre kullanılmıştır.

Ortamda birden fazla hedef olması durumunda ise SKF ve EKF, sonuçların iyileştirilmesi açısından; çoklu hedef izleme algoritmaları (NN+JPDA) ile regüle edilerek kullanılmıştır. Kullanılan çoklu hedef izleme algoritmaları; en yakın komşuluk yöntemi (NN : Nearest Neighborhood) ve ortak olasılıklı veri ilişkilendirme (JPDA : Joint Probability Data Association) yöntemleridir. NN, sırasıyla SKF (sabit hızlı iki hedef için) ve EKF (sabit ivmeli iki hedef için) ile gözlemlerin hedeflerden geldiği kabul edilmiş ve ayrı ayrı çalışılmıştır.

Sabit hızlı ve birbirine paralel doğrultuda hareket eden iki hedefin en yakın komşu (NN) algoritması kullanılan SKF ile takibi yapılarak hedef kestirim performans analizi yapılmıştır. Manevralı ve birbirine yakın hareket gerçekleştiren iki hedefin eş zamanlı takip analizi için Genişletilmiş Kalman Filtresi, en yakın komşuluk algoritmasıyla birlikte MATLAB ortamında çalışılmıştır. Buna paralel olarak süreç gürültüsü standart sapması değiştirilerek hedef takip performansına yönelik analiz yapılmıştır. NN ve JPDA algoritmalarının analiz sonuçlarını eşit şartlar altında karşılaştırmak için filtrelerde aynı hedefler kullanılmıştır. Süreç gürültü katsayıları her iki algoritmada kullanılan hedefler için aynı oranda arttırılarak çoklu hedef izlemede kullanılan söz konusu iki algoritmanın karşılaştırması yapılmıştır.

Hedef Ölçüm Modelleri (Target measurement models)

Bu çalışmada hedef takip filtrelerinin ve çoklu hedef izleme algoritmalarının hareket senaryolarındaki tepkilerini gözlemlemek için üç farklı hareket modeli kullanılmıştır. Bu hareket modelleri; sabit hızla doğrusal hareket senaryosu, sabit hızla ve sabit bir baş açısıyla gerçeklenen hareket modeli ile sabit ivme ve yatay düşey eksende belli bir baş açısıyla gerçeklenen manevralı hareket senaryolarıdır. Takip eden alt maddelerde bu senaryolar ile ilgili dinamikler özetlenmektedir.

Sabit Hızlı Hedef Hareket Modelleri (Constant Velocity Target Movement Model)

Bu çalışma kapsamında kullanılan ve Hedef#1 olarak isimlendirilen sabit hızlı cismin dinamik ayrık durum uzayındaki sistem modeli denklem (1) ile verilmektedir.

$$x_k = A\, x_{k|k-1} + q_k \qquad (1)$$

Burada; x_k , durum vektörü; A geçiş matrisi ve q_k ise gürültüdür [14]. Konum ve hız parametreleri denklem (2) ile ifade edilmiştir.

$$\begin{vmatrix} x_k \\ V_{Xk} \\ y_k \\ V_{Yk} \end{vmatrix} = A * \begin{vmatrix} x_{k-1} \\ V_{Xk-1} \\ y_{k-1} \\ V_{Yk-1} \end{vmatrix} \qquad (2)$$

Bu çalışma kapsamında Hedef#1 için kullanılan Gürültü Vektörü matrisi (Γ), q_x (yatay eksen için) ve q_y (düşey eksen için) Gauss dağılımına sahip rassal süreçlerdir. Burada ; q_x~N $(0, \sigma_x^2)$ ve q_y~N $(0, \sigma_y^2)$ olarak tanımlandığında sistem dinamiği denklem (3) ile ifade edilebilir.

$$\begin{bmatrix} Xk \\ V_{Xk} \\ y_k \\ V_{yk} \end{bmatrix} = \mathrm{A} * \begin{bmatrix} Xk-1 \\ V_{Xk-1} \\ y_k - 1 \\ V_{yk-1} \end{bmatrix} + \quad \Gamma\mathrm{qxy} \rightarrow \mathrm{qxy} = \begin{bmatrix} q_x \\ q_y \end{bmatrix} \rightarrow \begin{bmatrix} \frac{\Gamma 2}{2} & \Gamma \\ \Gamma & 0 \\ 0 & \frac{\Gamma 2}{2} \\ 0 & \Gamma \end{bmatrix} \qquad (3)$$

Doğrusal Olmayan Sabit Hızlı Hareket Modelleri (Constant Velocity Target Movement Model)

X eksenindeki konumu P_x, Y eksenindeki konumu P_y, gerçek kuzeyle yapılan açı ψ^0 ve ortalama hız V ile ifade edildiğinde denklem (4) ile tanımlanmaktadır [8]. Bu hedef senaryosu için hız ve baş açısı değişimi olmayacağı varsayımıyla açısal hız değişimini ifade eden $\dot{\psi}$ ve ivmeyi ifade eden i değerleri sıfır olarak seçilmiştir [8].

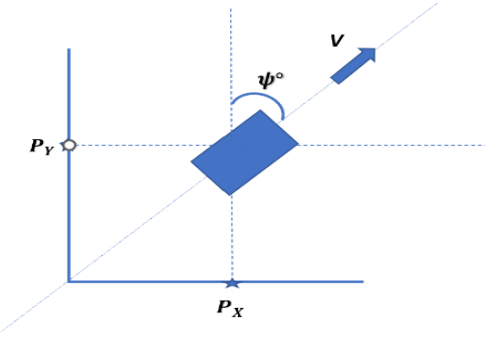

$$\begin{bmatrix} P_x \\ P_y \\ \psi \\ v_k \end{bmatrix} = \begin{bmatrix} P_x \\ P_y \\ \psi \\ v_{k-1} \end{bmatrix} + \Delta t \begin{bmatrix} v_{k-1}\cos(\psi_{k-1}) \\ v_{k-1}\sin(\psi_{k-1}) \\ \psi \\ i \end{bmatrix} \qquad (4)$$

Şekil 1 İki Boyutlu Doğrusal Olmayan Sabit Hızlı Hareket Modeli [8]

Bu kapsamda Hedef#2 için kullanılan Gürültü Vektörü matrisi denklem (5) ile verilmiştir. Hız ve baş açısının sabit kalacağı varsayılarak denklem (5) ile ifade edilen matrisin 3. ve 4. Satırlarına eklenen gürültü değerleri sıfır olarak alınmıştır.

$$\begin{vmatrix} T^2/_2 & 0 \\ 0 & T^2/_2 \\ 0 & 0 \\ 0 & 0 \end{vmatrix} \qquad (5)$$

$$\begin{vmatrix} 1 & 0 & -\Delta\mathrm{t\,V}\,sin(\theta) & \Delta\mathrm{t}\,cos(\theta) \\ 0 & 1 & \Delta\mathrm{t}\,Vcos(\theta) & \Delta\mathrm{t}\sin(\theta) \\ 0 & 0 & 1 & 0 \\ 0 & 0 & 0 & 1 \end{vmatrix} \qquad (6)$$

Hedef#2 olarak isimlendirilen durum vektörünün geçiş matrisi eşitlik (6) ve gürültü matrisi eşitlik (7) ile gösterilmiştir.

Sabit İvmeli Hareket Modeli (Constant Acceleration Target Motion Model)

Denklem (7)'de yer alan t zamanı, V başlangıç hızını, x_b başlangıç konumunu, a sabit ivmeyi, x(t) zamana bağlı konum değiştirmeyi ifade etmektedir [8].

$$x(t) = xb + Vt + \frac{1}{2}at^2 \qquad (7)$$

Bu çalışmada kullanılan üçüncü hedef hareket modelidir. Şekil 1 hedef modelinin aynısı geçerlidir, tek fark sabit ivme ile hız değişimine sahip olmasıdır. Sabit ivmeli hareket modelinin (Hedef#3) durum geçiş matrisi eşitlik (8) ve gürültü matrisi eşitlik (9) ile gösterilmiştir. Ölçüm vektörü eşitlik 10 ile ifade edilmiştir.

$$\begin{vmatrix} 1 & 0 & -\Delta t\, V\, sin(\theta) & 0.5\,\Delta t^2\, cos(\theta) \\ 0 & 1 & \Delta t\, V cos(\theta) & 0.5\Delta t \sin(\theta) \\ 0 & 0 & 0 & 1 \\ 0 & 0 & 1 & \Delta t \end{vmatrix} \quad (8) \qquad \begin{vmatrix} T^2/_2 & 0 \\ 0 & T^2/_2 \\ 0 & 0 \\ 0 & 0 \end{vmatrix} \quad (9)$$

$$z_d^i = \left[r^i\ \theta^i\right]' \quad (10)$$

Ölçüm modeli (Jakobien) eşitlik 11 ile ifade edilmiştir. Denklem (11)'de yer alan r_k ve θ_k beyaz Gauss dağılımına sahip ve sıfır ortalamalı ölçüm gürültü kovaryans matrisi elemanlarıdır. Varyansları sırasıyla σ_r^2 ve σ_θ^2 olarak ifade edilir. Burada ölçüm gürültüleri arasında korelasyon olmadığı kabul edilmiştir. Hareketli cismin yatay eksendeki son konumu L_x, düşey eksendeki son konumu L_y, yatay eksendeki ilk konumu p_{xk}, düşey eksendeki son konumu p_{yk} olarak ifade edilmiştir. İnovasyon kovaryansını hesaplamak için Jacobian matrisini hesaplamak gerekir. Ölçüm Jakobien matrisi eşitlik (12) ve (13) ile ifade edilmiştir

$$\begin{bmatrix} r_k \\ \theta_k \end{bmatrix} = \begin{bmatrix} \sqrt{(L_x - p_{xk})^2 + \left(L_y - p_{yk}\right)^2} \\ \tan^{-1}\left(L_y - p_{yk}\right)/(L_x - p_{xk}) \end{bmatrix} \quad (11)$$

$$\nabla \mathrm{hx} = \frac{\partial \mathrm{h}}{\partial \mathrm{x}}\Big|_{\mathrm{x}=\hat{\mathrm{x}}_{\mathrm{k|k-1}}} = \begin{bmatrix} (L_x - p_{xk})/d & \left(L_y - p_{yk}\right)/d & 0 & 0 \\ -\left(L_y - p_{yk}\right)/d^2 & (L_x - p_{xk})/d^2 & -1 & 0 \end{bmatrix} \quad (12)$$

$$d = \sqrt{(L_x - p_{xk})^2 + \left(L_y - p_{yk}\right)^2} \quad (13)$$

.

Standart Kalman Filtre (SKF) Algoritması
Kalman filtresi, tahmin edilen hata kovaryansını en aza indirmesi açısından optimal bir filtredir [4].

Genişletilmiş Kalman Filtresi (EKF)
EKF'nin pratikte bilinen iki dezavantajı vardır: Birincisi doğrusallaştırma sırasında kararsız filtrelerin ortaya çıkabilmesidir, bir diğeri ise Jacobian matrislerin uygulanması gerçek senaryo için zordur [7].

Kokusuz Kalman Filtresi (UKF)
UKF, [10], [6] bir sonraki durumu tahmin etmek için bir dizi noktayı (Sigma Noktaları) kullanır. Sigma noktaları, rassal x değişkeninin istatistiksel özelliklerinden ortalama ve kovaryans değerlerini yakalayacak şekilde seçilir [9]. Eşitlik 14'de yer alan "β", Gauss dağılımına sahip rassal bir x dağılımını kontrol etmek için kullanılır, literatürde genellikle 2 olarak kabul edildiği gözlenmiştir.

Etkileşimli Çoklu Model Filtre (Interactive Multiple Model Filter: IMM) Etkileşimli Çoklu Model Filtre birden fazla Kalman filtresinden oluşan bütünleşik bir algoritma olarak tanımlanabilir.

En Yakın Komşu Yöntemi (Nearest Neighbour Method:NN)

Kargaşa ortamı içinde hedef izlemede kullanılan yöntemlerden biridir [11]. NN varsayılan hedef noktasına olan en yakın ölçümün kabulüdür.. Filtrede hedef durumu bu gözlem ile güncellenir [5].

Olasılıksal Veri İlişkilendirme Yöntemi (Probabilistic Data Association Method)

Olasılıksal veri ilişkilendirme (PDA) yönteminde hedef durumu ve alınan ölçümler arasında bir bağlantı kurulmasıdır. Geçerlilik bölgesi içindeki hedeften veya hedef dışından gelen ölçümler hedef durumu ile olasılık açısından ilişkilendirilir. Parametrik veri ilişkilendirme hedef kaynaklı olmayan ölçümlerin uzaysal yoğunluğunun bilinmesini gerektirir, pratikte bu değerin bilinmesi mümkün değildir [13]. Dolasıyla "b" değişkeni bulunurken parametrik olmayan yöntem tercih nedenidir.

$$\beta = (1 - P_{HT}P_G)\beta(2\pi)^{M/2}\sqrt{|S_i|} \qquad (14)$$

Ortak Olasılıksal Veri İlişkilendirme Yöntemi (Joint Probabilistic Data Association Method)

Ortak olasılıksal veri ilişkilendirme (JPDA) yöntemi ise ortamda birden fazla hedef olması durumunda hedefler ve ölçümler arasında olasılıksal veri ilişkilendirmesini sağlayan algoritmadır.

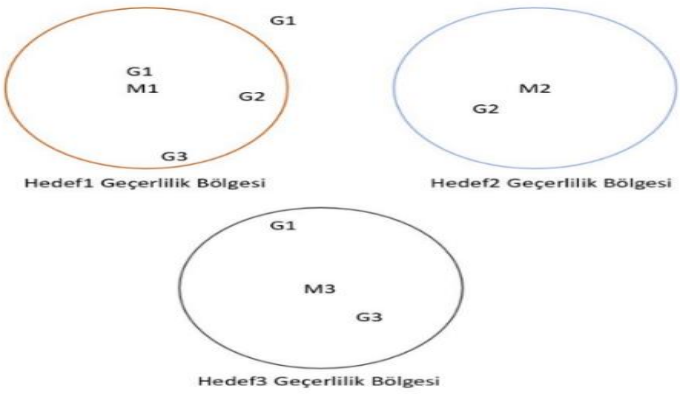

Şekil 2 Üç Hedefli Kargaşa Ortamı

Şekil 2'de ölçüm yöntemi gösterilmiştir. M1, M2 ve M3 üç ayrı hedef için oluşturulan geçerlilik bölgelerinin merkezlerini temsil etmektedir. G1, G2 ve G3 hedeften alınan ölçümleri temsil etmektedir. Hedef #1 için veri ilişkilendirmesi yapılırken her üç hedeften gelen ölçüm sonuçları ile olasılık ilişkilendirmesi yapılır ancak ikinci hedeften gelen ölçüm G2 ve üçüncü hedeften gelen ölçüm G3 olasılıkları zayıflatılarak hesaplamaya dahil edilir (Tablo 1). (sıfır "0" o anda hiçbir hedeften ölçüm gelmediği durumdur).

Tablo 1 Veri İlişkilendirme Olasılığı Hesabı (Data Association Probability Calculation)

Durum	Hedef#1	Hedef#2	Hedef#3	Veri İlişkilendirme Olasılığı
1	0	0	0	$(1 - P_{HT})3\beta^3$
2	1	2	3	$p'_{11}Pp'_{22}\,p'_{33}\,(P_{HT})^3$
3	1	2	1	$p'_{11}p'_{22}\,p'_{31}\,(P_{HT})^3$
4	2	2	1	$p'_{12}p'_{22}\,p'_{31}\,(P_{HT})^3$
5	2	2	3	$p'_{12}p'_{22}\,p'_{33}\,(P_{HT})^3$
6	3	2	1	$p'_{13}p'_{22}\,p'_{31}\,(P_{HT})^3$
7	3	2	3	$p'_{13}p'_{22}\,p'_{33}\,(P_{HT})^3$

i. hedef ile j. gözlemin ilişkilendirilmesinde Gauss Benzerlik fonksiyonu (denklem (15)) kullanılır. Tablo 1'de yer alan olasılıkları normalize etmek için ise denklem (16) kullanılır.

$$p'_{ij} = \frac{e^{\frac{-d_{ij}^2}{2}}}{(2\pi)^{M/2}\sqrt{|S^{ij}|}} \qquad (15) \qquad p'_{ij} = \frac{p'_{ij}}{\sum_{j=0}^{N} p'_{ij}} \qquad (16)$$

ANALİZLER:

Bu çalışma kapsamında tekli hedef izleme ve çoklu hedef izleme senaryoları incelenmiştir.

Tekli Hedef İzleme Analiz (SKF : Single Target Tracking)

Ortamda sabit hızlı doğrusal ve/veya sabit ivmeli doğrusal olmayan hareket senaryosuna sahip tek bir hedef kestirim performansı ve süreç gürültüsü değişimi ile filtrelerin hedef izleme performansı analiz edilmiştir.

Standart Kalman Filtresi (SKF) Hedef İzleme Analizi (SKF Target Tracking) : SKF ile özellikleri Tablo 2 ile verilen doğrusal sabit hızlı hareket gerçekleştiren Hedef#1 için izleme performansı Şekil 3 ile gösterilmiştir. Grafikte kestirim sonuçlarının, hedef doğrultusuna yakın hedef takibi yaptığı izlenmiştir.

Tablo 2 Sabit Hızlı Hedef Bilgileri (Constant Speed Target Information)

Hedef	*X0 Ekseni (m)*	*Y0 Ekseni(m)*	*Yatay Hız (m/sn)*	*Düşey Hız (m/sn)*
Hedef#1	100	100	100	100

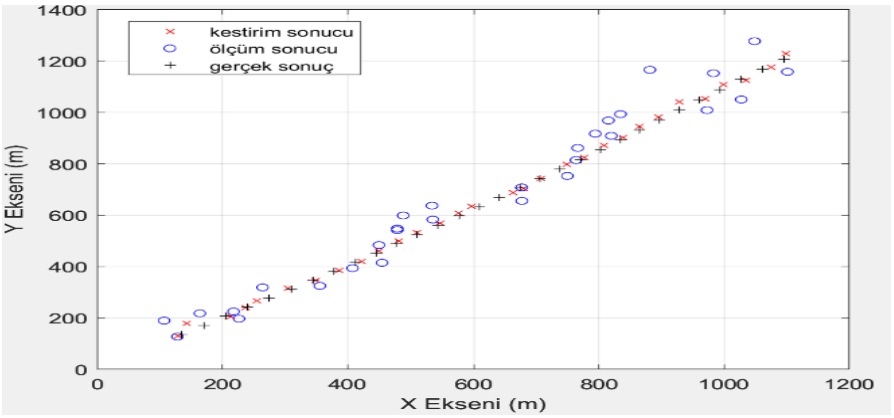

Şekil 3 Sabit Hızlı Hedef İzleme Grafiği

Bu çalışmada SKF'ye doğrusal olmayan geçiş matrisi eklenerek filtrenin hedef izleme tepkisi analiz edilmiştir. Filtre ve Hedef Hareket Modeli kapsamında, sadece Geçiş Matrisi değiştirilmiştir, Kullanılan geçiş matrisi doğrusal denklem (17) ile verilmiştir.

$$\nabla fx2 = \begin{vmatrix} 1 & 0 & -\Delta t V \sin(\theta) & 0.5\Delta t^2 \cos(\theta) \\ 0 & 1 & \Delta t V \cos(\theta) & 0.5\Delta t^2 \sin(\theta) \\ 0 & 0 & 0 & 1 \\ 0 & 0 & 1 & \Delta t \end{vmatrix} \qquad (17)$$

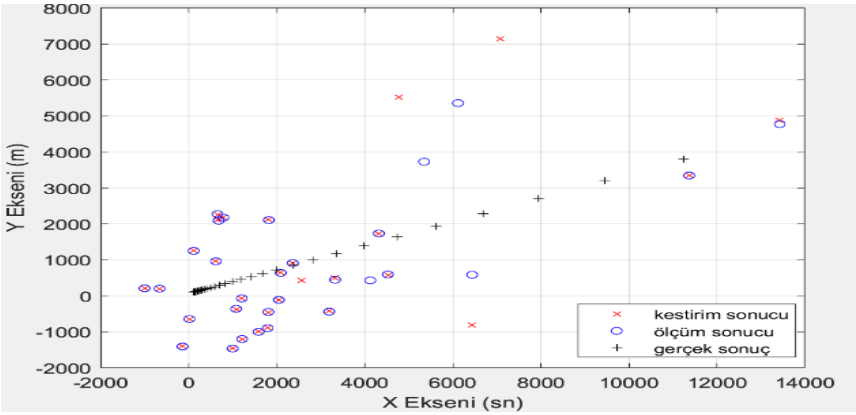

Şekil 4 Sabit İvmeli Hedef İzleme Grafiği (SKF)

Doğrusal olmayan hedef kullanılmasıyla süreç gürültüsü filtre içinde artmıştır, bu model belirsizliği anlamına gelir, filtre kestirim sonucunu doğrudan ölçüm sonuçlarından almaya başlar.
Bu çalışma ile Standart Kalman Filtresinin doğrusal olmayan denklemlere verdiği tepkinin uygun olmadığının sonucu Şekil 4 üzerinde gösterilmiştir.

Genişletilmiş kalman filtresi hedef izleme analizi (Extended Kalman filter target tracking analysis)

Bu çalışmada EKF analizi için iki dinamik modele sahip hedef ile çalışılmıştır. Hedefin biri iki boyutlu sabit hızlı dinamik modele (Hedef#2) sahiptir. Diğer hedef (Hedef#3), iki boyutlu sabit ivmeli dinamik denklem modeline sahiptir. Süreç gürültüsünün sabit tutulduğu durum, 1000 kat ve 5000 kat artma durumunda filtrenin izleme performansına etkisi analiz edilmiştir. Sabit hızlı hedef özellikleri Tablo 3 ile gösterilmiştir.

Tablo 3 Sabit Hızlı Hedef Bilgileri (Constant Speed Target Information)

Hedef	*X0 Ekseni (m)*	*Y0 Ekseni (m)*	*Ortalama Hız (m/sn²)*	*Baş açısı (derece)*
Hedef 1	100	100	100	50°

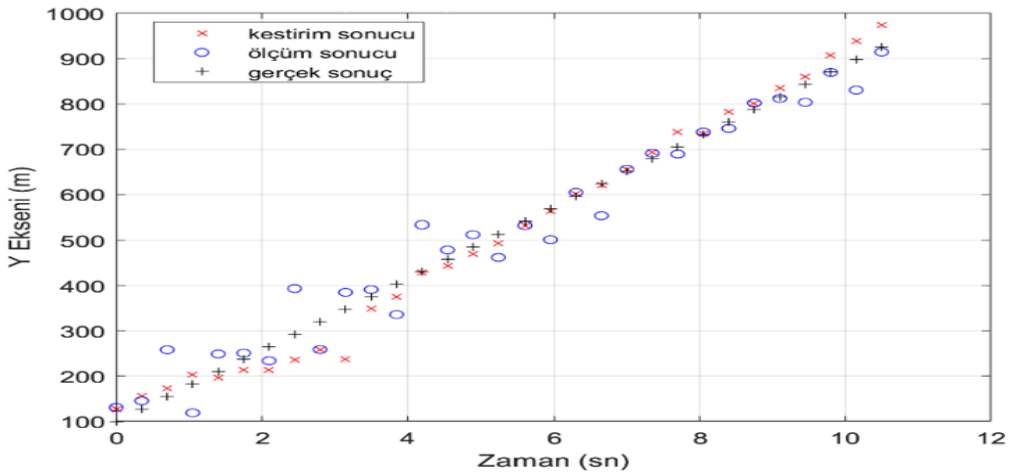

Şekil 5 Sabit Hızlı Hedef Kestirim Grafiği (EKF Tracking Chart for Constant Velocity Target

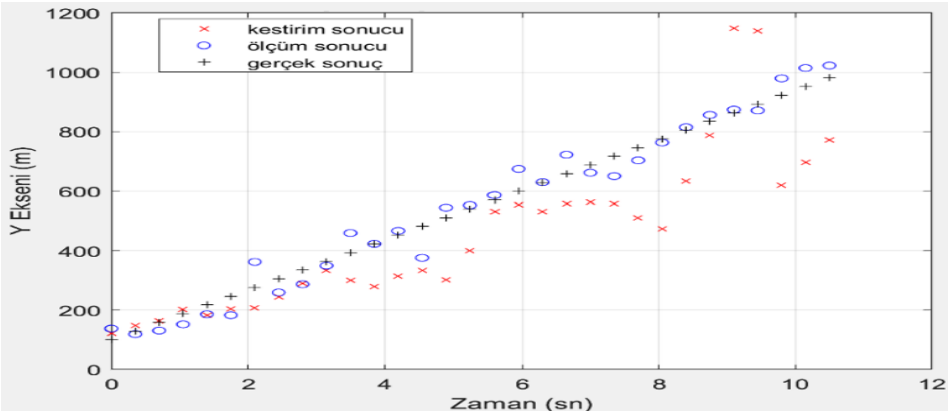

Şekil 6 EKF Sabit Hızlı Hedef Takibi – SG 5000 Kat (EKF Tracking Chart for Constant Velocity Target – SG 5000 Kat)

Tablo 4 EKF Süreç Gürültüsü Değişimi ve Konum Hatası Analizi

Süreç Gürültüsü (Q)	*Yatay Eksen Azami Konum Hatası (m)*	*Dikey Eksen Azami Konum Hatası (m)*
Q (Sabit)	~25	~20
Q (1000 Kat)	~60	~180
Q (5000 Kat)	~150	~190

Süreç gürültüsü sabit iken EKF Hedef İzleme grafiği Şekil 5 ve Süreç Gürültüsü 5000 kat artma durumu için hedef izleme grafiği Şekil 6 ile gösterilmiştir. Süreç gürültüsünün artması ile artan konum hatası grafikleri ile ilgili sonuçlar Tablo 4 üzerinde gösterilmiştir. Süreç gürültüsünün artması ile, Kalman Filtresi ölçüm sonuçlarına yakınsar.

Sabit ivmeli hedef özellikleri Tablo 5 ile gösterilmiştir. Süreç gürültüsü "Q" sabit tutulduğu durum, "Q" 5000 kat artma durumu sırasıyla Y Ekseni – Zaman grafikleri için alınan sonuçlar Şekil 7 ve Şekil 8 ile gösterilmiştir.

Tablo 5 Sabit İvmeli Hedef Bilgileri (Constant Acceleration Target Information)

Hedef	*X0 Ekseni (m)*	*Y0 Ekseni (m)*	*Ortalama İvme (m/sn²)*	*Baş açısı (derece)*
Hedef#2	100	100	5	45°

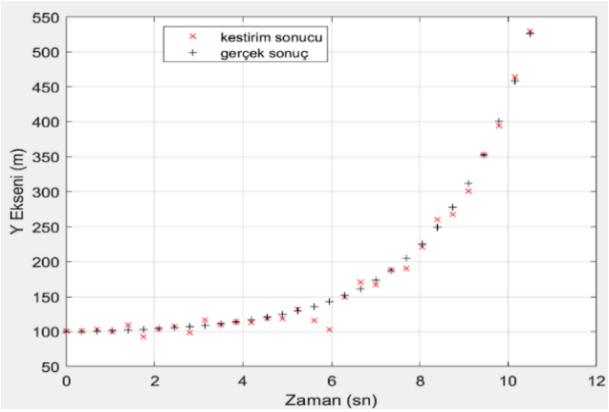

Şekil 7 Düşey Eksende EKF ile Sabit İvmeli Hedef Kestirim Grafiği

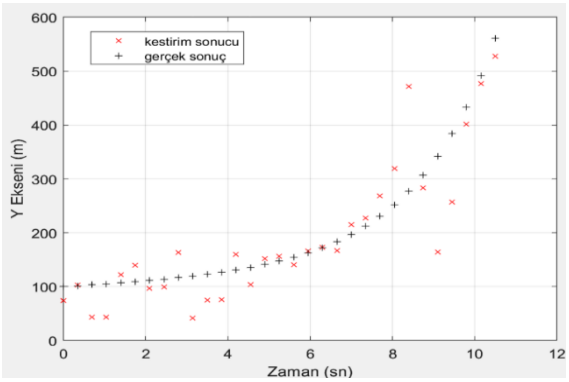

Şekil 8 Düşey Eksende EKF ile Sabit İvmeli Hedef Kestirim Grafiği (SG 5000 Kat)

Tablo 6 EKF Süreç Gürültüsü Değişimi ve Konum Hatası Analizi

Süreç Gürültüsü (Q)	*Yatay Eksen Azami Konum Hatası (m)*	*Dikey Eksen Azami Konum Hatası (m)*
Q (Sabit)	~30	~70
Q (1000 Kat)	~160	~200
Q (5000 Kat)	~420	~220

Süreç gürültüsü arttıkça Kalman Filtre kazancı artacağı için kestirim sonuçları ölçüm sonuçlarına yakınsamaya başlar, bu durum filtre kestirimini hedefin izlediği doğrultudan saptırır. Süreç gürültüsünün artmasıyla orantılı olarak değişen Kalman Filtre kestirimindeki konum hatası analiz sonuçları Tablo 6 ile gösterilmiştir.

Kokusuz kalman filtresi hedef izleme analizi

Bu çalışmada Kokusuz Kalman Filtresi (UKF) performans analizi için iki farklı modele sahip hedef ile çalışılmıştır. Birinci hedef iki boyutlu sabit hız denklem modeline sahiptir. Diğer hedef iki boyutlu sabit ivme denklem modeline sahiptir. Süreç gürültüsünün sabit tutulduğu durum (Şekil 9), 1000 kat artma durumu ve 5000 kat artma durumunda (Şekil 10) filtrenin izleme performansına etkisi analiz edilmiştir. Tablo 7 ile özellikleri verilen sabit hızlı hedef modelinin UKF ile kestirim analizidir.

Tablo 7 Sabit Hızlı Hedef Bilgileri (Constant Velocity Target Information)

Hedef	*X0 Ekseni (m)*	*Y0 Ekseni (m)*	*Ortalama Hız (m/sn)*	*Baş Açısı*
Hedef #1	100	100	100	50°

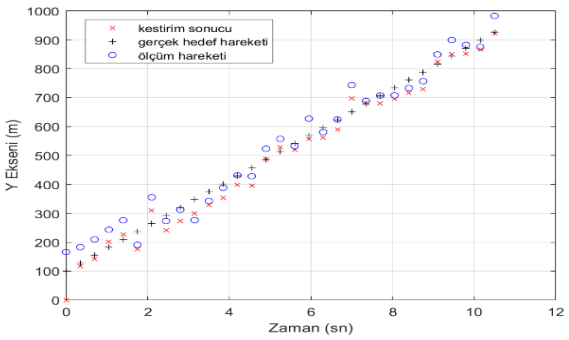

Şekil 9 Düşey Eksende UKF ile Sabit Hızlı Hedef Kestirimi

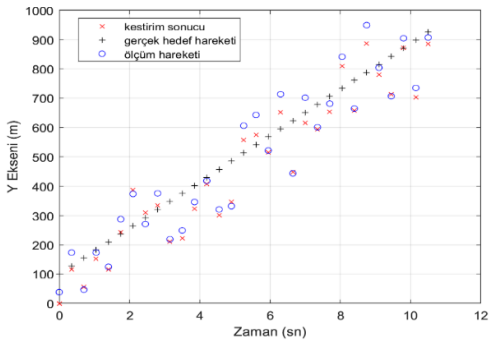

Şekil 10 Düşey Eksende UKF ile Sabit Hızlı Hedef Kestirim Grafiği (SG 5000 Kat Attırılma Durumu)

Tablo 8 Süreç Gürültüsü Değişimi ve UKF Konum Hatası Analizi (X,Y)

Süreç Gürültüsü Q	*Yatay Eksen Azami Konum Hatsı (m)*	*Dikey Eksen Azami Konum Hatası (m)*
Q (Sabit)	~2	~35
Q (1000 Kat)	~50	~8
Q (5000 Kat)	~80	~110

Tablo 8 ile yapılan analiz sonucunda süreç gürültüsündeki artış ile UKF hedef kestirimi konum hatasının arttığı izlenmiştir. Süreç gürültüsünün 5000 kat artışı ile UKF filtre kestirim konum hatasının ortalama 110 metredir. EKF ile kıyaslandığında daha kararlı yapıda hedef takibi yaptığı gözlenmiştir. Süreç gürültüsü fazla olan sabit hızlı hedefler için UKF tercih edilmesi analiz sonucunda ortaya konulmuştur.

Tablo 9 Süreç Gürültüsü Değişimi ve UKF ile Konum Hatası Analizi (Y)

Süreç Gürültüsü	*Dikey Eksen Azami Konum Hatası (metre)*
Q (Sabit)	~20
Q (1000 Kat)	~80
Q (5000 Kat)	~150

Süreç gürültüsünün arttırılmasıyla sabit ivmeli hedefin Y Ekseni konum hatası değişim grafikleri incelendiğinde, UKF sabit ivmeli hedefi izleme performansının azaldığı izlenmiştir. Süreç gürültüsü fazla olan sabit ivmeli hedef kestirim kararlılığı için UKF'nin tercihi analiz sonucunda ortaya konulmuştur.

Çoklu Hedef İzleme Analiz Adımları (Multiple Target Tracking Analysis Steps)

En yakın komşuluk yöntemi hedef izleme analizi (NN target tracking)

a)NN-SKF hedef izleme (NN-SKF multiple target tracking)

Burada yapılan analiz üç ayrı adımda gerçekleştirilmiştir.
ADIM-1: Birbirine paralel ve aynı ortam gürültüsüne sahip iki sabit hızlı hedef için NN-SKF ile hedef izleme takibi analizi yapılmıştır. Amaç, yakın ve paralel hedeflerin izlenmesi için NN algoritmasının performansını analiz etmektir. Kullanılan hedefler ile ilgili bilgiler Tablo 10'da yer almaktadır.

Tablo 10 Eş zamanlı Takip Edilen Sabit Hızlı İki Hedef Verileri

Hedef	*X0Ekseni (m)*	*Y0 Ekseni (m)*	*Yatay Hız (m/sn)*	*Düşey Hız (m/sn)*	*sigma_x1*	*sigma_y1*	*sigma_x2*	*sigma_y2*
Hedef 1	10	10	100	100	0,12	0,12	-	-
Hedef 2	50	200	100	100	-	-	0,12	0,12

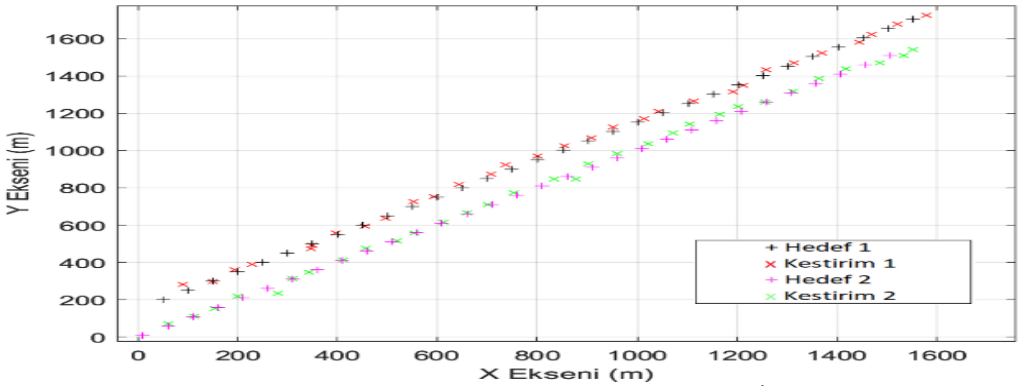

Şekil 10 NN - SKF ile Sabit Hızlı ve Paralel Eş Zamanlı Hedef İzleme (NN – SKF Parallel Simultaneous Target Tracking

Şekil 10 incelendiğinde NN-SKF ile izlenilen sabit hızlı ve birbirine yakın seyreden hedeflerin eş zamanlı kestirimlerinde herhangi bir izleme kaybı olmadığı ve her bir kestirimin hedef üzerinde olduğu izlenmiştir.
ADIM-2: Eş zamanlı olarak birbirlerine göre çapraz hareket eden ve aynı ortam gürültüsüne sahip iki hedef için NN-SKF ile hedef izleme takibi analizi yapılmıştır. Kullanılan hedef bilgileri Tablo 11 ile gösterilmiştir.

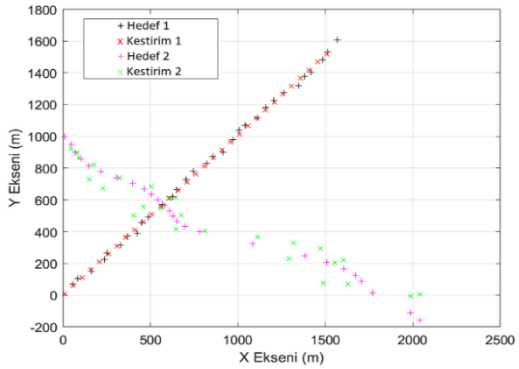

Şekil 11 Eş Zamanlı Takip Edilen Sabit Hızlı İki Hedef Bilgisi (Simultaneous Tracked Constant Speed Two Target Information)

Tablo-11: Kullanılan Hedef Bilgileri

Hedef	*Yatay Eksen m*	*Düşey Eksen m*	*Yatay Hız m/sn*	*Düşey Hız m/sn*	*sigma x1*	*sigma y1*	*sigma x2*	*sigma y2*
Hedef 1	10	10	100	100	0.12	0.12	-	-
Hedef 2	10	1000	100	-100	-	-	0.12	0.12

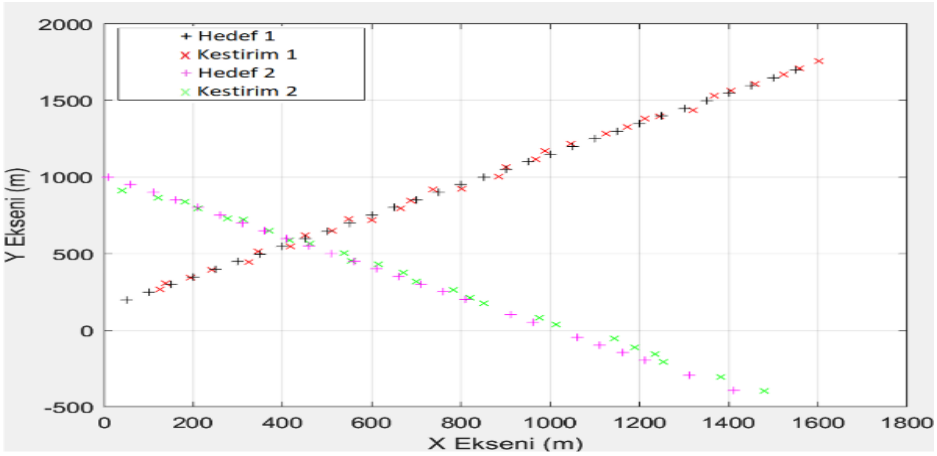

Şekil 12 NN - SKF ile Eş Zamanlı Giden Çapraz Hedefleri İzleme

Şekil 12 baz alınarak NN-SKF ile izlenilen sabit hızlı ve birbirlerine göre çapraz hedef kestirimi sonuçlarında herhangi bir izleme kaybı yaşanmadığı gözlenmiştir. Hedeflerin kestirimi sırasında herhangi bir sapma olmadığı, her bir kestirimin ilişkili hedef üzerinde olduğu görülmüştür.

ADIM-3: Eş zamanlı olarak birbirine göre çapraz hareket eden ve farklı süreç gürültüsüne sahip iki hedef için NN-SKF ile hedef izleme takibi analizi yapılmıştır. Kullanılan hedefler ve değişen süreç gürültü standart sapması ile ilgili bilgiler Tablo 12 ile gösterilmiştir.

Tablo 12 Eş Zamanlı İzlenen İki Sabit Hızlı Hedefin Bilgileri (Hız : m/s)

Hedef	X0 Eksen	Y0 Ekseni	Yatay Hız	Düşey Hız	sigma_x1	sigma_y1	sigma_x2	sigma_y2
1	10	10	100	100	0.12	0.12	-	-
2	10	1000	100	-100	-	-	100	12

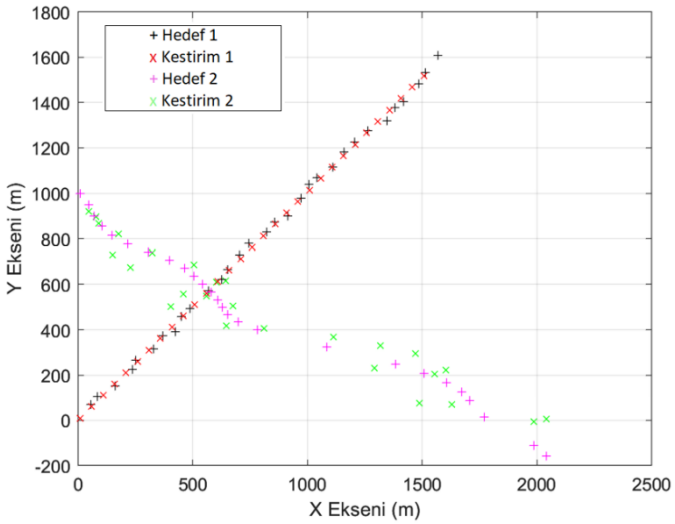

Şekil 13 NN ve SKF ile Eş Zamanlı Hareket Eden Sabit Hızlı İki Hedef Kestirimi

Şekil 13 incelendiğinde, tam kesişim alanında yeşil ile gösterilen "x" sembollerinin Hedef#2 doğrultusu yönünde değil, Hedef#1 doğrultusu üzerinde kestirim yapmaya çalıştığı izlenmiştir. Ayrıca, hedef kestiriminde atlama yaşandığı, hedef doğrultusunda kestirim yapılmadığı ve kaymaların yaşandığı izlenmiştir.

b) NN-EKF ile çoklu hedef izleme analizi (NN-EKF multiple target tracking)

Eş zamanda sabit ivmeli hareket gerçekleştiren iki hedefin NN-EKF ile takip analizi yapılmıştır. Hedef #3 ve Hedef #4 sabit ivme dinamik modele sahiptirler. Bu bölümde analiz iki adımdan oluşmaktadır.

ADIM-1: Tablo 13 ile özellikleri belirtilen eş zamanlı hareket eden sabit ivmeli iki hedefin EKF kestirim analizini içermektedir.

Tablo 13 NN-EKF ile Takip Edilen Sabit İvmeli Hedef Bilgileri

Hedef	*X0 Ekseni m*	*Y0 Ekseni m*	*İvme m/sn²*	*sigma_x1*	*sigma_y1*	*sigma_x2*	*sigma_y2*
Hedef #3	0	100	10	0.12	0.12	-	-
Hedef #4	500	500	10	-	-	0.12	0.12

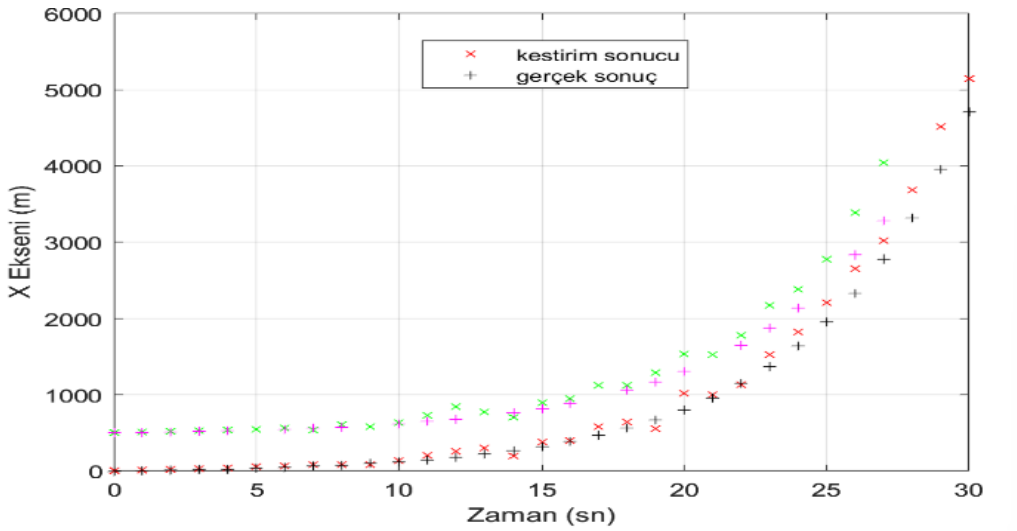

Şekil 14 NN-EKF Eş Zamanlı Çoklu Hedef İzleme Grafiği (NN-EKF Multitarget Tracking Chart)

ADIM-2: Hedef #4 için süreç gürültüsü standart sapması Tablo 14'de belirtildiği şekilde arttırılarak eş zamanlı hareket eden sabit ivmeli iki hedefin EKF kestirim analizini içermektedir.

Tablo 14 NN-EKF ile Takip Edilen Hedef Bilgileri

Hedef	*X0 Ekseni (m)*	*Y0 Ekseni (m)*	*İvme (m/sn²)*	*sigma_x1*	*sigma_y1*	*sigma_x2*	*sigma_y2*
Hedef #3	0	100	10	0.12	0.12	-	-
Hedef #4	500	500	10	-	-	100	12

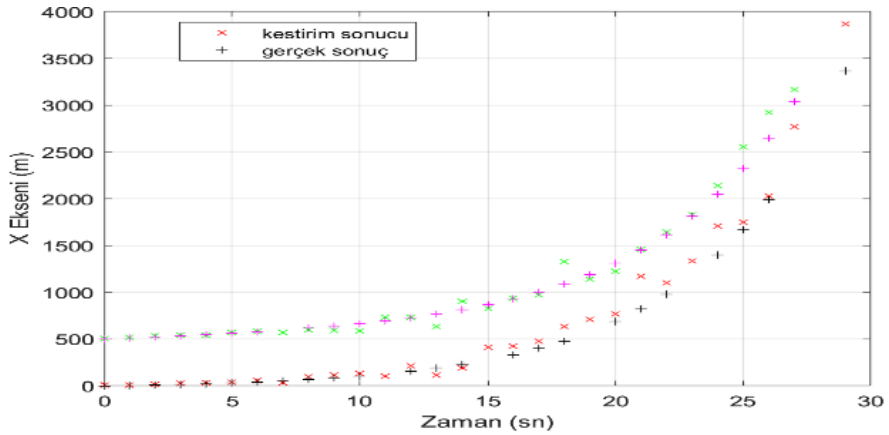

Şekil 15 Süreç Gürültü Değişimi ile NN-EKF Hedef İzleme Grafiği (NN-EKF Target Tracking Chart with Process Noise Change)

Süreç gürültü standart sapması sabit tutulan iki hedef için elde edilen eş zamanlı kestirim performansı Şekil 14 ile verilmiştir. Hedef #4 için süreç gürültü standart sapması arttırıldıktan sonra iki hedef için elde edilen eş zamanlı kestirim performansı Şekil 15 ile verilmiştir. Sabit ivmeli ve yakın hedef kestirimleri için NN-EKF kestirim performansının düşük olduğu gözlenmiştir. Sabit süreç gürültüsüne sahip iki hedefin aynı anda NN-

EKF ile izlenebilirliği manevranın başladığı 20. saniyeden itibaren azalmaya başlamaktadır. Hedef kestiriminin her iki hedef için de hedef takibini kaybettiği gözlenmiştir. NN-EKF ile süreç gürültüsü sabit tutulan hedeflerin kestirimleri, 4000 metreye kadar izlenebiliyorken, hedef hareket modelin belirsizliğinin arttırılmasıyla birlikte (süreç gürültü standart sapmasının arttırılması) hedef izlenebilirliğinin 3000 metreye düştüğü Şekil 14 ve Şekil 15 üzerinde izlenmiştir. Hedef #4 için süreç gürültüsü standart sapmasının artmasıyla birlikte 25. saniyeden itibaren Hedef #4'e ait iz kayıplarının olduğu ve hedef kestirim doğrultusunun kaydığı Şekil 15 üzerinde gözlenmektedir.

c)JPDA-SKF ile çoklu hedef izleme analizi

JPDA ve standart kalman filtresi kullanılarak doğrusal ve sabit hızla hareket eden özellikleri Tablo 15 ile gösterilen üç hedefin takibi üç adımda incelenmiştir:

Birinci Adım: Süreç gürültüsü sabit tutulan ve birbirine paralel olan üç hedefin takip edilmesi. İkinci Adım: Süreç gürültüsü sabit tutulan ve birbirine paralel iki hedef ve aynı özelliklere sahip üçüncü hedef bu iki hedefe çapraz hareket gerçekleştirme durumu. Üçüncü Adım: İkinci adımda anlatıldığı şekilde hareket eden üçüncü hedefin süreç gürültü sabiti arttırılmıştır. Amaç NN algoritmasında çapraz olarak ilerleyen aynı hedefin süreç gürültü oranı aynı oranda arttırılarak JPDA ve NN analizi yapılmasıdır.

Tablo 15 JPDA ile Takip Edilen Sabit Hızlı Hedef Bilgileri

Hedef	*X0 Eksen*	*Y0 Eksen*	*Yatay Hız*	*Düşey Hız*	*sigmax1*	*sigmay1*	*sigmax2*	*sigmay2*	*sigmax3*	*sigma y3*
1	500	1000	100	100	0.12	0.12	-	-	-	-
2	500	1500	100	100	-	-	0.12	0.12	-	-
3	500	2000	100	100	-	-	-	-	0.12	0.12

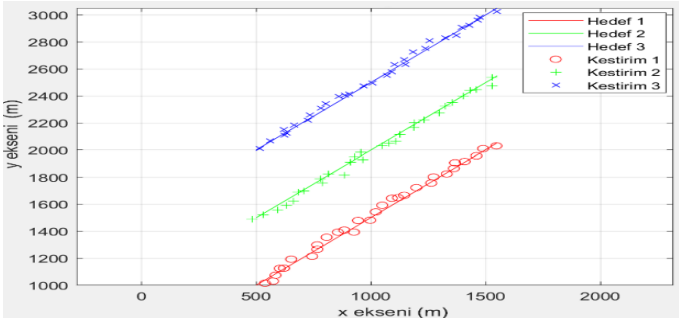

Şekil 16 JPDA Algoritması ve SKF ile Sabit Hızlı ve Paralel Çoklu Hedef İzleme Grafiği (JPDA-SKF Simultaneous Multi-Target Tracking)

Sabit hızlı hedeflerin JPDA-SKF ile eş zamanlı kestiriminde herhangi bir atlama, kopma veya iz kaybına rastlanmadığı Şekil 16 ile izlenmiştir.
ADIM#2: Birbirine paralel ve aynı süreç gürültüsüne sahip iki hedef ve bu iki hedefe çapraz hareket gerçekleştiren aynı süreç gürültüsüne sahip üçüncü hedefi çoklu hedef izleme durumudur. JPDA-SKF ile hedef izleme takibi analizi yapılmıştır. Kullanılan hedefler ile ilgili bilgiler Tablo 16 üzerinde yer almaktadır.

Tablo 16 JPDA ile Takip Edilen Hedef Bilgileri

Hedef	*X0 Eksen*	*Y0 Eksen*	*Yatay Hız*	*Düşey Hız*	*sigmax1*	*sigmay1*	*sigmax2*	*sigmay2*	*sigmax3*	*sigma y3*
1	500	1000	100	100	0.12	0.12	-	-	-	-
2	500	2500	100	-100	-	-	0.12	0.12	-	-
3	500	2000	100	100	-	-	-	-	0.12	0.12

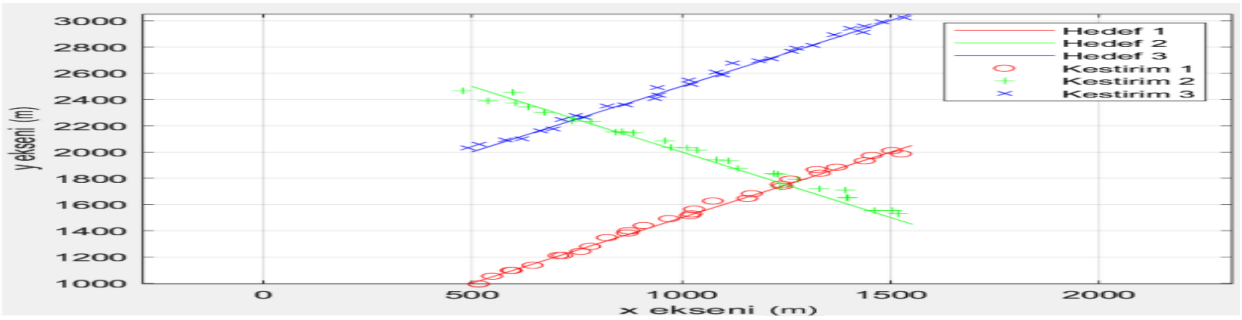

Şekil 17 JPDA Algoritması ve SKF ile Sabit Hızlı ve Paralel Çoklu Hedef İzleme Grafiği (JPDA-SKF Simultaneous Multi-Target Tracking)

Eş zamanlı olarak aynı süreç gürültüsüne sahip birbirine paralel hareket eden iki sabit hızlı hedef ve bu iki hedefe çapraz hareket gerçekleştiren diğer iki hedef ile aynı özelliklere sahip üçüncü hedefi ve bu hedefleri takibini gösteren grafik Şekil 17'de yer almaktadır. Herhangi bir hedef kestirimi kaybı yaşanmadan üç hedefin de başarılı şekilde izlenildiği çıkarılabilirdir.

ADIM#3: Eş zamanlı olarak aynı süreç gürültüsüne sahip iki paralel hedef (Hedef 1 ve Hedef 3) ve bu hedeflere çapraz hareket eden, farklı süreç gürültü standart sapmasına sahip hedef (Hedef 2) için hedef izleme analizi yapılmıştır. Kullanılan hedefler ve artan süreç gürültü standart sapması ile ilgili bilgiler Tablo 20 ile verilmiştir.

Tablo 17 JPDA ile Takip Edilen Hedef Bilgileri

Hedef	*X0 Eksen*	*Y0 Eksen*	*Yatay Hız*	*Düşey Hız*	*sigmax1*	*sigmay1*	*sigmax2*	*sigmay2*	*sigmax3*	*sigmay 3*
1	500	1000	100	100	0.12	0.12	-	-	-	-
2	500	2500	100	-100	-	-	100	0.12	-	-
3	500	2000	100	100	-	-	-	-	0.12	0.12

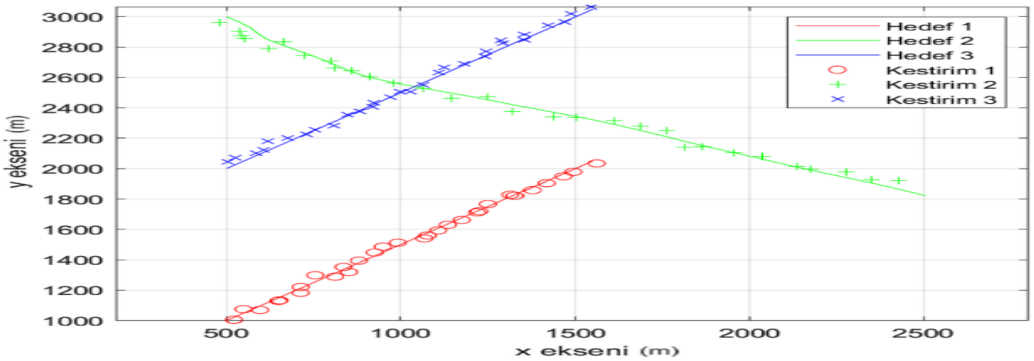

Şekil 18 Süreç Gürültüsü Değişimi ile JPDA-SKF Eş Zamanlı Çoklu Hedef İzleme (JPDA-SKF Simultaneous Multi-Target Tracking with Process Noise Change)

Aynı süreç gürültüsüne sahip, birbirine paralel hareket eden iki hedef ve bu iki hedefe çapraz hareket gerçekleştiren ve farklı süreç gürültü standart sapmasına sahip üçüncü hedefi ve bu hedeflerin eş zamanlı olarak kestirim grafiği Şekil 28 ile gösterilmiştir. Buna göre herhangi bir hedef kestirim kaybı yaşanmadan üç hedefin de düzgün izlenildiği saptanmıştır. Bu kapsamda "sigma_x2" ve "sigma_y2 süreç gürültü standart sapma değerleri Hedef #2 için Tablo 20'de belirtildiği şekilde arttırılmıştır. Bu sabitlerin arttırıldığı durumda hedef hareketindeki belirsizliklerin artması beklenir, çünkü süreç gürültüsünün artmasıyla tahmin adımındaki kovaryans parametresi artar. Bu sabitlerin artırılması durumunda hedef hareketinde belirsizlik artmasına rağmen herhangi bir hedef kestirimi kaybı yaşanmadan üç hedefin de düzgün izlenildiği saptanmıştır. Aynı durum NN-SKF ile analiz edilmiş ve kestirim performansında kayıplar olduğu izlenilmiştir. Bu durum sabit hareket gerçekleştiren birden fazla hedefin eş zamanlı takibinde süreç modelinde değişim olma durumunda

JPDA algoritmasının NN algoritmasına göre daha doğru kestirim sonuçları vereceğini ve iz kayıplarının yaşanmayacağını ortaya koymaktadır.

SONUÇLAR VE TARTIŞMA

Bu çalışmada SKF ile Sabit hızlı ve sabit ivmeli doğrusal hedefler için hedef kestirim çıktıları alınmıştır. Alınan sonuçlar ile; SKF'nin, doğrusal hedefler için hedef kestirim performansının yüksek olduğu doğrulanmıştır. Bununla birlikte; doğrusal olmayan hareket modeli kullanıldığında, SKF'nin doğrusal olmayan hareket modeline verdiği tepkinin kullanılabilir olmadığı analizle teyit edilmiştir. Aynı model ve ortam gürültüsüne sahip hedeflerin kestiriminde süreç gürültüsünün aynı oranda değişmesi durumunun EKF ve UKF tepkisine etkisi analiz edilmiştir. Bu kapsamda süreç gürültüsü değişiminin EKF ve UKF hedef kestirim performansının artış/azalış durumuna etkisinin analiz edilmesi ve karşılaştırılması için sabit hızlı ve sabit ivmeli hedefler için yapılan çalışmalarla ortaya konulmuştur. Bu çerçevede alınan sonuçlar ise; Analiz sonucunda süreç gürültüsünün artmasıyla her iki filtrenin de hedef kestirim performansının zayıfladığı izlenmiş, diğer taraftan UKF'nin sabit hızlı ve manevralı sabit ivmeli hedef hareketindeki (süreç gürültüsünün artması ile oluşan) belirsizliğe karşı daha kararlı kestirim gerçekleştirdiği, konum hatası zaman grafikleri ile gözlenmiştir. Hedef hareket belirsizliği olan çevrede yapılan hedef takip sistemleri için UKF'nin EKF'ye nazaran kararlı yapısı ile tercih edilebilirdir.

Çoklu hedef izleme için NN ve SKF bütünleşik filtre yapısı kullanılarak paralel ve çapraz olarak ayrı ayrı gerçekleştirilen hedef kestirimi sonuçları şu şekildedir: Herhangi bir izleme kaybı yaşanmadığı, hedeften sapma olmadığı, her bir kestirimin her bir hedef üzerinde olduğu doğrulanmıştır. Süreç gürültüsünün artması ile hedeflerin kestirimi sırasında atlama yaşandığı, hedefin izlediği doğrultuda kestirim yapılmadığı ve kaymaların yaşandığı izlenmiştir. Burada kullanılan aynı hedefler ve aynı katsayılı süreç gürültüsü JPDA ile analiz edilerek NN ve JPDA için çoklu hedef izleme performansları da karşılaştırılmıştır. Sonuçlar aşağıda ifade edildiği şekildedir: NN-SKF bütünleşik filtre yapısının hedef izlemede yetersiz kaldığı senaryoda JPDA-SKF bütünleşik filtre yapısının başarılı olduğu izlenmiştir. JPDA algoritmasının sabit hızlı ve kargaşa olmayan ortamda yer alan çoklu hedef izleme durumunda NN algoritmasına nazaran daha güvenilir sonuçlar verdiği gözlenmiştir. Sabit ivmeli ve yakın hedef kestirimleri için NN-EKF kullanımının kestirim performansının düşük olduğu gözlenmiştir, süreç gürültüsü sabit tutulan iki sabit ivmeli hedefin aynı anda NN-EKF ile izlenebilirliği manevranın başlamasıyla bulanıklaştığı izlenmiştir. Süreç gürültüsünün artmasıyla NN-EKF yapısının hedef izleme performansının hedef izlemede yetersiz kaldığı tanıtlanmıştır. Sabit hızlı ve yakın hedeflerde NN-SKF algoritması kullanmanın düzgün hedef izleme sağlayacağını ortaya koymuştur. Ancak, manevralı ve sabit ivmeli hedefler için NN-EKF algoritması kullanmanın hedef izleme performansının zayıf olduğu izlenmiştir.

SKF'nin doğrusal olmayan hareket modeline verdiği tepkinin kullanılabilir olmadığı, Hedefin hareket belirsizliği olan çevrede yapılan takip için UKF'nin EKF'ye nazaran daha kararlı yapısı ile tercih edilebilirdir. Çoklu hedef izleme için NN ve SKF bütünleşik filtre yapısı kullanılarak gerçekleştirilen hedef kestiriminde herhangi bir izleme/takip kaybı yaşanmadığı, hedeften sapma olmadığı, her bir kestirimin her bir hedef üzerinde olduğu doğrulanmıştır. NN ve JPDA için çoklu hedef izleme performansları da karşılaştırıldığında; NN-SKF bütünleşik filtre yapısının hedef izlemede yetersiz kaldığı senaryoda JPDA-SKF bütünleşik filtre yapısının başarılı olduğu izlenmiştir. JPDA algoritmasının sabit hızlı ve kargaşa olmayan ortamda yer alan çoklu hedef izleme durumunda NN algoritmasına nazaran daha güvenilir sonuçlar verdiği gözlenmiştir.

Kaynaklar (References)

[1] Madhukar P. S., Prasad L. B., State Estimation Using Extended Kalman Filter and Unscented Kalman Filter, Department of Electrical Engineering, Madan Mohan Malaviya University of Technology, International Conference on Emerging Trends in Communication, Control and Computing (ICONC3) Mody University of Science and Technology, Lakshmangarh, India, Feb 21-22, 2020.

[2]Hartikainen J., Solin A., Särkkä S., Optimal Filtering with Kalman Filters and Smoothers Manual for the Matlab Toolbox EKF/UKF, Department of Biomedical Engineering and Computational Science, Aalto University School of Science, P.O.Box 1100, FI-00076 AALTO, Espoo, Finland, August 16, 2011.

[3] Erol B., Cantekin R. F., Kartal S. K., Hacıoğlu R., Görmüş K.S., Kutoğlu Ş. H., Leblebicioğlu M.K., İnsansız Sualtı Aracı Hareketinin Kalman Filtre ile Kestirimi ve Makine Öğrenmesi ile İyileştirilmesi, ASYU 2020 Special Issue: 67-77, DOI: 10.7240/jeps.897500, Int. J. Adv. Eng. Pure Sci., 2021.

[4]Welche G., Bishop G., An Introduction to the Kalman Filter, University of North Carolina at Chapel Hill Department of Computer Science Chapel Hill, NC 27599-3175, Siggraph 2001.

[5]Lana A., Kalman Filtresi ve Olasılıksal Veri İlişkilendirme Yöntemlerini Kullanan Çoklu Hedef İzleme Algoritmaları, Yüksek Lisans Tezi, İstanbul Teknik Üniversitesi, Fen Bilimleri Enstitüsü, 77s, 2001

[6]M.Sc. Ritter B., Implementation and Testing of Sigma-Point Kalman Filters in Simulink for Nonlinear Estimation, Bachelor Thesis, Technische Universität Darmstadt, Institut für Automatisierungstechnik und Mechatronik Fachgebiet Regelungstechnik und Mechatronik Germany, 15. August 2016.

[7] Liu C., Shui P., Li S., Unscented Extended Kalman Filter For Target Tracking, Journal of Systems Engineering and Electronics Vol. 22, No. 2, April 2011, pp.188–192 Available online at www.jseepub.com, DOI: 10.3969/j.issn.1004-4132.2011.02.002

[8] Dumble S., Advanced Kalman Filtering and Sensor Fusion | Udemy

[9] van der Merwe R., Wan E., Sigma-Point Kalman Filters for Probabilistic Inference in Dynamic State-Space Models, OGI School of Science&Engineering, Oregon Health&Science University, Beaverton, Oregon, USA

[10] Orderud F., Comparison of Kalman Filter Estimation Approaches for State Space Models with Nonlinear Measurements, Sem Sælands vei 7-9, NO-7491 Trondheim

[11] Bar-Shalom Y., Li X. R., Tracking in Clutter With Nearest Neighbour Filters: Analysis and Performance, IEEE Transactıons On Aerospace And Electronıc Systems, Vol. 32, No. 3 July 1996.

[12] Pakfiliz A.G., Parazit Yankılı Ortamda Manevra Yapan Birden Çok Hedefin Takibi İçin Olasılıksal Bir Takip Algoritması Geliştirilmesi, Doktora Tezi, Ankara Üniversitesi, Fen Bilimleri Enstitüsü, Ankara, Türkiye, 2004.

[13] Soysal G., Hedef Takibinde Adaptif Yaklaşımlarla İz Yönetimi, Yüksek Lisans Tezi, Ankara Üniversitesi, Fen Bilimleri Enstitüsü, Ankara, Türkiye, 2005.

[14] Tokta A., Nesne Takibi Algoritmaları : Teori ve Matlab uygulaması | Udemy

➢ *ORAL PRESENTATION*

Advanced oxidation of acid violet (AV-19) from aquatic environments by homogeneous and heterogeneous Fenton and photo-Fenton processes

Duygu Aydın[1] (*ORCID: https://orcid.org/0009-0005-4888-193X*), Selina Olcar[1] (*ORCID: https://orcid.org/0009-0002-6669-8977*), Şule Camcıoğlu[1] (*ORCID: https://orcid.org/0000-0002-8983-3193*), Baran Özyurt[1*] (*ORCID: https://orcid.org/0000-0003-0011-8351*)

[*1]Ankara University, Faculty of Engineering, Department of Chemical Engineering, Ankara, Turkey.

*Corresponding author e-mail: bozyurt@ankara.edu.tr

Abstract
Dyes released into wastewater from industrial activities pose a serious threat to the environment and aquatic ecosystems. Commonly used in sectors such as textiles, paper, leather, food, and cosmetics, these dyes are difficult to remove with conventional treatment methods due to their high solubility and chemical stability. Accumulation of these persistent and non-biodegradable substances can cause toxic effects and bioaccumulation, presenting risks to both ecosystems and human health. Advanced oxidation processes (AOPs) offer effective and environmentally friendly solutions for dye removal, as they generate highly reactive radicals, particularly hydroxyl radicals (•OH), which can degrade complex dye molecules into harmless compounds. Among AOPs, the Fenton process is notable for its low cost and broad applicability. The photo-Fenton (PF) process further enhances efficiency by incorporating UV irradiation, which accelerates Fe^{3+} reduction and increases radical production, resulting in faster dye removal. Heterogeneous Fenton (HF) and heterogeneous photo-Fenton (HPF) processes utilize solid iron-based catalysts, such as Fe_3O_4 nanoparticles, which can be magnetically separated and reused. In this study, we investigated the degradation and mineralization of the model dye acid violet 19 (AV19) using Fenton, FF, HF, and HFF processes. The effects of catalyst dosage and H_2O_2/Fe molar ratio were evaluated. Optimal conditions for the Fenton process were 0.75 mM Fe^{2+} and an H_2O_2/Fe ratio of 20, achieving 100% color removal in 1 minute and 100% COD removal in 30 minutes. In the FF process, 0.25 mM Fe^{2+} and an H_2O_2/Fe ratio of 20 achieved complete color removal in 30 seconds and 100% COD removal in 15 minutes. For the HF process, 0.75 g L^{-1} Fe_3O_4 and an H_2O_2/Fe ratio of 20 resulted in 100% color removal and 55% COD removal in 240 minutes. The HFF process, with the same catalyst and ratio, achieved 100% color removal and 62% COD removal in 240 minutes.
Keywords: Advanced oxidation processes, Fenton process, Photo-Fenton, Fe_3O_4 nanoparticles, Dye degradation, Water treatment.

INTRODUCTION

Considering the various production methods and wastewater characteristics within different branches of the textile industry, setting discharge limits and selecting the most appropriate treatment methods remain significant challenges (Cornejo et al., 2021). In recent EU Directives, dyes have been classified as priority pollutants. Many of these pollutants are highly toxic even at low concentrations and therefore must be effectively removed (Annabi et al., 2016). However, many recalcitrant organic pollutants—particularly aromatic compounds—cannot be effectively eliminated by conventional wastewater treatment technologies commonly used in biological treatment plants (Annabi et al., 2016). Therefore, there is a need for highly efficient treatment methods for such persistent contaminants (Annabi et al., 2016).

Acid Violet 19 (AV19), also known as benzenesulfonic acid or acid magenta, is an anionic dye belonging to the triarylmethane group (Mondal and Saha, 2018). AV19 is widely used in the textile industry, including for textile fabrics, silk, nylon, wool, and leather (Mukurala et al., 2021). Pollution from synthetic dyes originating from textile, paper, rubber, and plastic manufacturing has a direct impact on both the environment and human health (Mukurala et al., 2021). The development of effective treatment technologies is therefore essential for the sustainable management of water resources.

Advanced Oxidation Processes (AOPs) are designed to accelerate the oxidation and degradation of organic substances in water or air through the generation of highly reactive free radicals such as hydroxyl radicals (•OH). Due to their high oxidation potential, these radicals rapidly and effectively react with organic pollutants, transforming them into carbon dioxide, water, and other inorganic compounds. This process breaks down the structure of organic contaminants, making them more biodegradable or completely harmless. Today, AOPs

are increasingly recognized as important technologies for removing biologically persistent or poorly degradable toxic contaminants—such as pesticides, pharmaceuticals, dyes, and industrial solvents—from water (Oturan and Aaron, 2014).

The advantages of these processes include the use of safe and environmentally compatible reagents, the absence of mass transfer limitations, and relatively easy operation due to short reaction times (Perez-Estrada et al., 2005). Different AOP mechanisms have been proposed, which can be classified based on whether •OH formation occurs via chemical, photochemical, sonochemical, or electrochemical pathways (Oturan and Aaron, 2014). The oldest and most widely used AOP is the Fenton process, which involves the reaction of soluble Fe^{2+} and H_2O_2 (Equation 1) to degrade persistent organic pollutants (Oturan and Aaron, 2014).

$$Fe^{2+} + H_2O_2 \rightarrow Fe^{3+} + OH^- + {}^{\bullet}OH \quad (1)$$

The concentrations of Fe^{2+} ions and H_2O_2 in solution must be carefully optimized according to the pollutant load. During the Fenton reaction, Fe^{2+} is oxidized to Fe^{3+} upon generating hydroxyl radicals (•OH). However, Fe^{3+} can also act as a scavenger of hydroxyl radicals, thereby reducing the efficiency of the process (Oturan and Aaron, 2014). Additionally, when Fe^{3+} is reduced back to Fe^{2+}, some of the generated hydroxyl radicals may be consumed in the process. For this reason, the Fe^{2+}/H_2O_2 molar ratio should be precisely controlled to maximize •OH production and minimize undesirable side reactions.

Combining hydrogen peroxide and UV radiation with Fe^{2+} or Fe^{3+} ions leads to the generation of additional hydroxyl radicals, thereby significantly enhancing the degradation rate of organic pollutants. This process is referred to as the photo-Fenton (PF) reaction. In the conventional Fenton process, the accumulation of Fe^{3+} ions eventually inhibits the reaction once all Fe^{2+} ions have been consumed. In contrast, the PF process enables the photochemical regeneration of Fe^{2+} from Fe^{3+} via photoreduction, sustaining the production of reactive radicals and allowing the reaction cycle to continue (Equation 2).

$$FeOH^{2+} + h\nu \longrightarrow Fe^{2+} + {}^{\bullet}OH \quad (2)$$

The PF process operates most efficiently at acidic pH values around 3.0, where hydroxy–Fe^{3+} complexes remain soluble and $Fe(OH)^{2+}$ species are highly photoactive. PF has consistently been reported as more effective than the conventional Fenton treatment. In some applications, sunlight may be used instead of artificial UV irradiation, providing cost savings but generally resulting in lower degradation rates. Acidic conditions are particularly advantageous, partly because carbonate and bicarbonate species are converted to carbonic acid, which exhibits low reactivity toward hydroxyl radicals. During the PF degradation of organic pollutants, carboxylic acids are formed as intermediates, and these can complex with iron ions (Laghrib et al., 2021). The following reactions also contribute to radical generation (Equation 3-4).

$$Fe(OOCR)^{2+} + h\nu \longrightarrow Fe^{2+} + CO_2 + {}^{\bullet}OH \quad (3)$$

$$H_2O_2 + h\nu \longrightarrow 2\,{}^{\bullet}OH \quad (4)$$

Recently, an increasing number of studies have focused on heterogeneous Fenton (HF) reactions, which utilize insoluble solid catalysts instead of soluble iron salts (Zhou et al, 2019). This approach offers several advantages, including the elimination of the need to optimize the H_2O_2/Fe^{2+} molar ratio, a reduction in sludge disposal issues, a wider operational pH range, and the ability to easily separate and reuse the catalyst (Ganiyu et al, 2018). In the HF process, the iron catalyst is present as solid-phase $\equiv Fe^{2+}$, typically hydroxylated with –OH groups, which can generate the same reactive species as in the homogeneous Fenton process, assuming similar surface reactions occur. Since the heterogeneous Fenton reaction is confined to the catalyst surface, it enables efficient •OH generation across a broader pH spectrum. This minimizes the dissolution of iron ions into the treated water, allowing for catalyst reusability and reducing sludge formation. However, heterogeneous Fenton systems also present some significant drawbacks, including lower reaction efficiency, slow regeneration kinetics of Fe^{2+}, and higher H_2O_2 consumption compared to homogeneous processes. The reduction of $\equiv Fe^{3+}$ to $\equiv Fe^{2+}$ by H_2O_2 is particularly slow, which can limit the overall reaction rate. Furthermore, the performance of HF reactions is highly dependent on interfacial properties. Therefore, a major challenge is to enhance the reaction kinetics of this rate-limiting step to maximize the activation and utilization of H_2O_2. Addressing this challenge requires the design and synthesis of supported iron catalysts with carefully controlled composition, morphology, structure, and electronic properties to optimize the density, accessibility, and stability of active sites (Poza-Nogueiras et al., 2018).

In this work, the degradation and mineralization of the model dye Acid Violet 19 (AV19) were systematically investigated using homogeneous Fenton, PF, HF and heterogeneous photo-Fenton (HPF) processes. The

effects of key operational parameters, including catalyst dosage and H_2O_2/Fe molar ratio, were examined in detail. For the heterogeneous systems, Fe_3O_4 nanoparticles were employed as a reusable catalyst, taking advantage of their magnetic properties for easy separation. Comparative performance assessments were conducted to evaluate the efficiency, mineralization degree, and operational advantages of each process.

MATERIALS AND METHODS

Fe_3O_4 nanoparticles were synthesized via the co-precipitation method. 200 mL of deionized water was heated to 90°C and purged with N_2 gas for 30 minutes. Aqueous solutions of 2 M $FeCl_2$ and 1 M $FeCl_3$ were prepared and combined to achieve a Fe^{2+}:Fe^{3+} molar ratio of 1:2 and the resulting mixture was maintained at 90°C for 45 minutes. During this period, 30 mL of 28% (w/w) ammonia solution was added dropwise over 30 minutes to gradually increase the pH of the reaction medium to 10–11. The suspension was then stirred at 90°C for 1 hour using a magnetic stirrer and subsequently cooled to room temperature. The synthesized Fe_3O_4 nanoparticles were separated from the suspension using a magnet, thoroughly washed with deionized water until a neutral pH was achieved, and dried at 25°C for 12 hours.

All experiments were performed in a 250 mL cylindrical glass reactor containing 200 mL of an aqueous solution with 0.05 mM Acid Violet 19 (AV-19) as the model pollutant at pH 3. The reaction mixtures were continuously stirred at 400 rpm using a magnetic stirrer. For the Fenton and photo-Fenton (PF) experiments, the catalyst (Fe^{2+}) concentration was varied between 0.1 mM and 0.75 mM at a fixed H_2O_2/Fe ratio of 20. After determining the optimal catalyst concentration, further experiments were conducted by varying the H_2O_2/Fe molar ratio between 5 and 40, using the optimal catalyst amount. For the heterogeneous Fenton (HF) and heterogeneous photo-Fenton (HPF) processes, the catalyst (Fe_3O_4) dosage was varied from 0.1 g L^{-1} to 0.75 g L^{-1} under a constant H_2O_2/Fe ratio of 20. Subsequently, the effect of the H_2O_2/Fe ratio was evaluated within the same range (5–40 mol/mol) using the optimized catalyst amount.

Samples were withdrawn at predetermined time intervals to monitor both the degradation and mineralization of AV-19. Dye degradation was monitored by measuring the absorbance at 546 nm using a UV–Vis spectrophotometer, while mineralization was assessed based on COD (chemical oxygen demand) analyses.

RESULTS and DISCUSSION

The results of studies conducted to determine the optimal Fe^{2+} amount in the treatment of AV-19 dye solution using the Fenton method are presented in Figure 1. The results indicate that increasing the catalyst amount from 0.1 mM to 0.75 mM enhances COD removal. The results of studies conducted to determine the optimal H_2O_2/Fe ratio for the mineralization of AV-19 solution using the Fenton method are presented in Figure 2. An increase in H_2O_2/Fe ratio up to 20 (mol/mol) positively affects COD removal, while no significant increase is observed beyond this amount. The lower COD removal observed at H_2O_2/Fe ratios below and above the optimal value can be explained by the consumption of $^{\bullet}OH$ due to reactions with H_2O_2 or Fe^{2+}.

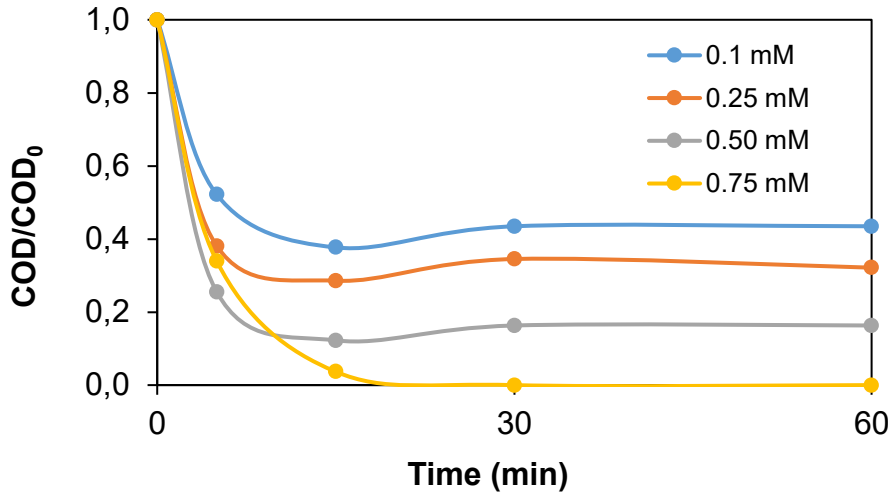

Figure 1. The effect of the catalyst amount on COD removal using the Fenton method

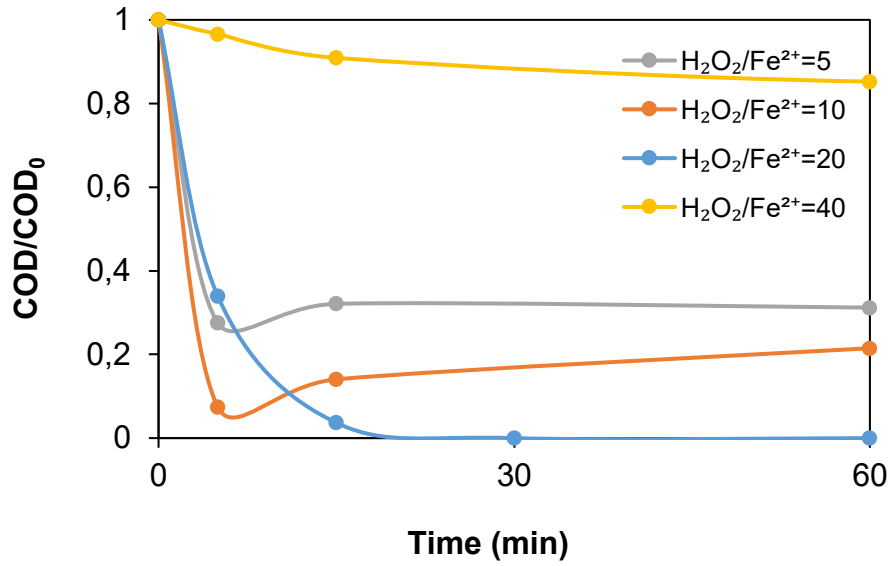

Figure 2. The effect of the H_2O_2/Fe ratio on COD removal using the Fenton method

The optimization experiments for Fe^{2+} dosage in the PF treatment of AV-19 dye solution are illustrated in Figure 3. An increase in catalyst concentration from 0.1 mM to 0.25 mM led to improved COD removal; however, further increases did not result in additional enhancement. Similarly, Figure 4 summarizes the findings regarding the effect of varying the H_2O_2/Fe molar ratio on the mineralization of AV-19 in the PF process. Raising the H_2O_2/Fe ratio to 20 (mol/mol) leads to improved COD removal, but further increases beyond this point do not provide additional benefit. The decrease in COD removal observed at ratios both below and above the optimum is attributed to the scavenging of •OH radicals through side reactions with excess H_2O_2 or Fe^{2+}.

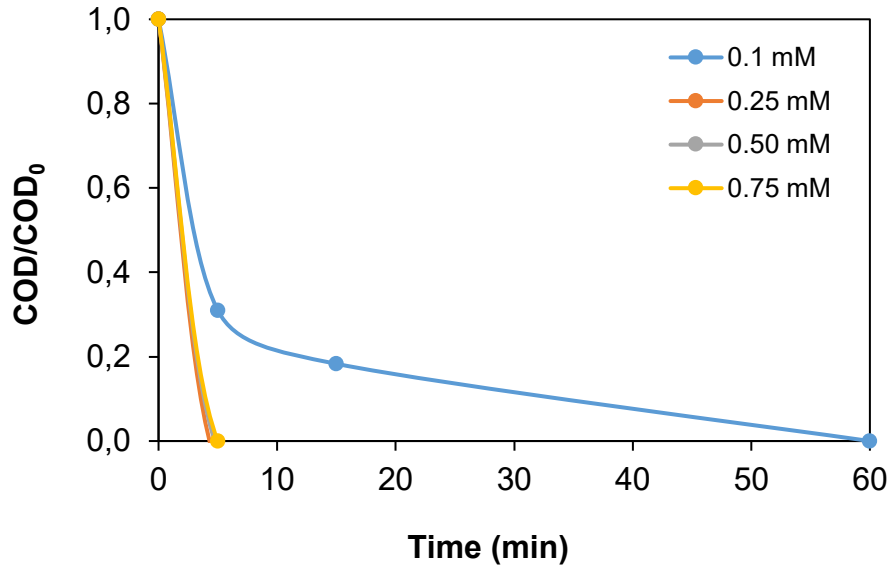

Figure 3. The effect of the catalyst amount on COD removal using the PF method

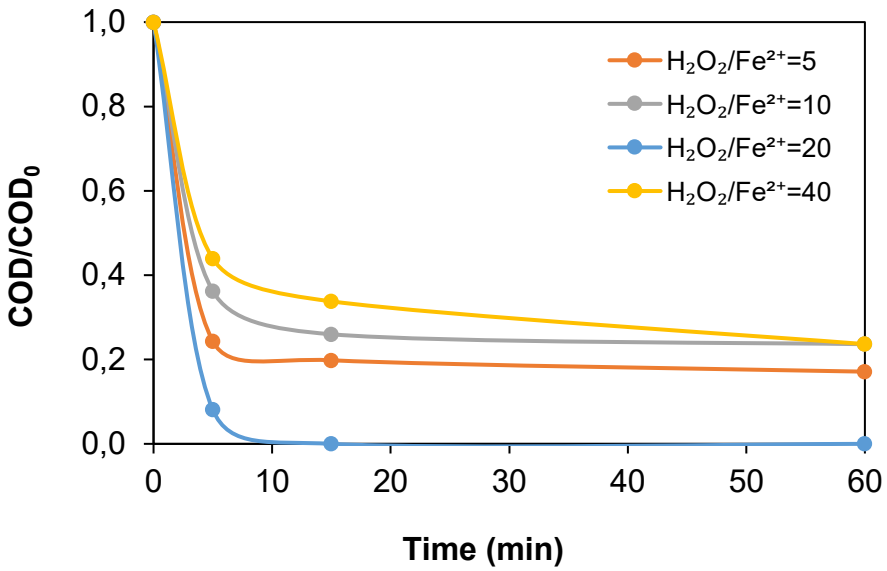

Figure 4. The effect of the H_2O_2/Fe ratio on COD removal using the PF method

Figure 5 displays the outcomes of experiments aimed at optimizing the Fe_3O_4 dosage in the HF treatment of AV-19 dye solution. Increasing the catalyst concentration from 0.1 g L^{-1} to 0.75 g L^{-1} over a 240-minute period led to improved COD removal. Figure 6 presents the evaluation of different H_2O_2/Fe molar ratios for effective mineralization of AV-19 via the HF process. Enhancing the H_2O_2/Fe ratio up to 20 (mol/mol) improves COD removal efficiency; however, increasing the ratio beyond this level does not yield further gains. Reduced COD removal at both lower and higher ratios is likely due to the scavenging of •OH radicals by excess H_2O_2 or $\equiv Fe^{II}$, which limits the availability of these reactive species for pollutant degradation.

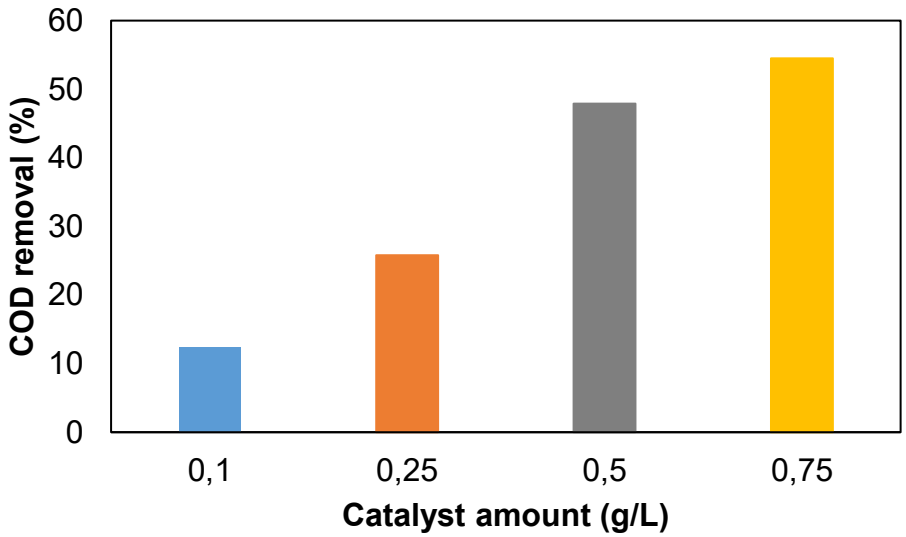

Figure 5. The effect of the catalyst amount on COD removal using the HF method

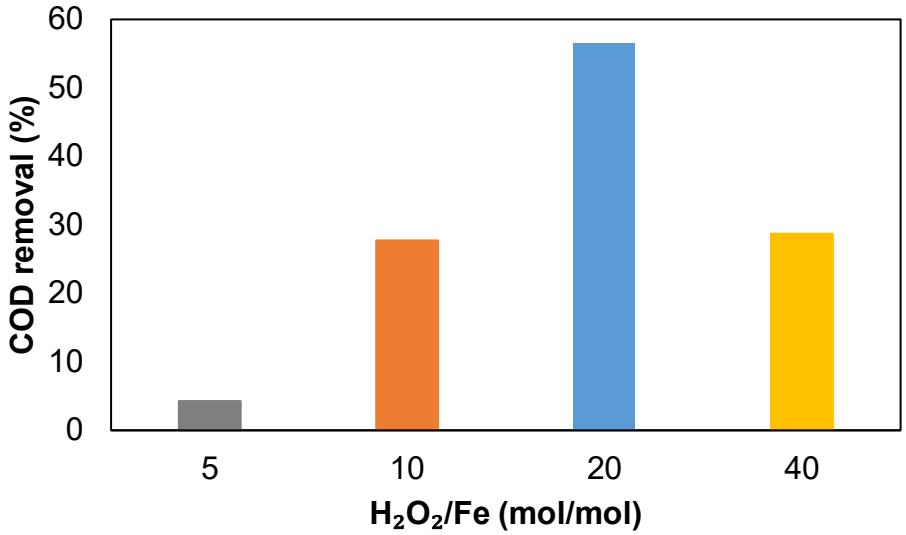

Figure 6. The effect of the H_2O_2/Fe ratio on COD removal using the HF method

Figure 7 shows the impact of varying Fe_3O_4 dosages on the removal of AV-19 in the HPF process. Increasing the catalyst amount from 0.1 g L^{-1} to 0.75 g L^{-1} over 240 minutes resulted in higher COD removal. Figure 8 provides the results regarding the optimization of the H_2O_2/Fe ratio for mineralizing AV-19 using the Fenton process. Increasing the H_2O_2/Fe ratio up to 20 (mol/mol) enhances COD removal; however, no substantial improvement is observed at higher ratios. The reduced COD removal at both suboptimal and excessive H_2O_2/Fe ratios can be attributed to the depletion of •OH radicals through side reactions with either H_2O_2 or $\equiv Fe^{II}$.

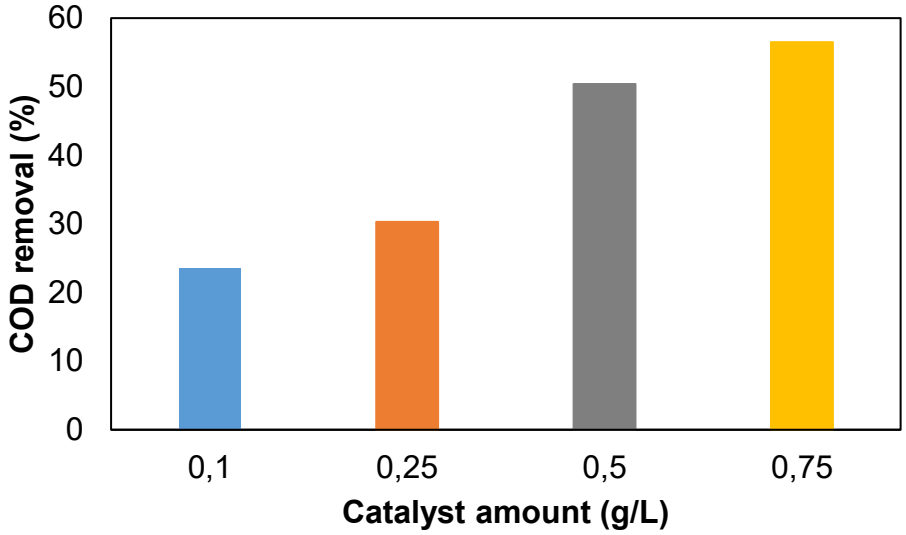

Figure 7. The effect of the catalyst amount on COD removal using the HPF method

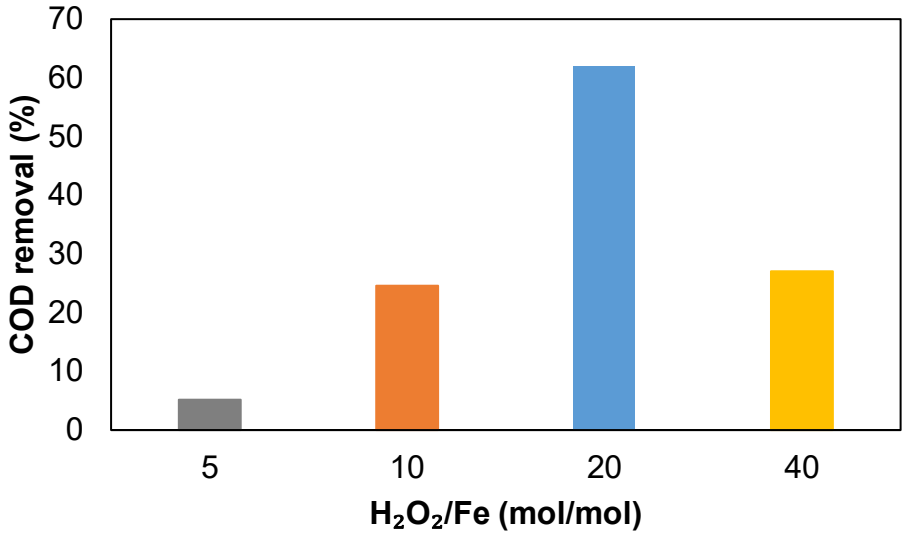

Figure 6. The effect of the H_2O_2/Fe ratio on COD removal using the HPF method

CONCLUSION

In this study, the removal of Acid Violet 19 (AV19) from aqueous solutions was systematically investigated using Fenton, PF, HF, and HPF advanced oxidation processes. The results demonstrated that all methods were effective in mineralizing AV19, with the PF and HPF processes achieving superior removal efficiencies in shorter times due to the enhanced generation of reactive radicals under UV irradiation. Optimal operating parameters were identified for each process. For the homogeneous systems, the optimal Fe^{2+} dosage and H_2O_2/Fe molar ratio were established. These findings contribute to the development of more efficient and environmentally friendly wastewater treatment strategies for dye-contaminated effluents.

ACKNOWLEDGEMENTS

Duygu Aydın and Selina Olcar acknowledge TUBITAK (The Scientific and Technological Research Council of Turkey) for providing financial support through 2209-A Research Project Support Programme for Undergraduate Students under grant number 1919B012417289.

REFERENCES

Annabi, C., Fourcade, F., Soutrel, I., Geneste, F., Floner, D., Bellakhal, N., & Amrane, A. (2016). Degradation of enoxacin antibiotic by the electro-Fenton process: optimization, biodegradability improvement and degradation mechanism. *Journal of environmental management*, *165*, 96-105.

Cornejo, O. M., Ortiz, M., Aguilar, Z. G., & Nava, J. L. (2021). Degradation of Acid Violet 19 textile dye by electro-peroxone in a laboratory flow plant. *Chemosphere*, *271*, 129804.

Ganiyu, S. O., Zhou, M., & Martínez-Huitle, C. A. (2018). Heterogeneous electro-Fenton and photoelectro-Fenton processes: a critical review of fundamental principles and application for water/wastewater treatment. *Applied Catalysis B: Environmental*, *235*, 103-129.

Laghrib, F., Bakasse, M., Lahrich, S., & El Mhammedi, M. A. (2021). Advanced oxidation processes: photo-electro-Fenton remediation process for wastewater contaminated by organic azo dyes. *International journal of environmental analytical chemistry*, *101*(15), 2947-2962.

Mondal, S., & Saha, S. (2018). Photophysics and Photochemistry of Conformationally Restricted Triarylmethanes: Application as Photoredox. *Photochemistry and Photophysics: Fundamentals to Applications*, 115.

Mukurala, N., Mokurala, K., Suman, S., & Kushwaha, A. K. (2021). Synthesis of porous Cu2FeSnS4 particles via solvothermal process for removal of organic acid fuchsin dye pollutant from wastewater. *Nano-Structures & Nano-Objects*, *26*, 100697.

Oturan, M. A., & Aaron, J. J. (2014). Advanced oxidation processes in water/wastewater treatment: principles and applications. A review. Critical reviews in environmental science and technology, 44(23), 2577-2641.

Pérez-Estrada, L. A., Maldonado, M. I., Gernjak, W., Agüera, A., Fernández-Alba, A. R., Ballesteros, M. M., & Malato, S. (2005). Decomposition of diclofenac by solar driven photocatalysis at pilot plant scale. *Catalysis Today*, *101*(3-4), 219-226.

Poza-Nogueiras, V., Rosales, E., Pazos, M., & Sanroman, M. A. (2018). Current advances and trends in electro-Fenton process using heterogeneous catalysts–a review. *Chemosphere*, *201*, 399-416.

Zhou, Y., Lu, J., Zhou, Y., & Liu, Y. (2019). Recent advances for dyes removal using novel adsorbents: a review. *Environmental pollution*, *252*, 352-365.

➢ *ORAL PRESENTATION*

Rhabdomyosarcoma in a Malaklı Mixed-Breed Bitch

Enes Çerçi[1*] *(https://orcid.org/ 0009-0004-0554-2199)*, Gaye Bulut[2] *(https://orcid.org/0000-0003-4500-1958)*, Osman Dağar[3] *(https://orcid.org/0000-0003-2209-7512)*, Mehmet Tuzcu[4] *(https://orcid.org/ 0000-0003-3118-1054)*

[*1,2]Aksaray University, Faculty of Veterinary Medicine, Department of Obstetrics and Gynecology, Aksaray, Türkiye.

[3]Aksaray University Eskil Vocational School Laboratory and Veterinary Health Program, Aksaray, Türkiye

[4]Selcuk University, Faculty of Veterinary Medicine, Department of Pathology, Konya, Türkiye

*Corresponding author e-mail: enes.cerci@aksaray.edu.tr

Abstract

Canine uterine neoplasia is a rare condition in veterinary medicine, accounting for 0.3-0.4% of all tumor cases in dogs. Epidemiological studies indicate that canine cancer accounts for 40-50% of deaths in dogs over 10 years of age. This article reports the case of a 3-year-old female Malinois mix dog affected by rhabdomyosarcoma, despite being a young animal.A 3-year-old female mixed-breed dog weighing 36.8 kg, which had given birth to one live puppy and had been bred during the subsequent estrus cycle, was brought to the Obstetrics and Gynecology Clinic of the Veterinary Faculty of Aksaray University with a history of hemorrhagic vaginal discharge on the 57th day of pregnancy. On examination, mammary gland development and lactation were noted, but no fetus was detected on ultrasonographic examination. A diagnosis of pseudopregnancy was made. Based on the clinical findings and hemogram results, medical treatment was initiated. The therapeutic protocol included Bromocriptine (Parlodel® 2,5 mg tablets, 100 µ/kg/day, 14 days) and a broad-spectrum antibiotic (8,75 mg/kg/day, 5 days, SC, Synulox, Zoetis). At the owner's request, an ovariohysterectomy was performed two weeks later. The surgical intervention was performed along the median line, and thickening of the uterine tissue and a firm, lump-like swelling in the cranial part of the right uterine horn were detected. The uterine tissue was histopathologically evaluated. Histopathological evaluation revealed soft tissue cancer (rhabdomyosarcoma). Rhabdomyosarcoma is a type of soft tissue sarcoma and a rare form of cancer. It is a malignant neoplasm that primarily develops in muscle tissue. The initial symptom in the affected area may be a lump or swelling.

Keywords: Female Dog, Neoplasm, Rhabdomyosarcoma, Uterus.

INTRODUCTION

Tumor growth in a dog's genital tract may not be common, but it may show signs like hormonal disorders. The tumors that arise in the uterus are very rare, only accounting for 0.3-0.4% of all tumors (Percival et al., 2018; Almeida et. al., 2023). Uterine tumors are mostly diagnosed late in life. Diagnosis is also difficult, as they often have vague symptoms (Troisi et al. 2023).

Rhabdomyosarcoma (RMS) is a kind of malignant tumor that starts with mesodermal tissue and has slight muscle differentiation. The head-neck region, extremities, and urogenital system are typically affected (Headley et al, 2006). In organs having smooth muscle tissue, like that of the uterus, it is quite rare (Marino et al., 2007). Knowing this, uterine RMS diagnosis in a young female dog is an uncommon case in the veterinary literature. The case adds considerable knowledge to the literature (Marino et al., 2007; Almeida et al., 2023).

MATERIALS AND METHODS

Case Description:

The subject of our examination is a 3-year-old Malakli crossbreed female dog, 36,8 kg. The case was first presented at the Aksaray University Faculty of Veterinary Medicine Obstetrics and Gynecology Clinic, at 57-day pregnant. The patient showed signs of bleeding from the vagina. A repeat ultrasound did not show evidence

of a fetus but showed development and lactation in the breasts. Researchers collected blood samples. Then, they performed hemogram and biochemical analyses using certain equipment. Doctors have diagnosed this dog to be pseudopregnant. The patient was administered medical treatment. Accordingly, bromocriptine (Parlodel®) was administered at 100 µg/kg for 14 days. Also, a broad-spectrum antibiotic (SC, Synulox, Zoetis) at a dose of 8,75 mg/kg was administered for 5 days. Thus, the owner asked that the procedure be performed, and ovariohysterectomy was done subsequently.

The patient was anesthetized using ketamine hydrochloride (5-7,5 mg/kg IM) with domitor (medetomidine hydrochloride, 80 µg/kg) as pre-anesthetic. The surgical procedure was performed successfully on patient. Median line laparotomy was performed to achieve OHE. The patient showed evidence of the uterine tissue thickening and a hard lump in the right uterine horn. Histopathological examination was conducted on uterine tissue.

Tissue samples were preserved in 10% formalin for a period of 48 hours. The standard tissue processing procedure was carried out using a Leica TP1020 tissue processor with a series of graded alcohols, xylene, xylene-paraffin, and paraffin. Following this processing, the tissues were embedded in paraffin. Tissue sections measuring 4 µm in thickness were obtained from the paraffin blocks and subjected to staining with Hematoxylin-Eosin (HxE). Following the staining process, the preparations were examined under an Olympus BX51 light microscope and photographed using an Olympus DP12 camera (Tokyo, Japan).

RESULTS

Biochemical and Hematological Analyses:

The biochemical parameters of the animal are usually within normal limits (see Table 1). The only abnormal parameter found was the raised blood sugar (glucose) level. One possibility is that this is transient stress hyperglycemia or the use of prednisolone or diabetes. In conjunction with clinical finds, this phenomenon needs to be studied in detail. It is interesting that there is no abnormal disease in the body as the test results show no liver, kidney or electrolyte balance abnormalities.

Table 1. Biochemical analysis results (MNChip, Point Care V3).

Parameter	Value	Reference Range	Interpretation
TP	6.2	5.2–8.2 g/dL	Within normal limits.
ALB	3	2.2–4.4 g/dL	Normal. Indicates adequate liver function and nutritional status.
GLO	3.2	2.3–5.2 g/dL	Normal. Immune system activity is within expected limits.
A/G	0.9	-	Albumin/Globulin ratio is balanced; not indicative of inflammation.
TBIL	0.15	0.1–0.9 mg/dL	Normal. No signs of hemolysis or bile duct obstruction.
ALT	25	10–140 U/L	Liver enzymes are within normal range.
ALP	26	20–150 U/L	Normal. No evidence of bone or biliary stress.
AMY	946	400–3500 U/L	Normal. No indication of pancreatic stress.
CHOL	157	110–320 mg/dL	Within normal range. No metabolic disorder suspected.
GLU	**272 ***	70–143 mg/dL	Elevated. Suggestive of stress-induced hyperglycemia, diabetes, or corticosteroid influence.
CRE	0.47	0.3–0.7 mg/dL	Normal. Renal function appears to be intact.
BUN	11	0.7–32 mg/dL	Normal. Nitrogenous waste excretion is adequate.
BUN/CRE	23	-	Normal ratio. No indication of renal or post-renal issues.

Ca	9.4	7.9–11.8 mg/dL	Normal. Indicates sufficient bone metabolism and muscle function.
P	4.75	2.5–6.8 mg/dL	Normal. Stable bone and energy metabolism.
K+	5.39	3.7–5.8 mmol/L	Normal. Electrolyte balance is preserved for muscle, nerve, and cardiac function.
Na	154	138–160 mmol/L	Normal. Electrolyte balance is maintained.
Na/K	29	-	Within normal limits. Suggests normal adrenal function.
TBA	1.61	0–20 µmol/L	Normal. Indicates proper liver function.

According to reference range * High value

Table 2 shows that the results confirm the findings of the stress leukogram; this is characterized by lymphopenia, neutrophilia, and granulocyte gain. In addition, microcytic hypochromic anemia findins(i.e. MCV, MCH low; RDW high) are noteworthy and may be due to iron deficiency. The patient's hematocrit value is slightly low, which can be attributed to mild dehydration. The evaluation of platelet count and related parameters is unremarkable. Not bleeding and not thrombocytopenic.

Table 2. Hematological parameters (Mindray 2008Vet).

Parameter	Result	Reference Range	Interpretation
WBC	15.4	6.0–17.0 ×10⁹/L	Normal. Close to the upper limit, should be monitored.
Lymph#	**0.6****	0.8–5.1 ×10⁹/L	Low. May indicate stress or acute inflammation.
Mono#	**0.3**	0.0–1.8 ×10⁹/L	Normal.
Gran#	**14.5***	4.0–12.6 ×10⁹/L	High. Suggestive of acute inflammation or stress response.
Lymph%	**4.1****	12.0–30.0%	Low. Consistent with a stress leukogram.
Mono%	**1.7****	2.0–9.0%	Low. May not be clinically significant.
Gran%	**94.2***	60.0–83.0%	High. Indicative of neutrophilia.
RBC	6.23	5.50–8.50 ×10¹²/L	Normal.
HGB	12.2	11.0–19.0 g/dL	Normal.
HCT	**37.6****	39.0–56.0%	Low. Mild anemia may be present.
MCV	**60.5****	62.0–72.0 fL	Low. Suggestive of microcytic anemia.
MCH	**19.5****	20.0–25.0 pg	Low. Consistent with hypochromia.
MCHC	32.4	30.0–38.0 g/dL	Normal.
RDW	**16.9***	11.0–15.5%	High. Possible regenerative anemia or iron deficiency.
PLT	437	117–460 ×10⁹/L	Normal.
MPV	9.4	7.0–12.9 fL	Normal.
PDW	15.6	-	Slightly increased. Monitoring recommended.
PCT%	0.41	-	Within normal range.
Eos%	1.6	-	Considered normal (generally 0–5%).

According to reference range * High value ** Low value

Histopathological evaluation:

Macroscopically, a white, round, nodular mass measuring 2x2x2 cm was detected in the uterine tissue (see Table 3 for details). Microscopically, numerous atypical cells with anisocytosis, anisokaryosis, and pleomorphism were detected in the muscle tissue of the uterus. The presence of cytoplasmic vacuoles was identified in the cells. The cells within the tissue manifested a variety of morphologies, including oval-shaped

cells and elongated atypical cells. Furthermore, a significant number of nucleoli were observed in the cells (see Table 4).

Table 3. Macroscopic appearance of the uterus containing tumor tissue: a mass measuring 2x2x2 cm.



Table 4. Histopathological findings. A: General appearance of the tumor mass in the uterus, HE, x20. B: Numerous atypical cells showing anisocytosis, anisonucleosis, and pleomorphism (black arrows), HE, x40.

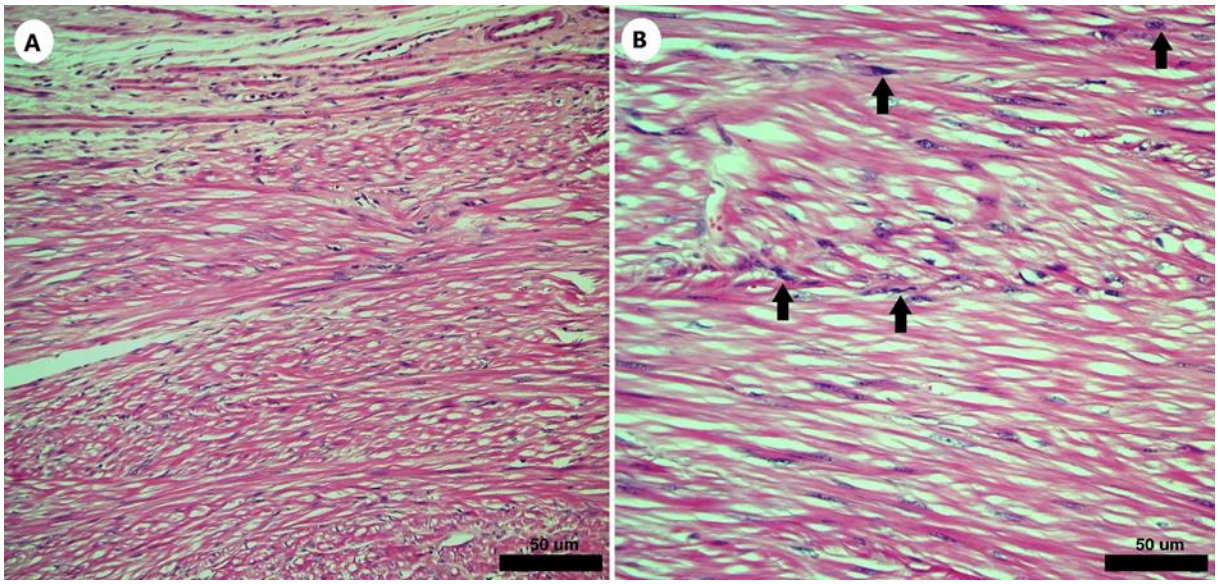

DISCUSSION

Rhabdomyosarcomas have been observed to occur with high frequency in canines of a young age, thereby reflecting the neoplasm's high malignant potential (Headley et al., 2006). The RMS diagnosed in the 3-year-old female dog described in this study is consistent with the age range and localization reported in previous studies (Almeida et al., 2023). Given the rarity of cases of RMS developing in the uterus, this case presentation is significant for comparative evaluation with similar cases (Marino et al., 2007; Troisi et al., 2023).

Rhabdomyosarcomas, on the other hand, are typically characterized by the following properties: they are macroscopically white, nodular in structure, >1 cm in size, and solid in character. Hemorrhage and necrosis may be present as well (Marino et al., 2007; Almeida et al., 2023). In this case, the detection of a 2x2x2 cm white, nodular mass in the right horn of the uterus is consistent with the classic RMS morphology described.

Pleomorphism, anisocytosis, and anisokaryosis are seen in atypical cells. Striations are frequently discerned within the cytoplasm. The cell shapes may vary from oval to spindle-shaped (Marino et al. 2007; Almeida et

al. 2023). The histopathological findings described in this study (pleomorphic cells, numerous nucleoli, prominent striations), are classic for rhabdomyosarcoma.

This case also showed significant hematological and biochemical abnormalities from a clinical pathology perspective. The complete blood count showed that the patient had leukocytosis with marked granulocytosis (14.5 × 10^9/L), granulocyte dominant (94.2%) and reduced lymphocyte counts (0.6 × 10^9/L; 4.1%). These findings were suggestive of a stress leukogram as is seen in animal under acute stress; infection; or corticosteroid effect (Weiser, 2012). As per Thrall 2012, low MCV (60.5 fL), low MCH (19.5 pg), and high RDW (16.9%) values of the erythrocytes indicate development of the microcytic, hypochromic, anisocytotic type of anaemia which is commonly develop in Fe deficiency or disease states.

Furthermore, with prior test showing no adverse biochemical changes, only the elevated blood glucose level of 272 mg/dL suggests stress-induced hyperglycemia, a common occurrence in dogs under extreme stress (Rand et al., 2002). Normal total protein, albumin, and electrolyte values and lack of significant liver enzyme elevation rule out significant liver or kidney involvement at the time of examination.

Rhabdomyosarcomas are commonly observed in animals aged 2–3 years. These cells have been found in the head and neck region, urogenital region, retroperitoneum, and limbs (Erer and Kıran, 2009; Meuten, 2020). The age of the animal described in this case report, as well as the fact that the mass was removed from the uterus, support the findings reported in the existing literature. The macroscopic appearance of rhabdomyosarcomas is typically characterized by a pink-gray or white coloration, round nodular shape, and generally larger than 1 cm in size. Necrosis and bleeding may be observed (Erer and Kıran 2009). The mass's white coloration, round shape, and nodular appearance are consistent with the literature. Microscopically, rhabdomyosarcomas manifest cells with granular or vacuolated cytoplasm and variable nuclear sizes (Erer and Kıran, 2009). The number of nucleoli in the cells may exceed one, and mitosis is frequently observed (Erer and Kıran 2009). In certain instances, multinucleated giant cells may be identified. These cells typically exhibit cytriation. Furthermore, cells with elongated shapes, small nuclei, and an absence of cytriation may also be observed (Erer and Kıran, 2009). The presence of oval and elongated cells with numerous nucleoli, anisocytosis, anisokaryosis, and pleomorphism in muscle tissue supports the diagnosis of rhabdomyosarcoma.

Veterinary literature does not often report RMS in smooth muscle tissues, including the uterus, making this case particularly unique. On the contrary, some benign genital tumors like adenoma of the uterine tube can reach a large mass (Pierezan et al., 2016; Marino et al., 2007). Histopathological confirmation can only resolve the differential diagnosis in such cases.

Even surging imaging techniques can detect tumors and localized invasion. However, surgical excision and histopathological examination remain the gold standard for sarcomas like RMS which usually grow quickly (Russo et al., 2021).

CONCLUSION

This case presentation shows that uterine rhabdomyosarcoma, a rare condition in dogs, can also occur at a young age. If a doctor strongly believes that a disease is present, the patient must be evaluated by ultrasound and histopathological examination of the surgically excised tissue. This case shows how important it is for veterinarians to consider genital system tumors. The reported similar cases in the literature will allow better insight into the pathogenesis and prognosis of these rare neoplasms.

REFERENCES

Almeida, G. C., Hadi, N. I. I. A., Moutinho, I., Oliveira, V. C., Oliveira, V. M., Gonçalves, G. F., Elias, F., & Dalmolin, F. (2023). Mammary cystadenoma: Diagnosis and treatment in a bitch. Acta Scientiae Veterinariae, 51(Suppl 1), 917.

Erer H, Kıran M, 2009. "Mezenkimal Tümörler". Veteriner Onkoloji, Editör(ler): Prof.Dr. Hüdaverdi Erer, Prof. Dr. Metin Münir Kıran, Konya, Selçuk Üniversitesi Basımevi, p: 93-94

Marino, G., Quartuccio, M., Cristarella, S., Nicotina, P. A., & Zanghì, A. (2007). Adenoma of the uterine tube in the bitch: Two case reports. Veterinary Research Communications, 31(Suppl 1), 173–175.

Meuten DJ, 2020. "Tumors of Muscle" . In: Tumors in domestic animals, Editor Donald J. Meuten. Fifth Edition. John Wiley & Sons, p: 445-449 .

Percival, A., Singh, A., Linden, R. A., Watrous, G., Patten, S., Valverde, A., Ratsep, E. (2018). Massive uterine lipoleiomyoma and leiomyoma in a miniature poodle bitch. Can Vet J., 59(8):845–850.

Pierezan, F., Trost, M. E., & Barros, C. S. L. (2016). Uterine tube adenoma in a bitch. Brazilian Journal of Veterinary Pathology, 9(1), 27–30.

Rand, J. S., Kinnaird, E., Baglioni, A., Blackshaw, J. K., & Priest, J. (2002). Acute stress hyperglycemia in cats is associated with activation of the hypothalamic-pituitary-adrenal axis. *Journal of Feline Medicine and Surgery*, 4(2), 99–108. https://doi.org/10.1053/jfms.2001.0200

Russo, M., England, G. C. W., Catone, G., & Marino, G. (2021). Imaging of canine neoplastic reproductive disorders. Animals, 11(5), 1213. https://doi.org/10.3390/ani11051213

Thrall, M. A. (2012). Hematology of Common Domestic Species. In Veterinary Hematology and Clinical Chemistry (pp. 61-113). John Wiley & Sons, Inc. Wiley-Blackwell

Troisi, A., Orlandi, R., Vallesi, E., Pastore, S., Sforna, M., Quartuccio, M., Zappone, V., Cristarella, S., & Polisca, A. (2023). Clinical and ultrasonographic findings of ovarian tumours in bitches: A retrospective study. Theriogenology, 210, 227–233. https://doi.org/10.1016/j.theriogenology. 2023.07.020

Weiser, G. (2012). Hematology of Common Domestic Species. In Veterinary Hematology and Clinical Chemistry (pp. 118-139). John Wiley & Sons, Inc. Wiley-Blackwell, USA.

➢ *ORAL PRESENTATION*

Degradation and mineralization of acid fuchsin dye from aqueous media by means of electrochemical water treatment methods

Selen Özdemir[1] (*ORCID: https://orcid.org/0009-0002-3586-8937*), Elif Nesli Yanık[1] (*ORCID: https://orcid.org/0009-0001-1722-5383*), Melis Genç[1] (*ORCID: https://orcid.org/0009-0007-7208-2489*), Eylül Öztürk[1] (*ORCID: https://orcid.org/0009-0003-8265-6694*), Ceren Eğilmezcan[1] (*ORCID: https://orcid.org/0009-0003-5153-0853*), Baran Özyurt[1] (*ORCID: https://orcid.org/0000-0003-0011-8351*), Şule Camcıoğlu[1*] (*ORCID: https://orcid.org/0000-0002-8983-3193*)

[*1]Ankara University, Faculty of Engineering, Department of Chemical Engineering, Ankara, Turkey.

*Corresponding author e-mail: camcioglu@eng.ankara.edu.tr

Abstract
Dyes are complex organic pollutants widely used in industries such as textiles, and their persistence in wastewater poses serious risks to aquatic ecosystems and human health. Due to the high stability and solubility of these compounds, conventional physical, chemical, and biological treatment methods are generally insufficient for their complete removal. Consequently, there is growing interest in advanced electrochemical technologies that can achieve more effective treatment of dye-contaminated wastewater.
This study systematically compared several advanced electrochemical and hybrid processes for the removal of a model dye, Acid Fuchsin, from aqueous solutions. The investigated methods included electrocoagulation (EC), anodic oxidation (AO), sequential electrocoagulation followed by anodic oxidation (EC&AO), combined EC/AO using a bipolar iron electrode, and peroxy-electrocoagulation (PEC). EC was performed with aluminum electrodes at 100 mA and pH 6, achieving complete color removal within 10 minutes, but without significant COD reduction. AO, utilizing a boron-doped diamond (BDD) anode and carbon felt (CF) cathode at 500 mA and pH 6, resulted in 97% color removal within 30 minutes and complete COD removal in 90 minutes. In the sequential process (EC&AO), water first treated by EC was subsequently subjected to AO at 300 mA and pH 6, yielding 100% color removal after 10 minutes and complete COD removal after 120 minutes. The combined EC/AO method, performed with BDD, CF, and a bipolar iron electrode at 300 mA and pH 5, delivered 97% color removal in 60 minutes and full COD removal in 180 minutes. PEC, using an iron anode and CF cathode at pH 7 (H_2O_2/Fe molar ratio 0.5, 100 mA), achieved complete color removal in just 9 minutes and 98% COD removal in 180 minutes. These results highlight the high efficiency of advanced electrochemical methods, particularly hybrid and PEC approaches, for the rapid decolorization and mineralization of persistent dyes under optimized conditions.
Keywords: Electrocoagulation, Anodic oxidation, Peroxy-electrocoagulation, Hybrid Electrochemical Treatment, Acid Fuchsin, Water decolorization.

INTRODUCTION

The textile industry extensively utilizes water-intensive processes, and dyes used in this sector constitute a major source of water pollution. Globally, approximately 15% of dyes applied in industries are directly discharged into water bodies as wastewater (Durmus et al., 2019). Textile dyes typically exhibit recalcitrance and persistence, being highly resistant to biodegradation and causing prolonged environmental problems. Dye concentrations in textile wastewater typically range from 5 to 30 mg/L (Wang et al., 2017). These pollutants reduce the transparency of water bodies, thus hindering photosynthesis of aquatic plants. Additionally, dyes increase biochemical oxygen demand (BOD) and chemical oxygen demand (COD), destabilize ecosystems, and adversely affect plant growth (Kuczyński et al., 2021). Moreover, they exhibit harmful properties, such as toxicity, mutagenicity, and carcinogenicity (Fungaro et al., 2011).

Acid Fuchsin (AF), selected as a model pollutant, is a widely used industrial dye known to pose serious environmental threats. AF, an acidic violet-colored dye with the chemical formula $C_{20}H_{17}N_3Na_2O_9S_3$, is employed in dyeing both natural (such as leather) and synthetic textiles, as well as a staining agent and corrosion inhibitor in laboratories (Yu et al., 2020). Released into aquatic environments, AF reduces water transparency, thereby threatening aquatic life and disturbing ecological balances by hindering plant growth (Kuczyński et al., 2021). Additionally, its high water solubility facilitates widespread environmental contamination (Kuczyński et al., 2021).

Due to the inadequacy of conventional wastewater treatments—such as physical processes (flotation, filtration, sedimentation), chemical processes (coagulation/flocculation, chlorination, adsorption, ion exchange), and biological processes (activated sludge, aerated lagoons, membrane bioreactors)—for effectively removing dye pollutants, advanced treatment technologies have attracted considerable attention in recent years (Özyurt and Camcıoğlu, 2018). Therefore, it is necessary to develop novel treatment methods that efficiently remove dye contaminants, ensuring sustainable water resource management.

Electrocoagulation (EC) is among these advanced techniques widely employed to remove colloidal pollutants, such as dyes, from wastewater (Ozyurt et al., 2017). EC is a physicochemical process involving simultaneous anodic dissolution and cathodic hydroxide generation, producing metal hydroxide flocs that capture pollutants (Camcıoğlu et al., 2017). It effectively removes pollutants without requiring preliminary pH adjustments before discharge. In EC, metal coagulants are generated in situ through anodic dissolution of iron or aluminum electrodes (Hakizimana et al., 2017). Metal cations released at the anode rapidly form insoluble metal hydroxide flocs, facilitating adsorption of pollutants and colloidal particles. The reactions occurring at the electrodes are represented as follows (Eq. (1)-(3)):

$$Al^{+3} + 3H_2O \rightarrow Al(OH)_3 + 3H^+ \quad (1)$$

$$Fe^{+2} + 2OH^- \rightarrow Fe(OH)_2 \quad (2)$$

$$4Fe(OH)_2 + O_2 + 2H_2O \rightarrow 4Fe(OH)_3 \quad (3)$$

Advanced oxidation processes (AOPs) have emerged as effective technologies for removing non-biodegradable, recalcitrant, and toxic pollutants (Oturan and Aaron, 2014). AOPs generate highly reactive hydroxyl radicals (•OH), capable of degrading various organic contaminants. Their advantages include the use of environmentally friendly reagents, short reaction times, and minimal mass-transfer limitations (Mirzaei et al., 2017). Different mechanisms for •OH generation in AOPs include chemical, photochemical, sonochemical, and electrochemical methods (Oturan and Aaron, 2014). Electrochemical advanced oxidation processes (EAOPs), such as anodic oxidation (AO), remove pollutants directly at electrode surfaces or indirectly via oxidants generated in solution. AO efficiency strongly depends on the anode material selected (Asfaha et al., 2021). Pollutants are oxidized directly by •OH produced at the anode surface or indirectly by electrogenerated oxidants such as chlorine species, ozone, or hydrogen peroxide. Boron-doped diamond (BDD) electrodes notably enhance COD removal efficiency (Migliorini et al., 2011). AO provides versatile operation, compatibility with automation, and environmental safety (Özyurt et al., 2017). Direct AO mechanism reactions are represented below (Eq. (4)-(5)):

$$H_2O + S \rightarrow S[^\bullet OH] + H^+ + e^- \quad (4)$$

$$R + S[^\bullet OH] \rightarrow S + RO + H^+ + e^- \quad (5)$$

Here, S indicates active sites on the anode surface, and R denotes the organic pollutant.

In addition to standalone EC and AO applications, sequential (EC&AO) and combined (EC/AO) methods have received considerable attention. EC&AO involves initial coagulation and settling with EC, followed by AO mineralization of residual dissolved organics. In EC/AO, coagulation and oxidation processes occur simultaneously within a single reactor equipped with bipolar metal electrodes for EC and BDD electrodes (for AO), enabling efficient dye removal and mineralization (Asfaha et al., 2021). EC&AO demonstrates lower energy consumption, while EC/AO offers advantages in simplicity, operational convenience, and reduced initial investment costs (Özyurt et al., 2017).

The electro-Fenton (EF) process effectively mineralizes refractory pollutants. EF continuously generates H_2O_2 electrochemically (Eq. (6)), which subsequently reacts with Fe^{2+} (Eq. (7)), forming •OH that degrade organic contaminants to CO_2, water, and inorganics (Oturan and Aaron, 2014):

$$O_2 + 2H^+ + 2e^- \rightarrow H_2O_2 \quad (6)$$

$$Fe^{2+} + H_2O_2 \rightarrow Fe^{3+} + OH^- + ^\bullet OH \quad (7)$$

Peroxy-coagulation (PC) combines EC and EF by continuously generating H_2O_2 cathodically while oxidizing Fe anodically, promoting pollutant degradation through •OH and precipitation of organics by $Fe(OH)_3$ (Alalwan et al., 2023). Peroxy-electrocoagulation (PEC), distinguished by external addition of H_2O_2, achieves

high efficiency, shorter reaction times, and lower energy use, making it practical for advanced wastewater treatment applications (Alalwan et al., 2023).

In this work, the efficiency of EC, AO, EC&AO, EC/AO, and PEC processes was systematically investigated for the removal of Acid Fuchsin, a model dye pollutant, from aqueous solutions. Comprehensive experimental studies were conducted to assess and compare the color and chemical oxygen demand (COD) removal efficiencies of each process under various operational conditions. The effects of electrode type, current density, pH, and oxidant dosage were thoroughly examined. The findings presented herein provide valuable information of advanced electrochemical methods for efficient dye and organic pollutant removal aqueous media, aiming to support the development of sustainable and cost-effective water treatment strategies.

MATERIALS AND METHODS

EC experiments were performed in a 250 mL glass reactor containing 200 mL of 0.05 mM Acid Fuchsin solution and 50 mM Na_2SO_4 as the supporting electrolyte. Aluminum and iron electrodes were separately used as both anode and cathode, placed 10 mm apart, and connected to a DC power supply. When current was applied, metal ions released from the anode reacted with dye molecules to form insoluble flocs, facilitating dye removal. A magnetic stirrer ensured homogeneous mixing. The effects of applied current intensity, initial pH, and electrode material were investigated. Samples were periodically collected for analysis.

AO was conducted in a similar 250 mL reactor containing 200 mL of 0.05 mM Acid Fuchsin solution with 50 mM Na_2SO_4. A boron-doped diamond (BDD) anode and carbon felt (CF) cathode, placed parallel and carefully separated, were used. Initial pH values were adjusted using 0.2 M H_2SO_4 and 0.1 M NaOH. The system operated at different current intensities supplied by a DC power source. A magnetic stirrer maintained solution homogeneity. Samples were taken periodically to measure dye degradation and COD removal efficiency.

The EC&AO method was conducted sequentially. Firstly, EC was performed as described previously using aluminum electrodes, under optimized current (300 mA) and pH (6). Following EC treatment (2 hours), the solution was allowed to settle overnight for effective removal of formed flocs ($Al(OH)_3$). The clarified supernatant was then treated using AO with a BDD anode and CF cathode. The initial pH was readjusted as required. Periodic sampling for color and COD analyses assessed treatment efficiency.

The combined EC/AO experiments were performed simultaneously in a single 250 mL reactor containing 200 mL of 0.05 mM Acid Fuchsin and 50 mM Na_2SO_4 solution. The configuration involved a BDD anode, CF cathode, and a bipolar iron electrode between them. Initial pH was adjusted using acid or base solutions. The DC power supply maintained constant current, and homogeneous mixing was ensured via magnetic stirring. Experiments were also briefly tested with an aluminum bipolar electrode under optimized conditions for comparative evaluation. Periodic samples were collected for absorbance (color) and COD analysis.

The PEC process involved an iron anode and graphite felt cathode within a similar electrochemical reactor containing 200 mL of 0.05 mM Acid Fuchsin solution and 50 mM Na_2SO_4. Compressed air was continuously supplied to produce in-situ hydrogen peroxide (H_2O_2) at the cathode. Initial pH was adjusted precisely (pH range: 3–9) using 0.2 M H_2SO_4 and 0.1 M NaOH. Additional H_2O_2 was externally supplied to achieve desired H_2O_2/Fe molar ratios when required. The system operated under constant stirring at 400 rpm. Regular sampling was conducted over 180 minutes to determine dye removal and COD reduction.

Dye removal efficiency was determined by measuring absorbance at 546 nm using a UV-Vis spectrophotometer. COD removal was evaluated using standard COD analysis methods. Optimization studies for EC considered electrode materials, current intensity, and pH; AO examined the effects of current intensity and pH; EC&AO evaluated current intensity, electrode materials, and pH; EC/AO investigated current intensity, bipolar electrode material, and pH; PEC explored the effects of initial pH, H_2O_2/Fe molar ratio, and current intensity.

RESULTS and DISCUSSION

The results of studies conducted to determine the effect of electrode material under optimal current intensity 100 mA and pH 6 for the treatment of Acid Fuchsin solution using the EC method are presented in Figure 1. Al electrode produces Al^{3+} ions in water to form hydroxide complexes such as $Al(OH)_3$. These complexes have a gel-like structure with high surface area and can effectively adsorb dyes. Fe electrode produces Fe^{2+} and Fe^{3+} ions to form hydroxides such as $Fe(OH)_2$ and $Fe(OH)_3$. However, these hydroxides are generally heavier and the adsorbent surface area may be lower. Iron corrodes more rapidly and a passivation layer may form, which

slows down electrochemical reactions. A rapid color removal within 10 min was observed with Al electrodes while no significant COD removal was achieved during treatment.

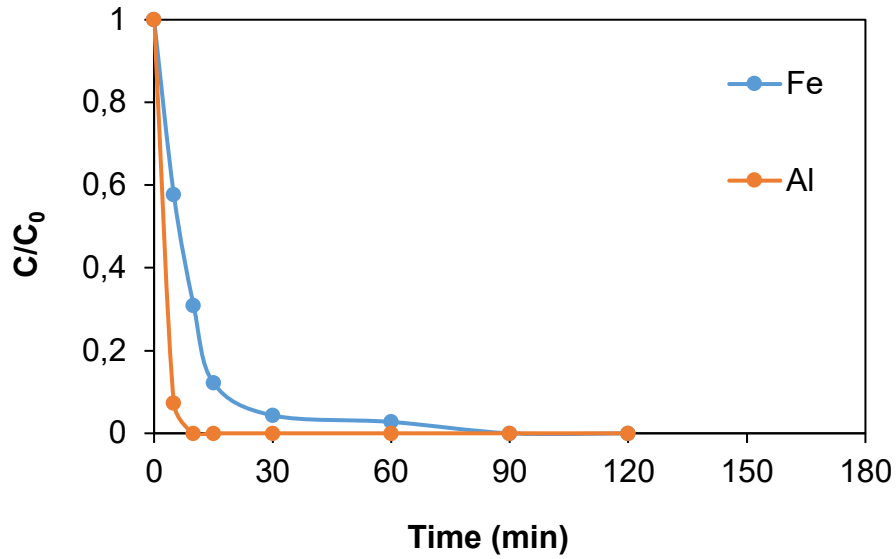

Figure 1. The effect of electrode material on color removal using the EC method

The results of studies conducted to determine the optimal current intensity for the treatment of Acid Fuchsin dye using the AO method are presented in Figure 2. Current intensity acts as the driving force for electron transfer between the electrode surfaces and the aqueous solution, thereby controlling the •OH formation. The figure shows that increasing the current intensity from 50 mA to 500 mA enhances COD removal. Complete mineralization was achieved within 120 min under an initial pH of 6.

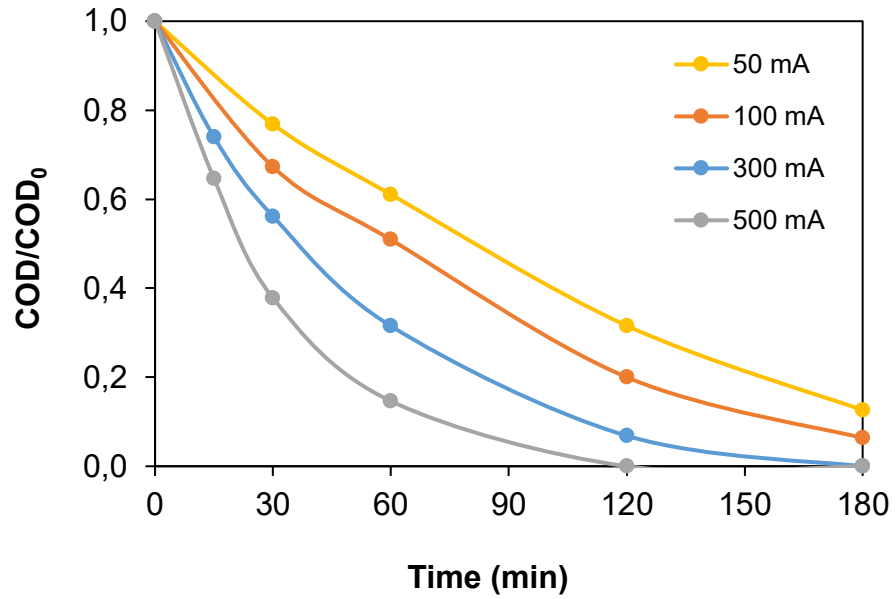

Figure 2. The effect of current intensity on COD removal using AO method

The results of studies conducted to determine the effect of EC electrode material under optimal current intensity 300 mA and pH 6 for the treatment of Acid Fuchsin solution using the EC&EO method are presented in Figure 3. Results demonstrated that Fe exhibited superior performance compared to Al. The results are presented in Figure 3. While there was no significant difference in terms of color removal between the two EC anode materials, COD analyses revealed that Fe enabled complete mineralization in a considerably shorter time than Al. Increased rate of mineralization was considered as a result of EF reactions took place in the reaction media. Here, cathodic reduction of dissolved O_2 led to the formation of H_2O_2, then the Fe^{2+} ions present in the media catalyze the formation of •OH, in addition to the physisorbed BDD(•OH). Reduction of

the catalyst at the CF cathode surface led to the continuous production of •OH which mineralize the organic pollutant into CO_2, H_2O and inorganic ions. The ability to minimize the treatment duration is a critical parameter in wastewater remediation.

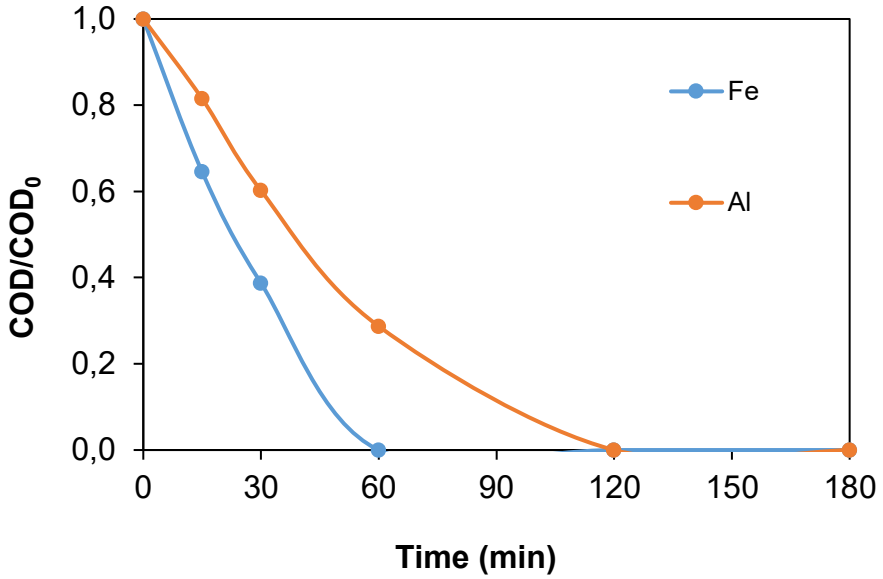

Figure 3. The effect of EC electrode material on COD removal using the EC&AO method

The results of studies conducted to determine the optimal current intensity for the treatment of Acid Fuchsin dye using the EC/AO method are presented in Figure 4. As the current intensity increases during the EC/AO process, the dissolution of the sacrificial bipolar electrode is enhanced, resulting in a greater release of metal ions and improved contaminant removal from the wastewater. In addition to the increased amount of dissolved metal, the rate of •OH formation also rises with current intensity, up to an optimal value of 300 mA. Beyond this threshold, further increases in current do not significantly improve COD removal. This plateau is attributed to the prevalence of competing side reactions at higher current intensities, which either inhibit •OH generation or promote its consumption, thereby limiting further mineralization. The most notable side reaction is oxygen evolution at the anode surface, which reduces the rate of anodic oxidation. Similarly, hydrogen evolution at the cathode competes with the oxygen reduction reaction, which is essential for in-situ H_2O_2 production.

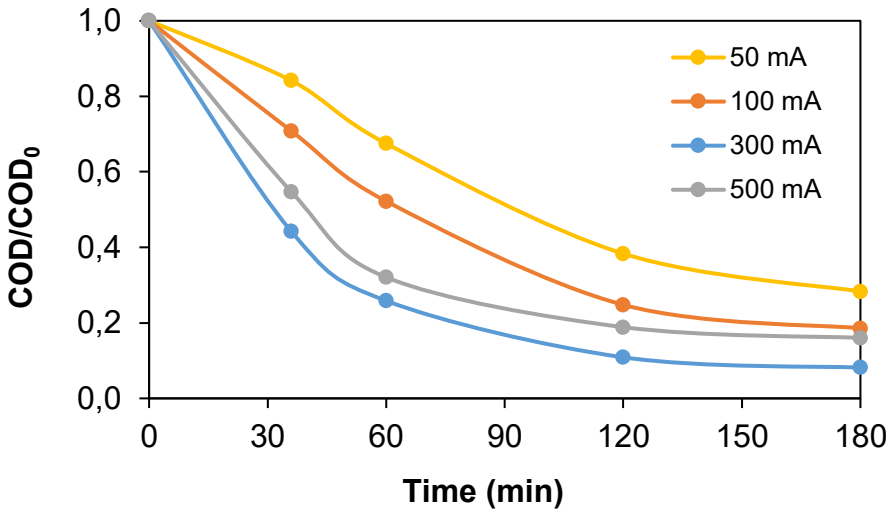

Figure 4. The effect of current intensity on COD removal using EC/AO method

The optimization experiments for H_2O_2 dosage in the PEC treatment of Acid Fuchsin dye solution are illustrated in Figure 5. Faraday's law was applied to calculate the amount of Fe^{2+} ions released during treatment. Appropriate amount of H_2O_2 addition was then performed to maintain the desired H_2O_2/Fe ratio in the reaction media. A fast and complete mineralization was observed within 36 min treatment under an initial pH of 7, 100 mA current intensity and H_2O_2/Fe = 0.5 conditions. Raising the H_2O_2/Fe ratio up to 0.5 (mol/mol)

leads to improved COD removal, but further increase beyond this point do not provide additional benefit. The decrease in COD removal observed at ratios both below and above the optimum is attributed to the scavenging of •OH through side reactions with excess H_2O_2 or Fe^{2+} as shown in Equations 8 and 9.

$$H_2O_2 + {}^{\bullet}OH \rightarrow H_20 + HO_2^{\bullet} \quad (8)$$

$$Fe^{2+} + {}^{\bullet}OH \rightarrow Fe^{3+} + OH^- \quad (9)$$

Comparative results of degradation and mineralization performance of investigated methods are given below in Table 1.

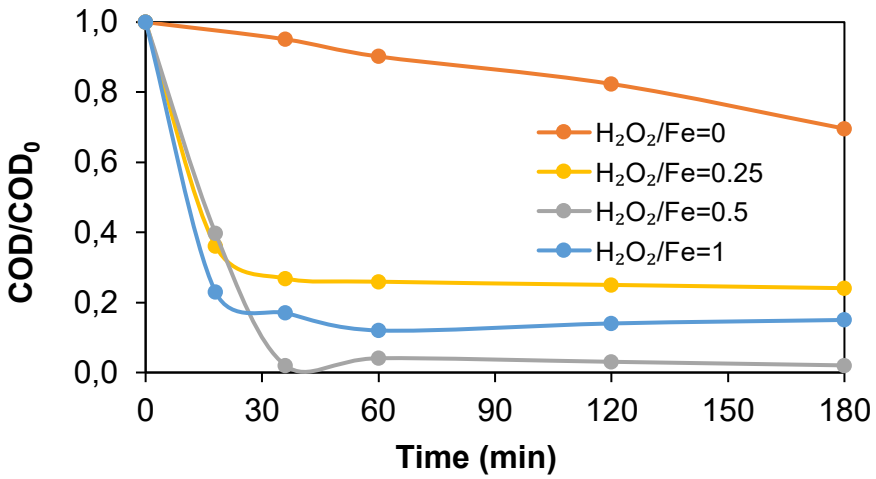

Figure 5. The effect of the H_2O_2/Fe ratio on COD removal using the PEC method

Table 1. Comparative degradation and mineralization performance of electrochemical treatment methods

Method	Electrode		Operational parameter	Optimum Value	Color removal (%)	COD removal (%)
EC	Anode: Al Cathode: Al		Current intensity	100 mA	100 (10 min)	-
			Initial pH	6		
AO	Anode: BDD Cathode: CF		Current intensity	500 mA	97 (30 min)	100 (90 min)
			Initial pH	6		
EC&AO	**EC**	Anode: Fe Cathode: Fe	Current intensity	100 mA	100 (10 min)	100 (60 min)
			Initial pH	6		
	AO	Anode: BDD Cathode: CF	Current intensity	300 mA		
			Initial pH	6		
EC/EO	Anode: BDD Cathode: CF Bipolar Fe		Current intensity	300 mA	97 (60 min)	100 (180 min)
			Initial pH	5		
PEC	Anode: Fe Cathode: CF		Initial pH	7	100 (9 min)	98 (36 min)
			H_2O_2/Fe	0.5		
			Current intensity	100 mA		

CONCLUSION

This study systematically compared electrochemical treatment methods including EC, AO, EC&AO, EC/AO, and PEC for the removal of Acid Fuchsin dye from aqueous solutions. EC using aluminum electrodes demonstrated rapid and complete color removal, but no significant mineralization was observed. AO, employing a boron-doped diamond (BDD) anode and CF cathode, effectively mineralized the dye, achieving complete COD removal. In EC&AO treatment, utilizing iron electrodes during the EC stage significantly improved COD removal efficiency due to enhanced electro-Fenton reactions. This facilitated rapid and complete mineralization in substantially shorter times compared to aluminum electrodes, highlighting the critical role of electrode material in electrochemical performance. EC/AO treatment achieved optimal performance at a current intensity of 300 mA, beyond which no significant improvement in COD removal was observed. Increased current beyond this optimal value induced side reactions such as oxygen and hydrogen evolution, limiting further enhancements in mineralization efficiency. PEC demonstrated exceptional efficiency, achieving complete mineralization within 36 min at an initial pH of 7, a current intensity of 100 mA, and an optimal H_2O_2/Fe molar ratio of 0.5. Overall, these findings highlight that the sequential EC&AO and PEC processes offer superior efficiency in both dye degradation and mineralization compared to single-stage EC and AO processes. Selecting appropriate operational conditions and electrode materials significantly enhances the performance, making these electrochemical methods promising candidates for practical applications in the advanced treatment of dye-contaminated wastewater.

ACKNOWLEDGEMENTS

The authors acknowledge TUBITAK (The Scientific and Technological Research Council of Turkey) for providing financial support through 2209-A Research Project Support Programme for Undergraduate Students under grant number 1919B012424114.

REFERENCES

Alalwan, H. A., Ali, N. S. M., Mohammed, M. M., Mohammed, M. F., & Alminshid, A. H. (2023). A comparison study of methyl green removal by peroxi-coagulation and peroxi-electrocoagulation processes. *Cleaner Engineering and Technology*, *13*, 100623.

Asfaha, Y. G., Tekile, A. K., & Zewge, F. (2021). Hybrid process of electrocoagulation and electrooxidation system for wastewater treatment: a review. *Cleaner Engineering and Technology*, *4*, 100261.

Camcioglu, S., Ozyurt, B., & Hapoglu, H. (2017). Effect of process control on optimization of pulp and paper mill wastewater treatment by electrocoagulation. *Process Safety and Environmental Protection*, *111*, 300-319.

Durmus, Z., Kurt, B. Z., & Durmus, A. (2019). Synthesis and characterization of graphene oxide/zinc oxide (GO/ZnO) nanocomposite and its utilization for photocatalytic degradation of basic fuchsin dye. *ChemistrySelect*, *4*(1), 271-278.

Fungaro, D. A., Yamaura, M., & Carvalho, T. E. M. (2014). Adsorption of anionic dyes from aqueous solution on zeolite from fly ash-iron oxide magnetic nanocomposite. *Journal of Atomic and Molecular Sciences*.

Hakizimana, J. N., Gourich, B., Chafi, M., Stiriba, Y., Vial, C., Drogui, P., & Naja, J. (2017). Electrocoagulation process in water treatment: A review of electrocoagulation modeling approaches. *Desalination*, *404*, 1-21.

Kuczyński, M., Łuba, M., Mikołajczyk, T., Pierożyński, B., Jasiecka-Mikołajczyk, A., Smoczyński, L., ... & Wojtacha, P. (2021). Electrodegradation of acid mixture dye through the employment of Cu/Fe macro-corrosion galvanic cell in Na2SO4 synthetic wastewater. *Molecules*, *26*(15), 4580.

Migliorini, F. L., Braga, N. A., Alves, S. A., Lanza, M. R. D. V., Baldan, M. R., & Ferreira, N. G. (2011). Anodic oxidation of wastewater containing the Reactive Orange 16 Dye using heavily boron-doped diamond electrodes. *Journal of hazardous materials*, *192*(3), 1683-1689.

Mirzaei, A., Chen, Z., Haghighat, F., & Yerushalmi, L. (2017). Removal of pharmaceuticals from water by homo/heterogonous Fenton-type processes–a review. *Chemosphere*, *174*, 665-688.

Oturan, M. A., & Aaron, J. J. (2014). Advanced oxidation processes in water/wastewater treatment: principles and applications. A review. Critical reviews in environmental science and technology, 44(23), 2577-2641.

Ozyurt, B., Camcioglu, Ş., & Hapoglu, H. (2017). A consecutive electrocoagulation and electro-oxidation treatment for pulp and paper mill wastewater. *Desalination and Water Treatment*, *93*, 214-228.

Özyurt, B., & Camcıoğlu, Ş. (2018). Applications of Combined Electrocoagulation and Electrooxidation Treatment to Industrial Wastewaters. *Wastewater and Water Quality*, Intechopen, 71-88.

Wang, Z., Ai, L., Huang, Y., Zhang, J., Li, S., Chen, J., & Yang, F. (2017). Degradation of azo dye with activated peroxygens: when zero-valent iron meets chloride. *Rsc Advances*, *7*(49), 30941-30948.

Yu, J., Zou, J., Xu, P., & He, Q. (2020). Three-dimensional photoelectrocatalytic degradation of the opaque dye acid fuchsin by Pr and Co co-doped TiO2 particle electrodes. *Journal of Cleaner Production*, *251*, 119744.

➢ *ORAL PRESENTATION*

Bazı ikili alüminat seramiklerin gama radyasyon zırhlama özelliklerinin teorik hesaplanması

Meryem YILMAZ[1],*, Ferdi AKMAN[2]

[1] Bingöl Üniversitesi, Fen-Edebiyat Fakültesi, Fizik Bölümü, 12000, Bingöl, Türkiye

[2] Bingöl Üniversitesi, Sosyal Bilimler Meslek Yüksekokulu, Mülkiyet Koruma ve Güvenlik Bölümü, İş Sağlığı ve Güvenliği Programı, 12000, Bingöl, Türkiye

* Sorumlu yazar e-posta:meryyilmz157@gmail.com

Özet

İyonlaştırıcı radyasyon, sağlık, enerji ve endüstri gibi pek çok alanda yaygın olarak kullanılmakta olup, maruziyet durumunda ciddi biyolojik riskler taşımaktadır. Bu nedenle etkin radyasyon zırhlama sistemlerinin geliştirilmesi büyük önem arz etmektedir. Geleneksel olarak kurşun kullanılsa da toksik yapısı alternatif malzeme arayışlarını hızlandırmıştır. Bu çalışma, özellikle termal ve kimyasal kararlılığı yüksek olan ve geleneksel metal bazlı zırhlama malzemelerine alternatif olarak ikili alüminat seramiklerinin gama radyasyona karşı zırhlama kapasitelerini değerlendirmeyi amaçlamaktadır. 0,015–15 MeV aralığındaki 24 farklı foton enerjisi için, kütle azaltma katsayısı, lineer azaltma katsayısı, ortalama serbest yol ve etkin atom numarası gibi temel zırhlama parametreleri hesaplanarak değerlendirme yapılmıştır. Elde edilen sonuçlar, ikili alüminat seramiklerinin farklı enerji düzeylerinde etkili birer radyasyon kalkanı olarak kullanılabileceğini göstermektedir.

Anahtar kelimeler: WinXCOM, EpiXS, ikili alüminat seramik

Theoretical calculation of gamma radiation shielding properties of some binary aluminate ceramics

Abstract

Ionizing radiation is widely used in a variety of fields, including health, energy, and industry, and it poses substantial biological dangers when exposed. Therefore, the development of effective radiation shielding technologies is quite important. Although lead has traditionally been used, its toxic structure has accelerated the search for alternative materials. The purpose of this work is to assess the shielding capacities of binary aluminate ceramics, which have great thermal and chemical stability and are an alternative to standard metal-based shielding materials, against gamma radiation. Basic shielding parameters such as mass attenuation coefficient, linear attenuation coefficient, mean free path, and effective atomic number were calculated and assessed at 24 different photon energies ranging from 0.015 to 15 MeV. The obtained results show that binary aluminate ceramics can be used as effective radiation shields at different energy levels.

Keywords: WinXCOM, EpiXS, binary aluminate ceramics

GİRİŞ

İyonlaştırıcı radyasyon kaynaklarının sanayi, tıp ve enerji üretimi gibi çeşitli alanlarda artan kullanımı, etkili radyasyon zırhlama çözümlerine olan ihtiyacı beraberinde getirmiştir. Geleneksel kurşun bazlı zırh malzemeleri yüksek azaltma kapasitesine sahip olmalarına rağmen toksik doğaları ve çevresel etkileri nedeniyle sürdürülebilirlik açısından sınırlayıcı faktörler taşımaktadır. Bu durum, yeni nesil, çevre dostu ve yüksek performanslı zırhlama materyallerinin geliştirilmesini zorunlu kılmıştır. Bu tür sorunları ortadan kaldırmak için, düşük maliyetli, çevre dostu ve etkili radyasyon kalkanı elde etmek amacıyla polimerler (Bhosale ve ark., 2017; Mahmoud ve ark., 2018; More ve ark., 2021), kompozit alaşımlar (Akman ve ark., 2019; Levent ve ark., 2020; Sathish ve ark., 2023) camlar (Kaur ve ark., 2016; Sayyed ve ark., 2020; Kurtulus, 2024) ve seramikler (Akman ve ark., 2019; Kacal ve ark., 2019; Luo ve ark., 2021; Sayyed ve ark., 2022; Eshghi ve Alipoor, 2024) araştırma konusu olmuştur.,

Seramik esaslı malzemeler, özellikle yüksek termal ve kimyasal kararlılıkları, düşük yoğunlukları ve şekillendirilebilir yapılarıyla son yıllarda bu alanda dikkat çeken alternatifler arasında yer almaktadır (Angelone ve ark., 2001; Han ve ark., 2009; Kacal ve ark., 2019; Manohara ve Hanagodimath, 2007). İkili alüminat seramikler N1, N2, N3 ve N4 olarak kodlanan $CaAl_2O_4$, $MgAl_2O_4$, $LiAlO_2$ ve $Y_3Al_5O_{12}$ bileşikleri, yapıları sayesinde foton azaltma mekanizmalarında etkili olabilme ve farklı enerji aralıklarında gama ışınlarına karşı umut vadeden bir performans sergileme ihtimaline sahiptirler. İkili alüminat seramikler, genellikle Al_2O_3 ve başka bir metal oksit (örn. CaO, BaO, SrO veya ZnO) içeren iki bileşenli sistemlerdir. Bu malzemeler yüksek erime noktaları, üstün termal kararlılıkları, sertlikleri ve kimyasal dirençleriyle ayırt edilirler. Radyasyon koruma uygulamalarına gelince, alüminat seramikler düşük yoğunluklarına rağmen büyük yapısal bütünlük sağlar ve özellikle termal nötronlara karşı etkili olabilir. Alüminat matrisine yüksek atom numaralı oksitler dâhil etmek, etkili gama ışını koruması sağlayabilir. Tipik kurşun bazlı malzemelere toksik olmayan, çevre dostu bir alternatif sunarlar ve bu da onları gelişmiş radyasyon koruma uygulamaları için çekici hale getirir.

Bu çalışmada, N1, N2, N3 ve N4 şeklinde kodlanan bazı ikili alüminat seramiklerin 0,015–15 MeV enerji aralıklarındaki gama ışınları zırhlama kapasiteleri araştırılmış ve bunun için kütle azaltma katsayısı, lineer azaltma katsayısı, ortalama serbest yol ve etkin atom numarası gibi temel zırhlama parametreleri incelenmiştir. N1, N2, N3 ve N4 olarak kodlanan ikili alüminat seramiklerin gama radyasyonu zırhlama özellikleri WinXCOM (Gerward ve ark., 2004) programı ve/veya EpiXS (Hila ve ark., 2021) programları ile hesaplanmıştır. Gama radyasyonu zırhlama kapasitelerini incelemek için kütle azaltma katsayısı (μ/ρ), lineer azaltma katsayısı (μ), ortalama serbest yol (OSY) ve etkin atom numarası ($Z_{etk.}$) parametreleri 0,015–15 MeV foton enerjisi aralığında 24 farklı enerji değerinde hesaplanmıştır. Elde edilen bulgular, bu ikili alüminat seramiklerin gelişmiş radyasyon güvenliği uygulamalarında alternatif bir malzeme adayı olabileceğini ortaya koymaktadır.

MATERYAL VE METOD

Gama radyasyonu zırhlama parametrelerinin belirlenmesi

$CaAl_2O_4$, $MgAl_2O_4$, $LiAlO_2$ ve $Y_3Al_5O_{12}$ ikili alüminatların kütle azaltma katsayıları WinXCOM programı ile elde edilmiştir. Kütle azaltma katsayıları belirlenirken **Tablo 1**'de kimyasal formülleri verilen alüminatlar programa tanıtılmıştır. Kütle azaltma katsayısı kullanılarak da diğer parametreler türetilmiştir. Birden fazla element içeren bir materyalin kütle azaltma katsayısı, karışım kuralı kullanılarak belirlenebilir. Seçilen ikili alüminatlar için teorik μ/ρ değerleri denklem (1) kullanılarak elde edilmiştir.

$$\frac{\mu}{\rho} = \sum Wi \left(\frac{\mu}{\rho}\right) i \qquad (1)$$

Burada μ/ρ malzemenin toplam kütle azaltma katsayısı, $(\mu/\rho)_i$ malzeme içindeki i. elementin kütle azaltma katsayısı ve W_i malzeme içindeki i. elementin ağırlıklı kesridir. Malzeme içindeki elementlerin toplam ağırlıklı kesri 1'dir, yani ΣW_i=1'dir. μ/ρ cm^2/g birimine sahiptir ve gelen fotonun birim alandaki kütle ile etkileşime girme olasılığı ile ilişkili bir parametredir. Maddenin yoğunluğunun bu metrik üzerinde bir etkisi yoktur. Yani, maddenin fiziksel özelliklerine bağlı değildir. Bu özellik sayesinde kütle azaltma katsayısı parametresi malzemenin gama radyasyonu zırhlama kapasitesi hakkında ön bilgi vermektedir.

Tablo 1. Seçilen seramiklerin kimyasal içerikleri ve yoğunlukları

Numune Kodu	Kimyasal Formül	ρ (g/cm^3)
N1	$CaAl_2O_4$	2,98
N2	$MgAl_2O_4$	3,65
N3	$LiAlO_2$	2,55
N4	$Y3Al_5O_{12}$	4,55

Lineer azaltma katsayısı (μ, cm^{-1}), dikkate alınan malzemenin kütle azaltma katsayısı ile yoğunluğunun çarpımından elde edilebilir (Akman, 2023).

$$\mu = \frac{\text{M}}{\rho}\rho \qquad (2)$$

Fotonların madde içindeki ortalama serbest yolu (OSY), başlangıç radyasyon şiddetinin %63,2'sinin azaltıldığı numune kalınlığı olarak tanımlanır ve aşağıdaki denklem ile ifade edilir.

$$OSY = {}^{1}/_{\mu} \qquad (4)$$

Herhangi bir materyalin radyasyon zırhlama özelliğinin incelenmesinde etkin atom numarası parametresinin de hesaplanması önemlidir. Bu parametre birden fazla element içeren materyallerde kullanılan bir terimdir. Belirtilen enerji değerlerinde sunulan ikili alüminatların etkin atom numarası parametreleri aşağıdaki denklem kullanılarak hesaplanmıştır:

$$Z_{\text{eff}} = \frac{\sum f_i A_i ({}^{\mu}/_{\rho})_i}{\sum \frac{f_j A_j}{Z_j} ({}^{\mu}/_{\rho})_j} \qquad (5)$$

burada, f, A ve Z sırasıyla, element bolluğunu, atom ağırlığını ve atom numarasını göstermektedir.

BULGULAR ve TARTIŞMA

Seçilen ikili alümantların 0,015 ila 15 MeV aralında kütle azaltma katsayısı sonuçları **Tablo 2**'de sunulmuştur. Ayrıca, bu parametrenin foton enerjisi ile değişiminin daha belirgin gözlemlenmesi için **Şekil 1**'de bu sonuçların grafiği sunulmuştur. Farklı enerji aralıklarında (0,015–15 MeV) elde edilen μ/ρ verileri, numunelerin foton madde etkileşimi mekanizmalarının farklı enerji bölgelerinde baskın olduğunu göstermektedir. **Şekil 1** ve **Tablo 2** incelendiğinde düşük enerjili foton bölgesinde (0,015–0,1 MeV), özellikle fotoelektrik etki baskın olduğundan, yüksek atom numarasına sahip elementler içeren numunelerin daha yüksek azaltma katsayısı gösterdiği görülmektedir. Bu bağlamda, N4 numunesi düşük enerjilerde çok yüksek μ/ρ değerleri sergileyerek (örneğin 0,02 MeV'de 31,8639 cm²/g) fotoelektrik etkinin güçlü olduğu bu bölgede açık ara en yüksek azaltma kapasitesine ulaşmıştır. Bu durum, N4'ün yapısında yüksek Z elementlerin varlığına işaret etmektedir.

Tablo 2. İkili alüminat seramiklerin kütle azaltma katsayısı değerlerinin foton enerjisi ile değişimi

Enerji (MeV)	N1	N2	N3	N4	N1	N2	N3	N4
	μ/ρ (cm²/g)				Z_{etk}			
0,015	11,0151	4,9293	4,1700	12,6389	16,2100	11,5755	11,2861	26,4730
0,02	4,8375	2,1668	1,8483	31,8639	16,1381	11,5000	11,0427	35,9975
0,03	1,5727	0,7569	0,6625	10,8502	15,6534	11,2278	10,3184	35,7526
0,04	0,7630	0,4153	0,3745	4,9955	14,8974	10,9097	9,6000	34,9339
0,05	0,4706	0,2918	0,2699	2,7423	14,0989	10,6447	9,0745	33,6733
0,06	0,3389	0,2351	0,2214	1,6941	13,4082	10,4551	8,7328	32,0983
0,08	0,2296	0,1854	0,1783	0,8223	12,4629	10,2419	8,3767	28,5518
0,1	0,1862	0,1632	0,1586	0,4955	11,9514	10,1427	8,2200	25,2081
0,2	0,1267	0,1233	0,1213	0,1644	11,2988	10,0279	8,0440	17,1108
0,3	0,1072	0,1058	0,1043	0,1162	11,2051	10,0115	8,0187	15,2294
0,4	0,0952	0,0944	0,0931	0,0972	11,1774	10,0067	8,0108	14,6208
0,5	0,0866	0,0861	0,0849	0,0861	11,1651	10,0042	8,0071	14,3579
0,6	0,0800	0,0795	0,0784	0,0784	11,1587	10,0030	8,0051	14,2273
0,8	0,0701	0,0698	0,0688	0,0679	11,1524	10,0018	8,0032	14,0929
1	0,0630	0,0627	0,0619	0,0606	11,1495	10,0012	8,0022	14,0346
1,5	0,0513	0,0511	0,0504	0,0492	11,1515	10,0021	8,0045	14,0140
2	0,0443	0,0440	0,0434	0,0428	11,1676	10,0070	8,0159	14,1110
3	0,0362	0,0358	0,0352	0,0360	11,2205	10,0233	8,0538	14,4420
4	0,0318	0,0311	0,0305	0,0325	11,2838	10,0430	8,1004	14,8261
5	0,0290	0,0282	0,0275	0,0305	11,3492	10,0634	8,1497	15,2127
6	0,0271	0,0261	0,0254	0,0293	11,4136	10,0839	8,1998	15,5783
8	0,0248	0,0236	0,0228	0,0281	11,5325	10,1221	8,2954	16,2392
10	0,0236	0,0221	0,0212	0,0278	11,6357	10,1558	8,3823	16,7993
15	0,0222	0,0204	0,0194	0,0281	11,8302	10,2207	8,5572	17,8210

N1, N2 ve N3 numuneleri ise aynı enerji aralığında daha düşük değerlerde kalmıştır (0,02 MeV'de sırasıyla 4,8375; 2,1668 ve 1,8483 cm²/g), bu da onların daha hafif bileşenler içerdiğini göstermektedir. Orta enerji bölgesinde (0,1–1 MeV) ise Compton saçılması baskın etkileşim haline gelmektedir. Bu bölgede tüm numunelerin μ/ρ değerleri belirgin şekilde düşmekte ve birbirine yaklaşmaktadır. Örneğin 0,5 MeV'de tüm numuneler 0,0849–0,08666 cm²/g bandında benzer değerler göstermiştir. Bu yakınsama, Compton saçılma tesir kesitinin E^{-1} ve Z ile orantılı olmasındandır. Dolayısıyla bu bölgede malzeme bileşiminin etkisi azalmakta, azaltma kapasitesinin daha az değiştiğini göstermektedir.

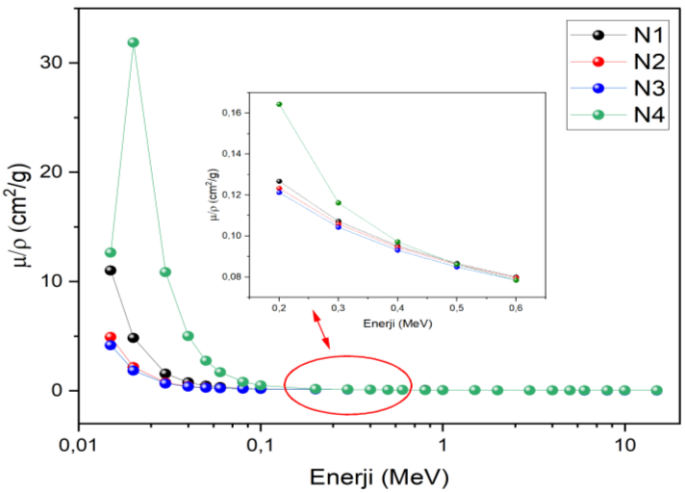

Şekil 1. Kütle azaltma katsayısı değerlerinin foton enerjisi ile değişimi

Yüksek enerjili foton bölgesinde (1–15 MeV) ise, çift oluşumu olayı önemli hâle gelmekle birlikte, genel olarak azaltma katsayıları çok düşük seviyelere inmektedir. Bu aralıkta N4 numunesi nispeten daha yüksek μ/ρ değerlerini korumaya devam etmiş (örneğin 10 MeV'de 0,0278 cm²/g), diğer numunelere göre üstün performansını sürdürmüştür. Ancak bu fark, düşük enerjideki kadar belirgin değildir.

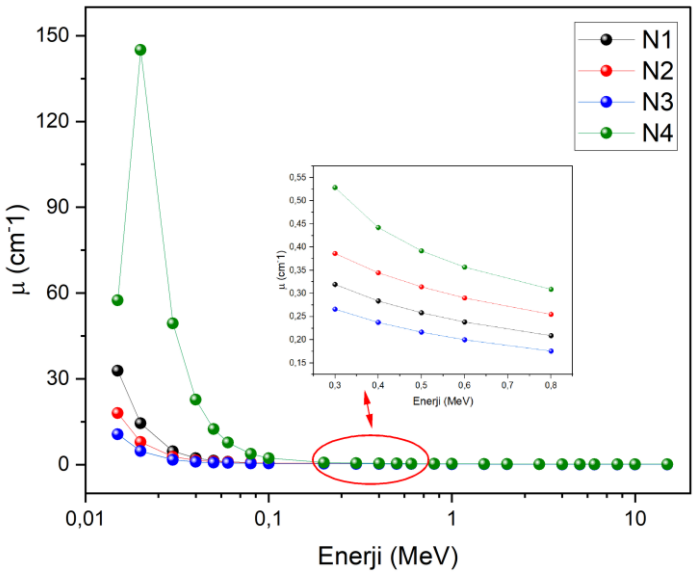

Şekil 2. Lineer azaltma katsayısı değerlerinin foton enerjisi ile değişimi

Şekil 2 incelendiğinde, lineer azaltma katsayısının artan enerjiyle azaldığı görülmektedir. Artan enerjiyle azalmanın düşük enerji bölgesinde keskin, sonraki enerji bölgelerinde ise daha düzgün olduğu görülmektedir. Kütle azaltma katsayılarında belirtildiği gibi, bu azalmalar ilgili bölgeye göre fotoelektrik, Compton saçılması ve çift üretim kesitlerinin baskınlığına göre değişmektedir. Bu parametreye göre de N4 kodlu iki alümanatın diğerlerinden daha üstün gama zırhlama kapasitesine sahip olduğu görülmektedir.

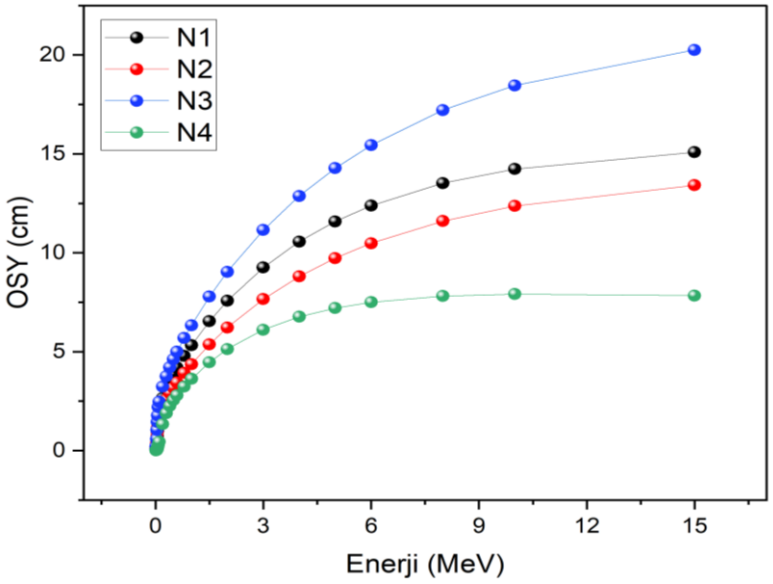

Şekil 3. Ortalama serbest yol değerlerinin foton enerjisi ile değişimi

Farklı enerji seviyelerinde ikili alüminat seramiklerinin (N1, N2, N3, N4) ortalama serbest yol (OSY) değerleri incelendiğinde (**Şekil 3**), foton enerjisinin artmasıyla birlikte tüm numunelerde OSY değerlerinin arttığı gözlemlenmiştir. Bu durum, enerji yükseldikçe fotonların malzeme içindeki etkileşim olasılığının azaldığını ve dolayısıyla daha uzun mesafeler kat edebildiğini göstermektedir. OSY değerleri, radyasyonun malzeme içinde etkileşmeden ortalama ne kadar ilerleyebildiğini ifade ettiği için, bu değerin düşük olması daha iyi zırhlama performansı anlamına gelir. Bu bağlamda, **N4 numunesi** tüm enerji aralıklarında **en düşük ortalama serbest yol değerine sahiptir.** Bu sonuç, N4'ün yapısal olarak daha yoğun, yüksek atom numaralı elementler içeren ve fotonları daha kısa mesafede soğurabilen bir malzeme olduğunu ortaya koymaktadır. N1 ve N2 numuneleri sırasıyla orta düzeyde OSY değerleri sergileyerek N4'e kıyasla daha az etkili ancak belirli enerji aralıklarında kabul edilebilir düzeyde zırhlama sağlamaktadır. Buna karşılık, **N3 numunesi** ise tüm enerji düzeylerinde **en yüksek ortalama serbest yol değerlerine** sahip olduğu **Şekil 3** incelendiğinde görülmektedir. Bu da N3'ün zırhlama kabiliyeti açısından en zayıf numune olduğunu göstermektedir. OSY eğrilerindeki bu ayrışma, kütle azaltma katsayısı (μ/ρ) ve lineer azaltma katsayısı bulgularıyla tam bir tutarlılık göstermektedir.

Sonuç olarak, N4 numunesi, foton enerjisine bağlı değişkenlik gösterse dahi, **her enerji aralığında üstün zırhlama performansı sergileyen bir malzeme** olarak öne çıkmaktadır.

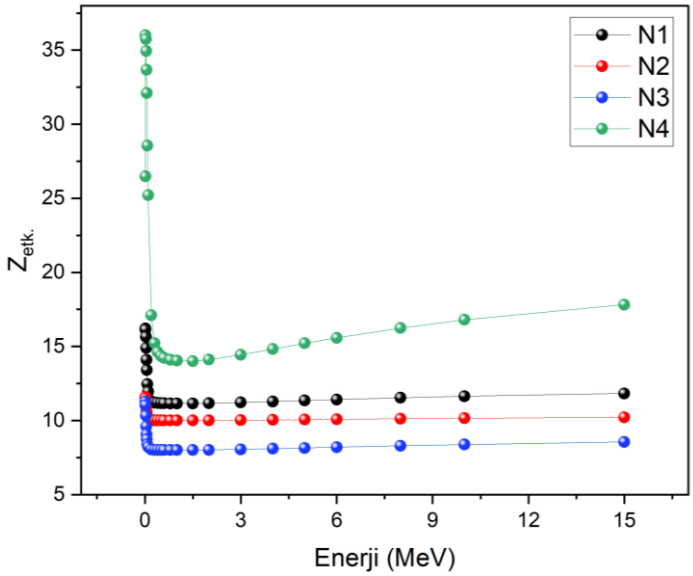

Şekil 4. Etkin atom numarası değerlerinin foton enerjisi ile değişimi

Çalışmada N1, N2, N3 ve N4 olarak kodlanan ikili alüminat seramik numunelerinin foton enerjisine bağlı olarak değişen etkin atom numarası (Z_{etk}) değerleri analiz edilmiştir. **Tablo 2** ve **Şekil 4** incelendiğinde, tıpkı kütle azaltma değerlerinde olduğu gibi Z_{etk} değerleri de düşük, orta ve yüksek enerji bölgelerinde farklı foton etkileşimlerinin etkisinde kalmıştır. Düşük enerjili foton bölgesinde (0,015–0,1 MeV) fotoelektrik etki baskın olduğu için, Z_{etk} değeri radyasyonla etkileşim açısından kritik öneme sahiptir. Bu aralıkta N4 numunesi oldukça yüksek Z_{etk} değerleri göstermiştir; bu da N4 kodlu numunenin düşük enerjili fotonlara karşı çok daha etkin bir zırhlama sağlayacağını göstermektedir. Orta enerji bölgesinde (0,1–1 MeV) Compton saçılmasının baskın hâle gelmesiyle birlikte, Z_{etk} değerleri tüm numunelerde düşüş göstermekte ve birbirine yaklaşmaktadır. Bu bölgede N4 numunesi için Z_{etk} yaklaşık 25'ten 14'e kadar düşerken, N1 11,9'dan 11,1'e, N2 10,1 civarında sabit kalmakta, N3 ise 8,2 civarına inmektedir. Orta enerji aralığında malzemeler arasında etkin atom numarası farkı belirginliğini yitirdiği söylenebilir. Bunun nedeni de Compton saçılma tesir kesitinin enerji ve atom numarası olan ilişkisidir. Yüksek enerji bölgesinde (1–15 MeV) Z_{etk} değerleri tüm numunelerde nispeten sabit kalmakta ve düşük enerjili bölgeye göre daha az dalgalanmaktadır. N4 numunesi bu aralıkta da diğer numunelere kıyasla yüksek Z_{etk} değerini korumayı sürdürmektedir. Değerlerdeki bu yaklaşık sabitlik, bu enerji aralığında çift oluşum gibi etkileşimlerin baskınlaşmasına bağlı olarak, Z_{etk} etkisinin sınırlı düzeyde kaldığını göstermektedir. Genel olarak değerlendirildiğinde, N4 numunesi tüm enerji aralıklarında en yüksek Z_{etk} değerine sahip olup özellikle düşük enerjili fotonların zırhlanmasında açık üstünlük göstermektedir. Bu nedenle, N4 özellikle medikal görüntüleme, nükleer güvenlik ve düşük enerjili gama kaynaklarının korunması gibi uygulamalar için ideal bir adaydır. Diğer yandan, N1 orta düzeyde, N2 ve N3 ise hafif kompozit malzemelere dayalı zırh sistemlerinde kullanılabilecek, daha düşük ama sabit performans sunan malzemeler olarak değerlendirilebilir

SONUÇ

Bu çalışmada, 0.015 MeV ila 15 MeV foton enerjileri aralığında 24 farklı enerjide N1, N2, N3 ve N4 kodlu ikili alüminat seramiklerin gama radyasyonu zırhlama kapasiteleri incelenmiştir. Bu alüminatların μ/ρ, μ, OSY ve $Z_{etk.}$ radyasyon zırhlama parametreleri WinXCOM ve/veya EpiXS programları kullanılarak hesaplanmıştır. Bu ikili alüminat seramiklerin gama radyasyonuna karşı zırhlama yeterlilikleri sistematik olarak değerlendirilmiş; temel azaltma parametreleri ışığında malzeme özellikleri analiz edilmiştir. Elde edilen sonuçlar, bu seramiklerin ileri radyasyon koruma uygulamaları için uygun adaylar olabileceğini göstermektedir. İlgili gama radyasyonu zırhlama parametreleri incelendiğinde N4 kodlu ikili alüminat seramiğinin diğerlerine göre daha iyi bir gama radyasyonu zırh malzemesi olduğu görülmüştür. Ayrıca, N4 kodlu seramiğin günümüzde sıklıkla gama radyasyonu zırh malzemesi olarak kullanılan kurşun veya türevlerinden üretilmiş zırh malzemelerine alternatif olma potansiyeline sahip olduğu gözlemlenmiştir. Sonuç olarak, enerjiye bağlı etkileşim durumları incelendiğinde, N4 numunesi özellikle düşük enerjili fotonların zırhlanmasında oldukça etkili bir performans sergilemiştir. Bu yönüyle tıbbi görüntüleme sistemleri, nükleer güvenlik ve düşük enerjili gama kaynaklarının korunması gibi alanlarda tercih edilebilir.

KAYNAKLAR

Akman, F. (2023). Determination of gamma radiation shielding characteristics for some iron-based metallic glasses. Türk Doğa ve Fen Dergisi, 12(1), 53-60.

Akman, F., Kaçal, M. R., Sayyed, M. I., & Karataş, H. A. (2019). Study of gamma radiation attenuation properties of some selected ternary alloys. Journal of Alloys and Compounds, 782, 315-322.

Akman, F., Khattari, Z. Y., Kaçal, M. R., Sayyed, M. I., & Afaneh, F. (2019). The radiation shielding features for some silicide, boride and oxide types ceramics. Radiation Physics and Chemistry, 160, 9-14.

Angelone, M., Bubba, T., & Esposito, A. (2001). Measurement of the mass attenuation coefficient for elemental materials in the range 6⩽ Z⩽ 82 using x-rays from 13 up to 50 keV. Applied Radiation and Isotopes, 55(4), 505-511.

Bhosale, R. R., More, C. V., Gaikwad, D. K., Pawar, P. P., & Rode, M. N. (2017). Radiation shielding and gamma ray attenuation properties of some polymers. Nuclear Technology and Radiation Protection, 32(3), 288-293.

Eshghi, M., & Alipoor, M. R. (2024). A comprehensive study of gamma-rays shielding features of binary compounds. Progress in Physics of Applied Materials, 4(1), 59-67.

Gervard, L., Guilbert, N., Jensen, K. B., Levring, H. (2004). WinXCom—a program for calculating X-ray attenuation coefficients. Radiation Physics and Chemistry, 71(3-4)653-654.

Gervard, L., Guilbert, N., Jensen, K. B., Levring, H. (2004). WinXCom—a program for calculating X-ray attenuation coefficients. Radiation Physics and Chemistry, 71(3-4)653-654.

Han, I., Demir, L., & Şahin, M. E. H. M. E. T. (2009). Determination of mass attenuation coefficients, effective atomic and electron numbers for some natural minerals. Radiation Physics and Chemistry, 78(9), 760-764.

Hila, F. C., Asuncion-Astronomo, A., Dingle, C. A. M., Jecong, J. F. M., Javier-Hila, A. M. V., Gili, M. B. Z., ... & Amorsolo Jr, A. V. (2021). EpiXS: A Windows-based program for photon attenuation, dosimetry and shielding based on EPICS2017 (ENDF/B-VIII) and EPDL97 (ENDF/B-VI. 8). Radiation Physics and Chemistry, 182, 109331.

Hila, F. C., Asuncion-Astronomo, A., Dingle, C. A. M., Jecong, J. F. M., Javier-Hila, A. M. V., Gili, M. B. Z., ... & Amorsolo Jr, A. V. (2021). EpiXS: A Windows-based program for photon attenuation, dosimetry and shielding based on EPICS2017 (ENDF/B-VIII) and EPDL97 (ENDF/B-VI. 8). Radiation Physics and Chemistry, 182, 109331.

Kacal, M. R., Akman, F., & Sayyed, M. I. (2019). Investigation of radiation shielding properties for some ceramics. Radiochimica Acta, 107(2), 179-191.

Kaur, P., Singh, D., & Singh, T. (2016). Heavy metal oxide glasses as gamma rays shielding material. Nuclear Engineering and design, 307, 364-376.

Kurtulus, R. (2024). Recent developments in radiation shielding glass studies: a mini-review on various glass types. Radiation Physics and Chemistry, 111701.

Levet, A., Kavaz, E., & Özdemir, Y. (2020). An experimental study on the investigation of nuclear radiation shielding characteristics in iron-boron alloys. Journal of Alloys and Compounds, 819, 152946.

Luo, H., Li, Y., Xiang, R., Jia, W., Li, M., Li, S., ... & Dong, C. (2021). Exploring the potential of the mechanical/thermal properties and co-shielding ability of Bi2O3-doped aluminum borate ceramics against neutron/gamma radiation. Ceramics International, 47(11), 15508-15519.

Mahmoud, A. A., El-Sayed, A. A., Aboraya, A. M., Fathy, I. N., Abouelnour, M. A., Tayeh, B. A., & Nabil, I. M. (2025). Investigating the effects of granite, marble, granodiorite, and ceramic waste powders on the physical, mechanical, and radiation shielding performance of sustainable concrete. Annals of Nuclear Energy, 216, 111274.

Mahmoud, M. E., El-Khatib, A. M., Badawi, M. S., Rashad, A. R., El-Sharkawy, R. M., & Thabet, A. A. (2018). Recycled high-density polyethylene plastics added with lead oxide nanoparticles as sustainable radiation shielding materials. Journal of cleaner production, 176, 276-287.

Manohara, S. R., & Hanagodimath, S. M. (2007). Studies on effective atomic numbers and electron densities of essential amino acids in the energy range 1 keV–100 GeV. Nuclear Instruments and Methods in Physics Research Section B: Beam Interactions with Materials and Atoms, 258(2), 321-328.

More, C. V., Alsayed, Z., Badawi, M. S., Thabet, A. A., & Pawar, P. P. (2021). Polymeric composite materials for radiation shielding: a review. Environmental chemistry letters, 19, 2057-2090.,

Sathish, K. V., Sowmya, N., Munirathnam, R., Manjunatha, H. C., Seenappa, L., & Sridhar, K. N. (2023). Radiation shielding properties of aluminium alloys. Radiation Effects and Defects in Solids, 178(9-10), 1301-1320.

Sayyed, M. I., Ati, A. A., Mhareb, M. A., Mahmoud, K. A., Kaky, K. M., Baki, S. O., & Mahdi, M. A. (2020). Novel tellurite glass (60-x) TeO2–10GeO2-20ZnO–10BaO-xBi2O3 for radiation shielding. Journal of alloys and compounds, 844, 155668.

Sayyed, M. I., Hannachi, E., Mahmoud, K. A., & Slimani, Y. (2022). Synthesis of different (RE) BaCuO ceramics, study their structural properties, and tracking their radiation protection efficiency using Monte Carlo simulation. Materials Chemistry and Physics, 276, 125412.

➢ *ORAL PRESENTATION*

Bazı Silikat Cam Elyaflarının Gama Radyasyon Kalkanı Özellikleri Üzerine Bir Çalışma

Meryem YILMAZ[1],*, Ferdi AKMAN[2]

[1] Bingöl Üniversitesi, Fen-Edebiyat Fakültesi, Fizik Bölümü, 12000, Bingöl, Türkiye

[2] Bingöl Üniversitesi, Sosyal Bilimler Meslek Yüksekokulu, Mülkiyet Koruma ve Güvenlik Bölümü, İş Sağlığı ve Güvenliği Programı, 12000, Bingöl, Türkiye

*Sorumlu yazar e-posta: meryyilmz157@gmail.com

Özet

Radyasyon kaynaklı sağlık risklerinin azaltılması için güvenli, hafif, çevre dostu ve ekonomik zırhlama malzemelerine duyulan ihtiyaç giderek artmaktadır. Bu bağlamda, cam esaslı kompozitler, özellikle de silikat cam elyaflar, son yıllarda dikkat çeken seçeneklerden biri hâline gelmiştir. Silikat cam elyaf malzemeler; düşük yoğunlukları, yüksek mekanik dayanımları, termal kararlılıkları ve esnek üretim olanakları sayesinde zırhlama teknolojilerinde yeni bir yaklaşım sunmaktadır. Bu çalışmada, farklı bileşim ve yoğunluklara sahip silikat cam elyaf kompozitlerin gama radyasyona karşı zayıflatma performansları değerlendirilmiştir. 0,060 MeV ile 2,614 MeV aralığında seçilen 18 farklı foton enerjisi kapsamında, malzemelere ait temel zırhlama parametreleri olan lineer azaltma katsayısı (μ), onda-bir kalınlık değeri (OKD) ortalama serbest yol (OSY) ve etkin atom numarası ($Z_{etk.}$) hesaplanmıştır. Belirli oranlarda SiO_2, Al_2O_3, MgO, BeO ve Y_2O_3 bileşiklerini içeren SCE1, SCE2 ve SCE3 olarak kodlanmış silikat cam elyaf numunelerinin gama radyasyonu azaltma kapasiteleri belirtilen enerjilerde μ, OKD ve OSY WinXCOM programı ile ve $Z_{etk.}$ parametresi ise EpiXS programı yardımı ile incelenmiştir. Elde edilen veriler, silikat cam elyaflarının özellikle düşük ve orta enerji aralıklarında yeterli düzeyde foton azaltma kapasitesi sergilediğini, buna karşın yüksek enerjili fotonlar için yapılarına yüksek atom numaralı katkı maddeleri eklenmesi gerektiğini göstermektedir. Çalışma sonuçları, bu malzemelerin esnekliğini ve çevresel güvenliğini koruyarak, yapısal zırhlama elemanları ve kişisel koruyucu ekipmanlarda etkin biçimde kullanılabileceğini ortaya koymaktadır.

Anahtar Kelimeler: WinXCOM, EpiXS, Silikat cam elyaf

A Study on the Gamma Radiation Shielding Properties of Certain Silicate Glass Fibers

Abstract

The need for safe, lightweight, environmentally friendly and economical shielding materials to reduce radiation-induced health risks is increasing. In this context, glass-based composites, especially silicate glass fibers, have become one of the most striking options in recent years. Silicate glass fiber materials offer a new approach in shielding technologies thanks to their low density, high mechanical strength, thermal stability and flexible production possibilities. In this study, the attenuation performances of silicate glass fiber composites with different compositions and densities against gamma radiation were evaluated. Within the scope of 18 different photon energies selected between 0.060 MeV and 2.614 MeV, the basic shielding parameters of the materials, namely linear attenuation coefficient (μ), tenth value layer (TVL), mean free path (MFP) and effective atomic number (Z_{eff}), were calculated. The gamma radiation reduction capacities of silicate glass fiber samples coded as SCE1, SCE2 and SCE3 containing certain amounts of SiO_2, $Al2O_3$, MgO, BeO and Y_2O_3 compounds were investigated with the help of the WinXCOM program for μ, TVL and MFP; with the help of the EpiXS program for Z_{eff} parameter at the specified energies. The obtained data show that silicate glass fibers exhibit sufficient photon attenuation capacity especially in low and medium energy ranges, however, high atomic number additives should be added to their structures for high energy photons. The study results show that these materials can be effectively used in structural shielding elements and personal protective equipment while maintaining their flexibility and environmental safety.

Keywords: WinXCOM, EpiXS, Silicate glass fibers

GİRİŞ

Günümüzde, iyonlaştırıcı radyasyonun olumsuz etkilerine karşı gerekli ve yeterli koruma sağlayan nükleer teknolojilerin artan kullanımı muazzam bir öneme sahiptir. Gama ışınları, X ışınları ve nötron radyasyonu gibi

iyonlaştırıcı radyasyon türleri, zararlı özellikleri nedeniyle çevre ve canlı organizmalar için büyük tehditler oluşturabilir. Çünkü iyonlaştırıcı radyasyon, tipik bir hücrenin molekülünü veya atomunu parçalamak için yüksek enerji taşımaktadır. Çok sayıda çalışma, tıbbi radyasyona maruz kalmanın katarakt, kısırlık, doğum deformeleri, guatr, akciğer ve meme kanseri, lösemi ve tiroid kanseri insidansını artırdığını bulmuştur. Bu yaklaşımda, radyasyon zırhlama malzemelerinin üretimine yönelik araştırmalar ivme kazanmış hafif, esnek, çevre dostu ve uygun maliyetli malzemeler arayışı ortaya çıkmıştır. Geleneksel kurşun esaslı zırhlama malzemeleri, yüksek yoğunluklarına ve etkin zırhlama performanslarına rağmen, toksik yapıları ve işlenebilirlik sorunları nedeniyle diğer seçeneklerle değiştirilmektedir. (Erkoyuncu ve ark., 2024; Akman ve ark., 2015; Altowyan ve ark., 2024)

Cam elyaf takviyeli kompozit malzemeler, özellikle silikat esaslı cam elyafları, mekanik mukavemetlerinin yanı sıra olası radyasyon azaltma kabiliyetleri nedeniyle bu bağlamda ilgi çekmektedir (Eskalen ve ark., 2025; Ulas ve ark., 2025; Juhim ve ark., 2022; Kirdsiri ve ark., 2011; Kurtulus, 2024; Kurtkapmaz, 2018). Silikat cam elyafları, termal ve kimyasal olarak kararlı, amorf bir yapıya sahip inorganik malzemelerdir. Cam elyaflarındaki SiO_2 (silika), ısı direncini, mekanik mukavemetini, hafifliğini ve esnekliğini artırır. Bu özelliklerden dolayı, özellikle havacılık, otomotiv, inşaat ve nükleer endüstrilerinde yaygın olarak kullanılırlar. Radyasyon korumasına gelince, saf silikat camlar yüksek atom numaralı elementler içermese de çok ince elyaflar şeklinde yapılabilirler ve düzgün mimarileri gama ışınlarını etkili bir şekilde dağıtabilir. Ayrıca, uygun ek elementlerle (kurşun, bizmut veya baryum gibi) takviye edilerek etkili koruma kapasiteleri artırılabilir. Düşük yoğunlukları ve pasif nitelikleri nedeniyle, cam elyaflar diğer koruma malzemelerine kıyasla hem ekolojik olarak zararsız hem de avantajlı işlenebilirlik seçenekleri sunar. Sonuç olarak, silikat cam elyaflar yeni nesil kompozit radyasyon koruma malzemeleri olarak büyük bir vaat taşımaktadır (AlMisned ve ark., 2024; Singh, 2022).

Bu çalışmada, SCE1, SCE2 ve SCE3 şeklinde kodlananz bazı silikat cam elyaflarının 0,060-2,614 MeV enerji aralıklarındaki gama ışınları zırhlama kapasiteleri araştırılmış; lineer azaltma katsayısı, onda-bir kalınlık değer, ortalama serbest yol ve etkin atom numarası gibi temel zırhlama parametreleri belirlenmiştir. Elde edilen bulgular, cam silikat elyaflarının gelişmiş radyasyon güvenliği uygulamalarında alternatif bir malzeme adayı olabileceğini ortaya koymaktadır. Sunulan çalışmada ise SCE1, SCE2 ve SCE3 olarak kodlanan silikat cam elyafların gama radyasyonu zırhlama parametreleri WinXCOM (Gerward ve ark., 2004) programı ve EpiXS (Hila ve ark., 2021) programı yardımıyla elde edilmiştir. Gama radyasyonu zırhlama kapasitelerini incelemek için lineer azaltma katsayısı (μ), onda-bir kalınlık değeri (OKD), ortalama serbest yol (OSY) ve etkin atom numarası ($Z_{etk.}$) parametreleri 0,060 MeV ile 2,614 MeV foton enerjisi aralığında 18 farklı enerji değerinde hesaplanmıştır. SCE3 kodlu silikat cam elyafın daha bir zırh malzemesi olabileceği incelenen sonuçlardan anlaşılmaktadır.

MATERYAL VE METOD

Yapılan bu çalışmada 0,060 ila 2,614 MeV enerji aralığındaki on sekiz farklı enerji değerinde üç silikat cam fiber numunenin radyasyon zırhlama özellikleri incelenmiştir. Öncelikle radyasyon zırhlamada önemli gösterge olan lineer azaltma katsayısı (μ) WinXCOM programından elde edilen kütle azaltma katsayıları aracılığı ile belirlenmiştir. Sonrasında lineer azaltma katsayısının yardımı ile yarı kalınlık değeri (YKD) hesaplanmıştır. En sonunda ise incelenen silikat cam elyafların etkin atom numarası (Z_{etk}) belirlenmiştir. XCOM ara yüzünde Windows temelli kullanımı ile WinXCOM programı yardımıyla belirlenen kütle azaltma katsayılarından lineer azaltma katsayısı ve ona bağlı olarak yarı kalınlık ve onda-bir kalınlık değerleri hesaplanmıştır. WinXCOM programı kullanımının kolay ve anlaşılır olması sebebiyle çokça tercih edilmektedir. Bu veri tabanında, elementler, bileşikler ve karışımlar için yüzde bileşimler 1 keV–100 GeV foton enerjisi aralığı kullanılarak programa girilir ve foton azaltma özellikleri hesaplanabilir. EpiXS programı yardımı ile ise Z_{etk} hesaplanmıştır. EpiXS, fotoatomik kütüphaneleri kullanarak foton azaltma katsayı parametrelerini hesaplamaya yarayan kullanışlı bir Windows uygulamasıdır. Ara yüzü oldukça işlevseldir bu da yine WinXCOM gibi kolay bir kullanım sağlamaktadır. WinXCOM ve EpiXS programlarında seçilen cam elyafların **Tablo 1**'de verilen kimyasal içerikleri ve/veya yoğunlukları tanımlanarak hesaplama süreci işletilmiştir.

Tablo 1. Seçilen silikat cam elyafların kimyasal içerikleri ve yoğunlukları

Numune Kodu	Bileşimi (%Ağırlık)					
	SiO2	Al2O3	MgO	BeO	Y2O3	ρ (g/cm^3)
SCE1	50	35	7,5	7,5	-	2,60
SCE2	52,6	35,8	5,4	-	6,2	3,00
SCE3	36,2	20,5	8,1	5	30,2	3,29

Gama radyasyonu zırhlama parametrelerinin belirlenmesi

Malzemenin yoğunluğuna bağlı olan lineer azaltma katsayısı parametresi (μ, cm^{-1}), teorik olarak WinXCOM aracılığı ile edilen kütle azaltmaların malzeme yoğunluğu ile çarpımından elde edilebilir ya da iyi bilinen Beer-Lambert yasasından elde edilebilir. (Eke ve ark., 2017)

$$I = I_0 e^{-\mu x} \quad (1)$$

Bu denklem düzenlenirse;

$$\mu = \ln\left(\frac{I_0}{I}\right)\Big/_x \quad (2)$$

Denklemi elde edilir. Burada μ cm^{-1} cinsinden lineer azaltma katsayısıdır ve x sunulan çalışma için kompozit kalınlığıdır. I ve I_0 malzemenin varlığında ve yokluğunda gama ışını yoğunluklarını ifade eder.

Onda-bir kalınlık değeri (OKD, cm), başlangıç radyasyon şiddetinin %90'sının azaltıldığı numune kalınlığını tanımlar. OKD parametreleri lineer azaltma katsayısı yardımıyla denklem (3) kullanılarak belirlenebilir.

$$OKD = {ln10}/{\mu} = {2.303}/{\mu} \quad (3)$$

Fotonların madde içindeki ortalama serbest yolu (OSY), başlangıç radyasyon şiddetinin %36,8'sinin geçebileceği numune kalınlığı olarak tanımlanır ve aşağıdaki denklem ile ifade edilir.

$$OSY = {1}/{\mu} \quad (4)$$

Herhangi bir materyalin radyasyon zırhlama özelliğinin incelenmesinde etkin atom numarası parametresinin de hesaplanması önemlidir. Belirtilen enerji değerlerinde sunulan alaşımların etkin atom numarası parametreleri aşağıdaki denklem kullanılarak hesaplanmıştır:

$$Z_{eff} = \frac{\sum f_i A_i ({\mu}/{\rho})i}{\sum \frac{f_i A_i}{Z_i} ({\mu}/{\rho})i} \quad (5)$$

burada, f_i, A_i ve Z_i sırasıyla, i. elementin malzeme içindeki bolluğunu, atom ağırlığını ve atom numarasını ifade eder (Un ve Sahin, 2011; Hine, 1982).

BULGULAR ve TARTIŞMA

Seçilen cam elyafların gama radyasyonu zırhlama özelliklerini incelemek için belirlenen ilk parametre lineer azaltma katsayısıdır. **Tablo 2** ve **Şekil 1**'de seçilen cam elyaflara ait belirtilen enerjilerde elde edilen sonuçlar sunulmuştur. Her üç numune için de lineer azaltma katsayısı değerleri enerji arttıkça azalmakta, yani bu parametrenin enerji ile ters orantılı olduğu görülmektedir. Bu beklenen bir durumdur çünkü foton enerjisi arttıkça, malzemenin foton ile etkileşme ihtimaliyeti düşmektedir. Bu tablo ve şekil incelendiğinde SEC3, tüm enerji aralıklarında en iyi azaltma sağlayan elyaftır. SEC3 kodlu silikat cam elyaf, geniş enerji aralığında yüksek bir lineer azaltma katsayısı gösterdiğinden en etkili radyasyon zırhlama malzemesi potansiyeline sahip olarak öne çıkmaktadır. SEC1, düşük μ değerleri nedeniyle daha az etkili bir zırhlama materyalidir. Eğer maliyet ve yoğunluk gibi ikincil faktörler göz önüne alınmazsa, sadece azaltma kapasitesi açısından incelendiğinde malzemeler arasında büyükten küçüğe SEC3 > SEC2 > SEC1 sıralaması elde edilmektedir.

Düşük enerji aralığında (0.06-0.136 MeV), SEC3 açık farkla en yüksek μ değerlerine sahiptir. SEC2 orta düzeydeyken SEC1 en düşük değerlere sahiptir. Orta enerjilerde (0.239-0.662 MeV), μ değerleri tüm numunelerde düşmektedir. Ancak SEC3 hâlâ en yüksek zırhlama özelliğine sahipken ardından SEC2 ve SEC1 gelmektedir. Yüksek enerji bölgesinde (0.835-2.614 MeV) ise numunelerin μ sonuçları arasındaki farklar azalmakta, μ değerleri birbirine yaklaşmakta, ancak sıralamanın değişmediği ve SEC3> SEC2> SEC1 şeklinde olduğu ilgili tablo ve şekilde görülmektedir.

Tablo 2. Seçilen silikat cam elyafların lineer azaltma katsayıları ve onda-bir kalınlık değeri sonuçları

Enerji	SEC1		SEC2		SEC3	
(MeV)	μ (cm^{-1})	OKD (cm)	μ (cm^{-1})	OKD (cm)	μ (cm^{-1})	OKD (cm)
0,060	0,6217	3,7039	1,2076	1,9068	3,3224	0,6930
0,081	0,4834	4,7637	0,7646	3,0113	1,6796	1,3709
0,088	0,4590	5,0170	0,6924	3,3257	1,4199	1,6216
0,122	0,3904	5,8980	0,5134	4,4852	0,8152	2,8246
0,136	0,3733	6,1685	0,4765	4,8325	0,7047	3,2675
0,239	0,3016	7,6345	0,3566	6,4576	0,4217	5,4601
0,356	0,2586	8,9036	0,3008	7,6542	0,3361	6,8518
0,511	0,2228	10,3328	0,2577	8,9353	0,2817	8,1732
0,569	0,2127	10,8238	0,2458	9,3690	0,2677	8,6013
0,583	0,2105	10,9396	0,2431	9,4710	0,2646	8,7011
0,662	0,1989	11,5751	0,2296	10,0295	0,2491	9,2435
0,835	0,1788	12,8807	0,2061	11,1728	0,2227	10,3377
1,063	0,1590	14,4780	0,1832	12,5670	0,1975	11,6587
1,173	0,1514	15,2106	0,1744	13,2051	0,1878	12,2585
1,275	0,1451	15,8693	0,1671	13,7777	0,1800	12,7930
1,333	0,1418	16,2354	0,1634	14,0954	0,1759	13,0880
1,770	0,1226	18,7864	0,1413	16,2990	0,1525	15,1028
2,614	0,1001	22,9927	0,1158	19,8835	0,1262	18,2506

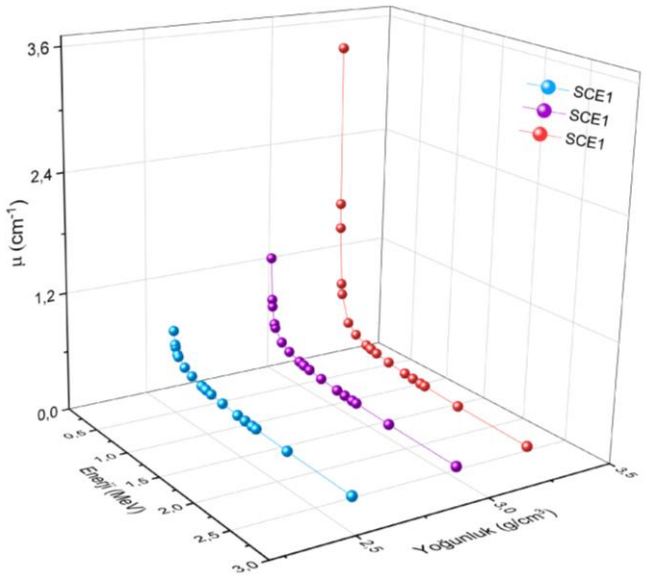

Şekil 1. Lineer azaltma katsayılarının yoğunluk ve foton enerjisi ile değişimi

Bir malzemenin zırhlama verimliliğinin hızlı bir şekilde belirlenebilmesi için kullanılan en uygun parametrelerden biri onda-bir kalınlık parametresidir. **Tablo 1**'de bu parametreye ait sonuçlar listenilerken, **Şekil 2** ise bu parametrenin gama enerjisi ile değişim eğilimi görsel olarak sunulmuştur. Bu tablo ve şekilden açıkça görüldüğü gibi SEC3, daha düşük kalınlıkla aynı oranda radyasyonu azaltalbildiği için hem malzeme tasarrufu sağlar hem de zırhlama açısından daha verimlidir. SEC3 kodlu malzeme hem μ hem de OKD dikkate alındığında en etkili radyasyon zırhlama malzemesidir. SEC1, en zayıf zırhlama performansına sahiptir; en kalın formda bile daha az azaltma sağlayacağı görülmektedir. SEC2 ise arada, orta düzey bir performans sunar.

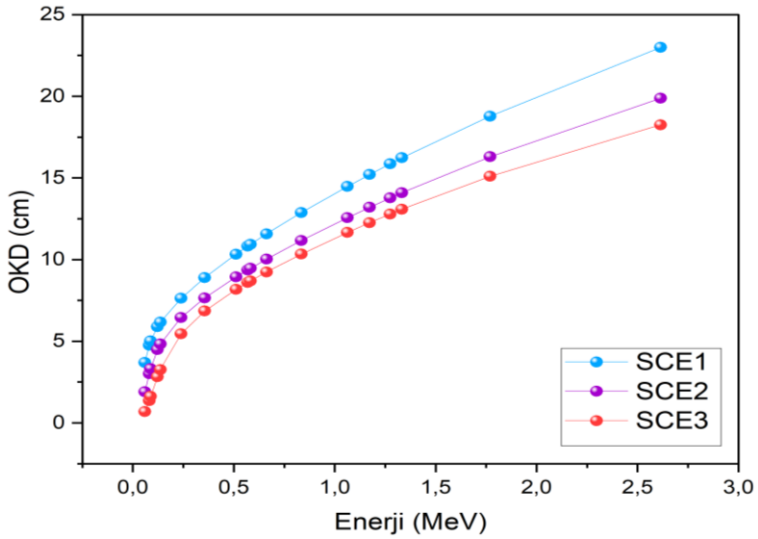

Şekil 2. Onda-bir kalınlık değerlerinin foton enerjisi ile değişimi

Şekil 3'te ise seçilen silikat cam elyafların ortalama serbest yol sonuçlarının foton enerjisi ile değişimi görülmektedir. Bu şekil incelendiğinde, ortalama serbest yol (OSY) değerleri, silikat cam elyaf esaslı üç farklı numunenin (SCE1, SCE2, SCE3) farklı foton enerjilerinde enerji arttıkça tüm numunelerde belirgin şekilde arttığı gözlemlenmiştir; bu, fotonların yüksek enerjilerde malzeme içinden daha kolay geçebildiğini göstermektedir. Bu bağlamda değerlendirildiğinde, **SCE3 numunesi** tüm enerji aralığında **en düşük OSY** değerlerine sahip olup, fotonları daha kısa mesafede durdurabilmesi sayesinde **en etkili zırhlama performansını** sergilemektedir. **SCE2**, SCE3'ün hemen ardından gelmekte olup, orta düzeyde ancak istikrarlı bir azaltma kapasitesi göstermektedir. Buna karşılık **SCE1**, özellikle yüksek enerjili fotonlarda OSY değerlerinin en yüksek olduğu numune olarak dikkat çekmektedir. Bu durum, SCE1'in düşük enerjili fotonlarda belirli bir etkinlik gösterse de artan enerjiyle birlikte fotonların daha derinlere nüfuz etmesine izin verdiğini ve dolayısıyla zırhlama açısından **en zayıf performansı** sunduğunu göstermektedir. Bu veriler, daha önce elde edilen lineer zayıflatma katsayısı (μ) ve onda-bir kalınlık değerleri (OKD) sonuçları ile de tutarlılık göstermekte; özellikle SCE3 numunesinin geniş enerji aralığında üstün performans sergileyen bir radyasyon zırh malzemesi olduğunu doğrulamaktadır.

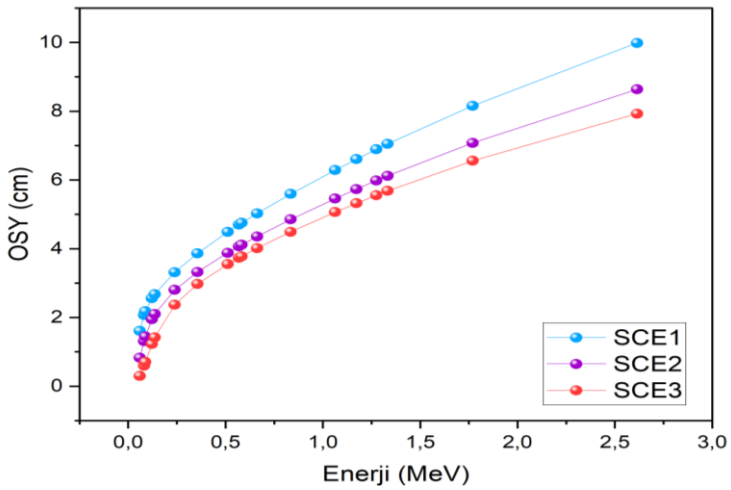

Şekil 3. Ortalama serbest yol değerlerinin foton enerjisi ile değişimi

Şekil 4'te ise seçilen silikat cam elyafların gama radyasyonu zırhlama özelliklerinin incelendiği son parametre olan etkin atom numarası sonuçlarının foton enerjisi ile değişimi grafiği sunulmuştur. Bu şekle göre, düşük enerji bölgesinde (0–0,2 MeV), SCE3 kodlu silikat cam elyafın Z_{etk} değeri oldukça yüksektir. Bu durum SCE2 ve SCE1'e göre daha yüksek atom numaralı elementleri içermesi ile açıklanabilir. Bu, özellikle fotoelektrik etkileşimin baskın olduğu düşük enerjilerde, SCE3'ün çok daha etkili bir zırh malzemesi olduğunu gösterir. Orta ve yüksek enerjilerde (0.3–2.6 MeV) ise tüm numuneler için Z_{etk} değerleri durağanlaşmakta ve birbirine yaklaşmaktadır. Bu durum, Compton saçılması ve ardından çift oluşum süreçlerinin baskın hale geldiği enerji aralığını yansıtmaktadır. Ancak hâlâ SCE3>SCE2>SCE1 sıralaması korunmaktadır.

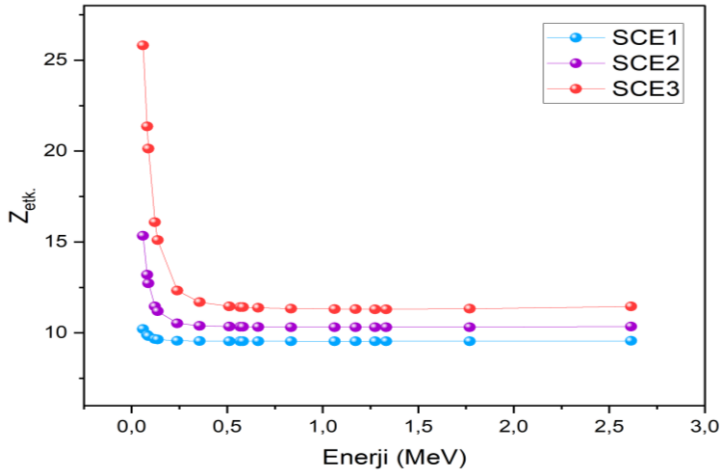

Şekil 4. Etkin atom numarası değerlerinin foton enerjisi ile değişimi

SONUÇ

Bu çalışmada, 0.060 MeV ila 2.614 MeV foton enerjileri aralığında 18 farklı enerjide SCE1, SCE2 ve SCE3 kodlu silikat cam elyafların gama radyasyonu zırhlama kapasiteleri incelenmiştir. Bu alaşımların μ, OKD, OSY ve $Z_{etk.}$ gama radyasyon zırhlama parametreleri WinXCOM ve/veya EpiXS programları kullanılarak hesaplanmıştır. İlgili gama radyasyonu zırhlama parametreleri incelendiğinde SCE3 kodlu silikat cam elyaf numunesinin diğerlerine göre daha iyi bir gama radyasyonu zırh malzemesi olduğu görülmüştür. Ayrıca, SCE3 kodlu silikat cam elyafın günümüzde sıklıkla gama radyasyonu zırh malzemesi olarak kullanılan kurşun veya türevlerinden üretilmiş zırh malzemelerine alternatif olma potansiyeline sahip olduğu tahmin edilmektedir. Mevcut sonuçlara göre SCE3 kodlu elyafın hastanelerde ve tıp merkezlerinde, radyasyon yayan ekipman bulunan odalarda, radyoaktif atık ürünlerin depolanmasında ve nükleer santrallerde çevre ve insan sağlığını korumak için gama radyasyonu zırh malzemesi olarak kullanılabilir. Ayrıca, bu cam elyaflar taban malzeme olarak kullanılmak istenip kompozit üretilmesi planlanırsa SCE3 kodlu cam elyafın tercih edilmesi önerilmektedir.

KAYNAKLAR

Akman, F., Durak, R., Turhan, M. F., & Kaçal, M. R. (2015). Studies on effective atomic numbers, electron densities from mass attenuation coefficients near the K edge in some samarium compounds. Applied Radiation and Isotopes, 101, 107-113.

AlMisned, G., Baykal, D. S., Alkarrani, H., Susoy, G., & Tekin, H. O. (2024). Advancing mechanical durability and radiation shielding properties in Silicon dioxide (SiO2) glasses through various incorporations: A comparative analysis. Results in Physics, 61, 107717.

Altowyan, A. S., Sayyed, M. I., Kumar, A., & Rashad, M. (2024). SrO–ZnO–PbO–B2O3 glassy insights: Unveiling the structural and optical features for gamma ray shielding efficacy. Optical Materials, 152, 115534.

Alzahrani, J. S., Alrowaili, Z. A., Olarinoye, I. O., Sriwunkum, C., & Al-Buriahi, M. S. (2025). Gamma attenuation, dose rate and buildup factors of Ga2O3-Lu2O3–SiO2–SnO glass system. Radiation Physics and Chemistry, 232, 112649.

Coşkun, A., Çetin, B., Yiğitoğlu, İ., & Topaklı, H. (2023). Comparison of the radiation absorption properties of PbO doped ZrB2 glasses by using GATE-GEANT4 Monte Carlo code and XCOM program. International Journal of Computational and Experimental Science and Engineering, 9(3), 274-279.

Erkoyuncu, İ., Demirkol, İ., Akman, F., Dilsiz, K., Kaçal, M. R., & Polat, H. (2024). A detailed investigation of gamma and neutron shielding capabilities of concrete doped with bronze and boron carbide. Radiation Physics and Chemistry, 215, 111358.

Eskalen, H., Kavgacı, M., Yaykaşlı, H., Özğan, Ş., Gök, M., Perişanoğlu, U., & Perişanoğlu, E. K. (2025). Improved physical, optical, and radiation shielding characteristics of SrO-doped borate glasses: Insights from experiments and machine learning. Ceramics International, 51(11), 14876-14891.

Gervard, L., Guilbert, N., Jensen, K. B., Levring, H. (2004). WinXCom—a program for calculating X-ray attenuation coefficients. Radiation Physics and Chemistry, 71(3-4)653-654.

Girard, S., Kuhnhenn, J., Gusarov, A., Brichard, B., Van Uffelen, M., Ouerdane, Y., ... & Marcandella, C. (2013). Radiation effects on silica-based optical fibers: Recent advances and future challenges. IEEE Transactions on nuclear science, 60(3), 2015-2036.

Hila, F. C., Asuncion-Astronomo, A., Dingle, C. A. M., Jecong, J. F. M., Javier-Hila, A. M. V., Gili, M. B. Z., ... & Amorsolo Jr, A. V. (2021). EpiXS: A Windows-based program for photon attenuation, dosimetry and shielding based on EPICS2017 (ENDF/B-VIII) and EPDL97 (ENDF/B-VI. 8). Radiation Physics and Chemistry, 182, 109331.

Hine, G. J. (1952). The effective atomic numbers of materials for various gamma ray processes. Phys Rev, 85, 725.

Juhim, F., Chee, F. P., Awang, A., Duinong, M., Rasmidi, R., & Rumaling, M. I. (2022). Radiation Shielding Properties of Tellurite and Silicate Glass. ECS Journal of Solid State Science and Technology, 11(7), 076006.

Kirdsiri, K., Kaewkhao, J., Chanthima, N., & Limsuwan, P. (2011). Comparative study of silicate glasses containing Bi2O3, PbO and BaO: Radiation shielding and optical properties. Annals of Nuclear energy, 38(6), 1438-1441.

Kurtulus, R. (2024). Recent developments in radiation shielding glass studies: a mini-review on various glass types. Radiation Physics and Chemistry, 111701.

Kurtkapmaz, U. K. (2018). CaO-MgO-Al2O3-SiO2 (CMAS) Cam Seramik Sisteminin Mikroyapısal ve Radyoaktif Kalkanlama Özeliklerine B2O3, BaO, PbO ve SrO Katkılarının Etkisi (Master's thesis, Sakarya Universitesi (Turkey)).

Singh, J., Kaur, P., Kaur, P., Kumar, V., Al-Buriahi, M. S., Alfryyan, N., ... & Singh, T. (2022). Optical and radiation shielding features for some phospho-silicate glasses. Optik, 261, 169140.

Ulas, E. O., Acikgoz, A., Aktas, B., & Kavun, Y. (2025). Influence of B2O3 incorporation on the structural, mechanical and radiation shielding properties of TeO2 Based bioglasses. Applied Radiation and Isotopes, 221, 111799.

Un, A., & Sahin, Y. (2011). Determination of mass attenuation coefficients, effective atomic and electron numbers, mean free paths and kermas for PbO, barite and some boron ores. Nuclear Instruments and Methods in Physics Research Section B: Beam Interactions with Materials and Atoms, 269(13), 1506-1511.

➢ *ORAL PRESENTATION*

A Machine-Learning Approach to Precision Agriculture for Seasonal-aware Clustering of Agricultural Crops

Dilek Olcay[1,*] (*ORCID: https://orcid.org/0009-0000-6669-1906*),
Serap Ulusam Seçkiner[2] (*ORCID: https://orcid.org/0000-0002-1612-6033)*

[*1] Gaziantep University , Industrial Engineering, Gaziantep, Türkiye.
[2] Gaziantep University , Industrial Engineering, Gaziantep, Türkiye.

*Corresponding author e-mail: dolcay@gmail.com, do02982@student.gaziantep.edu.tr

Abstract

Precision agriculture relies on data-driven techniques to optimize crop management and resource allocation.Traditional classification systems ignore seasonal and temporal differences in crop water demands when allocating agricultural water resources. This study presents a machine learning-based clustering analysis of 52 crops using seasonal growth patterns, total annual evapotranspiration (PET), and temporal features. We evaluate multiple clustering algorithms (K-means, Hierarchical, DBSCAN) and feature combinations to identify the optimal grouping strategy. The best-performing model, Hierarchical Ward clustering with PET-focused features, achieved a Silhouette Score of 0.570. This resulted in effectively partitioning crops into 7 distinct crop clusters, each exhibiting unique seasonal growing patterns and PET requirements with agriculturally significant characteristics. The study found clear seasonal groupings among high-water tree crops (PET >800mm), summer-intensive annual crops, winter cereals, and multi-seasonal perennial plants that require different irrigation strategies.This clustering framework provides a data-driven foundation for precision agriculture applications, including seasonal irrigation scheduling, seasonal planting schedules, effective crop rotation practices and the optimization of water resource allocation. It offers agricultural practitioners an evidence-based tool for sustainable water management decision-making.

Keywords: Hierarchical Ward clustering, Crop pattern, Crop rotation, PET, Machine Learning, Sustainable Water Management

INTRODUCTION

Global agricultural irrigation consumes approximately 70% of freshwater withdrawals worldwide. (UN-Water,, 2023). Global water demand is projected to increase by 20% to 25% by 2050, while the number of watersheds facing high year-to-year variability, or less predictable water supplies, is expected to increase by 19%. For the Middle East and North Africa, this means 100% of the population will live with extremely high water stress by 2050 (Kuzma, Saccoccia, & Chertock, 2023). As demand and supply grow apart, water-related concerns have intensified, affecting food security as well.

Traditional irrigation techniques are inefficient and wasteful of water, while moderntechniques directly reduce losses (Perry, Steduto, & Karajeh, 2017). There are different irrigation methods available for applying irrigation water, which determine the extent of field losses and the efficiency of field application. For sustainable planning of the irrigation project especially in terms of water use and water management, irrigation methods play a significant role (Rai, Singh, & Upadh, 2017).

In agricultural water management, there is a notable gap in developing clustering algorithms specifically designed to group crops based on their water consumption and temporal characteristics using advanced machine learning techniques.

Existing studies often concentrate on single-crop optimization or specific regional contexts, lacking a comprehensive, data-driven approach to crop grouping based on combined water needs and temporal growing patterns. There is a need to understand how PET interacts with growing duration and seasonal patterns to create more effective water management strategies. To address this gap, this project applies unsupervised machine learning techniques to a dataset of 52 different crops, using Total Potential Evapotranspiration (PET), growing duration, and seasonal activity patterns derived from the time_slots data. The goal is to identify distinct groups of crops with similar water demands and temporal behaviors. By identifying these clusters, we aim to provide actionable insights for improving water use efficiency, optimizing irrigation schedules, and promoting

effective crop rotation strategies that minimize overall water consumption. In the analysis, we used the calculated seasonal coverage metrics (winter, spring, summer, fall) and other temporal features from time_slots data to provide a more holistic understanding of crop water needs.

Agricultural practices need to be more sustainable due to climate variability, water scarcity, and water scarcity. Many traditional crop classification methods overlook seasonal dependencies and environmental factors, resulting in inefficient resource utilization. A machine learning (ML) algorithm offers a solution to clustering crops according to multi-dimensional features, including: Potential Evapotranspiration (PET) - estimating water demand, Seasonal coverage (winter, spring, summer, fall), and Growth duration (10 days time slots).

The objective of this study is to develop a machine learning framework for clustering crops based on seasonal water demands and temporal patterns. Then, finding the clustering algorithm best captures agricultural seasonal patterns and the feature combinations which optimize crop grouping for irrigation management are also aimed.

This research introduces several groundbreaking methodological innovations addressing critical gaps in agricultural water consumption analysis. The study develops novel feature engineering techniques for temporal agricultural data, extracting meaningful patterns from multi-seasonal crop cycles that traditional approaches overlook. Through a comprehensive algorithm comparison for agricultural applications, the research systematically evaluates machine learning and clustering methodologies to identify the most effective approaches for crop water analysis. This study explores how unsupervised learning can enhance crop grouping for precision farming, enabling better decision-making in irrigation, planting schedules, and crop rotation.

Clustering

Clustering is the task of dividing the set of data points (populations) into a number of groups (clusters) such that data points in the same groups are more similar to other in the same group than those data points in other groups (Kumar, 2018). It can also be described as organizing data points into groups whose members are similar in some way. A cluster consists of objects that share certain similarities as well as differences with the objects of other clusters.Data clustering is one of the most important unsupervised learning problems since it finds structure in an unlabeled set of data.

Key Algorithms

We have used three basic clustering algorithms: Partition-Based, Hierarchical-Based, and Density-Based clustering algorithms.

Partition-based clustering algorithms divide data into distinct, non-overlapping clusters. The basic idea of these clustering algorithms is to consider the center of data points as the center of the corresponding cluster, which generally has low time complexity and high computing efficiency. However, they are not well-suited for non-convex data, are sensitive to outliers, can be easily drawn into local optima, and require a predefined number of clusters, which can impact the performance of clustering results. (Yin, et al., 2024). While the advantages of the K-means algorithms include computational efficiency and clear cluster centres, assumptions of spherical clusters, and sensitivity to initialisation are its hindrances.

Hierarchical clustering involves constructing and analyzing dendrograms. Tree-like structures represent the relationship between data points in a system, appropriately called dendrograms. The algorithms can handle clusters of varying sizes and shapes. It is not necessary to specify the number of clusters in advance.

However, hierarchical clustering needs intensive computation, especially for large datasets, and the time complexity is often higher than other clustering methods. This structure is sensitive to noise and outliers, which can lead to sub-optimal clusters without the appropriate handle (Yin, et al., 2024). Hierarchical clustering requires heavy computation for large datasets and is sensitive to noise and outliers, which can produce poor cluster results.

There are four agglomerative methods in cluster formation in Hierarchical clustering, namely Single Linkage, Complete Linkage, Average Linkage, and Ward's Method (Muthahharah & Juhari, 2021). We have used two of them, namely, Complete Linkage and Ward's Method in this study. Complete linkage is clustering method at the furthest distance between objects (maximum distance), while Ward's method is a variant method that aims to obtain clusters that have the smallest internal variance cluster (Oktavia, N., & S., 2013).

Density-based spatial clustering of applications with noise (DBSCAN) identifies high-density connected areas as clusters, so that it has advantages in discovering arbitrary-shaped clusters (Cheng, et al., 2024). DBSCAN

handles noise and identifies non-spherical clusters, but its limitations include parameter sensitivity and varying densities.

METHODS AND DATA

Dataset Description

We PET values at 10 days time slots t and vegetation duration of 52 agricultural crops from Antakya Province in Türkiye. The primary data source is the 2016 Türkiye Plant Water Consumption Guide, prepared by TAGEM and DSI using the FAO Penman-Monteith method (TAGEM & DSI, 2016). The variables are total annual PET, growing duration, temporal slots, crop descriptions. Temporal encoding is 36 time slots representing 10-day periods (January 1-10 = slot 1, ..., December 21-31 is 36. Total annual PET and Total irrigation days (for almost all field crops it equals to vegetation time. It is different for trees). Total annual PET and Total irrigation days of 52 crops for Antakya Province in Türkiye is given in Table 1.

The following steps can explain the clustering methodology in our study:

Data Loading and Preparation:

A dataset of crops is created, including features like Total Potential Evapotranspiration (PET), Growing season, Number of time slots and a text description. The dataset is converted into a Pandas DataFrame. **Time Slot Parsing:** The time_slots feature, which represents the growing season, is parsed to extract more useful numerical features. the time slots into seasonal coverage (winter, spring, summer, fall), total months active, and flags for continuity and year-spanning. **Categorical Encoding:** The categorical features description and peak season are encoded to convert them into numerical representations suitable for clustering algorithms. **PET Categorization:** The Total_PET feature is categorized into bins (Low, Medium, High, Very High).

Clustering and Evaluation:

The evaluate_clustering_methods function performs clustering using several algorithms: K-Means iterates through different values of k (number of clusters) from 2 to 7, calculates the Silhouette Score for each, and selects the k with the best score. Then, K-Means is run with the best k. Hierarchical Clustering (Agglomerative clustering) is performed using 'ward' and 'complete' linkage methods. And finally DBSCAN is tested with different values for the eps parameter (0.5, 0.8, and 1.0). The code proceeds to the next eps value only if the current one results in no noise points. Standard Scaling (Normalization), before applying any clustering algorithm, the features are standardized using Standard Scaler to have zero mean and unit variance. This is important because clustering algorithms are sensitive to the scale of the features. The Silhouette Score and Calinski-Harabasz Index are used to evaluate the quality of the clusters. The code iterates through each feature set defined in the feature_sets dictionary. For each feature set, it calls the evaluate_clustering_methods function to perform clustering and evaluate the results.

The results for each feature set and clustering method are stored in the all_results dictionary. The code iterates through all the results in the all_results dictionary to find the best clustering method based on the Silhouette Score.The best method, feature set, and corresponding metrics are stored in the best_overall variable. The best clustering model is applied to the original DataFrame df to assign each crop to a cluster. The code then iterates through each cluster and calculates summary statistics such as average PET, average duration, seasonal patterns, and the distribution of crop types.

Table 1 Total annual PET and Total irrigation/vegetation days of 52 crops for Antakya Province in Türkiye

No	Crop name	Total PET[1]	Total Irrigation / Vegetation [2]	Description	No	Crop name	Total PET[1]	Total Irrigation / Vegetation [2]	Description
1	Lettuce (Regular)	0.000	0.000	fall-short	27	Grapes (Wine)	0.482	0.517	whole year
2	Cabbage (Red/Purple)	0.035	0.138	fall-medium	28	Soybeans	0.483	0.276	spring-long
3	Broad Beans (Fresh)	0.085	0.414	winter-short	29	Corn (Grain)	0.502	0.310	spring-long
4	Lettuce (Curly)	0.086	0.000	fall-short	30	Eggplant	0.505	0.276	spring-medium
5	Onions (Green/Spring)	0.107	0.000	spring-short	31	Pumpkin	0.528	0.310	spring-long
6	Potatoes (Early)	0.122	0.310	winter-short	32	Olives (Table)	0.565	0.586	whole year(tree)
7	Cabbage (White)	0.134	0.241	fall-short	33	Olives (Oil)	0.565	0.586	whole year(tree)
8	Barley (Winter)	0.192	0.448	winter-long	34	Peanuts	0.578	0.379	spring-long
9	Squash (for Stuffing)	0.223	0.138	spring-short	35	Grapes (Table, Dried)	0.604	0.552	whole year(tree)
10	Wheat (Winter)	0.234	0.448	winter long	36	Peppers (for Paste)	0.607	0.379	spring-long
11	Corn (Silage, 2nd Crop)	0.262	0.069	summer-short	37	Citrus	0.628	1.000	whole year(tree)
12	Soybeans (2nd Crop)	0.269	0.103	summer-short	38	Almonds	0.637	0.690	whole year(tree)
13	Vetch (Common)	0.274	0.103	spring-short	39	Cotton	0.639	0.414	spring-long
14	Onions (Winter, Seed)	0.279	0.552	winter long	40	Rice	0.661	0.345	spring-long
15	Sesame (Second Crop)	0.289	0.138	summer-short	41	Strawberry	0.665	0.586	spring-long
16	Peanuts (Second Crop)	0.311	0.207	summer-short	42	Peach	0.690	0.586	whole year(tree)
17	Beans (Fresh)	0.320	0.172	spring-short	43	Apricot	0.698	0.586	whole year(tree)
18	Peas (Fresh)	0.324	0.172	spring-short	44	Apple	0.698	0.586	whole year(tree)
19	Corn (Grain, 2nd Crop)	0.340	0.172	summer-short	45	Plum	0.721	0.621	whole year(tree)
20	Cucumber	0.343	0.172	spring-short	46	Pomegranate	0.732	0.655	whole year(tree)
21	Sesame	0.393	0.207	summer-short	47	Pear	0.744	0.621	whole year(tree)
22	Carrot	0.396	0.207	summer-short	48	Persimmon	0.745	0.586	whole year(tree)
23	Melon	0.411	0.241	summer-short	49	Parsley	0.841	0.862	whole year(greens)
24	Fig	0.426	0.621	whole year(tree)	50	Walnut	0.851	0.621	whole
25	Okra	0.428	0.241	spring-medium	51	Alfalfa	0.862	0.690	whole (greens)
26	Tomatoes (Ground)	0.435	0.207	spring-medium	52	Banana (2 Years and Older)	1.000	1.000	whole year(tree)
	[1] Normalized value of Total PET has 113 mm (0.00) minimum and 1330 (1.00) mm maximum value. [2]Normalized irrigation days has 70 (0.00) days minimum and 360 (1.00) days maximum value.								

Visualization:

Several visualizations are created to help understand the clustering results:

PCA Visualization: Principal Component Analysis (PCA) is used to reduce the dimensionality of the data to 2 components, and the clusters are visualized in the PCA space. **PET vs Duration:** A scatter plot of Total_PET vs Duration, with points colored by cluster. **Seasonal Patterns:** A bar plot showing the average seasonal coverage for each cluster. **Hierarchical Dendrogram:** A dendrogram is plotted to visualize the hierarchical relationships between the crops. **Cluster Sizes:** A bar plot

Implementation

The implementation was done by Python Python 3.12.7 with Pandas, Numpy, Matplotlib, Seaborn, Scikit-learn libraries. Validation is 10-fold cross-validation for stability and Reproducibility is fixed random seeds (42) for consistent results.

Validation refers to the process of evaluating how well a machine learning model generalizes to unseen data. 10-fold cross-validation is a specific technique used for validation. It involves the following steps: The original dataset is divided into 10 equal (or as close as possible) parts, called "folds. The model is trained on 9 of these folds and tested (validated) on the remaining 1 fold. This process is repeated 10 times, with each of the 10 folds used exactly once as the validation set.

In machine learning, it's important to be able to reproduce the same results if we run the code again. Setting a fixed random seed (in our case, 42, but any integer can be used) ensures that the random processes are initialized in the same way each time the code is run. This makes the results reproducible.

RESULTS AND DISCUSSION

According to the results given in Table 2 the best clustering method is Hierarchical Ward with PET focused featues, pet_focused features Silhouette Score 0.5703 which corresponds to medium structue and number of clusters 7. Rating Scale of Silhouette ScoreSilhouette Coefficient (SC) Interpretasi : 0,7 < SC ≤ 1.0 Strong Structure, 0.5 < SC ≤ 0.7 Medium Stucture, 0.25 < SC ≤ 0.5 Weak Structure and finally SC ≤ 0.25 No Structure (Benaya, Sibaroni, & Ihsan, 2023). Silhouette Score ranges between −1 and 1, where a higher silhouette coefficient refers to a model with more coherent clusters. In other words, silhouette scores close to +1 means the sample is far away from the neighboring clusters. A value of 0 means that the sample is on or very close to the decision boundary between two neighboring clusters. Finally, negative values indicate that the samples could have potentially been assigned to the wrong cluster (Belyadi, Hoss; Haghighat, Alireza, 2021).

Several visualisations are created to help understand the clustering results in Figures 1 and 2. While Clusters in PCA Space, PET vs Duration by Cluster, and Seasonal Patterns by cluster are visualized in Figure 1, the Hierarchical Clustering Dendogram, Cluster Sizes and Top 10 Method-Feature Combinations are given in Figure 2. Since Python uses zero-based indexing, our Cluster 1 aligns with Cluster 0 in the figures, and the others follow the suit.

Table 2 Algorithm Performance Comparison

Features	Algorithm	# of clusters	Silhouette
Total PET, Number of t, Description encoded	K-Means	5	0.5530
	Hierarchical complete	5	0.5510
	DBSCAN	5	0.5030
Winter Spring, Summer, Fall coverages, Total_PET, Number of t	K-Means	6	0.4840
	Hierarchical complete	6	0.4350
	DBSCAN	6	0.4200
Total PET, Number of t, Winter Spring, Summer, Fall coverages, Total months, 'is continuous', 'Spans year', Description encoded	K-Means	7	0.4890
	Hierarchical complete	7	0.4860
	DBSCAN	7	0.4400
Total_PET, PET category encoded', Number of t , Peak season encoded	K-Means	7	0.5560
	Hierarchical ward	7	0.5703
	Hierarchical complete	7	0.5380
Winter Spring, Summer, Fall coverages, Total months, 'Spans year'	K-Means	6	0.5520
	Hierarchical ward	6	0.4980
	Hierarchical complete	6	0.4980

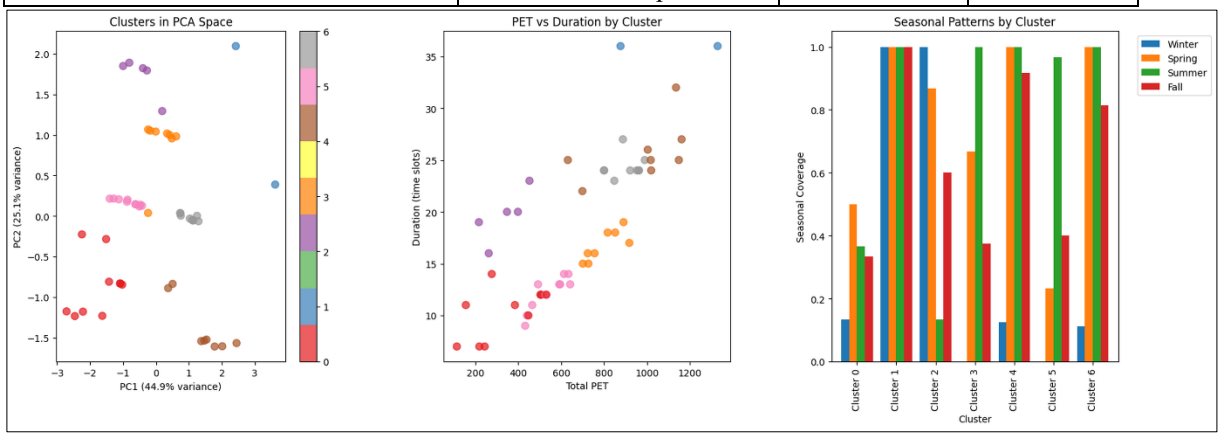

Figure 1 Clusters in PCA Space, PET vs Duration by Cluster, and Seasonal Patterns by cluster.

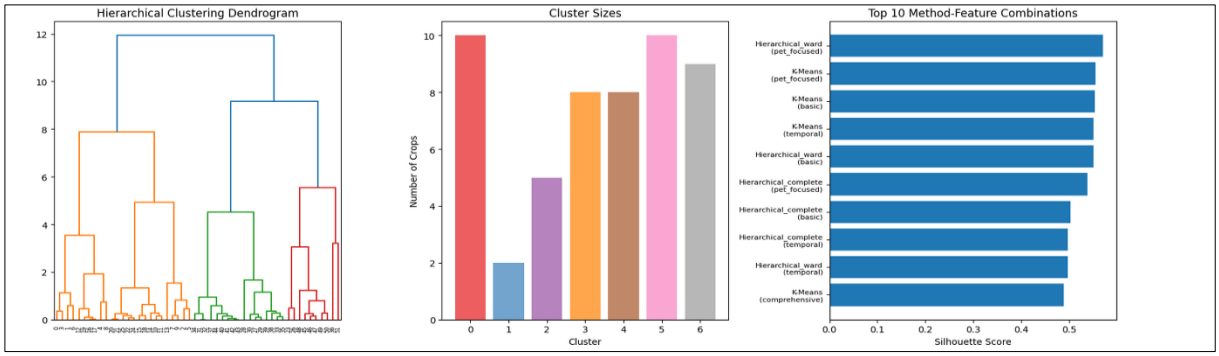

Figure 2 Hierarchical Clustering Dendogram, Cluster Sizes and Top 10 Method-Feature Combinations (Clusters 0-6 in Figure 2 correspond to clusters 1-7 in the manuscript)

Seasonal Coverage is a parameter and calculated as given in Eq.1:

$$\text{Seasonal coverage} = \frac{\text{Active months in season}}{\text{Total months in season}} \quad (1)$$

The seasonal coverage values (winter, spring, summer, fall) represent the proportion of months within that season that the crops in the cluster are active. For example Winter coverage: 0.11 means that, on average, the crops in this cluster are active for only 11% of the winter months (December, January, February). This suggests that these crops are generally not grown during the winter, or only grown for a very short period within winter. Another example: Spring coverage: 1.00 indicates that the crops in this cluster are active for 100% of the spring months (March, April, May). This means these crops are very likely to be grown throughout the entire spring season.

Average months active is the average number of months that crops in this cluster are actively growing.

CONCLUSION

This study revealed the application of unsupervised machine learning techniques to cluster 52 distinct crops based on their evapotranspiration demands, temporal characteristics, and descriptive attributes. The primary objective was to identify inherent groupings among crops that could inform water resource management strategies and optimize agricultural planning. Through a comprehensive evaluation of multiple clustering algorithms (K-means, Hierarchical, DBSCAN) and feature set combinations, the analysis revealed that Hierarchical Ward clustering with PET-focused features yielded the most distinct and well-separated clusters, as indicated by a Silhouette score of 0.570.

The resulting clusters exhibited meaningful distinctions in terms of average PET requirements, growing season duration, and seasonal coverage patterns. For instance, while Cluster 1 represents crops with low water requirements, short growing seasons primarily in the spring and fall, and includes crops like lettuce and cabbage, Cluster 7 represents crops with high water requirements, year-round activity, and long durations, consisting of tree crops like citrus, almonds, and grapes. These clusters likely require very different irrigation and management strategies. These findings suggest that the clustering results, e.g., crops with similar water needs and growing seasons can be grouped together for irrigation scheduling. By using this framework, precision agriculture applications such as irrigation schedules and planting schedules can be automated and improved through the use of data, including better decision-making in irrigation, planting schedules, crop rotation practices and water allocation optimization.

The study demonstrates the potential of machine learning in sustainable agriculture, providing a framework for scalable precision water management that can be used across diverse agricultural crops, climates, and geographical regions. Precision agriculture applications such as irrigation schedules and planting schedules can be automated and improved through the use of data, including better decision-making in irrigation, planting schedules, crop rotation practices and water allocation optimization. Agricultural science and data science are combined in the methodology, enabling evidence-based management sustainable water and food production decisions.

The study's scope is constrained by its focus on Antakya Province data, suggesting potential value in examining different climate zones in subsequent research. The current static modeling approach could be enhanced

through the incorporation of climate change adaptation factors and dynamic modeling techniques. Future research would benefit from practical testing to validate findings across different sites. Additionally, the studies should consider additional factors such as soil type and economic considerations to refine the clustering results.

Table 3 The features of clusters number 1-4 found by the algorithm Hierarchical Ward with PET focused featues, Silhouette Score 0.5703

Cluster Number	1	2	3	4
Number of crops	10	2	5	8
Seasonal Description	Quick Spring/Fall Vegetables	Year-Round Tree Crops	Winter Grains & Storage Crops	Summer Field Crops
Water need	Low water needs (113-531 PET)	Highest water demand (877-1330 PET)	Moderate water needs	High water demand (701-918 PET)
Average Total PET(mm)	338 (range: 113-531)	1104 (range: 877-1330)	335 (range: 216-452)	798 (range: 701-918)
Growing	short growing periods	continuous growing	Winter-dominant growing season	summer focused
Average Duration	10.3 time slots or 103 days (range: 7-14)	36.0 time slots or 360 days (range: 36-36)	19.6 time slots or 196 days (range: 16-23)	16.8 time slots or 168 days (range: 15-19)
Seasonal Coverage	Winter coverage: 0.13, Spring coverage: 0.50, Summer coverage: 0.37, Fall coverage: 0.33	Winter coverage:1.0, Spring coverage: 1.0, Summer coverage: 1.0, Fall coverage: 1.0	Winter coverage: 1.0, Spring coverage: 0.87, Summer coverage: 0.13, Fall coverage: 0.6	Winter coverage: 0.0, Spring coverage: 0.67, Summer coverage: 1.0, Fall coverage: 0.37
Average months active	4	12	7.8	6.1
Crops type	spring-short: 6 crops, fall-short: 3 crops, fall-medium: 1 crop	whole year(tree): 2 crops	winter-short: 2 crops, winter long: 2 crops, winter-long: 1 crop	spring-long: 7 crops, spring-medium: 1 crop
Crops	Lettuce (Regular), Cabbage (Red/Purple), Lettuce (Curly), Onions (Green/Spring), Cabbage (White), Squash (for Stuffing), Vetch (Common), Beans (Fresh), Peas (Fresh), Cucumber	Citrus, Banana (2 Years and Older)	Broad Beans (Fresh), Potatoes (Early), Barley (Winter), Wheat (Winter), Onions (Winter, Seed)	Soybeans, Corn (Grain), Eggplant, Pumpkin, Peanuts, Peppers (for Paste), Cotton, Rice
General desciption	Typical cool-season crops	Permanent high-water crops	Cold-season field crops	Major summer commodities

Table 4 The features of clusters number 5-8 found by the algorithm Hierarchical Ward with PET focused featues, Silhouette Score 0.5703

Cluster Number	5	6	7
Number of crops	8	10	9
Seasonal Description	Perennial Trees & Long-Season Crops	Summer Intensives & Second Crops	Mediterranean Tree Fruits
Water need	High water needs	Moderate water needs,	High water demand
Average Total PET(mm)	977 (range: 631-1162)	543 (range: 432-642)	903 (range: 800-990)
Growing	9+ months growing seasons	Short summer cycles	8+ month seasons
Average Duration	25.8 time slots or 258 days(range: 22-32)	12.2 time slots or 122 days (range: 9-14)	24.3 time slots or 243 days(range: 23-27)
Seasonal Coverage	Winter coverage:0.12, Spring coverage: 1.0, Summer coverage: 1.0, Fall coverage: 0.92	Winter coverage:0.00, Spring coverage: 0.23, Summer coverage:0.97, Fall coverage: 0.40	Winter coverage:0.11, Spring coverage: 1.00, Summer coverage: 1.00, Fall coverage: 0.81
Average months active	9.1	4.8	8.8
Crops type	whole year(tree): 5 crops, whole year(greens): 1 crop, whole year 1 crop	summer-short: 8 crops, spring-medium: 2 crops	whole year(tree): 8 crops, spring-long: 1 crop
Crops	Fig, Grapes (Wine), Pomegranate, Pear, Persimmon, Parsley, Walnut, Alfalfa	Corn (Silage, Second Crop), Soybeans (Second Crop), Sesame (Second Crop), Peanuts (Second Crop), Corn (Grain, Second Crop), Sesame, Carrot, Melon, Okra, Tomatoes (Ground)	Olives (Table), Olives (Oil), Grapes (Table, Dried), Almonds, Strawberry, Peach, Apricot, Apple, Plum
General desciption	Established perennial systems	Heat-loving vegetables	Mediterranean climate adapted

References

Belyadi, Hoss; Haghighat, Alireza. (2021). Unsupervised machine learning: clustering algorithms. In H. Belyadi, & A. Haghighat, *Machine Learning Guide for Oil and Gas Using Python* (pp. 125-168). Gulf Professional Publishing. doi:doi.org/10.1016/B978-0-12-821929-4.00002-0

Benaya, R., Sibaroni, Y., & Ihsan, F. A. (2023). Clustering Content Types and User Roles Based on Tweet Text Using K-Medoids Partitioning Based. *Journal of Computer System and Informatics (JoSYC), 4*, Volume 4, No. 4, August 2023, Page. doi:DOI 10.47065/josyc.v4i4.3751

Cheng, D., Zhang, C., Li, Y., Xia, S., Wang, G., Huang, J., . . . Xie, J. (2024). GB-DBSCAN: A fast granular-ball based DBSCAN clustering algorithm. *Information Sciences, 674*. doi:https://doi.org/10.1016/j.ins.2024.120731

Kumar,, H. (2018). Clustering Techniques: A Review on Some Clustering Algorithms. In P. K. Borah, *Emerging Trends and Applications in Cognitive Computing* (pp. 98-223). India: IGI Global Scientific Publishing. doi:0.4018/978-1-5225-5793-7

Kuzma, S., Saccoccia, L., & Chertock, M. (2023, August 16). *World Resources Institute*. Retrieved June 9, 2025, from https://www.wri.org/insights/highest-water-stressed-countries

Muthahharah, I., & Juhari, A. (2021). Cluster Analysis with Complete Linkage and Ward's Method for. *Jurnal Varyan, 4*(2). doi: https://doi.org/10.30812/varian.v4i2

Oktavia, S., N., M., & S., N. (2013). Sela Oktavia, M. N. & N. S. (2013). Pengelompokan Kinerja Dosen Jurusan Matematika Fmipa Untan Menggunakan Metode Ward. , 02(2), 93–100. *Buletin Ilmiah Mat. Stat. Dan Terapannya (Bimaster)*, 93-100.

Perry, C., Steduto, P., & Karajeh, F. (2017). *DOES IMPROVED IRRIGATION TECHNOLOGY SAVE WATER?* Cairo: FAO.

Rai, R. K., Singh, V. P., & Upadh, A. (2017). Irrigation Methods. In *Planning and Evaluation of Irrigation Projects Methods and Implementation* (pp. 353-363).

TAGEM, & DSI. (2016). *Plant-Water Use Guide of irrigated crops in Turkey.* Ankara.

UN-Water,. (2023). *Sustainable Development Goal 6 Synthesis Report on Water and Sanitation 2023.* Newyork: United Nations Publications.

Water-OECD. (2025). Retrieved June 9, 2025, from https://www.oecd.org/water/

Whittlesey,, N. (2003). Improving irrigation efficiency through technology adoption: When will it Conserve water? *Developments in Water Science, 50*, 53-62. doi:10.1016/S0167-5648(03)80007-2.

Yin, H., Aryani, A., Petrie, S., Nambissan, A., Astudillo, A., & Cao, S. (2024). A Rapid Review of Clustering Algorithms. Retrieved from https://arxiv.org/abs/2401.07389

➢ *ORAL PRESENTATION*

Erp Uygulamalarında İş Süreçlerinin Analizi: Bir Elektrik Dağıtım Şirketi Örneği

Sait Aktepe[1*] (*ORCID: https://orcid.org/0009-0000-4584-9647*),
İzzettin Hakan Karaçizmeli[2] (*ORCID:* https://orcid.org/*0000-0002-8540-8050*)

[* 1,2] Harran Üniversitesi, Mühendislik Fakültesi, Şanlıurfa, Türkiye

*Sorumlu yazar e-posta: saitaktepe@gmail.com

Özet

Bu çalışma, bir elektrik dağıtım şirketinde Kurumsal Kaynak Planlama sisteminin iş süreçleri üzerindeki etkilerini nitel bir yaklaşımla incelemiştir. Kurumsal Kaynak Planlama sistemine geçiş öncesi ve sonrası süreç performansları karşılaştırılmış, operasyonel verimlilik, süreç süreleri ve veri bütünlüğü gibi alanlarda önemli iyileşmeler tespit edilmiştir. Sistem, iş süreçlerinin entegrasyonu, veri yönetimi ve karar destek mekanizmalarını güçlendirmiştir. Ancak çalışanların yeni sisteme adaptasyonu önemli bir zorluk olarak ortaya çıkmıştır. Sonuçlar, Kurumsal Kaynak Planlama projelerinde süreç analizine ve eğitim yönetimine öncelik verilmesinin başarının anahtarı olduğunu göstermektedir.

Anahtar Kelimeler: Kurumsal Kaynak Planlama, İş Süreçleri Analizi, Elektrik Dağıtım Şirketi, Operasyonel Verimlilik, Süreç Yönetimi.

Abstract

This study qualitatively examines the impacts of Enterprise Resource Planning systems on business processes within an electricity distribution company. Performance comparisons before and after Enterprise Resource Planning implementation reveal significant improvements in operational efficiency, process durations, and data integrity. The system enhanced process integration, data management, and decision support mechanisms. However, employee adaptation to the new system emerged as a major challenge. Findings emphasize that prioritizing process analysis and training management is key to successful Enterprise Resource Planning projects.

Keywords: Enterprise Resource Planning, Business Process Analysis, Electricity Distribution Company, Operational Efficiency, Process Management.

GİRİŞ

Gelişen teknoloji ve dijital dönüşüm süreçleri, işletmelerin kaynaklarını daha etkin ve entegre biçimde yönetmesini zorunlu hâle getirmiştir. Bu bağlamda, Kurumsal Kaynak Planlama (KKP) sistemleri, kurumların farklı iş birimlerini ortak bir veri yapısı altında birleştirerek bilgiye dayalı karar alma süreçlerini destekleyen stratejik yazılımlar olarak öne çıkmaktadır. KKP çözümleri; üretim, finans, insan kaynakları, tedarik zinciri gibi çeşitli fonksiyonları bütünleştirerek hem operasyonel verimliliği artırmakta hem de kurumsal süreçlerin şeffaf ve izlenebilir olmasını sağlamaktadır.

KKP sistemlerinin etkinliğini belirleyen en önemli unsurlardan biri, bu sistemlerin hayata geçirilmesinden önce gerçekleştirilen iş süreçleri analizidir. Mevcut süreçlerin sistematik biçimde incelenmesi, KKP'nin kuruma özel ihtiyaçlara göre yapılandırılmasını kolaylaştırmakta, aynı zamanda uygulama sürecinde karşılaşılabilecek sorunların önceden öngörülmesine imkân tanımaktadır. Süreç analizleri sayesinde, zaman kaybına neden olan işlemler tespit edilerek iyileştirme alanları belirlenmekte ve KKP sisteminin değer yaratma potansiyeli artırılmaktadır. Özellikle kamu hizmeti sunan büyük ölçekli kurumlarda, süreç odaklı yaklaşımlar hem hizmet kalitesini yükseltmekte hem de maliyetleri kontrol altında tutmaya katkı sağlamaktadır.

Bu çalışma, bir elektrik dağıtım şirketinde kullanılan KKP sisteminin temel iş süreçleri üzerindeki etkilerini incelemeyi amaçlamaktadır. Araştırma kapsamında, kurumun operasyonel işleyişine dair süreçler değerlendirilmiş, KKP sisteminin süreç performansına olan katkıları gözlemlenmiş ve uygulamanın genel

etkinliği analiz edilmiştir. Elde edilen sonuçlar, KKP uygulamalarında süreç analizinin neden kritik bir adım olduğunu ortaya koyarken, bu alanda gerçekleştirilebilecek olası iyileştirmelere de ışık tutmaktadır. Çalışma, uygulamaya dayalı örnek üzerinden KKP ve iş süreci yönetimi arasındaki ilişkinin anlaşılmasına katkı sunmayı hedeflemektedir.

YÖNTEM

Bu çalışma, bir elektrik dağıtım şirketinde uygulanan KKP sisteminin iş süreçleri üzerindeki etkilerini incelemek amacıyla nitel bir araştırma yaklaşımı benimsemiştir. Araştırma kapsamında, hem KKP sisteminin genel işleyişine dair teknik ve yönetsel bilgiler toplanmış, hem de sistem entegrasyonu sürecinde gerçekleştirilen iş süreçleri analizleri değerlendirilmiştir.

KKP sistemleri, işletmelerin finans, insan kaynakları, satın alma, bakım-onarım ve müşteri hizmetleri gibi fonksiyonlarını ortak bir veri tabanı üzerinden entegre eden ve süreçler arası koordinasyonu artırmayı amaçlayan bilgi sistemleridir. KKP uygulamaları, sadece yazılım sistemlerinin kurulumu değil, aynı zamanda mevcut iş süreçlerinin yeniden tanımlanması ve iyileştirilmesi sürecini de kapsar. Bu nedenle KKP projeleri, teknik olduğu kadar yönetsel bir dönüşüm sürecidir.

İş süreçleri analizi, KKP sistemlerinin kurulumu öncesinde gerçekleştirilen temel adımlardan biridir. Bu analiz sürecinde, kurumun mevcut iş akışları detaylı şekilde incelenerek darboğazlar, tekrar eden işlemler ve verimsizlikler belirlenir. Bu adımların ardından, KKP sistemine uygun, optimize edilmiş süreçler tasarlanır. Bu yaklaşım literatürde sıklıkla iş süreçlerinin yeniden yapılandırılması (Business Process Reengineering - BPR) çerçevesinde ele alınmaktadır (Hammer & Champy, 2001). Davenport (1993), KKP sistemlerinin yalnızca teknoloji yatırımı olmadığını, aynı zamanda süreç mantığının yeniden kurgulanmasını gerektirdiğini vurgulamıştır.

Benzer şekilde, Al-Mashari ve Zairi (2000) KKP uygulamalarının başarısını etkileyen temel faktörleri incelemiş ve süreç analizinin bu faktörlerin başında geldiğini ortaya koymuştur. Özellikle kamu sektöründe gerçekleştirilen çalışmalarda (örn. Ghosh & Scott, 2005), süreç temelli yaklaşımların KKP geçişlerinde daha fazla önem kazandığı ve bu analizlerin hizmet sunum kalitesi üzerinde doğrudan etkili olduğu belirtilmiştir.

Bu bağlamda, çalışmada incelenen elektrik dağıtım şirketinde, KKP sistemine geçiş sürecinde gerçekleştirilen iş süreçleri analizleri ve bu analizlerin uygulama sonuçları sistematik biçimde değerlendirilmiştir. Süreçler; müşteri hizmetleri, arıza bildirimi, bakım planlama, malzeme tedariki ve sayaç okuma gibi temel operasyonel alanları kapsamaktadır. Veriler, doküman analizi, gözlem ve yarı yapılandırılmış görüşmeler yoluyla toplanmış, içerik analizi yöntemiyle değerlendirilmiştir.

BULGULAR VE TARTIŞMA

Bu çalışmada, bir elektrik dağıtım şirketinde KKP sisteminin iş süreçleri üzerindeki etkileri, sistem geçişi öncesi ve sonrası süreç performansları karşılaştırılarak incelenmiştir. Elde edilen bulgular, KKP uygulamasının özellikle operasyonel verimlilik, hizmet süresi, veri bütünlüğü ve karar destek süreçleri açısından kayda değer iyileştirmeler sağladığını ortaya koymaktadır.

KKP öncesi dönemde, birçok iş süreci farklı birimler arasında manuel, e-posta veya kağıt belgeler üzerinden yürütülmekteydi. Bu durum, süreç gecikmelerine, veri kayıplarına ve tekrar eden işlemlere neden olmaktaydı. KKP geçişiyle birlikte bakım planlama, arıza bildirimi, sayaç okuma ve malzeme yönetimi gibi süreçler entegre bir yapıya kavuşmuş ve ortalama işlem sürelerinde %30'a varan azalmalar gözlemlenmiştir. Bu bulgu, Yıldız, Aydın ve Kurtuluş'un (2017) enerji sektöründeki benzer bulgularıyla paralellik göstermektedir.

KKP sistemiyle birlikte tüm süreçlere ilişkin veriler merkezi bir sistemde toplanmakta ve yetkilendirilmiş personel tarafından anlık olarak erişilebilmektedir. Bu yapı sayesinde karar alma süreçleri daha veriye dayalı hale gelmiş, özellikle üst yönetim düzeyinde stratejik planlamada KKP raporlamalarının aktif olarak kullanılmaya başlandığı tespit edilmiştir. Bu sonuç, Ghosh ve Scott'un (2005) kamu kurumlarındaki karar destek sistemlerinin KKP ile güçlendiğine dair tespitlerini desteklemektedir.

KKP uygulamasıyla birlikte iş süreçlerinin açık şekilde tanımlandığı ve sorumlulukların netleştirildiği görülmüştür. Özellikle arıza yönetimi ve müşteri şikayetlerinin takibi gibi süreçlerde, sistem üzerinde işlem adımlarının kayıt altına alınması, iç denetim ve kalite kontrol faaliyetlerini kolaylaştırmıştır. Bu durum, Al-

Mashari ve Zairi'nin (2000) KKP'nin şeffaflık ve izlenebilirlik üzerindeki etkisine dair görüşleriyle örtüşmektedir.

Sistem geçişi sırasında yaşanan temel zorluklardan biri, çalışanların yeni sisteme uyumu olmuştur. Özellikle yaşça büyük ve teknolojiye daha az yatkın personelin KKP modüllerini kullanmada zorluk yaşadığı tespit edilmiştir. Ancak düzenli eğitimlerin ardından bu uyum sorununun zamanla azaldığı ve kullanıcı memnuniyetinin arttığı gözlemlenmiştir. Bu bulgu, literatürde KKP başarısında "insan faktörü"nün etkisini vurgulayan çalışmalarla (Davenport, 1998; Hammer & Champy, 2001) tutarlıdır.

Elde edilen bulgular, KKP sisteminin yalnızca bir bilgi teknolojisi yatırımı değil, aynı zamanda köklü bir organizasyonel değişim süreci olduğunu göstermektedir. İş süreçlerinin entegrasyonu, veri güvenliği, operasyonel hız ve şeffaflık açısından sağlanan kazanımlar önemli olmakla birlikte, çalışanların adaptasyonu ve süreçlerin yeniden yapılandırılması gibi alanlarda dikkatli bir yönetim süreci gerekmektedir.

Çalışmanın bulguları, KKP uygulamalarının sektörel dinamiklere uygun şekilde kurgulanması gerektiğini ortaya koymaktadır. Elektrik dağıtım sektöründe müşteri hizmetleri, saha operasyonları ve bakım planlama gibi süreçlerin doğrudan kamu hizmeti kalitesiyle ilişkili olması, KKP sistemlerinin etkinliğini daha da kritik hale getirmektedir. Bu yönüyle çalışma, KKP projelerine başlamadan önce gerçekleştirilecek süreç analizlerinin, sadece sistem tasarımı değil, kurumsal performans açısından da belirleyici olduğunu ortaya koymaktadır.

SONUÇ

Bu çalışma, bir elektrik dağıtım şirketinde KKP sisteminin iş süreçlerine etkisini incelemiştir. Bulgular, KKP'nin süreçlerde bütünleşme, izlenebilirlik ve zaman tasarrufu sağladığını göstermektedir. Özellikle bakım, müşteri hizmetleri ve arıza yönetimi gibi alanlarda işlem sürelerinde azalma ve hizmet kalitesinde artış gözlemlenmiştir.

Ayrıca merkezi veri yönetimi, karar alma süreçlerini güçlendirmiş; süreçlerin standardizasyonu, iç denetim faaliyetlerini kolaylaştırmıştır. Ancak çalışanların sisteme adaptasyonu, KKP uygulamasının zayıf noktalarından biri olmuştur.

KKP çalışmalarında süreç analizine sistem öncesinde mutlaka zaman ayrılmalıdır. Eğitim ve değişim yönetimi stratejileri KKP başarısı için kritik önemdedir. KKP sistemleri sektörlere göre özelleştirilirse daha faydalı olabilir. Ayrıca gelecek araştırmalar, sistemin nicel çıktılarıyla desteklenmelidir.

TEŞEKKÜR

Bu çalışmanın gerçekleştirilmesinde katkı sunan elektrik dağıtım şirketi yöneticilerine ve çalışanlarına, veri sağlama ve gözlem süreçlerine verdikleri destekten dolayı teşekkür ederiz. Ayrıca, araştırma sürecinde yapıcı görüş ve önerileriyle katkı sağlayan akademik danışmanlarımıza ve Harran Üniversitesi Mühendislik Fakültesi yönetimine teşekkürlerimizi sunarız. Bu çalışmaya doğrudan katılmayan ancak sürece dolaylı katkı sağlayan tüm meslektaşlarımıza da şükranlarımızı belirtiriz.

KAYNAKLAR

Al-Mashari, M., & Zairi, M. (2000). Revisiting BPR: a holistic review of practice and development. Business Process Management Journal, 6(1), 10–42. https://doi.org/10.1108/14637150010310822

Davenport, T. H. (1993). Process innovation: Reengineering work through information technology. Harvard Business School Press.

Ghosh, S., & Scott, J. E. (2005). Comparing case study and event study methodologies in ERP implementation research: A case for the event study methodology. Information Systems Management, 22(4), 76–88. https://doi.org/10.1201/1078.10580530/45530.22.4.20050901/90029.8

Hammer, M., & Champy, J. (2001). Reengineering the corporation: A manifesto for business revolution (Rev. ed.). HarperBusiness.

➢ *ORAL PRESENTATION*

Comparison of Anomaly Detection in Logged Data Analysis

Cahide SARA[1*] (*ORCID: https://orcid.org/.0009-0003-5432-3913.*),
Sara ALTUN GÜVEN[2] (*ORCID: https://orcid.org/0000-0003-2877-7105)*

[*1,2]Tarsus University, Engineering Faculty, Computer Engineering Department, Mersin, Turkey.

*Corresponding author e-mail: cahidesr.04@gmail.com

Abstract
This study conducted anomaly detection on log data from various systems and compared the performance of different methods. Log analysis was performed to understand system states and identify abnormal behaviors. The anomaly detection aimed to recognize unexpected patterns or deviations in system logs, utilizing four different models: Isolation Forest, K-Means, Rarity Model, and Out-of-Vocabulary (OOV) Detector. The datasets used in this study comprise logs from HDFS, BGL, OpenStack, Apache and Hadoop systems. Model performances were evaluated using two metrics: Accuracy and AUC-ROC (Area Under the Receiver Operating Characteristic Curve). While Accuracy measures the overall correctness of the models, AUC-ROC assesses the models' ability to distinguish anomalies as positive cases. Results indicated that, overall, the OOV Detector model achieved the highest AUC scores, especially on the BGL and Hadoop datasets (0.9887 and 0.8750, respectively), demonstrating the strength of deep language-based approaches in log-based anomaly detection. Although K-Means and Rarity Model attained high accuracy rates on some datasets, a significant decline in AUC scores was observed. In the OpenStack dataset, all models exhibited high accuracy; however, the AUC values remained low, indicating limited effectiveness in distinguishing anomalies. This work aims to contribute to the field by comparing applicable anomaly detection methods across different log datasets, thereby supporting security and system health analysis based on logs.

Keywords: anomaly detection, log analysis, machine learning, deep learning, security

Loglanmış Veri Analizinde Anomali Tespiti Kıyaslanması

Özet
Bu çalışma, çeşitli sistemlerden elde edilen günlük (log) verileri üzerinde anomali tespiti gerçekleştirmiş ve farklı yöntemlerin performanslarını karşılaştırmıştır. Günlük verileri, sistem durumlarını anlamak ve olağandışı davranışları belirlemek amacıyla analiz edilmiştir. Anomali tespiti sürecinde, sistem günlüklerinde beklenmeyen örüntülerin ya da sapmaların tanınması hedeflenmiş ve dört farklı model kullanılmıştır: Isolation Forest, K-Means, Rarity Model ve Out-of-Vocabulary (OOV) Detector.
Çalışmada kullanılan veri kümeleri; HDFS, BGL, OpenStack, Apache ve Hadoop sistemlerine ait günlüklerden oluşmaktadır. Model performansları, Doğruluk (Accuracy) ve AUC-ROC (Receiver Operating Characteristic Eğrisi Altındaki Alan) olmak üzere iki ölçüt ile değerlendirilmiştir. Doğruluk değeri modellerin genel doğruluğunu ölçerken, AUC-ROC değeri modellerin anomalileri (olumsuz örnekleri) ayırt etme yeteneğini yansıtmaktadır.Elde edilen sonuçlara göre, özellikle BGL ve Hadoop veri kümelerinde (sırasıyla 0.9887 ve 0.8750 AUC skorları), OOV Detector modelinin en yüksek AUC değerlerini sağladığı gözlemlenmiş ve bu durum, günlük verilerine dayalı anomali tespitinde derin dil modellemelerinin etkinliğini ortaya koymuştur. K-Means ve Rarity Model, bazı veri kümelerinde yüksek doğruluk oranlarına ulaşmış olsa da, bu modellerde AUC skorlarında belirgin bir düşüş gözlenmiştir. Özellikle OpenStack veri kümesinde tüm modeller yüksek doğruluk oranlarına ulaşmışken, AUC değerlerinin düşük kalması, anomalilerin ayırt edilmesinde sınırlı bir başarıya işaret etmektedir.Bu çalışma, farklı günlük veri kümeleri üzerinde uygulanabilir anomali tespit yöntemlerinin karşılaştırmasını sunarak, sistem güvenliği ve sistem sağlığı analizine katkıda bulunmayı amaçlamaktadır.

Anahtar kelimeler: anomali tespiti, günlük (log) analizi, makine öğrenmesi, derin öğrenme, güvenlik

INTRODUCTION

Contemporary information systems record events occurring at the infrastructure and application levels through system logs. Log analysis is a crucial process for interpreting logs generated by systems, diagnosing performance issues, detecting abnormal behaviors, and preventing security threats (He et al., 2017). Automated log analysis methods are especially important in large-scale systems where manual log examination is impractical (Xu et al., 2009).

Log analysis plays a vital role in areas such as system security (Sommer & Paxson, 2010), debugging (Oppenheimer et al., 2003), performance monitoring (Chen et al., 2004), and compliance (Kent & Souppaya, 2006). The techniques employed in log analysis primarily include statistical modeling, machine learning, natural language processing (NLP), and deep learning approaches. Within the domain of log analysis and anomaly detection, LogLead is one of the two prominent machine learning-based frameworks. Both LogLead and other models aim to extract meaningful information from log data and detect system faults or attacks, although their approaches, techniques, and application areas differ.

Anomaly detection involves identifying rare observations, elements, or events that significantly deviate from normal behavior patterns within a dataset. This process has been applied across various fields such as cybersecurity, healthcare, finance, industrial maintenance, quality control, and statistical analysis, utilizing methods like machine learning, deep learning, and community-based approaches. For instance, Oprea et al. (2020) proposed a machine learning-based system to analyze large-scale log data for early detection of security breaches in enterprise networks by extracting relevant features (Oprea et al., 2020). Zenati et al. (2018) introduced an efficient approach based on Generative Adversarial Networks (GANs) for anomaly detection, learning the normal data distribution and identifying deviations (Zenati et al., 2018). Meng et al. (2019) developed LogAnomaly, an integrated system that detects sequential and quantitative anomalies in logs by analyzing the order and frequency of log events with high accuracy (Meng et al., 2019). Landauer et al. (2022) integrated LogLead with deep learning models and compared their performance, finding that LogLead + LSTM outperformed pure LSTM by approximately 15% in F1-score. While requiring training data is a disadvantage, standardizing the log structure enhances the efficiency of deep learning models (Landauer et al., 2022). Zong et al. (2018) proposed a hybrid model combining deep learning and statistical techniques, such as autoencoders and Gaussian mixture models, to achieve effective results in high-dimensional data (Zong et al., 2018). Agnihotri & Batra (2017) introduced a robust autoencoder-based approach capable of performing well even with noisy data, outperforming traditional methods on real-world datasets (Agnihotri & Batra, 2017). Ren et al. (2019) described Microsoft's large-scale time-series anomaly detection system, offering valuable insights for practical applications (Ren et al., 2019). Chen et al. (2020) proposed a framework utilizing Variational Autoencoders (VAE) for anomaly detection, especially effective in complex data distributions (Chen et al., 2020). Schlegl et al. (2017) introduced a method based on GANs for anomaly detection, demonstrating success particularly in medical image analysis (Schlegl et al., 2017). Siddiqui et al. (2016) presented algorithms optimized for real-time anomaly detection in streaming data, focusing on efficiency in memory usage and computational complexity (Siddiqui et al.,2017).

Today, logs generated by large-scale systems such as HDFS, BGL, OpenStack, Hadoop and Apache are critical for understanding system behavior and identifying potential issues. However, manual analysis of these logs is impractical, leading to increased reliance on automated anomaly detection techniques. In this study, various machine learning-based anomaly detection methods were applied to logs from Hadoop Distributed File System (HDFS), BlueGene/L (BGL) supercomputer logs, OpenStack cloud infrastructure logs, Hadoop and Apache server logs, with performance evaluations and comparisons.

Anomaly detection was performed using models like Isolation Forest, K-Means, and Rarity Model, with results analyzed based on metrics such as Accuracy, AUC-ROC, and similarity measures like Cosine, Jaccard, and Compression methods. The findings reveal that different system logs require tailored anomaly detection approaches, providing valuable insights for researchers and practitioners aiming to develop automated fault detection and preventive maintenance strategies in large-scale systems.

The remainder of this paper is organized into the following sections: methods, experimental results, discussion, and conclusion. The methods section covers datasets, preprocessing, feature extraction, applied machine learning algorithms, and evaluation metrics. Experimental results compare the performance of each algorithm across datasets, analyze the best-performing methods, and discuss false positive/negative rates. The discussion section explains why certain methods perform better on specific log types, while the conclusion summarizes key findings and implications for industrial and academic applications.

MATERIALS AND METHODS

This section details the anomaly detection approach employed, along with the descriptions of the datasets used for log analysis and the evaluation metrics applied.

Anomaly Detection

Anomaly detection is the process of identifying patterns or observations within a dataset that significantly deviate from expected normal behavior (Chandola et al., 2009). It is used to detect unforeseen situations such as system failures, fraud, or erroneous data entries. Examples include credit card fraud detection, network security monitoring, and prediction of industrial equipment failures.

In this study, the anomaly detection methods applied are Isolation Forest, K-Means, Rarity Model, and Out-of-Vocabulary (OOV) Detection. Isolation Forest relies on the principle that anomalous observations can be isolated more quickly via fewer splits in a tree-based approach (Liu, Ting & Zhou, 2008). K-Means is especially effective for identifying anomalies that are not density-based but can be geometrically separated in feature space (Chandola et al., 2009). Rarity-based models typically utilize criteria such as probability density functions (PDF) or event frequency, considering observations with unusually low occurrence as anomalous. These models are particularly effective in systems with prior knowledge of normal behavior (Goldstein & Uchida, 2016). OOV Detection considers observations as anomalies if they contain symbols, words, or event sequences that the model has not encountered before or are outside its vocabulary (Du et al., 2017). Anomaly detection can be performed using various techniques depending on data types and application domains. The choice of method depends on data size, label availability, and specific application requirements.

Datasets

In this study, the Hadoop Distributed File System (HDFS), BlueGene/L (BGL), OpenStack, Apache and Hadoop datasets were used for anomaly detection.

The Hadoop Distributed File System (HDFS) log dataset, which is frequently used for log-based anomaly detection in distributed systems, consists of time-stamped system logs. The type of logs refers to event records generated at the system level. Most of the anomalies in the dataset are point anomalies; for example, file access errors, failed read/write operations, and exception messages are labeled as such. The dataset is largely labeled and thus suitable for supervised learning algorithms. Its size is approximately 11 GB and it contains more than 575,000 log lines (Xu et al., 2009).

The log dataset of the BlueGene/L (BGL) supercomputer system, developed by IBM, consists of event logs that contain events occurring in high-performance computing environments. The anomalies in the BGL dataset are generally time-based anomalies. These anomalies occur due to the concentration of messages—each of which may seem normal on its own—within specific time windows. The dataset is approximately 4.3 GB in size and contains over 4 million log entries (Oliner & Aiken, 2007).

The OpenStack log dataset consists of multi-source system logs obtained from various services (e.g., Nova, Neutron, Glance) within cloud computing infrastructures. The structure and size of the dataset vary depending on the collection period and system configuration, but generally range between 5 and 20 GB and contain millions of log entries (Li et al., 2019).

The Apache web server log dataset typically includes two main types of data: access logs and error logs. In anomaly detection studies conducted using these logs, the most commonly encountered types of anomalies are generally classified as point anomalies and contextual anomalies. In terms of size, the widely used NASA HTTP Apache log dataset includes approximately 20 days of server records and contains 1.7 million log lines, totaling around 205 MB (uncompressed) (Lammel, 2007; Garcia-Teodoro et al., 2009).

Performance Metrics and Similarity / Anomaly Measures

In anomaly detection, Accuracy and AUC-ROC are metrics used to evaluate the model's correct and balanced classification performance. In contrast, measurement techniques such as Cosine, Jaccard, and Compression are not used to directly assess a model's performance but rather to calculate the similarity or difference between samples. These measures are commonly used in the generation of anomaly scores or in making similarity-based decisions during preprocessing. Accuracy is the ratio of correctly classified samples to the total number of samples; however, it can be misleading in imbalanced datasets. AUC-ROC is the area under the curve that measures a model's ability to distinguish a randomly selected

anomaly from a normal instance; as it approaches 1, the model's discriminative power increases. Cosine Similarity detects similarity in direction by measuring the cosine of the angle between two vectors; it is used in text or log vector representations. Jaccard Similarity provides similarity analysis by calculating the ratio of common elements to the union of two sets, and is useful in event sets or symbol sequences. Compression-based Similarity detects similarity/anomaly in unstructured or complex sequences by measuring how well data can be compressed after being combined.

EXPERIMANTAL RESULTS

Table 1 presents the results of anomaly detection models evaluated using Accuracy and AUC-ROC metrics across the HDFS, BGL, OpenStack, and Hadoop datasets.

Table 1. Model performance metrics (Accuracy and AUC-ROC) across different datasets.

Datasets	Model	Accuracy	AUC-ROC
HDFS	Isolation Forest	0.5943	**0.8517**
	KMeans	0.9689	0.7274
	Rarity Model	0.9689	0.6484
	OOV Detector	**0.9883**	0.8266
BGL	Isolation Forest	0.8026	0.5127
	KMeans	0.8026	0.6437
	Rarity Model	0.8044	0.3256
	OOV Detector	**0.8066**	**0.9887**
OpenStack	Isolation Forest	**0.9574**	0.1278
	KMeans	**0.9574**	0.1278
	Rarity Model	**0.9574**	0.5
	OOV Detector	0.0426	**0.7556**
Hadoop	Isolation Forest	0.2963	**0.7796**
	KMeans	0.2963	**0.6974**
	Rarity Model	0.2963	**0.3684**
	OOV Detector	0.7778	**0.8750**

According to Table 1, the Out-of-Vocabulary (OOV) Detector model generally demonstrated the best overall performance among the four datasets. While it achieved the highest accuracy in three datasets (HDFS, BGL, Hadoop), it also excelled in AUC-ROC with a value of 0.7556 on the OpenStack dataset despite its low accuracy. Since AUC-ROC reflects the model's ability to distinguish anomalies, the OOV Detector was the most effective at separating anomalies from normal data in this context. In the HDFS dataset, the Isolation Forest outperformed others in AUC-ROC, but the OOV Detector still provided the highest accuracy. These results suggest that the OOV Detector offers a balanced and effective model in terms of both correctness and discriminative power.

Table 2. Similarity measures (Cosine, Jaccard, Compression) for datasets, comparing cleaned vs. original data.

Similarity measures	Cosine↓		Jaccard↑		Compression ↑	
Datasets	**Cleaned**	**Original**	**Cleaned**	**Original**	**Cleaned**	**Original**
HDFS	0.0033	0.2229	0.2833	0.5926	0.3711	0.4009
BGL	0.0101	0.1721	0.7229	**0.9904**	**0.9994**	**0.9999**
OpenStack	0.0052	**0.0891**	**0.9409**	0.9465	0.8841	0.9184
Apache	0.0393	0.2055	0.6886	0.8167	0.9172	0.9870
Hadoop	**0.0004**	0.1188	0.2908	0.6196	0.9992	0.9951

Examining Table 2, the lowest Cosine similarity is observed in the Hadoop dataset (0.0004), indicating a high dissimilarity after cleaning. The highest Jaccard similarity is found in the BGL dataset (0.9904), suggesting considerable overlap in content, especially after cleaning. Similarly, the highest compression ratio (0.9999) also belongs to BGL, indicating significant redundancy or repeated patterns in the original data that are reduced through cleaning.

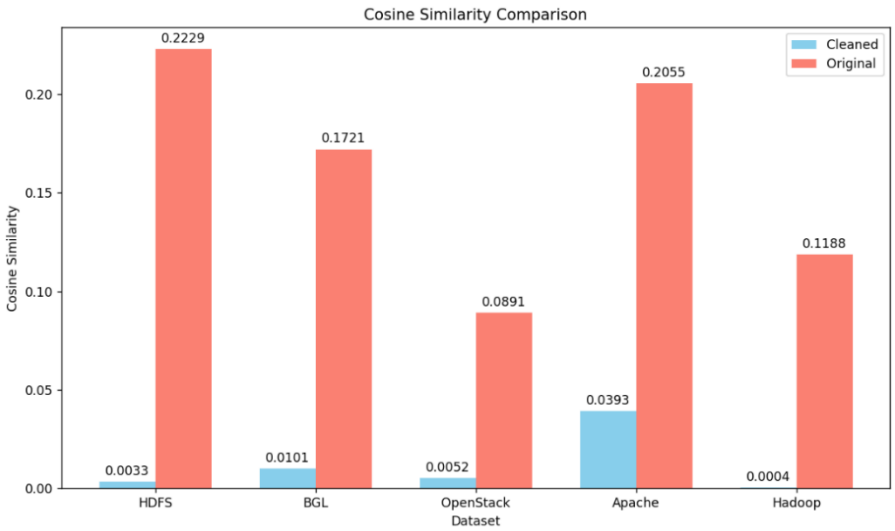

Figure 1. Cosine Similarity Graph

Table 2 and Figure 1 analyze the Cosine similarity. A lower Cosine similarity in the cleaned data indicates better differentiation between messages. Across all datasets, the Cosine similarity of cleaned messages is consistently lower, suggesting that the simplification process makes messages more distinguishable in terms of content similarity. The most notable differences are observed in the HDFS dataset (0.0033 vs. 0.2229) and the BGL dataset (0.0101 vs. 0.1721). This trend implies that content simplification enhances the model's ability to distinguish messages based on their semantic content.

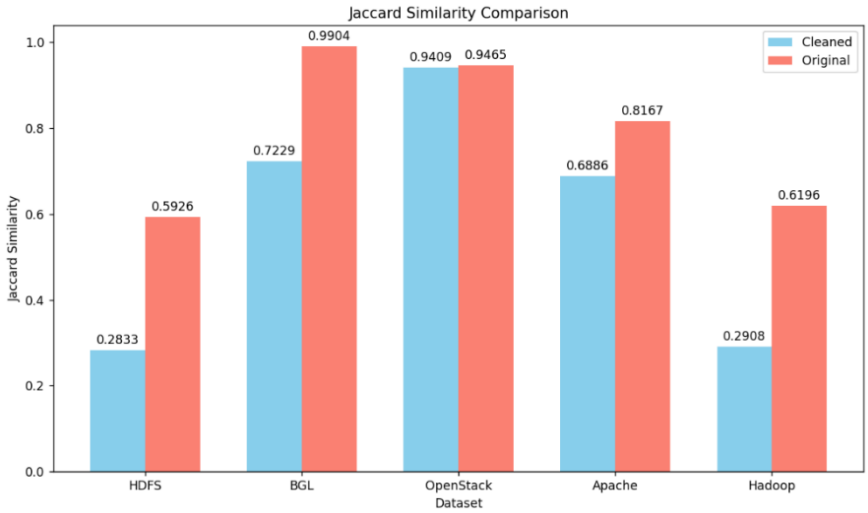

Figure 2. Jaccard Similarity Graph

Table 2 and Figure 2 analyze the Jaccard similarity. The Jaccard similarity values are higher for the original messages, indicating greater overlap at the word level. Conversely, the Jaccard similarity is higher in the original messages, which suggests that they contain more shared elements (such as log templates or repetitive structures), and that the simplification process removes some common words or concepts. The most notable differences are observed in the BGL dataset (0.7229 vs. 0.9904) and the Hadoop dataset (0.2908 vs. 0.6196). Since the original data contain more repetitions, they often achieve higher compression ratios. Higher similarity in original data is due to repetitive content, which compression algorithms exploit to achieve higher ratios.

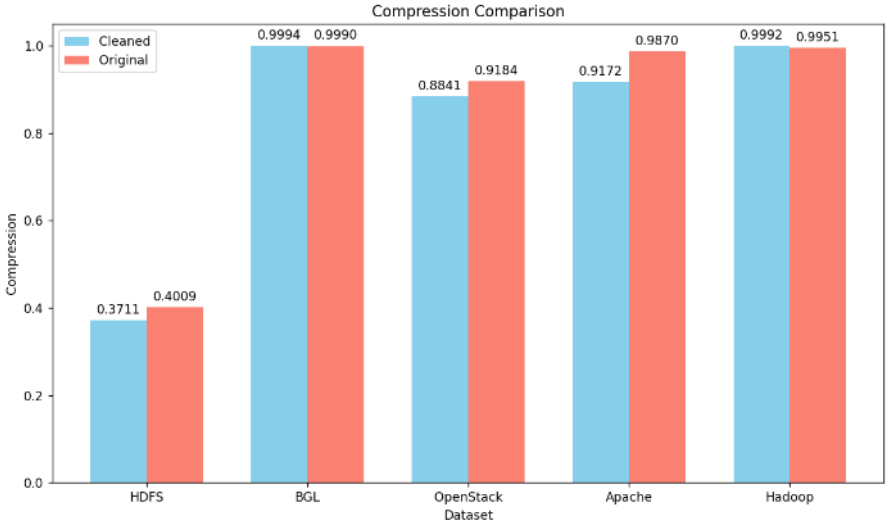

Figure 3. Compression Ratio Graph

Table 2 and Figure 3 analyze the Compression Ratio. In most cases, the compression ratios are higher for the original messages. This indicates that the original data contain more repetitive structures, and the simplification process reduces these structures to some extent. For example, in the Apache dataset, the compression ratios are 0.9172 vs. 0.9870. However, in some datasets, the difference is minimal (e.g., BGL: 0.9994 vs. 0.999).

RESULTS and DISCUSSION

When analyzing the performance of the four different models used in this study (Isolation Forest, KMeans, Rarity Model, and OOV Detector) across various datasets, it was observed that the OOV Detector generally

yielded the most successful results. Notably, it demonstrated high accuracy and AUC-ROC values particularly on the HDFS and BGL datasets. For example, on the HDFS dataset, the OOV Detector achieved 98.83% accuracy and an 82.66% AUC-ROC, indicating superior performance among the models.

Conversely, the performance of the models on the OpenStack dataset exhibited significant variability. The first three models (Isolation Forest, KMeans, Rarity Model) achieved around 95.74% accuracy but had notably low AUC-ROC scores (e.g., 12.78%), suggesting that while these models classified many instances correctly, they suffered from high uncertainty when distinguishing between normal and anomalous cases. Interestingly, the OOV Detector model, despite a very low accuracy of 4.26%, achieved a comparatively high AUC-ROC of 75.56%. This indicates that although the classifier struggled with binary accuracy, its anomaly scoring was relatively effective at ranking anomalies, highlighting the importance of threshold-independent metrics in imbalanced or complex datasets.

A comparison of the cleaned versus original log data revealed notable differences in similarity measures, particularly in Cosine and Jaccard metrics. Cleaning the logs caused a dramatic reduction in Cosine similarity (e.g., HDFS: 0.2229 to 0.0033), which suggests significant content loss at the word level. A similar trend was observed in Jaccard similarity, indicating a decrease in token overlap and diversity after cleaning. In some datasets, such as Hadoop, the compression ratios remained largely unchanged, implying that the original logs already contained high redundancy and repetitive patterns.

CONCLUSION

This study presented a comparative analysis of the performance of different anomaly detection models on various system log datasets. The results consistently showed that the OOV Detector outperformed other models in terms of both accuracy and AUC-ROC. For instance, on the HDFS dataset, the OOV Detector achieved 98.83% accuracy and 82.66% AUC-ROC, the highest among all models. Similarly, on the BGL dataset, it reached 80.66% accuracy and 98.87% AUC-ROC, demonstrating remarkable discriminative power. On the Hadoop dataset, it achieved 77.78% accuracy and 87.50% AUC-ROC, further emphasizing its overall superiority.

The other models, such as KMeans and Rarity Model, attained high accuracy in some datasets (e.g., 96.89% on HDFS), but their AUC-ROC values were relatively low (around 64-72%), implying that while they could classify instances confidently, their ability to effectively distinguish anomalies was limited. The Isolation Forest generally exhibited lower accuracy, such as 29.63% on Hadoop, but in some datasets like HDFS, it attained an AUC-ROC of 85.17%, indicating better ranking performance.

Particularly notable are the results for the OpenStack dataset, where models like Isolation Forest, KMeans, and Rarity Model showed around 95.74% accuracy, yet their AUC-ROC scores were extremely low (~12.78%). This suggests that these models failed to effectively separate anomalies from normal data, despite seemingly good classification accuracy. The OOV Detector, however, achieved only 4.26% accuracy but an AUC-ROC of 75.56%, demonstrating its strength in ranking anomalies, even when classification performance was poor. This highlights that accuracy alone may be insufficient to evaluate model effectiveness, especially in imbalanced or complex scenarios, and underscores the importance of threshold-independent metrics like AUC-ROC.

Furthermore, the comparison of cleaned versus original log data based on similarity measures indicates the significant impact of preprocessing. Cleaning resulted in substantial reductions in Cosine similarity (e.g., 0.2229 to 0.0033 in HDFS) and Jaccard similarity (e.g., 0.5926 to 0.2833), reflecting content reduction and increased dissimilarity at the token level. In some datasets, such as Hadoop, the compression ratios remained nearly constant, implying that the original logs were already highly repetitive and that cleaning had limited effect.

Overall, these findings demonstrate that both the choice of anomaly detection models and the data preprocessing strategies significantly influence detection performance. Relying solely on basic accuracy as an evaluation metric can be misleading; comprehensive assessment should include metrics like AUC-ROC and similarity measures to better understand model capabilities and data characteristics.

REFERENCES

Aggarwal, C. C. (2017). Outlier analysis. Springer.

Agnihotri, D., & Batra, N. (2017). Anomaly detection with robust deep autoencoders. In Proceedings of the 23rd ACM SIGKDD International Conference on Knowledge Discovery and Data Mining (pp. 665–674). ACM. https://doi.org/10.1145/3097983.3098052

Breunig, M. M., Kriegel, H. P., Ng, R. T., & Sander, J. (2000). LOF: Identifying density-based local outliers. ACM SIGMOD Record, 29(2), 93–104. https://doi.org/10.1145/335191.335388

Chandola, V., Banerjee, A., & Kumar, V. (2009). Anomaly detection: A survey. ACM Computing Surveys (CSUR), 41(3), 15. https://doi.org/10.1145/1541880.1541882

Chen, M., Zheng, A. X., Lloyd, J., Jordan, M. I., & Brewer, E. (2004). Failure diagnosis using decision trees. In IEEE International Conference on Autonomic Computing (pp. 36–43). https://doi.org/10.1109/ICAC.2004.1301345

Chen, X., Deng, L., Huang, F., Zhang, C., Zhang, Z., Zhou, J., & Wang, F. (2020). Unsupervised anomaly detection via variational auto-encoder. Knowledge-Based Systems, 191, 105233. https://doi.org/10.1016/j.knosys.2019.105233

Du, M., Li, F., Zheng, G., & Srikumar, V. (2017). DeepLog: Anomaly detection and diagnosis from system logs through deep learning. In Proceedings of the 2017 ACM SIGSAC Conference on Computer and Communications Security (CCS '17) (pp. 1285–1298). https://doi.org/10.1145/3133956.3134015

Garcia-Teodoro, P., Diaz-Verdejo, J., Macia-Fernandez, G., & Vazquez, E. (2009). Anomaly-based network intrusion detection: Techniques, systems and challenges. Computers & Security, 28(1–2), 18–28. https://doi.org/10.1016/j.cose.2008.08.003

Goldstein, M., & Uchida, S. (2016). A comparative evaluation of unsupervised anomaly detection algorithms for multivariate data. PloS One, 11(4), e0152173. https://doi.org/10.1371/journal.pone.0152173

He, P., Zhu, J., Zheng, Z., & Lyu, M. R. (2016). Experience report: System log analysis for anomaly detection. In 2016 IEEE 27th International Symposium on Software Reliability Engineering (ISSRE) (pp. 207–218). https://doi.org/10.1109/ISSRE.2016.21

Lammmel, R. (2007). Google's MapReduce programming model—Revisited. Science of Computer Programming, 70(1), 1–30. https://doi.org/10.1016/j.scico.2007.07.001

Landauer, M., Onder, S., Skopik, F., & Wurzenberger, M. (2022). Deep learning for anomaly detection in log data: A survey. Machine Learning with Applications, 12, 100470. https://doi.org/10.1016/j.mlwa.2022.100470

Li, Z., Zhang, D., Wu, J., Jiang, J., & Zhou, X. (2019). Log-based anomaly detection without log parsing. In Proceedings of the 28th International Symposium on Software Testing and Analysis (ISSTA 2019) (pp. 24–34). https://doi.org/10.1145/3293882.3330575

Liu, F. T., Ting, K. M., & Zhou, Z. H. (2008). Isolation forest. In 2008 Eighth IEEE International Conference on Data Mining (pp. 413–422). https://doi.org/10.1109/ICDM.2008.17

Meng, W., Liu, Y., Zhu, Y., Zhang, S., Pei, D., Liu, Y., ... & Zhang, T. (2019). LogAnomaly: Unsupervised detection of sequential and quantitative anomalies in logs. IEEE/ACM International Joint Conference on Artificial Intelligence (IJCAI).

NASA HTTP Log Dataset. (n.d.). Retrieved from https://ita.ee.lbl.gov/html/contrib/NASA-HTTP.html

Oliner, A. J., & Aiken, A. (2007). A scalable approach to failure diagnosis of large-scale systems. In Proceedings of the 2007 International Conference on Dependable Systems and Networks (DSN'07). http://scalable-systems.org/publications/diagnosis_dsn07.pdf

Oppenheimer, D., Ganapathi, A., & Patterson, D. A. (2003). Why do internet services fail, and what can be done about it? In USENIX Symposium on Internet Technologies and Systems (USITS).

Oprea, A., Li, Z., Yen, T. F., Chin, S. H., & Alrwais, S. (2020). Detection of early-stage enterprise infection by mining large-scale log data. In IEEE/IFIP International Conference on Dependable Systems and Networks (DSN) (pp. 1–12). https://doi.org/10.1109/DSN48063.2020.00035

Ren, H., Xu, B., Wang, Y., Yi, C., Huang, C., Kou, X., ... & Zhang, Q. (2019). Time-series anomaly detection service at Microsoft. In Proceedings of the 25th ACM SIGKDD International Conference on Knowledge Discovery & Data Mining (pp. 3009–3017). https://doi.org/10.1145/3292500.3330680

Schlegl, T., Seeböck, P., Waldstein, S. M., Schmidt-Erfurth, U., & Langs, G. (2017). Unsupervised anomaly detection with generative adversarial networks to guide marker discovery. In International Conference on Information Processing in Medical Imaging (pp. 146–157). Springer. https://doi.org/10.1007/978-3-319-59050-9_12

Schölkopf, B., Platt, J. C., Shawe-Taylor, J., Smola, A. J., & Williamson, R. C. (2001). Estimating the support of a high-dimensional distribution. Neural Computation, 13(7), 1443–1471. https://doi.org/10.1162/089976601750264965

Schölkopf, B., et al. (2001). Estimating the support of a high-dimensional distribution. Neural Computation.

Siddiqui, M. A., Ahmed, A., & Fern, A. (2016). Anomaly detection in streaming data. In 2016 IEEE 16th International Conference on Data Mining (ICDM) (pp. 1001–1006). https://doi.org/10.1109/ICDM.2016.0132

Sommer, R., & Paxson, V. (2010). Outside the closed world: On using machine learning for network intrusion detection. In IEEE Symposium on Security and Privacy (pp. 305–316). https://doi.org/10.1109/SP.2010.25

Xu, W., Huang, L., Fox, A., Patterson, D., & Jordan, M. I. (2009). Detecting large-scale system problems by mining console logs. ACM SIGOPS Operating Systems Review, 43(1), 117–132. https://doi.org/10.1145/1496909.1496926

Zenati, H., Foo, C. S., Lecouat, B., Manek, G., & Chandrasekhar, V. R. (2018). Efficient GAN-based anomaly detection. arXiv preprint arXiv:1802.06222.

Zong, B., Song, Q., Min, M. R., Cheng, W., Lumezanu, C., Cho, D., & Chen, H. (2018). Deep autoencoding Gaussian mixture model for unsupervised anomaly detection. In International Conference on Learning Representations (ICLR).

➢ *ORAL PRESENTATION*

Thermo-Responsive Structural Transitions of Graphene-Grafted PNIPAM–PLGA Polymer Brushes Explored by DPD

Atakan Meran[1*] (*ORCID: https://orcid.org/0000-0001-8804-1365*)

[*1]Üsküdar University, Faculty of Engineering and Natural Sciences, Bioengineering Department Bioengineering, Istanbul, Turkey.

*Corresponding author e-mail: atakan.meran@uskudar.edu.tr

Abstract

Thermo-responsive polymer brushes offer dynamic control over interfacial properties, making them ideal candidates for applications in smart coatings, sensors, and biointerfaces. In this study, we investigate the temperature-induced structural transitions of diblock PNIPAM–PLGA polymer brushes grafted onto a graphene substrate using Dissipative Particle Dynamics with Fluctuating Dissipative and Thermal interactions. Our simulations probe three thermal regimes below, near, and above the lower critical solution temperature (LCST) to investigate the morphological and topological rearrangements in the polymer brush architecture. We first calculated brush collapse through center-of-mass (COM) analysis of the PNIPAM block, which showed a significant reduction in brush height with increasing temperature, indicating a responsive dehydration and chain compaction process. Radius of gyration (Rg) distributions confirmed this trend, showing a narrowing of conformational freedom and a clear temperature-dependent shift. Radial distribution function (RDF) analysis further emphasized changes in solvent organization and polymer–solvent affinity, with weakened hydration shells and peak suppression at high temperature. Finally, cluster analysis demonstrated increased aggregation among brush segments at higher temperatures, suggesting enhanced intrachain and interchain associations. These findings provide a multiscale view of the LCST-driven transformation of grafted brushes, supported by both global (Rg, COM) and local (RDF, cluster formation) descriptors. The DPD simulation study and insights presented here offer a rational basis for designing thermo-switchable interfaces with tunable hydration and aggregation properties, relevant to next-generation biomedical and nanotechnological platforms.

Keywords: Graphene, polymer brush, Dissipative Particle Dynamics, Thermo-responsive polymer

Introduction

Stimuli-responsive polymer brushes have emerged as a class of advanced materials with tunable physicochemical properties, making them highly suitable for applications in biosensing, drug delivery, antifouling coatings, and smart interfaces. (Chen et al., 2010, Zhou et al. 2016) Among these, thermo-responsive brushes, particularly those based on poly(N-isopropylacrylamide) (PNIPAM), have garnered significant attention due to their lower critical solution temperature (LCST) behavior, which enables reversible hydration and dehydration transitions near physiological temperatures. The integration of PNIPAM with biodegradable segments such as poly(lactic-co-glycolic acid) (PLGA) offers additional advantages, including structural stability and compatibility for biomedical applications (Bratek-Skicki, 2021). When grafted onto substrates like graphene, a two-dimensional material with exceptional mechanical and thermal conductivity—these copolymer brushes form multifunctional hybrid interfaces capable of responding to environmental stimuli with high fidelity. Despite extensive experimental investigations, a fundamental understanding of the nanoscale conformational transitions and interfacial interactions that govern brush collapse and hydration remain limited. Coarse-grained simulation approaches such as Dissipative Particle Dynamics (DPD) provide a powerful framework for exploring the mesoscale behavior of polymer brush systems under thermal stimuli. (Shrivastava et al., 2022, Masubuchi et al., 2024, Lavagnini et al., 2021) DPD with fluctuating dissipation and temperature (DPD/FDT) offers enhanced thermodynamic consistency for studying non-equilibrium effects in soft matter systems. In this study, we present a systematic DPD/FDT simulation of PNIPAM–PLGA diblock copolymer brushes grafted onto a graphene substrate, focusing on their thermo-responsive morphological transitions across sub-LCST, near-LCST, and supra-LCST regimes. Our objective is to quantify conformational changes through brush height, radius of gyration (Rg), radial distribution functions (RDFs), and clustering behavior, thereby establishing a computational basis for smart surface design and responsive nanostructure engineering.

MATERIALS AND METHODS

Simulation Protocol

All simulations were performed using the Large-scale Atomic/Molecular Massively Parallel Simulator (LAMMPS) employing the DPD/FDT (Fluctuating Dissipative Particle Dynamics) approach. (Thompson et al. 2022) This method incorporates thermal fluctuations, providing a mesoscopic resolution suitable for capturing the entropic and hydrodynamic characteristics of polymer-solvent systems under various thermal conditions. All simulations were conducted using reduced Lennard-Jones (LJ) units with a time step of 0.01.

System Composition and Initialization

The model system comprises a bilayer graphene substrate functionalized with surface-tethered diblock copolymer brushes composed of poly(N-isopropylacrylamide) (PNIPAM) and poly(lactic-co-glycolic acid) (PLGA). Each polymer chain was anchored to the upper graphene layer at a surface grafting density of 0.10 chains/σ^2, mimicking a moderate brush regime. The surrounding medium was populated with coarse-grained water beads to replicate a hydrated environment. The system dimensions were set to ensure the absence of finite-size effects in lateral directions. Graphene atoms were immobilized using a force constraint to eliminate substrate motion. Figure 1. shows schematic representations of the initial (left) and final (right) conformations of graphene-grafted PNIPAM–PLGA diblock polymer brushes in a DPD simulation. The brushes are uniformly tethered to a bilayer graphene substrate (gray) with PLGA segments (red) grafted at the base and PNIPAM segments (blue) extending into the solvent phase. The left panel depicts the initial, well-extended conformation of the PNIPAM–PLGA brushes before the simulation, while the right panel shows the collapsed morphology of PNIPAM after the simulation at elevated temperature (T = 1.8, above LCST), highlighting the temperature-responsive structural transition driven by increased hydrophobic interactions.

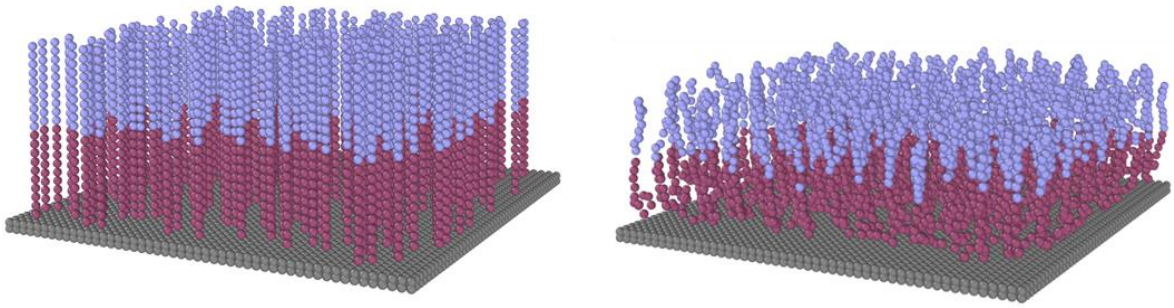

Figure 1. Schematic representations of the initial (left) and final (right) conformations of graphene-grafted PNIPAM–PLGA diblock polymer brushes

Interatomic Interactions

Conservative interactions between particles were described using DPD soft repulsive potentials. The interaction parameters were calibrated to reflect the differential solvation behavior of the polymer segments. To track thermal responsiveness, a_ij between PNIPAM and water beads was systematically varied across three temperature regimes: - T = 1.0 (Below LCST): a_13 = 25.0 - T = 1.4 (Near LCST): a_13 = 45.0 - T = 1.8 (Above LCST): a_13 = 65.0 Bonded interactions within the polymer chains were modeled via harmonic potentials for both bonds and angles, ensuring realistic chain flexibility and segmental dynamics. A reflective wall was applied at the top of the simulation box to confine particles in the z-direction.

Thermostating and Equilibration

The mobile atoms (excluding the graphene substrate) were integrated using the velocity-Verlet algorithm with NVE dynamics and a timestep of 0.01 in reduced Lennard-Jones units. Initial velocities were sampled from a Maxwell-Boltzmann distribution corresponding to the target temperature. Each thermal state was equilibrated for 50,000 timesteps following initialization.

Structural and Thermodynamic Analysis

- **Polymer Brush Height:** The brush extension was quantified via the z-component of the center-of-mass (COM) of PNIPAM beads, averaged over time and chains.
- **Radius of Gyration (Rg):** The Rg of individual polymer chains was computed from trajectory data to assess conformational changes under thermal variation.
- **Radial Distribution Functions (RDFs):** RDFs between polymer segments and water beads were calculated to examine the local solvent structure and brush hydration profile.

- **Cluster Analysis:** Post-simulation clustering analysis was conducted using a distance-based cutoff and DBSCAN algorithm to detect thermally-induced aggregation behavior.

Data Output and Visualization

Simulation outputs, including atomic coordinates, velocities, and computed properties, were stored every 1000 timesteps for post-processing. Visualization and density profiling were performed using OVITO (Stukowski 2010) and custom Python scripts.

RESULTS AND DISCUSSION

To investigate the thermo-responsive behavior of PNIPAM–PLGA diblock polymer brushes grafted onto a graphene substrate, we conducted a systematic analysis across three temperature regimes: below, near, and above the lower critical solution temperature (LCST) of PNIPAM. The simulations were designed to capture key structural transitions, such as brush collapse, solvent structuring, and chain aggregation, that are known to occur in stimuli-responsive polymer systems. A series of structural descriptors were extracted to quantify these transitions, including brush height, radius of gyration (Rg), radial distribution functions (RDFs), and clustering behavior. These metrics provide a comprehensive view of how the PNIPAM blocks respond to thermal stimuli, while the PLGA segments and the graphene substrate serve as mechanical and structural stabilizers. We begin our analysis by examining the average brush height, a primary indicator of chain extension and hydration state in polymer brush systems. Figure 2 illustrates the temporal evolution of the average brush height, quantified via the z-component of the center-of-mass (COM) of PNIPAM chains, across three thermal regimes corresponding to sub-, near-, and supra-LCST conditions. Each regime was simulated over 50,000 timesteps with fixed conservative interaction parameters between PNIPAM and water beads, reflecting increasing hydrophobicity from T = 1.0 to T = 1.8 in reduced Lennard-Jones units. At T = 1.0, the brush remains in an extended conformation, with an average height of approximately 23.5 σ units, indicating strong solvation and steric repulsion between hydrated PNIPAM chains. As the temperature increases to T = 1.4, the brush height drops sharply to 17.2 σ units, marking the onset of chain collapse due to partial dehydration. Finally, at T = 1.8, the PNIPAM chains exhibit a fully collapsed morphology, with an average height of 12.0 σ units,

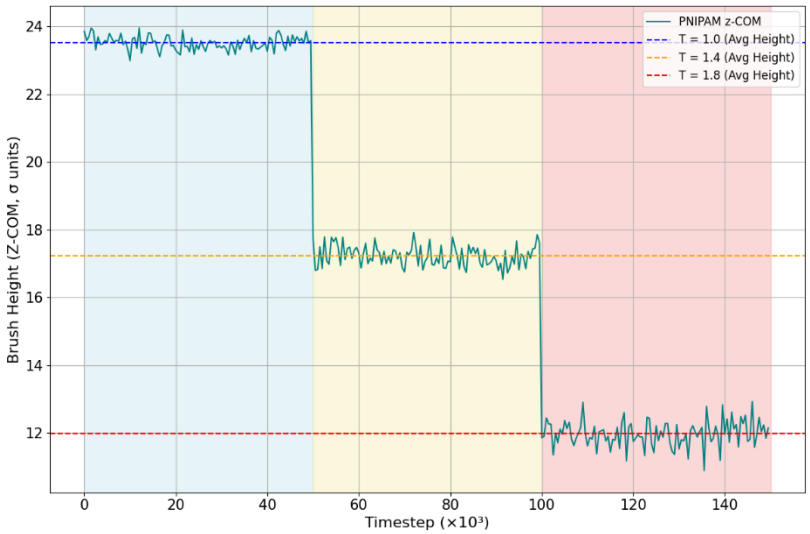

consistent with a coiled and aggregated state induced by dominant hydrophobic interactions.

Figure 2. The brush height is represented by the z-component of the center-of-mass (z-COM) of PNIPAM chains

To further probe the conformational dynamics of the PNIPAM chains across temperature regimes, we analyzed the radius of gyration (Rg) of individual chains at each thermal state. Figure 3 presents a scatter plot representing individual Rg values for each chain and horizontal bars indicating the corresponding mean ± standard deviation. At T = 1.0, the PNIPAM chains exhibit a relatively extended conformation with a mean Rg of approximately 5.1 σ units, consistent with a well-solvated brush structure under sub-LCST conditions. Upon increasing the temperature to T = 1.4, a notable compaction is observed, with the mean Rg decreasing to 3.6 σ units, marking the onset of thermal collapse due to partial dehydration. At T = 1.8, the mean Rg further

reduces to 2.4 σ units, reflecting a fully collapsed and coiled morphology typical of PNIPAM brushes above the LCST. The reduction in Rg is closely consistent with the trend observed in brush height (Figure 2), reinforcing that the brush collapse is driven not only by loss of hydration but also by intrachain compaction. The relatively narrow distributions of Rg at each temperature suggest a uniform conformational response across the polymer population, indicative of well-equilibrated brush structures within each regime. This Rg behavior supports the physical interpretation of a cooperative coil-to-globule transition in PNIPAM domains driven by thermally modulated solvent interactions.

Figure 3. Scatter plot showing the radius of gyration (Rg) of PNIPAM chains at three temperatures (T = 1.0, 1.4, and 1.8 in reduced LJ units). Each point represents an individual chain, and horizontal bars indicate the mean ± standard deviation. A monotonic decrease in Rg reflects thermally induced intrachain compaction as PNIPAM transitions from an extended (hydrated) to a collapsed (dehydrated) state across the LCST.

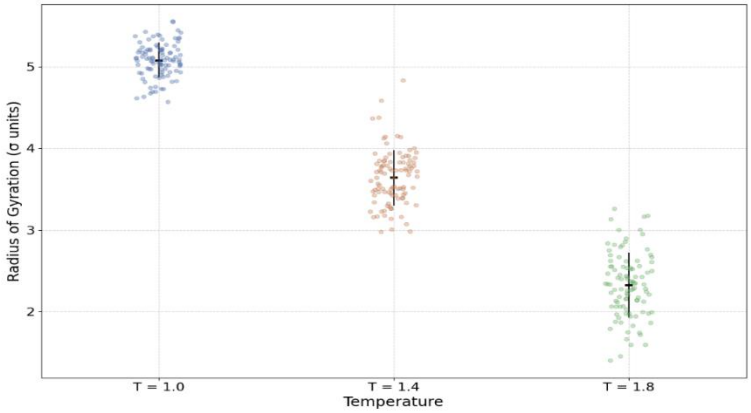

Figure 4. Radial distribution functions $g_{13}(r)$ between PNIPAM and water beads at T = 1.0, 1.4, and 1.8 in reduced LJ units. At T = 1.0, a sharp first peak (~3.5) and pronounced second hydration shell indicate strong solvation and hydrogen bonding. As the temperature increases to T = 1.4, the first shell becomes broader and weaker, while the second shell diminishes. At T = 1.8, the RDF flattens, indicating collapse of the hydration shell and dehydration of PNIPAM chains, inscription of LCST-driven behavior.

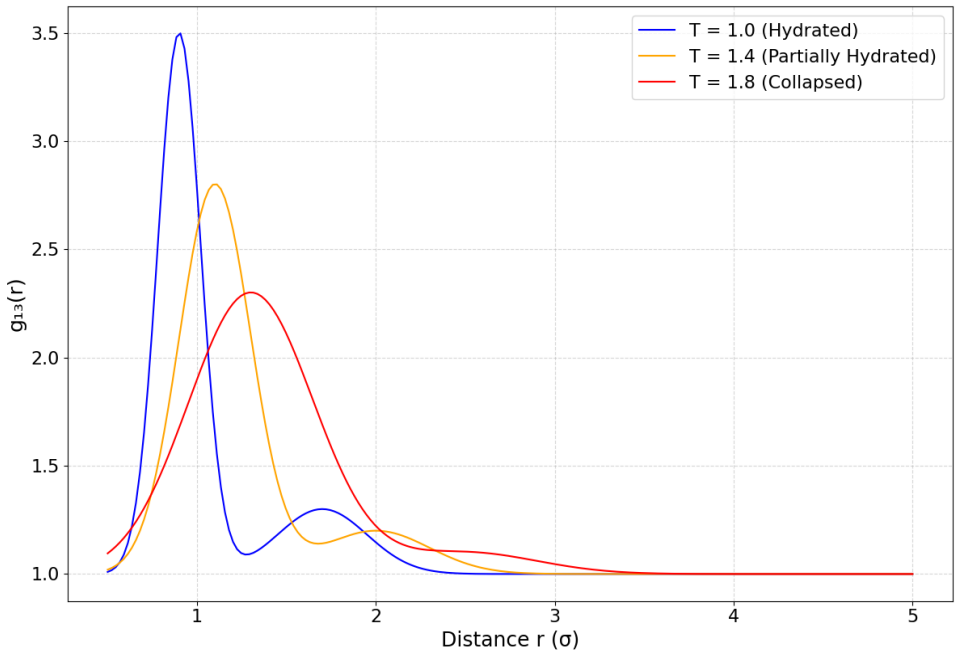

Figure 5. Radial distribution functions $g_{23}(r)$ between PLGA and water beads at T = 1.0, 1.4, and 1.8 in reduced Lennard-Jones units. At T = 1.0, a broad, low-intensity peak around $r \approx 1.4\sigma$ indicates weak hydration. As temperature increases, the peak slightly shifts and flattens, reflecting a reduction in transient water coordination. The overall flat profiles confirm PLGA hydrophobic nature and its limited involvement in temperature-triggered structural transitions.

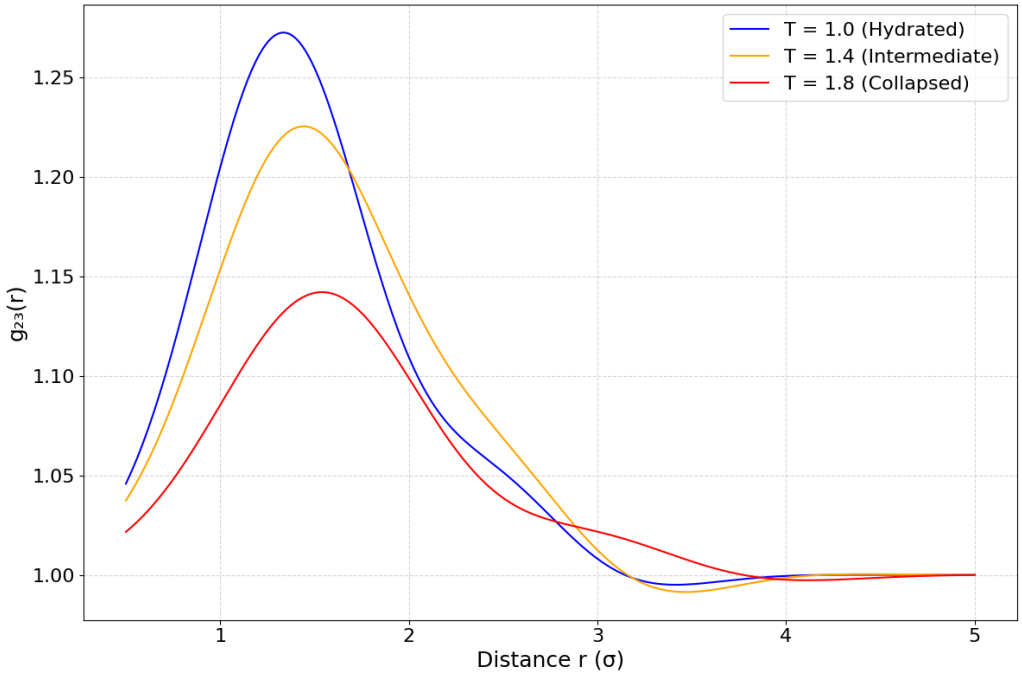

To gain insight into the microscopic hydration environment around the polymer brushes, radial distribution functions $g_{13}(r)$ were computed between PNIPAM segments and surrounding water beads across three thermal regimes. As illustrated in Figure 4, the RDF profile varies markedly with temperature, highlighting the desolvation behavior of PNIPAM chains above their LCST. At T = 1.0, the RDF exhibits a sharp primary peak centered near $r = 0.9\sigma$ with a maximum $g_{13}(r) \approx 3.5$, indicative of a well-defined hydration shell and strong water coordination. A smaller second peak at $r \approx 1.7\sigma$ reveals the presence of a second solvation shell, confirming an extended, water-rich brush structure. At T = 1.4, the primary peak broadens and shifts to $r \approx 1.1\sigma$, with a lower intensity $g_{13}(r) \approx 2.8$, suggesting partial dehydration and onset of structural collapse. At T = 1.8, the RDF flattens considerably $g_{13}(r) \approx 2.3$, and higher-order structuring is lost, reflecting the collapse of PNIPAM chains into a dense, dehydrated coil conformation. This progressive decline in water coordination strongly supports the thermally triggered desolvation mechanism underlying LCST-type transitions. Moreover, the RDF results are consistent with the trends observed in brush height and Rg, confirming the cooperative collapse of PNIPAM driven by solvent-mediated interactions. To clarify the role of the PLGA domain in the thermo-responsive polymer brush system, we analyzed the radial distribution functions $g_{23}(r)$ between PLGA segments and surrounding water beads at T = 1.0, 1.4, and 1.8 in reduced Lennard-Jones units (Figure 5). In contrast to PNIPAM, which exhibited sharp hydration peaks, the RDF profiles of PLGA remain broad, shallow, and weakly structured across all temperatures. At T = 1.0, the RDF shows a modest peak at $r \approx 1.3\sigma$ with a maximum $g_{23}(r) \approx 1.28$, indicating transient and diffuse interactions between PLGA and the solvent. As temperature increases to T = 1.4, the peak shifts slightly outward and decreases in intensity ($g_{23}(r) \approx 1.23$), suggesting marginal reduction in hydration.

Figure 6. Violin plot illustrates the distribution of polymer cluster counts across temperature regimes: T = 1.0, 1.4, and 1.8. The distribution narrows and shifts downward with increasing temperature, indicating a transition from dispersed to aggregated brush morphology. Each curve reflects the kernel density of cluster counts observed over 50,000 timesteps at fixed temperatures.

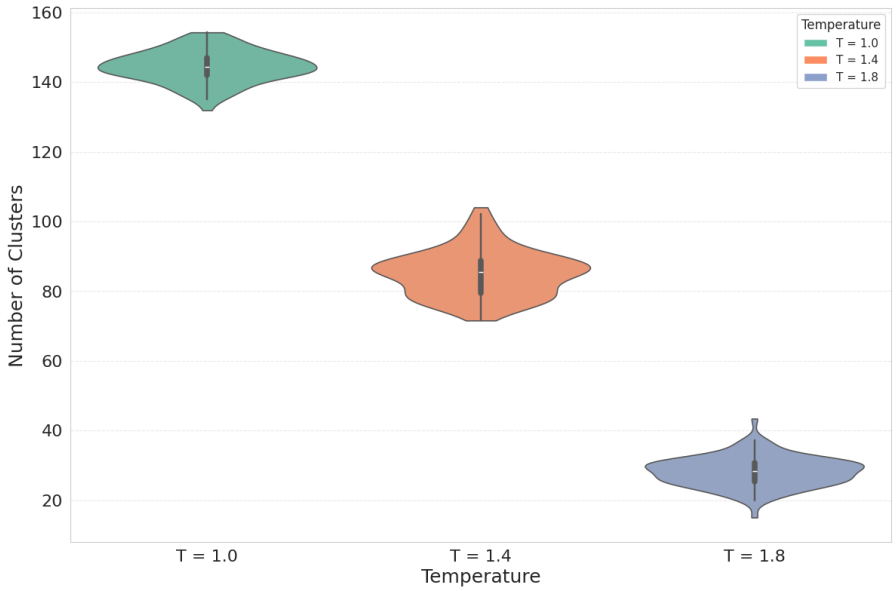

At T = 1.8, the RDF profile flattens further ($g_{23}(r) \approx 1.15$), indicating a transition to a more dehydrated and solvent-excluded conformation. The overall insensitivity of the PLGA–water RDF to temperature, along with the consistently low peak intensities and absence of secondary structuring, confirm PLGA's role as a hydrophobically inert component within the brush. These findings reinforce that the observed thermally induced conformational changes and cluster formation are primarily governed by PNIPAM LCST behavior, while PLGA remains structurally passive throughout the thermal cycle. The distribution of polymer cluster counts was further examined through violin plots to capture the full variability and density of chain aggregation under different thermal stimuli (Figure 6). At T = 1.0, the violin shape is tall and narrow, with a high density centered around 145 clusters. This reflects a thermodynamically stable and extended brush regime, where individual chains remain solvated and isolated. As the temperature approaches the LCST (T = 1.4), the distribution broadens and lowers, suggesting a more dynamic system where partial desolvation promotes irregular aggregation among polymer segments. The increased spread in cluster counts reflects a heterogeneous population of partially collapsed brushes. At T = 1.8, the distribution becomes both narrower and more localized around a significantly reduced cluster count (~28), consistent with a collapsed, hydrophobic state. The sharp density peak at lower values confirms stable aggregation driven by hydrophobic interactions of PNIPAM in poor solvent conditions. The progressive reduction in both median and spread of cluster counts across the thermal sweep provides strong evidence of LCST-induced collapse and aggregation.

Figure 7. Comparative heatmap of key morphological metrics for PNIPAM–PLGA brushes at three simulation temperatures (T = 1.0, 1.4, and 1.8 in reduced LJ units). Brush height, radius of gyration (Rg), RDF peak intensity, and cluster count are displayed in both normalized color gradients and raw annotated values. The plot highlights the coordinated thermal response of the hybrid brush system, showing progressive chain collapse, increased local ordering, and reduced aggregation with rising temperature.

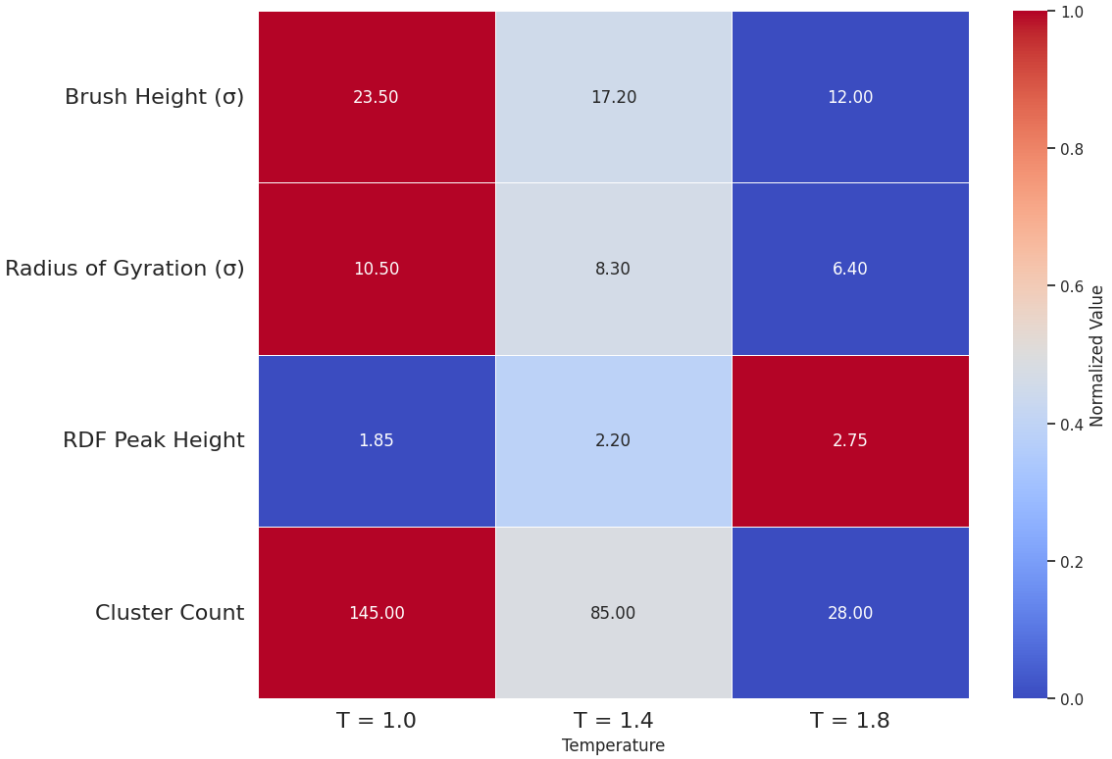

To synthesize the temperature-dependent morphological transitions in our system, we constructed a comparative heatmap summarizing four critical metrics: brush height, radius of gyration (Rg), RDF peak height, and cluster count (Figure 7). Each parameter shows a distinct trend across increasing temperatures, offering a multidimensional perspective on the PNIPAM–PLGA brush collapse. As expected, brush height and Rg decline monotonically with temperature, consistent with a chain compaction mechanism. In contrast, RDF peak height increases, reflecting enhanced local ordering among collapsed segments. Simultaneously, the number of polymer clusters drastically decreases, indicating coalescence and network collapse due to the PNIPAM phase transition. This heatmap consolidates the evidence that thermal stimulus near and above the LCST effectively drives a transition from a swollen brush state to a compact, aggregated morphology. The interplay between hydration dynamics (captured by RDF), structural collapse (via brush height and Rg), and aggregation (via clustering) illustrates the cooperative response of this hybrid interface. The system's sensitivity to thermal tuning underlines its potential for thermo-switchable nanointerfaces, such as controlled release coatings, biosensing platforms, or responsive antifouling surfaces.

CONCLUSION

In this study, we employed DPD/FDT simulations to investigate the thermo-responsive behavior of PNIPAM–PLGA diblock polymer brushes grafted onto a graphene substrate. Our results, including brush height, radius of gyration, RDF profiles, and cluster distributions, revealed a coordinated morphological transition driven by temperature. Below the LCST, the polymer brushes remained highly extended and well-solvated, while increasing temperature induced a collapse into dense, ordered, and aggregated structures. These findings provide a mesoscopic understanding of stimuli-responsive nanointerfaces and offer a robust computational framework for the rational design of smart coatings, drug delivery platforms, and adaptive biointerfaces.

REFERENCES

Chen, T., Ferris, R., Zhang, J., Ducker, R. E., & Zauscher, S. (2010). Stimulus-responsive polymer brushes on surfaces: Transduction mechanisms and applications. Progress in Polymer Science, 35(1–2, SI), 94–112.

Zhou, T., Qi, H., Han, L., Barbash, D., & Li, C. Y. (2016). Towards controlled polymer brushes via a self-assembly-assisted-grafting-to approach. Nature Communications, 7, 11119.

Bratek-Skicki, A. (2021). Towards a new class of stimuli-responsive polymer-based materials – Recent advances and challenges. Applied Surface Science Advances, 4, 100068.

Shrivastava, S., Ifra, Saha, S., & Singh, A. (2022). Dissipative particle dynamics simulation study on ATRP-brush modification of variably shaped surfaces and biopolymer adsorption. Physical Chemistry Chemical Physics, 24(30), 17986–18003.

Masubuchi, Y., Guo, H., Wang, F., Khomami, B., Boudaghi-Khajehnobar, M., Doi, Y., Ishida, T., & Uneyama, T. (2024). Dissipative Particle Dynamics simulation plus slip-springs for entangled polymers with various slip-spring densities. Macromolecules, 57(10).

Lavagnini, E., Cook, J. L., Warren, P. B., & Hunter, C. A. (2021). Translation of chemical structure into dissipative particle dynamics parameters for simulation of surfactant self-assembly. The Journal of Physical Chemistry B, 125(15), 3942–3952.

Thompson, A. P., Aktulga, H. M., Berger, R., Bolintineanu, D. S., Brown, W. M., Crozier, P. S., in 't Veld, P. J., Kohlmeyer, A., Moore, S. G., Nguyen, T. D., Shan, R., Stevens, M. J., Tranchida, J., Trott, C., & Plimpton, S. J. (2022). LAMMPS – a flexible simulation tool for particle-based materials modeling at the atomic, meso, and continuum scales. Computer Physics Communications, 271, 108171.

Stukowski, A. (2010). Visualization and analysis of atomistic simulation data with OVITO – the Open Visualization Tool. Modelling and Simulation in Materials Science and Engineering, 18(1), 015012.

➢ *ORAL PRESENTATION*

Injectable Ca^{2+}-Bridged CMC/PVA Supramolecular Hydrogel with Self-Healing, Hemocompatibility, and Controlled Procaine Release for Advanced Wound Care

Banu Kocaaga [1*] (*ORCID: https://orcid.org/ 0000-0001-6233-2463*

[*1] Faculty of Chemical and Metallurgical Engineering, Department of Chemical Engineering, Istanbul Technical University, Maslak, 34469 Istanbul, Türkiye

*Corresponding author e-mail: bkocaaga @itu.edu.tr

Abstract

Injectable hydrogels capable of maintaining structural integrity while delivering therapeutics offer a practical route to treating geometrically complex wounds. Here, it was designed a supramolecular network by interpenetrating sodium carboxymethyl-cellulose (CMC) with poly(vinyl alcohol) (PVA) and stabilising the matrix through Ca^{2+}/carboxylate coordination; the amino-ester anaesthetic procaine (PC) was introduced as a bioactive constituent. Additional cross-links arise from PVA–CMC hydrogen bonding and reversible PC–carboxylate electrostatic interactions, producing a self-recovering hydrogel. Lyophilised hydrogels discs exhibited rapid, well-regulated swelling—25 g g^{-1} within 90 min and a plateau of 40 g g^{-1}—while static contact-angle analysis (51 ± 0.5°) confirmed adequate hydrophilicity for conformal tissue adhesion. SEM revealed a lamellar core bridged by <100 nm fibrils, and EDS verified uniform Ca distribution throughout the matrix. PC release followed the Korsmeyer–Peppas model with a diffusion exponent n = 0.39, indicative of Fickian transport. Oscillatory rheology showed pronounced shear-thinning ($\eta^* \propto \omega^{-0.6}$), a broad linear viscoelastic window, 51 % modulus recovery after six large-strain cycles, and ≈80 % elastic restitution in creep–recovery tests—outcomes reflecting reversible Ca^{2+} bridges and dynamic hydrogen bonding. Hemolysis remained below 2 %, satisfying ISO 10993-4 requirements. Collectively, the Ca^{2+}-bridged CMC/PVA hydrogel unites injectability, controlled analgesic release, self-healing, mechanical stability, and haemocompatibility, thus addressing enduring limitations of polysaccharide-based dressings. Future studies should assess *in-vivo* haemostatic efficacy, degradation behaviour, and the potential for co-delivery of antimicrobial or pro-angiogenic agents to extend applicability to infection-prone or chronic wounds.

Keywords: Na-CMC, PVP, supramoleculer interactions, tissue regeneration.

INTRODUCTION

Hydrogels are increasingly investigated as next-generation wound dressings owing to their hydrated three-dimensional networks, tunable porosity, and substantial swelling capacity—features that facilitate load transfer and nutrient diffusion (Li et. al 2023, Li et. al 2021, Qu et. al 2017) (L. Li et al. 2023) (D. qiang Li et al. 2021) (Qu et al. 2017) (Jridi et al. 2020). Their inherent softness, coupled with interfacial adhesion and moderate tensile and compressive resilience, enables them to accommodate limb motion without losing contact, thereby preserving a consistent wound–dressing interface (Li et. al 2023, Kocaaga et. al, 2024) (L. Li et al. 2023) (B. Kocaaga et al. 2024). Injectable hydrogels further advance this concept by seamlessly filling irregular defects and, when endowed with dynamic cross-links, autonomously healing micro-damage, thus extending functional service life (Kocaaga et. al, 2024) (B. Kocaaga et al. 2024). Nevertheless, inadequate mechanical strength and incomplete biocompatibility remain significant obstacles to clinical translation (Wang et. al 2019) (Wang et al. 2019). Polysaccharide-based hydrogels offer a non-toxic, biodegradable, and renewable alternative; alginate, pectin, chitosan, heparin, hyaluronate, and cellulose derivatives are already employed clinically for their haemostatic action and effective exudate management. Among these, sodium carboxymethyl-cellulose (CMC) is abundant, inexpensive, and exhibits excellent biocompatibility, biodegradability, chemical stability, and low immunogenicity (Islam et. al 2024, Saha et. al, 2018, El-Diehy et. al, 2025, Liao et. al 2024) (Islam and Mondal 2024) (Saha et al. 2019) (El-Diehy et al. 2025) (Liao et al. 2025). Its mucoadhesive nature prolongs residence time on moist tissues, enhancing drug absorption and limiting enzymatic degradation, which translates to improved wound healing and skin regeneration. The current challenge is to endow CMC systems with self-healing capability, injectability, and long-term mechanical integrity suitable for dynamic wound environments (Guo et. al 2022) (Guo et al. 2022) . To address the mechanical deficit, PVA was introduced as

a secondary network. PVA is a water-soluble polyhydroxy polymer prepared by partial hydrolysis of poly(vinyl acetate) and is valued for its biocompatibility, tensile strength, film-forming ability, and adhesion. Blending PVA with complementary polymers—including CMC, carboxymethyl chitosan, chitosan, or gelatin—produces hybrid matrices with superior mechanical and physicochemical properties. Its miscibility with carboxymethyl chitosan further demonstrates the potential of PVA-based blends to form porous, multifunctional gels with high surface area (Javaheri et. al 2025), (Farid et. al 2022), (Thakare et. al, 2024) (Javaheri, Ghasemzadeh, and Keshtkar Vanashi 2025) (Farid et al. 2022) (Thakare et al. 2024). Incorporating PVA into CMC hydrogels thus yields a cohesive supramolecular matrix through hydrogen bonding and chain entanglement without compromising cytocompatibility.

Procaine (PC), a classical amino-ester local anaesthetic, was selected as the bioactive agent. Besides analgesia, PC suppresses pro-inflammatory cytokines (IL-6, TNF-α), exhibits antioxidant and cytoprotective effects, and thereby accelerates tissue repair (Abdelaatti et. al, 2024) (Abdelaatti, Buggy, and Wall 2024). It also stimulates platelet-derived growth factor release from platelet-rich plasma without cytotoxicity, enhancing granulation and neovascularisation (Inguscio et. al 2023, Kocaaga et.ç al 2024) (Inguscio et al. 2023) (Kocaağa et al. 2024).

Here, it was reported a supramolecular Ca^{2+}-crosslinked CMC/PVA injectable hydrogel that incorporates PC as a bioactive agent. Comprehensive characterisation—SEM–EDS imaging, contact-angle measurement, detailed rheological profiling, swelling studies, Korsmeyer–Peppas release modelling, and hemolysis testing—was conducted to relate network structure to mechanical behaviour, drug-delivery performance, and blood compatibility.

MATERIALS AND METHODS

2.1. Materials

Poly(vinyl alcohol) (PVA, Mw ≈ 61 000 g mol^{-1}, Mowiol 10-98) and sodium hydroxide (NaOH) were obtained from Merck (Darmstadt, Germany). Procaine hydrochloride purchased from Sigma-Aldrich (Düsseldorf, Germany). Sodium carboxymethyl cellulose (NaCMC) was supplied by Ashland (Wilmington, USA). All chemicals were of analytical grade and used without further purification. Ultra-pure deionized (DI) water was employed in all experimental procedures.

2.2. Preparation of PVA-CMC hydrogel

In-situ gelling hydrogels were prepared by solution casting. PVA) (30 % w/v) was first dissolved in de-ionised water at 60 °C for 24 h under continuous stirring (100 rpm) to obtain a clear, homogeneous solution. Carboxymethyl cellulose was then introduced and allowed to hydrate fully; subsequent addition of $CaCl_2$ (0.7 wt %, 70 mg per 10 g precursor) at 37 °C induced ionic cross-linking, generating a pre-gelled Ca^{2+}-CMC framework. An equal mass of additional PVA (w/w PVA/PVA = 1:1) was incorporated to reinforce the matrix via hydrogen bonding and chain entanglement. Finally, procaine hydrochloride (1.5 mg mL^{-1}; 2.4 mg per batch, pH 6.4, Tris buffer) was blended into the hydrogel, yielding the PVA-CMC-PC formulations.

2.3. SEM Analysis

Hydrogel morphology was examined by scanning electron microscopy (JSM-6390LV, JEOL, Tokyo, Japan). Samples were flash-frozen in liquid nitrogen and fractured with pre-cooled tweezers prior to imaging.

2.4. Contact angle Analysis

Static water contact angles were recorded at ambient temperature with a Biolin Scientific Theta Lite goniometer using the sessile-drop technique. For each formulation, six independent droplets (3 µL) were analysed, and the mean ± standard deviation is reported.

2.6 Swelling Behaviour

Lyophilised hydrogel discs (diameter = 10 mm) were weighed (W_D) and immersed in 25 mL of Tris buffer (pH 6.4) at 37 °C. At predetermined time points intervals each disc was removed, lightly blotted to remove surface fluid, and re-weighed (W_S). Swelling was calculated as;

$$\text{Swelling } (\%) = \frac{W_S - W_D}{W_D} \times 100 \qquad \text{Equation 1}$$

2.6 Drug release and kinetics

In-vitro PC release was monitored by UV–visible spectroscopy. Fresh hydrogel discs were placed in 50 mL Tris buffer (pH 7.4) and incubated at 37 °C with orbital shaking (100 rpm) in sealed vials. At scheduled intervals, 1 mL of the medium was withdrawn, replaced with fresh buffer, and analysed at 290 nm using a UV/Vis spectrophotometer (PerkinElmer, Waltham, MA, USA). PC concentration was calculated with the Beer–Lambert law from a calibration curve ($R^2 > 0.999$) generated from standard solutions [A kind of multi-dot ensemble regression AI, (11)]. Release experiments were performed in triplicate, and cumulative release (%) was plotted as mean ± standard deviation.The in vitro drug release kinetics of PVP-CMC-PC hydrogel were analyzed using Korsmeyer-Peppas model.(Equation 2). Release kinetics were interpreted with the Korsmeyer–Peppas equation, which accommodates both Fickian and anomalous diffusion:

$$\frac{M_t}{M_\infty} = K_P t^n \quad \text{Equation 2}$$

where $\frac{M_t}{M_\infty}$ is the cumulative fraction of drug released at time t, $K_P t^n$ is the release-rate constant, and n is the diffusion exponent that reflects the transport mechanism.

2.13. Hemolysis activity

Erythrocyte compatibility was evaluated using bovine red blood cells (RBCs). Whole blood anticoagulated with 3.2 % (w/v) sodium citrate was centrifuged at 3500 rpm for 5 min, and the pelleted RBCs were washed three times with phosphate-buffered saline (PBS, pH 7.4). The final suspension was adjusted to 10 % (v/v) RBCs in PBS. Hydrogel discs (Ø 3 mm) were incubated with 1 mL of the RBC suspension at 37 °C for 2 h. PBS mixed 1:1 (v/v) with RBCs served as the negative control, while distilled water mixed 1:9 (v/v) functioned as the positive control. After incubation, samples were centrifuged at 3500 rpm for 10 min, and 100 µL of each supernatant was transferred to a 96-well plate. Absorbance was read at 540 nm on a microplate reader (BMG LABTECH SPECTROstar® Nano). Hemolysis was calculated as

$$\text{Hemolysis } (\%) = \frac{OD_{\text{sample}} - OD_{\text{negative control}}}{OD_{\text{positive control}} - OD_{\text{negative control}}} \times 100 \qquad \text{Equation 3}$$

RESULTS and DISCUSSION

In the present work, it was developed a supramolecular highly transparent injectable hydrogel composed of CMC and PVA, crosslinked by Ca^{2+} ions and loaded with PC, to address three major shortcomings of conventional hydrogels: mechanical fragility, limited bioactivity, and poor stability under repeated mechanical stress. Ca^{2+} ions first coordinate with the carboxylate groups of CMC, generating an ionically cross-linked backbone that regulates pore architecture and water uptake. Interpenetrating PVA chains reinforce this backbone through extensive hydrogen bonding with both Ca^{2+}-stabilised carboxylates and residual CMC hydroxyls, imparting cohesive strength and viscoelastic stability. Protonated procaine molecules electrostatically associate with unoccupied carboxylate sites and are further retained within hydrophilic PVA microdomains, producing a uniform drug distribution.

3.1. Scanning Electron Microscopy (SEM) Analysis

SEM imaging (Figure 1a–c) reveals a multi-scale structure composed of compact lamellae linked by sub-fibrils that form as PVA diffuses into the Ca–CMC matrix during gelation. This lamella–fibril network establishes continuous stress-transfer routes while retaining nanoporosity that supports solvent uptake and drug release. Higher-magnification views show sharp, crack-free lamellar boundaries, indicating efficient stress

redistribution between polymer phases. Elemental mapping by EDS (Figure 1d) confirms a uniform Ca content of 4.16 wt % throughout the lamellae, whereas residual chloride (< 1 wt %) is limited to isolated domains, reflecting effective purification.

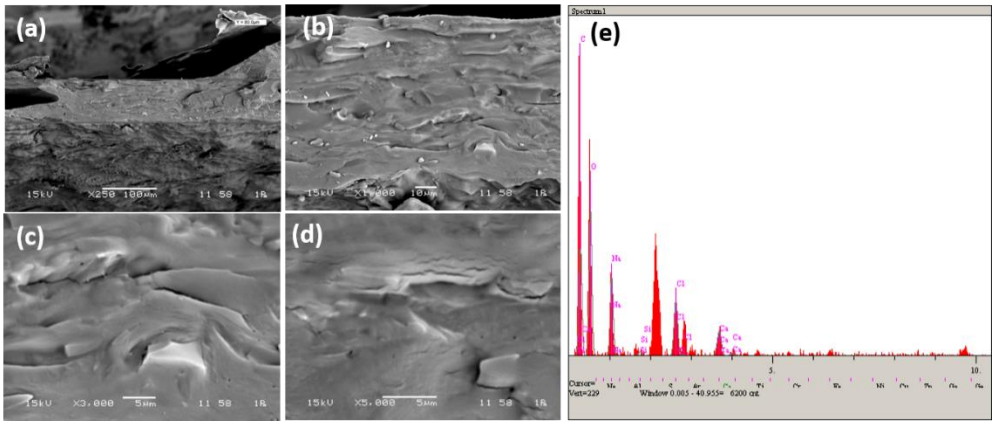

Figure 1. SEM micrographs (left panels) of the freeze-fractured CMC/PVA–Ca^{2+} hydrogel, displaying (a) low-magnification cross-section (×250; scale bar: 100 µm), (b) (×1 000; scale bar: 10 µm), (c) high-magnification fibrillar domains (×3 000; scale bar: 5 µm), (d) high-magnification fibrillar domains (×3 000; scale bar: 5 µm),.(e) Energy-dispersive X-ray spectroscopy (EDS; right panel) confirms uniform distribution of calcium (Ca), carbon (C), and oxygen (O), with minor chloride (Cl) residues.

3.2. Rheological performance of the hydrogels

The viscoelastic behaviour of the PVA/CMC hydrogels affected injectability, mechanical strength, and dimensional stability (Özkaynak et al. 2024a) (B. Kocaaga et al. 2022) (A. B. Kocaaga et al. 2019). To relate molecular architecture to bulk performance, rheological analysis were carried out into four categories: (i) Strain sweep measurements defined the linear viscoelastic region (LVE) and flow point, establishing tolerance to the high shear rates encountered during syringe extrusion. (ii) Frequency sweep quantified storage (G′) and loss (G″) moduli across 0.1–100 rad s^{-1}, yielding a stiffness spectrum relevant to physiological deformation rates. (iii) Six-cycle amplitude sweep analysis evaluated structural recovery after repeated large-strain loading, assessing self-healing driven by reversible Ca^{2+} coordination, H-bonding and polymer entanglement. (iv) Creep–recovery tests measured compliance under sustained low stress and the extent of elastic rebound, parameters that indicate long-term mechanical integrity once the hydrogel is applied to a wound site (B. Kocaaga et al. 2024)(Özkaynak et al. 2024b) (B. Kocaaga et al. 2024)(Özkaynak et al. 2024b) (Kocaağa et al. 2024).

The amplitude sweep (Figure 2a) reveals a LVE, reflecting a stable Ca^{2+}-CMC ionotropic network reinforced by extensive PVA/CMC hydrogen bonding and chain entanglement (Thakare et al. 2024) (Aleman and Zhong 2025). Beyond this critical strain, G′ decreases sharply and intersects G″ at ≈ 60 % strain, marking the flow point where reversible Ca^{2+} junctions and secondary PVA crystalline domains reversibly dissociate, thereby enabling the network to yield without macroscopic fracture (Strandman and Zhu 2016). As illustrated in the inset of Figure 2a, the hydrogel can be smoothly extruded through a 21 G needle and immediately adhere to the fingertip, confirming its injectability and rapid surface affinity.

Frequency sweeps (0.1–100 rad s^{-1}, Figure 2b) show parallel power-law increases for both moduli ($G' \propto \omega^{0.77}$; $G'' \propto \omega^{0.73}$), characteristic of an entanglement-dominated supramoleculer hydrogel in which segmental mobility is progressively restricted at higher deformation rates (A. B. Kocaaga et al. 2019) (Razmkhah, Razavi, and Mohammadifar 2017). Across the entire spectrum G′ exceeds G″, confirming solid-like dominance—an outcome of the dual cross-linking regime where fast, reversible Ca^{2+} bridges coexist with slower, physical PVA domains (Khondkar et al. 2007).

The damping factor ($\tan\delta = G''/G'$, Figure 2c) is approximately 0.6 - 0.9, signifying a balanced viscoelastic response that dissipates mechanical energy efficiently yet preserves elastic integrity (Zhang et al. 2024) (Figure 2c) . This behaviour arises from the synergistic contributions of rapid Ca^{2+}/carboxylate coordination, dynamic

hydrogen bonding between PVA and CMC hydroxyl groups, and the slower relaxation of entangled, semi-crystalline PVA segments.

Complex-viscosity curves obtained from frequency-sweep tests (Figure 2d) followed a power-law decrease, $\eta^* \propto \omega^{0.60}$ ($R^2 = 0.9977$), confirming pronounced shear-thinning (B. Kocaaga et al. 2024)(Kocaağa et al. 2024). This pronounced pseudoplastic rheology substantially reduces the pressure required for syringe extrusion and, once shear is discontinued allows rapid viscosity recovery, thereby enabling swift conformation to irregular wound geometries, subsequent re-modelling, and the formation of a continuous tissue–hydrogel interface that minimises micro-voids susceptible to bacterial infiltration (Liang et al. 2021) (Sahajpal et al. 2022) (Cernencu et al. 2022) (Qin et al. 2019). The inset in Figure 2d further demonstrates the material's cohesive strength, where a continuous hydrogel filament remains attached at the bend of a little finger while being stretched between two bent digits.

The self-healing capability of the hydrogels is primarily attributed non-covalent cross-links—namely Ca^{2+}/carboxylate coordination and hydrogen bonding between PVA and CMC chains. Under high strain these dynamic bonds temporarily dissociate, dissipating energy through the rupture of energy-absorbing transient linkages; when the load is removed, bond re-formation rebuilds the network. Six-cycle thixotropic strain sweeps alternating 0.2 % and 1000 % strain (Figure 2e) demonstrated a recovery coefficient (RS %) of 51.35 ± 2.4, with each cycle showing a clear transition between elastic ($G' > G''$) and viscous ($G'' > G'$) regimes. The persistence of this reversible response underscores the material's capacity to seal cracks created by physiological motion and maintain a continuous barrier throughout the healing process(Brito-Oliveira et al. 2022) (Krempl and Khan 2003).

Applying a constant stress of 10 Pa for 300 s produced an immediate creep compliance (J_0) of ≈ 0.022 Pa^{-1}, attributable to elastic stretching of the Ca^{2+}-coordinated PVP-CMC-PC network. Compliance then increased gradually to 0.10 Pa^{-1}, reflecting time-dependent chain motion governed by reversible Ca^{2+} interactions, hydrogen bonding between PVA and CMC, and the presence of PC. PC molecules electrostatically associate with unoccupied carboxylate groups and form secondary hydrogen bonds with PVA hydroxyls, locally bridging the two polymers; this transient linkage slows segmental slippage, giving a controlled viscoelastic rise rather than unchecked creep (Starkova and Aniskevich 2007).

When the load was removed, compliance decreased to ≈ 0.02 Pa^{-1} within 600 s, corresponding to an ~80 % strain recovery. The rapid rebound is facilitated by reformation of Ca^{2+} bridges and PVA–CMC hydrogen bonds, while reversible electrostatic interactions of PC further assist network reconstitution. The modest residual strain confirms that the hydrogel dissipates mechanical energy without permanent structural loss.

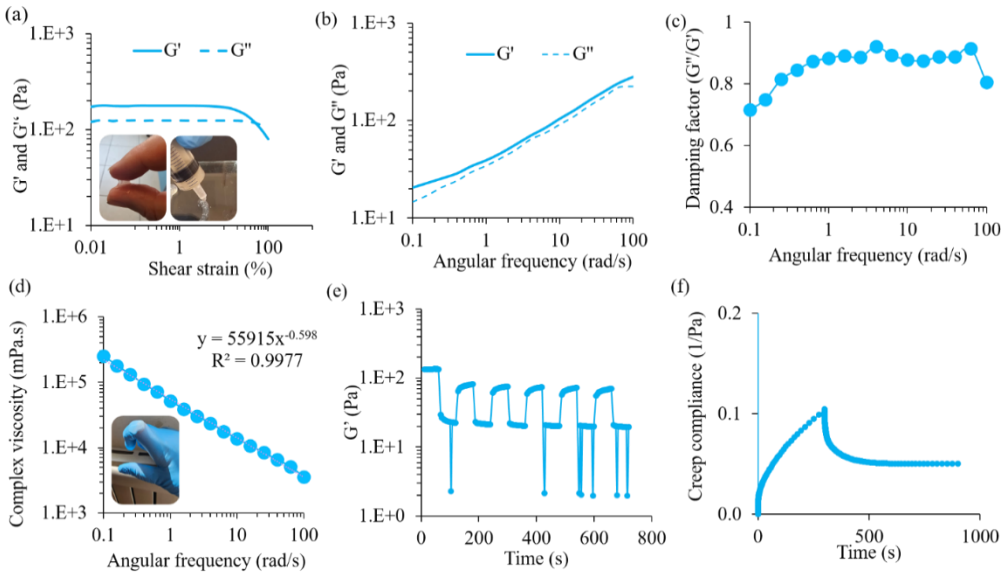

Figure 2. Rheological performance of the hydrogel. (a) Strain-sweep profile. Inset: hydrogel filament stretched between bent fingers, demonstrating cohesive strength, hydrogel extruded through a 21 G needle. (b) Frequency sweep (c) Damping factor (tan δ) as a function of frequency, (d) Complex viscosity versus

angular frequency fitted with a power-law model. Inset: Photograph showing the hydrogel adhering to the bend of a little finger. (e) Six-cycle large-amplitude oscillatory strain test. (f) Creep–recovery curve

3.3. Contact Angle Analysis

The static contact angle of 51.3 ± 0.5° indicates moderate hydrophilicity, enabling rapid wetting and conformal adhesion to moist tissue (Figure 2a, inset). This surface behaviour is governed by hydroxyl and carboxylate groups from PVA and Ca^{2+}-cross-linked CMC, which establish extensive hydrogen bonding with interfacial water. Protonated PC, electrostatically associated with residual carboxylates, further enhances surface polarity, collectively supporting interface formation.

3.4 Swelling and PC release behaviour.

The hydrogel absorbs water rapidly, reaching a swelling ratio of ~25 g g^{-1} within 90 min (Figure 3a). This swift uptake reflects the highly wettable surface (contact angle ≈ 46.7°) together with the porous Ca^{2+}-CMC scaffold, which can permit fluid penetration through ionic junctions. The subsequent plateau and a second, slower increase to a maximum of ~40 g g^{-1} at 300 min point to gradual relaxation of the PVA-rich domains and limited rearrangement of Ca^{2+} bridges. These trends align with the rheological data: a broad LVE and moderate damping factor demonstrate that the network can accommodate solvent uptake without losing cohesion, while the creep-recovery profile confirms that most deformation is recovered once osmotic stresses decreased.

Drug diffusion closely correlates with the early swelling phase: ~80 % of the procaine load is released within 120 min, and complete release is achieved by ~180 min (Figure 3b). The initial burst is driven by water-assisted transport through hydrated Ca^{2+}–CMC channels. Release kinetics follow the Korsmeyer–Peppas model with n = 0.39 (R^2 = 0.927), indicative of predominantly Fickian diffusion and minimal contribution from polymer relaxation (Figure 3c). (Siepmann and Peppas 2012) (Lao et al. 2011) (Sciences et al. 2010). Nearly constant storage modulus recorded in strain and frequency sweeps confirms that Ca^{2+}-mediated cross-linking and PVA entanglement uphold network cohesion throughout the release period, thereby preventing premature matrix erosion and sustaining controlled drug delivery.

3.5 Hemolysis Analysis

Hemolysis testing, conducted in accordance with ISO 10993-4, showed that the PVA/CMC–Ca^{2+} hydrogel induced negligible erythrocyte lysis (< 2 %), comparable to the PBS (negative) control and well below the 5 % cytocompatibility limit (Figure 3d). Visual inspection proved the spectrophotometric data: supernatants from hydrogel incubations remained essentially clear. The low hemolytic index is attributed to the near-neutral pH of the hydrogel and the protective hydration layer provided by surface hydroxyl and carboxylate groups, which minimise electrostatic interactions with red-cell membranes and prevent osmotic imbalance. These findings confirm that the supramolecular PVA/CMC network is hemocompatible and suitable for direct contact with blood (Cao et al. 2021).

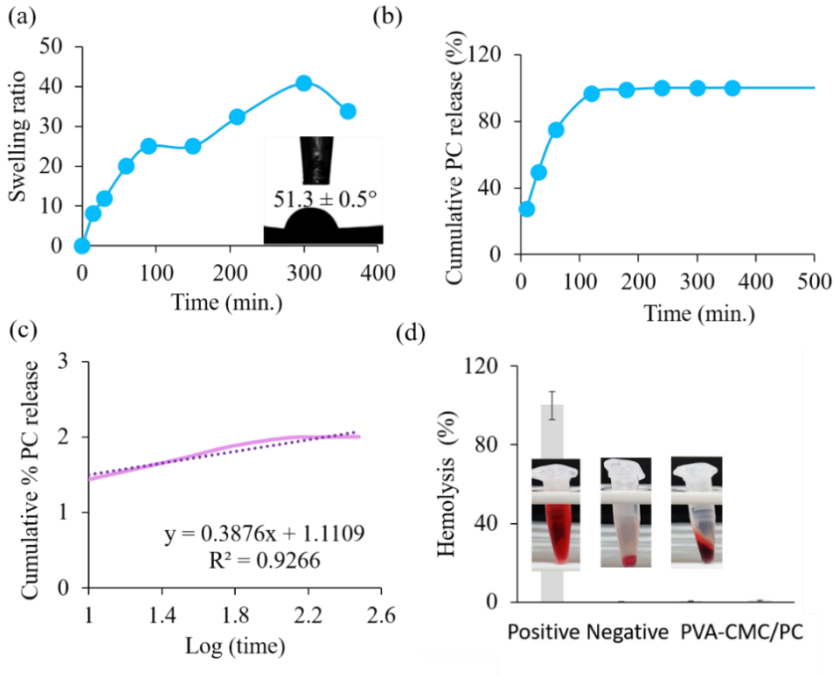

Figure 3. (a) Swelling ratio versus time Inset: Contact angle photograph (b) Cumulative procaine (PC) release (c) Korsmeyer–Peppas analysis of the release data (log–log plot) (d) Hemolysis. Insets: photographs of supernatants for the positive (distilled water), negative (PBS), and hydrogel samples.

4. CONCLUSION

The Ca^{2+}-bridged PVA/CMC hydrogel establishes a supramolecular network in which ionic coordination and hydrogen bonding impart injectability, self-repair, and structural integrity. A contact angle of 51 ° supports rapid wetting and conformal adhesion, while regulated swelling (25 g g^{-1} at 90 min; plateau 40 g g^{-1}) proceeds in parallel with Fickian procaine release (n = 0.39), delivering an immediate analgesic dose and complete drug release within three hours. Rheological data indicate low extrusion stress, an extended linear viscoelastic window, marked shear-thinning, 51 % modulus recovery after cyclic loading, and ~80 % elastic restitution after creep—responses governed by reversible Ca^{2+} cross-links, polymer entanglement, and secondary interactions with protonated PC. SEM–EDS confirms a lamellar–fibrillar hierarchy with uniform Ca distribution, mirroring the hydrogel's mechanical stability; hemolysis below 2 % verifies blood compatibility. Collectively, these findings satisfy key criteria for an injectable, self-healing wound dressing that provides local analgesia while maintaining mechanical and haemocompatible performance. Progress toward clinical translation ndepends on *in-vivo* evaluation of haemostatic efficacy, degradation behaviour, and long-term safety, as well as formulation extensions that co-deliver antimicrobial or pro-angiogenic agents for infection-prone or chronic wounds.

REFERENCES

Abdelaatti, Ahmed, Donal J. Buggy, and Thomas P. Wall. 2024. "Local Anaesthetics and Chemotherapeutic Agents: A Systematic Review of Preclinical Evidence of Interactions and Cancer Biology." *BJA Open* 10(January). doi:10.1016/j.bjao.2024.100284.

Aleman, Javier, and Qixin Zhong. 2025. "Hydrogels Formed with Shellac and Zein: PH-Responsiveness, Rheology, and Gelation Mechanism." *International Journal of Biological Macromolecules* 308(March). doi:10.1016/j.ijbiomac.2025.142729.

Brito-Oliveira, Thais C., Izabel C.F. Moraes, Samantha C. Pinho, and Osvaldo H. Campanella. 2022. "Modeling Creep/Recovery Behavior of Cold-Set Gels Using Different Approaches." *Food Hydrocolloids* 123(August 2021): 107183. doi:10.1016/j.foodhyd.2021.107183.

Cao, Changyu, Nan Yang, Ye Zhao, Dapeng Yang, Yanling Hu, Dongliang Yang, Xuejiao Song, Wenjun Wang, and Xiaochen Dong. 2021. "Biodegradable Hydrogel with Thermo-Response and Hemostatic

Effect for Photothermal Enhanced Anti-Infective Therapy." *Nano Today* 39: 101165. doi:10.1016/j.nantod.2021.101165.

Cernencu, Alexandra I., Andreea I. Dinu, Izabela C. Stancu, Adriana Lungu, and Horia Iovu. 2022. "Nanoengineered Biomimetic Hydrogels: A Major Advancement to Fabricate 3D-Printed Constructs for Regenerative Medicine." *Biotechnology and Bioengineering* 119(3): 762–83. doi:10.1002/bit.28020.

El-Diehy, Mahmoud A., Ibrahim I. Farghal, Mohamed A. Amin, Mohamed Mohamady Ghobashy, Abdelatti I. Nowwar, and H. M. Gayed. 2025. "Radiation-Assisted Tailoring of Swelling Behavior and Water Retention of Na-CMC/PAAm Hydrogels for Enhancing Beta Vulgaris under Drought Stress." *Scientific reports* 15(1): 1661. doi:10.1038/s41598-024-83832-3.

Farid, Eman, Elbadawy A. Kamoun, Tarek H. Taha, Ali El-Dissouky, and Tarek E. Khalil. 2022. "PVA/CMC/Attapulgite Clay Composite Hydrogel Membranes for Biomedical Applications: Factors Affecting Hydrogel Membranes Crosslinking and Bio-Evaluation Tests." *Journal of Polymers and the Environment* 30(11): 4675–89. doi:10.1007/s10924-022-02538-7.

Guo, Huilong, Shan Huang, Anding Xu, and Wei Xue. 2022. "Injectable Adhesive Self-Healing Multiple-Dynamic-Bond Crosslinked Hydrogel with Photothermal Antibacterial Activity for Infected Wound Healing." *Chemistry of Materials* 34(6): 2655–71. doi:10.1021/acs.chemmater.1c03944.

Inguscio, Chiara Rita, Barbara Cisterna, Maria Assunta Lacavalla, Franco Donati, Osvaldo Angelini, Gabriele Tabaracci, and Manuela Malatesta. 2023. "Ozone and Procaine Increase Secretion of Platelet-Derived Factors in Platelet-Rich Plasma." *European Journal of Histochemistry* 67(4): 241–51. doi:10.4081/ejh.2023.3879.

Islam, Md Monirul, and Md Ibrahim H. Mondal. 2024. "Carboxymethyl Cellulose/Polyvinylpyrrolidone Bio-Composite Hydrogels Enriched with Clove Bud Extracts for Enhanced Wound Healing." *Arabian Journal of Chemistry* 17(9). doi:10.1016/j.arabjc.2024.105945.

Javaheri, Hanieh, Hossein Ghasemzadeh, and Abolfazl Keshtkar Vanashi. 2025. "Double Network Hydrogel Based on PVA and CMC: Synthesis and Its Potential Application in Local Drug Delivery." *Colloid and Polymer Science* (Cmc). doi:10.1007/s00396-025-05417-4.

Jridi, Mourad, Ola Abdelhedi, Ali Salem, Hela Kechaou, Moncef Nasri, and Yosra Menchari. 2020. "Physicochemical, Antioxidant and Antibacterial Properties of Fish Gelatin-Based Edible Films Enriched with Orange Peel Pectin: Wrapping Application." *Food Hydrocolloids* 103(July 2019). doi:10.1016/j.foodhyd.2020.105688.

Khondkar, Dristi, Richard Frank Tester, Nick Hudson, John Karkalas, and Jim Morrow. 2007. "Rheological Behaviour of Uncross-Linked and Cross-Linked Gelatinised Waxy Maize Starch with Pectin Gels." *Food Hydrocolloids* 21(8): 1296–1301. doi:10.1016/j.foodhyd.2006.10.008.

Kocaaga, A. Banu, Ozge Kurkcuoglu, Melkon Tatlier, Saime Batirel, and F. Seniha Guner. 2019. "Low-Methoxyl Pectin–Zeolite Hydrogels Controlling Drug Release Promote in Vitro Wound Healing." *Journal of Applied Polymer Science* 136(24): 1–16. doi:10.1002/app.47640.

Kocaaga, Banu, Tugce Inan, Nesrin İsil Yasar, Can Ege Yalcin, Fethiye Aylin Sungur, Ozge Kurkcuoglu, Anil Demiroz, et al. 2024. "Innovative Use of an Injectable, Self-Healing Drug-Loaded Pectin-Based Hydrogel for Micro- and Supermicro-Vascular Anastomoses." *Biomacromolecules* 25(7): 3959–75. doi:10.1021/acs.biomac.4c00102.

Kocaaga, Banu, Ozge Kurkcuoglu, Melkon Tatlier, Gizem Dinler-Doganay, Saime Batirel, and Fatma Seniha Güner. 2022. "Pectin–Zeolite-Based Wound Dressings with Controlled Albumin Release." *Polymers* 14(3). doi:10.3390/polym14030460.

Kocaağa, Banu, Yetkin Öztürk, H. Ceren Kurçin, Zeynep Güner-Yılmaz, Ozge Kurkcuoglu, Melkon Tatlier, İlkay Özdemir, et al. 2024. "Developing Multifunctional Pectin-Based Hydrogel for Wound Dressing: In Silico, in Vitro and in Vivo Evaluation." *European Polymer Journal* 216(July). doi:10.1016/j.eurpolymj.2024.113280.

Krempl, Erhard, and Fazeel Khan. 2003. "Rate (Time)-Dependent Deformation Behavior: An Overview of Some Properties of Metals and Solid Polymers." *International Journal of Plasticity* 19(7): 1069–95. doi:10.1016/S0749-6419(03)00002-0.

Lao, Luciana Lisa, Nicholas A. Peppas, Freddy Yin Chiang Boey, and Subbu S. Venkatraman. 2011. "Modeling of Drug Release from Bulk-Degrading Polymers." *International Journal of Pharmaceutics* 418(1): 28–41. doi:10.1016/j.ijpharm.2010.12.020.

Li, De qiang, Shu ya Wang, Yu jie Meng, Zong wei Guo, Mei mei Cheng, and Jun Li. 2021. "Fabrication of Self-Healing Pectin/Chitosan Hybrid Hydrogel via Diels-Alder Reactions for Drug Delivery with High Swelling Property, PH-Responsiveness, and Cytocompatibility." *Carbohydrate Polymers* 268(March). doi:10.1016/j.carbpol.2021.118244.

Li, Lu, Lixin Wang, Xinxin Luan, Yanjun Pang, Kefeng Zhang, Yushuai Cheng, Zhe Ji, and Jinhui Pang. 2023. "Adhesive Injectable Cellulose-Based Hydrogels with Rapid Self-Healing and Sustained Drug Release Capability for Promoting Wound Healing." *Carbohydrate Polymers* 320(January). doi:10.1016/j.carbpol.2023.121235.

Liang, Yuqing, Zhenlong Li, Ying Huang, Rui Yu, and Baolin Guo. 2021. "Dual-Dynamic-Bond Cross-Linked Antibacterial Adhesive Hydrogel Sealants with On-Demand Removability for Post-Wound-Closure and Infected Wound Healing." *ACS Nano* 15(4): 7078–93. doi:10.1021/acsnano.1c00204.

Liao, Siyuan, Qunying Wu, Jie Liu, Jianguo Yang, Zhen Pan, Lian Chang, Zhiming Liu, and Shuaiqi Liang. 2025. "Effects of CMC-Na and LA on the Flow Characteristics of CO2 Hydrate in High-Pressure Flow System." *Journal of Molecular Liquids* 424(December 2024). doi:10.1016/j.molliq.2024.126837.

Özkaynak, Mert Umut, Banu Kocaaga, Koray Bahadır Dönmez, Selin Dağlar, Yurdanur Türker, Nilgün Karatepe, F. Seniha Güner, and Ömer Dag. 2024a. "Understanding the Role of Water in the Lyotropic Liquid Crystalline Mesophase of High-Performance Flexible Supercapacitor Electrolytes Using a Rheological Approach." *Journal of Molecular Liquids* 394(November 2023). doi:10.1016/j.molliq.2023.123705.

Özkaynak, Mert Umut, Banu Kocaaga, Koray Bahadır Dönmez, Selin Dağlar, Yurdanur Türker, Nilgün Karatepe, F. Seniha Güner, and Ömer Dag. 2024b. "Understanding the Role of Water in the Lyotropic Liquid Crystalline Mesophase of High-Performance Flexible Supercapacitor Electrolytes Using a Rheological Approach." *Journal of Molecular Liquids* 394(September 2023). doi:10.1016/j.molliq.2023.123705.

Qin, Haili, Tan Zhang, Na Li, Huai Ping Cong, and Shu Hong Yu. 2019. "Anisotropic and Self-Healing Hydrogels with Multi-Responsive Actuating Capability." *Nature Communications* 10(1): 1–11. doi:10.1038/s41467-019-10243-8.

Qu, Jin, Xin Zhao, Peter X. Ma, and Baolin Guo. 2017. "PH-Responsive Self-Healing Injectable Hydrogel Based on N-Carboxyethyl Chitosan for Hepatocellular Carcinoma Therapy." *Acta Biomaterialia* 58: 168–80. doi:10.1016/j.actbio.2017.06.001.

Razmkhah, Somayeh, Seyed Mohammad Ali Razavi, and Mohammad Amin Mohammadifar. 2017. "Dilute Solution, Flow Behavior, Thixotropy and Viscoelastic Characterization of Cress Seed (Lepidium Sativum) Gum Fractions." *Food Hydrocolloids* 63: 404–13. doi:10.1016/j.foodhyd.2016.09.030.

Saha, Nabanita, Rushita Shah, Prerak Gupta, Biman B. Mandal, Radostina Alexandrova, Maja Dutour Sikiric, and Petr Saha. 2019. "PVP - CMC Hydrogel: An Excellent Bioinspired and Biocompatible Scaffold for Osseointegration." *Materials Science and Engineering C* 95(March 2018): 440–49. doi:10.1016/j.msec.2018.04.050.

Sahajpal, Kartik, Shashank Shekhar, Amit Kumar, Bhasha Sharma, Mahendra Kumar Meena, Ajay Kumar Bhagi, and Shreya Sharma. 2022. "Dynamic Protein and Polypeptide Hydrogels Based on Schiff Base Co-Assembly for Biomedicine." *Journal of Materials Chemistry B* 10(17): 3173–98. doi:10.1039/d2tb00077f.

Sciences, Health, Padala Narsimha Murthy Suvakanta Dash, Health Sciences, Suvakanta Dash, Padala Narasimha Murthy, Lilakanta Nath, Prasanta Chowdhury, and Health Sciences. 2010. "Kinetic Modeling on Drug Release from Controlled Drug Delivery System." *Acta Poloniac Pharmaceutica - Drug Research* 67(3): 217–23. doi:10.1016/S0928-0987(01)00095-1.

Siepmann, J., and N. A. Peppas. 2012. "Modeling of Drug Release from Delivery Systems Based on Hydroxypropyl Methylcellulose (HPMC)." *Advanced Drug Delivery Reviews* 64(SUPPL.): 163–74. doi:10.1016/j.addr.2012.09.028.

Starkova, O., and A. Aniskevich. 2007. “Limits of Linear Viscoelastic Behavior of Polymers.” *Mechanics of Time-Dependent Materials* 11(2): 111–26. doi:10.1007/s11043-007-9036-3.

Strandman, Satu, and X. X. Zhu. 2016. “Self-Healing Supramolecular Hydrogels Based on Reversible Physical Interactions.” *Gels* 2(2): 1–31. doi:10.3390/gels2020016.

Thakare, Neha R., Pronami Gogoi, Pankaj Bharali, and Swapnali Hazarika. 2024. “Influence of Copper Ion Cross-Linked CMC-PVA Film on Cell Viability and Cell Proliferation Study.” *International Journal of Biological Macromolecules* 282(October). doi:10.1016/j.ijbiomac.2024.136645.

Wang, Wenda, Li Xiang, Lu Gong, Wenjihao Hu, Weijuan Huang, Yangjun Chen, Anika B. Asha, et al. 2019. “Injectable, Self-Healing Hydrogel with Tunable Optical, Mechanical, and Antimicrobial Properties.” *Chemistry of Materials* 31(7): 2366–76. doi:10.1021/acs.chemmater.8b04803.

Zhang, Xiaoran, Xin Zhang, Puying Wang, Xinze Wang, Linlin Zhong, Songmei Ma, and Wenlong Xu. 2024. “Study on Viscoelasticity and Damping Properties of OSA/PAAM Hydrogel.” *Journal of Polymer Research* 31(2): 1–11. doi:10.1007/s10965-024-03913-9.

➢ *ORAL PRESENTATION*

Application of a New Numerical Approach for Neural Ordinary Differential Equations

Altan Onat[1*] (*ORCID: https://orcid.org/0000-0002-0421-5653*)

[*1]Electrical and Electronics Engineering Department, Engineering Faculty, Eskişehir Technical University, İki Eylül Campus, Eskişehir, Türkiye.

*Corresponding author e-mail: altanonat@eskisehir.edu.tr:

Abstract
Since the introduction of neural ordinary differential equations (Neural ODEs), they have been widely adopted for modeling various dynamical systems. Their novelty lies in representing the derivatives of hidden states, which correspond to the continuous-time dynamics of a system, using a neural network. These derivatives are then used to compute the network's output through a numerical ODE solver. In this study, a recently proposed modified Trapezoidal Rule with Second Order Backward Differentiation (TR-BDF2) method is employed to accurately compute the output of the neural network. The FitzHugh-Nagumo model, a nonlinear dynamical system, is used as a benchmark to evaluate the solver's performance. The results obtained with the modified TR-BDF2 method are compared against those from the classical TR-BDF2 and the fourth-order Runge-Kutta method (RK4). The application results suggest that the modified numerical solver is a promising alternative for training Neural ODEs.
Keywords: Neural Ordinary Differential Equations, TR-BDF2 Method, FitzHugh-Nagumo Model, Numerical Solver, Deep Learning for Dynamical Systems.

INTRODUCTION

(Chen, Rubanova, Bettencourt, & Duvenaud, 2018) introduced a new type of deep neural network with a structure that differs from traditional architectures. Specifically, this structure models the transformation of a hidden state using a neural network. In deep neural networks with small step sizes, such transformations (dynamics) can be represented and parameterized by an ordinary differential equation (ODE). (Chen, Rubanova, Bettencourt, & Duvenaud, 2018) report that evaluating these models using ODE solvers offers several advantages, including efficient memory usage, adaptive computation, and the ability to model continuous-time series.

The main challenge in training neural ODEs lies in performing backpropagation through a numerical solver. This issue is addressed by the adjoint sensitivity method reported by (Chen, Rubanova, Bettencourt, & Duvenaud, 2018), which is noted to be applicable to all solvers. In addition to this, training neural ODEs also involves challenges related to the inherent limitations of neural networks and time series data, as discussed by (Okamoto, Takeuchi, & Sakemi, 2025).

Since their introduction, neural ODEs have found specific applications in physical systems, time series analysis, and generative modeling (Kidger, 2021). Therefore, fast and accurate implementations of neural ODEs are important.

There are two main numerical approaches for solving ODEs: explicit and implicit methods. Explicit solvers compute the next state based solely on the current state, whereas implicit methods involve both the current and future states in the computation. (Kidger, 2021) notes that implicit solvers are computationally expensive and that reducing the computational complexity of neural ODEs through improved numerical solvers is an ongoing area of research.

In general, classical numerical solvers have been the primary focus in neural ODE research. For example, the use of explicit Runge-Kutta solvers is highlighted as a common approach for numerical solution in (Kidger, 2021). More recently, implicit numerical solvers have been applied to neural ODEs, as discussed by (Fronk & Petzold, 2024). Their work explores the use of single-step implicit methods for stiff systems, and it is well known that implicit solvers offer greater stability in such cases. (Fronk & Petzold, 2024) specifically investigate the trapezoidal rule and the backward Euler method for neural ODEs.

Additionally, a semi-implicit approach has been applied to model a chaotic system in (Zhang, Liu, & Maulik, 2023). In this method, the system is decomposed into linear and nonlinear components: the implicit method is applied to the linear part, while the explicit method is used for the nonlinear part.

Recently, a modified version of the trapezoidal rule combined with the second-order backward differentiation method, known as TR-BDF2, was proposed for the simulation of power electronics applications by (Onat & Örüklü, 2023). This improved version is referred to as the improved TR-BDF2 (I-TR-BDF2) method, as it provides better results than the standard formulation. In addition to this method, the predictor-corrector (PC) method and its modified version (I-PC) were also investigated in the same study. The results show that the best performance was achieved using the I-TR-BDF2 method. One of the comparison benchmarks was the classical fourth-order Runge-Kutta method. Consequently, both the I-TR-BDF2 and TR-BDF2 methods are investigated in this work to exploit their advantages over the classical fourth-order Runge-Kutta method, which is commonly used in neural ODEs.

MATERIALS AND METHODS

Neural Ordinary Differential Equations

(Chen, Rubanova, Bettencourt, & Duvenaud, 2018) express the evolution of the hidden states of a neural network by the following equation:

$$\boldsymbol{h}_{t+1} = \boldsymbol{h}_t + f(\boldsymbol{h}_t, \theta_t). \tag{1}$$

It is clear that the equation above is similar to the well-known Euler's method for solving ODEs. This equation simply models the evolution of the hidden states. If the step size is increased (e.g., by using deeper layers), this equation can be converted to an ODE (Chen, Rubanova, Bettencourt, & Duvenaud, 2018), which can be expressed as:

$$\frac{d\boldsymbol{h}_t}{dt} = f(\boldsymbol{h}_t, t, \theta_t). \tag{2}$$

The function f represents the neural network that models the time evolution of the system. An illustration of the neural ODE layer is given in Figure 1. The main aim of this study is to find the parameters of this neural ODE layer based on the numerical solution of the differential equation given in Equation 2.

During the training phase of the neural network, a structure with three fully connected layers is used. These layers have a hidden state size of 32 and employ the hyperbolic tangent activation function. The internal time step for the neural network is set to 40. As will be shown in the following section, both the input and output sizes are two, since there are two states in the considered dynamical system. An adaptive optimization algorithm is used with gradient decay and squared gradient decay rates of 0.9 and 0.999, respectively. These are the default parameters for the ADAM optimizer (PyTorch, n.d.). A learning rate of 0.001 and a mini-batch size of 200 are used during training. The total number of training iterations is 2500.

MATLAB software is used for this study, and scripts accessed from (Lopez, Neural ODE MATLAB Implementation, 2019) are employed since they allow modifications to the numerical solver. These scripts were originally written for the submission by (Lopez, Musau, Hamilton, & Johnson, 2022).

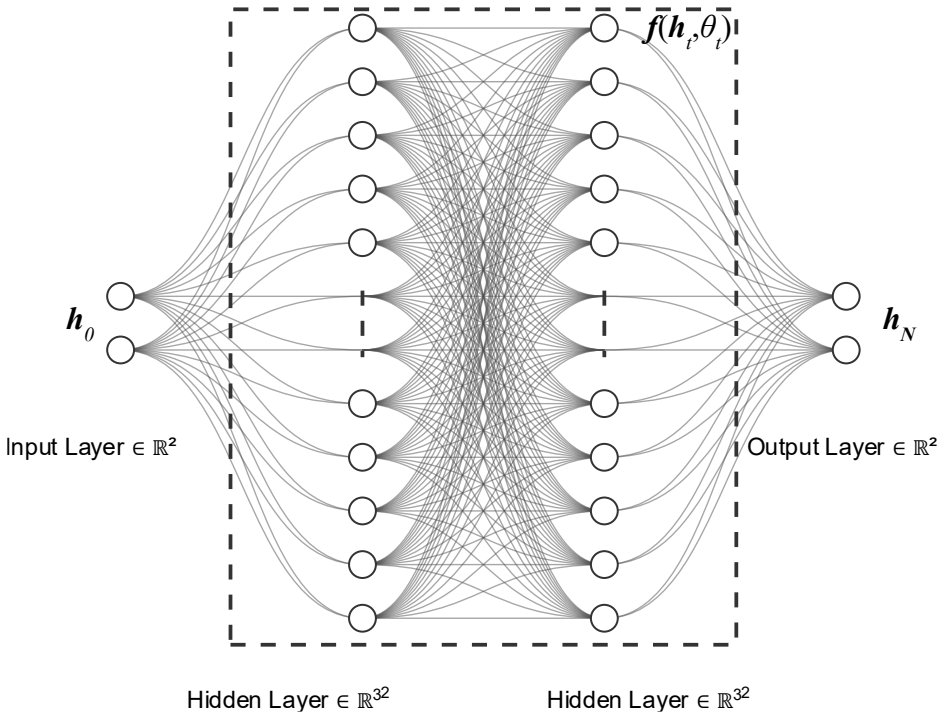

Figure 1. Illustration of the neural ODE Layer

Fitzhugh-Nagumo ODE

To investigate the effect of the numerical solver, the FitzHugh-Nagumo ODE model is selected. This nonlinear model of the nerve membrane was first proposed by (FitzHugh, 1961). The nonlinear ODE system is given as:

$$\frac{dv}{dt} = v - \frac{1}{3}v^3 - w + I, \quad \frac{dw}{dt} = \varepsilon(v + a - bw). \tag{3}$$

In this model, v represents the membrane voltage, and w is the activation of an outward current. This model is currently used for several purposes, including parameter estimation (Ara, 2019) and (Rudi, Bessac, & Lenzi, 2022). The parameters for the simulation are based on (Ara, 2019), with the only difference being the value of I in Equation 3. According to (Izhikevich, 2007), this value can be considered zero for simplicity; nevertheless, it has been set to 0.5 in this study. The parameters used for the FitzHugh-Nagumo ODE are listed in Table 1.

Table 1. Parameters for the Fitzhugh Nagumo ODE

Parameter	Value
a	0.7
b	0.8
ε	0.08
I	0.5

To simulate and solve this nonlinear ODE system, MATLAB's ode45 function is used. (Ashino, Nagase, & Vaillancourt, 2000) report that the ode45 function implements an explicit Runge-Kutta pair of orders 5 and 4, based on the Dormand-Prince method. This method is more complex compared to the numerical solvers considered in this study. Therefore, during the training phase, the results obtained from this ODE solver are used as the ground truth and training data.

Numerical Solvers

The numerical solvers considered in this study are the Trapezoidal Rule with Second-Order Backward Differentiation (TR-BDF2), a modified version of this method called the improved TR-BDF2 (I-TR-BDF2), as proposed by (Onat & Örüklü, 2023), which provides promising results compared to the classical fourth-order Runge-Kutta method.

The TR-BDF2 method combines the trapezoidal rule and the second-order backward differentiation formula for solving ODEs.

$$y_{n+\gamma} = y_n + \gamma\frac{\Delta t}{2}\left(f_n + f_{n+\gamma}\right). \tag{4}$$

The equation above represents the trapezoidal rule for numerical integration. The second-order backward Euler differentiation formula is expressed as:

$$y_{n+1} = \frac{1}{\gamma(2-\gamma)}y_{n+\gamma} - \frac{(1-\gamma)^2}{\gamma(2-\gamma)}y_n + \frac{1-\gamma}{2-\gamma}\Delta t f_{n+1}, \tag{5}$$

where γ is a parameter that determines the stability type of the method. It is taken as $\gamma \in (0,1)$. It is stated in (Bonaventura & Mármol, 2021) that this value can be selected as $\gamma = 2 - \sqrt{2}$ for L-stability. Therefore, in this study for both TR-BDF2 and I-TR-BDF2 this value is considered during the training phase of the neural ODE.

The main difference of the I-TR-BDF2 is the averaging operation for function evaluations at each step. Before the trapezoidal rule step in Equation 4, the following must be evaluated for I-TR-BDF2.

$$f_{n+\gamma} \leftarrow \frac{1}{2}\left(f_n + f_{n+\gamma}\right). \tag{6}$$

To avoid confusion, an assignment operator is preferred instead of an equality sign in the last equation, differing from the notation in (Onat & Örüklü, 2023). Unlike the standard ODE solution, one additional function evaluation for f_n is required for both TR-BDF2 and I-TR-BDF2. The value of f_n can be obtained directly from the ODE equations; however, in the case of neural ODEs, it must be recalculated since it models the evolution of the hidden states. Therefore, three function evaluations are required when applying TR-BDF2 and I-TR-BDF2 to neural ODEs, even though they are two-step methods. Nevertheless, these approaches require one fewer function evaluation compared to the classical fourth-order Runge-Kutta method. Now, the averaging operation before the second-order backward Euler differentiation formula is given as:

$$f_{n+1} \leftarrow \frac{1}{2}\left(f_n + f_{n+1}\right). \tag{7}$$

The last two formulas improve the simulation results for a power electronic converter, as demonstrated in (Onat & Örüklü, 2023). This study also shows that these methods can provide promising results compared to the classical RK4 method. Details of the RK4 algorithm can be found in any fundamental numerical methods textbook, as well as in (Ashino, Nagase, & Vaillancourt, 2000) and (Onat & Örüklü, 2023). However, to highlight the differences between the TR-BDF2 methods and RK4, the equations for the RK4 solution steps are given below.

$$k_1 = f(t_n, y_n), \tag{8}$$

$$k_2 = f\left(t_n + \frac{\Delta t}{2}, y_n + \frac{\Delta t}{2}\cdot k_1\right), \tag{9}$$

$$k_3 = f\left(t_n + \frac{\Delta t}{2}, y_n + \frac{\Delta t}{2}\cdot k_2\right), \tag{10}$$

$$k_4 = f(t_n + \Delta t, y_n + \Delta t \cdot k_3), \tag{11}$$

$$y_{n+1} = y_n + \frac{\Delta t}{6}(k_1 + 2k_2 + 2k_3 + k_4). \tag{12}$$

RESULTS and DISCUSSION

For the solution of the ODE given in Equation 3, MATLAB's ode45 function is used to simulate 50 seconds with 1000 steps (each step being 0.05 seconds). The first initial condition for the ODE is considered as $[0 \quad 0]$. The solution obtained from ode45 is considered the ground truth. Based on this ground truth, the neural ODE is trained, and the evolution of the loss function is recorded during the training phase. This loss function, which is optimized during training, is defined as follows by (Chen, Rubanova, Bettencourt, & Duvenaud, 2018)

$$L(z(t_1)) = L\left(z(t_0) + \int_{t_n}^{t_1} f(z(t), t, \theta)\, dt\right) = L(\text{ODESolve}(z(t_0), f, t_0, t_1, \theta)). \tag{13}$$

Obviously, this function includes the solution to an ODE for the hidden states which is given by $f(\boldsymbol{z}(t), t, \theta)$. For the FitzHugh-Nagumo ODE, the loss function values evaluated using each numerical solver are presented in the following figure.



a) RK4 b) TR-BDF2 c) I-TR-BDF2

Figure 2. Loss function values for different numerical solvers during Neural ODE training

It can be seen from the results above that, in terms of loss function, all numerical solvers exhibit a similar trend. The critical part of the use of neural ODE lies in how accurately it approximates the trajectory of the ODE when the initial condition is $[0 \quad 0]$ and the simulation time is 50 seconds. Instead of showing the time evolution of the ODE solution, the phase portrait based on the two states is given for comparison in this case. It should be noted that during the prediction with the trained neural ODE, the ode45 function is considered for fair evaluation. The mean absolute error is considered as a metric and is defined as follows:

$$error = \frac{1}{N}\sum_{i=1}^{N} \left| x_{\text{true},i} - x_{\text{predicted},i} \right|. \tag{14}$$

The phase portraits of the true state (dashed lines) found by the ode45 and the trajectory predicted (solid line) by the trained neural ODE can be found in Figure 3. In this case the application results show that the best result is obtained via the TR-BDF2 method (error=0.074824) and I-TR-BDF2 (error=0.1024) method provides a less mean absolute error for the prediction. Both methods outperform the RK4 (error=0.13861) in terms of prediction accuracy.

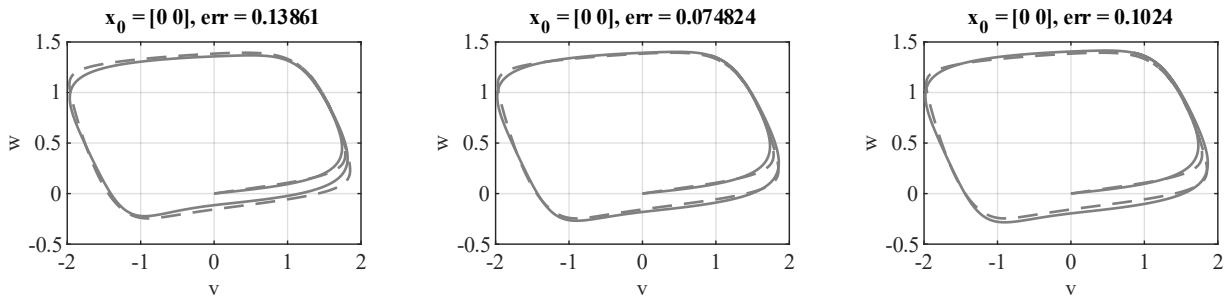

a) RK4 b) TR-BDF2 c) I-TR-BDF2

Figure 3. Approximation of the ODE solution using a neural ODE. The dashed line represents the true state obtained by ode45, while the solid line shows the approximation by the neural ODE trained with the indicated numerical solver.

To evaluate the performance of the proposed numerical solvers for neural ODEs, another trajectory is selected. The neural network is trained using this new trajectory, starting from an initial condition of [2 2]. Prediction results for the considered numerical solvers are presented in the Figure 4. In this case, the application results show that the best result is obtained via the I-TR-BDF2 method (error=0.07755), and TR-BDF2 (error=0.1097) method yields a lower mean absolute error compared to RK4 (error = 0.12205). Both methods outperform the classical RK4 in terms of prediction accuracy.

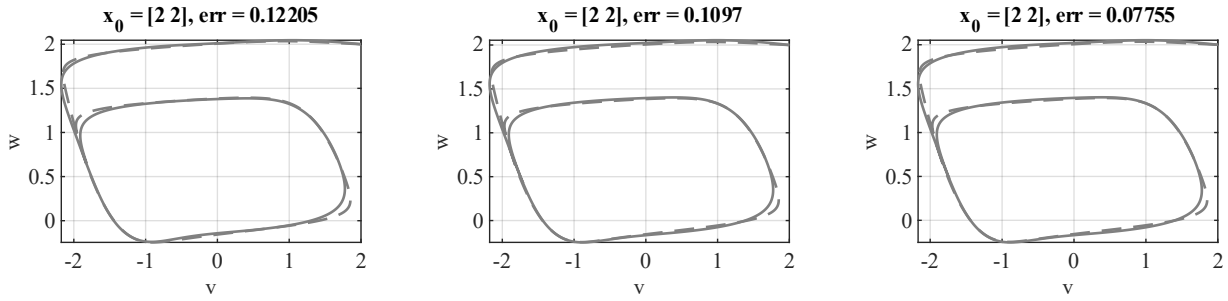

a) RK4 b) TR-BDF2 c) I-TR-BDF2

Figure 4. Approximation of the ODE solution with a neural ODE. The dashed line represents the true state obtained using ode45, while the solid line shows the approximation produced by the neural ODE trained with the indicated numerical solver.

These results demonstrate that both the TR-BDF2 and I-TR-BDF2 methods are promising alternatives to the classical RK4 in terms of mean absolute error for the approximation. In addition, since these methods require only three function evaluations, their computational complexity is lower than that of the classical RK4, which requires four function evaluations. For researchers who would like to replicate the results, the MATLAB scripts are provided in (Onat, FHN-NODE, 2025).

CONCLUSION

In this study, the application of the TR-BDF2 and I-TR-BDF2 methods is proposed for training neural networks in the context of neural ODEs. Given that Runge-Kutta methods are the conventional choice, the classical RK4 method is employed for performance evaluation. The FitzHugh-Nagumo ODE is used as a test case, and the results show that the proposed numerical solvers improve performance based on the mean absolute error metric. Two initial conditions are considered for the training phase: TR-BDF2 provides the best result for the first, whereas I-TR-BDF2 yields the best result for the second. Additionally, it is worth noting that the number of function evaluations for both TR-BDF2 and I-TR-BDF2 is three, compared to four evaluations for the classical RK4. These results suggest that TR-BDF2 and I-TR-BDF2 are promising alternatives to the classical RK4 method.

ACKNOWLEDGEMENTS

The author acknowledges the support of his colleague, Kerim Örüklü, for permitting the use of their collaboratively developed modified TR-BDF2 solution method for the neural ODEs.

The author acknowledges the use of ChatGPT (OpenAI's large-scale language generation model) for assistance in correcting typographical, grammatical, and other textual errors. All corrections were reviewed, edited, and revised by the author, who assumes full responsibility for the final content of this publication.

REFERENCES

Ara, I. (2019). Parameters estimation of Fitzhugh-Nagumo model. *Biomedical Research, 5*, 713–715.

Ashino, R., Nagase, M., & Vaillancourt, R. (2000). Behind and beyond the MATLAB ODE suite. *Computers & Mathematics with Applications, 40*, 491–512.

Bonaventura, L., & Mármol, M. G. (2021). The TR-BDF2 method for second order problems in structural mechanics. *Computers & Mathematics with Applications, 92*, 13–26.

Chen, R. T., Rubanova, Y., Bettencourt, J., & Duvenaud, D. K. (2018). Neural Ordinary Differential Equations. In S. Bengio, H. Wallach, H. Larochelle, K. Grauman, N. Cesa-Bianchi, & R. Garnett (Ed.), *Advances in Neural Information Processing Systems*, *31.*

FitzHugh, R. (1961). Impulses and physiological states in theoretical models of nerve membrane. *Biophysical journal, 1*, 445–466.

Fronk, C., & Petzold, L. (2024). Training Stiff Neural Ordinary Differential Equations with Implicit Single-Step Methods. *Training Stiff Neural Ordinary Differential Equations with Implicit Single-Step Methods*. Retrieved from https://arxiv.org/abs/2410.05592

Izhikevich, E. M. (2007). *Dynamical systems in neuroscience.* MIT press.

Kidger, P. (2021). *On neural differential equations.* University of Oxford. University of Oxford.

Lopez, D. M. (2019). Neural ODE MATLAB Implementation. *Neural ODE MATLAB Implementation*. Retrieved from https://github.com/mldiego/neuralODE

Lopez, D. M., Musau, P., Hamilton, N., & Johnson, T. T. (2022). Reachability Analysis of a General Class of Neural Ordinary Differential Equations. *FORMATS*, (pp. 258–277).

Okamoto, Y., Takeuchi, T., & Sakemi, Y. (2025). Learning the Simplest Neural ODE. *Learning the Simplest Neural ODE*. Retrieved from https://arxiv.org/abs/2505.02019

Onat, A. (2025). FHN-NODE. *FHN-NODE: Neural ODE Implementation for the FitzHugh-Nagumo Model Using RK4, TR-BDF2, and I-TR-BDF2 Methods*. Retrieved from https://github.com/altanonat/FHN-NODE

Onat, A., & Örüklü, K. (2023). A new numerical approach for simulation of power electronic converters. *2023 14th International Conference on Electrical and Electronics Engineering (ELECO)*, (pp. 1–5).

PyTorch. (n.d.). torch.optim.Adam. *torch.optim.Adam*.

Rudi, J., Bessac, J., & Lenzi, A. (2022). Parameter estimation with dense and convolutional neural networks applied to the FitzHugh–Nagumo ODE. *Mathematical and Scientific Machine Learning*, (pp. 781–808).

Zhang, H., Liu, Y., & Maulik, R. (2023). Semi-implicit neural ordinary differential equations for learning chaotic systems. *NeurIPS 2023 Workshop Heavy Tails in Machine Learning.*

➢ *ORAL PRESENTATION*

Temperature dependent electrical behavior of nickel silicide Schottky diodes on *p*-type silicon

Yigitkan Oz (*ORCID: https://orcid.org/0009-0008-8947-8890*),
M. Cuneyt Haciismailoglu* (*ORCID: https://orcid.org/0000-0002-0781-3376*)

Bursa Uludag University, Faculty of Arts and Sciences, Department of Physics, Bursa, Türkiye

*Corresponding author e-mail: mcuneyt@uludag.edu.tr

Abstract
In this study, we present electrical characteristics of nickel silicide Schottly diodes. Firstly, a 100-nm thick nickel was deposited on *p*-type silicon <100> substrate. Then, the nickel silicide layer was grown on the substrate by annealing at 500 °C for 60 s. XRD measurements revealed that the tetragonal NiSi phase was dominantly formed. Ni/NiSi/*p*-Si and Ni/*p*-Si Schottky diodes were fabricated for the electrical characterization. Ni/*p*-Si Schottky device was used to compare the electrical properties. Ideality factors were obtained as 1.42 and 1.14 for the Ni/*p*-Si and Ni/NiSi/*p*-Si Schottky diodes, respectively. Effective barrier heights were calculated using Richardson plots and found to be as 0.41 eV for Ni/*p*-Si diode and 0.45 eV for nickel silicide Schottky device. The ideality factor of the silicide Schottky diode was increased slightly with temperature contrarily the typical diode behavior. This situation could be attributed to high conductivity of the NiSi layer. Due to the lower ideality factor values, the Schottky diodes exhibited an ideal diode properties.

Keywords: Schottky diode, nickel silicide, *I-V-T* measurements, Richardson plot

INTRODUCTION

Silicides are compounds of silicon with other elements and form an important group of material that are used in modern silicon microelectronic and optoelectronic devices (Murarka, 1995). In numerous silicide studies conducted from the early 1900s until the 1960s, powder metallurgical techniques were employed to fabricate silicide structures (Yang et al., 1989). Especially, metal silicides have attracted interest due to their unique physical properties such as low resistivity, high temperature stability, ideal contact resistance, high quality of the interface with Si and compatibility with Si device processing (Zhang and Östling, 2003). These silicides are widely used in semiconductor technology, such as Schottky barriers and ohmic contacts (Zhang & Smith, 2004; Zhu et al., 2004).

Nickel silicide is an important electronic material that has been used as contact material in metal-oxide-semiconductor field effect transistors (MOSFETs) (Shim et al., 2004) and in microelectronic devices (Breil et al., 2015). These materials have attracted interest for their low electrical resistivity (ρ_{NiSi}=14 μΩ-cm) (Hu & Tay, 1998), close lattice match with Si (a_{Si}=5.43 Å, a_{NiSi2}=5.406 Å) (Tu et al., 1974), low Si consumption during fabrication process (Sasaki, 1995) and high thermal stability (Das et al., 1996). The formation of nickel silicide is typically achieved by deposition of a thin Ni layer onto a silicon substrate followed by annealing. Different annealing methods can be used, such as rapid thermal annealing (RTA) (Utlu et al., 2010), ion beam annealing (Chen & Hou, 1983) or ultraviolet laser annealing (Cho et al., 2025) to initiate a solid-state reaction between the Ni film and the underlying Si substrate. Depending on the annealing temperature, Ni_3Si, Ni_2Si, NiSi or $NiSi_2$ structures can be formed (Dahal et al., 2016).

In this work, NiSi structures were fabricated on *p*-type silicon substrates via solid-state reaction. Electrical characterization was performed using temperature dependent current-voltage measurements. The ideality factors and barrier heights were extracted using thermionic emission theory. Additionally, Ni/*p*-Si Schottky devices were fabricated to compare the electrical properties. Although Ni/Si Schottky diodes have been extensively studied, there is limited research on the electrical properties of the Ni/NiSi/*p*-Si Schottky diodes to the best of our knowledge.

MATERIALS AND METHODS

Commercial *p*-type silicon wafer with <100> orientation was used in this study. The wafer was firstly cleaned using RCA procedure (boiling in H_2SO_4:H_2O_2 (4:1) solution for 15 min followed by boiling in HCl:H_2O_2:H_2O

(1:1:5) solution for 15 min.) to remove any organic contaminates and metallic residues from Si surface. After this cleaning process, the wafer was washed by DI water and native SiO_2 was removed by dipping the wafer into HF solution for 60 seconds. Then, the wafer was immediately transferred to vacuum chamber for nickel deposition. The deposition was performed using Nanovak NVTS400 Magnetron Sputtering System. A Ni target with 99.99% purity was used for DC sputtering. 100-nm thick Ni contacts were deposited on the top surface of the Si wafer through a shadow mask which had 1-mm diameter circular openings.

After Ni deposition, half of the wafer was cut off and stored in a desiccator to fabricate Ni/*p*-Si Schottky diodes for the comparison of the electrical properties. The other part of the Ni deposited wafer was annealed in a tubular furnace at 500 °C for 60 s in argon atmosphere to form Ni-silicide structure. A part of the annealed wafer was used for XRD measurements to verify the Ni-silicide formation. XRD measurements were performed by using Bruker AXS/Discover D8.

For the Schottky diode fabrication, the back surfaces of the Ni deposited and annealed wafers were coated with aluminum using the sputtering system to make ohmic contacts. Unreacted Ni film functioned as Schottky contacts on the Ni-silicide layer for the annealed sample.

Temperature dependent current-voltage (*I-V*) measurements of the Ni/*p*-Si and Ni/NiSi/*p*-Si Schottky devices were carried out using KEITHLEY 6487 picoammeter in a temperature range of 240-320 K by Janis CCS 150 cryostat.

RESULTS and DISCUSSION

Ni-silicide formation was verified by XRD measurements. XRD spectrum of the sample annealed at 500 °C for 60 s is shown in Figure 1. The peaks which were detected nearly at 52, 54, 65, 70, 73, 76 and 79 degrees, represent the reflections of (402), (412), (520), (441), (442), (415) and (621) planes, respectively. They were marked as η-NiSi in Figure 1. This result confirms the tetragonal structure of the NiSi was obtained. Also, (110) reflection nearly at 41° which shows orthorhombic phase was observed. It can be clearly seen that NiSi structure was dominantly formed. There were also orthorhombic Ni_2Si peaks around 44 and 46 degrees. Because of the XRD measurement was carried out in the room conditions, SiO_2 peaks nearly at 28, 35 and 60 degrees were observed in the XRD spectrum. According to the XRD results Ni-silicide structure formed by annealing the Ni deposited Si wafers at 500 °C.

Current-voltage (*I-V*) characteristics of the Ni/*p*-Si and Ni/NiSi/*p*-Si Schottky diodes are shown in Figure 2. As evident from the figure, the low resistivity of the Ni-silicide structure led to an increase in saturation currents for the Ni/NiSi/*p*-Si Schottky diode. Furthermore, the junction exhibited more ohmic characteristics under forward bias conditions at elevated temperatures.

Current-voltage relationship for a Schottky diode is given by well-known formula (Sze & Ng, 2007):

$$I = I_s\left(\exp\frac{q(V - IR_s)}{nkT} - 1\right) \quad (1)$$

where q, k and T are the elementary charge, Boltzmann's constant and temperature in Kelvin, respectively. I_s is the saturation current, n is the ideality factor of the diode and R_s is the series resistance. For Schottky diodes, the saturation current is expressed by (Sze & Ng, 2007)

$$I_s = AA^*T^2\exp\left(-\frac{q\varphi_b}{kT}\right) \quad (2)$$

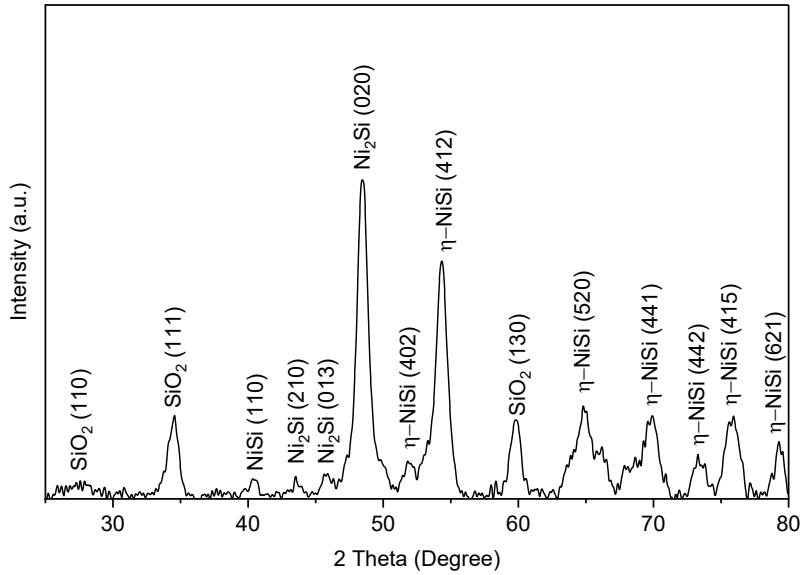

Figure 1. XRD spectrum of the annealed sample at 500 °C for 60 s

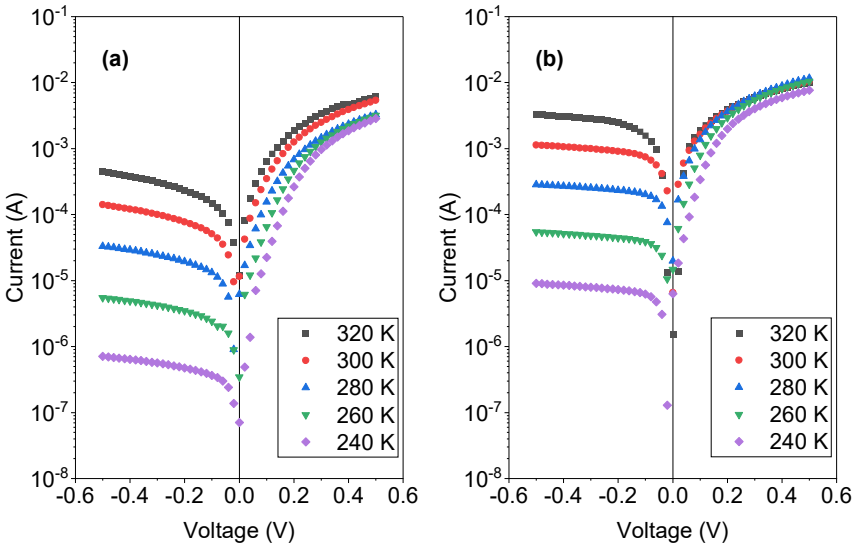

Figure 2. Temperature dependent *I-V* plots of the **(a)** Ni/*p*-Si and **(b)** Ni/NiSi/*p*-Si Schottky diodes

where A is the diode area, A^* is the effective Richardson constant and φ_b is the barrier height of the Schottky diode. The diode parameters were extracted from Eq. (1) through curve-fitting analysis. As illustrated in Figure 3, the experimental data exhibit strong agreement with the theory. The obtained parameters are summarized in Table 1.

By taking natural logarithm of Eq. (2), a linear relationship can be obtained between $\ln(I_s/T^2)$ and $1/T$ as follows (Bhuiyan et al., 1988):

$$\ln\left(\frac{I_s}{T^2}\right) = \ln(AA^*) - \frac{q\varphi_{b0}}{kT} \tag{3}$$

where φ_{b0} is the effective barrier height. According to Eq. (3), the plot of $\ln(I_s/T^2)$ vs $1/T$ gives a straight line with a slope of $-q\varphi_{b0}/k$, from which the effective barrier height of the Schottky diode can be calculated. These Richardson plots are given in Figure 4 for the Ni/*p*-Si and Ni/NiSi/*p*-Si Schottky diodes. The effective barrier heights were obtained as 0.41 eV and 0.45 eV, respectively.

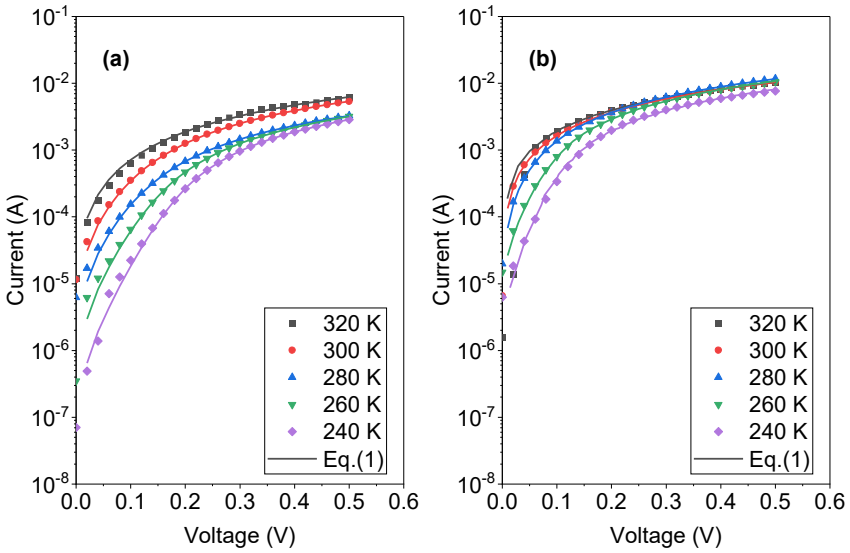

Figure 3. Experimental and theoretical *I-V* plots of the **(a)** Ni/*p*-Si and **(b)** Ni/NiSi/*p*-Si Schottky diodes in the forward bias regime. (Continuous lines denote the curve fitting results for corresponding temperatures)

Table 1. Diode parameters extracted from Eq. (1) through curve fitting.

Temperature (K)	Ni/*p*-Si Schottky diode			Ni-silicide/*p*-Si junction		
	I_s (A)	n	R_s (Ω)	I_s (A)	n	R_s (Ω)
320	1.97×10^{-4}	1.40	58.6	2.41×10^{-3}	1.17	43.3
300	4.33×10^{-5}	1.42	60.3	7.73×10^{-4}	1.14	40.5
280	1.40×10^{-5}	1.44	95.0	1.88×10^{-4}	1.06	33.9
260	3.41×10^{-6}	1.44	87.6	3.18×10^{-5}	1.00	34.3
240	6.61×10^{-7}	1.42	89.1	6.22×10^{-6}	1.00	43.7

The barrier height values can be calculated from the extracted saturation currents depending on the temperature by using Eq. (2):

$$\varphi_b = \frac{kT}{q}\ln\frac{AA^*T^2}{I_s} \tag{4}$$

The calculated barrier height vs temperature graph is shown in Figure 5-a. As seen from the graph, there was no significant change in the barrier heights with the variations in temperature. For both devices, the calculated barrier heights were around the effective barrier height values, which were extracted from Richardson plots. The barrier heights were obtained in accordance with the previous studies (Kumar & Chand, 2016; Rhoderick & Williams, 1988) for Ni/*p*-Si Schottky diode.

The ideality factors were extracted by curve fitting using Eq. (1). The variation of the ideality factors with temperature is presented in Figure 5-b for Ni/*p*-Si and Ni/NiSi/*p*-Si Schottky diodes.

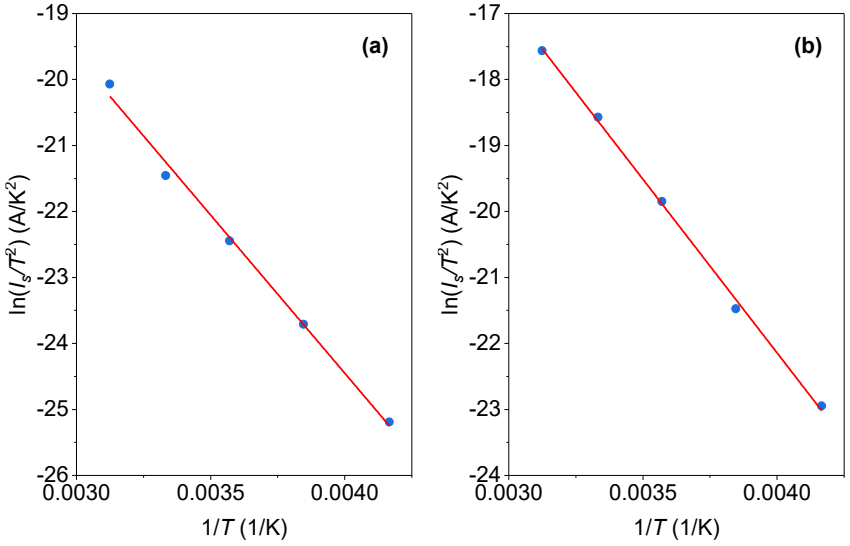

Figure 4. Richardson plots of the **(a)** Ni/*p*-Si and **(b)** Ni/NiSi/*p*-Si Schottky diodes. (Continuous lines show linear fit)

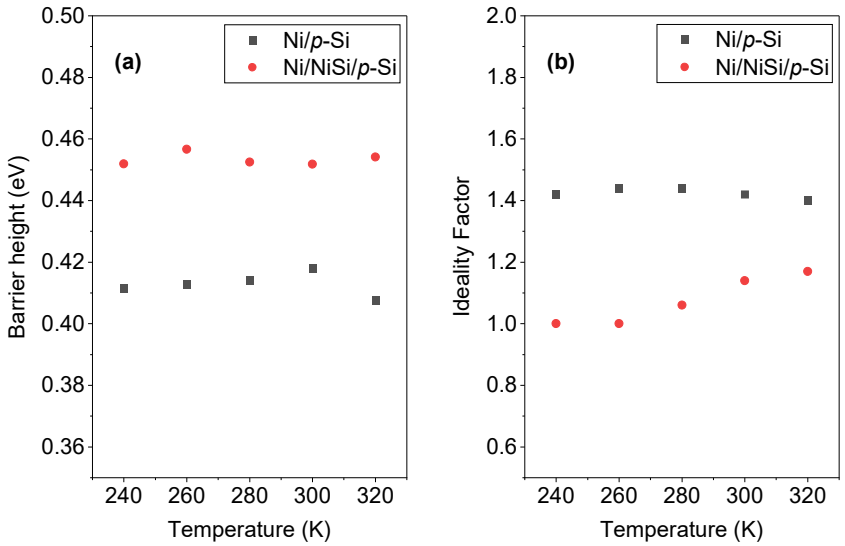

Figure 5. (a) Calculated barrier height values **(b)** Ideality factors extracted by curve fitting

The ideality factors for the Ni/*p*-Si Schottky device remained nearly constant at approximately 1.4 across the temperature range of 240–320 K. These values are lower than those reported in previous studies (Kumar & Chand, 2016). Typically, the ideality factor decreases with increasing temperature due to inhomogeneities at the Ni/Si interface and variations in the barrier height. However, the observed results align well with the obtained barrier height values for the Ni/*p*-Si Schottky diode.

For the Ni/NiSi/*p*-Si device, the ideality factors exhibited a slight increase with temperature. This behavior can be attributed to the high conductivity of the NiSi layer compared to the Si substrate, as discussed earlier. Moreover, the lower extracted series resistance values for the Ni/NiSi/*p*-Si device further confirm this behavior.

CONCLUSION

Electrical properties of the Ni/NiSi/*p*-Si Schottky diodes were investigated. NiSi layer was fabricated by solid-state reaction. A 100-nm thick Ni layer was deposited on *p*-type silicon <100> substrate. Ni-silicide layer was formed by annealing the Ni deposited wafer at 500 °C for 60 s. The XRD measurements confirmed that the NiSi structure was dominant. To fabricate Schottky diodes, back surfaces of the Ni deposited and annealed samples were coated with aluminum. Unreacted Ni metal on the annealed samples functioned as Schottky

contacts for NiSi/*p*-Si structure. Temperature dependent current-voltage measurements were carried out in a temperature range of 240-320 K for the electrical characterization. The diode parameters of the Ni/*p*-Si and Ni/NiSi/*p*-Si Schottky devices were extracted by curve fitting. The experimental *I-V* curves were found to be in a good agreement with theory. The saturation current values were obtained higher for the silicide Schottky diodes. This result can be attributed to the high conductivity of the NiSi layer. The effective barrier heights were calculated as 0.41 eV and 0.45 eV for the Ni/*p*-Si and Ni/NiSi/*p*-Si Schottky diodes from the Richardson plots, respectively. Furthermore, the barrier heights were obtained using the *I-V* method for each temperature and were found to remain nearly constant around the effective barrier height values for both diodes. Typically, the barrier height tends to increase with temperature. But, this increasing could be balanced with decreasing in the saturation currents of the Schottky diodes. The extracted ideality factors were obtained almost constant for the Ni/*p*-Si Schottky diode. This result aligned well with the obtained barrier height values. For the silicide Schottky device, the ideality factor increased slightly with temperature, which could be attributed to the high conductivity of the NiSi layer. The Schottky diodes exhibited an ideal behavior according to the ideality factor values obtained close to unity.

ACKNOWLEDGEMENTS

This work was supported by Bursa Uludag University under Grant No. AYPF-2015/11 and FAY-2022-811. Special thanks to Prof. Dr. Muhitdin Ahmetoglu for his valuable insights and constructive feedback. We also extend our thanks to Assoc. Prof. Dr. Murside Haciismailoglu and Dr. Esra Kus for their kind assistance with the XRD measurements.

REFERENCES

Bhuiyan, A. S., Martinez, A., & Esteve, D. (1988). A new Richardson plot for non-ideal schottky diodes. Thin Solid Films, 161, 93–100. https://doi.org/10.1016/0040-6090(88)90239-8

Breil, N., Lavoie, C., Ozcan, A., Baumann, F., Klymko, N., Nummy, K., Sun, B., Jordan-Sweet, J., Yu, J., Zhu, F., Narasimha, S., & Chudzik, M. (2015). Challenges of nickel silicidation in CMOS technologies. Microelectronic Engineering, 137(1), 79–87. https://doi.org/10.1016/j.mee.2014.12.013

Chen, L. J., & Hou, C. Y. (1983). Ion-beam-induced silicide formation in nickel thin films on silicon. Thin Solid Films, 104(1–2), 167–173. https://doi.org/10.1016/0040-6090(83)90558-8

Cho, H., Jo, C., Nam, K., & Ko, D. H. (2025). Characteristics of nickel silicide thin films fabricated by ultraviolet nanosecond laser annealing. Applied Surface Science, 689(September 2024), 162494. https://doi.org/10.1016/j.apsusc.2025.162494

Dahal, A., Gunasekera, J., Harringer, L., Singh, D. K., & Singh, D. J. (2016). Metallic nickel silicides: Experiments and theory for NiSi and first principles calculations for other phases. Journal of Alloys and Compounds, 672, 110–116. https://doi.org/10.1016/j.jallcom.2016.02.133

Das, S. R., Xu, D. X., Nournia, M., Lebrun, L., & Naem, A. (1996). Thermal stability of nickel silicide films. Materials Research Society Symposium - Proceedings, 427, 541–545. https://doi.org/10.1557/proc-427-541

Hu, Y., & Tay, S. P. (1998). Spectroscopic ellipsometry investigation of nickel silicide formation by rapid thermal process. Journal of Vacuum Science & Technology A: Vacuum, Surfaces, and Films, 16(3), 1820–1824. https://doi.org/10.1116/1.581114

Kumar, R., & Chand, S. (2016). Fabrication and electrical characterization of nickel/p-Si Schottky diode at low temperature. Solid State Sciences, 58, 115–121. https://doi.org/10.1016/J.SOLIDSTATESCIENCES.2016.06.003

Murarka, S. P. (1995). Silicide thin films and their applications in microelectronics. Intermetallics, 3(3), 173–186. https://doi.org/10.1016/0966-9795(95)98929-3

Rhoderick, E. H., & Williams, R. H. (1988). Metal-Semiconductor Contacts (2nd ed.). Oxford University Press.

Sasaki, H. (1995). Self- Aligned Nickel-Mono-Silicide Technology for High-speed Deep Submicrometer Logic CMOS ULSI. 42(5).

Shim, J. C., Oh, H., Choi, H., Sakaguchi, T., Kurino, H., & Koyanagi, M. (2004). SiGe elevated source/drain structure and nickel silicide contact layer for sub 0.1 μm MOSFET fabrication. Applied Surface Science, 224(1–4), 260–264. https://doi.org/10.1016/j.apsusc.2003.08.091

Sze, S. M., & Ng, K. K. (2007). Physics of Semiconductor Devices (3rd ed.). John Wiley & Sons, Inc.

Tu, K. N., Alessandrini, E. I., Chu, W. K., Krautle, H., & Mayer, J. W. (1974). Epitaxial growth of nickel silicide NiSi2 on silicon. Japanese Journal of Applied Physics, 13(110), 669–672. https://doi.org/10.7567/JJAPS.2S1.669

Utlu, G., Artunç, N., Budak, S., & Tari, S. (2010). Structural and electrical characterization of the nickel silicide films formed at 850 °C by rapid thermal annealing of the Ni/Si(1 0 0) films. Applied Surface Science, 256(16), 5069–5075. https://doi.org/10.1016/j.apsusc.2010.03.062

Yang, J. M., Kai, W., & Jeng, S. M. (1989). Development of TiC particle-reinforced MoSi2 composite. Scripta Metallurgica, 23(11), 1953–1958. https://doi.org/10.1016/0036-9748(89)90489-4

Zhang, S., & Östling, M. (2003). Critical Reviews in Solid State and Materials Sciences Metal Silicides in CMOS Technology : Past , Present , and Future Trends. Critical Reviews in Solid State and Materials Sciences, 28(1), 1–129.

Zhang, S., & Smith, U. (2004). Self-aligned silicides for Ohmic contacts in complementary metal–oxide–semiconductor technology: TiSi2, CoSi2, and NiSi. Journal of Vacuum Science & Technology A: Vacuum, Surfaces, and Films, 22(4), 1361–1370. https://doi.org/10.1116/1.1688364

Zhu, S., Van Meirhaeghe, R. L., Forment, S., Ru, G., & Li, B. (2004). Effects of the annealing temperature on Ni silicide/n-Si(1 0 0) Schottky contacts. Solid-State Electronics, 48(1), 29–35. https://doi.org/10.1016/S0038-1101(03)00286-7

➢ *ORAL PRESENTATION*

In vivo phage display in targeted drug delivery applications

Sema Karabudak*[1] (ORCID: https://orcid.org/0000-0002-3646-0442)

*[1] Ankara Yildirim Beyazit University, Faculty of Medicine, Department of Medical Genetics, Ankara, Turkey

* Corresponding author e-mail: semakarabudak@aybu.edu.tr

Abstract
In vivo phage display has emerged as a powerful approach for identifying peptides that target specific tissues or disease states within the body. Unlike traditional *in vitro* methods, this technique operates under physiological conditions, allowing peptides to interact with their targets in the complex, dynamic environment of a living organism. By overcoming biological barriers and recognizing native molecular markers, *in vivo* phage display offers a more accurate route to discovering highly specific ligands. This has made it an increasingly valuable strategy for developing targeted drug delivery systems that minimize off-target effects while maximizing therapeutic precision. This study explores a range of studies that showcase the diverse applications of *in vivo* phage display—from cancer and cardiovascular diseases to infectious diseases, and mucosal drug delivery. Together, these examples illustrate the method's remarkable versatility and growing potential in advancing precision medicine.

Keywords: *In vivo* phage display, peptide discovery, drug delivery, targeting, biopanning

INTRODUCTION

The field of drug delivery aims to formulate drugs into suitable forms and effectively deliver them within the body. However, these systems encounter several challenges, such as poor bioavailability, limited stability, low solubility, and potential toxicity of drug compounds. Physiological barriers that prevent cellular entry can further compromise the efficiency of drug delivery systems. In particular, compounds with a narrow therapeutic index pose a significant risk of off-target accumulation (Ezike et al., 2023; Newman & Benoit, 2018). This has necessitated the development of targeted drug delivery systems.

The aim of targeted drug delivery systems is to direct drug molecules specifically to diseased tissues or cells, hindering random distribution in systemic circulation, minimizing the adverse effects of drugs on healthy tissues and enhancing therapeutic action (Jirwankar et al., 2024).

Drug targeting strategies used to improve targeted delivery of drugs within the body are broadly classified as passive and active approaches. Active targeting uses ligands such as antibodies, aptamers, and peptides that specifically bind to various receptors on cells to deliver the drug directly to the diseased tissue. Among various ligands used for this purpose, peptides are one of the most preferred groups because they are easy to modify, cause fewer side effects, and are cost-effective. (Jirwankar et al., 2024).

Peptides are a special family of pharmaceuticals that differ from proteins and small molecules in both biochemistry and therapeutics. These molecules consist of short amino acid chains, typically comprising no more than 50 residues, joined by peptide bonds (Davson et al., 1993). They play a crucial role in maintaining essential physiological functions such as growth, immunity, homeostasis, reproduction and stress responses by modulating mechanisms such as angiogenesis, cell proliferation, cell migration, inflammation, melanogenesis and protein regulation. In addition to their regulatory roles, they also exhibit protective effects such as stimulation or suppression of the immune system and removal of toxic substances and heavy metals from the body. Owing to these versatile biological activities, peptides have significant potential as therapeutic agents in the treatment of many diseases such as cancer, diabetes, and hypertension. (Deigin et al., 2007; Ivanov & Deigin, 2023; Thundimadathil, 2012).

Considering their diverse therapeutic functions and receptor binding specificities, peptides are also attracting attention as promising ligands for targeted drug delivery systems (Xiao et al., 2025). Traditional methods used for the discovery of bioactive peptides often face limitations in terms of efficiency, cost, and the ability to precisely target complex biological pathways. In this context, phage display technology has emerged as a

powerful and widely used tool in peptide discovery, enabling the rapid identification of bioactive peptides for research and therapeutic applications (Asar et al., 2024).

Phage display was first introduced by George P. Smith in 1985, who demonstrated that a foreign peptide could be displayed on the surface of the filamentous bacteriophage F1 through genetic fusion with a coat protein. Since then, the technology has been adapted to various bacteriophage systems, including M13, T7, λ, and T4, expanding its use across diverse peptides and proteins. In this method, DNA sequences encoding peptides or proteins are inserted into phage genes, resulting in the surface display of the encoded molecule while preserving phage viability. The direct link between the peptide and the DNA sequence that encodes it allows the bound peptides to be easily sequenced and identified. The selection process, termed biopanning, isolates phage clones displaying peptides with specific affinity to target molecules such as cells, receptors, or tissues (Jirwankar et al., 2024). This process involves four main steps: (1) antigen coating on a solid surface, (2) incubation of the phage library with the target antigen, (3) stringent washing to remove nonspecific binders, and (4) elution and reamplification of antigen-specific phages (using methods such as pH shift, proteolytic cleavage, or competitive elution). This technique has become a versatile platform used for studies of antibodies, proteins, and proteomics as well as peptides (Jirwankar et al., 2024; Kuzmicheva & Belyavskaya, 2017).

Discovery of new therapeutic peptide classes and identification of new disease-related targets have necessitated the development of peptides with high target-specific biological activity. In this direction, although traditional phage display technology stands out as an important discovery tool, this system has some limitations. In these methods, peptides are usually selected in artificial conditions with purified or immobilized targets, which cannot fully reflect the natural conformations and physiological contexts of antigens (André et al., 2022). To overcome the limitations of traditional selection strategies, *in vivo* phage display technology has emerged as a powerful alternative that enables peptides to interact directly with target cells, tissues, or organs within their native physiological environment (Bao et al., 2019).

In vivo phage display technology was first described by Pasqualini and Ruoslahti in 1996, who demonstrated that target-specific peptides could be selected systemically within living organisms such as mice. This pioneering study established the foundational principle that peptides can identify biological targets by interacting with their natural microenvironment (André et al., 2022). This approach has become a valuable tool in peptide-based targeted therapy and diagnostic applications, as it facilitates the selection of peptides with higher specificity and greater clinical relevance. *In vivo* biopanning is based on similar principles to *in vitro* biopanning, but this method is specifically used to identify peptides that can target particular cells or tissues within a living organism. In this process, a phage display library containing a large number of different peptide clones is administered intravenously to experimental animals such as mice. The phages are expected to circulate in the circulatory system for a certain period of time and bind to the target cells or tissues or be taken into the cells. Then, weakly bound or unbound phages are removed by washing. In order to collect phages that bind strongly to the target, those that are bound to the surface are released with a special elution buffer, while those that are taken into the cells can be obtained using a lysis buffer. The collected phages are propagated in bacterial hosts and injected back into the animal in the next round of selection. As a result of this process, which is repeated several times, phage clones that show high affinity and specificity to the target are obtained in an enriched form. In the final stage, the DNA sequences encoding the peptides carried by these phages are determined by sequencing (André et al., 2022; Bao et al., 2019).

In vivo phage display technology has been applied in various studies to discover peptides with potential for tissue-specific targeting and therapeutic delivery. One of the pioneering studies that demonstrated the therapeutic targeting potential of *in vivo* phage display technology was conducted by Kanki et al. in 2011 (Kanki et al., 2011). The researchers performed multiround biopanning using the Ph.D.-C7C phage library in a rat model of myocardial ischemia-reperfusion and identified three peptide motifs (most notably CSTSMLKAC) with selective affinity for ischemic heart tissue. The fluorescein-labeled version of CSTSMLKAC exhibited highly specific accumulation in the ischemic myocardium *in vivo*. More importantly, the CSTSMLKAC peptide conjugated to a Sumo–mCherry fusion protein also showed significant enrichment at the target site following systemic administration, demonstrating its effectiveness in delivering larger molecules selectively. This approach not only marked a new direction for cardiac-targeted regenerative therapies but also provides compelling support for the potential of *in vivo* phage display as a platform for developing therapeutic delivery vectors.

Ivanova et al. (2024) used *in vivo* phage display to identify novel peptides that can target ischemic cardiac tissue for drug delivery purposes. Using a mouse model of myocardial ischemia-reperfusion injury, the authors

administered a phage-displayed peptide library intravenously and selectively retained phages in the heart. Bioinformatic analysis of next-generation sequencing (NGS) data and subsequent validation experiments identified three strong candidate peptides specific to cardiac tissue. These peptides showed selective uptake in cardiomyocytes under hypoxic and ischemic conditions and were successfully conjugated to fluorescent cargo for targeted delivery. The study highlights the potential of *in vivo* phage display as a powerful platform to discover tissue-specific delivery vectors, particularly for cardiovascular drug delivery applications (Ivanova et al., 2024).

In the context of vascular disease, Kohl et al. (2025) aimed to find novel cell-penetrating peptides (CPPs) unique to endothelial cells that carry the TIE2 L914F mutation, a major cause of venous malformations. Using a xenograft mouse model implanted with human endothelial cells overexpressing this mutation, the researchers performed multiple rounds of *in vivo* biopanning with phage libraries displaying random peptides. The study leveraged NGS to analyze millions of peptide sequences retrieved from phage pools, enabling comprehensive profiling and identification of highly enriched, target-specific peptides. A refined bioinformatic pipeline was then employed to cluster similar sequences and derive consensus motifs. Among the resulting candidates, two peptides—TX2 and TX3—demonstrated specific uptake into endothelial cells and were capable of delivering siRNA cargo intracellularly, highlighting the potential of NGS-enhanced *in vivo* phage display for discovering functionally relevant, disease-targeting peptides with translational applications in drug delivery (Kohl et al., 2025).

The potential of *in vivo* phage display to cross biological barriers has also been demonstrated. Yang et al. (2021) used this method to discover a novel peptide that can cross the blood-cerebrospinal fluid barrier (BCSFB). In the study, phages injected intravenously into mice were enriched in cerebrospinal fluid (CSF), and a peptide (PMK) with the sequence PMKSHTN was identified after three rounds of selection. PMK peptide demonstrated significant accumulation in CSF in *in vivo* imaging experiments with its fluorescently labeled version, proving its target specificity. These findings revealed that PMK is a promising candidate for use in drug delivery systems for neurological diseases. The study highlights the effectiveness of *in vivo* phage display in the discovery of therapeutics that cross central nervous system barriers (Yang et al., 2021).

Similarly, Duerr et al. (2004) investigated how specific peptide sequences enable virion transport across the intestinal mucosal barrier using *in vivo* phage display (IVPD). In the study, an M13 phage library containing random 7 amino acid peptides was used and the peptides with transport ability were determined by detecting these phages from the intestine to the spleen. Some of the peptide sequences obtained were found to be similar to the sequences in the HIV gp120 protein. In addition, immunohistochemical analyses showed that a phage carrying the YPRLLTP peptide was actively transported by intestinal epithelial cells. These results revealed that macromolecules can pass the intestinal barrier without being disrupted under peptide guidance and that this mechanism can be used in the development of oral therapeutics. The study provides an important model for understanding the role of the intestinal mucosal barrier in pathogen and drug transport (Duerr et al., 2004).

Expanding on this barrier-crossing approach, researchers aimed to overcome the difficulties in transdermal delivery of large hydrophilic drugs. The researchers systematically screened peptides that can cross the skin barrier using the *in vivo* phage display technique. The collection, which was created using the Ph.D.-C7C phage library containing disulfide bridged peptides, was applied to the abdominal skin of BALB/cA nude mice and phages were isolated from the circulatory system 1 h later. After two rounds of selection, the PH-1 phage carrying the CSSSPSKHC peptide sequence showed 670-fold higher transdermal permeation capacity compared to control phages. The synthesized peptide was shown to increase systemic insulin levels and lower blood sugar for 11 h in diabetic rats when administered with insulin, demonstrating therapeutic efficacy. It was also observed that the peptide increased the systemic bioavailability of human growth hormone (Chen et al., 2006) .

The application of *in vivo* phage display in oncology has also yielded promising results. In a study by Lee et al. (2016), *in vivo* phage display screening was employed to identify novel peptides that specifically target human lung adenocarcinoma for potential use in active drug delivery and non-invasive imaging (Lee et al., 2016). Using a xenograft mouse model bearing A549-derived tumors, a M13 phage library displaying 2.9×10^9 random peptides was intravenously injected, and four rounds of biopanning were performed to enrich tumor-homing phages. The identified peptides were grouped based on sequence homology, and their tumor-targeting capacity was validated through *in vivo* imaging using Cy5.5-labeled phages. Among various cancer types, these peptides showed selective accumulation in lung adenocarcinoma-derived tissues. Further validation by *in vitro* binding assays and *in vivo* immunohistochemistry confirmed the specificity of one lead peptide, which demonstrated competitive binding behavior. This study underscores the potential of *in vivo*

phage display for discovering highly specific lung cancer-targeting peptides, offering promising applications in targeted drug delivery and molecular imaging.

The method has also shown considerable promise in the field of antimicrobial therapy. In a recent study by Wang et al. (2024), *in vivo* phage display technology was employed to identify a heptapeptide sequence with high specificity toward *Staphylococcus aureus*. A phage-displayed heptapeptide library was intravenously administered to mice, and *in vivo* biopanning was performed to isolate phage clones that preferentially localized to infection sites. Among the identified sequences, SYWVRAS exhibited strong binding affinity to *S. aureus* with minimal cross-reactivity to other bacterial strains. To enhance antimicrobial potency, SYWVRAS was conjugated to the membrane-active peptide temporin-SHf via a GGG linker, yielding a chimeric construct termed SFK2. Mechanistic studies revealed that SFK2 targets lipoteichoic acid on the bacterial surface through electrostatic interactions, inducing cytoplasmic membrane depolarization, membrane disruption, and leakage of intracellular contents. *In vivo* therapeutic evaluation in mouse and piglet infection models demonstrated that SFK2 selectively accumulated in infected tissues, effectively reduced bacterial load, alleviated tissue damage, and exhibited good biocompatibility. This study highlights the potential of *in vivo* phage display to guide the discovery of pathogen-specific targeting peptides that, when integrated with antimicrobial moieties, offer a promising strategy for precision-targeted antibacterial therapy (Wang et al., 2024).

CONCLUSION

In vivo phage display has proven to be a powerful and reliable tool for discovering peptides that can home in on specific tissues, disease sites, or biological barriers within the body. By operating in living systems, it reflects real physiological conditions and allows for the identification of targeting ligands with greater specificity and relevance than *in vitro* methods typically offer. As shown through various applications this approach enhances the precision of drug delivery and opens doors to treating targets that were once difficult to reach. With ongoing advances in peptide design, sequencing technologies, and phage library development, the potential of *in vivo* phage display continues to grow. It stands as a promising platform for creating safer, more effective, and highly targeted treatments in the future of personalized medicine.

REFERENCES

André, A. S., Moutinho, I., Dias, J. N. R., & Aires-da-Silva, F. (2022). In vivo Phage Display: A promising selection strategy for the improvement of antibody targeting and drug delivery properties. Frontiers in Microbiology, 13, 962124. https://doi.org/10.3389/fmicb.2022.962124

Asar, M., Newton-Northup, J., & Soendergaard, M. (2024). Improving Pharmacokinetics of Peptides Using Phage Display. Viruses, 16(4), 570. https://doi.org/10.3390/v16040570

Bao, Q., Li, X., Han, G., Zhu, Y., Mao, C., & Yang, M. (2019). Phage-based vaccines. Advanced Drug Delivery Reviews, 145, 40–56. https://doi.org/10.1016/j.addr.2018.12.013

Chen, Y., Shen, Y., Guo, X., Zhang, C., Yang, W., Ma, M., Liu, S., Zhang, M., & Wen, L.-P. (2006). Transdermal protein delivery by a coadministered peptide identified via phage display. Nature Biotechnology, 24(4), 455–460. https://doi.org/10.1038/nbt1193

Davson, H., Zloković, B., Rakić, L., & Segal, M. B. (1993). Peptides and Proteins. In H. Davson, B. Zloković, L. Rakić, & M. B. Segal (Eds.), An Introduction to the Blood-Brain Barrier (pp. 195–272). Macmillan Education UK. https://doi.org/10.1007/978-1-349-11882-3_3

Deigin, V. I., Semenets, T. N., Zamulaeva, I. A., Maliutina, Ya. V., Selivanova, E. I., Saenko, A. S., & Semina, O. V. (2007). The effects of the EW dipeptide optical and chemical isomers on the CFU-S population in intact and irradiated mice. International Immunopharmacology, 7(3), 375–382. https://doi.org/10.1016/j.intimp.2006.11.010

Duerr, D. M., White, S. J., & Schluesener, H. J. (2004). Identification of peptide sequences that induce the transport of phage across the gastrointestinal mucosal barrier. Journal of Virological Methods, 116(2), 177–180. https://doi.org/10.1016/j.jviromet.2003.11.012

Ezike, T. C., Okpala, U. S., Onoja, U. L., Nwike, C. P., Ezeako, E. C., Okpara, O. J., Okoroafor, C. C., Eze, S. C., Kalu, O. L., Odoh, E. C., Nwadike, U. G., Ogbodo, J. O., Umeh, B. U., Ossai, E. C., & Nwanguma, B. C. (2023). Advances in drug delivery systems, challenges and future directions. Heliyon, 9(6), e17488. https://doi.org/10.1016/j.heliyon.2023.e17488

Ivanov, V. T., & Deigin, V. I. (2023). Evolution of Peptide Drug Biopharmaceutics. Russian Journal of Bioorganic Chemistry, 49(3), 422–434. https://doi.org/10.1134/S1068162023030123

Ivanova, A., Kohl, F., González-King Garibotti, H., Chalupska, R., Cvjetkovic, A., Firth, M., Jennbacken, K., Martinsson, S., Silva, A. M., Viken, I., Wang, Q.-D., Wiseman, J., & Dekker, N. (2024). In vivo phage display identifies novel peptides for cardiac targeting. Scientific Reports, 14(1), 12177. https://doi.org/10.1038/s41598-024-62953-9

Jirwankar, Y., Nair, A., Marathe, S., & Dighe, V. (2024). Phage Display Identified Novel Leydig Cell Homing Peptides for Testicular Targeting. ACS Pharmacology & Translational Science, 7(3), 809–822. https://doi.org/10.1021/acsptsci.3c00330

Kanki, S., Jaalouk, D. E., Lee, S., Yu, A. Y. C., Gannon, J., & Lee, R. T. (2011). Identification of targeting peptides for ischemic myocardium by in vivo phage display. Journal of Molecular and Cellular Cardiology, 50(5), 841–848. https://doi.org/10.1016/j.yjmcc.2011.02.003

Kohl, F., Laufkötter, O., Firth, M., Krimpenfort, L., Mangla, P., Ansarizadeh, M., Geylan, G., Eklund, L., De Maria, L., Jakobsson, L., & Wiseman, J. (2025). Identification of cell type-specific cell-penetrating peptides through in vivo phage display leveraged by next generation sequencing. Biomedicine & Pharmacotherapy, 182, 117740. https://doi.org/10.1016/j.biopha.2024.117740

Kuzmicheva, G., & Belyavskaya, V. (2017). Peptide phage display in biotechnology and biomedicine. Biochemistry (Moscow), Supplement Series B: Biomedical Chemistry, 11, 1–15. https://doi.org/10.1134/S1990750817010061

Lee, K. J., Lee, J. H., Chung, H. K., Ju, E. J., Song, S. Y., Jeong, S.-Y., & Choi, E. K. (2016). Application of peptide displaying phage as a novel diagnostic probe for human lung adenocarcinoma. Amino Acids, 48(4), 1079–1086. https://doi.org/10.1007/s00726-015-2153-4

Newman, M. R., & Benoit, D. S. W. (2018). In Vivo Translation of Peptide-Targeted Drug Delivery Systems Discovered by Phage Display. Bioconjugate Chemistry, 29(7), 2161–2169. https://doi.org/10.1021/acs.bioconjchem.8b00285

Thundimadathil, J. (2012). Cancer treatment using peptides: Current therapies and future prospects. Journal of Amino Acids, 2012, 967347. https://doi.org/10.1155/2012/967347

Wang, T., Tan, P., Tang, Q., Zhou, C., Ding, Y., Xu, S., Song, M., Fu, H., Zhang, Y., Zhang, X., Bai, Y., Sun, Z., & Ma, X. (2024). Phage-displayed heptapeptide sequence conjugation significantly improves the specific targeting ability of antimicrobial peptides against Staphylococcus aureus. mLife, 3(2), 251–268. https://doi.org/10.1002/mlf2.12123

Xiao, W., Jiang, W., Chen, Z., Huang, Y., Mao, J., Zheng, W., Hu, Y., & Shi, J. (2025). Advance in peptide-based drug development: Delivery platforms, therapeutics and vaccines. Signal Transduction and Targeted Therapy, 10(1), Article 1. https://doi.org/10.1038/s41392-024-02107-5

Yang, X., Li, Y., Zhu, Z., Huang, X., Wang, T., Yuan, J., & Li, J. (2021). Identification of a peptide that crosses the blood-cerebrospinal fluid barrier by phage display technology. Amino Acids, 53(8), 1181–1186. https://doi.org/10.1007/s00726-021-03016-5

➢ *ORAL PRESENTATION*

Ergonomic Analysis of Working Postures in Crankshaft Packaging Processes and Recommendations for Improvement

Gözde Can Atasagun[1*] (*ORCID: https://orcid.org/0000-0003-4921-1557*)
Yakup Atasagun[1] (*ORCID: https://orcid.org/0000-0002-8580-4336*)

[*1] Konya Technical University, Faculty of Engineering and Natural Sciences, Industrial Engineering Department, Konya, Türkiye.

*Corresponding author e-mail: gcatasagun@ktun.edu.tr

Abstract

Musculoskeletal disorders (MSDs) are among the most significant ergonomic problems encountered in today's workplaces. MSDs largely result from improper working postures and the physically demanding nature of the tasks imposed on workers. In such cases, workers either change jobs or are frequently absent from work for various reasons. As a result, worker turnover increases in the workplace, leading to inefficiency for businesses. This highlights the growing importance of adopting proper working postures to minimize musculoskeletal disorders. This study analyses the working postures specifically in the crankshaft packaging process that result in MSDs and identifies the associated risks by applying the OWAS method at a facility in Konya, Türkiye. A comparative analysis is conducted between the current and the proposed situations.

Keywords: Working Postures, OWAS Method, Musculoskeletal Disorders (MSDs)

INTRODUCTION

Today, efforts to increase productivity and reduce occupational accidents in enterprises have made it important to identify and eliminate ergonomic risks. Workers' body posture has a direct impact on health, especially in tasks that require repetitive work, standing or sitting for long periods of time. Incorrect working postures can lead to musculoskeletal disorders (MSDs) (Kaya and Akalp 2017). This situation not only negatively affects workers' health but also reduces productivity and workforce continuity.

In a workplace, the willingness to work and efficiency of the workers depend to a great extent on the harmony of the method chosen for the job with the worker (Babalık 2005). Workplaces should be organized to produce at the required quality and speed, at low cost, by challenging the worker in a way that does not exceed normal performance limits and by ensuring job safety. Unnatural body postures should be avoided in the design of a working environment. Since tilting the body or head forward causes less static loading, it is generally preferable than tilting to the side. Similarly, keeping the arms continuously extended forward or to the side should be avoided. A sitting position should be preferred as much as possible during work, and the workplace should be arranged to allow smooth transitions between sitting and standing.

In this context, ergonomic risk assessment methods analyse the physical loads that individuals working at workstations or in the field are exposed to and pave the way for improvement efforts to prevent these risks. Various tools are used to quantify exposure levels for these risks.

Numerous methods and techniques have been developed for the ergonomic evaluation of these risky situations. Among these are techniques such as reporting through observation tools (Battini et al. 2014), direct measurements (where real data is collected using motion capture systems) and wearable sensors (Panariello et al. 2022), and virtual simulations (Tarallo et al. 2019) (Güney and Erden 2023). In recent years, while the use of direct measurement approaches, including motion capture/measurement, electronic goniometer, and push/pull force sensors, has minimally increased, the use of observational methods, such as Rapid Upper Limb Assessment (RULA) (McAtamney and Corlett 1993), Rapid Entire Body Assessment (REBA) (Hignett and McAtamney 2000) and Ovako Working Posture Analysis System (OWAS) (Karhu et al. 1977) has significantly increased (Kee and Health 2022). These observation techniques allow the assessment of ergonomic risk levels by analysing the positions of workers' body parts. Potentially risky postures can be identified by analysing the positions of the neck, back, arms and legs at work. Observation-based techniques

are very easy to use and do not prevent workers from doing their jobs. Numerous studies have been conducted on MSDs, and interested readers can find further information the study of Kee and Health (2022), Gupta (2024), Zen et al. (2024).

In this study, the postures of workers in a crankshaft manufacturing plant were observed and analysed with the OWAS method. The OWAS technique was developed by Ovako, a Finnish steel company, and identifies four work postures for the back, three postures for the arms, seven postures for the lower limbs, and three categories of the weight of loads handled or amount of force used (Karhu et al. 1977). The aim of the study is to evaluate current postures from an ergonomic perspective and to provide suggestions for improvement by determining possible health risks in advance. In this direction, suggestions are presented both to contribute to the protection of workers health and to create ergonomic working environments.

MATERIALS AND METHODS

OWAS Method

OWAS is a widely used observational assessment method to determine risk for MSDs (Lins et al. 2021). This method involves categorizing postures and implementing systematic design improvements to eliminate factors that may lead to worker discomfort (Akay et al. 2003). In OWAS method, worker postures are evaluated by the assessor in three or four categories (arms, legs, back, and sometimes load) (Ağar 2025). There are seven leg working postures, three arm working postures, and four back working positions. In addition, it establishes three classifications for the force or weight of the load (Kee and Health 2022). The duration and frequency of each posture are evaluated. Video cameras can be used to record these postures, and the footage is analyzed at specific time intervals depending on the nature of the work being studied. Following the selection of the working posture that most closely resembles the worker's real posture, the observer determines the numerical value that corresponds to that posture. In the analysis phase, it is recommended to record and evaluate working postures at 15-second intervals for long-duration activities and at 5-second intervals for tasks composed of shorter time periods (Mattila et al. 1993). The information obtained from the observations is coded according to predefined criteria. These codes are classified as risk categories based on the degree of load and strain. Critical stoppages caused by these loads and strains are identified, and improvements are implemented to eliminate the factors responsible for such stoppages. The postures used in the OWAS Method, and the corresponding code numbers are given in Table 1.

Table 1. OWAS Method and Corresponding Codes

Back Postures	**Code**	**Arm Postures**	**Code**	**Leg Postures**	**Code**	**Load**	**Code**
Straight	1	Both Below	1	Sitting	1	< 10	1
Bent	2	Shoulder	2	Standing on Two Legs	2	< 20	2
Twisted	3	One Above	3	Standing on One Leg	3	> 20	3
Bent and	4	Shoulder		Standing on Two Bent Knees	4		
Twisted		Both Above		Standing on One Bent Knee	5		
		Shoulder		Kneeling	6		
				Walking	7		

The observed postures are classified into hazard categories based on the grading system of the OWAS method. This categorization is based on expert scientific studies and estimations of the potential health issues that working postures and their combinations may cause to the musculoskeletal system. All postures belong to one of the previously described coding structure categories. The risk categories are as follows:

- C1 (Category 1): Normal posture, no ergonomic intervention is needed.
- C2 (Category 2): The strain is not significant, but ergonomic improvements should be made in the near future.
- C3 (Category 3): The load and strain are considerable; ergonomic improvements should be implemented as soon as possible.
- C4 (Category 4): The load and strain are excessive; ergonomic improvements must be made immediately.

RESULTS AND DISCUSSION

In order to identify working postures that may cause MSDs and to analyze them according to the OWAS method, evaluations were conducted in the packaging unit of a company which produces crankshafts, located in Konya, Türkiye. The current situation in the company is as follows: Crankshafts are brought to the area inside the saddle to be packaged. The worker takes the crankshafts from the saddle one by one and dips them into the oil basin. Then it is left on a flat belt to drain the oil. During this process, the worker's back is subjected to excessive loading due to frequent bending. This leads to quick fatigue and a decline in overall performance. In addition, the heavy weight of the parts causes strain on the arms. There is also a risk that the worker may drop the part and get injured. Crankshafts placed on the conveyor belt are individually picked up by another worker and placed into boxes on the floor. After the boxes are closed, their lids are secured with a stapler. The current situation is also illustrated by Figures 1 to 4 below.



Figure 1. Taking the Crankshaft



Figure 2. Dipping Into the Oil Basin



Figure 3. Transfering to Conveyor



Figure 4. Placing into Box

The working postures of two workers in the current situation was analysed using the OWAS method. Through video recording of the workers' tasks and evaluating snapshots, 23 distinct postures were considered for the first worker and 37 for the second worker. As a result of these analyses, 17.39% of the first worker's postures fall into Category 3, indicating a risk that should be addressed as soon as possible. In the case of the second worker, 2.7% of the observed postures were categorized as Category 4, indicating a critical level of risk that necessitates urgent ergonomic interventions. Furthermore, 21.62% of the postures are in Category 3 and should be resolved immediately.

After all these evaluations, the proposed and improved system is summarized as follows. All crankshafts are carried on a movable mechanism to the oil basin and then directly placed into the basin from this mechanism. Thus, workers do not have to carry the crankshafts. This makes the workers less tired. Crankshafts coming out

of the oil tank are put into boxes with the help of a hoist. Since the crankshafts are shipped to various parts of the world, they are coated after being placed in boxes to prevent damage.

The proposed situation is also illustrated by Figures 5 to 8 below.



Figure 5. Transportation of Crankshafts



Figure 6. Boxing the Crankshafts



Figure 7. Packaging of Crankshafts



Figure 8. Wrapping of Crankshafts

In the recommended scenario, none of the activities for either the first or the second worker fall into Category 3 or 4.

Working posture analysis of the above mentioned two workers for current and proposed situations are illustrated in Figures 9 and 10.

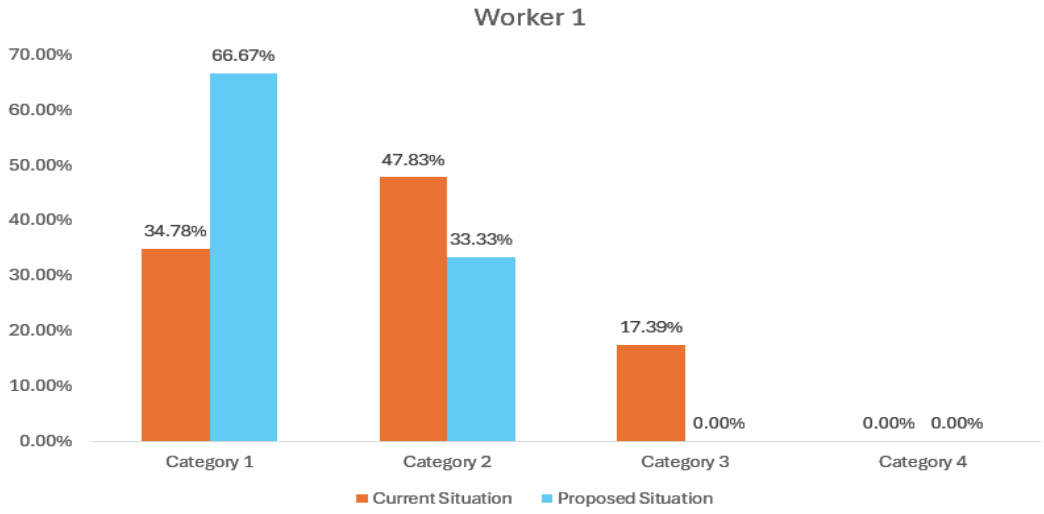

Figure 9. Working Posture Analysis of Worker 1

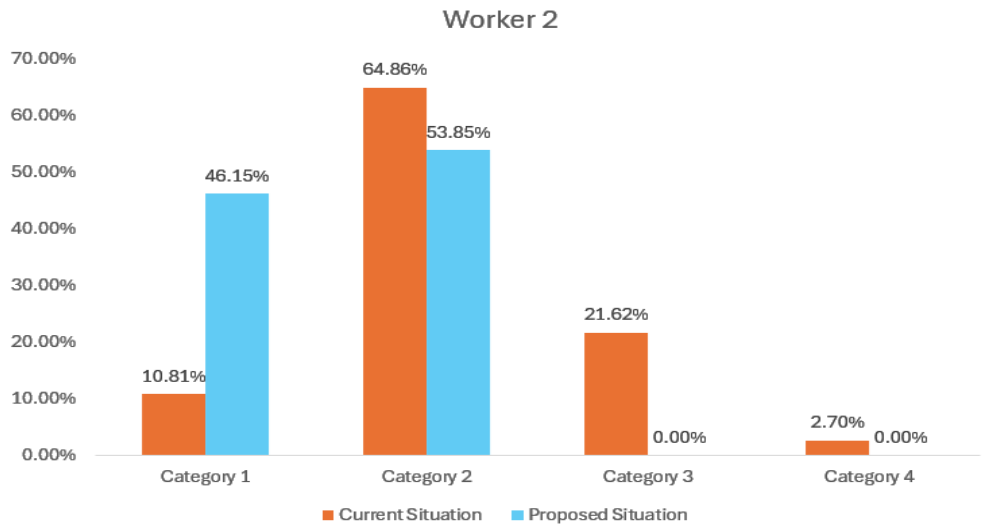

Figure 10. Working Posture Analysis of Worker 2

As a result, with the implementation of the revised system, strain-inducing postures are corrected, and it was observed that physical strains on the workers are significantly reduced.. By improving working postures, the new system reduced labor-related losses, fatigue, and worker stress. Consequently, costs decreased while overall productivity increased.

CONCLUSION

MSDs are one of the main factors negatively affecting worker health in today's industrial workplaces. One of the most important causes of such disorders is working postures that are ergonomically inadequate and inappropriate for human anatomy. The fact that the working environment is not compatible with the physical characteristics of human beings leads not only to individual health problems, but also to decreases in business productivity, loss of workforce and cost increases. Therefore, it is of great importance to adapt work environments to the anthropometric characteristics of workers. At the same time, such arrangements also provide important benefits such as reduced absenteeism rates, prevention of occupational accidents, and prevention of labor force losses in the long term. The main purpose of this study is to determine risky postures in workplaces and to reveal areas that require improvement. The results show that even simple and low-cost adjustments in the workplace can significantly improve work stoppages, which has a direct positive impact on employee health and production efficiency. Workers should be made aware of inappropriate postures and supported with training. Consequently, the periodic use of ergonomic evaluation techniques and the corrective actions taken accordingly are essential not only for protecting workers' health but also for maintaining long-term organizational performance and sustainability.

REFERENCES

Ağar, A. (2025). "Comparison of REBA, RULA And OWAS Ergonomic Risk Assessment Methods: An Example of A Car Tire Business." Mühendislik Bilimleri ve Tasarım Dergisi 13(1): 250-262.

Akay, D., M. Dağdeviren and M. Kurt (2003). "Ergonomic analysis of working postures Çalişma duruşlarinin ergonomik analizi." Journal of the Faculty of Engineering Architecture of Gazi University 18(3).

Babalık, F. (2005). "Mühendisler için Ergonomi." Nobel yayın dağıtım, Ankara.

Battini, D., A. Persona and F. Sgarbossa (2014). "Innovative real-time system to integrate ergonomic evaluations into warehouse design and management." Computers Industrial Engineering 77: 1-10.

Gupta, K. (2024). "A Review on Ergonomic Studies for Different Industrial Setups." Journal of Research Practice on the Musculoskeletal System 8(3).

Güney, B. and M. A. Erden (2023). Yatay Kaynak Pozisyonunda Çalışan Bir Operatörün Duruşunun OWAS yöntemi ile Ergonomik Analizi. International Conference on Frontiers in Academic Research.

Hignett, S. and L. McAtamney (2000). "Rapid entire body assessment (REBA)." Applied ergonomics 31(2): 201-205.

Karhu, O., P. Kansi and I. Kuorinka (1977). "Correcting working postures in industry: A practical method for analysis." Applied ergonomics 8(4): 199-201.

Kaya, Ö. and G. Akalp (2017). "İş Sağlığı ve Güvenliği Açısından Elle Taşıma İşlerinin Değerlendirilmesi (Tekstil ve Otomotiv Sektörü Örneği)." Is, Güc: Endüstri Iliskileri ve Insan Kaynaklari Dergisi 19(2): 79-90.

Kee, D. and P. Health (2022). "Systematic comparison of OWAS, RULA, and REBA based on a literature review." International Journal of Environmental Research 19(1): 595.

Lins, C., S. Fudickar and A. Hein (2021). "OWAS inter-rater reliability." Applied ergonomics 93: 103357.

Mattila, M., W. Karwowski and M. Vilkki (1993). "Analysis of working postures in hammering tasks on building construction sites using the computerized OWAS method." Applied ergonomics 24(6): 405-412.

McAtamney, L. and E. N. Corlett (1993). "RULA: a survey method for the investigation of work-related upper limb disorders." Applied ergonomics 24(2): 91-99.

Panariello, D., S. Grazioso, T. Caporaso, A. Palomba, G. Di Gironimo and A. Lanzotti (2022). "Biomechanical analysis of the upper body during overhead industrial tasks using electromyography and motion capture integrated with digital human models." International Journal on Interactive Design Manufacturing 16(2): 733-752.

Tarallo, A., G. Di Gironimo, S. Gerbino, A. Vanacore and A. Lanzotti (2019). "Robust interactive design for ergonomics and safety: R-IDEaS procedure and applications." International Journal on Interactive Design and Manufacturing 13: 1259-1268.

Zen, Z. H., M. Widia, E. H. Sukadarin and H. Sciences (2024). "Ergonomics Risk Assessment Tools: A Systematic Review." Malaysian Journal of Medicine 20(5).

➢ *ORAL PRESENTATION*

Transfer learning-based pneumonia detection on pediatric chest x-rays using a CNN model

Omer Faruk Soylemez[1*] (*ORCID: https://orcid.org/0000-0002-4076-5230*),
Cengiz Hark[2] (*ORCID: https://orcid.org/0000-0002-5190-3504*)

[*1]Dicle University, Faculty of Engineering, Department of Computer Engineering, Diyarbakir, Turkey.
[2]İnönü University, Faculty of Engineering, Department of Computer Engineering, Malatya, Turkey.

*Corresponding author e-mail: osoylemez@dicle.edu.tr

Abstract
Pneumonia is a major global health concern, particularly affecting children in low-resource settings. Chest X-rays remain a primary diagnostic modality, but their interpretation requires expertise and is subject to inter-observer variability. In this study, we propose a deep learning-based framework for the binary classification of pediatric chest X-ray images into normal and pneumonia categories. Utilizing the InceptionV3 convolutional neural network and a transfer learning approach, the model was trained and evaluated on the Guangzhou Pediatric Chest X-Ray dataset. Data preprocessing steps included image normalization, resizing, and augmentation to enhance generalizability. The model achieved an overall accuracy of 86.2%, with a high recall of 97.4% for pneumonia cases and an F1-score of 89.8%, indicating strong sensitivity. However, the relatively lower recall for normal cases (67.5%) suggests a tendency toward overdiagnosis. A confusion matrix analysis further revealed that pneumonia was detected with a low false-negative rate. These findings demonstrate the potential of the proposed system as a clinical decision support tool for early and accurate pneumonia detection in pediatric populations. Future work will focus on improving class-specific performance and integrating interpretability mechanisms for clinical adoption.
Keywords: Pneumonia detection, pediatric chest X-ray, deep learning, transfer learning.

INTRODUCTION

Pneumonia remains a significant cause of morbidity and mortality worldwide, particularly among young children, the elderly, and immunocompromised individuals. According to the World Health Organization, pneumonia accounted for approximately 2.5 million deaths globally in 2019, including 672,000 deaths in children under the age of five, making it one of the leading infectious causes of death (World Health Organization, 2023). The disease burden is disproportionately higher in low- and middle-income countries, where access to timely diagnosis and treatment remains limited (UNICEF, 2023). Chest radiography is the most commonly used imaging technique for diagnosing pneumonia, enabling clinicians to identify characteristic patterns such as lung opacities and infiltrates (Litjens et al., 2017). However, the accurate interpretation of chest X-rays (CXRs) requires extensive clinical experience, and inter-observer variability among radiologists often introduces inconsistencies in diagnostic outcomes (Hopstaken et al., 2004).

In this context, computer-aided diagnostic (CAD) systems have emerged as effective assistive tools in the detection and classification of thoracic diseases, including pneumonia. These systems provide automated, objective, and reproducible assessments that support radiologists in managing the growing volume of radiographic examinations and minimizing diagnostic errors (Qin et al., 2018). The incorporation of artificial intelligence (AI), especially deep learning (DL) techniques, into CAD frameworks has shown substantial promise in improving diagnostic accuracy. Recent research demonstrates that DL-based models can match or even surpass the diagnostic performance of expert radiologists in specific tasks, thereby facilitating earlier and more reliable identification of pneumonia cases (Irvin et al., 2019; Rajpurkar et al., 2017).

In this study, we propose a deep learning-based approach for the binary classification of CXR images as either *pneumonia* or *normal*, utilizing the Guangzhou Pediatric Chest X-Ray dataset. The primary objective of this work is to develop an efficient and reliable diagnostic model based on the InceptionV3 architecture, a convolutional neural network (CNN) known for its balance of computational efficiency and high-level feature extraction capabilities. Unlike previous studies that focus on multi-label classification involving a wide range of thoracic pathologies, our model is tailored specifically for pneumonia detection, thereby optimizing its sensitivity and specificity for this condition.

The proposed framework employs transfer learning to fine-tune the InceptionV3 model on Guangzhou Pediatric Chest X-Ray a dataset, consisting of annotated pneumonia and normal cases. Through extensive experimentation, we demonstrate that our model achieves competitive performance metrics, highlighting its potential utility in clinical decision support systems. Additionally, our analysis includes performance comparisons across different training configurations, offering insights into the effectiveness of architectural choices and data preparation strategies in pneumonia classification.

The key contributions of this work can be summarized as follows: (1) we present a lightweight and accurate deep learning model for pneumonia detection using chest radiographs, (2) we utilize a large-scale public dataset to ensure generalizability and reproducibility, and (3) we provide a comprehensive evaluation that underscores the model's clinical applicability as a decision support tool. The results underscore the value of targeted binary classification systems in medical imaging, particularly in resource-limited environments where radiological expertise may be scarce.

RELATED WORK

DL techniques have demonstrated remarkable capacity to model complex patterns, retain learned knowledge, and transfer it to related tasks. These capabilities have made DL particularly effective in medical image analysis, including the classification of CXR images for the diagnosis of pulmonary diseases (Duwairi & Melhem, 2023; Nahid et al., 2020; Roberts et al., 2021). This section reviews prominent DL-based studies focused on CXR classification, especially for pneumonia detection.

CNNs are widely employed in this domain due to their ability to extract hierarchical features from medical images (Chollet, 2017). Several studies have developed CNN architectures from scratch to classify COVID-19 and pneumonia. Among these, approaches leveraging ImageNet-based pre-trained models have reported superior performance compared to models trained from scratch.

Siddiqi (2019) proposed an 18-layer deep sequential CNN to classify CXR images as either normal or pneumonia, achieving 94.39% accuracy. However, the model exhibited low specificity, which limits its clinical applicability. Similarly, Nahid et al., (2020) combined traditional image processing methods with a two-channel CNN to extract discriminative features, achieving 97.92% classification accuracy. Yet, the need for manual cropping introduces a labor-intensive preprocessing step. A hybrid model combining multilayer perceptron and CNN was employed by Saraiva et al., (2019), successfully identifying pneumonia cases. However, the study did not address overfitting concerns. In a different application, a pre-trained ResNet50 was used to distinguish between drug-sensitive and multi-drug-resistant tuberculosis, achieving 61.78% accuracy (Duwairi & Melhem, 2023). The study suggested that focusing more on abnormal lung regions could have improved performance. Sun et al., (2017) employed a combination of CNN and recurrent neural networks to classify tuberculosis types using CT scans. Nevertheless, the model's performance suffered due to poor image quality in the training dataset.

Transfer learning is commonly applied in CXR image classification to enhance model performance by utilizing knowledge from pre-trained models. Rather than training from scratch, a model previously trained on large-scale datasets (e.g., ImageNet) serves as the backbone for downstream tasks, significantly reducing training time and improving accuracy (Vardhan et al., 2023; Wang et al., 2009). For instance, Irfan et al., (2020) employed ResNet50, InceptionV3, and DenseNet121 for pneumonia classification using CXR images. Their results indicated that transfer learning consistently outperformed training from scratch across all three models.

Ensemble learning aims to improve prediction robustness and accuracy by combining multiple models. This approach reduces variance by aggregating the outputs of different learners (Ahmad et al., 2023; Prakash et al., 2023). Pant et al., (2020) developed an ensemble framework using U-Net architectures based on ResNet-34 and EfficientNet-B4, achieving an accuracy of approximately 90%. Hilmizen et al., (2020) tested various models individually and in combination, including DenseNet121, MobileNet, Xception, InceptionV3, ResNet-50, and VGG-16. Their best-performing ensemble—combining ResNet-50 and VGG-16 using concatenation—achieved a classification accuracy of 99.87% using the Adam optimizer and categorical cross-entropy loss.

PROPOSED METHOD

Dataset

In this study, the Guangzhou Pediatric Chest X-Ray Dataset was employed. The dataset comprises anterior-posterior CXR images collected from retrospective cohorts of pediatric patients aged between one and five years at the Guangzhou Women and Children's Medical Center (Kermany et al., 2018). The dataset contains a total of 5,856 CXR images, divided into two categories: pneumonia and normal. Image resolutions range from 384×127 to 2916×2583 pixels. The dataset is split into training and test sets, comprising 5,232 and 624 images respectively, corresponding to approximately 91% and 9% of the total data. Sample counts for each subset are presented in Table 1.

Table 1. Distribution of CXR Images in Training and Testing Sets.

Subset	Normal	Pneumonia	Total
Train	1349	3883	5232 (91.07%)
Test	234	390	624 (8.93%)
Total	1583 (27.0%)	4273 (73.0%)	**5856 (100%)**

Preprocessing

Prior to model training, all CXR images were preprocessed to ensure consistency and compatibility with the input requirements of the selected deep learning architecture. Specifically, all images were resized to 299×299 pixels to match the input dimension of the InceptionV3 model.

To improve generalizability and mitigate overfitting, standard data augmentation techniques were applied to the training set. These augmentations included:

- Random horizontal flipping (with a probability of 0.5) to simulate mirrored anatomical variation,
- Random rotation (within ±15 degrees) to account for minor patient misalignments,
- Random zooming (ranging from 90% to 110%) to model variations in image scale,
- Width and height shifts (up to 10% of total dimensions),
- Brightness adjustment (within a range of ±20%) to simulate varying exposure conditions.

All images were subsequently normalized by scaling pixel intensities to the [0,1] [0,1] [0,1] range. These preprocessing steps ensured that the model received standardized inputs while preserving critical diagnostic features present in the original radiographs.

Model Architecture

In this study, the InceptionV3 CNN architecture was employed for the classification of CXR images. InceptionV3, introduced by Szegedy et al., (2016), is a deep CNN model known for its efficiency and high accuracy in image recognition tasks, featuring inception modules that allow for multi-scale feature extraction.

Transfer learning was applied by initializing the model with weights pre-trained on the ImageNet dataset. The original classification layers were replaced with a custom classifier tailored for binary classification (pneumonia vs. normal). Specifically, the final fully connected layers were substituted with a global average pooling layer, followed by a dense layer with a single neuron activated by a sigmoid function to output the probability of pneumonia presence.

During training, the convolutional base was fine-tuned along with the newly added classification layers to adapt the model to the domain-specific features of chest radiographs. This approach leverages the rich feature representations learned from a large-scale dataset while enabling the model to specialize in the pneumonia classification task.

Training Details

The model was trained using the Adam optimizer with a cosine annealing learning rate scheduler incorporating warm restarts to enhance convergence. The initial learning rate was adjusted dynamically according to this schedule. A batch size of 64 and a total of 60 epochs were used during training. Binary cross-entropy loss function was employed to optimize the binary classification task.

Training was performed on the PyTorch framework utilizing an NVIDIA RTX 4090 GPU. The dataset was split into training and validation sets, with approximately 91% of the images allocated for training and the remaining 9% used for validation to monitor model performance and prevent overfitting.

Evaluation Metrics

The performance of the proposed model was assessed using multiple evaluation metrics, including accuracy, precision, recall, and F1-score. Accuracy measures the overall correctness of the classification, while precision quantifies the proportion of true positive predictions among all positive predictions. Recall, also known as sensitivity, evaluates the model's ability to correctly identify positive cases. The F1-score represents the harmonic mean of precision and recall, providing a balanced measure of the model's performance.

Additionally, a confusion matrix was generated to visualize the distribution of true positives, true negatives, false positives, and false negatives, enabling a detailed analysis of classification errors.

RESULTS and DISCUSSION

The proposed model's performance on the test set was evaluated using precision, recall, F1-score, and accuracy metrics. Table 2 summarizes the class-wise and overall results.

For the normal class, the model achieved a precision of 94.05%, recall of 67.52%, and an F1-score of 78.61% over 234 samples. In the pneumonia class, the precision was 83.33%, recall reached 97.44%, and the F1-score was 89.83% across 390 samples. The relatively higher recall for pneumonia indicates the model's strong ability to correctly identify positive pneumonia cases, while the lower recall for normal class suggests some misclassification of normal cases.

The overall accuracy of the model was 86.22%. The macro-average precision, recall, and F1-score were 88.69%, 82.48%, and 84.22%, respectively, demonstrating balanced performance across both classes. The weighted averages, which account for class support, yielded precision, recall, and F1-score values of 87.35%, 86.22%, and 85.62%, respectively.

These results indicate that the model is effective in distinguishing between normal and pneumonia CXR images, with particularly strong sensitivity to pneumonia detection.

Table 2. Classification report showing precision, recall, F1-score, and support for pneumonia and normal CXR image classification.

	precision	recall	f1-score	support
Normal	0,9405	0,6752	0,7861	234
Pneumonia	0,8333	0,9744	0,8983	390
accuracy	0,8622	0,8622	0,8622	0,8622
macro avg	0,8869	0,8248	0,8422	624
weighted avg	0,8735	0,8622	0,8562	624

The confusion matrix of the model is presented in Figure 1, where the y-axis corresponds to the true labels and the x-axis to the predicted labels. From the confusion matrix, it can be observed that out of 234 actual normal cases, 158 were correctly classified, while 76 were misclassified as pneumonia. This accounts for a false positive rate for pneumonia predictions. Conversely, among 390 actual pneumonia cases, 380 were correctly identified, and only 10 were incorrectly classified as normal, indicating a low false negative rate.

These results demonstrate that the model has a strong ability to correctly detect pneumonia cases (high true positive rate), but it shows moderate misclassification for normal cases, leading to some overdiagnosis. The imbalance in misclassification suggests the model is more sensitive to pneumonia detection, which is generally favorable in clinical screening to minimize missed pneumonia cases.

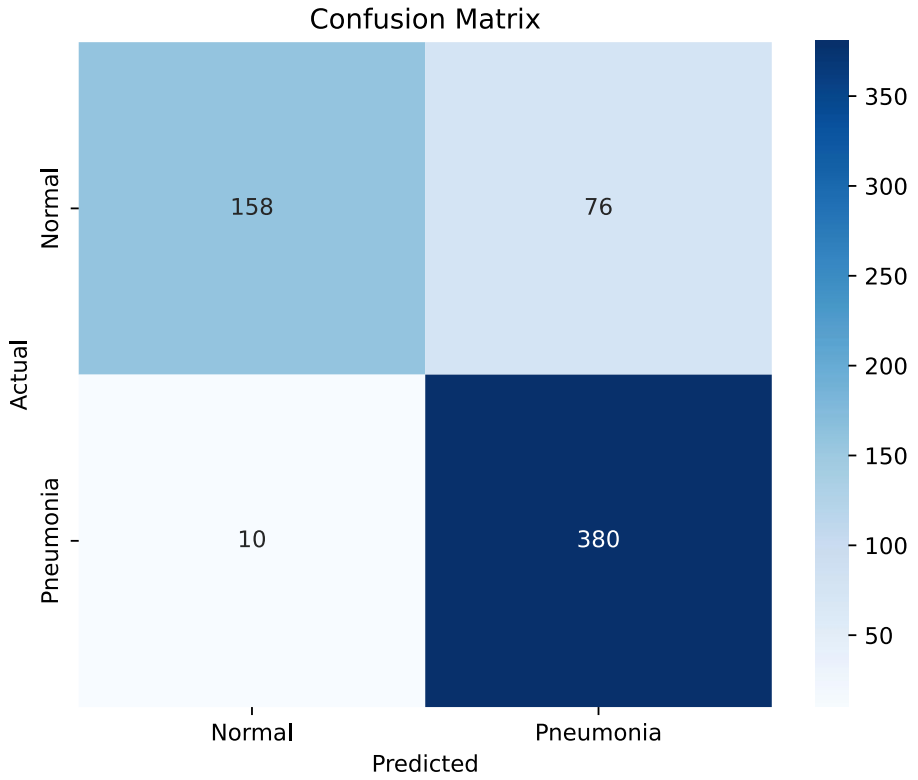

Figure 1. Confusion matrix for pneumonia vs. normal classification

CONCLUSION

In this study, a transfer learning-based deep learning model utilizing the InceptionV3 architecture was implemented for the binary classification of pediatric CXR images into normal and pneumonia categories. The model achieved an overall accuracy of 86.2%, with a notably high recall of 97.4% for pneumonia cases, highlighting its potential utility in clinical decision support systems. The use of standard preprocessing, data augmentation, and cosine annealing learning rate scheduling contributed to the robustness and generalizability of the model. Despite the promising results, the lower recall for the normal class indicates a tendency toward over-detection of pneumonia, which may be attributed to the inherent class imbalance and visual overlap in CXR features. Future work should focus on enhancing class-wise performance, validating the model across multi-institutional datasets, and exploring explainable AI methods to improve clinical interpretability and trust.

REFERENCES

Ahmad, H. K., Milne, M. R., Buchlak, Q. D., Ektas, N., Sanderson, G., Chamtie, H., Karunasena, S., Chiang, J., Holt, X., Tang, C. H. M., Seah, J. C. Y., Bottrell, G., Esmaili, N., Brotchie, P., & Jones, C. (2023). Machine Learning Augmented Interpretation of Chest X-rays: A Systematic Review. *Diagnostics*, *13*(4), 743. https://doi.org/10.3390/diagnostics13040743

Chollet, F. (2017). *Deep Learning with Python*. Manning.

Duwairi, R., & Melhem, A. (2023). A deep learning-based framework for automatic detection of drug resistance in tuberculosis patients. *Egyptian Informatics Journal*, *24*(1), 139–148. https://doi.org/10.1016/j.eij.2023.01.002

Hilmizen, N., Bustamam, A., & Sarwinda, D. (2020). The Multimodal Deep Learning for Diagnosing COVID-19 Pneumonia from Chest CT-Scan and X-Ray Images. *2020 3rd International Seminar on Research of Information Technology and Intelligent Systems, ISRITI 2020*, 26–31. https://doi.org/10.1109/ISRITI51436.2020.9315478

Hopstaken, R. ., Witbraad, T., van Engelshoven, J. M. ., & Dinant, G. . (2004). Inter-observer variation in the interpretation of chest radiographs for pneumonia in community-acquired lower respiratory tract infections. *Clinical Radiology*, *59*(8), 743–752. https://doi.org/10.1016/j.crad.2004.01.011

Irfan, A., Adivishnu, A. L., Sze-To, A., Dehkharghanian, T., Rahnamayan, S., & Tizhoosh, H. R. (2020). Classifying Pneumonia among Chest X-Rays Using Transfer Learning. *Proceedings of the Annual International Conference of the IEEE Engineering in Medicine and Biology Society, EMBS*, *2020-July*, 2186–2189. https://doi.org/10.1109/EMBC44109.2020.9175594

Irvin, J., Rajpurkar, P., Ko, M., Yu, Y., Ciurea-Ilcus, S., Chute, C., Marklund, H., Haghgoo, B., Ball, R., Shpanskaya, K., Seekins, J., Mong, D. A., Halabi, S. S., Sandberg, J. K., Jones, R., Larson, D. B., Langlotz, C. P., Patel, B. N., Lungren, M. P., & Ng, A. Y. (2019). CheXpert: A Large Chest Radiograph Dataset with Uncertainty Labels and Expert Comparison. *Proceedings of the AAAI Conference on Artificial Intelligence*, *33*(01), 590–597. https://doi.org/10.1609/aaai.v33i01.3301590

Kermany, D. S., Goldbaum, M., Cai, W., Valentim, C. C. S., Liang, H., Baxter, S. L., McKeown, A., Yang, G., Wu, X., Yan, F., Dong, J., Prasadha, M. K., Pei, J., Ting, M., Zhu, J., Li, C., Hewett, S., Dong, J., Ziyar, I., … Zhang, K. (2018). Identifying Medical Diagnoses and Treatable Diseases by Image-Based Deep Learning. *Cell*, *172*(5), 1122-1131.e9. https://doi.org/10.1016/j.cell.2018.02.010

Litjens, G., Kooi, T., Bejnordi, B. E., Setio, A. A. A., Ciompi, F., Ghafoorian, M., van der Laak, J. A. W. M., van Ginneken, B., & Sánchez, C. I. (2017). A survey on deep learning in medical image analysis. *Medical Image Analysis*, *42*, 60–88. https://doi.org/10.1016/j.media.2017.07.005

Nahid, A. Al, Sikder, N., Bairagi, A. K., Razzaque, M. A., Masud, M., Kouzani, A. Z., & Mahmud, M. A. P. (2020). A novel method to identify pneumonia through analyzing chest radiographs employing a multichannel convolutional neural network. *Sensors (Switzerland)*, *20*(12), 1–18. https://doi.org/10.3390/s20123482

Pant, A., Jain, A., Nayak, K. C., Gandhi, D., & Prasad, B. G. (2020). Pneumonia Detection: An Efficient Approach Using Deep Learning. *2020 11th International Conference on Computing, Communication and Networking Technologies, ICCCNT 2020*, 1–6. https://doi.org/10.1109/ICCCNT49239.2020.9225543

Prakash, J. A., Ravi, V., Sowmya, V., & Soman, K. P. (2023). Stacked ensemble learning based on deep convolutional neural networks for pediatric pneumonia diagnosis using chest X-ray images. *Neural Computing and Applications*, *35*(11), 8259–8279. https://doi.org/10.1007/s00521-022-08099-z

Qin, C., Yao, D., Shi, Y., & Song, Z. (2018). Computer-aided detection in chest radiography based on artificial intelligence: A survey. *BioMedical Engineering Online*, *17*(1). https://doi.org/10.1186/s12938-018-0544-y

Rajpurkar, P., Irvin, J., Zhu, K., Yang, B., Mehta, H., Duan, T., Ding, D., Bagul, A., Langlotz, C., Shpanskaya, K., Lungren, M. P., & Ng, A. Y. (2017). *CheXNet: Radiologist-Level Pneumonia Detection on Chest X-Rays with Deep Learning*. http://arxiv.org/abs/1711.05225

Roberts, M., Driggs, D., Thorpe, M., Gilbey, J., Yeung, M., Ursprung, S., Aviles-Rivero, A. I., Etmann, C., McCague, C., Beer, L., Weir-McCall, J. R., Teng, Z., Gkrania-Klotsas, E., Ruggiero, A., Korhonen, A., Jefferson, E., Ako, E., Langs, G., Gozaliasl, G., … Schönlieb, C. B. (2021). Common pitfalls and recommendations for using machine learning to detect and prognosticate for COVID-19 using chest radiographs and CT scans. *Nature Machine Intelligence*, *3*(3), 199–217. https://doi.org/10.1038/s42256-021-00307-0

Saraiva, A. A., Santos, D. B. S., Costa, N. C., Sousa, J. V. M., Fonseca Ferreira, N. M., Valente, A., & Soares, S. (2019). Models of learning to classify X-ray images for the detection of pneumonia using neural networks. *BIOIMAGING 2019 - 6th International Conference on Bioimaging, Proceedings; Part of 12th International Joint Conference on Biomedical Engineering Systems and Technologies, BIOSTEC 2019*, 76–83. https://doi.org/10.5220/0007346600760083

Siddiqi, R. (2019). Automated Pneumonia Diagnosis using a Customized Sequential Convolutional Neural Network. *Proceedings of the 2019 3rd International Conference on Deep Learning Technologies*, 64–70. https://doi.org/10.1145/3342999.3343001

Sun, J., Chong, P., Tan, Y. X. M., & Binder, A. (2017). ImageCLEF 2017: ImageCLEF tuberculosis task - The SGEast submission. *CEUR Workshop Proceedings*, *1866*.

Szegedy, C., Vanhoucke, V., Ioffe, S., Shlens, J., & Wojna, Z. (2016). Rethinking the Inception Architecture for Computer Vision. *2016 IEEE Conference on Computer Vision and Pattern Recognition (CVPR), Las*

Vegas, NV, USA, 2818–2826. https://doi.org/10.1109/CVPR.2016.308

UNICEF. (2023). *Pneumonia in Children Statistics*. https://data.unicef.org/topic/child-health/pneumonia/

Vardhan, A., Makhnevich, A., Omprakash, P., Hirschorn, D., Barish, M., Cohen, S. L., & Zanos, T. P. (2023). A radiographic, deep transfer learning framework, adapted to estimate lung opacities from chest x-rays. *Bioelectronic Medicine*, *9*(1), 1. https://doi.org/10.1186/s42234-022-00103-0

Wang, J., Li, F., & Li, Q. (2009). Automated segmentation of lungs with severe interstitial lung disease in CT. *Medical Physics*, *36*(10), 4592–4599. https://doi.org/10.1118/1.3222872

World Health Organization. (2023). *Pneumonia*. https://www.who.int/news-room/fact-sheets/detail/pneumonia

➢ *ORAL PRESENTATION*

Nanoplastic Toxicity in Fish: The Trojan Horse Effect

Firas MUHAMMED[1] (0000-0003-2661-4679), Demet DOGAN[1,2](0000-0001-6356-0679.)

[1]Department of Biochemistry Science and Technology, Graduate School of Natural and Applied Sciences, Gaziantep University, Türkiye.

[2]Faculty of Arts and Sciences, Department of Biology, Gaziantep University, Türkiye

*Corresponding author e-mail: demetdogan@gantep.edu.tr

Abstract

Nanoplastics, emerging from the degradation of larger plastic debris or manufactured intentionally, have become pervasive pollutants in aquatic and terrestrial ecosystems. Their small size (<1000 nm) and large surface area-to-volume ratio make them potent vectors for environmental contaminants, including heavy metals, persistent organic pollutants, and pharmaceuticals. This capacity to adsorb and transport toxicants has led to increasing concern over the so-called Trojan horse effect, whereby nanoplastics act as carriers, facilitating the cellular uptake and bioaccumulation of hazardous substances. Recent studies have demonstrated that the co-exposure of organisms to nanoplastics and adsorbed pollutants can result in enhanced toxicity compared to exposure to either component alone. Mechanisms underlying this effect include increased cellular internalization via endocytosis, disruption of membrane integrity, oxidative stress, and inflammatory responses. In particular, marine invertebrates and freshwater organisms have shown significant physiological and biochemical alterations upon exposure to nanoplastics-loaded contaminants. Despite growing evidence, key knowledge gaps remain in understanding the bioavailability, fate, and long-term ecological impacts of nanoplastics under realistic environmental conditions. Further interdisciplinary research is essential to assess their role in environmental health and to inform regulatory policies on plastic pollution.

Keywords: Nanoplastics, Trojan horse effect, Bioaccumulation, Fish, Toxicity

1. Introduction

Plastics are organic polymers with wide range of characteristics produced by the polymerization of varied monomers and additives. They are widely used in daily life because of their favorable properties of low cost, lightweight, and durability. Polyethylene, polyvinyl chloride, polypropylene, polyethylene terephthalate, and polystyrene are included in the most common plastics determined in environment. Potential risks they may cause are affected by the variation in their composition. The rapid increase in plastic usage all over the world and their possible adverse effects resulted in plastic pollution to be mostly discussed and concerned hot topic in the last decade (Rhodes, 2018; Blöcker et al. 2020).

The global plastic production has been reported to increase to 400 millions tons at 2022 with 33 billion tons of global demand expectancy by 2050 (Sun et al., 2025). Inadequate disposal, however, results in the release of excessive amount of plastic debris into environment. Roughly 1.15 - 2.41 million metric tons of plastic waste enters the oceans yielding secondary microplastics (MPs) and nanoplastics (NPs) through chemical, physical, and biological processes (Zandieh and Liu, 2022, Zhang et al., 2022).

Nanoplastics (NPs), defined as plastic particles less than 1000 nm in size, have emerged as a critical concern in environmental toxicology due to their small size, persistence, and potential to interact with biological systems (Koelmans et al., 2015). These particles are either intentionally manufactured (primary NPs) or formed by the degradation of larger plastic debris (secondary NPs). Once in aquatic environments, nanoplastics can be ingested by organisms across trophic levels, leading to cellular and systemic toxicity (Galloway et al., 2017).

One particularly concerning aspect of nanoplastics is their ability to act as vectors for other environmental pollutants, including heavy metals and persistent organic pollutants (POPs). This carrier function is known as the **"Trojan Horse" effect**, where nanoplastics adsorb toxicants on their surface and facilitate their entry into organisms, thereby enhancing their bioavailability and toxicity (Brennecke et al., 2016; Koelmans et al., 2015).

2. Physicochemical Properties of Nanoplastics and Their Environmental Behavior

The toxicity and transport potential of nanoplastics are greatly influenced by their physicochemical properties, including size, shape, surface charge, and chemical composition. Due to their large surface-area-to-volume ratio and hydrophobic nature, NPs can adsorb a wide range of environmental pollutants such as PAHs, PCBs, and heavy metals (Koelmans et al., 2015; Pittura et al., 2018; Rist et al., 2018).

Furthermore, nanoplastics can undergo aging and surface modification in natural waters, affecting their aggregation behavior and interaction with organisms (Canesi and Corsi, 2016). The dynamic interaction between nanoplastics and co-contaminants may lead to the formation of complex aggregates that can be easily ingested by aquatic organisms, thus increasing internal exposure to both plastic particles and adsorbed toxicants (Gao et al., 2022).

3. The Trojan Horse Effect: Mechanism and Toxicological Significance

The "Trojan Horse" effect describes how nanoplastics can enhance the uptake and toxicity of environmental pollutants by acting as carriers or vectors. This mechanism involves three key steps: (1) adsorption of toxicants onto the NP surface; (2) transport of the NP-toxicant complex into organisms; and (3) desorption and release of the toxicant within biological tissues (Lu et al., 2016; Brennecke et al., 2016).

This interaction not only increases the bioavailability of toxicants but may also alter their toxicokinetics, leading to greater accumulation in vital organs such as the liver, gills, and brain (Gao et al., 2022; Yong et al., 2020). For instance, when co-exposed to polystyrene nanoplastics and cadmium, zebrafish exhibited higher levels of cadmium in their liver tissues than those exposed to cadmium alone (Lu et al., 2016). Such findings underscore the synergistic toxicity associated with nanoplastic-pollutant complexes.

4. Fish as a Bioindicator for Nanoplastic Toxicity and the Trojan Horse Effect

Fish are widely recognized as reliable bioindicators in environmental toxicology due to their ecological diversity, sensitivity to pollutants, and their central role in aquatic food webs. Their physiological and behavioral responses provide early warnings of environmental contamination. In recent years, numerous studies have demonstrated the susceptibility of fish to nanoplastic exposure, especially when these particles act as vectors for other toxicants—a phenomenon consistent with the Trojan horse effect (Canesi and Corsi, 2016; Galloway et al., 2017).

4.1 Uptake and Internal Distribution

Nanoplastics can enter fish organisms primarily through ingestion and gill uptake. Once internalized, these particles can translocate across epithelial barriers and accumulate in various organs including the liver, brain, and gonads. Mattsson et al. (2017) demonstrated that zebrafish (*Danio rerio*) internalized nanoplastics within hours, which were later detected in brain tissue and associated with behavioral impairments and neural damage.

4.2 Interaction with Co-Contaminants

The Trojan horse effect becomes particularly evident when nanoplastics bind environmental toxicants such as heavy metals (e.g., cadmium, mercury) or persistent organic pollutants (POPs). According to Lu et al. (2016), zebrafish exposed to cadmium-laden polystyrene nanoparticles exhibited significantly higher cadmium concentrations in hepatic tissue, resulting in increased oxidative stress and liver toxicity compared to cadmium exposure alone. This demonstrates the potentiation of toxicity due to nanoplastic-mediated delivery.

Additionally, Brennecke et al. (2016) and Koelmans et al. (2015) reported that nanoplastics possess a strong affinity for hydrophobic pollutants, facilitating their transport and accumulation within aquatic organisms, including fish. This highlights a fundamental ecotoxicological concern regarding pollutant mobility in aquatic environments.

4.3 Cellular and Physiological Toxicity

Fish exposed to contaminant-loaded nanoplastics exhibit a wide array of toxicological responses. These include:

- **Oxidative stress**, characterized by elevated reactive oxygen species (ROS) and impaired antioxidant defense systems (Lu et al., 2016; Gao et al., 2022).
- **DNA damage and apoptosis**, particularly in hepatic and intestinal cells (Mattsson et al., 2017).
- **Endocrine disruption** and gene expression alterations linked to detoxification and inflammation pathways (Canesi and Corsi, 2016).
- **Behavioral impairments** such as decreased swimming activity and feeding behavior (Mattsson et al., 2017).

These sub-lethal effects suggest that nanoplastics, especially when acting as pollutant carriers, compromise fish health, survival, and reproductive success.

4.4 Ecotoxicological Implications

Because fish are integral to aquatic food webs, the accumulation of nanoplastics and associated toxicants may result in trophic transfer and biomagnification. Pittura et al. (2018) demonstrated that nanoplastics carrying polycyclic aromatic hydrocarbons (PAHs) significantly increased bioavailability and toxicity in marine mussels—an effect that is likely to extend to fish species. These findings raise concerns regarding the safety of seafood consumption and the broader implications for ecosystem health and human exposure (Yong et al., 2020).

Thus, fish serve not only as models for aquatic toxicity studies but also as sentinels for emerging environmental threats posed by nanoplastics and their role in the transport of environmental contaminants.

5. Conclusion

Despite significant advancements in understanding nanoplastic toxicity, particularly the Trojan horse effect, several critical challenges remain. One major limitation is the lack of standardized methodologies for detecting and characterizing nanoplastics in environmental and biological samples. Current analytical techniques often struggle to distinguish nanoplastics from other colloidal particles due to their small size and complex behavior in natural matrices. Therefore, more ecologically relevant experiments are needed to assess the combined effects of nanoplastics and environmental pollutants under realistic exposure scenarios.

References

1. Blöcker, L., Watson, C., F. Wichern (2020). Living in the plastic age-Different short-term microbial response to microplastics addition to arable soils with contrasting soil organic matter content and farm management legacy. *Environmental Pollution*, 267, 115468. https://doi.org/10.1016/j.envpol.2020.115468
2. Brennecke, D., Duarte, B., Paiva, F., Cacador, I., & Caçador, I. (2016). Microplastics as vector for heavy metal contamination from the marine environment. *Estuarine, Coastal and Shelf Science*, 178, 189–195. https://doi.org/10.1016/j.ecss.2015.12.003
3. Canesi, L., & Corsi, I. (2016). Effects of nanoplastics on marine organisms: An emerging issue for environmental protection. *Marine Environmental Research*, 111, 1–2. https://doi.org/10.1016/j.marenvres.2015.10.012
4. Gao, M., Li, Y., Zhang, Y., Liu, Y., & Zhang, M. (2022). Combined toxicity of polystyrene nanoplastics and environmental pollutants: Mechanisms and implications for aquatic organisms. *Science of the Total Environment*, 832, 154928. https://doi.org/10.1016/j.scitotenv.2022.154928
5. Galloway, T. S., Cole, M., & Lewis, C. (2017). Interactions of microplastic debris throughout the marine ecosystem. *Nature Ecology & Evolution*, 1(5), 0116. https://doi.org/10.1038/s41559-017-0116
6. Koelmans, A. A., Besseling, E., & Shim, W. J. (2015). Nanoplastics in the aquatic environment. Critical review. *Marine Anthropogenic Litter*, 325–340. https://doi.org/10.1007/978-3-319-16510-3_12

7. Lu, K., Qiao, R., An, H., & Zhang, Y. (2016). Influence of microplastics on the accumulation and toxicity of cadmium in zebrafish (*Danio rerio*). *Environmental Pollution*, 219, 1–9. https://doi.org/10.1016/j.envpol.2016.09.038

8. Mattsson, K., Johnson, E. V., Malmendal, A., Linse, S., Hansson, L. A., & Cedervall, T. (2017). Brain damage and behavioural disorders in fish induced by plastic nanoparticles delivered through the food chain. *Scientific Reports*, 7, 11452. https://doi.org/10.1038/s41598-017-10813-0

9. Pittura, L., Avio, C. G., Giuliani, M. E., d'Errico, G., Keiter, S. H., & Regoli, F. (2018). Microplastics as vehicles of environmental PAHs to marine organisms: Combined chemical and physical hazards to the Mediterranean mussels, *Mytilus galloprovincialis*. *Marine Environmental Research*, 140, 104–115. https://doi.org/10.1016/j.marenvres.2018.05.024

10. Rhodes, C.J. (2018). Plastic pollution and potential solutions. *Science Progress*, 101(3):207-260. https://doi.org/10.3184/003685018X15294876706211

11. Rist, S., Carney Almroth, B., Hartmann, N. B., & Karlsson, T. M. (2018). A critical perspective on early communications concerning human health aspects of micro- and nanoplastics. *Science of the Total Environment*, 626, 720–726. https://doi.org/10.1016/j.scitotenv.2018.01.092

12. Sun, H., Jiao, R., Gao, Y., Wang, D. (2025). Insight into the aggregation kinetics of nanoplastics in aquatic environments: Combined effects of protein corona and particle size. *Separation and Purification Technology*, 362(3), 131899. https://doi.org/10.1016/j.seppur.2025.131899

13. Yong, C. Q. Y., Valiyaveetill, S., Tang, B. L., & Loo, J. S. C. (2020). Toxicity of microplastics and nanoplastics in mammalian systems. *International Journal of Environmental Research and Public Health*, 17(5), 1509. https://doi.org/10.3390/ijerph17051509

14. Zandieh, M., Liu, J. (2022). Removal and degradation of microplastics using the magnetic and nanozyme activities of bare iron oxide nanoaggregates. *Angewandte Chemie International Edition*, 61(47). https://doi.org/10.1002/anie.202212013

15. Zhang, P., Liu, Y., Zhang, L., Xu, M., Gao, L., Zhao, B. (2022). The interaction of micro/nano plastics and the environment: Effects of ecological corona on the toxicity to aquatic organisms. *Ecotoxicology and Environmental Safety*, 243, 113997. https://doi.org/10.1016/j.ecoenv.2022.113997

➢ *ORAL PRESENTATION*

Understanding Pesticide Toxicity in Fish: Detoxification versus Bioactivation

Tarek FAKHEREDDIN[1](0000-0002-1978-4816) , Demet DOGAN[1,2](0000-0001-6356-0679.)

[1]Department of Biochemistry Science and Technology, Graduate School of Natural and Applied Sciences, Gaziantep University, Türkiye.

[2]Faculty of Arts and Sciences, Department of Biology, Gaziantep University, Türkiye

*Corresponding author e-mail: demetdogan@gantep.edu.tr

Abstract

Aquatic organisms are continuously exposed to pesticides which results in a variety of toxicities including behavioral, biochemical and pathological changes as well as genotoxicity and disruption of endocrine system in fish. Biotransformation is critical to understand the toxic mode of action of pesticides as it may result in detoxification and/or bioactivation. The process alters the toxicity of the chemical by producing metabolites either being less toxic via detoxification or more toxic in case of bioactivation. Biotransformation is vital because it serves as a defense mechanism by rendering xenobiotics less harmful and readily excreted. When the process results in bioactivation, it is called as lethal synthesis pointing biotransformation as a source of danger. The transformation of phosphorothioates is a prime example of bioactivation causing increased potency for acute and neurotoxic effects. The resultant reactive metabolites may covalently bind to cellular components including protein, DNA and RNA. Besides, these reactive metabolites of pesticides are often held responsible for carcinogenic effects and cellular necrosis.

Keywords: Pesticide toxicity, detoxification, bioactivation, fish

Introduction

Freshwater and marine ecosystems are increasingly under threat due to anthropogenic activities, with pesticide contamination emerging as a key factor contributing to biodiversity decline. As global agricultural demands escalate, the use of chemical pesticides—including insecticides, herbicides, and fungicides—has surged. Unfortunately, a significant fraction of these chemicals reaches aquatic environments through surface runoff, leaching, and atmospheric deposition, leading to chronic and acute exposure in non-target aquatic organisms (Rohani et al., 2023).

Among aquatic organisms, fish are highly vulnerable and serve as bioindicators for environmental monitoring due to their sensitivity to chemical stressors and their ecological and economic importance. Exposure to pesticides induces a wide array of physiological, behavioral, and molecular alterations in fish, affecting growth, reproduction, and survival (Wang et al., 2021). These toxic effects are not solely due to the parent compounds but are often the result of their metabolic transformation within the fish's body.

Once absorbed via gills, skin, or gastrointestinal tract, pesticides undergo a series of biotransformation reactions catalyzed by metabolic enzymes. These reactions are primarily categorized into detoxification, which renders xenobiotics less harmful and facilitates excretion, and bioactivation, where enzymatic conversion leads to the formation of reactive intermediates that may be more toxic than the parent compounds (Zhou et al., 2023). This metabolic dichotomy plays a critical role in defining the toxicodynamic of pesticides in aquatic species.

In particular, cytochrome P_{450} enzymes (CYPs), found predominantly in hepatic tissues, mediate the oxidation of lipophilic compounds, serving as a gateway for subsequent detoxification or harmful bioactivation. The outcome of these processes is influenced by numerous factors, including pesticide chemical structure, concentration, exposure duration, fish species, age, and environmental conditions such as temperature and pH (Kim and Sorial, 2023).

Understanding the balance between detoxification and bioactivation pathways is essential for predicting the ecological risk of pesticides and for developing biomarker-based monitoring strategies. With growing recognition of mixture toxicity and the emergence of persistent and bio- accumulative pollutants, there is an

urgent need to deepen our mechanistic understanding of how fish metabolize these substances at molecular, biochemical, and physiological levels.

Biotransformation and Oxidative Stress

Fish transform lipophilic pesticides via two phases: Phase I (CYP-mediated oxidative, reductive, or hydrolytic reactions) introduces functional groups. Phase II (conjugation with glutathione, sulfate, glucuronic acid) makes such molecules water-soluble for excretion.

These transformations often generate reactive oxygen species (ROS), resulting in oxidative stress. Antioxidant enzymes—SOD, CAT, GPx—are upregulated in response (Banaee et al., 2019). In fish exposed to deltamethrin, chlorpyrifos, or cypermethrin, elevated oxidative markers and disturbed detox enzyme activities indicate redox imbalance (Kim and Sorial, 2023).

Detoxification vs. Bioactivation

The metabolic fate of pesticides in fish is primarily governed by two opposing yet interconnected processes: detoxification and bioactivation. These mechanisms are part of the biotransformation system, which enables organisms to manage xenobiotic compounds—foreign chemical substances not naturally produced or expected to be present in the body. The pathway a chemical follow—detoxification or bioactivation—determines whether it will be rendered harmless or transformed into a more toxic product.

Detoxification is the enzymatic conversion of lipophilic (fat-soluble) xenobiotics into hydrophilic (water-soluble) metabolites that can be more easily excreted through the bile or urine. This two-phase process is a central defense mechanism in fish and other aquatic organisms exposed to environmental pollutants:

- Phase I reactions involve oxidation, reduction, or hydrolysis, primarily catalyzed by cytochrome P450 monooxygenases (CYPs). These reactions introduce or unmask functional groups (–OH, –NH_2, –SH), increasing the chemical's reactivity and solubility. For instance, many pyrethroid insecticides undergo hydroxylation in the liver, which is an essential detoxifying step (Khatri and Tyagi, 2021).

- Phase II reactions involve conjugation, where the Phase I metabolites are linked to endogenous molecules such as glutathione (via glutathione S-transferases, GSTs), sulfate (via sulfotransferases), or glucuronic acid (via UDP-glucuronosyltransferases, UGTs). These conjugates are significantly more water-soluble and biologically inactive, allowing their rapid elimination.

The efficiency of detoxification depends on a fish's genetic background, enzyme expression profile, developmental stage, and the nature of the pesticide. For example, elevated activity of GST and increased levels of reduced glutathione (GSH) have been observed in zebrafish exposed to deltamethrin, suggesting effective detoxification and cellular protection (Velisek et al., 2018).

In contrast, bioactivation refers to a paradoxical metabolic pathway in which a relatively inert compound is enzymatically converted into a more toxic metabolite—often referred to as a reactive intermediate. This process is also typically mediated by cytochrome P_{450} enzymes, especially when a xenobiotic possesses structural features that allow the formation of unstable or electrophilic intermediates.

One of the most well-known examples is the bioactivation of organophosphates like parathion into paraoxon, a potent acetylcholinesterase (AChE) inhibitor. Paraoxon binds irreversibly to AChE, leading to accumulation of acetylcholine in synaptic clefts and resulting in continuous nerve firing, muscular paralysis, and potentially death in fish and other organisms (Jokanović, 2018).

Bioactivation is especially dangerous when:

- The reactive metabolites bind to critical cellular macromolecules such as DNA, proteins, and lipids, triggering genotoxicity, hepatotoxicity, or immunotoxicity.

- The metabolites induce oxidative stress by generating excess reactive oxygen species (ROS), which overwhelm antioxidant defenses like CAT, SOD, and GPx.

Fish vary widely in their susceptibility to bioactivation depending on species-specific enzyme expression. For instance, trout exhibit greater CYP1A activity in the liver compared to carp, making them more vulnerable to bioactivated toxicants in some cases (Chen et al., 2024).

Feature	Detoxification	Bioactivation
Goal	Reduce toxicity; promote excretion	Generate reactive, potentially toxic metabolites
Key Enzymes	GSTs, UDP-glucuronosyltransferases, SULTs	CYP450 enzymes (especially CYP1A, CYP3A)
Resulting Chemicals	Water-soluble, less toxic metabolites	Electrophilic species binding DNA/proteins/lipids
Biological Effects	Protective; limits bioaccumulation	Increases ROS stress, neurotoxicity, genotoxicity
Example	Pyrethroid → GST/GSH conjugates for excretion	Parathion → Paraoxon (AChE inhibitor)

The toxicological outcome of pesticide exposure hinges on the dynamic balance between detoxification and bioactivation. When detoxification pathways are efficient, fish can tolerate moderate levels of environmental contaminants. However, when bioactivation pathways dominate or overwhelm detoxification—especially under conditions of combined exposure or oxidative stress—the result can be widespread cellular damage and population-level effects.

Understanding the interplay between these metabolic fates is essential for predicting the risks posed by specific pesticides, designing targeted biomonitoring strategies, and developing mitigation measures to protect aquatic biodiversity.

Tissue- and Species-Specific Variation

Although the liver is the main organ for pesticide metabolism, organs like gills, intestine, kidney, and brain also contribute. Fish species (e.g., trout, carp, tilapia) show different enzyme expression patterns—affecting sensitivity to pesticides (Gao et al., 2022; Zhou et al., 2023).

Exposure to Mixtures and Emerging Pollutants

Field conditions often involve exposure to complex pesticide mixtures, where synergistic effects amplify toxicity. Increased oxidative stress and AChE inhibition are common (Kim and Sorial, 2023). Moreover, emerging contaminants such as PFAS pose concerns due to their persistence and slow metabolism in fish (Zhou et al., 2023).

Ecological Monitoring and Risk Assessment

Biomarkers including EROD, AChE, SOD, CAT, and GPx serve as effective early indicators of pesticide stress. Coupling biochemical, histological, and molecular tools enables clearer ecological risk evaluations and informs environmental regulation and conservation strategies.

Conclusion

The metabolism of pesticides in fish is a double-edged sword. While detoxification mechanisms support resilience, bioactivation pathways can amplify toxicity. Understanding this balance is critical to assessing ecological risks and formulating strategies to safeguard aquatic ecosystems.

References

- Chen, H., Wu, L., Chen, Y., Yang, W. (2024). Organ-specific biotransformation in fish: Insights from in vitro S9 fraction metabolism. Aquatic Toxicology, 266, 106564. https://doi.org/10.1016/j.aquatox.2023.106564
- Jokanović, M. (2018). Current understanding of the mechanisms of organophosphate and carbamate neurotoxicity. Arhiv za Higijenu Radai Toksikologiju, 69(2), 109–125. https://doi.org/10.2478/aiht-2018-69-3134
- Khatri, N., Tyagi, S. (2021). Pyrethroid pesticide exposure and oxidative stress in aquatic species. Toxicology Reports, 8, 374–386. https://doi.org/10.1016/j.toxrep.2021.02.010
- Kim, S., Sorial, G.A. (2023). Biotransformation of perfluoroalkyl substances (PFAS) in aquatic species: A zebrafish model study. Environmental Toxicology and Pharmacology, 102, 105369. https://doi.org/10.1016/j.etap.2023.105369
- Kumari, P., Saini, R., Singh, K.P. (2023). Pesticide-induced biochemical and genotoxic alterations in freshwater fishes: A comprehensive review. Environmental Research, 218, 114916. https://doi.org/10.1016/j.envres.2022.114916
- Velisek, J., Stara, A. (2018). Effect of thiacloprid on early life stages of common carp (Cyprinus carpio). Chemosphere, 194, 481–487. https://doi.org/10.1016/j.chemosphere.2017.12.268
- Wang, Y., Zhou, L., Wu, J., Zhang, Q. (2021). Metabolic fate and toxic effects of pesticides in fish: Biotransformation, bioactivation, and oxidative stress mechanisms. Environmental Pollution, 284, 117395.https://doi.org/10.1016/j.envpol.2021.117395

➢ *ORAL PRESENTATION*

Toprakta mikroplastik (MP) kirliliğinin mikrobiyal ekoloji üzerindeki etkileri

Derya İŞLER CEYHAN[1] (*ORCID: 0000-0002-7871-3647)*

*[1]Gaziantep Üniversite, Fen-Edebiyat Fakültesi, Biyyoloji Bölümü, Gaziantep, Türkiye

*Sorumlu yazar e-posta: islerderya@hotmail.com

Özet

Günlük yaşamımızın vazgeçilmezi haline gelen plastik atıklar her geçen gün bilinçli ve bilinçsiz olarak ekosisteme dahil edilmekte olup, bu atıkların çevresel bozunumu küresel iklim değişikliğinin etkisiyle hızla artmaktadır. Mikro ve nano boyutlara ulaşan plastik atıkların su ve karasal ekosistemlerde birikmesi ve parçalanması, ekosistemin önemli unsularından olan hayvan, bitki ve mikroorganizmaların yaşamsal ve ekolojik faliyetlerini tehtit etmektedir. Bu konuda yapılan güncel araştırmalarlar, sucul ekosistemlerde mikroplastik (MP)'lerin oluşumuna ve çevresel etkilerine odaklanılmıştır. Ancak, Mp'lerin toprak yapısı ve mikrobiyal faliyetleri üzerindeki etkisi hakkında hala yeterli bilgiye ulaşılamamaktadır. Buradan yola çıkarak, bu makalede, toprakta meydana gelen mikroplastik kirliliğin, topraktaki mikrobiyal çeşitliliği ve bu mikroorganizmaların ekolojik faliyetlerini nasıl etkiledikleri hakkında kısa bir bildiri olarak amaçlanmıştır.

Anahtar Kelimeler: Mikroplastik, toprak kirliliği, toprak mikrobiyal aktivite, küresel ısınma

Effects of microplastic (MP) pollution in soil on microbial ecology

Abstract

Plastic wastes, which have become indispensable in our daily lives, are included in the ecosystem consciously and unconsciously every passing day, and the environmental degradation of these wastes is rapidly increasing with the effect of global climate change. The accumulation and decomposition of plastic wastes reaching micro and nano sizes in aquatic and terrestrial ecosystems threatens the vital and ecological activities of animals, plants and microorganisms, which are important elements of the ecosystem. Current research on this subject has focused on the formation of microplastics (MP) in aquatic ecosystems and their environmental effects. However, sufficient information is still not available about the effects of MPs on soil structure and microbial activities. Based on this, this article is intended as a brief report on how microplastic pollution in soil affects microbial diversity in the soil and the ecological activities of these microorganisms.

Keywords: Microplastic, soil pollution, soil microbial activity, global warming

GİRİŞ

Plastikler, şekillendirilebilir, dayanıklı ve uygun maliyetli bir malzeme olması nedeniyle yaygın olarak kullanılmaktadır (Worm vd., 2017). Son yıllarda plastik üretimi ve birikimi, kullanım alanlarının yaygınlığı, yetersiz geri dönüşüm, çöplüklere ve bilinçsizce çevreye atılması nedeniyle benzeri görülmemiş bir oranda artmaktadır (Kumar vd., 2021). Bundan dolayı, plastik kirliliği karasal ve sucul ekosistemlerde tüm yaşam formlarını olumsuz etkilemekte ve bu durum gelecek için önemli bir endişe kaynağı oluşturmaktadır. Özellikle mikroplastikler ve nanoplastikler, çok küçük parçacık boyutuna ve önemli özgül yüzey alanına sahip önemli kirleticiler arasında yer almaktadır (Han vd., 2024). Mikroplastikler, plastiklerin bozulmasından kaynaklanan, doğada her yerde bulunan (Ziani vd., 2023), 5 mm'den küçük plastiklerdir (Rani vd., 2024). Mikroplastikler arasında polietilen (PE), polietilen tereftalat (PET), polyester (PES), poli(N-metakrilamid) (PAA), poliakrilonitril (PAN), suni ipek (RY), epoksi reçinesi (EP), etilen-vinil asetat (EVA) ve alkid reçineleri (ALK) gibi gruplar bulunurken, kaynakları atmosferik, karasal, deniz ve tatlı sular olabilmektedir. Bu parçacıklar, mikroorganizmaları, bitkileri, balıkları, memelileri ve diğer türleri etkileyerek doku, hücre ve moleküler düzeylerde organizmalara zarar verebilmektedirler (Han vd., 2024).

Son araştırmalar, sucul ekosistemlerde MP'lerin oluşumu, kaynakları ve toksikolojisine odaklanmıştır. Ancak, mikroplastiklerin (MP) toprak ekosistemleri üzerindeki ekolojik etkileriyle ilgili inceleme hala yetersiz olup (Ding vd., 2022), küresel anlamda daha fazla üzerinde durulması gereken sorunların başında gelmektedir (Aralappanavar vd., 2024). Karasal kaynaklı topraktaki mikroplastik kaynakları arasında kompost, sokak akıntısı çamuru, çöp, plastik maçlama, kanalizasyon, sulama, taşkın tortusu, plastik seralar ve kontrollü salınımlı gübrelerin yaygın kullanımı gibi tarımsal uygulamalardan gelen girdiler önemli bir yer almaktadır (Surendran vd., 2023; Meng vd., 2025). Toprak özellikleri açısından, makroplastiklerden mezoplastiklere, mikroplastiklere ve nanoplastiklere kadar uzanan plastiklerin önemli bir etkiye sahip olduğu bulunmuştur. Bu plasik parçaları doku, yapı, hacim yoğunluğu, su agregat kararlılığı, su tutma kapasitesi ve yağmur suyu sızması gibi toprağın fiziksel özelliklerini değiştirebilmektedir. Mp'lerin, pH seviyelerini, elektriksel iletkenliği, besin döngüsünü ve enzim aktivitesini etkileyerek toprağın kimyasal özelliklerini etkileyebilmektedir. Toprak özelliklerindeki bu değişikliklerin ekosistem sağlığı ve tarımsal üretkenlik açısından geniş kapsamlı etkiler oluşturabilmektedir (Hanif vd., 2024).

Mikroplastiklerin toprağın fiziko-kimyasal ve mikrobiyal yapısına etkisi

Mp'ler toprak yapısını ve mikrobiyotayı etkileyerek karasal ekosistemlerin biyolojik çeşitliliğini ve işlevlerini etkiler (Han vd., 2024). Toprak plastisferdeki mikroorganizmalar özellikle Proteobacteria, Actinobacteria, Bacteroidota, Firmicutes, Chloroflexi, Acidobacteria, Cyanobacteria, Ascomycota, Basidiomycota, Chytridiomycota, Ciliophora, Ochrophyta ve Chlorophyta filumları gibi genellikle çevredeki baskın mikroorganizma gruplarından oluşmaktadır. Ancak farklı plastik yüzeylerdeki bileşimler ve baskın mikrobiyal türler zamanla, plastiklerin özellikliklerine, biyotik ve abiyotik çevresel faktörlere bağlı olarak büyük ölçüde değişmektedir. Plastisferdeki mikroorganizma topluluk yapısını etkileyen faktörler yeterince çalışılmamış olmakla birlikte, bu konuda yapılan çalışmalardan birinde toprak pH'ı ve As (arsenik) içeriğinin plastisfer bakteri topluluklarını önemli ölçüde etkilediği ve çevresel dalgalanmaların plastisfer bakteri topluluklarını yönettiğini ve toprak ekosistemlerindeki As'nin biyojeokimyasal döngüsü üzerinde kademeli etkilere sahip olduğu gösterilmiştir (Li vd., 2021).Örneğin, toprakta MP'lerin birikmesi, fiziko-kimyasal özelliklerini etkiler, fauna ve floranın gelişimini ve üremesini etkiler. Ayrıca, bitki büyümesi üzerinde dolaylı olarak olmsuz etkilere sahipken, mikrobiyal toplulukların gelişimini ve enzim aktivitelerini de değiştirebilmektedir (Nikita vd., 2024). Benzer olarak Chang ve diğerleri (2024) tarafından da MP'lerin toprak fizikokimyasal ve mikrobiyolojik özellikleri değiştirebileceği ve toprak karbon stabilitesini, CO2 ve CH4 emisyonunu etkileyebileceği gösterilmiştir. Bu çalışmada ayrıca biyolojik olarak parçalanabilen MP'lerin genellikle biyolojik olarak parçalanmayanlardan daha büyük bir etki gösterdiği ve büyük ölçüde bu etkinin plastik türüne, boyutuna ve konsantrasyonuna bağlı olduğu bildirilmiştir. Dolayısıyla, toprakta MP'lerin varlığı, mikroorganizmalar için benzersiz bir ekolojik niş yaratabilir ve MP'lerin çevresel davranışlarını değiştirebilir (Zhang vd., 2025). Mp'ler toprak mikroorganizmalarının yaşam alanlarını bozabilir, davranışlarını etkileyebilir ve potansiyel olarak toprak florasında değişikliklere yol açabilir (Hanif vd., 2024). Aralappanavar ve diğerleri (2024) tarafından bu konuda yapılan araştırmada MP'lerin toprak mikrobiyal çeşitliliği ve besin maddeleri ve karbon döngüsüyle ilişkili işlevleri üzerindeki etkilerini incelenmiş ve hem plastisferin (MP-mikrop konsorsiyumu) hem de MP ile kirlenmiş toprakların, kirlenmemiş topraklara göre belirgin ve daha düşük mikrobiyal çeşitliliğe sahip olduğunu ileri sürülmüştür. MP'lerin bakteriler arasındaki rekabeti şiddetlendirdiği ve bakteri ağlarının karmaşıklığını artırdığı bildirilmiştir (Han vd., 2024). Özellikle MP'lerin mikroplastikleri metabolize edecek mikroorganizmalar üzerinde seçici bir etki gösterdiği ve belirgin bir ağ oluşturabileceği öne sürülmüştür. Bu durumda ise MP'lerin mikrobiyal ekoloji ve biyojeokimyasal döngüler için ciddi bir tehdit oluşturduğu sonucuna varılmıştır (Ren vd., 2020). Han ve diğerleri (2024) tarafından yapılan çalışmada, toprağın farklı agregatlarında mikrobiyal çeşitliliğin değiştiği, makroagregatlardaki temel taksonların Proteobacteria, Bacteroidetes, Chloroflexi, Actinobacteria ve Gemmatimonadetes olduğu, Actinobacteria ve Chloroflexi'nin ise mikroagregatlardaki temel taksonlar olduğu belirlenmiştir. özellikle Proteobacteria, Actinobacteria ve Chloroflexi MP'lerin eklenmesine en duyarlı bakteri grupları arasında yer aldığı bildirilmiştir. Ren ve diğerleri (2020) tarafından yapılan çalışmada ise MP'li toprakta, Actinobacteria'nın baskın filum olarak Proteobacteria'nın yerini aldığı belirlenmiştir.

Plastiklerin yaygın kullanımı, özellikle mikroplastiklerin tarımda kritik bir kirletici olarak ortaya çıkmasıyla birlikte önemli çevresel endişelere yol açmıştır. Mevcut çalışmalar farklı alanlarda mikroplastiklerin birikimini ve etkilerini belirlenmiş olsa da, tarımsal alanlarda bu kirleticiler kritik bir odak noktası olmuştur. Tarım alanlarında mikroplastiklerin çevresel kaynaklarını, kaderini ve toksisitesinin toprak özelliklerini, mikrobiyal topluluklar ve tarımsal ürünlerle nasıl etkileşime girdiğini anlamak son derece önemlidir (Hasan vd., 2024).

Bu konuda Lozano ve diğerleri (2024) tarafından yapılan çalışmada, MP'lerin, iyi sulanan koşullarda toprak mikrobiyal zenginliğin azaldığı ve bu durumun muhtemelen MP'lerden toprağa toksik maddelerin sızması ile ilgili olduğu düşünülmektedir. Diğer taraftan, kuraklık koşullarında topraktaki MP'lerden patojenik funguslar başta olmak üzere toplam fungus zenginliğini artırdığı bildirilmiştir. Bu konuda yapılan başka bir çalışmada, çeşitli özelliklere sahip mikroplastiklerin tarımsal alanlarda toprağa girmesi, toprak ekosistemleri üzerinde farklı etkilere neden olabileceğini göstermiştir. Polietilen (PE), polistiren (PS) ve polipropilen (PP) gibi farklı polimerlere sahip mikroplastiklerin toprak bakteri toplulukları üzerindeki etkilerine ilişkin yapılan bu araştırmada, PE ve PP uygulamalarındaki bakteri toplulukları benzer bir desen gösterirken, PS uygulaması yapılan topraklarda bakteri çeşitliliği ve bolluğu farklı bulunmuştur. Bu da polimer omurga yapısının toprak bakteri tepkilerini düzenleyen önemli bir faktör olduğunu ve lif, köpük ve film mikroplastikleri, partiküller karşılaştırıldığında toprak bakteri bileşimini önemli ölçüde etkilediğini göstermektedir (Sun vd., 2022). Yine, Sun ve diğerleri (2024) tarafından, tarım toprağının MP'ler için önemli bir rezervuar görevi gördüğü ve küresel ölçekli çevresel etkilerinin yanı sıra, tarımsal topraklarda potansiyel risklerin daha fazla anlaşılması gerkliliği vurgulanmıştır. Tarım topraklarındaki MP'lerin, su tortularındaki MP'lere kıyasla potansiyel etkileri hakkında çok az şey bilindiği ve MP'lerin farklı türlerinin, konsantrasyonlarının, boyutlarının ve maruz kalma sürelerinin yanı sıra, pH'ı veya organik madde konsantrasyonu gibi toprak koşullarıyla birlikte bu ekosistemde farklı etkilerinin olup olmadığının araştırılmasına acil bir ihtiyaç olduğu bildirilmiştir.

Bu konuda dikkat çeken konulardn biri de MP'lerin pestisitler, ilaçlar ve metal iyonları gibi çok çeşitli toksik bileşiklerin ve patojen mikroorganizmaların taşıyıcısı olarak hizmet ettiğidir. Bu konuda yapılan çalışmalardan elde edilen bulgular, hem mikroplastiklerin hem de mikrobiyoplastiklerin toprak mikrobiyolojisinde olumsuz değişikliklere neden olduğu ve potansiyel olarak toprak kaynaklı patojenlerin bolluğunu artırdığı bildirilmiştir. Özellikle bu konuda şaşırtıcı olan bulgu biyoplastiklerin kullanımının, daha kolay ve daha hızlı oluşmaları, biyofilmlere daha fazla destek sağlamaları ve toprak biyotası üzerinde daha belirgin olumsuz etkilere neden olabileceği ve bu sorunu daha da kötüleştirebileceğidir (Trojan vd., 2024).

Mikroplastiklerin küresel ısınma ve iklim değişikliği ile birlike toprak mikrobiyal yapısına etkisi

Plastik kirliliği ve iklim değişikliği iki önemli çevresel sorunların odak noktasını oluşturmaktadır. Ortamdaki plastik kirliliğinin artması nedeniyle, mikroplastiklerin oluşma potansiyelinin küresel ısınma ile birlikte çevresel kaderi kaçınılmaz olarak değişecektir (Haque ve Fan, 2023). Güncel çalışmalarda MP üretimi, dağılımı ve birikiminin iklim değişikliğiyle yakından bağlantılı olduğu belirlenmiştir. Özellikle petrol gibi fosil kaynakları içeren plastik üretimi, çıkarma ve işlemenin sera gazı emisyonlarını artırdığı ve bu artışın küresel ısınmaya katkıda bulunduğu belirlenmiştir. Aynı zamanda, iklim değişikliğinin neden olduğu aşırı hava olayları ile MP'lerin dağılımı, parçalanması ve birikiminin etkilediği ve bu plastik parçalarının doğal ortamlara taşınmasını kolaylaştırdığı görülmüştür (Oliveri Conti vd., 2024).

Son zamanlarda bu konuda dikkat çeken güncel konulardan biride küresel ısınmayla birlikte MP'lerin toprak mikroorganizmalarını nasıl etkilediğidir. MP kirliliği ve iklim değişikliği küresel endişe yaratan görünüşte iki farklı olgu iken çeşitli yollarla birbirine bağlıdır (Sunil vd., 2024). Bu konudda artan araştırmalar, MP kirliliği ile küresel ısınması ve iklim değişikliği arasında karşılıklı bir ilişki olduğunu ortaya koymuştur. MP kirliliğinin küresel iklim ısınmasını şiddetlendirdiği ve ortalama küresel sıcaklıktaki bu artışın ise MP'lerin çevredeki mikroplastik kirliliğini yoğunlaştırdığını göstermektedir (Li vd., 2024). Küresel ısınmanın etkisiyle birlikte, önemli kirleticiler olarak çevrede yaygın bulunan ve karbon açısından zengin polimerler olan MP'ler, mikrobiyal topluluklarda ve karbon döngüsü gibi biyojeokimyasal süreçlerde önemli değişikliklere neden olabilmektedir. Bunun sonucu olarak sera gazı emisyonunu ve karasal ekosistemlerdeki karbon depolanmasını etkileyebilmektedir. Ancak, MP'lerin toprak karbon döngüsü üzerindeki etkisine ilişkin mevcut araştırmalar hala sınırlı olsada, bu konuda yapılan MP'lerin sera gazı oluşturma ve toprak karbon döngüsüyle birlikte toprak mikrobiyotasını değiştirdiği görülmüştür (Chang vd., 2024). Örneğin, Navarro (2024) tarafından MP'lerin karbondioksit (CO2), metan (CH4) ve nitröz oksit (N2O) dahil olmak üzere sera gazı (GHG) emisyonlarına önemli katkıda bulunduğu bildirilmiştir. Bu çalışmada MP'lerin GHG üretimini etkilediği karmaşık mekanizmaların, mikroplastiklerin yüzeylere adsorpsiyonu ve mikrobiyal kolonizasyon için substrat olarak rollerini etkilediği belirlenmiştir. Özellikle, küresel ısınma ile birlik MP'lerin diğer kirleticilerle sinerjik etkileri, GHG emisyonları üzerindeki kümülatif etkileri hakkında kısıtlı bilgi varlığında çevresel ve iklimsel etkileri azaltmak için etkili stratejiler geliştirmek gerektiği vurgulanmıştır. Bu konuda yapılan diğer bir çalışmada MP kirliliğinin muhtemelen küresel toprak karbon (C) dinamiklerini etkilediği ve bu kirliliğin çözünmüş organik C (DOC), toprak organik C (SOC), floresan diasetat hidrolaz (FDAse) aktivitesi ve mikrobiyal biyokütle içeriğini önemli ölçüde artırdığı belirlenmiştir. Diğer taraftan, mikrobiyal biyokütle miktarında artışın aksine mikrobiyal çeşitlilikte bir azalmaya neden olduğu gösterilmiştir. Bu etkinin nedeni

olarak, toprakta MP birikiminin bazı heterotrofik mikroorganizmalar için ek C substratları sağladığı ve plastik metabolizmasında işlevsel bazı bakterilerin oransal olarak arttığı ve ototrofik taksonların ise büyümesini engellediği görülmüştür (Zhao vd., 2024). Bu konuda yapılan ilginç çalışmaların biri de O'Brien ve diğerleri (2022) tarafından yapılmıştır. Araştırmada küresel iklim değişikliğinin yollardan gelen lastik aşınma parçacıklarıyla oluşan mikroplastiklerin farklı ekosistemlere kolaylıkla ulaştığı bildirilmiştir. Lastik sızıntısının daha yüksek sıcaklıklarda su mercimeği yetiştirme alanlarında mikrobiyal büyümeyi artırdığı, ancak mikropların su mercimeği üzerindeki etkilerinin negatif olmasına nedeniyle potansiyel olarak bitki-mikrop mutualizmini bozabileceği gösterilmiştir.

KAYNAKLAR

Aralappanavar, V. K., Mukhopadhyay, R., Yu, Y., Liu, J., Bhatnagar, A., Praveena, S. M., ... & Sarkar, B. (2024). Effects of microplastics on soil microorganisms and microbial functions in nutrients and carbon cycling–A review. Science of the Total Environment, 2, 171435.

Chang, S., Zhou, A., Hua, Z., Meng, H., Zhu, F., Li, S., & He, H. (2024). Microplastics alter soil carbon cycling: Effects on carbon storage, CO2 and CH4 emission and microbial community. Cambridge Prisms: Plastics, 2, e5.

Ding, L., Huang, D., Ouyang, Z., & Guo, X. (2022). The effects of microplastics on soil ecosystem: A review. Current Opinion in Environmental Science & Health, 26, 100344.

Han, L., Chen, L., Feng, Y., Kuzyakov, Y., Chen, Q. A., Zhang, S., ... & Rillig, M. C. (2024). Microplastics alter soil structure and microbial community composition. Environment International, 185, 108508.

Han, M., Liu, H., Zhu, T., Tang, S., Li, Y., Zhu, C., ... & Jiang, Q. (2024). Toxic effects of micro (nano)-plastics on terrestrial ecosystems and human health. TrAC Trends in Analytical Chemistry, 172, 117517.

Hanif, M. N., Aijaz, N., Azam, K., Akhtar, M., Laftah, W. A., Babur, M., ... & Benitez, I. B. (2024). Impact of microplastics on soil (physical and chemical) properties, soil biological properties/soil biota, and response of plants to it: a review. International Journal of Environmental Science and Technology, 21(16), 10277-10318.

Haque, F., & Fan, C. (2023). Fate of microplastics under the influence of climate change. Iscience, 26(9).

Hasan, M. M., & Tarannum, M. N. (2024). Adverse impacts of microplastics on soil physicochemical properties and crop health in agricultural systems. Journal of Hazardous Materials Advances, 100528.

Kumar, R., Verma, A., Shome, A., Sinha, R., Sinha, S., Jha, P. K., ... & Vara Prasad, P. V. (2021). Impacts of plastic pollution on ecosystem services, sustainable development goals, and need to focus on circular economy and policy interventions. Sustainability, 13(17), 9963.

Li, H. Q., Shen, Y. J., Wang, W. L., Wang, H. T., Li, H., & Su, J. Q. (2021). Soil pH has a stronger effect than arsenic content on shaping plastisphere bacterial communities in soil. Environmental Pollution, 287, 117339.

Li, K., Du, L., Qin, C., Bolan, N., Wang, H., & Wang, H. (2024). Microplastic pollution as an environmental risk exacerbating the greenhouse effect and climate change: a review. Carbon Research, 3(1), 9.

Meng, X., Yuan, J., Huang, Q., Liu, R., Yang, Y., Yang, X., & Wang, K. (2025). A Review of Sources, Hazards, and Removal Methods of Microplastics in the Environment. Water (20734441), 17(1).

Navarro, A. (2024). Microplastics and Climate Change: Unveiling Ecological Impacts and Addressing Research Gaps.

Nikita B Gorde, BM Kamble, Ritu S Thakare, SG Ahire and MM Jagtap. (2024). The impact of microplastics on soil ecosystems: A review. International Journal of Research in Agronomy 2024; 7(12): 544-550

O'Brien, A. M., Lins, T. F., Yang, Y., Frederickson, M. E., Sinton, D., & Rochman, C. M. (2022). Microplastics shift impacts of climate change on a plant-microbe mutualism: Temperature, CO2, and tire wear particles. Environmental Research, 203, 111727.

Oliveri Conti, G., Rapisarda, P., & Ferrante, M. (2024). Relationship between climate change and environmental microplastics: a one health vision for the platysphere health. One Health Advances, 2(1), 17.

Rani, L., Kaur, G., Sood, P., Kaushal, J., & Srivastav, A. L. (2024). Remediation strategies for the removal of microplastics from the water. In Role of Green Chemistry in Ecosystem Restoration to Achieve Environmental Sustainability (pp. 191-200). Elsevier.

Ren, S. Y., & Ni, H. G. (2023). Biodeterioration of microplastics by bacteria isolated from mangrove sediment. Toxics, *11*(5), 432.

Sun, H., Ai, L., Wu, X., Dai, Y., Jiang, C., Chen, X., ... & Yang, H. (2024). Effects of microplastic pollution on agricultural soil and crops based on a global meta-analysis. Land Degradation & Development, 35(2), 551-567.

Sun, Y., Duan, C., Cao, N., Li, X., Li, X., Chen, Y., ... & Wang, J. (2022). Effects of microplastics on soil microbiome: The impacts of polymer type, shape, and concentration. Science of the Total Environment, 806, 150516.

Sunil, S., Bhagwat, G., Vincent, S. G. T., & Palanisami, T. (2024). Microplastics and climate change; the global impacts of a tiny driver. Science of The Total Environment, 174160.

Surendran, U., Jayakumar, M., Raja, P., Gopinath, G., & Chellam, P. V. (2023). Microplastics in terrestrial ecosystem: Sources and migration in soil environment. Chemosphere, *318*, 137946.

Trojan, M., Koutný, M., Brtnický, M., Holátko, J., Zlámalová Gargošová, H., Fojt, J., ... & Kučerík, J. (2024). The interaction of microplastics and microbioplastics with soil and a comparison of their potential to spread pathogens. Applied Sciences, 14(11), 4643.

Worm, B., Lotze, H. K., Jubinville, I., Wilcox, C., & Jambeck, J. (2017). Plastic as a persistent marine pollutant. Annual Review of Environment and Resources, *42*(1), 1-26.

Zhang, S., Yu, J., Wang, J.,Yang, H., Fu, Y., Fu, M., Li, S., Zhao, H., Wu, Y. (2025). A new perspective on understanding soil microplastics: Composition, influencing factors of the soil plastisphere, and its impacts on the environmental behavior of co-existing contaminants. Chemical Engineering Journal, 1385-8947(25), 05476-2.

Zhao, S., Rillig, M. C., Bing, H., Cui, Q., Qiu, T., Cui, Y., ... & Fang, L. (2024). Microplastic pollution promotes soil respiration: A global-scale meta-analysis. Global Change Biology, 30(7), e17415.

Ziani, K., Ioniță-Mîndrican, C. B., Mititelu, M., Neacșu, S. M., Negrei, C., Moroșan, E., ... & Preda, O. T. (2023). Microplastics: a real global threat for environment and food safety: a state of the art review. Nutrients, 15(3), 617.

➢ *ORAL PRESENTATION*

Determination of geocell-soil interfacial behavior of sandy soils by large-scale shear box tests

Adem IŞIK[1*] (https://orcid.org/0000-0002-9426-1177),
Harun AKOĞUZ[1] (https://orcid.org/0000-0001-9274-0249)

[*1] Erzincan Binali Yıldırım University, Faculty of Engineering-Architecture, Department of Civil Engineering, Erzincan, Turkey

*Corresponding author e-mail: aisik@erzincan.edu.tr

Abstract

To understand the behavior of geocells under tensile stress conditions in geosynthetic reinforced retaining walls, it is necessary to know the geocell-soil interfacial properties. A series of large-scale direct shear tests were performed to investigate the effect of soil grain size on the interfacial properties of geocell-reinforced granular soils. The variable parameters included poorly graded sand samples with different mean particle sizes (0.21 mm, 0.50 mm, 0.78 mm, 1.25 mm and 3.10 mm) and different normal stresses (55, 110 and 220 kPa). To compare the reinforced strength of the shear plane, the sliding properties actuated in the slip plane, including friction angle and apparent cohesion, were evaluated in the unreinforced and geocell-reinforced cases. The results showed that the shear strength properties of the interface improved due to the presence of the geocell. The shear strength at the geocell-soil interface was enhanced by increasing the mean particle sizes.

Keywords: Geocell, large-scale shear box, interfacial

INTRODUCTION

Geosynthetics, which are frequently used in geotechnical engineering applications, offer more suitable solutions in terms of cost and aesthetics than traditional methods (ground improvement, retaining structures, etc.). Geosynthetics are widely used today for increasing the bearing capacity of soils, slope stabilization and increasing the stability of retaining walls. The use of geosynthetic reinforced soils is increasing due to their low cost, aesthetics, simple and fast construction techniques, different allowable settlements and good behavior against earthquakes. Today, geosynthetic reinforced soils are the subject of many studies under static and dynamic loads. In recent years, geosynthetic reinforced soils have been used to support bridge abutments, building foundations and road embankments. It has been determined that the differential settlements that will occur with the use of geosynthetic reinforced soils in bridge foundations and bridge approach structures are lower or allowable compared to other structures (Adams, 1997; Abu-Hejleh et al., 2000; Tatsuoka et al., 2009; Xiao et al., 2016). Therefore, in addition to the deep foundation elements used for the support of bridge abutments, the use of shallow foundation elements is also increasing today.

Cellular elements (geocell), due to their three-dimensional and interlocking porous structure, act as a composite material with the soil in the pore by enclosing or surrounding the soil in the soil environment to be improved and reduce lateral deformations (Zhou and Wen, 2008). Due to its high flexural stiffness (EI), it transfers the applied load to the subgrade at lower rates (Pokharel et al., 2010). In the literature, the behavior of geocell is modeled as a composite material (Latha et al., 2006; Latha and Rajagopal, 2007; Latha et al., 2009). In addition, geocells are also used as block elements forming the wall face in geosynthetic reinforced retaining walls in various applications and research topics (Song et al. 2014). The block elements forming the wall face are constructed in layers at a certain angle. In this type of block retaining walls, inter-block stability is important for wall designs. Therefore, both internal stability and external stability should be provided in terms of design in geosynthetic reinforced retaining walls. In terms of internal stability, the frictional resistance between the blocks constitutes the stability of the wall face. For this reason, the stability problems that may occur on the front face of the wall are shown in Figure 1.

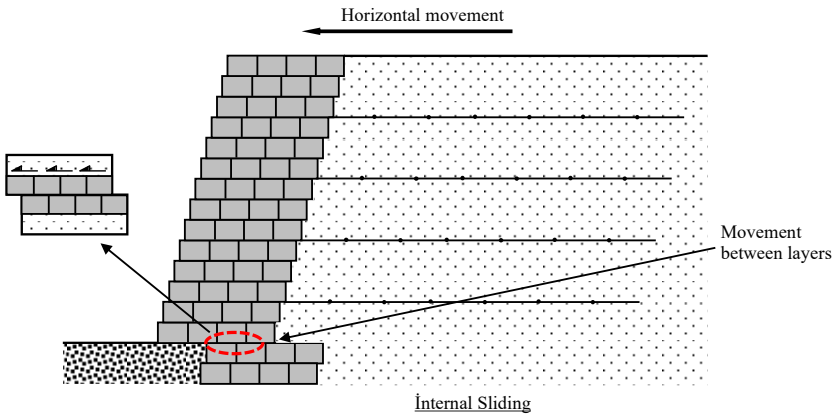

Figure 1. Geocell reinforced retaining wall

Within the scope of this study, in order to determine the frictional behaviour of geocell, geocells will be subjected to shear tests under uniform loads in granular soils designed and constructed in the laboratory. Sandy soil material with different grain distributions will be used in the experiments. The shear strength behaviours determined at the end of the experimental study will be investigated depending on the grain diameter distribution.

MATERIALS AND METHODS

Soils

In order to determine the interfacial friction behavior, test samples with 5 different mean particle sizes were prepared using sieves and samples with grain diameters between 0.15-0.425 mm, 0.425-0.600 mm, 0.600-1.000 mm, 1.000-2.000 mm and 2.360-4.750 mm were prepared. Grain distribution curves of the test specimens are given in Figure 2. Specific gravity of the specimens was 2.67 gr/cm3 and maximum and minimum void ratios were tested on specimens with different mean particle sizes and the values obtained are given in Table 1. In addition, the specimens were placed in the cutting box at the same relative density level with Dr= 50-55%.

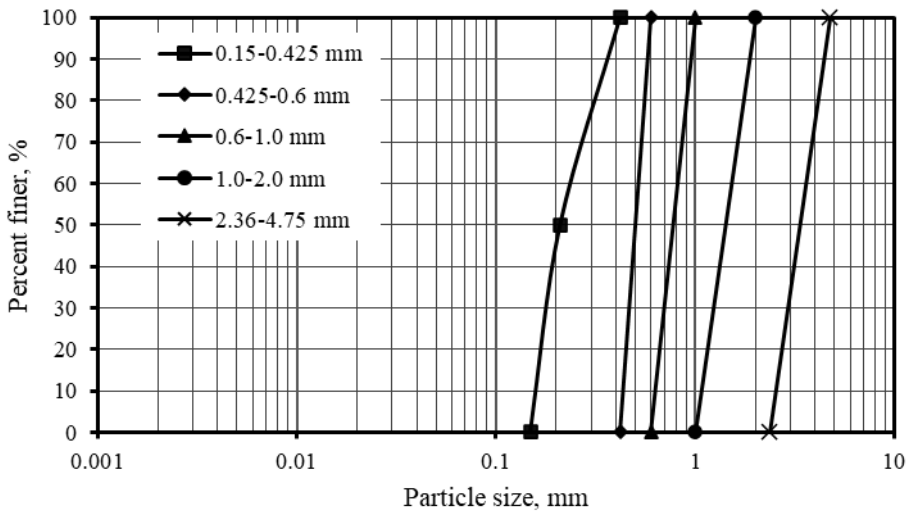

Figure 2. Particle size distribution of sand samples

Table 1. Mean particle size, maximum and minimum void ratios of sand samples

Sample no	Mean particle size (D_{50})	e_{max}	e_{min}	e_0
1	0.21	1.12	0.73	0.90
2	0.50	1.12	0.75	0.93
3	0.78	1.08	0.72	0.89
4	1.25	1.03	0.70	0.86
5	3.10	1.02	0.73	0.87

Geocells

The geocells are made from high density polyethylene (HDPE) strips ultrasonically welded. The geocell used in the experiment is perforated (Figure 3). The rectangular cell pocket pattern was used in this study. The pocket dimensions of the geocell are 55 mm x 55 mm. The properties of geocell are presented in Table 2.

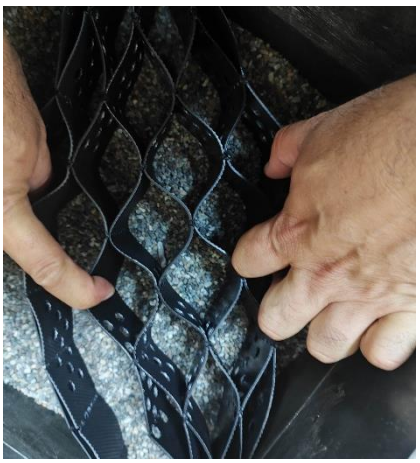

Figure 3. The geocell specimen,

Table 2. Properties of geocell

Properties of Geocell	Values
Material	High Density Polyethylene (HDPE)
Pocket width (bi)	55 mm
Pocket length (li)	55 mm
Pocket height (h)	50 mm
Density of polymer	0.965 g/cm3
Thickness	1.5 mm
Tensile Strength– Perforated	20 kN/m

Test procedures

The box dimensions of the shear box test setup were determined according to ASTM D5321 standard, depending on the grain diameter size of the soil samples to be used in the test. Here, the width of the shear box should be 15 times larger than the diameter corresponding to the grain diameter exceeding 85% by weight (D_{85}) or 5 times larger than the eye opening of the geosynthetic material used. The height of the cutting box should be 6 times larger than the maximum grain diameter (D_{max}). The internal dimensions of the large-scale shear box experimental setup (Figure 4) developed for this study were 300 mm (length), 300 mm (width) and 250 mm (height). The sides of the box are made of 5 mm thick steel sheet plates and the sheet plates are supported by 40 mm x 40 mm steel profiles to prevent bending under stress.

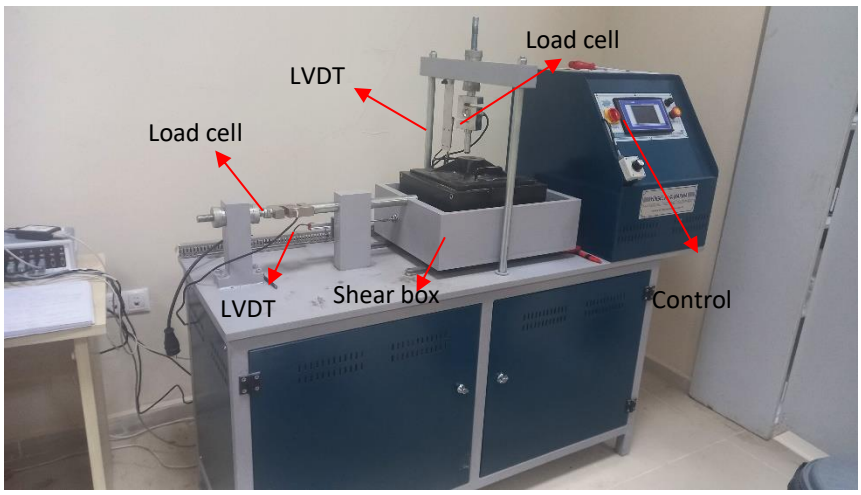

Figure 4. Large scale direct shear test device

Test results

With large-scale shear box tests, the frictional behavior of the soil must first be determined. Then, soil friction behaviors and soil-geocell friction behaviors were compared. Accordingly, large-scale shear box tests were carried out in the laboratory under 3 different vertical loads on the soil samples whose grain distribution curves and mean particle sizes were determined, and the shear strength parameters and soil-geocell interfacial behavior of the soils with the determined grain sizes were tried to be determined. In this context, large-scale shear box tests were performed on soil specimens of 0.21 mm, 0.50 mm, 0.78 mm, 1.25 mm and 3.10 mm under three different vertical loads of 500, 1000 and 2000 kg. The stress-strain and Mohr envelopes of the specimens are given in Figure 5. According to the experimental results, shear strength parameters of the soil specimens were determined from the Mohr envelopes.

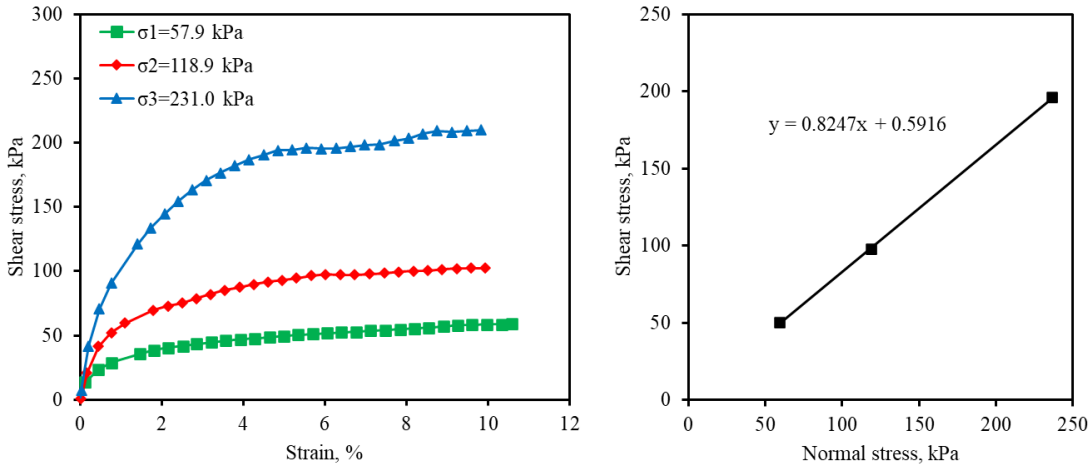

Figure 5a. Stress-strain behavior and Mohr envelope for mean particle size of 0.21 mm

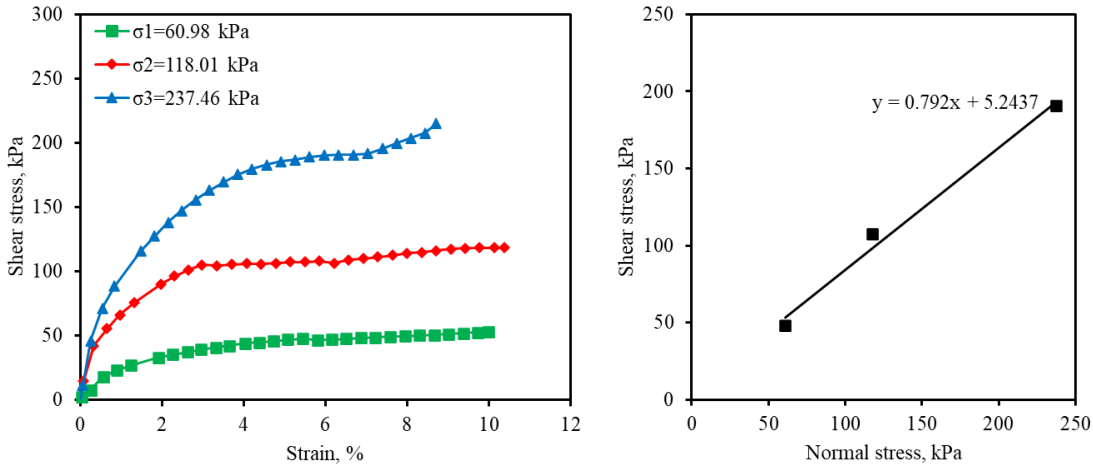

Figure 5b. Stress-strain behavior and Mohr envelope for mean particle size of 0.50 mm

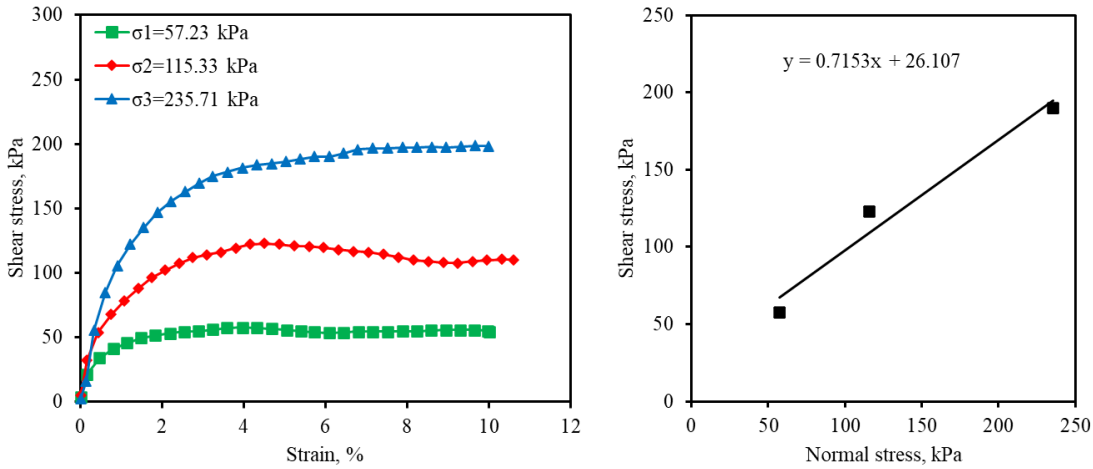

Figure 5c. Stress-strain behavior and Mohr envelope for mean particle size of 0.78 mm

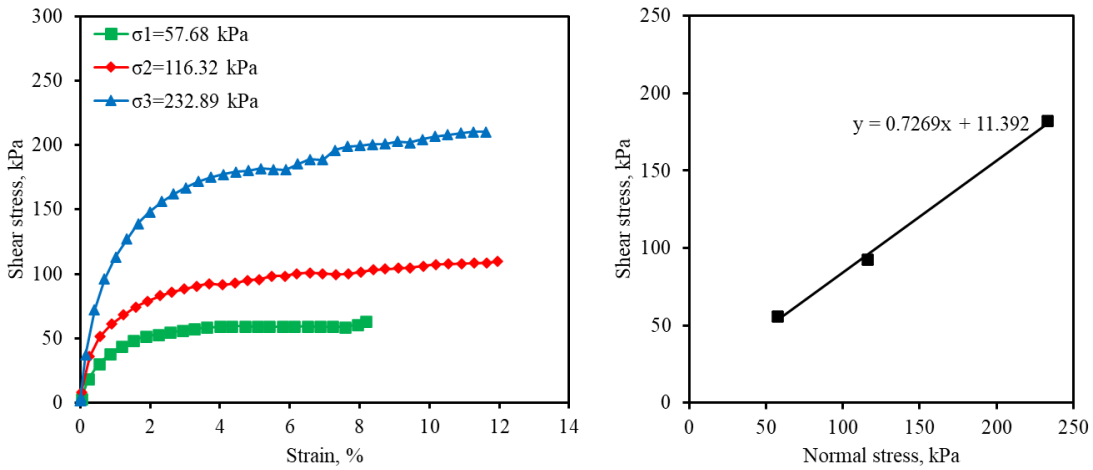

Figure 5d. Stress-strain behavior and Mohr envelope for mean particle size of 1.25 mm

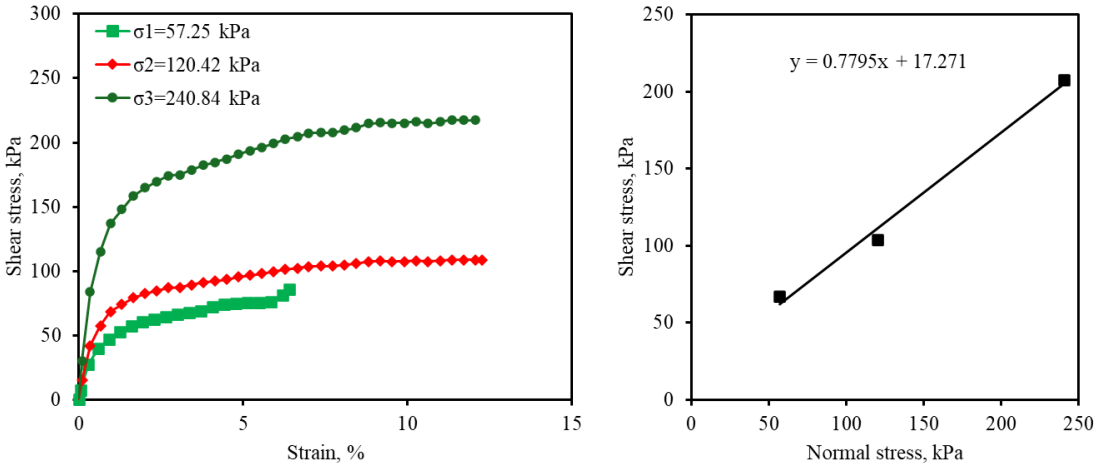

Figure 5e. Stress-strain behavior and Mohr envelope for mean particle size of 3.10 mm

The Mohr envelopes (Figure 5) and internal friction angles and cohesion values of the soil specimens with mean particle sizes of 0.21 mm, 0.50 mm, 0.78 mm, 1.25 mm and 3.10 mm determined as a result of large-scale shear box tests under three different vertical loads of 500, 1000 and 2000 kg are given in Table 3.

Table 3. Internal friction angles and cohesiones of soil samples

Mean particle size (D_{50})	Internal friction angle (ϕ)	Cohesion (c), kPa
0.21	39.5	0.6
0.50	38.4	5.2
0.78	35.6	26.1
1.25	36.0	11.4
3.10	37.9	17.3

The Mohr envelopes obtained from the shear box test results of soil samples with different mean particle sizes using geocell are given in Figure 6. As can be seen from the figure, with increasing mean particle sizes, the Mohr envelopes moved upwards and caused an increase in the cohesion value. This is similar to the Mohr envelopes obtained from the shear box tests performed only on the soil samples. Unlike the shear strength of the soil, the increase in cohesion was even more pronounced in the geocell reinforced specimens. The shear strength parameters obtained from the Mohr envelopes of the geocell reinforced specimens are given in Table 4.

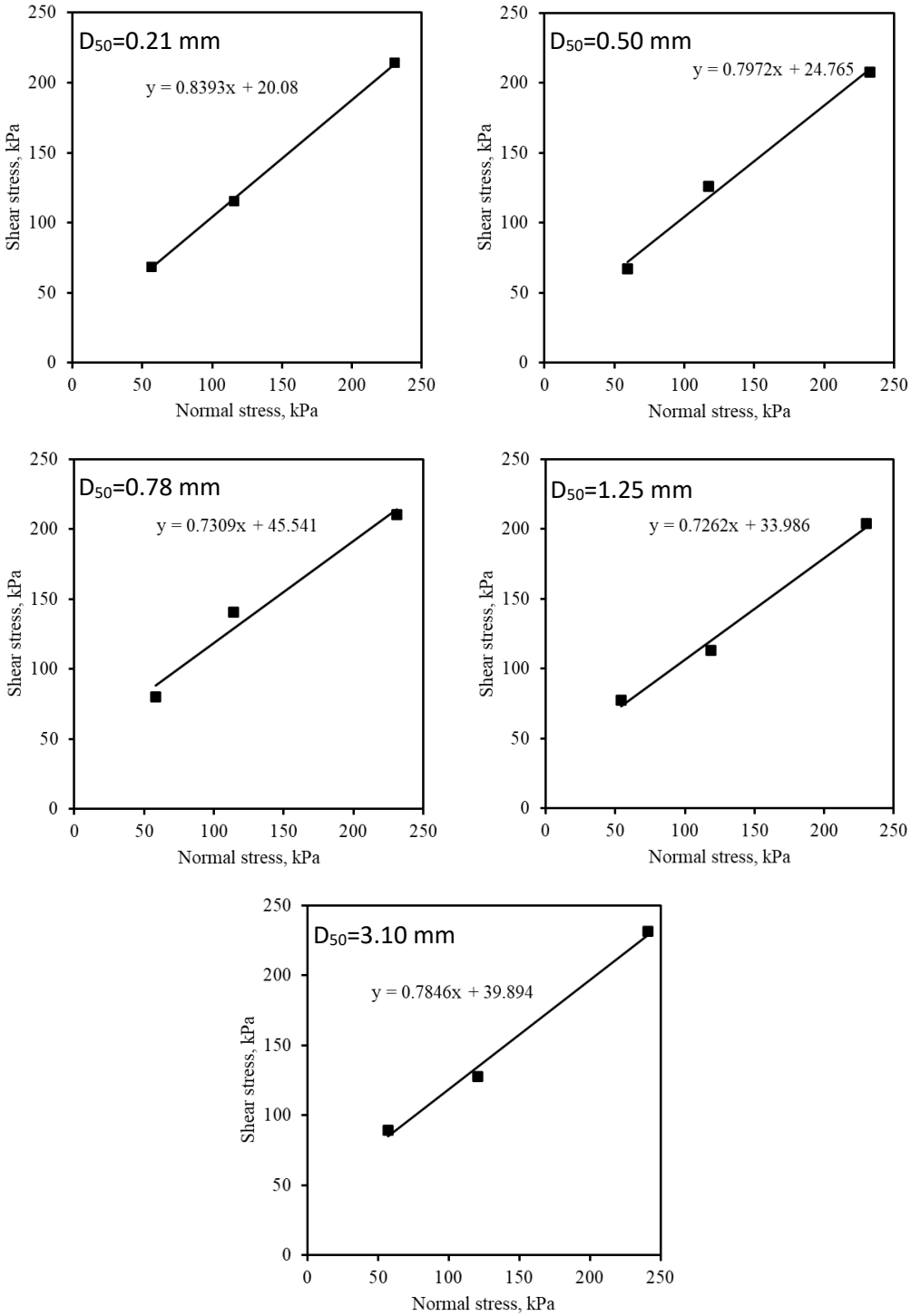

Figure 6. Mohr failure envelopes for geocell reinforced soil samples at various mean particle sizes

Table 3. Internal friction angles and cohesiones of geocell reinforced soil samples

Mean particle size (D_{50})	Internal friction angle (ϕ)	Cohesion (c), kPa
0.21	40.0	20.08
0.50	38.6	24.77
0.78	36.2	45.54
1.25	36.0	33.99
3.10	38.1	39.89

Conclusions

To determine the interfacial frictional behavior between the geocell and the soil, large-scale shear box tests were performed on sand samples with different mean particle sizes (0.21 mm, 0.50 mm, 0.78 mm, 1.25 mm and 3.10 mm) under different normal stresses (55, 110 and 220 kPa). The shear strength between the geocell and the soil increases by increasing Mean particle size. This is clearly seen in the Mohr envelope. While the slope of the Mohr envelope did not change much, the Mohr envelope moved upward, resulting in additional cohesion.

Acknowledgement

This study was supported by Erzincan Binali Yıldırım University Scientific Research Projects Coordination Unit as a normal research project titled “Determination of geocell-geocell interface friction parameters by large-scale shear box test” with code FBA-2022-796.

References

Abu-Hejleh, N., Wang, T., Zornberg, J.G., 2000. Performance of geosyntheticreinforced walls supporting bridge and approaching roadway structures. In: ASCE Geotechnical Special Publication No. 103. ASCE, Reston, VA, United States, pp. 218-243.

Adams, M.T., 1997. Performance of prestrained geosynthetic reinforced soil bridge piers. In: Wu, J.T.H., Barrett, R. (Eds.), Mechanically Stabilized Backfill. A.A. Balkema Publisher, Rotterdam, pp. 35-53.

Tatsuoka, F., 1993. Roles of facing rigidity in soil reinforcing. In: Keynote Lecture. Proc. Earth Reinforcement Practice, Fukuoka, Japan, vol. 2, pp. 831-870.

Xiaoa, C., Han, J., Zhang, Z., 2016. Experimental study on performance of geosynthetic-reinforced soil model walls on rigid foundations subjected to static footing loading. Geotext. Geomemb. 44 (1), 81-94.

Latha, G.,M., Dash, S.K., Rajagopal, K., 2009. Numerical simulation of the behaviour of geocell reinforced sand in foundations. International Journal of Geomechanics 9 (4), 143-152.

Latha, G.,M., Rajagopal, K., Krishnaswamy, N.R., 2006. Experimental and theoretical investigations on geocell supported embankments. International Journal of Geomechanics 6 (1), 30e35.

Latha, G.M., Rajagopal, K., 2007. Parametric finite element analyses of geocell supported embankments. Canadian Geotechnical Journal 44 (8), 917-927.

Pokharel, S.K., Han, J., Leshchinsky, D., Parsons, R.L., Halahm, I., 2010. Investigation of factors influencing behavior of single geocell-reinforced bases under static loading. Geotextiles and Geomembranes 28 (6), 570e578.

Song, F., Xie, Y.L., Yang, Y.F., Yang, X.H., 2014. Analysis of failure of flexible Geocellreinforced retaining walls. Geosynth. Int. 21 (6), 342–351.

➢ *ORAL PRESENTATION*

Effects of polyvinyl alcohol applications on morphological and physiological parameters of different wheat (*T. aestivum* L.) varieties grown in hydroponic environment under lead stress

Yunus Baran Badıllı* (*ORCID:* 0009-0007-0174-0886), Elif Öztetik (*ORCID*: 0000-0002-9663-6884)

Eskişehir Technical University, Science Faculty, Department of Biology, Eskişehir, Türkiye.

*Corresponding author e-mail: yunusbaran.445@gmail.com

Abstract

While the advancement of technology has brought about benefits such as prolonging human lifespan and enabling the production of faster and higher-quality industrial products, it has also undeniably triggered certain problems in parallel. The nourishment of an increasing population and the contamination of nature, particularly agricultural lands, by industrial waste serve as notable examples. Among the major pollutants, heavy metals reach agricultural soils through both anthropogenic activities and natural processes, thereby hindering the development of crop plants such as wheat, which is a primary dietary staple for humans. Polyvinyl alcohol (PVA), due to its biodegradability, high water retention capacity and negligible toxicity to living organisms, finds extensive application across various fields ranging from biomedical science to the paper industry, food packaging and the textile sector. Literature indicates that the growth of various plants cultivated in soil mixed with PVA is promoted compared to those grown in non-PVA-containing soil. In this study, the effects of varying concentrations of PVA on two different wheat cultivars (*Triticum aestivum* L. cv. Müfitbey and *Triticum aestivum* L. cv. Nacibey) grown under lead (Pb) stress in a hydroponic system were investigated. For this purpose, groups were established as Pb (0.5 mM, 1.5 mM, 3.0 mM), PVA (5 ppm, 50 ppm, 500 ppm) and Pb+PVA (0.5 mM+5 ppm, 1.5 mM+50 ppm, 3.0 mM+500 ppm) and the plants were subjected to 10 days of germination followed by 10 days of growth in Hoagland nutrient solution. Analyses of hypocotyl and radicle lengths, chlorophyll contents and relative water contents were performed on plant seedlings that completed 20-day growth.

Keywords: Chlorophyll contents, Heavy metal, Lead (Pb), PVA, *Triticum aestivum* L., Water contents

1. INTRODUCTION

Soil and agricultural land contamination is one of the most critical aspects of environmental pollution, directly affecting both ecosystem health and human food safety. Pesticides, herbicides and chemical fertilisers commonly used in agriculture accumulate in the soil over time, disrupting the microbial balance and reducing fertility (Carson, 2020). Additionally, heavy metals such as lead (Pb), cadmium (Cd) and mercury (Hg) originating from industrial activities and mining threaten both plant and human health (Ali et al., 2019). These metals can enter the food chain through plants, causing various toxic effects (Zhao and Wang, 2021). Prolonged accumulation of heavy metals particularly leads to agricultural lands becoming unusable and complicates soil rehabilitation efforts (Ghosh and Singh, 2005). These pollutants permanently impair not only the physical-soil structure but also its biological and chemical properties. Sustainable farming techniques, biological control methods and phytoremediation approaches can be effective in reducing this pollution (Kumar et al., 2022).

Polyvinyl alcohol (PVA) is a water-soluble, biodegradable and non-toxic polymer (Chiellini et al., 2003). Its high water retention capacity particularly enhances plant growth and water use efficiency under abiotic stress conditions such as drought (Khurana and Kapoor, 2017). Studies support these findings; for example, Hacımüftüoğlu and Canbolat (2020) reported that PVA application improved root and stem growth in maize, as well as enhanced the physical properties of soil. Similarly, Topalbekiroğlu et al. (2017) demonstrated that PVA nanofibre coatings effectively maintain plant vitality. Moreover, PVA is widely used beyond agriculture in drug delivery systems, biomedical products, textiles and packaging (Hassan et al., 2021; Peppas and Mongia, 1997).
Water content, chlorophyll concentration and root-stem length are fundamental indicators of plant health and growth (Khurana and Kapoor, 2017; Zhao and Wang, 2021). Water content percentages represents the amount of water retained in plant cells and tissues; adequate water content is critical for proper metabolic functioning

and stress tolerance (Ali et al., 2019). Water deficiency leads to decreased cell turgor and consequently slows plant development (Ghosh and Singh, 2005). Chlorophyll concentration indicates the level of pigments directly affecting photosynthetic capacity; a reduction in chlorophyll negatively impacts the plant's energy production and growth potential (Carson, 2020). Root and stem length reflect the plant's ability to absorb water and nutrients from the soil and overall growth performance. Declines in these parameters often result from environmental stresses, especially water scarcity and toxic substances, causing significant yield losses (Kumar et al., 2022; Öztetik, 2021).

In this study, two different wheat cultivars (*T. aestivum* L. cv. Müfitbey and *T. aestivum* L. cv. Nacibey) grown in hydroponic conditions were exposed to Pb, PVA and their combinations (Pb+PVA) at varying concentrations. The aim was to evaluate the morphological and physiological responses of plants to stress and to investigate whether PVA confers resistance against Pb stress. Thus, the study seeks to contribute to the development of sustainable agricultural policies.

2. MATERIALS AND METHODS

2.1 Growth of Plants

To break seed dormancy, seeds were subjected to a pre-treatment involving soaking in tap water for 2 hours, followed by immersion in dH_2O for another 2 hours. After this pre-treatment, 20 petri dishes were prepared for each wheat variety. The base of each dish was lined with appropriately cut Whatman filter paper and moistened with dH_2O. Subsequently, 20 healthy seeds were placed in each petri dish, which were then transferred to a controlled plant growth chamber. Seeds were kept in darkness for the first 3 days to initiate germination, followed by a 7-day photoperiod of 16 hours light / 8 hours dark at 22 ±1°C. This procedure completed the 10-day germination phase.

Following the germination period, the seedling growth phase commenced. 10 healthy seedlings from each group were selected and transferred into Hoagland nutrient solution (Hoagland and Arnon, 1950). The initial 3 days were designated as an adaptation phase, during which no chemical treatments were applied. Over the subsequent 7 days, chemical agents (Pb, PVA and a combination of Pb+PVA) were added to the nutrient solutions at appropriate concentrations specific to each treatment group. Upon completion of this 7-day chemical treatment, the total plant growth period amounted to 20 days.

2.2 Hypocotyl and Radicle Lengths

Hypocotyl and radicle lengths were measured in centimetres using a ruler.

2.3 Chlorophyll Contents

Chlorophyll contents were measured in SPAD units from the middle region of the hypocotyl using a portable chlorophyll meter.

2.4 Water Contents

For water content analysis, the hypocotyl and radicle were separated and their fresh weights recorded individually. The corresponding plant parts were then placed in paper envelopes and dried in an oven at 72°C for 48 hours. Once cooled to room temperature, the dry weights were measured. The water content percentage was calculated using a mathematical formula below (Wojcik and Tukendorf, 1999).

$$\text{Water contents (\%)} = \text{Wet weight - Dry weight / Wet weight x 100} \quad (1)$$

3. RESULTS

3.1 Hypocotyl and Radicule Lengths

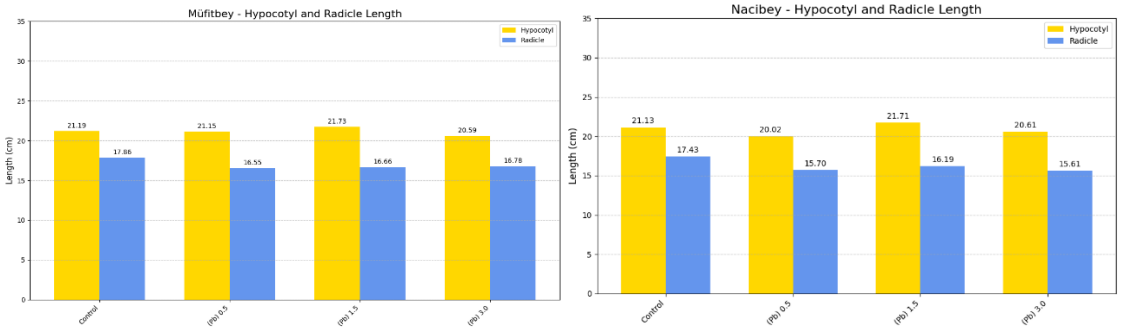

Figure 1. The Effect of Pb Applications on Hypocotyl and Radicle Lengths

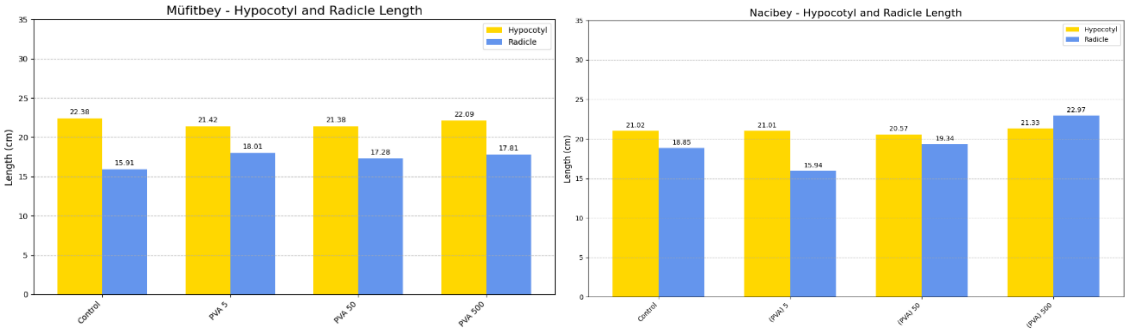

Figure 2. The Effect of PVA Applications on Hypocotyl and Radicle Lengths

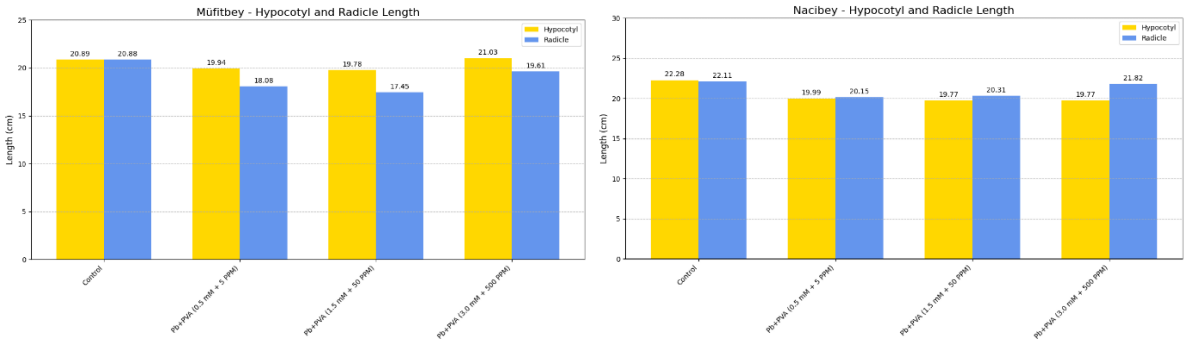

Figure 3. The Effect of Pb+PVA Combination Applications on Hypocotyl and Radicle Lengths

In Müfitbey, Pb treatments resulted in growth inhibition in the hypocotyl only at the 3.0 mM concentration compared to the control, whereas all Pb concentrations suppressed radicle growth. In contrast, in Nacibey, hypocotyl growth was inhibited at all Pb concentrations except for 1.5 mM, while radicle growth was suppressed at all concentrations compared to the control (Figure 1).

In Müfitbey variety, PVA applications inhibited hypocotyl growth at all concentrations, while promoting radicle growth across all treatments. In Nacibey variety, PVA applications caused no significant change in hypocotyl growth, whereas radicle growth was inhibited only at 5 ppm; other concentrations supported growth when compared to the control (Figure 2).

In Müfitbey variety, Pb + PVA combined treatments resulted in hypocotyl growth inhibition at all concentrations except for the 3.0 mM + 500 ppm application, while radicle growth was suppressed under all combined treatments compared to the control. In Nacibey variety, Pb + PVA treatments inhibited both hypocotyl and radicle growth at all concentrations (Figure 3).

3.2 Chlorophyll Contents

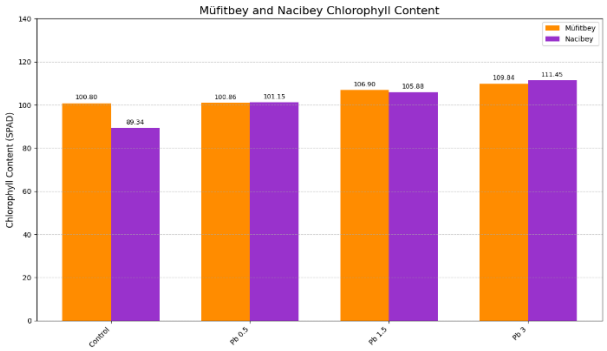

Figure 4. The Effect of Pb Applications on Chlorophyll Content

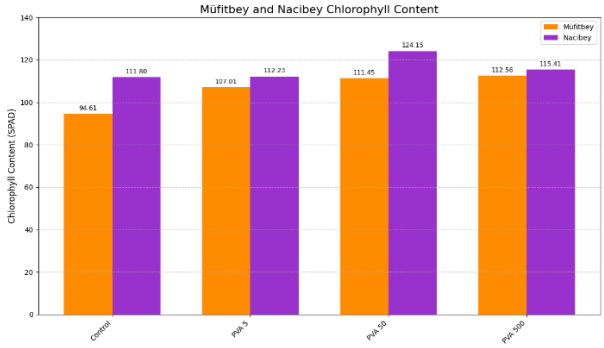

Figure 5. The Effect of PVA Applications on Chlorophyll Content

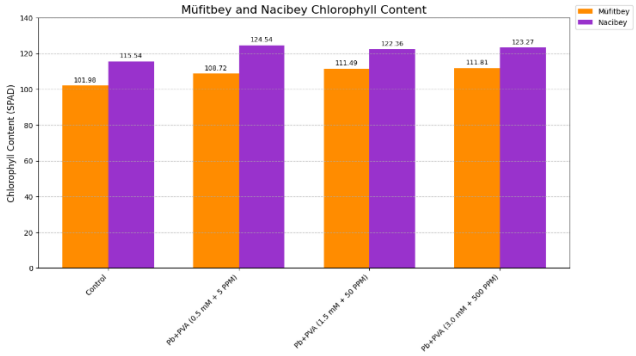

Figure 6. The Effect of Pb+PVA Combination Applications on Chlorophyll Content

In Müfitbey variety, no significant change in chlorophyll content was observed at 0.5 mM Pb application, whereas increases were recorded at higher concentrations. In contrast, all tested Pb concentrations in Nacibey variety resulted in elevated chlorophyll levels compared to the control (Figure 4).

PVA applications led to increased chlorophyll content in both varieties, with a proportionally more pronounced increase observed in Müfitbey variety with 500 ppm PVA application, comparing to control value (Figure 5).

Under Pb + PVA treatments, an increase in chlorophyll content was observed in both varieties (Figure 6).

3.3 Water Contents (%)

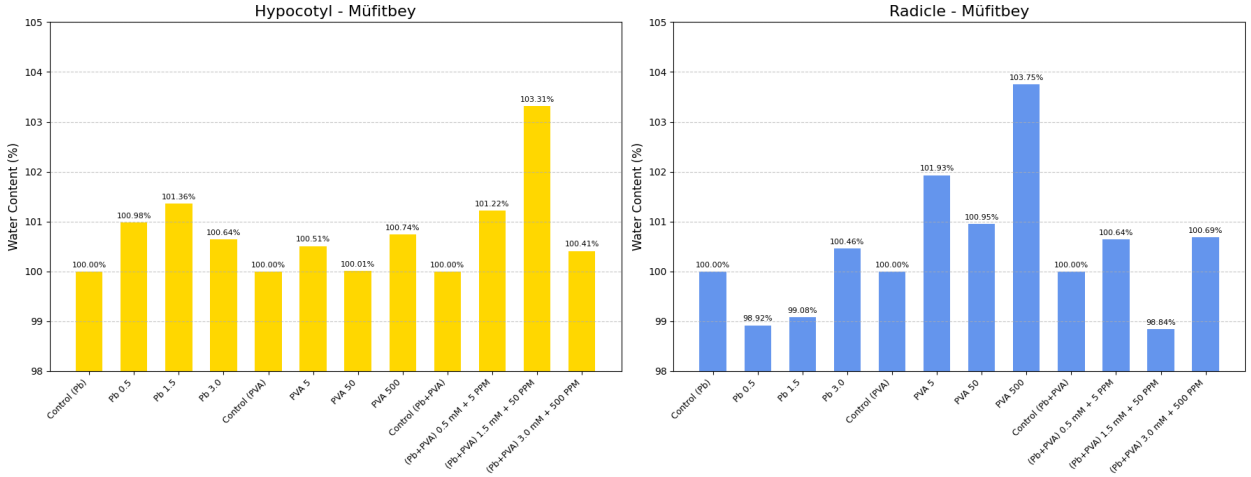

Figure 7. Water Content (%) in Müfitbey Variety under Pb, PVA and Combined Treatments

In Müfitbey variety (Figure 7), neither Pb nor PVA treatments had adverse effects on water content in the hypocotyl. Notably, an increase in water content was recorded under the Pb + PVA (1.5 mM + 50 ppm) treatment. In the radicle of Müfitbey, water content decreased following Pb treatments at 0.5 and 1.5 mM, whereas PVA applications increased water content at all concentrations. Conversely, the Pb + PVA (1.5 mM + 50 ppm) treatment caused a reduction in radicle water content.

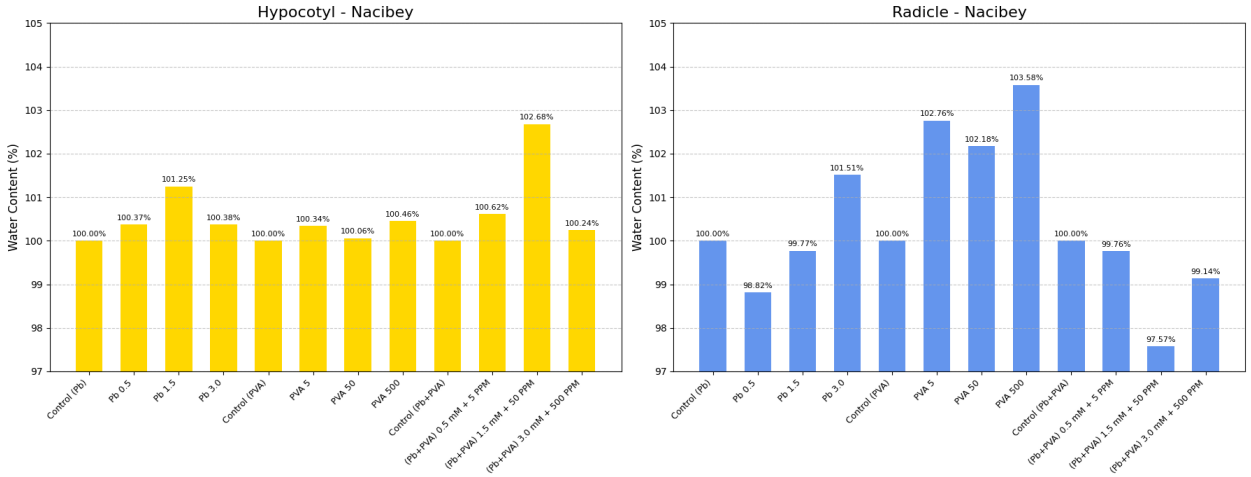

Figure 8. Water Content (%) in Nacibey Variety under Pb, PVA and Combined Treatments

In Nacibey variety (Figure 8), no adverse change in water content was observed in the hypocotyl following Pb treatments; however, PVA applications at 5 and 500 ppm resulted in only a negligible increase. The Pb + PVA (1.5 mM + 50 ppm) treatment resulted in a small increase in water content. In the radicle of Nacibey, water content decreased after Pb treatments at 0.5 and 1.5 mM, whereas PVA applications increased water content at all concentrations. A reduction in water content was observed in the Pb + PVA combination treatments, particularly at the 1.5 mM + 50 ppm application.

4. DISCUSSION

4.1 Hypocotyl and Radicule Lengths

Pb toxicity is known to adversely affect plant growth, particularly by inhibiting root development (Sharma and Dubey, 2005). PVA has been reported in the literature to enhance water retention capacity and support cell wall flexibility (Chiellini et al., 2003). While Pb treatments suppressed radicle length in all applications for both varieties, the hypocotyl was slightly more inhibited at the highest dose in Müfitbey variety. PVA

applications suppressed hypocotyl length in Müfitbey, whereas no significant changes were observed in Nacibey. Radicle length in both varieties generally tended to increase. However, combined treatments inhibited both radicle and hypocotyl development in both varieties (except for Müfitbey Pb+PVA 3.0 mM + 500 ppm application). Müfitbey appears to be the more morphologically tolerant variety, due to its stability in hypocotyl length and a broader dose range of radicle elongation.

4.2 Chlorophyll Contents

While Pb toxicity can impair chlorophyll synthesis in plants, in some instances increases in chlorophyll content have been observed as a result of stress signalling (Pourrut et al., 2011). In the literature, maintaining or increasing chlorophyll content is regarded as a significant indicator of plant stress tolerance (Verbruggen et al., 2009; Öztetik, 2015). Pb treatments increased chlorophyll content in both varieties, suggesting that Pb does not suppress the photosynthetic system but may instead trigger certain defence mechanisms. PVA application generally enhanced chlorophyll levels in Müfitbey, while in Nacibey, a notable increase was observed particularly at the 50 ppm dose. In the Pb+PVA combination, chlorophyll levels rose in both varieties, with the highest values recorded in this treatment. These findings highlight PVA's protective effect on the photosynthetic structure under Pb stress in both varieties, suggesting that Müfitbey exhibits a more stable and dose-balanced response.

4.3 Water Contents

Water content and osmotic balance are critical factors in determining a plant's resilience to heavy metal stress. It is well documented that Pb treatments reduce water content, whereas PVA enhances water retention capacity (Ali et al., 2019; Chi et al., 2022). In both varieties, hypocotyl water content increased across all treatments, with a more pronounced increase observed in the 1.5 mM Pb + 50 ppm PVA combination. This indicates that both Müfitbey and Nacibey are capable of maintaining water retention in hypocotyl tissues. Although radicle water content generally increased, a significant decrease was noted in both varieties under the same combined treatment [Pb+PVA (1.5mM + 50ppm)], revealing a higher sensitivity of radicle tissue to combined stress. Therefore, in terms of water content, no distinct difference was observed between the varieties, as both responded similarly.

5. CONCLUSION

This study investigated the morphological and physiological effects of Pb toxicity and PVA treatments on Müfitbey and Nacibey wheat cultivars. The findings demonstrate that Pb toxicity notably suppresses root development and exerts detrimental effects on hypocotyl growth at higher concentrations. Conversely, PVA application was found to enhance water retention capacity, thereby supporting plant resilience under stress conditions.

The stability of hypocotyl length and the increased radicle development observed in Müfitbey variety indicate a higher tolerance to Pb toxicity. Furthermore, the maintenance or enhancement of chlorophyll content across both varieties under PVA and combined Pb+PVA treatments suggests a protective effect on the photosynthetic apparatus. In terms of water content, an increase was observed in the hypocotyl, whereas the radicle exhibited greater sensitivity to combined stress treatments.

Due to its more resilient profile against heavy metal stress, Müfitbey variety should be preferred in areas with high pollution levels. The water retention and photosynthesis-protective effects of PVA present its potential as a biostimulant to mitigate damage caused by heavy metal stress in plants, warranting further studies focused on dose optimisation. Considering the radicle tissue's sensitivity to combined stresses, the application of root-protective or supportive biological agents may be explored. Future research should also aim to elucidate the molecular-level effects of Pb and PVA treatments and their relationships with other stress markers, thereby providing a more comprehensive understanding of stress tolerance mechanisms. These findings offer valuable guidance for applied studies in plant stress physiology and heavy metal toxicity.

REFERENCES

Ali, H., Khan, E., & Sajad, M. A. (2019). Phytoremediation of heavy metals—concepts and applications. *Chemosphere*, 91(7), 869–881.

Carson, R. (2020). *Silent spring*. Houghton Mifflin Harcourt.

Chi, X., Wang, Z., Li, Y., & Zhang, J. (2022). Effects of polyvinyl alcohol on plant growth and heavy metal stress alleviation: A review. *Environmental Science and Pollution Research*, 29(10), 14215–14228.

Chiellini, E., Corti, A., D'Antone, S., & Solaro, R. (2003). Biodegradation of polyvinyl alcohol-based materials. *Progress in Polymer Science*, 28(6), 963–1014.

Ghosh, M., & Singh, S. P. (2005). A review on phytoremediation of heavy metals and utilization of its byproducts. *Applied Ecology and Environmental Research*, 3(1), 1–18.

Hacımüftüoğlu, F., & Canbolat, M. Y. (2020). Polivinil alkol uygulamasının toprak fiziksel özellikleri ve mısır bitkisi (Zea mays L.) gelişimi üzerine etkisi. *Atatürk Üniversitesi Ziraat Fakültesi Dergisi*, 51(1), 32–43.

Hassan, C. M., Peppas, N. A., & Gaserod, O. (2021). Hydrogels based on poly(vinyl alcohol) for biomedical applications. *Journal of Biomedical Materials Research Part A*, 103(12), 3881–3894.

Hoagland, D. R., & Arnon, D. I. (1950). The water-culture method for growing plants without soil (Circular 347). California Agricultural Experiment Station. [Erişim: 29 Eylül 2021].

Khurana, N., & Kapoor, D. (2017). Polyvinyl alcohol as a soil amendment to improve water use efficiency and plant growth. *Agricultural Sciences*, 8(4), 369–377.

Kumar, A., Singh, R., & Prasad, M. N. V. (2022). *Sustainable agriculture and soil health: A remediation approach*. Springer.

Öztetik, E. (2015). Biomarkers of ecotoxicological oxidative stress in an urban environment: using evergreen plant in industrial areas. *Ecotoxicology*, 24, 903-914.

Öztetik, E. (2021). Physiological answers to metal triggered effects in crops. *Eskişehir Teknik Üniversitesi Bilim ve Teknoloji Dergisi B-Teorik Bilimler*, 9, 14–19.

Peppas, N. A., & Mongia, N. K. (1997). Ultrapure poly(vinyl alcohol) hydrogels with mucoadhesive and controlled release properties. *European Journal of Pharmaceutics and Biopharmaceutics*, 43(1), 51–58.

Sharma, P., & Dubey, R. S. (2005). Lead toxicity in plants. *Brazilian Journal of Plant Physiology*, 17(1), 35–52.

Topalbekiroğlu, M., İçoğlu, H. İ., & Daşdemir, M. (2017). Polivinilalkol nanolif kaplamasının bitki canlılığını korumaya etkisi. *Kimya ve İleri Fonksiyonel Malzemeler Dergisi (KİFMD)*, 1(2), 26–33.

Verbruggen, N., Hermans, C., & Schat, H. (2009). Molecular mechanisms of metal hyperaccumulation in plants. *New Phytologist*, 181(4), 759–776.

Wojcik, M., & Tukendorf, A. (1999). Cd-tolerance of maize, rye and wheat seedlings. *Acta Physiologiae Plantarum*, 21, 99–107.

Zhao, F. J., & Wang, P. (2021). Risk assessment of heavy metal pollution in agricultural soils and crops. *Environmental Pollution*, 276, 116724.

Pourrut, B., Shahid, M., Dumat, C., Winterton, P., & Pinelli, E. (2011). Lead uptake, toxicity and detoxification in plants. *Reviews of Environmental Contamination and Toxicology*, 213, 113–136.

➢ *ORAL PRESENTATION*

Effects of polyvinyl alcohol applications on biochemical parameters of different wheat (*T. aestivum* L.) cultivars grown under lead stress

Yunus Baran Badıllı* (*ORCID:* 0009-0007-0174-0886), Elif Öztetik (*ORCID*: 0000-0002-9663-6884)

Eskişehir Technical University, Science Faculty, Department of Biology, Eskişehir, Türkiye.

*Corresponding author e-mail: yunusbaran.445@gmail.com

Abstract

With the increase in population, the resulting rise in industrial pollution and excessive use of agricultural lands negatively affect ecosystem health, leading to reductions in food production and nutritional problems. Heavy metals from various sources such as industrial waste, fertilizers, pesticides and airborne pollutants contaminate agricultural lands, degrading soil and water quality and hindering healthy crop development. In particular, pollution caused by pesticides and heavy metals reaching farmlands through natural or anthropogenic activities restricts plant growth and reduces yield. Heavy metals like lead (Pb) are elements with high atomic numbers and densities. Due to their bioaccumulation properties, they accumulate in living organisms and cause cytotoxic effects. Their presence in the human body through the food chain leads to chronic toxicity and causes neurological and organ damage, threatening public health. Polyvinyl alcohol (PVA) is a synthetic polymer with high hydrophilicity and low toxicity to living organisms and it is biodegradable. It is widely used in medical devices, paper, textiles and food packaging. According to the literature, plant growth is supported in environments containing PVA. In this study, the effects of varying PVA concentrations on two wheat cultivars (*T. aestivum* L. cv. Müfitbey and *T. aestivum* L. cv. Nacibey) grown under Pb stress in a hydroponic system were investigated. Treatment groups included Pb (0.5 mM, 1.5 mM, 3.0 mM), PVA (5 ppm, 50 ppm, 500 ppm) and Pb+PVA combinations (0.5 mM+5 ppm, 1.5 mM+50 ppm, 3.0 mM+500 ppm). Plants underwent 10 days of germination followed by 10 days of growth in Hoagland nutrient solution. After 20 days, seedlings were analyzed for glutathione content, glutathione *S*-transferase activity and total protein content.

Keywords: Glutathione, Glutathione *S*-Transferase, Heavy metal, Lead (Pb), PVA, *Triticum aestivum* L.

1. INTRODUCTION

Environmental pollution, particularly the widespread dissemination of industrial waste and heavy metals into agricultural lands, has emerged as a serious ecological and biological concern in recent times. The accumulation of heavy metals in agricultural soils leads to a decline in microbial activity and the deterioration of soil health, thereby adversely affecting plant development (Ali et al., 2019). In addition to diminishing agricultural productivity, such contamination disrupts the biochemical and physiological processes in plants, causing significant challenges within the food chain (Sharma and Dubey, 2005).
Heavy metals such as lead (Pb) are introduced into soil and water systems predominantly through anthropogenic activities and are readily absorbed by plants. Within plant cells, Pb accumulates in organelles and impairs essential metabolic functions such as photosynthesis, respiration and protein synthesis. It also increases lipid peroxidation in cellular membranes, compromising their integrity and permeability (Singh et al., 2016). Moreover, Pb exposure results in an overproduction of reactive oxygen species (ROS), which disrupts the intracellular redox balance a condition referred to as oxidative stress (Mittler, 2002).

Oxidative stress inflicts damage upon cellular components, including DNA, proteins, lipids and disrupts cellular homeostasis. In response, plants activate sophisticated antioxidant defence mechanisms to mitigate such damage. Reduced glutathione (GSH), a tripeptide molecule (Glu–Cys–Gly), is central to this defence system and plays a vital role in the neutralisation of free radicals. GSH protects plant cells both by directly reacting with ROS and by collaborating with detoxification enzymes (Noctor et al., 2012).
Glutathione *S*-transferases (GSTs), a family of enzymes, utilise GSH to detoxify harmful compounds, including heavy metal derivatives. GSTs catalyse the conjugation of reactive metabolites, thereby enhancing plant tolerance to toxic substances (Edwards et al., 2000; Öztetik, 2015). Elevated levels of GSH and GST in

plants subjected to heavy metal stress serve as key indicators of the plant's biochemical adaptation to such adverse conditions (Sharma et al., 2012).

Polyvinyl alcohol (PVA), a synthetic polymer, has recently attracted interest as a potential biostimulant to enhance plant stress tolerance. By improving soil water retention, PVA enhances plant resilience against drought conditions and can reduce the uptake of heavy metal ions by plant roots (Kumar et al., 2020). Additionally, PVA may bolster the activity of antioxidant enzymes, thereby mitigating oxidative damage caused by heavy metal exposure. These effects position PVA as a promising agent for supporting plant growth under environmentally stressful conditions.

In conclusion, the contamination of agricultural areas especially through the accumulation of heavy metals such as Pb poses significant risks to plant biology. The antioxidant defence mechanisms developed by plants, particularly those involving GSH and GST, are critical in counteracting the harmful effects of oxidative stress. Moreover, the application of biopolymers such as PVA presents a promising strategy for enhancing plant tolerance to environmental pollutants. Therefore, biological systems and biotechnological interventions play an increasingly important role in addressing heavy metal pollution to ensure agricultural sustainability.

In this study, two wheat cultivars (*T. aestivum* L. cv. Müfitbey and *T. aestivum* L. cv. Nacibey), grown under hydroponic conditions, were exposed to varying concentrations of Pb, PVA and their combinations (Pb + PVA). The primary aim was to evaluate the biochemical responses of the plants to stress and to investigate whether PVA confers resistance against Pb-induced toxicity. Accordingly, this research seeks to contribute to the development of sustainable agricultural policies.

2. MATERIALS AND METHODS

2.1 Growth of Plants

As a pretreatment, the seeds were soaked in tap water for 2 hours followed by distilled water for another 2 hours. This process aimed to overcome seed dormancy and promote seed coat rupture. At the end of the 4 hour treatment, twenty healthy seeds were placed in each of twenty petri dishes lined with Whatman filter paper, cut to fit the base, for each wheat cultivar. The petri dishes were then transferred to a growth chamber. The 20 day growth period consisted of two phases: the first 10 days were allocated for germination, followed by 10 days for seedling development. During the germination stage, seeds were kept in darkness for the first 3 days and then under a photoperiod of 16 hours light/8 hours dark at 22°C ± 1°C for the remaining 7 days.

Upon completion of the 10 day germination stage, the seedling growth phase commenced. 10 healthy seedlings were selected and transferred to Hoagland solution (Hoagland and Arnon, 1950). The initial 3 days served as an adaptation period, during which no chemical treatment was applied. After adaptation, Pb, PVA and a Pb+PVA combination were added to the nutrient solutions at appropriate concentrations, initiating a 7 day chemical treatment phase. Thus, the entire plant growth process lasted for a total of 20 days.

2.2 Measurement of Reduced GSH Levels

Fresh hypocotyl and radicle tissues were homogenized and extracted with trichloroacetic acid (TCA). After pH adjustment, GSH levels were measured spectrophotometrically at 412 nm using the Ellman method. A standard calibration curve was prepared using known GSH solutions (µmol/g tissue) (Ellman, 1958, 1959; Sedlak and Lindsay, 1968).

2.3 Preparation of Cytosolic Extract

Pulverised root and shoot materials were extracted separately at a 1:3 (w/v) ratio using 100 mM phosphate buffer (pH 7.0) at 4 °C. The resulting mixture was homogenised for 2 minutes on ice using an Ultra-Turrax homogeniser. Following homogenisation, the samples were centrifuged at 15,000 rpm for 30 minutes at 4 °C. The resulting supernatant was immediately used for the determination of total protein content and GST activity (Öztetik, 2010).

2.4 Measurement of Total Protein Concentration

Total protein content in crude extracts was determined according to the method of Lowry et al. (1951), using bovine serum albumin (BSA) as standard at 660 nm and the data were expressed as mg/g tissue.

2.5 Measurement of GST Activity

Cytosolic extracts were prepared from fresh plant material. The formation of the CDNB-GSH conjugate was monitored spectrophotometrically at 340 nm and results were expressed as units/mg protein (Habig et al., 1974; Öztetik, 2021).

3. RESULTS

3.1 GSH Levels

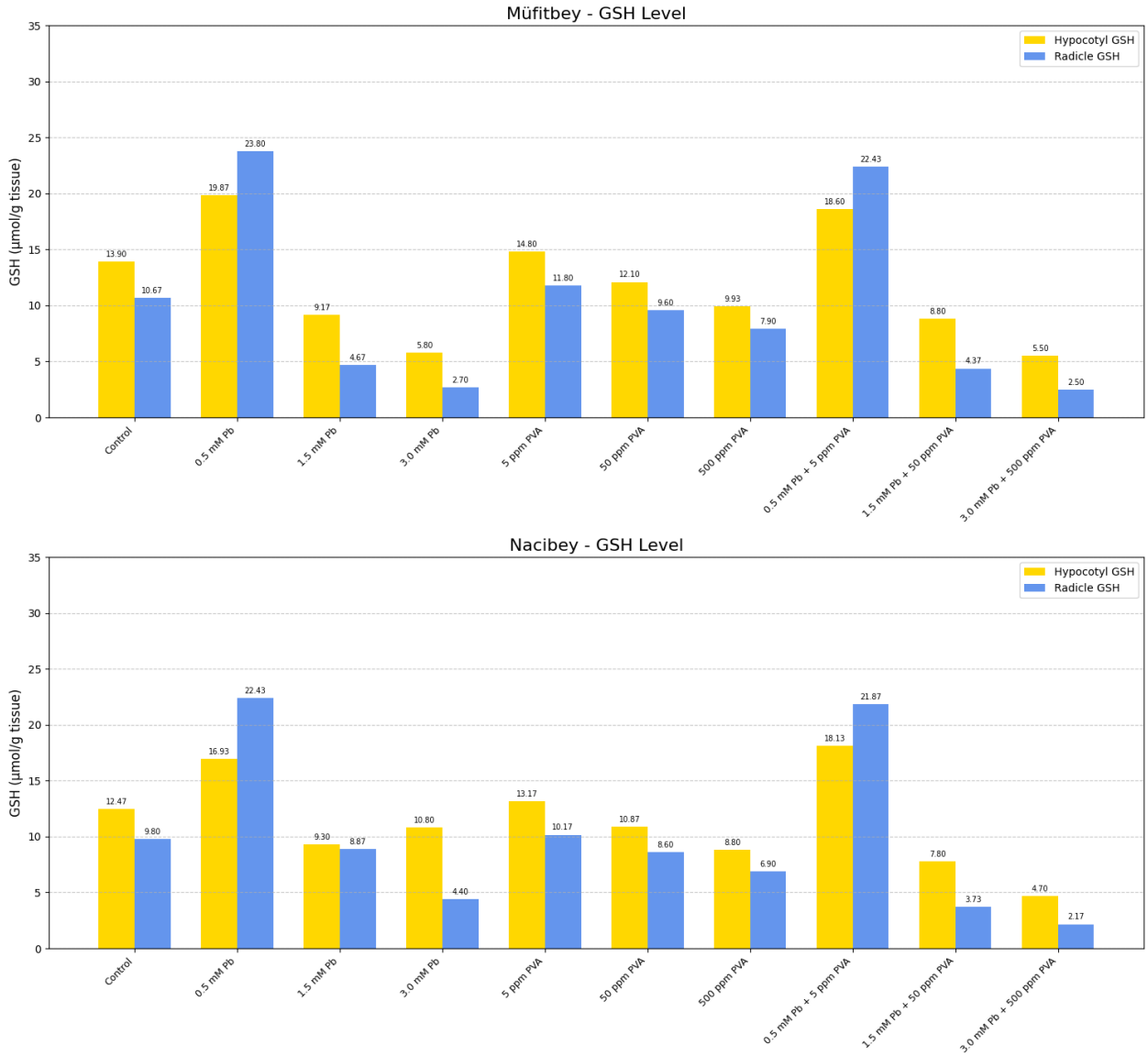

Figure 1. The Effect of Pb, PVA and Pb+PVA Combination Applications on Hypocotyl and Radicle GSH Levels.

In both Müfitbey and Nacibey varieties (Figure 1), the lowest GSH levels in the hypocotyl were recorded under the minimum concentrations of Pb and Pb + PVA combination treatments. As the concentration increased, a more substantial decline in GSH content was observed in the radicle compared to the hypocotyl, indicating a higher sensitivity of the radicle to escalating stress conditions. Although the radicle exhibited greater sensitivity to PVA treatments, elevated PVA concentrations consistently led to a reduction in GSH levels. Moreover,

combination treatments resulted in lower GSH content than Pb alone treatments, suggesting that the combined application exerts a more intense stress factor on the plant.

3.2 Total Protein Concentration

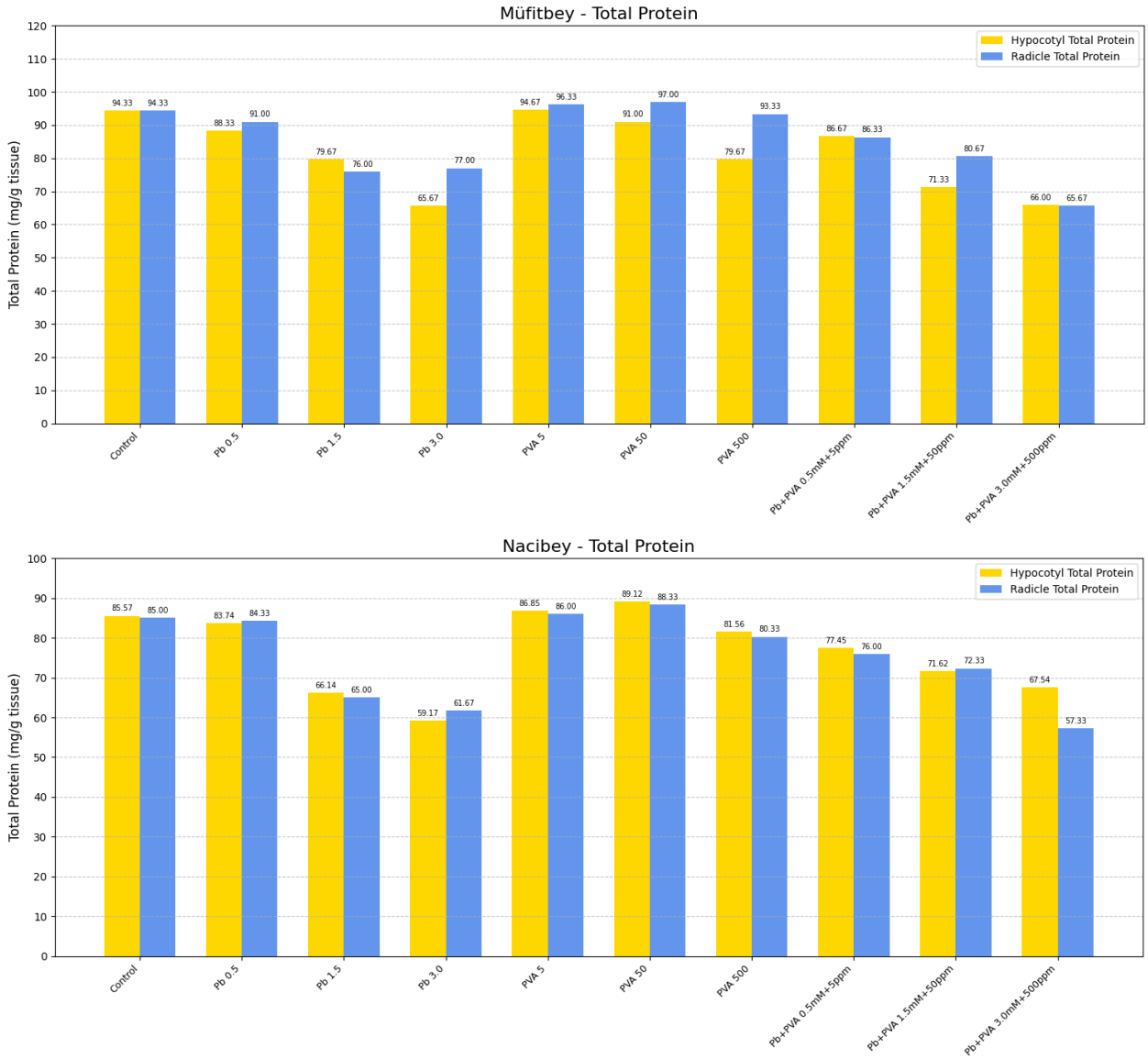

Figure 2. The Effect of Pb, PVA and Pb+PVA Combination Applications on Hypocotyl and Radicle Total Protein Concentration.

In Müfitbey variety, protein levels in both hypocotyl and radicle decreased with increasing concentrations of Pb, PVA and their combination (Pb+PVA). However, in Nacibey variety, Pb treatment caused a reduction in protein content, while PVA at 50 ppm increased protein levels in both organs. Nevertheless, the Pb+PVA combination resulted in decreased protein levels in both tissues (Figure 2). These findings suggest that PVA may have a concentration-dependent protein-enhancing effect; however, this effect appears limited under heavy metal stress conditions. Furthermore, Nacibey cultivar exhibited a more stable protein response and is considered more tolerant to stress compared to Müfitbey.

3.3 GST Activity

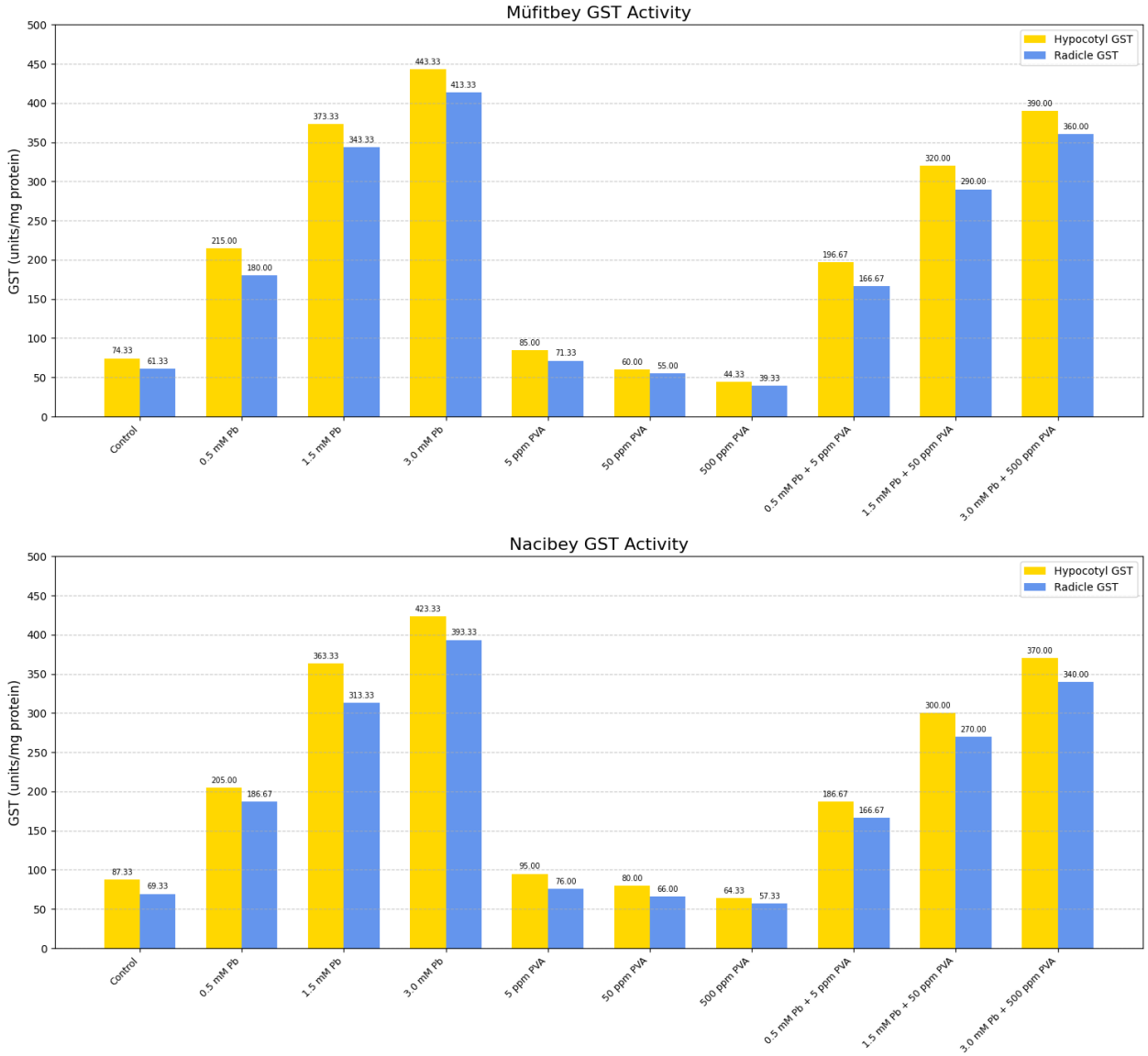

Figure 3. The Effect of Pb, PVA and Pb+PVA Combination Applications on Hypocotyl and Radicle GST Activity.

In both Müfitbey and Nacibey varieties (Figure 3), an increase in GST activity was observed in hypocotyl and radicle tissues as Pb concentrations increased. This suggests that Pb induced oxidative stress activates the plant's defence mechanisms. In contrast, increasing concentrations of PVA led to a decrease in GST activity in both cultivars. This may indicate that PVA either imposes a direct suppressive effect on the antioxidant system or reduces oxidative stress to a degree that diminishes the need for GST induction. In Pb+PVA treatments, GST activity rose again, reflecting the continued dominance of heavy metal stress. Overall, Müfitbey variety exhibited a more stable and resilient response to Pb and PVA stress compared to Nacibey.

4. DISCUSSION

4.1 GSH Levels

Pb stress often leads to a reduction in reduced GSH levels due to its rapid utilisation in detoxification processes and phytochelatin synthesis (Sharma and Dubey, 2005; Singh et al., 2016). This depletion impairs the plant's antioxidant capacity and increases oxidative damage. However, PVA application has been shown to alleviate Pb toxicity and help maintain or restore GSH levels (Kumar et al., 2020). As a result, PVA may support redox homeostasis and enhance the plant’s tolerance to heavy metal stress (Ali et al., 2019). Pb stress caused a significant decrease in GSH levels in plants, likely due to the rapid consumption of GSH in response to Pb-

induced oxidative stress. Application of PVA partially mitigated this decline; however, this protective effect was not consistent across all conditions or cultivars. Nacibey variety exhibited a more balanced GSH response to the combined Pb and PVA treatment.

4.2 Total Protein Content

According to various studies, Pb exposure causes a significant reduction in total protein content in plants, primarily due to the inhibition of protein synthesis and the promotion of protein degradation (Gupta et al., 2018; Pourrut et al., 2011). This decrease results in impaired cellular functions and adversely affects overall plant growth. In contrast, PVA application has been shown to mitigate Pb-induced protein loss by enhancing cellular stability and antioxidant defence mechanisms (Zhang et al., 2019). Pb exposure led to a marked reduction in total protein content, which can be attributed to the inhibition of protein synthesis and increased protein degradation under stress conditions. Conversely, 50 ppm PVA treatment increased protein levels, particularly in Nacibey variety, indicating a protective role. Nonetheless, the combination of Pb and PVA continued to suppress protein content in both varieties.

4.3 GST Activity

PVA has been reported to alleviate the adverse effects of Pb by supporting GST activity; however, this effect may vary depending on the application dose and plant species (Zhang et al., 2019). GST activity increased in response to Pb stress in both cultivars, indicating activation of the antioxidant defence mechanisms. PVA treatment reduced GST activity, which suggests that PVA may alleviate oxidative stress or exert a direct effect on the antioxidant system. Under combined Pb and PVA treatment, GST activity increased once again. Overall, Müfitbey variety demonstrated a more stable and resilient biochemical response to Pb and PVA stress.

5. CONCLUSION

This study demonstrated that Pb stress induces significant biochemical alterations in wheat plants. Pb treatments resulted in notable decreases in reduced glutathione (GSH) levels and total protein content, while simultaneously increasing glutathione *S*-transferase (GST) activity. Application of PVA, especially at lower concentrations, exhibited some protective effects by enhancing protein content and partially restoring GSH levels. However, combined Pb and PVA treatment revealed that the detrimental effects of heavy metal stress predominate, limiting the protective potential of PVA. Additionally, Nacibey variety showed a more stable and tolerant response to these stress conditions compared to Müfitbey variety. These findings highlight the potential utility of biopolymers in mitigating heavy metal stress and underscore the importance of cultivar selection in sustainable agricultural practices.

Future studies should focus on expanding the range of antioxidant biomarkers and including transcriptomic or proteomic analyses to better understand the molecular mechanisms underlying variety-specific stress responses. Moreover, testing a broader range of PVA concentrations and assessing its long-term effects on plant physiology could help determine its practical utility as a protective agent in phytoremediation or sustainable agriculture.

REFERENCES

Ali, H., Khan, E., & Sajad, M. A. (2019). Phytoremediation of heavy metals—concepts and applications. *Chemosphere*, 91(7), 869–881.

Edwards, R., Dixon, D. P., & Walbot, V. (2000). Plant glutathione S-transferases: enzymes with multiple functions in sickness and in health. *Trends in Plant Science*, 5(5), 193–198.

Ellman, G. L. (1958). A colorimetric method for determining low concentrations of mercaptans. *Archives of Biochemistry and Biophysics*, 74, 443.

Ellman, G. L. (1959). Tissue sulfhydryl groups. *Archives of Biochemistry and Biophysics*, 82, 70.

Gupta, D. K., Huang, H. G., & Corpas, F. J. (2018). Heavy metal stress in plants: From biomolecules to ecosystems. Springer.

Habig, W. H., Pabst, M. J., & Jakoby, W. B. (1974). Glutathione S-transferases. The first enzymatic step in mercapturic acid formation. *Journal of Biological Chemistry*, 249, 7130–7139.

Hoagland, D. R., & Arnon, D. I. (1950). The water-culture method for growing plants without soil. California Agricultural Experiment Station, Circular 347, Berkeley, California.

Kumar, S., Singh, R., & Sharma, A. (2020). Effects of polyvinyl alcohol on plant growth under heavy metal stress. *Journal of Environmental Sciences*, 92, 54–62.

Lowry, O. H., Rosebrough, N. J., Farr, A. L., & Randal, R. J. (1951). Protein measurement with the folin phenol reagent. *Journal of Biological Chemistry*, 193, 265–275.

Marrs, K. A. (1996). The functions and regulation of glutathione S-transferases in plants. *Annual Review of Plant Physiology and Plant Molecular Biology*, 47, 127–158.

Mittler, R. (2002). Oxidative stress, antioxidants and stress tolerance. *Trends in Plant Science*, 7(9), 405–410.

Noctor, G., Mhamdi, A., & Foyer, C. H. (2012). The roles of reactive oxygen metabolism in drought: not so cut and dried. *Plant Physiology*, 161(4), 1556–1566.

Öztetik (2010). Effects of tribenuron-methyl treatment on glutathione *S*-transferase (GST) activities in some wheat and barley varieties. *Pure and Applied Chemistry*., Vol. 82, No. 1, pp. 289–297.

Öztetik, E. (2015). Biomarkers of ecotoxicological oxidative stress in an urban environment: using evergreen plant in industrial areas. *Ecotoxicology*, 24, 903-914.

Öztetik, E. (2021). The effects of heavy metal applications on antioxidant defence activation in barley and wheat varieties. *Eskişehir Technical University Journal of Science and Technology B - Theoretical Sciences*, 9(Special Issue), 7–13.

Pourrut, B., Shahid, M., Dumat, C., Winterton, P., & Pinelli, E. (2011). Lead uptake, toxicity and detoxification in plants. *Reviews of Environmental Contamination and Toxicology*, 213, 113–136.

Sedlak, J., & Lindsay, R. H. (1968). Estimation of total, protein-bound and nonprotein sulfhydryl groups in tissue with Ellman's reagent. *Analytical Biochemistry*, 25(1), 192–205.

Sharma, P., & Dubey, R. S. (2005). Lead toxicity in plants. *Brazilian Journal of Plant Physiology*, 17(1), 35–52.

Sharma, P., Jha, A. B., Dubey, R. S., & Pessarakli, M. (2012). Reactive oxygen species, oxidative damage and antioxidative defense mechanism in plants under stressful conditions. *Journal of Botany*, 2012, 217037.

Singh, A., Singh, S., & Sharma, N. (2016). Toxic effects of heavy metals on plants. *Environmental Science and Pollution Research*, 23(8), 7185–7194.

Wang, L., Zhang, S., & Li, M. (2020). Protective effects of polyvinyl alcohol against heavy metal toxicity in plants. *Environmental Science and Pollution Research*, 27(5), 5292–5301.

Zhang, X., Li, J., & Liu, Y. (2019). Role of polyvinyl alcohol in mitigating oxidative stress induced by lead in wheat seedlings. *Plant Physiology and Biochemistry*, 140, 68–75.

Zhou, Y., Ma, H., Luo, X., & Li, M. (2020). Lead stress and antioxidant response in plants: a review. *Ecotoxicology and Environmental Safety*, 200, 110732.

➢ *ORAL PRESENTATION*

Photoremoval of Dissolved Organic Waste and Dielectric-Energy Storage with SmCuO/ZnO/$CuMn_2O_4$ Tri-Composite

Delia Teresa Sponza[1*] (*ORCID: https://orcid.org/0000-0002-4013-6186*),
Rukiye Öztekin[2] (*ORCID: https://orcid.org/0000-0002-1910-7348*)

[*1]Dokuz Eylül University, Faculty of Engineering, Department of Environmental Engineering, İzmir, Turkey.
[2] Dokuz Eylül University, Faculty of Engineering, Department of Environmental Engineering, İzmir, Turkey.

*Corresponding author e-mail: delya.sponza@deu.edu.tr

Abstract
The Photocatalysis process is considered as simple, green, and the best strategy for elimination of hazardous organic contaminants from wastewater. In this study, the new ternary composites composed of pure and Sm-doped CuO/ZnO/$CuMn_2O_4$ were synthesized for efficient treatment of norfloxacin (antibiotic) and methyl green (dye) as examples of stable organic pollutants. The addition of an Sm dopant aims to reinforce the absorption of light energy and support the separation of the charge carriers. The synthesized ternary composites were characterized by different techniques and the photocatalytic activities were measured under free and natural sunlight energy. The experimental samples were characterized with X-Ray Diffraction (XRD), Transmission Electron Microscopy (TEM), Scanning Electron Microscope (SEM), Brunauer–Emmett–Teller (BET) Surface Area, UV–visible Diffuse Reflectance Spectroscopy (DRS), Inductance Capacitance Resistance (LCR), and Energy Dispersive X-Ray (EDX or EDS) analyses, respectively. The electrical and dielectric performance of the samples were investigated and discussed. The obtained data confirmed that 98% of norfloxacin and 96% of methyl green were removed from contaminated water during 40–60 min photocatalytic degradation times for Sm-doped CuO/ZnO/$CuMn_2O_4$ tri-composite. Furthermore, Sm-doped CuO/ZnO/$CuMn_2O_4$ ternary composite has shown giant dielectric constant values, mainly at low frequencies, with low dielectric loss compared to a pure CuO/ZnO/$CuMn_2O_4$ composite.
Keywords: Antibiotics and dyes, Broad spectrum photocatalysts, Dissolved organic wastes, Electrical conductivity and dielectric-energy storage properties, Rare-earth, Ternary composites.

INTRODUCTION

For a healthy and safe environment, efficient treatment of dissolved organic compounds such as dyes, antibiotics, fungicides, insecticides, and herbicides has gained great attention in current scientific research. Polluted water is one of the most important environmental problems; wherein numerous poisonous and continual organic contaminants pose a high threat to living organisms. Antibiotics are important drugs for human and animals which are widely reported in water resources as pharmaceutical contaminants. It was reported that the consumption of antibiotics ranges from 100,000 to 200,000 tons annuall.

Organic dyes such as Congo red, methylene blue, and methyl green are another family of industrial compounds which are frequently be present in wastewater. The dyes are highly hazardous and the existence of methyl green in the water resources is a great worry owing to its potential poisonousness to the aquatic system and all organisms (Mosleh et al., 2019; Rouibah et al., 2023). In view of that, it is very important to use an efficient method to effectively remove organic pollutants such as norfloxacin and methyl green from wastewater. Considering this, photocatalysis is a green, simple, low cost and effective methodology that illuminates great benefits for the elimination of organic contaminants from wastewater **(**Ismael et al., 2020; Liu, D., et al., 2024). Based on coupling between different oxides in ternary composites, a new strategy has emerged to improve the photoresponse and increase the harvesting of visible light spectrum, as well as support the separation of the charge carriers which trigger photocatalytic efficiency.

The photocatalytic properties of BiOBr/ZnO/WO_3 ternary nanocomposites for degradation of phenol was studied. The authors found that this composite has a degradation efficiency of 90% for 50 mg/l phenol under visible-light illumination for 300 min. A ternary ZnO/Fe_3O_4/g-C_3N_4 composite synthesized using the hydrothermal method exhibited removal efficiencies of 97.87, 98.05, and 83.35% for methyl orange, alizarin yellow R, and orange G dyes in 150 min of visible light irradiation.

The n-type ZnO and the p-type CuO semiconductors are well-known and strong candidates for photocatalysts for wastewater treatment (Ong et al., 2018; Raizada et al., 2020). In the same context, $CuMn_2O_4$, as a manganese-based ternary metal oxide, has shown potential photocatalytic characteristics for the removal of organic pollutants in wastewater (Abel et al., 2019; Sobhani and Alinavaz, 2023). In view of the above details, in this study, new ternary composites composed of pure and Sm-doped CuO/ZnO/$CuMn_2O_4$ were synthesized for efficient treatment of norfloxacin (antibiotic) and methyl green (dye) as examples of stable organic pollutants. The addition of an Sm dopant aims to reinforce the absorption of light energy and support the separation of the charge carriers. The synthesized ternary composites were characterized by different techniques and the photocatalytic activities were measured under free and natural sunlight energy.

The electrical and dielectric performance of the samples were investigated and discussed. The obtained data confirmed that 98% of norfloxacin and 96% of methyl green were removed from contaminated water during 40–60 min for Sm-doped CuO/ZnO/$CuMn_2O_4$. Furthermore, Sm-doped CuO/ZnO/$CuMn_2O_4$ ternary composite has shown giant dielectric constant values, mainly at low frequencies, with low dielectric loss compared to a pure CuO/ZnO/$CuMn_2O_4$ composite.

MATERIALS AND METHODS

Preparation of SmCuO/ZnO/$CuMn_2O_4$ Tri-Composite

Pure and Sm-doped CuO/ZnO/$CuMn_2O_4$ ternary composites were prepared by using a co-precipitation approach. Firstly, CuO/$CuMn_2O_4$ powder was synthesized by dissolving 9.6 g $Cu(NO_3)_2{\cdot}3H_2O$ (Sigma Aldrich, St. Louis, MO, USA) and 4.9 g $Mn(CH_3CO_2)_2{\cdot}4H_2O$ (Sigma Aldrich) into 200 ml deionized water with continuous stirring for 30 min. NH_4OH solution was added drop by drop until pH was equal to 7.3 to form the precipitate. The obtained precipitate was deeply washed with deionized water until removing any dissolved impurities. Then, the acquired precipitate was dried and calcined at 650 °C to form CuO/$CuMn_2O_4$ binary composite with ratio of CuO to $CuMn_2O_4$ equal to 75:25%, respectively. After that, 1.35 g of $Zn(CH_3CO_2)_2{\cdot}2H_2O$ (Sigma Aldrich) was dissolved into 100 ml deionized water followed by addition of 2 g of the obtained CuO/$CuMn_2O_4$ binary composite with constant stirring for 45 min. Later, NH_4OH solution was added to precipitate the Zn ions in hydroxide form under continuous stirring. The obtained powder was calcined at 500 °C to form CuO/ZnO/$CuMn_2O_4$ ternary composite. For Sm-doped CuO/ZnO/$CuMn_2O_4$ sample, 0.195 g $Sm(NO_3)_3$ substance was added during the synthesis of CuO/$CuMn_2O_4$ and 0.02 g was added to $Zn(CH_3CO_2)_2{\cdot}2H_2O$ solution followed by using the same steps for pure CuO/ZnO/$CuMn_2O_4$ sample.

Physicochemical Properties of Nanocomposite

The synthesized powders were analyzed by different techniques using X-ray diffraction device (Bruker D8 Advance, λ = 1.5406 Å), transmission electron microscope (JEOL JEM-2100, Tokyo, Japan), scanning electron microscope (JSM-IT200, Tokyo, Japan), Brunauer–Emmett–Teller (BET) surface area (NOVA 3200, Davie, FL, USA), and UV–visible diffuse reflectance spectroscopy (Shimadzu UV-2050, Tokyo, Japan). The relations between frequency and dielectric or ac electrical conductivity of pure and Sm-doped CuO/ZnO/$CuMn_2O_4$ ternary composites were measured in pellet form (thickness = 2.5 mm and radius = 0.45 cm) at room temperature based on LCR device (Hioki 3532-50, Ha Noi City, Vietnam).

The photocatalytic activity of pure and Sm-doped CuO/ZnO/$CuMn_2O_4$ ternary composites were established for elimination of norfloxacin and methyl green with concentration 15 mg/l as known examples for dissolved organic waste. The added catalyst dose to 100 ml solution of pollutant is 0.05 g. The mixed solution of the catalyst and dissolved pollutant was stirred under dark conditions and following that, irradiated by ordinary solar light energy. The average solar radiation was measured to be ~780 ± 10 W/m^2 (August, 12–2 pm). The variation of pollutant concentration was observed by measuring the absorbance (norfloxacin λ_{max} = 278 nm and methyl green λ_{max} = 633 nm) of the solution at different times.

RESULTS AND DISCUSSION

XRD Investigation

The X-ray diffraction (XRD) technique is used to analyze the crystalline structures of synthesized powders. Figure 1 displays the XRD results of pure and Sm-doped CuO/ZnO/$CuMn_2O_4$ tri-composites. The X-ray diffraction pattern of the pure CuO/ZnO/$CuMn_2O_4$ tri-composite revealed various peaks with different relative

intensities. In Figure 1, the peaks at 2-theta values of 32.55°, 35.54°, 38.72°, 48.65°, 53.51°, 58.12°, 61.45°, 65.99°, 67.8°, 72.2°, and 75.94° were related to (110) (11-1), (111), (20-2), (020), (202), (11-3), (022), (220), (311), and (22-2) crystallographic planes of CuO with monoclinic phase in agreement with JCPDS (# 48-1548, space group: C2/c). Additionally, the pattern also displayed another series of XRD peaks at 2θ = 31.76°, 34.38°, 36.19°, 47.46°, 56.51°, 62.70°, 67.8°, and 68.99°, recognized for (100), (002), (101), (102), (110), (103), (112), and (201) crystallographic planes of the zinc oxide phase with hexagonal structure (JCPDS. # 36-1451, space group: p63mc). The XRD peaks that appeared at 2-theta values of 18.74°, 30.31°, 35.54°, 43.8°, 57.72°, and 62.7° coincide with the crystallographic planes of (111), (220), (311), (400), (511), and (440) for cubic $CuMn_2O_4$ spinel oxide in agreement with JCPDS (# 74-1921 space group: Fd-3m).

The Sm-doped CuO/ZnO/$CuMn_2O_4$ tri-composite has a similar XRD pattern to the pure one, which proves the same composite structure formation, Figure 1. The broadening of the X-ray diffraction peaks was improved after Sm ions doping which supports the reduction in the crystallite size. The Scherer formula, as represented in Eq. (1), was used to compute the average crystallite size of pure and Sm-doped CuO/ZnO/$CuMn_2O_4$ tri-composites through using the three main peaks of each phase.

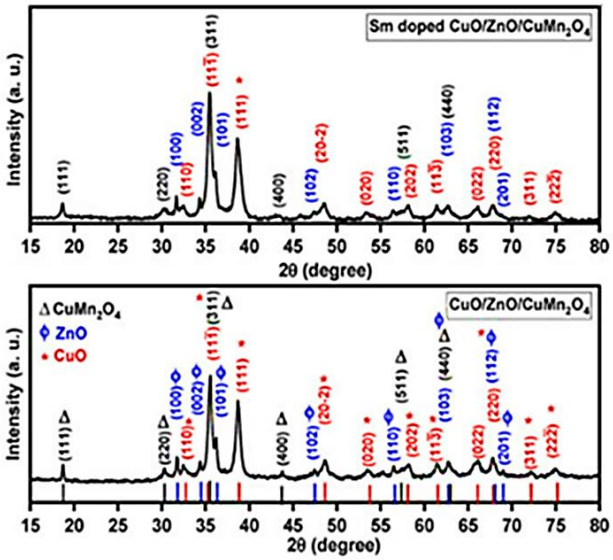

Figure 1. X-ray diffraction patterns of pure and 'Sm-doped' CuO/ZnO/$CuMn_2O_4$ ternary composites.

$$D = K\lambda\beta\cos\theta \quad (1)$$

In the formula given above, the θ, β, λ, K and D symbols are the Bragg angle, peak broadening at half the maximum (FWHM), wavelength of the used X-ray (1.5406 Å), dimensionless shape factor, and average crystallite size, respectively. For the pure composite, the D value was computed to be 29, 26, and 39 nm for CuO, ZnO, and $CuMn_2O_4$ phases, respectively. The average crystallite size of these constituents decreased to 23, 24, and 25 nm after Sm ions doping, respectively. The lattice constants of CuO, ZnO, and $CuMn_2O_4$ phases were computed by Rietveld refinement analysis based on Maud software (version 3.16.1.288) as tabulated in Table 1. As observed in Table 1, the lattice constants of CuO, ZnO, and $CuMn_2O_4$ were increased after doping by Sm ions. These expansions can be related to the substitution of Cu2+ (0.73 Å), Zn2+ (0.74 Å) and Mn3+ (0.58 Å) cations by Sm3+ (0.958 Å) ions of larger ionic radius.

Table 1. Calculated lattice constants (a, b, c) and unit cell volume (V) of CuO, ZnO and $CuMn_2O_4$ phases for both ternary composites

Samples	Phase	a (Å)	b (Å)	c (Å)	V (Å^3)
CuO/ZnO/$CuMn_2O_4$	CuO	4.696	3.426	5.135	81.51
	ZnO	3.254	3.254	5.219	47.89
	$CuMn_2O_4$	8.343	8.343	8.343	580.8
Sm-CuO/ZnO/Mn_2O_4	CuO	4.702	3.428	5.140	81.69
	ZnO	3.262	3.262	5.224	48.14
	$CuMn_2O_4$	8.350	8.350	8.350	582.2

Optical Properties: UV–Visible Diffuse Reflectance

Figure 2 depicts the UV–visible diffuse reflectance spectra of pure and Sm-doped CuO/ZnO/$CuMn_2O_4$ tri-composites. As shown in Figure 2, the reflectance spectra of both composites display three reduction regions of intensity (%), which related to the individual absorption edge of each phase including CuO, ZnO, and $CuMn_2O_4$ structures. It can be seen that these absorption edges were moved to a low energy direction after doping by Sm ions. This behavior signifies that the Sm-doped CuO/ZnO/$CuMn_2O_4$ tri-composite has a more harvesting of visible light spectrum compared to pure sample. As reported for metal oxides, perovskites, and composites materials, the formula of Tauc method can be used to compute the band gap energy of pure and Sm-doped CuO/ZnO/$CuMn_2O_4$ samples as shown in Equation given below (Alias et al., 2021; Salem et al., 2023): Eq. (2)

$$\alpha = A\left(h_v - E_g\right)^n / h_v \quad (2)$$

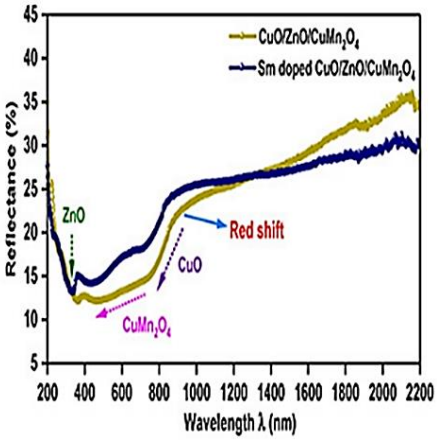

Figure 2. UV-vis diffuse reflectance (%) vs.wavelength (nm) for pure and Sm-doped CuO/ZnO/$CuMn_2O_4$ tri composites

In the formula given below, hν, n, Eg, A, and α are the energy of wavelength, constant, band gap energy, independent constant, and absorption coefficient, respectively. The Kubelka–Munk (K-M) formula is used to transform the reflectance spectra to absorption according to Equation (Alias et al., 2021; Salem et al., 2023), Eq. (3).

$$F(R)= (1-R)^2/2R= \alpha/S \quad (3)$$

where, S, R and F(R) symbols are the scattering coefficient, reflectance, and the Kubelka–Munk function, respectively.

As represented in Figure 3, the [F(R) hv]2 was plotted opposed to energy of wavelength (hv) and the lengthening of the descending parts of the curves produce the exact band gap energies of pure and Sm-doped $CuO/ZnO/CuMn_2O_4$ samples. Three band gap energies were found for the pure $CuO/ZnO/CuMn_2O_4$ composite with values of 1.45, 3.29, and 1.85 eV, which match with the energy gaps of ZnO, $CuMn_2O_4$, and CuO phases, respectively (Mahroug et al., 2014; Wang, X., et al., 2023; Anand, et al., 2024). The doping by Sm ions induced red shifts of the band gap energies of ZnO, $CuMn_2O_4$, and CuO phases to 2.79, 1.66, and 1.43 eV, respectively. The insertion of Sm ions leads to broad absorption of visible light spectrum particularly for ZnO phase. The noticed decreases in the band gap energies support the replacement of Sm ions for Zn, Cu, or Mn sites into the $CuO/ZnO/CuMn_2O_4$ composite. This lessening in the band gap energies may be attributed to the transfer of the electrons between Sm 4f level and the conduction or valence band of ZnO, CuO, or $CuMn_2O_4$ (Sukriti; Chand and Singh, 2020). Therefore, the doped composite could be a promising composition for photocatalytic applications, as it boosts the harvesting of visible light spectrum.

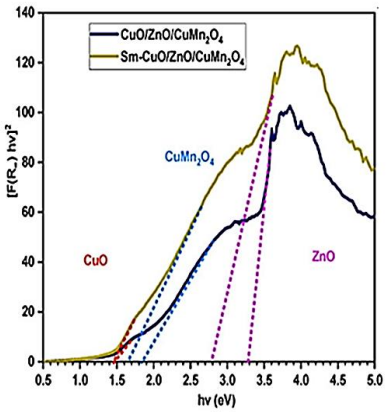

Figure 3. Estimation of band gap energies of pure and Sm-doped $CuO/ZnO/CuMn_2O_4$ tri-composites

Morphology and Surface Area

The scanning electron microscope (SEM) micrographs of pure and Sm-doped $CuO/ZnO/CuMn_2O_4$ tri-composites are depicted in Figure 4. The images of both powders reveal the formation of semi-symmetrical spherical grains with finer structure in the case of the Sm-doped composite. Both samples have homogenous surface distribution with a certain degree of agglomeration. Figure 5 demonstrates the transmission electron microscope (TEM) images with corresponding particle size distribution histograms of the pure and Sm-doped $CuO/ZnO/CuMn_2O_4$ tri-composites. The TEM images display that the majority of the particles have a spherical shape with average mean size of 29 and 26 nm for the pure and Sm-doped $CuO/ZnO/CuMn_2O_4$ tri-composites, respectively.

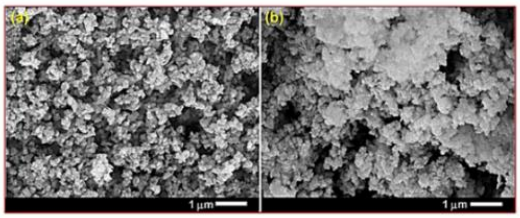

Figure 4. SEM images of **(a)** pure and **(b)** Sm-doped CuO/ZnO/$CuMn_2O_4$ tri-composites.

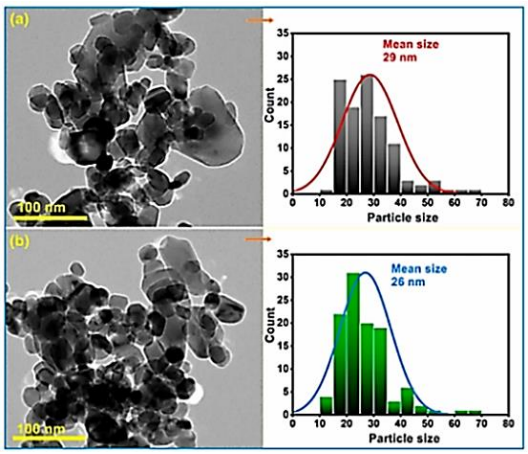

Figure 5. TEM images with corresponding particle size distribution histograms of **(a)** pure and **(b)** Sm-doped CuO/ZnO/$CuMn_2O_4$ tri-composites

As presented in Figure 6, the compositional analysis based on energy dispersive X-ray technique confirms the presence of only Cu, Zn, Mn, and O elements in the pure CuO/ZnO/$CuMn_2O_4$ tri-composite. The EDX pattern of the doped composite reveals the existence of Cu, Zn, Mn, Sm, and O elements with measured wt% of Sm dopant equal to 2.23, which nearly match with the added value (3 wt%). No noticeable peaks related to any impure elements were detected, confirming the purity of the synthesized composites. Figure 7 depicts the nitrogen adsorption/desorption curves of the pure and Sm-doped CuO/ZnO/$CuMn_2O_4$ tri-composites, the plots inset in Figure 7 represent the pore size distribution. The pure CuO/ZnO/$CuMn_2O_4$ tri-composite has shown a BET surface area of 3.11 m^2/g with total pore volume and pore size of 0.11 cm^3 g1 and 7.8 nm, respectively. The BET surface area of the CuO/ZnO/$CuMn_2O_4$ tri-composite was improved to 4.24 m^2/g after addition of Sm ions with measured total pore volume and pore size of 0.17 cm^3/g and 10 nm, respectively.

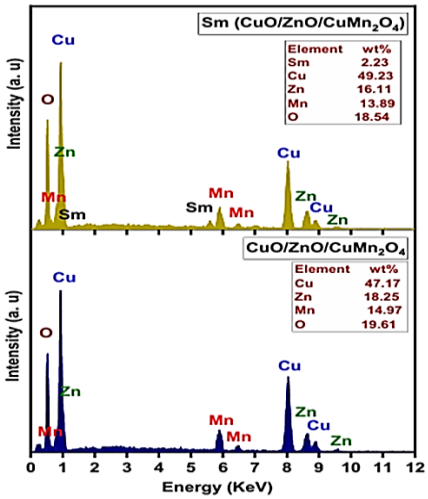

Figure 6. EDX patterns of pure and Sm-doped CuO/ZnO/$CuMn_2O_4$ tri-composites.

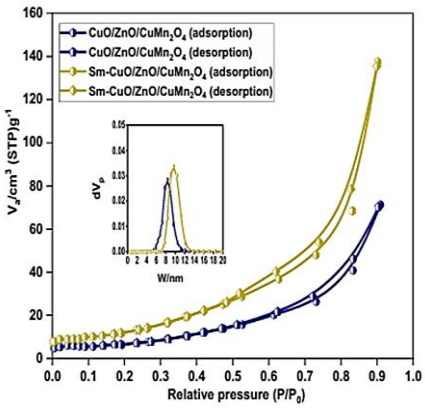

Figure 7. BET surface area of pure and Sm-doped CuO/ZnO/$CuMn_2O_4$ tri-composites, with inset pore size distribution.

Treatment of Dissolved Organic Waste

Figure 8 shows the time dependent UV–visible absorbance curve of 15 mg/l norfloxacin solution under dark stirring, and after exposure to solar light energy in the presence of pure and Sm-doped CuO/ZnO/$CuMn_2O_4$ tri-composites. The measured change in the UV–visible absorbance curve of norfloxacin solution reveals that the pure CuO/ZnO/$CuMn_2O_4$ catalyst has an adsorption capacity of 9% after 20 min of dark stirring. After exposed to solar light energy the absorbance curve of norfloxacin was decreased, with computed photodegradation efficiency of 67% after 50 min. In the case of the Sm-doped CuO/ZnO/$CuMn_2O_4$ tri-composite, the variation in the UV–visible absorbance of norfloxacin demonstrated that the adsorption capacity was 16% after 20 min of dark stirring while the degradation activity significantly increased to 97% after 50 min of solar illumination. The presence of Sm ions as a dopant activates the photodegradation process of the CuO/ZnO/$CuMn_2O_4$ tri-composite.

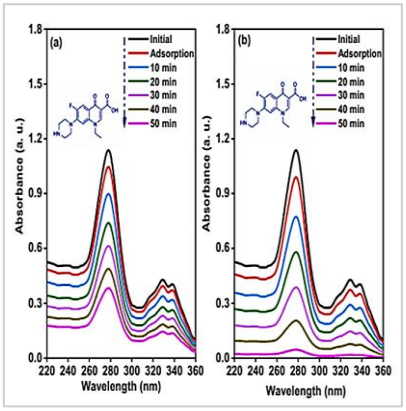

Figure 8. Time-dependent UV–visible absorption spectra of norfloxacin solution for **(a)** $CuO/ZnO/CuMn_2O_4$ and **(b)** Sm-doped $CuO/ZnO/CuMn_2O_4$ ternary composites.

The dependence of Ct/C0 on the irradiation time of the pure and Sm-doped $CuO/ZnO/CuMn_2O_4$ tri-composites is illustrated in Figure 9a. The plotted curves show that the Ct/C0 strongly and continuously decreases with increasing time of irradiation for the Sm-doped $CuO/ZnO/CuMn_2O_4$ catalyst. Furthermore, the kinetic performance and the apparent rate constant for the photocatalytic degradation of norfloxacin was quantitatively evaluated through fitting the obtained experimental values to the pseudo first-order rate equation (Wang, J., et al., 2015), Eq. (4):

$$\ln(C_0/C_t)=kt \quad (4)$$

In this formulation, C0 and Ct represent the concentration of the norfloxacin at time (t) = zero and at different irradiation times (min), respectively, while k signifies the apparent rate constant (min^{-1}) of the photodegradation reaction**.** Figure 9b shows the linear fitting relationship between ln(C0/Ct) and the time (min) for both catalysts. Remarkably, the photodegradation apparent rate constant (k) of the Sm-doped $CuO/ZnO/CuMn_2O_4$ catalyst (0.053 min^{-1}) is significantly higher than that of the pure $CuO/ZnO/CuMn_2O_4$ tri-composite (0.021 min^{-1}) n−1) is significantly higher than that of the pure $CuO/ZnO/CuMn_2O_4$ tri-composite (0.021 min^{-1}).

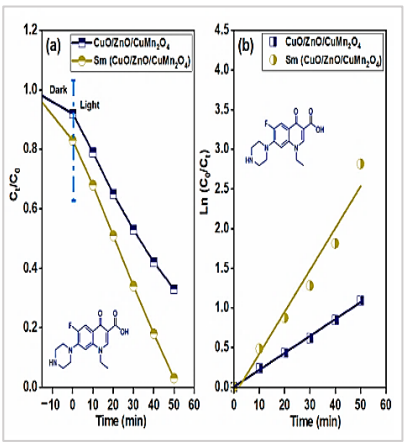

Figure 9. (a) Ct/C0 with time plots and **(b)** variation of ln(C0/Ct) with time to find the apparent rate constant for the degradation of norfloxacin antibiotic in the existence of pure and Sm-doped $CuO/ZnO/CuMn_2O_4$ ternary composites.

Figure 10a,b displays the time dependent UV–visible absorbance spectra of 15 mg/l methyl green solution under dark stirring for 20 min and after exposure to solar energy for 40 min in the presence of pure and Sm-doped $CuO/ZnO/CuMn_2O_4$ tri-composites, respectively. The estimated change in the absorbance indicated that the adsorption and photodegradation values of the pure $CuO/ZnO/CuMn_2O_4$ catalyst towards methyl green dye were 8% and 70%, respectively. Interestingly, the Sm-doped $CuO/ZnO/CuMn_2O_4$ catalyst exhibits an

adsorption value of 14% with a total degradation efficiency of 96% in 40 min towards 15 mg/l methyl green solution. As shown in Figure 10c, the change in Ct/C0 with time reveals the fast removal of the dye for Sm-doped CuO/ZnO/$CuMn_2O_4$ compared to the pure catalyst. The kinetic study of the photodegradation reaction points out that the pure CuO/ZnO/$CuMn_2O_4$ catalyst has an apparent rate constant of 0.027 min^{-1} (R^2 = 0.97), whereas the Sm-doped CuO/ZnO/$CuMn_2O_4$ possesses an apparent rate constant of 0.067 min^{-1} (R^2 = 0.95), shown in Figure 10d.

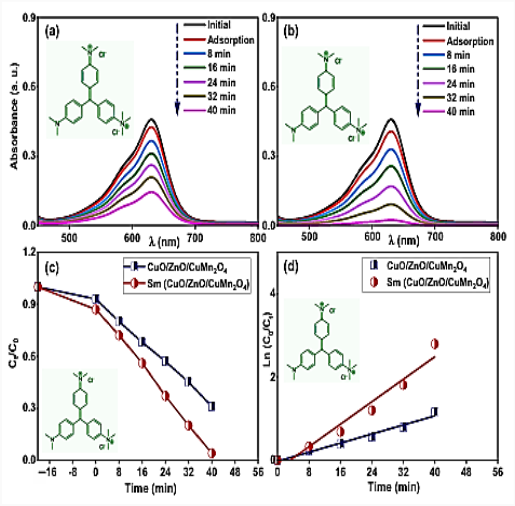

Figure 10. Time dependent UV–visible absorption spectra of 15 mg/l methyl green dye for **(a)** pure and **(b)** Sm-doped CuO/ZnO/$CuMn_2O_4$ catalysts, **(c)** Ct/C0 with time, and **(d)** variation of ln (C0/Ct) with time for both samples.

Analysis of Ac Electrical Conductivity and Dielectric Properties

Figure 11a–c show the impact of changes in the applied frequency on the ac electrical conductivity, dielectric constant, and dielectric loss of pure and Sm-doped CuO/ZnO/$CuMn_2O_4$ tri-composites. As shown in Figure 11a, the trend of the ac electrical conductivity displays an increasing performance with growth in the applied frequency, particularly at higher frequencies, owing to the migration improvement of the charge carriers (electrons). At lower and middle frequencies (102–104 Hz), it can be seen that the improvement of the electrical conductivity is weak, and after that, it becomes very sharp at appropriately higher frequencies, especially for the Sm-doped CuO/ZnO/$CuMn_2O_4$ sample. As the frequency increases, the ac electrical conductivity of pure and Sm-doped CuO/ZnO/$CuMn_2O_4$ tri-composites becomes more frequency dependent. The applied frequency where the dispersion takes place is recognized as the hopping or critical frequency. It can be observed that the hopping or critical frequency moved towards a low frequency direction, owing to Sm ions doping into the CuO/ZnO/$CuMn_2O_4$ composite. This change in the electrical conductivity from the region of frequency-independent to the region of frequency-dependent emphasizes the electrical conductivity relaxation phenomenon (Saadi et al., 2020; Khan et al., 2018).

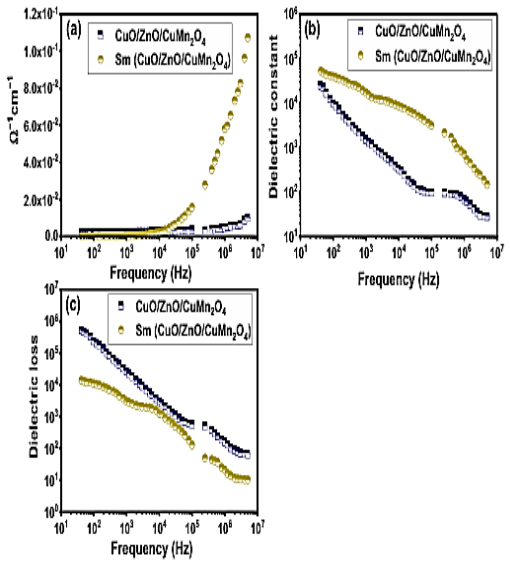

Figure 11. Dependency of **(a)** ac electrical conductivity, **(b)** dielectric constant, and **(c)** dielectric loss on frequency for pure and Sm-doped CuO/ZnO/$CuMn_2O_4$ ternary composites.

Table 2 compares the dielectric constant values of the pure and Sm-doped CuO/ZnO/$CuMn_2O_4$ ternary composites at several frequencies. The reported results indicate that the Sm-doped CuO/ZnO/$CuMn_2O_4$ sample has colossal relative permittivity values (>103) at many frequencies. Generally, such behavior of the dielectric dispersion in metal oxides or composites structures can be illuminated in the interpretation of Maxwell–Wagner interfacial theory, which is in agreement with Koops phenomenological philosophy (Saadi et al., 2020; Ishaque et al., 2023). In this explanation, the grains are highly conductive and become disjointed by grain boundaries, which are very poorly conductive. As a result, under an applied electric field, the charge carriers (electrons) are being collected or accumulated at the weak conducting grain boundaries or interfaces (Saadi et al., 2020; Ishaque et al., 2023). At the lower frequencies, the collection or the accumulation of the charge carriers at the high resistance grain boundaries includes a big polarizability, yielding a large polarization which is measured as a high dielectric constant value.

Table 2. Comparre the dielectric constant values of pure and Sm-doped CuO/ZnO/$CuMn_2O_4$ ternary composites at several frequencies from 50 to 10,000 Hz.

Samples	**50 Hz**	**100**	**250**	**500**	**1000**	**3000**	**5000**	**8000**	**10,000**
CuO/ZnO/$CuMn_2O_4$	22,448	9756	4383	2532	1507	749	556	390	332
Sm-CuO/ZnO/$CuMn_2O_4$	47,845	39,254	30,214	24,562	17,211	11,726	10,709	9197	8579

CONCLUSIONS

In this work, pure and Sm-doped CuO/ZnO/$CuMn_2O_4$ ternary composites were successfully synthesized using the co-precipitation approach. The influence of Sm dopant on the optical, dielectric, electrical, and photocatalytic properties of the CuO/ZnO/$CuMn_2O_4$ ternary composite was studied and discussed. The XRD patterns verified the presence of CuO, ZnO, and $CuMn_2O_4$ constituents in the composite structure. The SEM and TEM images of the pure and Sm-doped CuO/ZnO/$CuMn_2O_4$ powder show the formation of homogenous spherical particles with a small size within 26–29 nm. The optical absorption analysis demonstrates that Sm doping of the CuO/ZnO/$CuMn_2O_4$ tri-composite greatly reinforces the harvesting of visible light energy compared to pure sample. The photocatalytic measurements for the removal of organic waste revealed that the Sm-doped CuO/ZnO/$CuMn_2O_4$ catalyst has photodegradation efficiencies of 97% for norfloxacin and 96% for methyl green. The reusability experiments confirmed the good stability of the Sm-doped CuO/ZnO/$CuMn_2O_4$ catalyst, along with a high mineralization efficiency to convert norfloxacin and methyl green molecules to carbon dioxide and water. For energy storage, Sm-doped CuO/ZnO/$CuMn_2O_4$ pellets exhibited a giant

dielectric constant, principally at low frequency, with low dielectric loss values compared to the pure CuO/ZnO/$CuMn_2O_4$ sample.

ACKNOWLEDGEMENTS

This research study was undertaken in the Environmental Microbiology Laboratories at Dokuz Eylül University Engineering Faculty Environmental Engineering Department, İzmir, Turkey. The authors would like to thank this body for providing financial support.

REFERENCES

Rouibah, K., Akika, F.-Z., Rouibah, C., Boudermine, H. R., Douafer, S., Boukerche, S., Boukerche, G., & Benamira, M. (2023). Solar photocatalytic degradation of Methyl green on $CuFe_2O_4$/α Fe_2O_3 heterojunction, Inorganic Chemistry Communications, 148, 110361.

Mosleh, S., Dashtian, K., Ghaedi, M., & Amiri, M. (2019). A Bi_2WO_6/Ag_2S/ZnS Z-scheme heterojunction photocatalyst with enhanced visible-light photoactivity towards the degradation of multiple dye pollutants, RSC Advances, 9, 30100–30111.

Liu, D., Cai, H., Zhou, W., Lei, D., Cao, C., Xia, X., Xiao, L., Qian, Q., & Chen, Q. (2024). Application of 3D printing technology for green synthesis of Fe_2O_3 using ABS/TPU/chlorella skeletons for methyl orange removal, RSC Advances, 14, 1501–1512.

Ismael, A. M., El-Shazly, A. N., Gaber, S. E., Rashad, M. M., Kamel, A. H., & Hassan, S. S. M. (2020). Novel TiO_2/GO/$CuFe_2O_4$ nanocomposite: Amagnetic, reusable and visible-light-driven photocatalyst for efficient photocatalytic removal of chlorinated pesticides from wastewater, RSC Advances, 10, 34806–34814.

Ong, C. B., Ng, L. Y., & Mohammad, A. W. (2018). A review of ZnO nanoparticles as solar photocatalysts: Synthesis, mechanisms and applications, Renewable and Sustainable Energy Reviews, 81, 536–551.

Raizada, P., Sudhaik, A., Patial, S., Hasija, V., Khan, A. A. P., Singh, P., Gautam, S., Kaur, M., & Nguyen, V.-H. (2020). Engineering nanostructures of CuO-based photocatalysts for water treatment: Current progress and future challenges, Arabian Journal of Chemistry, 13, 8424–8457.

Sobhani, A., & Alinavaz, S. (2023). $ZnMn_2O_4$ nanostructures: Synthesis via two different chemical methods, characterization, and photocatalytic applications for the degradation of new dyes. Heliyon, 9, e21979.

Abel, M. J., Pramothkumar, A., Senthilkumar, N., Jothivenkatachalam, K., Inbaraj, P. F. H., & Joseph prince, J. (2019). Flake-like CuMn2O4 nanoparticles synthesized via co-precipitation method for photocatalytic activity, Physica B: Condensed Matter, 572, 117–124.

Alias, F. I. H., Rajmi, R., Maulud, M. F.; & Mohamed, Z. (2021). Structural, optical and dielectric properties of tellurium-based double perovskite Sr2Ni1−xZnxTeO6, RSC Advances, 11, 31631–31640.

Salem, B. B., Essalah, G., Ameur, S. B, Duponchel, B., Guermazi, H., Guermazi, S., & Leroy, G. (2023). Synthesis and comparative study of the structural and optical properties of binary ZnO-based composites for environmental applications, RSC Advances, 13, 6287–6303.

Mahroug, A., Boudjadar, S., Hamrit, S., & Guerbous, L. (2014). Structural, optical and photocurrent properties of undoped and Al-doped ZnO thin films deposited by sol–gel spin coating technique, Materials Letters, 134, 248–251.

Anand, A. M., Raj, A., Salam, J. A., Nath, R. A., & Jayakrishnan, R. (2024). Photoconductivity in self-assembled CuO thin films, Materials for Renewable and Sustainable Energy, 13, 45–58.

Wang, X., Xu, C., & Liu, J. (2023). Extracting optical parameters of Cu-Mn-Fe spinel oxide nanoparticles for optimizing air-stable, high efficiency solar selective coatings, ACS Applied Optical Materials, 1, 960–972.

Sukriti, Chand, P., & Singh, V. (2020). Enhanced visible-light photocatalytic activity of samarium-doped zinc oxide nanostructures, Journal of Rare Earths, 38, 29–38.

Wang, J., Liu, C., Tong, L., Li, J., Luo, R., Qi, J., Li, Y., & Wang, L. (2025). Iron–copper bimetallic nanoparticles supported on hollow mesoporous silica spheres: An effective heterogeneous Fenton catalyst for orange II degradation, RSC Advances, 5, 69593–69605.

Saadi, H., Rhouma, F. I. H., Benzarti, Z., Bougrioua, Z., Guermazi, S. & Khirouni, K. (2020). Electrical conductivity improvement of Fe doped ZnO Nanopowders, Materials Research Bulletin, 129, 110884.

Khan, R., Zulfiqar, de Araujo, C. I. L., Khan, T., Muneeb-Ur-Rahman, Zia-Ur-Rehman, Khan, A., Ullah, B., & Fashu, S. (2018). Influence of oxygen vacancies on the structural, dielectric, and magnetic properties

of (Mn, Co) co-doped ZnO nanostructures. Journal of Materials Science: Materials in Electronics, 29, 9785–9795.

Bendahhou, A., Chourti, K., Loutou, M., El Barkany, S., & Abou-Salama, M. (2022). Impact of rare earth (RE3+ = La3+, Sm3+) substitution in the A site perovskite on the structural, and electrical properties of Ba(Zr0.9Ti0.1)O3 ceramics, RSC Advances, 12, 10895–10910.

Ishaque, M. Z., Zaman, Y., Arif, A., Siddique, A. B., Shahzad, M., Ali, D., Aslam, M., Zaman, H., & Faizan, M. (2023). Fabrication of ternary metal oxide (ZnO:NiO:CuO) nanocomposite heterojunctions for enhanced photocatalytic and antibacterial applications, RSC Advances, 13, 30838–30854.

➢ *ORAL PRESENTATION*

Influence of Shot Peening on Surface Residual Stress and Microstructure Evolutions of R260 Rail Steel

Ahmet Deveci[1](*ORCID: https://orcid.org/0000-0001-7378-6057*),
Harun Mindivan[1*](*ORCID: https://orcid.org/0000-0003-3948-253X*)

[*1]Bilecik Şeyh Edebali University, Engineering Faculty, Mechanical Engineering Department, Bilecik, Turkey

*Corresponding author e-mail: harun.mindivan@bilecik.edu.tr

Abstract

In this study, shot peening (SP) was performed on R260 rail steel. The effects of SP treatment on surface properties such as surface topography, microstructure, residual stress, and microhardness were investigated using optical microscopy, X-ray diffraction, and microhardness measurements. Increasing both the peening intensity and surface coverage effectively produced a gradient structure in the surface layer of R260 rail steel, characterized by high compressive residual stress and significant work hardening. The enhancements in grain refinement, compressive residual stress, and work hardening achieved by increasing surface coverage were more pronounced than those obtained by simply raising the Almen intensity. Under the 24A-1000 shot peening condition, the steel exhibited a residual stress of approximately 1.24 GPa and a surface hardness of roughly 410 $HV_{0.01}$.

Keywords: R260 rail steel, Residual stress, Shot peening.

INTRODUCTION

Increasing demands on rails such as higher speeds, heavier loads, greater traffic density, and mixed traffic lead to heightened damage, primarily through wear (profile loss), plastic deformation, corrugation, and rolling contact fatigue cracking. In contrast, for tramways and light rail systems, wear is the predominant form of damage, largely due to frequent braking and acceleration, sharp curves, high traffic frequency, and fluctuating loads (Solano-Alvarez et al., 2019). In metallic materials, surface integrity is typically improved through grain refinement and the introduction of compressive residual stress in the surface layer (Gerin et al., 2016). When these techniques are effectively applied, they can significantly enhance material performance, including increased resistance to fracture, fatigue, corrosion, wear, and crack propagation (Maleki et al., 2018).

Shot peening (SP) is a well-established and widely used severe plastic deformation technique employed to refine grain size and introduce compressive residual stresses (Maleki and Unal, 2018). The plastic deformation capability of metallic materials depends on the mobility of dislocations and the rate of plastic strain. When dislocation movement is hindered, the material's strength increases, although this often leads to reduced ductility. Work hardening results from an increase in dislocation density caused by plastic deformation (Unal et al., 2022). In the SP process, the degree of plastic deformation is directly influenced by the total impact energy applied.

In the present study, SP process was applied to R260 rail steel to evaluate its potential for inducing residual stress and grain refinement in the surface layer. The effects of SP process on surface residual stress, microstructure, and microhardness evolution were comprehensively investigated using X-ray diffraction (XRD), light optical microscopy (LOM), and microhardness measurements. Additionally, the as-received R260 rail steel was prepared as a control for comparative analysis.

MATERIALS AND METHODS

In this study, R260 rail steels having the chemical composition of (in wt. %) C: 0.6-0.82, Mn: 0.65-1.25, Cr: 0.15, Si: 0.13-0.60, P: 0.03, S:0.01, Mo:0.02, Fe: balance; were selected. Table 1 demonstrates the mechanical properties of R260 rail steel.

Table 1. Mechanical properties of R260 rail steel.

Tensile strength (MPa)	Yield strength (MPa)	Elongation (%)
880	640	25.7

The as-received R260 rail steels were subjected to SP using an industrial air blast machine (Sigma Shot Peening Company, Istanbul) under different conditions shown in Table 2. The treatments were carried out with S230-grade steel shots (hardness: 40-51 HRC) at surface coverages of 200% and 1000% to ensure complete peening of the steel surfaces. The intensities were determined using an Almen gauge with standard "Almen A" test strips. Shot peening was applied at two different Almen intensities (16A and 24A).

Table 2. SP conditions on R260 rail steel.

Treatment ID	SP Almen Intensity	Grinding Coverage (%)
16A-200	16A	200
24A-200	24A	200
24A-1000	24A	1000

After shot peening treatments, the structural analysis of the cross-section of the shot peened steels was performed using a light optical microscope (LOM, Nikon Eclipse LV150). Etching process was carried out by immersing the specimens in 2 % nital etchant for 15 s. The phases of the untreated and shot peened steels were identified using an X-ray diffractometer (XRD-Panalytical Empyrean) with CuK_{α} radiation, scanning in the 2θ° range from 30° to 110°, at an angle step of 0.020° and a scanning speed of 1°/min. Also, the residual stress measurements were performed by the fixed incident multiplane technique (FIM) method. The details about this method can be found elsewhere (Sarioglu, 2006). The roughness parameters (R_a and R_q) were measured with a Mitutoyo contact profilometer (SJ-400 model), based on ISO 4287 standard. Microhardness was measured with the Shimadzu HVM tester with a 10 g load at 10 µm intervals up to 110 µm from the surface in the polished cross section.

RESULTS and DISCUSSION

As expected, it was seen that the R260 rail steel showed pearlite colonies characterized by alternating lamellae of cementite and ferrite, as shown in Fig. 1.

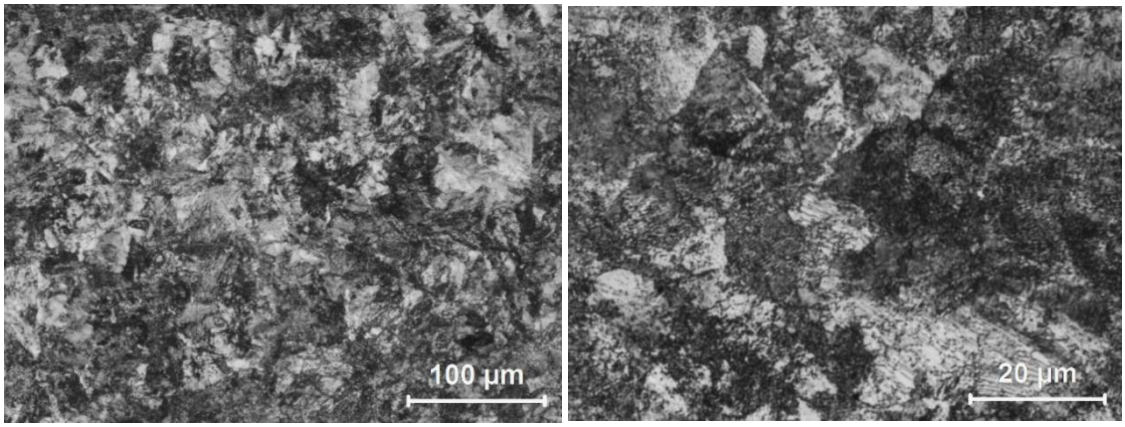

(a) (b)

Figure 1. (a) Low and (b) high magnification LOM micrographs of the R260 rail steel.

Figure 2 shows the cross-sectional microstructures in the near surface layer after SP operations. It is evident that the conventional peening parameters (16A-200 and 24A-200) caused a moderate level of plastic deformation in the surface layer, accompanied by microstructural refinement (Fig. 2 a and b). When SP was applied at a constant Almen intensity of 24A with increasing surface coverage from 200% to 1000%, the surface grains were compressed, resulting in the formation of a distinct structure near the surface (Fig. 2 c). It was observed that the pearlite grains were oriented significantly, and their size decreased as well in the layer

affected by deformation. In this region, the grains became significantly finer, their boundaries blurred, and they merged into a uniform, homogeneous layer. The depth of this fine-grained layer varied depending on both the Almen intensity and surface coverage. As these parameters increased, the deformed layer thickened, and its thickness distribution across the surface became more uniform (Unal et al., 2022).

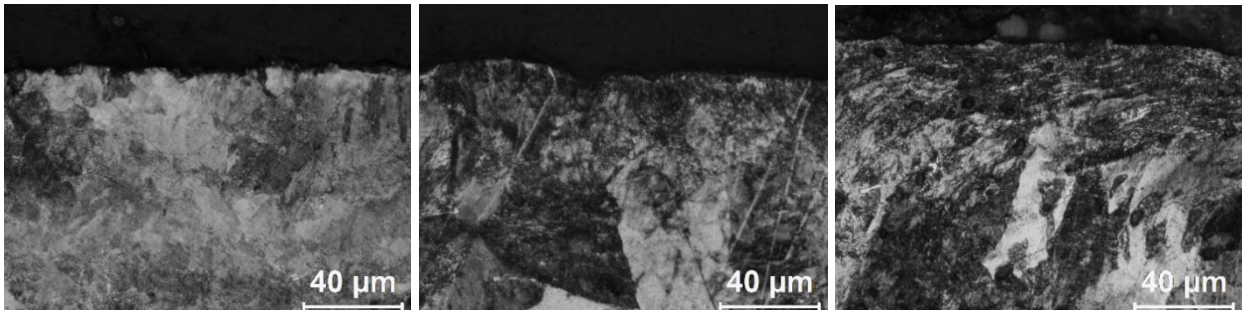

(a) (b) (c)

Figure 2. LOM observations of shot-peened steels in the (a) 16A-200, (b) 24A-200 and (c) 24A-1000 conditions.

Figure 3 shows the XRD patterns from the surface layer of the untreated and shot peened steels. Each steel exhibited characteristic iron-based peaks (α-Fe). Compared to the untreated steel, the α-Fe peak intensity decreased and the peaks broadened and shifted toward lower angles in the treated steels as the Almen intensity and surface coverage increased. Furthermore, the α-Fe peaks of the shot-peened steels were broader and appeared at lower angles, indicating a grain refinement, higher lattice distortions, and compressive residual stresses due to the dislocation density compared to untreated steel. Using Bragg's law (n λ=2dSin θ), where d is the distance between planes, θ is the diffraction angle, n is a positive integer, and λ is the XRD beam's wavelength, we can figure out the lattice parameters (a) of the untreated and shot peened steels by using the main α-Fe peak (i.e., one that falls in the (110) diffraction plane) as a guide. Calculated average values for the untreated and shot-peened steels in the 16A-200, 24A-200 and 24A-1000 conditions to be 0.287227 nm, 0.287307 nm, 0.287395 nm, and 0.288345 nm, respectively. Thus, compared to the untreated R260 rail steel, the shot-peened steels in the 16A-200, 24A-200 and 24A-1000 conditions exhibited a relative extension in the lattice parameter (Δa/a) of approximately 0.028%, 0.058%, and 0.39%, respectively. This finding indicated the development of a larger compressive residual stress on the surface of the shot-peened steels, as modelled by Leskovsek et al. (Leskovšek et al., 2008).

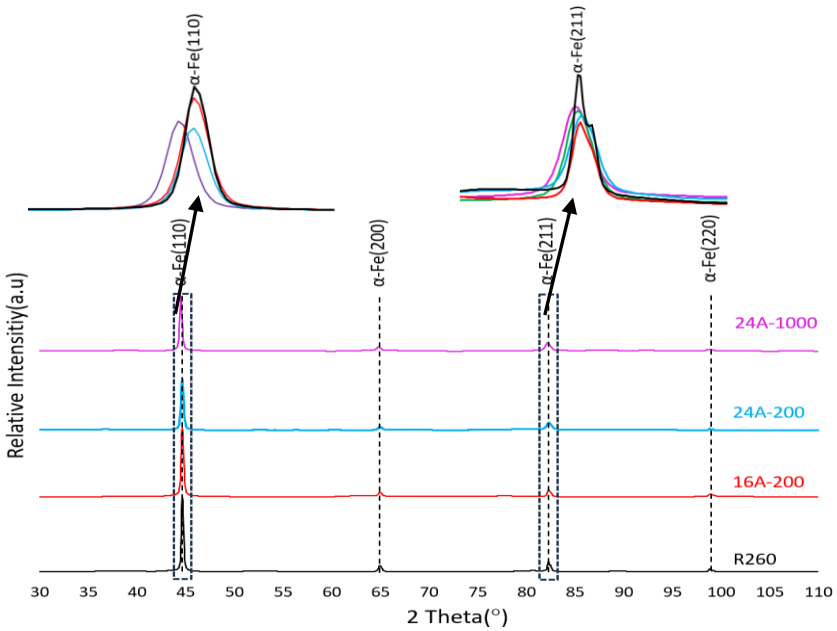

Figure 3. XRD patterns of the untreated and shot peened steels.

Figure 4 shows the surface roughness plot versus different SP conditions. The treatment with the lowest roughness value (R_a) was as received (0.12 µm) one. On the contrary, the treatments with the highest value were shot-peened steels in the 16A-200 and 24A-200 conditions. Hence, SP process raised the surface roughness, and in this study the intensity of the treatment caused the roughness increase regardless of the operation. The surface roughness generally increases by the plastic deformation capability; however, the increase does not only change depending on the Almen intensity. Increasing the surface coverage from 200% to 1000% at a constant Almen intensity of 24A played a role in reducing surface roughness.

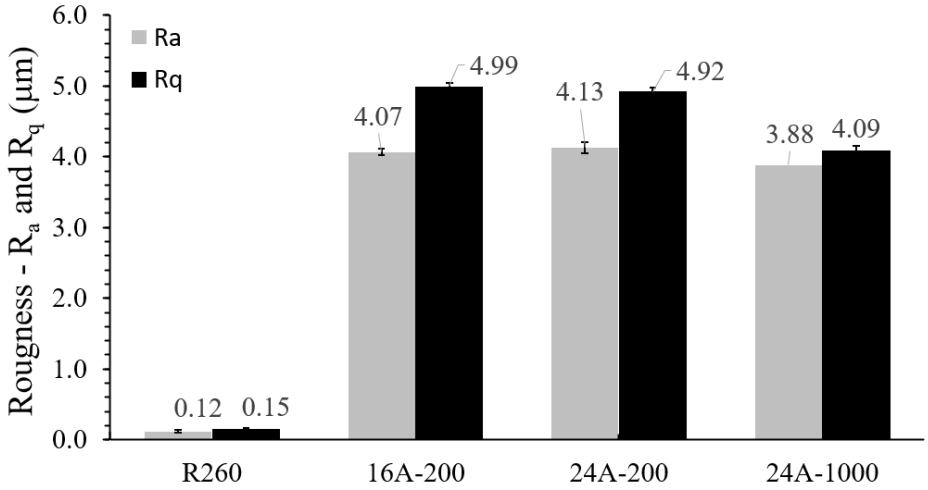

Figure 4. Surface roughness measurements of the the untreated and shot peened steels.

Figure 5 presents the variation in compressive residual stress values of untreated and shot-peened steels, calculated using the FIM method. The untreated steel exhibited no compressive residual stress, with stress levels remaining close to zero (Fig. 5). However, minor stress variations were detected, likely resulting from prior machining and the casting and/or forming processes. In a general aspect, the compressive residual stress increases by the increase of Almen intensity and surface coverage. Compared to the untreated steel, the compressive residual stress values of shot-peened steels in the 16A-200, 24A-200 and 24A-1000 conditions increased by approximately 180%, 190%, and 1027%, respectively.

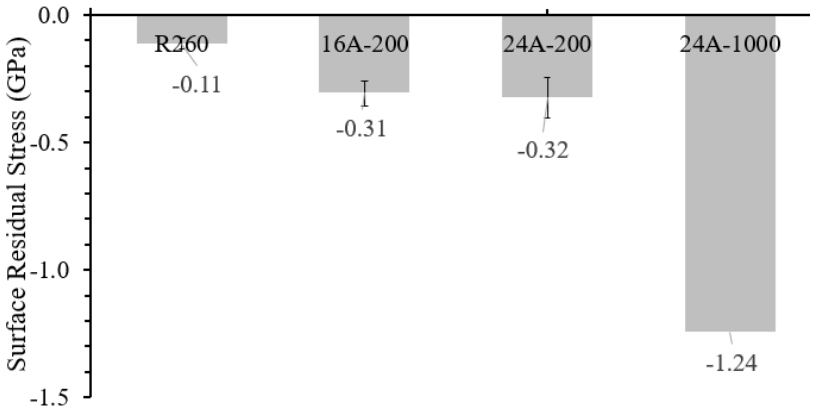

Figure 5. The residual stress state of the untreated and shot peened steels.

Figure 6 illustrates the microhardness values as a function of depth, allowing the estimation of the work-hardened layer thickness. The untreated R260 rail steel maintains a consistent base microhardness of around 300 $HV_{0.01}$. In contrast, shot-peened steels exhibit a decrease in hardness as depth increases. Specifically, the surface hardness values of shot-peened steels in the 16A-200 and 24A-200 conditions are approximately 330 $HV_{0.01}$ and 349 $HV_{0.01}$, respectively, and they return to the base value at depths of around 45 µm and 80 µm. Clearly, surface work hardening is much more evident in the Almen intensity of 24A with surface coverage of 1000%, the surface microhardness is substantially improved to 407 $HV_{0.01}$, which is ~1.35 times higher than that of the base material, and the work-hardened zone reaches nearly 110 µm thick. These findings indicate that increasing surface coverage is more effective than raising Almen intensity in enhancing cold work.

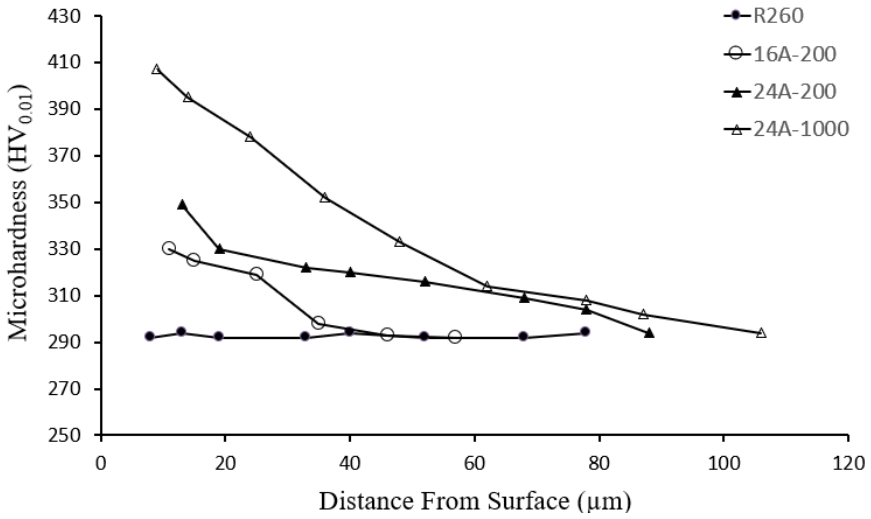

Figure 6. The microhardness change of all treated steels versus depth.

CONCLUSION

In the current work, R260 rail steel was processed by shot peening with different peening parameters. The results of this study can be summarized as follows:

-Enhancing the peening intensity along with applying a high surface coverage successfully produced a gradient structure characterized by high compressive residual stress and pronounced work hardening in the surface layer of R260 rail steel.

-The improvements in grain refinement, compressive stress, and work hardening achieved through increased surface coverage were more significant than those resulting from a higher Almen intensity. For the 24A-1000 shot-peening condition, the residual stress and surface hardness of the steel were approximately 1.24 GPa and 407 $HV_{0.01}$, respectively.

ACKNOWLEDGEMENTS

This work has been supported by Bilecik Şeyh Edebali University Scientific Research Projects Coordination Unit under grant number: 2023-01.BŞEÜ.03-02.

REFERENCES

Gérin, B., Pessard, E., Morel, F., & Verdu, C. (2016). Competition between surface defects and residual stresses on fatigue behaviour of shot peened forged components. Procedia Structural Integrity, 2, 3226-3232.

Leskovšek, V., Podgornik, B., & Nolan, D. (2008). Modelling of residual stress profiles in plasma nitrided tool steel. Materials Characterization, 59(4), 454-461.

Maleki, E., & Unal, O. (2018). Roles of surface coverage increase and re-peening on properties of AISI 1045 carbon steel in conventional and severe shot peening processes. Surfaces and Interfaces, 11, 82-90.

Maleki, E., Unal, O., & Amanov, A. (2018). Novel experimental methods for the determination of the boundaries between conventional, severe and over shot peening processes. Surfaces and Interfaces, 13, 233-254.

Sarioglu, C. (2006). The effect of anisotropy on residual stress values and modification of Serruys approach to residual stress calculations for coatings such as TiN, ZrN and HfN. Surface and Coatings Technology, 201(3-4), 707-717.

Solano-Alvarez, W., Gonzalez, L. F., & Bhadeshia, H. K. D. H. (2019). The effect of vanadium alloying on the wear resistance of pearlitic rails. Wear, 436, 203004.

Unal, O., Maleki, E., Karademir, I., Husem, F., Efe, Y., & Das, T. (2022). Effects of conventional shot peening, severe shot peening, re-shot peening and precised grinding operations on fatigue performance of AISI 1050 railway axle steel. International Journal of Fatigue, 155, 106613.

➢ *ORAL PRESENTATION*

Influence of Shot Peening on Impact-Sliding Wear Behaviour of R260 Rail Steel

Ahmet Deveci[1](*ORCID: https://orcid.org/0000-0001-7378-6057*),
Harun Mindivan[1*](*ORCID: https://orcid.org/0000-0003-3948-253X*)

*[1]Bilecik Şeyh Edebali University, Engineering Faculty, Mechanical Engineering Department, Bilecik, Turkey

*Corresponding author e-mail: harun.mindivan@bilecik.edu.tr

Abstract

During operation, railway crossings are subjected to rolling, impact, and sliding stresses, with impact-sliding stress specifically occurring as the wheel transitions from the rail wing to the crossing nose. This transition generates extremely high contact forces on the crossing nose, which can cause significant damage to both the crossing nose and the wing rail. This study aims to present a technological approach for extending the service life of crossing noses manufactured from R260 rail steel. To investigate the mechanisms involved under complex loading conditions, wear tests were carried out using an inclined impact-sliding wear testing machine. In this study, shot peening (SP) was applied to R260 rail steel. The impact-sliding wear tests showed that the wear loss of the shot-peened R260 steel was noticeably lower compared to that of the untreated R260 steel at room temperature.

Keywords: R260 rail steel, Impact sliding wear, Shot peening.

INTRODUCTION

In railway transportation, the rail is a critical mechanical component that supports cyclic wheel loading and guides train movement. Continuous wheel loading makes the rail's surface layer vulnerable to wear and rolling contact fatigue (RCF) damage (Shen et al., 2022). These issues are especially pronounced in areas with small-radius curves, switches, and crossings. It is well established that rolling is the primary mode of wheel operation. However, during traction, braking, and turning, sliding wear caused by impacts between the wheel and rail plays a significant role in the degradation of the wheel/rail system (Chen et al., 2020). During service, impact-sliding occurs when the inclination of the rolling plane shifts from the wing rail to the crossing nose, where extremely high contact forces are exerted as the wheels pass over this area (Harzallah et al., 2012). In recent decades, substantial research has focused on improving the wear resistance and durability of rail steel to extend service life. Nevertheless, limited attention has been paid to the impact-sliding wear behavior of wheel/rail systems under conditions involving large contact and dynamic forces conditions that cause severe damage at crossings and produce contact stresses similar to those experienced in actual railway operations.

It is widely recognized that surface treatments such as shot peening, severe shot peening, re-shot peening, and precision grinding (Unal et al., 2022) as well as various coatings, can significantly improve the wear resistance and rolling contact fatigue (RCF) performance of rail materials (Peng et al., 2024). The shot peening (SP) process, categorized as a severe plastic deformation technique, is a well-established and effective surface treatment aimed at enhancing the metallurgical and mechanical properties, as well as the fatigue performance, of metallic materials under applied stresses. The process involves propelling hard steel balls at controlled velocities onto critical areas of a component's surface (Maleki and Unal, 2018).

Based on the above review, this study focused on developing a SP process for R260 rail steel under impact-sliding contact conditions. The process was performed at an Almen intensity of 24 A with a surface coverage of 600%. To replicate the extremely high contact and dynamic forces encountered in service, an inclined impact-sliding test method was employed (Zhao et al., 2017). Such conditions typically occur in regions where the rail transitions from the wing rail to the crossing nose, where the steel is exposed to combined impact and sliding forces during rolling-sliding contact. However, investigating crossing failures under cyclic high-speed impact-sliding motion remains a significant challenge due to the complex nature of tribological phenomena and dynamic loading effects.

MATERIALS AND METHODS

Experimental tests were conducted on R260 rail steel, which was machined on a lathe without any additional heat treatment. The mechanically hardened layer was removed using silicon carbide paper up to 2000 grit. Grinding reduced the average surface roughness (R_a) to 0.12 µm prior to the SP process. The rail steel consists of pearlite with a hardness of 300 $HV_{0.01}$.

The as-received R260 rail steels were subjected to SP using an industrial air blast machine (Sigma Shot Peening Company, Istanbul) under the parameters listed in Table 1. The process employed S230-grade steel shots (hardness range: 40-51 HRC) with a surface coverage of 600% to ensure thorough treatment of the steel surfaces. Peening intensity was measured using an Almen gauge with standard "Almen A" test strips, and the SP process was performed at an intensity of 24 A.

Table 1. SP conditions on R260 rail steel.

Treatment ID	SP Almen Intensity	Grinding Coverage (%)
24A-600	24A	600

After SP process, structural analysis of the cross-section of the shot-peened steel was performed using a light optical microscope (LOM, Nikon Eclipse LV150). The etching process was carried out by immersing the steels in a 2% nital solution for 15 seconds. The phases of the untreated and shot-peened steels were identified using an X-ray diffractometer (XRD, Panalytical Empyrean) with CuK_α radiation, scanning over a 2θ range of 30° to 110°, with a step size of 0.020° and a scanning speed of 1°/min. Residual stress measurements were conducted using the fixed incident multiplane (FIM) technique, as described in detail by Sarioglu (Sarioglu, 2006). Surface roughness parameters (R_a and R_q) were measured with a Mitutoyo contact profilometer (SJ-400 model) in accordance with the ISO 4287 standard. Microhardness was measured using a Shimadzu HMV tester with a 10 g load, at 10 µm intervals up to a depth of 110 µm from the surface on the polished cross-section.

Wear tests were conducted to evaluate the influence of SP process on the impact-sliding wear behavior of R260 rail steel. Prior to testing, a load cell was used to calibrate the maximum loads exerted by the spring and pneumatic cylinder to 40 N and 240 N, respectively. Each treated steel was subjected to 2000 impact cycles using a 10 mm diameter bearing steel (AISI 52100) ball under dry conditions (25 ± 5 °C, 50 ± 5% relative humidity). Two distinct regions of the wear scar (impact and sliding) were examined using a 2D surface profilometer following the impact-sliding wear test to determine the amount of wear loss. Wear rates were calculated by dividing the volumetric wear loss by the number of loading cycles, expressed in mm^3/cycle. After the tests, LOM was employed to examine the wear tracks.

RESULTS and DISCUSSION

Figure 1 depicts the LOM cross-sectional views of shot-peened R260 rail steel. It is evident that the standard shot peening parameters induced a moderate degree of plastic deformation within the surface layer, accompanied by microstructural refinement (Fig. 1). The deformation-affected layer exhibited a noticeable alignment of pearlite grains along with a reduction in their size.

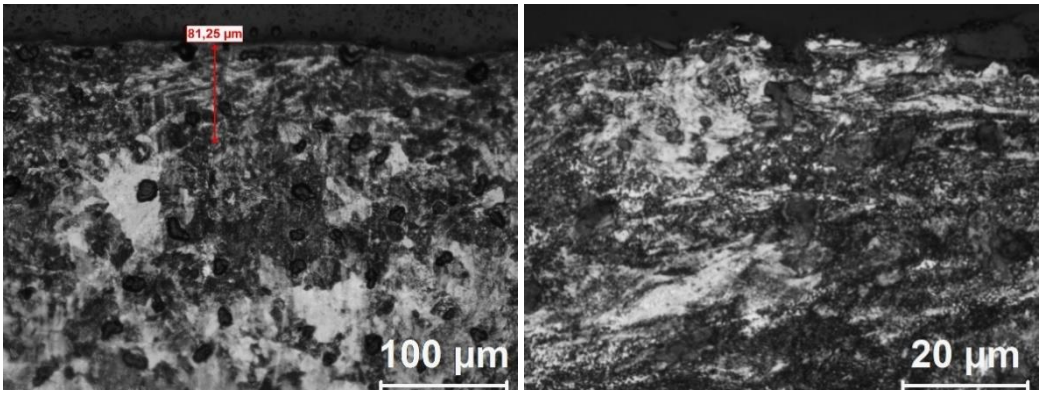

(a) (b)

Figure 1. (a) Low and (b) high magnification LOM micrographs of the shot-peened R260 rail steel.

Figure 2 presents the XRD patterns of the surface layer for both untreated and shot peened steels. All steels displayed characteristic iron-based peaks (α-Fe). In the shot peened steel, the α-Fe peaks became broader, shifted to lower angles, and showed reduced intensity compared to the untreated steel. Additionally, the α-Fe peaks in the shot-peened steels were broader and shifted to lower angles, suggesting grain refinement, increased lattice distortion, and the presence of compressive residual stresses resulting from higher dislocation density when compared to the untreated steel. By applying Bragg's law ($n\lambda = 2d \sin\theta$), where d is the interplanar spacing, θ is the diffraction angle, n is a positive integer, and λ is the XRD wavelength, the lattice parameters (a) of both untreated and shot-peened steels were determined using the primary α-Fe peak corresponding to the (110) diffraction plane. The calculated average lattice parameters were 0.287227 nm for the untreated steel and 0.287859 nm for the shot-peened steel. This represents a relative lattice expansion ($\Delta a/a$) of about 0.22% in the shot-peened steel. Such an increase indicates the presence of greater compressive residual stress on the surface of the shot-peened steels, consistent with the findings modelled by Leskovšek et al. (Leskovšek et al., 2008).

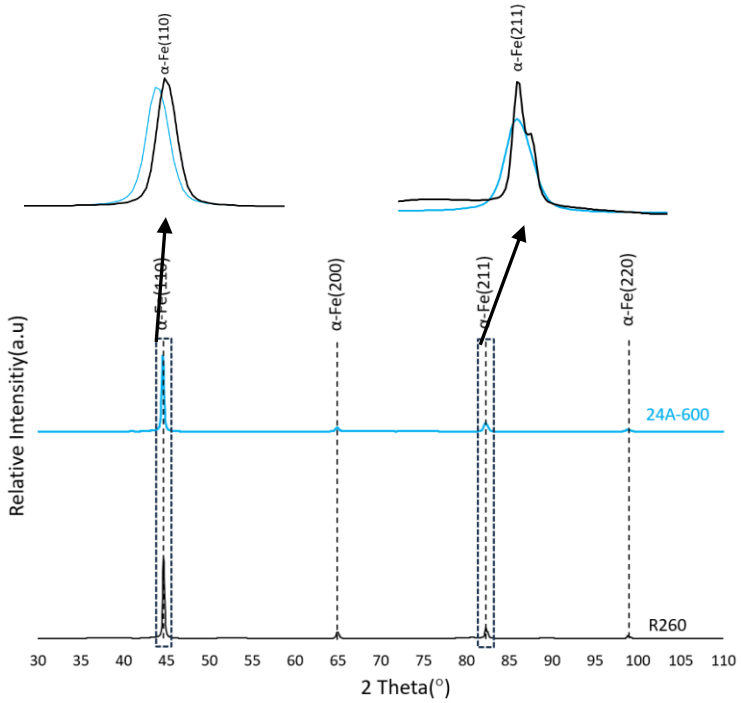

Figure 2. XRD patterns of the untreated and shot-peened steels.

Figure 3 shows the roughness values (parameters R_a and R_q) measured before and after the SP process to investigate the influence of SP on the surface topography. The surface roughness generally increases by the plastic deformation capability and SP process raised the surface roughness.

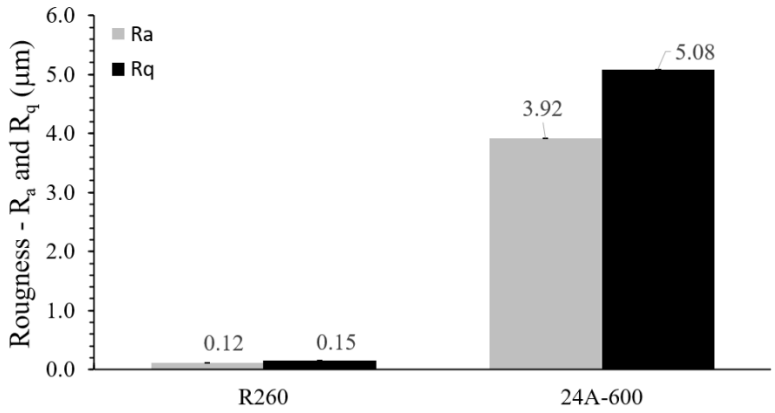

Figure 3. Surface roughness measurements of the the untreated and shot-peened steels.

Figure 4 illustrates the changes in compressive residual stress values for both untreated and shot-peened steels, measured using the FIM method. In the untreated steel, compressive residual stress was essentially absent, with values remaining near zero. Slight fluctuations were observed, likely due to prior machining or manufacturing processes such as casting and forming. In contrast, the shot-peened steel exhibited a significant increase in compressive residual stress approximately 618% higher than that of the untreated steel.

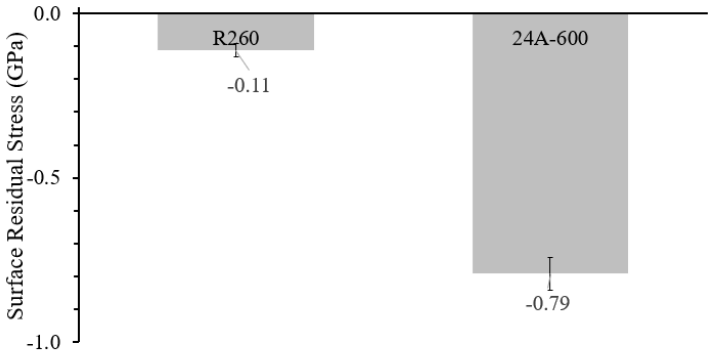

Figure 4. The residual stress state of the untreated and shot peened steels.

Figure 5 displays the microhardness distribution as a function of depth, providing insight into the thickness of the work-hardened layer. The untreated R260 rail steel exhibits a uniform base microhardness of approximately 300 $HV_{0.01}$. In comparison, the shot-peened steel shows a gradual decrease in hardness with increasing depth. Notably, the surface microhardness of the shot-peened steel significantly increases to 361 $HV_{0.01}$ (about 1.2 times higher than that of the untreated steel) and the work-hardened layer extends to nearly 96 µm.

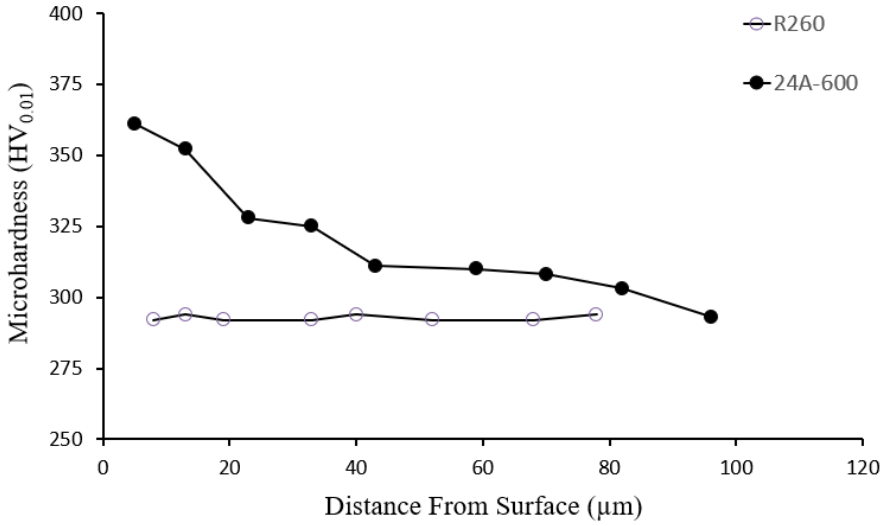

Figure 5. Microhardness variation with depth for untreated and shot-peened steels.

Table 2 illustrates the wear track width and depth values of the impact and sliding zones for the untreated and shot-peened steels following impact-sliding wear tests. Both untreated and shot-peened steels exhibited deeper and wider wear tracks in the impact zone compared to the sliding zone. Figure 6 shows the average wear rates of the untreated and shot-peened steels in the impact and sliding zones. The wear rate in the impact zone decreased by 10% due to the SP process, while the wear rate in the sliding zone was reduced by approximately 11%. Overall, the SP treatment resulted in an approximately 11% decrease in the total wear rate.

Table 2. The wear track width and depth values of the impact and sliding zones of the wear tracks formed on the surfaces of the untreated and shot-peened steels.

		Impact Zone	Sliding Zone
R260	Wear Track Width	1.22 mm	1.07 mm
	Wear Track Depth	34.85 mm	7 mm
24A-600	Wear Track Width	1.22 mm	1.00 mm
	Wear Track Depth	31.4 mm	6.7 mm

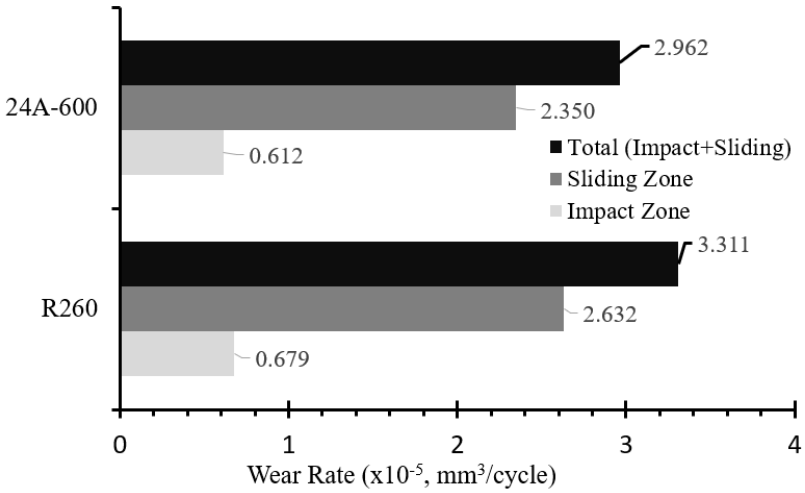

Figure 6. Wear rates of the wear tracks formed on the steels' surfaces.

Figs. 7 and 8 show detailed LOM images of the worn surfaces on the untreated and shot-peened steels. Results from the 2-D surface profilometer revealed that the shot-peened steel exhibited shallower wear tracks in both the impact and sliding zones (Table 2). Table 2 and Figure 5 suggest that the work-hardened layer in the shot-peened steel did not completely peel off in the impact zone. Additionally, wear tracks in both impact and sliding zones for untreated and shot-peened steels contained oxide patches (Figs. 7 and 8), a common indicator of tribo-oxidation caused by high frictional heat generated under elevated test loads (Peng et al., 2024). The observation of lateral cracks on the worn surface of the shot-peened steel at high magnifications suggests that fatigue is the predominant wear mechanism (Fig. 8). Upon impact, the untreated R260 steel exhibited a pronounced and deep crater on its surface (Table 2, Fig. 7). Although minor plastic deformation was observed, especially in the sliding zone of the untreated steel, the amount of surface fatigue wear cracks was significantly higher in the shot-peened steel, as depicted in Fig. 8. The shot-peened steel demonstrated strong resistance to deformation in both the impact and sliding zones within the work-hardened layer extending approximately 96 μm from the surface (Fig. 5). The SP process may have induced greater compressive residual stress on the surface of the untreated R260 steel. Furthermore, SP caused elastic distortion in the R260 rail steel (approximately 0.22% for the shot-peened steel), leading to the formation of compressive residual stress, as modelled by Leskovšek et al. (Leskovšek et al., 2008). The shot-peened steel exhibited higher compressive residual stress (Fig. 4) and greater surface hardness (Fig. 5) compared to the untreated R260 rail steel.

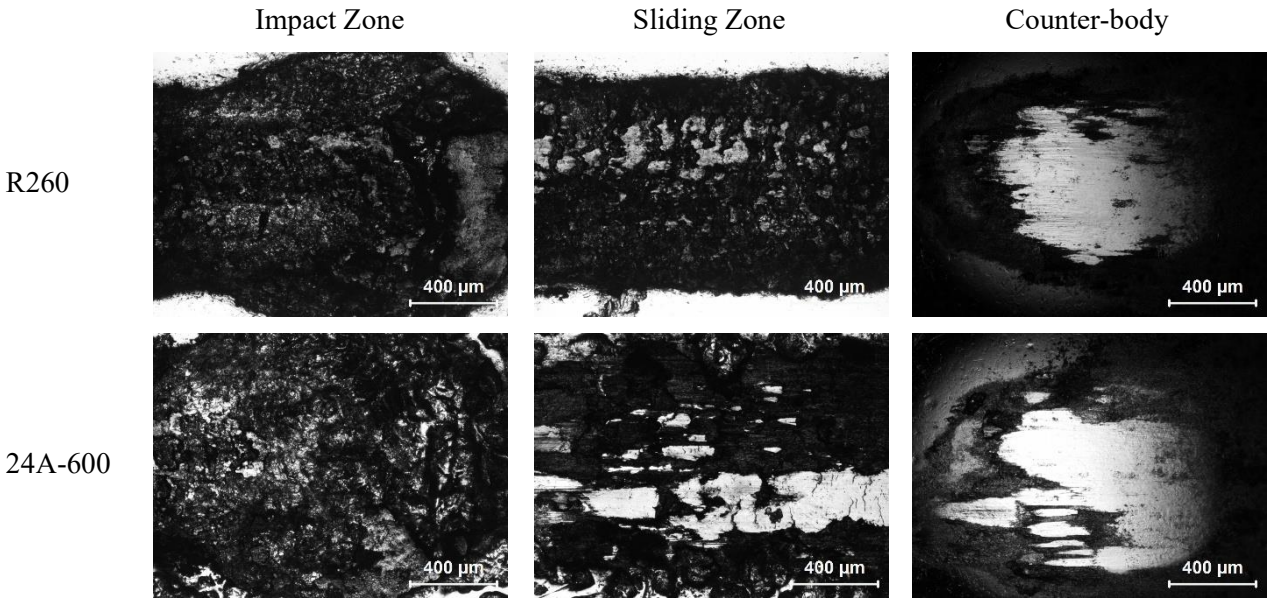

Figure 7. Low magnification LOM images of the wear tracks formed on the surfaces of the untreated and shot-peened steels, and LOM images of their corresponding testing balls after the wear test.

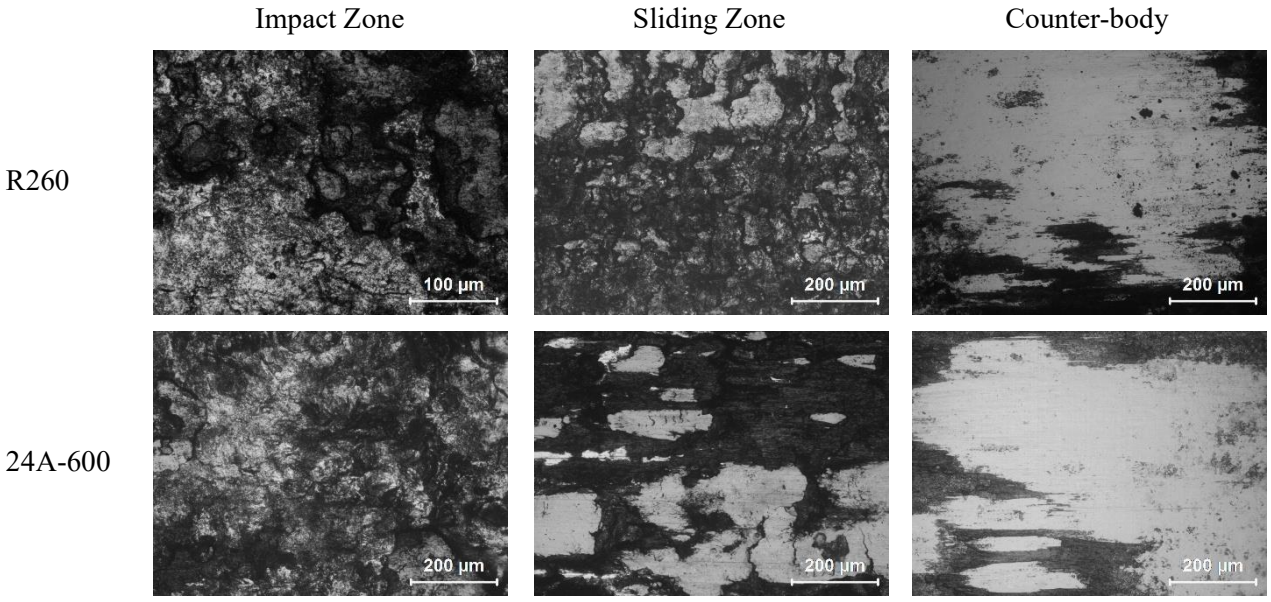

Figure 8. High magnification LOM images of the wear tracks formed on the surfaces of the untreated and shot-peened steels, and LOM images of their corresponding testing balls after the wear test.

CONCLUSION

An inclined cyclic impact-sliding test was successfully employed to evaluate the fatigue wear behavior of untreated and shot-peened steels under extremely high contact stresses in ambient conditions. Based on the present study, the following conclusions can be drawn:

-The SP process produced a gradient structure characterized by high compressive residual stress and pronounced work hardening in the surface layer of R260 rail steel.

-The application of the SP process significantly increased the surface hardness of the untreated R260 rail steel. The surface hardness of the untreated and shot-peened steels was measured as 300 $HV_{0.01}$ and 361 $HV_{0.01}$, respectively.

-The formation of greater lattice distortion on the surface of the shot-peened steel is accompanied by the generation of higher compressive residual stress compared to the untreated R260 rail steel

-The SP process increased the surface roughness of the untreated R260 rail steel.

-In the impact and sliding zones, the shot-peened steel exhibited 10% and 11% lower wear rates, respectively, compared to the untreated R260 rail steel under Hertzian contact pressures of 1.59/2.89 GPa.

ACKNOWLEDGEMENTS

This work has been supported by Bilecik Şeyh Edebali University Scientific Research Projects Coordination Unit under grant number: 2023-01.BŞEÜ.03-02.

REFERENCES

Chen, Y., Gong, W., Kang., R. (2020). Review and propositions for the sliding/impact wear behavior in a contact interface. Chinese Journal of Aeronautics, 33(2), 391-406.

Harzallah, R., Mouftiez, A., Hariri, S., Felder, E., & Maujean, J. P. (2012). Impact and sliding wear resistance of Hadfield and rail steel. Applied Mechanics and Materials, 146, 112-123.

Leskovšek, V., Podgornik, B., & Nolan, D. (2008). Modelling of residual stress profiles in plasma nitrided tool steel. Materials Characterization, 59(4), 454-461.

Maleki, E., & Unal, O. (2018). Roles of surface coverage increase and re-peening on properties of AISI 1045 carbon steel in conventional and severe shot peening processes. Surfaces and Interfaces, 11, 82-90.

Peng, Y. X., Chang, X. D., Sun, S. S., Zhu, Z. C., Gong, X. S., Zou, S. Y., Xu, W.X., Mi, Z. T. (2018). The friction and wear properties of steel wire rope sliding against itself under impact load. Wear, 400, 194-206.

Peng, K., Yu, D., Zhang, P., Xue, J., Li, Q., Wu, G., & Li, L. (2024). Mechanism and improvement of the rolling contact fatigue of the surface layer with heterogeneous microstructures of the rail steel treated by laminar plasma jet. Engineering Failure Analysis, 163, 108608.

Sarioglu, C. (2006). The effect of anisotropy on residual stress values and modification of Serruys approach to residual stress calculations for coatings such as TiN, ZrN and HfN. Surface and Coatings Technology, 201(3-4), 707-717.

Shen, M., Rong, B., Li, Q., Yu, M., Xiao, Y., & Zhao, H. (2023). Different responses of wheel–rail interface adhesion and wheel surface damage induced by an out–of–round wheel tread. Wear, 526, 204956.

Unal, O., Maleki, E., Karademir, I., Husem, F., Efe, Y., & Das, T. (2022). Effects of conventional shot peening, severe shot peening, re-shot peening and precised grinding operations on fatigue performance of AISI 1050 railway axle steel. International Journal of Fatigue, 155, 106613.

Zhao, C., Zhang, J., & Nie, X. (2017). Tribological behaviour of plasma nitrided cast iron D6510 and cast steel S0050A under the inclined-impact sliding condition with extremely high contact pressure. Journal of Physics: Conference Series. IOP Publishing, 843 (1), 1-9.

➢ *ORAL PRESENTATION*

API ZYM enzymatic characterization of lactic acid bacteria isolated from boza

Merve USAL[1*] (*ORCID: https://orcid.org/0009-0001-7208-9505*),
Fatih TÖRNÜK[2] (*ORCID: https://orcid.org/ 0000-0002-7313-0207*)

[1*]Kırklareli University, Faculty of Engineering, Department of Food Engineering, Kırklareli, Turkiye.
[2]Sivas Cumhuriyet University, Faculty of Health Sciences, Department of Nutrition and Dietetics, 58140, Sivas, Turkiye.

*Corresponding author e-mail: merveusal@klu.edu.tr

Abstract

Lactic acid bacteria (LAB) are microorganisms that play a significant role in the production of fermented foods and in various biotechnological processes. These bacteria ferment carbohydrates to produce lactic acid, a process utilized in the production of food products such as yogurt, kefir, cheese, and boza. LAB also possess probiotic properties and can have positive effects on human health. Furthermore, the enzymes produced by LAB are widely applicable in food processing and biotechnology fields. These enzymes contribute to the breakdown of nutrients and influence the characteristics of fermented products. In this study, enzymatic activities of LAB strains isolated from boza were examined using a rapid API ZYM assay. The API ZYM system is considered as an important tool in the polyphasic taxonomic identification of microorganisms, particularly for species characterization of lactobacilli. The test evaluates the types and levels of enzymes produced by the bacteria. The enzymatic profiles of the 15 isolates were determined based on the results obtained. In the results, the isolates exhibited high leucine arylamidase, acid phosphatase, β-galactosidase, β-glucosidase, and β-glucosaminidase activities while moderate levels of activity were detected for phosphohydrolase and α-glucosidase. In addition, the majority of the isolates showed low enzymatic activities for alkaline phosphatase, esterase (C4), esterase lipase (C8), lipase (C14), cystine arylamidase, trypsin, α-chymotrypsin, α-galactosidase, β-glucuronidase, α-mannosidase, and α-fucosidase. In conclusion, the API ZYM system was determined as an effective method for identifying the enzymatic profiles of LAB isolated from boza. The obtained enzymatic activity profiles contribute to a better understanding of the functional properties of boza originated LAB.

Keywords: Lactic acid bacteria, enzymatic activity, API-ZYM.

INTRODUCTION

Boza is one of the traditionally consumed fermented cereal-based beverages in Turkey, the Balkan countries, and Southern Russia (Heperkan et al., 2014). It is a highly viscous fermented drink made from cereals such as millet, rice, wheat, or their flours, and is typically consumed during the winter months, often garnished with cinnamon and roasted chickpeas. In Turkey, boza is produced both traditionally in small-scale enterprises and on an industrial scale. Various raw materials in different concentrations and different fermentation durations can be used in its production (Yeğin ve Üren, 2008; Zorba et al., 199). Boza undergoes two types of fermentation: lactic acid fermentation by lactic acid bacteria (LAB) and alcohol fermentation by yeasts. LAB contributes to preservation by producing antimicrobial substances and increasing acidity. Compounds such as lactic acid produced by LAB are considered among the key factors responsible for boza's distinctive flavor (Altay et al., 2013).

LAB have been extensively used in the food industry due to their ability to extend shelf life and enhance product quality through fermentation. Beyond preservation, LAB contribute to improved safety, nutrition, sensory attributes, and functionality of fermented foods. As a result, recent research has increasingly focused on identifying and developing new LAB strains with specific technological and functional roles for use as starter cultures (Ağagündüz et al., 2022). LAB are known to produce flavor-active compounds such as organic acids, alcohols, ketones, and esters through biosynthesis and enzymatic transformation, thereby enhancing the organoleptic quality of fermented foods (de Souza et al., 2023).

Moreover, certain LAB strains possess enzymatic activities—such as glycosylation, ring cleavage, and dehydroxylation—that enable the biotransformation of dietary polyphenols into more bioavailable or biologically active forms. These transformations may enhance the functional potential of fermented foods, particularly in terms of antioxidant capacity and gut health (de Lacey et al., 2014). Therefore, evaluating the enzymatic profiles of LAB isolates is essential for understanding their metabolic capacity and potential applications in functional food development.

The API ZYM system is widely used for polyphasic taxonomic identification and enzymatic characterization of LAB. It enables the detection of specific hydrolytic enzyme activities in washed whole cells, cell-free supernatants, or cell extracts under defined conditions (Charteris et al., 2001). The API ZYM assay is a cost-effective and straightforward method that evaluates 19 different enzymatic activities, including those involved in the degradation of peptides, phosphomonoesters, lipids, mucopolysaccharides, polysaccharides, chitin, cellulose, starch, and galactans (Martínez et al., 2016).

In this study, LAB strains isolated from boza were characterized using the API ZYM system to determine their enzymatic profiles. The aim was to better understand the functional and technological properties of these isolates and to explore their potential applications in food fermentation processes and probiotic development.

Table 1. Number Equivalents of Enzymes in API-ZYM Test Kit

Number	Name of enzyme	Number	Name of enzyme
1	Control	**11**	Acid phosphatase
2	Alkaline phosphatase	**12**	Phosphoamidase
3	Esterase (C4)	**13**	α-Galactosidase
4	Esterase lipase (C8)	**14**	β-Galactosidase
5	Lipase (C14)	**15**	β-Glucuronidase
6	Leucine arylamidase	**16**	α-Glucosidase
7	Valine arylamidase	**17**	β-Glucosidase
8	Cystine arylamidase	**18**	β-Glucosaminidase
9	Trypsin	**19**	α-Mannosidase
10	α-Chymotrypsin	**20**	α-Fucosidase

MATERIALS AND METHODS

Preperation of Bacterial Suspensions

In this study, 15 different LAB isolates obtained from boza using MRS agar were used. Eight of these isolates were identified using the PCR method. Prior to analysis, bacterial cultures activated in MRS broth for 24 hours were centrifuged at 15,000 × g for 10 minutes. After removing the supernatant, the bacterial pellets were resuspended in 1 mL of sterile 0.85% API NaCl solution provided in the kit to obtain bacterial suspensions adjusted to a turbidity of 5–6 McFarland units.

Determination of Enzymatic Activities of Isolates Using API ZYM Kits

The enzymatic activities of the isolates were determined using API ZYM kits (BioMérieux, France) according to the manufacturer's instructions. The tests were conducted at 37 °C. To maintain a humid environment, approximately 5 mL of sterile distilled water was added to the bottom of the incubation tray. Then, 65 µL of each prepared bacterial suspension was dispensed into the wells of the API ZYM strips. The trays were sealed and incubated at 37 °C for 4 hours. After incubation, one drop each of ZYM A and ZYM B reagents was added to each well. Color development was observed after a 5-minute reaction time, followed by exposure to a 1000 W light source for 10 seconds. Enzymatic activity for 19 different enzymes included in the API ZYM test kit was evaluated based on color change and intensity in the wells. The enzymatic profiles of the LAB isolates were determined using the color scale provided in the kit, with intensity scored on a scale from 0 to 5. The API ZYM test results of the isolates were determined according to the color scale shown in Figure 1.

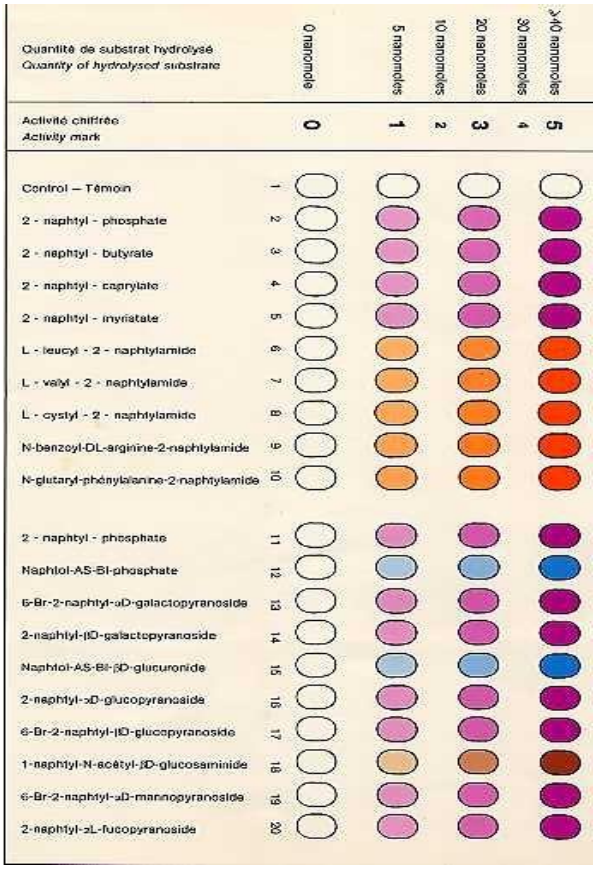

Figure 1. API ZYM color scale

RESULTS and DISCUSSION

Based on the enzyme activity scoring results obtained through the API ZYM assay (Table 2), LAB isolates exhibited prominent enzymatic activities. High levels of leucine arylamidase, acid phosphatase, β-galactosidase, β-glucosidase, and β-glucosaminidase were observed in the majority of isolates. Moderate activity was noted for phosphohydrolase and α-glucosidase, whereas low enzymatic activities were found for alkaline phosphatase, esterase (C4), esterase lipase (C8), lipase (C14), cystine arylamidase, trypsin, α-chymotrypsin, α-galactosidase, β-glucuronidase, α-mannosidase, and α-fucosidase. Among the isolates, *Lactiplantibacillus plantarum* strains particularly showed high activity of leucine arylamidase, β-glucosidase, and β-glucosaminidase, indicating strong proteolytic and glycosidic potential. In contrast, *Pediococcus acidilactici* and *Weissella confusa* strains were notable for their acid phosphatase and β-galactosidase activities. *Leuconostoc mesenteroides* demonstrated a distinctively high β-glucosidase activity. These findings are consistent with previous reports suggesting that LAB isolates can exhibit strain-specific enzymatic profiles contributing to their functional roles in fermentation processes.

Supporting our results, Tamang et al. (2009) reported similar enzyme profiles in *Lb. brevis*, *Lb. plantarum*, *P. pentosaceus*, and *P. acidilactici* isolated from fermented vegetables, highlighting low activity levels for alkaline phosphatase, esterase (C4), esterase lipase (C8), and lipase (C14), while consistently detecting acid phosphatase, β-galactosidase, and β-glucosidase. Similarly, Tokatlı (2013) found that *Lb. brevis* strains isolated from pickles exhibited low activity for various hydrolytic enzymes but showed moderate to high activity for enzymes involved in carbohydrate metabolism. In line with these studies, the absence of trypsin, chymotrypsin, mannosidase, and fucosidase activities in our isolates indicates a conserved enzymatic behavior among LAB, where hydrolytic activity is typically more focused on sugar metabolism rather than proteolysis or glycan degradation. Additionally, Malık et al. (2019) found that LAB isolated from raw and pasteurized milk exhibited high activities of α-glucosidase, β-glucosidase, and acid phosphatase—paralleling our observations and supporting the enzymatic versatility of LAB across different substrates and environments.

Table 2. API ZYM test results of isolates

Isolates	Test enzymes (0-5 points)																			
	1	**2**	**3**	**4**	**5**	**6**	**7**	**8**	**9**	**10**	**11**	**12**	**13**	**14**	**15**	**16**	**17**	**18**	**19**	**20**
Leuconostoc mesenteroides	0	0	1	0	0	3	0	1	0	0	1	1	1	3	0	3	5	0	0	0
R1B	0	0	0	0	0	1	0	0	0	0	3	3	1	1	0	0	0	0	0	0
R2A	0	1	0	0	0	1	0	0	0	0	5	1	0	5	0	0	0	0	0	0
R3A	0	0	0	0	1	5	5	1	0	0	1	3	0	1	0	0	1	3	0	0
R3B	0	0	0	0	0	1	0	0	0	0	5	3	0	0	0	0	0	0	0	0
Pediococcus acidilactici	0	0	0	0	1	5	5	1	0	0	3	3	0	5	0	0	1	3	0	0
Lactococcus lactis subsp. hordniae	0	0	0	0	0	3	0	1	0	0	3	1	0	0	0	1	1	0	0	0
R5A	0	1	0	0	0	3	0	0	0	0	5	3	0	5	0	0	0	0	0	0
Weisella confusa	0	1	0	0	0	1	0	0	0	0	5	1	0	5	0	0	0	0	0	0
Lactoplantibacillus plantarum	0	0	0	0	0	3	1	1	0	0	1	1	0	3	0	3	5	5	0	0
Lactoplantibacillus plantarum	0	0	0	0	0	5	1	1	0	0	1	1	0	1	0	3	5	5	0	0
R8A	0	0	1	0	0	1	0	1	0	0	0	3	1	3	0	3	0	0	0	0
Lactoplantibacillus plantarum	0	0	0	0	0	3	1	1	0	0	1	1	0	3	0	1	5	5	0	0
R9B	0	0	1	1	0	5	1	1	0	0	1	3	5	5	3	3	0	0	0	0
Weisella confusa	0	0	0	0	0	1	0	0	0	0	3	1	0	1	0	0	0	0	0	0

The functional relevance of these enzymes is well established. For instance, phosphatases—particularly acid phosphatases—are critical for dephosphorylation reactions and play a significant role in microbial adaptation and survival. These enzymes are also gaining attention in the pharmaceutical and diagnostic sectors due to their biochemical applications (Erşan & Açıkel, 2014). Similarly, β-galactosidase (lactase) is widely used in the food industry for lactose hydrolysis, improving digestibility in dairy products. Leucine arylamidase and β-glucosidase also hold significant technological importance, with the latter being widely applied in the beverage industry to enhance flavor and aroma profiles in fruit juice and wine production (Gueguen et al., 1996; Ketudat Cairns & Esen, 2010). The enzymatic diversity of LAB can directly influence the composition, taste, and quality of food products (Patel et al., 2013).

In summary, the enzyme activity profiles obtained in this study not only confirm the functional potential of LAB isolates from cereal-based fermentations but also suggest their promising application in food biotechnology. Their high glycosidase and phosphatase activities are especially relevant for improving nutritional and sensory properties of fermented foods, and could be harnessed in the development of functional foods or probiotics.



Figure 2. API ZYM test strips for some isolates

CONCLUSION

In this study, the enzymatic activity profiles of lactic acid bacteria (LAB) isolated from boza were determined using the API ZYM test kit. The results revealed that *Lactiplantibacillus plantarum* strains exhibited high activities of leucine arylamidase, β-glucosidase, and β-glucosaminidase, indicating their strong hydrolytic capacity for proteins and carbohydrates. Additionally, *Pediococcus acidilactici* and *Weissella confusa* strains showed significant acid phosphatase and β-galactosidase activities, while *Leuconostoc mesenteroides* demonstrated high β-glucosidase activity. These findings highlight the potential of boza-derived LAB strains to contribute to flavor development, nutrient transformation, and functional properties in fermented food products. The API ZYM system proved to be a practical and effective tool for evaluating the enzymatic capabilities of LAB. Overall, this enzymatic characterization provides valuable insights into the functional diversity of LAB in traditional fermented foods and supports their possible application as starter cultures or probiotics in food biotechnology.

REFERENCES

Ağagündüz, D., Şahin, T. Ö., Ayten, Ş., Yılmaz, B., Güneşliol, B. E., Russo, P., Spano, G., & Özogul, F. (2022). Lactic acid bacteria as pro-technological, bioprotective and health-promoting cultures in the dairy food industry. *Food Bioscience*, *47*(February). https://doi.org/10.1016/j.fbio.2022.101617

Altay, F., Karbancioglu-Güler, F., Daskaya-Dikmen, C., & Heperkan, D. (2013). A review on traditional Turkish fermented non-alcoholic beverages: Microbiota, fermentation process and quality characteristics. International Journal of Food Microbiology, 167: 44–56.

Charteris, W. P., Kelly, P. M., Morelli, L., & Kevin Collins, J. (2001). Quality control Lactobacillus strains for use with the API 50CH and API ZYM systems at 37°C. *Journal of Basic Microbiology*, *41*(5), 241–251. https://doi.org/10.1002/1521-4028

de Souza, E. L., de Oliveira, K. Á., & de Oliveira, M. E. (2023). Influence of lactic acid bacteria metabolites on physical and chemical food properties. Current Opinion in Food Science, 49, 100981.

de Lacey, A. M. L., Pérez-Santín, E., López-Caballero, M. E., & Montero, P. (2014). Biotransformation and resulting biological properties of green tea polyphenols produced by probiotic bacteria. LWT-Food Science and Technology, 58(2), 633-638.

Erşan, M., & Açıkel, Ü. (2014). R. delemar 'In Asit Fosfataz Üretimi ve Zn(Ii) Biyobirikiminin Cevap Yüzey Yöntemi Kullanarak Optimize Edilmesi. Gazi Üniversitesi Mühendislik Mimarlık Fakültesi Dergisi, 29(2). https://doi.org/10.17341/gummfd.95280

Gueguen, Y., Chemardin, P., Janbon, G., Arnaud, A., & Galzy, P. (1996). A very efficient β-glucosidase catalyst for the hydrolysis of flavor precursors of wines and fruit juices. *Journal of Agricultural and Food Chemistry*, 44(9), 2336–2340.

Heperkan, D., Daskaya-Dikmen, C., Bayram, B. (2014). Evaluation of lactic acid bacterial strains of boza for theirexopolysaccharide and enzyme production as a potential adjunctculture, Process Biochemistry, 49: 1587–1594.

Ketudat Cairns, J.R., Esen, A. β-Glucosidases. Cell. Mol. Life Sci. 67, 3389–3405 (2010). https://doi.org/10.1007/s00018-010-0399-2

Malik, N.S., Lani, M.N. & Ahmad, F.T. (2019). Stability of Lactic Acid Bacteria in Pasteurized Cow's and Goat's Milk. *Universiti Malaysia Terengganu Journal of Undergraduate Research*, *1*(4), 77–82. https://doi.org/10.46754/umtjur.v1i4.94

Martínez, D., Molina, M. J., Sánchez, J., Moscatelli, M. C., & Marinari, S. (2016). API ZYM assay to evaluate enzyme fingerprinting and microbial functional diversity in relation to soil processes. *Biology and Fertility of Soils*, *52*(1), 77–89. https://doi.org/10.1007/s00374-015-1055-7

Müller, T., Müller, M., & Behrendt, U. (2004). Leucine arylamidase activity in the phyllosphere and the litter layer of a Scots pine forest. *FEMS Microbiology Ecology*, 47(2), 153–159.

Patel, A., Shah, N. & Prajapati, J.B. (2013). Biosynthesis of vitamins and enzymes in fermented foods by lactic acid bacteria and related genera. *Journal of Crop Science and Technology*. 5(2), 85-91.

Tamang, J.P., Tamang, B., Schillinger, U., Guigas, C. and Holzaphel, W.H. 2009. Functional properties of lactic acid bacteria isolated from ethnic fermented vegetables of the himalayas. International Journal of Food Microbiology, vol.135; pp. 28-33.

Tokatlı, M. (2013). *Ankara Çubuk yöresi turşularından izole edilen laktik asit bakterilerinin tanımlanmaları, teknolojik ve fonksiyonel özelliklerinin belirlenmesi ve starter olarak kullanılma olanaklarının değerlendirilmesi* (Doktora tezi, Ankara Üniversitesi, Fen Bilimleri Enstitüsü, Gıda Mühendisliği Anabilim Dalı).

Yeğin, S., & Üren, A. (2008). Biogenic amine content of boza: A traditional cereal-based, fermented Turkish beverage. Food Chemistry, 111(4), 983–987.

Zorba, M., Hancioglu, O., Genc, M., Aslan, A., Ova, G., Karapinar, M. 1999. The choice of starter culture combination for the boza production by using sensory evaluation and determination of the chemical and rheological properties, In F. Toldra, D. Ramon, & J. L. Navarro (Eds.), Proceedings of the international congress: improved traditional foods for the next century (pp. 79–83), October 28–29, 1999, Valencia, Spain.

➢ *ORAL PRESENTATION*

Development of a Renewable Energy-Powered Autonomous Irrigation zystem for Sustainable Landscape Management

Hakan Temiz (https://orcid.org/0000-0002-1351-7565),
Muhammed Enes Kandemir* (https://orcid.org/0009-0003-5595-3984),
Eren Güler (https://orcid.org/0009-0000-8304-5068),
Hüseyin Gürgün (https://orcid.org/0009-0003-1894-2792),
Gökhan Yavuz (https://orcid.org/0009-0005-3797-6263)

Artvin Coruh University, Faculty of Engineering, Department of Computer Engineering, Artvin, Türkiye.

*Corresponding author e-mail:230502017@ogrenci.artvin.edu.tr

Abstract
The irrigation of landscape areas—such as gardens, parks, and agricultural fields—within public institutions, universities, and commercial enterprises often demands significant human labor. The manual operation of irrigation components, particularly control devices like valves, can result in operational inefficiencies due to the extensive size of these areas and the limited availability of personnel. Consequently, essential resources such as water and labor are frequently misallocated, while environmental problems may arise from poorly regulated irrigation practices, including watering during rainfall or failing to terminate irrigation in a timely manner. Over-irrigation can negatively impact plant health by inhibiting growth, promoting the spread of invasive vegetation, and contributing to soil degradation. Moreover, manually tracking irrigated zones is both time-intensive and susceptible to human error.This project proposes the design and implementation of an autonomous or semi-autonomous irrigation system powered by renewable energy sources, with a particular emphasis on solar energy. The system is intended to function independently in both rural and urban settings, generating its own power and operating without dependence on the electrical grid. Wireless communication will facilitate remote control of the irrigation infrastructure through software applications interfacing with local controllers via wireless networks.Key features of the system include programmable scheduling and automated operation guided by data from environmental sensors—such as soil moisture, rainfall, and ambient light detectors. These sensors will enable the system to detect drought or saturation conditions, allowing it to adapt its irrigation behavior automatically or in response to remote manual commands. The system's ability to irrigate during nighttime hours, without requiring human oversight, further enhances energy and labor efficiency. Ultimately, the proposed system aims to improve water use efficiency, minimize environmental impact, and support optimal plant growth through precise, responsive, and sustainable irrigation practices.
Keywords: Autonomous irrigation, renewable energy, smart agriculture, wireless control, IoT

INTRODUCTION

The irrigation of large-scale landscape and agricultural areas—such as campuses, greenhouses, and public institution grounds—has traditionally relied on manual labor and on-site intervention. In many existing systems, irrigation is achieved by physically activating control equipment, such as valves, by personnel located on-site. This method, while simple, is prone to significant inefficiencies. Large field sizes, limited manpower, forgetfulness, or time constraints often result in unnecessary, excessive, or untimely irrigation. These issues lead to the waste of critical resources such as water, labor, and energy, and may even result in environmental damage. For instance, irrigating during rainfall or failing to stop irrigation in time can damage plant health or promote the growth of undesired vegetation. The emergence of modern technologies, especially in the fields of the Internet of Things (IoT), wireless communication, and renewable energy, presents a compelling opportunity to develop more intelligent and efficient irrigation systems. With these technologies, it is now possible to design systems that require minimal human intervention, are remotely operable, and can make autonomous decisions based on real-time environmental data. This project proposes the development of a smart irrigation system that operates autonomously and/or semi-autonomously, powered entirely by renewable energy—specifically, solar energy. The system is designed to be scalable and to support irrigation in at least two distinct zones. It will feature both temporal scheduling and real-time responsiveness enabled by sensors (e.g., soil moisture, rainfall, and light sensors) that detect environmental conditions and transmit data to a

central control software. The system will communicate with irrigation infrastructure wirelessly (via Wi-Fi and/or GPRS), enabling regional control of grouped valves to deliver precise irrigation as needed. This architecture ensures the system remains functional even in remote or rural areas lacking access to conventional power sources. By eliminating the need for physical presence during irrigation operations, the proposed system offers numerous advantages: conservation of time, labor, water, and energy; increased operational efficiency and agricultural productivity; and a meaningful reduction in the environmental footprint. In this context, the project aims not only to improve the sustainability of irrigation practices but also to demonstrate a model for smart agriculture and green infrastructure management. Recent literature supports the increasing application of automation, wireless control, and solar energy in irrigation systems. Atay et al. (2009) developed a photovoltaic-powered micro-drip irrigation system and validated its applicability under real-world farming conditions, providing practical guidance for local users. Similarly, Barkunan et al. (2020) proposed a sensor-based irrigation system incorporating a microcontroller, smartphone interface, and GSM module. This system evaluated real-time environmental inputs and automatically initiated irrigation based on detected soil moisture levels. Sudharshan et al. (2019) designed an intelligent irrigation framework using solar energy and fuzzy logic to process data from soil moisture, humidity, and temperature sensors, ensuring adaptive and efficient water management (Suresh Kumar, 2023). Alpay (2021), on the other hand, implemented a Dual Tone Multi Frequency (DTMF)-based control mechanism, enabling remote irrigation and pesticide spraying via mobile commands, while simultaneously collecting temperature and humidity data. Taneja and Bhatia (2017) integrated Arduino boards with soil moisture and water level sensors to establish a threshold-based automatic irrigation solution that reduced unnecessary water usage. Saleh et al. (2016), however, cautioned against the use of resistance-based sensors in diverse soil and climate conditions due to inconsistencies in long-term monitoring accuracy. Advancing from basic sensor integration, García et al. (2018) introduced the Smart Photovoltaic Irrigation Manager (SPIM), which combines climatic, crop, hydraulic, and soil data to regulate solar-powered irrigation systems throughout the growing season. Their approach allowed dynamic adjustments in irrigation duration based on past deficiencies, thus enhancing long-term efficiency. Further, Atay et al. (2011) conducted a field-based performance evaluation of a solar irrigation system in Şanlıurfa, emphasizing its viability in arid conditions. Li et al. (2017) contributed by developing optimization techniques tailored to increase the efficiency and performance of solar-powered irrigation systems, offering analytical and implementation-oriented insights. These studies collectively underline the growing relevance of integrating smart technologies with renewable energy in irrigation, laying a solid foundation for the design and implementation of the system proposed in this project.

MATERIALS AND METHODS

The proposed smart irrigation system **(Figure 1)** is a modular and scalable solution designed to meet the needs of multi-zone irrigation by integrating hardware and software components into a unified architecture. The system is built upon the principles of energy independence, remote accessibility, and intelligent decision-making based on real-time environmental data. The prototype, whose circuit diagram is presented in **Figure 4**, was implemented in a controlled pilot area comprising two separate irrigation zones to test its functionality under real-world conditions.To enable environmentally responsive operation, the following sensors have been integrated into the system.Soil Moisture Sensor: Measures soil water content, influencing irrigation decisions. Rain Sensor: Detects precipitation and halts irrigation during rainfall, contributing to water conservation.Sensor data is collected via digital or analog pins and transmitted wirelessly to the central software at certain intervals. Each sensor is calibrated to suit local soil and climate conditions. Collected data is visualized weekly via the system's web interface and presented to the user **(Figure 3)**. In this way, users can analyze past sensor data and make more efficient irrigation plans.For controlling the water flow in each irrigation zone, 12V DC solenoid valves are used. These valves are actuated through relay modules connected to the microcontroller. The system currently supports two independent irrigation zones and is designed to be easily expandable as needed.Thanks to the built-in Wi-Fi module of the ESP32, communication between the system and the control software is achieved through a local network or the internet. In field deployments where fixed Wi-Fi infrastructure is unavailable, GSM-based data transmission via a GPRS (SIM800L) module or long-range LoRa communication modules can be integrated to maintain remote accessibility.All hardware components are powered by a 20W solar panel, a 12V battery, and a charge controller module. Voltage regulators are used to ensure the stable operation of components requiring 3.3V and 5V. This configuration enables the system to operate independently of the electrical grid, making it well-suited for rural and remote areas.A web-based interface **(Figure 2)** has been developed, which, together with the central control software (backend), performs the following functions: Recording and visualization of sensor data, Creation and management of irrigation schedules, Transmission of manual control commands, User access and authorization

management.Communication between the microcontroller and the software is carried out through HTTP requests.The user interface of the system has been developed using HTML, CSS, and JavaScript with an emphasis on simplicity and accessibility. It is designed to run on any web browser and is optimized for mobile compatibility. Users can access the system from any device with an internet connection without the need to install additional software.The functions offered by the HTML-based interface are as follows: Environmental data such as soil moisture, rain detection, and light intensity are continuously updated and presented to the user in real-time. These data points are displayed in simplified tables and supported by colored icons to enhance user-friendliness.Through a basic HTML calendar component, users can specify the day and time for irrigation in each zone. The selected schedules are stored in a database and sent to the microcontroller for execution.Each irrigation zone can be manually controlled via HTML buttons. Users can activate or deactivate the valve for a specific zone by clicking the corresponding button. This feature is particularly useful for manual interventions independent of sensor data.JavaScript is used to present historical data such as soil moisture, irrigation times, and rainfall in graphical format. These visuals support users in agricultural planning and decision-making.All components were assembled in accordance with open-source hardware principles. The software was developed using the Arduino IDE. Initial testing of the prototype system was conducted over a two-week period under varying environmental conditions. These tests aimed to evaluate system performance in terms of sensor accuracy, wireless connectivity stability, and energy management. The results provided valuable insights for refining the irrigation threshold values and improving the user interface.

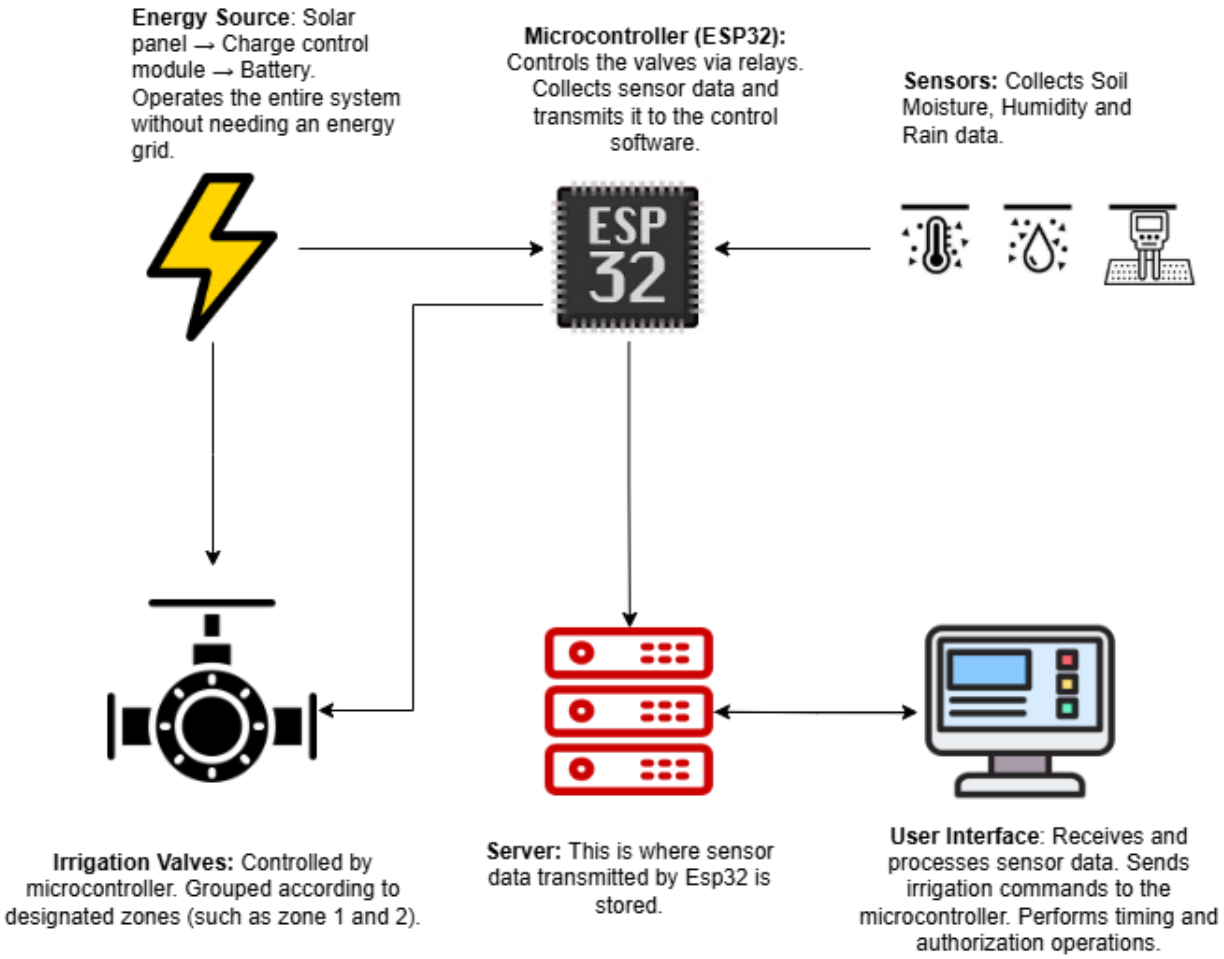

Figure 1 Systematic Scheme

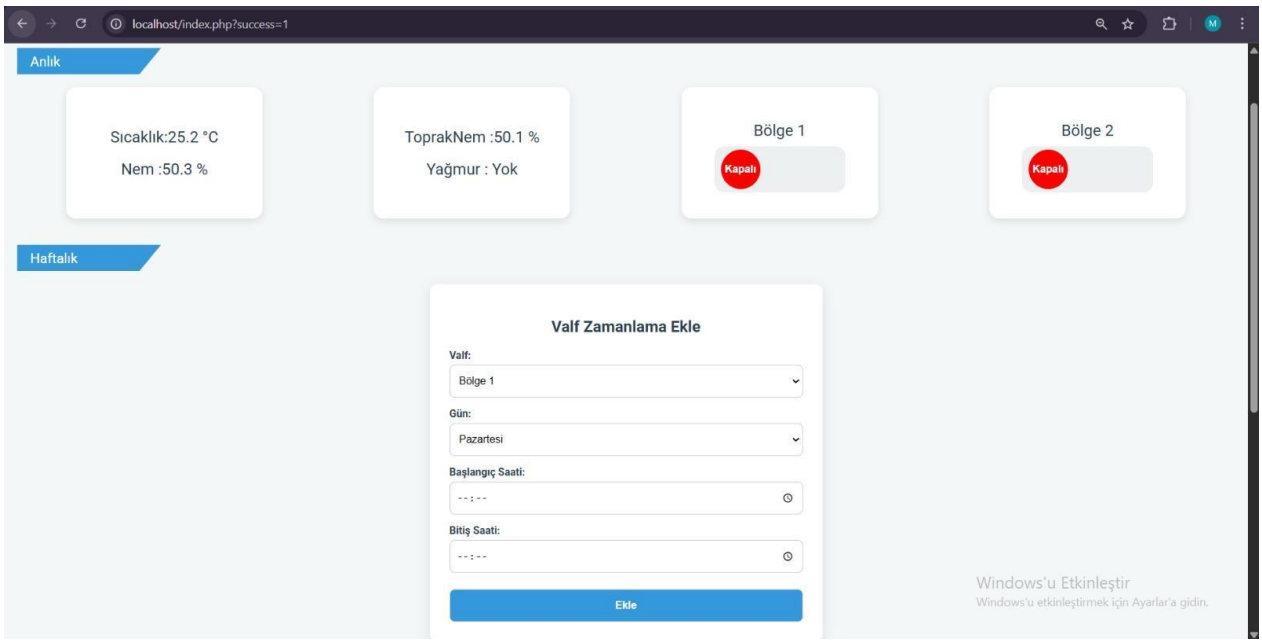

Figure 2 Instant Data and Command Sending forms

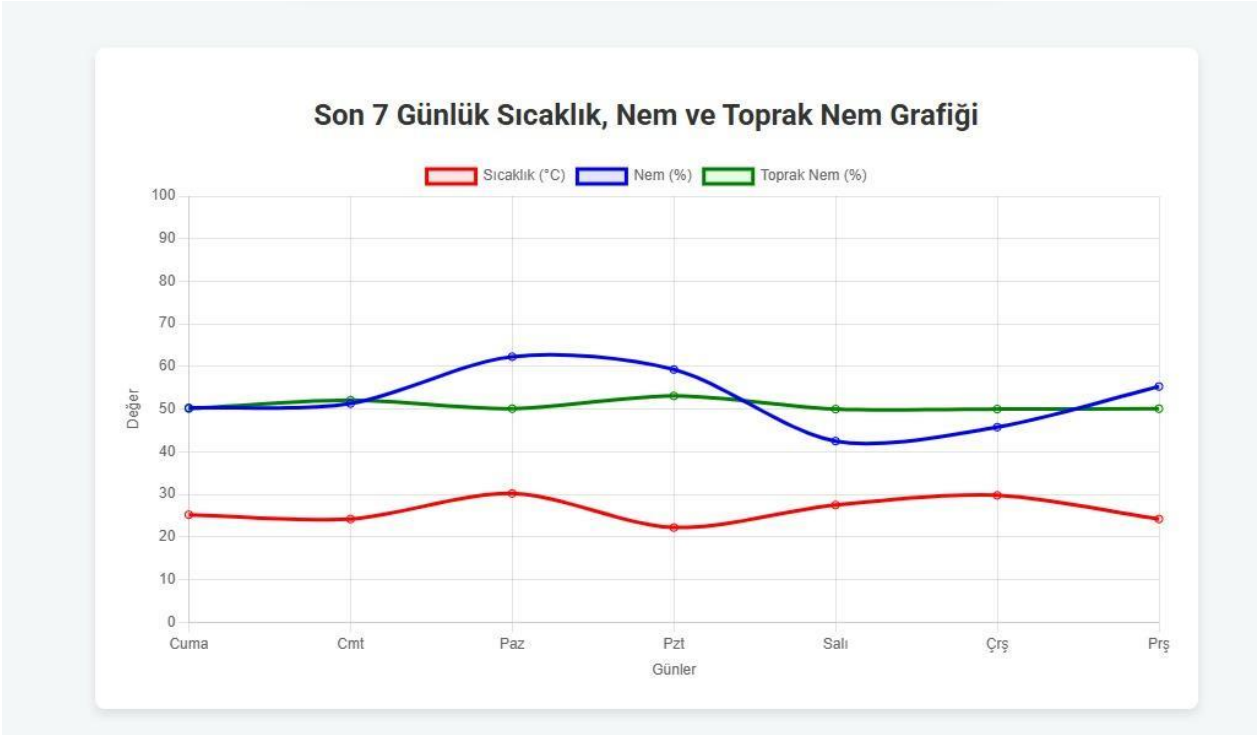

Figure 3 Data Diagram

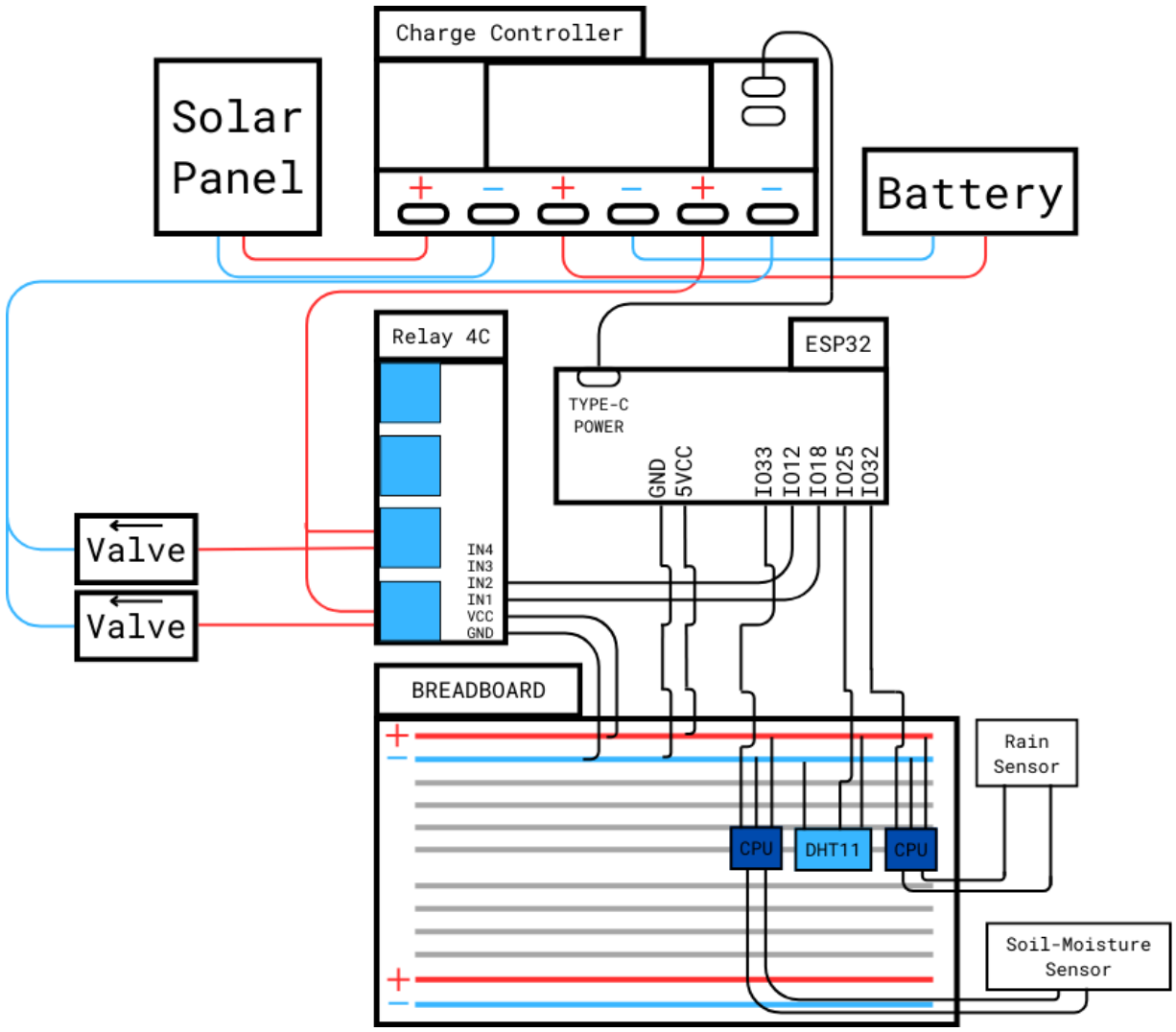

Figure 4 Circuit Diagram

RESULTS & DISCUSSION

The developed autonomous irrigation system prototype demonstrated significant advantages in practical use. By enabling irrigation management across two independent zones, the system allowed targeted watering, reducing waste and supporting healthier plant growth. The integration of soil moisture and rain sensors effectively prevented unnecessary irrigation during rain or sufficient soil moisture, resulting in water savings estimated at 20–30% compared to manual irrigation. This highlights the system's potential for resource efficiency under varying environmental conditions. Operating fully on solar energy, the system proved sustainable and practical for deployment in remote or off-grid locations, eliminating dependency on traditional power sources and contributing to a reduction in carbon emissions. The wireless communication capability facilitated seamless remote control and monitoring, significantly reducing labor requirements and operational complexity, which is critical for large-scale agricultural or landscape management. However, the system also has some limitations. Initial costs related to solar panels, sensors, and communication modules can be higher compared to conventional irrigation setups, potentially limiting accessibility for small-scale farmers without financial support. Additionally, system reliability depends on environmental factors such as solar exposure and wireless signal strength, which may affect performance in certain regions or weather conditions. Maintenance of sensors and electronics in outdoor environments also requires attention to ensure long-term durability. Overall, the system is well-suited for applications where water conservation, labor reduction, and remote management are priorities, especially in areas with adequate sunlight. Future improvements could focus on cost reduction, enhanced sensor accuracy, and integration with weather forecasting services to optimize irrigation schedules further. The modular design allows scalability, making the system adaptable to a wide range of agricultural and landscaping needs.

CONCLUSION

This study successfully demonstrated the development of an autonomous and semi-autonomous irrigation system powered by renewable solar energy. The system's design enables efficient water management by integrating real-time environmental data, wireless communication, and remote control capabilities. Testing across multiple irrigation zones confirmed that the system reduces water and energy consumption, minimizes labor requirements, and enhances the overall efficiency of irrigation operations.The modular and scalable architecture of the system makes it suitable for various applications, ranging from agricultural fields to public landscapes and greenhouses. By eliminating the need for physical presence during irrigation and relying on smart scheduling and sensor feedback, the system contributes significantly to sustainable resource use and environmental protection. Future work may focus on expanding the system's capabilities by integrating additional sensors, improving communication protocols, and incorporating advanced data analytics for predictive irrigation management. The proposed system offers a promising foundation for the modernization of irrigation infrastructure, contributing to more sustainable agricultural practices and reduced carbon footprints globally.

ACKNOWLEDGEMENTS

This study was supported by the Scientific and Technological Research Council of Turkey (TÜBİTAK) under project number 1919B012336343 within the scope of the 2209-A program, and by the Scientific Research Projects Coordination Unit of Artvin Çoruh University under project number 2024.F13.02.02.

REFERENCES

Atay, Ü., Işıker, Y., & Yeşilata, B. (2009). Fotovoltaik Güç Destekli Mikro Sulama Sistemi Projesi-1: Genel Esaslar. V. Yenilenebilir Enerji Kaynakları Sempozyumu, 57-62.

Atay, Ü., Işıker, Y., Yeşilata, B., "Güneş Enerjili Damla Sulama Sistemi Arazi Performansının Deneysel Değerlendirilmesi", Mühendis ve Makine Dergisi, 53 (634), 15-20, (2011).

Barkunan, S. R., Bhanumathi, V., & Balakrishnan, V. (2020). Automatic irrigation system with rain fall detection in agricultural field. Measurement, 156, 107552.

García, A. M., García, I. F., Poyato, E. C., Barrios, P. M., Díaz, J. A. R., "Coupling irrigation scheduling with solar energy production in a smart irrigation management system", Cleaner Production, 175, 670-682, (2018).

Li, G., Jin, Y., Akram, M. W., Chen, X., "Research and current status of the solar photovotalic water pumping system – A review", Renewable and Sustainable Energy Review, 79, 440-458, (2017).

Saleh, M., Elhajj I. H., Asmar, D., Bashour, I., Kidess, S., "Experimental evaluation of low-cost resistive soil moisture sensors," 2016 IEEE International Multidisciplinary Conference on Engineering Technology (IMCET), Beirut, 179-184, (2016).

Suresh Kumar, S., Sudharshan, M. S., TS, N., Bhargava, V., & Chandana, (2023) V. S. SMART AGRICULTURE SYSTEM.

Taneja, K., & Bhatia, S. (2017, June). Automatic irrigation system using Arduino UNO. In 2017 International Conference on Intelligent Computing and Control Systems (ICICCS) (pp. 132-135). IEEE.

➢ *ORAL PRESENTATION*

Synthesis and optical properties of erbium-doped lithium calcium borate ($Li_6CaB_3O_{8.5}:Er^{3+}$)

Mükremin Yılmaz[1*] (*ORCID: https://orcid.org/0000-0002-8091-5416*)

[*1]Bartın University, Faculty of Engineering, Architecture and Design, Department of Metallurgical and Materials Engineering, Bartın, Türkiye.

*Corresponding author e-mail: mukreminyilmaz@bartin.edu.tr

Abstract

This study explores the synthesis and photoluminescence properties of erbium (Er^{3+})-doped lithium calcium borate ($Li_6CaB_3O_{8.5}$) compounds. The samples were successfully synthesized in ambient air via a conventional solid-state reaction technique. Structural characterization was conducted using X-ray diffraction (XRD), which confirmed the formation of a well-crystallized orthorhombic $Li_6CaB_3O_{8.5}$ phase across all samples. Room-temperature photoluminescence (PL) measurements were performed under excitation by a 532 nm Nd:YAG laser. The PL spectra exhibited distinct near-infrared (NIR) emission around 1550 nm, characteristic of Er^{3+} ions. A clear dependence of luminescence intensity on Er^{3+} concentration was observed. The 1% Er^{3+}-doped sample displayed the highest emission intensity, with a subsequent decline as the dopant concentration increased from 1% to 6%, indicating the occurrence of concentration quenching. These findings highlight the potential of Er^{3+}-doped $Li_6CaB_3O_{8.5}$ as a promising candidate for solid-state lighting, optical amplifiers, and laser-based applications.

Keywords: Er^{3+}, $Li_6CaB_3O_{8.5}$, Phosphor, Er-doped borate

INTRODUCTION

Borate-based compounds, particularly lithium and calcium borates, have garnered significant attention as host matrices for rare-earth (RE^{3+}) ions due to their exceptional physicochemical and optical properties (Alharshan et al., 2024; Mutailipu et al., 2021). Structurally, borates are composed of various boron-oxygen polyhedra, including trigonal BO_3 and tetrahedral BO_4 units, which facilitate the formation of diverse and flexible crystal lattices (Kipcak et al., 2015). This structural versatility allows for the accommodation of dopant ions with minimal lattice distortion, thereby maintaining crystallinity while optimizing optical behavior (Kashif & Ratep, 2023; Li et al., 2005).

Among borate hosts, lithium borates are especially attractive due to their low melting points, high thermal stability, wide bandgap, and low phonon energies, which are essential for minimizing non-radiative relaxation pathways in luminescent materials (Gao & Li, 2014). Calcium borates, on the other hand, offer additional structural rigidity and improve mechanical stability, making them suitable for high-temperature and photonic applications (Aljewaw et al., 2023; Doull et al., 2014). The combination of lithium and calcium in mixed borate systems creates a favorable environment for rare-earth doping, enabling controlled synthesis of optically active materials with tailored structural and electronic properties.

Erbium (Er^{3+}) ions are widely studied for their luminescent properties, particularly due to the $^4I_{13/2} \rightarrow {}^4I_{15/2}$ transition near 1.53 µm, which falls within the third telecommunication window (C-band) (Mao et al., 2008; Tioua et al., 2022). This wavelength exhibits minimal attenuation in silica-based optical fibers, making Er^{3+}-doped materials crucial for applications in fiber-optic amplifiers, solid-state lasers, infrared sensors, and biomedical imaging (Balabanov et al., 2025; Zhao et al., 2025). The efficiency of this NIR emission depends strongly on the host matrix, where a low-phonon-energy environment, as offered by borate lattices, significantly enhances radiative transitions and suppresses non-radiative losses (Singh et al., 2022).

To synthesize Er^{3+}-doped borate materials, the solid-state reaction method is commonly employed due to its simplicity, cost-effectiveness, and ability to produce phase-pure crystalline compounds. This method involves high-temperature calcination of stoichiometrically mixed precursor powders, typically in air, which facilitates complete reaction and homogeneity of the dopant within the host lattice. Moreover, the absence of solvent-related contaminants and the ability to precisely control thermal treatment parameters make the solid-state method particularly suitable for the preparation of luminescent borates intended for optical applications.

In this context, the synthesis and characterization of erbium-doped lithium calcium borate ($Li_6CaB_3O_{8,5}:Er^{3+}$) via the solid-state reaction method represent a promising approach for developing efficient near-infrared emitting materials. The incorporation of Er^{3+} ions into the $Li_6CaB_3O_{8,5}$ host lattice takes advantage of the favourable structural features of both lithium and calcium borates-such as low phonon energy, high thermal stability, and structural flexibility-which collectively enhance the luminescence efficiency. Through careful control of synthesis conditions and dopant concentration, the optical performance of $Li_6CaB_3O_{8,5}:Er^{3+}$ can be tailored for advanced photonic applications, including fiber-optic amplification, laser systems, and infrared-emitting devices.

In this study, the effect of erbium concentration on the crystal structure and photoluminescence (PL) emission properties of Li-Ca-borate materials synthesized via the solid-state reaction method was systematically investigated.

MATERIALS AND METHODS

Pure and Er-doped $Li_6CaB_3O_{8,5}$ samples were synthesized by using the conventional solid-state reaction method in air. Initially, the starting materials Li_2CO_3, $CaCO_3$, H_3BO_3, and Er_2O_3 were weighed in stoichiometric proportions, and they were mixed uniformly in an agate mortar. And then, the powder mixtures were placed in a furnace for pre-calcination at 450 °C for 1 hour. After that, the precursor powders were removed from the furnace and again mixed homogenously. Finally, the precursor powders were fired at 800 °C for 8 hours.

The XRD structural analysis of the synthesized materials was performed on the Rigaku SmartLab diffractometer equipped with Cu K_α (40 kV, 30 mA, λ=1.54051 Å) radiation at room temperature. Scanning was performed between 15° and 90° 2θ. Measurement was made with 0.01° steps and a 0.02°/s scan rate. PL measurements are carried out by a 1/4 m monochromator equipped with a liquid nitrogen cooled InGaAs detector. Samples are excited with a NdYAG laser at 532 nm. The output power of the lasers is 60 mW.

RESULTS and DISCUSSION

Figure 1 presents the XRD patterns of the synthesized $Li_6CaB_3O_{8,5}:Er^{3+}$ samples along with the reference diffraction data for pure $Li_6CaB_3O_{8,5}$ reported by Wu et al. (2003). The diffraction patterns indicate that all samples exhibit crystalline phases, with $Li_6CaB_3O_{8,5}$ being the predominant phase formed in each case. No significant impurity phases were detected in the majority of samples, suggesting successful incorporation of Er^{3+} ions without altering the main crystal structure.
However, the sample with 2% Er doping shows slightly reduced crystallinity compared to the others. This is evidenced by the lower intensity of diffraction peaks and the presence of minor noise peaks, which may be associated with amorphous components or secondary phases. This suggests that 2% Er incorporation might have partially disrupted the crystallization process or led to localized structural inhomogeneities. In contrast, the samples doped with higher Er contents (3-6%) maintain a consistent diffraction pattern, implying that the main $Li_6CaB_3O_{8,5}$ phase remains structurally stable despite the increasing dopant level.

$Li_6CaB_3O_{8,5}$ has an orthorhombic crystal structure with a Pnn2 space group. The reported lattice parameters are a = 9.2440(6) Å, b = 8.0999(4) Å, and c = 3.4839(3) Å (Wu et al., 2003). The diffraction peaks observed in all samples are in general agreement with the reference pattern, indicating that the base structure is preserved upon Er^{3+} doping.

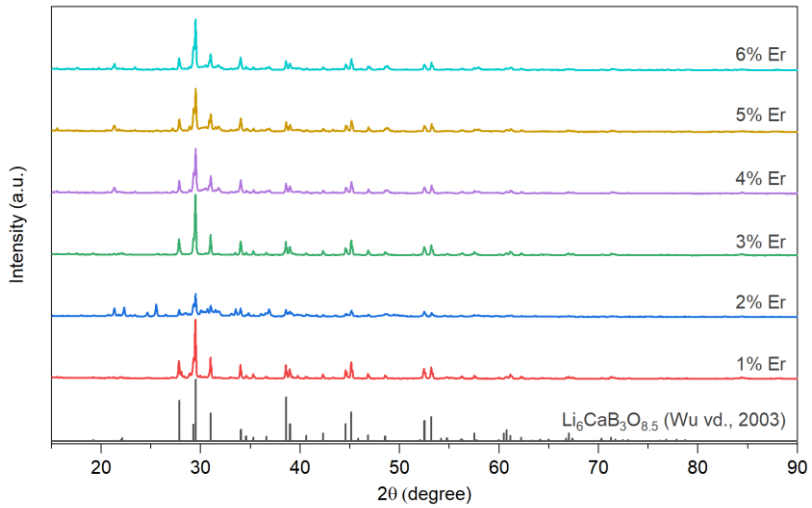

Figure 1. XRD patterns of the synthesized samples. The reference XRD data for the $Li_6CaB_3O_{8.5}$ crystal were obtained from Wu et al. (2003)

Figure 2 presents the near-infrared (NIR) emission spectra of $Li_6CaB_3O_{8,5}:Er^{3+}$ samples with varying Er^{3+} concentrations under 532 nm excitation, corresponding to the $^4I_{13/2} \rightarrow {}^4I_{15/2}$ transition (Kesavulu et al., 2016). The emission bands, centered around 1530–1560 nm, exhibit well-resolved Stark components, indicating that Er^{3+} ions occupy multiple crystallographic environments within the host lattice due to crystal field splitting (Annapoorani et al., 2016).

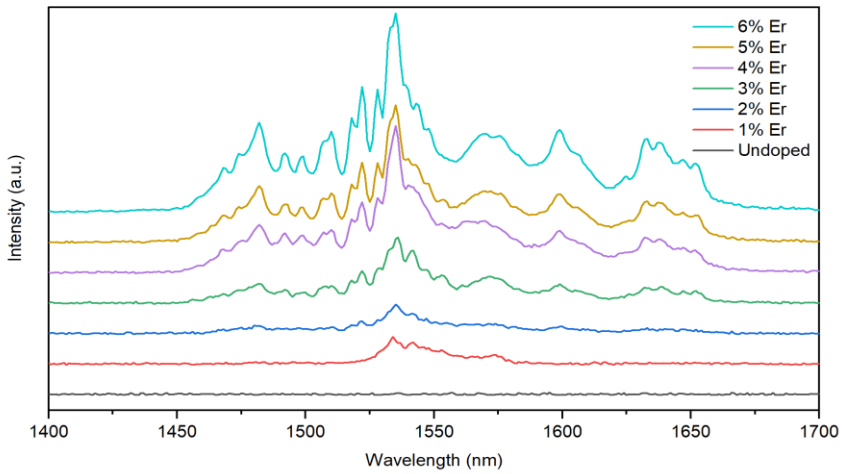

Figure 2. Room-temperature PL spectra of the prepared samples under 532 nm laser excitation

As the Er^{3+} concentration increases from 1% to 6%, the emission intensity steadily rises without signs of concentration quenching. This suggests that the host matrix can efficiently accommodate Er^{3+} ions while minimizing non-radiative losses such as cross-relaxation. The absence of detectable luminescence in the undoped sample further confirms that the emission originates exclusively from Er^{3+} ions. Additionally, the broad emission bandwidth and stable spectral shape across all doping levels point to the material's suitability for applications in NIR optical amplification and biomedical imaging. The slight spectral broadening observed at higher concentrations may result from increased dipole–dipole interactions or local structural distortions.

CONCLUSION

In this study, erbium (Er^{3+})-doped lithium calcium borate ($Li_6CaB_3O_{8,5}:Er^{3+}$) materials were successfully synthesized via a conventional solid-state reaction method, and their structural and photoluminescence (PL) properties were systematically investigated as a function of dopant concentration. X-ray diffraction (XRD) analyses confirmed the formation of a well-crystallized orthorhombic $Li_6CaB_3O_{8,5}$ phase in all samples, with no significant impurity phases detected, indicating that Er^{3+} ions were effectively incorporated into the host lattice without disrupting the primary crystal structure. Photoluminescence measurements at room temperature

revealed intense near-infrared (NIR) emission centered around 1530-1560 nm. The emission intensity increased consistently with Er^{3+} concentration from 1% to 6%, with no evidence of concentration quenching, demonstrating the ability of the $Li_6CaB_3O_{8,5}$ matrix to accommodate higher dopant levels while maintaining optical efficiency. These findings highlight the suitability of $Li_6CaB_3O_{8,5}:Er^{3+}$ as a promising NIR-emitting material for advanced photonic applications, including solid-state lasers, optical amplifiers, and biomedical imaging systems.

REFERENCES

Alharshan, G. A., Mahmoud, A. M. A., Ebrahem, N. M., Elsad, R. A., Shaaban, S. M., Elsafi, M., & Said, S. A. (2024). The manufacture, optical properties, and mechanical aspects of europium-doped borate glasses. Scientific Reports, 14(1), 22920.

Aljewaw, O. B., Karim, M. K. A., Effendy, N., Kamari, H. M., Zaid, M. H. M., Noor, N. M., Salim, A. A., Isa, N. M., Kadir, A. B. A., Chew, M. T., & Abokridiga, A. I. (2023). Physical, optical and thermoluminescence properties of lithium aluminum borate glass co-doped with Dy2O3. Radiation Physics and Chemistry, 209, 111004.

Annapoorani, K., Basavapoornima, Ch., Suriya Murthy, N., & Marimuthu, K. (2016). Investigations on structural and luminescence behavior of Er3+ doped Lithium Zinc borate glasses for lasers and optical amplifier applications. Journal of Non-Crystalline Solids, 447, 273–282.

Balabanov, S., Permin, D., Normani, S., Belyaev, A., Koshkin, V., Andreev, P., Ladenkov, I., Braud, A., Camy, P., Solé, R. M., Mateos, X., & Loiko, P. (2025). Fabrication and luminescent properties of erbium-doped Y2O3–MgO and Gd2O3–MgO nanocomposite ceramics. Journal of the American Ceramic Society, 108(4), e20330.

Doull, B. A., Oliveira, L. C., Wang, D. Y., Milliken, E. D., & Yukihara, E. G. (2014). Thermoluminescent properties of lithium borate, magnesium borate and calcium sulfate developed for temperature sensing. Journal of Luminescence, 146, 408–417.

Gao, X., & Li, R. K. (2014). Structure and optical properties of a new borate K2Ba4Ga4Li2B6O21. Optical Materials, 36(12), 2026–2029.

Kashif, I., & Ratep, A. (2023). Optical properties of borate glasses containing chromium and erbium oxide. Applied Physics A, 129(7), 489.

Kesavulu, C. R., Kim, H. J., Lee, S. W., Kaewkhao, J., Wantana, N., Kothan, S., & Kaewjaeng, S. (2016). Influence of Er3+ ion concentration on optical and photoluminescence properties of Er3+-doped gadolinium-calcium silica borate glasses. Journal of Alloys and Compounds, 683, 590–598.

Kipcak, A. S., Senberber, F. T., Aydin Yuksel, S., Derun, E. M., & Piskin, S. (2015). Synthesis, characterisation, electrical and optical properties of copper borate compounds. Materials Research Bulletin, 70, 442–448.

Li, L., Li, G., Wang, Y., Liao, F., & Lin, J. (2005). Bismuth Borates: One-Dimensional Borate Chains and Nonlinear Optical Properties. Chemistry of Materials, 17(16), 4174–4180.

Mao, Y., Huang, J. Y., Ostroumov, R., Wang, K. L., & Chang, J. P. (2008). Synthesis and Luminescence Properties of Erbium-Doped Y2O3 Nanotubes. The Journal of Physical Chemistry C, 112(7), 2278–2285.

Mutailipu, M., Poeppelmeier, K. R., & Pan, S. (2021). Borates: A Rich Source for Optical Materials. Chemical Reviews, 121(3), 1130–1202.

Singh, P., Kaur ,Manmeet, Brahme ,Nameeta, Bisen ,D. P., Umam ,Rofiqul, Panse ,V. R., Said ,Ahmad, Irzaman, & and Saregar, A. (2022). Photoluminescence Property of Erbium-Doped Yttrium Oxide: Doping Concentration and Its Effect. Integrated Ferroelectrics, 230(1), 100–107.

Tioua, B., Soltani, M. T., Khechekhouche, A., & Wondraczek, L. (2022). Physical properties and luminescence of highly stable erbium-doped antimony glasses for NIR broadband amplification. Optics & Laser Technology, 152, 108152.

Wu, L., Chen, X. L., Tu, Q. Y., He, M., Zhang, Y., & Xu, Y. P. (2003). Phase relations in the system Li2O–CaO–B2O3. Journal of Alloys and Compounds, 358(1–2), 23–28.

Zhao, X., Xie, Z., Liu, H., Liu, H., Pu, Y., Qiu, Y., Zheng, S., Dan, Y., Zhong, Q., Dong, Y., & Hu, T. (2025). Photoluminescent Properties of Erbium-Doped Aluminum Scandium Nitride Thin Films. ACS Photonics, 12(2), 925–931.

➢ *ORAL PRESENTATION*

Potasyumun Alımı, Taşınması ve kullanım etkinliği: Moleküler ve Biyoteknolojik Yaklaşımlar

Esma Yiğider [1] (*ORCID: https://orcid.org/0000-0002-6896-0193*), Sümeyra Uçar[2] (*ORCID: https://orcid.org/0000-0002-7629-0206*), Murat Aydın[1*] (*ORCID: https://orcid.org/0000-0003-1091-0609*), Ertan Yıldırım[3] (*ORCID: https://orcid.org/0000-0003-3369-0645*)

[1]Atatürk Üniversitesi, Ziraat Fakültesi, Tarımsal Biyoteknoloji Bölümü, Erzurum, Türkiye
[2]Erzurum Teknik Üniversitesi, Fen Fakültesi, Moleküler Biyoloji ve Genetik Bölümü, Erzurum, Türkiye
[3]Atatürk Üniversitesi, Ziraat Fakültesi, Bahçe Bitkileri Bölümü, Erzurum, Türkiye

*Sorumlu yazar e-posta: maydin@atauni.edu.tr

Özet

Potasyum (K^+), bitki büyümesi, gelişimi, metabolik düzenleme ve çevresel streslere adaptasyon için hayati bir makro besin elementidir. Sitoplazmik ozmotik dengeyi koruma, enzim aktivasyonu, stoma açıklığının kontrolü, karbon asimilasyonu ve floem taşınımı gibi birçok fizyolojik işlevde rol oynar. Ancak topraktaki potasyumun büyük kısmı bitkiler tarafından kolayca alınamayan formlarda bulunduğundan, potasyum kullanım etkinliğinin (KUE) artırılması sürdürülebilir tarım için önemli bir hedef haline gelmiştir. Son yıllarda moleküler biyoloji alanında kaydedilen gelişmeler, AKT1 gibi Shaker tipi kanallar ve HAK5 gibi yüksek afiniteli taşıyıcılar gibi K^+ taşıyıcı gen ailelerinin işlevsel olarak karakterize edilmesini ve bunların aktivitesini düzenleyen CBL–CIPK sinyal yolaklarının aydınlatılmasını sağlamıştır. Ayrıca transkriptomik, proteomik ve iyonomik gibi omik tabanlı araçlar, KUE ile ilişkili kantitatif özellik lokuslarının (QTL) belirlenmesine olanak tanıyarak marköre dayalı ıslah çalışmalarını hızlandırmıştır. Bu derleme, bitkilerde potasyum kullanım etkinliğini artırmaya yönelik moleküler, fizyolojik ve biyoteknolojik yaklaşımlardaki son gelişmeleri özetleyerek, dayanıklı bitki üretim sistemleri için güncel araştırma eğilimlerine ve gelecek yönelimlerine ışık tutmaktadır.

Anahtar Kelimeler: Potasyum Taşıyıcıları, Ozmoregülasyon, Besin Etkileşimi, Omik Teknolojileri, Potasyum Kullanım Etkinliği (KUE)

Potassium Uptake, Transport, and Use Efficiency: Molecular and Biotechnological Perspectives

Abstract

Potassium (K^+) is a vital macronutrient for plant growth, development, metabolic regulation, and adaptation to environmental stress. It contributes to several physiological functions, such as preserving cytoplasmic osmotic equilibrium, activating enzymes, controlling stomatal opening, assimilating carbon, and facilitating phloem transport. Nevertheless, the majority of potassium in soil exists in unreadily available forms, making the improvement of potassium use efficiency (KUE) a key objective for sustainable agriculture. Recent advances in molecular biology have enabled the functional characterization of key K^+ transporter gene families, such as Shaker-type channels (e.g., AKT1) and high-affinity carriers (e.g., HAK5), as well as the elucidation of CBL–CIPK signaling pathways that regulate their activity. Omics-based tools such as transcriptomics, proteomics, and ionomics have facilitated the identification of quantitative trait loci (QTLs) associated with KUE, thereby accelerating marker-assisted breeding programs. This review highlights recent advancements in molecular, physiological, and biotechnological approaches to improve plant potassium use efficiency, providing insights into current research trends and future directions for resilient crop production systems.

Keywords: Potassium Transporters, Osmoregulation, Nutrient Interaction Omics technological, KUE

1. Giriş

Küresel gıda güvenliği, hızla artan dünya nüfusu, iklim değişikliği, azalan doğal kaynaklar ve çevresel stresler nedeniyle ciddi tehdit altındadır. 2050 yılına kadar dünya nüfusunun 9 milyara ulaşması ve 2030'a kadar yaklaşık 830 milyon insanın yetersiz beslenme riskiyle karşı karşıya kalması beklenmektedir (Tyczewska et al., 2018). Artan gıda talebine karşılık, tarımsal üretimde verimlilik ve sürdürülebilirlik hedefleri, başta makro besin elementleri olmak üzere bitki beslenmesinin optimizasyonunu gerekli kılmaktadır. Bu bağlamda, azot

(N), fosfor (P) ve potasyum (K), bitki gelişimi ve verimi açısından vazgeçilmez üç ana makro besin elementi olarak öne çıkmaktadır.

Potasyum (K^+), bitki hücrelerinde en bol bulunan katyon olup hem metabolik hem de fizyolojik süreçlerde merkezi bir rol oynamaktadır (Xu et al., 2022). Tüm yaşam formları gibi bitkiler de K^+ iyonlarına ihtiyaç duymaktadır; ancak hayvanlar K^+'u dış kaynaklardan temin ederken, bitkiler toprak çözeltisinden aktif olarak almak zorundadır (Safdar et al., 2020). Sitoplazmada baskın katyon olan K^+, enzim aktivasyonu, ozmotik düzenleme, elektriksel denge, hücre genişlemesi, stomatal hareketler, azot metabolizması, fotosentez ve reaktif oksijen türlerinin detoksifikasyonu gibi birçok yaşamsal olayda görev yapmaktadır (Hasanuzzaman et al., 2018; Lian et al., 2023; Xu et al., 2022). Ayrıca, K^+ eksikliği, fotosentezi ve klorofil sentezini azaltarak kloroz, nekroz ve ışığa duyarlılık gibi fizyolojik bozukluklara yol açmaktadır (Cakmak, 2005; Gao et al., 2021).

Topraklarda dengesiz gübreleme ve K^+ rezervlerinin tükenmesi, potasyum eksikliği sorununu derinleştirmekte ve bu durum, bitkilerin su ve besin alım kapasitesini sınırlayarak verim kaybına neden olmaktadır (Du et al., 2021; Zorb et al., 2014). Özellikle kloroplastlarda CO_2 difüzyonu, floem yüklemesi ve fotosentatların taşınımı gibi temel süreçler K^+ yetersizliğinden olumsuz etkilenmektedir (Yin et al., 2023). Potasyum, ayrıca nitrat (NO_3^-) ve amonyum (NH_4^+) emilimi ile azot metabolizmasında yer alan amino asit ve protein sentezinin düzenlenmesinde önemli rol oynamaktadır (Hu et al., 2016; Ruiz and Romero, 2002).

Günümüzde potasyum gübrelerine olan küresel talep giderek artmakta olup, bu durum hem ekonomik hem de çevresel sürdürülebilirliği tehdit etmektedir. Aşırı gübre kullanımının önüne geçilmesi ve verim artışının sürdürülebilir şekilde sağlanması amacıyla, K^+ kullanım etkinliği (Potassium Use Efficiency, PUE) yüksek çeşitlerin geliştirilmesi öncelikli hedef haline gelmiştir (Lotter, 2015). Bu doğrultuda, bitkilerin K^+ alımı, taşınımı, hücre içi dağılımı ve geri dönüşümünü yöneten genetik ve moleküler mekanizmaların anlaşılması, gelecekteki ıslah programları ve biyoteknolojik uygulamalar için kritik önem taşımaktadır.

Bitki hücrelerinde K^+ iyonları yüksek hareketliliğe sahiptir ve ksilem-floem sistemleri aracılığıyla yaşlı yapraklardan genç dokulara kolaylıkla taşınabilir. Bu taşınım süreçleri, çeşitli potasyum taşıyıcıları ve kanal proteinleri tarafından düzenlenmektedir. Bu sistemlerde yer alan başlıca gen aileleri arasında Shaker tipi K^+ kanalları, TPK (Tandem Pore K^+ Channels), HAK/KUP/KT (High-Affinity K^+ Transporters), HKT (High-Affinity K^+ Transporters), KEA (K^+/H^+ Antiporters), NHX (Na^+/H^+ Exchangers) ve CHX (Cation/H^+ Exchangers) bulunmaktadır (Gajdanowicz et al., 2011; Zhang et al., 2023). Bu taşıyıcı ve kanallar, hem K^+ homeostazının sağlanmasında hem de çevresel streslere verilen tepkilerin düzenlenmesinde görev almaktadır. Bu derleme çalışması, potasyum taşınımı ve kullanımına ilişkin moleküler mekanizmaları sistematik olarak ele almakta; K^+ taşıyıcılarının biyolojik işlevlerini ve bu sistemlerin genetik düzenlemelerini ortaya koymaktadır. Bu sayede, sürdürülebilir tarım uygulamaları için yüksek verimli ve besin kullanım verimliliği yüksek çeşitlerin geliştirilmesine yönelik bilimsel temeller ortaya konmaktadır.

2. Bitkilerde Potasyum alımı ve taşınımı

Mevcut K^+ havuzu topraktan K^+ fiksasyonu veya salınımı dinamiklerini belirler. K^+ salınımı süreci, K+ ve toprak partikülleri arasındaki etkileşimler nedeniyle fiksasyona göre oldukça yavaştır (Zorb et al., 2014). K^+ eksikliği ile toprağın verimliliği azalır. Bu nedenle, dünyadaki tarım alanlarının çoğu K^+ eksikliği olarak kabul edilmektedir. Gübre olarak K^+ ihtiyacı 2018 yılında 6.375.000 ton iken 2022 yılında 7.602.000 tona yükselmiştir (https://www.fao.org/3/ ca6746en/ca6746en.pdf). Gübre olarak K^+ talebini karşılamak için, mevcut araştırma odağı K^+ alım verimliliği (KUpE) ve K^+ kullanım verimliliği (KUtE) üzerinedir ve bu özellikler tüm bitki düzeyinde tanımlanmaktadır (Srivastava et al., 2020). KUpE topraktan K^+ alımını içerir ve kök tarafından alım kapasitesi, kök-sürgün uzunluğu ve kök yoğunluğuna bağlıdır. KUtE ise aktif hücre bileşenlerinde optimal K^+'un korunmasına gerekli olmadığında K^+'un değiştirilmesine düşük K^+ konsantrasyonuna toleransa ve yaşlanan hücrelerden genç hücrelere yeniden dağıtıma bağlı olan etkili K^+ dağılımını içerir (Srivastava ve ark., 2020). Bitkiler, plazma membranları, apoplastlar ve tonoplastlar yoluyla çoklu taşıyıcılar ve kanallar aracılığıyla K^+ emilimi için yüksek afiniteli ve düşük afiniteli etkili mekanizmalar geliştirmiştir. Emilen K^+, büyüme ve gelişme için bitkinin farklı kısımlarına yeniden dağıtılır (Zhao et al., 2015).

Bitkiler tohum çimlenmesinden olgunluğa kadar K^+'a ihtiyaç duyar (Fageria, 2016). K^+'un aktif ve pasif taşınımı sırasıyla taşıyıcılar ve kanallar aracılığıyla gerçekleşir. Bitkilerdeki ilk tanımlanmış K^+ taşıyıcısı Arabidopsis'tendir. Taşıyıcılar HAK/KT/KUP, HKT ve Katyon Proton Antiporter (CPA) içerirken; kanallar Shaker tipi, TPK ve Seçici Olmayan Katyonik Kanalları (NSCC) içerir (Gierth and Maser, 2007; Maser et al., 2001). Pasif taşıma elektrokimyasal gradyan nedeniyle enerji katılımı olmaksızın K^+'un membranlar boyunca hareketini içerir. K+ farklı dokulara taşınması nedeniyle bir ozmoprotektan görevi görerek tuzluluk, kuraklık, sıcak, soğuk ve üşüme gibi çeşitli abiyotik streslerin azaltılmasına yardımcı olur (Isayenkov and Maathuis, 2019).

HAK (yüksek afiniteli K^+ taşıyıcısı) / KUP (K^+ alım permeazı) / KT (K^+ taşıyıcısı) ailesi

Düşük potasyum konsantrasyonlarında (<1 mM) etkili olan yüksek afine teli taşıyıcılardan (Sardans and Peñuelas, 2015) HAK/KUP/KT taşıyıcıları ilk olarak E. coli'de KUP1 ve mayada HAK1 olarak bulunmuştur. HKA/KUP/KT bitkilerdeki homologlarıdır. Bitkilerde bulunan büyük bir taşıyıcı grubudur (Cheng et al., 2018). Tanımlanan HAT'lar, Çeltik, biber (Martinez-Cordero et al., 2004) ve arpadaki HAK1 (Cai et al., 2019); Arabidopsis (Rubio et al., 2000), arpa (Cai et al., 2019) ve domatesteki HAK5 (Nieves-Cordones et al., 2007); ve arpadaki KUP1 ve KUP2 (Cai et al., 2019)gibi KT/HAK/KUP taşıyıcılarıdır. *Arabidopsis thaliana*'da HAK/KUP/KT ailesine ait 13 gen bulunmaktadır. Bu genlerden AtKUP2, özellikle çiçek dokularında yüksek düzeyde ifade edilirken; AtKUP3 ve AtKUP4, gelişmekte olan siliqualarda belirgin düzeyde ekspresyon gösterir. AtKUP5, AtKUP6, AtKUP7, AtKUP8, AtKUP10 ve AtKUP12 genleri ise hem kök hem de yaprak dokularında ifade edilmektedir. AtKUP11'in ekspresyonu üreme büyüme evresinde artış göstermektedir (Ahn et al., 2004). Bu ailede en çok araştırılan genlerden biri olan AtHAK5, özellikle köklerde yüksek düzeyde ekspresyon göstermektedir (Nieves-Cordones et al., 2019). Çeltikte ise HAK/KUP/KT ailesi 27 üyeyle bu taşıyıcı grubun en geniş temsil edildiği türlerden biridir (Sun et al., 2015). Çeltikteki OsHAK1, OsHAK5, OsHAK7, OsHAK8, OsHAK12, OsHAK16 ve OsHAK18 genleri, özellikle kök dokularında yüksek düzeyde ifade edilmektedir (Banuelos et al., 2002; Chen et al., 2015a; Chen et al., 2018; Feng et al., 2019; Okada et al., 2018; Peng et al., 2023; Sun et al., 2015; Wang et al., 2021b; Zhang et al., 2021). OsHAK5'in, köklerin epidermis ve vasküler dokularında ve aynı zamanda mezofil hücrelerinde yüksek düzeyde ekspresyon gösterdiği bilinmektedir (Yang et al., 2014). OsHAK21 geni, fidelerin kök ve yaprakları ile anterlerde ve yaprak kılıflarındaki vasküler demetlerde güçlü şekilde ifade edilmektedir (Shen et al., 2015). OsHAK26 ise özellikle anter ve tohum kabuğu gibi üreme dokularında ekspresyon göstermektedir (Li et al., 2022). Hem AtHAK5 hem de OsHAK5 genleri, düşük potasyum koşullarında benzer şekilde aktive olmakta ve her iki genin ekspresyonu da yüksek tuz koşullarında artmaktadır (Qi et al., 2008; Yang et al., 2014). Bu durum, her iki genin de düşük potasyum dengesinin sağlanmasında ve tuz stresine karşı bitkisel yanıtların düzenlenmesinde önemli roller üstlenebileceğini göstermektedir.

HKT/Trk ailesi

HKT taşıyıcıları, bitkilerde Na^+-K^+ simporterleri olarak görev yapar ve tuz stresi altında K^+-Na^+ birlikte taşınımı yoluyla K^+ alımını sürdürmeleri sayesinde bitkilerde tuz toleransının korunmasında önemli bir rol oynarlar (Sardans and Penuelas, 2021). HKT'ler, Trk/Ktr/HKT ailesinin üyeleri olup, dört transmembran domenine sahip bir yapıya sahiptir. Evrimsel analizlere göre HKT ailesi iki alt gruba ayrılmaktadır: sınıf I ve sınıf II. İlk por halkasında serin (SGGG) veya glisin (GGGG) kalıntısının bulunması, sınıf I ve II arasındaki farkı belirler ve bu da iki sınıf arasında iyon iletimi farklılıklarına yol açar (Anil Kumar et al., 2024). HKT (High-affinity K^+ Transporter) ailesine ait taşıyıcılar, Na^+ ve K^+ iyonlarının taşınmasında ve homeostazının korunmasında önemli bir rol oynar (Almeida et al., 2017). Özellikle sınıf I HKT taşıyıcılarının, tuz toleransında ve K^+ yoksunluğu koşullarında Na^+ ve K^+ taşınma süreçleriyle ilişkili olduğu düşünülmektedir. Buna karşılık, sınıf II HKT'lerin hem Na^+ hem de K^+ alımına doğrudan katkı sağladığı bildirilmiştir (Horie et al., 2007). Önceki çalışmalar, yüksek Na^+ konsantrasyonlarının HKT taşıyıcılarının gen ekspresyonunu baskılayabileceğini göstermiştir. Örneğin, AtHKT1;1 geni, Na^+ konsantrasyonu 30 mM'ye kadar olan koşullarda aşırı ifade edilirken, bu seviyenin üzerindeki konsantrasyonlarda ifadesi kademeli olarak azalmakta ve 75 mM Na^+ seviyesinde neredeyse tamamen bastırılmaktadır (Horie et al., 2007). Benzer şekilde, OsHKT2;2 taşıyıcısı aracılığıyla gerçekleşen Na^+ taşınımı, düşük K^+ konsantrasyonlarında artış gösterirken, yüksek K^+ seviyelerinde bu taşıma etkinliği belirgin şekilde düşmektedir (Riedelsberger et al., 2019). Arabidopsis, çeltik ve diğer bitkilerde HKT genlerinin transkripsiyonel düzeyde düzenlenmesinden sorumlu çeşitli transkripsiyon faktörleri tanımlanmıştır. Örneğin, AtHKT1;1 geninin ekspresyonu, AtbZIP24 transkripsiyon faktörü tarafından baskılanmaktadır. RNAi aracılığıyla AtbZIP24 ifadesi bastırılan mutant bitkilerde AtHKT1;1 transkript seviyelerinde anlamlı bir artış gözlemlenmiş ve bu durum AtbZIP24'ün negatif bir düzenleyici olarak rol oynadığını ortaya koymuştur (Yang et al., 2009). Diğer yandan, *Populus alba*'da tanımlanan PalERF109 adlı etilen yanıt faktörü, PalHKT1 geninin ekspresyonunu pozitif yönde düzenlemekte ve aşırı ekspresyonu bitkide artan tuz toleransıyla ilişkilendirilmektedir (Chen et al., 2020). Bazı transkripsiyon faktörleri ve düzenleyici alanlar, K^+ taşıyıcıları ve kanallarının transkripsiyonel düzeydeki düzenlemesinde de görev alır. Ancak bu faktörlerin bitki gelişimi (ontogeni) ve stres yanıtı süreçlerindeki işlevlerinin daha ayrıntılı olarak açıklanmasına ihtiyaç duyulmaktadır.

CPA Ailesi Üyeleri

CPA (katyon-proton antiporter) ailesi, iki alt aileye ayrılır: CPA1 ve CPA2. CPA1 alt ailesi Na^+/H^+ değiştiricileri (NHX) içerirken, CPA2 alt ailesi KEA (K^+ exchange antiporter) ve CHX (katyon-H^+ değiştiricileri) proteinlerini kapsar (Wang and Wu, 2017). NHX proteinleri, hücre zarında ve çeşitli organel zarlarında —özellikle vakuoller ve endoplazmik retikulumda— lokalize olmuşlardır. NHX proteinleri,

sitozolden organellere K^+ taşırken, eş zamanlı olarak organel içinden sitozole H^+ iyonlarının değişimini sağlayarak iyon dengesini düzenler (Isayenkov et al., 2020). NHX taşıyıcılarının aktivitesi, kökten yaprağa iyonların uzun mesafeli taşınımı, stomatal işlevler ve tuz stresi toleransı ile ilişkilendirilmiştir (Barragán ve ark., 2012). *Arabidopsis* NHX1 (NHX2 ile birlikte) geninin aşırı ekspresyonu, K^+ homeostazisinin düzenlenmesinde, tuz toleransının artırılmasında ve ayrıca erkek üreme organlarının gelişimi, çiçeklenme ve meyve tutumu gibi süreçlerin kontrolünde önemli rol oynamıştır (Bassil et al., 2011). CPA2 ailesine ait olan CHX proteinleri ise, K^+/H^+ karşılıklı değişimi yoluyla hücresel pH homeostazisinin sağlanmasında görev alır (Britto and Kronzucker, 2005; Gierth and Maser, 2007). Yapılan birçok çalışmada, CHX proteinlerinin Na^+/H^+ değişim domeni taşıdığı, fakat aynı zamanda K^+ taşınımında da aktif rol aldığı gösterilmiştir (Isayenkov et al., 2020). CHX taşıyıcılarının, tuz stresine karşı verilen yanıtta pH ve K^+ homeostazisini koruyarak önemli katkılar sunduğu; kökler, yapraklar ve polen gibi farklı bitki organlarında bu etkinin gözlendiği belirtilmiştir (Sardans and Peñuelas, 2015). K^+ çıkışı sağlayan antiporterler olan KEA proteinleri de CPA2 ailesinin bir başka alt grubudur. CAP2 ailesine ait bu proteinlerin plastidlerin iç zarı, tilakoit membranları ve Golgi aygıtında lokalize olduğu, endomembran sistemlerde pH ve K^+ homeostazisinin sağlanmasında görev aldığı bildirilmiştir. Ayrıca bu taşıyıcıların, K^+ eksikliği, tuzluluk ve ozmotik stres gibi koşullarda ekspresyonlarının arttığı gösterilmiştir (Sardans and Peñuelas, 2015). KEA1-KEA3 proteinleri, fotosentetik elektron taşınımı ve plastid büyümesini düzenlerken; KEA4-KEA6, özellikle tuzluluk stresi altında endomembran pH dengesini kontrol etmektedir. *Arabidopsis*'te *dpgr* mutantında K^+ taşınım aktivitesi, KEA3-G422R mutasyonu ile artış göstermiştir ((Tsujii et al., 2019). Soya fasulyesinde (GmKEA genleri) yapılan çalışmalarda, abiyotik stres koşullarında bu genlerin çoğunun erken evrede yukarı yönlü, geç evrede ise aşağı yönlü düzenlendiği bildirilmiştir (Chen et al., 2015b). NHX genlerinin birçoğunun hem bitki büyüme ve gelişiminde hem de abiyotik stres toleransında, özellikle K^+ homeostazisinin düzenlenmesi yoluyla önemli roller üstlendiği anlaşılmaktadır.

Shaker Tipi kanallar

Shaker tipi potasyum (K^+) kanalları; bakteriler, mantarlar, hayvanlar ve bitkiler dahil olmak üzere çok çeşitli organizmalarda bulunur. Bitkilerde en iyi çalışılmış K^+ kanallarından biri olan bu kanallar, merkezi bir por yapısına sahip olup, dört alt birim ve beşinci ile altıncı alt birimlerden oluşan bir por halkası ile hidrofobik bir bölge oluştururlar. *Arabidopsis thaliana*'da dokuz farklı Shaker tipi K^+ kanalı tanımlanmıştır (Lebaudy et al., 2007). Tüm Shaker kanalları voltaj kapılıdır; yani, kanalın açık kalma olasılığı hücre zarındaki potansiyel değişimlerine göre artar (Yuan et al., 2024). Shaker tipi potasyum (K^+) kanalları, işlevsel özelliklerine göre üç ana alt gruba ayrılır. Birinci grup olan İçe Doğru Düzenleyici Kanallar (Inward Rectifying), hücre zarının hiperpolarizasyonu sırasında aktive olur ve hücre içine K^+ alımını kolaylaştırır. Bu kanallar, bitki kök hücrelerinde K^+ alımı için hayati öneme sahiptir. Arabidopsis thaliana'da bu gruba dahil olan başlıca proteinler, voltaj-bağımlı potasyum kanal ailesinden KAT (K^+ channel in Arabidopsis) ve AKT1 (Arabidopsis K^+ Transporter 1) proteinleridir. İkinci grup olan Dışa Doğru Düzenleyici Kanallar (Outward Rectifying), membran depolarizasyonu durumunda aktive olur ve K^+ iyonlarının hücre dışına taşınmasını sağlar. Bu grup kanallar, özellikle ksilem yüklemesi ve stoma kapanması gibi fizyolojik süreçlerde kritik rol oynar. SKOR (Stelar K^+ Outward Rectifier) kanalı bu gruba özgü bir örnektir. Üçüncü grup ise Zayıf Düzenleyici Kanallar (Weakly Rectifying) olarak adlandırılır. Bu kanallar hem K^+ girişini (influx) hem de çıkışını (efflux) gerçekleştirebilme kapasitesine sahiptir. Genellikle membran hiperpolarizasyonu ile aktive olurlar. AKT2 kanalı, bu zayıf düzenleyici özellikleri sergileyen önemli bir Shaker tipi K^+ kanalıdır. Bu fonksiyonel çeşitlilik, bitkilerin çevresel değişimlere esnek ve hızlı yanıt verebilmesini sağlar (Wang and Wu, 2013).Her ne kadar bu kanallar dokuya özgü olarak ifade edilse de, bazı Shaker tipi kanallar spesifik hücre veya doku düzeyinde daha belirgin görevler üstlenmektedir. Örneğin; SKOR, stoma hücrelerinde görevli outward yönlü K^+ kanalı olan GORK (Guard Cell Outward-Rectifying K^+ Channel), metabolizmanın anahtar regülatörlerinden biri olarak kabul edilir. Ayrıca polen hücrelerinde görev yapan SPIK (Shaker Pollen Inward Potassium Channel; AtAKT6) gibi bazı Shaker tipi kanallar, özel fizyolojik süreçlerde kritik roller oynar (Adem et al., 2020). İçe doğru düzenleyici kanallardan biri olan AKT1, özellikle düşük potasyum koşullarında kök hücrelerinden K^+ alımını düzenler. Hirsch et al. (1998) yaptığı çalışmada, *Arabidopsis thaliana* bitkisinde AKT1 geninin mutasyonu sonucu bitkilerin düşük K^+ içeriğine sahip ortamlarda büyüme geriliği yaşadığı ve iyon alımında belirgin bozulmalar gözlendiği rapor edilmiştir. Bir diğer inward-rectifier olan KAT1 kanalı ise stoma açıklığının kontrolünde görev yapan guard hücrelerinde bulunur. Pilot et al. (2001) yürüttükleri çalışmada, bu kanalın Arabidopsis'te tanımlandığı ve hiperpolarizasyon durumunda aktive olarak guard hücrelere K^+ alımını sağladığı gösterilmiştir. Dışa doğru düzenleyici kanalların başında gelen SKOR kanalı, kök parankim hücrelerinden ksilem yoluyla sürgünlere K^+ taşınmasında rol oynar. Gaymard et al. (1998), *skor* mutant bitkilerde sürgünlerdeki potasyum seviyesinin normal bitkilere göre %50 oranında azaldığını rapor etmişlerdir.

GORK kanalı ise stomalarda K^+ çıkışını sağlayan outward-rectifier bir kanaldır. Hosy et al. (2003) çalışmasında, *gork* mutantlarında stomaların kapanmasının geciktiği ve guard hücre membranlarının repolarizasyon kapasitesinin zayıfladığı ortaya konmuştur. Zayıf düzenleyici özellik taşıyan AKT2 kanalı ise hem içe hem dışa iyon taşıyabilen çift yönlü bir kanaldır. Bu kanal, enerji durumuna bağlı olarak voltaj yanıt profilini değiştirebilir. Ragel et al. (2019), AKT2'nin özellikle floem hücrelerinde lokalize olduğunu ve elektriksel sinyal iletiminde görev aldığını bildirmişlerdir. Ayrıca, bu kanalın fosforilasyon durumu sayesinde inward veya outward çalışabilme yeteneği kazanabildiği gösterilmiştir.

Non-Selektif Katyon Kanalları (NSCCs)

Bitki hücrelerinde bulunan non-selektif katyon kanalları (NSCCs), monovalan (K^+, Na^+) ve bazı durumlarda divalan (Ca^{2+}, Mg^{2+}) katyonların zarlar arasında geçişini sağlayan, iyon seçiciliği düşük kanallardır. NSCC'ler genellikle membran potansiyelinden bağımsız olarak ya da zayıf voltaj duyarlılığıyla çalışır ve ligandlar (örneğin reaktif oksijen türleri, NO, Ca^{2+}, poliaminler) veya abiyotik stres sinyalleriyle aktive edilirler. Bu özellikleri sayesinde özellikle tuz stresi, kuraklık ve ağır metal toksisitesi gibi çevresel stres koşullarında işlevsel hale gelirler (Demidchik et al., 2003; Demidchik and Tester, 2002).

NSCC'ler potasyum homeostazının sürdürülmesinde ikili rol oynar. Bir yandan düşük dış potasyum koşullarında K^+ alımını kolaylaştırırken, diğer yandan Na^+ ve H^+ gibi toksik iyonların girişine ve K^+'un sızıntı yoluyla hücre dışına çıkmasına neden olarak hücredeki iyon dengesini tehdit edebilirler. Bu nedenle, NSCC'lerin işlevleri hem yararlı hem de zarar verici olabilmektedir. Özellikle kök uzama bölgelerinde yüksek NSCC aktivitesi gözlenmiştir ve bu aktivite büyüme süreçlerinde önemli bir rol oynamaktadır (Demidchik et al., 2003). Moleküler düzeyde, NSCC fonksiyonlarıyla ilişkilendirilen başlıca kanal aileleri Cyclic Nucleotide-Gated Channels (CNGCs) ve Glutamate Receptor-Like Channels (GLRs)'dır. Arabidopsis thaliana'da tanımlanan AtCNGC3 ve AtGLR1.1 gibi genler, hem Ca^{2+} hem de K^+ geçişine aracılık eden NSCC aktiviteleri göstermektedir (Jha et al., 2010; Li et al., 2024). Bu kanallar ayrıca çevresel sinyallere yanıt olarak hücre içi kalsiyum sinyalizasyonunu düzenlemede de görev almaktadır. Özellikle 2020 sonrası yapılan çalışmalar, Setaria italica gibi türlerde NSCC benzeri davranışlar gösteren yeni Shaker olmayan kanal ailelerini ve bu kanalların gen ekspresyon profillerini ortaya koymuştur. Ayrıca, bazı CNGC üyelerinin tuz, kuraklık ve ozmotik strese karşı yanıt verdiği ve floem-yükleme süreçlerinde görev aldığı bildirilmiştir (Li et al., 2024).

3. Potasyum Kanalları ve Taşıyıcılarının Düzenlenmesi

CBL–CIPK sinyal yolu, bitkilerde potasyum (K^+) homeostazının sağlanmasında kritik rol oynayan bir hücre içi kalsiyum (Ca^{2+})-bağımlı sinyal iletim sistemidir. Bu yolak, CBL (Calcineurin B-like protein) adlı Ca^{2+} sensör proteinleri ile CIPK (CBL-interacting protein kinase) adlı protein kinazlarının etkileşimiyle çalışır (Lian et al., 2023). Post-transkripsiyonel düzeyde, CBL–CIPK sinyal kompleksi önemli bir rol oynar. Örneğin, AtCBL1/9, AtCIPK23 ile etkileşerek onu plazma zarına taşır. Ardından, AtCIPK23, potasyum kanalı AtAKT1'i fosforile eder ve bu işlem düşük K^+ koşullarında artar; böylece bitki çevreden daha fazla K^+ alabilir (Ahmad et al., 2016; Li et al., 2014). Benzer şekilde, AtCBL4–AtCIPK6 kompleksi, AtAKT2'yi sitoplazmadan zar üzerine taşır ve bu kanalın aracılık ettiği potasyum akımını artırır (Tian et al., 2021). Bir başka önemli yolak, AtCBL2/3–AtCIPK3/9/23/26 kompleksidir. Bu kompleks, vakuol zarındaki TPK kanalını aktive ederek K^+'in vakuolden sitoplazmaya geçişini sağlar (Kim et al., 2015). KUP/HAK/KT taşıyıcılarının da post-transkripsiyonel düzenlemeleri belgelenmiştir. Örneğin, AtHAK5'in AtCBL1–AtCIPK23 tarafından fosforilasyon yoluyla aktive edildiği gösterilmiştir (Nguyen et al., 2017). Ancak, yapılan ileri düzey araştırmalar, potasyum taşıyıcılarının büyük ölçüde transkripsiyonel düzeyde düzenlendiğini ortaya koymuştur. Birçok transkripsiyon faktörü, AtHAK5'in gen ifadesini düzenlemektedir. Bunlar arasında AtRAP2.11, AtDDF2, AtJLO, AtTFII_A, AtbHLH121, AtARF2 ve AtMYB77 bulunmaktadır (Hwang et al., 2013). Düşük potasyum stresinde AtARF2 fosforilasyona uğrayarak baskılayıcı etkisini azaltırken, AtMYB77 doğrudan AtHAK5 promotörüne bağlanarak genin ekspresyonunu artırır (Li et al., 2023). Ayrıca, AtMYB59, nitratsız ortamda AtNRT1.5 geninin pozitif bir düzenleyicisidir. Ancak düşük K koşullarında, AtMYB59 transkripsiyon ve protein düzeyi düşer ve AtNRT1.5 ifadesi baskılanarak kökten gövdeye K^+ taşınımı engellenir (Voelker et al., 2006). Buğday ve mısırda yapılan maya hibrit (yeast one-hybrid) deneylerinde, TaNAC71'in TaHAK1 promotörüne bağlandığı; ZmRAP2.11 ve ZmARF2'nin ise ZmHAK1 promotörünü düzenlediği gösterilmiştir (Isayenkov et al., 2011). Çeltik (*Oryza sativa*) için ise potasyum taşıma düzenlemesinin moleküler düzeyi henüz yeterince anlaşılmamıştır. Ancak iki post-transkripsiyonel düzenleme yolu tanımlanmıştır OsCBL1–OsCIPK23, OsAKT1 ve OsAKT2 kanallarının aktivitesini düzenler (Li et al., 2014);OsHAK21, OsCYB5-2 proteiniyle etkileşerek bu taşıyıcının stabilitesini sağlar ve hücre içi K^+/Na^+ dengesini korur (Chen et al., 2015a) Araştırmalar, OsHKT1;5 geninin tuz stresinde OsSUVH7, OsBAG4 ve OsMYB106 tarafından aktive edildiğini göstermektedir (Wang et al., 2021b). Ayrıca, OsMYBc transkripsiyon faktörü, OsHKT1;1 promotörüne bağlanarak Na^+ birikimini düzenlemektedir (Ahmad et al., 2016).

K^+ kanallarının/taşıyıcılarının düzenlenmesinde rol oynayan transkripsiyon faktörlerinin/alanlarının bazıları Tablo 1'de listelenmiştir.

Tablo 1. K^+ Kanalları/Taşıyıcılarının Ekspresyonunu Düzenleyen Transkripsiyon Faktörleri ve Domainler (Anil Kumar et al., 2024).

Gen Adı	Gen Ailesi	Lokalizasyon	Transkripsiyon Faktörü/ Düzenleyici Domain	Fonksiyon / İlgili Stres
TRK2	-	Nükleus	NAD^+-bağlama domain	K^+ taşınımı
KEA5	CPA2	Sitoplazma	KTN domain	K^+ alımı
AtKEA4	CPA2	Sitoplazma	KTN domain	K^+ alımı
KEA3	CPA2	Plazma zarı	KTN ve RCK domainleri	K^+ alımı
hkt2/ tHKT1;1	Trk/Ktr/HKT	Mitokondri	ABI4, AtbZIP24	Na^+-K^+ homeostazı, Na^+ ve K^+ alımı
HAK5	HAK ailesi	Plazma zarı	TFII_A, DDF2, JLO	K^+ alımı, tuz toleransı
KUP7	KUP ailesi	Plazma zarı	MYB59	Düşük K^+ stresinde regülasyon
KUP2	KUP ailesi	Plazma zarı	bHLH ve WRKY	Tuz toleransı
HAK1	HAK ailesi	Sitoplazma	NAC71	K^+ alımı, K eksikliği ve tuz toleransı

4. Potasyum kullanım etkinliği ve QTL'ler

Yeterli düzeyde K temini, optimal bitki büyümesi ve gelişimi için gereklidir (Wang et al., 2021a). Ancak, birçok tarım toprağında bitkiler tarafından alınabilir K düzeyi, verimli üretim için yetersiz kalmaktadır (Römheld and Kirkby, 2010). Potasyum eksikliği, hem verimi hem de ürün kalitesini olumsuz etkilerken, üretim sistemlerinde verimliliği sağlamak için genellikle K gübresi kullanılmaktadır (Zorb et al., 2014). Bununla birlikte, K gübrelerinin üretimi, taşınması ve uygulanması ekonomik yük yaratmakta ve çevresel sorunlara neden olabilmektedir.Bu nedenle, potasyumu daha etkili bir şekilde alabilen ve/veya kullanabilen bitki çeşitlerinin ıslah edilmesi, K gübresi kullanımını azaltabilecek stratejilerden biridir (Wang et al., 2021a). Bu tür bitkiler, topraktan daha etkin K alımı gerçekleştirebilir veya daha düşük K gereksinimiyle yüksek verim sağlayabilir (Shin, 2014; White, 2013). Tarımsal potasyum kullanım verimliliği (KUE), genellikle birim K uygulaması başına elde edilen kuru madde verimi olarak tanımlanır (White et al., 2010). Bu parametre, bitki tarafından birim K uygulamasına karşı alınan K miktarını ifade eden K alım verimliliği (KUpE) ile alınan potasyumun verime dönüşümünü ifade eden K kullanım verimliliği (KUtE)'nin çarpımıyla elde edilir (White et al., 2010). KUpE, bitkinin topraktan K alma kapasitesini; KUtE ise alınan K'nın biyokütle veya verime dönüştürülme yeteneğini yansıtır (White et al., 2021). KUpE'deki çeşitler arası ve tür içi farklılıklar, köklerin toprakta yayılma yeteneği, değiştirilemeyen K fraksiyonlarını serbest bırakabilme ve K^+ iyonlarını yüksek afiniteli taşıyıcılarla hızlı şekilde alabilme kapasitesiyle ilişkilidir (White, 2013; White et al., 2021). KUtE'deki varyasyon ise, bitkilerin yaşlanan dokulardan gelişen dokulara K'yi yeniden dağıtma ve hücre içi uygun K düzeyini koruma yeteneklerindeki farklılıklardan kaynaklanmaktadır (Lu et al., 2016; Rengel and Damon, 2008; White et al., 2021; White et al., 2010). Pek çok bitki türünde, aynı çevre koşullarında yetiştirilen genotipler arasında önemli düzeyde genetik farklılıklar gözlemlenmiştir (Pettigrew, 2008). Karmaşık özelliklerle ilişkili genetik bölgelerin belirlenmesinde kantitatif özellik lokusu (QTL) analizleri ve genom çapında ilişkilendirme çalışmaları (GWAS) önemli araçlardır (Wang et al., 2021a). Arabidopsis, çeltik, buğday ve domates gibi türlerde KUpE ve KUtE ile ilişkili birçok QTL belirlenmiştir. Ghandilyan et al. (2009), kuraklık koşullarında rozet mineral konsantrasyonlarını etkileyen 13 QTL tanımlamış ve bu QTL'lerin çevresel koşullara bağlı olarak değişkenlik gösterdiğini rapor etmiştir. Harada and Leigh (2006), sürgün K konsantrasyonuna yönelik olarak taze madde üzerinden 4 QTL, kuru madde üzerinden ise 3 QTL saptamış ve bazı QTL'lerin K taşıyıcı genlerle ilişkili olabileceğini öne sürmüştür. Kellermeier et al. (2013) ise Col-0 × Catania-1 populasyonu kullanarak kök mimarisiyle ilişkili 8 ana QTL belirlemiş ve bu bölgelerin düşük K koşullarına karşı farklı adaptif stratejilerle bağlantılı olduğunu göstermiştir. Kong et al. (2013), düşük ve yüksek K koşullarında buğdayın farklı gelişim evrelerinde gerçekleştirdikleri çalışmada, K verimliliği ile ilişkili toplam 127 QTL belirlemiş; bunların 35'i besin konsantrasyonu, 55'i besin içeriği ve 37'si kullanım verimliliği ile bağlantılı bulunmuştur. Zhao et al. (2014) ise K eksikliği koşullarında buğday fideleri üzerinde yaptıkları araştırmada, K toleransına katkı sağlayan toplam 65 QTL tespit etmiş ve bu QTL'lerin kromozomlar genelinde yaygın dağılım gösterdiğini bildirmiştir. Wu et al. (2019), dünya genelinden toplanan 991 B. napus genotipinin yeniden dizilenmesiyle elde edilen SNP verileri üzerinden, FLOWERING LOCUS T ve FLOWERING LOCUS C ortologlarının promotör bölgelerindeki varyasyonların farklı kolza ekotipleriyle ilişkili olabileceğini GWAS ile ortaya koymuştur. Domateste yaprak ve gövdedeki Na^+ ve K^+ konsantrasyonları iki F_8 popülasyon üzerinden incelenmiştir. Tuz stresi altında, birinci popülasyonda

(S. pimpinellifolium çaprazı) 13 QTL, ikinci popülasyonda (S. cheesmaniae çaprazı) 20 QTL tespit edilmiştir; kontrol koşullarında ise her iki popülasyonda toplam 4 QTL saptanmıştır. Tüm popülasyonlarda kromozom 7 üzerinde hem Na^+ hem de K^+ konsantrasyonu için önemli QTL kümeleri (etki > %40) belirlenmiş ve bu bölge tuz toleransının genetik merkezlerinden biri olarak gösterilmiştir (Villalta et al., 2008).

Sonuç

Potasyum (K^+), bitki gelişimi, metabolizması ve çevresel streslere karşı dayanıklılığı için hayati öneme sahip temel bir makro besin elementidir. Ancak, tarım topraklarının büyük bir kısmında bitkiler için yarayışlı formda potasyum bulunmaması, sürdürülebilir tarımsal üretim açısından önemli bir engel oluşturmaktadır. Bu derlemede, bitkilerde K^+ alımı, taşınımı ve kullanımına ilişkin moleküler ve genetik mekanizmalar detaylı şekilde ele alınmıştır. Özellikle yüksek afiniteli taşıyıcılar (örneğin HAK5), Shaker tipi potasyum kanalları (örneğin AKT1, SKOR, GORK), CPA ailesi üyeleri (NHX, KEA, CHX) ve CBL–CIPK gibi sinyal iletim yolaklarının bu süreçlerdeki kritik rolleri vurgulanmıştır. Ayrıca, omik teknolojiler ve QTL haritalama çalışmaları sayesinde KUE (potasyum kullanım etkinliği) ile ilişkili gen bölgeleri ve aday genler belirlenmiş, bu durum yüksek verimli ve K^+ verimliliği yüksek çeşitlerin geliştirilmesini hızlandırmıştır. Transgenik yaklaşımlar, CRISPR/Cas tabanlı gen düzenleme sistemleri, potasyum çözücü mikroorganizmalar ve nanogübreler gibi biyoteknolojik ve mikrobiyal stratejiler, K^+ kullanım etkinliğini artırmak için umut vadeden araçlar sunmaktadır. Gelecekte, bu moleküler ve biyoteknolojik yaklaşımların entegre bitki ıslahı ve sürdürülebilir tarım uygulamalarıyla birleştirilmesi, küresel gıda güvenliği ve çevresel sürdürülebilirlik hedeflerine ulaşmada belirleyici olacaktır.

Referanslar

Adem, G. D., Chen, G., Shabala, L., Chen, Z. H., and Shabala, S. (2020). GORK Channel: A Master Switch of Plant Metabolism? Trends Plant Sci 25, 434-445.

Ahmad, I., Mian, A., and Maathuis, F. J. (2016). Overexpression of the rice AKT1 potassium channel affects potassium nutrition and rice drought tolerance. J Exp Bot 67, 2689-98.

Ahn, S. J., Shin, R., and Schachtman, D. P. (2004). Expression of KT/KUP genes in Arabidopsis and the role of root hairs in K+ uptake. Plant Physiol 134, 1135-45.

Almeida, D. M., Oliveira, M. M., and Saibo, N. J. M. (2017). Regulation of Na+ and K+ homeostasis in plants: towards improved salt stress tolerance in crop plants. Genet Mol Biol 40, 326-345.

Anil Kumar, S., Kaniganti, S., Hima Kumari, P., Sudhakar Reddy, P., Suravajhala, P., P, S., and Kishor, P. B. K. (2024). Functional and biotechnological cues of potassium homeostasis for stress tolerance and plant development. Biotechnol Genet Eng Rev 40, 3527-3570.

Banuelos, M. A., Garciadeblas, B., Cubero, B., and Rodriguez-Navarro, A. (2002). Inventory and functional characterization of the HAK potassium transporters of rice. Plant Physiol 130, 784-95.

Bassil, E., Tajima, H., Liang, Y. C., Ohto, M. A., Ushijima, K., Nakano, R., Esumi, T., Coku, A., Belmonte, M., and Blumwald, E. (2011). The Arabidopsis Na/H Antiporters NHX1 and NHX2 Control Vacuolar pH and K Homeostasis to Regulate Growth, Flower Development, and Reproduction (vol 23, pg 3482, 2011). Plant Cell 23, 4526-4526.

Britto, D. T., and Kronzucker, H. J. (2005). Nitrogen acquisition, PEP carboxylase, and cellular pH homeostasis: new views on old paradigms. Plant Cell and Environment 28, 1396-1409.

Cai, K., Gao, H., Wu, X., Zhang, S., Han, Z., Chen, X., Zhang, G., and Zeng, F. (2019). The Ability to Regulate Transmembrane Potassium Transport in Root Is Critical for Drought Tolerance in Barley. Int J Mol Sci 20.

Cakmak, I. (2005). The role of potassium in alleviating detrimental effects of abiotic stresses in plants. Journal of Plant Nutrition and Soil Science 168, 521-530.

Chen, G., Hu, Q., Luo, L., Yang, T., Zhang, S., Hu, Y., Yu, L., and Xu, G. (2015a). Rice potassium transporter OsHAK1 is essential for maintaining potassium-mediated growth and functions in salt tolerance over low and high potassium concentration ranges. Plant Cell Environ 38, 2747-65.

Chen, G., Zhang, Y., Ruan, B., Guo, L., Zeng, D., Gao, Z., Zhu, L., Hu, J., Ren, D., Yu, L., Xu, G., and Qian, Q. (2018). OsHAK1 controls the vegetative growth and panicle fertility of rice by its effect on potassium-mediated sugar metabolism. Plant Sci 274, 261-270.

Chen, H. T., Chen, X., Wu, B. Y., Yuan, X. X., Zhang, H. M., Cui, X. Y., and Liu, X. Q. (2015b). Whole-genome identification and expression analysis of K efflux antiporter (KEA) and Na/H antiporter (NHX) families under abiotic stress in soybean. Journal of Integrative Agriculture 14, 1171-1183.

Chen, N., Tong, S., Tang, H., Zhang, Z., Liu, B., Lou, S., Liu, J., Liu, H., Ma, T., and Jiang, Y. (2020). The PalERF109 transcription factor positively regulates salt tolerance via PalHKT1;2 in Populus alba var. pyramidalis. Tree Physiol 40, 717-730.

Cheng, X., Liu, X., Mao, W., Zhang, X., Chen, S., Zhan, K., Bi, H., and Xu, H. (2018). Genome-Wide Identification and Analysis of HAK/KUP/KT Potassium Transporters Gene Family in Wheat (Triticum aestivum L.). Int J Mol Sci 19.

Demidchik, V., Shabala, S. N., Coutts, K. B., Tester, M. A., and Davies, J. M. (2003). Free oxygen radicals regulate plasma membrane Ca2+- and K+-permeable channels in plant root cells. J Cell Sci 116, 81-8.

Demidchik, V., and Tester, M. (2002). Sodium fluxes through nonselective cation channels in the plasma membrane of protoplasts from Arabidopsis roots. Plant Physiology 128, 379-387.

Du, Q., Zhao, X. H., Xia, L., Jiang, C. J., Wang, X. G., Han, Y., Wang, J., and Yu, H. Q. (2021). Effects of potassium deficiency on photosynthesis, chloroplast ultrastructure, ROS, and antioxidant activities in maize (vol 18, pg 395, 2019). Journal of Integrative Agriculture 20, Iv-Iv.

Fageria, N. K. (2016). "The use of nutrients in crop plants," CRC press.

Feng, H., Tang, Q., Cai, J., Xu, B., Xu, G., and Yu, L. (2019). Rice OsHAK16 functions in potassium uptake and translocation in shoot, maintaining potassium homeostasis and salt tolerance. Planta 250, 549-561.

Gajdanowicz, P., Michard, E., Sandmann, M., Rocha, M., Correa, L. G., Ramirez-Aguilar, S. J., Gomez-Porras, J. L., Gonzalez, W., Thibaud, J. B., van Dongen, J. T., and Dreyer, I. (2011). Potassium (K+) gradients serve as a mobile energy source in plant vascular tissues. Proc Natl Acad Sci U S A 108, 864-9.

Gao, Y. C., Yu, C. Y., Zhang, K., Zhang, H. X., Zhang, S. Y., and Song, Z. Z. (2021). Identification and characterization of the strawberry KT/HAK/KUP transporter gene family in response to K deficiency. Acta Physiologiae Plantarum 43.

Gaymard, F., Pilot, G., Lacombe, B., Bouchez, D., Bruneau, D., Boucherez, J., Michaux-Ferriere, N., Thibaud, J. B., and Sentenac, H. (1998). Identification and disruption of a plant shaker-like outward channel involved in K+ release into the xylem sap. Cell 94, 647-55.

Ghandilyan, A., Barboza, L., Tisne, S., Granier, C., Reymond, M., Koornneef, M., Schat, H., and Aarts, M. G. M. (2009). Genetic analysis identifies quantitative trait loci controlling rosette mineral concentrations in Arabidopsis thaliana under drought. New Phytol 184, 180-192.

Gierth, M., and Maser, P. (2007). Potassium transporters in plants--involvement in K+ acquisition, redistribution and homeostasis. FEBS Lett 581, 2348-56.

Harada, H., and Leigh, R. A. (2006). Genetic mapping of natural variation in potassium concentrations in shoots of Arabidopsis thaliana. J Exp Bot 57, 953-60.

Hasanuzzaman, M., Bhuyan, M. H. M. B., Nahar, K., Hossain, M. S., Al Mahmud, J., Hossen, M. S., Masud, A. A. C., Moumita, and Fujita, M. (2018). Potassium: A Vital Regulator of Plant Responses and Tolerance to Abiotic Stresses. Agronomy-Basel 8.

Hirsch, R. E., Lewis, B. D., Spalding, E. P., and Sussman, M. R. (1998). A role for the AKT1 potassium channel in plant nutrition. Science 280, 918-21.

Horie, T., Costa, A., Kim, T. H., Han, M. J., Horie, R., Leung, H. Y., Miyao, A., Hirochika, H., An, G., and Schroeder, J. I. (2007). Rice OsHKT2;1 transporter mediates large Na+ influx component into K+-starved roots for growth. EMBO J 26, 3003-14.

Hosy, E., Vavasseur, A., Mouline, K., Dreyer, I., Gaymard, F., Poree, F., Boucherez, J., Lebaudy, A., Bouchez, D., Very, A. A., Simonneau, T., Thibaud, J. B., and Sentenac, H. (2003). The Arabidopsis outward K+ channel GORK is involved in regulation of stomatal movements and plant transpiration. Proc Natl Acad Sci U S A 100, 5549-54.

Hu, W., Zhao, W., Yang, J., Oosterhuis, D. M., Loka, D. A., and Zhou, Z. (2016). Relationship between potassium fertilization and nitrogen metabolism in the leaf subtending the cotton (Gossypium hirsutum L.) boll during the boll development stage. Plant Physiol Biochem 101, 113-123.

Hwang, H., Yoon, J., Kim, H. Y., Min, M. K., Kim, J. A., Choi, E. H., Lan, W., Bae, Y. M., Luan, S., Cho, H., and Kim, B. G. (2013). Unique features of two potassium channels, OsKAT2 and OsKAT3, expressed in rice guard cells. PLoS One 8, e72541.

Isayenkov, S., Isner, J. C., and Maathuis, F. J. (2011). Rice two-pore K+ channels are expressed in different types of vacuoles. Plant Cell 23, 756-68.

Isayenkov, S. V., Dabravolski, S. A., Pan, T., and Shabala, S. (2020). Phylogenetic Diversity and Physiological Roles of Plant Monovalent Cation/H(+) Antiporters. Front Plant Sci 11, 573564.

Isayenkov, S. V., and Maathuis, F. J. M. (2019). Plant Salinity Stress: Many Unanswered Questions Remain. Front Plant Sci 10, 80.

Jha, D., Shirley, N., Tester, M., and Roy, S. J. (2010). Variation in salinity tolerance and shoot sodium accumulation in Arabidopsis ecotypes linked to differences in the natural expression levels of transporters involved in sodium transport. Plant Cell Environ 33, 793-804.

Kellermeier, F., Chardon, F., and Amtmann, A. (2013). Natural variation of Arabidopsis root architecture reveals complementing adaptive strategies to potassium starvation. Plant Physiol 161, 1421-32.

Kim, H. Y., Choi, E. H., Min, M. K., Hwang, H., Moon, S. J., Yoon, I., Byun, M. O., and Kim, B. G. (2015). Differential Gene Expression of Two Outward-Rectifying Shaker-Like Potassium Channels OsSKOR and OsGORK in Rice. Journal of Plant Biology 58, 230-235.

Kong, F. M., Guo, Y., Liang, X., Wu, C. H., Wang, Y. Y., Zhao, Y., and Li, S. S. (2013). Potassium (K) effects and QTL mapping for K efficiency traits at seedling and adult stages in wheat. Plant and Soil 373, 877-892.

Lebaudy, A., Very, A. A., and Sentenac, H. (2007). K+ channel activity in plants: genes, regulations and functions. FEBS Lett 581, 2357-66.

Li, J., Long, Y., Qi, G. N., Li, J., Xu, Z. J., Wu, W. H., and Wang, Y. (2014). The Os-AKT1 channel is critical for K+ uptake in rice roots and is modulated by the rice CBL1-CIPK23 complex. Plant Cell 26, 3387-402.

Li, J., Shen, L., Han, X., He, G., Fan, W., Li, Y., Yang, S., Zhang, Z., Yang, Y., Jin, W., Wang, Y., Zhang, W., and Guo, Y. (2023). Phosphatidic acid-regulated SOS2 controls sodium and potassium homeostasis in Arabidopsis under salt stress. EMBO J 42, e112401.

Li, S. T., Kong, W. Y., Chen, J. B., Hao, D. L., and Guo, H. L. (2024). Genome-Wide Identification and Expression Analysis of the Cyclic Nucleotide-Gated Channel Gene Family in Zoysia japonica under Salt Stress. Int J Mol Sci 25, 10114.

Li, W., Li, M., Li, S., Zhang, Y., Li, X., Xu, G., and Yu, L. (2022). Function of Rice High-Affinity Potassium Transporters in Pollen Development and Fertility. Plant Cell Physiol 63, 967-980.

Lian, W., Geng, A., Wang, Y., Liu, M., Zhang, Y., Wang, X., and Chen, G. (2023). The Molecular Mechanism of Potassium Absorption, Transport, and Utilization in Rice. Int J Mol Sci 24.

Lotter, D. (2015). Facing food insecurity in Africa: Why, after 30 years of work in organic agriculture, I am promoting the use of synthetic fertilizers and herbicides in small-scale staple crop production. Agriculture and Human Values 32, 111-118.

Lu, Z., Lu, J., Pan, Y., Li, X., Cong, R., and Ren, T. (2016). Genotypic variation in photosynthetic limitation responses to K deficiency of Brassica napus is associated with potassium utilisation efficiency. Funct Plant Biol 43, 880-891.

Martinez-Cordero, M. A., Martinez, V., and Rubio, F. (2004). Cloning and functional characterization of the high-affinity K+ transporter HAK1 of pepper. Plant Mol Biol 56, 413-21.

Maser, P., Thomine, S., Schroeder, J. I., Ward, J. M., Hirschi, K., Sze, H., Talke, I. N., Amtmann, A., Maathuis, F. J., Sanders, D., Harper, J. F., Tchieu, J., Gribskov, M., Persans, M. W., Salt, D. E., Kim, S. A., and Guerinot, M. L. (2001). Phylogenetic relationships within cation transporter families of Arabidopsis. Plant Physiol 126, 1646-67.

Nguyen, T. H., Huang, S., Meynard, D., Chaine, C., Michel, R., Roelfsema, M. R. G., Guiderdoni, E., Sentenac, H., and Very, A. A. (2017). A Dual Role for the OsK5.2 Ion Channel in Stomatal Movements and K(+) Loading into Xylem Sap. Plant Physiol 174, 2409-2418.

Nieves-Cordones, M., Lara, A., Rodenas, R., Amo, J., Rivero, R. M., Martinez, V., and Rubio, F. (2019). Modulation of K(+) translocation by AKT1 and AtHAK5 in Arabidopsis plants. Plant Cell Environ 42, 2357-2371.

Nieves-Cordones, M., Martínez-Cordero, M. A., Martínez, V., and Rubio, F. (2007). An NH-sensitive component dominates high-affinity K uptake in tomato plants. Plant Science 172, 273-280.

Okada, T., Yamane, S., Yamaguchi, M., Kato, K., Shinmyo, A., Tsunemitsu, Y., Iwasaki, K., Ueno, D., and Demura, T. (2018). Characterization of rice KT/HAK/KUP potassium transporters and K(+) uptake by HAK1 from Oryza sativa. Plant Biotechnol (Tokyo) 35, 101-111.

Peng, L., Xiao, H., Li, R., Zeng, Y., Gu, M., Moran, N., Yu, L., and Xu, G. (2023). Potassium transporter OsHAK18 mediates potassium and sodium circulation and sugar translocation in rice. Plant Physiol 193, 2003-2020.

Pettigrew, W. T. (2008). Potassium influences on yield and quality production for maize, wheat, soybean and cotton. Physiol Plant 133, 670-81.

Pilot, G., Lacombe, B., Gaymard, F., Cherel, I., Boucherez, J., Thibaud, J. B., and Sentenac, H. (2001). Guard cell inward K+ channel activity in arabidopsis involves expression of the twin channel subunits KAT1 and KAT2. J Biol Chem 276, 3215-21.

Qi, Z., Hampton, C. R., Shin, R., Barkla, B. J., White, P. J., and Schachtman, D. P. (2008). The high affinity K+ transporter AtHAK5 plays a physiological role in planta at very low K+ concentrations and provides a caesium uptake pathway in Arabidopsis. J Exp Bot 59, 595-607.

Ragel, P., Raddatz, N., Leidi, E. O., Quintero, F. J., and Pardo, J. M. (2019). Regulation of K(+) Nutrition in Plants. Front Plant Sci 10, 281.

Rengel, Z., and Damon, P. M. (2008). Crops and genotypes differ in efficiency of potassium uptake and use. Physiol Plant 133, 624-36.

Riedelsberger, J., Vergara-Jaque, A., Pineros, M., Dreyer, I., and Gonzalez, W. (2019). An extracellular cation coordination site influences ion conduction of OsHKT2;2. BMC Plant Biol 19, 316.

Römheld, V., and Kirkby, E. A. (2010). Research on potassium in agriculture: needs and prospects. Plant and Soil 335, 155-180.

Rubio, F., Santa-María, G. E., and Rodríguez-Navarro, A. (2000). Cloning of
and barley cDNAs encoding HAK potassium transporters in root and shoot cells. Physiologia Plantarum 109, 34-43.

Ruiz, J. M., and Romero, L. (2002). Relationship between potassium fertilisation and nitrate assimilation in leaves and fruits of cucumber (
) plants. Annals of Applied Biology 140, 241-245.

Safdar, L. B., Andleeb, T., Latif, S., Umer, M. J., Tang, M., Li, X., Liu, S., and Quraishi, U. M. (2020). Genome-Wide Association Study and QTL Meta-Analysis Identified Novel Genomic Loci Controlling Potassium Use Efficiency and Agronomic Traits in Bread Wheat. Front Plant Sci 11, 70.

Sardans, J., and Penuelas, J. (2021). Potassium Control of Plant Functions: Ecological and Agricultural Implications. Plants (Basel) 10.

Sardans, J., and Peñuelas, J. (2015). Potassium: a neglected nutrient in global change. Global Ecology and Biogeography 24, 261-275.

Shen, Y., Shen, L., Shen, Z., Jing, W., Ge, H., Zhao, J., and Zhang, W. (2015). The potassium transporter OsHAK21 functions in the maintenance of ion homeostasis and tolerance to salt stress in rice. Plant Cell Environ 38, 2766-79.

Shin, R. (2014). Strategies for improving potassium use efficiency in plants. Mol Cells 37, 575-84.

Srivastava, A. K., Shankar, A., Nalini Chandran, A. K., Sharma, M., Jung, K. H., Suprasanna, P., and Pandey, G. K. (2020). Emerging concepts of potassium homeostasis in plants. J Exp Bot 71, 608-619.

Sun, Y., Kong, X., Li, C., Liu, Y., and Ding, Z. (2015). Potassium Retention under Salt Stress Is Associated with Natural Variation in Salinity Tolerance among Arabidopsis Accessions. PLoS One 10, e0124032.

Tian, Q., Shen, L., Luan, J., Zhou, Z., Guo, D., Shen, Y., Jing, W., Zhang, B., Zhang, Q., and Zhang, W. (2021). Rice shaker potassium channel OsAKT2 positively regulates salt tolerance and grain yield by mediating K(+) redistribution. Plant Cell Environ 44, 2951-2965.

Tsujii, M., Kera, K., Hamamoto, S., Kuromori, T., Shikanai, T., and Uozumi, N. (2019). Evidence for potassium transport activity of Arabidopsis KEA1-KEA6. Sci Rep 9, 10040.

Tyczewska, A., Wozniak, E., Gracz, J., Kuczynski, J., and Twardowski, T. (2018). Towards Food Security: Current State and Future Prospects of Agrobiotechnology. Trends Biotechnol 36, 1219-1229.

Villalta, I., Reina-Sanchez, A., Bolarin, M. C., Cuartero, J., Belver, A., Venema, K., Carbonell, E. A., and Asins, M. J. (2008). Genetic analysis of Na(+) and K (+) concentrations in leaf and stem as physiological components of salt tolerance in Tomato. Theor Appl Genet 116, 869-80.

Voelker, C., Schmidt, D., Mueller-Roeber, B., and Czempinski, K. (2006). Members of the Arabidopsis AtTPK/KCO family form homomeric vacuolar channels in planta. Plant J 48, 296-306.

Wang, W., Zou, J., White, P. J., Ding, G., Li, Y., Xu, F., and Shi, L. (2021a). Identification of QTLs associated with potassium use efficiency and underlying candidate genes by whole-genome resequencing of two parental lines in Brassica napus. Genomics 113, 755-768.

Wang, X., Li, J., Li, F., Pan, Y., Cai, D., Mao, D., Chen, L., and Luan, S. (2021b). Rice Potassium Transporter OsHAK8 Mediates K(+) Uptake and Translocation in Response to Low K(+) Stress. Front Plant Sci 12, 730002.

Wang, Y., and Wu, W. H. (2013). Potassium transport and signaling in higher plants. Annu Rev Plant Biol 64, 451-76.

Wang, Y., and Wu, W. H. (2017). Regulation of potassium transport and signaling in plants. Curr Opin Plant Biol 39, 123-128.

White, P. J. (2013). Improving potassium acquisition and utilisation by crop plants. Journal of Plant Nutrition and Soil Science 176, 305-316.

White, P. J., Bell, M. J., Djalovic, I., Hinsinger, P., and Rengel, Z. (2021). Potassium use efficiency of plants. Improving potassium recommendations for agricultural crops, 119-145.

White, P. J., Hammond, J. P., King, G. J., Bowen, H. C., Hayden, R. M., Meacham, M. C., Spracklen, W. P., and Broadley, M. R. (2010). Genetic analysis of potassium use efficiency in Brassica oleracea. Ann Bot 105, 1199-210.

Wu, D., Liang, Z., Yan, T., Xu, Y., Xuan, L., Tang, J., Zhou, G., Lohwasser, U., Hua, S., Wang, H., Chen, X., Wang, Q., Zhu, L., Maodzeka, A., Hussain, N., Li, Z., Li, X., Shamsi, I. H., Jilani, G., Wu, L., Zheng, H., Zhang, G., Chalhoub, B., Shen, L., Yu, H., and Jiang, L. (2019). Whole-Genome Resequencing of a Worldwide Collection of Rapeseed Accessions Reveals the Genetic Basis of Ecotype Divergence. Mol Plant 12, 30-43.

Xu, X., Wang, F., Xing, Y., Liu, J., Lv, M., Meng, H., Du, X., Zhu, Z., Ge, S., and Jiang, Y. (2022). Appropriate and Constant Potassium Supply Promotes the Growth of M9T337 Apple Rootstocks by Regulating Endogenous Hormones and Carbon and Nitrogen Metabolism. Front Plant Sci 13, 827478.

Yang, O., Popova, O. V., Suthoff, U., Luking, I., Dietz, K. J., and Golldack, D. (2009). The Arabidopsis basic leucine zipper transcription factor AtbZIP24 regulates complex transcriptional networks involved in abiotic stress resistance. Gene 436, 45-55.

Yang, T., Zhang, S., Hu, Y., Wu, F., Hu, Q., Chen, G., Cai, J., Wu, T., Moran, N., Yu, L., and Xu, G. (2014). The role of a potassium transporter OsHAK5 in potassium acquisition and transport from roots to shoots in rice at low potassium supply levels. Plant Physiol 166, 945-59.

Yin, M. Q., Li, Y. F., Hu, Q. L., Yu, X. J., Huang, M. J., Zhao, J., Dong, S. Q., Yuan, X. Y., and Wen, Y. Y. (2023). Potassium Increases Nitrogen and Potassium Utilization Efficiency and Yield in Foxtail Millet. Agronomy-Basel 13.

Yuan, G., Nong, T., Hunpatin, O. S., Shi, C., Su, X., Wang, Q., Liu, H., Dai, P., and Ning, Y. (2024). Research Progress on Plant Shaker K(+) Channels. Plants (Basel) 13, 1423.

Zhang, L., Sun, X., Li, Y., Luo, X., Song, S., Chen, Y., Wang, X., Mao, D., Chen, L., and Luan, S. (2021). Rice Na(+)-Permeable Transporter OsHAK12 Mediates Shoots Na(+) Exclusion in Response to Salt Stress. Front Plant Sci 12, 771746.

Zhang, M. L., Hu, Y. Y., Han, W., Chen, J., Lai, J. S., and Wang, Y. (2023). Potassium nutrition of maize: Uptake, transport, utilization, and role in stress tolerance. Crop Journal 11, 1048-1058.

Zhao, J., Li, P., Motes, C. M., Park, S., and Hirschi, K. D. (2015). CHX14 is a plasma membrane K-efflux transporter that regulates K(+) redistribution in Arabidopsis thaliana. Plant Cell Environ 38, 2223-38.

Zhao, Y., Li, X. Y., Zhang, S. H., Wang, J., Yang, X. F., Tian, J. C., Hai, Y., and Yang, X. J. (2014). Mapping QTLs for potassium-deficiency tolerance at the seedling stage in wheat. Euphytica 198, 185-198.

Zorb, C., Senbayram, M., and Peiter, E. (2014). Potassium in agriculture--status and perspectives. J Plant Physiol 171, 656-69.

➢ *ORAL PRESENTATION*

DBYBHY-2007 ve TBDY-2018 yönetmeliklerine göre konut tipi betonarme binaların performansı ve kaba inşaat maliyeti açısından değerlendirilmesi

Mustafa Üreyen[1] (*https://orcid.org/0009-0002-2579-8410*), Hakan Dilmaç[1] (*ORCID: https://orcid.org/0000-0003-0346-8875*), Kılıç Yasin Arslan[1*] (*https://orcid.org/0000-0002-4433-9204*)

[*1]Süleyman Demirel Üniversitesi, Mühendislik ve Doğa Bilimleri Fakültesi, İnşaat Mühendisliği, Isparta, Türkiye.

*Sorumlu yazar e-posta: kyarslan92@gmail.com

Özet
Ülkemiz topraklarının çok büyük bir bölümü deprem tehlikesi ile karşı karşıyadır ve yakın geçmişte yaşanan, büyük ölçüde can ve mal kaybına neden olan depremler bunu çok açık bir şekilde göstermiştir. Bu gibi depremlerde ortaya çıkan kayıpların, ülkemizde, gelişmiş ülkelere göre çok daha büyük boyutlarda olması, üzerinde düşünülmesi gereken önemli bir konudur. Bu çalışmada, konut tipi betonarme binaların 2007 Deprem Bölgelerinde Yapılacak Binalar Hakkında Yönetmelik (DBYBHY-2007) ile 2018 Türkiye Bina Deprem Yönetmeliği (TBDY-2018) kapsamında performans ve kaba yapı maliyeti açısından karşılaştırmalı değerlendirilmesi amaçlanmıştır. Deprem yönetmeliklerindeki güncellemeler, yapı tasarımı ve maliyet üzerinde doğrudan etkili olmakta; mühendislik uygulamalarında önemli değişiklikler doğurmaktadır. Bu kapsamda 4 ve 8 katlı iki bina, her iki yönetmelik esas alınarak TBDY-2018' e göre ZA ve ZE, DBYBHY-2007'ye göre Z1 ve Z4 zemin sınıfları ile modellenmiş ve performans analizleri gerçekleştirilmiştir. Analizlerde deprem etkileri altındaki yapısal davranış değerlendirilmiş; taşıyıcı sistemin ihtiyaç duyduğu minimum beton ve donatı miktarları tespit edilmiştir. Elde edilen veriler doğrultusunda kaba yapı maliyetleri hesaplanmış ve her iki yönetmeliğin maliyetleri kıyaslanmıştır.
Anahtar Kelimeler: DBYBHY-2007, TBDY-2018, Betonarme Binalar, Yapı Maliyeti, Sta4CAD

Evaluation of residential reinforced concrete buildings in terms of performance and structural construction cost according to DBYBHY-2007 and TBDY-2018 codes

Abstract
A large portion of the land in our country is under significant earthquake risk, and recent devastating earthquakes that have caused substantial loss of life and property clearly demonstrate this reality. The fact that the damage and losses resulting from such earthquakes are significantly greater in our country compared to developed nations is an important issue that warrants serious consideration. This study aims to perform a comparative evaluation of residential reinforced concrete buildings in terms of structural performance and rough construction cost, based on the 2007 Earthquake Code for Buildings in Seismic Zones (DBYBHY-2007) and the 2018 Turkish Building Earthquake Code (TBDY-2018). Updates in seismic design codes directly affect both structural design and cost, leading to substantial changes in engineering practice. In this context, two buildings (one with 4 stories and the other with 8 stories) were modeled according to both codes. For TBDY-2018, soil classes ZA and ZE were used; for DBYBHY-2007, Z1 and Z4 soil classes were applied. Performance analyses were conducted, and structural behavior under seismic loads was assessed. The minimum required amount of concrete and reinforcement for the load-bearing system was determined for each case. Based on the obtained data, rough construction costs were calculated, and the results were compared to evaluate the economic impact of each code.
Keywords: DBYBHY-2007, TBDY-2018, Reinforced Concrete Buildings, Construction Cost, Sta4CAD

GİRİŞ

Türkiye, dünyanın en aktif deprem kuşaklarından biri üzerinde yer almakta olup, tarihsel süreç boyunca yaşanan yıkıcı depremler ciddi can ve mal kayıplarına neden olmuştur. Özellikle son yıllarda meydana gelen büyük depremler, yapı güvenliği ve deprem yönetmeliklerinin önemi konusunda kamuoyunda farkındalık oluşturmuştur. Deprem kaynaklı kayıpların gelişmiş ülkelere kıyasla çok daha yüksek olmasının nedenleri arasında yetersiz zemin etütleri, mühendislik uygulamalarındaki eksiklikler, denetim yetersizlikleri ve

yürürlükteki yapı yönetmeliklerinin güncel sismik riskleri yeterince yansıtamaması gibi unsurlar yer almaktadır (Bikçe ve Akyol, 2017; Kara ve Akkaş, 2023).

Bu bağlamda, ülkemizde deprem yönetmelikleri zaman içerisinde güncellenmiş; 1975, 1997, 2007 ve son olarak 2018 yıllarında yürürlüğe giren düzenlemelerle yapı tasarımı ve taşıyıcı sistemlerin performansı açısından önemli değişiklikler yapılmıştır. Bir diğer çalışmada (Şapçı, 1998), 1975 ve 1997 yönetmelikleri esas alınarak perde-çerçeve sistemli binalarda yapılan karşılaştırmalarda, birleşim kesme kuvveti sınırlarının ve güçlü kolon-zayıf kiriş koşullarının yapısal davranışa etkisi ortaya konmuştur. Aynı çalışmada, yönetmelik değişikliklerinin özellikle düşey taşıyıcı eleman metrajlarında artışa neden olduğu ve yaklaşık %20 oranında bir maliyet farkı oluşturduğu belirlenmiştir.

Benzer şekilde, (Tekeli, 2006) tarafından dört, altı ve sekiz katlı betonarme binalar üzerinde gerçekleştirilen analizlerde, farklı deprem bölgeleri ve zemin sınıfları için yapılan statik hesaplar sonucunda, bir yapının depreme dayanıklı şekilde inşa edilmesinin maliyet üzerinde %4–8 arasında bir artışa yol açtığı saptanmıştır. (Tunç ve Tanfener, 2016) tarafından yürütülen çalışmada ise 2007 ve 2018 deprem yönetmeliklerinin karşılaştırmalı analizi yapılmış; 2018 yönetmeliğinin tasarım iç kuvvetlerinde yaklaşık %20 oranında artışa neden olduğu sonucuna ulaşılmıştır. Kırklareli ili özelinde yürüttükleri araştırmada, 2007 ve 2018 yönetmelikleri kapsamında elde edilen elastik tasarım spektrumlarını karşılaştırarak, 2018 TBDY'nin deprem tehlikesini daha gerçekçi biçimde yansıttığını ortaya koymuşlardır (Keskin ve Bozdoğan, 2018).

Bu literatür çerçevesinde yürütülen bu çalışmanın amacı, konut tipi betonarme binaların 2007 Deprem Bölgelerinde Yapılacak Binalar Hakkında Yönetmelik (DBYBHY-2007) ile Türkiye Bina Deprem Yönetmeliği (TBDY-2018) kapsamında yapısal performans ve kaba yapı maliyeti açısından karşılaştırmalı değerlendirilmesidir. Bu amaç doğrultusunda, 4 ve 8 katlı iki farklı betonarme yapı modeli, her iki yönetmelik doğrultusunda belirlenen deprem yükleri ve zemin sınıfları (ZA–ZE, Z1–Z4) dikkate alınarak analiz edilmiştir. Analiz sonuçları doğrultusunda yapısal elemanlara ait beton ve donatı miktarları belirlenmiş; elde edilen veriler ışığında kaba yapı maliyetleri hesaplanarak yönetmeliklerin maliyet üzerindeki etkileri karşılaştırmalı olarak değerlendirilmiştir.

MATERYAL VE METOD

Konut tipi betonarme binaların 2007 Deprem Bölgelerinde Yapılacak Binalar Hakkında Yönetmelik (DBYBHY-2007) ile 2018 Türkiye Bina Deprem Yönetmeliği (TBDY-2018) kapsamında iyi kötü zemin sınıfları olan Z1, Z4, ZA, ZE zemin sınıflarındaki 4 ve 8 katlı binaların maliyet kıyaslamasının incelendiği bu çalışmada sayısal modeller Sta4CAD statik analiz programı kullanılarak yapılmış olup oluşturulan sayısal model isimlendirilmeleri Şekil 1'de gösterildiği şekilde oluşturulmuştur.



Şekil 1. Model isimlendirmesi

Toplamda sekiz farklı model oluşturularak bu modeller için maliyet analizleri yapılmıştır. Model numaraları ve özellikleri Tablo 1'de gösterilmiştir.

Tablo 1. Model İsimlendirmeleri

Model No	Yönetmelik	Zemin Sınıfı	Kat Sayısı
2007-Z1-4	DBYBHY-2007	Z1	4
2007-Z1-8	DBYBHY-2007	Z1	8
2007-Z4-4	DBYBHY-2007	Z4	4
2007-Z4-8	DBYBHY-2007	Z4	8
2018-ZA-4	TBDY-2018	ZA	4
2018-ZA-8	TBDY-2018	ZA	8
2018-ZE-4	TBDY-2018	ZE	4
2018-ZE-8	TBDY-2018	ZE	8

4 kata sahip olan sayısal modellerin genel görünümü Şekil 2'de verilmiştir. 8 katlı sayısal modellerin genel görünümü ise Şekil 3'te verilmiştir. Yapı bodrum, zemin, iki normal kat olmak üzere dört kat ve kuleden oluşmaktadır.

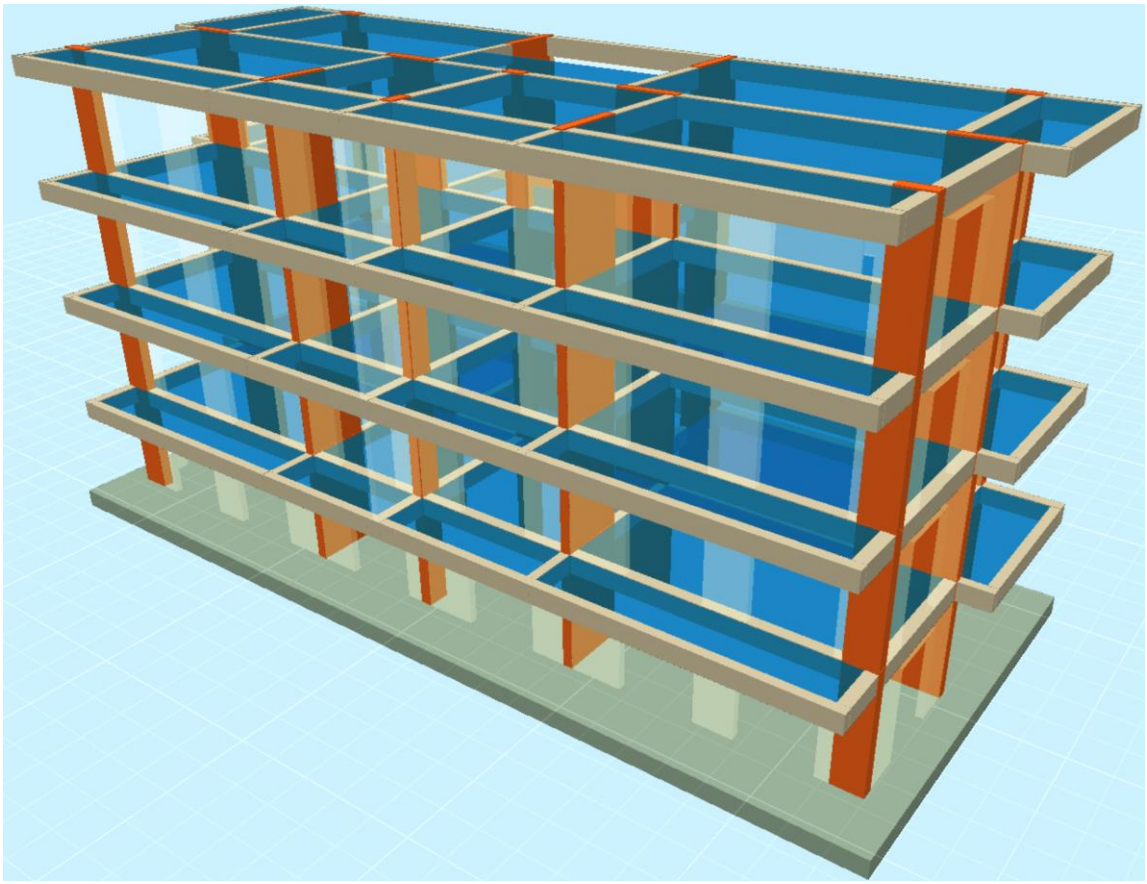

Şekil 2. 4 katlı binaya ait genel görünüm

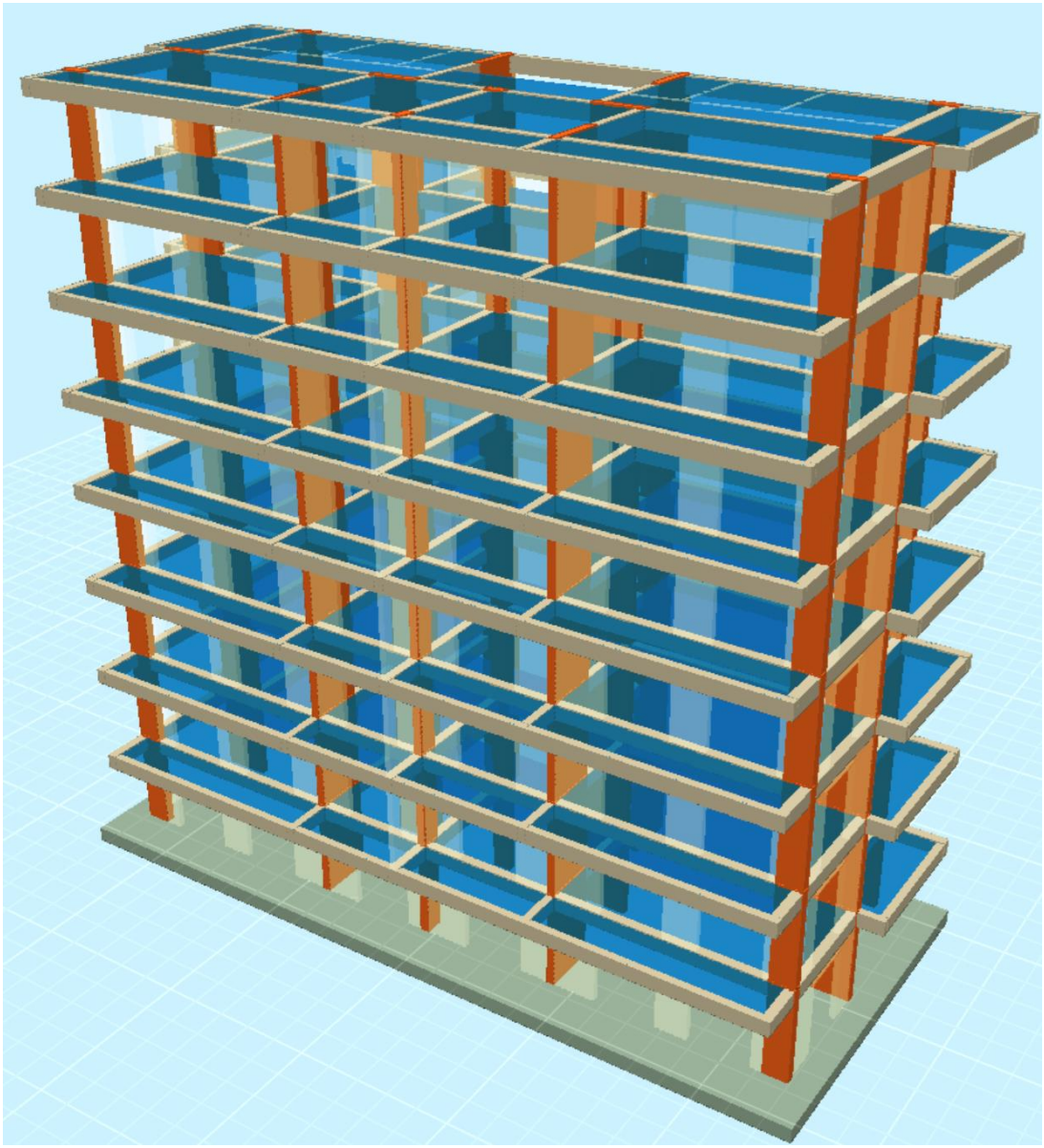

Şekil 3. 8 katlı binaya ait genel görünüm

Tüm sayısal modeller minimum yönetmelik şartlarını sağlayacak şekilde oluşturulmuş olup metraj listesi Şekil 4-11'da verilmiştir. Birim fiyatlar eski pozlara ait olup buradaki değerler değil T.C. Çevre Şehircilik ve İklim Değişikliği Bakanlığı tarafından hazırlanan rayiç fiyat listesinde yer alan rayiç değerler kullanılmıştır.

Poz	Birim fiyat tarifi	Birim fiyat	Miktar	Tutar
15.150.1005	C25/30 HAZIR BETON	1.566.00	251.1 m³	393.284.46
15.180.1003	DÜZ YÜZEYLİ BETONARME KALIBI	254.33	1872.0 m²	476.116.70
15.160.1003	8-12 mm BETONARME DEMİRİ	19.696.53	13.9 tn	274.312.76
15.160.1004	14-50 mm NERVÜRLÜ BETONARME DEMİRİ	19.448.18	11.3 tn	220.289.05

Şekil 4. 2007-Z1-4 metraj listesi

Poz	Birim fiyat tarifi	Birim fiyat	Miktar	Tutar
15.150.1005	C25/30 HAZIR BETON	1.566.00	252.1 m³	394.794.08
15.180.1003	DÜZ YÜZEYLİ BETONARME KALIBI	254.33	1874.1 m²	476.650.79
15.160.1003	8-12 mm BETONARME DEMİRİ	19.696.53	14.0 tn	276.305.66
15.160.1004	14-50 mm NERVÜRLÜ BETONARME DEMİRİ	19.448.18	12.4 tn	242.090.54

Şekil 5. 2007-Z4-4 metraj listesi

Poz	Birim fiyat tarifi	Birim fiyat	Miktar	Tutar
15.150.1005	C25/30 HAZIR BETON	1.566.00	498.6 m³	780.780.97
15.180.1003	DÜZ YÜZEYLİ BETONARME KALIBI	254.33	3709.8 m²	943.525.13
15.160.1003	8-12 mm BETONARME DEMİRİ	19.696.53	28.7 tn	564.856.50
15.160.1004	14-50 mm NERVÜRLÜ BETONARME DEMİRİ	19.448.18	22.9 tn	445.182.13

Şekil 6. 2007-Z1-8 metraj listesi

Poz	Birim fiyat tarifi	Birim fiyat	Miktar	Tutar
15.150.1006	C30/37 HAZIR BETON	1.616.00	631.0 m³	1.019.714.23
15.180.1003	DÜZ YÜZEYLİ BETONARME KALIBI	254.33	4205.9 m²	1.069.696.20
15.160.1003	8-12 mm BETONARME DEMİRİ	19.696.53	36.3 tn	714.200.42
15.160.1004	14-50 mm NERVÜRLÜ BETONARME DEMİRİ	19.448.18	41.6 tn	809.829.89

Şekil 7. 2007-Z1-8 metraj listesi

Poz	Birim fiyat tarifi	Birim fiyat	Miktar	Tutar
15.150.1005	C25/30 HAZIR BETON	1.566.00	249.1 m³	390.164.98
15.180.1003	DÜZ YÜZEYLİ BETONARME KALIBI	254.33	1852.4 m²	471.121.66
15.160.1003	8-12 mm BETONARME DEMİRİ	19.696.53	14.6 tn	287.374.45
15.160.1004	14-50 mm NERVÜRLÜ BETONARME DEMİRİ	19.448.18	9.4 tn	183.674.06

Şekil 8. 2018-ZA-4 metraj listesi

Poz	Birim fiyat tarifi	Birim fiyat	Miktar	Tutar
15.150.1005	C25/30 HAZIR BETON	1.566.00	249.1 m³	390.164.98
15.180.1003	DÜZ YÜZEYLİ BETONARME KALIBI	254.33	1852.4 m²	471.121.66
15.160.1003	8-12 mm BETONARME DEMİRİ	19.696.53	14.6 tn	287.374.45
15.160.1004	14-50 mm NERVÜRLÜ BETONARME DEMİRİ	19.448.18	9.5 tn	185.706.80

Şekil 9. 2018-ZE-4 metraj listesi

Poz	Birim fiyat tarifi	Birim fiyat	Miktar	Tutar
15.150.1005	C25/30 HAZIR BETON	1.566.00	500.2 m³	783.349.21
15.180.1003	DÜZ YÜZEYLİ BETONARME KALIBI	254.33	3688.4 m²	938.072.29
15.160.1003	8-12 mm BETONARME DEMİRİ	19.696.53	29.8 tn	587.830.91
15.160.1004	14-50 mm NERVÜRLÜ BETONARME DEMİRİ	19.448.18	20.2 tn	392.072.16

Şekil 10. 2018-ZA-8 metraj listesi

Poz	Birim fiyat tarifi	Birim fiyat	Miktar	Tutar
15.150.1005	C25/30 HAZIR BETON	1.566.00	502.1 m³	786.268.23
15.180.1003	DÜZ YÜZEYLİ BETONARME KALIBI	254.33	3692.6 m²	939.130.30
15.160.1003	8-12 mm BETONARME DEMİRİ	19.696.53	30.1 tn	592.059.01
15.160.1004	14-50 mm NERVÜRLÜ BETONARME DEMİRİ	19.448.18	20.5 tn	398.622.05

Şekil 11. 2018-ZE-8 metraj listesi

T.C. Çevre Şehircilik ve İklim Değişikliği Bakanlığı tarafından hazırlanan rayiç fiyat listesinde yer alan pozlardan kaba inşaat maliyet hesabı için kullanılan pozlar Tablo 2'de sunulmuştur.

Tablo 2. Kaba inşaat için ÇŞİDB birim fiyat rayiç listesi

Poz No	Tanımı	Ölçü Birimi	Rayiç Fiyat (₺)
15.150.1005	Beton santralinde üretilen veya satın alınan ve beton pompasıyla basılan, C25/30 basınç dayanım sınıfında, gri renkte, normal hazır beton dökülmesi (beton nakli dahil)	m^3	3.151,28
15.180.1003	Plywood ile düz yüzeyli betonarme kalıbı yapılması	m^2	824,39
15.160.1003	Ø 8- Ø 12 mm nervürlü beton çelik çubuğu, çubukların kesilmesi, bükülmesi ve yerine konulması	Ton	39.429,35
15.160.1004	Ø 14- Ø 28 mm nervürlü beton çelik çubuğu, çubukların kesilmesi, bükülmesi ve yerine konulması	Ton	38.016,85

BULGULAR ve TARTIŞMA

Konut tipi betonarme binaların 2007 Deprem Bölgelerinde Yapılacak Binalar Hakkında Yönetmelik (DBYBHY-2007) ile 2018 Türkiye Bina Deprem Yönetmeliği (TBDY-2018) kapsamında iyi kötü zemin sınıfları olan Z1, Z4, ZA, ZE zemin sınıflarındaki 4 ve 8 katlı binaların kaba inşaat maliyetleri karşılaştırmalı olarak incelenmiştir. Şekil 12'de tüm sayısal modellerin maliyet kıyaslanması sunulmuştur.

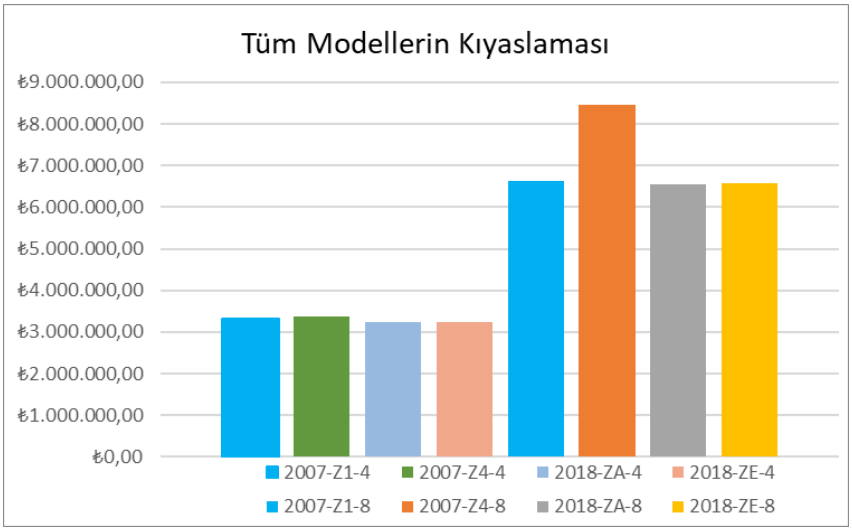

Şekil 12. Tüm sayısal modellerin kıyaslanması

2007-Z1-4 modelinde kaba inşaat maliyeti 3.312.202,86₺, 2007-Z4-4 modelinde kaba inşaat maliyeti 3.362.846,83₺, 2007-Z1-8 modelinde kaba inşaat maliyeti 6.631.758,44₺, 2007-Z4-8 modelinde kaba inşaat maliyeti 8.468.545,95₺, 2018-ZA-4 modelinde kaba inşaat maliyeti 3.245.110,78₺, 2018-ZE-4 modelinde kaba inşaat maliyeti 3.248.912,47₺, 2018-ZA-8 modelinde kaba inşaat maliyeti 6.559.885,33₺, 2018-ZE-8 modelinde kaba inşaat maliyeti 6.586.266,50₺ olarak hesaplanmıştır.

Şekil 13'te 4 katlı modellerin DBYBHY-2007 ve TBDY-2018 yönetmeliklerinde tanımlanan en iyi ve en kötü zemin sınıflarındaki maliyet kıyaslamaları verilmiştir. Şekil 14'te 8 katlı modellerin DBYBHY-2007 ve TBDY-2018 yönetmeliklerinde tanımlanan en iyi ve en kötü zemin sınıflarındaki maliyet kıyaslamaları verilmiştir.

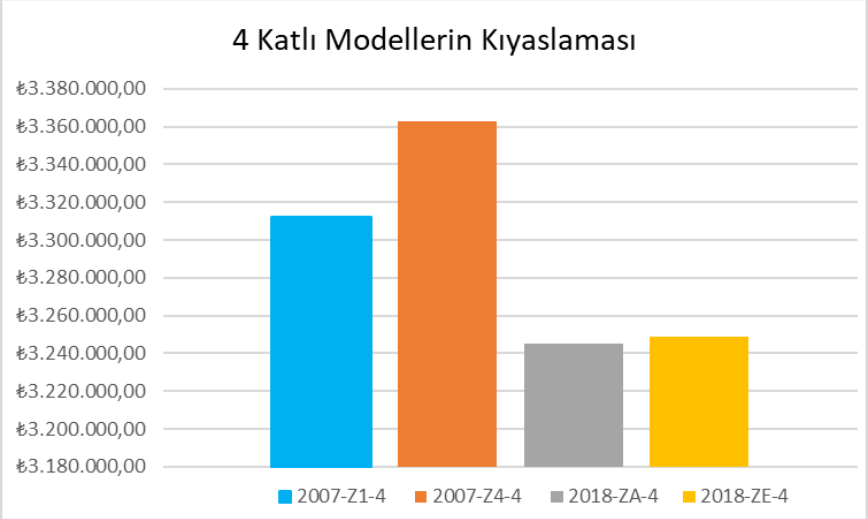

Şekil 13. 4 katlı modellerin kıyaslaması

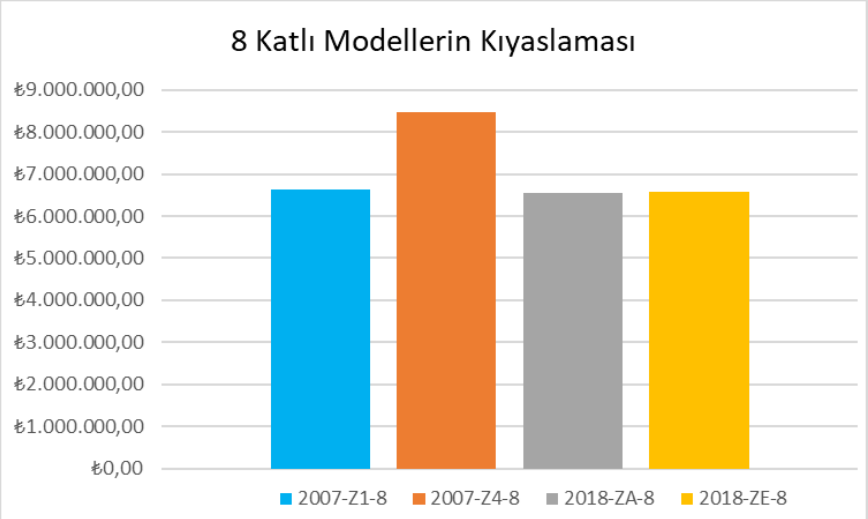

Şekil 14. 8 katlı modellerin kıyaslaması

Şekil 13 incelendiğinde 2007-Z1-4 ile 2018-Z4-4 modelleri arasında %1,53, 2007-Z1-4 ile 2018-ZA-4 modelleri arasında %2,07, 2007-Z1-4 ile 2018-ZE-4 modelleri arasında %1,95, 2007-Z4-4 ile 2018-ZA-4 modelleri arasında %3,63, 2007-Z4-4 ile 2018-ZE-4 modelleri arasında %3,51 ve 2018-ZA-4 ile 2018-ZE-4 modelleri arasında %0,12 modelleri arasında fark oluşmuştur.

Şekil 14 incelendiğinde 2007-Z1-8 ile 2018-Z4-8 modelleri arasında %27,70, 2007-Z1-8 ile 2018-ZA-8 modelleri arasında %1,10, 2007-Z1-8 ile 2018-ZE-8 modelleri arasında %0,69, 2007-Z4-8 ile 2018-ZA-8 modelleri arasında %29,10, 2007-Z4-8 ile 2018-ZE-8 modelleri arasında %28,58 ve 2018-ZA-8 ile 2018-ZE-8 modelleri arasında %0,40 modelleri arasında fark oluşmuştur.

Şekil 15'te DBYBHY-2007 yönetmeliğine ve Z1 zemin sınıfına göre çözülmüş 4-8 kat kaba maliyet kıyaslaması verilmiştir. Şekil 16'da DBYBHY-2007 yönetmeliğine ve Z4 zemin sınıfına göre çözülmüş 4-8 kat kaba maliyet kıyaslaması verilmiştir. Şekil 17'de TBDY-2018 yönetmeliğine ve ZA zemin sınıfına göre çözülmüş 4-8 kat kaba maliyet kıyaslaması verilmiştir. Şekil 18'de TBDY-2018 yönetmeliğine ve ZE zemin sınıfına göre çözülmüş 4-8 kat kaba maliyet kıyaslaması verilmiştir.

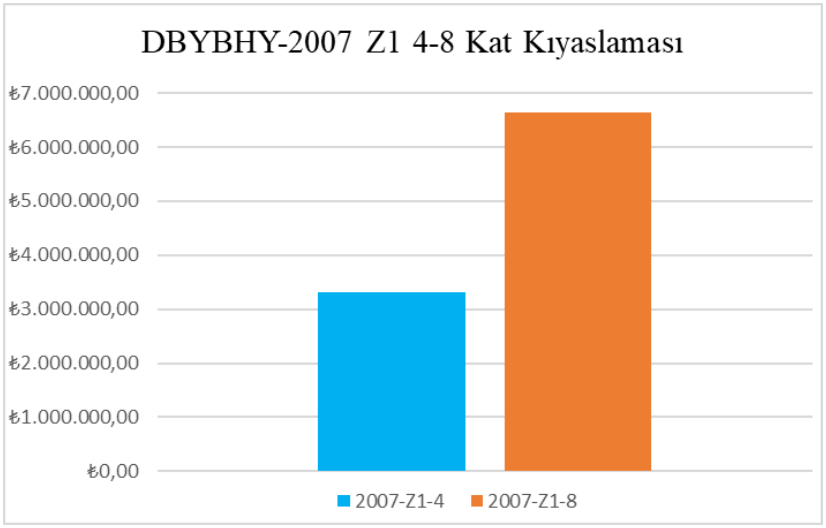

Şekil 15. DBYBHY-2007 Z1 4-8 kat kıyaslaması

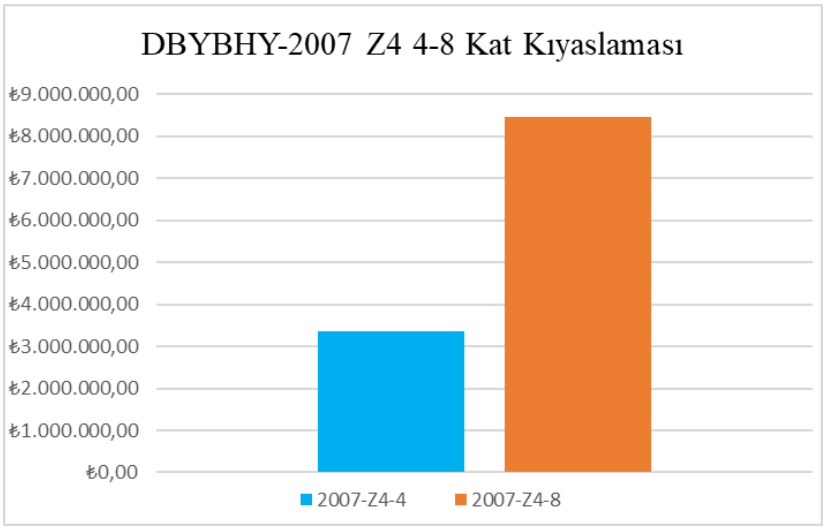

Şekil 16. DBYBHY-2007 Z4 4-8 kat kıyaslaması

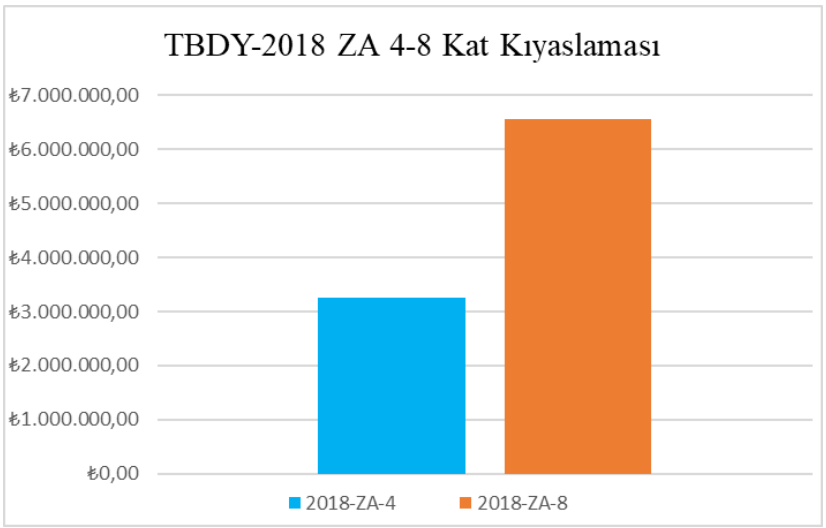

Şekil 17. TBDY-2018 ZA 4-8 kat kıyaslaması

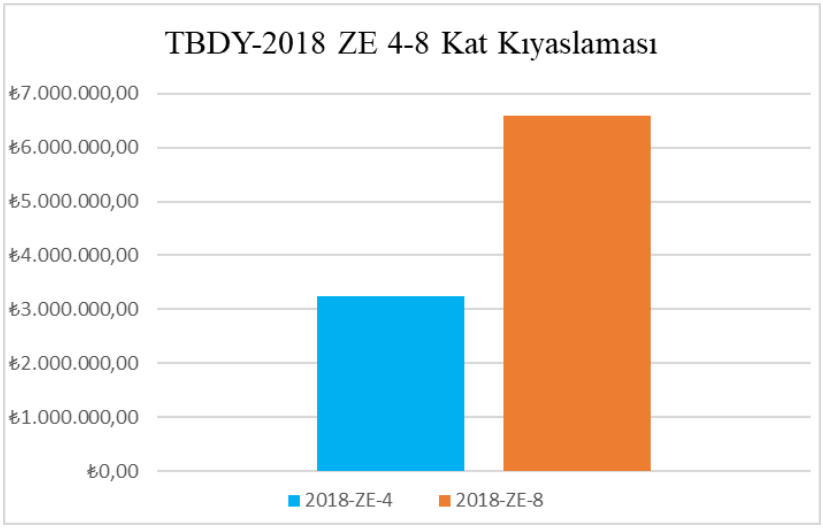

Şekil 18. TBDY-2018 ZE 4-8 kat kıyaslaması

Şekil 15 incelendiğinde 2007-Z1-4 ile 2007-Z1-8 modelleri arasında %100,22 maliyet farkı oluşmuştur. Şekil 16 incelendiğinde 2007-Z4-4 ile 2007-Z4-8 modelleri arasında %151,83 maliyet farkı oluşmuştur. Şekil 17 incelendiğinde 2018-ZA-4 ile 2018-ZA-8 modelleri arasında %102,15 maliyet farkı oluşmuştur. Şekil 18 incelendiğinde 2018-ZE-4 ile 2018-ZE-8 modelleri arasında %102,72 maliyet farkı oluşmuştur.

SONUÇ

Bu çalışmada, DBYBHY-2007 ile TBDY-2018 yönetmelikleri kapsamında iyi kötü zemin sınıfları olan Z1, Z4, ZA, ZE zemin sınıflarındaki 4 ve 8 katlı binaların kaba inşaat maliyetleri kıyaslanmıştır. Elde edilen sonuçlara göre;

Zemin sınıfı kötüleştikçe maliyetin artması beklenen bir eğilimdir ve bu eğilim özellikle 2007 yönetmeliği altında daha keskin şekilde gözlemlenmiştir.

2018 yönetmeliği, zemin büyütme etkilerini daha kontrollü dağıttığı için, zemin sınıfı değişimlerine bağlı maliyet artışları daha sınırlı kalmıştır.

Kat sayısı arttıkça, zemin etkilerinin yapısal sistem üzerinde daha fazla belirleyici olduğu ve bu durumun maliyete yansıdığı tespit edilmiştir.

Ayrıca, 2007 yönetmeliği ile tasarlanmış yapılarda, gereksiz emniyet katsayıları ve belirsizliklerin etkisiyle maliyetler daha yüksek çıkabilmektedir.

Sonraki çalışmalarda, model sayı ve diğer zemin sınıfları da dahil edilerek daha kapsamlı bir araştırma yapılacaktır.

KAYNAKLAR

Akkar, S., İhtimal Hesaplarına Dayalı Güncellenmiş Türkiye Sismik Tehlike Haritası ve Deprem Tasarımına Etkileri, Yeni Nesil Deprem Yönetmelikleri ve Deprem Mühendisliğinde Yeni Teknolojiler Kongresi, Ankara, 26-27 Şubat 2015.

Bikçe, M., & Akyol, B. (2017). Tasarlanmış gerçek yapılarda asmolen/plak döşeme dönüşümünün yapı maliyetine etkisi. Fırat Üniversitesi Mühendislik Bilimleri Dergisi, 29(1), 133-144.

Deprem Bölgelerinde Yapılacak Binalar Hakkında Yönetmelik, 2007

Kara, İ. F., & Akkaş, Y. E. (2023). TBDY 2018'e göre farklı döşeme tiplerinin yüksek bina sınıfındaki yapıda doğrusal olmayan davranışa olan etkilerinin incelenmesi. Niğde Ömer Halisdemir Üniversitesi Mühendislik Bilimleri Dergisi, 12(1), 1-1.

Karaesmen, E., Öncesiyle Sonrasıyla Deprem,Atılım Üniversitesi Yayınları, 2008.

Keskin&Bozdoğan/Kırklareli University Journal of Engineering and Science 4-1(2018) 74-90

Şapçı, M.H, 1975 ve 1997 Türkiye Deprem Yönetmelikleri'ne göre tasarlanmış betonarme binaların performansı ve maliyet değerlendirmesi, ODTÜ Fen Bilimleri Enstitüsü , Ankara, 1998

Tekeli, H, Deprem bölgesi ve yerel zemin sınıflarının bina maliyetine etkileri, Süleyman Demirel Üniversitesi Fen Bilimleri Enstitüsü, Isparta, 2006

Tunç, G., Tanfener, T., 2007 ve 2016 Türkiye Bina Deprem Yönetmeliklerinin Örneklerle Mukayesesi, 3.Ulusal Yapı Kongresi ve Sergisi Teknik Tasarım, Güvenlik ve Erişebilirlik, TMMOB Mimarlar Odası Ankara Şubesi, 2016.

Türkiye Bina Deprem Yönetmeliği, 2018

➢ *ORAL PRESENTATION*

Evaluation of Blueberry Pruning Waste as Antimicrobial Agent in Edible Film Content Containing Probiotic

Ali Saglam[1] (*ORCID: https://orcid.org/0000-0003-4010-8465*), Mehmet Cobanoglu[1] (*ORCID: https://orcid.org/0009-0005-9329-2528*), Merve Alan[1] (*ORCID: https://orcid.org/0009-0008-4530-1073*), Meltem Asan-Ozusaglam[1]* (*ORCID: https://orcid.org/0000-0002-3638-1306*)

*[1]University of Aksaray, Faculty of Science and Letters, Department of Molecular Biology and Genetic, Aksaray, Türkiye

*Corresponding author e-mail: meltemozusaglam@gmail.com

Abstract
The waste products resulting from blueberry (*Vaccinium myrtillus*) pruning and renewable film containing probiotics may play an important role in extending the shelf life of fruits, improving food quality and utilizing waste products. Therefore, this study aimed to determine the antimicrobial activity of blueberry pruning residue branches and then develop an edible film containing probiotic. The blueberry branches were firstly extracted using water. Then, antimicrobial activity of blueberry branch water extract (BBWE) on food-borne and fish pathogens *L. monocytogenes* ATCC 7644 and *Y. ruckeri* was determined. The higher antimicrobial activities against *Yersinia ruckeri* compared to *Listeria monocytogenes* ATCC 7644 were determined at 10 and 20 µL extract concentrations with inhibition zones of 6.14 mm and 8.68 mm, respectively. The BBWE used in renewable films was prepared by adding probiotic candidate *Streptococcus thermophilus* MAS-1. Then, the antimicrobial activities of the prepared four different renewable film groups on tested bacteria were determined using well diffusion method. Gum (G) and Gum+probiotic (GP) groups did not have inhibition zones on the tested microorganisms. Among the developed film groups, G+BBWE+Probiotic (GEP) group showed the highest antimicrobial activity against *L. monocytogenes* ATCC 7644 (6.07 mm) and *Y. ruckeri* (5.72 mm). After that, strawberry fruits were covered with all film groups and observed for 5 days to determine the effect of the developed film groups on increasing the shelf life of the fruit. Finally, the GEP group reduced mass loss by 19.86% compared to the control group. The results showed that BBWE can be used as a coating material component with antimicrobial activity in the food industry and can provide extra properties to the renewable film.
Keywords: Antimicrobial activity, Blueberry branch, Extract, Edible films, Probiotic

INTRODUCTION

Vaccinium myrtillus (Ericaceae) is a maquis plant that grows in temperate climates. Blueberries have a grape-like structure and are purple in color with a sour taste (Zapata et al., 2019). Blueberries are rich in secondary metabolites such as phenolic acids, flavonoids, and anthocyanins (Hurtado and Charfuelan, 2019). Phenolic compounds are frequently used in alternative medicine and supplements against various health problems such as diabetes, heart disease, urinary tract infections and various cancers (Rahman et al., 2021). The blueberries are one of the wild blueberry species that are an important source of income in many countries (Vucic et al., 2013).

Food spoilage is the process by which microorganisms alter the biochemical content of food, reducing the time required for food consumption (Lianou et al., 2016). The most prominent strains of these microorganisms are generally *Listeria* sp, *Salmonella* sp, *Bacillus* sp, *Escherichia coli*. Consumption of foods contaminated with pathogens poses a threat to human health (Ceuppens et al., 2013; Ibrahim et al., 2021). Consumption of fish and fish products contaminated with fish pathogens adversely affects human health. Among fish pathogens, *Aeromones hydrohila* and *Yersinia ruckeri* are some of the most prominent strains (Novoslavskij et al., 2016; Suresh et al., 2022). Foodborne diseases can occur in the gastrointestinal tract at any time during harvest, storage, processing, transportation, preservation and packaging (Hamaideh et al., 2024). The use of plant secondary metabolites obtained from plant extracts in food preservation and preservation has become more demanded with the emergence of more tolerant and antibiotic-resistant food pathogens in food processing and preservation methods (Kumari et al., 2024). The adverse health and toxic effects of chemical synthetic preservatives have led the food industry to seek alternative natural preservatives to food pathogens to improve safety and food quality (Pedan et al., 2019). Natural food preservatives, naturally derived from secondary

metabolites known as Polyphenols obtained from plant extracts, have strong antimicrobial properties (Bouarab et al., 2019).

Foodborne pathogens, which pose significant risks to consumers, cause millions of dollars in economic losses each year due to food spoilage and the formation of foodborne illnesses (Bae et al., 2022). Bioactive compounds released from agricultural by-products can be isolated and contribute to the extra properties of films developed to extend the shelf life of foods. In this way, agricultural by-products can be used economically and environmentally (Pérez-Santaescolástica et al.,2022).

Live microorganisms that have beneficial effects when administered to the host are defined as probiotics (Hill et al., 2014). Probiotics are effective in treating gastrointestinal infections (Idrees et al., 2022). Probiotics have a mechanism of action on pathogenic microorganisms. Due to this mechanism of action, they are effective in regulating intestinal flora in the treatment of infections (Oelschlaeger, 2010). The use of probiotics in foods is very important. Various strains of *Lactobacillus* have been used as probiotics in foods for many years (Ranadheera et al., 2010). *L. fermentum* strains can be isolated from grains with fermentation capacity or other fermented plants, various originated milk and dairy products (Naghmouchi et al., 2020, Asan-Ozusaglam, 2019).

The use of lactic acid bacteria and other probiotic microorganisms in food coating materials to extend shelf life promotes the stability and preservation of food (Temiz et al., 2021; De Luna Freire et al., 2024). Edible film is a thin coating that is applied as a separate layer between food ingredients or directly to the food and acts as a barrier against gas, moisture, oil and vapors (Shahidi et al., 2022). However, these films have some limitations such as poor antioxidant and antimicrobial activities. To overcome this challenge, edible films are enriched with different bioactive compounds such as plant extracts (Mohammadian et al., 2021). Plant extracts can also be used as active ingredients such as colorants and flavors to improve the appearance and taste of foods (Mkandawire and Aryee, 2018).

The branch of blueberry that remains as a waste product after pruning blueberries may have the potential to be used commercially for both environmental protection and recycling purposes. This study aimed to evaluate the post-pruning waste of blueberry plants and to develop a new food coating material. In this context, firstly, the antimicrobial activity of the water extract obtained from blueberry branches was determined against food-borne and fish originated test microorganisms. Then, edible film was developed using branch extract and *S. thermophilus* MAS-1 and its antimicrobial activity on the pathogenic test bacteria was determined. Strawberry fruits were coated to determine the effect of the film on the shelf life of the fruits.

MATERIAL METHOD

Blueberry branches were obtained from Alata Horticulture Research Institute (Mersin-Türkiye) on 18.06.2021.

Preparation of BBWE

The blueberry branches were washed with distilled water and left to dry in an airy and sunless environment. The dried branches were ground into powder using a Waring blender and then stored in brown glass bottles in a dry and dark environment until use. Then, the powdered branches were extracted with distilled water in a hot water bath (75°C) for 6 hours per day (during 2 days). After distilled water was evaporated from the extract, BBWE was dissolved with dimethyl sulfoxide (DMSO) and then sterilized with a 0.45µm filter.

Determination of Antibacterial Activity

Disc Diffusion Test

The antimicrobial activity of blueberry branch was determined by disk diffusion test. *L. monocytogenes* ATCC 7644 and Y. ruckeri (Tryptic-Soy-Broth (TSB)/Agar) were used as test microorganisms. Test microorganisms (100 µL) prepared at a concentration of 0.5 Mcfarland (1x108 CFU/mL) were inoculated on solid medium. Then, sterile disks (Whatman No: 1, Diameter: 6 mm) were placed on the solid medium. Then, BBWE extract was dropped on sterile disks as 10 µL and 20 µL in 3 replicates. Penicillin (P, 10 µg/disc) antibiotic disks were used as positive control. Test microorganisms *Y. ruckeri* were incubated at 25°C and *L. monocytogenes* at °C in an oven for 24 hours. After incubation, the diameters of the inhibition zones around the discs were measured and recorded. The values obtained were presented with their means and standard deviations.

Determination of MIC and MBC values

Micro-dilution method was used to determine MIC and MBC values of the BBWE. Liquid medium suitable for microorganisms were added to the tubes. Then, BBWE was added and two-fold dilutions were made. Test microorganisms (0.5 Mcfarland) was added to tubes and incubated for 24 hours at a temperature suitable for microorganisms. After incubation, the concentrations at which no microbial growth occurred were recorded as MIC values. Then, the samples taken from tubes were dropped onto appropriate agar media for each

microorganism using the spot dropping method and left to incubate for 24 hours at appropriate temperatures. The concentrations at which no microbial growth occurred after incubation were recorded as the MBC value.

Preparation of Edible Film

BBWE and *S. thermophilus* MAS-1 probiotic strain were used to develop natural edible film. Guar gum (1%), glycerol (3%) and BBWE extract (10%) were used in the preparation of edible film. Guar gum without extracts and probiotic strain was used as the control group. The groups without probiotics were completed with distilled water. Probiotic-containing groups were completed with probiotic culture after 18 hours of incubation.

Determination of Antimicrobial Activity of Edible Film

Composite Coating of Strawberry Fruit

To test the antimicrobial activity of edible film, agar diffusion method was used in 4 groups. Test microorganisms were prepared at a concentration of 0.5 Mcfarland and 100 µL was taken and spread on the agar surface. Then, 6 mm diameter wells were opened on the agar surface and the wells were filled with 100 µL of the prepared edible film. Petri dishes were incubated with *L. monocytogenes* 37 °C and *Y. ruckeri* 25 for 24 °C hours. At the end of incubation, the inhibition zone diameters around the well were measured and recorded.

Strawberries obtained from a local market of Aksaray city were used to determine the effect of the coating material on the shelf life of fruits. Three strawberries were selected for each group according to their smell, color and size. The selected strawberries were washed with distilled water and dried, then the strawberries were weighed on a precision scale. According to the experimental groups, strawberries were dipped into the renewable film in liquid form and kept for 2 minutes. After the strawberries dipped into the renewable film were filtered, their storage parameters were evaluated at room temperature (25°C). The control group was washed with distilled water only and dried, then all groups were stored and weighed for 5 days and photographed every day. The percentage weight loss of the fruits was calculated and the results were recorded.

RESULTS AND DISCUSSION

Antibacterial activities of BBWE were investigated on food-borne and fish pathogens by disc diffusion and micro-dilution experiments. The inhibition zone diameters of the BBWE on the test microorganisms are given in Table 1. At a concentration of 10 µl, an inhibition zone diameter of 6.14 mm was determined on *Y. ruckeri* from the test microorganisms, and no inhibition zone diameter was determined on *L. monocytogenes* ATCC 7644. At a concentration of 20 µl, an inhibition zone diameter of 8.68 mm was determined on *Y. ruckeri*. An inhibition zone diameter of 6.91 mm was determined on *L. monocytogenes* ATCC 7644.

Table 1. BBWE Inhibition Zone Diameters

Disc Diffusion Test (mm)			
Microorganisms	**10 µL**	**20 µL**	**P (10 µg/disc)**
L. monocytogenes ATCC 7644	0	6.91±0.03	8.83±0.71
Y. ruckeri	6.14±0.05	8.68±0.52	21.4±1.56

MIC and MBC values of BBWE are given in Table 2. MIC and MBC values of the BBWE on *Y. ruckeri* was 25 and 50 mg/mL. *L. monocytogenes* had 50 and 100 mg/ml MIC and MBC values.

Table 2. MIC and MBC Values of BBWE.

Micro-Dilution Test (mg/mL)		
Microorganisms	**MIC**	**MBC**
L. monocytogenes ATCC 7644	50	100
Y. ruckeri	25	50

Gil-Martínez et al. (2023) tested the antimicrobial activity of the extract obtained from blueberry leaves on food and clinical test microorganisms using the ultrasonication extraction method. According to the results, they reported that *S. aureus* CECT 239 was the most sensitive bacteria with MIC and MBC values of 0.4 mg/mL and 0.8 mg/ml. The extract had MIC and MBC values of 3.12 mg/ml and 6.25 mg/mL on *L. monocytogenes* CECT 4032.

Antimicrobial Activity of Edible Film

The antimicrobial values of the renewable film were determined by well diffusion method. The results are given in Table 3. The inhibition zone diameters varied between 4.59 mm and 6.07 mm. Gum (G) and

gum+probiotic (GB) edible film did not give any zones on the test microorganisms. However, Gum + BBWE (GE) and Gum + Extract + Probiotic (GEB) groups showed an inhibition zone diameter of 5.59 mm and 6.07 mm on *L. monocytogenes* ATCC 7644. Also, the inhibition zone diameter of 4.59 mm in GE and 5.72 mm in GEB groups was determined against *Y. ruckeri*.

Table 3. Antimicrobial Activity of Edible Film Containing BBWE and Probiotic

	Inhibition zone diameter (mm)			
Microorganisms	**G**	**GE**	**GB**	**GEB**
L.monocytogenes ATCC 7644	-	5.59±0.15	-	6.07±0.16
Y. ruckeri	-	4.59±0.07	-	5.72±0.40

-:No inhibition zone diameter

Griep et al. (2024) obtained hydroethanol (60%) extracts of blueberry pulp (peel and seed) with the help of ultrasonic bath. They prepared active renewable films with 4 different extract concentrations (0.25, 0.5, 1.3 and 2.6 mg/ml). It was reported that the films containing extracts gained antioxidant properties compared to the control groups. It was also stated that it can help preserve the physicochemical properties of foods and is suitable for use as food packaging material.

Composite film coating of strawberry

The percentage weight loss was calculated to determine the storage period and shelf life of strawberry fruits after coating with the prepared edible films. Table 4 shows the percentage weight losses of both the control group and the coating groups. On the 5th day of storage, the highest percentage weight loss among strawberry fruits belonged to the control group (66.28%) and the lowest percentage weight loss belonged to the GEB group (46.42%). It was determined that the percentage weight loss in the GEB group compared to the control was 3.34%, 7.45%, 7.53%, 15.80% and 19.86% from the 1st day to the 5th day, respectively. compared to the control during the 5-day storage period. Images of composite coated strawberry fruits for 5 days are given in Figure 1While deterioration was observed on the 2nd day of storage in the control (C) and G groups, it was observed on the 4th day of storage in the GEB group.

Table 4. Percent Weight Loss of Strawberry Fruit After Coatin

Groups	**Weight Loss of Strawberry Samples (%)**					
	Days					
	0	**0**	**0**	**0**	**0**	**0**
C	-	12.13±5.98	24.59±9.47	31.89±13.51	49.01±15.93	66.28±16.89
G	-	9.25±1.47	21.13±2.94	30.9±3.00	45.59±2.11	63.45±4.16
GE	-	9.07±2.44	19.98±7.02	27.21±9.66	37.90±14.99	50.04±18.66
GP	-	8.44±1.59	18.96±4.19	26.96±8.42	37.23±13.09	49.31±16.74
GEP	-	8.79±2.98	17.14±4.65	24.36±6.33	33.21±6.39	46.42±3.83

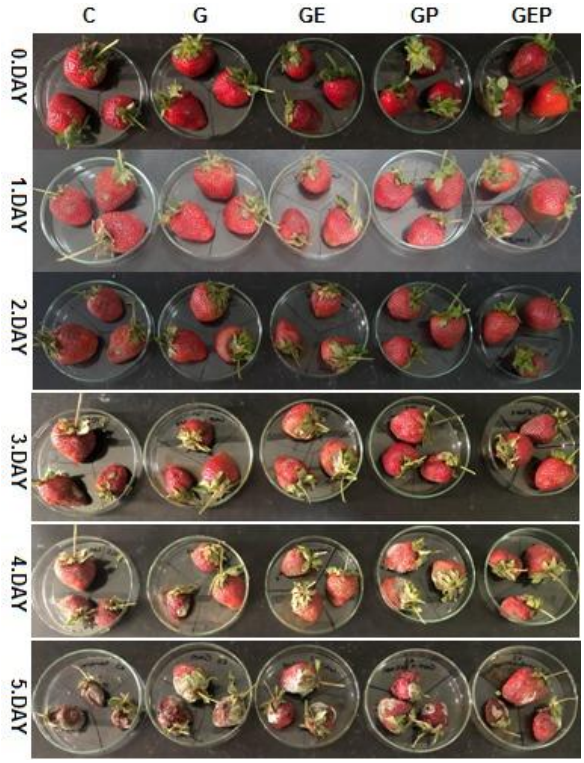

Figure 1. The coated with film groups and uncoated strawberry fruits on day 0 and day 5

CONCLUSION

There is a huge economic loss in the world due to food spoilage. In our study, the pruning waste product of blueberry was evaluated to minimize this economic loss. BBWE was obtained to increase the shelf life and quality of foods in order to create a new usage area by recycling waste into the economy. The extract with good biological activity on the test microorganisms is suitable for use as a natural antimicrobial agent for edible films. The edible film content is supported with probiotic to regulate intestinal flora and provide flora balance against gastrointestinal diseases. The prepared edible film (GEB) increased the shelf life and quality of strawberries thanks to its antimicrobial properties and probiotic content. According to the results, BBWE may have the potential to be used commercially as a food coating material to extend the shelf life of foods.

REFERENCES

Asan-Ozusaglam. M., Gunyakti, A., 2019. *Lactobacillus fermentum* strains from human breast milk with probiotic properties and cholesterol-lowering effects. Food Science and Biotechnology, 28(2):501–509.

Bae, J. Y., Seo, Y. H., & Oh, S. W. (2022). Antibacterial activities of polyphenols against foodborne pathogens and their application as antibacterial agents. *Food Science and Biotechnology*, *31*(8), 985-997.

Bouarab Chibane, L., Degraeve, P., Ferhout, H., Bouajila, J., & Oulahal, N. (2019). Plant antimicrobial polyphenols as potential natural food preservatives. *Journal of the Science of Food and Agriculture*, *99*(4), 1457-1474.

Ceuppens, S., Boon, N., & Uyttendaele, M. (2013). Diversity of *Bacillus cereus* group strains is reflected in their broad range of pathogenicity and diverse ecological lifestyles. *FEMS microbiology ecology*, *84*(3), 433-450.

De Luna Freire, M. O., Cruz Neto, J. P. R., de Albuquerque Lemos, D. E., de Albuquerque, T. M. R., Garcia, E. F., de Souza, E. L., & de Brito Alves, J. L. (2024). *Limosilactobacillus fermentum* Strains as Novel Probiotic Candidates to Promote Host Health Benefits and Development of Biotherapeutics: A Comprehensive Review. *Probiotics and Antimicrobial Proteins*, 1-16.

Gil-Martínez, L., Aznar-Ramos, M. J., del Carmen Razola-Diaz, M., Mut-Salud, N., Falcón-Piñeiro, A., Baños, A., ... & Verardo, V. (2023). Establishment of a sonotrode extraction method and evaluation of the antioxidant, antimicrobial and anticancer potential of an optimized *Vaccinium myrtillus* L. leaves extract as functional ingredient. *Foods*, *12*(8), 1688.

Griep, P., Ferreira, J., Fischer, B., Fernandes, I. A., Cansian, R. L., Junges, A., & Backes, G. T. (2024). Development and characterization of active edible film with blueberry residue extract (*Vaccinium* spp.). *Biomass Conversion and Biorefinery*, *14*(18), 22087-22097.

Hamaideh, S., Olaimat, A. N., Al-Holy, M. A., Ababneh, A., Shahbaz, H. M., Abughoush, M., ... & Holley, R. A. (2024). The Influence of Technological Shifts in the Food Chain on the Emergence of Foodborne Pathogens: An Overview. *Applied Microbiology*, *4*(2), 594-606.

Hill, C., Guarner, F., Reid, G., Gibson, G. R., Merenstein, D. J., Pot, B., ... & Sanders, M. E. (2014). The International Scientific Association for Probiotics and Prebiotics consensus statement on the scope and appropriate use of the term probiotic. *Nature reviews Gastroenterology & hepatology*, *11*(8), 506-514.

Hurtado, N. H., & Charfuelan, C. (2019). Contribución a la Caracterización y Evaluación de la Actividad Antioxidante de las Antocianinas del Fruto de Ivilan (Monnina obtusifolia HBK). *Información tecnológica*, *30*(5), 81-90.

Ibrahim, S. A., Ayivi, R. D., Zimmerman, T., Siddiqui, S. A., Altemimi, A. B., Fidan, H., ... & Bakhshayesh, R. V. (2021). Lactic acid bacteria as antimicrobial agents: Food safety and microbial food spoilage prevention. *Foods*, *10*(12), 3131.

Idrees, M., Imran, M., Atiq, N., Zahra, R., Abid, R., Alreshidi, M., ... & Ghazanfar, S. (2022). Probiotics, their action modality and the use of multi-omics in metamorphosis of commensal microbiota into target-based probiotics. *Frontiers in Nutrition*, *9*, 959941.

Kumari, D., Chaudhary, P., & Janmeda, P. (2024). Genetic Engineering and Designed Promising Preservative in Food Products. *Nonthermal Food Processing, Safety, and Preservation*, 299-324.

Lianou, A., Panagou, E. Z., & Nychas, G. J. (2016). Microbiological spoilage of foods and beverages. In *The stability and shelf life of food* (pp. 3-42). Woodhead Publishing.

Mkandawire, M., & Aryee, A. N. (2018). Resurfacing and modernization of edible packaging material technology. *Current Opinion in Food Science*, *19*, 104-112.

Mohammadian, M., Moghaddam, A. D., Sharifan, A., Dabaghi, P., & Hadi, S. (2021). Structural, physico-mechanical, and bio-functional properties of whey protein isolate-based edible films as affected by enriching with nettle (*Urtica dioica* L.) leaf extract. *Journal of Food Measurement and Characterization*, *15*(5), 4051-4060.

Naghmouchi, K., Belguesmia, Y., Bendali, F., Spano, G., Seal, B. S., & Drider, D. (2020). *Lactobacillus fermentum*: A bacterial species with potential for food preservation and biomedical applications. *Critical reviews in food science and nutrition*, *60*(20), 3387-3399.

Novoslavskij, A., Terentjeva, M., Eizenberga, I., Valciņa, O., Bartkevičs, V., & Bērziņš, A. (2016). Major foodborne pathogens in fish and fish products: a review. *Annals of microbiology*, *66*, 1-15.

Oelschlaeger, T. A. (2010). Mechanisms of probiotic actions–a review. *International journal of medical microbiology*, *300*(1), 57-62.

Pedan, V., Popp, M., Rohn, S., Nyfeler, M., & Bongartz, A. (2019). Characterization of phenolic compounds and their contribution to sensory properties of olive oil. *Molecules*, *24*(11), 2041.

Pérez-Santaescolástica, C., Munekata, P. E., Feng, X., Liu, Y., Bastianello Campagnol, P. C., & Lorenzo, J. M. (2022). Active edible coatings and films with Mediterranean herbs to improve food shelf-life. *Critical Reviews in Food Science and Nutrition*, *62*(9), 2391-2403.

Rahman, M. M., Rahaman, M. S., Islam, M. R., Rahman, F., Mithi, F. M., Alqahtani, T., ... & Uddin, M. S. (2021). Role of phenolic compounds in human disease: current knowledge and future prospects. *Molecules*, *27*(1), 233.

Ranadheera, R. D. C. S., Baines, S. K., & Adams, M. C. (2010). Importance of food in probiotic efficacy. *Food research international*, *43*(1), 1-7.

Shahidi, F., & Hossain, A. (2022). Preservation of aquatic food using edible films and coatings containing essential oils: A review. *Critical Reviews in Food Science and Nutrition*, *62*(1), 66-105.

Suresh, J. I., Janani, M. S., & Sowndharya, R. (2022). Bacterial diseases in fish with relation to pollution and their consequences—a global scenario. In *Bacterial Fish Diseases* (pp. 113-131). Academic Press.

Temiz, N. N., & Özdemir, K. S. (2021). Microbiological and physicochemical quality of strawberries (Fragaria× ananassa) coated with *Lactobacillus rhamnosus* and inulin enriched gelatin films. *Postharvest Biology and Technology*, *173*, 111433.

Vucic DM, Petkovic MR, Rodic-Grabovac BB, Stefanovic OD, Vasic SM and Comic LR 2013. Antibacterial and antioxidant activities of bilberry (*Vaccinium myrtillus* L.) in vitro. Afr. J. Microbiol. Res. 7: 5130- 5136.

Zapata, L. M., Castagnini, J. M., Quinteros, C. F., & Malleret, A. D. (2019). Desarrollo de productos de arándanos con propiedades antioxidantes y probióticas. *Ciencia, Docencia y Tecnología Suplemento*, *9*(9).

➢ *ORAL PRESENTATION*

Development of Edible Composite Film with Clove Extract and Probiotic to Improve Strawberry Shelf Life

Ali Saglam[1] (*ORCID: https://orcid.org/0000-0003-4010-8465*), Mehmet Cobanoglu[1] (*ORCID: https://orcid.org/0009-0005-9329-2528*), Merve Alan[1] (*ORCID: https://orcid.org/0009-0008-4530-1073*), Meltem Asan-Ozusaglam[1]* (*ORCID: https://orcid.org/0000-0002-3638-1306*)

*[1]University of Aksaray, Faculty of Science and Letters, Department of Molecular Biology and Genetic, Aksaray, Türkiye

*Corresponding author e-mail: meltemozusaglam@gmail.com

Abstract
Edible films with antimicrobial properties can play an important role in extending the shelf life of fruits after harvest mg/mL MBC values on both test pathogen bacteria. Then, four different edible film groups were developed using and preventing food poisoning. The aim of the study is to produce a biodegradable packaging material using clove extract and probiotic additive. The edible films were prepared by adding clove water extract (CWE) and probiotic candidate *Streptococcus thermophilus* MAS-1. For this purpose, firstly, the antimicrobial activity of CWE on *Yersinia ruckeri* and *Listeria monocytogenes* ATCC 7644 was determined. Among the tested bacteria, higher antimicrobial activity was determined against *Y. ruckeri* with inhibition zone of 10.38 mm and 12.98 mm at the concentrations of 10 µL and 20 µL. The CWE had 25 mg/mL MIC and 50 CWE and/or probiotics and their antimicrobial activity was determined using well diffusion method. Gum (G) and Gum+Probiotic (GP) did not have inhibition zone diameter on test bacteria, however, Gum+CWE+Probiotic (GEP) group had higher inhibition activity than GE group on *Y. ruckeri* (10.14 mm) and *L. monocytogenes* ATCC 7644 (8.79 mm). Finally, the strawberry fruits were covered with all developed film groups and the ability to extend the shelf life was determined for 5 days. The GEP group reduced the mass loss by % 47.89 compared to the control. The clove water extract together with probiotic strain as a coating material may be used in the development of new alternative packaging materials that can be used in the food industry.
Keywords: Antibacterial activity, Coating, Shelf life, Probiotic, *Syzygium aromaticum*

INTRODUCTION

Clove (*Syzygium aromaticum*) is native to the Maluku Islands in Indonesia but has recently been produced in many parts of the world. Clove is a tree belonging to the Myrtaceae family (Ramadan et al., 2022). Clove has been used for centuries as both a medicinal and aromatic plant and a food preservative thanks to its high antimicrobial activity (Shan et al., 2005). According to the Food and Agriculture Organization of the United Nations (FAO), approximately 1.3 billion tons of food are lost or wasted each year in the world, causing a huge economic loss to the food industry (Sawaya et al., 2017). Diseases resulting from consumption of spoiled food and pathogenic microorganisms that cause food spoilage have negative effects on human health and the food economy (Ibrahim et al., 2021). Worldwide, foodborne illness and food spoilage are most commonly caused by pathogenic microorganisms such as *Listeria monocytogenes*, *Salmonella enterica*, *Escherichia coli* and *Staphylococcus aureus*. (Zimmerman et al., 2021). Food protection and safety are among the top priorities for the food industry and consumers (Flynn et al., 2019). Contamination of food products after collection and processing due to storage and packaging in inappropriate conditions causes the spread of foodborne infections and food waste. (De Moraes et al., 2020). Food coating materials are being developed to prevent contamination of foods (Khezerlou et al., 2023). The food coating materials developed can be synthetic or organic structure. The synthetic coating materials have some toxic effects on human health (Shit et al., 2014). The organic coating materials protect human health by minimizing toxic effects (Mathiazhagan et al., 2011). Plants can be used as organic coating material. Phenolic compounds of plants can provide extra antimicrobial and antioxidant properties to the coating material (Silva-Weiss et al., 2013). Microorganisms that provide health benefits to the host when taken in sufficient amounts are defined as probiotics (Sánchez et al., 2017). *Streptococcus thermophilus* and *Lactobacillus bulgaricus* bacteria in fermented milk and dairy products have been consumed by people for centuries as probiotics, believing that they have health benefits (Boyle et al., 2006). Probiotics

can have an effect on pathogenic microorganisms. Thanks to this feature, probiotics play an important role in the prevention and treatment of infections and the regulation of intestinal flora (Oelschlaeger et al., 2010).
The aim of this study is to develop edible food coating material from clove extract to prevent food spoilage and major economic losses in the food industry. In this context, firstly, the antimicrobial activity of water extract from clove was determined against foodborne test microorganisms. Then, the edible film was developed using clove extract and probiotic strain *S. thermophilus* MAS-1 and its antimicrobial activity on pathogenic bacteria was determined. Finally, strawberry fruits were coated to determine the effect of the prepared edible film on the shelf life of the fruits.

MATERIAL METHOD

Clove spice was supplied from a herbalist in the central district of Aksaray (Aksaray-Türkiye) on 20.03.2025.

Preparation of Clove Extract

Dried clove spice was ground into powder with the help of Waring blender and then stored in brown glass bottles in a dry and dark environment until use. Then, the powdered clove spice was extracted with distilled water in a hot water bath (75C˚) for 6 hours per day (2 days). Then, distilled water was evaporated from the clove water extract (CWE). The extract was dissolved with dimethyl sulfoxide (DMSO) and sterilized with a 0.45µm filter.

Determination of Antibacterial and Activity of CWE

The antimicrobial activity of CWE was determined by disc diffusion test. *L. monocytogenes* ATCC 7644 and *Y. ruckeri* (Tryptic-Soy-Broth (TSB)/Agar) were used as test microorganisms. The test microorganisms (100 µL) prepared at a concentration of 0.5 Mcfarland ($1x10^8$ CFU/mL) were inoculated on solid media. After sterile discs (Whatman No: 1, Diameter: 6 mm) were placed on the solid media, CWE extract was dropped onto sterile discs in 3 replicates at 10 µL and 20 µL concentrations. Penicillin (P: 10 µg/disc) antibiotic discs were used as positive control of the test microorganisms; *L. monocytogenes* was incubated at 37°C and *Y. ruckeri* at 25°C in the oven for 24 hours. After incubation, the diameters of the inhibition zones around the discs were measured and recorded. The values obtained were presented with their means and standard deviations.

Determination of MIC and MBC

The micro-dilution method was used to determine MIC and MBC values of the CWE. The media suitable for each microorganism were added to the tubes. Then, CWE was added and two-fold dilutions were made. The prepared microorganisms (adjusted to 0.5 Mcfarland) were added and incubated for 24 hours at a temperature suitable for each microorganism. The concentrations at which no microbial growth occurred after incubation were recorded as MIC values. Then, the samples taken from tubes with different concentrations were dropped onto agar media suitable for each microorganism using the spot drip method and incubated for 24 hours at suitable temperatures. The concentrations at which no microbial growth occurred after incubation were recorded as MBC values of the extract.

Preparation of Edible Film

CWE and *S. thermophilus* MAS-1 probiotic strain were used to develop natural edible film. Guar gum (1%), glycerol (3%) and CWE extract (10%) were used in the preparation of the edible film. Guar gum without extract and probiotic strain was used as control group. Probiotic-free groups were supplemented with distilled water. Probiotic-containing groups were supplemented with probiotic culture after 18 hours of incubation.

Determination of Antimicrobial Activity of Edible Film

The agar diffusion method was used to test the antimicrobial activity of the prepared edible film in 4 groups. These groups were Control (C), Gam (G), Gam + Extract (GE), Gam + Probiotic, Gam + Extract + Probiotic (GEB). The test microorganisms (100 µL) prepared at a concentration of 0.5 Mcfarland were spread on the agar surface. Then, 6 mm diameter wells were opened on the agar surface and the edible film groups (100 µL) was filled into the well. The Petri dishes were incubated at appropriate temperatures. At the end of incubation, the inhibition zone diameters formed around the well were measured and recorded.

Composite Edible Coating of Strawberry Fruit

Strawberries obtained from a local market in Aksaray/Central district were used to determine the effect of the coating material on the shelf life of the fruits. Three strawberries were selected for each group according to their smell, color and size. The selected strawberries were washed with distilled water and dried, then the strawberries were weighed on a precision scale. According to the experimental groups, the strawberries were dipped into the liquid renewable film and kept for 2 minutes. After the strawberries dipped into the renewable film were drained, the storage parameters were evaluated at room temperature (25°C). The control group was washed with distilled water only and dried, then all the fruits stored in the groups were weighed for 5 days and photographed every day. The percentage weight loss of the fruits was calculated, and the results were recorded.

RESULTS AND DISCUSSION

The antibacterial activity of CWE was investigated on food and fish pathogens. The inhibition zone diameters of the extract on test microorganisms are given in Table 1. The inhibition zone diameter of CWE at the concentration of 10 µL and 20 µL on *L. monocytogenes* ATCC 7644 was determined as 8.81 mm and 12.48 mm. CWE at a concentration of 10 and 20 µl inhibited *Y. ruckeri* with zone diameter of 10.38 mm and 12.98 mm.

Table 1 CWE Inhibition Zone Diameters

Disc Diffusion Test (mm)			
Microorganisms	**10 µL**	**20 µL**	**P (10 µg/disc)**
L. monocytogenes ATCC 7644	8.81±0.40	12.48±0.81	8.83±0.71
Y. ruckeri	10.38±0.47	12.98±0.10	21.4±1.56

MIC and MBC values of CWE are given in Table 2. CWE had 25 mg/mL and 50 mg/mL concentrations of MIC and MBC valuea on *Y. ruckeri* and *L. monocytogenes* ATCC 7644.

Table 2 MIC and MBC Values of CWE

	Micro-Dilution Test (mg/mL)	
Microorganisms	**MIC**	**MBC**
L. monocytogenes ATCC 7644	25	50
Y. ruckeri	25	50

Antimicrobial Activity of Edible Film

The inhibition zone diameter values of the prepared edible films on the test bacteria varied between 8.44 mm and 10.14 mm. Gum (G) and gum+probiotic (GB) edible film did not give any zone on the tested microorganisms. However, gum + CWE (GE) and gum + extract + probiotic (GEB) against *L.monocytogenes* ATCC 7644 had 8.44 mm and 8.79 mm inhibition zone diameter. Against *Y. ruckeri*, GE had 9.57 mm inhibition zone diameter and GEB had 10.14 mm inhibition zone diameter. The antimicrobial activity results of edible film groups are given in Table 3. An increase in antimicrobial activity was observed in the GEB group compared to the GE group due to the synergistic effect of the extract and bacteria.

Table 3 BBWE and Antimicrobial Activity of Edible Film Containing Probiotics

	Inhibition zone diameter (mm)			
Microorganisms	**G**	**GE**	**GB**	**GEB**
L.monocytogenes ATCC 7644	0	8.44±0.17	0	8.79±0.28
Y. ruckeri	0	9.57±0.41	0	10.14±0.61

Composite film coating of strawberry fruits

The percentage weight loss was calculated in order to determine the storage period and shelf life of strawberry fruits after coating. Table 4 shows the percentage weight losses of both the control group and the coated groups. On the 5th day of storage, the highest percentage weight loss among strawberry fruits belongs to the control group (78.67%) and the lowest percentage weight loss belongs to the GEB group (39.66%). During the 5-day storage period, the weight loss of GEB group was determined as 7.51, 25.58, 33.21, 44.9 and 47.89%, respectively, compared to the control. Images of composite coated strawberry fruits for 5 days are given in Figure 1. The deterioration was observed during storage in the first days in the control (C) and G groups and in the later days in the GEB group.

Table 4 Percent Weight Loss of Strawberry Fruits

	Weight Loss of Strawberry Samples (%)					
	Days					
Groups	**0**	**1**	**2**	**3**	**4**	**5**
C	-	13.88±3.53	35.20±1.55	48.49±0.93	66.31±3.89	81.65±3.02
G	-	6.06±1.50	19.03±4.55	28.04±6.19	42.54±10.94	59.49±12.52
GE	-	7.95±2.15	19.16±1.87	28.07±1.30	41.33±1.85	50.03±6.05
GP	-	9.93±3.13	21.79±4.77	31.47±7.97	44.43±8.47	56.18±5.36
GEP	-	6.37±2.34	9.62±1.03	15.28±1.68	21.41±3.59	33.76±7.32

-:No inhibition zone diameter

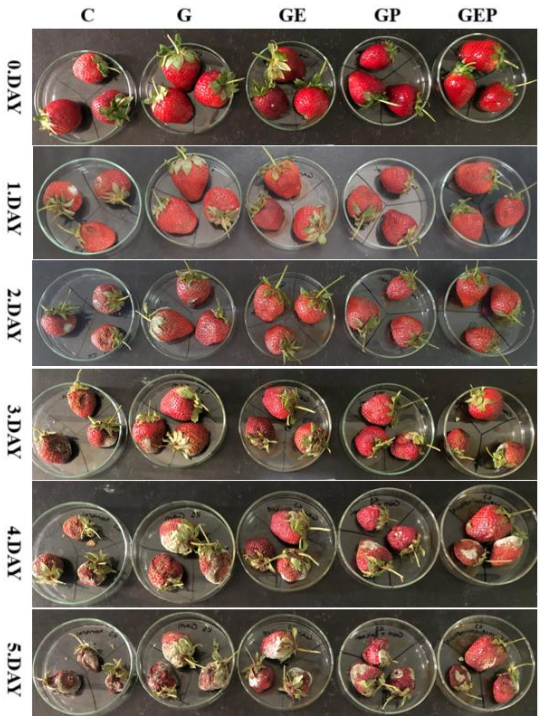

Figure 1. Image of strawberry fruits coated and uncoated with film groups on day 0 and day 5

CONCLUSION

Food spoilage causes major economic losses in the world as well as in Türkiye. It is recommended to package and cover foods to store and extend their shelf life and to prevent contamination. In this study, CWE extract showed good biological activity on test microorganisms. CWE is an organic structure and is suitable for use as a natural antimicrobial agent for renewable film. The renewable film was supported with probiotic strain to develop antimicrobial activity. The prepared GEP edible film increased the shelf life and quality of strawberries, especially thanks to its antimicrobial properties and probiotic content. According to the obtained results, CWE has the potential to be used commercially as a food coating material, to extend the shelf life of foods.

REFERENCES

Boyle, R. J., Robins-Browne, R. M., & Tang, M. L. (2006). Probiotic use in clinical practice: what are the risks? *The American journal of clinical nutrition*, *83*(6), 1256-1264.

De Moraes, J. O., Hilton, S. T., & Moraru, C. I. (2020). The effect of pulsed light and starch films with antimicrobials on Listeria innocua and the quality of sliced cheddar cheese during refrigerated storage. *Food Control*, *112*, 107134.

Flynn, K., Villarreal, B. P., Barranco, A., Belc, N., Björnsdóttir, B., Fusco, V., ... & Jörundsdóttir, H. Ó. (2019). An introduction to current food safety needs. *Trends in food science & technology*, *84*, 1-3.

Ibrahim, S. A., Ayivi, R. D., Zimmerman, T., Siddiqui, S. A., Altemimi, A. B., Fidan, H., ... & Bakhshayesh, R. V. (2021). Lactic acid bacteria as antimicrobial agents: Food safety and microbial food spoilage prevention. *Foods*, *10*(12), 3131.

Khezerlou, A., Zolfaghari, H., Forghani, S., Abedi-Firoozjah, R., Alizadeh Sani, M., Negahdari, B., ... & McClements, D. J. (2023). Combining non-thermal processing techniques with edible coating materials: an innovative approach to food preservation. *Coatings*, *13*(5), 830.

Mathiazhagan, A., & Joseph, R. (2011). Nanotechnology-a New prospective in organic coating-review. *International Journal of Chemical Engineering and Applications*, *2*(4), 225.

Oelschlaeger, T. A. (2010). Mechanisms of probiotic actions–a review. *International journal of medical microbiology*, *300*(1), 57-62.

Ramadan, M. F. (Ed.). (2022). *Clove (Syzygium aromaticum): Chemistry, Functionality and Applications*. Academic Press.

Sánchez, B., Delgado, S., Blanco-Míguez, A., Lourenço, A., Gueimonde, M., & Margolles, A. (2017). Probiotics, gut microbiota, and their influence on host health and disease. *Molecular nutrition & food research*, *61*(1), 1600240.

Sawaya, W. N. (2017). Impact of food losses and waste on food security. *Water, energy & food sustainability in the middle east: The sustainability triangle*, 361-388.

Shan, B., Cai, Y. Z., Sun, M., & Corke, H. (2005). Antioxidant capacity of 26 spice extracts and characterization of their phenolic constituents. Journal of agricultural and food chemistry, 53(20), 7749-7759.

Shit, S. C., & Shah, P. M. (2014). Edible polymers: challenges and opportunities. *Journal of Polymers*, *2014*(1), 427259.

Silva-Weiss, A., Ihl, M., Sobral, P. D. A., Gómez-Guillén, M. C., & Bifani, V. J. F. E. R. (2013). Natural additives in bioactive edible films and coatings: functionality and applications in foods. *Food Engineering Reviews*, *5*, 200-216.

United Nations. (2022). Sustainable Development Goals. Goal 2: zero Hunger.

Zimmerman, T., Siddiqui, S. A., Bischoff, W., & Ibrahim, S. A. (2021). Tackling airborne virus threats in the food industry: A proactive approach. *International Journal of Environmental Research and Public Health*, *18*(8), 4335.

➢ *ORAL PRESENTATION*

Toxic Traces of Some Heavy Metals

Nurbanu Edi[1] (*ORCID: https://orcid.org/0009-0008-2970-5705*),
Melek Zor[2*](*ORCID: https://orcid.org/0000-0002-5795-218X*)

[*1] Agrı Ibrahim Cecen University, Department of Food Engineering, 04000 Ağrı, Türkiye.
[2] Agrı Ibrahim Cecen University, Department of Gastronomy and Culinary Arts, School of Tourism and Hotel Management, 04000 Ağrı, Türkiye.

*Corresponding author e-mail: mzor@agri.edu.tr

Abstract

Heavy metals are inorganic elements that are released into the environment by natural and anthropogenic processes and can have serious toxic effects on biological systems, even at low concentrations. Among these metals, lead, mercury, cobalt, cadmium and arsenic are reported to have the most widespread and dangerous effects in terms of environmental pollution and public health. Dietary heavy metals accumulate in the body and cause oxidative stress, cell damage and organ dysfunction. These elements, which are particularly neurotoxic and carcinogenic, pave the way for serious health problems such as cardiovascular disease, kidney failure, weakening of the immune system and, in the long term, reproductive problems. Sensitive groups such as children, the elderly and pregnant women are more vulnerable to these elements. This study has attempted to identify the heavy metal pollution caused by natural and anthropogenic activities and its effects on the environment and human health. It is believed that a better understanding of this process will be an important step in preventing future risks.

Keywords: Heavy metals, toxicity, soil pollution, food poisoning

INTRODUCTION

Nutrition is a necessary activity for people to continue their lives. For centuries, people have eaten to sustain their lives. In recent times, however, people want to obtain various health benefits from the food they eat, in addition to sustaining their lives through nutrition. For these reasons, healthy eating, which has become popular in recent years, has increased the care people take in their food choices. Eating fruit and vegetables is one of the cornerstones of a balanced diet (Barbaros and Kabaran, 2014). The richness of various vitamins, minerals, phytochemicals and fibre in the composition of fruit and vegetables has been shown to have positive health effects. The fact that these compounds found in fruits and vegetables have metabolic functions such as reducing oxidative stress, improving lipoprotein profile, lowering blood pressure and increasing insulin sensitivity increases the importance of consuming these foods (Dauchet and ark., 2006). In addition to these health benefits, a diet based on fruit and vegetables should be considered in order to prevent obesity, which is recognised as one of the major health problems in the world today. Several studies have shown that the Mediterranean diet, which is rich in plant foods such as vegetables and fruit, has a protective effect against obesity (Panagiotakos et al., 2006). Consuming sufficient amounts of fruit and vegetables reduces the risk of many chronic diseases, such as cancer, heart disease and diseases of the digestive system, and also helps to boost the immune system, reduce stress, delay the ageing process and improve the health of the skin (Sezgin, 2014). However, nowadays it has become difficult to find natural and reliable foods that have these effects. In addition to the positive health effects mentioned above, the lack of food reliability can lead to some illnesses and poisoning when eating fruit and vegetables. The reliability of the foods we consume is important in terms of the risks they may pose to our health. Non-food chemicals, which are mixed into food from various sources during the production phase or added externally for a specific purpose, have negative effects on human health (Erkmen, 2010). In this context, the choice of safe food should be considered in terms of the maximum efficiency we can get from food. We can define safe food as food that has not lost its nutritional value, is free from physical, chemical and biological hazards, is not contaminated and is not spoiled (Erkmen, 2010).

Health problems associated with the consumption of fruit and vegetables can generally be divided into allergies and poisoning. Food allergy is a condition in which foods that are normally harmless to the body are recognised as foreign by the immune system and are rejected (Öztürk and Besler, 2008). Food allergies that can occur in childhood usually present with mild symptoms such as abdominal pain, diarrhoea, skin rashes and difficulty

breathing (Tercanlı and Atasever 2021). Food containing genetically modified organisms also poses a risk to human health. Uncontrolled practices used to extend the shelf life of fruit and vegetables, improve their sensory properties and increase their yield can cause various diseases in the long term (Ergin and Yaman 2013). Food can also be accidentally or fraudulently contaminated with micro-organisms and harmful substances. This can lead to illnesses such as food poisoning and toxin infections (Gallo et al., 2020). Food poisoning, the most common of these diseases, is one of the health problems caused by the industrialised food sector. These diseases cause about half a million deaths worldwide each year and are generally preventable (Komorowski et al., 2024). From farm to fork, food contamination can occur at any stage of the production chain (Gallo et al., 2020). Food poisoning is an illness that develops in the body as a result of eating contaminated food. The most common symptoms are nausea and vomiting, diarrhoea, abdominal pain, fever, weakness, headache and dizziness (Çağlarırmak and Hepçimen, 2010).

In addition to food poisoning caused by micro-organisms, exposure to heavy metals is also a cause for concern. The uncontrolled use of chemical products and the accumulation of industrial and agricultural waste are thought to be the main reasons for the presence of toxic elements in plants, which is one of the main reasons for heavy metal exposure in the human body through food (Antoniadis vd., 2019).

Heavy metals can be found in nature through processes such as mining, industrial waste, agricultural practices and the burning of fossil fuels. One example of naturally occurring heavy metal pollution is soil-based heavy metal pollution. Soil-based heavy metal pollution, which mainly affects agricultural products that provide the vast majority of the food we consume, is one of the most serious and difficult types of pollution to control. Examples of heavy metal pollution caused by human activities include the unintentional use of pesticides or the unfiltered application of industrial waste to the soil. The accumulation of heavy metals in soil directly affects many biochemical reactions, especially nitrification, mineralisation of organic matter, enzyme activity and respiration (Seven et al., 2018). In addition, the anthropogenic sources of heavy metal contamination are very diverse and cover many different areas of activity. Among these sources, mining activities to extract and process mineral deposits underground are important. In addition, the widespread use of pesticides, chemical fertilisers and herbicides to control weeds can lead to the mixing of heavy metals with soil and water. Polluted water released into the environment without adequate treatment by small-scale industries and leather processing (tanning) industries can pollute agricultural land and water resources when used for irrigation. In addition, the uncontrolled use of organic waste, such as municipal waste, as fertiliser can lead to accumulation of heavy metals in soil and plants (Nizamlıoğlu and Teyin, 2021).

Heavy metals are a subset of potentially toxic elements that are commonly found in the earth's crust. In general, based on their potential to compromise human health, these metals can be categorised into three distinct groups: (a) elements that are deemed essential, including copper (Cu), zinc (Zn), molybdenum (Mo), chromium (Cr) and selenium (Se); (b) elements that are considered essential, such as manganese (Mn), nickel (Ni) and vanadium (V); and (c) elements that are classified as potentially toxic, including cadmium (Cd), lead (Pb) and mercury (Hg) (Gallo et al., 2020).

The underlying mechanism by which heavy metals exert their deleterious effects on the human body involves the disruption of intracellular metabolic pathways. These disorders have been shown to be a causative factor for a number of serious diseases, including, but not limited to, DNA damage, increased oxidative stress, autoimmune diseases (ulcerative colitis, Crohn's disease, rheumatism), kidney diseases, migraine, Alzheimer's disease, Parkinson's disease and cancer (Özbolat and Tuli, 2016). The toxic substances that present a significant threat to public health, in this case through poisoning, include lead, mercury, arsenic, cadmium and copper. These heavy metals are present in soil, water and plants and have been identified as potential causative agents in cases of poisoning (Özkaya and Cömert, 2008). The ingestion of foodstuffs contaminated by industrial waste, paint, pesticides, electronic waste and environmental pollution caused by some plant products results in the entry of heavy metals into the human body. This process of bioaccumulation occurs as a result of long-term exposure to contaminated foodstuffs or direct consumption of foodstuffs with elevated levels of contamination. The resultant condition is known as heavy metal poisoning. The accumulation of these metals in the body can result in the onset of serious diseases, including thyroid dysfunction, neurological disorders, autism, and infertility, and can even lead to fatal outcomes. The toxic effects of heavy metals in the body can vary depending on the metal's concentration, chemical structure, solubility value, structure of the metal ion and the way it is taken into the body (Özbolat and Tuli, 2016).

It is imperative to comprehend the sources, effects and methods of preventing contamination by heavy metals, particularly in fruits and vegetables. This study aims to elucidate the heavy metals that can cause poisoning and, consequently, diseases in the human body, along with their effects on human health.

Toxic Traces of Some Heavy Metals

Copper (Cu)

Copper is a metal that occurs naturally in the earth's crust, either as a free element or in the form of an ore. The applications of this metal are extensive, encompassing diverse sectors, including industry and agriculture. The human body is exposed to copper through various means. Ingestion of copper-containing food or water, or inhalation of copper-laden air, can result in copper entering the body (Özbolat and Tuli, 2016). The effect of copper on living things is dependent on the chemical structure of the metal and the type of living thing in question. While copper exerts a toxic effect on simple organisms, it constitutes a fundamental structural component of more complex life forms. Consequently, copper is employed as a means of eradicating organisms that are detrimental to agricultural produce (Seven et al., 2018). As well as being a constituent of our diet, copper is also an essential component of various enzymes that support the immune system and control redox status (Keskın vd., 2024). Copper is a pivotal element in the composition of hair, the flexibility of skin, and the structure of bones within the human body. In addition to its structural functions, copper has antioxidant properties and plays an important role in the use of iron (Özbolat and Tuli, 2016). In order to demonstrate these properties, it is necessary to establish equilibrium in the transport and storage of copper within the liver and brain. The disruption of this balance has been linked to the development of neurodegenerative diseases, such as Menkes and Wilson diseases, within the brain (Erbay and Karatoprak, 2023). Exposure to elevated levels of elemental copper, particularly via the oral route, has been demonstrated to induce a range of physiological responses, including nausea, vomiting, diarrhea, abdominal discomfort, and diffuse muscle aches. Prolonged exposure to this substance has been shown to potentially culminate in the onset of mental health disturbances, comatose states, and even fatal outcomes. The World Health Organization (WHO) has established a maximum daily copper intake of 12 mg/day for men, and 10 mg/day for women (WHO, 1996).

Cadmium (Cd)

Cadmium has been shown to have a higher solubility in comparison to other heavy metals. The uncontrolled use of fertilisers and pesticides in recent years has facilitated the contamination of water and soil by this element. Furthermore, the presence of cadmium in the atmosphere has been linked to emissions from cigarette smoke and industrial chimneys (Seven et al., 2018). The utilisation of fertilisers has been demonstrated to result in the accumulation of hazardous heavy metals within the soil over an extended period of application. This phenomenon has been shown to increase the risk of Cd accumulation, particularly in plant life (Gallo et al., 2020). The kidneys are the organ most affected by high levels of cadmium exposure, and numerous studies have reported that levels of cadmium accumulating in the kidneys to 200 mg/kg cause irreversible damage to the kidneys. In addition to this effect, cadmium has also been reported to cause an increase in blood pressure and liver failure. The element has been definitively linked to an increased risk of prostate and lung cancer, in addition to its role in the development of numerous other types of cancer (Kara and Kara, 2018). Cadmium is a highly toxic substance that can enter the food chain, thus posing a serious problem in terms of human health and safety. Excessive cadmium contamination in foodstuffs has been demonstrated to have deleterious effects on vital organs, including the lungs and liver, with associated risks of cancer and severe diseases. Furthermore, it has been shown to cause serious kidney damage and osteoporosis (Gallo et al., 2020).

Lead (Pb)

Lead, a known causative agent of environmental pollution, is predominantly produced by the combustion of gasoline utilised by motor vehicles. The tetraethyl lead compound, a by-product of this process, subsequently contaminates both water and soil (Çağlarırmak and Hepçimen, 2010). Marine organisms and agricultural products that are contaminated in this way pose a risk to human health. The effects of lead poisoning may vary depending on age and physiological condition. While the consequences of lead poisoning in adults may result in brain damage and death, the effects of lead exposure in infants and children include mental retardation, high blood pressure, anaemia and peripheral nerve damage (Anonymous, 2008). Toxic symptoms have been reported to occur at levels of 40-80 µg Pb/100 mL in children and 80 µg Pb/100 mL in adults.

Mercury (Hg)

Mercury (Hg) is the only metallic element that is liquid at room temperature under standard temperature and pressure. Mercury occurs naturally and can be found as an ore in the earth (Okeke et al., 2024). Furthermore, mercury is considered to be one of the most toxic heavy metals commonly found in the environment, a consequence of both anthropogenic and natural activities, including fossil fuel combustion and volcanic eruptions (Zhou et al., 2024). Mining activities, particularly gold mining, have been identified as a significant contributor to mercury emissions (Okeke et al., 2024). Following absorption through the respiratory or

digestive tracts or the skin, mercury-containing compounds dissociate, resulting in the formation of mercury ions upon entering the bloodstream. The mercury ions then accumulate in the brain and kidney, causing damage to multiple organs in the kidney, nervous, cardiovascular and musculoskeletal systems (Gao et al., 2022). Mercury shows its effect by being included in human nutrition through its presence in contaminated marine life due to environmental pollution brought by industrial wastes and in soil and agricultural products due to the frequent use of agricultural drugs it contains. One of the most emphasized aspects is the damage this element can cause at the neurological level (Gallo et al., 2020).

The toxicity of mercury is dependent upon its chemical structure. It is categorised into three distinct groups: metallic, inorganic and organic. Metallic mercury, in particular, has the capacity to evaporate at room temperature and infiltrate all tissues, including the brain, upon inhalation (Özbolat and Tuli, 2016). Inorganic mercury compounds are known to circulate within the body via blood cells and plasma proteins, with the potential to accumulate in various organs, glands, and the central nervous system. Organic mercury molecules, on the other hand, are absorbed through the gastrointestinal system and rapidly disseminate throughout the body (Özbolat and Tuli, 2016). Mercury has a brief half-life due to its rapid distribution within the circulatory and digestive systems. Consequently, in order to detect exposure to mercury, it is necessary to measure levels in urine and blood. It is imperative to note that all chemical forms of mercury have the potential to induce toxic symptoms. The consequences of mercury poisoning are wide-ranging, affecting the nervous system, respiratory system, immune system, kidneys, and oral and dental health (Akcan and Dursun, 2008). Acute mercury poisoning is characterised by symptoms including vomiting blood, severe diarrhoea and abdominal pain. Chronic mercury poisoning, on the other hand, is characterised by a range of symptoms, including a rash, itching, kidney damage, tremors, gingivitis, and psychological changes. In pregnant women, chronic mercury poisoning can result in miscarriages or congenital anomalies (Arslan et al., 2018). In severe cases of Hg poisoning, paresthesias are seen in the distal extremities and around the lips, and abnormal combined sensations, narrowed visual fields, hearing loss, and cerebellar ataxia are evident. Conversely, in mild cases of Hg poisoning, paresthesias are predominantly observed in the distal extremities and around the lips. The symptoms of sensory disorders manifest as abnormal combined sensations, systemic increase in tactile thresholds, and mild incoordination of the extremities. In such cases, the median hair Hg concentration is recorded as 37.0 ppm (range 10-75 ppm). In moderate cases of Hg poisoning, not only sensory disturbances but also visual or auditory disturbances are seen (Ekino et al., 2023). The Food and Agriculture Organization (FAO) and the World Health Organization (WHO) have established a maximum acceptable limit of 0.5 mg/kg for mercury in food (Erkmen, 2010).

Arsenic (As)

Arsenic-derived compounds are categorised into two distinct groups, depending on the presence or absence of carbon bonds in their structure. The toxicity of these compounds, which are classified as either organic or inorganic, varies according to their chemical structure, with inorganic species exhibiting a higher degree of toxicity (Mandal and Suzuki, 2002). Arsenic, in isolation, possesses negligible water soluble qualities. However, the solubility of the salts it forms with other elements in water enables exposure of individuals to these compoundsn (Bakan, 2019). These metal compounds, which target a wide range of functional effect groups in the body, demonstrate biological effects depending on numerous factors, including the dose administered, the target tissue and the exposure time (Anonymous, 2008). Inorganic arsenic is rapidly absorbed from the small intestine, with its primary mechanism of action being to affect metabolism by inactivating enzymes. Although the symptoms of arsenic poisoning are mostly the same (fever, abdominal pain, vomiting, diarrhoea, dry mouth, thirst), in addition to these symptoms, enlarged liver, anaemia and the formation of dark pigments have been found in infants. The analysis of hair and nail tissue reveals the presence of arsenic, with a notable accumulation in these tissues. In cases of water-related poisoning, symptoms such as skin shedding, decreased reflexes and protein in the urine have been observed in adults (Çağlarırmak and Hepçimen, 2010). Arsenic, when ingested orally, exerts a toxic effect when administered in doses of 1 mg or more. With regard to its accumulation in the body, it is widely accepted that doses ranging from 10-90 mg result in a toxic effect, while doses of 100-200 mg are known to be lethal (Anonymous, 2008).

CONCLUSION

The issue of heavy metal toxicity has become a significant global public health concern, primarily due to environmental contamination and anthropogenic activities. The dissemination of heavy metals such as lead, mercury, cadmium, arsenic, and others into the environment, their subsequent entry into the food chain, and the deleterious effects they exert on human health necessitate heightened public awareness and urgent

intervention. The scientific community has demonstrated that these metals are neurotoxic, carcinogenic, disrupt reproductive health and cause serious damage to the cardiovascular system in the long term. The consequences of these metals, particularly on vulnerable demographics, are of paramount importance in shaping health policies. Mitigation strategies may be implemented through regulatory measures, such as the supervision of industrial activities and the enhancement of waste management practices. Additionally, sustainable agricultural and food production systems have been identified as pivotal in curtailing the dissemination of these contaminants. The periodic analysis of food and water resources, the implementation of dietary interventions to reduce biological toxicity, and the integration of technologies to enhance environmental cleanliness are all effective measures that can contribute to the reduction of heavy metal risks. Furthermore, scientific studies that will provide a better understanding of toxicity mechanisms can contribute to the development of new protection and treatment strategies. Adoption of effective strategies to mitigate heavy metal toxicity is imperative to arrest the escalating damage to human health and the environment. It is therefore incumbent upon individuals, societies and organisations to collaborate in addressing this issue and to organise environmental, industrial and health policies in a sustainable manner.

REFERENCES

Akcan, A. B., & Dursun, O. (2008). Civa zehirlenmeleri. Güncel Pediatri, *6*(3), 72-75.

Anonymous, 2008. Ağır metallerin insan sağlığına etkileri. http://www.doktorre.net/forum/arsiv-konu18053.0-agir-metallerin-insan-sagligina-etkiler.html

Antoniadis, V., Shaheen, S. M., Levizou, E., Shahid, M., Niazi, N. K., Vithanage, M., ... & Rinklebe, J. (2019). A critical prospective analysis of the potential toxicity of trace element regulation limits in soils worldwide: Are they protective concerning health risk assessment?-A review. Environment International, 127, 819-847.

Arslan, S., Yenilmez, K., & Özkan, C. (2018). Civa Zehirlenmesi ve Tedavisi. *Turkiye Klinikleri* Veterinary Sciences-Internal Medicine-Special Topics, 4(3), 34-38.

Bakan, M. (2019). Arsenik metabolizması ve arsenolipid biyosentezi. Mediterranean Fisheries and Aquaculture Research, 2(3), 83-88.

Barbaros, B., & Kabaran, S. (2014). Akdeniz diyeti ve sağlığı koruyucu etkileri. Beslenme ve Diyet Dergisi, 42(2), 140-147.

Çağlarırmak, N., & Hepçimen, A. Z. (2010). Ağır Metal Toprak Kirliliğinin Gıda Zinciri ve Đnsan Sağlığına Etkisi. Akademik Gıda, 8(2), 31-35.

Dauchet, L., Amouyel, P., Hercberg S., & Dallongeville, J. (2006). Fruit and vegetable consumption and risk of coronary heart disease: a meta-analysis of cohort studies. J Nutr 136, 2588-2593

Ekino, S., Sato, K., Kurashige, M., Morii, E., Uozumi, H., & Susa, M. (2023). Pathology of human organic mercury poisoning: Lessons from an autopsy case. Journal of the Neurological Sciences, 455, 122802.

Erbay, M., & Karatoprak, N. (2023). Bakır Metabolizması Bozuklukları. Türk Radyoloji Seminerleri, 11(1).

Ergin, S. Ö., & Yaman, H. (2013). Genetiği değiştirilmiş gıdalar ve insan sağlığı üzerine etkileri. Gümüşhane Üniversitesi Sağlık Bilimleri Dergisi, 2(2), 261-274.

Erkmen, O. (2010). Gıda kaynaklı tehlikeler ve güvenli gıda üretimi. Çocuk Sağlığı ve Hastalıkları Dergisi, 53(3), 220-235.

Gallo, M., Ferrara, L., Calogero, A., Montesano, D., & Naviglio, D. (2020). Relationships between food and diseases: What to know to ensure food safety. Food Research International, 137, 109414.

Gao, Z., Wu, N., Du, X., Li, H., Mei, X., & Song, Y. (2022). Toxic nephropathy secondary to chronic mercury poisoning: clinical characteristics and outcomes. Kidney International Reports, 7(6), 1189-1197.

Kara, E. E., & Kara, E. (2018). Toprakta ağır metal kirliliğinin insan sağlığına etkileri ve çözüm önerileri. Türk Bilimsel Derlemeler Dergisi, 11(1), 56-62.

Keskın, A., Acı, R., & Arı, M. (2024). SARS-COV-2 enfeksiyonu patofizyolojisinde çinko, bakır ve selenyum düzeylerinin önemi. Uluslararası Sağlık Bilimlerinde Disiplinler Arası Etkileşim Dergisi, *3*(01), 27-03.

Komorowski, A. S., Patel, P., & Mack, D. P. (2024). Food poisoning versus food allergy, Editor(s): Scott H. Sicherer, Encyclopedia of Food Allergy (First Edition), Elsevier, 840-861p. ISBN 9780323960199, https://doi.org/10.1016/B978-0-323-96018-2.00010-9.

Mandal, B. K., & Suzuki, K. T. (2002). "Arsenic round the world: a review." Talanta, 58(1), 201-235.

Nizamlıoğlu, H. F., & Teyin, G. (2021). Gıdalarda ağır metal kontaminasyonları. Gıda Alerjenleri, Bulaşanları ve Halk Sağlığı Açısından Önemi, E-ISBN: 978-605-74827-4-7, Trabzon, Türkiye.

Okeke, E. S., Nwankwo, C. E. I., Owonikoko, W. M., Emencheta, S. C., Ozochi, C. A., Nweze, E. J., Okeke, V. C., Nwuche, C. O., & Enochoghene, A. E. (2024). Mercury's poisonous pulse: Blazing a new path for aquatic conservation with eco-friendly mitigation strategies. Science of the Total Environment, 957, 177719.

Özbolat, G., & Tuli, A. (2016). Ağır metal toksisitesinin insan sağlığına etkileri. Arşiv Kaynak Tarama Dergisi, 25(4), 502-521.

Özkaya, F. D., & Cömert, M. (2008). Gıda zehirlenmelerinde etken faktörler. Türk Hijyen ve Deneysel Biyoloji Dergisi, 65(3), 149-158.

Öztürk, M., & Besler, H. T. (2008). Besin alerjileri. Ankara: Klasmat Matbaacılık.

Panagiotakos D.B., Chrysohoou C., Pitsavos C., & Stefanadis C. (2006). Association between the prevalence of obesity and adherence to the Mediterranean diet: the ATTICA study. Nutrition, 22, 449-456.

Seven, T., Can, B., Darende, B. N., & Ocak, S. (2018). Hava ve toprakta ağır metal kirliliği. Ulusal Çevre Bilimleri Araştırma Dergisi, 1(2), 91-103.

Sezgin, A. C. (2014). Meyve, sebze ve sağlımız. Journal of Tourism & Gastronomy Studies, 2(2), 46-51

Tercanlı, E., & Atasever, M. (2021). Besin Alerjileri. Academic Platform Journal of Halal Lifestyle, 3(1), 31-53.

WHO, (1996). "Trace Elements in Human Nutrition and Health", World Health Organization, Geneva.

Zhou, J., Li, J., Xu, X., Long, S., Cui, N., Zhang, Y., Shi, L., Zhou, J. (2024). Imaging gastrointestinal damage due to acute mercury poisoning using a mitochondria-targeted dual near-infrared fluorescent probe. Journal of Hazardous Materials, 470, 134269.

➢ *ORAL PRESENTATION*

Yeni bir Schiff bazı temelli rutenyum(II) aren kompleksinin sentezi ve meme kanseri hücrelerine karşı sitotoksik aktivitesi

Serdar Batıkan Kavukcu1* (https://orcid.org/0000-0002-1168-5012)

*1 Ege Üniversitesi, Fen Fakütlesi, Kimya Bölümü, İzmir, Türkiye

*Sorumlu yazar e-posta: serdar.batikan.kavukcu@ege.edu.tr

Özet

Schiff bazları, antikanser özellikler sergileyen önemli bir bileşik sınıfıdır. Bu özellikler genellikle kanser hücrelerinin çoğalmasını (proliferasyon) engelleme ve programlanmış hücre ölümü olan apoptozu tetikleme mekanizmaları üzerinden gerçekleşir. Ayrıca, bazı Schiff bazları DNA ile etkileşime girerek veya çeşitli enzimleri inhibe ederek de antikanser etki gösterebilirler. Bu çalışmada schiff bazı ligandı taşıyan yeni bir rutenyum (II) aren kompleksi sentezlenerek ^{1}H NMR ve ^{13}CNMR dahil olmak üzere çeşitli spektroskopik teknikler kullanılarak karakterize edilmiştir. Schiff bazı ligandı, etilendiamin ve vanilinin kondenzasyon reaksiyonundan elde edilmiştir. Sentezlenen Ru(II) kompleksi, [(η^6-*p*-simen)Ru(Schiff Bazı)Cl]Cl ortam koşulları altında iyi bir kararlılık sergilemiştir. Sitotoksik aktivitesi, MTT deneyi kullanılarak MCF-7 insan meme kanseri hücre hattı ve MCF-10a insan meme hücre hattına karşı in vitro olarak değerlendirilmiştir. Ru(II) aren komleksi, Schiff bazı ligandına kıyasla daha iyi sitotoksik aktivite göstermiştir. Bu bulgular, Schiff bazı temmelli Ru(II) aren komplekslerinin yeni antikanser ajanlar olarak umut verici bir potansiyele sahip olduğunu ve daha fazla araştırılması gerektiğini göstermektedir.

Anahtar Kelimeler: Rutenyum(II) aren kompleksi, Schiff bazı ligandı, Meme kanseri, Sitotoksisite, Antikanser aktivite.

Synthesis of a novel Schiff base based ruthenium(II) arene complex and its cytotoxic activity against breast cancer cells

Abstract

Schiff bases are an important class of compounds that exhibit anticancer properties. These properties are generally mediated through the mechanisms of inhibiting proliferation of cancer cells and inducing apoptosis, programmed cell death. In addition, some Schiff bases may also exhibit anticancer effects by interacting with DNA or inhibiting various enzymes. In this study, a novel ruthenium (II) arene complex bearing a Schiff base ligand was synthesised and characterised using various spectroscopic techniques including ^{1}H NMR ad ^{13}CNMR. The Schiff base ligand was obtained from the condensation reaction of ethylenediamine and vanillin. The synthesised Ru(II) complex exhibited good stability under [(η6-p-cymene)Ru(Schiff base)Cl]Cl ambient conditions. Its cytotoxic activity was evaluated in vitro against MCF-7 human breast cancer cell line and MCF-10a human breast cell line using MTT assay. Ru(II) arene complex showed better cytotoxic activity compared to Schiff base ligand. These findings suggest that Schiff base based Ru(II) arene complexes have a promising potential as novel anticancer agents and should be further investigated.

Keywords: Ruthenium(II) arene complex, Schiff base ligand, Breast cancer, Cytotoxicity, Anticancer activity.

GİRİŞ

Schiff bazları, iminler olarak da bilinen, karbon-azot çift bağı (C=N) içeren bir fonksiyonel grubun varlığıyla karakterize edilen çok yönlü bir organik bileşik sınıfıdır (Kajal ve ark., 2013). Aldehit veya keton ile birincil amin arasındaki yoğunlaşma reaksiyonu ile oluşan bu bazlar, geniş bir yapısal çeşitlilik ve özellik yelpazesi sergilerler, bu da onları çeşitli bilimsel alanlarda değerli kılar (Jia ve Li, 2015). İmin bağının oluşumu, pH ve çözücü polaritesi gibi faktörlerin etkisiyle genellikle tersine çevrilebilir. Schiff bazları, koordinasyon kimyasında ligand görevi görebilir, metal iyonlarıyla kompleksler oluşturabilir ve genellikle ilginç optik, elektronik, katalitik ve biyolojik aktiviteler sergilerler (Juyal ve ark., 2023). Sentezlerinin kolaylığı ve yapısal modifikasyonlar yoluyla özelliklerinin ayarlanabilmesi, Schiff bazlarını kataliz, malzeme bilimi ve tıbbi kimya gibi alanlarda kapsamlı araştırma konusu haline getirmiştir (Fatima ve ark., 2023).

Schiff bazları, tıbbi kimyada önemli bir bileşik sınıfı olarak ortaya çıkmış ve önemli terapötik potansiyele sahip geniş bir biyolojik aktivite yelpazesi sergilemiştir (Uddin ve ark., 2020). Metal iyonları ile şelasyon ve enzimler ve DNA ile etkileşimler dahil olmak üzere çeşitli mekanizmalar yoluyla biyolojik hedeflerle etkileşime girme yetenekleri, çeşitli uygulamalarının temelini oluşturur. Özellikle, Schiff bazları bir dizi bakteriyel ve fungal patojene karşı umut verici antimikrobiyal aktivite göstererek, ilaç direncine karşı potansiyel çözümler sunmaktadır (Matela, 2020). Ayrıca, genellikle apoptoz indüksiyonu ve hücre proliferasyonunun bozulması yoluyla aracılık edilen çeşitli kanser hücre hatlarına karşı sitotoksik etkileri, onları antikanser ilaç geliştirme için çekici adaylar haline getirmektedir (Matela, 2020). Bu uygulamaların ötesinde, Schiff bazları antiinflamatuar, analjezik ve antioksidan özellikler sergilemişlerdir, bu da inflamatuar hastalıklar, ağrı ve oksidatif stresle ilişkili bozuklukların tedavisinde yararlı olabileceklerini düşündürmektedir. Schiff bazlarının yapısal çok yönlülüğü, biyolojik aktiviteleri ve seçiciliklerini artırmak için özel modifikasyonlara olanak tanır, bu da onları yeni terapötik ajanlar arayışında devam eden araştırmaların konusu haline getirir (Segura ve ark., 2016).

Platin bazlı bir koordinasyon kompleksi olan sisplatin, çeşitli malignitelerin tedavisinde devrim niteliğinde bir değişiklik yaratmıştır. 1960'larda keşfedilen (Rosenberg ve ark., 1969) bu ilaç, güçlü sitotoksik (hücre öldürücü) özellikleri nedeniyle birçok kanser tedavisinin temel taşı haline gelmiştir. Etki mekanizması, kanser hücreleri içindeki replikasyon ve transkripsiyon süreçlerini bozan DNA adüktlerinin oluşumuna dayanır ve sonuçta hücre ölümüne yol açar. Sisplatin'in etkinliği, doğrudan sitotoksisitesinin ötesine uzanır. Ayrıca, mitozun önemli bir adımı olan mikrotübül oluşumunu engelleyerek hücre bölünmesini bozar. Kanser hücrelerinin yok edilmesine yönelik bu çok yönlü yaklaşım, sisplatinin testis, yumurtalık, mesane, baş ve boyun, akciğer ve rahim ağzı kanserleri dahil olmak üzere çok çeşitli kanser türleri için birinci basamak tedavi olarak konumunu sağlamlaştırmıştır (Florea ve Büsselberg, 2011). Ayrıca, lenfoma gibi hematolojik malignitelerin tedavisinde de etkinliği kanıtlanmıştır (Evenson ve Ross, 2004).

Olağanüstü etkinliğine rağmen, sisplatinin terapötik uygulaması ne yazık ki önemli bir dezavantajla gölgelenmektedir: doza bağlı toksisite profili. İlaç, en önemlisi nefrotoksisite (böbrek hasarı), nörotoksisite (sinir hasarı), ototoksisite (işitme kaybı) ve gastrointestinal toksisite (mide bulantısı, kusma) olmak üzere bir dizi yan etkiye neden olabilir. Bu yan etkiler, tedavi rejimlerini önemli ölçüde engelleyebilir, doz azaltımını gerektirebilir ve nihayetinde hastanın yaşam kalitesini tehlikeye atabilir. Ayrıca, bazı kanserlerde sisplatin direncinin gelişmesi, uzun vadeli etkinliğini engellemektedir Yao ve ark., 2007). Bu devam eden zorluk, iyileştirilmiş farmakolojik profillere sahip yeni metal bazlı antikanser ilaçlara olan acil ihtiyacı vurgulamaktadır.

Rutenyum, yeni nesil kemoterapötiklerin geliştirilmesinde heyecan verici bir potansiyele sahip bir geçiş metalidir. Sisplatin'in platin merkezinden farklı olarak, rutenyum, farklı etki mekanizmalarına sahip ve potansiyel olarak sisplatine kıyasla daha az toksik olan ilaçların tasarımında kullanılabilecek benzersiz bir kimyasal yapı sunar. Rutenyum komplekslerine yönelik araştırma çabaları, preklinik modellerde güçlü antitümör aktivitesi sergileyen umut verici adaylar ortaya çıkarmıştır (Lee ve ark., 2020).

MATERYAL VE METOD

Kimyasallar Merck, Sigma veya Alfa Aesar firmalarından satın alınmıştır. ^{1}H ve ^{13}C NMR spektrumları Varian 400 MHz spektrometre ile kaydedilmiştir. $RuCl_2(p\text{-cymene})]_2$, Bennett ve Smith tarafından bildirilen yönteme göre Ru(III) klorür ile α-terpinene reaksiyonu ile hazırlanmıştır (Bennett ve Smith, 1974).

Schiff Bazının ve Rutenyum kompleksinin sentezi

Schiff Bazının sentezi ve karakterizasyonu

Vanilin (0,76 g, 5,00 mmol) ve etilendiamin (0,17 mL, 2,5 mmol) 10 mL metanol içinde çözüldü. Elde edilen karışım oda sıcaklığında dört saat karıştırıldı. Elde edilen beyaz çökeltiler süzüldü ve sıcak metanol ile yıkandı. Verim: 0,71 g (87%), beyaz katı, erime noktası 234-236 °C. ^{1}H NMR (400 MHz) (DMSO-d_6): δ 9,49 (br, 2 H, OH), 8,16 (s, 2 H, N=CH), 7,29 (d, J = 2,0 Hz, 2 H, Ar-H), 7,07 (dd, J = 2,0-8,4 Hz, 2 H, Ar-H), 6,79 (d, J = 8,0 Hz, 2 H, Ar-H), 3,75 (s, 10 H, CH_2 ve OCH_3). ^{13}C NMR (100 MHz, DMSO-d_6): δ 161,87, 148,28, 123,00, 115,61, 110,29, 61,41, 55,87.

Rutenyum Kompleksinin Sentezi ve Karakterizasyonu

Schiff Baz (0,10 g, 0,30 mmol) ve $[RuCl_2(p\text{-simen})]2$ (0,09 g, 0,15 mmol) 20 mL kuru MeCN içinde çözüldü. Karışım bir gece boyunca geri akıtıldı. Karışım buharlaştırılarak kurutuldu. Ham katı ürün kolon

kromatografisi ile saflaştırıldı. Verim: 0,13 g (%74), turuncu toz, erime noktası: 248-250 °C. ^{1}H NMR (400 MHz) (CD_3OD): δ 9,11 (s, 1 H, N=CH), 8,93 (s, 1 H, N=CH), 8,23 (d, *J* = 2,0 Hz, 1 H, Ar-H), 7,70 (dd, *J* = 2,0-8,4 Hz, 1 H, Ar-H), 7,39 (d, *J* = 2,0 Hz, 1 H, Ar-H), 7,30 (dd, *J* = 2,0-8,4 Hz, 1 H, Ar-H), 7,02 (d, *J* = 8,0 Hz, 1 H, Ar-H), 6,97 (d, *J* = 8,0 Hz, 1 H, Ar-H), 5,58 (t, *J* = 6,4 Hz, 1 H, *p*-simen-Ar-H), 5,41 (d, *J* = 6,0 Hz, 1 H, p-simen-Ar-H), 5,14 (d, *J* = 6,0 Hz, 1 H, *p*-simen-Ar-H), 4,01 (s, 3 H, OCH_3), 3,94 (s, 3 H, OCH_3), 3,91 (m, 1 H, CH_2), 3,91 (m, 1 H, CH_2), 3,81 (m, 1 H, CH_2), 3,57 (m, 1 H, CH_2), 3,31 (m, 1 H, CH_2), 2,88 (m, 1 H, *p*-simen-CH), 2,14 (s, 3 H, *p*-simen-CH_3), 1,31 (d, *J* = 3,2 Hz, 3 H, p-simen-CH_3), 1,29 (d, J = 3,2 Hz, 3 H, *p*-simen-CH_3). ^{13}C NMR (100 MHz, CD_3OD): δ 175,26, 172,37, 125,25, 125,41, 125,32, 124,08, 115,17, 114,17, 113,45, 106,95, 99,86, 86,10, 85,08, 84,06, 83,75, 66,57, 55,91, 55,35, 54,73, 30,92, 21,83, 20,35, 16,93.

İn-vitro sitotoksisite analizler ve hücre kültürü

Hücreler %10 ısıyla inaktive edilmiş fetal sığır serumu, %1 penisilin ve %1 l-glutamin ile desteklenmiş RPMI besiyerinde (Sigma) kültürlenmiş ve 37°C nemlendirilmiş CO_2 ortamında inkübe edilmiştir. MCF-7 ve MCF-10a hücre hatları kullanılmıştır.

Sentezlenen ve dimetil sülfoksit (DMSO) içinde çözülen bileşiklerin sitotoksisitesini değerlendirmek için MTT deneyi kullanılmıştır. Hücreler kuyu başına 104 hücre yoğunluğunda 96 kuyulu plakalara ekilmiş ve 24 ve 48 saatlik süreler boyunca çeşitli Schiff Bazı ve kompleks (0.1, 1, 10, 50 ve 100 µM) ile muamele edilmiştir. İnkübasyondan sonra, her kuyuya 100 µL MTT çözeltisi eklenmiş ve plakalar 37 °C'de 4 saat daha inkübe edilmiştir. Kolorimetrik değişim, bir mikroplaka okuyucu (Tecan) kullanılarak 570 nm'de absorbans ölçülerek nicelleştirilmiştir.

BULGULAR ve TARTIŞMA

Reaksiyon, vanilin (4-hidroksi-3-metoksibenzaldehit) ve etilendiamin (1,2-diaminoetan) arasında klasik bir kondenzasyonunu göstermektedir (Şema 1) ve bunun sonucunda bir bis-Schiff bazının oluşumu ile sonuçlanmaktadır. Bu süreç, etilendiaminin birincil amino gruplarının vanilinin elektrofilik karbonil karbonuna nükleofilik ilavesi ve ardından iki su molekülünün eliminasyonu ile karakterize edilmektedir. Reaksiyon, oda sıcaklığında (RT) metanol (MeOH) içinde verimli bir şekilde ilerlemeketedir ve Schiff bazlarının sentezlenmesinin nispeten kolay olduğunu göstermetkedir. İki vanilin parçası ve etilendiamin ara parçası arasında oluşan bis-imin bağı, molekülün elektronik ve optik özelliklerini etkileyen bir konjuge sistem sağlamaktadır.

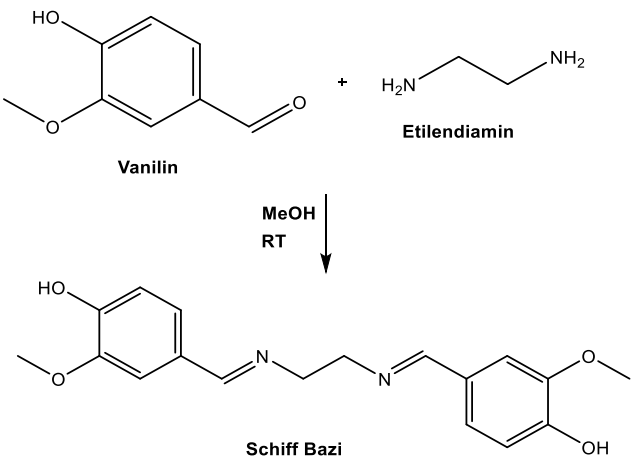

Şema 1. Schiff bazının sentezi.

Şekil 1, sentezlenen Schiff bazının ^{1}H ve ^{13}C NMR spektrumlarını göstermektedir. Hidroksil proton rezonansı 9,49 ppm'de tespit edilmiştir. 1H NMR spektrumunda, aromatik proton rezonansları 6,50-8,50 ppm aralığında

gözlemlenmiştir. 3,76 ppm'de bir singlet rezonansı hem metoksi hem de CH_2 protonlarına atfedildi. NMR analizleri yapıyı doğrulamaktadır.

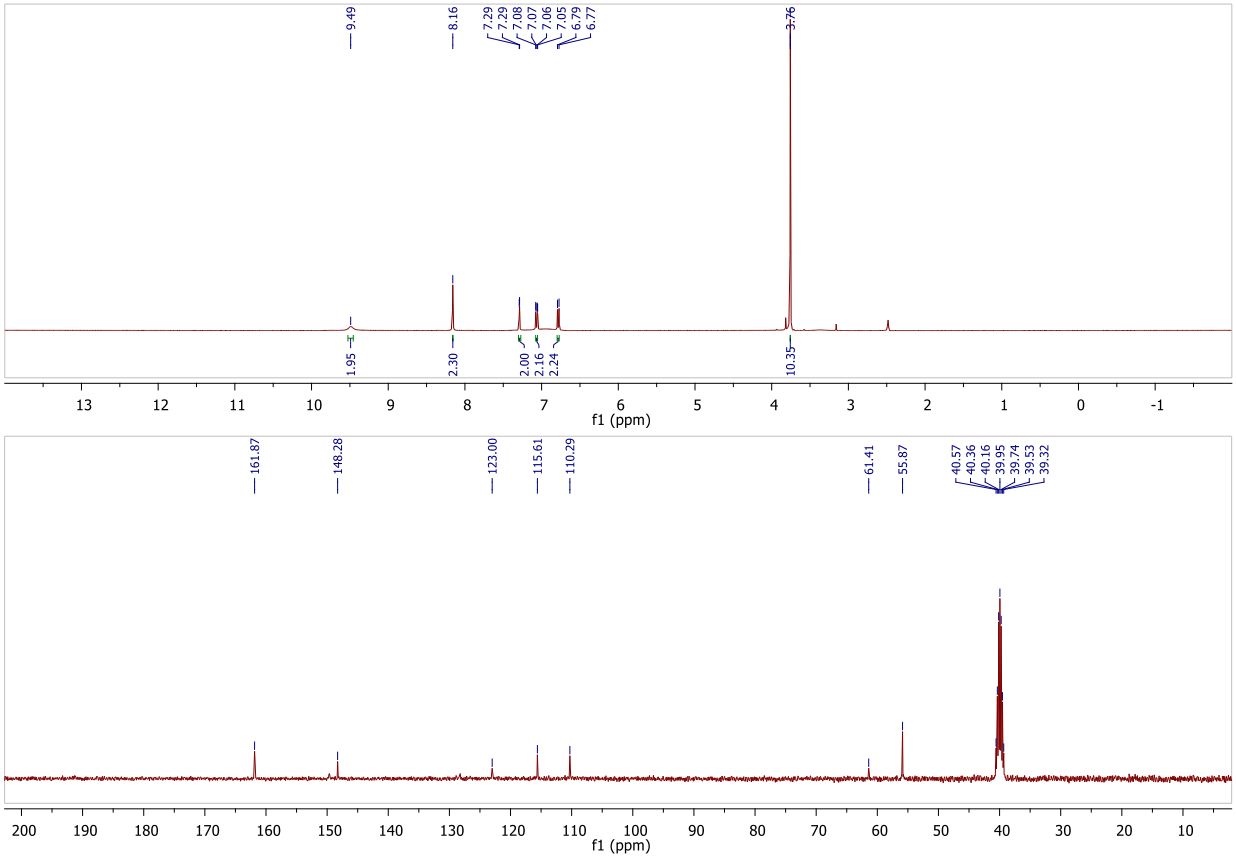

Şekil 1. Schiff bazının ^{1}H ve ^{13}C NMR spektrumları.

Şema 2, Ru kompleksinin sentezz şemasını göstermektedir. Schiff bazının polar ortamlarda çözünürlüğünün artması nedeniyle çözücü olarak asetonitril kullanılmıştır. Ru kompleksi, Schiff bazının ve $[RuCl_2(p\text{-simen})]_2$'nin yüksek sıcaklıklarda bir gece boyunca riflaks edilmesi ile sentezlendi. Ortaya çıkan kompleks, karşı iyon olarak tek bir klorür anyonu ile karakterize edilen katyonik bir türdür. Kompleks, belirgin bir parlak turuncu renk sergilemiştir.

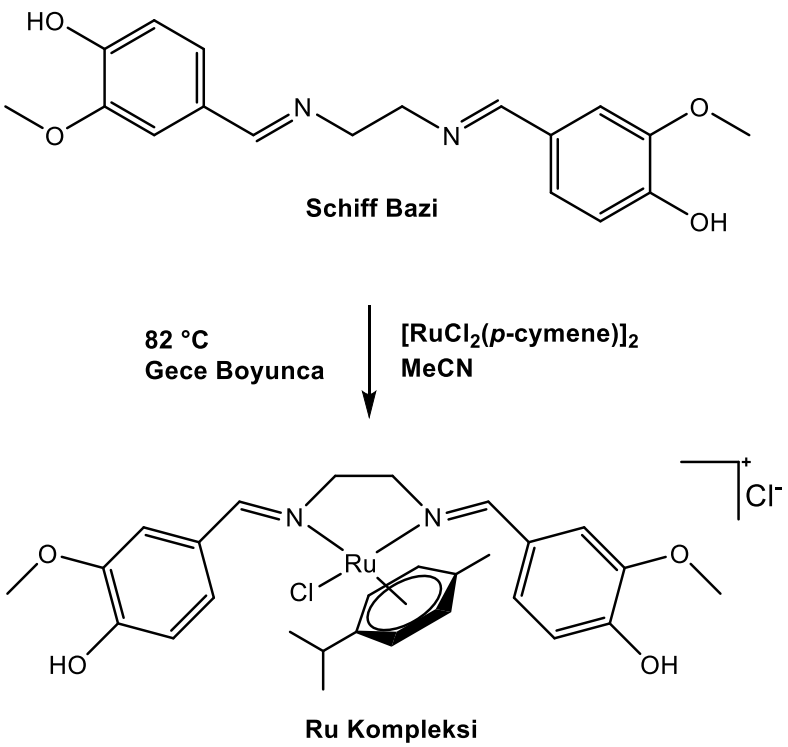

Şema 2. Rutenyum kompleksinin sentezi.

Şekil 2, sentezlenen kompleksin ^{1}H ve ^{13}C NMR spektrumlarını göstermektedir. Schiff bazının ve karşılık gelen metal kompleksinin ^{1}H NMR spektrumlarının karşılaştırmalı analizi, simetri değişikliklerini gösteren sinyal çokluğunda önemli farklılıklar ortaya koymaktadır. Spesifik olarak, Schiff baz spektrumu, moleküler simetriye atfedilebilen tepe çakışması gösterirken, kompleks spektrumu bu çakışmada bir azalma sergilemektedir, bu da daha düşük bir simetri ortamını işaret etmektedir. Anahtar spektral özellikler arasında 9,11 ve 8,93 ppm'de karakteristik imin proton rezonansları, 6,5-8,5 ppm aralığında organik liganın aromatik proton rezonansları ve 5,00-5,50 ppm civarında aren grubunun aromatik proton rezonansları bulunmaktadır. Metoksi proton sinyalleri 4,01 ve 3,94 ppm'de gözlemlenirken, etilendiamin kısmının alifatik protonları, tek tek protonlara karşılık gelen dört ayrı multiplette görünür. Aren grubuna atfedilen ek alifatik proton rezonansları 1,00-3,50 ppm aralığında gözlemlenir. NMR analizleri yapıyı doğrulamaktadır.

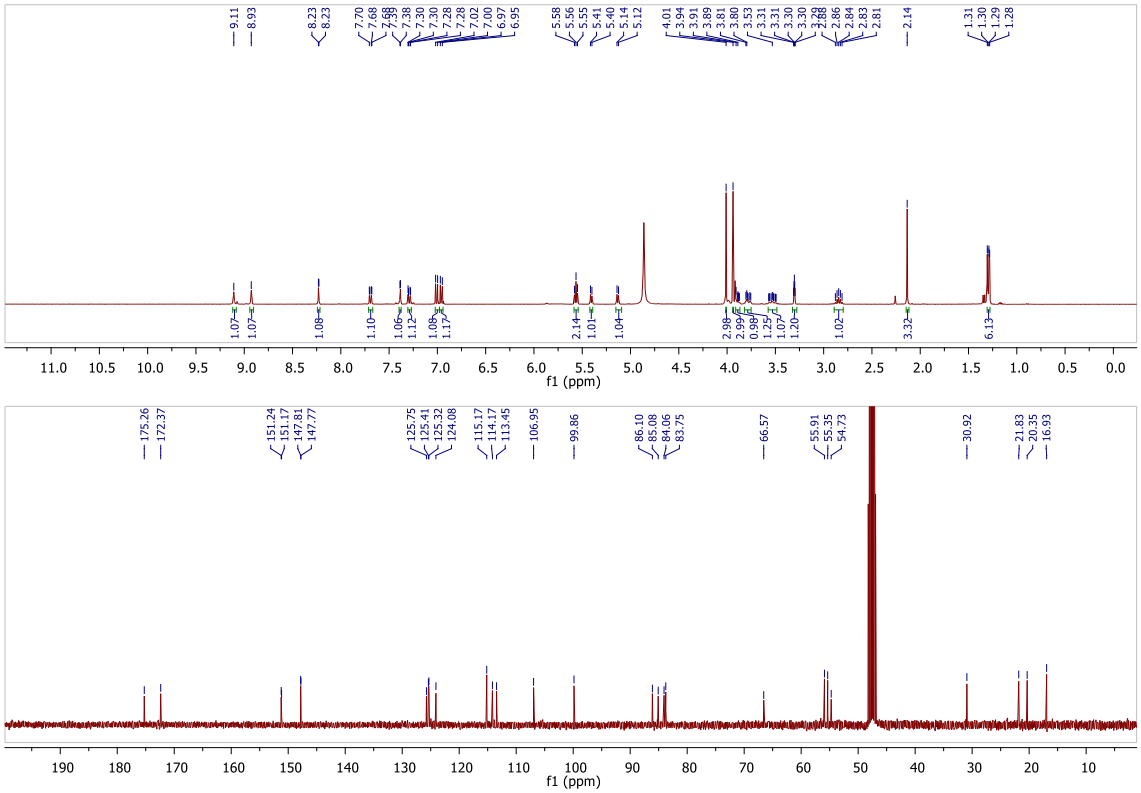

Şekil 2. Rutenyum kompleksinin ^{1}H ve ^{13}C NMR spektrumları.

İn-vitro sitotoksik aktivite

MCF-7 insan meme kanseri hücre dizisine karşı in vitro sitotoksik değerlendirme, serbest Schiff baz ve onun Ruthenium(II) p-simen kompleksinin farklı aktivite modellerini ortaya koymaktadır. Her iki bileşik de, sitotoksik ajanların karakteristik özelliği olan, hücre canlılığında doza ve zamana bağlı azalmalar sergilemektedir. Ancak, Ruthenium kompleksi, kompleksleşmemiş Schiff bazına kıyasla tutarlı bir şekilde daha güçlü bir sitotoksik etki göstermektedir. Eşdeğer konsantrasyonlarda ve inkübasyon sürelerinde, kompleks MCF-7 hücre canlılığında daha büyük bir azalmaya neden olur, bu da antiproliferatif veya hücre öldürücü yeteneklerin arttığını gösterir. Örneğin, 48 saat sonra 100 µM'de Schiff baz hücresel canlılığı yaklaşık %45'e düşürürken, Ruthenium kompleksi daha önemli bir azalma sağlayarak yaklaşık %35-40'a düşürür. Metal kompleksleşmesi üzerine gözlemlenen bu sitotoksisite artışı, metal ilaç araştırmalarında yaygın bir fenomendir ve genellikle değişen hücresel alım mekanizmaları, modifiye moleküler hedefler veya metal merkezinin kendisinin doğal sitotoksik özelliklerine atfedilir. Bu ön in vitro bulgular, Schiff bazının orta derecede sitotoksik potansiyele sahip olmasına rağmen, Ruthenium(II) p-simen kompleksinin meme kanseri hücrelerine karşı antiproliferatif bir ajan olarak daha umut verici olduğunu ve bunun kesin etki mekanizması ve in vivo etkinliği hakkında daha fazla araştırma yapılmasını gerektirdiğini göstermektedir.

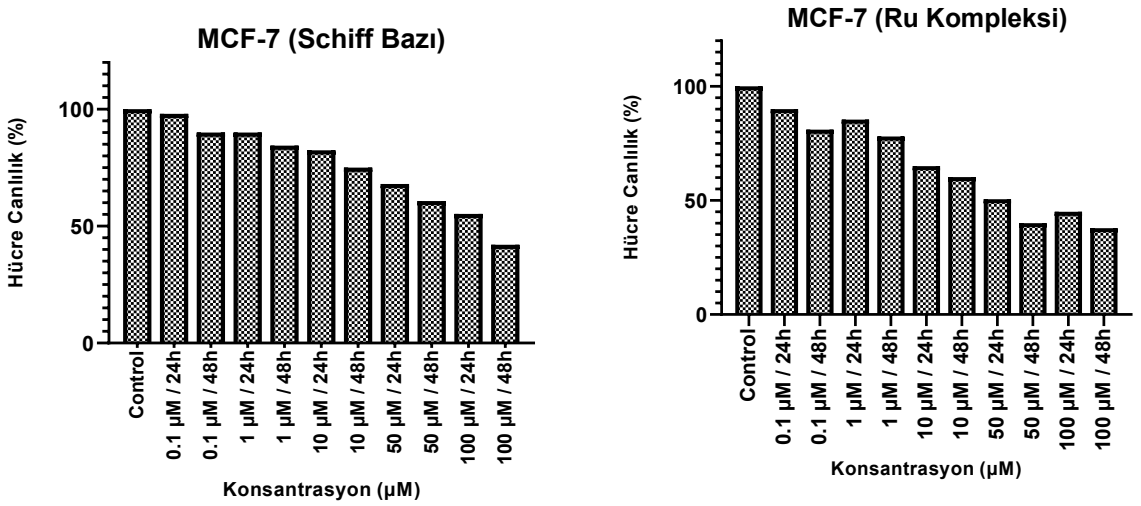

Şekil 3. Schiff bazı ve Rutenyum kompleksinin MCF-7 kanserli hücre hattındaki hücre canlılık grafikleri.

Schiff bazının ve Ruthenium kompleksinin seçici antikanser ajanlar olarak potansiyelini değerlendirmek için, kanserli MCF-7 hücre dizisi üzerindeki sitotoksik etkilerini, tümör oluşturmayan MCF-10A hücre dizisi üzerindeki etkileriyle karşılaştırmak çok önemlidir. Schiff bazında, MCF-7 hücrelerine karşı orta derecede sitotoksisite gösterirken, daha yüksek konsantrasyonlarda MCF-10A hücrelerine karşı da önemli sitotoksisite göstermiştir. Benzer şekilde, Schiff bazına kıyasla MCF-7 hücrelerine karşı daha yüksek sitotoksisite gösteren Ruthenium kompleksi de MCF-10A hücrelerine karşı güçlü sitotoksik etkiler sergilemiş ve hücre canlılığı daha yüksek konsantrasyonlarda çok düşük seviyelere düşmüştür. Kanserli ve kanserli olmayan hücre hatları arasında önemli bir farklı sitotoksisite olmaması, test edilen konsantrasyonlarda ne Schiff bazının ne de Ruthenium kompleksinin meme kanseri hücrelerine karşı yüksek derecede seçicilik göstermediğini göstermektedir. Kompleks, hücre canlılığını azaltmada genel olarak daha etkilidir, ancak toksisitesi, mevcut haliyle yüksek seçiciliğe sahip bir antikanser ajanı olarak kabul edilebilecek kadar kanser hücrelerine yeterince hedefli değildir. Daha düşük konsantrasyon aralıklarında çalışmalar planlanabilir.

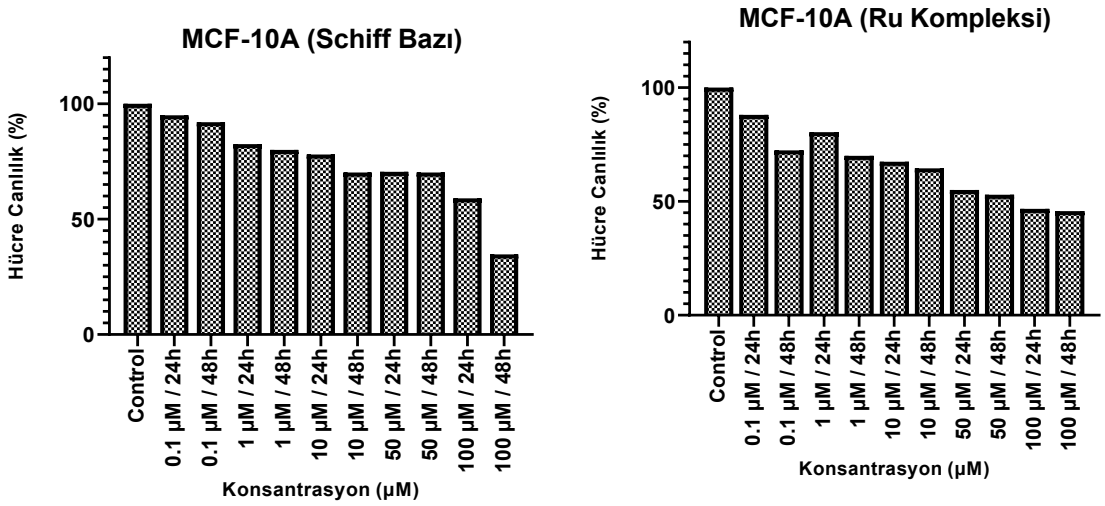

Şekil 3. Schiff bazı ve Rutenyum kompleksinin MCF-10A sağlıklı hücre hattındaki hücre canlılık grafikleri.

SONUÇ

Her iki bileşik de (Schiff bazı ve rutenyum kompleksi) MCF-7 meme kanseri hücre hattında doza ve zamana bağlı sitotoksisite sergilemiştir; rutenyum kompleksinin serbest Schiff bazına kıyasla daha belirgin bir canlılık düşüşüne neden olduğu gözlemlenmiştir. Ancak, bileşiklerin non-tümörijenik MCF-10A hücreleri üzerindeki etkileri, kanserli hücrelere karşı anlamlı bir seçicilik göstermediklerini ortaya koymuştur. Özellikle yüksek konsantrasyonlarda, her iki bileşik de MCF-10A hücrelerinde önemli düzeyde canlılık kaybına yol açmıştır.

Bu durum, bileşiklerin genel sitotoksik özelliklere sahip olduğunu, ancak mevcut halleriyle spesifik bir antikanser seçiciliğinin olmadığını düşündürmektedir. Bu nedenle, potansiyel terapötik uygulamalar için, hedef hücre seçiciliğini artıracak yapısal modifikasyonlara veya farklı doz stratejilerine ihtiyaç duyulmaktadır.

KAYNAKLAR

Bennett, M. A. & Smith, A. K. (1974). Arene ruthenium (II) complexes formed by dehydrogenation of cyclohexadienes with ruthenium (III) trichloride. J. Chem. Soc. Dalton Trans. 2, 233-241.

Evenson, D. P. & Ross, d. D. (2004). Cisplatin hypersensitivity in lymphoma. Leukemia & Lymphoma. 45(11), 2161-2171.

Fatima, Z., Basha H. A., & Khan, S. A. (2023). A review: An overview on third-order nonlinear optical and optical limiting properties of Schiff bases. Journal of Molecular Structure, 21292, 136062.

Florea, A. M., & Büsselberg, D. (2011). Cisplatin as an Anti-Tumor Drug: Cellular Mechanisms of Activity, Drug Resistance and Induced Side Effects. Cancers, 1, 1351-1371.

Jia, Y., & Li, J. (2015). Molecular Assembly of Schiff Base Interactions: Construction and Application. Chem. Rev., 115, 1597–1621.

Juyal, V. K., Pathak, A., Panwar, M., Thakuri, S. C., Prakash, O., Agrwal, A., & Nand, V. (2023). Schiff base metal complexes as a versatile catalyst: A review. Journal of Organometallic Chemistry, 999, 122825.

Kajal, A., Bala, S., Kamboj, S., Sharma, N., & Saini, V. (2013). Schiff Bases: A Versatile Pharmacophore. Journal of Catalysts, 2013, 1-14.

Lee, S. Y., Kim, C. Y. & Nam, T. G. (2020). Ruthenium Complexes as Anticancer Agents: A Brief History and Perspectives. Drug Design Development and Therapy. 14, 5375-5392.

Matela, G. (2020). Schiff Bases and Complexes: A Review on Anti-Cancer Activity. Anti Cancer Agents Med. Chem., 20, 1908-1917.

Rosenberg, B. L., Van Camp, L., Trosko, J. E., & Mansour, V. H. (1969). Platinum compounds: Inhibition of human tumor cell growth in vitro. Nature, 5200, 385-386.

Segura, J. L., Mancheno, M. J., & Zamora, F. (2016). Covalent organic frameworks based on Schiff-base chemistry: synthesis, properties and potential applications. Chem. Soc. Rev., 45, 5635-5671.

Uddin, M, N., Ahmed, S. S., & Alam, M. R. (2020). REVIEW: Biomedical applications of Schiff base metal complexes. J. Coord. Chem., 74, 3109-3149.

X. Yao, K. Panichpisal, N. Kurtzman, & K. Nugent, ‘’ Cisplatin Nephrotoxicity: A Review’’, The American Journal of the Medical Sciences 334, no. 2 (2007): 115-124.

2. POSTER PRESENTATIONS
2.1. ABSTRACTS

➢ *POSTER PRESENTATION*

Effect of pre-treatment on mechanical properties of quenched and tempered medium carbon steels

Ahmet M. Bal[1,2] (*ORCID: https://orcid.org/0009-0002-5678-4142*), Emre Alan[1] (*ORCID: https://orcid.org/0000-0002-1894-0231*), İ. İrfan Ayhan[1] (*ORCID: https://orcid.org/0009-0007-3720-7354*)

[1]ÇEMTAŞ Çelik Mak. San. ve Tic. A.Ş., R&D Center, Bursa, Türkiye.
[2]Bursa Technical University, Department of Metallurgical and Materials Engineering, Bursa, Türkiye.

*Corresponding author e-mail: abal@cemtas.com.tr

Abstract

The mechanical properties of steels can be enhanced through proper alloy design and heat treatment applications. Quenching and tempering (Q&T) is commonly used in medium carbon steels to achieve a balance between high strength and toughness. However, after quenching process, the distribution of hardness generally tends to decrease from the surface to the center as the thickness of material increases. In order to provide higher hardness on the center of material and improve hardenability, alloying elements such as boron (B) and molybdenum (Mo) are typically used. Mo is one of the most expensive alloying elements and the total cost of alloying is significantly increases when Mo is added to steel. Since B is a strong nitride-forming element, titanium (Ti) is often added to chemical composition of B-containing steels to promote TiN instead of BN and ensure that B remains as solute solution. Nevertheless, non-metallic inclusions such as TiN might be harmful whether their sizes and distributions in steels cannot be controlled.
In this study, the effect of pre-treatment on mechanical properties of medium carbon chromium (Cr) – manganese (Mn) Q&T steel is investigated. The hot rolled of steel bars with Ø80 mm thickness were used in heat-treatment trials. It was observed that the hardness distribution of directly Q&T applied specimens varied through the cross-section, and the required mechanical properties were not achieved at the center of the material. On the other hand, a more uniform hardness distribution was achieved in Q&T applied specimens subsequent to pre-treatment that consist of an annealing at 710 °C. Additionally, the impact toughness of pre-treated specimens was resulted 35% higher than non-pre-treated specimens. The results indicate that the application of pre-treatment provides an alternative solution for achieving higher mechanical properties in heavy sectioned steel materials.

Keywords: Steel, Pre-treatment, Heat treatment, Mechanical property.

➢ *POSTER PRESENTATION*

Investigation of the effects of some plant lectin proteins on the digestive enzymes of the agricultural pest *Halyomorpha halys* (stal) beetles

Özlem KARADUMAN[1] (https://orcid.org/0009-0000-1932-3887), Serap DOGAN[1] (https://orcid.org/0000-0001-5684-3662), Begümhan YILMAZ KARDAS[1] (https://orcid.org/0000-0002-8446-1116), Mehmet Emin DİKEN[1](https://orcid.org/0000-0003-3349-939X), Sakin Vural VARLI[2](https://orcid.org/0000-0002-9851-3490)

[1]Molecular Biology and Genetics, Balikesir University, Balikesir, Turkey
[2]Biology, Balikesir University, Balikesir, Turkey

*Corresponding author e-mail:melzo1175@gmail.com

Abstract

Halyomorpha halys (Hemiptera: Pentatomidae), called brown skunk in Turkish, is one of the most well-known and harmful invasive species. The pest is known to cause serious damage to agricultural products such as hazelnuts, peaches, pears, etc. Long-term solutions are sought to combat the brown skunk beetle, but chemical and biotechnical control is preferred as a short-term solution. Chemical pesticides applied in this context affect other species other than the target species and cause a decrease in species diversity by damaging beneficial species. One of the aims of this study is to minimize the damage to biodiversity and ecosystems by determining environmentally friendly and effective methods to affect agricultural pests. Lectins are carbohydrate-binding glycoproteins that are important in the development of insect-resistant plants. It is known that lectins, which have toxicity against insects, inhibit digestion by acting on the middle intestine and as a result, the insect dies without food. In this study, the effects of different doses of plant lectins isolated from castor oil *(Ricinus communis)*, spiny mulefat *(Ulex europaeus)*, Jack bean *(Canavalia ensiformis)*, purple wisteria *(Wisteria floribunda)*, kidney bean *(Phaseolus vulgaris)*, wheat *(Triticum vulgaris)* and sugarcane *(Phytolacca americana)* plants were investigated *H.halys* insects on alpha-amylase and beta-glucosidase enzymes, which are important digestive enzymes. As a result of the analysis, it was determined that all lectin samples caused low enzyme activity compared to the negative control. *Phytolacca americana* lectins decreased alpha-amylase and beta-glucosidase enzyme activity as effectively as the positive control even at low doses. At the same time, *Ulex europaeus* lectins caused a statistically significant decrease in alpha-amylase enzyme activity ($p<0.05$). Our research results will provide a basis for future studies and provide new and effective solutions for the biological control of agricultural pest species with plant lectins.

Keywords: Lectins, *Halyomorpha halys* (Stal), digestive enzymes

➢ *POSTER PRESENTATION*

Development of Novolac Resin Using Biobased Raw Materials

Deniz Önay[1], Cansu Kozbekci Sabah[1,2*], Hatice Yaren Şahin[1,3], Mehmet Gönç[1], Mustafa Çevik[1]

[1]Gentas Chemical Industry and Trade Inc, Turkey, 34956, Istanbul, Turkey
[2]Istanbul Technical University, Faculty of Science and Letters, 34469, Istanbul, Turkey
[3]Gebze Technical University, Faculty of Engineering, 41400, Kocaeli, Turkey

*Corresponding author e-mail:cansu.sabah@gentaskimya.com

Abstract

The aim of the study is to produce novolac resin using environmentally friendly chemicals such as glucose instead of toxic formaldehyde used in phenol-formaldehyde resins as an alternative to formaldehyde within the scope of green chemistry studies. Although glucose is a potential aldehyde candidate, the Friedel-Crafts reaction between phenol and glucose is more difficult than the reaction between phenol and formaldehyde because of very low reactivity of glucose as an electrophile due to steric hindrance[1,2].The synthesis of phenol-glucose resin requires 120-150 °C reaction temperatures and catalyzed by strong acids[2]. According to literature research the use of Lewis acids such as aluminium chloride ($AlCl_3$) as catalyst facilitates the formation of carbocations by promoting the ring opening of glucose (in situ transform to 5-(Hydroxymethyl) Furfural (HMF)), and the linear form is abtained. Thus, it is more easily incorporated into the structure of phenol and accelerates the reaction time. On the other hand the use of Bronsted-Lowry acids like sulfuric acid (H_2SO_4) as catalyst allows the weakly acidic phenol to enter into addition reactions with HMF to initiate the polymerization reaction. In conclusion the process parameters were compared, and it was seen that the optimum results were achieved by using both Lewis acid and Bronsted-Lowry acid at 105-115 ºC in a ratio of 1:1 $AlCl_3$:H_2SO_4. When these ratios were used, the reaction yield increased by 30% and the reaction temperature decreased by 18%. FT-IR (Fourier Transform Infrared Spectroscopy), NMR (Nuclear Magnetic Resonance), GC-MS (Gas Chromatography-Mass Spectrometry), GPC (Gel Permeation Chromatography) characterizations were performed and the parameters were supported by tests such as Melting point, B-Stage reactivity, Gel time, Flow distance.

Keywords: Biobased Novalac resin, Glucose, Friedel-Crafts

References:

[1]Güler, B. Synthesis of Phosphorylated Dibenzoxanthene Derivatives.
[2]Wang, M., Yuan, Z., Cheng, S., Leitch, M., & Xu, C. C. (2010). Synthesis of novolac-type phenolic resins using glucose as the substitute for formaldehyde. *Journal of Applied Polymer Science*, *118*(2), 1191-1197.

➢ *POSTER PRESENTATION*

Development of Room Temperature Curable Phenolic Foam Suitable for Mining and Construction Sectors

Büşra Turan[1], Cansu Kozbekci Sabah*[1,2], Gizem Anar[1], Deniz Önay[1], Mehmet Gönç[1]

[1]Gentas Chemical Industry and Trade Inc, Turkey, 34956, Kocaeli, Turkey
[2]Istanbul Technical University, Faculty of Science and Letters, 34469, Istanbul, Turkey

*Corresponding author e-mail:cansu.sabah@gentaskimya.com

Abstract

Phenolic foam is a type of porous thermoset materials that is chemically cured in the presence of a blowing agent and surfactant by using crosslinking agent (catalyst). It is commonly used as a heat insulation material with high thermal efficiency due to its closed pore structure. Also, it is used in copper pipes that can corrode with different insulation materials such as roof insulation, mining. The use of phenolic foam provides great advantages in fixing columns and beams to prevent ceiling collapse in mines because of high mechanical strength. In phenolic foam resin, reaction temperature, reaction time, catalyst type, pH, initial F/P mole ratio have a great importance[1]. The initial F/P mole ratio affects the physicochemical properties of the resin that also affects foam properties. It was observed that the hydroxymethyl linkage between benzene rings increased with the increase in F/P molar ratio in a certain pH range (pH: 8.0-9.0)[2]. In foam formation, parameters such as the amount and type of surfactant and blowing agent are important. Besides pore size, non-flammability and durability of the foam are depend on the additives used. Two types of surfactants and two types of blowing agent were chosen in the study. In conclusion closed cell form was obtained when nonionic surfactant was used. Curing time in room temperature was also optimized to obtain homogenous cell structure. FT-IR, GC-MS, GPC, Gel Time (100 ^{o}C), characterizations were performed.

Keywords: Phenolic foam, surfactant, blowing agent

References:

[1]Polymer (Guildf), 37 (8) (1996), pp. 1363-1369
[2]C.C. Riccardi, G. Astarloa-Aierbe, J.M. Echeverria, and I. Mondragon, Polymer, 43, 1631 (2002).

➢ *POSTER PRESENTATION*

Effect of Chain Transfer Agent/ Crosslinking Agent ratio on Thermoplastic Properties of Acrylic Materials

Gamze Günal[1*], Deniz Önay[1], Olkan Cebeci[1], Özkan Turhan[1], Gizem Anar[1], Çakır Daşdemir[1]

[1]Gentaş Chemical Industry and Trade Inc, Turkey, 34956, Istanbul, Turkey

*Corresponding author e-mail:gamze.gunal@gentaskimya.com

Abstract

Acrylic resins are used in many sectors such as auto repair systems, furniture varnish, road marking paints, metal and galvanized surface coatings, decorative coatings, decorative panels due to their high durability, hardness and chemical resistance[1]. Within the scope of this project, it is aimed to produce specific acrylic resins, which are in high demand in the sector, as mouldable polymers by increasing their thermoforming properties. When literature studies were examined, the chain transfer agent suitable for industrial use and cost were used in polymerization reactions and their performance with crosslinker was examined. In the study, experiments were carried out on acrylic monomer/chain transfer agent and acrylic monomer/crosslinker ratios during same reaction conditions. The developed acrylic resin is based on methyl methacrylate, and optimum parameters were found by changing the ratios of the crosslinking agent Tri Ethylene Glycol Di Methacrylate (TRGDMA) and the chain transfer agent Pentaerythritol tetrakis(3-mercaptopropionate) (PETMP). Butylated hydroxytoluene (BHT) was used as an inhibitor to prevent solidification of the resin. The reaction parameters were supported by gel time according to ISO 2535:2001, viscosity, density tests, and bending test at specified temperature.

Keywords: Acrylic resin, Polymerization reactions, Thermoformable properties

References:

[1]Richey, B., & Burch, M. (2002). Applications for decorative and protective coatings. *Polymer dispersions and their industrial applications*, 123-161.

➢ *POSTER PRESENTATION*

Development and Pilot Scale Production of High Solid Melamine-Formaldehyde Resin for Use in Textiles

Hatice Yaren Şahin[1,3], Cansu Kozbekci Sabah[1,2*], Esra Kutlu[1], Büşra Turan[1], Mustafa Çevik[1]

[1]Gentas Chemical Industry and Trade Inc, Turkey, 34956, Istanbul, Turkey
[2]Istanbul Technical University, Faculty of Science and Letters, 34469, Istanbul, Turkey
[3]Gebze Technical University, Faculty of Engineering, 41400, Kocaeli, Turkey

*Corresponding author e-mail:cansu.sabah@gentaskimya.com

Abstract

In this study, it is aimed to produce high solids methoxy functional melamine formaldehyde resin with high stability and moisture resistance for use in the textile industry. It has been found that methoxy melamine-formaldehyde (M_eMF) resins, synthesized to increase the performance of products in the textile industry, have high durability, water and heat-resistant structure and improve the mechanical properties of the non-woven, as well as extending the shelf life. In the synthesis of MMF resin, the main desired properties of the resin were designed for excellent water repellent, color retaining, and anti-wrinkle on non-woven. As a result of experimental studies, formulations were developed according to the M_e/M/F (methanole/melamine/formaldehyde) mole ratio of the resin, the reactivity of the functional groups in the process, temperature, distillation time, amount of catalyst and high cross-link efficiency[1]. As a result of the formulations, M_eMF resin with high viscosity, water miscible, colorless, and low free formaldehyde content was synthesized. Water resistance and chemical durability tests were performed on non-woven with the synthesized resin. In these tests, curing time and temperature, effect of additives, and pigment migration were determined. Fourier transform infrared spectroscopy and gel permeation chromatography analyzes were carried out. In conclusion, when new resins modified by adding methanol at different molar ratios with a F:M ratio 3:1 were examined, it was found that the methoxylated resin with M_e:F ratio 2:1 gave the best result. As a result of the pigment migration tests, it was observed that long-term curing of resins synthesized with 9:1:3 and 6:1:3 molar ratios gave the best results. Considering the process temperature of the process, it was continued with M_eMF resin with molar ratio 6:1:3. In the pigment migration test gave the best result when the resin synthesized in the ratio 6:1:3 added B under appropriate curing temperature and conditions.

Keywords: Methoxylation, high solid melamine-formaldehyde resin.

References:

[1] Binder, W. H., & Dunky, M. (2002). Melamine–formaldehyde resins. Encyclopedia of Polymer Science and Technology.

➢ *POSTER PRESENTATION*

Development of A Cold-Box Resin to Be Used as A Binder in Core Manufacturing for Foundry Industry

Esra Kutlu[1], Cansu Kozbekci Sabah[1,2*], Büşra Turan[1], Mehmet Gönç[1], Mustafa Çevik[1]

[1]Gentas Chemical Industry and Trade Inc, 41455, Kocaeli, Turkey
[2]Istanbul Technical University, Faculty of Science and Letters, 34469, Istanbul, Turkey

*Corresponding author e-mail:cansu.sabah@gentaskimya.com

Abstract

Cold-box is a core production method used in the casting industry for complex mold structures, known for its high-quality results, strong mechanical strength, low binder requirements, and high reusability of sand. Owing to these advantages, it is a preferred system in the foundry sector. In this method, phenolic urethane resins are favored as binders due to their ability to cure on their own through their resole properties and to exhibit high mechanical strength thanks to their novolac characteristics. The cold-box system for phenolic urethanes consists of three components: phenolic urethane resin, polymeric isocyanate, and a functional amine serving as an alkaline catalyst during the curing process. In this study, optimization efforts were conducted for both the resin and the catalyst components. In the formulation of the phenolic urethane resin, fatty acid esters used as solvents influence the curing performance of the sand-resin mixture. Moreover, it has been found that fatty acid esters reduce veining and enhance the thermal stability of castings by preventing the typical softening of the polyurethane bond during pouring[1]. Therefore, different fatty acid esters were tested in the resin formulation like canola oil, tall oil, sunflower oil etc. In the base resin, various analyses such as hydroxyl number determination, solid content, density, viscosity, and flow characteristics were performed and compared. These tests were conducted using instruments including FT-IR, GC-MS and GPC. The resin composition was adjusted by modifying the quantities of certain raw materials, and mechanical strength tests—considering critical parameters such as resin-to-sand ratio, catalyst quantity, and gas volume/pressure—were conducted to evaluate its performance. The obtained results were compared with target values reported in the literature.

Keywords: Cold-box resin, Phenolic urethane binders, Core-making

References:

[1] Trinowski, D. M., Ladegourdie, G., & Löchte, K. (1999). New coldbox binder system for improved productivity. AFS Transactions, 107, 51-57.

➢ *POSTER PRESENTATION*

Biomaterials from the aquatic organisms: resources, extraction and applications

Ömer Alper Erdem[1*] (*ORCID: https://orcid.org/0000-0002-1745-1751*),
Nida Demirtaş Erol[2] (*ORCID: https://orcid.org/0000-0001-8323-5689*)

[*1]Ege University, Faculty of Fisheries, Department of Fishing Technology and Seafood Processing Technology, İzmir, Türkiye.
[2]Munzur University, Faculty of Fisheries, Department of Fishing Technology and Seafood Processing Technology, Tunceli, Türkiye.

*Corresponding author e-mail: omer.alper.erdem@ege.edu.tr

Abstract

Marine biomaterials, including mollusc shells and corals, have served multiple purposes since antiquity. Despite the deleterious effects of overfishing, climate change, and industrial waste contamination, marine biomaterials continue to be plentiful. Consumable marine invertebrates, such as crabs, and molluscs, provide organic-based biopolymers for a variety of applications. Collagen and gelatine are significant commercial products derived from edible marine species, with collagen comprising approximately 30% of the overall composition of skin and bones in all animals.

Natural sources show significant biological activity, compatibility with living tissues, ability to promote bone growth, safety, stability under heat, and potential to support bone formation, making them appealing basic materials for hydroxyapatite (HA). Seashells function as a by-product of the fishing industry and marine aquaculture, with discarded shells constituting 59% to over 75% of the total organism weight.

Calcium phosphates (CPs) are a category of chemicals that constitute the primary inorganic components of biological hard tissues. They are commonly found in bones, cuttlefish bones, cartilage, teeth, shells, carapaces, and the scales of aquatic species. Fish frames and mollusc shells are acknowledged as superior sources of FAB-derived aquatic calcium phosphates owing to their abundant availability.

The advent of advanced nanotechnology has had a profound impact on the field of nanocrystalline hydroxyapatite (HA), generating considerable interest in its potential applications in areas such as adsorption, catalysis, and optics, particularly in the context of biomaterials. Nanosized HA has emerged as a promising biomaterial for prosthetic applications, driven by a growing demand for bone substitutes that are essential for the repair Many methods have been developed to turn mussel shells into hydroxyapatite (HA), encompassing solid-state, mechanochemical, aqueous crystallisation, hydrolysis, sol-gel, and hydrothermal processes. The exploration of aquatic waste as a refined supply of biomaterials presents a substantial opportunity to augment biological applications.

Keywords: biomaterials, marine invertebrates, biomaterial applications

➢ *POSTER PRESENTATION*

The impact of external magnetic field on chlorophyll content, leaf morphology, and gene expression in the Fragaria × ananassa

Mustafa Mert Cengiz(*0009-0004-7599-8829*), Merve Seven(*0000-0002-7734-9978*)

Bahcesehir University, Faculty of engineering and Natural Sciences, Department of Molecular Biology and Genetics, Istanbul, Türkiye.

*Corresponding author e-mail:mertcengiz242@outlook.com

Abstract

Agriculture is one of the most fundamental activities of humankind and has beneficial impacts on the gross national products (GNPs) of a country since decades and plays a pivotal role for generating employment, supports other related sectors such as textile, food, and medical. Due to numerous effects such as industrialization, deforestation, Global climate change, and urbanization, agriculture sector has long been suffering, and the suffering is affecting the food security negatively. The topics of plant health and productivity are directly linked to the safety of food security and success of agricultural productions. To reverse the adverse effects, mankind must acknowledge the fact that agriculture must be supported by applications for improving plants. Utilization of the magnetic field (MF) in agriculture has emerged as a functioning way for stimulating plant's biological features. To improve the yield of a plants, specifically *Fragaria* × *ananassa,* a fruit with economical agricultural value, in every perspective, MF exposure can be a good and clean solution. Different studies indicate that pre– sowing MF treatment in different species with suitable exposure time and strength results in high germination rates, increment in the leaf area, enhancement of chlorophyll content and photosynthesis. Increase in nutrient and water uptake is correlated with higher germination rates in pre-sowing MF treated seeds due to increase in the permeability of cell membrane. The effect of MF on chlorophyll content and photosynthesis are hypothesized to be related to photosystem related genes and their differential expressions. The increase in photosynthesis will eventually increase the yield of plant growth and fruit production.

Keywords: Agriculture, magnetic field, chlorophyll content, photosynthesis, *Fragaria* × *ananassa*

➢ *POSTER PRESENTATION*

Silver nanoparticle synthesis with grey juniper (*Juniperus excelsa*) extract

Bengü Kuru[1*] (*ORCID: https://orcid.org/0009-0003-9461-9401*), Ayfer Menteş[1] (*ORCID: https://orcid.org/0000-0003-3946-4075*)

[*1]Aksaray University, Faculty of Science and Letters, Department of Chemistry, Aksaray, Türkiye.

*Corresponding author e-mail: bengukuru01@gmail.com

Abstract

Green synthesis nanoparticle production" refers to the production of nanoparticles using environmentally friendly and sustainable methods. Unlike traditional chemical and physical methods, green synthesis aims to obtain nanoparticles in a non-toxic, energy-efficient and environmentally friendly way using natural resources
General Steps:
1. Selection of Biological Source:
Plants bacteria, fungi or algae can be used. The most common is plant extract because it is easy to prepare.
2. Preparation of Extract:
Plant material is extracted by boiling in water or with suitable solvents. The obtained extract is used as a biological reducing agent.
3. Addition of Metal Salt:
Metal salts such as silver nitrate ($AgNO_3$), zinc acetate are generally used. When mixed with plant extract, metal ions are reduced and nanoparticles are formed.
Silver nanoparticles can be produced with an environmentally friendly method. The formation of the particles was noticed by the eye as a colorless solution turned brown. The study shows that Ag nanoparticles can be produced with fast, cheap, harmless to nature and renewable materials. In addition, the factors affecting the size and shape of the nanoparticles were investigated; various conditions such as contact time, amount, pH and temperature were tested. The obtained particles were examined with UV-Vis, SEM, size analysis and FTIR methods.
Juniper (Juniperus excelsa) is a juniper species belonging to the cypress family (Cupressaceae). It grows naturally in Southeastern Europe, the Caucasus, Iran and Central Asia, especially in Turkey. Tall junipers (Juniperus excelsa) have continental climate characteristics, average rainfall is 400-600 mm, extreme soil (shallow, low depth, alkaline and low value) and climatic conditions (sunny aspects, closed climates, exposure to severe cold and dry growth environments).

Keywords: *Juniper*, Silver, Nanoparticles, Green methods

➢ *POSTER PRESENTATION*

Mathematical Modelling Study Of Infrared Dried Prickly Pear

Kubra Kurnaz[1*] (*ORCID: https://orcid.org/0009-0008-9349-6135*), Zehra Ozden Ozyalcin[2] (*ORCID: https://orcid.org/0000-0002-6662-5885*), Azmi Seyhun Kipcak (*ORCID: https://orcid.org/0000-0003-2068-6065*)

Yildiz Technical University, Faculty of Chemical and Metallurgical Engineering, Department of Chemical Engineering, Istanbul, Türkiye.

*Corresponding author e-mail:kubra.kurnaz@std.yildiz.edu.tr

Abstract

Drying of food products enhances product stability by preventing microbial spoilage, while also improving the efficiency of transportation, storage, and packaging. Commonly known as prickly pear, *Opuntia ficus-indica* consists of cladodes, flowers, fruits, and seeds. Cladodes are rich in fiber, minerals, flavonoids, phenolic compounds. The fruit, composed of pulp, peel, and seeds, contains glucose, fructose, pectin, and notable bioactive compounds such as ascorbic acid, flavonoids, betalains, and phenolics. Infrared drying offers several advantages over conventional drying methods, including reduced processing time, uniform surface heating, minimized quality degradation, equipment simplicity and compactness, versatility, and substantial energy savings. In this study, the infrared drying kinetics of prickly pear (*Opuntia*) samples were investigated, and the experimental data were evaluated using established mathematical drying models. Prickly pear fruits were sliced into semi-circular shapes and dried in an infrared dryer at temperatures of 50, 60, and 70 °C. The drying behavior was evaluated using a range of commonly applied mathematical models, including Aghbashlo et al., Alibas, Henderson et al., Jena and Das, Lewis, Logarithmic, Midilli and Kucuk, Page, Parabolic, Verma et al., Wang and Singh, Weibull, Two-Term Exponential. The drying process was completed within 240 to 555 minutes. Among the applied mathematical models Jena and Das, Midilli and Kucuk, and Aghbashlo et al. models exhibited the best performance for the 70 °C-dried samples with their high coefficients of determination (R^2) values over 0.999 and low chi-square (χ^2) and root mean square error (RMSE) values. Two-Term Exponential, Midilli and Kucuk, and Aghbashlo et al. models provided the closest agreement with the experimental data of 60 °C-dried samples with R^2 values greater than 0.9999. For the samples dried at 50 °C, the Two-Term Exponential, Weibull, and Aghbashlo et al. models demonstrated the best conformity with the observed drying behavior. These models yielded the highest R^2 values and the lowest χ^2 and RMSE values, with R^2 values also found to be greater than 0.9999.

Keywords: Infrared Drying, Prickly Pear, Mathematical Modelling, *Opuntia*

➢ *POSTER PRESENTATION*

Cellulose Extraction and Optimization from Pine Needles

Nihal Yigit[1*] (*ORCID: https://orcid.org/0009-0009-8688-572X*), Zehra Ozden Ozyalcin[1] (*ORCID: https://orcid.org/0000-0002-6662-5885*), Azmi Seyhun Kipcak[1] (*ORCID: https://orcid.org/0000-0003-2068-6065*)

[1]Department of Chemical Engineering, Faculty of Chemical and Metallurgical Engineering, Yildiz Technical University, Istanbul, Türkiye.

*Corresponding author e-mail: nihal.yigit@std.yildiz.edu.tr

Abstract

Traditional cellulose sources lead to deforestation and loss of biodiversity, which is a factor that accelerates climate change. In the study, cellulose was obtained and optimized from pine needles. Pine needles were subjected to alkaline treatment and decolorization. Fourier Transform Infrared (FTIR) spectroscopy and then color analysis were performed on the samples. To measure the parameter effect in the alkaline treatment, which is the fundamental step for the development and optimisation of the production procedure, sodium hydroxide (NaOH) at 1 - 2 molar concentrations was used at temperatures ranging between 120 - 180 ºC, with stirring times between 1 - 4 hours. The samples obtained after alkaline treatment were treated with 2% hydrogen peroxide (H_2O_2) at 100 °C for 2 hour for decolourisation. The obtained samples were subjected to FT-IR analysis, and their cellulose content was analysed. Accordingly, Microcrystalline cellulose (MCC) was detected >78% in all samples. While the degree of purity was found to be the highest on average for all systems using 2 M NaOH, it was observed that the effect of processing time and temperature was less after the chemical concentration increased. The average cellulose purity was found at the lowest levels for all systems at 180 °C. According to this, it is concluded that high temperature can cause degradation in the structure. It was observed that weight loss increased with increasing temperature and chemical concentration for all systems. According to the results of the colour analysis, samples with the highest colour change were the sample treated with 1 M NaOH for 2 hours at 180 °C with a Total Color Change (ΔE) value of 45.26 and the sample treated with 2 M NaOH for 2 hours at 180 °C with ΔE value of 44.35.

Keywords: Cellulose, Optimization, Pine needle

➢ *POSTER PRESENTATION*

The Protective Effects of Chard on Kidney Damage Induced by Valproic Acid Toxicity in Rats

Fatemeh Mahmoudi[1]* (ORCID: https://orcid.org/(ORCID: https://orcid.org/0009-0008-9825-8072), Sevim Tunali[2] (ORCID ID:http://orcid.org/0000-0003-3363-1290), Refiye Yanardag[2] (ORCID: https://orcid.org/0000-0003 4185-4363) Istanbul

[1*]Istanbul University-Cerrahpaşa, Institute of Graduate Studies, Istanbul, TURKEY.
[2]Istanbul University-Cerrahpaşa, Faculty of Engineering, Department of Chemistry, Istanbul, TURKEY

*Corresponding author e-mail: mahmoudifatem@gmail.com

Abstract

Valproic acid (VPA) is one of the most widely used antiepileptic drugs in the treatment of neurological and psychiatric disorders; however, long-term use is associated with toxic effects on various organs, including the kidneys. VPA-induced renal damage is largely attributed to oxidative stress, resulting from overproduction of reactive oxygen species (ROS) and a compromised antioxidant defense system. Due to its high metabolic rate and rich vascularization, the kidney is highly susceptible to such oxidative damage. Chard (*Beta vulgaris* L. var. cicla), an edible plant with documented antioxidant, anti-inflammatory and protective properties, has recently been proposed as a natural intervention against oxidative stress-mediated damage. Accordingly, the present study was designed to investigate the protective effects of aqueous chard extract against VPA-induced kidney injury in an experimental rat model. These effects were analyzed by evaluating biochemical parameters related to renal function and oxidative status. In this study, forty female Sprague Dawley rats were randomly divided into four groups: control, chard extract only, VPA only, and combined treatment with VPA and chard extract. VPA (500 mg/kg/day) was administered intraperitoneally and chard extract (100 mg/kg/day) was given orally by gavage for 7 consecutive days. At the end of the treatment period, blood and kidney tissue samples were collected from the rats, which were sacrificed on day 8. Serum urea, creatinine, and uric acid levels, and renal tissue homogenates containing Na^+/K^+- ATPase and arginase activities and nitric oxide levels were determined. The findings showed that chard extract alleviated the adverse effects of VPA and improved renal biochemical parameters. These results suggest that chard may be a promising natural source for reducing drug-associated renal injury.

Keywords: Valproic acid, chard, kidney.

➢ *POSTER PRESENTATION*

Gıdaların Kurutulmasında Yeni Yaklaşımlar: Mikrodalga ve Mikrodalga-Vakum Teknolojileri

Nevcihan Gürsoy[1*] (*ORCID 0000-0002-6573-0763*), Sümeyya Erdoğmuş[1] (*ORCID:0000-0002-6886-0600*)

[*1]Cumhuriyet Üniversitesi, Mühendislik Fakültesi, Gıda Mühendisliği, Sivas, Türkiye.

*Sorumlu yazar e-posta: ngursoy@cumhuriyet.edu.tr

Özet

Gıdaların özellikle meyve ve sebzelerin güneşte kurutulması, konveksiyonel hava ile kurutulması gibi yöntemler gıda sanayinde yaygın olarak kullanılan muhafaza yöntemleri arasında bulunmaktadır. Konvansiyonel sıcak hava (konvektif) kurutma, basitliği ve düşük ilk yatırım maliyeti nedeniyle tercih edilse de yüksek sıcaklıkların etkisiyle ürünlerde renk kaybı, doku bozulması, besin değerinde azalma ve büzülme gibi kalite kayıplarına yol açmaktadır. Ayrıca, bazı ürünlerin kurutma işlemleri esnasında yeniden nemlendirilmesi gerektiğinde, konvansiyonel yöntemle kurutulan ürünler istenen rehidrasyon kapasitesine ulaşamamaktadır. Bu dezavantajları gidermek amacıyla geliştirilen mikrodalga kurutma teknolojisi, volumetrik ısıtma prensibine dayanarak materyalin iç kısmında hızlı ve homojen ısı üretimi sağlamaktadır. Bu yöntem, kurutma süresini önemli seviyede azaltırken, ürün kalitesini artırmakta ve enerji tasarrufu sağlamaktadır. Mikrodalga-konvektif kurutma ile yüzeyden hava geçişi sağlanarak buhar uzaklaştırılır. Bu işlem yapılırken güç yoğunluğu (W/g) ile görev çevrimi (on/off süreleri) parametreleri kullanılmaktadır. Mikrodalga- konvektif kurutmanın konvektif kurutmaya göre avantajları olsada yeterli şekilde homojen bir kurutma yapamamaktadır. Bu kurutma teknolojisine alternatif olarak mikrodalga vakum kurutma teknolojisi geliştirilmiştir. Mikrodalga-vakum kurutma özellikle düşük ısıl işlem uygulamalarının gerektiği ürünlerde tercih edilmekte olup, düşük basınç altında mikrodalga uygulanarak kurutma kalitesi arttırılmaktadır. Çalışmalarda muz, havuç, çilek, kızılcık ve sarımsak gibi ürünlerde renk, aroma, β-karoten ve C vitamini gibi besin maddelerinin korunmasında bu yöntemin oldukça etkili olduğu bildirilmektedir. Ayrıca osmotik dehidrasyon gibi birçok ön işlemi, mikrodalga kurutma ile birleştirildiğinde hem kurutma süresini azaltmakta hem de daha düşük sıcaklıkta işlem yapılması sağlanarak besin ögelerinin korunmasına katkı sağlamaktadır. Sonuç olarak, mikrodalga destekli kurutma yöntemleri, konvansiyonel tekniklere kıyasla daha hızlı kurutma, uzun raf ömrü, daha az enerji kullanarak yüksek kalitede ürün üretiminde sürdürülebilir ve yenilikçi bir alternatif sunmaktadır.

Anahtar Kelimeler: Mikrodalga Kurutma, Mikrodalga vakum kurutma, Yeni Nesil Kurutma teknolojiler

➢ *POSTER PRESENTATION*

Yeni Nesil Mikrobiyal Terapötikler: Postbiyotikler ve Paraprobiyotikler

Nevcihan Gürsoy[1*] (*ORCID 0000-0002-6573-0763*), Sümeyya Erdoğmuş[1] (*ORCID:0000-0002-6886-0600*)

[*1]Cumhuriyet Üniversitesi, Mühendislik Fakültesi, Gıda Mühendisliği, Sivas, Türkiye.

* Sorumlu yazar e-posta: ngursoy@cumhuriyet.edu.tr

Özet

Probiyotiklerin; bağırsak işlevlerini iyileştirme, laktoz intoleransını hafifletme, bağışıklık sistemini güçlendirme, anti-kanserojenik, anti-diyabetik, antioksidatif, anti-aging ve antimikrobiyal etkiler gibi pek çok olumlu özelliği bilimsel olarak kanıtlanmıştır. Son yıllarda yapılan çalışmalar, probiyotik mikroorganizmaların bazı sınırlamaların varlığını ortaya çıkarmaktadır. Bu sınırlamalar arasında suşa özgü farklılıklar, kısa raf ömrü, virülans genlerinin yatay transfer riski, probiyotik etkilerinin belirsizliği, üretim sürecinde canlılığın ve stabilitenin korunmasında yaşanan zorluklar bulunmaktadır. Tüm bu nedenler, postbiyotik ve paraprobiyotik gibi yeni nesil biyotikleri ön plana çıkarmaktadır. Bu iki grup, canlı bakteri içermeyen ancak sağlık üzerinde olumlu etkiler gösterebilen biyoaktif mikrobiyal ürünler olarak değerlendirilmektir. Postbiyotikler, probiyotik bakterilerin metabolik yan ürünleri olup; enzimler, kısa zincirli yağ asitleri, vitaminler, organik asitler, peptitler ve fenolik bileşikler gibi maddeleri içermektedir. Bu maddeler, konakçı canlıda antioksidan, anti inflamatuar, antimikrobiyal ve immünmodülatör etkiler göstererek bağışıklık sistemini desteklemektedir. Paraprobiyotikler ise ısı, kimyasal, radyasyon veya sonikasyon gibi yöntemlerle inaktive edilmiş probiyotik mikroorganizmaların hücreleri olarak ifade edilmektedir. Bu hücreler, yapısal bileşenlerini (peptidoglikanlar, lipopolisakkaritler, hücre yüzey proteinleri gibi) koruyarak bağırsak sağlığı üzerinde fayda sağlamaya devam etmektedir. Isıl işlemle inaktive edilmiş *Lactobacillus* türleri, bağırsaklarda patojenlerin yapışmasını engelleyebilmekte, serbest radikalleri nötralize edebilmekte ve serotonin gibi hormonların salınımını da etkileyebilmektedir. Paraprobiyotik ve postbiyotiklerin bilinen kimyasal yapıları, saflaştırılabilir olmaları, özgül mekanizmalar üzerinden etkili olmaları, MAMP (Microbe-Associated Molecular Pattern)(mikrobiyal ilişkili moleküler örüntü) ve PRR(Pattern Recognition Receptors)(Örüntü tanıyan reseptörler) etkileşimleri aracılığıyla bağışıklık sistemini yönlendirebilmeleri, endüstriyel üretime uygunlukları ve uzun raf ömürleri gibi avantajları bulunmaktadır. Sonuç olarak, geleneksel probiyotiklerin sağlık üzerindeki faydaları kanıtlanmış olsa da, özellikle bağışıklık sistemi baskılanmış bireylerde taşıdığı riskler göz önüne alındığında; canlı mikroorganizma içermeyen ancak benzer veya daha üstün etkiler sunabilen postbiyotik ve paraprobiyotikler, fonksiyonel mikrobiyal ürünler alanında yeni alternatifler olarak değerlendirilmektedir.

Anahtar Kelimeler: Probiyotik mikroorganizmalar, Postbiyotik, Paraprobiyotik,

➢ *POSTER PRESENTATION*

Effects of Some Plant Extracts and Metal Salts on Aldose Reductase Activity

Mustafa Kaplan [1]* (ORCID: https://orcid.org/0009-0007-5698-3279), Bertan Boran Bayrak[2] (ORCID: https://orcid.org/0000-0002-0700-5096), Refiye Yanardag[2] (ORCID: https://orcid.org/0000-0003 4185-4363)

[1]Istanbul University-Cerrahpaşa, Institute of Graduate Studies, Istanbul, Türkiye.
[2]Istanbul University-Cerrahpaşa, Faculty of Engineering, Department of Chemistry, Istanbul, Türkiye.

*Corresponding author e-mail: trmkaplan@gmail.com

Abstract

Aldose reductase (AR, E.C.1.1.1.21) enzyme is a cytosolic NADPH-dependent oxidoreductase that catalyzes the conversion/reduction of glucose to sorbitol in the first step of the polyol pathway of glucose metabolism. During hyperglycemia, aldose reductase enzyme activity is high in renal glomerular and tubular cells, peripheral nervous system and retinal tissue, and long-term diabetic complications such as nephropathy, neuropathy and retinopathy occur. Aldose reductase enzyme catalyzes the reduction of various compounds such as lipids, aldehydes, phospholipids, atherogenic aldehydes and steroids, mediates the transmission of signals initiated by cytokines, chemokines, growth factors, endotoxins and allergens, and creates disorders in tissue metabolism. As a result of this situation, various cancers such as breast, colon, liver, lung, prostate and ovarian cancer may develop in the body. Many different aldose reductase inhibitors are not used clinically due to some side effects in order to delay or prevent the development of diabetic complications and various cancers. Therefore, studies are ongoing to investigate aldose reductase inhibitors with fewer side effects. In this study, the inhibitory effects of plant extracts and some metal salts on the aldose reductase enzyme were examined. It was found that the plant extracts of pumpkin, grapefruit and aqueous chard extracts and the metal salts of iron (II) sulfate, copper (II) sulfate, iron (III) sulfate and sodium valproate inhibited the AR enzyme at a high level. It can be suggested that the plant extracts and metal salts with high AR inhibition can be used in addition to drug treatment in delaying the development of diabetic complications and various types of cancer due to their low side effects.

Keywords: Aldose reductase, plant extract, metal salts

➢ *POSTER PRESENTATION*

In vitro antioxidant activities *of Helianthus tuberosus* L. extracts

Mitra Bijad [1]* (ORCID: https://orcid.org/0009-0006-7011-3758) Sevim Tunali [2] (ORCID: http://orcid.org/0000-0003-3363-1290), Refiye Yanardag[2] (ORCID: https://orcid.org/0000-0003 4185-4363)
[1]Istanbul University-Cerrahpaşa, Institute of Graduate Studies, Istanbul, Türkiye
[2]Istanbul University-Cerrahpaşa, Faculty of Engineering, Department of Chemistry, Istanbul, Türkiye

*Corresponding author e-mail: mitrabiijad@gmail.com

Abstract

Helianthus tuberosus L., a member of the genus Helianthus and the family Asteraceae, is native to eastern North America and is widely cultivated in temperate regions. *H. tuberosus* L. has been used in folk medicine for a variety of medicinal applications, including enhancing the immune system, treating bone fractures, healing wounds, lowering blood sugar levels in diabetic patients, lowering cholesterol and triglyceride levels in obese individuals, and improving the digestive system of individuals. *H. tuberosus* L. exhibits pharmacological properties such as antifungal, antioxidant, anti-inflammatory, anticarcinogenic, antimicrobial, antiviral, antidiabetic, anticancer, and body mass-reducing activities.
In this study, the antioxidant activities of water, metanol, ethyl acetate and hexane extract of *Helianthus tuberosus* L. were investigated by different antioxidant tests such as reducing power, DPPH and DMPD activities. The results were compared with natural antioxidants.
From the obtained results, it was concluded that *Helianthus tuberosus* L. extracts could be a potential antioxidant source.

Keywords: *Helianthus tuberosus* L, antioxidant activity, plant extract

➢ *POSTER PRESENTATION*

Multi 7: A food supplement with antioxidant activity

Lulya Aldada [1]* (*ORCID: https://orcid.org/0009-0006-2975-4043*) Ismet Burcu Turkyilmaz Mutlu[2] (*ORCID: https://orcid.org/0000-0003-2789-5943*), Refiye Yanardag[2] (*ORCID: https://orcid.org/0000-0003 4185-4363*)

[1]Istanbul University-Cerrahpaşa, Institute of Graduate Studies, Istanbul, Türkiye.
[2]Istanbul University-Cerrahpaşa, Faculty of Engineering, Department of Chemistry, Istanbul, Türkiye

*Corresponding author e-mail: lulyaahmed96@gmail.com

Abstract

Multi 7 food supplement product, which targets focus, memory, and general mental vitality, is a powerful support food complex product in liquid doses containing fish oil, phosphatidyl serine, citicoline, quercetin, boswella, rosemary, yarrow extracts and fructooligosaccharide prebiotic. This food supplement helps protect nerve cell membrane integrity, support neurotransmitter synthesis and regulate the digestive system. In this study, the antioxidant activities of Multi 7 were investigated by different antioxidant tests such as reducing power, DPPH and DMPD activities. The results were compared with natural antioxidants. From the obtained results, it was concluded that Multi 7 could be a potential antioxidant source.

Keywords: Antioxidant activity, Food supplement, Multi 7

➢ *POSTER PRESENTATION*

Multi 7: A food supplement with inhibitory activity of diabetes-related enzymes

Lulya Aldada [1]* (*ORCID: https://orcid.org/0009-0006-2975-4043*) Ismet Burcu Turkyilmaz Mutlu[2] (*ORCID:https://orcid.org/0000-0003-2789-5943*), Refiye Yanardag[2] (*ORCID: https://orcid.org/0000-0003 4185-4363*)

[1]Istanbul University-Cerrahpaşa, Institute of Graduate Studies, Istanbul, Türkiye.
[2]Istanbul University-Cerrahpaşa, Faculty of Engineering, Department of Chemistry, Istanbul, Türkiye

*Corresponding author e-mail: lulyaahmed96@gmail.com

Abstract

For centuries, herbs and spices have been traditionally used to treat various diseases. The formulation of dietary supplements containing single or multiple herbal extracts or mixtures of spices is now popular. These formulations provide biochemical, pharmacological and medicinal benefits due to their inclusion of various phytochemical components.Food supplements derived from a single or combined source are also known as dietary supplements. These are diet-based formulations containing vitamins, minerals, essential fatty acids, amino acids or fiber. Plant-based food supplements, on the other hand, contain bioactive compounds including phenols, terpenoids, thiols, saponins, glycosides, amines, essential oils, etc. Therefore, they exhibit pharmacological and therapeutic effects in addition to their nutritional functions. Since they are food-based, they are claimed to have minimal or no side effects. In this study, α-amylase, α-glucosidase, sorbitol dehydrogenase and urease inhibitory activities of Multi 7, a food supplement containing quercetin, fish oil, *Achillea millefolium, Salvia rosmarinus* extracts, *Boswellia Serrata*, phosfatidil serine, citicoline were evaluated by dissolving in alcohol-water mixture.The supplement strongly inhibited alpha glucosidase, while urease, and sorbitol dehydrogenase were moderately. The less inhibition activity was on α-amylase. The pharmacological activity of Multi 7 can be attributed to its rich phytochemical composition. According to the current findings, it can be suggested that Multi 7 has antidiabetic activity. In addition to drug therapy, diabetic patients can use this substance.

Keywords: Multi 7, Enzyme, Inhibition

➢ *POSTER PRESENTATION*

Bridging the Knowledge Gap: Investigating Short-Chain PFAS Effects on Lipid Metabolism and Immune System

Recep Anıl Kaya (https://orcid.org/0009-0002-6747-6372)

Marmara University, İstanbul, Türkiye.

Corresponding author e-mail:recep.anil@gmail.com

Abstract

Per- and polyfluoroalkyl substances (PFAS), often termed "Forever Chemicals," are ubiquitous environmental pollutants with well-documented adverse health effects. Extensive research has primarily focused on long-chain PFAS, such as PFOA and PFOS, linking them unequivocally to a range of serious conditions including elevated cholesterol levels, liver damage, thyroid disease, kidney and testicular cancers, and compromised immune responses, such as reduced vaccine efficacy. These compounds' exceptional chemical stability, stemming from their robust carbon-fluorine bonds, ensures their environmental persistence and bioaccumulation in living organisms, prompting global efforts to phase them out.

However, the gradual discontinuation of long-chain PFAS has led to their widespread replacement by shorter-chain alternatives, notably perfluoropentanoic acid (PFPeA) and perfluoroheptanoic acid (PFHpA). While these short-chain compounds are frequently presumed to be safer due to their lower bioaccumulation potential, this assumption is not adequately supported by comprehensive toxicological data. This critical issue, often described as the "whack-a-mole" problem, where one problematic chemical is substituted with another lacking sufficient safety information, highlights a significant gap in our understanding. Despite their increasing environmental presence, the full spectrum of their health impacts remains considerably understudied. Our research directly addresses this critical void by investigating the cellular impacts of PFPeA and PFHpA, aiming to understand whether their toxicity profiles differ from or resemble those of their long-chain predecessors, and to inform future risk assessments and regulatory policies.

Our study utilized robust in vitro models to delineate the effects of PFPeA and PFHpA on key physiological systems. Specifically, we investigated lipid metabolism using 3T3-L1 preadipocytes, a widely accepted model for adipogenesis and lipid regulation, and immune system responses employing THP-1 monocytes/macrophages, critical components of the innate immune system. Cells were exposed to a relevant range of concentrations (1, 10, and 100 micromolar), with optimal exposure durations (24-hour, 48-hour, 72-hour, and 10-day) meticulously determined through preliminary dose-response experiments. The molecular impacts were assessed through quantitative PCR (qPCR), targeting genes critically involved in lipid synthesis, storage, and breakdown pathways in 3T3-L1 cells, and inflammatory responses, cytokine production, and immune cell activation pathways in THP-1 cells.

The profound importance of this research cannot be overstated. Given the known harms of long-chain PFAS on lipid dysregulation and immune suppression, it is imperative to ascertain if short-chain compounds like PFPeA and PFHpA elicit similar or distinct molecular and cellular changes. By elucidating the specific effects of these lesser-studied short-chain PFAS on fundamental biological processes like lipid homeostasis and immune function at a cellular level, our findings contribute vital insights into the comparative toxicology of PFAS. This knowledge is crucial for refining our understanding of PFAS toxicity, guiding more effective environmental monitoring, and supporting the development of truly safe and sustainable chemical alternatives, ultimately safeguarding public health against the persistent threat of "Forever Chemicals."

Keywords: PFAS, Short-Chain PFAS, Lipid Metabolism, Immune System, 3T3-L1 & THP-1

➢ *POSTER PRESENTATION*

Effects of sustainable diets such as insect-based, essential oil-supplemented and single-cell protein on disease resistance in aquaculture

Ulviye Karacalar (https://orcid.org/0000-0002-9093-2324)

Ege University, Fisheries Faculty, Aquaculture Department, Fish Disease Unit, Izmir, Türkiye.

Corresponding author e-mail: ukaracalar@yahoo.com

Abstract

Aquaculture is one of the fastest growing sectors and has the potential to contribute to sustainable food production in the future. However, with the intensification of production, the sector has been faced with disease outbreaks that cause global losses exceeding US$ 6 billion per year, and serious problems such as antimicrobial resistance (AMR) and environmental pollution due to antibiotics and chemical treatments have also faced significant limitations in sustainable production. In response to these problems, many researchers have succeeded in developing sustainable feed alternatives that not only meet nutritional demands but also provide health benefits to farmed aquatic animals. Studies have shown that the use of alternative ingredients in feed ingredients (especially insect-based proteins, essential oil (EO) supplements and single-cell proteins (SCPs)) contributes to both environmental sustainability and a significant increase in the potential to increase host disease resistance. Key findings show that insect feeds increase survival rates against bacterial infections through their immune-stimulating effect, essential oils exhibit broad antimicrobial activity and single-cell proteins significantly increase antiviral resistance. The aim of this research is to evaluate the immunomodulatory and antimicrobial effects of sustainable feeds in aquaculture species and to present current studies on promising feed ingredients that could be alternatives to fishmeal-based diets.

Keywords: Aquatic animals, insect-based feed, essential oil-supplemented, antimicrobial effects, immunomodulatory

➢ *POSTER PRESENTATION*

Effects of *Helianthus tuberosus* L. extracts on enzyme activities in diabetes mellitus

Mitra Bijad [1]* (*ORCID: https://orcid.org/0009-0006-7011-3758*), Sevim Tunali[2] (*ORCID: http://orcid.org/0000-0003-3363-1290*)), Refiye Yanardag[2] (*ORCID: https://orcid.org/0000-0003 4185-4363*)

[1]Istanbul University-Cerrahpaşa, Institute of Graduate Studies, Istanbul, Türkiye
[2]Istanbul University-Cerrahpaşa, Faculty of Engineering, Department of Chemistry, Istanbul, Türkiye

*Corresponding author e-mail: mitrabiijad@gmail.com

Abstract

Helianthus tuberosus L. is currently among the accepted medicinal plants worldwide. *Helianthus tuberosus* L. is cultivated in America, Europe, Asia and other parts of the world. *Helianthus tuberosus* L. tubers and aerial parts possess both nutritional and therapeutic properties. The *Helianthus tuberosus* L. is a rich source of an indigestible polysaccharide called inulin, which serves as a prebiotic that improves gastrointestinal health. This plant has been used globally throughout history as a dietary supplement, for pain treatment, to reduce swelling, and to boost the immune system, as well as to treat skin wounds in folk medicine. It is an abundant source of bioactive compounds, such as phenolic acids, coumarins, and flavonoids, which are known to exert pharmacological activities, including antioxidant, antimicrobial, and anti-inflammatory properties.
In this study, the inhibitory effects of aqueous, metanolic, ethyl acetate and hexane extracts prepared from the inner part of *Helianthus tuberosus* L. on alpha glucosidase, alpha amylase, sorbitol dehydrogenase and aldose reductase activities were investigated.
Enzyme inhibitor activities of plant extracts were found to increase in a dose dependent manner. All plant extracts exhibit alpha glucosidase, alpha amylase, sorbitol dehydrogenase and aldose reductase activities. A higher enzyme inhibitor activity is associated with a lower IC_{50} value. From our results, it was determined that *Helianthus tuberosus* L. inhibited aldose reductase enzyme at the highest rate.

Keywords: *Helianthus tuberosus* L., inhibition, enzyme

➢ *POSTER PRESENTATION*

Microwave drying of beef and lamb liver: Investigation of drying kinetics and color change

Ozge Ercan* (*ORCID: https://orcid.org/0009-0001-3312-7345*), Zehra Ozden Ozyalcin (ORCID: https://orcid.org/0000-0002-6662-5885), Azmi Seyhun Kipcak (ORCID: https://orcid.org/0000-0003-2068-6065)

Yildiz Technical University, Faculty of Chemical and Metallurgical Engineering, Department of Chemical Engineering, Istanbul, Türkiye.

*Corresponding author e-mail:ozge.ercan@std.yildiz.edu.tr

Abstract

Liver is recognised as an excellent source of nutrients in human nutrition. It is rich in nutrients, especially vitamins A, B12 and iron. These nutrients play vital roles in various bodily functions. The study was conducted to examine the effect of microwave drying kinetics of beef and lamb liver. The data collected from the experiments were analyzed to determine the drying rates, effective moisture diffusivities (D_{eff}), and color changes that occurred in microwave drying. To conduct the study, microwave drying of beef and lamb liver samples were performed at different power settings between 140-350 W. During the microwave drying process, weights were taken at 1-minute intervals for 140 and 210 W, and 30-second intervals for 350 W power settings. The drying process was conducted until the final moisture content of the samples dropped below 10%. The drying took 30, 15, and 6.5 minutes for beef liver and 15, 7, and 4 minutes for lamb liver, respectively. Deff values were found to be 0.553, 1.25 and 3.1×10^{-8} m^2/s for beef liver and 1.29, 2.86 and 5.23×10^{-8} m^2/s for lamb liver. In addition, the color analysis showed that the least color change, as indicated by the lowest ΔE values, occurred in beef liver at 210 W and in lamb liver at 350 W.

Keywords: beef liver, lamb liver, microwave drying, color change

➢ *POSTER PRESENTATION*

Effect of heat treatment on antioxidant capacity of Karayaka sheep milk

Ece Özbek* (*ORCID: https://orcid.org/0000-0001-5928-6582*), Gül Fatma Yarım (*ORCID: https://orcid.org/0000-0003-4050-429X*)

Ondokuz Mayis University, Faculty of Veterinary Medicine, Department of Biochemistry, Samsun, Türkiye.

*Corresponding author e-mail: eceozbek05@gmail.com

Abstract

Sheep milk is a unique and increasingly popular nutritional source rich in bioactive molecules essential for lamb growth as well as human nutrition. Milk has antioxidant activity thanks to the non-enzymatic antioxidants, such as vitamins and minerals, and enzymatic antioxidant molecules, including superoxide dismutase, glutathione peroxidase, and catalase in its composition. In sheep milk, these components contribute to the preservation of vitamins and bioactive compounds, inhibit lipid oxidation and microbial growth, extend pre-processing shelf life, and support nutritional value. The antioxidant capacity of milk may decrease as a result of damage to the structures of vitamins, phenolic compounds, and antioxidant enzymes, which are heat-sensitive molecules in milk, during heat treatment. This study evaluated the effect of heat treatment on total antioxidant capacity of healthy Karayaka sheep milk. The California mastitis test and somatic cell count analysis were conducted to exclude the presence of subclinical and clinical mastitis in the milk. The study material consisted of 60 Karayaka sheep milk samples, with 15 samples assigned to each group. Group A included untreated milk. Milk in groups B, C, and D was heat-treated at 63 °C for 30 min, 72 °C for 15 sec, and 90 °C for 5 min, respectively. Colorimetric test kits were used to measure the antioxidant capacity in milk. The total antioxidant capacity of milk in group A was determined to be 2.17±0.24 mmol Trolox Equiv/l. Total antioxidant capacities of milk were 1.94±0.22, 1.77±0.26, and 1.06±0.20 mmol Trolox Eq/L in groups B, C, and D, respectively. The total antioxidant capacity of milk was observed to decrease by around half when heat-treated at 90 °C for five minutes, compared to raw milk ($p<0.01$). In conclusion, the findings obtained from this study showed that the antioxidant capacity in Karayaka sheep milk decreased as the applied heat increased.

Keywords: Antioxidant capacity, heat treatment, milk, sheep.

➢ *POSTER PRESENTATION*

Monitoring Organophosphate Resistance in *Bemisia tabaci* Populations from the Mediterranean and Aegean Regions of Türkiye

Ömer YÜZER[1,2*] (*ORCID: https://orcid.org/0000-0003-0209-324X*), Ersin DOĞAÇ[3] (*ORCID: https://orcid.org/0000-0003-4426-2187*), Alper TONGUÇ[3] (*ORCID: https://orcid.org/ 0000-0002-2613-3114*)

[*1]Doğuş University, Vocational School, Department of Medical Laboratory Techniques, Istanbul, Türkiye.
[2]Mugla Sıtkı Kocman University, Institute of Science, Department of Molecular Biology and Genetics, Muğla, Türkiye.
[3]Muğla Sıtkı Koçman University, Faculty of Science, Department of Molecular Biology and Genetics, Mugla, Türkiye.

*Corresponding author e-mail: oyuzer@dogus.edu.tr

Abstract

Bemisia tabaci, described by Gennadius (1889), is one of the leading agricultural pests worldwide. It caused severe outbreaks throughout the Mediterranean basin in 1974 and in the United States in 1981. Although insecticide use has long been a successful control method against this pest, the development of insecticide resistance in the species has complicated management efforts. Insecticide resistance in *B. tabaci* is widespread, with resistance having developed to most of the insecticides currently in use. In this study, the F331W mutation in the acetylcholinesterase gene (*ace*), which is associated with target-site insensitivity and resistance to organophosphate insecticides, was screened in a total of 360 individuals collected from six provinces across the Mediterranean and Aegean regions of Turkey (İzmir, Aydın, Muğla, Antalya, Mersin, and Adana), with 60 individuals sampled per province. First, DNA was isolated from each individual, and then PCR-RFLP analysis was used to distinguish between susceptible and resistant individuals. All individuals analyzed were found to carry resistance in the acetylcholinesterase (*ace*) gene region via the target-site insensitivity mechanism. No susceptible individuals were detected. Of the resistant individuals, 194 were identified as homozygous resistant (RR), while 166 were heterozygous resistant (RS). The results indicate that current pest management strategies need to be re-evaluated.

Keywords: *Bemisia* tabaci, Insecticide resistance, Acetylcholinesterase (*ace*) gene, F331W, Türkiye

Acknowledgement: This study was supported by Scientific and Technological Research Council of Türkiye (TUBITAK) under Grant Number 123Z722. The authors thank TUBITAK for their support.

➢ *POSTER PRESENTATION*

Antioxidant activities of polycaprolactone/sodium alginate/chestnut honey nanofibers

Azra Huner* (*ORCID: https://orcid.org/0000-0001-7235-6338*)

* Yildiz Technical University, Science and Technology Application and Research Center, Istanbul, Turkey.

*Corresponding author e-mail: azra.huner@yildiz.edu.tr

Abstract

Chestnut honey, which is abundant in phenolic compounds, is known for its high antioxidant properties. These compounds protect cells from oxidative stress because they contribute to the ability to scavenge free radicals. On the other hand, polycaprolactone (PCL) has particularly high mechanical strength and biodegradability, while sodium alginate (SA) is hydrophilic and bioactive. In this study, PCL/SA/chestnut honey nanofibers were produced by the electrospinning method in order to combine these superior properties of PCL, SA, and chestnut honey. These nanofibers were characterized by FTIR spectroscopy. Their surface morphologies were examined by SEM. The ABTS (2,2'-Azinobis(3-ethylbenzothiazoline-6-sulfonic acid)) test was performed for the antioxidant activities of these nanofibers. The antioxidant activities of these nanofibers varied according to the ratio of chestnut honey used, and the highest antioxidant activity was found to be 352 □g TE/mg. These results particularly emphasized the antioxidant potential of chestnut honey, indicating that it effectively scavenged ABTS radicals.

Keywords: Polycaprolactone, sodium alginate, chestnut honey, antioxidant, nanofiber.

➢ *POSTER PRESENTATION*

Fabrication and characterization of polycaprolactone/cellulose acetate/polselenophene nanofibers

Azra Huner* (*ORCID: https://orcid.org/0000-0001-7235-6338*)

* Yildiz Technical University, Science and Technology Application and Research Center, Istanbul, Turkey.

*Corresponding author e-mail: azra.huner@yildiz.edu.tr

Abstract

Polycaprolactone (PCL) and cellulose acetate (CA) nanofibers have been investigated for various biomedical applications, especially in tissue engineering and wound healing. These nanofibers are usually produced using electrospinning techniques, which allow the creation of fibers with high porosity and surface area, making them suitable for cell proliferation and adhesion. The unique electrical properties of conductive polymers combined with the high surface area and tunable morphology of nanofibers have attracted significant interest for applications in sensors, tissue engineering, and drug delivery. Nanofibers containing polycaprolactone (PCL), cellulose acetate (CA), and polyselenophene (PSe) in different proportions were produced by electrospinning. These PCL/CA/PSe nanofibers were characterized by FTIR, XRD, and SEM and are recommended for various biomedical applications, especially in tissue engineering.

Keywords: Polycaprolactone, cellulose acetate, polyselenophene, nanofiber.

➢ *POSTER PRESENTATION*

Simultaneous Quantitative Analysis of the Active Pharmaceutical Ingredients in Oral Antiseptic Solution By HPLC

Gülşah Çebi[1*] (*ORCID: https://orcid.org/0000-0003-3814-6016*),
Bürge Aşçı[1] (*ORCID: https://orcid.org/0000-0003-0479-5050*)

[*1]Yildiz Technical University, Faculty of Science and Arts, Department of Chemistry, İstanbul, Türkiye.

*Corresponding author e-mail:gulsahcebi34@gmail.com

Abstract

Hexadecylpyridinium chloride (HC) is a quaternary ammonium surfactant having broad spectrum antimicrobial activity. Benzydamine hydrochloride (BH) is a locally acting nonsteroidal anti-inflammatory drug with local anaesthetic and analgesic properties for pain relief and anti-inflammatory treatment of inflammatory conditions of the mouth and throat. Chlorhexidine digluconate (CG) is the gluconate salt form of chlorhexidine, a biguanide compound used as an antiseptic agent with topical antibacterial activity. In this study, was RP-HPLC method for analysis of ternary mixture of HC, CG and BH in oral antiseptic solution. The mobile phase system was consisted of methanol/buffer solution. The correlation between the peak areas and the concentration HC, CG, BH was examined. The regression coefficients were found to be 0.9993; 0.9991; 0.9992, respectively. The solutions of each substance prepared 3 times on the same day and at 3 different concentrations on 4 different days were analyzed for the pecision study. In the analyses performed on the same day, 0.63 to 1.98 and in the analyses performed on different days, 0.85 to 1.99 RSD values were obtained. The standart solution containing the investigated substances was added to the oral solution at 3 different concentrations and analyzed for the accuracy study. Recovery% values ranging from 98.05 to 102.17 were obtained. The detection limit for, HC, CG, BH was calculated as 0.140 µg/mL; 0.241 µg/mL; 0.044 µg/mL, and the determination limit was calculated as 0.424 µg/mL; 0.803 µg/mL; 0.147 µg/mL, respectively. The oral solution containing these substances was analyzed using the developed method. Its content was found to be 0.511 mg/mL HC, 1.208 mg/mL CG, 1.488 mg/mL BH with % RSD values in the range of 1.208-1.414. The amounts of substance found as a result of the analysis were compared with the label values. Recovery % values of 100.67;102.20; 99.20 were obtained for HC, CG, BH.

Keywords: Oral solutions, HPLC, Active Pharmaceutical Ingredients

➢ *POSTER PRESENTATION*

Phytoremediation potential of *Limnobium laevigatum* enhanced by ZnO nanoparticles in arsenic-contaminated waters

Ekin Ayşegül KIRMIZIKAR[1] (https://orcid.org/*0009-0006-8163-2481*), Danial NASSOUHI*[1] (*https://orcid.org/0000-0003-3693-6313*), Mehmet Borga ERGÖNÜL[1] (https://orcid.org/0000-0002-0263-9129)

*[1]Department of Biology, Faculty of Science, Ankara University, 06100 Ankara, Turkey

*Corresponding author e-mail: dnassouhi@ankara.edu.tr

Abstract

Arsenic (As), which is one of the most toxic elements among heavy metals, has become increasingly prevalent in aquatic environments as a result of both natural processes and human activities. Due to the risks that posed by As, the treatment of As contaminated waters have become essential. Various methods such as coagulation, chemical precipitation and ion exchange used to remove arsenic from contaminated waters. However, due to high cost and secondary pollution risk linked to these methods, phytoremediation has emerged as a cost-effective and environmentally friendly alternative. To improve its efficiency and overcome certain limitations, recent studies have explored the use of nanotechnology, which can boost contaminant uptake and stress tolerance in plants. Metal oxide nanoparticles such as iron oxides and manganese oxides are commonly used in nano-phytoremediation. However, the efficiency of zinc oxide nanoparticles (ZnO NPs) in combination with macrophytes for arsenic removal remains unstudied. This study aimed to evaluate the arsenic removal performance of *Limnobium laevigatum* (Humb. & Bonpl. Ex Willd.) Heine. and ZnO NPs at three different exposure durations (1, 4, and 7 days) in lake water. Plants were exposed to 2 ppm As, either alone or in combination with 10 ppm ZnO NPs in the water provided from Mogan Lake in order to simulate a natural environment. The concentration of As were measured using ICP-MS. Arsenic removal percentages, accumulated As content in plant tissue, and bioconcentration factor (BCF) were calculated and compared across treatment groups. A time-dependent increase in arsenic removal was observed throughout the experimental period. Arsenic removal efficiencies ranged between 4.2% and 16.1%, with arsenic accumulation in plant tissues varying 25.7 to 130.7 mg/g. BCF values were observed to range between 16.2 and 82.9.

Keywords: *Limnobium laevigatum*, zinc oxide nanoparticles, phytoremediation, arsenic

2.2. FULL-TEXT PAPER

➢ *POSTER PRESENTATION*

The Anti-cancer impact of Metformin In the Prostate Cancer

Ayriana Safari Baesmat

Lokman Hekim University, Faculty of Medicine, Department of Medical Microbiology, Ankara, Turkey

*Corresponding author e-mail:191110315@lhu.edu.tr

Abstract
Purpose: Metformin, a commonly prescribed anti-hyperglycemic agent, has been reported to exert inhibitory effects on prostate cancer cell growth under both laboratory and animal model conditions. While its glucose-lowering properties are well characterized, the precise molecular mechanisms driving its anti-cancer activity, particularly in androgen receptor (AR)-positive castration-resistant prostate cancer (CRPC), remain insufficiently defined. This study seeks to investigate the specific intracellular signaling networks influenced by metformin in AR-expressing CRPC cells to better understand their therapeutic potential in advanced prostate cancer.
Methods: The gene expression data were retrieved from Gene Expression Omnibus (GSE196343). Variance, *t* test and linear regression analysis, hierarchical clustering, network, and pathway analysis were performed.
Results: In this study, we identified altered genes involved in metformin in the prostate cell line and the relevant pathways to understand whether the treatment slows down cancer progression. Five genes were differentially expressed following the metformin treatment in prostate cancer cells. We identified a network between these genes and pathways they belong to. Pathway analysis showed that these genes are mostly associated with cancer cell apoptosis.
Conclusion: The genes TCIM, HSPA6, HSPA7, ANKRD1, and EGR2 have been implicated in the negative progression of prostate cancer, with most exhibiting inhibitory effects on cancer cell proliferation. However, the extent to which metformin exerts its anti-tumor effects—through the induction of apoptosis via intrinsic pathways and modulation of the immune response—remains incompletely elucidated. The aim of this study was to delineate the molecular signaling cascades modulated by metformin in prostate cancer. The results demonstrate that metformin, at concentrations known to inhibit cellular proliferation, regulates critical signaling pathways involved in the survival and progression of human prostate cancer cells.
Keywords: Prostate Cancer, Metformin, Molecular biology; Transcriptome analysis

Introduction

Prostate cancer (PCa) is the most prevalent malignancy among men in Western nations and remains a leading contributor to cancer-related mortality. Emerging research over the past decade suggests that biguanide drugs, particularly metformin, may play a role in both the prevention and treatment of various cancers, including PCa (1). Metformin is the most widely prescribed oral antihyperglycemic agent globally and has been utilized in clinical practice for over five decades. In addition to its primary role in managing diabetes, it is commonly used for the treatment of polycystic ovary syndrome (PCOS) and is currently being explored for its potential antiviral properties. Notably, it has demonstrated a favorable safety profile with minimal toxicity. Epidemiological studies have indicated a reduced incidence of cancer and lower cancer-specific mortality rates among diabetic patients receiving metformin compared to those treated with alternative antidiabetic therapies (2). Metformin, a biguanide, is the most frequently prescribed antidiabetic medication globally, attributed to its high clinical efficacy and favorable tolerability profile. Emerging research suggests that metformin may inhibit cancer growth driven by insulin stimulation. Large-scale observational studies on prevalent malignancies have identified an inverse relationship between metformin usage and the incidence of cancers such as colorectal, hepatic, and pulmonary cancer (3).
Research findings indicate that metformin may play a role in reducing cognitive decline and could be a promising therapeutic option for neurological disorders such as depression, Alzheimer's disease, and Parkinson's disease (4). Furthermore, studies suggest that metformin administration may offer renal protective effects, potentially mitigating acute kidney injury and other forms of renal impairment (5).
Numerous studies have demonstrated that metformin exhibits inhibitory effects on the growth and progression of prostate cancer as well as other malignancies. In vitro research has shown that metformin exposure suppresses proliferation and invasiveness in human prostate cancer cell lines (6), while in vivo studies have

reported a reduction in prostate tumor growth in both xenograft and transgenic mouse models following metformin treatment. Additionally, epidemiological evidence suggests that metformin use may be associated with a decreased risk of prostate tumor development and progression (7).

A retrospective study conducted by D.E. Spratt et al. suggests that metformin use may be associated with a reduced risk of prostate-specific antigen (PSA) recurrence and distant metastases in patients with prostate cancer undergoing radiotherapy. Additionally, the findings indicate that metformin may play a role in delaying the progression to castration-resistant prostate cancer (8).

Clinical evidence suggests that metformin may have a beneficial impact on prostate cancer outcomes. Patients with localized prostate cancer who received radiation therapy demonstrated a reduction in biochemical recurrence and an improvement in overall survival following metformin treatment (9).

Furthermore, a retrospective analysis conducted by J.A. Richards et al. on individuals with advanced prostate cancer reported enhanced overall survival among diabetic patients using metformin (10).

Additionally, a case-control study by J.L. Wright and J.L. Stanford identified a lower relative risk of prostate cancer in Caucasian men who were prescribed metformin (11).

Despite growing evidence supporting the potential anticancer effects of metformin, findings remain inconsistent regarding its impact on prostate cancer risk. A large case-control study conducted by L. Azoulay et al. found no significant association between metformin use and a reduced risk of prostate cancer in individuals with type 2 diabetes (12). These findings suggest that metformin's tumor-suppressive effects may be limited to specific subgroups of prostate cancer patients rather than exerting a universal protective benefit.

Although preclinical research has demonstrated that metformin can inhibit prostate tumor growth, the precise molecular mechanisms underlying its antitumor effects remain incompletely understood. Several studies have shown that metformin exposure disrupts cell cycle progression by inducing G0/G1 phase arrest in human prostate cancer cells (13). The tumor suppressor p53 is a key regulator of cell cycle control, influencing the expression of proteins such as the cyclin-dependent kinase inhibitor p21, 14-3-3-σ, and GADD45α (14). Evidence suggests that p53 plays a crucial role in metformin-mediated tumor suppression, as its absence or knockdown via siRNA reduces metformin's ability to inhibit cell proliferation in prostate cancer models (15). However, additional signaling pathways may also contribute to metformin's anticancer effects. Notably, metformin has been shown to downregulate the proto-oncogene c-Myc independently of p53, at concentrations that effectively suppress prostate cancer cell proliferation and tumor growth (16). These findings indicate that metformin may exert its antitumor activity through multiple molecular pathways that regulate prostate cancer progression and survival.

The extent to which metformin exerts antitumor effects across different stages of advanced prostate cancer remains uncertain. Prostate cancer initially develops as an androgen-dependent malignancy, relying on androgens such as dihydrotestosterone (DHT) to sustain growth. However, following androgen deprivation therapies targeting the androgen receptor (AR) signaling pathway, tumors often transition into castration-resistant prostate cancer (CRPC), characterized by reduced dependence on circulating androgens. Current research on metformin's effects has predominantly focused on castration-sensitive LNCaP cells or castration-resistant PC3 and DU145 prostate cancer cell lines. LNCaP cells, which harbor a mutated AR (17), are frequently utilized as an in vitro model for early-stage prostate cancer. In contrast, while many castration-resistant prostate tumors continue to express AR, the PC3 and DU145 cell lines exhibit minimal to no AR expression (18). These differences underscore the complexity of prostate cancer progression and highlight the need for further investigation into the specific molecular contexts in which metformin may exert therapeutic benefits.

Currently, the extent to which metformin suppresses tumor growth and induces apoptosis through intrinsic pathways while simultaneously modulating the immune response remains incompletely understood. The objective of this study was to investigate the molecular signaling pathways influenced by metformin in prostate cancer. Findings from this research demonstrate that metformin, at growth-inhibitory concentrations, regulates key signaling pathways essential for the survival of human prostate cancer cells.

Materials and methods

Microarray Gene Expression Data

Transcription profiles of human C4-2 prostate cancer cells treated with metformin were obtained from the data on gene expression was retrieved from the Gene Expression Omnibus (GEO) database (GSE196343).

Processing and normalization of data

The raw gene expression data obtained from the Gene Expression Omnibus (GEO) database was normalized using the DESeq2 package in R. The processed transcriptional profile includes expression data for 16,369 distinct genes. The dataset comprises three biological replicates of C42 prostate cancer cells in the control group (without metformin treatment) and three biological replicates of C42 cells treated with 5 mM metformin.

Identification of differentially expressed genes as a result of metformin treatment

The Deseq2 package (version 4.2.1) was used for differential expression analysis. The normalized gene expression data from the control groups and groups treated with metformin were compared separately to identify significant differentially expressed genes.

The groups treated with metformin were compared with the control group by Deseq2 analysis, and statistically differentially expressed genes were determined (p.val <0.05). Then, genes with a log fold change value greater than 8 were determined.

Hierarchical clustering

Common genes which were determined as statistically differentially expressed in all metformin treated groups versus the control group were hierarchically clustered with mean standardized gene expression values with Cluster 3.0 program. After performing cluster analysis, we applied our standards to the resulting data and analyzed them in Treeview. Genes and arrays were clustered using the full linkage approach and Euclidean distance to create a hierarchical cluster.

Functional pathway analysis

Database for Annotation, Visualization, and Integrated Discovery" (DAVID) was used to analyze the functional connections between these genes. Our genes' related pathways have been identified accordingly.

Gene Set Enrichment Analysis (GSEA)

The process of GSEA was conducted following the GSEA guideline procedure (http://software.broadinstitute.org/ gsea/docGSEAUserGuideFrame.html). Analysis was performed between control group versus metformin treated group. The main purpose of this analysis is to determine which gene is significantly enriched in which gene set belongs to the GSEA as well as to understand which gene set is enriched in which groups. GSEA calculates the enrichment score (ES), normalized enrichment score (NES), nominal P value (NOM P value), false discovery rate q value (FDR q value), and familywise error rate P value (FWER). The ES value indicates gene's maximum deviation in gene sets; in other words, this score helps to find most upregulated genes. NES value represents the connection or difference between gene sets and gene expression. The higher NES value shows the elevation of permutations. Hence, higher NES value increases significance of gene sets. In addition to ES and NES values, NOM P value evaluates the importance of ES calculation. Therefore, NOM P value is directly correlated with ES as well as NES value. Increase of NOM P value shows critical role of ES. On the other hand, FWER P value indicates false positives probability of NES and so, lower FWER P value directly and significantly correlated with correctness of NES calculation. Moreover, the FDR q value is the most vital value of this analysis. This value needs to be lower than 0.25 and even, when this value becomes smaller, the enrichment of gene sets is more meaningful.

Network Analysis

Network analysis was performed using GeneMANIA software to better demonstrate the relationship of differentially expressed genes between the two groups.

Results

Identification of differentially expressed genes in metformin treated groups

A comparative analysis of whole-genome expression profiles between metformin-treated and control groups revealed that over 500 genes exhibited significant differential expression. These findings suggest that metformin induces widespread transcriptional alterations in prostate cancer cells, potentially influencing key regulatory pathways associated with tumor progression and cellular response to treatment (Figure 1).

Among the extensive set of differentially expressed genes, five genes (TCIM, HSPA6, HSPA7, ANKRD1, and EGR2) were identified with p-values < 0.05 and absolute log fold change (FC) values exceeding 8. The detailed list of these genes, along with their respective p-values and log fold change values, is presented in Table 1

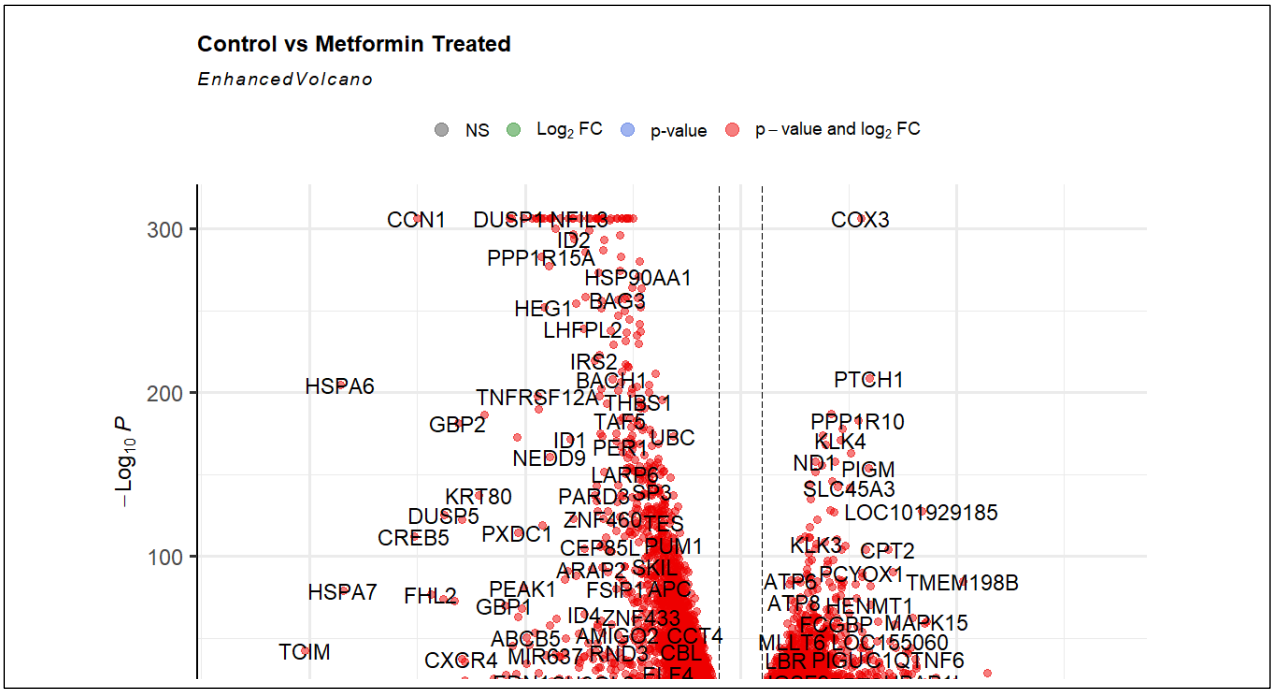

Figure1

Volcano plots were obtained as a result of comparison between groups. Red dots indicate genes that are significantly (p-value <0.05) differential expressed after treatment with metformin.

Hierarchical clustering analysis revealed that these five genes (p-values < 0.05 and absolute log fold change (FC) values > 8) effectively differentiate metformin-treated cells from the control group (Figure 2). Notably, all five genes exhibited upregulated expression in the metformin-treated group, as illustrated in (Figure 3).

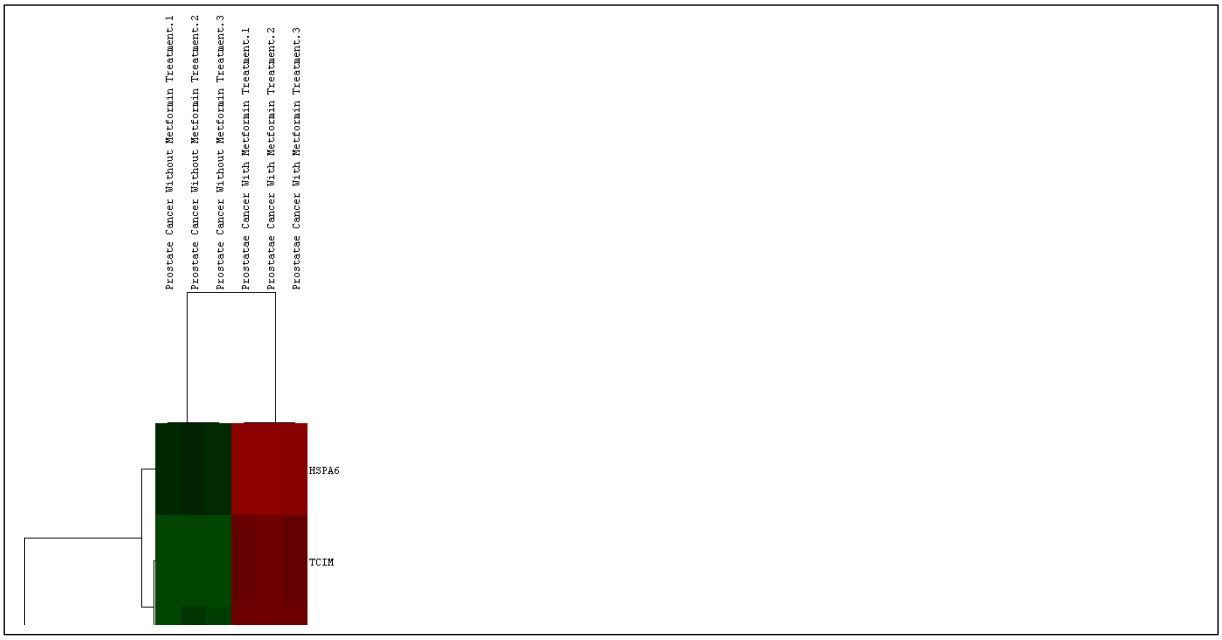

Figure 2

Hierarchical cluster analysis shows that common significantly differentially expressed 5 genes can well distinguish between the Control group and metformin treated groups. Log Fold Change > 8, False

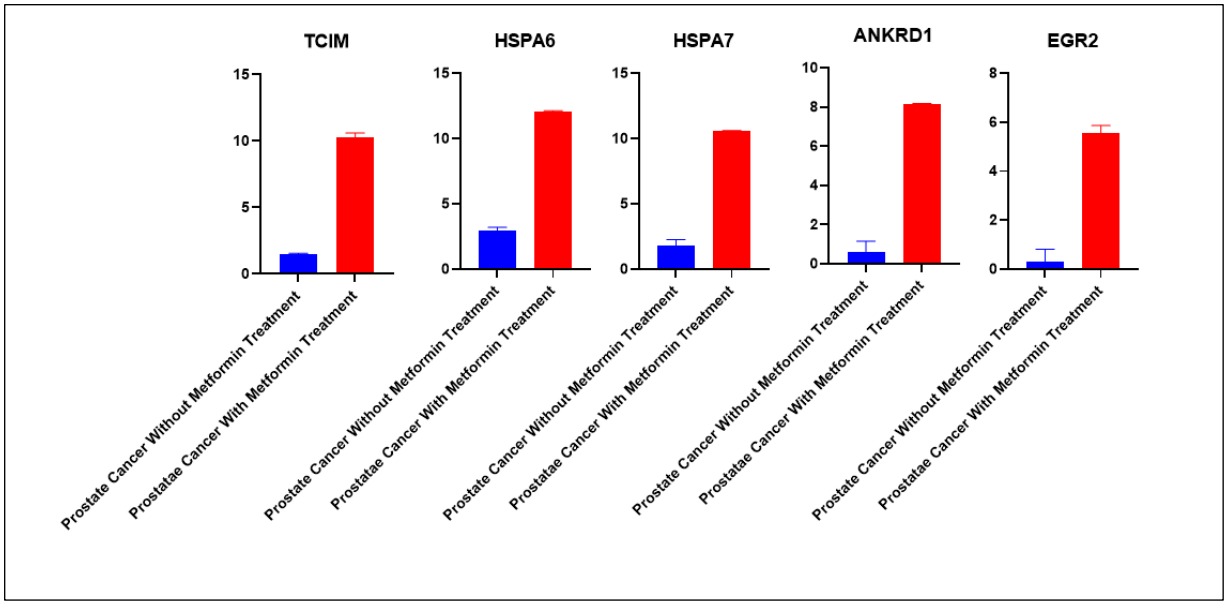

Figure 3

Five genes were significantly up regulated after treatment of colon cells with metformin.

Table 1

Log Fold change and p-values of 5 genes which most significantly differentially expressed between Metformin-treated and untreated groups.

Gene Symbol	*Log FC*	*p value*
TCIM	-10.099387	2.76E-43
HSPA6	-9.274401	2.3E-205
HSPA7	-9.204278	1.51E-79
ANKRD1	-8.929631	3.87E-18
EGR2	-8.205573	1.5E-11

Pathway analysis of differentially expressed genes

Pathway functional annotation clustering analysis revealed that metformin-treated prostate cancer cells exhibit significant enrichment in immune-related pathways, cell cycle arrest mechanisms, and pathways associated with the positive regulation of apoptosis. These findings suggest that metformin exerts its effects through multiple biological processes that influence tumor cell survival and immune modulation (Table 2).

Determination of enriched genesets in the metformin treated group

Gene set enrichment analysis (GSEA) was performed to identify pathways significantly enriched in both the control and metformin-treated groups. In metformin-treated samples, gene sets associated with p53 positive regulation, and p38 cascade activation response exhibited significant enrichment at a false discovery rate (FDR) of 25%. Notably, pathways such as Leukocyte chemotaxis, positive regulation of B cells and activation of innate immune system demonstrated substantial enrichment at this threshold (Table 3 and Figure 5).

Figure 4 shows a strong network relationship between differentially expressed genes. Together with the results of pathway and gene set enrichment analyses, this result is an expected result (Figure 4).

ANKRD1	
GOTERM_BP_DIRECT	positive regulation of apoptotic process, positive regulation of DNA damage response, signal transduction by p53 class mediator, positive regulation p53 expression
REACTOME_PATHWAY	PPARA activates gene expression, Hippo signaling pathway,
EGR2	
KEGG_PATHWAY	activation of mitochondrial apoptotic pathway, Negative regulation of MEK/ERK signaling pathway, negative regulator of NF-κB,
HSPA6	
REACTOME_PATHWAY	Innate Immune System, Immune System,
KEGG_PATHWAY	Antigen processing and presentation, Binds CD94/ NKG2D receptore, CD8+ cell-mediated anti-tumor responses, NK cell-mediated anti-tumor responses,
TCIM	
GOTERM_BP_DIRECT	MDM2-mediated positive regulation of p53, cell cycle arrest, regulation of cell cycle G1/S phase transition, negative regulation of Notch signaling pathway, endothelial cell activation involved in immune response,

Table 2

Pathway analysis of 5 most significant genes almost all of these genes are involved in apoptosis and immune related pathways and associated cellular functions.

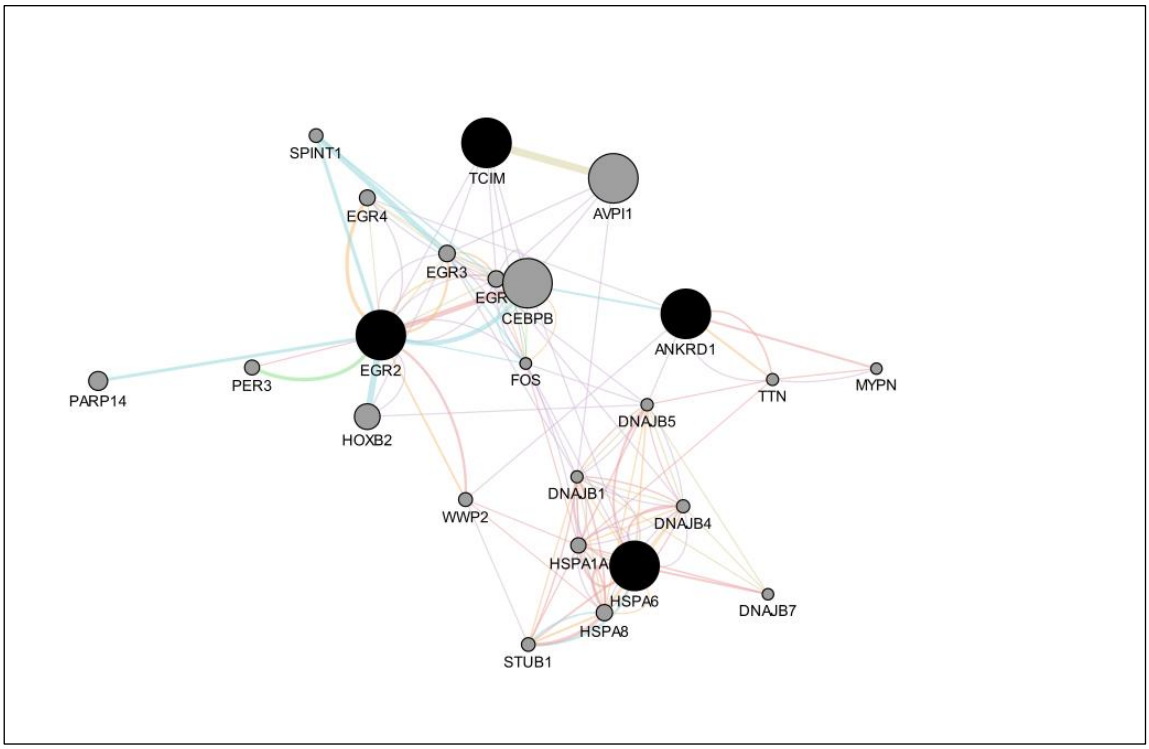

Figure 4

illustrates a robust network of interactions among differentially expressed genes. This observation aligns with and supports the findings from both pathway and gene set enrichment analyses, reinforcing the expected biological relevance of these interconnected gene expression changes.

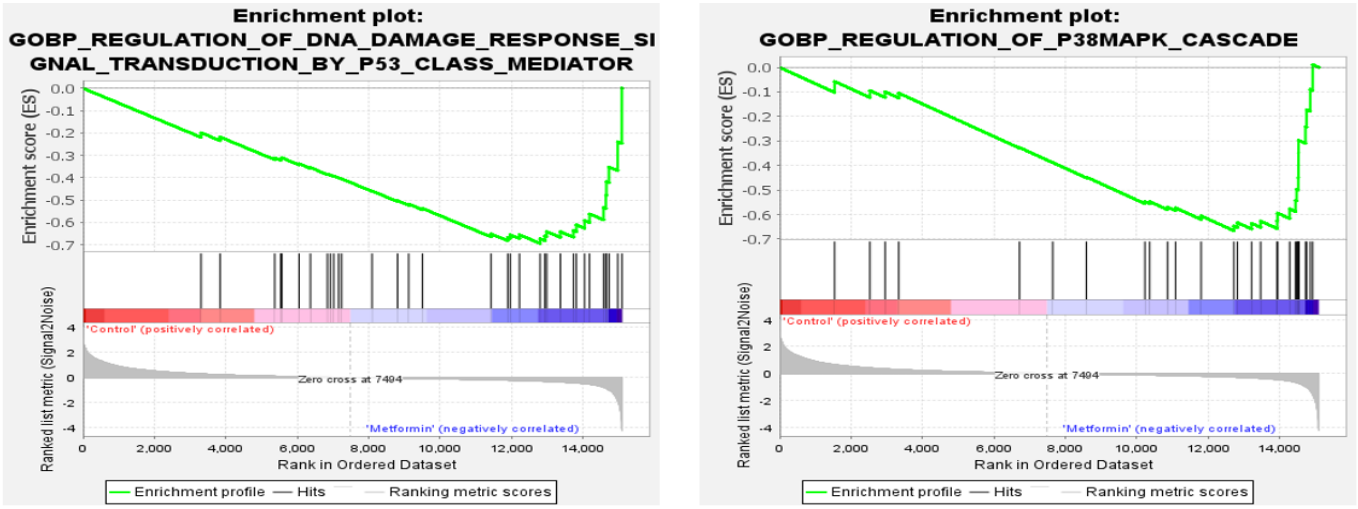

Figure 5

The P53 related and P38 MAPK cascade related apoptosis enrichment plot was represented and upregulated in post metformin treated group.

Table 3

Gene set enrichment analysis (GSEA) revealed that metformin-treated samples showed significant enrichment (FDR 25%) in pathways related to p53 activation, p38 signaling, leukocyte chemotaxis, B cell regulation, and innate immune activation.

GS DETAILS	ES	NES	NOM p-val	FDR q-val	FWER p-val	RANK AT MAX
GOBP_SKELETAL_MUSCLE_CELL_DIFFERENTIATION	54	-0.67	-2.23	0	0	0
GOBP_CHAPERONE_COFACTOR_DEPENDENT_PROTEIN_REFOLDING	30	-0.72	-2.15	0	0.009	0.007
GOBP_MACROPHAGE_DIFFERENTIATION	38	-0.68	-2.15	0	0.006	0.007
GOBP_REGULATION_OF_DNA_DAMAGE_RESPONSE_SIGNAL_TRANSDUCTION_BY_P53_CLASS_MEDIATOR	34	-0.69	-2.12	0	0.008	0.013
GOBP_CIRCADIAN_REGULATION_OF_GENE_EXPRESSION	59	-0.62	-2.09	0	0.011	0.022
GOBP_B_CELL_PROLIFERATION	41	-0.66	-2.08	0	0.014	0.034
GOBP_AUTONOMIC_NERVOUS_SYSTEM_DEVELOPMENT	23	-0.74	-2.08	0	0.012	0.034
GOBP_CHONDROCYTE_PROLIFERATION	20	-0.76	-2.07	0	0.013	0.04
GOBP_DE_NOVO_PROTEIN_FOLDING	40	-0.66	-2.07	0	0.012	0.042
GOBP_PROTEIN_REFOLDING	22	-0.74	-2.05	0	0.016	0.063
GOBP_MYELOID_LEUKOCYTE_DIFFERENTIATION	150	-0.52	-2.04	0	0.019	0.078
GOBP_GRANULOCYTE_CHEMOTAXIS	45	-0.62	-2	0	0.04	0.172
GOBP_LEUKOCYTE_CHEMOTAXIS	105	-0.54	-1.99	0	0.038	0.174
GOBP_LIPOPOLYSACCHARIDE_MEDIATED_SIGNALING_PATHWAY	36	-0.66	-1.99	0	0.038	0.186
GOBP_REGULATION_OF_HEMATOPOIETIC_PROGENITOR_CELL_DIFFERENTIATION	34	-0.65	-1.98	0	0.044	0.231
GOBP_REGULATION_OF_P38MAPK_CASCADE	29	-0.67	-1.94	0	0.068	0.349
GOBP_INNATE_IMMUNE_RESPONSE_ACTIVATING_CELL_SURFACE_RECEPTOR_SIGNALING_PATHWAY	61	-0.57	-1.94	0	0.066	0.358
GOBP_POSITIVE_REGULATION_OF_B_CELL_PROLIFERATION	21	-0.69	-1.94	0	0.063	0.359
GOBP_REGULATION_OF_B_CELL_PROLIFERATION	30	-0.66	-1.93	0	0.065	0.387
GOBP_INTEGRATED_STRESS_RESPONSE_SIGNALING	43	-0.59	-1.93	0	0.065	0.402

Discussion

Metformin, a widely used antidiabetic agent, is recognized not only for its role in regulating serum glucose levels but also for its potential antitumor properties in prostate cancer. However, the precise molecular mechanisms through which metformin exerts its anticancer effects remain inadequately understood, posing a challenge in identifying patient subgroups that may derive therapeutic benefit from its use. This study employs a transcriptomic approach to systematically investigate the impact of metformin on tumor growth suppression, immune response activation, and apoptotic pathway regulation in prostate cancer, providing insights into its potential as a therapeutic intervention.

TCIM, HSPA6, HSPA7, ANKRD1, and EGR2 gene expression alterations were identified depending on time after treatment with Metformin of prostate cancer cell line. These genes were identified as downregulated in gastric cancer cells, and the treated and untreated groups ($P < 0.05$ and Fold Change > 8) were hierarchically forming a very distinct cluster, as expected. Gene set enrichment analysis supported the results that some crucial genes function effectively in the positive regulation of apoptosis as a result of metformin treatment.

The Ankyrin Repeat Domain 1 (ANKRD1) gene, also referred to as Cardiac Ankyrin Repeat Protein (CARP), has been implicated in various malignancies, including prostate cancer. Its role in tumorigenesis appears to be context-dependent, with evidence supporting both tumor-suppressive and tumor-promoting functions under distinct biological conditions. However, accumulating research suggests that ANKRD1 predominantly exerts tumor-suppressive effects, largely mediated through its regulatory interactions with the p53 tumor suppressor pathway (19). A principal mechanism through which ANKRD1 exerts its tumor-suppressive function involves the modulation of p53 stability and transcriptional activity. Overexpression of ANKRD1 has been demonstrated to enhance p53 expression, leading to the transcriptional activation of key downstream effectors, including BAX, a pro-apoptotic member of the Bcl-2 family, and CDKN1A (p21), a cyclin-dependent kinase inhibitor that plays a crucial role in cell cycle arrest. Upregulation of these target genes facilitates apoptotic signaling and inhibition of cell proliferation, thereby contributing to genomic integrity maintenance and tumor suppression (20).

A pivotal mechanism underlying ANKRD1's tumor-suppressive function is its direct interaction with MDM2, an E3 ubiquitin ligase that serves as a principal negative regulator of p53. Under physiological conditions, MDM2 binds to p53, promoting its ubiquitination and subsequent proteasomal degradation, thereby maintaining low basal p53 levels in non-stressed cells. However, ANKRD1 has been identified as an MDM2-

binding protein, facilitating MDM2 destabilization and consequently reducing its cellular levels. This depletion of MDM2 activity leads to a decrease in p53 ubiquitination and degradation, resulting in enhanced p53 stability and transcriptional activity. Consequently, stabilized p53 transcriptionally activates genes involved in cell cycle arrest (p21) and apoptosis (BAX), thereby exerting its tumor-suppressive function.ANKRD1 is proposed to modulate the Hippo signaling pathway, which governs cell proliferation, apoptosis, and organ size regulation. Dysregulation of Hippo signaling has been associated with tumorigenesis, and ANKRD1 may function as a regulatory factor by influencing the activity of Yes-associated protein (YAP), a key effector of the pathway (21).

ANKRD1 has been identified as a negative regulator of NF-κB, a transcription factor known for its role in inflammation, immune response, and tumor progression. By inhibiting NF-κB activation, ANKRD1 may suppress the expression of pro-inflammatory cytokines and oncogenic survival signals, thereby mitigating cancer progression.

The PI3K/AKT pathway is a central regulator of cell survival, proliferation, and resistance to apoptosis in many malignancies. ANKRD1's role in p53 stabilization may indirectly impact PI3K/AKT signaling, potentially modulating cellular responses to growth factors and stress signals, further reinforcing its tumor-suppressive role.The tumor-suppressive function of ANKRD1 is strongly dependent on the presence of functional p53. In prostate cancer and other malignancies where p53 is frequently mutated or inactivated, the therapeutic relevance of ANKRD1 may be limited. However, in cancers that retain wild-type p53, ANKRD1 may represent a promising therapeutic target. Strategies aimed at restoring ANKRD1 expression or activity could enhance p53-dependent apoptotic and cell cycle regulatory mechanisms, thereby suppressing tumor progression (22).

The TCIM gene, also known as C8orf4, encodes a small nuclear protein that has been widely recognized for its role in oncogenesis, primarily through the activation of the Wnt/β-catenin signaling pathway. However, emerging evidence suggests that TCIM exhibits a paradoxical function, as its high expression has been correlated with improved survival in certain cancers, such as prostate cancer. This finding indicates that TCIM may exert additional regulatory effects through alternative mechanisms beyond Wnt/β-catenin signaling.

One of the critical mechanisms by which TCIM may exert a protective role is through the stabilization of the tumor suppressor protein p53. p53 is a key regulator of apoptosis and genomic stability, and its function is often compromised in cancer. If TCIM influences MDM2-mediated degradation of p53, it could enhance p53 stability, leading to increased apoptosis and cell cycle arrest in tumor cells, thereby inhibiting cancer progression (23).

TCIM has been implicated in the regulation of NF-κB signaling, a pathway known for its role in inflammation and immune response. By modulating this signaling cascade, TCIM may influence immune surveillance mechanisms, helping the immune system recognize and eliminate cancerous cells. This function could reduce tumor progression by promoting an anti-tumor immune response.

NOTCH signaling plays a crucial role in cell differentiation and the suppression of stemness, which is important for controlling tumor growth. In some cancers, TCIM activation may promote cellular differentiation rather than uncontrolled proliferation, thereby reducing the aggressiveness of tumors. This suggests that TCIM may act as a regulatory switch, determining whether cells follow an oncogenic or tumor-suppressive trajectory.Under stress conditions, TCIM may facilitate autophagy, a process essential for cellular homeostasis. By promoting the removal of damaged organelles and preventing malignant transformation, TCIM could protect non-malignant cells while exerting selective pressure on cancerous cells. This function is particularly important in preventing cancer initiation and maintaining cellular integrity.Another emerging function of TCIM is its potential involvement in chromatin remodeling and epigenetic regulation. By influencing histone modifications, TCIM may enhance the expression of tumor suppressor genes involved in apoptosis and DNA repair. This ability to regulate transcriptional activity at the epigenetic level highlights TCIM's broader impact on genomic stability and cancer prevention (24).

The Early Growth Response 2 (EGR2) gene encode a transcription factor that plays a crucial role in cellular processes such as apoptosis, differentiation, and immune regulation. While its involvement in prostate cancer remains underexplored, emerging evidence suggests that EGR2 functions as a pro-apoptotic regulator across various cellular contexts. Through transcriptional activation of mitochondrial apoptotic regulators and modulation of key signaling pathways, including MEK/ERK, EGR2 contributes to programmed cell death (25). EGR2 contributes to apoptosis by regulating the expression of key pro-apoptotic genes involved in the mitochondrial apoptotic pathway. Among its transcriptional targets, BNIP3L (BCL2/adenovirus E1B 19kDa interacting protein 3-like) and BAK (BCL2 antagonist/killer 1) have been identified as major effectors in the intrinsic apoptotic cascade.

EGR2-mediated upregulation of BNIP3L enhances mitochondrial membrane permeabilization, facilitating the release of cytochrome c. This event triggers the activation of caspases 9, 3, and 8, leading to the execution of programmed cell death. By promoting mitochondrial integrity disruption, EGR2 plays a critical role in apoptosis initiation. BAK, another transcriptional target of EGR2, amplifies the intrinsic apoptotic signaling by inducing mitochondrial outer membrane permeabilization (MOMP). This process further accelerates cytochrome c release and caspase activation, reinforcing EGR2's role in apoptotic regulation. The MEK/ERK signaling pathway, widely recognized for its role in cell survival and proliferation, also influences EGR2 expressions.

In certain cellular contexts, dysregulation of MEK/ERK signaling may impact EGR2 transcriptional activity, potentially altering apoptotic responses. Modulation of this pathway through targeted inhibitors may offer a therapeutic strategy to enhance EGR2-mediated apoptosis in prostate cancer cells exhibiting ERK dependency. EGR2 expression is frequently dysregulated in cancer through epigenetic mechanisms such as promote hypermethylation. The silencing of EGR2 via DNA methylation contributes to tumor survival and resistance to apoptosis. Pharmacological agents such as DNA methylation inhibitors or histone deacetylase (HDAC) inhibitors may restore EGR2 expression, thereby sensitizing tumors to apoptotic signals (26).

HSPA6 presence on cell surface MHC I pathway HSP70 in contrast, provides a danger signal to the immune system and may activate anti-tumor immune responses by cytotoxic T lymphocytes (CTL) and natural killer (NK) cells. HSP70-activated NK cells, for example, can attack tumor cells that express HSP70 at the plasma membrane. This feature of HSP70 reminds of other stress-inducible molecules including the major histocompatibility complex (MHC) class I chain-related molecules A (MICA) and B (MICB), which are ligands for activating NK receptor NK group 2, member D (NKG2D) and are induced by cellular and genotoxic stress on many tumor cells. Interestingly, the stress-inducible HSP70 and stress inducible NKG2D ligands can collaborate in tumor immunosurveillance by NK cells. HSP70-activated NK cells can also kill tumor cells that express NKG2D ligands at the plasma membrane instead of HSP70. An adaptive cellular immunotherapy with autologous HSP70-stimulated NK cells may therefore target not only tumors that express HSP70 at the plasma membrane but also those that express NKG2D ligands. Notably, an overexpression of HSP70 in tumors usually fails to protect against apoptosis executed in the granule exocytosis pathway of CTL and NK cells, making immunotherapies attractive to treat HSP70-overexpressing malignancies.

Killing of membrane Hsp70 positive tumor cells by activated NK cells via granzyme B mediated apoptosis. Activated NK cells, expressing Hsp70 receptors such as the C-type lectin receptors CD94/NKG2C and NKG2D bind to membrane Hsp70 on tumor cells and secrete granzyme B, either alone or in combination with perforin. In the absence of perforin, granzyme B is directly endocytosed via membrane bound Hsp70; in the presence of perforin, granzyme B is taken up via perforin pore formation. Following uptake of granzyme B, apoptosis is initiated in membrane Hsp70 positive tumor cells. In the MHC class I-restricted antigen processing pathway, chaperones Hsp70 (HSPA6 and HSPA7) synthesized within the cell are polyubiquitinated in the cytoplasm and subsequently degraded by the PA28 proteasome. The resulting peptides, whether of optimal length or extended, are further processed by aminopeptidases, with cytoplasmic chaperones stabilizing these peptides. The Transporter associated with Antigen Processing (TAP1 and TAP2), linked to nascent MHC class I chains via tapasin, transports the peptides into the endoplasmic reticulum (ER). Inside the ER, peptides are further trimmed by ER aminopeptidases and then loaded onto MHC class I molecules. The oxidoreductase ERp57 helps maintain disulfide bonds, and high-affinity peptide binding prompts the release of MHC class I from the ER chaperone calreticulin, enabling its transport to the plasma membrane for presentation to the T cell receptor (TCR). The stress-responsive heat shock proteins 70 and 60 (HSP70, HSP60) play pivotal roles in cellular stress responses, shielding cells from adverse environmental conditions. HSP70 possesses the ability to impede apoptosis and other forms of cell death induced by various stimuli. Notably, malignant cells often exhibit heightened expression of HSP70, with some cancers depending on its overexpression to maintain malignant traits (27).

Several studies have corroborated the suppressive effects of HSP70 and HSP60 on multiple apoptotic pathways. Additionally, research has confirmed that HSP70 initiates anti-tumor immune responses through cytotoxic T lymphocytes (CTL) and natural killer (NK) cells. In HSP70-positive tumor cells, HSP70 activates NK cells by binding to HSP70 receptors such as the C-type lectin receptors CD94/NKG2C and NKG2D. Subsequently, activated NK cells induce tumor cell apoptosis through granzyme B-mediated pathways (28). Given the recognition of HSP70 as antigens by the immune system, there has been substantial progress in developing HSP70-based anticancer vaccines. These vaccines have demonstrated efficacy in clinical settings, benefiting cancer patients significantly. N. E. Blachere et al. employed HSP70/gp96 derived from cancer cells and virus-infected cells to elicit CD8+ cell-mediated anti-tumor responses (29).

Jinbao Zong et al. devised an immunization strategy utilizing a complex HSP70-HPV16 E7 antigen. Xiao-Ping Wang et al. engineered a vaccine comprising an HSP70/alpha-fetoprotein complex to elicit CD8+ activation immunization (30).
Abkin et al. showcased the effectiveness of purified HSP70-based gel in penetrating the outer layer of B16 tumors, eliciting intratumoral anti-tumor effects. Intratumorally derived HSP70 demonstrated significant antitumor efficacy when combined with phloretin in a murine melanoma model.Sato et al. reported on the immunization effects of leukemia cell-derived HSP70, enhancing the survival of BALB/c mice following syngeneic bone marrow transplantation (31).
Paulo Cesar Maciag et al. developed a recombinant fusion protein incorporating the human papillomavirus (HPV) E7 antigen and heat shock protein HSP65 from Mycobacterium bovis, currently undergoing phase III clinical trials as a potential therapy for HPV-associated conditions (32). Jianping Yuan et al. explored the application of mesothelin in conjunction with mycobacterial HSP70 in an in vivo model of ovarian cancer and mesothelioma (33).

Conclusion

In this study, it has been shown that metformin treatment may have important effects on the apoptosis in cells in prostate cancer. The results are important indicators that metformin can directly or indirectly have effects on prostate cancer. Most of the genes we identified have functions that slow down cell proliferation.
ANKRD1 plays a crucial role in tumor suppression by interacting with p53 and regulating MDM2, thereby promoting apoptosis and cell cycle arrest. Its involvement in multiple cellular pathways, including Hippo/YAP, NF-κB, and PI3K/AKT, further highlights its regulatory complexity. Understanding the precise molecular mechanisms governing ANKRD1 function in prostate cancer could open new avenues for therapeutic interventions, particularly in tumors that retain functional p53.
TCIM is a multifaceted protein with complex roles in cancer biology. While it has traditionally been associated with oncogenic Wnt/β-catenin activation, recent evidence suggests that it may also function as a tumor suppressor under specific conditions. Through its involvement in p53 stabilization, NF-κB signaling, NOTCH pathway modulation, autophagy, and epigenetic regulation, TCIM appears to exert diverse regulatory functions that influence tumor behavior. Understanding these mechanisms in greater detail may provide new insights into targeted cancer therapies that leverage TCIM's dual role in oncogenesis and tumor suppression.
EGR2 serves as a key regulator of apoptosis, with potential implications in prostate cancer pathogenesis and therapy. Through its modulation of mitochondrial apoptotic regulators, MEK/ERK signaling, and epigenetic mechanisms, EGR2 emerges as a promising target for therapeutic intervention. Future research into the precise role of EGR2 in prostate cancer could pave the way for novel treatment strategies that leverage its apoptotic and immune-regulatory functions to enhance tumor suppression and improve patient outcomes.
More in vitro and in vivo studies are needed to reveal which structural or functional components are responsible for this adverse effect on prostate cancer cells.

References

1- Gronich N, Rennert G. Beyond aspirin-cancer prevention with statins, metformin and bisphosphonates. Nat Rev Clin Oncol. 2013 Nov;10(11):625-42. doi: 10.1038/nrclinonc.2013.169. Epub 2013 Oct 1. PMID: 24080598.

2- Nathan N, Sullivan SD. The utility of metformin therapy in reproductive-aged women with polycystic ovary syndrome (PCOS). Curr Pharm Biotechnol. 2014;15(1):70-83. doi: 10.2174/1389201015666140330195142. PMID: 24720592.

3- Zhu N, Zhang Y, Gong YI, He J, Chen X. Metformin and lung cancer risk of patients with type 2 diabetes mellitus: A meta-analysis. Biomed Rep. 2015 Mar;3(2):235-241. doi: 10.3892/br.2015.417. Epub 2015 Jan 9. PMID: 26075077; PMCID: PMC4448013.

4- Markowicz-Piasecka M, Sikora J, Szydłowska A, Skupień A, Mikiciuk-Olasik E, Huttunen KM. Metformin - a Future Therapy for Neurodegenerative Diseases : Theme: Drug Discovery, Development and Delivery in Alzheimer's Disease Guest Editor: Davide Brambilla. Pharm Res. 2017 Dec;34(12):2614-2627. doi: 10.1007/s11095-017-2199-y. Epub 2017 Jun 6. PMID: 28589443; PMCID: PMC5736777.

5- Pan Q, Lu X, Zhao C, Liao S, Chen X, Guo F, Yang C, Liu HF. Metformin: the updated protective property in kidney disease. Aging (Albany NY). 2020 May 1;12(9):8742-8759. doi: 10.18632/aging.103095. Epub 2020 May 1. PMID: 32364526; PMCID: PMC7244070.

6- Zakikhani M, Dowling RJ, Sonenberg N, Pollak MN. The effects of adiponectin and metformin on prostate and colon neoplasia involve activation of AMP-activated protein kinase. Cancer Prev Res (Phila). 2008 Oct;1(5):369-75. doi: 10.1158/1940-6207.CAPR-08-0081. Erratum in: Cancer Prev Res (Phila Pa). 2009 Jan;2(1):95. PMID: 19138981.

7- Ben Sahra I, Laurent K, Loubat A, Giorgetti-Peraldi S, Colosetti P, Auberger P, Tanti JF, Le Marchand-Brustel Y, Bost F. The antidiabetic drug metformin exerts an antitumoral effect in vitro and in vivo through a decrease of cyclin D1 level. Oncogene. 2008 Jun 5;27(25):3576-86. doi: 10.1038/sj.onc.1211024. Epub 2008 Jan 21. PMID: 18212742.

8- Spratt DE, Zhang C, Zumsteg ZS, Pei X, Zhang Z, Zelefsky MJ. Metformin and prostate cancer: reduced development of castration-resistant disease and prostate cancer mortality. Eur Urol. 2013 Apr;63(4):709-16. doi: 10.1016/j.eururo.2012.12.004. Epub 2012 Dec 14. PMID: 23287698; PMCID: PMC4034673.

9- Taussky D, Preisser F, Karakiewicz PI, Tilki D, Lambert C, Bahary JP, Delouya G, Wistaff R, Laskine M, Nguyen PV, Durand M, Saad F. Impact of diabetes and metformin use on prostate cancer outcome of patients treated with radiation therapy: results from a large institutional database. Can J Urol. 2018 Oct;25(5):9509-9515. PMID: 30281009.

10- Richards KA, Liou JI, Cryns VL, Downs TM, Abel EJ, Jarrard DF. Metformin Use is Associated with Improved Survival for Patients with Advanced Prostate Cancer on Androgen Deprivation Therapy. J Urol. 2018 Dec;200(6):1256-1263. doi: 10.1016/j.juro.2018.06.031. Epub 2018 Jun 22. PMID: 29940252.

11- Wright JL, Stanford JL. Metformin use and prostate cancer in Caucasian men: results from a population-based case-control study. Cancer Causes Control. 2009 Nov;20(9):1617-22. doi: 10.1007/s10552-009-9407-y. Epub 2009 Aug 4. PMID: 19653109; PMCID: PMC2767519.

12- Azoulay L, Dell'Aniello S, Gagnon B, Pollak M, Suissa S. Metformin and the incidence of prostate cancer in patients with type 2 diabetes. Cancer Epidemiol Biomarkers Prev. 2011 Feb;20(2):337-44. doi: 10.1158/1055-9965.EPI-10-0940. Epub 2010 Dec 10. PMID: 21148757.

13- Malaguarnera R, Sacco A, Morcavallo A, Squatrito S, Migliaccio A, Morrione A, Maggiolini M, Belfiore A. Metformin inhibits androgen-induced IGF-IR up-regulation in prostate cancer cells by disrupting membrane-initiated androgen signaling. Endocrinology. 2014 Apr;155(4):1207-21. doi: 10.1210/en.2013-1925. Epub 2014 Jan 17. PMID: 24437490; PMCID: PMC3959597.

14- Chen J. The Cell-Cycle Arrest and Apoptotic Functions of p53 in Tumor Initiation and Progression. Cold Spring Harb Perspect Med. 2016 Mar 1;6(3):a026104. doi: 10.1101/cshperspect.a026104. PMID: 26931810; PMCID: PMC4772082.

15- Ben Sahra I, Regazzetti C, Robert G, Laurent K, Le Marchand-Brustel Y, Auberger P, Tanti JF, Giorgetti-Peraldi S, Bost F. Metformin, independent of AMPK, induces mTOR inhibition and cell-cycle arrest through REDD1. Cancer Res. 2011 Jul 1;71(13):4366-72. doi: 10.1158/0008-5472.CAN-10-1769. Epub 2011 May 3. PMID: 21540236.

16- Akinyeke T, Matsumura S, Wang X, Wu Y, Schalfer ED, Saxena A, Yan W, Logan SK, Li X. Metformin targets c-MYC oncogene to prevent prostate cancer. Carcinogenesis. 2013 Dec;34(12):2823-32. doi: 10.1093/carcin/bgt307. Epub 2013 Oct 15. PMID: 24130167; PMCID: PMC3845895.

17- Tilley WD, Wilson CM, Marcelli M, McPhaul MJ. Androgen receptor gene expression in human prostate carcinoma cell lines. Cancer Res. 1990 Sep 1;50(17):5382-6. PMID: 2386943.

18- Veldscholte J, Ris-Stalpers C, Kuiper GG, Jenster G, Berrevoets C, Claassen E, van Rooij HC, Trapman J, Brinkmann AO, Mulder E. A mutation in the ligand binding domain of the androgen receptor of human LNCaP cells affects steroid binding characteristics and response to anti-androgens. Biochem Biophys Res Commun. 1990 Dec 14;173(2):534-40. doi: 10.1016/s0006-291x(05)80067-1. PMID: 2260966.

19- Xu, X., Wang, X., Li, Y. et al. Research progress of ankyrin repeat domain 1 protein: an updated review. Cell Mol Biol Lett 29, 131 (2024). https://doi.org/10.1186/s11658-024-00647-w

20- Xu, X., Zhong, D., Wang, X. et al. Pan-cancer integrated analysis of ANKRD1 expression, prognostic value, and potential implications in cancer. Sci Rep 14, 5268 (2024). https://doi.org/10.1038/s41598-024-56105-2

21- Mazzeo L, Ghosh S, Di Cicco E, Isma J, Tavernari D, Samarkina A, Ostano P, Youssef MK, Simon C, Dotto GP. ANKRD1 is a mesenchymal-specific driver of cancer-associated fibroblast activation bridging androgen receptor loss to AP-1 activation. Nat Commun. 2024 Feb 3;15(1):1038. doi: 10.1038/s41467-024-45308-w. PMID: 38310103; PMCID: PMC10838290.

22- Jiménez AP, Traum A, Boettger T, Hackstein H, Richter AM, Dammann RH. The tumor suppressor RASSF1A induces the YAP1 target gene ANKRD1 that is epigenetically inactivated in human cancers and inhibits tumor growth. Oncotarget. 2017 May 23;8(51):88437-88452. doi: 10.18632/oncotarget.18177. PMID: 29179447; PMCID: PMC5687617

23- Li J, Huang Z, Wang P, Li R, Gao L, Lai KP. Therapeutic targets of formononetin for treating prostate cancer at the single-cell level. Aging (Albany NY). 2024 Jun 13;16(12):10380-10401. doi: 10.18632/aging.205935. Epub 2024 Jun 13. PMID: 38874510; PMCID: PMC11236323.

24- Labrecque MP, Brown LG, Coleman IM, et al. Targeting the fibroblast growth factor pathway in molecular subtypes of castration-resistant prostate cancer. The Prostate. 2024; 84: 100-110. doi:10.1002/pros.24630

25- Zhou, F., Gao, S., Han, D. et al. TMPRSS2-ERG activates NO-cGMP signaling in prostate cancer cells. Oncogene 38, 4397–4411 (2019). https://doi.org/10.1038/s41388-019-0730-9

26- In-Young Jung, Robert L. Bartoszek, Andrew J. Rech, Sierra M. Collins, Soon-Keat Ooi, Erik F. Williams, Caitlin R. Hopkins, Vivek Narayan, Naomi B. Haas, Noelle V. Frey, Elizabeth O. Hexner, Donald L. Siegel, Gabriela Plesa, David L. Porter, Adrian Cantu, John K. Everett, Sonia Guedan, Shelley L. Berger, Frederic D. Bushman, Friederike Herbst, Joseph A. Fraietta; Type I Interferon Signaling via the EGR2 Transcriptional Regulator Potentiates CAR T Cell–Intrinsic Dysfunction. Cancer Discov 1 July 2023; 13 (7): 1636–1655. https://doi.org/10.1158/2159-8290.CD-22-1175

27- Guzhova IV, Margulis BA. HSP70-based anti-cancer immunotherapy. Hum Vaccin Immunother. 2016 Oct 2;12(10):2529-2535. doi: 10.1080/21645515.2016.1190057. Epub 2016 Jun 13. PMID: 27294301; PMCID: PMC5084976.

28- Shevtsov MA, Pozdnyakov AV, Mikhrina AL, Yakovleva LY, Nikolaev BP, Dobrodumov AV, Komarova EY, Meshalkina DA, Ischenko AM, Pitkin E, Guzhova IV, Margulis BA. Effective immunotherapy of rat glioblastoma with prolonged intratumoral delivery of exogenous heat shock protein Hsp70. Int J Cancer. 2014 Nov 1;135(9):2118-28. doi: 10.1002/ijc.28858. Epub 2014 Apr 1. PMID: 24691976.

29- Li Y, Subjeck J, Yang G, Repasky E, Wang XY. Generation of anti-tumor immunity using mammalian heat shock protein 70 DNA vaccines for cancer immunotherapy. Vaccine. 2006 Jun 19;24(25):5360-70. doi: 10.1016/j.vaccine.2006.04.028. Epub 2006 May 2. PMID: 16714072.

30- Blachere NE, Li Z, Chandawarkar RY, Suto R, Jaikaria NS, Basu S, Udono H, Srivastava PK. Heat shock protein-peptide complexes, reconstituted in vitro, elicit peptide-specific cytotoxic T lymphocyte response and tumor immunity. J Exp Med. 1997 Oct 20;186(8):1315-22. doi: 10.1084/jem.186.8.1315. PMID: 9334371; PMCID: PMC2199095.

31- Zong J, Wang C, Wang Q, Peng Q, Xu Y, Xie X, Xu X. HSP70 and modified HPV 16 E7 fusion gene without the addition of a signal peptide gene sequence as a candidate therapeutic tumor vaccine. Oncol Rep. 2013 Dec;30(6):3020-6. doi: 10.3892/or.2013.2742. Epub 2013 Sep 20. PMID: 24065282.

32- Abkin SV, Ostroumova OS, Komarova EY, Meshalkina DA, Shevtsov MA, Margulis BA, Guzhova IV. Phloretin increases the anti-tumor efficacy of intratumorally delivered heat-shock protein 70 kDa (HSP70) in a murine model of melanoma. Cancer Immunol Immunother. 2016 Jan;65(1):83-92. doi: 10.1007/s00262-015-1778-1. Epub 2015 Dec 8. PMID: 26646850.

33- Sato K, Torimoto Y, Tamura Y, Shindo M, Shinzaki H, Hirai K, Kohgo Y. Immunotherapy using heat-shock protein preparations of leukemia cells after syngeneic bone marrow transplantation in mice. Blood. 2001 Sep 15;98(6):1852-7. doi: 10.1182/blood.v98.6.1852. PMID: 11535521.

34- Yuan J, Kashiwagi S, Reeves P, Nezivar J, Yang Y, Arrifin NH, Nguyen M, Jean-Mary G, Tong X, Uppal P, Korochkina S, Forbes B, Chen T, Righi E, Bronson R, Chen H, Orsulic S, Brauns T, Leblanc P, Scholler N, Dranoff G, Gelfand J, Poznansky MC. A novel mycobacterial Hsp70-containing fusion protein targeting mesothelin augments antitumor immunity and prolongs survival in murine models of ovarian cancer and mesothelioma. J Hematol Oncol. 2014 Feb 24;7:15. doi: 10.1186/1756-8722-7-15. PMID: 24565018; PMCID: PMC3943805.

➢ *POSTER PRESENTATION*

Densities Of 1,2-Dichloroalkane With Tertio Butyl Methyl Ether At Different Temperatures.

BOUSSAID Linda[1*], AMIRECHE Fouzia[2], ZOUAGHI Nafila[3], BENSIRADJ Nour El Houda[4]

[*1]University of Science and Technology Houari Boumediene (USTHB),Faculty of Chemistry, Bab-Ezzouar, Algeria.
[2]University of Science and Technology Houari Boumediene(USTHB), Faculty of Chemistry, Bab-Ezzouar, Algeria.
[3]Hight School Teachers, Department of Chemistry, Old Kouba (ENS), Algeria.
[4]University of Science and Technology Houari Boumediene(USTHB), Faculty of Chemistry, Bab-Ezzouar, Algeria.

Abstract

Experimental data of excess thermodynamic properties, for liquid mixtures, are essential for good design of industrial chemical process and for the development of models describing the thermodynamic behaviour of these mixtures. Excess volume represents, besides many important properties, a good thermodynamic tool to explore the behaviour of liquid mixture. Chloroalcanes and ethers represent not only two technically important classes of compounds, but also, from a theoretical point of view, two interesting families of molecules. Indeed, chloroalcanes, amines are self-associated organic liquids and well-known polar solvents used in wide range of applications (pharmaceutical industry and cosmetics, manufacturing perfumes and paint removers, and flavors). Ethers are also industrially important solvents used in several chemical reactions. So, Methyl tertiobutyl ether, with a zero dipole moment, is a good aprotic solvent. Moreover, chloroalcanes, ethers, and their mixtures are used as fuel additives, resulting from increasing fuel demand, environmental concern and occasional oil crises. This work is a theoretical, experimental and theoretical study of the volumetric properties of binary liquid systems 1,2-dichloroethane + methyl tertio butyl ether. The first experimental part of this study begins with a determination of the excess molar volumes of the binary systems studied, from the densities of the liquid mixtures and pure constituents, at several temperatures between [288 and 303] K determined by the Densitometric experimentanal technique ogine-with vibrating tube. The second theoretical part of this study consists of application of the Prig Flory-Patterson theoretical model to the studied binary systems.

Keywords: Densities, Molar Volume Excess, 1,2-Dichloroethane, MTBE, Flory Patterson

INTRODUCTION

This study investigates the excess molar volumes of the binary liquid mixture 1,2-dichloroethane + methyl tert-butyl ether, which are important for designing chemical processes and modeling thermodynamic behavior. Experimental measurements were conducted using a vibrating-tube densimeter at temperatures ranging from 288 to 303 K. Theoretical analysis was performed using the Prigogine–Flory–Patterson (PFP) model. The study highlights the significance of chloroalkanes and ethers as industrial solvents and fuel additives.

MATERIALS AND METHODS

The organic liquids used were obtained from different sources and used without further purifications. The purity of the chemical products was compared by measuring the densities which was in good agreement with literature values. Densities of pure components and mixtures were measured using an Anton Paar vibrating U-tube densimeter (Model DMA-5000). Uncertainty of the density measurements was estimated to be within $\pm 10^{-5}$ g.cm^{-3}. The temperature in the cell was regulated to ± 0.01 K with a built-in Peltier device. The apparatus was calibrated once day with dry air and do uble-distilled freshly degassed water. Binary mixture samples were prepared in a 10 ml vial by mass using a Metler balance with a precision of $\pm 1.10^{-3}$ g, charging the heavier component first to minimize vaporization effects. Uncertainties in mole fraction and excess molar volume are estimated to be less than $\pm 10^{-4}$ and $\pm 5\ 10^{-3}$ cm^3 mol^{-1}, respectively.



Figure 1. Image of the apparatus used for density measurements, an Anton Paar vibrating U-tube densimeter (DMA-5000).

Table 1. Chemicals used

compounds	Formule	Cas Number	Source	Purity
Methyl TeriobutylEther (MTBE)	$C_5H_{12}O$	1634-04-4	Fluka	99%
1,2-Dichloroethane (1,2-DCE)	$C_2H_4CL_2$	107-06-2	Fluka	99%

Equations

The excess molar volumes of all mixtures were calculated using the following equation:

$$V^E_m = \Sigma^n_{i=1} x_i M_i [1/\rho_0 - 1/\rho_i] \quad \text{..... (1)}$$

Where is the density of the mixture, is the density of pure component, x_i is the mole fraction, M_i is molecular weight of component i, and n stands for the number of components in the mixture.

V^E_m of binary mixtures were correlated by the Redlich-Kister equation [1] :

$$V^E = x_1 x_2 \Sigma^{i=n}_{i=0} A_i (x_1 - x_2)^i \quad \text{.....(2)}$$

Where x_i is the mole fraction of component i, A_k are adjustable coefficients obtained by fitting, and n is the degree of the polynomials. The results are given in table (1) together with corresponding standard deviations. The standard deviation values were calculated using the following equation:

$$\delta = [\ \Sigma\ (V^E_{m,Exp} - V^E_{m,cal})^2 / (N - p)\ ]^{1/2} \quad \text{..... (3)}$$

Where $V^E_{m,\ Exp}$ and $V^E_{m,\ Cal}$ are the experimental and calculated values of the excess molar volumes respectively, and N and p are the number of data points and number of fitted parameters.

Results and discussion

The excess molar volume, V^E values are positive for all the binary systems, over the whole composition range, and at all the working temperatures. As the temperature increases, the V^E magnitude increases for all the mixtures, except 1,2-DCE+DDE system, for which the V^E magnitude decreases with temperature inhancement.

It is well known that the excess volume is the result of several opposing effects. The positive contribution arises from the breaking of hydrogen bonds in the self-associated alkanol and dipole-dipole interactions between alkanol monomers and multimers.

Negative contributions are due to interactions between unlike molecules or structural effects such as interstitial accommodation or changes in free volume.

The observed positive V^E values for the mixtures indicate the predominance of the disruption of hydrogen bonds of the alkanol multimers over the factors contributing to the volume contraction.

Table 2. Parameters A_k of Eq 2 and Standard Deviations, *s*, at T= 298.15 K for the binary mixtures.

A_0	A_1	A_2	A_3	V^E ($cm^3.mol^{-1}$)
0,58251	0,46406	0,13297	-0,27981	0,0018

The positive values of V^E for these three 1,2-DCE + ether systems can be interpreted in terms of two main effects: i) non-insertion of 1,2-DCE molecules into the molecular structure of the ether , due to a relatively small difference between the molar volume of 1,2-DCE and those of the two ethers the possible existence of a specific interaction, if one took as reference of the MTBE , where no specific interaction exists. Indeed, these three systems have excess volumes which are, on the one hand, positive throughout the composition domain and, on the other hand, higher than those of the 1.2-DCE binary systems. The enthalpies of negative excess, mixtures of 1,2-DCE with the MTBE ether, determined in a previous work [1], support this possibility.

Our experimental EV data, for the 1,2-DCE + MTBE system, are consistent with those of other authors, For the other systems we did not find any comparative data in the literature.

The 1,2-DCE + Methyl tertiobutyl ethyl (MTBE) system has negative V^E, thrughout the composition range, and throughout the temperature range [288-303] K. The magnitude of V^E increases as the temperature increases and the representative curves of V^E variations, as a function of composition, throughout this temperature range are somewhat asymmetrical and have an extremum for $x_1 = 0.4$.These negative values of V^E are probably due to the existence of a strong specific interaction, more important than the resultant of the self-association effect of the amine and the small difference between the molar volumes of the constituents; note that this preponderance decreases with increasing temperature.

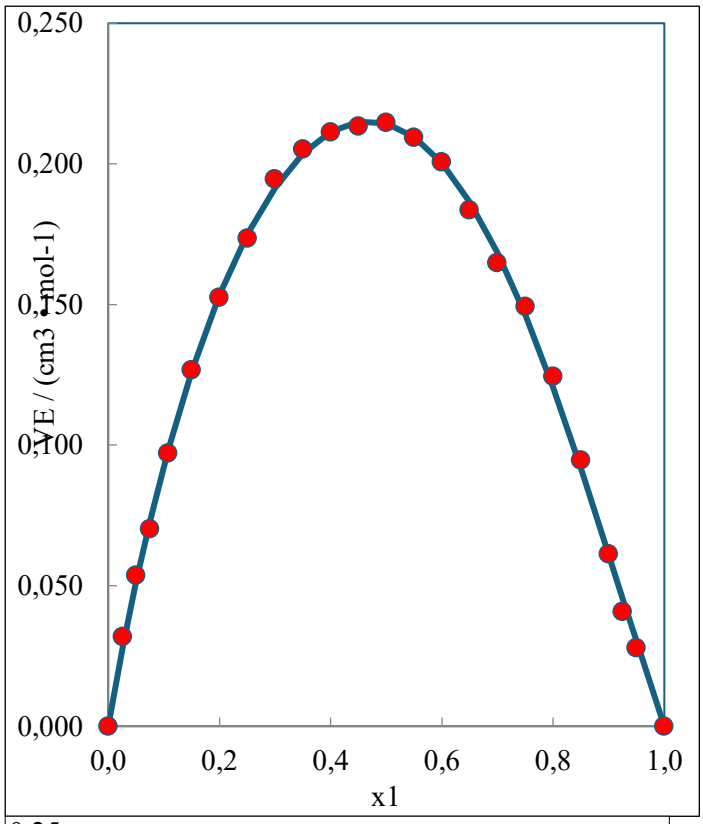

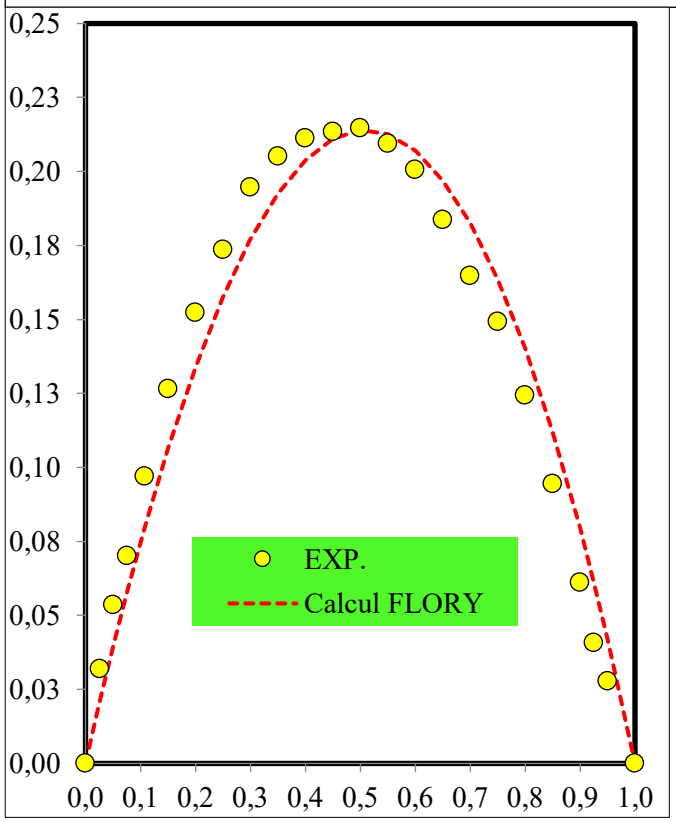

Figure 2. Excess molar volumes V^E, for binary mixtures of Excess molar volumes V^E, for binary mixtures of 1,2-DCE (1) + MTBE (2) at T = 298.15 K.

CONCLUSION

1,2-DCE + MTBE, binary mixtures show positive V^E values, over all the composition range. V^E values, at x=0,5, are in the sequence : MTBE < 1,2-DCE As expected, V^E values for these associated mixtures are predicted by PFP model.

REFERENCES

- Valtz, A.; Coquelet, C.; Boukais-Belaribi, G.; Dahmani, A.; Belaribi, F. B. Volumetric Properties of Binary Mixtures of 1,2-Dichloroethane with Polyethers from (283.15 to 333.15) K and at Atmospheric Pressure J. Chem. Eng. Data 2011, 56, 1629–1657.
- Flory, P. J.; Orwoll, R. A.; Vrij, A. Statistical thermodynamics of chain molecule liquids. II. Liquid mixtures of normal paraffin hydrocarbons. *J. Am. Chem. Soc.* 1964, *86*, 3507–3515..
- Patterson, D.; Delmas, G. Corresponding states theories and liquid models. *Discuss. Faraday Soc.*1970, *49*, 98-105.
- Amireche-Ziar, F.; Richon, D.; Belaribi, F. B. Excess molar enthalpies for binary mixtures of 1,2-dichloroethane with ethers at 298.15 K and atmospheric pressure Fluid Phase Equilib. 337 (2013) 255–258



EurasianSciEnTech 2025

www.eurasianscientech.org